

PROCEEDINGS

VOLUME 1

**PERMAFROST**

Sixth International Conference

# PERMAFROST

Sixth International Conference

PROCEEDINGS (Vol. 1)

July 5—9, 1993

Beijing China

Organized by

Lanzhou Institute of Glaciology and Geocryology,  
Chinese Academy of Sciences & Chinese Society of  
Glaciology and Geocryology

South China University of Technology Press

[粤]新登字12号

Permafrost Sixth International Conference Proceedings (Vol. 1)

Published by South China University of Technology Press

(Wushan Guangzhou China)

First Published 1993

ISBN 7-5623-0484-X/P·1

## Preface

About one-fifth of the land area of the earth is underlain by perennially frozen ground, or permafrost. It affects many human activities, causing unique problems in the environment, ecosystem, resource development and constructions in cold regions. Since permafrost is a thermal condition, it is very sensitive to changes in climate. Global warming could result in permafrost degradation, causing resultant ecological and socioeconomic consequences. Thus, permafrost has become more and more important in the development of polar and high altitude regions which occupy key positions in the global system.

It is necessary to give scientists and engineers an opportunity to meet regularly in order to discuss the state of the art of science and technology in their fields, and to gain the impetus for further work, as well as to compare permafrost conditions with other regions of the world, particularly regions where only seasonally frozen soils currently exist. The International Conferences on Permafrost are organized to serve this purpose.

The First International Conference on Permafrost was therefore held in the United States at Purdue University, in 1963; the Second in Yakutsk, Siberia, 1973; the Third in Edmonton, Canada, 1978; the Fourth in Fairbanks, Alaska, 1983; and the Fifth in Trondheim, Norway, 1988.

The Sixth International Conference on Permafrost was co-sponsored by several national scientific and technical organizations, and was held under the auspices of the Chinese Society of Glaciology and Geocryology (CSGG), which is in the Adhering National Body of the International Permafrost Association (IPA), and was organized by the Lanzhou Institute of Glaciology and Geocryology (LIGG), Chinese Academy of Sciences, with the collaboration of the State Key Laboratory of Frozen Soil Engineering, LIGG. The support and the guidance of the International Permafrost Association were extremely important for us in preparation for the conference.

A total of 189 contributed papers are included in this first volume of the proceedings which contains almost all the papers accepted for presentation at the paper sessions. A second volume containing reports of Special Sessions, additional contributed papers, poster papers, etc. will be published at a later date. Many scientific and engineering disciplines were represented, including physics, chemistry and mechanics of frozen soil, geophysics, periglacial geomorphology, soil science, climatology, hydrology, ecology, civil and mechanical engineering. The high quality of the papers was the result of hard work by the authors, as well as from the assistance given by the Editorial Committee of the International Permafrost Association, and by the numerous reviewers in the member countries.

Finally, the Chinese Organizing Committee wishes to acknowledge all of you that have participated in the preparation for this conference: the authors of the papers, the reviewers, the sponsors, the publisher, and the staff of many institutions that have been working to make it a successful conference.

Cheng Guodong  
Chairman  
Chinese Organizing Committee  
Sixth International  
Conference on Permafrost

## Contributing Sponsors

The Financial Support to the Sixth International Conference on Permafrost is mainly contributed by the following organizations.

### Governmental

Commission of National Natural Science Foundation of China;  
Chinese Academy of Sciences;  
Geography Society of China.

### Nongovernmental

The First Highway Survey & Design Institute, Ministry of Communication;  
Cold Regions Development & Research Society of China;  
Central Coal Mining Research Institute, Ministry of Coal Mining of China;  
Heilongjiang Provincial Institute of Water Conservancy Science;  
The First Survey & Design Institute, Ministry of Railway of China;  
Heilongjiang Provincial Institute of Cold Region Construction Science;  
Heilongjiang Provincial Institute of Communication Science;  
Northwest Institute of Railway Science, Ministry of Railway of China;  
Gansu Provincial Institute of Water Conservancy Science;  
Northeast Survey & Design Institute, Ministry of Water Conservancy;  
Mining Industry University of China;  
Inner Mongolia Institute of Water Conservancy Science;  
Jilin Provincial Institute of Water Conservancy Science.

## Chinese Honorary Committee

Chairman: Zhou Guangzhao      President of Chinese Academy of Sciences,  
Academician.  
Vice-Chairmen: Sun Honglie      President of Natural Resources Expedition  
Commission of China, Academician.  
Liu Tungsheng      President of International Union for Quaternary  
Research, Academician.  
Sun Shu      Vice-President of the National Natural Science  
Foundation of China, Academician.  
Zhu Lilan      Vice-President of the State Science and  
Technology Commission of China, Academician.  
Liu Shu      Professor, the State Science and Technology  
Association of China.  
Members: Li Jiejun      Li Yusheng      Wang Sijing  
Zheng Du      Xu Shaoxing

### Consultative Committee

Chairman: Shi Yafeng      Academician  
Vice-Chairmen: Dai Moan      Vice-Governor of Heilongjiang Province.  
Yang Shengfu      Director of Engineering Administration,  
Department of the Ministry of Communications  
of China.  
Zhang Xiangong      Professor, Geology University of China  
Members: Zhu Xuan      Dai Dingzong      Xu Ronglie  
Ouyang Ziyuan      Xue Shiying      Weng Shida  
Zhang Jiazhen      Zhao Chunian      Cui Zijiu

### Organizing Committee

Chairman: Cheng Guodong  
Vice-Chairmen: Wu Ziwang      Zhou Youwu      Yu Xiang  
Ge Qihua      Zhang Jie  
Secretary-General: Zhu Yuanlin  
Associate Secretary-Generals: Xu Xiaozu      Chen Xiaobai      Tong Boliang  
Huang Yizhi      Qiu Guoqing      Tong Changjiang  
Gu Zhongwei  
Members: Wu Jingming      Yu Qun      Liu Hongxu  
Huang Xiaoming      Jia Jianhua      Zhu Qiang  
Dai Huiming      Xie Yingqi      Xu Bomong  
Lu Guowei  
Overseas Members: J. Brown      H.M. French      N.A. Grave

### Review Process

The review of abstracts and manuscripts for this pre-Conference publication was conducted under the supervision of the Chinese Organizing Committee and the IPA Editorial Committee. Approximately 450 abstracts were received from 24 countries. It was necessary to limit the number of papers from Russia and China. These countries were asked to invite a more limited number of appropriate papers. A review form was agreed to and each paper received two or more reviews. Some papers were rejected; in other cases the authors simply did not submit manuscripts. Individuals without papers were encouraged to submit posters and have their abstracts published in a post-Conference volume. In order to save time and to employ native languages in the reviews, all Chinese and Mongolian papers were reviewed in China and all Russian papers were reviewed in Russia, employing the standard review form. All Russian and Chinese reviewed papers were available in English in August 1992 when members of the Editorial Committee met in Washington, D.C., during the IPA Council meeting. The papers and review forms were examined and discussed at that time, and members of the IPA Council were asked to assist with additional reviews.

Review of the 100 non-Chinese or -Russian papers involved reviewers from many of the IPA member countries. This review process was conducted by

the Chair, IPA Editorial Committee, in consultation with members of the Committee. Below is a list of all individuals who provided these reviews. The IPA Editorial Committee and the Chinese Organizing Committee express their appreciation to all those who devoted their valuable time and expertise to this process. Deserving particular thanks for their assistance in selecting reviewers and following up with many of them are Alan Heginbottom, Geological Survey of Canada; Nikolai Grave and Valery Volgina, Russian Academy of Sciences; Eugene Marvin, Cold Regions Research and Engineering Laboratory, representing the American Society of Civil Engineers; and John Zarling, University of Alaska, representing the American Society of Mechanical Engineers. The Cold Regions Research and Engineering Laboratory is gratefully acknowledged for furnishing instructions, samples and layout sheets for preparation of final camera copy for the proceedings volumes. Members of the IPA Editorial Committee are:

Jerry Brown, Chair, USA  
H.M. French, Canada  
N.A. Grave, Russia  
Cheng Guodong, China  
L. King, Germany  
E.A. Koster, The Netherlands  
T.L. Péwé, Ex Officio, IPA Executive Committee

### Reviewers

H. Jonas Akerman, University of Lund, Lund, Sweden  
Donald Albert, Cold Regions Research and Engineering Laboratory, Hanover, New Hampshire, USA  
Bernard Alkire, Michigan Technological Institute, Houghton, Michigan, USA  
Duwayne Anderson, Texas A&M University, College Station, Texas, USA  
Ronald Atkins, West Lebanon, New Hampshire, USA  
Abdul Aziz, Gonzaga University, Spokane, Washington, USA  
T.H.W. Baker, National Research Council of Canada, Ottawa, Ontario, Canada  
Richard Berg, Cold Regions Research and Engineering Laboratory, Hanover, New Hampshire, USA  
Patrick Black, Cold Regions Research and Engineering Laboratory, Hanover, New Hampshire, USA  
George Blaisdell, Cold Regions Research and Engineering Laboratory, Hanover, New Hampshire, USA  
Steven Blasco, Geological Survey of Canada, Dartmouth, Nova Scotia, Canada  
Jerry Brown, Arlington, Virginia, USA  
Margo M. Burgess, Geological Survey of Canada, Ottawa, Ontario, Canada  
Chris Burn, Carleton University, Ottawa, Ontario, Canada  
Nel Caine, University of Colorado, Boulder, Colorado, USA  
L. David Carter, U.S. Geological Survey, Anchorage, Alaska, USA  
Edward Chacho, Jr., Cold Regions Research and Engineering Laboratory, Hanover, New Hampshire, USA  
Edward Chamberlain, Cold Regions Research and Engineering Laboratory, Hanover, New Hampshire, USA  
Ian D. Clark, University of Ottawa, Ottawa, Ontario, Canada  
Gary Clow, U.S. Geological Survey, Menlo Park, California, USA  
Bill Connor, Alaska Department of Transportation and Public Facilities, Fairbanks, Alaska, USA  
Scott Crowther, Crowther Associates, Anchorage, Alaska, USA  
Scott Dallimore, Geological Survey of Canada, Ottawa, Ontario, Canada  
Larry Dingman, University of New Hampshire, Durham, New Hampshire, USA  
Jean-Claude Dionne, Université Laval, Québec City, Québec, Canada  
Francesco Dramis, Università di Camerino, Camerino, Italy  
Larry Dyke, Geological Survey of Canada, Ottawa, Ontario, Canada  
Robert Eaton, Cold Regions Research and Engineering Laboratory, Hanover, New Hampshire, USA  
P.A. Egginton, Geological Survey of Canada, Ottawa, Ontario, Canada

David Esch, Alaska Department of Transportation and Public Facilities, Juneau, Alaska, USA

K.R. Everett, Ohio State University, Columbus, Ohio, USA

Oscar Ferrians, U.S. Geological Survey, Anchorage, Alaska, USA

Kaare Flaate, Norwegian Road Administration, Oslo, Norway

D.C. Ford, McMaster University, Hamilton, Ontario, Canada

Stephen Forman, Ohio State University, Columbus, Ohio, USA

Hugh M. French, University of Ottawa, Ottawa, Ontario, Canada

Masami Fukuda, Hokkaido University, Sapporo, Japan

John R. Giardino, Texas A&M University, College Station, Texas, USA

Odd Gregersen, Norwegian Geotechnical Institute, Oslo, Norway

George Gryc, U.S. Geological Survey, Menlo Park, California, USA

Wilfried Haerberli, Versuchsanstalt für Wasserbau, Hydrologie und Glaziologie, Zurich, Switzerland

Bernard Hallet, University of Washington, Seattle, Washington, USA

Stuart A. Harris, University of Calgary, Calgary, Alberta, Canada

William D. Harrison, University of Alaska, Fairbanks, Alaska, USA

David G. Harry, Energy, Mines and Resources, Ottawa, Ontario, Canada

Donald W. Hayley, EBA Engineering Consultants, Ltd., Edmonton, Alberta, Canada

Beez Hazen, Northern Engineering and Scientific, Anchorage, Alaska, USA

J. Alan Heginbottom, Geological Survey of Canada, Ottawa, Ontario, Canada

Karen Henry, Cold Regions Research and Engineering Laboratory, Hanover, New Hampshire, USA

Christopher E. Heuer, Exxon Production Research Co., Houston, Texas, USA

Ken Hinkel, University of Cincinnati, Cincinnati, Ohio, USA

Larry Hinzman, University of Alaska, Fairbanks, Alaska, USA

Pieter Hoekstra, Blackhawk Geosciences, Inc., Golden, Colorado, USA

Vincent Janoo, Cold Regions Research and Engineering Laboratory, Hanover, New Hampshire, USA

Thomas Jenkins, Cold Regions Research and Engineering Laboratory, Hanover, New Hampshire, USA

Nils Johansen, University of Alaska, Fairbanks, Alaska, USA

G.H. Johnston, Ottawa, Ontario, Canada

Alan S. Judge, Geological Survey of Canada, Ottawa, Ontario, Canada

Douglas Kane, University of Alaska, Fairbanks, Alaska, USA

B.D. Kay, University of Guelph, Guelph, Ontario, Canada

G. Peter Kershaw, University of Alberta, Edmonton, Alberta, Canada

Stephen Ketcham, Cold Regions Research and Engineering Laboratory, Hanover, New Hampshire, USA

John Kimble, Soil Conservation Service, Lincoln, Nebraska, USA

Lorenz King, Justus Liebig Universität, Giessen, Germany

Eduard Koster, University of Utrecht, Utrecht, The Netherlands

William B. Krantz, University of Colorado, Boulder, Colorado, USA

Raymond A. Kreig, RA Kreig & Associates, Anchorage, Alaska, USA

Pavel J. Kurfurst, Geological Survey of Canada, Ottawa, Ontario, Canada

Arthur H. Lachenbruch, U.S. Geological Survey, Menlo Park, California, USA

Branko Ladanyi, Université de Montréal, Québec, Canada

J.P. Lautridou, Centre de Géomorphologie, Caen, France

Antoni G. Lewkowicz, Erindale College, University of Toronto, Mississauga, Ontario, Canada

B.H. Luckman, University of Western Ontario, London, Ontario, Canada

Virgil Lunardini, Cold Regions Research and Engineering Laboratory, Hanover, New Hampshire, USA

Phillip Marsh, National Hydrology Research Institute, Saskatoon, Saskatchewan, Canada

Terry McFadden, University of Alaska, Fairbanks, Alaska, USA

J.D. McKendrick, University of Alaska, Palmer, Alaska, USA

Brainerd Mears, University of Wyoming, Laramie, Wyoming, USA

Michael Metz, GeoTech Services, Inc., Golden, Colorado, USA

Bruce Molnia, U.S. Geological Survey, Reston, Virginia, USA

Yoshisuke Nakano, Cold Regions Research and Engineering Laboratory, Hanover, New Hampshire, USA

F.E. Nelson, Rutgers University, New Brunswick, New Jersey, USA

J.F. Nixon, Nixon Geotech, Calgary, Alberta, Canada

Walter Oechel, San Diego State University, San Diego, California, USA

Kevin O'Neill, Cold Regions Research and Engineering Laboratory, Hanover, New Hampshire, USA

Thomas Osterkamp, University of Alaska, Fairbanks, Alaska, USA

Samuel I. Outcalt, University of Michigan, Ann Arbor, Michigan, USA

Kim Peterson, University of Alaska, Anchorage, Alaska, USA

Troy L. Péwé, Arizona State University, Tempe, Arizona, USA

J.A. Pilon, Geological Survey of Canada, Ottawa, Ontario, Canada

Wayne Pollard, McGill University, Montréal, Québec, Canada

Vern Rampton, Terrain Analysis and Mapping Services Ltd., Carp, Ontario, Canada

W.R. Rouse, McMaster University, Hamilton, Ontario, Canada

Frank Sayles, Cold Regions Research and Engineering Laboratory, Hanover, New Hampshire, USA

D.C. Sego, University of Alberta, Edmonton, Alberta, Canada

Paul V. Sellmann, Cold Regions Research and Engineering Laboratory, Hanover, New Hampshire, USA

Gaius Shaver, Marine Biological Laboratory, Woods Hole, Massachusetts, USA

Sally Shoop, Cold Regions Research and Engineering Laboratory, Hanover, New Hampshire, USA

Yuri Shur, RA Kreig & Associates, Anchorage, Alaska, USA



Michael Smith, Carleton University, Ottawa, Ontario, Canada

C. Tarnocai, Agriculture Canada, Ottawa, Ontario, Canada

Rupert G. Tart, Jr., Golden Associates, Inc., Anchorage, Alaska, USA

J.C.F. Tedrow, Rutgers University, New Brunswick, New Jersey, USA

Howard Thomas, America North Inc., Anchorage, Alaska, USA

Clement Tremblay, Ministry of Transport, St. Foy, Québec, Canada

Rein Vaikmae, Estonian Academy of Sciences, Tallinn, Estonia

Robert O. Van Everdingen, Arctic Institute of North America, Calgary, Alberta, Canada

Brigitte van Vliet-Lange, Centre de Géomorphologie, Caen, France

Theodore Vinson, Oregon State University, Corvallis, Oregon, USA

John Vittek, Oklahoma State University, Stillwater, Oklahoma, USA

Donald A. Walker, INSTAAR, University of Colorado, Boulder, Colorado, USA

James Walters, University of Northern Iowa, Cedar Falls, Iowa, USA

Baolai Wang, University of Ottawa, Ottawa, Ontario, Canada

A. Lincoln Washburn, University of Washington, Seattle, Washington, USA

Kathleen D. White, Cold Regions Research and Engineering Laboratory, Hanover, New Hampshire, USA

Sidney White, Ohio State University, Columbus, Ohio, USA

Peter J. Williams, Carleton University, Ottawa, Ontario, Canada

Ming-Ko Woo, McMaster University, Hamilton, Ontario, Canada

John Zarling, University of Alaska, Fairbanks, Alaska, USA

Bai Chongyuan, LIGG, Chinese Academy of Sciences, China

Chen Xiaobai, LIGG, Chinese Academy of Sciences, China

Cheng Guodong, LIGG, Chinese Academy of Sciences, China

Gu Zhongwei, LIGG, Chinese Academy of Sciences, China

Guo Dongxing, LIGG, Chinese Academy of Sciences, China

Huang Yizhi, LIGG, Chinese Academy of Sciences, China

Kang Ersi, LIGG, Chinese Academy of Sciences, China

Li Guoliang, Northwest Institute of Railway Science, Ministry of Railway, China

Li Shude, LIGG, Chinese Academy of Sciences, China

Liu Tieliang, Northwest Institute of Railway Science, Ministry of Railway, China

Qiu Guoqing, LIGG, Chinese Academy of Sciences, China

Sheng Zhongyan, LIGG, Chinese Academy of Sciences, China

Tong Boliang, LIGG, Chinese Academy of Sciences, China

Tong Changjiang, LIGG, Chinese Academy of Sciences, China

Wu Bangjun, LIGG, Chinese Academy of Sciences, China

Wu Ziwan, LIGG, Chinese Academy of Sciences, China

Xu Xiaozu, LIGG, Chinese Academy of Sciences, China

Zeng Zhonggong, LIGG, Chinese Academy of Sciences, China

Zhang Changqing, LIGG, Chinese Academy of Sciences, China

Zhou Youwu, LIGG, Chinese Academy of Sciences, China

Zhu Qiang, Gansu Provincial Institute of Water Conservancy Science, Ministry of Water Conservancy, China

Zhu Linnan, LIGG, Chinese Academy of Sciences, China

Zhu Yuanlin, LIGG, Chinese Academy of Sciences, China

V.T. Balobaev, Permafrost Institute, Siberian Branch of the Russian Academy of Sciences, Yakutsk, Russia

L.N. Chrustalev, Moscow State University, Moscow, Russia

V.P. Chernjadiev, Institute of Engineering Construction Survey, Moscow, Russia

G.I. Dubikov, Institute of Engineering Construction Survey, Moscow, Russia

A.D. Frolov, Russian Humanities University, Moscow, Russia

B.U. Genadinnik, Institute of Cryosphere of the Siberian Branch of the Russian Academy of Sciences, Tyumen, Russia

N.A. Grave, Russian National Permafrost Committee, Russian Academy of Sciences, Moscow, Russia

S.E. Grechishev, Institute of Hydrogeology and Engineering Geology, Moscow, Russia

I.E. Gurianov, Permafrost Institute, Siberian Branch of the Russian Academy of Sciences, Yakutsk, Russia

I.V. Klimovsky, Permafrost Institute, Siberian Branch of the Russian Academy of Sciences, Yakutsk, Russia

A.A. Mandarov, Permafrost Institute, Siberian Branch of the Russian Academy of Sciences, Yakutsk, Russia

N.G. Moskalenko, Institute of Hydrogeology and Engineering Geology, Moscow, Russia

A.V. Pavlov, Institute of Hydrogeology and Engineering Geology, Moscow, Russia

O.P. Pavlova, Institute of Engineering Construction Survey, Moscow, Russia

N.N. Romanovsky, Moscow State University, Moscow, Russia

G.E. Rosenbaum, Moscow State University, Moscow, Russia

A.V. Sadovsky, Institute of Basements and Underground Constructions, Moscow, Russia

N.V. Tumel, Moscow State University, Moscow, Russia

K.F. Voitkovsky, Moscow State University, Moscow, Russia

S.S. Vyalov, Moscow Engineering Construction Institute, Moscow, Russia

Yu.K. Zaretsky, Institute "Hydroproject," Moscow, Russia

Jerry Brown  
Chairman of the  
IPA Editorial Committee

Zhu Yuanlin  
Secretary-General of the  
Chinese Organizing Committee

## Contents

Plastic Frozen (Saline) Soil as Bases Aksekov V.I. and Bruskov A.V.	1
Quaternary Geology and Geocryology in Nunavik, Canada Allard Michel, Tremblay Clement, Pilon Jean A. and Frydecki Janusz	5
Influence of Climate Change on Highway Embankment Stability and Permafrost in the Permafrost Region of the Qinghai-Xizang Plateau An Weidong, Wu Ziwang, Zhu Yuanlin and Judge A.S.	11
Temperature Variations in the Active Layer of Permafrost Aziz A. and Lunardini V.J.	17
Sixth International Conference on Permafrost Towards A Permafrost Information and Data System Barry R.G. and Brennan A.M.	23
Active Rockglaciers and the Lower Limit of Discontinuous Alpine Permafrost in the Khumbu Himalaya, Nepal Barsch Dietrich and Jakob Matthias	27
Seasonal Changeability of Physicochemical Properties of Permafrost Active Layer Waters in the Recherche Fiord Region (Western Spitsbergen) Bartoszewski Stefan A., Michalczyk Zdzislaw and Magierski Jan	32
Distribution of Permafrost, Glaciers, and Rock Glaciers in the Italian Mountains and Correlations with Climate: An Attempt to Synthesize Belloni S., Carton A., Dramis F. and Smiraglia C.	36
Time Dependent Displacement of Piles in Saline Permafrost Biggar Kevin W., Hivon Elisabeth G. and Sego Dave C.	42
Sudden Drainage of A Thaw Lake on the Alaskan Arctic Coastal Plain Brewer M.C., Carter L.D., Glenn R. and Murray D.F.	48
Monitoring of Engineering-Geological Processes along Pipeline Routes in Permafrost Terrain in Mackenzie River Valley, Canada and Nadyin Area, Russia Burgess M.M., Grechishev S.E., Kurfurst P.J., Melnikov E.S. and Moskalenko N.G.	54
Stage-Discharge Relations in the Mackenzie Delta during Winter and Development of Intrusive Ice in Lake-Bottom Sediments Burn C.R.	60
Cooperative Russia-Canadian Geophysical Investigations of Permafrost on the Yamal Peninsula, Western Siberia Burns R.A., Goriainov N.N., Hunter J.A., Judge A.S., Skvortsov A.G., Todd B.J., Timofeev V.M.	66
Research on Rock Glaciers in the Central Italian Alps (Valtellina, Sondrio, Northern Italy) Calderoni G., Guglielmin M., Lozej A. and Tellini C.	72
Late Pleistocene Stabilization and Reactivation of Eolian Sand in Northern Alaska: Implications for the Effects of Future Climatic warming on An Eolian Landscape in Continuous Permafrost Carter L. David	78
Permafrost Around CGWS, Antarctica Chen Xiaobai	84
Structure and Texture Formation of Frozen Sapropel Chuvilin E.M., Ershov E.D. and Murashko A.A.	89
Unfrozen, High-Salinity Intervals Within Ice-Bearing Permafrost, North Slope of Alaska Collett Timothy S. and Bird Kenneth J.	94
Simulation of Hydrocarbon Spills in Permafrost Corapcioglu M. Yavuz and Panday Sorab M.	100

\*The latter part of the book is the papers received after the deadline; see general subject and author indexes for additional information.

Administering Countermeasures on Embankment Thaw Settlements of Permafrost along Qinghai Xizang Highway Cui Jianheng, Xu Dongzhou and Chen Hongzhe	105
Periglacial Phenomena and Environment Since the Late Period of Late Pleistocene, Daqingshan Area, Inner Mongolia Cui Zhijiu and Song Changqing	111
Vegetation in Permafrost Region and the Division of Forest Management in Da Hinggan Ling Forest Region Dai Chuntian, Dai Baoguo, Du Chengxian, Liu Qingren and Dai Pin	116
Frost Heave Susceptibility of Highway Bridge Foundation Soil in Seasonal Frost Regions Dai Huimin and Wang X.L.	120
Permafrost Conditions along An Onshore-Offshore Transect of the Canadian Beaufort Shelf Dallimore S.R. and Taylor A.E.	125
A Primary Study on Composition of Methane Hydrate Deng Yousheng, Xu Xiaozu and Zhang Lixin	131
Geothermal Regime of Cryolithozone of West Siberia Devjatkin V.N., Duchkov A.D. and Sokolova L.S.	134
Application of Thermalpile to Culvert Engineering in Permafrost Region Ding Jingkan, Wu Jinming, Lou Anjin and Zhang Jingzhao	138
An Application Limit for Reducing Heave of Sulphate Saline Soil by Mixing Sodium Chloride Ding Yongqin and Chen Xiaobai	143
Creep Effects on A Laterally Loaded Pile Domaschuk L., Kwok R. and Shields D.H.	149
Deformed Embankments on Mari and the Ways of Their Stabilization Dydyshko P.I., Kondratyev V.G., Vasilyev M.L., Prigoda V.Ya., Sadakova M.N., Valuyev A.S.	155
Peculiarities of Gas Hydrate Formation in Sands Ershov E.D., Lebedenko Yu.P., Chuvilin E.M. and Yakushev V.S.	160
Detection of Frozen Soils and Soil Moisture Changes Beneath Highway Pavements Esch David C.	164
Influence of Pore Fluid Salinity on Electromagnetic Wave Propagation Parameters in Soil at Permafrost Temperatures Fediukin Igor V. and Frolov Anatoly D.	170
Aspects of Natural Recovery of Soils, Hydrology and Vegetation at An Abandoned High Arctic Settlement, Baffin Island, Canada Forbes Bruce C.	176
Monitoring Thawing Front Movement by Self-Potential Measurement Fortier Richard, Allard Michel and Seguin Maurice-K.	182
A Numerical Technique for Solving Temperature Field of Frozen Wall Gao Xingwang	188
Karst Morphology and Hydrology in A Permafrost Environment: The Case of Akpatok Island, Ungava Bay, Eastern Arctic Canada Gray James T. and Lauriol Bernard	192
Development of Physical-Chemical Model for Cryogenic Heaving and Enlargement of Segregated Ice in Freezing Sandy-Clayey Soils Grechishchev Stanislav E. and Shankov Vladimir V.	198
Permafrost Features and Their Changes in Amur Area, Daxinganling Prefecture, Northeastern China Gu Zhongwei, Zhou Youwu, Liang Fenxian, Liang Linheng and Zhang Qibin	204
A Preliminary Research of Solifluction Terraces in Fenghuoshan Pass Basin on Qinghai-Xizang Plateau Guo Dongxing, Huang Yizhi and Zhao Xiufeng	210

Monitoring the Long-Term Evolution of Mountain Permafrost in the Swiss Alps Haerberli Wilfried, Hoelzle Martin, Keller Felix, Schmid Willy, Vonder Muhll D.S., Wagner S.	214
Rock Temperatures from Livingston Island (Maritime Antarctic): Implications for Cryogenic Weathering Hall Kevin J.	220
Calculation of the Thermal Conductivity of Unsaturated Frozen Soil near the Melting Point Hallet B. and Rasmussen L.A.	226
Micromorphological Investigations of Active-Layer Detachment Slides, Ellesmere Island, Canadian Arctic Harris Charles and Lewkowicz Antoni G.	232
Palsa-Like Mounds Developed in A Mineral Substrate, Fox Lake, Yukon Territory Harris Stuart A.	238
Frost Heave Predictions for Alaskan Soils Hazen Beez, Nixon J.F., Heuer C.E., Caldwell J.B., Brudie E.L.	244
Dynamic Elastic Modulus and Strength of Saturated Frozen Silt He Ping, Zhu Yuanlin, Zhang Jiayi, Sheng Zhongyan and Yu Qihao	250
A New Permafrost and Ground Ice Map for the National Atlas of Canada Heginbottom J. Alan and Dubreuil Marie-Andree	255
Near-Surface Summer Heat-Transfer Regimes at Adjacent Permafrost and Non-Permafrost Sites in Central Alaska Hinkel Kenneth M., Outcalt Samuel I. and Nelson Frederick E.	261
Hillslope Hydrology in An Arctic Setting Hinzman Larry D., Kane Douglas L. and Everett Kaye R.	267
Application of BTS-Measurements for Modelling Mountain Permafrost Distribution Hoelzle Martin, Haerberli Wilfried and Keller Felix	272
Experimental Study of the Effects of Impurities on Ice creep at -1°C Huang Maohuan, Li Gang, Miao Lina and Jin Zhengmei	278
The Desertification in the Permafrost Region of the Qinghai-Xizang Plateau and Its Influences on the Environment Huang Yizhi, Guo Dongxing and Zhao Xiufeng	282
The Construction of Electrical Substations in Discontinuous Permafrost Regions Huneault P.A., Ares R., Garneau R.R. and Iordanescu M.	286
Measurement of Thermal Stresses in Asphalt Concrete Mixtures Janoo Vincent, Jr Bayer John, Walsh Michael and Tomita Hsiao	292
Countermeasures to Prevent Canal Structures from Frost Damage Jian Gong	298
Research of Frost Heave Property of Soil in Daqing Region Jang Hongju and Cheng Enyuan	302
Thermal Regime of Alpine Permafrost in the Upper Reach of Urumqi River, Xinjiang, China Jin Huijun, Qiu Guoqing, Zhao Lin, Wang Shujuan and Zeng Zhonggong	307
Study of the Prevention of Ice Damage of Structures in Water in Cold Regions Jin Naichui, Qu Xiangming, Zhang Yuanyou and Lin Ying	312
Use of Snow Capture for Land Rehabilitation in Arctic Oilfields Jorgenson M. Torre, Cater Timothy C., and Joyce Michael R.	316
Gas Pipe-Line Mastakh-Yakutsk and Environment Kamensky Rosteslav M., Konstantinov Innokentii P., Popov Viktor A.	322
Use of Spatially Distributed Data to Model Arctic Hydrologic Processes Kane D.L., Hinzman L.D. and Lilly E.K.	326

Interaction Between Snow Cover and High Mountain Permafrost Murtel/ Corvatsch, Swiss Alps Keller Felix and Hansuelli Gubler	332
Microclimatic Characteristics of Palaas along An Altitudinal Gradient, Mackenzie Mountains, NWT, Canada Kershaw G. Peter and Skaret Kevin D.	338
Examples of Geomorphological Changes in Glacially Sculptured High Arctic Permafrost Areas from Svalbard and the Queen Elizabeth Islands, Canada King Lorenz	344
The Influence of Relief and Lithology on Soil Formation in West Spitsbergen Klimowicz Zbigniew, Melke Jerzy, Uziak Stanislaw	350
Co-Operative Russian-Canadian Engineering Geology Investigations of Permafrost on the Yamal Peninsula, Western Siberia Kurfurst P.J., Melnikov E.S., Tarasov A.M., Tschervova E.I.	356
Arctic Well Drilling and Completion Problems Kutasov I.M.	362
A Model of Elastic Wave Propagation in Frozen Media Comparison with Experiment Leclaire P., Tenoudji F. Cohen and Aguirre-Puente J.	368
The Significance of Permafrost in the Formation and Appearance of Push Moraines (Examples of the Canadian Arctic and Spitsbergen) Lehmann Rainer	374
Hydrogeological Aspects of Cryogenic Slides on the Yamal Peninsula Leibman M.O., Rivkin F.M., Saveliev V.S.	380
Study of Forecast of Frost Heave on Canals Li Anguo, Li Hao and Cheng Qinghua	383
Application of Remote Sensing Images to the Investigations of the Changes of Permafrost Environment in Burned Forest Regions, Da Hingganling, China Liang Fengxian and Gu Zhongwei	388
The Characteristics of the Distribution of Snow Cover and Its Warm Effect on the Temperature of Permafrost, Amuer Region, Da Hinggan Ling Liang Linheng and Zhou Youwu	393
The Denudation by Gelifraction and Influential Factors in the Periglacial Environment of Tianshan Mountains, China Liu Gengnian, Xiong Heigang and Cui Zhijiu	397
Discussion on the Distribution of the Tangential Frost-Heaving Forces along the Lateral Surfaces of Pile Liu Hongxu	403
Study of the Law of the Distribution of Permafrost and Vegetation in Da Hingganling, Northeast of China Liu Qingren, Sun Zhenkun, Cui Yongsheng	407
Cryogenic Processes and Phenomena in Mongolia Lomborinchen R.	411
Research on Tangential Heaving Force and Frictional Resistance Against Pulling up of Pile Lu Xingliang, Yu Shengqing, Xu Bomeng and Hu Shicai	416
Permafrost Formation Time Lunardini Virgil J.	420
Origin and Treatment of the Icings in Gulian Region, Northern Da Hinggan Ling, Northeast China Luo Minru, Zhou Xinqing and Na Yunlong	426
Effects of Snow Cover on Thermal Regime of Frozen Soils Ma Hong, Liu Zongchao and Liu Yifeng	429
Strength and Yield Criteria of Frozen Soil Ma Wei, Wu Ziwang and Zhang Changqing	432

Geological-Engineering Conditions of Yamal Peninsula along Designing Railroad Mamzelev Anatoly P. and Are Felix E.	436
Infiltration of Meltwater into Frozen Soils in A Continuous Permafrost Environment Marsh Philip and Woo Ming-Ko	443
Critical Polygon Size for Ice-Wedge Formation in Svalbard and Antarctica Matsuoka Norikazu and Hirakawa Kazuomi	449
Peculiarities of Formation and Thawing of Ice Originated from Colloid Solutions and Regulating of the Phase Conditions of Water in the Cryosphere Melnikov Vladimir and Smorygin Gennadi	455
The Change of the Artificial Permafrost Table Under the Roadbed and Effect on the Roadbed Mi Haizheng and Wang Shaoling	461
Phenomenological Modelling of Frost-Susceptible Soils Michalowski Radoslaw L.	465
Trans Alaska Pipeline Reinsulation in Atigun Pass Mobley Keith F. and Ferrell John E.	471
Cast in Place Concrete Piles in Permafrost Molmann Truls and Senneset Kaare	477
Sand Wedges and Permafrost History, Crumbling Point, Pleistocene Mackenzie Delta, Canada Murton Julian B. and French Hugh M.	482
Effects of Climatic Warming on the Active Layer Nakayama T., Sone T. and Fukuda M.	488
Uplift Resistance of Pipelines Buried in Frozen Ground Nixon J.F. (Derick) and Hazen Beez	494
Potential Occurrence of Permafrost and Gas Hydrates in the Continental Shelf Near Lonely, Alaska Osterkamp T.E. and Fei T.	500
The Ion Exchange Intensity between Soil and Snow Ostroumov V.E., Demidov V.V., Butsenko A.N., Makeev O.V. and Gershevich V.D.	506
Quantitative Estimation of Mass-Transfer in Landscape Complexes of Northern Russia Pavlov A.V.	511
Soil Classification and Climatic Zones of Alaska Ping C.L. and Moore J.P.	517
Dilatometry of Porous Limestones Undergoing Freezing and Thawing Pissart A., Prick A., Ozouf J.Cl.	523
Discussion of Destructive Cause on the Soil Dam Bank of Reservoirs and Its Preventative Steps Qiso Dianshi, Xu Jingguang and Zhang Xikun	529
Development Condition of Alpine Permafrost in the Mt. Tianshan, China Qiu Guoqing	533
Repair of A Road Built on Permafrost at Kilpisjarvi, Northern Finland Sarrelainen Seppo	539
Global Climatic Change and Some Possible Geomorphological and Ecological Effects in Arctic Permafrost Environments, Isfjorden and Liefdefjorden, Northern Spitsbergen Schmitt Elisabeth	544
Correct Use of the Segregation Potential Concept for Two-Dimensional Frost Heave Simulation Shen Mu and Konrad J.M.	550

A Model of Migration Potential for Moisture Migration during Soil Freezing Sheng Yu, Ma Wei and Hou Zhongjie	556
Effect of Soil Thaw on Off-Road Vehicle Traction Shoop Sally A.	559
N-Factor Maps of Russian Permafrost Region Shur Y.L., Slavin Borovskiy V.B.	564
Aluminas in Quaternary Sedimentary Rocks of Yakutia: New Findings Concerning Mineral Formation in Permafrost Regions Siegert Christine	569
Hydrologic and Water Quality Characteristics of A Degrading Open- System Pingo Slaughter Charles W. and Hartzmann Ronald J.	574
Laboratory Simulation of Dolomite and Limestone Dissolution: Rates, Yield, and Mineralogy of Fine-Grained Residue Sletten Ronald S.	580
Analysis of Temperature Effects on the Flexural Behavior of Frozen Soil Soo Sweanum and Fang Tsung Ping	586
The Method of Determined Design Values of Horizontal Heave Force on Retaining Walls in Seasonally Frozen Ground Area Sui Tieling, Na Wenjie, Li Dazhou and Jiang weiqiang	592
Critical Segregation Potential-Frost Heave Upper Limit Svec Otto J. and Chang Yen	596
Calculation of Frost Heave Stress Acting on the Foundation Bottom Tang Shuchun	602
Experiment and Application of Heavy Tamping Method to Prevent a Highway from Frost Heaving and Boiling Tang Xiaobo	605
A Method to Measure Heat Conductivity With A Heat Flow Meter Tao Zhaoxiang, Zhang Lixin and Hou Zhongjie	608
Ultrasonic Measurements in Frozen Soils to -120°C: Results and Interpretation Using Different Theoretical Models Thimus J.F., Aguirre Puente J., Cohen Tenoudji F. and Leclaire Ph.	611
Ice Wedges in Northeastern China Tong Boliang	617
Shallow Foundation in the Region of Frozen Ground Tong Changjiang and Luo Mingru	622
Influence of Mountain Permafrost on Construction in the Zugspitze Mountains, Bavarian Alps, Germany Ulrich Roland and King Lorenz	625
Permafrost and Periglacial Forms in the Romanian Carpathians Urdea Petru	631
A Multi-Lingual Index of Permafrost Terms Van Everdingen Robert O.	638
Periodic Ice-Wedge Formation and Weichselian Cold-Climate Floodplain Sedimentation in the Netherlands Vandenberghe J. and Kasse C.	643
Pavement Permafrost and Low Temperature Cracking of Subarctic and Arctic Airfields Vinson Ted S., Jung Duhwoe, and Rooney James W.	648
Geophysical and Photogrammetrical Investigation of Rock Glacier Muragl I, Upper Engadin, Swiss Alps Vonder Muhll Daniel S. and Schmid Willy	654

Rapid Solifluction as A Stage of the Transition from Covered Solifluction to the Free Solifluction Vtyurina E.A., Guevorkian S.G. and Poznanin V.L.	660
A Numerical Simulation of Coastal Retreat and Permafrost Conditions, Mackenzie Delta Region, Canada Wang Baolai	664
Correlation of Freeze-Thaw Action to the Formation and Exploration of Quaternary Gold Placers Wang Chunhe	670
Influence of Porous Characteristic of Material on Displacement during Freezing Wang Jiacheng and Cheng Guodong	675
Three-Dimensional Finite Element Analysis of Stress and deformation of Frozen Walls in Deep Thick Clay layers. Wang Jianping, Wang Zengting and Wu Qijian	678
The Prevention, Control and Evaluation of Frost Damage on the Buildings of Canal Systems in Seasonal Frozen Ground Areas Wang Wenkai and Lin Chuanwei	685
Profiles of Freezing Point and Unfrozen Water Content Around CGWS, Antarctica Wang Yaqing and Chen Xiaobai	689
Permafrost and Periglacial Winds Around the Wisconsinan Ice Margin in the Northern Plains of the USA Wayne William J. and Guthrie Robert S.	694
Microstructural Alteration of A Frost Heave Susceptible Soil Adjacent to A Buried Chilled Pipeline White T.L. and Williams P.J.	700
Influence of Salinity on the Compressive Strength Behavior of Frozen Soils Wijeweera Harsha and Joshi Ramesh C.	706
Effects of Terrain Disturbance on Arctic Slope Hydrology Woo Mingko and Young Kathy L.	712
The Relationship Between the Lake and Forming Environment of Permafrost, North Region, Kekexili, Qinghai Wu Qingbai and He Yixiang	718
Experimental Research on Deformation in Model of Artificially Frozen Wall Wu Ziwan, Ma Wei, Zhang Changqing, Chang Xiaoxiao and Liu Yongzhi	722
Active Layer Thaw Calculations Using Simplified Thermal and Hydrological Parameters Xia Zhaojun and Woo Mingko	725
Problems of Permafrost in Development of Water Resources of the Henguna and Heilongjiang River Xu Bomeng, Wang Zeren, Kagan A.A. and Krivonogova N.P.	730
A Primary Study on Interface Conditions of Ice Saturated Clay Xu Xiaozu and Wang Jiacheng	734
The Role of Snow in Streamflow Generation from An Alpine Permafrost Basin in Tianshan, Northwestern China Yang Daqing, Woo Mingko, Liu Fengjing and Yang Zhenniang	738
Permafrost Hydrological Processes in Binggou Basin of Qilian Mountains Yang Zhenniang, Yang Zhihuai, Liang Fengxian and Wang Qiang	744
Estimation and Measurements of Transport Properties of Frozen Soils Yen Yinchao and Nakano Yoshisuke	750
The Degeneration of Permafrost in Upstream Valley Region of Heilong River Yu Shengqing and Wang Zhanchen	755
Use of Ground Penetrating Radar for the Detection of Permafrost and Delineation of Its Distribution under the Asphalted Road of Qinghai-Xizang Highway Zeng Zhonggong, Huang Yizhi and Xia Zhiying	758



The Problems of Water Transfer from South to North China over Western Permafrost Areas Zhang Changqing, Zhu Linnan, Zhang Jianming and Liu Yongzhi	764
Mechanism of the Attenuation of Strength for Loess-Cement under Cyclical Freezing and Thawing Zhang Huyuan, Feng Ke, Zhang Lixin, Wang Yinmei and Zhang Xianggong	768
Analysis of the Second Phase Transition of Sodium Chloride Solution in Freezing Soil Zhang Lixin, Xu Xiaozu, Tao Zhaoxiang and Deng Yousheng	773
Plant Community Ordination and Its Environmental Interpretation Following the Disastrous Fire in Amur Area, Da Xingganling Prefecture, Northeastern China Zhang Qibin, Zhou Youwu, Wang Jiachen, Liang Linhen and Gu Zhongwei	778
Changing Climate and Permafrost Temperatures in the Alaskan Arctic Zhang T. and Osterkamp T.E.	783
Random Characteristics of Frost Heave and Application to the Design of Anti-Frost Lift Reliability of Grouting Pile at Building Site Zhang Xin, Zhang Duo and Feng Yanhui	789
The Formation Characteristics of Frozen-Area Bogs in China Zhang Zeyou	793
Instantaneous-State Deformation and Strength Behaviour of Frozen Soil Zhang Zhaoxiang, Yi Qun, Xen Zhenyao and Lu Heiyen	797
Climate Fluctuation and the Process of Permafrost Formation Since Last Glaciation in the Source Area of Urumqi River, Tianshan, China Zhao Lin, Qiu Guoqing and Jin Huijun	803
The Loess and Its Climate Records in Kunlun Shan Region Since the Late Pleistocene Zhao Xiufeng, Guo Dongxing and Huang Yizhi	809
Protein Changes and Functions during Cold Acclimation of Winter Wheat Zhao Yutain and Zhao Jun	813
Effects of Forest Fire on the Hydro-Thermal Regime of Frozen Ground, The Northern Part of Da Hinggan Ling, China Zhou Youwu, Liang Linheng, Gu Zhongwei, Liang Fengxian and Zhang Qibin	819
A Development Model of the Periglacial Landforms on Slope Land- Taking the Phenomena of Periglacial Landforms in the Tianshan Mountains, West Antarctica and the Andes as Examples Zhu Cheng	826
The Research of the Fossil Ice-Wedges and Periglacial Involutions in the Eastern Piedmont of the Greater Xingan Ranges, China Zhu Jinghu, Song Changqing, Tang Zhonghai and Wang Guangzhou	832
Simulated Analysis on A Modeling Test for Soil Freezing-Thawing Process Without Pressure Zhu Linnan, Li Dongqing and Guo Xingming	835
Frost Heave Prevention Measures for the Rigid Canal Linings Zhu Qiang	838
Permafrost in the North of Korean Peninsula An Viktor	843
Forecasting of River Bed Deformations in the Permafrost Zone Are Felix E. and Savitsky Victor A.	846
Prediction of Stability of Solifluction Slopes and Structures on them Bondarenko G.I.	851
Creation of Water-Impervious Frozen Screens in Earth Dams in Central Yakutia Chang Rudolf V. and Alexeeva Olga I.	855

Evolution of Permafrost Zone of North Eurasia in Late Cenozoic and Neotectonic Movements Danilov Igor D. and Roujansky Vladislav E.	858
Stress-Strain State of Frozen Rocks at their Thawing Around Excavations Dubina Mikhail M. and Chernyakov Yurii A.	862
The Temperature Effect on the Re-distribution of Microelements in the Soil Massif Fedoseeva Valentina I. and Streltsova O.A.	865
The Microbiological and Biogeochemical Research in Permafrost: Paleocological Implications Gilichinsky David A., Rivkina Elizaveta M., Samarkin Vladimir A.	869
Construction of Buildings Erected on Surface-Type Space Foundations Designed for Permafrost Goncharov Ju. M.	875
Mechanisms of Layer Structures Growing During Ground Freezing Gorelik Yakov and Kolunin Vladimir	879
Optimal Parameters of Internally Pressurized Opening in Permafrost Guryanov Igor E.	885
Dynamics of Permafrost-Hydrogeological Medium at Primary (Ledge) Diamond Deposit Development Klimovsky Igor V. and Gotovtsev Semyon P.	891
Isotopic and Chemical Composition of Ground Ice in West Siberia Kritsuk L.N. and Polyakov V.A.	897
On the Study on Nival Deposits in Yakutia Kunitsky Viktor V.	903
Complex Technology for Preparation of Perennially Frozen Placers to Dredging Kurilchik A.F., Samyshin V.K. and Perlshtein G.Z.	909
Technogenic Geochemical Fields in the Permafrost Zone on the Example of Yakutia Makarov Vladimir N.	911
Phyto-Ecological Mapping and Biogeocoenosis Stability of the West-Siberian Permafrost Zone Meltzer Liya I.	914
Role of Climate on Active Layer Variations, Svalbard Migala Krzyzstof	919
Degradation of Cryogenic Strata in Large Water Storage Areas Olovin Boris A. and Kamensky Rostislav M.	923
Regularities of Perennially Frozen Ground Forming in Southern Zabaikalie Salnikov P.I.	927
Massive Ice Beds of Western Siberia: Structure and History in Pleistocene Shpolyanskaya N.A.	930
Borehole Electrometry of Permafrost Zone Snegirev A.M.	934
Stratigraphy, Age and Origin of Massive Ice, Yamal Peninsula, West Siberia Solomatin V.I., Koniakhin M.A.	937
Peculiarities of Pile Behavior in Thawing Soils Torgashov Y.Y.	941
Northern Asia Cryolithozone Evolution in Late Quaternary Vasil'chuk Yuriy K.	945
Engineering and Geocryological Peculiarities of Using Pile Foundations in Magadan Area Vlosov Vladimir P.	951

Ensuring Structural Stability and Durability in Permafrost Ground Areas at Global Warming of the Earth's Climate Vyalov S.S., Gerasimov A.S., Zolotar A.J., Fotiev S.M.	955
Author Index	961
General Subject — Senior Author Index	963

## PLASTIC FROZEN (SALINE) SOIL AS BASES

V. I. Aksenov and A. V. Bruskov

Industrial and Research Institute for Engineering Investigations of Construction, 18, Okruznoy, Moscow, Russia

The paper presents the wide complex of original information on saline frozen soil, methods of testing, properties, experience of construction.

The frozen soils frequently met in the North of Russia and their mechanical properties should be thoroughly investigated when determining their boundaries. The saline frozen soils (SFS) are known to have lower strength and higher deformability compared with nonsaline soils. They also have a lower temperature of freezing. In addition, the SFS are in a plastic frozen state in a large range of sub-zero temperatures. Therefore, the information on SFS occurrence is very topical when solving the problems of engineering geocryological survey and design.

The major part of cryolithozone along the Arctic coast is characterized by SFS and cool sediments containing layers of saline water below 0°C and highly mineralized ground water with sub-zero temperature. Although the solutions in those soils, chemically and in concentration, are not homogeneous, they are stable for large territories and are connected with the formation conditions and perennial freezing (cooling) of the sediments causes the occurrence of two main types of salinization: marine and continental.

The main type of salinization mostly occurs in the soils of cryogenic thickness of Northern territories - along the Arctic coast and on the islands. For instance, on the Yamal Peninsula, SFS occur everywhere to the North of the latitude of the settlement of Novii Port and considerably increase northward. The changing of dominating ion salt composition of soils is observed in the same direction from sulfate-hydrocarbonate-sodium to chloride-sodium. The maximum salinization (average 1.1%) occurs in the sediments on the Northern and Western coast of Yamal.

The soils are saline in the region of the settlements of Amderma, Dikson and Tiksi. The frozen soils on the Cape Schmidt and on the Chukotka Peninsula contain salts. The salinization of the soils on the Arctic coast totals 0.1-1.5% rarely 2% (1) and with depth the salinization increases from 0.2-0.3% (at a depth of 1-2 m) to 1.5% (in the depth of 10-15 m and below).

The Northern region of the Centre Russia as well as the Magadan Region and Yakutia are frequently characterized by hydrocarbonic mineralization of soils referring to the continental type of salinization. The increased salinization of soils is characteristic of the Yakutia territory and it is observed in the valleys of the rivers Lena, Vilyuya and other. According to Carpunina

(1974) over 10% of the territory of Central Yakutiya is presented by the saline soils.

One can observe the similarity of cation composition in the atmospheric water, ground water and soils. The soil and ground water in the continental regions determine the degree and character of saline soils. Based on the data of engineering survey obtained by Dubikov and Ivanova (1990) published the boundaries of SFS on the territory of Russia have been mapped in the scale 1:10,000,000, and the salinization map of the Yamal Peninsula on the scale of 1:500,000 has been made.

The complete data on the properties of frozen soils are required to carry out the foundation analyses when designing. The values of design pressure on the frozen soil R (normal shear strength of frozen soil) and Rat (shear strength of frozen soil on the adfreezing surface with the foundation) are usually used and are determined in the laboratory in uniaxial compression tests or pressing in a ball stamp and shear tests using special equipment. The available methods of tests do not apply to SFS. The experimental work with frozen soils enabled us to determine the test peculiarities of saline frozen soils.

The method of soil testing by means of the ball stamp applies to various SFS with massive, fine-grained, thin-layer cryogenic texture in the range of temperatures from  $T=T_{bf}+(-1^{\circ}\text{C})$  to  $T=-10^{\circ}\text{C}$ . It does not apply to large-sized clods of soil and large-sized sand and soil with ice content  $L_b > 0.2$  or with cryogenic texture in which the visible particles of ice are commensurable with the diameter of ball stamp.

The analysis of experimental data when testing SFS by means of the ball stamp makes it possible to recommend for testing the stamp diameter of 2.6 cm or more.

The dependence of adequate cohesion upon the amount of load enables us to recommend for SFS the conditions of its selection within the range of settlements for clayey soils depending on the stamp diameter e. g. for 8 hours  $s < (0.02-0.04)d$ .

For practical analysis of long cohesion value, according to 8 hours test, one can use the transition factor: for the saline sands 0.34-0.4 and clayey soils 0.55-0.7. In order to determine long cohesions, the duration of the test can be 15-40 days and more.

The method of uniaxial compression test of

frozen soils at fixed load is the direct method of normal pressure determination under the base of foundation and applies to SFS tests with any cryogenic texture as in the case of uniform distribution of ice streaks in the sample in the same range of subzero temperatures as the ball stamp.

The relationship between short and long-term strength which is typical of SFS is considerably lower than for frozen nonsaline soils and makes it up 5-20 with salinization of 0.2% and 20-40 with higher salinization.

When the duration of tests on the samples of SFS is under 3 days the approximate parameters of long-term strength formulas and deformation formula by Vyalov may differ from the values determined during long-term tests. Therefore, it is recommended to make tests for 3-10 days.

According to Velli (1973), the SFS are distinguished by high plastic flow under load. However, the main regularities of deformation and deformation characteristics of SFS of different geological types have been insufficiently studied.

The soil investigation carried out at uniaxial compression tests with different loading history showed that the SFS have the same features as the deformation of usual frozen soils. However, there are essential differences mentioned below.

As a rule, the frozen soil has three deformation stages: damping creep, flow at constant rate and the flow at increasing rate. The method of soil viscosity factor is based on the property of frozen soils with ice content to flow approximately at constant rates and used when designing the structure stability. The peculiarity of saline frozen dispersive soils is damping creep at high loads. The typical curves of creep for supes\* and suglinok\*\* are given in Figure 1, 2. The deformation reaches the values of 20% and more without noticeable stabilization of flow rates under load. This peculiarity of deformation of saline frozen soils is not typical and not always observed for slightly salted soils and sands.

The above-said should be taken into account when making test method by incremental loading; it turns out that the value of failure load depends upon the load value on the increments (if

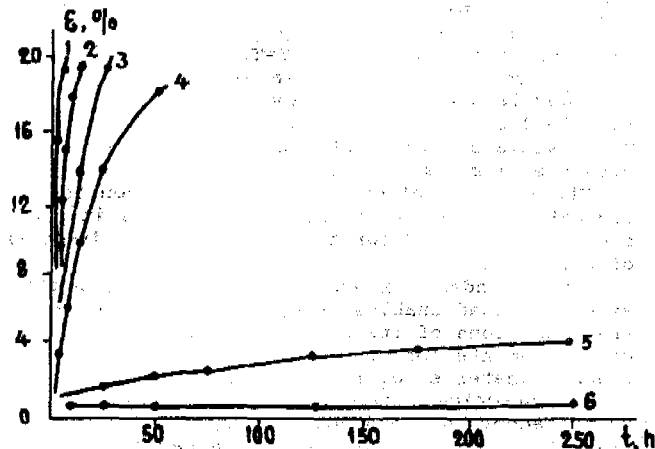


Figure 1. Creep curves of frozen sand at salinization and temperature  $-2^{\circ}\text{C}$ : 1-0.4; 2-0.3; 3-0.25; 4-0.2; 5-0.15; 6-0.1 MPa

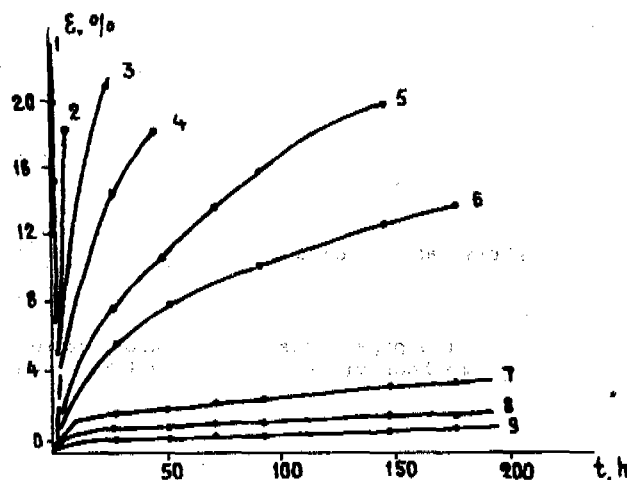


Figure 2. Creep curves of frozen suglinok at salinization and temperature  $-6^{\circ}\text{C}$ : 1-0.5; 2-0.6; 3-0.7; 4-0.9; 5-1.0; 6-1.1; 7-1.2; 8-1.4; 9-1.6 MPa

deformation value 20% or so is taken for the failure criterion) incredible.

In order to predict deformation there is necessary to make approximation of deformation process based on the formulas of experimental creep curves. The known formulas by Vyalov have been used:

$$\delta = \xi \cdot t^{-\alpha} \cdot \varepsilon^m$$

where  $\delta$  - load;  $t$  - time;  $\varepsilon$  - deformation;  $\xi$ ,  $\alpha$ ,  $m$  - parameters. For description of failure:

$$\delta_p = \frac{\beta}{m \cdot \frac{t_p}{B}}$$

where  $\delta_p$  - failure load;  $t_p$  - failure time;  $\beta$  and  $B$  - parameter.

It turned out when processing the test data, the approximation of the obtained curves of creep and long-term strength is quite satisfactory, with a correlation factor about 0.9. However, that may be possible on condition that the creep curves are divided into two parts, the independent approximation being on each of the parts.

The process of deformation and destruction of saline frozen soils is influenced by the density, ice content, cryogenic structure etc. The increase of ice content of saline soil at high subzero temperatures causes the increase of strength and decrease of deformation (Fig. 3).

The mechanical properties of saline frozen soils are influenced by the salt composition as well. The soils of chloride-sodium salinization type are characterized by the least strength and that may be explained from the point.

Special attention was paid to the research of shear resistance on the freezing surface of SFS with the foundation material - concrete and steel. That is very significant for designing the stability of pile foundations widely spread in the North and Siberia. Previously, such experimental work was carried out at the Amderna permafrost station headed by Velli in order to obtain some necessary data for practical recommendations for the construction on permafrost (SNiP

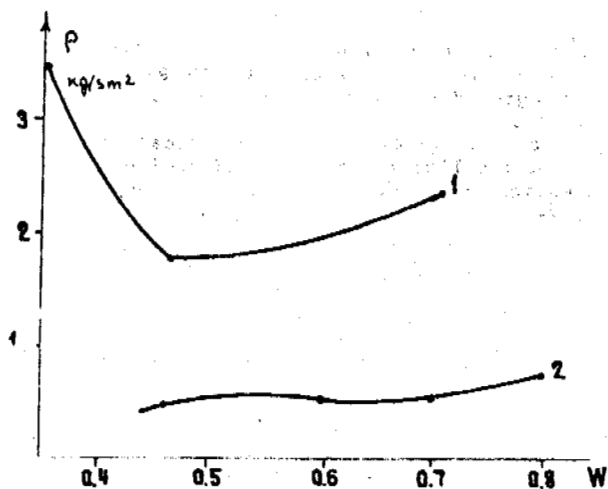


Figure 3. Dependence of uniaxial compression strength (P) and surface adfreezing shear with concrete of frozen saline (1-0.5%; 2-1%) suglinok at temperature of  $-3^{\circ}\text{C}$  upon humidity.

Building Norms and Regulations 11-18-76). It was worked out that SFS of the Arctic coast (where chloride-sodium, marine type of salinization is observed) have much lower shear resistance characteristics than average ones for saline soils. Some attempts have been made to study the influence of some factors on adfreezing strength: normal pressure, adfreezing temperature of sample and material, ice content etc. Some data are given in Table 1. The research has been carried out only with some types of soils at definite temperature and salinization. Therefore, under some other conditions, the influence of the above-mentioned factors on the shear strength on the adfreezing surface may be completely different.

In order to ensure reliable construction on the SFS and provide grounds for the prediction of foundation stability, much attention should be given not only to the mechanical properties of soils, but also to the salt diffusion at possible temperature changes due to the construction and maintenance of engineering structures. The tests have been made for about a year, at temperature gradient about  $0.05-0.1^{\circ}\text{C}/\text{cm}$  with the samples at salinization 0.5%. The experiments have been conducted in the underground laboratory of the Amerma permafrost station ensures long and reliable observance of experimental conditions. The moisture and salt distribution according to the experiment is presented in Table 2. Thus, for the conditions which are characteristic of the frozen saline thickness the salt diffusion under the temperature gradient proved to be practical.

We suggest that we use the relative temperature as a common parameter reflecting the state of SFS. The temperature is equal to the relationship of actual soil temperature (T) and temperature of freezing at the very beginning (Tb. fr.). Thus, for example, one can assume  $T/\text{Tb. fr.} = 5$  for the division frozen state of saline suglinok with salinization of chloride type.

Unfortunately, the construction experience on SFS despite their frequent occurrence on the Arctic coast is not sufficient enough and is caused by comparatively minor construction under such conditions. The Arctic settlement of Amerma

Table 1. Adfreezing with concrete of saline frozen soils from different sites of Yamal.

Soil	Salinization, %	Temperature, $^{\circ}\text{C}$	Adfreezing strength, R, kg/cm	Recommended R, kg/cm, CNiP 11-18-76
Sand	0.05		0.60	1.50
(r. Ero-uta-Yacha)	0.20	-2	0.14	0.80
	0.03		0.03	0.50
	0.15	-6	1.10	1.60***
Supes (r Se-Yacha)	0.76		0.46	0.90
	0.50		0.13	0.60
	0.50	-3.8	0.60	1.20
Suglinok (lake Tibeit-To)	0.50		0.23	0.50
	0.75	-2	0.13	0.45
	1.00		0.04	0.40
	0.60		2.20	1.10***
	1.00	-6	0.90	1.00***
	1.20		0.60	-

\*\*\*  $t = -4^{\circ}\text{C}$

Table 2. Moisture distribution and salinization in the sample four years after the beginning of the experiment (on the left temperature  $-2^{\circ}\text{C}$ , on the right  $-3^{\circ}\text{C}$  sample space about 1.3 cm)

Layer number	1	2	3	4	5	6	7	8
W, %	37.5	40.5	15.1	30.4	38.5	38.2	37.6	35.5
Dsol, %	0.48	0.50	0.46	0.67	0.49	0.37	0.47	-

located on the Yugov Peninsula is the zone of typical thickness saline marine. There are 268 buildings in Amerma and about 40% of them (108 buildings) have been deformed (deflections, cracks, settlements) which exceeds the standards established in SNiP (Construction Norms and Regulations), 12% of the buildings are in emergency service. The stone buildings turn out to be deformed frequently (32 buildings of 66 i.e. 20% in emergency service which partially accounts for considerable loading on the foundation and less permissible deformations). Of 19 boiler and diesel power stations, 2 have small deformations and 10 have impermissible ones which lead to collapse. Most of the deformed buildings were built 5-7 years ago.

Thus, neither design analysis nor construction conditions and maintenance on the Arctic coast might be evaluated satisfactory. The recent research results considered in the present report make it possible to recommend some certain test techniques of SFS and establish some peculiarities of their behavior under mechanical loads. The authors hope that the research work done will contribute to the improvement of construction along the Arctic coast.

\* Silty sand with some clay, sandy silty loam; contains 3 to 10% of clay by weight with particles less than  $0.005\text{ mm}$ ,  $0.005$  being the dividing line between clay and silt in the Soviet soil classification (Russian-English Glossary of Permafrost Terms, prepared by V.N. Poppe Canada Institute for Scientific and Technical Information National Research Council of Canada, Technical Memorandum No. 117, Ottawa, April, 1976)

\*\* Clayed silt with some sand, clayey silty loam; contains 10 to 30% clay by weight with par-

ticles less than 0.005 mm, 0.005 being the dividing line between clay and silt in the Soviet soil classification (see above).

**REFERENCES**

Velly Ju.Ya. (1973). Stability of buildings and constructions in Arctic. Leningrad, Stroyizdat, 39 -112.

Dubikov G.I., Ivanova N.V. (1990). Saline frozen ground and its expansion in the USSR. In: Salin frozen ground as bases for construction, Nauka, M., 3-9.

Karpunina A.A. (1974). Physical-chemical properties of frozen saline soils. Study of engineering site investigations. Candidate thesis, unpublished, M., 2-19

## QUATERNARY GEOLOGY AND GEOCRYOLOGY IN NUNAVIK, CANADA

Michel Allard<sup>1</sup>, Clément Tremblay<sup>2</sup>, Jean A. Pilon<sup>3</sup> and Janusz Frydecki<sup>1</sup>

<sup>1</sup>- Centre d'études nordiques, Université Laval,  
Sainte-Foy, Québec, Canada, G1K 7P4

<sup>2</sup>- Nirliq inc., 230 2ième Avenue, Aéroport de Québec,  
Sainte-Foy, Québec, Canada, G2E 5W1

<sup>3</sup>- Terrain Sciences Division, Geological Survey of Canada,  
601 Booth st., Ottawa, Ontario, Canada, K1A 0E8

In Nunavik (Northern Québec), permafrost knowledge has increased considerably over the last five years thanks to a joint government-university task force set up to carry out a comprehensive research program within the framework of airport construction in 12 villages. Patterned ground types and geocryological facies are closely related to the various types of surficial deposits laid by the Wisconsinan glaciation and, subsequently, by the post-glacial marine inundation and emergence on the coastal fringe of the Peninsula. Tundra polygons and low-center mudboils are the dominant periglacial features on glacial landforms such as moraines and drumlins, on glaciofluvial outwash plains and eskers, on fluvial terraces and on raised beaches. Both soil wedges and ice wedges can be found beneath the edges of the polygonal structures. Interstitial ice dominates in these coarse, gravelly and sandy, sediments. The dominant periglacial features on post-glacial marine silty clays are cryogenic mounds and fields of high-center mudboils. In these fine-grained sediments, segregated ice is abundant in warm permafrost (0°C to -2°C) in the first few meters below permafrost table. Massive icy beds over 11 m thick occur in cold permafrost (-5°C) in the northernmost part of the territory. Other features such as palsas in bogs, frost blisters, icings, bedrock heaved features and aggrading permafrost under tidal marshes are also significant in the region.

### INTRODUCTION

Most of Nunavik, the Inuit territory of northern Quebec, is underlain by permafrost (Figure 1). The state of knowledge of permafrost distribution and characteristics in this region was presented and discussed by Allard and Seguin (1987a); a new map of the permafrost zones, quite different from the previous ones by Brown (1979) and Ives (1979), was then proposed. Since that time, extensive new research has been carried out in the region, thanks to the setting up of a comprehensive, university-government, joint research program conducted within the framework of construction of airstrips in twelve coastal Inuit villages. The aims of the research project were to gain new regional knowledge on permafrost characteristics, to test existing and new tools for permafrost surveys and to develop a suitable methodology for terrain assessment prior to construction activities.

In the vicinity of each village where airports were to be built, periglacial landforms and patterned ground features were observed in the field after identification on air photographs. Test pits were dug with hand shovels, back-hoes and large mechanical shovels. Frozen cores were recovered with two types of portable drills; thermistor cables were installed vertically in drill-holes in bedrock and also in all major soil types present in the surroundings. Four geophysical methods were tested: (1) vertical electrical resistivity profiles using the Schlumberger array, (2) bi-dimensional electrical resistivity,

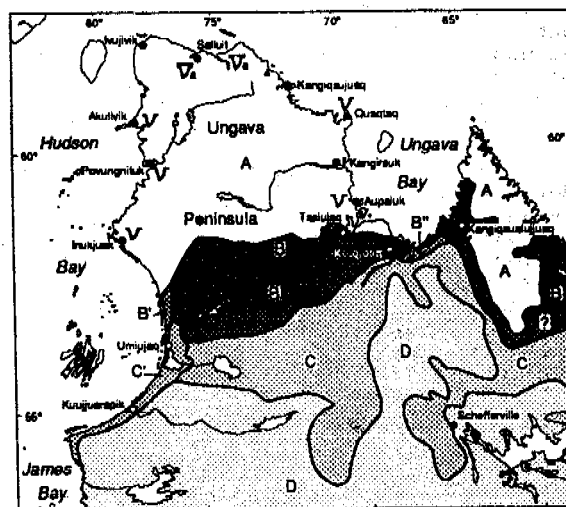


Figure 1. Permafrost map of Nunavik. A) Continuous permafrost. B) discontinuous and widespread (more than 50% of the land area) permafrost. Sub-zone B1 is a major concentration area of cryogenic mounds in marine silts. Sub-zone B2 is a concentration area of palsas over marine silts. C) Discontinuous and scattered permafrost. Subzone C' has abundant palsas D) Sporadic permafrost (less than 2% of territory) mainly in bogs and under high hills. The dotted line is the northern limit of palsas. V<sub>1</sub>) Areas of active ice wedges; V<sub>2</sub>) Areas of inactive ice wedges. Modified from Allard and Seguin (1987a).



(3) induced polarization profiling in the dipole-dipole configuration and (4) ground probing radar (GPR) profiling (Allard et al., 1991; Seguin and Lévesque, 1990; Seguin et al. 1988).

The results were twofold: 1- The gathered observations and thermal data lead to the establishment of a terrain evaluation key relating Quaternary geology, landforms, patterned ground and permafrost cryofacies, 2- an assessment of the applicability of geophysical tools to preliminary ground evaluation surveys. The latter lead to GPR being chosen as the most useful technique for probing the near surface soil layers on which structures are to be built. This paper summarizes the permafrost conditions in Nunavik in the light of the recent findings.

#### PERMAFROST DISTRIBUTION AND TEMPERATURE

The permafrost map of Nunavik has not changed since 1987, because most of the new research was done within the continuous zone. On this map (Figure 1), however, permafrost distribution in Nunavik appears very differently than on previously published maps of eastern North America (e.g. A.G.C.R., 1988). For one thing, the continuous zone extends much further southward along the Hudson Bay coast south of Inukjuak and southwest of Ungava Bay, between Tasujaq and Kuujuaq. Since a strong relationship has been observed between forest cover, snow cover thickness and permafrost absence over many years of field work (Allard and Seguin, 1987b; Thom, 1969), the southern limit of the discontinuous zone is believed to follow the forest limits quite closely.

Our coldest site is Salluit, at the extreme north of the region; at the depth of zero annual temperature (ca. 20 m), the temperature is  $-6.5^{\circ}\text{C}$ . Minimum soil surface temperature is about  $-26.5^{\circ}\text{C}$  at the southern limit of the discontinuous zone, permafrost temperature at depth is between  $-1^{\circ}\text{C}$  and  $0^{\circ}\text{C}$  (Lévesque et al., 1990). In the discontinuous zone, permafrost in Quaternary sediments reaches maximum thicknesses of between 15 and 30 m. This is currently the case in tills under drumlins and under cryogenic mounds in silty clays (Lévesque et al., 1988a, 1988b, Fortier et al., 1991). In bedrock, depths to 120 m have been measured under snow-free, windswept ridges in Schefferville (Thom, 1969) and to 180 m near Kuujuaaraapik (Poitevin and Gray, 1982). In the continuous zone, permafrost depths can reach over 500 m (Seguin, 1978; Taylor and Judge, 1979).

#### QUATERNARY GEOLOGY AND PERMAFROST CONDITIONS

The amount and type of ground ice in permafrost was found to be closely related to the type of Quaternary sediments into which the permafrost has aggraded. Deglaciation of the region started by about 10,000 years BP along the Hudson Strait coast and the whole Québec-Labrador peninsula was ice-free by 6500 BP (Dyke and Prest, 1987). Permafrost aggraded in the region as new territory was gradually uncovered from glacier ice and exposed to periglacial climate. It is also possible that permafrost already existed under cold glacier ice in the central part of the Ungava peninsula during the Wisconsin; however, climatic reconstruction by thermal modelling leaves this question open (Taylor and Judge, 1979).

Although the climate above the actual tree line was certainly cold enough to generate permafrost shortly after deglaciation, many Holocene climatic reconstructions suggest that permafrost was less abundant during the Hypsithermal and expanded during the Neoglacial period starting at about 3000 B.P. (Allard and Seguin, 1987b).

Since a marine transgression immediately followed deglaciation in the coastal regions, it was only after emergence that exposure to the cold atmosphere allowed permafrost aggradation on the fringes of Nunavik peninsula. As post-glacial uplift took place gradually during the Holocene, permafrost progressively invaded the newly emerged land, a process still taking place at present along the coastal areas.

Bedrock (mostly granitic) outcrops over a very large portion of the land surface. In some regions, the cover of morainic sediments is either sparse or consists of a veneer a few meters thick. In the region above the marine limit, till is the dominant surficial deposit. This generally sandy and bouldery material is found in such types of landforms as Roggen and De Geer moraines as well as in vast drumlin fields. Glaciofluvial sediments are also abundant in the form of sandurs and eskers. Below the marine limit, there are coarse, gravelly and sandy sediments in raised beach ridges and fluvial terraces. In permafrost within all these coarse sediments, pore ice dominates and excess ice is very scarce.

Thick fine, clayey and silty sediments extend in valley bottoms that were formerly marine basins (Figure 2). Around Ungava Bay, large tidal ranges during the postglacial marine episode were responsible for strong currents and wide intertidal zones; this resulted in a variety of sedimentary facies including intertidal bouldery muds now forming diamictic soils with a fine matrix, sand veneers over deep deposited clays and raised boulder flats and boulder barricades. As the fine sediments are prone to ice segregation, these geological variations lead to numerous lateral and stratigraphic changes in cryofacies. Since all the existing Inuit villages are located along the coast, the need for precise permafrost surveys and improved construction project design is greatest where the distribution and stratigraphy of the soil materials is the most complex in the region.

#### DOMINANT PERMAFROST LANDFORMS, PATTERN GROUND AND CRYOFACIES

##### A) Sandy and gravelly soils.

Tundra polygons are the most widespread periglacial features associated with the coarse grained materials. Over till and other diamicts, frostboils are also abundant and they often pit the interior of the polygons (Jetchick and Allard, 1990).

The polygons, with four to eight sides, are from 10 to 30 m in diameter. In the southern part of the widespread discontinuous permafrost zone (Figure 1), the polygonal cells are either flat or only slightly domed; the sides are marked by shallow linear furrows that contain active layer soil wedges. As yet, no ice wedges have been found underneath the sides of these extensively distributed features. In the continuous permafrost zone, active layer soil wedge polygons are also found at a few dry sites; however, most frost

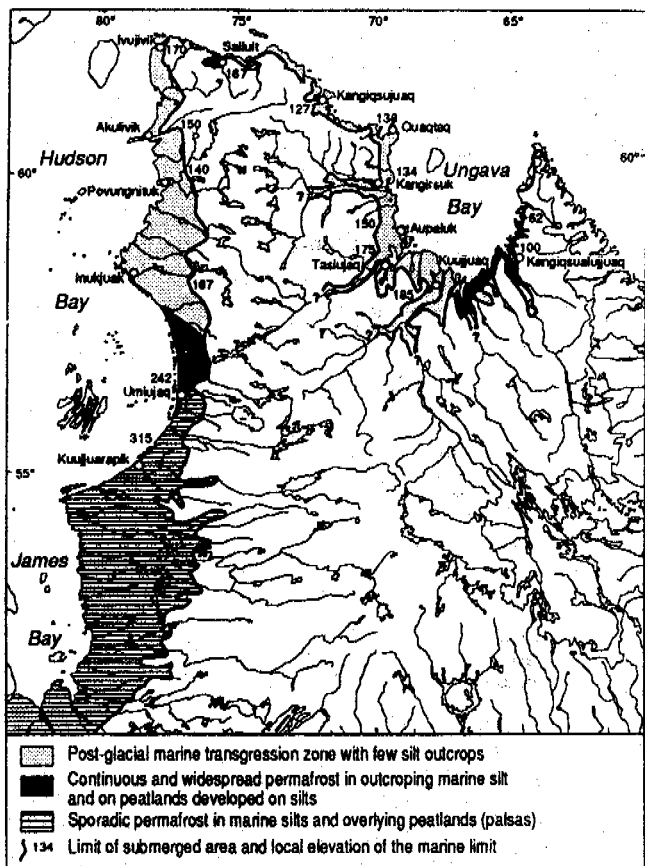


Figure 2- Geographical extension of the post-glacial marine transgressions.

cracks and polygon sides contain ice wedges. The ice wedge polygons are found mainly on flat terraces and most of them are low centered due to the formation of double ridges over recently grown wedges. Two areas of active frost cracking were recently documented: Salluit (Kasper, 1992; Moisan, 1988) and Deception Bay (Seppälä et al., 1992). Both sites are at the extreme northern tip of the Ungava peninsula where mean annual air temperature is in the order of  $-10^{\circ}\text{C}$ .

Ice wedges were also found at four localities during airstrip construction work, while ditching and by drilling. The top of these ice wedges was found to coincide with permafrost table according to thermal measurements but the absence of actual ice veins and open cracks in the active layer indicate that they are either inactive or rarely active under the present climatic conditions (Mackay, 1992). They very likely formed during a Holocene interval colder than the present. Many ice wedges were imaged with ground probing radar (Figure 3).

Other patterned ground features over coarse or diamictic soils comprise frostboils, soil stripes and turf hummocks. Most of the frostboils on tills and on raised, coarse tidal sediments are low center, being rimmed by turf banks. Vast expanses of terrain dominated by these pattern types can be seen on air photographs; they are clear indicators of permafrost containing both pore ice and a very small amount of segregated ice in a soil material that has a slight silt content. The soil

stripes on slopes appear to be the equivalent of the low center, turf sided, frost boils found on the same soil types on flat terrains. The turf hummocks, from 30 cm to 1 m high and about 1.5 m in diameter, occur in poorly drained lowlands over the same types of soils.

Pore ice dominates in sandy and gravelly materials of glacial, glaciofluvial, fluvial or beach origin. When the matrix of the till contains a fraction of silt (variable up to 10%), very fine, hair thin segregation ice can be seen in very fresh samples.

#### B) Silty and clayey soils.

In the discontinuous permafrost zone, ice segregation in the fine marine sediments has provoked the heaving of cryogenic mounds. The sediments consist in average of 65% silt, 23% clay and 12% sand; their unfrozen plasticity index is about 13%. Laboratory and site measurements revealed that their thaw settlement coefficient, 25-30%, is comparable to other similar soils as studied by McRoberts et al. (1978). The mounds vary in size from a few meters to over 100 m in diameter. Their height varies from 2-3 m to 10 m. Each one contains a permafrost nucleus that may reach depths down to 30 m; the average depth, as measured by electrical resistivity soundings (Lévesque et al., 1988a and b) and thermistor cables (e.g. Allard et al., 1988; Fortier et al., 1991) is about 20 m. Core extraction revealed very high ice contents, thick ice lenses (Leroueil et al., 1991) and also large reticulated or erratic cryostructures. In most cases, the temperatures fluctuate widely over one year in the near-surface ice-rich layer while it varies very little in the lower part of the profile, at temperatures warmer than  $-2^{\circ}\text{C}$ , due to the thermal inertia induced by a high unfrozen water content. Usually, ice rich layers are found from the permafrost table down to 3-4 meters, with the volumetric ice contents varying from 50 to 80% (Allard et al., 1988; Leroueil et al., 1991).

Surface electrical resistivity soundings using the Schlumberger array (Seguin and Allard, 1984) provide general information on permafrost thickness in these cryogenic mounds. However experience has shown that real permafrost thickness can sometimes be underes-

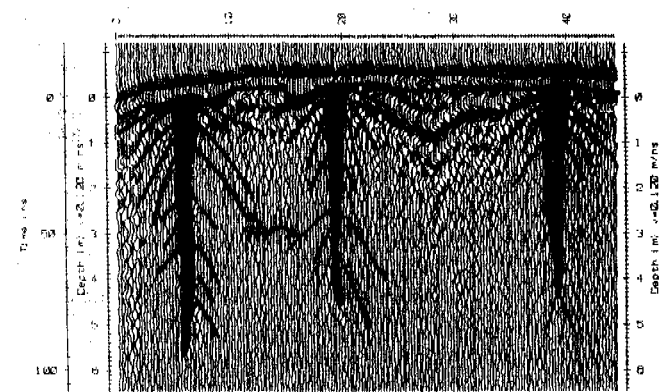


Figure 3. GPR section across ice-wedge polygons near Salluit. S= surface; PT= permafrost table; PR= parabolic reflectors. Pulse Ekko IV; 200 Mhz; 0.5 m separation; 0.25 m step size; constant gain.

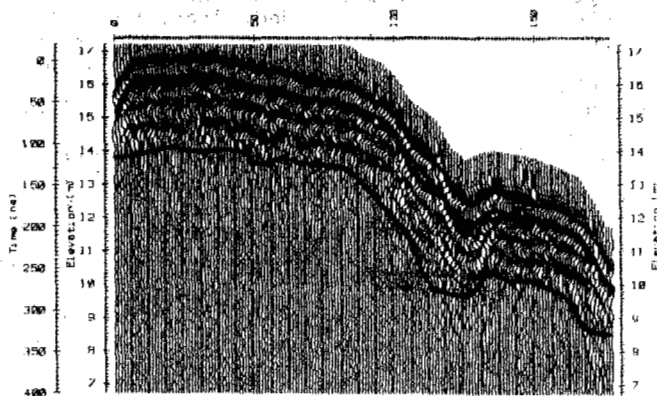


Figure 4. GPR section of a clayey cryogenic mound near Kangiqsualujuaq, with topography. Although the thermally measured depth of permafrost base is 23 m, signal returns are limited to the first 2-3 m below permafrost table.

S= surface; PT= permafrost table. Pulse Ekko IV radar; 50 Mhz; 2 m antenna separation; 1 m step size; automatic gain control.

timated with this method because of low resistivity contrasts in the basal permafrost layers. Near permafrost base temperatures are only a few tenths of a degree below 0°C and the soil is ice-poor or unfrozen as a result of overburden pressure and salt concentration resulting from extrusion during freezing. In contrast, recent interpretation of vertical electrical resistivity profiles along electrode cables in drill-holes indicate that ice-rich layers may in fact be present at the base of the permafrost in the discontinuous zone in areas where the water table can supply ice formation, leaving an ice-poor layer in between (Fortier et al., 1991). GPR profiles run across cryogenic mounds typically show the presence of the ice-rich layer below the permafrost table. At greater depths, the strong signal attenuation in the ice-poor, partly frozen fine grained sediments prevents any returns (Figure 4).

The ground surface on the cryogenic mounds is pitted with high center frostboils that affect the entire thickness of the active layer. On the sides of the mounds, the frostboils tend either to stretch out parallel to the slope or to merge into terracettes. Near depressions and thermokarst hollows, active layer detachment failures occur on the flanks of the mounds (Seguin and Allard, 1984; Allard et al., 1986). In areas of extensive marine silts in the discontinuous zone, past climatic variations and the warming of the XXth century have induced thermokarst resulting in innumerable ponds which coexist with the permafrost mounds (Allard and Seguin, 1987b).

In the continuous permafrost zone, definite mounds do not form in the marine silts although large surfaces of terrain have been heaved by the aggradation of abundant ground ice. High center frostboils are also widespread over these frozen fine sediments. Coring and observations in natural sections in river banks as well as in small retrogressive thaw slumps revealed that the permafrost contains massive icy beds within which ice amounts to over 80% per volume. A site near

Salluit along the access road to the new airport was studied. Drilling showed that the massive icy layer is 11 m thick, a value corroborated by a change of polarity sign on an induced polarization survey. In the same region, at greater depths, ice lenses 10 cm thick and 50 cm apart form a reticulated network with ice veins 3 cm wide in one section. The mean permafrost temperature at the 5 m depth is about -5°C.

#### OTHER PERMAFROST FEATURES

The geographical distribution of palsas and peat plateaus in northern Québec has been studied by Lagarec (1982), Allard et al., (1986) and Allard and Seguin (1987a). The northern limit of their distribution area corresponds well to the present tree line (Figure 1). Icings and frost blisters are particularly abundant along the Hudson Bay coast between Kuujjuarapiik and Nastapoca river. Near the community of Umiujuag, two large icings (one nearly 500 m wide) made it necessary to select a more suitable site for the airport. Heaved bedrock landforms (Dionne, 1983) form over permafrost where the geological structure is favourable to partitioning of blocks that are differentially heaved by hydraulic forces induced in the active layer during annual freeze-back. The basaltic formations along the eastern coast of Hudson Bay are particularly favourable to this phenomenon (Michaud and Dyke, 1990).

Finally, in the coastal regions with a very large tidal range, such as Ungava Bay, aggrading permafrost has been found under higher marshes that are inundated by large tides and onto which the ice-foot freezes to the bottom in winter. A recent study of the thermal regime of this intertidal permafrost has shown that it is brackish (salinity ca. 15 per mil), has a freezing point depression of about 0.9°C and that tidal submersions in summer induce convective heat transfer by infiltration in the active layer. Ground ice in this permafrost consists of very thin reticulated ice lenses and veins (Allard et al., 1992).

#### CONCLUSION

Table 1 summarizes the correlations between Quaternary sediments, periglacial landforms, patterned ground features and permafrost characteristics in Nunavik. The extensive knowledge of these relationships makes it possible for land management project planners and engineers to use it as a key for mapping probable areas of ice rich permafrost, planning geophysical surveys and drilling operations at reduced costs and making decisions prior to undertaking construction projects involving cutting, digging, insulating and designing foundations. Our improved geographic knowledge is also helpful in planning further research, by identifying areas and phenomena most sensitive to geomorphic and ecological variations in the context of natural or man-induced climatic changes.

#### ACKNOWLEDGEMENTS

The authors express their thanks to Transports Québec for financial and logistic support of research in the framework of the Nunavik airports construction program and, also, to the Geological Survey of Canada for

Table 1. Correspondences between landforms, patterned ground features, surficial geology and ground ice types in Nunavik.

Landforms and pattern ground	Minimal air photo scale	Surficial geology	Texture	Permafrost regions	Ground ice types
Permafrost mounds	1:40,000	Marine silts and clays, sand (lower mounds)	Clayey silts, Fine and medium sand	Widespread, scattered	Segregated
Palsas	1:40,000	Peat, peat/silts peat/sand peat/till (scarce)	Fibrous or humic peat over fine soils	Widespread, scattered	Segregated
Thermokarst ponds (are associated with palsas and mounds)	1:40,000	All formations, mostly fine and peaty	Peat, silts, sands	Widespread, scattered sporadic	Nil
Ice-wedge polygons	1:20,000	Tills, sandy fluvial terraces, raised beaches, Fens	Peat, fine to coarse sands	Continuous	Wedge ice, interstitial within polygons
Soil-wedge polygons	1:20,000	Tills (on moraines and drumlins), Glacio-fluvial deposits (sandurs and deltas)	Coarse and poorly sorted sand and gravel	Continuous, widespread	Interstitial
Rimmed frost-boils (often associated with ice ground wedges and gelifluxion lobes)	1:10,000	Tills and other diamicts (raised stony tidal flats)	Sandy and gravelly soils with a fraction of silt	Continuous, widespread	Interstitial, a little segregated ice
High-centre frost-boils	1:20,000	Marine and lacustrine fine sediments	Fine sands and clayey silts	Continuous, widespread, scattered	Segregated
Soil stripes	1:40,000	Tills and slope deposits	Bouldery with matrix	Continuous	Interstitial
Gelifluxion lobes	1:40,000	Tills, slope deposits, sands	Poorly sorted soils with matrix	Continuous, widespread, scattered, sporadic	Interstitial
Thufurs	1:10,000	Tills and diamicts on poorly drained terrains	Poorly sorted soils with matrix	Continuous, widespread	Interstitial
Icings and frost blisters	1:10,000	All types	All including organics	Continuous, widespread	Intrusive
Heaved bedrock	1:5000	Jointed bedrock		Continuous, widespread, scattered	Intrusive? segregated?

financial, professional and logistic help. The principal author also benefited from grants from the Natural Sciences and Engineering Council of Canada and the «Fonds F.C.A.R.» of the Québec Department of Higher Education. Comments on a preliminary version of the manuscript by Dr Alan Judge and two other reviewers of the conference proceedings were very helpful. This work could not have been done without the precious help of Mr. Richard Lévesque. Many students also contributed.

#### REFERENCES

- A.C.G.R. (Associate committee on geotechnical research) 1988: Glossary of permafrost and related ground ice terms. National Research Council of Canada, Technical memorandum n° 142, 156 pp.
- Allard, M., Fortier, R. and Seguin, M.K. 1992. The thermal regime of intertidal permafrost, George River estuary, Québec. Canadian Journal of Earth Sciences, 29 (2), 249-259

- Allard, M., Lévesque, R., Seguin, M.K. and Pilon, J.A. 1991. Les caractéristiques du pergélisol et les études préliminaires aux travaux de génie au Québec nordique. Rapport au ministère des transports du Québec, non publié, 94 p.
- Allard, M. and Seguin, M.K. 1987a. Le pergélisol au Québec nordique: bilan et perspectives. *Géographie physique et Quaternaire*, 41: 141-152
- Allard, M. and Seguin, M.K. 1987b. The Holocene evolution of permafrost near the tree line along the eastern coast of Hudson Bay, northern Quebec. *Canadian Journal of Earth Sciences*, 24: 2206-2222
- Allard, M., Seguin, M.K. and Lévesque, R. 1986. Palsas and mineral permafrost mounds in northern Quebec. In *International Geomorphology, Part II*, Edited by V. Gardiner, John Wiley and Sons Ltd, London, pp. 285-309
- Allard, M., Seguin, M.K. and Pelletier, Y. 1988. Shoreline permafrost in Kangiqsualujjuaq Bay, Ungava, Quebec. In *Permafrost, Fifth International Conference on Permafrost Proceedings*. Edited by K. Senneset. Tapir Publishers, Trondheim, Norway, 1, pp. 113-118
- Brown, R.J.E. 1979. Permafrost distribution in the southern part of the discontinuous zone in Quebec and Labrador. *Géographie physique et Quaternaire*, 33: 279-290
- Dionne, J.C. 1983. Frost-heaved bedrock features: a valuable permafrost indicator. *Géographie physique et Quaternaire*, 33: 241-251
- Dyke, A.S. and Prest, V.K. 1987. Late Wisconsinan and Holocene history of the Laurentide ice sheet. *Géographie physique et Quaternaire*, 41: 237-264
- Fortier, R., Lévesque, R., Seguin, M.K. and Allard, M. 1991. Caractérisation du pergélisol de buttes cryogènes à l'aide de diagnostics électriques au Nunavik, Québec. *Permafrost and periglacial processes*, 2: 79-93
- Ives, J.D. 1979. A proposed history of permafrost development in Labrador-Ungava. *Géographie physique et Quaternaire*, 33: 233-244
- Jetchick, E. and Allard, M. 1990. Soil wedge polygons in northern Québec: description and paleoclimatic significance. *Boreas*, 19: 353-367
- Kasper, J.N. 1992. Les coins de glace comme indicateurs climatiques au Québec nordique. Association québécoise pour l'étude du Quaternaire, colloque des 27-28 février 1992, Ottawa, Résumé des communications.
- Lagarec, D. 1982. Cryogenic mounds as indicators of permafrost conditions, northern Québec. In *Proceedings Fourth Canadian Permafrost Conference*, the Roger J.E. Brown Memorial Volume, Ottawa, National Research Council of Canada, pp. 43-48
- Leroueil, S., Dionne, G. and Allard, M. 1991. Tassement et consolidation au dégel d'un silt argileux à Kangiqsualujjuaq. *Canadian Geotechnical Journal*, 28: 678-689
- Lévesque, R., Allard, M. and Seguin, M.K. 1988a. Le pergélisol dans les formations quaternaires de la région des rivières Nastapoca et Sheldrake, Québec nordique. Centre d'études nordiques, Université Laval, *Nordicana* n°51, 23 pp.
- Lévesque, R., Allard, M. and Seguin, M.K. 1988b. Regional factors of permafrost distribution and thickness, Hudson Bay coast, Québec. In *Permafrost, Fifth International Conference on Permafrost Proceedings*. Edited by K. Senneset. Tapir Publishers, Trondheim, Norway, 1, pp. 199-204
- Lévesque, R., Allard, M., Seguin, M.K. and Pilon, J.A. 1990. Données préliminaires sur le régime thermique du pergélisol dans quelques localités du Nunavik, Québec. In *Permafrost-Canada, Proceedings of the Fifth Canadian Permafrost Conference*, Centre d'études nordiques, Université Laval, *Nordicana* n° 54, pp.207-214
- Mackay J.R. 1992 The frequency of ice-wedge cracking (1967-1987) at Garry Island, western Arctic coast, Canada. *Canadian Journal of Earth Sciences*, 29:236-248
- McRoberts, E.C., Law, T.C. and Moniz, E. 1978. Thaw settlement studies in the discontinuous permafrost zone. *Proceedings of the Third Int. conference on Permafrost*, National Research Council of Canada, p. 701-706
- Michaud, Y. and Dyke, L. 1990. Mechanisms of bedrock frost heave in permafrost regions. In *Permafrost-Canada, Proceedings of the Fifth Canadian Permafrost Conference*, Centre d'études nordiques, Université Laval, *Nordicana* n° 54, pp.125-130
- Moisan, Y. 1988. Etude de trois sites de polygones à coins de glace dans la région de Salluit, Québec arctique. Université Laval, Département de géographie, Mémoire de baccalauréat, 71 pp.
- Poitevin, S. and Gray, J.T. 1982. Distribution du pergélisol dans le bassin de la Grande Rivière de la Baleine, Québec. *Naturaliste canadien*, 109: 445-455
- Seguin, M.K. 1978. Temperature-electrical resistivity relationship in continuous permafrost at Purtunig, Ungava peninsula. *Proceedings of the Third International Permafrost Conference*, National Research Council of Canada, pp. 137-144
- Seguin, M.K. and Allard, M. 1984. Le pergélisol et les processus thermokarstiques de la région de la rivière Nastapoca, Nouveau-Québec. *Géographie physique et Quaternaire*, 38: 11-25
- Seguin, M.K., Gahé, E., Allard, M. and Ben-Miloud, K. 1988. Permafrost geophysical investigation at the new airport site of Kangiqsualujjuaq, northern Québec, Canada. In *Permafrost, Fifth International Conference on Permafrost Proceedings*. Edited by K. Senneset. Tapir Publishers, Trondheim, Norway, 2, pp. 980-988
- Seguin, M.K. and Lévesque, R. 1990. Détection, par méthodes géophysiques, de sols gélifs à l'emplacement de pistes d'atterrissage au Nunavik, Québec. In *Permafrost-Canada, Proceedings of the Fifth Canadian Permafrost Conference*, Centre d'études nordiques, Université Laval, *Nordicana* n° 54, pp. 239-245
- Seppälä, M., Gray, J.T. and Ricard, J. 1992. Development of low-centre ice-wedge polygons in the northernmost Ungava peninsula, Québec, Canada. *Boreas*, 20: 259-282
- Taylor, A. and Judge, A. 1979. Permafrost studies in northern Québec. *Géographie physique et Quaternaire*, 33: 245-252
- Thom, B. 1969. New permafrost investigation near Schefferville, P.Q. *Revue de géographie de Montréal*, 23: 317-327

# INFLUENCE OF CLIMATE CHANGE ON HIGHWAY EMBANKMENT STABILITY AND PERMAFROST IN THE PERMAFROST REGION OF THE QINGHAI-XIZANG PLATEAU

An, Weidong<sup>1</sup>, Wu, Ziwang<sup>2</sup>, Zhu, Yuanlin<sup>3</sup> and A.S. Judge<sup>1</sup>

1 Lanzhou Institute of Glaciology and Geocryology, Academia Sinica, China;  
Centre D'études Nordiques, Université Laval, Québec, Canada G1K 7P4

2 Lanzhou Institute of Glaciology and Geocryology, Academia Sinica, China

3 Terrain Science Division, Geological Survey of Canada, Ottawa, Canada K1A 0E8

This paper presents a numerical prediction of the influence of climate change on the thaw stability of asphalt-surfaced embankments constructed on permafrost along the Qinghai-Xizang Highway, China, if predictions based on global climate change models for the Qinghai-Xizang Plateau region are correct. With climate warming, the major highway stability problems and the foundations of other engineered structures can be expected in areas of ice-rich soils due to thaw subsidence and pothole formation. Special measures or new designs may be needed to protect such structures against thaw settlement damage owing to present geocryological variations and future climate change. Substantial increase in the depth of seasonal thaw will lead to degradation of permafrost and the formation of frigid and arid areas on the plateau, especially where the annual precipitation is low at present. Thus the problems related to environmental change in the permafrost regions of the Qinghai-Xizang Plateau present broader social and economic issues than solely those of infrastructure engineering.

## INTRODUCTION

In the northwestern section of the Qinghai-Xizang Plateau (QXP), the Qinghai-Xizang highway crosses, at elevations of 4200 m and above, a region of continuous permafrost and experiences mean annual ground temperatures of  $-1.0$  to  $-4.5^{\circ}\text{C}$ . This region located from  $30$  to  $37^{\circ}\text{N}$  and  $90$  to  $100^{\circ}\text{E}$  may experience additional problems if predicted climate change of the globe influences permafrost and structures constructed on permafrost.

Because of the accumulation of  $\text{CO}_2$  and other radiatively active gases in the atmosphere and the resulting enhanced greenhouse factor, a climate warming may occur in the QXP (Houghton et al., 1990), leading to a rise in the air temperature of  $2.0$  to  $6.0^{\circ}\text{C}$  by the year 2035. If steady warming takes place in this permafrost region, ground temperature at depth will slowly respond. Obviously, future structures should incorporate some consideration of climate change in the design, but existing structures in this alpine permafrost area contain no allowance for climate change. Some countermeasures, however, may be necessary to prevent their settlement and deterioration.

The stability of the asphalt-surfaced fill embankments of the Qinghai-Xizang highway, one of the two roads into Xizang, is a major engineering concern. To date, many methods have been proposed to prevent or minimize degradation of permafrost beneath embankments around the world, such as thermopiles, air duct venting, polystyrene foam insulation, and embankment fills (Hildebrand, 1983, Vita, 1983, Zhu et al., 1983, Wu, 1988, Esch, 1990). However, the most simple and cost-effective method of construction of the highway on continuous permafrost in the QXP is to use embankment fill structures (Yu, 1986, Wu, 1988, An, 1989). Heat absorption by the asphalt pavement, loading to

increased seasonal thaw and difficulties of drainage of the thaw basin formed beneath, has resulted in embankments suffering serious degradation through inhomogeneous differential thaw settlement and pothole formation. This has been caused by embankment heights being much lower than the critical heights especially in areas with ice-rich soils or massive ground ice near the permafrost table, and has sometimes led to temporary suspension of transportation since reconstruction in 1982.

In addition, a more general problem may be triggered through the influence of climate change on the permafrost of the QXP. At present, the mean annual precipitation varies regionally from a low of 100mm in the western areas to excess of 400mm in the southern areas around Mount Tanggulashan. Strong winds and high levels of solar radiation on the plateau cause considerable evaporation of surface moisture (Tong and Li, 1983). Thus, except for some very localised areas with moderated microclimates, the greater part of the northern and western regions of plateau, such as the Mount Konglongshan area along the Qinghai-Xizang Highway, possess an arid climate and sparse vegetation. Clearly, the existence of the permafrost is the decisive factor in preserving ground moisture, supporting the vegetation and preventing the plateau surface from becoming a frigid desert.

The nature and magnitude of climate change, especially on a regional basis is still a debatable problem, and so far there have been no completely satisfactory theoretical models to link increased concentration of greenhouse gases in the atmosphere with climate change. Thus whether or not a permanent long-term climate warming will take place and the rate and magnitude of the change remains uncertain. The effect of climate warming on the permafrost and on engineering structures of the QXP will

be serious. This paper presents a preliminary numerical study of those predicted effects of surface warming on the ground temperatures beneath both the virgin permafrost and the highway embankments at the Kekexili and Wudaoliang sites. These sites lie in a continuous permafrost environment, 4700m above sea level, with a mean annual air temperature of  $-5.6^{\circ}\text{C}$ . Over the next forty years these sites are assumed to be subject to global warming at a rate of  $0.08^{\circ}\text{C}/\text{year}$ . The numerical prediction showed that the effects of climate warming on asphalt-surfaced embankments are increased depth of thaw, and greater thaw settlement of an embankment constructed on an ice-rich foundation. Comparison of the ground temperature variation between the current climate condition (i.e. in the modelling  $0.08^{\circ}\text{C}$  mean annual air temperature increment) and the future condition shows that 1) for a moderate air temperature increase (i.e. less than  $1.5^{\circ}\text{C}$ ), the influence of the climate change on the stability of embankments is not serious if the embankment height is maintained above the critical height; 2) with an air temperature rise higher than this value, the effect of the asphalt pavement will be the most critical factor in the stability of the Highway.

## MATHEMATICAL MODEL AND NUMERICAL SCHEME

### 1. Mathematical model

For the mathematical modelling of freeze-thaw cycle in permafrost, we will assume: soils are isotropic and homogeneously layered; soil particles and water are incompressible; diffusive dispersal fluxes of both water and gas masses are negligible and local fluid and solid temperatures are equal. Furthermore we will neglect thaw consolidation, moisture migration, additional heat sources, and chemical potentials. The heat conduction through soil particles and water, ice-water phase-change and convection only are considered. Thus the governing equation of the phase-change temperature,  $T(t, x, y, z)$ , of permafrost can be given by the following:

$$C \frac{\partial T}{\partial t} = \text{div}(\lambda \text{grad } T) + C_w \rho_w \text{div}(\vec{V}T) + L\rho_i \frac{\partial \theta_i}{\partial T} + q \quad (1)$$

The relationships between ice content and temperature in the freezing region can be considered. Thus, equation (1) is simplified as

$$\bar{C} \frac{\partial T}{\partial t} = \text{div}(\lambda \text{grad } T) + C_w \rho_w \text{div}(\vec{V}T) \quad (2)$$

where

$$\bar{C} = C + L\rho_i \frac{\partial \theta_i}{\partial T} \quad (3)$$

$$C = C_s \theta_s + C_w \theta_w + C_i \theta_i \quad (4)$$

$$\lambda = \lambda_s^* \lambda_w^* \lambda_i^* \quad (5)$$

unfrozen water content is a function of the ground temperature; and the ice content is written as

$$\theta_i = \theta - \theta_u \quad (6)$$

Equations (1)-(6) can be solved for the initial conditions and boundary conditions. Generally, the initial conditions are

$$T(x, y, z, t)_{t=0} = f(x, y, z) \quad (7)$$

and the boundary conditions are expressed as

$$T_{(x,y,z) \in \Gamma} = \phi(x, y, z, t) \quad (8)$$

$$\left( \frac{\partial T}{\partial t} + \rho(T)T \right)_{(x,y,z) \in \Gamma} = \phi_2(x, y, z, t) \quad (9)$$

where

$T$	Temperature
$\bar{C}$	Apparent volumetric heat capacity of the soils
$C^*, C$	Volumetric heat capacities of thawed and frozen soils
$L$	Volumetric latent heat of fusion of bulk water
$V$	Velocity flux
$\rho_i, \rho_w$	Ice and water densities
$\lambda, \lambda^*, \lambda'$	Thermal conductivity of the soils, thaw and frozen soils, respectively
$\theta_u, \theta_i$	Unfrozen water content
$\theta$	Total content of water and ice
$x, y, z$	Cartesian coordinates
$t$	time

The equations (2) to (6) describe mathematically the temperature field in freezing and thawing permafrost or frozen ground. The convection term in equation (2) is so small that it is omitted (Nixon, 1978). Because of temperature-dependent thermal properties in equations (1) and (2), the equations are nonlinear, and the phase-change temperatures and critical heights of the embankments in the Kekexili and Wudaoliang sites were represented using the conventional finite difference equation.

### 2. Numerical scheme

Using the law of energy conservation and a conventional finite difference scheme of alternating-direction, the two dimensional problems of equations (2) to (6) are given as

$$\begin{aligned} [B^n] [T^{n+1/2}] &= [F^n] \\ [B^{n+1/2}] [T^{n+1}] &= [F^{n+1/2}] \end{aligned} \quad (10)$$

$$\begin{aligned} \Delta x_{j+1/2} &= \Delta x_j (\Delta x_{j+1} + \Delta x_j) / 2 \\ \Delta x_{j-1/2} &= \Delta x_j (\Delta x_j + \Delta x_{j-1}) / 2 \end{aligned} \quad (11)$$

With the similar definition to  $\Delta z$   
Initial condition:

$$T_{i,j}^0 = \Psi_0(x_j, z_j) \quad (12)$$

Boundary condition:

$$T_{i,0}^n = f_1(x_j, \tau), \quad T_{i,n}^n = f_2(x_j, \tau) \quad (13)$$

$$T_{i,j}^{n+1/2} = T_{i,j}^{n+1/2}, \quad T_{i,j}^{n+1/2} = T_{i,j}^{n+1/2}$$

$$T_{i,j}^{n+1} = T_{i,j}^{n+1}, \quad T_{i,j}^{n+1} = T_{i,j}^{n+1} \quad (14)$$

$i=1, 2, 3, \dots, N; j=1, 2, 3, \dots, M; n=1, 2, 3, \dots$   
 The difference equations are permanently stable and convergent. Initial conditions can be determined from the monitored data or calculated from the characteristics of the particular problem using the Laplace equation.

**DETERMINATION OF THE CRITICAL HEIGHT FOR AN ASPHALT SURFACED FILL EMBANKMENT**

Except for asphalt-surfaced pavement, the embankments are generally constructed from local materials and built directly on the original ground surface. To safeguard the frozen state of permafrost and to prevent instability of the embankment due to thaw deterioration of the underlying permafrost, the maximum depths of the seasonal active layer of both the undisturbed permafrost and the embankment foundation should remain at the same level. The computed height of embankment to meet this requirement is termed the critical height.

The effects of the thawing indices of the various ground surface covers at different sites were considered. These combine the actions of the ambient air temperature and solar radiation on the ground surface represented by fine-grained soils, coarse-grained soils, and asphalt pavement (Wu, 1988, An, 1989). Representative local ambient air temperature for any time of year is calculated by the following equation:

$$f(\tau) = -15.7832 - 1.7623E-1\tau + 4.2239E-3\tau^2 - 1.8758E-5\tau^3 + 2.32903E-8\tau^4 \quad (15)$$

Where  $\tau$  is the Julian day.

Initial conditions were determined using the ground temperatures monitored in observation drillholes before thawing and numerically with the Laplace equation.

The top time-dependent boundary condition is given as:

$$f_0(\tau) = \begin{cases} \Delta t_1 + f(\tau) + \Delta T & J < J_1 \\ \Delta t_1 + J \cdot (\Delta t_1) + f(\tau) + \Delta T & J_1 \leq J \leq J_2 \\ \Delta t_2 + f(\tau) + \Delta T & J > J_2 \end{cases} \quad (16)$$

where

$$\Delta t_1 = \begin{cases} D_n \cdot \sin(\tau - \tau_0) + D_m & f(\tau) > T_b \\ D_m & f(\tau) \leq T_b \end{cases}$$

$$\Delta t_2 = \begin{cases} D_s \cdot \sin(\tau - \tau_0) + D_m & f(\tau) > T_0 \\ D_m & f(\tau) \leq T_0 \end{cases}$$

The lower boundary condition as

$$f_1(\tau) = T_b \quad (17)$$

where  $\Delta T$  is the mean annual air temperature increment.

The relationship between unfrozen water content and temperature is expressed (Xu, 1985):

$$W_u = W(1 - R(T))$$

$$\text{where } R(T) = 0.605446 - 0.35881T + 0.144879T^2 - 2.89856E-2T^3 + 2.60897E-3T^4 - 8.78246E-5T^5 \quad T < -7.0^\circ\text{C} \quad (18)$$

for the coarse-grained soils; and

$$W_u = \begin{cases} W = R_3(T - T_0) & T_1 \leq T \leq T_0 \\ 0.0775 \cdot \exp(0.0656T) & T < T_1 \end{cases} \quad (19)$$

for the fine-grained soils.

The correlation coefficients of both equations are 0.96 and 0.98 and the  $T_0$ ,  $T_1$  and the constant  $T_b$  are 0.0, -0.75 and -0.20°C, respectively.

The unfrozen water content also affected by the soil density, decreasing with increasing soil density  $\rho_d$ . As the values of  $\rho_d$  change from 1600, 1550 to 1500, the constant  $R_3$  varies from 0.1333, 0.162 to 0.313, respectively; the constants  $D_n$ ,  $D_{wn}$ ,  $D_a$ ,  $D_{wa}$  are 1.35, 1.1, 6.9, 1.5, respectively.

The time and space steps used for the computation were

$$\Delta \tau = 4.0 \text{ to } 8.0 \text{ h}; \Delta z = 0.10 \text{ m}; \Delta x = 0.15 \text{ to } 0.25 \text{ m}$$

The relevant soil and thermal parameters are shown in table 1; and a cross-sectional sketch of the embankment is shown in figure 1.

Table 1. The Soil and Thermal Parameters Used for Model Computations.

Soil*	Dry Density $\rho_d$ (kg/m <sup>3</sup> )	Water Content W (g/g)	C <sub>v</sub> (KJ/m <sup>3</sup> .K)	C <sub>s</sub> (KJ/m <sup>3</sup> .K)	$\lambda$ (W/m.K)	$\lambda_{eq}$ (W/m.K)
C.S.G.	1900	6	2227.4	1913.4	1.919	1.982
S.L.G.M.	1800	10	2185.5	1695.6	1.919	2.616
Loam	1600	13	2210.6	1976.6	0.982	0.912
	1550	14	2202.3	1942.7	0.976	0.908
S.G.S.	1500	20	2512.1	2072.5	1.093	1.221
	1600	14	2210.6	1641.2	1.642	2.151

\* Coarse Sand and Gravel (C.S.G.)  
 Sandy Loam and Gravel Mixture (S.L.G.M.)  
 Sandy Gravel Soil (S.G.S)

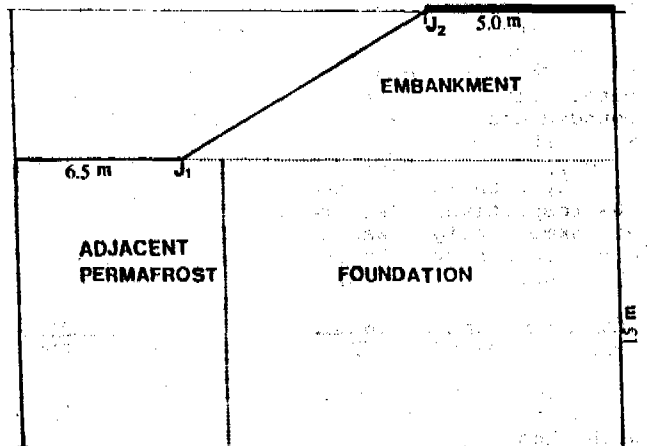


Figure 1. Cross-section of an asphalt-surfaced embankment.



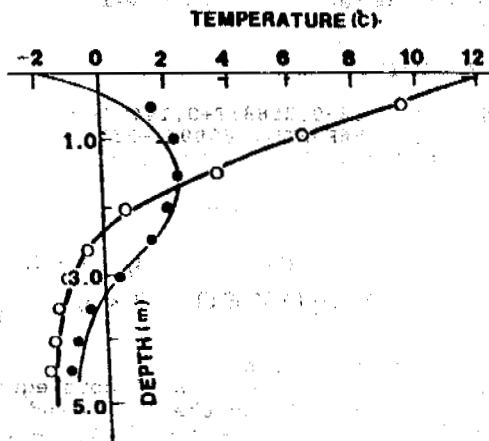


Figure 2 Temperature distribution in the vertical direction along the center line of the embankment.  
 — computed results  
 •, o monitoring data from the last ten days of October 1986 and the middle ten days of July, 1987 respectively

For the fine-grained soil foundation of the embankment at the Kekexili site, Figure 2 shows the vertical temperature profiles derived from the numerical solution and from the drillhole data beneath the center of the paved embankment. The maximum depths of seasonal thaw on a cross-section of the embankment are presented in Figure 3. Comparisons of the monitored and numerically predicted values of both ground temperature and depths of maximum seasonal thaw on the cross-section of embankment and on adjacent permafrost agree quite well. Figure 4 gives monitored results from a drillhole at the center of the embankment showing the depth of zero degree isotherm during seasonal thaw.

While the minimum critical height, on the one hand, was the important calculated result for the thermal stability of the embankment, the drainage, consolidation and mechanical properties of the embankment were also of concern. Considering all of the factors, the computed critical height was 2.1 m for a compounded coarse-grained fill of dry density, with water content of 1800 kg/m<sup>3</sup> and 8% respectively, and the fine-grained foundation of dry density with water content of 1550 kg/m<sup>3</sup> and 10% respectively (Figure 3). The observed embankment height was 2.0m after 7.0 years of continuous service testifying to the reasonable success of the predicted performance.

PREDICTION OF THE INFLUENCE OF CLIMATE CHANGE ON THE PERMAFROST AND THE HIGHWAY EMBANKMENT

To contrast the results of the present ground temperature profiles and variations with those predicted for the next forty years, the current seasonal thaw variations with time in both the fine-grained and coarse-grained soils beneath the undisturbed permafrost are computed, and these results shown to fit the observed data (Figure 5). With an increase of mean annual air temperature, the corresponding increasing depths of thaw are demonstrated by the temperature profiles for depths beneath the embankment (Figure 6) and in cross-section along the embankment (Figure 7). The parameters used for the calculation were those for

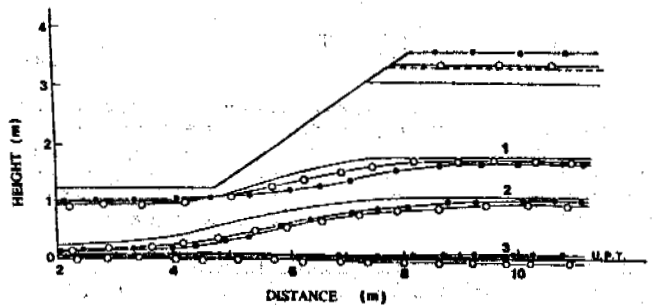


Figure 3. Critical heights of the embankment with three different fills.  
 U.P.T. Upper undisturbed permafrost table monitored  
 - - - the test embankment height (monitored)  
 —, •, o computation results for different properties of fill;  
 —  $\rho_d=1600 \text{ kg/m}^3, W=13\%$   
 o  $\rho_d=1800 \text{ kg/m}^3, W=10\%$   
 •  $\rho_d=1900 \text{ kg/m}^3, W=6\%$   
 1, 2, 3 the results of the mid-May, mid-July and early-September, respectively

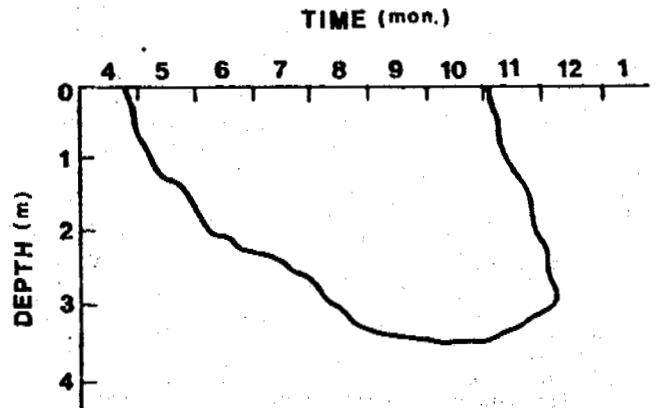


Figure 4. Variation of depth of thaw with time (0.0°C isotherm) in the center drillhole of the embankment (monitored April 1986 to May 1987).

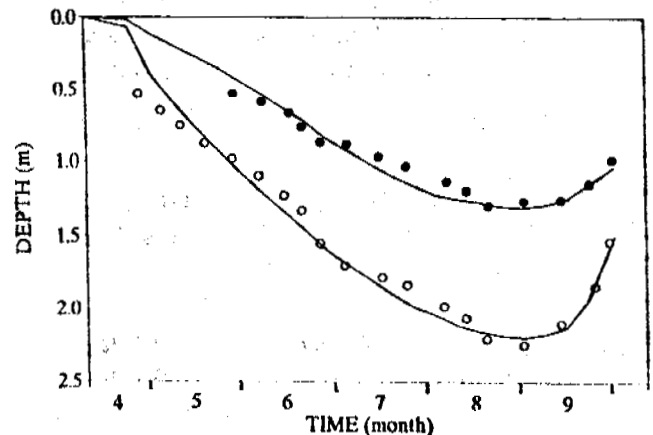


Figure 5. Variation of depth of thaw with time in two types of the undisturbed permafrost soils.  
 •, o Monitored data in fine and coarse-grained soils respectively  
 — Calculated results in the fine-grained and coarse-grained soils

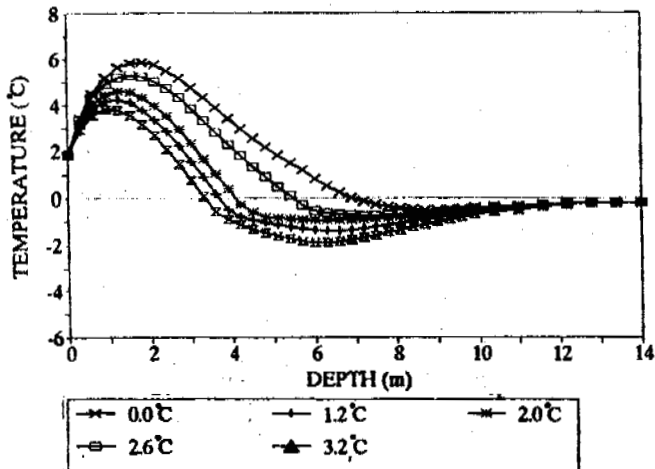


Figure 6. Temperature variation with depth at the center point of the embankment resulting from increments of annual air temperature.

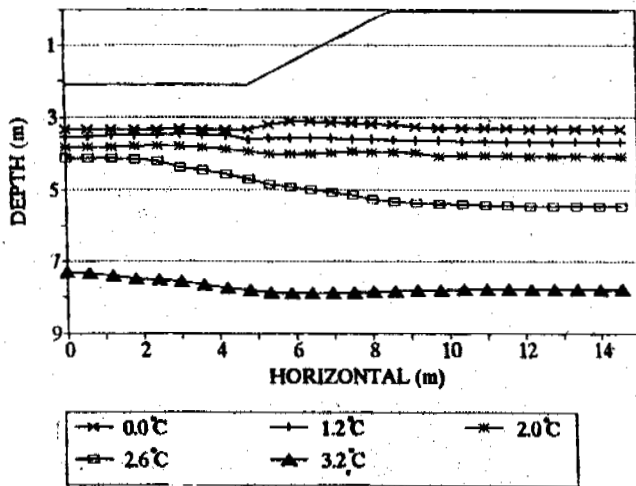


Figure 7. Variation of depth of thaw along the cross-section of the embankment resulting from various mean annual air temperature increments.

the field situation (i.e. an embankment 2.1m high constructed of compounded coarse-grained fill on a fine-grained soil). Increases in air temperature of up to 3.2°C have been considered in according with the maximum warming predicted by the Intergovernmental Panel on Climate Change (IPCC) (Houghton et al., 1990) for the QXP.

In response to such a gradual warming occurring over forty years the maximum seasonal depth of thaw is calculated to increase from 3.3m at present to as much as 8m beneath the embankment and from 1.3m to 5.2m beneath the adjacent undisturbed permafrost. The depth of thaw beneath the asphalt-surfaced embankment is obviously the greatest while that beneath the fine-grained soils is less at any given time (Figure 8).

From the prediction of the numerical results, as shown in Figure 7, the depth of thaw in the embankment will increase slowly while the mean annual air temperature increase is less than 1.5°C. The maximum depths of thaw beneath the undisturbed permafrost and the embankment nearly remain in same level, and

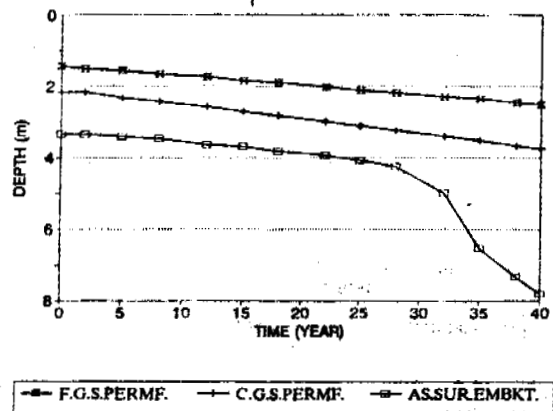


Figure 8. Comparison of the variation of depth of thaw with time beneath the undisturbed permafrost and the center of the embankment. Fine-grained soils (F.G.S.); Coarse-grained soils (C.G.S.) Asphalt-surfaced embankment (AS.SURBT.)

the interfaces between frozen and unfrozen soils at the maximum seasonal thaw maintain a slightly convex shape, if the embankment is kept at the critical height. An important conclusion is derived from these results, that is, in the short-term, even if the air temperature increases by as much as 1.5°C, the critical height of the embankment could be maintained as a necessary condition for preventing serious thaw settlement and to extend the "design life". When the mean annual air temperature increases by more than 1.5°C, however, a thaw basin could form in the foundations of the embankment and adjacent permafrost. The thawing of ice-rich sediment, combined with vehicle loading and traffic frequency and vibration will exacerbate the settlement and general deterioration of the highway embankment will result. The major consequence of deeper seasonal thaw is thaw subsidence in the underlying ice-rich soils resulting in loss of support and the formation of potholes in the Highway.

It can be seen from Figure 9 that, even with a constant increment of mean annual air temperature, the much stronger solar radiation in QXP and the effects of heat absorption by the asphalt pavement are responsible for the rapid increase of the seasonal thaw beneath the embankment and for the consequent problems associated with thaw settlement. Obviously, a reduction of heat absorption properties of the asphalt pavement of embankments, while maintaining the high quality of the pavement, is particularly significant for the continuous permafrost regions of the Qinghai-Xizang Highway, especially under conditions of climate warming.

The problems of the influence of climate warming are important to other cold region engineering and permafrost specialists as well as to highway engineers. A potentially serious problem exists in areas of arid climate north and west of QXP. Increased seasonal thaw could cause increased water seepage to greater depths, especially in the coarse-grained or highly permeable soils, leading to a substantial decline in the ground water table and a marked deterioration of the vegetation cover (especially shallow-rooted species) if the total precipitation remains at the present

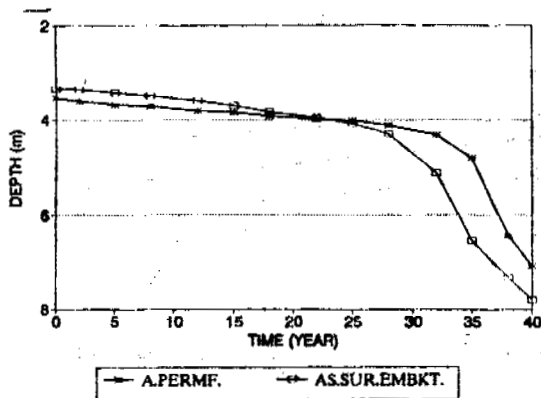


Figure 9. comparison of the variations of depth of thaw beneath the asphalt-surfaced embankment and adjacent permafrost with time. Adjacent permafrost (A. PERMF) Asphalt-surfaced embankment (AS.SURBKT.)

level. In addition the combination of winds along the plateau surface, further development of animal grazing and other agricultural activities could result in further permafrost degradation and cause these areas to become a frigid desert.

In fact, the depth of seasonal thaw could be much deeper than those computed because thaw consolidation, seepage and heat and mass transfer were neglected. Moreover, the permafrost degradation would extend over the vast areas of the QXP where the mean annual air temperature is already above  $-5.6^{\circ}\text{C}$ , and especially near the margins of the permafrost. Thus, monitoring and research into climate change is a more significant issue than just protection of the engineering infrastructures and should include the ecology, environmental protection as well as economic development in these cold alpine regions.

#### CONCLUSION

1. In the short-term, when the air temperature increase are less than  $1.5^{\circ}\text{C}$  in the QXP the critical heights of the asphalt-surfaced fill embankments could continue to provide the essential condition for preventing rapid deterioration of permafrost foundation and thaw settlement of the embankment.

2. If air temperature increases are greater than  $1.5^{\circ}\text{C}$  a thaw basin could form beneath the asphalt-surfaced embankment foundation and the adjacent permafrost, particularly after air temperature increases above  $2.5^{\circ}\text{C}$ . If the foundation is in ice-rich soils, it will result in serious thaw settlement of the embankment and pothole formations in the highway. Furthermore, ground water could flow into the basin from the surrounding area where the depth of thaw is less causing water accumulation and thus accelerating thaw settlement.

3. If steady climate warming occurs over the next forty years as predicted, the effects of heat absorption of the asphalt pavement will be a critical factor in the "design life" of the highway embankment. Reduction of these effects would solve a considerable number of problems for highway design and maintenance in the permafrost regions in the QXP.

4. More attention should be given to the monitoring of and research into climate change

in the QXP, in an effort to understand and perhaps to prevent the plateau surface advancing towards a frigid desert. This could become a main issue for environmental protection and economic development.

#### ACKNOWLEDGEMENT

The authors wish to gratefully acknowledge the assistance and valuable suggestions of Dr. Michel Allard and Mr Etienne Girard, Centre D'études Nordiques, Université Laval, Canada; The senior author gratefully acknowledge the Terrain Sciences Division, Geological Survey of Canada for hospitality at the Ottawa office during a one-year visiting scholarship. We gratefully thank the Lanzhou Institute of Glaciology and Geocryology, Academia Sinica, in particular the Department of Geocryological Engineering, for their support of this research and for providing the data cited in this paper.

#### REFERENCE

- An, Weidong, 1989. Numerical simulation of the critical height of the highway embankment with double medium, Proceedings of the 2nd National Conference on Frozen Soil, China, pp.34-49.
- An, Weidong, 1989. Interaction among temperature, moisture and stress fields in frozen soils, Lanzhou University Publishing House, Lanzhou, pp. 21-71. (Chinese)
- Esch, D.C., 1990. 20 years permafrost history of first insulated roadway on permafrost in Alaska, Proceedings of the 5th Canadian Permafrost conference, Quebec, pp. 335-340.
- Hildebrand, E.E., 1983. Thaw settlement and ground temperature model for highway design in permafrost areas, Proceedings of the 4th International Conference on Permafrost, Fairbanks, pp. 492-497.
- Houghton, J.T., Jenkins, G.J., and Ephraim, J.J., 1990. Climate change-the IPCC scientific assessment, Cambridge University press, New York, pp. 364.
- Nixon, J.F., 1978. The role of convective heat transport in the thawing of frozen soils, Can. Geotech. J., Vol.12, No.44, pp. 425-429.
- Tong, Boliang and Li, Shude, 1983. Some characteristics of permafrost on Qinghai-Xizang Plateau and a few factors affecting them, Professional papers on permafrost studies of Qinghai-Xizang Plateau, Science Press, Beijing, pp 1-11. (Chinese)
- Vita, C.L., 1983. Thaw plug stability and thaw settlement evaluation for arctic transportation routes; A probabilistic approach, Proceedings of the 4th International Conference on Permafrost, pp. 1321-1325.
- Wu, Ziwang, 1988. Roadbed engineering, Lanzhou University Publishing House, Lanzhou, pp. 34-86. (Chinese)
- Xu, Xuezu, 1985. Soil water potential, unfrozen moisture and temperature, Journal of Glaciology and Geocryology, 7(1), pp.1-14. (Chinese)
- Yu, Wenxue, 1986. The problems of the asphalt paved embankment height of the Qinghai-Xizang Highway in permafrost regions, Journal of Xian Highway Institute.
- Zhu, Xuewen, et al., 1983. Stability of highway subgrade in plateau permafrost region of China, Proceedings of the 4th International Conference on Permafrost, Fairbanks, pp. 1502-1506.

## TEMPERATURE VARIATIONS IN THE ACTIVE LAYER OF PERMAFROST

A. Aziz

Department of Mechanical Engineering  
Gonzaga University, Spokane, WA 99258

V.J. Lunardini

Applied Research Branch  
U.S. Army Cold Regions Research and Engineering Laboratory  
Hanover, New Hampshire 03755

Permafrost is controlled by the temperature variations and heat flow in the active layer, as well as by geothermal heat flow. The temperature of the bottom of the active layer is of particular interest because it can be used as a boundary condition for the permafrost thermal regime. A finite element numerical model was used to predict the temperature of the active layer subjected to a sinusoidal surface temperature variation. The predictions of the purely conductive heat transfer model demonstrated such basic characteristics of the active layer bottom temperature as the zero curtain effect. A simple analytic model based on the assumption of a homogeneous system was devised to predict the temperature variations in the active layer. The analysis, which combines phase-change and non-phase-change time spans for one year, yields temperature predictions that are within 6% of the numerical model. The approach is potentially adaptable to a surface energy boundary condition that can be used to evaluate the effect of short-term atmospheric changes on permafrost.

### NOMENCLATURE

c	specific heat
C	$\rho c$ specific heat capacity
G	geothermal gradient
k	thermal conductivity, W/m·K
$k_{1,2}$	$k_1/k_2$
$\ell$	latent heat
L	volumetric latent heat
P	$2\pi/\omega$ , period of surface temperature oscillation
t	time
T	temperature
T	initial constant temperature
$T_o'$	initial temperature of active layer at start of thaw
$T_o$	$T(o,t)$ , surface temperature
$T_{s1}$	surface temperature at start of decrease of
$T_B$	depth
$x_a$	maximum thickness of active layer
$x_t$	thaw depth, m
$\alpha$	thermal diffusivity
$\epsilon$	lag angle
$\rho$	density, kg/m <sup>3</sup>
$\sigma$	dimensionless depth, $x(2\pi/P\alpha_u)^{1/2}$
$\tau_s$	$(t-t_s)$
$\omega$	frequency of surface temperature oscillation

### Subscripts

1,2	different phases of soil
f,u	frozen, thawed

### INTRODUCTION

In permafrost regions the seasonal variation of the ground surface temperature causes an upper layer of the soil to thaw and freeze as the

temperature fluctuates around the freezing temperature of soil water (nominally 0°C). Since the properties of frozen and thawed soils are significantly different, the study of this layer, called the "active layer," is very important in cold regions engineering research and practice. Many cold regions phenomena such as frost heave, ice wedges, patterned ground, and others are related to the presence of the active layer, (Lunardini, 1981). A proper understanding of the thermal behavior of the active layer is vital to the safe design and construction of roads, pavements, airfields, utilities, and other structures in cold regions.

The recognition of global warming and its possible severe consequences in the permafrost regions has further accentuated the need to predict accurately the behavior of the active layer. It is reasonable to expect that an increase in mean annual air temperature due to global warming would cause the mean annual ground surface temperature to increase. As a result, the active layer will increase in thickness with attendant changes in its thermal regime (Kane et al., 1991). Over decades the phenomenon can also affect the thermal stability of the permafrost that lies underneath the active layer. The basic input for calculating the thaw depth is the seasonal variation of the surface energy balance, which controls the ground surface temperature. This information is rarely available; however, the annual variation of air temperature is routinely monitored by meteorological stations at many sites. The relationship between the air and surface temperatures is difficult to establish because it is affected by the highly complex surface energy exchanges that take place in the contact layer covering the soil system (Lunardini, 1981). The energy balance must include the net radiation at the surface,

atmospheric convection, latent heat effects (evaporation, snow melting, etc.), and energy generation or absorption due to biochemical and other processes. Each of these depends upon a host of other factors that are difficult to quantify. An engineering approach that has proved somewhat satisfactory is the theory of n-factors, which relates the mean air temperature to the mean surface temperature (Lunardini, 1978). But even the n-factor for a given site varies with time, from month to month and year to year. The best strategy therefore may be to measure the average daily surface temperatures at the site of interest and establish a curve that best fits the data; Kane et al. (1991) presented such a curve based on the measurements over a four-year period at a field site near Toolik Lake, Alaska. The curve resembles a sine curve but with several distinguishing features.

Aziz and Lunardini (1992) made a comparative assessment of various analytic approaches for predicting the thickness of the active layer. The analytical predictions were compared with a finite element solution generated using a code developed at CRREL (Frag et al. 1988, Coutermarsh and Phetteplace 1991). Since that paper was in a general comparison of the analytical and numerical predictions, and not for a specific site, a sinusoidal surface temperature variation was assumed instead of a site-specific temperature pattern. The purpose of this paper is to study the same problem, the focus being on predicting the yearly temperature variations in the active layer, particularly the temperature variation at the bottom of the active layer because it establishes the upper boundary condition for studying permafrost thermal regimes. A simple analytic model for the temperature variation is presented and its predictions are compared with finite element calculations obtained using the aforementioned code.

### THERMAL REGIME OF ACTIVE LAYER

We will consider the thermal response of a homogeneous medium due to a sinusoidal surface temperature, taking into account phase change. The system initially has a linear temperature distribution established as a consequence of a constant geothermal heat flux. It is assumed that the surface temperature oscillates around the mean value  $T_0$  with an amplitude of  $A_0$  and a period of one year or  $P$  hours. Further, the soil medium changes phase at a well-defined temperature,  $T_c$ . Once phase change occurs, there will be two distinct regions: frozen and thawed, each with different thermal properties. Based on one-dimensional conduction, the transient response of the system can be modeled as follows:

$$\frac{\partial^2 T_j}{\partial x^2} = \frac{1}{\alpha_j} \frac{\partial T_j}{\partial t} \quad (1)$$

$$T_j(x_t, t) = T_f \quad (1a)$$

$$T(0, t) = T_s(t) = T_0 + A_0 \sin\left(\frac{2\pi t}{P}\right) \quad (2)$$

$$T(x, 0) = T_0 + Gx \quad (2a)$$

$$k_1 \frac{\partial T_1(x_t, t)}{\partial x} - k_2 \frac{\partial T_2(x_t, t)}{\partial x} = \begin{cases} +\rho_1 \ell dx_t/dt & \text{during freeze} \\ -\rho_2 \ell dx_t/dt & \text{during thaw} \end{cases} \quad (3)$$

where the subscript  $j = 1, 2$  denotes the frozen and thawed zones and the other symbols are as defined in the nomenclature. The thermal properties of the soil are spatially uniform but differ for the thawed and frozen states of the material. Since the problem does not admit an exact analytical solution, we consider two approaches: a fully numerical solution and an approximate analytic solution.

### A. Numerical Solution

The numerical solution was generated using a finite element code developed at CRREL and referred to in the Introduction. The code can handle arbitrary boundary conditions and nonhomogeneous soils. The problem was run for the specific soil and climatic conditions shown in Table 1. The non-saturated case consists of a homogeneous sand with a water content of about 7.4%, in a moderately warm permafrost location (ground temperature of  $-3^\circ\text{C}$  at 20 m). All the soil moisture is assumed to change phase at  $0^\circ\text{C}$ . The soil used was arbitrary; it is not felt that this particular choice of soil or temperature will affect the analytic method. The spatial increments, over a depth of 50 m, varied from 1 cm for the upper 2 m to 50 cm for the lowest 34 m, while the time increment was 12 hours. The lower boundary condition was that of a constant geothermal gradient of  $0.0344^\circ\text{C}/\text{m}$ . The numerical program has been tested for a phase-change problem with an exact solution (Neumann problem) and found to be accurate within a few percent; the sinusoidal surface temperature was tested for a problem without phase change and was accurate within 3% (Coutermarsh and Phetteplace 1991).

Table 1. Properties of soils for analysis.

	Non-saturated case 1		Saturated* Case 2	
	Frozen	Thawed	Frozen	Thawed
$k$ ( $\text{W}/\text{m}^\circ\text{C}$ )	1.56	1.73	3.399	1.98
$c \frac{J}{\text{kg}^\circ\text{C}}$	784.8	940.32	928.8	1378.8
$\rho$ ( $\text{kg}/\text{m}^3$ )	1836	1836	1960	1994
$\alpha$ ( $\text{m}^2/\text{hr}$ )	0.0039	0.00361	0.00672	0.00259
$L, \frac{J}{\text{m}^3}$		$45.35 \times 10^6$		$126 \times 10^6$
$P, \text{hr}$	8760		8760	
$T_0$ ( $^\circ\text{C}$ )	-3.6		-11.0	
$A_0$ ( $^\circ\text{C}$ )	9.4		18	
$G$ ( $^\circ\text{C}/\text{m}$ )	0.0344		0.0286	

\*Soil and temperatures for Prudhoe Bay, Alaska.

Starting with the linear initial temperature, the program was run for five cycles of one year (total of 43,800 hr) with the given surface temperature fluctuations. Yearly freeze/thaw was calculated and the maximum thaw penetration after the fifth year was evaluated as  $x_a = 173$  cm. Figure 1 shows the temperature variations at the bottom of the active layer ( $x_a =$

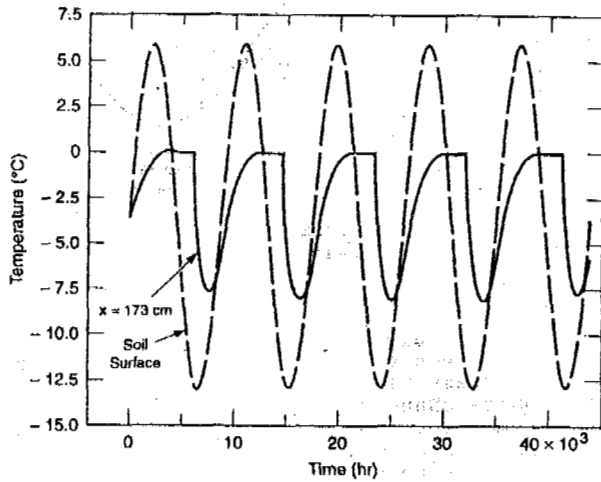


Figure 1. Temperature of soil during five yearly cycles, numerical model.

173 cm) and also the imposed surface temperature variation ( $x = 0$ ). Figure 2 shows the temperature variation at the bottom of the active layer for the fifth year in greater detail. The profile exhibits the familiar zero curtain effect wherein the temperature remains at or near the phase change temperature for a large part of the year, approximately 2458 hours in this case. The temperature at the bottom of the active layer tended to oscillate slightly just below the freezing value instead of remaining exactly at  $0^\circ\text{C}$ . This is partly due to the effect of the surface sinusoidal temperature and partly due to the numerical method when there is a thick zone nearly at the freezing temperature. The temperature changes of about  $0.1^\circ\text{C}$  do not seriously affect the overall results.

It is of interest to examine the maximum depth reached by the  $T_f$  isotherm for this soil with no phase change. The solution to this problem is readily available for homogeneous and layered soils (Lachenbruch 1959, Lunardini 1981). The results of those studies can be used to calculate the "active layer depth" for a homogeneous soil without phase change. Here, the active layer is meant to be the depth at which the soil temperature never exceeds  $T_f$ . The active layer for the particular soil is 304.4 to 316.5 cm, depending upon the use of either the frozen or thawed property values. Thus the ratio of the non-phase-change active layer to that of the actual active layer is about 1.8. The effect of freeze/thaw tends to greatly reduce the depth to which the phase-change temperature penetrates into the soil mass.

#### B. Analytic Solution

As was mentioned earlier, an exact solution to Eqs. 1-3 is not available. However, it is possible to approximately predict the annual temperature variation at the base of the active layer. Figure 3 is a sketch of the surface temperature and active layer bottom temperature during the fifth year of a five-year cycle, obtained from the numerical model. Time commences at the end of the fourth year when  $t_0 = 35,040$  hours.

The calculation method involves four steps:

i. Assume a frozen block exists at  $t = 0$  hours ( $t_0 = 35,040$  hr). While the surface

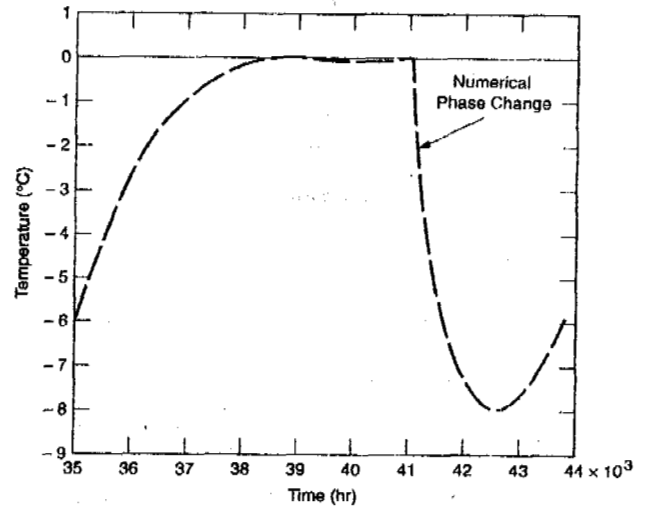


Figure 2. Temperature at bottom of active layer during fifth year.

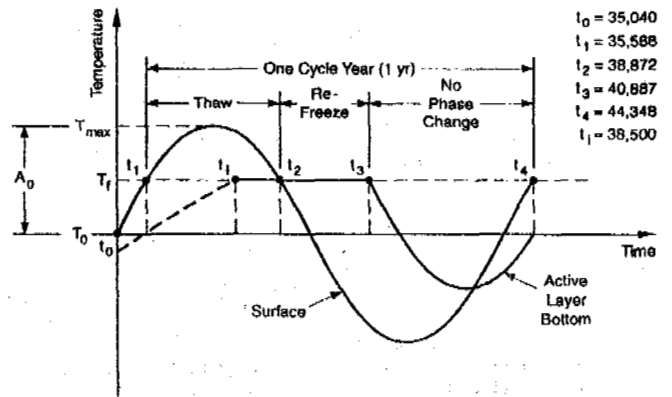


Figure 3. Sketch of surface and active layer bottom temperature for one year.

temperature is above freezing,  $t_1 \leq t \leq t_2$ , thaw occurs. Thaw depth is then calculated; initially start as if  $T_0 = 0^\circ\text{C}$ . Clearly  $T_0 < 0^\circ\text{C}$ , but this will be addressed later.

ii. Calculate the time needed to completely refreeze the thawed layer when  $t = t_3$ .

iii. Calculate the temperature drop at the active layer bottom with time until  $T_f$  is again at  $0^\circ\text{C}$ . This is a non-phase-change problem and occurs for  $t_3 < t < t_4$ .

iv. Calculate the temperature rise of the active layer bottom for  $t > t_4$ . This is again the thaw part of the cycle but the calculation originally started at  $t_1 = 548$  hr, not  $t = 0$ , and we now consider the fact that  $T_0 < 0^\circ\text{C}$ .

#### 1. Thaw Depth

From the sinusoidal surface temperature, Eq. 2, the length of the surface thaw season and the mean surface temperature during thaw can be obtained:

$$\omega t_1 = \sin^{-1} \left( \frac{T_f - T_0}{A_0} \right) \quad (4)$$

Table 2. Thaw depth using Neumann and Stefan solutions.

Case	$T_i$	$\gamma_t$	$\sigma$ (cm)	Percent Error*
Neumann	0°C	0.262	180.4	+4.3
Stefan	0°C	0.268	184.5	+6.6
Neumann	-1°C	0.251	172.9	-1

\*Compared to numerical solution.

$$\omega(t_2 - t_1) = \pi - 2\sin^{-1} \left( \frac{T_f - T_0}{A_0} \right) \quad (5)$$

$$\bar{T}_S = T_0 - \frac{A_0}{\omega(t_2 - t_1)} [\cos \omega t_2 - \cos \omega t_1] \quad (6)$$

For this problem  $t_1 = 547.95$  hr,  $\Delta t = t_2 - t_1 = 3284.1$  hr,  $\bar{T}_S = 3.77^\circ\text{C}$ . It is well known that the Neumann solution will yield a close estimate of the thaw depth if the average surface temperature  $\bar{T}_S$  and the time increment  $\Delta t$  are used (Lunardini 1991). The Neumann solution is

$$x_t = 2\gamma_t \sqrt{\alpha_1 \Delta t} \quad (7)$$

$$\frac{e^{-\gamma_t^2} - k_{21} \sqrt{\alpha_{12}} \phi e^{-\alpha_{12} \gamma_t^2}}{\text{erf } \gamma_t} = \frac{\gamma_t \sqrt{\pi}}{S_T} \quad (8)$$

where region 1 is thawed

$$S_T = C_1 \left( \frac{\bar{T}_S - T_f}{L} \right), \quad \phi = \frac{T_f - T_i}{\bar{T}_S - T_f}$$

$T_i$  = the initial temperature of the frozen medium.

Table 2 shows that the Neumann solution agrees quite well with the numerical results. Clearly with an initial temperature of  $-1^\circ\text{C}$ , the Neumann solution would agree even more closely with the numerical results. We can check later on the validity of  $T_i = -1^\circ\text{C}$ , but the mean value of  $T_i$  will be something less than  $0^\circ\text{C}$  at the start of thaw.

### ii. Re-freeze Time

The time needed to refreeze the thawed layer,  $t_3 - t_2$ , can be found by again using a Neumann solution. We can now assume  $T_i = 0^\circ\text{C}$  since the nature of the sinusoidal temperature changes will assure that the thawed soil layer will be close to the freezing temperature. The thickness of the layer to freeze is known and is  $x_t$ . Thus

$$x_t = 2\gamma_f \sqrt{\alpha_f (t_3 - t_2)} \quad (9)$$

$$\frac{e^{-\gamma_f^2}}{\text{erf } \gamma_f} = \frac{\gamma_f \sqrt{\pi}}{S_T} \quad (10)$$

$$\bar{T}_S = T_0 - \frac{A_0}{\omega(t_3 - t_2)} [\cos \omega t_3 - \cos \omega t_2] \quad (11)$$

where  $S_T = \frac{C_f}{L} (T_f - \bar{T}_S)$ . Solving these equations yields  $\bar{T}_S = -6.38^\circ\text{C}$ ,  $\gamma_f = 0.3083$ ,  $S_T = 0.2026$ , and  $t_3 = 5847$  hr. This is close to the numerical value of  $t_3 = 5960$  hr.

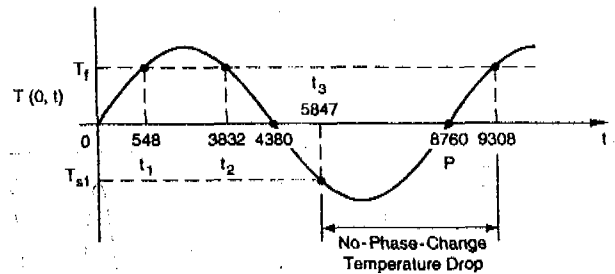


Figure 4. Surface temperature sketch for one year.

### iii. Non-Phase-Change Active Layer Temperature

Once the active layer has completely refrozen, its temperature will change without phase change as long as the surface temperature remains below the freezing value. Figure 4 shows that the active layer temperature will change without phase change for

$$t_3 \leq t \leq P + t_1 \quad (12)$$

or, in this case,  $5847 \leq t \leq 9308$ .

For convenience we will shift the time so that the non-phase-change temperature change starts at

$$r_s = t - t_3 = 0 \quad (13)$$

Thus

$$T(0,t) = T_0 + A_0 \cos \left( \frac{2\pi r_s}{P} - \epsilon \right) \quad 0 < r_s < 3461 \quad (14)$$

where  $\epsilon = \frac{\pi}{2} - \frac{2\pi t_1}{P}$ . The surface temperature at  $r_s = 0$  (or  $t_3 = 5847$  hours) is  $T_{s1} = -11.76^\circ\text{C}$ . Since the bottom of the active layer starts at  $T_f$ , we assume a linear initial temperature distribution in the active layer:

$$T_i = \begin{cases} g(x - x_a) & 0 \leq x \leq x_a \\ T_f & x > x_a \end{cases} \quad (15)$$

where  $g = \frac{-T_{s1}}{x_a}$ . The problem to be solved is that of a homogeneous soil mass with a sinusoidal surface temperature and an initial temperature distribution given by Eq. 15. The transient response of the soil is required for  $0 < r_s < 3461$ . The method of solving this problem has been described in Carslaw and Jaeger (1959) and it is only necessary to adopt the solution to the particular initial temperature variation.

With  $v = T - T_0$ , the problem can be split into two parts. The surface and initial temperatures are given by:

$$v_1(0, r_s) = 0 \quad (16)$$

$$v_1(x, 0) = \begin{cases} V + gx = f(x) & x \leq x_a \\ T_0 & x > x_a \end{cases} \quad (17)$$

$$v_2(0, r) = A_0 \cos \left( \frac{2\pi r_s}{P} - \epsilon \right) \quad (18)$$

$$v_2(x, 0) = 0 \quad (19)$$

where  $V = T_{s1} - T_0$ . The solutions to both of these linear problems can be written down immediately as

$$v_1 = \frac{1}{2\sqrt{\pi\alpha_f\tau_s}} \left\{ \int_0^{\infty} f(x') e^{-(x-x')^2/4\alpha_f\tau_s} dx' - \int_0^{\infty} f(x') e^{-(x-x')^2/4\alpha_f\tau_s} dx' \right\} \quad (20)$$

$$v_2 = A_0 e^{\frac{xK}{P}} \cos\left(\frac{2\pi\tau_s}{P} - xK - \epsilon\right) - \frac{2A_0}{\sqrt{\pi}} \int_0^{\infty} \cos\left[\frac{2\pi}{P} \left(\tau_s - \frac{x^2}{4\alpha_f\mu^2}\right) - \epsilon\right] e^{-\mu^2} d\mu \quad (21)$$

After some manipulation the temperature can be written as

$$T - T_0 = V \operatorname{erf} a + \frac{1}{2} [V - (T_f - T_0)] (\operatorname{erf} b - \operatorname{erf} c) - e^{-c^2} - e^{-b^2} + \frac{g}{2} x (\operatorname{erf} b + \operatorname{erf} c) + \frac{\sqrt{\alpha_f\tau_s}}{\pi} g + \frac{2A_0}{\sqrt{\pi}} \int_0^{\infty} \cos\left[m \left(\frac{1}{a^2} - \frac{1}{\mu^2}\right) - \epsilon\right] e^{-\mu^2} d\mu \quad (22)$$

$$\text{where } a = \frac{x}{2\sqrt{\alpha_f\tau_s}}, \quad b = \frac{x_a - x}{2\sqrt{\alpha_f\tau_s}}, \quad c = \frac{x_a + x}{2\sqrt{\alpha_f\tau_s}}, \quad m = \frac{x^2}{\alpha_f P}, \quad K = \frac{\pi}{\sqrt{\pi} P \alpha_f}$$

The temperature at any depth and time can now be evaluated. In particular the temperature of the bottom of the active layer can be predicted as a function of time. Table 3 shows the calculated values using Eq. 22, and also lists the numerical results. Over much of the time without phase change the differences are less than 6%.

Table 4 shows the temperature distribution of the upper 3 m of soil at the beginning of surface thaw ( $\tau_s = 3461$ ), calculated from Eq. 22. The average temperature of the active layer at this time is  $-2.0^\circ\text{C}$  while the average temperature of the upper 3 m is  $-2.8^\circ\text{C}$ .

#### Active Layer Temperature During Melt

Eq. 22 is valid only until the surface temperature reaches the phase change value at  $\tau_s = 3461$ , beyond this time the calculated values are shown in Table 3. These denote an active

Table 3. Active layer bottom temperature during non-phase change.

$\tau_s$ (hr)	t (hr)	Active layer bottom temperature $^\circ\text{C}$		Percent error
		Eq. 22	Numerical	
0	5847	0	0	--
100	5947	-2.39	0	--
500	6347	-5.38	-4.56	19.1
1000	6847	-7.14	-6.90	3.6
1500	7347	-7.80	-7.91	1.4
1600	7447	-7.82	-7.91	1.1
2313	8160	-7.09	-7.35	3.5
3000	8847	-5.17	-5.47	5.5
3461*	9308	-3.53	-4.0	11.8
4000	9847	-1.42	--	--
4300	10147	-0.34	--	--
4400	10247	0	--	--

$x = 1.739$  m,  $g = 6.76$ ,  $T_s = -11.76^\circ\text{C}$ ,  $\tau_s = 3461$  hr,  $\alpha_f = 8.16$   $^\circ\text{C}$ .

\* Surface thaw starts, Eq 22 not valid after this time.

layer bottom temperature,  $T_B(t)$ , which increases too rapidly to the phase change value. The correct procedure is to evaluate the active layer bottom temperature while thaw is occurring. Once again, the Neumann solution can be used for this. Starting with  $T_B(3461) = -3.53^\circ\text{C}$  will result in an initial temperature of  $T'_0 = -2.77^\circ\text{C}$  (average noted in Table 4). The bottom temperature is then given by

$$T_B = T'_0 - \frac{(T'_0 - T_f)}{\operatorname{erfc}\gamma/\alpha_{uf}} \operatorname{erfc} \frac{x_a}{2\sqrt{\alpha_f\Delta t}} \quad (23)$$

where  $\alpha_{uf} = \alpha_u/\alpha_f = .926$  and  $x_a = 1.74$  m.  $\gamma$  is evaluated using Eq. 8, while the mean surface temperature during  $\Delta t$  is found from Eq. 6. The mean surface temperature is recalculated for each  $\Delta t$ . The calculated results are shown in Table 5. This shows that the initial temperature must be less than  $T_s$  during the thaw process but the value does not agree with the initial assumption of  $T_s = -1^\circ\text{C}$ .

Figure 5 shows the results of the complete calculation and comparison to the numerical profile. It is clear from these figures that the simple calculation scheme detailed here can calculate the temperature of the active layer over a yearly cycle with reasonable accuracy, for this particular case, without resorting to complicated numerical codes.

Figure 6 shows the results for case 2: a saturated soil with properties and meteorological conditions connected with Prudhoe Bay, Alaska, (see Table 1). The main difference for this case is that the bottom of the thawed zone tends to freeze much faster than for the previous one.

Table 4. Soil temperature at beginning of thaw.

Depth (m)	T ( $^\circ\text{C}$ )
0.0	0.0
0.25	-0.76
0.50	-1.42
0.75	-1.99
1.0	-2.48
1.25	-2.89
1.50	-3.23
1.75	-3.50
2.0	-3.72
2.25	-3.87
2.50	-3.98
2.75	-4.04
3.00	-4.06

Table 5. Active layer bottom temperature during initial thaw.

$\tau_s$	$T_s$ ( $^\circ\text{C}$ )	$\phi_0$	$S_T$	$\tau_f$	$\Delta t$ (hr)	$T_B$ ( $^\circ\text{C}$ )
35,588	0	--	--	--	0	-3.53
36,000	1.22	2.27	0.047	0.1219	412	-2.18
37,000	3.45	0.803	0.131	0.2386	1412	-0.65
38,000	4.27	0.649	0.163	0.2459	2412	-0.24

Note: Used  $T'_0 = -2.77^\circ\text{C}$  instead of  $-3.53$  to evaluate  $\gamma$ , not much difference.



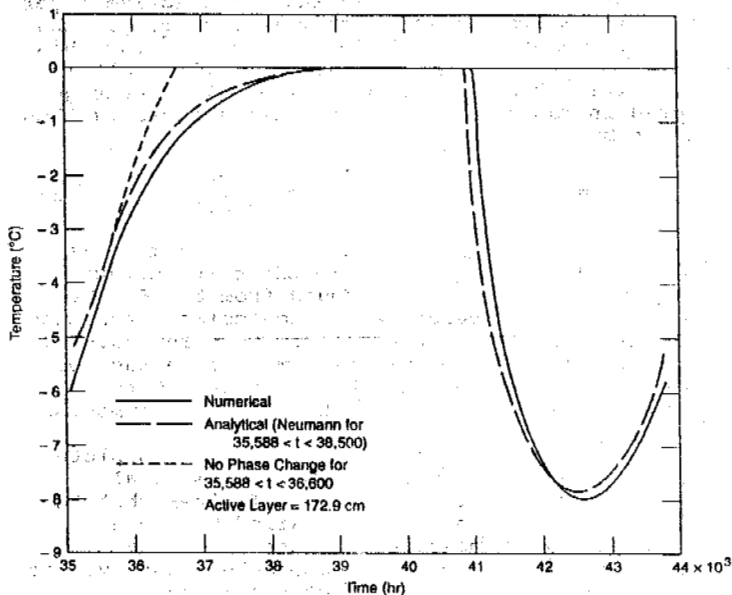


Figure 5. Active layer bottom temperature during fifth year, non-saturated soil model,  $x_a = 172.8$  cm.

Nevertheless, the active layer bottom temperature prediction is still quite accurate.

#### CONCLUSIONS

The problem of temperature variation in the active layer due to sinusoidal fluctuation of surface temperature has been studied both analytically and numerically. Particular attention was paid to the yearly temperature variation at the bottom of the active layer, although the method applies to any depth. An approximate analytic solution strategy developed for the problem compared well with the finite element predictions. The analytical approach employed the well-known Neumann solution in conjunction with the non-phase-change transient conduction solutions for the sinusoidal surface temperature. A judicious application of these solutions to the different portions of the cycle has demonstrated that such a strategy provides an effective alternative to the fully numerical computations. The method is applicable to any periodic surface temperature function amenable to Fourier analysis, but with increased computational effort. Phenomena such as the zero-curtain effect are explainable simply with conductive heat transfer theory with phase change.

#### REFERENCES

- Aziz, A. and Lunardini, V.J. (1992). Assessment of methods to predict the thickness of the active layer in permafrost regions. *Proceedings OMAE 1992*, Paper No. OMAE-92-209, Calgary, Canada.
- Aziz, A. and Na, T.Y. (1984). *Perturbation Methods in Heat Transfer*. Hemisphere Publishers, New York.
- Carslaw, H.W. and J.C. Jaeger (1959). *Conduction of Heat in Solids*. Oxford: Clarendon Press, 2nd edition.
- Cotta, R.M., Ozisik, M.N., and Menning, J. (1990). Coupled integral equation approach for solving phase-change problems in a

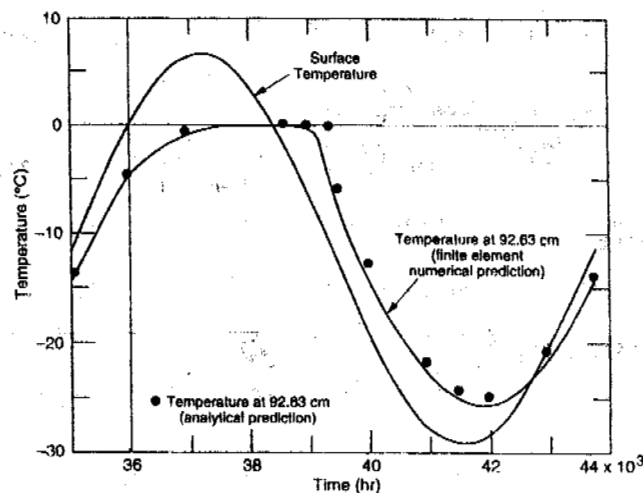


Figure 6. Active layer bottom temperature during fifth year, Prudhoe Bay model,  $x_a = 92.6$  cm.

- finite slab. *J. Franklin Inst.*, Vol. 327, pp. 225-234.
- Coutermarsh, B. and G. Phetteplace, (1991). Numerical analysis of frost shields. *Proceedings of Sixth Cold Regions International Specialty Conference TCCP/ASCE*, West Lebanon, NH, February 26-28, 1991.
- Farag, I., G. Buzzell and G. Phetteplace (1988). A phase change heat transfer program for microcomputers. *International Symposium on Phase Change Heat Transfer*, Chongqing, China, May.
- Gutman, Lev N. (1986). On the problem of heat transfer in phase-change materials for small Stefan numbers. *Int. J. Heat Mass Transfer*, Vol. 29, pp. 921-926.
- Kane, D.L., Hinzman, L.D., and Zarling, J.P. (1991). Thermal response of the active layer to climatic warming in a permafrost environment. *Cold Regions Science and Technology*, Vol. 19, pp. 111-122.
- Lachenbruch, A.H. (1959). Periodic heat flow in a stratified medium with application to permafrost problems. *U.S. Geological Survey Bulletin* 1083-A.
- Lock, G.S.H. (1968). On the use of asymptotic solutions to plane ice-water problems. *J. Glaciology*, Vol. 8, pp. 285-300.
- Lock, G.S.H., Gunderson, J.R., Quon, D., and Donnelly, J.K. (1969). A study of one-dimensional ice formation with particular reference to periodic growth and decay. *Int. J. Heat Mass Transfer*, Vol. 12, pp. 1343-1352.
- Lunardini, V.J. (1991). *Heat Transfer with Freezing and Thawing*. Elsevier Science Publishers, Amsterdam, The Netherlands.
- Lunardini, V.J. (1981). *Heat Transfer in Cold Climates*. New York: Van Nostrand Reinhold.
- Lunardini, V.J. (1978). Theory of N-Factors and correlation of data. *Proc. Third Int. Conf. on Permafrost*, Edmonton, Alberta, Vol. 1, pp. 40-46.
- Menning, J. and Ozisik, M.N. (1985). Coupled integral equation approach for solving melting or solidification. *Int. J. Heat Mass Transfer*, Vol. 28, pp. 1481-1485.
- Ozisik, M.N. (1983). *Heat Conduction*. John Wiley and Sons, New York.

## SIXTH INTERNATIONAL CONFERENCE ON PERMAFROST

### TOWARDS A PERMAFROST INFORMATION AND DATA SYSTEM

R.G. Barry and A.M. Brennan

World Data Center-A for Glaciology  
University of Colorado, Boulder, CO 80309-0449 USA

Research on ground ice, permafrost and the active layer is rapidly expanding as shown by literature citations in the permafrost bibliographies compiled by World Data Center-A for Glaciology (WDC-A)/National Snow and Ice Data Center (NSIDC) since 1978 and the approximately 25,000 permafrost-related entries dating back to 1900 in the COLD bibliography. Requirements for permafrost information and data vary considerably according to the user's purpose, however, and the subject identifiers (keywords) commonly used are inadequate for some needs.

Approaches to developing a permafrost data system initiated by the International Permafrost Association Working Group on Permafrost Data and WDC-A for Glaciology involve: (1) the preparation of a preliminary inventory; (2) distribution of this information for comment and updating by the community; (3) assembly of selected, readily available data sets and their distribution to interested users; and (4) interaction between data center(s) and scientists holding data to ensure consistent documentation and quality control. This work and future plans are described.

#### INTRODUCTION AND BACKGROUND

A workshop on permafrost data and information was held on 2 August 1988 in conjunction with the Fifth International Conference on Permafrost in Trondheim, Norway (Barry, 1989). Approximately 50 participants from nine countries discussed the need for inventories and catalogues of existing permafrost data sets as a prelude to facilitating scientific access to such data for global change research. A proposal was also submitted to the Council of the International Permafrost Association to form a Working Group on Permafrost Data; this group was established in fall 1988 and has met subsequently on several occasions. The Working Group, in conjunction with WDC-A for Glaciology, is taking a series of steps toward development of a permafrost data system and the plans and progress to date provide the basis for this report.

#### DATA TYPES

Sources of data include published literature, maps, direct measurements (e.g., drill holes, geophysical surveys), and indirect or proxy indicators of permafrost occurrence (Barry, 1988). Their characteristics are discussed briefly.

#### Literature

The most widespread source of data is published literature in papers, monographs, and books, as well as 'grey literature', technical reports, and maps published by national and local agencies. Literature citations in the

quinquennial permafrost bibliographies compiled by WDC-A for Glaciology totalled 4,400 titles for 1978-82 and 3,300 for 1983-87 (Brennan, 1983; 1988). However, communication with Russian colleagues indicates that less than 20 percent of articles published in Russia on ground ice and permafrost are incorporated in these bibliographies (Y.K. Vasil'chuk, pers. commun., 1992) and the situation for Chinese and Japanese materials is unknown. The COLD bibliography, compiled by the Cold Regions Bibliography Project at the Library of Congress and now available on the "Arctic and Antarctic Regions" CD-ROM prepared by the NISC Corporation, contains over 25,000 permafrost-related entries dating back to 1900. The usefulness of these sources is limited, however, by the degree to which subjects of interest can be identified through key descriptors in use. In particular, at present there is no easy way to identify studies that have significant tabulations of data or maps published in books, reports or journal articles. More generally, searches by author present a particular problem with transliterated Russian and Chinese names having different punctuation and rendering. Thus, the Scott Polar Research Institute (SPRI) bibliography spells out Chou Wanxi in the Chinese manner whereas the Cold Regions Research and Engineering Laboratory (CRREL) bibliography records Chou, W.X. The CRREL bibliography transliterates the Russian name Ershov, where SPRI uses Yershov according to the pronunciation. The fact that keywords are assigned subjectively may create difficulties in retrieving citations. For example, a search of the SPRI data base for 1989 found 218 citations

on permafrost or frozen ground through a keyword search, but 467 by using a 'global' search (i.e., a search of all elements in a record, including title and abstract). Also, in several instances, a keyword search would not have picked up a reference in a particular data base. These two items indicate that cataloging and indexing are very individual tasks and that an intimate knowledge of a data base is required to retrieve the maximum number of references. Experience obtained at WDC-A for Glaciology in attempting to compile a comprehensive bibliography on permafrost and frozen ground indicates that none of the polar bibliographies is complete; each records some percentage of unique entries.

A comparative study has been made of results of bibliographic searches conducted on several data bases: four that are included on the "Arctic and Antarctic Regions" CD-ROM - ASTIS (Arctic Institute of North America, Calgary, Canada), CRREL (Cold Regions Research and Engineering Laboratory, Hanover, NH, USA), SPRI (Scott Polar Research Institute, Cambridge, UK), and WDC (World Data Center-A for Glaciology, Boulder, CO, USA). The fifth data base discussed is GEOREF (Bibliography of Geology), also on CD-ROM. Because of the volume of permafrost data, one year, 1989, was chosen for comparison. This was the most recent year that could be expected to be reasonably completely indexed. The search terms used were 'permafrost' or 'frozen ground' in the keyword field. Table 1 gives an overview of what was found.

Table 1. Permafrost or Frozen Ground. <sup>(1)</sup>

Data Base	# of Citations		Unique		Comparison
	KW	Global	#	%	
ASTIS	8	14	6		
CRREL	301	312	172	57	ASTIS-4 C-CORE-3 SPRI-118 WDC-49
SPRI	218	467	67	31	ASTIS-4 C-CORE-3 SPRI-147 WDC-50
WDC	51	53	7	14	ASTIS-4 CRREL-40 SPRI-40
GEOREF	134		45	34	ASTIS-4 C-CORE-3 CRREL-67 SPRI-67 WDC-16

<sup>(1)</sup> See text for explanations.

Column 1 is the data base name; column 2 is the number of citations found using only the keyword field and then using the global search feature; column 3 lists the number of citations found only in a particular data base and as a percentage of the data base total; the last column shows the duplication among data bases. C-CORE is a data base maintained by the Centre for Cold Ocean Resources Engineering, St. John's, Newfoundland, Canada. The percentage of unique entries is as high as 57% in the CRREL data base, but the percentage is significant in all the data bases searched. For this reason, we

think that continuing the compilation and publication of the Permafrost Bibliography is useful to the community since it provides citations from a wide variety of sources.

#### Maps

Maps of permafrost distribution for national territories (1:10 million to 1:25 million) and smaller-scale global maps present other problems (Heginbottom, 1984). The distribution of data used to construct them, and the data quality, are seldom documented in detail. Until recently, the map was seen as an end product rather than as a potential source of input for other correlative studies. Yet for this purpose it is essential to have digital geo-referenced data files. Issues of appropriate sampling resolution, grid interpolation schemes and map coordinate systems have to be addressed, however, in order to provide such digitized versions.

A further problem is the awareness of the existence of maps, especially those published as supplements to monographs or journal articles. The latter may not be readily identifiable in bibliographies. J.A. Heginbottom (pers. commun., 1992) is compiling a catalogue of national permafrost maps.

#### Data Sets

Data on permafrost and ground ice conditions are collected by various organizations - national and state agencies, university research groups, and the private sector. They include measurements of permafrost extent, thickness of the active layer and of ice-bearing sediment, the 0°C depth, temperature profiles, and ice content, as well as data on different physical, mechanical, thermal, chemical, and electrical properties of frozen sediments (see Barry, 1988; Table 1). The most extensive data sets known to exist in the public domain are those collected in Canada by the Geological Survey of Canada in the Mackenzie Valley (Proudfoot and Lawrence, 1976) and geophysical well data collected by the Earth Physics Branch of the Department of Energy, Mines and Resources (Taylor and Judge, 1974; Geotech Engineering Ltd., 1983; Hardy Associates (1978) Ltd., 1984). Other examples are cited in Barry (1988).

#### PLANNING A PERMAFROST DATA SYSTEM DATA INVENTORY

In order to lay the ground work for a permafrost data system, a preliminary inventory of existing data sets has been carried out. WDC-A for Glaciology mailed a letter and brief questionnaire to members of the permafrost community worldwide in February 1992. Names were selected from the mailing list of the International Permafrost Association and from the attendees at the V International Conference on Permafrost held in Trondheim, Norway, in 1988. The survey asked four basic questions as shown in Table 2.

Table 2. Permafrost Data Questionnaire.

1. Do you as an individual or group hold permafrost data?  
If yes, in what format do the data reside?  
What type of data are they?  
What geographic area do they cover?  
Time period?
2. Do you know of any major sources of permafrost data that we could contact?
3. If you hold data would you be willing to make them available through a central coordination office?
4. Would "publishing" the data, e.g., on CD-ROM, possibly together with the Permafrost Bibliographies, be of interest?

One-hundred and twenty-five responses (37 percent) had been received to the 340 letters distributed, representing 14 countries: Argentina, Canada, China, Denmark, Germany, Japan, the Netherlands, Norway, Poland, South Africa, Sweden, Switzerland, the UK, and USA. Of the 125 respondents: 76 hold data, 58 would be willing to make these data available through a coordination office and 50 would be interested in "publishing" their data. Most responders indicated the availability of ground temperature records, in some cases dating back to the 1950s, but mostly beginning in the 1980s. The areas represented included Canada, Alaska, Scandinavia, Svalbard, Greenland, China and the Andes. Other records contained data on permafrost and active layer thickness, electromagnetic properties, hydrochemistry, frost heave and geomorphic features. The questionnaire also asked for referrals to other known or potential sources of data and those will be followed up.

#### Data Assembly

The second step in our planned activity will be to use the survey results to establish a simple data base containing information on the investigator, institution, data type, time period, and geographic area covered. This information will be distributed to the responders and a wider community for corrections, updating and additions. The third step that we plan is to assemble selected data sets from those offered for publication, on appropriate media (diskettes, tapes, CD-ROMs) and to distribute them to interested potential users. The wishes of the researchers about release of the data for general use will, of course, be taken into consideration. A designated period of exclusive use by the collector can be accommodated. One publication option would be a CD-ROM sampler, such as the "Arctic Multisensor Data Sampler" recently issued by the National Snow and Ice Data Center (NSIDC, 1992), to illustrate the potential variety of data. The scope of this activity will be determined by the level of interest of the community, their capability to utilize particular media, the assessed usefulness of the data, particularly for baseline of global change studies, and, of course, the availability of funding to assemble, format, reproduce, and distribute the data. It is hoped to make a start on this process through the "data rescue" program of the Earth Science Data and Information Management component of the National Oceanic and Atmospheric Administration. This program is designed to ensure that valuable data sets are not irretrievably lost. Examples of activities under this program include: (1) migrating digital data sets onto media approved for long term archival storage (e.g., 3480 tape cartridges); and (2) transferring analog documents to digital files using Optical Character Recognition technology.

A further necessary step in the development of high-quality data sets will be the interaction between data center(s) and scientists collecting or assembling data to ensure careful documentation and screening procedures for quality control.

#### Data Distribution

There are advantages of storage size, distribution cost, longevity and increased audience to be gained by archiving permafrost data on CD-ROM discs. CD-ROM (Compact Disc - Read Only Memory) has become an accepted medium for data archive and distribution, with CD-ROM drives available at a cost compatible with most research grant funding levels. CD-ROMs are small, compact and inexpensive to produce. As one current-generation CD-ROM stores about 600 megabytes of data, the comparison of delivery on tape versus delivery on CD-ROM shows a clear advantage for the latter medium; 600 megabytes of data require 3-6 tapes recorded at 6250 bits per inch, depending on the block size. NSIDC distributes such high-density tapes for \$115 per reel; 600 megabytes of data on magnetic tape would be billed at \$345 - \$575. Blank tapes cost \$12 each, whereas one CD-ROM costs about \$9.00, if mastering cost is prorated. CD-ROM drives for microcomputers are widely available commercially costing well under \$1000, and are therefore within the reach of most scientific investigators.

CD-ROM drives can also be shared by a networked system of microcomputers. Organizations with budget limitations can maximize return on investment in a CD-ROM drive and a CD-ROM library by providing networked CD-ROM access to many individuals within the organization.

CD-ROM is an ideal medium for long-term archival of stable data sets. Unlike tapes, which must be exercised at least once a year and have a shelf life under ten years, CD-ROMs are thought to be stable for at least fifty years (Nimbus Information Systems, 1989, p. 22). Therefore, a small stock of unopened CD-ROMs containing permafrost data, stored in a safe location, would assure a secure archive for the foreseeable future. In addition, each CD-ROM in the hands of a user can serve as a backup archive, should the need arise.

Distributing CD-ROMs by mail is much less expensive than mailing magnetic tapes, and CD-ROMs are not subject to damage or destruction by being dropped or x-rayed. Inexpensive, easy-to-distribute, well-documented data on a CD-ROM are likely to be used by investigators outside the original group of Principal Investigators. Ease of distribution coupled with ease of use could widen the audience for permafrost data, generating increased cross-discipline investigations. The opportunity to make temporal and geographical comparisons could be enhanced depending on the variety and scope of the data available on the CD; new applications might be found for data collected years ago in corroborating and augmenting recently collected data. The ability to store and distribute a large volume and variety of permafrost data in a compact and inexpensive format will greatly enhance the value of the data to the permafrost community and more widely to those involved in global change research.

#### CD-ROM Data Preparation

Preparation of data for placement on a CD-ROM includes a series of steps:

- a. Identifying target data sets for inclusion. Consideration should be given to deciding which data sets are appropriate (based on stability, data quality, importance of the data set, or perhaps even obscurity, among other factors) from the permafrost data available.
- b. Defining suitable archive formats. Existing standard formats should be used where available and feasible. Data should be placed on the CD-ROM(s) in ASCII-coded form rather than binary, to assure portability among various types of hardware, and for ease of use by investigators in various disciplines with myriad applications.

It is not generally recommended that application software be developed for distribution either on or with the CD-ROM(s) since each investigator will prefer a different approach to data analysis.

- c. Working with scientists to produce complete documentation. Documentation is the key to successful data use beyond the originating scientist. A description of the data must be clearly written such that any researcher would be able to read and manipulate the data without further information.

Complete documentation includes, but is not limited to, the following: location of the data in time and space, sampling interval, definition of all data fields (variable name and definition), Fortran format, data type (integer, real, alpha-numeric, etc.), unit of measurement, location of any implied minus sign or decimal point, brief description (or name) of analysis technique(s) used, level of precision, name and locating information for all investigators involved in the data collection or analysis process, and references to published data reports or analyses.

d. Verifying data submissions. Data must be checked for integrity on receipt by the archive center. In addition, quality checks based on community consensus must be defined and performed for all data that will be archived and distributed on the CD-ROM(s). The level of quality control need not be excessive as long as it is documented rigorously and that documentation is provided to data users.

#### Benefits of Data Archives to the Scientific Community

Ease of distribution coupled with ease of use could widen the audience for permafrost data, generating increased cross-disciplinary investigation. The opportunity to make temporal and geographical comparisons could be enhanced depending on the variety and scope of the data available on the CD. New applications might be found for data collected years ago, particularly in corroborating and augmenting recently collected data. The availability of CD as a distribution medium may encourage the release of proprietary data, particularly where the economic incentive for maintaining such data bases has declined. The ability to store and distribute a large volume and variety of permafrost data in a compact and inexpensive format will greatly enhance the value of the data to the permafrost community and, more widely, to those involved in global change research.

#### CONCLUDING REMARKS

NSIDC, with its permafrost data inventory, has begun the process of establishing a system "to improve and standardize the collection, archiving, documentation and dissemination of permafrost data." (Barry, 1989, p. 123). Our initial survey has revealed that a significant amount of permafrost data is held by the research community and that there is considerable willingness to make these data widely available. The demands of global change research and the increasing need for interdisciplinary science make it imperative that such a cooperative effort move forward. By the VII International Conference (1998) we plan, with the cooperation of all permafrost researchers, to have a system in place and operational.

#### ACKNOWLEDGMENTS

We wish to thank Dr. Jerry Brown for his encouragement of this work which is supported by NOAA under task NA90RAH00076 and the U.S. Army Cold Regions Research and Engineering Laboratory for their support for preparation of the permafrost bibliographies.

#### REFERENCES

- Barry, R.G., 1988. Permafrost data and information. Status and needs. In: *Fifth International Conference on Permafrost Proceedings Vol. 1.* (Ed., K. Senneset), Tapir Publishers, Trondheim, pp. 119-122.
- Barry, R.G., 1989. Workshop on Permafrost Data and Information. In: Brennan, A.M. and R.G. Barry, eds. *Ice Core Update, 1980-1989; Permafrost Data Workshop.* Glaciological Data, Report GD-23, World Data Center-A for Glaciology, University of Colorado, Boulder, CO, pp. 107-126.
- Brennan, A.M., compiler, 1983. *Permafrost: a bibliography, 1978-1982.* Glaciological Data, Report GD-14, World Data Center-A for Glaciology, University of Colorado, Boulder, CO, 334 p.

Brennan, A.M., compiler, 1988. *Permafrost Bibliography Update, 1983-1987.* Glaciological Data, Report GD-21, World Data Center-A for Glaciology, University of Colorado, Boulder, CO, 224 p.

Brennan, A.M. and M. Andrews, eds., 1988. Twelfth Northern Libraries Colloquy, 5-9 June 1988. *Glaciological Data, Report GD-22, World Data Center-A for Glaciology, University of Colorado, Boulder, CO, 331 p.*

Geotech Engineering Ltd., 1983. *Subsurface temperature data from Arctic wells.* Earth Physics Branch, Energy, Mines and Resources, Canada, Open File 83-11, pp. 1-401.

Hardy Associates (1978) Ltd., 1984. *A study of well logs in the western Northwest Territories and Yukon to outline permafrost thickness and/or gas hydrate occurrence.* Earth Physics Branch, Energy, Mines and Resources, Canada, Open File 84-27, pp. 1-290.

Heginbottom, J.A., 1984. *The mapping of permafrost.* Canadian Geographer 28, pp. 78-83.

National Snow and Ice Data Center, 1992. *Arctic Multisensor Data Sampler.* Boulder, CO, CD-ROM.

Nimbus Information System, 1989. *The Road to CD-ROM.* Nimbus Information Systems, Guildford Farm, SR 629, Ruckersville, VA 22968.

Proudfoot, D.A. and D.E. Lawrence, 1976. *Mackenzie Valley Geotechnical Data Bank Tape Description Manual.* Geological Survey of Canada, Open File 350.

Taylor, A.E. and Judge, A.S., 1974. *Canadian geothermal data collection - northern wells, 1955 to February 1974.* Geothermal Series no. 1, Earth Physics Branch, Energy, Mines and Resources, Canada, pp. 1-171.

# **Active Rockglaciers and the Lower Limit of Discontinuous Alpine Permafrost in the Khumbu Himalaya, Nepal**

Dietrich Barsch<sup>1</sup> and Matthias Jakob<sup>2</sup>

<sup>1</sup>Department of Geography, University of Heidelberg, Im Neuenheimer Feld 348, 6900 Heidelberg, Germany

<sup>2</sup>Department of Geography University of British Columbia, 217-1984 West Mall, Vancouver, B.C. V6T 1Z2, Canada

Rockglaciers, a common phenomenon in the Khumbu Himalaya, are located between 4,950 and 5,400 m asl. Climate and intense weathering promote development. Refraction seismic measurements reveal a depth of the unfrozen layer between 0.6 and 3.9 m. Discontinuous alpine permafrost (DAP) has its lower limit between 5,400 and 5,500 m on slopes with a southern aspect. On western orientated slopes the lower limit of DAP is located around 5,150 m. The ELA ranges only 100 to 250 m higher.

Rockglaciers play a significant role in mass transport and can be seen as a proof for intense weathering in the research area. Rock weathering intensities above the rockglaciers in the study area seem to be in the same order of magnitude as in the Swiss Alps. Future climatic warming and thus melting permafrost can trigger mass movements by mobilisation of formerly frozen debris which causes natural hazards.

## **Introduction**

Active rockglaciers are periglacial phenomena of subnival belts in cold and relatively dry mountain environments. Barsch (1978) has shown them to be indicators of discontinuous alpine permafrost (DAP).

The Khumbu Himalaya is an example of a subtropical high mountain environment (ca. 28°N) in which active rockglaciers have not been studied systematically so far. During February to May 1991, rockglacier studies were carried out around the Pokalde massif, about five kilometers southwest of Mount Everest (Fig. 1). Sledge hammer refraction seismic was used to determine the depth of the active layer on four hitherto unnamed active rockglaciers and on adjacent ground to determine the lower limit of DAP (Table 1, cf. also Jakob in press).

Relative dating was employed to differentiate morphological units and to determine a possible correlation with climatic changes. Vertical mass transport by rockfall, calculated using rockglacier age and volume, was compared with Jäckli's (1957) results from the Swiss Alps.

## **Climate**

Several climatological and meteorological data sets exist for the Khumbu Himalaya and its adjacent areas (Sen and Chatterjee 1934, Müller 1958, Pugh 1961, Dhar and Narayan 1965, Ageta 1976, Häckel et al. 1970, Kraus 1970, Inoue 1976, Fuji and Higuchi 1976). The climatic conditions are dominated by the summer monsoon, which is limited from June to September. Because of rainshadow effects, the mean annual precipitation (MAP) ranges between 400 and 500 mm at an altitude of 4,900 m (Müller 1958, Inoue 1976, Ageta 1976).

Kraus (1970) monitored radiation near Chukung (4750 m). Extreme values exceeded the solar constant because cumulus clouds increased the initial radiation. Insolation maxima occur in May. Increasing cloud cover was

responsible for a decrease in insolation in June. The daily appearance of convectional clouds create high insolation values on slopes with eastern and southern aspect, whereas north and west oriented slopes experience severely less insolation. The daily valley wind system is responsible for convection and cloud build-up which in turn influences radiation and temperatures.

## **Rockglacier description**

The four tongue-shaped rockglaciers which have been studied in detail were identified on the topographic map of Schneider (1957). His observations allow the distinction between rockglaciers and debris-covered glaciers. Three of the rockglaciers cover the southern half of the cirque or side valley in which they are found. This asymmetrical position results from differences in exposure and thus differences in weathering. The source areas are found between 5,100 and 5,400 m, and toes are located at altitudes between 4,950 and 5,240 m. The lengths range between 410 and 1100 m. Rockglacier Lingten (LI on fig. 1) consists of at least two morphologically differentiated parts. The lower one is now inactive because the front has been stabilized and plants grow on it. Detailed lichen analysis support this observation. At an altitude of about 5,150 m an inactive part is being overridden by an active section. Rockglacier Dugla (DU), Kongma (KO) and Nuptse (NU) seem to display a single-unit morphology (Barsch 1992). Ridge and furrow topography and well-developed active fronts are found on all of them.

## **Results of sledge hammer seismic measurements and the lower limit of discontinuous alpine permafrost**

A Bison portable hammer seismograph was used for geophysical measurements of the existence and depths of the unfrozen surface layer. In the research area 44 seismic profiles were recorded. The depths to the

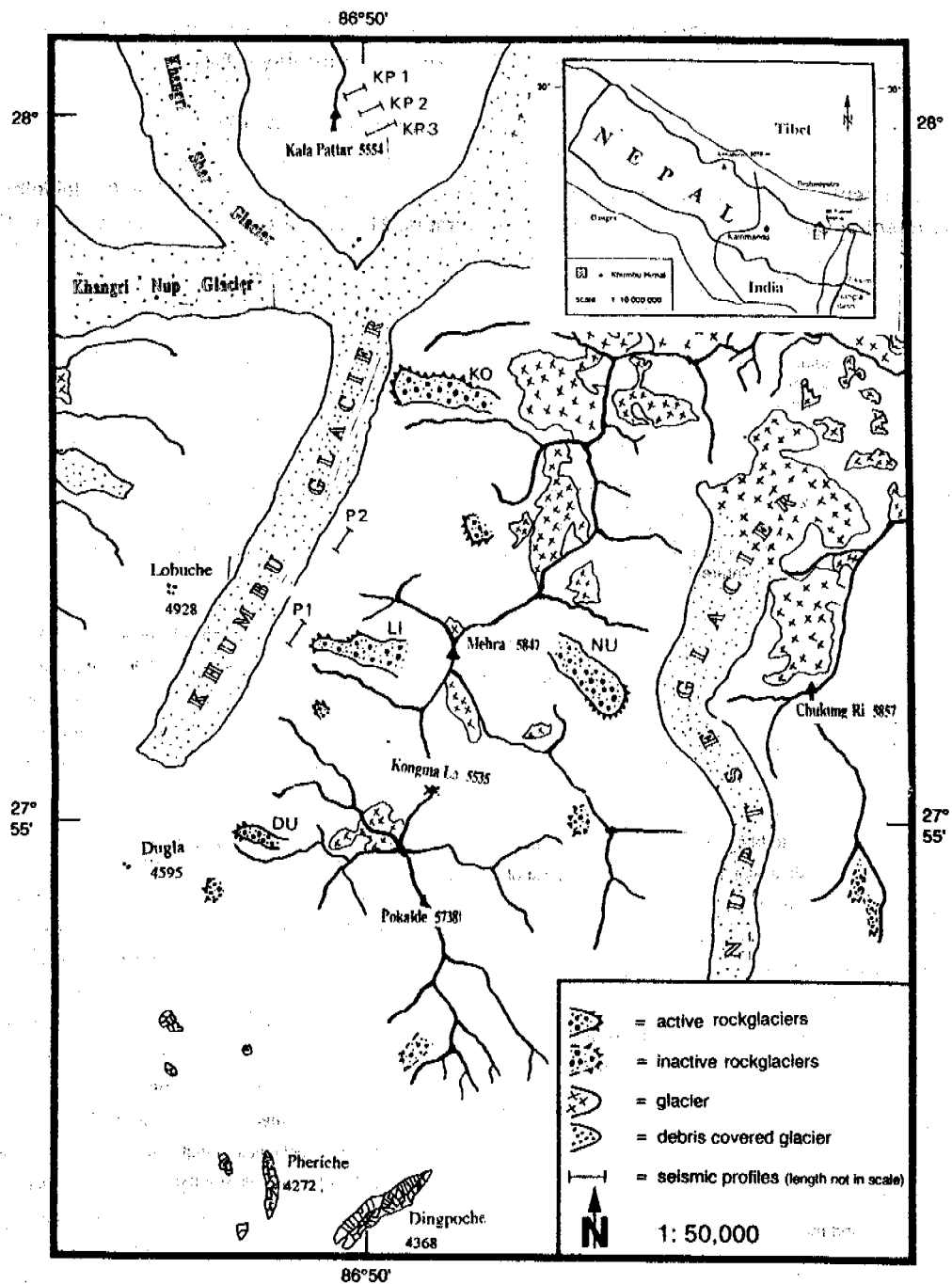


Figure 1: The location of active and inactive rockglaciers, glaciers, debris covered glaciers and seismic profiles in the research area, Khumbu Himalaya. Map drawn from Schneider (1957) 1:50,000.

position and number	altitude (m)	direction of strike	profile length(m)	profile orientation	v1 (m/s)	v2 (m/s)	d1 (m)	d2 (m)
Lingten rgl (1)	4960	y	50	NO-SW	871	2530	2.4	17.1
Lingten rgl (2)	5000	y	40	NO-SW	687	2200	2	14.7
Lingten rgl (3)	5040	y	40	NO-SW	586	2250	2.9	15.6
Lingten rgl (4)	5170	y	40	NO-SW	500	3330	1.6	11.3
Lingten rgl (5)	5200	y	40	NO-SW	500	1378†	0.5	7.7
Kongma rgl (1)	5120	x	40	W-O	238	1630	1.3	15.8
Kongma rgl (2)	5160	x	50	W-O	424	2700	1.1	15.5
Kongma rgl (3)	5160	y	40	N-S	633	2500	2.7	14.4
Kongma rgl (4)	5180	z	40	NO-SW	254	2296	2	14.4
Kongma rgl (5)	5230	y	40	N-S	420	2830	1.2	12.3
Kongma rgl (6)	5260	x	40	W-O	300	2313	0.6	13.3
Kongma rgl (7)	5320	y	40	NO-SW	400	2670	0.9	13.4
Kongma rgl (8)	5340	x	40	W-O	433	4250	2.1	8.8
Nuptse rgl (1)	5315	y	40	N-S	926	2500	4.7	16
Nuptse rgl (2)	5315	y	40	N-S	804	3000	2.8	13.1
Nuptse rgl (3)	5320	y	40	N-S	750	3100	2.3	12.4
Nuptse rgl (4)	5320	y	40	N-S	719	2625	2.2	13.7
Nuptse rgl (5)	5340	x	40	O-W	396	4000	3.4	10.7
Nuptse rgl (6)	5350	x	40	O-W	712	2564	2.5	14.7
Nuptse rgl (7)	5372	x	40	O-W	738	2891	3	14.3
Nuptse rgl (8)	5400	x	40	O-W	605	2667	2.1	13.5
Nuptse rgl (9)	5400	y	40	N-W	663	1834	2.9	16.5
Nuptse rgl (10)	5420	y	40	N-S	1125	3367	3.4	17.2
Nuptse rgl (11)	5460	y	50	N-S	835	2584	3.9	18.1
Nuptse rgl (12)	5480	y	40	N-S	585	3250	3.2	12.4
Mehra rgl (1)	5230	y	40	NO-SW	833	3084	2.8	12.9
Mehra rgl (2)	5260	x	30	NW-SO	572	3214	1.7	9.0
Mehra rgl (3)	5265	y	30	NO-SW	353	3330	1.3	8.5
Dugla rgl (1)	5150	y	40	N-S	482	2434	1.7	13.8
Dugla rgl (2)	5170	x	40	W-O	510	2750	2.6	13.6
Dugla rgl (3)	5170	y	40	N-S	608	2750	2.8	13.8
Kala Pattar (1)	5360	y #	30	NO-SW	382	1000	1.5	13.7
Kala Pattar (2)	5560	y #	23	NO-SW	914	3100	2.6	8.2
Kala Pattar (3)	5600	y #	46	NO-SW	250	5800	1.1	-----
Pokalde (1)	4950	y #	40	N-W	300	750	2.1	19.1
Pokalde (2)	5050	y #	40	N-S	430	860	6.1	22.0
Lhotse debris. gl. (1)	4770	y	40	N-S	810	-----	16.0*	-----
Lhotse debris. gl. (2)	4790	y	40	N-S	707	4476	2.8	8.6
Lhotse gl. endm. (1)	4800	y	40	N-S	342	2400	18.2*	-----
Tauroglacier (1)	4250	y	30	NO-SW	285	507	3.6	16.6
Tauroglacier (2)	4500	x	30	NW-SO	250	3000	0.7	8.7
Ama Dablam gl. endm.	4750	y	50	W-O	640	2400	2.4	17.6

\* P-wave-velocities of potentially underlying ice were assumed as 3600 m/s

x in flow direction of the rockglacier

† three layer case with 3800 m/s as the P-wave velocity of the third layer

y 90° to flow direction

z 45° to flow direction

y # 90° to slope

Table 1: The data of all seismic profiles in the study area

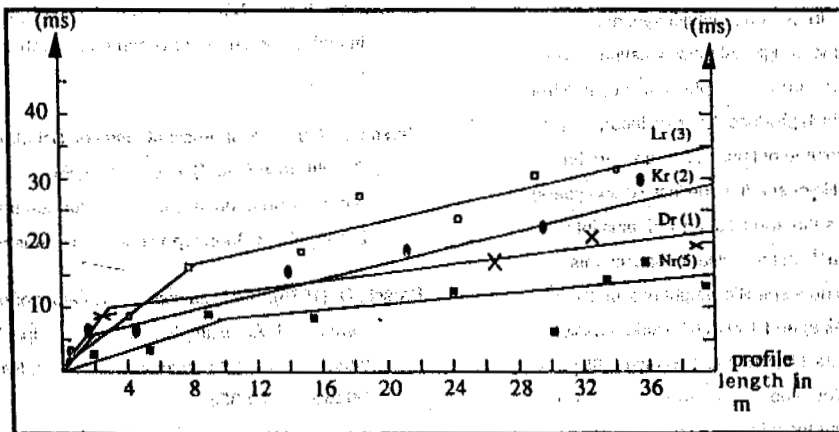


Fig. 2: Examples of seismic profiles of Lingten rockglacier (Lr), Kongma rockglacier (Kr), Dugla rockglacier (Dr) and Nuptse rockglacier (Nr).



supersaturated permafrost varied between 0.6 m on the uppermost part of Lintgen and 3.9 m near the active front of Nuptse rockglacier. Figure 2 shows some examples of the profile curves. Table 1 displays the results of all seismic measurements carried out on active rockglaciers as well as on adjacent terrain.

Regarding the lower limit of discontinuous alpine permafrost (DAP), the following results are obtained: On slopes with southern aspect, the DAP ranges between 5,400 and 5,500 m. On slopes with western aspect it is located around 5,150 m.

The equilibrium line altitude (ELA), determined to exist between 5,600 m on south facing slopes and 5,400 m on west and east facing slopes, agrees well with Müller's (1978) and William's (1983) results. The vertical difference between the DAP and the ELA is, therefore, only 100-250 m. This is a very low value which can only be explained by the special climate in the Khumbu area. Here large rockwalls and rockslopes well above the ELA are free of snow throughout the greater part of the year, which is caused by the intense radiation. The same observation can be made in the relatively dry Argentine Andes (Schrott 1991). The high altitude belts of these areas are characterized by a dry periglacial climate which comprises possible source areas for talus which can be incorporated into the rockglaciers. The effective cryogenic belt is, therefore, much larger than the difference between the lower limit of DAP and the ELA. In comparison to the relative wet Alps, active rockglaciers are only developed in parts where the difference between ELA and DAP is larger than 400 m.

Fuji and Higuchi (1976) have measured ground temperatures in the Khumbu region and Hidden Valley. Their measurements indicate the possibility of permafrost above 4,900 m in the Khumbu Himalaya and above 5,000 m in the Hidden Valley. Guodong (1983) calculated the altitude of the lower limit of DAP as a function of latitude as 5,080 m at 25°22' N. Although somewhat lower, their findings do not differ markedly from our results.

It can be concluded that discontinuous alpine permafrost can be expected above 5,100 to 5,500 m in the Khumbu Himalaya. Comparable limits are found in mountain ranges on the Tibetan plateau (Gorunov 1983) or in the Andes of Mendoza (Schrott 1991).

### The importance of rockglaciers for mass wasting

Barsch (1977 a,b) showed that active rockglaciers play a significant role in mass transport in the Swiss Alps. In general, rockglaciers are responsible for about 15-20 % of all alpine periglacial mass wasting in the Swiss Alps (Barsch 1977 a). Rockglaciers are very helpful in calculating the mean annual weathering of rockwalls which produce the talus incorporated in the rockglaciers. Accepting that the volume of talus in rockglaciers has been produced continuously during the Holocene (i.e. the last 10,000 years), it can be estimated that in the Swiss Alps the annual supply of talus into talus rockglaciers is about  $30 \cdot 10^3 \text{ m}^3 \text{ a}^{-1}$ . In the Pokalde massif, this value amounts to  $1 \cdot 10^3 \text{ m}^3 \text{ a}^{-1}$ . Assuming a specific weight of  $2.65 \text{ t} \cdot \text{m}^{-3}$  and a vertical distance of 75 m (Swiss Alps) and 100 m (Pokalde massif), the vertical mass transport according to Jäckli (1957) and Barsch (1981) can be calculated to  $6 \cdot 10^6 \text{ m}^3 \text{ a}^{-1}$  (Swiss Alps) and  $2.7 \cdot 10^6 \text{ m}^3 \text{ a}^{-1}$  (Pokalde massif). Related to the area which contributes talus into the rockglaciers

(Swiss Alps:  $50 \text{ km}^2$ ; Pokalde massif:  $2.4 \text{ km}^2$ ) the specific vertical mass transport amounts to  $120 \cdot 10^3 \text{ m}^3 \text{ a}^{-1} \text{ km}^{-2}$  (Swiss Alps) and  $85 \cdot 10^3 \text{ m}^3 \text{ a}^{-1} \text{ km}^{-2}$  (Pokalde massif).

These values are based on the vertical transport only. Similar important horizontal transport has not been discussed. If only the vertical transport is used, then the change in potential energy can be expressed by these values transformed in the SI-unit Watt (c.f. Calne 1976). The change in potential energy amounts to  $37 \text{ W} \cdot \text{km}^{-2}$  in the Swiss Alps and to  $26 \text{ W} \cdot \text{km}^{-2}$  in the Pokalde massif.

Regarding the difficulties to obtain these values and considering that the number of rockglaciers in the Pokalde massif is small, both values are in the same order of magnitude. This demonstrates the fact that active rockglaciers in the Pokalde massif are of the same importance as talus transport systems as in parts of the Alps.

### Conclusions

Low precipitation, high radiation, low temperatures and intense weathering in an extreme relief, all favor rockglacier development in the Khumbu Himalaya. Mountain permafrost, a common and widespread phenomenon of the periglacial belt of the study area, is indicated by talus rockglaciers of considerable lengths. The rockglaciers attest to intensive periglacial mass wasting. Upon estimating the volume of rock debris incorporated in rockglaciers, the annual production of talus in the rock sheds above the rockglaciers are in the same order of magnitude in the Swiss Alps and in the Pokalde massif.

If global warming maintains its current trend, the lower rockglaciers studied will tend toward inactive status. Other places, now being covered by glaciers above the ELA, might become new rooting areas for rockglaciers assuming that precipitation does not increase significantly. Reduction in permafrost, however, may initiate catastrophic failures in the form of debris flows and rock avalanches which would threaten natives, trekkers, and mountaineers.

### Bibliography:

- Agata, Y. (1976): Characteristics of precipitation during the monsoon season in Khumbu Himal. *Seppyo* 38: 84-88.
- Barsch, D. (1977a): Nature and importance of mass-wasting by rock glaciers in alpine permafrost environments. *Earth Surface Processes* 2: 231-245.
- Barsch, D. (1977): Eine Abschätzung von Schuttproduktion und Schutttransport im Bereich aktiver Blockgletscher der Schweizer Alpen. Wirthmann, A. (ed.): *Hangformen und Hangprozesse*. Zeitschrift für Geomorphologie, Supplementband 28: 148-160.
- Barsch, D. (1978): Rock glaciers as indicators of discontinuous Alpine Permafrost. An example of the Swiss Alps. *Proceedings, Third International Conference on Permafrost, National Research Council, Ottawa* 1: 349-352.

- Barsch, D. (1981): Studien zur gegenwärtigen Geomorphodynamik im Bereich der Oobloyah Bay, N- Ellesmere Island, N.W.T., Kanada. *Heidelberger Geographische Arbeiten* 69: 69-90
- Barsch, D. (1992, in press): Permafrost creep and rockglaciers. Situation report. *Permafrost and Periglacial Processes*.
- Caine, N. (1976): A uniform measure of subaerial erosion. *Geological Society of America Bulletin* 87: 137-140.
- Dhar, O.N. and Narcyanca, J. (1965): A study of precipitation distribution in the neighbourhood of Mount Everest. *Indian Journal of Meteorology and Geophysica* 16 (2): 229-240.
- Fuji, Y. and Higuchi (1976): Ground temperature and its relation to permafrost occurrences in the Khumbu Himal and Hidden Valley. *Seppyo* 38: 125-141.
- Guodong, Ch. (1983): Vertical and horizontal zonation of high-altitude permafrost. *Proceedings, Fourth International Conference on Permafrost*. National Academy Press, Washington D.C.: 136-141.
- Gorunov, A. P. (1983): Rock glaciers of the mountains of middle Asia. *Proceedings, Fourth International Conference on Permafrost*. National Academy Press, Washington D.C.: 359-362.
- Häckel, H., Häckel, K. and Kraus, H. (1970): Tagesgänge des Energiehaushaltes der Erdoberfläche auf der Alp Chukung im Gebiet des Mount Everest. *Khumbu Himal* 7: 42-64.
- Inoue, J. (1976): Climate of the Khumbu Himal. *Seppyo* 38: 66-73.
- Jäckli, H. (1957): *Gegenwartsgeologie des bündnerischen Rheingebietes- ein Beitrag zur exogenen Dynamik alpiner Gebirgslandschaften. Beiträge zur Geologie der Schweiz, Geotechnische Serie* 36: 126 p.
- Jakob, M. (in press): Rock glaciers as indicators for discontinuous alpine permafrost in the Khumbu Himalaya, Nepal. *Permafrost and Periglacial Processes*.
- Kraus, H. (1970): Freie und bedeckte Ablation. *Khumbu Himal* 7: 203-235.
- Müller, F. (1958): Eight months of glacier and soil research in the Everest region. *The Mountain World 1958/59*, Swiss Foundation for Alpine Research, George Allen and Unwin Ltd., London: 191-208 pp.
- Pugh, L.G.C.E. (1961): Science in the Himalaya. *Nature* 4787: 429-430.
- Schneider, E. (1957): *Topographic map Khumbu Himal 1:25.000 and 1:50.000*. Kartographische Anstalt Freytag-Berndt und Artaria, Vienna, Austria.
- Schrott, L. (1991): Global solar radiation, soil temperature and permafrost in the Central Andes, Argentina: a progress report. *Permafrost and Periglacial Processes* 2: 59-66.
- Sen, S.N. und Chatterjee, N.P. (1934): *Everest 1933*. Hugh Rutledge (Ed.), Hodder & Stoughton Ltd., London: 352 p.

SEASONAL CHANGEABILITY OF PHYSICO-CHEMICAL PROPERTIES OF PERMAFROST ACTIVE LAYER WATERS  
IN THE RECHERCHE FIORD REGION (WESTERN SPITSBERGEN)

Stefan A. Bartoszewski<sup>1</sup>, Zdzislaw Michalczyk<sup>1</sup> and Jan Magierski<sup>2</sup>

<sup>1</sup>Institute of Earth Sciences, Maria Curie-Skłodowska University, Lublin, Poland

<sup>2</sup>Institute of Soil Sciences, Agricultural College, Lublin, Poland

The paper discusses the results of hydrological investigations carried out in the southern shore of Bellsund in 1986-90. It was noted that the active layer retention is slight mainly because of the small thickness of the saturation zone. The air temperature affects hydrological and hydrochemical processes. All waters in the studied area are characterized by poor mineralization, weak alkaline reaction and low temperature.

## INTRODUCTION

The aim of the investigations were to study the hydrological and physicochemical features of the area. The collected materials were used to obtain the characteristics of spatial and seasonal differentiations of physicochemical properties of water in different circulation phases. The studies were carried out in the central Western Spitsbergen. Measurements and field studies were made in the region of the Calypsobyen settlement situated above Recherche Fiord (Fig.1).

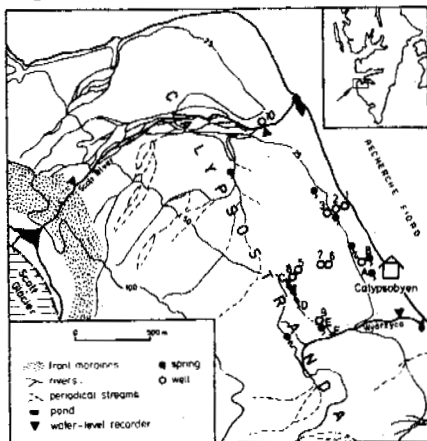


Fig.1. Situation of the investigation area

## STUDY AREA

The western part of the study area consists the Hecla Hoek formation of the Upper Proterozoic Age (Dallmann et.al.1990). Tillites, phylites and quartzites constitute the main types

of rocks. The region of the Van Keulen Fiord is built of a series of Upper Paleozoic and Mesozoic sediments. In the western region are found gypsum and dolomites, sandstones, shales and mudstones are typical in the eastern region.

The central sector is dominated by a mountain massif of 550-800 m a.s.l. with glaciers occupying the valleys. The coastal plains are built of unconsolidated Quaternary sediments in the form of gravels, sands, boulder clays and marine silts. Infiltration coefficients of sand-gravel formations determined by means of Burger cylinders range between 0.0006-0.0023 m s<sup>-1</sup>.

## GROUND WATERS

The analysis of hydrological and hydrochemical phenomena occurring in the permafrost active layer is based on stationary observations. A hydrometric measurements system was developed included 10 wells, 3 springs, 8 water gates and the Wydrzyca River (Skua River) where a water-level recorder was installed.

Underground waters of Calypsotranda form a water-bearing level fitted to the upper part of the permafrost. The depth of the water table and the thickness of the non-saturated zone are related to dynamics of permafrost active layer. The observations of wells was based from the period of 18 July-8 September, 1989 formed a basis for analysis. In the summer-autumn period a gradual decrease of water resources retention in the permafrost active layer takes place. The amount of water loss due to drainage and evapotranspiration is greater than current atmospheric input and ground ice melt contribution. The potential evaporation in the studied period

in 1989 was 87 mm and the precipitation sum was 52.3 mm. The water table decreases gradually.

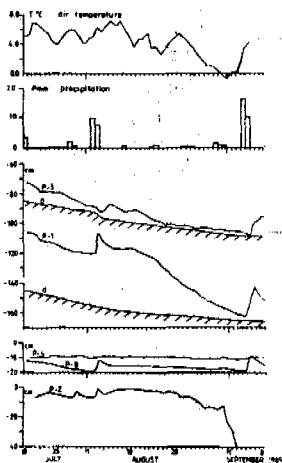


Fig.2. Situation of the ground waters in 1989). (0-depth of the frost table occurrence in wells).

The curves from various years are very similar. Intense rain fall can slow down a decrease tendency but does not change a general trend.

#### SPRINGS

By the end of the spring after the snow melted, some small springs began to flow from the terrace 20-25 m a.s.l. The waters originated from the ground ice melt and the rain. The spring observed for the longest period of time is found near the base camp of the UMCS Expedition. The spring basin area is 0.009 km<sup>2</sup>. Its yield for the period of 21 July - 17 August in successive years is as follows:

Year	1986	1987	1988	1989
Yield (dm <sup>3</sup> s <sup>-1</sup> )	0.107	0.089	0.044	0.127

The course of the spring yield is similar to the changes of water storage in the permafrost active layer, particularly in its area of regular water saturation. Maximum yields of the spring are recorded after heavy rainfalls with a lag of 2-4 day. The highest yield of 0.186 dm<sup>3</sup>s<sup>-1</sup> was recorded on the 5 August, 1989, and was due to a 17.4 mm rainfall on 2-3 August. During the field studies period between 5 July-8 September, 1989 the unit outflow from the spring basin was 12 dm<sup>3</sup>s<sup>-1</sup>km<sup>-2</sup> which corresponds to the outflow index 67 mm (Michalczyk 1990).

#### SURFACE WATERS

The water-bearing level of the active layer in Calypsotranda is drained by a few small rivers of which Wydrzyca (Skua River) has been observed for the longest period-5 years (Bartoszewski et.al.1988, Michalczyk 1990). Its left

tributary, with a drainage area of 0.103 km<sup>2</sup> is the object of this present analysis. The basin covers an almost flat area of difficult surface and underground outflows. The studied stream is fed by thawing ground ice, melting snow and rainwaters. Spring meltwaters constitute 2/3 of the total outflow. The maximum outflow recorded in this period was 224 dm<sup>3</sup>s<sup>-1</sup>km<sup>-2</sup> in 1990. After the disappearance of the snow cover, the only source of outflow alimentation is thawing ground ice in the active layer and precipitation. The pattern of the daily flow in the summer of 1989 was similar to changes of spring yield and of ground water level fluctuations. During the period of investigation 7000 m<sup>3</sup> of water was discharged, which corresponds to the outflow index 69 mm (Michalczyk 1990.)

#### WATER TEMPERATURE

The course and intensity of hydrochemical and hydrological processes was strongly dependent on changes of air and water temperatures. Regular studies of yield, temperature and some hydrochemical features were carried out in the spring close to the base in Calypsobyen in 1986-1989 (point A in Fig.1).

According to our observations the temperature of water remained at 0.5-6.4°C, it was dependent on the depth of the frost table, the thickness of aeration and the saturation zone. The curve of the water temperature course in this spring shows a general relation to the air temperature course (Fig.3).

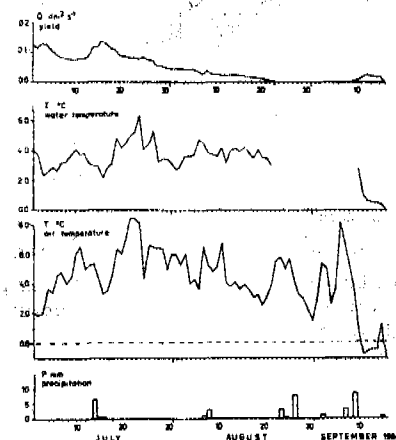


Fig. 3. Yield of spring in Calypsobyen and temperature in 1988

In the first days of July 1988 water temperatures exceeded those of air temperatures due to the faster heating of soil surface layers. Water temperature was more stable than that of air temperature. The seasonal values of spring water and air amplitudes were 5.9 and 9.2°C respectively. The average water temperature in the period of the investigations was 3.4°C and that of air was 4.3°C. Outflow decline in the period of 23 August-9 September, 1988 was due

to the reduction in active layer storage. There was still some water in the spring basin as a static resource. The renewed increase of retention took place after precipitation on the turn August and September 26.1 mm in total. At first the water temperature was 2.8°C but as a result of sudden cooling it dropped to 0.5°C and then the spring got frozen with a several centimeter soil layer.

#### WATER CHEMISTRY

The water ionic composition was determined in the field hydrochemical laboratory in Calypsobyen by means of the classical titration method. General mineralization was determined as a sum of ions and on the basis of electrical conductivity. The elemental composition of waters in the region of studies is slightly differentiated (Fig.4).

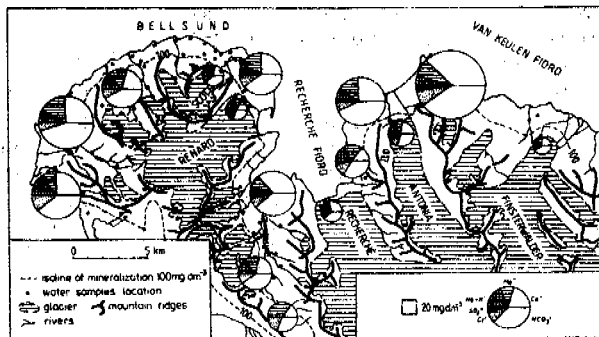
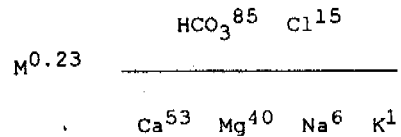


Fig. 4. Chemical composition of water in the Recherche Fiord region

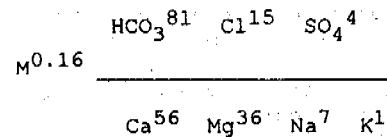
There is a common occurrence of tillites and phyllites as well as rocks containing calcium and magnesium on the surface. The inland waters of this part of Spitsbergen are poorly mineralized and most frequently are classified as ultrasweet. The lowest mineralization of several  $\text{mg dm}^{-3}$  was found in the waters coming from surface glacial ablation. The waters in the proglacial zone enriched themselves in the dissolved substances reaching mineralization of the range 50-70  $\text{mg dm}^{-3}$ . The mountain massifs and adjacent elevated areas over 150 m a.s.l. had 100  $\text{mg dm}^{-3}$  of mineralization during the summer. The coastal terrace plains as a rule had higher ground water mineralization from 100 to 300  $\text{mg dm}^{-3}$ .  $\text{HCO}_3^-$  ion constituting 68-83% of millival sums of anions was predominant in most analyzed samples of water. The share of  $\text{Cl}^-$  ion was from several to 25% and of  $\text{SO}_4^{2-}$  ion, as well as to a few percent of millival sums of an-

ions.  $\text{Ca}^{2+}$  ion takes up at least half of the millival sums of cations. The share of  $\text{Mg}^{2+}$  ion is 20-40% and that of  $\text{Na}^+$  about 10%. The chemical composition of waters of permafrost origin and its seasonal differentiation was most carefully studied in the Calypsotranda region.

Mineralization of waters circulating in the zone of active exchange was from 180 to 300  $\text{mg dm}^{-3}$ ; water reaction was weakly alkaline, pH was in the range 7.6-8.5. The typical chemical composition of waters is represented by the spring A in Calypsobyen:



The composition of water of the unglaciated basin is represented by the Wydrzyca River:



Both surface and ground waters are characterized by a similar chemical composition of  $\text{HCO}_3^-$  - Ca - Mg type. During the investigations this composition was relatively stable. Its changes are caused by temperature and inflow of meltwater and rainfall. Meltwaters in the spring season cause a general mineralization decrease. Mineralization decrease of waters also occurred after intense rainfalls which to some extent modified the chemical composition through the increased participation of ions coming from marine aerosol i.e.  $\text{Na}^+$ ,  $\text{Cl}^-$ ,  $\text{Mg}^{2+}$  and  $\text{SO}_4^{2-}$ . Temperature is also a modifying agent of the water chemical composition through the increase of  $\text{Ca}^{2+}$ ,  $\text{Mg}^{2+}$  and  $\text{SO}_4^{2-}$ . During the polar summer permafrost water mineralization increases. The air temperature below zero caused an accelerated increase of total mineralization which is due to the cryochemical effect. As analyses show  $\text{Ca}^{2+}$  and  $\text{HCO}_3^-$  ions and partially  $\text{Mg}^{2+}$  ions are responsible for total mineralization (Fig.5). The exception was well P-2 in which a contrary tendency, was observed i.e. mineralization decrease from the spring period for which  $\text{Ca}^{2+}$  ion is responsible. This spot is situated on the terrace slope at the basset of marine silts. It should be supposed that at the beginning of the active hydrological season in June there took place an outflow of more mineralized waters stagnating in the permafrost upper part than in the previous year.

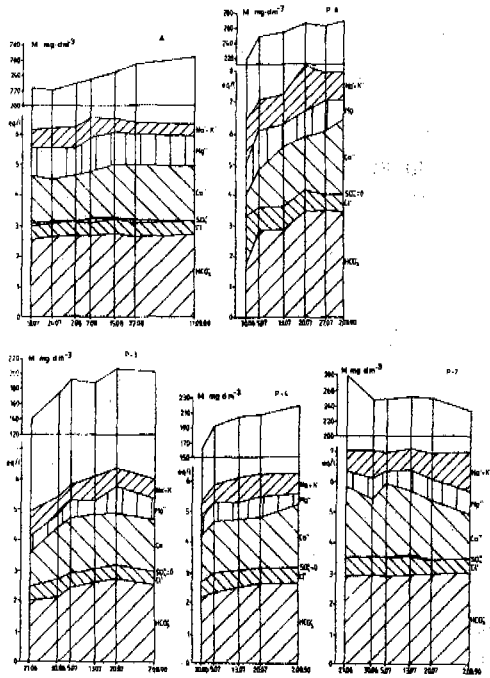


Fig. 5. Changes of water chemical properties in the Calypsostranda region (spring A in 1988, 2, 3, 4, 5 - wells in 1990)

#### CONCLUSIONS

In the permafrost active layer between its upper part and terrain surface there is formed a water-bearing level systematically fed by waters coming from ground ice melting and partially by rainfalls infiltrating the background. The active layer retention is slight of the tens of millimeters order mainly because of the small thickness of the saturation zone. In spite of this character of the river outflow, spring yield and fluctuations of ground water table are highly dynamic. These processes affect the changeability of ground water physical and chemical features. A slight petrographic change of under surface rocks causes quantitative but not qualitative character of chemical composition differences. All waters in a given area are weakly mineralized, of a weak alkaline reaction and low temperature. The analysis of water chemical composition shows that independent of alimentation source, the hydrogen carbonate ion is predominant among anions and calcium and magnesium ions among cations. The greatest changes of chemism are observed at the beginning and in the end of the active hydrological season. With the air temperatures below zero there was an accelerated increase of general mineralization which can be associated with the effect of cryochemical phenomena. During the polar summer the chemical composition of the studied ground waters became stabilized.

#### REFERENCES

Bartoszewski S., Rodzik J., Wojciechowski K. (1988) The outflow of water in permafrost environment -

Spitsbergen. Proc. 5th ICOP, 543-545, Trondheim.  
 Buk E.M. (1988). Hydrochemistry of rivers in mountain permafrost at 33° L.S., Mendoza-Argentina. Proc. 5th ICOP, 294-298, Trondheim.  
 Dallmann W.K., Hjelle A., Ohta Y., Salvigsen O., Bjornerud M.B., Hauser E.C., Maher H.D., Craddock C. (1990). Geological map of Svalbard 1:100 000, Sheet B 11G Van Keulenfjorden. Norsk Polarinst., Oslo.  
 Everett K.R., Ostendorf B. (1988). Hydrology and geochemistry of a small drainage basin in upland tundra, Northern Alaska. Proc. 5th ICOP, 574-579, Trondheim.  
 Michalczyk Z. (1990). Hydrological characteristics of Calypsostranda. Spitsbergen Geographical Expeditions of UMCS, 75-91, Lublin.

DISTRIBUTION OF PERMAFROST, GLACIERS, AND ROCK  
GLACIERS IN THE ITALIAN MOUNTAINS AND CORRELATIONS  
WITH CLIMATE: AN ATTEMPT TO SYNTHESIZE.

S. Belloni <sup>1</sup>, A. Carton <sup>2</sup>, F. Dramis <sup>3</sup> and C. Smiraglia <sup>1</sup>

1. Department of Earth Sciences, University of Milan, Italy
2. Institute of Geology, University of Modena, Italy
3. Department of Earth Sciences, University of Camerino, Italy

On the two Italian mountain chains, the Alps and the Apennines, the lowermost limit of discontinuous permafrost has been determined by examining rock glacier distribution. From aerial photographs and field surveys, more than a thousand forms were identified in the Alps, and a few dozen in the Apennines. The mean elevation of the active rock glacier fronts was found to be 2527 m a.s.l. The mean altitude of inactive rock glaciers is 2261 m a.s.l.. The lower limit of active rock glaciers runs on average along the  $-1.5^{\circ}\text{C}$  isotherm, while that of the inactive ones is at  $0.3^{\circ}\text{C}$ . The mean elevation of the present equilibrium line for the Italian Alps glaciers is at 2890 m a.s.l., with a distribution conditioned by whether the climate is more or less continental. Also the drop in elevation of the equilibrium line during Late Glacial (mean value 280 m) and the corresponding thermic variations ( $-1.7^{\circ}\text{C}$ ) have been estimated.

## INTRODUCTION

Rock glaciers are not only one of the most widespread and interesting landforms in the Alpine environment, and presently the most discussed feature in periglacial morphology, but they are as well certainly one of the most important and significant indicators of mountain permafrost. In fact, in those regions with a large number of rock glaciers, they can be used for identifying and mapping the permafrost lowermost limit (Barsch, 1978; King et al., 1992). Although rock glacier research began in Italy during the first half of the 20th Century, it has been relatively neglected until a short time ago. This recent revival in rock glacier research has been focused on two themes: 1) to verify the presence, distribution and frequency of rock glaciers along the Italian side of the Alps, and 2) to collect data for improving our knowledge of their genesis, evolution and relation with climate.

For the former theme, about 1000 landforms have been identified as rock glaciers by means of photointerpretation and field surveys (Smiraglia, 1985; Carton et al., 1988; Guglielmin, 1991; Smiraglia, 1992). Moreover, many active rock glaciers have been identified and correlated with climatic parameters (Belloni et al., 1988). Then, topographic and geophysical surveys have been carried out on selected rock

glaciers to determine surface movement rate and identify the presence of internal ice.

During the last years, the research has continued on these two themes, and has been extended to the Apennines (Dramis and Kotarba, in press).

## AIMS AND METHODS

The objectives of the study were: 1) to enlarge the knowledge of permafrost distribution along the whole of the Italian side of the Alps and in the Apennines, using the rock glaciers as indicators, and 2) to verify the relationship between climate and altitude of permafrost, rock glaciers and glaciers.

Following the methods adopted in the previously cited works, photointerpretative analyses were revised and extended to all the Italian Alps and the Apennines (Figure. 1). Rock glaciers were identified, distinguishing between active and inactive, mostly taking into account morphology and vegetation cover. To achieve this aim, numerous morphological, topographic and geophysical surveys were carried out on a sample of rock glaciers to determine the presence of ice and the degree of activity (Smiraglia, 1989; Resnati and Smiraglia, 1990; Evin, 1992; Calderoni et al., in press).

To examine the relationships between rockglaciers, glaciers, and climate, three

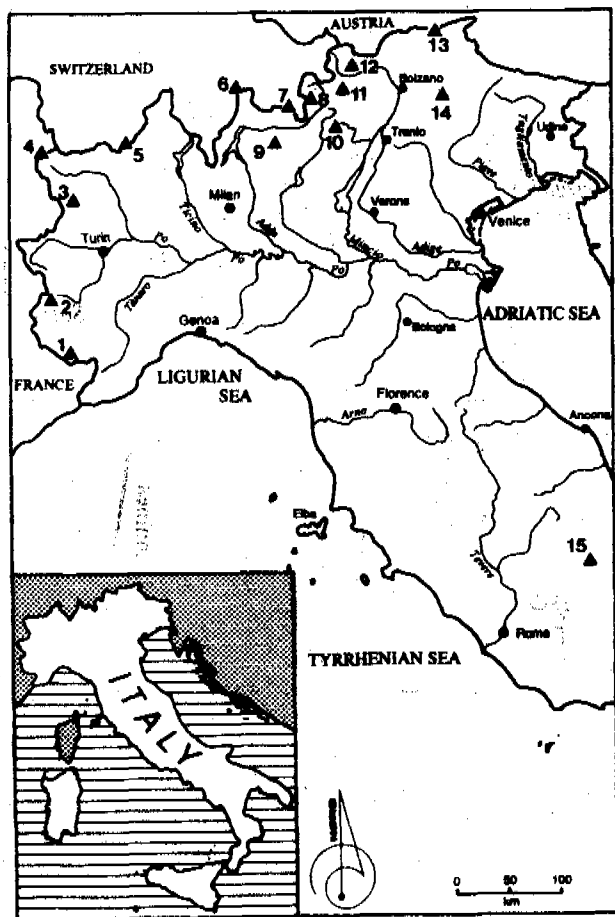


Figure 1. Location of the mountain sectors. 1) Marittime Alps; 2) Cottian Alps; 3) Gran Paradiso Group; 4) Monte Bianco Group; 5) Monte Rosa Group; 6) Tambò-Suretta Group; 7) Bernina Group; 8) Piazzzi-Campo Group; 9) Orobie Alps; 10) Adamello-Presanella Group; 11) Ortles-Cevedale Group; 12) Venoste Alps; 13) Noric Alps; 14) Dolomites; 15) Central Apennines

parameters were chosen: 1) the elevation of the rock glacier fronts (determined by applying information from aerial photographs to large-scale maps); 2) the glacier equilibrium line (ELA) (derived from unpublished data collected by the Italian Glaciological Committee for the World Glacier Inventory, Catasta and Smiraglia, unpublished); 3) the main annual average temperature (MAAT) recorded at several meteorological stations located in different mountain sectors. Of course, many limitations are implicit in this method, most of which concern the distinction between active and inactive forms, and the selection of meteorological stations and of climate parameters.

With regard to the first point, as already mentioned this was partly effected by means of topographic and geophysical surveys of sample forms in various sectors of the Italian Alps. As to the second point, it is known that permafrost distribution (and also that of rock glaciers) is connected, in addition to the annual average temperature of the air, to numerous other parameters such as the layer of winter snow, solar radiation, vegetation, geothermal flux, and topography. The MAAT is thus a parameter affording results that are hardly satisfactory for comparisons on a worldwide scale, but which can be useful for regional studies (Cheng Guodong and Dramis, 1992). Bearing in mind the scale of our research, we therefore consider that the collected data are homogeneous enough and the results adequately valid.

LOWER LIMIT OF ROCK GLACIERS AND EQUILIBRIUM LINE OF GLACIERS. VALUES AND DISTRIBUTION

The collected data are synthesized in Tab. 1, which reports the average elevation of both inactive (RGi) and active (RGa) rock glacier fronts and the equilibrium line of present-day glaciers (ELA), divided according to mountain sector.

Table 1. Elevation of rock glaciers fronts and of the glacier equilibrium line in the Italian mountains

Mountain Sector	AVERAGE ELEVATION	AVERAGE ELEVATION	AVERAGE ELEVATION
	RGi in m	RGa in m	ELA in m
Maritime Alps	2075	2320	2670
Cottian Alps	2292	2579	3010
Gran Paradiso	-	2768	3050
Monte Bianco	2298	2530	3063
Tambò-Suretta	-	2327	2806
Bernina	2261	2406	2865
Piazzzi-Campo	2380	2560	2904
Ortles-Cevedale	2432	2823	3074
Orobie Alps	-	2407	2503
Adamello-Presanella	2093	2488	2890
Venoste Alps	2393	2603	2999
Noric Alps	2199	2637	2888
Dolomites	2130	2287	2641
Central Apennines	2135	2539	2900

In the figure 2 are represented the various sectors of the Alps (and also those of the central Apennines) going from west to east with the highest peaks in each sector and the elevation of the equilibrium lines on present-day glaciers and of the active and inactive rock glacier fronts.



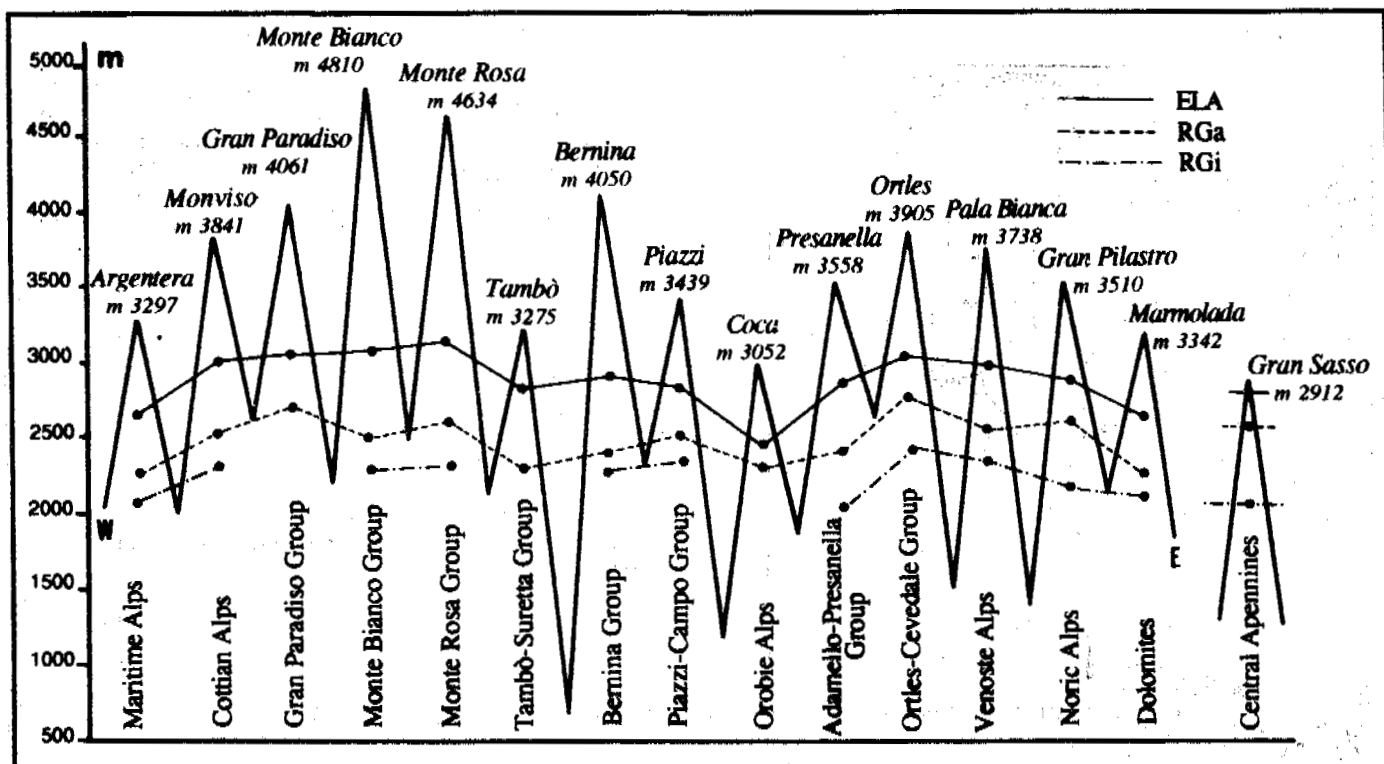


Figure 2. Sectors of the Alps with the highest peaks and the elevations of the equilibrium lines (ELA), of the active rock glaciers (RGa) and of the inactive rock glaciers (RGi).

Lower limit values of the equilibrium line are found in the end of the chain, i.e. in the Dolomites and Carnian Alps (2641 m a.s.l.) and in the Maritime Alps (2670 m a.s.l.). These elevations tend to be higher in the innermost sectors of the chain, remaining above 2800 m in almost all the groups, with the highest values in the Monte Rosa (3112 m), Monte Bianco (3063 m), Gran Paradiso (3050 m), and Ortles-Cevedale groups. Thus, at a regional scale, the influence is evident of the continental and maritime climates on the ELA distribution, to which should be added the position of the individual mountain groups with respect to the Paduan plain. The most notable exception is that of the Orobic Alps which, despite being situated in the central sector of the Italian Alps, have the lowest ELA altitude of all (2806 m a.s.l.). In fact, this mountain group is situated longitudinally to the south of the main watershed and forms the first notable orographic obstacle to the north of the Po plain.

Instead, what is not clear is how the continental climate influences the altitudinal distribution of the rock glacier fronts. It is generally held that the increase of this climate has led to a decrease of the lowermost limits of permafrost (Haerberli, 1978; King, 1986; Guodong and Dramis, 1992).

From Table 1 and Figure 2, it can be seen that the altitudinal differences between ELA and

RGa (the average of which is 357.9 m) are rather reduced in the outermost sectors such as the Maritime Alps (350 m) and the Dolomites (354 m), and also in the Apennines (361 m), whereas some of the inner groups like those of Monte Rosa (465 m) and Bernina (459 m) display high values. The exceptions, however, are numerous, such as the Gran Paradiso and Ortles-Cevedale with fairly limited values (282 and 251 m, respectively), despite their being characterized by a more continental climate compared to other Alpine groups. The minimum difference between ELA and RGA (96 m) was recorded for the Orobic Alps.

These exceptions may derive from numerous factors: 1) local situations of maritime climate (as in the case of the Orobic Alps); 2) the presence of permafrost at altitudes lower than those of the rock glacier fronts (the fact of this not being identified leads to an underestimate of the altitudinal difference between ELA and RGA); and 3) active rock glaciers being considered inactive (which leads to an overestimate of the ELA-RGA difference).

However, it should be emphasized that the concept of continental climate in the Italian Alps, where the distance from the sea never exceeds 300 km, is a very relative one and can be used only for local situations. Further proof of this can be had by utilizing the Gorbunov (1978) Index of Continentality (the difference

in the average height in kilometers of the equilibrium line on the glacier and the lowermost limit of permafrost). When taking as the lowermost limit of permafrost the altitude of the rock glacier fronts, the values are all below 0.6, with a minimum in the Orobic Alps of 0.1.

With regard to inactive rock glaciers, as appears from Fig. 2, the curve of their frontal altitudes follows fairly faithfully the trend of that for active ones (the difference in altitude between active and inactive rock glacier fronts averaging 285 m).

#### CLIMATIC DATA

Taking into account the experience obtained from previous research on the relationship between glacial dynamics (or rock glacier distribution) and climatic parameters, some meteorological stations were selected in ten mountain sectors. For these stations, data on average annual temperature (MAAT) for the period 1955-1985 were collected. Using a gradient of 0.6 °C/100 m, for each of the sectors average annual temperatures were calculated both at the present-day average of the active and inactive rock glacier fronts and for ELA.

The results of this calculation are synthesized in Table 2, where mountain sectors, the name and elevation of meteorological stations, and average annual temperature (in °C) measured at the stations (MAAT st) and calculated for elevation both of active (MAAT RGa) and inactive (MAAT RGi) rock glacier fronts, and for the ELA (MAAT ELA), are shown.

On the basis of the data reported in Table 2, average values are obtained of -1.5 °C for the fronts of Italian active rock glaciers, 0.3 °C for those of inactive ones, and -3.8 °C for ELA. It is shown that the value -1.5 °C falls in the interval of about -1 to -2 °C, that is supposed to represent the large-scale climatological boundary conditions for the existence of active rock glaciers (Barsch, 1978; Evin, 1983; King,

1983; Haerberli, 1985, and in press); the same isotherm of -1 to -2 °C of average air temperature should also indicate the lowermost limit of discontinuous permafrost distribution (Cheng Guodong, 1983).

#### FURTHER ELABORATIONS

From the data contained in Table 2, and with the present-day distribution of glaciers and rock glaciers on the Italian mountains, an average temperature difference of 2.3 °C can be obtained between the ELA and the active rock glacier fronts (and thus between ELA and the lowermost limit of discontinuous permafrost). The average difference between ELA and inactive rock glacier fronts is, instead, 4.1 °C, whereas that between active and inactive rock glaciers is 1.7 °C (the same values can, of course, also be obtained merely from the altitudinal data of Table 1, using the well-known formula

$$T = (E1 - E2) \cdot 0.6/100$$

where T is the difference in average annual temperature, E1 and E2 are the elevations of the two parameters in question, i.e. ELA and RGi, and where 0.6/100 is the vertical thermal gradient; the slight differences depend on the fact that in Table 2 not all the mountain groups of Table 1 have been included.

The differences between temperatures at the fronts of active and inactive rock glaciers may also infer paleoclimatic factors (Kerschner, 1985). By generically attributing the genesis of today's inactive rock glaciers to the most recent phases of Late Glacial, on the Italian mountains there would be, as mentioned previously, a mean decrease of 1.7 °C in average annual temperature, with a maximum of 2.4 °C in the Ortles-Cevedale and Adamello sectors and a minimum of 0.9 °C in the Bernina sector.

Presupposing in addition that altitude intervals between ELA and rock glacier fronts

Table 2. Thermic conditions in the Italian mountains

Mountain Sector	Meteo-Station	Elevation in m	MAAT st	MAAT RGa	MAAT RGi	MAAT ELA
Monte Bianco	Aosta	508	10.8	-1.3	0.1	-4.5
Monte Rosa	Gressoney S.J.	1400	5.3	-2.2	-0.2	-5.0
Bernina	Sondrio	307	11.1	-1.5	-0.6	-4.2
Piazzzi-Campo	Bormio	1225	7.9	-0.2	1.0	-2.2
Ortles-Ceved.	S. Caterina Valf.	1740	3.1	-3.4	-1.0	-4.9
Adamello-Pres.	Pantano	2328	0.7	-0.3	2.1	-3.1
Venoste Alps	S. Valentino	1500	3.5	-3.1	-1.8	-5.5
Noric Alps	Anterselva	1236	6.1	-2.3	0.3	-3.8
Dolomites	Cortina d'Amp.	1211	6.7	0.2	1.2	-1.9
Apennines	Isola Gr. Sasso	418	12.3	-0.4	2.0	-2.6

have not undergone significant modification, even though climatic changes have occurred, it can therefore be hypothesized that spatial relationships between ELA and altitudes of rock glacier fronts (and therefore of the lowermost limit of discontinuous permafrost) were relatively constant, and that the present-day figures for the different portions of the Alps are not very different (on a regional scale) from those of the past.

Thus, the altitude of the equilibrium line in the past (the most recent phases of Late Glacial?) can be obtained from the formula

$$ELAf = RGi + (ELAp - RGA)$$

where ELAf is the altitude of the former ELA, ELAp that of the present-day one, and RGi and RGA are those of the inactive and active rock glacier fronts.

Table 3 reports the altitudes of the former ELA, the altitudinal differences with respect to the present-day ELA (ELAp), and the thermal differences calculated with the gradient mentioned above. From this Table an average ELAf altitude of 2627 m is obtained with a mean difference of 291 m compared to that of ELAp, which corresponds to a thermal variation of 1.7 °C.

Table 3. Altitudes of the former ELA, altitudinal differences respect to the present-day ELA (ELAp), thermal differences calculated with the gradient.

Mountain sector	ELAf (m)	ELAp-ELAf (m)	ELAp-ELAf (°C)
Maritime Alps	2425	245	1.5
Cottian Alps	2723	287	1.7
Monte Bianco	2753	310	1.9
Monte Rosa	2786	326	1.9
Bernina	2720	145	0.9
Piazzzi-Campo	2724	180	1.1
Ortles-Cevedale	2683	391	2.3
Adamello-Presanella	2495	395	2.4
Venoste Alps	2789	210	1.3
Noric Alps	2442	438	2.6
Dolomites	2484	157	0.9
Central Apennines	2496	404	2.4

As a term of comparison, it may be recalled that according to Kerschner (1985) in the Tyrolean Alps during Late Egesen the ELA was lower than the current one by 350 m (in the maritime zone), 240 m (in the transitional one), and by 200 m (in the continental one).

#### CONCLUSION

In conclusion, it has been stated that along the Italian side of the Alps, the active rock glacier fronts, which should indicate the

lowermost limit of discontinuous permafrost, are on average located around an altitude of 2527 m a.s.l. (a figure slightly different from the one presented by Belloni *et al.* (1988), when the photointerpretative revision had not yet been completed), with values ranging from a minimum of 2287 m a.s.l. in the Dolomites to a maximum of 2823 m a.s.l. in the Ortles-Cevedale sector. In the Apennines, the only rock glacier classified as possibly active has a front located at an altitude of 2539 m a.s.l. (Dramis and Kotarba, *in press*). The meteorological station data yield an average annual temperature of -1.5 °C for the altitude of the active rock glacier fronts.

The average elevation of the Alpine inactive rock glaciers is 2261 m a.s.l., while that of the Apenninic fronts is 2135 m.

Altitudinal difference between the fronts of active and inactive rock glaciers, on an average 285 m, ranges from a minimum of 145 m in the Bernina sector to a maximum of 438 m in the Noric Alps.

The increase in altitude of the rock glacier belt corresponds to a rise in average annual temperature of about 1.7 °C.

The average altitude of the equilibrium line for present-day glaciers in the Italian Alps is around 2890 m a.s.l.. The altitudinal difference between present-day and former ELA in the Alps is on average slightly less than 300 m (as opposed to 404 m in the Apennines), and corresponds to a rise in the average annual temperature of about 1.7 °C.

#### ACKNOWLEDGEMENTS

The present study has been carried out in the framework of research projects undertaken by the Glaciology Section of the National Physical Geography and Geomorphology Group, with the collaboration of G.B. Castiglioni, G. Catasta, M. Guglielmin, L. La Guardia, V. Maggi, U. Mattana, M. Meneghel, A. Onorati, C. Ottone, G. Palmentola, B. Parisi, G.B. Pellegrini, M. Pelfini, P. Petruzzelli, U. Sauro, P. Sansò, C. Tellini, V. Toniello, C. Vannuzzo, C. Voltolini.

#### REFERENCES

- Barsch, D. (1977). *Alpiner Permafrost-ein Betrag zur Verbreitung, zum Charakter und zur Ökologie am Beispiel der Schweizer Alpen*. *Abhandlungen der Akademie der Wissenschaften, Göttingen, Math.-phys. Kl.*, 3, 118-141.
- Barsch, D. (1978). *Rock glaciers as indicators for permafrost. An example from the Swiss Alps*. *Proc. Third Int. Conf. on Permafrost, Ottawa, NRC, I*, 349-352.

- loni, S., Pelfini M., and Smiraglia C. (1988). Morphological features of the active rock glaciers in the Italian Alps and climatic correlations. Proc. Fifth Int. Conf. on Permafrost. Trondheim, Norway, I, 678-682.
- deroni, G., Guglielmin, M., Lozej, A. and Tellini, C. (in press). Researches on rock glaciers in the Italian Central Alps (Valtellina, Sondrio, Italy). same volume.
- ton, A., Dramis, F. and Smiraglia C. (1988). A first approach to the systematic study of the rock glaciers in the Italian Alps. Proc. Fifth Int. Conf. on Permafrost. Trondheim, Norway, I, 712-717.
- tasta, G. and Smiraglia, C. (unpublished). Data on Italian glaciers (Lombardy Alps) for World Glacier Inventory.
- eng Guodong (1983). Vertical and horizontal zonation of high-altitude permafrost. Proc. Fourth Int. Conf. on Permafrost. Washington, D.C., 136-141.
- eng Guodong and Dramis, F. (1992). Distribution of mountain permafrost and climate. Proc. Int. Workshop on Permafrost and Periglacial Environments in Mountain Areas, Interlaken, 1991. Permafrost and Periglacial Processes, 3, 83-91.
- ramis, F. and Kotarba, A. (in press). Southernmost limit of relict rock glaciers in the Central Apennines (an example from the Maiella Mountains). Permafrost and Periglacial Processes.
- evin, M. (1983). Structure et mouvement des glaciers rocheux des Alpes du Sud. Université de Grenoble I, Institut de Géographie Alpine, Thèse de 3e cycle, 343 pp.
- evin, M. (1992). Glaciers rocheux et sondages géoelectriques sur le versant nord du Viso (Alpes Cottienes, Italie). Comité National Français de Géographie, Commission pour l'Etude des Phénomènes Periglaciaux, Réunion annuelle de la Commission, 10 pp.
- Gorbunov, A.P. (1978). Permafrost investigations in high-mountain regions. Arctic and Alpine Research, 10, 283-294.
- Guglielmin, M. (1991). I rock glaciers del Passo del Foscagno (Livigno, Sondrio). Natura Bresciana. Ann. Mus. Civ. Sc. Nat. Brescia, 26, 35-47.
- Haerberli, W. (1978). Special aspects of high mountain permafrost methodology and zonation and zonation in the Alps. Proc. Third Int. Conf. on Permafrost, Ottawa, 1, 379-384.
- Haerberli, W. (1985). Creep of Mountain Permafrost: Internal Structure and Flow of Alpine Rock Glaciers. ETH, Zürich, 142 pp.
- Haerberli, W. (in press). Scientific, environmental and climatic significance of rock glaciers. Proc. 75° Congress of the Italian Geological Society, Milano, 1990.
- Kerschner, H. (1985). Quantitative palaeoclimatic inferences from lateglacial snowline, timberline and rock glaciers data, Tyrolean Alps, Austria. Proc. Symposium on Climate and Paleoclimate of Lakes, Rivers and Glaciers, Igls, 1984, Zeitschrift für Gletscherkunde und Glaziologie, 21, 363-369.
- King, L. (1983). High mountain permafrost in Scandinavia. Proc. Fourth Int. Conf. on Permafrost, Washington D.C., 612-617.
- King, L. (1986). Zonation and ecology of high mountain permafrost in Scandinavia. Geografiska Annaler, 68 A, 131-139.
- King, L., Gorbunov, A. and Evin, M. (1992). Prospecting and mapping of mountain permafrost and associated phenomena. Proc. Int. Workshop on Permafrost and Periglacial Environment in Mountain Areas, Interlaken, 1991. Permafrost and Periglacial Processes, 3, 71-72.
- Resnati, C. and Smiraglia, C. (1991). Determinazione della struttura interna del rock glacier di Val Pisella (Alta Valtellina) attraverso sondaggi elettrici verticali. Risultati e problemi. Geografia Fisica e Dinamica Quaternaria, 13, 171-177.
- Smiraglia, C. (1985). Contributo alla conoscenza dei rock glaciers delle Alpi Italiane. I rock glaciers del Monte Confinale (Alta Valtellina). Rivista Geografica Italiana, 92, 117-140.
- Smiraglia, C. (1992). Observations on the rock glaciers of Monte Emilius (Valle d'Aosta, Italy). Proc. Int. Workshop on Permafrost and Periglacial Environment in Mountain Areas, Interlaken, 1991. Permafrost and Periglacial Processes, 3, 163-168.

TIME DEPENDENT DISPLACEMENT OF PILES  
IN SALINE PERMAFROST

Kevin W. Biggar<sup>1</sup>, Elisabeth G. Hivon<sup>2</sup>, and Dave C. Segó<sup>3</sup>

<sup>1</sup>Royal Military College of Canada, Kingston, Ontario

<sup>2</sup>EBA Engineering Consultants Ltd, Edmonton, Alberta

<sup>3</sup>University of Alberta, Edmonton, Alberta

The widespread distribution of saline permafrost has only recently been acknowledged, and reduced pile capacities in saline permafrost has been an area of growing concern. Recent studies at the University of Alberta have examined the behavior of various saline frozen soils, and pile behavior in saline soils. This paper summarizes some of the results of these studies, and proposes guidelines for pile design in saline permafrost.

INTRODUCTION

Recent studies have found naturally occurring frozen soils with salts in the pore water. Gregerson *et al.* (1983) describe marine saline permafrost in Spitzbergen. A discussion on the distribution of saline permafrost in the Canadian Arctic is provided by Hivon and Segó (1991) and in the Soviet Union by Dubikov *et al.* (1988).

Reduced pile capacities in saline permafrost in Arctic communities have recently been identified as a problem (Hoggan 1985, Nixon 1988, and Miller 1990) for which there is little information available. Soviet experience (Karpov and Velli 1968, and Velli *et al.* 1973) generally provides maximum adfreeze bond capacities for different pile materials and various soils, but does not address the issue of time dependent displacement. Generally, the strength of the bond between frozen soils and the steel pile surface is dramatically reduced by the presence of dissolved solutes in the soil pore water. It appears that a film of unfrozen water may form at the interface reducing the effective frozen bond area and/or reducing the strength of the ice which has bonded. Adfreeze bond strengths are reduced by at least 50% at salinities as low as 5 ppt, by 60% to 75% at 10 ppt, and by as much as 90% at 15 ppt.

Nixon and Neukirchner (1984) provided the first design guidelines for piles in saline permafrost considering time dependent displacement, based upon constant stress test results on ice-rich saline silty sand reported by Nixon and Lem (1984). Recent work has been completed at the University of Alberta pertaining to the behavior of three different saline ice-poor frozen soils (Hivon 1991), and the behavior of model piles in one of these soils was studied by Biggar (1991). This paper will examine the time-dependent displacement of piles in ice-poor saline soil based upon the work of these two authors. It does not address the reduction in adfreeze bond strength due to salinity.

BEHAVIOR OF SALINE SOILS

Background

Ice crystals are formed of fresh water excluding impurities, such as salt ions, from the pure crystalline ice structure into the remaining unfrozen water. As the temperature decreases the salt ions are excluded into the remaining unfrozen brine, further depressing its freezing point. This process continues until the pore solution becomes a matrix of ice crystals and salt ions with no liquid brine at the eutectic temperature, which for a sodium chloride solution is  $-21.3^{\circ}\text{C}$ . This is illustrated in the phase diagram for a NaCl solution shown in Figure 1.

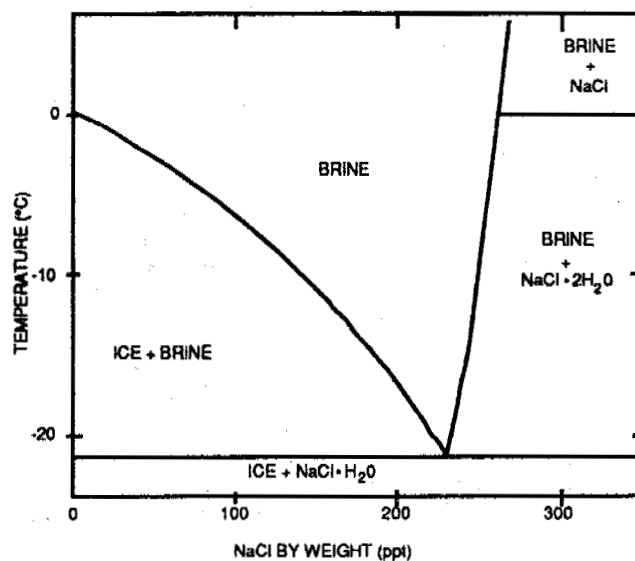


Figure 1. Sodium Chloride (NaCl) Water (H<sub>2</sub>O) Binary Phase Diagram

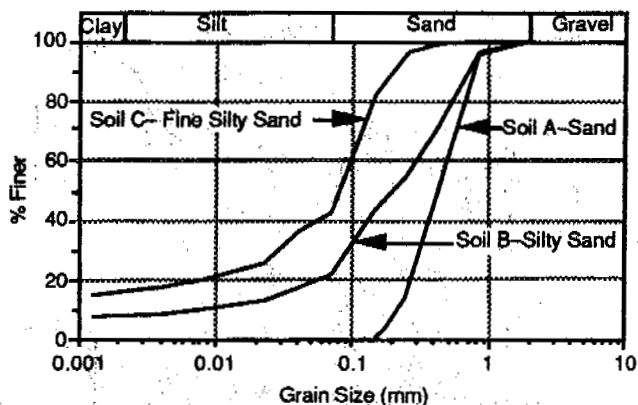


Figure 2. Grain size distribution of soils tested

At a specified temperature the unfrozen water in the pore space of frozen soils increases with the addition of dissolved solutes. The greatest compressive strength reduction has been observed in cohesionless soils at low values of salinities ( $S < 10$  ppt) due to the loss of cohesion between the ice and the soil grains (Tsytovich et al. 1973, and Sego et al. 1982). The compressive strength of saline frozen cohesionless soils have been related to the percentage of unfrozen water (Ogata et al. 1983, Nixon and Pharr 1984, and Pharr and Merwin 1985). Strength reduction is less pronounced and more gradual in cohesive soils where unfrozen water is already present in the form of adsorbed water. The relationship between unfrozen water content and unconfined compressive strength has been shown to be valid for individual soil types, but could not be applied to unify the behavior of different soil specimens (Ogata et al. 1983).

Time dependent soil deformation under constant stress is increased many times by the presence of solutes in the pore fluid. Creep strains in alluvial sand increase dramatically with increasing salinity from 0 to 10 ppt (Ogata et al. 1983). In fine-grained saline soils increases in uniaxial creep strain rates of 10 to 100 times may occur for salinities near that of sea water ( $S=30-35$  ppt) at temperatures applicable in foundation engineering (Nixon and Lem 1984).

Although creep behavior of fine-grained ice-rich saline soil has been studied by Nixon and Lem (1984), the behavior of fine-grained ice-poor saline soils has not been addressed. Work by Sayles and Haines (1974) has shown that the creep behavior of ice-poor non-saline frozen soils continues to attenuate with time as interparticle contact increases and the load is transferred to the soil particles from the ice matrix. It was desirable to determine if ice-poor saline soil would behave in the same manner.

#### Constant stress tests in ice-poor saline soils

A total of 43 unconfined constant stress compression tests were conducted to examine the time dependent deformation response of three different soils at four different salinities: a fine uniform sand (soil A), a silty sand (soil B), and a very fine silty sand (soil C) with pore water salinities of 0, 5, 10, and 30 ppt. The grain size distribution of the soils tested is shown in Figure 2. The average densities and moisture contents for soils A, B, and C

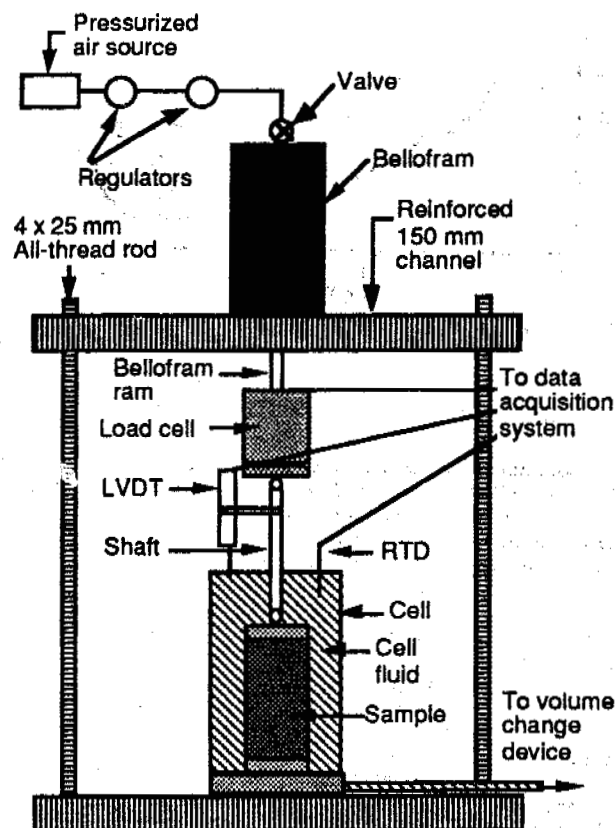


Figure 3. Schematic diagram of constant stress compression test set-up

are shown in Table 1. All tests were conducted at a temperature of  $-7^{\circ}\text{C} \pm 0.4^{\circ}\text{C}$ .

TABLE 1  
Soil average bulk densities and moisture contents

Soil	Density ( $\text{Mg}/\text{m}^3$ )	MC (%)
A	2.06	17.1
B	2.06	16.8
C	1.96	22.1

Load was applied to the 100 mm by 200 mm specimens via compressed air applied to a bellofram filled with oil. Load was measured using a load cell, displacement was measured using a linear voltage displacement transducer (LVDT), and temperature was measured with a resistance temperature device (RTD) (Figure 3). Readings of time, load, displacement and temperature were recorded on an electronic data logging apparatus.

In order to determine the time to failure (defined as the onset of an accelerating strain rate) the tests results were plotted with the strain rate versus time in log-log coordinates, illustrated in Figure 4.

The minimum strain rate is more easily defined in this manner, however some judgement and a close examination of the test data is required to determine the time of failure, particularly at times greater than 100 hours. The individual test results from the

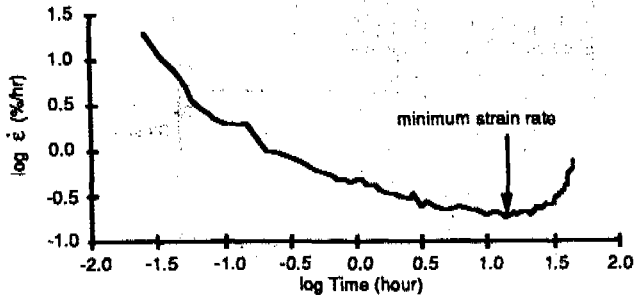


Figure 4. Typical plot of log strain rate versus log time for constant stress tests

42 constant stress compression tests are contained in Hivon (1991).

#### Model pile tests in saline ice-poor soil

A total of 65 constant load model pile tests were conducted in soil B detailed above, maintained at a temperature of  $-5^{\circ}\text{C} \pm 0.3^{\circ}\text{C}$ , using sandblasted steel pipe piles with either a clean sand or a cementitious cold temperature grout as a backfill material. Soil salinities of 0, 10 and 30 ppt were used, and test durations varied from instantaneous failure to as long as 76 days without failure.

The test cell (Figure 5) was placed in the same frame as shown in Figure 4. Load, displacement, and temperature were recorded as discussed for the constant stress compression tests. The pile displacement rate was plotted against time in log-log coordinates, and determination of the time to failure was the same as that detailed above for the constant stress compression tests. Further details of the specimen preparation, test procedures and individual test results are contained in Biggar (1991).

#### Comparison of creep parameters from constant stress and model pile tests

At the stress ranges examined in the constant stress compression tests, none of the tests displayed a constant strain rate. Either a decelerating rate followed by an accelerating rate was observed or, for soils B and C at salinities of 30 ppt, an attenuating displacement rate was displayed to accumulated strains in excess of 20%. In the model pile test program however, lower stress ranges were applied and constant displacement rates were observed. Hence a constant displacement rate formulation for pile time dependent displacement is proposed as discussed below.

A constitutive relationship to describe the constant strain rate deformation of frozen soils may be expressed as a simple power law of stress and time (after Ladanyi 1972 and Ladanyi and Johnston 1974), and may be written as:

$$\dot{\epsilon}_0 = B \sigma_0^n \quad (1)$$

where  $\epsilon_0$  and  $\sigma_0$  denote the von Mises equivalent strain and stress respectively,  $n$  is the stress exponent and  $B$  is a material and temperature dependent parameter. For uniaxial compression (1) may be modified to:

$$\dot{\epsilon}_1 = D (\sigma_1/\sigma_r)^n \quad (2)$$

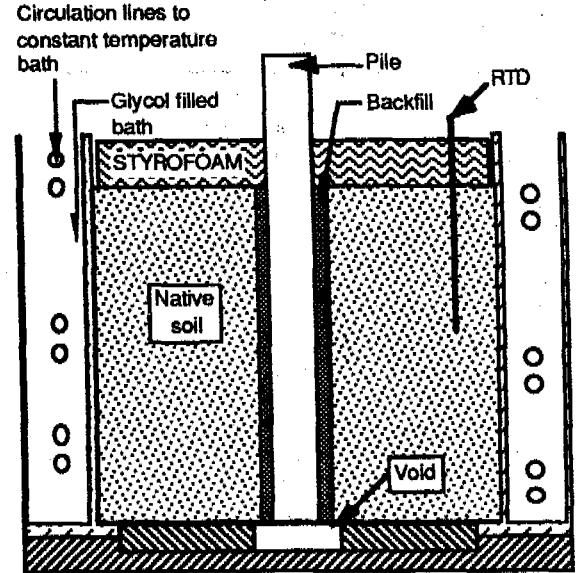


Figure 5. Constant load test apparatus for model piles

In (2) the applied stress,  $\sigma_1$ , is normalized by dividing by  $\sigma_r$ , a value of stress representative of the stress range being tested. A value of  $\sigma_r$  equal to 1000 kPa was used for the constant stress tests. The parameter  $B$  has been changed to  $D$  to reflect that it will have a different value due to the normalization of the stress term.

As previously mentioned, a constant strain rate was not observed during the constant stress tests, however a practical value which may be used is the minimum observed strain rate. Plotting the minimum observed strain rates versus the normalized stresses in log-log coordinates a linear relationship was observed, and the values  $n$  and  $D$  were determined. The variation of  $n$  with salinity for the three soils is shown in Figure 6. It can be seen that using a value of  $n=3$ , as is done for ice and non-saline ice-rich soils, is incorrect. The variation in  $\log(D)$  with salinity is shown in Figure 7.

Regression analysis of the data provided the following relationships (note the values of salinity of 0 ppt had to be omitted to calculate  $D$  since  $\log 0$  is undefined):

$$\text{Soil A} \\ n = \text{constant} = 5.2 \quad \text{for } S \neq 0 \quad (3a)$$

$$\log(D) = -3.13 + 3.11 \log(S) \quad R^2 = 0.987 \quad (4a)$$

$$\text{Soil B} \\ n = 13.8 - 0.29(S) \quad R^2 = 0.987 \quad (3b)$$

$$\log(D) = -9.39 + 7.48 \log(S) \quad R^2 = 0.987 \quad (4b)$$

$$\text{Soil C} \\ n = 23.1 - 0.69(S) \quad R^2 = 0.947 \quad (3c)$$

$$\log(D) = -11.4 + 8.98 \log(S) \quad R^2 = 0.947 \quad (4c)$$

where  $S$  is the pore water salinity in ppt. These values are valid only for the temperature of  $-7^{\circ}\text{C}$ , and the units of  $D$  are %/hour at  $\sigma_r$  equal to 1000 kPa.

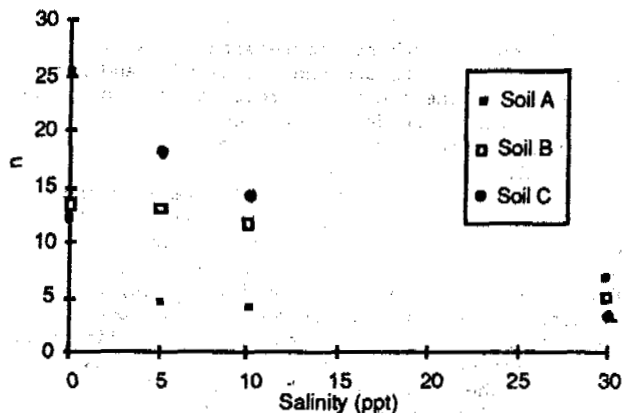


Figure 6. Flow law parameter  $n$  versus salinity

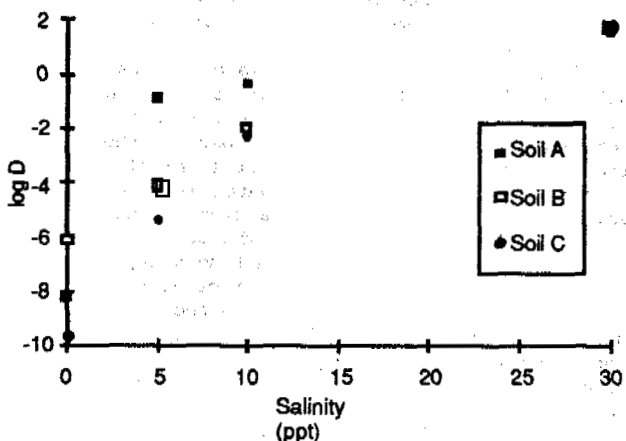


Figure 7. Flow law parameter  $D$  versus salinity

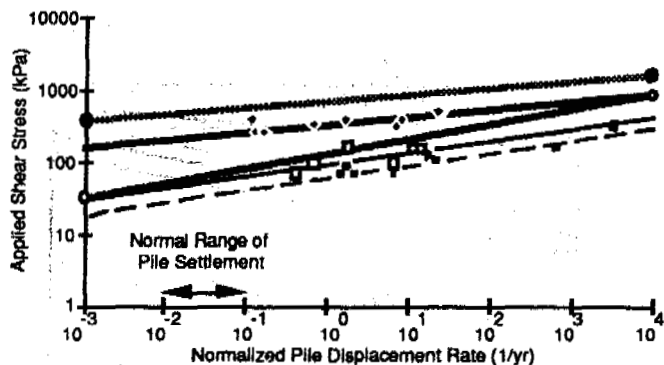
For constant displacement rate of piles, which may be encountered in ice and ice-rich permafrost (Johnston and Ladanyi 1972, Nixon and McRoberts 1976; and Morgenstern et al. 1980), (1) may be written as :

$$\frac{\dot{u}}{a} = \frac{u}{at} \frac{\sqrt{3}^{(n+1)}}{(n-1)} B \tau^n \quad (6)$$

where  $\dot{u}$  is the pile constant displacement rate which has been normalized to the pile radius,  $a$ ,  $u$  is the pile displacement,  $t$  is the time,  $\tau$  is the applied shear stress,  $n$  is the stress exponent, and  $B$  is a temperature and material dependent parameter. In this formulation the value of the stress exponent,  $n$ , is the same as that in (2). The parameter  $B$  may be related to  $D$  by:

$$B = D \sigma_r^{-n} = D(1000)^{-n} \quad (7)$$

The only model pile tests which were considered for comparison to the constant stress compression tests were those in which failure occurred at the backfill/native soil interface, as in these cases the creep of the native soil was studied and creep within the backfill material was not significant. These tests include grout backfilled piles in soil with salinities of 10 and 30 ppt, and sand backfilled piles in soils with salinities of 30 ppt. The values



Native Soil Salinity	Backfill Material	Model Pile Test Results	Model Pile Regression	Prediction from Const Stress Tests
10	Grout	◆	—	—
30	Grout	□	—	—
30	Sand	■	—	—

Figure 8. Comparison of results from model pile tests conducted in Soil B at  $-5^{\circ}\text{C}$  with predicted performance based upon constant stress tests at  $-7^{\circ}\text{C}$ .

of  $n$  and  $B$  obtained for the model pile tests in this study are contained in Table 2. In the model pile tests, as in the compression tests, the values of  $n$  also differed from 3. By comparison, the calculated values of  $n$  for 10 and 30 ppt salinity, using (3b), are 10.9 and 5.1 respectively.

TABLE 2  
Values of  $n$  and  $B$  parameters from regression analysis of model pile data

Soil Salinity	Backfill Material	$n$	$B$ ( $\text{yr}^{-1} \text{kPa}^{-n}$ )
10	Grout	9.5	$4.59 \times 10^{-26}$
30	Grout	6.1	$1.07 \times 10^{-13}$
30	Sand	5.9	$3.94 \times 10^{-12}$

Figure 8 compares the results from the model pile load test program to the predicted performance based upon the results of the constant stress compression tests, by substituting the values of  $n$ , and  $D$  from (3b) and (4b), into (7) and (6). As expected the allowable shear stress values from the model pile tests at  $-5^{\circ}\text{C}$  are lower than those predicted from the compression tests at  $-7^{\circ}\text{C}$ . For piles in ice, given a temperature decrease from  $-5^{\circ}\text{C}$  to  $-7^{\circ}\text{C}$ , the increase in allowable shear stress may be expected to be approximately 20-50% (Morgenstern et al 1980). For fine-grained ice-rich soil at 35 ppt salinity, the allowable shear stress may increase by approximately 100-200% for the same temperature decrease (Nixon and Neukirchner 1984). Over the stress range tested, at a salinity of 10 ppt the predicted allowable shear stress at  $-7^{\circ}\text{C}$  is approximately 100% greater than that observed at  $-5^{\circ}\text{C}$ , which is slightly greater than expected therefore unconservative. At a salinity of 30 ppt, the predicted allowable shear stress at  $-7^{\circ}\text{C}$  is approximately 50-100% greater than that observed at  $-5^{\circ}\text{C}$ , which is less than expected therefore conservative.

At displacement rates similar to those which may be tolerated under field conditions, at a salinity of 10 ppt there is little change in the relative



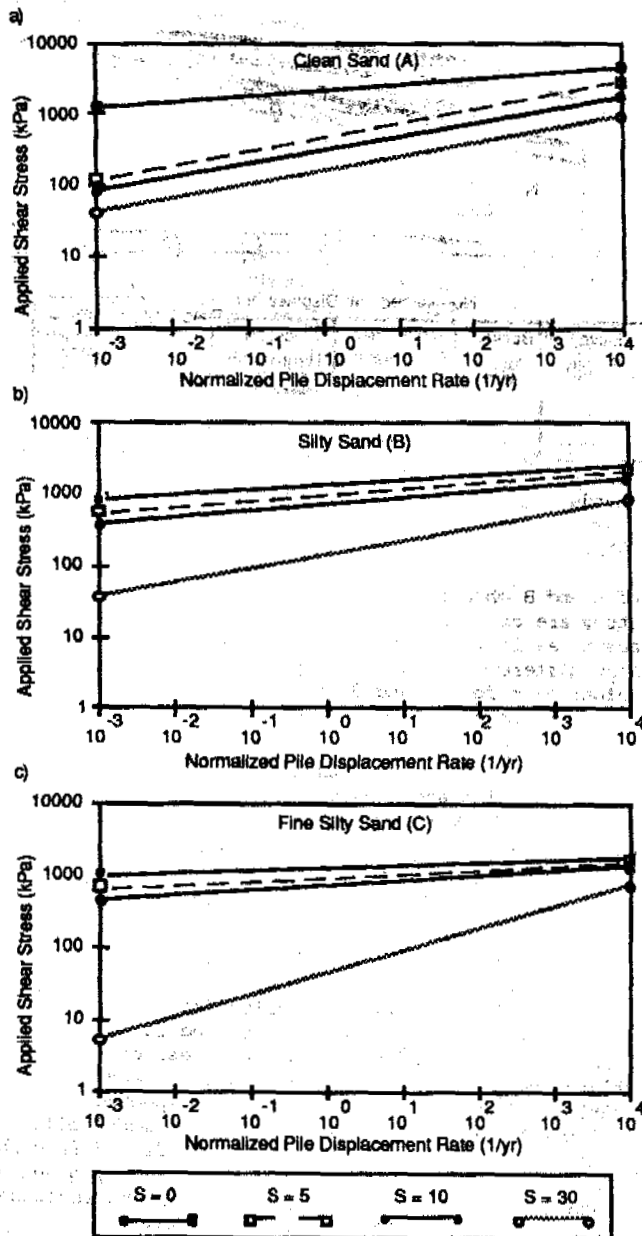


Figure 9. Applied shear stress versus normalized pile displacement rate for piles in soils with salinities (S) of 0, 5, 10, and 30 ppt. at a temperature of  $-7^{\circ}\text{C}$

- a) Clean sand (Soil A)
- b) Silty sand (Soil B)
- c) Fine silty sand (Soil C).

difference in allowable shear stress based on the two different tests due to the large value of  $n$ . At a salinity of 30 ppt however, due to the difference in the values of  $n$ , the allowable shear stresses predicted by the two different tests converge, and are nearly equal.

Considering the difference in testing methodology, the similarities in the predicted pile behavior is reasonable. This lends credence to the formulation in (6) to predict pile behavior based

upon the constant stress compression tests. It is therefore proposed to use the values of  $n$  and  $D$  from the results of the constant stress compression tests to predict time dependent displacement of piles in the three different saline soils tested.

#### Proposed Design Guidelines

Figure 9 shows the relationships between the normalized pile displacement and the applied shear stress for the three different soils tested, using the values of  $n$  and  $D$  from (3) and (4) in (7) and (6). Unlike most previously published work, the lines for different salinities are not parallel because the slope of the line ( $1/n$ ) increases as the salinity of the soil increases for the silty soils. At lower salinities the values of  $n$  are large so the normalized displacement is not highly dependent on the applied stress. At salinities of 30 ppt the value of  $n$  approaches that for ice ( $n=3$ ), and the normalized displacement is highly dependent on the applied stress.

It is seen that there is a large decrease in the pile capacity for the clean sand (soil A) when the salinity increases from 0 to 5 ppt. This is anticipated, as discussed above, because the change from an absence of unfrozen water (non-saline sand) to a small amount of unfrozen water (sand at a salinity of 5 ppt) results in a significant decrease in the ice-sand bond strength. The decrease in pile capacity for the silty sand and fine silty sand (soils B and C) as the salinity increases from 0 to 5 ppt is much less pronounced due to the presence of unfrozen water at a salinity of 0 ppt. For soils B and C the most dramatic decrease in resistance is observed when the salinity increases from 10 to 30 ppt.

#### CONCLUSIONS

The results from constant stress compression tests and model pile tests on ice-poor saline soil have shown that it is inappropriate to use a constant value of the stress exponent,  $n$ . The value of  $n$  has been shown to decrease with increasing salinity, and approaches the value used for design in ice-rich soils ( $n=3$ ) as soil salinities approach 30 ppt.

Large reductions in pile capacity can be expected in sandy soils with values of salinity as low as 5 ppt. The reduction in pile capacity in silty sandy soil is less marked at low salinities because unfrozen water is already present at zero salinity.

At salinities of 30 ppt (similar to sea water) the allowable applied shear stress is very low for the normal range of acceptable pile settlements for foundation design for ice-poor soils.

#### REFERENCES

- Biggar, K.W. (1991) Adfreeze and grouted piles in saline permafrost. Unpublished Ph D. Thesis, University of Alberta, Edmonton, Alberta, p. 342.
- Dubikov, G.I. et al. 1988. Pore solutions of frozen ground and its properties. Proc., 5th International Conference on Permafrost, Trondheim, Norway, pp. 333-338.
- Gregerson, O., Phukan, A., and Johansen, T. 1983. Engineering properties and foundation design alternatives in marine Svea clay, Svalbard. Proc., 4th International Conference on Permafrost, Fairbanks Alaska, USA, pp. 384-279.

- Hivon, E.G. and Segó, D.C. 1991. Distribution of saline permafrost in the Northwest Territories. Proc., 44th Canadian Geotechnical Conference, Sept 29 - Oct 2, Calgary, pp. 38-1 to 38-10.
- Hivon, E.G. 1991. Behavior of saline frozen soils. Unpublished Ph D. Thesis, University of Alberta, Edmonton, Alberta, p. 435.
- Hoggan Engineering and Testing (1980) Ltd. 1985. Pile load tests, Arctic Bay multi-purpose hall and school extension, report submitted to the Department of Public Works, Government of the Northwest Territories.
- Ladanyi, B. 1972. An engineering theory of creep in frozen soils. Can. Geotech. J., 9: pp. 63-80.
- Johnston, G.H., and Ladanyi, B. 1972. Field tests on grouted rod anchors in permafrost, Canadian Geotechnical Journal. 9: 176-194
- Ladanyi, B. and Johnston, G.H. 1974. Behavior of circular footings and plate anchors embedded in permafrost. Can. Geotech. J., 11: 531-553.
- Karpov, V., and Velli, Y. 1968. Displacement resistance of frozen saline soils. Soil Mechanics and Foundation Engineering (English Translation), 4(July/August): pp.277-279.
- Miller, D.L. and Johnson, L.A. 1990. Pile settlement in saline permafrost: a case history. Proc., 5th Canadian Permafrost Conference. Quebec City, Quebec, pp. 371-378.
- Morgenstern, N.R., Roggensack, W.D., and Weaver, J.S. 1980. The behavior of friction piles in ice and ice-rich soils. Can. Geotech. J., 17: pp. 405-415.
- Nixon, J.F. 1988. Pile load tests in saline permafrost at Clyde River, Northwest Territories, Can. Geotech. J., 25: pp. 24-31.
- Nixon, J.F., and Lem, G. 1984. Creep and strength testing of frozen saline fine-grained soils. Can. Geotech. J., 21: pp. 518-529.
- Nixon, J.F., and McRoberts, E.C. 1976. A design approach for pile foundations in permafrost. Can. Geotech. J., 13: pp. 40-57.
- Nixon, J.F., and Neukirchner, R.J. 1984. Design of vertical and laterally loaded piles in saline permafrost. Proc., 3rd International Specialty Conference on Cold Regions Engineering, Edmonton, Alberta, CSCE, 1-6 April, pp. 131-144.
- Nixon, M.S. and Pharr, G.M. 1984. The effects of temperature, stress and salinity on the creep of frozen soil. Transactions of the ASME Journal of Energy Resources Technology, 106: pp. 344-348.
- Ogata, N., Yasuda, M. and Kataoka, T. 1983. Effects of salt concentration on strength and creep behavior of artificially frozen soils. Cold Regions Science and Technology, 8: pp 139-153.
- Pharr, G.M. and Merwin, J.E. 1985. Effects of brine content on the strength of frozen Ottawa sand. Cold Regions Science and Technology, 11: pp 205-212.
- Sayles, F.H., and Haines, D. 1974. Creep of frozen silt and clay. US Army Cold Regions Research and Engineering Lab, Hanover, New, Hampshire, Technical Report 252, p. 51.
- Segó, D.C., Schultz, T., and Banasch, R. 1982. Strength and deformation behavior of frozen saline sand. Proc., 3rd International Symposium on Ground Freezing, Hanover, New Hampshire, pp. 11-19.
- Tsyтовich, N.A., Kronik, Y.A., Markin, K.F., Aksenov, V.I., and Samuel'son, M.V. 1973. Physical and mechanical properties of saline soils. Proc., 2nd International Conference on Permafrost, USSR Contribution, Yakutsk, USSR, pp. 238-247.
- Velli, Y.Y., Lenzniep, and Karpunia, A.A. 1973. Saline permafrost as bearing ground for construction. Proc., 2nd International Conference on Permafrost, USSR Contribution, Yakutsk, USSR, pp. 545-550.

## SUDDEN DRAINAGE OF A THAW LAKE ON THE ALASKAN ARCTIC COASTAL PLAIN

M.C. Brewer<sup>1</sup>, L.D. Carter<sup>1</sup>, R. Glenn<sup>2</sup>

<sup>1</sup> U.S. Geological Survey, 4200 University Drive,

<sup>2</sup> Arctic Slope Consulting Group, P.O. Box 6

<sup>3</sup> University of Alaska Museum, 907 Yukon Drive,

The sudden natural drainage of a small, 5-meter-d local interest in the possibility that the drainage warming effects in ice-rich, continuous permafrost possibility seemed strengthened by reports that warm, as well as unusually wet in some areas. The lake drainage had been very rapid, eroding a new deep as 10 m. Exposures of longitudinal sections indicate that the erosion occurred along a system most likely immediate cause of the sudden drainage rainfall during July and August, which apparent a swale at the north end of the lake. Subsequent wedge troughs in the swale resulted in rapid eroded frozen sediments. Lake drainage by this mechanism cycle on the Arctic Coastal Plain in Canada, has been described. If the climate were to become warmer, it might become more frequent.

### INTRODUCTION

The disturbance of arctic Alaskan tundra terrain, its potential for recovery, and the degradation of the underlying permafrost have generated considerable controversy in recent years. Generally, the discussions have involved disturbances caused by people and equipment in the course of road and pipeline construction and oilfield development, rather than modification of the terrain by natural processes. The importance of these natural processes, and of variations in their rates, has been recently emphasized by concern over the possibility of global warming and what its effects might be on permafrost and arctic tundra. Of particular importance are those natural processes involved in the formation and drainage of thaw lakes (the thaw lake cycle of Britton, 1967), which are among the most conspicuous landscape features of the Arctic Coastal Plain. At elevations less than about 100 m, these lakes may occupy from 15 to more than 50 percent of the coastal plain between the Sagavanirktok (148° W.) and Utukok (162.5° W.) rivers in Alaska. On the Tuktoyaktuk Peninsula in Canada, thaw lakes drained at the rate of about 2 per year during the period 1950-1986 (Mackay, 1988); and at least 10 lakes drained during the summer of 1989 in the Prudhoe Bay area, Alaska (R.D. Reger, Alaska Division of Geological and Geophysical Surveys, oral commun., 1989). In spite of these frequent occurrences, lake drainage rarely has been witnessed, and only a few published descriptions exist of recently drained lake basins and of the mechanisms and effects of their drainage (Mackay, 1988 and references therein).

Thus, the North Slope Borough's Department of Wildlife Management noted with much interest the sudden natural drainage, in the late summer of 1989, of a small but relatively deep (5 m)

lake that eroded a 10-meter-deep gully in permafrost. That Department arranged for a field inspection of the drained lake basin, the eroded gully, and the immediate surroundings by a group of scientists on 19 September, prior to the area being obscured by snow, and more importantly, prior to any modifications that might be caused by runoff waters the following spring during breakup. This note presents the results of that examination, and the rationale for the authors' interpretation that the most likely immediate cause of the lake drainage was unusually high rainfall during July and August. We discuss the implications of this for the lake-dotted wetlands of the Arctic Coastal Plain if the regional climate were to become warmer, as predicted by some scenarios for global warming.

### REGIONAL SETTING

The drained lake, at 69°48.2'N, 155°31.5'W and 1.3 km north of East Oumalik Test Well No. 1 (Fig. 1), is located in the southernmost portion of the Arctic Coastal Plain Province (Wahrhaftig, 1965), and is within the zone of continuous permafrost (Ferrians, 1965). By extrapolating from temperature data (Lachenbruch et al., 1987) obtained from wells at similar latitude and not too distant from the lake, it would appear that the permafrost thickness in the area is approximately 300 m. The drained lake is in an area with fewer lakes and greater relief than the coastal plain a few kilometers to the north and to the east and is characterized by broad, gently rolling, concordant interfluvial elevations of up to 90 m that separate terraced valleys with floors as much as 50 m below the interfluvial crests. A number of large, flat-floored thermokarst basins as deep as 20 m have developed on the interfluvial crests as a result of melting of syngenetic ice wedges, which formed as wind-blown silt (loess)

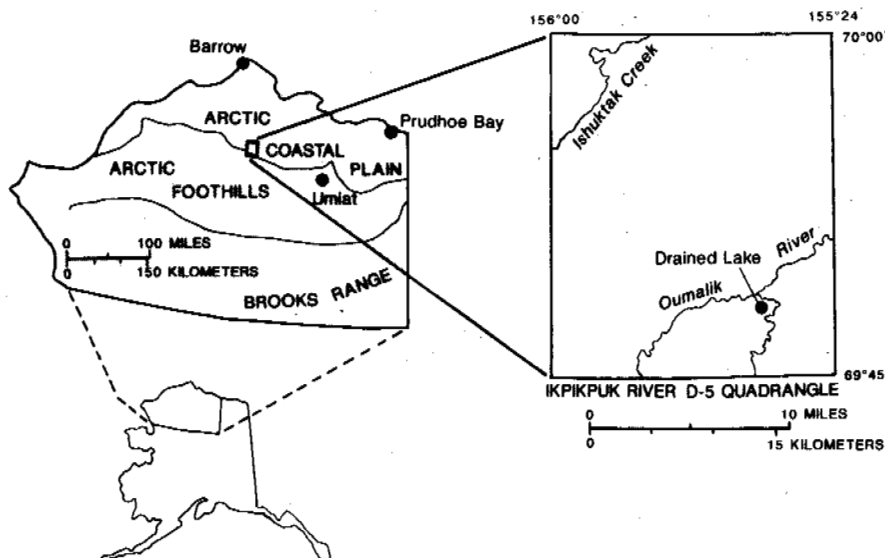


Figure 1. Location of the drained lake and other features mentioned in the text.

accumulated during the last glacial cycle (Carter, 1988). The loess is locally more than 30 m thick, and, in the vicinity of the drained lake, probably rests on bedrock (Lawson, 1986). Sand beds occur locally within the silt, and were most likely derived from sandstone exposed to the south of the loess and deposited by north-flowing streams as the loess accumulated. The loess was called the foothill silt by O'Sullivan (1961), included in the Gubik Formation by Black (1964), and more recently included within map units called "upland silt" by several authors (Carter and Galloway, 1988).

The surface pattern of ice-wedge polygons is subdued but typical of tussock-covered tundra areas on the Arctic Slope. A relatively large older basin, tundra-covered and exhibiting the deeply incised outlet of a lake that also was suddenly drained, occurs about 1 km southeast of the site. The meandering south fork of the Oumalik River, into which the lake water rushed, passes within 315 m of the northern bank of the drained lake.

The essentially continuous vegetation of this low rolling landscape is dominated by tussock tundra, typical of such settings all across the Arctic Slope of northern Alaska. The tussock-forming sedge *Eriophorum vaginatum* L. is the primary species, and gives the vegetation its characteristic form and texture. Additionally, there are several shrub species and a number of forbs. The willow *Salix pulchra* Cham. is locally prominent. Tussock tundra is absent on the summits, in swales, and along the river margins where it is replaced, respectively, by grass-sedge-forb communities, sedge mats of *Carex aquatilis* Wahlenb., and thickets of willows in which *Salix pulchra* is dominant.

#### DESCRIPTION OF THE LAKE SITE

The lake basin occupies the central, flat-floored part of a swale that transects an interfluvium. The basin is oval-shaped with a width of about 160 m and a north-trending long axis of about 235 m (Fig. 2). Rather pronounced, parallel, vegetated, east-west

trending troughs, on the order of 2 m in depth, extend as much as 60 m away from the lake bank on the western side, suggesting the possibility that gradual headward thermal erosion of the underlying ice wedges is occurring. Similar parallel troughs are present, but not nearly as pronounced, on the eastern bank of the lake. The wind-protected troughs contain willows as much as a meter tall.

The lake bed slopes gently to a relatively flat central area that occupies about 80 percent of the basin and is approximately 5 m below the former shoreline. Relief on the central deep consists of broad mounds about 10 m in diameter separated by troughs about 2 m wide and 1 m deep that form a pronounced polygonal pattern. This pattern suggests the former presence of ice wedges, which could not have formed beneath the recently drained lake because it was too deep to freeze to the bottom. The troughs could indicate that deeper parts of the syngenetic ice wedges that underlie this region had not completely melted prior to lake drainage.

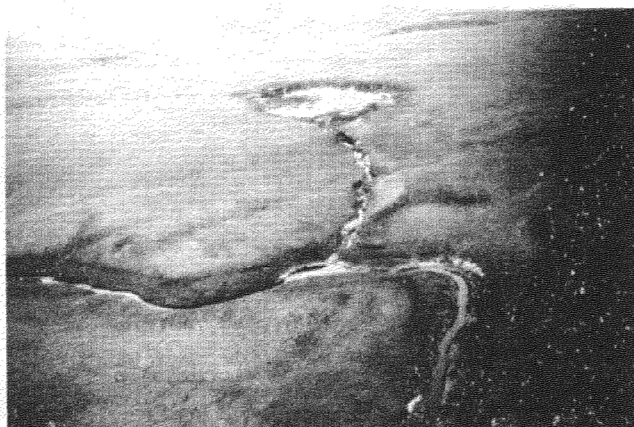


Figure 2. Aerial view of the drained lake basin and the gully cut during drainage.

Channels as much as 5 m deep in the northern portion of the basin formed during drainage of the lake. On 19 September, the slope was lightly frost-encrusted, while portions of the central basin had a thin skin of snow-covered ice overlying the ponded areas. The shallow shelf, out to a previous water depth of about 1 m, had remnants of rooted vegetation; scattered small tussock-sized clumps, primarily of mud-encrusted organic material, were found between the 1 and 1.5-m depths. Desiccation cracks, to a depth of about 15 cm and enclosing soil blocks about 30 cm in the longer direction, extended over portions of the shelf to depths of about 1.5 m below the original lake surface. Unfrozen, undrained, low-bearing capacity, highly-organic sediments extended beyond that point. These lacustrine sediments may be no more than a few meters thick, since the mounds on the basin floor appear to reflect the pattern of ice wedge polygons that were present prior to lake formation. Immediately south of the lake, high-centered, ice-wedge polygons are well developed on the floor of the broad swale in which the lake developed.

The depth of the thaw bulb beneath the bottom of the central portion of the basin would be subject to numerous variables, including the length of time the lake had existed with water depths greater than 2 m, the ice content of the sediments predating formation of the lake, and the degree of inhomogeneity of those sediments. However, a maximum thaw bulb depth on the order of 30 to 50 m, as measured from the water surface before lake drainage, would be a reasonable estimate. This estimate is based on information from Lachenbruch's (1957a) paper on heat conduction in permafrost beneath heated buildings, his calculations concerning the thermal effects of the ocean on permafrost (Lachenbruch, 1957b), and on the temperature measurements obtained from beneath Imikpuk Lake near Barrow (Brewer, 1958). In the latter instance, a measured thaw bulb depth of 57.8 m from the water surface was found where the water depth was 2.6 m, about 130 m basinward of the 2-m depth contour. The difference in depths of the two lakes would not be expected to cause significant differences in average water temperatures at the bottom, or in the thickness of the resulting thaw bulbs. However, the smaller size of the drained lake (60-65 m from the 2-m depth contour to its center), and its possibly younger age than Imikpuk, would be expected to provide a somewhat shallower thaw bulb.

#### DESCRIPTION OF THE DRAINAGE CHANNEL

Erosion during lake drainage cut an essentially straight gully about 315 m long down the axis of the swale between the former lake and the south fork of the Oumalik River. The gully is about 30 m wide where it leaves the basin, but it narrows quickly to a width of 2 to 5 m. Shortly beyond the basin the gully reaches its maximum depth of 10 m and then shallows as the ground surface slopes downward. The headward 3/4 of the gully has nearly vertical walls with tundra-capped overhangs as much as 1 m across. The overhangs locally have collapsed, obscuring the gully floor and walls. Undercut niches occur at the bases of exposed ice masses in the deeper and commonly narrower portions of the channel. No measurements were

obtained for the thickness of the thawed layer, which was at its maximum depth for the year. From the location of icicles hanging along the channel walls, which elsewhere have been observed to coincide with the base of thaw at the time of freeze up, and from the depth to the tops of the highest ice wedges, which provides a maximum depth of the active layer (Fig. 3), it would appear that the depth of seasonal thaw varies between 50 and 60 cm. This depth is about that to be expected in vegetated areas at this distance inland, and it is consistent with observations at the nearby East Oumalik wellsite on 26 July 1978 (Lawson, 1982).

About 250 m downslope from the head of the gully, a portion of the 20 to 50-cm thick tundra mat and the subjacent sediment remains intact across the subsurface channel eroded during drainage. Tundra plants on this surface are bent downstream, showing that flow occurred both above and below the mat. The depth of flow across this surface probably was at least 1 m, the maximum height of the bushes, because silt was left clinging to the highest leaves. Immediately downstream, blocks of the tundra mat and attached sediment rest where they collapsed into the channel.

At the gully terminus and for about 100 m down the south fork of the Oumalik River, willow shrubs and other tundra plants as much as 3.2 m above river level were coated with silt, and bent downstream by the force of the flow. Lake drainage must have been rapid to produce such a rise in water level. Remarkably little sediment was deposited by the floodwaters at the terminus of the gully and along the river, considering the size of the gully excavated during lake drainage.

Ground ice and frozen silt and sand are well exposed in the gully walls. Organic remains consist of rootlets in the silt and coarser plant material in the upper meter or so of the sediments. An occasional exposure of a deep pocket of organic material suggests the encroachment of organics into and the consequent filling of ponds or potholes.

Sediment exposed in the gully walls is predominantly silt, but a considerable amount

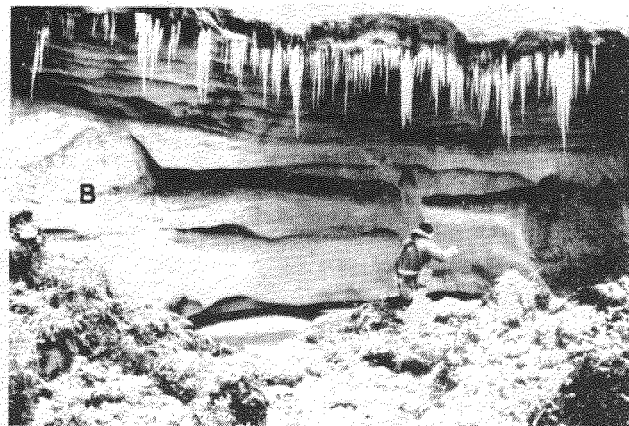


Figure 3. Gully wall composed of ice-wedge ice (A), and silt (B), with an overhang consisting mostly of tundra. Niche at base of gully formed by undercutting during drainage of the lake.

of sand is also present. The silt was initially deposited as loess (Carter, 1988), but much of it may have been redeposited in ponds in the swale or by a stream. The sand exhibits trough cross-bedding and was most likely deposited by a through-flowing stream, because the only source of sand during deposition of the loess was to the south in the foothills.

Extensive sections of the gully walls, except for the active layer, are composed completely of ice-wedge ice (Fig. 3). These walls are clearly longitudinal sections along large ice wedges. Some ice wedges may be syngenetic, as determined for other sites in the loess (Carter, 1988), and there are at least two generations of ice wedges exposed here. Laterally extensive buried ice masses with horizontal tops were observed, but their bases were not exposed. These are most likely also ice wedges, although Lawson (1983) has reported a large ice sill at the nearby East Oumalik wellsite.

Large volumes of ice in the gully walls are not surprising. Williams and Yeend (1979) calculated a total ice volume of 78% for a 20 m-high exposure along the Topagoruk River near the inner edge of the coastal plain, about 35 km northwest of the gully. This is in general agreement with an estimate by Livingstone et al. (1958) of 68% by volume in loess about 4 km east of the gully. Lawson (1982) measured ice volumes of 40 to nearly 100%, with a mean of 85%, in samples obtained by drilling in the East Oumalik area, 1.3 km south of the gully. He estimated that large ice lenses and ice wedges compose 60% by volume of the upper 10 m of upland permafrost.

#### TIME AND RAPIDITY OF DRAINAGE

During discussions with North Slope Borough pilots, it was learned that the drained lake was first noted on 1 September, a bright sunny day. The pilots were attracted to the lake, a very minor feature on a coastal plain dotted with many larger lakes, by its "glistening and shiny" appearance. Such an "appearance" is indicative of water saturation at the surface for very fine or silty sand. Considering the surface materials, the degree of slope in the shallower portion of the lake bottom, its small size, and the fact that it was a sunny day, which would result in rapid evaporation, one would not expect that a shiny or glistening appearance would prevail for more than a few hours. Thus the lake probably drained only hours earlier. Further credence for this interpretation is provided by Tom Albert's memorandum of 11 September in which he states that, when he visited the site on 8 September (7 days after the discovery), "drainage occurred long enough ago that the mud on the lake bottom dried out to the extent that some cracking has occurred" (i.e., desiccation cracks).

Rapid drainage is suggested by evidence for a large, transient increase in the water level of the south fork of the Oumalik River. This evidence consists of silt-covered, deformed willows 3.2 m above river level found immediately downstream from, but not upstream from, the gully. Sudden drainage is also suggested by the generally vertical gully walls and the undercut niches. Major slumping does not appear to have occurred until after the

gully was cut to its full depth, which implies that cutting of the gully was very rapid. The length of time required to drain the lake down to the point where the outflow was reduced to a modest trickle and to cut the channel observed, probably did not exceed a few hours once the organic mat over its pathway was broken. This conclusion is based on accounts of lake drainage in Canada (Mackay, 1981, 1988), observations by John B. O'Sullivan (oral communication, 1963) of a lake that drained into the Meade River south of Barrow about 1963, observations by Adam Leavitt about drainage of a large lake elsewhere on the Alaskan Arctic Coastal Plain in 1930 (R. Gal, U.S. Park Service, written commun., 1985) and personal observations concerning the annual spring drawdowns and channel cutting at Middle Salt Lagoon near Barrow. The latter drawdown occurs overnight, even though the lagoon has about 50 times the surface area of the drained lake; there is less massive ice in the involved sediments; and the head at the lagoon is usually less than 2 m compared to the perhaps 15-m head between the lake surface, before drainage, and the nearby stream.

#### CAUSE AND MECHANISM OF DRAINAGE

According to Mackay (1988), sudden lake drainage is usually associated with the erosion of a channel along interconnecting ice wedge systems. The longitudinal sections of ice wedges exposed in the gully walls suggest that this was indeed what had occurred. Furthermore, erosion primarily of ice would explain why so little sediment was deposited in and along the nearby stream during lake drainage. This erosion could have been initiated by either a lowering of the surface of an ice-wedge trough at the lake margin to below lake level by thermal degradation of the underlying ice, or by the overtopping of an ice-wedge trough by higher-than-normal lake levels. Thus, lake drainage could have been initiated by conditions that were either warmer or wetter than normal.

Weather records are available only for two distant localities: Barrow, a coastal environment 150 km to the north, and Umiat, an inland foothills site 120 km east-southeast of the drained lake. As mentioned in Dr. Albert's memorandum of 11 September, "this summer has seemed both warmer and wetter than usual." The weather records for Barrow support Dr. Albert's observations. The degree days above freezing for the June-August period established a new record (563 centigrade degree days, about double the average and about 20 percent greater than for the particularly warm summers of 1951 and 1954), with the July and August temperatures averaging 3.7 and 4.9°C, respectively, above average. Summer precipitation (13.3 cm) was 2.4 times average, with the month of July setting a new record for rainfall of 8.2 cm, 3.7 times the monthly average. However, the weather records for Umiat show a total June-August precipitation of only 2.5 cm, which is believed to be below normal, whereas the July and August average temperatures were 1.6 and 3.3°C above average.

These records reflect the highly variable character of rainfall across the Arctic Slope, but do not provide any direct indication of summer rainfall at the drained lake site during

Table 1. Thaw indices and some maximum depths of thaw, beneath various surface environments, during warm and cool summers near Barrow, Alaska. USGS Arctic Ice and Permafrost Project.

Surface Environment	Year, Thaw Index (centigrade degree days), and Maximum Depth of Thaw (cm)			
	1953 cool, 186 degree days	1954 warm, 474 degree days	1956 cool, 122 degree days	1957 warm, 324 degree days
1. Grass-covered, flat-lying, moist tundra	38.1	47.8	---	---
2. Red grass-covered, ponded, low-centered polygon	27.2	34.3	25.4	33.0
3. Sphagnum-covered, flat-lying, very wet meadow	29.2	26.7	28.7	28.7
4. Unvegetated pea gravel, well-drained beach	---	---	79.2	100.8
5. Bare, silt-covered, recently drained, shallow lake bed	63.5	64.8	*66.0	*94.5
6. Grass-covered, well-drained, high-centered polygon	29.7	38.1	39.9	*52.1
7. Grass-covered, wet trough adjacent to high-centered polygon	36.7	---	---	**35.6

\*Wet surface 1956, dry surface 1957

\*\*1958, warm summer, 384°C days above freezing

1989. They indicate, however, that the summer of 1989 was warmer than normal. Nevertheless, we do not believe that warmer temperatures resulted in significant degradation of ground ice and lowering of the swale surface for two reasons: (1) observations of the ground surface and gully walls during our investigation, and (2) past observations of the effects of summer temperature variations on the depths of seasonal thaw near Barrow.

1. Thermal degradation of ice wedges causes irregular subsidence of the ground surface, and had it occurred during 1989, it should have been relatively widespread. No subsidence due to recent ice wedge degradation was observed in the vicinity of the drained lake, and no evidence of thermal degradation of ground ice was observed in the gully walls. Furthermore, the active layer was not unusually deep for this type of environment.

2. Temperature data (unpublished) from the Barrow area, accompanied by thaw depth measurements determined by probing, were obtained for a number of surface/subsurface environments by the Geological Survey's Arctic Ice and Permafrost Project in the 1950s. That was a decade that included several unusually warm summers (1951, 1954, 1957, and 1958) and three unusually cool summers (1953, 1955, and 1956). The June-August precipitation during that 10-year period departed remarkably little from "normal". Table 1 provides the cumulative centigrade degree days above freezing (thaw index) for the summers for two of the warm and two of the cool summers, with the corresponding maximum depths of thaw beneath various surface environments. Several general conclusions, useful in evaluating potential parameters in the drainage of the lake under discussion, are suggested by these data:

a. Year-to-year changes in the depths of thaw in generally breezy arctic environments

appear to be far more responsive to changes in composition of the surface cover, soil moisture content, and to evaporative cooling than to major changes in the average summer air temperatures.

b. The maximum depth of thaw was (and is) only modestly affected by large changes (doubling or tripling) of the cumulative degree days above freezing (thaw index) in vegetated, permanently-saturated soils with water at or very near the surface, including the wet troughs above ice wedges.

It is thus concluded that a warmer-than-normal summer was not the cause of the sudden drainage of the lake. Overtopping of an ice-wedge trough by a higher-than-normal lake level therefore would appear to be the most likely cause. This agrees with Mackay's (1988) observation that erosion along an ice-wedge system is generally associated with high lake levels during the snowmelt period or following heavy summer rains. At this locality, drainage occurred long after the snowmelt period, and evidence suggests that erosion was initiated by a rise in lake level produced by heavy, late-summer rains.

The former shoreline is clear and distinct as there is an abrupt change in vegetation from tussock tundra to mats of the sedge *Carex aquatilis*, emergent aquatics such as *Arctophila fulva* (Trin.) Anders. and *Hippuris vulgaris* L., and dense growths of the moss *Drepanocladus brevifolius* (Lindb.) Warnst. (determined by Barbara M. Murray, University of Alaska Museum, Fairbanks). Not only do these plants mark the shoreline, but also they indicate that water levels had been stable for a very long time prior to lake drainage. The increase in the water level that led to failure of the impoundment is not recorded by the vegetation above the shoreline, hence the increase was probably both rapid and transient.

## CONCLUSION

The sudden draining of this thaw lake, and the drainage of several lakes in the Prudhoe Bay area during the summer of 1989, aroused local interest in the possibility that the drainings could be a manifestation of the type of global warming predicted for the Arctic by many climatologists and climate modelers. Those predictions are based on general circulation models of the atmosphere that suggest the presently increasing concentrations of radiatively active gases will intensify the "greenhouse effect" and produce global climatic warming (Ramanathan, 1988), including changes in precipitation. Predicted precipitation increases for northern Alaska range from 10 to 40 percent, depending upon the circulation model used (Etkin, 1990), and could lead to generally higher lake levels and more frequent lake drainage via rapid cutting of an outlet along an ice-wedge system between lakes, or between a lake and a stream such as occurred at the drained lake discussed herein. Furthermore, increased precipitation could result in increased stream discharge and thus increased bank erosion. That could also increase the rate of sudden lake drainage by breaching barriers between streams and thaw lakes, or by exposing, and thereby causing to melt, ice wedges that extend to adjacent thaw-lake basins. Of the lakes that drained in the summer of 1989 in the Prudhoe Bay area, one was drained by lake waters eroding an ice wedge and at least two were triggered by stream erosion (R.D. Reger, Alaska Division of Geological and Geophysical Surveys, oral commun., 1989). The drained lake described in this paper, and at least some of the lakes that drained in the Prudhoe Bay area thus resulted from processes that could be expected to become more frequent as a result of global climatic change. However, there is as yet no evidence to determine if the unusually large number of lakes that drained in 1989 is the beginning of a long-term trend or the consequence of an isolated, unusually wet summer.

## ACKNOWLEDGEMENTS

The authors wish to acknowledge the assistance and information provided by Dr. Thomas Albert, by Borough pilots Charles Caldwell, Randy Crosby, and Price Brower, and to thank the North Slope Borough for the logistical support provided.

## REFERENCES

- Black, R.F. (1964) Gubik Formation of Quaternary age in northern Alaska. U.S. Geological Survey Professional Paper 302-C. p. 59-91.
- Brewer, M.C. (1958) Some results of geothermal investigations of permafrost in northern Alaska. Transactions, American Geophysical Union 39, 19-26.
- Britton, M.E. (1967) Vegetation of the arctic tundra, in Hansen, H.P., ed., Arctic Biology (second edition). Corvallis, Oregon State University Press. p. 67-113.
- Carter, L.D. (1988) Loess and deep thermokarst basins in arctic Alaska, in Proceedings Fifth International Conference on Permafrost. Trondheim, Tapir Publishers. p. 706-711.
- Carter, L.D. and J.P. Galloway (1988) Engineering-geologic maps of northern Alaska, Ikpikpuk River quadrangle. U.S. Geological Survey Open-File Report 88-375. 2 sheets. Scale 1:250,000.
- Etkin, D. (1990) Greenhouse warming: Consequences for Arctic climate. Journal of Cold Regions Engineering 4, 54-66.
- Ferrians, O.J., Jr. (1965) Permafrost map of Alaska. U.S. Geological Survey Miscellaneous Geological Investigations Map I-445. Scale 1:2,500,000.
- Lachenbruch, (1957a) Three dimensional heat conduction in permafrost beneath heated buildings. U.S. Geological Survey Bulletin 1052-B, p. 51-69.
- \_\_\_\_\_ (1957b) Thermal effects of the ocean on permafrost. Geological Society of America Bulletin 68, 1515-1529.
- Lachenbruch, A.H., J.H. Sass, L.A. Lawver, M.C. Brewer, B.V. Marshall, R.J. Munroe, J.P. Kennelly, Jr., S.P. Galanis, Jr. and T.H. Moses, Jr. (1987) Temperature and depth of permafrost on the Alaskan Arctic Slope, in Tailleux, I. and P. Weimer, eds., Alaskan North Slope Geology. Bakersfield, Calif., Society of Economic Paleontologists and Mineralogists, Pacific Section, v. 2, p. 545-558.
- Lawson, D.E. (1982) Long-term modifications of perennially frozen sediment and terrain at East Oumalik, northern Alaska. Hanover, New Hampshire, U.S. Army Cold Regions Research and Engineering Laboratory, CRREL Report 82-36. 33p.
- \_\_\_\_\_ (1983) Ground ice in perennially frozen sediments, northern Alaska, in Proceedings Fourth International Conference on Permafrost. Washington, D.C., National Academy Press, p. 695-700.
- \_\_\_\_\_ (1986) Response of permafrost terrain to disturbance: A synthesis of observations from northern Alaska, U.S.A. Arctic and Alpine Research 18, 1-17.
- Livingstone, D.A., K. Bryan, Jr., and R.G. Leahy, (1958) Effects of an Arctic environment on the origin and development of fresh water lakes. Limnology and Oceanography 3, 192-214.
- Mackay, J.R. (1981) An experiment in lake drainage, Richards Island, Northwest Territories: A progress report, in Current Research, Part A. Geological Survey of Canada, Paper 81-1A, p. 63-68.
- \_\_\_\_\_ (1988) Catastrophic lake drainage, Tuktoyaktuk Peninsula area, District of Mackenzie, in Current Research, Part D. Geological Survey of Canada, Paper 88-1D, p. 83-90.
- O'Sullivan, J.B. (1961) Quaternary geology of the Arctic coastal plain, northern Alaska. Ames, Iowa, Iowa State University of Science and Technology, Ph.D. Dissertation. 191 p.
- Ramanathan, V. (1988) The greenhouse theory of climate change: a test by an inadvertent global experiment. Science 240, 293-299.
- Wahrhaftig, C. 1965. Physiographic divisions of Alaska. U.S. Geological Survey Professional Paper 482. 52 p.
- Williams, J.R., and W.E. Yeend, (1979) Deep thaw lake basins of the inner Arctic Coastal Plain, Alaska. U.S. Geological Survey Circular 804-B, p. B35-B37.



# MONITORING OF ENGINEERING-GEOLOGICAL PROCESSES ALONG PIPELINE ROUTES IN PERMAFROST TERRAIN IN MACKENZIE RIVER VALLEY, CANADA AND NADYM AREA, RUSSIA

M.M. Burgess<sup>1</sup>, S.E. Grechischev<sup>2</sup>, P.J. Kurfurst<sup>1</sup>, E.S. Melnikov<sup>2</sup> and N.G. Moskalenko<sup>2</sup>

<sup>1</sup>Geological Survey of Canada, Ottawa, Ontario, Canada

<sup>2</sup>Committee of Geology of Russia, VSEGINGEO, Moscow, Russia

Joint Canada-Russia field investigations of engineering-geological processes, which develop and act along the routes of oil and gas pipelines in permafrost terrain, were carried out during summer 1991 in the Nadym region of Western Siberia, Russia and in the Mackenzie River Valley, Canada. In both study areas active processes are monitored at specific observation sites along the pipeline rights-of-way. Field observations and measurements have been carried out for 10 to 18 years in USSR and 5 to 8 years in Canada. Detailed measurements, utilizing either fully automatic or manual observations, include ground temperatures to 20 m depth, depth of seasonal thaw and thaw settlement. Monitoring results in various landform units and geological conditions are described and recommendations made for future pipeline monitoring programs.

## INTRODUCTION

The development of oil- and gas-bearing regions within permafrost terrain in the former USSR, in the USA and in Canada has raised a number of problems related to the interaction between engineering structures and frozen soils. One of the most serious concerns is the impact of construction and operation of pipelines and rights-of-way (ROW) upon permafrost and environmental conditions in the ROW and the adjacent terrain. These problems are important not only in environmental terms, but also in geotechnical terms, because many engineering-geological processes can lead to deformation of the pipe. Should a breach occur, the geotechnical problems also have an ecological impact.

Considerable experience in monitoring of engineering-geological processes along pipeline ROW in permafrost terrain has been gained by the Geological Survey of Canada, which has conducted research along the Norman Wells pipeline, and by VSEGINGEO Institute, Committee of Geology of Russia, which has performed systematic investigations along pipeline routes in Western Siberia (Fig. 1).

The approaches and methods used by Canadian and Russian specialists for design, construction and geotechnical monitoring of pipeline routes were studied jointly by the authors of this paper as part of the Canada USSR Agreement on Scientific Research Cooperation in Arctic, Theme 1, Project 7 "Geocryological Conditions and Development of Oil- and Gas-Bearing Areas in Arctic". Several of the joint field investigations in July and August 1991, in the Nadym area, Russia, and along the Norman Wells pipeline in the Mackenzie River Valley, Canada.

This paper presents background information on pipeline design, construction, operation and monitoring in both countries, and observations on the development of engineering-geological processes along pipeline ROW. Conclusions and recommendations are made about effective approaches to pipeline route monitoring.

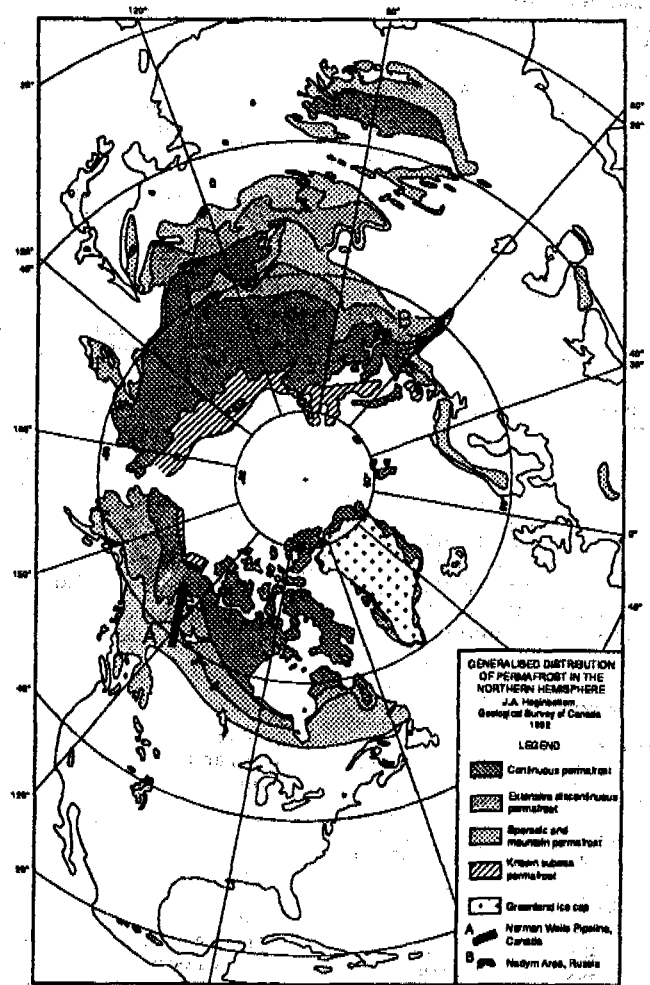


Figure 1. Location of Nadym area, Russia, and Mackenzie Valley, Canada, in relation to permafrost zones.

## PIPELINE DESIGN, CONSTRUCTION AND OPERATION

In the Nadym area, 1600 km of natural gas pipelines (Fig. 2), 142 cm in diameter, are buried at 1 m depth, in ROW which may contain from 4 to 10 lines and range up to 500 m in width. Construction of the lines took place during the winters of 1971-1991; operation began in 1977. Throughput is 1.5 billion m<sup>3</sup>/day. The pipelines operate with a gas input temperature of +20°C with no refrigeration along the lines. No mitigative measures such as revegetation, insulation of thaw-sensitive terrain, or drainage and erosion control structures were used during construction to reduce thermal or erosional impacts.

By contrast, the 869 km long Norman Wells pipeline is the first completely buried oil pipeline built in the discontinuous permafrost zone of Canada. It is a single small diameter line (328 mm) buried at 1 m depth within a 25 m-wide ROW. Construction took place during the winters of 1983-1985 and operation began in 1985. Throughput is 5000 m<sup>3</sup>/day. The design philosophy was to minimize terrain disturbance and assure pipe integrity under possible conditions of frost heave, thaw settlement and slope instability. An ambient thermal design was selected to minimize heat input from the pipe, so that permafrost degradation would be largely due to the removal or disturbance of vegetation. The oil is chilled to -1 to -2°C before entering the line. A layer of wood chips, 0.5 to 1.8 m thick, was used to insulate 56 thaw-sensitive slopes. The insulation was designed to retard thaw, thus preventing build-up of excess pore water pressure. Additional features included an uninsulated pipe (except at sag bends), winter ROW clearance maximizing the use of existing cutlines, revegetation of mineral soils with seeds and fertilizer, and drainage and erosion control measures. Details of the engineering and environmental considerations are summarized by MacInnes et al. (1989).

## ENGINEERING-GEOLOGICAL PROCESSES ALONG THE NADYM AREA PIPELINE RIGHTS-OF-WAY

Specialists from VSEGINGEO have been monitoring engineering-geological processes at a number of study sites along gas pipelines in the Nadym region, Western Siberia (Fig. 2) for up to 18 years. The ROW are periodically inspected by helicopter as part of an effort to determine proper monitoring methodology. Results of these investigations have been published elsewhere (Grechishev, 1983; Melnikov, 1983a, 1983b and 1988; Melnikov and Dubikov, 1986).

The gas pipelines run north to south across the following zones, shown in Fig. 2, and discussed below:

(1) Southern tundra of the western part of Tazovskaya Peninsula (zone T<sup>2</sup>) is characterized by a deeply dissected relief and gently sloping hummocky terrains. Marine, glacial marine and coastal marine clays and silts of Middle and Upper Pleistocene age are widespread, although sandy and sand-loam lacustrine-fluvial sediments are also present. Depth of continuous permafrost ranges from 200 to 700 m

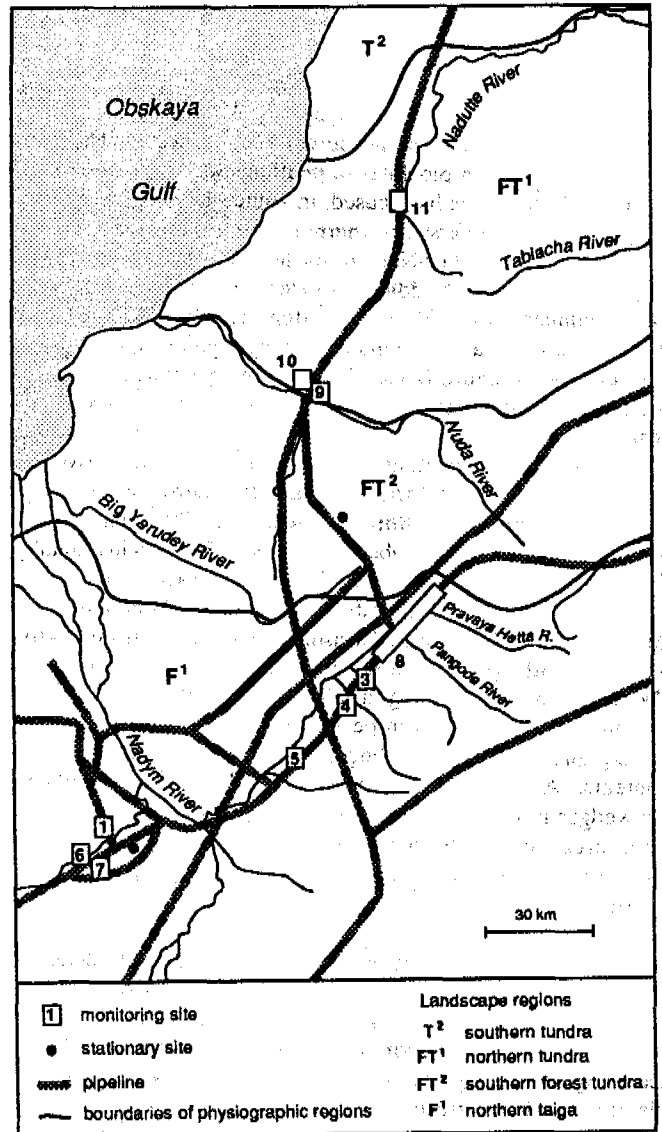


Figure 2. Location of pipeline ROW and study sites in Nadym area. "Monitoring" sites are those used for engineering-geological monitoring. "Stationary" sites are those used for geocryological monitoring.

although taliks occur under large rivers and lakes. Depth of seasonal thaw varies from 0.4 to 2m. Permafrost temperatures are typically -4° to -5°C; and range from 0 to -1°C below lakes to -6 to -7°C below snow-free valley areas.

The highest volumetric ice content (40%) occurs in the top 3 m of mineral soils; relative thaw subsidence reaches 0.1-0.3 m. The lowest volumetric ice content has been observed in the 3-10 m depth interval where relative subsidence is < 0.1 m. The upper parts of peatbogs and flooded lowlands, composed of biogenic Holocene sediments, have high volumetric ice contents (50 to 90%); their relative thaw subsidence is 0.3 to 0.4 m. Massive ground ice occurs only in fluvial and lacustrine sediments as ice wedges, ice lenses and thin icy layers, mainly to depths of 2-4 m, where average

volumetric ice content is 10%.

The most widely occurring cryogenic processes are thermokarst, and seasonal and perennial frost heave. The installation of buried pipelines in peatbogs with ice wedges and on ice-rich slopes has caused, in some places, an initiation of thermokarst and thermo-erosion processes.

(2) Most of the Pur-Nadym northern forest tundra (zone FT<sup>1</sup>) is covered by a Middle Pleistocene marine loamy and clayey sediments with infrequent, often dissected hilly, lacustrine-bog terrain. A similar landscape typifies the southern forest tundra (zone FT<sup>2</sup>), where typical soils are sands and sandy loams, in places overlain by up to 2.5 m of peat.

Permafrost is discontinuous with taliks under lakes, river and stream valleys and forested areas. Permafrost is 50 to 100 m thick with temperatures between 0 to -5°C. The highest temperatures are observed in river flood-plains, small flat-bottom valleys, forested areas of river terraces and swamps. The lowest temperatures are typical of flat and hilly peatbogs. Depth of seasonal thaw ranges from 0.3 to 0.5 m in peatbogs to 2.5 m in sandy areas of river terraces. Depth of seasonal freezing in taliks is 1-2 m.

Only the soils of frozen peatbogs and swampy areas of flood-plains and lacustrine-boggy terrains have high ice contents. A wide variety of ground ice types occur, including ice wedges in peatbogs and ice-cored frost mounds in the outer areas of river terraces and in the bottoms of drained lake basins. Volumetric ice content may exceed 10% only in lacustrine-bog terrains of the northern forest tundra.

The most widely occurring cryogenic processes are thermokarst along ice wedges in northern areas, aggradation of permafrost, and seasonal and perennial frost heave in drained lake bottoms and in river flood-plains. Pipeline construction initiates thermokarst and thermo-erosion along ice wedges, and aggradation of permafrost following tree clearing on river terraces.

(3) The Nadym northern taiga in the valleys of the Nadym River and its large tributaries (zone F<sup>2</sup>) is characterized by flood-plains composed of fine silty sands. A small percentage of the area is covered by low flat river terraces and gently sloping lacustrine-fluvial plains of an Upper Pleistocene age where hummocky terrains and large areas of eolian deposits are also encountered.

Permafrost is associated only with areas of extensive peatbogs and floodplain terraces; its depth ranges from 5 to 20 m. The average ground temperatures vary from -0.5 to -1.5°C; however, they range from -3.5° to -4°C within hummocky peatbogs to -0.2° to -1.0°C in wooded swamps. At sand dune sites, the temperatures reach +1° to +3°C. Volumetric ice content may reach 50% in organic and underlying mineral soils while in sandy soils it does not exceed 20-25%.

Thaw subsidence of sandy soils does not exceed 0.15-0.2 m, however in areas overlain by a thick peat cover (2-4 m), the subsidence of a 10 m thick profile can reach 2.6 to 3 m due to the high compactability of thawed peat. Widely developed geomorphic processes include aggradation of permafrost, perennial and seasonal frost heave, and eolian processes. Disturbance of natural cover due to human activity intensifies these processes.

#### Ground Thermal Regime

The largest changes in ground temperature regime are observed in drained sandy areas. In the forest tundra zone, permafrost originally consists of individual frozen layers of sediments. Following removal of the vegetation cover, seasonal freezing gradually reaches these layers. Eight years after the disturbance, the frozen layers have coalesced and permafrost extends to the surface. No permafrost is present beneath forested sand deposits in the northern taiga but depth of seasonal freezing increases following disturbance.

The smallest ground temperature changes due to anthropogenic impact are observed in fens and peatbogs. Surface disturbance causes a slight increase in ground temperature, which is observed both in the forest tundra and the northern taiga zones. The peatbogs, unlike the drained areas, do not show stabilization of the temperature regime and depth of seasonal thaw for a long time. The temperature changes observed in peatbogs during the first several years after construction are insignificant; later the temperature increases more noticeably as thaw depths reach as much as 5 m within 20 years (Fig. 3). Changes in the depth of seasonal thaw are thought to depend on changes in thermo-physical properties of peat, caused by its subsidence and compaction, and on flooding of disturbed peatbogs (Fig. 4).

#### Inventory of the Disturbed Surface Area

Data obtained by remote sensing and aerial photography,

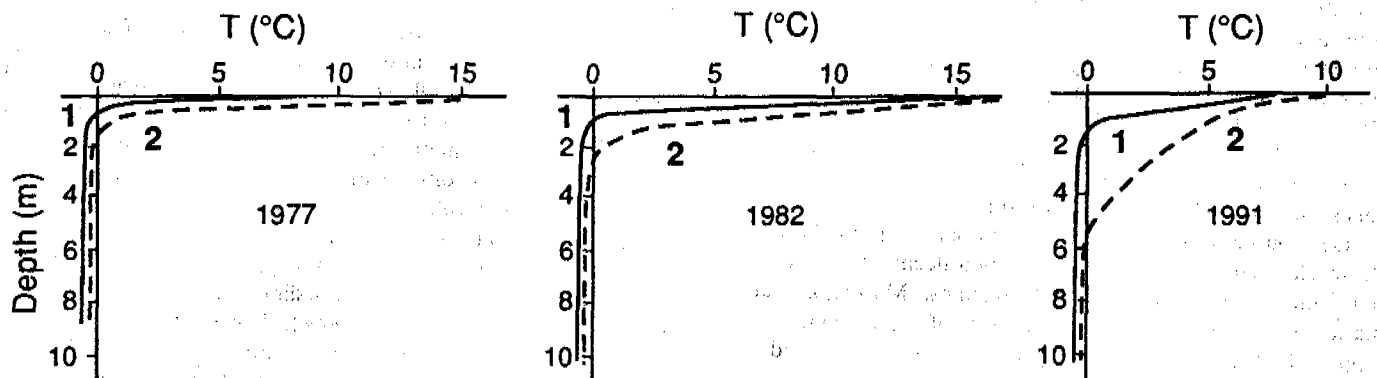


Figure 3. Changes in soil temperature with depth at a site in the northern taiga zone, Nadym area, in peatbog in natural (1) and disturbed (2) conditions for different years.

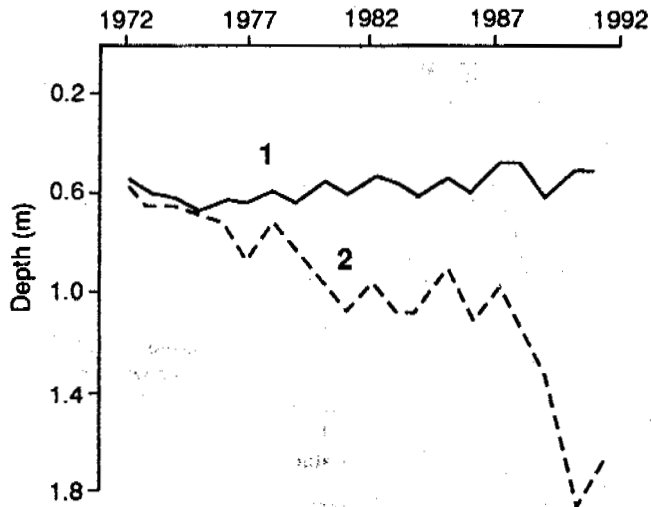


Figure 4. Maximum thicknesses of seasonal thaw at a site in the northern taiga zone, Nadym area in peatbog in natural (1) and disturbed (2) conditions.

and visual airborne observations and ground surveys before and during each of three years after construction, were used to compile large-scale landscape maps of the ROW and to make an inventory of anthropogenic disturbances at the gas fields and along gas pipelines in Western Siberia.

The repeated mapping enabled evaluation of the dynamics of disturbed zones and of the consequences of direct anthropogenic impacts. The width of the disturbed zone in different terrain units varies from 40 m to 400 m for one gas pipeline. This zone is narrowest (<50 m) in drained areas. In swampy areas, bogs and areas with frost mounds the width of this zone increases to 150-250 m; it reaches 300 to 400 m when periodic new disturbances cause flooding and create swamps. The width of the disturbed zone also increases due to formation of thermokarst. All these changes are caused by modification in surface run-off and ground-water movement due to pipeline installation. Slopes in river valleys are affected by actively developed erosion processes leading to the formation of deep ravines.

Calculation of disturbed areas, based on the landscape maps, has shown that the disturbed area can increase initially by up to 30% due to development of swamps, thermokarst, and erosion. The width of the disturbed zone then gradually broadens, increasing by 35-60% over 20 years.

In the tundra zone, thermokarst and erosion processes are of greatest concern. In the northern taiga, where large areas are covered by unfrozen, water-logged swamps, the construction of pipelines alters the surface water run-off, rapidly activating flooding processes which then affect the adjacent, initially undisturbed landscape complexes.

#### ENGINEERING-GEOLOGICAL PROCESSES ALONG THE NORMAN WELLS PIPELINE RIGHT-OF-WAY

The Geological Survey of Canada (GSC) is one of several agencies which participate in the Canadian government's Permafrost and Terrain Research and Monitoring Program

(PTRM) for the Norman Wells pipeline. In 1984-1985 23 study sites were established at 13 locations along the pipeline route (Fig. 5) and instrumented with temperature cables to record changes in the pipe external thermal regime, on the ROW and off-ROW. These sites were selected to represent the terrain types of greatest concern, to examine thaw settlement, and mitigative and design measures. Most sites are located on level terrain. The pipeline company (IPL) also established a geotechnical monitoring program which initially focused on instrumentation of 26 slopes.

From eight to twelve PTRM monitoring trips have been carried out annually, using helicopters, since the pipeline began operation. These trips allow reconnaissance of the overall ROW, temperature data collection and other surveys such as surface topography and snow depth. Over the years, loggers and additional instrumentation have been installed.

Permafrost underlies approximately 75% of the ROW in the northern portion of the pipeline route, and extends to depths <50 m with temperatures ranging from -1 to -3°C. Along the southern portion of the route, permafrost is discontinuous, <20 m thick, and warm with temperatures between -1 and 0°C. Some 25% of the ROW is underlain by permafrost and transitions from frozen to unfrozen are numerous, reaching several per kilometer over the southernmost 200 km. Lacustrine and moraine sediments predominate in the north, organic terrain characterizes the south; the frozen soils are often ice-rich and thaw-sensitive.

Several papers and reports have been published to date describing the observations and results of the program (Burgess, 1992; Burgess and Harry, 1990; Burgess and Allen, 1991; MacInnes et al., 1990).

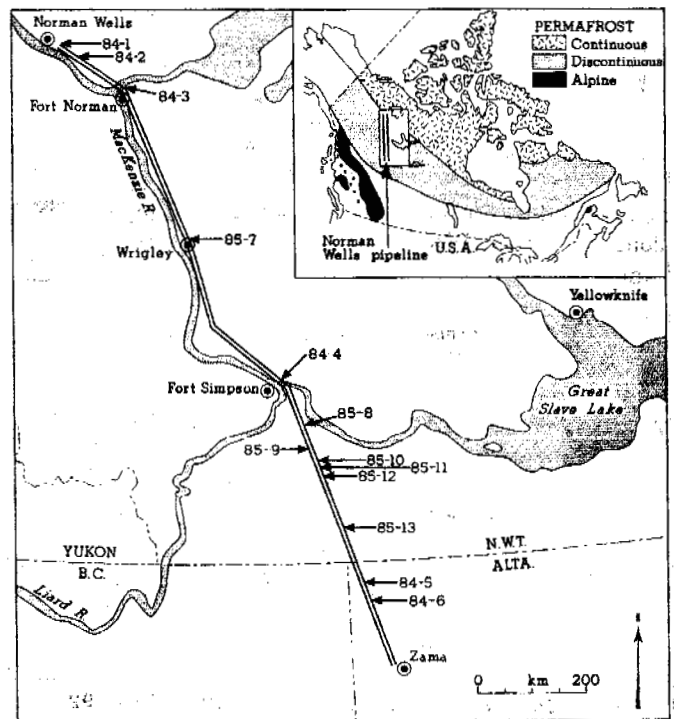


Figure 5. Norman Wells pipeline and monitoring sites location.

### Pipe Thermal Regime

Within the first 20 km, the pipeline is greatly influenced by the chilling of the oil at Norman Wells, as mean annual pipe temperatures range from 0 to  $-1^{\circ}\text{C}$ . Over this distance the pipe operates close to ambient ground temperature. Elsewhere mean annual pipe temperatures are greater than  $0^{\circ}\text{C}$  and reach as high as  $7^{\circ}\text{C}$ , with a general increase from north to south (Fig. 6). Mean annual pipe temperature has gradually increased over the years (Fig. 6), both in response to increases in ground temperature in the disturbed ditch area on the ROW, resulting from clearing and construction, and in response to a gradual increase in oil throughput.

### Ground Thermal Regime

In permafrost terrain, pipe temperatures are generally warmer than ground temperatures on the ROW at a similar depth; these in turn are warmer than those off ROW. Figure 7 illustrates these relationships as well as the warming trend in on-ROW ground temperatures. Off-ROW ground temperature warming has been more variable, generally of lower magnitude and related to ROW disturbance extending

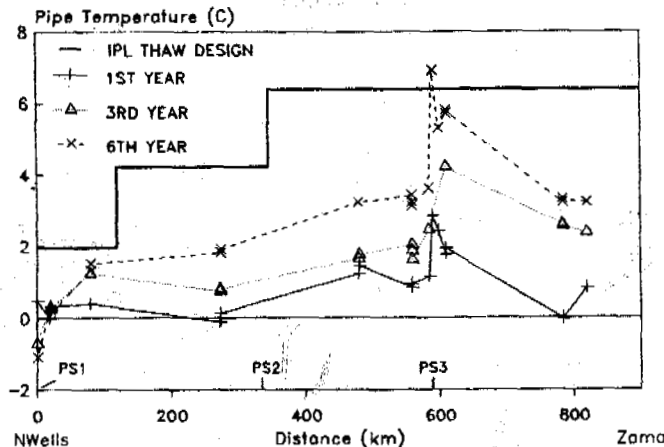


Figure 6. Mean annual pipe temperatures at monitoring sites along the Norman Wells pipeline. PS = pump station.

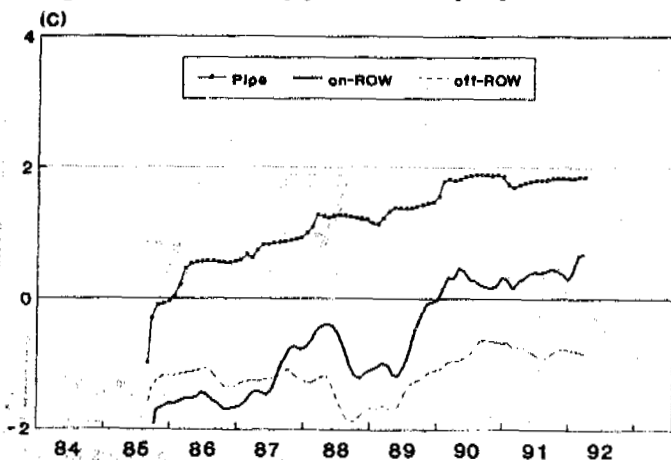


Figure 7. Running mean annual pipe and ground temperatures at pipe burial depth on-ROW and off-ROW, ice rich lacustrine plain, km 272.3, Norman Wells pipeline.

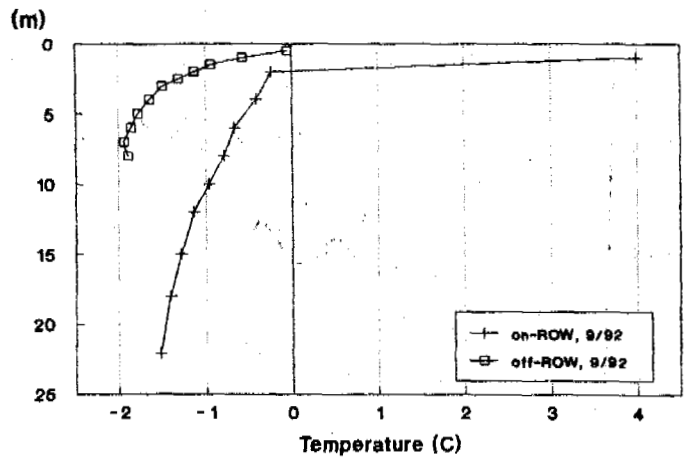


Figure 8. Comparison of fall 1992 temperature profiles on-ROW and off-ROW along the Norman Wells pipeline, km 79.2, ice-rich alluvial terrace deposits.

off the ROW, disturbance due to the installation of off-ROW instrumentation, and climate warming.

Figure 8 compares temperature-depth profiles on-ROW and off-ROW for the fall of 1992; the on-ROW temperatures are those measured furthest from the pipe. These plots illustrate the increase in the depth of thaw on-ROW and the depth of warming 7-8 years after ROW clearing. Changes in ice-rich peat plateaus have been small and slow. Thaw depths have increased at more rapid rate than had been predicted beneath some wood chip insulated slopes and in the vicinity of the pipe in organic terrain.

### Wood Chip Insulated Slopes

Biological heating within the wood chip insulation occurred, as predicted, in the first year. However, on many slopes the heating has either persisted in localized "hot spots", recurred after several quiescent years, or only flared up in recent years. These unexpected results indicate the complexity and diversity of biological activity involved. Remedial actions for cooling off the hot spots and the ground beneath have included, with varying degrees of success, removal of snow, removal, thinning or watering of chips, and the installation of ventilation pipes.

The thermal design of slopes considered the pipe to be passive thermally. The observed pipe temperatures however indicated growth of a thaw bulb around the pipe. This greater than expected warming was confirmed by increased settlement and probing the depth of thaw, and by development of tension cracks along the ditchline. A re-evaluation of factor of safety undertaken by IPL in 1992 indicated that portions of 7 slopes had factors of safety less than their original design. Re-assessment of slope stability is currently a priority issue and involves detailed evaluations, analyses, further field investigations and instrumentation.

### Ground Surface Settlement

Immediately after construction, surface settlement occurred along the ditchline due to the use of ice-rich or snow-contaminated uncompacted backfill. In the first few years

after construction, 50 cm or more of settlement was recorded in the trench at over half of the study sites. Some 100 km of trench, in areas that could be affected by erosion, were re-filled by IPL during winter maintenance programs in 86-88.

Continued subsidence along the ditchline is related to increased depth of thaw around the pipe. This has become increasingly marked in thick organic terrain, where subsidence has exceeded 1 m, with development of tension cracks and collapse in the trench on peat plateaus. Surface settlement of the remainder of the ROW has been ongoing and ranges from 0 to 100 cm. Variable surface settlement has also been recorded off-ROW in relation to ground temperature warming.

Settlement facilitates the diversion of water along the ROW on sloping terrain, in particular along the subsided trench, and can lead to increased erosion along the ditchline. A reduction in depth of cover over the pipe may result in increasing incidence of pipe exposures.

#### Ground Surface Erosion

ROW surface erosion has generally been limited by erosion control structures. However, in the first few years after construction remedial action was required due to inappropriately designed, sized or located structures. Irregular subsidence, particularly in the ditch area and along low angle slopes with no control structures, led to erosion problems following major precipitation and run-off events. Two major stream crossings had to be completely reconstructed following erosion related to summer storms in 1988.

Ground water flow and subsurface erosion have been noted at a number of wood chip covered slopes. The Great Bear River south bank insulated slope underwent extensive remedial work in 1992 to backfill a lengthy subsurface cavity over the ditchline beneath the chips.

#### CONCLUSIONS

The approach to monitoring pipeline ROW in permafrost areas in both Russia and Canada is based on landscape (terrain) type, i.e. selecting a number of critical landscape types for monitoring the response to disturbance, followed by a further selection of a number of observation sites for instrumentation and detailed, long-term monitoring.

The principle pipeline design approach adopted in the Nadym area was to minimize geotechnical and environmental impacts of construction by routing the pipeline through the most suitable landscape types, least sensitive to disturbance. The monitoring program thus placed great emphasis on geocryological conditions and observations. In addition to this approach, the Norman Wells pipeline design also emphasized novel design, construction and mitigative measures to minimize impacts of pipeline construction and related activities. The Norman Wells pipeline studies thus put more emphasis on detailed monitoring of pipeline design and mitigative measures.

The Norman Wells approach will likely be the one applied to any future pipeline construction project in either country. The experience gained during the Norman Wells pipeline program over the last 8 years shows the necessity for

flexibility in the monitoring program, particularly when novel techniques have been used. Over the lifetime of the pipeline, issues and priorities related to operation and maintenance of pipeline may change, thus requiring changes in location of research areas, observation sites, and type and frequency of measurement techniques and equipment.

#### ACKNOWLEDGMENTS

The PTRM program is coordinated by Indian and Northern Affairs Canada (INAC). Funding for the program has been received from the Northern Affairs Program of INAC, the Northern Oil and Gas Action Program, the Geological Survey of Canada, the Federal Panel on Energy, Research and Development, Agriculture Canada, the National Research Council and IPL. Logistic support for the pipeline monitoring trip around Nadym was provided by Dr. V. Dubrovin and Mr. A. Kostigin. The authors are grateful to J.A. Heginbottom and T.W.H. Baker for their excellent comments. This paper is GSC contribution #36292.

#### REFERENCES

- Burgess, M.M. 1992. Analysis of the pipe and ditch thermal regime, Norman Wells pipeline. Proc., 11th Int. Conf. Offshore Mechanics and Arctic Engineering, p.575-584.
- Burgess, M.M. and Allen, V.S. 1991. Notes on the use and performance of thermal instrumentation: experience from the Norman Wells pipeline ground temperature monitoring program. Geological Survey of Canada, Paper 91-1E, p. 337-345.
- Burgess, M.M. and Harry, D.G. 1990. Norman Wells pipeline permafrost and terrain monitoring: geothermal and geomorphic observations, 1984-1987. Canadian Geotechnical Journal, Vol. 27, p. 233-244
- Grechischev, S.E. (Editor) 1983. Geocryological prediction for West-Siberian gas-bearing province. Publ. House "Nauka", Novosibirsk, 180 p.
- MacInnes, K.L., Burgess, M.M., Harry, D.G. and Baker, T.W.H. 1989, 1990. Permafrost and Terrain Research and Monitoring: Norman Wells Pipeline. Volume I. Environmental and Engineering Considerations. Volume II Research and Monitoring Results: 1983-1988. Environmental Studies Report No. 64. Indian and Northern Affairs Canada, Northern Affairs Program, 132 pp and 204 pp.
- Melnikov, E.S. (Editor) 1983a. Landscapes of the cryolithozone in West-Siberian gas-bearing province. Publ. House "Nauka", Novosibirsk, 166 p.
- Melnikov, E.S. (Editor) 1983b. Geocryological conditions of West-Siberian gas-bearing province. Publ. House "Nauka", Novosibirsk, 198 p.
- Melnikov, E.S. 1988. Natural Geosystems of the Plain Cryolithozone. Proc., 5th Int. Conf. on Permafrost, pp. 208-212.
- Melnikov, E.S. and Dubikov, G.I. (Editors) 1986. Methods of regional engineering-geocryological investigations for plain terrains. Publ. House "Nedra", Moscow, 208 p.

## STAGE-DISCHARGE RELATIONS IN THE MACKENZIE DELTA DURING WINTER AND DEVELOPMENT OF INTRUSIVE ICE IN LAKE-BOTTOM SEDIMENTS

C.R. Burn<sup>1</sup>

Department of Geography, University of British Columbia,  
Vancouver, BC, Canada V6T 1Z2

<sup>1</sup>Present address: Department of Geography, Carleton University,  
1125 Colonel By Drive, Ottawa, ON, Canada K1S 5B6

The discharge of northern rivers declines in fall and winter, but water levels rise during freeze-up as the ice cover impedes flow, forcing an increase in channel storage. Water levels in the Mackenzie Delta may rise throughout winter as distal channels freeze through, blocking discharge. The hydrologic regime of a Delta lake connected to East Channel of Mackenzie River was monitored during winter from 1987 to 1992. During 1987-88 and 1988-89, ice on the lake rose after November. The increases in ice elevation were similar to changes on East Channel at Inuvik. Observations confirmed that in winter water may re-enter the lake from East Channel. While inflow occurred, water pressure was sufficient to raise ice and frozen sediment and led to the growth of intrusive ice in the lake bottom. No inflow was measured from 1989 to 1992: the lake-sill elevation has risen so that the stream connecting the lake and East Channel freezes through.

### INTRODUCTION

The hydrologic regime of Mackenzie Delta lakes during winter is significant for: management of aquatic populations which reside there such as muskrats and various fish and plants; the water balance of the Delta; and the extent of frost penetration in lake-bottom sediments (Burn 1990). Winter field surveys of lake-ice conditions have been conducted between 1987 and 1992 at a site in the Mackenzie Delta 16 km downstream from Inuvik, N.W.T. The site, called Lake 2, is one of a cluster of lakes adjacent to East Channel of Mackenzie River, bounded to the east by the Caribou Hills (Figs 1 and 2). Surface elevation and ice thickness have been monitored at the lake, and samples of ice and water have been collected for determination of electrical conductivity from the lake and from East Channel. This paper presents evidence for lake refilling during winter, and accounts for the development of intrusive ice in lake-bottom sediments.

### HYDROLOGIC REGIME OF MACKENZIE DELTA

#### Channel regime in the Delta

Figure 3 indicates the stage (water level) and discharge between April 1987 and April 1988 of East Channel of Mackenzie River at Inuvik. Stage measurements at Inuvik are made by manometer and are reliable within  $\pm 1$  cm. Discharge in winter is interpolated from the stage between direct, i.e. velocity-area, measurements taken at intervals. The precise relationship between stage and discharge during this season depends in part on assumptions regarding the form of the rating curve. However, the pattern shown on Figure 3 has been repeated every year since 1973, when continuous records began.

Gerard (1990) describes the stage-discharge relationship during freeze-up when frictional resistance of an irregularly developing ice

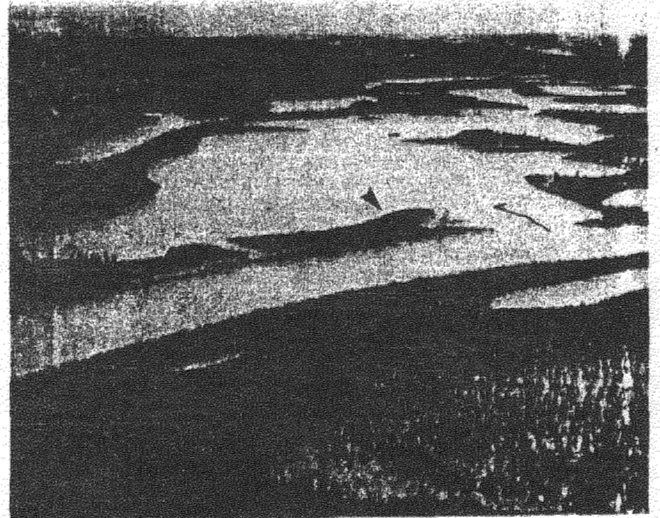


Figure 1. Oblique aerial photograph eastward over Lake 2, 14 November 1990. Note that the outlet to East Channel is not frozen over. The arrow indicates the survey line (Fig. 4). East Channel is approximately 50 m wide. The Caribou Hills form the upper portion of the photograph.

cover impedes flow, reduces discharge and forces an increase in channel storage, i.e. water level. This effect is small on East Channel, which carries less than one per cent of the Mackenzie's discharge, but can be observed in mid-October 1987. Discharge and stage decrease in November while freeze-up occurs upstream, farther south. By mid-

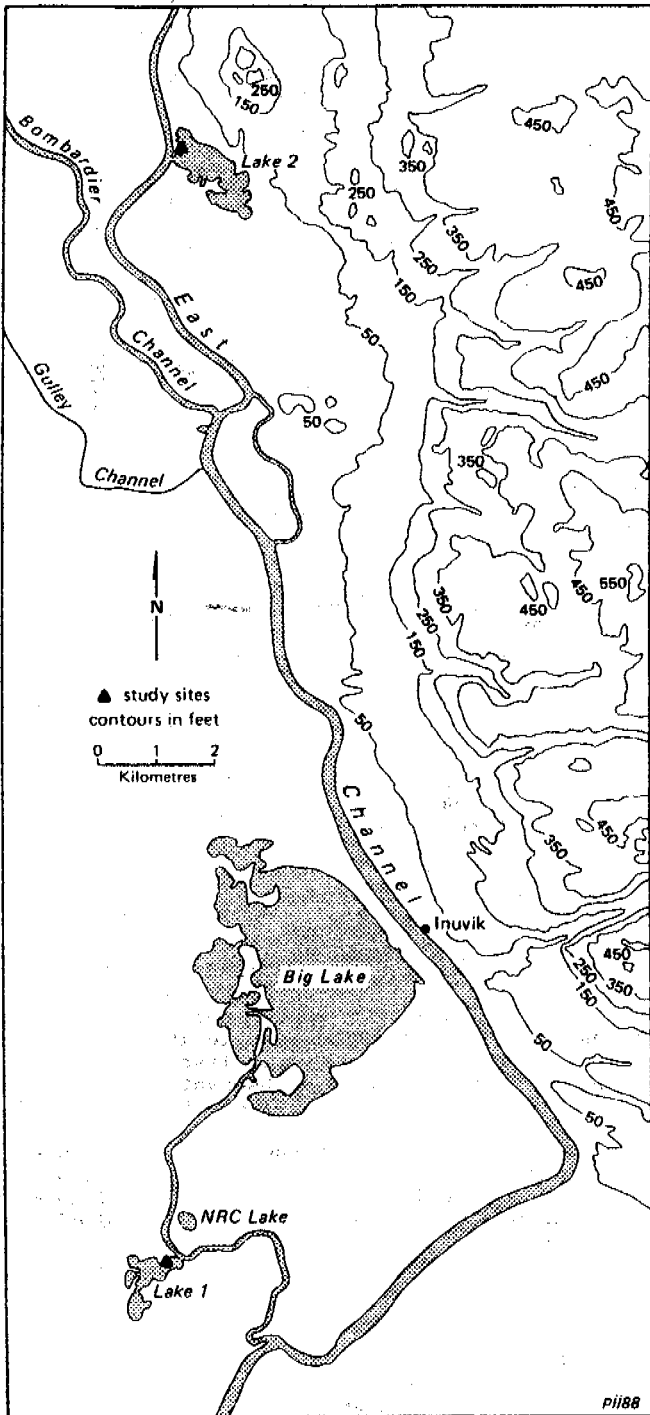


Figure 2. Location of study sites, near Inuvik, Mackenzie Delta, Northwest Territories (68°22'N 133°43'W; Burn 1989, Fig. 1). Observations reported in this paper are from Lake 2.

December freeze-up is completed over most of Mackenzie River. As the base of the ice cover smooths over, water comes out of channel storage, and both stage and discharge rise.

The water level of East Channel continues to rise throughout winter although discharge declines after mid-January. Unpublished gauge height and discharge records for stations in the Mackenzie Delta which operated in the mid-1970s indicate that the winter rise in water level is not restricted to East Channel. The gradual and constant increase in stage may be a result of shallow parts of channels in the outer Delta freezing through (Jenner and Hill 1991), diverting discharge from smaller channels and increasing storage in the main distributaries.

#### Lake Regime

Lakes cover up to one-half of the alluvial plain which comprises the Mackenzie Delta (Mackay 1963, Fig. 39). Marsh and Hey (1989) quantified the classifications proposed by Mackay (1963, p. 133) of no-, low- and high-closure for seasonal hydraulic connection of lakes to Mackenzie River. "No-closure" lakes, connected to distributary channels of the Delta at the end of summer, comprise 12% of the 132 lakes in Marsh and Hey's study area on the east side of the Delta near Inuvik. This paper is concerned with the hydrologic regime of a "no-closure" lake in winter.

#### SITE CONDITIONS

During summer a small boat can enter Lake 2 without difficulty. During freeze-up, as the Mackenzie stage falls, water drains from the lake into East Channel. Figure 3 indicates that between September and December the water level in East Channel may decline by over a metre.

Oblique aerial photographs taken in 1935 (A5023-25C,26C) indicate that Lake 2 used to be partially separated from East Channel by a small island. Before 1987 the stream between the lake and East Channel north of the island was filled by sediments and organic debris. Now, only one outlet permits unimpeded flow of surface water between East Channel and the lake most of the year. Lake drainage ceases when the outlets freeze through or the Mackenzie stage rises and discharges into the lake.

There is active sedimentation in the lake near the main outlet. Lake-bottom aggradation has not been measured directly, but it is likely on the order of cm/yr because: (1) East Channel has greater flow and sediment transport than the distributary channel at another lake near Inuvik (Lake 1 on Fig. 2) where Ferguson (1990) recorded more than 5 mm of lake-bottom aggradation near the mouth of the lake over one summer; and (2) 47 cm of sediment were deposited in the summers of 1988 to 1991 near an oil drum stranded upright on a bar at the mouth of the lake. The mean sedimentation rate of 12 cm/yr measured near the drum is of the same order as high rates reported by Mackay (1963, p.134). Observations in November 1992 confirmed this rate for summer 1992.

During the period of observation, greatest lake-ice thicknesses were measured in March 1991 and 1992, when lake water had frozen through, after winters with low snow accumulation (Table 1) and no lake refilling. In other years the water column in the centre of the lake did not freeze through.



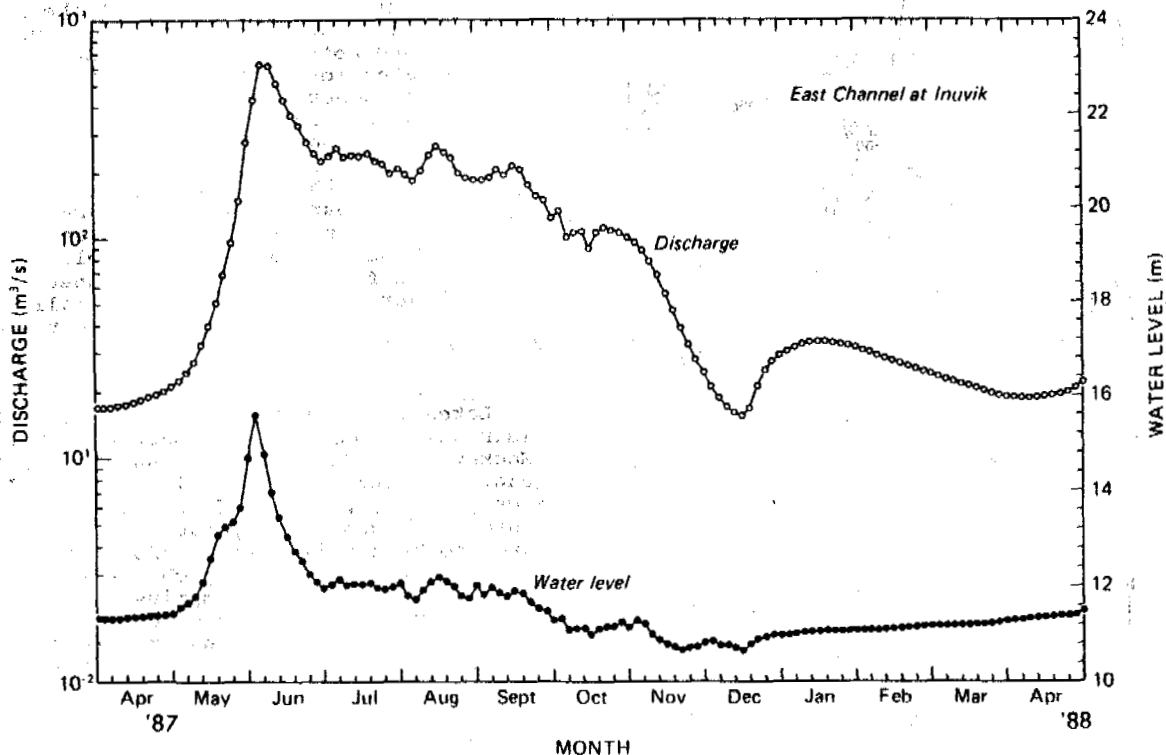


Figure 3. Water level and discharge of Mackenzie River (East Channel) gauged at Inuvik, WSC Station 10LC002, April 1987 - April 1988. Subtract 10 m from water level for reference to Geodetic Survey of Canada datum. Data from Water Survey of Canada (1988, 1989).

Table 1. Snow depths and late winter ice thicknesses, 1987-88 to 1991-92, Mackenzie Delta study site.

	Snow (cm)	Ice (cm)	Date
1987-88	27	89	16 March
1988-89	37	77	15 April
1989-90	42	83	3 April
1990-91	30	125	21 March*
1991-92	30	126	10 March*

\* Water column froze through

#### FIELD METHODS

Lake-ice thickness and surface elevation were measured by chiselling holes in the ice and by levelling from a benchmark installed in permafrost. The benchmark is a 1.25 cm steel rod, 3.5 m long, covered in the active layer and near-surface permafrost by a 2 m-long sleeve of close-fitting aluminum tubing. Collars on the rod protrude into permafrost. Field checking in August 1992 indicated that the benchmark had not heaved in five years.

Lake-ice elevation was levelled at points marked by dowels along a 200 m transect from shoreline. Tin cans frozen to the lake surface

provided a stable reference position at each site. Changes in lake-surface elevation were also measured with sets of concentric heave tubes (Mackay et al. 1979), and magnet heaveometers (Mackay and Leslie 1987). The precision of measurement by levelling was approximately 1 cm, but observations of  $\pm 0.1$  mm were obtained from the heave tubes, and  $\pm 0.5$  mm from magnets.

Icing (aufeis) at the lake was measured on stakes installed during the first visit of each year. Lake sediments were drilled to determine intrasedimental ice content at the end of each season.

#### RESULTS

During 1987-88 surveys were made in late November, January and March (see Burn 1989). During the two months preceding 23 January the lake surface at sites where ice was not grounded rose by 38 cm. Eighteen cm of icing formed in the same period. In the subsequent two months the ice surface rose by a further 11 cm. Table 2 indicates the change in ice thickness between November and March. The 71 cm of ice measured on 20 March below the icing comprised: 30 cm present in November; 11 cm from freezing of 10 cm of water in the November column; and 30 cm added to the ice cover below the lake surface. The icing and 30 cm added to the ice cover below the surface imply that 44 cm water (48 cm ice) were added to the lake over the period.

In 1988-89, drainage of the lake during November and early December lowered the level of the main body of the lake (Fig. 4). However, between 10 December and 18 February the ice surface, at points where the ice was not grounded, rose by 34 cm. The ice surface continued to rise after 18 February, but more slowly. The change in lake ice and water column thickness during 1988-89, reported in Table 2, is in general agreement with the levelled change in lake elevation. The agreement is not precise, probably due to undulations in the lake-bottom, since holes were not reopened for measurement. The ice surface in mid-April was approximately 10 cm higher than during early November.

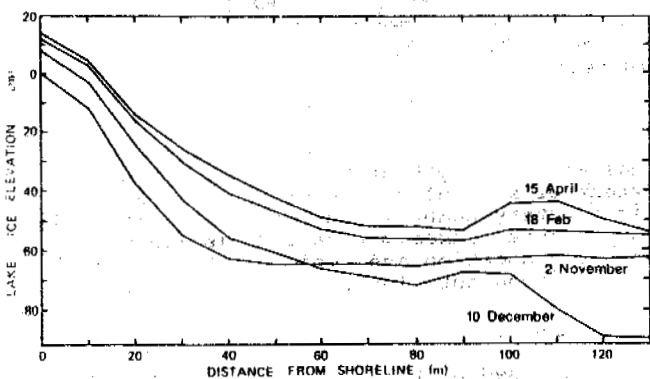


Figure 4. Changes in elevation of the ice surface at the study site, winter 1988-89. Elevations are with reference to shoreline on 2 November.

Lake level declined throughout winter 1989-90 and 1990-91. On 3 April 1990, the ice surface was 22 cm below its elevation on 8 November 1989. In 1990-91 the ice surface dropped 9 cm between 15 November and 21 March.

#### Conductivity in the lake and in East Channel

Changes over winter in the electrical conductivity of water from the lake and from East Channel are documented in Table 3. Lake water increases in conductivity by an order of magnitude during winter as a result of solute exclusion during freezing (Lesack et al. 1991). The ice cover had a conductivity of less than 10  $\mu\text{mhos/cm}$  in April 1990. The increase in lake-water conductivity was twice as high in 1989-90 as in 1988-89, although ice thicknesses were comparable. East Channel water maintains a conductivity of about 300  $\mu\text{mhos/cm}$  throughout winter, similar to the value of 274.5  $\mu\text{mhos/cm}$  reported by Reeder et al. (1972) for a sample collected from Mackenzie River above Arctic Red River in summer 1970.

#### DISCUSSION

Burn (1989) tentatively attributed lake refilling during winter to groundwater discharge from an aquifer flowing off the Caribou Hills. However, Water Survey of Canada records indicate that the Mackenzie stage rose continuously during winter 1987-88 after 14

Table 2. Lake ice thicknesses and water depths, Mackenzie Delta study site, 1987-88 and 1988-89.

	23 Nov.	20 March	Change
-----			
1987-88			
Direct measurement			
Icing	-	18	+18
Ice	30	71	+41
Water	15	5	-10
Total	45	94	+49
-----			
Levelling	-315	-267	+48
=====			

	10 Dec.	15 April	Change
-----			
1988-89			
Direct measurement			
Icing	-	-	-
Ice	47	77	+30
Water	17	14	-3
Total	64	91	+27
-----			
Levelling	-295	-259	+36
=====			

All measurements in cm.

Table 3. Electrical conductivity of lake and Channel water ( $\mu\text{mhos/cm}$ ) and ice thickness (cm), 1988-89 to 1990-91.

Date	Lake 2		East Channel	
	Ice	Cond.	Ice	Cond.
-----				
Winter with lake refilling (1988-89)				
02/11	28	280	-	-
11/12	47	490	-	-
18/02	62	460	-	-
15/04	77	1250	-	-
-----				
Winter with minimal refilling (1989-90)				
10/11	26	380	-	-
02/12	36	560	-	300
15/02	61	1740	49	320
07/04	83	2400	60	310
-----				
Winter without lake refilling (1990-91)				
15/11	43	400	40	290
04/12	52	600	53	265
18/02	102	4850	76	310
21/03	125	-*	100	310
=====				

\* Water column froze through.

December (Fig. 3), after 8 December in 1988-89, 27 November in 1990-91 and 25 November in 1991-92. Comparison of the stage records for 1987-88 with lake-surface surveys indicates a close correspondence (Table 4). The increase in surface elevation of the lake may be due to refilling by channel water. During these winters a sub-ice channel would have connected the lake and East Channel for most of the season.

Discharge from the lake can be observed in the outlet channel (see Fig. 1), which in autumn and early winter is sufficiently shallow for turbulence to prevent freezing, e.g. on 4 November 1992 the channel was 5 cm deep with a surface velocity of 0.7 m/s.

Table 4. Measured changes in lake level and in stage of East Channel, 1987-88 and 1988-89.

Date	Mackenzie stage (m)	Change (m)	Lake level (m)	Change (m)	Change (m H <sub>2</sub> O)
<b>1987-88</b>					
23 Nov	10.67	-	-3.15	-	-
23 Jan	11.07	+0.40	-2.77	+0.38	+0.35
20 Mar	11.20	+0.13	-2.67	+0.10	+0.09
Total		+0.53		+0.48	+0.44
<b>1988-89</b>					
10 Dec	10.96	-	-2.95	-	-
18 Feb	11.22	+0.26	-2.61	+0.34	+0.31
15 Apr	11.27	+0.05	-2.59	+0.02	+0.02
Total		+0.31		+0.36	+0.33

Mackenzie stage from Water Survey of Canada (1988, 1989).  
Lake level with respect to benchmark in permafrost.

On 30 November 1989, water was observed flowing out of the lake towards East Channel. The 8-cm-deep stream had no ice cover. On 2 December an ice cover had formed over the channel, but about 10 cm above the previous water level and water was flowing from the river into the lake. This observation confirms that East Channel water may have entered the lake during winter as the stage rose. However, in 1989-90, refilling did not last as long as in previous years, for the outlet channel was frozen through at a thickness of 28 cm when it was excavated on 18 February 1990. Since the lake level continued to decline between 2 December 1989 and 3 April 1990, there was no net input to the lake from groundwater. Instead, the lake lost water by seepage throughout the winter. Unfortunately the Water Survey gauge at Inuvik was not in operation for winter 1989-90, so it is impossible to determine whether the observed reversal in flow in the outlet channel corresponded to an increase in stage at Inuvik.

In order for the lake to be recharged by the Mackenzie in winter, the outlet channel should not freeze through, and the water level in East Channel should remain above the lake sill. Both conditions were met in 1987-88 and 1988-89. However, active sedimentation in the outlet channel has raised the sill enough to stop this process on a regular basis (1989-92).

Further support for the interpretation of lake-surface dynamics may be derived from conductivity measurements of lake water collected at various stages of the winter (Table 3). The conductivity of lake water increased in 1988-89 by an order of magnitude during the winter as a result of solute exclusion during growth of lake ice. However, during 1990, when lake refilling from the Channel was minimal, the total increment in conductivity was double that of 1989. The dilution of lake water by water from East Channel in 1988-89 is apparent (Table 3).

It has not been possible to determine the regional extent of lake refilling in winter. Inspection of the east side of the Delta during travel from Inuvik to Richards and Garry Islands in November 1990, 1992 and December 1991 revealed only one other lake with an open outlet. However, such observations merely

indicate the depth of the outlet, not the extent of hydraulic connection between distributary channels and adjacent lakes. Many "no-closure" lakes may have sills low enough to ensure connection and refilling beneath an ice cover throughout winter.

#### INTRUSIVE ICE

Lake sediments along the transect, where ice was frozen to the bottom, were drilled at the end of each winter. In 1988, close to the lakeward limit of grounded ice, an ice lens 14 cm thick was observed in sediments, 13 cm below lake bottom. The lens comprised columnar vertical crystals 1 cm in diameter, with elongated bubbles up to 1 cm long. The lens was devoid of mineral inclusions. The appearance of the ice was similar to S2 ice (Michel and Ramseier 1971). Seven cm of ice-bonded sediments lay below the ice lens. When these were penetrated, water rose to within 8 cm of the lake-ice surface. The hydrostatic head in the lake-sediments and the nature of the lens suggest it was intrusive ice, formed from water injected towards the freezing front. The large columnar crystals imply that the ice formed from bulk water, rather than by ice segregation. The suggestion is that in February or March 1988, after lake-bottom sediments at the drill site had begun to freeze, the rising stage lifted lake ice and frozen sediment together, and injected water into underlying sediments. Only traces of columnar ice, in lenses less than 1 cm thick, were recovered during drilling at similar locations in 1989, and none were observed in 1990 or 1991. These observations are similar to those from central Alaska of Kane (1981), who has described intrusive ice in the banks of small streams where icings are common.

Lesack et al. (1991) describe a ruptured ice cover at "NRC" Lake (Fig. 2) with water overflowing onto the ice surface during rising water level preceding break-up. No intrusive ice has been observed at NRC Lake, suggesting that in combination, the rate of increase in water level and the depth of frozen sediment led to rupture of the ice cover rather than intrusion of water into frozen ground.

## CONCLUSION

In summary, observations presented in this paper indicate that some lakes of the Mackenzie Delta may be recharged in winter by flow from channels where downstream blockage by ice causes a rise in water level. Some distributary channels in the outer Delta may freeze through over the season, diverting discharge and increasing storage in the main distributaries. Pressures sufficient to rupture ice over 30 cm thick, leading to icing, and to develop intrusive ice in freezing lake-bottom sediments may develop beneath the ice cover.

## ACKNOWLEDGEMENTS

The fieldwork has been supported by NSERC, the Geological Survey of Canada, Imperial Oil Limited and the Science Institute of the Northwest Territories. Unpublished stage and discharge data were kindly supplied by Paul Squires, Water Survey of Canada, Yellowknife, and by the late Herb Wood, Wade Hanna and Moe Hansen, Water Survey of Canada, Inuvik. Field measurements have been made in winter by Gary White and Les Kutny of the Inuvik Research Laboratory, Science Institute of the Northwest Territories. Numerous colleagues from the University of British Columbia have provided field assistance. Valuable comments on the manuscript were received from M. Conly, D.L. Kane, J.R. Mackay, P. Marsh and the referees.

## REFERENCES

- Burn, C.R. (1989) Frost heave of subaqueous lake-bottom sediments, Mackenzie Delta, Northwest Territories. Geological Survey of Canada Paper 89-1D, 85-93.
- Burn, C.R. (1990) Frost heave in lake-bottom sediments, Mackenzie Delta, Northwest Territories. Proc. 5th Can. Permafrost Conf. 103-108.
- Ferguson, M.E. (1990) Sediment movement in lakes in the central area of the Mackenzie Delta, N.W.T. M.Sc. thesis, Univ. Saskatchewan, Saskatoon. 85 pp.
- Gerard, L. (1990) Hydrology of floating ice. NHRI Science Report 1, 103-134.
- Jenner, K. A. and Hill, P.R. (1991) Sediment transport at the Mackenzie Delta - Beaufort Sea interface. Proc. Workshop on the Mackenzie Delta, NHRI Symposium 4, 39-51.
- Kane, D.L. (1981) Physical mechanics of aufeis growth. Canadian Journal of Civil Engineering 8, 186-195.
- Lesack, L.F.W., Marsh, P. and Hecky, R.E. (1991) Ice-cover growth and freeze-out of solutes in a Mackenzie Delta lake. Proc. Northern Hydrology Symp. NHRI Symposium 6, 219-236.
- Mackay, J.R. (1963) The Mackenzie Delta area, N.W.T. Geographical Branch Memoir 8, 202 pp. Dept. of Mines and Technical Surveys, Ottawa.
- Mackay, J.R., Lewis, C.P., MacKay, D.K., and Ostrick, J. (1979) Frost heave at ground temperatures below 0°C, Inuvik, Northwest Territories. Geological Survey of Canada Paper 79-1A, 403-406.
- Mackay, J.R. and Leslie, R.V. (1987) A simple probe for the measurement of frost heave within frozen ground in a permafrost environment. Geological Survey of Canada Paper 87-1A, 37-41.
- Marsh, P. and Hey, M. (1989) The flooding hydrology of Mackenzie Delta lakes near Inuvik, N.W.T., Canada. Arctic 42, 41-49.
- Michel, B. and Ramseier, R.O. (1971) Classification of river and lake ice. Canadian Geotechnical Journal 8, 36-45.
- Reeder, S.W., Hitchcock, B., and Levinson, A.A. (1972) Hydrogeochemistry of the surface waters of the Mackenzie River drainage basin, Canada - I. Factors controlling inorganic composition. Geochimica et Cosmochimica Acta 36, 825-865.
- Water Survey of Canada (1988) Surface water data, Yukon and Northwest Territories 1987. 110 pp. Inland Waters Directorate, Water Survey of Canada, Ottawa.
- Water Survey of Canada (1989) Surface water data, Yukon and Northwest Territories 1988. 114 pp. Inland Waters Directorate, Water Survey of Canada, Ottawa.

# COOPERATIVE RUSSIA-CANADIAN GEOPHYSICAL INVESTIGATIONS OF PERMAFROST ON THE YAMAL PENINSULA, WESTERN SIBERIA

R.A. Burns<sup>1</sup>, N.N. Goriainov<sup>2</sup>, J.A. Hunter<sup>1</sup>,  
A.S. Judge<sup>1</sup>, A.G. Skvortsov<sup>2</sup>, B.J. Todd<sup>1</sup>, and V.M. Timofeev<sup>2</sup>

<sup>1</sup> Geological Survey of Canada, 601 Booth Street, Ottawa, Ontario, Canada K1A 0E8

<sup>2</sup> Ministry of Geology, VSEGINGEO, 142452 Zeleny Village, Moscow, Russia

Geophysical field studies were carried out at a site on the Yamal Peninsula of Russia as part of a joint Russia-Canada program of geotechnical investigations of permafrost for engineering purposes. The site was selected for its known variability of soil types and ground ice conditions. Several different electrical, electromagnetic, seismic, and ground probing radar (GPR) surface techniques were tested in unison to detect the presence/absence of ground ice, lithologic variations, and the presence of saline permafrost. In addition, twelve boreholes were drilled to depths ranging from 10 to 20 meters. Borehole geophysical logging was conducted in all boreholes; the techniques consisted of gamma-gamma (density), neutron-neutron (volume % water), natural gamma (lithology), electrical conductivity, and longitudinal (P) and transverse (S) wave seismo-acoustics. Surface seismic profiling and soundings were carried out on representative areas of the survey site in order to observe seismic velocity structure. A new seismic reflection profiling technique was developed, using transverse SH waves; it was successfully tested over an area of massive ground ice. The various geophysical surveys were able to successfully delineate anomalous zones of ground ice and saline permafrost. Recommended procedures and techniques were developed for use in geotechnical investigations in permafrost areas.

## INTRODUCTION

As part of a joint Russia Canada program of geotechnical investigations of permafrost for engineering purposes, geophysical studies were carried out at a site on the Yamal Peninsula of Western Siberia in July, 1991, (see also Kurfurst et al., 1993, fig. 1). The site selected is in the center of the developing Bovanenkovo oil and gas field, where there is a known variation in permafrost soil types and ground ice conditions.

Surface electrical and electromagnetic surveys are most efficiently performed to obtain a regional overview of permafrost conditions and to identify anomalies which may require further examination. Such anomalies may include change in lithology of near-surface sediments, occurrence of massive ground ice, and the occurrence of saline (or, non ice-bonded) permafrost. Surface electromagnetic surveys are most cost efficient and should be one of the primary reconnaissance geophysical tools used in any route or site investigations.

In a similar manner, a reconnaissance form of seismic refraction surveying can also be used to detect changes in lithology and to delineate the presence of talik zones.

Ground probing radar and seismic reflection techniques can be applied to obtain information on structural changes within the shallow permafrost section. Such variations include the detailed delineation of massive ice and lithological boundaries.

The application of combinations of geophysical techniques often result in the identification of variations of geophysical properties which may indicate potential geotechnical problems. Many of the geophysical anomalies can be directly related to surface geomorphology (i.e. presence of lakes, streams, thaw

slides, etc.), and are self evident. It is the presence of geophysical anomalies which do not correlate with obvious surface geomorphological features which justify the application of these techniques.

After completion of surface geophysical surveys at a geotechnical site, drilling may be necessary to examine geophysical anomalies. At this stage of the program, borehole geophysics can be of value in assessing the geophysical and geotechnical properties of the anomalous zones. The judicious use of borehole geophysics can substantially reduce the cost of a borehole program; that is, geophysics can replace, in part, the necessity of continuous sample recovery.

The following discussion is a review of current geophysical techniques used in geotechnical site evaluations with specific examples derived from the Russia/Canada test site at Bovanenkovo. The complete geophysical data set for this site can be found in Kurfurst (1992).

A detailed description of the Bovanenkovo field site has been given by Kurfurst et al. (1993), and will not be repeated here. Also, figures 1, 2 and 3 of that paper show the location of the site, landforms, geophysical survey lines, and boreholes to which reference will be made in this paper.

Although each geotechnical site in permafrost presents its own unique problems, it is hoped that the results presented here will be a useful guide for future workers in the field.

## ELECTRICAL AND ELECTROMAGNETIC METHODS

Three different electrical and electromagnetic techniques were applied to the survey site. Each technique was applied

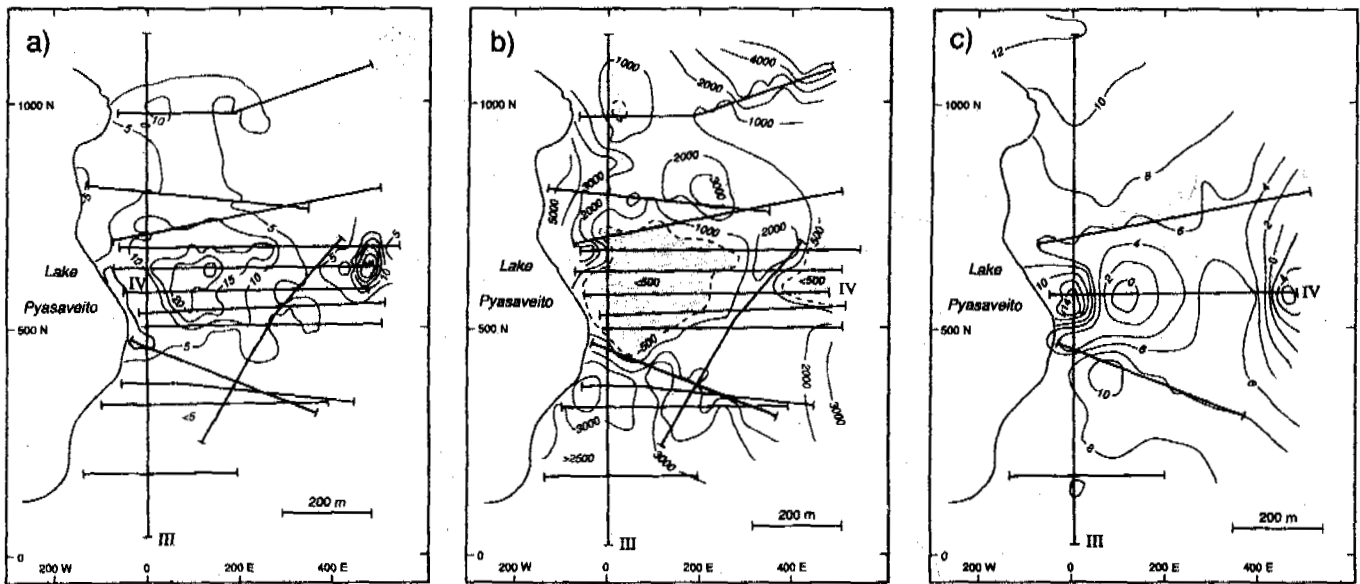


Figure 1 - Electrical conductivity maps for the Bovankovo field site: (a) EM-31, at 39.2 kHz, vertical dipole at ground level. Contours are conductivity in milliSiemens/meter. (b) VCHEP, inductive electrical system at 8 kHz. Contours are resistivity in Ohm-meters. (c) MaxMin EM, vertical dipole, quadrature component, at 7040 Hz. Contours are % of the total field.

along a series of survey lines (see Kurfurst et al., 1993, figure 3), and the data were compiled and contoured in map form.

An electrical technique designed at VSEGINGEO, known as VCHEP, is a capacitive-coupled line antenna system which measures the electrical field of a transmitted low-frequency EM signal. The transmitter and receiver electrode configurations are similar to that used in DC electrical surveying; however, the advantages of this method lie in its ability to electrically couple to resistive earth materials and to obtain reliable measurements at high resistivities. The system as used at the test site was configured as a dipole-dipole arrangement of transmitter and receiver with a 30 meter spacing between transmitter and receiver electrode pairs and a 6 meter spacing between electrodes. The transmitter frequency was 8 kHz. Measurements were made at 10 meter intervals along survey lines. With this transmitter-receiver spacing, the maximum depth of penetration is approximately 15 meters.

Two inductive frequency-domain EM units were tested at the Bovankovo site. Instruments of this type employ a local transmitter coil to generate a time varying magnetic field that induces small eddy currents in the earth. These eddy currents produce a secondary magnetic field which is detected, along with the primary field, by a receiver coil. This secondary field and its depth of penetration are a function of the intercoil spacing, the orientation of the coils, and to a lesser extent, the operation frequency, and the layering in the ground. Under certain constraints, the ratio of the secondary to the primary magnetic field is linearly proportional to the terrain conductivity (resistivity).

The two EM units used for shallow permafrost mapping at this site were the Geonics EM-31 and the Apex MaxMin I.

The Geonics EM-31 operates at 39.2 kHz with a fixed intercoil spacing of 3.66 meters. Three measurements with the instrument provide three effective depths of exploration. A horizontal dipole at ground level corresponds to 2.1 meters

effective depth; a horizontal dipole at 1 m elevation has a 3.7 meter effective depth; and a vertical dipole at ground level has a depth of penetration of 4.6 meters.

The Apex MaxMin I is a multifrequency horizontal loop EM system which operates at 110, 220, 440, 880, 1760, 3520, 7040, and 14080 Hz. The lowest frequency provides the deepest penetration and the highest frequency provides the shallowest. Readings of in-phase and quadrature components of the secondary magnetic field were made using a coil spacing of 50 meters. The effective depth of penetration is approximately 25 meters. In this permafrost terrain, negative quadrature values are indicative of conductive ground.

Figure 1(a), 1(b), and 1(c) show some of the results in map form for EM-31, VCHEP, and MaxMin respectively (shallowest to deepest penetration). Although EM-31 and MaxMin are in units of conductivity, whereas the VCHEP results are in units of resistivity, all three systems have indicated anomalies which are correlatable from map to map. Several anomalies can be correlated with geomorphological surface features as seen on Figures 2 and 3 of Kurfurst et al. (1993) (topographic lows and areas of healed retrogressive thaw slides generally show conductivity highs or resistivity lows). In general, the northern portion of the map area has lower resistivities. A broad resistivity low (conductivity high) centered at 600 N, 100 E is associated with a thick layer of clayey silt as determined from drilling (Kurfurst et al., 1993). From the EM-31 results, the high conductivity values suggest that the active layer is thicker in this area than elsewhere in the survey area, or, that there is high salinity groundwater near the surface. High resistivities in the southern portion of the map area result from the occurrence of near-surface ice-rich sands.

Figure 2 shows the results of EM-31, VCHEP, and MaxMin along profile III. Anomalies can be correlated with the geological interpretation as shown in figure 4 of Kurfurst et al. (1993).

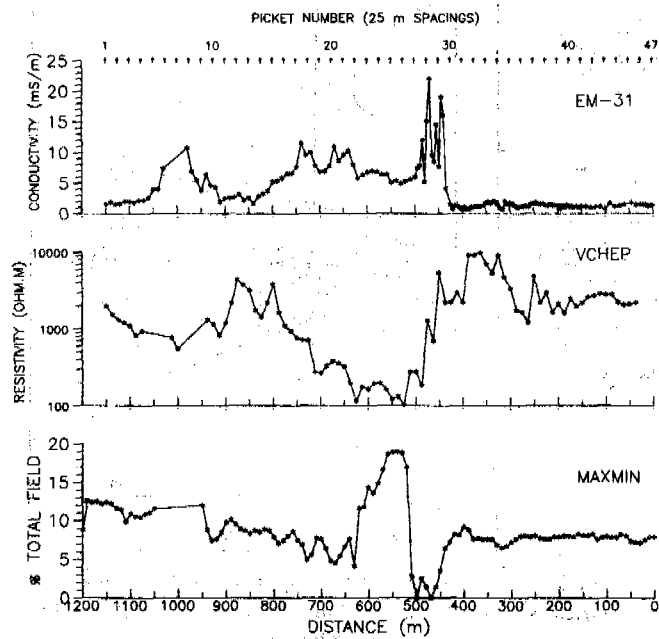


Figure 2 - Electromagnetic profiling along profile III. The instrument parameters are as given in figure 1.

The high conductivity anomaly situated at 450 E and 550 N can be seen on the EM-31, VCHep, and MaxMin maps (figure 1), and also in profile form in figure 3 (profile IV, see also Kurfurst et al., 1993, figure 4). The results suggest that the conductivity anomaly persists at depth and could represent

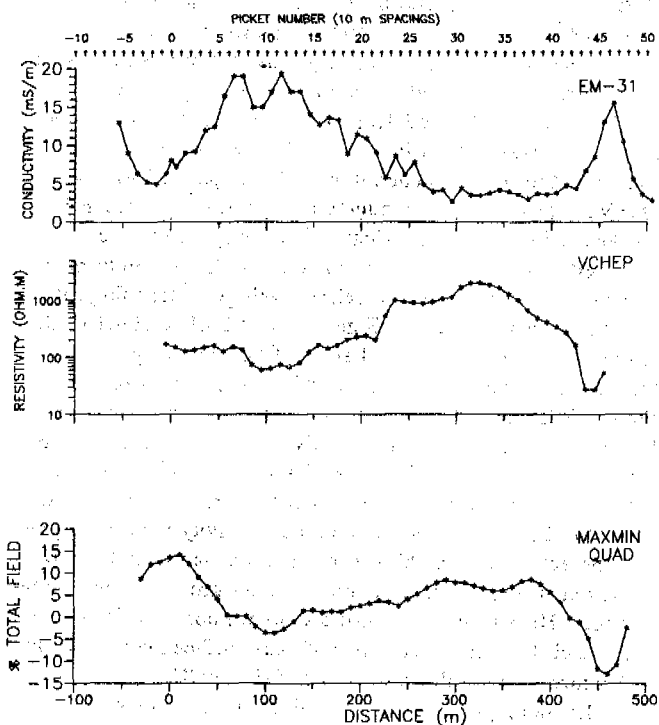


Figure 3 - Electromagnetic profiling along profile IV. The instrument parameters are as given in figure 1.

either a talik zone or a saline permafrost zone. This area represents a potential drilling target; a borehole was subsequently drilled to examine the anomaly (BH-7K).

### SEISMIC REFRACTION METHODS

A two channel seismic refraction method was applied along profile III to obtain changes of average P-wave velocity. The separation between geophones was 10 meters, and the source offset for forward and reverse shooting was 25 meters. The source used was a steel rod inserted through the active layer and seated on frozen ground. The refraction arrivals from forward and reverse shots were averaged to obtain a velocity which is unaffected by structure beneath the geophone locations. The choice of offset determines the depth of measurement of the average velocity. The offset for this survey was chosen to obtain measurements of velocities beneath the thermal effect of the near surface. Figure 4 shows a section along profile III, and should be compared with the geological profile given in figure 4 of Kurfurst et al. (1993). High P wave velocities are observed at the north end of the profile where massive ice is present at shallow depth beneath the silty clay. At distances between 400 and 700 meters along the profile, there is no indication of massive ice, and the velocity values are in the range of 2000-2400 meters/sec, typical of those for silty clay at  $-5^{\circ}\text{C}$ . At the south end of the profile, the velocity values increase to the range of 2500-3000 meters/sec in the area of ice-rich sand.

This form of refraction profiling can be a rapid cost-effective method to obtain additional information on variation of geophysical properties; its application should be considered in the early reconnaissance phase of surveying.

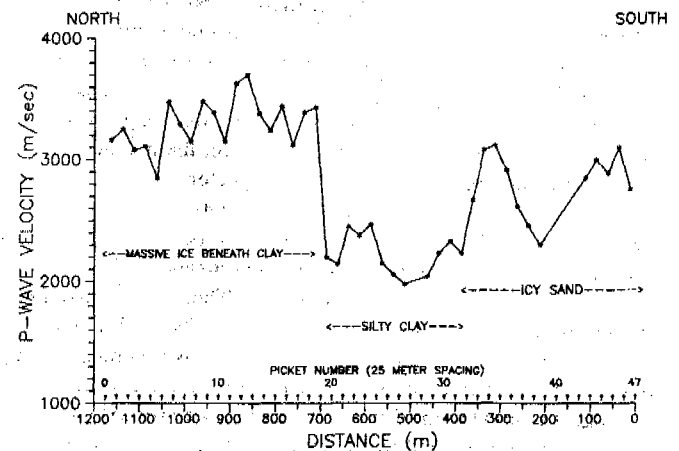


Figure 4 - The results of the two-channel P wave seismic refraction surveying along profile III. Measurements were made at 25 meter intervals.

### GROUND PROBING RADAR

Several kilometers of line were surveyed at Bovankovo using a pulseEKKO IV ground probing radar (GPR) system.

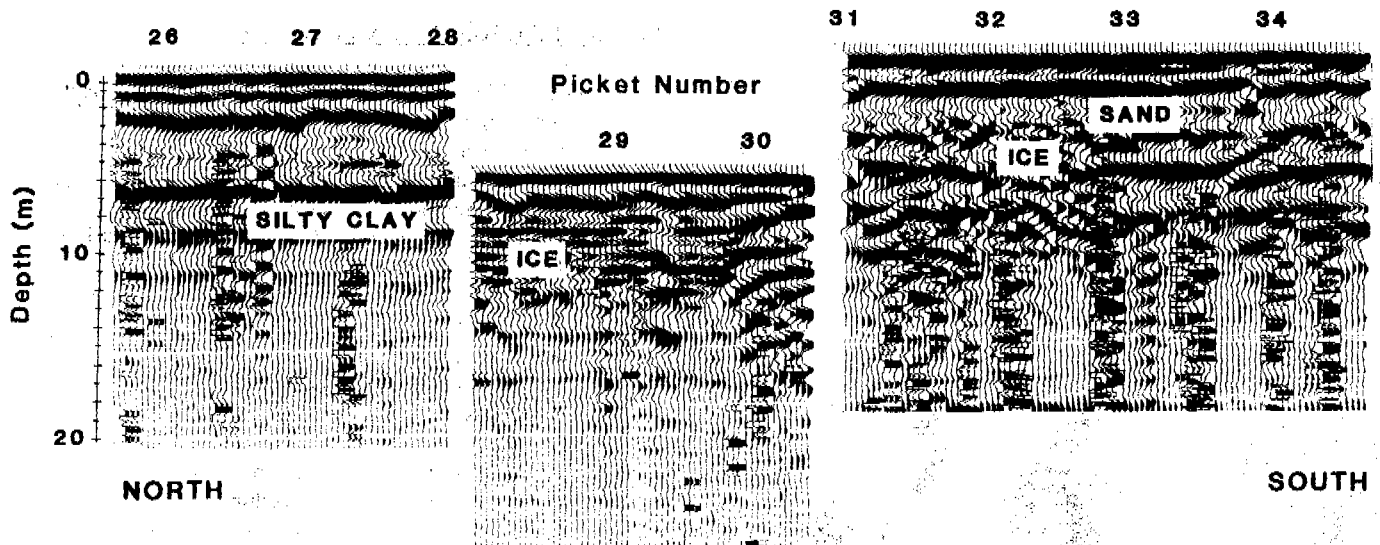


Figure 5 - An example of ground probing radar along a portion of profile III. The measurements were made at 1 meter intervals.

The system is a lightweight, fully digital, radar developed in Canada by Sensors & Software Ltd. for the Geological Survey of Canada. These test surveys were conducted to evaluate GPR as a sounding tool with which to compliment geotechnical drilling evaluation in the very complex surficial geology conditions of the Yamal Peninsula in general and the Bovanenkovo area in particular. GPR, with its high resolution, in the range of 10 to 30 cm, and a depth of penetration in the range of 10 to 30 meters, was considered a useful tool in resolving near-surface characteristics posed by particular problems of a wide range of soil types, extensive ground ice, and saline permafrost.

The survey lines were carried out using three different frequencies of 50 MHz, 100 MHz, and 200 MHz, each yielding different effective depths of penetration and near-surface resolution. Two types of survey were used:

- 1) the transmitter and receiver moving progressively along a survey line at a constant separation of either 1 or 2 meters; and
- 2) step-wise increase of separation between transmitter and receiver.

The former was the standard reflection survey mode, while the latter was used to determine the near-surface signal velocity. Since limited time was available for surveys, several type localities were chosen to represent transitions between sands and clays, icy sands in contrast with non-icy sands, saline frozen sediments, and massive ice bodies within both sand and clay sequences.

Figure 5 demonstrates some of the major features observable on the radar profiles. It shows approximately 200 meters of section (325 to 525 m N - between pickets 34 and 26) along profile III at a major transition zone from frozen sands to clays. The survey was conducted with 50 MHz antennas at trace spacings of 1 meter. Depth is expressed on the vertical axis using the measured ground wave velocity of 0.090 meters/ns. Approximate corrections for topography have been made by vertical shifts in the traces. Materials on

the south part of the profile are mainly sands containing massive ice; on the northern part of the profile, the materials are mainly silty clays which are frozen but do not contain thick ice sequences over the section and depth intervals shown. The edge of the sand body is readily seen on the south side of the topographic low, in the center of the section.

#### SEISMIC REFLECTION METHODS

High resolution P wave reflection techniques often cannot be applied in permafrost areas for the delineation of shallow structure because of the necessity for very high frequencies (> 1000 Hz), and problem of high-velocity ground roll interference. However previous tests in the Yamal Peninsula (A. Skvortsov, 1990, pers. comm.) indicated the possibility of utilizing shear wave techniques.

Offset vertical seismic profiling tests were conducted in BH-2K (Skvortsov et al., 1992) to determine optimum reflection geometry and to correlate reflection events with known geology.

A test survey using the shear wave reflection technique was conducted between pickets 10 and 25 on profile III (see Kurfurst et al., 1993, figure 4). The surface array consisted of 50 Hz horizontal geophones oriented transversely to the survey line to maximize the detection of SH waves. The source was a steel rod and a 5 kg hammer; the rod was also oriented transverse to the survey line. Using a digital enhancement seismograph it was possible to stack signals from several blows. By changing the orientation of the source by 180 degrees, switching the polarity of the geophone, and stacking equal number of blows from the two directions, it was possible to substantially improve the signal to noise ratio (a standard technique for polarized shear wave investigations).

Figure 6 shows an optimum offset section from the survey using a 10 meter source-geophone offset with 2 meter spacings.



## BOREHOLE GEOPHYSICAL LOGGING

Geophysical logging in boreholes can often compliment borehole sampling programs by either providing additional information between sampling locations within a borehole or corroborating the laboratory testing of samples. Often a geophysical borehole tool provides an average value of a physical property since measurements are made from a large volume of material surrounding the tool.

Several different types of borehole logs were obtained at the Bovankovo test site:

The natural gamma log measures the natural radiation from a formation (generally composed of radiation from uranium, thorium and potassium). High count rates are associated with fine-grained materials, including organic-rich zones. Low count rates are associated with sands and gravels. In a permafrost setting, count rates approaching zero indicate the presence of excess ice or massive ice. Usually most of the measured radioactivity is within 0.3 meters of the detector in the hole.

The conductivity tool measures electrical conductivity of a surrounding formation using a high frequency (39 kHz) inductive electromagnetic technique similar to those used on surface. In ice-rich sediments, the response from this tool can be minimal, and it is not recommended for accurate discrimination of lithology. However, the tool is an excellent one for the detection of saline zones within the permafrost section. Conductivities less than 10 mS/m are indicative of high ice-content materials; conductivities in the range of 10-20 mS/m can be correlated with fine-grained materials with some unfrozen water content. Conductivities above 20 mS/m are associated with substantial unfrozen water content and/or saline conditions. This tool is averaging conductivities from at least 1 meter into the surrounding formation.

The gamma-gamma log measures the density of the material surrounding the borehole (to approximately 0.3 m penetration) by the absorption and scattering of gamma rays from a radioactive source. When properly calibrated for

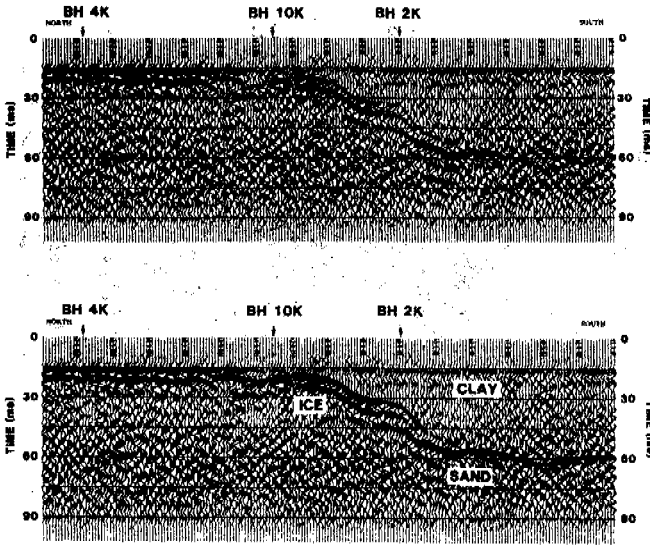


Figure 6 - An example of shear wave reflection surveying along a portion of profile III. The measurements were made at 2 meter intervals.

between traces. One major reflection package is observed rising from south to north. For most of the section this event is correlated with the top of massive ice, as determined by drilling (see Kurfurst et al., 1993, figure 4).

From borehole velocity measurements the average shear wave velocity for the silty clay is 750 m/s, and for both massive ice and icy sand is on the order of 2000 m/s. The large velocity contrast between these units results in a large reflection coefficient. This reflection technique cannot discriminate between reflections from the clay/ice boundary versus the clay/sand boundary; however, the structure of the units are well defined where large velocity contrasts exist. It is suggested that this technique can be utilized in many areas of permafrost soils, although field experience, to date, is limited.

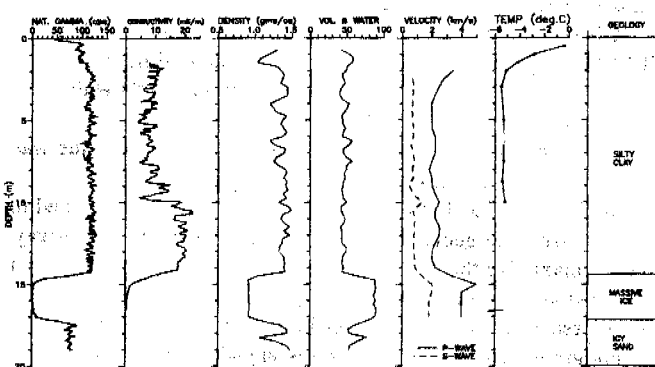


Figure 7 - Combined geophysical logs and generalized geology for hole BH-2K. Natural gamma and conductivity measurements are at 2.5 cm intervals, density (gamma-gamma) and volume % water (neutron-neutron) are at 25 cm intervals, and seismic velocities are at 0.5 meter intervals.

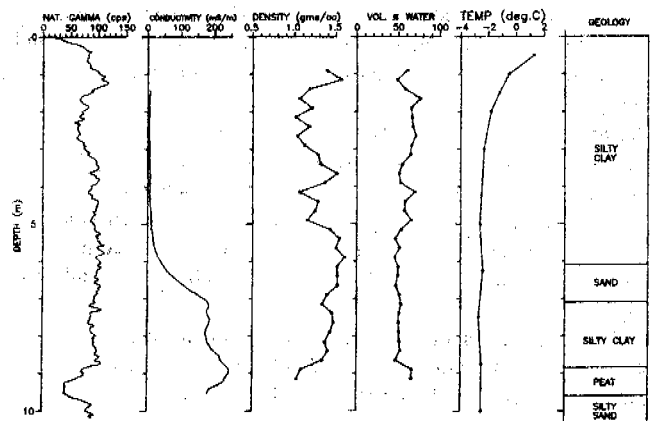


Figure 8 - Combined geophysical logs and generalized geology for hole BH-7K. Measurement parameters are as given in figure 7.

borehole size, this tool can provide accurate bulk densities of materials.

The neutron-neutron tool measures the absorption of neutrons from a radioactive source in the hole. The count rate is inversely proportional to the amount of hydrogen atoms in the materials, hence it can be calibrated to volume-percent water content. This tool can provide excellent indication of excess ice and massive ice.

Seismic downhole logs measure both compressional and shear wave velocities, which can be used to estimate the dynamic elastic moduli of materials. The tool consists of a three-component seismometer clamped at intervals down the hole. The source (a hammer and rod) is on surface at the borehole. Measurements of arrival times of both P and S waves over a minimum of three locations can be used to compute interval velocities.

Figure 7 shows a complete suite of geophysical logs for BH-2K on profile III. Most logs identify the major lithological boundaries. The conductivity log shows little contrast between massive ice and icy sand beneath; however the increase in conductivity within the silty clay unit suggests increasing unfrozen water content with depth.

Figure 8 shows the available borehole logs for BH-7K, located at the geophysical conductive anomaly on profile IV. The large conductivity anomaly identified in the surface electrical profiling is correlated to the highly conductive materials beneath the silty clay at depths greater than 6 meters.

## GROUND TEMPERATURE MEASUREMENTS

Ground temperature measurements were made to depths of 10 meters in seven of the holes drilled during the Bovanenkovo field survey of July 1991. The results in two of the boreholes are shown in figures 7 and 8. Each of the measurements were made at least two days after completion of the drilling, and were obtained by suspending a 10 sensor multithermistor cable in the hole for a period of four hours, or, in several cases, overnight. Since the holes were air-filled, with the exception of BH-7K, which contained unfrozen saline water in its lower half, there was some concern regarding their overall thermal stability. In short-term tests, the boreholes proved stable if the surface casing was plugged to prevent air exchange with the atmosphere. Measurements in air-filled holes are, in fact, standard practice in Russia. The cable used for these measurements was of Canadian manufacture using YSI 44033 thermistors and a 5-digit Fluke DMM for resistance measurement.

The two examples given demonstrate that, although this area is in continuous permafrost and arctic tundra, ground temperatures, even at 10 meters depth, vary by several degrees between different locations. Measured ground temperatures at a depth of 10 meters in all of the boreholes ranged from -2.1 to -6.7°C with a mean value of -4.5°C. The coldest sites were beneath the upland sandy soils with an average temperature of -6.7°C.

## SUMMARY

Geophysical methods can be used effectively in geotechnical sites surveys in permafrost to compliment and expand surface geomorphological and geological studies through the application of such rapid cost-effective surface surveys as electromagnetic, electrical, seismic and ground probing radar. Such surveys should be conducted as early as possible in the site program so that any anomalies that are identified can be compared to known surface features; those that cannot be so explained may become priorities for primary drilling programs.

Borehole geophysics can be extremely useful to compliment geotechnical testing from borehole sampling. Even in the case of continuous coring of boreholes, geophysical logging can be used to identify zones within a sampled hole where geotechnical testing should be carried out.

Finally geophysical surface techniques can be applied on a detailed scale where geotechnical drilling has identified structures which require delineation in three dimensions.

In conclusion, geophysical techniques can be effectively used in all stages of geotechnical assessment of a site in permafrost. Some techniques are refined enough to yield accurate geotechnical properties for direct use, others may be able to delineate structure of materials at depth without the ability to accurately assess properties, and still others may only be able to identify a geophysical anomaly integrated over a large volume of material. However, a combination of techniques used in concert is a most powerful and effective tool which should be an integral part of geotechnical surveying.

## REFERENCES

- Kurfurst, P.J., (ed.), (1992), Canada-Russia geotechnical studies of permafrost, Bovanenkovo test site, Yamal Peninsula, Western Siberia, July 1991; Geological Survey of Canada, Open File 2546, 402 pp.
- Kurfurst, A.G., Melnikov, E.S., Tarasov, A.M., and Tschervova, E.I., (1993), Co-operative Russian-Canadian engineering geology investigations of permafrost on the Yamal Peninsula, Western Siberia; Proceedings, 6th International Conference on Permafrost, Beijing, China, (this volume).
- Skvortsov, A.G., Hunter, J.A., Goriainov, N.N., Burns, R.A., Tsarov, A.M., and Pullan, S.E., (1992), High resolution shear-wave reflection technique for permafrost engineering applications: New results from Siberia; in Expanded Abstracts with Biographies, 1992 Technical Program, 62nd Annual International Meeting of the Society of Exploration Geophysicists, October 25-29, 1992, New Orleans, LA, p. 382-384.

RESEARCH ON ROCK GLACIERS IN THE CENTRAL ITALIAN ALPS  
(VALTELLINA, SONDRIO, NORTHERN ITALY)

Calderoni G. (\*), Guglielmin M. (\*\*), Lozej A. (\*\*\*) and Tellini C. (\*\*)

(\*) Dept. of Earth Sciences, University of Rome, P.le A. Moro, 5 00100-Rome, Italy

(\*\*) Institute of Geology, Paleontology and Geography, University of Parma, Viale delle Scienze, 78 43100-Parma, Italy

(\*\*\*) Dept. of Earth Sciences, University of Milano, Via Cicognara, 7 20128-Milano, Italy

**SYNOPSIS** This paper reports the preliminary results of a continuing multidisciplinary research aimed at determining the distribution and implementing the classification of the rock glaciers spread in the Upper Valtellina (Sondrio, Italian Alps). Also reported are the first data of radiocarbon chronology, yielded by the paleosols underlying the studied rock glaciers, which are herein used to obtain a tentative time scale of the main glacial stages occurred in the area. Results provide evidence of phases of rock glacier expansion that can be assigned to Larstig, Goschenen I and Goschenen II stages and to the Little Ice Age.

#### INTRODUCTION

During the last decade the concern about periglacial alpine environments increased in Italy following the first stimulating studies on rock glaciers carried out by Italian researchers (Gruppo Nazionale Geografia Fisica e Geomorfologia CNR, 1987; Smiraglia, 1989; Guglielmin, 1991; Guglielmin and Tellini, in press).

This paper provides new data on the distribution of rock glaciers in the Upper Valtellina (Sondrio, Northern Italy) along with a tentative chronologic framework. A multidisciplinary approach has been chosen to accomplish the task, including electric sounding, radiocarbon dating and measurement of both shallow temperature of ground in summertime (SGT) and bottom temperature of winter snow cover (BTS).

#### GEOLOGIC AND GEOMORPHOLOGIC SETTING

The study area (Fig. 1) extends over 620 km<sup>2</sup> at altitudes ranging from 900 to 3439 m a.s.l. and is located in the central Lombard Alps (Sondrio, Northern Italy). The geology of the area is dominated by different tectonic units of the Upper Austroalpine structural domain; the most spread terranes being represented by low to medium metamorphic grade gneisses and schists. The sedimentary cover, lacking over most of the area, only occurs in the N apex where carbonate rocks of Mesozoic age predominate. The country rocks show impressive tectonic deformations and joints, this resulting in enhanced congelifraction effects. The whole study area, at present submitted to glacial and periglacial processes, also shows morphologic evidence of both late- and post-glacial stages. In this respect Figure 2 shows that in the Upper Foscagno Valley the geomorphologic survey pointed out that six glacial stages occurred. Here, an end moraine at 2000 m a.s.l. is assigned to the oldest glacial event (Daun stage),

while the maximum expansion of the Egesen stage is recorded by an end moraine at 2030 m a.s.l. Concerning the succession of the events it has been claimed that the end moraine of the first Holocene stage (Larstig stage?) reached 2190 m a.s.l. (Heuberger, 1988). The subsequent Goschenen I event (Burga, 1987) is recorded by the end moraine laid down at 2375 m a.s.l. by the glacial tongue of the Sattaron glacier as well as by the front of the Larstig (?) moraine of Mt. Foscagno. Both end and lateral moraines of Sattaron cirque, at about 2500 m a.s.l., are assigned to the Little Ice Age.

The new chronologic data for Mt. Foscagno and the nearby La Foppa and Mt. Vago cirques (Fig. 2 and 3, respectively) fit the above glacial sequence.

#### ROCK GLACIERS DISTRIBUTION IN NORTHERN VALTELLINA

Aerial photo interpretation and subsequent field survey led to identify, on morphologic basis, seventy nine rock glaciers, mostly lying on late- and post-glacial deposits. Figure 1 shows the location of the rock glaciers, assigned to the active, inactive, complex and uncertain groups according to the suggestions after Barsch (1978). In particular, active rock glaciers, besides lacking vegetation cover, showed an overall convex morphology, transverse ridges and furrows at the surface along with steep slopes at the front. Ultimate classification, however, relies also on the results of morphometric, physico-chemical and geophysical measurements, as well as occurrence of permafrost and downwards movement.

The rock glaciers were analysed for most morphologic features according to the guidelines after Carton et al. (1988). It has been found that glacial cirques and slopes account for 67 and 30%, respectively, of the host geomorphologic features. Only 14% of the surveyed rock glaciers show small size glaciers at the back side. Only

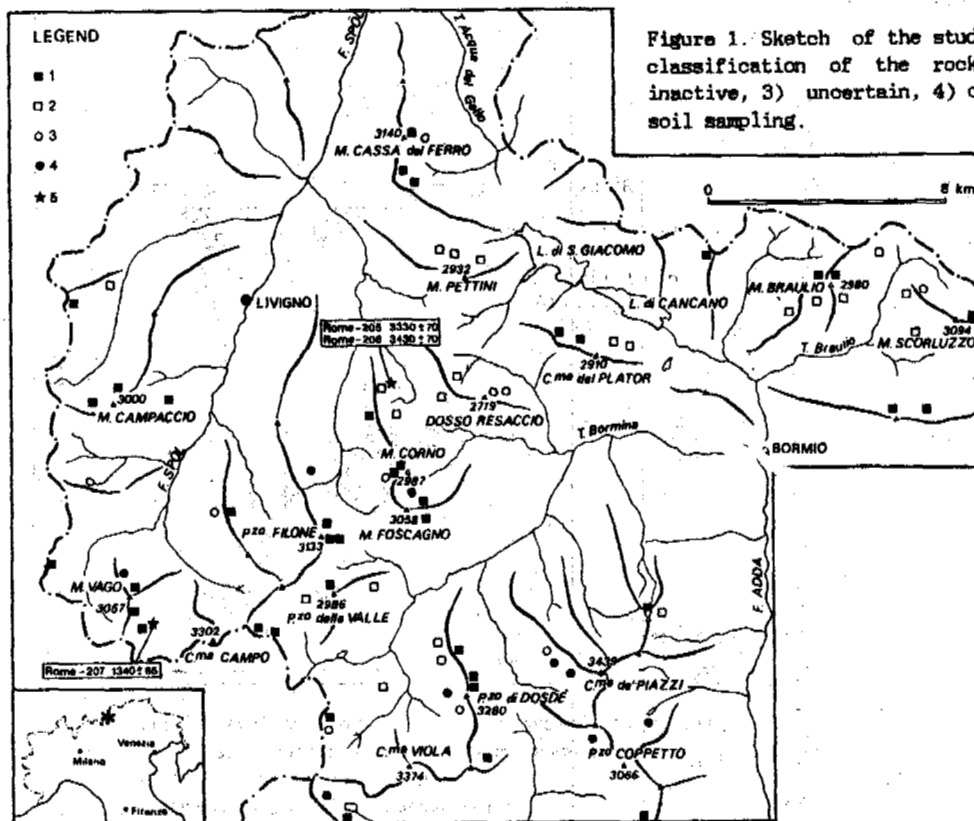


Figure 1. Sketch of the study area showing location and classification of the rock glaciers. 1) active, 2) inactive, 3) uncertain, 4) complex, 5) sites of buried soil sampling.

35 and 50% of the upslope deposits are represented by snow banks and moraines, respectively. Rock glaciers on metamorphics (82%) are 4-fold predominant over those on carbonate rocks (18%). Also by taking into account the relative distribution of the two lithotypes the preferential clustering of rock glaciers on metamorphics only drops to a 3-fold excess. Such distribution could suggest that lithology controls to some extent the rock glacier formation, in response to the differences in cliff morphology, thermal and mechanical properties of the involved rocks.

#### CLIMATOLOGIC CONSTRAINTS ON ROCK GLACIERS DISTRIBUTION

The climatic constraints on the presence of active rock glaciers are mean annual temperature and annual precipitation less than  $-1^{\circ}\text{C}$  and 2500 mm, respectively (Haeberli, 1985). Although meteorologic records for the study area are meagre, it has been estimated that the  $-1^{\circ}\text{C}$  isotherm falls between 2370 and 2742 m a.s.l. and the mean annual rainfall ranges from 750 to 1150 mm (Belloni, 1969). The climatologic control of the area can be inferred by surveying the lowest altitudes reached by the front of the rock glaciers. Active rock glaciers lie at 2325 through 2890 m a.s.l. (mean: 2617 m a.s.l.), thus altitudes consistent with the  $-1^{\circ}\text{C}$  isotherm, while the fronts of inactive rock glaciers are at 2115 through 2795 m a.s.l. (mean: 2457 m a.s.l.), that is ca 150 m below those of the active rock glaciers.

#### EXPERIMENTAL

Three glacial cirques at Mt. Foscagno, La Foppa (Fig. 2) and Mt. Vago (Fig. 3) (Sondrio, Northern Italy),

facing north and/or northeastwards and lying above 2300 m a.s.l., were analysed in detail. Mt. Foscagno cirque hosts the largest active rock glaciers (more than 1000 and 300 m in length and width, respectively) known throughout the area. At La Foppa six active rock glaciers occur, the larger one, named La Foppa I, being 500 m long and 200 m wide. The cirque of Mt. Vago, ca. 3 km west of La Foppa, contains, close to the moraine of 14-18th centuries ( $\approx$  Little Ice Age after Porter, 1986), two active rock glaciers facing northeastwards.

#### Measurements

**Water analysis:** Temperature, electric conductivity and total hardness were measured for runoff from the front of active rock glaciers to ascertain the occurrence of buried ice and/or permafrost. According to Evin (1984), the runoff temperature from active rock glaciers is  $< 2^{\circ}\text{C}$ .

**Shallow temperature of ground in summertime (SGT):** In 1991 summer simultaneous measurements of ground and air temperatures were made by a thermistor probe. Ground temperature and vertical thermal gradient were measured in shallow boreholes in rock glaciers and other deposits.

**Bottom temperature of winter snow cover (BTS):** BTS measurements were first introduced by Haeberli (1973) and since then have been extensively used (Haeberli and Patzelt, 1983). BTS values are thought to reflect permafrost occurrence and distribution; in fact, in winter time, under snow cover thicker than 1 m, BTS is almost constant up to the melting period and its value reflect the heat stored by the rock glacier active layer during the past summer (Haeberli, 1973). According to literature data  $\text{BTS} < -3$ , from  $-3$  to  $-1.7$  and  $> -1.7^{\circ}\text{C}$

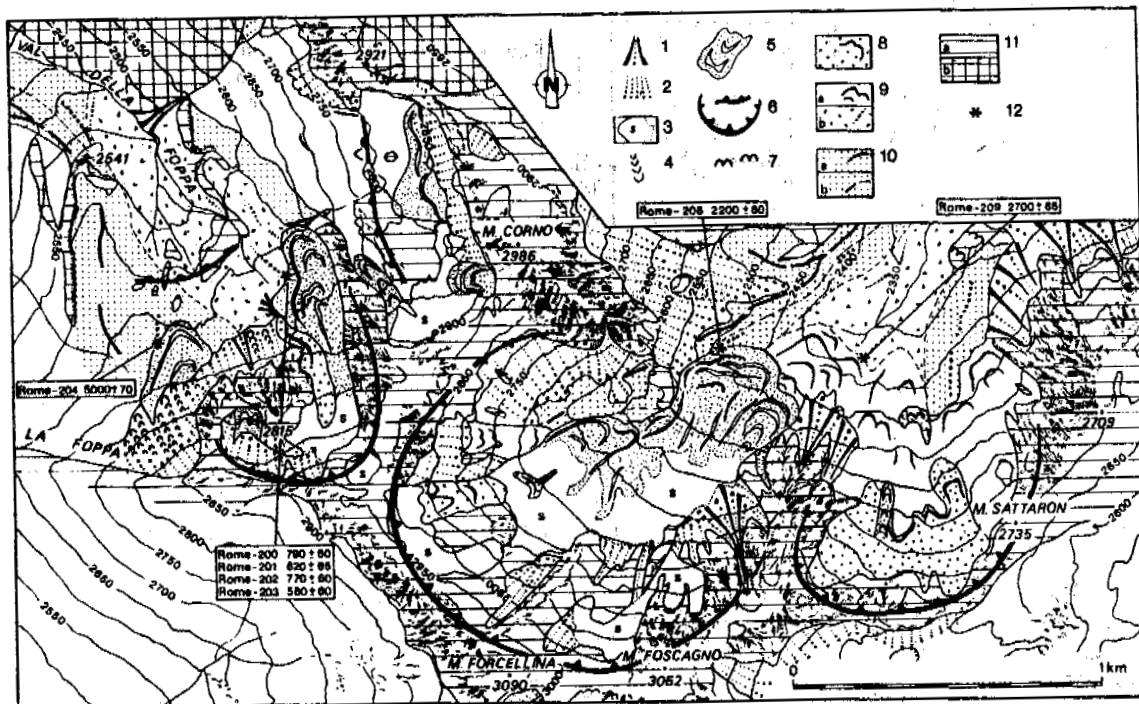


Figure 2: Geomorphologic map of the upper Foscagno and La Foppa valleys. Legend: 1) polygenetic alpine cone; 2) scree slope; 3) snow bank; 4) solifluction lobe; 5) active rock glacier; 6) edge of cirque and step of trough; 7) roches moutonnées; 8) Little Ice Age moraines; 9) Post-glacial moraines: a) Goschenen I stage ?, b) Larstig stage ?; 10) Late-glacial moraines : a) Egesen stage, b) Daun stage; 11) a) metamorphic bedrock; b) "En masse" collapsed slope; 12) sites of buried soils sampling.

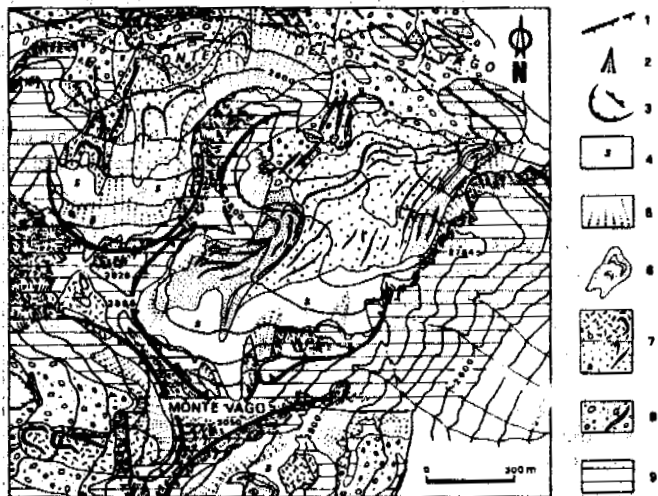


Figure 3. Geomorphologic map of Mt. Vago cirque. Legend: 1) gravitative deformational trench; 2) avalanche cone; 3) edge of cirque and step of trough; 4) snow bank; 5) scree slope; 6) active rock glacier; 7) Little Ice Age moraines: a) Fernau stage ?, b) 19-20th centuries age; 8) Late- and Post-glacial moraines.

points to permafrost, possible permafrost and lack of permafrost, respectively. Therefore these data were used to determine whether permafrost was present. Eighty BTS measurements were run with a thermistor probe from March

through April, 1982. Data record for each station also included snow thickness and air temperature 3 m above the topographic surface.

Electric soundings: The field equipment consisted of a georesistivimeter with 400 V of power supply. Besides the difficulties stemming from the irregular topographic surface, it was difficult to insert the electrodes into the coarse debris cover and establish reliable contact between the electrodes. The glaciologic interpretation of the model used relies upon the data after King et al., 1987; Evin and Assier (1980) and Evin et al. (1990) for permafrost and glacial ice.

Radiocarbon dating: Radiocarbon dating was performed with the liquid scintillation counting (LSC) technique using benzene as a counting medium. Chemical procedures and criteria of statistical evaluation of counting data are reported elsewhere (Calderoni and Petrone, 1992).

#### RESULTS AND DISCUSSION

Electric conductivity and temperature data for the measured runoffs show that the temperature of runoff from active rock glaciers was  $< 1.5^{\circ} \text{C}$  whereas that of outpourings from other aquifers exceeded  $2^{\circ} \text{C}$ . Both electric conductivity and total hardness data, however, failed to discriminate among the investigated aquifers. This being likely accounted for by the homogeneous lithology of the study area.

SGT values are listed in Table 1 along with the corresponding air temperatures. At Foscagno site SGT, measured at depths ranging from 37 to 110 cm (the clastic

character of the deposits prevented surveying at constant depth), discriminates the active rock glacier (SGT = 1.8° C) from inactive rock glacier, moraines and patterned ground (SGT = 8.5, 3.1 and 3.8° C, respectively).

BTS values were used for a rough zonation between permafrost areas (BTS < -3° C) and uncertain permafrost areas (-1.7° < BTS < -3° C): the resulting mapping and the sites of measurement are reported in Figure 4. The relationships BTS vs. snow cover thickness and altitude (not shown), though showing a low correlation, point out that all BTS's for deposits other than active rock glaciers are > -1.7° C. The few BTS values exceeding -1.7° C measured on active rock glaciers are reasonably accounted for by discontinuous permafrost occurrence. According to the distribution of BTS values, however, it appears that permafrost is mostly located at the front of active rock glaciers. Future research will be concerned with studying the relationships among BTS,

climate and thickness of active layer.

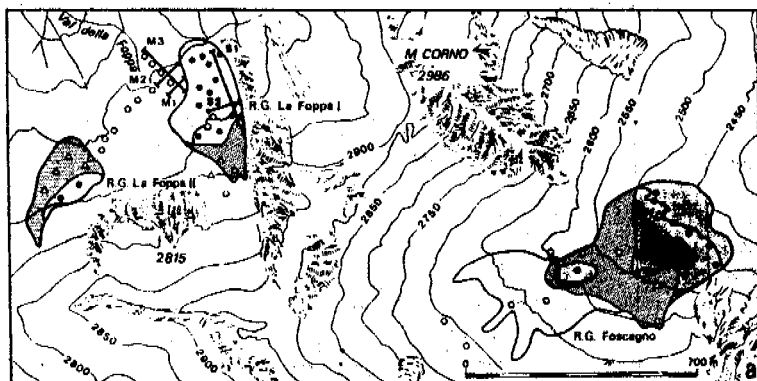
Results of the 1991 geoelectric campaign (sites are shown in Fig. 4) along with corresponding electric model and glaciologic interpretation are given in Figure 5 (a and b) and 6. Electric soundings on the morainic ridge at La Foppa I (M1, M2 and M3) revealed that the deposit includes several layers notably differing in thickness and lithology. Geoelectric sounding M2 is of particular concern in that suggests the occurrence, 10 m deep, of either a small body of buried ice or an ice-rich permafrost. Electric soundings for the active rock glacier La Foppa I revealed quite different stratigraphy, the layers being thicker and higher in resistivity than those in the morainic edge. Resistivity patterns provided by S1 and S2 soundings are hardly interpretable, for the occurrence of a thick level interbedded within the active layer and the ice-enriched permafrost.

Results of <sup>14</sup>C dating and <sup>δ13</sup>C measurements for the most representative humic matter fraction preserved in the sampled paleosols (PAs) are listed in Table 2. Although the younger, geochemically mobile carbonaceous compounds were previously removed, ages yielded by <sup>14</sup>C dating of humic matter in soils and sediments are referred to as "mean apparent ages" (Ferrin et al., 1984 and references therein). Thus, because a soil is a dynamic system subjected to continuing, unpredictable renovation, <sup>14</sup>C chronology may only provide the minimum age of the soil humic matter. The studied PAs, buried by rock glacier deposits, formed at 2300 through 2700 m a.s.l. in the alpine environment, characterized by low rainfall (< 1150 mm/yr) and mean annual temperature from 1.5 to -1.5° C (Gruppo Nazionale Geografia Fisica e Geomorfologia CNR, in press). Under such conditions the pedogenetic processes, including litter production, are only effective over 4-5 months per year. The PAs, formed on comparable bedrock assemblage, are from 20 to 40 cm thick and generally lack differentiation into horizons. Such latter feature could be a primitive character of the parent soil, developed under severe climatic conditions greatly affecting downwards migration of the soil particles. However, also soil reworking for cryoturbation and/or slow movement of the overlying rock glaciers could have been effective in overshadowing the

TABLE 1  
Shallow temperatures of ground in summertime (SGT)

	a	b	c	d	e	f	g
1 Mt. Foscagno	2540	+18	+3.0	37	0.40		
1 Mt. Foscagno	2540	+18	-2.0	80	0.25		
1 Mt. Foscagno	2560	+22	+2.5	30	0.65		
1 Mt. Foscagno	2615	+22	+6.5	40	0.39		
1 Mt. Foscagno	2615	+22	-1.0	73	0.31		
2 Mt. Foscagno	2380	+22	+9.0	51	0.25		
2 Mt. Foscagno	2460	+18	+8.0	40	0.25		
3 Mt. Foscagno	2550	+22	+5.5	49	0.33		
3 La Foppa I	2665	+20	+0.8	110	0.17		
4 Mt. Foscagno	2560	+22	+8.0	40	0.35		
5 Mt. Foscagno	2390	+18	+3.0	55	0.23		
5 Mt. Foscagno	2410	+18	+6.5	70	0.13		
5 Mt. Foscagno	2650	+22	+2.0	32	0.62		

a) geomorphic features: 1- active rock glaciers; 2- inactive rock glaciers; 3- moraines; 4- scree slopes; 5- patterned grounds. b) measurement sites; c) altitude (m a.s.l.); d) air temperature (°C); e) ground temperature (°C); f) depth of measurement (cm); g) negative thermal gradient (°C/cm).



LEGEND

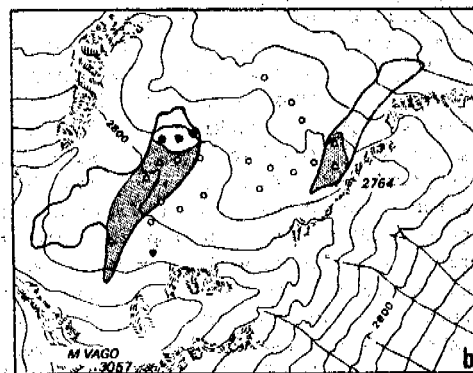
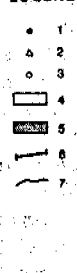


Figure 4. Preliminary permafrost zonation at La Foppa (a) and Mt. Vago (b) cirques (Upper Foscagno valley). Legend: 1) BTS < -3°C; 2) -1.7 < BTS < -3°C; 3) BTS > -1.7°C; 4) permafrost; 5) doubtful permafrost; 6) electric soundings location; 7) rock glaciers boundary.

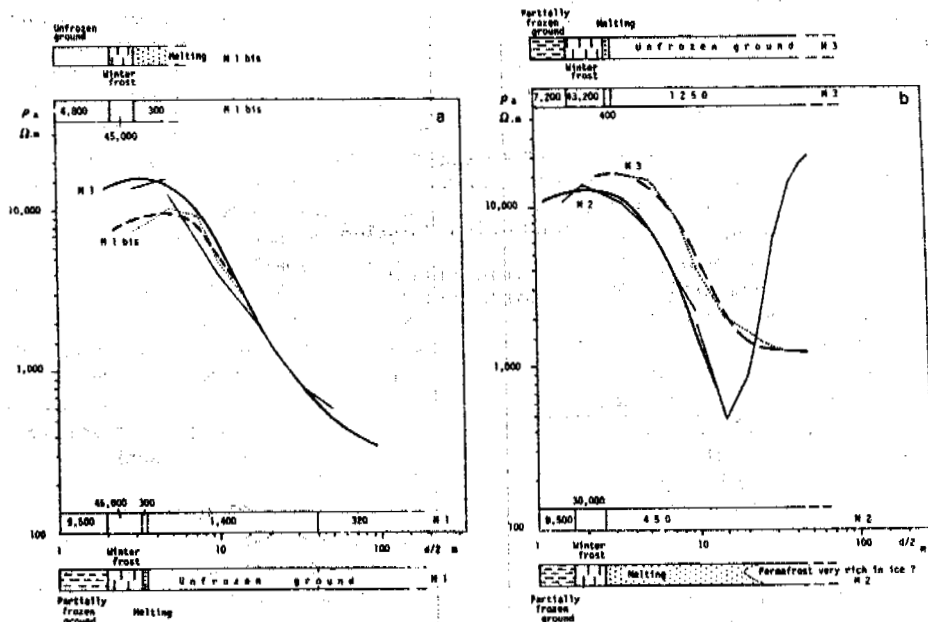


Figure 5. Geoelectric soundings on the Holocene morainic ridge at La Foppa I site: a) M 1 (fine and thick solid lines) and M1 bis (dashed and dotted lines) soundings; b) M2 (fine and thick solid lines) and M3 (dashed and dotted lines). The corresponding models are also shown.

primitive soils structure. For a better understanding of  $^{14}\text{C}$  ages three PAs were measured both on the topmost 1 cm (samples Rome-201, -203 and -206) and on the whole profile (samples Rome-200, -201 and -205). The results for the pair samples (Table 2) were quite comparable, thus pointing to an homogeneous C-isotopes distribution through the PAs profile, this being accounted for only by intensive reworking. Paleosols were sampled as far upglacier as possible to minimize the risk of considering soil spots buried by local slope collapses unrepresentative of the rock glacier movement. In this respect the measured  $^{14}\text{C}$  levels (Table 2), significantly lower than that of the reference "modern carbon", support the assumption that the analysed samples refer to a fossil pedosphere, not in steady-state with the atmospheric C-reservoir.

Radiocarbon dating of PAs is intended to provide the first maximum radiometric ages for the overlying deposits. Additional interpretation of the ages is beyond the scope of this paper, as glaciologic studies throughout the study area are just beginning and radiometric ages are lacking. The PAs submitted to  $^{14}\text{C}$  dating were collected from the five sites listed, along with the results, in Table 2; sample locations are shown in Figures 1 and 2. Ages for the four samples (Rome-200 through Rome-203) from la La Foppa I site, from beneath an active rock glacier at 2760 m a.s.l. and overlying a Holocene morainic ridge, bracket a 790 to 560 yr B.P. time-span. Thus inference is made that at La Foppa I site the rock glacier was also active over the 13-14th centuries (= Little Ice Age). The PA sample Rome-204, dated at 5000 yr B.P., underlies the inactive rock glacier La Foppa II and rests on glacial deposits not far from La Foppa I site. The measured age represents the only fixed point in the time-scale for the former

activity of La Foppa II rock glacier. North of Mt. Foscagno (Fig. 2) PA sample Rome-206, from beneath an active rock glacier overlying a Late-glacial morainic ridge was dated at 2200 yr B.P., whereas a PA (Rome-209) interbedded within two post-glacial morainic deposits and underlying the same active rock glacier postdated at 2700 yr B.P.. About 1 km northwards, near Foscagno Pass, samples Rome-205 and Rome-206 dated at 3330 and 3430 yr B.P., respectively, an overlying inactive rock glacier. Finally, the active rock glacier at Campo Valley (Fig. 1) postdates 1340 yr B.P. (sample Rome-207).

According to the simplified glacial time-scales after Heuberger (1968), Mair (1968) and Burga (1987), the  $^{14}\text{C}$  ages provide the following preliminary indications on

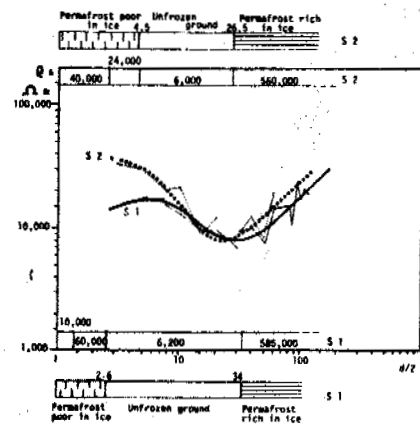


Figure 6. Electric soundings at La Foppa I active rock glacier. S1 (fine and thick solid lines) and S2 (dashed and dotted lines). The corresponding models are also shown.

TABLE 2

Conventional radiocarbon ages and carbon isotope data for the dated paleosol samples.

1	2	3	4	5
<b>Active rock glaciers</b>				
La Foppa I	Rome-200	780±60	-27.6	-93.21±7.4
La Foppa I	Rome-201	620±65	-27.5	-73.8±7.5
La Foppa I (*)	Rome-202	770±60	-27.2	-91.8±6.7
La Foppa I (*)	Rome-203	580±80	-27.0	-89.9±7.0
Campo Valley	Rome-207	1340±65	-26.6	-153.6±8.7
Mt. Foscagno	Rome-208	2200±60	-26.4	-239.7±8.1
<b>Inactive rock glaciers</b>				
La Foppa II	Rome-204	5000±70	-25.1	-463.4±5.0
Foscagno Pass	Rome-205	3330±70	-26.3	-339.1±6.0
Foscagno Pass (*)	Rome-206	3430±70	-26.6	-347.7±5.8
<b>Post-glacial moraines</b>				
Mt. Foscagno	Rome-209	2700±70	-26.2	-265.3±6.35

(\*) Topmost 1 cm.; (1) Sampling site; (2) Lab code; (3) Conventional  $^{14}\text{C}$  age (yr B.P.); (4)  $\delta^{13}\text{C}$  (‰); (5)  $\delta^{14}\text{C}$  (‰).

the main glacial stages recorded in the study area:

-LARSTIG stage. Site La Foppa II, sample Rome-204, 5000 yr B.P.

-GOSCHENEN I stage. Mt. Foscagno, samples Rome-208 and Rome-209, 2200 and 2700 yr B.P., respectively, and Foscagno Pass, samples Rome-205 and Rome-206, 3330 and 3430 yr B.P., respectively.

-GOSCHENEN II stage. Campo valley, sample Rome-207, 1340 yr B.P..

-XII-XVth centuries cold phase (= Little Ice Age), La Foppa I site, samples Rome-200 through Rome-203, spanning from 790 to 580 yr B.P..

#### CONCLUSION

Measurements of BTS and SGT, physicochemical analyses of water runoff and electric soundings were carried out for some rock glaciers in Upper Valtellina (Italian Alps). Results confirmed permafrost occurrence above 2500 m a.s.l.. Radiocarbon dating of paleosols buried by rock glaciers provided a preliminary chronologic framework for the glacial activity in the area.

#### REFERENCES

- Barsch D. (1978) - "Rock glacier as indicator for discontinuous alpine permafrost. An example from the Swiss Alps." Proc. 3rd Intl. Conf. on Permafrost, Edmonton, Alberta, Canada. Natl. Res. Con. Canada, Ottawa, 1, 348-352.
- Belloni S. (1969) - "Il clima della Valtellina in relazione alla difesa del suolo", Mem. Sc. Mat. Ist. Lon., XXVI, pp. 1-76.
- Burga C.A. (1987) - "Gletscher und Vegetationsgeschichte der Sudratischen Alpen seit der Spateiszeit", Mémoires de la Société Helvétique des Sc.Nat., 101, p. 184; Birkhauser, Basel.
- Calderoni G. and Petrone V. (1992) - "Department of Earth Sciences at the University of Rome radiocarbon dates I", Radiocarbon, 34,1, 105-113.
- Carton A., Dramis F., Smiraglia C. (1988) - "A first approach to the systematic study of the rock glaciers

in the Italian Alps", Proceed. Fifth Int. Conf. Permafrost, Trondheim, Norway, pp. 712-717.

- Evin M. (1984) - "Caractéristiques physico-chimiques des eaux issues des glaciers rocheux des Alpes du sud (France)", Zeit.Gletscher. und Glazial., 20, pp. 27-40.
- Evin M. and Assier A. (1990) - "The distribution of Permafrost in Rock Glaciers of the Southern Alps (France)", Geomorphology, 3, pp. 57-71.
- Evin M., Assier A. and Fabre D. (1990) - "Les glaciers rocheux du Marinét (Haute-Uri, France)", Rev.Geom.Dynamique, pp. 139-154.
- Gruppo Nazionale "Geografia Fisica e Geomorfologia" del CNR (1987) - "Nuovi dati per lo studio dei rock glaciers del Gruppo Ortles-Cevedale (Alpi)", Riv. Geogr.It., 94, pp. 425-450.
- Gruppo Nazionale "Geografia Fisica e Geomorfologia" del CNR (a cura di Mortara G., Orombelli G., Pelfini M. e Tellini C.) - "Suoli e suoli sepolti olocenici per la datazione di eventi geomorfologici in ambiente alpino: alcuni esempi tratti da indagini preliminari in Val d'Aosta" (in press).
- Guglielmin M. (1991) - "I rock glaciers del Passo del Foscagno (Livigno, Sondrio)", Natura Bresciana, 26, pp. 35-47, Brescia.
- Guglielmin M. and Tellini C. (in press) - "Contributo alla conoscenza dei rock glaciers nelle Alpi italiane. I rock glaciers del Livignasco, della Val Viola e dello Stelvio. (Sondrio, Italia)", Riv.Geogr. It., in press.
- Haerberli W. (1973) - "Die basis temperatur der winterlichen Schneedecke als möglicher, indikator für die verbreitung von permafrost in den alpen", Zeit. Gletscher. und Glazial., IX (1-2), pp. 221-227.
- Haerberli W. and Patzelt G. (1983) - "Permafrostkartierung in Gebiet der Hochebenkar Blockgletscher, Obergurgl, Otzal", Zeit. Gletscher. und Glazial., 18, 2, pp. 127-150.
- Haerberli W. (1985) - "Creep of mountain permafrost: internal structure and flow of alpine rock glaciers", Mitt. der Versuch. Wasserbau, Hydrol.und Glaziol., 77, Zurich, p. 142.
- Heuberger H. (1968) - "Die Alpengletscher in Spät- und Postglazial", Eiszeitalter und Gegenwart, 19, pp. 270-275.
- Lozej A. and Guglielmin M. (in press) - "Prospezioni geoelettriche sul rock glacier de "La Foppa", Livigno, Sondrio, Italia". Ass. Min. Subalpina (TO).
- Mair F. (1968) - "Postglacial Glacier Fluctuations and Correlative Phenomena in the Stubai Mountains, Eastern Alps, Tyrol", Earth Sciences, 7,167-177.
- Perrin R.M., Willis E.H. and Hodge C.A.H. (1964) - "Dating of humus podzols by residual radiocarbon activity", Nature, 202, 165-168.
- Porter S.C. (1986) - "Pattern and Forcing of northern hemisphere glacier variations during the last millennium." Quaternary Res., 26, 27-28.
- Smiraglia C. (1988) - "Misura di velocità superficiale al rock glacier orientale di Val Pisella (Gruppo del Cevedale, Alta Valtellina)", Geog.Fis. Dinam. Quat., 12, pp.41-44.



LATE PLEISTOCENE STABILIZATION AND REACTIVATION OF EOLIAN SAND IN NORTHERN ALASKA: IMPLICATIONS FOR THE EFFECTS OF FUTURE CLIMATIC WARMING ON AN EOLIAN LANDSCAPE IN CONTINUOUS PERMAFROST

L. David Carter

U.S. Geological Survey  
Anchorage, Alaska 99508-4667, USA

During the last glacial maximum, when climate in northern Alaska was cooler and drier than today, active dunes occupied about 11,600 km<sup>2</sup> of the Alaskan Arctic Coastal Plain. The climate warmed as the ice age ended, and the dunes were stabilized from about 12 to 11 ka, when summers were warmer and wetter than at present. Stabilization of the dunes is recorded by a paleosol, which was buried when eolian sand accumulation resumed abruptly about 11 ka. Renewed eolian sand-transport occurred in response to a decrease in surface moisture, but summer temperatures remained warm. Future climatic warming could enhance the present stability of this eolian landscape, or cause its reactivation, depending on changes in surface moisture. General circulation models predict that in Alaska climatic warming will be accompanied by an increase in precipitation, which may increase surface moisture and promote continued landscape stability. However, the depth to permafrost is an important control on drainage and surface moisture. If mean annual air temperatures become warm enough to lower the permafrost table and thereby facilitate drainage, then drier surface conditions and renewed eolian sand-transport could accompany an increase in rainfall.

**INTRODUCTION**

Perennially frozen eolian sand dunes and sand sheets form the surficial materials over much of the western part of the Alaskan Arctic Coastal Plain (Figure 1; Black, 1951; Carter and Galloway, 1988, and maps cited therein). This sand is highly susceptible to wind erosion if the stabilizing tundra vegetation and underlying permafrost are disturbed by human activities, or by processes such as natural or anthropogenic climatic change. Over the past 20 k.y., natural climatic change has caused the repeated stabilization and reactivation of the dunes and sand sheets (Carter and others, 1984). One of these cycles occurred during the termination of the last glacial event and the inception of the present interglacial, and is identified by a thin, discontinuous but widespread paleosol that is a stratigraphic and geomorphic marker horizon. The paleosol records a brief period of landscape stability when ice-age dunes were stabilized as surface moisture increased and summers became warmer than they are now. The paleosol was buried when renewed eolian sand movement occurred in response to a return to dry surface conditions, although summers remained warmer than at present. This cycle of dune stabilization and reactivation provides insight into how these now-stabilized dunes and sand sheets might respond to future climatic warming.

**ICE AGE DUNES**

During the last glacial maximum (about 18 ka), when summers were cooler and surface conditions drier than at present, extensive deposits of eolian sand accumulated in most of the lowland areas of Alaska (Hopkins, 1982; Lea and Waythomas, 1990). On the western Arctic Coastal Plain, an active sand sea occupied about 11,600 km<sup>2</sup>, and barren sand plains and sand sheets extended at least 100 km northeast of the

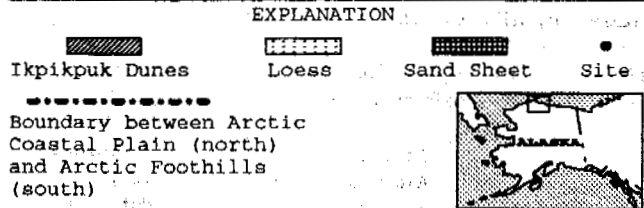
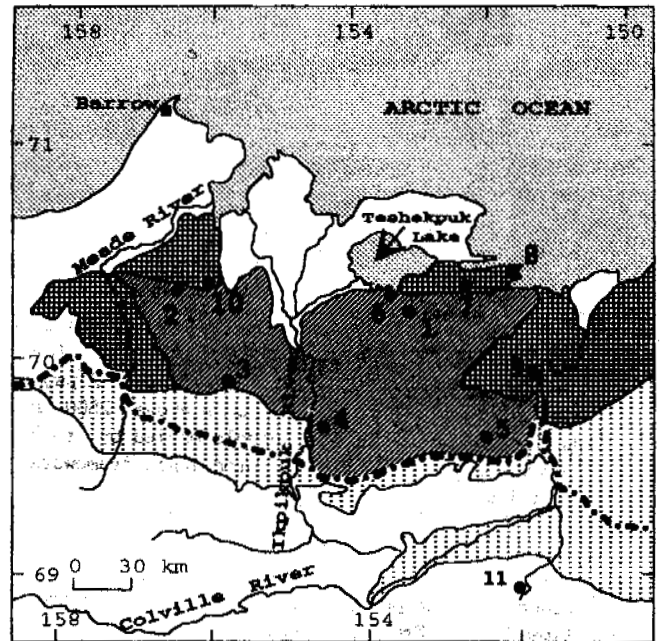


Figure 1. Map showing distribution of eolian deposits and location of sites discussed in text. Entire land area is within the zone of continuous permafrost (Ferrians, 1965).

dunes (Carter, 1981, 1983). The dunes, sand plains, and sand sheets were part of a system of eolian sediment transport that extended about 400 km from outwash plains and fans in the east to where waning winds deposited loess along the margin of the Arctic Foothills (Carter, 1988). In this report, the dunes are informally referred to as the Ikpikpuk dunes.

Between the Colville and Ikpikpuk Rivers, the Ikpikpuk dunes are composed of large, linear dunes as much as 20 km long, 1 km wide, and 30 m high. Dune forms between the Ikpikpuk and Meade Rivers are more complex and are difficult to classify. Dominant winds during dune formation, as determined by bedding attitudes, climbing adhesion ripples, and dune ridge orientations, were easterly to northeasterly, similar to the modern prevailing winds (Carter, 1981). Sand wedges, rather than ice wedges, formed upwind of the dunes and locally within the dune field (Carter, 1983). The sand wedges and dunes record a dry, barren, and windswept landscape across a significant part of the Alaskan Arctic Coastal Plain during middle and late Wisconsin time. Downwind of the dunes in the loess belt, however, more moist conditions prevailed and deep, syngenetic ice wedges formed (Carter, 1988).

#### DUNE STABILIZATION AND PALEOSOL FORMATION

Stabilization of the Ikpikpuk dunes is recorded by a thin, discontinuous but widespread, organic soil-complex (Figure 2). Nine  $^{14}\text{C}$  ages on humus and peat from this paleosol, and on shrubs rooted in it, at six sites show that peak soil development occurred between 12 and 11 ka (Table 1). Four of these sites are described in detail to illustrate the consistency of the age and stratigraphic setting of the paleosol, and the variety of its character and complexity. The sites are topographic highs that preserve the uppermost sediments of the Ikpikpuk dunes because they have been buried by younger eolian sand. They were chosen to minimize the complexities of soil development introduced by slope processes, thaw lake processes, and the development of

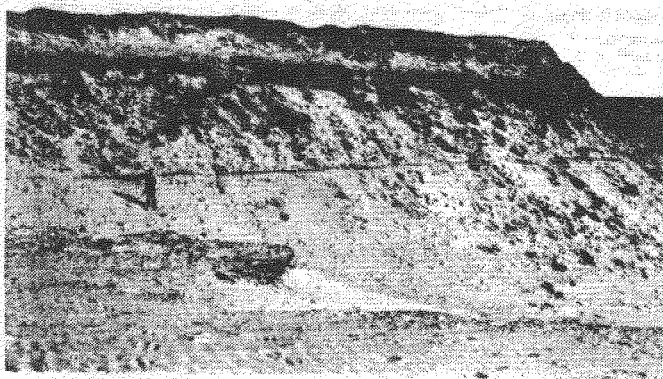


Figure 2. Eolian sand and paleosols at site 1. Dark band at height of man's shoulder is the late Pleistocene paleosol that records an episode of landscape stability between episodes of eolian sand movement.

low-centered polygons noted by Everett (1979) in his description of the modern soil-landscape of this region.

Site 1 (figs. 2 and 3A) is a blowout in a 27 m-high east-facing river bluff cut through one of the large, Pleistocene linear dunes. Wind erosion has produced an excellent exposure of the Pleistocene dune sand and the interbedded organic soils and eolian sand that overlie it. The lowest organic-bearing horizon occurs about 16.5 m above the base of the bluff; it is a paleosol composed of humus-rich sand 5 to 10 cm-thick that grades laterally into a zone 40 to 60 cm thick composed of thin interbeds of sand and humic sand with abundant woody roots, and with shrubs (probably willow (*Salix*)) in growth position at the top of the zone. The paleosol is only slightly cryoturbated, and no ice-wedge pseudomorphs were observed over approximately 50 m of continuous exposure. A  $^{14}\text{C}$  age on roots from the base of the wood-rich zone is  $11,430 \pm 170$  yr B.P. (Table 1), which provides an approximate age for stabilization of the Ikpikpuk dunes at this locality. Roots identified as willow (R.C. Koeppen, U.S.D.A., written commun., 1978) at the top of the wood-rich zone gave a  $^{14}\text{C}$  age of  $10,980 \pm 80$  yr B.P. (Table 1).

Site 2 (Figure 3B) is a 9 m-high west-facing lake bluff. Stabilization of the Ikpikpuk dunes at this site is recorded by an organic-bearing zone about 40 cm thick 5 m above the base of the bluff that consists of several thin, slightly cryoturbated, humus rich sand beds. The thickest of these humic horizons has yielded a  $^{14}\text{C}$  age of  $11,300 \pm 170$  yr B.P. (Table 1). No ice-wedge pseudomorphs were observed to be associated with this paleosol.

Stabilization of the Ikpikpuk dunes at Site 3 (Figure 3C) is marked by a paleosol that grades laterally from a single, 16 cm-thick humic horizon into numerous thin, humic horizons and sand beds that together are about 50 cm thick. The central humic horizon in this zone has yielded a  $^{14}\text{C}$  age of  $11,300 \pm 160$  yr B.P., and a shrub rooted in the upper humic horizon has been dated at  $11,240 \pm 160$  yr B.P. (Table 1). Again, no ice-wedge pseudomorphs were observed beneath this soil over about 50 m of excellent exposure along this south-facing river bluff.

Site 4 (Figure 3D) is a south-facing river bluff about 24 m high that exposes 21.5 m of eolian sand and interdunal lake deposits of the Ikpikpuk dunes, overlain by 2.5 m of interstratified organic-rich beds and eolian sand. A zone 50 cm thick containing thin beds of slightly cryoturbated humic sand separates sand of the Ikpikpuk dunes from younger eolian sand. The thickest humic horizons are at the base and top of the zone, and they have yielded  $^{14}\text{C}$  ages of  $12,070 \pm 100$  and  $11,190 \pm 60$  yr B.P. respectively (Table 1).

The other two localities within the Ikpikpuk dunes for which  $^{14}\text{C}$  ages for this paleosol have been obtained are Sites 5 and 6 (Figure 1). Site 5 is a north-facing river bluff 20 m high that exposes 17 m of dune sand overlain by 3 m of interbedded peat, lacustrine sand and eolian sand. About 5 cm of fibrous autochthonous peat occurs at the top of sand of the Ikpikpuk dunes and is overlain by lacustrine sand. A  $^{14}\text{C}$  age determined for this peat is  $11,040 \pm 170$  yr B.P. (Table 1). Site 6 is an 8.2 m-high north-facing bluff on the south shore of Teshekpuk Lake that exposes 6.4 m of eolian sand of the

Table 1. Radiocarbon ages pertaining to late Pleistocene stabilization and reactivation of eolian sand on the Alaskan Arctic Coastal Plain.

Site (Fig. 1)	Latitude	Longitude	Sample	Material	Laboratory Number	Age 14C yr B.P.	Description
<b>Late Pleistocene paleosols in the Ikpikpak dunes</b>							
1	70° 22.4'	153° 12.2'	77ACrII002A	Wood	USGS-377	10,980±80	Roots at top of paleosol (fig. 3A)
1			80ACrII016A	Wood	I-11,675	11,430±170	Roots at base of paleosol (fig. 3A)
2	70° 28.0'	156° 30.1'	90ACr029D	Humus	I-17,014	11,300±170	Cryoturbated paleosol (fig. 3B)
3	70° 09.9'	153° 55.7'	78ACrII100C	Humus	I-10,878	11,240±160	Wood in growth position (fig. 3C)
3			78ACrII100B	Wood	I-10,876	11,300±160	Central humic horizon in zone of interbedded sand and humic sand (fig. 3C)
4	69° 49.4'	154° 24.9'	79ACr078C	Humus	USGS-1155	11,190±60	Upper humic horizon in zone of interbedded sand and humic sand (fig. 3D)
4			78ACr078B	Humus	USGS-823	12,070±100	Lower humic horizon in zone of interbedded sand and humic sand (fig. 3D)
5	69° 44.7'	152° 18.3'	83ACr251D	Peat	I-13,490	11,040±170	Peat 5 cm thick underlain by eolian sand and overlain by lacustrine sand
6	70° 26.1'	153° 28.9'	78ACrII050C	Humus	I-10,814	11,230±170	Humic horizon 5 cm thick underlain and overlain by eolian sand
<b>Late Pleistocene paleosols near the Ikpikpak dunes</b>							
7	70° 26.6'	152° 33.6'	80ACrII018C	Humus	I-11,674	11,500±170	Humic horizon 7 cm thick underlain by marine sand and overlain by eolian sand
8	70° 33.2'	151° 51.6'	78ACrII042B	Humus	USGS-629	10,980±70	Humic horizon 10 cm thick underlain by marine sand and overlain by eolian sand
9	70° 03.9'	151° 34.4'	83ACr197	Humus	I-13,323	11,460±170	Humic horizon 3 cm thick underlain and overlain by eolian sand
10	70° 28.6'	156° 05.9'	82ACr155	Rootlets	I-13,442	12,300±190	Root zone 13 cm thick in eolian sand
<b>Other radiocarbon ages for sites 1 through 4</b>							
1	70° 22.4'	153° 12.2'	77ACrII002D	Peat	USGS-380	940±110	Peat underlain and overlain by eolian sand (fig. 3A)
1			77ACrII002C2	Peat	USGS-379	5250±80	Top of 25 cm thick peat (fig. 3A)
1			77ACrII002C1	Peat	USGS-448	8180±75	Base of 25 cm thick peat (fig. 3A)
1			77ACrII002B	Wood	USGS-378	10,700±120	Wood in growth position in eolian sand (fig. 3A)
2			82ACr159E	Peat	I-13,173	1400±80	Peat underlain and overlain by eolian sand (fig. 3B)
2			82ACr159D	Peat	I-13,172	4490±100	Top of 25 cm thick peat (fig. 3B)
2			82ACr159C	Peat	I-13,162	7800±130	Base of 25 cm thick peat (fig. 3B)
3			78ACrII100E	Peat	I-10,887	8665±145	Base of 40 cm thick peat (fig. 3C)
4			79ACr078G	Peat	I-11,420	8010±130	Base of 30-cm thick peat (fig. 3D)
4			79ACr078E	Rootlets	I-11,418	10,820±170	Root zone in eolian sand (fig. 3D)
<b>Other pertinent radiocarbon ages</b>							
11	69° 01.3'	151° 56.7'	79ACr138C	Wood	I-11,601	7730±120	From discontinuous woody peat
11			79ACr138A	Wood	I-11,599	11,700±175	From detrital peat within swale filling
11			79ACr138B	Wood	I-11,600	11,800±170	From tundra mat (peat) that forms surface underlain by fossil ice wedges

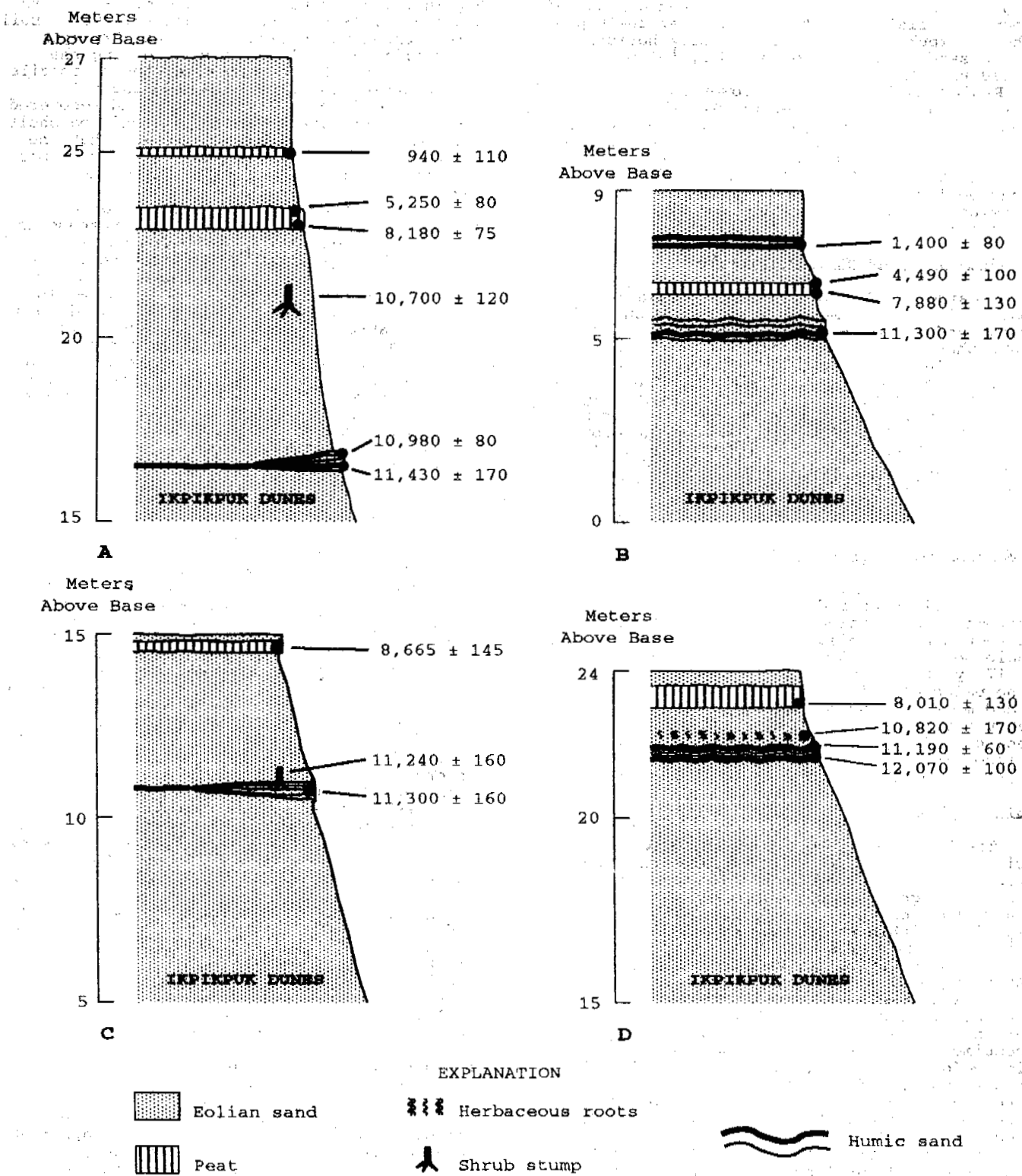


Figure 3. Stratigraphy and radiocarbon ages (in yr B.P.) at: A, site 1; B, site 2; C, site 3; and D, site 4. All of the materials are perennially cryotic except for a surficial active layer that is generally less than 1 m thick.

Ikpikpuk dunes overlain by interbedded peat and younger eolian sand. The paleosol at the top of the Ikpiuk dunes is a 10 cm-thick horizon of humic sand that has been dated by  $^{14}\text{C}$  at  $11,230 \pm 170$  yr B.P. (Table 1).

Radiocarbon ages on the lower and upper humic horizons at Site 4 either bracket or are analytically indistinguishable from all of the  $^{14}\text{C}$  ages from other sites that were measured on the paleosol that formed during stabilization of the Ikpiuk dunes. It thus appears that the peak period of landscape stability and soil development within the dune field was between 12 and 11 ka.

#### CORRELATIVE PALEOSOLS OUTSIDE THE DUNEFIELD

Outside the Ikpiuk dunes, correlative paleosols have formed in eolian sand and marine sand, and are overlain by a sheet of eolian sand that also blankets the Ikpiuk dunes. These paleosols, like those described for the Ikpiuk dunes, generally consist of a 4 to 10 cm-thick zone of humic sand. Radiocarbon ages on these paleosols have been obtained for Sites 7, 8, 9, and 10 (Figure 1). They range from  $10,980 \pm 70$  to  $12,300 \pm 190$   $^{14}\text{C}$  yr B.P. All of these ages are either bracketed by or analytically indistinguishable from the  $^{14}\text{C}$  ages for the lower and upper humic horizons at Site 4.

#### RENEWED EOLIAN SAND MOVEMENT

A closely limiting age on the cessation of soil development and the renewal of eolian sand movement was obtained for Site 4. At this site, a root zone in eolian sand 20 cm above the paleosol (Figure 3D) yielded a  $^{14}\text{C}$  age of  $10,820 \pm 170$  yr B.P. Considering the minimum ages on the paleosols, it is clear that renewed eolian sand movement and burial of the paleosols began abruptly about 11 ka. Radiocarbon ages for the end of this episode of eolian sand movement range from  $8,665 \pm 145$  yr B.P. at Site 3 to  $7,880 \pm 130$  yr B.P. at Site 2 (Table 1).

#### SIGNIFICANCE

The broad distribution of the paleosols within and near the Ikpiuk dunes that date from 12 to 11 ka indicates that this was a period of general landscape stability over a large part of the Arctic Coastal Plain. A locality within the Arctic Foothills for which  $^{14}\text{C}$  dates are available also indicates a period of landscape stability centered on 12 to 11 ka. At this locality (Site 11, Figure 1), a 12 m-high river bluff exposes 7 m of colluvium over 5 m of river gravel. About 1 m above the base of the colluvium is a fossil tundra mat a few centimeters thick that is underlain by small ice wedges up to 0.5 m across. A sample of the tundra mat yielded a  $^{14}\text{C}$  age of  $11,800 \pm 170$ . These are the only ice wedges exposed in the section other than those associated with the modern surface. The tundra mat and ice wedges record a cessation of colluvial sedimentation and an episode of landscape stability. It seems likely that the interval 12 to 11 ka was a period of regional landscape stability on the Alaskan Arctic Slope.

A late Pleistocene to early Holocene warm period in northern Alaska and northwestern Canada is well documented (McCulloch and

Hopkins, 1966; Ritchie and others, 1983; Burn and others, 1986; Harry and others, 1988). Soil formation and stabilization of the Ikpiuk dunes from 12 to 11 ka occurred during the early part of this warm period. Insect fossils from organic pond silt formed during this interval of landscape stability, and recovered from cores obtained from the Chukchi Sea shelf, have been interpreted as indicating that the climate at that time was substantially warmer than the modern climate (Elias and others, 1992).

Soil formation and stabilization of the Ikpiuk dunes indicate either an increase in surface moisture to allow the growth of stabilizing vegetation, or a decrease in the supply of eolian sand to the dunes. Inasmuch as the area upwind (northeast) of the dunes for more than 100 km was composed largely of loose sand, an abrupt decrease in the supply of eolian sand seems unlikely to be the sole cause. An increase in surface moisture seems to have been necessary to stabilize the dunes. Such an increase is supported by preliminary results of analyses of fossil lacustrine ostracodes from Arctic Slope lake deposits dated to the interval 12 to 11 ka. These analyses suggest that summers then were warmer and wetter than those of the present (Carter and others, 1984; R.M. Forester and L.D. Carter, unpublished data). Surface moisture apparently increased as climate warmed at the end of the last glacial cycle.

An increase in surface moisture could have promoted a decrease in the thickness of the active layer, in spite of a warmer climate, because the heat capacity of sand increases with increasing moisture content (Williams and Smith, 1989). A decrease in the active layer thickness might have impeded drainage, thereby providing a positive feedback effect on surface moisture.

The absence of ice wedge pseudomorphs and minimal cryoturbation associated with the 12- to 11-ka paleosol in excellent exposures is interesting. Ice wedges were forming during this period in the Arctic Foothills as shown by the fossil ice wedges at Site 11, and, at favorable localities, ice wedges were forming on the Arctic Coastal Plain by at least 14 ka (Brown, 1965). Mackay (1978) noted that at Garry Island in the Mackenzie Delta area, ice wedges rarely crack when snow cover on the ground approaches 1 m. Limited growth of ice wedges on the Arctic Coastal Plain during the period 12 to 11 ka could have been caused by a thicker winter cover of insulating snow than the 50 cm-thick cover characteristic of modern winters.

Renewed eolian sand movement at about 11 ka coincides with the beginning of the 11- to 10-ka Younger Dryas Chronozone, which, in the North Atlantic region and in some other areas, was a period of pronounced climatic cooling (e.g., Berger, 1990; Engstrom and others, 1990). In northern Alaska and northwestern Canada, however, summer temperatures apparently remained warm, as indicated by pollen, lacustrine ostracode assemblages, beetle faunas, and plant macrofossils (Ritchie and others, 1983; Carter and others, 1984; Nelson and Carter, 1987; Anderson, 1988). The ostracode assemblages also indicate greater evaporative concentration of lake water than occurs today, which suggests relatively dry,

cloud-free air masses. Drier climatic conditions would tend to strengthen the effect of warm air temperatures on ground temperatures, by decreasing soil moisture and heat capacity. This would favor a lowering of the permafrost table, which would facilitate surface drainage and promote the dry surface conditions necessary for a renewal of eolian sand movement.

#### IMPLICATIONS FOR FUTURE CLIMATIC WARMING

Wetter surface conditions than at present evidently would promote continued stabilization of the eolian dunes and sand sheets of the Arctic Coastal Plain, whereas drier conditions would favor reactivation of these surfaces. Global climatic warming is expected to result from the buildup of anthropogenic greenhouse gases in the atmosphere, and this warming is expected to be amplified in polar regions by various feedback processes (Etkin, 1990). Present general circulation models (GCMs) predict that in Alaska this warming will be accompanied by cloudy skies and an increase in precipitation, which may increase surface moisture and promote the continued stability of the dunes and sand sheets. However, these GCMs are still under development, and are presently weak in their ability to predict cloud cover. Moreover, drier surface conditions could accompany an increase in rainfall if mean annual temperatures become warm enough to lower the permafrost table and thereby facilitate drainage. Reactivation of dunes and sand sheets over a large part of the Arctic Coastal Plain cannot be excluded as a possible result of the predicted global warming.

#### ACKNOWLEDGMENTS

Helpful comments on earlier drafts of this paper were received from O.J. Ferrians, Jr., J.P. Galloway, and two anonymous reviewers. Assistance in the field was provided by J.P. Galloway. This research was part of the Global Change and Climate History Program of the U.S. Geological Survey (USGS), and was partially funded by the USGS National Mineral Resource Assessment Program.

#### REFERENCES CITED

- Anderson, P.M. (1988) Late Quaternary pollen records from the Kobuk and Noatak River drainages, northwestern Alaska. *Quaternary Research* 29, 263-276.
- Berger, W.H. (1990) The Younger Dryas cold spell - a quest for causes. *Palaeogeography, Palaeoclimatology, and Palaeoecology* 89, 219-237.
- Black, R.F. (1951) Eolian deposits of Alaska. *Arctic* 4, 89-111.
- Brown, Jerry (1965) Radiocarbon dating, Barrow, Alaska. *Arctic* 18, 36-48.
- Burn, C.R., F.A. Michel, and M.W. Smith (1986) Stratigraphic, isotopic, and mineralogical evidence for an early Holocene thaw unconformity at Mayo, Yukon Territory. *Canadian Journal of Earth Sciences* 23, 794-801.
- Carter, L.D. (1981) A Pleistocene sand sea on the Alaskan Arctic Coastal Plain. *Science* 211, 381-383.
- Carter, L.D. (1983) Fossil sand wedges on the Alaskan Arctic Coastal Plain and their paleoenvironmental significance, in *Permafrost: Fourth International Conference Proceedings*. Washington, D.C., National Academy Press, 109-114.
- Carter, L.D. (1988) Loess and deep thermokarst basins in arctic Alaska, in *Permafrost: Fifth International Conference Proceedings*. Trondheim, Norway, Tapir Publishers, 706-711.
- Carter, L.D., R.M. Forester, and R.E. Nelson (1984) Mid-Wisconsin through early Holocene changes in seasonal climate in northern Alaska. *American Quaternary Association Eighth Biennial Meeting, Program and Abstracts*, 13 through 15 August, 1984, 20-22.
- Carter, L.D., and J.P. Galloway (1988) Engineering-geologic maps of northern Alaska, Ikpikpak River quadrangle. U.S. Geological Survey Open-File Report 88-375, 2 sheets, scale 1:250,000.
- Elias, S.A., S.K. Short, and R.L. Philips (1992) Paleocology of late-glacial peats from the Bering Land Bridge, Chukchi Sea shelf region, northwestern Alaska. *Quaternary Research* 38, in press.
- Engstrom, D.R., B.C.S. Hansen, and H.E. Wright, Jr. (1990) A possible Younger Dryas record in southeastern Alaska. *Science* 250, 1383-1385.
- Etkin, David (1990) Greenhouse warming: Consequences for Arctic climate. *Journal of Cold Regions Engineering* 4, 54-66.
- Everett, K.R. (1979) Evolution of the soil landscape in the sand region of the arctic coastal plain as exemplified at Atkasook, Alaska. *Arctic* 32, 207-223.
- Ferrians, O.J., Jr. (1965) Permafrost map of Alaska. U.S. Geological Survey Miscellaneous Geological Investigations Map I-445, scale 1:2,500,000.
- Harry, D.G., H.M. French, and W.H. Pollard (1988) Massive ground ice and ice-cored terrain near Sabine Point, Yukon Coastal Plain. *Canadian Journal of Earth Sciences* 25, 1846-1856.
- Hopkins, D.M. (1982) Aspects of the paleogeography of Beringia during the late Pleistocene, in Hopkins, D.M., Matthews, J.V., Jr., Schweger, C.E., and Young, S.B., eds., *Paleogeography of Beringia*. 3-28, Academic Press, New York.
- Lea, P.D. and C.F. Waythomas (1990) Late Pleistocene eolian sand sheets in Alaska. *Quaternary Research* 34, 269-281.
- Mackay, J.R. (1978) The use of snow fences to reduce ice-wedge cracking, in *Current Research, Part A: Geological Survey of Canada Paper 78-1A*, p. 523-524.
- McCulloch, D.S., and D.M. Hopkins (1966) Evidence for an early Recent warm interval in northwestern Alaska. *Geological Society of America Bulletin* 77, 1089-1108.
- Nelson, R.E., and L.D. Carter (1987) Paleoenvironmental analysis of insects and extralimital *Populus* from an early Holocene site on the Arctic Slope of Alaska. *Arctic and Alpine Research* 19, 230-241.
- Ritchie, J.C., L.C. Cwynar, and R.W. Spear (1983) Evidence from north-west Canada for an early Holocene Milankovitch thermal maximum. *Nature* 305, 126-128.
- Williams, P.J., and M.W. Smith (1989) *The frozen earth*. 306 p., Cambridge University Press, New York.

## PERMAFROST AROUND CGWS, ANTARCTICA

Chen Xiao-bai

Lanzhou Institute of Glaciology and Geocryology,  
Chinese Academy of Sciences, China

Except for some thawing areas under large lakes, the permafrost is distributed continuously with a thickness of 20 m to 100 m and with a maximum thawing depth of 0.5 m to 1.8 m in the Great Wall Station, Antarctica, which mainly depends on the landform, the thickness and elapsed time of snow cover, soil, as well as its moisture. There is a mass ground ice with a thickness of 30 cm and an ice wedge with a height of 15 cm developed at a small hill. As well, a thawing intercalation is found in permafrost.

### INTRODUCTION

The China Great Wall Station, Antarctica, (CGWS) is located at the Fildes Peninsula, of the south of King George Island, Antarctica (58°17'51"9W, 62°12'59"7S). The landform of the area around the CGWS is a hilly region without any ice cover, and with an elevation of less than 165 m a.s.l. It is a sub-Antarctic maritime climate zone with an annual air temperature of -3°C and precipitation of more than 600 mm. About 10% of the total area in Fildes Peninsula is covered by seasonal snow accumulation which will melt in early or mid January (Chen, 1991). Further more, the ground surface will start thawing under the action of the solar radiation, sensitive heat and convection exchange between air and earth. Except the thawing areas under some Large Lakes, the permafrost is distributed continuously. Many geocryologists (Vkunin, 1985; Xie, 1988; Zhu, 1991) were and are engaging in the investigation of permafrost here. However, it is difficult to study in detail because the working time is very limited and some special equipment was lacking. The author completed a preliminary investigation and observation of the permafrost by using a small drilling machine, an electric pick, temperature gauges and their collectors with the support of the 5th China Antarctic Expedition. As a result, some geocryological profiles including some sedimental cores with a maximum thickness of 7.76 m, the maximum thawing depth data, typical thawing processes as well as ground temperature profiles, 0 m to 3 m to 6 m in depth, at various landforms were measured. After calculated, the thickness of permafrost is 20 m to 100 m. Further more, the reconstruction of the climate and environment in Late Pleistocene is being conducted at present.

### TYPICAL GEOLOGICAL PROFILES

Generally speaking, the types of landforms

here could be divided as follows: frost weathering rock and hill, steep slope, gentle slope, marshland, glacial-fluvial deposit hill, and marine terrace. As well, the lakes are rather developed.

1. Glacial-fluvial deposit hill. As a typical profile with an elevation of 22.9 m a.s.l., as shown in Fig.1, is located at the top of West Hill. It is mainly developed sandy clay with stone formed by glacial-fluvial deposits. There is a medium sand layer and a sand lens developed at the depth of 0.55 m to 0.60 m and 2.75 m to 2.78 m respectively. The direction of the layer is almost parallel to the slope surface and slopes down to the sea. The moisture profile is correspondant to the density and depends on the cryogenic structures.

2. Gentle slope, east to the West Lake. The geological profile is shown in Fig.2 with an elevation of 17.6 m a.s.l., the soil is almost the same as that of Fig.1. There is a sandy gravel layer developed at the depth of 0.95 m to 1.20 m.

3. Marine terrace. The current meteorological station is built at the third terrace, 10 m a.s.l. in elevation, with a thickness of sandy gravel of more than 1.8 m. However, the rockbed is buried at the depth of about 1.1 m beneath the sandy gravel layer at the first terrace.

4. Gentle slope and marshland. The sandy clay with stone is developed within 0 to 1 m in depth all over the region. It is saturated while melting.

5. Yenu Lake. The elevation of the lake surface is about 14.6 m a.s.l. Its geological profile is shown in Fig.3. The diluvial-slope deposit, sandy clay with stone, is developed at the depth of 0 to 1 m and somewhere below 1 m. The lacustrine and marine deposits are developed beneath the depth of 1 m. The fossil shells were found at different levels, 1.90 m to 2.20 m and 5.60 m to 6.50 m in depth. The moisture content is correspondant to its cryogenic structure.

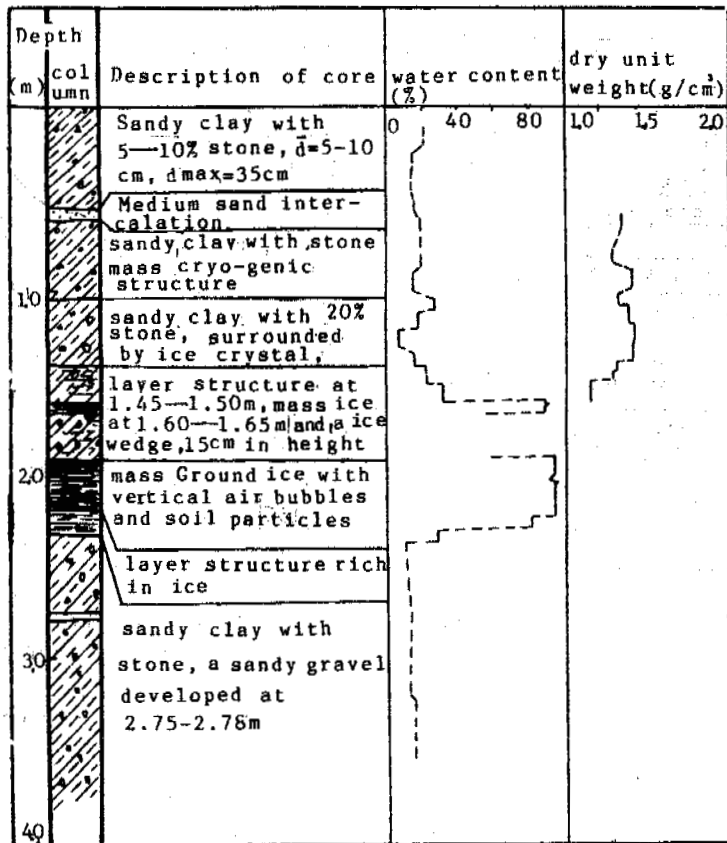


Figure 1. Comprehensive column of sedimental core collected from West Hill

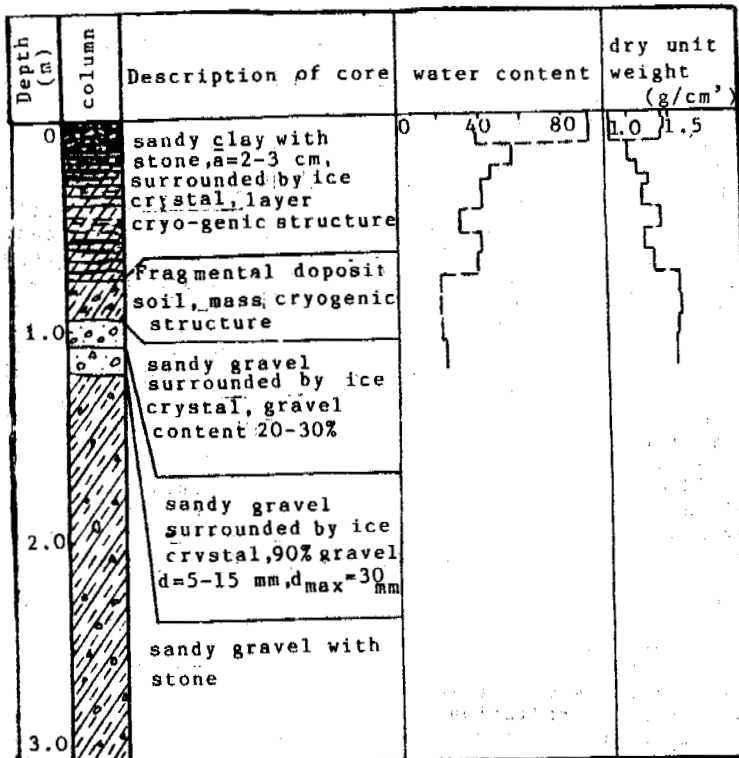


Figure 2. Comprehensive column of sedimental core collected from the East side of West Lake



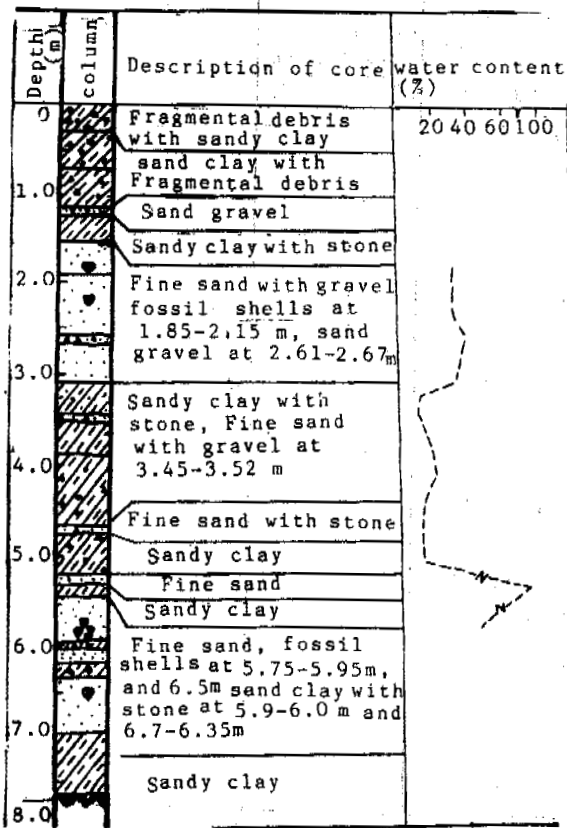


Figure 3. Comprehensive column of sedimental core collected from Yenwu Lake

### SEASONALLY THAWING LAYER

#### 1. Seasonally thawing-freezing processes.

The seasonally thawing-freezing processes and the thawing index curve of China Antarctic Meteorological Station is shown in Fig.4. From that we know the positive air temperature accumulation started at the middle of December while snow cover disappeared and the ground began thawing. During the middle of November to the middle of December, the snow cover was melting in the day time while air temperature was above 0°C which caused a ground surface phase change with a temperature of 0°C. The thawing depth will be near the maximum in early March while the ground surface starts freezing, from unstable to stable gradually. The maximum thawing depth occurs at the end of March with an extreme index of 190.8°C·day. And then the freezing processes of earth will appear in two directions, i.e. from the surface downwards and from the permafrost table to the surface. The thawing layer will be frozen completely at the end of April and meanwhile connected with the permafrost.

Fig.5 shows that the seasonally thawing-freezing process at the gentle slope, at the east side of West Lake. There is more thickness of snow cover and shorter solar radiation compared with that of the meteorological station. The melting process started at the end of December and the maximum thawing depth occurred at the middle or the end of March while freezing started in two directions. The thawing layer

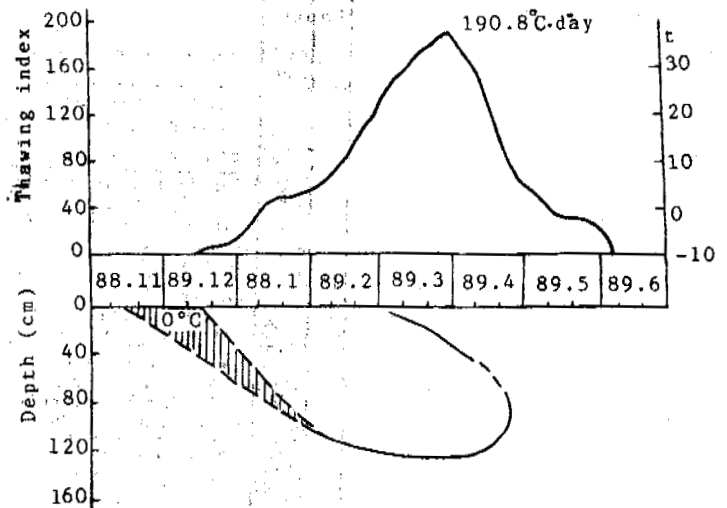


Figure 4. The positive air temperature accumulation and thawing-freezing process of the meteorological station, CGWS

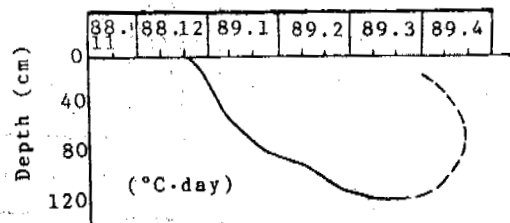


Figure 5. Thawing-freezing process of gentle slope at the East side of West Lake

will be frozen in the middle of April.

#### 2. Cryogenic structures of the seasonally thawing-freezing layer.

(1) For the hill of glacial-fluvial deposit. Because it is located at the top of the hill with good drainage and less water content of soil, in common cases, almost all of the frozen ground layer is a mass structure, except for a layer structure and ice crystals surrounding gravel and stones near the permafrost table.

(2) For Gentle slope of the east side of West Lake. The situation here is very similar to that of the other gentle slope. Due to sufficient water supply and thicker snow cover producing a lower frost penetration rate during freezing, the layer cryogenic structure has a thicker ice lens and ice crystals surrounding the surface of gravel and stone, which were formed with a water content of 40% to 90%. As a result, the bearing capacity of the layer will be lost. The dehydrated layer forms at the depth of 0.75 m to 1.05 m because of water migrating up towards the frost front and down the permafrost table side. The density variation of soil along the depth is correspondent to that of its moisture condition (see Fig.2).

(3) For the marine terrace. The upper part, 0 to 20 cm in depth, is gravel without any sand contained in it which provides an excellent drainage condition. It was in a dry and loosened state in the middle and the end of November,

1988, with a snow cover of 15 to 20 cm in thickness. The snow melt water penetrated down in the day time and frozen in the night forming ice crystals surrounding the surface of gravel. A 0°C zone occurs easily in the gravel layer, rich in ice both during freezing and thawing. The maximum thawing depth was 0.85 m to 0.95 m at the first marine terrace with ice crystals surrounding the surface of frost weathering rocks near the permafrost table.

3. The maximum seasonally thawing depth.

After detailed investigation and observation around Fildes Peninsula, the maximum seasonally thawing depth at different landforms was compiled and listed in Table 1 including the conditions of soil, vegetation, and the disappearing date of snow cover.

Table 1. The maximum thawing depth of different landforms in Fildes Peninsula

Landform unit	Soil type	Earth surface condition	Date without snow cover	Max. thawing depth (m)
Top of hill	Sandy clay with stone	No vegetation and dry	End of Nov.	1.4 to 1.5
Top of hill	Sand clay with stone	Liken and Marsh and wet	End of Nov. Early Dec.	0.9 to 1.0
3rd terrace	Sandy gravel	No vegetation	End of Dec.	1.2 to 1.2
2nd terrace	Gravel	No vegetation	End of Dec. Early Jan.	1.6 to 1.8
1st terrace	Gravel	No vegetation	End of Dec. Early Jan.	0.85 to 0.95
Gentle slope	Sand clay with stone	Sorted circle developed	End of Dec. Early Jan.	0.6 to 0.7
Gentle slope	Sandy clay with stone	Marsh and wet	Early Jan.	0.6 to 0.7
Marsh-land	Sand clay	Marsh and wet	Middle of Jan.	0.55 to 0.65
Marsh-land	Sandy clay	Lots of marsh & wet	Middle of Jan.	0.5 to 0.6
The side of lake	Sandy clay with stone	No vegetation No water discharge	Middle of Jan.	1.0 to 1.1
The side of lake	Sandy clay with stone	No vegetation Water discharge	Middle of Jan.	1.2 to 1.3

1989, and after regression analysis, the ground temperature at the depth of 6 m is -1.25°C, the annual ground temperature is around -1.3°C to -1.5°C and the calculated thickness of permafrost is 50 m to 30 m.

For the West Hill, after regression analysis of the tendency of the ground temperature profile, measured in situ with little snow cover, the annual ground temperature was calculated as -2.1°C with a level of zero annual amplitude of temperature of about 10 m. And the calculated permafrost thickness here is near 80 m. The snow cover at the gentle slope, at the east side of West Lake, is rather thick, so the level of zero annual amplitude of temperature is near 6 m with annual ground temperature of -1.0°C and permafrost thickness of about 40 m. Consequently, it could be assumed that the thickness of permafrost in the area without any snow cover might be more than 100 m.

PERMAFROST

1. Ground temperature profiles and thickness of permafrost. The ground temperature profile of the side of Yenwu Lake is shown in Fig.6 where the temperature profile below the depth of 3.5 m is kept stable. Meanwhile the ground temperature will rise with the increase in the depth. The gradient of ground temperature was calculated with an average of 36 m/°C. Based on the above, the thickness of permafrost here is about 22 m with an annual average ground temperature of -0.45°C.

The ground temperature profile of the glacial-fluvial deposit gentle slope, east side of West Lake, is shown in Fig.7. Based on the basic ground temperature profile measured on March 2,

2. Ground ice. In common cases, there is a layer of ice lens developed near the permafrost table and ice crystals surrounding gravel and stone. However, in the drilling core collected from West Hill (Fig.1), there is a mass ice, 10 cm in thickness, developed at the depth of 1.60 to 1.75 m with many vertical air bubbles and few soil particles. As well, an ice wedge with a height of 15 cm developed at the same level. A mass ground ice, 30 cm in thickness, exists at the depth of 1.9 to 2.3 m with some vertical air bubbles and few soil particles also. Below the level developed mass ice, there is a layer with a layer cryogenic structure, rich in ice. What should be pointed out is that the elevation of the West Hill is 22.9 m a.s.l. which is 6.9 m higher than that of the Lake surface. So the existence of the mass ice could reflect an occurrence of a sedimental environment because it could not be formed recently without

Ground temperature (°C)

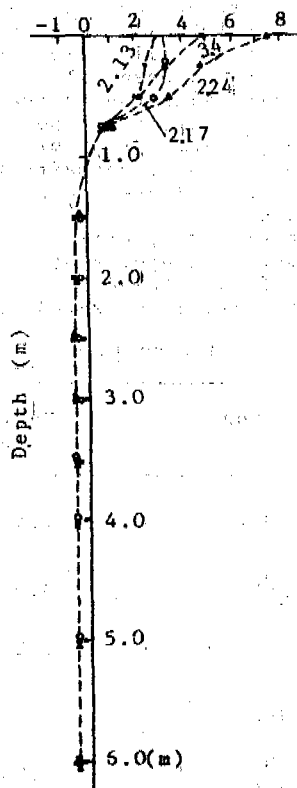


Figure 6. The ground temperature profile of the side of Yenwu Lake

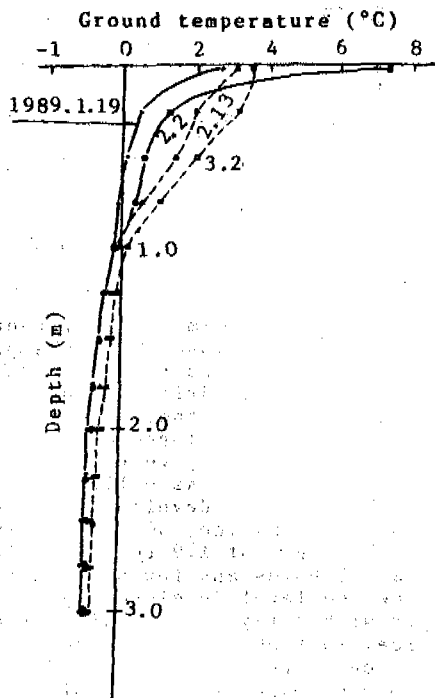


Figure 7. The ground temperature profile of a gentle slope, the East side of West Lake

sufficient water supply.

Besides above, the cryogenic structure of fine sand layers in the core collected from Yenwu Lake (Fig.3) is a mass one with much more water content than that of the saturated one.

3. Thawing intercalation — During the investigation of a sorted circle near the scientific building, a thawing intercalation was found at a depth below 0.87 m with a water content of 28 to 34%. However, the water content of the upper part, 0 to 0.87 m in depth, was more than 50% by weight and the cryogenic structure was a thick layer, the freezing point  $T_f$ , 0 to 0.87 m in depth, is near 0°C, except -0.015°C, -0.036°C and -0.012°C at the depth of 0.34 m to 0.36 m, 0.74 m to 0.16 m and 0.81 m to 0.83 m respectively. But, at a depth over 0.87 m, its  $T_f$  was -0.08°C to -0.13°C which is much lower than that of the upper part. The relatively high ground temperature produced by snow cover, 1.5 m to 2 m in thickness, and rather low freezing point makes the lower part of the sorted circle formed a thawing intercalation.

During the construction of CGWS, Antarctica, the thawing intercalations were found by the expedition members while digging the trench of the building base.

This phenomenon will be discussed in detail while reconstructing the ancient climate and environmental conditions here.

#### CONCLUSIONS

1. Except for some large lakes, permafrost is continuously distributed at the Fildes Peninsula, King George Island, Antarctica. The thickness of permafrost is 20 m to 100 m which depends on landform, soil, moisture and snow cover.

2. There is a layer of mass ground ice with a thickness of 10 to 30 cm, and an ice wedge at the West Hill, and a thawing intercalation within the permafrost which was produced in ancient climate and environmental conditions.

#### ACKNOWLEDGMENT

This project was supported by The China Antarctic Expedition Committee.

#### REFERENCES

- Chen Xiaobai and Zhang Yongping, (1991) Snow accumulation and Melting Processes at the Great Station, Antarctica, ANTARCTIC RESEARCH, Vol.3, No.3, p8-14.
- Vkunin, V.I. and Moskalevskii, M.U., (1985) Cryogenico-Geomorphic Phenomena at South Shetland Island, geomorphology, Vol.1, Academia of Sciences, USSR, OTTISK Branch, p73-79.
- Xie Youyu, (1988) Chemical Weathering in Permafrost Regions of Antarctica — Great Wall Station, Casey Station and Davis Station Areas, ANTARCTIC RESEARCH, Vol.1, No.2, p8-14.
- Zhu Cheng, et al., (1991) An Analysis of Periglacio-Geomorphic Processes on Fildes Peninsula, King George Island, Antarctica, ANTARCTIC RESEARCH, Vol.3, No.3, p25-38.

## STRUCTURE AND TEXTURE FORMATION OF FROZEN SAPROPEL

E.M. Chuvilin, E.D. Ershov and A.A. Murashko

Department of Geocryology, Faculty of Geology  
Moscow State University, Russia

Based on lab modelling and analyses of the processes of structural and textural formation in frozen high humid lake organogenous sediments has been carried out. Experimental data shows, that the process of freezing of organogenous high humid grounds causes humidity transfer from this zone into the frozen one, and its local redistribution in the boundaries of freezing and frozen zones appearing to extend differently depending on the conditions of heat exchange. In conditions where low intensive heat exchange prevails, humidity transfers from the thawed zone of organogenous ground into the frozen one with the subsequent freezing of migrated water presenting segregational layers of ice. Local redistribution of water mainly appears in conditions of intensive heat exchange at a high speed of freezing and is the result of expression and subsequent freezing of the connected water during the process of dehydration of the organomineral frame and of coagulation of the organic components of the rock.

### INTRODUCTION

Exploitation of lacustrine organogenic sapropel sediment as a valuable natural raw material, working all year round through technologies of their recovery in areas with stable winter freezing is impossible without taking into account the mass-exchange, physico-chemical and texture formation process caused by cryogenic phenomena. The efficiency of the existing technology of de-watering sapropel by way of freezing in precipitation tanks depends to a significant extent on the character of transformation of the texture of sapropel as a result of freezing. Unlike mineral soils, the processes which occur in frozen sapropel have not been thoroughly studied. A series of problems need further study. The most important of them are the following: study of the mechanisms and regularities of cryogenic texture- and structural formation, discovery of qualitative and quantitative relations of thermal and mass-exchange and cryogenic texture- and structural formation, predicting changes of structure and properties during freezing, and choosing the optimal freezing modes.

In accordance with the above mentioned the aim of this study was the research of formation and transformation of cryogenic macro- and microtexture of sapropel in a vast range of thermodynamic conditions of freezing, taking into account the mass-exchange, physico-chemical and physico-mechanical processes on the basis of laboratory modelling.

### THE TECHNIQUES OF RESEARCH

Modelling of thermal- and mass- transfer processes, cryogenic texture- and structural formation in sapropel was conducted on the basis of use of laboratory equipment and instruments. The main feature of this set was a laboratory installation (Brovka, Murashko, 1989). Its construction ensures the maintenance of a one-dimension temperature field during the freezing of ground

samples with a diameter of 140 mm and 300 mm in height. The installation allowed us to conduct a comprehensive study of thermal- and mass-transfer parameters in the freezing dispersal systems with automatic changing and regularity of temperature, and alteration of swelling degree.

The experiments were conducted on the sapropel samples of the upper- quaternary age with irregular composition patterns, different initial water content which did not undergo seasonal freezing in natural conditions. Sapropel of different compositions have been studied during modelling: organic, carbonate, siliceous, mixed- collected from the deposits of Byelorussia (Table 1).

Table 1. Characteristics of the studied sapropel of natural composition

Type of ground	Density of ground, $\gamma$ , g/cm <sup>3</sup>	Density of matrix (skeleton) $\gamma_f$ , g/cm <sup>3</sup>	Natural humidity W, %	Ash content A <sup>c</sup> , %
Organic sapropel	1.03	0.042	2000	12.7
Carbonate sapropel	1.22	0.49	142-183	84.0
Siliceous sapropel	1.1	0.39	379	75.8
Mixed sapropel	1.08	0.47	340	57.0

Sapropel samples were frozen at given boundary conditions to the depth of 100 mm. After one-side freezing of samples they were cut in slices and the humidity and density were

determined. The results were used in drawing a diagram of curves reflecting the pattern of water distribution along the height of the samples at different time intervals. Thermal- and mass-transfer parameters were calculated. Cryogenic macro- and microstructures were studied in samples of organogenic soil prepared by means of vacuum sublimation, in replicas and thin sections with the use of optical and electron microscopy (Ershov, 1988). The universal digital system of image analysis IBAS-2000 produced by "Opton" which was capable to conduct various measurements, transformation and classification of the studied objects was used in order to perform comprehensive analysis of the processes of texture- and structure formation depending on the parameters of heat and mass transfer.

Application of the method of image analysis for research of the cryogenic structure of frozen organogenic soils enabled us to calculate a series of object- and field specific textures and structural parameters which reflect the form, dimensions, orientation in space, location with respect to one another, and pattern of distribution of ice and organomineral constituents. The following object-specific parameters were calculated: area (S), perimeter (P), maximal and minimal diameter of ground particles ( $D_{max}$ ,  $D_{min}$ ), their orientation (X, Y,  $\psi$ ) and form coefficients ( $K_f$ ,  $K_{el}$ ). Determination of field specific parameters with respect to the ice constituent allowed the calculation of voluminous schlieren ice content in the rock  $i_t$ , and, separately, the ice content due to horizontal and vertical schlieren of ice. The application of the image analysis system let us obtain the data on water content of aggregates of organomineral matrix of soil  $W_{ra}$ . The volume distribution pattern ( $W_{vol}$ ) down the frozen zone of samples was determined layer-by-layer by means of thermostatic drying. Afterwards, ice content was calculated with the image analyser according to the image of the cryogenic structure obtained from the replica. The density of organomineral layers was calculated as:

$$W_{ga} = \frac{W_{vol} - i_t}{1 - i_t}$$

The mentioned parameters helped to establish the quantitative relationship of processes of re-distribution of water and formation of cryogenic macro- and microstructure of freezing sapropels.

## THE RESULTS AND THEIR ANALYSIS

The result of experiments on one-sided freezing show that the physical and chemical processes in sapropels depends a lot on the availability of organic components of the rock matrix. It stimulates the coagulation processes during freezing, influences the water transfer mechanism and cryogenic texture and structural formation on the whole. Despite the anomalously high natural water content in sapropels, the character of re-distribution of water in them is similar as in mineral soils. Ice was also observed here in the frozen zone as well as the dehydration in the thawed zone which is due to the gradient of general thermodynamic potential causing the flow of water from the thawed zone to the frozen one. The dynamics of freezing is characterised by the most significant water re-distribution in conditions of low-intensity thermal exchange at low

velocities as the velocity of the division boundary between the phases, decrease of temperature gradient in the frozen zone and the density of migrating flow of water (Fig.1).

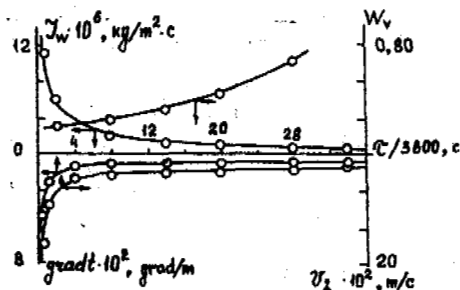


Figure 1. The character of the density of water migration flow ( $J_w$ ), temperature gradient ( $grad\ t$ ), humidity ( $W_{vol}$ ) and velocity of freezing ( $V_{fr}$ ) temporal changes in the carbonate sapropel.  $W_{vol}=0.71$ ;  $\gamma_f^0=0.51\ g/cm^3$ ,  $t_0=-3.4^\circ C$ .

The results of experimental studies confirm that texture- and structural formation during freezing of sapropel occurs in conditions of two mechanisms of mass-transfer: migration of water from the thawed zone of the freezing ground into the frozen one with subsequent freezing in the form of layers consisting of segregation ice (migration-segregation mechanism) and local re-distribution of water withing the freezing and frozen zones during the process of driving off combined water and its subsequent freezing with the dehydration of organomineral aggregates and coagulation of organic components (coagulation mechanism). Cryogenic texture- and structural formation in freezing sapropel occurs in several stages in correspondence with the alteration of the prevailing mechanism of mass transfer during freezing.

At the initial stage of freezing which is characterised by high values of  $grad\ t$ , the process of texture formation is regulated by the laws of free water crystallization which corresponds to the prototrope stage of crystallization. At the following stage the forming ice matrix promotes oriented growth of ice crystals which constitutes vertical schlieren. They thicken with depth and pull the associates of organomineral matrix apart while deforming and consolidating it. The process of consolidating the sapropel matrixes accompanied by dehydration with driving the combined water off which freezes at the periphery of ground aggregates. Dewatering of the matrix causes activation of the process of aggregation and coagulation of organomineral component. Height contents of the organic component in the sapropel which possesses high adhesion characteristics, promotes combining material particles into organo mineral aggregates. Their formation is accompanied by the nearing of particles and the increase of their surface and it causes still more deep dewatering of the organomineral matrix. The vertical ice schlieren were formed during this process which is due to the driving off and subsequent freezing of combined water during dehydration of organo-mineral matrix and coagulation of the organic component of the rock (coagulation-segregation mechanism of ice formation). As the front goes forward and the rate of freezing beside the coagulation-segregation mechanism of ice formation, the role of migration-segregation factor increases which

leads to the occurrence of horizontal schlieren of ice of second generation and while having the higher importance is the lower rate of freezing.

Relation between the mechanism of mass transfer and ice formation is determined by the conditions of freezing (Fig.2) and the composition of organogenic soil. The rate of freezing is higher, temperature gradient in the frozen zone and lower the ash content of sapropel, the more intense is the coagulation-segregation mechanism and the lesser role belongs to the migration-segregation mechanism. The influence of the altering rate of freezing  $V_{fr}$  and the temperature gradient in the frozen zone  $grad\ t$  on the processes of texture- and structural formation can be seen in the example of carbonate sapropel (initial humidity  $W_0=183\%$ ,  $\gamma_f=0.42\text{ g/cm}^3$  frozen in a closed system with changing thermostat temperatures of the surface of the sample from  $t_0=-2.1^\circ\text{C}$  to  $t_0=-9.9^\circ\text{C}$ . The laboratory modelling has shown that total ice content due to schlieren ice formation regularly decreases as the  $grad\ t$  increases in the frozen zone. The effect of horizontal  $i_h$  and vertical  $i_v$  components of the schlieren ice formation on changing total ice content are not equal and also depends on  $grad\ t$  values in the frozen sapropel zone. At  $grad\ t$  values below  $1.5\text{ grad/cm}$  the schlieren ice formation sharply increases due to segregation layers  $i_h$  while  $i_v$  features the opposite tendency. Increase of temperature gradient up to  $grad\ t > 1.5\text{ grad/cm}$  leads to monotonous augmenting of the contribution of the vertical due to segregation. At the values of  $grad\ t$  exceeding  $12\text{ grad/cm}$  the ice content caused by the vertical layers becomes predominant (Fig.2). Temperature of thermostat conditions influences the distribution of components of schlieren ice formation to the depth of the sample while tracing the zone of changing the prevailing mechanism of mass transfer (Fig.3).

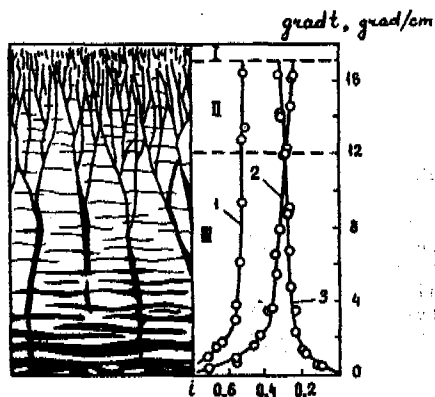


Figure 2. The character of the cryogenic texture, schlieren ice content in the rocks component and the prevailing mechanism of ice segregation changes due to the freezing conditions of the carbonate sapropel ( $W_0=183\%$ ,  $\gamma_f=0.42\text{ g/cm}^3$ ):

- I - the zone of prototrope crystallization;
- II - the zone of prevailing coagulation-segregation ice formation;
- III - the zone of prevailing migration-segregation ice formation;
- 1) - the total schlieren ice content;
- 2) - the ice content due to horizontal schlieren;
- 3) - the ice content due to vertical schlieren.

Total structural ice content and ice caused by the horizontal schlieren increases with the

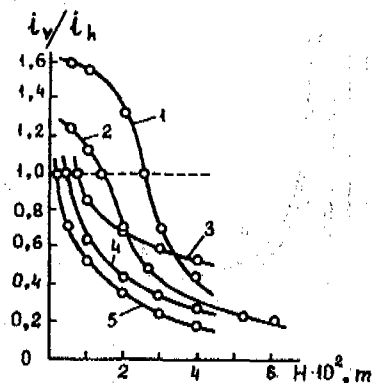


Figure 3. Changes of relations between schlieren ice segregation depth of the carbonate sapropel sample due to the temperature - humidity freezing conditions:

- 1 -  $t_0=-9.9^\circ\text{C}$ ,  $W_0=110\%$ ,  $\gamma_f=0.60\text{ g/cm}^3$ ;
- 2 -  $t_0=-5.1^\circ\text{C}$ ,  $W_0=122\%$ ,  $\gamma_f=0.56\text{ g/cm}^3$ ;
- 3 -  $t_0=-9.9^\circ\text{C}$ ,  $W_0=183\%$ ,  $\gamma_f=0.42\text{ g/cm}^3$ ;
- 4 -  $t_0=-5.1^\circ\text{C}$ ,  $W_0=183\%$ ,  $\gamma_f=0.42\text{ g/cm}^3$ ;
- 5 -  $t_0=-2.1^\circ\text{C}$ ,  $W_0=183\%$ ,  $\gamma_f=0.42\text{ g/cm}^3$ .

increasing of initial water content of organogenic soil. The predominance of the contribution of the horizontal schlieren formation to the process of structure formation begins at lower  $grad\ t$  values for the less humid sample than for the sample with high  $W_0$  and the transfer point moves inside the frozen zone (Fig.3).

The cryogenic microstructure of sapropel shows regular and monotonous transformation with the changing of temperature conditions of freezing. As the temperature gradient lowers so does the freezing rate, the microstructure of high-ash containing sapropel changes from nearly massive with few subvertical layers to incompletely lattice-like and lattice-like (at domination of the vertical component), then at further lowering of the temperature gradient to the lattice-like with prevalence of the horizontal lenses and schlieren, horizontal-layered, and at significant slowing down of the freezing front to ataxitic with a sharp predominance of ice component. Dimensions of ice schlieren and organomineral blocks tend to increase as the temperature gradient decreases in the frozen zone (Fig.4) connected with the extending of the time of migration ice accumulation in the frozen and dewatering thawed part of soil when the migration water flows, predominantly form macro- and micro-structures.

The main re-structuring of the organomineral matrix of sapropel occurs within the limits of the frozen and freezing zones depending on the intensity of the local water migration processes, dehydration of the matrix and coagulation of the organic component. Increase of the freezing rate and temperature gradient in the frozen zone causes significant subsidence gradients of the frozen organogenic rock and intensive development of local dewatering process which results in the formation of a more compact microtexture.

The texture formation processes in sapropels of different types occur according to the general scheme while at the same time having significant differences. The research of freezing of carbonate sapropel ( $A_C=84\%$ ) has shown that the texture formation process begins in the thawed and continues in the freezing and frozen zones.

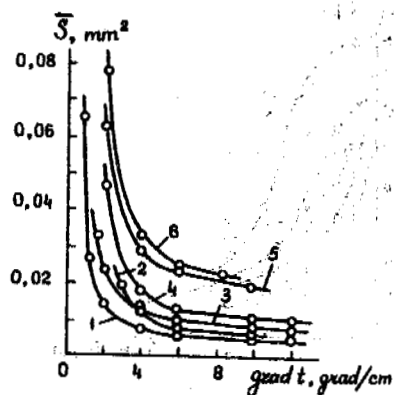


Figure 4. Correlation between the area organo-mineral layers and the temperature gradient in the frozen zone of various types of sapropel: Organic sapropel: 1-  $W_0=2000\%$ ,  $\gamma_f=0.048 \text{ g/cm}^3$ ; 2-  $W_0=710\%$ ,  $\gamma_f=0.13 \text{ g/cm}^3$ ; Siliceous sapropel: 3-  $W_0=379\%$ ,  $\gamma_f=0.24 \text{ g/cm}^3$ ; Mixed sapropel: 4-  $W_0=340\%$ ,  $\gamma_f=0.27 \text{ g/cm}^3$ ; 5-  $W_0=225\%$ ,  $\gamma_f=0.38 \text{ g/cm}^3$ ; Carbonate sapropel: 6-  $W_0=183\%$ ,  $\gamma_f=0.42 \text{ g/cm}^3$ .

The most significant transformations of texture in the thawed zone occurs at low rate of freezing. Due to dewatering the particles of the organomineral matrix become nearer, the porosity decreases, regular texture starts to form with larger aggregates and blocks. A fast rate of freezing consolidation of the matrix goes on within the freezing and frozen zones. The forming ice framework deforms aggregates on the organo-mineral matrix caused by ice crystal growth which caused their local dehydration with driving part of the weakly combined water into the interstices and its subsequent freezing. Local dewatering is accompanied by aggregation and coagulation of the organo-mineral phase and formation of consolidated humus substances, water-resistant aggregates due to intensive cementing action.

Research of the microtexture of organomineral matrix of carbonate sapropel has shown its rather insignificant transformation in the changing of the temperature of freezing. So, at grad t values in the frozen zone equal to 10.2 grad/cm and 1.7 grad/cm respectively in the roof and floor of the sample and significant difference of microstructure, the texture of the organomineral matrix remains unchanged and is characterized by a uniform pattern of distribution of aggregates with sizes 5 to 15 microns with predominantly isometric shapes. Parts of weakly aggregated material 2-3 microns in size were also seen. Pores are not larger than 10 microns and their distribution pattern is uniform. Ice in cement is of a porous type.

The scheme of physico-chemical and texture formation processes in siliceous and mixed sapropel is qualitatively similar to their character in the carbonate sapropel. However, the higher humus content and, as a result, high natural humidity increases the significance of coagulation effects during the process of texture formation.

Cryogenic microstructure of the siliceous sapropel ( $AC=75.8\%$ ) is characterized by two main specific features. Formation of soil microstructure by means of differentiation of the system into ice and organomineral constituents depends to a significant extent on the freezing condi-

tions. At the same time the microtexture of the soil component varies rather inconsiderably within the given range of temperature - humidity conditions and is determined by the processes of local migration of water within the frozen zone. Microtexture of organomineral layers is characterized by uniform distribution of non-oriented aggregates 5 to 10 microns in size covered with a film of coagulation formations. The interstitial space is filled with fine-dispersed weakly oriented organomineral material with the size of 1-2 microns with tabular and flaky shapes. Ice in cement is presented by the porous type. Pore dimensions vary from 3 to 10 microns.

High water content characteristics of the mixed sapropel ( $AC=57.0$ ) in natural conditions leads to the formation of a cryogenic structure of an ataxitic type in it with the characteristic uniform distribution of organomineral grains at grad t > 4 grad/cm (Fig.4). Microtexture of the organomineral grains is characterized by coagulation forms in the form of films surrounding quartz grains and calcite crystals, the presence of large grains (10-15 microns) cemented by consolidated and a dewatered fine-dispersed fraction. Interstitial pores filled with ice cement do not exceed 5 to 15 microns.

In low-ash organic sapropel ( $AC=12.7\%$ ) the formation of the texture of organomineral matrix is totally dependent on the coagulation effects. Consolidation of the matrix due to crystallization pressure causes dewatering of organomineral blocks, the occurrence of single flaky and filmy textural grains oriented along the surface of voluminous deformation of the block during local dewatering forming concentric casings surrounding mineral grains or ice crystals. The highest changes of the dimensions of structural grains occur at grad t values below 2.5 grad/cm at a slow rate of freezing (Fig.4). Ataxitic cryogenic structure is characteristic of the occurrence of wide ice fields with "floating" organomineral layers which change orientation from subvertical to subhorizontal as the grad t values decrease.

Research of re-distribution of water content as a result of freezing of sapropels has shown that the humidity of the organomineral constituent can be regarded as near to the constant irrespective of the freezing conditions (Fig.5). That is why the sharp increase of ice content due to intensive schlieren formation at freezing with low temperature gradients which significantly reduces the content of matrix-mineral component in the frozen sapropel is the main factor which decreases the efficiency of dewatering. Analysis of changes of organomineral constituent to the depth of the frozen zone has shown that after reaching certain (critical) values of temperature gradient grad t the complete elimination of organomineral layers and formation of a solid ice field occur. The grad t value is determined by the initial humidity of the sapropel and has higher values with an increase of  $W_0$ . For organic sapropel samples at initial humidity  $W_0=2000\%$ ,  $W_0=836\%$ ,  $W_0=710\%$ , grad t values are equal to 1.13; 0.82 and 0.73 grad/cm respectively. For mixed sapropel at  $W_0=340\%$ , grad t = 0.46 grad/cm, for siliceous sapropel at  $W_0=379\%$  and 315%, grad t = 0.55 and 0.41 grad/cm.

The obtained values of grad t allow the determination of the optimal temperature and humidity conditions of freezing of organogenic soils at which the freezing mainly influences the matrix-mineral component of soil until the formation of ice horizon, as well as for

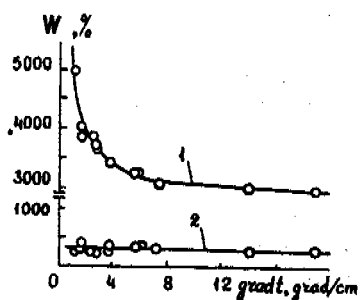


Figure 5. Correlation between the total humidity (1), the organomineral layers humidity (2) and the temperature gradient in the organic sapropel frozen zone  $W_0=2000\%$ ,  $\gamma_f=0.048 \text{ g/cm}^3$ ,  $A^C=12.7\%$ .

calculating the optimal depth of freezing for industrial purposes.

#### REFERENCES

1. Brovka, G.P. and Murashko, A.A. (1989) Laboratory complex for geocryologic investigations. Engineering-geocryologist investigations on permafrost: Proceedings of the 5th Scientific-Techn. Conference, Magadan, p.111-112.
2. Chuvilin, E.M. and Yazynin, O.M. (1988) Frozen soil macro- and micro-texture formation. 5th International Conference on Permafrost. Proc. v.1, Tapir publisheim. Norway, p.320-323.
3. Ershov, E.E. (1988) Microstructure of frozen rocks. Moscow, 183pp.



UNFROZEN, HIGH-SALINITY INTERVALS WITHIN  
ICE-BEARING PERMAFROST, NORTH SLOPE OF ALASKA

Timothy S. Collett<sup>1</sup> and Kenneth J. Bird<sup>2</sup>

<sup>1</sup>U.S. Geological Survey, Denver Federal Center, Box 25046,  
MS-940, Denver, Colorado 80225, USA

<sup>2</sup>U.S. Geological Survey, 3475 Deer Creek Road,  
Palo Alto, California 94304, USA

The review of available well-logs from the Prudhoe Bay and Kuparuk River oil fields on the North Slope shows that the ice-bearing permafrost interval is not vertically continuous, but interrupted by numerous intervals in which the ice content is greatly diminished or absent. The most prominent unfrozen interval occurs within 50 to 250 m of the surface, it is laterally continuous over at least 1,000 km<sup>2</sup>, and ranges in thickness from 15 to 100 m. This prominent interval occurs within a conglomeratic section and extends into the upper part of an underlying relatively clay-rich sequence. Well logs further indicate that this interval occurs at temperatures as low as -8 °C and the pore-water (bulk) salinity within this interval is calculated to be at least 130 ppt.

#### INTRODUCTION

Geophysical well logs, which can be used to detect the presence of ice within the subsurface, indicate that the thickness of the North Slope ice-bearing permafrost sequence ranges from about 130 to 650 m (Osterkamp and Payne, 1981; Collett and others, 1989). The base of ice-bearing permafrost usually lies at a shallower depth than the 0°C isotherm (permafrost). This discrepancy has been attributed to the phenomenon of freezing-point depression (Collett and Bird, 1988). Geophysical well logs from the North Slope Prudhoe Bay oil field show that the ice-bearing permafrost interval is not vertically continuous, but interrupted by anomalous units or zones in which the ice content is greatly diminished or absent. The primary purpose of this paper is to document the occurrence of these anomalous, possibly unfrozen, zones and assess the physical and chemical parameters controlling their distribution. This paper will focus on the most prominent anomalous unit in the northeastern part of the Prudhoe Bay oil field.

#### WELL-LOG EVALUATION OF ICE-BEARING PERMAFROST

In this study the term, ice-bearing permafrost refers to the strata which contains or is interpreted to contain a sufficient volume of ice to be detected on geophysical well logs without the aid of temperature data. The minimum amount of ice necessary for

detection by well-logging devices is unknown. Desai and Moore (1968) were the first to report that ice-bearing sediments exhibit physical characteristics that can be detected with well logs. Howitt (1971) observed log responses similar to those described by Desai and Moore (1968) in a well from the Prudhoe Bay oil field (BP-12-10-14A) in which the permafrost interval was extensively cored. He reported that ice was observed in these cores to a measured well depth of 1,858 ft (566 m below the ground surface). The log-determined base of ice-bearing permafrost is at 1,885 ft well depth (562 m below the ground surface). The 4-m discrepancy between the log determinations and observed ice is not considered significant because Howitt (1971) reported that the core-identified base of ice is accurate only within plus or minus 9 m. These observations of ice-bearing cores in relation to log response for this well represents the only direct evidence that verifies the accuracy of well logs as ice-detection devices. Unfortunately, no information was provided on the limits or sensitivity of well logs to ice detection. Based on our analyses of the resistivity and acoustic log response in this well, we have assigned "cutoff" log values to discriminate between ice-bearing and non-ice-bearing sediments. The value of the electrical-resistivity "cutoff" is 9.0 ohm-m, while the acoustic transit-time "cutoff" is 130 µs/ft.

In a previous study (Collett and others, 1989), well logs from 156 wells were used to map the depth to the base of the ice-bearing

permafrost on the North Slope. The depth of ice-bearing permafrost ranges from less than 200 m in the National Petroleum Reserve in Alaska to more than 600 m in the Prudhoe Bay area. Of the well logs commonly available, the electrical-resistivity and acoustic transit-time logs were found to be the most useful in detecting the presence of ice in a rock sequence. For further discussion of ice-bearing permafrost well-log evaluation techniques see Osterkamp and Payne (1981), and Collett and others (1989).

#### GEOLOGIC NATURE OF THE ANOMALOUS INTERVALS

The review of 156 well-log suites from the Prudhoe Bay-Kuparuk River area reveals the occurrence of numerous laterally continuous intervals in which the resistivity and acoustic transit-time logs suggest that the ice content is greatly diminished or missing within the permafrost sequence. Well logs from the Foggy Island-1 well (figure 1) show the distribution of several of the more prominent anomalous intervals. These intervals exhibit resistivities ranging from 0.5 to 3.0 ohm-m compared to 500 to 1,000 ohm-m in the surrounding ice-bearing rocks. As previously discussed, a rock unit that exhibits electrical-resistivities of 0.5 to 3.0 ohm-m indicates that the interstitial pore-waters are likely unfrozen. Similarly, low acoustic velocities recorded on the acoustic transit-time well logs also suggest that these anomalous intervals are unfrozen, with recorded acoustic transit-time values ranging from about 250 to 200  $\mu$ s/ft (acoustic-velocity of  $\approx$ 1.0-1.5 km/s). In figure 1, ice-bearing to non-ice-bearing "cutoff" log values, established in the BP-12-10-14A well, have been added to the electrical-resistivity and acoustic transit-time log plots. A comparison of the resistivity and acoustic transit-time logs from the Foggy Island-1 well (figure 1) reveals inconsistencies between these logs in their ice-detection capabilities. These inconsistencies are likely caused by poor wellbore conditions, such as an enlarged borehole, which would more adversely affect the transit-time device. Thus, we favor utilizing the resistivity log.

No direct evidence, such as core observations, conclusively proves that these anomalous intervals are unfrozen. An oil- or gas-bearing interval within ice-bearing permafrost would exhibit similar low acoustic velocities but resistivities would be higher than observed. No indications of oil or gas are reported for these intervals. A completely dry interval, one in which the rock pores are filled with air, would show low velocity but high resistivity. Thus for lack of a better explanation, we conclude that these anomalous

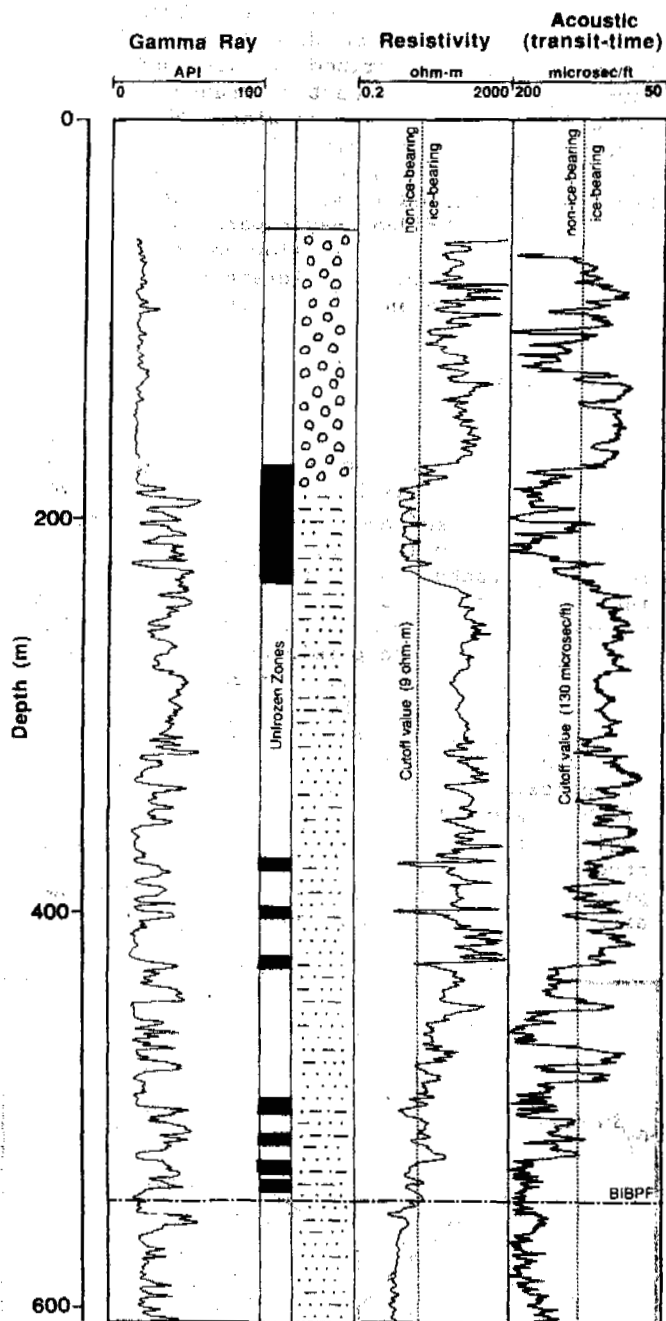


Figure 1. Selected well logs from within the ice-bearing permafrost sequence of the Foggy Island-1 well on the North Slope of Alaska. The base of ice-bearing permafrost (BIBPF) is at  $\approx$ 530 m. The resistivity-log suggests the occurrence of eight zones in which the ice content is greatly diminished (unfrozen), including a prominent 60-m-thick zone at a depth of about 170 m. Ice-bearing to non-ice-bearing "cutoff" log values have been added to the resistivity and transit-time log plots.

intervals are unfrozen and water saturated.

The most prominent of these anomalous intervals, first described by Osterkamp and Payne (1981) in wells east of Prudhoe Bay, is about 50-m-thick and occurs within 200 m of the surface in the Foggy Island-1 well (figure 1). This, the thickest unfrozen interval observed, has been identified in most of the wells drilled in the Prudhoe Bay-Kuparuk River area that have well logs at shallow depths and it lies within the same stratigraphic interval. The gamma-ray log and drill-cuttings analysis indicate that this anomalous interval includes an upper sandstone and conglomerate part and a lower interbedded clay-rich mudstone and sandstone part. Within the area of well control, the depth to the top of this interval varies from 50 m in the southwest to 250 m in the northeast, it is laterally continuous over at least 1,000 km<sup>2</sup> and it ranges in thickness from 15 to 100 m (figures 2, 3, and 4). The regional structure of this prominent unfrozen interval conforms to the regional geology which is characterized by a 1 to 2 degree dip to the northeast. Both the prominent unfrozen interval and the overlying frozen conglomeratic section thicken from the southwest to the northeast across the study area, with the unfrozen interval obtaining maximum thicknesses of approximately 100 m in the area of the offshore Endicott oil field (figure 2). Regional subsurface stratigraphic correlation studies suggest that the distribution of this prominent unfrozen interval is limited to the area of the Prudhoe Bay and Kuparuk River oil

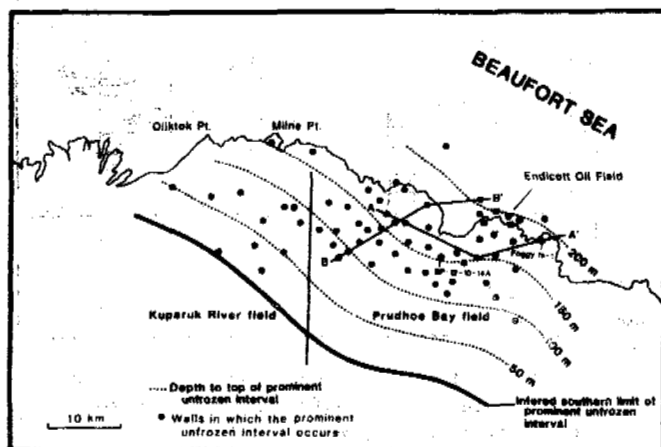


Figure 2. Distribution of the laterally continuous, near-surface, prominent unfrozen interval in the Prudhoe Bay-Kuparuk River area of northern Alaska. Also shown is the approximate depth to the top of this prominent unfrozen interval. The locations of cross sections A-A' (figure 3) and B-B' (figure 4) are shown.

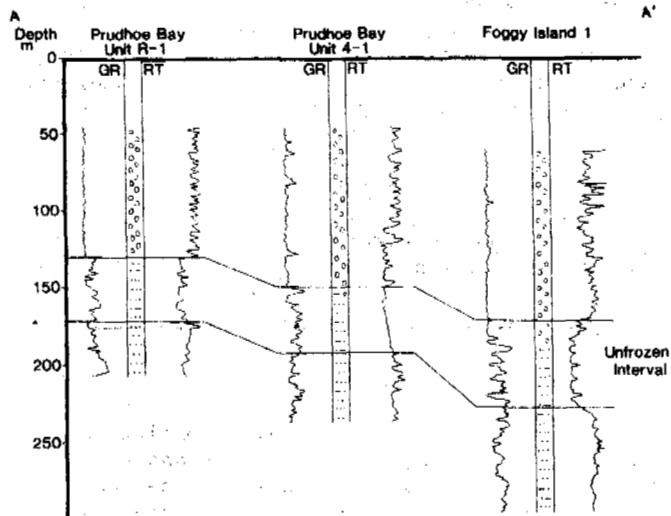


Figure 3. A generalized west to east well-log cross section (A-A') illustrating the vertical and lateral nature of the most prominent unfrozen interval. GR = gamma ray log, RT = resistivity log

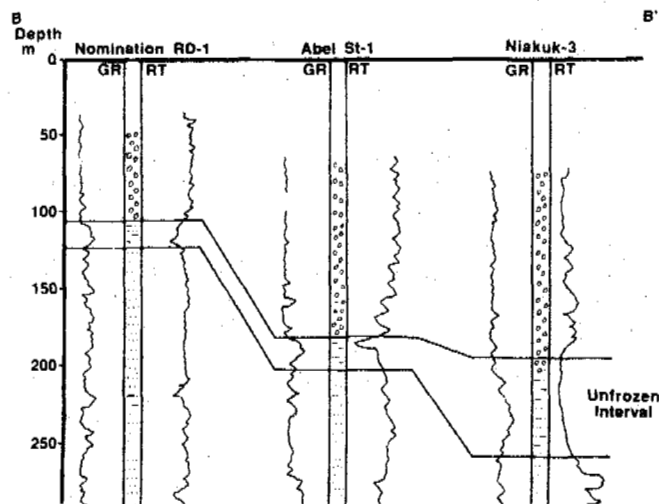


Figure 4. A generalized southwest to northeast well-log cross section (B-B') illustrating the vertical and lateral nature of the most prominent unfrozen interval. GR = gamma ray log, RT = resistivity log

fields, and it is likely absent to the south and west of the inferred truncation line in figure 2. The northern offshore extent of the unfrozen intervals beyond the barrier-islands is uncertain for lack of well control.

The less prominent (thinner) unfrozen intervals exhibit similar well-log characteristics and also occur at lithologic contacts between clay-rich mudstones and

relatively porous, coarse-grained rock sequences. These relatively thinner unfrozen intervals are often laterally continuous, however, they rarely cover an area of more than several square kilometers. The remainder of the paper will only deal with the most prominent unfrozen interval described earlier in the Foggy Island-1 well.

#### PHYSICAL/CHEMICAL CONTROLS ON FREEZING-POINT-DEPRESSION

High-resolution equilibrated-wellbore temperature surveys from nine oil wells in the Prudhoe Bay field (reviewed in Collett and others, 1989) suggest that the most prominent unfrozen interval is characterized by formation temperatures that range from about -7 to -9°C. Such low temperatures require geologic or geochemical conditions that would depress the freezing-point of the pore-water within this interval.

Factors that influence the freezing-point of water include pore-fluid salinity (total dissolved solids), pore-pressure, and sediment grain-size (Osterkamp and Payne, 1981; Collett and Bird, 1988). The cumulative effect of these factors is expressed in the following equation, reviewed by Osterkamp and Payne (1981).

$$T_o = 0.0100 - T_c - T_p - T_s \quad (1)$$

The term  $T_o$  represents the freezing-temperature of the system being analyzed, 0.0100 is the triple-point of water and  $T_c$ ,  $T_p$ , and  $T_s$  are the temperature effects of chemical composition (salts), pore-pressure, and soil/rock particle-size effect, respectively.

The effect of pore-pressure ( $T_p$ ) on the freezing-point of water can be calculated from the following equation if pore-pressure (P) is known.

$$T_p = BP \quad (2)$$

The variable B is the Clausis-Clapeyron Slope (0.00751 °C atmos<sup>-1</sup>). Since this unfrozen interval lies at shallow depths (<300 m) the maximum freezing-point depression that may be attributed to the effect of pore-pressure, assuming a hydrostatic pore-pressure gradient (0.097 atmos/m), would be no greater than about 0.2°C. The theoretical maximum pore-pressure gradient (lithostatic; 0.223 atmos/m) would still only produce a -0.5 °C freezing-point depression. There is no indication of overpressuring within the permafrost sequence of the Prudhoe Bay area (Collett and Bird, 1988).

Osterkamp and Payne (1981) suggest that the particle effect of clay-sized material could suppress the freezing-point by several degrees

Celsius, but for coarser material, such as silts and sands, the particle effect is negligible. It is generally accepted, that within the relatively coarse-grained clastic sediments that dominate the permafrost sequence in the Prudhoe Bay area, grain-size should have little or no effect on the freezing-point of water (Collett and Bird, 1988). Furthermore, the comparison of available gamma-ray (used for lithologic characterization) and resistivity well logs from the Prudhoe Bay area show that the clay-rich mudstone rocks beneath the unfrozen intervals are often ice-bearing; thus, the grain-size particle effect on freezing-point depression within this area is considered negligible.

We used the following equation reviewed in Collett and Bird (1988) to calculate the volume of salt required to depress the freezing-point by -8°; this equation yields accurate values for waters containing seawater-type salt (mostly NaCl) in concentrations ranging from 124.68 to 230.77 ppt.

$$T_c = 6.05326 - 97.00732(S_p/1,000 - S_b) \quad (3)$$

To depress the freezing-point of water ( $T_c$ ) by -8.0 °C requires a pore-water salinity ( $S_b$ ) of 127 ppt. Therefore, by process of elimination, pore-fluid salinity may be the principal factor controlling the freezing-point of the pore-water within this unfrozen interval.

Water chemistry data from cores and petroleum production tests on the North Slope show that the predominant pore-water salt is NaCl (Collett and Bird, 1988). Water samples collected below the permafrost sequence have pore-water salinities (total dissolved solids) in the range from 0.5 to 19.0 ppt (Collett and Bird, 1988). Water samples in the ice-bearing-cores from the BP-12-10-14A well in the Prudhoe Bay Oil Field have salinities in the range of 0.15 to 0.50 ppt (Howitt, 1971; Collett and Bird, 1988). However, the usefulness of these analyses to this study are uncertain because none of these ice/water samples were from the unfrozen intervals within the ice-bearing permafrost sequence. The highest pore-water salinity measured on the North Slope (19.0 ppt) would depress the freezing-point of water to about -1.0°C.

The maximum cumulative freezing-point depression that can be attributed to the observed salinities, pore-pressures, and grain-sizes is about -1.0 to -2.0 °C, a temperature far above the -8°C of the most prominent unfrozen interval in the Prudhoe Bay area. Of these factors, only salinity offers the possibility of freezing-point depression of a magnitude large enough to account for these observations.

Although we have no salinity data from the anomalous unfrozen intervals, it is possible to

calculate pore-fluid salinities within these intervals with conventional well-log interpretation techniques. The following equation (reviewed by Schlumberger Educational Services, 1989) uses recorded well-log resistivities ( $R_t$ ) to calculate pore-water resistivities ( $R_w$ ) which can then be converted to pore-water salinities (NaCl equivalents).

$$R_t = \frac{F_R R_w}{S_w^n} \quad (4)$$

If we assume the rock pore-space is 100% water saturated ( $S_w = 100\%$ , no hydrocarbon or ice), the term  $S_w^n$  is equal to 1 and the equation can be rewritten into the following form.

$$R_w = \frac{R_t}{F_R} \quad (5)$$

The term  $F_R$  is referred to as the formation resistivity factor which can be calculated in a sandstone sequence by using the following empirically derived so-called Humble equation (reviewed by Schlumberger Educational Services, 1989).

$$F_R = 0.62 \phi^{-2.15} \quad (6)$$

Porosities ( $\phi$ ), calculated from the neutron well logs, within the conglomeratic portion of the most prominent unfrozen interval, average about 40%; thus, the formation resistivity factor ( $F_R$ ) for this interval is 4.5. The log calculated porosity of 40% is close to the core values reported by Howitt (1971) for the permafrost sequence in the Prudhoe Bay area. The electrical-resistivity ( $R_t$ ) of the conglomeratic part of the prominent unfrozen interval in 43 of the surveyed wells averages about 1.0 ohm-m. Only the conglomeratic rock portion of the unfrozen interval (determined by gamma-ray log response) was examined because these calculations are only accurate within clean, relatively non-clayey (<10% clay), rocks. By assuming a formation resistivity factor ( $F_R$ ) of 4.5 and a rock resistivity ( $R_t$ ) of 1.0 ohm-m, the resistivity of the pore-water ( $R_w$ ) within the most prominent unfrozen interval is calculated to be 0.22 ohm-m. The Schlumberger water-resistivity versus salinity (NaCl) comparison graph (reviewed by Schlumberger Educational Services, 1989) indicates that a pore-water with a electrical resistivity of 0.22 ohm-m at a formation temperature of  $-8.0^\circ\text{C}$  has a salinity (total dissolved solids in NaCl equivalents) of approximately 130 ppt. These calculations are correct only if the studied intervals are ice-

free, because even a small amount of ice increases the electrical-resistivity of a rock unit. An ice-induced electrical-resistivity increase, however, would shift the calculated salinities to lower apparent values. Thus, the well-log calculated (bulk) pore-water salinity of 130 ppt for the most prominent unfrozen interval is a minimum value. A pore-water salinity ( $S_p$ ) of 130 ppt would depress the freezing-point of water ( $T_f$ ) by  $-8.4^\circ\text{C}$ .

Because the prominent unfrozen interval is at a formation temperature of about  $-8^\circ\text{C}$ , and the well-log calculated salinities closely agree with those salinities necessary to depress the freezing-point of water by the required  $-8.0^\circ\text{C}$ , it can be reasonably assumed that this interval is unfrozen by virtue of the presence of high-salinity pore-waters.

#### ORIGIN OF HIGH-SALINITY, UNFROZEN INTERVALS

It is generally believed that thermal conditions conducive to the formation of permafrost have persisted in northern Alaska since the end of the Pliocene ( $\approx 1.65$  Ma). However, temperature fluctuations during the Pleistocene ( $\approx 1.65$  to 0.01 Ma) have been great enough to repeatedly thicken and thin the permafrost sequence (Carter and others, 1986). The magnitude and duration of these temperature changes for the North Slope are not well documented. It is also known that deep surface water bodies may prevent the formation of permafrost or induce thawing when permafrost already exist. Therefore, the paleo-position of the Arctic Ocean coastline is important in understanding the history of permafrost development. At this time, inadequate data exist on climatic or geologic changes on the time scale necessary to assess the history of permafrost formation in northern Alaska. It is possible, however, that the most recent period of renewed permafrost development in the coastal area of northern Alaska started at the end of the last interglacial stage, Sangamonian ( $\approx 0.07$  Ma), as a response to falling temperatures and sea level.

It is possible, that the mechanism responsible for the occurrence of these unfrozen intra-permafrost intervals was initiated at the end of the Sangamonian when the present land surface in the Prudhoe Bay area was likely covered by the Arctic Ocean (Carter and others, 1986). The relatively warm ocean waters would have prevented the formation of permafrost and the pore-water of the sediments lying beneath the unfrozen seabed would have had a chemical makeup similar to that of sea water. As temperatures and sea level fell during the ensuing Wisconsinan glacial stage, the Prudhoe Bay area would have been subareally exposed and permafrost development would have commenced. Solute

exclusion associated with the deepening ice-bearing permafrost sequence would have concentrated the pore-water salts along the freezing-front. As the freezing-front moved downward through the surficial conglomeratic sequence and encountered the relatively impermeable underlying clay-rich mudstone, the solute material was unable to penetrate the clay-rich rocks, thus trapping the high-salinity waters between the overlying ice and the underlying mudstone. With continued freezing conditions, the permafrost sequence would have deepened and a new freezing-front was developed below the unfrozen salt-water-bearing interval.

Clays are known to act as barriers to  $\text{Na}^+$  and  $\text{Cl}^-$  ions in aqueous solutions. However, due to the lack of water samples or cores, the assumption that the underlying clay-rich rock sequence of the unfrozen interval has acted as a solute filter cannot be verified. The examination of the less conspicuous unfrozen intervals deeper in the permafrost sequence of the Prudhoe Bay area appears to support the assumption that clays act as solute filters, because these more deeply buried unfrozen sequences also occur at the base of permeable rock sequences which are directly underlain by clay-rich rocks. The effectiveness of these clay-rich rock sequences as semipermeable membranes is purely speculative and warrants further study.

#### CONCLUSION

Anomalous well-log resistivities and acoustic characteristics in the permafrost sequence of the Prudhoe Bay-Kuparuk River area of northern Alaska reveal the occurrence of numerous laterally continuous intervals that are unfrozen, brine-rich zones within an otherwise solid ice-bearing section as much as 600-m-thick. The most prominent unfrozen interval is about 100-m-thick and has pore-water salinities, calculated from well logs, about three times greater than normal sea water. Such a salinity is sufficient to lower the freezing-point of these waters so they remain unfrozen. It is postulated that these elevated salinities are the result of the combination of solute exclusion during permafrost development and by trapping the density-driven downward-flowing salt-waters of the freezing-front above a regional semipermeable relatively clay-rich rock sequence.

#### REFERENCES

Carter, L.D., Brigham-Grette, Julie, Marincovich, Louie, Jr., Pease, V.L., and Hillhouse, J.W., 1986, Late Cenozoic Arctic

Ocean sea ice and terrestrial paleoclimate: *Geology*, v. 14, p. 675-678.

Collett, T.S., and Bird, K.J., 1988, Freezing-point depression at the base of ice-bearing permafrost on the North Slope of Alaska: in *Proceedings of the Fifth International Conference on Permafrost*, Trondheim, Norway, August 2-5, p. 50-55.

Collett, T.S., Bird, K.J., Kvenvolden, K.A., and Magoon, L.B., 1989, Map of the depth to the base of the deepest ice-bearing permafrost as determined from well logs, North Slope, Alaska: U.S. Geological Survey Oil and Gas Map OM-222, 1 sheet, Scale 1:1,000,000.

Desai, K.P., and Moore, E.J., 1968, Well log interpretation in permafrost: *The Log Analyst*, v. 10, no. 1, p. 13-25.

Howitt, Frank, 1971, Permafrost geology at Prudhoe Bay, Alaska: *World Petroleum*, v. 42, no. 8, p. 28-38.

Osterkamp, T.E., and Payne, M.W., 1981, Estimates of permafrost thickness from well logs in northern Alaska: *Cold Regions Science and Technology*, v. 5, p. 13-27.

Schlumberger Educational Services, 1989, *Log interpretation principles/applications*: Schlumberger, Houston, Texas, 120 p.

## SIMULATION OF HYDROCARBON SPILLS IN PERMAFROST

M. Yavuz Corapcioglu  
Department of Civil Engineering  
Texas A&M University  
College Station, TX 77843-3136 USA

Sorab M. Panday  
HydroGeoLogic, Inc.  
1165 Herndon Parkway, Suite 900  
Herndon, VA 22070 USA

The increasing potential of soil and groundwater contamination by petroleum products in the Arctic regions demands an enhanced understanding of the governing processes that determine their fate. The Arctic system has unique features requiring special attention due to low temperatures and the presence of ice. Even the most comprehensive compositional models for isothermal conditions do not address many crucial factors, chiefly the influence of freezing and thawing on the thermal and flow regime, and the influence of temperature and ice on flow and phase behavior for the fluids in the porous medium and the component species of the fluids. This study develops a model to simulate the transport and fate of petroleum products in Arctic soils and groundwater. The model is based on identification and quantification of the significant physical, thermal, chemical and biological processes and construction of mathematical representations of these phenomena, with simplifying assumptions facilitating a numerical solution to the complex set of equations. Results of a one-dimensional simulation for a hypothetical gasoline spill scenario are also presented.

### INTRODUCTION

In view of the large number of oil spills that have occurred in Arctic regions (Mackay, 1985), it is necessary to understand and quantify the significant processes that act on a hydrocarbon contaminant in frozen soils. The thermodynamic aspects of the problem involve quantification of phase transfer of the contaminant's condition into soil air and soil water at the various states of temperature, pressure, and composition that exist in the system. Melting and freezing of the contaminated soil water solution is also quantified by equilibrium thermodynamic relations. Flow aspects of the problem include quantification of movement of all phases in the soil, as well as transport of individual contaminant species within all phases. Energy transport within the soil is also quantified, since variations in the thermal regime govern freezing, melting, phase partitioning of components and flow properties of the phases. Biodegradation by indigenous microorganisms and other reactions may be quantified as sources or sinks in the governing equations. Numerous wording assumptions and sophisticated numerical techniques are required for solution to the set of governing equations that describe the fate of a petroleum contaminant on frozen soils.

Vast amounts of literature have been published on each of the aspects concerning the problem discussed above. Phase behavior and thermodynamic relations for phase partitioning are explained by Walas (1985) and summarized by Reid *et al.* (1987). Phase behavior of petroleum products have further been researched by the petroleum industry. Partitioning calculations have evolved from evaluating the equilibrium partition coefficients,  $K$ , as functions of pressure and temperature (Kazemi *et al.*, 1978), to using a generalized equation of state (EOS) to calculate  $K$ -values along with other physical properties as a single consistent source (Coats, 1980). Non-equilibrium partitioning has been discussed by Pistiner *et al.* (1989). Phase behavior and water transport of dissolved solutes in water with a

freezing porous medium have been modeled by Panday and Corapcioglu (1991). The numerous processes that interact in the freezing and melting of Arctic soils are described by Kay and Perfect (1988). Biodegradation in Arctic regions is discussed by Atlas (1975). Flow of multiphases in a porous medium has been extensively studied by the petroleum industry. Recently, there is an increased interest in the groundwater community on multiphase flow behavior due to the rising incidents of groundwater contamination by immiscible hydrocarbons. Forsyth (1988) presents a model for three-phase flow in a porous medium for a single component contaminant. Compositional simulators involving numerous components have been developed by Coats (1980), and Corapcioglu and Baehr (1987). A recent model for examining the fate of hydrocarbon products on frozen soils developed by integrating the concepts discussed above has been presented by Panday and Corapcioglu (1992). The various balance equations, constraints, and relationships for the governing processes are developed therein and the simplifying assumptions that can be made for solution to the complex set of equations are noted. Robust numerical techniques required to solve the highly non-linear system of coupled governing equations are provided by Corapcioglu and Panday (1991).

### MATHEMATICAL MODEL

A mathematical model is presented to simulate the processes occurring during multicomponent petroleum contamination of a frozen soil. The governing equations that have been simplified for a vertical one-dimensional soil column are listed in Appendix A. Quantification of the transport of each component is achieved by employing the conservation of mass equation (A1) for every component within the system. Equation (A1) states that the rate of change of the mass of a component in all phases of a representative elementary volume is due to advection and dispersion within all phases, subject to biodegradation loss.

Equilibrium thermodynamic relations determine the partitioning of components among these phases. Constitutive relations determining relative permeabilities of the flowing phases and capillary pressure-saturation functions for all phases are extended from two-phase relationships, since multiphase relationships are difficult to obtain. The thermal regime of the system is quantified by the energy conservation equation (A2), which states that the rate of change of internal energy in a representative elementary volume is due to the net conduction and convection of heat into it within all phases present. Quantification of the change of internal energy due to solubility of compound species in the water phase and volatilization is negligible compared to the large contribution to the internal energy due to ice-water phase change and advective and dispersive heat transport. Heats related to biodegradation and dispersive heat flux are also neglected in Equation (A2). The thermal conductivity and heat capacity of the system are dependent on phase saturations and compositions, and on thermal properties of the individual components. Densities and viscosities of all phases are functions of temperature, pressure, and composition of the respective phases. A non-deforming porous medium has been assumed in the above transport equations, and ice lensing and its effects have been neglected. The Clapeyron equation (A3) provides the general equilibrium relationship between ice and water. The mole fraction constraints (A4) and the saturation constraint (A5) complete the set of governing equations.

The unknowns of solution are the spatial distributions and temporal variations of mole fractions of each of the components in the system,  $x_{MP}^k$ , the temperature  $T$ , the phase pressures  $p_{\alpha}$ ,  $\alpha = wp$  (water phase),  $fw$  (frozen water),  $np$  (non-aqueous),  $ap$  (air phase), and their saturations  $S_{\alpha}$ . These equations are solved simultaneously for a one-dimensional soil column, subject to appropriate initial and boundary conditions. A Newton-Raphson linearization and an implicit iterative procedure for the non-linearities are applied on the equations over a domain discretized by finite differences. Underrelaxation formulas are used to assist convergence of the solution scheme. The numerical methods are discussed further by Panday and Corapcioglu (1991).

## NUMERICAL PROCEDURE

The transport equations (A1) and the energy equation (A2) are written in general form as

$$\frac{\partial}{\partial t} A = \frac{\partial}{\partial x} \left( B \frac{\partial C}{\partial x} \right) + D \quad (1)$$

For a Newton-Raphson scheme, each term is expanded as a function of all the primary variables. The Newton-Raphson scheme enhances convergence for the set of highly non-linear equations encountered. Each term of the equation (1) for the transport and energy equations is expanded and rearranged to have only incremental terms on the left-hand side. The remaining equations (A3)-(A-5) that comprise the primary set are also expanded in a similar fashion, and rearranged. The right-hand side contains all the known terms. These terms are then added to their respective locations in a coefficient matrix  $J$  and a force vector  $V$  such that the system is defined as

$$J \delta P_m = V \quad (2)$$

where the change of the primary unknowns,  $\delta P_m$  is to be solved for. An explicit treatment is given to all coefficient terms by expressing them at the latest iteration level. All partial derivatives appearing in the expansion of the equations with respect to the primary unknowns are calculated using a cord-slope method. The cord is taken as the difference between the latest known iterate value and the previous time step. If this cord is below a certain prescribed minimum, the minimum value is taken as the cord for determining the slope. The matrix equation (2) is a block matrix equation containing all simultaneous equations (A1)-(A5) at each node within the domain. Exceptions occur in special cases wherein this set does not represent the physical situation and needs to be substituted by other equations. The resulting matrix is block tri-diagonal and is solved at each non-linear iteration using a method parallel to the Thomas Algorithm, wherein operations are performed on block matrices instead of variables.

## RESULTS

A homogeneous unsaturated soil column, initially frozen to  $-3^{\circ}\text{C}$  with ice and water saturation of equilibrium conditions shown in Figure 1, is subject to a simulated gasoline spill at the surface, which increases the surface temperature to  $5^{\circ}\text{C}$  during the period of the spill. Surface temperatures remain at  $5^{\circ}\text{C}$  thereafter. The simulated gasoline is a mixture of benzene, N-butane, cyclohexane and N-octane, with mass fraction ratios of 0.2, 0.1, 0.3, and 0.4, respectively. Transport of these components and of water and air within the soil column are simulated for this scenario over a period of time, using the one-dimensional model discussed above. Figure 1 shows the temperature and saturation profiles for all phases within the simulated soil column at various times. Saturation of water increases as ice melts due to application of warmer gasoline. Thermal effects were substantial for this simulation, and all ice within the 3 m column was melted within 12 days. Gasoline displaces air, percolating down the column by more than 1 m after 12 days. Figure 2 shows the distribution of mole fraction of water as a component in the water phase and of oxygen and the pseudo-component ( $\text{N}_2 + \text{CO}_2$ ) in the air phase. Mole fraction of water in the water phase is reduced near the soil surface due to gasoline components dissolving in the water. Water mole fraction is unity, 1.8 m down the column at 12 days, beyond which only water exists in the water phase. Gasoline has drained about 1.3 m during this time period. Contaminants present in the water phase below this region are transported mainly by diffusion. Advection of water and air are small and, hence, dispersion is also negligible. Volatization of contaminants accounts for reduction of the mole fractions of oxygen and ( $\text{N}_2 + \text{CO}_2$ ) in the air phase in the upper regions of the column. Aerobic reactions are neglected in this simulation and, hence, oxygen mass is conserved. The effect of contaminants on the freezing temperature is not noticed here since the zero degree isotherm has moved down the column quicker than the solutes.

## CONCLUSIONS

A model is developed to predict the fate of a simulated gasoline spill in frozen soils. The governing equations for multi-component, multi-phase transport, the energy conservation equation, and numerous constitutive functions and thermodynamic relations that constitute the model are solved for



a vertical one-dimensional soil column. The gasoline phase has flowed down the column approximately 1.3 m for the case examined. Components of the gasoline were transported further down the column by diffusion in the air and water phases. Various other scenarios, including refreezing after the gasoline spill, may also be examined by the model to study the fate of a gasoline spill on frozen soils.

There have been a large number of accidental oil spillages in the Arctic tundra since the development of Alaskan oil fields and the construction of the trans-Alaska pipeline. Understanding and predicting the migration, biodegradation and immobilization of petroleum contaminants in soils and groundwater will improve recovery and clean-up of these substances as well as improving assessment of potential accidents in Arctic regions. The results of this study can be used by water resources planners, regulatory agencies, permit issuing officials, and engineers at federal and state levels involved with groundwater resources and hazardous wastes.

## REFERENCES

- Corapcioglu, M.Y. and A. Baehr (1987) A compositional multiphase model for groundwater contamination by petroleum products, I. Theoretical considerations. *Water Resources Research*, 23, 191-200.
- Corapcioglu, M.Y. and S. Panday (1991) Compositional Multiphase Flow Models. *Advances in Porous Media*. Elsevier, Amsterdam, The Netherlands, 1, 1-79.
- Coats, K.H. (1980) An equation of state compositional model. *Society of Petroleum Engineers Journal*, 363-376.
- Forsyth, P.A. (1988) Simulation of nonaqueous phase groundwater contamination. *Advances in Water Resources*, 11, 74-83.
- Kazemi, H., C.R. Vestal and G.D. Shank (1978) An efficient multicomponent numerical simulator. *Society of Petroleum Engineers Journal*, 355-368.
- Kay, B.D. and E. Perfect (1988) State of the art: Heat and mass transfer in freezing soils. *Proc. Fifth Intl. Symp. on Ground Freezing*, Balkema, Rotterdam, The Netherlands, 3-21.
- Mackay, D. (1985) The physical and chemical fate of spilled oil. *Petroleum Effects in the Arctic Environment*, Elsevier, Amsterdam, The Netherlands, 37-61.
- Panday, S. and M.Y. Corapcioglu (1991) Solute rejection in freezing soils. *Water Resources Research*, 27, 99-108.
- Reid, R.C., J.M. Prausnitz, and B.E. Poling (1986) *The Properties of Gases and Liquids*. 4th edition, McGraw-Hill, New York.
- Walas, S.M. (1985) *Phase Equilibria in Chemical Engineering*. Butterworth Publishers, London.

## Nomenclature

- $[AMW]_{\alpha}$  = apparent molecular weight of phase  $\alpha$
- $C_{\alpha}^k$  = concentration of component k in phase  $\alpha$
- $D_{\alpha}^k$  = hydrodynamic dispersion of k in phase  $\alpha$
- $g$  = gravitational acceleration
- $h_{\alpha}$  = enthalpy of phase  $\alpha$
- $K_{\alpha,\beta}^k$  = equilibrium partition coefficient for component k between phase  $\alpha$  and phase  $\beta$
- $k_o$  = intrinsic permeability to phase  $\alpha$
- $k_{ra}$  = relative permeability to phase  $\alpha$
- $L_{M,\alpha}^k$  = latent heat of transfer of component k from phase M to phase  $\alpha$
- $[MW]^k$  = molecular weight of component k
- $n$  = porosity of the medium
- $p_{\alpha}$  = pressure in phase  $\alpha$
- $R$  = universal gas constant
- $R_{bio,\alpha}^k$  = rate at which component k is biodegraded from phase  $\alpha$
- $S_a$  = degree of air phase saturation
- $S_o$  = degree of hydrocarbon phase saturation
- $S_w$  = degree of water phase saturation
- $S$  = degree of ice saturation
- $T$  = temperature
- $t$  = time
- $U_{\alpha}$  = internal energy of phase  $\alpha$
- $U_a$  = internal energy of phase  $\alpha$
- $x_{\alpha}^k$  = mole fraction of component k in phase  $\alpha$
- $z$  = vertical coordinate
- $\lambda_m$  = net thermal conductivity of the soil
- $\rho_{m\alpha}$  = molar density of phase  $\alpha$
- $\theta_{\alpha}$  = volumetric content of phase  $\alpha$
- $\mu_{\alpha}$  = viscosity of phase  $\alpha$

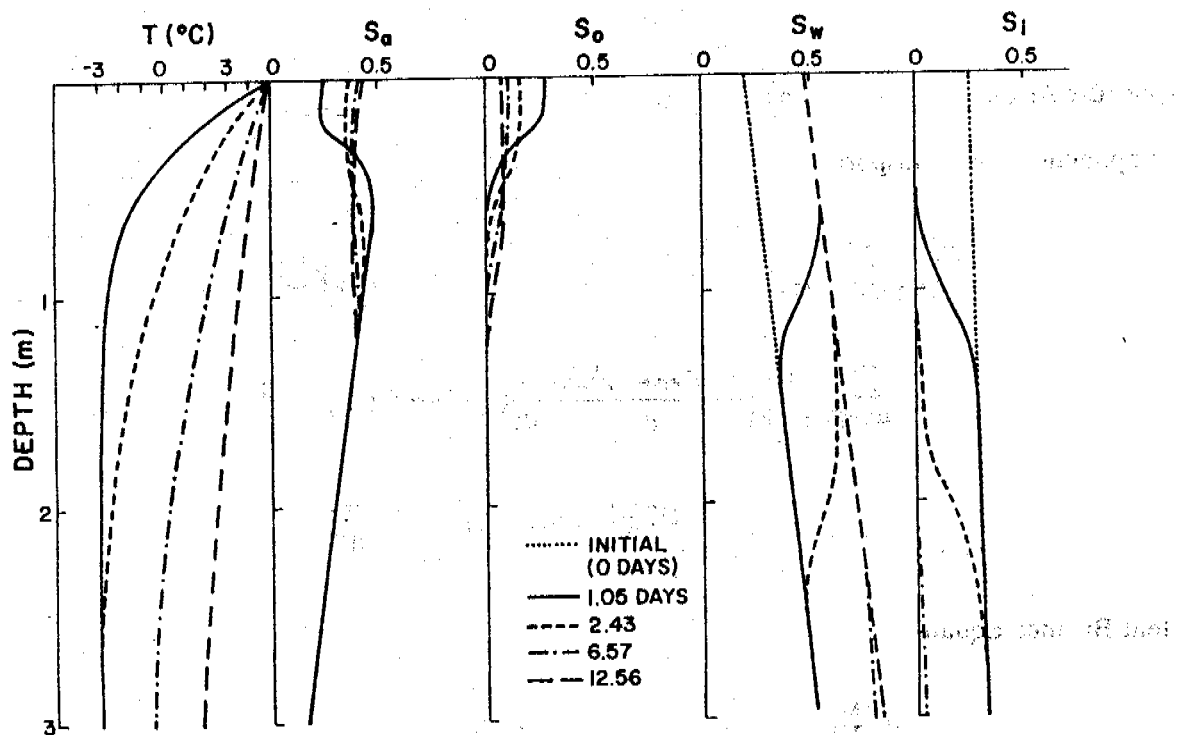


Fig. 1. Temperature and saturation profiles along the soil column

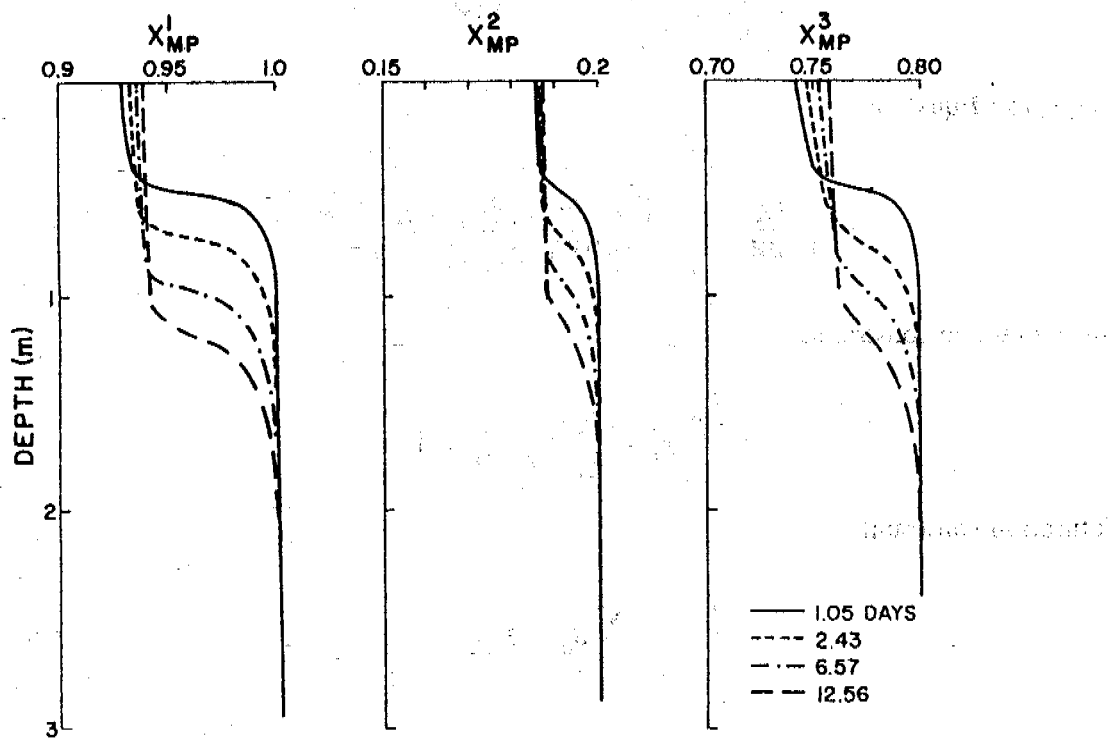


Fig. 2. Mole fraction of water component in the aqueous phase, and of oxygen and ( $N_2 + CO_2$ ) in the air phase throughout the soil column

## Appendix A: Governing equations

### Component Mass Transport Equations

$$\begin{aligned}
 & \frac{\partial}{\partial t} \left( \sum_{\alpha=np,wp,ap} (nS_{\alpha} \rho_{m_{\alpha}} K_{mp;\alpha}^k + K_{wp;\alpha}^k \rho_{m_{wp}} \rho_{ss} (1-n) K_{mp;wp}^k) x_{mp}^k \right) \\
 & - \sum_{\alpha=np,wp,ap} \left[ \frac{\partial}{\partial z} \left( \frac{\rho_{m_{\alpha}} K_{mp;\alpha}^k x_{mp}^k k_o k_{ra}}{\mu_{\alpha}} \frac{\partial}{\partial z} (p_{\alpha} - [AMW]_{\alpha} \rho_{m_{\alpha}} gz) \right) \right] \\
 & - \sum_{\alpha=np,wp,ap} \left[ \frac{\partial}{\partial z} \left( D_{\alpha}^k \frac{\partial}{\partial z} (\rho_{m_{\alpha}} K_{mp;\alpha}^k x_{mp}^k) \right) \right] - \frac{R_{bio}^k}{[MW]^k}
 \end{aligned} \tag{A1}$$

### Heat Balance Equation

$$\begin{aligned}
 & \frac{\partial}{\partial t} \left( \sum_{\alpha=1}^{NP} (nS_{\alpha} \rho_{m_{\alpha}} U_{\alpha}) \right) + \rho_{ss} (1-n) U_{ss} - \frac{\partial}{\partial z} \left( \lambda_m \frac{\partial T}{\partial z} \right) \\
 & - \sum_{\alpha} \left[ \frac{\partial}{\partial z} \left( \frac{h_{\alpha} \rho_{m_{\alpha}} k_o k_{ra}}{\mu_{\alpha}} \frac{\partial}{\partial z} (p_{\alpha} - [AMW]_{\alpha} \rho_{m_{\alpha}} gz) \right) \right] = 0
 \end{aligned} \tag{A2}$$

### Clapeyron Equation

$$\frac{p_{f_w}}{[AMW]_{f_w} \rho_{m_{f_w}}} - \frac{(p_{wp} - RT \rho_{m_{wp}} x_{wp}^c)}{[AMW]_{wp} \rho_{m_{wp}}} - \frac{L_{f_w} (T - T_o)}{T_o} = 0 \tag{A3}$$

### Mole Fraction constraints

$$\sum_{k=1}^{NC} x_{\alpha}^k - \sum_{k=1}^{NC} K_{mp;\alpha} x_{mp}^k = 1 \tag{A4}$$

### Saturation constraint

$$\sum_{\alpha} S_{\alpha} = 1 \tag{A5}$$

ADMINISTERING COUNTERMEASURES ON EMBANKMENT THAW SETTLEMENTS  
OF PERMAFROST ALONG THE QINGHAI XIZANG HIGHWAY

Cui Jianheng, Xu Dongzhou and Chen Hongzhe

The First Survey and Design Institute of Highway,  
The Ministry of Communications, Xian, China

The thermal unstabilities and engineering complexities of permafrost along the Qinghai-Xizang Highway are determined by special engineering geological conditions, climatic environment and permafrost development characteristics. The paper analyzes the embankment temperature regime under asphalt pavement on Qinghai-Xizang Highway, discusses the development regulations and tendency of embankment thaw settlement and the way of improving embankment thermal regime, and presents the synthetic countermeasures to be administered.

SOME CHARACTERISTICS OF PERMAFROST ALONG THE QINGHAI-XIZANG HIGHWAY

The Qinghai-Xizang Plateau is in a low latitude and high elevation area, the permafrost has some special characteristics in this climatic environment and development regimes of permafrost compared with the permafrost of high latitudes.

1. The Climatic Environment Characteristics

The special geographic position determines the intense solar radiation on the Qinghai-Xizang Plateau, the total annual radiation amount is about 170 Kcal/cm<sup>2</sup> per year (Kao Youguan, 1982) and more than 1.5 times of Xian's and 2.0 times of Yakutsk's. The radiation equilibrium amount is always at a plus for the whole year. Table 1 shows that the difference values between ground temperature and air temperature is always a value more than 95% of radiation equilibrium amount and is transferred into atmospheric layer (Kao Youguan).

Because of high elevations and low latitudes, there are special low temperature conditions in the Qinghai-Xizang Plateau. The permafrost is developed well due to location in the center of three low temperature centres between Fenghuo Mountain and Tanggula Mountain (Xie Yingqin, 1983). The curves in Fig.1 indicate that the mean annual ground temperatures are higher than the mean annual air temperature at Wu Daoliang and Tuotuo River meteorological stations in the last ten years. The ratios between the mean air freezing index and thawed index of the years are about 5.8 at Wu Daoliang and 3.32 at Tuotuo River. But the ratios between mean ground surface freezing index and thawing index of the years are about 1.65 at Wu Daoliang and 1.16 at Tuotuo River. This is different from the temperature regime in high latitude permafrost areas. Therefore, the mean annual air temperature is not equal to the mean annual ground surface temperature and ground temperature. It is not suitable to evaluate the permafrost temperature environment by using an air freezing index and air

Table 1. The temperature difference between ground and air at some meteorological stations along the Qinghai-Xizang Highway

Month	1	2	3	4	5	6	7	8	9	10	11	12	Year
Stations													
Wu Daoliang	0.0	-0.6	-1.2	-2.2	-1.5	-3.7	-4.2	-4.2	-3.5	-2.2	-0.8	-0.2	-1.8
Tuotuo River	-0.1	-0.6	-1.5	-2.8	-3.4	-4.1	-4.6	-4.5	-3.9	-2.4	-0.9	-0.2	-2.4
Wen Quan	-0.5	-0.5	-1.4	-2.4	-3.0	-3.9	-4.5	-4.3	-3.7	-2.6	-1.4	-2.0	-2.5
An Duo	1.5	-0.5	-2.4	-3.1	-5.9	-5.3	-4.5	-4.5	-3.9	-2.1	-2.5	-0.6	-2.7

thawing index.

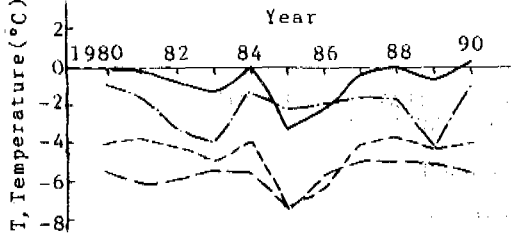


Figure 1. The temperature curves of air and ground surface at the meteorological stations of Wu Daoliang and Tuotuo River (— and - - - are the annual mean temperature of ground surface, - - - and . . . are the annual mean air temperatures at Tuotuo River and Wu Daoliang stations)

The precipitation for the whole year in Qinghai-Xizang Plateau is concentrated in the warm season. The precipitation from June to September is about 80% of whole year's precipitation (see Table 2). The seasonally thawed depth mainly depends on the summer precipitation. The curves of the maximum thawed depth, annual precipitation and mean monthly plus temperature accumulation in the warm season are shown in Fig.2. It is shown that the change of the maximum thawed depth depends mainly on the annual precipitation because of the water carrying ground surface heat into permafrost table. Therefore the precipitation is one of the important effect factors on seasonally thawed depths in Qinghai-Xizang Plateau permafrost area.

2. Some Characteristics of Permafrost Development

2.1. The unstability of permafrost thermal regime

The stable condition of permafrost is that ground surface heat flow ( $q_p$ ) is greater than or equal to under ground heat flow ( $q_c$ ). i.e.

$$\lambda = \frac{t_{cp} - t_B}{h_{cp}} \geq \lambda_0 g_c$$

or  $t_B \leq t_{cp} - \frac{\lambda_0}{\lambda} g_c \cdot h_{cp}$

where,  $\lambda$  and  $\lambda_0$  are heat conductivities of upper and lower tables of the annual change layer,  $t_{cp}$  and  $t_B$  are permafrost temperatures and mean annual ground surface temperature,  $h_{cp}$  is annual change depth of ground temperature,  $g_c$  is a ground temperature gradient.

It is known from above, the permafrost stable condition is that the mean annual ground surface temperature is less than the permafrost temperature. But the ground surface temperature on

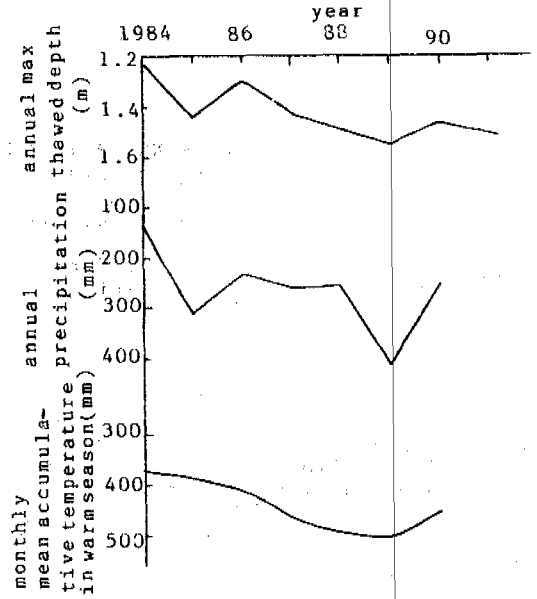


Figure 2. The curves of annual maximum thawed depths beneath natural ground surfaces, annual precipitation and monthly mean accumulative temperature at Kekexili Mountain Station

Qinghai-Xizang Plateau is not very low. The mean annual ground temperature and permafrost temperature in the last ten years have been about  $-2.2^\circ\text{C}$  and  $-3^\circ\text{C}$  at Wu Daoliang meteorological station. Most permafrost areas on Qinghai-Xizang Plateau are in an unstable retreating state, for example, the north boundary of permafrost near Xidatan and the south boundary near Anduo are retreating. Under the intense solar radiation conditions, the ground surface condition causes the heat flow to change greatly. From the observation data in 1991, the differences in the natural permafrost table were up to 1.0 m at the same area with different cover conditions.

2.2 Subground ice development characteristics

The formation of subground ice is closely related to geological deposits and permafrost development histories. Based on the formation process, the subground ice can be classified into intergrowth ice and secondary ice.

The intergrowth ice, formed in a geological deposit process, exists in poor drainage conditions in high-plateau areas. The existing type is generally a lentoid uncontinuous ice layer. The secondary ice is formed in a freezing-thawing cyclical process, near the permafrost table, and

Table 2. Annual mean precipitation at Wu Daoliang and Tuotuo River Stations (mm)

Station	Month												Whole year
	1	2	3	4	5	6	7	8	9	10	11	12	
Wu Daoliang	1.0	1.7	2.5	6.8	22.5	46.5	70.0	65.4	40.4	7.0	0.9	1.0	265.7
Tuotuo River	1.3	1.4	1.5	5.0	16.9	50.7	85.5	65.4	40.1	11.7	0.5	1.1	281.1

exists in fine soil layers. The existing type of secondary ice is generally in steady continuous ice layers.

### THE THAW SETTLEMENT ANALYSES OF HIGHWAY FOUNDATIONS

#### 1. Thermal Regime Analyses

##### 1.1 The temperature field of the highway foundation

The surface of asphalt pavement absorbs a large amount of solar radiation and restrains moisture from evaporating. Therefore the surface temperature of asphalt pavement is higher than the natural ground surface's. Table 3 shows at the south of Chumaer River, the temperature difference between the asphalt pavement and natural ground surface was 4.5°C in the warm season of 1985. The difference decreases with degradating solar radiation from July to October. But in the winter the temperature differences increase slightly due to the high reflective ratio of snow cover on natural ground surfaces.

The mean ground temperature curve beneath the asphalt pavement at Kekexili Mountain in 1980, shown in Fig.3, indicates that the mean temperature at 0.5 m depth was at a plus and the thawing index of asphalt pavement was greater than

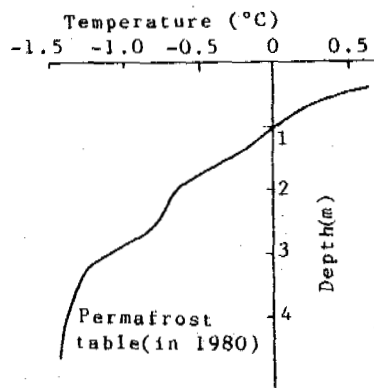


Figure 3. Annual mean ground temperature beneath asphalt pavement

Table 3. The temperatures of the asphalt pavement and the natural ground surface in the south of Chumaer

Month	6				7				8				9				10				11	
	last	first	middle	last	last	first	middle	last	last	first	middle	last	last	first	middle	last	last	first				
Natural ground surface temperature (°C)	10.6	10.3	12.6	12.3	12.7	12.6	10.1	7.7	3.3	4.0	3.4	1.9	-6.1	-9.4								
Asphalt pavement temperature (°C)	13.8	15.8	18.9	18.9	18.9	18.3	15.1	11.8	6.8	/	/	4.7	-3.0	-6.1								
Increasing value of temperature (°C)	3.2	5.5	6.3	6.6	6.2	5.7	5.0	4.1	3.5	/	/	2.8	3.1	3.3								

the freezing index, the potential seasonally thawed depth was greater than seasonally frozen depth in 1980. Therefore an unfrozen sandwich structure exists in the highway foundation. The temperature regimes of embankment in a cross section beneath the asphalt pavement at the south of Xieshui River in 1987, are shown in Fig.4. Fig.4(a) shows there is a plus temperature zone in the unthawed soil layer. This is remanent unfrozen parts in thawed depth of the last year. Fig.4 also shows that at same depth the temperature of the embankment centre is always higher than the temperature of both sides of the embankment. According to the observation date in 1991, the existence of the unfrozen sandwich structure in the highway foundation was a common phenomenon. The seasonally frozen depth beneath the asphalt pavement is about 3-4.5 m at different highway sections.

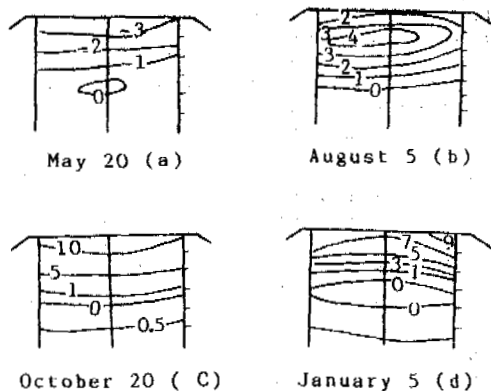


Figure 4. Isotherms of embankment section

Because the seasonally thawed depth is greater than the seasonally frozen depth, an "unfrozen core" or unfrozen sandwich structure is formed. This means that in the annual heat cycles there exists a remanent heat amount.

### 1.2 Thermal stability of the embankment

The temperature field of the highway foundation can be expressed by a two-dimensional temperature field. There is a high-temperature zone beneath the asphalt pavement. In this thermal regime, not only vertical temperature gradients exist, but also horizontal temperature gradients exist. Based on the heat conduction theory, the horizontal heat flow equals the horizontal conductivity times the horizontal temperature difference, the vertical heat flow equals the vertical conductivity times the vertical temperature difference. The ratio of horizontal heat flow to vertical heat flow is called the lateral radiation heat coefficient.

If the heat flow of the upper boundary only thaws the seasonally frozen layer, the thermal stability of highway foundation will exist.

### 1.3 The effect factors on the embankments thermal stability

The highway foundation stability depends on the surface absorbing condition (solar radiation, environment temperature, pavement condition), lateral radiation condition and water on the frozen layer. For special climate conditions of Qinghai-Xizang Plateau, the directly influencing factors of the highways foundation thermal stability are as follows:

#### 1.3.1 Pavement material

The asphalt pavement with a low reflectivity and high heat absorbance makes its surface temperature higher than natural ground temperature, it is an important factor in causing the permafrost table to descend.

#### 1.3.2 Embankment filling material

Because different soil types have different thermal characteristics and moisture characteristics the influences of water content and transfer water ability of soil on heat flow are very large.

#### 1.3.3 Superpermafrost water

Atmospheric rainfall is the main resource of superpermafrost water. The rainfall is an important effect factor on the seasonally thawed depth change in Qinghai-Xizang Plateau. The seasonally thawed depth in water logged years is greater than in dry years. The seepage flow carries not only its own heat amount, but also natural ground surface radiation heat into the permafrost table. This causes permafrost thawing and "unfrozen core" development.

#### 1.3.4 A cross section of types and heights of embankments

The vertical geothermal gradient decreases with the increasing embankment height. The thermal effect on the embankment increases with the increasing pavement width. It is advantageous to form a horizontal geothermal gradient, decreasing vertical heat flow and reinforcing lateral radiation heat by putting in a berm and a gentle slope.

## 2. Analyses of Embankment Thaw Settlement

### 2.1 Thaw settlement state

Because of the instability of engineering geology and the sensitivity of the thermal regime on the Qinghai-Xizang Plateau, there are different types and degrees of thaw settlement. The types of thaw settlement can be classified as follows:

#### 2.1.1 "Large wave" shape thaw settlement along the highway

It is widely distributed in the ranges of one meter to ten meters in the rich content lenticular underground ice section on high plateaus and poor drainage areas. The settlement depth is different from 1 cm to 60 cm.

#### 2.1.2 "U" shape thaw settlement on a cross section

It is mainly distributed in rich-content continuous underground ice sections over mountain areas with a length of ten meters to one hundred meters. In the gentle terrain area, it is the symmetric "U" shape settlement, the largest settlement amount is at the embankment center. In the slope terrain area the non-symmetric "U" shape settlement, as shown in Fig.5, is formed.



Figure 5. Thaw settlement in highway slope section

#### 2.1.3 The berm slumping

It occurs in poor-drainage sections. Because of poor-drainage at both sides of the highway, the serious thaw settlement and slumping happen on the sloped berm.

#### 2.1.4 Integral thaw settlement

It may occur in parts of the sections of rich content underground ice and poor drainage areas (in Fig.6).

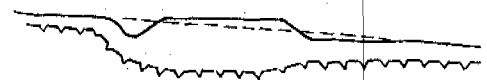


Figure 6. Embankment thaw settlement

In the vertical section, the artificial permafrost table in the area with low-content ice is deeper than in the area with rich-content ice. The reason is the different thawing latent heat and the settlement coefficient between rich-content ice permafrost and poor-content ice permafrost. The permafrost table in slight thaw settlement areas is deeper than in serious thaw settlement areas.

### 2.2 Development tendency of the embankment thaw settlement

From a thermal view, the stability tendency of the embankment exists in the deeper permafrost table and low-content ice of the permafrost highway. There are two reasons, one is to form a vertical heat flow equilibrium easily, another is the relatively little settlement amount on low-content ice permafrost.

Generally speaking, because of the difference of permafrost temperatures and climatic conditions, the thawing settlement speed of the embankment will be slow for high elevation areas and quick for low elevation areas. The sections

of thaw settlement in the highway will increase with the increasing operating time. "Unfrozen core" beneath asphalt pavement will be a common phenomenon.

## ADMINISTERING COUNTERMEASURES TO THAW SETTLEMENT

### 1. The Way of Improving the Embankments Thermal Regime

#### 1.1 Improve the absorbing heat conditions of pavement

Because an extra amount of heat is absorbed by asphalt pavement it is the basic reason for embankment thaw settlement. It is necessary to improve the absorbing heat condition of pavement by paving with white-colour pavement. Based on experiments, APP pavement is easily polluted, its surface becomes black gradually with increasing operating time. The concrete pavement is easily destroyed due to the repeated freezing-thawing cycles, temperature stress of the concrete slab and inhomogeneous settlement of the embankment. Because the embankment settlement is caused by an artificial permafrost table degradation and will be stagnant about three years, it is necessary to solve remanent settlement of embankments by using concrete pavement. The steel fibre concrete pavement is well administered material with a high anti-torsion strength, but is in an engineering experimental period.

#### 1.2 Increasing vertical heat-resistance

The non-equilibrium vertical heat flow is a very important thermal condition for thawing permafrost. It is a effective countermeasure for increasing vertical heat-resistance or decreasing vertical heat-flow. Because of the low-anti-compression strength and high elasticity deformation, the PVC slabs easily fail due to the large settlement amount of the pavement. The materials to be used must solve the problems of pavement structure combination and construction method. It should be a low-cost durable material and a good thermal insulation filling material.

#### 1.3 Improving the thermal diffusion condition

Engineering experiments indicate that the permafrost table beneath the culvert remains at almost a stationary state. This is because that the culvert not only obstructs the solar radiation, but also ventilates and diffuses heat. The embankment with ventilation ducts is an effective countermeasure to control permafrost degradation.

#### 1.4 Improving lateral thermal diffusion

From an embankment thermal stability view, lateral thermal diffusion would be advantageous for decreasing the vertical heat flow. It is a reasonably administered countermeasure to set the berm with a certain height, width and gentle slope ratio, to improve lateral thermal diffusion to restrain superpermafrost water from penetrating into the embankment and improve the embankments thermal regime.

#### 1.5 Raising the embankment height and degradating the vertical ground temperature gradient

At present the method to raise the embankment height is used effectively to protect the permafrost. But, the present embankment height is not at the height at which the embankment is in a thermal steady state.

#### 1.6 Improving drainage conditions on ground

#### surface

Cutting off rainfall penetration and draining superpermafrost water does not only degradate heat conductivity of the embankment but also decrease thermal convection.

### 2. Synthetically Administered Countermeasures

At present, there are no embankment filling materials with the conditions of "unidirectional conduction", or "low-temperature conduction heat and high-temperature insulation". Because the seasonally thawed depth is greater than the seasonally frozen depth, the formation of an "unfrozen core" is inevitable. Therefore the synthetically administered countermeasures to raise embankment height for decreasing the vertical ground temperature gradient, to set a berm with a certain height and width and gentle slope protection for improving lateral thermal diffusivity and to avoid water penetrating into permafrost, are necessary.

#### 2.1 Raising embankment height

The determination principle of embankment height is to reduce vertical heat-flow to make the embankment in heat equilibrium and permafrost table up to maximum thaw depth. Table 5 is the reference taken value of a embankment-height.

Table 5. The reference value of depth of permafrost table

The type of frozen soil	With poor-content ice	With rich-content ice	With saturated ice	Ice layer with soil
Embankment height	1.5 m	1.8 m	2.2 m	2.6 m

#### 2.2 Setting a gentle slope for protection and increasing the height and width of berm

Based on engineering experiments, the thaw settlement is slight in the highway sections with installed berm. There are two aspects to this reason, one is superpermafrost water is prevented from penetrating into permafrost table, another is to form horizontal ground temperature gradient to improve lateral thermal diffusion. The designed height of berm is 2-3 m in common sections and 5 m in poor drainage sections. The slope ratio of slope protection is taken from 1:2.5 to 1:3.

The comparison curves of ground temperature beneath the berm and the highway centre on Kekexili Mt. highway section in 1980, shown in Fig.7, indicate that the berm ground temperature has a increasing tendency and the effectiveness of berm lateral thermal diffusion is good when the berm height is below the range of 1 m. Therefore it is suitable that the berm height is lower than 1 m at the embankment height.

#### 2.3 Improving drainage installation

The permafrost on Qinghai-Xizang Plateau is sensitive to rainfall. It is a important countermeasure to eliminate water seepage. The wider and more shallow side ditches are constructed. Seepage-proof and insulation countermeasure must be taken in the side ditches. The drainage ditch must be set to avoid the foot slope accumulating water in the slope section of the highway. The drainage along the roadbed foot slope must be reinforced.



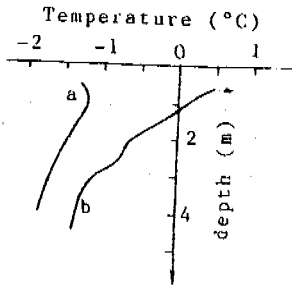


Figure 7. The curves of ground temperature beneath the berm and the highway center  
 a. Ground temperature of right berm;  
 b. Ground temperature of highway center.

### CONCLUSION

Based on the analysis of the engineering geology condition and embankment thermal regimes in Qinghai-Xizang Plateau permafrost area, the following conclusions can be obtained.

1. The mean annual air temperature is not equal to the mean annual ground surface temperature and the mean annual ground temperature. It is not suitable to evaluate the permafrost temperature environment by using an air freezing index and a thawing index.
2. The permafrost of Qinghai-Xizang Plateau is a sensitive area to the thermal stability. The seasonally thawed depth depends on precipitation. The different developing histories of permafrost leads to the different subground ices developing.
3. The formation of an "unfrozen core" beneath asphalt pavement is inevitable tendency.
4. It is a basic countermeasure for thaw settlement of embankments to improve embankment absorbent heat conditions and drainage conditions, reinforce lateral thermal diffusion and degradate the vertical ground temperature gradient.

### ACKNOWLEDGEMENTS

The authors would like to thank very sincerely the valuable help given by Profs. Wu Jingming and Yu Wenxue.

### REFERENCES

- Kao Youguan, (1982) Research of Radiation on Qinghai-Xizang Plateau. Memoirs of Lanzhou Institute of Glaciology and Geocryology, Chinese Academy of Sciences, No.3, Published by Science Press House.
- Kao Youguan, (1982) Research of Radiation Equilibrium on Qinghai-Xizang Plateau. Memoirs of Lanzhou Institute of Glaciology and Geocryology, Chinese Academy of Sciences, No.3, Published by Science Press House.
- Xie Yingqin and Zeng Qunzhu, (1983) Climatic Conditions for the Development of Permafrost on Qinghai-Xizang Plateau. Proceeding of Second National Conference on Permafrost, China, pp.13-20.

PERIGLACIAL PHENOMENA AND ENVIRONMENT SINCE THE LATE PERIOD  
OF LATE PLEISTOCENE, DAQINGSHAN AREA, INNER MONGOLIA

Cui Zhijiu and Song Changqing

Department of Geography, Peking University, Beijing 100871

There are plentiful periglacial phenomena of the late period of late Pleistocene including periglacial involutions, sand wedges, block fields, patterned grounds, nivation hollows, taluses and so on in wide area of Inner Mongolia. The products of weak periglacial action, stone lines\*, gelifluction lobes, taluses and hummocks etc., were developed during Holocene. In addition the fact that the temperature was 7-8°C lower has been recognized recently by using the methods of <sup>14</sup>C dating, periglacial phenomena, chemical elements, archaeology etc. during the late period of Late Pleistocene. On the other hand, four cold climatical stages can be divided during Holocene according to four stone lines with <sup>14</sup>C ages. The lowest annual mean temperature was 2.0-2.5°C lower than today and the highest was 1-2°C higher during Holocene in the wide area of Inner Mongolia. The fluctuation of vertical vegetation belts was about 200-600 m during the Holocene.

INTRODUCTION

Inner Mongolia is located in the north of China, 38-52°N and 102-122°E. The relief features belong to plateau with mountain, the eastern Daxingan Range is above 1500 m a.s.l. and the middle Daqingshan Mountain of Yinshan Mountain system is above 2300 m a.s.l.. This area is temperate climatical zone and a transitional zone of semiarid to arid climate from east to west. In terms of phytogeography, it is a transitional zone of forest-steppe. However, there are differences of periglacial phenomena between the plateaus and mountains. Both ancient and present periglacial phenomena occur a lot in mountain areas, where only ancient periglacial phenomena is distributed on the plateau.

The present periglacial processes are weak in both the middle and eastern mountains. In Daqingshan Mountain areas, processes such as physical weathering and mass movement occur between 1300 and 2000 m a.s.l., while frost heaving is more important above 2000 m a.s.l.. In addition, the boundary between the mountainous cold-temperate forest steppe and subalpine meadow occurs at the same altitude as the 1°C annual mean temperature isotherm. In the other hand, the periglacial processes in the Daxingan Range is obviously stronger than that in Daqingshan and the low periglacial limit falls gradually from south to north because of the altitudinal and latitudinal actions. A lot of materials have been supplied by physical weathering and mass movement due to cold weather and formed classical periglacial landforms such as taluses, block slopes etc., while some landforms such as block field, stone circles, hummocks etc. were formed by serious frost heave.

The relic periglacial phenomena in Inner Mongolia has formed since the last glaciation. They are of two ages.

Pre-Holocene Periglacial Phenomena

The ancient periglacial phenomena such as involutions as well as sand wedges are widely distributed on the Inner Mongolia Plateau. According to the morphology of sand wedges, they can be divided into three kinds: (1) a narrow shape with two straight symmetrical sides with a burying depth of 0-10 cm, height of 50-150 cm, width of 15-30 cm and ratio of height to width is 2.0-3.3. (2) a wide shape with large scale, wide mouth of wedge, un-symmetrical and bent sides with a burying depth of 0-10 cm, height of 70-150 cm, and the ratio of 0.9-2.3. (3) variation shape the second wedge invaded into a larger one and produces a double layered structure at the depth of 10-50 cm, height of 40-200 cm, width of 30-110 cm, the ratio of 0.7-5 cm, for example, the sand wedge that is 200 cm high becomes wide at a depth of 70-80 cm under ground and there is the small wedge in the sand wedge itself.

In addition, the wedges can be divided into sand wedges and ice wedge casts, the former is distributed in the western part of Inner Mongolia and is reflected in arid-cold climatic conditions and the later is in the eastern part and is represent by a wet-cold climate.

On the other hand, the periglacial processes in mountain areas was stronger than the plateau. There were ancient block fields, patterned ground, involutions, sand wedges, nivation hollows and taluses in the Daqingshan Mountain during the late period of Late Pleistocene with its lower limit of periglacial action down to 1300 m a.s.l.. For example, involutions and sand wedges occur between 1600 and 1700, a.s.l. on Chayouzhongqi, while ancient block fields and patterned ground on Manhanshan and ancient block fields, nivation hollows, sand wedges and involutions on Caoduoshan are above 2000 a.s.l.. Thus, the periglacial environment was more extensive

\* Stone line: One kind of weak periglacial phenomena formed by frost weathering.

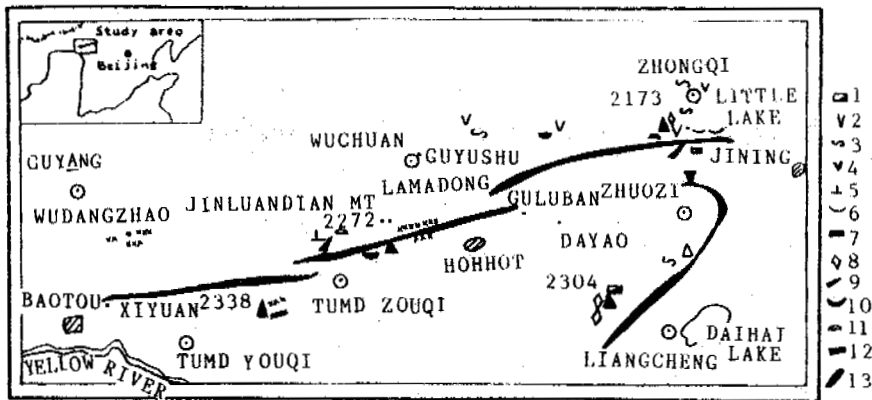


Fig.1 Sketch map of periglacial in Daqingshan Mountains  
 Legend: 1.ancient block field; 2.ancient talus; 3.involution;  
 4.sand wedge; 5.tor; 6.nivation hollow; 7.stone line;  
 8.patterned ground; 9.creep turf; 10.solifluction lobe;  
 11.hummock; 12.small layers; 13.mountain

during the late period of Late Pleistocene in Daqingshan Mountains (Fig.1). Especially, at Yitulihe in the northern Daxingan Range, there exists inactive ice wedges besides those types in the Daqingshan Mountain area.

#### Holocene Periglacial Phenomena

Some periglacial phenomena like stone lines and gelifluction lobes only developed in mountains. They are simpler than those formed before the Holocene. In Daqingshan area, four stone lines (Fig.2) buried at a depth of 25-170 cm, are distributed widely on the piedmont at about 1000, a.s.l.. They reflect four cold climatic stages. Ancient gelifluction with 4-5 m in length, 3-4 m in width and 1-2 m thick are located between the present soil and an ancient soil above 1800, a.s.l.. The speed of accumulation of the ancient soil, 0.416 mm/yr is roughly calculated by the thickness of 60 cm and a soil-forming period of 1444 years base on two <sup>14</sup>C dates (2926±74-1482±70 years B.P.).

#### ENVIRONMENTAL RECONSTRUCTION

##### The Environmental Reconstruction During the Late Period of Late Pleistocene

According to the features of periglacial phenomena, loess, pollen and mammoth, the late period of Late Pleistocene can be divided into the following stages.

(1) 80-53 ka.B.P. was first cold stage since the last glaciation. The Malan loess began to first deposit at 80 ka.B.P. and end at 53 ka.B.P. western China (Li, 1990).

(2) 53-35 ka.B.P. is a warm stage during the last glaciation. The Malan loess sediment became weak, the forming soil action became strong and the pollen of trees rose. All of these features reflect good climate at the time from 53-35 ka. B.P.. The mammoth began to appear after 35 ka. B.P. in northern China.

(3) 35-10 ka.B.P. was cold climatic environment with fluctuations of wet-dry. During 35-26 ka.B.P. was the coldest stage of the Last Glaciation and a lot of sand wedges grew in Inner Mongolia. The annual mean temperature was 7-8°C lower than today (Cui, 1984). The climate was wet-cold between 26-23 ka.B.P., and the pollen

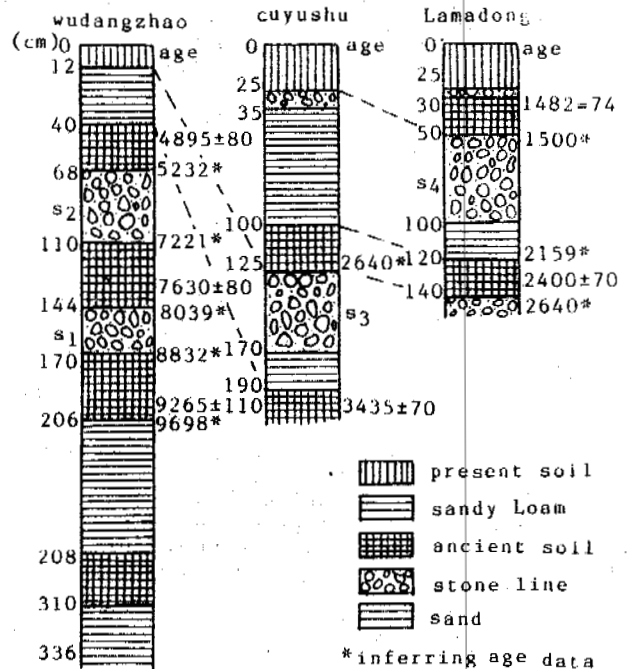


Fig.2 Stratigraphic columns indicating locations of stone line and ancient soil profiles, Daqingshan Mountains

content of abies and picea rose. About 13 ka.B.P. pollen of abies and picea appeared again and climate changed to a wet-cold tendency when pollen of grasses such as Ephedra, Artemisia, Compositae etc. rose and that of the conifer fell and that reflected arid-cold climate (Kong, 1982; Zhou, 1987).

##### Environmental Reconstruction During Holocene

During the Holocene, the dominant periglacial phenomena were stone lines and gelifluction lobes. The stone lines, about 25 cm thick, occur between the ancient soil layers (Fig.2). They

are extensively on the peidmont and consist of gravels, 10-15 cm in diameter, with sharp edges and AB planes of about 10°. Generally speaking, stone lines reflect an arid and cold climatic environment which resulted in the weathered bed-rock creeping downslope. Stone lines in Daqingshan are of the following ages, about 8500 years B.P.(S1), 6000 years B.P.(S2), 3500 years B.P.(S3) and 1500 years B.P.(S4). In addition, gelifluction lobes evolved above 2200 m a.s.l. with radiocarbon ages of 2926±73 and 1482±70 years B.P.. These correspond to stone line S4. Five ancient soil-forming periods, reflecting temperate and wet environment, are inferred: 9600-8800 years B.P., 8000-7200 years B.P., 5200-4500 years B.P. 2500-2000 years B.P. and 1500-800 years B.P..

The features of climatic change during the Holocene can be recognized by analysing the chemical composition, humus content, the features of quartz sand grains and chemical leaching. For example, the features of low CaCO<sub>3</sub>, low humus content and high ba [ $ba = (K_2O + Na_2O + CaO) / Al_2O_3$ ] in the sand layer 2, stone lines 2, 4 (Fig. 3) reflect weak chemical weathering, weak leaching, weak humification process, and a colder climatic environment than today. On the contrary, the ancient soil layers 3, 5, 7 (Fig. 3) indicate warm and wet climatic environments. In addition, the surface features of quartz sand grains indicate a short distance of movement, and in situ weathering.

Four cold-warm fluctuations during the Holocene have been identified in Daqingshan by the study of stone lines and ancient soil profiles

in Wudangzhao, Guyushu and Lamadong and of gelifluction lobes in Jinluandian. Each fluctuation is from 2500-3000 years to 1500-2000 years indication. A warm stage about 7000 years B.P. corresponds to a warm stage in the Weihe river basin (Huang, 1989). A cold stage appeared about 5500 years B.P. not only in Daqingshan but also in the Weihe river basin (Huang, 1989). A cold stage appeared about 5500 years B.P. and in Japan (Yutaka Sakaguchi, 1983). A warm stage about 4500 years B.P. occurred in the Daihai basin (Liu, 1989), Weihe river basin (Huang, 1989) and Xingjiang (Han, 1990). This corresponds to the lake level rising at Issky-Kul (Shi, 1990). The last two cold stages at about 3000 years B.P. and 2000-1500 years B.P. correspond to advances in the southeaster Qinghai-Tibet plateau since the middle Holocene (Li, 1988).

The environmental changes indicated by periglacial phenomena are substantiated by palaeobotanic data. About 7500 years B.P. pollen composition included Pinus, Betula, Ulmus, at Little Lake on the Huitenglian (about 2000 m a.s.l.) (Fig. 4). This assemblage indicates the climate was temperate and semihumid, between 7000 and 5500 years B.P., Pinus, Betula, Ulmus, Tilia and Quercus were the main species, with a few Abies, Picea and Ephedra. This means that the climatic environment changed from temperate, cold and wet to cold and dry. This corresponds to stone line S2 in the Wudangzhao profile. Between 4500 and 3500 years B.P., the climate changed from temperate and dry to wet, as reflected by the spore and pollen composition, which included Pinus, Betula, Quercus and a few Artemisia, Com-

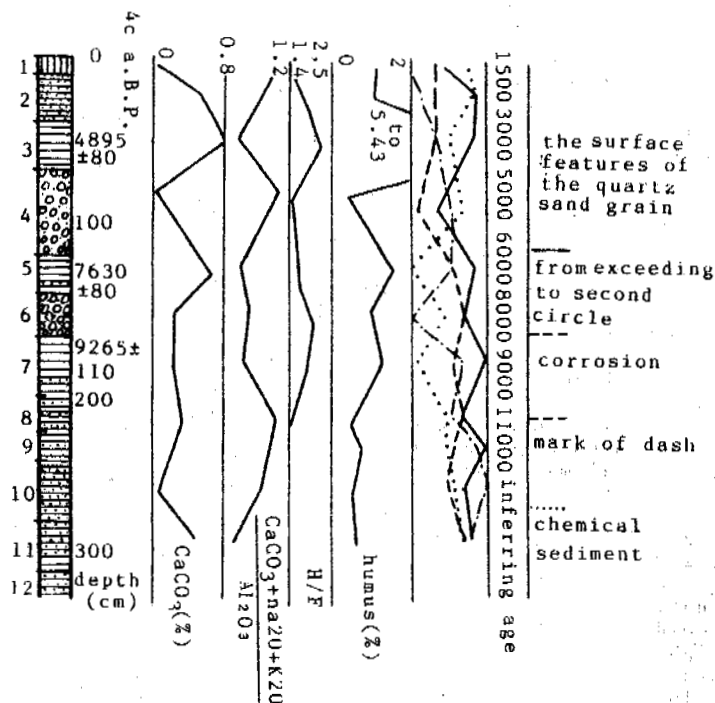


Fig. 3 Graph showing changes with depth of chemical substances, the surface features of quartz sand grains and <sup>14</sup>C age of stone lines in the ancient soil profile at Wudangzhao, Daqing Mountains

Legend: 1. light sandy loam (modern soil); 2. light sandy loam; 3. silty loam (ancient soil); 4. stone line; 5. sandy loam (ancient soil); 6. stone line; 7. sandy loam (ancient soil); 8. silt; 9. light silty loam; 10. light sandy loam; 11. sandy loam; 12. sand

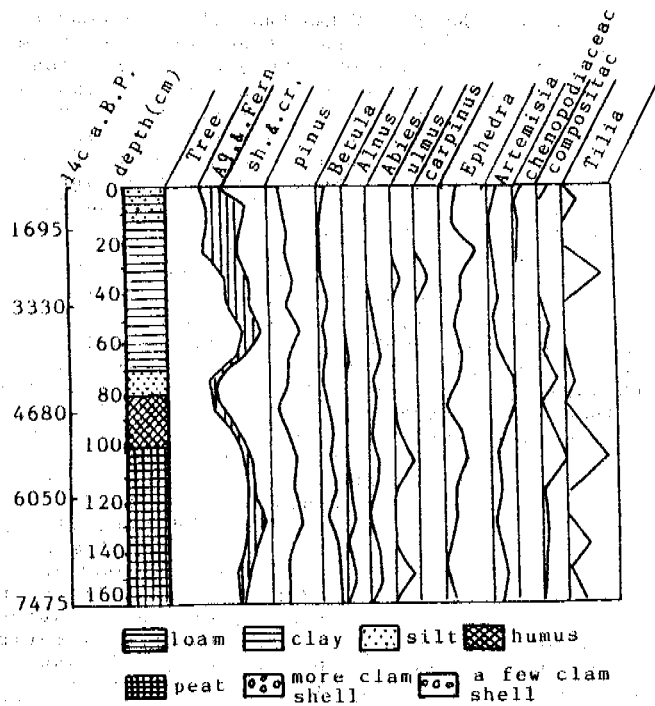


Fig.4 Pollen diagram from little lake in Daqingshan Mountain

positae, Ephedra at low places. A pollen assemblage including Pinus, Quercus and some Artemisia and Ephedra show a temperate cold semiarid climate at about 3000 years B.P. that corresponds to stone line S3 in the Guyushu profile. A later temperate semihumid climate is reflected by a pollen composition including Pinus, Ulmus, Tilia and Quercus at about 2500 years B.P.. The temperate cold semiarid climate at about 2000 years B.P. is reflected by an increase in Ephedra, Chenopodiaceae and Artemisia and a decrease in Pinus, Quercus and Betula. This corresponds to the stone line S4 in the Lamadong profile and the gelifluction lobes on Jingluandian. The temperate arid semihumid climate since 1500 years B.P. is reflected by a pollen composition which includes Pinus, Quercus and increasing Picea, Cupressaceae, Betula and Herbs.

Four vertical vegetation belts in Saqingshan can be identified (1) mountainous warm temperate steppe (1000-1200 m a.s.l.), (2) mid-temperature deciduous forest with temperate coniferous forest (1200-1800 a.s.l.), (3) cold temperate coniferous forest (1800-2100 m a.s.l.) and (4) subalpine meadow (above 2100 m a.s.l.). The altitude of these vegetational belts changed with the climatic fluctuation during the Holocene. For example, the cold temperate coniferous forest belt was 300 m higher 7500 years B.P.. The annual mean temperature at the same time was 1.8°C higher (i.e. 2.4°C lower than today in this area).

During the early Yangshao to early Longshan cultural period (6000-4000 years B.P.) polished stone tools found at Xiyuan and Guluban cultural locations indicate human occupation. Hence, the natural environment at that time was mild and suitable. In the Bronze Age (4000-2500 years B.P.), the climate became cold and suitable only to pastoral development under temperate cold

dry-wet conditions. During the Warring States-Han Dynasty (2500-1700 years B.P.), the climate became warmer and more suitable to agricultural development. During the Northern and Southern Dynasties (1700-400 years B.P.), pastoralism was more important under the temperate cold and dry temperate conditions. In the Sui and Tang Dynasty (400-1000 years B.P.), agriculture became more important under the warm and wet climate. Today, vegetation has been destroyed by human activities at low altitude in Daqingshan and has caused a decrease in forest, grass degeneration and soil erosion increases.

#### CONCLUSIONS

The annual mean temperature was about 7-8°C lower at the end of the Late Pleistocene, 1-2°C higher during the middle Holocene 8000-7000 years B.P. and 2.0-2.5°C lower than today during recent glaciation (3000 years B.P.).

The elevation change of the vertical vegetation belts was 200-600 m during the Holocene in mountainous area.

#### REFERENCES

- Cui Zhibiu (1984) On the southern boundary of permafrost and periglacial environment during the late period of Late Pleistocene in north and northeast China. ACTA Geologica Sinica, 2, 165-175 (in Chinese).
- Washburn, A.L. (1979) Geocryology. Edward Arnold London, pp279-320.
- Pewe, T.L. (1960) Ice-wedges in Alaska--classification, distribution and climatic significance. In Proceedings, 1st International Permafrost Conference. Natl. Acad. Sci-Natl. Res. Council Publ. 1287, pp676-81.
- Huang Chuhchang (1989) The loess and environmental changes of Holocene in the Weihe river basin. Geographical Research 1, 20-31.
- Yutaka Sakaguchi (1983) Warm and cold stages in the past 7600 years in Japan and their global correlation--especially on climatic impacts to the global sea level changes and the ancient Japanese history. Bulletin of the Department of Geography University of Tokyo, 15, 1-33.
- Liu Qingsi (1989) Holocene environmental change and using in Daihai basin. Journal of Arid Land Resources and Environment, 3, 37-45.
- Han Shutí (1990) Preliminary study of Holocene environmental evolution in the Balikun Lake. Marine Geology and Quaternary Geology, 3, 90-98.
- Shi Yafeng (1990) Glacier recession and lake shrinkage indicating the climatic warming and drying trend in central Asia. Acta Geographica Sinica, 1, 1-13 (in Chinese).
- Zhu Kezhen (1973) A preliminary study on the climatic change during the last 5000 years in China. Scientia Sinica (B), 16, 226-256 (in Chinese).
- Li Jijun (1988) The Glaciers of Tibet. Science Press, Beijing, China.
- Kong Zhaochen (1982) The vegetation development and climatic change in Beijing areas since 10000 a.B.P., ACTA Vegetation Sinica, Vol.24, No.2 (in Chinese).
- Li Wenyi (1985) The vegetation and environment during the Hypsithermal eastern Hebei Province, ACTA Vegetation Sinica, Vol.27, No.2 (in Chinese).
- Li Jijun (1990) The comparison between loess

profiles and antarctic ice core since the last glaciation, *Scientia Sinica* (B), No.16 (in Chinese).

Qiu Shanwen (1982) The glaciation of Late Pleistocene and paleoclimate in Northeast China, Collection on glacier and permafrost, Chinese Geographical Society (in Chinese).

VEGETATION IN PERMAFROST REGION AND THE DIVISION OF FOREST  
MANAGEMENT IN DA HINGGAN LING FOREST REGION

Dai Chuntian, Dai Baoguo, Du Chengxian, Liu Qingren and Dai Pin  
Heilongjiang Institute of Forestry, Heilongjiang Province, China

The permafrost in Chinese northeast lies within 47°28'N in China and it occupies 80% area of the whole northeast region. It is the continuous permafrost from Bergunayouqi in northwest part to Bishui and Mehe. Its depth is 50-80 m. The other regions are sporadic permafrost with depth of about 15 m. The vegetation in Da Hinggan Ling belongs to boreal flora and the vegetation species is simple. According to the division rules of regional geomorphology, ecological factors, cover types, vegetation similarity within a area and the differences among the areas, we divide the forest in Da Hinggan Ling into five management zones. From the experience in Hongxin and Weihe areas about the practice of amelioration in swamp in spordic region. We present the ways to improve and utilize permafrost.

PERMAFROST DISTRIBUTION

Frozen ground and permafrost are mainly distributed in the northern part of Heilongjiang Province and Hulongbeier League of Chinese Mogoia. The range of distribution is 47°28'-53°31' 40"N and 119°52'30"-125°45'. Its eastern extension is to the Yuchong and Heijiang areas and it appears in a triangle form. The rule of the distribution is that it is continuous permafrost with depth of 50-70 m in northern part and there is sporadic permafrost with depth of 3-7 m in southern part. The formation, development and deterioration of permafrost is not only determined by geology, geomorphology, climate, soil and latitude but also by the types of vegetation, fire, road and residential construction, cultivation and other human activities.

The temperature of the continuous permafrost area distributed in northern part of Da Hinggan Ling is that the mean annual air temperature is below -5°C (the minimum air temperature is -5.5°C), the mean annual temperature is -2°C. The permafrost area occupies 80% of all the region except for in the areas of river beds, alluvial flats and faults areas, which is permafrost-free. The depth of continuous permafrost is 50-80 m, and the depth of sporadic permafrost is within 15 m, and within 3-7 m in the southern part of 47°N. Its ground temperature is -0.5 - -1.5°C (See Figure 1).

From the distribution of permafrost in Da Hinggan Ling, we can estimate that the southern limit of permafrost is in the belts from Longzheng, Helongmeng to Aer mountain. Sporadic permafrost is distributed in the moutches of branch rivers and swamps in the belts from Alihe to Dayangshu. Its depth is 3-7 m. We didn't find permafrost from Dayangshu to Long River. It is our main tasks to ameliate and utilize permafrost, improve forest productivity and make a healthy ecological environment.

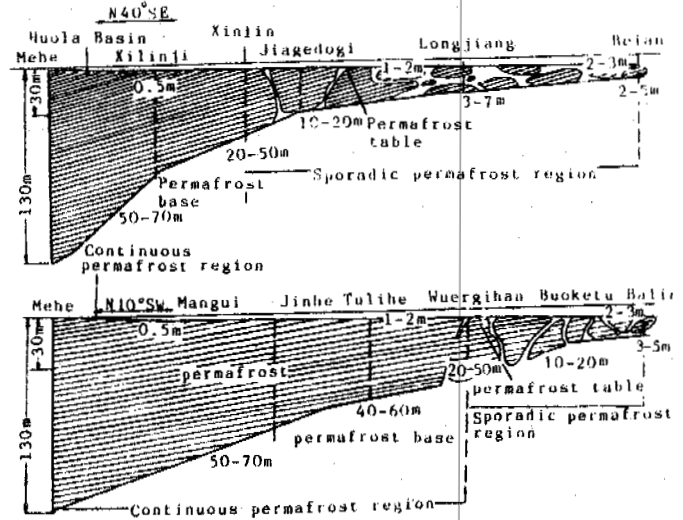


Figure 1. The scheme diagram of the changing depth of permafrost in Da Hinggan Ling forest region

THE CHARACTERISTIC OF FOREST DISTRIBUTION AND FOREST DIVISIONS

The forest in Da Hinggan Ling belongs to boreal flora. According to the natural economic divisions in "Scheme and planning of forest in Da Hinggan Ling", the region is divided into five economic zones (See Figure 2).

Division one: Upland tundra and forest area in northern part of Da Hinggan Ling. The vegetation is used as a protection forest. The hull area is 4.0 millions hectares and the timber

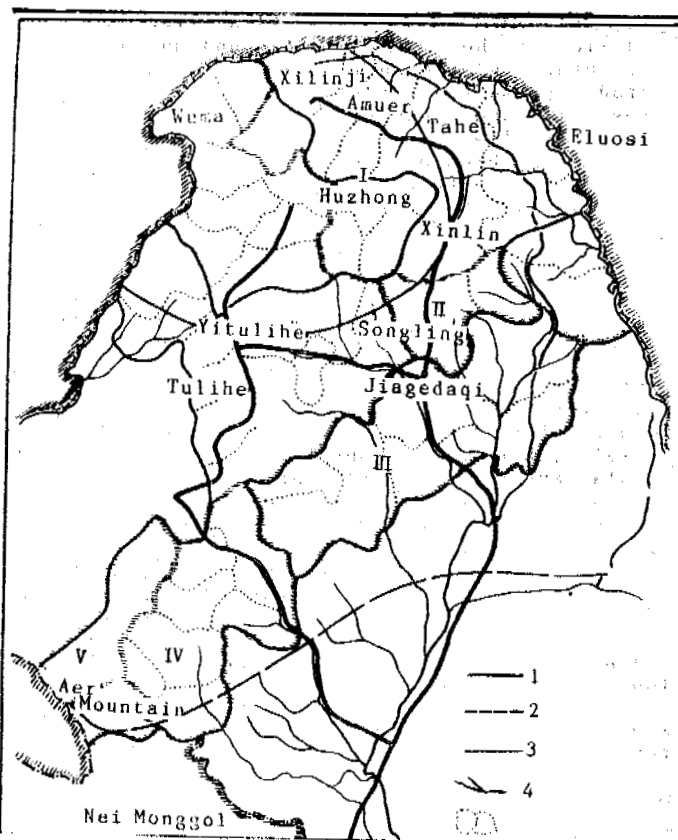


Figure 2. Forest division and distribution of permafrost

1. Southern limit of continuous permafrost;
2. Southern limit of sporadic permafrost;
3. Railway;
4. River;
5. A foresting Bureau limit

reserve is close to 400 millions  $m^3$ . The unit reserve is  $88.1 m^3/ha$ . The region belongs to denudated plateau and the altitude is 800-1000 m. Mean annual air temperature is  $-4 - -6^\circ C$  and the annual accumulated air temperature is 1000-1600  $^\circ C$ . The frost-proof period is 80-90 days. The yearly precipitation is about 400 mm. The soil is brownish stone soil, peat and humus. The depth of permafrost is 50-70 m. The main species of vegetation is *Larixgmelinii* which constitutes 73% of all the forest, next is *betula platyphylla* and *Pinus sylvestris* var. *mongolica*. The dominant vegetation types are *Rhododendron dauricum-Larixgmelinii*, *Ledum palustre* var. *angustum-Larixgmelinii*, and *Pinus pumila-Larixgmelinii* (Zhang, 1986). Because of the late exploitation of the region, the forest is basically in its virgin state. The region lies in the source area of Eerguna River, Huma River and Amuer River. It is the base for protected forest and timber resources. There are eleven forest bureaus such as Huzhong, Huma, Wuma, Magui etc. in this region.

The timber reserve in this area is greatest in Da Hinggan Ling forest region. The unit timber reserve is  $88.1 m^3/ha$ . The management policy is mainly to protect forests. In the condition of protecting the ecological system, reasonably utilizing forest resource and bringing forest into full play, we should mainly manage the

species of *Larixgmelinii*. Since this region it belongs to is continuous permafrost with a thickness of 60-70 m and has a shallow seasonally thawed depth and low ground temperature, the depth of the descending axis is shallow. Thus, the nutrient space is not enough and the productivity is low. In the later exploitation, we ought to give artificial interruption, drain surface water, lower the permafrost table in addition to its natural succession in order to maintain recent forest structure and prevent it from a reversed succession.

Division two: The area of the forest in the middle of Da Hinggan Ling in this area is 1000 millions hectares. Timber reserve is 600 millions  $m^3$ . It is the biggest forest area and the timber reserve and the production is the biggest too. The unit forest reserve is  $62 m^3/ha$ . The region belongs to denudated and eroded area. The elevation is 1000-1200 m. The mean annual air temperature is  $-2 - -4^\circ C$ . Warm index is  $35-45^\circ C$ . Accumulated air temperature is 1400-1800  $^\circ C$ . The frost-free period is 80-100 days. The yearly precipitation is 400-450 mm. It is brownish crushed gravel. *Larixgmelinii* is about 70%, next are *Betula platyphylla*, *Pinus sylvestris* and a little *Picea*. The vegetation types are tussock-*Larixgmelinii*, *Rhododendron dauricum-Larixgmelinii*, *Ledum palustre* var. *angustum-Pinus sylvestris*, *Rhododendron dauricum-betula platyphylla* and *Bryophta-Picea*. The region had been exploited earlier, but the unit forest reserve is a little less than the division one. At present, it is a naturally important timber base. The region has fourteen forest bureaus which belong to the continuous permafrost region. Because the soil layer is effected by low temperature in the long term it has formed a barrier to prevent the activities of microorganisms and the release of nutrition. The depth of permafrost is 20-60 m. It has a considerable effect on the regional exploitation and forest resources. But the region has a great forest reserve and it is a large area, the natural conditions, are suitable for forest growth. Forest industry and transportation are well developed. From this, we should well manage the destination species of *Larixgmelinii* and *Pinus sylvestris* in order to bring the forest into full play. In the western part of this region, in the prairie, we should develop it in animal husbandry.

Division three: The region lies in low ridges of the southern slope of Da Hinggan Ling. The area is 5.50 million hectares and forest reserve is about 160 million  $m^3$ . Unit reserve is  $29.3 m^3/ha$ . The geomorphology belongs to eroded and denudated mountain area and plateau. Elevation is 400-800 m. The mean annual air temperature is  $0-2^\circ C$ . Warm index is  $45-55^\circ C$ . Accumulated air temperature is 1600-2000  $^\circ C$ . The frost-free period is 90-120 days. Yearly precipitation is 450-500 mm. The soil is brownish stone soil and peat.

The condition of climate and soil is suitable for vegetation to grow. The region has mainly grown *Larixgmelinii*. Through frequently destruction, it has succeeded into a secondary vegetation of *Quercus mongolica*, *Betula davurica* and *Populus davidiana*, in addition to *Fraxinus mandshurica* and a few *Larixgmelinii*. The forest types are tussock-*Betula platyphylla*, *Lespedeza michx-Quercus mongolica*, *Corylus-Betula davurica* and tussock-*Larixgmelinii*. The region has thirteen bureaus. The yearly timber production is 2.00 million  $m^3$ . In the southern part of the



region, the exploitation of the area began very early. Because of the man-made and fire effects, the forest is severely destroyed. Thus, unit forest reserve is 29.3 m<sup>3</sup>/ha. The forest belongs to secondary forest of low-production and less value. Through the measures of raising, remaking and utilizing the secondary forest, we can raise rapidly the growing species of *Populus davidiana* and *Pinus sylvestris* being used for industry. The region belongs to spodic permafrost and its depth is 20-40 m. We ought to remake and utilize it.

Division four: Southern Da Hinggan Ling timber region. (The characteristics of the division are omitted here).

Division five: The area of seed-reserved *Pinus sylvestris*.

#### IMPROVEMENT OF SWAMPY LAND IN THE PERMAFROST REGION

Continuous and sporadic permafrost has a great effect on vegetation. The succession vegetation in the permafrost areas appears to be in a reversed succession. The growth percentage is low and it will probably become "dwarf old men", in the local dialect. The reason is that the root system is hindered by permafrost and the nutrition space is less, which prevents vegetation growth. For example, the growth characteristics of *Larix melinii* in permafrost-dominated and permafrost-free areas are listed in the following table.

Table 1. The growth characteristics of *Larix melinii* in different soil types

Soil type	Degree of soil status	Vegetation type	Height of trees(m)	Diameter (cm)	Timber reserve per tree (m <sup>3</sup> )
Continuous permafrost	V	Cryophyta & <i>Larix melinii</i>	5.5	5.0	0.02058
Sporadic permafrost	VI	<i>Ledum p.</i> var <i>Larix melinii</i>	17.0	15.0	0.1865
Permafrost-free	III	Dauricum & <i>rhododendron Larix melinii</i>	20.0	20.0	0.3260

In the area of seed-reserved trees, we should take artificial methods to aforest *Pinus sylvestris*, *Populus davidiana* and *Larix melinii*. In good drainage and humid areas, we ought to aforest quickly growing trees of less circulation period (about 20 years) in order to increase productivity and the coverage degree of forest land. In low land, the drainage is bad. In this area, we should take drainage, aforesting and cutceating methods to increase ground surface temperature, decrease the depth of sporadic permafrost and shrink the range of permafrost.

From the information of Hongxing and Weihe bureaus and through drainage of wet land and swamp to aforest *Larix melinii* and *Populus davidiana*, the ground surface temperature has raised 2-3°C and the increment percent increased by 20%.

The wet land and swamp in Xiao Xinan Ridges are widely distributed. In this area, there is sporadic permafrost. Reasons to exploit this area and increase forest coverage and forest reserve have significant importance.

Hongxing forest bureau (48°-19'43"44"N) is located in Xiao Xinan Ridges. The bureau has wet

According to this, we should utilize the condition of the increase of ground surface temperature and the shrinking of the range of sporadic permafrost area due to the June 6, 1987 forest fire and speed the recovery of vegetation and improve low production and low value forest and swamps, which are the key technological measures for us to spread the forest area.

The continuous and sporadic permafrost is widely distributed and occupies 80% of the hull region. The sporadic permafrost is mainly on the river terraces in valleys, swamp or wet land, such as the valleys of the upper reaches of Huma River and Hailaer River drainage areas. Except for the Huma River drainage area, other areas have been exploited earlier and human activity has been frequent. The species of vegetation is in a reverse succession and the forest's form isn't integrated. The vegetation is mainly *Betula platyphylla*, *Quercus mongolica*, *Betula dauverca* and a few *Larix melinii*. In this region, the conditions of water, soil and heat is good. Precipitation is enough and soil is fertile.

The accumulated temperature higher than 10°C is 1600-2000°C. This deteriorates the permafrost and shrinks the range of sporadic permafrost. The region has good conditions for quick growing and high-yielding species and the remaking of low-yield and less valuable forest. Therefore, not only do the conditions for a destination species exist, the modes of the recovery and regeneration are both artificial and natural.

land and swamp area of 50000 hectares in which the wet land is 38000 hectares and swamp is 12000 hectares. There is small *Larix melinii* in the swamp. Timber reserve is 30000 m<sup>3</sup>, unit forest reserve is 39.4 m<sup>3</sup>/ha. Water occupies the swamp all year long. The plants are mosses and other grasses and its thickness is up to 40 cm. Under the plant layer is permafrost. The trees in this region are called "dwarf old men" in local dialect. In order to improve the forest form and the soil quality, the bureau has been giving drainage tests since 1965 and has obtained good results. The main mean is to dig cross drainage channels in length and breadth of 25 m and 50 m. There have been good results three years later after the drainage. The results are below:

1. The form of standing body of trees becomes better and bark becomes smooth. Trunks and leaves are exuberant. The color appears fresh. Root systems become thicker. The key root is deeper into ground. The "dwarf old men" disappear.

2. Swamp deteriorates. The coverage degree of peat decrease, trees such as *Betula sylvestris*

and *Deyeuxia angustifolia* appear.

3. The quality of physical chemistry of soil becomes better. The water content decreases, soil temperature rises and the permafrost table decreases. The thickness of the layer of moss becomes less. The ground water level becomes lower. Soil fertility becomes better. All of the changes are results of the effects of drainage.

4. Economic benefits increase. The unit timber reserve before the drainage test is 39.4 m<sup>3</sup>/ha. It has become 63.4 m<sup>3</sup>/ha 15 years after the drainage test, it has increased 2.6 times. According to 1985's calculation, the unit timber reserve becomes 180 m<sup>3</sup>/ha 30 years later after the drainage. The tree's diameter is up to 24-32 cm. The maturing of the trees occur 10 years earlier than the ordinarily afforesting *Larix gmelinii*. The research in Hongxing forest bureau provides a successful experience for the ameliorating of wet land and swamp. This would improve the crisis of forest resource.

From the introduction of "Swamp becomes forest", there is 10.0 million hectares of swamp in Finland which occupied one fourth of the country's land. The area for drainage to afforest is more than 5 million hectare. They yearly timber production is 6.0 million m<sup>3</sup> but one Finland officer said that 3.0 million hectares swamp would remain in order to keep an ecological balance. Keeping some swamp area will adjust climate, increase humidity and protect living things in swamps.

Due to this, we ought to learn from Finland in its ameliorating swamps.

#### REFERENCE

Zhang Wanru, (1986) Chinese Forest and Soil, Published by Chinese Sciences.

## FROST HEAVE SUSCEPTIBILITY OF HIGHWAY BRIDGE FOUNDATION SOIL IN SEASONAL FROST REGIONS

Dai Huimin and X.L. Wang

Heilongjiang Institute of Highway and Transport,  
40 Qingbin Road, Harbin, 150080, China

With the purpose of further investigation and discussion on frost heave susceptibility of highway bridge foundation soil in seasonal frost region and to determine its judging criteria so as to solve frost damages of highway bridge, extensive in-situ experiments on clayey soil, silty soil and fine sand which are frost susceptible and more common in highway bridge and culvert engineering have been carried out since 1980 by Heilongjiang Institute of Highway and Transport. In the paper, after a brief introduction to the testing approaches, the effects of water content and ground water level on frost heave susceptibility are systematically analysed. And with mathematical treatment of the data obtained in a 5-grade classification and its criteria for seasonal frost soil of highway bridge are presented, which have been taken into standard specifications of use.

### INTRODUCTION

Seasonal frost soil is distributed widely in China, covering more than 10 cities and provinces in the North with an area of around 5.14 million square kilometers. 53.5 percent of the total area of the nation is involved. Its frost heave, especially the strong and severe frost heave of clayey soil has led to great damage to highway bridges culverts and other engineering structures. And these damages have a great influence on the highways and transportation, and heavy losses to the national economy. In this regard experimental studies on frost susceptibility of highway bridge foundation soil were carried out in Qingan Frozen Ground Experimental Station by Heilongjiang Institute of Highway and Transport. Our research is directed towards fully understanding and scientifically judging the frost susceptibility of soil so as to solve the frost damage of highway bridges.

### FROST SUSCEPTIBLE EXPERIMENTS OF SOILS

It is well known that the frost susceptibility of soils is dependant upon many factors, such as grain composition, mineralogical composition, moisture, density, temperature and the gradient of soils, etc. But there are usually three main factors, i.e., soil, water and temperature. For the foundation soil of bridges and culverts which allows water to pass through water is the most important factor to influence frost heave, and the quantity of water is a crucial condition to determine strength or weakness of frost heave. Hence in research of the frost heave of highway bridge foundation soil we concentrate upon water consideration, particularly on the effect of ground water level on frost heave.

To make clear the frost susceptibility of highway bridge foundation soil we chose clay, clayey loam and fine sand which are commonly adopted and the frost-susceptibility is rather strong in situations under different water

content and different ground water levels.

Table 1 shows the physical properties of samples.

### EXPERIMENTAL RESULTS AND ANALYSIS

#### Frost Susceptibility

Table 2 shows the results of experiments with clayey soil and fine sand.

It is apparent from Table 2 that (a) the highway bridge foundation soil (equivalent to that of No.1 and No.2 testing section) is of high water content, high ground water level, and thus has a strong frost susceptibility. For example, the frost heave of clayey soil may reach 397 mm (437 mm for the maximum), and the frost heave ratio of it is 34.4% (38.2% for the maximum); and the frost heave of fine sand is 219 mm, its ratio 15.7%. (b) frost heave is affected obviously by ground water. With a drop of the ground water level, the frost susceptibility becomes weakened apparently. From Table 2 the corresponding frost heaving ratio is 34.4%, 19.2%, 6.2% and 2.3% when the ground water level is 23.3, 56.6, 108.0, and 182.0 cm, respectively. And is more apparent in the fine sand: the frost heave ratio is 15.7% when the ground water level is 38.6 cm, 4.9% when the level drops to 64.7 cm, and 0.3% when the level keeps on dropping to 113 cm.

#### Dependence of the Frost Susceptibility on Water Content of Soils

It can be seen from the results of many domestic experiments that the frost susceptibility is affected by the water content before freezing, but not in all the water involved, it refers only to the part beyond initial water content of frost heaving. Generally their relationship is expressed as follows.

$$K_d = a (W - W_p) \quad (1)$$

Table 1. Grain composition analysis of testing soils

Soil sam. No.	Liquidity limit (%)	Plastic limit (%)	Plastic exponent Ip	Grain size (mm)						
				>2.0	2.0-0.5	0.5-0.25	0.25-0.1	0.1-0.05	0.05-0.005	<0.005
1	43.0	23.0	20.0					17.7	57.8	24.5
2	35.7	22.4	13.3					17.0	53.5	29.5
3				-5.0	18.3	11.2	46.0	19.5		

The designation of soil sample numbered with 1,2 and 3 is clayey soil, clayey loam and fine sand, respectively.

Table 2. Results from frost heave experiments

Testing sections	i	ii	iii	iv	v	vi	Mean value
Clayey soil							
1	34.4	23.3	155.0	397	115.3	34.4	7-year datum
2	28.8	56.6	183.0	295	153.5	19.2	
3	31.0	129.0	221.0	110	210.0	5.2	
4	36.3	113.0	206.0	105	195.5	5.4	3-year datum
5	32.3	108.0	206.0	121	193.9	6.2	
6	32.0	113.3	206.0	96	196.4	4.9	
7	34.7	137.7	212.0	82	203.8	4.0	
8	31.8	121.7	209.7	67	203.0	3.3	
9	35.1	141.7	216.0	87	207.3	4.2	
10	37.0	162.3	212.7	52	207.5	2.5	
11	30.5	144.0	230.3	98	210.5	4.7	
12	33.8	162.7	222.3	47	317.6	2.2	
13	34.0	182.0	222.0	49	217.1	2.3	
Fine sand							
1	23.0	38.6	161.8	219	139.9	15.7	6-year datum
2	17.5	64.7	169.8	79	161.9	4.9	
3	12.3	115.8	180.2	14	178.8	0.8	
4	15.7	113.0	178.3	6	177.7	0.3	3-year datum

i-refers to water content of soils before freezing in %; ii-is ground water level before freezing in cm; iii-is thickness of frozen layer of soils in cm; iv-represents frost heave of soils in mm; v-is frost penetration in cm; vi-is frost heave ratio in %.

where Kd is frost heave ratio in %; W is the mean water content of soils before freezing in %; Wp is initial water content of frost heave (equivalent to plastic limit of soil) in %; and a is a coefficient.

In this connection we still adopt the relation by Eq.(1) to analyse data obtained from our field experiments (Table 3). As a result, the arithmetic mean  $\bar{a}=0.36$ ; the standard deviation  $S=0.068$ ; the coefficient of variation  $C_v=0.189$ ; and the magnitude of a under the confidence level of 95% is 0.47.

Hence, we obtain

$$K_d = 0.47(W - W_p) \quad (2)$$

Calculating the critical water content for the frost heave classification of clayey soil, and making reference to related literature to amend, we finally obtain the critical water content in conformance with each grade of the classification as follows. (I) For non-heaving soil,  $K_d \leq 1$ . Thus  $W \leq W_p + 2.1$ ; use  $W \leq W_p + 2$ . (II)

Weak-heaving soil,  $1 < K_d \leq 3.5$ . Thus  $W_p + 2.1 < W \leq W_p + 7.5$ ; use  $W_p + 2 < W \leq W_p + 8$ . (III) Medium-heaving soil,  $3.5 < K_d \leq 6$ . Thus  $W_p + 7.5 < W \leq W_p + 12.8$ ; use  $W_p + 8 < W \leq W_p + 15$ . (IV) Strong-heaving soil,  $6 < K_d \leq 15$ . Thus  $W_p + 12.8 < W \leq W_p + 31.9$ ; use  $W_p + 15 < W \leq W_p + 32$ . (V) Severe-heaving soil,  $K_d > 15$ ; use  $W > W_p + 32$ .

#### Effect of Ground Water Level on Frost Susceptibility

As afore mentioned the level of the ground water will yield great influence on frost heave susceptibility, as was dwelt upon in detail in the literature (X.R. Wang, 1980; X.B. Chen and Y.Q. Wang, 1986). For the purpose of quantitative analysis of the relationship between the ground water and the frost heave of bridge foundation soil we proceeded with mathematical treatment of the experiment data (including 159 samples of data on clayey soil and 51 on fine sand) observed since 1982 in Qingan Frozen Ground Experimental Station.

For clayey soil the result of regression analysis on the relation between ground water

Table 3. Values of a for clayey soil

No. of data	Z (cm)	Kd (%)	W <sub>1</sub> -W <sub>p</sub>	a <sub>1</sub>	No. of data	Z (cm)	Kd (%)	W <sub>1</sub> -W <sub>p</sub>	a <sub>1</sub>
1	120	4.8	16.7	0.29	20	170	2.9	9.1	0.32
2	120	5.1	16.7	0.31	21	171	3.1	6.8	0.46
3	120	5.4	16.7	0.32	22	171	3.2	6.8	0.47
4	135	5.5	11.1	0.50	23	125	5.0	17.5	0.29
5	135	5.4	11.1	0.49	24	125	5.0	17.5	0.29
6	135	5.0	11.1	0.45	25	125	4.6	17.5	0.26
7	129	3.6	13.9	0.26	26	110	6.0	12.3	0.49
8	129	3.6	13.9	0.26	27	138	5.0	13.4	0.37
9	121	4.8	13.8	0.35	28	138	4.9	13.4	0.37
10	121	5.0	13.8	0.36	29	138	4.4	13.4	0.33
11	121	5.3	13.8	0.38	30	113	3.5	10.9	0.32
12	155	2.5	6.8	0.37	31	113	3.5	10.9	0.32
13	155	2.3	6.8	0.34	32	113	3.7	10.9	0.34
14	155	2.0	6.8	0.29	33	134	4.9	15.2	0.32
15	150	2.5	6.3	0.40	34	134	5.2	15.2	0.34
16	150	2.7	6.3	0.43	35	134	5.0	15.2	0.33
17	150	3.0	6.3	0.48	36	141	4.8	14.2	0.34
18	170	3.0	9.1	0.33	37	141	4.6	14.2	0.32
19	170	3.0	9.1	0.33	38	141	5.1	14.2	0.36

and frost susceptibility is expressed by Eq.(3) and shown in Fig.1.

$$K_d = a \exp^{bz} = 35.1 e^{-0.019z} \quad (R=0.88) \quad (3)$$

And for the fine sand the result is that as expressed by Eq.(4) and shown in Fig.2.

$$K_d = a + b \ln z = 24.2 - 5.2 \ln z \quad (4)$$

$$R = 0.87 \quad F = 391.62 > F_{0.01} = 7.2$$

in which z refers to ground water level from the earth surface before freezing in cm and other symbols are the same as explained above.

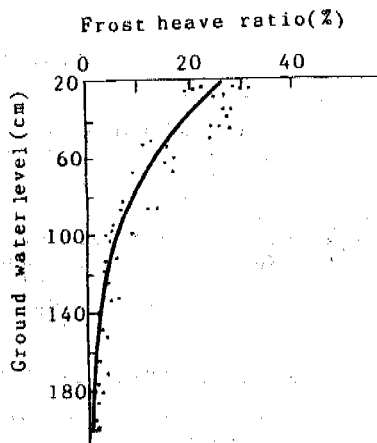


Figure 1. Relation of frost heave ratio vs. ground water level for clayey soil

Both proposed and calculated critical values of ground water levels on the basis of Eqs.(3) and (4) are listed in Table 4.

Seasonal Frost Soil Classification for Highways and Bridges

To sum up the experiments with consideration of the influences of ground water and water

Frost heave ratio (%)

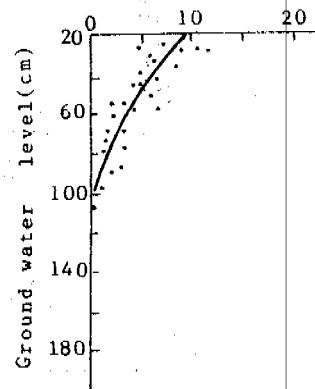


Figure 2. Relation of frost heave ratio vs. ground water level of fine sand

content of soil before freezing and with reference to the experiences related to frost soil classification (X.R. Wang, 1980; Tong, 1983; Z.Q. Wang, 1981; JTJ 024-85, 1985; TJ 7-74, 1974) we, from the convenient and applicable point of view, present a 5-grade classification for the seasonal frost soil of highway bridges in accordance with the frost susceptibility (here represented with frost heave ratio). Namely they are non-heaving soil ( $K_d \leq 1\%$ ), weak-heaving soil ( $1 < K_d \leq 3.5\%$ ), medium-heaving soil ( $3.5 < K_d \leq 6\%$ ), strong-heaving soil ( $6 < K_d \leq 15\%$ ), and severe-heaving soil ( $K_d > 15\%$ ). The judging criteria are shown in Table 5.

SUMMARY AND CONCLUSIONS

After mathematical treatment and the reference and adoption of the advantages of related frost soil classification published domestically and abroad, the seasonal frost soil classification is developed from 7-years of field experi-

Table 4. Critical values of ground water (m) in classification

	Grade of classification				
	Non-heaving	Weak	Medium	Strong	Severe
<b>Clayey soil</b>					
Calculated	1.87	1.21	0.93	0.45	<0.45
Proposed	>2.0	>1.5	>1.0	>0.5	≤0.5
<b>Fine sand</b>					
Calculated	0.87	0.54	0.33	0.06	<0.06
Proposed	>1.0	>0.6	>0.4	>0.1	≤0.1

Table 5. Classification of seasonal frost soil

Designation of soil	Natural water content of soil before freezing W(%)	Ground water level from earth surface before freezing Z(m)	Classification of frost soil
(i)	omitted	omitted	Non-heaving
(ii)	W≤12	>1.5	Weak
	(Sr≤0.5)	≤1.5	Medium
	12<W≤18	>1.5	Strong
	(0.5<Sr≤0.8)	≤1.5	Severe
	W>18	>1.5	Severe
	(Sr>0.8)	≤1.5	Severe
Fine sand silty sand	W≤14	>1.0	Non-heaving
		1.0≥Z>0.6	Weak
		0.6≥Z>0.4	Medium
		0.4≥Z>0.1	Strong
	14<W≤19	≤0.1	Severe
		>1.0	Weak
		1.0≥Z>0.6	Medium
		0.6≥Z>0.4	Strong
	W>19	≤0.4	Severe
		>1.0	Medium
		1.0≥Z>0.6	Strong
		≤0.6	Severe
Clayey soil	W≤Wp+2	>2.0	Non-heaving
		2.0≥Z>1.5	Weak
		1.5≥Z>1.0	Medium
		1.0≥Z>0.5	Strong
	Wp+2<W≤Wp+8	≤0.5	Severe
		>2.0	Weak
		2.0≥Z>1.5	Medium
		1.5≥Z>1.0	Strong
	Wp+8<W≤Wp+15	≤1.0	Severe
		>2.0	Medium
		2.0≥Z>1.5	Strong
		≤1.5	Severe
Wp+15<W≤Wp+32	>2.0	Strong	
	≤2.0	Severe	
	omitted	Severe	
	omitted	Severe	

Note: 1. Wp indicates water content of soil to plastic limit; W is natural water content (i.e., the mean value of water content within standard frozen depth of soils before freezing; Sr is saturated degree of soil; (i) includes rock, crushed stone, gravelly coarse and middle sand (less than 15% of clay and silt fractions); (ii) means crushed stone, gravelly, coarse, and the middle sand (more than 15% of clay and silt fractions).  
2. Consideration of lower grade is necessary relating to 0.5% or more of salt content.

ments on common bridge and culvert foundational soil under different ground water levels as well as different water content. Therefore the classification is rational and its judging criteria is reliable, suitable for the objective reality of seasonal frost soil of highway bridges.

#### REFERENCES

- Bureau of the National Architecture of P.R.China, (1974) TJ7-74, Standard Specifications for Foundation Designs of Industrial and Civil Architecture: 15 pp.
- Chen, X.B. and Wang, Y.Q., (1986) Frost heave of soils under different ground water levels. Lanzhou Institute of Glaciology and Geocryology of Chinese Academy of Sciences, (unpublished).
- Ministry of Communications, P.R. China, (1985) JTJ 024-85, Standard Specifications of the Foundation designs of Highway and Bridge: 63 pp.
- Tong, C.J., (1983) Frost heave classification for permafrost regions. Proceedings of Frozen Ground Research in Qinghai and Tibet Regions: 73-78.
- Wu, Z.W. et al, (1981) On the frost heave susceptibility of soils. Journal of Glaciology and Geocryology, 2: 127pp.
- Wang, X.R., (1980) Frost heave susceptibility of different soils under different ground water levels. Journal of Glaciology and Geocryology, Vol.II, No.3: 50 pp.
- Wang, Z.Q., (1981) The characteristics and classifications of fine sand frost heave. Harbin Architectural and Civil Engineering College, (unpublished).
- Xu, Y.Z. and Wang, Z.Q., (1980) Discussions on foundation designs in seasonal frost region. Harbin Architectural and Civil Engineering College, (unpublished).

## PERMAFROST CONDITIONS ALONG AN ONSHORE-OFFSHORE TRANSECT OF THE CANADIAN BEAUFORT SHELF

S.R. Dallimore and A.E. Taylor,  
Terrain Sciences Division,  
Geological Survey of Canada,  
Ottawa, Canada

In 1990, a drilling program was carried out along a 25km transect in an area of active marine transgression across an arctic permafrost landscape. Six boreholes were drilled to depths between 42 and 103m from onshore on northern Richards Island to offshore on the Beaufort Shelf; the four offshore sites were in water depths of 3 to 10m. Marine transgression is the principal event shaping the character of this offshore region and its permafrost and geothermal regime. Sediment grain size and salinity are the principal properties governing the presence or absence of ice-bonding. Permafrost is degrading in the offshore due to the transgression. The depth to the top of ice-bonded sediments is about 90m below the present seabed inshore, but lies only 11m below the seabed 25km offshore. At present, this is attributed to a reduced rate of sea level rise and warmer sea water temperatures in the past millennium. A continuity of four major geologic units was established between the onshore and offshore. A marine unit arising from the present transgression was documented in the coastal area.

### INTRODUCTION

During March and April of 1990, the Geological Survey of Canada conducted a geotechnical investigation of permafrost conditions along a 25km transect from northern Richards Island along a proposed offshore pipeline route (Fig. 1). For the first time, boreholes 40 to 100m deep were drilled specifically to recover cores and to delineate the permafrost regime and geology along the coastal margin of the Beaufort Shelf. Program description and preliminary results of the geology, geotechnical properties and ground thermal regime can be found in Dallimore (1991). The present paper describes the permafrost conditions along the transect as they relate to geological processes which have been ongoing since the area was transgressed by the sea.

### MARINE TRANSGRESSION AND OFFSHORE PERMAFROST

Marine transgression in arctic regions represents a major thermal event, as sea water near its freezing point encroaches on a colder permafrost landscape developed in a terrestrial setting. Nearshore permafrost distribution is primarily controlled by three major factors: the initial ground temperatures and ground ice distribution prior to transgression, the temperature history experienced after transgression, and the rate at which transgression took place. At present, typical permafrost thicknesses on Richards Island are in the order of 400 to 700m with mean annual ground surface temperatures of approximately  $-6^{\circ}$  to  $-9^{\circ}\text{C}$ ; similar thicknesses of relict Pleistocene permafrost are reported offshore (Judge et al., 1987). Seabottom temperatures of shallow coastal areas of the Beaufort Sea (<10m water depth) in the vicinity of the Mackenzie Delta are influenced by large seasonal outflows of relatively warm river water, resulting in positive mean annual

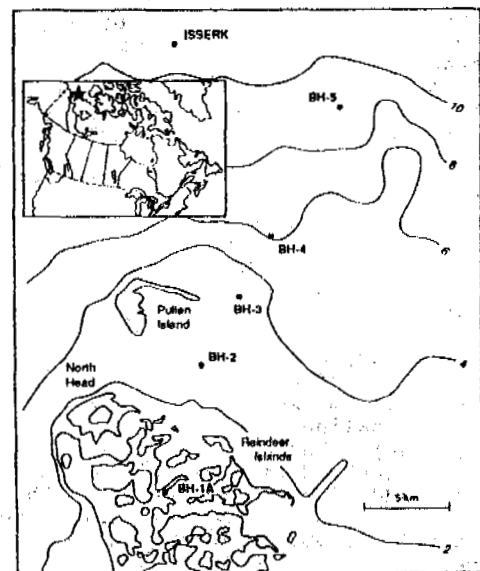


Figure 1. Location of onshore-offshore drilling transect. Boreholes are labelled BH-x. Bathymetry is in metres and tenths.

seabottom temperatures and permafrost degradation (Hunter, 1988; Hunter et al., 1988). Further offshore in areas remote from the influence of the Mackenzie River, negative mean annual seabottom temperatures are reported (Taylor and Allen, 1987).

The rate of transgression is determined by the rise in relative sea level, the geology and topography of the coast, and coastal sedimentation. Investigations of relative sea level for the southern Beaufort Sea (Forbes, 1980; Hill et al., 1985; 1991) suggest that a



significant decline in the rate of rise has occurred during the late Holocene period. Depending on the sea level curve selected, estimated rates vary from 0.6 to 1.0 mm/a during the early Holocene and decline to 0.2 to 0.4mm/a for the past 3500 years. Rates during the past few centuries have possibly been even slower as shown by a flat portion of most global sea level curves for this period. These trends are reflected in the rate of coastal retreat during the Holocene. Pelletier (1984) shows two possible offshore beach ridges dated at 14,500 and 8,500 years BP, occurring approximately 140km and 90km offshore. While these features would imply average retreat rates up to 10m/a since their deposition, the Tuktoyaktuk Peninsula and Richards Island areas have been retreating at average rates of 0.3 to 2m/a for the past 40 years (Harper et al., 1985).

#### PRELIMINARY RESULTS OF THE GSC ONSHORE-OFFSHORE TRANSECT

##### 1. Geology

Although the technical challenges presented in offshore drilling did not allow continuous coring, downhole geophysical logs (natural gamma, conductivity and seismic) were run in each borehole; this allowed interpolation of the stratigraphy between sampling horizons (Hunter et al. in Dallimore, 1991). A simplified geological model of the upper hundred metres along the transect is summarized on Figure 2a. Five major stratigraphic units can be traced from onshore areas to the farthest borehole offshore. Both an onshore-based stratigraphy (e.g. Rampton, 1988) and an offshore-based stratigraphy (O'Connor, 1980; Blasco et al., 1990) are shown in the figure.

The oldest unit encountered in the offshore transect can be correlated on land with the Kendall sediments, while offshore it is called Unit E. Although only sampled intermittently, this unit was quite uniform in character, consisting of medium-grained sand with relatively low moisture content. The Kendall sediments are overlain by a 10 to 14m thick, low plastic clay, called the Hooper clay on land and Unit D offshore. The Hooper clay forms a critical marker horizon since it is a fine grained, saline clay of marine origin (Rampton, 1988), that occurs between two relatively thick and well described sand sequences. Additional information on the continuity of the Unit D is available from marine seismic surveys (Blasco and Lewis, in Dallimore, 1991) and from boreholes drilled by industry (Blasco, pers. comm. 1990). The Hooper clay is overlain by a 20 to 40m thick sand sequence which has been described as Unit C offshore. Detailed mineralogy and sedimentology investigations suggest that it is in fact composed of two or possibly three sub-units which correlate with the Kittigazuit and Kidluit formations described on land (Rampton 1988). Unit C is overlain in nearshore areas by Unit B, a marine silt thought to be deposited during the present marine transgression. On this transect Unit B occurs exclusively in water depths of about 2 to 9m, reaching a maximum thickness of about 15m in 3m of water. It is absent in BH-5 and in shallow coastal waters less than 2m deep. Unit A (Blasco et al., 1990) occurs farther offshore and was not encountered along the transect.

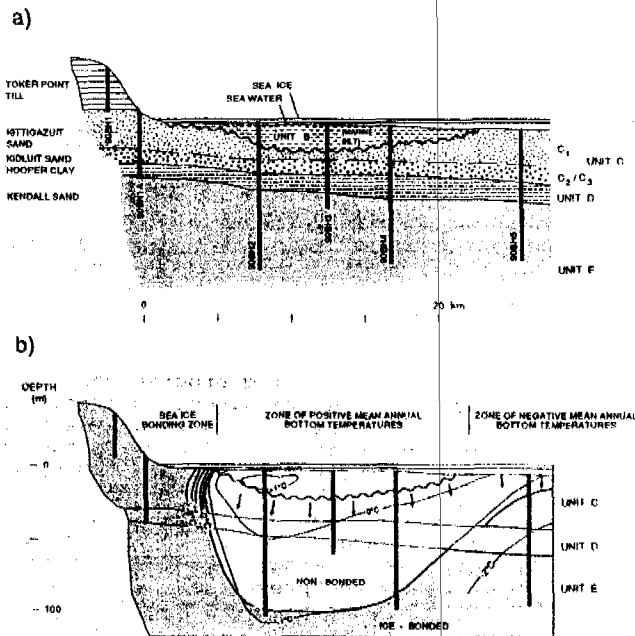


Figure 2. Cross-sections of onshore-offshore transect: a) stratigraphy, and b) geothermal regime and ice-bonding (short arrows show direction of movement of saline porewater).

##### 2. Seabed temperatures and thermal properties

Ground temperature cables, with 15 thermistors, were installed in each borehole upon completion; a data logger monitored the recovery of the thermal conditions from the drilling disturbance (Taylor and Allen, in Dallimore, 1991). Figure 3 shows the ground temperatures measured at the end of April, 1990 and also temperatures from previous offshore work at the Isserk site (Fig. 1).

Late winter seabed temperatures at all sites are below 0°C. Below the seasonal influence that extends to 10m. Below 10m, temperatures decrease with depth and extrapolation suggests that mean seabed temperatures decrease seaward from above 0°C at BH-2, BH-3 and BH-4 to below 0°C at BH-5 and Isserk. Only subtle differences in the slope (the temperature-depth gradient) of the profiles are apparent.

Some 700 thermal conductivity measurements were made on core maintained in freezers as close to in-situ temperatures as possible (Wilkinson and Taylor, in Dallimore, 1991). These, with the various other geotechnical properties reported in this paper, will permit various quantitative analyses to be undertaken.

##### 3. Permafrost and ice-bonding conditions

A major focus of the transect drilling was to quantify the geotechnical properties, including ice-bonding, of the various stratigraphic units. Downhole electrical conductivity logs and measured pore water salinity values provide an overview of conditions from the onshore borehole to the farthest offshore borehole (Fig. 4).

##### Borehole BH-1a

Borehole BH-1a shows the physical properties of terrestrially exposed sediments prior to transgression. Ground temperatures

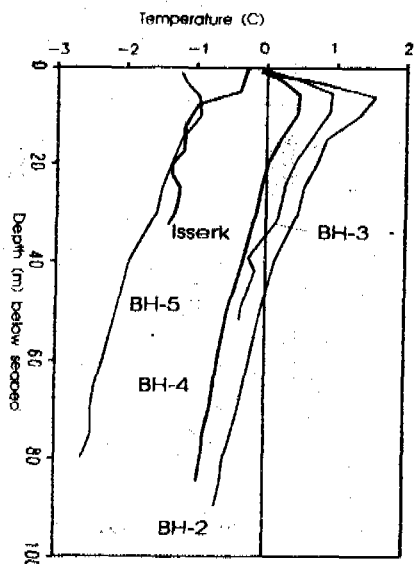


Figure 3. Temperature profiles versus depth below present seabed.

are consistently below  $-7^{\circ}\text{C}$  and sediments are well ice-bonded. Ice contents are generally quite high (range 10-40% excess ice by volume) in the upper 5m especially immediately below the active layer. Salinity measurements on pore water extracted from core samples and downhole conductivity measurements characterize the very low porewater salinity of the Kittigazuit, Kidluit and Toker Point sediments indicating emplacement of pore water during terrestrial exposure. An abrupt rise in salinity and conductivity within the Hooper clay confirms a marine environment during deposition. The Kendall sediments were not penetrated to a sufficient depth to accurately determine their properties.

#### Borehole BH-2

Borehole BH-2, in 3m of water, illustrates the dramatic change in physical properties resulting from transgression. The  $0^{\circ}\text{C}$  isotherm is approximately 46m below the sea floor and the majority of the borehole intersected unbonded sediments (Fig. 2b). Unit B is approximately 15 m thick. Unlike the Kittigazuit/Kidluit at BH-1a, Unit C has high salinities up to 60 ppt with high downhole conductivities throughout (Fig. 4). It is postulated that the elevated salinities have resulted from the movement of saline porewater from the sea floor as thawing occurred after submersion. Also, the salinities are substantially higher than those found in Unit B (15 to 40 ppt). The abrupt decrease in downhole conductivity at the top of Unit D, and the almost identical salinities in this unit to those observed in BH-1a, suggest that saline migration from the sea floor did not penetrate Unit D.

While most sediments in BH-2 are unbonded, a partially ice-bonded zone was encountered at 88m. Although marginal ice-bonding is often difficult to detect in deep boreholes, three independent lines of evidence appear to confirm this partially ice-bonded zone: observations of partial ice-bonding in core samples, variable drilling resistance and

mud pressure registered through the zone, and downhole seismic velocity measurements above 2.0 km/s, a value generally accepted as indicative of partial ice-bonding (see Hunter et al., in Dallimore, 1991).

#### Borehole BH-5

Borehole BH-5, in approximately 10m of water, was sited specifically in a zone of widespread shallow permafrost identified from seismic refraction surveys (Hunter, pers. comm. 1990). Unlike the boreholes closer inshore, Unit B sediments are absent at this site and Unit C occurs at the sea floor (Fig. 2a). Ground temperatures are consistently below  $-1^{\circ}\text{C}$  and ice-bonding conditions are variable (Fig 2b). A thin layer of ice-bonding encountered at the seabed is interpreted as seasonally frozen sediments responding to cold winter bottom temperatures. This condition was also observed at other sites in the area (Kurfurst and Dallimore, 1991). Salinities in the top of Unit C just beneath the sea floor are elevated to 20 to 40 ppt (Fig. 4). Unlike BH-2, however, there is an abrupt drop in salinity and downhole conductivity at approximately 15m to values similar to those observed in the Kittigazuit/Kidluit sediments onshore in BH-1a. Ice-bonding appears to be controlled entirely by salinity, with an unbonded zone in the upper part of Unit C, a partially bonded transitional zone from 11 to 16 m, and a well bonded zone beneath 16m where the salinities are near zero. Three discrete layers of ground ice, 10 to 35cm thick, were observed from 17 to 19m. Ice contents ranged from 60 to 80% by volume and oxygen isotope ratios determined on two samples from the ice were  $-29.4$  and  $-28$  ‰ (SMOW), suggesting ice formation from terrestrial water at climatic conditions somewhat colder than today.

An abrupt rise in salinity to 20 to 40 ppt for Unit D follows a similar trend to that observed in BH-1a. However, in BH-5 because of the relatively warm ground temperatures (approximately  $-1.5^{\circ}\text{C}$ ), high pore water salinity and the fine grain size, Unit D was unbonded. In contrast, Unit E which had slightly lower salinities and is coarse grained was well bonded.

#### DISCUSSION

Three permafrost zones, each with different temperature and ice-bonding conditions, occur in the coastal zone in the vicinity of the borehole transect (Fig. 2b).

#### Sea ice contact zone

This zone occurs adjacent to the shoreline where water depths are less than 2m. Although none of the deep boreholes were placed in this zone, it has been well documented by cone penetration testing along the transect (Kurfurst and Woeller in Dallimore, 1991) and at other nearshore sites in the North Head area (Kurfurst, 1986, 1987). A dominant influence in this area is the formation of landfast sea ice which freezes to the bottom during the winter. As described by Dyke (1991), this zone experiences unique ground surface temperatures. Permafrost is generally preserved close to the surface but is warmer than onshore. A thick active layer forms during the summer in response to relatively warm surface waters. In some cases the active layer at the top of

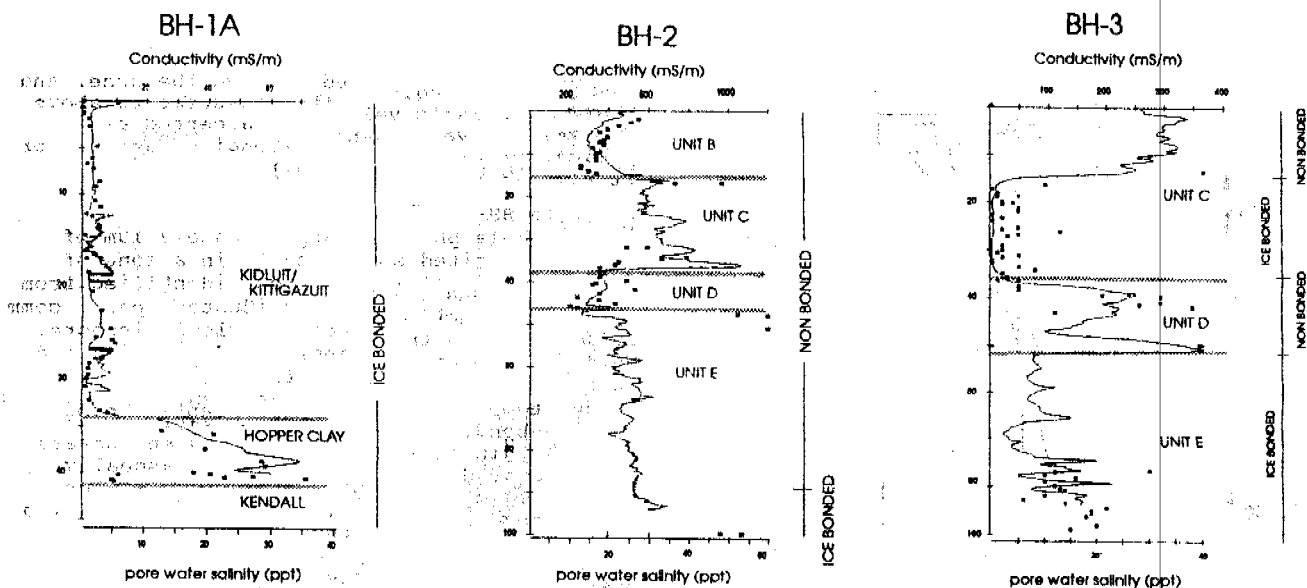


Figure 4. Composite logs for boreholes 1a, 2 and 5 showing downhole electrical conductivity and pore water salinity measurements.

permafrost may become highly saline as a result of processes such as salt rejection from sea ice or concentration through evaporation.

#### Zone of positive mean annual seabottom temperatures

A zone of degrading permafrost occurs in water depths of 2 to 9 m where mean annual seabottom temperatures vary from 1.2°C (BH-2) to 0.5°C (BH-4) farther offshore. These temperatures reflect the mean sea water temperatures in an area dominated by the seasonal warm plume of the Mackenzie River. This area is characterized by thick inshore accumulations of Unit B sediments (Fig. 2a). The ice-bonding interface, confined to submerged terrestrial sediments, parallels the contact between Unit B and Unit C and the -1°C isotherm; it occurs almost 90m deep at the 3m isobath (BH-2) and approximately 80m deep at the 9m isobath (BH-4). Thawing of sediments is ongoing and settlement in the seabottom results from the liberation of excess pore water. If the water contents and bulk densities found in BH-1a are used as an example, settlement in the order of 1m is likely to occur for every 10m thawed. In contrast, if a massive ice layer such as that described by Dallimore et al. (1988) for North Head were present, settlement could exceed 10m for upper 30m thawed. In association with the thawing is the emplacement of saline pore water into unfrozen sediments from the seafloor or from the base of Unit B. This process is apparently controlled by the permeability of the thawing sediments since it has been observed to elevate the salinities of the coarse grained high permeability sediments of Unit C but not the finer grained, lower permeability sediments of Unit D.

#### Zone of negative mean annual seabottom temperatures

This zone occurs in waters deeper than 9m where mean annual seabottom temperatures are below 0°C (BH-5). Unit B sediments are absent or very thin. Unit C is unbonded just below the sea floor and has elevated salinities

similar to those observed in the zone of positive mean annual seabottom temperatures. A 4m thick partially ice-bonded zone corresponds with a decrease in salinity and is underlain by well bonded Unit C with still lower pore water salinities. Permafrost beneath is interpreted as relict in origin since it has similar pore water salinities and isotopic characteristics to those observed on land. The continuity of ice-bonding with depth is interrupted in this zone by an unbonded interval of some 12m, correlating with the fine-grained, highly saline Unit D (Fig. 4).

#### Origin of shallow ice-bonding in the vicinity of Borehole BH-5

Observations of shallow ice-bonded sediments at similar water depths to BH-5 have been reported by other researchers (e.g. Fortin, 1987) and widespread islands of elevated ice-bonded sediments have been reported farther offshore (Morack et al., 1983; Blasco, 1984). Frozen sediments were detected only 11m below the seafloor at BH-5. Following transgression, ice-bonding may have re-established in these sediments in response to sub-0°C seabottom temperatures observed today at this location. However, our data show that these shallow ice-bonded sediments are unlikely to have been thawed by the transgression, since they have identical salinities and isotopic character to sediments exposed on land. Thawing of Unit C from the sea bed inevitably would be associated with emplacement of some saline pore water which upon freezing would be redistributed ahead of the freezing front. If the present transgression were to continue until the BH-2 site reached the colder water at the 10m isobath, refreezing would occur at the seabed and the ice-bonding and geologic conditions would be completely different to those observed today in BH-5.

We conclude that the ice-bonding conditions observed at BH-5 reflect a different history since transgression from those areas farther inshore. Dyke (1991) suggests two possible scenarios which could account for shallow ice-

bonding of this nature: (1) A past, cooler climate and lower sea temperatures prior to 1500 years ago, with a subsequent decrease in the rate of coastal retreat, (2) recent erosion of an ancient island.

In the first case thawing is accelerated inshore because of the warmer water and longer residence time while the depth of ice-bonding remains more stable farther offshore in the deeper, cooler water. Dyke's general model of the top of ice-bonding (Fig. 9b in Dyke, 1991) resembles qualitatively the shape of the ice-bonded surface (Fig. 2b), and as discussed previously, trends in relative sea levels during the late Holocene support a decrease in the rate of transgression.

In the second case Dyke suggests that the rolling low relief of Richards Island would favour the formation of islands as inundation proceeds (Fig. 11a in Dyke, 1991). This would have the effect of decreasing the transgression time and possibly lowering the applied seabottom temperatures. A number of shoals are seen in the vicinity of the transect (Fig. 1).

#### Geologic and thermal modelling

Pending further modelling and quantitative analysis of our data, Dyke's first scenario may be the best working hypothesis for the shallow offshore permafrost at BH-5. Transgression is the main thermal event, but seabottom temperatures, retreat rates, erosion, sedimentation and the history of the Mackenzie River plume are key variables.

Figure 5 illustrates a possible progression of ground temperatures at BH-2 following marine transgression, from an equilibrium with a long-term sub-aerial environment based on a simple analytic technique developed by Lachenbruch et al. (1982). Measured temperatures are shown only below the top of Unit C (the assumed transgression surface) and are plotted at depths adjusted for the measured variations in sediment thermal conductivity. The agreement suggests BH-2 was transgressed some 900 years ago. Similar analyses yield times of 900 to 1000 years at BH-3, BH-4 and BH-5. Time resolution is poor after a few hundred years with this particular model; also, these time intervals are minima, as the simple model does not consider the latent heat of melting that would delay the impact of the inundation on deeper temperatures.

More sophisticated numerical analyses may overcome these restrictions and accommodate the diverse quantitative data obtained in this project. The measured temperature profiles and the depth to the top of ice-bonding represent tight constraints on any analysis. This work is underway and will be reported elsewhere.

#### CONCLUSIONS

Two onshore and four offshore boreholes were drilled, cored and logged along a 25km transect across the Mackenzie Delta and Beaufort Shelf (Fig. 1). Based on preliminary quantitative analysis, the following observations may be made:

1. Stratigraphic onshore-offshore equivalences have been established between Richards Island and the adjacent Beaufort Shelf, i.e. the Kittigazuit/Kidluit sands and Unit C, Hooper Clay and Unit D, and Kendall sands and Unit E (Fig. 2a). Up to 15m of marine, post-transgressive sediments (Unit B) are present in the nearshore zone.

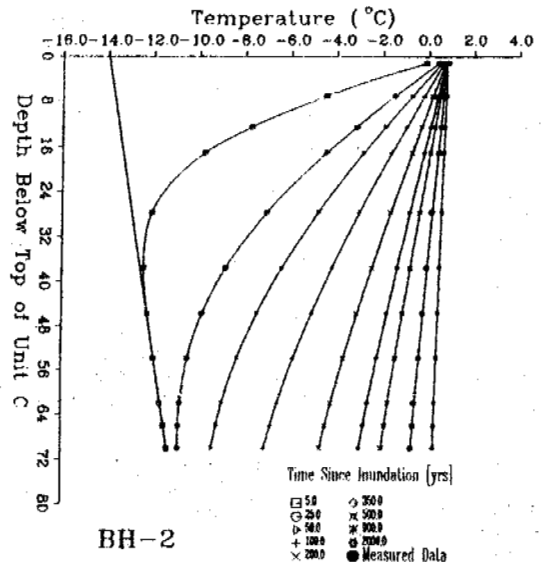


Figure 5. Temperature profiles calculated at various times following marine transgression across a landscape initially at  $-14^{\circ}\text{C}$ .

2. Sand units in the offshore have low salinities similar to their onshore equivalents except below surfaces that are at present, or are interpreted to have been in the past, in contact with saline marine conditions. Clay units are of intermediate salinity and are interpreted to date from earlier marine transgressions.
3. Ice-bonding is controlled by grain size, salinity and marine transgression history. Top of ice-bonded permafrost (Fig. 2b) is 90m below the seabed at BH-2 (<10km from present shoreline) but only 11m at BH-5 (~25km from shore). The latter appears to be relict, not refrozen. A major unbonded horizon in the latter is confined to the fine-grained, saline marine Unit D.
4. Marine transgression is the principal event shaping the character of the offshore and the observed permafrost and geothermal regime. Quantitative analysis is required to deduce the most probable transgressions history consistent with the regional geology and under the tight constraints presented by data measured in this project.

#### ACKNOWLEDGEMENTS

This project was funded by the Panel for Energy Research and Development (EMR), The Northern Oil and Gas Action Program (DIAND) and by the Geological Survey of Canada. Advice and logistic support were provided by Gulf Canada Resources and Esso Resources. Laboratory facilities at the Inuvik Research Centre were provided the Science Institute of the Northwest Territories. The authors drew freely on the diverse data presented by some two dozen participants in the initial project report (Dallimore, 1991) and acknowledge their valuable contribution to this preliminary synthesis. Constructive comments provided by M. Burgess and P. Kurfurst and two critical reviewers are gratefully acknowledged.

## REFERENCES

- Blasco, S.M. 1984. Perspective on the distribution of subsea permafrost on the Canadian Beaufort continental shelf. In: Proceedings, 4th International Conference on Permafrost, Fairbanks, Alaska, pp. 83-86.
- Blasco, S.M., Fortin, G., Hill, P.R., O'Connor, M.J. and Brigham-Grette, J. 1990. The late Neogene and Quaternary stratigraphy of the Canadian Beaufort continental shelf. In: A. Grantz, L. Johnson and J.F. Sweeney, editors, The Arctic Ocean region, Boulder, Colorado, Geological Society of America, The Geology of North America, vol. L, pp. 491-502.
- Dallimore, S.R. editor 1991. Geological, geotechnical and geophysical studies along an onshore-offshore transect of the Beaufort Shelf. Geological Survey of Canada, Open File Report 2408, 263p.
- Dallimore, S.R., Kurfurst, P.J. and Hunter, J.A.M. 1988. Geotechnical and geothermal conditions of near-shore sediments, southern Beaufort Sea, Northwest Territories, Canada. In: Proceedings, 5th International Conference on Permafrost, Tapir, Trondheim, Norway. Vol 1, pp. 127-131.
- Dyke, L.D. 1991. Temperature changes and thaw of permafrost adjacent to Richards Island, Mackenzie Delta, N.W.T. Canadian Journal of Earth Sciences, Vol. 28, pp. 1834-1842.
- Forbes, D.L. 1980. Late Quaternary sea levels in the southern Beaufort Sea. In: Geological Survey of Canada, Ottawa, Canada. Paper 80-1B, pp. 75-87.
- Fortin, G. 1987. Interpretation of Beaufort Sea 1985 high resolution refraction/reflection data. Geological Survey of Canada, Open File Report 1350.
- Harper, J.R., Reimer, P.D. and Collins, A.D. 1985. Canadian Beaufort Sea physical shore-zone analyses. Geological Survey of Canada, Open File Report 1689, 105p.
- Hill, P.R., Mudie, P.J., Moran, K. and Blasco, S.M. 1985. A sea level curve for the Canadian Beaufort Shelf. Canadian Journal of Earth Sciences, Vol 22, pp. 1383-1393.
- Hill, P.R., Hequette, A., Ruz, M.-H. and Jenner, K.A., 1991. Geological investigations of the Canadian Beaufort Sea Coast, Northwest Territories-Yukon Territory. Geological Survey of Canada Open File Report 2387, 365p.
- Hunter, J.A.M., Neave, K.G., MacAulay, H.A., and Hobson, G.D. 1978. Interpretation of sub-seabottom permafrost in the Beaufort Sea by seismic methods, Part I, seismic refraction methods. In: Proceedings, 3rd International Conference on Permafrost. Edmonton, Alberta, Vol. 1, pp.514-520.
- Hunter, J.A.M. 1988. Permafrost aggradation and degradation on arctic coasts of North America. Proceedings, 5th International Conference on Permafrost, Trondheim, Norway, Vol. 3, pp. 27-34.
- Hunter, J.A., MacAulay, H.A., Pullan, S.E., Gagné, R.A., Burns, R.A. and Good, R.L. 1988. Thermal evidence for an active layer on the seabottom of the Canadian Beaufort Sea Shelf. In: Proceedings, 5th International Conference on Permafrost, Trondheim, Norway, Vol. 2, pp. 948-956.
- Judge, A., Pelletier, B.R. and Norquay, I., 1987. Permafrost base and distribution of gas hydrates. In: B.R. Pelletier, ed., Marine Science Atlas of the Beaufort Sea: Geology and Geophysics. Geological Survey of Canada, Miscellaneous Report 40, p. 39.
- Kurfurst, P.J. editor. 1986. Geotechnical investigations of the nearshore zone, North Head, Richards Island, N.W.T. Geological Survey of Canada, Open File Report 1376, 147p.
- Kurfurst, P.J. editor. 1987. Geotechnical investigations off Richards Island, N.W.T. Geological Survey of Canada, Open File Report 1078.
- Kurfurst, P.J. and Dallimore, S.R. 1991. Engineering geology of nearshore areas off Richards Island, N.W.T.: a comparison of stable and actively eroding coastlines. Canadian Geotechnical Journal, Vol. 28, pp. 179-188.
- Lachenbruch, A.H., Sass, J.H., Marshall, B.V. and Moses, T.H. 1982. Permafrost, heat flow and the geothermal regime at Prudhoe Bay, Alaska. Journal of Geophysical Research, Vol 87, pp. 9301-9316.
- Morack, J.L., MacAulay, H.A. and Hunter, J.A.M. 1983. Geophysical measurements of seabottom permafrost in the Canadian Beaufort Sea. In: Proceedings 4th International Conference on Permafrost, Fairbanks, Alaska, pp. 866-871.
- O'Connor, M.J. 1980. Development of a proposed model to account for the surficial geology of the southern Beaufort Sea. Geological Survey of Canada, Open File Report 954. 129p.
- Pelletier, B.R., editor. 1984. Marine science atlas of the Beaufort Sea, Geology and Geophysics. Geological Survey of Canada, Miscellaneous Report 40.
- Rampton, V.N. 1988. Quaternary geology of the Tuktoyaktuk Coastlands. Geological Survey of Canada, Memoir 423, 98 p.
- Taylor, A.E. and Allen, V.S., 1987. Shallow sediment temperature perturbations and sediment thermal conductivities, Canadian Beaufort Shelf. Canadian Journal of Earth Sciences Vol 24, pp. 2223-2234.
- Taylor, A. and Judge, A. 1988. Reconstruction of marine transgression history from an offshore ground temperature profile, Esso Angasak L-03 wellsite, Beaufort Sea. In: Current Research, Geological Survey of Canada, Paper 88-1D, pp. 137-142.

## A PRIMARY STUDY ON COMPOSITION OF METHANE HYDRATE

Deng Yousheng, Xu Xiaozu and Zhang Lixin

State Key Laboratory of Frozen Soil Engineering, IGGAS, Chinese Academy of Sciences

A crystalline hydrate, which is called as methane hydrate, can be formed when methane gas and water are mixed together under certain conditions of pressure and temperature. Its molecular formula can be written as  $CH_4 \cdot nH_2O$ . The methane hydrate is composed under pressures 2.7 to 9.0 MPa in corresponding to temperature from 0.2 to 9.8°C. The relationship between pressure and temperature for composition can be expressed as  $P_c = AB^{T_c}$ . The methane hydrate is decomposed under pressure from 3.0 to 9.0 MPa in corresponding to temperature from 1.75 to 11.7°C and the relationship between them can also be expressed as  $P_d = CD^{T_d}$ . Analysis shows that the conditions for composition of methane hydrate is different with those for decomposition and there is a hysteresis phenomenon. The ratio of gas to water for hydrate changes from 1:6.3 to 1:6.6 and the density changes from 0.910 to 0.905 g/cm<sup>3</sup>.

### INTRODUCTION

With the development of science and technique, the problem of energy source becomes serious day by day so that it is more important to find out the new energy source for the mankind. The discovery of gas hydrates makes us hopeful for the further energy source. But many problems still exist in exploitation and utilization of gas hydrates. First of all, there are many difficulties in exploitation and reclamation because of the complex existence conditions of gas hydrates. Secondary, the formation of gas hydrates will stop the gas pipe or valve. Therefore, many people are doing research work on utilization of gas hydrates and prevention of its harmness. The gas hydrates can only be formed under a certain thermodynamic conditions (lower temperature and higher pressure) (Davidson D.W. et al. 1987). It is well known that methane is the principle composition of natural gas. The methane hydrate is a kind of solid crystal with molecular formula of  $CH_4 \cdot nH_2O$  in which  $n$  is the number of water molecular depending on the composition conditions such as temperature and pressure. The properties and composition of methane used in our test is shown in Table 1.

Table 1 Physical properties and substance content of methane

Physical properties of methane gas		methane gas and substance content	
molecular weight	16.042	CH <sub>4</sub>	>99.99%
gaseous density	0.6678Kg/m <sup>3</sup>	C <sub>2</sub> H <sub>2</sub>	<25vpm
liquid density	426Kg/m <sup>3</sup>	O <sub>2</sub>	<20 vpm
boiling point	111 K	N <sub>2</sub>	<40vpm
melting point	90.65K	H <sub>2</sub> O	<15vpm
critical pressure	4.58MPa		
critical temp.	190.7K		
explosion limit	5-15(v%)		

The purpose of this paper is to describe the conditions and properties of methane hydrate composed in the laboratory.

### EXPERIMENTAL DEVICE

The experimental device as shown in Fig.1 is

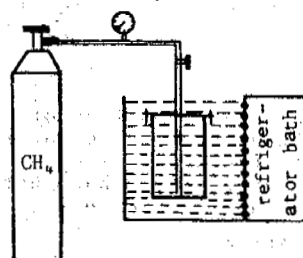


Fig.1 Device for hydrate composition

consists of a tank with methane gas, a refrigerator bath, a higher pressure container, a gauge and a thermometer. The test procedure is as follows: first, 50-100 g of water is poured into the pressure container and the container is connected with the tank and sealed. Afterwards, the pressure container is put into the refrigerator bath and set the pressure and temperature according to the requirement and shaken periodically to enlarge the connected areas between water and gas. Then, after several days to allow water and gas composed sufficiently, the pressure in the container is decreased to the atmospheric and opened in the low temperature condition. Finally, the methane hydrate is taken out of the container and determined.

Fig.2 shows the device used for determining the equilibrium parameters of methane hydrate (decomposed pressure and temperature). The composed methane hydrate is put into the plexiglass

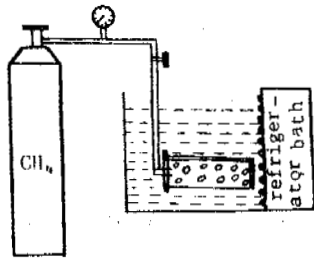
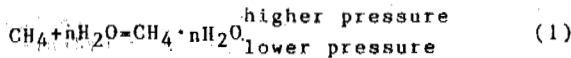


Fig.2 Device for hydrate decomposition

cylinder and the decomposed pressure is determined by the way of keeping temperature constant and decreasing the pressure and the decomposed temperature determined by keeping pressure constant and increasing the temperature. When there is the first bubbles are appeared under conditions mentioned above, the decomposed pressure or temperature is determined.

DETERMINATION OF COMPOSITION CONDITION AND PARAMETERS OF METHANE HYDRATE

Methane hydrate can be spontaneously formed under a certain conditions of pressure and temperature.



From equation (1) it can be seen that the methane gas saturated by water vapor can be spontaneously composed as hydrate when the pressure of methane gas in the system is greater than the pressure of hydrate decomposition, i.e.,

$$p_{\text{hydrate decomposition}} < p_{CH_4}^{\text{system}} < p_{CH_4}^{\text{saturation}}$$

For the spontaneous composition of methane hydrate, not only the gas must be saturated by the vapor, but also the pressure of water vapor in the system must be greater than that of crystal surface of methane hydrate, e.e.,

$$p_{H_2O}^{\text{hydrate}} < p_{H_2O}^{\text{system}}$$

The composition temperature of methane hydrate must be lower than the decomposition temperature of hydrate, mainly,

$$T_{\text{hydrate}}^{\text{system}} < T_{CH_4}^{\text{hydrate}}$$

From the analysis mentioned above it is known that the composition temperature and the pressure of methane gas are the important factors for the composition of methane hydrate. By the composition test using the device shown in Fig. 1, we obtain the minimum pressure of composition of methane hydrate when the temperature is constant and the maximum temperature when the pressure is constant. The results are shown in Table 2. The relationship between the pressure and the temperature for composition can be expressed as

$$P = AB^T$$

where A and B are the coefficients of methane hydrate, A=2.660 and B=1.1335. Fig.3 shows the

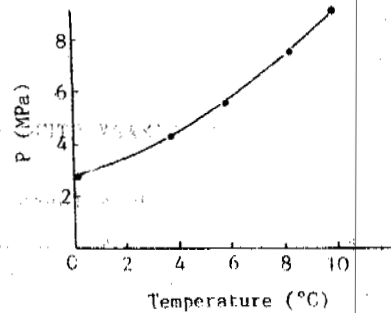


Fig.3 Curve of pressure vs. temperature of hydrate composition

curve of pressure of methane hydrate vs. temperature.

Table 2 The thermodynamic conditions and physical parameters for the composition of methane hydrate

pressure of composition MPa	temperature of composition °C	number of water molecule	density of hydrate g/cm <sup>3</sup>
2.7	0.2	6.624	0.9053
4.2	3.6	6.588	0.9061
5.6	5.8	6.521	0.9058
7.5	8.3	6.357	0.9090
9.0	9.8	6.305	0.9104

When the methane hydrate is stable, it is in the condition of solid crystal. When unstable, it is decomposed as gas and water. Therefore, it is necessary for us to determine its equilibrium parameters, including the decomposition pressure and temperature. By using the device shown in Fig.2, we obtain the equilibrium parameters shown in Table 3. The relationship between the pressure and temperature of decomposition can be written as

$$P_{\text{decomposition}} = CD^{T_{\text{decomposition}}}$$

Where C and D are the coefficients. C=2.4745, D=1.1165.

Table 3 Values of equilibrium parameters of methane hydrate

decomposition pressure, MPa	3.0	4.2	5.6	7.5	9.0
decomposition temperature, °C	1.75	4.8	7.4	10.1	11.7

Fig.4 shows the curve of decomposition pressure vs. temperature. The hydrate in the zone above the curve is stable and below the curve unstable. From Fig.3 and 4 it can be seen that the temperature of composition is lower than that of decomposition when the pressure is constant and the pressure of composition is higher than that of decomposition when the temperature is constant. It means that there is a hysteresis phenomenon. The reason may be as follows: the temperature for hydrate composition and decomposition not only depend on the pressure condition but also depend on the concentration of water vapor in the system (the composition of hydrate is conducted in the system with three

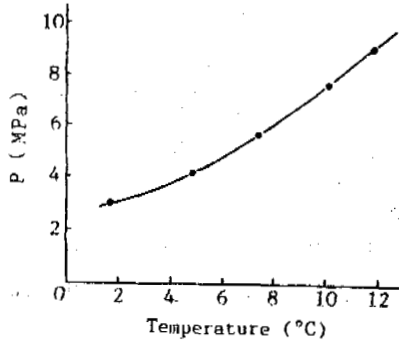


Fig. 4 Curve of pressure vs. temperature of hydrate decomposition

phases but the decomposition is in the system with two phases and the difference of vapor concentration between the systems of two and three phases induces this hysteresis.

Determination of Molecular Number (n) of Water in Methane Hydrate

The hydrate composed under the conditions of a certain temperature and pressure is taken out from the pressure container in the environment with the temperature lower than that corresponding to the decomposition pressure equal to the atmosphere and weigh it in a weighing bottle. Then, the methane hydrate is decomposed in a environment with positive temperature and weighed again. The molecular number (n) can be calculated by the following formula:

$$n = \frac{16(x-y)}{18y} \quad (2)$$

Where x is the weight of methane hydrate; y is the weight of methane gas and 16 and 18 are the molecular weights of methane gas and water, respectively. The values of molecular number of water are listed in Table 2. From Table 2 it can be seen that the value of n slightly decreases with the increase in composition temperature and pressure because of the bonding water content decreasing with increasing in temperature and gas filling in the pores increasing with increasing in pressure.

Determination of Density of Methane Hydrate

The density of methane hydrate is determined in the environment with temperature lower than its decomposition temperature by suspension method. Results are shown in Table 2. It can be seen that the density of methane hydrate increases with decreasing of molecular number of water and the relationship between them can be written as:

$$D = D_i \left( 1 + \frac{CH_4}{nH_2O} \right) \quad (3)$$

Where D is the density of hydrate;  $D_i$  is the density of ice.

Substituted the density of hydrate obtained from the determination into equation (3), we calculate the density of ice equal to 0.7989 g/cm<sup>3</sup>. This value is lower than that of pure ice. It implies that there are many holes in the ice.

CONCLUSIONS

(1) The methane hydrate can only be composed under certain conditions of temperature and pressure. The relationship between composed temperature and pressure can be expressed as  $P=AB^T$  and also the relationship between decomposed temperature and pressure can be written in  $P_d=CD^U$ . There is a hysteresis phenomenon between composition and decomposition.

(2) The density of methane hydrate increases with increasing in pressure or temperature. The molecular number of water, n, decreases with increasing in temperature or pressure.

(3) The study on conditions of composition and decomposition of hydrate may forecast the zones existed hydrate in our contrary.

REFERENCE

Davidson D.W., Desando M.A., Gough S.R., Handa Y.P. (1987) Some physical and thermophysical properties of clathrate hydrates, Journal Incl. Phenom, V.5, N.2, pp219-223.



## GEOHERMAL REGIME OF CRYOLITHOZONE OF WEST SIBERIA

V.N.Devjatkin<sup>1</sup>, A.D.Duchkov and L.S.Sokolova<sup>2</sup>

<sup>1</sup>Institute of Cryosphere of Earth of Russian Academy of Sciences p.b.1230 Tyumen 625000 Russian Federation

<sup>2</sup>Institute of Geophysics of Russian Academy of Sciences University prospekt 3, 630090 Novosibirsk Russian Federation

The report analyzes the permafrost-geothermal information on the exposure of the present heat condition of the West Siberia lithosphere at the depth from 20 to 5000 m

### INTRODUCTION

The main part of the West Siberia occupies the same name plate, which represents the largest epihercynian platform. The mesocainosic sedimentary cover in West Siberia has a thickness of 8-10 km on the north decreasing on the boards, up to disappearance. The heterogenous fundament of the plate is presented by the complicated displaced metamorphical rocks of the different ages (from the Pre-Cambrian to the Paleozolic). The separate fragments of the fundament are releaved to the surface of the Earth in the plicated mountains, framing a plate. On the fundament of the plate stands out the network of the graben-rifts, from those the Koltogor-Urengoian graben-rift is most representative. The central part of the plate is characterized by the anomal reduced crust (Nesterov et al., 1988). In the deep horizon of the lithosphere is observed the anomal distribution of the speeds of the seismic waves, testifying the warming-up of the lithosphere. The all those peculiarities of the lithosphere structure of the West-Siberian plate correlated with the tectonic-magmatical activity of this region in the beginning of the Mesozoic, evidently are accompanied by the introducing of the treat heat amount in the lithosphere. The spatial and temporary variations of the temperature on the earth's surface influence the temperature regimes of the stratum of the subsurface (Balobaev and Levchenko, 1988).

### DISCUSSION OF RESULTS

#### Temperature at the depth of 20 m, the cryolithozone, the geothermal gradient

The modern average annual temperature of the rocks at the depth of 15-25 m. drops up to -12°C on the northern part of the West Siberia. The zero isotherm is situated near the Polar circle, but to the south the temperature becomes positive and raises up to +8°C in the west-southern part of the region (Figure 1). It follows to accentuate, that the average annual temperature of the air is about 3-5° lower than the mentioned values in the region.

The permafrost of the West Siberia spreads southward to the latitude 61° N. on the west and

to the latitude 59° N. on the east of the region (Figure 1). The upper limit of the Permafrost lies directly below the Earth surface in the area northward from the Polar Circle. It sinks southward to the different depths. The low limit of the permafrost with a temperature of 0° C is observed at the depth of 500-600 m in the north, 100 m and less in the western part and 380 m in the central part of the Siberian Uvals. The thickness of permafrost decreases from 600 m in the north up to total it's disappearance near the southern boundary of the cryolithozone. On the

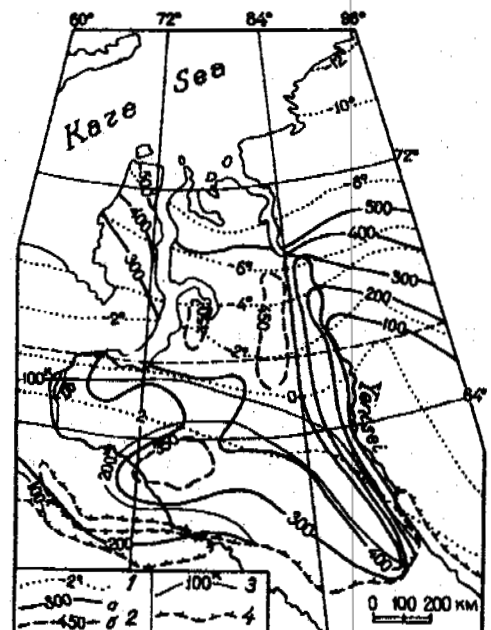


Figure 1. Permafrost-geothermal parameters of West Siberia 1 - isolines of rock's temperature on depth of 20 m (°C); 2 - isolines of lower limit of permafrost (m); a - main, b - intermediate; 3 - isolines of the upper limit of permafrost (m); 4 - southern boundary of cryolithozone (Geocryology..., 1988)

south cryolithozone has the insular distribution: permafrost islands and open taliks (Geocryology..., 1989).

The geothermal gradients of the permafrost change from 3 to 0° per 100 m from the northern areas to the Polar circle and change its sign on the equality on the suprapermafrost taliks, where the temperature decreases up to the upper limit of the permafrost with the zero isotherm. The gradient in frozen rocks from the Polar circle to the southern boundary of the cryolithozone is equal to zero. In the open taliks on the depth's intervals from 20 to 200-400 m has been registered the gradual increasing of the temperature with the relatively small value of the gradient, which is about 1.5° per 100 m. Below of this layer and in the upperpermafrost horizons of the lithosphere the gradient increases up to 3-5° per 100 m.

#### The heat flow

For the composition of the map of the hypogene heat flow ( $q_+$ ) have been used the data on about 700 geothermal lots (figure 2) (Duchkov, Sokolova, 1974; Heat-physical..., 1983; Kataloge..., 1985; Heat field..., 1987; Kurchikov and Stavitchki, 1987). The range of the measured parameters ( $q_+$ ) is very wide - from 15-20 to 80-90  $mW/m^2$  under an average value of about 52  $mW/m^2$ . As the whole the standart of the average  $q_+$  corresponds to the average continental value of the heat flow of the hercynian structures (Smirnov, 1980). In the practice the all area of distribution of the Mezo-Cainozoic deposits  $q_+$  is limited by the isoline of 50  $mW/m^2$  to the north of the latitude 56° N. except of the eastern parts, next to the Siberian platform. The north-western and the south-eastern parts of the plate are distinguished by the relatively high  $q_+$  - more than 70-80  $mW/m^2$ . Such a heat flow is typical for the Beresovo dislocations, the Sherkalin synclinoriums. In the limits of the enumerated parts the fundament, composed by the metamorphic and intrusive igneous rocks, sinks monoclinary from the west to the east from 0.5-1 to 3-4 km. The higher heat flow (up to 70  $mW/m^2$ ) is registered in the Jamal peninsula by the deep bedding of the plicate fundament (more than km). The number of the comparatively small anomalies of the heat flow by areas more than 70  $mW/m^2$  are registered on the latitudinal part of the Ob river and to the south. The structures, surrounding the West-Siberian plate from the west, east and south are characterized by the lowering heat flow of 30-40  $mW/m^2$  (Kataloge..., 1985; Bulashevitch and Shapov, 1987; Hurtig et al., 1991).

The main factors, forming the heat field of the earth crust come out from the change of the mantle heat flow at the time and the space and the spacial variation of the radio-active heat appropriated to the rocks of the earth crust. The conformity of the average levels of the heat flow to its average values in the continental structures of the definite age testifies the regional stability of the temperature conditions of the entrails of the Earth. At same time the non-stationary heat field in the region is evident because of the temperature variations on the earth surface in the Holocene, which have caused the forming of the permafrost. It is especially noticeable under a comparison of the heat flow, observing on the frozen  $q_-$  and, laying unfrozen

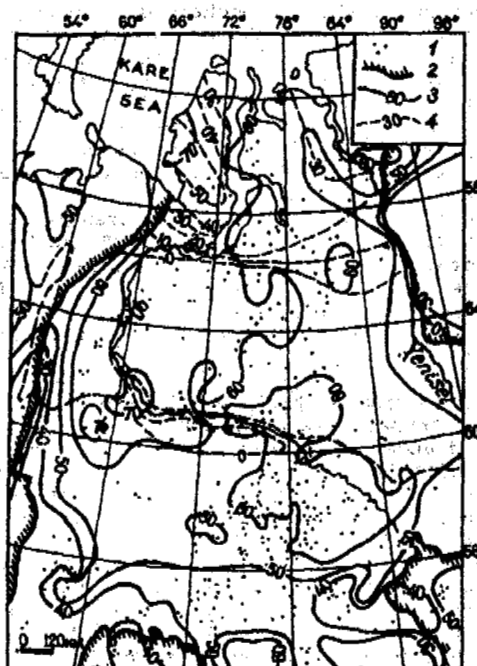


Figure 2. Map of West-Siberian heat flow. 1 - geothermal lots; 2 - boundary of West-Siberian plate; 3 - isolines of hypogene heat flow ( $mW/m^2$ ); 4 - isolines of heat flow in permafrost ( $mW/m^2$ ).

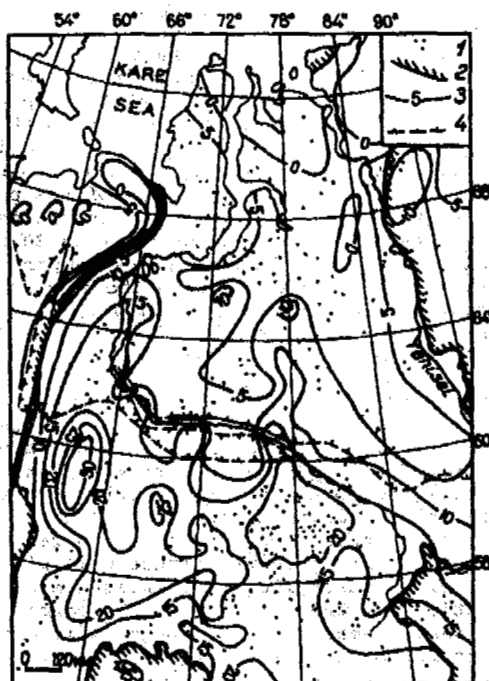


Figure 3. Map of temperature distribution at the depth of 0.5 km. Conditional marking 1 and 2 see figure 2; 4 see figure 1; 3 - isolines of temperature (°C). [Isotherms in limit at latitude 72-60° N. and 84-96° E. according to Balobaev V.T., Volodjko B.V., Rusakov V.G. - Permafrost Institute of SB RAS].

thickness of the lithosphere  $q_0$  (Devjatkin, 1990). The value of the  $q_0$  is less noticeable than  $q_1$  or is equivalent to zero in the cryolithozone (figure 2). This fact testifies about a modern nonstationary heat regime of the degrading permafrost. The investigation of the permafrost dynamics requires several years observation of the changes of the temperature on the boundary.

Between the frozen and unfrozen rocks, in the Institute of the Geophysics of SB RAS has been elaborated the comparatively simple electronic system (geothermal autonomous station GETAS) for the automation of the regional measurement of the chinks and the reservoirs (Heat field..., 1983).

#### The temperature at the depth of 0.5 km

The temperature distribution at this depth is formed under the interaction of the hypogene heat flow with the climatic processes in the Holocene. As a whole the temperature at the depth of 0.5 km changes from the north to the south from 0 to 20-25°C (Figure 3) by the average values for the regions of about 10°C. In the northern part of the region have been observed the lowest temperatures of the rocks from the negative up to +5°C, here and there up to +10°C, comparatively weak differentiated of the field and the latitudinal orientation of the isolines.

The western and southern parts of the region are warmed up to 20-35°C. Those are characterized by the complicated differentiated field of the temperature and the various orientation of the anomalies.

#### The temperature at the depth of 1 km

At the depth in the region the temperature changes from 9 to 57°C, average 29°C. The original diagonal disposition of the main isotherms unlike the temperature distribution at the depth of 0.5 km, and the difference between the north and the south, became apparent here only at the level of 1 km (25 and 34°C accordingly). The western, south-western and central parts of the plate are most warmed-up and in those places the temperatures exceed the average value by 29-30°C. In the local parts of the territory the temperature rises up to 40°C and more. On the south the high temperatures are distinguished only for depressions of the plate and for the Altai-Saijan area. The north-eastern and eastern parts of the plate, and joining regions of the Siberian platform, mountain ranges of the Altai-Saijan area, Kokchetav mountain-mass of the Northern Kazakhstan and the Ural are regarded to the cooled parts (where the temperatures are no more than 30°C). The outlined north-eastern - south-western orientation of the main isolines, the isolation of two high temperature zones on the south-west and north-east are corrected rather well with the field of the heat flow. The influence of the variations of the climate and the permafrost was decreased essentially, although it is apparent, in the regional plane, for the entrails of the northern parts at this depth too.

#### The temperature at the depth of 2 km

The temperature changes at this depth in the region from 33 to 96°C (average is 60°C). The temperatures near to the average values are common for the northern and southern parts of the region and they are 57 and 65°C accordingly. At

the depth of 2 km it keeps the configuration of the temperature's field, which has begun to form at the depth of 1 km. The temperature above an average of 60°C is typical for the western part of the plate. On the south the warmed zone propagates up to 84° E, but to the north it narrows and occupies only the narrow zone on the Jamal peninsula. In this zone there is a number of the parts, where the temperature of the entrails can exceed 80-90°C. On the southern part of the region the high temperature of the entrails is typical for the depressions of the West-Siberian plate and for the Altai-Saijan area. The great territories on the north and east of the plate and the adjoining parts of the Siberian platform, the Ural, the Northern Kazakhstan and the Altai-Saijan area are characterized by the low temperature up to 50°C and below.

#### The temperature at the depth of 3 km

The average temperature at the depth of 3 km is 92°C, but in the range of the measured values they are changing from 44 to 147°C. The western part of the plate is characterized by the heightened values of the temperature. Here is observed a large number of the anomalous parts, partly with the complicated configuration, within the limit of those the temperature increases and exceeds by 100-120°C. On the south such temperatures are typical for the depressions of the Altai-Saijan area, the Irtysh caving and the Bi-Barnaul depression. The eastern part of the plate, the Siberian platform and the mountains on the south and on the west are cooled by 40-80°C. The main peculiarities of the temperature distribution at the depth of 3 km correspond to the heat flow. As a rule, the parts with the high values of the heat flow are characterized by the high temperatures and vice versa.

#### The temperature at the depth of 5 km

The temperature conditions at the depth of 5 m should be predicted because of the small number of the data. In the region the average temperature is 141°C (88-197°C in the range of the measured values). According to the prognosis the greater part of the plate is characterized by the temperature above 140°C. In the limit of this territory have been distinguished the parts (the Beresovo dislocations, the Shaim anticlinorium, the Surgut and the Salym arches, and the other structures on the latitudinal part of the Ob river), where the temperature on the entrails exceeds 160°C. The parts in the outlying district of the region were cooled to 100-120°C. There are parts, where the temperatures at the depth of 5 km are lower, up to 70-80°C.

In general, the distribution of the temperature at the depth of 5 km corresponds to the changes of the heat flow, moreover its value is 50 mW/m<sup>2</sup> and confirms with the temperature of 120°C and the value of 60 mW/m<sup>2</sup> - with 140°C.

The statistical data testify that the specific density of the potential resources of the hydrocarbons are on direct dependence on the density on the geothermal regime (Map..., 1987). The high level of the geothermal parameters of the West Siberia (a heat flow, a temperature and its gradient) promotes at the same time with other factors the generation of the hydrocarbons and the forming of the permafrost with the non-stationary heat regime. The latter is necessary to

take into account under the development of the oil-gas-fields on exploring region.

#### CONCLUSIONS

1. The West-Siberian plate is distinguished concerning to the contiguous territories by the higher values of the hypogene heat flow ( $q_0$ ) and of the rocks temperature. The main peculiarities of the heat flow are formed in the consequence with the addition of the two compounds: a heat flow from the mantle and the radiogenous isolation of the heat flow from the earth crust. In the supra-surface stratum the  $q_0$  becomes transformed under the influence of the surface relief, the moving of the ground-water, the variations of the heat-conductivity of the rocks and the surface temperature (it is a climatic factor). For the West Siberia the last factor is of particular significance in connection with the broad distribution of the permafrost. The analysis testified that the influence of the paleo- and the modern permafrost is observed at the depth of 1.5-1.7 km. By the interpretation of the geothermal data it is necessary to make the climatic corrections.

2. Concerning the heat flow in the cryolithozone ( $q_0$ ), the territory of the West Siberia should be subdivided into two geocryological zones: A - a zone to the North from Polar circle with  $q_0 > 0$ ; B - a zone from the Polar circle to the southern boundary of the permafrost with  $q_0 = 0$ . The correlation of the heat flow  $q_0/q_1$  is less than 1 or equally to zero; it testifies that the modern non-stationary heat regime of the cryolithozone is of the degrading type practically on the whole territory of the West Siberia.

#### REFERENCES

Balobaev V.T. and Levchenko A.I. (1988) The deep freezing and the dynamic of the heat flow of the upper part of the West Siberian earth crust:

- oil-geological interpretations of the heat-regime of the West-Siberian entrails - Tyumen, pp.31-45.
- Bulachevitch Ju.P. and Shapov V.A. (1987) About the anomal low heat flow in the Tagil anticlinorium: Nuclear-geophysical and geothermal investigations.-Sverdlovsk, pp.4-12.
- Cataloge of the data on the heat flow of Siberia (1985) Novosibirsk, 82 pp.
- Devjatkin V.N. (1990) The heat flow of the West-Siberian permafrost: Linear constructions on the perennially frozen grounds.-Moscow, Nauka, pp.50-55.
- Duchkov A.D. and Sokolova L.S. (1974) The geothermal investigation in the Siberia.- Novosibirsk, Nauka, 288pp.
- Geocryology of the USSR - Moscow, Nedra: a - European territory of USSR, 1988, 358 pp.; b - West Siberia 1989, 454pp.
- Heat field of the Siberian entrails (1987) / Duchkov A.D., Lysak S.V., Balobaev V., T. et al./- Novosibirsk, Nauka, 196pp.
- Heat-physical investigations of the cryolithozone (1983). Novosibirsk, Nauka, 215 pp.
- Hurtig E., Cernak V., Haenel R., Zui V.I. \*) (Editors) (1991) Geothermal atlas of Europe. - Goth.Publishing House, Potsdam.
- Kurchikov A.R. and Stavitchki B.P. (1987) The geothermy of the oil-gas areas of the West Siberia.- Moscow, Nedra, 134 pp.
- Map of the useful minerals of USSR (1987) (scale 1:5 000 000) - Moscow.
- Nesterov I.I., Kurchikov A.R., Stavitchki B.P. (1988) The main peculiarities of the West-Siberian geothermy's field: oil-geological interpretation of the heat regime of the West-Siberian entrails.- Tyumen, pp.5-24.
- Smirnov Ja.B. (1980) The heat field of the USSR territory: the explanatory transaction to the maps of the heat flow and the hypogene temperatures in a scale 1: 10000000, 150p.

\*) - in English; others - in Russian

## APPLICATION OF THERMALPILE TO CULVERT ENGINEERING IN PERMAFROST REGION

Ding Jingkang<sup>1</sup>, Wu Jinming<sup>2</sup>, Lou Anjin<sup>1</sup> and Zhang Jingzhao<sup>2</sup>

<sup>1</sup>Northwest Institute of Chinese Academy of Railway Sciences

<sup>2</sup>The First Designing Institute of Highway, The Ministry of Communications

In culvert engineering, particularly the building of the entrance/exit of the culvert, the damage is mainly due to the thaw settlement of the foundation in permafrost regions. Cooling the foundation of the entrance/exit with thermalpile can effectively prevent buildings from frost heave and thaw settlement, increase the stability of the foundation, improve the culvert condition and extend the running period of the culvert.

### INTRODUCTION

There are two principles for designing the base of the foundation of a culvert: 1) Maintain the permafrost within the foundation to be in the stipulated frozen form; 2) Allow the permafrost under the base to thaw.

When the first principle is selected, the base of the culvert should be buried below the synthetic stable upper limit, the base of the middle section should be buried below the synthetic upper limit of more than 0.25 m, and the base of the transition section and the entrance/exit boundary should be buried below the synthetic upper limit of more than 0.5 m (Criterion in Ministry of Railway, 1986).

In the permafrost region of Qinghai-Tibet Plateau, the buried depth of the culvert base does not meet the above conditions. The buried depth of the base is determined according to following principles in the design of highway culverts: the buried depth of the base in the middle section is 0.7 times more than that of the permafrost table; the buried depth of the culvert base at entrance/exit has a range of 2 m and the base of "A"-type wall is 0.4 more than that of the middle section (Chen Zhuohuai, 1983). Sometimes the buried depth does not meet the first principle. After a culvert is built, the original balances of heat and mass change greatly. So do the physical and dynamic properties of the permafrost within the foundation. The soil temperature rises, the permafrost within the foundation thaws and the permafrost table lowers. As a result, a lot of culverts are damaged due to the thaw settlement. According to the report in October, 1990, along the Qinghai-Tibet Highway, with length of 560 km in a permafrost region, 119 culverts were damaged seriously, about 15.4% of the total culverts; generally damaged culverts were 163, about 21.1% of the total culverts, the other 490 culverts were about 63.5%.

The most seriously damaged spot is the entrance/exit buildings. 212 culverts of the 282 damaged culverts were damaged at the entrance/exit.

Therefore, this is the key to prevent the culvert from being destroyed at the foundations and base at entrance/exit, and to maintain the structures in permafrost regions. In order to research the treatment measures for the damaged culverts and provide a basis of culvert design in permafrost regions, we selected a representative culvert to test the method which is the application of thermalpile at the entrance/exit for cooling the foundation of permafrost.

### TEST DESIGN

After the foundation of the culvert is treated with thermalpile, the temperature of the permafrost within the foundation will decrease, its strength will increase and the permafrost table will rise, so that the stability of the frozen foundation is improved and the frost heave and thaw settlement are reduced. The culvert is located in Kekexili, close to Wudaoliang. It is designed on the principle of maintaining the foundation in a frozen state. The culvert was rebuilt in 1984. For the purpose of studying the thermal state of the foundation of the culvert and verifying the reasonableness of the design, five tubes were buried along the central axis of the culvert to measure the temperature field of the foundation, and measuring points for strain were set up on the plate and the "A"-type wall of the culvert. Detailed observations for the temperature field of the foundation and the strain of the culvert began in 1984.

The foundation of the culvert is the permafrost, which consisted of ice-rich loam. There exists an ice layer with soil with a thickness of about 0.2-1.0 m. The permafrost table is about 1.5 m. After the culvert was built, we discovered that the permafrost table lowered 20-25 cm in

the middle section of the culvert, and 30-90 cm at the entrance/exit. As a result, all the sections of the culvert were damaged, particularly at the site of the exit, where the bottom liner had dropped more than 20 cm and had become a water puddle, and the "A"-type wall had inclined inwards obviously and separated 10 cm from the body of the culvert. The entrance was also damaged where the crevasse between the "A"-type of wall and the body of the culvert was more than 6 cm. Due to a badly-distributed settlement, a 2 cm width of crevasse occurred at the bottom of the middle culvert. The crevasse cut the bottom liner into two parts. From the crevasse the surface water flowed into the ground and passed through the foundation and flowed out from the bottom of the liner at the exit. Half a culvert had ceased to be effective. The main reason for the damage to the exit was that water permeated the foundation.

By way of the meteorological information, the thermal properties of the recent thermalpiles and the geological condition, we found that single thermalpile conducts about 0.23 million kilocalorie of cold energy, and the freezing radius is 1.2 m. In order to effectively freeze the foundations of the entrance/exit and the "A"-type wall, the most appropriate interval between thermalpiles is about 2.5-3.0 m. Because of the limitations of the structural condition and the requirement of the stability of the liner at the bottom of the entrance/exit of the culvert, we planned to bury 4 thermalpiles outside the culvert wall at entrance/exit (the buried depth was 4.5 m), and bury 4 thermalpiles in the "A"-type wall and the water resisting wall. The arrangement of the thermalpile is shown in Fig.1. The actual interval between thermalpiles is about 3.0-3.5 m. Although the interval is comparatively great, the running of the thermalpile can reduce the temperature of the foundation at the entrance/exit by 5-7°C.

In order to determine the effectiveness of the frozen foundation with thermalpiles and observe the temperature field of the foundation, another five boreholes with depths of 3.5 m for measuring temperature were drilled outside the "A"-type wall at the entrance/exit. To compare with natural soil temperature, a borehole for measuring natural soil temperature was buried outside, 10 m apart from the "A"-type wall at exit, and its depth was 1 m. The observation spots for strain were set up on the "A"-type wall.

#### TESTING RESULTS

Thermalpiles and pipes were buried on Sept. 27, 1989 and the observation began in Oct. 2 years later, the thermalpiles worked well and the freezing foundation was effective. The temperature at entrance/exit of the culvert was about -5°C lower than natural soil temperature in the cold season, and the maximum temperature of the foundation of the culvert was about 0.5-0.8°C lower than the natural soil temperature in the warm season. The permafrost table in 1990 under the base increased averagely by 0.19 m than that in 1989. The permafrost table in 1991 increased slightly than that in 1990. The culvert strain to utilize the thermalpile to fix the foundation at entrance/exit of the culvert, prevents the building from thaw settlement and frost heave and improves the stability of the foundation.

#### The Effective Decreased Temperature and the Effected Radius of the Thermalpile for the Foundation

After the thermalpiles were set up, there was a quick reaction, and the temperature of the foundation at the entrance/exit of the culvert reduced quickly in the cold season in 1989. From Fig.2 and Fig.3, it can be concluded that the temperature in every borehole was lower than the

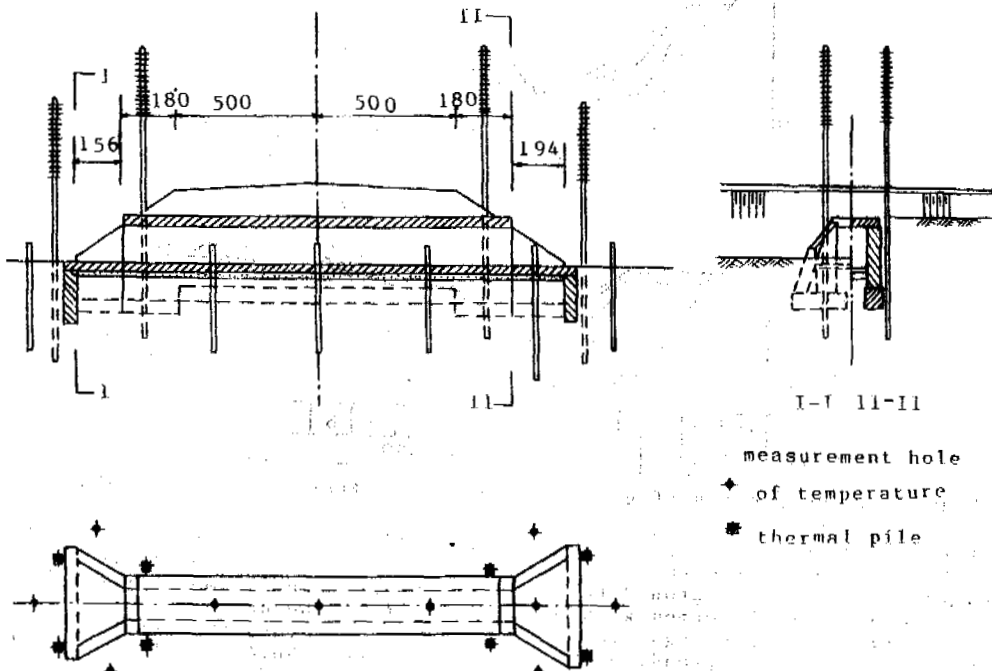


Figure 1. The test culverts in thermalpile foundation

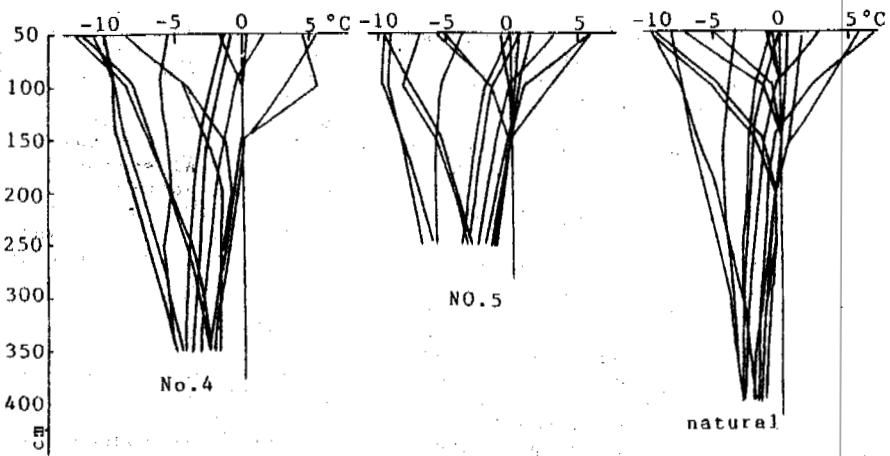


Figure 2. The curves of ground temperatures after thermalpiles were buried

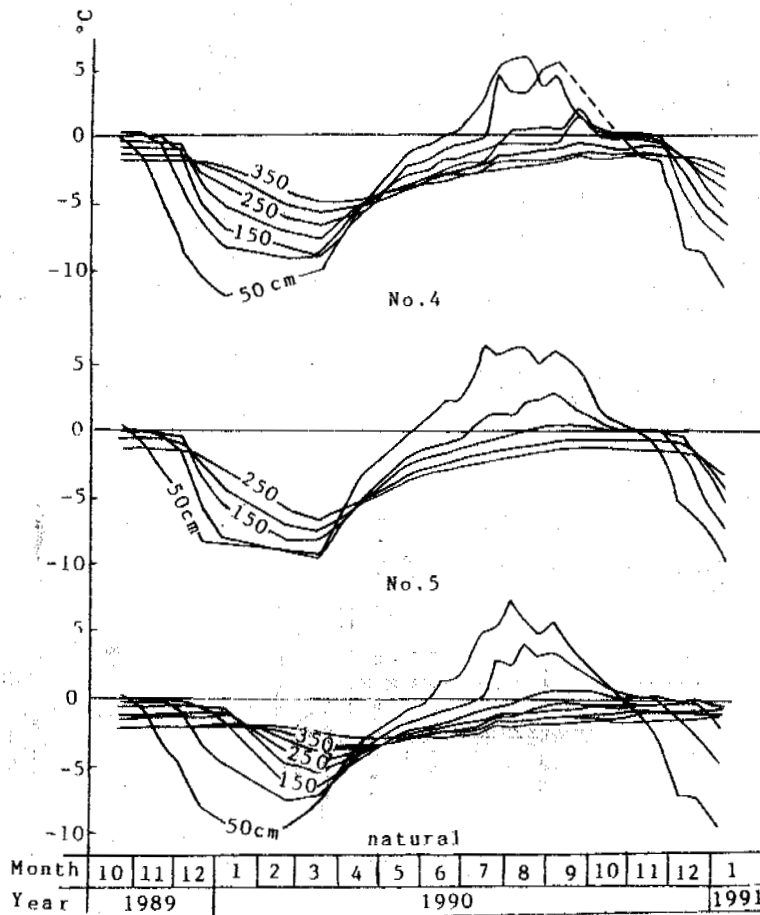


Figure 3. The process of ground temperature after thermalpiles were buried

natural temperature, except for that in borehole No.3 which was too far apart from the thermalpile. In comparison with natural ground temperature, the amplitude of every observed ground temperature rised obviously in a negative direction and all the curves have a spreading tendency.

Comparing the temperature in borehole No.4

and No.5 with natural soil temperature, the effectiveness of the thermalpiles was obvious. The mean monthly temperatures in the three boreholes within the depth of 2 m are listed in Table 1. Table 2 lists the mean monthly temperatures in borehole No.4 and the natural borehole within the depth of 3.5 m.

It is illustrated from Table 1 that the mean

Table 1. Comparison of mean monthly temperatures within the depth of 2.5 m

Date	1989					1990					1991										
	10	11	12	1	2	3	4	5	6	7	8	9	10	11	12	1	5	6	7	8	9
Hole No. 4	-0.20	-0.98	-4.53	-7.30	-8.38	-8.58	-5.56	-2.80	-1.79	-0.07	1.57	1.43	-0.21	-0.72	-4.56	-7.12	-2.79	-1.44	0.36	1.72	0.45
Hole No. 5	0.05	-0.89	-3.16	-5.68	-7.98	-8.36	-5.14	-1.56	-1.37	0.09	0.85	1.08	-0.17	-0.68	-2.81	-6.04	-2.44	-1.32	0.42	1.25	1.42
Natural	-0.20	-0.75	-2.07	-3.44	-6.40	-6.40	-3.96	-2.12	-1.35	0.19	1.40	1.39	0.19	-0.60	-2.10	-3.58	-1.86	-0.57	0.59	2.58	1.68

Table 2. Comparison of mean monthly ground temperature within the depth of 3.5 m

Date	1989					1990					1991										
	10	11	12	1	2	3	4	5	6	7	8	9	10	11	12	1	5	6	7	8	9
Hole No. 4	-0.60	-1.16	-3.77	-5.96	-7.37	-7.67	-5.43	-3.14	-2.18	-0.77	0.64	0.40	-0.58	-0.93	-3.77	-5.89	-3.05	-1.86	-0.50	-0.03	-0.19
Natural	-0.66	-1.02	-1.96	-2.89	-5.34	-5.62	-3.87	-2.40	-1.76	-0.51	0.53	0.59	-0.24	-0.71	-1.79	-2.84	-2.04	-1.03	-0.12	1.42	0.81

monthly temperature in borehole No.5 is lower than that in the natural borehole. The maximum temperature that occurred in Sept. was 0.3°C lower than the natural ground temperature at that moment. The temperature in borehole No.4 was higher than the natural ground temperature in Aug. and Sept. 1989, and the reason was that borehole No.4 was inside the water resisting wall at the exit where permeating surface water from the liner crevasse at the bottom of the culvert accumulated. After the crevasse was stopped up in the warm season of 1991, the above phenomenon disappeared.

It is indicated from Table 2 that owing to the freezing action of thermalpiles, the temperature of foundation inside the "A"-type wall at the exit of the culvert within a depth of 3.5 m was 3°C lower than the natural ground temperature, and the temperature in Aug., when the temperature reached the maximum value, was 1.45°C lower than the natural ground temperature.

The following is the comparison of the temperatures of permafrost below the permafrost table, so that the effective decrease of temperature in the foundation with thermalpile can be seen.

The mean monthly temperatures of the permafrost in borehole No.4 and No.5 within the depth from permafrost table to 2.5 m and 3.5 m are listed respectively in Table 3 and Table 4.

Figure 4 shows the process of the soil temperature obtained from Table 3 and Table 4. We find that under the influence of thermalpile, the temperature of the permafrost foundation decreases obviously. The maximum decreased mean monthly temperature in borehole No.5 from the permafrost table to the depth of 2.5 m occurs in Jan. and the decreased temperature is 3.35°C. The minimum decreased temperature occurred in June and its value is 0.43°C. Owing to the influence of ground water, the mean monthly temperature in borehole No.4 is higher than natural ground temperature. However, the maximum decreased temperature is still 0.45°C lower than that in borehole No.5. It is shown in Figure 4 that the temperature of the permafrost foundation under the influence of thermalpile begins to decrease in Oct., while the natural ground temperature is increasing. In early Nov., the natural ground temperature of permafrost reaches a maximum, while the ground temperature with

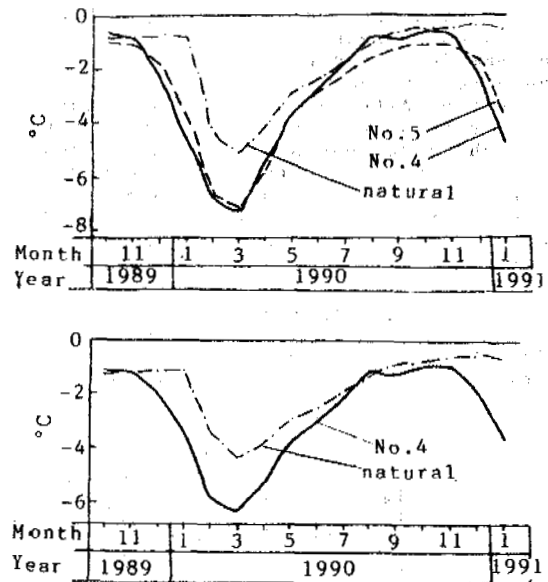


Figure 4. The process of the mean monthly temperature of permafrost

thermalpiles has decreased about 1.3 - 2.0°C. This is very effective in improving the bearing capacity of the foundation. The bearing capacity of the permafrost foundation doubled. The stability of the permafrost foundation rises rapidly.

The maximum ground temperature of foundation generally occurs in early Nov., the maximum ground temperature of the foundation with thermalpiles occurs in mid Oct. The difference between the two maximum ground temperature is the effective decrease in temperature and it equals 0.8°C for this test. The effective decrease in temperature is an important parameter in the design of the foundation with thermalpile which is the basic index to determine the bearing force and inspect the anti-frost heaving stability of the foundation.

What we must point out is that borehole No.4 and No.5 are at a distance of 2 m from the thermalpile. So the change of temperature is



Table 3. Comparison of mean monthly temperatures of permafrost from permafrost table to the depth of 2.5 m

Date	1989			1990										1991		
	10	11	12	1	2	3	4	5	6	7	8	9	10	11	12	1
Hole No. 4	-0.60	-0.75	-2.15	-4.55	-6.75	-7.35	-5.50	-3.70	-2.73	-1.82	-0.75	-0.85	-0.60	-0.70	-2.48	-4.75
Hole No. 5	-0.95	-1.00	-1.80	-3.75	-6.60	-7.20	-5.70	-3.60	-2.80	-2.12	-1.52	-1.18	-1.08	-1.10	-1.65	-3.90
Natural	-0.80	-0.75	-0.75	-0.80	-4.35	-5.10	-4.10	-2.80	-2.37	-1.67	-0.98	-0.58	-0.50	-0.45	-0.30	-0.55

Table 4. Comparison of mean monthly temperatures of permafrost from permafrost table to the depth of 3.5 m

Date	1989			1990										1991		
	10	11	12	1	2	3	4	5	6	7	8	9	10	11	12	1
Hole No. 4	-1.10	-1.18	-2.01	-3.58	-5.80	-6.38	-5.30	-3.85	-2.99	-2.17	-1.23	-1.38	-1.08	-1.08	-2.14	-3.78
Natural	-1.30	-1.23	-1.21	-1.15	-3.53	-4.40	-3.88	-2.95	-2.57	-1.97	-1.32	-0.99	-0.90	-0.73	-0.65	-0.78

more distinct around the thermalpile and the date when the temperature of permafrost foundation begin to decrease will move up to late Sept. The maximum decreased temperature will increase, and the effective decreased temperature will increase too. After discussing the observed data, it is found that the ground temperature in every borehole decreases under the influence of thermalpile. This indicates that the heat-transfer radius effected by thermalpile reaches to every borehole outside of borehole No.3. The maximum transfer radius measured from Figure 1 is about 3 m.

Change of the Permafrost Table within the Foundation of Culvert

Under the influence of thermalpile, the change of permafrost table within the foundation of the culvert is shown in Figure 5.

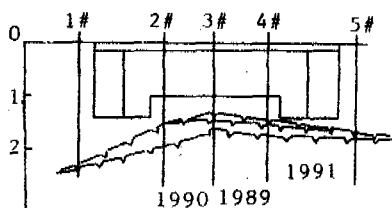


Figure 5. The change of permafrost table within the foundation of culvert

It is illustrated that by means of the freezing action of thermalpile, the permafrost table within the foundation of the culvert tends to rise. The mean annual rise was about 0.19 m in 1990, and there was a slight rise in the middle section of the culvert in 1991. It can be predicted that the permafrost table rises to the natural permafrost table.

The Strain of the Culvert

Owing to the freezing action of the thermalpile, the frost heave of foundation decreases greatly in a vertical direction. The strain of the culvert decreases clearly and tends to stabilize. Before the thermalpiles were buried, the frost heave of the "A"-type wall at the exit

was comparatively greater. After the thermalpiles were set up, the maximum frost heave was 10 mm in the winter 1989, and the maximum thaw settlement is 8 mm in the warm season 1990. The strains of the culvert wall and the "A"-type wall have a tendency to stabilize. The maximum frost heave was only 5 mm in the winter of 1990.

CONCLUSIONS

Based on the results of field tests, the following may be concluded:

1. By treating the foundation with thermalpiles at the entrance/exit of the culvert, the temperature of the permafrost foundation decreases. As a result, the strength and stability of the permafrost foundation are increased, the permafrost table is raised and the thickness of changing layer is decreased. The foundation treated with thermalpile is one of the most effective foundations in cold regions, which can prevent the permafrost from declining and thawing, decrease frost heave and deformation of the foundation, improve the running condition of the culvert and extend the running time of the culvert.
2. Under the field test condition, the effected radius of the heat-transfer of thermalpile is 3 m, the effective decreased temperature is 0.8°C in the permafrost foundation.

REFERENCES

Chen Zhuohuai, (1983) The foundation of railway culvert on frost soil. Proceedings on Second National Conference on Frozen Soil.  
 Criterion in Ministry of railway, (1986) TBJ2-85: "The design of culvert on railway" Ministry of Railway. People's republic of China.

## AN APPLICATION LIMIT FOR REDUCING HEAVE OF SULPHATE SALINE SOIL BY MIXING SODIUM CHLORIDE

Ding Yongqin and Chen Xiaobai

Lanzhou Institute of Glaciology and Geocryology,  
Chinese Academy of Sciences, China

Some new test results are presented in the paper: The total amount of heave for saline soil increases with the enlargement of  $\text{Na}_2\text{SO}_4 \cdot 10\text{H}_2\text{O}$  crystallized during cooling from  $25^\circ\text{C}$  down to  $-15^\circ\text{C}$ . Additional content of  $\text{NaCl}$  in the soil could restrain the crystallization of  $\text{Na}_2\text{SO}_4$ , which will reduce the heave amount, during cooling from  $25^\circ\text{C}$  down to  $15^\circ\text{C}$ . While the ratio of  $\text{NaCl}$  to  $\text{Na}_2\text{SO}_4$  by weight exceeds a critical one, all of  $\text{Na}_2\text{SO}_4 \cdot 10\text{H}_2\text{O}$  and, consequently, heave will disappear. However, while soil temperature is below  $15^\circ\text{C}$  and the ratio exceeds a critical value, the amount of  $\text{Na}_2\text{SO}_4 \cdot 10\text{H}_2\text{O}$  and  $\text{NaCl} \cdot 2\text{H}_2\text{O}$  crystallized will be produced with the increase of  $\text{NaCl}$ . Consequently, the salt heave will get stronger. As the ratio exceeds the critical value, there are two salt-frost heave peaks in the temperature zones of  $15^\circ\text{C}$  to  $13^\circ\text{C}$  and  $-5^\circ\text{C}$  to  $-12^\circ\text{C}$ , respectively.

### INTRODUCTION

The alkalization-salinization of soils is one of the causes of heavy natural disasters, which are widely distributed in the world. The crystallization of  $\text{Na}_2\text{SO}_4$  from the solution in soil during cooling produces mirabilite ( $\text{Na}_2\text{SO}_4 \cdot 10\text{H}_2\text{O}$ ) and meanwhile makes soil volume expand, which is harmful for roads, railways, buildings as well as hydraulic structures. Many researchers in this field have been studying the characteristics of saline soils and found some treatment methods for dealing with them. So far the methods usually used in saline subgrade can be divided into two types: First, the physical methods include: a) replacing saline soil with non-saline soil, b) covering with a sandy gravel mat, c) setting up a drainage system, d) covering with geotextiles, etc. All of above could be used effectively for controlling saline damage in the subgrade, but the project cost is relatively expensive. Secondly, chemical methods include: a) setting lime-sand piles, b) mixing chemical additives with the saline base such as  $\text{NaCl}$ ,  $\text{CaCl}_2$ ,  $\text{BaCl}_2$  and  $\text{Ca}(\text{OH})_2$ , etc. The chemical methods have wider application prospects with a low cost and a small amount of work. Furthermore, the latter is more effective in northwest China, because of the wide distribution of  $\text{NaCl}$  and lack of non-saline soil in these areas. Recently civil engineering departments in China have found out that mixing the additional content of  $\text{NaCl}$  in sulphate saline soil could reduce the amount of salt heave in a given condition. In order to explore the mechanism and application limit of above treatment, some salt-frost susceptibility tests of Lanzhou loess mixed with different percentages of  $\text{Na}_2\text{SO}_4$  and  $\text{NaCl}$ , by weight, were conducted. With the help of the illustrated isothermal phase diagrams, the mechanism of salt-frost heave has been explained preliminarily. The authors hope that the results will be helpful for the treatment of saline

subgrade.

### SAMPLES AND TEST METHOD

Lanzhou loess was selected as the test material. Its original physico-chemical properties are listed in Table 1. Based on the classification for saline soil, Lanzhou loess is a subsulphate saline and mid-saline soil because its total content of salt is  $1.47 \text{ g}/100 \text{ g}$  soil. Before the test, the loess has been fully washed in order to obtain non-saline soil. After washing, the physico-chemical properties are shown in Table 2. Comparing Table 2 with Table 1, we know that the particle size before and after washing is very close. But the total salt content of washed loess is  $0.221 \text{ g}/100 \text{ g}$  soil which is 5.65 times less than the original one. It is said that when salt content in soil is below  $0.5 \text{ g}/100 \text{ g}$ , the salt has no effect on the physical and mechanical properties of soil (Bozniyak, 1956).

#### Preparation of Samples

Four samples were compounded with washed loess mixed with an over-saturated solution of different percentages of  $\text{NaCl}$  to  $\text{Na}_2\text{SO}_4$ , by weight. They were named sample 86-1, 86-2, 86-3 and 86-4. The basic physico-chemical properties are in Table 3.

#### Cooling Test Apparatus and Conditions

The samples mixed well with the given content of salt were compacted in layers and put into plexiglass cylinder cells,  $11.76 \text{ cm}$  in inner diameter at the top,  $10.95 \text{ cm}$  in inner diameter at the bottom and  $13.68 \text{ cm}$  in height, lined with plastic membranes. The samples' temperature along the depth was measured by thermocouples collected by HP-3054S Automatic Data Acquisition/Control System with a resolution of  $\pm 1\mu\text{V}$ , and the amount of heave was determined by means of a displacement gauge with a sensitivity of

Table 1. The Physico-chemical Properties of Lanzhou Loess Particle

Percentage of following size (mm) by weight (%)					Liquid limit (%)	Plastic limit (%)	Classification
0.1-0.05	0.05-0.01	0.01-0.005	0.005-0.002	<0.002	(%)	(%)	
11.36	63.50	6.80	4.15	14.19	22.6	15.3	Loam
Chemical composition (me/100 g soil)							Total (g/100g soil)
HCO <sub>3</sub> <sup>-</sup>	Cl <sup>-</sup>	SO <sub>4</sub> <sup>2-</sup>	Ca <sup>2+</sup>	Mg <sup>2+</sup>	Na <sup>+</sup>	K <sup>+</sup>	
0.74	9.43	12.50	9.11	1.86	11.63	0.07	1.47

Table 2. The Physico-chemical Properties of Lanzhou Loess Particles after Washing

Percentage of following size (mm) by weight (%)					Liquid limit (%)	Plastic limit (%)	Classification
0.1-0.05	0.05-0.01	0.01-0.005	0.005-0.002	<0.002	(%)	(%)	
10.84	62.88	8.43	3.1	14.76	23.0	16.8	Loam
Chemical composition (me/100 g soil)							Total (g/100g soil)
HCO <sub>3</sub> <sup>-</sup>	Cl <sup>-</sup>	SO <sub>4</sub> <sup>2-</sup>	Ca <sup>2+</sup>	Mg <sup>2+</sup>	Na <sup>+</sup>	K <sup>+</sup>	
1.002	0.087	1.947	2.558	0.312	0.207	0.069	0.221

Table 3. The Basic Physico-chemical Properties of Samples

No.	Percentage concentration of solution (%)		Salt content (g/100g soil)		Dry density (g/cm <sup>3</sup> )	Water content (%)	Liquid limit (%)	Plastic limit (%)	
	NaCl	Na <sub>2</sub> SO <sub>4</sub>	Total	NaCl					Na <sub>2</sub> SO <sub>4</sub>
86-1	0	25.20	4.68	0	4.68	1.60	13.90	22.80	15.80
86-2	8.52	22.95	7.08	1.92	5.16	1.57	15.42	22.00	14.50
86-3	19.69	19.75	9.85	4.92	4.93	1.52	15.12	18.70	13.00
86-4	40.09	15.08	17.36	12.62	4.75	1.41	14.11	18.60	12.00

±0.001 mm. Cooling plates connected to refrigerated circulating baths with an accuracy of 0.1°C were placed at the top and bottom of each sample, and the entire assembly was placed in an insulated box. So evaporation wasn't a consideration. During cooling from +25°C down to -15°C, a temperature gradient was always propagated downwards through the sample. The tests lasted for 565.82 hr.

**Test Results**

Figure 1 and Figure 2 show the curves of the cooling process at the top and the bottom of samples and salt-frost heave vs elapsed time, respectively.

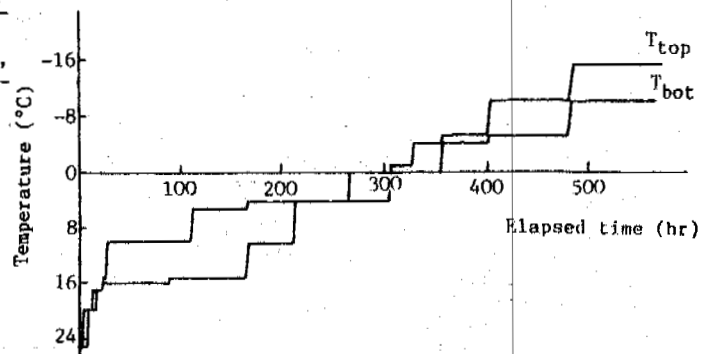


Figure 1. Boundary temperature vs Elapsed time

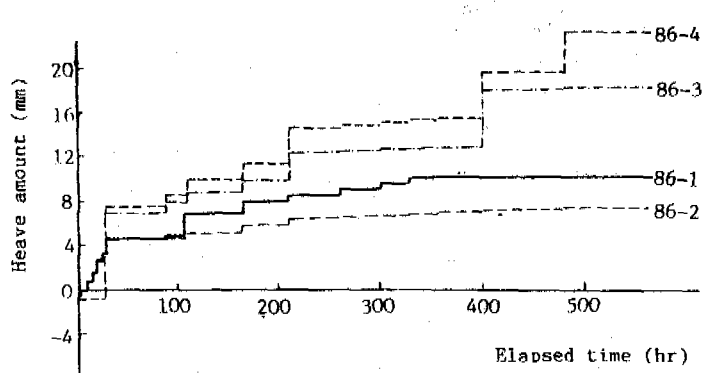


Figure 2. The amount of salt-frost heave vs Elapsed time

### EXPERIMENTAL RESULTS AND DISCUSSION

The initial system values and the concentration of pore solution in samples are listed in Table 4. From Fig.2 we know that the total amount of heave in the four samples depresses in order of Sample 86-4, 86-3, 86-1 and 86-2. It is obvious that while the ratio of NaCl to  $\text{Na}_2\text{SO}_4$  by weight,  $R$  is less than a critical value, as an example of Sample 86-2 with  $R=0.37$ , the total amount of heave is minimum. While  $R$  increases, for instance  $R=1$  for Sample 86-3 and  $R=2.66$  for Sample 86-4, the total amount of heave will not decrease and will get higher and higher which is 1.8 and 2.4 times than that of Sample 86-1 with zero additional content of NaCl.

Table 4. The Initial Parameters of Four Samples

No.	Initial system values (g)				Concentration (%)	
	Water	$\text{Na}_2\text{SO}_4$	NaCl	Total	$\text{Na}_2\text{SO}_4$	NaCl
86-1	323.05	108.84	0	431.89	25.20	0
86-2	360.72	120.80	44.85	526.37	22.95	8.52
86-3	354.62	115.65	115.30	585.57	19.75	19.69
86-4	333.86	112.30	298.55	744.71	15.08	40.09

The crystallization of  $\text{Na}_2\text{SO}_4$  from the solution in soil during the cooling produces mirabilite ( $\text{Na}_2\text{SO}_4 \cdot 10\text{H}_2\text{O}$ ) and makes the soil volume expand (Chen et al, 1988). This theory is approved by many scientists in engineering projects and applied widely in saline subsoil or geotechnical engineering in practice. In this paper, the authors will give some further explanations about the relationship between the crystallization amount of  $\text{Na}_2\text{SO}_4$  and restraining the heave after mixing with additional NaCl. The change mechanism of the crystallization amount of  $\text{Na}_2\text{SO}_4$  in pore solution and crystallization amount after mixing with NaCl during cooling could be explained by the principle of  $\text{Na}_2\text{SO}_4$ -NaCl- $\text{H}_2\text{O}$  water-salt system phase diagram. The isothermal phase diagrams at different temperatures of 25°C, 10°C, 5°C, -5°C and -15°C are illustrated by means of chemical analyses and the drawing rule of the phase diagram. Based on the corresponding concentration of initial system values in Table 4, corresponding system

points can be found out respectively in the phase diagrams mentioned above. In line with the rules of the diagram, corresponding solidoid amounts, liquidoid amounts and concentration of system values in each phase diagram can be calculated separately. The calculated solidoid amount at the above temperatures are listed in Table 5. Because the compounded solution in each sample was an over-saturated solution at 25°C. For instance,  $\text{Na}_2\text{SO}_4 \cdot 10\text{H}_2\text{O}$  crystallized in Sample 86-1 and 86-2,  $\text{Na}_2\text{SO}_4$  crystallized in Sample 86-3 and  $\text{Na}_2\text{SO}_4$  and NaCl crystallized in Sample 86-4 (Table 5). Thus we can assume that well-crystallized solidoid at 25°C from pore solution is regarded as solid particles and consequently, the recrystallization of  $\text{Na}_2\text{SO}_4 \cdot 10\text{H}_2\text{O}$ , NaCl·2H<sub>2</sub>O and ice below 25°C produces the heave of the samples if we neglect the effect of recrystallized  $\text{Na}_2\text{SO}_4$  and NaCl on the porosity of the sample. Thus, we count the corresponding relationship between the recrystallized amounts of  $\text{Na}_2\text{SO}_4 \cdot 10\text{H}_2\text{O}$ , NaCl·2H<sub>2</sub>O and ice during different cooling intervals in the pore solution and the heave of the samples, which are listed in Table 6.

It is shown in Table 6 that the isothermal phase diagram interval zone from 25°C down to 10°C, the  $\text{Na}_2\text{SO}_4 \cdot 10\text{H}_2\text{O}$  of the four samples has been crystallized, and the more the crystallized  $\text{Na}_2\text{SO}_4 \cdot 10\text{H}_2\text{O}$ , the stronger the heave amount will become. The situation is the same at the interval of 10 to 5°C. In the interval of 5 to -5°C, because a large amount of crystallized ice formed in sample 86-1, frost heave occurred. Since a small amount of crystallized  $\text{Na}_2\text{SO}_4 \cdot 10\text{H}_2\text{O}$  was separated out in Sample 86-2, the heave amount was relatively small. As a large amount of crystallized NaCl·2H<sub>2</sub>O and a small amount of crystallized  $\text{Na}_2\text{SO}_4 \cdot 10\text{H}_2\text{O}$  were developed in Sample 86-3, and the volume expansion produced by NaCl hydrating a molecule into NaCl·2H<sub>2</sub>O is much larger than that of a molecule of H<sub>2</sub>O changing into ice, so the total heave of Sample 86-3 was much stronger than that of Sample 86-1 in the interval. Because the amount of crystallized NaCl·2H<sub>2</sub>O in Sample 86-4 was much more than that in Sample 86-3, the heave amount of Sample 86-4 was stronger than that of Sample 86-3. In the interval of -5 to -15°C, because of the lack of crystals in Sample 86-1, its heave hardly occurred. Since ice in Sample 86-2 only formed in the beginning, and ice crystals were few, as a result, the heave was little. The  $\text{Na}_2\text{SO}_4 \cdot 10\text{H}_2\text{O}$  and NaCl·2H<sub>2</sub>O in Sample 86-3 were also few, so the total heave was not obvious. Although the crystallization of NaCl·2H<sub>2</sub>O and  $\text{Na}_2\text{SO}_4 \cdot 10\text{H}_2\text{O}$  in Sample 86-4 was rather small, its heave became stronger and stronger. The reason can be described as follows: In the interval of 5 to -5°C, because NaCl·2H<sub>2</sub>O crystallized in Sample 86-4 numerously, it took a longer time to produce displacement, until the interval -5 to -15°C.

Generally speaking, during cooling processes (from 25°C down to -15°C), the total amount of heave in the four samples increased with the increase of  $\text{Na}_2\text{SO}_4 \cdot 10\text{H}_2\text{O}$  crystallized. While the ratio of NaCl to  $\text{Na}_2\text{SO}_4$  ( $R$ ) was less than the critical one, an additional content of NaCl in the samples could restrain the crystallization of  $\text{Na}_2\text{SO}_4 \cdot 10\text{H}_2\text{O}$ , and consequently reduce the heave. For instance, the amount of crystallization in Sample 86-2 ( $R=0.37$ ) was less than that in Sample 86-1 ( $R=0$ , i.e. the content of NaCl is zero) and the heave of the former was less than that of the latter consequently. Conversely,

Table 5. The Amount of Solidoid Crystallization from Solution in Samples at Given Temperatures

No.		86-1	86-2	86-3	86-4
Initial system values (g)		431.89	526.37	585.57	744.71
IDS under 25°C (g)	S	0	0	80.59	80.35
	S <sub>10</sub>	66.15	129.49	0	0
	Cl	0	0	0	189.73
	Cl <sub>2</sub>	0	0	0	0
	Ice	0	0	0	0
	Total	66.15	129.49	80.59	270.08
IDS under 10°C (g)	S	0	0	0	0
	S <sub>10</sub>	198.77	254.85	236.61	232.31
	Cl	0	0	40.35	229.60
	Cl <sub>2</sub>	0	0	0	0
	Ice	0	0	0	0
	Total	198.77	254.85	276.96	461.91
IDS under 5°C (g)	S	0	0	0	0
	S <sub>10</sub>	215.94	261.79	246.96	239.76
	Cl	0	0	41.13	229.79
	Cl <sub>2</sub>	0	0	0	0
	Ice	0	0	0	0
	Total	215.94	261.79	288.09	469.55
IDS under -5°C (g)	S	0	0	0	0
	S <sub>10</sub>	246.24	269.01	256.60	252.85
	Cl	0	0	0	0
	Cl <sub>2</sub>	0	0	89.67	475.06
	Ice	185.65	0	0	0
	Total	431.89	269.01	346.27	727.91
IDS under -15°C (g)	S	0	0	0	0
	S <sub>10</sub>	246.24	270.70	260.41	253.79
	Cl	0	0	0	0
	Cl <sub>2</sub>	0	0	100.11	477.62
	Ice	185.65	8.85	0	0
	Total	431.89	279.55	360.52	731.41

Note: S — Na<sub>2</sub>SO<sub>4</sub>, S<sub>10</sub> — Na<sub>2</sub>SO<sub>4</sub>·10H<sub>2</sub>O, Cl — NaCl, Cl<sub>2</sub> — NaCl·2H<sub>2</sub>O  
IDS — Isothermal diagram system

Table 6. Relationship between crystallization Amount of S<sub>10</sub>, Cl<sub>2</sub> and Ice in Given Temperature Zone vs. Heave Amount of samples

Temp. interval	25°C — 10°C		10°C — 5°C		5°C — -5°C			-5°C		-15°C		
	ΔS <sub>10</sub> (g)	Δh (mm)	ΔS <sub>10</sub> (g)	Δh (mm)	ΔS <sub>10</sub> (g)	ΔCl <sub>2</sub> (g)	ΔIce (g)	Δh (mm)	ΔS <sub>10</sub> (g)	ΔCl <sub>2</sub> (g)	ΔIce (g)	Δh (mm)
86-1	132.62	8.77	17.17	0.54	30.30	0	185.65	1.12	0	0	0	0.01
86-2	125.36	6.55	6.94	0.10	7.22	0	0	0.71	1.69	0	8.85	0.29
86-3	236.61	14.65	10.35	0.27	9.64	89.67	0	3.51	7.18	10.44	0	0.42
86-4	232.31	13.12	7.45	0.22	13.09	475.06	0	7.55	0.94	2.56	0	3.70

Note: S<sub>10</sub> — Na<sub>2</sub>SO<sub>4</sub>·10H<sub>2</sub>O Cl<sub>2</sub> — NaCl·2H<sub>2</sub>O

while R exceeded the critical value, the amount of Na<sub>2</sub>SO<sub>4</sub>·10H<sub>2</sub>O crystallized became stronger with the increase of NaCl. As a result, the salt heave was getting stronger and stronger because of the development of hydrate (NaCl·2H<sub>2</sub>O) caused by the excessive content of NaCl near 0°C. For

instance, during the interval of 25 to 10°C, the amount of Na<sub>2</sub>SO<sub>4</sub>·10H<sub>2</sub>O crystallized in sample 86-3 (R=1) and Sample 86-4 (R=2.66) was about twice as much as that in Sample 86-1. Consequently the heave amount of Sample 86-3 and 86-4 increased correspondingly. It is obvious that it

is necessary to find out the critical ratio of NaCl to  $\text{Na}_2\text{SO}_4$  for controlling the salt-frost heave. As well as the temperature interval which is very important for chemical reaction, in the interval of 25 to 15°C, an additional amount of NaCl mixed in the samples restrains  $\text{Na}_2\text{SO}_4 \cdot 10\text{H}_2\text{O}$  crystallized from the solution and while the ratio exceeds the critical one, all of  $\text{Na}_2\text{SO}_4 \cdot 10\text{H}_2\text{O}$  and, consequently, the heave disappears (see Fig.3). However, after cooling down to 15°C, the situation is quite different. This is because mixing NaCl reduces the hydrate energy of  $\text{Na}_2\text{SO}_4 \cdot 10\text{H}_2\text{O}$  crystallized and makes  $\text{Na}_2\text{SO}_4 \cdot 10\text{H}_2\text{O}$  crystallized dehydrated into forming  $\text{Na}_2\text{SO}_4$  crystals. The minimum temperature limit of keeping  $\text{Na}_2\text{SO}_4$  crystals in  $\text{Na}_2\text{SO}_4$ -NaCl- $\text{H}_2\text{O}$  water-salt system is 17.9°C. The value of the hydrate energy changes with the temperature interval. While soil temperature is below 17.9°C, the absolute value of reducing hydrate energy by mixing with NaCl ( $\Delta E_{\text{NaCl}}$ ) is less than that produced by cooling ( $\Delta E_r$ ), i.e.

$$|\Delta E_{\text{NaCl}}| < |\Delta E_r| \quad (1)$$

In the interval of 32.38 to 17.9°C, the situation mentioned above is just the opposite, i.e.

$$|\Delta E_{\text{NaCl}}| > |\Delta E_r| \quad (2)$$

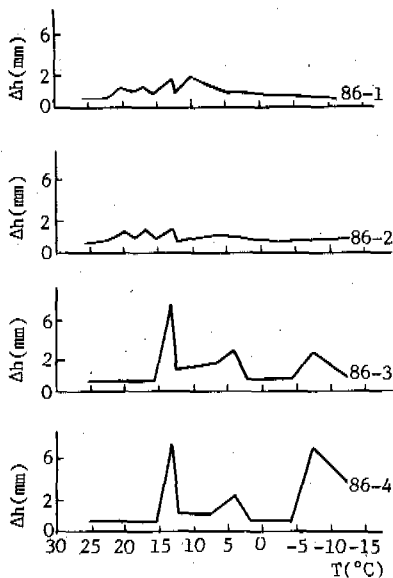


Figure 3. The distribution of heave peak in samples vs temperature intervals

In conclusion, restraining heave by mixing with NaCl is easily accomplished only in the temperature zone between 32.38°C and 17.9°C. The photos' identification results, by using a polarizing microscope for the solidoid crystals at 25°C, shows that in the solution with a given  $\text{Na}_2\text{SO}_4$  concentration, while adding a little NaCl, crystallized  $\text{Na}_2\text{SO}_4 \cdot 10\text{H}_2\text{O}$  dehydrated into recrystallized  $\text{Na}_2\text{SO}_4$  partially. The more NaCl added, the more the crystallized  $\text{Na}_2\text{SO}_4 \cdot 10\text{H}_2\text{O}$  dehydrated into  $\text{Na}_2\text{SO}_4$  until the extra NaCl is left in the solution. In the cooling process from 25 down to 15°C, the amount of heave was 3.11 mm

(Sample 86-1), 3.4 mm (Sample 86-2) and zero (Sample 86-3 and Sample 86-4), respectively. It can be explained as follows: because the ratio of NaCl to  $\text{Na}_2\text{SO}_4$  in Sample 86-3 and Sample 86-4 exceed the critical value and no crystallized  $\text{Na}_2\text{SO}_4 \cdot 10\text{H}_2\text{O}$  solidoid exists in the pore solution, so the heave amount was not observed. After cooling below 15°C, the heave amount will suddenly become stronger in sample 86-3 and 86-4 caused by crystallized  $\text{Na}_2\text{SO}_4$  rehydrating into  $\text{Na}_2\text{SO}_4 \cdot 10\text{H}_2\text{O}$ .

It is also obvious that the heave peaks in Sample 86-1 appear in a positive temperature zone and mainly in the interval of 22 to 5°C (see Fig.3). In this zone, the heave amount will increase with the increase of crystallized  $\text{Na}_2\text{SO}_4 \cdot 10\text{H}_2\text{O}$ . The heave peaks in Sample 86-2 appear in the interval of 22 to 12°C. The heave peaks in sample 86-3 and 86-4 appear in the interval of 15 to 13°C and -5 to -12°C. This is because in the interval 15 to 13°C, the crystallized  $\text{Na}_2\text{SO}_4$  hydrated forming  $\text{Na}_2\text{SO}_4 \cdot 10\text{H}_2\text{O}$ , meanwhile in the saturated solution  $\text{Na}_2\text{SO}_4 \cdot 10\text{H}_2\text{O}$  crystal separated out, so the amount of  $\text{Na}_2\text{SO}_4 \cdot 10\text{H}_2\text{O}$  crystallized in Sample 86-3 and Sample 86-4 was more than that in Sample 86-1 and 86-2. In the interval of -5 to -12°C, because NaCl crystallized hydrated forming  $\text{NaCl} \cdot 2\text{H}_2\text{O}$  and the extra  $\text{NaCl} \cdot 2\text{H}_2\text{O}$  crystal separated out from the saturated solution, the amount of heave will appeared in another peak.

#### CONCLUSIONS

1. The total amount of heave in the saline soil will increase with the increase of  $\text{Na}_2\text{SO}_4 \cdot 10\text{H}_2\text{O}$  crystallized during cooling from 25°C down to -15°C. Additional content of NaCl in the soil could restrain the crystallization of  $\text{Na}_2\text{SO}_4 \cdot 10\text{H}_2\text{O}$ , which reduces heave amount. However, while the ratio of NaCl to  $\text{Na}_2\text{SO}_4$  by weight exceeds a critical value, the extra amount of  $\text{Na}_2\text{SO}_4 \cdot 10\text{H}_2\text{O}$  and  $\text{NaCl} \cdot 2\text{H}_2\text{O}$  crystallized will be produced with the increase of NaCl. As a result, the salt heave will become stronger.
2. An additional amount of NaCl mixed in the soil will restrain  $\text{Na}_2\text{SO}_4 \cdot 10\text{H}_2\text{O}$  crystallized from the solution during the cooling from 25°C down to 15°C. While the ratio of NaCl to  $\text{Na}_2\text{SO}_4$  exceeds a critical one, all of  $\text{Na}_2\text{SO}_4 \cdot 10\text{H}_2\text{O}$  and, consequently, the heave will disappear.
3. The amount of  $\text{Na}_2\text{SO}_4 \cdot 10\text{H}_2\text{O}$  and, consequently, salt heave will increase gradually with  $\text{Na}_2\text{SO}_4$  in saline soil during cooling. While an additional amount of NaCl is mixed in the soil, and the ratio of NaCl to  $\text{Na}_2\text{SO}_4$  exceeds the critical value, there are two heave peaks in the temperature zones from 15 to 13°C and from -5 to -12°C respectively.

#### ACKNOWLEDGMENT

This study was supported by Chinese Natural Science Foundation. The authors are grateful to Madam Sen Wenkun and Wang Yaqing, and the engineers in our institute, for their help in the laboratory.

#### REFERENCES

- Boznyiay, H.M., (1956) Road engineering in saline soil region. People's Transportation Pressing House, Beijing.  
Chen Xiaobai, Qiu Guoqing, Wang Yaqing, Sen Wenkun, Tao Zhaoxiang and Tian Linxiang,

- (1988) Physico-chemical and mechanical properties of heavy saline soil during cooling. SCIENTIA SINICA, A(2):245-254.
- Liang Baomin, (1986) The principle of water-salt system phase diagram and its application. Light Industry Pressing House, Beijing.
- Lo Weipu, (1980) Highway engineering in saline soil region, People's Transportation pressing House, Beijing.

## CREEP EFFECTS ON A Laterally LOADED PILE

L. Domaschuk<sup>1</sup>, R. Kwok<sup>2</sup> and D.H. Shields<sup>1</sup>

<sup>1</sup>Department of Civil Engineering, University of Manitoba  
Winnipeg, Manitoba, R3T 2N2, Canada

<sup>2</sup>Department of Civil Engineering Technology, Red River Community College  
Winnipeg, Manitoba, R3H 0J9, Canada

A rectangular pipe pile embedded in a frozen sand was subjected to lateral loading. The pile was instrumented with a series of load cells and strain gages. A lateral load was applied and maintained constant for a period of 70 days. The load was then removed and the pile was allowed to equilibrate. The load was reapplied in three approximately equal increments. Each increment was maintained constant for a period of 1 day. The load was then increased and maintained constant for an additional 76 days. The total pile head displacement consisted of instantaneous and creep components. Creep under constant lateral load resulted in redistribution of the reactive soil pressures. Generally, pressures near the soil surface decreased with additional displacement. Pressures increased with additional displacement at deeper depth.

### INTRODUCTION

A pile embedded in frozen soil undergoes creep displacements and deflections when subjected to a lateral load. The creep displacement causes a redistribution of the lateral soil reactive forces acting on the pile. The nature of the initial distribution of the forces and their redistribution associated with the creep displacements, depends on the magnitude of the applied load and the relative stiffness of the pile to that of the frozen soil. Very little experimental work has been carried out to determine the creep effects on the lateral reactive soil pressures. Domaschuk et al. (1991) reported some results of reactive soil pressures along a pile embedded in a frozen sand when subjected to incremental increases in lateral load. The instrumentation was limited to load cells positioned along the upper bearing face of the pile only and so the reaction along the entire pile length could not be determined. However, they did establish that as a result of creep a significant redistribution of soil reactive forces along the bearing face occurred. Generally, reactive forces near the soil surface decreased while those at depth increased as a result of creep. The decreases were as much as 25% while the increases exceeded 100%. Thus the redistribution is important when analyzing pile deflections, moment distribution and displacements.

This paper presents the results of a second series of tests in which a pile was instrumented more extensively.

### TEST SETUP

#### Test Facility

The test facility consisted of a pit formed by insulated reinforced concrete walls and floor, housed in a refrigerated cold room. Plate-coil refrigeration panels were placed

along the insides and the bottom of the pit to control soil temperatures.

#### Soil

The sand used in the test consisted of medium sized particles with a uniformity coefficient of approximately 2. The sand was placed in a loose saturated state by a process of sedimentation. The sand was then frozen unidirectionally upward by maintaining a cold temperature in the bottom refrigeration panels. Strings of thermocouples were placed vertically at several locations to monitor soil temperatures. Details of the procedure for placing and freezing the sand are presented in Domaschuk et al. (1988).

Samples of the frozen sand were recovered by coring prior to the load test. The density and water content profiles are given in Figure 1. The dry unit weights ranged between 13.4 and 15.5 kN/m<sup>3</sup>. The water contents varied from about 23.2% to 24.8% which corresponds to saturation levels of 78% and 100%. There was no visual evidence of ice segregation in the cores.

#### Test Pile

The test pile was a rectangular pipe, 203 mm x 154 mm in section, and 1800 mm long. The wall thickness was 11 mm. The embedded length of pile was 1267 mm. Load cells were mounted along the frontside of the pile from the soil surface to a depth of about 1000 mm, and from the bottom of the pile to a height of about 700 mm along the backside of the pile. A description of the fabrication and mounting of the load cells is given by Domaschuk et al. (1991). Strain gages were attached to the pile at intervals along the frontside of the pile. The locations of the load cells and strain gages is shown in Figure 2. The stiffness, (EI), of the pile was  $7.82 \times 10^3$  kNm<sup>2</sup> in the direction of loading. The modulus of subgrade reaction, k, of the frozen sand based on previous tests



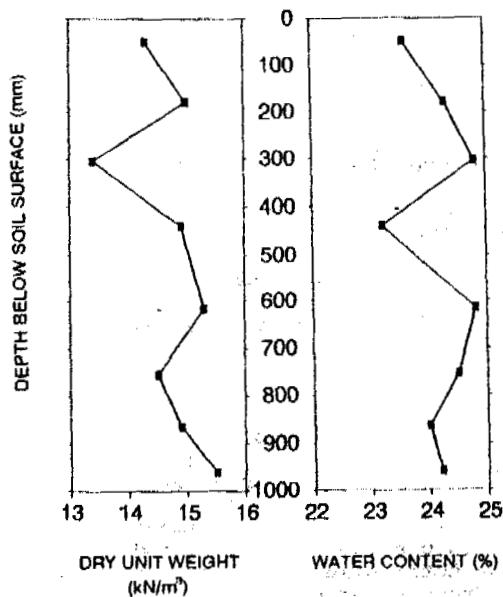


Figure 1. Profiles of sand densities and water (ice) contents.

conducted under similar temperature conditions, Domaschuk et al. (1991) ranged between 2 and 8 GN/m<sup>3</sup> depending on the magnitude of reactive pressure. The corresponding range of

dimensionless length,  $\beta L$ , in which  $\beta = \sqrt{kD/4EI}$  and  $L$  is the embedded pile length, is 2.24 to 3.17 which suggests that the pile behaves as a flexible pile, Broms (1965).

#### Loading Assembly

A large beam spanning the pit and supported by columns located just outside the pit walls was used as the reaction for the applied lateral load. The lateral load was applied through a hydraulic ram connected to an Enerpac air-on-oil pump system. Loadings provided by the pump system were regulated by controlling the air pressure, which maintained the load at a reasonably constant magnitude throughout the test. A load cell placed between the ram and the pile, at 203 mm above the soil surface, measured the applied load.

An LVDT was used to measure the pile displacement at 203 mm above soil surface.

#### TEST PROCEDURE AND RESULTS

An instantaneous lateral load of approximately 103 kN was applied in the direction of the long axis and maintained for a period of 70 days. This magnitude of load was chosen because it represented an approximate design load for this particular pile, based on previous test data. The load was then removed and the pile was allowed to equilibrate. The same load was then reapplied in stages of 32, 75 and 103 kN to examine stage-loading effects. Each load was maintained for a period of 1 day. The load was then increased to 170 kN, which had been estimated to be close to the failure load, and was maintained constant for a further period of 76 days. The load was then removed. Load cell, displacement and temperature readings were taken frequently throughout the test with the

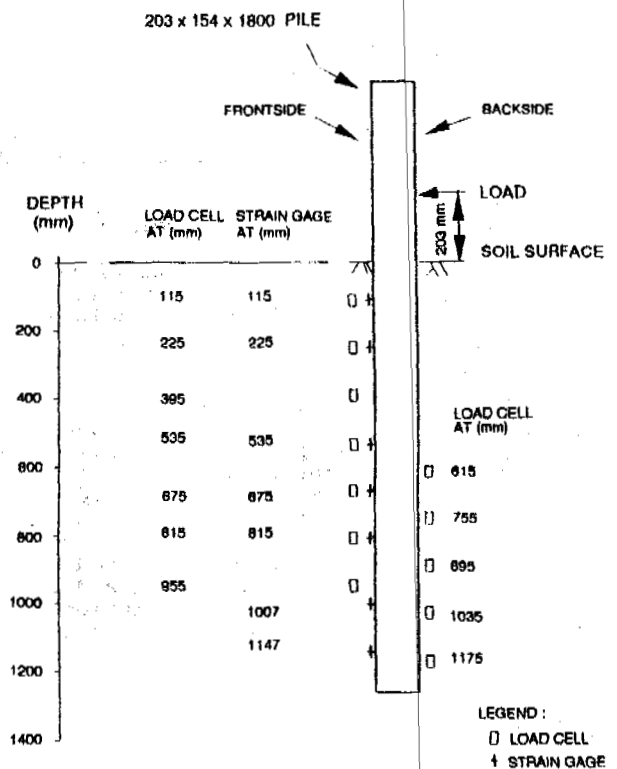


Figure 2. Pile showing location of load cells and strain gages.

aid of an electronic data acquisition system.

#### TEST RESULTS

##### Displacements

The pile head displacements versus time are shown in Figure 3. Upon the application of each load, an instantaneous displacement occurred which was followed by creep displacement. The initial application of the 103 kN load caused an instantaneous displacement of 2.0 mm and creep displacement of 2.6 mm over a period of 70 days. However the creep displacement had not attenuated completely and the average displacement rate over the final 45 days was 0.01 mm/day. Unloading resulted in an instantaneous recovery of 2.0 mm followed by a 0.8 mm creep recovery. Thus the initial instantaneous displacement was fully recovered upon unloading.

Reloading the pile to 103 kN resulted in a cumulative instantaneous displacement of about 2.6 mm and a creep displacement of 0.4 mm.

Increasing the load to 170 kN and maintaining it for 76 days resulted in an additional 1.0 mm of instantaneous and 4.7 mm of creep displacements. When the test was terminated the average displacement rate was 0.02 mm/day. The total instantaneous displacement was 3.6 mm and the total creep displacement was 6.9 mm.

Unloading the pile resulted in an instantaneous recovery of 4.5 mm and a creep recovery of 0.6 mm. Thus the total recovery is made up of 3.6 mm of pile deflection and 1.5 mm of soil rebound. The permanent displacement of the pile was 5.4 mm. The displacements for the entire test are summarised in Table 1.

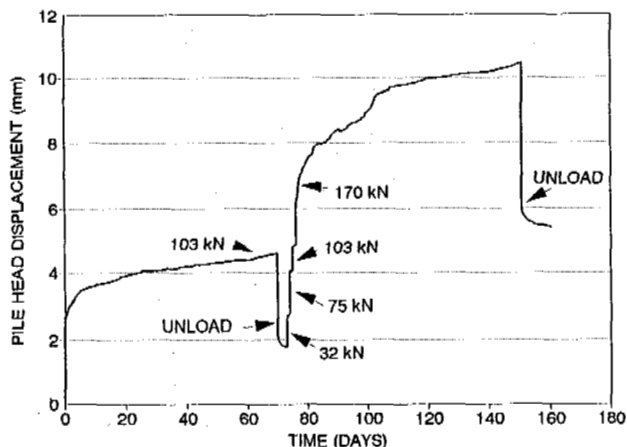


Figure 3. Pile head displacements versus time.

Table 1 Pile head displacements

Load (kN)	Instant. Disp. (mm)	Elapsed Time (days)	Creep Disp. (mm)
103	2.0	70	2.6
0	-2.0	3	-0.8
32	0.8	1	0.2
75	1.2	1	0.1
103	0.6	1	0.1
170	1.0	76	4.7
0	-4.5	10	-0.6
Total displacement			= 10.5 mm
Residual displacement			= 5.4 mm

### Reactive Forces

#### 103 kN Load

Plots of the applied load and the soil reactive forces as a function of time are shown in Figure 4a for the load cells along the frontside of the pile and in Figure 4b for those along the backside. Unfortunately the upper load cell, LC-1 and the load cell at the 895 mm depth indicated continual drift in readings and therefore their data were discarded. As can be seen in the figures, the applied load varied between 100 and 106 kN during this phase. Along the frontside of the pile, (Figure 4a), the soil reactive forces extending to a depth of 675 mm, increased during the first 10 days and then remained constant. The load cell at the 815 mm depth basically indicated no reactive force, and the cell at the 955 mm depth registered a small negative load. Along the backside of the pile, (Figure 4b), the reactive forces were slightly negative at the 615 and 755 mm depths, were positive at the 1035 and 1175 mm depths and increased with time at these latter depths.

Soil reactive pressures were computed from the reactive forces and the size of the bearing face of the load cell. The distributions of the reactive pressures at the start and end of the

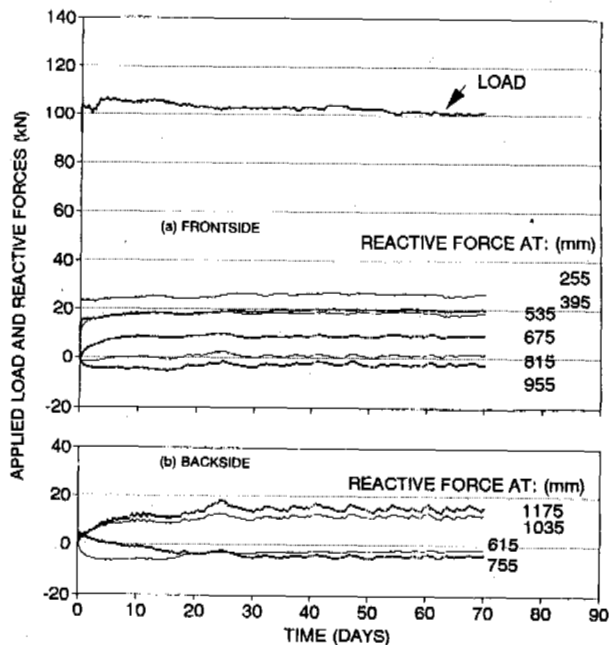


Figure 4. Applied load and reactive forces versus time:  $P = 103$  kN, (a) frontside, (b) backside.

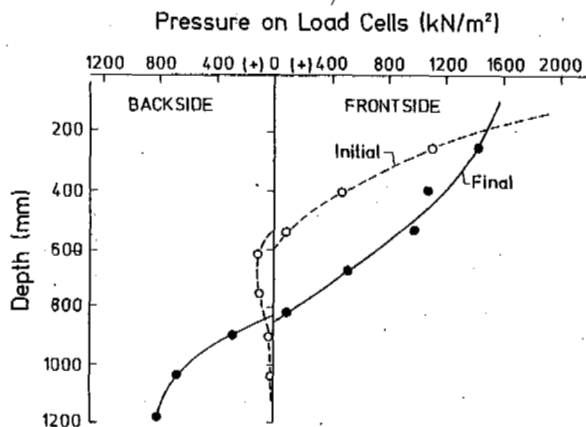


Figure 5. Distributions of reactive soil pressures:  $P = 103$  kN.

application of the 103 kN load are shown in Figure 5. A substantial redistribution of pressures occurred along the entire pile length due to creep within the frozen soil. The final distribution on each side of the pile was non-linear. Overlap of pressures near the point of transition from frontside to backside pressures occurred because the pile has a rectangular section and so each face rotates about a separate point.

#### 0-32-75-103 kN Loads

The reactive forces for the unload-reload phase are shown in Figure 6a for the frontside cells and in Figure 6b for the backside cells. During the unload period, (days 70 to 73), some cells, notably those at depths of 675 and 815

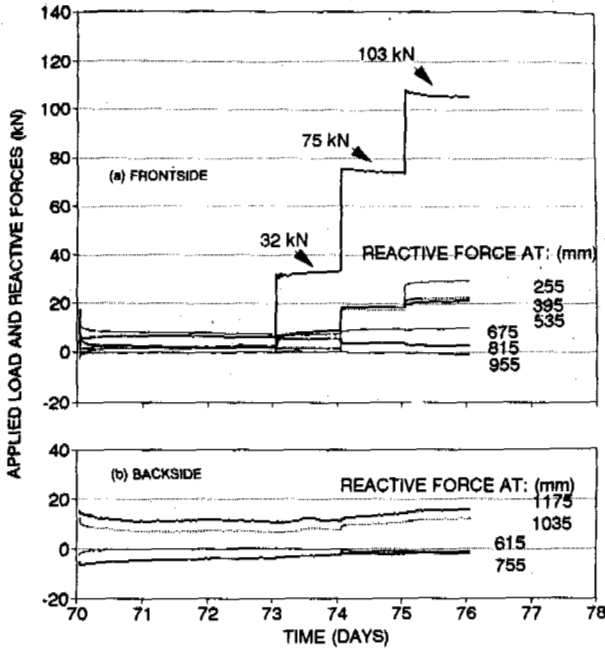


Figure 6. Applied loads and reactive forces versus time: unload-reload, (a) frontside, (b) backside.

mm on the frontside, and 1035 and 1175 mm on the backside, retained significant residual forces. As noted earlier, unloading the pile resulted in a residual displacement of the pile and therefore associated residual reactive forces were expected.

The distributions of the reactive pressures at the end of each load increment are shown in Figure 7. The retention of residual reactive pressure in the vicinity of mid-depth of the pile is illustrated. Applying a load of 32 kN brought about little change in reactive pressures and the distribution remained unusual in that the reactive pressures near the ground surface were small. This was probably caused by the development of a gap in front of the pile during unloading. The pile then behaves as a beam cantilevered at some depth below the ground surface. Increasing the load to 75 kN brought the upper portion of the pile into contact with the soil. Under a load of 103 kN the distribution was more conventional. However because this load was only applied for 1 day, the distribution differed somewhat from that achieved at the end of the single application of the 103 kN load for a period of 70 days.

#### 170 kN Load

The applied load and load cell reactive forces for the 170 kN load are shown in Figure 8. Generally there was a significant increase in all the reactive forces during the first few days and thereafter the uppermost and lowest cells continued to indicate a small increase with time while the other loads remained essentially constant. Upon unloading, load cells at depths of 815 and 955 mm on the front face, and 1035 and 1175 mm on the backside indicated a residual load as large as 10 kN.

The changes in the reactive pressure dis-

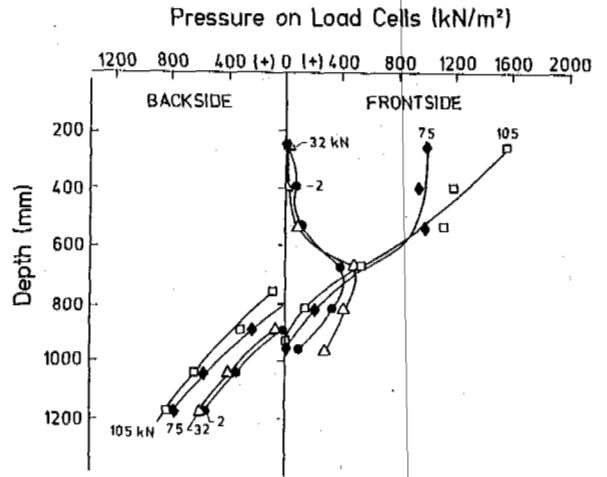


Figure 7. Distributions of reactive soil pressures:  $P = 0, 32, 75, 103$  kN.

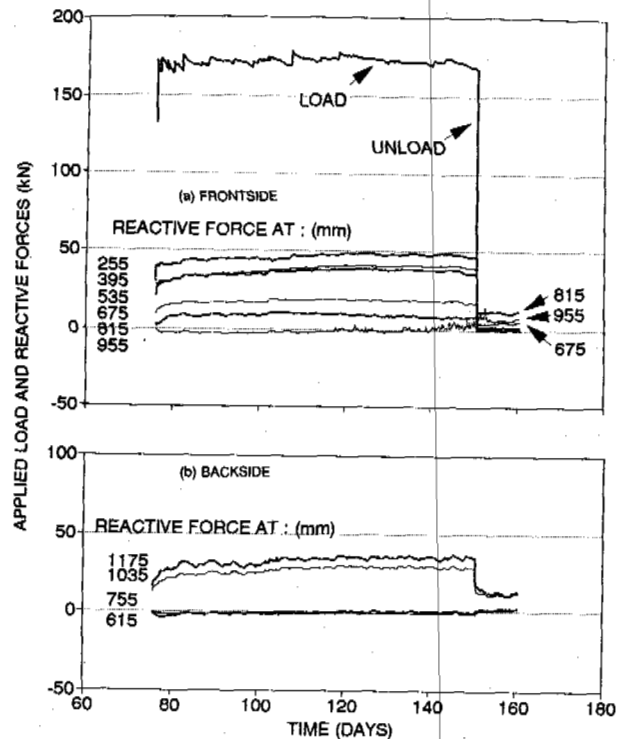


Figure 8. Applied load and reactive forces versus time:  $P = 170$  kN, (a) frontside, (b) backside.

tribution due to creep are shown in Figure 9. The changes are particularly significant near the top and near the bottom of the pile. The distributions are nonlinear reflecting the effects of pile deflection on the reactive pressures.

#### Pile Deflection Shapes

From the strain gage readings the bending stresses and moments along the pile were deter-

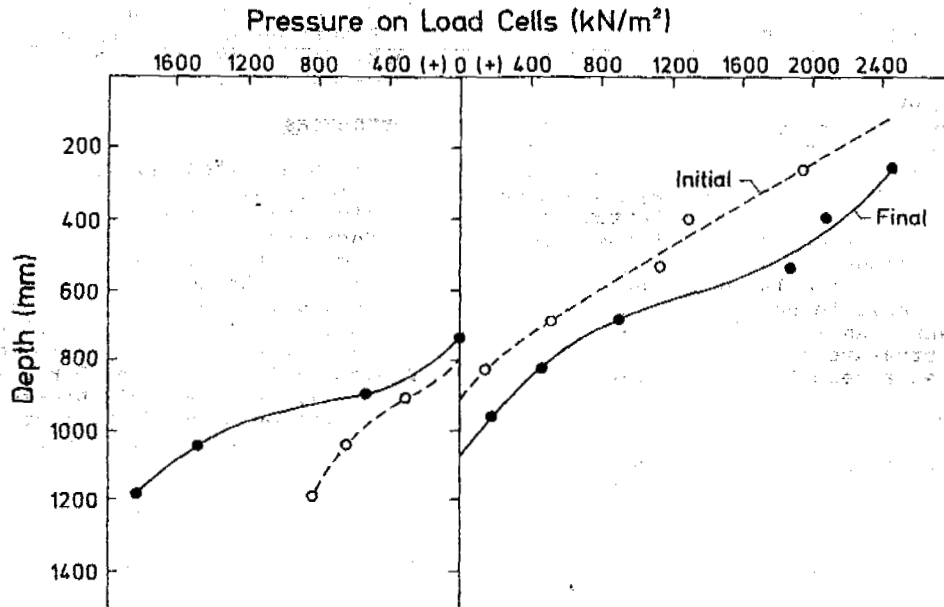


Figure 9. Distributions of reactive soil pressures:  $P = 170 \text{ kN}$ .

mined. Unfortunately strain gage 7 at a depth of 1,150 mm showed a continual drift of readings and they were discarded. Based on the moment-area method, pile deflections were determined for the 103 kN and 170 kN loads, after an elapsed time of 1 hour and at the end of the loading periods. These are shown in Figure 10. The deflection curves were nonlinear in all instances and the overall curvature increased significantly as a result of creep.

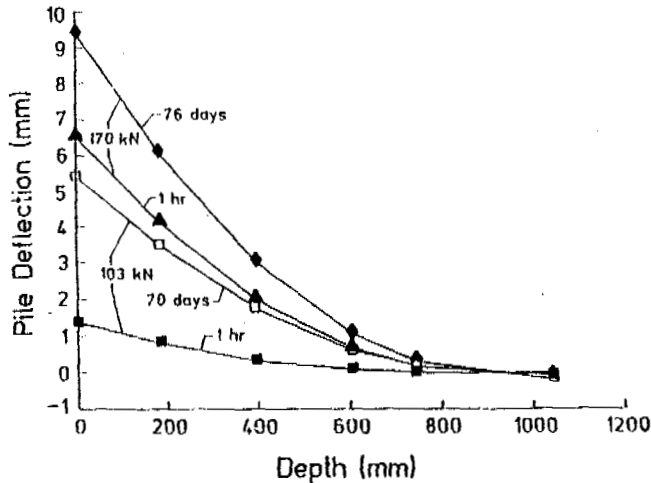


Figure 10. Pile deflection shapes.

#### Soil Temperatures

As mentioned earlier, soil temperatures were monitored by means of four vertical strings of thermocouples. Figure 11 shows the temperatures at the surface, the 400 and the 800 mm depths. The temperatures were not constant with time and also decreased with soil depth. The decrease in temperature with soil depth is attributed to the fact that only the bottom

refrigeration panel was used for controlling soil temperatures. The side refrigeration panels developed problems at the start of the test and were shut off. This also affected the automatic temperature controls which meant that the controls had to be operated manually, making it difficult to maintain constant soil temperatures. The temperatures varied between  $-4^\circ\text{C}$  and  $-6^\circ\text{C}$  for the most part. These variations however did not appear to affect the pile displacements nor the reactive pressures significantly.

#### OBSERVATIONS AND CONCLUSIONS

1. The creep displacement of a laterally loaded pile in frozen sand was about 1.5 times greater than the magnitude of the instantaneous displacement under a 103 kN load, and was 4.5 times as large as the instantaneous displacement under a 170 kN load. The displacements had not ceased

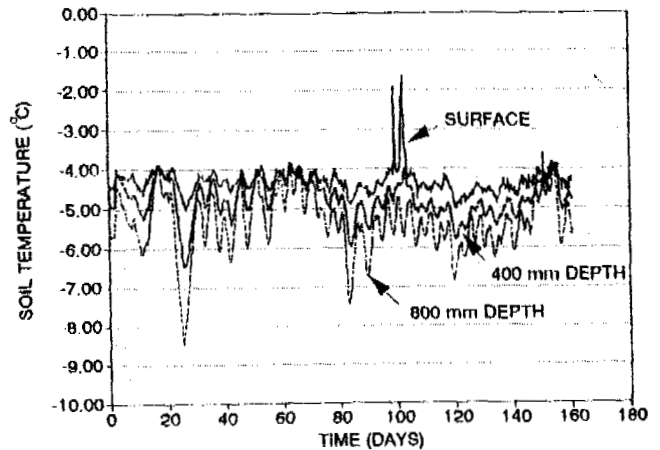


Figure 11. Soil temperatures versus time.

entirely under each load but had attenuated to rates of 0.01 and 0.02 mm/day respectively. Most of the attenuation occurred in the first 10 days.

2. There were radical changes in the reactive soil pressures associated with creep displacements (Figures 5 & 9). Pressures near the ground surface decreased with increasing displacement; below this they increased with a maximum increase at the bottom of the pile. The pressure distributions were generally nonlinear.
3. Pile deflections calculated on the basis of the reactive soil forces indicated that the pile did behave as a flexible pile with the degree of curvature significantly increasing as a result of pile creep.

#### ACKNOWLEDGEMENTS

The writers wish to acknowledge the

assistance of M. Green, B. Turnbull, and N. Piamsalée in carrying out the experimental work. The study was financed through an NSERC research grant.

#### REFERENCES

- Broms, B.B. (1965) Design of laterally loaded piles. Journal of the Soil Mechs. and Fdn. Div., Proc. American Society of Civil Engineers, Vol. 91, No. SM3, 79-99.
- Domaschuk, L., Fransson, L., and Shields, D.H. (1988) Interaction between a laterally loaded pile and frozen sand. Proc. 5th Intl. Conf. on Permafrost, 2, 1060-1065, Tapir Publishers, Trondheim, Norway.
- Domaschuk, L., Shields, D.H., and Fransson, L. (1991) Reactive soil pressures along a pile in frozen sand. Journal of Cold Regions Engineering, 5(4), 174-194.

## DEFORMED EMBANKMENTS ON MARI AND THE WAYS OF THEIR STABILIZATION

P. I. Dydyshko<sup>1</sup>, V. G. Kondratyev<sup>2</sup>, M. L. Vasilyev<sup>2</sup>, V Ya. Prigoda<sup>3</sup>, M. N. Sadakova<sup>4</sup>, A. S. Valuyev<sup>4</sup>

<sup>1</sup>All-Union Research Institute of Railway Transport, Mytishenskaja str. 10, Moscow, 129851, Russia

<sup>2</sup>Moscow State Design and Survey Institute of Transport Construction, P. Korchaguin str. 2, Moscow 129278, Russia

<sup>3</sup>All-Union Research Institute of Transport Construction, Kolskay str. 1, Moscow, 129329, Russia

<sup>4</sup>Moscow Institute for Engineers of Railway Transport, Obraztsov str. 15, Moscow, 101475, Russia

The paper illustrates the Bajkal-Amur Main Line roadbed state. The types of roadbed deformations considered. A complex of investigation and regime observations has been carried out within the limits of engineering and geocryological monitoring. We have also ascertained the cause and effect interrelations of the going of nature processes. Optimum measures have been elaborated for elimination of construction deformations.

Constructive and termophysical characteristics of a railway bed, as linear structure determine special features of its operation in the regions of permafrost. In the southern zones of these regions the permafrost under embankments as a rule does not drain. In cuts we observe its full and partial degradation, what in its turn leads to accelerated disintegration of bedrocks, weakened by cryogenic weathering and formation of new weathering crusts.

After construction and putting into operation of the Bajkal-Amur Main Line the following deformations, defects and damages of the roadbed became apparent:

many-year settling and sliding apart of the embankments of the thawing base soils;

thermoerosion lowering on the adjacent to the embankment sections of mari and water-diversion ditches;

icing of hill-sides, in cuts and beds of water courses;

thermoerosive ravines on the slopes of cuts and hill-sides;

soil heaving and subsidence of track in cuts and zero places;

ballast pockets and beds on the subgrade; erosion wash-out and wash-offs of embankments and cut slopes, talus in cuts;

slide of embankments and cut slopes;

silting or washing-out of water-diversion ditches at embankments, hill-side ditches and roadside ditches in cuts and on hill-sides, stagnation of water in water-ways and near roadbed.

The first four kinds of processes are typical for the regions of permafrost spreading. The rest are observed in permafrost as well as in conditions of seasonal freezing of soils; the character of their manifestation and measures of their elimination and prevention have been studied in details (Technical Instructions, 1987)

Icing, especially in cuts, presented the greatest danger during the first 3-4 years after

construction of the roadbed. The following measures for their elimination have been undertaken for the period of temporary service; drilling and blasting drainage, catchment and removal of the underground water sources, water lowering by holes, deep tube drainage, warmth-keeping chutes, ice-holding ditches and banks etc. made it possible, that in due course this problem become less urgent (Vasiliev et al., 1989).

Cryogenic deformations in the subgrade zone, caused by seasonal freezing and thawing of soil (heaving at subsidence of track, ballast pockets etc.) are mainly in cuts at zero points. Total length of places with these deformations makes approximately 60 kilometers.

Thermoerosion destruction of cut slopes, made in icy soils, practically ceased after fulfillment of strengthening works (fixing of slopes by rocks).

The most frequent character has settling of embankments with the attendant defects. Over 700 kilometers of tracks are effected by these defects. In connection with the above-stated and also taking into account insufficient knowledge of the cause and effect interrelations, the present paper is devoted to this type of roadbed deformations.

The settlings are irregular on sections from 100 to 1000 metres and more. It often happens so that on the general background of considerable in length lowerings (depressions) there are places of greater settling intensity. In due course, if there is no adequate compensational track raising on ballast, the longitudinal profile is distorted, especially on approaches to buildings and structures (Figure 1). In places of embankment settling the shoulders are unevenly lowering, the height of the ballast section increases up to 1 m and more. The ends of the sleepers become bare. Ballast sections don't place on the subgrade and its slope turns into the slope of embankment.

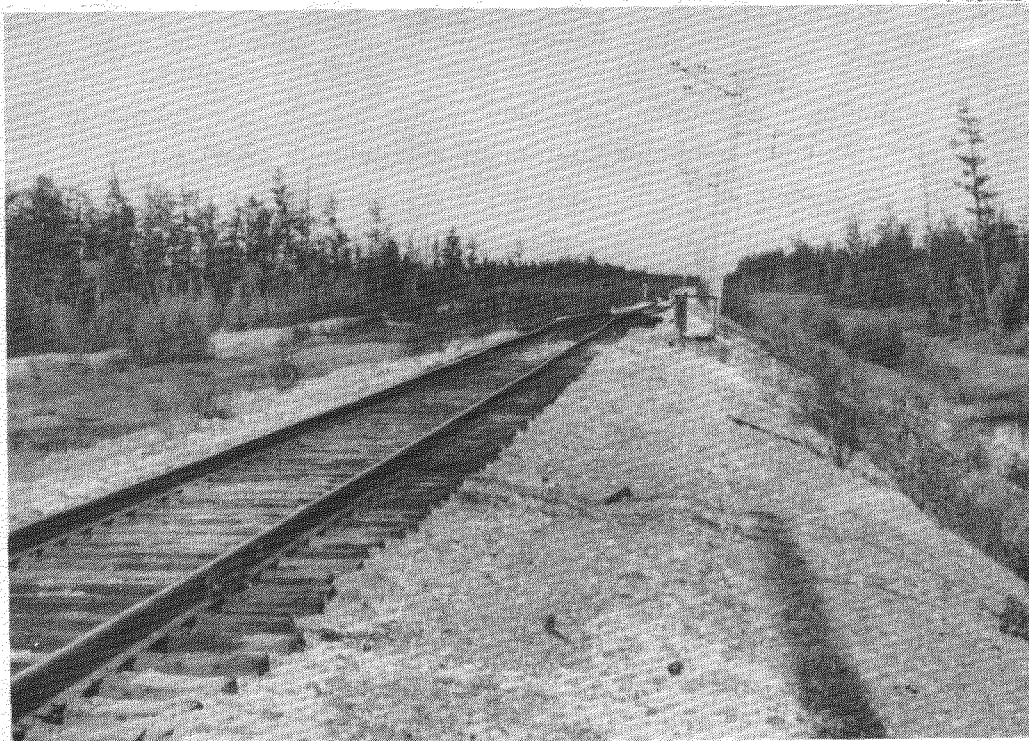


Fig. 1. Embankment settlements on approaches to a bridge.

The berms submerge into the base and in some places go into the water. The thermokarst lowerings are filled with water. At their further development the thermokarst lakes appear along the embankment.

As a result of local lowerings with nonallowable gradients and other geometric deformations of track and also because of quick development of the deformations the speed of the train operation is limited up to 15-40 km/h. Maintenance of track in working order needs considerable labour and material resources: consumption per 1 kilometre of track with settlements is by an order of magnitude greater, than of stable sections. The railway capacity lowers because of a large number of deformations.

The problem of the embankment stability insurance on the Bajkal-Amur Main Line is very urgent (Dydyshko, 1991, Ashpiz, 1989). At present the works, fulfilled within the limits of engineering and geocryological monitoring of roadbed are aimed at its solution. Institutes of Transport Construction, Railway Transport, Russian Academy of Science and other Departments take part in these works.

The works on monitoring include the following (Kondratyev et al., 1988a, b):

- 1) engineering and geological investigations, revealing of deformations, including potential ones, determination of the cause and effect interrelations in the nature-construction system and detailed engineering surveys on the unstable sections;

- 2) installation of experimental sections and fulfillment of nature regime observations under changes of the temperature, strength and other soil characteristics of the embankment and base,

hydrogeological conditions, speed and value of the deformations;

- 3) geocryological forecast with design - theoretical analysis, mathematical and physical modelling of nature processes at technogenic influence of the engineering conditions;

- 4) elaboration and carrying out of the anti-deformation measures and structures on the basis of heat and mass transfer process control;

- 5) determination of the fulfilled measures efficiency on roadbed stability.

Prevalence of the embankment settling deformations over other deformations depends upon the fact that on considerable length (up to 30%) of the BAM the roadbed base is laid by soils of the III-IV-th category of subsidence ( $\delta > 0,1$ ), such as: peat, icy sand and loam, sand of different genesis, here and there with seam and vein ice.

Total thickness of the strongly subsidiary layer during thawing varies from 1.5-2.0 to 5-6 m, rarely to 10 m. High icing of the Quarternary period deposits is the most typical for marsh sections with weak discharge of high flood-plain lands and over-flood-plain benches of the river valleys bottoms of temporary water-courses, plane water sheds. However in some cases the embankment settlements are intensively developing not only on highly icy soils of the base, but on the weakly subsidiary ones as well.

Since 1987 we have been carrying out investigations on experimental sections of the Zeisk Fervralsk line, which are on embankments with different type of bases. Section I (km 2908-2909) is located on local lowering of the Dugda shed with mossy and moss-hummock mari. The geological section (Figure 2, a) from the surface to 6-7 m depth is represented by strongly icy thickness of

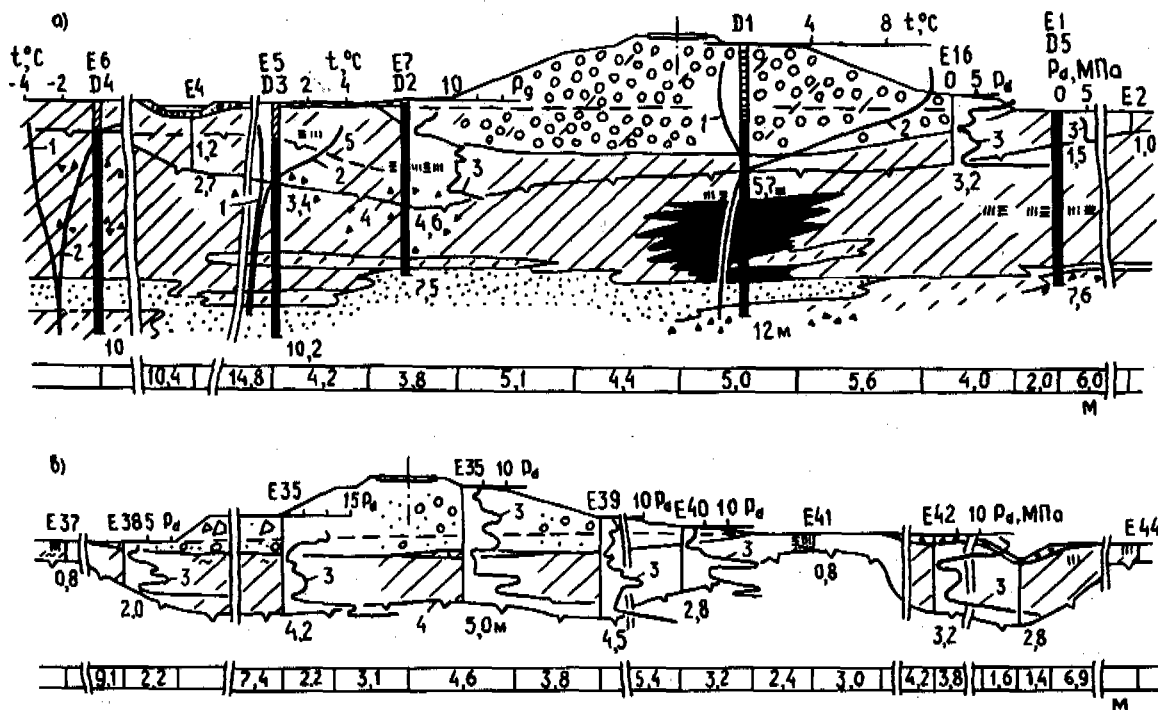


Fig. 2. Engineering-geological sections on experimental sections: 1 (2908 km) - a) and 5 (2744 km) - b); 1 and 2 - soil temperature distribution in spring and autumn period, 1991; 3 - distribution of conventional dynamic resistance  $P_d$  in thawed soils; 4 - permafrost upper bound in 1991; 5 - ditto before mari filling with mineral soil in 1988.

the diluvial-solifluction deposits: loams often landwasted, with content of grass soils with loam filling up to 30%, with interlayers of peat of 0.1-0.25 m thickness along the whole layer. Lower occur alluvial deposits of the flood-plain facies: interlaid solty sand loam, fine and silty sand, often with thin interlayers of loam, loam with gravel and pebble and sand thin interlayers. The cryotexture of frozen soil is layered, net lense-layered, seldom massive (in sand). Icing of diluvial-solifluction deposits is up to 50%. Drill hole 1 has broken-up under the embankment 3.2 m thick reformed ice wedges.

Embankment of up to 3 m height is laid by gravel and pebble soil with sand loam sandy filling. At a moment of observation (1987) its bottom was 1.5-2.0 m lower than the natural surface.

Section 2 (km 2858) is located on the slope of the North-North-East exposition of the Tungala river valley. The slope is divided by the ravines with temporary water courses. The 2 m high embankment of weathered shales is laid at the foot of a slope on grass-moss-hamrock mari. Base soils up to 2.0-3.5 m depth are represented by diluvial sand loams and light loams with up to 20% of grass and broken-stone, grass sand, than: alluvial-diluvial grass and broken-stone loams, grass soils with sand loam and loam filling up to 30%. From the slope upper side and under the deposits are overlapped by 0.7 m thick peat. Permafrost soils are characterized by layered, occasional-reticular cryotexture at 15% of icing ( $\delta = 0.05-0.10$ ) and for alluvial-diluvial deposits: massive and crust cryotexture ( $\delta < 0.01$ ). In 1987 the total embankment settling was equal to 1.0 m.

Experimental section 3 is located on the gentle slope of the Bolshaja Elga river. The slope surface is represented by grass-moss-hamrock mari sometimes with met oppressed larsh.

The embankment is made of alluvial loams with grass and strongly weathered rock. The base soils up to 2,5 - 4,0 m depth are represented by diluvial-solifluction peated loam, clay sand loam, with broken-stone inclusions, with peat interlayers and lenses along the whole layer, and from the surface overlapped by up to 0,6 m thick peat. Frozen soil is characterized by a layered, occasionally rectangular and massive cryotexture with icing from 10 to 60%. Lower lay alluvial-diluvial broken-stone and grass soils with sand loam filling, grass sand and alluvial clay. Their cryotexture is mainly massive. In 1987 the total embankment settling reached 1,5 m.

Engineering-geological investigations and observations have also been fulfilled for some other sections of the Tynda-Unral and Tynda-Berkhakit line (2435, 2535, 2715, 2744, 211-212 km etc.).

As a result of the embankment filling on mari from mineral soil the heat exchange conditions have changed: shadowing of surface and moisture evaporation by vegetation are excluded; embankment soil thaws and freezes quickly because of low moisture content and therefore, low latent heat of ice formation. During the day time of the warm period of the year the ground surface as well as flooded mari heats up several times higher than shadowed mari. Measured temperatures during the day period are the following: on mari between the hummockes - 0,4 to 6,4°C; air in shadow - 7,8 to 14,8°C; on embankment under



gravel - 7,0 to 16,0°C; under water on mari surface - 4,0 to 12,8°C. Difference in temperatures reaches 2-15 times. During thawing the embankment and also filled with mineral or flooded surface of mari interacts with permafrost as a heated block. Several years after filling of the embankment the temperature regime of the embankment and base soils will stabilize in accordance with the changed conditions of heat exchange, if there do not appear additional factors strengthening the thawing process (cross filtration under the embankment, the climate gets warmer, redistribution of snow cover etc.). On sections 1-3 at 0.8-1,5 m depth of seasonal layer in natural conditions and new quazi-stationary state the permafrost upper under the embankment reaches 4,7-5,7 m depth (from the embankment top). If base soils are less dispersed, the depth of the permafrost upper bound reaches 6,2-8,2 m (2715 km). Within the berms the permafrost upper bound reaches 2,5 to 4,5 m depth, and on mari sections, filled with 0,1-0,5 m layer of mineral soil it is on 2,0-3,4 m depth (Fig. 2). Heat action of the heated roadbed surface, as an additional source of heat (17), spread over small distance, which does not exceed 2 m from the embankment edge (see D 5 Fig. 2a and E 41 Fig. 2b).

Thus, a typical thawing bed is formed under the embankment, adjacent mari sections, filled with mineral soils, and draining ditches. The depth of trawing practically does not depend upon the thickness of this soil layer.

The first year of the five-year period of observations (the roadbed was filled in 1983) is characterized by approximately average many-year degree day sum of air positive and negative temperatures (1950 and 3800 correspondingly); next summers and winters were warmer on 18-27%. The depth of soil seasonal freezing along the roadbed center line from the given period on section I made 4,3 - 4,6 m talik thickness - 1,0 m; on section 2 - 3,5 m and 1,3 m correspondingly. On section 3 the permafrost upper bound lowered during the period of observations from 4,65 to 4,95 m, talik was not registered.

If flooded mari surface is filled with mineral soil, the permafrost upper bound lowers with maximum intensity up to 1 m per year during the initial period (see D 3 and E 5, Fig. 2, a).

Thus, for low embankments on mari with weak drainage the optimum embankment structure has minimum width at the bottom, no berm, filling of mineral soil on the adjacent section and along the draining ditches profile is not carried out. Otherwise, there is increase of zone width with violation of temperature regimes, as well as flooding along the thawing bed. Filtration of surface and overpermafrost water through the embankment can promote local thawing.

The considered processes of temperature regime formation don't account the outlined lately tendency for the climate getting warmer in this region.

A weak layer of soils ( see Fig. 2, b) has been revealed by a method of electrocontact dynamic probing, which combines in itself penetration and resistively logging (18) under the embankment and berm foot along their whole width. These data have been received as a result of engineering-geological survey of ten sections of the Tynda-Zeisk-Fevral'sk and Tynda-Berkhakit lines. The layer is characterized by conventional dynamic resistance  $P_d$  from 0.5 to 1.0 Mpa, what

corresponds to soil conditions from fluidal to soft plastic (Fig. 3). The weak layer thickness makes 0.1-0.5 m. Less value of  $P_d$  corresponds to greater value of embankment settling intensity.

According to electrocontact dynamic probing data on some sections (2435, 2715 km) there were ascertained zones of disconsolidated soils in the embankment body ( $P_d$  value lowers up to 1.5-2 Mpa). The disconsolidation is stipulated by influence of vibrodynamic loads from trains, peculiarities of rolling stock and temperature-moisture regime of embankment soils. The ascertained state of soils considerably determines the going embankment deformations.

The initial period of formation of embankment settling new temperature regime takes place mainly because of ice melting and soil consolidation of the base, it makes 80-300 to 350-500 mm per year. In due course their intensity lowers.

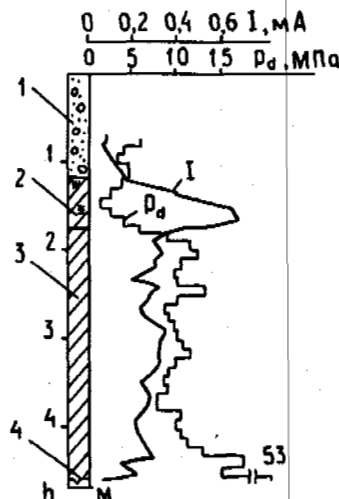


Fig. 3. Diagrams of changes of current  $I$  and conventional dynamic resistance  $P_d$ , depending on structure, state and properties of soils: 1 - sand and gravel mix; 2 - peated loam; 3 - loam; 4 - permafrost upper bound.

After reaching quazistationary regime the character and reasons of settling change. On the experimental sections the embankment and base deformations have been determined according to the results of planned and altimetric survey with the help of geodetic methods by fixed points on the rail heads and by marks during maximum freezing and thawing period (6,14). Increased in comparison with general background settlings become apparent as a rule in one and the same place (Fig. 4, a). For the period of four years the subgrade lowered here up to 70 cm. On section 1 this value was equal to 30 cm. Maximum year settling on sections 1-3 were equal to 280, 90 and 200 mm correspondingly. Lowerings along the rail heads with taking into account fulfilled track raising reached 80-200 mm per year. Lagging of tempo of track raising on ballast from settling led to lowering of the rail head level up to 50 cm within three years of observation (section 1). The settlings take place from July to December; at the beginning of cold period the moisture migrates from the underlying thawed layer to the

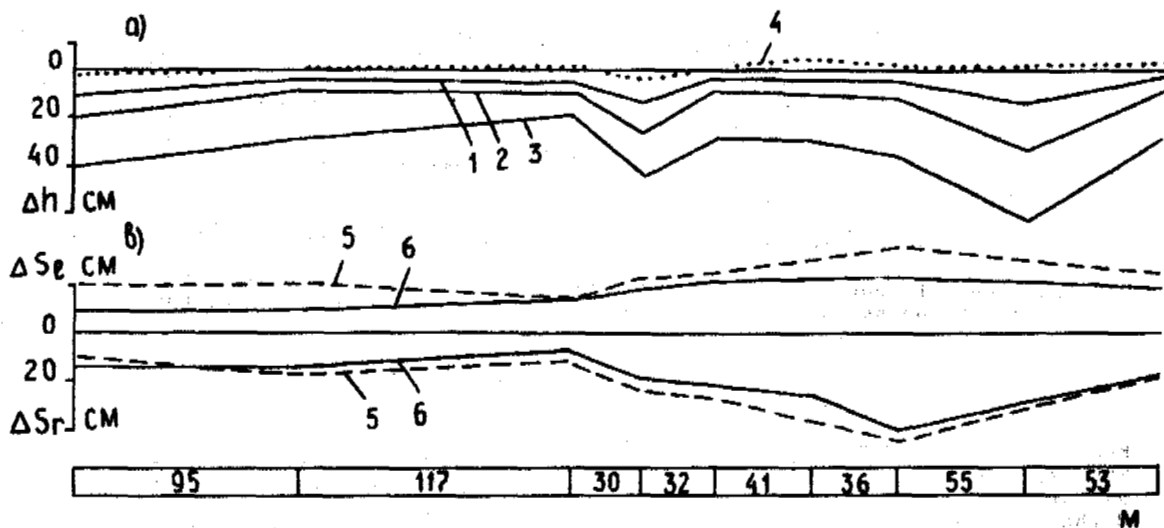


Fig. 4. Curve of vertical  $\Delta h$  - a) and horizontal forces (to the left  $\Delta S_1$  and right  $\Delta S_2$ ) - b) displacements: during one (1), two (2) and four (3) years; 4 - during winter of the first year of observations; 5 and 6 -  $\Delta S$  along the shoulders and berms for four years (experimental section 3).

embankment foot (19). This leads to overmoistening of boundary layer and intensification of settling as a result of geological processes. Instrumental observation also showed horizontal displacement of the marks of the similar value as that of the settlements (Fig. 4, b). Summary vectors of displacements are directed down and to the sides from the centreline of the roadbed. The embankment blocks slide apart autonomously, including with formation of cracks on the shoulders, moving on the berms and their displacement in the direction of field side. In a number of cases the base soils are squeezed out from under the embankment and at the berm edges, burst of clay soil suspension along flaw ways through the berm soils.

On the basis of the received data we have come to the conclusion, that the main reason of settlements and other embankment deformations on mari before achievement of quasi-stationary temperature regime is squeezing out of the fluidal soils of the boundary layer from the embankment. At temperature regime reaching a steady state the measures of deformations stabilization are to be aimed at creation of barrier against squeezing out of base soils from under the embankment or on change of its physical and mechanical properties. The first is achieved by regulation of the permafrost upper bound position under the berms or along the embankment edges by freezing of these soils, change of embankment loam soils in this zone for drainage ones up to permafrost upper bound, mechanical strengthening of soils under the berms and etc. The second - consolidation, drain, chemical and mechanical fixing of base soils directly under the embankment.

If temperature regime has not reached a steady state and there is a considerable thickness of III-IV type of soil substance in the base, it is necessary to fulfill measures on soil temperature regime control together with measures, preventing from base soil flooding and cross filtration under the roadbed.

Experimentally and in industrial scale the Bajkal-Amur Railway used selected rock filling of

weakly weathered rock, cooling devices like tubes and coverings of different structures, heat insulation from peat and foam plastic etc. In order to eliminate the unfavourable vibrodynamic effects from trains on the embankments stability it is necessary to construct counter-banquettes and other supporting facilities. Anti-deformation measures are fulfilled in combination with reclamation of the expropriation zone, which includes filling of the expropriation zone, which includes filling of the thermokarst lowerings by peat and peated loam soils and also drainage of water.

#### REFERENCES

- Ashpiz. 1989. The results of the roadbed survey of the Bajkal-Amur Railway eastern section and suggestions on its stabilization//Materials of scientific-technical conference Ensurance of the railway roadbed operational reliability. M.:NIIT, 87-89 pp.
- Dydysko P. I. 1991. Deformation of embankments on mari, their elimination and prevention//Railway Transport. Track and Track Service. TSNITTEI MPS issue 4. 17-32 pp.
- Kondratyev V. G., Korolev A. A. 1988a. State and tasks of the construction geocryological ensurance//Transport Construction. N 6, 9-11 pp.
- Kondratyev V. G., Korolyev A. A. 1988. Permafrost protection. The way it should be//Transport Construction. N 11. 3-4 pp.
- Technical instructions on elimination of railway track heaving and settling. 1987. - M.:Transport, 65 p.
- Vasilyev M. L., Lavrisheva L. G. 1989. Peculiarities of icing formation and comparison estimation of control methods for icing during railway construction//The results of investigations in the field of hydrogeology, engineering geology and cryology.VNII-Gidrogeologia i inzhenernaja geologia. M.: p. 48-59, deposited with VNIIT, N 2015-1389.

## PECULIARITIES OF GAS HYDRATE FORMATION IN SANDS

E.D. Ershov<sup>1</sup>, Yu.P. Lebedenko<sup>1</sup>, E.M. Chuvilin<sup>1</sup> and V.S. Yakushev<sup>2</sup>

<sup>1</sup>Department of Geocryology, Geologic Faculty of Moscow State University, Russia

<sup>2</sup>All-Union Research Institute of Natural Gases Moscow Region, Russia

Results of experiments concerning gas hydrate formation in sands are presented. The experiments were made in a special hermetic cell at static conditions of hydrate formation. Samples of sands with different granularity were used. Methane was the hydrate-forming gas. Some physical and petrographic properties of samples obtained were studied. Results obtained showed close similarity of gas hydrate accumulation processes with such processes of ice in sands. Sand particles cementing, water transfer and gas hydrate texture formation were fixed. A microscopic study of hydrate-saturated sands showed that gas hydrate accumulates in porous space in forms of fine separate crystals, hydrate films at particle surfaces and snow-like accumulations. Hydrate formation in sands accompanied by water transfer from inner parts of samples to their surface. Preliminary observations showed that water transfer was in film and vapor forms. Fixed processes can take place in permafrost regions, where hydrate-containing deposits are present.

### INTRODUCTION

Recent investigations showed that gas hydrates are rather widespread in nature (Panaev, 1987; Collet, 1983; Yakushev, Collet, 1992). Being nonstoichiometric compounds of gas and water, gas hydrates possess physical properties fairly similar to that of ice, and hydrate-formation and ice-formation processes have certain similar features. During the gas hydrate formation, as well as during the ice formation, water acquires the crystalline texture, therefore the influence of these two processes in the rock in which they occur is very similar. Humidified dispersed rocks during the freezing or during the hydrate formation are cemented, and undergoing some lithogeneous transformations they acquire the additional strength. The study of subaqueous hydrate-containing deposits showed that gas hydrates can form local accumulations in outward homogeneous rocks. Such accumulations were found in many samples of hydrate-containing rocks lifted from the bottom of seas and oceans (Gas Hydrates..., 1985). These accumulation which can be named "hydrate textures" suggest the possibility of mass transfer during the hydrate formation. The nature and mechanism of mass transfer during the hydrate formation are very poorly studied. There are only studies concerning the problem of the mass exchange during the hydrate formation, mostly its theoretical aspects (Groisman, et al, 1977; Tcherskiy, Tsarev, 1977). However the factual data (both experimental and field) on this problem were absent. Therefore the further investigations of the hydrate-containing rock genesis will surely require the reproduction of the process of the hydrate accumulation. Such reproduction is impossible without the consideration of the mass exchange in rocks.

### METHODS

The series of experiments with the sand of

various granulometric composition, was made to reveal the conditions and reasons promoting the hydrate texture formation. Washed fine- and mid-grained quartz sands picked from the upper 100 m of the permafrost zone of Tasovskiy peninsula and quartz-feldspar large grained sands from the Moscow moraine were used (The grain gradation is given according to classification of E.M. Sergeev). The sands were humidified by distilled water until their humidity reached 0.5 from the humidity of the capillar moisture capacity. During the experiment the sand was loaded into the cylindrical container, 10 cm in length and 4 cm in diameter made from the chromium-plated copper. The inner walls of the container were covered by a layer of plastic heavy clay in order to prevent gas flow along the walls. The bottom of the container possessed a hole, 0.5 cm in diameter, for gas supply into the rock. The container was put into the experimental pressure cell into which methane flowed. The cell was closed hermetically, the pressure was increased up to 8 Mpa at a temperature of 20°C. After that the cell was separated from the gas cylinder and was placed into the air freezer with temperatures about +2° to +4°C. The scheme of the installation is shown on the Fig.1.

The hydrate formation process was fixed with pressure decreasing in the cell. The pressure decreased until all free water in the cell was transformed into hydrate. The temperature in the freezer and the cell came into equilibrium, the pressure in the cell during 1-3 minutes was lowered to the atmospheric value. The cell was opened, the container with the frozen hydrate-saturated sample was taken out and was cut into 5 pieces along the the length. Each part humidity were measured.

Due to the self-preservation effect of gas hydrate at temperatures below 0°C discovered earlier, the study of the hydrate-saturated samples was conducted using methods developed for the frozen soils (Ershov et al, 1990, 1991).

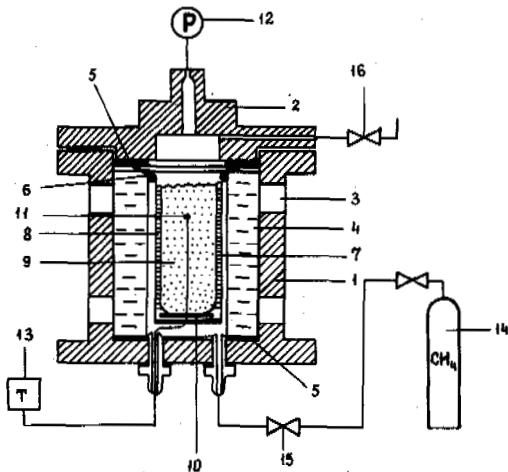


Figure 1. Scheme of experimental cell  
 1-cell body; 2-flange cap;  
 3-window; 4-plexiglass cylinder;  
 5-teflon; 6-rubber;  
 7-container of rock; 8-clay;  
 9-humid sands; 10-piston;  
 11-thermocouple; 12-manometer;  
 13-microvoltmeter; 14-gas cylinder;  
 15-admitting valve; 16-outlet valve.

### RESULTS AND ANALYSIS

The visual study permitted us to ascertain that in the sand rocks methane hydrates can form a texture resembling the cryotexture in the permafrost rocks. Massive, crust-like, porphy-like, lense-like and layered textures were fixed (Fig.2). The essential difference of hydrate textures from cryotextures in permafrost rocks is that the most diversity of the hydrate texture types is observed in large-grained sands and in fine-grained sands the massive cryotexture was only established. At the same time for cryotextures the most diversity of types is observed in most high-dispersed soils, i.e. in heavy sandy loams, loams, clays. The hydrate texture formation as a rule occurs in the places of the heterogeneity in the soil, i.e. along the boundaries of organic and inorganic material inclusion, along the contacts of the soils with different dispersion (e.g.-sand-clay contact), and in the places of incompact packing of sandy particles. The primary heterogeneity in the soil providing more favourable conditions for the hydrate formation than the neighbouring areas appears to be necessary for the hydrate texture formation

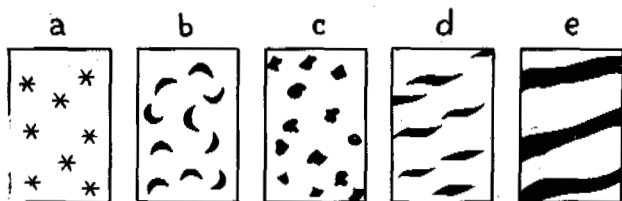


Figure 2. Types of hydrate textures established during the experiment of the hydrate saturation of sands

- a-massive, b-cryst-like,
- c-porphyr-like, d-lense-like,
- e-layered.

Microscopic study of the permafrost hydrate saturated sandy soils allowed us to ascertain the fact of the hydrate accumulation in the pore space forming films on the subface of mineral particles, accumulations of separate small crystals within the pore space and especially along the contacts of mineral particles and small (with a thickness of 1-2 mm) streaks of the solid semitransparent hydrate (Fig.3). Hydrate schlierens were filled predominantly by accumulations of small needle-like crystals resembling the solid snow, the thickness of the crystal streaks did not exceed 3 mm. As a rule hydrate inclusions in the pore space of the soils have the porous structure which permits the free filtration of the gas. However at the same time we observed pores completely filled by the white-coloured hydrate which had no visible porosity. Such pores completely filled by the hydrate were observed relatively rarely and they neighbored with areas of the good filter capacity.

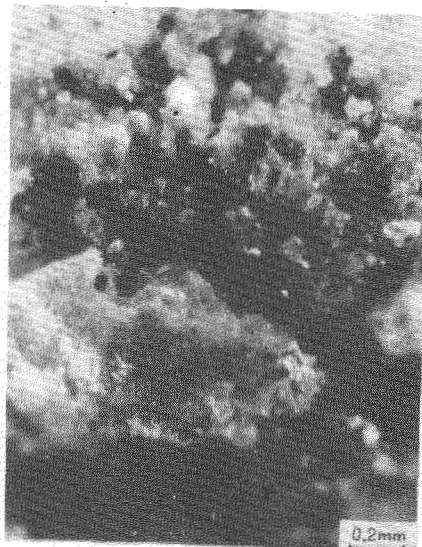


Figure 3. Methane inclusion in the sample of the fine-grained sands

The study of the humidity distribution in samples showed that during the process of the hydrate formation there was water transfer from the central areas of samples to their edges (Fig.4). The most differentiated distribution of humidity was observed in fine grained sands. After getting samples out from the cell the edges of them possessed the peculiar hydrate "caps" composed of separate elongated needle-like crystals and of crystalline crust and accumulations. The bottom of the container possessing a relatively small hole and the preliminary methane blowing of the sample being directed upwards, the hydrate "cap" near the bottom was considerably smaller than at the top where the humid rock had free contact with volume of the hydrate-forming gas along the larger area. This was reflected in the diagrams of the water balance in samples (Fig.4). Water accumulation above the upper edge was considerably larger than under the lower one. The difference in weights of the water accumulated on the different edges of the sample appears to be related with the consequences of the preliminary

blowing of samples, because the humidity changes along the sample- from the centre to edges- are approximately the same in both directions.

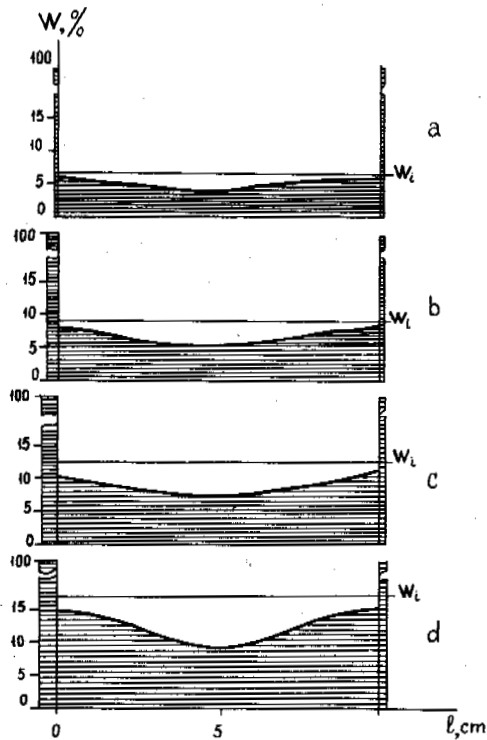


Figure 4. Water balance in the samples of the sand with different dispersion after the hydrate formation  
a, b, c, d - large-, mid-, fine-grained sand, respectively.  
 $W_i$  and  $W$  - the humidity of the samples before and after the experiment, respectively.

Based on the results of investigations conducted we can imagine the following way of the formation of hydrate "caps" on the exposed surfaces of the rock samples and of the hydrate accumulation in the places where the rock is heterogeneous (the hydrate texture formation). After the beginning of the hydrate-formation process the active formation of the hydrate crystalline embryos begins in the areas where the rock is heterogeneous and on its exposed surface, i.e. where is: a free space for the crystal growth and an access to the hydrate-forming gas. While the hydrate film in the inner parts of the samples almost isolates the gas from the water, the possibility of the crystal growth is confined by the pore walls and the gas filtration to the centre of the sample is made difficult by the rock, crystals in places of heterogeneity and on exposed surfaces of the gas-water contact have more favourable conditions for their growth.

Active growth of crystals on the edges results in the establishment in the inner part of the samples of the constant flow of moisture from the centre toward the exposed surface of the samples. Migration seems to occur in the form of a film from both sides of the hydrate crust covered mineral particles. At the same

time a rather low gradient of gas concentration, causing the gas migration inside the sample, must be established between central and sub-surface parts of the sample. The hydrate formation in the system being continued, the filtrating gas simultaneously transforms into gas hydrate and only a small amount of it reaches the central inner parts of the sample. Therefore the hydrate formation has the lowest intensity here and the process of dehydration is most significant. The film migration of the moisture in sandy deposits during the hydrate formation results in the formation of hydrate textures. These textures arise in rocks possessing heterogeneities. If there are some ways of the gas migration in the geological section e.g. tectonic fractures, penetrative zones, the rise of two oncoming migrating flows can be expected in the interval of the gas hydrate stability zone. One of them (gas flow) will be directed from the penetrative zone to the thickness of sandy rocks, another (water flow) will be directed from the bed toward the penetrative zone, where the most intensive hydrate formation will occur.

Analysis of results of the experimental study conducted permits us to make a number of conclusions concerning the peculiarities of the mass transfer during the process of the hydrate formation in dispersed rocks.

During the gas hydrate accumulation in sandy rocks the migration of the moisture toward the areas of active growth of hydrate formations takes place. Water migrates in vapour and liquid states and the moisture transfer appears to occur principally in the liquid state, i.e. the film mechanism of the migration takes place. It must be noted that not only water firmly tied on the hydrate surface but also weakly tied, lying under the isolating hydrate film, seems to be able to migrate.

The presence of different heterogeneities (organic remains, unconsolidated areas, inclusions of soil of another granulometric composition) causes the hydrate-texture formation in the places of heterogeneities.

The presence of clay particles in pore spaces of sandy rocks considerably reduces the potential of the hydrate formation and makes the moisture transfer and gas exchange within the rocks difficult.

Hydrate formation in consolidated sandy rocks stops in places of the transition from the light sandy loams (the content of clay particles is 2-5%) to heavy ones (the content of clay particles is 5-10%). We believe that further investigations of the mass transfer during the hydrate formation in dispersed rocks should be aimed at the determination of the quantitative regularities of the gas and water migration.

Urgent tasks in this field are to determine the dependence of the mass transfer intensity from the thermobaric conditions, humidity and mineralisation of the pore water, the gas composition and a number of other factors. The separate special task is to clarify the nature of the mass-transfer motive forces.

Further experiments should be correlated with the examination of the natural hydrate-containing rocks reproducing the natural conditions of the hydrate formation.

#### REFERENCES

- Cherskiy, N.V., Tsarev, V.P., (1977) Nekotorye novye napravleniya izutchenia fiziko-khimitcheskikh osobennostei sistem voda-gas-

gidrat i ispolsovanie gazovykh gidratov. Poiski i otsenka resursov gasa v gasogidratnykh zalezkhakh. (Some new directions in the study of physical and chemical peculiarities of the water-gas hydrate systems and utilization of gas hydrates. Prospecting and evaluation of gas resources in gas hydrate accumulations). Yakutsk.

Collet, T.S., (1983) Direction and evaluation of natural gas hydrates from well logs, Prudhol Bay, Alaska. M.S. Thesis. University of Alaska. Fairbanks. 78p.

Ershov, E.D., Lebedenko, Yu.P., Chuvilin, E.M., Istomin, V.A., Yakushev, V.S., (1991) Osobennosti sushchestvovaniya gazovykh gidratov v kriolitozone. (Peculiarities of the gas hydrate existence in the permafrost zone). Doklady Akademii Nayk S.S.S.R. V. 321. No.4, p.788-791.

Ershov, E.D., Lebedenko, Yu.P., Chuvilin, E.M., Yakushev, V.S., (1990) Experimentnye issledovaniya mikrostroeniya aglomerata lyodgidrat metana. (Experimental study of the methane hydrate-ice agglomerate microstructure). Inzhenernaya Geologia. No.3, p.38-44.

Gas Hydrates, (1985) METC. Topical report, No. SP-218. Morgantown. U.S.A. 31p.

Groisman, A.G., Evseev, M.S., Tsikel, M.A., (1977) O migratsii vlagi v dispersnykh sredakh pri obrasovanii gasovykh gidratov. (On the migration of the moisture in the dispersed media during the gas hydrate formation). in: Teplofizicheskie i massoobmennyye svoystva gigroskopicheskikh materialov. Yakutsk. p.102-106.

Panaev, V.A., (1987) Gazogidraty v mirovom okeane. (Gas hydrates in the world ocean). Bulletin Moskovskogo Obtshestva ispytatelei prirody. Otdel Geologicheskiiy. V.62. Iss.3 p.66-72.

Yakushev, V.S., Collet, T.S., (1992) Gas hydrates in arctic regions: rick to drilling and production. Proc. of the second. Internat. Offshore and Polar Engineering Conference, San-Francisco, 1992. p.669-673.

DETECTION OF FROZEN SOILS AND SOIL MOISTURE CHANGES  
BENEATH HIGHWAY PAVEMENTS

David C. Esch

Alaska Department of Transportation  
Headquarters Engineering Standards  
Juneau, Alaska 99801-7898

Instrumentation types for the determination of soil moistures and frozen layer positions were reviewed and systems selected for two 1991-92 field pilot study installations of different sensor types. Literature reviews and laboratory evaluations were also done to answer questions about sensor designs and the capability of different systems to detect frozen layers. Trial systems were installed at two Strategic Highway Research Program highway pavement sites, located in Idaho and New York. Sensors included thermocouples and encapsulated thermistors, soil electrical resistance probes, and soil dielectric constant measurements with time-domain (TDR) and frequency shift probe logging techniques (Sentry 200). The trial TDR probes included both two and three prong, and flat and curved probe types.

The advantages and disadvantages of each system are discussed from the standpoints of readability, calibration needs and installation difficulties in boreholes. Based on the observations made in this study, final plans were developed for the instrumentation and monitoring of 62 additional highway pavement study sites. The field subsurface monitoring of climatic effects on pavement structural layers will be continued on a monthly basis for several years, and will include measurements of pavement response to loads, pavement roughness, and frost heaving.

## INTRODUCTION

One of the research objectives of the Strategic Highway Research Program (SHRP) as conducted by the United States' National Research Council, is the measurement of frozen soil layer boundaries and other seasonal changes which can affect the structural behavior of highway pavements. To evaluate alternative methods of detecting frozen soil boundaries, frost heave, and moisture content changes in thawed soils at the lowest possible costs, a panel of experts was asked to recommend the most economical and reliable instrumentation types for field trials. A final plan was approved for field trial installations at two highway locations, and five sensor types were installed in the Fall of 1991. The primary requirements were that instrumentation be installed in boreholes through paved highway traffic lanes, and that equipment be reasonably low in cost. Saline soils from highway de-icing salt applications present additional problems of freezing point depressions and electrical resistance changes in the soil, which had to be considered in frozen layer detection.

The systems chosen for field evaluations were based on electrical measurements of temperatures, electrical resistances and the di-electric constants of soils. Temperatures were determined from Type T thermocouples and from thermistors. Electrical resistance measurements were obtained from soil contact rings wired onto plastic rods at 5 cm intervals, with AC resistances measured in both 2 and 4-wire modes. The most innovative portion of the study involved the installations for measurements of the di-electric constants of the soil layers, using time-domain and frequency-shift, resonant circuit measurement systems. The measurement of the di-electric constant of soils appears to be ideally suited to determinations of the frozen or thawed state of soils since this value is directly related to the unfrozen moisture content. Significant changes in the di-electric constant at temperatures at or below zero degrees will indicate that phase change has occurred, and the indicated moisture contents provide a measure of the unfrozen moisture content of the soil.

## MOISTURE SENSOR BASICS

In the judgement of the experts guiding the field monitoring work, the most reliable moisture measurement systems are based on the soil's di-electric constant, which is related to the "electrical capacitance" of the soil. The di-electric constant ( $\epsilon$ ) of a material is defined as the square of the ratio of the velocity of travel of an electromagnetic wave in a vacuum to the velocity of travel in that material, or:

$$\epsilon = (c/v)^2$$

Where:  $c$  = speed of EM wave in free space  
 $v$  = speed of wave in soil  
 $\epsilon$  = dielectric constant (dimensionless)

The dielectric constant varies from about 3 to 5 for soil with no water, to 80 for pure water. The values in soil at water contents between these two extremes are directly related to the volumetric percentage of unfrozen water in the soil, through an empirical equation as developed and reported by Topp, Davis and Anan (1980), or through dielectric mixing theory based on the constants for soil, air and water as described by Roth et. al.. The ability of TDR soil probe systems to detect the unfrozen water contents of partially frozen soils was demonstrated in studies reported by Smith and Patterson (1980).

As mentioned above, two methods of field measurement of the dielectric constant of a soil layer are currently available in commercial form, and both were included in the field studies. The first and most common is the time domain reflectometry (TDR) method, using the Tektronix model 1502 system, as reported on by many researchers. The second is the frequency shift measurement technique using a soil probe system from Troxler Electronics, Model Sentry 200, termed the "S200" in discussions herein.

### TDR Moisture Sensor Design Considerations

Time domain reflectometry (TDR) equipment was originally developed for measuring electromagnetic wave travel times to detect breaks or shorts in electrical conductors, and has been adapted to the measurement of soil moisture by agricultural researchers. The field trials discussed herein, as well as all research reports found in the literature, were performed with and are specific to the wave frequencies of the Tektronics Model 1502, (series B and C) cable testers.

The principle of the TDR system is similar to a radar system, in that an electromagnetic (EM) wave is transmitted and the reflected waveform is recorded and analyzed to measure the distances to objects which reflect the waves. In the TDR method the wave is transmitted along a shielded coaxial metallic cable (commonly of type RG-58, 50 ohm type) which connects to the soil probe rods. The cable and probe rods act as a waveguide, although the wave actually is transmitted through the medium surrounding the conductors. The wave velocity is a function of the dielectric constant ( $\epsilon$ ) of that medium. Sudden changes in the dielectric, as well as open or short circuits in the cable, will create wave reflection or wave loss points as indicated by slope changes in the return wave pulse, which is plotted on the screen and recorded on the chart recorder of the TDR.

For soil moisture applications, the co-axial cable center conductor from the TDR is connected to one of the two or more metallic rods which are inserted in parallel into the soil to be measured. The cable's outer shield is connected to the outer (3-prong) or second (2-prong) rods of the soil probe. The TDR screen displays a rise and fall in the return signal strength as the EM wave enters the probe rods, followed by a second rise in the return signal as the wave hits the end of the probes (Fig. 1). The apparent or "electrical" length of the probes is measured from the TDR chart record, and compared mathematically to the actual length to calculate the dielectric constant, according to the following equation:

$$\epsilon = (L_a/V_p \cdot L)^2$$

Where:  $\epsilon$  = di-electric constant  
 $L_a$  = apparent length of probe (from chart of TDR)  
 $L$  = actual length of probe  
 $V_p$  = phase velocity setting on TDR (normal=.99)

Usage of a TDR to measure moisture contents beneath highways was studied by Stott, Patterson and Phang (1983). The application to measurement of frost depths below roadways was reported by Kane (1986), who tested both straight and curved 2-prong TDR probes. In 1989 a new TDR probe type, using 3 prongs to create a balanced waveform, was developed in Australia (North, 1989); creating a stronger return signal and increased accuracy.

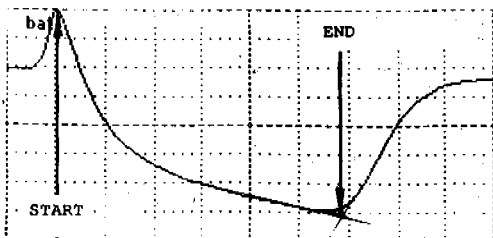


Figure 1. Typical TDR trace for 3-prong probe

### TDR Probe Design Factors

Knowledge of the area of influence of soil moisture around the probe rods is an important consideration in TDR sensor design, and in installation and calibration work, particularly for installation in boreholes. According to the literature, the influence area of a TDR probe set is frequency dependent but is roughly equal to an ellipse surrounding the probe rods as shown by Figure 2 for the two prong type. For 3-prong probes the pattern is similar except that majority of the EM wave energy follows the center conductor. When flat probes are installed horizontally at various depths in a borehole, the moisture measurements will be entirely confined to the backfill material, while for curved probes positioned around the wall of the borehole, the moisture sensed will be half in the surrounding soil and half in the backfill.

In a review of the literature, a confusing array of soil probe designs, dimensions and materials will be seen. However, because the probe rods only guide the direction of the waveform, the probe material, diameter and whether they are hollow or solid, do not matter. The spacing between the probe centers should always be smaller than a tenth of the wavelength of the EM signal (Stein and Kane, 1983). Since the TDR system transmits a variety of wavelengths from frequencies between 1 and 1000 MHz, adequate signal return strength will be obtained with any reasonable probe spacings that can be accommodated in a borehole installation. In practice, probe rod spacings of 25 to 50 mm are most commonly used, while probe lengths vary from 150 to 500 mm. Wider probe spacings result in measurement of a larger volume of material, at the expense of signal clarity and strength. Similarly, longer probes measure more volume and permit more accurate readings.

In saline soils the signal strength will be lowered and eventually lost as the probe length is increased, due to cumulative electrical shorting of the probe rods. For this reason, shorter probes will be required as salinity levels increase. An alternative for saline soils, which was not tested, is to apply a layer of electrical insulation to one of the probe rods to counteract the shorting effects of salinity. Unfortunately this invalidates the normal calibration equations for TDR probes. The probe design length and rod spacings must be a compromise between the desires for increased measurement volume and the reality of decreased strength and eventual loss of the return signal.

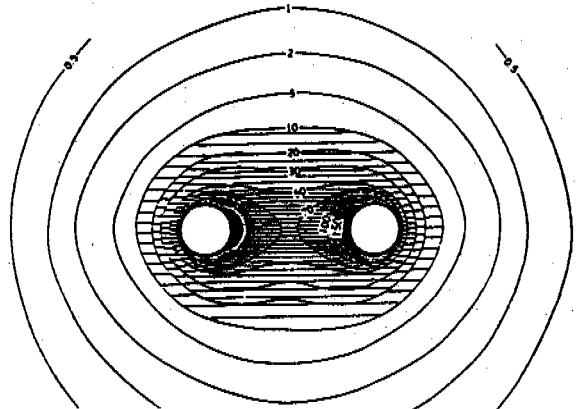


Figure 2. Influence zones for 2-prong TDR soil probe. Based on contours of equal power density. Note maximum effect of soil between probe rods. After North (1989)



#### Field Placement of TDR Probes

A primary purpose of the field pilot studies was to investigate the feasibility of and time requirements for placing probes in a borehole at a series of depths to 1.8 m below the surface. This avoids the problems of test pits which cannot be exactly restored, and of coarse granular soils where the probes cannot be driven.

The SHRP trial installations were designed to evaluate the benefits of straight 20 cm long TDR probes which were placed flat on the bottom of the borehole at 15 cm intervals of depth during the backfilling operation; versus the use of 30 cm probes curved to fit around the side of a 25 cm diameter borehole. The benefits of 2 versus 3-prong probes were determined by alternating between 3 and 2-prong systems in each borehole, with a total installation at each site of two TDR boreholes and 10 probes per hole. All probe rods were of 6.35 mm outside diameter stainless steel tubing, held in alignment with Lexan plastic spacers and nylon screws. For installation, pavement cores 0.3 m in diameter were first cut with diamond type core barrels and set aside for later replacement. Auger borings were then made to the 2 m depth. All materials were removed and stored in sealed containers to avoid moisture loss. Soil layers were then replaced in original positions and drop-weight compacted to prepare for each of the flat probes, which were placed at the required depths in a thin layer of loose soil. Moisture samples were taken at each probe location for calibration purposes. Curved probes were held against the side of the borehole while compacting the soil in layers. Both probe types withstood the compaction process with few problems. Following installation, the pavement was sawcut for the extension cables leading from each probe to a roadside junction box from which readings were made. Finally, after backfilling the pavement cores were bonded back into place with pourable plastic sealants to prevent water infiltration.

#### FREQUENCY SHIFT (S200) SYSTEM:

As an alternate to the TDR system for soil dielectric and moisture measurements, a new downhole probe type logging system as conceived and tested by Selig and Wobschall (1975) and further developed and marketed by Troxler Electronic Laboratories as the "Sentry 200" model (S200), shown in the photo in Figure 3. In this system the moisture sensing probe, which is 48 mm in diameter by 150 mm in length, measures the capacitance between a pair of electrodes separated by a plastic spacer and fabricated to serve as the tip of a probe rod. This probe is lowered inside a non-metallic casing which has been placed in intimate contact with the soil, either by driving it or by tamping the soil as backfill around the casing after augering a larger hole. The S200 system operates on a frequency shift measurement technique in which the sensor electrodes and the surrounding soil become parts of a resonance circuit whose frequency of oscillation is a function of the circuit components. Primary factors in the resonant frequency are the dielectric constant of the surrounding medium, and the geometry of the probe itself. From the measured resonant frequencies in the soil and in an electronic calibration medium, the frequency difference or "shift" is recorded. The probe readout system then computes the moisture content based on material-specific, internally stored calibration equations.

Unfortunately, the soil's electrical resistance is also a factor affecting the calibration equation. This becomes a problem when salinity changes occur in the porewater, as when a highway is salted for ice control, and the surface seal allows water intrusion.

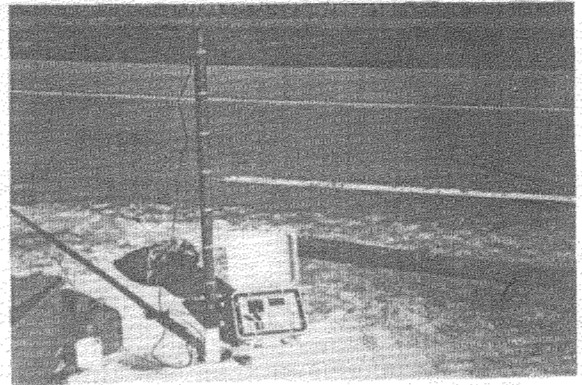


Figure 3. Photo of Troxler Sentry 200 probe system.

#### Influence Zone of S200 System

According to the manufacturer, the area of soil moisture influence on an S200 probe inserted inside a 50 mm ID PVC plastic pipe casing, extends radially 100 mm into the soil surrounding the casing. This relatively large influence zone, as compared to the TDR probe method, will result in measurement of soil moistures outside of the borehole backfill material, making it very important that the backfill soil be as closely matched as possible to the surrounding undisturbed soil, since different materials may have differing calibration equations, and lead to errors when a measurement combines two materials.

The vertical extent of the moisture influence zone was extensively evaluated in laboratory trials by compacting and freezing soils in cylindrical containers 300 mm in diameter, with PVC plastic casings for access by the S200 probe. The vertical influence zone of a thaw interface was found to be 250 mm in thickness as discussed below.

#### Laboratory Tests of S200 Probe in Frozen Soils Detection

Laboratory tests were run at the Federal Highway's Fairbank Laboratory to observe the responses of this system to soil freezing and thawing. Two waxed cardboard column forms, 750 mm in length by 300 mm in diameter, were used as sample containers. A center casing of 50 mm diameter PVC pipe represented a typical probe access tube. Two typical soil types were used; a silt-clay soil with gravel particles as a typical subgrade material, and a crushed rock with silt, used as a highway base layer.

For the laboratory trials, soils were placed and compacted around the center casings in thin layers, using a hollow pipe compactor with a flat plate bottom which slipped over the casing. After the sample containers had been half filled with compacted soil, they were tested with the S200 and then placed in a freezer for several days at  $-12^{\circ}\text{C}$  (Fig. 4). The tubes, now half filled with frozen soil, were removed from the freezer and the remainder of the tubes filled with the same soil and compacted in a thawed state. The resultant tubes provided a frozen interface at a known position, to judge the ability of this system to detect such frozen boundaries in silty gravels (Fig. 5) and in a silty clay (Fig. 6). The tubes were again logged and allowed to thaw, with S200 measurements taken at intervals to observe the changes in indicated moisture contents with temperature (Fig. 7). This final plot demonstrates the ability of this system to indicate unfrozen moisture contents at subfreezing temperatures, but the accuracy needs further evaluations.

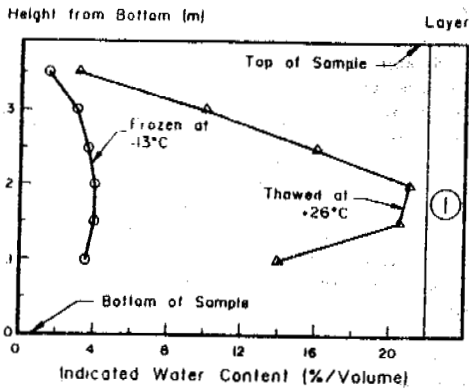


Figure 4. Indicated S200 moisture contents in single layer, silty clay with gravel; before and after freezing.

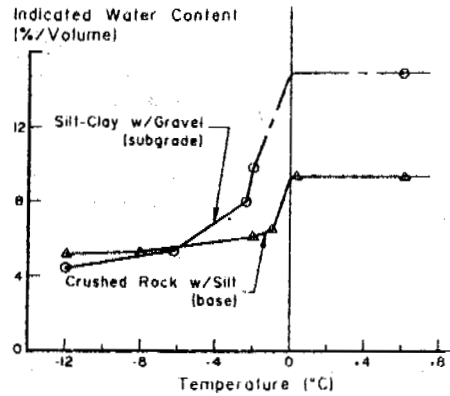


Figure 7. Effects of temperature and freezing on S200 indicated moisture contents of soils

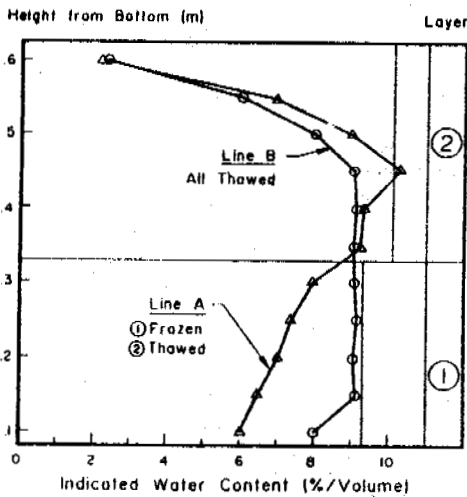


Figure 5. Laboratory indicated moisture contents for silty gravel base layers with thawed layer of same soil placed over frozen layer. Sentry 200 logging system.

### Salinity Effects

In a second series of tests, a small tube was installed to mid-depth of the sample container to provide an access point for injecting a saline porewater solution with a concentration of 20,000 parts per million (ppm). Approximately 1/2 liter of this solution was injected into a 100 kg soil sample mass, to study the effect of changing porewater salinity. TDR probes of the two and three prong types were also installed in these tests, to compare the effects of salinity on both systems. In summary, the S200-indicated soil moisture content climbed by roughly 10% over two days, as the saline porewater diffused around the center casing. However, the TDR probes indicated little or no change in moisture. The effective increase in soil moisture from the saline water added was calculated to be less than 1%. The major effect of salinity on the S200 comes from the contribution of the soil's electrical resistance to the frequency shift values indicated by this moisture measurement system. Use of measured soil resistance values to correct for soil salinity appears possible, but was not attempted.

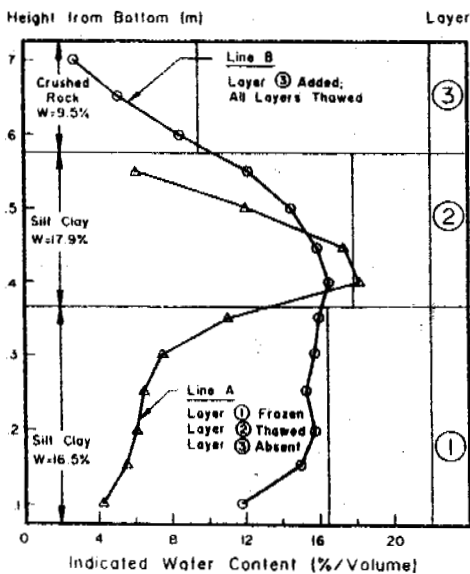


Figure 6. Indicated S200 moisture contents with thawed layer (2) placed over frozen layer; and after layer (1) was thawed, and silty crushed rock layer (3) was added.

### Conclusions on S200

Conclusions drawn from these laboratory studies include the following:

- \* Soil porewater salinity changes can cause excessively large errors in indicated moistures
- \* Different calibration equations are needed to predict actual moisture contents for soil
- \* Field or laboratory calibration checks are necessary for best accuracy.
- \* The soil moisture influence area is relatively much larger than that for the TDR test method. The center of the probe must be at least 150 mm below the soil surface for readings to be free of surface effects.
- \* Sensing of moisture contents in base course layers which lie closer than 150 mm to the bottom of a pavement is not possible.
- \* Moisture readings made within 150 mm of the bottom of the casing will not be accurate.
- \* Layers thinner than 300 mm cannot be measured with accuracy.
- \* The transition zone around a frozen/thawed layer contact is again approximately 300 mm in width.
- \* The potentials exist for use of a much smaller probe of this type to measure thinner layers and to more accurately sense thaw interfaces.

## Field Installations of S200

The S200 method of moisture measurement was included in the field studies by installing 50 mm inside diameter by 1.5 m long plastic (PVC) pipe casings through 150 mm diameter coreholes made through the pavement. Two field installation methods for placing the soil casings were tested, as follows:

Method A; useable in any soil type, was to auger a 150 mm borehole to the maximum depth of measurement. The PVC casing was then capped on the bottom and placed and held in the center of the borehole while alternately pouring in small portions of the soil backfill and compacting with a hollow soil tamper which was dropped down over the casing. Moisture content samples were taken from the backfill soil at frequent intervals to provide field calibration factors. This placement technique worked extremely well. The primary precaution needed is to assure that the moisture content, soil type and density of the backfill match those of the surrounding soil.

Method B; useable only in fine-grained soils which are not excessively dense, was to place the casing by alternately driving it into the soil with a hammer and wood block, and augering ahead with an auger small enough to slip down inside the casing. This method was tried unsuccessfully at the Syracuse site, due to stoppage by rock particles. It was used at the Boise, Idaho site in a dense sand which allowed only slow and difficult advancement of the casing, and which so constricted the PVC casing that it had to be reamed out to allow the probe to be inserted. This method may be very limited in sub-roadway applications due to the high soil densities commonly present there.

To complete the installations, watertight cases with removable covers were installed and bonded in place to seal the pavement and to thereby prevent additional water infiltration around the borehole.

The primary benefits of the S200 system are that the field installation is greatly simplified, and that measurements may be made at any desired increments of depth. However, the road must be closed to traffic for readings to be made, while TDR readings can be made remotely through any reasonable length of coaxial connection cable. It should be noted that separate probes of the S-200 type can also be permanently installed and remotely read. However, their high cost makes this approach prohibitive on a low budget installation.

## TEMPERATURE SENSORS

The two most common sensor types for soil temperatures were chosen for the field installations. The first was the Type T thermocouple, using the best available "special limits of error" thermocouple wire. Field readings were made using an ice-bath reference junction and a digital multi-meter reading to one micro-volt which provides a resolution of .03°C and an accuracy of perhaps 0.2°C under ideal conditions. The second was the glass bead thermistor, matched to use a single calibration equation and providing a field accuracy of about ±0.1°C.

The thermistor string assemblies were purchased as prefabricated assemblies containing 15 thermistors, which had been sealed inside a 25 mm O.D. Lucite tube containing an internal switching circuit so that all sensors could be read through a three-wire connection cable. This system, manufactured by the Measurement Research Company (MRC) of Bellevue, Washington is read by a small hand-held digital device, which provides a direct temperature readout to 0.01°C.

Advantages and disadvantages exist in both sensor types, as discussed in detail by Each (1989). The primary

advantages of thermocouples are their consistency of calibration, their extreme durability and freedom from drift over time, and their very low cost when lead wire lengths are kept short. Thermocouple disadvantages primarily come from the difficulty in obtaining accurate measurements of their very small output voltages under field conditions, and the problems of maintaining a stable reference junction temperature or voltage under these conditions. In practice, erratic temperature data from thermocouples frequently results in a scattering of indicated temperatures over a range of ±0.3°C, as shown by long term comparisons of deeply buried thermocouple/thermistor pairs (Fig. 8).

Thermistor advantages come primarily from their very high temperature/resistance relationships, which may equal 500 Ω/°C. This makes the field measurements of temperature much more accurate than for thermocouples, as low cost readout equipment which is relatively insensitive to temperature can be utilized. The primary disadvantage is that thermistor beads are subject to calibration shifts with moisture absorption and temperature cycling. This type of sensor drift over time is indicated by temperatures which do not reflect the normal and expected progressive temperature variations with depth, as in Figure 9. Such drift problems have not yet been noted in the MRC sealed thermistor assemblies. However, in summary, thermistors should be regarded as sensors of higher accuracy but of shorter field lives than thermocouples, which have continued to provide apparently good data after 25 years in-situ.

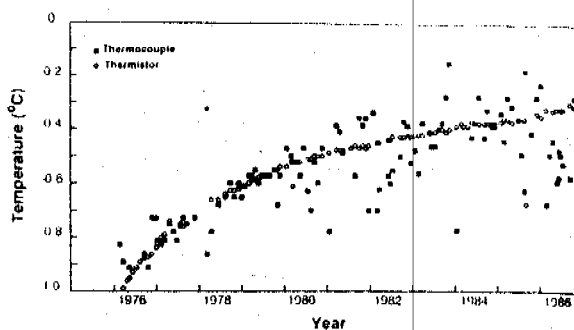


Figure 8. Comparison of field temperature measurements from paired thermocouples and thermistors buried in permafrost at 6 m depth, over a 10 year period.

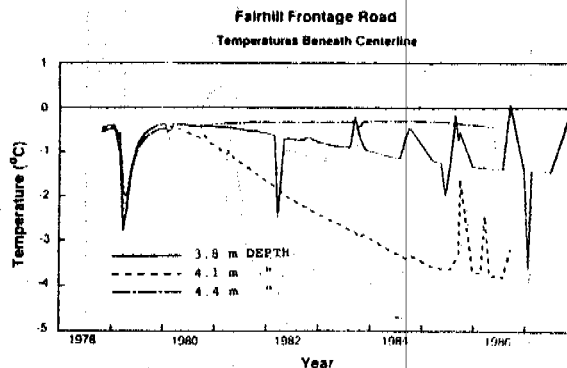


Figure 9. Temperature versus time plots of adjacent thermistors in permafrost. Indicates drift and erratic calibrations of thermistors at 3.8 and 4.1 m depths.

## SOIL ELECTRICAL RESISTANCE PROBES

The determination of frozen layer positions from measurements of the AC electrical resistance between a series of copper rings assembled on a vertical probe rod has been described by Atkins (1989). The SHRP probes were assembled to the design as developed by USA-CRREL, and had a length of 1.83 m with soil contact rings spaced at 50.8 mm intervals; each ring being connected to a separate conductor in a commercial multi-conductor cable. The cable is embedded into a slot milled into the side of a 32 mm PVC plastic rod. Conductors are soldered to each of the soil contact rings which are made by circling the rod with three wraps of #12 gauge copper wire.

The probes were installed in the same .25 m diameter boreholes as the curved TDR probes. Impact compaction and rodding were used to assure soil contact with the resistance rings. Field readings were made with an AC voltage and current source attached to each ring pair in sequence. Additional readings were made with the more technically correct 4-wire hookup, in which a voltage is imposed and current flow measured between the two outer rings of sequential 4-ring sets, and the voltage drop is measured between the two inner rings. This method eliminates the contact resistances between the soil and the rings, and will be further evaluated in future work.

At the test sites, freezing occurred only at Syracuse. There, two test dates indicated soil freezing, which reached a maximum of 0.5 m in late January of 1992. Except in the relatively dry gravel and crushed rock layers, the probes otherwise performed well. Resistance values in fine grained soils typically doubled upon freezing. The resistance values did not react to freezing of the gravels in the upper 0.1 m below the pavement. It is apparent that some judgement is needed in the interpretation of soil resistance versus depth profiles, as the values are variable in time and with material types. Better results are obtained when frequent observations are made. However, the resistance probes were judged useful in frozen layer determinations, and included in the final monitoring equipment plan.

## SUMMARY AND RECOMMENDATIONS

Based on sensor evaluations and field installation trials as described above, recommendations for simplified field installations at 62 North American highway study sites to be instrumented during 1993, were as follows:

- \* Temperature monitoring will be done at all sites using encapsulated thermistor probe assemblies, which provided the most consistent and accurate temperature measurements under field conditions with a variety of operators. Frost depths will be inferred from the temperature data.
- Soil electrical resistance probes will be installed at those sites and depths where significant soil freezing is anticipated. These probes will supplement soil temperature data for frost depth determinations and are particularly necessary in saline soil conditions.

- \* Soil moisture monitoring will be done using the TDR procedure at sites subjected to salt intrusion potentials from de-icing chemicals. The TDR method also provides good indications of the frozen/thawed state of soils up to salinities so high that the TDR signals are lost due to electrical shorting of the probes. If shorting becomes a problem in the field, the use of electrical insulating coatings on the center probe rods will be tested in future installations.
- \* TDR probes of both flat and curved types worked well in the field. The 3-prong probe designs proved slightly superior in signal strength and quality, and will be utilized in a flat configuration, with probes 200 mm in length and spaced at 38 mm apart. Up to ten TDR probes will be placed at intervals of depth in 254 mm diameter auger holes made through the pavement at the outer wheelpath.
- \* The pavement will be resealed above the probes by the reinsertion and re-bonding of the pavement core which was cut out in preparation for the borehole. All temperature, soil resistance and TDR probes will be placed in a single borehole to minimize time and costs.

## REFERENCES

- Atkins, R.T., 1989. Determination of Frost Penetration by Soil Resistivity Measurements. in: USA CRREL Special Report 89-23, State of the Art of Pavement Response Monitoring Systems for Roads and Airfields pp. 87-100
- Esch, D.C., 1989. Temperature and Thaw Depth Monitoring of Pavement Structures. in: USA CRREL Special Report 89-23, (Title as above) pp.78-86
- Kane, D.L., 1976. Soil Moisture Monitoring Under Pavement Structures using Time Domain Reflectometry. Alaska Department of Transportation, Report RD-87-08
- North, A.H., 1989. Evaluation of the TDR Technique for Volumetric Soil Water Content in Australian Soils. THESIS for BS Degree, University of New England
- Roth, K., Schulin, R., Fluhler, H., and Attinger, W., 1990. Calibration of Time Domain Reflectometry -Using a Composite Dielectric Approach. J. of Water Resources Research, Vol.26, No.10, Oct. pp.2267-2273
- Selig, E.T., and Wobschall, D.C., 1975. Capacitance Sensor for Soil Moisture Measurement, Transportation Resch. Rcd.#532 USA National Research Council, pp. 64-76
- Stott, M.G., Patterson D.E., and Phang, W.A., 1983. Developments in-Situ Monitoring of Moisture in Pavement Structures by Time Domain Reflectometry (TDR) R&D Report, Ontario (Canada) Ministry of Transportation
- Topp, G.C., Davis, J.L., and Annan, A.P., 1980. Electromagnetic Determination of Soil Water Content: Measurements in-coaxial transmission lines. Water Resources Research, 16: pp. 574-582

# INFLUENCE OF PORE FLUID SALINITY ON ELECTROMAGNETIC WAVE PROPAGATION PARAMETERS IN SOILS AT PERMAFROST TEMPERATURES.

Igor V. Fediukin and Anatoly D. Frolov

Russian State H. University, Miusskaja Sq. 6, Moscow, 125267, Russia

Basing on the our experimental data for the dielectrical properties of the frozen sand saturated with NaCl and KCl solutions ( with various initial concentrations  $10^{-5}$  - 1 mole/l ), there were evaluated the principal electromagnetic wave propagation parameters: complex refractive indexes, reflective coefficients, surfase impedance, wave velocities, absorption coefficient ect. The values of all parameteres have been obtained for the frequency range  $10^2$  -  $10^5$  Hz at positive and negative temperatures below and above of the eutectic point  $t_{eu}$  of the pore fluid. The paper presents the prime results and principal regularities that allow first to see the specificity of the influence of permafrost salinity on the electromagnetic wave propagation parameteres important for geophysical investigations, radiocommunications ect. in the Arctic coast regions.

## INTRODUCTION

The solution to many scientific and practical problems connected with the design and field realization of geophysical electromagnetic methods at permafrost areas, to remote radio wave research for construction, electro-magnetic sounding, radionavigation, and ground and underground radiocommunications in Northern regions needs clarification of conditions for electromagnetic wave propagation in frozen earth materials (Frolov 1977, 1978, Gussev et al. 1978).

In the Arctic shore regions saline frozen sandy and loamy soils are widespread (Dubikov 1990). Therefore the influence of the concentration and ionic composition of the pore fluids on the electromagnetic wave propagation parameters is very important. These data are practically absent at present. Data on the electrical properties of saline soils over a wide frequency range are very poor and as a rule, they have been obtained or at very low or at very high frequencies (Van Loon 1991, Pandit and King 1978, Zykov et al. 1990).

Therefore it is expedient to evaluate electromagnetic wave propagation parameters and estimate the essential laws of its dependence upon the salinity, the soil temperature and the field frequency. This is based on the our laboratory results (Fediukine et al. 1979, Frolov and Fediukine 1983) of studies of the real  $\epsilon'$  and imaginary  $\epsilon''$  parts of complex dielectric permittivity of frozen sand samples saturated with NaCl and KCl solutions.

As the principal parameters we have picked out real  $n'$  and imaginary  $n''$  parts of the complex refractive index, the surface impedance  $Z$ , the electromagnetic wave velocity  $V$ , the phase angle  $\varphi$ , the absorption coefficient  $\beta$ , the complex reflection coefficient  $R^*$  as well as the principal incidence angle  $i_0$  (the analogy of the Brewster angle for dielectrics).

All parameters were calculated in the frequency range  $10^2$  -  $10^5$  Hz, and for various concentrations of saturating pore solutions from 0 to 1 N at positive and negative temperatures below and above of the eutectic temperature  $t_{eu}$  of the pore fluid. The calculations were carried out for a uniform media and for some two-layer models. The optimum frequencies for underground radiocommunications and the radiointrosopy of the permafrost were evaluated and analysed too.

A number of results obtained need detailed analysis. In this paper we discuss only preliminary information about the most important characteristics.

## BACKGROUND

The experimental studies (Frolov 1978, Frolov and Fediukine 1983) has shown that it is impossible to calculate the values of electrical parametres  $\epsilon'$  and  $\epsilon''$  for moist sandy-argillaceous soils from additive mixture equations. The difference between the experimental and mixture equation calculated data is especially significant at relatively small water content (< 5 %) and low frequencies (<  $10^5$  Hz). This is conditioned by forming of the semi - isolated

quasibounded liquid phase domains (cells) linked by the very thin films. In these domains the ions migrating under influence of applied electrical field forms the electrical macrodipoles. The values of electrical moments of these macrodipoles and its contribution to the total polarisation of medium is greater, the greater the degree of domain discreteness and ion mobility and the lower the exciting field frequency. For the present there is only qualitative description of this phenomenon (Frolov 1978, Frolov and Fediukine 1983, Frolov 1991). Therefore the evaluation of the electrical (and derivative from its) properties of moist porous-capillary media must be based upon the experimental data.

Thus influence of pore fluid salinity on the electromagnetic wave propagation parameters was evaluated on the basis of our experimental data for the temperature ( $t^\circ$ ) and frequency ( $f$ ) dispersions of  $\epsilon'$  and  $\epsilon''$  of the specimens. The lows obtained on the influence of the pore fluid salinity on  $\epsilon'(f, t^\circ)$  and  $\epsilon''(f, t^\circ)$  must have some effect on the calculated wave parameters, and it is necessary to keep this in the mind during the analysis.

The characteristics obtained of  $\epsilon'$  and  $\epsilon''$  are (Fediukine et al. 1979, Frolov and Fediukine 1983, Frolov 1991):

1. Presence of a critical (bound) concentration of the pore solutions  $C_{cr} = (0.5 - 1) \cdot 10^{-2}$  N, which determines an abrupt change in the regularities governing the kinetics of freezing of soils, the unfrozen pore fluid and the saline pore ice contents and consequently, the values of  $\epsilon'$  and  $\epsilon''$ .

2. The electrical and the other physical properties of the frozen soils with  $C < 10^{-3}$  N are practically identical to the properties of the nonsaline soils.

3. If  $C > C_{cr}$ , the essential distinctions appear to be: the temperature interval of the phase changes is more extended. When  $C \geq 0.1$  N the intensive phase changes take place down to eutectic temperature  $t_{eu}$  of saturating pore solution and below.

In the last case the saline frozen sand become the analogy of the nonsaline one ( $C \leq 10^{-3}$  N) by the values of  $\epsilon'(f, t^\circ)$  and  $\epsilon''(f, t^\circ)$  at temperatures about 15 - 20° C below of  $t_{eu}$ . When  $C \sim 10^{-2}$  N the same state appeared at temperatures about 5 - 10° C below  $t_{eu}$ , especially at frequencies lower than 1 kHz.

During the analysis of the influence of the pore fluid salinity on the electromagnetic wave propagation parameters we distinguish the next most important cases:

a) frozen soil saturated with the low concentration solution ( $C < 10^{-3}$  N); and b) frozen soil saturated with the high concentration solution ( $C \geq 10^{-2}$  N) in particular cases: ba) temperatures  $t > t_{eu}$ ; and bb) temperatures  $t < t_{eu}$ .

## GENERAL EQUATIONS

The real  $n'$  and imaginary  $n''$  parts of the complex refractive index  $n = n' - j \cdot n''$  were calculated from the complex dielectric permittivity

$$\epsilon^*(f, t^\circ) = \epsilon^* = \epsilon' - j \cdot \epsilon''$$

using the relations:

$$n' = \sqrt{0.5 \cdot (\epsilon + \epsilon')} \quad n'' = \sqrt{0.5 \cdot (\epsilon - \epsilon')}$$

where  $\epsilon = [(\epsilon')^2 + (\epsilon'')^2]^{1/2}$  - the modulus of the complex dielectric permittivity. These equations as well as all underlying were obtained in the approximation that the relative magnetic permeability  $\mu = 1$ .

The absolute value of the surface impedance  $Z$ , the phase velocity  $V$  and the phase angle  $\varphi$  were calculated on the basis of the equations (Dolukhanov 1960, Von Hippel 1954, Kessenikh 1952):

$$Z = \frac{Z_0}{n} \quad V = \frac{c}{n'} \quad \varphi = \arctan \frac{n''}{n'}$$

where:  $Z_0 = 377$  Ohm - the impedance of the freespace,  $c = 3 \cdot 10^8$  m/s - the light velocity in the freespace,  $n = [(n')^2 + (n'')^2]^{1/2}$  - the modulus of the complex refractive index. To calculate the linear absorption coefficient  $\beta$  we used the expression:

$$\beta = \text{Re} \cdot \{ j \cdot \omega \cdot \sqrt{\epsilon^* \cdot \mu^*} \} = 2 \cdot \pi \cdot f \cdot \sqrt{\epsilon_0 \cdot \mu_0} \cdot n'' = 2.09 \cdot 10^{-8} \cdot f \cdot n'' \text{ (m}^{-1}\text{)}$$

where the frequency  $f$  is expressed in Hz.

The expressions for the complex amplitude reflection coefficients of the electromagnetic waves at a plane boundary of the frozen soils were obtained from the Fresnel formulas (Dolukhanov 1960, Von Hippel 1954, Kessenikh 1952). The reflection coefficient  $R_{En}^*$  for the wave electrical component normal to the incidence plane between medium 1 and 2 is:

$$R_{En}^* = R_{En} \cdot e^{j\psi_n}$$

where

$$R_{En} = \sqrt{\frac{[\sqrt{\epsilon_1} \cdot \cos i - A \cdot \cos \theta_n]^2 + [A \cdot \sin \theta_n]^2}{[\sqrt{\epsilon_1} \cdot \cos i + A \cdot \cos \theta_n]^2 + [A \cdot \sin \theta_n]^2}}$$

and

$$\tan \psi_n = \frac{\epsilon_1 \cdot A^2 \cdot \sin 2\theta_n}{\epsilon_2 \cdot \cos i - \epsilon_1 \cdot A^2 \cdot \cos 2\theta_n}$$

The reflection coefficient for the wave electrical component parallel to the incidence plane is

$$R_{Ep} = R_{Ep} \cdot e^{j\psi_p}$$

where

$$R_{Ep} = \sqrt{\frac{[\epsilon_2 \cos i - \sqrt{\epsilon_1} A \cos \theta_p]^2 + [\sqrt{\epsilon_1} A \sin \theta_p]^2}{[\epsilon_2 \cos i + \sqrt{\epsilon_1} A \cos \theta_p]^2 + [\sqrt{\epsilon_1} A \sin \theta_p]^2}}$$

$$\text{and } \tan \psi_p = \frac{\epsilon_1 A^2 \sin 2\theta_p}{\epsilon_2 \cos i - \epsilon_1 A^2 \cos 2\theta_p}$$

Here  $\epsilon_1$  and  $\epsilon_2$  are the absolute values of the complex dielectric permittivity for the upper and lower soils respectively,  $i$  is the incident angle and

$$A = [(\epsilon_2' - \epsilon_1' \cdot \sin^2 i)^2 + (\epsilon_2'' - \epsilon_1'' \cdot \sin^2 i)^2]^{1/4}$$

$$\theta_n = 0.5 \cdot \left\{ \arctan \frac{\epsilon_2'' - \epsilon_1'' \cdot \sin^2 i}{\epsilon_2' - \epsilon_1' \cdot \sin^2 i} - \arctan \frac{\epsilon_1''}{\epsilon_1'} \right\}$$

$$\text{and } \theta_p = \theta_n + \arctan \frac{\epsilon_1''}{\epsilon_1'} - \arctan \frac{\epsilon_2''}{\epsilon_2'}$$

## RESULTS AND DISCUSSION

The refractive index  $n'$  (fig.1) in the frequency range  $10^2 - 10^5$  Hz is characterized by strong frequency dispersion - it decreases 3-5 times for soils with  $C < C_{cr}$  over whole our temperature range and for the soils with  $C > C_{cr}$  at temperatures  $t < t_{eu}$ . Decreasing the temperature of the soil with  $C < C_{cr}$  from  $-3^\circ\text{C}$  to  $-25^\circ\text{C}$  diminishes  $n'$  100-300% in the frequency range  $10^2 - 10^4$  Hz. There is no effect on the value of  $n'$  at the frequencies  $> 10^5$  Hz (fig.1 a).

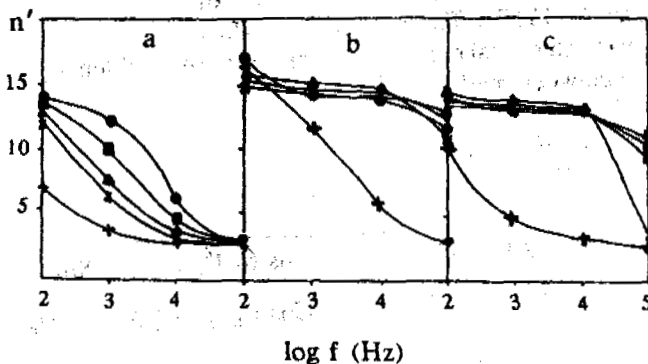


Fig.1. Frequency dependence of the refractive index of the specimens saturated with: a) NaCl  $C=10^{-3}$  N; b) NaCl  $C=0.1$  N; c) KCl  $C=0.1$  N.  
 ● -  $2.9^\circ\text{C}$ ; ■ -  $6^\circ\text{C}$ ; ▲ -  $9.4^\circ\text{C}$ ; × -  $13.5^\circ\text{C}$ ; + -  $25^\circ\text{C}$

In soils with  $C > C_{cr}$ , decreasing the temperature from  $-3^\circ\text{C}$  to  $t_{eu}$  has practically no influence on the value of  $n'$  (fig. 1 b,c).

It is interesting to note that the pore fluid ionic composition at the temperatures greater than  $t_{eu}$  feebly influence the  $n'$  value as well as its frequency and temperature dependence.

The curves in fig. 1a are typical for the soils saturated with NaCl and KCl solutions at concentrations  $C < 10^{-3}$  N. The curves in fig. 1 b,c are typical for soils saturated with highly concentrated ( $C > 10^{-1}$  N) NaCl and KCl solutions.

The imaginary part  $n''$  of the refractive index (fig. 2) has extreme frequency dependence, with the peak displacing to the low frequency region when the temperature drops.

For the soils with  $C < C_{cr}$  (fig. 2 a), the frequency of the maximum  $n''$  lie in the range  $10^3 - 10^4$  Hz at  $t > -9^\circ\text{C}$ , and in the range  $10^1 - 10^2$  Hz at  $t < -16^\circ\text{C}$ . The highest value of  $n''$  remains practically constant.

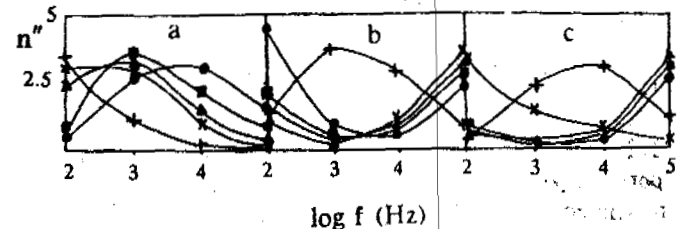


Fig.2. Frequency dependence of the imaginary part of the refractive index. (Designation see fig.1)

For the soils with  $C > C_{cr}$  (fig. 2 b,c) in the frequency range  $10^3 - 10^4$  Hz, the minimum of  $n''$  occurs at  $t > t_{eu}$  and the maximum at  $t \leq t_{eu}$ , which displaces to the lower frequency  $10^1 - 10^2$  Hz (fig. 2 c) when the temperature drops.

The surface impedance  $Z$  and phase velocity  $V$  have similar frequency and temperatures dependences. The surface impedance  $Z$  increases slowly from 25-40 Ohms at the low frequencies (fig. 3) to 100-130 Ohms at the high frequencies for the soils with  $C < C_{cr}$  and for the soils with  $C > C_{cr}$  at  $t < t_{eu}$ . The lower the temperature, the higher is  $Z$ . The impedance of the soils with  $C > C_{cr}$  at  $t > t_{eu}$  remain practically the same ( $\sim 20-30$  Ohm) over all of our frequency range (fig. 3 b,c).

Similarly, the phase velocity  $V$  changes from  $(2-3) \cdot 10^7$  m/s to  $(8-11) \cdot 10^7$  m/s when the frequency increase from  $10^2$  Hz to  $10^5$  Hz in the soils with  $C < C_{cr}$  and at the temperatures below eutectic in the soils with  $C > C_{cr}$ . But in the soils with  $C > C_{cr}$  at  $t > t_{eu}$  the phase velocity  $V$  is practically independent from the frequency and remain at the limits  $(2-3) \cdot 10^7$  m/s till the frequencies  $10^5 - 10^6$  Hz.

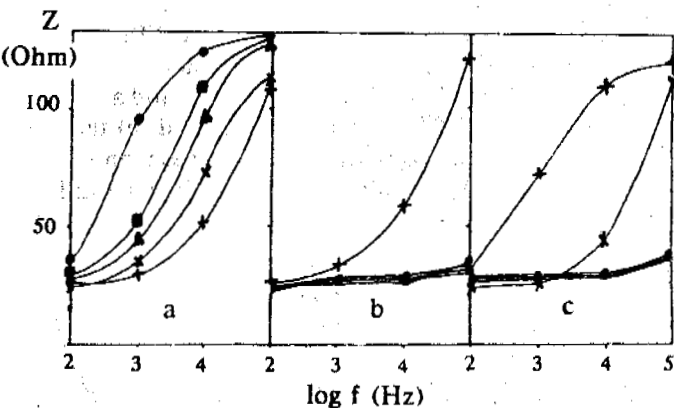


Fig. 3. Frequency dependence of the surface impedance (Designation see fig. 1)

The phase angle  $\varphi$ , as does  $n''$ , has a strong dependence on the frequency, changing in the limits from  $2^\circ$  to  $50^\circ$  (fig. 4).

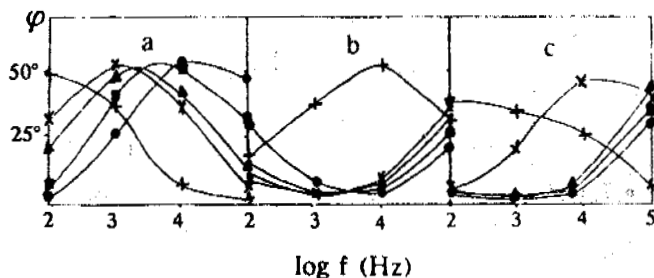


Fig. 4. Frequency dependence of the phase angle (Designation see fig. 1)

In the soils having low concentration of pore fluid the frequency of the maximum value of  $\varphi$  at temperatures near  $0^\circ\text{C}$  lies around  $5 \cdot 10^4$  Hz; at  $t = -25^\circ\text{C}$  it is three orders lower.

Increasing the saturating pore solution salinity above critical displaces the frequency of the maximum at  $t > t_{eu}$  in the high frequency region ( $\sim 10^6$  Hz). Decreasing the temperature below  $t_{eu}$  causes the frequency of the maximum to return to the frequency range ( $10^2 - 10^3$  Hz).

We think that the large difference between the values of  $\varphi$  at the frequencies  $10^3 - 10^4$  Hz at the temperatures below and above  $t_{eu}$  ( $3^\circ - 5^\circ$  and  $50^\circ$ ) may be used for the geophysical studies of the high saline frozen soils.

The absorption coefficient  $\beta$  (fig. 5) increases practically in proportion to the frequency from  $10^{-6} - 10^{-5}$  1/m to  $5 \cdot 10^{-4} - 7 \cdot 10^{-3}$  1/m except for the low saline soils at the low temperatures ( $t < -25^\circ\text{C}$ ), where  $\beta$  increase only by 10 times when the frequency rises three orders.

It is very interesting that the decrease of the temperature may cause the absorption coefficient to

increase. It was obtained for the soils with  $C < C_{cr}$  at the frequencies below  $10^3$  Hz and for the soils with  $C > C_{cr}$  in the frequency range  $10^3 - 10^4$  Hz.

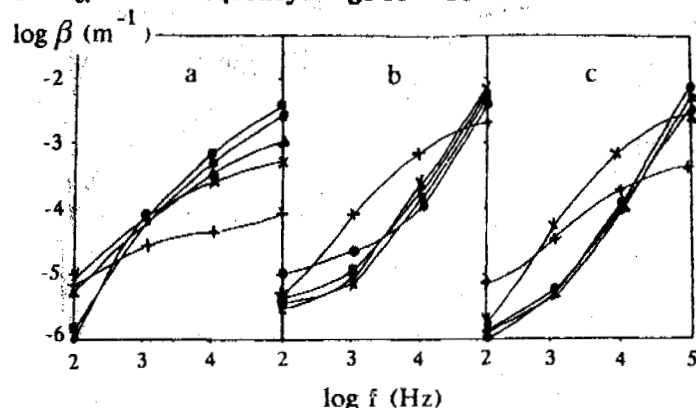


Fig. 5. Frequency dependence of the absorption coefficient  $\beta$  (Designation see fig. 1)

The existence of optimal frequencies for underground radiocommunications is caused by the fact that the increasing of the frequency on the one hand leads to an antennas effectivity increase, but on the other hand, to an increase of wave absorption. Expressions for the effectivity of underground radiocommunications in absorbing media were obtained from the literature (Rjevsky 1978). It has been shown that if the conduction currents are much greater than the displacement currents ( $\sigma \gg \omega \cdot \epsilon'' \cdot \epsilon_0$ ), the optimal frequencies for radiocommunications are inversely proportional to the square of the distance with the coefficient A depending on the geometrical parameters of the antennas and on the conductivity of a media such that

$$f_{opt} = A \cdot r^{-2} \quad (1)$$

We have calculated the frequency dependence of the effectivity of the radiocommunication taking into consideration  $\epsilon'$  and  $\epsilon''$  of the frozen saline sands. We found that in the high saline soils at the temperatures above the eutectic, the optimal frequencies diminish slowly with the distance as predicted by relation (1).

At the same time, if the concentration  $C < C_{cr}$ , the optimal frequencies at the temperatures near  $0^\circ\text{C}$  decrease with the distance much faster than that given by equation (1). For example, in the frozen sands with  $C = 0.5\text{N}$  at  $-3^\circ\text{C}$  the optimal frequency for radiocommunication at the distance  $r > 10^3$  m given by the formule (1) is ten times less than that given by the exact calculation.

The absolut value of the reflection coefficient  $R_{Ep}$  of the electromagnetic waves at the boundary of the air with the frozen soils have a clear minimum that corresponds to the changing of the phase of the reflected wa-



ve to  $\pi$ . This takes place at the incidence angle  $i_b$  (fig. 6).

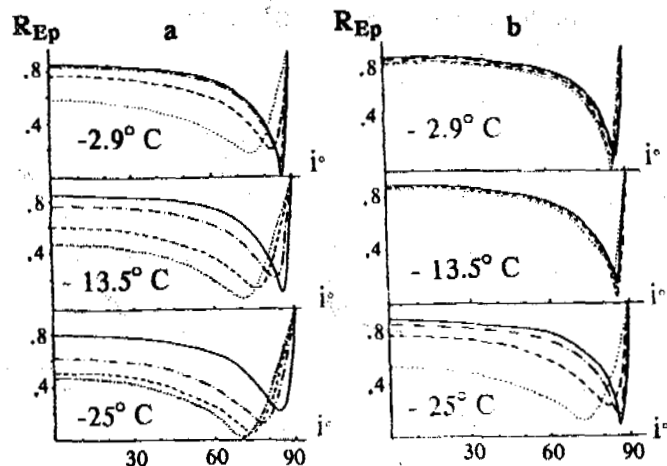


Fig. 6. Reflection coefficients vs incident angle for the air-soil boundary: a) nonsaline; b) saline NaCl  $C=0.1$  N. —  $10^2$  Hz; ---  $10^3$  Hz; - - -  $10^4$  Hz; ····  $10^5$  Hz.

It has been noted that the values of  $R_{Ep}$  and  $i_b$  decrease with increasing frequency and decreasing temperature. The minimal value of  $R_{Ep}$  grows at the low frequencies and diminishes at the high frequencies when the temperature decreases. The diminution of  $i_b$  with decreasing temperature becomes more visible at the high frequencies.

The comparison between the dependencies of  $R_{Ep}$  upon the incidence angle at the boundary of the air and nonsaline sands (Gussev et al. 1978) with the saline one shows that:

1. With increasing frequency the reflection coefficient from the saline sands decreases far more slowly than from the nonsaline sands.
2. The principal reflection angle  $i_b$  for the saline soils is greater at all frequencies and temperatures than that for the nonsaline soils.
3. The principal reflection angle for the high salinity soils at  $t > t_{eu}$  is practically independent of the temperature.

At  $t < t_{eu}$  the saline values of  $R_{Ep}$  and  $i_b$  and its frequency and temperature dependencies are close to a those for the nonsaline values.

The absolute value of  $R_{En}$  uniformly increases with the incidence angle from the same value for  $R_{En}$  and  $R_{Ep}$  for normal incidence to 1 for the waves parallel to the boundary and hasn't any interesting particularities.

The absolute values of the reflection coefficients of the electromagnetic waves at the boundary of the frozen soils with the different properties were also calcu-

lated. In fig. 7 examples for two models are given: a) the upper layer is the nonsaline sand at different temperatures (the seasonal layer in summer and in winter) and the lower layer is the nonsaline sand at the fixed temperature  $2.9^\circ$  C (permafrost); and b) the upper layer is the same as in the preceding case, and the lower one is the high saline ( $C=0.1$  N) frozen sand at  $-2.9^\circ$  C.

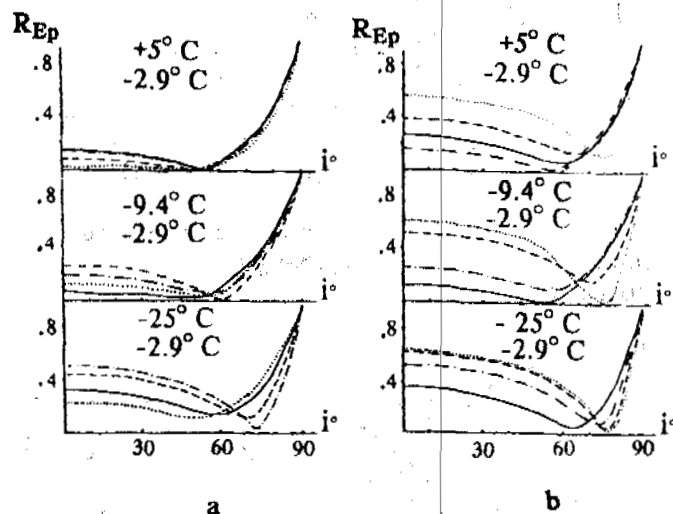


Fig. 7. Reflection coefficients vs incident angle for two layers models: a) and b) see in the text (Designations see fig. 6.)

The reflection parameters in these two models are very different and appears to be a good physical base for the mapping of a saline frozen soil layer by electromagnetic methods. The differences in the values of  $R_{Ep}$  and  $i_b$  between models a and b increase with rising frequency and reach the highest sizes at  $10^5$  Hz. Supposing that this trend remains up to the range  $10^7 - 10^8$  Hz, then there is a very good outlook for the sounding of saline soils by radiolocation methods.

It is to be noted that unlike the air-soil boundary case (fig. 6), in this model the inverse dependence of  $R_{Ep}$  at the high and low frequencies takes place, as well as does the other range of the incidence angles nearby of which occurs the changing of the reflected wave phase.

During the estimation of the optimal frequency for the radiointrospection of the boundary of the soils at the negative temperatures, besides the dependence of the effectivity of the antennas and the absorption coefficient from the frequency, an important role play the reflection coefficient at the boundary of the soils.

We found that if at least one of two soils is highly conducting and the depth of the boundary is small, the values of the optimal frequencies may be well described by the formulas of the type (1). However, to so-

und, the boundary of the nonsaline sands with the saline one at the temperature near  $-3 \pm 5^{\circ}\text{C}$ , the value of the optimal frequency for distances more than 100 m may be 10 times greater, given formula (1). This deviation of the frequency from the optimum value may diminish the amplitude of the signal by 100 - 500 times.

## CONCLUSION

We have presented and discussed calculated electromagnetic wave propagation parameters to see for the first time the specific influence of the permafrost salinity. We obtained principal characteristics that must be taken into consideration for the design and realisation of the geophysical methods for the Arctic coast regions, construction and exploitation of the radio-communication and radionavigation systems, power transmitting systems, etc. Moreover, the data obtained, especially for the reflection coefficients for the two-layer models, contain useful information for the further development and perfection of the electromagnetic geophysical sounding of the saline permafrost and cryopegs.

## ACKNOWLEDGEMENT

The authors gratefully acknowledges the contribution to our common studies of dielectric properties of saline frozen soils made by Dr. Boris V. Gussev, who met an untimely death.

## REFERENCES

- Dolukhanov M.P. 1960. "Radio wave propagation", 491 pp., Sviaz Press, Moscow.
- Dubikov G.I., Ivanova N.V. 1990. "Saline frozen soils and their distribution on the USSR territory", Coll. "Saline frozen soils as the foundations of constructions", Nauka Press, Moscow, 3 - 9.
- Fediukine I.V., Frolov A.D., Gussev B.V. 1979. "Influence of salinity on the electrical properties of frozen soils", Doklady Acad. Sci. USSR, v. 244, N4, 941 - 944.
- Frolov A.D. 1977. "Dynamic properties of frozen soils and areas of their applications to the solution of mining and geological problems". Izvestia VUZov, Geol. and Razvedka, N10, Moscow, 122 - 127.
- Frolov A.D. 1978. "Basic regularities of forming and changing of the electric and elastic properties of frozen earth materials". Doct.Sci.Thesis, Moscow Mining Inst, 310 pp.
- Frolov A.D., Fediukin I.V. 1983. "On the polarization of frozen soils in the time various electric fields". Izvestia VUZov, Geol. and Razvedka, Moscow, 90 - 96.
- Frolov A.D. 1991. "Peculiarities of phase changes in quartz sand saturated with salt solutions at  $0^{\circ}\text{C} - 40^{\circ}\text{C}$ ". Proc. III intern. Symp. on Cold Regions Heat Transfer, U.A.F., Fairbanks, Alaska, USA, 293 - 301.
- Gussev B.V., Fediukine I.V., Frolov A.D. 1978. "Some electromagnetic wave characteristics in frozen soils". Materials for III ICP, Edmonton, Canada, Coll. N2, Engineering Geocryology, Novosibirsk, Nauka Press, 273 - 278.
- Hippel A.R. von. 1954. "Dielectrics and waves". U. Wiley and sons INC., New York, 430 pp.
- Kessenikh V.N. 1952. "Radio wave propagation". GITTL Press, Moscow, 488 pp.
- Loon W.K.P. Van. 1991. "Heat and mass transfer in frozen porous media". Ph.D.Thesis, Agric Univ., Wageningen, Netherland, 204 pp.
- Pandit B.I., King M.S. 1978. "Influence of pore fluid salinity on seismic and electrical properties of rocks at permafrost temperatures". Proc. III Int. Conf. on Permafrost, vol. 1, NRC, Ottawa, Canada, 553 - 559.
- Rjevsky V.V., Korenberg E.B. 1978. "Mining radio-introsopy and radiocommunication". Nedra Press, Moscow, 273 pp.
- Zykov Y.D. et al 1990. "Electrical and acoustic properties of the saline frozen soils". Coll. "Saline frozen soils as the foundations of constructions". Nauka Press, Moscow, 128 - 135.

ASPECTS OF NATURAL RECOVERY OF SOILS, HYDROLOGY AND  
VEGETATION AT AN ABANDONED HIGH ARCTIC SETTLEMENT,  
BAFFIN ISLAND, CANADA<sup>1</sup>

Bruce C. Forbes

Department of Geography, McGill University  
Montreal, Quebec, Canada H3A 2K6

Vehicular traffic is a mechanical impact associated with land-based resource development of all kinds, as well as recreation and military activities. 21 years after it was abandoned, a small, coastal settlement has resulted in surface disturbances among soils, vegetation and hydrology which have both similarities and differences when compared to low arctic disturbances of comparable proportions. Reported here are patterns of local response, with the emphasis on substrate effects. Soils in single- and multi-pass vehicle tracks often exhibited altered moisture regimes which, in turn, has affected surface albedo. Organic layers were typically compacted or lacking, thus affecting active layer processes. Tracks perpendicular to the local slope have channelled surface and subsurface flow from snowmelt runoff and, as a result, have had significant effects on downslope plants and soils, including species composition and cover, soil moisture, surface albedo, active layer processes and soil chemistry.

#### INTRODUCTION

Beginning winter 1969-70 the settlement of Clyde River (70°26'N, 68°31'W) was dismantled and moved to a new location (70°28'N, 68°34'W) on the western shore of Patricia Bay, NE Baffin Island (Fletcher 1975). The abandoned settlement provided the opportunity to investigate more than two decades of unassisted recovery among high arctic vegetation and soils. Biotic aspects of these disturbances have been reported elsewhere (Forbes 1992b, 1993a, b). The purpose of this paper is to provide details on some abiotic substrate effects, in particular cumulative hydrological changes associated with vehicular traffic, including shifts in surface reflectance, soil moisture, pH and active layer development.

The literature of high arctic disturbance ecology provides an extremely limited amount of data on responses to anthropogenic disturbances of any scale, intensity or age. Particularly lacking are long-term data on the community-level recovery potential of the most productive wet and mesic sedge-moss meadow habitats, mainly occurring in coastal lowlands, which are of minimal extent and thus of critical importance to the region's herbivores (Anonymous 1972; Bliss 1977). Long-term and cumulative impacts resulting from large-scale development have been addressed in the Low Arctic (Lawson 1986; Walker et al. 1986, 1987), but data from the High Arctic have not been forthcoming. It is well known that the High Arctic differs considerably from the Low Arctic in terms of its floristics, vegetation, climate, soil development and hydrology (Young 1971; Moore 1978; Maxwell 1981; Woo 1986; Edlund 1990), yet we have no long-term data on anthropogenic disturbance by which to compare these two regions. Taken together, the extant

applied studies of disturbance in the High Arctic of North America treat mostly short-term vehicle damage and fertilization effects (cf. Kevan 1971b; Babb 1972; Babb & Bliss 1974; Barrett 1975; Barrett & Schultén 1975; Bliss 1975; Addison & Bell 1976; Henry et al. 1987; Bliss & Grulke 1988).

Both intentional and inadvertent obstruction of groundwater flow by roads and other barriers can have profound effects in permafrost regions through either impoundment, in areas upslope from the barrier, or drainage in downslope areas (cf. Pomeroy 1985; Woo 1986; Forbes 1992a). Studies of the spatial, temporal and chemical variability of spring runoff in the High Arctic have shown that late-lying snow banks provide much of the moisture and often many of the nutrients critical to the maintenance of the limited number of well-vegetated lowlands (Rydén 1977; Woo & Steer 1986; Buttie & Fraser 1992). As much as 80% of the annual precipitation can be lost into the atmosphere through evaporation, leaving only 20% for runoff, which occurs mostly during and immediately after the melt period (Ohmura 1982). Because of this limited window of moisture availability, researchers have long warned of the need to prevent obstruction of the lateral flow of surface and subsurface waters across tundra sedge-meadows. Kevan (1971a), for example, speculated that "on gently sloping wet meadows vehicles may (*italics mine*) press the vegetation into shallow troughs, which then direct water that would normally percolate over a wide area, thus draining all or part of the meadow and reducing its biotic productivity over many years". Until now there have been no data to either support or refute such predictions, given that the only such studies from Alaska (cf. Walker et al. 1987) are of an entirely different scale in a different biogeographic region.

Woo (1986:218) noted that "off-road vehicles can gouge the soil if used *repeatedly* (*italics mine*), and the tracks can develop into rills or depressions that promote and concentrate surface

<sup>1</sup> This paper is dedicated to the memory of Jopi Tassugatt, who assisted in the collection of the data presented here.

flow". Similarly, Dyke (1985:1), testing light tracked vehicles in central Keewatin peatlands, found that "little degradation takes place with a single trip under any terrain conditions". The present data show that even a single passage of a tracked vehicle on mesic, sloped high arctic tundra may be sufficient to induce several aspects of the changes discussed by Kevan, Woo and others (cf. Haag & Bliss 1974).

## STUDY SITE

The study area at 'Old' Clyde River (henceforth 'CR') is considered representative of the gently-sloping (ca. 3-4°) and hummocky lowlands of eastern Baffin Island, where disturbance of this nature has not previously been documented. The actual slope on which the abandoned settlement sits has a westerly aspect, facing into the prevailing winds during much of the year (Fletcher & Young 1976). A J.I. Case™ 1000D excavator was brought to the site of Clyde ca. 1965 and its use over the following 4-7 yr resulted in a number of surface disturbances (Forbes 1992b). Late-lying snow banks provide moisture to ungrazed, *Sphagnum*-dominated transitional-poor fens (*sensu* Sjörs 1952) during spring runoff, which was more or less complete by the first week of July 1990. This site falls within the High Arctic as delineated by, Woo (1986) and Bliss & Matveyeva (1992), and within Young's (1971) Zone 3 based on vascular floristics. Most of the eastern Baffin lowlands, including the Kogalu Lowland where CR is located, are within the 4°C bioclimatic zone as mapped by Edlund (1990). The actual July temperature mean was closer to 4.6°C, with average summer precipitation of 6.5 cm, during the course of this study and during the period 1948-1972 (Forbes, unpublished data; Fletcher & Young 1976; see also sources in Andrews et al. 1980). Seasonal thaw depths of 1 m were rare and restricted to areas such as late-melting snow patches where the vegetation and organic mat are thin and relatively dark in color.

## METHODS

A series of archival, black and white vertical airphotos from the period 1960 to 1983 were obtained from the National Airphoto Library in Ottawa and enlarged five times to a scale of 1:1200 to help construct a chronology of disturbance and to judge the spatial extent of surface impact, including hydrological change. Vertical airphotos were analyzed with a Macbeth QuantaLog™ RD-400 Reflection Densitometer, which provides a measure of diffuse density on a scale from -0.5 (white body) to 0.5 (black body). Density measurements from photos were made along transects matching as closely as possible those made during stratified random quadrat sampling in the field (see Forbes 1992b). These transects included both water tracks (or channels) and adjacent interfluves, similar in appearance and function to those reported for the Low Arctic by Walker et al. (1989).

Soil cores 5 cm in diameter (volume 100 cm<sup>3</sup>) were extracted once from just outside each of ca. 260 permanent quadrats (25 x 50 cm) over a precipitation-free 48 hr period from 7-9 July 1989. Several stands were resampled 5-7 July 1990 for comparative purposes. In each case sampling took place ca. three weeks after most of the study site was snow-free. These were taken between 5-10 cm (rooting depth) below the mineral

soil/organic layer interface, the depth of which was noted in each case and photographed in many, or 5-10 cm below the surface in the event the organic mat had been removed. Standard methods were followed to obtain measurements of gravimetric water and bulk density (Klute 1986). In 1990 the pH of mineral (and occasionally highly organic) soils and surface waters (if any) was measured in the field once a month for each quadrat using a Cole Parmer model 5985-80 Digi-Sense™ meter accurate to ±0.05 according to methods given in Sheldrick (1984).

Seasonal development of the active layer was measured using a 1 cm x 1 m steel probe calibrated with 10 cm etched increments. Readings were taken once daily during 1988 by probing randomly just outside a chosen edge of each quadrat. In 1989 these readings were made from 10 June to 15 July. After 15 July, sampling frequency was reduced to twice weekly and continued until 30 August. In 1990, readings were made 2-3 times weekly until 21 July and once weekly thereafter.

## RESULTS

Analysis of surface reflectance in the July 1969 airphoto revealed that vehicle tracks running perpendicular and diagonal to local slope had already impeded local drainage and altered surface albedo prior to abandonment (Fig. 1). Changes were evident in tracks, both single- and multi-pass, and in drained peatlands downslope. At the time, reflectance was apparently increased in multi-pass tracks and decreased in single-pass tracks. In a separate set of multi-pass tracks, where the organic mat was mostly destroyed but portions of the sedge mat remained intact, albedo was decreased at the time of abandonment (Fig. 2). However, within four years the rapid regeneration of rhizomatous graminoids in the tracks had resulted in a substantial increase in albedo compared to adjacent controls. Over twenty years later, mid-season gravimetric water measurements have shown that the drained peatlands remain drier, often significantly, than the controls upslope. Relative to upslope control areas, reductions of 3.5-5% were measured 2 m downslope from single-pass tracks and 12.5-15% 2 m below multi-pass tracks. Measurements made at distances of 10 m below the same sets of tracks yielded similar results. In the airphoto analysis, wet areas appear dark because of the high radiation absorption and generally register tone densitometer values of >0. Drained areas appear lighter due to the low moisture and relatively high reflectivity of these areas and generally provide values of <0. It is notable that the changes in reflectance in drained areas induced by single- and multi-pass tracks were essentially equivalent (Fig. 1), and that soil pH tended to become more basic in each of the drained and tracked areas relative to control areas upslope (Fig. 3).

Sampling of vegetation composition and cover (Forbes 1993b) has shown that, in the long-term, both vascular and non-vascular plants have responded to the changes in hydrology. In general, cover/abundance and frequency of *Sphagnum* spp. and rhizomatous aquatic sedges (e.g. *Carex aquatilis* var. *stans*, *Eriophorum angustifolium*) were reduced or eliminated altogether in drained areas, while *Salix arctica* and other dwarf shrubs and caespitose graminoids (i.e. *Luzula nivalis*) were increased. Rhizomatous sedges and grasses (e.g. *Carex*, *Dupontia fisheri*

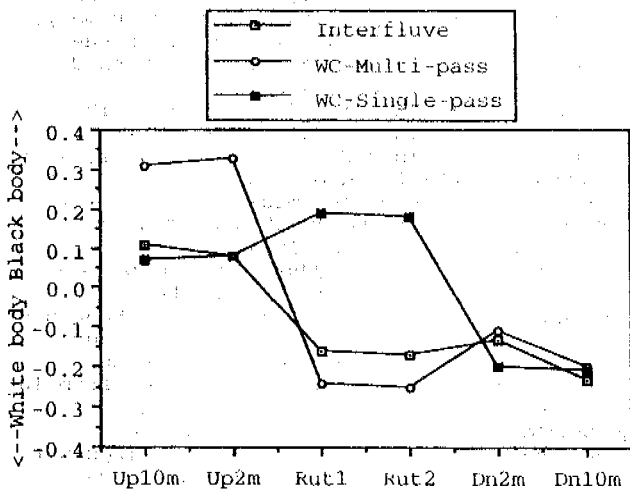


Figure 1. Surface reflectance from vehicle tracks, drained peatlands and upslope controls at Clyde River. Abbreviations are: Up=upslope from ruts; Dn=downslope from ruts; WC=water channel. Local slope=3-4°. Source=B/W airphoto No. A21157-157.

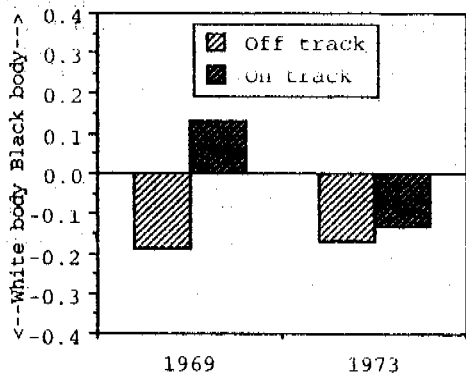


Figure 2. Surface reflectance from multi-pass tracks and adjacent controls at Clyde River. Source=B/W airphotos Nos. A21157-157 and A23500-46.

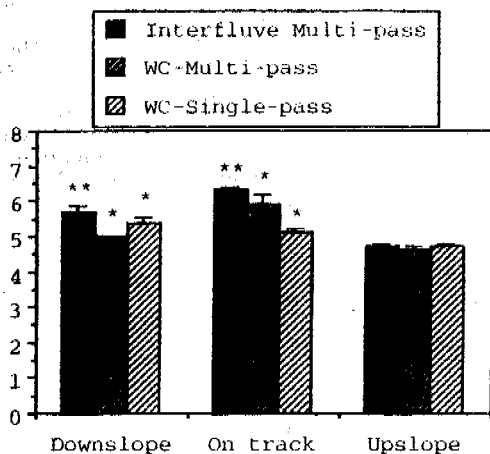
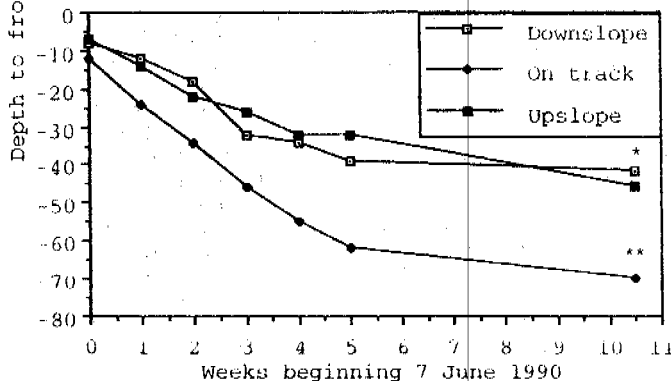
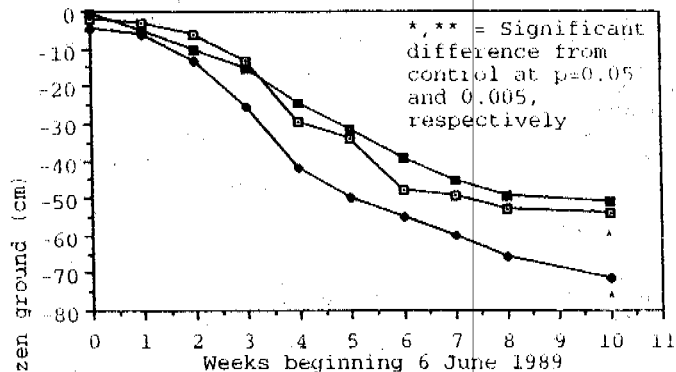
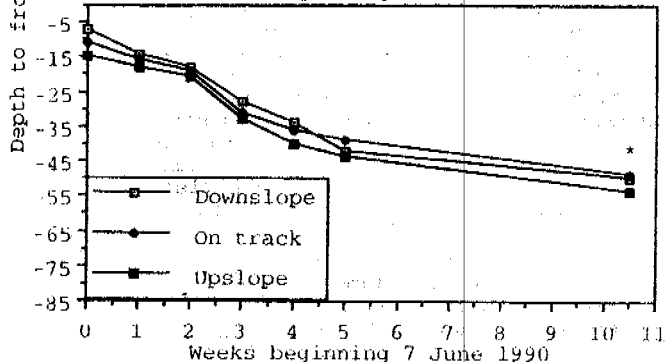
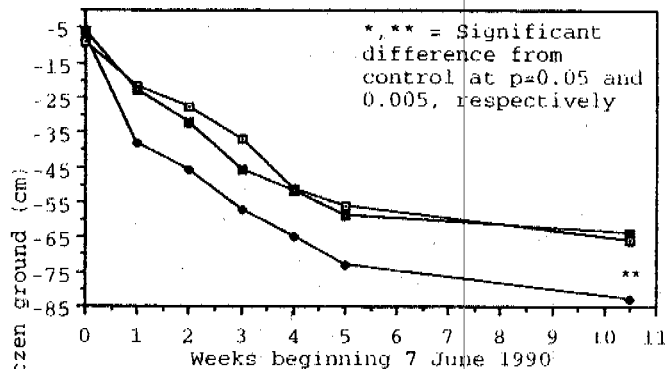


Figure 3. Mid-season pH of mineral soils along the same transect sampled in Fig. 1. WC=water channel; n=10; \*, \*\* = 0.005 and 0.0005, respectively.



Figures 4 (above) and 5 (below). Active layer development at Clyde River, Baffin Island in multi-pass tracks, drained peatlands and upslope controls.



Figures 6 (above) and 7 (below). Active layer development at Clyde River, Baffin Island in multi- (above) and single-pass tracks (below), drained peatlands and upslope controls.

ssp. *psilosantha*, *Eriophorum*) predominated in ruts, where woody species remained significantly reduced or were lacking altogether (see Forbes 1992b).

The microtopographic differences between multi-pass tracks and adjacent controls is attributed to the destruction of the organic mat, soil compaction, and a loss of fines (Forbes, unpublished data). Active layer development remained consistently enhanced in multi-pass vehicle tracks, a pattern which is repeated each year (Figs. 4, 5, 6). Single-pass tracks, on the other hand, did not thaw as rapidly nor to as great depths as adjacent controls (Fig. 7). There, the organic mat remained largely intact but noticeably compressed (Forbes, unpublished data). Active layer development remained retarded in drained peatlands below both single- (Fig. 7) and multi-pass (Figs. 4, 5, 6) tracks, at least in the earlier part of the growing season. This pattern was also repeated in each of the three years for which measurements were made, although the differences at the thermal maximum in late August were more variable among years.

#### DISCUSSION

Despite the increase in reflectance on multi-pass tracks after 4 yr (Fig. 2), presumably because of the invasion of rhizomatous graminoids (cf. Forbes 1992b), active layer development remained significantly enhanced in the tracks after 221 yr. The tracks also remained significantly wetter than adjacent undisturbed terrain and the organic mat failed to regenerate. The original hummock-forming *Sphagnum* spp. were replaced by bryophytes typical of more aquatic and/or calcareous habitats (i.e. *Bryum cryophilum*, *Hypnum hambergeri*, cf. Vitt 1975), which were lacking in the adjacent mesic, undisturbed vegetation. In a study of seasonal heat flux in low arctic Alaskan tundra soils, Jorgenson (1986) revealed that surface moisture accounted for 64% of the variation, organic matter depth 13%, and tundra vegetation only 5% (see also Rouse 1984). In light of both sets of findings, the enhanced active layer development is not surprising. What is unusual and perhaps more critical for the status of the lowland is the extent to which the disturbance spread across the landscape in a short period of time. Many thousands of square meters of drained peatlands are evident in the older airphotos and were still evident during an overflight in 1989. Thus, a second critical characteristic of these disturbance regimes is the persistence of their effects.

The seasonal variation in albedo appears somewhat similar to that reported for winter roads in the Low Arctic by Haag & Bliss (1974), because even slight depressions from a single pass of a tracked vehicle are apparently capable of acting as small snow catchment basins. The snow certainly works to increase albedo in the tracks early in the season. However, once snowmelt is complete the level of reflectance of the various tracks is linked to the extent to which moisture persists through the growing season, the degree of vegetation cover, and whether exposed soils are organic and thus relatively dark or mineral and relatively light. Haag (1974) found a general increase in albedo was correlated with the growth and development of plant cover and that the seasonal maximum albedo corresponded to the time of maximum standing crop of vegetation.

Little snow accumulates on the lowland's windward slopes where most sampling took place, especially close to the shore. Moisture percolation across the drained areas is thus minimal or lacking, leaving the tundra surface dry through much of the remainder of the growing season. Precipitation events were uncommon after June and typically left only traces of moisture. Given this situation, it is unlikely that seasonal albedo flux is great in the drained peatlands. What variation exists is perhaps due more to vegetation growth than the local moisture regime. We may infer indirectly, based on the active layer development profiles (Figs. 4-7), that seasonal soil heat flux is apparently more variable. By this reasoning, drained soils should be cooler early in the season, as reflected by the shallower active layers seen in the first few weeks along the transects. These differences were reversed in three of the four transects by week five. It was highly significant that a single passage of a vehicle across a water channel during summer was able to induce responses so similar to multi-pass tracks in terms of altering local drainage and its effects on downslope reflectance and active layer development. These findings contrasted with Woo's (1986) assertion that repeated passes are necessary to gouge the tundra and effectively direct surface flow.

Changes in vascular and non-vascular plant composition and cover associated with vehicle tracks corroborate the earlier assertion by Shaver et al. (1983), based on work in the Low Arctic, that retention of the organic mat is critical in terms of directing vegetation dynamics on disturbed patches. However, whereas they emphasized the organic mat's importance in relation to the extensive seed bank and store of nutrients it potentially provides, in the High Arctic its retention in a wetland of any kind (ranging from oligotrophic to minerotrophic) invariably means that some rhizomatous and/or viviparous graminoids have resisted the impact (Forbes 1992b) and will be at an advantage when the disturbance ceases and regrowth begins. The emergence of seedlings of any kind from disturbed peat was extremely rare. In general, rhizomatous sedges responded favorably to 'pulse' disturbances (i.e. single-pass vehicle tracks) that left the organic mat intact (Forbes 1992b). In contrast to the more gradual and perhaps subtle shifts in dominance within the vascular canopy in tracked and drained areas, the cryptogamic understory may exhibit much more rapid and dramatic changes in composition (Forbes 1993b). The retention of the organic mat in tracked areas, and subsequent response of vegetation, also has a profound effect upon surface reflectance, soil pH and active layer development. The patterns of recolonization among both herbaceous and woody species differ appreciably from those reported by Chapin & Shaver (1981) and others working in the Low Arctic. For example, Gartner et al. (1983) showed that natural revegetation of a disturbed Alaskan tussock grassland, mainly from buried seeds, resulted in a cover of only two of the original species after four years. Similarly, Ebersole (1985) and Hernandez (1973) found seedlings of up to 35 taxa on disturbed mesic substrates, including many *Salix* spp. Only a few seedlings from among a much more limited number of taxa were observed on tracked ground in the High Arctic, even after two decades (Forbes 1992b). In drained areas, desiccated and dying aquatic plant communities continue to be replaced by those

tolerant of more mesic conditions.

#### CONCLUSION

Both field sampling and remote sensing have provided evidence of cumulative impacts which have extended far beyond the areas of initial anthropogenic disturbance, apparently quite rapidly ( $\leq 4$  yr), and have persisted to the present ( $\geq 21$  yr). The long-term nature of these effects contrasts with results from short-term studies of vehicular impact in the High Arctic by Babb & Bliss (1974:561), who concluded that such disturbances "do not appear to extend beyond the areas immediately affected". Egginton & Ferris (1980) came to similar conclusions in the Low Arctic. The extent of vegetation recovery in tracked areas was minimal compared to the Low Arctic and the effects of peatland drainage were of a much smaller scale than those reported for Alaska, yet still locally significant. This appears to limit somewhat the applicability of findings from the studies outside the High Arctic. Given that the ruts from single- and multi-pass tracks (Fig. 8) continued to alter the snowmelt runoff regime on these slopes, it is unlikely that either the drained peatlands or the tracks themselves will regain thermal equilibrium in the foreseeable future. It was a surprise to find that hydrological changes resulting from single-pass tracks were capable of substantially reducing soil moisture and surface albedo, altering active layer development, increasing soil pH and affecting significant changes in downslope plant communities. These findings serve to increase the level of caution necessary when planning developments in wet to mesic, well-vegetated areas of the High Arctic. Particular

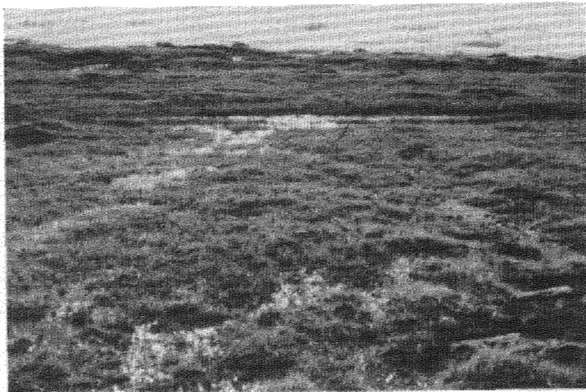


Figure 8. View looking down a  $3^\circ$  slope from the center of a water channel during the beginning of snowmelt runoff. Note the inability of the water to reach the shoreward areas beyond the tracks, leaving these downslope areas extremely desiccated after  $\geq 21$  yr. This has resulted in the extreme reduction in cover/abundance of many aquatic plants and the extinction of thousands of square meters of *Sphagnum* hummocks. In almost two decades of disuse, a significant amount of fines have been washed from the exposed mineral soils in the tracks, leaving a compacted sandy surface with few plants other than three aquatic graminoids. One of these, *DuPontia fisheri* ssp. *psilosantha*, is a colonist not present in the adjacent control area. Photo date: 12 June 1990

caution is advised where local slope exceeds  $3^\circ$ , given the extremely limited extent of wetlands in the High Arctic, many of which are gently-sloping (Babb & Bliss 1974; Tarnocai & Zoltai 1988). Even gentle slopes have the potential for serious cumulative hydrological impacts resulting from ostensibly low-intensity individual or 'pulse' disturbances. Cumulative effects of drainage on plant community productivity and nutrient uptake of dominant graminoids and deciduous shrubs, as well as further details on soil heat flux, will be discussed in a future paper.

#### ACKNOWLEDGMENTS

Financial and/or logistical support for this research were provided by: the Arctic Institute of North America; Department of Indian and Northern Affairs; McGill University; Northern Heritage Society/Science Institute of the Northwest Territories; Polar Continental Shelf Project; and G.W. Wenzel. I would like to thank field assistants C.C. Earnshaw, H. Whitaker and the late J. Tassugatt, and the Hamlet of Clyde River for permitting the work on the abandoned settlement.

#### REFERENCES

- Addison, P.A. and K.A. Bell (1976) Plant growth in relation to surface disturbances, King Christian Island, ALUR Report 75-76-73, DINA, Ottawa, 24 p.
- Andrews, J.T., W.N. Mode and P.T. Davis (1980) Holocene climate based on pollen transfer functions, eastern Canadian Arctic, *Arct. Alp. Res.*, 12:41-64
- Anonymous (1972) Arctic ecology map series - critical wildlife areas, 1:1000000, Lancaster Sound (2036), NTS Nos. 48 & 58, Prepared by Renewable Resources Consulting Services for the Canadian Wildlife Service, Ottawa
- Babb, T.A. (1972) The effects of surface disturbance on vegetation in the northern Canadian Arctic Archipelago, M.Sc. thesis, Univ. of Alberta, Edmonton
- Babb, T.A. and L.C. Bliss (1974) Effects of physical disturbance on high-arctic vegetation in the Queen Elizabeth Islands, *J. Appl. Ecol.*, 11:549-562
- Barrett, P.E. (1975) Preliminary observations of off-road vehicle disturbance to sedge-meadow tundra at a coastal lowland location, Devon Island, N.W.T., ALUR 73-74-71, DINA, Ottawa, 34 p.
- Barrett, P.E. and Schultén, R. (1975) Disturbance and the successional response of arctic plants on polar desert habitats, *Arctic*, 28:70-73
- Bliss, L.C. (ed.) (1975) Plant and surface responses to environmental conditions in the western High Arctic, ALUR 74-75-73, DINA, Ottawa, 72 p.
- Bliss, L.C. (1977) Introduction, IN: L.C. Bliss (ed.) Truelove Lowland, Devon Island, Canada: a high-arctic ecosystem, Univ. of Alberta Press, Edmonton, pp. 1-11
- Bliss, L.C. and N.E. Grulke (1988) Revegetation in the High-Arctic: its role in reclamation of surface disturbances. IN: G.P. Kershaw (ed.), Northern environmental disturbances, Occ. Pub. No. 24, Boreal Institute for Northern Studies, Edmonton, pp. 43-55
- Bliss, L.C. and N.V. Matveyeva (1992) Circumpolar arctic vegetation, IN: F.S. Chapin III, R.L. Jefferies, J.F. Reynolds, G.R. Shaver and J. Svoboda (eds.) Arctic ecosystems in a changing

- climate: an ecophysiological perspective, Academic Press, N.Y., pp. 59-89
- Buttle, J.M. and K.E. Fraser (1992) Hydrochemical fluxes in a high arctic wetland basin during spring snowmelt, *Arct. Alp. Res.*, 24:153-164
- Chapin, F.S. III and G.R. Shaver (1981) Changes in soil properties and vegetation following disturbance of Alaskan arctic tundra, *J. Appl. Ecol.*, 18:605-617
- Dyke, L.D. (1985) Terrain disturbance due to summer off-road vehicle use in central Keewatin, N.W.T., Canada, *Environmental Studies No. 36, LAND*, Ottawa, 47 p.
- Ebersole, J.J. (1985) Vegetation disturbance and recovery at the Oumalik oil well, arctic coastal plain, Alaska, Ph.D. thesis, Univ. of Colorado, Boulder
- Edlund, S.A. (1990) Bioclimatic zones in the Canadian Arctic Archipelago, IN: C.R. Harrington (ed.) *Canada's missing dimension: science and history in the Canadian Arctic Islands*, Vol. II, Canadian Museum of Nature, Ottawa, pp. 421-441
- Egginton, P.A. and J.P. Ferris (1980) Terrain disturbance resulting from vehicle movement, Lone Gull Lake, central Keewatin; IN: *Current Research, Part B, Geological Survey of Canada Paper 80-1B*, pp. 69-74
- Fletcher, R.J. (1975) Settlements of northern Canada: a gazetteer and index, *Occ. Pub. No. 11*, Boreal Institute for Northern Studies, Edmonton, 136 p.
- Fletcher, R.J. and G.S. Young (1976) Climate of arctic Canada in maps, *Occ. Pub. No. 13*, Boreal Institute for Northern Studies, Edmonton, 48 p.
- Forbes, B.C. (1992a) History, ecology and biogeography of anthropogenic disturbance along the upper Steese Highway, interior Alaska, *J. No. Sci.*, 4:1-15
- Forbes, B.C. (1992b) Tundra disturbance studies. I. Long-term effects of vehicles on species richness and biomass, *Env. Conserv.*, 19:48-58
- Forbes, B.C. (1993a) Tundra disturbance studies. II. Plant growth forms of human-disturbed ground in the Canadian Far North, Musk-ox (in press)
- Forbes, B.C. (1993b) Tundra disturbance studies. III. Classification of high arctic ruderal vegetation and the problem of character taxa (submitted to *J. Veg. Sci.*)
- Gartner, B.L., F.S. Chapin III and G.R. Shaver (1983) Demographic patterns of seedling establishment and growth of native graminoids in an Alaskan tundra disturbance, *J. Appl. Ecol.*, 20:965-980
- Haag, R.W. (1974) Nutrient limitations to plant production in two tundra communities, *Can. J. Bot.*, 52:103-116
- Haag, R.W. and L.C. Bliss (1974) Energy budget changes following surface disturbance to upland tundra, *J. Appl. Ecol.*, 11:355-374
- Henry, G.H.R., B. Freedman and J. Svoboda (1987) Effects of fertilization on three tundra plant communities of a polar desert oasis, *Can. J. Bot.*, 64:2502-2507
- Hernandez, H. (1973) Natural plant colonization of surficial disturbances, Tuktoyaktuk Peninsula region, N.W.T., *Can. J. Bot.*, 51:2177-2196
- Jorgenson, M.T. (1986) Biophysical factors influencing the geographic variability of soil heat flux near Toolik Lake, Alaska: implications for terrain sensitivity, M.Sc. thesis, Univ. of Alaska, Fairbanks
- Kevan, P.G. (1971a) Oil under the tundra in the Mackenzie Delta region, *Can. Field Nat.*, 85:99-100, 122
- Kevan, P.G. (1971b) Vehicle tracks on high arctic tundra: an 11 year case history around Hazen Camp, Ellesmere Island, N.W.T., Defence Research Board, Ottawa, Hazen 41, 17 p.
- Klute, A. (ed.) (1986) *Methods of soil analysis*, Pt. 1, Physical and mineralogical methods, 2nd edition, American Society of Agronomy/Soil Science Society of America, Madison, WI.
- Lawson, D.E. (1986) Response of permafrost terrain to disturbance: a synthesis of observations from northern Alaska, USA, *Arct. Alp. Res.*, 18:1-17
- Maxwell, J.B. (1981) Climatic regions of the Canadian Arctic Islands, *Arctic*, 34:225-240
- Moore, T.R. (1978) Soil formation in northeastern Canada, *Ann. Assoc. Amer. Geogr.*, 68:518-534
- Ohmura, A. (1982) Evaporation from the surface of the arctic tundra on Axel Heiberg Island, *Water Res. Res.*, 18:291-300
- Pomeroy, J.W. (1985) An identification of environmental disturbances from road developments in subarctic muskeg, *Arctic*, 38:104-111
- Rouse, W.R. (1984) Microclimate at arctic tree line. 1. Radiation balance of tundra and forest, *Water Res. Res.*, 20:57-66
- Rydén, B.E. (1977) Hydrology of Truelove Lowland, IN: L.C. Bliss (ed.) *Truelove Lowland, Devon Island, Canada: a high arctic ecosystem*, Univ. Alberta Press, Edmonton, pp. 107-136
- Shaver, G.R., B.L. Gartner, F.S. Chapin III and A.E. Linkins (1983) Revegetation of arctic disturbed sites by native tundra plants, IN: *Proc. 4th International Permafrost Conf.*, National Academy of Sciences, Washington, D.C., pp. 1133-1138
- Sheldrick, B.H. (ed.) (1984) *Analytical methods manual*, Research Branch, Agriculture Canada, Ottawa
- Sjörs, H. (1952) On the relation between vegetation and electrolytes in north Swedish mire waters, *Oikos* 2(1950):241-258
- Tarnocai, C. and S.C. Zoltai (1988) Wetlands of arctic Canada, IN: C. D. A. Rubec (ed.) *Wetlands of Canada*, Polyscience, Montreal, pp. 27-53
- Vitt, D.H. (1975) A key and synopsis of the mosses of the northern lowlands of Devon Island, N.W.T., Canada, *Can. J. Bot.*, 53:2158-2197
- Walker, D.A., P.J. Webber, M.D. Walker, N.D. Lederer, R.H. Meehan and E.A. Nordstrand (1986) Use of geobotanical maps and automated mapping techniques to examine cumulative impacts in the Prudhoe Bay oilfield, Alaska, *Env. Conserv.*, 13:149-160
- Walker, D.A., P.J. Webber, E.F. Binnian, K.R. Everett, N.D. Lederer, E.A. Nordstrand and M.D. Walker (1987) Cumulative impacts of oil fields on northern Alaskan landscapes, *Science*, 238:757-761
- Walker, D.A., E.F. Binnian, B.M. Evans, N.D. Lederer, E. Nordstrand and P.J. Webber (1989) Terrain, vegetation and landscape evolution of the R4D research site, Brooks Range foothills, Alaska, *Holarct. Ecol.*, 12:238-261
- Woo, M.-K. (1986) Permafrost hydrology in North America, *Atmos.-Ocean*, 24:201-234
- Woo, M.-K. and P. Steer (1986) Runoff regime of slopes in continuous permafrost areas, *Can. Water Res. Journ.*, 11:58-68
- Young, S.B. (1971) The vascular flora of St. Lawrence Island with special reference to floristic zonation in the arctic regions, *Contributions to the Gray Herbarium No. 201*, Harvard Univ., pp. 11-115



## MONITORING THAWING FRONT MOVEMENT BY SELF-POTENTIAL MEASUREMENT

Richard Fortier, Michel Allard and Maurice-K. Seguin

Centre d'études nordiques, Laval University, Sainte-Foy (Québec) Canada G1K 7P4

Natural electrical potentials developing in the active layer and in permafrost during the thaw period in 1990 were measured with a millivoltmeter for two different soils (a fine sandy silt and a sand) near Umiujaq in Nunavik (Canada). For each site, a 4 m long electrical cable with multiple stainless steel electrodes distributed regularly every 10 cm was driven into the ground. Each electrode was linked to a contact box at the ground surface by an individual electrical conductor. Self-potential measurements were taken every week over a two month period during the thawing season.

Measurements of the potential difference between two electrodes were made with a special arrangement. The positive terminal of the millivoltmeter was connected to the deepest electrode on the electrical cable which was used as the permanent reference electrode. At this depth, the ground temperature does not change much; consequently, the unfrozen water content remained virtually stable and the ion concentration in water was constant too. This electrode was therefore used as a constant reference for potential measurements along the array. These particular conditions provided a stable potential reference for measurement. The negative terminal was then connected successively to the electrodes along the cable from the surface downwards by increments of 10 cm. The variation of the electrical potential relative to this moving electrode reflected an increase or a decrease in electrolyte concentration in relation with the changes in phase composition and temperature in the active layer and the upper permafrost layer. When compared with the thermal measurements, it was observed that the electrical potential difference between the moving electrode and the reference electrode roughly locates the thawing front.

For example, in the silty soil, from late April to early July of 1990, the active layer thaw and the permafrost warming were well illustrated by an increase of self-potential. The active layer was loading negatively in relation to permafrost because the electrolyte dilution was induced by the phase change. At depths greater than 300 cm, self-potential remained stationary. For sandy soil, the electrical behavior was quite different; the active layer loaded positively during this period because the soil drying induced electrolyte concentration. In this case, the self-potential variations were more difficult to interpret since the electrical potential relative to the reference electrode did not remain stable with time.

### INTRODUCTION

Self-potential (SP) or spontaneous potential measurement in freezing and thawing soils is a recent geophysical method in geocryology. A natural electrical potential difference appears spontaneously between two metallic electrodes when they are buried in the ground. The electrical potential difference varies from formation to formation, usually within few hundred millivolts (mV). SP polarity and intensity depend upon various parameters such as temperature, water content and migration, type of soil, type of ions in solution and their concentration, and type and distance between electrodes. Natural electrical potentials also change considerably over time.

The self-potential method was first used in petroleum logging (Kallenburg, 1984; Serra, 1984). Electrical potential differences were measured between a moving electrode in a borehole filled with a drilling mud and a surface reference electrode. This method provides a lithology log sensitive to sand and shale beds. The SP curve allows us to differentiate

between porous, permeable beds where petroleum is found and shales. In nonpetroleum logging (engineering geophysics and hydrogeology), SP is used to distinguish between permeable and impermeable zones. Seguin (1977), in his original research work at Schefferville (Québec, Canada) conducted for mining purposes, delimited the contact between a permafrost zone and a talik zone with the help of SP logging. The contacts were marked by an abrupt change in self-potential. In each case mentioned above, the measurements were punctual and the SP variation over time was not investigated.

Spontaneous potentials are also measured along surface profiles for the investigation of hydrogeologic units (Ernstson and Scherer, 1986) and landslide areas (Bogoslovsky and Ogilvy, 1977). The distribution patterns and polarities of electrical potential differences are influenced by hydrogeologic factors and by the lithology of the soil. The effect of time on self-potential is closely related to water movement in layers of different permeability (Ernstson and Scherer, 1986). Streaming potentials (Bogoslovsky and Ogilvy, 1972), induced

by water flow through soil, are considered the basic source of natural electrical potentials. In certain cases, a change in the intensity of the spontaneous potential indicated the locations of areas where landslide movement was imminent (Bogoslovsky and Ogilvy, 1977).

Freezing potential has been studied extensively in the laboratory (Borovitskii, 1975; Hanley and Ramachandra Rao, 1982; Kelsh and Taylor, 1988; Yarkin, 1973 and 1986; Zongchao, 1990). When soil freezes, abrupt changes occur in the electrical potential difference between electrodes buried in frozen and unfrozen parts of the soil. Freezing potential behavior is complex and not well understood. It is clear, however, that moisture migration and ion expulsion from pore water during freezing are the principal mechanisms that cause these potentials.

Only a few field studies of freezing and thawing potential variation as a function of time are found in the literature (Borovitskii, 1975; Gahé et al., 1987 and 1988; Outcalt and Hinkel, 1989 and 1990; Parameswaran et al., 1985; Parameswaran and Mackay, 1983), and the results are sometimes confusing and difficult to rationalize. Experimental results indicate that self-potential depends on so many parameters that it is impossible to determine their individual contribution. Parameswaran and Mackay (1983) presented original results on SP variation with time in a mud hummock. They concluded that: "It is possible to locate and study the advancing freezing front and water migration at different levels below the surface as ground freezes and thaws by suitably modifying electrode probes and improving measuring techniques". However, their results did not demonstrate this possibility. Outcalt and Hinkel (1989 and 1990) used self-potential measurements in the upper 15 cm of mineral soil in Michigan to calculate a parameter, the C-index, linked with the electrolyte concentration of the pore water. Their field observations demonstrated that rainfall-dewfall induced electrolyte dilution while evaporation induced electrolyte concentration. Indeed, an increase in electrolyte concentration produced a potential decrease and a C-index value increase and a dilution produced the opposite effect. Soil freezing, associated with ion expulsion from the pore water, created electrolyte dilution and a C-index decrease.

The purpose of this paper is to present our field instrumentation and the self-potential measurement techniques we used to follow the thawing front movement in response to temperature changes. Some examples of thawing potential developed in both a silty and a sandy soils on permafrost during the thaw period of 1990 at Umiujaq (Nunavik, Canada) are also given to demonstrate the relevance of the self-potential method in geocryology. The SP data are compared with the thawing front progression determined by the measurement of ground temperature profiles and the interpretations of our results are given.

## SELF-POTENTIAL

Spontaneous potentials arise from an unbalanced distribution of ions caused by many mechanisms. The two principal mechanisms involving the movement of ions appear to be :

- 1) streaming potentials and
- 2) freezing potentials.

These processes can alter the balance of ion concentrations and cause potential differences.

### 1) Streaming potentials

Streaming potentials are produced by water flow through permeable soil. Normally, clay particles are characterized by a negatively charged surface (Mitchell, 1976). The negative charges on the surface are compensated by the accumulation of an equivalent number of cations in the adjacent solution. The cations from the solution are attracted by the negative charge on the clay surface. The first few molecular layers are hydrodynamically immobile and form the "fixed layer" (Mitchell, 1976). A little farther from the clay surface is the "diffuse layer" (Mitchell, 1976). Liquid can move through this layer, which has an excess of positive ions. Next to these two layers, the bulk solution (pore water) is finally reached and the pore liquid is electrically neutral. When hydraulic differential pressure is applied across a soil, fluid flow takes place (see Figure 1). Fluid flow occurs both in the pores of the soil and in the diffuse layer around clay particles. This flow in the diffuse layer carries along the excess pore cations. The movement of charges then creates an electrical potential difference across the length of the pores and across the soil. This potential results in current flow back through the soil, and a resultant potential drop through the liquid in the soil (see Figure 1). Ernstson and Scherer (1986) have found a close relation between self-potential and such hydrogeologic parameters as hydraulic head and permeability.

### 2) Freezing potentials

During the freezing process in soil, electrical potentials appear between frozen and unfrozen zones. The amplitude and dynamic of these freezing potentials vary under different conditions and depend on soil type and moisture content, the nature and concentration of electrolytes, and the freezing rate. Yarkin (1973 and 1986) has noted this phenomenon. When soil freezes without noticeable redistribution of moisture (i.e.: sandy soil or clayey

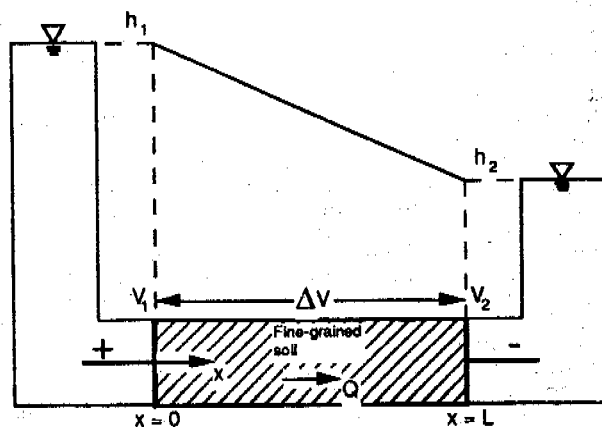


Figure 1. Diagram of system for measuring electrical streaming potentials ( $h$  is hydraulic head,  $Q$  is flow,  $V$  is electrical potential and  $L$  is length) due to passage of water through soil.

soil with a low moisture content and a fast freezing rate), the frozen part of the sample charges negatively in comparison with the unfrozen part. When soil freezes with significant redistribution of moisture (i.e.: clayey soil with a slow freezing rate), the frozen part of the sample charges positively in comparison with the unfrozen part. These effects are attributed to the degree to which various ions are excluded from the ice structure (Kelsh and Taylor, 1988). The interrelation between freezing potential amplitude and moisture redistribution is very important.

The development of a spontaneous potential during freezing of a sample is explained in the following way. During freezing, water migrates toward the freezing front. In soil with a high water content and slow freezing rate, several electrokinetic effects (such as streaming potential) appear as a result of the relative movement between water, ions in solution and the solid phase (Parameswaran and Mackay, 1983). In this case, the frozen zone charges positively in agreement with the moisture migration. The development of this electrical potential difference between the unfrozen and frozen zones causes a migration of water to the freezing front (Borovitskii, 1975), like those observed in the process of electro-osmosis (movement of water takes place in the direction of the negatively charged electrode). For soil without noticeable redistribution of moisture, cations are preferentially rejected at the freezing front from the frozen part into the unfrozen part (Hanley and Ramachandro Rao, 1982). In this case, the frozen part charges negatively relative to the unfrozen part. The rearrangement of the structure of water from the liquid to the crystalline state and vice versa can also develop electrical potential (Borovitskii, 1975). When the soil thaws, electrical potential variation is also noted (Parameswaran et al., 1985). The development of this potential is due to water movement.

#### FIELD INSTRUMENTATION

Monitoring the self-potential variations due to thawing (or freezing) of the active layer required an electrical multi-wire cable with electrodes at incremental depth intervals. The electrical contact with the soil was provided by metallic electrodes. For each site investigated, a 4 m long electrical cable with 41 stainless steel electrodes distributed regularly every 10 cm was driven vertically into the ground. The depths of the first and last electrodes were respectively 5 and 405 cm. The electrode shape was a circular band fixed around the electrical cable, 1 cm wide and 2 cm in diameter with a thickness of 1 mm. Each electrode was linked to a contact box at the ground surface by an individual electrical conductor. It was assumed that the electrodes and cable were electrically inactive. In parallel with the electrodes, 21 UUB31J1 thermistors (1000 Ohm at 25°C), from Fenwal Electronics Ltd, distributed regularly every 20 cm along another electrical cable provided a temperature control. The pair of electrodes and thermistors cables constituted the thermo-electrical cable. An electrical cable is similar to thermoelectrical cable without the thermistors.

Self-potentials were measured with a Terrameter ABEM SAS 300 from Atlas Copco,

Geophysics. The Terrameter precision is about 10  $\mu\text{V}$  ( $10^{-5}$  V) and its input impedance was 10 MOhm ( $10^7$  Ohm). This special millivoltmeter had enough precision and impedance to avoid measurement problems.

Only one electrode arrangement was used to measure self-potentials: the referential array. It was made with a downward moving electrode along the electrical cable and a stationary electrode. This fixed electrode corresponded to the deepest electrode on the electrical cable, at a depth of 405 cm in permafrost, which was used as the permanent reference electrode. At this depth, the ground temperature does not change much; consequently, the unfrozen water content stays virtually stable. Thus, the electrical potential relative to this reference electrode remains constant. These particular conditions provide a reliable reference for self-potential measurement. Ideally, the reference electrode should be located in permafrost at a depth where the annual amplitude of the ground temperature is zero in order to eliminate all the electrical potential variations due to temperature variations to the level of the reference electrode. For the referential array, the measuring depth was considered to be the level of the downward moving electrode.

Self-potentials in the active layer and in permafrost during the thaw period of 1990 (from April 30 to July 9) were measured at two different sites in Umiujaq (Nunavik, Canada): a silty permafrost mound and a sandy marine terrace. The thermoelectrical cables were driven into the ground in August 1989. The holes were drilled with a portable drill and a CRREL coring auger kit. After the cable was installed in the hole, the latter was filled with silty or sandy mud from the cuttings. For the silty soil, a thermoelectrical cable (#1) and an electrical cable (#2) were buried in two holes 50 cm apart. For the sandy soil, only one thermoelectrical cable (#3) was installed in the ground. Self-potentials in silt and ground temperature were measured every day on the thermoelectrical cable (#1). For the self-potential measurement, the positive terminal of the Terrameter was always connected to the deepest electrode on the thermoelectrical cable. The negative terminal was connected successively to the electrodes along the cable from the surface downwards at 10 cm intervals. Respect for polarity is extremely important because significant information on electrical charge distribution is gained from it. For the electrical cable (#2) in silt and the thermoelectrical cable (#3) in sand, measurements were taken every week during the 1990 thaw period. The electrical potential variations observed in the active layer and upper permafrost layer reflected changes in temperature, phase composition, moisture migration in the ground and electrolyte concentration.

#### SELF-POTENTIAL MEASUREMENT - RESULTS

The variations of temperature (°C) and of self-potential (mV) as a function of depth below the ground surface and time are shown in Figures 2a and 2b for the silty soil. The air temperature variation is also plotted on these figures. The contour lines were made with the SYSTAT program (Wilkinson, 1984) on Macintosh. Although the temperature increased by 3 or 4°C (from -7 to -3°C) to a depth greater than

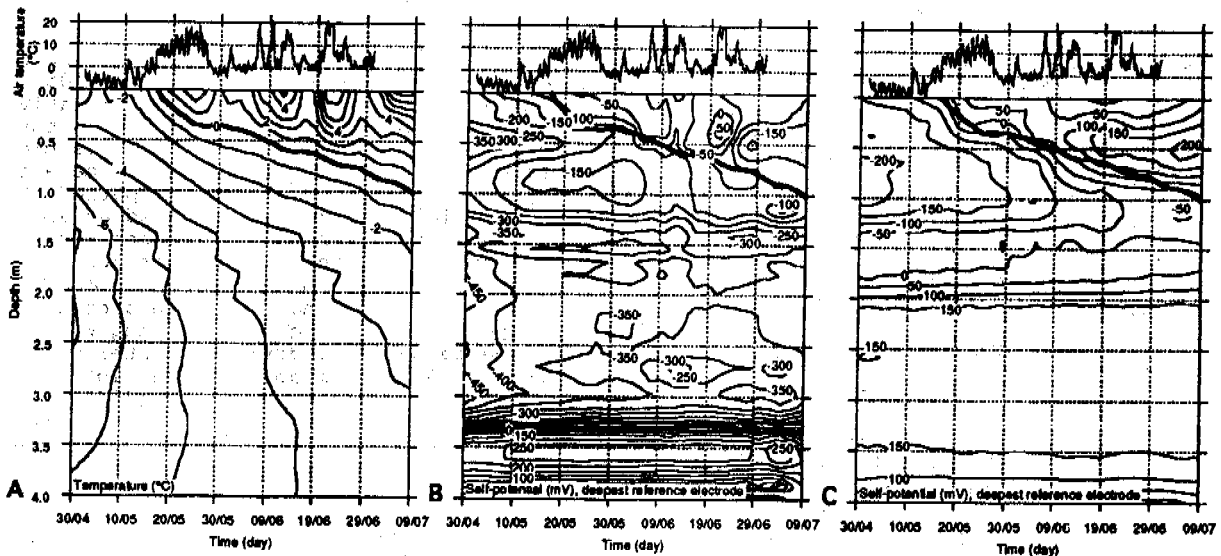


Figure 2: Umiujaq (1990), silty permafrost mound. A) thermoelectrical cable 1: ground temperature vs depth and time; B) thermoelectrical cable 1: self potential vs depth and time; C) electrical cable 2: self potential vs depth and time.

300 cm during the study period (Figure 2a), the self-potential values remained stable in permafrost during this time (Figure 2b). The choice of the reference electrode position at 405 cm depth was therefore appropriate. For a temperature under  $-3^{\circ}\text{C}$ , the unfrozen water content in permafrost does not vary much (Anderson et al., 1973) and this situation allows a constant electrical potential relative to the reference electrode. The active layer thickness in the silt was about 120 cm. The active layer/permafrost contact was characterized by a marked increase in ice content. This contact was easy to locate during drilling from the appearance of horizontal lenses of segregated ice in the core. Between the 120 and 300 cm depths in permafrost, the self-potential values did not change significantly and the variations were attributed to an increase in the unfrozen water content with temperature. For a given day, different electrical potential values were noted on the vertical profile of the active layer and permafrost. SP variation in the permafrost indicated a difference in the direction of moisture migration and ion concentration distribution in the soil during permafrost mound formation. The thawing front position at  $0^{\circ}\text{C}$  is also underlined by a thick contour line on Figure 2a and it is transferred and underlined by a thick contour line on Figure 2b. The thawing front progression in silt was evaluated at 2 cm per day. The thawing front position determined by the  $0^{\circ}\text{C}$  contour line (see Figure 2a) corresponds roughly to the  $-100$  mV contour line (Figure 2b). This correspondence is remarkable considering the method of measurement. The  $-100$  mV value can change from year to year because it depends on moisture migration and ion concentration distribution during the last freezing period. The self-potential values in the active layer increased during the study period. From May 8 to June 12 of 1990, the ground temperature at a depth of 55 cm increased by  $3^{\circ}\text{C}$  (from  $-3.2$  to  $0.1^{\circ}\text{C}$ ) while self-potential increased by 230 mV (from  $-290$  to  $-60$  mV). For a self-potential increase and a constant reference potential, the elec-

trode in the active layer loaded negatively because the potential relative to this electrode decreased with time. Streaming potentials generated by downward migration of water toward the thawing front and freezing potentials produced by water freezing beneath the thawing front are the probable causes of the self-potential increase in the active layer. Downward water migration and freezing at the base of the active layer during the thaw period were well explained by Mackay (1983). He has shown substantial field evidence of this phenomenon. Parameswaran et al. (1985) and Borovitskii (1975) have also observed self-potential variation in the active layer during thawing and freezing. They used the hypothesis of water migration and refreezing to explain this variation. The active layer has a polyhedral cryotexture and this cryofacies produced an increase in soil permeability. Thus, water migration was facilitated, even beneath the thawing front, allowing streaming potentials to be generated. Before the thaw period, when the active layer temperature was close to  $0^{\circ}\text{C}$  and the unfrozen water content was high, water migration was possible and self-potential values also increased. Furthermore, water migration and phase change created an electrolyte dilution which affected self-potential values. According to Outcalt and Hinkel (1989 and 1990), an increase in self-potential is produced by electrolyte dilution. For the thawed zone, the self-potential variation is linked to desiccation and moisturizing cycles.

The self-potential contour lines plotted on Figure 2c are derived from the electrical cable (#2) data. The pattern observed in Figure 2c is quite similar to that in Figure 2b for the thermoelectrical cable (#1) but the values are completely different. This dissimilarity is due to the difference in ion concentration distribution between the two vertical profiles. The backfill of the drilling hole after the electrical cable is driven into the ground can change the physical properties of the ground and the ion concentration distribution. The 0 mV contour line corresponds roughly to the thawing front position.

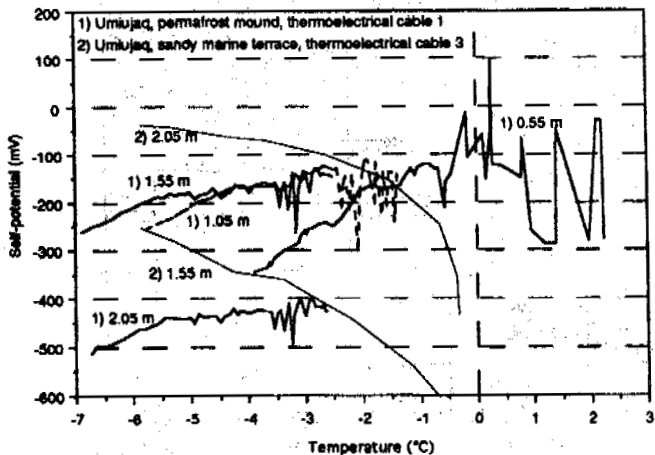


Figure 3. Self-potential vs ground temperature.

For the frozen silty soil, the self-potential variation with temperature changes was greater close to the surface in the active layer than in the permafrost (Figure 3). Beneath 0°C, the SP gradient at a depth of 55 cm was about 70 mV-°C<sup>-1</sup> while it was 25 mV-°C<sup>-1</sup> at a depth of 205 cm. Water migration was stronger in the active layer and generated higher streaming potential values.

In the case of the sandy soil, the electrical behavior was quite different. Temperature and self-potential contour lines are plotted in Figures 4a and 4b. The thawing front progression was more rapid in the sand than in the silt: 3 cm per day. The exact active layer thickness is not known for this site but a value between 200 and 300 cm appears to be reasonable. The self-potential values at the basal electrode in permafrost did not remain stable because the ground temperature increased to close to 0°C, the porosity was

high and the water content was low. Therefore, the reference electrode position at 405 cm was not deep enough and the potential relative to this electrode became unstable during the study period. In spite of this, it is clear that the self-potential values in the active layer decreased during the thaw period. Values between -400 and -350 mV provided an approximate location of the thawing front. The SP gradient at a depth of 155 cm is about -60 mV-°C<sup>-1</sup> (Figure 4a) while it is 25 mV-°C<sup>-1</sup> at the same depth in the silt. The decrease of self-potential during soil warming was probably due to the soil drying as water migrated downward. Sand permeability was high, facilitating water migration. The negative charges on the surface grains should be compensated by an accumulation of cations in the adjacent solution. This accumulation created an electrolyte concentration and a self-potential decrease (Outcalt and Hinkel, 1989 and 1990). The active layer in the sandy marine terrace loaded positively and the self-potential decreased during the thaw period.

#### CONCLUSION

The thawing front movement was monitored by means of self-potential measurement in a silty permafrost mound and a sandy marine terrace at Umiujaq (Canada, Nunavik) during the thaw period of 1990. SP variations corresponded roughly with the thawing front movement determined by ground thermal profiles. The electrode arrangement used was the referential array. To eliminate all undesirable potential variations relative to the reference electrode induced by temperature changes, this electrode had to be located in permafrost at a depth where the annual temperature amplitude is zero, the phase change is avoided and the electrolyte concentration is constant.

The active layer in the silty soil loaded negatively during the thaw period while it loaded positively in the sandy soil. The self-

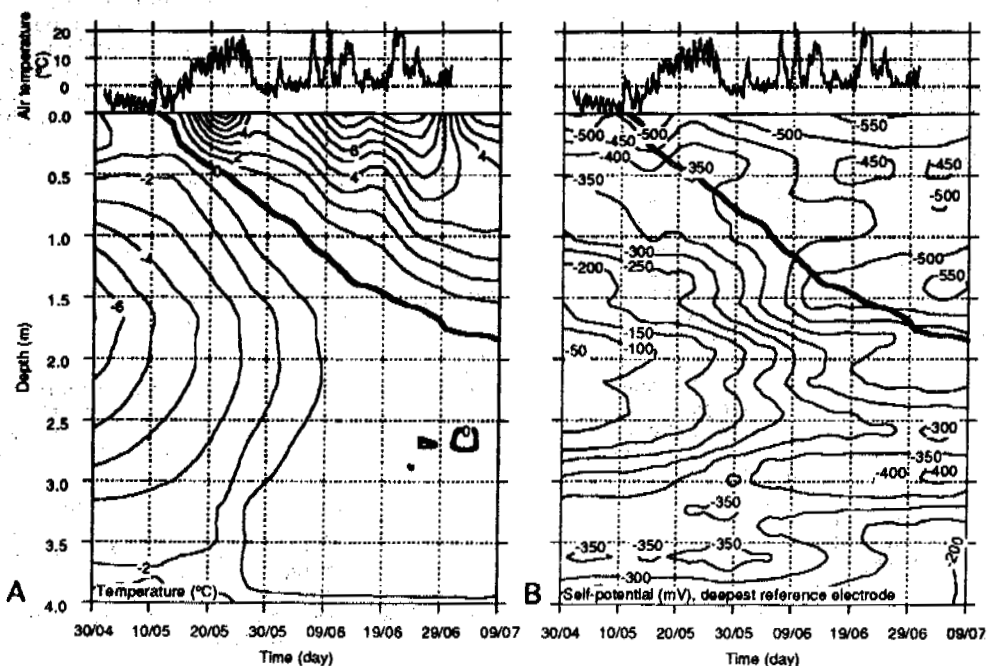


Figure 4. Umiujaq(1990), sandy marine terrace, thermoelectrical cable 3. A) ground temperature vs depth and time; B) self-potential vs depth and time.

potential increase in silty soil was due to streaming potentials generated by water migration toward the thawing front and to electrolyte dilution created by phase change. Freezing potentials produced by water freezing beneath the thawing front also created observable potential variations. Temperature and unfrozen water content increase before reaching the thawing temperature (0°C) also affected the natural electrical potentials. The self-potential decrease in sandy soil was due to the soil drying as water migrated downward. The electrolyte concentration increase was related to the accumulation of cations in the adjacent solution around sand particles to compensate the negative charge on the surface grains.

Monitoring self-potential changes in the active layer and in permafrost offers good possibilities for assessing changes in temperature, water content and migration, and in ion concentration distribution. Self-potential measurement could be useful for studying and predicting landslides and detachment failures induced by ice melting in permafrost terrain.

#### ACKNOWLEDGMENT

The authors owe sincere thanks to the Inuit community of Umiujaq and to Willie Kumarluk for their hospitality and friendly support. We gratefully acknowledge Energy, Mines and Resources Canada for the loan of an all-terrain vehicle and a CRREL coring auger kit. Thanks are due to Jocelyn Lauzon for his help in the field and to Jean Pilon from the Geological Survey of Canada for his logistical support. The research was supported by grants from the National Sciences and Engineering Research Council of Canada (NSERC), the Québec Fonds FCAR, and Indian and Northern Affairs Canada.

#### REFERENCES

- ANDERSON, D. M., TICE, A. R. and H. L. McKIM (1973). The unfrozen water and the apparent specific heat capacity of frozen soils. Proceedings Second International Conference on Permafrost, Yakutsk, USSR, North American Contribution Volume: 289-295.
- BOGOSLOVSKY, V. A. and A. A. OGILVY (1972). The study of streaming potentials on fissured media models. *Geophysical Prospecting*, vol. 20: 109-117.
- BOGOSLOVSKY, V. A. and A. A. OGILVY (1977). Geophysical methods for the investigation of landslides. *Geophysics*, vol. 42, no. 3: 562-571.
- BOROVITSKII, V. P. (1975). The development of inherent electrical fields during the freezing of rocks in the active layer and their role in the migration of trace elements. *Journal of Geochemical Exploration*, vol. 5: 65-66.
- ERNSTSON, K. and H. U. SCHERER (1986). Self-potential variations with time and their relation to hydrogeologic and meteorological parameters. *Geophysics*, vol. 51, no. 10: 1967-1977.
- GAHÉ, É., ALLARD, M. and M. K. SEGUIN (1987). Géophysique et dynamique holocène de plateaux palsiques à Kangiqsualujjuaq, Québec nordique. *Géographie physique et Quaternaire*, vol. XLI, no. 1: 33-46.
- GAHÉ, É., ALLARD, M., SEGUIN, M. K. and R. FORTIER (1988). Measurements of active layer and permafrost parameters with electrical resistivity, self potential and induced polarization. Proceedings, V International Conference on Permafrost in Trondheim, Norway: 148-153.
- HANLEY, T. O'D. and S. RAMACHANDRA RAO (1982). Electrical freezing potentials and the migration of moisture and ions in freezing soils. Proceedings, Fourth Canadian Permafrost Conference: 453-458.
- KALLENBERG, J. K. (1984). *Geophysical logging for mineral and engineering applications*. Pennwell Books, 254 p.
- KELSH, D. J. and S. TAYLOR (1988). Measurement and interpretation of electrical freezing potential of soils. Cold Regions Research & Engineering Laboratory (CRREL) Report 88-10, 15 p.
- MACKAY, J. R. (1983). Downward water movement into frozen ground, western arctic coast, Canada. *Canadian Journal of Earth Sciences*, vol. 20: 120-134.
- MITCHELL, J. K. (1976). *Fundamentals of soil behavior*. John Wiley & Sons, Inc., 422 p.
- MITCHELL, J. K. (1991). *Conduction phenomena: from theory to geotechnical practice*. Géotechnique, 31st Rankine Lecture, vol. 41, no. 3: 299-340.
- OUTCALT, S. I. and K. M. HINKEL (1989). Night-frost modulation of near-surface soil-water ion concentration and thermal fields. *Physical Geography*, vol. 10, no. 4: 336-348.
- OUTCALT, S. I. and K. M. HINKEL (1990). The soil electric potential signature of summer drought. *Theoretical and Applied Climatology*, vol. 41: 63-68.
- PARAMESWARAN, V. R., JOHNSTON, G. H. and J. R. MACKAY (1985). Electrical potentials developed during thawing of frozen ground. Proceedings, Fourth International Symposium on Ground Freezing, Sapporo: 9-15.
- PARAMESWARAN, V. R. and J. R. MACKAY (1983). Field measurements of electrical freezing potentials in permafrost areas. Proceedings, Fourth International Conference on Permafrost, Fairbanks, Alaska: 962-967.
- SEGUIN, M. K. (1977). Détermination de la géométrie et des propriétés physiques du pergélisol discontinu de la région de Schefferville. *Canadian Journal of Earth Sciences*, vol. 14: 431-443.
- SERRA, O. (1984). *Fundamentals of well-log interpretation*. 1: The acquisition of logging data. Elsevier, 423 p.
- VEDER, C. (1981). *Landslides and their stabilization* (with contribution by R. Hilbert). New York: Springer-Verlog, 247 p.
- WILKINSON, LELAND (1989). SYGRAPH. Evanston, IL: SYSTAT, Inc., 600 p.
- YARKIN, I. G. (1973). Effect of natural electric potentials on water migration in freezing soils. Proceedings, Second International Conference on Permafrost, Yakutsk, U. S. S. R. Contribution, U. S. National Academy of Sciences, Washington, D. C.: 359-361.
- YARKIN, I. G. (1986). Natural electrical potentials that arise when soils freeze. Cold Regions Research & Engineering Laboratory (CRREL) Report 86-12, 28 p.
- ZONGCHAO, L. (1990). Freeze and thaw point of wet clay and its determination. *Cold Regions Science and Technology*, vol. 18: 183-189.

# A NUMERICAL TECHNIQUE FOR SOLVING TEMPERATURE FIELD OF FROZEN WALL

Gao Xingwang

Lanzhou Institute of Glaciology and Geocryology,  
Chinese Academy of Sciences, China

The heat conduction problem with a phase-change is a weak intermission nonlinear problem. After the governing differential equations were transformed into equations with non-dimensional spatial variable by means of mathematical transformations, it is convenient to numerically solve the equations by a three-time level implicit finite difference scheme (Bonacina, 1973). In this paper we use this technique to solve the temperature field of the frozen wall. But this technique is only used for coarse soil which freezes at zero and in which moisture migration can be neglected. This technique can not be used for clay with a different phase-change temperature zone.

## INTRODUCTION

As is known, the strength of frozen ground is closely related to its temperature. In the sinking of a frozen wall in the artificially frozen ground, for the temperature field of the frozen wall should be solved as it is an important meaning in estimating the strength of frozen wall and in controlling the construction processes. Because of the heat absorption from the soil by the dozens of freeze-pipes arranged in a circle and the existence of two frozen-thawed interfaces in the inside and the outside of the freeze-pipes circle, the complexity of solving this kind of problems is greatly increased.

In order to transform nonlinear governing differential equations into linear equations, the writer used a mathematical transformation to make the space variable non-dimensionalized. In the obtained non-dimensional equations, the fronts of the phase-change interface were fixed. The equations were numerically solved by choosing a three-time level difference scheme and the temperature dependent coefficients were estimated at an intermediate-time level. Meanwhile, the heat balance equation of the interfaces were numerically treated by difference methods and the interface positions were determined by the predictor-corrector algorithm (Feng, 1978). In that way, the nonlinearity of the original problems and troubles caused in determining interface coefficients could be entirely avoided. Since the equations to be solved are linear algebra equations, the calculation accuracy can be improved. This technique is named "severing singularity" or "moving coordinate" technique in mathematics (Zhu, 1980).

This paper presents the technique of solving the temperature field of the sunken frozen wall in the artificially frozen ground in the Liang-Huai area of CHINA and discusses the rationality and feasibility of the severing singularity technique in treating phase-change problems.

## SYMBOLS

- $t$  — temperature of the original differential equations, °C;
- $t_f$  — phase-change temperature °C;
- $t_0$  — initial temperature °C;
- $\tau$  — time, h;
- $T$  — temperature of non-dimensional differential equations °C;
- $r$  — radial coordinate of frozen shaft, M;
- $\xi$  — position of the phase-change interface, M;
- $R_0$  — radius of the freeze-pipes circle, M;
- $R_H$  — influence radius of outer melting zone of freeze-pipes circle, M;
- $C$  — volumetric heat capacity  $J/M^3 \cdot ^\circ C$ ;
- $\lambda$  — thermal conductivity  $W/M \cdot ^\circ C$ ;
- $L$  — phase-change latent heat per unit volume  $J/M^3$ ;
- $Q_1$  — heat flux on inside surface of freeze-pipes circle  $W/M^2$ ;
- $z$  — non-dimensional space variable;
- $Q_2$  — heat flux on outside surface of freeze-pipes circle  $W/M^2$ ;
- $g$  — initial temperature function of original differential equations °C;
- $G$  — initial temperature function of non-dimensional differential equations °C.

## SUPERSCRIPIT

- "+", "-" — thawing and freezing;
- "·" — change rate of phase-change interface with respect to time.

## SUBSCRIPT

- "1", "2" — interior and exterior of freeze-pipes circle.

## FORMULATION OF THE PROBLEM

In the artificial freezing sinking, a few frozen deep shafts need assistant freeze-pipes

installed in the inner shallow layer of the main freeze-pipes circle because of its large diameter and for the purpose of saving construction time by advanced digging. Generally, the single-circle freeze-pipes technique is used. The freezing process of the single-circle in the shallow layer, when the inclination of freeze-pipes may be neglected, can be described as follows.

The energy equations of the freezing-thawing region inside and outside the freeze-pipes circle:

$$C_j^i(r, \tau) \frac{\partial t_j^i}{\partial \tau} = \frac{1}{r} \frac{\partial}{\partial r} (r \lambda_j^i(r, \tau) \frac{\partial t_j^i}{\partial r}) \quad (1)$$

The initial conditions:

$$t = t_j^i(r); \quad \varepsilon_j(\tau) = \varepsilon_j(0) \quad (2)$$

When  $i=+$ ,  $j=1$ ,  $0 < r < \varepsilon_1(\tau)$ ,  $\tau \geq 0$ .

When  $i=-$ ,  $j=1$ ,  $\varepsilon_1(\tau) < r < R_0$ ,  $\tau \geq 0$ .

When  $i=-$ ,  $j=2$ ,  $R_0 < r < \varepsilon_2(\tau)$ ,  $\tau \geq 0$ .

When  $i=+$ ,  $j=2$ ,  $\varepsilon_2(\tau) < r < R_H$ ,  $\tau \geq 0$ .

The connecting conditions at the freezing-thawing interface:

$$\text{When } \tau \geq 0, \text{ at } r = \varepsilon_1(\tau), \quad t_1^+ = t_1^- = t_f \quad (3)$$

$$\lambda_1^-(r, \tau) \frac{\partial t_1^-}{\partial r} - \lambda_1^+(r, \tau) \frac{\partial t_1^+}{\partial r} = L \frac{d\varepsilon_1}{d\tau} \quad (4)$$

$$\text{When } \tau \geq 0, \text{ at } r = \varepsilon_2(\tau), \quad t_2^+ = t_2^- = t_f \quad (5)$$

$$\lambda_2^-(r, \tau) \frac{\partial t_2^-}{\partial r} - \lambda_2^+(r, \tau) \frac{\partial t_2^+}{\partial r} = L \frac{d\varepsilon_2}{d\tau} \quad (6)$$

The boundary conditions

$$r=0, \quad \frac{\partial t_1^+}{\partial r} = 0; \quad r=R_0, \quad -\lambda_1^- \frac{\partial t_1^-}{\partial r} = Q_1; \quad (7)$$

$$r=R_0^+, \quad \lambda_2^- \frac{\partial t_2^-}{\partial r} = Q_2; \quad r=R_H, \quad t_2^+ = t_0. \quad (8)$$

In order to non-dimensionalize the space variable, the following mathematical transformations were used for four freezing-thawing regions inside or outside the freeze-pipes circle:

$$\text{Inner thawing region: } z = \frac{r}{\varepsilon_1(\tau)}; \quad 0 \leq r \leq \varepsilon_1(\tau) \quad (9)$$

$$\text{Inner frozen region: } z = \frac{r - \varepsilon_1(\tau)}{R_0 - \varepsilon_1(\tau)}; \quad \varepsilon_1(\tau) \leq r \leq R_0 \quad (10)$$

$$\text{Outer frozen region: } z = \frac{r - R_0}{\varepsilon_2(\tau) - R_0}; \quad R_0 \leq r \leq \varepsilon_2(\tau) \quad (11)$$

$$\text{Outer thawing region: } z = \frac{r - \varepsilon_2(\tau)}{R_H - \varepsilon_2(\tau)}; \quad \varepsilon_2(\tau) \leq r \leq R_H \quad (12)$$

Let  $t(r, \tau) = T(z, \tau)$

$$\frac{\partial t(r, \tau)}{\partial \tau} = \frac{\partial T(z, \tau)}{\partial z} \frac{\partial z}{\partial \tau} + \frac{\partial T(z, \tau)}{\partial \tau} \frac{\partial \tau}{\partial \tau} = \quad (13)$$

$$\frac{\partial z}{\partial \tau} \frac{\partial T(z, \tau)}{\partial z} + \frac{\partial T(z, \tau)}{\partial \tau} \quad \left( \frac{\partial \tau}{\partial \tau} = 1 \right) \quad (13)$$

$$\frac{\partial t(r, \tau)}{\partial r} = \frac{\partial T(z, \tau)}{\partial z} \frac{\partial z}{\partial r} + \frac{\partial T(z, \tau)}{\partial \tau} \frac{\partial \tau}{\partial r} = \quad (14)$$

$$\frac{\partial T(z, \tau)}{\partial z} \frac{\partial z}{\partial r} \quad \left( \frac{\partial \tau}{\partial r} = 0 \right) \quad (14)$$

$$\frac{\partial^2 t(r, \tau)}{\partial r^2} = \frac{\partial}{\partial r} \left[ \frac{\partial t(r, \tau)}{\partial r} \right] = \frac{\partial}{\partial z} \left[ \frac{\partial T(z, \tau)}{\partial z} \frac{\partial z}{\partial r} \right]$$

$$\frac{\partial z}{\partial r} + \frac{\partial}{\partial \tau} \left[ \frac{\partial T(z, \tau)}{\partial z} \frac{\partial z}{\partial r} \right] \frac{\partial \tau}{\partial r} = \left( \frac{\partial z}{\partial r} \right) \cdot \frac{\partial^2 T(z, \tau)}{\partial z^2}$$

$$\left( \frac{\partial \tau}{\partial r} = 0 \right) \quad (15)$$

The first derivatives with respect to  $r$  and  $\tau$  from equations (9)-(12) were substituted into equations (13)-(15), then equations (13)-(15) were substituted into (1)-(8). Hence, the original equations were transformed to the equations with non-dimensional space variables.

For the inner thawing region:

$$C_1^+(z, \tau) \xi_1(\tau) \frac{\partial T_1^+(z, \tau)}{\partial \tau} = (C_1^+(z, \tau) \cdot z \cdot \xi_1^+(\tau) + \frac{\lambda_1^+(z, \tau)}{\xi_1(\tau)z} \frac{\partial T_1^+(z, \tau)}{\partial z} + \frac{1}{\xi_1(\tau)} \frac{\partial}{\partial z} (\lambda_1^+(z, \tau) \frac{\partial T_1^+(z, \tau)}{\partial z}))$$

$$(0 < z < 1; \quad \tau > 0) \quad (16)$$

For the inner frozen region

$$C_1^-(z, \tau) (R_0 - \varepsilon_1(\tau)) \frac{\partial T_1^-(z, \tau)}{\partial \tau} = (-C_1^-(z, \tau) \xi_1^-(\tau) (z-2) + \frac{\lambda_1^-(z, \tau)}{(z-1)(R_0 - \varepsilon_1(\tau)) + \varepsilon_1(\tau)} \frac{\partial T_1^-(z, \tau)}{\partial z} + \frac{1}{R_0 - \varepsilon_1(\tau)} \frac{\partial}{\partial z} (\lambda_1^-(z, \tau) \frac{\partial T_1^-(z, \tau)}{\partial z}))$$

$$(1 < z < 2; \quad \tau > 0) \quad (17)$$

The connecting conditions at the inner interface:

$$\lambda_1^-(z, \tau) \frac{1}{R_0 - \varepsilon_1(\tau)} \frac{\partial T_1^-(z, \tau)}{\partial z} - \lambda_1^+(z, \tau) \frac{\partial T_1^+(z, \tau)}{\partial z} = L \frac{d\varepsilon_1(\tau)}{d\tau}$$

$$(z=1; \quad \tau \geq 0) \quad T_1^+ = T_1^- = t_f \quad (18)$$

The inner initial conditions:

$$T_1^+ = G_1^+(z), \quad 0 < z < 1; \quad T_1^- = G_1^-(z), \quad 1 < z < 2 \quad (20)$$

The inner interface position is always at  $z=1$ .

The inner boundary conditions:

$$z=0, \quad \frac{1}{\xi_1(\tau)} \frac{\partial T_1^+(z, \tau)}{\partial z} = 0 \quad (21)$$

$$z=2^-, \quad -\lambda_1^-(z, \tau) \frac{1}{R_0 - \varepsilon_1(\tau)} \frac{\partial T_1^-(z, \tau)}{\partial z} = Q_1 \quad (22)$$

For outer frozen region:

$$C_2^-(z, \tau) (\varepsilon_2(\tau) - R_0) \frac{\partial T_2^-(z, \tau)}{\partial \tau} = (C_2^-(z, \tau) \cdot \xi_2^-(\tau) (z-2) + \frac{\lambda_2^-(z, \tau)}{(z-2)(\varepsilon_2(\tau) - R_0) + R_0} \frac{\partial T_2^-(z, \tau)}{\partial z} + \frac{1}{\varepsilon_2(\tau) - R_0} \frac{\partial}{\partial z} (\lambda_2^-(z, \tau) \frac{\partial T_2^-(z, \tau)}{\partial z}))$$

$$(2 < z < 3; \quad \tau > 0) \quad (23)$$

The outer thawing region:



$$C_2^+(z, \tau)(R_H - \xi_2(\tau)) \frac{\partial T_2^+(z, \tau)}{\partial \tau} = (-C_2^+(z, \tau) \cdot \xi_2^+(\tau) (z-4) + \frac{\lambda_2^+(z, \tau)}{(z-3)(R_H - \xi_2(\tau)) + \xi_2(\tau)}) \frac{\partial T_2^+(z, \tau)}{\partial z} + \frac{1}{R_H - \xi_2(\tau)} \frac{\partial}{\partial z} (\lambda_2^+(z, \tau) \frac{\partial T_2^+(z, \tau)}{\partial z}) \quad (24)$$

(3 < z < 4; \tau > 0)

The connecting conditions at the outer interface:

$$\lambda_2^-(z, \tau) \frac{1}{\xi_2(\tau) - R_0} \frac{\partial T_2^-(z, \tau)}{\partial z} - \lambda_2^+(z, \tau) \frac{1}{R_H - \xi_2(\tau)} \frac{\partial T_2^+(z, \tau)}{\partial z} = L \frac{d\xi_2(\tau)}{d\tau} \quad (25)$$

$$(z=3; \tau > 0) \quad T_2^- = T_2^+ = t_f \quad (26)$$

The outer initial conditions:

$$T_2^- = G_2^-(z), \quad 2 < z < 3; \quad T_2^+ = G_2^+(z), \quad 3 < z < 4 \quad (27)$$

The outer interface position is always at z=3.

The outer boundary conditions:

$$z=2^+: \quad \lambda_2^-(z, \tau) \frac{1}{\xi_2(\tau) - R_0} \frac{\partial T_2^-(z, \tau)}{\partial z} = Q_2 \quad (28)$$

$$z=4: \quad T_2^+(z, \tau) = t_0 \quad (29)$$

In equations (16)-(29), their space variables are dimensionless and the positions of phase-change interface inside or outside the circle are fixed in form. If the differences of the equations at the interface are also made, it is convenient to solve numerically equations (16)-(29) by means of the predictor-corrector algorithm. This is for reasons that boundaries of equations obtained by transformations are given, therefore the non linearity of the original problems and the troubles of treating the interface coefficients can be avoided.

#### DETERMINATION OF INITIAL AND BOUNDARY CONDITIONS AND ANALYSIS OF CALCULATED RESULTS

In artificial freezing sinking, if the temperature field of the frozen wall is determined by the axisymmetric model, we should consider the unaxisymmetric temperature distribution in the start of freezing (e.i. before the coincidence of a frozen circle formed by the single freezing-pipes). Even when the frozen circles had connected, there still is a temperature difference between the main plane and nodepoint plane. There will be no strictly axisymmetric temperature distribution unless the frozen wall on the main plane and nodepoint plane have become smooth. Based on this understanding, the severing singularity technique used in this paper demands a certain thickness of the frozen wall at the beginning of the calculation, which coincides with our consideration.

In this paper, the thickness and temperature of the frozen wall observed at the depth of 140 m, on May 20th, 1984, in an assistant well at TAOYUAN were chosen as the initial conditions for calculating.

The treating of the boundary condition at  $r=0$ , according to the given condition  $\partial t / \partial r = 0$ , was approximately described by the combination of temperatures at three points. Accuracy of

the approximate treatment was relatively higher and agreed with that of the difference equations (which is also of the second order). At  $r=R_0$ , that is to say, in the circle of freeze-pipes, its unknown temperature asks for a supplemented difference equation in the same form as all difference equations to obtain it. However, the second-kind of boundary condition on the inner surface and the outer surface of the freeze-pipes circle is only approximately expressed by a formula of first-order accuracy, this may cause certain errors in the calculating results. The temperature at the boundary of the thawing region outside of the circle of freeze-pipes, i.e. at the influence radius, was 19.1°C. This is based on the basic distribution rule of the primitive ground temperature in Liang-Huai zone, i.e. the temperature at 15 m below ground surface is 15°C, the temperature in the region below 15m increases at a gradient of 3.3°C/100 m and the 19.1°C was gained by the above method.

The comparison between the calculated results and observed results for the frozen wall thickness are listed in Table 1.

Table 1. The comparison between the calculated and observed values of frozen wall thickness

Thick.(m)		Time(d)			
		30	60	90	120
Calculated	Inner	0.94	1.55	2.16	2.77
	Outer	0.91	1.33	1.75	2.15
	Total	1.85	2.88	3.91	4.92
Observed	Inner	1.30	1.75	2.40	2.80
	Outer	1.05	1.40	1.65	1.96
	Total	2.35	3.15	4.05	4.75

It can be seen from Table 1 that the differences at the starting stage of freezing are larger, this was related to the average heat flux chosen in the practical calculation. With time increasing the differences between the calculated and observed values become smaller and smaller and errors are within 8 percent, this accuracy is acceptable for practical engineering.

The comparison between calculated and observed values for temperature are listed in Table 2.

It can be seen from Table 2 that due to choosing the average heat flux at the circle in the calculation, the frozen wall development was slow in starting, this could cause larger temperature differences. If a exponential attenuation curve had been used for the boundary values in the calculation, these differences would be eliminated.

From above, it is obvious that solving numerically problems with phase-changes by means of the severing singularity technique is rational and applicable.

Its characteristics are as follow:

1. Clear mathematical derivation and reliable theoretical base;
2. Avoided the problem of treating interface coefficients in calculation processes because the phase-change interfaces are fixed in form;
3. Avoided the crossover-intermission difference in the difference equations for the phase-change interface in the difference equations is always treated as a node;

Table 2. Comparison between calculated and observed temperatures

Position (m)	Time(d) 30		60		90	
	Obs.	Cal.	Obs.	Cal.	Obs.	Cal.
6.0	6.9	7.2	3.4	4.1	1.1	1.5
7.1	1.3	2.6	-1.1	-0.5	-5.9	-3.9
8.1	-5.0	-3.7	-9.0	-7.2	-9.1	-10.1
9.1	-4.2	-3.5	-7.4	-6.6	-9.8	-9.9
10.3	5.5	4.9	2.6	2.1	0.1	-1.1
11.1	9.7	9.2	6.8	5.9	5.3	3.5
12.1*	13.8	13.2	10.0	10.2	2.6*	7.9

\*Because of water poured into the observed hole, the value is not true to the original.

4. Avoided the troubles of solving a set of nonlinear algebra equations at every time-level because the temperature dependent coefficients are estimated at intermediate-time level by a three-time level implicit scheme.

REFERENCES

Feng Kang, et al., (1978) Numerical Calculation Method, National Defence Industry Publishing House, pp.476-480  
 O. Bonacina and G. Comini, (1973) Numerical solution of phase-change problems, Int. J. Heat and mass transfer 16, pp.1825-1832.  
 Zhu Youlan, et al., (1980) The Difference Method on Initial and Boundary Value Problems and Wind-flow, Science Publishing House, pp.1-10.

KARST MORPHOLOGY AND HYDROLOGY IN A PERMAFROST ENVIRONMENT:  
THE CASE OF AKPATOK ISLAND, UNGAVA BAY, EASTERN ARCTIC CANADA.

James T. Gray<sup>1</sup> and Bernard Lauriol<sup>2</sup>

<sup>1</sup>Département de Géographie, Université de Montréal  
Montréal, Québec, H3C 3J7, Canada

<sup>2</sup>Département de Géographie, Université d'Ottawa,  
Ottawa, Ontario, K1N 6N5, Canada

Akpatok Island, in north-western Ungava Bay, is an outlier of horizontally disposed Ordovician limestones. Sink-holes, seasonally disappearing lakes and resurgences, indicate an extensive network of subterranean karst drainage, of special interest because the island is situated in the continuous permafrost zone, with a mean annual temperature of  $-7^{\circ}\text{C}$ . A thermal profile indicates a permafrost thickness in excess of 30 m. Resurgences are infrequent, suggesting the existence of submarine springs. At the surface, mechanical frost weathering processes predominate and rates of postglacial cliff retreat were estimated from volumes of talus debris accumulated on dated raised beaches. A subterranean water circulation model within a permafrost environment is proposed, which takes into account 1) paleo-environmental conditions, 2) the highly fissured bedrock, and 3) the thermal and kinetic energy of penetrating waters.

## INTRODUCTION

In this paper periglacial and karst weathering and the evolution of subterranean drainage are discussed for Akpatok Island in Ungava Bay (figure 1). Despite being situated well within the continuous permafrost zone, adjacent to the Ungava Peninsula where permafrost thicknesses of circa 200 m have been measured (Gray et al., 1979), surface water penetrates into the limestone bedrock to a depth in excess of 100 m (Lauriol and Gray, 1990). How could such drainage develop through a thick continuous permafrost layer? In order to answer this question, the surface drainage pattern and the geothermal regime are examined, and a model for water circulation presented.

## PHYSICAL FRAMEWORK

Akpatok Island forms an uneven plateau 100 - 275 m high, and is surrounded by cliffs. The plateau edge has been dissected by fluvial processes, particularly in the south-eastern sector where a network of narrow gorges has been partly infilled by glacial and marine deposits. Marine deltas and raised beaches characterise parts of the western, northern and north-eastern coasts up to elevations of 80 - 100 m (figure 2). Geologically, the island is composed of a sequence of 600 m of thinly bedded and densely jointed Ordovician limestones (Cox, 1932; Workum et al., 1976), unconformably overlying the Pre-cambrian crystalline rocks of the Canadian Shield at about 300 m below sea-level. Most of the plateau surface is veneered with glacial till derived both locally and from the Quebec-Labrador Peninsula (Loken, 1978; Gray et al., 1990).

Climatic data for Akpatok Island can be reasonably estimated on the basis of records from the Cape Hope's Advance (Quaqtaq) weather station, situated at the north-eastern tip of

the Ungava Peninsula, 60 km to the west. The mean annual precipitation is 160 cm, two thirds in the form of snow-fall (Villeneuve, 1967). The winter snow-cover is approximately 70 cm (Gray, 1983). The mean annual air temperature is  $-7^{\circ}\text{C}$ , reaching  $6^{\circ}\text{C}$  in July, and descending to  $-21^{\circ}\text{C}$  in January. From these temperature values, and bearing in mind that the south-eastern Ungava Peninsula, immediately to the west, is characterised by continuous permafrost, with locally measured thicknesses in excess of 200 m (Gray et al., 1979), it is clear that the whole of Akpatok Island must be underlain by a thick permafrost body. The low summer temperatures, and the wind-swept nature of the plateau, allied to edaphic conditions provoked by the alkaline and permeable limestone bedrock, support a sparse herbaceous tundra vegetation, which becomes almost continuous, however, on glacial soils enriched in minerals derived from the Canadian Shield.

## KARST HYDROLOGY AND MORPHOLOGY

### Water Infiltration and Resurgence

The south-west of Akpatok Island is characterised by the general absence of an integrated surface drainage network, by the presence of numerous small lakes and depressions, many without surface outlets, and by perched dry valleys truncated by back-wearing of the coastal cliffs. Stream-beds did generally exist at the outlets of the larger lakes, but at the time of the field visit in August 1989, these outlets were dry, despite the presence of water in the lakes. The absence of vegetation and rock lichens indicates that these stream-beds are occupied ephemeraly by surface run-off, probably during the spring snow-melt, when the underground drainage capacity through open joints is either exceeded, or impeded near the surface by ground freezing. The northern and central parts of the island display a generally more integrated pattern of

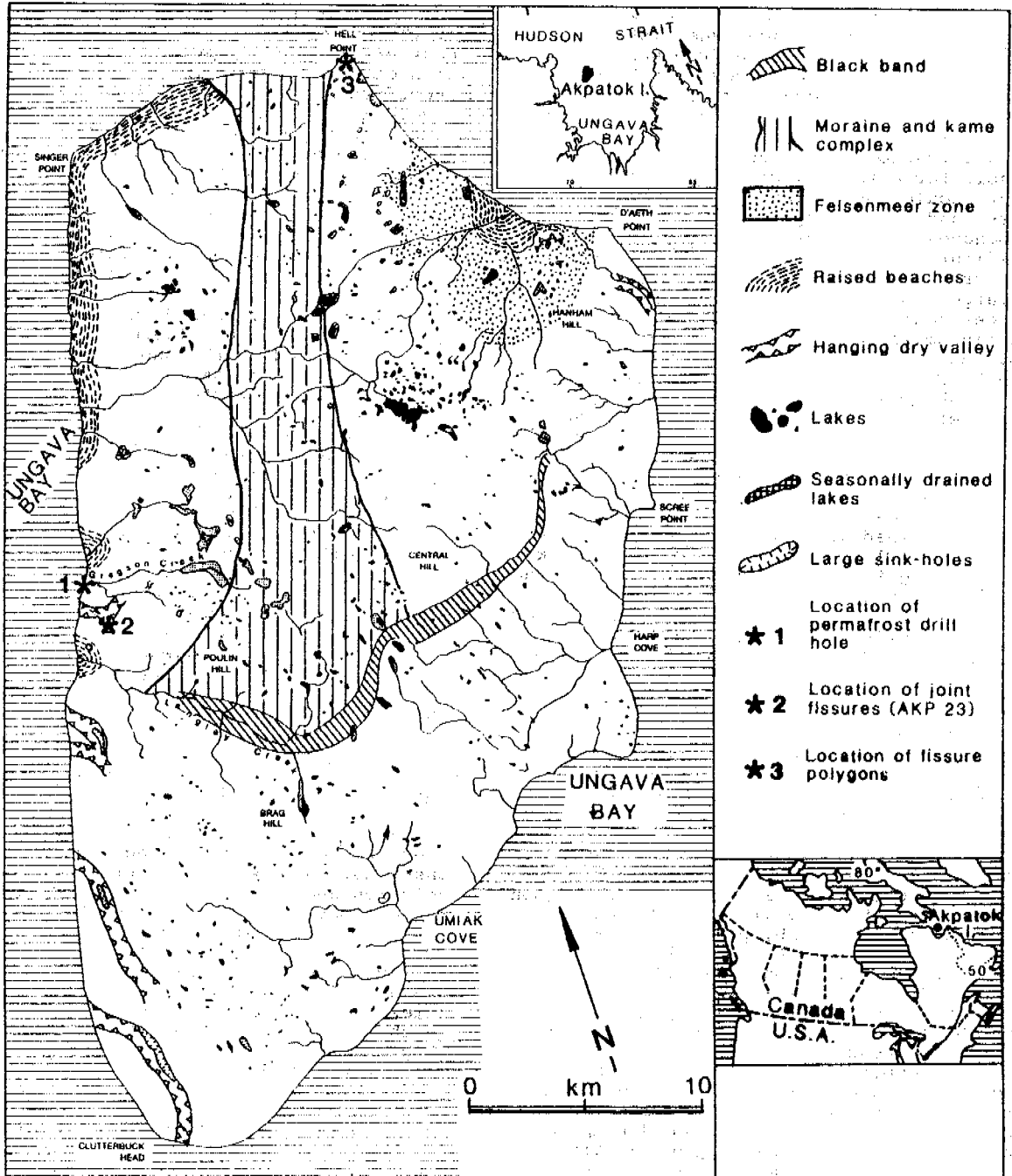


Figure 1. Location and geomorphological features of Akpatok Island, Arctic Canada.

surface drainage. Higher surface retention of water due to a thicker till cover occurs, with blockage of vertical joints by debris. It was possible to distinguish drained lakes on the basis of trimlines (figure 3) from lakes with slight sub-surface drainage. The small number of springs at the edge of the plateau, and low stream discharge at the bottom of even the deepest gorges, suggests that most ground-water travels through joint passages deep into the limestone bedrock, re-emerging from submarine springs. At observed resurgences, discharges of less than 100 litres/second were estimated.

#### Karst landforms

The infiltration of surface drainage has been responsible for a variety of karst land-forms. At a micro-scale, suffusion depressions up to 50 cm across, and 30 cm deep, have developed on cobble beaches, where late lying snow beds have melted (figure 2). They may owe their formation to beach gravels being funnelled down into solution enlarged joint openings (Ford, pers. comm). At a larger scale are linear open fissures, which drain small streams, and marshy hollows in till covered valley floors, and rarely exceed 1 m in width. These fissures cannot be penetrated far, although in one case a descent of 16 m was possible, before progress was blocked by debris.

Many sink-holes occur on the plateau surface, particularly in south-western Akpatok Island. They vary in diameter from 10 - 150 m, and in depth from 3 - 20 m, and are found at intervals along open vertical joints on the plateau surface, or in drained lake bottoms. Cliff retreat 200 m east of Hell Point truncated such a sink-hole, displaying a 200 m cut-away section of the former vertical conduit. Traces of a former horizontal conduit in the vadose zone, near sea-level, were observed at Umiak Cove (figure 4). Vertical erosion has caused collapse of the conduit roof, but its tubular profile remains etched in the bedrock at the base of the gorge.

#### PERMAFROST AND PERIGLACIAL ENVIRONMENT

##### Ground temperatures

Thermocouple profiles were obtained in order to shed light on the problem of subterranean water circulation in a permafrost environment. Measurements were made with a nominal precision of 0.1°C, down to the level of blockage by ice at a depth of 30 m in an old borehole at Gregson Creek on August 9th, 1989 (figure 5), and in four fissures on the nearby plateau surface on August 6th, 1989 (figure 6).

For the Gregson Creek borehole minimum temperatures of -2.4°C at 5 m depth, close to the transition between beach gravels and bedrock, indicate the level of penetration of seasonal warming for mid-August. The depth of 10 m at which ground temperatures begin to increase at a slow constant rate, reflects the level of minimal annual amplitude. Extrapolation to the surface suggests a mean annual ground temperature of -2°C, about 5°C warmer than the air temperature postulated from the weather station at Cape Hope's Advance. Probably the local topographic situation at the base of a 100 m cliff, favouring winter snow accumulation, and reduced exposure to wind-induced heat loss, explain the large differential between ground and air temperatures. Ground temperatures on the wind-swept plateau are likely to be much colder, however. Because of blockage of the borehole by ice, it can be affirmed that permafrost on the Gregson

Creek terraces at least 30 m thick, with a temperature at the point of blockage of -1.7°C. Tentative extrapolation of linearly increasing temperatures suggests, however, that the base of the permafrost is at a depth of circa 100 m, with a geothermal gradient of about 25°C/km.

The presence of ice in the borehole, well below the level of the active layer/permafrost interface is intriguing. The borehole was capped at the end of operations in 1966, and is cased to bedrock. Snow-melt, precipitation and circulation of ground-water in the active layer are therefore not responsible for this ice. The ice level, in fact, corresponds to sea-level at low tide, and represents the hydrostatic head created in the borehole by a salt water reservoir - Ungava Bay - which is only 200 m distant. Open fissures in the limestone bedrock within, or more likely, beneath the permafrost and within the vadose zone acted as conduits for sea water, allowing it to freely penetrate into the borehole, and to rise to its present level before freezing.

Temperatures measured in the four joint fissures on the plateau (figure 6) showed major contrasts, related to the supply of run-off from the surface. Sites AKP 23A and AKP 23B show a decline from about 8°C at the surface, down to 1°C at a depth of 10 m. In the case of AKP 23A, ice blocked the base of the joint. There was no evidence that these two fissures were occupied by stream run-off. By contrast, fissure AKP 23C received a small stream, with a discharge of 1 litre/sec at a temperature of 13°C during the August visit, and fissure AKP 23D had received water from an ephemeral meltwater stream earlier in the summer. As a result of this mass transfer of heat to the base of these fissures, resultant temperatures are much higher than at the base of AKP 23A and AKP 23B. Indeed a descent into AKP 23C was blocked at a depth of 15 m, not by ice, but rather by an infilling of glacial debris. The temperature profile in this fissure was isothermal in nature, with temperatures of -8°C.

##### Periglacial features and rates of weathering

Despite the local presence of karst land-forms, the thin-bedded and close-jointed nature of the limestone bedrock, allied to the lack of a vegetation cover, and to a near surface permafrost table, have permitted frost weathering and mass wasting processes to predominate over dissolution and fluvial processes. On steep bedrock slopes, postglacial frost weathering occurs at a much accelerated rate, aided by gravity. Along the base of an old sea-cliff on the west coast considerable volumes of talus debris have accumulated (figure 7). Bedrock and talus slope profiles were surveyed for four sections on the north side of Gregson Creek (figure 8). Mean values of 4.5 to 9.3 m were estimated for linear retreat of the cliff, on the basis of the talus volumes present, using an average bulking factor of 30% (Fraser, 1935). An important assumption in the method is that the cliff angle of about 85° can be extrapolated to the base of the slope beneath the talus debris. This assumption is considered valid by virtue of the almost vertical and linear profiles observed at the base of actively sapped cliffs (figure 9). A curve of postglacial land emergence, constructed on the basis of radiocarbon dated shells (figure 10), permitted rates of cliff retreat to be estimated since the cessation in the late Holocene of continuation and removal at the cliff-base by wave action. For the last 5 KA, cliff recession has

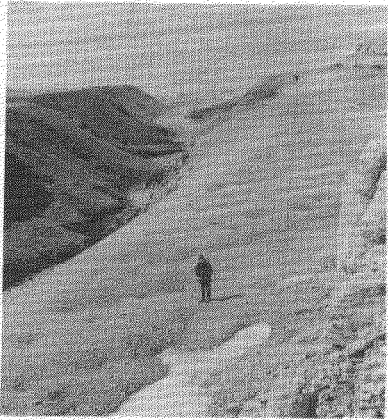


Figure 2. Raised beaches and suffusion hollows at Gregson Creek.

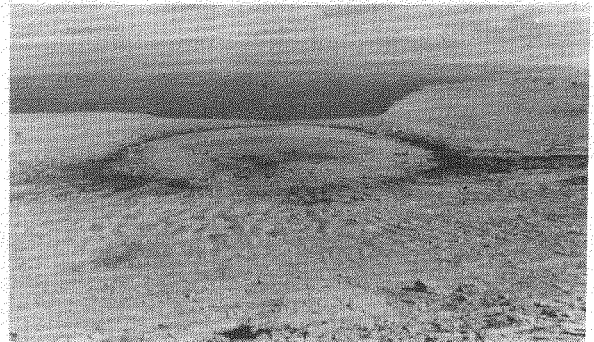


Figure 3. Disappearing lake above Gregson Creek.

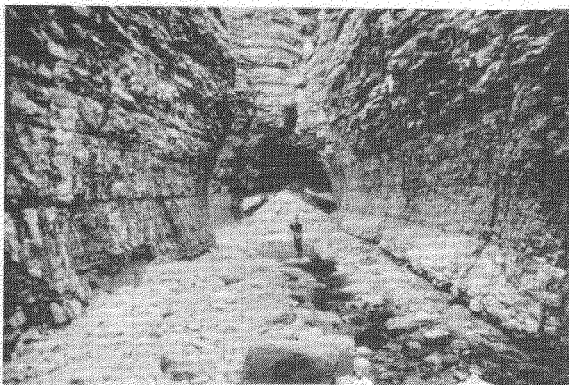


Figure 4. Former horizontal conduit, Umiak Cove.

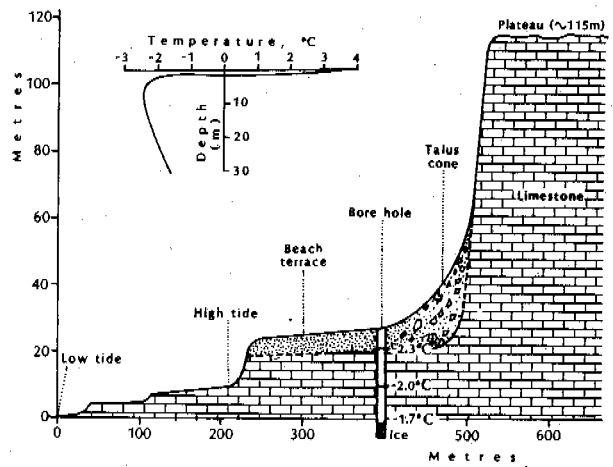


Figure 5. Thermal profile, Gregson Creek borehole.

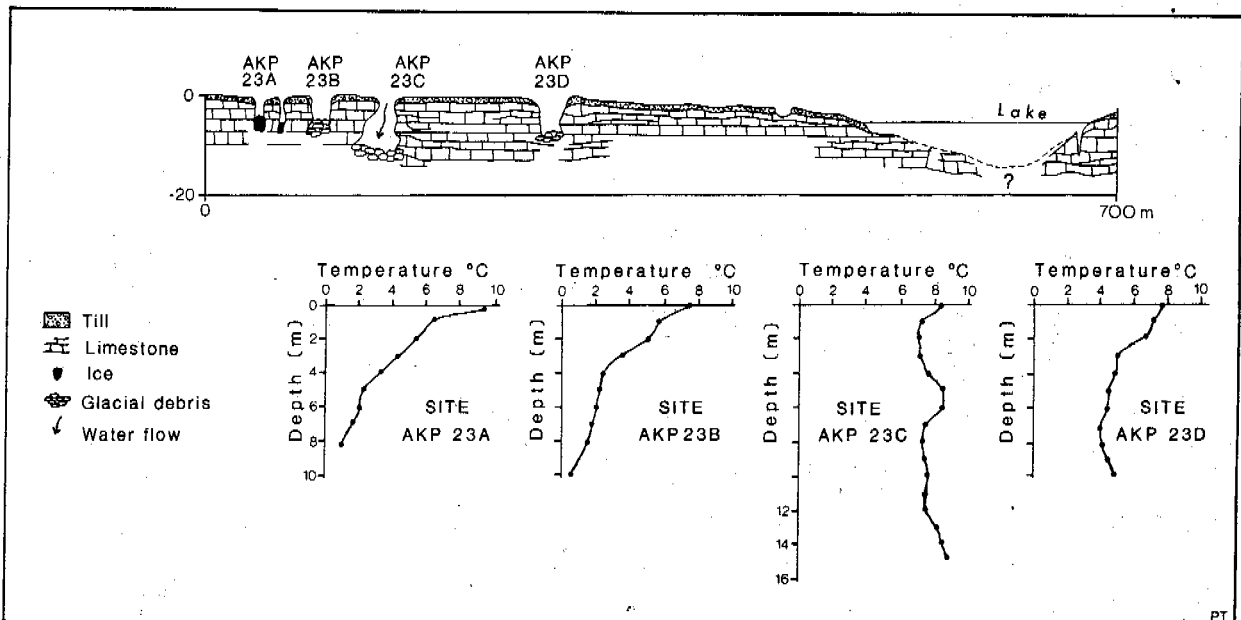


Figure 6. Temperature profiles in joint fissures on plateau south of Gregson Creek.

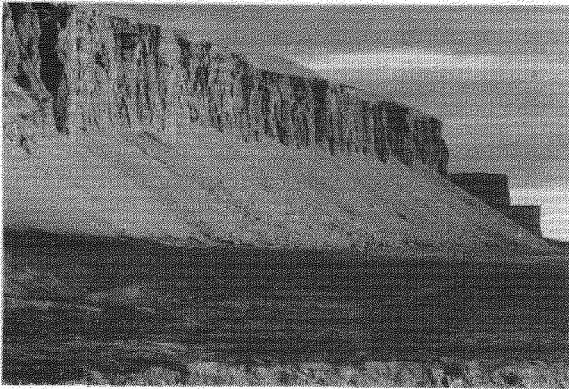


Figure 7. Old sea-cliff at Gregson Creek.

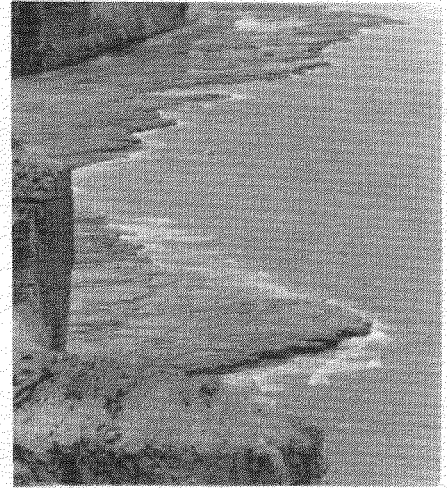


Figure 9. Actively sapped cliff on south-east coast.

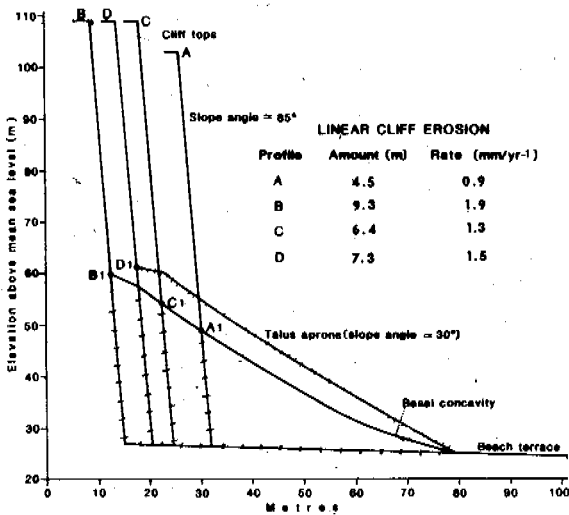


Figure 8. Old sea-cliff and talus slope profiles and recent recession, Gregson Creek.

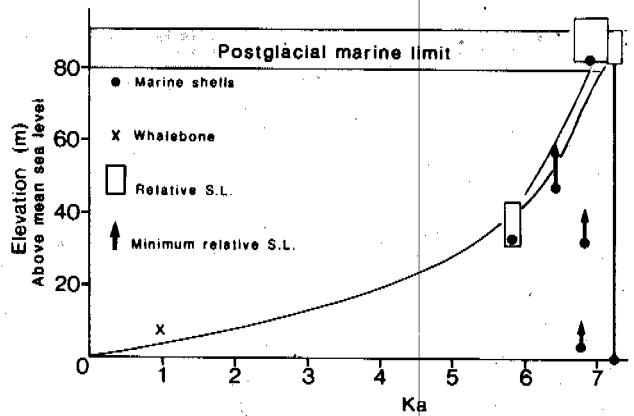


Figure 10. Postglacial emergence curve for western Akpatok Island.

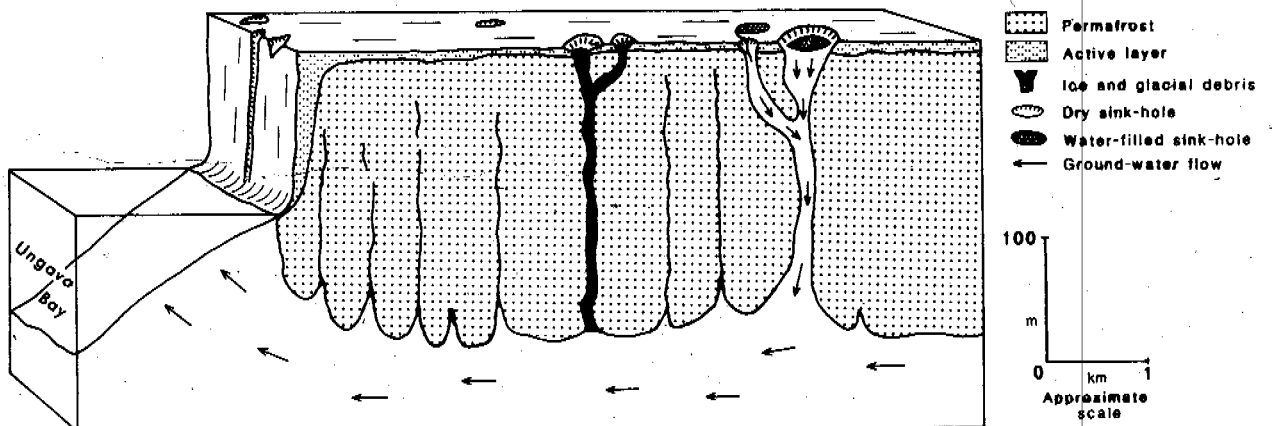


Figure 11. Model for subterranean drainage in a continuous permafrost environment on Akpatok Island.

been in the order of 1 to 2 mm/yr. This rate of erosion is five times more rapid than rates for rock-walls on limestones, cherts and sandstones in Spitsbergen by Rapp (1960), and ten to fifty times more rapid than rates for metasedimentary rocks in the Yukon Territory by Gray (1972). The friable nature of the shaly unmetamorphosed limestones on Akpatok Island, the lack of horizontal contrasts in rock strength, as well as the originally vertical nature of the cliffs, are all factors which explain such rapid recession.

#### MODEL FOR DRAINAGE THROUGH CONTINUOUS PERMAFROST

A water circulation model is proposed in figure 11, which shows why 1) underground drainage is so dominant despite the thick permafrost body on Akpatok Island, and 2) sub-aerial re-surgences of water are so infrequent. In this model water enters the bedrock rapidly through sink-holes leading to vertical passages which traverse the permafrost. Such passages transport the water rapidly beyond the base of the permafrost, to an ultimate base-level represented by sea-level. In this sub-permafrost zone the water can flow under hydrostatic pressure to the sea, the permafrost close to the surface serving as a roof for the water table.

Several factors favour the maintenance of circulation of water in the vertical joints by hindering the development of ice plugs. In the first place, relatively warm permafrost occurs where cliffs, ravines and gorges permit a thick winter snow cover, average near surface ground temperatures of  $-2^{\circ}\text{C}$  being noted at a drill-hole site in such a location. In the second place, surface water can penetrate into the ground, through sink-holes in lake floors. In the third place, those lakes which do not drain completely before winter freeze-up should be underlain by a thinner and slightly warmer permafrost layer, than the surrounding areas. Even the lakes which drain completely in late summer, leave hollows which probably fill up with an insulating layer of snow in early winter, which should also induce warmer underlying permafrost. In the fourth place the penetrating water at temperatures attaining maximum values of approximately  $13^{\circ}\text{C}$ , and possessing considerable kinetic energy convertible to frictional heating, should be able to maintain a relatively positive thermal regime in the largest vertical joint passages. Finally, a necessary precondition for such a drainage model is sufficient topography with the initial development in a non-permafrost environment of a large interconnected network of joint passages by dissolution and/or tectonism.

How and when such drainage passages developed is unknown, but fragmentary evidence for both vertical and horizontal conduits, exposed respectively by cliff retreat and roof collapse, indicates their existence. These conduits must have developed either during non-permafrost intervals, associated with either 1) a warmer interglacial or pre-glacial climate, or 2) a thick warm-based ice sheet. They clearly follow an initial horizontal and vertical jointing pattern in the limestones. The opening of the joints into conduits may be related to 1) erosion by chemical dissolution and mechanical corrosion, or 2) dilatation of joints by neo-tectonism. The latter process has been described by Schroeder et al. (1986, 1990) from Southern Quebec, and seems viable for Akpatok Island. There postglacial isostatic rebound, in excess of 80 - 100 m,

associated with the melting of the last main Laurentide and local Akpatok Island ice sheets (figure 10), may be responsible for crustal decompression with accompanying dilatation of at least the horizontal joints.

#### CONCLUSIONS

Akpatok Island, a Paleozoic limestone outlier in Ungava Bay, is underlain by continuous permafrost greater than 30 m in thickness, with ground temperatures varying between  $-2^{\circ}\text{C}$  and  $-7^{\circ}\text{C}$ . The periglacial climate, in association with the friable nature of the bedrock, has led to extremely rapid cliff recession of 1 - 2 mm/yr, during the late Holocene. Special environmental conditions favour sub-surface drainage through the permafrost. These are, 1) relatively warm ground temperatures; and 2) the heat energy associated with rapid infiltration of surface waters into large vertical conduits developed during non-permafrost intervals in the past.

#### REFERENCES

- Cox, I. (1932) The physical geology of Akpatok Island. *Geographical Journal*, 29:224-227.
- Fraser, H.J. (1935) Experimental study of the porosity and permeability of clastic sediments. *Journal of Geology*, 43:910-1010.
- Gray, J.T. (1972) Postglacial rock-wall recession in the Ogilvie and Wernecke Mountains, Central Yukon Territory. In Adams, W.P. and Helleiner (eds). *International Geography*, University of Toronto Press.
- Gray, J.T., J.A. Pilon, and J. Poitevin (1979) Le pergélisol et la couche active dans la toundra forestière au sud de la Baie-aux-Feuilles, Nouveau-Québec. *Géographie Physique et Quaternaire*, 33:253-264.
- Gray, J.T. (1983) Extraction and compilation of available temperature and snow-fall data in the Ungava Peninsula as input to geothermal modelling of Quaternary paleoclimates. *Earth Physics Branch, Open File Report*, 33 pp.
- Gray, J.T., B. Lauriol, and V. Sloan (1990) Geomorphological evidence for the partial overriding of Akpatok Island, Ungava Bay by two lobes of Laurentide ice. Abstract of 19th Arctic Workshop: 27-30. INSTAAR, University of Colorado.
- Lauriol, B. and J. Gray (1990) Drainage karstique en milieu de pergélisol: le cas de l'île d'Akpatok, T.N.O., Canada. *Permafrost and Periglacial Processes*, 1:129-144.
- Løken, O.H. (1978) Postglacial tilting of Akpatok Island, Northwest Territories. *Canadian Journal of Earth Science*, 15: 1547-1553.
- Rapp, A. (1960) Talus slopes and mountain walls at Tempelfjorden, Spitsbergen: *Norsk Geologisk Tidsskrift*, 119: 1-96.
- Schroeder, J., M. Beaupré, and M. Cloutier (1986) Ice push caves in platform limestones of the Montreal area. *Canadian Journal of Earth Sciences*, 23:1842-1851.
- Schroeder, J., M. Beaupré, and M. Cloutier (1990) Substrat glaciotectonisé et till syngénétique à Port Rouge, Québec. *Géographie Physique et Quaternaire*, 44:33-42.
- Villeneuve, G.O. (1967) *Sommaire Climatique du Québec*, (Vol 1), Min. Rich. Nat. Québec, Publ. M24: 168 pp.
- Workum, R., T. Bolton and C. Barnes (1976). Ordovician geology of Akpatok Island, Ungava Bay, District of Franklin. *Canadian Journal of Earth Sciences*, 13:157-178.



DEVELOPMENT OF PHYSICAL-CHEMICAL MODEL FOR CRYOGENIC HEAVING AND ENLARGEMENT OF SEGREGATED ICE IN FREEZING SANDY-CLAYEY SOILS

Stanislav E. Grechishchev and Vladimir V. Shankov

All-Russian Institute of Hydrogeology and Engineering Geology, Zeleny-Village, Noginsk district, Moscow region, 142452, Russia

The kinetic physical-chemical model for cryogenic heaving and water migration was proposed by one of the authors of this report some years ago. Now the development of this physical-chemical model into complete one-dimensional mathematical model for water saturated soils is proposed. It includes conductive heat transport with water-ice phase transfer in frozen region, conductive heat transport and water filtration in thawed region, and growth of ice on boundary between frozen and thawed regions. Kinetic equations of icing on the freezing front describing behavior of different soils are included. Computer model is developed. Proposed numerical method is described. Freezing different soils is analyzed. The validity of the model is checked against the results of laboratory experiment. New fundamentals of frost heaving are discussed.

INTRODUCTION

In a number of publications by one of the authors of the present report (Grechishchev 1980, 1983) the kinetic physical-chemical model of porous dispersing water saturated medium with water-ice phase transfer was developed. This model was called by the author "thermoreological" and was based on the following observations and assumptions. (1) Thawed soils have thin and large pores which so differ that in thin pores opposite pore walls are in state of force interaction, and in large pores such interaction is absent. (2) In connection with capillary effects of the 1-st and 2-nd kind freezing of water in pores of different size take place under different temperature and, hence, at different time moments: the greater the pore diameter, the sooner and under higher temperature freezing of pore moisture takes place; the thinner the pore, the lower the water freezing point in it. (3) Unfrozen water in frozen soil is situated along all the surface of mineral particles in thin pores and in that part of large pores which remains unfrozen under given temperature in connection with capillary effects of the 1-st kind.

Thermodynamic analysis of interaction between soil matrix, ice and pore water on phase boundary in freezing water saturated dispersing soil, taking into account listed assumptions, enabled to obtain two kinetic equations (Grechishchev 1980, 1983):

$$I_g = \kappa_g [-T_f/T_0 - (\rho_i^{-1} - \rho_w^{-1}) (P_f - P_0) - \rho_i^{-1} \sigma_f^s] \quad (1)$$

$$I_t = \kappa_t [-T_f/T_0 - (\rho_i^{-1} - \rho_w^{-1}) (P_f - P_0)], \quad (2)$$

where  $I_g$  and  $I_t$  are the rate of water freezing in thin and large pores, respectively;  $\kappa_g$  and  $\kappa_t$  are some kinetic coefficients;  $L$  is

latent heat of water-ice phase transfer;  $T_0 = 273.15$  °K is the temperature of phase equilibrium;  $\rho_i$  and  $\rho_w$  are ice and water densities;  $T_f$  is the temperature of phase transfer on the freezing front;  $P_f$  is the pressure in pore moisture on the freezing front,  $P_0 = 0.1$  MPa is the atmospheric pressure;  $\sigma_f^s$  is the effective stress in soil skeleton normal to the freezing front.

Equation (1) expresses the rate of water freezing in thin pores and first of all in a gap between mineral particle and ice. Equation (2) describes the rate of water freezing in large pores including the largest, where capillary effects influence the phase transfer weakly and, hence, kinetic coefficient  $\kappa_t$  may be considered in first approximation as constant for water in free state. As for the kinetic coefficient  $\kappa_g$ , it appears to be connected with both the kinetics of phase transfer of film water into ice in the gap between particle and ice and with water flow from large pores into this gap, what provides ice enlargement near the particle. Flux from the large pore into the gap may be described by the simplest expression

$$q_{fg} = \frac{\rho_w h^3}{2\mu_w S} (P_f - P_g), \quad (3)$$

Where  $q_{fg}$  is the flux from the large pore into the gap between ice and mineral particle,  $h$  is the width of the gap,  $\mu_w$  is water viscosity,  $S$  is the area of transversely cross section of the particle.

It can be shown that kinetic coefficient  $\kappa_g$  is connected with  $\kappa_t$  by the following expression

$$\kappa_g^{-1} = \kappa_t^{-1} + \frac{2\mu_w S}{\rho_w h^3} \quad (4)$$

For modelling of principle importance is to stand out possible dependence of any parameter on unfrozen water content  $W_u$  which strongly depends on the temperature. In the same time width of the gap  $h$  can be taken proportional to  $W_u$  under temperature  $T_f$ . That is why the coefficient  $\kappa_g$  will be expressed in the following form

$$\kappa_g = \kappa_t W_u^3 / (W_u^3 + B), \quad (5)$$

where  $B$  is considered as new empirical coefficient dependent mainly on the soil particle size distribution and its specific surface.

Added equations describe kinetic thermodynamic conditions on the water-ice phase transfer boundary. The full system of equations of kinetic one-dimensional model of freezing soil is formulated below.

#### DIFFERENTIAL EQUATIONS

Soil specimen is assumed to consist of two regions: a thawed region of thickness  $H_{th}$  and a frozen region of thickness  $H_{fr}$ , (Figure 1). The thawed region underlies the frozen one. The thawed region contains water only in the liquid phase. The soil matrix is permeable and filtration is possible. The frozen region contains ice, unfrozen water, and soil formation. It is assumed impermeable.

The heat transport in the frozen region is governed by the equation

$$\frac{d}{dt}(\rho c T + L \rho_w \phi S_w) = \frac{\partial}{\partial z}(\lambda \frac{\partial T}{\partial z}), \quad (6)$$

where  $\rho$ ,  $c$ ,  $\phi$ , and  $\lambda$  are density, heat capacity, porosity, and heat conductivity of the specimen, respectively;  $S_w$  is unfrozen water saturation,  $T$  is the temperature,  $L$  is the latent heat of phase transfer.

The heat transport in the thawed region is described by the equation. (6) with  $S_w = 1$ ,  $\phi = \text{const}$ .

The filtration in the thawed region is described by the equation

$$\beta \frac{d}{dt} P = \frac{\partial}{\partial z} \left( \frac{k \rho_w}{\mu_w} \left( \frac{\partial P}{\partial z} - \rho_w g \right) \right), \quad (7)$$

where  $\beta$  and  $k$  are water capacity and permeability of the specimen,  $p$  is pore pressure,  $g$  is the acceleration of gravity.

The stress,  $\sigma$ , in the frozen region is described by the equation

$$\frac{\partial \sigma}{\partial z} = \rho g \quad (8)$$

The influence of stress on filtration in the thawed region is not considered in the present study and corresponding equations are omitted.

The equation of mass conservation on the

freezing front has the form (for obviousness see Figure 1)

$$I_g = F - (\rho_w - \rho_i) \omega_t \frac{\partial H_{th}}{\partial t}, \quad (9)$$

where  $I_g$  is the rate of icing in the ice-soil gap  $p$  the water mass flux on the front,  $\omega_t$  is the portion of front area occupied by ice tenons.

The equation of energy conservation on the freezing front has the form

$$I_g \omega_g + I_t \omega_t = \Delta Q / L, \quad (10)$$

where  $I_t$  is the rate of icing on the ice tenons,  $\omega_g$  is the portion of front area occupied by ice-soil gap,  $\Delta Q$  is the rate of cold supply to the front determined by

$$\Delta Q = -\lambda \frac{\partial T}{\partial z} |_{H_{th}=0} + \lambda \frac{\partial T}{\partial z} |_{H_{th}=L} \quad (11)$$

The pressure in pore water on the front  $P_f$  is supposed to obey restrictions:

$0 \leq P \leq \sigma_f$ , where  $\sigma_f$  is the stress on the frozen side of the front.

Three possible cases are distinguished:

- 1) The case of water shortage, when  $P_f = 0$ ,
- 2) The case of water balance, when  $Q \leq P_f \leq \sigma_f$
- 3) The case of water abundance, when  $P_f = \sigma_f$

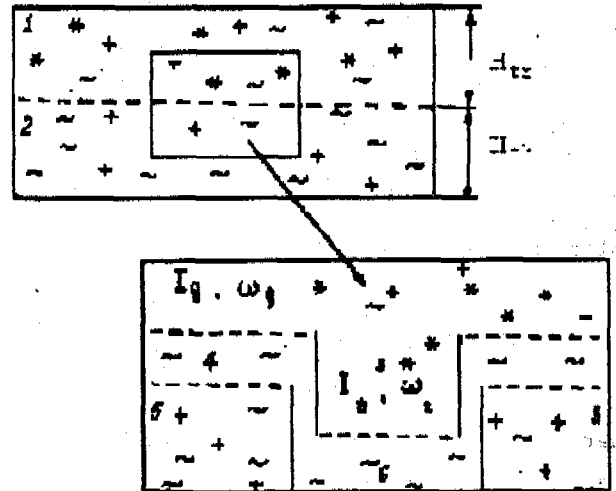


Figure 1. Schematic cross section of the freezing specimen.

1 - frozen region, 2 - thawed region, 3 - ice tenon, 4 - ice-soil gap, 5 - soil formation with unfrozen pores, 6 - freezing pore, \* - ice, ~ - water, + - soil formation.

The thickness of the frozen and thawed regions are governed by equations

$$\frac{\partial H_{th}}{\partial t} = (I_g - I_t) / \rho_i, \quad (12)$$

$$\frac{\partial H_{th}}{\partial t} + \frac{\partial H_{fr}}{\partial t} = I_g / \rho_i. \quad (13)$$

In the case of water balance the rate of

icing on the ice tenons is described by equation. (2) with kinetic coefficient of icing  $\kappa_t$  given by the following empirical relationship

$$L\kappa_t/\rho_i = 0.0273 \text{ m/s} \quad (14)$$

The rate of icing in the ice-soil gap is described by equation (1) with effective stress of soil matrix given by

$$\sigma_f = \sigma_f^s + P_f, \quad (15)$$

kinetic coefficient of icing in the ice-soil gap  $\kappa_g$  is given by equation. (5) in the following form

$$\kappa_g = \kappa_t \omega^3 / (\omega^3 + C_s) \quad (16)$$

where  $\omega$  is the portion of front area occupied by unfrozen water,  $C_s$  is soil parameter.

Functions  $\omega$ ,  $\omega_t$ , and  $\omega_g$  depend on soil, composition, front temperature and pressure; they are defined by

$$\omega = (1 - \omega_0) \rho_{sg} W_u / \rho_w, \quad (17)$$

$$\omega_t = \omega_0 - \omega, \quad (18)$$

$$\omega_g = 1 - \omega_t, \quad (19)$$

where  $W_u = M_w / M_{sg}$  is mass content of unfrozen water.  $M_w$  and  $M_{sg}$  are mass of unfrozen water and soil grains,  $\omega_0$  is the portion of cross section occupied by water in initial unfrozen soil, equals to its porosity,  $\rho_{sg}$  is the density of soil grain.

Thus all functions  $\omega$ ,  $\omega_t$  and  $\omega_g$  are defined through function  $W_u$  which may be determined experimentally. In the present study the following rough approximation for  $W_u$  is used

$$W_u = \begin{cases} 0, & T \leq T_{cr} \\ W_u^0 (1 - T/T_{cr}), & T_{cr} < T < 0 \\ W_u^0, & T \geq 0 \end{cases} \quad (20)$$

where  $W_u^0$  is mass water content of initial thawed soil  $T_{cr}$  is soil parameter.

In the cases of water shortage and water abundance the rate of icing on the ice tenons is given by equation (2), but the rate of icing in the ice-soil gap is given by equations (9) and (12).

In frozen region porosity and unfrozen water saturation are described by

$$\frac{\partial \phi}{\partial t} = -(1 - \phi)^2 \rho_{sg} (\rho_i^{-1} - \rho_w^{-1}), \quad (21)$$

$$\phi S_w = (1 - \phi) \rho_{sg} W_u / \rho_w. \quad (22)$$

On the external boundary of the frozen region the boundary condition for the heat transport problem is imposed. On the external boundary of the thawed region the boundary conditions for both the heat transport and

filtration equations are imposed.

#### NUMERICAL DEVELOPMENT

To solve eqs. (6)-(8) the frozen and thawed regions are divided into a sets of cells  $\Delta_i$ . In each cell the temperature, pore pressure, and properties of water, ice, and soil formation are assumed uniform.

Equations (6) and (7) are rewritten in the flux form

$$a \frac{d}{dt} U = - \frac{\partial}{\partial z} W, \quad (23)$$

$$W = -b \frac{\partial}{\partial z} U + d. \quad (24)$$

Integrating of equation (23) along the cell  $\Delta_i$  and displacing time derivative by finite difference one obtains

$$a_i (U_i - \bar{U}_i) \Delta_i / \Delta t = W_i - W_{i+1}, \quad (25)$$

where  $U_i$ ,  $a_i$  are the values of functions in the  $i$ th cell,  $W_i$  is the value of flux at the left end of  $i$ th cell,  $\Delta t$  and  $\Delta_i$  are the time and space increments,  $\bar{U}_i$  is the value of  $U_i$  on the previous time layer.

Dividing equation (24) by  $b$  and integrating between the middle points of the neighboring cells, where the flux is assumed to be uniform, one obtains:

$$\left( \frac{\Delta_{i-1}}{b_{i-1}} + \frac{\Delta_i}{b_i} \right) W_i = 2 (U_{i-1} - U_i) + \frac{d_{i-1} \Delta_{i-1}}{b_{i-1}} + \frac{d_i \Delta_i}{b_i}, \quad (26)$$

Substituting  $U_{i-1}$ , and  $U_i$  from (25) into (26) one obtains the system of equations with unknown flux  $W_i$  which is solved by Thomas method. Discrete analogue of equation. (8) is obtained by integrating over the cells of the frozen region.

#### BASIC PROCEDURE OF NUMERICAL METHOD

The proposed methods based on the finite-difference technique, proceeds as follows.

On each time step heat transport and filtration problems are solved iteratively. In the case of water balance one starts iteration with step I. In the cases of water shortage and water abundance one starts iteration with step II. To begin the time step with the regime of water balance is supposed to take place. STEP I.

Heat transport problem is solved. In the case of water balance one simultaneously solves equation. (6) both in frozen and thawed regions with the front boundary condition given by equations (10), (11), (2), and (1); the front pressure is that obtained on the previous iteration; after the problem has been solved one proceeds to step II. In the cases of water shortage and water abundance one simultaneously solves equation (6) both in the frozen and the thawed regions with the front boundary condition given by eqns. (9), (10), (11), (12), and (2); the front pressure is that obtained on

the previous iteration; the water mass flux on the freezing front is that calculated in step II of the current iteration; after the problem has been solved one proceeds to step IV.

STEP II

Filtration problem is solved. In the case of water balance the front temperature is that obtained on the step I; after the problem has been solved one proceeds to step III. In the cases of water shortage and water abundance after the problem has been solved one proceeds to step I.

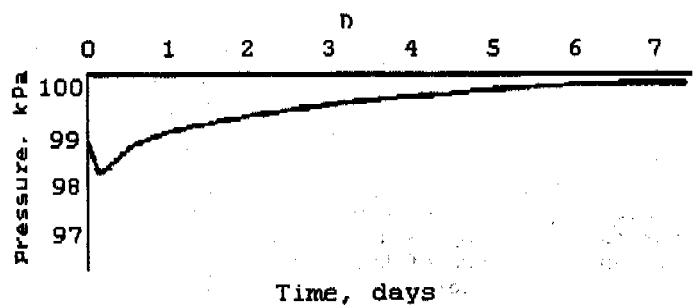
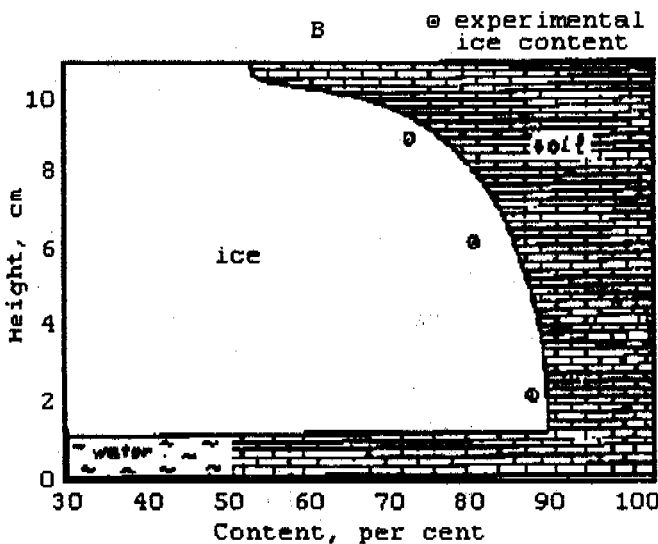
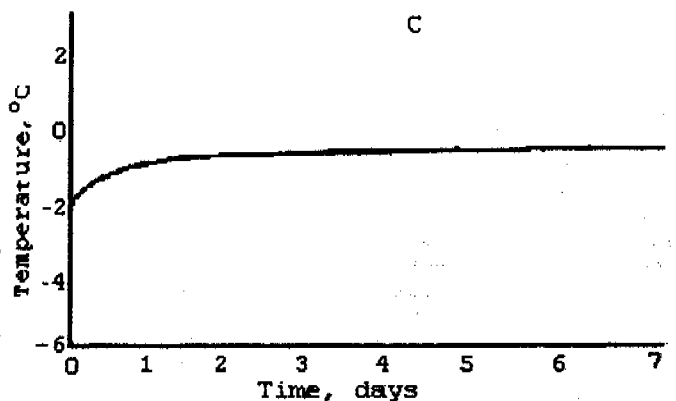
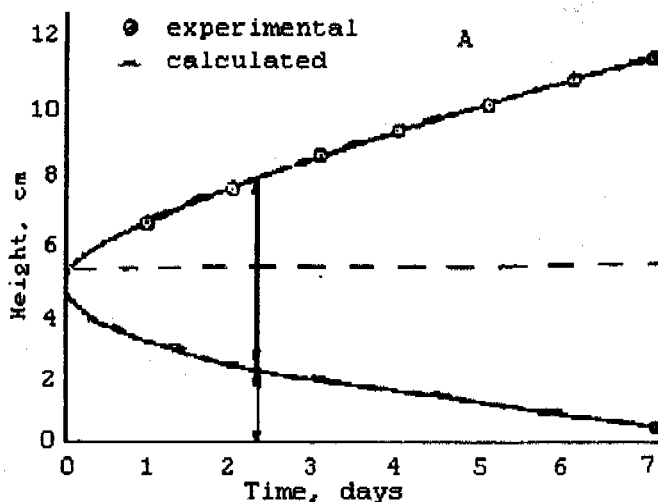
STEP III

The front pressure is analyzed. If the front pressure is less than or equal to zero then the regime of water shortage is supposed to take place the front pressure is set equal to zero, and one returns to step II to perform another

returns to step II to perform next iteration. If the front pressure is greater than zero and less than the stress on frozen side of the freezing front, then it is compared against the front pressure on the previous iteration. If the deviation is greater than a preset value, then the regime of water balance is supposed to take place and one proceeds to step I to reiterate. Otherwise, if the deviation is less than or equal to the preset value, then heat transport and filtration problems are assumed to be solved for the current time step and one proceeds to step IV.

STEP IV

The icing rate on the ice tenons is calculated from eqn. (2). In the case of water balance the rate of icing in the ice-soil gap is determined from eqn. (1). In the cases of water shortage



iteration. If the front pressure is greater than or equal to the stress on the frozen side of the freezing front, then the regime of water abundance is supposed to take place the front pressure is set equal to the stress on the frozen side of the freezing front, and one

Figure 2. Simulation of freezing and frost heaving of silt (details and notation are in the text) A and B - comparison of simulated results with laboratory measurements; C - calculated temperature on the freezing front; D - calculated pressure in pore moisture on the freezing front.

and water abundance the icing rate in the ice-soil gap is determined from equations (9) and (12).

#### STEP V

The increments of the thawed and frozen regions are calculated from eqns. (12) and (13).

The calculated increments are analyzed. If they are greater than a preset value, then time step is recalculated with smaller time increment  $\Delta t$ . If the increments are less than the preset value, they are added to the near front cells and mean soil content in the near front frozen cell is calculated.

#### STEP VI

The discretization is analyzed. If it is unsufficiently good, then new grid is generated and corresponding values of functions are obtained by averaging.

#### STEP VII

The stress on the frozen side of front is calculated from discrete analogue of equation (8).

### COMPUTER MODEL

The finite difference computer model SCHLIERE is developed for simulating laboratory freezing of specimens. It is menu driven and provided with graphical modules. This permits the User to control the process of modeling and display the main characteristics of the process as functions of time or space coordinate on the screen. The program is written in elementary FORTRAN-77. Detailed description of subroutines is available.

### COMPARISON WITH LABORATORY DATA

To test the model laboratory experiments by Dr Sheshin Y.B. were chosen. Experiments were carried out on water saturated sandy-clayey soil specimens 50 MM height and 70 MM in diameter. The system was open: lower specimen's surface was in contact with water saturated sand under atmospheric pressure and temperature about 0°C which was achieved by heating of water. All clip in thermal-insulator was placed into the cooling chamber with given negative air temperature. The upper specimen's butt-end was in direct contact with the air of the chamber. During heaving the upper specimen's part was crawling out of the clip. That is why the side surface of crawled out part was always under the same temperature as the butt-end. Heave and thickness of the lower thawed part were measured. After an experiment the density, the total moisture content, and the concentration of mineral particles by photoes of diameter cross section were measured. Figure 2 compares the simulated results with the experimental measurements for light silt with the following initial parameters: porosity  $\omega_0=0,49$ , soil skeleton density  $\rho_s=1700 \text{ kg/m}^3$ . Freezing was carried out under temperature equal to -3°C. After 7-day freezing the "muddy"

schliere (or ice-soil) was generated: total heave was approximately equal to 7 CM, total moisture content of the frozen part was equal to 105%, density of frozen part  $\rho_{fr}=1300$

$\text{kg/m}^3$ , heat conductivity of frozen part was found to be low  $\lambda_{fr}=0.4 \text{ W/(M}^\circ\text{C)}$ .

To simulate this experiment, in addition to the listed, the following tabular values of parameters, also included in the model, were adopted:  $k=10^{-14} \text{ m}^2$ ,  $\omega_0=0.49$ ,  $\lambda_{th}=1.0 \text{ W/(M}^\circ\text{C)}$ ,  $\lambda_{fr}=0.4 \text{ W/(M}^\circ\text{C)}$ ,  $T_{cr}=-0.1^\circ\text{C}$ . The best approximation was achieved with the fitting parameter of the model  $C_s=0.5$ .

Data on Fig. 2 (A, B) indicate good agreement between simulated and experimental results. For the same specimen Fig. 2 (C, D) also shows calculated values for two hardly measurable quantities: the temperature and pore pressure on the moving freezing boundary. They have comparable values with known in literature experimental data.

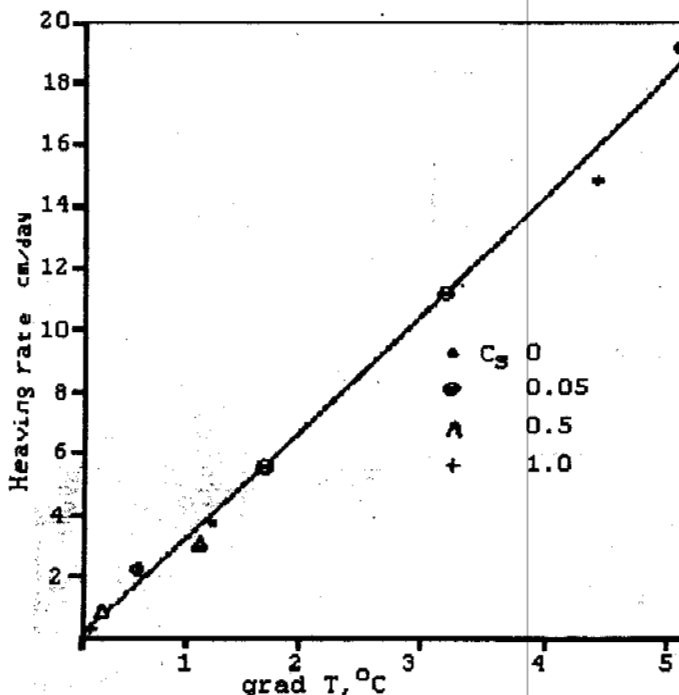


Figure 3. Heaving rate dependence on grad T (simulated).

One of the important results of numerous modeling calculations for sandy-loam and loam soils is the conclusion about inevitable generation of "muddy" ice, i.e. ice including soil particles which are as if torn off from the thawed soil region and taken with by growing ice schliere.

The test with known Penner model in accordance with which heaving rate is proportional to the temperature gradient in frozen region was also carried out. Calculations were made for light silt with

$k=10^{-14}m^2$ ,  $\omega_0=0.4$ ,  $T_{cr}=-1^\circ C$ , specimen's sizes and conditions of the experiment were the same as described before, the temperature of the upper surface was varied from  $-0.5^\circ C$  to  $-5.0^\circ C$ , the parameter  $C_s$  was also changing. Results are depicted on Figure 3. They confirm that for the same soil and under the same external load the heaving rate is actually proportional to the temperature gradient.

Wider possibilities of kinetic model in comparison with others are also to be mentioned. Besides heaving, migration fluxes, and schliere growth it enables also to calculate the pore pressure ahead freezing front, and the temperature on the freezing front (what permits to give concrete meaning to such concept as content of unfrozen moisture on the freezing front). For kinetic model there is no need to use such hardly explicable concepts as "suction" and it contains natural thermodynamic restrictions for the conditions of phase equilibrium, what directly follows from equations (1)-(2).

#### CONCLUSIONS

Proposed kinetic model of cryogenic heaving and cryogenic moisture migration in freezing soils enables to calculate moisture flux, pore pressure, effective stress of soil matrix, temperature of overcooling on the boundary of phase transfer. The model includes only one fitting coefficient (parameter of the model) which depends on the soil particle size distribution and density of soil matrix and can be determined by results of one experimental soil freezing by any scheme. The model well agrees with the experiment.

Practical calculations by kinetic model revealed geocryologically important phenomenon that enlargement of segregated ice schlieres is inevitably accompanied by tearing mineral particles off from the thawed region and their inclusion into the ice. Calculations of soil particles concentration show that it depends on the soil properties and freezing conditions. One may assume that "muddy" ice is the evidence of its segregated origin.

#### REFERENCES

- Grchishchev, S.E. On the thermoreological fundamentals of frost heaving of soils. "Second International Symposium. Frost and Soil. Trondheim, Norway, 1980, Proceed.", 1980.
- Grchishchev, S.E. Fundamentals of thermoreology of cryogenic soils. "Forth Internat. Conf. on permafrost. Proceed.", 198S.

PERMAFROST FEATURES AND THEIR CHANGES IN AMUR AREA,  
DAXINGANLING PREFECTURE, NORTHEASTERN CHINA\*

Gu Zhongwei, Zhou Youwu, Liang Fenxian,  
Liang Linheng and Zhang Qibin  
Lanzhou Institute of Glaciology and Geocryology,  
Chinese Academy of Science, China

Three sections can be divided as follows: 1) Permafrost section at the foot of the slope and the swamp wetland. 2) Permafrost section in the gentle slope before the mountain. 3) Permafrost section in the terrace of the river. The permafrost in Amur area is degenerating presently. The seasonally thawing depth has deepened at least 30 cm while the thickness of permafrost has reduced at least 52-17 m. The ground temperature at the depth of 20 cm has gone up at least 0.8°C, and the mean annual ground temperature has increased 2.1°C-0.7°C. The area of talik is expanding. The reasons for such changes are analyzed in this paper, which can be summed up as follows: 1) Climate warming. The mean annual air temperature of the last 30 years has increased about 1.6°C. 2) Influence of increasingly intense human activity.

INTRODUCTION

Mt. Daxinganling is the high-latitude large stretch of permafrost distribution area in China. The existence of permafrost bring up the greatest forest resource in China, but its degeneration and disappearance directly influence forest growth and the changes of ecological environment. Amur is in one of the coldest and well-developed permafrost areas. So, it has good representatives for us to study. Supported by the National Natural Science Foundation of China since 1990, the authors have given extensive investigations and site observations about the changes of permafrost environment after forest fire in this area, and same time, collected a lot of information on the features and changes of permafrost. The following discussed permafrost change are mainly concerned with climate warming and human activities.

PHYSIOGRAPHIC AND GEOLOGIC OUTLINE OF THE STUDY AREA

Amur lies in the northern part of Mt. Daxinganling in China, where the geographical position is 123°11'E and 52°50'N. The Amur Forest Bureau and Jintao Town are located here (Fig.1).

Amur belongs to the region of low mountains and hilly lands. The Amur River (the tributary of the Heilongjiang River), which develops sinuously with a wide bed, flows through the southern side of the area from southeast to northwest. On the northern side of the Nenlin Railway, there is a wide stream valley which is called the North Gully, and the stream flows into the Amur River. The study area is mainly concentrated in the right bank terraces of Amur River and the North Gully that are near the Amur Forest Bureau and Jintao Town.

\*The research project is supported by the National Natural Science Foundation of China.

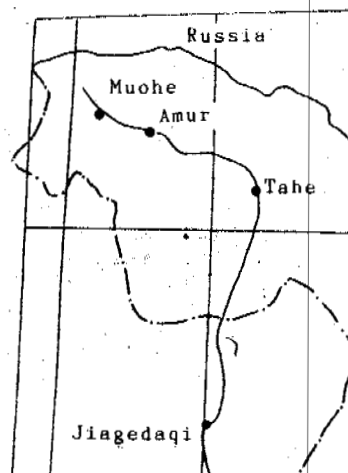


Figure 1. Location of Amur

It is a frigid-temperate zonal continental climate in the study area. The mean annual air temperature is -2.1 -- -6.3°C, of which the average is -4.7°C. The maximum air temperature is 35°C while the minimum is -49.7°C. The mean annual precipitation is 443.9 mm and is mainly concentrated in May-Sept. The major wind direction is WN. The frigid period (daily mean air temperature  $\leq 0^\circ\text{C}$ ) is 211.3 days (1975-1981). The snow-covered period lasts 187.2 days (1975-1981). The snow thickness is usually 15-30 cm and the thickest can reach 36 cm. The snow density is 0.153-0.170 g/cm<sup>3</sup>.

The stratum of the study area is relatively simple. The upper layers are distributed with loose layers of the Holocene epoch. There are

mainly alluvial pluvial layers, slope was pluvial layers and slope wash alluvial layers, etc. and their thicknesses are different. The lower layers are turf breccia of the Cretaceous period in the Mesozoic era.

Many places in the study area have been exploited and become locations of administrative organs, streets, factories, schools and dwelling houses. The original ground surfaces have suffered severe damage. Before exploitation, the terraces of the river and valley terrain were characterized by damp ground surface with logging water, and also by well-developed gully ponds in other places. On the ground surfaces there is exuberant vegetation. On the mountain slope terrain, the ground surface is dry and the plants grow vigorously. The turbulent forest fire in 1987 burned away a large area of vegetation at a varying degree and only left patches of natural larch and pine trees on the left slope of the North Gully. In the heavy burning section, there are currently sprouted birch, Rhododendron, Ledum and other pioneer plants and they grow perfectly well.

#### PERMAFROST FEATURES

Mt. Daxinganling is the high-latitude large stretch of permafrost distribution area in China. Based on the characteristics of permafrost distribution in the study area, the sections can be divided as follows: permafrost section in the foot of the slope and swamp wetland, permafrost section in the gentle slope before the mountain, and permafrost section in the terrace of the river.

1. Permafrost section in the foot of the slope and swamp wetland: It is situated in the foot of the slope on two sides of North Gully and in the bottom of valley. The North Gully is in the direction of NE-SW with 600 m in opening width and 2000 m in length. The section is characterized by a smooth terrain and low-lying land with logging water on the ground surface. There is a stream in the middle of valley, which runs through the valley bottom and flows into the Amur River. Presently growing are *Eriophorum vaginatum* Sphagnum spp. *Ledum palustre* and *Betula fruticosa* etc. on the ground surface. Beside the stream are clumps of willows. There existed a few larch trees here before the fire in 1987.

The stratum is simple. The upper slope wash pluvial layer is more than 10 m in thickness which is composed by round gravel mixed with subclay soil. The lower part is a weathering breccia layer (Fig.2).

The permafrost develops the best in this section. The mean annual ground temperature of the permafrost is low (-4.2 -- -1.7°C); the thickness is great (more than 60 m in general, 100 m or so, at the maximum); the annual change depth is about 15 m (Table 1); and the maximum seasonal thawing depth is shallow (less than 80 cm in the 1970s, and 125 cm in 1991). The permafrost structure is described from the surface to the bottom as follows. Under the surface layer of mosses is a layer of ground water, with 10 cm in thickness, penetrating into the layer of ice of which the ice is pure. Beneath the ice layer is the integral frozen soil structure or thin-layer structure. In the vicinity of the permafrost upper table is a straticulate or straticulate-like structure, and an ice layer of 2-15 mm in thickness can be seen, of which the volume water content is 40-80% while the weight water

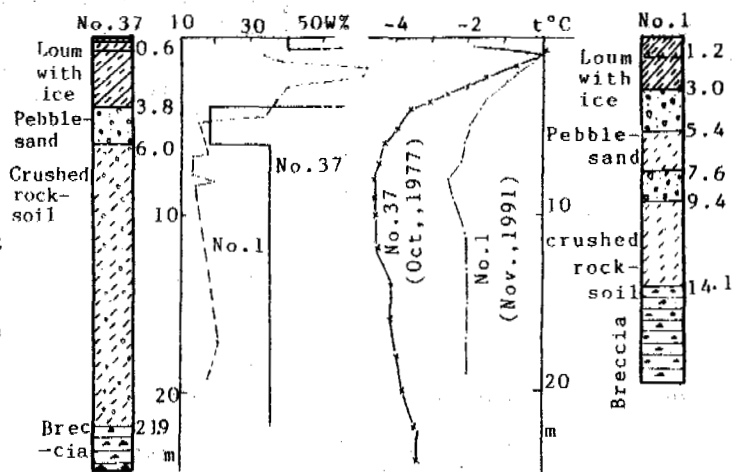


Figure 2. Geological columnar figure and ground temperature, water content curves for No.37 drilling (from Dai Jinbo, 1982) and No.1 drilling

content is 36.7-64.5%. Toward the lower part, it is straticulate or the straticulate-like structure of fine grained soil, whereas it is the package structure in coarse grained soil and the water content decreases.

2. Permafrost section in the gentle slope before the mountain. It is situated on the slopes of the two sides of the North Gully. The right side of the slope faces southeast and is 5-10° in a natural slope. The natural ground surface suffered severe damage from the turbulent fire in 1987 that burned away large areas of forest and only left patches of pines, and further more, some of the slope places have been exploited into residential quarters. In the unexploited places there are currently growing *Betula Platyphylla*, *Rhododendron dauricum*, *Vaccinium vitis-idaea*, *Carex* spp. *Deyeuxia angustifolia* etc. The upper lithological property is crushed rock soil. The permafrost only exists in the lower part of the mountain slope and becomes developed towards the inside of the gully. The altitude of permafrost distribution is below 530 m at the gully mouth and ascends to 560 m at the hinterland of the gully, while the other places above the altitude are the seasonally frozen ground section. According to the three boreholes' temperature observing data from the third IRED in 1982, the ground temperature at a depth of 4.5-10.0 m was 0°C. The permafrost was characterized by high temperature and a thin layer that is about 10 m in thickness. The records of some borehole indicated straticulate-like or integral structured ice content frozen soil in which the ice content was 10-15 percent. The maximum seasonal thawing depth was 1.8-3.5 m.

The left side of the mountain slope faces northwest with 10-20 degrees in slope which is a little steeper than that of the right side. In 1987, the northern part of the slope suffered severe damage from the forest fire, while the middle and southern parts were only burned slightly or experienced no fire at all. These areas are now growing mixed forest of larch, pine and birch. The lithological property is mainly crushed rock soil that belongs to the weathering residual layer of the Quarternary period.

Situated on the half-shady slope, the permafrost



Table 1. Features of temperature and the thickness of permafrost in the section of the foot slope and swamp wetland

Drilling number	Geomorphological position	Time measured	Mean annual ground temperature (°C)	Thickness of permafrost (m)	Annual change depth (m)	Source of information
37	Low-lying wetland	1978-1979	-4.2	120*	15.0	Third IRED
16	Low-lying wetland	1978-1979	-2.8	85.4**	15.4	
0	Low-lying wetland near the stream	1978-1979	-1.9	62.0**	15.0	
26	Low-lying wetland	1975	-3.7	107.5*	15.0	
39	Foot of slope	1978-1979	-1.7	57.5*	14.0	
1	Low-lying wetland with larch	1991	-2.1	67.5*	15.0	
2	Low-lying wetland without larch following the fire	1991	-2.0	65.0*	15.0	Authors

Note: \* The thickness of permafrost is the calculated value from the Third Inst. of Railway Exploration and Design (Third IRED).  
 \*\*The thickness of permafrost is the measured value from the borehole observation.

in this section, should have been well-developed. but in fact, the thickness of permafrost is thin and temperature high (Fig.3). From Fig.3, we can see that minus temperature occurred at a depth of 8-12 m in No.38 drilling and 8-10 m in No.3 drilling, and the temperature was only 0 - -0.2°C. The frozen depth here was about 4-5 m. Hence we can conclude that it is an unconnective frozen layer and is mainly caused by the effect of underground water. It is just the thermal action of ground water that causes frozen ground to become thin and ground temperature high, and consequently forms an unconnective frozen soil layer.

II-level terrace or in the boundary of the I and II-level terraces on the right bank of Amur River. It is characterized by a smooth terrain with a slope of 5-10 degree gently inclining to the west. Amur Forest Bureau and Jintao town are located in this section. Before exploitation, the humid ground surface harboured exuberent vegetation. Presently the natural ground surfaces has been injured and most have been occupied by roads, streets, houses and wood storage yards etc. The lithological property is mainly alluvial-pluvial deposits.

The frozen ground at the boundary of the I and II level terraces is as thin as 0.9-5.6 m in thickness and usually appears to be integral or straticulate-like or a reticulated structure. It has a relatively high ground temperature. Influenced by the intense human activities and forest fires in recent years, the permafrost in this region has been degenerating.

In the II-level terrace and the back terrain of it, permafrost develops well. It is mostly a layered structure interspersed with ice dense body of fine grained soils, and can be divided into rich ice, saturated ice and ice content frozen soil, in accordance with the amount of ice content. The pure ice layer is 1-70 mm in thickness, the rich ice frozen soil layer usually numbers ten centimetres in thickness and occasionally to 2.2 m. In coarse grained soils, the permafrost is usually integrally structured and there are saturated, rich or less ice content ones due to the difference of ice content. The depth of the active layer varies greatly at different sites. It is 0.5-1.0 m at the site of humid ground surface with exuberent vegetation while 1.5-4.5 m at the site of dry ground surface with no vegetation. The permafrost temperature in this region is usually -1.0°C or so, and the minimum is -4.0°C (Fig.4). According to the ground temperature curve, we can obtain that the permafrost thickness is usually 30-50 m and the maximum can reach 100 m or so. It is notable

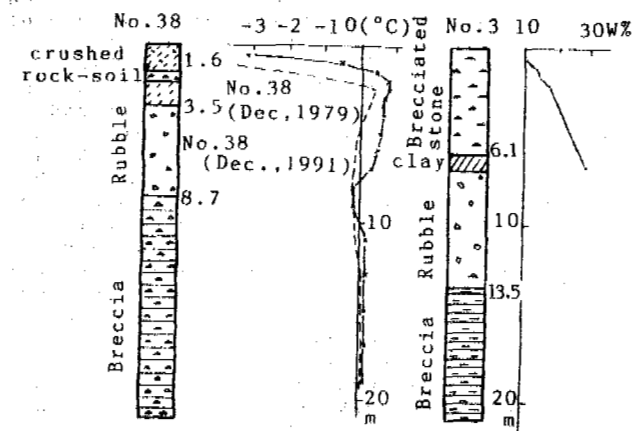


Figure 3. Geological columnar figure and ground temperature, water content curves for No.38 drilling (from Dai Jinbo, 1982) and No.3 drilling

3. Permafrost section in the terrace of the river. It is situated in the back sector of the

that in the vicinity of the filling petrol station, 3.8 km to the southeast of Jintao town, a thawing layer was found at the depth of 7.8-9.0 m, together with pressed ground water which belongs to the permafrost interlayer water. The occurrence of such a double layer structured permafrost is due to its location at the gentle slope before the mountain and hence related with the activity of ground water.

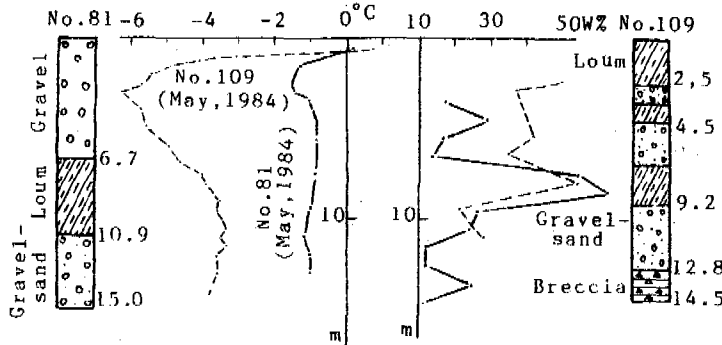


Figure 4. Geological columnar figure and ground temperature, water content curves for No.81 and No.109 drillings

Overall, the permafrost in Amur area has a large variation in both ground temperature and thickness. Its development condition is controlled by many interrelated and interactive factors such as topography, geomorphology, slope-aspect, river, stream, gully snow-cover, vegetation, forest fire as well as human activities, etc.

#### CHANGES OF PERMAFROST

In recent years, there have been many papers to discuss the changes of permafrost in Mt. Daxinganling in Northeastern China. The following discussed permafrost changes are mainly concerned with climate warming and human activity. As for the effect of fire, it will be elucidated in other papers.

In the permafrost of Mt. Daxinganling, there appears a tendency of regional degeneration from south to north. The island talik is expanding. The upper table of permafrost is declining, whereas the lower table is ascending. In our study area, the permafrost also presents an obvious degeneration trend.

#### The Seasonal Thawing Depth is Increasing

In 1970s, the maximum seasonal thawing depth was usually 50-70 cm in a sector covered with a thick moss layer. According to the observation of the natural site by Jintao Frozen Soil Experiment Station of the Third IRED\*, the measured thawing depth of frozen soil in the humid wetlands covered with thick mosses was 0.68 m and the soil temperature at depth of 20 cm was 0.8°C on the afternoon of Sept. 27, 1978. We made contrastive measurements in the natural swamp wetland of the same ground surface condition and obtained the following data. On the morning of

Sept. 17, 1991, the thawing depth of frozen ground was 0.8-0.95 m and the soil temperature at depth of 20 cm was 2.0-2.4°C. On the morning of Sept. 27, 1991, the thawing depth increased to more than 1.0 m (the steel probe was too short to reach the frozen soil) and the soil temperature at the same depth was 1.6°C on Oct. 18, 1991, the measured thawing depth was 1.25 m. Thus it can be concluded that the seasonal thawing depth, under the above conditions, increased at least 0.3 m and the soil temperature at the depth of 20 cm increased at least 0.8°C during 1978-1991.

#### The Changes of Permafrost Ground Temperature

The observational data of No.26, 37, 16 and 0 drillings have been used to make contrastive analysis with that of No.1 drilling that was drilled in 1991, which were situated at the same bottom of the North Gully (Fig.5). From the Fig. 5, we can see that the mean annual ground temperature rose from -3.7°C to -2.1°C (a rise of 1.6°C) based on the comparison of No.26 drilling with No.1 drilling, if calculated by the same method, the thickness of permafrost would be reduced from 107.0 m to 67.5 m. If compared with the No.16 drilling and No.37 drilling, the mean annual ground temperature would have a rise of 2.1°C and 0.7°C respectively, while the thickness of permafrost would be reduced 52.5 m and 17.0 m respectively. Judging from this, we can see that in the last ten years, or so, permafrost shows an obvious trend of degeneration even in the most developed sections of the swamp wetland and at the foot of the slope. It is only the No.0 and No.1 drillings that are relatively the same in ground temperature. This is likely created by the thermal action of ground water in the stream near the No.0 drilling and thus made the ground temperature higher than that of No.26, 37, and 16 drillings (refer to Table 1).

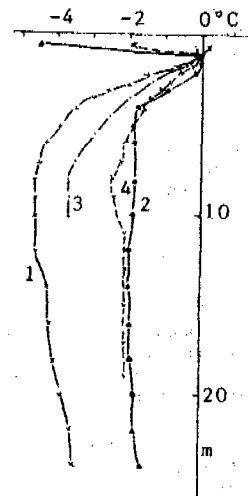


Figure 5. Contrastive curves of ground temperature in boreholes at the same region in different time  
1 - No.37 (Oct. 1977), 2 - No.0 (Dec. 1978)  
3 - No.26 (Nov. 1975), 4 - No.1 (Nov. 1991)

The authors made further comparisons of the ground temperature-curve of the No.38 drilling of 1977 with that of the No.3 drilling of 1991

\* (The changing law of ground temperature in permafrost area of northern part of Daxinganling prefecture) June, 1981, manuscript.

(Fig.3). Both boreholes were situated at the same altitude and within a short distance of the half shady slope of the left side of the North Gully. We can see that the ground temperature has also risen, No.38 drilling revealed that the minus temperature zone was between 5-12 m while No.3 drilling revealed it to be between 8-10 m. This suggests that the permafrost upper table has declined whereas the lower table has ascended. Finally it results in the formation of un-connective permafrost. The permafrost also appears to have a degenerating tendency, however, the degenerated amplitude is not as prominent as that in the swamp wetland. This is mainly caused by the influence of ground water, of which the intense thermal action controls the development conditions of permafrost in this region and makes the effect of climate warming on permafrost less significant.

#### The Extent of Talik is Expanding

Along with the development of production and increasing population, many different kind of buildings equipped with heating installation have been built on sites of perfect geological engineering conditions such as the I and II-level terraces and the sunward slope terrains. Also influenced by other factors, the high temperature and thin stratum permafrost get into ablation gradually and finally leads to talik. The permafrost boundary in the North Gully declined about 80 metres towards the bottom of Gully in the last ten years and this leads to the disappearance of permafrost on the mountain slopes where it existed in the past.

#### Reasons of the Permafrost Changes

(1) Climate warming. The gradual rising of air temperature is a major contributor to the regional degeneration of permafrost in Daxinganling prefecture. Fig.6 is the mean 5-year running curves of mean annual air temperature at Amur Meteorological Observatory (1975-1991) and the adjacent Muohe Meteorological Observatory (1959-1991). The figure reflects that the mean annual air temperature presents an apparent rising trend in the past three decades. The average value of a 5-year running of mean annual air temperature was about  $-5.0^{\circ}\text{C}$  during 1959-1976, about  $-4.8^{\circ}\text{C}$  during 1973-1980, rising to about  $-4.4^{\circ}\text{C}$  during 1973-1980, rising prominently to  $-3.4^{\circ}\text{C}$  during 1986-1991. The mean annual air temperature has increased about  $1.6^{\circ}\text{C}$  over thirty years with an average of  $0.5^{\circ}\text{C}$  rise during each decade. Amur Meteorological Observatory also has such a trend, and the rising amplitude is larger during 1984-1989 and 1987-1991. In the yearly accumulated value of minus temperature there appears the same rising trend (Fig.7). It fluctuated at about  $-125$  -  $-130^{\circ}\text{C}$  during 1959-1977, about  $-120^{\circ}\text{C}$  during 1978-1986, and rising prominently to about  $-105^{\circ}\text{C}$  after 1987. The absolute value decreased at least  $20$  -  $25^{\circ}\text{C}$  in the last thirty years.

Climate warming can also lead to a rise in the amount of snowfall in winter (Table 2). The maximum thickness of snowcover in Amur in Jan. is presently 25-26 cm, which, based on our calculations, can cause a rising of  $3.8$  -  $4.0^{\circ}\text{C}$  for mean annual ground surface temperature compared with the places without snowcover. If the thickness of snowcover increases 4-5 cm again, the mean annual ground surface temperature will increase  $4.3$  -  $4.5^{\circ}\text{C}$ . That is, the rising rate of mean annual ground surface temperature and the thickness of snowcover is

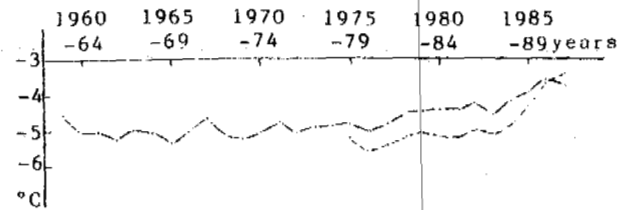


Figure 6. Five-year running curves of mean annual air temperature in Muohe (1959-1991) and Amur (1975-1991)

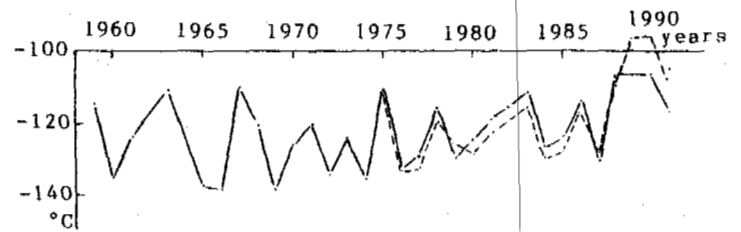


Figure 7. Yearly accumulated curves of minus temperature in Muohe (1959-1991) and Amur (1975-1991)

Table 2. Maximum thickness of snowcover in Amur in January during 1987-1992

Year	1987	1988	1989	1990	1991	1992
Thickness (cm)	15	23	18	25	27	30

$0.5^{\circ}\text{C}/4$  -  $5$  cm. This suggests that the increase of snowcover thickness would also contribute to the degeneration of permafrost.

(2) Influence of increasingly intense human activity. Before 1965, this region was full of exuberant primeval forest without people. Beginning from the late 1960s, with the construction of the railway, large areas of forest cutting and a gradual increase of population, many towns were founded. There is presently a population of about 500,000 in the Daxinganling prefecture, Heilongjiang Province, and about 40,000 in Jintao Town, where there are many roads, schools, administrative organs, factories, dwelling houses and other buildings. This increasingly intense human activity has led to a rising of permafrost ground temperature, a deepening of the active layer and degeneration or disappearance of permafrost, as can be illustrated by an example of house heating. Compared with the house-heating after three years with the natural state before construction, the permafrost mean annual ground temperature went up from  $-3.7^{\circ}\text{C}$  to  $-2.5^{\circ}\text{C}$ . This means the house heating within three years contributed to a rise of  $1.2^{\circ}\text{C}$  in ground temperature (Fig.8). By inference in the permafrost section in the terrace of the river of which the mean annual ground temperature is usually  $-1.0^{\circ}\text{C}$  (where most of the areas have been occupied by different kinds of buildings), the permafrost under buildings has experienced ablative action and become talik at present.

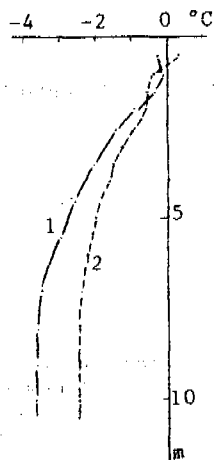


Figure 8. Comparison of ground temperature curves in natural state (1) with that following house-heating after construction (2) (from the 3rd IRED)

#### CONCLUSION

The permafrost in Amur area, can be divided into the following three sections: Permafrost section at the foot of the mountain slope and the swamp wetland, permafrost section in the gentle slope before the mountain and permafrost section in the terrace of the river. The permafrost in this region shows an apparent tendency of degeneration with the active layer deepening, the mean annual ground temperature rising and the talik expanding. The degeneration of permafrost is mainly created by climate warming and intense human activity.

#### REFERENCES

- Dai Jinbo, (1982) Characteristics of ground temperature in permafrost region of northern part of Mt. Daxinganling. *Journal of Glaciology and Geocryology*, 4(3), 53-62.
- Research Group of Permafrost in Northeastern China. (1983) Basic characteristics of permafrost distribution in northeastern China. *Proceedings of 2nd Chinese National Conference on Permafrost*, pp.36-42.
- W. Haeberli, (1990) Glacier and permafrost signals of 20th-century warming. *Annals of Glaciology*, 14, pp.99-101.
- Yuan Haiyi, (1989) Degenerating permafrost in the Daxinganling Mountain. *Proceedings of 3rd Chinese National Conference on Permafrost*, pp.54-58.

A PRELIMINARY RESEARCH OF SOLIFLUCTION TERRACES IN FENGHUOSHAN  
PASS BASIN ON QINGHAI-XIZANG PLATEAU

Guo Dongxing, Huang Yizhi and Zhao Xiufeng

Lanzhou Institute of Glaciology and Geocryology, Chinese Academy of Sciences

Solifluction is one of the most prevalent periglacial processes in the Fenghuoshan region. According to analyses of the investigation and the dynamic observations in 1984 and 1990, the formation and movement of the solifluction which is situated on the WS-slope in Fenghuoshan Pass Basin may be attributed to the actions of temporary water flow on the ground surface, gravity, the pressurization caused by bidirectional freezing etc..

INTRODUCTION

The Fenghuoshan region is located in the interior of the Qinghai-Xizang Plateau where the permafrost is well developed and typically distributed. Due to the practical needs of the investigation and the design of Qinghai-Xizang railway and exploitation of the Qinghai-Xizang Plateau, much research and fixed position observations on the formation, distribution and developing regularities of the permafrost and on the physiomechanical properties of frozen soil and ground ice have been done in the region from the beginning of the 1960s. Other experimental works on the embankment, cutting, culvert, retaining wall and slope protection have also been carried out for engineering needs. Though the research work in the region is much more detailed than those in other regions along the Qinghai-Xizang highway, only little attention was paid to the cryogenetic down-slope processes, and discussions on the cryogenetic landforms and periglacial sediments did not cover their formation mechanisms, developing processes and dynamics.

Solifluction is one of the main cryogenetic downslope processes in the Fenghuoshan region. Based on the data collected from topographic surveying, investigations and fixed position observations in 1984 and 1990, we present some results of our research on the formation mechanisms, developing processes and dynamics of the 12-stage solifluctional terraces developed on the WS-oriented slope in Fenghuoshan Pass Basin.

THE DEVELOPMENT BACKGROUND OF THE SOLIFLUCTIONAL TERRACES

Located in the interior of the Qinghai-Xizang Plateau and characterized by low mountains and hills on the high plateau, Fenghuoshan is in the eastern stretch of the Hoh Xil Mts. with an elevation of 4750 to 5100 m a.s.l.. According to the

data at Wudaoliang Meteorological station in the adjacent region, the mean monthly temperature in the region from June to Sept. is above zero degree centigrade and the active layer of permafrost is formed in this seasonal thawing period. About 90% of the annual precipitation also is concentrated in this period (Table 1), most of which flows into the gullies from the shallow ditches on the slope and drains away. But a part of it seeps into the seasonal thaw layer and increases the natural soil moisture content, which makes the thawing layer near or reach its plastic flow state and thus provide a favourable condition for the development of solifluction.

Table 1 The temperature and precipitation at Wudaoliang Meteorological Station in the Adjacent region(1961-1970)

Month	Jan.	Feb.	Mar.	Apr.	May.	June	
Air Tem. (°C)	-17.3	-15.2	-10.9	-5.2	-0.8	2.4	
P.(mm)	0.8	1.8	2.9	4.5	18.1	47.4	
Month	July	Aug.	Sep.	Oct.	Nov.	Dec.	Total
Air Tem. (°C)	5.4	4.9	1.5	-5.6	-13.3	-16.2	-5.9
P.(mm)	74.3	70.6	39.1	6.6	1.4	0.2	267.6

Fenghuoshan is at the eastern fringe of the Cenozoic Hoh Xil depression. In the Paleocene and Oligocene epoch, it was a fault lake basin and thick sediments of purple mudstone, mud-siltstone and marl were deposited. In the transitional period from the Oligocene to Miocene epoch and accompanied by the Himalaya Movement, the region uplifted strongly and stopped its inland lake basin sediments and formed the modern geomorphological landscape. During the Quaternary period, there was a slow but continuous wide-ranging uplifting. The primary moun-

tainous plateau morphology, formed in the initial period of the Miocene epoch, was denuded and sculptured by various exogenic forces and the slope-frost creeping sediments accumulated on the slope with a thickness of 3-6 meters (Fig.1) and provided the material source of the later solifluction development.

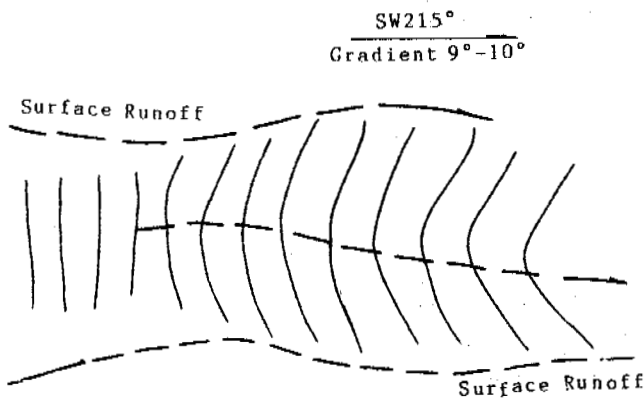


Fig.1 The front edge shape of the solifluctional terraces in 1984

As a result of the Neotectonic properties, the processes of denudation by exogenic forces and the transportation of its products were moderate. Therefore the sediments had a long time and opportunity to be exposed near the ground surface, enduring the reforming action of exogenic forces. The grain-size became finer which was more favourable for the later solifluction development.

Compared with other regions along the Qinghai-Xizang highway, the permafrost and ground ice in the Fenghuoshan region is best developed and the permafrost in Fenghuo Pass basin is better developed than that of other places in Fenghuoshan region. According to the available temperature data measured in a drill-hole, the mean annual ground temperature at the bottom of the basin is  $-3.8^{\circ}\text{C}$  and the estimated thickness of permafrost may surpass 100 to 120 m. The maximum seasonal thaw depth, affected by the slope-aspect and vegetation, ranges from 1.2 to 2.0 m. The maximum seasonal thaw depth where the solifluction has developed is 1.3 m which was determined by the drill-hole. The layer from the ground surface to the depth of 0.6 m in the seasonal frozen layer presents a homogeneous frozen texture or fine ice layered texture with a volumetric ice content of around 15-25%; From 0.6 m down to the upper table of permafrost, a fine ice layered or thin and thick layered texture appears with volumetric ice content amounts from 25-60% and the soil layer is in a plastic flow state when melted. The aspect of the slope where the solifluctional terraces are located is  $\text{SW}215^{\circ}$ , of which the gradient is between  $10-11^{\circ}$ . The solifluctional terraces are situated in the concave part of the concave slope. And over the highest terrace there are four linear ditches in which the precipitation accumulates and flows across the sides and the middle part of the terraces.

#### THE TWO INVESTIGATION RESULTS OF THE SOLIFLUNCTIONAL TERRACES

When doing research work in Fenghuoshan on

June 29th 1984, the writers carefully investigated the solifluctional terraces. After more than six years, on July 21st to 26th, 1990, surveying and dynamic observation work on the tenth solifluctional terrace were done including the topographic surveying.

According to the investigation results in June, 1984, the 12-stage solifluctional terraces existing on the slope has a total length of about 300 m. The width of each terrace is between 12-27 m, and the height of the terraces is about 0.4-1.2 m, the aspect of the slope faces  $\text{SW}215^{\circ}$ , the slope gradient is  $10-11^{\circ}$ . The number of each terrace was counted downwards.

We discovered that the edges of the 1st to 5th terraces were nearly leveled and straight, parallel with the slope contour line. The middle parts of the 6th to 12th terrace edges, which culved upwards and were arranged like a series of arcs, was the place where the surface water passed through and after rainfall or snow melting a temporary brook was formed. The mountain meadow and the scarcely scattered mound-like vegetation occupied the surface of the slope and the solifluctional terraces. Due to the erosion by temporary water flow, the integrity of the vegetation at the edge of terraces was destroyed. The vegetation and the soil beneath slanted or collapsed down on the terrace surfaces below. Some block or mound-like sods had been removed by flowing water.

The exiting temporary water which flows at the culved edges of the solifluctional terraces and the movement of the collapsed sod demonstrated that the culved front edges of the terraces was the results of water headward erosion at this place.

In 1990 from July 21st to 25th, topographic surveying and investigation on the solifluctional terraces were again carried out and a series of dynamic observation points were set up on the terraces. The results of the investigation six years after 1984 showed a great deformation of the front edges of the terraces.

The front edges of 1st to 3rd terraces protruded downward slightly, and the terrace heights were no more than 0.2-0.3 m. The step of 4th terrace was nearly gone, and the 4th terrace connected with the 5th terrace composed a slope. The former shape of the front edges of the 6th-10th terraces no longer existed. Some of them projected downward in the middle area, some of

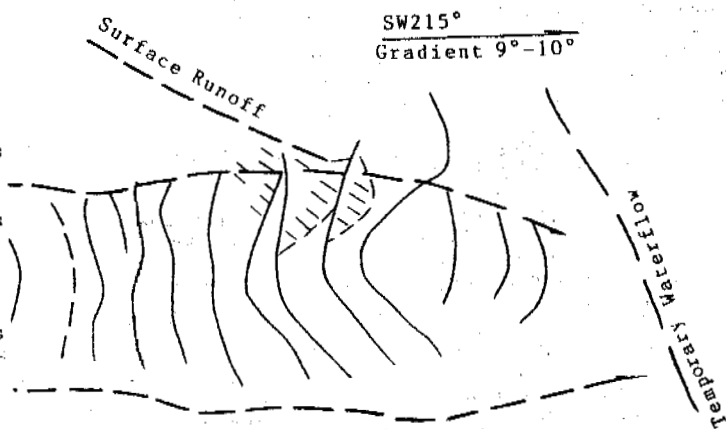


Fig.2 The front edge shape of the solifluctional terraces in 1990

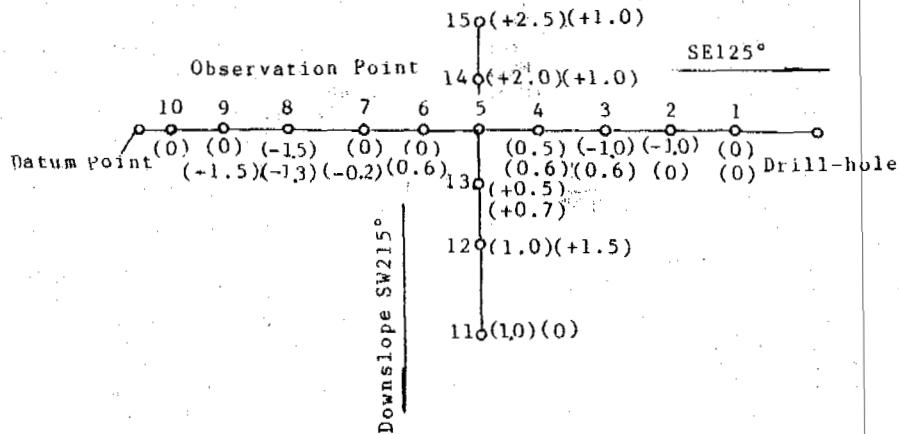


Fig.3 The dynamic observation points on the tenth terrace and its movement

Notes:

- A) 1,2,3,...15, Numbers of the observation points.
- B) (0),(+1.5),(-1.0)..., The first measured movements.
- (0),(+1.5)..., The second measured movements. Plus signs showing down slope movements, minus signs showing upward movement. Measuring Unit:cm.

them were S-shaped and some of them curved irregularly. A small-scale diluvial fan had developed in the right part of 9th to 12th terraces due to the silt-subclayey sediments deposited here by water flow. Some sod blocks or mounds were scattered on the surface of the fan (Fig.2). Though the front edge of 11th and 12th terraces still projected upward, they had a sharper curve than that of six years ago. Another important difference of the terraces compared with their shape of six years ago was that three mudflowing tongues appeared below the 12th terrace. The upper two mudflow tongues had obvious steps and thick green grasses grew on their surfaces. The lowest mud tongue was embryonic in form and the sparse grass indicated that the tongue had been formed recently.

In July, 1990, we arranged sixteen observation points (Fig.3) in the downslope direction or the widthwise direction on the tenth terrace surface and on June 25th, 1991, the first observation was made. Five of the six points in the widthwise direction showed downslope movements, the maximum moving distance was 2.5 cm, the minimum was 0.5 cm. Five of the nine points arranged on the 10th terrace in the downslope direction showed no movement, three of them moved upwards and one moved downslope.

ANALYSIS ON THE FORMATION AND MOVEMENT MECHANISMS OF THE SOLIFLUCTIONAL TERRACES

To discuss the formation of the solifluctional terraces in more detail, we need to trace back the development history of the solifluctional sediments. The permafrost in the region in its geological history has undergone several fluctuation. Correspondingly, the cryogenic geomorphology and cryogenic sediments have also undergone several reformations. H.H.HomHovski suggests that in the formation, development and evolution processes of permafrost, there are great differences in the cryogenic action and cryogenic sediments in different developing periods (V.A.Kudryavtsev et al.,1978; E.D.Ershov et al.,1989; E.D.Ershov et al.). In the cold

period, the permafrost developed and the frost thaw weathering, frost heaving, frost cracking, etc., were prevalent. The corresponding sediments and periglacial phenomena such as block fields, stone streams, debris slopes, cavity ice, pingos and ice core were formed. In the warm period, permafrost retreats in area and in thickness, the preceding cryogenic action and its sediments are restrained. Contrary to the cold period, thermokarst, solifluction, thermokarst erosion become dominant and the corresponding periglacial phenomena and sediments are solifluctional terraces or tongues, thermokarst settlements, ice wedge casts and thermokarst slumping.

In "The formation and its history of the thick ground ice in Fenghuoshan Region"(Guo Dongxing, 1982), author showed that the solifluctional terraces on the slope in Fenghuoshan region are the products of the warm climate after the Late Pleistocene. The view is based on stratum analyses when discussing the formation history of the thick ground ice.

The investigation of the solifluctional sediment in 1990 to 1991 revealed that there were five or six greyish black humus layers at the depth of 1.6 to 2.7 m with a single thickness of about 0.5-2.0 cm.

As mentioned above, the sod at the front edge of the solifluctional terraces was tilted and would be buried when the terrace was further developed. So the humus layers were obviously the result of accumulation of the solifluctional sediments in the geological period, the <sup>14</sup>C dating of the humus layers was 15380±620 a B.P. and showed that the formation was after the Late Pleistocene Glaciation in the climate transitional period.

According to the comparisons of the topographic surveys on solifluctional terraces and the available data of dynamic observation, the solifluction develops in a rather complex process. The forces of solifluction development comes from three aspects: The first is the erosion and depositing action of water sheet and linear water flow, which is the main force for changing the shape of the terraces and the mic-

rotography of the terraces surface. The upward curving shape of the terraces edge in 1984 was due to the erosion of a steady linear stream formed in the middle part of the terraces immediately after rainfall or snow melting. After 1984, the water sheet and stream changed their direction to the left side of the SE and the increasing precipitation in the autumn of 1989 caused the water sheet and stream to carry more mud, thus the shape of the terraces edge was gradually changed to its present shape. Secondly, in seasonal melting periods when the melting soil layer developed to a certain depth, generally 30 to 60 cm, the melted ground ice in the seasonal thawed layer causes the soil to be in a plastic flowing state, and the layer creeps downward along the frost-thaw table because of its gravity. Based on reports and available materials, the velocity of the solifluction movement is from 1-2 cm/y to several centimetres a year, and the velocity of this solifluction is 1-2 cm/y. Thirdly, in the transitional period from autumn to winter, the seasonal thaw layer becomes frozen. With the downward movement of the frost front, the thawed layer between frozen soil layers, which is in a plastic flow state, is pressed and forms a complex mechanical system and the complexity is enhanced by the difference of ground surface microtopography. The soil layer under the forces not only moves downward, which is also caused by its own gravity, but moves upward and in other directions. The dynamic observation of the 15 points which showed 6 points moving down the slope, 3 upward, 6 in their original-places, coincided with our suggestion. More long term observation material is needed for supporting this theory because it is based on the analysis of the preliminary observations.

#### REFERENCES

- V.A.Kudryavtsev et al.(1978) General Geocryology. P270-282. MSU Press (in Russian).
- E.D.Ershov et al.(1989) Geocryology of USSR (Middle Siberia). P74-80. "Nedra" Press (in Russian).
- E.D.Ershov et al.Geocryology of USSR (The Southern Mountains).P77-126. "Nedra" Press (in Russian).
- Guo Dongxin, Li shude (1982) The Formation and History of the Thick Ground Ice Layer at Fenghuoshan District in the Qinghai-Xizang Plateau. "Proceedings of the Symposium on Glaciology and Cryopedology Held by Geographical Society of China" (Cryopedology) P60-66. Beijing: Science Press (in Chinese).



## MONITORING THE LONG-TERM EVOLUTION OF MOUNTAIN PERMAFROST IN THE SWISS ALPS

Wilfried Haeberli, Martin Hoelzle, Felix Keller,  
Willy Schmid, Daniel S. Vonder Muehll and Stephan Wagner

Laboratory of Hydraulics, Hydrology and Glaciology,  
VAW -ETH Zentrum  
CH - 8092 Zürich, Switzerland

Attempts are presently being made to establish a measurement network for monitoring the long-term behaviour of mountain permafrost in the Swiss Alps, especially in view of warming trends. Methods applied include aerial photogrammetry of permafrost creep within selected rock glaciers, borehole measurements for permafrost deformation and temperature, data archiving from geophysical surface soundings for later repetition and qualitative analysis of infrared aerial photography. The investigated permafrost is typically several decameters to more than 100m thick and has mean annual surface temperatures between the melting point and about  $-3^{\circ}\text{C}$ . Heat flow within the uppermost 60m of bedrock-reaching permafrost indicates more or less stable surface temperatures between about 1950 and 1980. As a consequence of the exceptionally warm 1980s, permafrost temperatures in the uppermost 10 meters below surface now seem to be rising at rates of 0.5 to more than  $1^{\circ}\text{C}$  per decade. Annual rates of thaw settlement from melting of ground ice in Alpine permafrost may have more than doubled since the 1970s.

### INTRODUCTION

Snow, glaciers and permafrost react sensitively to changes in atmospheric temperature because of the proximity to melting conditions. In addition, mass wasting is most intensive in high mountain areas with steep slopes. As a consequence, climatic changes cause pronounced effects in the glacial and periglacial belts of mountain areas (Haeberli 1990, Wood 1990). The 20th century has seen striking changes in glacierized areas of mountain ranges and, hence, in the extension of periglacial mountain belts all over the world. The changes in surface and ground ice conditions caused a corresponding shift in geomorphic processes such as debris flow activity in freshly exposed or thaw-destabilized moraines and talus. In the Alps, this development was accompanied by increasing human activities. The combination of atmospheric warming and human impact have, in fact, introduced the most striking changes in high mountain landscapes.

Coordinated long-term monitoring of glaciers in the Swiss Alps started as early as 1893. The significance of glaciers as key parameters for climate-system monitoring is now widely recognized and the results of long observational series represent convincing evidence of fast climatic change at a global scale (IPCC 1992). Systematic monitoring of seasonal snow started considerably later. Because of the large amplitude of year-to-year variations and the lacking "memory" function of seasonal snow as compared to glaciers or permafrost, snow monitoring is more important in view of the ecological and economic consequences of potential changes (water cycle, energy production, tourism) than as a signal of climate change (VAW 1990). Systematic long-term monitoring of permafrost only started recently and is still being developed as part of a combined observational programme on changes in the Alpine cryosphere. The goal of the long-term project discussed here on mountain permafrost in the Swiss Alps is to

- (a) adequately document ongoing changes;
- (b) better understand the processes involved;
- (c) improve the basis for assessing consequences of potential warming trends in the near future.

### CONCEPTS AND TECHNIQUES

Changes in permafrost take place at various scales of time and space. Along vertical profiles with depth at individual points, reactions of permafrost to climatic changes are supposed to take place in three main forms:

(1) changes in active layer thickness and thaw settlement/frost heave in supersaturated material at the permafrost table as an immediate response (time scale: year(s);

(2) disturbance of temperature profiles within the permafrost, i.e. between the permafrost table and the permafrost base, as an intermediate response (time scale: years to decades); and

(3) displacements of the permafrost base as a definitive response (time scale: decades to centuries or even millennia).

With regard to the 3-dimensional dynamics of complex landscapes, two more types of reactions at highly variable time scales can be envisaged:

(4) modification of permafrost distribution patterns, involving

(5) adjustment of geomorphic, hydrological and nivo-glaciological processes such as permafrost creep, frost heave/thaw settlement, thermokarst, erosion and slope instability on thaw-destabilized slopes, runoff variations in time, drainage characteristics, snow cover evolution and metamorphism, and avalanche formation.

Hence, the most important parameters to be observed are the surface altitude in permafrost areas and the depth to the permafrost table beneath the surface, the vertical temperature profile within the permafrost, the local/regional distribution pattern of permafrost, the

horizontal and vertical deformation of ice-bearing ground, geomorphic forms, and runoff characteristics in the periglacial belt. Evidently, a combination of methods must be applied (cf. King et al. 1992) to appropriately document this entire set of phenomena and associated changes.

The depth to the permafrost table can be measured with thermistors in boreholes and with geophysical surface soundings. Seismic refraction and geoelectrical resistivity soundings are best applied in non-consolidated sediments with a high ice content. The permafrost table in such cases often consists of almost pure ice and gives sharp contrasts in P-wave velocity and specific resistivity. The resolution of active layer thickness determination by such measurements may not be better than a meter or two. The commonly encountered coarse, blocky surface layer makes exact definition of surface geometry difficult and introduces considerable

heterogeneity in near-surface physical properties over the considered profile. For logistic and economic reasons, borehole temperatures can be monitored at a few sites only, whereas geophysical soundings may cover a number of profiles and areas. Fast changes can be expected to exceed the methodological uncertainty range within the time scale of decades. Melting of pure ice at the permafrost table, however, leads to surface lowering rather than to increased active layer thickness.

The vertical profile of permafrost temperature should be observed in boreholes (Fig. 1) reaching beyond the depth of seasonal temperature variations and - if possible - even penetrating the permafrost base into non-frozen sub-permafrost ground. Periodic recalibration of the installed thermistors by repeated measurements with a thermistor chain lowered into the borehole is essential for assuring measurement accuracy in the  $0.1^{\circ}\text{C}$  range over long

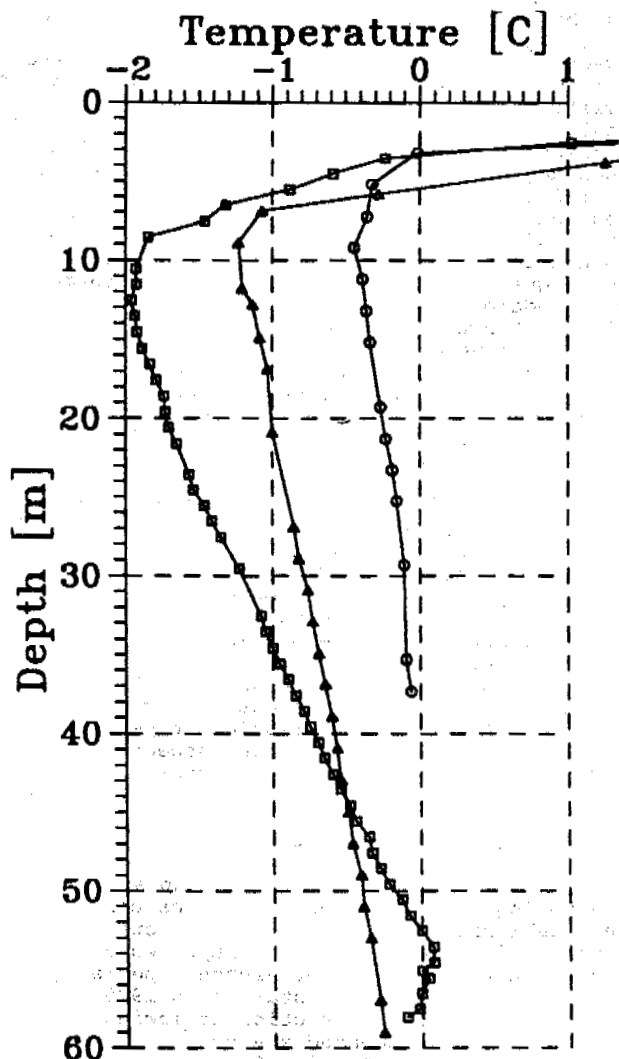


FIGURE 1. Temperature profiles in the permafrost boreholes Murtèl (squares), Ursina 1 (triangles) and Ursina 2 (circles). The date is September 1991.

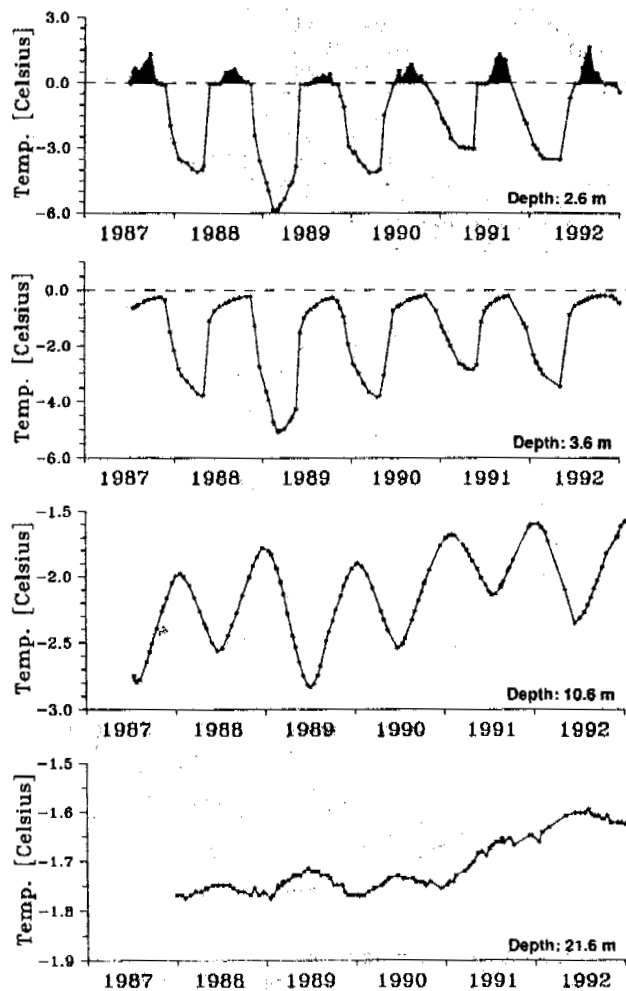


FIGURE 2. Borehole temperatures in the permafrost of the active rock glacier Murtèl/Corvatsch (Grisons) at various depths. The permafrost table is between 2.6 and 3.6 m depth. Recent warming trends from the exceptionally hot 1980s and early 1990s are most clearly visible at 10.6 and 21.6 m depth. The accuracy of the measurements is about  $\pm 0.05^{\circ}\text{C}$ .

time-periods. (Vonder Mühll and Haeberli 1990, Vonder Mühll 1992). Clear signals can be observed after a few years (Fig.2). Interpretation can be based on heat conduction theory as long as water flow remains negligible. The vertical temperature profile in permafrost is, indeed, the clearest information available at present but the representativity of observations in a few expensive boreholes must be assessed using complementary methods. Interpretation of geophysical soundings with respect to displacements of the permafrost base are difficult and uncertain (cf. Haeberli 1985). Long-term changes are, therefore, only detectable with precise borehole temperature measurements. Even with this method, problems exist due to borehole depths not reaching the permafrost base, slow and small rates of change at the considered depth range, and effects of freezing-point depressions or complicated influences of groundwater (Vonder Mühll 1992).

Patterns of permafrost distribution in mountain areas with a thick enough cover of winter snow are best mapped using the BTS method (Fig. 3) if possible in combination with geophysical soundings at representative sites. The great number of point measurements collected in this way enables the development of statistically calibrated models of permafrost occurrence as a function of energy balance parameters and topographic effects on snow redistribution by avalanches and wind (cf. Hoelzle et al. 1993). Such models can also be used to simulate spatial effects of changing climatic conditions

for various scenarios and, thus, point to the most sensitive sites. Repetition of regional mapping could reveal marked changes in the observed patterns of permafrost existence within time intervals of decades.

Thaw settlement and frost heave as related to permafrost degradation and aggradation cause changes in surface altitude which can be mapped using geodetic and photogrammetric techniques. Direct photogrammetric comparison of specially flown large-scale aerial photographs also serves for monitoring the flow field in creeping rock glacier permafrost (Fig.4). The concepts and procedures have been introduced and illustrated by Haeberli and Schmid (1988). The slow displacement of a coarse, blocky surface with a roughness of the meter scale is the main limitation to the resolution of altitude change determination within a regular grid remaining fixed in time. Averaging over larger areas helps to reduce this uncertainty and gives significant results about marked changes within a time period of a few years to several decades. More detailed interpretation of the observed changes requires that one distinguishes between the "climatic signal" (settlement/heave from melting/freezing) and the "dynamic signal" (vertical strain from 3-dimensional flow) by analysing in detail the fields of vectors and horizontal strain rates. Uncertainties with such detailed calculations are caused mainly by poor local information about permafrost thickness and complex variations of vertical strain rates with depth. Horizontal and vertical borehole deformation using borehole inclinometry and magnetic rings offers essential information with regard to these difficulties (cf. Wagner 1992) but are available for only a few sites.

The evolution of geomorphic phenomena associated with Alpine permafrost can be recorded and documented using aerial photographs. High-altitude/small-scale infrared photography is especially suitable for mapping large areas in view of changes in vegetation cover at rock glacier margins (flow activity), scree slopes and cones (rockfall activity), debris flow traces (frequency of occurrence), size and water-level variations in thermokarst lakes (permafrost hydraulics), and growth/disappearance of perennial ice patches. Repetition of mapping seems reasonable at time intervals of one to a few decades. Monitoring the processes of water runoff in areas of mountain permafrost requires classical hydrological equipment with the main difficulty being its maintenance during winter. Monitoring snow characteristics at permafrost sites may also be an important aspect of observing long-term changes at high altitudes (cf. Keller and Gubler 1993).

#### PROGRAMME AND FIRST RESULTS

The initial step for building up a long-term monitoring system in the Swiss Alps consisted in establishing survey nets at selected rock glaciers in conjunction with repeated high-precision photogrammetry. At Gruben, special flights at low altitude started in 1970 in connection with flood protection following two lake outbursts. Repeated analyses in 1975 and 1979 (Haeberli and Schmid 1988) showed that growth and degradation of permafrost can take place simultaneously at different places within the same rock glacier but that an overall thinning tendency of a few centimeters per year occurred in the purely periglacial part of the

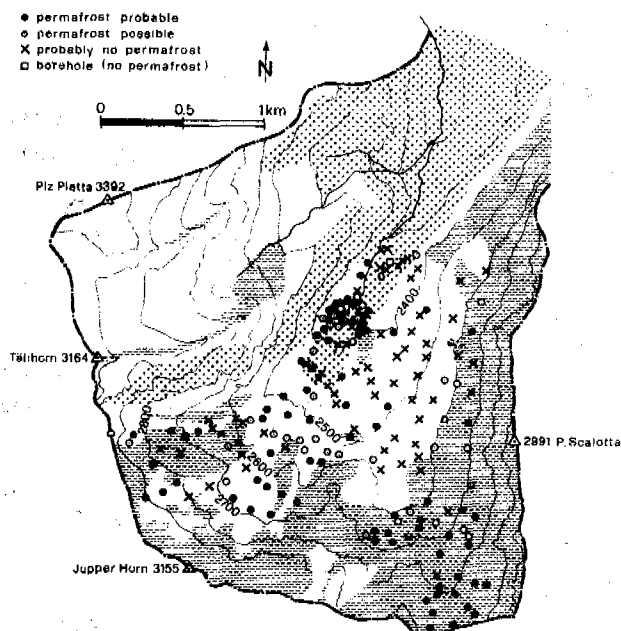


FIGURE 3. Permafrost mapping in the Val Bercla (Grisons) using BTS-measurements. The stippled and dashed screens give permafrost-free areas and areas with probable permafrost as estimated from the empirical "rules of thumb" developed earlier in a nearby test area (cf. Hoelzle et al. 1993). The reliability of the rules is reduced particularly in historical glacier forefields with a complicated recent thermal history (cf. the cirque between Tällhorn and Jupper Horn).

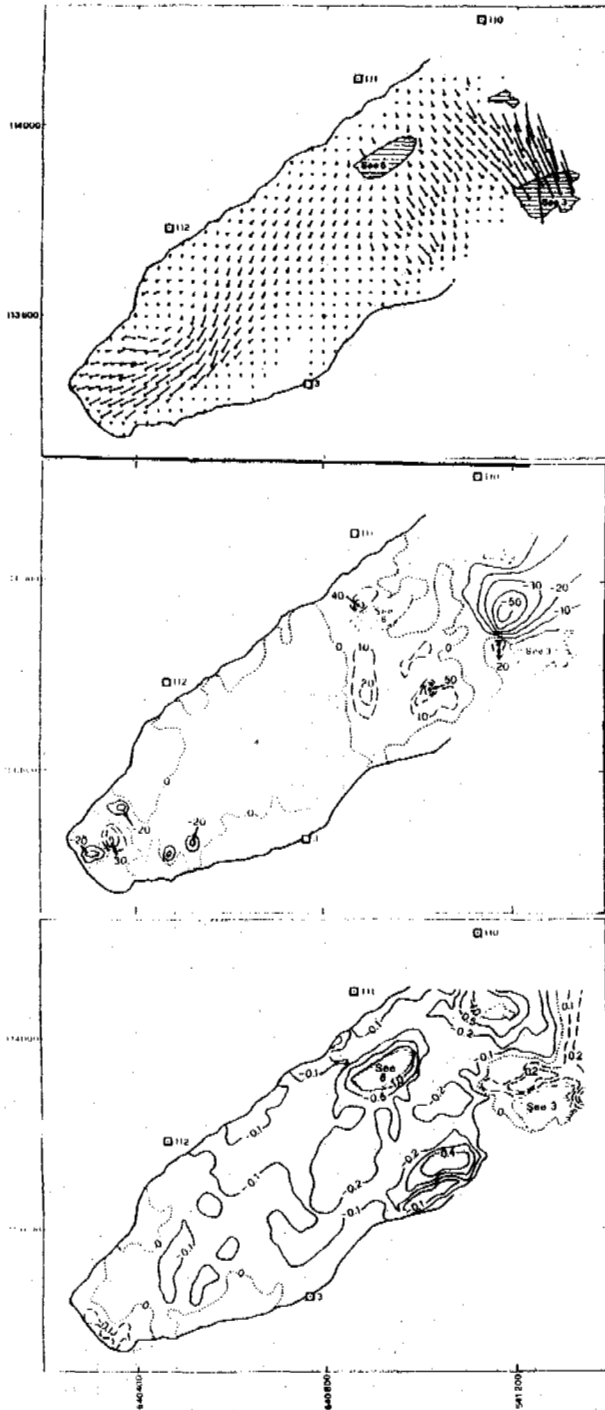


FIGURE 4. Photogrammetrical analysis of creeping permafrost at Gruben rock glacier: (a) vector field 1985-1991, (b) changes in surface altitude (1979-1991, cm/year) and (c) changes in flow velocity 1979-1985/1985-1991 (m/year). Accuracy is about 0.1 to 0.2 m/year. The part to the west of lake 6 is a purely periglacial feature, whereas the remaining parts have been influenced by a glacier advance during the Little Ice Age and carry relics of dead ice on top of the permafrost (cf. Haerberli and Schmid 1988 for more details on the method and the site).

rock glacier and of about 1 decimeter per year in the formerly glacier-covered part with remains of dead ice buried on top of the permafrost. New analyses were carried out from aerial photographs taken in 1985 and 1991 (Fig. 4). The number of grid points has now been increased greatly by reducing the mesh width (25m) to half its original value. In comparison with the 1970s, annual thinning rates have accelerated by a factor of 2 to 3 in the warm 1980s to early 1990s (Fig. 5). This is probably caused by increased melting of ice at the permafrost table and may therefore be superimposed onto an assumed long-term trend of slow melting at the permafrost base. Results from similar surveys since 1981 are available from Muragl rock glacier in the Grisons (Vonder Mühll and Schmid 1993) and confirm the generally small rates of geometric change in Alpine permafrost. Additional results from repeated photogrammetry can soon be expected from the rock glaciers Réchy, Furggen/Gemmi and Gufer/Aletsch in the Valais and from Murtèl/Corvatsch and Ursina/Pontresina in the Grisons (Fig. 6).

With the 1987 drilling through the permafrost

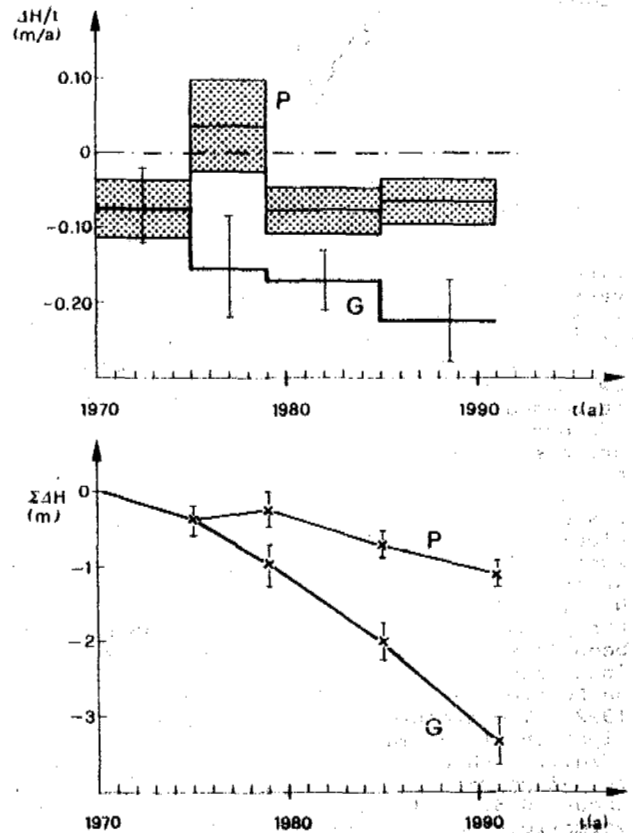


FIGURE 5. Changes in surface altitude at Gruben rock glacier from aerial photogrammetry since 1970: annual velocities (top) and cumulative effect (bottom). P = periglacial part, G = glacier-affected part with dead ice remains. Surface lowering (thaw settlement) is significant in both parts and considerably faster in the warm 1980s than in the 1970s.

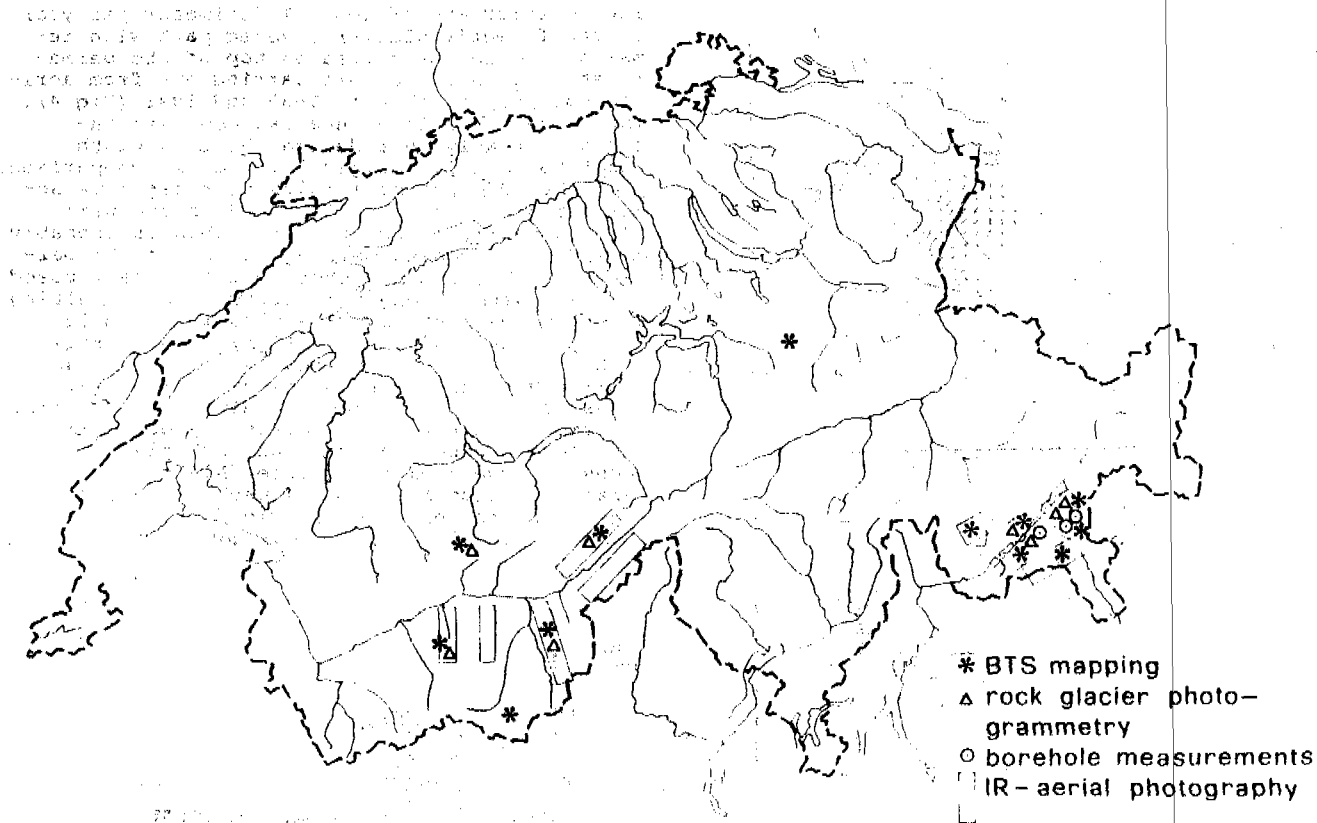


FIGURE 6. Location map of permafrost monitoring activities in the Swiss Alps.

within the active rock glacier Murtèl/Corvatsch, the first borehole was equipped for long-term observations in the Swiss Alps (Haeberli et al. 1988, Vonder Mühli and Haeberli 1990). Up to 1992, permafrost temperatures between the permafrost table and 10m depth have increased at rates of a few tenths to nearly 2°C per decade. This fast warming of near-surface permafrost is a consequence of the especially warm late 1980s and early 1990s. Results of bore-hole deformation measurements are discussed by Wagner (1992). Horizontal and vertical strain rates vary with depth in an unexpectedly complicated and still poorly understood way but remain fairly constant in time. No significant effects of thaw settlement at the permafrost base or permafrost table have been detected so far. Two more boreholes were installed in 1990 at the nearby site of Ursina/Pontresina (cf. Vonder Mühli and Holub 1992). Temperature profiles measured after dissipation of thermal disturbance from drilling (Fig.1) within all three boreholes give mean annual permafrost temperatures at 10m depth of about -0.5, -1.3 and -2°C with corresponding permafrost thicknesses of 40, 70 and possibly more than 100m. The last value is a rough estimate based on a discussion of groundwater influence in a talik at 53m depth, which can also be assumed to be the cause of the strongly elevated value for the overall temperature gradient and vertical heat flow in the Murtèl borehole (Vonder Mühli 1992). The less disturbed temperature gradients in the two Ursina boreholes indicate vertical heat flow values close

to steady state conditions and, hence, point to relatively stable surface temperatures between about 1950 and the early 1980s.

Systematic permafrost mapping has been carried out in a number of test areas (Fig.3, cf. Haeberli 1992, King 1990, Hoelzle 1992, Tenthorey 1992). The corresponding information is being stored in the data archive GIS/Kryo (Keller 1992) enabling comparison with later repetitions of mapping and sounding programmes.

Collection of infrared aerial photography flown at high altitude started in the Goms (Upper Valais) and the Poschiavo regions (Grisons) as part of a governmental research programme on debris flows from the 1987 flood catastrophes and continued in the Upper Engadin (Grisons, 1988/1990) and in the Saas, Turtmann and Réchy/Lona valleys (Valais, 1991). First steps to investigate the long-term evolution of runoff characteristics using discharge measurements and tracer experiments in Alpine mountain areas have been undertaken recently in the Réchy area (Monbaron and Tenthorey 1989). The goal of such studies is to assess the influence of Alpine permafrost and its potential future changes on flow paths and discharge variations of water in non-glacierized areas at high altitudes.

**CONCLUSIONS AND RECOMMENDATIONS**

First attempts to document climate-induced permafrost changes at various scales in time and space in the Swiss Alps indicate accelerated warming and degradation of Alpine permafrost

since about 1980. Long-term monitoring efforts, expansion of similar observations to other countries, and systematic comparison with already existing measurements in other mountain ranges are needed to assess whether information from Switzerland is representative in the more general context of ongoing global warming trends. It is recommended that international coordination encourage and strengthen such efforts.

#### REFERENCES

- Haeberli, W. (1985): Creep of mountain permafrost: internal structure and flow of Alpine rock glaciers. Mitteilung No.77 der Versuchsanstalt für Wasserbau, Hydrologie und Glaziologie, ETH Zürich, 142p.
- Haeberli, W. (1990): Glacier and permafrost signals of 20th-century warming. *Annals of Glaciology* 14, p. 99-101.
- Haeberli, W. (1992): Possible effects of climatic change on the evolution of Alpine permafrost. In: *Landscape-Ecological Impact of Climatic Change, International Symposium at Amsterdam 1989, Catena Supplement 22, p. 23 - 35.*
- Haeberli, W. and Schmid, W. (1988): Aerophotogrammetrical monitoring of rock glaciers. V International Conference on Permafrost, Proceedings Vol. 1, p.764-769.
- Haeberli, W., Huder, J., Keusen, H.-R., Pika J. and Röthlisberger, H. (1988): Core drilling through rock glacier permafrost. V Internat. Conference on Permafrost, Proceedings Vol.2, p. 937-942.
- Hoelzle, M. (1992): Permafrost occurrence from BTS measurements and climatic parameters in the Eastern Swiss Alps. In: *Permafrost and Periglacial Environments in Mountain Areas; International Workshop at Interlaken 1991. Permafrost and Periglacial Processes 3/2, p. 143 - 147.*
- Hoelzle, M., Haeberli, W. and Keller, F. (1993): Application of BTS measurements for modelling mountain permafrost distribution. VI Internat. Conference on Permafrost at Beijing 1993.
- IPCC (1992): *Climate change 1992-the supplementary report to the IPCC scientific assessment.* WMO/UNEP, Cambridge University Press, 200p.
- Keller, F. (1992): Automated mapping of mountain permafrost using the program PERMAKART within the geographical information system ARC/INFO. In: *Permafrost and Periglacial Environments in Mountain Areas; International Workshop at Interlaken 1991. Permafrost and Periglacial Processes 3/2, p. 133 - 138.*
- Keller, F. and Gubler, H.U. (1993): Interaction between snow cover and high mountain permafrost at Murtèl/Corvatsch, Swiss Alps. VI International Conference on Permafrost at Beijing 1993.
- King, L. (1990): Soil and rock temperatures in discontinuous permafrost: Gornergrat and Unterrothorn, Wallis, Swiss Alps. *Permafrost and Periglacial Processes 1/2, p. 177-188.*
- King, L., Gorbunov, A.P. and Evin, M. (1992): Prospecting for mountain permafrost and mapping of associated phenomena. In: *Permafrost and Periglacial Environments in Mountain Areas; International Workshop at Interlaken 1991. Permafrost and Periglacial Processes 3/2, p. 73 - 81.*
- Monbaron, M. et Tenthorey, G. (1989): Hydrologie en zone périglaciaire au Vallon de Réchy (VS) - essai de coloration sur un glacier rocheux. *Bulletin de la Société neuchâteloise de géographie, N° 32-33, p. 117-128.*
- Tenthorey, G. (1992): Importance of perennial névés and their meltwater in the hydrology of rock glaciers. In: *Permafrost and Periglacial Environments in Mountain Areas; International Workshop at Interlaken 1991. Permafrost and Periglacial Processes 3/3.*
- VAW (1990): *Schnee, Eis und Wasser in einer wärmeren Atmosphäre.* Internationale Fachtagung in Zürich 1990. Mitt. 108 der VAW/ETHZ, 135p.
- Vonder Mühl, D. (1992): Evidence of intrapermafrost groundwater flow beneath an active rock glacier in the Swiss Alps. In: *Permafrost and Periglacial Environments in Mountain Areas; International Workshop at Interlaken 1991. Permafrost and Periglacial Processes 3/2, p. 169 - 173.*
- Vonder Mühl, D. and Haeberli (1990): Thermal characteristics of the permafrost within an active rock glacier (Murtèl/Corvatsch, Grisons, Swiss Alps). *Journal of Glaciology 36, 123, p.151-158.*
- Vonder Mühl, D. and Holub, P. (1992): Borehole logging in Alpine permafrost, Upper Engadin, Swiss Alps. In: *Permafrost and Periglacial Environments in Mountain Areas; International Workshop at Interlaken 1991. Permafrost and Periglacial Processes 3/2, p. 125 - 132.*
- Vonder Mühl, D. and Schmid, W. (1993): Geophysical and photogrammetrical investigation of Muragl rock glacier, Engadin, Swiss Alps. VI International Conference on Permafrost at Beijing 1993.
- Wagner, S. (1992): Creep of Alpine permafrost, investigated on the Murtèl rock glacier. In: *Permafrost and Periglacial Environments in Mountain Areas; International Workshop at Interlaken 1991. Permafrost and Periglacial Processes 3/2, p. 157 - 162.*
- Wood, F.B. (1990): Monitoring global climate change: the case of greenhouse warming. *Bulletin of the American Meteorological Society 71/1, p.42-52.*

ROCK TEMPERATURES FROM LIVINGSTON ISLAND (MARITIME ANTARCTIC):  
IMPLICATIONS FOR CRYOGENIC WEATHERING

Kevin J. Hall

Geography Department, University of Natal,  
Pietermaritzburg, 3200, South Africa.

The present-day understanding of cryogenic weathering of rock is constrained not so much by theory as by actual field data regarding the controlling factors (rock properties, rock temperatures and rock moisture content, chemistry and distribution). Attempting to overcome this limitation, the British Antarctic Survey has initiated a series of undertakings, at various locations in the Antarctic, in which these parameters are monitored. The rock temperature component of the information data base is presented for three sites on the ice-free Byers Peninsula of Livingston Island in the South Shetland Islands.

At these study sites, on different aspects, rock temperatures were monitored several times each day. In addition, climatic data regarding air temperature, radiation, humidity, wind speed and direction and moisture availability were also monitored. This information made it possible to undertake within and between site comparisons plus to consider the relationship of the various rock temperatures to climatic conditions.

#### INTRODUCTION

In a discussion regarding frost shattering, McGreevy (1981, p. 71) concluded that "Priority ought to be given...to measurements of rates, amplitudes and magnitudes of temperature oscillations around freezing point on and below rock surfaces...". Seven years later, Thorn (1988, p.13), following a detailed discussion by McGreevy and Whalley (1982), was still led to state that "...there is a pressing need for field records of bedrock temperature..." and four years further on to state "Foremost among...problems has been uncertainty concerning the thermal and moisture regimes which actually prevail within natural bedrock..." (Thorn, 1992, p.10). Many studies rely on air temperature records and yet these are of no use with respect to rock weathering (McGreevy, 1985) and so it is imperative that actual rock temperatures are obtained. Whether the older notions of rock damage due to a 9% volumetric increase resulting from the phase change of water during freezing or the newer hypothetical models based on segregation ice growth within rock as the disruptive influence (e.g. Hallet, 1983) are considered, then without such data it is impossible to determine the mode of frost weathering in the field or to undertake meaningful laboratory simulations. In fact, without data on both temperature and moisture the presumption of frost action as the main cause of rock breakdown in cold regions may itself be erroneous (Thorn, 1992). Rock temperature data are, in general, relatively rare although McGreevy (1985) has examined the role of the thermal properties of rocks on weathering processes. For cold regions there are some data, of varying degrees of longevity and complexity, relating to rock temperatures and considering the extent and diversity of such regions it is still an extremely small data base.

As part of a recent study of weathering processes in a maritime Antarctic environment, rock temperature data were collected for part of the summer period. Data were collected for various aspects, allowing comparison with the controlling climatic factors of radiation, humidity, air temperature, wind speed and direction. In much the same vein as papers by Jenkins and Smith (1990) for the Canary Islands and Balke *et al.* (1991) for the continental Antarctic, the aim here is to show the variability of rock surface temperatures that can occur as a function of aspect and to discuss the findings in the context of the generally perceived nature of weathering for this region. Data on ancillary factors pertinent to the consideration of weathering, such as rock moisture content and rock properties have been collected but are presented in detail elsewhere (Hall, In press).

#### STUDY AREA

The study was undertaken on the Byers Peninsula, located at the western extremity of Livingston Island. The Byers Peninsula is the largest (c. 50 km<sup>2</sup>) ice-free area in the South Shetland Islands (Lat. 62°40'S, Long. 61°00'W). According to John and Sugden (1971) this area has a mean annual temperature of -3°C and annual precipitation is in the order of 100 to 150 cm water equivalent. Thom (1978) states that for most years the mean daily temperature from December to March is above freezing and that permafrost is present below an active layer of 0.3 to 0.7m thickness. However, whether there is truly permafrost, as opposed to seasonally frozen ground, has not been verified.

The bulk of upstanding rock outcrops in the landscape comprise volcanic dykes, sills or plugs. By providing a major obstruction to the snow-bearing winds, these outcrops collect a

substantial lee-side accumulation of snow, predominantly on the south-facing side. In addition to the presence of snow the southerly aspect also has low radiation receipts, is influenced by the cooling effect of occasional cold, southerly winds and is protected from rain-bearing northerly winds during summer. Thus different aspects have markedly different microclimatic environments and these are reflected by the observed differences in weathering (Hall, 1992, In press).

With respect to weathering, several authors have argued strongly in favour of freeze-thaw action dominating in the South Shetlands. Simonov (1977) indicated that despite a mean annual air temperature of  $-2.9^{\circ}\text{C}$  the rock surfaces experience frequent crossings of  $0^{\circ}\text{C}$ . Blümel (1986) showed that in 1979 there were 286 frost days consisting of 164 when no thaw occurred and 122 with both freezing and thawing. These were with respect to the air, however, and thus take no cognisance of rock heating due to insolation. However, the extensive cloud cover in this region limits the effect of direct radiation although Simonov (1977) did find that with solar heating the rock surface temperature could rise to  $20^{\circ}\text{C}$  whilst the shadow-side remained below  $0^{\circ}\text{C}$ . These temperatures do not necessarily mean effective frost action occurred as, in addition to subzero temperatures, there must be water available in the rock to freeze. Nevertheless, with respect to the South Shetlands, Araya and Hervé (1966), Corté and Somoza (1957), Olsacher (1956), Vtyurin and Moskalevskiy (1985), Simonov (1977), Ståblein (1983), Blümel (1986), Dutkiewicz (1982) and Blümel and Eitel (1989) all cite freeze-thaw as the major agent in modifying the landscape.

#### METHODOLOGY

Rock temperature data were collected during January and February of 1991 from three sites: an E-W trending dyke, a volcanic boss and on a raised beach. On the dyke, temperatures were recorded, by means of thermocouples (with an accuracy of  $\pm 0.2^{\circ}\text{C}$ ) for the north- and south-facing aspects at the rock surface and at a depth of 2 cm at c. 0900, 1300 and 1800 hrs each day plus at others times as the opportunity arose. On the volcanic boss, rock surface temperatures were monitored simultaneously on the four cardinal aspects. At these two sites rock moisture content was ascertained for each rock face at the same time the temperature measurements were taken. At the raised beach site two logging systems were used. A Campbell logger was utilised to record air (at 1 m above the ground surface), ground surface and 5 cm depth temperatures, together with wind speed and direction, humidity, and radiation. Being a site exposed though the full  $360^{\circ}$  the raised beach served as a control site to give the general meteorological conditions against which the other sites could be compared. Data were collected at 30 minute intervals for the first 25 days (Julian days 7 to 31) and then at 5 minute intervals for the remaining 20 days. Cobbles of local rock were used at this site to monitor non-aspect controlled variability in rock moisture content. In addition to the Campbell, sporadic use was made of a Grant "Squirrel" system to monitor the differences between the top surface and north-facing surface of a cobble. Although the two sensors were only  $\pm 2$  cm apart they showed distinctly different

thermal regimes on the two faces. Both the Campbell and the Squirrel loggers used thermistors with an accuracy of better than  $0.1^{\circ}\text{C}$ .

Ancillary data on factors such as rock properties (Hall, in press) and the nature of the sorted pattered ground (size and orientations) were also obtained as these provide information that is useful in determining the weathering regime (Hall, 1992).

#### RESULTS AND DISCUSSION

At the dyke, the mean surface temperature for the northern aspect was  $3.1^{\circ}\text{C}$  whilst that for the southern aspect was  $1.6^{\circ}\text{C}$ . The minimum for the south ( $0^{\circ}\text{C}$ ) was lower, but not substantially so, than for the north ( $1^{\circ}\text{C}$ ) whilst the maximum for the north ( $19^{\circ}\text{C}$ ) was much greater than that for the south ( $9^{\circ}\text{C}$ ). Despite the disparity in ranges between the two sites ( $18^{\circ}$  vs.  $9^{\circ}\text{C}$ ) a comparison of sample means indicates the two samples come from the same population (with  $p = 0.05$ ). Although the north has a larger spread of values, the concentration of temperatures is mainly in the range  $2.5^{\circ}$  to  $4.5^{\circ}\text{C}$  whilst that for the south is in the range  $3.5^{\circ}$  to  $5.5^{\circ}\text{C}$ .

For the rock boss, the mean temperature of the northern aspect ( $6^{\circ}\text{C}$ ) was higher than that of the southern ( $3.9^{\circ}\text{C}$ ) but not so different from the values for the east and west aspects (which were both the same at  $5.3^{\circ}\text{C}$ ). A comparison of sample means with meaningfully paired observations for the north and south aspects showed that (with  $p = 0.05$ ) they could not be considered to be from the same population. The temperature range for the north was the greatest ( $16^{\circ}\text{C}$ ) whilst that for the south was the least ( $7^{\circ}\text{C}$ ) with that for the west and east both being  $13^{\circ}\text{C}$ . Statistically, the observations for the west and east showed no difference (with  $p = 0.05$ ).

Rock surface temperatures for the dyke are different from those for the boss (Fig. 1). The mean temperature for the northerly aspect of the boss was only  $1^{\circ}\text{C}$  higher than for the dyke but a comparison of sample means with meaningfully paired observations indicated that the two could not be considered to come from the same population ( $p = 0.05$ ). Similarly, the southern samples from the dyke and the boss were statistically different but here the mean for the dyke ( $4.6^{\circ}\text{C}$ ) was greater than that for the boss ( $3.9^{\circ}\text{C}$ ). The main reason for the southern aspect of the boss having lower temperatures than that of the dyke is that the former is overshadowed by a large rock outcrop that protects it from much of the late-day, low-angled sun. The slight difference between the northern aspects at the two sites is a result of the angles of their respective faces. Whilst the dyke had a vertical to slightly overhanging face, that of the boss was at  $\pm 50^{\circ}$  and so received radiation at a more perpendicular angle. However, at both sites rock surface temperature maxima correspond to peaks in received radiation with, at the dyke (Fig. 1), the southern face experiencing a higher temperature than the northern face in the afternoon.

At the open site, the ground surface temperatures broadly replicate that of the air (Fig. 2) but with highs closely mirroring peaks in received radiation. The effect of the incoming radiation in heating the ground is clearly expressed by the difference in



temperatures between the air and the ground surface with the maximum ground surface temperature (14.1°C) substantially greater than that for the air (4.9°C). Conversely, the minimum values show radiative cooling from the ground surface with the air temperature (1.2°C) being greater than that for the ground surface (0.45°C). The mean wind speed (22 km hr<sup>-1</sup>, s=4) reflects a continuous wind throughout the day, with only 2% of observations below 14.4 km hr<sup>-1</sup> but with 56% above 21.6 km hr<sup>-1</sup> and 6% above 29 km hr<sup>-1</sup>. The strongest winds were between 0030hrs and 1000hrs, the lowest between 1230hrs and 1530hrs.

At the open site, measurements on the top and

north-facing sides of a stone show differences of >1°C despite their having been taken only 2cm apart from each other. On January 8 (Fig. 3) the north-facing side of the stone was marginally (±0.6°C) warmer than the top surface until g.1445hrs when the top became warmer, culminating in a peak at 1510hrs (when it was 1°C hotter). The two sides then attained similar temperatures during the cooling phase until g.1900hrs, when the north face became marginally (0.1°C to 0.4°C) warmer than the top surface. Another example of the marked difference between these two aspects is given by the data for February 5 (Fig. 4). On this day the northern aspect became warmer than the stone

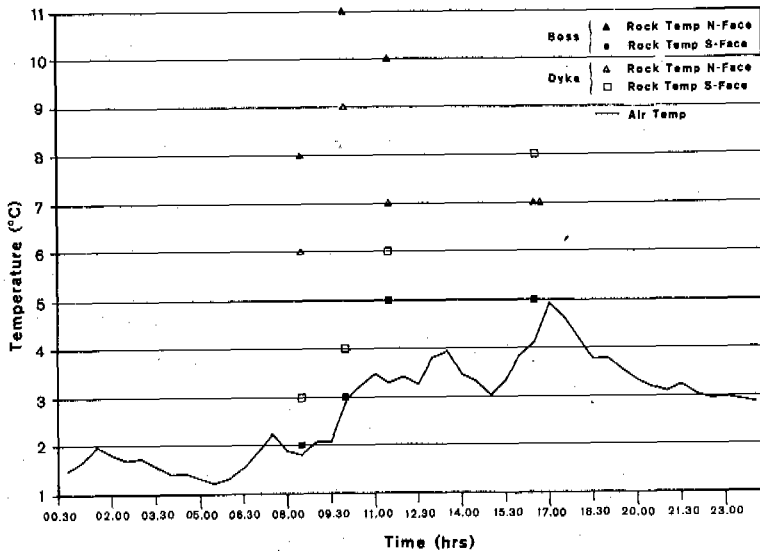


Fig.1: North and south face rock temperatures as measured at the dyke and the rock boss together with the air temperature record for January 8th, 1991.

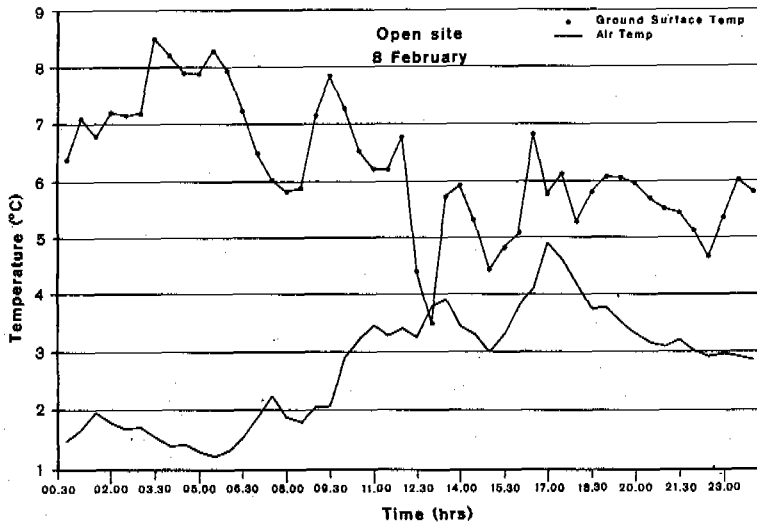


Fig.2: Temperatures recorded for the air and soil surface at the open site on January 8th, 1991.

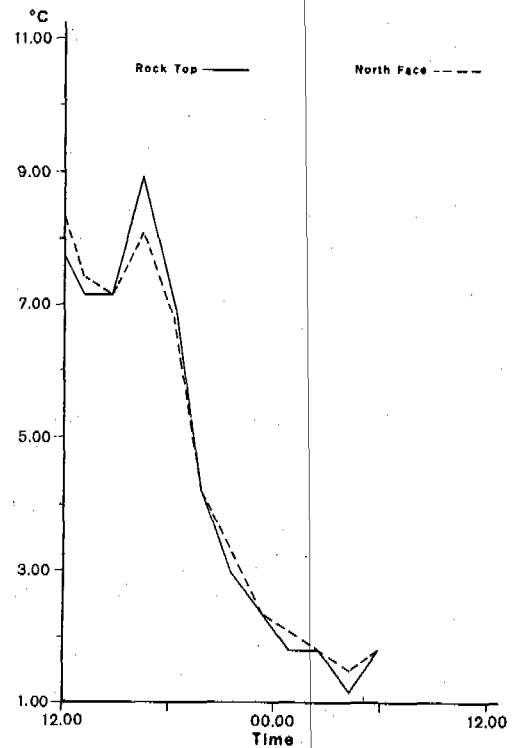


Fig.3 : Temperature measurements for the top and north-face of the stone at the open site for January 8th, 1991.

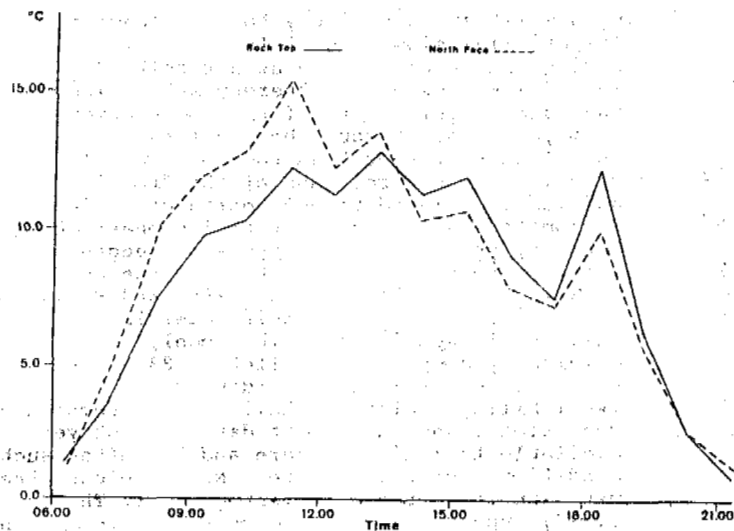


Fig. 4 Temperature measurements for the top and north-face of the stone at the open site for February 5th, 1991.

top at 0630hrs, after which the difference between these two faces continued to increase until a peak at 1120hrs when there was a 3°C difference (14.6°C vs. 11.6°C) between the two faces. After this peak the two records begin to coincide until at 1340hrs they cross over and the rock top attains the higher temperature with the maximum differences at 1510hrs (1.4°C) and 1815hrs (2.1°C). Subsequently the two curves coincide once more with the northern face becoming marginally warmer ( $\pm 0.1^\circ\text{C}$ ) after 2015hrs.

The importance of these data are twofold. First, marked differences in temperature can occur over very short distances and this, in turn, could have an influence on the character and rate of the operative weathering processes. Second, high recorded temperatures could be conducive to chemical, rather than physical, weathering. Clearly the above effects are the result of heating of the rock by incoming radiation and night-time heat loss due to radiative cooling. The northern face has the greatest receipts in the first part of the morning but is superseded by the top in the afternoon when the north face is in shadow. The night-time crossover is a result of radiative cooling affecting the upper surface of the rock more than the vertical northern face. In addition, as with the data from the dyke and the rock boss, it shows how much higher rock temperatures can be as compared to the air. On February 5 when the north face attained a temperature of 14.6°C, the air was only 4.9°C. Later, at 1815hrs when the top surface of the rock was 11.6°C the air was 4°C. Conversely, as night approached and the air temperature dropped to 2.3°C (@2100hrs) the stone was  $\pm 0.9^\circ\text{C}$  as a result of radiative cooling.

Another attribute shown by the detailed data from the logger at the open site is the difference in the rate of change of temperature. During the cooling phase from 1810hrs to 2010hrs on February 5 the rate of change of temperature of the rock surface was  $4.8^\circ\text{C hr}^{-1}$  for the first hour and  $4.5^\circ\text{C hr}^{-1}$  for the second whilst that for the air showed no temperature decline during the first period and only  $1.2^\circ\text{C hr}^{-1}$  during the

second. Thus the rock is clearly cooling more rapidly than the air, mainly as a result of the loss of incoming radiation. Although this was not a freezing event it is interesting to note that the recorded rate of change of temperature for the rock ( $0.08^\circ\text{C min}^{-1}$ ) was very close to the  $0.1^\circ\text{C min}^{-1}$  suggested by Battle (1960) to be necessary for effective frost action, i.e. it could be that rates of cooling are more conducive to the hypothesis of Battle (1960) rather than the slow rates required by the model of Walder and Hallet (1985). However, as argued later, slow rates of fall of temperature in line with the suggestion of Walder and Hallet (1985) are more likely to occur when autumn snow provides some insulation, which slows the penetration of the winter freeze.

Thus it can be seen that the air temperature record does not indicate what is happening to the rock. Consequently, the air temperature record of frost events as cited by Blümel (1986) for the South Shetlands may grossly overestimate the role of freeze-thaw weathering and underestimate other processes. Another noticeable fact is the differences in rock temperature that can occur as a function of aspect, including over very short distances. These temperature differences may be important with respect to weathering processes such that, temporally and spatially, different processes may be operating. As moisture variability was often less than temperature variability during the period of record it would seem that the former exerts a stronger influence on weathering than the latter. One exception was the presence of snow on the lee side of obstacles that acted as a moisture source during warm, dry periods. This availability of moisture combined with high rock temperatures resulted in weathering not usually considered with respect to the Antarctic environment, namely chemical weathering.

The presence of rock moisture combined with the relatively high (5–15°C) rock temperatures indicates that chemical weathering may be active during the summer, a suggestion also made by Balke *et al.* (1991) for the ice-free areas of the continental Antarctic. Evidence for the action of chemical weathering was provided by the presence of weathering rinds on both the dyke and rock boss. It was found that the rinds were consistently thicker on the snow accumulation side of obstacles (Hall, *In press*). Thus, as recently suggested by Balke *et al.* (1991) with respect to the Antarctic continent, it may be that chemical weathering is far more active, although limited to the summer period, than has been considered previously. Certainly the wet summer conditions combined with the relatively high rock temperatures experienced on Livingston Island explain the presence of weathering rinds and chemically altered bedrock outcrops.

It is noticeable that despite the number of authors who cite freeze-thaw as the major process in the South Shetlands, no frost events with negative temperatures lower than  $-1^\circ\text{C}$  took place during the 45 days of record. Rather than freeze-thaw, it was wetting and drying that was the most commonly recorded event, largely as a result of the frequent rain and strong, desiccating winds. Wetting and drying is a mechanical weathering process about which very little is known (Hall, 1988), but experiments currently in progress on samples of bedrock from this area have shown that a mass loss of 3.2g resulted from 82 wetting and drying cycles

applied to a 917.9g block (Hall, unpublished data). Considering that it is estimated that more than 100 wet-dry cycles could occur in one year (Hall, 1992) then this mechanism may be a major cause of rock breakdown in its own right. In addition, wetting and drying can operate synergistically with other mechanisms to facilitate rates of breakdown greater than would otherwise occur.

What then of the role of freeze-thaw as cited by so many authors? The available evidence indicated no events during the January-February period, essentially the end of summer to start of autumn. This does, though, leave the rest of the year, particularly the early winter and spring periods plus the annual winter cycle. However, two indirect lines of evidence suggest that freeze-thaw may still not be as frequent an event as has been previously thought. First, upon arrival on the island at the start of January the bulk of the area was still snow covered, with substantial accumulations (>3m depth) in the lee of most obstacles. Thus, as this was well into summer it implies that any freeze-thaw that took place during the spring was insulated from the rock by the snow cover. As the landscape was once more beginning to be covered by snow by late February, the potential for effective frost cycles during the autumn to early winter period was also limited. A second line of evidence supports this supposition. Observations of the sorted patterned ground, particularly the sorted stripes that occur in abundance in this area, suggest that few freeze-thaw cycles of any magnitude are experienced by the ground as miniature sorted features predominate. In addition, the stripes were found primarily on the snow-free northern aspects of slopes with very few occurrences on the southern, snow-accumulation sides even when such surfaces were melted free by early January. The lack of frost penetration may also help explain the extensive thaw slumps now occurring on the island.

Thus, freeze-thaw weathering that does occur is constrained to those snow-free northern outcrops when moisture is present. Whether moisture is readily available during freezing is still unknown. However, it would seem likely that some moisture would be present at that time as a result of the extensive snowmelt and rainfall that occurs during the summer. This would explain the suggestion by Hall (1992), based on Schmidt hammer, indentor tests and weathering rind measurements, that mechanical weathering predominates on the northern aspect whilst chemical weathering predominates on the southern.

Hallet *et al* (1991, p.295) in a discussion regarding the results of a laboratory experiment designed to test the segregation ice theory of rock disruption, suggest that the depth this process is most likely to operate at is "...the base of the active layer or the top of the permafrost...". On the Byers Peninsula, Thom (1978) described the disruption of bedrock by the growth and collapse of ice lenses at a position close to the top of the permafrost. This process occurred on near-horizontal wave cut benches not affected by aspect and where moisture was readily available due to drainage from snowbanks on higher levels further inland. This would appear to be possible confirmation of the ice segregation theory, particularly as Thom (1978, p.573) suggests that the ice was of segregation origin. Certainly these sites are

both moist and are likely to experience a (relatively) slow rate of fall of temperature during the annual freeze as a result of the insulating snow cover, thereby satisfying two of the major requirements of the segregation theory. Thus, it would be the annual cycle that is effective rather than the, more usually cited, frequent crossings of the freezing point and its associated 9% volumetric expansion concomitant upon the water to ice phase change. However, it would be premature to suggest that this information is supportive of the contention by Walder and Hallet (1985, 1986) and Hallet *et al.* (1991, p.295) that their model is universally applicable. The model, as originally proposed by Hallet (1983), has very specific requirements regarding moisture availability, moisture chemistry and temperature conditions, and sufficient data are not yet available to indicate where and how often such conditions occur in nature. Nevertheless, the wet, exposed sites as investigated by Thom (1978) appear to be conducive to the formation of segregation ice but they differ markedly in terms of moisture (Hall, unpublished data) and temperatures from the vertical bedrock exposures.

As of yet there are insufficient data to really test theoretical models and so the nature of the freezing-induced breakdown processes on the rock outcrops of the Byers Peninsula, as with most other areas, remain conjectural. However, it is the obtaining of data such as presented here that is required for both the testing of hypothetical models and the verification of what role frost action really plays in the destruction of rock in cold regions. It is possible that in some situations, as on the Byers Peninsula, that chemical weathering and mechanical processes such as wetting and drying may play a far greater role than was thought hitherto.

#### CONCLUSIONS

The general perception of weathering in cold environments is that mechanical processes, particularly freeze-thaw, predominate and certainly the literature for the South Shetland Islands reflects this opinion. However, with very few exceptions these judgements are based on the occurrence of angular clasts and the recording of atmospheric freeze-thaw cycles. It would seem, however, that wetting and drying may be the predominant mechanical weathering mechanism during the brief summer. In addition, the rock temperature data here presented suggest that chemical weathering processes can also be active during the summer period and that the rock property and weathering rind data from ancillary studies support this contention. Aspect is shown to exert an influence upon temperature but water availability is more important for promoting chemical weathering such that it is on the snow-accumulation lee-side of obstacles where the greatest amount of weathering occurs. It is possible that on the Byers Peninsula freeze-thaw weathering is much less active than was hitherto thought. Temperature variability is marked, even over very short distances (<2cm), and may exert a control upon mechanical weathering mechanisms to the extent that sweeping judgements as to what process takes place in a particular area are unrealistic.

Although the information presented here

indicate a change in the perception of weathering for this area, nevertheless it is still insufficient to make any sound detailed judgements. However, this is a universal problem with respect to cold regions and epitomises both the need for more data and the care that should be accorded in simply assuming the action of freeze-thaw.

#### ACKNOWLEDGEMENTS

I would like to express my sincere thanks to Dr David Drewry and Dr David Walton of the British Antarctic Survey for allowing my participation in the 1990-91 Antarctic field season. Dr Cynan Ellis-Evans kindly made available all the Campbell logger climatic data and provided the Squirrel logger. The Master and crew of the R.R.S. John Biscoe are thanked for all their effort. The help of the University of Natal Cartographic Unit in finishing the diagrams is acknowledged.

#### REFERENCES

- Araya, R. and Hervé, F. 1966. Estudio geomorfológico y geológico en las Islas Shetland del Sur Antártica. Instituto Antártico Chileno, Publicación, 8, 76pp.
- Balke, J., Haendel, D. and Krüger, W. 1991. Contribution to the weathering-controlled removal of chemical elements from the active debris layer of the Schirmacher Oasis, East Antarctica. *Zeitschrift für Geologische Wissenschaften*, 19, 153-158.
- Battle, W.R.B. 1960. Temperature observations in a bergschrund and their relationship to frost shattering, *In* W.V. Lewis (ed.): *Norwegian Cirque Glaciers*. Royal Geographical Society Research Series, 4, 83-95.
- Blümel, W. D. 1986. Beobachtungen zur Verwitterung an vulkanischen Festgesteinen von King-George-Inland (S-Shetlands/W-Antarktis). *Zeitschrift für Geomorphologie, N. F., Supplementband*, 61, 39-54.
- Blümel, W. D. and Eitel, B. 1989. Geocological aspects of maritime-climatic and continental periglacial regions in Antarctica (S-Shetlands, Antarctic Peninsula and Victoria-Land). *Geökodynamik*, 10, 201-214.
- Cortés, A. E. and Somoza, A. L. 1957. Observaciones criopedológicas y glaciológicas en las Islas Decepcion, Media Luna y Melchior. Instituto Antártico Argentino, Publicación, 4, 65-131.
- Dutkiewicz, L. 1982. Preliminary results of investigations on some periglacial phenomena on King George Island, South Shetlands. *Biuletyn Peryglacjalny*, 29, 13
- Hall, K.J. 1988. The interconnection of wetting and drying with freeze-thaw: some new data. *Zeitschrift für Geomorphologie, N.F., Supplementband.*, 71, 1-11.
- Hall, K.J. 1992. Weathering processes on the Byers Peninsula, Livingston Island, South Shetlands Islands, Antarctica Proceedings of the Sixth International Symposium on Antarctic Earth Sciences, Tokyo, Japan.
- Hall, K.J. In press. Enhanced bedrock weathering in association with late-lying snowpatches: Evidence from Livingston Island (Antarctica). *Earth Surface Processes and Landforms*.
- Hallet, B. 1983. The breakdown of rock due to freezing: A theoretical model. *Proceedings of the Fourth International Conference on Permafrost, National Academy of Sciences, Washington, D.C.*, 433-438.
- Hallet, B., Walder, J.S. and Stubbs, C.W. 1991. Weathering by segregation ice growth in microcracks at sustained subzero temperatures: verification from an experimental study using acoustic emissions. *Permafrost and Periglacial Processes*, 2, 283-300.
- Jenkins, K.A. and Smith, B.J. 1990. Daytime rock surface temperature variability and its implications for mechanical rock weathering: Tenerife, Canary Islands. *Catena*, 17, 449-459.
- John, B.S. and Sugden, D.E. 1971. Raised marine features and phases of glaciation in the South Shetland Islands. *British Antarctic Survey Bulletin*, 24, 45-111.
- Kerr, A., Smith, B.J., Whalley, W.B. and McGreevy, J.P. 1984. Rock temperatures from southeast Morocco and their significance for experimental rock-weathering studies. *Geology*, 12, 306-309.
- McGreevy, J.P. 1981. Some perspectives on frost shattering. *Progress in Physical Geography*, 5, 56-75.
- McGreevy, J.P. 1985. Thermal properties as controls on rock surface temperature maxima, and possible implications for rock weathering. *Earth Surface Processes and Landforms*, 10, 125-136.
- McGreevy, J.P. and Whalley, W.B. 1982. The geomorphic significance of rock temperature variations in cold environments: a discussion. *Arctic and Alpine Research*, 14, 157-162.
- Olsacher, J. 1956. Contribucion al conocimiento geológico de la Isla Decepcion. Instituto Antártico Argentino, Publicación, 2, 1-78.
- Simonov, I. M. 1977. Physical-geographic description of the Fildes Peninsula (South Shetland Islands). *Polar Geography*, 1, 223-242.
- Stäblein, G. 1983. Formung von Hängen, Halden und Wänden. Beobachtungen im Bereich der Antarktischen Halbinsel, *In* H. Poser and E. Schunke (eds): *Mesoformen des Reliefs im heutigen Periglazialraum*. Vandenhoeck and Ruprecht, Göttingen, 160-170.
- Thom, G. 1978. Disruption of bedrock by the growth and collapse of ice lenses. *Journal of Glaciology*, 20, 571-575.
- Thorn, C.E. 1988. Nivation: A geomorphic Chimera, *In* M.J. Clark (ed.): *Advances in Periglacial Geomorphology*. John Wiley, Chichester, 3- 31.
- Thorn, C.E. 1992. Periglacial geomorphology: what, where when? *In* J.C. Dixon and A.D. Abrahams (eds.): *Periglacial Geomorphology*. John Wiley, Chichester, 1-30.
- Vtyurin, B. I. and Moskalevskiy, M. Yu. 1985. Cryogenic landforms on King George Island, South Shetland Islands. *Polar Geography and Geology*, 9, 62-69.
- Walder, J.S. and Hallet, B. 1985. A theoretical model of the fracture of rock during weathering. *Geological Society of America Bulletin*, 96, 336-346.
- Walder, J.S. and Hallet, B. 1986. The physical basis of frost weathering: toward a more fundamental and unified perspective. *Arctic and Alpine Research*, 18, 27-32.

# CALCULATION OF THE THERMAL CONDUCTIVITY OF UNSATURATED FROZEN SOIL NEAR THE MELTING POINT

B. Hallet and L. A. Rasmussen

Quaternary Research Center and Department of Geological Sciences  
University of Washington  
Seattle, Washington 98195, USA

The thermal conductivity of frozen soil, the key parameter in heat transfer analyses for cold regions, is fundamental to a number of issues of both practical and scientific interests. Very few reliable data are available, however, particularly for temperatures near the melting point and for frost-susceptible soils that are unsaturated. Herein, we develop a model of the thermal conductivity founded on a physically sound geometric arrangement of water, ice and air in soil pores, and of ice lenses perpendicular to the heat flow direction. The model provides a means of calculating the conductivity of soil as a function of temperature, moisture and amount of segregation ice, and hence, is ideally suited for analyses of the thermal evolution of freezing and frozen soils.

## INTRODUCTION

The analysis of heat transfer processes in frozen soils, particularly in the active layer (the upper  $\approx 1$  m of soil that thaws and freezes annually in permafrost areas) is central to a number of subjects of both scientific and practical interest. Scientific subjects include active layer dynamics (Kane et al., 1991) and geomorphic development in periglacial environments, both under present climatic conditions and under future conditions with higher atmospheric concentrations of greenhouse gases. In the context of global warming and the growing interest in interpreting permafrost temperature profiles as faithful long-term records of surface temperature in high latitudes -- precisely where "anthropogenic climatic change is expected to be greatest and first observable" (Lachenbruch et al., 1988) -- heat transfer through the active layer has received renewed attention because it constitutes the vital but complex and imperfectly understood thermal link between the atmosphere and the permafrost.

Measurements of thermal conductivity are exceptionally difficult near  $0^\circ\text{C}$  because most techniques require finite temperature perturbations, which confound the conductivity determination by inducing water transport, freezing/melting, and associated latent heat effects (Penner, 1970; Kay et al., 1981), and by introducing significant spatial inhomogeneities. Most available data for frozen soils are for temperatures well below  $0^\circ\text{C}$  and for soils that are saturated with ice or water but lack considerable segregation ice. In addition the few *in situ* conductivity measurements, which may under favorable conditions be available, are seldom sufficient to reflect the temporal and spatial variations in ice or water content, amount of segregation ice, and temperature that are all likely to be substantial in the active layer over a seasonal cycle.

Thus, there is considerable need to model precisely the conductivity of soil at subfreezing temperatures with various degrees of saturation, and relative amounts of ice and water. Such modeling is essential near  $0^\circ\text{C}$  because slight temperature variations cause large changes in phase composition and configuration, leading to a particularly sensitive temperature dependence of the conductivity, as illustrated for saturated soils by Penner (1970) and by Williams and Smith (1989, p. 88). A series of empirical conductivity models have been proposed with various degrees of success Farouki (1981). These models do not, however, generally reflect the geometric arrangement of mineral grains,  $\text{H}_2\text{O}$  phases and air in frozen soils, such as the phase geometry proposed by Miller (1973). We present a

rational physical model, similar to Gori's (1983), that explicitly includes the phase geometry and its calculated variation with temperature. The model is ideally suited for tracking quantitatively the thermal conductivity while the temperature, and the amount of ice and water, change in soils under either natural or artificial conditions.

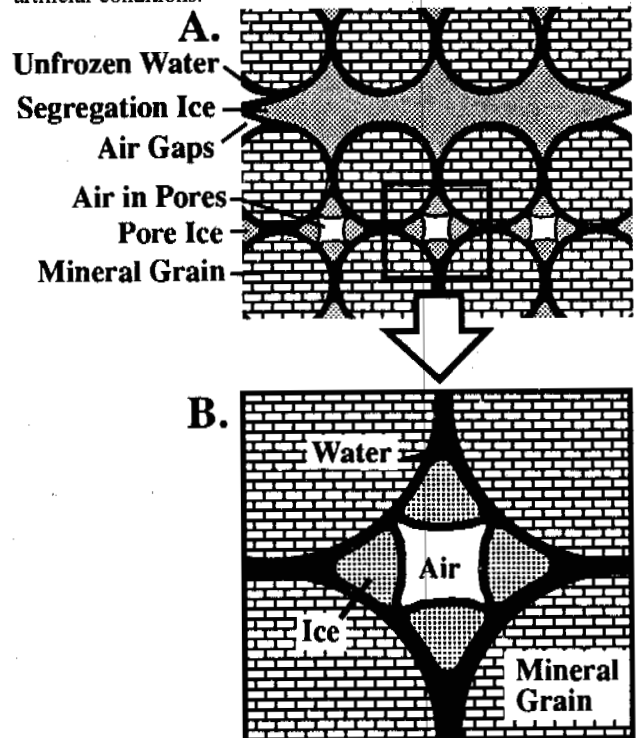


Fig. 1. (A) Geometric idealization of unsaturated soil with segregation ice. (B) Enlarged cross section of the soil matrix.

## CONDUCTIVITY MODEL

Below the melting temperature, the amount of unfrozen water in any soil is taken to be strictly a function of temperature. The total ice content is subdivided into ice in soil pores and ice in lenses, since these contrasting geometries affect heat conduction differently. Similarly, the air content is partitioned between pores in the soil matrix, and gaps between ice lenses and the matrix.

For each mineral constituent and  $H_2O$  phase, the conductivity and heat capacity are calculated as published functions of temperature (Appendix). The matrix conductivity is then computed from a series-parallel integration of the individual components in accord with their configuration in the matrix. The global conductivity reflects the series arrangement of the soil matrix and ice lenses, and hence is the reciprocal of the sum of the individual thermal resistances of each major phase: soil matrix, segregation ice, and intervening air gaps.

### Frozen Ground Geometry

We consider vertical heat flow in a column of frozen ground with unit cross section. A unit volume is taken to consist of a cubical soil matrix of volume  $V_s$ , generally accompanied by a horizontal layer of segregation ice of volume  $V_x$ , which itself may be partially separated from the soil matrix by air gaps having a volume  $V_e$  (Fig 1a). The soil matrix is subdivided into polyhedral elements with volumes  $V_m$  of mineral grains,  $V_w$  of unfrozen water,  $V_y$  of ice, and  $V_a$  of air. A representative cross section of the idealized soil matrix is shown in Figure 1b. Ice and air in pores are separated from the mineral grains by a film of unfrozen water of uniform thickness. Ice occupies interstices between grains, and air occupies the central part of pores. The total amount of ice in the ground  $V_i$  is subdivided into segregation ice  $V_x$  and pore ice  $V_y$ .

Specified variables are temperature  $T$  (Celsius), soil porosity  $P$ , and total amount of ice in the ground  $V_i$ . Also specified are the maximum fraction  $S_{\max}$  of the pore volume that may be filled with water or ice and the ratio  $\eta = V_e/V_x$ , which relates the volume of air gaps to that of segregation ice. For any particular soil at  $T < 0^\circ C$ , the amount of unfrozen water is taken to be a function of  $T$  alone. For example, for the fine-grained soil in sorted circles at our Spitsbergen site (Hallet et al., 1988; Anderson, 1988), nuclear magnetic resonance (NMR) measurements indicate that the unfrozen water content is given by

$$\frac{V_w}{V_s} = 8.72 \times 10^{-6} \rho_m (1-P) (-T)^{-0.32} \quad (1)$$

When this is combined with the pore saturation condition,

$$V_w + V_y \leq S_{\max} P V_s$$

the amount of segregation ice  $V_x$ , if any, is given by

$$V_x = \max \left[ 0, \frac{V_i - V'}{1 - (1+\eta)V'} \right] \quad (2)$$

in which

$$V' = S_{\max} P - V_w / V_s$$

Once  $V_x$  is determined, the other volumes are given directly by the definitions  $V_y = V_i - V_x$ ,  $V_e = \eta V_x$ , and  $V_s = 1 - V_x - V_e$ ; then  $V_w$  is obtained from Equation (1).

Local coordinates are assigned so that one quadrant (Fig. 2) of the representative cross section lies in the square  $0 \leq \lambda \leq 1$ ,  $0 \leq \mu \leq 1$ . The relative areas represent the relative volumes in the three-dimensional soil matrix:  $V_m/V_s$  for the mineral grains; and, in the pore,  $V_w/V_s$  for the unfrozen water,  $V_y/V_s$  for the ice, and  $V_a/V_s$  for the air, the last three summing to the porosity  $P$ . Effective grain-to-grain contacts are specified to have a fractional length of  $1 - \lambda_m$ . The vertex coordinates giving the prescribed areas are

$$\mu_m = P / \lambda_m \quad (3)$$

$$\begin{pmatrix} \lambda_w \\ \mu_w \end{pmatrix} = \sqrt{P - V_w/V_s} \begin{pmatrix} \lambda_m / \sqrt{P} \\ \sqrt{P} / \lambda_m \end{pmatrix} \quad (4)$$

$$\lambda_y = \frac{V_a}{\mu_w V_s} \quad (5)$$

The symmetry of the soil matrix (Fig. 2) permits simplification of the notation, because the mineral vertex and unfrozen-water vertex both lie on the axis of symmetry  $\mu = \lambda$ . Although  $\mu$  is the ordinate, the  $\lambda$  coordinate will be identified sometimes in terms of  $\mu_m$ , sometimes in terms of  $\mu_w$  to avoid introducing new  $\lambda$  variables for quantities that are numerically equal to  $\mu_m$  and  $\mu_w$ . Accordingly, the slope of the mineral grain face is given by

$$\tan \theta = \frac{\mu_m}{\lambda_m - \mu_m} = \frac{\mu_w}{\lambda_w - \mu_w} = \frac{P}{\lambda_m^2 - P} \quad (6)$$

The vertex formulations vary continuously and accommodate the extreme cases. When the pore is devoid of ice,  $V_a/V_s = P - V_w/V_s$  and  $\lambda_y = \lambda_w$ . When the pore is filled with water, so that  $V_w/V_s = P$ , then  $\lambda_w = \mu_w = \lambda_y = 0$ . The relative lengths  $L_m + L_w + L_y + L_a = 1$  of the individual phases in the vertical direction are readily computed for any  $\lambda$  in terms of  $b$  and the vertex coordinates.

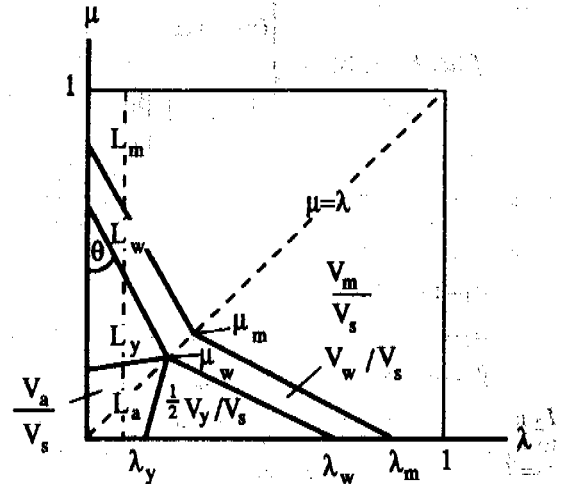


Fig. 2. Representative cross section of the upper right-hand quadrant of the idealized soil matrix (Fig. 1-B). Locations of the vertices are determined (Eq. 3,....,6) in the local coordinate system  $(\lambda, \mu)$ . Relative areas in the representative cross section are equal to the volume ratios  $V_m/V_s$ ,  $V_w/V_s$ ,  $V_y/V_s$ ,  $V_a/V_s$  assumed for the three-dimensional soil matrix. The line  $\mu = \lambda$  is an axis of symmetry, and the length of the effective grain-to-grain contact is  $1 - \lambda_m$ .

### Conductivity Integration

The total conductivity for the soil matrix is computed on the assumption that the heat flow is strictly unidirectional (Gori, 1983). Taking the heat flow to be vertical, in the direction of the  $\mu$  axis, conductivities for individual phases combine in series,

$$\frac{1}{k(\lambda)} = \frac{L_m}{k_m} + \frac{L_w}{k_w} + \frac{L_y}{k_i} + \frac{L_a}{k_a} \quad (7)$$

according to their lengths in that direction (Fig. 2). Here  $k_m$ ,  $k_w$ ,  $k_i$ , and  $k_a$  are the conductivities of mineral, water, ice, and air; their reciprocals are the resistivities  $R_m$ ,  $R_w$ ,  $R_i$ , and  $R_a$ . Empirical relations for the conductivity of each phase as a function of temperature (Appendix) are used. Along the  $\lambda$  axis they are combined in parallel to give the total value  $k_s$  for the entire cross section.

$$k_s = \int_0^1 k(\lambda) d\lambda \equiv \sum_{j=1}^6 I_j \quad (8)$$

The incremental integrals  $I_j$  span successive intervals of the  $\lambda$  axis. The specific intervals depend on the relative sizes of  $\lambda_y$ ,  $\mu_w$ ,  $\mu_m$ , and  $\lambda_w$ . The first integral  $I_1$  spans the interval from 0 to  $b_1$ , the integral  $I_2$  the interval from  $b_1$  to  $b_2$ , and so on; therefore, in the following results, only the upper limit is mentioned for integrals  $I_2, I_3, \dots, I_6$ . In general, because the lengths  $L$  vary linearly with  $\lambda$  over each interval -- as expressed by the quantity  $\alpha_j + \beta_j \lambda$  -- they all have identical functional forms

$$I_j = \int_{a_j}^{b_j} k_j(\lambda) d\lambda = \int_{a_j}^{b_j} \frac{d\lambda}{\alpha_j + \beta_j \lambda} = f(a_j, b_j, \alpha_j, \beta_j) \quad (9)$$

in which

$$f(a, b, \alpha, \beta) = \begin{cases} (b-a)/\alpha & (\beta=0) \\ \frac{1}{\beta} \ln \frac{\alpha + \beta b}{\alpha + \beta a} & (\beta \neq 0) \end{cases} \quad (10)$$

$I_1$  is the air-ice-water-mineral integral from  $\lambda = 0$  to  $\lambda = \lambda_y$  if  $\lambda_y \leq \mu_w$  or to  $\mu_w$  if  $\lambda_y > \mu_w$ . If  $\lambda_y = 0$ ,  $I_1 = 0$ ; otherwise,  $a_1 = 0$  and

$$\begin{aligned} b_1 &= \min(\lambda_y, \mu_w) \\ \alpha_1 &= R_m + \lambda_w(R_w - R_m) + \lambda_w(R_i - R_w) + \lambda_y(R_a - R_i) \quad (11) \\ \beta_1 &= (R_a - R_i)(1 - \lambda_y/\mu_w) + (R_m - R_i)/\tan\theta \end{aligned}$$

$I_2$  is the air-ice-water-mineral integral to  $\lambda = \mu_w$  if  $\lambda_y < \mu_w$ , to  $\lambda_y$  if  $\mu_w < \lambda_y < \mu_m$ , or to  $\mu_m$  if  $\mu_m \leq \lambda_y$ . If  $\lambda_y = \mu_w$ ,  $I_2 = 0$ ; otherwise,  $a_2 = b_1$  and

$$\begin{aligned} b_2 &= \begin{cases} \mu_w & (\lambda_y < \mu_w) \\ \min(\lambda_y, \mu_m) & (\lambda_y > \mu_w) \end{cases} \\ \alpha_2 &= R_m + \lambda_w(R_w - R_m) + \begin{cases} \lambda_w(R_i - R_w) + \gamma_2 \mu_w & (\lambda_y < \mu_w) \\ \lambda_w(R_i - R_w) \tan\theta + \gamma_2 \lambda_y & (\lambda_y > \mu_w) \end{cases} \quad (12) \\ \beta_2 &= -\gamma_2 + \begin{cases} (R_m - R_i)/\tan\theta & (\lambda_y < \mu_w) \\ (R_w - R_i) \tan\theta + (R_m - R_w)/\tan\theta & (\lambda_y > \mu_w) \end{cases} \end{aligned}$$

in which

$$\gamma_2 = \frac{(R_a - R_i) \min(\lambda_y, \mu_w)}{|\lambda_y - \mu_w|} \begin{cases} 2 - \lambda_y/\mu_w & (\lambda_y < \mu_w) \\ 1 & (\lambda_y > \mu_w) \end{cases}$$

$I_3$  is the air-ice-water-mineral integral to  $\lambda = \mu_m$  if  $\lambda_y < \mu_m < \lambda_w$ , to  $\lambda_w$  if  $\lambda_y < \lambda_w \leq \mu_m$ , or to  $\lambda_y$  if  $\lambda_y > \mu_m$ . If  $\lambda_y = \mu_m$ ,  $I_3 = 0$ ; otherwise,

$$\begin{aligned} a_3 &= \begin{cases} \max(\lambda_y, \mu_w) & (\lambda_y < \mu_m) \\ \mu_m & (\lambda_y > \mu_m) \end{cases} \\ b_3 &= \begin{cases} \min(\lambda_w, \mu_m) & (\lambda_y < \mu_m) \\ \lambda_y & (\lambda_y > \mu_m) \end{cases} \quad (13) \end{aligned}$$

$$\alpha_3 = R_m + \lambda_w(R_i - R_w) \tan\theta + \begin{cases} \lambda_m(R_w - R_m) & (\lambda_y < \mu_m) \\ \lambda_m(R_w - R_m) \tan\theta + \gamma_3 \lambda_y & (\lambda_y > \mu_m) \end{cases}$$

$$\beta_3 = \begin{cases} (R_w - R_i) \tan\theta + (R_m - R_w) / \tan\theta & (\lambda_y < \mu_m) \\ (R_m - R_i) \tan\theta - \gamma_3 & (\lambda_y > \mu_m) \end{cases}$$

in which

$$\gamma_3 = (R_a - R_i) \mu_w / (\lambda_y - \mu_w)$$

$I_4$  is the ice-water-mineral integral to  $\lambda = \mu_m$  if  $\lambda_w < \mu_m$ , or to  $\lambda_w$  if  $\mu_m < \lambda_w$ . If  $\lambda_w = \mu_m$ ,  $I_4 = 0$ ; otherwise,  $b_4 = \max(\lambda_w, \mu_m)$  and

$$a_4 = \begin{cases} \lambda_w & (\lambda_w < \mu_m) \\ \max(\lambda_y, \mu_m) & (\lambda_w > \mu_m) \end{cases}$$

$$\alpha_4 = R_m + \begin{cases} [\lambda_m(R_w - R_m) + \lambda_w(R_i - R_w)] \tan\theta & (\mu_m < \lambda_w) \\ \lambda_m(R_w - R_m) & (\mu_m > \lambda_w) \end{cases} \quad (14)$$

$$\beta_4 = \begin{cases} (R_m - R_i) \tan\theta & (\mu_m < \lambda_w) \\ (R_m - R_w) / \tan\theta & (\mu_m > \lambda_w) \end{cases}$$

$I_5$  is the water-mineral integral to  $\lambda = \lambda_m = b_5$  and

$$\begin{aligned} a_5 &= \max(\lambda_w, \mu_m) \\ \alpha_5 &= R_m - \beta_5 \lambda_m \quad (15) \end{aligned}$$

$$\beta_5 = (R_m - R_w) \tan\theta$$

$I_6$  is the mineral integral to  $\lambda = 1$ .

$$I_6 = (1 - \lambda_m) k_m \quad (16)$$

The variation of soil geometry in the third dimension of the cube, along the the  $v$  axis, may be taken either to vary linearly or to have constant cross section. In the linear case, the phase areas in the cross section are scaled by a factor that varies from  $2/\lambda_m$  at  $v=0$ , to 0 at  $v=\lambda_m$ . The same grain-to-grain contact length  $1-\lambda_m$  is assumed to exist in the  $v$  direction as in the  $\lambda$  and  $\mu$  directions. The  $v$  integral of the scaled areas, therefore, is consistent with the volumes prescribed for the cubical soil matrix. The cross section through the pore, for example, is taken to have an area that declines linearly from  $2P/\lambda_m$  at  $v=0$  to zero at  $v=\lambda_m$ , and is zero over  $\lambda_m \leq v \leq 1$ ; the integral of the area from  $v=0$  to  $v=1$  is thus  $P$ . A simpler, alternative approach is mentioned below.

At any particular point along the  $v$  axis, the value given by Equation (8) is regarded as being  $k(v)$ . Because of the very steep slope of  $k(v)$  versus  $v$  (Fig. 3), numerical integration along  $v$  is difficult. An algebraic result for this integral would be difficult to obtain. An alternative approach is provided by the assumption that the pore geometry is unvarying over  $0 \leq v \leq \lambda_m$ . This constant cross section has areas that over  $0 \leq v \leq \lambda_m$  are obtained by scaling up the relative volumes by  $1/\lambda_m$ , and that over  $\lambda_m \leq v \leq 1$  are zero; their integrals from  $v=0$  to  $v=1$  are thus equal to the relative volumes. The conductivity  $k_s$  of the segment  $0 \leq v \leq \lambda_m$  is calculated from Equations 8, ..., 16 by using the scaled up values for the areas. It is then combined in parallel with  $k_m$  to give the conductivity of the entire soil matrix

$$k_s = (1-\lambda_m)k_s + \lambda_m k_m \quad (17)$$

The advantage of making this assumption is that no arduous  $v$  integration is needed and it affords a close approximation, within about 5 percent, of the result obtained from the physically more realistic linear formulation. The difference between the two formulations is inconsequential in view of the effect of

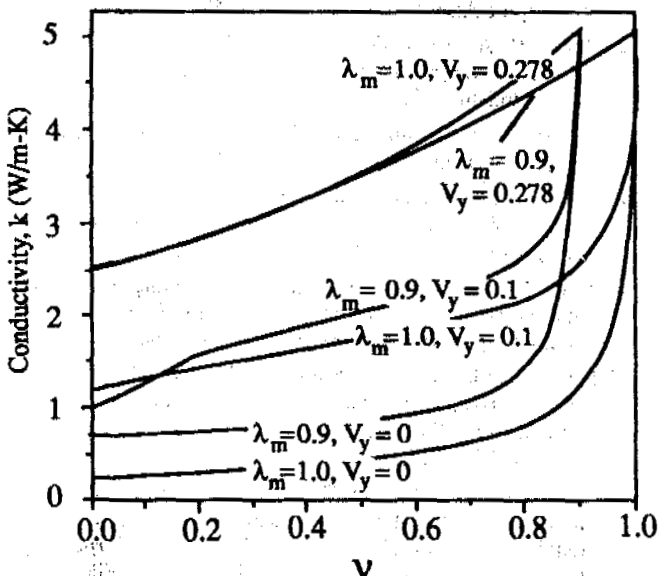


Fig. 3. Conductivity variation in the third dimension  $k(v)$  for selected amounts of pore ice  $V_y$  and for selected grain-to-grain contact lengths  $1-\lambda_m$ . Except when the pore is filled entirely with ice and unfrozen water, conductivity declines rapidly as  $v$  drops below  $\lambda_m$ , because of the strong insulating effect of air. The conductivity shown is that for the soil matrix only. Porosity  $P$  is 0.3, which gives  $V_w/V_s = 0.022$  at  $-0.5^\circ C$ .

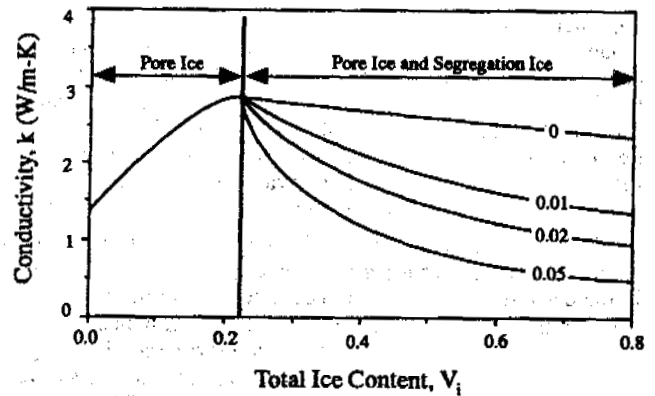


Fig. 4. Conductivity variation with ice content  $k(V_i)$ , including local air gaps between ice lenses and the soil matrix, and both pore ice  $V_y$  and segregation ice  $V_x$ . Here pores are permitted to fill with ice and water only to 0.8 of the pore volume; additional ice  $V_i$  forms segregation ice  $V_x$ . For a porosity of 0.3, the maximum  $H_2O$  volume in pores is thus 0.24; at  $-0.5^\circ C$ , it is divided between  $V_w = 0.022$  and  $V_y = 0.218$ . The dependence of  $k$  on  $V_i$  is shown for selected ratios of air gaps to segregation ice ( $\eta = V_e/V_x$ ).

other uncertainties in the internal geometry of the soil such as its precise phase geometry, the porosity, etc.

Once  $k_s$  has been found, it is combined serially with the conductivities for the segregation ice  $V_x$  and air in gaps  $V_e$  according to

$$\frac{1}{k} = \frac{V_s}{k_s} + \frac{V_x}{k_i} + \frac{V_e}{k_a} \quad (18)$$

The three volumes sum to unity. Although in Equation (18) volumes constitute the numerators whereas in Equation (7) lengths do so, the two equations are consistent because, for a soil column of unit cross section, the volume of an increment is proportional to its vertical length. The linear-formulation curve is elaborated in Figure 4, in which  $S_{max}$  is reduced to 0.8, and  $V_i$  is increased past the capacity of the pores, so that it produces  $V_x$  according to Equation (2). Here,  $k(V_i)$  is obtained from Equation (18) for four different values of  $\eta = V_e/V_x$ , specifying various amounts of air in gaps.

Before discussing how the calculated thermal conductivity values are used in a geomorphic context, we note that heat transfer calculations require a specification of the volumetric heat capacity as a function of temperature and degree of saturation. Empirically based estimates of these heat capacities (Appendix) are used.

### GEOMORPHIC CONTEXT

Our motivation for developing the conductivity model and for calculating heat capacity per unit volume stems from a desire to analyze data obtained with extensive instrumentation installed to monitor active layer properties in western Spitsbergen in a study of the dynamics of exceptionally well developed sorted circles (Hallet et al., 1988). We have developed a heat budget model using detailed temperature measurements to calculate how much ice formed as a function of time and depth. The amount and distribution of ice in the active layer at the onset of the thaw season is of interest because it controls to a large extent whether the soil layer is gravitationally stable or tends to overturn (Hallet and Waddington, 1991), which has



important implications regarding the formation of patterned ground and involutions. In that model, the principal variable being evaluated is the divergence of the heat flux, which requires precise estimates of soil thermal properties. We can calculate the apparent rate of latent heat production as a function of depth and evaluate the combined rates of freezing-melting (e.g., Anderson, 1988) or evaporation-condensation, and the mass fluxes accompanying these phase transitions.

Initial results of the heat budget model yield clear thermal anomalies that represent pervasive latent heat input to melt ice in the early summer and latent heat output from the freezing of water in the fall (Smith, 1990). The sum of all nonconductive processes in the soil for the bulk of the thaw period is negligible at our sorted circle study site. This suggests that advective heat transport in the thawed active layer is insignificant, bringing into question its inferred importance in possibly initiating soil patterning by inducing spatially periodic variations in the thaw rate of permafrost, as proposed by Krantz (1990). Thus, analyzing temperature profiles by using a model of thermal conductivities can provide insights into heat transfer processes that pertain directly to geomorphic development in periglacial areas.

### CONCLUSION

We suggest that high resolution soil thermal records, which are relatively common, provide much more than detailed temperature histories. As McGaw et al. (1978) and Hinkel et al. (1990) have also shown, they constitute rich sources of information on thermal properties, mass transfer and phase transformations in the active layer. Careful calculations of thermal properties as functions of water and ice content and of temperature, now pave the way to quantifying the conductive and non-conductive heat transfer processes by using simple temperature data in appropriate heat transfer models. Because the  $H_2O$  content of soil, which strongly influences the thermal conductivity, generally varies in both space and time under natural conditions, continuous measurement of the  $H_2O$  content of soil would significantly complement temperature measurements. Thus, thorough heat transfer studies in the field ought to include moisture measurements by time domain reflectometry or other suitable technique, and direct measurements of heat flow or thermal conductivity.

Testing the conductivity model stands out as the next item on our research agenda. We intend to compare our model results with published data on measured conductivities. Initial efforts to do so with the data of Penner et al. (1975), for example, were hampered by the lack of information about the amount and distribution of segregation ice in the frozen soils. An alternative approach we are also pursuing is to verify whether the computed conductivities are consistent with the heat budget in intensively instrumented frozen soils in the field. With this aim in mind, we have complemented our ongoing study of the temperature in the active layer at our Spitsbergen site with independent measurements of heat flow and thermal conductivity.

Our approach to the analysis of heat transfer properties near  $0^\circ C$  hinges on the separation of heat conduction from non-conductive effects. It diverges from earlier work in which the diverse effects of heat flow near the melting point -- conduction, mass transfer, phase transition -- are effectively grouped into empirically observable "effective" thermal parameters such as the apparent thermal diffusivity (Hinkel et al., 1990) or apparent heat capacity (Anderson et al., 1973). Its virtue, how-

ever, is that it permits quantitative assessment of, and hence more precise insight into, specific thermal processes.

### ACKNOWLEDGMENTS

This work was supported by the U. S. Army Research Office (Grant No. DAAL03-87-K-0058). We thank Suzanne Prestrud Anderson and Jacquie Smith for their productive involvement in the early phases of our study of heat transfer in the active layer. The Norsk Polarinstittutt provided logistical support for our field work. We are also grateful to F. Gori for instructive correspondence and to A. Tice of the U. S. Army Corps of Engineers Cold Regions Research and Engineering Laboratory for conducting the NMR determinations of the amount of unfrozen water in soil samples.

### REFERENCES

- Anderson, D. M., Tice, A. T., and McKim, H. L., 1973, The unfrozen water and the apparent specific heat capacity of frozen soils. *Second International Conference on Permafrost*. p. 289-295.
- Anderson, S. P., 1988, Upfreezing in sorted circles, Western Spitsbergen. *Fifth International Conference on Permafrost*. V. 1, p. 666-671.
- Berman, R. G., and Brown, T. H., 1985, Heat capacity of minerals --  $Na_2O$ ,  $K_2O$ ,  $CaO$ ,  $MgO$ ,  $FeO$ ,  $Fe_2O_3$ ,  $Al_2O_3$ ,  $SiO_2$ ,  $TiO_2$ ,  $H_2O$ ,  $CO_2$  -- representation, estimation, and high temperature extrapolation. *Contributions to Mineralogy and Petrology*, V. 89, p. 168-183.
- Clark, S. P., 1966, Thermal conductivity. in *Handbook of physical constants: Memoir 97*, S. P. Clark, Editor, Geological Society of America, New York, p. 459-482.
- De Vries, D. A., 1963, Thermal properties of soils. in *Physics of plant environment*, W. R. Van Wijk, Editor, North Holland Publishing Co., Amsterdam
- Eisenberg, D., and Kauzmann, W., 1969, *Structure and Properties of Water* Oxford University Press, 296 p.
- Farouki, O.T., 1981, Thermal properties of soils. *U. S. Cold Regions Research and Engineering Laboratory, Monograph 81-1*, 136 p.
- Gori, F., 1983, A theoretical model for predicting the effective thermal conductivity of unsaturated soils. *Fourth International Conference on Permafrost*, p. 363-368.
- Hallet, B., Anderson, S. P., Stubbs, C. W., and Gregory, E. C., 1988, Surface soil displacements in sorted circles, western Spitsbergen. *Fifth International Conference on Permafrost*. V. 1, p. 1770-1775.
- Hallet, B., and Waddington, E. D., 1991, Buoyancy forces induced by freeze-thaw in the active layer: implications for diapirism and soil circulation. in *Periglacial Morphology*, J. C. Dixon and A. D. Abrahams, Editors, John Wiley and Sons, New York
- Hinkel, K. M., Outcalt, S. I., and Nelson, F. E., 1990, Temperature variation and apparent thermal diffusivity in the refreezing active layer, Toolik Lake, Alaska. *Permafrost and Periglacial Processes*, V. 1, p. 265-274.

- Kane, D. L., Hinzman, L. D., and Zarling, J. P., 1991, Thermal response of the active layer to climatic warming in a permafrost environment. *Cold Regions Science and Technology*, V. 19, p. 111-122.
- Kay, B. D., Fukuda, M., Izuta, H., and Sheppard, M. I., 1981, The importance of water migration in the measurement of thermal conductivity of unsaturated frozen soils. *Cold Regions Science and Technology*, V. 5, p. 95-106.
- Krantz, W. B., 1990, Self-organization manifest as patterned ground in recurrently frozen soils. *Earth-Science Reviews*, V. 29, p. 117-130.
- Lachenbruch, A. H., Cladouhos, T. T., and Saltus, R. W., 1988, Permafrost temperature and the changing climate. *Fifth International Conference on Permafrost*. V. 3, p. 9-17.
- McGaw, R. W., Outcalt, S. I., and Ng, E., 1978, Thermal properties and regime of wet tundra soils at Barrow, Alaska. *Third International Conference on Permafrost*. p. 48-53.
- Miller, R. D., 1973, Soil freezing in relation to pore water pressure and temperature. *Second International Conference on Permafrost*. p. 344-352.
- Penner, E., 1970, Thermal conductivity of frozen soils. *Canadian Journal of Earth Sciences*, V. 7, No. 3, p. 982-987.
- Penner, E., Johnston, G. H., and Goodrich, L. E., 1975, Thermal conductivity laboratory studies of some MacKenzie Highway soils. *Canadian Geotechnical Journal*, V. 12, No. 3, p. 271-288.
- Sass, J. H., Lachenbruch, A. H., and Munroe, R. J., 1971, Thermal conductivity of rocks from measurements on fragments and its application to heat-flow determinations. *Journal of Geophysical Research*, V. 76, No. 14, p. 3391-3401.
- Smith, J., 1990, Extracting soil thermal properties and phase change phenomena on the basis of temperature measurements. Masters Thesis, University of Washington, Seattle, Washington, U.S.A.
- Williams, P. J., and Smith, M. W., 1989, *The Frozen Earth*, Cambridge University Press, 306 p.

#### APPENDIX. Conductivities and heat capacities

Conductivities of individual constituents are taken from published sources. They are given as weak functions of temperature, which have been scaled here to give  $k$  values in  $Wm^{-1}K^{-1}$ . Farouki (1981) gives for water (p. 75) and for ice (p. 76)

$$k_w = -0.5818 + 6.357 \times 10^{-3} T_{abs} - 7.9663 \times 10^{-6} T_{abs}^2 \quad (A-1)$$

and

$$k_i = -0.21286 + 670 / T_{abs} \quad (A-2)$$

For air, De Vries (1963) gives  $k_a = 0.024 Wm^{-1}K^{-1}$ . The absolute temperature is denoted by  $T_{abs}$  and the Celsius temperature is denoted by  $T$ . For particular minerals, including those making up the soil at the Spitsbergen site, the weak temperature dependence evident in the data (Clark, 1966, p.470) can be expressed as polynomials:

$$\begin{aligned} k_c &= 3.6649 - 0.010893T + 2.9914 \times 10^{-5} T^2 - 3.1401 \times 10^{-8} T^3 \\ k_d &= 4.9790 - 0.016701T + 7.4266 \times 10^{-5} T^2 - 1.6039 \times 10^{-7} T^3 \\ k_q &= 8.0881 - 0.030058T + 8.0575 \times 10^{-5} T^2 - 8.7546 \times 10^{-8} T^3 \end{aligned} \quad (A-3)$$

in which  $c, d, q$  refer to calcite, dolomite, and quartz. The combined conductivity of the mineral component is obtained from a formula given by Sass et al. (1971). For the particular individual minerals in the Spitsbergen soil, it yields

$$k_m = k_c^{\phi_c} k_d^{\phi_d} k_q^{\phi_q} \quad (A-4)$$

where  $\phi_c, \phi_d, \phi_q$ , which sum to unity, are relative volume fractions of individual minerals. This formulation is appropriate for arbitrary mixtures of constituents, provided they have similar conductivities. It is used here for obtaining the average conductivity of mineral grains because we have no reason to suspect that soil grains are arranged according to mineralogy. In contrast, our model for the overall thermal conductivity of the soil is founded on physically reasonable  $H_2O$  phase geometry. The model can explicitly treat the presence of air gaps and air in pores because it is not restricted to phases of similar conductivity. Of course for other soils, relations similar to Equations (A-3) can be obtained readily for the appropriate minerals from Clark (1966) or other sources.

Heat capacities of individual constituents are weak functions of temperature taken from published sources. The total heat capacity of the ground is given by

$$\rho c = V_m \rho_m c_m + V_w \rho_w c_w + V_i \rho_i c_i + (V_a + V_e) \rho_a c_a \quad (A-5)$$

The mineral component is summed over its constituents. In the case of the carbonate soil from Spitsbergen it takes the form

$$\rho_m c_m = \phi_c \rho_c c_c + \phi_d \rho_d c_d + \phi_q \rho_q c_q \quad (A-6)$$

For these constituents Berman and Brown's (1985) expression yields, in  $J kg^{-1}K^{-1}$

$$\begin{aligned} c_c &= 1.9307 \times 10^3 - 2.0391 \times 10^4 T^{-1/2} + 1.9928 \times 10^9 T^{-3} \\ c_d &= 1.9956 \times 10^3 - 2.0338 \times 10^4 T^{-1/2} + 9.8032 \times 10^8 T^{-3} \\ c_q &= 1.3322 \times 10^3 - 4.0010 \times 10^3 T^{-1/2} - 5.9053 \times 10^7 T^{-2} + 8.1846 \times 10^9 T^{-3} \end{aligned} \quad (A-7)$$

Densities are taken to be  $\rho_c = 2700$ ,  $\rho_d = 2900$ ,  $\rho_q = 2650 kg m^{-3}$ . The heat capacity for water is  $4.182 MJm^{-3}K^{-1}$ , independent of temperature. For ice, a simple linear extrapolation from the freezing point to  $0^\circ K$  is reasonable (Eisenberg and Kauzmann, 1969); it implies

$$\rho_i c_i = 7.065 \times 10^{-3} T_{abs} \quad (A-8)$$

**MICROMORPHOLOGICAL INVESTIGATIONS OF ACTIVE-LAYER  
DETACHMENT SLIDES, ELLESMERE ISLAND, CANADIAN ARCTIC**

Charles Harris<sup>1</sup> and Antoni G. Lewkowicz<sup>2</sup>

<sup>1</sup> Department of Geology, University of Cardiff, P.O. Box 914,  
Cardiff CF1 3YE, U.K.

<sup>2</sup> Department of Geography, University of Toronto, Erindale Campus,  
Mississauga, Ontario, L5L 1C6, Canada.

Active-layer detachment slides are widespread on the Fosheim Peninsula, Ellesmere Island, where they are developed in low-plasticity fine-grained sediments. Undisturbed soil samples were collected for micromorphological investigation from excavated sections through displaced active layer slide blocks. Slide blocks consist of a sandy colluvial surface layer overlying strongly structured, hard, sandy or silty clay. In many cases a vertical blocky or prismatic structure is present, structural units becoming smaller towards the surface. It is concluded that drying of the active layer, due to the combined effect of summer evaporation and water migration during two-sided freezing, leads to hardening, and this is responsible for maintaining the integrity of slides. The generally noncohesive nature of the sediment is reflected in the fact that displacement often occurs over a basal shear zone up to several centimetres in thickness, rather than a polished slickensided slip surface.

### INTRODUCTION

Shallow planar slope failures caused by mobilization of unfrozen active layer sediments which slide downslope over the frozen substrate, are common on the Fosheim Peninsula of Ellesmere Island (Figure 1), and have been described by Lewkowicz (1990, 1992) and Harris & Lewkowicz (submitted). Slides are between 0.5 and 0.75 m thick, produce a scar in which isolated displaced blocks are scattered, and a depositional area in which the main displaced unit comes to rest. Compression in the toe and along the sides of the slide frequently results in a series of frontal transverse ridges and lateral berms.

It was concluded by Lewkowicz (1992) that the particularly warm summer climate of the Fosheim Peninsula compared to other parts of the Canadian Arctic Archipelago is a major factor leading to frequent slide activity in the area, since failures are thought to be triggered by rapid thaw penetration late in the summer when the active layer is close to its maximum thickness. Lewkowicz (1990) showed that in the valley known as Black Top Creek, slide frequencies ranged from 0.2 to 5 per year between 1950 and 1987, but that 75 slides were triggered during an unusually warm late-summer period in 1988.

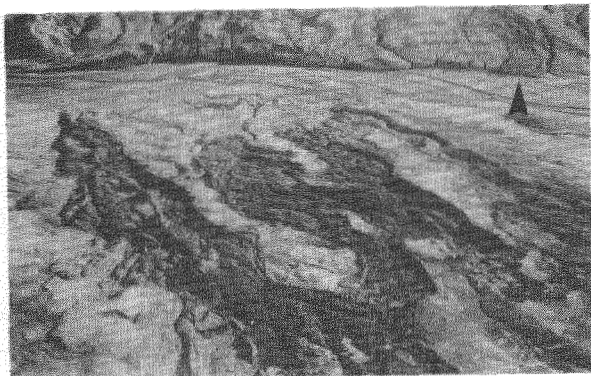


Figure 1. Active-layer detachment slides, Black Top Creek. Slides are c. 150 m in length. Slide 1, on the opposite valley side is arrowed.

In this paper field observations on the structure and composition of active-layer detachment slides are augmented by micromorphological investigations, allowing more precise conclusions to be drawn concerning the mechanisms of active-layer slope failures on the Fosheim Peninsula. Microscopic analysis of thin sections has been used previously to describe the disturbed fabric of landslide materials and slip surfaces (e.g. Chandler, 1972; Skempton et al., 1991). In addition, there is a large literature on the micromorphological effects of soil freezing and thawing (see, for instance the review by Van Vliet-Lanoe, 1985)

### STUDY SITES

The morphology and structure of active-layer detachment slides was investigated in three areas (Figure 2): Black Top Creek (79°58'N, 85°40'W), Hot Weather Creek (79°58'N, 84°28'W) and Big Slide Creek (unofficial name, 79°42'N, 85°23'W). Slide 1, at Black Top Creek, is 140 m long, 20-30 m wide and has an average gradient of about 9.5° (pp. 238-239 and Figure 10.9, Lewkowicz, 1992). It extends from a mid-slope location to the valley floor (Figure 1) and dates to 1987 (Lewkowicz, 1990). The slip scar has a corrugated surface and lies at a depth of around 0.6 m. The main slide block occupies the lower third of the landslide and shows considerable compressional deformation, but two other blocks lie farther upslope and these have suffered little disturbance during sliding. An excavated face within the upper slide block (Figure 4a) is discussed in detail below.

At Hot Weather Creek the study slide, which occurred in 1988 (Lewkowicz, 1990), is 60 m long and up to 17 m wide, with an overall gradient of around 20°. The single displaced unit shows a series of transverse compression ridges in the toe zone formed over highly folded active layer sediments, but upslope from this the displaced slide shows little internal disturbance (Figure 4b). At both Black Top Creek and Hot Weather Creek, the active layer is formed of clay, silt and sand, apparently largely derived from underlying shales, mudstones and sandstones, though these sites lie below the Quaternary marine limit.

The third site is on a slope of gradient 4°-11.5° immediately adjacent to the stream at Big

Slide Creek. Here there is no topographic evidence for recent landslide activity, but excavation revealed that active-layer detachment failures have probably occurred at this location in the past. The site lies above the marine limit, and the active layer is developed in silts and clays derived from the underlying Cretaceous shale bedrock.

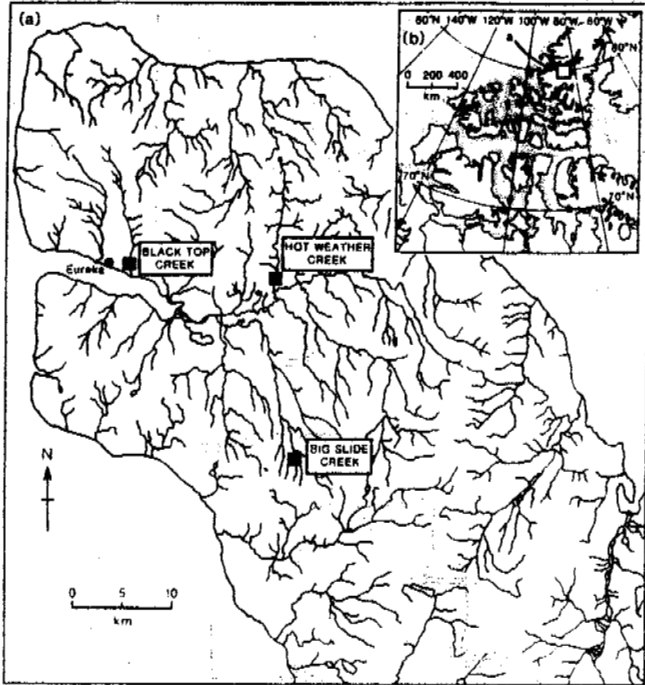


Figure 2. Location map. (a) Fosheim Peninsula, (b) Canadian Arctic Islands

#### CLIMATE

Records are available from the Eureka weather station, and indicate mean annual temperature and precipitation (1951-80) of  $-19.7^{\circ}\text{C}$  and 64 mm respectively (Atmospheric Environment Service, 1984). Permafrost is continuous, with active layer depths generally less than 70 cm. The mean July temperature of  $+5.4^{\circ}\text{C}$  is anomalously high compared with similar latitudes in the Canadian arctic, and there is evidence that summer temperatures inland from the Eureka station are even higher (Edlund et al., 1989, Lewkowicz, 1992).

#### METHODS

Trial pits were excavated through displaced slide units in late July and early August 1990. Excavation extended to the frozen subsurface, at a general depth of around 60 cm, just above the permafrost table. Clean vertical faces oriented along the line of greatest slope were prepared for field description and undisturbed sampling. Samples were collected by carefully pushing 6 cm square, 4 cm deep open-ended plastic boxes horizontally into the face. Samples were sealed and transported to the laboratory where they were air dried for several months prior to impregnation with epoxy resin. Oriented thin sections were then prepared, with samples cut in the vertical plane, parallel to the sampled face.

A control site, some 750 m south of slide 1 at Black Top Creek, was also excavated to provide information on soil structures developed where active layer detachment sliding is unlikely to have occurred in the past. The control was

located on the plateau surface above the valley, where the local slope gradient was  $2^{\circ}$  towards the east.

#### STRATIGRAPHY AND MICROMORPHOLOGY

##### Control Site

The profile consisted of a 3 cm thick dry sandy yellowish brown vesicular crust that graded downwards into an underlying very dark greyish brown clay (Figure 3). This clay was dry and hard to a depth of 0.3 m, below which it became progressively moister and softer. The thaw depth at the time of excavation was 51 cm. The drier upper unit displayed a strong fine angular blocky structure (Figure 5A), with pedes increasing in size from 1-2 mm at the top to 3-4 mm at the base. Under crossed polarizers, weak birefringence was noted in the outer parts of some pedes, indicating the presence of clay particles aligned parallel to the ped surfaces. Below 0.3 m the active layer was structureless and uniform.

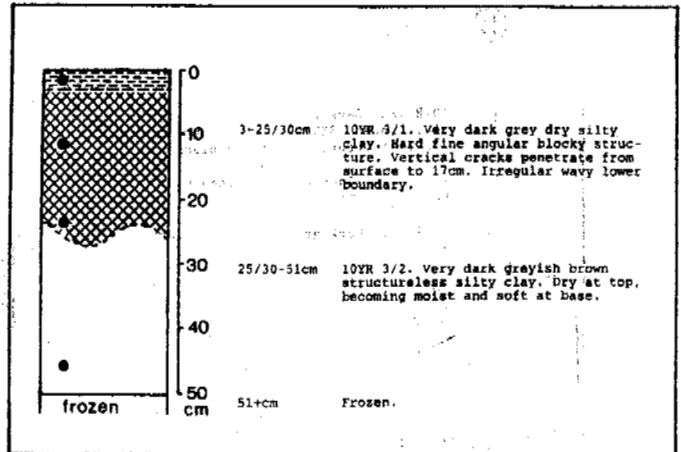


Figure 3. Soil profile, control site, Black Top Creek. Large dots mark locations of undisturbed samples.

##### Black Top Creek, Slide 1

Three layers were identified within the upper displaced unit (Figure 4a), layer 1 consisting of sandy surface colluvium, layer 2, a strongly structured dense silty clay and layer 3, a softer sandy clay with vertical jointing in its upper parts. These layers were traced into the toe zone where they became increasingly deformed.

The uppermost colluvial layer consists of alternating lighter sandy laminae up to 3 mm in thickness and darker silty and clayey laminae which are generally thinner and less continuous. Laminations are deformed into wavy and flame-like involutions (Figure 5B), either as a result of cryoturbation or disturbance during sliding, and a weak platy structure probably results from ice segregation during soil freezing. Also prominent are vesicles (Figure 5B), 500-1000  $\mu\text{m}$  in diameter, thought to result from structural collapse of the soil during thaw consolidation, when trapped soil air forms bubbles in the wet thawing soil mass (Harris, 1985; Van Vliet-Lanoë, 1985). Vesicles are common in the near-surface horizons of many arctic soils.

In layer 2, a strongly-developed vertical prismatic structure is clearly apparent both in the field and in thin sections (Figures 5C). Pedes are angular, with long axis lengths up to 18 mm near the base of the layer, decreasing

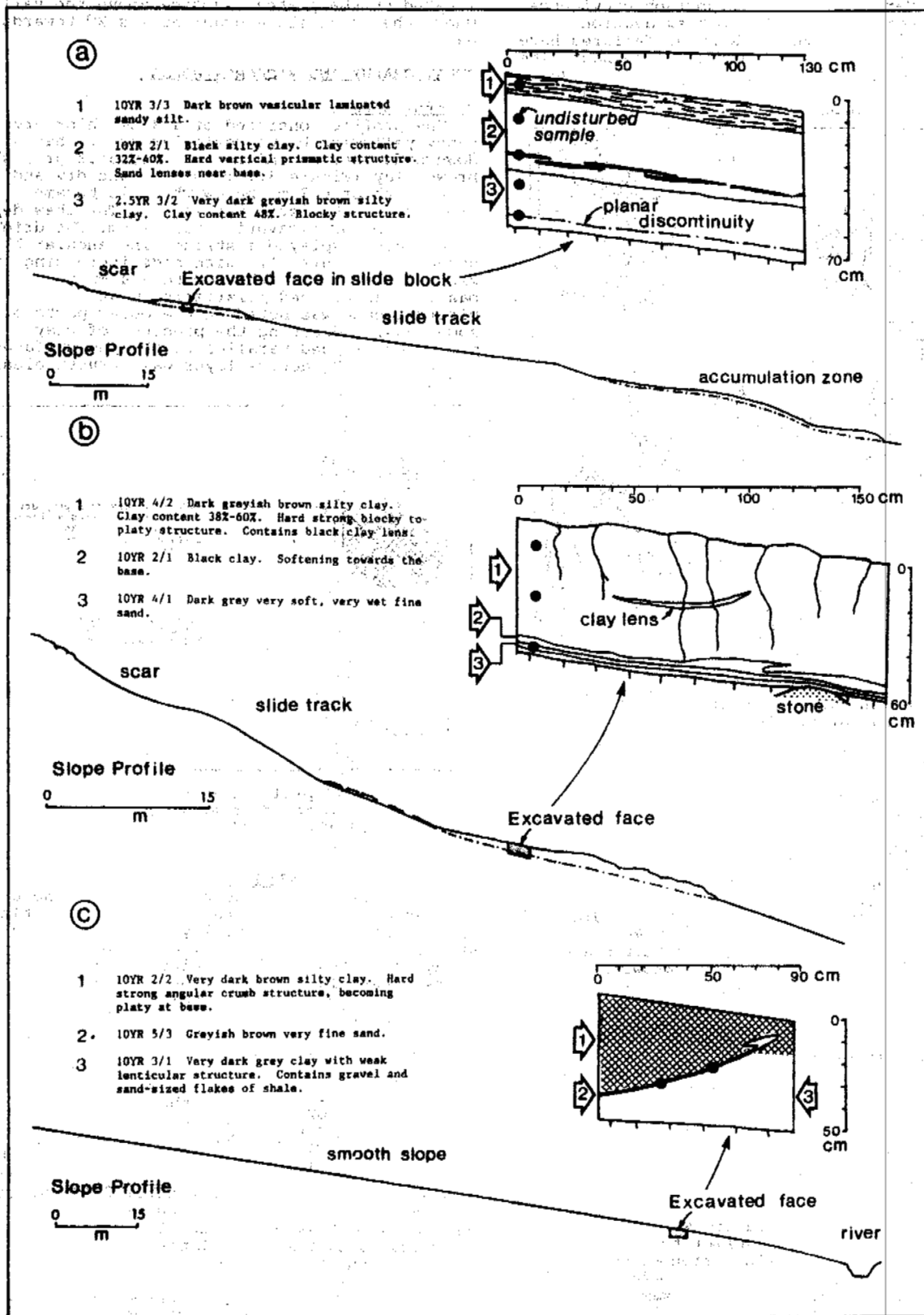


Figure 4. Slope profiles and section descriptions. (a) Black Top Creek, (b) Hot Weather Creek, (c) Big Slide Creek

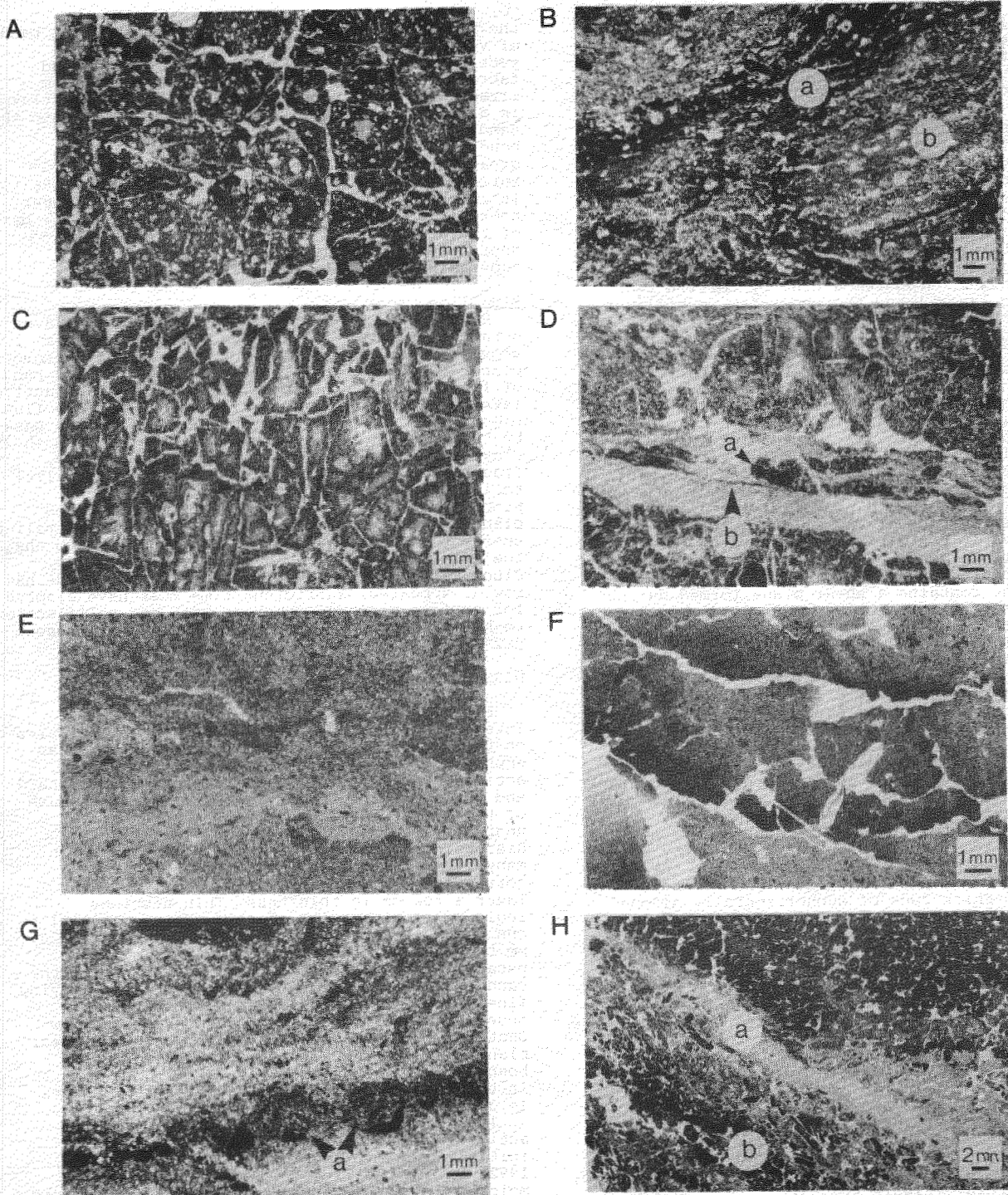


Figure 5. (A) Control site, 10-14 cm depth. Note planar voids forming angular blocky structure. (B) Layer 1, Black Top Creek, 4-6 cm depth. (a) deformed clay laminae, (b) vesicles. (C) Layer 2, Black Top Creek, 20-24 cm depth. Note strong vertical prismatic structure. (D) Sheared sand layer, Layer 2, Black Top Creek. Lenses of clay (a) are sheared and form lining of slip surface (b). (E) Layer 3, Black Top Creek, 64-66 cm depth. Sheared sand with wavy perturbations due to fluidization. (F) Layer 1, Hot Weather Creek, 28-30 cm depth. Dense peds form a strong blocky structure. (G) Layer 2, Hot Weather Creek, 58-60 cm depth. Sheared basal sand layer. Silt incorporated at the base of the sheared zone is deformed into ball-like boudins (a). (H) Big Slide Creek, 25-30 cm depth. Emergent shear zone (a). Note oriented shale fragments (b).

to a maximum of 5 mm near the top. Thin sections reveal dense peds containing scattered fine sand grains, though in some samples more sandy zones also occur. Roughly orthogonal irregular planar voids produce a crazed pattern across thin sections (Figure 5B), with spacing of vertical voids ranging from 750  $\mu\text{m}$  to 3000  $\mu\text{m}$ .

The planar voids in layer 2 are generally clean and open, but in the uppermost part of the layer peds are subangular, widely spaced, reoriented, and set in a silty clay groundmass with no open voids. The groundmass contains vesicular pores, though these are not present within the peds. This reorganisation of peds and infilling of intervening voids may be due to annual thaw-induced remoulding by solifluction affecting layer 1 and the upper few cm of layer 2. Such modification of the soil structure is absent in the plateau location of the control site.

Near the base of layer 2, lying parallel to the ground surface at a depth of 0.4 m, a 4 cm thick sandy horizon was noted during field description (Figure 4a). The horizon consisted of discontinuous lenticular units comprising alternating bands of fine sand and silty clay. Thin section analysis shows that the uppermost sand layer is abruptly truncated by a clay-lined surface (Figure 5D). Sand grains immediately below this surface lie parallel to it, and the sand above it contains lenses of silty clay that are apparently sheared out to form the lining of the discontinuity. It is concluded that this sandy zone contains a shear plane formed during displacement of the active-layer slide block, though it is not thought to represent the main basal slip surface.

The basal silty clay layer (layer 3, Figure 4a) shows strong vertical prismatic to blocky structure to a depth of c. 55 cm, below which the sediment is massive and structureless. In the structured upper zone, vertical joints are open, planar and crack-like, with spacing 15-40 mm. Near the base of the excavation, thin sections reveal an irregular groundmass containing diffuse sand-rich and clay-rich patches. These show cryoturbation-like deformations apparently extending upwards from a thin sandy horizon. This sandy horizon forms a planar discontinuity lying parallel to the ground surface close to the base of the active layer (Figure 4a) and consists of a wavy 4 mm thick zone of subhorizontally aligned sand grains. Its upper surface contains perturbations forming flame-like structures extending upwards into the overlying sandy silty clay (Figure 5E). It is concluded that active layer detachment and subsequent sliding took place over this basal zone of sediment fluidization. The main zone of deformation was probably concentrated in the 4 mm thick band of sand, but fluidization extended upwards into the base of the slide block, into which excess pore water escaped.

#### Hot Weather Creek

The excavated section revealed a thin superficial sandy colluvial horizon, similar to that of Slide 1 at Black Top Creek, overlying hard, dark grey clay (Figure 4b). The clay displayed a strong angular blocky to platy structure with peds up to 6 mm thick and 40 mm wide. In thin section peds are shown to consist of dense silty clay, but to include some zones of fine silty sand. Voids resemble irregular open cracks (Figure 5F). They contain no redeposited translocated clay and there are no signs of stress cutans in the surfaces of peds. The hard, dry, strongly structured silty clay extended to a depth of 55 cm, and between this and the frozen substrate the active layer was softer and moister. Lying immediately above the surface of

the underlying frozen ground was a 5 cm thick band of very wet and very soft medium sand. Thin sections of this sand layer reveal a disturbed fabric with inclusions of silty clay that form irregular wavy structures (Figure 5G). Silty clay is also observed to have been incorporated into the sand from the layer below, and deformed into boudinage structures (Figure 5G), reflecting greater stiffness in the silty clay than the surrounding sand during deformation (Hills, 1963). It is concluded that sliding of the active layer took place over this soft sandy horizon at the base of the active layer and that the structures described reflect shearing of the sand in a supersaturated fluidized state.

#### Big Slide Creek

Here a trench was dug through the active layer on a smooth lower valley-side slope, some 50 m above the stream. The section revealed an emergent planar discontinuity marked by a 3-4 mm thick band of fine sand (Figure 4c). The upper 20 cm of active layer consists of very dark brown clay with a fine blocky structure. This was truncated from the base by the emergent discontinuity (Figure 5h). In the clay immediately underlying the discontinuity, fragments of shale were strongly aligned parallel to it, suggesting reorganisation of fabric, probably as a result of shearing. The observed planar discontinuity apparently represents a relict emergent shear zone, probably formed close to the toe of a former active-layer detachment slide. Since all topographic evidence of such a slide has now disappeared, sufficient time must have elapsed for surface processes such as wash and solifluction to have smoothed the slope to produce its present day profile.

#### DISCUSSION

Excavation and micromorphological investigation of active-layer detachment failures on the Fosheim Peninsula, Ellesmere Island, has emphasised two major characteristics. Firstly, active-layer sediments are for the most part hard and strongly structured. Secondly, near the base of the active layer, sediments become moist, unstructured and soft, and contain a planar discontinuity marking the basal shear zone. In many if not all cases, this shear zone corresponds with the presence of a fine sandy layer a few cm in thickness. Thin sections indicate reorientation of sand grains parallel to the plane of the shear zone in a layer up to 20 mm thick, though local fluidization and water escape may have disturbed both the fabric of the sandy layer and that of the immediately overlying fine-grained sediment. This contrasts with observations of shear surfaces beneath shallow Quaternary clayslides in Britain, in which shear planes are associated with polished surfaces bounded by zones no more than a millimetre or so in thickness containing aligned clay aggregates (e.g. Skempton et al., 1991).

The high ice contents at the base of the active layer, thought to be responsible for initiating active layer detachment (Lewkowicz, 1992) may result from downward migration of moisture from the thawed upper active layer into the still-frozen lower parts during spring and early summer (Parmuzina, 1978, 1979; Mackay, 1983). Such migration would be encouraged by the strong thermal gradient that exists immediately below the thaw plane at this time. In addition, upward freezing from the permafrost table in early autumn may also lead to concentration of segregation ice near the base of the active layer (Mackay et al., 1979). In the Fosheim Peninsula, ice contents near the base of the active layer are often in excess of the liquid limit of the host sediment (ice contents by volume 40-100%,

Liquid Limits 25-55%, Lewkowicz, 1992). Thus, slope failures are associated with the sliding of coherent masses of active layer over a basal shear zone in which thaw-induced high porewater pressures reduce effective stresses and therefore frictional strength to low values.

The coherence of slide blocks during slope failure cannot be attributed to cohesion due high clay contents, since geotechnical measurements indicate low cohesive and high frictional strength for active layer soils (Harris and Lewkowicz, in press). However, drying of the soil layer by evaporation over the summer and by two-sided freezing during autumn reduces moisture contents to below the plastic limit, so that during sliding the active layer behaves as a rigid block. The strong prismatic and blocky structure may result largely from soil shrinkage during desiccation, or alternatively, may reflect ice segregation and the formation of reticulate ice veins during active layer freezing. The fine blocky structure observed in the upper 0.3 m at both the control site and in the excavated slide blocks suggests little alteration of the near-surface active layer during sliding. The larger-scale jointing between c. 0.3 m and 0.5 m, widely observed in displaced active layer slide blocks, but absent in the control site, may reflect active-layer desiccation, the formation of reticulate ice during freezing, or fracturing of a dry, brittle soil during translational sliding.

#### CONCLUSIONS

Micromorphological investigations of active layer detachment slides on the Fosheim Peninsula in Ellesmere Island, Canada, have demonstrated that during sliding the middle and upper part of the displaced active layer behaves as a rigid block and that translational sliding takes place over a sheared basal layer a few cm in thickness. The coherence of the displaced slide blocks results from lowering of moisture content in the upper and middle active layer to below the plastic limit, and the development of a relatively rigid soil mass. The observed soil structure may reflect desiccation, though cryogenic moisture migration associated with ice segregation may also be a factor. Downward migration of moisture into the lower part of the active layer apparently leads to the development of high basal ice contents, and when late-summer thaw penetration is rapid, thaw consolidation causes high porewater pressures in the basal zone, triggering active layer detachment. Sliding was observed to occur over a fine sandy basal layer rather than a slickensided shear surface.

#### ACKNOWLEDGEMENTS

The authors acknowledge support from the NATO Scientific Affairs Division, the Natural Sciences and Engineering Research Council of Canada (A.G.L.) and a Research Agreement with Energy, Mines and Resources, Canada (A.G.L.). Logistical support was provided by the Canadian Continental Polar Shelf Project.

#### REFERENCES

- Atmospheric Environment Service (1984) Eureka, Principal Station Data, Volume 79, Environment Canada, Downsview, Ontario.
- Chandler, R.J. (1972) Lias clay: weathering processes and their effect on shear strength. *Geotechnique* 22, 403-431.
- Edlund, S.A. Alt, B.T. & Young, K. (1989) Interaction of climate, vegetation and soil hydrology at Hot Weather Creek, Fosheim Peninsula, Ellesmere Island, Northwest Territories. *Current Research, Part D, Geological Survey of Canada, Paper 89-1D*, 125-133.
- Harris, C. (1985) Geomorphological applications of soil micromorphology with particular reference to periglacial sediments and processes. Richards, K.S., Arnett, R.R. & Ellis, S. (eds.), *Geomorphology and Soils*, pp. 219-232, George Allen & Unwin, London.
- Harris, C. & Lewkowicz, A.G. (submitted) Form and internal structure of active-layer detachment slides, Fosheim Peninsula, Ellesmere Island, N.W.T. Canada. *Canadian Journal of Earth Sciences*.
- Hills, E.S. (1963) *Elements of Structural Geology*. Methuen, London.
- Lewkowicz, A.G. (1990) Morphology, frequency and magnitude of active-layer detachment slides, Fosheim Peninsula, Ellesmere Island, N.W.T. Proceedings of the 5th Canadian Permafrost Conference, Quebec, pp. 111-118, *Collection Nordicana 54, Centre d'études nordiques de L'Université Laval, Quebec*.
- Lewkowicz, A.G. (1992) Factors influencing the distribution and initiation of active-layer detachment slides on Ellesmere Island, Arctic Canada. Dixon, J.C. & Abrahams, A.D. (eds.), *Periglacial Geomorphology*, pp. 223-250. Wiley, Chichester.
- Mackay, J.R. (1974) Reticulate ice veins in permafrost, northern Canada. *Canadian Geotechnical Journal*, 11, 230-237.
- Mackay, J.R. (1979) An equilibrium model for hummocks (non-sorted circles), Garry Island, North West Territories. *Geological Survey of Canada*, 79-1A, 165-167.
- Mackay, J.R. (1983) Downward water movement into frozen ground, western arctic coast, Canada. *Canadian Journal of Earth Sciences*, 20, 120-134.
- Mackay, J.R., Ostrick, J. Lewis, C.P. & MacKay, D.K. (1979) Frost heave at ground temperatures below 0°C, Inuvik, Northwest Territories. *Current Research Part A, Geological Survey of Canada, Paper 79-1A*, 403-406.
- Parmuzina, O. Yu. (1978) Cryogenic texture and some characteristics of ice formation in the active layer. (In Russian). *Problems of cryolithology*, Vol. 7, A.I. Popov (ed.), pp. 141-164. Moscow University Press, Moscow.
- Paruzina, O. Yu. (1979) An approach to the question of the redistribution of moisture in frozen soil (according to full scale observations). (In Russian). *Problems of cryolithology*, Vol. 8, A.I. Popov (ed.), pp. 194-197. Moscow University Press, Moscow.
- Skempton, A.W., Norbury, D. and Petley, D.J. (1991) Solifluction shears at Carsington, Derbyshire. *Quaternary Engineering Geology: Proceedings of the 25th Annual Conference of the Engineering Group of the Geological Society of London*, 381-388.
- Van Vliet-Lanoe, B. (1985a) Frost effects in soils. Boardman, J. (ed.), *Soils and Quaternary Landscape Evolution*, pp. 115-156, Wiley, Chichester.
- Van Vliet-Lanoe, B. (1985b) From frost to solifluction: a new approach based on micromorphology, its application to arctic environment. *Inter Nord* 17, 15-20.



PALSA-LIKE MOUNDS DEVELOPED IN A MINERAL SUBSTRATE,  
FOX LAKE, YUKON TERRITORY

Stuart A. Harris

Department of Geography, University of Calgary  
Calgary, Alberta, Canada T2N 1N4

Palsa-like mounds at the south end of Fox Lake, southwestern Yukon Territory consist of a long-lived series of icy mounds that develop in the mineral substrate in marshes. They pass through 5 developmental stages, commencing with low, grassy mounds and followed by invasion by shrubs (*Betula* spp., *Arctostaphylos* spp., and *Salix* spp.) and by *Picea glauca*. The sere takes at least 380 years to reach stage V and some of the mounds may be considerably older. Once shrubs appear, an  $A_h$  develops and thereafter saprophytic lichens. The mounds can reach almost 3 m in height and look superficially like palsas. Ice is interstitial or in the form of narrow lenses and ultimately reaches about 65-70% by volume in the permafrost core. The ice appears to be primarily meteoric in origin. Stages I and V are the most susceptible to the effects of climatic change.

These mounds differ from true palsas in the absence of aquatic, fen or sphagnum peat at the surface in all stages; therefore the heat exchange processes will be different. The name "lithalsa" is suggested for palsa-like mounds such as these that develop in areas where the relative humidity is too low in summer for the development of a luxuriant growth of mosses.

#### INTRODUCTION

Palsas were first described morphologically by Fries and Bergström (1910), and since then many more descriptions have been added to the literature, together with theories as to their origin. Unfortunately there are few detailed studies of the nature and development of individual fields of palsa-like mounds, so there is still considerable debate regarding their nature and classification (Dionne, 1978; Washburn, 1983; Seppälä, 1988).

This paper describes the nature and probable history of a field of palsa-like mounds developed in mineral substrates at the south end of Fox Lake, southwestern Yukon Territory, Canada. It is followed by a discussion of their relationship to true palsas and minerogenic palsas.

#### STUDY AREA

The Fox Lake palsa-like mounds occur at the south end of Fox Lake, 80 km north of Whitehorse, Yukon Territory (Fig. 1). They are developed in both lacustrine silts and in colluvial and alluvial deposits along Richthofen Creek. Their elevation is 800 m, i.e., some 100 m higher than Whitehorse. The climate is noticeably cooler (estimated MAAT =  $-2^{\circ}\text{C}$ ) than the latter and pronounced cold air drainage events are common during the winter months. Since the end of 1986, air temperatures have been unusually warm, but the main palsa-like mounds are surviving. The thawing index averaged 1771.5  $^{\circ}\text{days/year}$  between 1987 and 1991, while the freezing index averaged 2362  $^{\circ}\text{days/year}$ . This period included one of the warmest years on record.

The vegetation consists of Boreal Forest with more open areas on south-facing forested slopes where soils are thin and there has been interference by fire or anthropogenic disturbances. The valley floors are occupied by grassy fens with willow thickets, except where mature palsas occur and white spruce dominates.

Soils are generally poorly developed and the area was heavily glaciated during the Late Wisconsinan period. Subsequently, the hill slopes have been washed by glacial lakes so that frequently the glacial till has been largely removed. The lower slopes and valley floors have appreciable thicknesses of lacustrine sediments, often overlain by alluvial fans and overbank deposits of streams, e.g.,

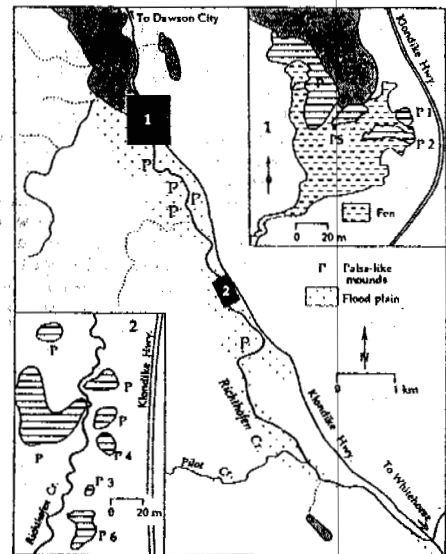


Figure 1. Location of the palsa-like mounds at the south end of Fox Lake, S.W. Yukon Territory. The mounds with P numbers are those referred to in the text.

along Fox Creek. The White River ash (Capps, 1915) is commonly found just below the surface, indicating that the valley sides have been stable for the last 1200 years (Hughes et al., 1972).

The palsa-like mounds occur around the southern margin of Fox Lake and along the flat floor of Fox Creek (Fig. 1). They show a range from low grassy mounds, through shrub covered mounds, to extensive, mature mounds with tall, white spruce trees. The latter stand out as islands amongst the surrounding fens occupied by sedges and grasses. Permafrost was encountered on the surrounding hills during investigations for the Dempster Lateral Gas Pipeline (Harris, 1983).

## METHODS USED

During the summer of 1984, access holes were drilled to a depth of over 5 m in two readily accessible palsalike mounds (P1 and P2) using a hot water drill modified after Napoleon and Clarke (1978). The holes were aligned in north-south transects and were immediately cased with PVC tubing, sealed shut at the lower end. Rubber bungs were placed in the holes to keep out precipitation and the tubes froze into place. Four tubes on each mound were used as access tubes for the neutron moisture probe and four were used for ground temperature cables. The latter consisted of YSI 44033 thermistors placed in 16 pair geophysical cable. Manual readings with a Biddle Wheatstone Bridge confirmed that the ground was frozen, but it was next Spring before the ground had recovered from the input of heat during the drilling process. The readings were taken to the nearest 0.01°C. Next year, mounds P3, P4 and P5 were drilled in a similar way. A neutron probe (Campbell Pacific Nuclear Model 503) was used to measure the moisture content at 10 cm. intervals. The actual count at each depth was divided by the standard count, and the resulting ratio was calibrated by comparing gravimetrically determined moisture in samples of known volume removed with a SIPRE corer with the results of neutron probe measurements through the PVC tube. The results are expressed as % by volume H<sub>2</sub>O. From 1976, ground temperatures were measured every two weeks in summer and whenever possible in winter. Neutron probe measurements were also made every two weeks in summer for four years. Thereafter the frequency of measurements was reduced.

Samples of the material in the mounds were collected using a power SIPRE auger and the walls of cracks were examined and sampled for grain size analysis in the laboratory and for study of the distribution of ice. The latter appeared to form narrow lenses throughout the mounds, based on the changes in speed of drilling with the hot water drill.

Plant collections were made at all sites and both vascular plants and lichens were collected. These plants were identified at the Herbarium of the University of Calgary, with the exception of the *Salix* spp., which were determined by G. W. Argus at the National Herbarium in Ottawa.

The mounds were surveyed by chain, compass and plane table, and levelling surveys were carried out so as to map their contours. A levelling survey was carried out in 1988, using a bench mark on the road, to see whether the palsas changed elevation during the summer, but this did not occur.

Problems were encountered with frost jacking of the access tubes in the grassy mounds, and the height above ground of all access tubes was noted at each visit in order to document these changes. The cracks were mapped in 1987 and measurements made of the changes in distance from reinforcing bars driven down into the permafrost on either side of a given crack. To further document the movements, monthly recording charts were used to log the progress of the movement in the same way as records were made of diurnal heaving and soil creep at Kananaskis (Harris, 1973). Magnet wire was also stretched across the cracks between reinforcing bars and the ends wired to electric watches so that when the wire broke, the watch would stop.

Soil pits were dug in the active layer of each mound and the soils described and sampled. Back in Calgary, grain size was determined on the soil samples using the pipette method of Kilmer and Alexander (1949), with pretreatment with hydrogen peroxide to remove organic matter. Calgon was used as a dispersing agent and the results expressed in terms of USDA classes of sand, silt and clay.

A weather station was set up on mound P1 in 1984 and moved to the nearby Rocking Horse Ranch in 1986. A continuously recording Lambrecht 3-level Temperature Recorder was used; it was calibrated by using a thermistor and the Biddle Bridge. The data for 1985 and 1986 was

Table 1. Characteristics of the different stages of palsalike mounds.

Stage	I	II	III	IV	V		
Dominant Vegetation	Grasses	Shrubs	Shrub <i>Picea glauca</i>	<i>Picea glauca</i> (regenerating)	<i>Picea glauca</i> (old)		
Height (m)	1.2	2.4	2.5	2.7	2.25		
Active Layer Thickness (cm)	290-410	Shrub 60 Grass 230	N. 60 S. 80	N. 60 S. 120	130		
Permafrost Thickness (m)	1.9 - 3.1	5.4	2.7	5.5	5.0	4.8	4.2
L <sub>10</sub> /A <sub>10</sub> (cm)	0-2	2-20	10-60	5-35	3-15		

incomplete, but those years appear to be the last two with weather typical of the last few decades. Since then, the climate has become very unpredictable, but a complete temperature record has been made.

Good quality aerial photographs are available for 28 July, 1971, at a scale of 1:17340. These were used to check the longevity of the youngest mounds, and for mapping purposes.

## RESULTS

### 1. Vascular Plants

The palsalike mounds can be divided into five groups based on the vegetation cover, apparently forming a developmental sequence or sere (see Table 1). Stage I consists of low mounds with gentle slopes, and is characterized by a vegetation association dominated by grasses which provide a 30-60% cover. P6 and P3 can be recognized on aerial photographs taken in 1970, so this stage can persist for at least 20 years. In Stage II, shrubs appear and displace the grasses. *Arctostaphylos uva-ursi* may form a dense ground cover, but ultimately *Betula glandulosa*, *B. nana*, and *Salix* spp. become dominant. During the eight years of data collection, the *Betula* and *Salix* shrubs have encroached about 30 cm on average into the areas of *Arctostaphylos* and grasses on P4. These taller shrubs are trimmed back in winter by snowshoe hares in the two years when the hares are most abundant in their cycle (e.g., 1990 and 1991), but otherwise grow with little hindrance.

As the grasses disappear from the mounds, small, scattered *Picea glauca* seedlings appear among the shrubs (Stage III). These gradually grow into trees, but on P2 there are still only about 12 spruce trees on a mound of 840 m<sup>2</sup>. The oldest tree was established by 1906 A.D., and the ages of the trees, based on tree rings (Fig. 2A) suggest that germination is uneven and that conditions in

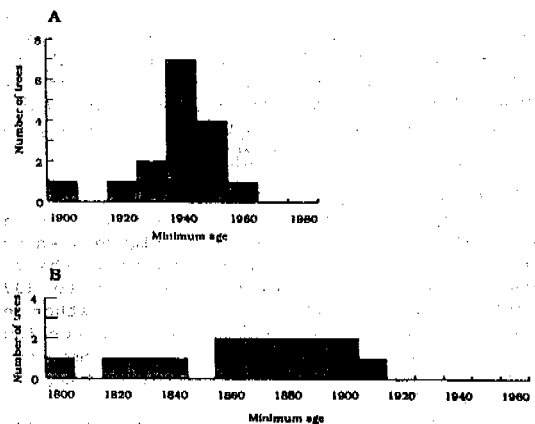


Figure 2. Histograms showing the number of trees that had become established in a given decade for A. Mound P2 and B. Mound P1.

1940-1950 were best for seedling establishment. Seedlings are still appearing, but the young seedlings were not cut down to determine their age. Grasses are rare.

Stage IV is where *Picea glauca* forms a continuous cover with some shrubs such as *Salix* spp. forming an understory. P5 is an example where the spruce trees are of different ages and are also regenerating. However, in the case of P4, the spruce trees are of a more even size, and when they die, they leave an opening in the forest cover. The oldest tree cored had reached breast height in 1801 A.D., but coring shows that there was regular replacement until about 1920 A.D. (Fig. 2B). Since then, there has been no regeneration, i.e. the mound has been in Stage V.

This sequence is accompanied by a series of changes in subordinate species of vascular plants and is also closely related to the other characteristics of the mounds (Table 1).

## 2. Substrate

The mounds form in calcareous, lacustrine silts and in colluvium and alluvium. Grain-size analysis shows that they are silt loams, loams, and sandy loams containing less than 10% clay (Fig. 3). Stones may occur in the colluvium.

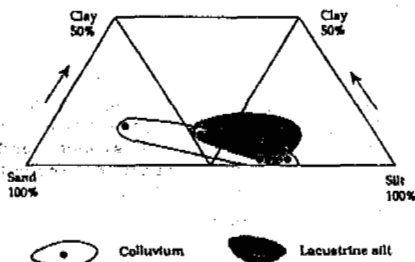


Figure 3. Grain size of the mineral substrate in the Fox Lake palsa-like mounds.

## 3. Morphology

As indicated in Table 1, the stable, grassy mounds are low (up to 1.2 m) with gentle slopes and little surface cracking. In stage II, the mounds rapidly increase in height, the growth apparently occurring rapidly as the shrubs spread over its surface. Large cracks appear in the ground during this process and measurements with constant recording machines and magnet wire stretched across the crack and wired to electric watches show that the movement is most prevalent in winter and spring, but continues throughout the year. The movement may be gradual, punctuated by sudden spurts, or it may be episodic between spells with no movement. In stage III, the mounds become more consistent in height and cracking decreases. By now the side slopes may be over 20°. In stage IV, cracking is absent and the maximum elevation about the fen is achieved. In both stages III and IV, the height may vary across the mound. Stage V is somewhat lower (2.2 m), but cracking does not reappear unless the mound starts to disappear. That process will be discussed elsewhere.

## 4. Ground Temperatures

The permafrost body is too shallow to have constant temperatures within 5 m of the surface. Figure 4 shows a typical series of observations made manually at the four temperature cables installed in P2 from 1975 to 1977. These pre-date the substantial changes in weather experienced since then, but the seasonal pattern continues much the same in spite of the substantial temperature swings of the last few years. Similar seasonal changes are found at all the palsas.

Figure 5 shows a comparison of the ground temperatures recorded in late July 1987, for stages II to V with those for P6 (stage I) in late June 1990. It will be seen that the coolest temperatures are found in stages III-IV.

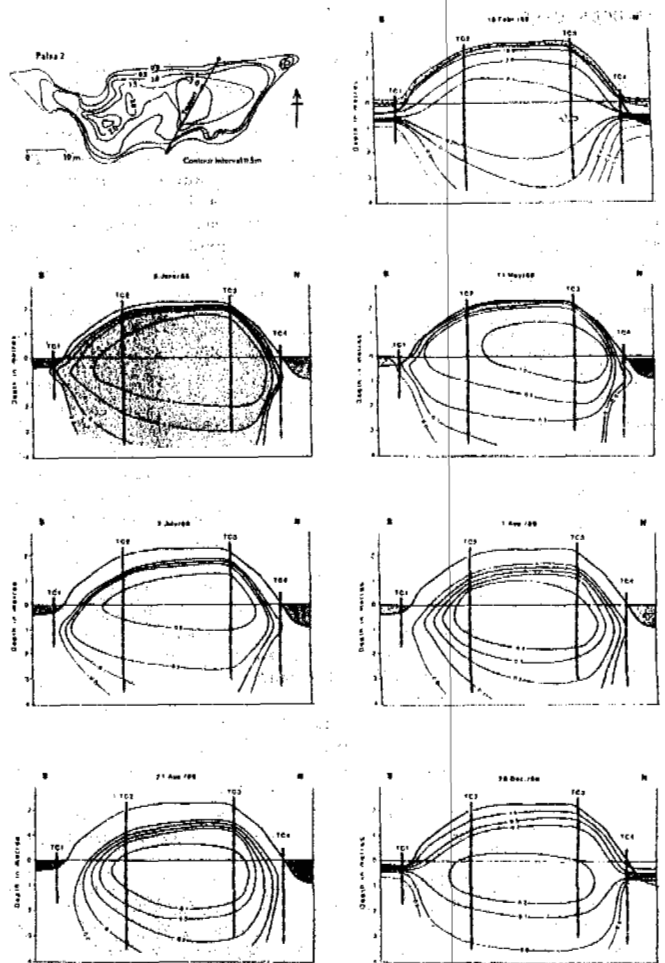


Figure 4. Seasonal changes in ground temperature distribution in Mound P2 between 1985 and 1987.

In stage II, colder temperatures are encountered under the shrub vegetation than under the residual grassy patches. Stage I shows much warmer ground temperatures, even though the data are for late June rather than late July.

## 5. Active Layer Thickness

The lowest active layer thickness (60 cm) is encountered on north-facing slopes in stages II-IV under shrub or *Picea* vegetation (Table 1). Actual values vary from year to year, and those in Table 1 are values for the warmest years within the eight year study period. In stage V, the active layer doubles in thickness, while it is thickest in stage I (up to 4 m) and in the grassy portions of the mounds in stage II. Thus the vegetation cover plays a key role in the heat exchange process. Active layer thickness is generally inversely related to permafrost temperature in the sequence of stages, but the relationship is not linear (Fig. 6).

## 6. Permafrost Thickness

The base of the permafrost in all mounds is rather similar (Fig. 5), but the level of the permafrost table varies enormously according to the vegetation cover. The thickest permafrost occurs in stages II to IV, but is least in stage I. General relationships exist between permafrost thickness and mound height (Fig. 7) for the sequence, but surveying bench marks at regular intervals during a season showed no seasonal changes in height of the mounds.

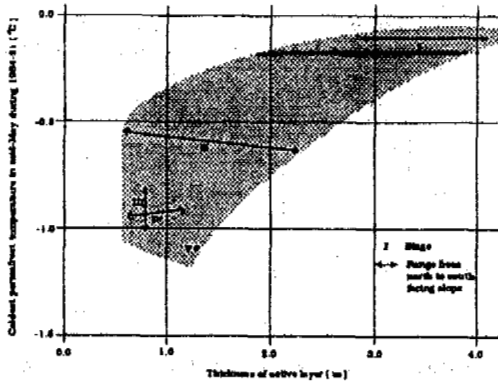


Figure 5. Relationship between minimum ground temperature recorded in the mounds in late July with active layer thickness.

### 7. H<sub>2</sub>O Distribution

Regular measurement of the distribution of total H<sub>2</sub>O using the neutron probe in the access tubes shows that the total moisture content of the permafrost is fairly constant, but a perched water table can be shown to move downwards as the thawing front descends in summer.

Figure 8 compares the total moisture distribution in the main body of permafrost in P2, 4, 5 and 6. The data for stage I (P6) was collected when the thawing front was at about 2 m and it will be seen that the moisture content increases with depth from about 45% by volume to 60% at the base of the permafrost layer. Similar results are seen in Stage II, but thereafter the maximum values are found in the upper portion of the permafrost mass, where they may reach between 65 and 70% by volume (Harris, 1988). This zone increases in thickness in Stage IV until most of the permafrost contains over 60% total H<sub>2</sub>O by volume.

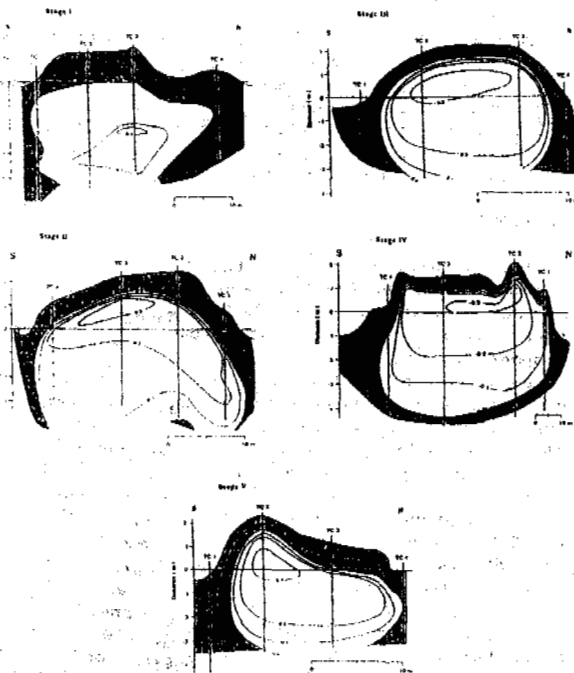


Figure 6. Comparison of the ground temperatures recorded in late July, 1987, for Stages II to V with those for Stage I (P6) in late June 1990.

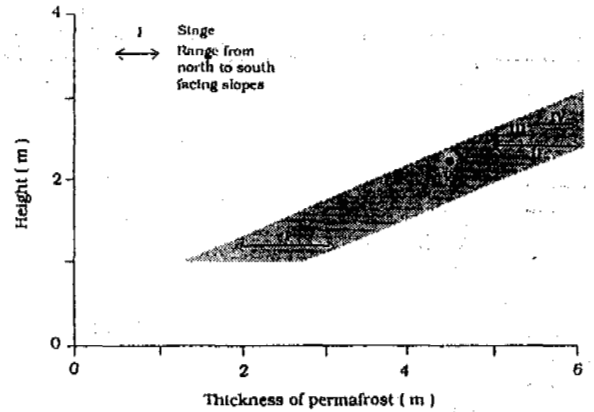


Figure 7. Relationship between mean permafrost thickness of the mounds between 1985 and 1991 and mound height.

### 8. Soils

The soil profiles in the mounds in stage I show minimal profile development. However, once the shrubs appear in stage II, a marked LFH A<sub>h</sub> sequence appears due to the large production of dead leaves each fall. As cracking occurs and the slopes steepen, there tends to be movement of the A<sub>h</sub> downslope, producing thickening of the A<sub>h</sub> away from the crest. By stage III, the A<sub>h</sub> may be over 50 cm thick on the lower slopes of the mound, so that the mounds resemble palsas. Litter production is reduced once the *Picea glauca* becomes dominant and thereafter the A<sub>h</sub> decreases in thickness into stage V (Table 1).

### 9. Lichens

The distribution of lichens in the various stages is shown in Table 2. With the appearance of a marked litter layer in stage III, at least nine species of lichens make their appearance. Most are saprophytes found on the surface of the soil. With the development of a closed canopy in stage IV, the species change somewhat, some of the newcomers living directly on the bark of the trees. By stage V, the variety of lichens is greatly reduced.

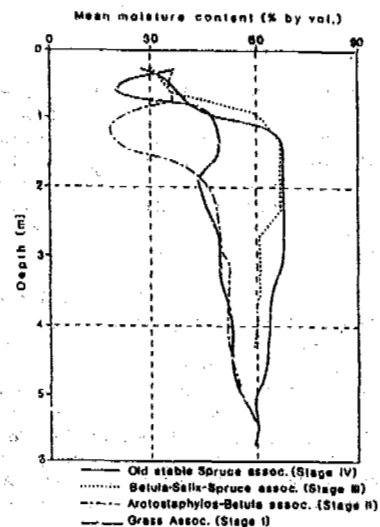


Figure 8. Comparison of the total moisture content (% by volume) for Stages I to IV as determined by the neutron probe using 10 cm intervals.

Table 2. Distribution of lichens on the five stages of palsa-like mounds (classification after Hale, 1979).

FAMILY	SPECIES	STAGE				
		I	II	III	IV	V
Atactoriaceae	<i>Myoria fuscescens</i>					X
Cladoniaceae	<i>Cladonia arbuscula</i> ssp. <i>arbuscula</i>			X		
	<i>C. mitis</i>			X		
	<i>C. zameliformis</i>			X		
	<i>Cladonia chlorophaea</i>			X	X	X
	<i>C. flabellata</i>			X	X	
	<i>C. gracilis</i> var. <i>dilatata</i>			X	X	
	<i>C. pleurota</i>			X	X	
	<i>C. pyrenosa</i>			X	X	
	<i>C. scabrilobula</i>			X	X	
Hypogymnaceae	<i>Hypogymnia physodes</i>			X	X	X
Lecanoraceae	<i>Lecanora imputens</i>				X	
Parmeliaceae	<i>Catocria nivalis</i>					X
	<i>G. pinastri</i>			X	X	
	<i>Parmelia sulcata</i>			X	X	X
	<i>Parmeliopsis ambigua</i>			X	X	
Peltigeraceae	<i>Peltigera aphthosa</i>				X	
	<i>P. polydactyla</i>				X	
	<i>P. venosa</i>				X	
Teloschistaceae	<i>Xanthoria fallax</i>				X	X
	<i>X. polycarpa</i>				X	X
	Number of species	0	0	11	16	7

Table 3. Estimated minimum duration of each stage of the palsa-like mounds at Fox Lake, Yukon Territory.

Stage	Estimated Minimum Duration - Years	Method
I	20	Aerial photographic interpretation
II	70	Growth rates of shrubs
III	100	Tree rings
IV	120	Tree rings
V	70	Tree rings
Total minimum age	380 years	

## DISCUSSION

### 1. Developmental Sequence

The vegetational sequence seen on these mounds represents a sere where there is no interruption by fire. This is unusual and fire has passed through the vegetation of icy mounds in nearby sites on the other side of Richthofen Creek.

The complete mound sequence probably extends through a minimum period of 380 years (Table 3) and the presence of all stages suggests that from about 1600 A.D. until 1987, conditions had been suitable for their growth and survival. Some of the mature mounds may be substantially older.

The permafrost in the mounds is most susceptible to adverse environmental changes in Stage I where the active layer is very deep and the permafrost is warm. However, once the shrub vegetation develops in stage II, the active layer is greatly reduced in thickness and the permafrost becomes colder. This is followed by an increase in total moisture content, especially in the upper layers of the permafrost (stage III) and this increase slowly spreads downwards. This suggests that the input of meteoric moisture following the seasonal cooling moves downwards (see Harlan, 1974; Burn & Smith, 1985a & b; Harris, 1988). This moisture input may be responsible for dilation cracking in stages II and III, as is suggested by the occurrence of widening of the cracks in winter and spring when the ground temperature gradients are steep and the cooling wave is descending into the ground, followed by warming. Any flow of interstitial ice that might occur should be minimal at the lower surface temperatures in winter.

The development of an LFH A<sub>h</sub> sequence undoubtedly alters the heat exchange processes at the surface of the ground and these effects are currently under investigation. They also provide a suitable substrate for lichens which are common in stages III and IV. Limited supplies of litter in stages IV and V are probably the cause of the thinning of the A<sub>h</sub> layer with time, while the absence of an appreciable shrub or herb layer in stage V may cause a minor decline in the permafrost thickness. Alternatively, the difference in permafrost thickness between P5 and P1 may be original.

### 2. Comparison With Palsas and Minerogenic Palsas

Palsa-like mounds developed on a purely mineral substrate have been previously referred to as "cryogenic mounds" (e.g. Payette & Seguin, 1979; Lagarec, 1982) or

"mineral palsas" (e.g. Åhman, 1975, 1976, 1977; Dionne, 1978, 1984), but both terms are problematic (Seppälä, 1988). There is little data on the growth stages of aggradational examples, and until more examples of mounds in each stage have been examined, the range of results shown in Table 1 must be regarded as a general guideline. The mounds are very similar to palsas in many ways, but lack true fen, sphagnum, or aquatic peat. Since the name "palsa" means a frozen peat mound (Seppälä, 1988), those who object to calling mounds such as those at Fox Lake "minerogenic palsas" have a strong case. Undoubtedly the rates of heat exchange will be different in these mounds compared with true palsas (see Romanov, 1968), although the overall pattern of development is similar. "Cryogenic mounds" is a term that is also applied collectively to many different permafrost mounds. For this reason, the term "lithalsas" is suggested for palsa-like mounds developed in mineral substrates such as these. Undoubtedly, they can grade into palsas where there is thin peat overlying a mineral substrate, but the heat exchange processes of such features will be dominated by the effects of the surface peat with its low density and high insulating properties when dry. It would seem to this author that such cases can justifiably be called "minerogenic palsas". The vegetational and soil sequences of both "minerogenic palsas" and true palsas are quite different to those found on lithalsas.

Lithalsas occur in a broad zone across southwestern Yukon Territory between Carmacks and Marsh Lake, where the relative humidity in summer is too low for the luxuriant growth of mosses, or for peat formation on the marshy valley floors. To the north and east, where the relative humidity in summer is higher, the mosses flourish and lithalsas are replaced by minerogenic palsas and true palsas, the latter being dominant.

## CONCLUSIONS

The palsa-like mounds at the south end of Fox Lake and along Richthofen Creek in southwestern Yukon consist of a long-lived series of mounds that develop in a mineral substrate in marshes. They go through a series of five developmental stages commencing with low grassy mounds, followed by invasion of shrubs, and ultimately of white spruce. The sere takes at least 380 years to complete the stages and some of the mounds may be much older. They develop an A<sub>h</sub> horizon in the soils once shrubs are present, so they look superficially like palsas, but lack the aquatic, *Sphagnum* and fen peats at the surface of true palsas. The mounds can reach a height of nearly 3 m and up to 60-70% by volume of ice in the permafrost. The ice is interstitial and in the form of narrow lenses. The moisture appears to be meteoric in origin and enters from above. The mounds with a shrub or regenerating *Picea glauca* vegetation are the most stable and the coldest, and have the thinnest active layers. Cracking occurs during the periods of rapid growth of the icy core. The latter is fed by meteoric waters descending following the cooling wave.

Given the different heat exchange processes that must occur at the surface of these mounds compared with that on

the peat of true palsas, the name "lithalsas" is suggested for these mounds. They develop in a belt from Marsh Lake to Carmacks where the relative humidity is too low in summer for luxuriant growth of mosses. However, saprophytic lichens do occur in the later stages of lithalsas after the litter and A<sub>h</sub> horizons become sufficiently developed. Lithalsas are replaced by palsas in the wetter areas to the north and east in southern Yukon Territory.

#### ACKNOWLEDGEMENTS

The work was carried out using funds from NSERC operating grant A 7843 and also Northern Training Grants to a succession of students. W. K. Blumstengel, J. Brydon, L. Kirkham, G. McDermid, K. Olson, J. Pedersen, L. Piet, I. H. Schmidt, and T. Waller all helped with the field work. Bonnie Smith helped with plant identification in the Herbarium. Dr. G. W. Argus of the National Museum of Natural History in Ottawa identified the *Salix* spp., while Mrs. K. Wilkinson identified the grasses. The author is indebted to Art and Linda Hutchinson of the Rocking Horse Ranch for their logistical help and for collecting the weather data since 1986.

#### REFERENCES

- Åhman, R. (1975) Pal strukturer och palsmorfolog: i Nordnorge. Svensk Geografisk Årsbok 51, 223-232.
- Åhman, R. (1976) The structure and morphology of minerogenic palsas in northern Norway. *Buletyn Peryglacjalny* 26, 25-31.
- Åhman, R. (1977) Palsar i Nordnorge. Meddelanden från Lunds Universitets, 165 pp. Geografiska Institution, Avhandlingar, #78.
- Burn, C. R. & M. W. Smith (1985a) Comment on "Water movement into seasonally frozen soils" by D. L. Kane and J. Stein. *Water Resources Research* 21, 1051-1052.
- Burn, C. R. & M. W. Smith (1985b) On the origin of aggradational ice in permafrost. In: *Freezing and Thawing of Soil-Water Systems*. D. M. Anderson & P. J. Williams, Eds. Technical Council on Cold Regions Engineering Monograph, American Society of Civil Engineers, New York, pp. 77-84.
- Capps, S. R. (1915) An ancient volcanic eruption in the upper Yukon Basin. U.S. Geological Survey Professional Paper #95, pp. 59-64.
- Dionne, J. C. (1978) Formes et phénomènes périglaciaires en Jamésie, Québec subarctique. *Géographie Physique et Quaternaire* 32, 187-247.
- Dionne, J. C. (1984) Palses et limites méridionales du pergélisol dans l'hémisphère nord: le cas de Blanc-Sablon, Québec. *Géographie Physique et Quaternaire* 38, 165-184.
- Fries, T. and E. Bergström (1910) Några iakttagelser öfver palsar och deras förekomst i nordligaste Sverige. *Geol. Fören. Förhandl. Bd. 32, vol. 1, Stockholm*.
- Hale, M. E. (1979) How to Know the Lichens. 246 pp. Wm. C. Brown, Co., Dubuque, Iowa. 2nd Ed.
- Harlan, R. L. (1974) Dynamics of water movement in permafrost: A review. In: *Permafrost Hydrology: Proceedings of a Workshop Seminar*. Environment Canada, Ottawa, pp. 67-77.
- Harris, S. A. (1973) Studies in soil creep, Western Alberta, 1970-1972. *Arctic & Alpine Res.* 5, A171-A180.
- Harris, S. A. (1983) Comparison of the climatic and geomorphic methods of predicting permafrost distribution in Western Yukon Territory. In: *Permafrost: Fourth International Conference, Proc.*, pp. 450-455. 1524 pp. National Academy Press, Washington.
- Harris, S. A. (1988) Observations on the redistribution of moisture in the active layer and permafrost. *Proc. 5th International Permafrost Conference, Trondheim, Norway*. Tapir Press, Trondheim. 1: 364-369.
- Hughes, O. L., V. N. Rampton & N. W. Rutter (1972) Quaternary geology and geomorphology, southern and central Yukon (Northern Canada). 24th International Geological Congress, Montreal. Guidebook to Excursion All. 59 pp. McAara Ltd., Calgary.
- Kilmer, V. J. & L. T. Alexander (1949) Methods of making mechanical analyses of soils. *Soil Sci.* 68, 15-24.
- Lagarac, D. (1982) Cryogenic mounds as indicators of permafrost conditions, northern Quebec. In: *Proc. 4th Can. Permafrost Conf., N.R.C., Ottawa*, pp. 43-48.
- Napolsoni, J. P. & G. K. C. Clarke (1978) Hot water drilling in a cold glacier. *Can. J. Earth Sciences* 15, 316-321.
- Payette, S. & M. K. Seguin (1979) Les buttes minérales cryogènes dans les bosses terres de la rivière au Feuilles, Nouveau-Québec. *Géographie Physique et Quaternaire* 33, 339-358.
- Romanov, V. V. (1968) Hydrophysics of bogs. Israel Program for Scientific Translations. Cat. # 1967. 299 pp. Jerusalem.
- Seppälä, M. (1988) Palsas and related forms. In: *Advances in Periglacial Geomorphology*, M. J. Clark, Ed. J. Wiley & Sons, Toronto, pp. 247-278.
- Washburn, A. L. (1983) What is a palsa? In: *Mesoformen des reliefs im heutigen Periglazialraum*. H. Poser & E. Schunke, Eds. *Abhandl. Akad. Wiss. in Göttingen*. Vanderhoeck & Ruprecht, Göttingen, pp. 34-47.

## FROST HEAVE PREDICTIONS FOR ALASKAN SOILS

Beez Hazen<sup>1</sup>, J.F. (Derick) Nixon<sup>2</sup>, G.E. Heuer<sup>3</sup>, J.B. Caldwell<sup>3</sup>, E.L. Brudie<sup>1</sup>

<sup>1</sup> Yukon Pacific Corporation, Anchorage, Alaska, USA

<sup>2</sup> Nixon Geotech, Calgary, Alberta, Canada

<sup>3</sup> Exxon Production Research Company, Houston, Texas, USA

Results from one-dimensional frost heave tests and comparisons with predictions are given. Tests were conducted using soil from a lacustrine deposit near the Coldfoot, Alaska, area, along the proposed route of the Trans-Alaska Gas Pipeline. A new temperature control system and environmental enclosure were developed to allow tests to be conducted at very low cooling rates and temperature gradients. A new test cell was also developed to improve the quality of one-dimensional tests.

### INTRODUCTION

Yukon Pacific Corporation (YPC) and Exxon Production Research Company (EPR) formed a Joint Industry Project in 1991 to collaborate on frost heave laboratory testing and data analysis. Both companies were interested in developing test procedures and data necessary for frost heave predictions of large-diameter (≈1 meter) chilled pipelines.

Several objectives were defined for the joint project:

- test at thermal conditions closer to field conditions than typically obtained by other investigators. Use boundary temperatures closer to freezing (0 °C) and lower boundary temperature ramp rates (e.g., -0.02 °C/day) to get lower temperature gradients, cooling rates, and freezing rates.
- study one soil type in detail to understand the relationship between heave rate and thermal parameters such as temperature gradient, cooling rate and freezing rate.
- compare different testing methods to ensure that test results are independent of test method and to select the best method for production testing.
- improve data quality by improving control of thermal boundary conditions and test cell design.

### TESTING APPARATUS

#### One-Dimensional Test Cells

Two types of test cells were used. Most tests were conducted in conventional frost heave test cells as shown in Myrick (1982). EBA Engineering supplied three such cells, developed for the proposed Northwest Alaskan Pipeline Project. Figure 1 shows a new test cell developed by EPR and YPC which was introduced at the end of the testing program. It was designed to operate as a table-top unit, not requiring a cold room. Additional performance requirements for the new cell included minimizing radial thermal gradients (relative to a conventional cell operated in a cold room), limited use of metal fasteners to avoid extraneous thermal influences, improved coolant flow pattern in end-plates to provide uniform end temperatures, and improved modularity, serviceability and durability.

#### End Plate Temperature Control

It is common practice for the temperature of the top and bottom of the soil sample to be controlled by pumping a coolant supplied by a controlled-temperature refrigerated bath through

channels in both end-plates of the test cell. In most cases, influences such as bath temperature stability, environmental temperature fluctuations, and system thermal time constants frustrate efforts to maintain tight tolerances on end-plate temperatures. Thermal noise in the end-plates and the environment propagates into the soil which complicates data analyses.

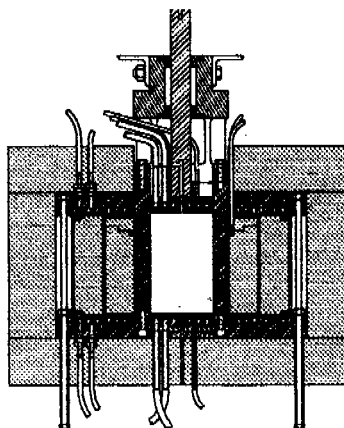


Figure 1 - EPR / YPC Test Cell

After attempts to modify conventional test equipment failed to produce good end-plate temperature stability, an active-control system was developed from a concept offered by Mr. Wilson Lamb, EPR, called an IFTCS (in-line feedback temperature control system). The concept was simple: 1) send coolant to the IFTCS colder than it should be when it arrives at a given reference location, such as the warm plate; and 2) heat the coolant while it is en route so it arrives at the temperature required. This strategy was used because it was possible to control the amount of heating very accurately.

The IFTCS is shown schematically in Figure 2. The warm and cold end-plates operated as independent systems with separate baths, pumps, and IFTCS. Each IFTCS had two Stages. Each Stage was comprised of an electric heater and downstream thermal well (or end-plate). Stage 1 performed primary temperature control, generally raising the coolant temperature to within approximately -0.05 °C, ± 0.005 °C, of the setpoint of the end-plate; Stage 2 raised the coolant to within ±0.002 °C of the prescribed test conditions. A Digilink 4C Plus SCADA (Supervisory Control and Data Acquisition) system manufactured by Kaye Instruments was used to control the IFTCS.

PID control logic (proportional, integral, derivative) was used to regulate IFTCS heaters.

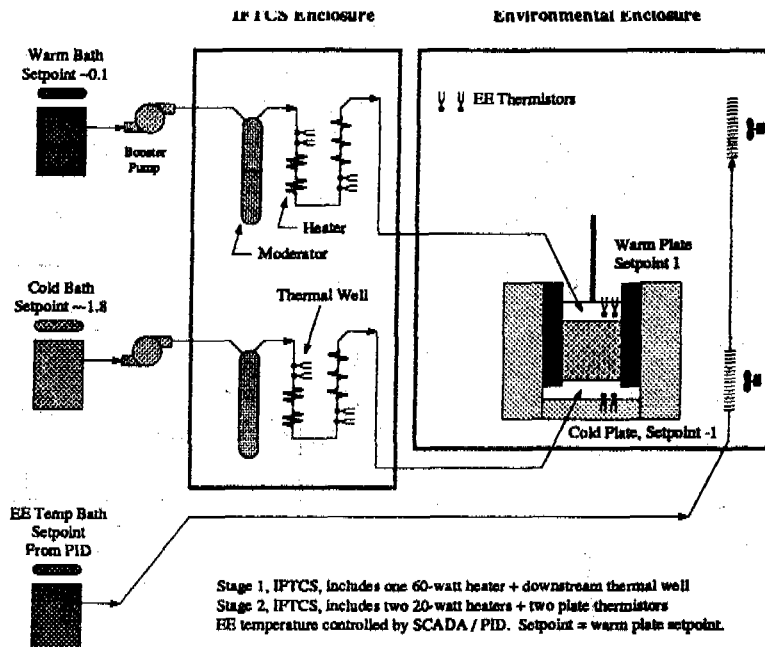


Figure 2 - Schematic of Testing Apparatus

The PID circuit was programmed to slowly raise or lower heater output depending upon the (instantaneous) average temperature of two thermistor sensors located downstream of the heater. The performance of the IFTCS / PID system was very good, yielding a standard deviation of the difference between actual and setpoint of approximately 0.0005 °C. A PC computer was used to monitor the SCADA system and record test data.

NESLAB RTE-110D circulation baths, manufactured by NESLAB Instruments, Portsmouth, New Hampshire, were used for the project. These baths consistently maintained a stability of  $\pm 0.015$  °C near 0 °C and were easy to control with the SCADA system. Time-slice proportional controllers for IFTCS heaters and voltage controllers for NESLAB baths were manufactured by Oven Industries, Mechanicsburg, Pennsylvania.

#### Testing Environment

Early tests were conducted by submerging the test cell and load frame in a circulating ice water bath. This technique relied upon the latent heat of the ice to maintain a stable environmental temperature ( $\pm 0.1$  °C) around the test cell. This technique was superseded by a PID-controlled air cooling system for the last two tests. The air cooling system allowed easier test cell setup (no bags to wrap the test cell and load frame), better visibility of the test cell during testing, and a far lower chance of moisture contamination of instruments. The stability of the air temperature in the environmental enclosures was approximately  $\pm 0.05$  °C. This enclosure and IFTCS is depicted in Figure 2.

#### Loading System

Most samples were tested with an overburden stress of 50 kPa. Loads were attained using a combination hydraulic and dead load system developed by EBA Engineering. The system used an approximately 8.3 cm diameter Bellofram cylinder/piston mounted above the test cell and a 5.1 cm diameter cylinder/piston mounted in a load frame located on the floor outside of the environmental enclosure. The two cylinders were connected with a small diameter hydraulic line. The difference in piston diameters served as a load

multiplier: a 25 kg dead load applied to the 5.1 cm piston caused the 8.3 cm piston to exert a 66 kg load on the top cap. Loads were monitored with an in-line strain-gauge load cell which was read by the SCADA system.

#### Displacement Measurement

Displacement of the top cap was measured by a Mitutoyo model 3058-01 dial gauge and by a Sensotec model MDLC-1000 LVDT (linear voltage displacement transducer). Output of the LVDT was read by the SCADA system.

#### Water Supply System

Samples were given free access to distilled water during tests. A burette configured as a Mariotte's bottle was used to provide a constant head of 10 cm of water on the top of the soil sample. The height of the bottle was adjusted daily to match the frost heave of the soil sample.

#### Calibrations

All thermistor sensors were calibrated before each test at 0 °C using a guarded and stirred distilled ice / distilled water bath. A slow-actuation mechanical stirring system was used to agitate the ice-water bath. This apparatus was placed in the 0 °C air-cooled environmental enclosure during sensor calibrations. LVDT instruments were calibrated with a micrometer. Load cells were calibrated with a dead-load hanger system.

#### CONTROL SOIL

All tests used a homogenized sample of a lacustrine deposit excavated near Coldfoot, Alaska. Grain-size data are presented in Figure 3. Unfrozen moisture content data measured using TDR, Smith (1992), are shown in Figure 4.

#### TEST MATRIX

Eleven tests were conducted. Most tests had multiple test segments where boundary temperatures and/or loads were changed (see Table 1).



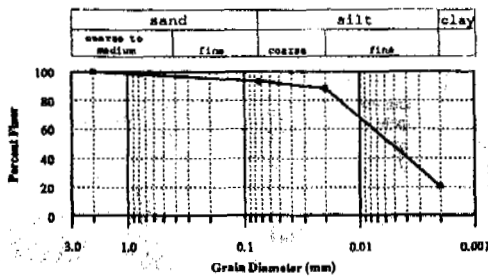


Figure 3 - Grain Size Distribution

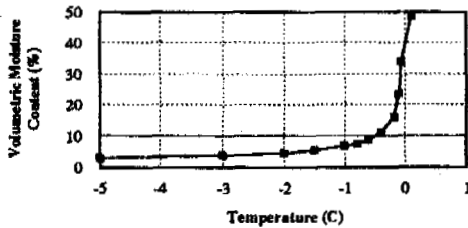


Figure 4 - TDR Unfrozen Moisture Content

Tests 1, 2, 5, 6 and the first segment of test 7 were constant-end temperature tests. Test 3, and most segments of test 7 were ramped-end temperature tests. Test 4 was an insulated warm end (IWE) test. The insulation was used to cause the frost front to move closer to the warm end during the test, thereby decreasing the unfrozen sample length and suction.

Table 1 - Test Matrix

Test	Stress (kPa)	Boundary Temperatures
1	50	+1/-1 -> +0.6/-1 -> +0.2/-1
2	50	+0.6/-1 -> +0.2 /-1
4	50	+1/-1 (IWE)
5	50	+1/-1 -> +0.2/-1 -> +0.05/-1 -> +0.01/-1 -> +0.002 /-1
6a	50	+1/-0.6 (remolded)
6b	50	+1/-0.6 (refrozen)
6c	50	+1/-0.6 (refrozen)
6d	100	+1/-0.6 (refrozen)
6e	180	+1/-0.6 -> +1/-1 (refrozen)
3	50	-0.1 °C/day -> -0.02 °C/day -> -0.01 °C/day
7	50,100,200	+1/-0.6 -> -0.02 °C/day

note: the symbol -> indicates a change to another test segment.

#### OBSERVATIONS

Typical test plots are shown in Figures 5 to 8. Figure 5 shows heave and frost-penetration over time. Frost penetration is based upon the location of the -0.15 °C isotherm as calculated from thermistor sensors located on 0.6 to 1.2 cm

intervals along the sidewalls of the test cells. This isotherm was chosen because it represents the approximate temperature that lenses formed in the sample, based upon post-test observations of lens locations.

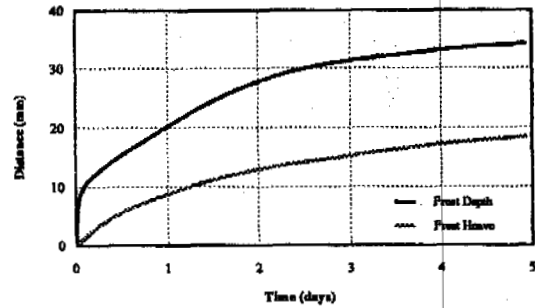


Figure 5 - Heave and Frost Penetration, Test 6a

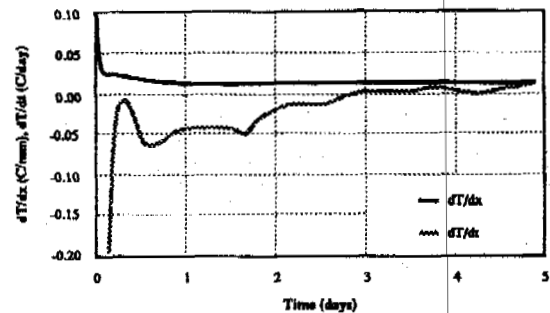


Figure 6 - dT/dx and dT/dt, Test 6a

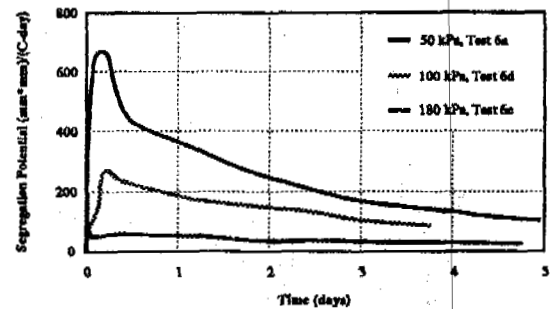


Figure 7 - SP, Tests 6a, 6d & 6e

Figure 6 shows frozen soil temperature gradients (dT/dx) and cooling rate (dT/dt) evaluated using the position of the -0.15 °C isotherm. The temperature gradient, dT/dx, was calculated from the derivative of a quadratic equation fitted through sidewall thermistor data. Cooling rate, dT/dt, was calculated from smoothed frost penetration (dx/dt) data (evaluated at the -0.15 °C isotherm), heave rate (dh/dt) and dT/dx data using

$$dT/dt = dT/dx * (dh/dt - dx/dt). \quad (1)$$

Figure 7 shows the segregation potential, SP, over time. SP, developed by Konrad and Morgenstern (1982) was calculated using

$$SP = dh/dt / (1.09 * \text{grad } T). \quad (2)$$

Figure 8 shows suction over time calculated from

$$\text{Suction} = (dh/dt * L_t / k_h) * kPa/cm. \quad (3)$$

Where  $dh/dt$  = heave rate;  $k_h$  = unfrozen soil hydraulic conductivity measured before each test (cm/hr);  $L_t$  = thawed length given in cm; and  $kPa/cm$  is a conversion factor.

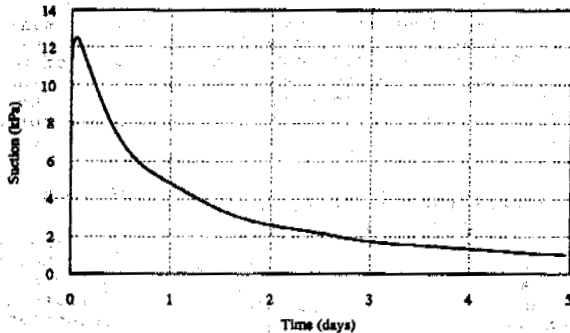


Figure 8 - Suction, Test 6a

#### Repeatability

Repeatability between tests was very good. Tests 6a, 6b and 6c, all conducted with the same soil sample in the same test cell and with the same boundary conditions produced SP values of 273, 295 and 310  $mm^2/(^{\circ}C\text{-day})$ , respectively. Frost heave comparisons between these tests are shown in Figure 9. The constant end-plate temperature segment of Test 7, with the same plate temperatures and overburden stress as 6a, 6b and 6c, produced an SP of 315.

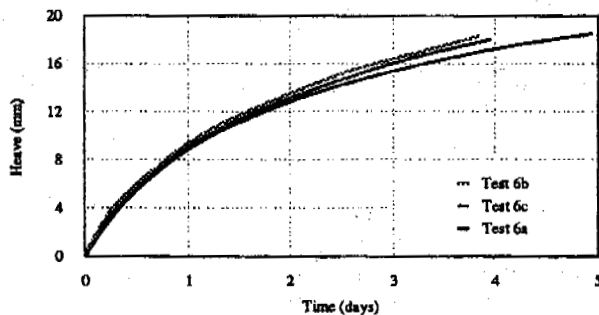


Figure 9 - Heave, Remolded & Refrozen 50 kPa Tests

#### Effect of Refreezing

Measurements by Konrad (1989) on Calgary silty clay showed that repeat freezing of soil samples caused a corresponding decrease in the SP of the soil. Similar results were not obtained with the Coldfoot sample. Three tests were conducted. Test 6a used a remolded sample; Test 6b used the same soil as Test 6a after it had been frozen completely (frozen from the bottom up after the heave test, maximum soil temperature  $-1^{\circ}C$ ), thawed, reconsolidated and rebounded. The soil sample was not otherwise disturbed between tests. Test 6c used the same soil sample as 6b (hence 6a). Between 6b and 6c the sample was again frozen, thawed, reconsolidated and rebounded. Heave over time data are shown in Figure 9. Unfrozen soil hydraulic conductivity tests were conducted between each test segment after re-consolidation and rebound.

#### Effect of Pressure

Frost heave in the Coldfoot sample was influenced by overburden pressure. Figure 10 shows heave over time for Tests 6b, 6d, and 6e, conducted at pressures of 50, 100 and 180 kPa, respectively. The values of SP extracted from these tests are shown in Table 2. The time and SP values shown in Table 2 for Tests 6a, 6b and 6c represent an arithmetic average of values calculated for individual tests.

Table 2 - SP Interpreted at Different Pressures

Test	Stress (kPa)	Time (days)	SP ( $mm^2/(^{\circ}C\text{-day})$ )
6a, 6b, 6c	50	1.7	290
6d	100	1.7	155
6e	180	2.3	35

Two techniques were used to extract values of SP from a test. One technique was based upon cooling rate ( $dT/dt$ ) and the other on the natural transition during a test between segregational freezing and net heat flux controlled freezing. SP values in Table 2 were derived using the cooling-rate technique.

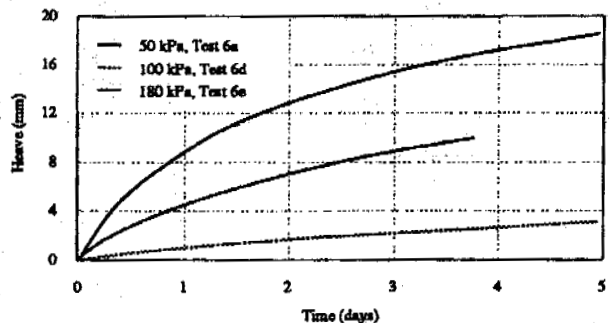


Figure 10 - Heave for 50, 100 & 180 kPa

In the cooling-rate technique, measurements of the height and thickness of the final ice lens (after the sample is cut longitudinally to expose the interior ice-lens profile) and heave over time data are used to identify the time when the final ice lens began to form; this time is used to select values of SP and the corresponding cooling rate.

In the net-heat flux / segregational freezing break-over technique a value of SP is taken from a plot of SP versus  $dx_u/dt$ , the frost-penetration rate into unfrozen soil. The break-over technique is designed to find the SP when the sample transcends from segregational freezing to net-heat flux controlled freezing. In calculation of frost heave using SP, SP only applies until the final ice-lens begins to grow; subsequently, water migration is controlled by a balance of heat and mass transfer.

The break-over technique is attractive because it is relatively easy to pick a value of SP from the SP versus  $dx_u/dt$  plot. But from the few tests in this program, it is not clear if the break-over time is consistent with the physical evidence of the tests such as the location of lenses and time when the final ice lens begins to grow (i.e., the break-over appears to occur too early, when lenses were still forming). Future tests are proposed to be simpler and are expected to increase

confidence in this technique. Values of SP reported herein rely upon the cooling-rate technique,  $dT/dt = -0.01$  °C/day, because it seems to be more consistent with physical observations.

#### Effect of Type of Test

Two primary types of tests were conducted in the current Series: constant end-plate temperature tests (also referred to as quick-freeze and step tests) and ramped end-plate temperature tests. Comparisons between the two types of tests were needed to see if test results were independent of test method and to help choose the best method for production testing. Constant end-plate tests are generally short duration, lasting 4 to 6 days. Ramped end-plate tests are considerably longer, lasting up to 30 days.

One test, #7, was conducted initially as a constant end-plate temperature test, then was continued as a ramped end-plate test. It was postulated that if step tests and ramp tests produced equivalent information, an equation fitted with data from a step test should reasonably predict a ramp test and visa versa. To evaluate test data an equation was fitted to  $dT/dx$  and overburden stress data using the multi-variate, nonlinear NONLINWOOD code (Daniel & Wood, 1980). To compare the step and ramp segments of test 7, the same general equation was fitted to different segments of the test. First an equation was fitted to the all segments of the test (step, ramp, multiple gradients and multiple loads). Next the same equation was re-fitted to the step segment of the test and finally the equation was fitted to the ramp segments of the test. The general form of the equation was

$$dh/dt = a + b*dT/dx + c*dT/dx^d - e*stress^f \quad (4)$$

Goodness-of-fit comparisons between measured and predicted heave varied considerably. Where data from the ramp and step segments were used (0.5 to 16 days), comparisons are generally good. Parameters fit to the step-portion of the test did not closely predict the ramp portion: the predicted heave rate was approximately twice as high as measured data. Similarly, parameters fit to the ramp segment did not closely predict the step segment.

The underlying assumption in these comparisons was that test 7 was still forming ice lenses (in segregational freezing mode as opposed to net-heat flux controlled mode) during the ramp segment of the test -- DILT simulations (see Modeling below) suggest it was, but there was no physical evidence. Data from test 7 do not provide clear evidence that step tests and ramp tests produce equivalent results. If test 7 had been a simpler test (i.e., one load, one gradient, such as defined for future tests) a more definitive comparison would have been possible.

#### Cyclical Values of SP for Slow Ramp Rates

Konrad (1988) reported results of freezing tests conducted at the Canadian National Research Council and compared his results to slow ramped end-plate tests reported by Penner (1986). Tests were conducted on a silty clay soil, 2% clay size, referred to as "Soil Mix 1". Penner's test #3 was a ramp test, at a rate of  $-0.02$  °C/day, the same as YPC/EPR test 7. Penner observed a near constant frost penetration and heave rate, similar to that observed in test 7. At this very slow ramp rate, values of SP showed cyclical behavior, ranging between approximately 70 and 105 mm<sup>2</sup>/(°C-day), with a period of approximately 3 days. Results for the Coldfoot sample do not show this cyclical behavior. It is possible, however, that test 7 was building a final ice lens during most of the ramp segments of the test; consequent-

ly, ice-lens formation would be governed by heat-flux, not by segregational freezing so cyclical behavior would not be expected.

#### Characteristic Frost Heave Surface

The SP theory (Konrad, 1984) posits the existence of a unique relationship between SP, rate of cooling and suction for a given soil. This is referred to as the Characteristic Frost Heave Surface. Konrad's frost heave tests on Devon silt were done with zero applied load. Tests were generally done at 50 kPa, which is a load of more interest to predictions for large-diameter chilled-pipelines. At this stress level, the postulated characteristic unique frost heave surface does not appear to exist for the Coldfoot sample.

#### MODELING

Comparisons between measured and predicted frost heave, frost penetration and ice lens patterns were made to gain insight to the mechanics of frost heave and to improve selections of appropriate boundary conditions for future testing programs. Predictions were made using a computer model based upon the Discrete Ice Lens Theory (DILT), Nixon (1991).

#### Model Input Parameters

Several parameters were needed for the DILT model. Most of them were conventional, such as soil density and thermal conductivity, but the DILT model also needed a relationship between unfrozen moisture content and temperature in frozen soil, and a relationship between hydraulic conductivity and temperature in frozen soil.

Calculation of unfrozen moisture content data used the standard relationship

$$W_u = (a/w_{tot}) * (-T)^b \quad (5)$$

$W_u$  = fraction of total water content remaining unfrozen at temperature T

$a = 0.052$ , unfrozen moisture content at  $-1$  °C (from TDR, dim.)

$T$  = freezing temperature (°C)

$b = -0.503$ , a constant (from TDR, dim.)

$w_{tot}$  = total moisture content (dim.)

Calculation of hydraulic conductivity in frozen soil used the relationship

$$K_{hf} = K_o / (-T)^\alpha \quad (6)$$

$K_{hf}$  = frozen soil hydraulic conductivity (cm/sec)

$K_o$  = hydraulic conductivity at  $-1$  °C (cm/sec)

$T$  = freezing temperature (°C)

$\alpha$  = dimensionless constant

Few published data are available for values of  $K_o$  and  $\alpha$  and no standard test has been widely used. Nixon (1991) proposed a technique for extracting  $K_o$  and  $\alpha$  values using results from three frost heave tests, each conducted at different pressures. Using data from tests 6a (at 50 kPa), 6d (at 100 kPa) and 6e (at 180 kPa), Nixon derived values of  $\alpha = 1.848$  and  $K_o = 6.6 \cdot 10^{-11}$  for the Coldfoot sample.

Other miscellaneous soil properties used for simulations included

unfrozen soil hydraulic conductivity  $1.2 \times 10^{-6}$  (cm/sec), but varied for each test  
 soil porosity = 0.491  
 soil dry density = 1.427 gm/cc  
 soil saturation = 100%  
 soil separation pressure (DILT parameter) = 25 kPa.  
 soil specific gravity = 2.803  
 measured unfrozen soil thermal conductivity = 1.39 W/m-°C; frozen = 2.55 W/m-°C.

#### Comparisons with Measurements

Comparisons between measured and predicted frost penetration and frost heave are shown in Table 3 below. In general, predictions show good agreement with measured values.

Table 3 - Comparisons Between Measured and Predicted Frost Depth and Frost Heave, End of Test

Test	Overburden Stress (kPa)	Frost Depth (mm)		Frost Heave (mm)	
		Meas.	DILT	Meas.	DILT
6a	50	44	43	19	27
6d	100	40	41	11	13
6e	180	39	41	3	7

#### CONCLUSIONS

A new temperature control system, called an In-line Feedback Temperature Control System, was developed for frost heave testing. This active temperature control system consistently produced stable end-plate temperatures and was capable of ramp rates as low as 0.004 °C/day.

A new frost heave test cell was also developed. This cell was designed to operate as a laboratory "table top" unit, not requiring a cold room. It was further designed to have lower radial temperature gradients than conventional cells in cold rooms, even when operating on a table top.

Data have been published for Calgary silty clay showing that repeated freezing of soils causes a reduction in heave in each successive refreeze. Data collected during this program do not show this behavior.

It was not resolved whether ramped end-plate and constant end-plate temperature tests produce equivalent information. Data from test 7, a combination step and ramp test, suggest the test methods do not produce equivalent information, but it is not clear if the test was in segregation mode during the ramp segments of the test.

Comparisons between measured and predicted frost heave and frost penetration show good agreement. Predictions were made using a model based upon the Discrete Ice Lens Theory. This finding shows that the technique proposed by Nixon to extract frozen-soil hydraulic conductivity data from frost heave tests produces reasonable values and it shows the DILT model can be used to give considerable insight into the mechanics of frost heave.

Eleven tests were conducted by YPC and EPR using a homogenized soil sample. Many of these tests had multiple segments, e.g., beginning with

an initial warm plate temperature of +1 °C, then to +0.6 °C after a few days, etc. In some cases the duration of these segments was not long enough to form a final ice lens for the segment. This complicated analyses of test data and lessened the value of post-test observations of ice lens patterns and thicknesses. It is generally considered that segregation frost heave (at very low cooling rates, just before final ice formation) is the dominant mode of frost heave relevant in the analysis of chilled pipelines. It is, therefore, particularly important for laboratory test data to clearly show a transition between segregation heaving, before final ice lens formation, and heat-flux controlled heaving. Future lab tests will be proceeded with bounding simulations using the DILT model to look closely at proposed boundary conditions before and during laboratory tests.

#### ACKNOWLEDGMENTS

The work reported herein was funded by a joint industry project between Yukon Pacific Corporation and Exxon Production Research Company. The support of Mr. P. DeMay, Mr. J. Swanson and Mr. M. Metz with Yukon Pacific, Mr. K. Croasdale with Esso Resources Canada Limited, and Mr. R. Haring and Mr. W. Lamb with Exxon Production Research is gratefully acknowledged. Contributions by Dr. J.-M. Konrad to our testing effort have been greatly appreciated. The authors also gratefully acknowledge the tireless work of Mr. C. Pelz and Mr. K. Schacht in development of apparatus prototypes and the experience and dedication of EBA Engineering, particularly Mr. R. Caron, in laboratory testing.

#### REFERENCES

- Daniel, C and Wood, F.S., 1980. Fitting Equations to Data, John Wiley & Sons, Inc., ISBN 0-471-05370-8.
- Holden, J., Piper, D., and Jones, R., 1985. Some Developments of a Rigid-ice Model of Permafrost Heave. Proceedings, 4th International Symposium on Ground Freezing, Sapporo, Japan, pages 93-99.
- Konrad, J.M. and Morgenstern, N.R., 1983. Frost Susceptibility of Soils in Terms of Their Segregation Potential, Proceedings, Fourth International Conference on Permafrost, Fairbanks, Alaska.
- Konrad, J.M. and Morgenstern, N.R., 1984. Frost Heave Prediction of Chilled Pipelines Buried in Unfrozen Soils, Canadian Geotechnical Journal, Vol. 21: 100-115.
- Konrad, J.M., 1988. Influence of Freezing Mode on Frost Heave Characteristics, Cold Regions Science and Technology, 15 (1988): 161-175.
- Myrick, J.E., Isaacs, R.M., Liu, C.Y. and Luce, R.G., 1982. The Frost Heave Program of the Alaskan Natural Gas Transportation System. Proceedings of the ASME Conference on Offshore Mechanics and Arctic Engineering, Phoenix, Arizona.
- Nixon, J.F., 1989. Ground Freezing and Frost Heave -- A Review. The Northern Engineer, Vol. 19, No. 3 & 4, pages 8 - 18.
- Nixon, J.F., 1991. Discrete Ice Lens Theory for Frost Heave in Soils, Canadian Geotechnical Journal, 28 Mo. 6, pages 843 - 859.
- Penner, E., 1986. Aspects of Ice Lens Growth in Soils. Cold Regions Science and Technology, 13 (1): 91-100.
- Smith, M.W., 1992. TDR Results for Coldfoot Control Soil for YPC and EPR.

## DYNAMIC ELASTIC MODULUS AND STRENGTH OF SATURATED FROZEN SILT

He Ping, Zhu Yuanlin, Zhang Jiayi Shen Zhongyan and Yu Qihao

State Key Laboratory of Frozen Soil Engineering, Lanzhou Institute of  
Glaciology & Geocryology, Chinese Academy of Sciences, China

A series of vibration tests were conducted on saturated frozen silt at constant dynamic loading parameters (maximum stress, minimum stress and frequency) and constant temperature. The test results indicated that dynamic elastic modulus decreases with increasing strain and increases with increasing frequency and descending temperature. The influence of maximum stress on dynamic elastic modulus is negligible. The strength increases with the descending frequency. The influence of frequency on strength depends on the inherent frequency of frozen soil. The influence of minimum stress on the strength is negligible. The regression equations of dynamic elastic modulus and dynamic strength depending on various factors are presented.

### INTRODUCTION

The research on dynamic elastic modulus and dynamic strength is an important content of the mechanics of frozen soil. Vinson (1983) had initially done the work and pointed out that dynamic elastic modulus increases with descending temperature, increasing frequency and decreasing strain amplitude. In order to further study the basic law of dynamics of frozen soil, a series of uniaxial compressive dynamic tests were conducted on saturated frozen silt (Lanzhou loess) at constant dynamic loading parameters (maximum stress, minimum stress and frequency) and constant temperatures. The test temperature were  $-10^{\circ}\text{C}$ ,  $-5^{\circ}\text{C}$  and  $-2^{\circ}\text{C}$ . The test frequencies were 5Hz, 1Hz and 0.1Hz, respectively.

### TEST METHOD

The test specimens were made of silt (Lanzhou loess). The specimens with a dry density of  $1.47 \text{ g/cm}^3$  and a water content of 27% were 6.18 cm in diameter and 15 cm long. Before loaded, the specimens were at a constant temperature for 24 hours. Loading and collecting data were automatically done by means of a series of devices made by MTS Company. Figure 1 shows the variation of dynamic stress with strain (test conditions:  $T=-5^{\circ}\text{C}$ ,  $f=5\text{Hz}$ ,  $\sigma_{\min}=0.272 \text{ MPa}$ , and  $\sigma_{\max}=1.786 \text{ MPa}$ ).

In a cycle of vibration the dynamic elastic modulus is calculated by

$$E = \frac{\sigma_2 - \sigma_1}{\epsilon_2 - \epsilon_1}$$

where  $\epsilon_2$  and  $\epsilon_1$  are the maximum and minimum strains during the unloading process in a cycle of vibration, and  $\sigma_2$  and  $\sigma_1$  are the stresses in MPa corresponding to  $\epsilon_2$  and  $\epsilon_1$  (see Fig.2).

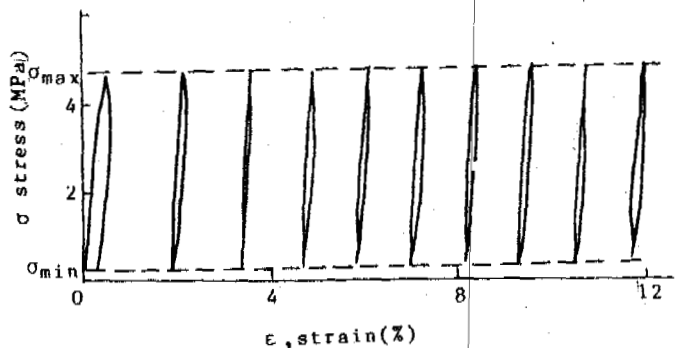


Figure 1. Dynamic stress vs. strain

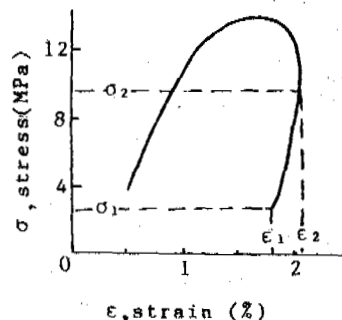


Figure 2. Dynamic stress vs. strain in a cycle of vibration

**RESULTS AND DISCUSSION**

**Dynamic Elastic Modulus**

Based on a large number of tests, the influence of various factors on dynamic elastic modulus is analyzed as follows.

**Influence of maximum stress**

Figure 3 and Figure 4 show that the influence of maximum stress on dynamic elastic modulus is negligible in the condition that the minimum stress is close to zero.

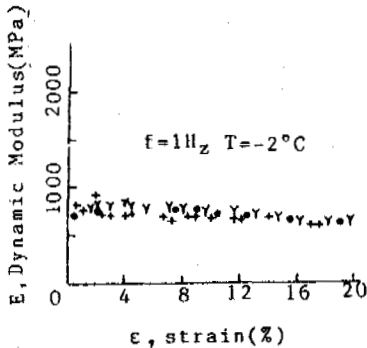


Figure 3. Dynamic elastic modulus vs. strain under different maximum stress

- — 0.088-0.679 MPa
- Y — 0.107-0.984
- + — 0.051-1.259

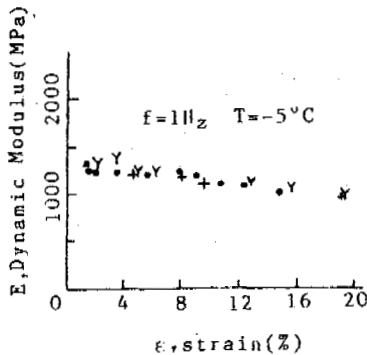


Figure 4. Dynamic elastic modulus vs. strain under different maximum stress

- — 0.076-2.218 MPa
- Y — 0.145-4.711
- + — 0.157-6.100

**Influence of strain**

The relationship between dynamic elastic modulus and strain is shown in Figure 5. It is noted that dynamic elastic modulus decreases linearly with increasing strain. The decrease ratio depends on the temperature of frozen soil. The lower the temperature is, the greater the decrease ratio is (see Fig.8 and Fig.9).

**Influence of frequency**

Figure 6 shows the dynamic elastic modulus increases logarithmically with increasing frequency.

**Influence of temperature**

Dynamic elastic modulus increases with descending temperature. The increase ratio is from

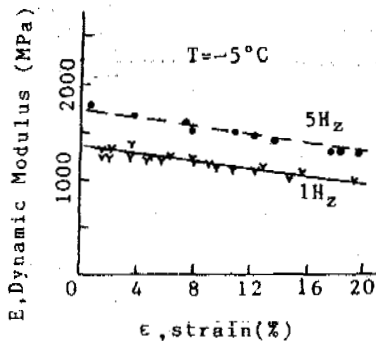


Figure 5. Dynamic elastic modulus vs. strain

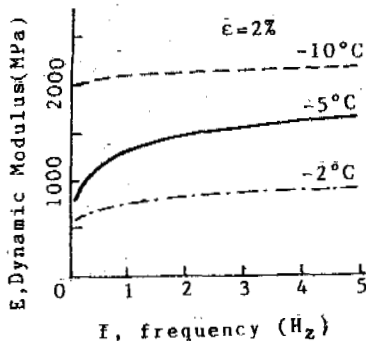


Figure 6. Dynamic elastic modulus vs. frequency

quick to slow in the state of high frequency (5Hz) and from slow to quick in the state of low frequency (0.1Hz) (see Fig.7).

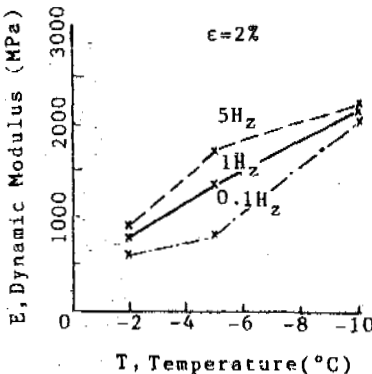


Figure 7. Dynamic elastic modulus vs. temperature

**Regression equation**

The regression equation was put forward by analyzed test data as follows:

$$E = A + B \cdot \ln(f) + C \cdot \epsilon \tag{1}$$

where, E is dynamic elastic modulus (MPa), f is frequency (Hz), ε is strain (%), and A, B and C are parameters depending on temperature (see Table 1).

Figure 8, Figure 9 and Figure 10 show that the values calculated by equation (1) (expressed in terms of lines) coincide with the test values (expressed in terms of symbols) very well.

Table 1. Parameter values in equation (1)

Temperature (°C)	A	B	C	Mean square deviation	Regression coefficient
-10	2201.1	45.266	-47.266	84	0.965
-5	1359.9	229.212	-22.101	46	0.980
-2	781.0	80.865	-8.292	58	0.89

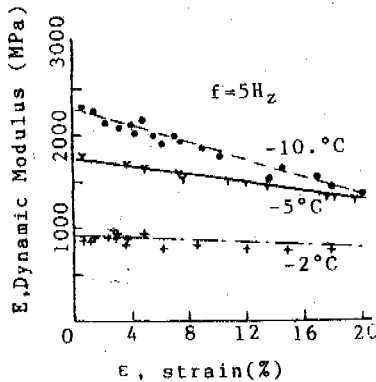


Figure 8. Dynamic elastic modulus vs. strain

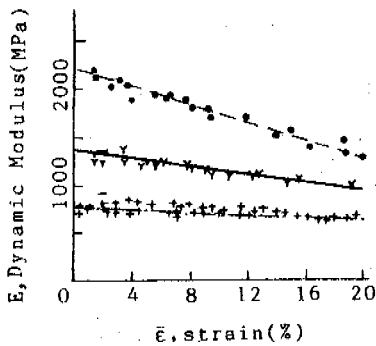


Figure 9. Dynamic elastic modulus vs. strain

f=1Hz  
 -10°C=---(•)  
 -5°C=---(γ)  
 -2°C=---(+)

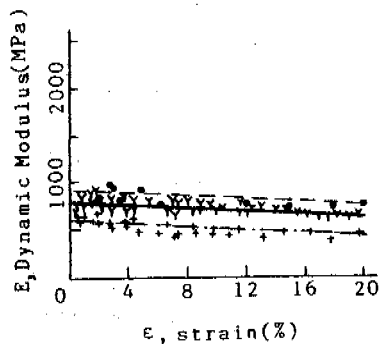


Figure 10. Dynamic elastic modulus vs. strain

T=-2°C  
 5Hz=---(•)  
 1Hz=---(γ)  
 0.1Hz=---(+)

Dynamic Strength

Because of the creep property of frozen soil, a constant dynamic load (constant maximum stress, constant minimum stress and constant frequency) may also cause the failure of frozen soil. It is considered that the creep failure occurs when the creep rate reaches its minimum value. The time to the minimum rate is defined, as the failure time ( $t_f$ ). The maximum stress is the creep failure strength ( $\sigma_f$ ). The influences of various factors on failure strength are analyzed as follows.

Influence of minimum stress

A large number of test results show that the influence of minimum stress on frozen soil failure is slight (see Fig.11), therefore the influence is negligible.

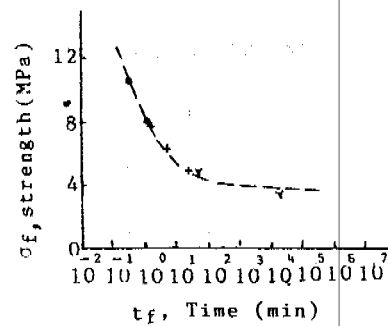


Figure 11. Strength vs. failure time

f=1Hz T=-10°C  
 $\sigma_{min} < 0.2MPa$  (+)  
 $1MPa < \sigma_{min} < 3MPa$  (γ)  
 $\sigma_{min} > 3MPa$  (•)

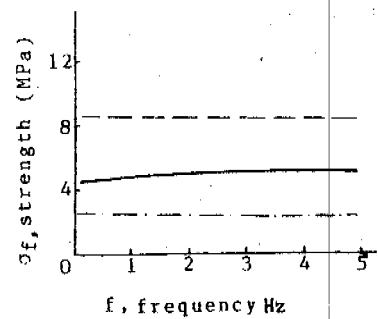


Figure 12. Strength vs. frequency

t = 1 MPa  
 -10°C = ---  
 -5°C = ---  
 -2°C = ---

Influence of frequency

According to the resonant theory, when dynamic frequency is equal to the inherent frequency of the specimen, the resonance happens, so that the specimen is broken very easily. The property of resonance can be reflected in the curve of relationship between strength and frequency, that is, the strength corresponding to the frequency defined as resonant frequency is minimum. Fig.12 shows that in the frequency of 2.9Hz the strength is at a minimum when the temperature of the

specimen is  $-2^{\circ}\text{C}$ . Because of a few number of frequencies (5Hz, 1Hz and 0.1Hz), resonant property is not reflected in the curves of  $-5^{\circ}\text{C}$  and  $-10^{\circ}\text{C}$ .

Influence of temperature

Figure 13 shows that the strength increases with descending temperature in different frequency.

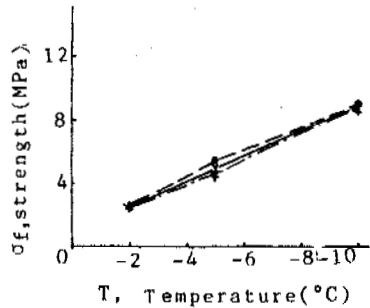


Figure 13. Strength vs. temperature  
 $t=1$  MPa  
 0.1Hz ----  
 1Hz ———  
 5Hz - - - -

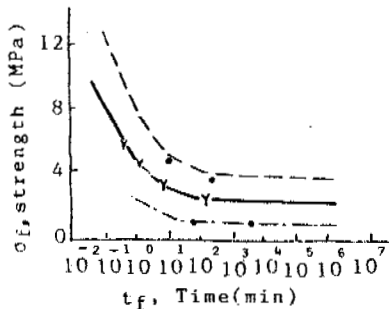


Figure 14. Strength vs. failure time ( $f=5\text{Hz}$ )  
 $f=5\text{Hz}$   
 $-10^{\circ}\text{C}$  ---- (•)  
 $-5^{\circ}\text{C}$  ——— (Υ)  
 $-2^{\circ}\text{C}$  - - - - (+)

Regression equation

A large number of test data were analyzed. The relationships between creep strength and failure time, temperature and frequency are given by

$$\sigma_f = A + B \cdot f + C \cdot f^2 + D \cdot \ln\left(1 + \frac{1}{\sqrt{t_f}}\right) \quad (2)$$

where  $t_f$  is failure time (min),  $f$  is frequency (Hz),  $\sigma_f$  is creep strength (MPa), and A, B, C and D are parameters depending on Temperature (see Table 2).

Figure 14, Figure 15 and Figure 16 show the values calculated by equation (2) (expressed in the terms of curves) coincide with the test values (expressed in the terms of symbols) very well.

Table 2. Parameters values in equation (2)

Temperature( $^{\circ}\text{C}$ )	A	B	C	D	Mean square deviation	Regression coefficient
-2	0.709	-0.187	0.032	2.740	0.119	0.937
-5	1.331	0.329	-0.040	4.626	0.308	0.984
-10	3.770	-0.112	0.010	6.985	0.239	0.994

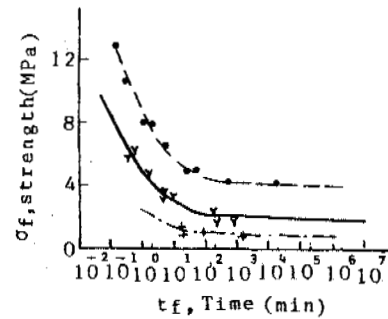


Figure 15. Strength vs. failure time  
 $f=1\text{Hz}$   
 $-10^{\circ}\text{C}$  ---- (•)  
 $-5^{\circ}\text{C}$  ——— (Υ)  
 $-2^{\circ}\text{C}$  - - - - (+)

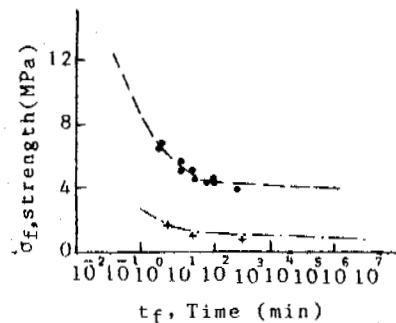


Figure 16. Strength vs. failure time  
 $f=.1\text{Hz}$   
 $-10^{\circ}\text{C}$  ---- (•)  
 $-2^{\circ}\text{C}$  - - - - (+)

CONCLUSIONS

- It can be concluded from this study that:
1. Dynamic elastic modulus increases with descending temperature and increasing frequency, and decreases with increasing strain. The influence of maximum stress on dynamic elastic modulus is negligible.
  2. Equation (1) can be used to calculate the dynamic elastic modulus depending on temperature, frequency and strain.
  3. The strength increases with descending temperature. The influence of minimum stress on failure of frozen soil is negligible.
  4. The influence of dynamic frequency on the strength depends on the inherent frequency of the specimen. When dynamic frequency is equal to the inherent frequency, the strength is minimum.
  5. Equation (2) can be used to predict the creep strength.



ACKNOWLEDGEMENTS

The authors are grateful to Peng Wanwei, Miao Lina, Liu Yongzhi, Chang Xiaoxiao, Zhang Xuezheng and Hou Zhongjie for their help in this study.

REFERENCES

Vinson, T.S., (1983) Dynamic properties of silt:  
In Proceeding of the Fourth International  
Conference on Permafrost, pp.1315-1320.

## A NEW PERMAFROST AND GROUND ICE MAP FOR THE NATIONAL ATLAS OF CANADA

J. Alan Heginbottom<sup>1</sup> and Marie-Andrée Dubreuil<sup>2</sup>

<sup>1</sup>Geological Survey of Canada and <sup>2</sup>National Atlas of Canada,  
Energy, Mines and Resources Canada, Ottawa, Canada

A new map of Canada, at a scale of 1:7.5 M, illustrating the extent of permafrost and ground ice conditions, has been prepared for the fifth edition of the National Atlas of Canada. Physiographic units are used as the basic framework for compilation of the geocryological data. The map shows the estimated extent of permafrost, in five classes; estimated relative abundance of ground ice in the upper 10-20m of the ground as percent volume, in four classes; relative abundance of ice wedges, massive ice bodies and pingos, in three classes; and, at selected localities, values of permafrost thickness and shallow permafrost temperatures. A brief description of the preparation process and a discussion of the data used in the compilation are included on the map, along with explanations of technical terms and general notes on permafrost in Canada.

### INTRODUCTION

From society's point of view, the main difficulty with permafrost is not so much the temperature of the ground, but the fact that most of the water in the ground exists as ice (Ferrians and Hobson, 1973; Heginbottom 1983). Throughout the circum-arctic countries, considerable resources and effort have been devoted, for many decades, to addressing problems of engineering and development arising from the extent and variability of ground ice within permafrost. As a further complication, society today demands a high degree of protection for the way of life of local inhabitants within permafrost regions, and for the natural environment of frontier areas. Finally, there is the threat of global climatic warming in response to anthropogenic changes to atmospheric composition. Most global climate models not only suggest a general-warming of the world's atmosphere over the next several decades, but also that such warming will first become evident in subarctic and low arctic latitudes. This warming is anticipated to lead to a warming of permafrost and a melting of much shallow ground ice which, in turn, will lead to the release into the atmosphere of large quantities of greenhouse gasses, especially methane and carbon dioxide.

This new map of permafrost and ground ice conditions in Canada is designed to contribute to the resolution of the problems associated with resource development of the permafrost region of Canada. Information is presented, for the first time, on the distribution of ground ice as well as of permafrost for the whole country, using a single legend and mapping approach.

### BACKGROUND

The compilation of this map built on experience gained from the preparation of several other maps: permafrost and ground ice maps of two small areas in the western arctic coast of Canada (Heginbottom, 1989), trial maps at a scale of 1:250,000 (Heginbottom, 1983), and a map of permafrost and ground ice conditions of northwestern Canada at a scale of 1:1 M (Heginbottom and Radburn, 1991). It is believed that this map of northwestern Canada is the first map at a 'medium' scale (1:1 M) for any part of North America to show the distribution of ground ice in a systematic manner. Previously, North American maps have shown either the distribution of specific types of ice bodies, such as pingos (Mackay, 1963) or, on a large scale map (1:24K) of the Fairbanks area, the actual distribution of individual ground ice bodies (Péwé and Bell, 1974).

The only comparable map from the former Soviet Union is a "Map of the cryological regions of the West Siberian Plain" (Baulin, ed., 1982), which shows the ice content of the ground as 'high' or 'low' in relation to the age, texture and peat cover of surficial geology map units. An inset map shows the distribution of ice wedges and three categories of ground ice for the same region. Other Russian maps show either the typical distribution of selected ground ice features, such as ice wedges or massive ice (Melnikov, 1966), or details of the cryotexture of the ground (Popov et al. 1985, 1990) but give no data on the quantity of ground ice. Recent medium scale Chinese maps (Tong et al., 1982; Shi and Mi, 1988) include little or no data on ground ice.

## PRINCIPLES OF COMPILATION

The permafrost region of Canada encompasses some 5,000,000 km<sup>2</sup>, within a country of some 10,000,000 km<sup>2</sup>. A major problem in the compilation of maps of complex natural phenomena over such large areas is variations in the level and accuracy of the source information available. In the case of permafrost, the variations relate both to disparities in the level of research effort from region to region, and to variations in the environmental and geological factors that control the distribution and attributes of permafrost.

The Mackenzie Valley and Delta and the Tuktoyaktuk Coastlands of northwestern Canada are geocryologically the best known part of the country, with research in this area dating back nearly 50 years. By contrast, the geocryology of parts of the east-central arctic, such as the Foxe Basin area and sections of the Canadian Shield, is known in only the most general way. Unlike the Mackenzie and Tuktoyaktuk regions, these areas are difficult of access, commonly have limited or poor natural exposures, and have not been of interest for resource development.

In view of the relatively small scale of the map (1:7.5 M) and the large area to be covered, the present compilation is based on a framework of physiographic units. The "Physiographic Regions of Canada" map (Bostock, 1970a) was selected as the base map for the compilation. This is the only physiographic map covering the whole of Canada at a suitable scale and level of detail, and compiled in a reasonably consistent manner. While better maps exist for parts of Canada, none are available for northern, central and eastern Canada. For our purposes, it was assumed that the variability in all geological conditions within a physiographic map unit was less than the variability between adjacent units. This assumption was modified with regard to the distribution of permafrost within some of Bostock's larger units. For instance, the Kazan Upland unit, covering northern Manitoba, northern Saskatchewan and southeastern Northwest Territories, extends from the continuous permafrost zone in the northeast to the southern limit of the sporadic discontinuous permafrost zone in the southwest. In this case, the map unit has been subdivided into the various permafrost zones; these intercalated boundaries are specified on the map as being 'gradational' in nature. The same procedure was followed for a number of other map units in the southwestern and southern parts of the Canadian Shield. Again for the purposes of the map, some units were combined, particularly in the non-permafrost region. Hence, from the original 141 units derived from Bostock's map, a final set of 171 thematic map units was created.

All pertinent and readily available data related to permafrost and ground ice distribution were assembled in a computer data base. Information on geological and environmental factors known to control the distribution of permafrost and the occurrence of ground ice was also included. The data were organised in direct relation to the physiographic map units.

This rigorous procedure highlighted a number of gaps in the source data, particularly in the case of ground ice

conditions. These information gaps were completed by using the data base as a form of expert system. Thus the ground ice conditions for a particular map unit were determined by assessing the full suite of other attributes for the unit and comparing them to adjacent units, and to other units with similar suites of attributes. This procedure constituted a rational and consistent mechanism for extrapolating from the known to the unknown and for 'predicting' permafrost and ground ice conditions in areas with limited field data.

## MAP DESIGN AND THEMATIC CONTENT

The map is a comprehensive summary of permafrost and ground ice conditions in Canada. The basic map units are each described in terms of the extent of permafrost, the quantity of ground ice, and the relative abundance of larger bodies of ground ice: pingos, ice wedges and bodies of massive ice. Note that no distinction is made between massive ice of intrasedimental origin (Mackay and Dallimore, 1992) and massive ice resulting from the burial of ice formed at the ground surface, such as buried glacier, river or icing ice. Information on permafrost thickness and ground temperatures is given for selected localities across the country. Details of the classes, colours and symbols used are given in Figure 1. This new National Atlas map has been produced almost entirely by computer mapping techniques. Exceptions are the plotting of the isotherms of mean annual ground temperature on the inset map and the placement of labels and symbols on the main map, which were done by hand.

The information on the map and the legend follows closely the format developed for the forthcoming "Circum-Arctic Map of Permafrost and Ground Ice Conditions" sponsored by the International Permafrost Association (IPA) (Brown et al., in prep.).

### Permafrost Extent

The estimated extent of permafrost in each map unit is presented in five classes, based on the percentage of the ground that is underlain by permafrost (90-100%, 50-90%, 10-50%, 0-10%, 0%). The class definitions are based on those developed for the IPA map. Areas generally free of permafrost are also indicated.

### Ground Ice

Information on the relative abundance of ground ice in each map unit is presented in the form of qualitative estimates of the percentage of ice in the upper 10-20m of the ground. The estimates are for segregation ice, injection ice and reticulate veined ice only; large identifiable ice bodies are treated separately. Four classes are used for ground ice content (>20%, 10-20%, 0-10%, 0%); their definitions are also based on those developed for the IPA map. The general distribution and relative abundance of known occurrences of the large bodies of ground ice (pingos, ice wedges and bodies of massive ice) is depicted by means of symbols. A simple, three step scale of "abundant, sparse and absent" is used.

### Ground Temperature

Values of mean annual ground temperature (MAGT) observed in the upper 15m of the ground, are shown for about 75 selected localities across northern and central Canada. These data are drawn from a more extensive data set held at the Geological Survey of Canada (Taylor et al., 1982; Young, 1985; Young and Judge, 1985, 1986). The localities selected were chosen so as to present a general picture of the distribution of ground temperatures across Canada. In cases where a number of MAGT determinations within a small area show a range of temperature conditions, this is indicated by quoting the actual range of temperature values.

In addition, isotherms of MAGT are shown on a small scale (1:30 M) inset map. The location of the data points is also indicated on the inset, but the actual temperature values are quoted only on the main map. A 5°C isotherm interval, from +5°C to -15°C, has been used, with supplementary isotherms at +2°C and -2°C. In plotting the isotherms, maps of the distribution of mean annual air temperature (Atmospheric Environment Service, 1984) were used to guide the trend of the isotherms in areas of sparse data, such as the coastal zones of Baffin Island and Labrador.

### Permafrost Thickness

The thickness of permafrost is provided for some 75 localities in northern Canada (Figure 1). These data are also drawn from a data set held at the Geological Survey of Canada (Taylor et al. 1982). The most precise data, shown by a point symbol labeled with a thickness value (in metres), are for sites where the thickness has been determined by interpolation between temperature measurements in stable, long established boreholes that penetrate through the permafrost body. Where the thickness of permafrost has been derived by downward extrapolation from a borehole that does not penetrate through the permafrost body, from a calculated equilibrium temperature profile, or from the depth of a diagnostic 'kick' on a geophysical log, the depth value appears in parentheses. At a few localities, where the data are insufficient for extrapolation or the calculation of an equilibrium temperature profile, the thickness of permafrost is indicated as being greater than the stated value. A separate symbol is used for the thickness of permafrost beneath the continental shelf of the Beaufort Sea, as this body of permafrost is a relic from the periods of low sea level that occurred during the Quaternary glacial maxima.

### Ground Temperature Profiles

Representative ground temperature profiles for eight selected sites are presented as an inset diagram. These profiles complement the point data on permafrost temperature and thickness depicted on the main and inset maps.

### Legend, Notes and Sources

The explanation of the conventions of the map, the colour scheme and the symbols are given in the map legend (Table 2). The digital base map was developed by the National Atlas Information Service, and the general design

and overall layout of the map (Figure 2) follow the standards of the National Atlas of Canada. As well, the map includes a brief description of the general nature and characteristics of permafrost and ground ice in Canada and a summary of the compilation methodology. The text provides explanations of the technical terminology used on the map, so as to make this National Atlas sheet more accessible to non-specialist users. The principle sources relied on in the compilation of the map are listed.

## REGIONAL DISTRIBUTION AND CHARACTERISTICS OF PERMAFROST AND GROUND ICE IN CANADA

The map illustrates how the regional distribution of permafrost and the nature and extent of ground ice within the permafrost region of Canada vary not only with latitude and altitude, but also in response to variations in climate, topography, bedrock geology, and surficial geology. The Quaternary history of Canada, with alternating episodes of glaciation and deglaciation, and phases of marine and lacustrine submergence and emergence of the land, also had a significant effect on the nature and distribution of both permafrost and ground ice. Seven distinct regions can be recognized from the patterns appearing on the National Atlas sheet.

The map indicates that permafrost is continuous in the Western Arctic, with temperatures between -3 and -13°C and a thickness of 100 to >600m. Ground ice is widespread and extensive, with massive-ice cored landforms common. Some ground ice is deformed, apparently by glacial thrusting, and is presumed to be pre-last-glacial in age (Rampton and Mackay, 1971). Pore and segregation ice are common, ice wedges are very common, reticulate vein ice is common and pingos are locally very common. This is the most researched area of permafrost in Canada.

In the Queen Elizabeth Islands, permafrost is continuous and very cold, with temperatures of -10 to -20°C. Thickness ranges from <300m near the coasts to >600m in the interiors of the islands. The occurrence of ground ice is highly variable with strong geological controls. Ice wedges are locally common, pingos are rare, segregated ice occurs in bedrock and massive ice is locally very significant, some of which is known to be buried surface ice, probably of Wisconsinan age (Lorrain and Demeur, 1985).

Permafrost conditions of the Eastern Arctic and Canadian Shield are not well known. Permafrost is continuous in the north, with temperatures between -2 and -12°C, and discontinuous in the south, with temperatures of 0 to -2°C. Thicknesses of 400 to 500m have been determined for localities in central Keewatin, northern Ungava and the Baffin region (Taylor et al., 1982). Ground ice occurrences are of limited extent except in peatlands; some ground ice has been reported in bedrock locally.

There are two basins within the Canadian Shield with very different geological conditions from the Shield itself. In Foxe Basin, permafrost is continuous, with a temperature of about -9°C; ground ice conditions are poorly known. In the Hudson Bay Lowlands, permafrost is discontinuous (extensive to isolated patches) and shallow, with temperatures of

**A: Extent of permafrost and ground ice content**

Extent of permafrost (% of land area underlain by permafrost)	Ground ice content in the upper 10-20 m of the ground (% by volume visible ice) Includes segregation, injection ice, reticulate ice veins, ice crystals and ice coatings on particles						
	H*	M-H	M	L-M	L	N-L	N
Continuous permafrost (>90%)	Ch very dark purple	Cmh dark purple	Cm purple	Clm light purple	Ci very light purple		
Discontinuous permafrost			Em dark blue	Elm blue	Ei light blue	Enl very light blue	
	Extensive (50-90%)			Slm green	Sl light green	Snl very light green	
Sporadic (10-50%)				IIm dark yellow	Ii yellow	Inl light yellow	In very light yellow
Isolated (0-10%)							
No permafrost (0%)							U light tan
Subsea permafrost				Olm maroon			

\* Key to ice content classes: H = high, M-H = medium to high, M = medium, L-M = low to medium, L = low, N-L = nil to low, N = nil.

**B: Ground ice bodies**

**C: Temperature and thickness of permafrost**

General distribution of known occurrences of large bodies of ground ice (Note does not include surface icings)		Mean annual ground temperature (°C)	● -7
Ice wedges (sparse, abundant)		Range of typical shallow temperatures mean annual ground (°C)	● -2 .. -4
Massive ice bodies (sparse, abundant)		Thickness of permafrost (m) (measured or interpolated, extrapolated or calculated)	■ 100 ■ (120)
Pingos (sparse, abundant)		Thickness of subsea permafrost (m)	◆ 60

Figure 1. Atlas map summary legend.

0 to -2°C. Ground ice is extensive in peatlands, occurring as ice wedges and as thick ice lenses at the base of the peat cover.

Permafrost conditions in the Mackenzie Valley and Interior Plains are relatively well known. Permafrost distribution ranges from extensive in the north to isolated patches in the south. Permafrost temperature and thickness range from 0 to -5°C and from near 0 to about 150m, respectively. Ground ice is extensive in fine grained soils and peatlands. Reticulate vein ice is common, pingos are rare in the north and absent elsewhere in the region, ice wedges occur but are generally inactive.

Within the Cordillera, permafrost conditions are particularly variable, due to the complex nature of the geology and topography of this large region. Permafrost distribution is strongly controlled by altitude. In Yukon, western Mackenzie District and northern British Columbia, permafrost is continuous to sporadic, with temperatures of -1 to -6°C and thicknesses of 0 to 100m. Ground ice conditions are complex; open-system pingos are common in west central Yukon, and ice wedges are locally common. In southern British Columbia and southwestern Alberta, permafrost is sporadic to isolated in distribution and occurs only at higher elevations. Temperatures range from 0 to -4°C; ground ice is of limited occurrence.

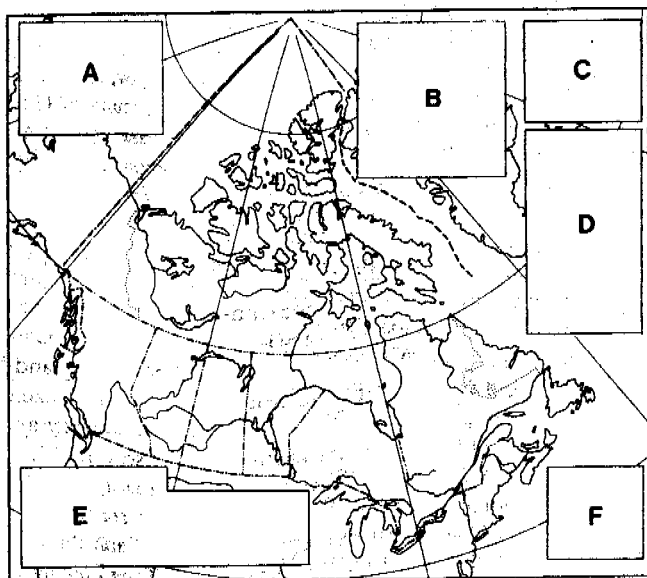


Figure 2: Atlas map layout: A = Ground temperature profiles; B = Inset map of ground temperature isotherms; C = Title block; D = Notes; E = Legend; F = Principle sources.

Subsea permafrost beneath the Beaufort Sea Continental Shelf of the Western Arctic has a thickness of 400 to 800m and temperatures of 0 to  $-2^{\circ}\text{C}$ . Ground ice generally occurs as crystals and lenses; some ice bodies, in the form of massive ice and truncated ice wedges, are known from the near-shore zone in areas of rapid coastal retreat.

Isolated outliers of permafrost are also present at particularly favourable localities in the non-permafrost region of southern Canada, such as peatlands near the southern limit of permafrost and high mountain tops in the Appalachians, including the Chic-Choc Mountains of Quebec and in western Newfoundland.

#### CONCLUSIONS

In preparing this new map, conclusions were drawn about the distribution of permafrost and ground ice and on the available permafrost data in Canada.

#### Permafrost and Ground Ice Distribution

The present map differs significantly from earlier atlas sheets of permafrost in Canada (Brown, 1967, 1973, 1978). First, this map presents information on the extent and distribution of permafrost in relation to landscape units, rather than in terms of zonal soil climate (Heginbottom, 1984). The major changes in permafrost distribution from that appearing on the earlier maps are found in the northern Cordillera and the Labrador-Ungava Peninsula. In the former area, the work

of S.A. Harris has illustrated the effects of mountains on the distribution of permafrost (Harris, 1983, 1986). In eastern Canada, work at the Centre d'études nordiques, Laval University, Quebec, has elucidated the relationships between landscape, Quaternary history and geocryology (Allard and Seguin, 1987). Secondly, the present map also shows, for the first time, information on the distribution and extent of ground ice for all of Canada. These data are also presented in relation to the landscape units. In addition to being published in the National Atlas of Canada, the map will comprise the Canadian contribution to the "Circumarctic Map of Permafrost and Ground Ice Conditions" being compiled under the aegis of the International Permafrost Association.

#### Permafrost Data

As has been known for many years, there is considerable variability in the amount, distribution and reliability of data on permafrost and ground ice in Canada. These variations reflect real differences in geocryological conditions, particularly in ground ice extent and distribution. They also reflect, however, the different amount of research undertaken in the regions of the country, differences in accessibility, natural exposures, and resource development activity.

#### ACKNOWLEDGMENTS

The authors thank J. Bjornson and K. Ruhland for assistance in compiling the computer data base, I. Rose and A. Caron for assistance in producing the map manuscript, two anonymous reviewers for helpful comments on the draft manuscript, and S. Parnham for preparation of the camera ready copy. This paper is GSC Contribution number 33692.

#### REFERENCES

- Allard, M. and M.K. Seguin (1987) Le pergélisol au Québec nordique: bilan et perspective. *Géographie physique et Quaternaire*, XLI (1), 141-152.
- Atmospheric Environment Service (AES) (1984) Climatic Atlas -- Canada: Map Series 1, Temperature and Degree Days. Environment Canada, Canadian Climate Program.
- Baulin, V.V. (editor in chief) (1982) [Map of] Geocryological regions of the West Siberian Plain. USSR Ministry of Geology, VSEGINGEO, scale 1:5 M (in Russian).
- Bostock, H.S. (1970a) Physiographic regions of Canada. Geological Survey of Canada, Map 1254A, scale 1:5 M.
- Brown, J., O.J. Ferrians, Jr., J.A. Heginbottom and E.S. Melnikov (in prep.) Circum-Arctic map of permafrost and ground ice conditions: a status report. Permafrost, Sixth International Conference, Proceedings.
- Brown, R.J.E. (1967) Permafrost in Canada. National Research Council Publication 9769, and Geological Survey of Canada, Map 1246A, scale 1:7,603,200.
- Brown, R.J.E. (1973) Permafrost. National Atlas of Canada, 4th ed. Plate 11-12, scale 1:15 M.
- Brown, R.J.E. (1978) Permafrost/Pérgelisol. Hydrological Atlas of Canada, Plate 32 (Ottawa, Canada: Department of Fisheries and Oceans).

- Ferrians, O.J., Jr. and G.D. Hobson (1973) Mapping and predicting permafrost in North America: a review, 1963-1973. Permafrost, the North American Contribution to the Second International Conference, Proceedings, 479-498.
- Harris, S.A. (1983) Comparison of the climatic and geomorphic methods of predicting permafrost distribution in western Yukon Territory. Permafrost, Fourth International Conference, Proceedings, 450-455.
- Harris, S.A. (1986) Permafrost distribution, zonation and stability along the eastern ranges of the Cordillera of North America. *Arctic* 39 (1), 29-38.
- Heginbottom, J.A. (1983) Problems in the cartography of ground ice: a pilot project for northwestern Canada. Permafrost, Fourth International Conference, Proceedings, 480-485.
- Heginbottom, J.A. (1984) The mapping of permafrost; Canadian Geographer, XXVIII (1), 78-83.
- Heginbottom, J.A. (1989) Permafrost and ground ice conditions of the areas around Illisarvik (Richards Island) and Tuktoyaktuk, District of Mackenzie, N.W.T. Geological Survey of Canada, Open File Report 1970; scale 1:50,000.
- Heginbottom, J.A. and L.K. Radburn (1991) Permafrost and ground ice conditions of northwestern Canada. Geological Survey of Canada, Map 1691A; 2 sheets, scale 1:1 M.
- Lorrain, R.D. and P. Demeur (1985) Isotopic evidence for relic Pleistocene glacier ice on Victoria Island, Canadian Arctic Archipelago. *Arctic and Alpine Research*, 17 (1) 89-98.
- Mackay, J.R. (1963) The Mackenzie Delta area, Northwest Territories. Canada, Department of Mines and Technical Surveys, Geographical Branch, Memoir 8, 202 pp. (Reprinted in 1974 as Geological Survey of Canada Miscellaneous Report 23).
- Mackay, J.R. and S.R. Dallimore (1992) Massive ice of the Tuktoyaktuk area, western Arctic coast, Canada. *Canadian Journal of Earth Sciences* 29 (6), 1235-1249.
- Melnikov, P.I. (1966) Schematic geocryological map of the Yakutsk A.S.S.R. (Moscow: Akademia Nauk), scale 1:5 M (in Russian).
- Péwé, T.L. and J. Bell (1974) Map showing the distribution of permafrost in the Fairbanks D-2 SW quadrangle, Alaska. U.S. Geological Survey, Miscellaneous Investigations Series, Folio I-829-B, scale 1:24,000.
- Popov, A.I. et al. (1985) Map of cryolithology of the USSR. Faculty of Geography, M.V. Lomonosov University, Moscow, scale 1:4 M (in Russian).
- Popov A.I. (1990) Cryolithology map of North America. Faculty of Geography, M.V. Lomonosov University, Moscow, scale 1:6 M (in Russian).
- Rampton, V.N. and J.R. Mackay (1971) Massive ice and icy sediments throughout the Tuktoyaktuk Peninsula, Richards Island and nearby areas, District of Mackenzie. Geological Survey of Canada, Paper 71-21, 16 pp.
- Shi Yafeng and Mi Disheng (editors) (1988) Map of snow, ice and frozen ground in China. Lanzhou Institute of Glaciology and Geocryology, Academia Sinica, Lanzhou, scale 1:4 M.
- Taylor, A.E., M.M. Burgess, A.S. Judge and V.S. Allen (1982) Canadian geothermal data collection - northern wells 1981. Earth Physics Branch, Geothermal Series No. 13, 153 pp.
- Tong Boliang et al. (1982) Map of permafrost along the Qinghai-Xizang highway [China]. Lanzhou Institute of Glaciology and Geocryology, Academia Sinica, Lanzhou, scale 1:600,000.
- Young, S.E. (1985) Shallow ground temperature data collection for northern Canada. Earth Physics Branch, Unpublished Data Report, 2 vols., 93 pp. + 100 pp.
- Young, S. and A.S. Judge (1985) A ground temperature data collection for northern Canada. Paper prepared for presentation at McGill Workshop on Climate and Thermal Regimes in Northern Canada, November 8, 1985, 17 pp.
- Young, S. and A.S. Judge (1986) Canadian permafrost distribution and thickness data collection: a discussion. in Student Research in Canada's North: Proceedings of the National Student Conference on Northern Studies, November 18-19, 1986 (ed. W. Peter Adams and Peter G. Johnson), 223-229.

NEAR-SURFACE SUMMER HEAT-TRANSFER REGIMES AT ADJACENT PERMAFROST AND  
NON-PERMAFROST SITES IN CENTRAL ALASKA

Kenneth M. Hinkel<sup>1</sup>, Samuel I. Outcalt<sup>2</sup> and Frederick E. Nelson<sup>3</sup>

<sup>1</sup>Department of Geography, University of Cincinnati  
Cincinnati, Ohio 45221-0131, USA

<sup>2</sup>Department of Geological Sciences, University of Michigan  
Ann Arbor, Michigan 48109, USA

<sup>3</sup>Department of Geological Sciences, Cornell University  
Ithaca, New York 14853 USA

Observations on soil temperature and a surrogate index of soil water ion concentration were collected during late summer from the upper 50 cm of soil at two adjacent sites in the discontinuous permafrost zone of central Alaska. One site is above permafrost while the other, 13 m away in an area of weak groundwater discharge, appears to have no underlying permafrost. At the permafrost site, temperatures at the surface of the organic mat experienced large diurnal variation, but temperature amplitude was strongly attenuated with depth. At the seep site, pore water saturation is maintained by groundwater seepage, which effectively damps temperature variation over time and depth. In late summer, infiltration of precipitation is an effective method of transporting heat to the base of the active layer and extending seasonal thaw depth above permafrost, but where the soil is consistently saturated it has little impact.

## INTRODUCTION

The potential for permafrost nascence and maintenance in the discontinuous permafrost zone is determined by many local factors including mean annual temperature, aspect, shading, elevation, and physical properties of the soil. Soil properties exert a particularly important influence on the distribution of permafrost in the discontinuous zone. The oft-cited insulating effect of an organic mat with low thermal conductivity is considered crucial for the development and maintenance of permafrost bodies near their southern margins; peat-covered palsas provide an excellent example (Nelson 1986). Conversely, owing to the large heat content and thermal inertia of large water masses, permafrost is usually absent beneath streams and standing bodies of water in such regions.

In the discontinuous permafrost zone, temperatures below the annual damping depth remain near the freezing point for the ice-soil solution system. The growth of a moss mat, for example, favors permafrost aggradation since relatively dry, porous material inhibits summer heat transfer by conductive and nonconductive mechanisms. Conversely, ponded or flowing water mitigates against permafrost growth or maintenance. Frozen and unfrozen materials can coexist proximally below the surface, but equilibrium conditions can change over time and space. Alterations in the ground cover or surface drainage patterns strongly impact the evolution of the subsurface thermal regime, and have important ramifications for complete understanding of permafrost distribution. This paper reports results from a high-frequency, small-scale program of soil temperature and soil water ionic concentration measurements at two proximal but dissimilar sites in an area of discontinuous permafrost near Fairbanks, Alaska, discusses the impact of soil physical properties on heat transfer and utilization at the micrometeorological scale, and relates them to

the presence/absence of permafrost.

## SITE DESCRIPTION AND INSTRUMENTATION

The study area, located in the Caribou-Poker Creeks Research Watershed (65° 10' N, 147° 30' W), is approximately 50 km north of Fairbanks, Alaska, in the Yukon-Tanana Upland physiographic province (Wahrhaftig 1965), and is well within the discontinuous permafrost zone (Ferrlians 1965). Haugen et al. (1982) reported a mean annual air temperature of -3.8° C at a nearby location for the period 1975-79.

Two instrumented sites, separated by a distance of about 13 m, were established on a south-facing slope (4°) at an altitude of about 250 m. The first, situated over a body of permafrost encountered at a depth of 47 cm by probing in early August, is hereafter referred to as the PF site. Vegetation cover is composed of sparse black spruce, shrubs, and a thick (27 cm) organic mat of sphagnum moss. A layer of mixed silt and partially decomposed moss extends from 27-41 cm, and is underlain by a silt loam of colluvial origin (Rieger et al. 1972). The second site is located in a water-saturated zone of weak groundwater discharge, and is referred to as the SEEP site. Probing to a depth of 2.0 m in the immediate area revealed no permafrost bodies. Cotton grass is the prevalent species; trees and mosses are absent. A thin (1.0 cm) mixed organic-silt layer grades sharply downward into a colluvial silt loam. Situated near the center of a shallow valley and lacking channelized flow, discharge from the subsurface may be derived from ascending springs (see Lawson et al. 1991). The vegetation differences between these sites suggest that contrasting hydrological and thermal conditions have persisted for an appreciable period.

The data acquisition systems, identical at the two sites, are built around 19-channel Squirrel 1204 data loggers, with a resolution of 5 ohms over a range of 0-20,000 ohms. Yellow



Springs thermistors (#44020) were employed. The system has a precision of  $0.02^{\circ}\text{C}$  at  $5^{\circ}\text{C}$ , which increases to  $0.01^{\circ}\text{C}$  at  $-10^{\circ}\text{C}$ . Thermistors were repeatedly calibrated in an ice slush bath prior to installation. Each logger is connected to eight thermistors encased in stainless steel tubes (40 mm x 6 mm OD). An additional eight channels are each connected to a coated copper wire, the stripped end of which was wrapped tightly around each thermistor casing.

To install the probes, a square (0.4 m) pit was dug to a depth of 0.55 m. Care was taken to remove the organic mat and soil as an intact block and to rapidly return exhumed material to its original sequence, although some thermal and mechanical disruption was inevitable. Probes were inserted horizontally into the pit wall, beginning at a depth of 1 cm, and separated vertically by 7 cm. A copper ground spike, separated from the probe stack by a horizontal distance of 0.40 m, was driven into the soil to a depth of about two meters. Two stripped copper wires, one connected to the data logger and one soldered to the ground spike, were immersed in a non-precipitating, electrolytic reference solution. The data logger and reference solution are housed in an instrument shelter.

Electric potential measurements, made between each probe wire and the ground spike reference solution, are used to derive the "C-Index," a relative measure of the soil water ionic concentration (Outcalt et al. 1989; 1990). Evaporation, the penetration of a freezing front toward the probe level, or advection of a relatively ion-rich solution, are reflected as increases in the C-index (Outcalt and Gray 1988; Outcalt and Hinkel 1989; 1990; Gray and Outcalt 1990). Conversely, soil water dilution induced by precipitation, soil water advection, or condensation at the probe level will reduce the C-index (Outcalt and Hinkel 1990; Outcalt et al. 1990).

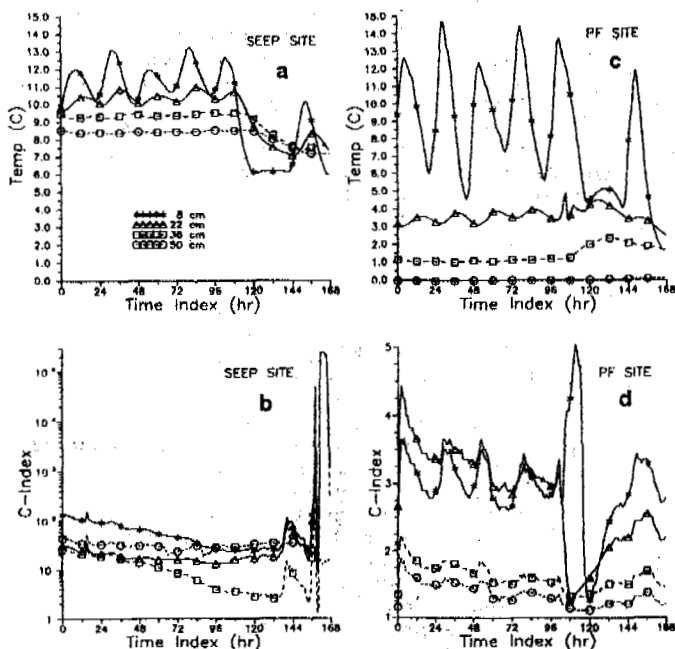


Figure 1. Hourly thermal and C-index records for the period 13-20 August 1991, beginning at 1200 hours, for adjacent sites. Only alternate probe levels are plotted. Line symbols every 12 hours.

## ANALYSIS

After allowing ten days for the thermal disturbance induced by installation to dissipate and to test the system, data recording began. Two sequential data sets at hourly and five-minute intervals, respectively, were collected from each site several days after an intense rain event. The high measurement frequency allows for detailed examination of heat-transfer processes within the active layer during thaw (Outcalt and Hinkel 1992). The subsurface measurements at the study area are supplemented by hourly air temperature and precipitation readings collected at a long-term meteorological station located about 300 m away, referred to subsequently as the INF met station.

### Hourly Data

Temperature and C-index readings were recorded at hourly intervals for a seven-day period beginning at 1200 hours AST on 13 August 1991 (Figure 1). Clear, dry conditions prevailed during the first five days, with daily air temperature maxima around  $20^{\circ}\text{C}$  and nighttime lows ranging from  $-4^{\circ}\text{C}$  to  $7^{\circ}\text{C}$  at the INF met station. Heavy rains fell during the fifth and sixth diurnal cycle; 71 mm were recorded at the INF met station over a 24-hr period beginning around time index (TI) 101.

The influence of local soil conditions is evident in the thermal record. At the SEEP site (Figure 1a) the temperature ranged over about  $7^{\circ}\text{C}$  throughout the soil column. Although temperature gradients were shallow, a diurnal temperature wave train is apparent at all probe levels. The C-index (Figure 1b) does not respond to solar forcing, remaining relatively constant prior to the precipitation event. Although maximum concentrations were recorded at the near-surface probe, the pattern at depth is complicated.

Conversely, the PF site (Figure 1c) experienced steep thermal gradients in the upper 50 cm. Large daily temperature fluctuations were recorded at the surface of the dry organic mat, but the temperature wave was attenuated rapidly with depth. Peak temperatures at depth are lagged to a greater degree than at the SEEP site, indicating lower effective thermal diffusivity values. The extreme attenuation of the diurnal temperature waves between the 8- and 22-cm levels, and the fact that the wave trains are nearly out of phase over 14 cm, illustrates the effectiveness of the organic mat as a thermal insulator.

During clear sky conditions, soil water ionic concentrations at the PF site were slightly greater at the upper probe levels (Figure 1d), suggesting preferential evaporative concentration of solutes near the surface. The diurnal cycle is apparent at all levels and, although attenuated with depth, the peaks and troughs are not lagged with depth. Furthermore, peaks along the C-index traces correspond with peaks in the temperature trace of the 1-cm probe level (not shown). These patterns are produced by midday evaporation and vapor flow from depth toward the surface, i.e., down the osmotic and matric potential gradients. The rapid upward movement of water vapor accounts for the quick response observed within the active layer (Outcalt and Hinkel 1989).

The extent to which temperature amplitude is damped with depth can be appreciated by extracting the daily minimum and maximum

temperatures recorded for each probe from the first four days of the time series. This daily temperature amplitude (one-half the temperature range) is plotted on the y-axis in Figure 2 against the "daily temperature ratio," defined as the daily temperature amplitude at the individual probe divided by the daily temperature amplitude at the 1-cm level. The daily temperature ratio decreases with depth, and resembles the temperature amplitude ratio described in Sellers (1965; p. 136). Although inter-site patterns appear similar, the scale of the y-axes differ by nearly an order of magnitude. The insulating efficiency of the organic mat at the PF site is apparent, while the modulating influence of water-filled pores at the saturated SEEP site is pronounced. The SEEP site is more exposed and thus receives a greater solar radiation load. Additionally, saturated soil has a greater thermal conductivity than its desiccated equivalent. However, it appears that a greater proportion of the surface radiation flux is expended on evaporating and warming near-surface pore water. Continual replenishment of this water by groundwater seepage may also limit large temperature variations.

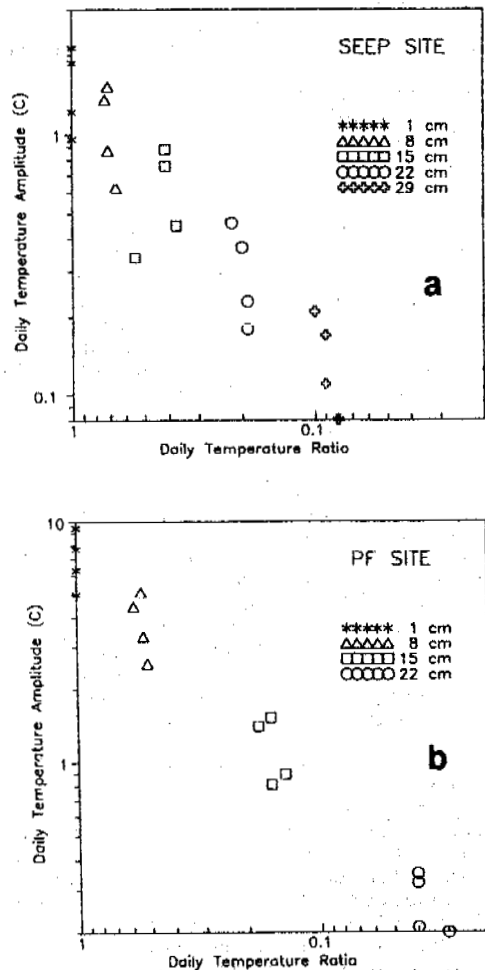


Figure 2. Daily temperature amplitude for each probe level plotted against the "daily temperature ratio" at (a) SEEP and (b) PF sites for the first four days of record. Note differences in scale of y-axes.

### Impact of Precipitation

During the first two weeks of August, the frost table remained at a depth of about 47 cm. Temperatures near the base of the active layer were approximately constant, indicating that the lowest probe was near the diurnal thermal damping depth. During the first 4.5 days of record, the mean daily air temperature at the INF met station was about 11°C, with an average daily variation of 9°C. Over the same period, the temperature at the 50-cm level rose gradually from -0.06°C to -0.03°C, warming at a constant rate of about 0.007°C day<sup>-1</sup>.

Late summer thickening of the active layer below the insulating organic mat occurred during an intense precipitation event in the fifth diurnal cycle (71 mm over a 24-hr period beginning around TI 101). Air temperature at the INF met station remained fairly constant at about 4°C throughout the event. Assuming the rain has a similar temperature, infiltration would cause surface cooling and concurrent warming at the base of the active layer. At the PF site, infiltration produced dramatic temporary warming at the 22-cm level (spike in Figure 1c) and more gradual warming at deeper levels. At depth, and especially within the mixed organic-silt substrate below 27 cm, the impact is discernible as a gradual increase in temperature at all levels. Although not readily detectable at the scale of Figure 1, the temperature at the lowest probe (50 cm) rose above freezing, reflecting thaw at the base of the active layer enhanced by an influx of relatively warm water from above. Over a 1.5-day period, the temperature at 50 cm rose from about -0.03°C to 0.06°C, warming at a rate of 0.06°C day<sup>-1</sup>. Despite the lower air temperature (and thus thermal gradient), this warming rate exceeded that existing during the previous precipitation-free period by nearly an order of magnitude; it does not, however, account for the additional energy required to make the solid-liquid phase transition (0.334 MJ kg<sup>-1</sup>).

Within the organic mat, soil water ion concentration exhibited precipitation-induced perturbations. Infiltration at the PF site initially increased the C-index at the 8-cm level, probably owing to the downward flushing of soluble salts precipitated near the surface during periods of evaporation. By TI 120 ion gradients are largely destroyed within the active layer, but are slowly re-established as clear sky conditions and surface evaporation resumed near the end of record. The impact of infiltration on the soil water ionic concentration, as measured by the C-index, is minimal at the PF site below the organic mat. This may be attributable to the relatively low hydraulic conductivity of the substrate, or to the presence of significant pore water prior to the onset of precipitation.

Although the temperature field was disrupted by the precipitation event, the ionic concentration field at the SEEP site remained largely unaffected (Figure 1b). However, 30 hours after the event, the C-index at the upper probe levels increased nearly an order of magnitude, fell gradually back to "original" values over a 24-hour period, then increased sharply by about four orders of magnitude. Since these ascensions are not in phase with the surface temperature wave, they may have resulted from the delayed impact of groundwater discharge into the SEEP area. A system of north-south trending bedrock fractures has been identified

tentatively as subsurface groundwater conduits (Lawson et al. 1991). Fed by precipitation at higher elevations, groundwater reemerges into weathered bedrock or colluvium. Since the SEEP site occupies a north-south depression, groundwater emergence may explain the observed time lag and C-index pattern.

The period during and immediately following the rainfall event provides an opportunity to examine the hydrothermal impact of infiltrating water on the active layer. Since the effect was concentrated in the organic mat, the following discussion centers on the upper four probes (1-22 cm). Figure 3 shows hourly temperature, precipitation, and C-index measurements for the 24-hour period beginning noon August 17 at the PF site. The prolonged rainfall event began around TI 101 (1700 hours; P on Figure 3). Nocturnal cooling had already begun at the surface of the organic mat, although temperatures were still rising within the organic mat. Rainfall intensity peaked around TI 104 (14 mm), after which temperatures at the 1- and 8-cm levels were nearly equivalent. From TI 104-110, temperature at the upper two probes decreased at the same rate. Air temperature remained near 4°C throughout the precipitation event.

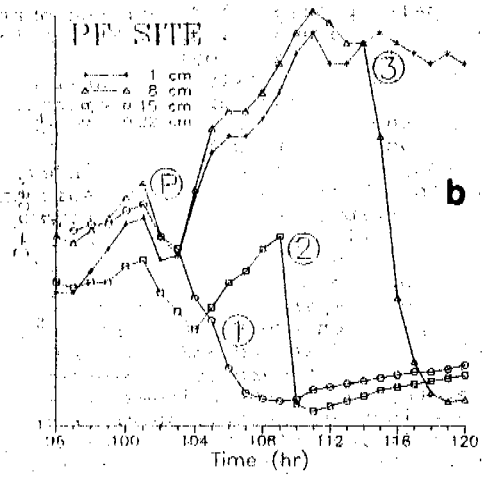
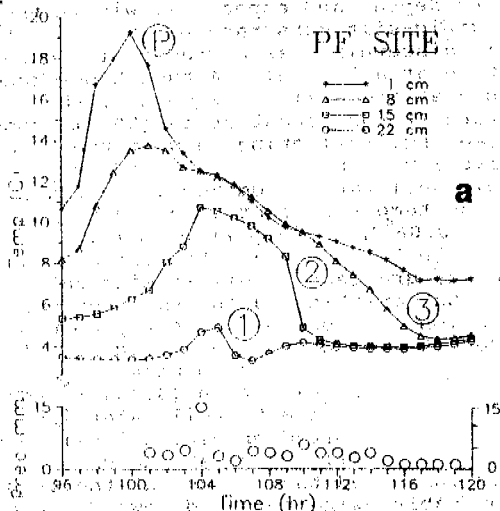


Figure 3. (a) Temperature/precipitation (mm) and (b) C-index values for upper four probes at the PF site for the 24-hour period beginning at noon August 17. (P) = precipitation event, circled numbers indicate stages referenced in text.

Precipitation began around TI 101 as a drizzle. The C-index at all probe levels underwent an immediate reduction. This may, however, reflect the cessation of midday evaporation as the sky became overcast because 4 mm of rain is unlikely to affect the entire soil column and no thermal effect was registered at depth. Around TI 104 (14 mm), the C-index at the upper two probes increased in response to downward flushing of ions from the surface where they had been deposited during the earlier evaporative regime. This effect was also recorded at the 15-cm level after TI 104. To facilitate further discussion, three "stages" were delineated and are referenced in Figure 3.

STAGE 1: Near the base of the organic mat the thermal impact of the infiltrating water was not registered until TI 106. The 22-cm trace shows a reduction in the C-index, from the relatively high pre-rain value of 3.00, to 1.25. By TI 107, dilution by infiltrating water at this level resulted in uniform C-index values at the lowermost five probes.

STAGE 2: As precipitation continued, flooding of the organic mat progressed upward from the frost table. By TI 109-110, rising soil water reached the 15-cm level and the C-index dropped rapidly as the probe came into contact with dilute water. The impact of soil saturation can also be seen in the temperature trace for the 15-cm probe; between TI 109-110 the temperature dropped rapidly and approached that at the 22-cm probe level. The temperature at these levels was about 4°C, which approximates the air temperature during the precipitation period.

STAGE 3: By TI 114-115, a rapid drop in both the C-index and the temperature indicated that saturated conditions had progressed to the 8-cm level. By TI 117, both the temperature and the C-index at the 8-, 15-, and 22-cm levels (and the deeper probes) were nearly uniform; the thermal and chemical gradients have been destroyed. Shortly thereafter, cessation of rain prevented saturation from extending up to the 1-cm level, and the soil water perched above the frost table drained slowly. The rate at which the subsurface became saturated appears, therefore, to have been 1.0-1.5 cm hr<sup>-1</sup>.

#### High-frequency data

To increase the temporal resolution, temperature and C-index readings were collected at 5-minute intervals at the sites beginning at 1200 hours on 20 August 1991 (Figure 4). This 44-hr time series is a continuation of the previous data sets, collected at higher frequencies following a brief hiatus. The weather during this period was clear and dry, though a cooling trend is evident. Daily air temperature maxima at the INF met station reached 19°C with nighttime lows of around -6°C; mean daily temperatures were about 5°C cooler than the pre-rain period.

At the PF site, the pronounced damping of the diurnal temperature amplitude continued within the organic mat (Figure 4c). C-index readings are in phase with the surface temperature cycle and are attenuated, though not lagged, with depth (Figure 4d). Ionic concentrations increased toward the surface, reflecting the influence of evaporation. At the SEEP site, the saturated condition effectively diverted the heat flux, and daily temperature variation is reduced (Figure 4a). Ionic concentrations appear not to have been forced significantly by temperature, and showed little temporal

variation. The vertical pattern does, however, contain sharp gradients and appears to reflect complexities introduced by spring discharge (Figure 4b).

### Advection

The C-index can also be used to recognize the hydrothermal impact of frost at the surface (Outcalt and Gray 1988; Outcalt and Hinkel 1989; Outcalt et al. 1990). These effects are best observed at the PF site by plotting the temperature and C-index as time-space fields (Outcalt et al. 1990). Figure 5 shows that soil water ionic concentrations are closely correlated with temperature patterns during the day, when evaporation dominates; gradients in the temperature field are associated with similar gradients in the C-index field. Shortly before sunrise on 21 August (TI 250), however, air temperature fell to about  $-7^{\circ}\text{C}$ , and surface frost may have augmented vertical advection by increasing the local soil water tension.

The frost event can be observed as a pronounced "ridge" centered near TI 230 in Figure 5b; relatively cold, dilute water from near the base of the active layer was drawn toward the drier freezing near-surface zone. The advection event also perturbed the temperature field as the entire soil column became nearly isothermal around TI 234, a pattern not observed in the seven-day data set. Extremely rapid warming at the surface (Figure 5a, TI 250) after sunrise truncated the advection event and, as strong evaporation resumed, the C-index increased near the surface. At depth, gradients in the C-index field collapsed with the cessation of advection as ions diffused down local concentration gradients.

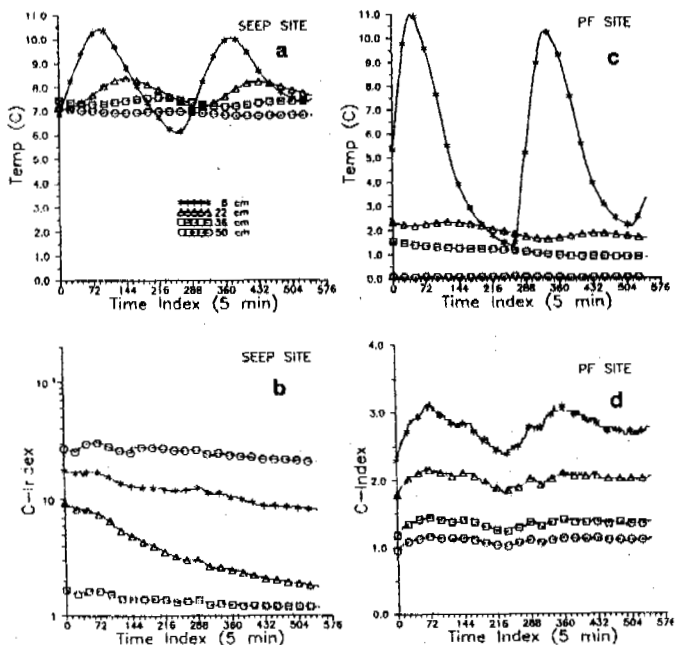


Figure 4. Thermal and C-index records for the 44-hr period 20-22 August 1991, collected at 5-minute intervals beginning at 1200 hours. Only alternate probe levels are shown. X-axis labels are at 6-hr intervals, line symbols every 2 hrs.

### CONCLUSIONS

Despite close spatial proximity, soil properties and groundwater patterns maintain permafrost at one site and prevent it at another. A dry organic mat above the permafrost body experiences large temperature variations at the surface, but effectively damps penetration of the diurnal temperature wave. Conversely, the saturated medium in the nearby groundwater seep zone experiences little near-surface thermal variation over time and depth, owing to the modulating effect of water-filled pores.

Precipitation appears to be an effective method of transporting sensible heat to the base of the active layer and deepening seasonal thaw above permafrost bodies. Intense rain events can result in rapid saturation of the active layer, significantly increasing the enthalpy. Owing to limited infiltration, precipitation had little immediate impact at the saturated site although rainfall may have an indirect effect by subsequently increasing discharge from springs. The impact of rain events on the spatial and temporal variability of active layer thickness needs further study so as to separate this component from the long-term climate signal.

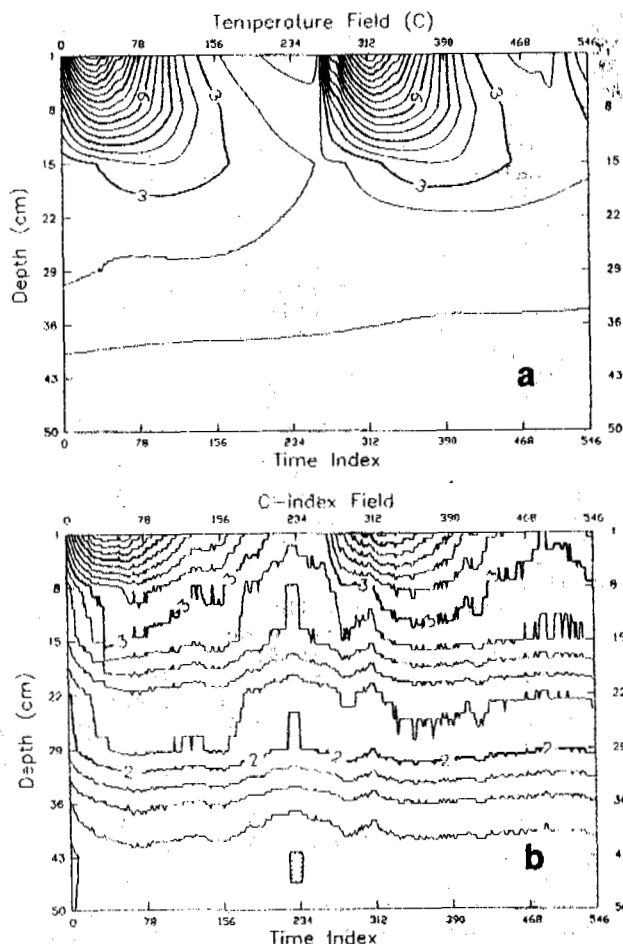


Figure 5. Contour maps showing (a) temperature and (b) C-index fields for PF site using same data and time scale as Figure 4. Contour intervals are  $1.0^{\circ}\text{C}$  and  $0.2$  C-index units.

#### ACKNOWLEDGMENTS

This research was supported by the U.S. National Science Foundation, Grant #SES-9008771. We gratefully acknowledge the assistance from field staff at the Institute of Northern Forestry and especially the efforts of Mr. Ron Hartzman.

#### REFERENCES

- Carson, J.E. (1963). Analysis of soil and air temperature by Fourier techniques. *Journal of Geophysical Research* 68, 2217-2232.
- Ferrians, O.J., Jr. (1965). Permafrost Map of Alaska. U.S. Geological Survey Miscellaneous Geological Investigations, Map I-445, (1:2,500,000).
- Gray, D.H., and Outcalt, S.I. (1990) Thermally driven electrical coupling effects and pore water advection in soils. *Transportation Research Record* 1288, 10-14.
- Haugen, R.K., Slaughter, C.W., Howe, K.E., and Dingman, S.L. (1982). Hydrology and Climatology of the Caribou-Poker Creeks Research Watershed, Alaska. U.S. Army Cold Regions Research and Engineering Laboratory, CRREL Report 82-26, 42 pp.
- Hinkel, K.M., Outcalt, S.I., and Nelson, F.E. (1990). Temperature variation and apparent thermal diffusivity in the refreezing active layer, Toolik Lake, Alaska. *Permafrost and Periglacial Processes* 1(4), 265-274.
- Lawson, D.E., Arcone, S.A., and Collins, C.M. (1991). Geophysical Investigations of an Anomalous Unfrozen Zone, Caribou Peak, Alaska. U.S. Army Cold Regions Research and Engineering Laboratory, CRREL Report 91-17, 29 pp.
- Nelson, F.E. (1986). Permafrost distribution in central Canada: applications of a climate-based predictive model. *Annals of the Association of American Geographers* 76(4), 550-569.
- Outcalt, S.I., and Gray, D.H. (1988). Two electric potential signatures of serial diurnal frost. *Physical Geography* 9(4), 354-360.
- Outcalt, S.I., Gray, D.H., and Benninghoff, W.S. (1989). Soil temperature and electric potential during diurnal and seasonal frost. *Cold Regions Science and Technology* 16(1), 37-43.
- Outcalt, S.I., and Hinkel, K.M. (1989). Night frost modulation of the near-surface soil water ion concentration and thermal fields. *Physical Geography* 10(4), 336-348.
- Outcalt, S.I., and Hinkel, K.M. (1990). The soil electric potential signature of summer drought. *Theoretical and Applied Climatology* 41(1), 63-68.
- Outcalt, S.I., and Hinkel, K.M. (1992). The fractal geometry of thermal and chemical time series from the active layer, Alaska. *Permafrost and Periglacial Processes*, (in press).
- Outcalt, S.I., Nelson, F.E., and Hinkel, K.M. (1990). The zero-curtain effect: heat and mass transfer across an isothermal region in freezing soil. *Water Resources Research* 26(7), 1509-1516.
- Rieger, S., Furbush, C.E., Schoephorster, D.B., Summerfield, H., and Gieger, L.C. (1972). Soils of the Caribou-Poker Creeks Research Watershed, Alaska. U.S. Army Cold Regions Research and Engineering Laboratory, CRREL Technical Report 236, 14 pp.

Sellers, W. (1965). *Physical Climatology*. University of Chicago Press, Chicago, 272 pp.

Wahrhaftig, C. (1965). Physiographic Divisions of Alaska. U.S. Geological Survey Professional Paper 482, 52 pp.

## HILLSLOPE HYDROLOGY IN AN ARCTIC SETTING

Larry D. Hinzman<sup>1</sup>, Douglas L. Kane<sup>1</sup> and Kaye R. Everett<sup>2</sup>

<sup>1</sup>Water Research Center, University of Alaska  
Fairbanks, Alaska 99775 U.S.A.

<sup>2</sup>Byrd Polar Research Center, Ohio State University  
Columbus, Ohio 43210 U.S.A.

The interaction of hillslope surface flow and the underlying soils is a topic of great interest in arctic environments because of the shallow nature of the active layer overlying the permafrost. For eight years, hillslope processes have been studied in a small northern Alaskan watershed, Imnavait Creek. Both the thermal and moisture regimes were monitored at three scales, including four runoff plots (89 m<sup>2</sup>) that collect both downslope runoff through the organic soils and overland flow, water track (0.026 km<sup>2</sup>) and watershed levels (2.2 km<sup>2</sup>). Downslope water movement is controlled by the hydraulic conductivities of the soils; the organic soils have relatively high conductivities compared with the mineral soils. A typical scenario is for the organic layer to become saturated, both during snowmelt and major rainfall events, and runoff is generated by water moving either through or over the organic soils.

### INTRODUCTION

Horton (1937) first described the classic model of hillslope hydrology over fifty years ago. Although the equations he developed to quantify rates of water movement are no longer widely used, the basic premises defined in his infiltration theory are useful in a discussion of processes associated with hillslope hydrology in the Arctic. His essential premise was that precipitation is divided into two components at the soil surface depending upon the infiltration capacity of the soil. The slower component of streamflow arose due to the baseflow of soil moisture and groundwater while the more rapid component was due to the runoff of precipitation in excess of the rate of infiltration. Several investigators have shown that often only a portion of a watershed may be contributing such rapid overland flow (Betson, 1964; Hewlett and Hibbert, 1967; Dunne and Black, 1970) leading to a separate theory of saturated flow. These inter-related processes are complex in any environment; however, the presence of permafrost both simplifies and complicates mechanisms in arctic regions. Ice-rich permafrost is essentially an impermeable barrier which prevents any percolation of soil moisture or supra-permafrost groundwater to sub-permafrost groundwater.

The active layer is that portion of the soil profile above the permafrost which proceeds through the freeze/thaw cycle annually. The thickness of this layer ranges from 10 cm to 150 cm but is typically about 40 cm or 50 cm at the study site described in this paper. The permafrost table also maintains a perched water table within the active layer which frequently rises to the surface with a great deal of spatial variability. This causes an irregular oscillation between surface and subsurface flow and is one of the major difficulties associated with simulating hillslope hydrology in the Arctic. This runoff pattern shares

characteristics of both the Horton (1937) concept and that of Dunne and Black (1970).

### SITE DESCRIPTION

Field research was conducted in a small (2.2 km<sup>2</sup>) headwater watershed called Imnavait Creek (Figure 1) located in the foothills on the north side of the Brooks Range on the North Slope of Alaska, U.S.A. (Latitude 68°37'N, Longitude 149°17'W). This site is located in a zone of continuous permafrost approximately 250 km north of the Arctic Circle and 200 km south of the Arctic Ocean. Hydrologic and biologic research was conducted in this small watershed as a component of a large ecologic study entitled "Response, Resistance, Resilience and Recovery from Disturbance" between 1984 and 1992.

The soils in this watershed appear to be at least 11,500 years old (40 years (Walker et al., 1989) and are mostly silty colluvium and residual material of glacial origin. The predominant soils have been classified as Histic Pergelic Cryaquepts (Rieger et al., 1979). There is a thick layer of organic matter on the surface consisting of partially decomposed mosses, sedges and other associated plants. The thickness of this peat layer varies from as thin as 5 cm near ridge tops to over 50 cm in the valley bottom. The surficial organic layer is quite porous and saturates and drains quickly; however, the underlying mineral soil is usually saturated with water. Such soils are the most common on the North Slope (Rieger, 1983). The dominant vegetation is tussock tundra and is mostly water tolerant plants such as sedges and mosses, but they are accompanied by lichens and shrubs such as willows, alder and dwarf birch. Tussock sedges are common on the ridge tops and slopes but do not occur in the lowest, wettest areas (Walker et al., 1989).

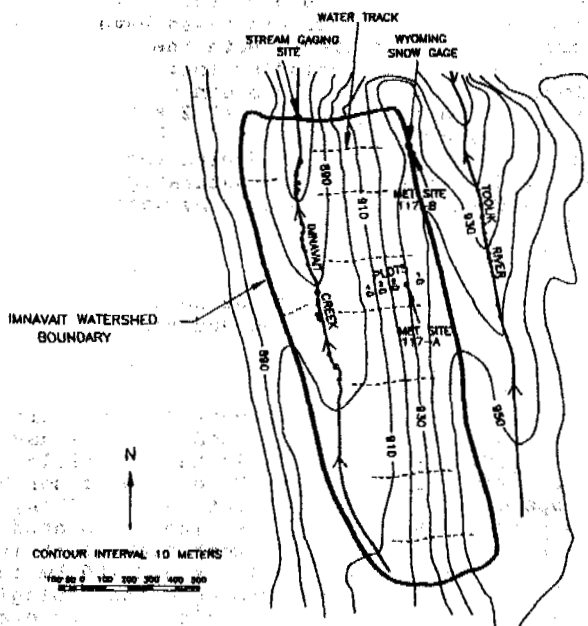
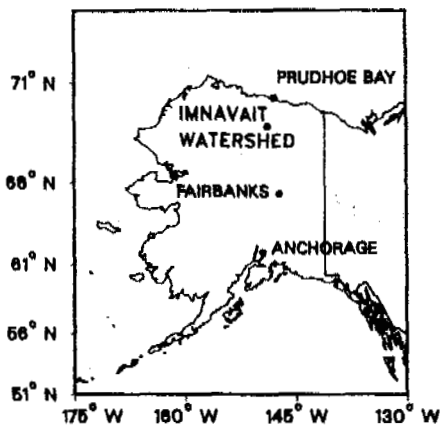


Figure 1. Map showing location of research watershed, location of plots and topography.

#### METHODS

Hydrologic processes were examined on three different scales, i.e., plot (89 m<sup>2</sup>), water track (0.026 km<sup>2</sup>) and basin (2.2 km<sup>2</sup>) (Figure 1). Runoff plots were installed in the autumn at the time of maximum depth of thaw. Borders of wood and plastic were utilized to isolate the plots from the surrounding hillside. A system of collection gutters was installed at the bottom of the plot to collect all overland and subsurface flow. This discharge was routed to a holding tank instrumented with a water level recorder. Flows from the plots were monitored during the spring snowmelt (1985-1989) and occasionally during summer precipitation events. A stilling well, water level recorder and compound weir were installed near the bottom of a water track. Water track flows were monitored during the spring snowmelt (1986-1992) and during summer precipitation events

(1986-1992). We measured discharge in Imnavait Creek from 1985 through 1992. A continuous recorder was installed in the stream channel in 1986 and a 1.3 m H flume was installed in 1987 (Figure 1). Measurements of soil moisture were made in a transect across the hillside using time domain reflectometry probes (TDR) and shallow wells. Additionally, two complete meteorologic stations were established within the watershed to measure air and soil temperatures, relative humidity, radiation components, wind speed and direction, barometric pressure, precipitation, and soil heat flux. Periodically throughout the winter and just prior to spring melt, detailed snow surveys were conducted adjacent to the runoff plots and in a transect parallel to the water tracks across the valley. During springmelt, snow surveys were conducted daily near the plots to determine rates of snowpack ablation.

#### DISCUSSION

Many deficiencies exist in our ability to model many of the basic arctic hydrologic processes; premier among these are knowledge of mechanisms and pathways of water movement through the active layer. Physical parameters which control or influence these processes include the thickness of the active layer or depth to permafrost, the soil type and properties, vegetation, slope morphology, and gradient. Primary mechanisms of water flow include subsurface flow through the mineral soil, subsurface flow through the organic layer at and above the organic/mineral interface, surficial inter-tussock flow, surficial diffuse flow through mosses, water track flow, and streamflow. Woo and Marsh (1990) discuss the importance of similar lateral flows in maintaining high moisture contents in fens at a High Arctic site.

The hydrologic characteristics of this watershed were somewhat different from that of a basin in the High Arctic studied by Edlund et al. (1990) due primarily to soil and vegetation differences. The highly organic soils of Imnavait Creek are common in arctic regions and strongly influence the hydrologic processes. The soils consist of live vegetation rooted in roughly 10 cm of partially decomposed, highly porous organic matter (Figure 2). Below this is a somewhat denser, substantially more decomposed organic layer which overlies a glacial till (Hinzman et al., 1991). The organic layer is thickest in the valley bottoms and thinnest on the ridgetops, which directly impacts the thermal regime and the depth of thaw. Maximum active layer thickness is about 60 cm near the ridge tops but can be as thin as 20 cm in the valley bottoms. The hydraulic conductivities of the organic soils range from 10 to 1000 times greater than the underlying mineral soils (Hinzman et al., 1991); consequently pathways of downslope subsurface water movement are frequently above the mineral soils through the organic layers. This mechanism impacts rates of water movement and sources of soil water chemistry.

Vertical hydraulic conductivities into an unsaturated organic layer are so great, surficial runoff seldom occurs due to precipitation in excess of infiltration, but rather is due instead to complete saturation of the organic layer caused by both precipitation and lateral movement of water. Dingman (1971) noted a similar process in a subarctic watershed

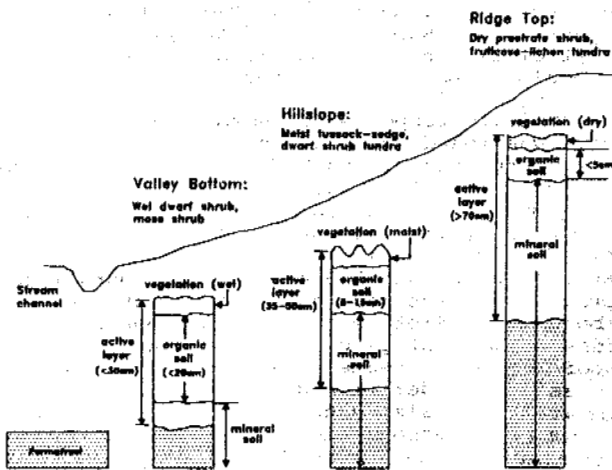


Figure 2. Relative changes in vegetation, active layer thickness and soil type as a function of position on hillslope.

partially underlain by permafrost. The implications of this process is that the active layer becomes saturated from the bottom up, rather than from the top down as in the vadose zone of more temperate regions.

The ice-rich permafrost maintains a saturated zone within the active layer throughout the summer (Hinzman et al., 1991). The depth of this perched water table depends upon recent weather patterns and position within the watershed (Figure 3). In the valley bottom where the thawed zone is thin and hydraulic gradients are low, the water table is frequently near the soil surface. On the hillsides, the water table is usually located within the mineral soil. The data presented in Figure 3 appear typical of the eight years that we have observed.

#### WATER TABLE DEPTHS ALONG BASIN TRANSECT

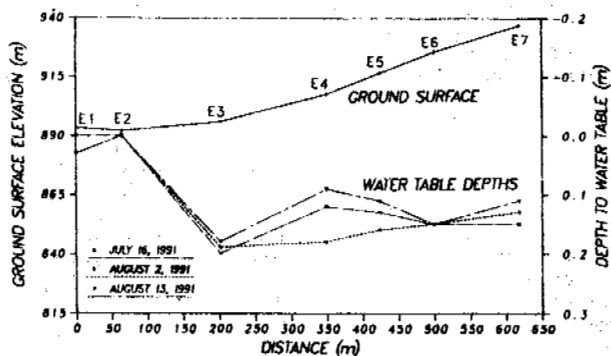


Figure 3. Distance from ground surface to water table across basin.

Water tracks are small channels which are formed on slopes as permafrost features (Walker et al., 1989). They can be quite subtle and are often distinguished more by changes in vegetation rather than topography (Hastings et al., 1989); i.e., a visible channel is not always obvious. These drainage features form about every 50 m perpendicular to the slope and are quite efficient at draining excess water from the hillslope (Kane et al., 1991). They originate near the top of the hillslope usually

just below the shoulder of the hill and diffuse near the toe of the slope (Figure 4). Depth of-thaw is significantly greater in water tracks (Hastings et al., 1989).

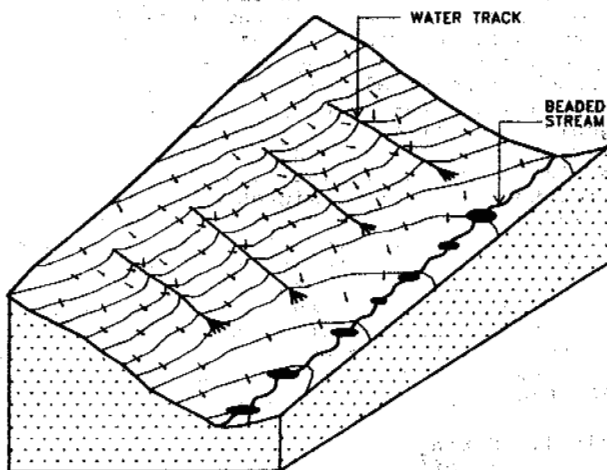


Figure 4. Cross-section of hillside displaying water tracks and beaded stream.

Water tracks form on hillsides among tussock tundra. Whereas the presence of the peat layer is the primary influence on subsurface flows, the vegetation and surface conditions dictate the rates of surficial flow. Rates of inter-tussock flow can be relatively high and during snowmelt or rainfall events, the primary source of water feeding water tracks is inter-tussock flow. At the base of the water track, flow must diffuse through the moss, slowing significantly and occasionally rising above the surface during snowmelt and heavy rainfall.

Due to the relatively close spacing of water tracks, they generally have small drainage areas compared to the basin scale. The water track described in this paper was one of the larger sub-drainages in the basin, but still represented only about 1% of the entire watershed. Similar to plot and basin scale hydrographs, flow in the water tracks is quite flashy, rising quickly to peak flow and falling quickly through recession (Figure 5). We have measured peak water velocities of 0.2 m/s in the water track; due to the high density of water tracks in the basin, this explains the rapid response of the main stream.

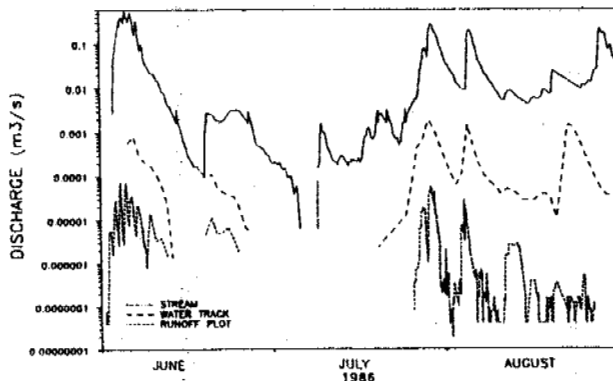


Figure 5. Stream, water track, and plot hydrographs on a log scale during the summer of 1986.



Runoff plots were quite useful in studying the amount of runoff generated in response to snowmelt or rainfall (Table 1). The plots reveal that snow accumulation, runoff and evaporation were quite variable throughout the watershed. Evaporation, calculated as the remainder term in a water balance (Table 1), gave values similar to those calculated using an energy balance approach (Kane et al., 1990). The amount of moisture which was required to re-wet the organic layer prior to downslope movement of water was estimated to be 1.5 cm. Throughout the winter, the surficial organic mat becomes desiccated as moisture migrates across the thermal gradient into the overlying snowpack forming hoar frost crystals. During the summer, the surficial soils are dried through evapotranspiration. Through direct field measurements, and plot and basin water balance calculations, it was estimated that about 1.5 cm of water must be absorbed by a dry organic layer before runoff will begin (Kane and Hinzman, 1988; Kane et al., 1989). This is quite

consistent after desiccation over the winter, but during the summer it is dependent upon the amount of time since a previous rainfall event and would probably vary according to hillslope position.

Hydrologic response to snowmelt and rainfall events was found to be different at each level (plot, water track, and basin) both in response time and nature of runoff (Table 2). During spring melt, the hydrologic response was found to be greatly impacted by the distribution of snow (Kane et al., 1991). Plot measurements also indicated that the amount of evaporation from the snow was related to the thickness of the snowpack. Plots with thinner snowpacks lost a greater percentage of water to evaporation, probably due to greater absorption of solar radiation by underlying soil and vegetation. Evaporation is also enhanced on snow-free spots such as high tussocks due to the ample supply of moisture from the surrounding snow and the greater absorption of solar radiation. Consequently the total abstraction to runoff by evaporation and soil storage was somewhat variable.

Table 1. Spring snowmelt water balance for runoff plots and Innavait Creek watershed.

Site	Snowpack Water Equivalent (cm)	Snowmelt Runoff (cm)	Evaporation (cm)	Soil Storage (cm)
<b>1985</b>				
Plot 1	13.8	10.9	1.4	1.5
Plot 2	11.7	4.4	5.7	1.5
Plot 3	9.7	2.1	6.1	1.5
Plot 4	10.6	3.3	5.8	1.5
Basin	10.2	6.6	2.0	1.5
<b>1986</b>				
Plot 1	14.7	10.0	3.2	1.5
Plot 2	12.4	6.2	4.7	1.5
Plot 3	8.1	4.3	2.3	1.5
Plot 4	10.2	5.1	3.6	1.5
Basin	10.9	5.7	3.7	1.5
<b>1987</b>				
Plot 1	9.8	6.7	1.6	1.5
Plot 2	10.7	3.5	5.7	1.5
Plot 3	*	*	*	*
Plot 4	10.0	6.5	2.0	1.5
Basin	10.8	7.1	2.2	1.5
<b>1988</b>				
Plot 1	*	*	*	*
Plot 2	7.3	1.2	4.6	1.5
Plot 3	8.4	3.6	3.3	1.5
Plot 4	6.9	2.5	2.9	1.5
Basin	7.8	3.9	2.4	1.5
<b>1989</b>				
Plot 1	*	*	*	*
Plot 2	11.6	4.2	5.9	1.5
Plot 3	11.7	8.2	2.0	1.5
Plot 4	*	*	*	*
Basin	15.5	9.5	4.7	1.5

\* not collected

Table 2. Ratio of runoff/snowpack during spring melt for plot, water track and watershed scales.

	Plot 1	Plot 2	Plot 3	Plot 4	Plot Avg.	Water -shed	Water Track
1985	0.79	0.39	0.22	0.31	0.43	0.65	*
1986	0.68	0.50	0.29	0.50	0.49	0.52	0.79
1987	0.69	0.33	*	0.20	0.41	0.66	*
1988	*	0.17	0.44	0.38	0.33	0.50	*
1989	*	0.57	0.81	*	*	0.61	*
1990	*	*	*	*	*	0.60	*
1991	*	*	*	*	*	0.68	0.48

\* not collected

Snowpack had even greater impact upon flow in the main stream (Hinzman and Kane, 1991). Redistribution of snow throughout the winter left major accumulations on the lee side of slopes, in depressions such as water tracks and in the valley bottom along the stream. Along the hillside, where the hydraulic gradients were highest, the damming effect of the snowpack was not of major importance; however, in the valley bottom, storage of water in the snowpack could delay initiation of streamflow for many days. The amount of snow damming was related not only to the amount of snow, but also to the shear strength of the snowpack which was dependent upon snowpack density formed during winter wind events and daily temperature during snowmelt.

Due to the very limited storage capacity in the active layer, the timing of the recession component of plot, water track and stream hydrographs are quite brief. Plots have the least capacity for downslope subsurface flows because they are isolated from an external source of soil water. Consequently, after a rainfall or snowmelt event, the hydrograph returns to zero flow almost immediately (Figure 5). Soil samples from the hillslopes prior to spring melt reveal ice contents which are much greater than the saturation level of thawed soils due to existence of ice lenses. However, after the very quick recession following snowmelt, there is no baseflow from the plots because the plants utilize almost all excess water in the active layer for transpiration. This differed from the results

of Edlund et al. (1990) primarily because of vegetation patterns. The baseflow from the water track will also cease within a few days after a precipitation event. Although the baseflow of the main stream can be very low, it normally continues throughout the summer. We believe this demonstrates the increasing importance of baseflow as the scale increases.

#### SUMMARY

The hillslope hydrology of Imnavait basin was studied on three scales (plot, water track and watershed) between 1985 and 1992. The plots were designed to collect all surface and subsurface flow. Water tracks are surface drainage features which act to quickly route excess water off hillsides to the valley bottom. Many of the hydrologic processes are directly or indirectly controlled by the presence of the permafrost and its impacts upon active layer thickness. The mechanisms and pathways of downslope water flow are controlled primarily by soil type, vegetation and gradient. Most subsurface water movement occurs through the organic layer along the organic/mineral interface. This organic layer is quite porous and therefore saturates and drains quickly leading to the rapid hydrologic response. Because the mineral soils are frozen for most of the year and the hydraulic conductivities are relatively low, water movement downslope through the mineral soils is minimal. Usually the mineral soils are near saturation throughout the summer, except during periods of extended drought. The runoff response is fairly rapid and likewise the recession of runoff is fairly quick. The dominant surface runoff mechanisms consist of inter-tussock flow and water track flow. At all scales, flows are flashy and recessions are brief due to the limited soil moisture storage capacity. Snowpack distribution had an important impact upon timing of spring melt runoff and the amount of runoff and evaporation from the plots. In valley bottoms, where wind transported snow accumulated, snow acted as a dam often delaying initial stream flow for several days after initial plot flow.

#### ACKNOWLEDGMENTS

This research was sponsored by the U.S. Department of Energy's Office of Health and Environmental Research, Ecological Research Division as part of the R4D program in Arctic Tussock Tundra. We would like to acknowledge Elizabeth K. Lilly and Robert E. Gieck for assistance in data collection, reduction and analysis.

#### REFERENCES

- Betson, R.P. (1964) What is watershed runoff? *Journal of Geophysical Research*, 68:1541-1552.
- Dingman, S.L. (1971) Hydrology of Glenn Creek watershed Tanana River basin, central Alaska. U. S. Army, Cold Regions Research and Engineering Laboratory, Research Report 297.
- Dunne, T. and R.D. Black (1970) Partial-area contributions to storm runoff in a small New England watershed. *Water Resources Research*, 6:1296-1311.
- Edlund, S.A., M.K. Woo and K.L. Young (1990) Climate, hydrology, and vegetation patterns, Hot Weather Creek, Ellesmere Island, Arctic Canada. *Nordic Hydrology*, 21(4/5):273-286.
- Hastings, S.J., S.A. Luchessa, W.C. Oechel and J.D. Tenhunen (1989) Standing biomass and production in water drainages of the foothills of the Phillip Smith Mountains, Alaska. *Holarctic Ecology*, 12(3):304-311.
- Hewlett, J.D. and A.R. Hibbert (1967) Factors affecting the response of small watersheds to precipitation in humid regions. in: Forest Hydrology, W.E. Sopper and H.W. Lull (eds.) Pergamon Press, Oxford. pp. 275-290.
- Hinzman, L.D. and D.L. Kane (1991) Snow hydrology of a headwater arctic basin 2. Conceptual analysis and computer modeling. *Water Resources Research*, 27(6):1111-1121.
- Hinzman, L.D., D.L. Kane, C.S. Benson, and K.R. Everett (1991) Hydrologic and Thermal Properties of the Active Layer in the Alaskan Arctic. *Cold Regions Science and Technology*, 19(2):95-110.
- Horton, R.E. (1937) Hydrologic interrelations of water and soils. *Proc. Soil Science Society of America*, 1:401-429.
- Kane, D.L., R.E. Gieck, and L.D. Hinzman (1990) Evapotranspiration from a Small Alaskan Arctic Watershed. *Nordic Hydrology*, 21(4/5):253-272.
- Kane, D.L., and L.D. Hinzman (1988) Permafrost hydrology of a small arctic watershed. K. Senneset (ed.) *Proc. Fifth International Conference on Permafrost*, Trondheim, Norway. Tapir, pp. 590-595.
- Kane, D.L., L.D. Hinzman, C.S. Benson, and K.R. Everett (1989) Hydrology of Imnavait Creek, an arctic watershed. *Holarctic Ecology*, 12:262-269.
- Kane, D.L., L.D. Hinzman, C.S. Benson and G.E. Liston (1991) Snow hydrology of a headwater arctic basin 1. Physical measurements and process studies. *Water Resources Research*, 27(6):1099-1109.
- Rieger S. (1983) The genesis and classification of cold soils. Academic Press, New York. 230 p.
- Rieger, S., D.B. Schoephorster and C.E. Furbush (1979) Exploratory soil survey of Alaska. U.S.D.A. Soil Conservation Service. Washington D.C. 213 p.
- Walker, M.D., D.A. Walker and K.R. Everett (1989) Wetland soils and vegetation, Arctic Foothills, Alaska. U.S. Fish and Wildlife Service. Biological Report 89(7). 89 pp.
- Woo, M.K. and P. Marsh (1990) Response of soil moisture change to hydrologic processes in a continuous permafrost environment. *Nordic Hydrology*, 21(4/5):235-252.

**APPLICATION OF BTS-MEASUREMENTS FOR MODELLING  
MOUNTAIN PERMAFROST DISTRIBUTION**

Martin Hoelzle, Wilfried Haerberli and Felix Keller

Laboratory of Hydraulics, Hydrology and Glaciology, VAW - ETH Zentrum  
CH-8092 Zurich, Switzerland

In the early 1970s, rules of thumb to predict local permafrost occurrences in the Swiss Alps were based on a considerable number of field measurements and the assumption that the main governing factors were (1) mean annual air temperature (altitude, regional scale), (2) solar radiation (slope aspect, local scale) and (3) snow redistribution by wind and avalanches. Information from a large number of BTS-measurements and potential direct solar radiation as calculated from digital terrain models can now be used for improving the model. Mean annual air temperature and potential direct solar radiation can now be introduced explicitly, replacing 'altitude' and 'slope aspect' in the original rules of thumb. This important result helps to explain permafrost existence at low-altitude sites with extremely reduced solar radiation (well below the 0°C-isotherm). It also makes simulation of effects from various future climatic scenarios more realistic.

**INTRODUCTION**

Modelling distribution patterns of discontinuous mountain permafrost at a regional scale (e.g., Dingman and Koutz 1974, Harris 1981, Greenstein 1983, Gorbunov 1978, Jorgenson and Kreig 1988) is a basic tool in connection with the planning of human activities in these especially sensitive environments (Haerberli 1992). Furthermore, the simulation of permafrost distribution for past and future climatic conditions in view of ongoing warming trends and their effects on natural hazards in high mountain areas has become increasingly important. The present contribution discusses the basic concept of predicting permafrost occurrences in the Swiss Alps as a function of topographic and climatic parameters. It presents results from tests of existing models and discusses ongoing efforts to further improve such tools.

**MOUNTAIN PERMAFROST AND THE ENERGY BALANCE**

On a worldwide scale, permafrost characteristically occurs in cold regions at high latitudes ('polar permafrost') and high altitudes ('mountain permafrost'). However, it must be emphasized that air temperature does not 'cause' permafrost (Williams and Smith 1989), even though it is the result of the energy exchange processes. In particular, the local pattern of discontinuous permafrost distribution can only be explained through an understanding of these processes involved.

The energy balance governing the existence or absence of permafrost is determined by radiative and mass fluxes. It is the driving factor for heating/cooling, evaporation/condensation and the acceleration/delay of chemical processes. The relative magnitude of the different energy balance components varies greatly in space and time as an effect of atmospheric (climatic) and site-specific (microclimatic) factors, which are linked together via intensive interactions and feedback mechanisms. A basic step is to determine which parameters in the energy balance are important to permafrost distribution in mountain areas and to assess their influence. The energy balance equation can be written:

$$Q_R + Q_H + Q_{LE} + Q_G = 0 \quad (1)$$

- $Q_R$  = Net radiation
- $Q_H$  = Sensible heat flux
- $Q_{LE}$  = Latent heat flux
- $Q_G$  = Ground heat flux

Modelling permafrost distribution for a given area must be based on consideration of the energy balance as a function of space and time. Due to the limited information available about the critical parameters and about the complex boundary conditions influencing them, index models consisting of easily-measurable or computable parameters are in most cases applied as reliable tools (Abbey et al. 1978).

Solar radiation ( $K\downarrow$ ) is a climatic factor, which depends on latitude, time (year, day), clouds and atmospheric turbidity. The site-specific effects of the local topography (slope angle, aspect and shading effects of the horizon) are very important, especially in mountain areas where the orientation of a surface with respect to the solar beam is a powerful variable in determining energy income. This effect can lead to considerable differences in the entire energy balance (Oke 1987 p.175). The great variability of  $K\downarrow$  and of the albedo ( $\alpha$ ) strongly influences the local occurrence of permafrost (cf. measurements by Ohmura 1981 or Abbey et al. 1978 for Arctic regions or Schrott 1990, Happoldt and Schrott 1992 for the Andes). Radiation is even of great importance beyond the meso-scale: Cheng (1983) described the worldwide permafrost distribution as a function of latitude and altitude in relation to net radiation. Sensible heat flux  $Q_H$  is determined by eddy conductivity (index for the turbulent transfer) which depends on windspeed (climatic factor), surface roughness (site-specific factor) and the difference between surface and air temperature. The short-term variability of the heat flux can be very large but will be smaller over time scales of years. The overall influence of the air temperature on the energy balance is considerable (Ng and Miller 1977). In comparison with solar radiation and sensible heat, latent and ground heat fluxes are usually considered to be smaller (Oke 1987).

**BTS-MEASUREMENTS**

The temperature at the bottom of the winter snow cover (BTS) is a reliable tool to investigate the distribution of permafrost in areas where the winter snow cover is thick enough (0.8 meter). The method was introduced by Haerberli (1973) and has often been applied since then (e.g. Haerberli and Patzelt 1982, King 1983, Stingl and Veit 1988, Hoelzle 1992). The snow cover with its low heat transfer capacity insulates the soil from short-term variations in the surface energy balance (Keller and Gubler 1993). During the months of February and March, when the snow cover in the Alps is about

one meter thick or more and surface melting is negligible, the BTS remains nearly constant and is mainly controlled by the heat transfer from the upper ground layers, which in turn is strongly influenced by the presence or absence of permafrost (cf. Haeberli 1985, Stoop 1990, Vonder Mühll and Haeberli 1990).

The BTS-measurements used in the present work were performed in six different areas at altitudes between 1800 and 3400 m a.s.l. Five areas are situated within or near the Upper Engadin (eastern Swiss Alps) and one region lies in the northern Swiss Alps (cf. Haeberli et al. 1993).

#### THE EXISTING RULES OF THUMB

##### The original model and its implementation for automated mapping

The original model for predicting permafrost distribution patterns in the Alps was developed as part of the first systematic study on Alpine permafrost in the region of Flüelapass/Piz Grialetsch in the Grisons (Haeberli 1975). On the basis of visual inspection of natural outcrops, active-layer temperatures, ramsonde profiles, seismic refraction, geoelectrical resistivity, temperatures of spring water in late summer/fall, BTS-measurements in high winter, head areas of active rock glaciers, collapsed frontal parts of fossil/relic rock glaciers and bergschrunds above glaciers, about 150 point observations were collected. One important finding was the fact that permafrost mainly occurred in vegetation-free areas (75%) or in the transition zone of pioneer vegetation/alpine meadows (25%) and that permafrost occurrences in areas with well-developed vegetation were rare. In order to differentiate this general picture and to interpolate information from the point observations, empirical *rules of thumb* were derived. Altitude as the parameter reflecting the influence of air temperature and slope aspect as the parameter representing the influence of solar radiation were considered together with the following typical topographic situations representing the influence of snow redistribution:

- slopes steeper than 5 to 10°,
- sites at the foot of high and steep slopes (avalanche runout zones with long-lasting snow),
- flat and wind-protected depressions (cirque floors, etc.) with increased accumulation of winter snow and
- flat and wind-exposed crests and summits with reduced winter snow cover.

The basic assumption behind this procedure was that the sensible heat flux (mean annual air temperature) determines permafrost occurrence at a regional scale (altitudinal belts), that radiation predominantly influences the permafrost distribution pattern at a local scale and that the snow cover with its influence on sensible heat and radiative fluxes (thermal insulation against winter cold, protection against summer heating due to latent heat of fusion, albedo) is being redistributed by wind and avalanches as a function of general topography. A first and rather qualitative but nevertheless quite successful test of the applicability of these *rules of thumb* was the mapping of permafrost distribution patterns in the Hochebenkar region, Austrian Alps (Haeberli and Patzelt 1982) using mainly BTS measurements and seismic refraction soundings. It became evident from this study that the inclusion of surface characteristics (vegetation, fine/coarse material, etc.) could give additional information and that a larger number of BTS measurements would greatly increase the size of the statistical sample for developing more

sophisticated models. Based on the generally encouraging experience, a transformation of altitudinal limits into temperature limits was made for better application in paleoclimatic studies (Haeberli 1982) and written recommendations were handed out to earth scientists and engineers in Switzerland as a help for practical work in mountain areas of the Alps (VAW/ETH 1985). A graphic presentation of the *rules of thumb* is shown by Keller (1992).

A computer program 'PERMAKART' was recently developed to map permafrost distribution in Alpine regions by implementing the *rules of thumb* in the Geographical Information System ARC/INFO (Keller 1992). The basic input for using 'PERMAKART' is a digital terrain model (DTM) which must exist as an ARC/INFO coverage in the form of a contour map or a set of x,y points with the identification code representing z-values. Surface analyses will then create a data base of surface parameters, whereas aspect, slope and elevation values can directly be computed using the triangulated irregular network of the DTM. The significance of the general morphology has to be adjusted for considering sites at the foot of slopes, which receive long-lasting deposits of avalanche snow in spring: a square grid with a mesh-width of 100 meters is calculated taking the concavity of topographic forms into account. With regard to the resolution of the presently available DTM Rimini, a better determination of avalanche deposits would not yield better results. An important task in connection with the data base is the management of the topology, i.e., the mathematical procedure for defining spatial relationships. The data base furnishes the data for the application of the *rules of thumb*. In connection with the topologically determined spatial relationships, the permafrost item can be organized in a triangulated irregular network which represents a thematic permafrost surface. The map of the supposed permafrost distribution is the result of interpolating polygons ranged into three classes separated by the lower limits of possible and probable permafrost respectively (cf. Keller 1992 for more details of the computing procedure). Implementation of the *rules of thumb* in a Geographical Information System now enables fast assessments of plausible permafrost distribution over large mountain areas with complex topography. It also facilitates simulation of possible past and future scenarios of permafrost distribution (for instance: Late glacial time, Little Ice Age, 21st century).

##### Test with BTS measurements

The numerous BTS measurements collected during the past years offer the possibility of investigating the reliability of the original *rules of thumb*. After elimination of soundings on glaciers and lakes, 701 measurements remained for testing.

Figure 1 demonstrates the relation between permafrost occurrence and vegetation cover, confirming that 89% of the investigated permafrost sites are more or less free of vegetation and that 71% of the permafrost-free areas are covered with alpine meadows or forest. Table 1 shows the results of the comparison between the BTS measurements and the *rules of thumb*. According to the original definition of the permafrost zones and boundaries, an unsuccessful prediction was defined as a contradiction to the *rules of thumb* (permafrost found in areas predicted as permafrost-free and permafrost-free sites found in areas with permafrost existence predicted to be probable). The uncertainty range (permafrost possible) was excluded from the test. The mean (weighted) rate of unsuccessful predictions is 25%. In

view of the fact that no topographic differentiation was applied to the test sample, the mean error probability in predicting permafrost areas and permafrost-free areas from the original rules of thumb can be estimated at less than 25%. The safety of the prediction is, however, a function of aspect. Permafrost terrain is especially well predicted for slopes exposed to W, NW, N and NE (12 to 24% error) and permafrost-free terrain can quite safely be delineated on slopes exposed to W, SW and NE (9 to 18% error). Problems mainly exist for permafrost terrain on SW-exposed slopes and in permafrost-free areas exposed to S, SE, E and N, NW, respectively. Such uncertainties have obvious reasons. Concerning SW-exposures, the sample is still too small and does not reach high-enough altitudes to safely predict permafrost areas. In southern to eastern exposures, the special condition of the foot of slopes with long-lasting avalanche snow is responsible for the high error rate in the test when predicting permafrost-free terrain (the full application of the rules of thumb with the topographic differentiation would give considerably better success). On slopes exposed to N and NW, special conditions of extremely reduced solar radiation make predictions of permafrost-free terrain uncertain. Eliminating from the test sample all sites at altitudes below 1900 m a.s.l. which were not considered in the original rules of thumb would reduce the error probability for slopes exposed to N from 50% to 20%. The phenomenon of low-altitude permafrost sites is, however, real and must be dealt with by more appropriate consideration of the energy balance parameters involved.

Table 1. Comparison between the BTS-measurements and the rules of thumb. The test shows the errors from permafrost (BTS < -3°C) areas predicted as permafrost-free and permafrost-free (BTS > -2°C) areas predicted as probable permafrost. The uncertainty range (BTS between -2°C to -3°C: possible permafrost) is excluded from the test.

Exposure	errors (no permafrost in probable permafrost areas)	number of sites
N	18%	34
NE	12%	28
E	-	
SE	-	
S	-	
SW	59%	12
W	13%	62
NW	24%	118
Total	21%	

Exposure	errors (probable permafrost in permafrost-free areas)	number of sites
N	50% (20%)	8
NE	12%	9
E	45%	20
SE	41%	46
S	31%	64
SW	18%	22
W	9%	33
NW	44%	34
Total	32%	

#### DIRECT USE OF POTENTIAL RADIATION AND ESTIMATED AIR TEMPERATURE

Permafrost as well as the BTS are functions of the mean annual surface temperature (MAST) and therefore a result of the entire energy balance at the surface. In the spatial relation between permafrost and energy balance parameters, permafrost can be represented by BTS-measurements and the energy balance by a combination of the mean annual air temperature (MAAT) and the potential direct solar radiation (PR). MAAT and PR can be determined. PR represents the potential energy income as a function of the local topography. Especially in mountain areas, the local topography gives the largest variability of the energy income which, in turn, strongly influences the distribution patterns of discontinuous permafrost. MAAT describes the sensible heat flux.

In order to statistically analyze the relation between permafrost/BTS and the most important energy balance parameters, MAAT was determined for each BTS-point from 27 meteorological stations and by using typical regional values for gradients of air temperature with altitude (Gensler 1978, Hoelzle 1989): values of 0.56°C/100m were chosen in the Upper Engadin, and of 0.60°C/100m in the Northern Alps. In addition, mean daily PR between July to October was computed (during this time interval the investigated areas are more or less free of snow and the radiation has its strongest effects on the surface) for each BTS-point on the basis of a digital terrain model with a mesh-width of 100 meters (Funk and Hoelzle 1992). The uncertainty with respect to estimates of MAAT is about ± 100 meters (± 0.5 to 0.6 °C). The error of the calculated PR is mainly determined by the resolution of the digital terrain model. A higher resolution of the DTM with more precise determination of the surface topography would lead to significant improvements. The first result

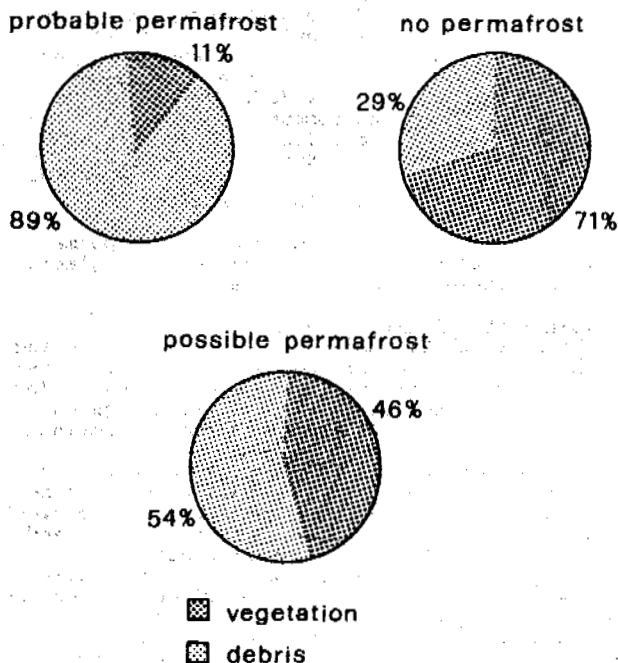


Figure 1. Permafrost distribution and surface characteristics (debris and vegetation). The sample size is N = 701 whereas n = 311 probable permafrost (BTS < -3°C), n = 151 possible permafrost (BTS between -2°C to -3°C) and n = 239 permafrost-free sites (BTS > -2°C).

of statistical analysis with these data was a significant relation between BTS and PR (Hoelzle 1992).

Next the BTS-measurements were grouped into three classes according to their significance with respect to permafrost occurrence:

- A) permafrost probable: BTS equal to or colder than  $-3^{\circ}\text{C}$
- B) permafrost possible (uncertain information): BTS warmer than  $-3^{\circ}\text{C}$  and colder or equal to  $-2^{\circ}\text{C}$
- C) probably no permafrost: BTS warmer than  $-2^{\circ}\text{C}$

The BTS-points which are located in Class B (possible permafrost) were considered to be in a climatic environment where the conditions are just marginal for permafrost existence. MAAT and PR were averaged for all BTS points in this BTS class and for altitude intervals of 100 meters: Figure 2 shows the corresponding relation between MAAT, PR for BTS (Class B). From MAAT =  $-1^{\circ}\text{C}$  (approx. 2300 m a.s.l.) to  $-2.7^{\circ}\text{C}$  (approx. 2800 m a.s.l.) the sample size can be considered representative. Because of avalanche risks and difficult access, the sample is still small for altitudes above 2800 m a.s.l. At altitudes below 2300 m a.s.l., suitable permafrost sites for measuring BTS are not numerous. Nevertheless, a permafrost site at 1800 m a.s.l. was found in the northern Swiss Alps and BTS-values could be measured (Funk and Hoelzle 1992). Two other sites of low-altitude permafrost were found in the north-eastern Swiss Alps (Alpstein group: Bächler 1930) and in the Jura mountains (Creux du Van: Pancza 1988). For each of these sites, PR was calculated and the results plotted on Figure 2.

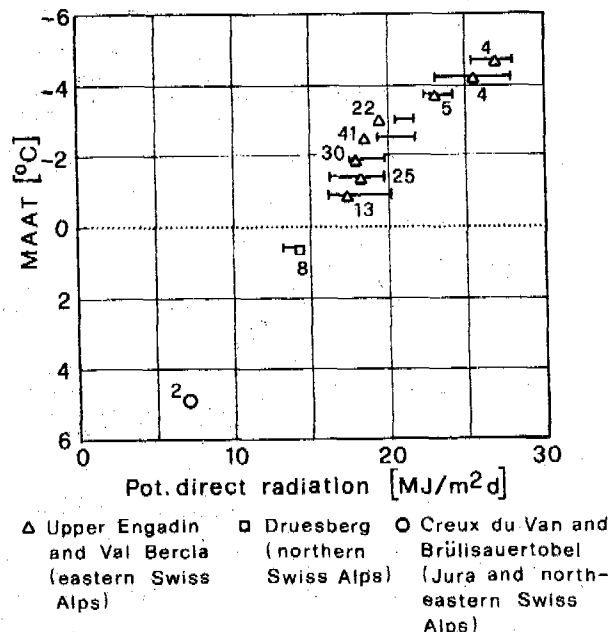


Figure 2. Relation between potential direct solar radiation (PR) and mean annual air temperature (MAAT) at the limit of permafrost existence (BTS between  $-2^{\circ}\text{C}$  to  $-3^{\circ}\text{C}$ : possible permafrost). The numbers represent the count of measurements. The symbols indicate mean values (PR and MAAT) in this BTS-class for altitude intervals of 100 meters. Double bars represent the range where indications of permafrost presence (BTS  $< -3^{\circ}\text{C}$ ) and absence (BTS  $> -2^{\circ}\text{C}$ ) overlap.

Both sites are exposed to the North and have a MAAT of  $4.9^{\circ}\text{C}$  (altitude is around 1150 m a.s.l.) but strongly reduced solar radiation income. Such extreme sites greatly help in extrapolating and assuring the statistically significant relation found within the periglacial belt at higher altitudes. An independent method for checking the relation of Figure 2 consists in calculating the overlap range between the BTS class with no permafrost (C) and the one with probable permafrost (A). By definition of the uncertainty zone (possible permafrost), this zone of mixed information also represents the limits of permafrost existence and should thus be equivalent to the sample used so far. The corresponding overlap ranges are marked by double bars on Figure 2. They indeed confirm the significance of the previously derived relation.

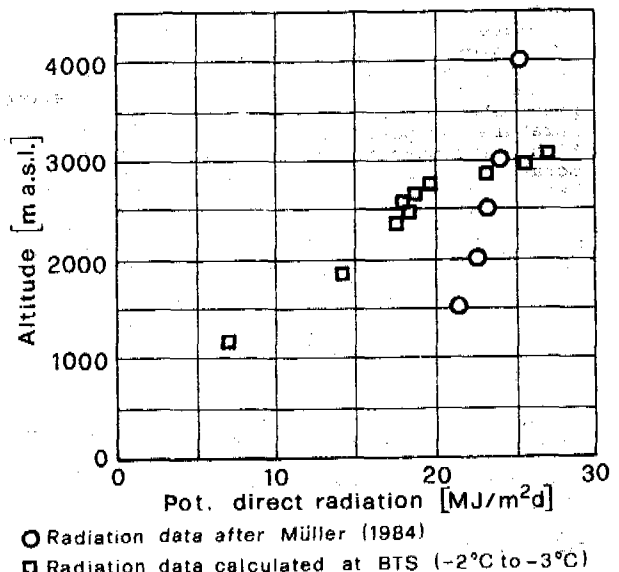


Figure 3. Potential direct radiation and altitude: comparison between measurements on horizontal surfaces after Müller (1984) and values calculated for limits of permafrost existence (BTS between  $-2^{\circ}\text{C}$  to  $-3^{\circ}\text{C}$ : possible permafrost).

Figure 3 shows that the effect of altitudinal increase in incoming direct radiation (circles, Müller 1984, Funk 1985) cannot be responsible for the relationship shown in Figure 2 (squares): the gradients differ by almost an order of magnitude.

With respect to modelling present-day distribution patterns and possible effects of climatic changes on mountain permafrost, the relation found in Figure 2 is an important step forward insofar as altitude and slope aspect of the original rules of thumb can now explicitly be replaced by careful estimates of air temperature and solar radiation as two important energy balance parameters. Transfer of the model to other mountain ranges should thus be possible and modelling effects of climatic changes become more realistic.

BTS, MAST and permafrost are results of the entire energy balance involving the whole set of climatic as well as site-specific factors:

$$\text{BTS} = f(\text{MAST}) = f(Q_R, Q_H, Q_{LE}, Q_G) \quad (2)$$

They are strongly influenced by surface

characteristics such as snow cover, vegetation and debris. The distribution and height of the snow cover are especially significant (Smith and Riseborough 1983, cf. Keller and Gubler 1993): the accumulation of snow in autumn, for instance, heavily influences mean annual ground temperatures (Goodrich 1982, Haerberli 1985, Keller and Gubler 1993). Further improvement of predictive models for mountain permafrost distribution can, therefore, be expected from more realistic treatment of snow redistribution by wind and avalanches in winter and spring, of snow cover duration in early summer (remote sensing) and of ground surface characteristics (water content, coarse debris, bedrock, etc.).

#### CONCLUSIONS

The often-used rules of thumb for predicting permafrost distribution in high mountain areas of the Swiss Alps were tested with a great number of BTS measurements and have been used in the Geographical Information System for automated mapping of permafrost distribution over large mountain areas with complex topography. Further analysis of the large BTS sample showed that a close relationship exists between permafrost occurrence, mean annual air temperature and potential direct solar radiation. With computer-derived estimates for air temperature and solar radiation, more physically-based modelling of present-day permafrost distribution patterns (plus effects from past and potential future climatic changes) are possible. Further progress towards consideration of the full energy balance could be made by taking into account the snow-cover and ground surface characteristics as well as by using higher-resolution digital terrain models.

#### ACKNOWLEDGEMENTS

The investigations described in the present paper were funded by the Federal Institute of Technology Zurich (ETH). The assistance of a number of colleagues is gratefully acknowledged. Bruno Nedela prepared the drawings.

#### REFERENCES

Abbey, F.L., D.M. Gray, D.H. Male, and D.E.L. Erickson (1978) Index models for predicting ground heat flux to permafrost during thawing conditions. Third International Conference on Permafrost. NRC-Ottawa. 1, 4-9.

Bächler, E. (1930) Der verwünschte oder verhexte Wald im Brüeltobel. Appenzeller Kalender. 209.

Cheng, G. (1983) Vertical and horizontal zonation of high-altitude permafrost. Fourth International Conference on Permafrost. Fairbanks. 1, 136-141.

Dingman, S.L. and F.R. Koutz, (1974) Relations among vegetation, permafrost, and potential insolation in Central Alaska. Arctic and Alpine Research. 6(1), 37-42.

Funk, M. (1985) Räumliche Verteilung der Massenbilanz auf dem Rhonegletscher und ihre Beziehung zu Klimaelementen. Zürcher Geographische Schriften. Geographisches Institut ETH Zurich. 24, 183pp.

Funk, M. and M. Hoelzle (1992) Application of a potential direct solar radiation model for investigating occurrences of mountain permafrost. Permafrost and Periglacial Processes. 3(2), 139-142.

Gensler, G.A. (1978) Das Klima von Graubünden. Habilitationsschrift an der Universität Zurich. Schweizerische Meteorologische Anstalt Zurich. 112pp.

Goodrich, L.E. (1982) The influence of snow

cover on the ground thermal regime. Canadian Geotechnical Journal. 19, 421-432.

Gorbunov, A.P. (1978) Permafrost investigations in high-mountain regions. Arctic and Alpine Research. 10(2), 283-294.

Greenstein, L.A. (1983) An investigation of midlatitude alpine permafrost on Niwot ridge, Colorado Rocky Mountains. Fourth International Conference on Permafrost. Fairbanks. 1, 380-383.

Haerberli, W. (1973) Die Basis-Temperatur der winterlichen Schneedecke als möglicher Indikator für die Verbreitung von Permafrost in den Alpen. Zeitschrift für Gletscherkunde und Glazialgeologie. 9, 221-227.

Haerberli, W. (1975) Untersuchungen zur Verbreitung von Permafrost zwischen Flüelapass und Piz Grialetsch. Mitteilung der Versuchsanstalt für Wasserbau, Hydrologie und Glaziologie ETH Zurich. 17, 221pp.

Haerberli, W. (1982) Klimarekonstruktion mit Gletscher-Permafrost-Beziehungen. Materialien zur Physiogeographie. 4, 9-17.

Haerberli, W. and G. Patzelt, (1982) Permafrostkartierung im Gebiet der Hochebenkar-Blockgletscher, Obergurgl, Oetztales Alpen. Zeitschrift für Gletscherkunde und Glazialgeologie. 17, 127-150.

Haerberli, W. (1985) Creep of mountain permafrost: internal structure and flow of alpine rock glaciers. Mitteilung der Versuchsanstalt für Wasserbau, Hydrologie und Glaziologie ETH Zurich. 77, 142pp.

Haerberli, W. (1992) Construction, environmental problems and natural hazards in periglacial mountain belts. Permafrost and Periglacial Processes. 3(2), 111-124.

Haerberli, W. M. Hoelzle, F. Keller, W. Schmid, D. Vonder Mühli, and St. Wagner (1993) Monitoring the long-term evolution of mountain permafrost in the Swiss Alps. Sixth International Conference on Permafrost. Beijing. This volume.

Happoldt, H. and L. Schrott (1992) Ground thermal regime and global radiation exemplified by an active rock glacier, High Andes of Argentina. Permafrost and Periglacial Processes. In press.

Harris, S.A. (1981) Climatic relationships of permafrost zones in areas of low winter snowcover. Arctic. 34(1), 64-70.

Hoelzle, M. (1989) Untersuchungen zur Permafrostverbreitung im Oberengadin. Diploma thesis ETH Zurich. 79 pp.

Hoelzle, M. (1992) Permafrost occurrence from BTS-measurements and climatic parameters in the Eastern Swiss Alps. Permafrost and Periglacial Processes 3(2), 143-147.

Jorgenson, M.T. and R.A. Kreig (1988) A model for mapping permafrost distribution based on landscape component maps and climatic variables. Fifth International Conference on Permafrost. Trondheim. 1, 176-182.

King, L. (1983) High mountain permafrost in Scandinavia. Fourth International Conference on Permafrost. Fairbanks. 1, 601-605.

Keller, F. (1992) Automated mapping of mountain permafrost using the program PERMAKART within the geographical information system ARC/INFO. Permafrost and Periglacial Processes. 3(2), 133-138.

Keller, F. and H.U. Gubler (1993) Interaction between snow cover and Alpine permafrost. Sixth International Conference on Permafrost, Beijing. This volume.

Müller, H. (1984) Zum Strahlungshaushalt im Alpenraum. Mitteilungen der Versuchsanstalt für Wasserbau, Hydrologie und Glaziologie ETH Zurich. 71, 167 pp.

Ng, E. and C. Miller (1977) Validation of a model of the effect of tundra vegetation on soil temperature. Arctic and Alpine Re-

- search. 9(2), 89-104.
- Ohmura, A. (1981) Climate and energy balance on Arctic Tundra. Zürcher Geographische Schriften. Geographisches Institut ETH Zurich. 3, 183 pp.
- Oke, T.R. (1987) Boundary layer climates. Second edition. Cambridge University Press. 435 pp.
- Pancza, A. (1988) Un périgelisol actuel dans le Jura Neuchâtelois. Bulletin de la Société neuchâteloise. 32/33, 129-140.
- Schrott, L. (1991) Global solar radiation, soil temperature and permafrost in the Central Andes, Argentina: a Progress Report. Permafrost and Periglacial Processes. 2, 59-66.
- Smith, M.W. and D.W. Riseborough (1983) Permafrost sensitivity to climatic change. Fourth International Conference on Permafrost. Fairbanks. 1, 1178-1183.
- Stingl, H. and H. Veit (1988) Fluviale und solifluidale Morphodynamik des Spät- und Postglazials in den südlichen Hohen Tauern im Raum um Kals/Osttirol. Deutscher Arbeitskreis für Geomorphologie. Exkursionsführer Osttirol-Dolomiten, Bayreuth. 5-69.
- Stoop, P. (1990) Ueber den Wärmehaushalt eines alpinen Permafrostgebietes. Diploma thesis ETH Zurich. 79 pp.
- VAW/ETHZ, (1985) Tips und Faustregeln für die Abschätzung der Permafrostverbreitung in den Alpen. Unpublished.
- Vonder Mühl, D. and W. Haeberli (1990) Thermal characteristics of the permafrost within an active rock glacier. Journal of Glaciology. 36(123), 151-158.
- Williams, P.J. and M.W. Smith (1989) The Frozen Earth. Fundamentals of Geocryology. Cambridge University Press. 306 pp.



## EXPERIMENTAL STUDY OF THE EFFECTS OF IMPURITIES ON ICE CREEP AT $-1^{\circ}\text{C}$

Huang Maohuan, Li Gang, Miao Lina and Jin Zhengmei  
State Key Laboratory of Frozen Soil Engineering, Lanzhou Institute of  
Glaciology and Geocryology, Chinese Academy of Sciences, China

Polycrystalline ice specimens were prepared with carborundum powder, ranging in size from  $6\phi$  to  $7\phi$ , and soluble impurities.

Specimens with different impurity concentrations were experimented with uniaxial compressive creep apparatus under  $0.42\text{ MPa}$  constant stress at  $-1^{\circ}\text{C}$ . As compared with the creep of the ice without impurity it is found that solid impurities are able to drag the creep development of ice, to postpone the appearance of minimum creep rate, and to slightly increase the minimum creep rate, where as chemical impurities in the concentration magnitude of  $\text{mg/g}$  are able to increase the minimum creep rate more significantly.

### INTRODUCTION

An enhanced flow rate is always observed in the dirty basal ice beneath a glacier, for example, under Camp Century in Greenland (Shoji & Langway, 1984). Observations in a tunnel excavated close to the bed of Urumqi Glacier No.1, China, also discovered that the effective viscosity of a debris-laden basal layer,  $0.35\text{ m}$  in depth, is more than two orders of magnitude less than the overlying clean ice (Echelmeyer & Wang, 1987). These in site observations give rise to the conclusion that solid impurities in ice cause substantially higher flow rates. But there is little laboratory support for the conclusion (Budd & Jacka, 1989). There were not many experiments, especially of long-term creep, about this. Li et al (1992a) have taken debris-laden ice at the position near the tunnel for constant stress creep experiments under  $-1^{\circ}\text{C}$ , but no observable change was revealed when debris concentrations was less than 2.5% by volume. Again Li et al (1992b) prepared ice specimens with carborundum powder ranging from  $4\phi$  to  $6\phi$  and sent them to experiment under the same conditions. It was found that the creep rates have increased by a factor of 3, at the most. Budd and Jacka (1989) pointed out that because of the disparity of the various laboratory results reported, the flow rates for ice with a wide range of solid impurities needs extensive further study, including possible chemical effects associated with the solid impurities. This time we dispersed much finer carborundum, and prepared ice specimens from distilled and non-distilled water. Experiments reveal that solid impurities are able to enhance creep rates of ice slightly, where as chemical impurities enhance it significantly.

Our experiments are characterized by high temperature, fine solid impurities and a large strain.

### SPECIMEN PREPARATION

Specimens were prepared in two stages. In the first stage artificial polycrystalline ice was made stratified with carborundum powder layers in a plate. In a cold room at the temperature of about  $-12^{\circ}\text{C}$  a thin layer of distilled water was poured into the plate. When the water was frozen, a little carborundum powder was casted on the ice, and again poured a thin layer of water. After the ice was formed, we again casted powder. This procedure was repeated. In the second stage, the stratified ice prepared in the first stage was crushed and sifted with a  $5\text{ mm}$  sieve, and then put into a specific mould,  $61.8\text{ mm}$  in diameter, mixed with a little carborundum powder. Distilled water at  $0.5^{\circ}\text{C}$  was injected from the bottom of the mould in such a way that the water level rose slowly in order to drain the air away from the porosity, as far as possible. To minimize the grain being washed away by injected water, the mould bottom had a porous plate covered by filtered paper. When the mould was full it was removed to a cold room and frozen at  $-12^{\circ}\text{C}$ . The mould could draw off one day late. The specimen was cut to  $150\text{ mm}$  in length required for testing. Its two ends were carefully polished and strictly oriented perpendicular to the specimen axis. The prepared specimens have relative homogeneous dispersion of powder. A specimen was cut in three and their powder concentrations were determined. What was determined showed that the powder concentration of the lower piece was higher than the upper piece, with a relative error of 2.5%. Ice crystal size was less than  $5\text{ mm}$  and c-axis randomly oriented because the ice grains were put into the mould randomly.

Particle-size analysis by pipet method revealed that the mixed carborundum powder, No.M1, ranged in size from  $6\phi$  (64.42%, medium silt) to  $7\phi$  (28.36%, fine silt).

## METHOD OF EXPERIMENT

The experiment was conducted on a compressive creep apparatus with constant stress. It was loaded by a weight, which drew a specific cam through a wire rope and then compressed the specimen. The constant stress error was  $\pm 1\%$ . The applied constant stress was 0.42 MPa. The displacement between the upper and lower die blocks was measured by a high resolution displacement sensor. There was a load cell on the upper die block. The sensor and cell were connected to a data logging corrector. The apparatus was installed in an ordinary room. The testing section of the apparatus was encased in a chest, in which the temperature was kept constant by a temperature controlling system which was connected to a refrigerator. The refrigerator supplied cold air to the chest when it was in operation. The temperature was controlled at  $-1 \pm 0.1^\circ\text{C}$  during the experiment. The specimens were cased by rubber to avoid evaporation when they were ready. Before loading they were kept in the constant temperature chest for 24 hours to insure their temperature state was constant. We began by loading the variations in load, displacement and temperature into the data logging collector which was connected with the load cell, displacement sensor and thermometer. In case of loading departure, the weight was regulated to correct it. The experiment was concluded as 10% axial strain was obtained.

Chemical analysis of specimens was performed in an ion chromatograph.

## RESULTS AND ANALYSES

Eight specimens were tested successfully. Two of them (No.15 and 16) as a standard were prepared from distilled water without carborundum. Other six contained dispersed carborundum powder of 5.4%, 8.7%, 15.1%, 9.8%, 12.5% and 14.3% by volume, i.e., 17.9%, 28.2%, 49.8%, 32.2%, 41.4% and 47.3% by weight, respectively. Two of them (No.19 and 20) were prepared from non-distilled water containing a few chemical impurities.

The experimental results are given in Table 1.

Table 1. Summary of creep experiments

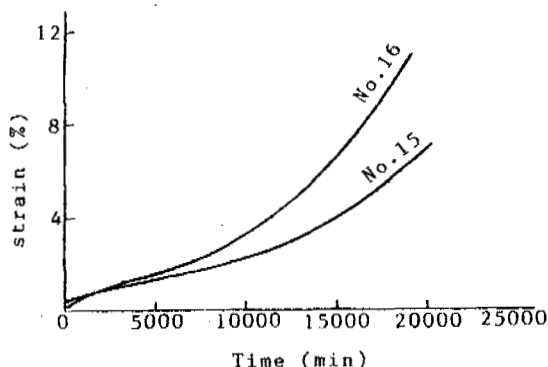
No	Concentration of Carborundum (% by volume)	Density ( $\text{kg}/\text{m}^3$ )	Time to minimum (min)	$\dot{\epsilon}$ ( $10^{-6} \text{S}^{-1}$ )		
				$\dot{\epsilon}_{\min}$ ( $\epsilon_{\min}$ )	$\dot{\epsilon}_{10\%}$	$\dot{\epsilon}_{\text{end}}$ ( $\epsilon_{\text{end}}$ )
15	0	892	3960	0.026 (1.2%)		0.115 (7.0%)
16	0	900	2650	0.053 (1.0%)	0.196	0.200(11.0%)
17	5.4	956	2640	0.098 (2.3%)	0.144	0.144(11.1%)
18	8.7	1058	4370	0.082 (2.7%)	0.105	0.105(10.8%)
21	12.5	1316	11730	0.035 (4.6%)		0.110 (9.7%)
22	14.3	1360	8300	0.078 (6.6%)	0.120	0.120(10.1%)
19	15.1	1391	2500	0.26 (7.4%)	0.28	0.33 (10.5%)
20	9.8	1173	880	1.10 (7.4%)	1.19	1.60 (23.4%)

The creep curves of specimens with carborundum and from non-distilled water (No.19 and 20) are shown in Figure 3. Their  $\dot{\epsilon}_{\min}$  are enhanced by a factor of at least 5, as compared with ice from distilled water (Table 1).

After, experiment specimens without carborundum (No.15) and from non-distilled water

including the minimum creep rate,  $\dot{\epsilon}_{\min}$ , creep rate at the end of the experiment,  $\dot{\epsilon}_{\text{end}}$ , their strain,  $\epsilon_{\min}$  and  $\epsilon_{\text{end}}$  and the appearance time of  $\dot{\epsilon}_{\min}$ , respectively. When  $\epsilon_{\text{end}} > 10\%$ , creep rate at  $\epsilon = 10\%$ ,  $\dot{\epsilon}_{10\%}$ , is given.

The creep curves of specimens without carborundum (No.15 and 16) are shown in Figure 1. A creep curve of initially isotropic polycrystalline ice, as shown in Figure 1, can be distinguished into three stages: primary, secondary and tertiary.  $\dot{\epsilon}_{\min}$  occurs in the secondary stage, and then the creep is followed by an accelerating phase to an asymptotic steady state, tertiary stage, when tertiary creep rate,  $\dot{\epsilon}_{\text{ter}}$ , occurs.  $\dot{\epsilon}_{10\%}$  is approximated to  $\dot{\epsilon}_{\text{ter}}$  (Budd & Jacka, 1989, Li et al, 1992a, b). A similar result has been found to apply for the creep of frozen soil (Ting, 1983).



The creep curves of specimens with carborundum (No.17, 18, 21 and 22) are shown in Figure 2. In Figure 2 no relation between solid impurity concentration and creep rate has been demonstrated. The appearance of  $\dot{\epsilon}_{\min}$  for every curve was postponed to  $\epsilon_{\min} = 2.3\%$ , event to 6.6%. The three stages are not so obvious as in Figure 1, except No.21.  $\dot{\epsilon}_{10\%}/\dot{\epsilon}_{\min}$  for No.21 is 3.1, but 1.5, 1.3 and 1.5 for the others.  $\dot{\epsilon}_{10\%}$  appears to have not reached  $\dot{\epsilon}_{\text{ter}}$  yet.

(mixture of No.19 and 20) were sent to analyse their concentrations of chemical impurities (Table 2). From Table 2 we can see that the total soluble concentration of the mixture of specimens No.19 and 20 is increased by a factor of 10. The main ion is  $\text{SO}_4^{2-}$ .

It will be noted that the experimental results

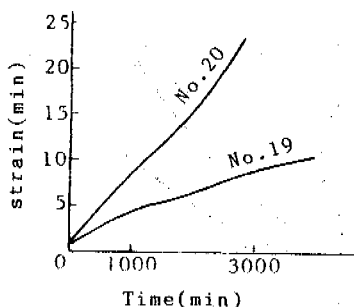
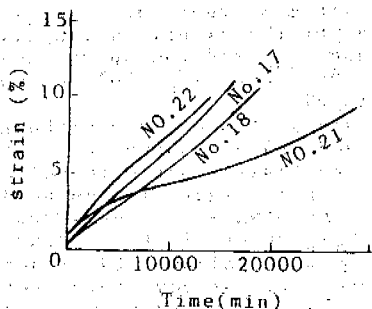


Table 2. Concentration of soluble impurities (mg/g)

No.	Na <sup>+</sup>	K <sup>+</sup>	Cl <sup>-</sup>	SO <sub>4</sub> <sup>2-</sup>	NO <sub>3</sub> <sup>-</sup>	Total
15	0.061	0.000	0.092	0.005	0.000	0.158
Mixture of 19, 20	0.109	0.438	0.021	1.027	0.000	1.595

are comparable for the specimens that were prepared with the same technological process, and tested with the same apparatus under the same temperature and load conditions. However, the repetition for every set of specimens is poor, as shown in Table 1 and Figures 1-3. There must be something else at work.

## DISCUSSION

1. From Table 1 we can see first that impurities postpone the appearance of  $\dot{\epsilon}_{min}$ , correspondingly  $\epsilon_{min}$  increased two or more times. The steady-state  $\dot{\epsilon}_{ter}$  is also postponed and  $\epsilon_{10\%}$  has not reached  $\dot{\epsilon}_{ter}$  yet. Impurities appears to drag the recrystallization of ice. In the creep experiment of ice containing ultrafine (150 Å) amorphous silica (Nayar et al, 1971) the drag could also be recognized. In another creep experiment of ice with sand (Gao, 1989) it also can be seen that the appearance time of  $\dot{\epsilon}_{min}$  is 4.5-9 times longer than with clean ice, correspondingly  $\epsilon_{min}$  increases to 2.8% on the average, even to 4.2%.

2. We can see secondly that  $\dot{\epsilon}_{min}$  of ice dispersed with impurities is higher than that

without impurities, and the same with  $\dot{\epsilon}_{ter}$ . But  $\epsilon_{10\%}$  of the former is no higher than that of the latter, because  $\epsilon_{10\%}$  of the latter is approximated to its  $\dot{\epsilon}_{ter}$ , and  $\epsilon_{10\%}$  of the former has not reached its  $\dot{\epsilon}_{ter}$  yet. Of the initial isotropic polycrystalline ice,  $\dot{\epsilon}_{ter}/\dot{\epsilon}_{min}$  is usually about 3 for compression (Budd & Jacka, 1989). According to this most  $\epsilon_{10\%}$  in Table 1 have not reached  $\dot{\epsilon}_{ter}$  yet. Furthermore many researchers would like to use  $\dot{\epsilon}_{min}$  to distinguish whether the creep rate is enhanced by impurities (cf. Nayar et al, 1971; Hooke et al, 1972; Ting, 1983).

In a creep experiment on ice containing dispersed fine sand under -9.4 - -7.4°C Hooke et al (1972) found that creep rate in ice with low sand concentrations were in some case higher, and in other case lower than in clean ice. However with high sand concentrations, say higher than 10% by volume, the creep rate decreases exponentially with increasing volume fraction sand.

In their experiment Nayar et al (1971) discovered that silica dispersion strongly decreases creep in ice, resulting in steady state creep rates in a 1-volume % dispersion 10-30 times slower than in pure ice. They also pointed out that the influence of the dispersed phase in ice is stronger at lower temperatures, -11.9°C, than at higher temperatures, -4.8°C. From the experimental results at -3.3°C of Gao (1989) it also can be seen that  $\dot{\epsilon}_{min}$  slightly decreases in the ice with 11% of sand by volume. In experiments at -1°C conducted by Li et al (1992a, b), as mentioned above, no observable change, or at the most a 3 times increase in the creep rate, has been found.

To sum it up, in the discussed concentration range, solid impurities are able to decrease creep rate at lower temperature (<-10°C), there is no observable influence in general, and a slightly increased creep rate at high temperatures (>-1°C). Ice at high temperatures appears to reduce its melting point, enhancing its flow owing to dispersion of solid impurities associated with chemical impurities.

A summary of relevant studies is give in Table 3.

3. Two forms of chemical impurities have been shown to affect the flow of ice. First, trace concentrations of certain dopants, such as HF, have been found to increase the ice flow rate substantially. Second, relatively larger concentrations of more common natural chemicals, such as sea salt, can increase the flow rates of ice (Budd & Jacka, 1989). We have not made a trace analysis, but from Table 1 we can see that a larger enhancement of the creep rate may be attributed to the latter. However, salinity of 1 mg/g appears to have less of an increase on the creep rate of artificial frozen alluvial sand according to an experiment at -10°C carried out by Ogata (1983). Chemical impurities may become active near the melting point, such as -1°C we made experiments at.

The more than 5 times enhancement of  $\dot{\epsilon}_{min}$  of specimens No.19 and 20 over ice from distilled water may be attributed to combination of solid and chemical impurities, of which the mechanism needs further investigation. The discovery in Urumqi Glacier No.1 (Echelmeyer and Wang, 1987) can be explained by the combination of solid and chemical impurities, which may create lower melting point in high stress zones around the solid inclusions, resulting in enhancing creep rate.

Table 3. Summary of relevant studies

Worker(s)	Method	Temperature of experiment or observation (°C)	Impurities and concentration (by volume)	Change in strain rate relative to clean ice
Echelmeyer & Wang (1987)	1	-2	mainly gravel, 40%	115 times increase
Hooke et al (1972)	3	-9.4 - -7.4	fine sand, <10%, >10%	in some case increase & in other case decrease $\dot{\epsilon}_{\min}$ decrease exponentially
Nayar et al (1971)	3	-22 - -2	ultrafine silica, <1%	$\dot{\epsilon}_{\text{ter}}$ 10-30 times decrease
Gao (1989)	3	-3.3	sand, <11%	$\dot{\epsilon}_{\min}$ slightly decrease
Li et al (1992a)	2	-1	mainly medium sand <2.5%	no observable
Li et al (1992b)	3	-1	silt, <11%	1.5-2.4 times increase
This paper	3	-1	silt, <15% silt & chemical	$\dot{\epsilon}_{\min}$ slightly increase $\dot{\epsilon}_{\min}$ increase >5 times

Note Method: 1 — observation in ice tunnel; 2 — experiment on glacial ice;  
3 — experiment on laboratory prepared ice.

### CONCLUSION

- (1) Solid impurities are able to drag the creep development of ice, and postpone the appearance of  $\dot{\epsilon}_{\min}$  and of  $\dot{\epsilon}_{\text{ter}}$ .
- (2) Under  $-1^{\circ}\text{C}$  solid impurities alone enable ice to increase its creep rate slightly.
- (3) Chemical impurities enable ice to increase its creep rate significantly.
- (4) Extensive further study is needed to verify whether chemical impurities alone or associated with solid impurities contribute to the enhanced creep rate that was observed in the experiments on ice containing carborundum powder prepared from non-distilled water.

### ACKNOWLEDGEMENTS

We thank Deng Yousheng and Sun Weizhen for chemical and particle-size analyses.

### REFERENCES

- Budd, W.F. and T.H. Jacka (1986) A review of ice rheology for ice sheet modelling. *Cold Regions Science and Technology*, 16(2), 107-144.
- Echelmeyer, K. and Wang Zhongxiang (1987) Direct observation of basal sliding and deformation of basal drift at subfreezing temperatures. *Journal of Glaciology*, 33(113), 83-98.
- Gao Xiangqun (1989) Laboratory studies of the development of anisotropic crystal structure and flow properties of ice. Ph. D. Thesis, Meteorology Department, The University of Melbourne.
- Hooke Roger LeB., Brian B. Dahlin and Michael T. Kouper (1972) Creep of ice containing dispersed fine sand. *Journal of Glaciology*, 11(63), 327-336.
- Li Gang, Huang Maohuan, Wang Maohai and Wang Wenti (1992a) Constant stress experiments on

- dirty glacial ice. Annual Report on the Work at Tianshan Glaciological Station (In Chinese).
- Li Gang, Wang Maohai, Huang Maohuan and Wang Wenti (1992b) Experimental study of the influence of mixing silt on ice creep. *Chinese Science Bulletin*, 37(21), 1827-1830.
- Nayar H.S., F.V. Lenel and G.S. Ansell (1971) Creep of dispersion of ultrafine amorphous silica in ice. *Journal of Applied Physics*, 42(10), 3786-3789.
- Ogata N., M. Yasuda and T. Katsoka (1983) Effects of salt concentration on strength and creep behavior of artificially frozen soils. *Cold Regions Science and Technology*, 8(2), 139-153.
- Shoji, H. and C.C. Langway (1984) Flow behaviour of basal ice as related to modelling considerations. *Annals of Glaciology*, 5, 141-148.
- Ting John M. (1983) On the nature of the minimum creep rate-time correlation for soil, ice and frozen soil. *Canadian Geotechnical Journal*, 20(1), 176-182.

THE DESERTIFICATION IN THE PERMAFROST REGION OF THE QINGHAI-XIZANG PLATEAU AND ITS INFLUENCES ON THE ENVIRONMENT\*

Huang Yizhi, Guo Dongxing and Zhao Xiufeng

Lanzhou Institute of Glaciology and Geocryology,  
Chinese Academy of Sciences, China

Desertification has been caused by the special geographical and geological conditions in the permafrost region in the Qinghai-Xizang Plateau. The widespread sand deposits results in a great decline of the permafrost upper table, an increase in ground temperature and the retreat of permafrost, which in turn provides favourable conditions for desertification. A special periglacial process—the process of sand-erosion slumping developed in most sand-covered regions is also discussed in this paper.

THE LANDFORM TYPES OF THE SAND DEPOSITS

The desertification problems in permafrost regions especially the influences of sand deposits on frozen ground have gradually caught specialists' attention in recent years (Wang Shaoling, 1989, Huang Yizhi, 1991). The sand deposits in the permafrost region on the Qinghai-Xizang Plateau can be divided into three types according to their geomorphic forms: The sand deposit of the first type covers a large area as a layer of sand but with no apparent wind-drift sand landforms. It is wide-spread in all the areas except the middle and upper part of high mountains and part of the mountainous region. This type of sand deposit developed relatively early and can be dated back to 21.7 Ka B.P. according to Wang Shaoling (Wang Shaoling, 1989, C<sub>14</sub> dating of the humus layer in the sand in the sand deposit near a little river in the north of Wudaoliang). The vegetation in the sand distribution area of this kind is relatively good; The second sand deposit type is presented as non-active or sub-active sand dunes on which drought-enduring plants grow sparsely such as the *Stipa sabulosa* Turca and the *Cyperaceae*. This type of sand deposit occurs mostly in high plateaus, River valleys and basins, and mostly develops in the regions such as from Budongquan, Qingshui River, Wudaoliang basin and nearby areas, from Xiushui River to Beilu River and Tuotuo River basin. These sand covered areas are characterized by undulated topography and the developing age of these sand covers is later than that of the first type. The third type of sand deposit appears mainly in the valleys and some footslopes as modern active dunes, longitudinal dunes, etc. The dunes are very active. This can be shown by the dune in the north of Xidatan which moved a distance of 88.4 m in 22 years and the dune on the south bank of Hongliang River which has

moved more the 50 m across the highway from west of east.

THE NATURAL CONDITIONS RESULT IN DESERTIFICATION IN THE PERMAFROST REGION ON THE QINGHAI-XIZANG PLATEAU

In a high latitude permafrost region, the well-developed vegetation, relatively high precipitation and snow cover in winter and spring can resist desertification. Contrary to this, the following conditions on the Qinghai-Xizang Plateau, which is located in a middle latitude, are most favourable for the formation and development of desertification:

1). Abundant sand source. Glacial and glacio-fluvial deposits caused by glaciation in the Quaternary period and modern times, are wide spread on the Qinghai-Xizang Plateau. Combined with the cryogenic weathering processes in the periglacial environment, they provide a rich sand source for desertification. 2) Strong wind action, high evaporation, low and unequally distributed precipitation. According to Wudaoliang and Tuotuo River Meteorological Stations in the interior of the plateau, the mean annual wind velocity is about 5 m/s and the mean month wind velocity from Dec. to March is above 6 m/s. The gale days in a year are above 140 d. The maximum wind velocity is 28 m/s. The sand storm days in a year are between 15-22 days and can reach 28 days in some years. The annual precipitation is about 200 mm which is higher than that of arid desert regions in China, but 85 percent of the precipitation is concentrated in the warm period (from June to Sept.). Almost no precipitation occurs from Nov. to March with the maximum monthly precipitation no more than 2 mm during this period. The continual no-recorded precipitation days in many years are 102 days. The mean annual evaporation is 1421.0 mm which is about seven times that of the mean annual precipitation. No stable snow cover exists in

\*This work is supported by the NSFC.

winter and spring and the surface ground is extremely arid. This arid period coincides with the gale period on the plateau. 3) The small and sparse, slowly growing vegetation with short growing season due to the cold-arid climate on plateau. Only a little drought and cold-enduring herbaceous species grow in the short warm period from July to Sept. Their resistance to desertification is weak and the vegetation is difficult to recover when destroyed.

#### THE INFLUENCES OF SAND COVER ON FROZEN GROUND

The mean annual air temperature in the permafrost region on the Qinghai-Xizang Plateau is about  $-3 - -6^{\circ}\text{C}$  and the permafrost is continuously distributed in most of the region. But the high solar radiation and special geological tectonics result in unstable permafrost with high temperatures and a thin thickness. The permafrost is sensitive to environmental changes and the permafrost changes are easily caused by the changes of ground surface conditions.

The existing permafrost layer prevents the seepage of the water in the shallow layer and thus increases the soil moisture which is favorable for plants. That is why desertification in the permafrost region is under control. However, for the reasons as mentioned above, the desertification on the Qinghai-Xizang Plateau is prevalent. In unstable permafrost regions especially where the mean annual ground temperature is above  $-1.5^{\circ}\text{C}$ , the temperature range and the depth of seasonal thawed layer are increased and the soil layer near the ground surface become drier because of water seepage if the ground surface is covered by sand. That is unfavorable for plants and makes the wind drifts more active. Fig.1 shows the comparative observation data of ground temperature in an observation field located in the desert area of the Qumar high plateau. (a) The ground temperature distribution where the natural ground surface is occupied by sparse vegetation. The maximum seasonal thaw depth is 3.0 m. (b) The ground temperature distribution where man-made sand cover with a depth of 0.2 m is made. The maximum seasonal thaw depth is 4.95 m. Obviously the seasonal thawed depth is increased by 60 percent in sand cover areas. Fig.2 shows the ground temperature distribution near the above field. a. In natural ground surfaces near a dune. b. Drill-hole observation data under the center of the non-active dune which is 1.6 m high and its diameter is 20 m. The same thermometer was used. The similar changing trend of the permafrost upper table can be seen and the mean annual ground temperature under the dune is  $0.2^{\circ}\text{C}$  higher than that under the nearby natural ground surface.

This trend was also verified by former observation data. In mountainous regions not covered by sand the permafrost was characterized by a thin seasonal thawed depth, low ground temperature and thick permafrost layer, while under the sand cover a different trend exists. This can be shown by the following examples: In Tuotuo River basin where a paleosand deposit was developed, almost all the permafrost under the paleosand dune has disappeared, but the permafrost with a certain thickness still exists in depressive areas among the dunes. The above phenomena can be seen more clearly near permafrost limits as in Fig.3. The data was collected in Liangdao River to the south of the Tanggula Mts. (a) On a swamp land with developing vegetation. (b) On a sand covered area within 2 km from the former

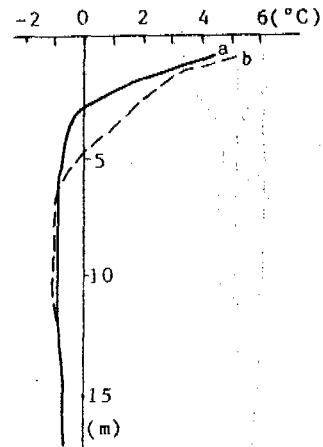


Figure 1. The observation on seasonal thawed depth in a man-made sand covered field

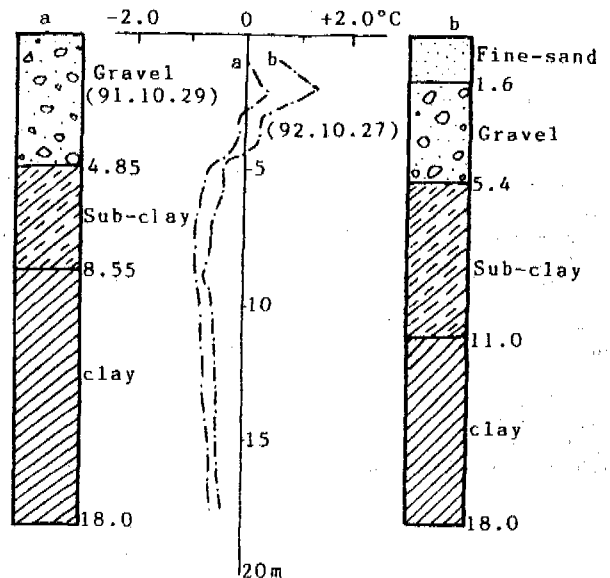


Figure 2. The influences of non-active dunes on frozen ground temperature

location. The thickness of permafrost can be about 60 meters, but in sand cover areas the permafrost disappeared.

The influences of sand cover on frozen ground can be clearly seen by the above facts. The sand cover accelerates the degradation of permafrost which is more evident in high temperature permafrost regions.

#### A SPECIAL FROST-THAW GEOMORPHOLOGICAL PROCESS CAUSED BY SAND DEPOSIT-SAND EROSION SLUMPING

The sand-drifts greatly changed the landscape in permafrost regions. It may also cause special frost-thaw processes as the sand erosion slumping.

The linear step stretching from several hundred meters to several kilometers with a height from tens of centimeters to above 3 meters is often distributed along the Qinghai-Xizang highway. Their genesis is undiscussed. We discovered from investigation that they are all located

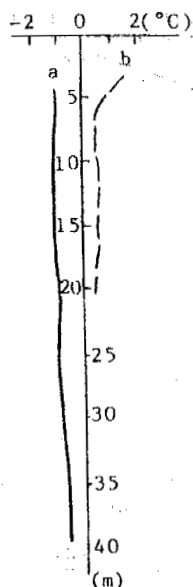


Figure 3. The influences of sand cover on frozen ground

above the sand layer and are caused by the water erosion on sand deposits. Their retreat velocity can be more than 1 m/y.

A sand erosion slumping has developed at the footslope of a arc-like hill to the south of Beiluhe. Its strike is NE-SW and it stretches more than 3 km. The height of the step is from 1 m to 3 m. The slumping material is relatively pure fine sand. The slope of the slumping is about 3-5° and is covered by vegetation whose coverage is above 70 percent. The sand layer of the slumping seems like the first sand type based on their landform. The thickness of the sand is 3.5-4.0 m according to radar prospection (Fig.4).

The origin of this kind of slumping is obviously different from the common slumping which is caused by exposed ground ice, for no obvious ground ice had been found. A over-saturated layer may be seen at the lower part of the step from which ground water seeps out. According to this, the slumping is caused by the concentration of melted water near the frozen layer and the water brings out the sand in its flow thus causing the upper sand layer to lose support and slump down. The sand that is slumped down is again brought away by spring water and the slumping is in continuous development. As the slumping material is sand and the motivating force comes from the erosion of seasonal thaw water on sand, we call this kind of slumping sand erosion slumping. This slumping process strongly changed the landforms and vegetation. According to the observation data, the retreat velocity is about 1.3 m/y and the velocity is different each year. The minimum velocity observed in 1990 and 1991 was only 5 cm/y. This can be attributed to different water flowing velocity and the water velocity has a controlling action on the slumping development. The vegetation above the slumping is mainly the drought-enduring cyperaceae but below the slumping hygrophytes can be always found.

#### DISCUSSION

1). About the history and formation conditions of the wind-drift sand action on the Qinghai-Xizang Plateau. According to the  $C_{14}$  dating of the first type of sand deposit (12.7 Ka B.P.), its formation age was after the maximum period of the Last Glaciation (18-15 Ka B.P.) and coincided with the cold-wet fluctuation period (Before 12 Ka B.P.) showed in the loess profile in Baxie, Gansu Province (An Zhisheng, 1990). In the maximum period of the Last Glaciation, the mean annual air temperature then, in middle and eastern China, was 10-12°C lower than that of today and the permafrost on the Qinghai-

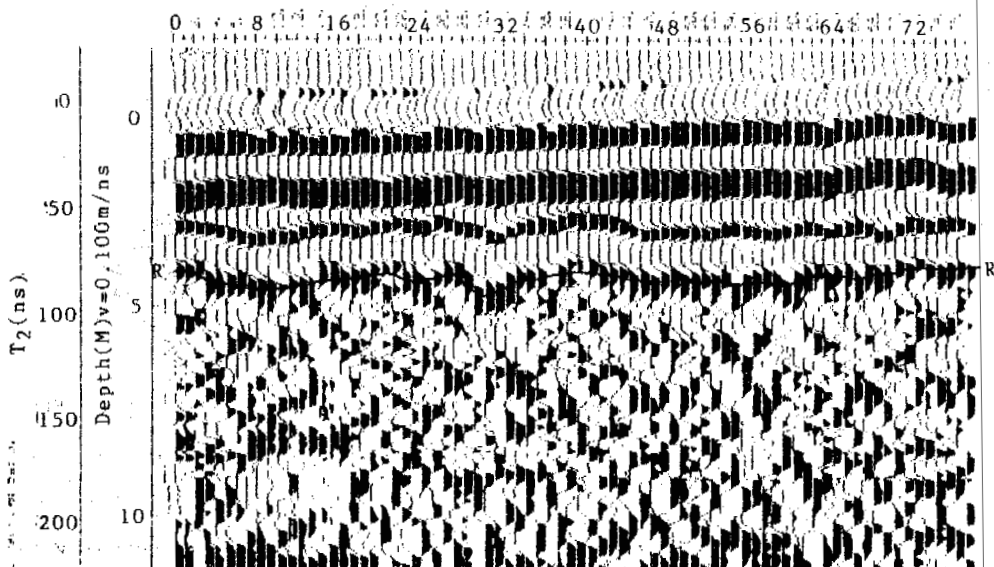


Figure 4. The radar prospecting record of the sand erosion slumping below the arc-like hill

Xizang Plateau was most developed. It was unsuitable for strong wind-drift sand action during this period. According to the  $C_{14}$  dating of this sand type, its formation age coincides with the high susceptibility section during 13-12 Ka B.P. of Baxie loess profile. This shows that this sand deposit was developed in the above warm-moist period. The second type of sand deposit was formed in the warm period of the Holocene according to the  $C_{14}$  dating on plant remnants at a depth of 1.5-2.0 m in the longitude dune north of Wudaolian (Wang, 1989). The interlaced sand and plant remnants indicated a relatively warm and wet climate condition. That also coincided with the analysis results derived from the above loess profile. The third type of sand deposit is the product of a modern warm period and its age is not more than several hundred years. The mean annual temperature in the optimum period in the Holocene was 2-4°C higher than that of today and the permafrost retreated strongly in areas. A strong sand drift action was estimated to appear in this period which needs more materials to identify it, and if the estimation is true, then the sand drift action may be divided into four periods.

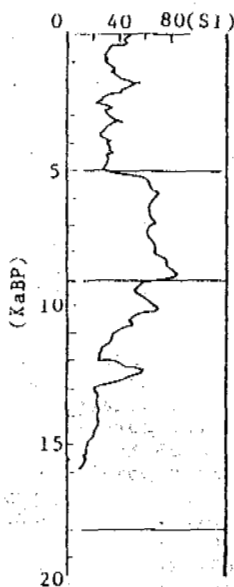


Figure 5. The susceptibility curve of the loess profile in Baxie

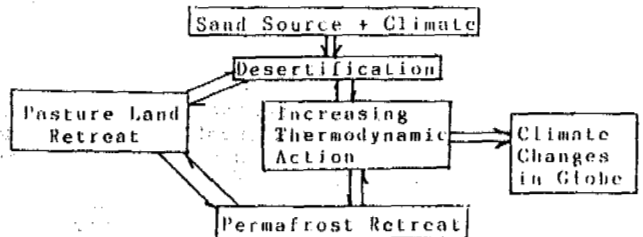
According to the above analysis, the sand deposit on the Qinghai-Xizang Plateau is mainly formed during the warm period in which the permafrost retreated strongly.

2). The influences of desertification on the environment. The Qinghai-Xizang Plateau has strong influences on the climate changes of the whole world. Its thermodynamic action and its influences on general circulation are well-known facts. Kuhle, M. proposed (Kuhle, 1987) that the Qinghai-Xizang Plateau can be the trigger for climate fluctuation. This showed one side of the important role of the plateau. But the changes of the ground surface condition can not be ignored. It is obvious that if the desertification area on the plateau expands to a certain degree and thus causes all the permafrost to disappear, the thermodynamic action of plateau will greatly increase. Its influences on climate

has an important meaning especially on the climate condition in the Northern Hemisphere.

The desertification in the permafrost region resulted in the descending of the permafrost upper table, the permafrost receding and a more arid ground surface. This in turn caused the desertification be stronger, and thus caused the limited pastureland in harsher conditions.

We can show the relationship between desertification and environmental factors by the following pattern. The abundant sand source, strong wind action and arid climate causes desertification, then permafrost and grass land degrade



which in turn causes stronger desertification. The permafrost and grass land degrading interact on each other. At last, the increased thermodynamic action causes the global climate to change.

#### REFERENCES

- An Zhisheng, (1990) Paleoenvironment evolution in China since 18000 a B.P. *Natural Science Progress*, No.2, 167-173.
- Huang Yizhi, (1991) Desertification in permafrost region on Qinghai-Xizang Plateau, *Encyclopedic knowledge*, 1991, 6, 48-49.
- Matthias, Kuhle, (1987) Subtropical Mountain --- and Highland -- Glaciation as Ice Age Triggers and the waning of the Glacial periods in the Pleistocene, *Geojournal* 14, 4 pp.393-412.
- Wang Shaoling, (1989) Formation and Evolution of Permafrost on the Qinghai-Xizang Plateau since the Late Pleistocene, *Glaciology and Geocryology*, Vol.11, No.1, 69-75.



THE CONSTRUCTION OF ELECTRICAL SUBSTATIONS  
IN DISCONTINUOUS PERMAFROST REGIONS

P.A. Huneault<sup>1</sup>, R. Arès<sup>1</sup>, R.R. Garneau<sup>1</sup> and M. Iordanescu<sup>2</sup>

<sup>1</sup>Rousseau, Sauvé, Warren inc.  
Montréal, Québec, Canada

<sup>2</sup>IREQ, Hydro-Québec Research Institute  
Varenes, Québec, Canada

This paper concentrates on various aspects of site selection and permafrost engineering appropriate for the design and construction of electrical substations in discontinuous permafrost regions. Focus is on the discontinuous permafrost regime in northern Québec. The long term creep of foundations, frost heave, equipment grounding and various thermal aspects including heat losses from a power transformer, from cables in ground conduits, from the grounding net in the case of a short-circuit and from buildings, are important design considerations.

#### INTRODUCTION

A major portion of the electricity generated in Québec comes from Northern Québec following extensive development over the last two decades of the La Grande River watershed flowing to James Bay, now better known as the La Grande Complex. Hydro-Québec is currently planning to develop the hydroelectric potential of the Great Whale river watershed leading to Hudson's Bay, and must now start to contend with the permafrost regime of Northern Québec. Preliminary studies have hence been undertaken to guide construction activities in these areas.

This paper discusses various issues related to the construction of substations in discontinuous permafrost zones, most of which are general in nature.

#### POWER SUBSTATIONS

Substations associated with hydroelectric power generating plants boost the operational voltage of the alternators to higher levels in order to reduce losses while transmitting electricity to areas of consumption. Other substations serve to reduce voltage in the conductors stepwise to distribute electricity to end users.

Substations may occupy an area up to 0.75 x 0.75 km of practically level terrain. Typically, internal and peripheral trenches help drain the site. To avoid short-circuiting with the earth, transmission cables rest on four-legged towers or a combination of H-framed lattice structures which tolerate little differential settlement at their base. Hundreds of foundations support various equipment dedicated to modifying and monitoring the transmission as well as providing shut-off or rerouting power capability for servicing. Most of the equipment is light and carried on tall single shaft structures to avoid grounding problems. Critical loads for foundations supporting light

equipment are transient lateral loads associated with wind, ice, short-circuit or seismic forces and vertical frost heave loads. Other equipment such as shunt inductance or power transformers are bulky and heavy and induce a self-weight critical loading of the foundation ranging up to 300 metric tons.

A network of conduits as well as trenches also exist in-ground, within the substation infrastructure, for housing a multitude of cables. Control cables monitoring current or voltage pass underground, from the appropriate equipment, to the surface, and lead to instrumentation within the command post building. Other cables lead underground from the command post for lighting purposes or pneumatic control of equipment. A 25 kV in-ground line may distribute auxiliary power within the substation. Trenches may also contain grounding cables.

All installations in a substation must be grounded. Copper wires are woven following a two dimensional grid pattern into an equipotential net. This net typically lies 50 cm below the finished grade of the substation. Drop lines from the equipment and steel structures are then bolted on to the net as required. Usually site selection is such that soil conditions offer good grounding capacity allowing the equipotential net also to serve as a grounding net. The net must also extend beyond the outer fence perimeter in order to ground the fence as well.

#### THE DISCONTINUOUS PERMAFROST REGIME OF NORTHERN QUEBEC

Brown (1960) gives an interesting overview of the evolution, since 1928, of the permafrost map of Canada. Three maps presently exist detailing Québec's permafrost regime, those of Brown (1975, 1979), Allard and Séguin (1987) and Lagarec and Dewez (1990).

Allard and Séguin's (1987) proposal, influenced by the work of Payette (1983), is shown in Figure 1. Regions denoted A correspond to continuous and B, C, D to discontinuous permafrost, specifically B, to the extended type (>50 % of territory), C, to the dispersed type (<50 % of territory) and D, to the sporadic type (<2 % of territory). For regions south and west of Ungava Bay and for those rivers flowing towards it, region B corresponds closely to the watershed of the Rivière aux Feuilles, the limit between regions B and C, to that of the Rivière aux Mélèzes and for that part of region D sandwiched between C, to that of Rivière Caniapiscou and Rivière à la Baleine. The final major hydrographic basin situated in discontinuous permafrost is that of Grande rivière de la Baleine, slated soon for development, which flows through region D and empties into Hudson's Bay at Kuujjuarapik.

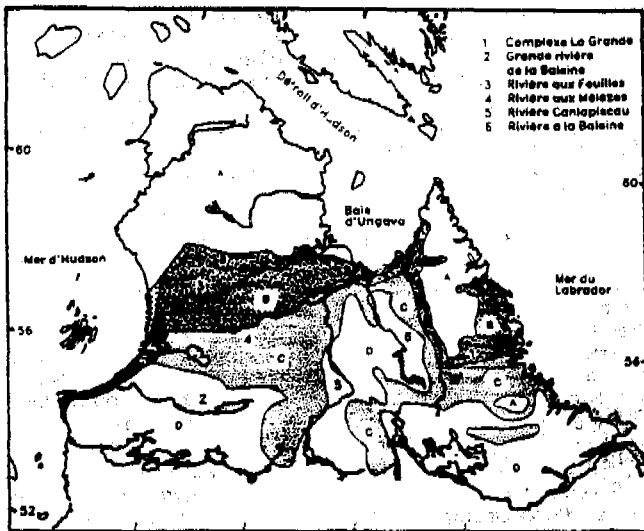


Figure 1 : The discontinuous permafrost of northern Québec (modified from Allard et Séguin (1987))

For our purposes, the southern and northern limits of the discontinuous permafrost zone correspond broadly with latitudes 54° and 58° respectively. Permafrost thickness varies, on average, from 0 to 20 m in depth from south to north; although depths up to 180 m have been reported near the coasts (Allard and Séguin (1987)). The average annual air temperature ranges from -4 to -7° C from south to north, with a west to east cooling trend associated with an increase in terrain altitude from 0 to 600 m (SDBJ (1974)). The length of the frost season ranges from 200 to 220 days and that of the thaw season, from 145 to 165 days. Fluctuations for the mean daily air temperatures correspond to a yearly amplitude of 18° C, which remains mostly constant throughout the discontinuous permafrost zone. The respective average freezing indices are roughly 2500 to 3333° C days to which, on a preliminary basis, 400° C days can be added for extreme values (Johnston (1981)); or 800° C days on the basis of a 100-year period of return (McCormick (1991)).

As will be shown later, discontinuous permafrost is relatively warm, one of its most outstanding engineering features. Probably the two most important factors affecting its distribution is the presence or not of snow and peat in any given region. It is well known that the variation of thermal properties of peat due to freezing can lead to a heat pump or cooling effect of the ground below whereas the seasonal presence of snow layer leads to an insulating effect.

Climatological atlases normally provide data on the total precipitation including the snow fraction but not the snow accumulation at a site. The latter is necessary for quantifying the thermal influence of snow and may vary according to topography, average wind speed and direction, etc. The best available estimates of snow depth for Northern Québec are those of Hydro-Québec's meteorological service. Data for most regions is scarce and not statistically significant but should improve in the future. The best data comes from close to existing reservoirs on the southern fringe of the discontinuous zone. Given these limitations, maximum yearly average snow levels are estimated at 75 cm for the southern limit and 50 cm for the northern limit with an average snow density of 0.25 g/cc. Near the Hudson Bay coast, maximum accumulations drop to 30 cm with an increase in density to 0.33 g/cc due to wind effects. Snow depths are reached rapidly with heaviest precipitations early in the frost season.

Construction on warm discontinuous permafrost offers many challenges. In order to adequately choose a site for a substation, the extent of potential problems must first be evaluated. We first consider thermal, mechanical and then grounding aspects relative to substation operation, and finally site selection.

#### TEMPERATURE RANGE OF DISCONTINUOUS PERMAFROST

The discontinuous permafrost is expected to be relatively warm.

Based on an interpretation of the work of Kudryavtsev (1977) concerning solar radiation on flat terrain, the relative warming of the ground regime, to that of the ambient air, is expected to be 2° C at the latitudes involved.

Further, the relative warming of the annual ground temperature due to snow cover is evaluated at

$$\Delta T_n = A (Z_n) / 4$$

where

$\Delta T_n$  : increase in annual average ground temperature relative to air temperature, (° C),

A : yearly amplitude of the average daily air temperatures (° C),

$Z_n$  : maximum depth of snow cover (m).

Equation (1) is a simplified fit to considerations presented by Kudryavtsev (1977), is applicable for average values of snow densities and assumes that average snow depths are half the maximum values.

For example, for the data relating to Northern Québec, equation (1) predicts a

relative warming of ground temperatures of 3.4 and 2.3° C at the southern and northern discontinuous permafrost boundaries, respectively. By comparison, based on numerical simulation, Chekhovskiy and Zenova (1989) propose a warming gradient due to snow effects of 3.2° C per meter accumulation, independent of air temperature amplitude, whereas Goodrich (1982) arrives at considerably greater values. In this regard, continuation of the work of Jordan (1991) holds much interest.

On a preliminary basis then, considering average annual air temperatures, solar and snow effects, the annual average ground temperatures in the discontinuous permafrost zone are estimated at +1.4 and -2.7° C at the southern and northern limits respectively.

In the case of terrain initially covered by a layer of peat, the placement of a fill or other construction practices may negate or destroy the cooling properties of peat and lead to an additional warming of the ground of the order of +1° C (see Kudryavtsev (1977), Goodrich (1982)).

If a maximum ground regime temperature of -1° C is warranted to preclude extraordinary creep, it is not expected that preserving discontinuous permafrost as a construction base will constitute a viable option in the southern two thirds of Québec's discontinuous permafrost zone.

#### OPERATIONAL ASPECTS

Operational aspects in a substation that potentially affect a site's thermal regime include a grounding event, heat loss from buried cables, the pouring of mass concrete, thermal losses from power transformers and the heating of a command post.

Although admissible currents in grounding cables are limited, cable temperatures may rise to 500° C for a 60 Hz current applied over a 0.5 second time span. It can be shown however that the grounding event is so transient that cooling of a cable in a typical fill material limits significant heat diffusion to a restricted concentric zone about the cable, negligible for a typical 20 mm diameter grounding cable.

Other cables used for lighting and auxiliary power generate heat and are typically placed within the substation infrastructure. For a continuous heat source and ignoring phase change, an analysis reworked from Lunardini (1981) may be applied. Cables are grouped together within an area of radius,  $r_0$ , centered a distance,  $h_0$ , below grade. The temperature of the cables is  $T_c$  along the outer perimeter,  $r_0$ , while the surface grade maintains an average annual temperature of  $T_g$ . Steady state intermediate isotherms,  $T$ , are circular within the infrastructure, of radius  $r$ , centered at a depth  $h$  and calculated as follows:

$$G = h_0/r_0 \quad (2a)$$

$$C_0 = (G + \sqrt{G^2 - 1})^2 \quad (2b)$$

$$C = C_0 (T - T_g) / (T_c - T_g) \quad (2c)$$

$$r = \frac{2\sqrt{C}}{(C-1)} \frac{(C_0-1)}{(C_0+1)} h_0 \quad (2d)$$

$$h = \frac{(C+1)}{2\sqrt{C}} r \quad (2e)$$

The maximum depth of influence of the  $T$  isotherm is  $Z = h+r$ . The composition of various cable networks may vary substantially. Depending on the above, they may best be placed in reinforced conduits at grade or insulated at the base.

In non permafrost zones, power transformers and shunt inductance normally rest upon mass concrete foundations. Considering the exothermic curing of concrete and its limited thermal diffusion capacity, temperatures within a large mass may rise substantially, affecting the thermal regime in permafrost areas. Modelling the exact process is involved: it varies with the type of concrete, the fineness of cement, ambient temperature, the temperature of the concrete when poured as well as the physical dimensions of the concrete element. For relatively small foundations, the temperature within the concrete will normally rise and start cooling off within its first week. In order to characterize the temperature rise within a given mass, ACI (1979) proposes to reduce adiabatic temperature rise by coefficients taking into account the volume to surface ratio of the mass. Having determined the heating curve of the mass, Schmidt's method (a central difference finite difference scheme) is applied to arrive at the heating of the surrounding environment. As an example, consider a foundation 3 m high, 7 m wide and 9 m long, including the thermal equivalence in concrete of the wood formwork, and a type 3 early strength concrete placed at 21° C as a worst case scenario. Assuming a typical granular fill (diffusivity of 0.0045 m<sup>2</sup>/hour), one dimensional heat transfer beneath the center of the foundation leads to a maximum warming of the foundation/fill interface of 7.5° C and 3 m below, of approximately 1° C. For type 1 normal concrete placed at 10° C, these temperatures are sharply reduced (by up to one half or more) such that they hardly influence the surrounding thermal regime.

Approximately 1 % of a transformer's nominal power is dissipated through heat loss. Furthermore, some manufacturers now prefer reinforcing a transformer base by direct thickening of its base plate instead of using reinforcement doubling as skids (Plante (1992)). This leads to direct heating of the foundation; the soil directly beneath the transformer would then respond by reducing heat flow to the environment during periods of frost. This could lead to a warming and possible melting of the permafrost.

A transformer is made up of a series of massive copper windings centrally housed in a container filled with oil that circulates through convection to peripherally mounted radiators. Temperature of the oil is restricted to 65° C above ambient whereas normal operation leads to oil temperatures, relative to ambient, of 40 ± 15° C, i.e. 55° C at the top and 25° C at the base of the transformer. If the transformer is allowed to sit directly on the infrastructure, then insulation is required during the thaw season to limit the depth of thaw while artificial cooling is required

beneath the installation to reduce temperatures in the soil. Nixon (1978) concentrates on ventilated pad design whereas Lunardini (1981) limits thaw depth beneath heated insulated rectangular surfaces. To limit the thaw depth in a typical granular fill (thermal conductivity  $2.0 \text{ W/m}^2 \text{ K}$ ) to the half width of the transformer under a 3 m square transformer surface, approximately 0.5 m of rigid polystyrene insulation is required if average ground temperatures are  $-0.5^\circ \text{ C}$ , and 0.15 m of insulation for  $-1.5^\circ \text{ C}$ . Since artificial cooling in cold periods would also be required, consideration should be given to simply raising the transformer base by avoiding mass concrete and using a naturally ventilated supported slab design (Staudzs (1991)).

Similar considerations can be made for the foundations of a heated command post. However, for an arbitrarily small building (8 m square), heated at a constant  $20^\circ \text{ C}$ , 1.3 m of insulation would be required to limit the thaw depth to 4 m, the half width of the building, for an average soil temperature of  $-0.5^\circ \text{ C}$ . Given the size of command posts and the relative warmth of discontinuous permafrost, design of an insulated and refrigerated pad becomes cumbersome and not at all practical. An elevated structure is a more attractive alternative.

#### MECHANICAL ASPECTS

Issues touched on briefly are laterally and vertically loaded foundations as well as frost heave.

With the exception of towers which must resist a permanent lateral load, lateral loading of most foundations is associated with transient wind, seismic or short-circuit loads; hence, long term creep effects are usually negligible. Design proceeds as in non permafrost areas with a possible increase in short term strength associated with permafrost.

Most foundations support light loads and are very prone to frost heave. Use of spread footings for anchoring normally require that their base rest below the level of maximum frost penetration to avoid frost heave pressures. For medium to coarse grained permafrost soils, the foundation may rest on the permafrost surface if its preservation and adequate drainage at this level is assured. However, for fine to medium grained warm permafrost, as seasonal frost penetrates below the permafrost table, fluctuations in a potentially initially high unfrozen water content may lead to development of normal frost heave forces, and anchoring may be required within the permafrost. Consideration should always be given to protecting vertical surfaces from tangential heave, through use of a buffer layer with low shear resistance placed next to the surfaces. This can possibly be achieved in combination with the use of coatings such as polyethylene, polystyrene or polyvinyl chloride due to their relatively low ice adhesion (Sayward (1979)). In this regard, a concrete caisson type foundation protected by cardboard and a buffer zone may shortly be retained as a Hydro-Québec standard for substations in non permafrost zones (Garneau (1982), Iordanescu (1991)). This design has performed well, for some time now, at an Alaskan substation built on permafrost (Wyman and Haagenson (1991)). Floating slabs

are also elegant solutions to frost heave problems if sufficient lateral stability can be guaranteed by extending the slab surface to multiple equipment (Staudzs (1991)).

As seasonal frost propagates towards the permafrost table, drying of the layers beneath the frost front leads to development of the maximum frost heave force, in a first approximation, at a depth corresponding to  $2/3$  the maximum frost depth (Tsyrovich (1960)).

Furthermore, given the presence of a relatively impermeable lower permafrost boundary, particular attention should be given to peripheral drainage trenches which ultimately could intercept all lateral water flow to the substation. These and trenches internal to the substation would help reduce water content values to a minimum thereby preventing frost heave problems.

Foundations for heavy equipment may experience creep. Power transformers and shunt inductance may weigh up to 300 metric tons. Normalized foundations (mass concrete) have been designed in southern regions for this equipment type on the basis of a 150 kPa loading of the soil.

In order to evaluate the potential creep of these foundations, the creep response of various permafrost soils have been investigated. For pure ice, the creep properties are those given by Morgenstern et al. (1980), for a poor MacKenzie Valley permafrost, those related by McRoberts (1988), and for Suffield clay, Bat-Baioss clay, Hanover silt, Callovian sandy silt, Manchester fine sand, Ottawa sand nos. 1 and 2, those given by Weaver and Morgenstern (1981). For preliminary purposes, an initial elastic stress distribution following Boussinesq for a square foundation was applied and stress redistribution was neglected thereafter. Creep settlements were obtained below the foundation center by discrete summation of creep deformations on a layer by layer basis up to a depth of approximately 12 times the foundation width. Permafrost is warm, at a temperature of  $-1^\circ \text{ C}$ , over a 25 year service life.

All soils undergoing hardening performed relatively well, i.e. all except pure ice and the MacKenzie Valley permafrost. Nevertheless, only three soils (Hanover Silt, Callovian sandy silt and Ottawa sand no.2) performed acceptably under a 150 kPa loading on the basis of a total creep settlement to foundation width ratio ( $S/L$ ) less than 0.02. For a thick layer of permafrost, a good probability exists then, unless maintenance frequency and costs are increased, that foundation pressure may have to be reduced by avoiding mass concrete, by increasing surface area, by adding piles or by a combination of these methods. For pure ice and poor MacKenzie Valley permafrost, global creep deformation values ( $S/L$ ) are up to 7 orders of magnitude too high! These soils do not harden as they creep and indicate that unless the permafrost layer is thin or that a stable layer is available at depth, warm soils with high ice content should be avoided at all costs.

#### ELECTRICAL GROUNDING IN PERMAFROST

Murmann (1973), McNeill (1980a), Smith (1986) and Henry (1987) discuss the electrical

conductivity and grounding in soils in the frozen or unfrozen state.

Currents in soils are generally associated with ionic mobility due to a general lack of electrons or metallic elements. The concentration and mobility of ions then determine the electrical conductivity of soils. In turn, these depend on the porosity, the water content and the physical state of water in the soil.

Minerals making up sand and silt are electrically neutral and excellent insulators. On the other hand, the considerable specific surface area of clays retain numerous ions such that the conductivity of soil also becomes a function of its clay content.

When a soil freezes, the unfrozen water content drops off at a rate which is a function of the soil type. While ionic mobility decreases proportionally, ionic concentration increases following expulsion or exclusion from the ice matrix. Ions absorbed on soil particles interact with water molecules nearby, hindering their phase change. As a result, the conductivity of silty and clayey soils decrease more steadily, with decrease in temperature below freezing, than a more granular soil which would have an abrupt decrease in conductivity.

In general, the resistivity of permafrost is so great that it precludes the use of the most simple and economic grounding techniques, i.e. an equipotential net 50 cm below grade that also serves as a grounding net. The latter is normally conceived for summer conditions and in seasonal frost zones, has to be complemented by a regular number of rods penetrating 6 m into the earth. Rock is highly resistive and site selection normally confines it to considerable depths. In the case of small rock outcrops, the grid must be buried at least 1.8 m below grade so as to limit surface or walking voltages to acceptable values. These techniques may be envisaged for thin permafrost layers by establishing a grid deeper in the active layer or augmenting the fill depth and using rods to pierce through the permafrost layer. Given the constraints on number of rods and burial depth however, it may be more economical, in any case, to simply abandon the concept of grounding at site. Rather, a minimum grid could be established close to grade, sufficient only to pick up the various drop lines from the installations, from which two conductors would emerge and lead to electrodes immersed in an appropriately sized lake that does not freeze to the bottom. Techniques employed in arid zones to limit grounding current such as adding resistance to the neutral of transformers should also be given due consideration (Marquis (1992)).

#### SITE SELECTION

As has been shown, there are no benefits associated with constructing on warm discontinuous permafrost and site selection should be geared to avoiding it. Since the advantage of obtaining suitable grounding in "loose" soil deposits is for the most part lost, rock outcrops close to lakes now become very attractive sites (Staudzs (1991)).

The backbone of site reconnaissance is air-photo interpretation. Color photographs scaled 1:15 000 along with magnification should be sufficient for detecting all but the smallest

forms associated with cryotic ground (Lévesque (1992)). Interpretations should yield extent, depth to, thickness and type of permafrost. Field trips to the sites should be made in summer to better take note of the topography, vegetation and drainage patterns and in winter, for snow and ice accumulation patterns.

The temperature profile of all prospective sites should be obtained through use of portable thermistor cables placed in cased and sealed boreholes filled with viscous anti-freeze. These temperatures will help confirm the airphoto interpretation which may be less accurate for coarse grained soils. The maximum temperature profile occurring in the fall is of the most interest.

The boreholes allow for soil description and classification following ASTM D4544-86 and ASTM D2607-69 for peat, ASTM D4083-89 for frozen soils and ASTM D2487-85, ASTM D422-63 and ASTM D2217-85 for non frozen soils. Physical properties of interest include total water content (ASTM D2216-80), unfrozen water content (see graphs in Tsytovich (1960) or Smith (1986)), frozen and dry soil density, porosity, Atterberg limits (ASTM D4318-84), organic content (ASTM D2974-87), salinity (ASTM D4542-85) and quartz content (visual estimate). Quartz content forms the basis for obtaining the thermal conductivity of mineral soils following Johansen's method (table 24, Farouki (1981)) while salinity adversely affects the mechanical properties of frozen soils. The effects of salinity have been widely reported in both the North American and former Soviet (now C.I.S.) literature but on a different basis. The conversion from one system to the other can be made using

$$Z_{CIS} = W (1+W) Z_{ASTM} / 10 \quad (3)$$

where :

$Z_{CIS}$  : salinity following Sarkisyan et al. (1983), expressed in ‰,

$W$  : total water content,

$Z_{ASTM}$  : salinity expressed in o/oo following ASTM D4542-85.

When required, better mapping of a discontinuous permafrost site can best be obtained using ground-penetrating radar or an electromagnetic technique as well as localized temperature soundings. Third generation, fully digitized GPR provides better data interpretation in medium to coarse grained soils (Judge et al. (1991)). Electromagnetic techniques are reserved for relatively conductive fine grained soils (McNeill (1980b)). These geophysical methods should be calibrated on site by drilling and sounding between additional boreholes. A portable temperature probe consisting of a long rod with a thermistor at its tip can also be used to sound the active layer for the permafrost table (Pilon et al. (1979)).

#### ACKNOWLEDGEMENTS

Over the course of this study, the authors have had the privilege to meet with northern engineering experts, professors Branko Ladanyi, Michel Allard, Tom Kinney, Gerald Walker, researchers Fred Crory, Dr. Jean Pilon,

Dr. George Palacky, engineers Andy Staudzs, Gregory Wyman, Steve Haagenson and geomorphologist Richard Lévesque. The receptiveness of the Golden Valley Electrical Association, Fairbanks, and Manitoba Hydro, Winnipeg is gratefully acknowledged. Discussions with RSW personnel Joe Hanson, Alain Mérand and Émile Marquis have been most helpful. Comments by reviewers are also appreciated.

## REFERENCES

- ACI (1979), Effect of restraint, volume change, and reinforcement on cracking of massive concrete, report no. ACI 207.2R-73, in ACI Manual of Concrete Practice, Part 1,
- ALLARD, M. and SÉGUIN, M.K. (1987), Le pergélisol au Québec nordique: bilan et perspectives, *Géogr. Phys. Quater.*, Vol.XLI, no.1, p.141-152,
- BROWN, R.J.E. (1960), The distribution of permafrost and its relation to air temperature in Canada and the U.S.S.R., *Arctic*, Vol.13, no.3,
- BROWN, R.J.E. (1975), Permafrost investigations in Québec and Newfoundland (Labrador), Technical paper no.49, DBR, NRCC,
- BROWN, R.J.E. (1979), Permafrost distribution in the southern part of the discontinuous zone in Québec and Labrador, *Géogr. Phys. Quater.*, Vol.XXIII, nos.3-4, p.279-289,
- CHEKHOVSKIY, A.L. and ZENOVA, O.A. (1989), Nomographs of soil annual average temperature, Frost in geotechnical engineering, VTT symp. 94, Vol.1, p.219-231,
- FAROUKI, O.T. (1981), Thermal properties of soils, Monograph 81-1, CRREL, Hanover, 35 pp.,
- GARNEAU, R.R. (1982), Rapport d'études des fondations à action latérale pour les postes, Bureau d'Études des Lignes de Transport Inc. (BELT), décembre, 107 pp.,
- GOODRICH, L.E. (1982), The influence of snow cover on the ground thermal regime, *Can. Geotech. J.*, Vol.19, p.421-432,
- HENRY, K. (1987), Electrical grounding in cold regions, *Cold Regions Technical Digest* no.87-1, CRREL, Hanover, 17 pp.,
- IORDANESCU, M. (1991), Etude du soulèvement par gel adhésif des fondations à action latérale, de type caisson en béton armé, pour les postes, Vol.2: recommandations de conception et de construction, rapport 91-134, IREQ, Hydro-Québec,
- JOHNSTON, G.H. (1981), Permafrost/Engineering design and construction, ACGR, NRCC, John Wiley & Sons, 540 pp.,
- JORDAN, R. (1991), A one-dimensional temperature model for a snow cover, Special report 91-16, CRREL, Hanover, 49 pp.,
- JUDGE, A.S., TUCKER, C.M., PILON, J.A. and MOORMAN, B.J. (1991), Remote sensing of permafrost by ground-penetrating radar at two airports in Arctic Canada, *Arctic*, Vol.44, supp.1, p.40-48,
- KUDRYAVTSEV, V.A. (Ed.) (1977), Fundamentals of frost forecasting in geological engineering investigations, Draft translation 606, CRREL, Hanover, 489 pp.,
- LAGAREC, D. and DEWEZ, V. (1990), Dynamique du pergélisol discontinu et changements globaux dans le Nord du Québec, *Proc. 5th Can. Permafr. Conf.*, Collection Nordicana, no.54, Université Laval, Québec, p.215-222,
- LÉVESQUE, R. (1992), Personal communication, Polygéo Inc., Montréal,
- LUNARDINI, V.J. (1981), Heat transfer in cold climates, Van Nostrand Reinhold Co., 731 pp.,
- MARQUIS, É. (1992), Personal communication, Electrical engineering, RSW Inc., Montréal,
- MCCORMICK, G. (1991), Freezing and thawing indices in northern Canada, *Can. Geotech. J.*, 28, p.899-903,
- MCNEILL, J.D. (1980a), Electrical conductivity of soils and rocks, Technical note TN-5, Geonics Ltd, Mississauga, Ont., October, 22 pp.,
- MCNEILL, J.D. (1980b), Electromagnetic terrain conductivity measurement at low induction numbers, Technical note TN-6, Geonics Ltd, Mississauga, Ont., 15 pp.,
- MCRBERTS, E.C. (1988), Secondary creep interpretations of ice rich permafrost, *Proc. 5th Int. Conf. Permafr.*, Trondheim, p.1137-1142,
- MORGENSTERN, N.R., ROGGENSACK, W.D. and WEAVER, J.S. (1980), The behaviour of friction piles in ice and ice rich soils, *Can. Geotech. J.*, Vol.17, p.405-415,
- MURMANN, R.P. (1973), Ionic mobility in permafrost, *Proc. 2nd Int. Conf. Permafr.*, North American Contr., p.352-359,
- NIXON, J.F. (1978), Geothermal aspects of ventilated pad design, *Proc. 3rd Int. Conf. Permafr.*, Vol.1, Edmonton, p.841-846,
- PAYETTE, S. (1983), The forest tundra and present tree lines of the northern Québec-Labrador Peninsula, *Tree-line Ecology*, Proc. Northern Québec Tree-Line Conf., Morissette, P. and Payette, S. (Eds.), Collection Nordicana, no.47, Université Laval, Québec, p.3-23,
- PILON, J.A., ANNAN, P.A., DAVIS, L.J. and GRAY, J.T. (1979), Comparison of thermal and radar active layer measurement techniques in the Leaf Bay area, Nouveau-Québec, *Géogr. Phys. Quater.*, Vol.XXIII, nos.3-4, p.317-326,
- PLANTE (1992), Personal communication, Mechanical engineering, Asea Brown Boveri, Varennes, Québec,
- SARKISYAN, R.M., NERSESOVA, A.Z., VYALOV, S.S. and ZATSARNAYA, A.G. (1983), Handbook on the determination of the physical, thermal and mechanical properties of frozen soils, Technical Translation TT-2064, NRCC, Ottawa, ISSN 0077-5606,
- SAYWARD, J.M. (1979), Seeking low ice adhesion, Special report 79-11, CRREL, Hanover,
- SDBJ (1974), Etudes climatologiques, dans Etudes sur l'environnement, Territoire de la Baie James, Rapport Synthèse 1972-1979, Société de développement de la Baie James-Environnement Canada,
- SMITH, D.W., (Ed.) (1986), Electrical Resistance, appendix J, Cold Regions Utilities Manual, CSCE, Montréal,
- STAUDZS, A. (1991), Personal communication, Civil engineering, Manitoba Hydro, Winnipeg,
- TSYTOVICH, N.A. (1960), Bases and foundations on frozen soil, Highway Research Board, Special report 58, NRC, NAS publ. no.804, Washington, 98 pp.,
- WEAVER, J.S. and MORGENSTERN, N.R. (1981), Pile design in permafrost, *Can. Geotech. J.*, Vol.18, p.357-370,
- WYMAN, G. and HAAGENSON, S. (1991), Personal communication, Engineering, Golden Valley Electrical Association, Fairbanks, Alaska.

## MEASUREMENT OF THERMAL STRESSES IN ASPHALT CONCRETE MIXTURES

Vincent Janoo<sup>1</sup>, John Bayer, Jr.<sup>1</sup>, Michael Walsh<sup>1</sup> and Hsiao Tomita<sup>2</sup>

<sup>1</sup>Cold Regions Research and Engineering Laboratory  
Hanover, NH, USA 03755

<sup>2</sup>Federal Aviation Administration  
Washington DC, USA. 20591

Asphalt concrete (AC) pavements in permafrost and seasonal frost regions are prone to thermal cracking. There are two theories for predicting thermal cracking of AC pavements. The first is that the thermal stress in the pavement structure at some low winter temperature exceeds the tensile strength of the mixture. This is the more likely scenario in permafrost areas. The second hypothesis is that the AC mixture fails due to thermal fatigue; the cracks are generated from repetitive daily high and low temperature cycling. As part of the development of guidance for the selection of asphalt concrete mixtures that will resist thermal cracking in cold regions, CRREL developed a thermal stress test device for measuring thermal induced stresses in AC beams in the laboratory. The test device attempts to simulate the thermal strain in the longitudinal direction of the in-situ AC layer. The device is capable of subjecting the test specimen to temperature change rates that vary between 1° and 30°C/hr. Test specimens in the device can be subjected to both monotonic and cyclic thermal loading. This paper describes the thermal stress test device. Typical results from the test are also presented.

### INTRODUCTION

Thermal cracking is a serious problem in seasonal frost and permafrost areas. Thermal cracks are usually seen to run transversely across the road and airfield pavements. Related distresses caused by thermal cracking are increased pavement roughness, localized loss of support, voids under the pavement and foreign object damage to aircraft such as from chipped pavements. Thermal cracking occurs when the thermal stress (due to low temperatures) in the asphalt concrete (AC) pavement exceeds the tensile strength of the AC mixture. This form of cracking is called *low temperature cracking* (Figure 1). The temperature at which failure occurs is referred to as the fracture temperature. In fairly new pavements, cracks have been observed to appear at greater than 30-m spacing. As the pavement ages or more extreme temperature drops occur, the crack spacing has been observed to decrease to 3-6 m.

Thermal cracks can also occur when AC pavements are subjected to diurnal temperature cycling. The thermal cycling of the pavement structure is due to the daily daytime high and nighttime low temperatures. This cycling can cause *thermal fatigue*, a concept similar to load-induced fatigue.

Factors that influence the initiation and frequency of thermal cracking are asphalt grade, asphalt temperature susceptibility, aggregate type, type of subgrade, traffic and even pavement thickness (Janoo, 1990a). Most research has concentrated on the stiffness of the asphalt cement, which has a strong influence on thermal cracking. The major thrust of past efforts has been to relate asphalt cement properties and indices, such as viscosity and penetration, to low temperature performance of asphalt concrete. The viscosity and/or penetra-

tion values are used to derive two temperature susceptibility indices. These are the penetration index (PI) and the penetration viscosity number (PVN). They are used extensively to characterize the performance of asphalt concrete at low temperatures. However, there are several drawbacks in using these indices. First, the indices are dependent on either the crude oil refining technique or on the amount of wax present in the asphalt. Second, these indices are developed from tests conducted at temperatures of 4°, 25° and 135°C. Therefore it becomes necessary to extrapolate from the measured data to estimate the asphalt properties at below-freezing temperatures.

The U.S. Army Cold Regions Research and Engineering Laboratory (CRREL) in conjunction with the Federal Aviation Administration (FAA), is conducting research on characterizing the performance of asphalt concrete pavements in cold regions. The aim is to provide guidance to pavement engineers in cold regions on the selection of asphalt concrete that will minimize low temperature cracking. The study includes a field study on the performance of low viscosity asphalt concrete mixtures in cold climates (Janoo, 1990a), development of a laboratory test method for characterizing asphalt mixture properties at low temperature and a test program for studying the engineering properties of unmodified and modified asphalt concrete mixtures at low temperatures. The test program has been started, but not completed. This paper describes the testing apparatus for measuring the thermal loads in an asphalt concrete mixture.

### PREDICTION OF LOW TEMPERATURE CRACKING

The predicted parameter that is commonly sought in low temperature performance of asphalt concrete mixtures is the fracture temper-

ature. The thermal stress in the asphalt concrete is calculated using analytical methods. Most often the stresses are calculated using the pseudoelastic equation put forth by Hills and Brien (1966). The equation is as follows:

$$\sigma_x(t) = \int_{t_0}^t \alpha(T) S(\Delta t) T dT(t) \quad (1)$$

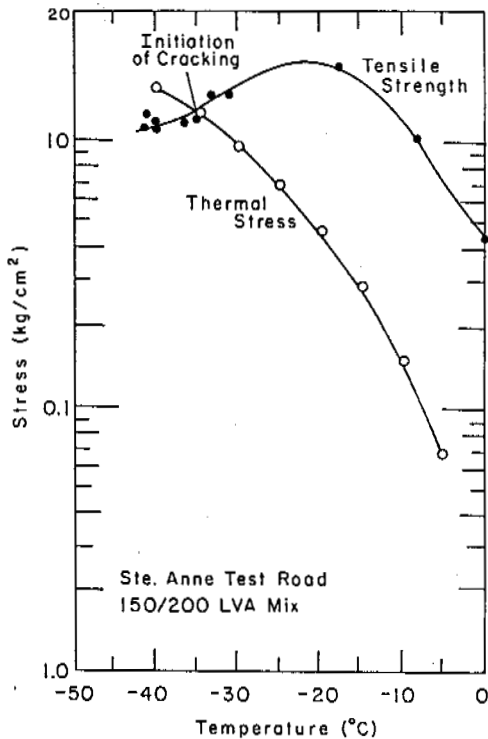


Figure 1. Prediction of fracture temperature.

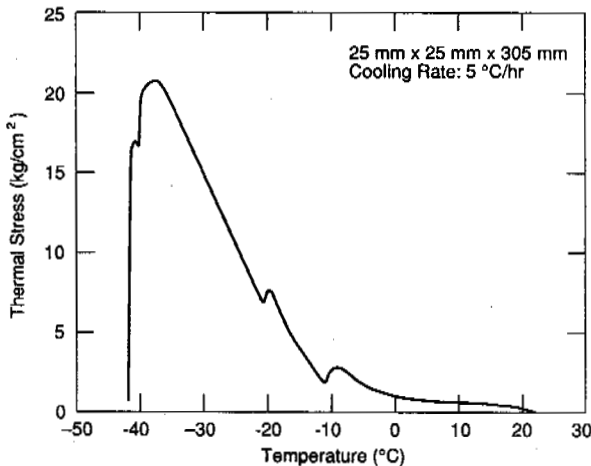


Figure 2. Typical stress-temperature curve.

where  $\sigma_x(t)$  = accumulated thermal stress  
 $\alpha(T)$  = coefficient of thermal contraction  
 $S(\Delta t, T)$  = asphalt mix stiffness, function of time and temperature  
 $dT(t)$  = temperature drop (cooling rate).

Equation 1 can be solved numerically using the finite difference method. Typical values of a range between  $1.7 \times 10^{-5}$  and  $3 \times 10^{-5} \text{ } ^\circ\text{C}$  (Janoo et al. 1990b, 1992);  $\alpha$  is usually held constant in the analysis. The stiffness ( $S$ ) of the AC mixture can be estimated from laboratory tests or with nomographs such as Van der Poel's nomograph (1955) in conjunction with the Heukelom and Klomp (1964) or Bonnaure (1977) nomographs. The calculated thermal stress is then compared with the tensile strength of the AC mixture. The tensile strength can be determined from indirect or direct tension tests. A summary of the various tests is given in Janoo et al. (1990b, in prep.).

#### DIRECT MEASUREMENTS OF THERMAL STRESS

Attempts to measure the thermally induced loads in asphalt concrete started in the mid 1960s. The direct measurement of low temperature failure stresses and temperatures have been reported by Monismith et al. (1965), Hills and Brien (1966) Tuckett et al. (1970) Chipperfield and Fabb (1971), Fabb (1974), Sugawara et al. (1982, 1984), and Arand (1987). Currently, as part of its mixture characterization research, the Strategic Highway Research Program (SHRP) has also developed a device for measuring the thermally induced load in a restrained asphalt concrete specimen. CRREL was a consultant to SHRP in the development of this test device. A summary of the test and the test variables are given in Janoo et al. (1990b, in prep.).

The thermal stress test simulates the in-situ condition of plane strain in the longitudinal direction of the AC layer ( $\epsilon_{\text{long}} = 0$ ). This is done by restraining the long axis of an AC beam specimen between two rigid frames. The thermally induced load is measured by a load cell attached between the rigid frame and the test specimen. The specimen, or in some cases the frame and the specimen, is then placed in an environmental chamber. The temperature in the chamber is dropped and the load cell monitored. With the temperature drop, the AC beam attempts to contract in the longitudinal direction. However, since it is restrained to the rigid frame, it is unable to shrink and thus tensile stresses develop in the specimen. As the temperature drops further, the stress increases up to a level when it reaches its tensile strength. At this time fracture occurs. A typical load temperature response from this type of test is shown in Figure 2.

#### CRREL THERMAL STRESS TEST (CTST)

The following criteria were used to develop the thermal stress device:

1. The thermal stress, thermal fatigue and creep compliance tests conducted in the test equipment should not require additional modifications to the system.

2. The system should provide accurate data on low temperature cracking, thermal coefficient of contraction, creep compliance and thermal fatigue.



3. The cooling system should provide values of temperature drop and low temperatures likely to be seen in the field.

4. The monotonic and cyclic cooling rates should be microprocessor controlled.

There are two versions of the CTST at CRREL (Figures 3 and 4). A brief description of these devices is presented in this paper; complete details can be found in Janoo et al., in prep. Both test systems consist of three components: 1) a specimen loading system (SLS), an environmental chamber and 3) a data acquisition system. A specially designed air cooling unit was used for cooling or warming the specimen. This unit was capable of producing temperatures between  $-100^{\circ}$  and  $+100^{\circ}\text{C}$ . With the aid of a programmable temperature controller, the cooling unit was capable of producing cooling rates up to  $27^{\circ}\text{C/hr}$ . The data acquisition/control system consisted of a personal computer, a data acquisition board, temperature load and deformation measurement sensors.

#### System 2

One of the SLS fixtures consisted of a frame of four Invar-36 bars between two end plates, with a load cell and a specimen mounting plate in between (Figure 3). Stresses on the sample caused by thermally induced strains in the SLS fixture were minimized by using Invar for most of the critical components in the fixture. Invar was chosen for this application because of its very low mean thermal coefficient of expansion ( $9 \times 10^{-7}/^{\circ}\text{C}$ ) and relatively high modulus of elasticity (148 GPa). Some steel was used to compensate for the Invar shrinkage, although this was not the basis of the design. The similar thermal conductivity and masses of the steel and Invar components ensured that the

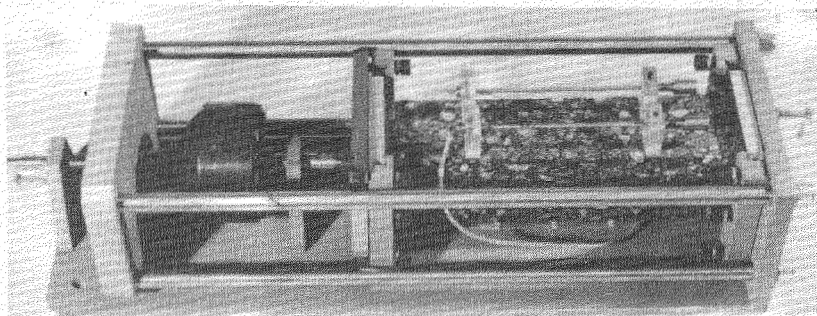


Figure 3. Thermal stress device (Invar rod system).

Figure 3. Thermal stress device (Invar rod system).

thermal responses of the different components would be comparable, thus reducing the stress-strain fluctuations that occurred with a prior SLS design.

The latest device was our second attempt in the development of an SLS fixture. This device is referred to as system 2 in the graphs presented later. The improved system has been found to work very well with 25-mm-square and 305-mm-long beams. In AC mixtures, the maximum stone size can be as large as 19 mm and therefore the question of specimen homogeneity was raised with the 25-mm-square beams. Larger sample cross sections (up to 76 mm square) were also tested with this device. Two major results were found from this study:

1. The thermal stresses in a 25-mm-square specimen were much higher than in larger samples (Janoo et al, 1990b). This suggested that sample size was a critical element in the test procedure. Based on the results, the minimum specimen size that was considered acceptable for the thermal stress test was 50 mm square. The rate of change in the thermal stress decreased substantially above a 50-mm square

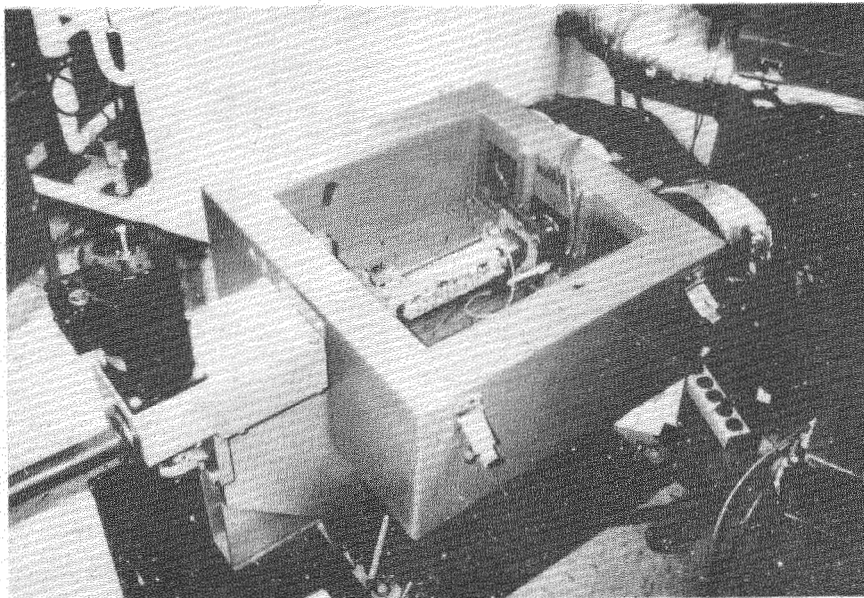


Figure 4. Thermal stress device (step motor system).

cross section. This cross section was also adopted by SHRP.

2. As the specimen size increased, so did the compliance of the system. The larger (76 mm square) specimens did not show any signs of fracture at temperatures down to  $-40^{\circ}\text{C}$ . This rather inexpensive and simple device would benefit from greater reduction in its compliance. The effect of this compliance will be illustrated in the results presented later. This device is suitable to evaluate fine AC mixtures where the cross section could be as low as 25 mm square.

### System 3

To decrease the problem of sample inhomogeneity and overcome the compliance problems in the previous design, a larger SLS fixture with a massive, rigid steel frame specimen holder was developed. To reduce the compliance of the system, a closed-loop feedback linear positioning device was installed on the system to more closely control the length of the specimen, (Figure 4). The control system employed a servo motor and drive in conjunction with a jack-screw. The drive system consists of a computer controlled driver and motor with resolver.

The interaction of the instrumentation with the servo drive provides the feedback control necessary to maintain the sample length over varying parts of the test (Figure 5). As the temperature in the environmental chamber falls, the sample attempts to shrink, resulting in a force in the sample constraining structure (frame, jack screw, load cell, etc.). This force causes distortion in the support structure that, if not compensated for, will allow the sample to shrink axially and thus partially unload. When the sample shortens, the length control linear variable differential transform-

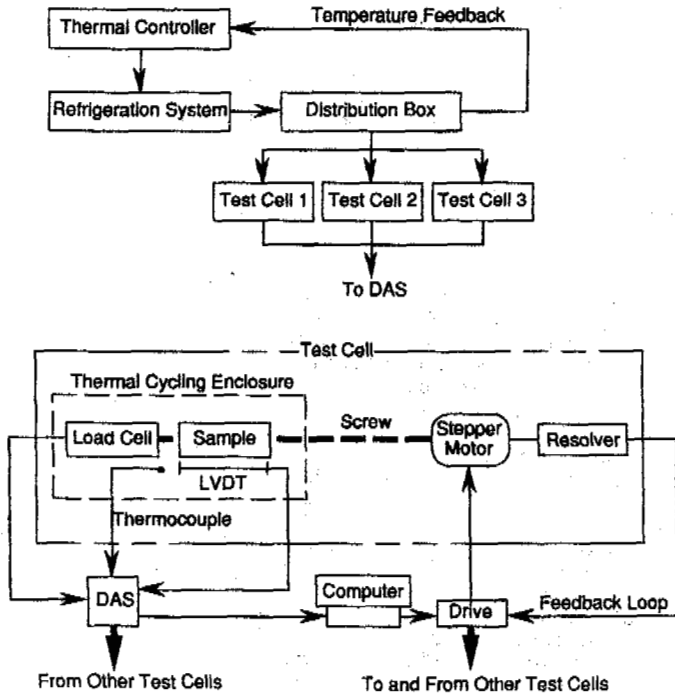


Figure 5. Schematic of feedback control system.

er (LVDT) registers a decrease in length by varying its output voltage. This length differential analog signal is compensated for the ambient temperature (derived from a thermocouple in near proximity to the LVDT) and is fed into the servo drive for the jack screw positioning stepper motor. A command to move a fixed number of pulses is sent to the stepper motor to correct for this length differential. A resolver, connected to the drive motor, returns to the driver the number of steps taken during the scan interval of the driver. Any difference between the two is considered an error and the motor is commanded to make up the difference. This feedback control loop will thus maintain the sample length whether the sample is shrinking or expanding, thus compensating for both decreasing and increasing temperatures.

Another modification was made to avoid fracture close to the end caps. Swivel joints were added to connect the test specimen to the load cell as well as the screw jack in order to reduce any noncentric loading near the end of the samples. The swivel joints were used in the monotonic load tests; however, they were replaced with rigid joint fixtures for thermal cycling tests. In the cycling tests, during the warming cycle, the specimen tended to expand. Rigid joints were necessary because as the specimen expanded, the step motor applied a compressive load on the specimen. With a swivel joint, this load was applied nonuniformly.

### TEST RESULTS

Some typical test results are presented from the two specimen loading systems. The results are from the SHRP program, studies conducted for Quebec Ministry of Transportation, and in-house studies.

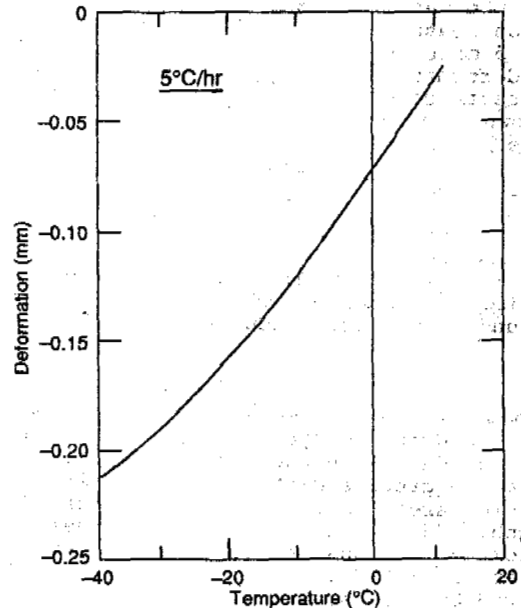


Figure 6. Typical results of deformation caused by temperature changes in AC specimens.

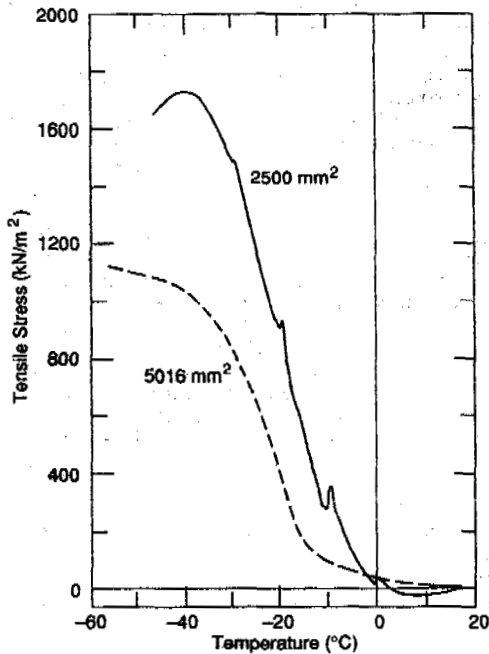


Figure 7. Typical thermal stress test results from Invar rod system.

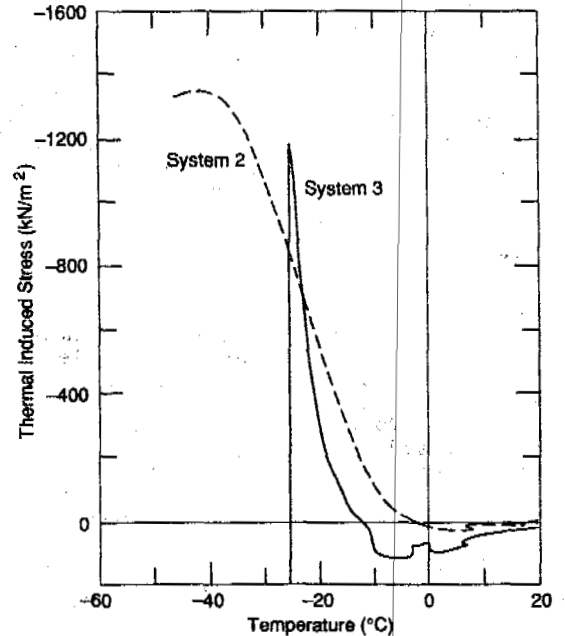


Figure 8. Comparison of failure temperatures from Invar rod and step motor system.

#### Coefficient of thermal contraction (k)

The coefficient of thermal contraction for asphalt concrete was determined between a temperature range of 20°C and -50°C. The tests were conducted at cooling rates of 5°C/hr, 10°C/hr and 20°C/hr. Four LVDTs were attached to the test specimen and deformation measurements were taken every 5 minutes. An average of all the deformation temperature shrinkage tests conducted at 5°C/hr is shown in Figure 6. The slope of the deformation temperature curve is not constant over the entire range. This difference becomes more apparent at very low temperatures. The coefficient of thermal contraction (k) varies from  $29 \times 10^{-6}$  to  $18 \times 10^{-6}$  °C as the temperature drops from 10 to -40°C. Similar values were found from tests conducted at 10° and 20°C/hr.

#### Thermal Stress

Thermally induced loads were measured under both monotonic temperature drop and cyclic temperatures. Studies were conducted on the effect of asphalt grade, asphalt-aggregate mixtures and specimen cross section areas on fracture temperature and strength. Additional information on the results from the various studies can be found in Janoo et al. (1992). A typical result from the Invar rod thermal stress test devices is shown in Figure 7. The influence of specimen size on the failure temperature is also shown in this figure; the 70- x 70-mm specimen did not reach a failure condition.

The effect of the compliance in the systems under monotonic test is shown in Figure 8. Two

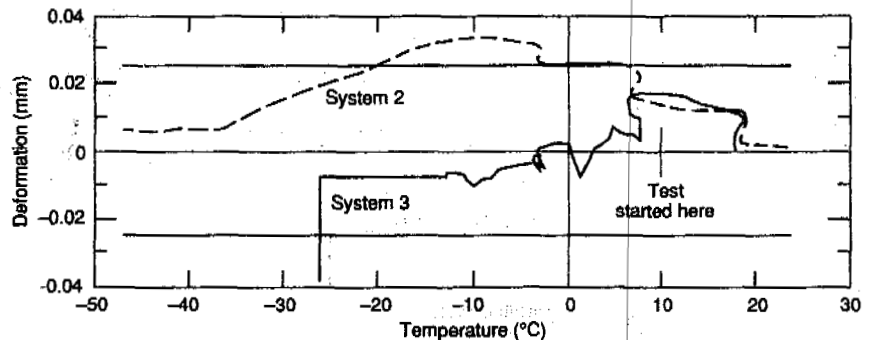


Figure 9. Variation in displacement in AC sample as measured in Invar rod and step motor systems.

50- x 50-mm<sup>2</sup> test samples were tested simultaneously in the two systems. System 2 is the Invar rod system that did not have a step motor system to maintain the longitudinal deformation at zero. Even though the failure stresses were similar, the sample in System 3 (step motor system) failed at a higher temperature (-26° vs. -40°C). With respect to the amount of deformation allowed in the test specimen, the difference in compliance of the two systems during thermal loading is shown in Figure 9. An ideal system would show no movement during the test. The horizontal lines at  $\pm 0.0254$  mm shown in the figure are the limits suggested by Fabb (1972) who felt that large errors in the fracture temperature would occur if deformations in the specimen were not held below  $\pm 0.0254$  mm. It appears that these limits need to be further reduced. A suggested value is  $\pm 0.01$  mm. The initial compression seen in System 3 occurred because the step motor was off. The step motor

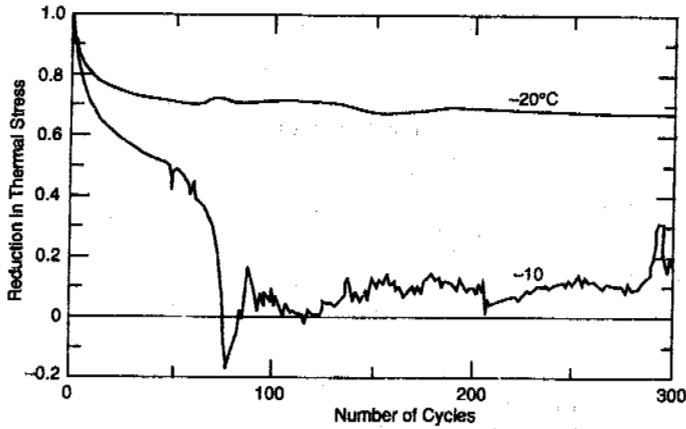


Figure 10. Reduction in strength caused by temperature cycling.

was turned on when the temperature had dropped to 10°C; it was then able to control the expansion to the  $\pm 0.01$ -mm level. Since this experiment, better control of the deformation has been attained. At this time, in system 3, the movement is controlled to  $\pm 0.01$  mm.

Thermal cycling tests were performed in both SLS fixtures. For the SHRP study, the tests were conducted in system 3. The 50 x 50-mm<sup>2</sup> samples were prepared in the laboratory and provided to CRREL by SHRP. Based on results obtained by Sugawara (1989), our initial assumption was that failure would occur at approximately 100 cycles. The results show (Figure 10) that although there was a reduction in strength quite early in the cycling process, the strength level remained fairly constant after that. The thermal stress at -10°C drops to zero after approximately 70 cycles, indicating the specimen has "failed." However, visual inspection of the specimen at the end of the test showed no failure planes. At present, the hypothesis of thermal cracking due to temperature cycling cannot be confirmed in the laboratory. The failures reported by Sugawara (1989) may have been specimen size dependent. Sugawara used a 25- x 25-mm<sup>2</sup> specimen for the thermal cycling tests. Also the temperatures he used were very close to the monotonic failure temperatures. Further research in this area needs to be done.

#### CONCLUSIONS

Two thermal stress devices have been developed at CRREL for studying the low temperature and thermal fatigue performance of any asphalt concrete mixture. Both monotonic and cyclic thermal loads can be applied to the specimen. The cooling system is capable of generating cooling rates between 3 and 27°C/hr. A minimum temperature of -60°C can be achieved in this apparatus. The step loading device is capable of restraining movements in the test specimen to less than  $25 \times 10^{-5}$  mm.

The results from the laboratory test need to be correlated with field experience. The results of the SHRP field tests are being analyzed and preliminary results show a good correlation. The effect of thermal cycling on

asphalt concrete fracture needs to further be searched.

#### REFERENCES

- Arand, W. (1987) Influence of bitumen hardness on the fatigue behavior of asphalt pavements of different thickness due to bearing capacity of subbase, traffic loading and temperature. Proceedings, 6th International Conference on Structural Behavior of Asphalt Pavements, U. of Michigan.
- Bonnaure, F., G. Gest, A. Gravois and P. Uge (1977) A new method of predicting the stiffness of asphalt paving mixtures. Proceedings of the Association of Asphalt Paving Technologists.
- Chipperfield, E.H. and T.R.J. Fabb (1971) Development of more durable road surfacing. Proceedings of the Canadian Technical Asphalt Association.
- Fabb, T.R.J. (1974) The influence of mix composition, binder properties and cooling rates on asphalt cracking at low temperatures. Proceedings of the Association of Asphalt Paving Technologists.
- Haas, R., H. Lee, F. Meyer, and G. Argue (1987) Cold climate performance of Canadian airport pavements. Mini Workshop 3, Paving in Cold Areas, vol.1, p. 303-332., Ottawa, Ontario, July 20-22.
- Heukelom, W. and A.J.G. Klomp (1964) Road design and dynamic loading. Proceedings, Association of Asphalt Paving Technologists.
- Hills, J.F. and D. Brien (1966) The Fracture of bitumens and asphalt mixes by temperature induced stresses. Discussion (p. 293), Proceedings, Association of Asphalt Paving Technologists.
- Janoo, V.C. (1990a) Use of soft grade asphalts in airfields and highway pavements in cold regions. USA Cold Regions Research and Engineering Laboratory, Special Report 90-12.
- Janoo, V.C. J. Bayer Jr., T. Vinson and R. Haas (1990b) Test methods to characterize low temperature cracking. Proceedings of the 4th Workshop in Paving in Cold Areas, Sapporo, Japan.
- Janoo, V.C., J. Bayer Jr., and M. Walsh (in prep.) Thermal stress measurements in asphalt concrete. USA Cold Regions Research and Engineering Laboratory, CRREL Report in preparation.
- Monismith C.L., G.A. Secor and K.R. Secor (1965) Temperature induced stresses and deformation in asphalt concrete. Proceedings, Association of Asphalt Paving Technologists.
- Sugawara, T., H. Kubo and A. Moriyoshi (1982) Low temperature cracking of asphalt pavements. Proceedings, Paving in Cold Areas Mini-Workshop.
- Sugawara, T. and A. Moriyoshi (1984) Thermal fracture of bituminous mixtures. Proceedings, Paving in Cold Areas Mini-Workshop.
- Tuckett, G.M., G.M. Jones and G. Littlefield (1970) The effects of mixture variables on thermally induced stresses in asphaltic concrete. Proceedings, Association of Asphalt Paving Technologists.
- Van der Poel, C. (1954) A general system describing the viscoelastic properties of bitumens and its relation to routine test data. Journal of Applied Chemistry, Vol. 4.

## COUNTERMEASURES TO PREVENT CANAL STRUCTURES FROM FROST DAMAGE

Jian Gong

Northwestern Hydraulic Science Institute of Water Resources  
Ministry, Yangling, Shaanxi, 712100, P.R. China

Most of the canal seepage prevention structures in northeastern, central and northwestern cold areas of China are in thin-plate types with extensive areas exposed to the air. Being frequently in contact with water under minus temperatures in the winter, the canal structures will suffer severe damage from frost heaving, thereby affecting the full benefit of the engineering structures. In order to prevent and eliminate such types of frost heaving damages in engineering structures, the author presents some concrete countermeasures to prevent and control the frost damage in the aspects of design, construction and management of the seepage prevention structures. This has been the basis of recent years of experience in editing the "Technical Specifications of Canal Seepage Prevention Engineering" and some valuable reference materials combined with the characteristics of the structures.

### INTRODUCTION

The contradiction between the supply and requirement of water resources is getting severer in China. In order to reduce seepage water losses and increase the water utilization efficiencies of the canals, a great deal of canal lining projects have been completed in past decades. They have played active roles in alleviating the water shortage problem, controlling the salinization of soils and ensuring the safety of canals. But owing to the severe frost damage problems in the three cold areas (northeast, north central and northwest of China), incidences like frost heaving, cracking, mislapping and collapsing are frequently happening to the canal lining structures, resulting in not only the reduction of the benefits of engineering investments, the life of the structures and outcome of water conservation practices, but also severe accidents are affecting the normal operation of irrigation canal systems. For example, according to our investigation on canal lining structures in the irrigation districts of Shaanxi Province, owing to the frost damages, 75.3% of the lining plates on the shadow side of the canal have cracked, and on the sun shine side it is 27%. More cracks were found in the pre-casted plates than in the site-casted plates. Another example is the Xinliu main canal in the Xinjiang Autonomous Region. The canal was lined with a plastic membrane for seepage prevention and paved with pre-casted concrete plates as a protection layer. Because of the higher water table in the canal foundation and the action of minus temperatures in the winter, the un-uniform frost heaving occurred in the canal, where the concrete plates were cracked, bodies of the plastic membrane and the concrete plate collapsed after the frozen layer was melted (Tong Changjiang et al., 1985). As for the earth protected membrane-lining structures, due to a lack of frost damage consideration in the design, the melting-sliding of the

protection layer has been more common. In order to prolong the life of canal lining structures and ensure better outcomes from investment of construction and lining of the canals, many institutions of scientific research, design, construction and management and related universities in the country have been actively studying the mechanisms and the controlling measures of frost damages. And fruitful achievements have been made in this area. This paper will introduce some countermeasures for the prevention of frost damages on the basis of the research (Water Resources Ministry of China, 1992; Water Resources Ministry of China, 1991; Tong Changjiang et al., 1985).

### COUNTERMEASURES FOR THE CONTROL OF FROST DAMAGES TO CANAL LINING STRUCTURES

Based on the recognition of the protruding role that water plays in the process of frost damages to canal lining structures and from the consideration of characteristics of the lining structures, control and prevention of frost damages should stress the reduction of soil moisture in the canal base, isolating the water supply from the outside, and lowering the water table. These measures had been applied in practice and proved to be realistic and feasible in controlling the frost damages to the canals.

#### Measures to Reduce Soil Moisture Content in the Canal Base

Experimental results show that when the soil moisture content in the base is less than the starting water content of frost heaving the soil will be free of frost damage. Therefore, if the soil water content in the base is greater, the following measures should be taken to reduce frost damages:

(1) For new construction of canal lining structures: Excavate the earth canal 15 or more days ahead of the construction of the lining;

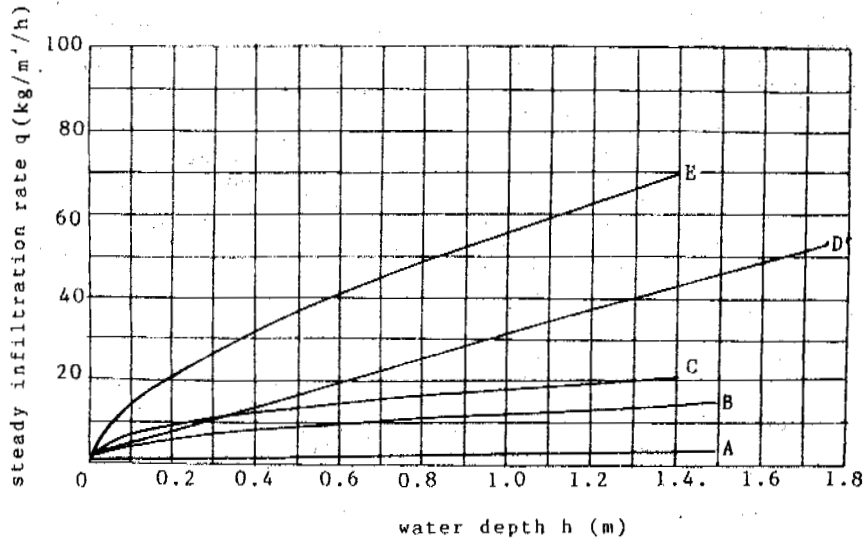


Fig.1 Generalized steady infiltration curves of the canal lined with different materials (A-membrane; B-site-casted concrete; C-precast concrete; D-mortar-lined stones; E-earth)

Leave a 3-5 cm thickness of soil before the designed cross section is formed so as to let the soil moisture evaporate under natural conditions; At the time of construction, carefully clear away a 3-5 cm thickness of top soil so as to make the soil surface a natural wet condition which will be favourable for the lining of concrete or other seepage prevention materials.

(2) For the improved use of structures: Soils below the used structures are often in a saturated condition, and it is necessary to refill the canal base, re-excavate and re-form the designed cross section before lining. In these processes, the following measures should be taken to reduce the soil moisture content in the foundation: (a) Before lining, stop transporting water through the canal as early as possible and loosen the base soil and let it dry out naturally; (b) If the lining is necessary when the canal has just stopped transporting water (this means that the base soil is probably saturated), the pumping method should be adopted to extract the water from the canal base; (c) If the former two methods are still unable to meet the design requirements, mix the base soil with low water-content soils to a uniform soil moisture content, approximately to the plastic limit of the soil,

and then refill the canal base. For large scale or important project structures, or structures designed to shift the base soils so as to prevent frost damages, remove the base soils and refill with ideal water-content soils or sands, gravel and stone materials. The depth of excavation depends on the depth of frozen and/or the criteria of design.

(3) Planting trees on the levee of canal to extract water in the base soil. According to the experience in Xinjiang Autonomous Region, planting water-loving trees like the willow will cause biological drainage. Measurements of the same canal indicated that soil water content in the tree-planted levee was 14-16% less than that in the bare levee.

#### Measures to Prevent Outside Water Sources From Entering the Canal Base

The outside water sources can infiltrated from the canal water, from surface water on top of the levee and from nearby mountain slopes and farm fields. To prevent these water sources from entering the canal base, the following measures should be taken respectively:

(1) Designing the seepage prevention structures with advanced technologies:

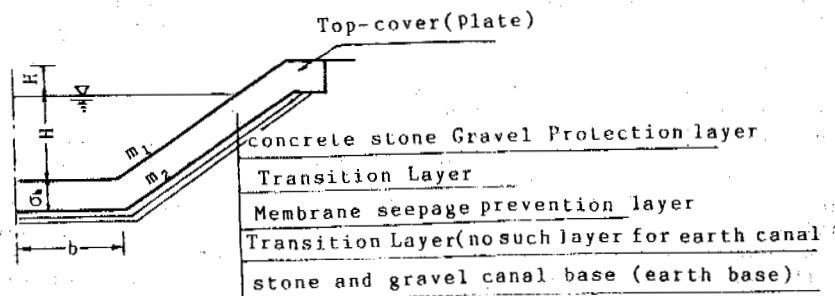


Fig.2 Top-cover (plate) of the lined canal

(a) First choose the membrane lining material. Field tests in Shanxi Province proved (in Fig.1) that under the same canal water depths the membrane materials reduced seepage the most, compared with the site-casted concrete lining and the pre-casted concrete lining. Therefore, the membrane lining should be actively adopted and extended in practice;

(b) Choose a better crack filler. Experience has proved that crack fillers for the inflexible lining materials like concrete should be adopted. A new type of crack filler, the Tar Plastic Daub, has been developed in the Northwestern Hydraulic Science Institute, with great binding strength (under-15°C) up to 8.9 kg/cm<sup>2</sup> and good stretching strain (under-12°C) in the range of 46.7-260%. For large scale project structures, the plastic (or rubber) seepage stop belt is recommended;

(c) Extend the top-cover layer to prevent outside water from entering the canal base. A horizontal top-cover plate of 25-30 cm wide, as shown in Fig.2, should be designed. When there is a gravel shifting-pad layer under the lining plate, the width of the top-cover should be 10 cm greater than the combined width of the gravel-pad and the lining plate. And if the lining depth is less than the canal depth, the top-cover should be extended into the levee. The material of the top-cover is generally the same as that of lining plate or the protection layer of the membrane;

(d) For membrane lining, the top-cover should be laid as shown in Fig.3. The connection of the membrane with building structures should be designed as shown in Fig.4:

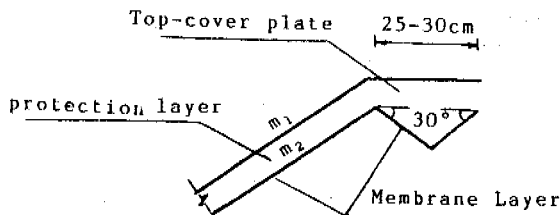


Fig.3 Top treatment of the membrane layer

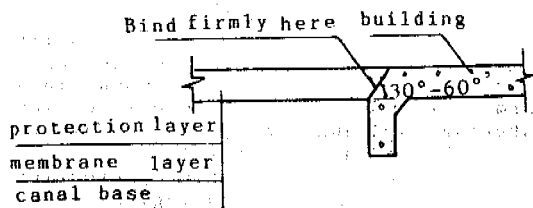


Fig.4 Connecting of membranes with buildings

(e) Seepage prevention canals should be constructed having a sideways slope of 1/100-1/200. If the canal bank is beside a high-rising slope, a drainage ditch should be constructed along the foot of the slope to let the water flow out the levee or into the canal.

(2) Constructing carefully to ensure the quality of the canal lining

The following procedures should be carefully followed to ensure the quality of the canal lining engineering:

(a) Consolidate the canal base. According to regulations in reference (Water Resources Minis-

try of China, 1991), the pressed density degree of the canal base should not be less than 0.98, and the unit dry weight of the base soil should not be less than 1600 kg/m<sup>3</sup> or less than 1.05 times that of the original natural soil. This has provided a sound base not only for the canal lining but also for prevention of frost damage. For the solid canal base can also obstruct soil moisture from migrating to the frost front area, thereby protecting the soil from frost heaving;

(b) Precisely determine the mixing proportion of concrete and other raw materials, carefully do the mixing and casting. And especially pay attention to the filling of the cracks. Binding the crack filler firmly and meeting the design criteria;

(c) Membrane lining should be conducted carefully from downstream to upstream and from one bank to another so as to prevent any damage to the membrane. If damages are found, re-mend them quickly with a membrane 10-20 cm wider on each side than that of the broken hole. Overlapping of the different size of membranes and their connection to other buildings should be well designed and well treated;

(d) Construction of top-cover, levee and drainage ditches should be strictly in accordance with the design.

#### Measures To Lower the Water Table

In places along the canal where the original water table is relatively high due to various reasons including the intrusion of outside water, the canal structures are threatened by frost damage or affected by the floating forces from the ground water. The following measures should be taken to lower the water table:

(1) In the initial planning and designing, the canal lining structures should be considered as far as possible to be of an earth filling type, so as to increase the height of the canal and to prevent or alleviate the uprising of ground water to the frozen front area in the process of freezing. The minimum distance between the frozen line and the water table in China are mainly determined by the capillary action of various soils. According to reference (Tong Changjiang et al., 1985), the minimum distance for the clay soil containing montmorillonite and hydromica stroma is 3.5 m; for the clay, and clay-loam soils containing kaolinite stroma 2.5 m; for the sandy loam and fine sandy loam soils 1.5 m, for the sandy and fine sandy soils 1.0 m; for the fine sands 0.6 m; and for the coarse sands 0.4 m.

(2) In places where the earth-filling canal is not possible or the height of the canal to the water table is within the frost damage range, drainage ditches along the canal banks can be built (as is seen in Xinjiang) to lower the water table, while the earth-filling plan should also be considered simultaneously.

(3) For the improvement of canals or for new canals where the above methods of lowering the water table are not applicable, the longitudinal and transverse drainage systems should be built beneath the canal base so as to lower the water table and alleviate frost damages. In places where the land topographic conditions allow for the drainage of ground water, the water can be directly drained out of the canal. Otherwise, the water should be drained into the downstream of this canal. Fig.5,6, and 7 are the illustrative diagrams of longitudinal and transverse drainage systems.

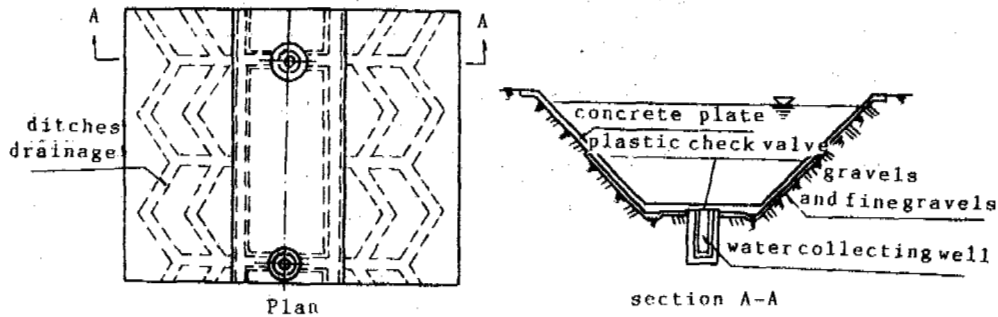


Fig. 5 Combined drainage system beneath the canal

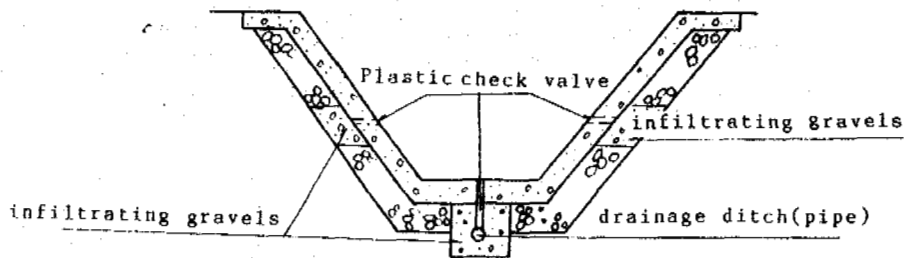


Fig. 6 Drainage system diagram

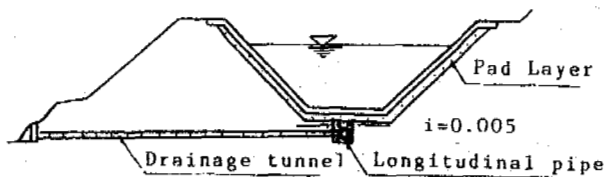


Fig. 7 Longitudinal and transverse drainage system

#### REFERENCES

- Water Resources Ministry of China (1992) Technical Regulations for Canal Seepage Prevention Structures SL18-91. Hydraulic and Hydro-power Publishing House.
- Water Resources Ministry of China (1991) Design Regulations for the Frost Heaving Prevention in Structures of Canal System (SL 23-91). Hydraulic and Hydro-power Publishing House.
- Tong Changjiang and Guan Fennian (1985) Frost heaving of soils and control of frost damages to the structures, Hydraulic and Hydro-power Publishing House.

#### Management Measures For the Control of Frost Damages

In order to alleviate frost damages to the canal lining structures, engineering management work should be stressed on the the following aspects:

(1) Irrigation of farm lands and tree belts adjacent to the excavated canals should be stopped at least 15-20 days before the temperature decreases to the minus.

(2) Canals which that will not be operated in the winter should stop transporting water well before the air temperature decreases steadily below  $0^{\circ}\text{C}$ . And only if the air temperature is steadily above  $0^{\circ}\text{C}$  can the canal return to operation. Winter-operative canals should keep a continuous transport of water and a greater water level well above the winter minimum level.

(3) Before irrigation (especially the fall irrigation) or after rainstorms, the lined canals should be completely checked to ensure the completeness, safety and reliability of the seepage prevention layer, the shrinkage and construction junctures, the top-cover, and the above mentioned drainage systems. If there is any damage, crack, mis-lap, obstruction and other out-of-repair parts, prompt mending should be provided. As it is well known that the canal seepage prevention structures should never be operated under ill condition.



## RESEARCH OF FROST HEAVE PROPERTY OF SOIL IN DAQING REGION

Jiang Hongju and Cheng Enyuan

Daqing Oilfield Design Academy, China

Since 1960, in order to meet the needs of oilfield engineering construction, more than 50 observation points of frost heave have been set up in Daqing region and the observations and experimental research of soil frost heave, freezing depth and ground temperature etc. under natural conditions have been conducted. In this paper, the main characteristics of frost heave property of natural soil in Daqing region will be introduced.

### INTRODUCTION

The region lies at 125 degrees east longitude and at 46 degrees north latitude. It is located in the middle of Harbin and Qiqihar on the Songnen plain and it is an alluvial plain with the two river systems of Songhua River and Nenjiang River. Its geological structure belongs to the northwest part of the central depression in Songliao basin. The landform type belongs to the first grade of terrace of Songhua River and Nenjiang alluvial plain. Its terrain is on the low side in the southwest and on the high side in the northeast. Its altitude is in the range of 126-165 m. Its landform appears in the low plain like an undulating wave. From the mini-landform, there are three main types of landform: the mound area is like an isolated hill, the plain area is like an undulating wave and damp low marsh and a small lake area.

The mound area like an isolated hill: the area is relatively 4-8 m higher than the small lake area. A layer of aeolian weak loam covers the upper part. One side of a large part of the mound faces a small lake. The condition of surface runoff is good. The water contents of surface soils within the freezing depth are almost lower than the plastic limit. The highest underground water level is usually below 4 m and the annual changeable scope of the underground water level is between 1.2-1.8 m. The surface vegetation grows poorly.

The plain area like an undulating wave: almost all parts of Daqing area are of this type of region. Its terrain is even but there are some rises and falls. The surface soil within the freezing depth are fine sand, weak loam and loam respectively. The condition of surface runoff is bad. A large amount of rainfall permeates underground. The highest underground water level is within 1.0-2.5 m. Its annual changeable scope is 2.5-2.9 m. The surface of this area is farmland and grass cover.

The damp low lying marsh and small lake area: the damp low lying marshes are almost linked with the small lake. It has perennial or seasonal stored water areas. The surface soil of this area consists of weak loam, loam and a little cohesive soil. The highest underground water level is within 0.0-1.5 m. The annual changeable extent of underground water is between 2.2-2.4 m. The ground is covered in reed grass.

No matter what the type of area in Daqing region, the soil layer distribution and structure within the soil freezing depth are basically homogeneous or even single. Its main soil layers are fine sand, weak loam and loam.

The underground water level in Daqing region changes with the change of season. The highest underground water level occurs during September and October and the lowest level is during March and April. Its changeable rule shows basically the change in a line curve.

This region belongs to continental, semi-arid, severe cold, prairie climate. Winter is long, with severe cold and is arid. Summer is short and warm. According to the 28 years of statistics from 1957 to 1984, annual precipitation varies from 267.3 to 664.3 mm. 50 per cent of precipitation is distributed in the three months of July, August and September. Precipitation is an important resource of underground water supply. Because of the need for oilfield development and construction, two large reservoirs were built on the edge of the oilfield and the diversion canals were dug. To a certain degree, the reservoirs resulted in the changes of underground water levels in Daqing. In addition, the bankments of complicated highway nets are high and make ground drainage more blocked. Besides its effect on underground water levels, it also caused the enlargement of soil water content.

The highest monthly average temperature of summer in the region is 22.8°C. The lowest monthly average temperature of winter is -19.6°C.

The annual average temperature is 3.26°C. The annual freezing index is 1936.3°C day which was the 27 year average value from 1951 to 1983. The ground begins freezing from the middle of November and reaches the largest freezing depth until the middle of March of the next year. From the beginning of thawing ground in the middle of March to the complete melting of the frozen soil layers in the middle of June, frozen soil will continue for 7 months. The biggest annual freezing depth is 1.7-2.3 m. It belongs to deep seasonal frozen soil region.

#### THE TYPES OF SOIL FROST HEAVE IN DAQING REGION

On the basis of the different soil constituents, underground water level, soil water content and saline content etc., more than 50 observation points of frost heave were set up in the area of 400 km<sup>2</sup>. The frost heave in different layers (at the depths of 0.0, 0.5, 1.0, 1.5 and 2.0 m under ground) were observed in the typical region. Meanwhile the freezing depth, underground water level and ground temperature were conducted. Through analyses of observation data, the following frost heave types have been discovered in Daqing region:

##### Frost and Contracting Area

The area located in the flat and slightly low area. It has less growth of weeds. The soil within the freezing depth appears black brown in colour. Plastic index is about 12 or more. The soil classification is loam or cohesive soil. The particle percentages of less than 0.005 mm are more than 30-40%. The dry density of the soil is 1.7 g/cm<sup>3</sup>. The total saline content is 0.32 g/100 g dry soil. The underground water level at the beginning of winter is 1.5 m below the ground. Fig.1 shows the curves of frost heave and freezing depth vs elapsed time (note: frost and contracting curves mean the altitude changes relative to sea level). From Fig.1, we can see that the soil layer above 1.0 m contracts, but the soil below 1.0 m expands. Moreover, the contracted amount of the soil layer between 0.5-1.0 m is more than the contracted amount between 0.0-0.5 m. Until the middle of March, the thawing of the soil layer is between 0.0-0.5 m and results in expansion, and then recovers to the initial elevation. The soil layer between 0.5-1.0 m also recovers to the initial elevation. The soil layer below 1.0 m begins expanding from the middle of November until January, the layer produces little contraction. It begins expanding again during the beginning of February, but the amount of expansion is small.

##### No Frost Heave Area (the Average Frost Heave Ratio $\eta \leq 1\%$ within the Freezing Depth of Soil)

The area located in the flat fine sandy area or isolated hill and high mound zones. The isolated hill and high mound zones are almost all weak loam and yellowish loam. The underground water level before winter is below 4 m. The condition of surface runoff is good. The soil water content within the freezing depth is equal to or less than the plastic limit. The total saline content in the fine sand area is about 0.053 g/100 g dry soil. The total saline content in the high mound area is about 0.088 g/100 g soil. Fig.2 shows the curve of soil frost heave in each layer in winter. From Fig.2, we can see: The soil produces only several millimetres of

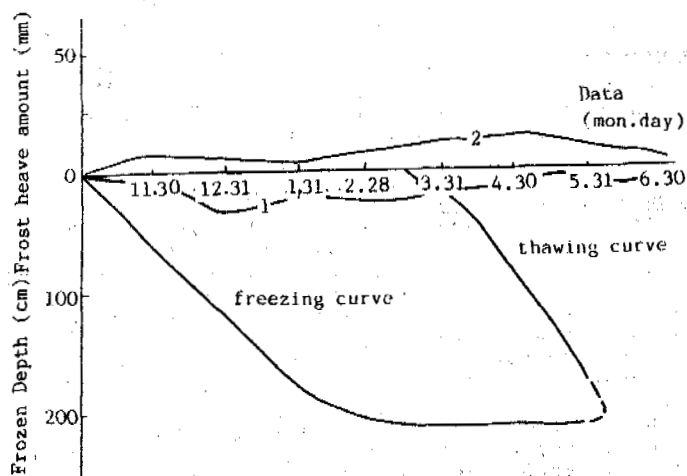


Figure 1. The curves of Point 7 frost heave observation in each layer (in the winter, 1983-1984, frost and contracting area)

Note: Buried depth of observation points  
1. Buried depth 50 cm;  
2. Buried depth 150 cm.

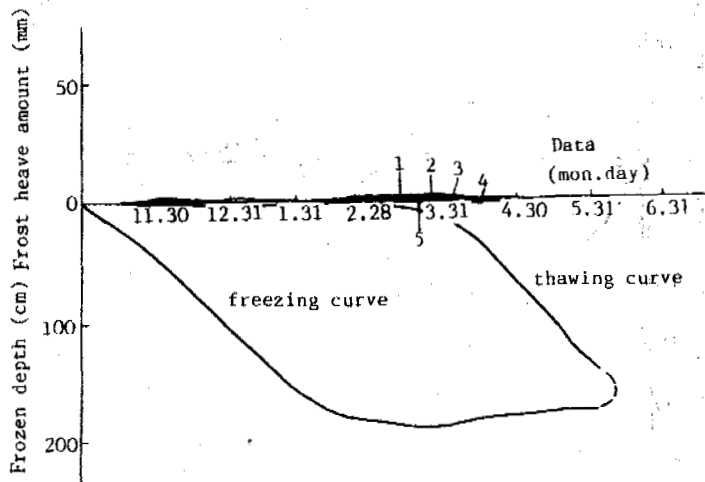


Figure 2. The curves of Point 8 frost heave observation in each layer (in the winter, 1982-1983, no frost heave area)

Note: Buried depth of observation points  
1. On the ground;  
2. Buried depth 50 cm;  
3. Buried depth 100 cm;  
4. Buried depth 150 cm;  
5. Buried depth 200 cm.

deformation. It is very small. So it is considered as neither producing frost heave nor contracting.

##### The Soil of Frost Heave

The soil can be classified on the basis of the method of a now generally recognized classification in China and can be divided into four kinds i.e. (Design Standard of the Foundation of Industrial, 1974):

Soil name	Average frost heave ratio
Weak frost heave soil	$1\% < n \leq 3.5\%$
Frost heave soil	$3.5\% < n \leq 6.0\%$
Stronger frost heave soil	$6.0\% < n \leq 12.0\%$
The strongest frost heave soil	$n > 12.0\%$

#### Weak frost heave soil

The soil distributed on the flat area of the slightly high relief. The underground water level before winter is near 2 m in the depth. The water content of the soil is small. Large parts of the soil are weak loam or loam, which has a wide distribution. The soil is more compacted. The total saline content of this soil is about 0.068 g/100 g-dry soil. Fig.3 shows the curve of frost heave distribution of the soil. A characteristic of this area is the bigger freezing depth of the soil. The curves of frost heave in each layer vs elapsed time are nearly parallel. When thawing and subsiding, the upper layer of soil thaws and subsides more quickly than the lower. If a change takes place in the ground conditions of the soil or the surface stores of water, the frost heave grade would result in a change.

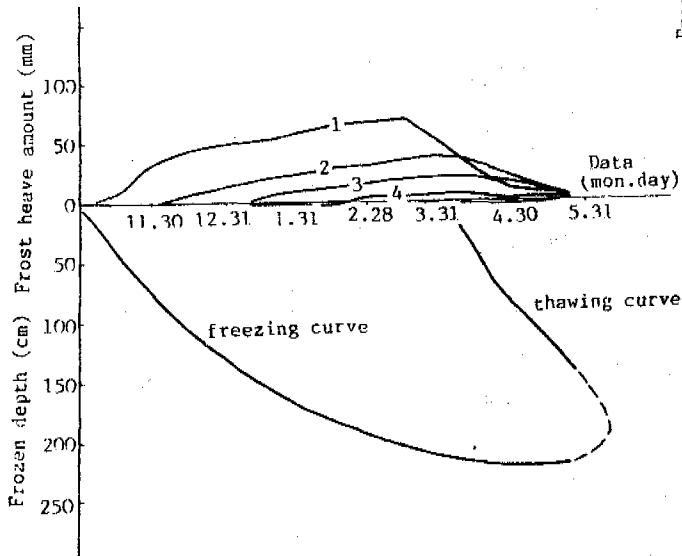


Figure 3. The curves of Point 9 frost heave observation in each layer (in the winter, 1982-1983, weak frost heave)

Note: Buried depth of observation points

1. On the ground;
2. Buried depth 50 cm;
3. Buried depth 100 cm;
4. Buried depth 150 cm;
5. Buried depth 200 cm.

Average frost heave ratio  $\bar{n}=3.3\%$

#### Frost heave soil

The soil has a wide distribution in Daqing region. Its relief is flat. It is made from weak loam or loam. The dry weight of the sample is between 1.5-1.6 g/cm<sup>3</sup>. The water content of the soil is medial. The underground water level before freezing is between 1.0-1.5 m. The initial void ratio is within 0.6-0.7. The total saline content of the soil is about

0.063 g/100 g-dry soil. Fig.4 shows the curve of frost heave in each layer. A characteristic is the smaller freezing depth than that of the weak frost heave area. The curves of frost heave in each layer are also parallel. After thawing of the total frozen layers, the location of each layer recovers to the initial elevation.

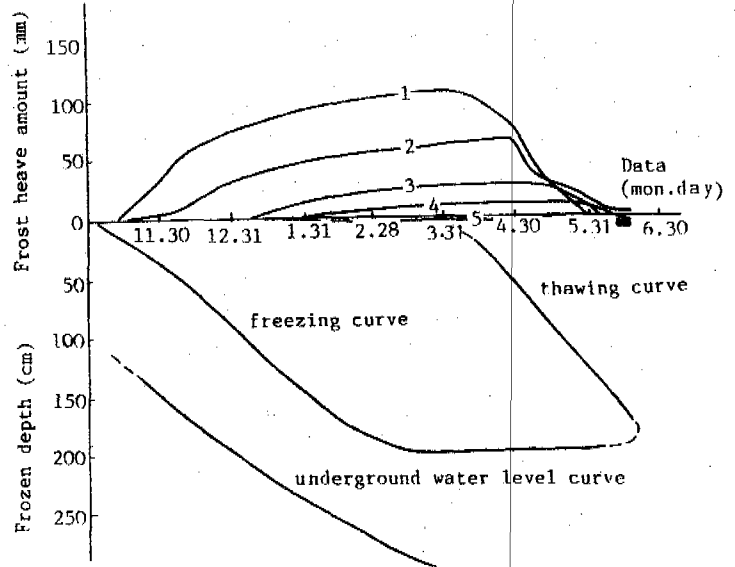


Figure 4. The curves of Point 10 frost heave observation in each layer (in the winter, 1983-1984, frost heave area)

Note: Buried depth of observation points

1. On the ground;
2. Buried depth 50 cm;
3. Buried depth 100 cm;
4. Buried depth 150 cm;
5. Buried depth 200 cm.

Average frost heave ratio  $\bar{n}=5.3\%$

#### Stronger frost heave soil

The soil is located in flat and in small low reliefs. It is weak loam or loam of yellow-brown colour. The dry density of the soil is 1.5-1.6 g/cm<sup>3</sup>. The void ratio is between 0.6-0.7. The underground water level is within 1.0-1.5 m. The water content of the soil is slightly large. The total saline content is about 0.055 g/100 g-dry soil. Its curve of frost heave can be seen in Fig.5. The freezing depth of the soil is lower than frost heave soil.

#### The strongest frost heave soil

The soil is distributed in shallow and flat areas, which are almost all weak loam or loam with a yellowish brown colour. The dry density of the soil is 1.45-1.6 g/cm<sup>3</sup>. Initial void ratio is more than 0.7. It is easy to store water. The underground water level before winter is within 0.3-0.8 m. The total saline content of the soil is about 0.092 g/100 g-dry soil. Fig.6 shows the curve of frost heave in each layer. A characteristic is that the soil below 1.5 m won't produce frost heave (when the frost heave ratio is more than 17%). The freezing depth is obviously low. The soil layers when frozen will not produce frost heave.

The theory about the frost heave of frozen soil has been generally recognized and testified to with a lot of experiments. We don't doubt the theory's correctness. However, according to

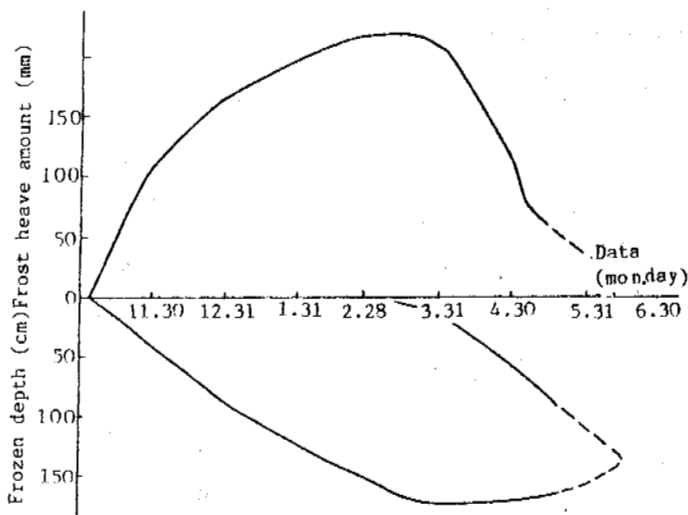


Figure 5. The curves of Point 11 frost heave observation in each layer (in the winter, 1963-1964, strong frost heave area)

Ground frost heave observation,  
Average frost heave ratio  $\bar{\eta}=12.5\%$

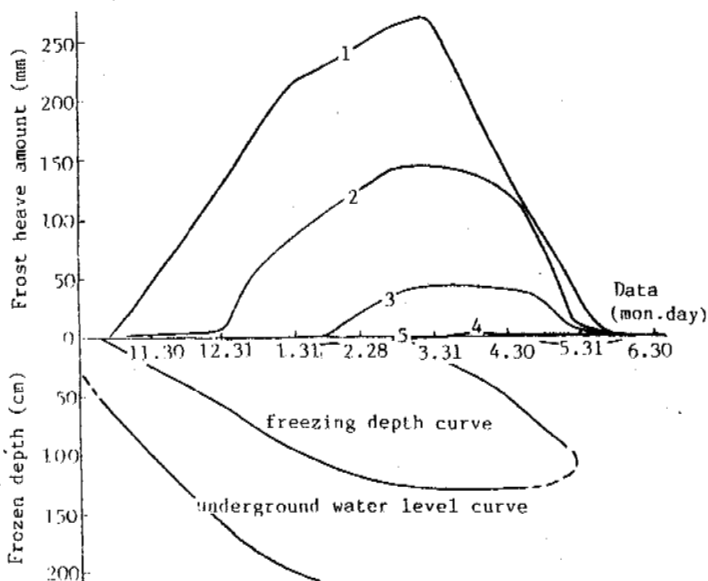


Figure 6. The curves of Point 12 frost heave observation in each layer (in the winter, 1983-1984, strong frost heave area)

Note: Buried depth of observation points

1. On the ground;
2. Buried depth 50 cm;
3. Buried depth 100 cm;
4. Buried depth 150 cm;
5. Buried depth 200 cm.

Average frost heave ratio  $\bar{\eta}=20.1\%$

the field observations of many points and various types in Daqing region, we have found out: No matter what type of frost heave there is, in frozen soil there hardly occurs any frost heave during the frost heave process. Under the conditions of the climate and geology in Daqing region, the frost heave of the soil produced mainly in the front of the freezing and the frost heave

of frozen soil is very small and couldn't be observed. The frost heave of the soil can't be considered in engineering construction.

#### THE CHARACTERISTICS OF SOIL FROST HEAVE RATIO ALONG THE DEPTH DISTRIBUTION

On the problem of frost heave ratio of foundation soil along the depth distribution, three kinds of opinions have been mentioned currently: First, the frost heave ratio from the surface to the lower layer reduces gradually. Secondly, the frost heave ratio from the surface increases gradually. Thirdly, the frost heave ratio is the same along the depth. On the basis of the field observations of many points and many years in Daqing region, under the conditions of climate and engineering geology, our conclusion is: The frost heave ratio decreases gradually from the ground to lower layers (see Table 1 and Fig.7). From the statistical points, the data in Table 1 it can be seen that: The amount of frost heave in the layer 0-50 cm is 49.9% of the total amount of frost heave. The amount of frost heave in the layer 50-100 cm is 32.3% of the total amount of frost heave. The amount in the layer 100-150 cm is 12.8% of the total amount. The amount in the layer below 150 cm is 5% of the total amount. The average values of frost heave ratio in each layer are 12.1%, 9.2%, 3.6% and 0.84% respectively. So our conclusion is correct. However, the soil layer below 10 cm from the surface has a small frost heave ratio because of wind drying and evaporating. So the soil layer can be omitted because there is no effect on engineering construction.

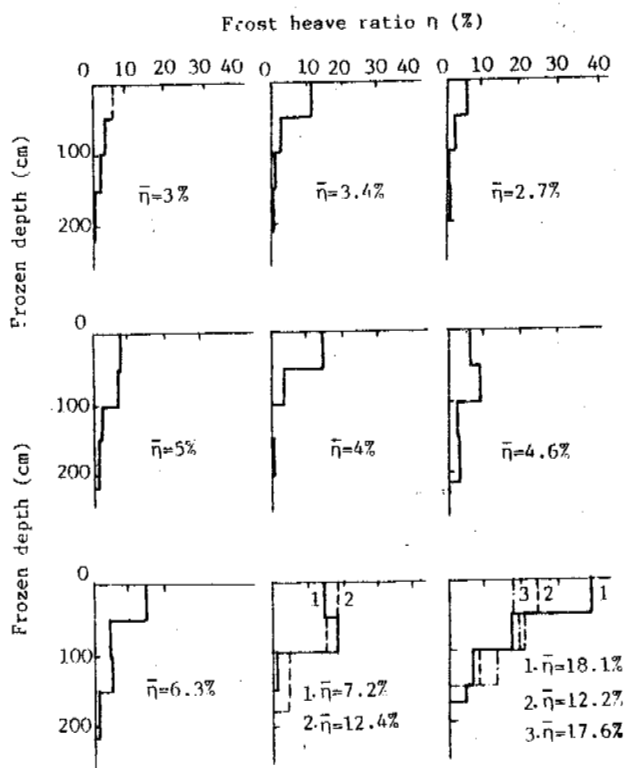


Figure 7. The distribution of frost heave ratio along the depth

Table 1. The observation values of frost heave amount (ratio) along the depth

Observation points	Freezing depth (cm)	Total frost heave amount H (mm) Average frost heave ratio (%)	Frost heave amount in each layer $\Delta h$ and frost heave ratio $\eta$ (%)											
			0-50 (cm)			50-100 (cm)			100-150 (cm)			below 150 (cm)		
			$\Delta h$ (mm)	$\frac{\Delta h}{\Delta H}$ %	$\eta$ (%)	$\Delta h$ (mm)	$\frac{\Delta h}{\Delta H}$ %	$\eta$ (%)	$\Delta h$ (mm)	$\frac{\Delta h}{\Delta H}$ %	$\eta$ (%)	$\Delta h$ (mm)	$\frac{\Delta h}{\Delta H}$ %	$\eta$ (%)
Point 10(1)	184	$\frac{53}{2.9}$	27	50.9	5.4	10	18.9	2.0	12	22.7	2.4	4	7.5	1.1
Point 9	214	$\frac{64}{3.0}$	29	45.3	5.8	17	26.5	3.4	14	21.9	2.8	4	6.3	0.6
Point 14	205	$\frac{70}{3.4}$	52	74.2	10.4	14	20	2.8	2	2.8	0.4	2.1	3.0	0.4
Point 20(2)	205	$\frac{94}{4.6}$	29	30.9	5.8	42	44.7	8.4	10	10.6	2.0	13	13.8	2.4
Point 10(2)	207	$\frac{103}{5.0}$	39	37.9	7.8	36	34.9	7.2	14	13.6	2.8	14	13.6	2.4
Point 25	198	$\frac{81}{4.1}$	62.5	77.1	12.5	16.5	20.4	3.3	0	0	0	2	2.5	0.4
Point 10(3)	195	$\frac{170}{8.7}$	72	42.4	14.4	93	54.7	18.6	5	2.9	1.0	0	0	0
Point 27	192	$\frac{135}{7.0}$	73	54.1	14.6	54	40.0	10.8	8	5.9	1.6	0	0	0
Point 10(4)	203	$\frac{128}{6.3}$	72	56.2	14.4	22	17.2	4.4	24	18.8	4.8	10	7.8	1.9
Point 12	149	$\frac{266}{17.8}$	122	45.9	24.4	103	38.7	20.6	41	15.4	8.2	0	0	0
Point 29	150	$\frac{255}{17.0}$	88	34.5	17.6	100	39.2	20.0	67	26.3	13.4	0	0	0
Average				49.9	12.1		32.3	9.2		12.8	3.6		5.0	0.84

REFERENCE

Design Standard of the Foundation of Industrial, (1974) Publishing House of Building Industry, China.

Thermal Regime of Alpine Permafrost in the Upper  
Reach of Urumqi River, Xinjiang, China\*

Jin Huijun, Qiu Guoqing, Zhao Lin Wang Shujuan and Zeng Zhonggong

Lanzhou Institute of Glaciology and Geocryology,  
Chinese Academy of Sciences, China

The distribution and ground temperature of alpine permafrost have a very close relation to the altitude in the middle section of East Tian Shan. The lower limit of permafrost is at 3250 m a.s.l. on the south-facing slope and at 2900 m a.s.l. on the north-facing slope where the mean annual air temperature is about  $-2.0^{\circ}\text{C}$ . The mean annual ground temperature decreases from  $-0.7^{\circ}\text{C}$  to  $-4.9^{\circ}\text{C}$  and permafrost thickness increases from about 50 m to 230 m as the altitude rises from 3300 to 3500 m a.s.l. The thawing starts in late April at 3450 m a.s.l., reaches 3.5 m in mid-Oct. and refreezing begins in early Nov. and is finished in mid-Feb.; whereas the thawing starts in mid-June at 3540 m a.s.l., reaches 2.3 m in mid-Oct. and immediately the refreezing starts and is finished in late Dec.

## INTRODUCTION

Systematical studies on alpine permafrost in East Tian Shan (Tian Shan in Chinese territory) were started in the early 1970's. Much work on permafrost distribution and thermal regime have been undertaken in the Kuixian Daban (Pass) region (Qiu and Zhang, 1981). In the early 1980's, permafrost investigations were carried out at the source area of the Urumqi River for engineering purposes and in some alpine areas from west to east of East Tian Shan for an understanding of permafrost distribution. The results of the above work were presented at the Second Chinese National Conference on Permafrost, Lanzhou, China, 1981 and at the Fourth International Conference on Permafrost, Fairbanks, Alaska, U.S.A., 1983 (Qiu et al., 1983a, b). Study on rock glaciers were conducted by Cui and Zhu (1988). Recently, the project of Alpine Permafrost Studies in Central Asia supported by the National Natural Science Foundation of China and the Tian Shan Glaciological Station of Academia Sinica, provided an opportunity for further investigation in the middle section of East Tian Shan. As part of the results of the project, this paper is designed to discuss the thermal regime of alpine permafrost in the region, especially in the upper reach of the Urumqi River ( $43^{\circ}06'N$ ,  $86^{\circ}50'E$ ) (Fig.1).

## THE STUDY REGION

Many ridges and fault basins in East Tian Shan are controlled by the WNW and ENE tectonic lines and other factors. Most of East Tian Shan, in the middle section, consists of Paleozoic granite and metamorphic system. The crest eleva-

\*This project is supported by the National Natural Science Foundation of China and the Research Foundation of Tian Shan Glaciological Station, Academia Sinica.

tion varies from 4000 to 4300 m a.s.l., the Tiangel Peak in the south is 4562 m a.s.l., while the Bogda Peak in the northeast is 5445 m a.s.l. The present snowline is at about 4000 m a.s.l.; the modern glacier terminals are at about 3700 m a.s.l. and the glaciated area in the Last Glaciation was down to an elevation of 3000 m.

The climate in the East Tian Shan is characterized by the cold-humid belt across the semi-arid region of the Xinjiang Uygur Autonomous Region, which depends upon high altitudes. The precipitation increases upward, westward and northward. In the alpine permafrost regions it will be 200-500 mm per year, while at the snow line — 600-700 mm or more. It concentratively falls in June, July and August. In the Tian Shan Mountain area, the air temperature decreases with a gradient of about  $0.33-0.37^{\circ}100\text{ m}^{-1}$  from 1830 to 3000 m a.s.l. and  $0.61-0.66^{\circ}100\text{ m}^{-1}$  from 3000 to 4000 m a.s.l. The period with a mean diurnal air temperature lower than  $0^{\circ}\text{C}$  exceeds 130 days per year.

A series of landscapes are encountered with altitude, namely deserts and semi-deserts (below 1700 m a.s.l.), forest steepes (1700 or 1800 to 2800 m a.s.l.), subalpine meadows (2800 or 3300 to 3500 m a.s.l.) and an alpine glacio-periglacial zone (above 3300 or 3500 m a.s.l.). Their boundaries vary with slope orientation, latitude, longitude and other factors.

## RESULTS OF TEMPERATURE MEASUREMENTS

Based on the previous work in the middle section of East Tian Shan, five boreholes with depths from 14 m to 60 m were drilled at an elevation from 3300 to 3900 m a.s.l. in the upper reach of Urumqi River in the summers of 1990 and 1991. Ground temperatures were recorded twice a month since August of 1990 at borehole No.2 and No.4, and since September of 1991 at borehole No.1, No.3 and No.5.

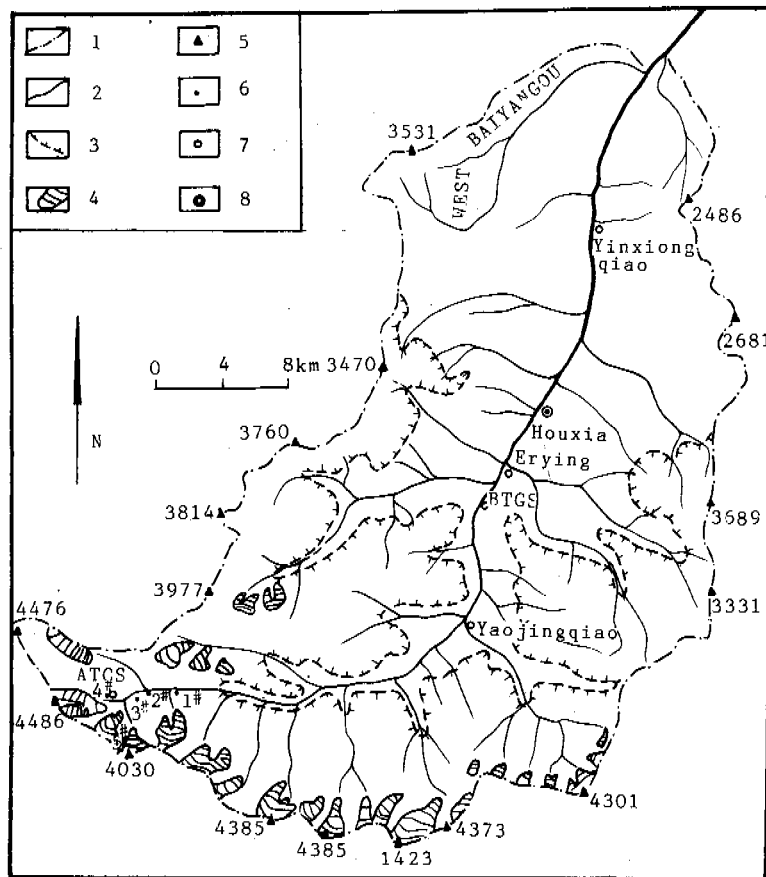


Figure 1. Distribution of modern glaciers alpine permafrost and location of boreholes in the Urumqi River basin

The borehole No.3 (3500 m a.s.l.) is located on a gentle swampy low land which is composed of clayey sand and gravels with a high ice content above the depth of 10.7 m and the diabase is below 10.7 m. The profile of borehole No.5 (3900 m a.s.l.) on the east-facing gneiss slope is covered by the coarse sand and gravels 3.3 m in thickness, borehole No.1 sets itself on a morainic deposits with loose materials above the depth of 16 m and diabase below 10.7 m. The profile of borehole No.4 is composed of detritus and clayey sand within 16.4 m and the loose material layer is 12.3 m in thickness at borehole No.2 on turf-bound boggy marshland and both of them cut into the diabase.

Fig.2 illustrates the ground temperature profiles of borehole No.1, No.3, and No.5; Fig.3 shows the isotherms of ground temperature with the depth of 9.0 m below the ground surface at borehole No.2 and No.4. Some observed characters of permafrost regime and estimated permafrost thickness based on the gradient of ground temperature of borehole No.3 are given in Table 1:

#### THERMAL ANALYSIS

##### Geothermal gradient and Permafrost Thickness

The obtained data of ground temperature at the deepest borehole, No.3, shows that ground

temperature remains at about  $-1.6^{\circ}\text{C}$  from 10 to 25 m and changes into  $-0.8^{\circ}\text{C}$  at the depth of 59 m, so the geothermal gradient is about  $1^{\circ}43\text{ m}^{-1}$  from 25 m to 59 m (Fig.2, ). Thus the thickness of permafrost here should be about 95 m if ground temperature increased with depth at a same gradient below 59 m. The ground temperature stays at  $-1.8^{\circ}\text{C}$  from 13.0 to 15.5 m and show no change in borehole No.4. If this isothermal layer is ended at a depth of 25 m as in borehole No.3 and ground temperature increases with depth also at a gradient of  $1^{\circ}43\text{ m}^{-1}$ , the permafrost thickness at borehole No.4 would exceed 100 m. The ground temperature is about  $-4.9^{\circ}\text{C}$  at the depth of 18 m, permafrost thickness should be about 230 m calculated by the gradient of  $1^{\circ}43\text{ m}^{-1}$ . Here, it is problematical that the underlain bedrock is gneiss, not as same as that underlain in other boreholes. The ground temperature is  $-0.9 - -1.0^{\circ}\text{C}$  at the depth of 11 m at borehole No.2. The permafrost would be 60 m in thickness if the MAGT were  $-1.0^{\circ}\text{C}$  at the depth of 15 m and it increased with depth at a gradient of  $1^{\circ}43\text{ m}^{-1}$ . The mean annual ground temperature is  $-0.7^{\circ}\text{C}$  at 17 m, so permafrost would be nearly 50 m at borehole No.1 calculated by the geothermal gradient of  $1^{\circ}43\text{ m}^{-1}$  (Table 1).

Table 1. Some observed data of thermal regime of permafrost and estimated thickness of permafrost in the upper reach of Urumqi River

Borehole	Depth (m)	Elevation (m a.s.l.)	MAGT (°C)	Permafrost table (m)	Depth of zero annual amplitude (m)	Estimated thickness of permafrost (m)
No.5	20	3900	-4.9	2.4	18	230
No.4	16	3540	-1.8	2.3	13	100
No.3	60	3500	-1.6	2.0	10	95
No.2	14	3450	-1.0	3.5	15	60
No.1	25	3300	-0.7	3.0	17	50

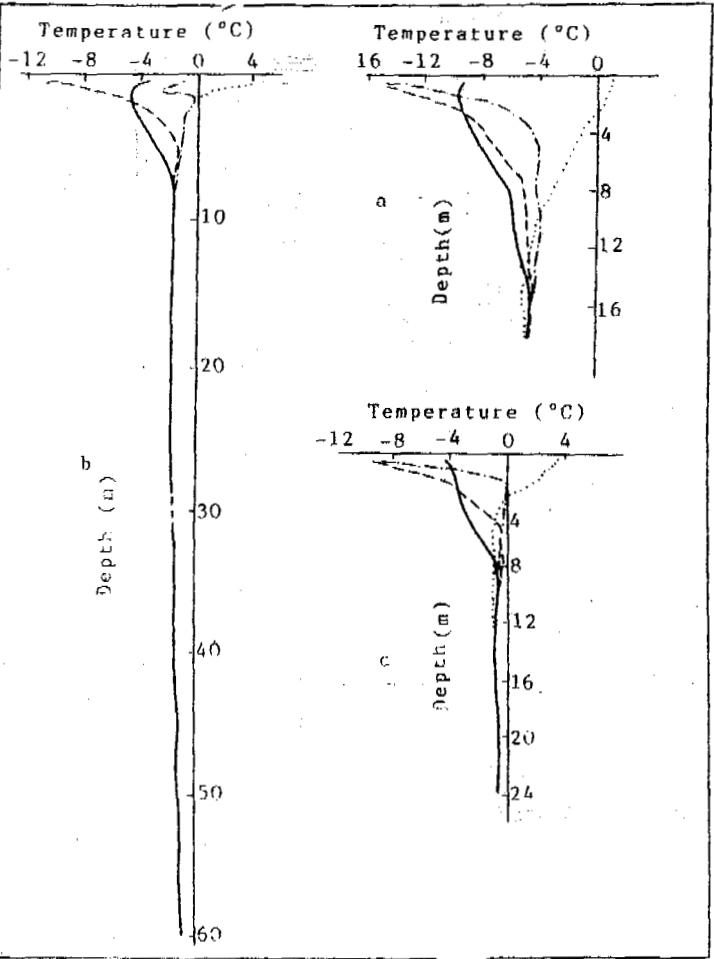


Figure 2. Ground temperature profiles of borehole No.2, No.3 and No.5 in the upper reach of Urumqi River

..... Sept. 28, 1991  
 - - - - Dec. 27, 1991  
 - · - · Feb. 17, 1992  
 ——— Apr. 13, 1992

a — at borehole No.5 (3900 m a.s.l.)  
 b — at borehole No.3 (3500 m a.s.l.)  
 c — at borehole No.1 (3300 m a.s.l.)

The Thermal Regime of the Active Layer

From Fig. 3, downward seasonal thawing begins in mid-June and reaches the maximum seasonally thawing depth of 2.3 m, then the downward re-freezing begins while the upward re-freezing

begins in the early December and re-freezing is finished at the end of December in borehole No.4, downward seasonal thawing begins at the end of April and reaches the maximum seasonally thawing depth of 3.5 m, then begins the downward re-freezing at the end of October and upward in the early February of the next year, re-freezing is finished in late February at borehole No.2.

From Table 1 and Fig.3, one can see that the process of seasonally thawing is characterized by:

1) The maximum depth of seasonally thawing is bigger in the vicinity of the lower limit of alpine permafrost. The maximum depth of seasonally thawing is 3.0 m at borehole No.1 (3300 m a.s.l.), 2.0 m at borehole No.3 (3500 m a.s.l.), 2.3 m at borehole No.4 (3540 m a.s.l.), and 2.4 m at borehole No.5 (3900 m a.s.l.). As an exception, it is 3.5 m at borehole No.2 (3450 m a.s.l.) due to thermal disturbance of the Luobodogou creek.

2) Slowly thawing and quickly re-freezing. The thawing process lasts 4 months and re-freezing only 2 months and upward re-freezing only one month at borehole No.4. The thawing process lasts as long as 8 months, re-freezing — only 4 months, and upward re-freezing — only one month at borehole No.2. Three months are delayed in the upward thawing than the downward thawing at borehole No.2 may also be due to the thermal disturbance of the Luobodogou creek.

3) The zero curtain. Isotherm of 0°C remains unchanged at the depth of about 2.30 m (i.e. the permafrost table) for 3 months from October to December at borehole No.4, at the depth of about 3.5 m for 4.5 months from October, 1990 to mid-February, 1991 and 2 months from mid-December, 1991 to mid-February, 1992. Washburn (1979) pointed out that zero curtain indicates the high moisture at the depth slightly higher than the permafrost table. Also two other steps of 0°C isotherm occurred at the depth of 2.0 and 3.0 m at borehole No.2 and at the depth of 1.0 and 1.5 m at borehole No.4 both in the processes of seasonally thawing and re-freezing, implying a higher energy budget during phase changes at these depths. The findings of an ice-rich layer in the active layer during excavation supports such an implication.

Fig.4 illustrates the ground temperatures of seasonally frozen ground at and in the vicinity of the Base of the Tian Shan Glaciological Station (2133.4 m a.s.l.). It shows that the gravels covered by a sparsely vegetated flat have a maximum depth of seasonally freezing as deep as 3.2 m and that of the humus soil on the solifluction tongue at 2238 m a.s.l. in the vicinity of the Base of the Tian Shan Glaciological Station it is only 1.6 m. Also, the ground temperature



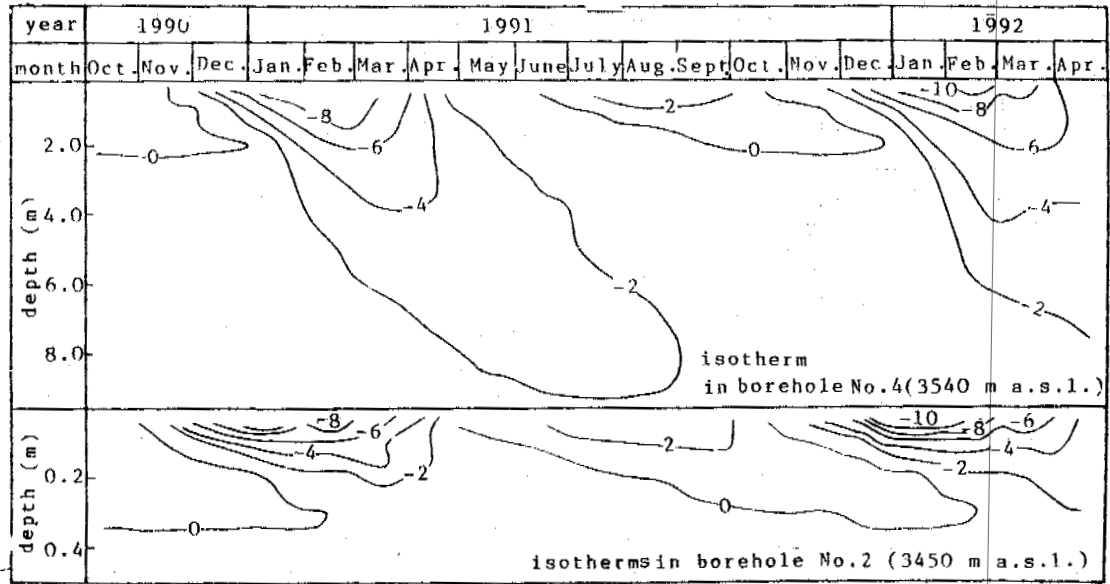


Figure 3. Isotherms of ground temperature in the upper reach of Urumqi River

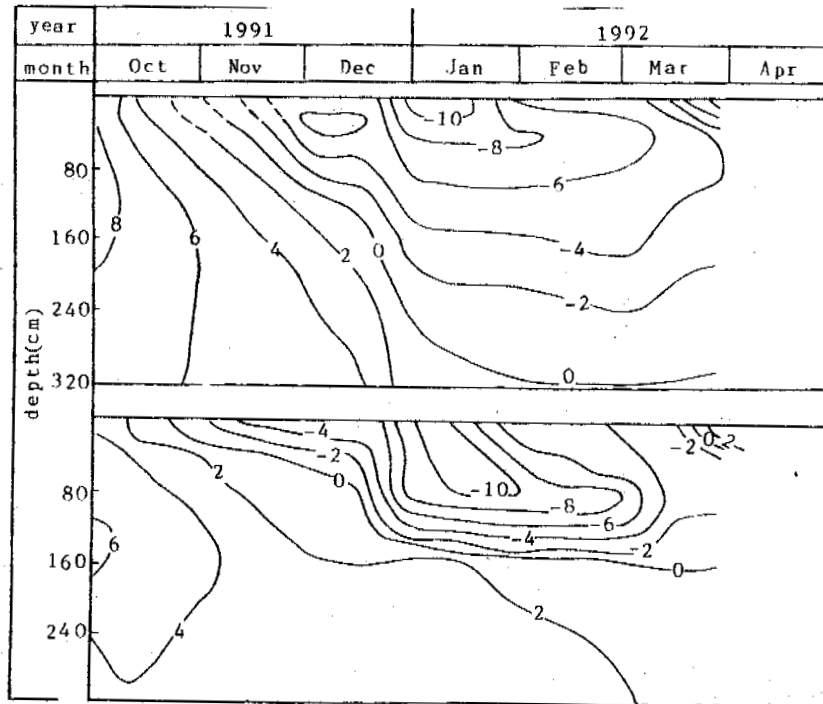


Figure 4. Isotherms of ground temperature at and in the vicinity of the Base of Tian Shan Glaciological Station  
 a — in gravels at the BTGS (2133.4 m a.s.l.)  
 b — in humus soil of solifluction tongue on northwestern slope (2238 m a.s.l.)

in the humus soil changes at a gradient much higher than in gravels.

#### CONCLUSION

1. The thermal regime of alpine permafrost in the middle section of East Tian Shan is strictly controlled by the altitudinal zonation and other factors including lithology, topography, moisture, and cover conditions. The altitudinal zonation of permafrost is mainly charac-

terized by that the permafrost increases in thickness, decreases in the mean annual ground temperature, postpones in seasonally thawing and antedates in re-freezing with elevation rising.

2. The geothermal gradient is  $1.43 \text{ m}^{-1}$  from 25 m to 59 m in the diabase. The thickness of permafrost based on the gradient displays an altitudinal zonation, which increases from 50 m at borehole No.1 (3300 m a.s.l.) to 230 m at borehole No.5 (3900 m a.s.l.).

3. The permafrost in the upper reach of Urumqi

River basin is warmer and thinner than that of in the Kuixian Daban region 22 km to the south. At about 3300 m in Kuixian Daban the ground temperature is  $-2.0^{\circ}\text{C}$  and permafrost is 110 m in thickness; while in the upper reach of Urumqi River — only  $-0.7^{\circ}\text{C}$  and 50 m.

#### REFERENCES

Cui Zhijiu and Zhu Cheng, (1988) Commentaries and prospects of the study on periglacial geomorphology, the Journal of Glaciology and Geocryology, Vol.10, No.3, p.304-311.

Qiu Guoqing and Zhang Changqing, (1981) The characteristics of alpine permafrost distribution in Kuixian Pass nearby, in Memoirs of the Lanzhou Institute of Glaciology and Geocryology, Academia Sinica, No.2, Beijing, Science Press, p.1-16.

Qiu Guoqing, Huang Yizhi and Li Zuofu, (1983a) Basic characteristics of permafrost in Tian Shan, China, Proceedings of Second National Conference on Permafrost, Gansu People's Publishing House, p.21-29.

Qiu Guoqing, Huang Yizhi and Li Zuofu, (1983b) Alpine permafrost in Tian Shan, China, Proceedings of Fourth International Conference on Permafrost, July 17-22, 1983, Fairbanks, Washington, National Academy Press, p.1020-1023.

Washburn, A.L., (1979) Geocryology, Edward Arnold (Publishers) Ltd, p.58-59.

## STUDY OF THE PREVENTION OF ICE DAMAGE OF STRUCTURES IN WATER IN COLD REGIONS

Jin Naichui<sup>1</sup>, Qu Xiangming<sup>1</sup>, Zhang Yuanyou<sup>2</sup> and Lin Ying<sup>2</sup>

<sup>1</sup>Heilongjiang Hydraulic Research Institute, Harbin, China

<sup>2</sup>Heihe Hydraulic Bureau, Heilongjiang, China

The authors constructed a water tower surface insulating layer with polystyrene foam plates, preventing ice damage of the water tower at the power station for three years. Through practical freeze-thaw cycle tests, the thermal effect value in the freeze-thaw process was obtained. The ice layer thickness under the polystyrene foam insulating plate (abbreviated name is insulation plate) was decreased, the ice damage was dispelled through construction of an ice cover, this has ensured that the water tower will run normally. This way of preventing ice damage is technologically simple and economically beneficial, and has an advantage over the artificial breaking of ice. This has initiated a new way for preventing ice damage in seasonally frozen ground areas.

### INTRODUCTION

In regions near the latitude of forty-five degrees north, the weather is cold in the winter, a larger thickness of ice is formed in rivers, lakes and reservoirs. Under ice pressure action there are stability and failure problems for bank slopes, and sluice gates of dam and water tower structures in reservoirs. To make structures run safely, they have to be maintained and reinforced every year. Thus, causing an economic waste.

There are many ways to prevent ice damage of structures in water at home and abroad. Besides increasing the strength and rigidity of structures, there are ways of dispelling ice pressure and freezing forces that are usually employed during operation. For example, thermo-electricity, the breakage of ice and the use of water surface wave motion. The above methods don't obtain the ideal effect specially the practise of breaking the ice, since this is very difficult in cold circumstances. The authors present an effective method of preventing ice damage in this paper.

### MECHANISM OF THE INSULATING METHOD

For solving the problem of structural damage caused by ice pressure.

There are many structures built in rivers, lakes and reservoirs, these structures suffer failure from ice pressure in winter. For this reason we studied the mechanism of changing water to ice.

0°C is a boundary value of changing water into ice. So 0°C potential energy field (Qin, 1991) can be used for solving structural failure problems caused by ice pressure. For this aim it is necessary to choose material with a small heat conductivity, this kind of material can insulate heat radiation to decrease the thickness of ice cover, thus, the ice damage is dispelled. Among all the insulation materials

polystyrene foam plate has the most favourable insulation and mechanical properties, when polystyrene plates are spread around the structure in water, the partial temperature field of water is changed, and forms a 0°C temperature field with the shape "Ω" under ice cover, i.e. there is water not ice around the structure, therefore the aim, i.e. preventing ice damage is achieved.

### NATURAL GEOGRAPHY CONDITIONS OF THE TEST ENGINEERING AND TEST METHOD

#### Natural Geography Conditions

Weniuhe reservoir is located at the northern latitude of 50°18'16" and the eastern longitude of 127°30'0". It is a hilly area reservoir.

The region has a long winter, low air temperature, larger air temperature range, and it belongs to a continental climate of a cold-temperature zone. The lowest air temperature reached in history was -42°C. The longest frozen period was from October 20 to May 1, about 170 days. Mean annual air temperature is -1°C - -2°C, the coldest month is January, the largest thickness of ice cover is about 1.48 m.

#### Test Method

#### Physical properties of insulation materials

Polystyrene foam plate is a highly efficient insulation material, its heat conductivity coefficient is 0.027-0.039 W/m·°C. It is a kind of obturator construction and a small density material ( $P=20-40 \text{ kg/m}^3$ ), bulk weight is about 1/50-1/100 of that of gravel and sand, polystyrene is a light material. Because polystyrene foam plate has the properties of light bulk weight, high strength, and chemical resistance for preventing ice damage, it is chosen first as the material for preventing ice damage. Its physical indexes are given in Table 1.

Table 1. Physical indexes of polystyrene foam plate

Item	Values
Compression strength (KPa)	100-130
Heat-resistant temperature (°C)	80.0
Linear coefficient ( $\times 10^{-5}/^{\circ}\text{C}$ )	5.0-7.0
Absorbing water rate (g/100 cm <sup>2</sup> )	0.15-0.20

Distribution of the temperature observation points

The test engineering was the water tower of Weniuhe reservoir, the insulation plate size was 8.0x8.0 m, the plates were spread on the water surface around the water tower. When the ice cover thickness reached 20 cm, we then fixed the plates on the ice cover around the water tower. The plates were 15 cm in thickness and 30 cm in width. At the same time the ice cover temperature field was measured by a thermistor bolometer (see Fig.1, Fig.2).

TEST RESULT ANALYSIS

Through the test studies in three winters (1988-1991) we found the temperature field of the ice layer under the insulation plate and the process of development and change of the ice layer. According to the observation data the relationship curves of temperature and freezing depth were plotted (Fig.3). From the tests it was confirmed that this method is economically beneficial.

Test Observations

Ice layer temperature observation

Test observations were conducted for three winters. Ice point temperature was the same, i.e.  $-0.43^{\circ}\text{C}$ , but  $0^{\circ}\text{C}$  was the boundary value of ice point. Table 2 gives the temperatures of the ice layer profiles.

From Table 2, it was seen that the ice layer temperature at the plate centre is more than that of the plate edge. This shows the effect of the insulation plate on the temperature of the ice layer is significant.

Ice layer thickness observations

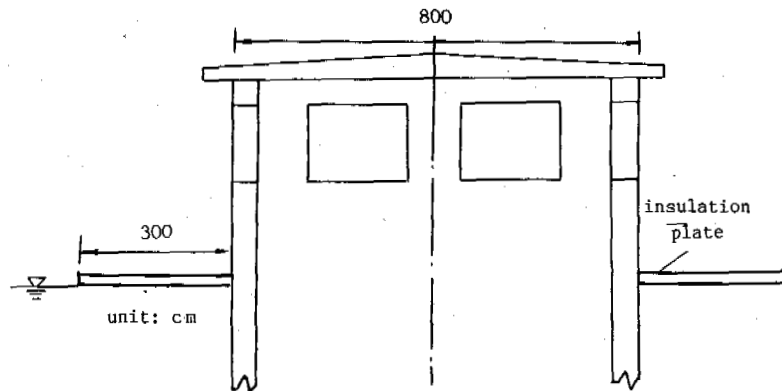


Figure 1. Profile of insulation plates distribution

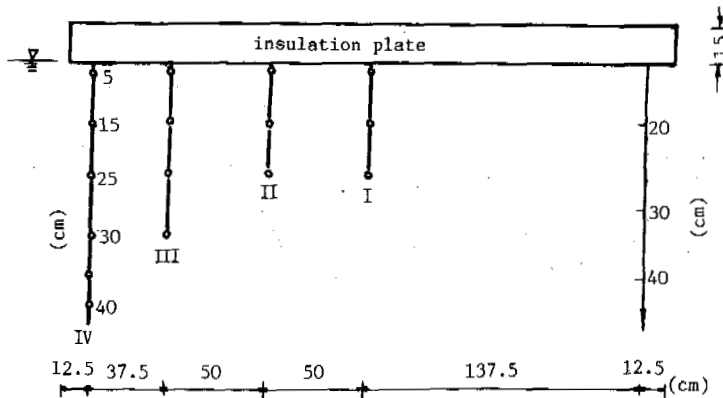


Figure 2. Distribution of thermistor bolometers

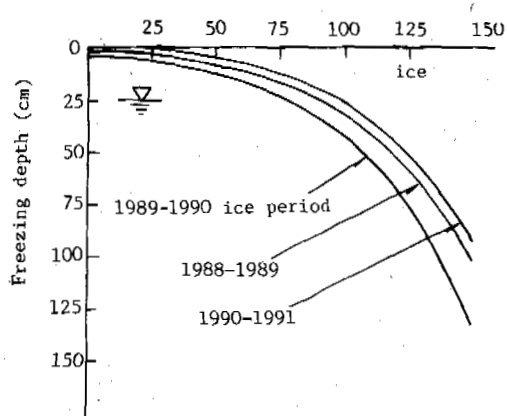


Figure 3. Freezing curves

Table 2. Temperature values of ice layer profiles under the plates

Sections	Point number				
	1	2	3	4	5
Area IV temperature in ice (°C)	-2.17	-1.3	-0.87	-0.43	0
Area III temperature in ice (°C)	-2.17	-1.3	-0.87	0	
Area II temperature in ice (°C)	-0.43	-0.43	0		
Area I temperature in ice (°C)	-0.43	-0.43	0		

The change of the ice layer thickness was measured for three years. When the natural ice layer thickness reached the maximum, the ice layer thickness under the plate was measured. The results are given in Table 3.

Table 3. The maximum ice layer thickness under the insulation plate

Horizon distance (cm)					Lowest air temp.	Maximum thickness (cm)
	12.5	50	100	150		
Winter						
1988-1989	80.0	25.0	2.0	1.30	-32.4°C	100
1989-1990	130.0	40.0	12.5	5.0	-38.9°C	130
1990-1991			0		-33.6°C	89

From Fig.3 it was shown that the ice layer shape under the plate formed a "Ω" type (Fig.4). The ice layer thickness under the plate centre reached the minimum.

#### Test Results Comprehensive Analysis

Under natural conditions the ice layer thickness is dependent on the negative air temperature. When atmospheric radiation heat, water latent heat and ground heat don't reach a balance freezing or thawing will occur in the ice layer, the frozen front of the ice layer moves forward during the frozen period and the water changes into ice. If there were other effecting factors the natural ice layer will have a continuous and

Figure 4. Profile of the ice layer under the insulation plate

uniform thickness. Our study purpose is to change the freezing conditions of the ice layer and to dispel the ice pressure on the structures.

According to the tests the authors draw the following conclusions:

#### 1. Insulation plates can partially change the freeze-thaw conditions of the ice layer

From the test result it can be seen that the temperature field of the ice layer under the insulation plates is not the same as that of the natural ice layer. After the insulation plates were laid on the water surface, the ice layer thickness decreased from 20 cm in natural conditions to 5-0 cm, at the time the temperature of the ice-water interface was 0°C - -0.43°C.

The tests show that when the air temperature rises in spring, the thaw rate of the ice layer under the insulation plates is quicker than that of the natural ice layer. In March the lowest air temperature is -13.77°C, the highest air temperature is 11.2°C, the mean thaw rate of the ice layer under the insulation plates is 0.4 cm/day. At the end of this month the ring shape water range has been formed around the water tower. However, the natural ice layer thickness changes less. From this fact it can be shown that the insulation plates can change the freeze-thaw conditions of the ice layer.

#### 2. There is a "Ω" formation water range under the insulation plate, the water range cuts off the pressure of the ice layer on the water tower

Before the ice layer thickness reaches 20 cm, the ice pressure does not cause damage on the structures. So, when the ice layer thickness reaches 20 cm the insulation plates were spread on the ice surface, the test was conducted at this time.

At the in situ test the ice point temperature was -0.43°C, the magnitude of the boundary of water and ice was plotted in Fig.4, the curve appears as a quadric curve, and the ice cover with a "Ω" shape was formed.

The minimum thickness of the ice layer was 5 cm and in the plate centre, the ice was high temperature ice where the ice strength was decreased. So, the pressure from the natural ice layer will break down the high temperature and lower strength ice layer then the pressure will be dispelled and will not cause ice damage on the structure.

#### 3. Calculation of the insulation plate thickness and insulation range design

The test insulation plate sizes were: thickness 15 cm width 300 cm. The plate size is a key factor, it effects the formation of the "Q" shape range of high temperature ice or water, so that the insulation plate size must be calculated with the following demands.

1) The insulation plates should be spread around the structure, the plate width should not be less than three times the maximum thickness of the natural ice layer.

2) The insulation plate thickness can be calculated with the heat transfer formula. Usually the thickness can be estimated as 1/10 of the maximum thickness of the natural ice layer.

### ECONOMIC BENEFITS

The ice breaking time is about 135 days every year for this water tower. The cost of artificial ice breaking is 1755 Yuan (Renminbi) for a winter.

The insulation plate has the following advantages:

It has a light unit weight, high strength, simple construction, lower loss and it can be used repeatedly for several years. So the method is economical, the cost is only 1/3 of that of artificial ice breaking (Table 4).

Table 4. Cost comparison table

Plate size (mXmXm)	Material amount (m <sup>3</sup> )	Unit price Yuan/m <sup>3</sup>	Total cost (Yuan)	Use time (year)	Mean year cost (Yuan)	Save ratio (%)
30.0X3.0X0.15	13.50	436.28	5889.78	5	1177.96	32.88
30.0X2.5X0.15	11.25	"	4908.15	5	981.63	44.88
30.0X2.0X0.15	9.00	"	3926.52	5	785.30	55.25

### CONCLUSION

The practical engineering tests were conducted under natural conditions and the following conclusions were obtained:

(1). For the 3 years of field work the test data and results -- were good, reliable, it was confirmed that the freezing characteristics of the ice layer under the insulation plates and the test results were identical.

(2). The movement rate of the freezing line on the ice-water interface correlates with the insulation plate sizes. The design parameters given by this paper may be consulted.

(3). The results are not only confined to reservoir engineering, but have widespread application prospects for preventing ice damage of all structures in rivers and lakes.

### REFERENCE

- Qin Dabe, (1991) Developing and physical characteristics of first-year sea ice in Great Wall Bay and its adjacent area by King George Island, Antarctica, Vol.13, No.2, Science Publishing Press.

## USE OF SNOW CAPTURE FOR LAND REHABILITATION IN ARCTIC OILFIELDS

M. Torre Jorgenson<sup>1</sup>, Timothy C. Cater<sup>1</sup>, and Michael R. Joyce<sup>2</sup>

<sup>1</sup>Alaska Biological Research, Inc.,  
PO Box 81934, Fairbanks, Alaska 99708 USA

<sup>2</sup>ARCO Alaska, Inc., PO Box 100360, Anchorage, Alaska 99510 USA

Low summer precipitation in arctic Alaska leads to low soil moisture on gravel fill and mine overburden and is problematic for rehabilitating lands degraded by oil development. To increase moisture, berms at three sites captured snow and increased meltwater. Berms were perpendicular to prevailing winter storm winds. Small berms were constructed on a gravel pad and topsoil was added to increase water-holding capacity. Moderate berms were built on another gravel pad, troughs stored meltwater, and topsoil was added. Large berms were constructed on mine overburden and impoundments were used to create aquatic wetlands. Small and moderate berms increased soil moisture during June, when rainfall was lacking. Addition of topsoil increased soil moisture throughout the summer. Consequently, plant growth was better inside berms than in flat treatments and was much better in the berm-with-topsoil treatments. Large berms allowed creation of aquatic wetlands by adding more snowmelt than evaporated.

### INTRODUCTION

Oil exploration and development in arctic Alaska have created a wide variety of terrain disturbances that eventually will require rehabilitation: mine pits, overburden stockpiles, gravel roads and pads, reserve pits, spills of fuel and other contaminants, gravel spray from snow removal, road washouts, road dust, impoundments, and scraped tundra. Gravel fill for roads and pads is the most widespread type of terrain disturbance within the Prudhoe Bay and Kuparuk oilfields and is particularly difficult to revegetate without treatment, because its hydrologic and pedologic conditions are drastically different from those of the original tundra.

Poor growth of plants on gravel fill is attributed to low soil moisture, which affects the water balance of plants, the movement of nutrients through the soil, and the availability of nutrients (Johnson 1981; McKendrick 1986; Jorgenson 1988). In addition, growth of plants is affected by the thickness of the fill, which is one factor limiting the capillary rise of groundwater (Jorgenson 1988).

To compensate for the deficiency of moisture in thick gravel fill in a region where rainfall is low, three experiments evaluated the use of soil berms to capture drifting snow and increase the amount of water available from snowmelt. In 1988, an experiment initiated at Mine Site D in the Kuparuk Oilfield used small berms (0.5 m high) to capture drifting snow and impound meltwater. In 1989, an experiment at Drill Site 13 in the Prudhoe Bay Oilfield expanded the concept of hydrologic manipulation by creating moderate berms (1 m high) for greater capture of snow and by excavating troughs to provide storage during snowmelt. Finally, in 1990, the concept was expanded again by creating two perched ponds on a large overburden stockpile at Mine Site D in the Kuparuk Oilfield, by constructing large berms (4 m high). In all experiments, the berms were situated perpendicular to the direction of

prevailing winds during winter storms (northeast to southwest).

Collection of drifting snow has been used for many purposes in the Arctic. Snow fences were considered for augmenting water supplies for Barrow (Slaughter et al. 1975). Snow was used routinely for making snow roads during construction of the Trans-Alaska Pipeline (Brown and Berg 1980) and for access to exploratory well sites (personal observation). In addition, numerous snow fences (4-6 m high) have been constructed throughout the oilfields during the last decade, to reduce snow-clearing requirements near facilities (personal observation). Ice pads (which start with snow) have been used for temporary exploratory pads and, more recently, they have been used for temporary stockpiling of overburden that subsequently is used for capping buried reserve pits.

### STUDY AREA

The three study sites are located within the two largest oilfields in the USA, the Prudhoe Bay Oilfield and the Kuparuk Oilfield, which are located on the Arctic Coastal Plain of northern Alaska. The Kuparuk Oilfield lies approximately 50 km west of the Prudhoe Bay Oilfield (Figure 1).

Terrain features in the Prudhoe Bay and Kuparuk oilfields encompass a landscape dominated by thaw lakes and include the floodplains of the Sagavanirktok and Kuparuk rivers. In general, the area is flat and poorly drained and has been influenced by thaw-lake cycles, fluvial processes along rivers and streams, and coastal processes of erosion, sediment deposition, and flooding. Aeolian transport of sand and silt from the river deltas has influenced landforms, soil chemistry, and vegetation (Walker and Webber 1979).

Winters on the Arctic Coastal Plain are cold and summers are cool; the summer thaw period lasts only about 90 days. The average

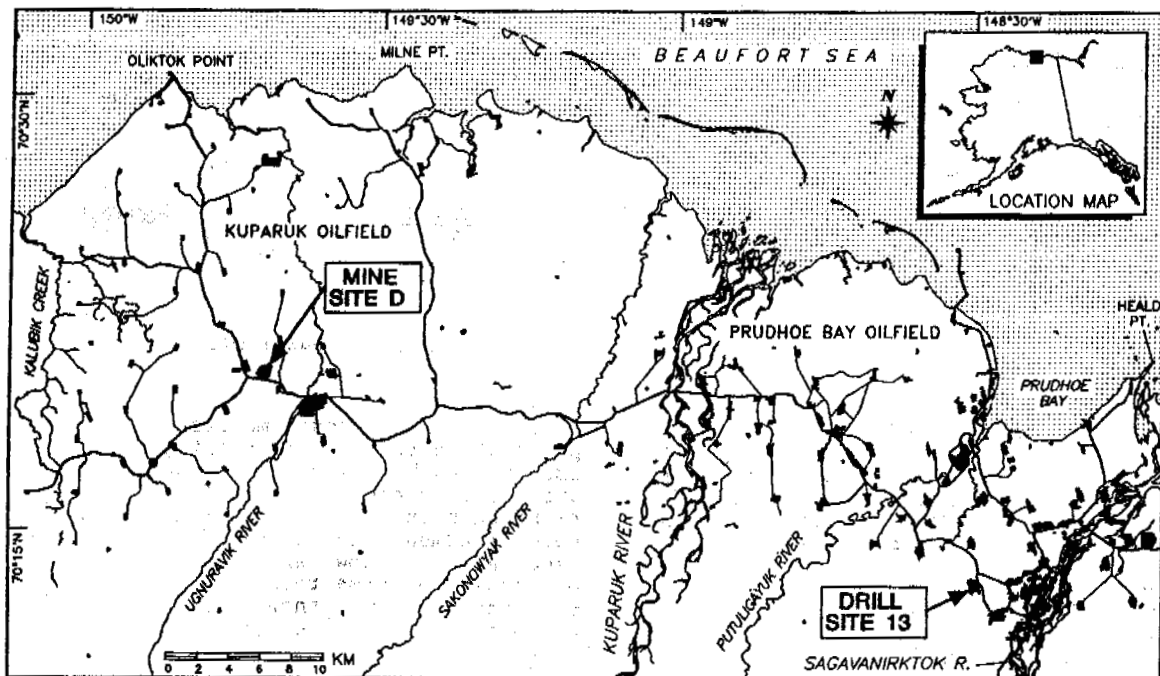


Figure 1. Locations of Drill Site 13 and Mine Site D in the Prudhoe Bay and Kuparuk oilfields, Arctic Coastal Plain of Alaska.

precipitation for summer in the Prudhoe Bay Oilfield is 67 mm (Thoman 1990) and in the Kuparuk Oilfield is 64 mm (U.S. Dept. of Commerce, National Oceanic and Atmospheric Admin., unpubl. data; Figure 2). Snow cover varies widely because of strong winds; however, drifts are common in low-lying areas. In the Kuparuk Oilfield, the average temperature of the warmest month (July) is 8.2°C. The average sum of thawing-degree-days over the summer is 618°C (range = 472-974°C), compared with approximately 3000°C for Anchorage, Alaska (Johnson and

Hartman 1969). Prevailing wind directions during summer in this region are from the northeast or the southwest.

#### SMALL BERMS: MINE SITE D

The experiment initiated in 1988 at Mine Site D in the Kuparuk Oilfield was designed to evaluate three site-preparation treatments for modifying the hydrologic regime of a thick (1.7 m) gravel pad. These treatments included a "control" area of flat gravel (flat), an area with small gravel berms (0.5 m high) to trap blowing snow and runoff during snowmelt (berm), and an area in which organic topsoil was added inside the berms to increase water-storage capacity (berm-with-topsoil). Within each of these site-preparation treatments, four standard plant-cultivation techniques were applied: (1) natural (control); (2) fertilized; (3) fertilized and seeded with a mixture of native grasses (70% *Poa glauca* and 30% *Festuca rubra*); and (4) fertilized, seeded, and mulched (mulch).

Snow depth and density were measured along a permanent transect. Numerous physical, chemical, and biological responses were monitored during 1989-1991, including percent snow cover, profiles of soil moisture, water balance at the surface, physical and chemical properties of soil, and plant cover. Soil moisture was determined gravimetrically at two stations in each site-preparation treatment, and plant cover was measured with a point frame within 10 permanent quadrats (1 m<sup>2</sup>) in each of the 12 treatment combinations. Only a subset of those data are presented here.

Although the berms were not very efficient at capturing snow, they did increase the input

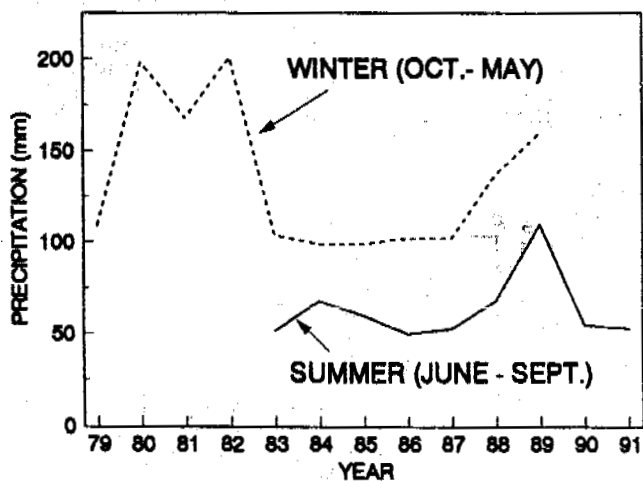


Figure 2. Mean precipitation in the Prudhoe Bay and Kuparuk oilfields, Alaska, during winter (Prudhoe Bay) and summer (Kuparuk).



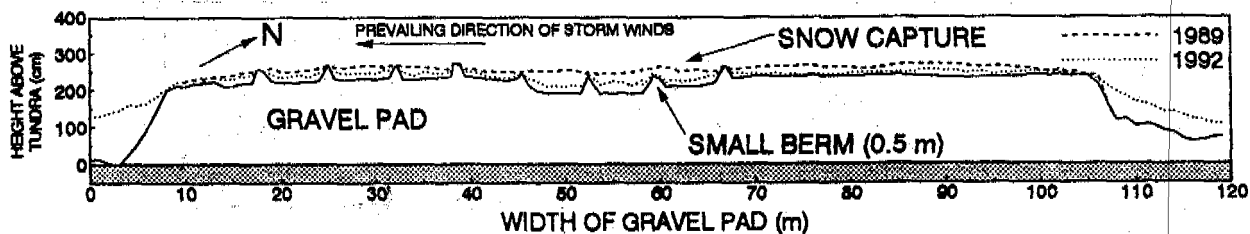


Figure 3. Depth of snow capture (dashed lines) at Mine Site D in the Kuparuk Oilfield, Alaska, in 1989 and 1992.

of water to the pad (Figure 3). In 1989, the berm treatment accumulated more snow (mean = 45.6 cm; standard deviation [SD] = 13.4; n = 11) than did the flat (22.7 cm; SD = 8.7; n = 24) and the berm-with-topsoil (25.5 cm; SD = 11.5; n = 14) treatments. In 1990, a relatively dry winter, no snow accumulated in the flat and berm-with-topsoil treatments, and the berm treatment accumulated only 5 cm of snow. In 1991, a moderately snowy winter, the berm treatment again accumulated more snow (mean = 42.0 cm; SD = 17.9; n = 32) than did the flat (25.7 cm; SD = 9.5; n = 15) and the berm-with-topsoil (23.2 cm; SD = 12.5; n = 35) treatments. During snowmelt, water remained impounded within the berm treatment at depths up to 10 cm for about a week (Figure 4).

Soil moisture profiles indicated that berms increased soil moisture during early summer, whereas topsoil increased soil moisture during the entire summer (Figure 4). In 1989, snowmelt in the berm treatment added 158 mm of water to the gravel (summer precipitation added 135 mm), whereas only 75 mm of water were added in the flat area. Because water storage at field capacity ranged from 45 to 60 mm of water in the top 0.5 m of gravel (unpublished data), the amount of snowmelt added exceeded the storage capacity and was lost as throughflow. Thus, increased water-holding capacity by addition of organic matter was more important to water balance than was increased input of water.

After three years of growth, it was clear that berm establishment, topsoil application, and mulching had beneficial effects for plant growth (Figure 5). The addition of topsoil,

however, was the most important site-preparation technique: plant growth was improved by both higher availability of water and higher concentrations of nutrients. Although plant cover was slightly higher in the berm treatment than in the flat treatment, the importance of snow capture berms appeared to decrease over time relative to the flat treatment, because snow also was trapped by the upright grasses. The addition of mulch also made a large contribution toward improving plant growth, particularly in the flat area, which did not benefit from the increased moisture from berms and added topsoil. The mulch probably was most important during the seed germination phase. Overall, this experiment showed that, with proper site preparation and plant cultivation, vigorous plant growth can be achieved on the extreme environment created by thick gravel pads in the Arctic.

#### BERMS AND TROUGHS: DRILL SITE 13

To expand the experimental design for hydrologic manipulation on gravel pads, more snow was captured on a gravel pad (Drill Site 13 in the Prudhoe Bay Oilfield; Figure 1) with moderate berms (1 m high) and troughs (0.5 m deep) to store the large volumes of meltwater. This design allowed most of the surface to drain freely. Also, topsoil was added to increase soil-water storage and nutrient availability. Potential benefits of increasing water storage capacity included irrigation of the higher portions of the pad, increased heat

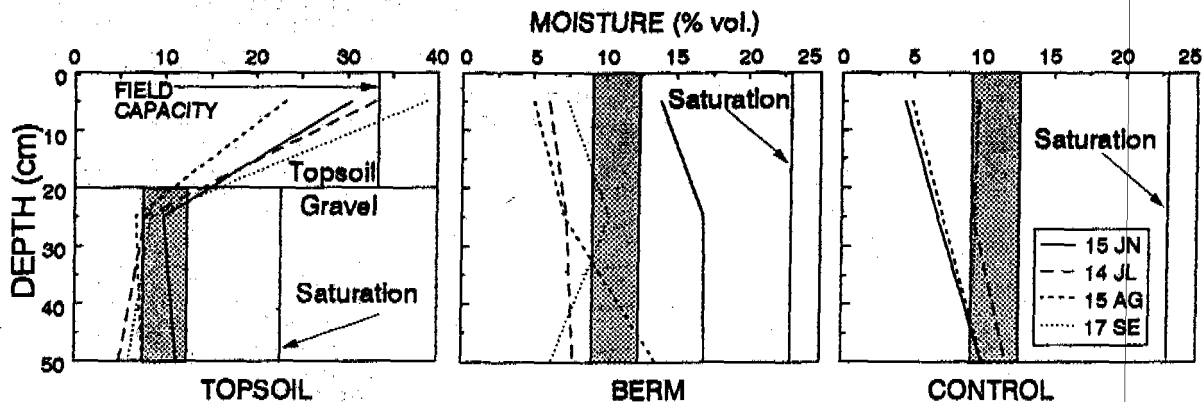


Figure 4. Effect of treatment on soil moisture profiles at Mine Site D in the Kuparuk Oilfield, Alaska, during the summer of 1989.

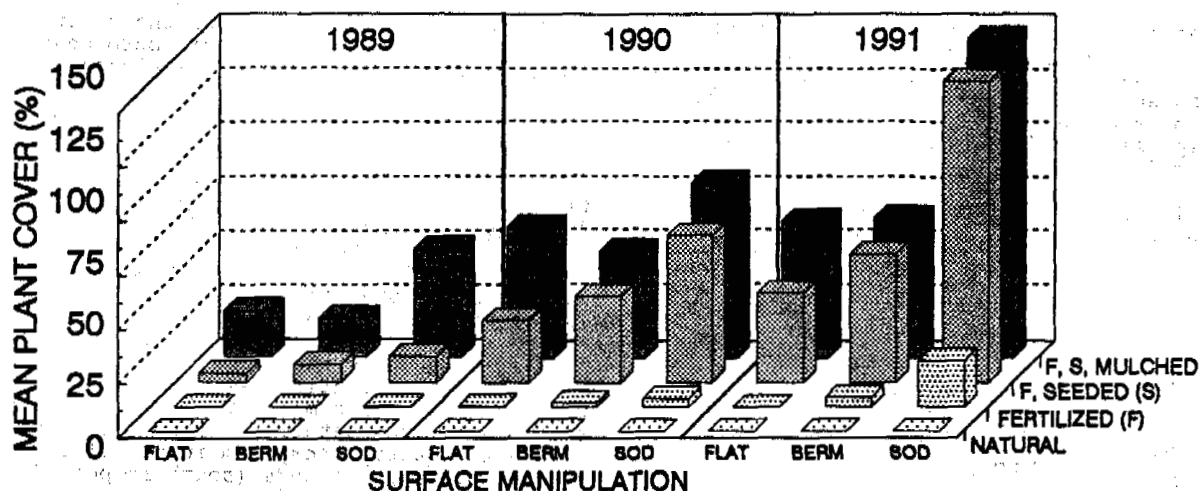


Figure 5. Summary of effects of surface manipulation and plant cultivation treatments on plant cover at Mine Site D in the Kuparuk Oilfield, Alaska 1989-1991.

gain to the underlying permafrost (Jorgenson 1986), which may result in permanent impoundments, and reduced leaching of soil nutrients. Under these conditions, habitat might be created for wetland flora and fauna. To test the design, half of the gravel pad was graded to create berms and troughs, while the other half of the pad remained flat (Figure 6). Within these two surface-contouring treatments, topsoil was added in half of the area; thus, four treatment areas were created. The entire surface then was scarified to provide a rough seedbed for enhancing seed germination. Finally, five native grass cultivars (40% *Festuca rubra*, 20% *Poa glauca*, 20% *Deschampsia beringensis*, 15% *Arctagrostis latifolia*, and 5% *Calamagrostis canadensis*) were sown on the entire pad; seed was applied at  $33 \text{ kg ha}^{-1}$ . A

hydrophytic grass (*Beckmannia syzigachne*) was applied to the troughs at  $5.5 \text{ kg ha}^{-1}$ .

During two winters (1990-1991 and 1991-1992), snow accumulated between the berms, and especially in the troughs. As the captured snow melted during early spring, standing water (up to 25 cm) persisted in troughs up to two weeks. Levels of groundwater were similar in both the flat and berm-trough areas after the pad thawed entirely in mid-June (Figure 7). Thus, much of the snow melt recharge was lost to evaporation and drainage through the gravel pad because of the gravel's low storage capacity. After two years, little difference in plant cover was evident among treatments (range = 11.2-16.8%); however, plant cover was not fully developed, and differences should become evident. In addition, plant growth in

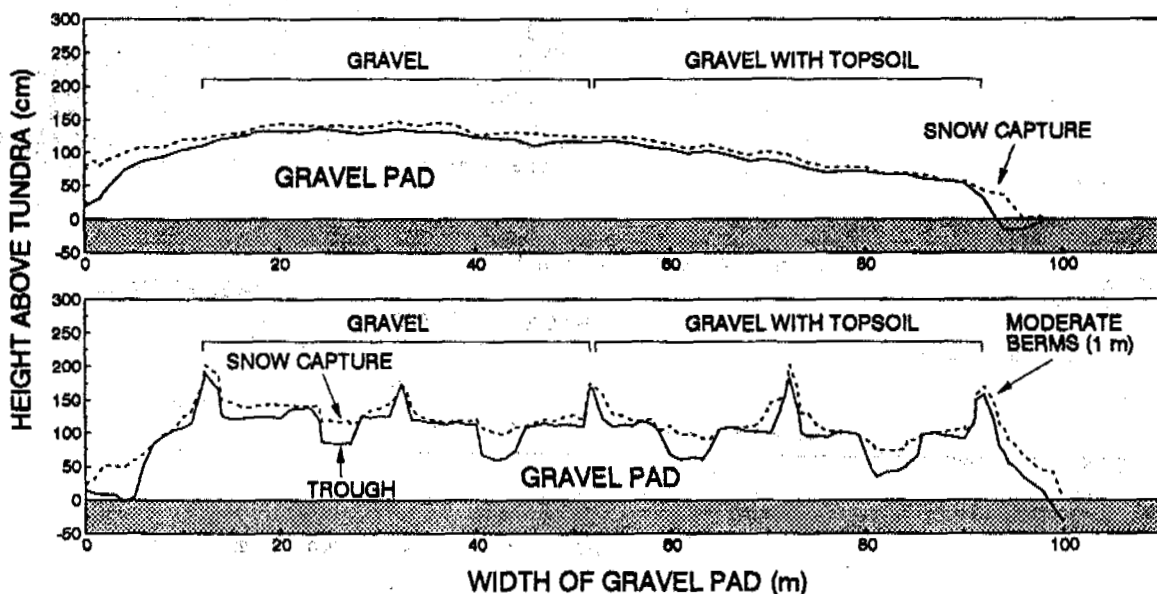


Figure 6. Snow capture in 1992 at Drill Site 13 in the Prudhoe Bay Oilfield, Alaska. The upper profile went across the flat treatment; the lower profile went across the berm-with-trough treatment.

the troughs (not sampled separately) appeared more vigorous than it did on the benches, probably because of increased soil moisture: the troughs accumulated more snow than the benches did, and the thinner fill allowed greater capillary rise of groundwater than did the thicker fill.

After 3 years, thaw settlement has been minimal, although thaw depth below the surface of the tundra was deeper in the troughs (54-66 cm) than in the flat (control) area (44-54 cm). Both indicators suggest that the

troughs will remain stable for the short-term and will not subside and become permanent impoundments, as originally was planned.

LARGE BERMS AND IMPOUNDMENTS: MINE SITE D

Creation of freshwater wetlands on previously dry overburden at gravel mine sites is important because it can increase habitat diversity and provide high-value habitat to shorebirds and waterfowl. Also, natural communities of plants and invertebrates appear to establish more readily in wet areas (Jorgenson et. al. 1992). An experiment to create wetlands (two perched ponds) on a 29.6-ha overburden stockpile began in 1990 at Mine Site D by creating large berms (4 m high) to capture snow and moderate berms (1-2 m high) to store the meltwater. In 1991, techniques to create an aquatic ecosystem in one of the 2.6-ha (6.5-ac) wetlands (southern pond) included cultivation of emergent grasses and sedges and transfer of approximately 19 m<sup>3</sup> of water from a natural pond that contained phytoplankton, bacteria, sediments, detritus, and aquatic invertebrates; aquatic invertebrates also were transplanted by hand.

The berms successfully captured snow drifts during the winters of 1990-1991 and 1991-1992 (Figure 8). During 1991, water level increased by 63 cm during snowmelt. In 1992, approximately 3050 m<sup>3</sup> of water were added to the pond by snowmelt. Areal coverage of the water in the southern pond increased from 0.2 ha in 1990 to 1.2 ha in 1991 (Figure 9).

Sprigs of *Arctophila fulva* were transplanted (785 in 1991, 2000 in 1992) in the southern pond to establish emergent vegetation, and seeds of indigenous hydrophytic grass and sedge species (*Carex aquatilis*, *C. membranacea*, *Eriophorum angustifolium*, *E. scheuchzeri*, *Dupontia fisheri*, and *Alopecurus alpinus*) were sown (Jorgensen et. al. 1992). By late summer 1992, nearly 100% of the transplanted sprigs had survived, and provided a small amount of cover. In 1991, mean phytoplankton biomass was high (range = 15-22 µg L<sup>-1</sup>), because of high nutrient levels in the water. In addition, a variety (25 taxa) of aquatic invertebrates was introduced in July 1991; however, only Chironomidae (midge larvae) were found after 6 weeks (mean = 5339 m<sup>-2</sup>; n = 3); they already were present before introduction of indigenous

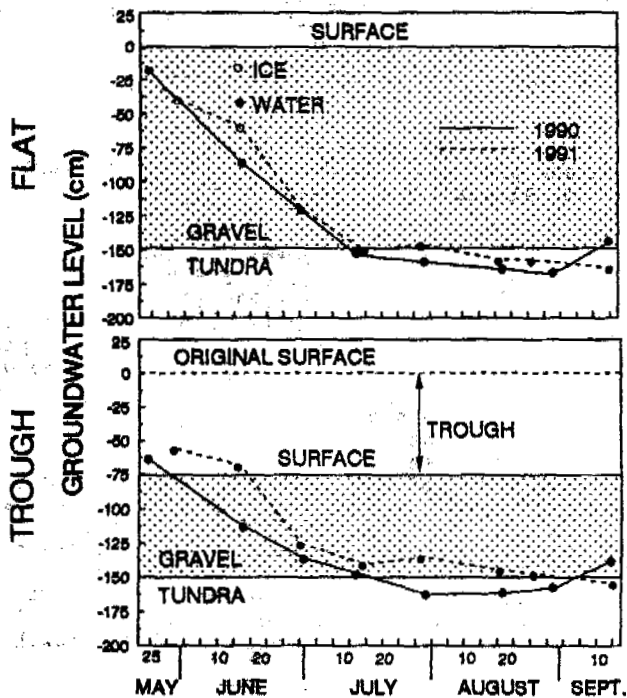


Figure 7. Effect of surface manipulation treatments on groundwater level at Drill Site 13 in the Prudhoe Bay Oilfield, Alaska, in the summers of 1990 and 1991.

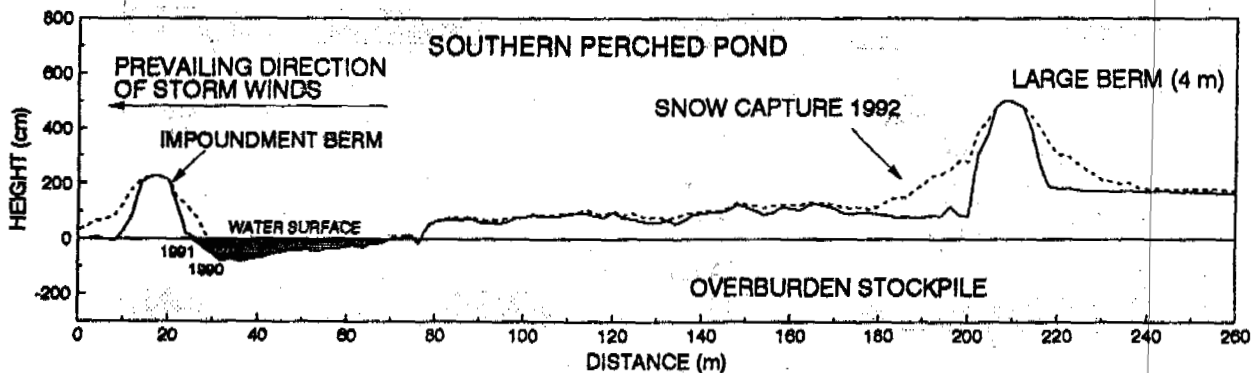


Figure 8. Depth of snow capture (dashed line) at the southern perched pond at Mine Site D in the Kuparuk Oilfield, Alaska, in 1992.

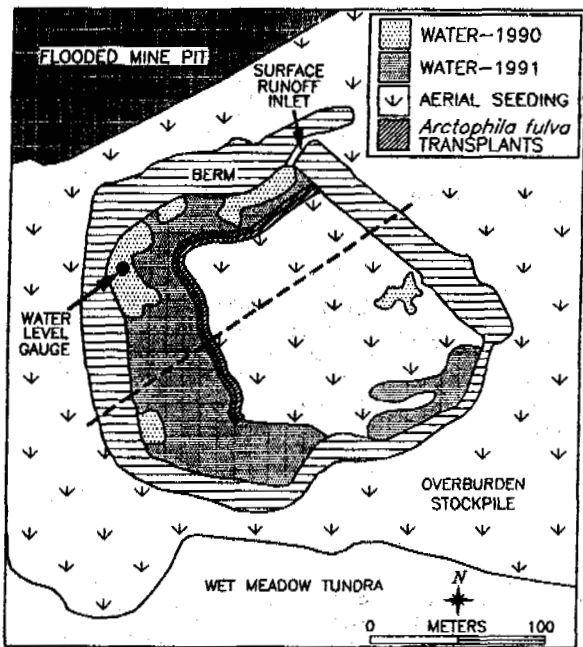


Figure 9. Layout of southern perched pond at Mine Site D, Kuparuk Oilfield, Alaska, with berms and impounded water on the overburden stockpile.

invertebrates, so their abundance was due primarily to natural colonization. Low survival of the introduced invertebrates was attributed to high pH (near 9) and insufficient development of emergent vegetation. Use of the pond by wildlife was evident; a few shorebirds, usually semipalmated sandpipers (*Calidris pusilla*), were flushed from the shoreline during each visit, and greater white-fronted geese (*Anser albifrons*) and northern pintails (*Anas acuta*) often were seen feeding and resting along the shoreline.

#### CONCLUSION

The experiments show that, although the soil berms were not very efficient at the capture of snow, they added a significant amount of water and, hence, altered the water balance of gravel and overburden stockpiles. This addition of water can be particularly important to the growth of plants early in the summer, when rainfall is negligible and solar radiation is greatest. On gravel pads, the added snowmelt can persist for 1-2 weeks and can add more water than the gravel is able to store. Berms may be preferred over snow fences, because they are permanent, are inexpensive to construct, and require no maintenance. However, increasing the amount of snowmelt on pads is not as important for the growth of plants as is increasing water storage capacity. In reality, plant growth on thick gravel pads is best when berms are created and topsoil is added.

On overburden stockpiles, which remain permanently frozen at depth beneath the thin active layer, large berms are effective at adding more water from snowmelt than can evaporate during the summer. The ability to create ponds on an otherwise arid environment

can provide a wide diversity of habitats to benefit shorebirds and waterfowl.

#### ACKNOWLEDGMENTS

These studies were funded by ARCO Alaska, Inc., Anchorage, AK. Roger Mechon, Construction Engineer, ARCO, supervised site preparation work at Mine Site D. We thank T. Davis, L. Jacobs, B. Lance, M. Smith, and G. Zusi-Cobb for help in the field, A. Zusi-Cobb for help with the graphics, and R. H. Day for help with the manuscript.

#### REFERENCES

- Brown, J., and R. L. Berg (1980) Environmental engineering and ecological baseline investigations along the Yukon River-Prudhoe Bay Haul Road. U. S. Army Cold Regions Research and Engineering Laboratory, Hanover, NH, CRREL Report 80-19. 187 pp.
- Johnson, L.A. (1981) Revegetation and selected terrain disturbances along the Trans Alaska Pipeline. U. S. Army Cold Regions Research and Engineering Laboratory, Hanover, NH, CRREL Report 81-12. 115 pp.
- Johnson, P.R., and C.W. Hartman (1969) Environmental atlas of Alaska. Alaska Environmental Information Data Center, University of Alaska, Fairbanks, AK. 111 pp.
- Jorgenson, M. T. (1986) Biophysical factors influencing the geographic variability of soil heat flux near Toolik Lake, Alaska: implications for terrain sensitivity. University of Alaska, Fairbanks, AK, MS Thesis. 109 pp.
- Jorgenson, M. T. (1988) Rehabilitation studies in the Kuparuk Oilfield, Alaska, 1987. Final Rep. prepared for ARCO Alaska, Inc., Anchorage, AK, by Alaska Biological Research, Inc., Fairbanks, AK. 90 pp.
- Jorgenson, M. T., T. C. Cater, L. L. Jacobs, M. R. Joyce (1992) Wetland creation and revegetation on overburden in arctic Alaska. Pages 265-275 in S. Bandopadhyay and M. G. Nelson, eds. Mining in the Arctic. A. A. Balkema, Rotterdam.
- McKendrick, J. D. (1986) Final cleanup at selected (1975-1981) well sites, sampling and testing of waters and bottom muds in the reserve pits and the recording of tundra plant responses on the National Petroleum Reserve in Alaska. Vol. III: Recording of Plant Responses. Report prepared for U. S. Geological Survey, Anchorage, AK, by Nueria Reclamation Co., Anchorage, AK. 225 pp.
- Slaughter, C., M. Mellor, P. Sellmann, J. Brown, and L. Brown (1975) Accumulating snow to augment the freshwater supply for Barrow, Alaska. U. S. Army Cold Regions Research and Engineering Laboratory, Hanover, NH, CRREL Report 217. 21 pp.
- Thoman, R. L., Jr. (1990) The climate of Prudhoe Bay, Alaska. U. S. Department of Commerce National Weather Service, Anchorage, AK, NOAA Technical Memorandum NWS AR-40. 33 pp.
- Walker, D. A., and P. J. Webber (1979) Relationships of soil acidity and air temperature to the wind and vegetation at Prudhoe Bay, Alaska. Arctic 32:224-236.

## GAS PIPE-LINE MASTAKH-YAKUTSK AND ENVIRONMENT

Rosteslav M. Kamensky, Innokentii P. Konstantinov, Viktor A. Popov

Permafrost Institute, Russian Academy of Sciences  
Yakutsk, 677018, Russia

The paper presents the data on the permafrost situation both in natural conditions and disturbed ones as a result of the gas pipe-line construction Mastakh-Yakutsk in the region of Central Yakutia. The temperature change regularities of the transported gas have been set by field research; the degree of soil thaw at the gas pipe-line base and its displacements have been specified. It has been noted that the consequences of natural conditions disturbances in the cryolithozone presents the hazard for operating and being constructed pipe-lines.

In the fuel energy balance of Yakutia gas is of considerable importance which is delivered by two gas pipe-lines from the Mastakh deposit located 380 km to the north-west of Yakutsk. The initial gas pressure at the head gas facilities is 5.5 MPa, at the gas distribution station in Yakutsk - 2.5 MPa. The gas pipe-line comprises the pipes 529 mm in diameter and pipe branches 273 and 377 mm.

The gas pipe-line has been laid through the continuous permafrost 300-350 m thick. The climate of the region is sharp continental characterized by a short hot summer and long cold winter, a small amount of precipitation (250-300 mm per year). The mean annual temperature in the town of Yakutsk is  $-10.3^{\circ}\text{C}$ .

The cold season with below-zero air temperatures lasts 7 months a year (from October to April).

The gas pipe-line crosses the northern-eastern part of the Lena-Vilyuisk watershed including three sites different in the geomorphologies structure; the complex of over-flood-lands terraces of the Lena and Vilyui rivers, accumulative-denudation and denudation plains.

The upper part of the geological section of the Lena-Vilyuisk watershed comprises the Quaternary deposits presented by different genetic types: alluvial, eluvial, deluvial, lake-swampy and technogenic formations. The thickness of alluvial deposits depending on the watercurrent amount ranges from 305 m to 20-30 m.

The eluvial and deluvial formations are deposited on the watershed within the limits of their slopes and river valleys. The formation composition is determined by the composition of the underlying bedrocks. They are represented by sand and supes, seldom supes-suglinok formations rarely exceeding 3 m thick.

The lake-swampy deposits occur within the limits of river valleys, marec sites and alases. The peat supes and suglinoks prevail in their composition.

The lake-studded and swampy territory through which the gas pipe-line Mastakh-Yakutsk has been laid comprises about 10%. The closed taliks are

widely spread; they deposit under the river beds and lakes, under tukuluns (massifs of modern and ancient eolian sands) occurring on the area 33-95 km. The ground ice occur as repeatedly-vein ice formations 3-4 m thick and segregated ice forming layered and reticulate cryogenic texture.

The soil temperature varies from 1.1 to  $-5.5^{\circ}\text{C}$  at the depth of 10-15 m. The lowest temperatures are characteristics of the swampy sites of flood-lands and over flood-lands terraces composed of ice-rich suglinoks from the surface. The average annual temperature of the soils is considerably higher and is equal to  $-2...-3^{\circ}\text{C}$  on the well-drained sites with pine and pine-deciduous woods having underdeveloped topsoil.

The highest temperatures (to  $1.1^{\circ}\text{C}$ ) are noted on the sites of development of ancient and modern eolian sands. These specific natural formations represent the typical desert landscape characterized by dunes, barkhans, interbarkhan depressions.

The seasonal thawing depth varies along the pipeline depending on the lithological soil composition, their moisture, the character of the vegetative cover and exposition of the country sites.

The maximum seasonal thawing depth (to 4.5 m) are fixed on the sites of sand deposits with moisture 0.03-0.05. The minimum seasonal thawing (0.4-0.5) are observed on the depressed insufficiently drained sites composed of ice rich peat and suglinoks from the surface. The thawing of frozen soils starts in the first half of May. By the end of May 15-20% of the entire layer gets thawed, at the end of June the thawing reaches 50%, by the end of August 85%. The maximum soil thawing occurs at the end of September when the soil freezing already begins from the surface.

The soil freezing occurs both from above and below, on the part of permafrost, the soil freezing rate being different on various sites and depending upon the average annual soil temperature, the composition and moisture of freezing deposits. The minimum rate of soil freezing from below is observed on the heavily irrigated sites and averages 1.2-2.4 cm per day. The higher rates

(4.8-7.2 cm pd) are noted on the woody sites composed of supes-suglinok deposits with moisture 0.2-0.3. The high rates of soil freezing of seasonally thawed layer (0.5-0.6 cm pd) are characteristics of dry well-drained sites composed of supes.

The change of conditions of heat exchange within the limits of the opening has led to the increase of seasonal depth of thaw practically on all the country types. The exception is massifs of flowing about sands (tukulans). The disturbance of soil conditions within the limits of construction has not caused somewhat noticeable changes of seasonal thawed soil layers (STL) and seasonal frozen soil layers (SFL); one of the reasons for that is the lack of vegetative cover.

As one can see from the data of Table I the thickness of STL increased 2-2.2 times on the relatively dry sites and 1.3-1.5 times on the sites with high moisture. A slight change of thickness of STL (1.1-1.2 times) is observed on the sites with grass vegetation.

From the exogenetic geological processes and phenomena one should note ravine erosion thermokarst, solifluction mud flow of seasonal thawed layer and deflation reducing the reliability of the gas pipe-line maintenance due to uncovering, possible sagging and impermissible pipe displacement. The abovesaid makes difficulties for motor transport along the pipe-line road.

The main gas pipe-line Mastakh-Yakutsk is one of the first built in the zone of permafrost. The expediency and reliability of the three methods of laying pipe-lines - overground, ground and underground - have been verified in the course of construction.

A long period of observation on the gas pipe-line showed that the underground method of pipe laying is the most proper for the conditions of Central Yakutia ensuring the stable temperature regime of the gas pipe-line.

The overground pipe laying excluding the thermal effect of the pipes on the frozen soils completely requires some device of pile support resistant to the frost heaving forces and horizontal loads.

Under conditions of sharp continental climate of Yakutia the open pipe-lines are subjected to considerable tensile and compressive stresses, therefore, the breakdowns on the open pipe-lines are more likely to happen rather than on the underground ones.

The ground pipe laying (on the ground surface with soils falling) has been employed on the swampy sites (Figure 1). Its essential drawbacks are springing surface and supra-permafrost waters, failure of falling, heaving and pipe uncovering, probability of breakdown situations.

At the Mastakh gas deposit the method of low temperature separation is used ensuring the temperature  $-14^{\circ}\text{C} \dots -20^{\circ}\text{C}$  at the inlet to the main gas pipe-line. To the last point located at the distance of 380 km (Yakutsk) the gas comes warmed up to above-zero  $0.5 \dots 2.5^{\circ}\text{C}$  (in summer) and to below-zero  $6.7 \dots 7.6^{\circ}\text{C}$  (in winter). The character of temperature change of the transported gas along the pipe-line depends upon the pipe-laying method, intensity of heat exchange between the pipe and environment, the gas pipe-line capacity and other factors. The largest day and seasonal temperature fluctuations are noted on the first kilometers of the underground section and vice versa.

The data on the temperature changes of the wall and surrounding soils show that at the distance of 20 km the wall temperature (of the gas) gets equal to the soil temperature as a result of the heat exchange between the gas pipe-line and soils. This difference makes to  $60^{\circ}\text{C}$  between the underground sections and to  $24^{\circ}\text{C}$  between the overground and underground ones.

On the sites where the underground gas pipe-line goes out to the surface the wall temperature (of the gas) equalizes with the air temperature in summer in 1.7 km, in winter in 6.6 km.

Taking into accounts the fact that the gas pipe-line over 1.7 km are subjected to the amplitude of annual temperature fluctuations exceeding considerably the standards ( $58-70^{\circ}\text{C}$ ), at present the overground pipe laying of great extent is not recommended in Yakutia.

The depth of soil thaw near the gas pipe-line does not practically differ from the depth of soil thaw on the opening and does not exceed 2.5 m including 1.45 m under the pipe laid at the depth of 0.4-0.5 m. With the increase of depth of pipe laying to the design depth (0.8 m) the soil thawing decreases. At overground laying (in the embankment and falling) the total depth of soil thawing of the gas pipe-line base is 1.5-1.8 times more than at the underground laying which is accounted for the effect of filled soil in the thermal regime of the bedrocks.

Along the gas pipe-line the depth of soil-thaw under the pipe ranges from 0.73 to 1.45 m, the annual and seasonal values being practically identical. The soils under the pipe thawed in the summer period completely freeze in winter. That results in seasonal vertical displacements of the pipe-line - heaving (in the period of soil freezing) and settlement (in the period of thawing).

The vertical displacements of the ground pipe-line caused by the temperature deformations and heaving processes reach the maximum values to 230 mm (on the mari). The annual heaving of the underground sections on the pipe-line ranges from 10 to 100 mm which is compared with the total heaving of the surrounding soil and exceeds tenfold their displacement in the horizontal and longitudinal directions.

In summer the pipe-line returns to its original state. The residual heaving of the pipes is watched not in the frost-susceptible soils, as it was expected, but on the sections of the pipe-line in the sand desert (tukula-nam) due to its flexure increase resulting in the cavity formation which are filled with sand and the gas pipe-line cannot return to its original state.

In the cohesive soils the cavities (20-50 mm) arising around the pipe remain open serving as a compensator.

In connection with the further development of gas and oil deposits in Yakutia a question arises concerning the use of large diameter pipes for which conventional methods of pipe laying are likely to be improper. In this case much attention should be drawn to the choice of optimum depth of pipe laying and prediction of stressed state when combining different methods of pipe laying and the impact on the environment.

The previous pipe-laying construction experience in the zone of permafrost cannot give all the answers for the deposits development located, for instance, in the tundra or in the mountains. Besides, the designs lack the forecast of natural conditions change and the technical

Table 1. Seasonal thawed layer (STL) and seasonal frozen layer (SFL) in natural conditions and on the opening along the gas pipe-line Mastakh-Yakutsk

Relief element	Country type	Vegetative cover	Lithology	Moisture	Depth of STL and SFL	
					in natural conditions	on the opening
II over floodlands terrace of r. Vilyui	Heavily irrigated bottom of the alas, 20km	Moss, various grass deciduous wood	Peat 0.5 m supes heavy	1.2-1.7	1.1-1.3	2.0
	Interalas, 20 km	Cow-berries, various grass, deciduous wood	Supes heavy	0.25-0.3	1.5-1.6	3.0
III over-floodlands terrace of r. Vilyui	Modern eolin sands-dune crest-depression of flowing about, 81 km	Lacks	Medium sand	0.02-0.03	4.5-5.5	4.5-5.5
				0.03-0.05	3.5-4.5	3.5-4.5
Accumulative-denudation plain	Mari, 99 km	Moss, various grass depressed deciduous-birch wood	Slightly decomposed peat 0.3 m supes	1.7-1.9	1.5-1.6	2.2
Denudation plain	Southern slope of the valley of r. Kenkeme, 350 km	Deciduous-birch low forest	Supes heavy	0.15-0.25	1.5	2.2
	High floodlands of r. Kenkene, 350 km	Grass vegetation	Supes peat	0.3-0.45	1.3	1.7



Figure 1. The first part of the gas pipe-line Mastakh-Yakutsk on the swampy site.

decisions are made on the basis of the conditions before the construction which leads to the wrong engineering decisions concerning the linear part of the pipe-lines. In some cases, there is double insurance e. g. the substitution of frost-susceptible soils for non-susceptible ones or the thermal protection of frost-susceptible soils under the pipe-line from its heat (cold) emission. Occasionally, the engineering conception of the ecological construction plan is not developed and engineering-geocryological reasons for the changes of technical state of the pipe-lines are not specified.

In our opinion the further scientific research should be carried out along with the production

activities. It is necessary that the long-term plans of the enterprises should envisage the preliminary work concerning the preproject preparation of the future gas and oil pipelines including the geocryological survey with scale 1:100,000 for a large territory and 1:25000 for the key sites.

In addition to this, according to the contract with enterprises the long-term regime observation on the key sites (monitoring) should be carried out with a view to study the effect of construction and the reverse influence of this effect on the building structures.



## USE OF SPATIALLY DISTRIBUTED DATA TO MODEL ARCTIC HYDROLOGIC PROCESSES

D. L. Kane, L. D. Hinzman and E. K. Lilly

Water Research Center, University of Alaska  
Fairbanks, Alaska 99775 U.S.A.

Past interest in arctic hydrologic processes has been dictated by resource development. However, there is renewed curiosity in arctic hydrologic science because of the issue of climate change. The need to understand the interaction of climate, hydrology and both aquatic and terrestrial processes has increased the need for better quality hydrologic data and physically based hydrologic models. Discussed here is the development of a spatially distributed hydrologic model that addresses the dominant hydrologic processes and has been applied to a small arctic watershed. To test and verify this model, we need both point and spatially distributed data. Soil moisture, snowpack water content, and surface temperature are all useful forms of spatially distributed data that we are using to help construct a better understanding of hydrologic processes. Also, digital terrain data are used to determine drainage paths in this permafrost environment.

### INTRODUCTION

General circulation models (GCMs) predict that greater climatic warming will occur in the Arctic than in lower latitudes (Manabe and Stouffer, 1980; Schlesinger and Mitchell, 1985; and Etkin, 1990) and that warming will be greatest in the winter months. A warmer climate would trigger numerous hydrologic feedback mechanisms that could augment climatic warming; for example, earlier spring snowmelt and delayed snow accumulation in the autumn would significantly change the surface albedo and hence, the energy balance. Increased or decreased precipitation amounts could also alter the hydrologic response, particularly of the active layer. Our concern related to climatic warming has accentuated the facts that we have a poor hydrologic data base in northern latitudes and we lack both an understanding of and the capability to model basic arctic hydrologic processes.

In the past, we have relied on lumped parameter models. However, if we are going to understand hydrologic interactions with biogeochemical processes, we must develop spatially distributed hydrologic models. Woo (1986) stresses that these models must also have a good physical basis. Beven (1989) discusses the pros and cons of physically based models. To ensure that the modeling results are realistic it is imperative that good input data be used to drive these models. Finally, there are still reservations about the generated output of GCMs; this deficiency could be partially offset by developing mesoscale distributed models, particularly of the hydrologic processes.

This paper describes the formulation of a physically based, spatially distributed hydrologic model for use in the Arctic. Also discussed is how spatially distributed data are utilized in this model.

### HYDROLOGIC MODEL

Numerous physically-based hydrologic models are in existence with wide ranging characteristics (Beven and O'Connell, 1982; and Grayson et al., 1992). Discussed here is a physically based, spatially distributed hydrologic model with the following algorithms (Figure 1): snowmelt, subsurface active layer flow, soil thermal regime, overland flow, channel routing, and evapotranspiration.

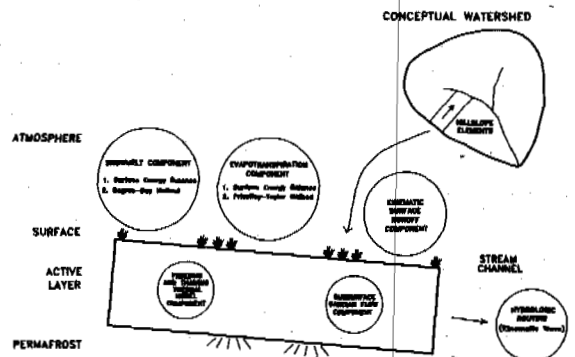


Figure 1. Components of a physically-based spatially-distributed hydrologic model.

This model is being developed because most existing models do not adequately address snowmelt and soil thermal regime. Snowmelt is the major hydrologic event each year in the Arctic and therefore it is essential that we have models that adequately predict ablation and take spatial distribution of the snowpack into consideration. Also, since the active layer is continually thawing throughout the summer period, the transient nature of the active layer depth is important in quantifying subsurface flow.

Runoff for a given landscape unit (element) is based upon calculations of overland flow, sub-surface flow and channel flow. During each time step, it is necessary to determine if the flow within the element is subsurface or both subsurface and overland flow. When the volume of water exceeds the total soil moisture storage capacity, then both surficial and subsurface flow must be calculated for that element. The subsurface flow is modeled using a Darcian approach and both the overland flow and channel flow are routed with kinematic equations. Snowmelt, evapotranspiration and depth of thaw are modeled with a surface energy balance (Hinzman et al., 1991a; Kane et al., 1991b). There is an option to model evapotranspiration with the Priestly-Taylor equation and snowmelt by the degree-day method (Kane et al., 1990; Kane et al., 1992). Presently, the thermal regime of the active layer is modeled using a heat-diffusion equation incorporating phase change.

Spatially distributed models have many positive features; however, these models require considerable data. Distributed models are used when spatial variation of some input parameter significantly alters the output response. An example would be where we are interested in tracing water movement from the top of the slope to a channel and the resistance to flow varies along the route. There are numerous examples where spatial variation should be considered when trying to model an arctic hydrologic system. During snowmelt, there is considerable variation in the water content of the snowpack caused by redistribution throughout the winter by the wind. There are also significant differences in surface temperatures or energy balance due to slope and aspect. This difference in energy balance impacts both snowmelt and evapotranspiration and to a lesser degree, active layer thickness. Obviously, vegetation differences impact transpiration, but it is difficult to obtain information necessary to incorporate this process into a hydrologic model.

As this model is being developed, various algorithms are being tested on data from Imnavait Creek watershed near Toolik Lake, Alaska, U.S.A. (lat. 68°37', long. 149°17'). This small watershed (2.2 km<sup>2</sup>) which is underlain by continuous permafrost has been the focus of an intense hydrologic study since 1985 (Kane and Hinzman, 1988; Everett et al., 1989; Kane et al., 1989; Kane et al., 1991a; Hinzman et al., 1991b; Kane et al., 1991b; Hinzman and Kane, 1991; Hinzman and Kane, 1992). Imnavait Creek would generally be considered a first order stream, but flow does cease during the winter months as the active layer completely refreezes, usually by the end of December.

Although there are numerous sites in the Alaskan Arctic where basic meteorologic measurements such as temperature, wind speed and relative humidity are measured, there are very few sites where any radiation or atmospheric profile measurements are made. This presently restricts the application of our model to one small watershed. This model is continually evolving and simpler algorithms are being developed for areas where there are limited data. This does compromise the physical integrity of this hydrologic model. It is anticipated that the addition of a few critical meteorologic and hydrologic stations and data obtained by remote sensing will in the near future allow us to apply this model to a much

larger area such as the entire Kuparuk River drainage (8140 km<sup>2</sup>).

## APPLICATION OF SPATIAL DATA

### Digital Terrain Model

To accurately model the hydrologic response of a watershed it is critical that the surface drainage be accurately depicted. For first order streams and higher this is not too difficult with available topographic data for the Alaskan Arctic. However, characteristic features of many arctic watersheds are water tracks, which carry water off the slopes and feed the first order streams (Walker et al., 1989). These water tracks are very efficient at transporting water during snowmelt and major rainfall events during the summer. To obtain accurate simulations of hydrologic processes such as runoff, it is imperative that these features be included in the drainage network. Our first objective was to develop a Digital Terrain Model (DTM) of the watershed showing the pathways of water movement out of Imnavait Creek. Topographic maps and aerial photography of the basin show the major drainage features; however, we lack knowledge about the pathways of water off the slopes. Close inspection, both in the field and of aerial photographs, reveals that the water tracks carry water off the slopes during the spring ablation and during major rainfall events.

A selected watershed is sub-divided into a number of smaller, theoretically uniform, regions called elements. A water balance considering each component described in Figure 1 is calculated for each element during each time step. During pre-processing, the direction of flow for each element is determined (i.e., if flow is into a channel or to one or two neighboring elements). It is only necessary to determine the pathways of flow for each element once for each drainage. The direction of flow is determined using vector calculus and the gradient of each element (Silfer et al., 1987). If flow from one element enters two others, then the proportion entering each element is algebraically determined based upon partial areas. If two elements share a common outflow side, then that boundary is a water track or stream channel.

Detection of a water track is dependent upon both the resolution of the digital elevation data and element size; in this application, it was not always possible to distinguish an entire water track from beginning to end. Once a water track was identified by the model, we forced the water track to continue downslope until it reached the main stream channel.

Water tracks are very efficient at carrying water off the slopes during snowmelt and periods of substantial precipitation and into the riparian area adjacent to the stream. These water tracks are a direct result of the area being underlain by continuous permafrost at shallow depths (25 to 60 cm). Could these water tracks, at least some of them, be reproduced by a digital terrain model (DTM) from the topographic data available? The answer to this question depends upon the resolution of the elevation data. For Imnavait Creek, we have available a 1:6000 map with a contour interval of 5 m. We superimposed a triangular grid network over the entire watershed (Figure 2). To get the elevation at the corner of each

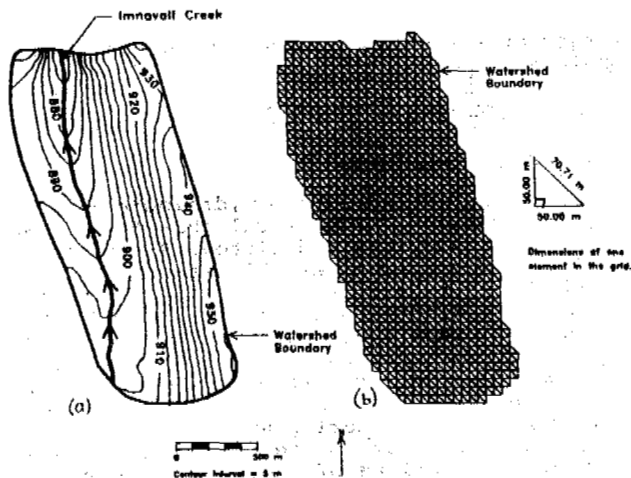


Figure 2. Innavait Creek drainage (a) and elements (b) used in digital terrain model.

triangular element, we used a kriging routine from commercially available software. Assuming that the topography could be utilized to predict surface drainage features, the pathway for each element was determined by calculating the slope of steepest descent.

Digital terrain models (DTMs) or digital elevation models (DEMs) have been used recently to determine watershed drainage area and drainage networks (Fairfield and Leymarie, 1991; Van Blargan et al., 1990; Band, 1986; and Jones et al., 1990). There are numerous difficulties one can encounter when using such models. First, some form of a grid network needs to be formulated. There are a number of options here; in our case, for convenience, we used a uniform triangular grid with each element having a base and height of 50 m (Figure 2). For Innavait Creek watershed, this approach produced approximately 1800 triangular elements.

The next step was to utilize the digital elevation data and a kriging technique to determine the elevation at each node of all the triangular elements. Next, the slope of steepest descent was determined. If the flow between two elements is toward the common boundary, then a channel is assumed to exist. Once a channel is initiated, it must be continuous and connect with other channels. In our model, we assumed if the angle between two adjacent paths of descent was less than  $5^\circ$ , they were parallel and no channel would form.

During the process of determining the elevation of each node, it is possible to find a point that is lower than all the surrounding nodes. This implies that there is no outlet and that a depression or pond exists. Depressions are a problem commonly faced in hydrologic modeling using DEMs (Chou, 1992). In a natural situation, if a depression exists, water will drain into it until it is filled and a new gradient will develop to carry the water away. In this case though we are trying to establish the drainage pattern based upon topography alone. To handle this case, we developed a technique similar to that of Fairfield and Leymarie (1991) by establishing the general direction of flow by looking at a number of other points around, but removed from the problem area and then forcing the flow to go through the area in the direction determined.

The next problem is that channels are only allowed to form along boundaries of the triangular elements. If the elemental boundaries coincide with the stream channel then everything is fine. If they do not coincide, then the flow is forced to take a different route; for our elements this could be off by as much as  $45^\circ$ . In Figure 3, a comparison is made between those water tracks that were clearly visible on 1:9000 aerial photography and those generated by our digital terrain model from digital elevation data used to create a 1:6000 contour map at a 5 m contour interval. First,

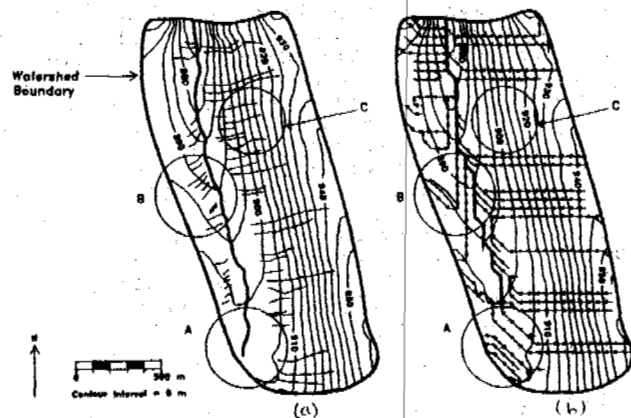


Figure 3. Actual (a) and modeled (b) water tracks for Innavait Creek, circled areas A, B, and C discussed in text.

we wanted to test the model to see if we could generate both the main drainage and also some of the water tracks. The stream was represented fairly well in the digital terrain model except in the area highlighted as A in Figure 3. This area at the top of the watershed is relatively flat; south of this area water flows from east to west and is carried to the Kuparuk River, which parallels Innavait Creek to the west. The digital terrain model actually routes some of the water that should be included in Innavait Creek drainage over to the Kuparuk River (7% of watershed area). This problem can only be overcome by obtaining higher resolution elevation data; the 5 m contour interval is too crude. In highlighted area B of Figure 3, we have a number of small water tracks draining to the northeast. In the results from the digital terrain model, we have generated water tracks that flow parallel to Innavait Creek in a northerly direction. What occurs here is that the orientation of the boundary of the elements restricts the direction of flow. This problem could be overcome by using a different design for the elements. For the arrangement of elements used here, the direction of flow could be off by  $45^\circ$  (Figure 4); the design shown in Figure 4b would reduce the maximum directional error to  $22.5^\circ$ .

There are some areas where we show no water tracks from the digital terrain model results, but they are apparent in the aerial photography (highlighted area C in Figure 3). The resolution of the vertical data is such that these water tracks are not detected. Again, part of the problem is related to the size of the elements; smaller elements would approximate the terrain better.

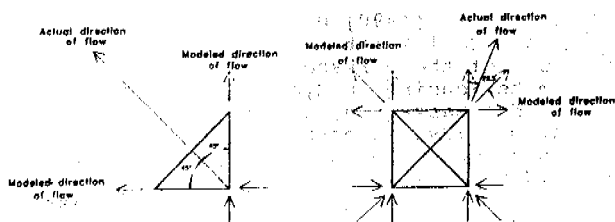


Figure 4. Worst case scenario for element configuration (a) in digital terrain model and improved option (b) that reduces the maximum directional error from 45° to 22½°.

#### Hydrologic and Meteorologic Data

A grid network such as that shown in Figure 2 is especially useful for incorporating hydrologic properties which vary spatially, such as soil hydraulic conductivity, surface temperature, active layer thickness, snowpack water content, or vegetation patterns. Through Geographical Information Systems (GIS), it is quite easy to utilize spatial data, such as a snow distribution map, as model input.

It is more difficult to obtain spatially distributed data which varies on short time scales such as meteorologic measurements. Many methods exist to estimate spatial variability in precipitation based upon point measurements and in some cases elevation (Gupta, 1989). Certain algorithms can be useful in calculating changes in temperature with elevation (Bergström, 1976), or the effect of slope on incident radiation (Hinzman et al., 1992); however, for some variables, such as wind speed, it is difficult to estimate spatial variation and one is forced to assume uniform conditions everywhere.

Soil moisture distribution as predicted by the hydrologic model for the Innavait Creek area, is shown in Figure 5. In general, this figure shows that the valley bottoms are wetter than the hillslopes; but even on the hillslopes there are wet areas along the water tracks.

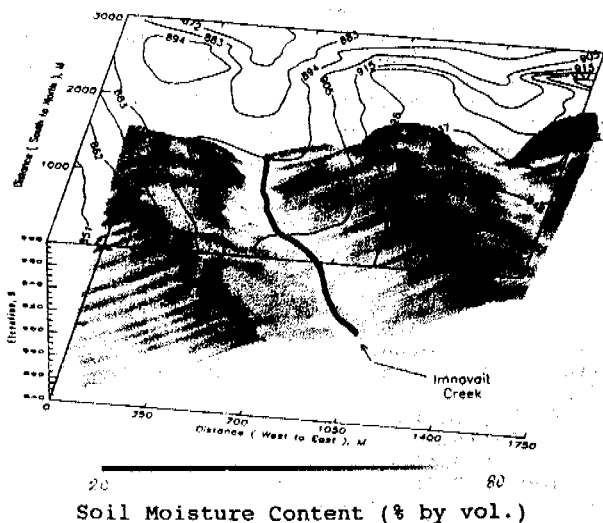


Figure 5. Three-dimensional, spatially distributed, modeled soil moisture for Innavait Creek on August 24, 1991.

#### Synthetic Aperture Radar Data

Microwave imagery has been used in a number of hydrologic applications. Rott (1984) investigated the potential of using various SAR systems for monitoring seasonal snow cover and glaciers. Josberger and Beauvillain (1989) used passive microwave with visual images to map snowcover in the upper Colorado River basin in United States. Foster et al. (1991) also used passive microwave radiometry to determine the snow water equivalent in a boreal forest. Blanchard and Chang (1983) used Seasat Synthetic Aperture Radar to determine if the imagery could be used to estimate soil moisture. Engman (1990) discusses the coupling of microwave remotely sensed soil moisture data with hydrologic models.

The rationale for using microwave imagery for determining soil moisture contents is that the return signal is sensitive to changes in the complex dielectric constant of the soil water system. The complex dielectric constant of liquid water is about 20 times higher than either soil or ice, therefore liquid water changes in the soil-water system may significantly impact this constant. Attenuation of the microwave signal as emitted from the satellite is of interest. Blanchard and Chang (1983) found that the geometry of the terrain and the electrical properties of the soil are the two major factors that influence the microwave backscattering response the most.

Vegetation on the surface can also influence the backscatter signal. In the Arctic, the limited size and low density of the natural vegetation should help to minimize this problem; but dew or the remnants of rain on the vegetation could significantly impact the backscatter response. One additional problem is the lack of knowledge about the depth of penetration of the microwaves into the soil. Because permafrost limits vertical drainage and the mineral soils above the permafrost are near saturation, there can exist relatively dry organic soils at the surface and saturated mineral soils at very shallow depth.

In 1991, the European Space Agency (ESA) put into polar orbit the European Remote Sensing satellite (ERS-1). On board is an active microwave instrument, operating at a frequency of 5.3 GHz (C-band) in which one of the subsystems is Synthetic Aperture Radar (SAR) in the image mode. Numerous images of the North Slope of Alaska, including Innavait Creek, are available for 1991. We are attempting to use these satellite images for determining the spatial variation of the near-surface soil moisture contents of the active layer. Assuming that this is possible, then the results from the SAR imagery can be used to compare with the predicted soil moisture distribution from the hydrologic model.

This last step is very significant because it allows us to check the spatial performance of the hydrologic model. In the past, hydrologic model performance has been evaluated by comparing the modeled hydrograph with the measured values. This technique is not useful for making spatial adjustments to the modeling parameters.

There is a definite need to develop hydrologic models that are compatible with the output from remote sensors. Once it has been calibrated, the SAR imagery could be utilized to initialize a hydrologic model or to compare with the modeled soil moisture.

## CONCLUSIONS

The need exists for more physically based hydrologic models that consider spatial variability. Demonstrated in this paper is a digital terrain model that is capable of generating the stream channel of a small headwater arctic watershed; in addition, it also detected a number of smaller drainages referred to as water tracks. A physically based, spatially distributed hydrologic model is described. This model uses the output from the digital terrain model to establish drainage patterns. Using either rainfall or calculated snowmelt as input, the hydrologic model determines changes in soil moisture, evapotranspiration, and stream discharge. SAR imagery will be utilized to estimate soil moisture levels and these data will be used to initialize the model and to appraise the spatial and temporal soil moisture distribution for a small arctic watershed. If successful, this imagery can also be used to extrapolate model results to larger areas. Arctic watersheds have physical features that help to simplify efforts to model the hydrology. First, the existence of continuous permafrost guarantees that the subsurface flow will be restricted to the shallow active layer. Second, the vegetation in this harsh environment is limited to mosses, grasses and small shrubs. However, there are several complicating factors for system hydrology in the Arctic; the likelihood that the active layer will become saturated and overland flow will occur is increased, the active layer is continually increasing in depth throughout the summer, and winter winds significantly redistribute snow on the ground.

## ACKNOWLEDGMENTS

This research was sponsored by the U.S. Department of Energy's Office of Health and Environmental Research, Ecological Research Division as part of the R&D program in Arctic Tussock Tundra and the National Aeronautics and Space Administration. We would like to acknowledge Yuwu Zhang, Hao Chen and Robert E. Gieck for assistance in modeling, data collection, reduction and analysis.

## REFERENCES

- Band, L. E. (1986) Topographic Partitions of Watersheds with Digital Elevation Models. *Water Resources Research*, 22(1):15-24.
- Bergström, S. (1976) Development and Application of a Conceptual Runoff Model for Scandinavian Catchments. Swedish Meteorological and Hydrological Institute, Norrköping, Sweden, Report No. RHO7. 118 pp.
- Beven, K. (1989) Changing Ideas in Hydrology-The Case of the Physically-based Models. *Journal of Hydrology*, 105:157-172.
- Beven, K. J. and P. E. O'Connell (1982) Physically Based Models in Hydrology. Rep. 81, Inst. of Hydrology, Wallingford, Oxon, England.
- Blanchard, B. J. and A. T. C. Chang (1983) Estimation of Soil Moisture from Seasat SAR Data. *Water Resources Bulletin*, 19(5):803-810.
- Chou, Y. H. (1992) Slope-line Detection in a Vector-based GIS. *Photogrammetric Engineering and Remote Sensing*, 58(2):227-233.
- Engman, E. T. (1990) Use of Microwave Remotely Sensed Soil Moisture in Hydrologic Modeling. Proc. of the Workshop on Applications of Remote Sensing in Hydrology, Environment Canada, Saskatoon, Saskatchewan, pp. 279-292.
- Etkin, D. (1990) Greenhouse Warming: Consequences for Arctic Climate. *Journal of Cold Regions Engineering*, 4(1):54-66.
- Everett, K. R., G. M. Marion and D. L. Kane (1989) Seasonal Geochemistry of an Arctic Tundra Drainage Basin. *Holarctic Ecology*, 12(3):279-289.
- Fairfield, J. and P. Leymarie (1991) Drainage Networks from Grid Digital Elevation Models. *Water Resources Research*, 27(5):709-717.
- Foster, J. L., A. T. C. Chang, D. K. Hall and A. Rango (1991) Derivation of Snow Water Equivalent in Boreal Forests Using Microwave Radiometry. *Arctic*, 44(1):147-152.
- Grayson, R. B., I. D. Moore and T. A. McMahon (1992) Physically Based Hydrologic Modeling 1. A Terrain Based Model for Investigative Purposes. *Water Resources Research*, 28(10):2639-2658.
- Gupta, R. S. (1989) *Hydrology and Hydraulic Systems*. Prentice Hall, Englewood Cliffs, New Jersey. 739 pp.
- Hinzman, L. D. and D. L. Kane (1991) Snow Hydrology of a Headwater Arctic Basin 2. Conceptual Analysis and Computer Modeling. *Water Resources Research*, 27(6):1111-1121.
- Hinzman, L. D., D. L. Kane and R. E. Gieck (1991a) Regional Snow Ablation in the Alaskan Arctic. in *Northern Hydrology, Selected Perspectives*, NHRI Symposium No. 6, T.D. Prowse and C.S.H. Ommanney (eds). National Hydrology Research Institute, Saskatoon, Saskatchewan. pp. 121-140.
- Hinzman, L. D., D. L. Kane, R. E. Gieck and K. R. Everett (1991b) Hydrologic and Thermal Properties of the Active Layer in the Alaskan Arctic. *Cold Regions Science and Technology*, 19:95-110.
- Hinzman, L. D. and D. L. Kane (1992) Potential Response of an Arctic Watershed During a Period of Global Warming. *Journal of Geophysical Research*, 97(D3):2811-2820.
- Hinzman, L. D., G. Wendler, R. E. Gieck, and D. L. Kane (1992) Snowmelt at a Small Alaskan Arctic Watershed, 1. Energy Related Processes. Northern Research Basins Conference. Whitehorse, YT, Canada.
- Jones, N. L., S. G. Wright and D. R. Maidment (1990) Watershed Delineation with Triangle-Based Terrain Models. *Journal of Hydraulic Engineering*, 116(10):1232-1251.
- Josberger, E. G. and E. Beauvillain (1989) Snow Cover of the Upper Colorado River Basin from Satellite Passive Microwave and Visual Imagery. *Nordic Hydrology*, 20:73-84.
- Kane, D. L. and L. D. Hinzman (1988) Permafrost Hydrology of a Small Arctic Watershed. Proc. of Fifth International Permafrost Conference, Trondheim, Norway, Tapir Publishers, pp. 590-595.
- Kane, D. L., L. D. Hinzman, C. S. Benson and K. R. Everett (1989) Hydrology of Imnavait Creek, an Arctic Watershed. *Holarctic Ecology*, 12:262-269.
- Kane, D. L., L. D. Hinzman, C. S. Benson and G. E. Liston (1991a) Snow Hydrology of a Headwater Arctic Basin 1. Physical Measurements and Process Studies. *Water Resources Research*, 27(6):1099-1109.

- Kane, D. L., R. E. Gleck, and L. D. Hinzman (1990) Evapotranspiration from a Small Arctic Watershed. *Nordic Hydrology*, 21:253-272.
- Kane, D. L., L. D. Hinzman and J. P. Zarling (1991b) Thermal Response of the Active Layer to Climatic Warming in a Permafrost Environment. *Cold Regions Science and Technology*, 19:111-122.
- Kane, D. L., R. E. Gleck, G. Wendler and L. D. Hinzman (1992) Snowmelt at a Small Alaskan Arctic Watershed, 2. Energy Related Modeling Results. Northern Research Basins Conference. National Hydrologic Research Institute. Whitehorse, YT, Canada.
- Manabe, S. and R. J. Stouffer (1980) Sensitivity of a Global Climate Model to an Increase in CO<sub>2</sub> Concentration in the Atmosphere. *Journal Geophysical Research*, 85:5529-5554.
- Rott, H. (1984) Synthetic Aperture Radar for Snow and Glacier Monitoring. *Advance Space Research*, 4(11):241-246.
- Schlesinger, M. E. and J. F. B. Mitchell (1985) Model Projections of the Equilibrium Climatic Response to Climate Effects of Increasing Carbon Dioxide. U. S. Dept. of Energy, Report DOE/ER 0237, Wash. D. C., pp. 81-147.
- Silfer, A. T., G. J. Kinn and J. M. Hassett (1987) A Geographic Information System Utilizing the Triangulated Irregular Network as a Basis for Hydrologic Modeling. Autocarto 8. Proceedings of the Eighth International Symposium on Computer-Assisted Cartography. Baltimore, Maryland. March 29-April 3, 1987. pp 129-136.
- Van Blarigan, E. J., R. M. Ragan and J. C. Schaafe (1990) Hydrologic Geographic Information System. *Transportation Research Record*, No. 1261, pp. 44-51.
- Walker, D. A., E. Binnian, B. M. Evans, N. D. Lederer, E. Nordstrand and P. J. Webber (1989) Terrain, Vegetation and Landscape Evolution of the R4D Research Site, Brooks Range Foothills, Alaska. *Holarctic Ecology*, 12:238-261.
- Woo, M. K. (1986) Permafrost Hydrology in North America. *Atmosphere-Oceans*, 24(3):201-234.

INTERACTION BETWEEN SNOW COVER AND HIGH MOUNTAIN PERMAFROST  
MURTEL/CORVATSCH, SWISS ALPS

Felix Keller<sup>1</sup> and Hansueli Gubler<sup>2</sup>

<sup>1</sup>Laboratory of Hydraulics, Hydrology and Glaciology, VAW - ETH Zentrum  
CH-8092 Zurich, Switzerland

<sup>2</sup>Swiss Federal Institute for Snow and Avalanche Research,  
CH-7270 Weissfluhjoch/Davos, Switzerland

Structural avalanche control in avalanche release zones cause a redistribution of the snow and therefore local disturbances to the heat balance at the ground/snow interface. An attempt was therefore made to evaluate the influence of the snow cover on the ground temperature field and to determine permafrost-specific characteristics of snow cover processes. In the Murtel rock glacier area 90 snow pits were selected and the snow and soil temperatures measured. Thermal resistance of and heat flux through the winter snow cover are calculated at two locations with and at two without permafrost. As a consequence of low temperature gradients within the snow cover over permafrost, snow metamorphism differs from locations without permafrost. Snow related cooling processes in autumn could be important for the existence of permafrost near the permafrost limit and should be further investigated.

## INTRODUCTION

In the Swiss Alps, high mountain permafrost often occurs above 2500 m a.s.l. on steep slopes with avalanches and debris flow hazards (Haeberli 1975, Roesli & Schindler 1990). Some villages are located in risk areas below these permafrost regions. This study is part of a protection project in an area with difficult geotechnical conditions and snow forces (Salm 1977). Improved knowledge about the interactions between snow cover and high mountain permafrost is required in order to develop a sound avalanche protection concept for steep slopes with creeping mountain permafrost (Haeberli 1985).

With differences in altitude of more than 1000 m within a horizontal distance of 2 km, the topography in the Alps strongly influences the distribution of the discontinuous high mountain permafrost. Topographic effects on radiation and air temperature determine primarily the energy balance at the surface (Oke 1987, Hoelzle et al. 1993). The snow cover is a leading factor in protecting the ground from heat loss in winter (Williams and Smith 1989). In polar regions the influence of snow cover on the distribution of discontinuous permafrost is recognized along with factors such as aspect and vegetation (Nicholson and Granberg 1973). Granberg (1988) investigated thermal resistance, short-wave transmissivity and thermal buffering of the seasonal snow cover for its significance with respect to the ground temperature field in woodland and alpine tundra (Schefferville, Canada). In the non-polar regions encountered in the Alps, snow depths of more than 75 cm do not indicate an absence of permafrost (Haeberli and Epifani 1986). However, redistribution of snow by avalanches and wind alter the thermal regime in the ground significantly (Haeberli 1975). The following aspects are currently being investigated:

(1.) In winter, the thermal regime in the active layer and at the ground/snow interface is assumed to depend primarily on the existence of

permafrost and the characteristics of snow cover and ground (porosity and thermal conductivity). In order to investigate the effects involved, the thermal resistance of the snow cover, snow and ground temperatures, heat fluxes near the ground/snow interface and snow profile stratification have to be determined;

(2.) Measurements of the Bottom Temperature of Snow cover (BTS) is a method to map the existence of permafrost (Haeberli 1975). Attempts are made to improve the knowledge about the influence of the build-up of the snow cover on the BTS;

(3.) the influence of permafrost on the snow stratigraphy is being analyzed.

## THERMAL EFFECTS

BTS, as used for mapping permafrost, is defined here as the Bottom Temperature of the winter snow cover in February and March by a seasonal snow depth > 0.8 m. Snow, with its low thermal conductivity, is a high-frequency thermal filter between the atmosphere and the earth's surface. Therefore, the BTS value is mainly controlled by heat flux in the uppermost part of the ground. When permafrost is absent the BTS value is warmer than -2 °C (Haeberli 1975). A cold Alpine permafrost body in the ground reduces the heat flux to the base of the snow cover and keeps the BTS value in general below -3 °C. Haeberli and Patzelt (1982) assumed that in the presence of permafrost the BTS value in February depends on summer temperatures of the active layer.

The effects used by the BTS method correspond to a numerical study of the effects of snow cover on the ground thermal regime of Goodrich (1982). Furthermore, Goodrich concluded that the thermal resistance of the snow cover is a critical factor affecting ground temperatures and cannot easily be modeled. To improve the understanding of temperature distribution in the active layer and the seasonal snow above, heat fluxes and thermal resistances have to be calculated using field measurements of snow density and snow temperatures.

The empirical formulation by Devaux (1933) mentioned by Mellor (1977) relates thermal conductivity,  $k_{eff}$  to snow density:

$$k_{eff} = 2.93(\rho^2 10^{-6} + 0.01) \text{ in } (\text{Wm}^{-1}\text{C}^{-1}) \quad (1)$$

where:  $k_{eff}$  = eff. thermal conductivity ( $\text{Wm}^{-1}\text{C}^{-1}$ )  
and:  $\rho$  = density ( $\text{kgm}^{-3}$ )

The steady-state unidirectional heat flux  $q$  is calculated as:

$$q = -k_{eff} \frac{d\theta}{dz} \quad (\text{Wm}^{-2}) \quad (2)$$

where:  $\frac{d\theta}{dz}$  = temperature gradient

The thermal resistance  $\Omega$  of the snow cover is as defined by Cranberg (1988) as:

$$\Omega = \frac{d}{k_{eff}} \quad (\text{m}^2\text{C}\text{W}^{-1}) \quad (3)$$

where:  $d$  = snow depth

Due to their influence on vapor transport, temperature gradients in the snow cover not only affect ground temperatures, but also snow metamorphism. Since the very beginning of snow research, metamorphism is one of the topics researchers have focused on. Basic laws of snow metamorphism were discovered and the importance of their qualitative dependence on the temperature gradient were pointed out (Seligman 1936, de Quervain 1963). Giddings and LaChapelle (1962) and Colbeck (1983) estimated growth rates of snow grains exposed to high temperature gradients from theoretical considerations. Gubler (1985) established a model for dry snow metamorphism by interparticle vapor flux. Empirical relationships for growth rates as a function of temperature and temperature gradients were determined by Marbouty (1980).

## INVESTIGATIONS

Since 1973 the rock glacier area of Murtèl (0.4 km<sup>2</sup>, 2600 m a.s.l.) at Piz Corvatsch in the Upper Engadin of the eastern Swiss Alps has been investigated. The active layer is a few meters thick and consists mainly of porous debris ( $\phi=15-100$  cm) with only a small proportion of fine material ( $\phi < 2$  mm) and nearly without vegetation. Based on a total of about 300 BTS measurements from the years 1983, 1987 and 1990, the permafrost distribution in the area (8 km<sup>2</sup>) around the rock glacier has been determined. The ice content of the frozen ground varies between 10% and extreme supersaturation (Vonder Mùhl and Holub 1992).

During the winters of 1989/90 and 1990/91, snow profiles were measured every two weeks (Fig. 1) and classified according to the international snow classification (Colbeck et al. 1990) at four Locations. Location 1 is atop the rock glacier about

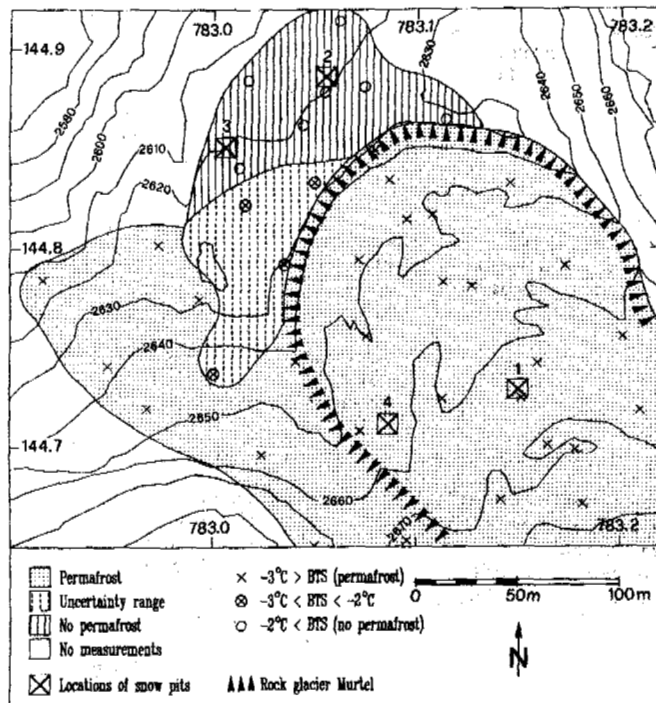


Fig. 1. Rock glacier area Murtèl at Piz Corvatsch, Upper Engadin, eastern Swiss Alps: Permafrost distribution, BTS measurements of February 26 1990 and locations of the snow profiles in winter 1989/90 and 1990/91.

10 m from the borehole of 1987 (Vonder Mùhl and Haeberli 1990). Locations 2 and 3 are situated outside the permafrost area in front of the rock glacier. Location 2 is in a wind-protected depression with greater snow accumulation than at location 3 which is exposed to wind and characterized by an undulating terrain. Location 4 is within the permafrost area at the border of the rock glacier. The non-porous ground at location 4 contains a high proportion of fine material ( $\phi < 2$  mm) typical for areas outside rock glaciers. At locations 3 and 4, wind erosion of snow is an important mechanism that reduces snow depth. At all sites the ground is generally dry in autumn. A recording system based on a CAMPBELL CR10 Logger was used to measure snow ( $n=5$ ) and ground ( $n = 3$  or 4) temperatures every 3 hours at an accuracy of  $\pm 0.1$  °C. These measurements were taken during the period of snow cover from December to June at the four locations. The snow sensors were located in the snow 5, 30, 45, 60 and 100 cm above the ground. At location 2, the ground sensors were placed 20, 50, 90 and 130 cm below the ground. The sensors at location 1 were between boulders ( $\phi > 50$  cm) with advective heat transport by air circulation. Because these temperatures are mainly determined by air circulation, data at the levels of 30, 65 and 110 cm below ground were not used for the heat conduction calculations.



## RESULTS

### Thermal resistance

The thermal resistance of each snow layer was calculated (Eq. 1 and 3) for each snow profile. These values were added together to determine the thermal resistance of the snow cover (Fig. 2).

A notable difference between the permafrost (heavy lines) and permafrost-free sites cannot be recognized. The influence of permafrost on the thermal resistance is minor as compared to the influence of snow removal by wind erosion (broken lines). In early winter, the thermal resistance increases greatly due to snow accumulation. New snow causes an additional layer with low thermal conductivity. In January and February, thermal resistance is mainly determined by snow depth. Because of a cold dry period without precipitation, snow settlement reduced the snow depth whereas the snow density increased and the thermal resistance generally decreased. This fact is responsible for the temporal heat flux maximum (Fig. 5). In spring, mean snow densities were lower (i.e. lower thermal conductivity) at permafrost sites due to reduced melting. Thus, in March, the thermal resistances were higher in the permafrost areas even though the snow depths were similar at all locations. Maximum snow depths were observed during April/May. Nevertheless thermal resistance in April/May was lower than in January owing to a low-density snowpack (precipitation forms, fragmented particles and rounded grains).

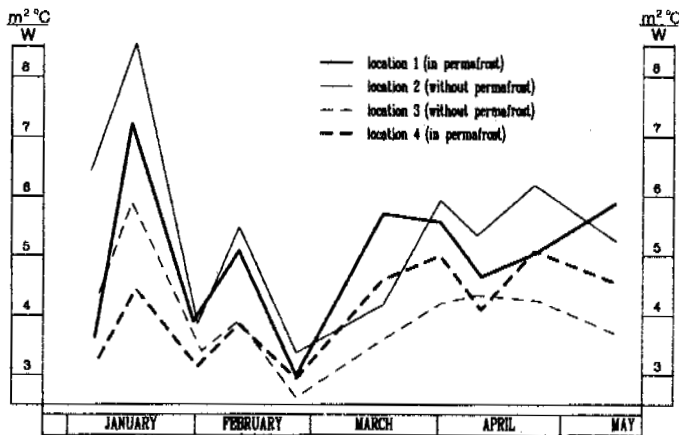


Fig. 2. Thermal resistance during the winter of 1990/91. Heavy lines are used to represent permafrost (Locations 1 and 4), broken lines for locations with a reduced snow depth (Locations 3 and 4).

### Temperatures

At the four locations, the observed thermal regime of the ground/snow interface is significantly different between permafrost and non-permafrost areas.

Measured ground and snow temperatures at Location 2 in front of the Murtèl rock glacier are plotted as 48h-averages in Fig. 3. The snow temperature sensor located in the snow 5 cm above the ground shows the development of the BTS (snow depth > 0.8 m) which is between  $-1^{\circ}\text{C}$  and  $0^{\circ}\text{C}$  during the entire winter. This confirms the ab-

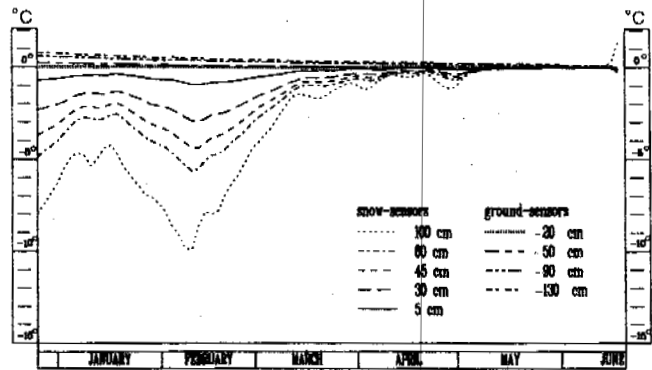


Fig. 3. Snow and ground temperatures at Location 2 (without permafrost) in winter 1990/91

sence of permafrost. During the observation period, ground temperatures were never colder than  $0^{\circ}\text{C}$  and they did not vary significantly. The variations of snow temperatures are damped with increasing snow depth. Only in February, during a cold period, did the snow temperatures at heights of 45, 80 and 100 cm above ground decrease by several degrees. The temperature gradient never reversed except in a few situations at the 100 cm sensor in April due to warmer air temperatures.

Fig. 4 shows the 48h-averages of measured ground and snow temperatures at Location 1 (permafrost location). Obviously the temperatures at all levels differ significantly from those measured over permafrost-free ground (Fig. 3). All the temperatures at this permafrost location (1) are generally about  $5^{\circ}\text{C}$  colder than at Location 2. Until the beginning of June, the temperatures within the porous debris as well as the 'BTS sensor' at the 5 cm level in the snow cover, remained below  $-3.5^{\circ}\text{C}$ . At Location 1, with the highly porous debris layer, the variations of the snow temperatures at the 5 cm level are significantly higher than at all the other locations even though the thermal resistance of the snowpack is nearly the same (Fig. 2). At this permafrost location, the large temperature difference between the 5 cm snow

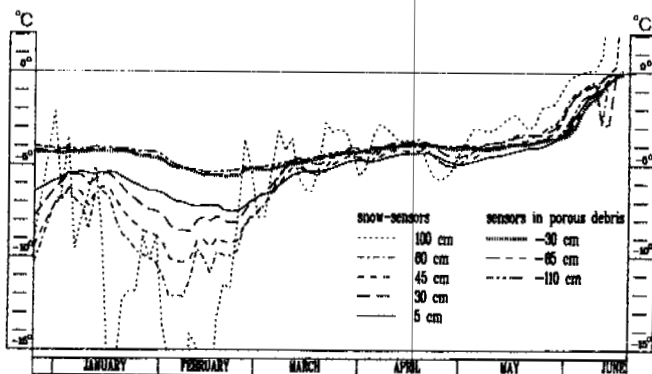


Fig. 4. Snow and ground temperatures at Location 1 (in permafrost) in winter 1990/91. Until March the sensor at the 100 cm level was not within the snowpack.

level and the -30 cm level in the porous debris is remarkable. On the other hand temperature gradients are greatly reduced in the basal snow layers between the 5 cm and 30 cm level. At the beginning of March, the temperature gradient reversed in the snow cover close to the ground/snow interface.

#### Heat fluxes

Linear interpolation methods were used to obtain density, layer thickness and grain shape between the dates of the snow pits. The heat flux between 15 and 30 cm with a resolution of two days (Fig. 5) is determined by the effective thermal conductivity and the temperature field (Eq. 1 and 2). Permafrost sites (heavy lines) are characterized by a small heat flux in January and February (approximately  $-1 \text{ W/m}^2$ ). Due to warmer ground temperatures outside the permafrost area, the increased temperature differences between the ground and snow surface cause increased heat fluxes for sites with comparable thermal resistances. For example, in January the heat flux at Location 2 is higher than at Location 1 even though the thermal resistance is greater at Location 2. In spring the snow cover warms up, so that the heat flux approaches approximately  $0 \text{ W/m}^2$ , except at Location 1 where heat flows from the snowpack into the ground.

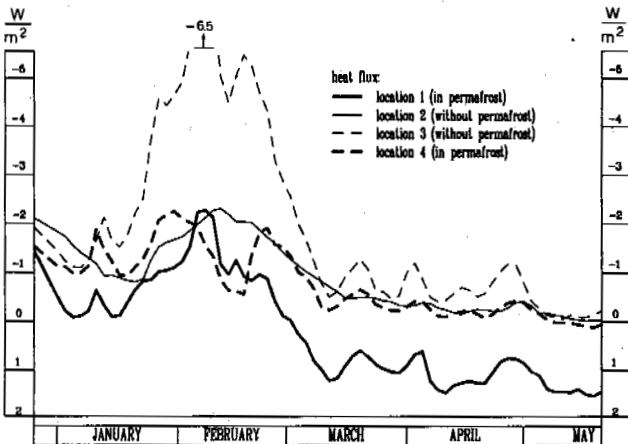


Fig. 5. Heat flux through the snow cover in winter 1990/91. Heavy lines are used to represent permafrost (Locations 1 and 4), broken lines for locations with a reduced snow depth (Locations 3 and 4).

#### Snow stratification

The interpolated snow profiles at Location 1 and 2 contain data from about 200 observed snow layers. Based on this data the statistics of grain shapes were calculated for every month.

In the wind-protected depression at permafrost-free Location 2 in front of the rock glacier, the snow depth reached 150 cm in December (Fig. 6). During the almost precipitation-free period until February, snow settling took place. A full 80% of the snowpack metamorphosed to solid-faceted crystals or depth hoar. In March, snowfall increased the snow depth again until the maximum snow depth was reached in May. The occurrence of wet grains

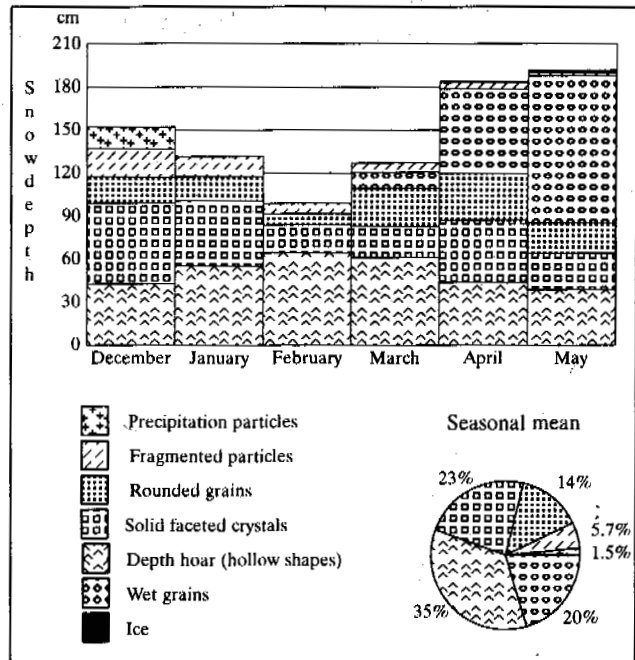


Fig. 6. Snow stratification at location 2 (without permafrost) in winter 1990/91.

at the beginning of March marks the onset of melting. Analysis of all grain shapes averaged over the entire winter revealed that depth hoar was the most frequently observed (35%).

At Location 1 the snow depth was  $< 1 \text{ m}$  until March (Fig. 7). Rounded grains dominated the entire winter (39%). The small proportion of depth hoar crystals (4%) proves that high vapor fluxes inducing high recrystallisation rates seldom occurred at this site. The high proportion of rounded grains in April and May caused an increased strength of the snowpack in spring (Keller, in prep.). The maximum snow depth was reached in May and was comparable to the permafrost-free site (Location 2). At Location 1 snow temperatures at the 5 cm level reached the melting point roughly one month later than at Location 2 (Fig. 3 and Fig. 4). Thus, meltwater runoff at the permafrost site started considerably later and less intensively.

#### INTERPRETATION

##### Temperatures near the ground/snow interface

Two observations need to be explained:

a) Very low temperature near the ground/snow interface at the end of December at Location 1,

b) Temperature and temperature variations near the ground/snow interface in the permafrost area with a porous active layer at Location 1.

a) The cold ground temperature at the end of December can be explained as follows: Before the first seasonal snow covers the ground, the active layer (snow free) starts to cool because of cool

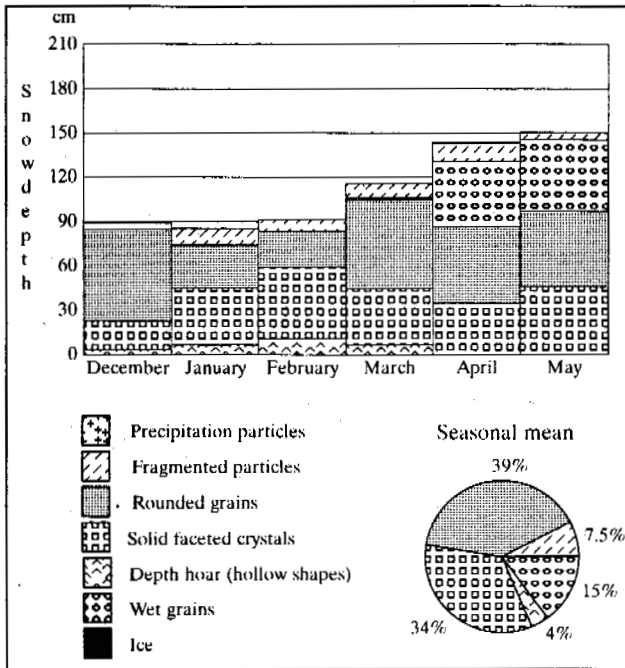


Fig. 7. Snow stratification at Location 1 (in permafrost) in winter 1990/91

autumn temperatures and reduced incoming radiation. In autumn, Locations 1 and 4 often retain a shallow snow cover as a result of a lack of direct radiation, whereas outside the permafrost area (Fig. 1) the snow usually melts again in this season. Once a shallow snow cover has built up (snow depth:  $d < 15$  cm), long-wave emissivity  $E$  at the surface increases significantly ( $E_{\text{rubble}} = 0.8$ ,  $E_{\text{snow}} = 0.97$ ). Short wave absorption decreases (albedo:  $\alpha_{\text{rubble}} < 0.5$ ,  $\alpha_{\text{snow}} = 0.9$ ). The new energy balance causes snow-surface temperatures below  $-10$  °C (Bader and Weillenmann 1992), whereas ground-surface temperatures remain initially between 0 and 5 °C. The resulting large temperature gradient in the shallow snow cover strongly increases heat flux from the ground to the atmosphere. This cooling process now depends on the further build-up of the snow cover. With further snow accumulation the thermal resistance of the snow cover will increase. As a result, the cooling process of the active layer decreases. In winter 1990/91 a snowfall of about 50 cm in November strongly reduced the cooling process by forming a layer with a significant thermal resistance. The only exception was at Location 1, where the debris with diameters of 50–100 cm prevented the build-up of a continuous snow cover. Thus the active layer continued to cool down to  $-4.5$  °C until a continuous snow cover formed in December. The assumed reinforced ground cooling processes due to thin snow cover could affect the distribution of high mountain permafrost.

b) An indication for the processes involved at the porous active layer in the permafrost area are the vertical funnels through the snow cover (Fig. 8) observed near Location 1 on the rock gla-

cier with its very rough surface. These funnels could allow direct heat exchange between the atmosphere and the active layer. They could be responsible for the significant temperature variations at the base of the snow cover at the begin of January (Fig. 4). It is likely that cold air flows into the active layer and warm air leaves the active layer through the funnels. The observed fast growth of large crystals in the funnels could support this assumption. Funnels were observed only in the first part of the two winters, when the snow depths were less than about 70 cm. In spring advective air currents in the porous active layer provided an explanation for the observed heat flux from the snowpack into the ground at Location 1.

#### Snow metamorphism

Temperature gradients and snow temperatures co-determine snow metamorphism, grain shapes and the snow stratification. In contrast to polar regions (Benson 1969), in the Alps the influence of water vapor migration from the ground is negligible (de Quervain 1963). The following factors are responsible for the different snow stratigraphy at Locations 1 and 2: The difference between air and ground temperatures as well as snow depth influences temperature gradients in the snow cover. In January at Location 1, the low temperature at the 5 cm level and the assumed thermal coupling by funnels reduced the difference between snow surface temperatures and snow temperatures at the lower levels significantly. Heat flux through the snow cover was reduced. Even though the snow depth at Location 1 was smaller than at Location 2, the temperature gradients at the low snow levels were

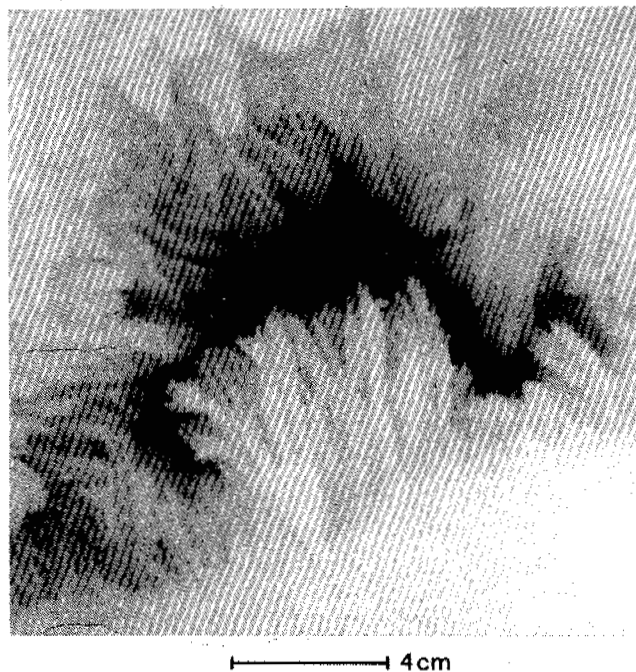


Fig. 8. Vertical funnel through the snowpack over the active layer of the Murtel rock glacier, Upper Engadin, eastern Swiss Alps with fast growth of large crystals (January, 1990).

significantly lower. Low snow temperatures (low vapor density) also reduce recrystallisation rates. Therefore, low temperature gradients and low snow temperatures slowed down metamorphic processes. This explains the high proportion of rounded grains at Location 1 whereas at Location 2 faceted crystals and depth hoar were dominant.

#### CONCLUSIONS

Investigation during two winters (1989-1991) of snow cover characteristics at four Alpine sites, two with permafrost and two without, showed that:

thermal resistance of the snow cover does not differ notably between permafrost and permafrost-free sites;

temperature gradients and heat flux are greatly reduced in basal snow layers over permafrost;

in contrast to permafrost-free sites with abundant formation of depth hoar in basal snow layers, snow over permafrost sites contains high proportions of rounded grains giving clear evidence of reduced temperature metamorphism;

meltwater runoff from the snow cover over permafrost starts significantly later (roughly one month) than in permafrost-free areas;

effects of direct thermal coupling between the atmosphere and the active layer through funnels in the snow cover as well as reinforced ground cooling processes in early winter due to thin snow cover could be important for the existence of permafrost near the permafrost limit and should be further investigated.

Avalanche protection installations may alter the natural snow distribution. As a consequence thermal ground characteristics may change. Modified ground temperatures may alter mechanical properties of the ground with consequences for the installations. The magnitude of disturbance of the ground heat balance by changing the snow distribution can now be assessed.

#### ACKNOWLEDGEMENTS

This paper is part of a research and consulting project funded by the Swiss Federal Office of Environment Forest and Landscape (BUWAL), the government of Grisons and the village of Pontresina (Grisons).

#### REFERENCES

- Bader, H.-P. and P. Weilenmann (1992) Modeling temperature distribution, energy and mass flow in a (phase changing) snowpack: *Cold Regions Science and Technology*, 20(1992), 157-181.
- Benson, C. (1989) The seasonal snow cover of Arctic Alaska. The Arctic Institute of North America; research paper, 51, 47 pp.
- Colbeck, S. C. (1983) Ice crystal morphology and growth rates at low supersaturations and high temperatures: *J. Appl. Phys.*, 54, 2677-2682.
- Colbeck, S. C., E. Akitaya, R. Armstrong, H. Gubler, J. Lafeuille, K. Lied, D. McClung, and E. Morris (1990) The international classification for seasonal snow on the ground. Wallingford, Oxfordshire, IAHS and ICSI, 23 pp.
- de Quervain, M. R. (1963) On the metamorphism of snow: *Ice and Snow*, ed. by W. D. Kingery, 377 pp. MIT Press, Cambridge.
- Giddings, J.C. and E. LaChapelle (1962) The formation rate of depth hoar: *J. Geophys. Res.*, 67(6), 2377-2383.
- Goodrich, L.E. (1982) The influence of snow cover on the ground thermal regime. *Can. Geotechn. J.*, (19), 421-432.
- Granberg, H.B. 1988 : On the spatial dynamics of snowcover-permafrost relationships at Schefferville: *Proc. 5nd Int. Conf. on Permafrost*, Trondheim, 159-163
- Gubler, H. (1985) Model for dry snow metamorphism by interparticle vapor flux: *J. Geophys. Res.*, 90(C8), 8081-8092.
- Haerberli, W. (1975) Untersuchungen zur Verbreitung von Permafrost zwischen Fluelapass und Piz Grialetsch (GR). Eidg. Tech. Hochschule, Zurich. Versuchsanst. Wasserbau, Hydrol. Glaziologie. Mitt. 17, 221 pp.
- Haerberli, W. (1985) Creep of mountain permafrost: Internal structure and flow of alpine rock glaciers. Eidg. Tech. Hochschule, Zurich. Versuchsanst. Wasserbau, Hydrol. Glaziologie. Mitt. 77., 142 pp.
- Haerberli, W. and F. Epifani (1986) Mapping of the distribution of buried glacier ice: An example from Lago delle Locce, Monte Rosa, Italian Alps: *Ann. Glaciol.*, 8, 79-81.
- Haerberli, W. and G. Patzelt (1982) Permafrostkartierung im Gebiet der Hochebenkar-Blockgletscher, Obergurgl, Oetztaler Alpen: *Z. Gletscherk. Glazialgeol.* 18(2), Innsbruck, 127-150.
- Hoelzle, M., W. Haerberli, and F. Keller (1993) Application of BTS-measurements for modelling mountain permafrost distribution: *Proc. 6th International Conference on Permafrost*, Beijing.
- Keller, F. (in prep.) Permafrost und Lawinenschutz: eine Grundlagenstudie im Oberengadin. Ph D thesis ETH Zurich.
- Marbouty, D. (1980) An experimental study of temperature-gradient metamorphism: *J. Glaciol.*, 26(94), 303-312.
- Mellor, M. (1977) Engineering properties of snow: *J. Glaciol.*, 19(81), 15-66.
- Nicholson, F. H. and H. B. Granberg (1973) Permafrost and snowcover relationships near Schefferville: *Proc. 2nd Int. Conf. on Permafrost*, Washington, 159-164.
- Oke, T. R. (1987) *Boundary Layer Climates*. 2nd edition. Cambridge University Press., 435pp.
- Roesli, U. and C. Schindler, (1990) Debris flows 1987 in Switzerland: geological and hydrogeological aspects: *IAHS Publ.* 194, 379-386.
- Salm, B. (1977) Snow forces: *J. Glaciol.*, 19(81), 67-99.
- Seligman, G. (1936) *Snow structure and ski fields*. 555 pp. Macmillan and Co., limited, St. Martin's street, London.
- Vonder Muehll, D. and W. Haerberli (1990) Thermal characteristics of the permafrost within an active rock glacier (Murtel/Corvatsch, Grisons, Swiss Alps): *J. Glaciol.*, 36(123), 151-158.
- Vonder Muehll, D. and P. Holub (1992) Borehole logging in Alpine permafrost, Upper Engadin, Swiss Alps: *Permafrost and Periglacial Processes*, 3(2), 125-132.
- Williams, P.J. and M. W. Smith (1989) *The Frozen Earth. Fundamentals of Geocryology*, 306 pp. Cambridge University Press.

**MICROCLIMATIC CHARACTERISTICS OF PALSAS ALONG AN ALTITUDINAL GRADIENT,  
MACKENZIE MOUNTAINS, NWT, CANADA**

G. PETER KERSHAW AND KEVIN D. SKARET

Department of Geography, University of Alberta  
Edmonton, Alberta, T6G 2H4, Canada

Three of 4 automated microclimatic stations operated on palsas for a year in a research area extending for 30 km over an altitudinal gradient of approximately 410 m relief (1250 to 1660 m asl). Rainfall and wind speed data were similar for the study features with 113 to 142 cm rain and mean annual wind speeds of 2.35 to 2.68 m s<sup>-1</sup>. Mean annual air temperatures were similar, despite elevation differences: -7.4°C at 1250 and 1660 m and -6.7°C at 1480 m. The coldest mean annual palsa core temperatures (-150 cm) were at the lower elevations (-1.5°C at 1660 m, -2.8°C at 1480 m and -2.5°C at 1250 m). The accumulated thawing-degree-days for the highest elevation feature were lower or equal to the other sites but the highest station had fewer days above 0°C. The extreme minimum air temperature of -44.6°C was recorded at the lowest elevation feature while at the highest palsa it only dropped to -34.5°C. Cold air drainage is a significant factor in the microclimate of palsas in the mountainous environment of northwestern Canada.

**INTRODUCTION**

Since 1910, when the term was first used in the scientific literature (Fries and Bergström 1910 as cited in Åhman 1977), few geomorphological phenomena have been shrouded in terminological ambiguity comparable to that referring to palsas. Despite relatively clear definitions of the phenomena early in the history of systematic investigations, the term has been frequently misapplied. Insights into the problem are provided by review papers by Lundqvist (1969), Seppälä (1972), Washburn (1983), Nelson et al. (1991). We use the term as Lundqvist and Seppälä did. Seppälä (1988) maintained that "real palsas, [are] updomed by ice segregation" and that these aggradational forms occur only in the discontinuous permafrost zone. Pollard's (1988) classification system is similar. This is the definition that Canadian researchers have used e.g. Zoltai (1972) and Zoltai and Tarnocai (1971; 1975) in western Canada; Allard and Seguin (1987), Allard et al. (1987), Cummings and Pollard (1989; 1990), Dionne (1978; 1984), Lagarec (1982), Payette et al. (1976) and Seguin and Crépault (1979) east of Hudson Bay.

Few studies have been published on the climate and microclimate of permafrost bodies in the discontinuous permafrost zone: peat plateaus (Allard and Fortier 1990) and palsas (Lundqvist and Mattsson 1965). Considerable work has been done to extrapolate palsa field temperatures from regional weather stations (for example Brown, 1967 for western Canada; Lagarec and Dewez, 1990 and Dionne, 1984 for Quebec, Canada; Åhman, 1977 for northern Norway; Priesnitz and Schunke, 1978 for Iceland).

There have been a number of studies of palsas that have included internal or core temperatures (Cummings and Pollard 1990, Kershaw and Gill 1979; Seguin and Allard 1984). Data that are available for these short time periods or spot measurements confirm that, during the thaw season, palsa core temperatures from a variety of depths are generally between -2.0°C and 0.0°C. There is little data available for core temperatures during winter. In the peat plateau investigated by Allard and Fortier (1990) temperatures dropped to approximately -8°C at -85 cm and to approximately -13°C at -185 cm in mid-winter. Lundqvist and Mattsson (1965) recorded approximately -3°C as the minimum at -150 cm when at -200 cm the mean annual palsa temperature was -0.47°C. In the wetlands surrounding palsas, Seppälä (1990) measured temperatures of -10°C at about -20 cm and of about -3°C at -150 cm.

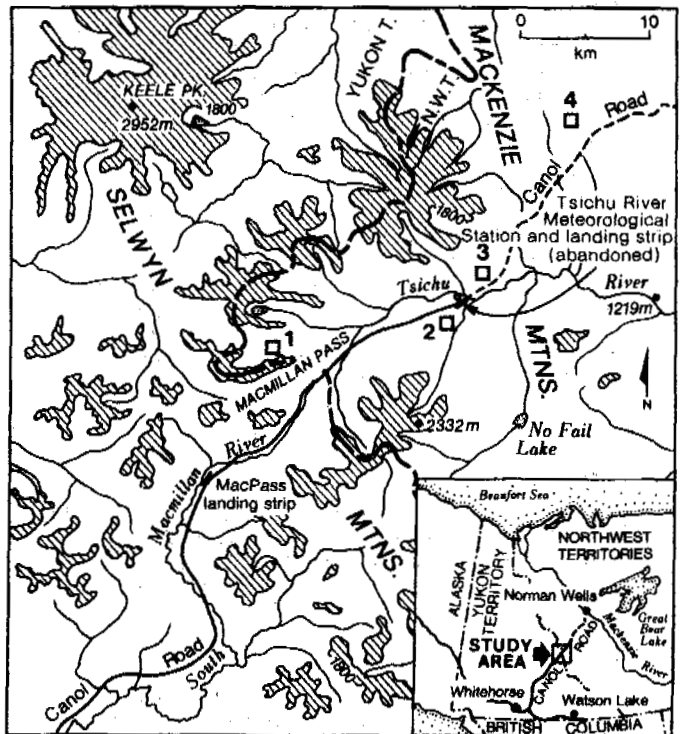


Figure 1: The study area is just east of the Yukon border in the Northwest Territories; the transition area between the Mackenzie and Selwyn Mtns. Palsas are found in valley bottom locations and in wetlands on the plateau of the Mackenzie Mountain Barrens (shading denotes >1800 m asl). Palsa study areas - 1: Dale Creek, 2: Beaver Pond, 3: Hare Foot, and 4: Goose Flats

The lack of data on the microclimatic characteristics of palsas and their site conditions provided the impetus for this study. The objective was to quantify selected microclimatic attributes on a year-round basis and to attempt to explain the expected differences in these characteristics

dictated by site conditions and variations in elevation (e.g. topographic position, elevation change).

#### Study Area

In the Mackenzie Mtns. palsas were first described by Porsild (1945) during botanical studies shortly after the CANOL Project was completed. He referred to them as pingos but subsequent investigations proved them to be palsas, a term not in common usage in North America in 1944-5. Kershaw and Gill (1979) conducted detailed investigations in several palsa fields within the study area. They determined that these permafrost bodies had been reduced in area by between 34% and 100% over a 30- to 34-year period ending in 1978.

This paper is a product of recent investigations in an area larger than that reported on by Kershaw and Gill (1979) but centred in the Macmillan Pass - Tsichu River area just across the Yukon border in the Northwest Territories, Canada (Figure 1). Four palsa fields were selected for study after air photo and site reconnaissance. Each palsa field consisted of at least several features, so the instrument installation was done on the one subjectively selected as representative of the variety of forms present. The highest elevation site (1660 m) was named after the Mountain Indian name for the plateau on which they were found - Goose Flats. The plateau had little relief, but wherever depressions occurred palsas and peat plateaus were common. The feature (h: 2.2 m; d: 59 m) selected for study was dominated by a sedge, lichen and moss cover. The Dale Creek site (h: 3.7 m; d: 45.15 m) was at 1480 m in a 1.5-km-wide valley approximately oriented along the prevailing wind direction (WSW) and was dominated by lichens with moss and a sparse sedge cover. The Beaver Pond site (h: 4 m; d: 90.5m) was at 1270 m in the 5-km-wide Tsichu River valley and was dominated by a dense lichen mat with a sparse shrub cover. Unfortunately shortly after leaving the field the Beaver Pond station was damaged when an animal cut the solar cell connected to the power supply, consequently this station was dropped from the analysis. The lowest site at 1250 m was the Hare Foot palsa (h: 4.9 m; d: 54 m) which was 3.5 km down the Tsichu River valley from Beaver Pond Palsa. Hare Foot palsa had a similar plant cover to that at Beaver Pond except the shrub cover was denser.

The term *core temperature* is used in this paper when referring to the internal or central portion of a palsa. Core temperature does not differ from a normal ground temperature except that palsas are commonly well-defined, meso-scale features distinct (as defined by morphology, surface cover and internal composition) from surrounding landforms. In this context the core temperatures relate to the interior of an individual feature and are not representative of conditions outside the palsa where mean annual ground temperatures are above 0°C.

#### METHODS

The instrument package consisted of an automated datalogger (Campbell Scientific CR10), 3 cup anemometer (0.447 m·s<sup>-1</sup> offset), thermocouples (at least at +150 cm, 0.0 cm, -2.5 cm, -5 cm, -150 cm at the highest point of the palsa top and -5 cm and -150 cm in the adjacent fen). Thermocouple leads were constructed of 16 ga type TX, copper constantan wire connected to fine (0.1 mm) type T thermocouples. Lead lengths to bare peat substrates (generally on the palsa edges) and to the fens did not exceed 35 m. The dominant surface cover on palsa tops had a thermocouple at -5.0 cm with as many as 3 others in common surface covers (bare peat always, tussock base, tussock top, thin snowpack slope as determined by the shrub leader kill zone, moss polster, lichen mat). Three sites (except Hare Foot) also had rain gauges and pyranometers. Output frequency was 8 h for much of the year but only the 24 h summary data will be presented here.

Overall reference junction accuracy was < 0.1°C in the -33°C to +48°C range and ≤ 1.0°C in the -40°C to +56°C range (Campbell Scientific Inc. 1991).

There were 288 readings each day (5 min. scan interval) used to determine the mean daily values. Data gaps were left as blanks on illustrations and the length of the record noted in Table 1.

Analysis was based on one 365-day period beginning 1 August 1990 and ending 31 July 1991. Annual thawing and freezing-degree-day totals were calculated by summing all > or < 0°C temperature values, respectively for the year. The number of days for each were also counted to determine the duration of the freeze and thaw periods.

#### RESULTS

At the lowest site, Hare Foot, an animal tore out sensors from the fen in mid-April. At the mid-elevation site, Dale Creek, a grizzly bear overturned the anemometer mast in mid-June. In late-July an animal uprooted the fen sensors at the higher elevation site, Goose Flats and no rain was recorded between 3 July and 5 August 1991 when the severed cable was repaired.

#### Air Temperature

Mean annual air temperatures for the palsa sites were similar (Table 1). A range of only 0.7°C separated Dale Creek, the warmest, from the other two palsas which had virtually identical means at -7.4°C. A relatively rapid switch from <0°C to >0°C occurred in the spring at the low elevation, Hare Foot site but was stretched over as much as a month at the high elevation Goose Flats site (Figure 2). The fall freeze-back period for all 3 locations was approximately a month long, commencing in late August 1990.

The extreme minimum air temperature of -44.6°C and the extreme maximum temperature of 15.8°C were both recorded at the low elevation Hare Foot palsa (Table 1). The differences in maximum temperatures were minor (2.1°C), however, there was a 10°C difference between the minimums with Goose Flats at 410 m above Hare Foot, experiencing the warmer minimum temperatures.

#### Palsa Surface and Near-surface Temperature

Mean annual surface temperatures were 3 to 4°C warmer than air temperatures (Table 1). On the palsa top the -5 cm mean annual temperature was similar to the surface temperature at the 3 palsa sites. Bare peat temperatures were warmer than palsa top values at the lower elevation sites but cooler at the Goose Flats site.

#### Palsa Core Temperature

A difference of 1.3°C separated the warmest from the coldest mean annual palsa core (-150 cm) temperature (Table 1). Although not a great difference it should be noted that internal temperatures for all 3 palsas only varied over 7.0°C and in this context a 18.6% variation was considered a large difference. The higher elevation Goose Flats palsa had the warmest mean annual core temperature and the highest maximum temperature when it alone of the 3 sites experienced >0°C (Figure 3). This palsa also had the greatest variability in core temperature when compared to the other, lower elevation features.

#### Fen Temperature

The mean annual fen temperature at -150 cm varied little (1.1°C) among the 3 palsa sites (Table 1 and Figure 3). Only the fen adjacent to Goose Flats palsa, the highest site, experienced freezing at this depth and this condition persisted from mid-May to early July 1991, achieving a minimum of -1.1°C. Goose Flats also had the greatest range in temperature varying over 4.8°C.

#### Thawing and Freezing Indices

The accumulated thawing-degree-days were highest for the 0.0 cm and +150 cm sensors on all palsas (Table 1). In general, the deeper into the feature, regardless of the surface cover, the lower the thawing-degree-day totals (Figure 4). At -5 cm thawing-degree-day totals were a result of warmer conditions for bare peat surfaces than for the dominant surface cover types on all the palsas

Table 1: Summary of several microclimatic parameters measured on three palsas over the 1 August 1990 to 31 July 1991 period in the Mackenzie Mtns., NWT.

	Annual Temperature							Wind (m·s <sup>-1</sup> )	Total Rain (mm)
	Air on Palsa Top	Palsa Top with Plants	Bare Peat	Palsa Core	Fen				
	+150 cm	Surface	-5.0 cm	-5.0 cm	-150 cm	-5.0 cm	-150 cm		
<b>Goose Flats (1660 m)</b>									
Mean	-7.37	-3.43	-3.31	-4.01	-1.55	1.37	0.87	2.68	142.24
Maximum	13.6	12.4	10.9	12.95	0.5	13.2	3.7	7.1	
Minimum	-34.5	-20.9	-19.4	-23.5	-3.7	-1.1	-1.1	NA	
Days of record	365	364	365	365	365	365	365	357	
Thawing-deg- ree-days	695.3	747.2	654.9	781.4	7.9	556.2	343.6		
Thawing days	123	133	136	134	38	197	263		
Freezing- degree-days	3385.2	1996.7	1862.9	2243.4	572.2	69.4	32.3		
Freezing days	242	231	229	231	327	159	94		
<b>Dale Creek (1480 m)</b>									
Mean	-6.69	-3.18	-3.1	1.14	-2.85	1.83	1.98	2.35	113.03
Maximum	15.4	13.6	11.8	15.4	-0.7	13.1	3.1	10.2	
Minimum	-42.7	-22.2	-20.8	-6.8	-6.5	-1.0	0.0	NA	
Days of record	365	365	365	365	365	365	365	345	
Thawing- degree-days	906.8	797.6	715.2	946.0	0.0	753.3	720.1		
Thawing days	139	131	132	142	0	154	364		
Freezing- degree-days	3354.8	1963.7	1853.4	537.6	1038.4	96.6	0.0		
Freezing days	226	234	233	223	365	210	0		
<b>Hare Foot (1250 m)</b>									
Mean	-7.37	-4.25	-3.43	-2.73	-2.52	0.97	1.49	2.39	NA
Maximum	15.8	18.6	13.9	14.95	-0.6	14.3	3.5	11.1	
Minimum	-44.6	-30.9	-22.0	-12.6	-6.5	-1.9	0.1	0	
Days of record	365	365	365	287	365	287	287	365	
Thawing- degree-days	1041.5	1176.0	917.1	351.2	0.0	500.0	428.8		
Thawing days	146	147	148	56	0	71	287		
Freezing- degree-days	3731.6	2728.3	2162.7	1134.8	920.8	221.8	0.0		
Freezing days	219	218	217	231	365	216	0		

except at Hare Foot where values were lower because the sensor was out of action for 78 days. Freezing-degree-day totals indicate warmer conditions beneath bare peat surfaces compared to the dominant surface plant cover types on all palsas except the Goose Flats feature where the lichen- and moss-dominated surface cover of the palsa top was warmer.

The trend was for higher values of air and surface freezing and thawing indices with lower elevation (Figure 4). Comparing fen and palsa core indices, they were almost mirror images of each other. Positive mean daily temperatures were essentially absent at -150 cm in the palsa while in the fens only at the Goose Flats site did temperatures drop below 0°C for a freezing-degree-day total that was a factor smaller than the magnitude of the thawing-degree-day total for this depth in the fen (i.e. -32.26 vs 343.58, Table 1).

#### Wind Speed

With the Dale Creek anemometer out of commission for 19-20 days, one must be cautious interpreting the wind data. However, if one assumes average conditions then annual means would only be 0.1 to 0.2 m·s<sup>-1</sup> larger for this site. Mean annual wind speeds were similar for all 3 palsa sites (Table 1). Maximum wind speeds were similar for the lower sites but 3-4 m·s<sup>-1</sup> slower at the highest elevation palsa. During the period between mid-November and mid-January the Goose Flats site was relatively calm compared with the lower elevation palsas.

#### Rain

A month of data missing from the Goose Flats palsa resulted in an unknown underestimate of the total value for this station. Despite this problem there was still more rain collected at this high elevation site than at the lower Dale Creek palsa (Table 1).

#### DISCUSSION

##### Air Temperature

The effects of elevation on the cooling of air temperatures should have amounted to approximately 4°C, however measured mean annual air temperatures were identical for the upper and lower elevation stations. Thaw season adiabatic cooling was evident (Table 1). In winter, pronounced cooling at lower elevations confirms that air density stratification is an important phenomenon. Minimum temperatures were 10°C cooler less than 15 km away in the 410 m lower Taichu River Valley and at this scale, synoptic weather systems should be similar throughout this mountainous study area. A severe event of density stratification has been reported by Harris (1983), during which extremely cold air temperatures were generated in valley bottom locations. Furthermore, it has been reported that cold air drainage can promote the distribution of permanent frost bodies in valley bottom locations in mountainous terrain (Brown 1980; Jeckel 1988; Zamolotchikova 1988) and this is confirmed by our results (Table 1).

##### Palsa Surface and Near-surface Temperature

The difference between air and surface temperatures reflected the insulative effects of snowpack in winter (Steppuhn 1981) when heat loss from the palsa core was reduced by the snow cover. It was also due to boundary layer effects that promote warmer temperatures at heights below 150 cm within the plant canopy (Cernusca and Seeber 1981). At the Goose Flats site the colder mean annual -5 cm temperature under bare ground as well as the more extreme maximum and minimum values confirm the importance of the plant canopy in controlling the distribution of snow and heat flux on the palsa top. Temperature data from beneath bare peat for the other palsas were significantly influenced by micro-site characteristics since at the Dale Creek and Hare Foot sites snow drifts blanketed these palsa margin sites in winter and the aspect (south-east) of these palsa edges enhanced heating during the

thaw season.

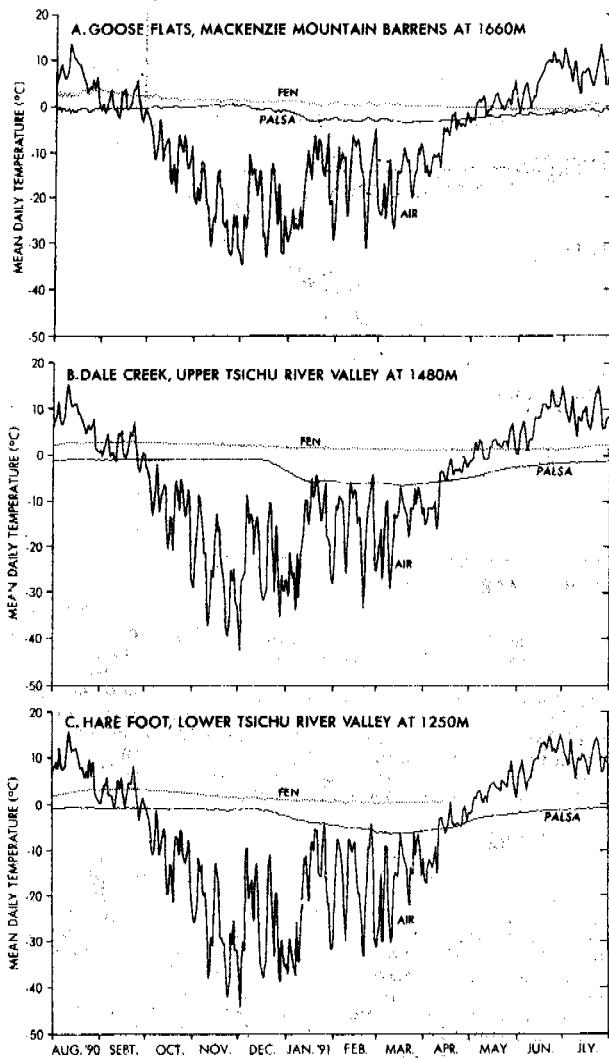


Figure 2: Air, fen and palsa temperature data for 3 palsa study sites in the Mackenzie Mtns., NWT.

#### Palsa Core Temperature

The palsas with the coldest mean annual core temperature were the ones in valley bottom sites where cold air accumulated. The Dale Creek site had little suitable plant cover to retain snow, whereas the Hare Foot palsa (230 m lower) had a thick lichen mat and a low shrub cover capable of retaining snow and insulating the core and thus reducing heat loss. The Hare Foot feature which experienced the lowest mean annual and minimum air temperature of the 2 sites had warmer core temperatures due to this surface insulation enhancement. Other factors may include shading influences of the erect shrub cover during the thaw season and the consequent reduction in surface heating and heat flux into the palsa core.

A difference of 1.3°C for the mean annual temperature in the air column would not be that noteworthy, however, at -150 cm into the Goose Flats palsa which had an annual fluctuation less than 4.5°C, this degree of difference should be discussed. It appears that elevation differences and cold air drainage influences have a role to play here as with the minimum air temperatures. The winter season brings extreme cooling events to lower elevations and apparently the heat loss from palsas at these times exceed the gains during the

thaw season to the extent that mean annual core temperatures at high elevations are warmer.

Goose Flats palsa was the only one to exhibit evidence of the zero curtain effect. Although temperatures rose above 0°C, they did not exceed +0.5°C. This palsa had less relief than the other study features (2.2 vs 3.7 and 4.9 m) and should be less prone to wind erosion of its snowpack in winter. A thicker, lower density snowpack (less wind packing) will provide better insulation in winter. In this manner, this morphology can contribute to the warm core temperature and high degree of temperature fluctuation observed for the Goose Flats feature compared to the other palsas. Further study is needed and is underway to determine the validity of this hypothesis, including snowpack, vegetation, internal composition (organic, moisture and mineral content) and morphological changes.

#### Fen Temperature

Variations in the thermal characteristics of the fens may be explained by water depth and through flow, peat volume differences and other physical characteristics of the sites that were not measured.

The high degree of variation in temperature for the highest elevation Goose Flats fen (Figure 3) reflects the smaller thermal mass of the fen segment that was instrumented (relatively low heat capacity) and its rapid responses to ambient conditions. The thermocouples were in an isolated area of only a few square metres above the main fen. The fens at Dale Creek and particularly at Hare Foot had greater water depth and horizontal extent, although volume estimates could not be attempted without detailed probing. The Dale Creek fen had the warmest mean annual and minimum temperatures and was the only fen to have sheet and channelized flow through it (no volume estimates conducted). It may be that the Dale Creek fen is fed by groundwater sources that keep the temperature warmer and more stable than the other palsa sites.

#### Thawing and Freezing Indices

Palsa cores remained frozen with accumulated degree-days somewhat larger than the magnitude of the thawing indices for the adjacent fens. Where bare peat was exposed, the dark surface colour enhanced heat penetration (measured at 5.0 cm) and these areas were consequently warmer (Table 1). Bare peat sites on 2 palsas had south-east exposures and when free of snow should experience enhanced heating. Freezing indices also indicate warmer conditions for bare peat surfaces in winter when these palsa edge sites probably had more snow than palsa top positions. At the Goose Flats site the bare peat thermocouple was adjacent to the palsa top sensors, so snowpack differences between the microsites would have been minimal. Thus a difference in plant cover was the most important factor affecting heat loss in winter.

#### Wind Speed

The 2-month, early winter period of calm conditions at the Goose Flats site may reflect a lack of wind or it is possible that the anemometer cups were prevented from functioning due to fine or frost accumulations. Without observations during this period it is impossible to tell. Notwithstanding this possibility, the higher mean annual maximum wind speeds at lower elevations may reflect katabatic breezes associated with cold air drainage, however, the differences are slight. Furthermore, the palsa sites were not aligned with the main valley, a prerequisite to properly test for the role of air density stratification in the generation of winds. No summertime chinook winds or diagnostic cloud formations were observed during this study or during previous investigations in the area (Ion and Kershaw 1989) but this phenomena may play a role in the region if such events occur. Wind characteristics at the 3 palsa sites were not significantly different. Mean annual wind speeds were similar among the sites and there were only minor differences (4.01 m<sup>2</sup>) in maximum speeds. Therefore differences in microclimatic factors such as snowpack characteristics, evaporative heat losses and boundary layer thickness would not vary among



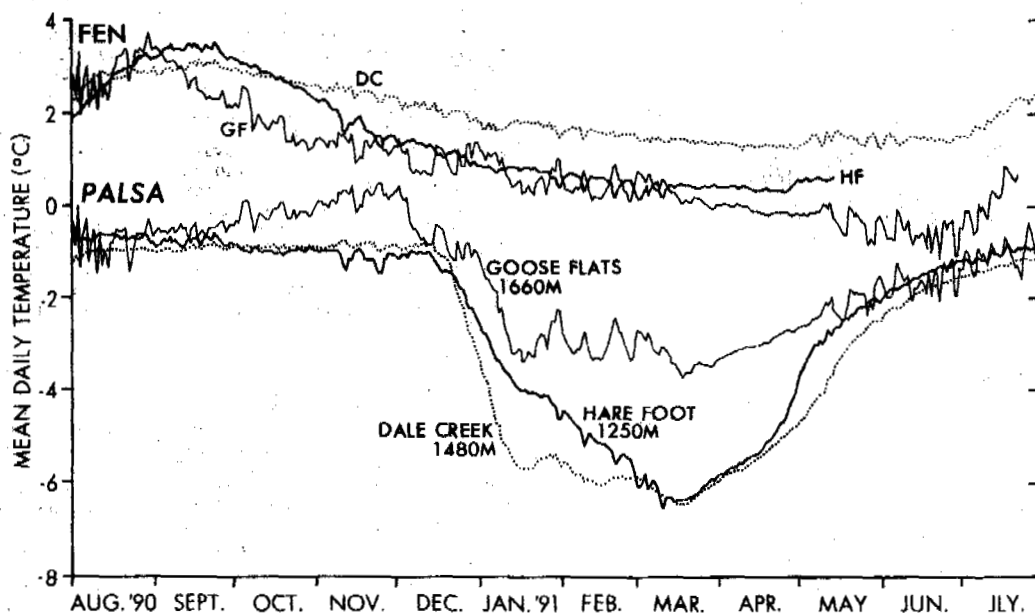


Figure 3: Mean daily palsa core and fen temperatures at -150 cm for the 3 palsa stations in the Mackenzie Mtns., NWT. Goose Flats and Hare Foot fen sensors were disabled by animals near the end of the record.

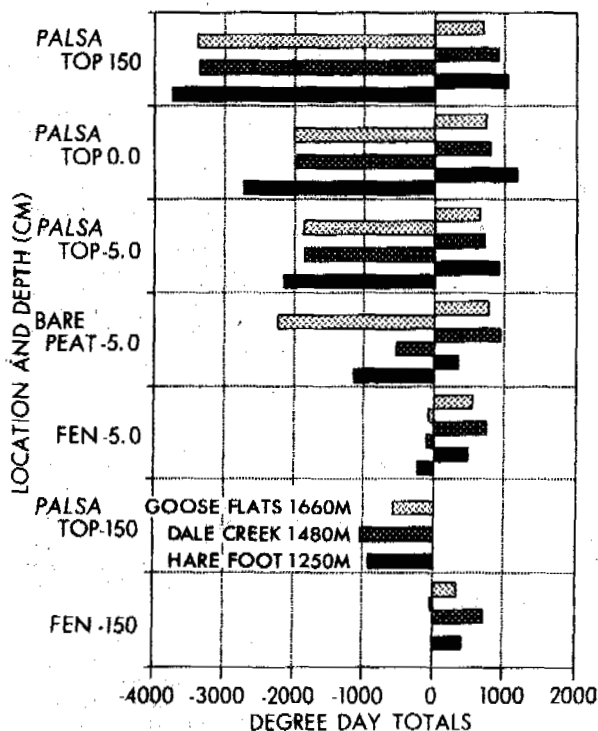


Figure 4: Thawing and freezing indices at various heights and depths for 3 palsas and adjacent fens in the Mackenzie Mtns., NWT.

the palsas due to wind.

Rain  
With one month of missing thaw-season data at the Goose Flats site it was difficult to compare

results between the 2 palsas. However, the rainfall appears to be typical of mountainous terrain and orographic precipitation. Precipitation data collected year-round in the 1974 to 1981 period indicate that summer is when most precipitation falls (Kershaw and Kershaw 1983).

CONCLUSIONS

The influence of elevation on palsa microclimate in the study area was not restricted to affecting the regional environmental lapse rate. Instead, the influence of elevation was mostly effected through cold air drainage in winter and consequently the higher sites were warmer. Other factors such as the insulative properties of the snowpack and the internal boundary layer associated with different plant communities appear to influence microclimate characteristics where they vary on a site-specific basis over individual palsa surfaces. These relationships are currently under more detailed investigation in the study area.

REFERENCES

Ahman, R. 1977. Palsar i Nordnorge. *Meddelanden från Lunds Universitets, Geografiska Institution, Avhandlingar LXXVIII*, 165pp.  
 Allard, M. and Seguin, M.K. 1987. The Holocene evolution of permafrost near the tree line, on the eastern coast of Hudson Bay (Northern Quebec). *Canadian Journal of Earth Sciences*, 24:2206-2222.  
 Allard, M., Seguin, M.K. and Lévesque R. 1987. Palsas and permafrost mounds in northern Quebec. In V. Gardiner (ed.) *International Geomorphology, Part II*. John Wiley and Sons, Chichester: 285-309.  
 Brown, G. 1980. Palsas and other permafrost features in the lower Rock Creek Valley, West-Central Alberta. *Arctic and Alpine Research*, 12(1):31-40.  
 Brown, R.J.E. 1967. Permafrost Investigations in British Columbia and Yukon Territory. *Technical Paper No. 253*, National Research Council of Canada, Division of Building Research.  
 Campbell Scientific Inc. 1991. *10TCRT Thermocouple Reference Instruction Manual*. Campbell Scientific Canada Corp., Edmonton. 2pp.  
 Cernusca, A. and Seeber, M.C. 1981. Canopy structure, microclimate and the energy budget in different alpine communities. In J. Grace, E.D.

- Ford and P.G. Jarvis (eds.) *Plants and their Atmospheric Environment*, 21st. Symposium of the British Ecological Society. Blackwell Scientific Publications, Oxford: 75-81.
- Cummings, C.E. and Pollard, W.H. 1989. An investigation of palsas in the Schefferville area, Quebec. *The Musk-Ox*, 37:8-18.
- Cummings, C.E. and Pollard, W.H. 1990. Cryogenetic categorization of peat and mineralcored palsas in the Schefferville area, Quebec. Fifth Canadian Permafrost Conference, *Collection Nordicana*, 54:95-102.
- Dionne, J.C. 1978. Formes et phénomènes périglaciaires en Jamésie, Québec subarctique. *Géographie physique et Quaternaire*, 32: 187-247.
- Dionne, J.C. 1984. Palses et limites méridionales du pergélisol dans l'hémisphère nord: le cas de Blanc-Sablon, Québec. *Géographie physique et Quaternaire*, 38:165-184.
- Fries, T. and Bergström, E. 1910. Några iakttagelser öfver palsar och deras förekomst i nordligaste Sverige. *Geol. Fören. Förhandl.* 32(1).
- Harris, S.A. 1983. Cold air drainage west of Fort Nelson, British Columbia. *Arctic*, 35:539-541.
- Ion, P.G. and Kershaw G.P. 1989. The selection of snowpatches as relief habitat by woodland caribou (*Rangifer tarandus caribou*), Macmillan Pass, Selwyn/Mackenzie Mountains, N.W.T., Canada. *Arctic and Alpine Research*, 21(2):203-211.
- Jeckel, P.P. 1938. Permafrost and its altitudinal zonation in N. Lapland. In *Proceedings, Fifth International Conference on Permafrost*, Tapir Publishers, Trondheim, Vol. 1:170-175.
- Kershaw, G.P. and Gill, D. 1979. Growth and decay of palsas and peat plateaus in the Macmillan Pass-Tsichu River area, Northwest Territories, Canada. *Canadian Journal of Earth Sciences*, 16(7):1362-1374.
- Kershaw, G.P. and Kershaw, L.J. 1983. *Geomorphology and Vegetation of the MacTung Study Area, Yukon/NWT*. Report prepared for AMAX Northwest Mining Co. Ltd., Vancouver.
- Lagarec, D. 1982. Cryogenic mounds as indicators of permafrost conditions, Northern Quebec. In *Proceedings of the Fourth Canadian Permafrost Conference*, Calgary. National Research Council of Canada, Ottawa: 43-48.
- Lagarec, D. and Dewez, V. 1990. Dynamique du pergélisol discontinu et changements globaux dans le nord du Québec. Fifth Canadian Permafrost Conference, *Collection Nordicana*, 54:215-222.
- Lindqvist, S. and Mattsson, J.O. 1965. Studies on the thermal structure of a palsa. *Svensk Geographisk Årsbok* 41: 38-49.
- Lundqvist, J. 1969. Earth and ice mounds: a terminological discussion. In T.L. Péwé (ed.), *The Periglacial Environment: Past and Present*, McGill-Queen's University Press, Montreal, pp. 203-215.
- Nelson, P.E., Hinkel, K.M. and Outcalt, S.I. 1991. Palsa-scale frost mounds. In J.D. Dixon and A.D. Abrahams (eds.), *Periglacial Geomorphology, Proceedings of the 22nd Annual Binghamton Symposium in Geomorphology*. John Wiley & Sons, Chichester, pp. 305-325.
- Payette, S., Samson, H. and Lagarec, D. 1976. The evolution of permafrost in the taiga and in the forest-tundra, Western Quebec-Labrador peninsula. *Canadian Journal of Forest Research*, 6(2):203-220.
- Pollard, W.H. 1988. Seasonal frost mounds. In M.J. Clark (ed.) *Advances in Periglacial Geomorphology*, John Wiley and Sons Ltd. 201-229.
- Porsild, A.E. 1945. The alpine flora of the east slope of Mackenzie Mountains, Northwest Territories, *National Museums of Canada, Bulletin* 101 (*Biological Series*, No. 30), Edmond Cloutier, Printer, Ottawa.
- Priesnitz, K. and Schunke, E. 1978. An approach to the ecology of permafrost in central Iceland. In *Proceedings of the Third International Conference on Permafrost*, National Research Council of Canada, Ottawa, Vol. 1:474-479.
- Seguin, M.K. and Allard, M. 1984. Le pergélisol et les processus thermokarstiques de la région de la Rivière Nastapoca, Nouveau-Québec. *Géographie Physique et Quaternaire*, 38:11-25.
- Seguin, M.K. and Crépault, J. 1979. Étude géophysique d'un champ de palses à Poste-de-la-Baleine, Nouveau-Québec. *Géographie physique et Quaternaire*, 33:327-337.
- Seppälä, M. 1972. The term 'palsa'. *Zeitschrift für Geomorphologie*, 16:463.
- Seppälä, M. 1988. Palsas and related forms. In: M.J. Clark (ed.), *Periglacial Geomorphology*. John Wiley and Sons, Chichester. 247-278.
- Seppälä, M. 1990. Depth of snow and frost on a palsa mire, Finnish Lapland. *Geografiska Annaler*, 72A:191-201.
- Steppuhn, H. 1981. Snow and agriculture. In D.M. Gray and D.H. Male (eds.) *Handbook of Snow: Principles, Processes, Management and Use*. Pergamon Press, Toronto: 60-125.
- Washburn, A.L. 1983. What is a palsa? *Abhandlungen der Akademie der Wissenschaften in Göttingen, Mathematisch-Physikalische Klasse*, Dritte Folge 35:34-47.
- Zamolotchikova, S.A. 1988. Mean annual temperature of grounds in East Siberia. In *Proceedings, Fifth International Conference on Permafrost*, Tapir Publishers, Trondheim, Vol. 1:237-240.
- Zoltai, S.C. 1972. Palsas and peat plateaus in Central Manitoba and Saskatchewan. *Canadian Journal of Forest Research*, 2:291-302.
- Zoltai, S.C. and Tarnocai, C. 1971. Properties of a wooded palsa in northern Manitoba. *Arctic and Alpine Research*, 3:115-129.
- Zoltai, S.C. and Tarnocai, C. 1975. Perennially frozen peatlands in the western Arctic and Subarctic of Canada. *Canadian Journal of Earth Sciences*, 12:28-43.

#### ACKNOWLEDGEMENTS

A number of individuals contributed to the success of the field component of the Palsa Evolution in Alpine Tundra (PEAT) project: Brent Ambrose, Linda and Eric Kershaw, Dave Milton, Craig Olsen, Elaine Seier, Kim Winnicky. Jim Hickling, our neighbour, provided much appreciated 4x4 lifts just when they were needed most. Stan Simpson donated dietary supplements that provided a 'fresh' change from canned stuff. Sam Miller and later, Norm Barichello and George Calef of Old Squaw Lodge permitted us to use their trailer at Camp 222 and helped with equipment lifts onto the Barrens whenever they could. This research has been supported through a Natural Sciences and Engineering Research Council of Canada (NSERC) operating grant to Kershaw; the Canadian Circumpolar Institute (CCI) and the Royal Canadian Geographical Society. The SEED programme of the federal government helped with salary subsidies for field assistants.

EXAMPLES OF GEOMORPHOLOGICAL CHANGES  
IN GLACIALLY SCULPTURED HIGH ARCTIC PERMAFROST AREAS  
FROM SVALBARD AND THE QUEEN ELIZABETH ISLANDS, CANADA

Lorenz King

Geographisches Institut, Justus Liebig Universität  
D-6300 GIESSEN, Germany

The glacial geomorphology of selected areas in NW-Spitzbergen and in the Queen Elizabeth Islands has been mapped and geomorphological changes measured with geodetical and photogrammetrical techniques covering a time span of up to 28 years. The recorded summer climates and measured ground and ice temperatures help explain significant differences of the geomorphological processes.

The investigated areas in NW-Spitzbergen (MAAT = about  $-5^{\circ}\text{C}$ ) show perennially frozen moraines that often have push features at their outer margins and debris covered dead glacier ice in the central parts. Thermoerosion starts at favoured places but erosion may be stopped after a few years due to the debris cover.

The Thompson Glacier push moraine in the Queen Elizabeth Islands (MAAT = about  $-19^{\circ}\text{C}$ ) consists of stacked, frozen gravel blocks. The glacier front and the adjoining moraine complex were moved horizontally for up to 500 meters within 28 years. The dislocation rate during this time span decreased from 20 m/year to 10 m/year. The main structures of the moraine have been preserved in spite of the displacement. Thermal erosion is comparatively rare, even at investigated push moraines in front of a stagnant glacier (Oobloyah Bay) and of a receding glacier (Hare Fiord). In spite of the differences between the Norwegian and Canadian areas, ecological similarities due to their location in a climatologically favoured "inner fiord region" are evident.

## INTRODUCTION

### Aim and methods

During the Pleistocene, vast regions have been glacially sculptured under cold climate conditions (e.g. in Canada or northern Europe). The geomorphology of these landscapes may be better interpreted, if the geomorphological changes in today's glacially sculptured areas are recorded. The areas selected for this study belong to the continuous permafrost zone. Special interest was put to push moraines and thermo-erosion features as two dominant forms. Modern photogrammetrical and geodetical techniques supplied the data for the evaluation of long term changes during the formation and transformation of these dominant features. Changes within a time span between one summer season and up to 28 years could thus be accurately measured. The photogrammetric data collection was often done with semi-metric cameras.

Additionally, the investigation areas have been mapped in a scale of 1:5000 and a vast range of data (summer climates, glacier ice temperatures, snow cover, ablation values, ecological maps) supplied additional help for the interpretation of the observed geomorphological processes. This paper concentrates on a geomorphological comparison, and the climatological/ecological background data for the understanding of the involved geomorphological processes is presented where necessary. Lehmann (1993) presents additional geomorphological information (morphological description, inner structure, genetical conclusions). The geodetical details are given in King & Hell (1993).

### Location, climate and geomorphology

In NW-Spitzbergen, the area Liefdefjorden/Bockfjorden has been visited every year between 1989 and 1992. The Queen Elizabeth Islands have been visited in 1975, 1978 and 1988 (Expedition Fiord area at the west coast of Axel Heiberg Island and Oobloyah Bay, Ellesmere Island, respectively). The investigation areas are located at a latitude of about  $80^{\circ}\text{N}$ . However, the average permafrost thickness in non-coastal areas is about 150 m in Svalbard and 500 m in Axel Heiberg or Ellesmere Island (Judge et al. 1981). Whereas the mean annual air temperature at Liefdefjorden, Svalbard, is about  $-4^{\circ}\text{C}$ , the

MAAT in Eureka (Ellesmere Island) is about  $-19^{\circ}\text{C}$ . These mean values may vary locally, especially along the coast. Our BTS measurements (cp. Jeckel, 1988, for methodological comments) hint to even higher ground temperatures and probably very thin permafrost in a 200 m wide stretch along the investigated coast of Liefdefjorden (results in King et al. 1993). However, both investigation areas experience similar mean summer air temperatures between  $+5^{\circ}$  and  $+6^{\circ}\text{C}$  for July. The occurrence of Dryas and Cassiope dominated plant communities in both research areas also hints to climatologically favoured locations with a high global radiation typical for protected "inner fiord areas" (Schmitt 1993, Edlund 1986). Table 1 gives a comparison of long term temperature means for inner (Longyearbyen, Eureka) and outer fiord stations (Isfjord Radio, Alert).

In both areas medium-sized and large glaciers originate in glacial cirques or even in vast icefields reaching up to more than 1000 m a.s.l. The glaciers often end close to sea level and their moraines often show push features in the perennially frozen sediments of the valley floors or in near-shore marine sediments. These mutual geomorphological characteristics formed a good starting point for the comparative research of geomorphological changes in these glacially sculptured permafrost areas.

Table 1: Characteristical mean annual and mean summer air temperatures (National Weather Services) for inner and outer fiord areas in Spitzbergen and the Queen Elizabeth Islands.

	MAAT	June	July	August
Longyearbyen, N	-5.8	+2.8	+6.3	-5.1
Isfjord Radio, N	-4.7	+1.7	+4.7	+4.3
Eureka, CDN	-19.3	+2.3	+5.5	+3.6
Alert, CDN	-18.0	-0.6	+3.9	+0.9

## RESULTS FROM SPITSBERGEN

### Area, investigated topics and morphological results

The main parts of our studies were focused on the snouts of Glopgreen and Erikbreen in the Liefdefjord area and at Børrebreen and Karlsbreen in the Bockfjord area (Figure 1). The findings have been compared then with the proglacial areas of Adolfbreen and Schjelderupbreen. Most glaciers are strongly receding since about 1920, leaving vast debris covered intramorainic areas that easily experience thermal erosion (cf. King & Schmitt 1993). The surrounding moraine ridges are usually very impressive features in size, covering an area of 0.8 km<sup>2</sup> at Erikbreen or over 1 km<sup>2</sup> at Karlsbreen, respectively. They are quite often composed of huge boulders (e.g. at Adolfbreen, Kvamsbreen, Takryggbreen). In contrast, the outermost, usually smaller ridges consist often of fine grained sediments. A closer examination reveals, that strongly tilted sediment layers are present and that the folded and thrustured push features must have been formed by glacial push when the sediments were frozen.

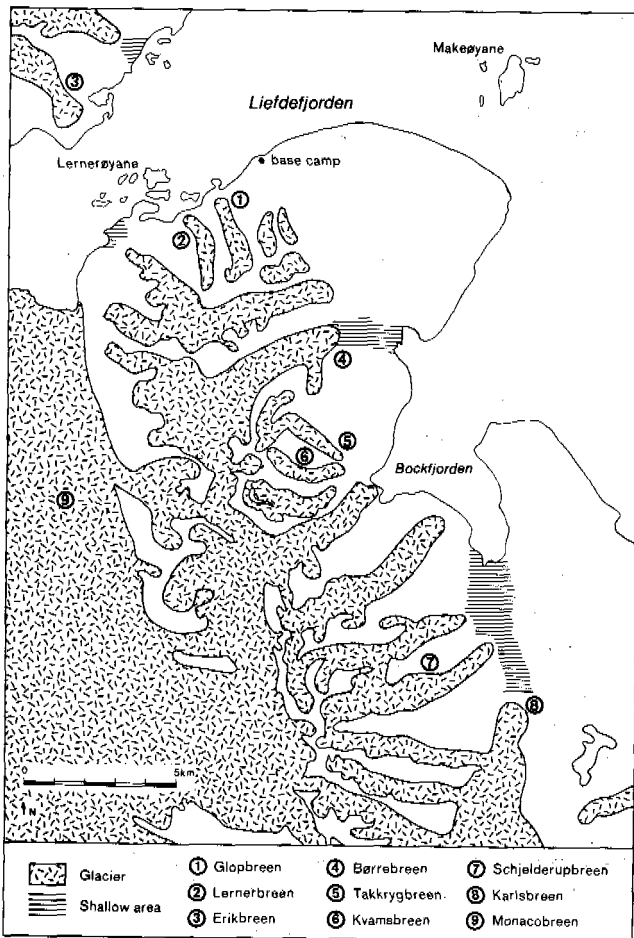


Figure 1: Liefdefjord and Bockfjord (Northern Spitsbergen) with investigated glaciers described in the text. Four map sheets 1:25.000 cover the area and have been developed during the German Spitsbergen Expeditions SPE90-92 by Hell & Brunner (1991).

These features are restricted to near coastal sites with the mentioned relatively warm ground temperatures (0°C to -1°C) Geomorphological details of this "coastal type" of arctic push moraines are given by Lehmann (1992, 1993). The sequence described from Holsteinbreen by van der Wateren (1992: 127) can be transferred to the glaciers in NW-Spitsbergen (exposed glacier, ice-cored moraine zone, glacially pushed sediment zone, proglacial outwash zone), even if the push moraine is restricted to one or two fine grained ramparts that surround the extended boulder moraine. Their age is mainly Neoglacial, but older moraine ridges may originate from several Subatlantic glacier advances (Furrer 1991, Salvigsen et al. 1982).

### Observed processes and measured changes

Terrestrial observations show, that many of the mentioned impressive moraine complexes consist of a debris covered core of dead glacier ice that may be preserved under permafrost conditions for long periods. The distinction between massive ground ice and dead glacier ice is usually possible in these relatively young features. However, it can be well understood that this distinction may pose problems, e.g. in older intramorainic areas (cp. French et al. 1990, Rampton 1991) or in the case of Glopgreen in some proglacial parts where glacier ice is closely linked with icings (Lauriol et al. 1991).

In the intramorainic slopes of the Glopgreen moraines (Figure 2), thermal erosion is especially dominant in its eastern parts. A weather station located in the wind protected and bowl shaped thermal erosion area showed significantly higher air (and surface) temperatures than the main station located on an exposed ridge (cp. Table 2). Eight other stations recorded a great number of ecological parameters during the summer 1990. The surficial movement of boulders was repeatedly measured between July 1990 and August 1992 (mean value = 100 cm) and the calculated rates of thermal erosion (vertical movement) were up to 5-10 cm per year (Table 3). The temperature sums of the three expedition years may be correlated with the yearly erosion rate.

Even larger thermo-erosive areas exist at Erikbreen or Karlsbreen. The approximately 20 km long Karlsbreen with its 900 m long and 900 m broad push moraine complex (Figure 3), displays a vast intramorainic area close to the glacier front with fast degradation due to thermal erosion. However, the impressive push moraine itself remained mostly unchanged between 1960 and 1990.



Figure 2: Rollei metric 6006 photograph of the intra-morainic area at Glopgreen with strong thermo-erosive activity; the weather station (arrow) registers the meso- and microclimatic parameters. Surface movements were measured in the central part of the picture (July 1991).

Table 2: Examples of maximum air and surface temperatures and corresponding windspeed and radiation (hourly mean) from a protected thermo-erosion site TS1 and an exposed site nearby (SP1), July 1990.

	21.07.	22.07.	23.07.	24.07.
<b>TS1</b>				
air temp. (2.0m)	12.5°	11.3°	11.1°	11.7°
air temp. (0.5m)	14.6°	12.4°	12.3°	13.7°
soil temp. (-1cm)	22.6°	19.1°	19.3°	24.2°
windspeed (m/sec)	1.6	3.3	12.5	1.5
radiation (W/m <sup>2</sup> )	333	375	387	435
<b>SP1</b>				
air temp. (2.0m)	12.1°	9.8°	10.5°	10.2°
air temp. (0.5m)	14.2°	10.8°	11.6°	11.2°
soil temp. (-1cm)	20.7°	15.7°	16.6°	18.6°
windspeed (m/sec)	1.6	8.8	5.7	7.1
radiation (W/m <sup>2</sup> )	238	346	375	363

Table 3: Average rates of horizontal boulder movement, thermal erosion rates and positive temperature sums in 14 cm depth (mid-July to mid-August)

	horiz.	vertic.	temp. sum
summer 1990	40 cm	4 cm	281,4°C (37 days)
summer 1991	55 cm	3 cm	221,1°C (32 days)
summer 1992	45 cm	4 cm	247,2°C (35 days)

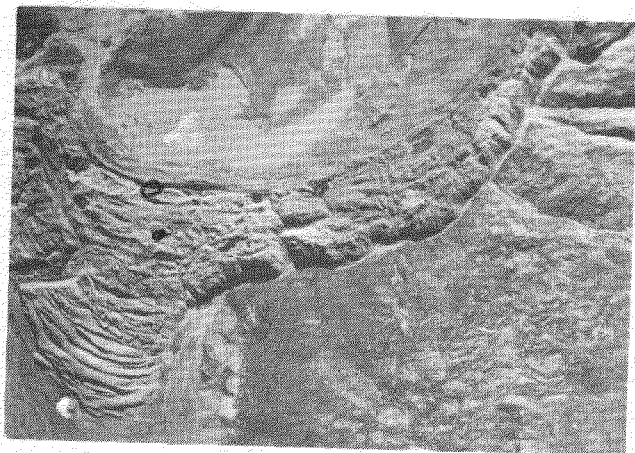


Figure 3: The glacier front of Karlsbreen, Bockfjorden: In the lower half of the figure, the width of the push moraine is 650 meters (photo by Norsk Polarinstitutt, Oslo, taken in 1967).

In contrast to the intramorainal parts, the outer parts of the moraines usually have a debris cover sufficiently thick to better protect its core from melting. However, even these areas may undergo fast changes from year to year. Melting may start at the proglacial lake or its run-off, followed by partial or complete drainage (e.g. Børrebreen and Takryggbreen). Glacial ice has thus been exposed sometimes even in the outermost ridges that were thought to consist of frozen ablation material. At the most prominent boulder moraines, often sufficient thickness and slope exists for permafrost creep of the deposit. A rockglacier-like movement is then expressed by surficial flow structures or is visible at the steep instable front. It amounts to 2 cm per year in the case of Globbreen (Priesnitz in King & Schmitt 1992).

Due to the glacier retreat, no active push moraine could be found in the visited areas. However, observations in July/August 1992 give hints to new advances or even surges of Monacobreen and maybe Erikbreen. According to Hagen & Liestl in van der Wateren (1992) 90% of the glaciers in Svalbard are regularly surging. Future observations are recommended here.

#### QUEEN ELIZABETH ISLANDS: OBSERVED PROCESSES AND DATES

##### Oobloyah Bay and Hare Fiord, Ellesmere Island

The studied features are located close to sea-level and push moraines are again common in all researched places. The push moraine of Carl Troll Glacier is located north of Greely Fiord, just 2 km away from the head of Oobloyah Bay. It has a semi-circular shape and surrounds the eastern half of the glacier front, where it reaches a relative height of about 25 m above the outwash plain and a width of 200 to 300 m. In its western part, the glacier front rides over a small moraine consisting of ice-rich shear and ablation material. The glacial history of the area is described in King (1983).

The glacier was visited and photographed in 1978 (Barsch & King, eds. 1981) and a triangulation network was established (Hell 1981). In 1988, a terrestrial survey showed strong fluvial erosion in the eastern part due to undercutting. Strong deflation could repeatedly be observed and shapes especially the moraine tops. Additional aerial photographs were taken with semi-metric cameras at an altitude of about 750 m a.s.l. (Figure 4) and compared with photographs taken in 1978 and in 1959/60 by the National Air Photo Library, Ottawa (scale = about 1:50 000). The evaluation method is described in King & Hell (1993).

The comparison of the pictures (1960/1978/1988) shows a dislocation of the glacier surface of probably several hundred meters over 18 and 28 years, respectively, but only hardly visible changes at its more or less stagnant front and in large parts of the moraine.

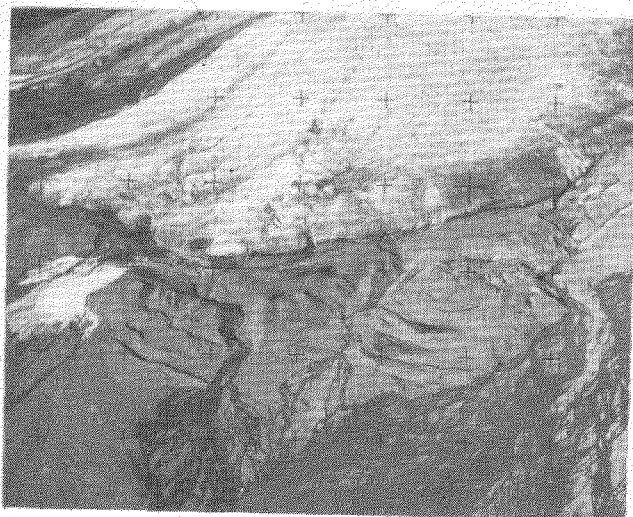


Figure 4: Rollei metric 6006 photograph of frontal area of Troll Glacier. It was taken from an altitude of about 750 m a.s.l. in 1988 and used for the stereo compilation. The picture shows the investigated push moraine to the right, in the left (not visible), the glacier overrides its own moraine, consisting mainly of sheared subglacial debris. The extent of the Aufeis (left margin) varies from year to year (July 1988).

Changes exist in the western part of the moraine due to thermal erosion. In the central part, the outermost moraine ridges in 1988 consisted of about 4 m thick frozen sediment plates that have been sheared out of the outwash plain (Figure 5) and folded and dislocated horizontally for about 3 to 5 meters (cp. Klassen 1982), this in spite of an almost stagnant behaviour of the glacier front.

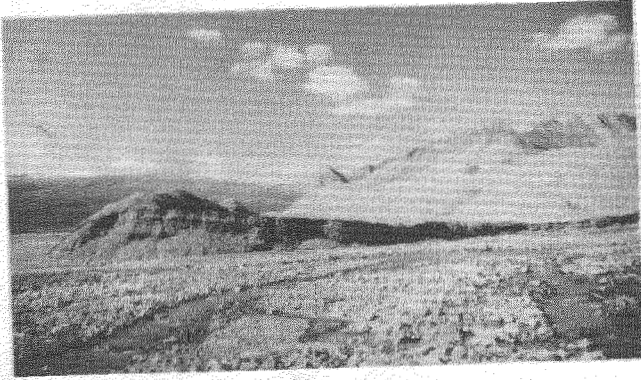


Figure 5: Fresh looking 4 m high frozen plate of sediments pushed up in the frontal part of the Troll Glacier moraine, visible in the right half of the picture (July 1988).

Three geoelectrical soundings were done 500 to 800 m in front of the moraine. The graphs show an active layer of about 50 cm, followed by a high-resistivity horizon (permafrost) of 10 m, 6 m and 4 m respectively (resistivity relation 1:100 for the first two soundings). All graphs show low apparent resistivities in greater depths that hint to unfrozen sediments or, if permafrost is present, unfrozen pore water in the fine grained marine sediments. Although the total permafrost thickness may be more than 4 to 10 m, it is reasonable to assume that relatively thin permafrost occurs in this near-shore area of young sediments and strong isostatic rebound (King, 1981).

In the Hare Fiord area an unnamed glacier was photographed in 1958 and 1978 by NAPL, Ottawa (cf. Figure 6b). A differential map shows a glacier retreat of 200 m between these 20 years (Hell ed. 1986). Aerial photographs were also taken in June 1988. They reveal a further glacier retreat of 500 m (Figure 6a). Photogrammetrical calculations show, that the push moraine, however, has been very well preserved even in the parts situated in the fiord. The low energy environment (short fetch of the waves, long ice covered periods and isostatic rebound) certainly has contributed to the preservation of the moraines (King 1985).

#### Thompson Glacier, Axel Heiberg Island

Thompson Glacier is bulldozing up an impressive push moraine that is more than 2 km long and 700 m wide (Figure 7). It rises generally about 45 m and in places even more than 100 m above the outwash plain! First maps based on aerial photographs and a geodetic determination of control points have been produced already in 1960 by Haumann. Aerial photographs were taken again with semi-metric cameras in 1988. The comparison gives the following results: (1) The advancing glacier front and the adjoining 500 m broad push moraine complex form a morphological unit that has been dislocated 400 m to 500 m within a time span of 28 years (cf. Figure 7 in King & Hell 1993); (2) The dislocation of the push moraine was more than 20 m per year in the sixties, decreased to an average of about 14 m per year in the last 20 years and to about 10 m per year in the eighties. (3) The main structures have been preserved surprisingly well within the moraine complex, e.g. the relative location of sediment blocks and lakes (Figure 8). (4) Most changes occurred in the outermost parts, where relatively thin new sediment plates are sheared from the perennially frozen outwash plane and incorporated into the moraine.

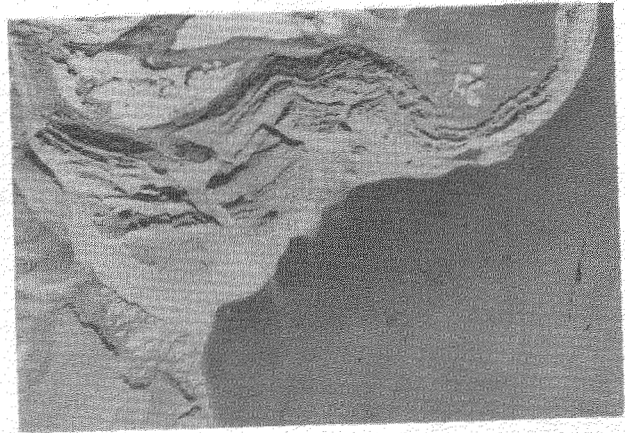
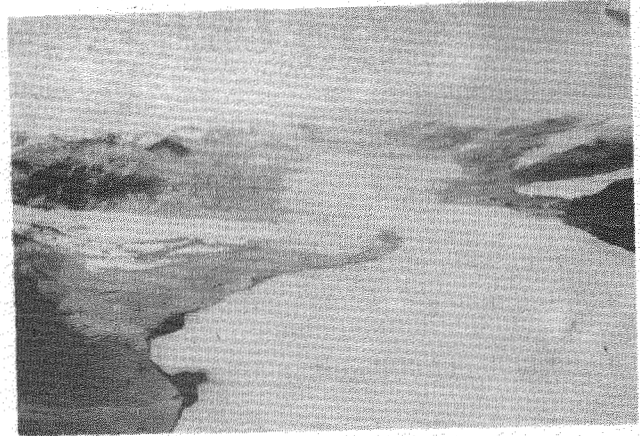


Figure 6a: Oblique aerial photograph of a push moraine in the Hare Fiord area taken in 1988 (upper photograph). In comparison with the situation in 1958 and 1978, the glacier tongue retreated a distance of about 500 m and 700 m, and the area of debris rich medial moraines melted down about 35 m and 65 m, respectively, but the push moraine itself (cf. vertical photograph 6b, taken in 1978) shows hardly any changes during these 30 years.

Terrestrial surveys showed the following: In June 1975 and again in June 1988, the respective outermost, youngest ridges must have recently been lifted 4 to 5 m above the valley floor and fresh radial cracks with a width of a few cm to dm extended to the outwash plain (Figure 9). In its western part, the Thompson Glacier front showed a steep ice cliff in 1988 and at the glacier base large ice blocks seemed to be overridden by the advancing front. The eastern and highest part of the moraine showed signs of surficial melting and mass wasting. The glacier seems even to run onto the moraine. Fluvial erosion at its outer edge further reduces here the width of the moraine. These combined processes lead to the growth of the push moraine in the frontal parts and limit the growth in the lateral parts.

Our geoelectrical sounding, although done about 1 km west of Kälin's soundings, supported his results (1971: 33-41), but a quantitative interpretation is difficult, probably due to local thermal anomalies (warm springs) and low resistivity materials (e.g. gypsum). Due to this, the existence of structurally weak layers serving as shear planes in a few meters depth in the frozen outwash plain cannot be varified with this method.

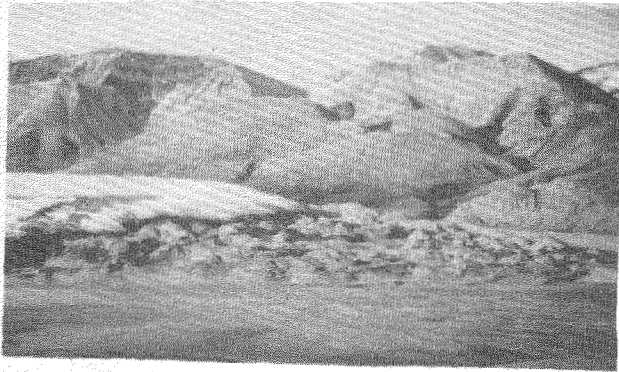


Figure 7: The snout of Thompson glacier with its push moraine taken in July 1988.



Figure 8: Old, frozen and tilted sediment plates in the central part of the push moraine complex and younger fluvial terraces.

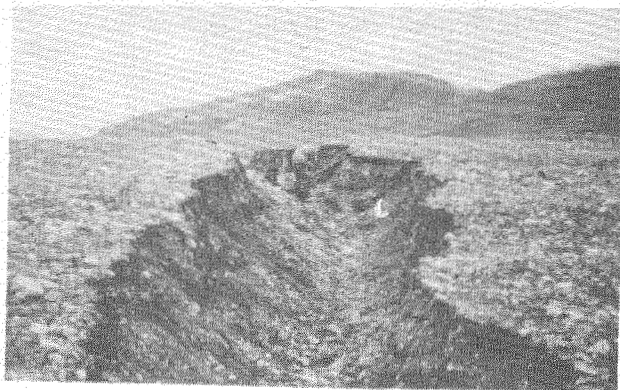


Figure 9: A fresh radial crack has been formed in front of the Thompson Glacier push moraine (view towards the outwash plain). The vertical crack in the slightly tilted frozen blocks of glacio-fluvial and marine sediments is the first sign that these areas are being incorporated into the growing push moraine complex (July 1988).

## CONCLUSIONS

A comparison of the two research areas, the Queen Elizabeth Islands, Canada, and NW-Spitzbergen shows that the dominant *geomorphological forms* differ. Push moraine features occur frequently in both regions. In Svalbard, the usually very impressive Neoglacial moraine complex consists of a large portion of glacier ice, covered with thick debris (often boulders). With a few exceptions (e.g. Karlsbreen), push moraines are limited to a few ridges outside the large boulder moraine and consist of relatively thin pushed-up and folded plates of frozen glaciofluvial/marine sediments. In the Queen Elizabeth Islands, push moraines usually consist of large complexes of stacked frozen sediment blocks. A detailed geomorphology of the "coastal type" (Svalbard) and the "arctic type" of push moraines is presented by Lehmann (1993). The processes have been described in the present paper.

The most important *geomorphological processes* are different as well. In Svalbard, thermal erosion dominates in many intramorainal areas and may lead to extensive landscape transformation. It is often connected with partial or complete drainage of proglacial lakes. Permafrost creep and solifluction are widespread if the necessary conditions exist. Ecological differences lead to great variations in the ground temperature regimes of the active layer. The intensity of the mentioned processes is very different over short distances.

In the Canadian areas investigated, the geomorphological effects of thermal erosion are limited (smaller ice content of morainic deposits, deeper permafrost temperatures). Push moraines show little deformation, even in marine environments. Deflation and fluvial erosion are the main transforming processes in inactive moraines.

*Push moraines* are by definition formed in front of advancing glaciers or the margins of an icesheet. It has to be realized, however, that the term "push moraine" is often used differently, considering the existence of permafrost:

- 1: in unfrozen or seasonally frozen sediments (Haefeli in Haeberli 1979, Eybergen 1987),
- 2: in perennally frozen sediments, e.g. in the Alps (Haeberli 1979) or the Arctic (Kálin 1971, or more recently by Van der Meer & Boulton 1986, Boulton & Van der Meer, eds. 1989, Riezebos et al. 1986).
- 3: as Pleistocene push moraines, e.g. from areas of Quaternary ice margins in Europe, e.g. the Netherlands, North Germany, Poland, but also in North America (Chamberlain 1894, Gripp 1929, Mackay et al. 1964).

Van der Wateren (1992) states in the last paragraph of a larger study, that a frozen substratum is not a prerequisite of folding and overthrusting of unlithified sediments. According to his theory (concept of accretionary wedges) the formation of a push moraine does not require a weak layer, but if exists, the formation is facilitated (p. 169). In our research areas, a frozen substratum is undoubtedly present. It has very low permafrost temperatures (and a higher viscosity) in Canada and at least 10°C higher permafrost temperatures (and a lower viscosity) in Svalbard. The effect of permafrost on viscosity is difficult to evaluate, especially when the viscosity lowers greatly with depth over short distances. In the researched areas in Svalbard, the sediments gradually change from a frozen state into an unfrozen state in the layers involved in push moraine formation (cf. results of BTS measurements). Our results may help to explain at least some of the differences. Future research on the role of permafrost for the formation of push moraines is certainly needed.

## ACKNOWLEDGEMENTS

Sincere thanks are given to the members of the expeditions for their cooperation. The Svalbard expeditions (1989 to 1992) and the Kanarktis expeditions (1978 and 1988) were mainly financed by the Deutsche Forschungsgemeinschaft, Bonn. In Canada, the Polar Continental Shelf Project, Ottawa gave precious logistical support. On Axel Heiberg Island the camp facilities of McGill University, Montreal, could be used.

## REFERENCES

BARSCHE, D. & L. KING, eds., (1981): Results of the Heidelberg Ellesmere Island Expedition 1978. - Heidelberg Geographische Arbeiten 69: 573 pp.

BOULTON, G.S. & J.J.M. VAN DER MEER, eds. (1989): Preliminary report on an expedition to Spitsbergen in 1984 to study glaciotectionic phenomena (Glacitecs '84). - Rapport No. 37, Fysisch Geografisch en Bodemkundig Laboratorium, Universiteit van Amsterdam: 195 pp.

CHAMBERLAIN, T.C. (1894): Proposed genetic classification of Pleistocene glacial formations. - J. Geol. 2: 517-538.

EDLUND, S. (1986): Modern Arctic vegetation distribution and its congruence with summer climate patterns. - In: FRENCH, H.M., ed.: Proc. Climate change impacts in the Canadian Arctic, Canadian Climate Program Workshop, March 3-5, 1986: 84-99.

EYBERGEN, F.A. (1987): Glacier snout dynamics and contemporary push moraine formation at the Turtmannglacier, Wallis, Switzerland. - In: VAN DER MEER, J.J.M., ed., Tills and Glaciotectionics, Rotterdam: 217-231.

FRENCH, H. & D.G. HARRY (1990): Observations on Buried Ice and Massive Segregated Ice, Western Arctic Coast, Canada. - Permafrost and Periglacial Processes 1, 1: 31-43.

FURRER, G. (1991): Zur Gletschergeschichte des Liefdefjords. - Stuttgarter Geographische Studien, 117: 267-278.

GRIPP, K. (1929): Glaciologische und geologische Ergebnisse der Hamburgischen Spitzbergen-Expedition 1927. - Abh. Naturw. Ver. Hamburg, XXII: 147-249.

HAEBERLI, W. (1979): Holocene push moraines in alpine permafrost. - Geogr. Ann., 61A: 43-48.

HAGEN, J.O. (1987): Glacier Surge at Usherbreen, Svalbard. - Polar Research 5: 239-252.

HELL, G. (1981): Geodätische und photogrammetrische Arbeiten an der Oobloyah Bay, N-Ellesmere Island, N.W.T., im Rahmen der Heidelberg Ellesmere Island Expedition. - Heidelberg Geographische Arbeiten 69: 35-46, and map 1:25.000 (48 cm x 103 cm).

HELL, G., ed. (1986): Veränderungen der Zunge eines Gletschers am Harefjord (NWT, Kanada) zwischen 1958 und 1978. - (Maps 1:20.000), Karlsruhe.

JECKEL, P.P. (1988): Permafrost and its altitudinal zonation in N.Lapland. - In: Permafrost Fifth International Conference, August 2-5, 1988, Trondheim, Proc. Vol. 1: 170 - 175.

JUDGE, A.S., A.E. TAYLOR, M. BURGESS & V.S. ALLEN (1981): Canadian Geothermal Data Collection, Northern Wells 1978-1980. - EMR, Earth Physics Branch, Geothermal Service of Canada, Geothermal Series 12, Ottawa.

KÄLIN, M. (1971): The active Push Moraine of the Thompson Glacier, Axel Heiberg Island, Canadian Arctic Archipelago. - Axel Heiberg Island Research Reports, McGill University, Montreal. Glaciology 4: 68 pp.

KING, L. (1981): Studies in glacial history of the area between Oobloyah Bay and Esayoo Bay, Northern Ellesmere Island, N.W.T., Canada. - In: BARSCHE, D. & L. KING, eds.: Results of the Heidelberg Ellesmere Island Expedition: 233-268.

KING, L. (1983): Contribution to the glacial history of the Borup Fiord area, northern Ellesmere Island, N.W.T., Canada. - In: Schroeder-Lanz, H., ed.: Late- and postglacial oscillations of glaciers: glacial and periglacial forms, Rotterdam: 305-323.

KING, L. (1985): Land-sea interactions in an arctic marine low energy environment, northern Ellesmere Island, N.W.T., Canada. - 14th Arctic Workshop, Arctic Land-sea Interaction, Nov. 6-8, Dartmouth N.S., Canada: 144.

KING, L. & G. HELL (1993): Photogrammetry and geomorphology of high arctic push moraines, examples from Ellesmere Island, Canadian Arctic and Spitsbergen, Svalbard Archipelago. - Zeitschrift für Geomorphologie N.F., Suppl.-band 92: 21-38.

KING, L. et al. (1993): Geomorphologische und geoökologische Daten der Gießener Arbeitsgruppe der SPE'90-Expedition zum Liefdefjorden, Spitzbergen. - "Basler Datenband", in print.

KING, L. & E. SCHMITT (1993): Solifluction and thermal erosion in High Arctic ecosystems, Northern Spitsbergen: Processes and effects. - In: FRENZEL, B., ed.: Palaeoclimate Research, Vol. 7. Special Issue: ESF Project "European Palaeoclimate and Man", European Science Foundation Strasbourg.

KLASSEN, R.A. (1982): Glaciotectionic thrust plates. Bylot Island, district of Franklin. - In: Current Research, Part A. Geological Survey of Canada, Paper 82-1A: 369-373.

LAURIOL, B.J. CINO MARS & I.D. CLARK (1991): Localisation, Genèse et Fonte de Quelques Naleds du Nord du Yukon (Canada). - Permafrost and Periglacial Processes 2, 3: 225-236.

LEHMANN, R. (1992): Arctic Push Moraines, a case study of the Thompson Glacier Moraine, Axel Heiberg Island, N.W.T., Canada. - Zeitschrift für Geomorphologie, Supplementband 86: 161-171.

LEHMANN, R. (1993): The Significance of Permafrost in the Formation and Appearance of Push Moraines. Examples of the Canadian Arctic and Spitsbergen. - This volume.

MACKAY, J.R. & W.H. MATHEWS (1964): The Role of Permafrost in Ice-Thrusting. - J. of Geol. 72: 378-380.

MACKAY, J.R. & SCOTT, R.D. (1992): Massive Ice of the Tuktoyaktuk Area, Western Arctic Coast, Canada. Canadian Journal of Earth Sciences 29 (6): 1235-1249.

RAMPTON, V.N. (1991): Observations on Buried Glacier Ice and Massive Segregated Ice, Western Arctic Coast, Canada: Discussion. Permafrost and Periglacial Processes 2, 2: 163-165.

RIEZEBOS, P.A., G.S. BOULTON, J.J.M. van der MEER et al. (1986): Products and effects of modern eolian activity on a nineteenth-century glacier-pushed ridge in West Spitsbergen, Svalbard. - Arctic and Alpine Research 18: 389-396.

SALVIGSEN, O. & OSTERHOLM, H. (1982): Radiocarbon dated raised beaches and glacial history of the northern coast of Spitsbergen, Svalbard. - Polar Research 1: 97-115.

SCHMITT, E. (1993): Global climatic change and some possible geomorphological and ecological effects in arctic permafrost environments, Isfjorden and Liefdefjorden, northern Spitsbergen. (This volume).

VAN DER MEER, J.J.M. & G.S. BOULTON (1986): Hernieuwde belangstelling voor onderzoek van stuwwallen. Eerste resultaten van de Glacitecs 1984 Expeditie naar Spitsbergen. - In: K.N.A.G. Geografisch Tijdschrift XX, 3: 236-244.

VAN DER WATEREN, D. (1992): Structural Geology and Sedimentology of Push Moraines. - Diss., Faculteit der Ruimtelijke Wetenschappen, Universiteit van Amsterdam: 230 pp.



THE INFLUENCE OF RELIEF AND LITHOLOGY ON  
SOIL FORMATION IN WEST SPITSBERGEN

Zbigniew Klimowicz, Jerzy Melke, Stanisław Uziak

Department of Soil Science, Maria Curie-Skłodowska University,  
Lublin, Poland

The present studies have been conducted on coastal terraces in the Bellsund region of West Spitsbergen. In the field research the method of soil cross-sections has been applied. A significant dependence between the soil cover and its properties on one hand and lithology and terrain relief on the other is reported. Relief influences erosion processes, deluvial and striped soils and partial water relations as well as plant cover. Lithology influences mainly soil thickness, grain-size distribution and some chemical properties.

INTRODUCTION

Studies in arctic regions allow for a better understanding of the conditions of soil formation in the sectors with moderate climates once subjected to periglacial processes. Literature concerning the arctic region is substantial (e.g. Brown, 1964, 1967; Everett et al., 1981; Jahn, 1946, 1975; Linell and Tedrow, 1981; Rieger, 1983; Schunke, 1981; Tedrow, 1977). Spitsbergen occupies a special place in these studies (Forman and Miller, 1984; Klimowicz and Uziak, 1988; Lag, 1980; Mann et al., 1986; Melke and Uziak, 1989; Melke et al., 1990; Szeszeń, 1974; Ugolini and Sletten, 1988).

Our studies were carried out on Spitsbergen from 1986 to 1990 within the framework of the scientific expedition project of the Institute of Earth Science of Maria Curie-Skłodowska University in Lublin. The aim of these studies was, among others, to estimate the influence of the terrain relief and lithology on the soil properties.

STUDY AREA

The investigated area is situated in the western part of Spitsbergen in the Bellsund region (about 78°N and 20°E). The studies were carried out on the Calypsostranda and Reinsletta terraces of the southern Bellsund Coastal Plain. The largest areas on the Calypsostranda as well as on Reinsletta occupy terraces of 20-30 m and 10-15 m A.S.L. (Pełkala, 1987).

Bedrock consists of old metamorphic rocks of Hecla Hoek formation developed mainly as tillites with limestone and quartzite inclusions, and as grey limestone and dolomite (Dallmann et al., 1990).

The Calypsostranda plain is formed mainly of sandstone and Tertiary mudstone with some coal which in turn are covered with a series of Quarternary sediments - marine, glacial, and fluvioglacial. Material of the lower terraces consists mainly of gravel and sandy deposits, but on the raised terraces lithology is more complex, consisting mainly of clay and sand with marine fauna plus boulder clay and gravel-sand mixtures (Pełkala, 1987). The Reinsletta surface formation consists mainly of glaciofluvial sands with an admixture of aeolian silt.

The studied region belongs to the subpolar zone

(Tedrow, 1977). The yearly mean temperature approximates -4°C and the yearly mean precipitation is 350-400 mm. In the region of the southern Bellsund coast there are three predominating types of flora: dry tundra, covering the largest areas, mezophyllic moss and lichen, and wet moss (Swigs, 1988). The character of wet areas depends mainly on the relief and lithology (Michalczyk, 1990).

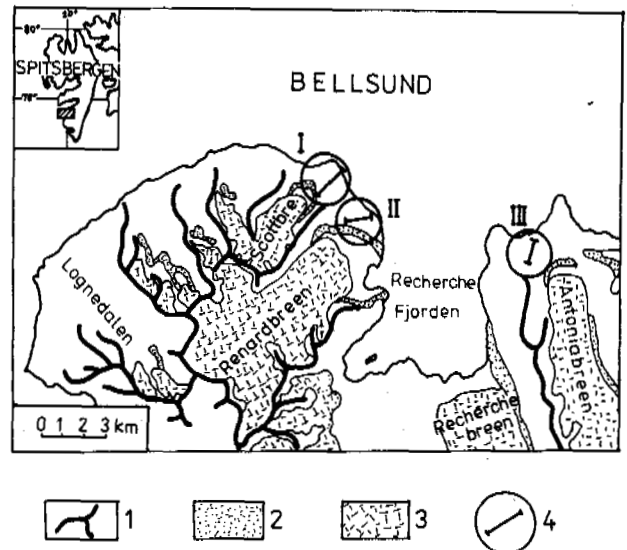


Fig.1. Location of study area in Bellsund region. 1 - mountain ridges, 2 - ice-moraine ridges, 3 - glaciers, 4 - cross-sections.

RESEARCH METHODS

In the field investigations the method of soil cross-sections was applied. Topographic sections were made by the use of levelling-instrument. The above method has

not been applied in the arctic studies before. The cross-sections (I, II - on Calypsostranda, III - in the region of Reinsletta; Fig.1) were carried out in the areas representing various terrain forms, different types of bedrock, wetness and plant cover. The soil morphology was studied in the active layer (study sites 1-66) during the summer months. Samples were collected from 15 soil pits for analysis.

Grain-size distribution was estimated by means of the areometric Bouyoucos-Casagrande method as modified by Prószyński (particles distribution after Polish Society of Soil Science: 1-0.1 mm - sand, 0.1-0.02 mm - silt, 0.02-0.002 mm silty clay, < 0.002 mm - clay), reaction - in 1N KCl, CaCO<sub>3</sub> - by means of Scheibler apparatus, organic carbon - by means of Tiurin method, total nitrogen - by means of Kjeldahl method, easily available phosphorus and potassium - by means of Egner-Riehm method, exchangeable cations - in 0.5 N NH<sub>4</sub>Cl (pH 8.2). These methods were described by Lityński et al. (1976).

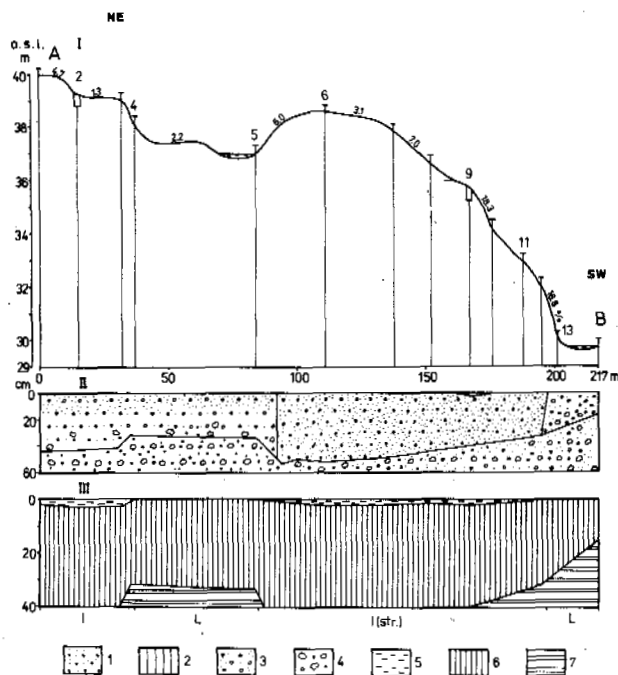


Fig.2. Cross-section I(A-B) - The foreland of Scott-glacier (Calypsostranda).

I - topographic section, II - geological section, III - pedological section; 1-14 - soil pits, 1 - loam, 2 - silt, 3 - gravel, 4 - stones, 5 - transitional horizon AC, 6 - parent rock C, 7 - underlying material D; I - initial soil, I(str.) - initial striped soil, L - lack of soil cover.

The results of field studies are illustrated in Figs. 2-4, and laboratory results in Tab. 1.

## RESULTS AND DISCUSSION

### Cross-section I

The predominant forms of terrain relief are the following: overflowed terrace (soil pits 1-3) and a slight convex form that is a part of a loamy ground moraine (soil pits 6-12), Fig.2. The terrace is covered by sparse vegetation (about 30% cover) in which the following species are predominant: *Salix polaris*, *Saxifraga oppositifolia*, *Silene acaulis* L., and lichens (*Cetraria* sp.).

Plant cover on the ground moraine is greater than on the terrace (about 50%) with the predominance of moss, lichens (*Cetraria* sp.) and *Salix polaris*. The soil is often striped (in places where the slope is greater).

### Cross-section II (A-B-C)

The section contains three main morphological forms: an undulating plain (soil pits 26-35), a rather steep slope (soil pits 36-43) and a low ridge top (soil pits 44-45), Fig.3.

On the new storm bar (sites 26-28) there is no vegetation and no genetic soil present. The old, partly washed out storm banks (sites 29-35) are covered by sparse vegetation (10-20%) with *Saxifraga oppositifolia*, *Papaver arcticum*, *Silene acaulis*, and *Cetraria* sp. predominating. There are initial soils with gley soils in the depressions having a more dense plant cover and a shallow frost table (20-30 cm).

Plant cover on the slope is quite differentiated (from about 20% in the polygon regions to 100% on some flat terrain). Vascular plants such as *Saxifraga oppositifolia*, *Salix polaris*, *Silene acaulis*, *Polygonum viviparum* together with mosses and lichens predominate.

The top part of the slope is covered with rather continuous vegetation (similar to the plant cover on the more gentle slopes) and with a similar type of species composition. There are brown soils with frost fissures and with well developed A and B horizons.

### Cross-section III (A-B-C-D)

Terrain consists of a prominent plain in the central section (soil pits 53-60), bordered by steeper slopes (soil pits 47-52 and 60-65), Fig.4.

Contrary to the two previously discussed sections, plant cover, especially on the plain, is nearly complete and in places forms a dense sod. Vegetative cover on the slope and on top of the landform itself is discontinuous (from about 60% on the slope to 20% near the top).

Plant cover on the plain, especially in the more wetted parts, consists mainly of grasses. There are also some other vascular plants such as: *Salix polaris*, *Silene acaulis*, *Saxifraga oppositifolia*, *Polygonum viviparum* present. The contribution of grasses on the slope is small, and on the top of the landform *Orvas octopetala*, *Silene acaulis*, and *Salix polaris* are predominant.

Where there is a richer vegetation soil development is quite good, especially on the plain. On the plain, brown soils, and peat soils in the shallow depressions predominant, but on steeper slopes, eroded brown soils are present.

The soils of West Spitsbergen are being formed under the influence of three groups of factors. These are 1) cryogenic processes, 2) soil formation processes, that are usually overlapping and 3) lithology, the last of which influences the mineral composition and grain-size distribution.

The most important soil processes are those associated with the initial stages of development, soil browning, gleying, peat formation, and deluvial process. Cryogenic processes induce many forms of structural soils (Klimowicz, Uziak 1988; Meike, Chodorowski, Uziak, 1990). Structural soils are extensively reported in the papers by Jahn (1946,1975), Brown (1964), Tedrow (1977) and others.

As a rule, the soils are poorly developed from a morphological viewpoint, with very shallow profile development and very thin humus layer (about 2 cm; but in Reinsletta about 3-5 cm). Many of the soils can be grouped as initial soils, i.e. Regosols. There are also gley and brown soils, and other undifferentiated varieties plus deluvial deposits present. The above mentioned soils show the character of polygonal soils on the surface (stone circles, frost fissures, loamy outflows) or they are non-differentiated. Moreover, the so-called striped soils developed as a result of solifluction processes on sloping ground.

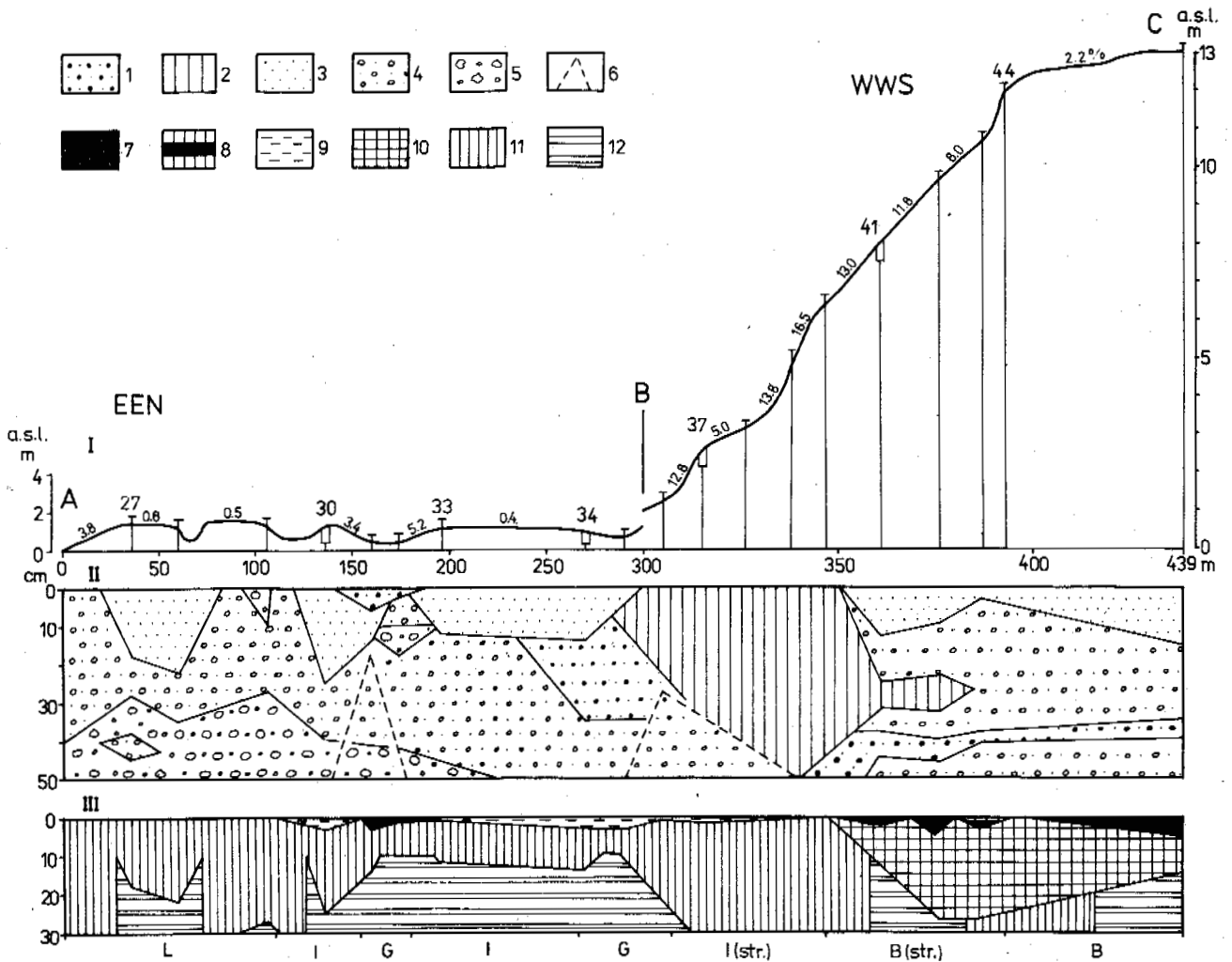


Fig.3. Cross-section II(A-B-C) - The foreland of Renard-glacier (Calypsostranda).

I - topographic section, II - geological section, III - pedological section; 26-46 - soil pits, 1 - loam, 2 - silt, 3 - sand, 4 - gravel, 5 - stones, 6 - depth of seasonal thaw, 7 - humus horizon A, 8 - transitional horizon AB, 9 - transitional horizon AC, 10 - browned horizon B, 11 - parent rock C, 12 - underlying material D; B - brown soil, B(str.) - brown striped soil, G - gley soil, I - initial soil, I(str.) - initial striped soil, L - lack of soil cover.

Grain-size distribution is varied, from sands (loose, light loamy, and loamy sands), through loams (light, medium, and heavy) to silty material. Nearly all of these soils contain up to 80% skeletal material. Some of profiles contain considerable amounts of silty fractions especially the A horizons, which is typical of Tundra soils (the results of frost processes and possibly some aeolian activity). The clay fraction is small (up to several per cent) but sometimes it reaches 25%.

Lighter texture of parent rocks predispose for the formation of the soils with frost fissure nets or undifferentiated on the surface. Soils with heavier granulometric composition favor soils with polygons and stone circles.

In the conditions of dry Tundra and on the sandy deposits and silty marine terraces, brown soils with nets of frost fissures, are generally present. They are covered by moss, and some vascular plants.

Gley soils, often with polygons and stone circles,

are formed mainly in wetter sites under grass-mossy vegetation. The gleying process is usually associated with heavier textures and shallow permafrost causing better moistening of the upper layers. Peat with shallow permafrost is formed under the compact vegetation cover of the very wet Tundra.

On the slopes striped soils are formed, i.e. polygonal soils that are solifluctionally extended. On the steeper slopes water erosion process can be observed. Water erosion decreases thickness of the already very thin soil cover. At the foot of the slopes deluvial soils are formed.

The character of the parent rock, terrain relief and the type of plant cover together with the compactness of this cover influence the thickness of the soils. Under a dense vegetation cover soils are, as a rule, thicker and better developed.

In many locations neither plant cover nor soil cover was noticed. The reason for this phenomenon are young sediments as parent rocks. Also initial soils - Regosols -

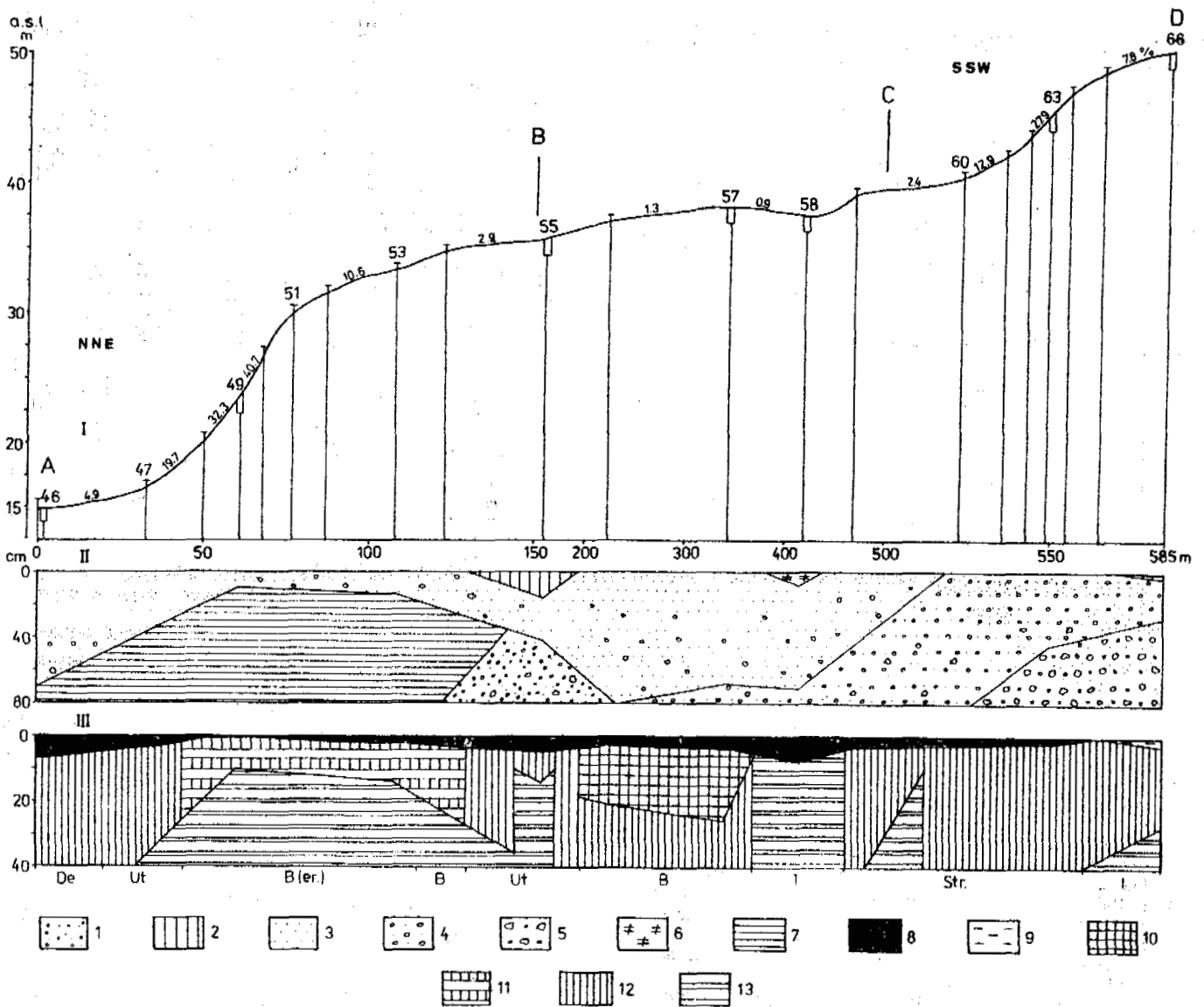


Fig. 4. Cross-section III(A-B-C-D) - The Malbukta Gulf (Reinsletta).

I - topographic section, II - geological section, III - pedological section; 46-54, 55-59, 60-66 - soil pits, 1 - loam, 2 - silt, 3 - sand, 4 - gravel, 5 - stones, 6 - peat, 7 - black schists of Hecla Hoek formation, 8 - humus horizon A, 9 - transitional horizon AC, 10 - browned horizon B, 11 - transitional horizon BC, 12 - parent rock C, 13 - underlying material D; B - brown soil, B(er.) - brown eroded soil, I - shallow peat soil, Ut - soil of underfined typology, Str. - striped soil, De - deluvial soil.

are connected with this type of parent rocks. The short duration period of soil formation process together with cryogenic disturbances results in only slight soil development.

Mineral soils of this region are usually have an alkaline or neutral reaction. The pH value, as a rule, increases slightly with the increased depth of the soil, and is generally associated with the presence of  $\text{CaCO}_3$ .

The quantity of organic matter in the soil as a rule is not high as evidenced by 0.5% to 5% of carbon in the A horizon. Organic content usually decreases markedly with depth. Organic substances have a total N content of up to 0.40%. C:N ratios range from 6 to 16.

The sorptive capacity, as well as the exchangeable cation composition have a considerable range. As a rule, they are related to the quantity of particles  $< 0.02$  and to the colloidal fractions. The exchangeable cation ratios are generally:  $\text{Ca} > \text{Mg} > \text{Na} > \text{K}$ . In several profiles however, the pattern is different, i.e.  $\text{Ca} > \text{Na} > \text{Mg} > \text{K}$ . Total amount of exchangeable cations (S) is lower in the soils of the III cross-section than in the remaining cross-sections.

The soils in general showed very low contents of available phosphorus and potassium. This condition results from limited chemical weathering and poor biochemical reactions. The mineralogical composition of these

Tab.1. Granulometric composition and some chemical properties of the soils studied.

Cross-section, Profile Soil*	Horizon, depth, cm	Color**	Fraction content, %				CaCO <sub>3</sub> , %	pH KCl	Org. C %	N %	C:N	available mg/100 g		meq/100 g					Ca:Mg		
			ske-leton >1 mm	1-0.1	0.1-0.02	<0.02						<0.002	P <sub>2</sub> O <sub>5</sub>	K <sub>2</sub> O	Ca <sup>++</sup>	Mg <sup>++</sup>	Na <sup>+</sup>	K <sup>+</sup>		S (Ca+Mg+Na+K)	
I 2	AC	0-3	2.5Y 6/1	80	86	7	7	1	27.7	8.0	0.41	0.05	8.2	0.6	0.6	17.1	0.8	2.10	0.04	20.0	21.4
I	C	10-20	2.5Y 6/2	80	86	9	5	1	32.0	8.2	0.24	-		0.4	1.0	19.7	0.8	2.15	0.03	22.7	24.6
9	AC	0-2	5Y 6/2	25	24	44	32	7	27.3	8.0	0.51	0.06	8.5	0.3	1.2	40.3	2.2	4.35	0.08	46.9	18.3
I(str.)	C1	10-20	5Y 6/2	9	21	33	46	12	28.5	7.8	0.25	0.03	8.3	0.3	0.8	41.2	2.0	4.50	0.08	47.6	20.6
	C2g	30-40	5Y 6/1	15	11	33	56	24	21.5	7.7	0.52	0.06	8.7	0.4	1.5	39.1	2.8	4.25	0.17	46.3	14.0
II 34	AC	0-3	2.5Y 5/2	20	50	32	18	0	16.1	7.3	2.85	0.25	11.4	0.9	1.3	18.4	7.1	1.70	0.08	20.6	8.8
G	Cg	5-12	5Y 5/2	15	48	35	17	0	28.1	7.8	0.98	0.09	10.9	0.6	0.8	22.2	1.1	2.25	0.05	25.6	20.2
	Dp	20-30	7.5Y 6/3	9	31	37	32	2	31.8	8.0	0.32	-		0.3	0.4	32.4	0.5	3.05	0.05	36.0	64.8
37	Ac	4-1	2.5Y 4/1	-	-	-	-	-	21.5	7.2	5.15	0.41	12.6	-	-	24.7	5.1	2.75	0.24	32.8	4.8
I(str.)	AC	0-2	7.5Y 6/2	25	27	47	26	3	28.9	7.8	0.66	0.07	9.4	0.3	0.6	34.9	1.4	3.05	0.06	39.4	24.9
	C	25-35	5Y 6/2	30	30	42	28	4	28.3	8.0	0.52	0.05	10.4	0.6	0.4	39.4	1.6	3.80	0.06	41.1	24.6
41	AB	0-2	10YR 5/3	40	75	13	12	0	14.4	7.5	1.22	0.12	10.2	0.5	0.7	15.2	1.6	1.90	0.05	18.7	9.5
B(str.)	B	5-10	10YR 4/4	45	73	12	15	0	18.1	7.6	1.03	0.09	11.4	0.6	0.4	17.8	1.2	2.05	0.03	21.1	14.8
	D	15-25	2.5Y 6/2	70	83	8	9	1	20.8	8.0	0.30	-		0.9	0.3	25.4	0.7	2.65	0.02	29.0	36.3
III 55	A	0-5	10YR 4/2	1	34	62	4	1	18.2	7.3	2.11	0.19	11.1	0.3	1.7	12.1	4.5	1.45	0.05	18.1	2.7
Ut	C	8-15	10YR 6/2	1	46	49	5	1	17.1	7.3	1.63	0.13	12.5	0.3	1.2	8.9	3.9	1.20	0.02	14.0	2.3
	D1	30-40	10YR 5/3	4	60	32	8	4	12.3	7.5	0.93	0.08	16.6	0.9	1.0	7.0	3.4	0.75	0.03	11.2	2.1
	D2	45-55	10YR 4/3	45	44	28	28	9	2.5	7.8	1.53	0.10	15.3	1.7	1.6	10.8	4.2	1.00	0.17	16.2	2.6
57	A	0-4	10YR 4/2	2	59	34	7	0	5.0	7.1	2.25	0.21	10.7	0.7	1.0	11.0	4.1	1.10	0.06	16.3	2.7
B	B	10-20	10YR 4/4	1	87	9	4	0	0.8	7.1	0.62	0.07	8.8	0.6	0.6	4.8	1.6	0.45	0.02	6.9	3.0
	C	40-50	10YR 5/4	1	78	9	13	1	0.8	7.2	0.18	-		1.4	0.8	4.4	1.2	0.40	0.02	6.0	3.7
58	D1	9-13	10YR 4/2	2	57	37	6	0	0.0	5.1	1.79	0.15	11.9	0.3	0.6	5.7	1.7	0.60	0.02	8.0	3.3
I	D2	15-25	10YR 5/2	1	69	25	6	0	0.2	6.3	1.31	0.11	11.9	0.6	0.6	4.4	1.8	0.65	0.02	6.9	2.4
	D3	30-40	10YR 4/3	2	63	29	8	0	0.3	6.5	2.50	0.21	11.9	0.6	0.4	8.9	2.8	1.30	0.04	13.0	3.2
63	A	0-3	2.5Y 6/2	55	44	35	21	1	16.3	7.4	0.76	0.08	9.5	0.4	0.5	9.5	4.1	0.90	0.06	14.6	2.3
Str.	C	10-20	2.5Y 6/3	55	39	39	22	2	17.8	7.6	0.46	0.05	9.2	0.3	0.5	8.9	4.3	0.90	0.06	14.2	2.1

\* I - initial soil, I(str.) - initial striped soil, G - gley soil, B(str.) - brown (striped) soil, Ut - soil of undefined typology, B - brown soil, I - peat soil, Str. - striped soil.  
 \*\* after Standard Soil Color Charts (by M. Oyama, H. Takehara, 1967).

soils may also influence the general low level of available nutrients.

CONCLUSIONS

1. There is a significant dependence between the soil cover and terrain relief, as well as wetness and plant cover.
2. Lithology influences soil thickness, grain-size distribution and some chemical properties (the content of CaCO<sub>3</sub>, soil reaction, basic cations, and others).
3. Lithology also influences soil typology indirectly (initial soils, brown and gley soils) and structural soils.
4. Erosion processes, deluvial and striped soils, and partial water relations as well as plant cover are related to terrain relief. Also relief influences the formation of certain soil varieties such as gley soils and peat soils.
5. Wetness of the site influences development of the plant cover as well as gley and organogenic soils. Plants influence mainly the organic matter content of the soils.

REFERENCES

Brown, J., J.C.F. Tedrow (1964) Soils of the Northern Brooks Range, Alaska: 4. Well-drained soils of the glaciated valleys. Soil Sci. 97, 187-195.  
 Brown, J. (1967) Tundra soils formed over ice wedges, Northern Alaska. Soil Sci. Soc. Amer. Proc. 31, 686-691.  
 Dallman, W.K., A. Hjelle, Y. Ohta, O. Salvigsen, M.B. Bjørnerud, E.C. Hauser, H.D. Maher, C. Craddock (1990) Geological Map of Svalbard 1:100 000, sheet B 11G, Van Keulenfjorden. Norsk Polarinstittutt, Oslo.  
 Everett, K.R., V.D. Vassilyevskaya, J. Brown, B.D. Walker (1981) Tundra and analogous soils. In: Tundra ecosystems: a comparative analysis. Univ. Press, Cambridge pp 139-179.  
 Forman, S.L., and G.H. Miller (1984) Time-dependent

soil morphologies and pedogenic processes on raised beaches, Brøggerhalvøya, Spitsbergen, Svalbard Archipelago: Arctic and Alpine Research 16(4), 381-394.  
 Jahn, A. (1946) O niektórych formach gleb strukturalnych Grenlandii Zachodniej (About some forms of structural soil markings in West Greenland). Przegl. Geogr. 20, 73-89.  
 Jahn, A. (1975) Problems of Periglacial Zone. PWN, Warszawa, 223 pp.  
 Klimowicz, Z., S. Uziak (1988) Soil-forming processes and soil properties in Calypsostranda, Spitsbergen. Polish Polar Research 9/1, 61-71.  
 Lag, J. (1980) Special peat formation in Svalbard. Acta Agric. Scand. 30, 205-210.  
 Linell, K.A., J.C.F. Tedrow (1981) Soil and permafrost surveys in the Arctic. Clarendon Press, Oxford, 279pp.  
 Mityński, T., H. Jurkowska, E. Gorlach (1976) Chemical and agricultural analysis (in polish). PWN, Warszawa, 330 pp.  
 Mann, D.H., R.S. Sletten, F.C. Ugolini (1986) Soil development at Kongsfjorden, Spitsbergen. Polar Research 4, 1-16.  
 Melke, J. S. Uziak (1989) Dynamics of moisture, redox potential and oxygen diffusion rate of some soils from Calypsostranda, Spitsbergen. Polish Polar Research 10/1, 91-104.  
 Melke, J., J. Chodorowski, S. Uziak (1990) Soil formation and soil properties in the areas of Lyellstranda, Dyrstad and Logne in the region of Bellsund (West Spitsbergen). Polish Journal of Soil Science XXIII(2), 213-222.  
 Michalczyk, Z. (1990) Hydrological characteristics of Calypsostranda. Wyprawy Geograficzne na Spitsbergen, UMCS, Lublin, 75-92.  
 Oyama, M., H. Takehara (1967) Revised Standard Soil Color Charts.  
 Pekała, K. (1987) Rzeźba i utwory czwartorzędowe przedpola lodowców Scotta i Renarda (Spitsbergen). XIV Sympozjum Polarne, Lublin, 84-87.  
 Rieger, S. (1983) The genesis and classification of cold soils. Academic Press. New York, London, 230 pp.

- Schunke, E. (1981) Zur kryogenen Bodendynamik der Arktischen Tundren Nordamerikas und Nordeuropas. *Polarforschung* 51(2), 161-174.
- Szerszeń, L. (1974) Wpływ czynników bioklimatycznych na procesy zachodzące w glebach Sudetów i Spitsbergenu (Effect of bioclimatic factors on the processes occurring in the soils of the Sudety Mountains and Spitsbergen). *Roczn. Glebozn.* 25(2), 53-95.
- Świąś, F. (1988) Zróżnicowanie geobotaniczne tundry na południowym wybrzeżu Bellsundu (Zachodni Spitsbergen). *Wyprawy Geograficzne na Spitsbergen, UMCS, Lublin*, 215-228.
- Tedrow, J.C.F. (1977) *Soils of the polar landscapes*. Rutgers Univ. Press. New Brunswick, 638 pp.
- Ugolini, F.C., R.S. Sletten (1988) Genesis of arctic brown soils (Pergelic Cryochrept) in Svalbard. *Proc.: V Int. Conf. on Permafrost Trondheim, Norway* 478-483.

# CO-OPERATIVE RUSSIAN-CANADIAN ENGINEERING GEOLOGY INVESTIGATIONS OF PERMAFROST ON THE YAMAL PENINSULA, WESTERN SIBERIA

P.J. Kurfurst<sup>1</sup>, E.S. Melnikov<sup>2</sup>, A.M. Tarasov<sup>2</sup> and E.I. Tschervova<sup>2</sup>

<sup>1</sup>Geological Survey of Canada, 601 Booth Street, Ottawa, Ontario, Canada K1A 0E8

<sup>2</sup>Committee of Geology of Russia, VSEGINGEO, 142452 Zeleny Village, Moscow region, Russia

Extensive geotechnical field studies were carried out on the Yamal Peninsula, Russia in July 1991 as a part of a joint Canada-Russia program of scientific studies in the Arctic regions, in order to compare existing methodology and field techniques and to test new techniques and equipment for detection and delineation of massive ground ice and saline permafrost. Results of the field and laboratory studies provided basis for detailed geological and permafrost profiles and maps and led to selection and recommendation of effective methods and techniques of geotechnical mapping in different permafrost terrains, required by the oil and gas exploration and construction industries working in the Arctic.

## INTRODUCTION

Major oil and gas discoveries in the arctic areas of Canada and Russia have created an urgent need for regional and site specific knowledge of geological, geotechnical and geothermal conditions of these areas. This information is essential especially for the design, construction and maintenance of engineering structures such as pipelines and related facilities.

In this paper the methodology and preliminary results of geotechnical studies of the Bovanenkovo oil and gas field on the Yamal Peninsula, Western Siberia are described. The selection of the site for detailed field studies was based on evaluation of existing geological and landform maps of the northern Yamal Peninsula and results of drilling. Field studies included geological mapping, geotechnical drilling and borehole sampling, standard and experimental surface geophysical profiling and mapping, standard and experimental downhole logging, ground probing radar, and topographical surveys.

This investigation, based on preliminary interpretation of field and laboratory results, produced detailed profiles and maps of the distribution and extent of surficial materials, various bodies of massive ground ice, and zones of saline permafrost.

### Geological Setting

The Yamal Peninsula is located in Western Siberia in the northern part of the West Siberia basin (Fig. 1). The peninsula is 750 km long and 240 km wide and lies between the Obskaya and Baydaratskaya Gulfs of the Kara Sea (Fig. 1 - inset). The West Siberian Basin deepens northward, with several kilometres of sediments beneath the Yamal Peninsula. The sedimentary cover is composed of marine and terrestrial deposits of Jurassic, Cretaceous, Tertiary and Quaternary age. Bovanenkovo oil and gas field, shown in Fig.1, lies within the North-Central Gas District. The surface relief, developed in late Quaternary, consists mainly of the late Pleistocene and Holocene terraces (Ershov, E.D., editor, 1989). The terraced

surface of the region is cut by V-shaped river valleys. The slopes of these valleys are dissected by short ravines with steep slopes, partly caused by thermal erosion of ice-rich sediments. Polygon relief is widespread in the depressions and on the elevated and flat parts of the terraces. The study area is located within two major landscape units, first marine terrace (ImV) and recent river flood plain (OaA). A detailed map of the Bovanenkovo study site, showing the landscapes, land units and sub-units present, is presented in Fig. 2.

### Field Studies

The field studies of the Bovanenkovo area were carried out by scientists from the VSEGINGEO Institute in Moscow between 1987 and 1990. Based on preliminary 1:50 000 maps of landscape units and results from drilling, site KU-2-90 within the Bovanenkovo oil and gas field was selected for detailed investigations. Results of preliminary mapping and

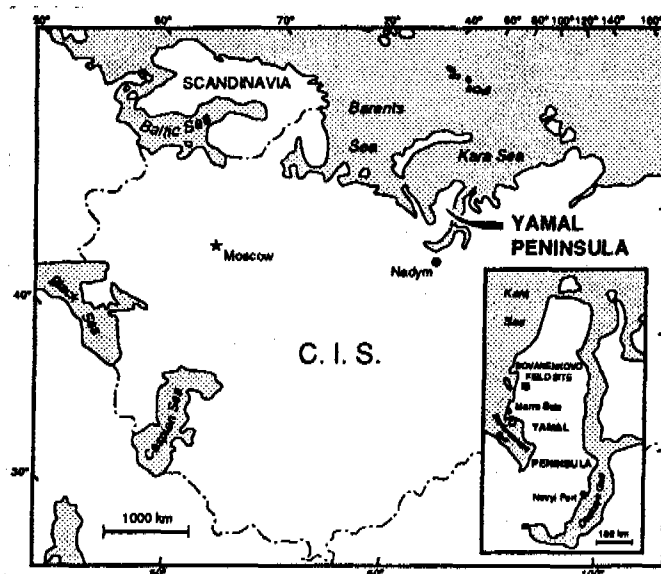


Figure 1. Location of the study site.

the 1990 drilling along four profiles (Fig. 2 - I to IV) indicated the presence of sediments ranging from clays to sands with varied ice contents. The study area was also underlain by large body of massive ice up to 12 meters thick. After studying the available maps and profiles, locations of geotechnical boreholes and geophysical surveys were selected by the scientists from the Geological Survey of Canada (GSC); all field work described in this paper was conducted by the joint VSEGINCEO/GSC team during July 1991.

#### Surface Mapping

Surface studies included detailed mapping of various surficial exposures and associated vegetation cover within two landscape types (OaA and ImV). The field results were combined into a landscape map of the study site showing land units and sub-units (Fig. 2). Surface mapping was complemented by a detailed topographic survey. Results of this survey, showing elevations and topographic contours, are summarized in Fig. 3.

#### Geotechnical Drilling and Sampling

Fourteen boreholes (1K-14K) ranging in depth from 10 to 24 m were drilled along profiles I, III and IV in locations where additional information on lithology or massive ice was required or in areas where geophysical anomalies were detected. In addition, two boreholes drilled in 1990 (34 and 36) were reamed out to allow downhole logging using Canadian equipment. Locations of the 1990 boreholes (1-44) and the 1991 boreholes (1K-14K) are shown in Fig. 2.

A small hand-held portable drill was used to drill 75 mm diameter boreholes and collect continuous soil and ice samples with spoon sampler. A total of 97 samples were collected for future laboratory analyses. All samples were logged for lithology, ice content and cryogenic structures and prepared for shipping. This information was combined into four profiles (I to IV) showing detailed geology and extent of massive ice (Fig. 4).

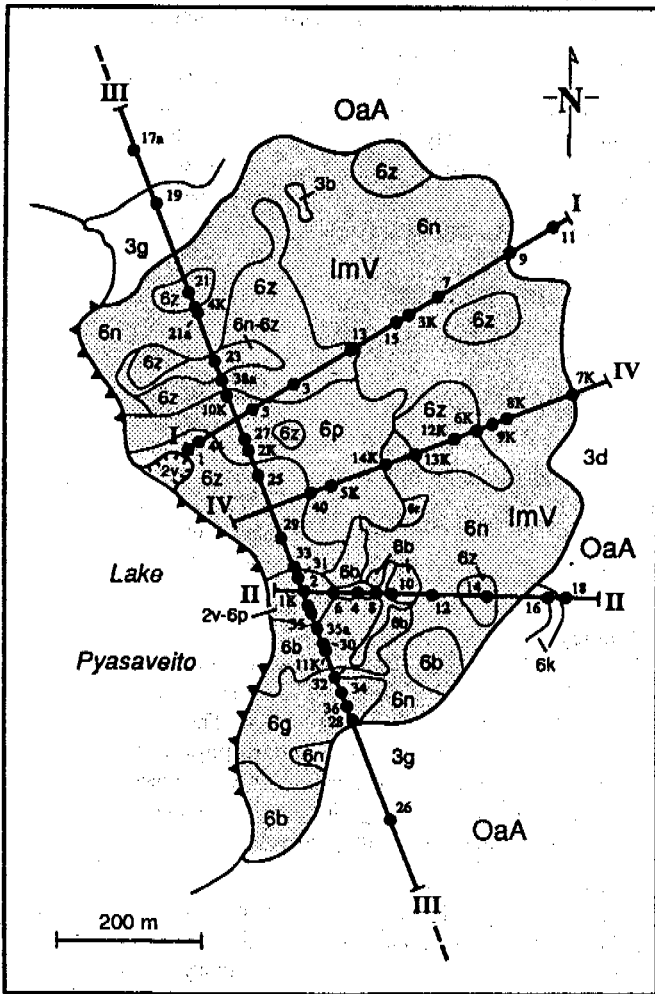


Figure 2. Landform map of the study site.

#### LEGEND

- I — I geological profiles
- 6K boreholes
- OaA / ImV boundaries of landscapes
- 3g (6n) boundaries of land sub-units
- ▲ shore scarps
- ∩ gullies

#### LANDSCAPES

- Im first marine terrace
- Oa recent river flood plain

#### LAND UNITS

- A lacustrine, bog, flat
- V solifluction / landslides, hilly

#### LAND SUB-UNITS

- First Marine Terrace**
- 2v ravines, gully
- 3b swamps, flat
- 6b terraces, polygonal, well drained
- 6g terraces, polygonal, poorly drained
- 6n terrace slopes
- 6p terraces, eroded
- 6z terrace slopes, micro-polygonal
- Recent River Flood Plain**
- 3d swamps, polygonal
- 3g swamp complex
- 6k low area of flood plain



Borehole bottom temperatures were recorded to provide detailed information on the geothermal regime at the study site; these temperatures are also presented in geology/ice profiles in Fig. 4.

#### Surface Geophysical Surveys

Surface geophysical surveys included standard electromagnetic (EM) surveys (EM-31 and Max-Min I portable EM units) and high frequency electrical profiling (VCHEP). These techniques were used to detect and map the horizontal distribution of shallow sediments with a high ice content or of massive ice. The EM surveys were run along 14 profiles totalling 7.8 km in length; their locations are shown in Fig. 3.

An experimental common depth point (CDP) shallow seismic shear wave reflection technique was also used to determine vertical and horizontal extent of massive ice bodies. Approximately 300 m of profile III were surveyed between boreholes 2K and 4K.

#### Standard Downhole Logging

Two passive (natural gamma, conductivity) and two active (gamma-gamma, neutron) downhole logs were run in all the 1991 boreholes (1K to 14K). Seismic downhole logging was conducted only in boreholes 1K, 2K, 4K, 10K and 11K.

The natural gamma tool detects amount of gamma radiation in subsurface materials in counts per second (cps).

Count rates range from up to 150 cps for clay to less than 50 cps for coarse-grained sand and gravel; count rates approaching 0 cps are indicative of large ice lenses or massive ice.

The conductivity tool measures conductivity of the formation directly in millisiemens per meter (mS/m). Conductivity values below 10 mS/m were found to correspond to ice bonding or excess ice in sediments. Higher conductivities are indicative of an increase in unfrozen water content, the presence of saline brine, or both. The gamma-gamma tool detects gamma radiation which is a measure of the density and mineralogy of the formation. In general, densities of ice-rich sediments are in 1.3-1.6 g/cm<sup>3</sup> range while density of massive ice is around 0.9 g/cm<sup>3</sup>.

The neutron tool measures neutron count rate in the formation and can be used as an indicator of water content in subsurface materials. The water content of ice-rich sediments is in range of 45-60%, while values for massive ice reach close to 100%.

Seismic downhole techniques were used in the boreholes to measure both compressional and shear wave velocities of the sediments, to complement the surface seismic reflection and refraction surveys done in the area.

Compressional wave velocities were in excess of 2000 m/s for all frozen materials and reached well over 3000 m/s in massive ice. Shear wave velocity variations correlate well with those of compressional wave velocity. Fine-grained sediments had shear wave velocities below 1000 m/s, while velocities in the range of 1000-2000 m/s were associated with ice-rich sediments and massive ice.

#### Ground Penetrating Radar

Several kilometers of line along profiles III, IV, A and D were surveyed using a pulse EKKO IV ground penetrating radar system developed in Canada. The system, which has a high resolution (10-30 cm) and a depth penetration of 10 to 30 m, was considered the most suitable for characterization of contrasting lithology and for the detection of zones of saline permafrost and massive ice.

Details description of the geophysical equipment and techniques used, field results and their interpretation are discussed by Burns, et al. (1992).

#### Laboratory Studies

Laboratory tests of soil, ice, water and organic samples collected from the Bovanenkovo field site were carried out both by the VSEGINGEO and GSC laboratories. The measurements included determination of standard physical properties (grain size, Atterberg limits, water content, density, salinity), geochemistry (clay mineralogy, ion content, stable isotopes) and age determination (radiocarbon dating).

#### Physical Properties

Detailed study of the physical properties was carried out to further delineate the stratigraphic and lithological boundaries of the sediments which had been tentatively established on the basis of detailed core logging in the field.

The gravimetric water content for all samples ranged from 18% in some silts and sands to nearly 100% in massive ice; the average value, excluding those of massive ice, was 42%.

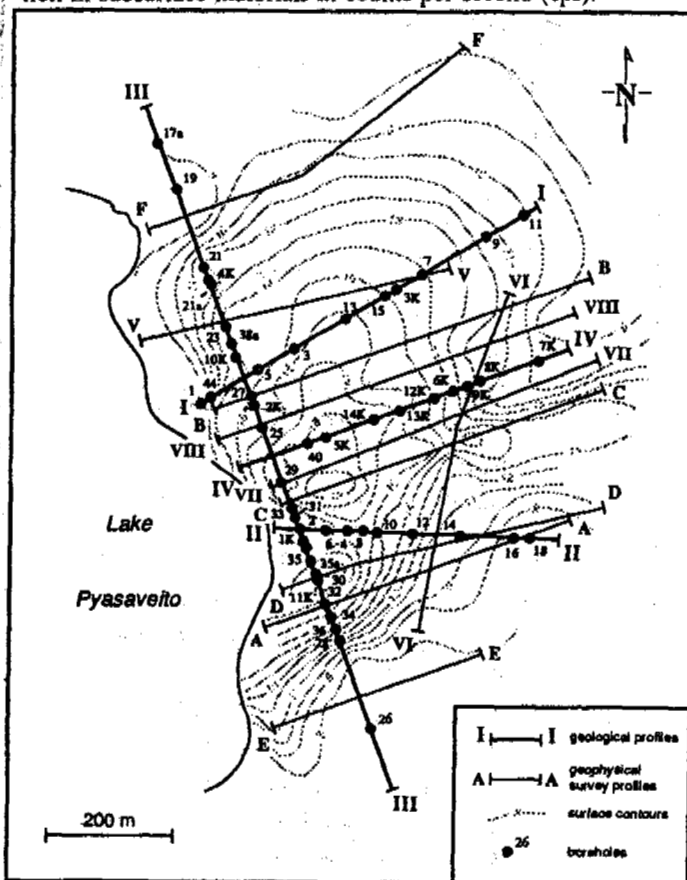


Figure 3. Topography map of study site with locations of geological and geophysical profiles.



Values of bulk density varied between 0.76 g/cm<sup>3</sup> for samples with high content of organic material to 1.77 g/cm<sup>3</sup> with average value 1.30 g/cm<sup>3</sup>.

Salinity values of massive ice and soil samples were very low (less than 3 ppt), with the exception of samples of clay from horizons between 3.8 and 4.1 m in boreholes 2K and 10K, which were 18 and 20 ppt respectively. A sample of water seepage, collected from borehole 7K, had an exceptionally high salinity value of 61 ppt. A typical borehole profile (borehole 1 K), summarizing the physical properties, is shown in Fig. 5.

#### Geochemistry and Mineralogy

Detailed chemical and mineralogical analyses of the samples were carried out to complement the results of the physical properties tests. The X-ray diffraction technique was used on 53 samples from eleven boreholes to determine clay mineralogy. Major clay minerals present included smectite, illite, kaolinite and chlorite. Smectite was the most frequently present clay mineral (from 29 to 75%), followed by illite (from 23 to 45%). Combined content of kaolinite and chlorite varied between 11 and 22%. All samples also contained traces of quartz and feldspar.

Thirteen samples from several boreholes were selected for detailed studies using the X-ray diffraction technique to analyze the unoriented powder samples of soils and of fractions larger than 0.1 mm. The results of these analyses of mineral content confirmed that various soil types (sands, clays and aleurites) are of same origin, i.e. their source is from same area, and their conditions of deposition were similar.

Water extracted from 63 samples was tested for pH and ion content (HCO<sub>3</sub><sup>-</sup>, Cl<sup>-</sup>, SO<sub>4</sub><sup>-2</sup>, Ca<sup>+</sup>, Mg<sup>+</sup>, Na<sup>+</sup> + K<sup>+</sup>). Samples from all 1991 boreholes had pH values between 7.15 and 8.13, with the exception of samples from borehole 7K, where pH varied between 5.15 and 7.05. The results showed that water samples from clayey soils deposited above the massive ice contained mainly ions Cl<sup>-</sup> and Na<sup>+</sup>. Samples of sandy soils, both from above and below the massive ice, showed the predominant presence of ions HCO<sub>3</sub><sup>-</sup>, Na<sup>+</sup> and Ca<sup>+</sup>, while mainly ions HCO<sub>3</sub><sup>-</sup>, Mg<sup>+</sup> and Na<sup>+</sup> were present in samples from the active layer.

Results of the chemical analysis of water from borehole 7K showed very high content of ions Na<sup>+</sup> and Cl<sup>-</sup> and presence of elements such as Br, I and others, typical of a marine environment. Over 100 samples of massive ice and of ice from the underlying and overlying sediments from boreholes 27, 32, 35, 1K, 2K, 3K, 4K, 6K, 10K and 11K and two samples of water seepage from borehole 7K were tested for isotope content (δ<sup>18</sup>O and δD). Values of δ<sup>18</sup>O and δD for massive ice ranged from -17.11 to -20.5 SMOW, and from -134.0 to -152.0 SMOW respectively, showing little variation with depth. The average values of δ<sup>18</sup>O and δD of massive ice from various boreholes were similar and ranged from -18.2 to -19.5 SMOW and from -138.9 to -147.5 SMOW respectively. Values of δ<sup>18</sup>O and δD of ice samples from deposits below and above massive ice show almost no difference from those of massive ice, with the exception of samples from ice and clay at shallow depths in borehole 2K

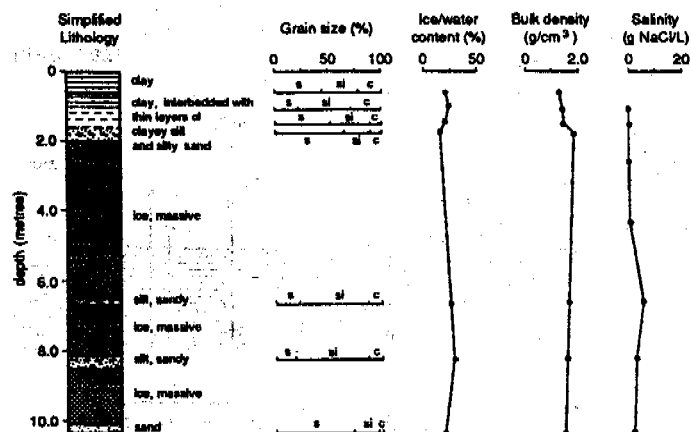


Figure 5. Typical log of physical properties.

where values of δ<sup>18</sup>O and δD are very high and similar to those of sea water. Two independent measurements of the seepage water produced δ<sup>18</sup>O values of -14.1 and -14.9 SMOW and δD values of -102.5 and -79.0 SMOW. For comparison, samples of precipitation, lake and sea water were also tested.

#### Discussion of Results

Surficial mapping and surveying provided detailed delineation of the extent and boundaries of land sub-units within two major, previously established landscapes; and of the soils and vegetation types, surface expression, the thickness of active layer, and ground temperatures associated with them. Seven and three land sub-units were recognized within the first marine terrace complex and recent river flood plain complex respectively.

Geotechnical drilling, sampling and field core logging were the bases for the identification of major lithological units and bodies of massive ice. Fine sands, sandy silts, and silty clays are three major types of sedimentary deposits within the study area. Organic material, from several centimetres to several meters thick, was commonly found in the core samples. The major body of massive ice was also identified in the study area. Its thickness ranged from 5 to 12 m and its width and length varied between 150 and 400 m. The massive ice was overlain by several meters of fine sand or silty clay and was underlain by a very thin layer (1-3 cm) of clayey silt gradually changing into sand. The ice was mainly clear, horizons near clay or sand deposits contained small inclusions (1-5 mm) of sediment material however. The ice often contained air bubbles, 1 to 2 mm in diameter.

Massive ground ice is commonly present in sediments on Yamal Peninsula. Although it has been studied by many experts (i.e. Melnikov et al., 1990), there is no consensus on its origin and growth mechanism. The following results from the VSEGIN GEO/GSC field and laboratory studies confirmed marine origin of deposits with massive ice:

- high content of NaCl was measured in clayey deposits;
- shells of marine molluscs were found in clay overlying massive ice (borehole 10K) as well as in the underlying silty sands (borehole 2K);

- grain size analyses of the overlying and underlying sediments confirmed that their mineral content is similar (sands and clays).

It has been suggested that some of the massive ice on Yamal Peninsula may be buried glacier ice. This seems unlikely, since the isotope content of massive ice and winter precipitation is similar. Winter precipitation was the major source in formation of massive ice. This precipitation fell into marine deposits during warmer periods, seeped through coarse-grained deposits (sands, silty sands) and then, during the cooler periods, refroze and formed lenses of ground ice. Values of  $\delta^{18}\text{O}$  and  $\delta\text{D}$  do not vary with depth (i.e. borehole 11K), thus suggesting that formation of ice occurred within the open system with a steady supply of water. Strong supportive evidence for formation of massive ice within soils is provided by presence of ice diapirs extending from ice into surrounding sands (i.e. borehole 11K). Similar diapirs extending from massive ice into overlying clays have been documented in other areas of Bovanenkovo field.

Interpretation of results of the surface electromagnetic surveys (EM-31, Max-Min) delineated distinct areas of high conductivity along about 100 m on profiles IV and VII and about 500 m along profiles VIII and B. These areas of high apparent conductivity correspond well with areas of low apparent resistivity mapped by other surface electrical method (VCHEP); they also coincide with areas of highest elevations. Results of drilling in these areas showed that the surface sediments were not underlain by ice. The high conductivity values hence suggested that either the active layer thickness increased or high salinity ground water was present near surface. Laboratory tests confirmed presence of highly saline water near surface in borehole 7 K (profile IV). Drilling also confirmed wet, unfrozen sediments in the area of a topographic low near a small lake at the end of profiles VIII and B. Low apparent conductivity values measured along the remaining profiles suggested that shallow permafrost table is present within 1-2 m of the ground surface.

The experimental shallow seismic shear wave reflection technique clearly detected clay/ice or clay/sand interfaces. It also successfully delineated the steeply dipping surfaces of the massive ice as well as its bottom. This technique was able to delineate the depth, shape and extent of the massive ice except in the areas where the interface between the massive ice and overlying frozen fine-grained sediments was shallow. The ground penetrating radar technique was able to detect boundaries between different lithologies and between massive ice and various types of sediments as well as to outline zones of saline permafrost. The downhole logging tools (natural gamma, conductivity, seismic, gamma-gamma, neutron) provided high resolution information on the extent and boundaries of various lithological units and massive ice. They also permitted qualitative differentiation within individual units of factors such as amount of ice in frozen sediments, inclusions in massive ice and the presence of saline horizons. The interpreted results also gave an excellent indication of the water content and density of the sediments.

## CONCLUSIONS

Field studies and their results reviewed in this paper show that in situ geotechnical and geophysical techniques, combined with surficial mapping and shallow geotechnical drilling and sampling, do provide a reliable approach to establishing detailed stratigraphic and lithological boundaries, detecting the presence and extent of ice-bonded sediments and massive ice, and delineating zones of saline permafrost. Results of the laboratory tests confirmed the validity and accuracy of the in situ measurements and provided information required for the detailed interpretation and increased resolution of the field results.

Complex geotechnical investigations of permafrost on Yamal Peninsula showed that:

- Maps of landforms and vegetation provide a good areal indication of various sedimentary materials and of the presence or absence of massive ground ice;
- Small, light portable drills are capable of drilling beyond 20 m depth and producing the quality of core samples of frozen materials and massive ice required for detailed logging and laboratory tests;
- Surface seismic techniques such as shear wave reflection provide a very good indication of the shape, extent and upper and lower boundaries of massive ice bodies;
- Surface electrical and electromagnetic techniques are suitable for the delineation of areas containing sediments with high ice content and salinity; and
- The combined use of surface mapping, geotechnical drilling and appropriate geophysical surveys will allow the quick and relatively inexpensive geotechnical characterization of permafrost conditions, especially for site specific investigations.

## Acknowledgements

The Canadian contribution to the field studies was supported by the funds provided by the Panel on Energy Research and Development. The authors wish to thank their Canadian and Russian colleagues participating in the field work on the Yamal Peninsula for stimulating discussions and comments. Special thanks are due to Mr. J.A. Heginbottom for his suggestions and comments to improve this paper. The reviewers provided useful advice on areas of the paper which required clarification. This is contribution of the Geological Survey of Canada #16792.

## REFERENCES

- Burns, R.A., Goriainov, N.N., Hunter, J.A., Judge, A.S., Skvortsov, A.G., Timofeev, V.M. and Todd, B.J., 1992. Cooperative USSR-Canadian geophysical investigation of permafrost on the Yamal Peninsula, Western Siberia. Submitted to Proceedings, 6th International Conference on Permafrost, Beijing, China.
- Ershov, E.D., Editor. 1989. Geocryology of USSR, West Siberia (in Russian). Nedra, Moscow, USSR.
- Melnikov, E.S., Kritzuk, L.N. and Pavlov, A.V., 1990. Geocryological and engineering-geological problems of development at Yamal (in Russian). VJEMS, Moscow, USSR, 53p.

## ARCTIC WELL DRILLING AND COMPLETION PROBLEMS

I.M. Kutasov

Consultant, 1444 S. Centinela  
W. Los Angeles, California 90025, USA

Drilling through permafrost raises some unique difficulties: washouts, caving of frozen soils, fill on the bottom, stuck pipe, poor primary cement jobs. When the well is shut-in, it will be subjected to potential hazards of external freezeback pressures, internal freezeback pressures, thaw consolidation. The main objective of this study is to demonstrate the impact of frozen soils present in well drilling and completion. In this paper the results of field and analytical investigations are presented which will allow one to find effective methods to control hole enlargement during drilling, to estimate the shut-in period of time during which the water based drilling mud would be free from freezing, and predict the radius of thawing. Some practical recommendations are proposed for drilling operators.

### INTRODUCTION

The development of oil and gas reserves in permafrost areas has required new drilling and well completions technology to deal with the impact of frozen soils. Drilling through permafrost raises some unique difficulties: intensive washouts, caving of frozen soils, fill on the bottom, stuck pipe, and poor primary cement jobs. When the well is shut-in, it will be subjected to the potential hazards of external freezeback pressures, internal freezeback pressures, and thaw consolidation. The drastic changes of mechanical properties of permafrost during thawing and refreezing is an important factor influencing the designs of producing wells. As permafrost is not homogeneous but varies in thickness, lithology, mechanical and thermal properties, it often happens that drilling methods successful in one area cannot be used in another.

The main objective of this study is to demonstrate the impact of frozen soils on well drilling and completion. In this paper the results of field and analytical investigations are presented which allow one to find effective methods to control hole enlargement during drilling, to estimate the shut-in period of time during which the water based drilling mud would be free from freezing, and to predict the radius of thawing. Some practical recommendations are proposed for drilling operators.

### RADIUS OF THAWING

When wells are drilled through permafrost, the natural temperature field of the formations (in the vicinity of the borehole) is disturbed, and the frozen rocks thaw out for some distance from the borehole axis. For frozen soils, ice serves as a cementing material, and therefore the strength of frozen soils is significantly reduced at ice-water transition. If the thawing soil

cannot withstand the load of overlying layers, consolidation will take place, and the corresponding settlement can cause significant surface shifts.

The settlement in the vertical direction has a greater significance when the shear stress acts downward on the casing causing compressive stresses which can deform the casing (Palmer 1978). The approximate estimates show that the magnitude of the settlement (the center displacement of the thawing soil ring) and the axial compressive stress are proportional to the squared values of the radius of thawing (Palmer 1978). Thus, for long term drilling, the radius of thawing should be estimated to predict platform stability and the integrity of the wellbore. The radius of thawing value also has significant effect on the thermal regime of wells during drilling and cementing. This circumstance has to be taken into account when selecting the oil well cement and mud.

To estimate the radius of thawing we will assume that the mud temperature at a given depth during drilling is equal to its mean value in time. The results of field and analytical investigations provide support for this assumption if the circulation period is more than several hours (Kutasov 1976). If the temperature of the permafrost is taken to be equal to the melting temperature of ice-bounded permafrost,  $0^{\circ}\text{C}$ , the heat flow into the frozen zone ring during drilling can be neglected. We will also assume a steady state temperature distribution in the thawed zone. In this case the well known solution of the Stefan equation is

$$\frac{I_t}{I_1} = \frac{H^2}{2} \ln H - \frac{1}{4} (H^2 - 1) \quad (1)$$

$$I_c = \frac{t a_t}{r_w^2}; \quad I_1 = \frac{a_c L w}{T_m k_t}; \quad H = \frac{h}{r_w}$$

where  
 $t_c$  = dimensionless mud circulation time  
 $l$  = dimensionless latent heat of the formations  
 $H$  = dimensionless radius of thawing  
 $h$  = radius of thawing  
 $t$  = mud circulation time at a given depth  
 $a$  = thermal diffusivity of thawed formation  
 $k_t$  = thermal conductivity of thawed formation  
 $r_w$  = borehole radius  
 $T_m$  = circulation mud temperature in the drill pipe - formation annulus at a given depth  
 $l$  = 80 kcal/kg - latent heat of ice  
 $w$  = ice content per unit of formation volume

Let us assume that the depth of the surface casing shoe (below the permafrost base) is  $l$ , and  $v$  is the average penetration rate. The duration of mud circulation at the given depth  $z$  is equal to:

$$t = \frac{l - z}{v} \quad (2)$$

From formulas (1.2) we obtain

$$\frac{v}{T_m} = \frac{4B_c(l - z)}{2H^2 \ln H - (H^2 - 1)} \quad (3)$$

$$B_c = \frac{k_t}{r_w^2 L W}$$

The results of calculations after Formula 3 for one example are presented in Fig. 1. For this example:  $w = 370 \text{ kg/m}^3$ ,  $k_t = 2.4 \text{ kcal/(m}\cdot\text{hr}\cdot^\circ\text{C)}$ ,  $z = 305 \text{ m(1000 ft)}$ ,  $r_w = 0.222 \text{ m}$ ,  $l = 671 \text{ m(2200 ft)}$

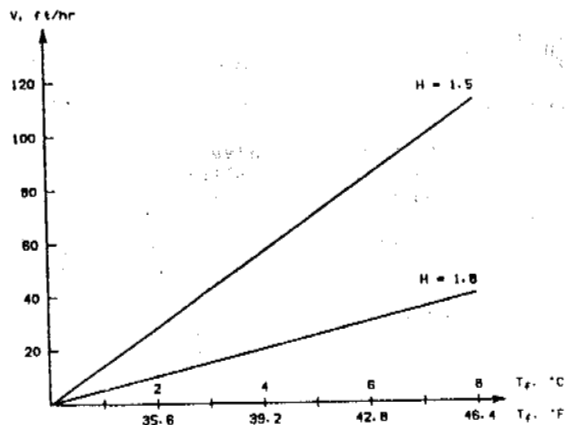


Figure 1. Penetration rate versus drilling mud temperature at  $H = 1.5$  and  $H = 1.8$

As shown by Fig. 1 the most effective way to reduce the permafrost thawing is lowering the drilling mud temperature. Indeed, to maintain the value of  $H = 1.8$  at a mud temperature of  $6.0^\circ\text{C}$  ( $42.8^\circ\text{F}$ ) the penetration rate should be  $9.14 \text{ m/hr}$  ( $30 \text{ ft/hr}$ ) or higher. Lowering the mud temperature to  $2.0^\circ\text{C}$  ( $35.6^\circ\text{F}$ ), the penetration rate of only  $3.05 \text{ m/hr}$  ( $10 \text{ ft/hr}$ ) will produce the same effect.

Now we will briefly discuss the use of brines with inlet temperatures below  $0^\circ\text{C}$  as drilling fluids. It is obvious that in order to prevent thawing, the annular mud temperature must be maintained below  $0^\circ\text{C}$ . High penetration rates while drilling the permafrost interval require high power inputs on the bit. It is commonly assumed that during drilling, more than 99 percent of the mechanical energy (rotary and pump input) is transformed into thermal energy. Experience in the Russian Federation, where conventional water base muds were used, has shown that the outlet drilling mud temperature was, in many cases, close to or even higher than that the inlet mud temperature when drilling permafrost (Gryaznov 1978).

In the McKenzie Delta area (Canada), the XKB (XC polymer, KCl, bentonite) system was applied to drilling permafrost (Hanni 1973). The original concept was to use KCl in the mud system to lower the mud freezing point below  $0^\circ\text{C}$ . It was hoped that by using a super-cooled mud, the thawing of permafrost could be prevented. During drilling it was found virtually impossible to maintain the annular mud temperature below  $0^\circ\text{C}$  (Hanni 1978). The main point is that at high rates of heat generation on the bit, the small variations in the inlet mud temperature (which can be achieved by using brines) have an insignificant effect on permafrost thawing around the well. From this point of view, only with reverse mud circulation should the possibility of using brines be considered.

It is also known that ice disintegrates if it is exposed to brines. With the passage of time the soil's cohesion will be significantly reduced due to breaking off bonds between ice and soil particles. Under this condition it is very difficult to make a good cementing job. Because of this, fresh water has to be used (causing thawing) to clean up the well before cementing.

#### WASHOUTS AND CAVING

A number of problems occur during Arctic drilling: hole and surface instability, and poor cementing jobs intimately associated with washed out formation. During drilling, the formation is heated by circulation of a warm drilling fluid. As a result, the strength of soils around the well is significantly reduced by the melting of the ice. Heating of frozen soils without thawing also sharply reduces the shear strength of soils and results in the initiation of washouts. Experimental investigations have shown that the shear strength of permafrost depends mainly on the negative temperature, the value of external pressure, and the time of load action. During drilling operations, the increase of the temperature of permafrost (increase of the unfrozen water content) can result in a significant reduction of cohesion, which accounts for a substantial part of the total shear strength of frozen soils. Thus the hole enlargement due to caving of frozen soils is possible even when the temperature of the drilling mud is maintained below  $0^\circ\text{C}$ .

The field experience and experimental data have shown that three main causes may be responsible for hole enlargement in permafrost areas (Kutasov et al. 1977; Goodman 1978; Kutasov and Bates 1980):

- a. Frozen soil impermeability, which hinders filter cake build-up and limits differential pressure (overbalance) needed for well bore

- support.
- b. Filtration of fluid from drilling mud into the thawed zone, which reduces the intergranular cohesion forces and tends to fluidize thawed soils.
  - c. Caving of frozen soils due to sharp reduction of their strength properties with the increase of temperature during drilling.

Experience has shown that consolidated frozen soils are not susceptible to washouts problems. Caliper logs at the Prudhoe Bay Field have shown that a gauge hole could not be obtained when drilling the permafrost interval (Perkins et al. 1974). The interval 100-450 ft. (mostly well graded gravel with some strata of silty sand) was especially sensitive to washout (Fig. 2).

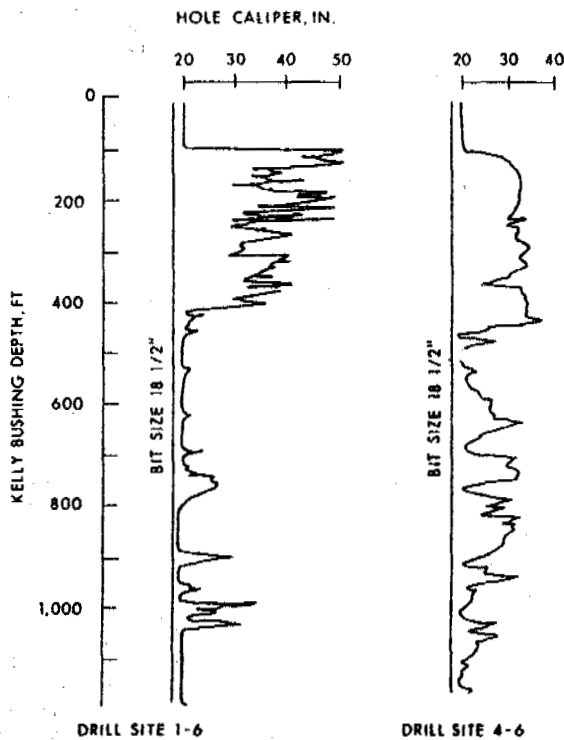


Figure 2. Caliper logs through permafrost at Prudhoe Bay (Perkins et. al 1974).

The Soviet experience (Gryaznov 1978; Kutasov and Bates 1980) has shown that washout can present a severe problem even in areas where the main body of the permafrost is at temperatures below  $-3^{\circ}\text{C}$  and where the predicted radius of thawing was quite small.

Especially extensive washouts occur in high-temperature permafrost (Kutasov and Bates 1980), where the temperatures of unconsolidated frozen soils (shaley sands with about 20% of ice content) are close to  $0^{\circ}\text{C}$ . For example, typical wells in the Medvezhe gas field (Russia, Tyumen region) completely filled the reserve pit (150 m) with cuttings in a matter of days. Solids control systems were easily overloaded. Computations indicated that the volume of material removed was up to four times greater than would be indicated by the radius of thawing (Equation 1). This can only be explained by additional volume of material added to the hole by caving of frozen

soils due to reduction of their strength with an increase of the temperature during drilling. It is interesting to note that in many cases the drilling operators in the Medvezhe field observed crystals of ice in the cuttings. The hole enlargement caused caving of the soil around the well head during drilling through permafrost. In some long drilling wells, the derricks were repositioned (Kutasov and Bates 1980).

To estimate the radius of washouts, we considered an extreme case when ice is the only cementing material of frozen soils, and the initial temperature of the formation is equal to the temperature of ice melting ( $0^{\circ}\text{C}$ ). We also assumed that during drilling the thawed material is removed from the borehole by the mud circulation system. In this case the radius of washouts will be equal to the maximum radius of thawing, and the position of the moving mud-frozen soils interface can be obtained from the Stefan equation:

$$\frac{Lw}{2} \frac{dd_h}{dt} = h_c T_m$$

where

$T_m$  = circulation mud temperature in the drill pipe-formation annulus at a given depth,  $^{\circ}\text{C}$   
 $t$  = mud circulation time  
 $h_c$  = the convective heat transfer coefficient  
 $d_h$  = thawed hole diameter = washout diameter

The values of the convective heat transfer coefficients for laminar and turbulent flow were taken from the literature.

For laminar flow:

$$h_c = \frac{4k_m}{d_h - d_p}$$

where

$k_m$  = thermal (molecular) conductivity of drilling mud  
 $d_p$  = drill pipe (outer) diameter

For the turbulent flow the value of  $h_c$  was calculated from the Dittus-Boelter equation. We obtained formulas which allow one to predict the maximum value of the washouts diameter (Kutasov and Caruthers 1988). For laminar flow:

$$K = \frac{1}{D} + \sqrt{\left(1 - \frac{1}{D}\right)^2 + \frac{16T_m k_m t}{Lw d_p^2}} \quad (4)$$

Where the washout coefficient, the bit diameter and drill pipe outside diameter ratio are defined by

$$K = \frac{d_h}{d_b} \quad D = \frac{d_b}{d_p}$$

where

$d_b$  = bit diameter

Thus, for laminar flow in the annulus, the hole enlargement can be minimized when the thermal conductivity of the drilling fluid is low, the penetration rate is high, and the temperature is maintained as close to  $0^{\circ}\text{C}$  as possible.

For turbulent flow:

$$\frac{Bt_D}{I_1} = F(KD) - F(D) \quad (5)$$

$$F(x) = \frac{5}{14} (x+1)^{2.0} - \frac{10}{9} (x+1)^{1.0}$$

$$B = 0.046 \left( \frac{4q}{\pi v d_p} \right)^{0.8} \left( \frac{v}{a} \right)^{0.4}$$

$$t_D = \frac{at}{d_p^2} \quad I_1 = \frac{Lwa}{T_m k_m}$$

where

$t_D$  = dimensionless mud circulation time

$I_1$  = dimensionless latent heat of the formations

$a$  = thermal diffusivity of drilling mud

$v$  = kinematic viscosity of drilling mud

$q$  = volumetric flow rate

As can be seen from the last expression, the washout coefficient decreases with reduction in flow rate and increasing fluid viscosity. Both the minimum annular fluid velocity and fluid viscosity are controlled by the ability of drilling fluids to carry cuttings out of the hole. It is also clear that the reduction in the time of mud circulation (increasing the penetration rate) is not a controllable factor.

At first blush, it would appear that the use of drill pipes with large diameters would have a significant impact on the hole enlargement, but this is not a case, because the function  $F$  is strongly dependent on the value of  $D$  (bit diameter to drill pipe overall dimension ratio). It can be shown that for turbulent flow in the annuli, the lowering of drilling fluid parameters (temperature, density and specific heat) is most effective in reducing the washout diameter. The field data and results of analytical and experimental investigations (Kutasov et al. 1977; Kutasov and Caruthers 1988) have shown that several options are available to drilling operators to control hole enlargement while penetrating the permafrost interval:

a. Fluid infiltration into the thawed zone plays a dominant role in hole enlargement. The diameter of washouts can be reduced when water base drilling muds have small water losses or when oil base fluids are used. The density of the drilling muds should be minimal.

b. The caving of frozen soils can be mainly responsible for hole enlargement when one is penetrating nonconsolidated high temperature permafrost. In this case, chilled muds and high density drilling muds should be used.

c. The most effective way to reduce permafrost thawing and hence the washout diameter is lowering of temperature, density and specific heat of drilling muds and increasing mud viscosity. Minimal flow rates should be used to reduce the heat exchange between the frozen soils and drilling muds and to minimize the mechanical erosion.

d. A bentonite mud can be designed for use only when one is penetrating low ice content permafrost. This is the only case when the mud cake is built up.

## SAFETY PERIOD

If a well is shut-in during drilling, the water base fluids in casing-casing, drill pipe-casing or tubing-casing annuli will refreeze and generate radial loads in the borehole. This process, termed internal freezeback, is distinguished from external freezeback of thawed permafrost and water base fluids outside of the casing (Goodman 1978). In some cases, high enough pressures may develop to cause casing and drill pipe damage (Gryaznov 1978; Kutasov and Bates 1980).

In Siberia collapsed casing and collapsed production strings were observed both in wells in which drilling has been temporarily suspended and in wells which have been completed and were awaiting production. Collapsed casing were not observed at depths greater than 150 m nor at temperatures warmer than  $-2.0^\circ\text{C}$  (Gryaznov 1978).

If the water in permafrost soils freezes at  $0^\circ\text{C}$ , the internal freezeback starts only when the external freezeback is completed. It is known, however, that in the freezing of soils, and especially in fine soils, by no means does all of the pore water change to ice at the freezing temperature of the soils, but only part of it. With further lowering of temperature ( $^\circ\text{C}$ ), phase transition of water continues, but at steadily decreasing rates (Tsytoovich 1975).

Freezeback could be a problem if it becomes necessary to temporarily abandon drilling operations. The drilling engineer needs to be able to determine the amount of time he can suspend fluid circulation without the drilling mud freezing. If the shut-in period is more than the "safety period" (free from freezing of drilling mud in the well), the water base mud in the permafrost section has to be replaced by oil mud or a low freezing-point fluid.

An empirical formula is presented below which allows one to predict the safety shut-in time ( $t_{sp}$ ) at various drilling times and permafrost temperatures ( $T_f$ ). Let us assume that the well is temporarily shut-in and the mud circulation is stopped at the moment of time  $t = t_d$  (Fig. 3).

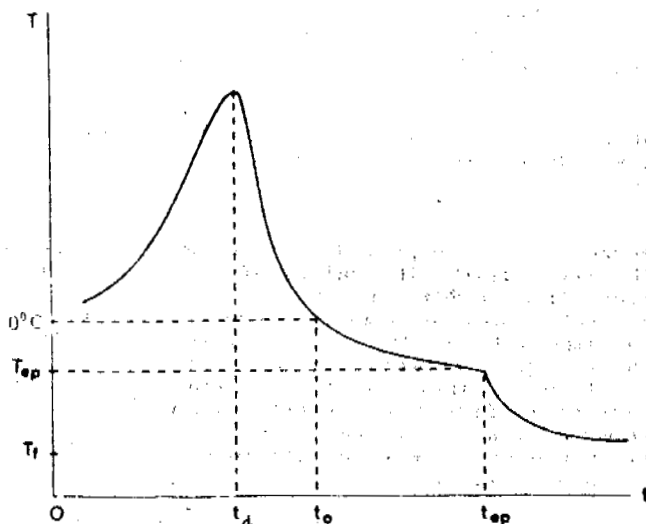


Figure 3. Downhole temperature versus time for a given depth - schematic curve.



From physical considerations it is clear that the radius of thawing will increase for a definite period of time ( $t_0 - t_d$ ) at the expense of heat stored in the thawed zone during drilling. This period of time may be called the safety shut-in period. During this time the temperature of the drilling mud in the wellbore will be greater than  $0^\circ\text{C}$ , and drill pipe will not freeze with mud.

The question may arise, "why not consider the period of time ( $t_{ep} - t_d$ ) as a safety period" (Fig. 3). It should be noted that at the moment of time  $t - t_{ep}$ , the phase transition between water and ice is practically completed. As was mentioned above, the presence of unfrozen water at temperatures less than  $0^\circ\text{C}$  leads to the conclusion that only a part of water freezes at  $0^\circ\text{C}$ . Therefore, it is possible that for moments of time  $t < t_{ep}$ , a significant amount of water in the formation will remain unfrozen and in the same time the drilling mud may be in a frozen state, because it was assumed that the drilling mud freezes at  $0^\circ\text{C}$ . Geothermal investigations in permafrost areas have shown that even at  $-1^\circ\text{C}$  the freezing of formations continues for a large section of permafrost.

The magnitude of the "safety period" depends mainly on the duration of the thermal disturbance (drilling time) and on the static temperature of permafrost (Kutasov 1976; Kutasov and Strickland 1988). Precise temperature measurements (61 logs) conducted by the Geothermal Service of Canada in 32 deep shut-in wells in Northern Canada were used to estimate the values of  $t_{sp}$  (Kutasov and Strickland 1988). The total drilling time ( $t_t$ ) for these wells ranged from 4 to 404 days, the total vertical depth ( $h_t$ ) ranged from 1356 m (4,450 ft) to 4704 m (15,430 ft), and the depth of permafrost ( $h_p$ ) ranged from 74 m (243 ft) to 726 m (2,380 ft).

We have found that the duration of the "safety period"  $t_{sp}$  for a given depth can be approximated with sufficient accuracy as a function of two independent variables: time of thermal disturbance at the given depth (drilling time) and permafrost static temperature ( $T_1$ ). A regression analysis computer program was used to process field data. We have found that the following empirical formula can be used to estimate the safety shut-in period:

$$t_{sp} = 3.06 t_d^{0.017} (-T_1)^{-1.5} \quad (6)$$

where  $t_d$  is the thermal disturbance time at a given depth. The value  $t_d$  is:

$$t_d = t_t - t_h$$

where  $t_h$  is the period of time needed to reach the given depth. The values of  $t_h$  can be determined from drilling records.

A safety factor of 2 was introduced in Equation 6 to compensate for the largest differences between observed and calculated values of  $t_{sp}$ . The accuracy of the results (Equation 6 without the safety factor) is  $\Delta(\ln t_{sp}) = 0.664$  and was estimated from the sum of squared residuals. It should be remembered that in Equation 6, time is in days and temperature in  $^\circ\text{C}$ .

Example: A well is drilled offshore in the Beaufort Sea near Prudhoe Bay. The temperature-depth curve is presented in Fig. 4. Only three days were spent penetrating the permafrost section of the well. After 40 days drilling has to

be discontinued at the depth 8,000 ft. Can the well be shut-in for 2 weeks?

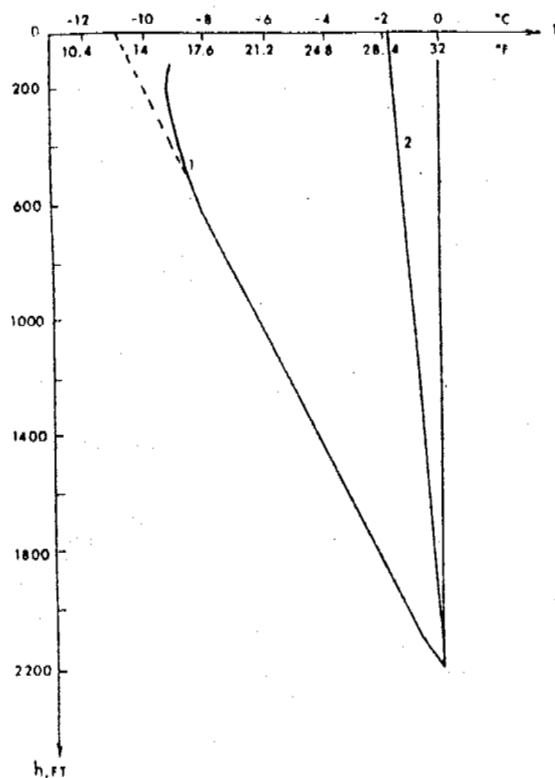


Figure 4. Permafrost temperature versus depth: 1 - Prudhoe Bay (Gold and Lachenbruch 1973); 2 - Beaufort Sea (estimated).

Step 1. From Fig. 4 one can determine that the surface permafrost temperature is  $-1.8^\circ\text{C}$ .

Step 2. Assuming that for the upper permafrost section  $t_d \approx t_t = 40$  days

From Formula 6 one can estimate that the value of  $t_{sp} = 26$  days. Thus, the well can be shut-in for 2 weeks and the drilling fluid will not freeze.

## CONCLUSIONS

Analytical and empirical formulas are presented which will allow one to control hole enlargement during drilling, to evaluate the safety shut-in period, and to predict the radius of thawing. The application of suggested recommendations may reduce the cost of drilling and completion operations in permafrost areas.

## REFERENCES

- Gold, L.W., and A.H. Lachenbruch (1973) Thermal Conditions in Permafrost - A Review of North American Literature. Permafrost (North American Contribution), Second International Conference, July 13-28, 1973, Yakutsk, USSR National Academy of Sciences, Washington, D.C., 10.
- Goodman, M.A. (1978) World Oil's Handbook of Arctic Well Completions. Gulf Publishing Company, Houston, 8-10.

- Gryaznov, G.S. (1973) Designs of Gas Wells in Permafrost Areas. Nedra, Moscow, 1978, 136p.
- Hanni, G. (1973) Drilling the Permafrost. Baroid News Bulletin, April, 21-23
- Kutasov, I.M. (1976) Thermal Parameters of Wells Drilled in Permafrost Regions. Nedra, Moscow, 119p.
- Kutasov, I.M. Tarasov, A.A., and Kononov, Yu.I. (1977) Experimental Study of Washouts in Frozen Rocks Using Models of Drilling Wells. Neftianoe Khoziaistvo, June, 1977 21-33
- Kutasov, I.M., and T.R. Bates (1980) Arctic Drilling Technology in the Soviet Union. Paper 80-Pet-73, Presented at the 1980 ASME Energy Technology Conference and Exhibition, New Orleans, February 3-7
- Kutasov, I.M. and D.G. Strickland (1988) Allowable Shut-in is Estimated for Wells in Permafrost. Oil & Gas Journal, Sept. 5, 55-60.
- Kutasov, I.M. and R.M. Caruthers (1988) Hole Enlargement Control During Arctic Drilling. Proceedings of the SPE California Regional Meeting, Long Beach, March 23-25. 393-400.
- Palmer, A. (1978) Thawing and the Differential Settlement of the Ground Around Oil Wells in Permafrost. The USSR Contribution to the Second International Conference, July 13-28, Nat. Acad. Sci., Washington, D.C., 619-624
- Perkins, T.K., J.A. Rochon, and C.R. Knowles (1974) Studies of Pressure Generated Upon Refreezing of Thawed Permafrost Around a Well Bore. Journal of Petroleum Technology, October, 1159-1166
- Tsyrovich, N.A. (1975) The Mechanics of Frozen Ground. Scripta Book Company, Washington, D.C., 8-250

A MODEL OF ELASTIC WAVE PROPAGATION IN FROZEN MEDIA  
COMPARISON WITH EXPERIMENT.

P. Leclaire\*, F. Cohen Tenoudji\* and J. Aguirre-Puente\*\*

\* LUAP, Université D. Diderot (Paris 7), Paris, France  
\*\* Laboratoire d'Aérothermique du CNRS, Meudon, France

A model is developed within the framework of Biot's theory of elastic wave propagation in porous media. In the case of ground freezing, three constituents are present in finely dispersed soils under 0°C: the soil solid grains, ice particles and liquid water. After modelization of interactions between the three constituents, elastic potential and kinetic density functions and an energy dissipation term are obtained leading to the equations of propagation. The resolution of these equations allows the calculation of velocities and attenuations of several longitudinal and transverse waves which are functions of the unfrozen water content and depend upon frequency. A thermodynamical argument is used to evaluate the unfrozen water content with temperature; it is then possible to predict the velocity and attenuation of the waves at a given temperature. Experiments are performed with longitudinal and transverse waves in through transmission experiments on both consolidated and unconsolidated media. The results are discussed in comparison with the present theory.

## INTRODUCTION

Mechanical properties of soaked soils at temperatures below 0°C are strongly dependent upon the respective proportions of frozen and unfrozen water contents, quantities which vary with temperature. These proportions are functions of the soil granulometry and porosimetry: In fact a medium with very fine porosity will tend to have a higher unfrozen water content at a given temperature than a coarse medium. Acoustic wave propagation provides a non destructive method to evaluate mechanical properties and could be used with the objective to deduce the soil thermodynamical state from the acoustical measurements. A model of acoustic propagation in this multicomponent medium is necessary in order to interpret the experimental results. It has been shown [1-3] that the simple semi-empirical approaches were unable to explain the totality of experimental results: the model of weighted average of constituents bulk moduli would apply better for a non consolidated soil (with a low frame stiffness compared to the constituents moduli) and the average slowness model for a consolidated one (the moduli of the solid frame are of the same order than the constituents moduli), but today no theory of acoustic wave propagation in frozen grounds has been given.

The frame of the exact theory of acoustic propagation in porous media has been established by Biot [4,5]. Applied to a biphasic medium, this theory provides the values of both wave velocities and attenuations for the different types of waves propagating in the medium [6,7]. It has been successfully applied for the interpretation of seismic signals in geophysical research [8]. The aim of this work is to apply Biot's approach to ground freezing where three constituents coexist: solid particles, ice particles and unfrozen liquid water. The expected results would give the possibility of predicting the different acoustic waves velocities for both consolidated and unconsolidated media and the attenuations of

these waves starting from the mechanical properties of the three constituents. The final objective is the possibility to extract soil state parameters such as unfrozen water content from interpretation of experimental results. The problem treated here considers only the case of total saturation of the solid by water when it is unfrozen.

Experiments have been performed on selected consolidated and unconsolidated samples in order to back up the fundamental aspects of the study.

## THEORETICAL ARGUMENTS

The results presented here are part of the doctoral work of one of us [9]. Only the general guidelines will be given here. The details of the theory will be published elsewhere.

Biot's theory deduces the wave propagation equations from the Hamilton's least action principle applied to the effective continuous medium, equivalent to the real inhomogeneous mixture. This approach is valid when wavelengths are much greater than the sizes of heterogeneities within the medium, a condition satisfied in most measurements. Three energy densities are used: the potential energy density  $V$ , the kinetic energy density  $C$ , and a dissipation potential density  $D$ .

### Potential energy density $V$

The elastic potential energy density  $V$  may be written as a sum of several terms. Some terms are relative to the movements of one constituent, the others being fixed: this defines the concept of an effective constituent. Other terms contain the combination of movements of two constituents; these are coupling terms between the effective constituents.

In our case, three constituents are present. In order to render the problem more practicable, the important assumption has been made that unfrozen water exists between the solid and ice particles such as there is no direct coupling between these

two phases. Indeed it is well known that unfrozen water tends to form films on the solid particles isolating them from the ice [17].

For small amplitudes of deformations and variations of temperature from the equilibrium state and in the absence of external forces, the potential energy may be developed to the second order. Using the indexes: 1 for the effective solid, 2 for the effective fluid and 3 for the ice as a second effective solid one may write:

$$V = \mu_1 d_1^2 + \frac{1}{2} K_1 \theta_1^2 + C_{12} \theta_1 \theta_2 + \frac{1}{2} K_2 \theta_2^2 + C_{23} \theta_2 \theta_3 + \frac{1}{2} K_3 \theta_3^2 + \mu_3 d_3^2 \quad (1)$$

where the bulk compression moduli are respectively  $K_1$ ,  $K_2$  and  $K_3$  and the shear moduli of the two solids are  $\mu_1$  and  $\mu_3$ . In a classical way for an isotropic medium, the strain tensors have been decomposed in spherical parts describing the dilatations  $\theta_i$  and in deviators  $d_{ij}^{(1)}$  and  $d_{ij}^{(3)}$  (with  $d_{ij}^{(1)} \cdot d_{ij}^{(1)} = d_1^2$  and  $d_{ij}^{(3)} \cdot d_{ij}^{(3)} = d_3^2$ ). The crossed terms  $C_{12}$  and  $C_{23}$  characterize the elastic coupling between the solid and water and between the water and ice; The term  $C_{13}$  is missing according to the assumption that there is no direct coupling between solid and ice.

In our case in a first step we need to calculate the elastic constants of the three constituents taken separately. For the two solids, we need to know if they form skeletons and the elastic constants of these skeletons. We treat differently the media where the solid is consolidated or unconsolidated at ambient temperature. We use for the solid matrix at all temperatures the constants evaluated at ambient. Doing so we make the hypothesis that ice formation does not affect the rigidity of the solid frame. We have tested a different assumption in the paper published in collaboration with J.F. Thimus presented also at this Conference [10]. For the solid matrix where the porosity  $\epsilon$  is generally less than 0.4, the Kuster and Tökösz model [11] is used to evaluate the solid matrix constants when the solid is consolidated at ambient temperature. For ice, we have made the assumption that the ice skeleton is completely connected at low temperatures. The apparent porosity is greater than  $1 - \epsilon$  and the Kuster and Tökösz model may be applied at low temperatures but is not relevant when the ice content is very small. A percolation model is used to describe the evolution of the elastic constants as ice forms and the bonds between ice particles occur progressively in the material bulk when temperature decreases. In a general manner, the percolation theory can be used to describe the transition of a system or a material between the continuous state and the discontinuous state. In the paper presented in collaboration with J.F. Thimus [10] a second percolation effect of the solid particles is described. The percolation threshold of the ice matrix has been arbitrarily taken at 0°C. The elastic constants of the ice matrix have been written as:

$$\begin{cases} K_{im} = K_{imMax} \left( \frac{\phi_i}{\epsilon} \right)^\tau \\ n_{im} = n_{imMax} \left( \frac{\phi_i}{\epsilon} \right)^\tau \end{cases} \quad (2)$$

where  $\phi_i$  is the ice volume fraction and  $\epsilon$  is the porosity. We take the same critical exponent  $\tau$  for the bulk modulus  $K_{im}$  and the shear modulus  $n_{im}$ . For a tridimensional system and for elasticity, the chosen value has been 3.8 [12, 13]. The maximum values  $K_{imMax}$  and  $n_{imMax}$  are determined with the use of the elasticity model of Kuster and Toksöz.

Given the elastic properties of each constituent the next step is the evaluation of the constants of the effective media appearing in equation (1). For the case of a two constituent mixture, Biot and Willis [14,15] have given a physical significance of these effective elastic coefficients by conceptual experiments. They have been able to formulate those in terms of the elastic coefficients of the constituents taken separately. We have applied their arguments and expressed the coefficients in (1). The shear strength induced by the viscosity of water at the measurement frequency has been included (Ref[9]).

#### Kinetic energy density C

The kinetic energy density C may be expressed as a function of the local velocities  $\dot{u}_i$  of the three effective phases. It contains also crossed coupled terms where a mass term multiplies the product of the velocities of the two phases; this mass coefficient expresses the additional inertial mass when the movement of one phase carries along the movement of the other. One may write:

$$C = \frac{1}{2} \rho_{11} \dot{u}_1^2 + \rho_{12} \dot{u}_1 \dot{u}_2 + \frac{1}{2} \rho_{22} \dot{u}_2^2 + \rho_{23} \dot{u}_2 \dot{u}_3 + \frac{1}{2} \rho_{33} \dot{u}_3^2 \quad (3)$$

The terms  $\rho_{12} \dot{u}_1 \dot{u}_2$  and  $\rho_{23} \dot{u}_2 \dot{u}_3$  characterize the inertial coupling between the solid and water and the ice and water. As above this expression does not contain a term in  $\dot{u}_1 \dot{u}_3$ ; this results from the assumption of absence of mechanical contacts between solid and ice. The expressions for the inertial coefficients have been found using the results given by Biot [15].

#### Dissipation energy density D

The dissipation potential may be written as the sum of two contributions:

$$D = \frac{1}{2} b_{11} |\dot{u}_1 - \dot{u}_2|^2 + \frac{1}{2} b_{33} |\dot{u}_2 - \dot{u}_3|^2 \quad (4)$$

where  $u_i$  are the effective velocities of solid, water and ice;  $b_{11}$  and  $b_{33}$  are real coefficients respectively defined as the friction coefficients between the solid and water and between ice and water; they are proportional to the water viscosity and volume fraction and inversely proportional respectively to the permeability of the solid frame and of the ice matrix.

The dynamical equations are obtained from Lagrange's equations which express the relationship between the stresses and the generalized momentum. The propagation equations are deduced in a three by three matrix form (three constituents) with the use of the different energy densities to evaluate the stresses and momentum. The complexity of the obtained expressions makes a numerical solution mandatory.

#### Relationship between temperature and unfrozen water content

With the help of Thomson's formula [17] and porosimetric distribution, it is possible to determine a thermodynamical relationship between the unfrozen water content and temperature. For a given medium, one may then obtain velocities as function of temperature.

Thomson's formula gives the equilibrium temperature T at the ice-water interface in a capillary pore with radius r:

$$\ln \frac{T}{T_0} = - \frac{2 \sigma_{iw}}{r \rho_i L_w} \quad (5)$$

where  $\sigma_{iw} = 3.5 \cdot 10^{-2} \text{ N.m}^{-1}$  is the surface tension at the interface,  $\rho_i = 920 \text{ kg.m}^{-3}$ ,  $L_w = 3.337 \cdot 10^5 \text{ J.kg}^{-1}$

is the latent ice fusion heat and  $T_0 = 0^\circ \text{C} = 273 \text{K}$ . The unfrozen water content  $\phi_w$  may be written as the product of the porosity  $\epsilon$  and of the distribution function  $F(r)$ ; this last function gives the pore fraction of which radii are greater than  $r$ :  $\phi_w = \epsilon F(r)$ . Let us write  $r_0 = 2 \sigma_{iw} / \rho_i L_w$ , then

$$\phi_w = \epsilon F(r) = \epsilon \int_{-\infty}^{r_0 / \ln(r/r_0)} f(r) dr. \quad (6)$$

with  $f(r)$  the probability density function being the derivative of  $F(r)$ . Assuming a Gaussian porosimetric repartition, we evaluate in figure 1, the unfrozen water content for an average radius  $r_{ave} = 0.1 \mu\text{m}$ , for several standard deviations, and for a porosity  $\epsilon = 0.3$ .

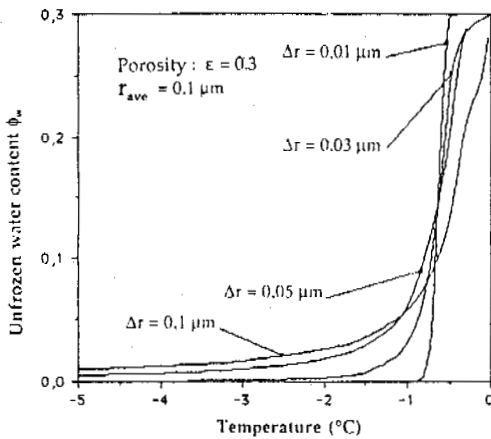


Figure 1.- Unfrozen water proportion calculated with Thomson's formula for a Gaussian porosimetric distribution.  $r_{ave}$  and  $\Delta r$  are respectively the average value and the standard deviation of the pore radius distribution.

### NUMERICAL RESULTS

Using Newton's complex method the numerical resolutions of the characteristic equations give the velocities and attenuations of the different modes as functions of the volumic proportions of liquid water. The three longitudinal modes are labeled  $L_1$ ,  $L_2$ ,  $L_3$ , and the two transverse  $T_1$ ,  $T_2$ . These modes are associated with the presence in the frozen medium of solid, unfrozen water and ice taken as effective phases. Nevertheless, because of the existence of elastic and inertial coupling, each mode does not propagate in the phase labeled with the same index as it may be thought but must be considered as an eigen mode propagating independently in a fictitious material support. Hence the waves indexed 1 can be considered as principal waves and the others as secondary (the subscripts 1, 2 and 3 do not refer to solid, water and ice).

For a two phase medium Biot [4,5] has obtained the velocity and attenuation of the different modes of propagation: two longitudinal modes and one transverse for a consolidated medium and one longitudinal for an unconsolidated soil. A first test of the validity of the results is the convergence of our results to those obtained by this author when only the solid and the liquid water are present.

Figure 2 shows the calculated velocities of the different modes at 0.5 MHz for an unconsolidated medium with the mechanical coefficients of a fine glass powder saturated with water. As expected, when the unfrozen water content tends to porosity, the velocities of  $L_2$ ,  $L_3$ ,  $T_1$  and  $T_2$  tend to zero and one finds back the unique mode of propagation predicted by Biot.

The attenuation curves for  $L_1$  and  $T_1$  for the same sample are shown in figure 3. The peculiar shape of these curves is explained qualitatively by a maximum of absorption when the water layer around the solid grains is in the order of magnitude of the viscous skin depth around them at that frequency.

Porosity:  $\epsilon = 0.305$ ,  $\rho_w = 1000 \text{ kg/m}^3$ ,  $K_w = 2.25 \cdot 10^9 \text{ Pa}$ ,  
 Water viscosity  $\eta_w = 1.8 \cdot 10^{-3} \text{ kg}\cdot\text{m}^{-1}\cdot\text{s}^{-1}$  (at  $0^\circ \text{C}$ )  
 $\rho_i = 920 \text{ kg/m}^3$ ,  $K_i = 8.5 \cdot 10^9 \text{ Pa}$ ,  $\mu_i = 3.6 \cdot 10^9 \text{ Pa}$  ([16])  
 Initial permeability of the ice matrix (for  $\epsilon = 0.305$ ):  $\kappa_i = 5 \cdot 10^{-4} \text{ m}^2$   
 $\rho_s = 2480 \text{ kg/m}^3$ ,  $K_s = 5 \cdot 10^{10} \text{ Pa}$ ,  $\mu_s = 3 \cdot 10^{10} \text{ Pa}$ ,  
 $K_{sm} = 0 \text{ Pa}$ ,  $\mu_{sm} = 0 \text{ Pa}$ , Solid permeability  $\kappa_s = 5 \cdot 10^{-11} \text{ m}^2$   
 Average radius of solid grains:  $60 \mu\text{m}$ , Frequency:  $f = 500 \text{ kHz}$

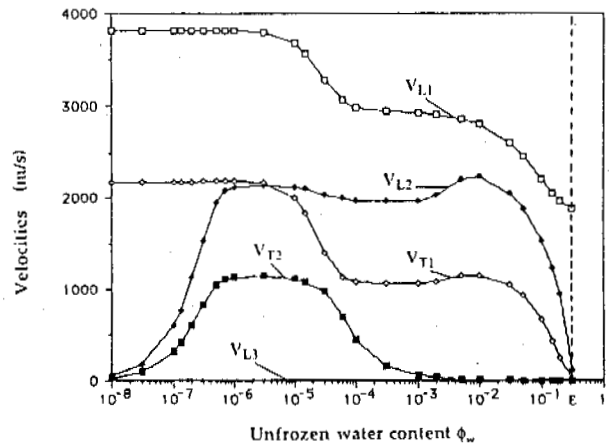


Figure 2.- Longitudinal ( $V_L$ ) and transverse ( $V_T$ ) wave velocities as functions of unfrozen water content for an unconsolidated medium (glass powder).

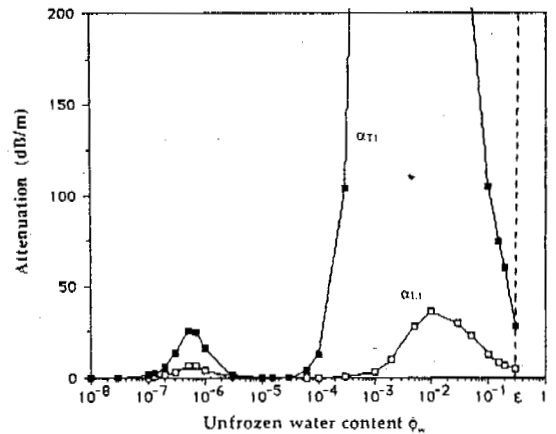


Figure 3.- Attenuation coefficients ( $\alpha$ ) of  $L_1$  and  $T_1$  modes as functions of unfrozen water content for an unconsolidated medium (glass powder).

In figure 4 and 5 are plotted the results for a consolidated medium made of sintered bronze beads saturated with water. In figure 4, the maximum velocities obtained at low temperatures are smaller than in the glass powder. This is a consequence of the higher densities of the bronze particles compared to that of glass. We may remark also the relatively small variation of the modes and, as expected, a non zero velocity for modes  $L_2$ , and  $T_1$  for the completely defrosted medium.

The behaviour difference of the two media types appears again in figure 6, where are shown the calculated Poisson's ratio resulting from the  $L_1$  and  $T_1$  velocities. The range of variation for the consolidated medium appears relatively small. The Poisson's ratio of the unconsolidated medium tends to 0.5 as expected when the ice is no longer present to give a shear strength to the medium.

Porosity :  $\epsilon = 0.30$ ,  $\rho_w = 1000 \text{ kg/m}^3$ ,  $K_w = 2.25 \cdot 10^9 \text{ Pa}$ ,  
 Water viscosity  $\eta_w = 1.8 \cdot 10^{-3} \text{ kg.m}^{-1}.\text{s}^{-1}$  (at  $0^\circ \text{C}$ )  
 $\rho_i = 920 \text{ kg/m}^3$ ,  $K_i = 8.5 \cdot 10^9 \text{ Pa}$ ,  $\mu_i = 3.6 \cdot 10^9 \text{ Pa}$  ([16])  
 Initial permeability of the ice matrix (for  $\epsilon = 0.30$ ):  $\kappa_i = 10^{-3} \text{ m}^2$   
 $\rho_s = 8774 \text{ kg/m}^3$ ,  $K_s = 1.46 \cdot 10^{11} \text{ Pa}$ ,  $\mu_s = 4.01 \cdot 10^{10} \text{ Pa}$ ,  
 $K_m = 1.28 \cdot 10^{10} \text{ Pa}$ ,  $\mu_m = 8.84 \cdot 10^9 \text{ Pa}$ ,  
 Solid permeability  $\kappa_s = 3 \cdot 10^{-11} \text{ m}^2$   
 Average radius of solid grains:  $70 \mu\text{m}$ , Frequency:  $f = 500 \text{ kHz}$

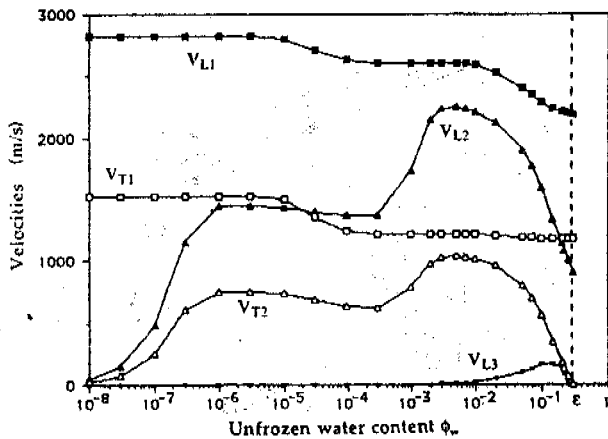


Figure 4.- Longitudinal ( $V_L$ ) and transverse ( $V_T$ ) wave velocities as functions of unfrozen water content for a consolidated medium (sintered bronze).

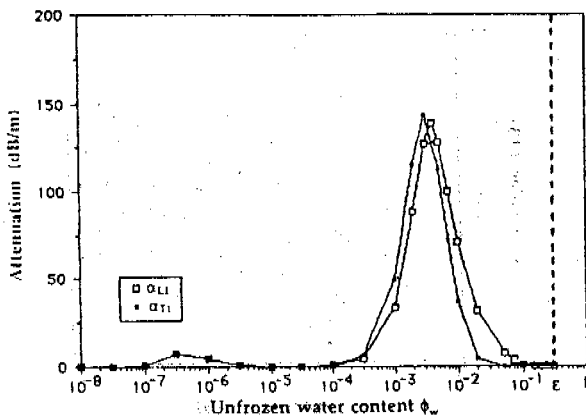


Figure 5.- Attenuation coefficients ( $\alpha$ ) of  $L_1$  and  $T_1$  modes as functions of unfrozen water content for a consolidated medium (sintered bronze).

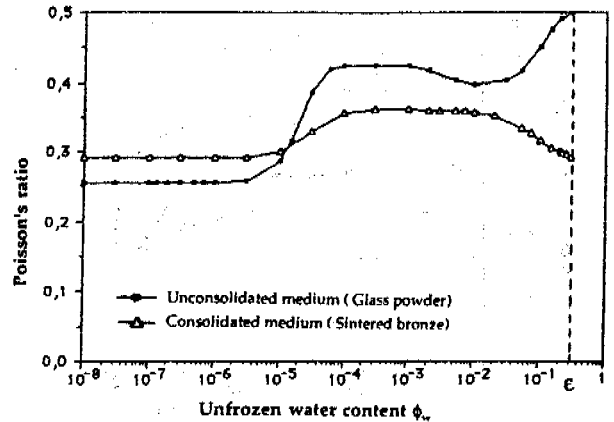


Figure 6.- Poisson's ratio for an unconsolidated medium (glass powder) and for a consolidated medium (sintered bronze) calculated from the  $L_1$  and  $T_1$  modes velocities.

## EXPERIMENTS

Experiments are performed in laboratory as through transmission experiments of short acoustical pulses. For measurements in unconsolidated media, the soil is put in a plastic cell (described in Ref[1]), on which two pairs of commercially available broad band transducers for longitudinal and transverse waves are bonded on two opposite faces. The transducers' nominal frequency is 0.5 MHz and the ultrasonic path length in the sample is 2 cm. For consolidated media, the smaller size of the samples required the use of smaller transducers with nominal frequency of 5 MHz. The signals are displayed on a sampling oscilloscope whose output is a low frequency replica of the ultrasonic signals. This output is digitized with an 8-bit A/D converter and recorded on a microcomputer. The analysis is then done either in time or frequency domain after Fourier Transformation. The fairly large frequency content of the brief acoustical pulses (0.05 to 0.7 MHz for the 0.5 MHz nominal transducers) allows the study of the frequency dependence of velocities and attenuations of the transmitted waves.

The sample's temperature is monitored by a thermocouple located in or upon the sample. For the preparation of an experiment, the sample is quickly taken from ambient to  $-30^\circ \text{C}$ . The acoustical measurements are performed during a slow reheating during 10 hours of the sample to a positive temperature.

### Velocity measurements

Figure 7 represents, the experimental longitudinal and transverse velocities of the fastest modes as function of temperature for three water soaked samples: glass powder, Caen silt and sintered bronze. In the case of glass powder the experimental velocities at low temperature are comparable to the value calculated with the theoretical model for complete freezing; For complete defreezing, the velocity has not been measured, the waves attenuation was extreme and surely caused by a small volume of air in the sample. For sintered bronze, the measured velocities are smaller than those in glass powder sample, as expected. Nevertheless the range in velocity variation between the totally frozen and unfrozen media is larger for the experimental curves than for theoretical ones. This phenomenon is unexplained.

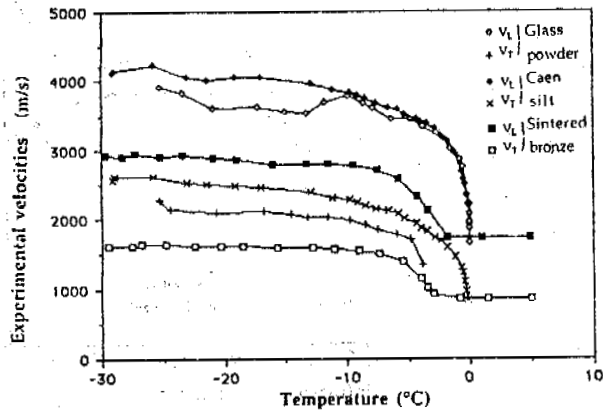


Figure 7.- Experimental velocities of the fastest longitudinal and transverse modes as functions of temperature.

Poisson's ratios calculated from the experimental velocities are shown in figure 8 as function of temperature. The variation for the sintered bronze is rather small as expected, the sample is consolidated by sintering and has always a fairly high shear modulus. For the glass powder and Caen silt sample the Poisson's ratio shows an important increase for temperature higher than  $-6^{\circ}\text{C}$ . Poisson's ratio appears to be a good parameter of identification between a consolidated or unconsolidated medium, and frosted or defrosted medium in either case.

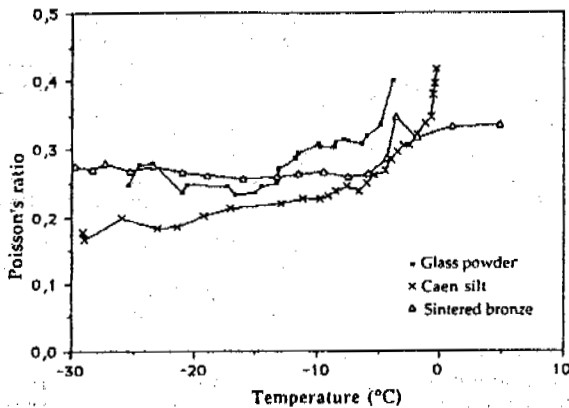


Figure 8.- Poisson's ratio for different materials as a function of temperature.

#### Attenuation measurements

At the measurement frequency, the wavelengths are small compared to heterogeneity sizes and wave attenuation is dominated by viscous drag. Attenuation is an increasing function of frequency as may be seen in figure 9 for longitudinal (a) and transverse (b) waves in the case of glass powder. The amplitudes have been normalized to the values obtained at the lowest available temperature of  $-30^{\circ}\text{C}$ . We also remark the greater relative attenuation of the transverse waves.

The two frequency regimes of attenuation given by Biot's theory may be observed in figure 10. In this sample of glass powder, the attenuation is plotted as function of frequency in a log-log plot. At low frequencies the average slope is 2.1 (2 in Biot's theory) and in the higher frequency regime the average observed slope is 0.34 (0.5 in Biot's theory). We may remark that the transition

frequency between the two regimes (whose locus is given by the dotted curve), decreases as temperature increases. This is conform to Biot's theory where, as the capillary pore dimension increases, the transition frequency shifts to lower frequencies. In our case this role is played by the thickness of the unfrozen water film around the solid grains, which increases with temperature.

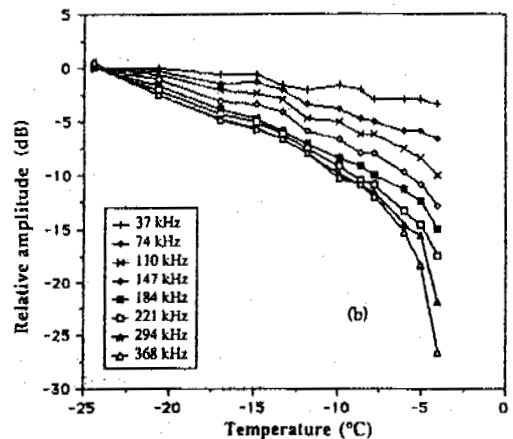
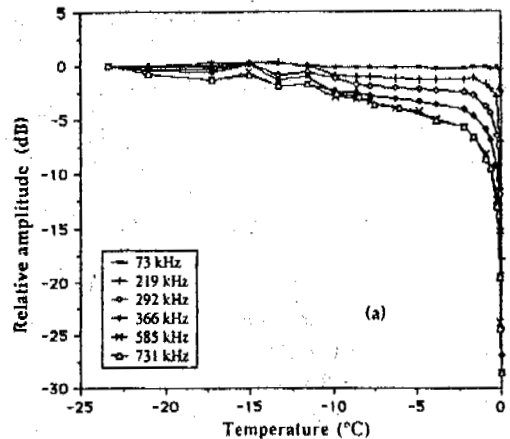


Figure 9.- Normalized amplitudes of longitudinal (a) and transverse (b) waves for different frequencies as functions of temperature (in glass powder).

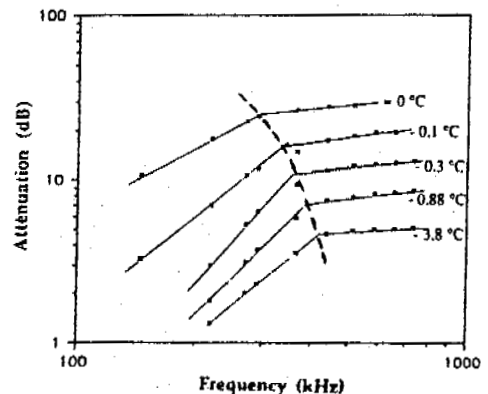


Figure 10.- log-log plot of frequency variations of longitudinal wave attenuation in glass powder as functions of temperature.

## CONCLUSION

The theoretical model of elastic wave propagation in frozen ground based on Biot's theory of sound propagation in porous media presented here shows the possibility to treat in an unified way the different cases resulting from diverse consolidation states met in practical situations. The calculations were made more practicable by making the physical assumption of no direct contact between the two solid phases: ice and solid particles. The equations of propagation obtained from the continuous media mechanics are solved numerically. Three longitudinal modes and two transverse modes of propagation appear possible; their velocities and attenuations are calculated as function of the unfrozen water content.

Experiments are performed in consolidated and unconsolidated samples.

A simple thermodynamical argument has been presented which, used in conjunction with the mechanical model may lead to the calculus of mechanical properties as function of the thermodynamical state of the soil. Experimental results are in good agreement with the theoretical ones, although some improvements to the model appear necessary. The comparison of acoustical results with those given by different methods such as calorimetry or NMR are desirable and will be performed in a near future.

## REFERENCES

1. Deschatres M. H., Cohen-Ténoudji F., Aguirre-Puente J. and Thimus J. F., "Ultrasonic propagation through frozen porous media. Liquid phase content determination", Ultrasonic Int. Conf. Proc., pp. 158 - 163 (1989).
2. Deschatres M. H., "Propagation des ultrasons dans les milieux finement dispersés. Application à la métrologie des sols gelés", Thèse de Doctorat de l'Université Pierre et Marie Curie, Paris 6 (1990).
3. Thimus J. F., Aguirre-Puente J. and Cohen-Ténoudji F., "Determination of unfrozen water content of an overconsolidated clay down to -160°C by sonic approaches. Comparison with classical methods", Proc. Vith Int. Symp. on Ground Freezing, Beijing, China, pp. 83 - 88 (1991).
4. Biot M. A., "Theory of propagation of elastic waves in a fluid saturated porous solid. Part I - Low frequency range", J. Acoust. Soc. Am., 28(2), pp. 168 - 178 (1956 a).
5. Biot M. A., "Theory of propagation of elastic waves in a fluid saturated porous solid. Part II - Higher frequency range", J. Acoust. Soc. Am., 28(2), pp. 179 - 191 (1956 b).
6. Johnson D. L. and Plona T. J., "Acoustic slow waves and the consolidation transition", J. Acoust. Soc. Am., 72(2), pp. 556 - 565 (1982).
7. Plona T. J. and Johnson D. L., "Experimental study of the two compressional modes in water-saturated porous structures", Proc. IEEE Ultrasonics Symp., pp. 868 - 871 (1980).
8. See Bourbié T., Coussy O. et Zinszner B., "Acoustique des milieux poreux", Technip, Paris (1986).
9. Leclaire P., "Propagation acoustique dans les milieux poreux soumis au gel. Modélisation et expérience", Thèse de Doctorat en Physique, Université Paris 7, Paris (1992).
10. Thimus J. F., Aguirre-Puente J., Cohen-Ténoudji F. and Leclaire P., "Sonic determination of unfrozen water content in frozen soils. Critical comparison of the use of different models", Presented in this Conference.
11. Kuster G. T. and Toksöz N., "Velocity of seismic waves in two phase media. Part I, Theoretical formulation", Geophys., 39(5) pp.587-606 (1974).
12. De Gennes P. G., "On a relation between percolation theory and the elasticity of gels", J. Physique Lett., 37, pp. L1 - L2 (1976).
13. Deptuck D., Harrison J. P. and Zawadzki P., "Measurement of elasticity and conductivity of a three-dimensional percolation system", Phys. Rev. Lett., 54(9), pp. 913 - 916 (1985).
14. Biot M. A. and Willis D. G., "The elastic coefficients of the theory of consolidation", J. Appl. Mech., 24, pp. 594 - 601 (1957).
15. Biot M. A., "Mechanics of deformation and acoustic propagation in porous media", J. Appl. Phys., 33(4), pp. 1482 - 1498 (1962).
16. Roethlisberger H., "Seismic exploration in cold region", C.R.R.E.L. Monograph II, A2A (1972).
17. Aguirre-Puente J. et Bernard J. J., "Comportement au gel des matériaux de construction", (Le comportement thermique des matériaux de construction), Editions du Batiment et des Travaux Publics, pp. 29 - 72 (1978).



THE SIGNIFICANCE OF PERMAFROST IN THE FORMATION  
AND APPEARANCE OF PUSH MORAINES  
Examples of the Canadian Arctic and Spitsbergen

Rainer Lehmann

Geographisches Institut, Universität  
Heidelberg, Im Neuenheimer Feld 348,  
D/W-6900 Heidelberg, Germany

The term push moraine is applied to some moraine like features with different development. The existence of permafrost effects the formation significantly. On the basis of investigated push moraines of the Canadian Arctic and Spitsbergen two main types can be presented. The arctic push moraine in a continuous permafrost environment is formed by faulting and thrusting whereas the coastal (or Spitsbergen) push moraine developed by a large scale underpush of glacier ice below marine sediments. Although a lot of differences separate the two moraine types, some similarities can be determined. The important role of permafrost in the development of the moraines is shown in this paper. The morphological constitution of the permafrost itself is changing due to stacking, deformation, degradation and growth.

INTRODUCTION

Push moraines are formed from sediments deformed in front of an advancing glacier. Development occurs in different environments. CHAMBERLIN (1890) gives the first description, and a division into four types is presented by LEHMANN (1992 a). The investigation of push moraines in Spitsbergen and the Canadian High Arctic gave the opportunity for a comparison of the formation of arctic push moraines under different environmental conditions.

Central questions of the research were: do push moraines show different development in different arctic environments, and what is the role of permafrost in the formation.

In the Canadian Arctic Archipelago the Thompson Glacier push moraine (Expedition Fiord, Axel Heiberg Island, 79°50' N) and the Carl Troll Glacier push moraine (Borup Fiord, Ellesmere Island, 80°50' N) were explored (Fig.1). Thompson Glacier and moraine are still active, the Carl Troll Glacier moraine shows light activity. Erikbreen push moraine (Liefdefiord, 79°36' N) and the Børrebreen push moraine (Bockfiord, 79°31' N) are investigated in Northwest Spitsbergen. While Børrebreen is stagnant to little retreating, Erikbreen has been retreating for about 70 years (WORDIE 1921, in HAMBREY 1984).

Environmental distinctions concern climate, permafrost, location to the sea, size and activity of glaciers. Climate as the most important environmental difference controls development and depth of permafrost. Mainly West Spitsbergen is influenced by relative warm Atlantic waters of the West Spitsbergen Current. The most important consequence is a relatively high mean annual air temperature of about -5.8 °C (representative station at Ny

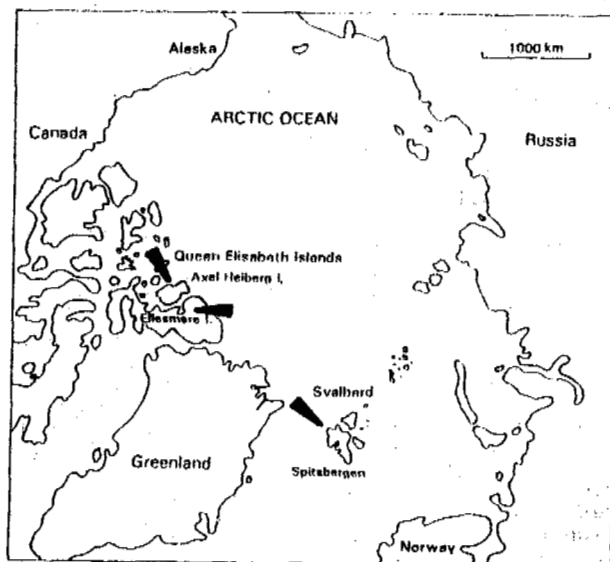


Fig.1. Map of the arctic region, showing the locations of investigated push moraines.

Alesund) and the absence of sea ice for at least 8 months per year at the west coast. In 5 of 10 years sea ice with concentrations above 4/10 covers the surrounding sea of Svalbard from January to March (STEFFENSEN 1982). During southerly or southwesterly air currents mild Atlantic air masses are transported to Svalbard. Even February and March as the coldest months (mean temperatures of -13.9 resp. -13.1 °C, Ny Alesund) may show positive temperatures

during short periods. The climate is classified as polar, but under strong marine influence. The term marine-arctic may describe the climate. Sea ice covers the waters of the Canadian Arctic Archipelago for about 9 to 10 months (see also KING 1981). The mean annual air temperature is reduced to  $-19.3^{\circ}\text{C}$  (Eureka) and temperatures stay below  $0^{\circ}\text{C}$  for about 8 months. Weather is characterised by continentality (see also THOMPSON 1967). Precipitation is scarce in Spitsbergen with a mean annual amount of 200 to 400 mm. Eureka as the representative weather station of Axel Heiberg Island and Ellesmere Island gets only 58 mm precipitation per year. But OHMURA (1981) pointed out that this value may be exceeded in one summer month.

Permafrost developed in valley floors and beaches after they became ice-free or raised over sea level. Thickness of permafrost is estimated to be 20-30 m in front of Thompson Glacier due to a short time of a few thousand years for developing. The moraine is composed of outwash sediments 12 km behind the shore line and at a height of about 30 m over present sea level. In contrast the Spitsbergen moraines are close to sea level and are build up of marine and glaciofluvial sediment. Marine silt and clay may be dominant. The studied moraine of Erikbreen developed on the shore line. Frozen permafrost here is estimated not more than about 1 m during formation.

The size of push moraines does not always correlate with the size of pushing glaciers. But it seems, that maximum elevations of the push moraine above the outwash plain is a function of glacier size. In most cases the moraines of the Canadian Arctic cover some hundred thousand  $\text{m}^2$  to  $\text{km}^2$ , while the glacier snouts are 1 to 3 km wide. Thompson Glacier covers about 225  $\text{km}^2$ . Peaks of ridges inside the moraine reach 100 m over the valley floor. In contrast, Spitsbergen's investigated glaciers are smaller. Areas range between 5 and 12  $\text{km}^2$  and glacier snouts are 500 to 1000 m in width. The highest elevations of the push moraines are raised 25 m over the surrounding ground. Relating to the small glacier size, the moraines cover a conspicuous large area compared to Canadian push moraines.

#### METHODS

Inner structures of push moraines are the key to understanding formation and dynamics. Fluvial erosion inside the moraine and thermo-erosion cut niches and create bluffs. Denudation and transportation of thawed sediment by water show exposed "open" permafrost. Such steep slopes give view of layering and displacement of the sediments. Questions of movement between separate blocks may be clarified with the help of visible faults and different tilted blocks. Sediments and attitudes give information of general environment of formation and development of the inner structure of the push moraine in time. Correlations of internal constitution and outward appearance help to explain the kind of push moraine and its development.

Research methods are therefore based on geomorphological mapping and investigation to understand and survey outward appearance. Analysis

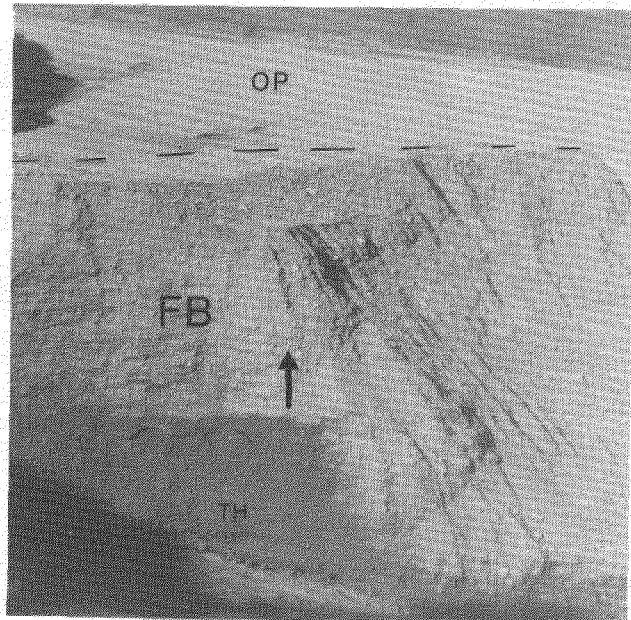


Photo 1. Large frozen thrust block (FB) at the lateral outermost front of Carl Troll Glacier. Please note the preserved original bedding and the inclination of the block. Approximate height is 7 m. In the foreground river water causes thermoerosion (TH). The outwash plain (OP) is situated to the right and in the background, the glacier is to the left.

of aerial photographs and, if available, topographic maps ascertains change of glaciers and moraines with time. In the case of Thompson Glacier and Carl Troll Glacier a photographic aerial survey could be carried out (HELL & ZICK in prep.). Inner structures and sediments were surveyed at few but important bluffs. Findings of shells and driftwood had particular consideration. The geomorphological mapping on a scale of 1:10 000 is based on the mapping key of the German Association on Geomorphology (LESER & STÄBLEIN 1975) and was tested before in an arctic region by MAÜSBACHER (1981).

The results of both methods give answer to questions of surface and subsurface processes and activity, and the significance and effects on permafrost. Most important questions are: Does permafrost affect internal constitutions and/or outward appearances? What are the consequences of absence or presence of permafrost?

#### RESULTS

The results will be focussed on three main points of interest: 1. outward appearance, inner structure and materials, 2. the formation of both kinds of push moraines, and 3. role and condition of permafrost.

Push moraines of the Canadian High Arctic develop in outwash gravel and sediments modified by fluvial, lacustrine or marine action (see also KÄLIN 1971). The closer to the

sea, the more marine sediment may be incorporated, but fluvio-glacial material is still dominating. Carl Troll Glacier push moraine is a good example for it is situated 2.5 km behind the shore. Frozen blocks of coarse gravel are cemented by ice. The ice content in the sediments may reach 80 %. Concordant bedding and cross-bedding is visible on exposures, showing that the entire and intact blocks are raised, turned and tipped (Photo 1). Surface cracks indicate vertical faults, which can be seen sometimes on steep bluffs. Thrust sheets are sheared at a weakness layer in the underground. At least one thrust plane is to be expected under every frozen block (Photo 2). Shear planes of first order underlie the outwash gravel and turn into shear planes second order when the blocks and plates are incorporated in the moraine (Fig.2). For active glaciers, the moraine may be subdivided into different subsurface activity zones characterised by outward appearance. Fresh fractures and cuesta-like forms indicate young heaved blocks in the outer zone of the moraine and the very active zone. The areas in front of the glacier snout are mostly reshaped by erosion and of a rounded character. They are less active to inactive. The zone between active and inactive area shows still activity. Some blocks are in motion. But denudation, sedimentation and fluvial action cause smoothing and aging of the sharp forms. The moraine is advancing as a whole, acting as one unit with the glacier snout.



Photo 2. Thompson Glacier push moraine. Fresh fractures and cuesta-like structures indicate active pushing in the outermost parts.

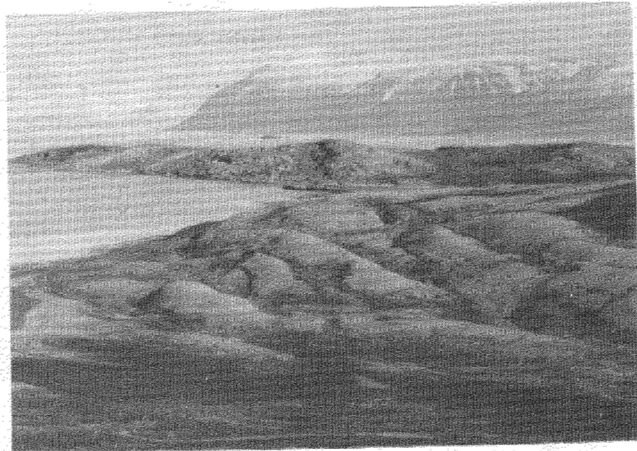


Photo 3. Eastern push moraine complex of Erikbreen. Development occurred in fine marine sediments, covered partly with outwash gravel and beach pebbles. Folding is almost correlating with the small ridges.

The material of coastal push moraines of Spitsbergen consist of marine and fluvio-glacial sediments (LEHMANN 1992 b). In parts the silty to clayey material dominates. It shows signs of folding also in a large scale, corresponding with ridge and valley positions. Even in the youngest and outermost areas of the moraine, forms are rounded (Photo 3). The fine and malleable material do not build up cuesta-like slopes, except at locations of massive fluvial erosion. Frozen raised blocks and vertical faults are absent despite stress during pushing. It is to be expected, that thrust sheets are sheared more or less at the bedrock. Because of the retreat of Erikbreen since about 70 years, glacier-faced retrogressive thaw slumping at the location of the former contact-zone of glacier and moraine allows views of the inner structure of the moraine (Photo 4). It is obvious, that the moraine is underlain by glacier ice at least in part. The most important phenomenon is, that driftwood and shells could be found in the mudflow-area between moraine and glacier at Erikbreen. Undisturbed concordant marine sediments with shells are situated directly on the glacier ice of Børrebreen (Photo 5). Any zonation of subsurface activity is impossible. Traces of activity like fresh fractures are obliterated by surface aging processes.

Permafrost is an important distinguishing feature in the development of both moraine-types. Cementing the coarse gravel in case of the outwash moraine, it allows creation of thick and rigid blocks or plates. The outwash plain acts as an abutment to lift out the blocks of the plain. In the coastal environment, frozen ground is subordinate and thickness reaches only 1 m. This is concluded by the absence of faults and the folding of the sediments without superimposed load. Permafrost may have existed but probably it was not frozen due to the freezing-point depression of saline pore water (marine cryopeg, hydrochemical talik). Sediment packets did not function as blocks.

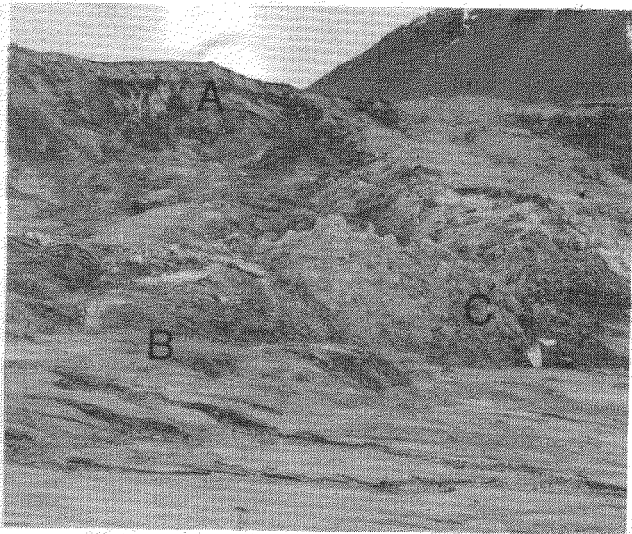


Photo 4. Erikbreen, glacier faced retrogressive thaw slumping. The retreating glacier is to the right. Push moraine is situated to the left and behind the sediment covered ice cliff (A). Thawing glacier ice and sediment form numerous mudflows (B). Driftwood, bedded marine sediment and shells are found within the area (C).

The formation of the push moraines develop as different as the environment. Inner structure, material and outward appearance indicate two simplified general models; in the outwash environment the glacier pushes frozen blocks and plates in front of the glacier snout. It is comparable with bulldozing. During the advance more and more blocks are incorporated at the front of the moraine. They are raised and the whole moraine is formed by stacking of frozen blocks (Fig.2). Against that, the coastal push moraine is formed by a large scale underpush of glacier ice below marine sediments, mainly indicated by marine silt and clay, driftwood and shells located on the ice (Fig.3). They are pushed onto the glacier ice partially. During that process, the folding forms small ridges and valleys. Investigations of the large Holmstrømbreen push moraine in Ekmanfiord (VAN DER MEER & BOULTON 1986) show similar foldings on exposures of up to 10 m height. The advance of the glacier causes an ice heaving process which raises the marine sediment cover. Abutments are not observed. Development took place between roches moutonnées in case of Erikbreen.

#### CONCLUSIONS AND DISCUSSION

The first impression of Holocene push moraines show similar appearances. They are build up of ridges and troughs with a semicircular shape around the push center, in most cases the middle of the glacier snout. It is obvious that the moraines grow at the outermost front in contact with the outwash plain. That means the youngest parts are incorporated at the edges of the moraine. The possibility of overpush and

underpush (LEHMANN 1992 a) is given in both cases. But the moraines are distinguished in detail. They show significant differences due to environment and permafrost which verify two kinds of formation as seen above. This important result contrast with conclusions of VAN DER WATEREN (1992) because permafrost conditions do control the developments of different types. The most important distinguishing features are the bulldozing in front of the glacier and the elevation of sediments by glacier ice respectively. Even after a time of pushing a bulldozed moraine may be overrun by the glacier during one advance. That seems impossible in the case of the coastal push moraine. The missing dissection into fault blocks and depressions indicate "soft" compression in principally nonfrozen, malleable material, comparable with results of KÖSTER (1958, Abb.1a). That is why moraine and glacier are not advancing as one unit like the described outwash moraine. There, the boundary between glacier and moraine is discernible, whereas the formation of an ice core under coastal moraines allows only suppositions of a separation. The differences in the development can be clearly put down to different environmental conditions. Permafrost is very important to the kind of formation and appearance of the moraines. But the morphological constitution of the permafrost itself is changing. Bulldozing causes a stacking of frozen gravel blocks and therefore a stacking of permafrost, but folding is of minor significance for it. On the basis of a thickness of 20-30 m in the outwash plain, the thickness amounts to a maximum of 120 -130 m and a mean value of about 90 m. Permafrost is deformed by movement of sediments in the moraine. Thermoerosional processes and denudation at edges and river channels cause degradation, but accumulations for example under slopes cause growth of the permafrost thickness.

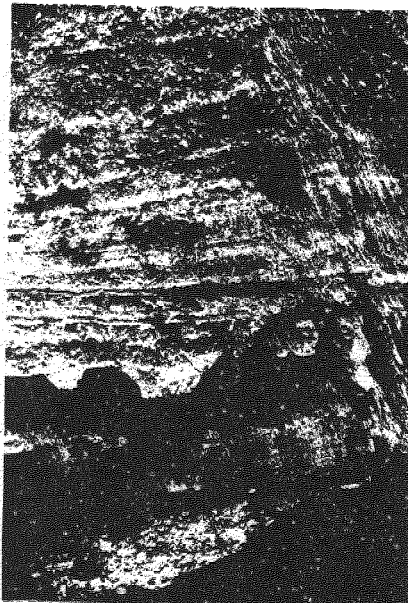


Photo 5. Close-up of originally bedded marine sediments with shells (A), overlying glacier ice of Børrebreen (B).

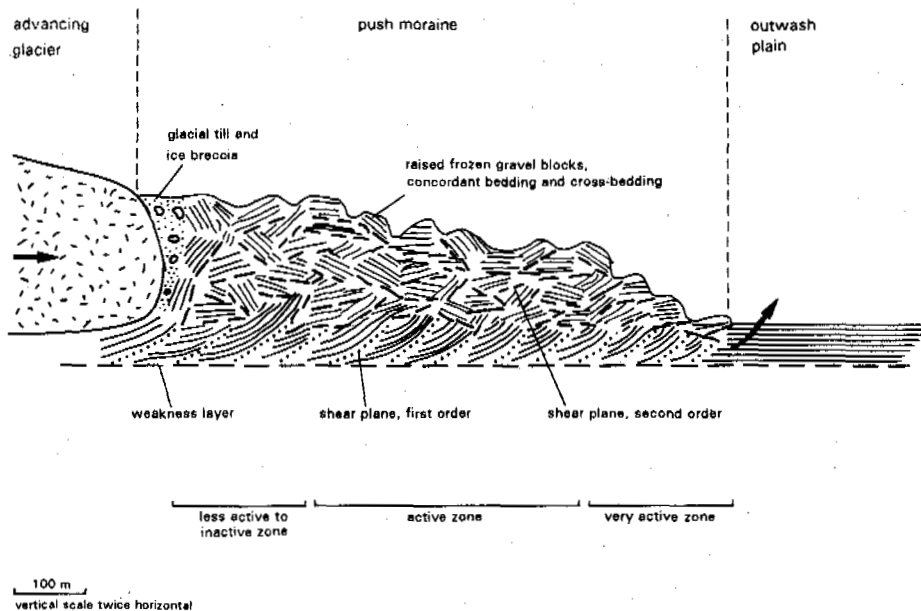


Fig. 2. Cross-section of Thompson Glacier push moraine. Simplified model of an outwash push moraine formed under permafrost conditions (see also LEHMANN 1992 a).

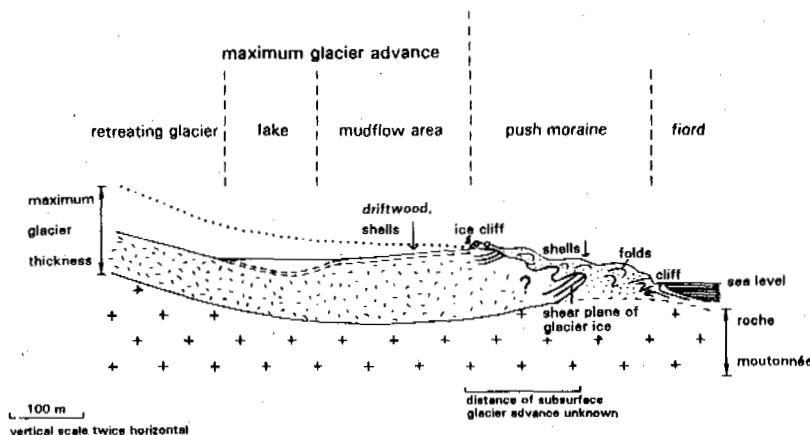


Fig. 3. Cross-section of Erikbreen push moraine. Simplified model of a coastal push moraine formed mainly in non-frozen ground.

Remaining questions are: what causes the glacier to push sediment? Is the conclusion of a large scale underpush actually possible? A cold based glacier snout may be bonded with the frozen gravel. The existence of a decollement layer within or below permafrost supports the formation of a push moraine in front of a glacier. Both prerequisites are not applicable on Spitsbergens coastal push moraines. Following VAN DER WATEREN (1985), three factors control their formation: the velocity of the advancing glacier, the critical combination of

ice thickness and depth of a decollement layer, the age of the raised beaches and because of that, the development, thickness and condition of permafrost. At least MULLER (1947, in MACKAY & MATHEWS 1963) pointed out the influence of pore water on shearing strength. Specific combinations of these factors may lead to push moraine formation. The mechanics of underpush of glacier ice under marine sediments are not completely understood yet. On balance the conclusion is to subdivide the phenomenon of the arctic push moraine into two characters:

the coastal arctic and the outwash arctic push moraine. Ice-bonded permafrost is probably a prerequisite for the development of outwash moraines but obviously of minor importance in case of coastal moraines.

#### ACKNOWLEDGEMENTS

The author is grateful to Prof. Dr. L. King (Giessen) and Prof. Dr. H. Leser (Basel) for being able to participate in the Kanarktis 2 Expedition 1988 and the Spitsbergen Expedition 1990 (SPE90), during which these observations were made. Thanks are also due to Deutsche Forschungsgemeinschaft (DFG) and Swiss National Foundation (SNF) for financial support.

#### REFERENCES

- CARLE, W. (1938) Das innere Gefüge der Stauch-Endmoränen und seine Bedeutung für die Gliederung des Altmoränengebietes.- Geologische Rundschau, Bd. 29, H. 1/2: 27-51.
- HAMBREY, M.J. (1984) Sedimentary Processes and Buried Ice Phenomena in the Pro-Glacial Areas of Spitsbergen Glaciers.- Journal of Glaciology, Vol.30, No. 104, p. 116-119.
- HELL, G. & ZICK, W. (in prep.) Geodätische und photogrammetrische Arbeiten im Rahmen der Kanarktis Expedition 1988 in die Queen Elizabeth-Inseln.
- KÄLIN, M. (1971) The active push moraine of the Thompson Glacier.- Axel Heiberg Island Research Report, Glaciology No. 4, McGill University, Montreal.
- KING, L. (1981) Die Meeresentwicklung im Innern des östlichen kanadischen Arktisarchipels und ihre Bedeutung für die Arbeiten der Heidelberg-Ellesmere Island-Expedition an der Oobloyah Bay, N-Ellesmere Island, N.W.T., Kanada.- Heidelberger Geograph. Arb. 69: 521-540.
- KÖSTER, R. (1958) Schuppung und Faltung im Glazialtektonischen Experiment.- Geologische Rundschau, Bd. 46: 564-571.
- LEHMANN, R. (1992 a) Arctic push moraines, a case study of the Thompson Glacier Moraine, Axel Heiberg Island, N.W.T., Canada.- Z. Geomorph. N.F., Suppl.-Bd. 86:161-171.
- LEHMANN, R. (1992 b) Beobachtungen zum Stauchmoränenproblem an Gletschern Spitzbergens.- Stuttgarter Geographische Studien, Bd. 117, p. 279-290. Stuttgart.
- LESER, H. & STÄBLEIN, G. (1975) Geomorphologische Kartierung. Richtlinien zur Herstellung geomorphologischer Karten 1:25 000. 2. veränderte Aufl., Berliner Geogr. Abh., SH 1-39.
- MACKAY, J.R. & MATHEWS, W.H. (1964) The role of permafrost in ice-thrusting.- The Journal of Geology, Vol. 71, p. 378-380. Discussion.
- MÄUSBACHER, R. (1981) Geomorphologische Kartierung im Oobloyah-Tal, N-Ellesmere Island, N.W.T., Kanada.- Heidelberger Geograph. Arb. 69: 413-440.
- OHMURA, A. (1981) Climate and Energy Balance on Arctic Tundra.- Zürcher Geograph. Schriften, H. 3. Zürich.
- STEFFENSEN, E. (1982) The climate at Norwegian Arctic stations. Klima Nr.5. 44 pp., Det norske meteorologiske institutt, Oslo.
- THOMPSON, H.A. (1967) The Climate of the Canadian Arctic.-The Canada Year Book 1967, Ottawa.
- VAN DER MEER, J.J.M. & BOULTON, G.S. (1986) Hernieuwde belangstelling voor onderzoek van stuwwallen - Eerste resultaten van de Glacitecs '84 expeditie naar Spitsbergen.- K.N.A.G. Geografisch Tijdschrift XX, Nr. 3.
- VAN DER WATEREN, D. (1985) A model of glacial tectonics, applied to the ice-pushed ridges in the Central Netherlands.- Bull. Geol. Soc. Denmark 34, 55-74.
- VAN DER WATEREN, D. (1992) Structural Geology and Sedimentology of Push Moraines.- Amsterdam.

## HYDROGEOLOGICAL ASPECTS OF CRYOGENIC SLIDES ON THE YAMAL PENINSULA

M.O. Leibman, F.M. Rivkin, V.S. Saveliev

Industrial and Research Institute for Engineering Investigations of Construction, 18, Okruzhnoy, Moscow, Russia

As a result of field research in cryogenic slides the dependencies of expanding and display forms of cryogenic shearing slides (CSS) on some natural factors were ascertained. The main factors are climatic and hydrogeologic territorial particularities. They show themselves as the ground water behaviour and soil filtration properties. That is indirectly evidenced by the unprecedented activity of CSS in 1989 which was notable for the maximum related to the sites with more moistened slopes. One could draw the conclusion about the difference of CSS mechanisms in different lithologic conditions.

### INTRODUCTION

A station was established on the Yamal Peninsula between the rivers Se-Yacha and Mordy-Yacha for studies of hazardous cryogenic processes, including cryogenic slides (Fig. 1). As a result of field research in cryogenic slides the dependencies of expanding and display forms of CSS on geostructural, morphological, lithologic, climatic and hydrogeological territorial particularities were ascertained. The cyclic character of CSS is due to climatic conditions.

The observations of the past years showed that the active increase of CSS was observed on the Yamal Peninsula in 1989. The 1989 season was rather warm (the sum of positive temperatures was 705 centigrade days, at the meteorological station Marre-Sale and the maximum values for the period starting in 1961 was 810 centigrade days, and minimum of 315 centigrade days). At the same time in 1989, maximum precipitation were observed (239 mm for the previous winter and 198 mm in summer, close to values observed only in 1966). The prevailing numbers of CSS were observed on the sites of surface and underground flow thereby illustrating the moisture influence on the occurrence of CSS.

The essential difference in sizes of CSS are due to the lithologic soil composition with different filtration properties. Our observations show that larger CSS are formed on sandy soils of STL than on loamy soils. These observations prove the stability of analysis of slopes, carried out by method of Saveliev (1989). The different sizes of CSS are largely connected with the filtration properties of STL (Seasonal thaw layer).

The present paper is devoted to the investigation of important factors influencing the slope stability: the amount of atmospheric and soil moisture, ground water behavior in STL and filtration properties of STL soils.

### METHODS

In order to assess the ground water behavior in STL, the piezometric observations and stability analysis of slopes were performed. The

analysis made for a deliberately slide hazardous slope that the instability is possible only when the piezometric level is above earth surface which in turn is possibly due to a number of factors. It is necessary that one should have low filtration soils (moisture is not pressed upward but creates buoyancy pressure), large ice content soils in STL which upon thawing provide water

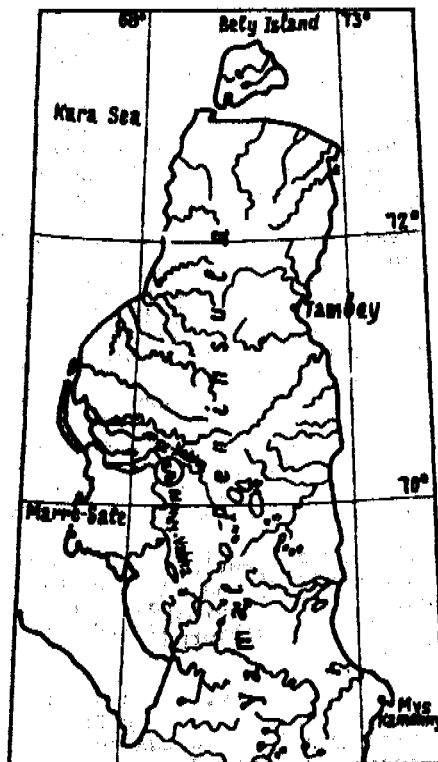


Figure 1. Location map. Station for studies of hazardous cryogenic processes on Yamal Peninsula ("S" - the station)

saturation of the STL and a considerable amount of precipitation to provide recharge of ground water. The piezometric observations made in the dry summer of 1991 showed that little atmospheric precipitation is not sufficient to maintain high piezometric level even if there is high ice content in STL soils nor the melted ice from STL soils. As a result, one could not observe CSS in 1991 on a large territory of about 90 km<sup>2</sup> even on the sufficient sites with fissures in the turf.

In order to analyse the influence of STL filtration properties on CSS the laboratory and field filtration tests were performed. They proved the suggestion that the results of the filtration factor determination in the soil sample and in the massif differ for some reasons:

firstly, the considerable anisotropy of filtration properties being observed on the territory under investigation and determining the behavior of the ground water in the STL were not considered in laboratory tests;

secondly, it is impossible to take into account the large fissures which are formed as a result of cryogenic transformation of STL soils, especially, clayey soils.

#### EXPERIMENTS

In the performing tests, we choose the dominant lithologic sections for STL, which are known to be subjected to CSS different scale; mainly in sandy and mainly in clayey soils. Two representative sites within the station were chosen with sandy and clayey sections of STL. The determination of filtration factor was made by pouring water into the pit (modification of method by Boldyrev, see Sergeev, 1984), the seepage factor by pouring water into cylinders (method of Nesterov, Sergeev, 1984). The results of permeability tests on STL soils are given in Table 1.

The results given in Table 1 makes it possible to speak about anisotropic permeability of soils in STL. It was observed in sandy soils that the seepage factor (Fs2) equal to 2.1 m per day considerably exceeds the filtration factor down the slope (Ff1) equal to 0.02 m per day. The dependence is reversed for clayey soils. The seepage factor (Ff2 equal to 0.07 m per day) in clayey soils is much less than the filtration factor down the slope along the STL (Ff1 is equal to 19.4 m per day). These data for permeability of clayey and sandy soils determine to a great extent the regional specificity of CSS formation; therefore it is necessary to provide it theoretically.

In sandy soils the high values of seepage factor are likely to be the result of STL soils transformation in the process of frequent freezing and thawing. All sandy soils from the investigated area contain a great amount of silty particles. The fraction less than 0.5 mm comprises up to 36%. This decreases the soil filtration, which was established when determining the filtration factor in field test and in laboratory test of the soils having disturbed structure. In the first case Ff1 is equal to 0.02 m per day. In the second case, Ff is equal to 0.12 m per day. Considerably higher values of seepage factor in silty sands are probably due to the presence of active vertical porosity which is much larger than active porosity down the slope. The similar

Table 1. The results of field and laboratory permeability tests on STL soils

Soil N composition	Natural conditions			Disturbed conditions
	Ff1*	Ff2**	Ff1/Ff2***	Ff****
	m per day			m per day
1 silty sand	0.02	2.1	0.0062	0.12
2 clay	19.4	0.07	281	-
3 loamy sand	-	0.4	-	0.03

\* - filtration factor; \*\* - seepage factor;  
\*\*\* - filtration factor/seepage factor ratio;  
\*\*\*\* - filtration factor.

distribution of porosity is characteristic of loess. One of the reasons for vertical porosity in loess is lining of capillars coming in place the plants' root system. In our case the formation of vertical porosity is due to multiple cycles of thawing and freezing which stimulate the moisture movement in the vertical direction. This phenomenon possibly caused the formation of active vertical porosity. The high content of salts in STL soils (there are some data on the dry residual up to 300mg/l) is likely to contribute to the fixing of capillars similar to those in loess. Thus, the considerable increase of seepage factor compared with ground water filtration factor along the STL is understandable although requires detailed investigations.

This is the reverse dependency in clayey soils, connected with the fact in field we determine the filtration factor of whole layer in clayey STL, having expressive post-cryogenic structure. It differs from the determination of filtration factor of clayey soil sample. During the tests it was established that the water dynamics within the STL occur in this case along large post-cryogenic fissures and along the contact of ice/soil in the lower part of STL. The main amount of water is filtrated in the lower part of STL and the thickness of permeable layer is not more than 10 cm. In the process of the investigations this part of layer became wet very quickly (23 minutes after the beginning of the experiment) and the percolation of ground water began on the soils of the pit. In comparison the percolation in sandy soil began 2 hours 15 minutes after the beginning of the experiment. After 1 hour 15 minutes the percolation of water in the intake pit had turned into water flow from one pit into the other one, water jets, leaking from post-cryogenic fissures. Thus, Ff1 which is equal to 19.4 m per day is conditioned by the system of post-cryogenic fissures, formed as a result of thawing of clay in STL with reticulated and layered thick-streaked cryogenic structure. It follows that this value can vary from year to year depending on cryogenic structure of STL which is determined by soil moisture before freezing and by the autumn freezing regime.

The water saturation ability of sandy massif leads on one hand to a considerable increase of their weight, and on the other hand to the decrease of shearing strength of the solids. The specific shearing resistance of water saturated silty sand is very little. It was 0.6 to 0.7 kg per square meters at the beginning of the experiment with natural moisture equal to 22%, and it was practically equal to 0.0 at complete saturation.



tion. Thus, the ability of STL soils to shearing greatly increases under complete water saturation.

The main result of specific filtration ability of silty sand soils in STL is the formation of large shearing slides, with weights of 150000 tons. The high seepage ability of sands makes it possible for high rate of percolation of atmospheric precipitation to the base of the STL. We have preliminarily data that the average rate of seepage (100 m per day) exceed several times the average intensity of summer precipitations for the area under consideration. The precipitation was 60 to 90 mm per month even during the year with the most active shearing. If the whole volume of precipitation had fallen during 24 hours, it could have percolated into the STL. Thus, practically the whole volume of summer atmospheric precipitation (except the evaporation) contributes to STL. The CSS are under the control of its intensity.

The formation of slides, having not great weight (mainly to 5000 tons) was noted on sites with STL formed from clayey soils. It is determined by the fact that ground and surface water flow down the slope and accumulate as lenses in the middle and lower parts of the slope. It is due to the different permeability which is determined by cryogenic formation of CSS. Specific shearing strength of clayey soils after the experiment was 0.6 to 0.7 kg per/cm<sup>2</sup>. This is considerably more than the similar value for sandy

soils. This is one of the causes why the CSS of small weight are characteristic of the slopes formed by clayey soils.

#### CONCLUSION

The preliminary results after the filtration investigations in the massif are reasons for more frequent measurements of filtration factor in massif. This will make it possible to find the transition from the filtration factors obtained in the laboratory test to those obtained in field.

The conclusion could be drawn about the difference of CSS mechanisms in different lithologic condition. The leading factor of such mechanism on the sites with STL soils of clayey composition is the buoyancy pressure of ground water. As to the sites with sandy soils the abrupt lowering of contact layer strength because of its' water saturation is valuable in CSS mechanism.

#### REFERENCE

- Saveliev V. S. (1989) Influence of ground waters on slope and constructions stability in permafrost regions. In: Construction in East Siberia and Far North regions, N 4, 5 pp.
- Sergeev E. M. (1984) Methodical textbook on engineering study of rocks. V. 2. 423 pp.

## STUDY OF FORECAST OF FROST HEAVE ON CANALS

Li Anguo<sup>1</sup>, Li Hao<sup>2</sup> and Cheng Qinghua<sup>1</sup>

<sup>1</sup>Northwest Hydrotechnical Science Research Institute,  
Yangling Town, China

<sup>2</sup>Ningxia Hydrotechnical Science Research Institute,  
Yinchuan, China

The systematic experiments were carried out to test the relationship between frost heave and various soil, different groundwater table, as well as different canal direction on the test canals in Yinchuan field station. Based on the geographical condition in situation soil types, groundwater table and initial moisture content before the unfreezing and observation data of air temperature and frozen depth. The method to predict frozen depth and frost heave in canal section is given in the article.

### INTRODUCTION

In order to study the frost heave principles and explore the method to predict frost heave on canal subsoil, a field testing station was set up at Yinchuan, Ningxia. The groundwater table underlying the station was artificial. The station had four test canals in different directions. The canals were lined with concrete slabs, 15 m long, 1.85 m depth, 3.1 m wide in bottom and 1:1.35 slope coefficient. Sandy loam was refilled in these canals with 1.7 m groundwater table (from the canal bottom). The station had 25 test units lined with concrete slabs in an area of 10x15 m<sup>2</sup> each of the units is 2x3 m<sup>2</sup>. Five types of soil (heavy silty loam, silty loam, sandy loam 1, sandy loam 11 and fine sand) were refilled on the units with five kinds of groundwater tables (1.7, 2.2, 2.7, 3.2, 3.7 m). The dry density of subsoil was about 1.6 g/cm<sup>3</sup>.

The observation contents in the station consisted of air temperature, ground temperature, frozen depth, soil water content, groundwater table, subsoil deformation of freezing and thawing and precipitation. The systematic data had been collected during the freezing period from 1988 to 1990.

### THE BASIC PRINCIPLE OF THE CANAL SUBSOIL DURING FREEZING

#### The Changing Characteristics of Temperature Field in Canal Subsoil

The differences of ground temperatures along the canal sections mainly depended on canal directions, types of soil and the groundwater table. The negative temperature indexes, taken from observation data during the freezing period in 1988, 1989 and 1990, were 627.3°C·day, 456.8°C·day and 493.9°C·day, respectively. The isotherms of canal section at a typical time are shown in Figure 1. It is noted that the ground temperature increases successively from

E-W direction, NE45°, N-S to NW45° direction at #1 and #5, and descends at #7 and #11. The ground temperature at #6 has a small change in different direction canal under a given groundwater table. The ground temperature difference of symmetry section at #6 is the highest in E-W direction, the higher temperature difference is in EW45° and NW45° direction. And the lowest temperature difference is in N-S direction canal. The isotherms of canal section shows an "M" shape in NE45° and NW45° directions.

The ground temperatures of testing units depend on the types of soil and the groundwater table. The ground temperature decreases with the increasing of the depth of the groundwater table.

#### The Changing Characteristic of Frozen Depth

It was found that the frozen depth, not only in the shape but also in the value, is identical with 0°C isotherms along the canal sections. The maximum frozen depth was observed during February 2-4, at various observation points. The frozen depths at #1 and #5 decrease and increase at #7 and #11 with the change of canal direction from E-W, NE45°, N-S to NW45°. The frozen depth for a given groundwater table has no or little change when changing canal direction. The frozen depth difference of symmetry section at #6 reduces successively with the change of direction from E-W, N-E, NW45° to N-S. The frozen depths along canal section were extended in an "M" shape in NE45° and NW45° direction of canals.

#### The Relation between Frozen Depth and Negative Temperature Index

Based on above results, it is found that the relationship between the maximum frozen depth and negative temperature index of the surface can be expressed as following empirical equation.

$$H = A \sqrt{F_0} \quad (1)$$

The effect coefficient,  $K_z$ , of groundwater table on frozen depth can be expressed as following:

$$K_z = \frac{a+be^{-Z_0}}{a+be^{-Z_1}} \quad (3)$$

Where,  $Z_0$  - the depth of groundwater table (from the ground surface) (m)

$Z_1$  - the depth of groundwater table (from the canal section) (m)

If the depth of groundwater table is 2.2 m from the ground surface, the values of  $K_z$  obtained with formula (3) shown in Table 3.

Table 3. The values of  $K_z$

Position	#3	#6	#9	Note
E - W	88s' year	1.0499	0.9179	1.0499
	89s' year	0.9890	0.8086	0.9890
	90s' year	0.9352	0.7230	0.9352
	Average value	0.9914	0.8165	0.9914
NE45°	88s' year	1.0499	0.9179	1.0499
	89s' year	0.9352	0.7230	0.9352
	90s' year	0.9352	0.7230	0.9352
	Average value	0.9734	0.7880	0.9734
N - S	88s' year	1.0499	0.9179	1.0499
	89s' year	0.9890	0.8086	0.9890
	90s' year	0.9352	0.7230	0.9352
	Average value	0.991	0.8165	0.9914
NW45°	88s' year	1.0499	0.9179	1.0499
	89s' year	0.9352	0.7230	0.9352
	90s' year	0.9352	0.7230	0.9352
	Average value	0.9734	0.7880	0.9734

$Z_c=2.2m$

#### The Determination of the Degree Coefficient of Sunshine and Sun Shade along the Canal Section

The value,  $K_d$  of degree coefficient of sunshine and sun shade is a basic parameter for predicting frozen depth in the design of canal anti-frost heave. In order to get the value of total solar radiation along the canal section and on the ground surface, based on geographical condition, terrain condition, canal direction and section size of canal engineering, the climatology method is used to sum the solar radiation per day during freezing period. Then, the total solar radiation amount,  $\Sigma Q_{\beta\alpha}$ , for each part of the canal section, and the total solar radiation amount,  $\Sigma Q$ , for horizontal surface ground can be obtained during the frozen period. In the period the increasement of accumulating temperature, which each part of the canal corresponds to horizontal surface ground, is:

$$\Delta F_{\beta\alpha} = \frac{\Sigma Q_{\beta\alpha} - \Sigma Q}{\beta} \cdot a_s \quad (4)$$

Where,  $\beta$  - Thermal diffusive coefficient determined by average wind velocity.

$a_s$  - Thermal absorbing coefficient, it takes 0.65 for a concrete surface.

Therefore, the degree of sunshine and sun shade is considered by using stefen formulation,

the value  $K_d$  of revised coefficient of frozen depth at each part of the canal could be computed as:

$$K_d = \frac{H_{\beta\alpha}}{H_0} = \frac{a \cdot \sqrt{F_{\beta\alpha}}}{a \cdot \sqrt{F_0}} = \sqrt{\frac{F_0 - \Delta F_{\beta\alpha}}{F_0}} = 1 - \sqrt{\frac{(\Sigma Q_{\beta\alpha} - \Sigma Q) \cdot a_s}{F_0 \cdot \beta}} \quad (5)$$

Where,  $F_0$  - frozen index.

$H_{\beta\alpha}, H_0$  - frozen depth value of each part of canal section and ground surface.

Table 4. The values of  $K_d$

Position	#3	#6	#9	
E - W	88s' year	1.365	1.064	0.586
	89s' year	1.474	1.090	0.274
	90s' year	1.441	1.083	0.391
	Average value	1.427	1.079	0.417
NE45°	88s' year	1.270	1.072	0.792
	89s' year	1.356	1.097	0.687
	90s' year	1.330	1.090	0.719
	Average value	1.319	1.086	0.733
N - S	88s' year	1.061	1.073	1.061
	89s' year	1.078	1.097	1.078
	90s' year	1.072	1.089	1.072
	Average value	1.070	1.086	1.070
NW45°	88s' year	0.792	1.072	1.270
	89s' year	0.687	1.097	1.356
	90s' year	0.719	1.090	1.330
	Average value	0.733	1.086	1.319

Based on the geography latitude, height above sea level, strike of canal and the size of the canal section in frost-heave testing field using above method, the average wind velocity is 1.84 m/s in freezing periods, the values of  $K_d$  are given in Table 4. The frozen periods are from Nov. 20 to Mar. 8 in the year of 1988 to 1989, from Nov. 19 to Feb. 27 in the year of 1989 to 1990, from Nov. 20 to Feb. 28 in the year of 1990 to 1991.

#### The Calculation of Frozen Depth along Canal Section

The frozen depth along canal section,  $H_d$  can be determined by the following equation:

$$H_d = K_z \cdot K_d \cdot H_0 \quad (6)$$

Where,  $H_d$  - frozen depth along canal section (cm).

$H_0$  - frozen depth from ground surface (cm).

It can be taken from observation of average datas for years, or from equation (1) and (2) by using average frozen index for years.

The calculation values compared with observation values of frozen depth along canal section are shown in Table 5. It is clear that calculation values are approximately equal to observation

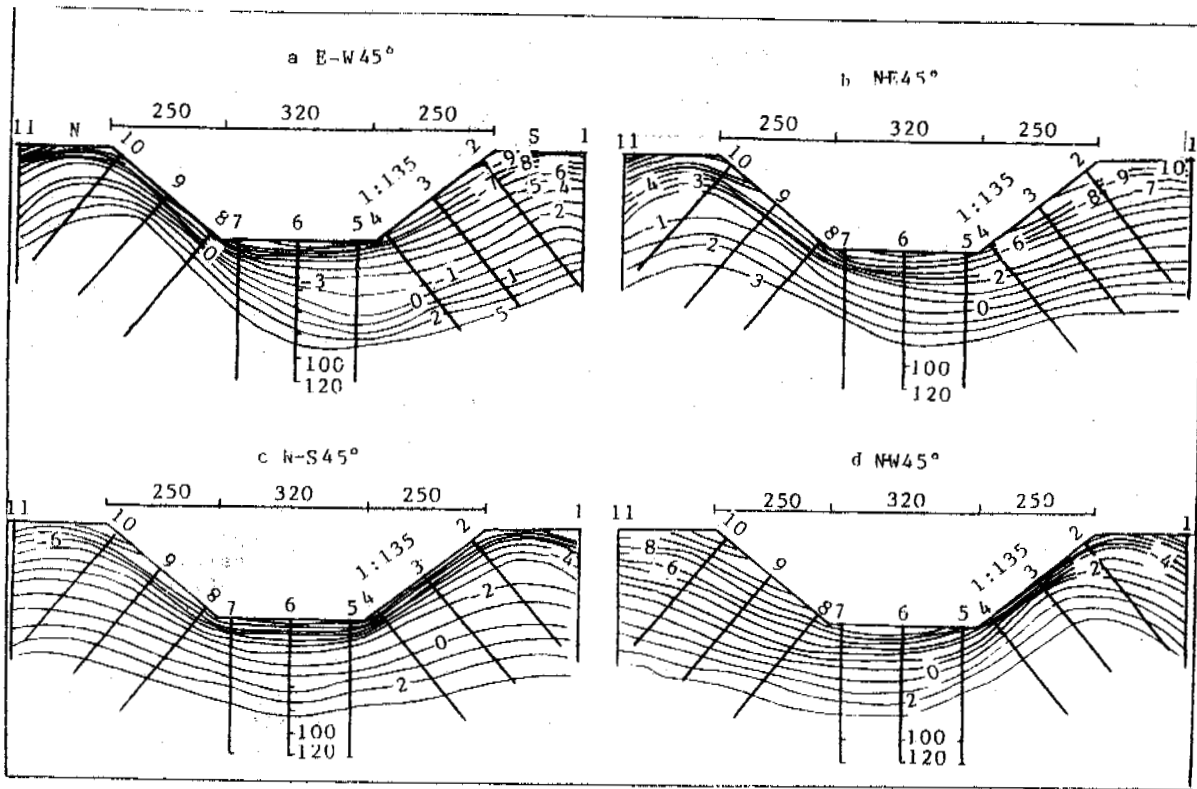


Figure 1. The isotherms of canal section at typical time (cm) (February 2, 1990)

Table 1. The values of A at various observation point

Observation point	#1	#2	#3	#4	#5	#6	#7	#8	#9	#10	#11
E - W	4.4063	5.1095	4.4485	3.4843	3.1493	2.7443	1.9227	1.4100	0.945	2.3914	3.5525
NE45°	3.3999	4.9913	3.8905	2.9516	2.5386	2.5323	1.9566	1.7672	1.6255	3.6257	3.9187
N - S	4.3375	4.6200	3.3414	2.4876	2.3818	2.6135	2.3569	2.5473	3.3457	4.5149	4.2913
NW45°	4.1147	3.4509	1.6409	1.5925	1.9675	2.4663	2.5555	3.0081	4.0206	5.1230	4.4449

Where, H - the maximum frozen depth (cm)  
 $F_0$  - negative temperature index ( $^{\circ}\text{C}\cdot\text{day}$ )  
 A - parameters of frozen depth (see Table 1)

The values of A are affected by many factors. These factors consist of types of soil, dry density of soil, soil water content, groundwater table, solar radiation, heat exchange of ground surface and so on. It may be seen that there is very small change for A in different canal direction at #6 when frozen index and the depth of groundwater table do not change.

The Relation between Frozen Depth and Types of Soil as well as Groundwater Table

The influence of the groundwater table on the freezing process is significant. Based on the observations, it is clear that the depth of groundwater table increases with decreasing frozen depth under a given soil type and the frozen depth is fine sand > sandy loam > heavy silty loam > silty loam at a given groundwater table. That is to say, the values of frozen

depth is inversely proportional to the flux of water migration.

The relationship between the value of A and the depth of groundwater table can be presented as the following empirical equation:

$$A = \frac{1}{a+be^{-Z}} \quad (2)$$

Where, Z - the depth of groundwater table (m)  
 a, b - parameters (see Table 2)

Table 2. The values of a and b

Soil types	a	b	Regression coefficient
Heavy silty loam	0.3179	0.5158	0.884
Silty loam	0.3298	0.5347	0.847
Sandy loam	0.2983	0.4302	0.850
Fine sand	0.2759	0.4112	0.823

values. The equation (6), can be used in canals engineering design.

Table 5. The values of frozen depth (cm)

Position		#3	#6	#9	
Direction	E - W	Observation value	101.5	62.9	32.7
		Calculated value	93.8	58.4	27.4
	NE45°	Observation value	89.2	58.4	47.3
		Calculated value	85.1	56.7	47.3
	N - S	Observation value	76.8	59.9	76.9
		Calculated value	70.3	58.8	70.3
	NW45°	Observation value	47.5	56.8	92.0
		Calculated value	47.3	56.7	85.1

## THE FROST HEAVE REGULATION OF CANAL SUBSOIL

### The Change of Characteristic of Frost Heave Deformation

Based on the test result, it is found that the frost heave deformation along the canal section mainly depends on soil water content. The frost heave increases with the decrease of water table depth and increase of soil water content. The frost heave deformation from big to small are arranged as the bottom, down-slope and up-slope.

It is known that the frost heave damage on the lining canal is produced by the uneven frost heave along the canal section. The unevenness may be expressed by a uneven coefficient, K, the ratio of the difference of frost heave deformation in two points to the distance in same two points. The result, Table 6, points out that the position of maximum frost heave may not be in the position of maximum value of K. The maximum K is close to slope angle. This is because there are restraints in slope-angle. It is necessary in anti-frost heave design to restrain the frost heave of subsoil, to optimize the shape canal section and lining structure, to eliminate the unevenness of frost heave deformation along canal section.

### The Relationship between Frost Heave Deformation and Subsoil Water Content

Table 6. The uneven coefficient along the canal section

Position		#2 -#3	#3 -#4	#4	#5	#5 -#6	#6 -#7	#7	#8	#8 -#9	#9 -#10	
Direction	E - W	88s' year	0.0	0.0	0.0	2.33	-0.08	-0.21	-1.17	0.0	0.0	0.0
		89s' year	0.04	0.21	0.40	0.40	0.17	-0.63	-1.00	-0.20	-0.08	0.0
		90s' year	0.21	1.25	1.00	2.40	0.63	-2.21	-3.40	-0.20	-0.08	0.0
	NE45°	88s' year	0.0	0.0	0.0	0.50	0.04	-0.04	-0.50	0.0	0.0	0.0
		89s' year	0.17	0.71	1.4	3.80	1.5	-2.13	-4.4	-0.60	-0.29	0.0
		90s' year	0.08	0.46	1.00	2.80	1.88	-1.38	-4.4	-1.20	-0.19	-0.13
	N - S	88s' year	0.0	0.0	0.0	3.33	0.17	-0.33	-2.67	0.0	0.0	0.0
		89s' year	0.08	0.21	0.20	1.00	0.71	-0.71	-2.2	-0.60	-0.13	-0.08
		90s' year	0.08	0.63	0.60	3.20	1.46	-1.25	-4.0	-1.20	-0.50	-0.04
NW45°	88s' year	0.0	0.0	0.0	2.00	-0.17	0.08	-1.0	0.0	0.0	0.0	
	89s' year	0.0	0.38	1.40	3.80	1.38	-1.42	-1.60	-0.60	-0.46	-0.06	
	90s' year	0.0	0.21	0.80	5.0	1.71	-1.79	-2.6	-1.60	-0.88	-0.04	

The frost heave is resulted from freezing of the subsoil water and expanding of the subsoil volume. Therefore, the subsoil water content is one of basic factors determining the degree of subsoil frost heave. Based on the testing frost heave ratio (the ratio of the maximum frost heave deformation and the corresponding frozen depth) and subsoil water content, using the least square method, the relationship between frost heave ratio and subsoil water content during unfreezing and freezing can be written:

$$\eta = \alpha_1 (W_1 - \beta_1 W_p) \quad (7)$$

$$\eta = \alpha_2 (W_2 - \beta_2 W_p) \quad (8)$$

Where,  $\eta$  - the frost heave ratio (%)

$W_1$  - subsoil water content before freezing (%)

$W_2$  - subsoil water content during freezing (%)

$W_p$  - water content of liquid limit (%)

$\alpha_1, \alpha_2$  and  $\beta_1, \beta_2$  - parameters (see Table 7)

Because the subsoil frost heave mainly depends on subsoil water content, it is necessary in engineering design to prevent the water source from seeping into the subsoil and to decrease the subsoil water content to achieve the goal of eliminating heave action.

### The Relation between the Frost Heave and the Depth of Groundwater Table

Table 7. The value of  $\alpha_1$  and  $\beta_1$  in different soil

Soil types	$\alpha_1$	$\alpha_2$	$\beta_1$	$\beta_2$	Regression coefficient
Sandy loam	0.7572	0.4474	0.625	0.702	$R_1=0.584$ $R_2=0.766$
Silty loam	1.8756	0.9397	1.158	1.414	$R_1=0.778$ $R_2=0.942$
Heavy silty loam	1.1792	0.6564	1.226	1.365	$R_1=0.913$ $R_2=0.968$

From the testing result, it is known that groundwater is one of the water sources causing frost heave. The relationship between the frost heave ratio and the depth of groundwater table, using the analysis of the least square method, can be written as follow:

$$\eta = De^{-BZ} \quad (9)$$

Where,  $\eta$  - the frost heave ratio (%).  
 $Z$  - the depth of groundwater table (cm).  
 $D, B$  - parameters (see Table 8).

Table 8. The values of  $D, B$  in different soils

Soil types	$D$	$B$	Regression coefficient
Sandy loam	21.972	0.02202	0.802
Silty loam	44.326	0.01087	0.957
Heavy silty loam	59.254	0.01599	0.949

The above formula shows that frost heave ratio increases with decrease of the depth of groundwater table and rapidly increases when the depth of groundwater is lower than a certain range. When the depth of groundwater is more than a certain range, the influence of groundwater on frost heave ratio is slight and negligible.

It is defined that the frost heave ratio is not affected by groundwater when the  $|\frac{d\eta}{dZ}|$  is less than 0.05. The depth of groundwater is defined as critical depth. It is obtained the critical depths of groundwater for silty loam, silty loam and sandy loam are 1.84 m, 2.08 m and 1.03 m respectively.

#### REFERENCES

- Li Anguo, (1992) The study of calculation method on frozen depth in the canal design, Northwest Water Resources and Water Engineering, Vol.3, No.1, pp1-11.  
 Water resources ministry of China, (1991) Design regulations for the frost heaving prevention in structures of canal system (SL23-91), Water Resources and Electric Power Press, pp3-9.

# APPLICATION OF REMOTE SENSING IMAGES TO THE INVESTIGATIONS OF THE CHANGES OF PERMAFROST ENVIRONMENT IN BURNED FOREST REGIONS, DA HINGGAN LING, CHINA

Liang Fengxian and Gu Zhongwei

Lanzhou Institute of Glaciology and Geocryology,  
Chinese Academy of Sciences, China

From the indications of aerial and satellite images, we made a field investigation on the typical burned forest area, and established interpretation signs about the degree of burned forest, types of vegetation species, and vegetation recovery. The results are as follows: 1. After the forest fire of May 6, 1987, the forest environment of slightly and moderately burned areas has approximately recovered. 2. The recovering plants in burned areas in the 1960s, 1970s and 1990s are mainly *Larix gmelinii* and *Pinus sylvestris* mingled with broad-leaved forests. 3. The effects caused by the forest fire on the permafrost environment is obvious. There is displayed a warming effect which presents the variation of plant species and the later phenomenon of vegetation growing period of the TM remote sensing images. The warming effects decrease with the depth.

## INTRODUCTION

The disastrous forest fire area lies in Da Hinggan Ling, Northeast of China. The area belongs to low rolling ridges whose altitude is about 400-800 m. The slope is less than 15 degrees generally. The area experiences a frigid-temperate climate. The mean annual air temperature is between  $-4.7^{\circ}\text{C}$  and  $-5.2^{\circ}\text{C}$ . The yearly precipitation is between 400 mm and 500 mm, and it is mainly during the period from June to September. The area is dominated by continuous or widespread and sporadic permafrost, and is the coldest area in China. The types of vegetation are comparatively simple. The main species are *Larix gmelinii*, *Pinus sylvestris* and *Betula platyphylla*, *Larix gmelinii* are in a steady climax in the climatic conditions of this area. *Pinus sylvestris* is in a climax in impoverished and drought conditions, *Betula platyphylla* is always the pioneer at burned forest sites or cutting sites. The characteristics of the local configuration of vegetation in Da Hinggan Ling has a close relation with the distribution and the development degree of permafrost. The types of vegetation have the effect of indicating permafrost. In swamp, straw mattress has an effect of indicating thick layered ground ice. *Larix gmelinii* indicates low temperature permafrost, and *Pinus sylvestris* indicates high temperature or the sporadic permafrost (Liang Fengxian, 1990). The permafrost-ecological environment is weak, because the area is located on the southern Eurasia border with high latitude continuous permafrost. After the big forest fire, the steady permafrost-ecological environment changed. This paper presents the application of remote sensing technology and the analysis of the changes of the permafrost-ecological environment in burned forest regions in and before 1987.

## RESOURCES OF REMOTE SENSING INFORMATION

1. Panchromatic aerial image of 1:60000 in local region in 1960.
2. Mss allochromatic synthetic landsat image of 1:1000000 before 1979's forest fire in the local region.
3. The mosaic figure of TM image in burned forest region, Da Hinggan Ling, May 6, 1987.
4. TM allochromatic synthetic landsat imagery of 1:500000 after 1987's forest fire on 7 Oct., 1988 (sheet 122/23), 4 Nov., 1988 (sheet 121/23) and 13 May, 1990 (sheet 123/23).

## INTERPRETATION AND ANALYSES OF THE IMAGERY

On the basis of burned forest land and ecological characteristics of vegetation, successional cycles and the relation between vegetation and permafrost, we analyzed the imagery mainly on visual interpretation, established interpretations signs about the burned degree of forest fire, vegetation types, the recovery of the burned forest after the forest fire and the changes of permafrost environment respectively, and at the same time, gave field investigation and observations about the burned forest region in the 1950s, especially the burned forest region on 6 May, 1987.

## INTERPRETATION ABOUT BURNED FOREST REGIONS AND BURNED DEGREE

There are some different imagery characteristics about burned forest regions on different remote sensing imagery. We distinguish them according to strong chromatic observation in color cast about burned and unburned regions.

1. It is a black color cast in burned regions on the panchromatic aerial images and greyish white granular and rough feeling and a solid perception. There is a white fog on the image in the burned forest region.
2. On standard allochromatic synthetic landsat images, the burned forest region appears

brownish black and the unburned forest region appears fresh red.

3. We color TM 7, 3 and 4 bands into red, green and blue, and make the landsat imagery approximately into natural colors. The burned region appears black-black red-red, and the unburned forest region appears green (see Fig.1).

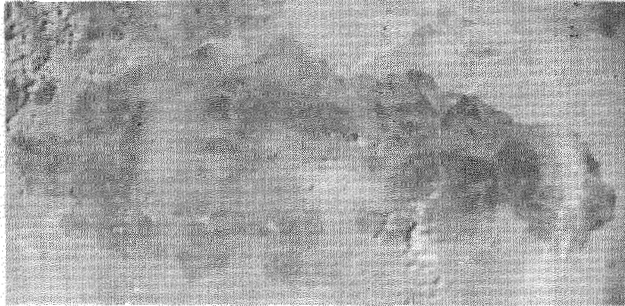


Figure 1. The mosaic figure of TM imagery in burned forest region in Da Hinggan Ling on June 1987

Figure 1 audio-visually illustrates the full view of 1987's big forest fire and the burned degree. On the basis of Figure 1 and the color cast and vegetation shadow lines characteristics, we divide the burned degree into three types. Severely burned, moderately burned and slightly burned, and compose a taxonomic figure (see Fig. 2) of the burned degree of 1987's forest fire in Da Hinggan Ling. The imagery characteristics of each burned type and landscape see Table 1.

Table 1. Imagery characteristics of burned degree and landscape

Burned degree	Imagery characteristics and landscape
Severely burned	It appears blackish red and red on landsat imagery, no information about green vegetation, landscape is dead plats. There are naked stands in spotted forms in local ground surface.
Moderately burned	It appears blotted black-red with uncontinuous green bands like flimsy yern on landsat imagery. Ground surface is covered by 30% high-forest and 60% dead plants (Young trees and grass). Most highforest is alive except for scorched part within 1/3 high of the trees from ground. The canopy of the high forest is green.
Slightly burned	It appears blotted black-red on the widespread green background on landsat imagery. Most vegetation is still alive. The dead plants are shrub and grass.

#### THE INTERPRETATION OF VEGETATION TYPES

As described above, the main vegetation in Da Hinggan Ling is *Larix gmelinii*, *Pinus sylvestris* and *Betula Platyphylla*. Owing to the simple species, the chromatic observation information on the allochromatic synthetic landsat image and phenological information on the multitemporal landsat image can distinguish the dominant species. From spectrum research, the reflectances

of *Larix gmelinii*, *Pinus sylvestris* and *Betula Platyphylla* increase in order of succession. So, on the parchromatic aerial imagery, *Pinus sylvestris* appears black, *Larix gmelinii* appears greyish black and *Betula platyphylla* appears greyish white; on standard allochromatic synthetic summer landsat imagery, the three species appear browish red, red and yellowish red successively; on approximate natural chromatic synthetic landsat imagery, the three species appear blackish green, green and yellowish green. As the chromatic aberration of vegetation is less in its growing season, it is difficult to divide demarcation line of vegetation types. But by combining the analysis of winter landsat imagery, we are able to obtain good interpretative results. Because of the fact that *Larix gmelinii* and *Betula platyphylla* are deciduous trees, there appear grey or greyish green on standard allochromatic synthetic landsat imagery. *Pinus sylvestris* is green all year, it appears as a reddish blotted block on standard synthetic landsat imagery. On grass or shrub land, it appears bright red in summer and greyish white in winter.

#### THE INTERPRETATION OF VEGETATION RECOVERY REGIMES IN THE BURNED FOREST AREA

##### Vegetation Recovery Regimes in the Burned Forest Area

On the allochromatic synthetic landsat image of 1:500000, sheet 123/23 and TM 2, 3 and 4 bands on 3 Oct., 1988, the burned area appears red not only in the river valley, but also on the slope. According to the image characteristics of even and fine, and no stereoscopic sensation red with that the more severely the burned, the better the connected stretches on the image, we found that the first recovered plant is tussock in the second year after the forest fire. Through field investigation in 1990/1991, the plant coverage was up to 80-90%. There are mainly young *Betula Platyphylla* and *Populus devidiana* which are about 2-3 meters high and make up the main recovered plants.

On the analyses of TM 2, 3 and 4 bands synthetic landsat image on sheet 121/23 on 4 Nov., 1989 and TM 7, 4 and 3 bands synthetic landsat image on sheet 123/23 on 13 May, 1990, the color casts of moderately burned forest regions appear basically the same as the unburned forest region in these two periods. They appear in a bathochromatic hue. This illustrates that the arborous layer in moderately and slightly burned regions is not destroyed by the fire, and this result is verified from the field investigation. But it appears in a yellow or yellowish white hypsochromatic hue in severely burned regions in the two periods. This hue has an obvious contrast with the bathochromatic hue, and appears as a characteristic of "forest window". Since the vegetation in the severely burned region is almost all dead, the recovered vegetation is tussock and shrub. In the withering period, the reflectance of the litter layer increases. It appears as a hypsochromatic hue in the germinating season, the lower grass is covered by high dead grass, and appears as a hypsochromatic hue as well. This characteristic of "forest window" is correspondent with the results of field investigation.

##### The Analysis of Forest Recovery in Past Recorded Forest Fires



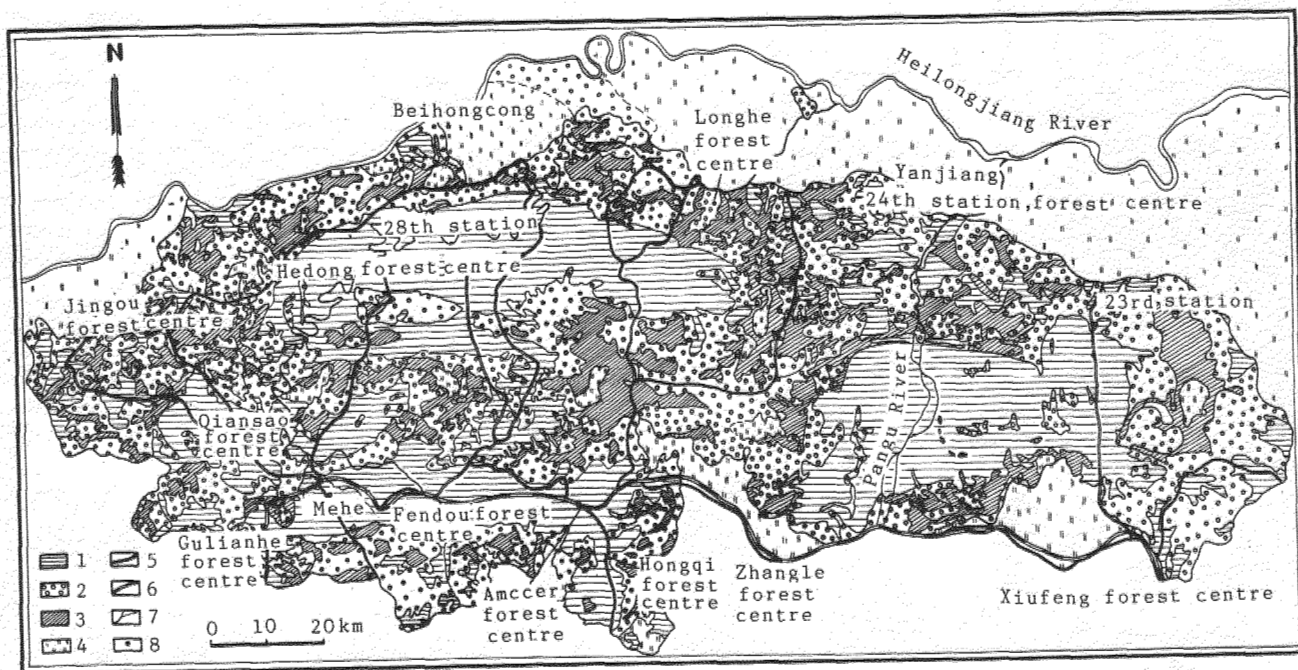


Figure 2. The interpretation figure of TM imagery about burned degree in burned forest region in Da Hinggan Ling on 5 June, 1987

Legend Scale: 1. Severely burned forest land; 2. Moderately burned forest land; 3. Slightly burned forest land; 4. Unburned forest land; 5. Railway; 6. Road; 7. River; 8. Residential area.

Forest fires occur frequently in Da Hinggan Ling. In order to investigate the recovery characteristics, we inspect 12 burned forest sites with vegetation recovery regimes since the 1950's (see Table 2).

As described in Table 2, the spatial distribution sequence of recovered vegetation at the burned sites illustrates the successional sequence of vegetation in time series. The recovered vegetation in the 1950's burned areas are mainly pine-birch forest assemblage and in the 1980's the burned areas are mainly birch and poplar. From Table 2, we see that anthropogenic afforestation can reconstruct the rational forest structure and accelerate the formation of a climax, especially in severely burned regions where there is no resource-seed trees alive, i.e. the severely burned region at the Eighteenth Station Forest Bureau in 1975.

#### INTERPRETATION OF THE CHANGES OF PERMAFROST ENVIRONMENT

The effect of forest fire on the permafrost environment is mainly the warming effect. Its presentation is the increase of air and ground surface temperatures. Their synthetic effects cause an increase in the seasonally thawed depth. Since vegetation is sensitive to those factors, we give analyses about the changes of permafrost environment according to the abnormal information on imagery.

Figure 1 shows leaf-form shallow green blotted black abnormality in the Northern Hongcong region. The abnormality has a strong contrast with the adjacent deep green. From field inves-

tigation, the abnormality is caused by 1965's forest fire whose effects made the changes of radiation, increased ground temperature and evaporation, decreased water content and increased the seasonally thawed depth, etc. The warming effect has an advantage to vegetation succession. We verified the warming effect through field investigation in June 1990. From the observation of ground temperature and thaw depth at 20 burned sites and 10 unburned sites, we found that the average ground temperatures at a depth of 20 cm at burned and unburned sites are 5.1°C and 0.8°C respectively, and the thaw depths at the same time at burned and unburned sites are 48 cm and 27.8 cm respectively. The burned site is 20.2 cm deeper than at the unburned site.

From borehole information in the northern valley of Amuer in Oct. 1991, the maximum seasonally thawed depth at the burned site, 50 m apart from the unburned site, and unburned site are 2.5 m and 1.25 m respectively in swamp, the difference is great. From the measured temperatures in boreholes, the difference of ground temperatures in the two boreholes at burned and unburned sites is distinct within the depth of 5 meters. The range of the difference is 0.5-0.8°C, the maximum is 2.0°C. With the increase of the depths, the difference of the temperatures in the two boreholes become little. At depth of 20 cm, they are correspondent. As described above, it is the warming effect caused by forest fires on the permafrost environment that is obvious and significant.

#### CONCLUSIONS

Table 2. Vegetation recovery of past recorded burned forest regions

No.	Region	Burned time	Mode of Regeneration	Recovered Constitution
1	Kuduer Forest-Bureau	Before 1950	Natural	Larix gmelinii and Picea asperata with diameter of 20-30 cm
2	Testing Forest Centre	1988	Natural	Larix gmelinii and Betula platyphylla
3	Yanshan Forest Centre	1960	Natural	Betula platyphylla and Larix gmelinii
4	Beihong County	Before 1965	Natural	Betula platyphylla and Larix gmelinii
5	Yanshan Forest Centre	1966	Natural	Larix gmelinii and Betula platyphylla
6	Yanshan Forest Centre	1966	Natural	Larix gmelinii and Betula platyphylla
7	Xinlin Forest Centre	1972	Anthropogenic	Larix gmelinii and Betula platyphylla with ratio of 8:1
8	Linlan	1972	Natural	Betula platyphylla and Larix gmelinii
9	Tahe Forest Bureau	1978	Natural and Anthropogenic	Betula platyphylla, Larix gmelinii and Pinus sylvestris with ratio of 7:4:1
10	Neighteenth Forest Bureau	1975	1. Natural	All broad-leaved trees (no reserved-seed trees)
			2. Natural	Larix gmelinii and Betula platyphylla (have reserved-seed trees)
			3. Natural	Pinus sylvestris and Betula platyphylla (have reserved-seed trees)
			4. Anthropogenic	All pinus sylvestris with hight of 3-4 m
11	Kuduer Forest Bureau	1980	Natural	The secondary forest of Betula platyphylla
12	Tuqiang Forest Bureau	1982	Natural and Anthropogenic	All pinus sylvestris

With the analyses of remote sensing imagery and field investigation, the results are as follows:

(1) Remote sensing imagery has a good interpretative results about burned forest areas, the burned degree of forest fires vegetation types, the regime of vegetation recovery as well as the information about the permafrost environment. Those results illustrate a prospective application of remote sensing technology in permafrost environment and vegetation.

(2) Vegetation has good recovery conditions. The vegetation in 1987's forest fire land has recovered rapidly. The first recovered species is grass with coverage up to 80-90%. The grass has an effect on soil and water conservation, and makes the ecological environment have a positive developing tendency. The vegetation in lightly and moderately burned forest areas has been recovering considerably, although the recovered species are broad-leaved trees such as Betula Platyphylla, Populus devidiana, etc., which create a better condition for further succession. It is noticeable that there is only grass in the severely burned areas in which there are no seed-reserve trees alive. In these regions, we have to afforest in order to speed the succession.

(3) From field investigation of past recorded forest fires, the results indicate that the burned forest has a steady successional rule. The secondary forest such as Betula Platyphylla finally succeeds to a climax (pine) only through a long successional process in which it needs 100-200 years. Because of the steady ecological

system and strong ability to resist disturbance of pine communities, the succession is very slow. The regular pattern of the succession of burned forest in Da Hinggan Ling is correspondend with the successional pattern of coniferous forest illustrated by K.V. Ckee (Zhou Youwu, 1991). From this, we can see that the recovery of the burned forest on May 6, 1987 may need more than a half century for the significant succession.

(4) Forest and permafrost are the two major factors whose interaction maintains the ecological balance in permafrost regions. Therefore, the recovery of the permafrost environment must depend on the vegetation recovery. The speed of the recovery of the permafrost environment relates not only to the burned degree, but also to the climatic conditions and the vegetation types. Viereck's conclusion indicates that the thawed depth reaches the maximum thaw depth in lower temperature regions earlier than in higher temperature regions in burned areas (Gu Zhongwei, 1989). C.H. Raccine's results illustrate that when the burned vegetation types differ, the degree of its recovery and the effects on permafrost differs distinctively. In tundra, the thaw depth reaches its maximum two years after a fire and it returns to the prefire depth two years later. But in forest region it need about 15 years for the thaw depth to reach its maximum after a fire and needs about 25-50 years to return to the pre-fire level (Zhou Youwu, 1991). In accordance with this, we analyze that the recovery of the permafrost environment after a fire in swamp which has the

lowest annual ground temperature and thick layered ground ice is the quickest, in the Larix gmelinica region whose annual ground temperature is higher than in swamp it is slow and in the Pinus sylvestris region it is the lowest and has a possibility of forming a talik.

(5) Larix gmelinii has a good adaptability to the permafrost environment over a long period of time; its distribution has a close relationship with permafrost. But we ought to look at the relationship again. We don't conclude that permafrost is the only or optimum condition for Larix gmelinii to grow and to protect forest. Like other vegetation, Larix gmelinii's growing is limited mainly by three factors, water, radiation and heat. Through field investigation, Larix gmelinii grows best on the southern slope on which the three factors are at an optimum, next best is on the northern slope. In swamp which has low temperature and high water content, Larix gmelinii growth is worst. In Chinese dialect, it is called "old dwarf man". This indicates that the well-developed permafrost region does not have optimum conditions for Larix gmelinii to grow. But the litter layer when slightly burned and cleaned can increase radiation in forest, soil temperature and thaw depth, which improves the growing conditions of vegetation in high water content land.

(6) Although forest fire is frequent in Da Hinggan Ling, the two extreme tendencies of desertification and swamping are not obvious. Through analysis, the reasons are as following:

A. The reason that the desertification phenomenon is not clear is owing to the fact that the region belongs to a frigid-temperate zone and has a semi-humid climate. The burned forest area is only a small part of Da Hinggan Ling and it doesn't cause the change of atmospheric circulation. Under this condition, burned vegetation has good recovery and covers the ground surface quickly.

B. There is no sand resource.

C. The mean annual wind velocity is small and the days of large winds are few. In the conditions of no sand resource, less wind power, good recovery climate, the tendency of desertification is little.

The swamping tendency is not obvious because of the fact that:

A. Fire burned litter layer, causes the decrease of water capacity and improved water drainage.

B. Burned forest layer formed a "forest window" which lets more radiation into the forest, increases evaporation and water content in the active layer except for the increase in local swamp land (Zhou Youwu, 1991). The amplitude of the decrease of water content is up to 50-70% (Liang Linheng, et al, 1981).

C. From pit tests, this region has a layer of weathering elastic granite that has strong water permeability which create a good condition for the water of thawed ground ice to penetrate. This can interpret the degree of the decrease of water content in the seasonally thawed layer with the increase of seasonally thawed depth.

The effect of forest fires on the permafrost environment and vegetation is a complex subject. The recovery of vegetation and permafrost environment require a long process. In order to evaluate the effects of forest fires on vegetation and to know well the rules of vegetation succession and the recovery of permafrost environment, we ought to use the real time and

dynamic state of remote sensing information completely in addition to paying attention to the contrast observation and pit tests in burned and unburned forest regions, give long term monitoring to the burned forest region forest fire on June 5, 1987, and supply a scientific basis in order to establish a steady forest-permafrost ecological environment.

#### ACKNOWLEDGMENT

The project was funded by Chinese Committee of National Sciences. The authors would like to thank Prof. Zhou Youwu and Assoc. Wang Jiacheng and also thanks are due to Zhang Qiping, Liang Linheng and Lou Guowei.

#### REFERENCES

- Guo Yongchong, (1986) Forest Resource in Da Hinggan Ling. Restricted Publication.
- Gu Zhongwei, (1989) The Changes of Permafrost and Plants after Tundra Fire. Translated Reports of Glaciology and Geocryology (in Chinese), 6(2).
- Liang Fengxian, (1990) The Application of Multi-Temporal Landsat Imagery in the Interpretation of Permafrost and Vegetation. Fourth National Conference on Permafrost.
- Liang Linheng, (1989) The Changes to the Permafrost Environment after Forest Fire, Gulian Mining Area, Chinese Da Hinggan Ling.

THE CHARACTERISTICS OF THE DISTRIBUTION OF SNOW COVER AND ITS WARM EFFECT  
ON THE TEMPERATURE OF PERMAFROST, AMUER REGION, DA HINGGAN LING

Liang Linheng and Zhou Youwu

Lanzhou Institute of Glaciology and Geocryology, Chinese Academy of Sciences

This paper presents the characteristics of the distribution, depth, density and temperature of snow cover and the regime of shallow ground temperature in different vegetation zones and geomorphological position, Amuer region, Da Hingan Ling, Northeast of China in 1991-92. The results indicate that the depth of snow cover in swamp is thicker than on slope in general, the depth in burned forest site is 1-3 cm thicker than unburned forest site in the same geomorphological position and same vegetation conditions, the naked site (cutting site) is the thinnest. The thickest depth of snow cover in this region is more than 60 cm in this time of investigation. The characteristic of the density of snow cover is that the density at naked site is the biggest, and at unburned site is the least. From calculation, the depth of snow cover from 21 to 36 cm can increase mean annual ground surface temperature 2.8-5.0°C.

INTRODUCTION

The depth and density of snow cover and its distribution are very important to the study of permafrost and hydrology. Many scholars studied the problem, such as C.A. Troendle, R.A. Schmit (1980) and D.A. Toews (1988) who had studied snow deposition process in a forest. UNSCO/IASH/WMO (1970) in the study of seasonal snow cover concerned the distribution of snow cover and etc.. Dai Jinbo (1981) had observed the depth of snow cover in swamp in our study region. This paper discusses the characteristics of the depth, density and the temperature of snow cover in different geomorphological positions and different types of vegetation zones (natural, naked and burned forest zone) in Amuer region, Da Hingan Ling, Northeast of China.

SITE CONDITION

Amuer forest region (122°38'30"E, 52°15'3"N) lies in the northern part of the Da Hingan Ling continuous permafrost region (Guo Dongxin, 1981) (see Fig.1) and near the China-pre-USSR border. The climate is influenced by cold air masses from Siberia and Mongolia. The mean annual air temperature is -5.1°C (1959-1987), the annual air temperature range is 47.6°C, and the yearly precipitation is about 394.9 mm. It begins to snow at the end of September or the beginning of October, and it ends to snow to the beginning of May next year. Snow cover remains for seven months, which is correspondent with yearly frozen period. The depth of mean annual snow cover is 20-30 cm. The region also is the typical boreal forest area, and the area of forest is

Table 1 The characteristics of vegetation, geomorphology and lithology in each site

site No.	geomorphological position	the type of the site	vegetation	lithology
A	footslope(2-3°C) E.S.exposure	natural	dense young pinus pumila	crushed-rock loam & sand
B	ditto	burned	burned young Pinus pumila	ditto
C	crest E.S.exposure	lightly burned	dense pine- birch com- munity	crushed stone loam
D	side-slope E.S.exposure	naked	pine and birch cutting site	crushed stone loam
E	swamp	burned	tussock hum- mocks & shrub	peat & humus & sandy loam
F	ditto	natural	small pine, tussock hum- mocks & shrub	ditto

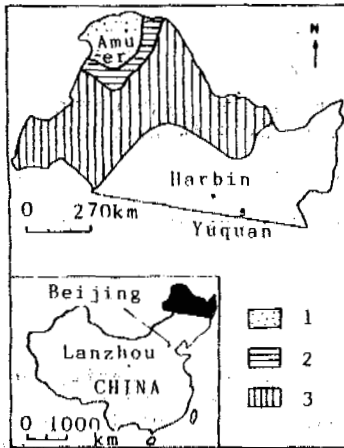


Fig.1 Geographical position in research area  
 1--Continuous permafrost;  
 2--Wide spread continuous permafrost;  
 3--Spodaic permafrost.

more than 91%. The forest was severely burned by forest fire in this region in 1987. We established observation sites for the changes of permafrost environment after the fire in 1990. This investigation is the continuing of 1990's work. The vegetation, geomorphological position and lithology at each observation site is in Tab.1.

DISTRIBUTION OF THE DEPTH OF SNOW COVER

In the process of monitoring the depths of snow cover from site A to E in March 1991, the depth at each site is the average of five depths measured.

From the observation, the depths of snow cover are different on the different types of vegetation and geomorphological positions (Table 2). As described in Tab.2, the difference between site A (natural) and site B (burned) in Northwest slope is that site B is 3.3 cm deeper than site A. The depth at site C (Pine-birch) at crest is the twice deeper than site D (naked) in Northeast side-slope. In swamp, the depth at site E (burned) is deeper than site F (unburned).

Table 2 The thickness of snow cover at different sites(17-20.03.1991)

date	17	19	20
site No.	A B C D E F		
depth(cm)	30.2 33.5 30.3 21.0 37.0 34.8		

Generally speaking, the depth of snow cover in swamp is deeper than the depth on slope, and the depth at burned site is deeper than at unburned site, in which the difference between naked and forest sites is the most distinct.

From field investigation, the main reasons which caused the difference of the of snow cover are the forest, wind and topogaphy. Forest can not only protect the snow under it from being moved by wind, but also can resist snow-fall to the ground. Part of the snow on forest canopy can be thrown up by wind and transferred. This maybe is the one reason that made the difference of the depths of snow cover between burned and unburned sites in the same geomorphological

position.

The interaction of wind and topography maybe is another reason that caused the difference of the depths of snow cover. In this survey, that the depth in swamp is deeper than on slope except for the naked site is probable the results of the interaction, but in the conditions of ground surface, the naked site differs from the other sites which either have shrub and tussock or dense or sparse pine trees. Thus, the snow cover at site C is easiest for wind to transfer, and the monsoon of northern direction in winter increased the transfer. Finally the depth of snow cover at naked site (site C) is thinnest.

The depth listed in Table 2 is not the maximum depth of snow cover. After heavy precipitation in March 22nd and 23rd, the depth at site B is 61 cm and site A is 51.5 cm. In April, the snow begins to thaw slowly.

THE CHARACTERISTIC OF SNOW DENSITY

The densimeter used in this time was made by Lanzhou Institute of Glaciology and Geocryology, Chinese Academy of Sciences. It is 10cm high and its diameter is 5 cm. Through investigation, we found the snow density has reversal distribution at each site to the depth (Fig.2, Tab.2). The density in figure 1 at each site is the average of the density of each layer along the depth. From figure 1, we can see the density at sites A and C (dense forest sites) is the minimum (172.0 Kg/m<sup>3</sup>), and the density at site D (naked site) is the maximum (203.7 Kg/m<sup>3</sup>). The sequence of the density is site A(C)>B>D>E>F. The reasons for the density differences probably are the forest and wind except for the natural factors of its weight, deformation and etc.. Wind can move surface snow, help to destroy the loose structure, break off protuberances and increase density. Those promote metamorphism and hardening of the snow (Albert F.Wuori, 1963). Forest can protect the snow cover from being disturbed by wind.

The densitification of fresh snow is very quick. The density of fresh snow (as soon as snow fall stopped) measured during this observation is 19.1 kg/m<sup>3</sup>. Two days late, the density becomes 114.6 Kg/m<sup>3</sup>. In the same time and at the same site, snow density changes greatly along the depth. Fig.3 presents the changes of snow density along the depth at sites A and B after snow fall. Within the depth of 0-20 cm, the difference is not obvious; under this, the difference is clear.

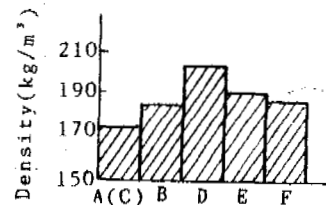


Fig.2 Density of snow cover at each site

REGIME OF SNOW TEMPERATURE AND ITS WARM EFFECTS ON GROUND AND GROUND SURFACE TEMPERATURE

During the survey, we measured snow temperatures at each site in different vegetation zones and geomorphological positions. In swamp, the temperature (Fig.4) at site E (burned) is higher

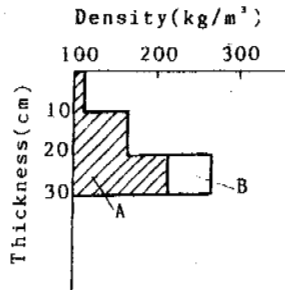


Fig. 3 The change of density of snow cover with depth at site A & site B

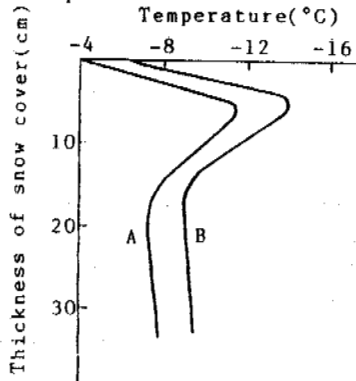


Fig. 4 The change of snow temperature with depth at site A & site B

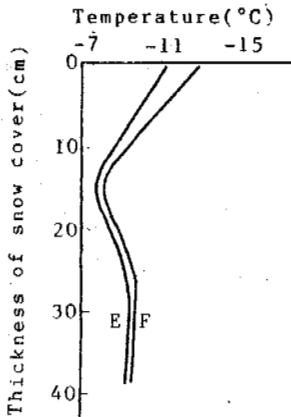


Fig. 5 The change of snow temperature with depth at site E & site F

than at site F, which is correspondent with the depth of snow cover at each site. But the Fig. 5 appears that the temperature at burned site (site B) is lower than at unburned site (site A), the reason is probably the effect of vegetation. Through micro-climatic observation at sites A and B from October 1991 to March 1992 during cold period, the results are that the daily air temperature at site A (in natural forest) is 0.5°C lower than site B (burned), but the snow surface temperature at site A is 0.3°C higher than at site B during the observation. This made the temperature of snow cover at site A higher than at site B. The difference of snow temperatures made the difference of ground temperatures. The monitored ground temperatures in two shallow boreholes at sites A and B, similar to the regime of snow temperature, are that the tempera-

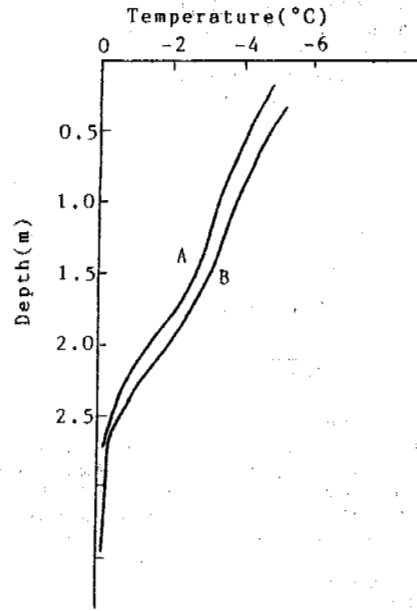


Fig. 6 Temperature in borehole at site A & site B

ture at site A is higher than at site B (see Fig. 6) from ground surface to the depth of 2.2m, and the temperatures appears same at the depth of 2.2 m at both sites. From this, we can see that the vegetation is a important factor to affect the snow and ground surface and snow temperatures.

#### THE EFFECTS OF SNOW COVER ON THE RISE OF TEMPERATURE

There are no exact answers about how much the intensity of heat-shield effect of snow cover is or how much degree the snow cover can increase ground surface temperature. Following is the proximate caculation about this questions. The parameters used in formula come mainly from the observation this time.

According to Amuer meteorological data, the maximum depth of snow cover in 1991 is deeper than before. In caculation, the depths are from Table 2, in which the data is proximate to the average of years running maximum depths.

From other scholars' study, the heat conductivity of snow cover is mainly determined by its density whether it is in theory, in test or in field observations (Schwerdtfeger, 1963; Yen, 1981; Lang, 1985, etc.), Yen (1981) derived a general formula from other researchers' information in laboratory and field about the relation between the thermal conductivity and the desity of snow cover,

$$\lambda = 2.22362 \cdot \rho^{1.885} \quad (1)$$

the units of  $\lambda$  and  $\rho$  are respectively w/m.k and Mg/m<sup>3</sup>. To substitute the  $\lambda$  in  $K = \lambda / \rho \cdot C$ , the result is:

$$K = (2.22362/C) \rho^{0.885} \quad (2)$$

where C is the specific heat of snow cover. It only has relation with temperature (Yen, 1981). During this observation, the parameter can be regarded as constant,  $2009 \times 10^3$  J/Mg.k (S.B. Pater-

son, 1981). Put the data of snow density at each site into formula (2), the calculated results of K are listed in Table 3. The values of K and other

Table 3 Thermal conductivity of snow cover at each site

site	A (C)	B	D	E	F
density (kg/m <sup>3</sup> )	171.9	184.6	203.7	191.0	186.7
thermal conductivity (m/hr)	0.8387	0.8933	0.9746	0.9207	0.9023

parameters combined with V.A. Kydryavtsev's para-empirical formula:

$$\Delta T = A/2(1 - e^{-Z\sqrt{\pi KT}}) \quad (3)$$

where T is the one year's time (hour), Z is the depth of snow cover (m), A is the mean annual air temperature range (47.6°C) (From Amuer meteorological station from 1975 to 1987) and ΔT is the raised degree of mean annual ground surface temperature. So far, we obtained the final results (see Table 4) about snow raised annual ground surface temperatures. The data in Table 4 is correspondent with the results calculated by V.A. Kydryavtsev's formula.

Table 4 The increased annual ground surface temperatures at each site

site	A	B	C	D	E	F
thickness of snow cover (m)	0.302	0.335	0.363	0.210	0.370	0.348
increased temperature (°C)	4.3	4.6	5.0	2.6	4.9	4.7

From Table 3 and 4, it is distinct that the thinner the depth of snow cover, the bigger the value of K, and the less the warm effect (i.e. site D), and same time we can see the value of ΔT is mainly determined by the depth of snow cover when the ranges of K doesn't change greatly. Especially, Table 4 presents that the warm effect at burned sites (sites B and E) is stronger at unburned sites. The effect at site C is the strongest. As for the effect of snow cover on the regime of ground surface temperature we ought to consider common effects of it and vegetation.

The conclusion above is only characteristics of snow and its effect to ground surface temperature in 1991, but it presents the general results about the distribution of snow cover, the reason which causes difference of the distribution and the degree of the influence of snow cover to ground surface temperature. The aim of this is to emphasize the importance of snow cover.

According to the depth of snow cover in winter in 1992, its depth (about 30 cm in March) is comparatively thinner than the depth in 1991, but the characteristics of its distribution and its effect to ground surface temperature are similar to the 1991's, only in the difference about the intensity and ranges of the effects.

## CONCLUSIONS

The depth of snow cover related to geomorphological position and the types of vegetation (naked, burned and unburned). The depth in swamp

is thicker than on slope. In the same geomorphological position and vegetation condition, the depth at burned site is thicker than at unburned site. The depth at naked site is the thinnest.

The density of snow cover decreases by sequence: naked site > burned site > unburned site, the value is 100-200 Kg/m<sup>3</sup>.

The effect of snow cover on increase of ground surface temperature is mainly determined by the depth. In the same geomorphological position, the effect at burned site is stronger than at unburned site. Owing to the effect of vegetation on the temperature, the temperature of the layer of snow cover and ground temperature become complex.

## REFERENCES

- Albert F. Wuori (1963) Snow stabilization Studies. Ice and Snow Properties, Processes and Application, 438-458.
- Guo Dongxin (1981) Diversion of Permafrost in Da Hinggan Ling, Northern China (In Chinese). Journal of Glaciology and Geocryology. 3(3), 1-9.
- Lang M.A. (1985) Measurements of Thermal Parameters in Antarctic Snow and Firn. Annuals of Glaciology, 6:100-104.
- Paterson W.S.S. (1981) Temperature Distribution in Glacier and Ice Cap. Glaciological Physics. p116
- Schwerdtfeger P. (1963) Theoretical Derivation of the Thermal Conductivity and Diffusivity of Snow. IASH PZ Publ. 61:75-81.
- Toews D.A.A. and Gluns D.R. (1988) Translating Snow Hydrology Research Results Into Guidelines for Frost managers: Gaps Between Theory and Practice. 56th Annual Meeting of Western Snow Conference.
- UNESCO/IASH/WMO (1970) Seasonal Snow Cover. A Contribution to the International Hydrological decade. Technical Papers in Hydrology.
- V.A. Kydryavtsev and et al. (1974) Foundation of Geocryology Forecast in the Researches of Engineering (In Russian).
- Yen Y.C. (1981) Review of Thermal Properties of Snow. Ice and Sea Ice, CRREL Report 81-10.

# THE DENUDATION BY GELIFRACTION AND INFLUENTIAL FACTORS IN THE PERIGLACIAL ENVIRONMENT OF TIANSHAN MOUNTAINS, CHINA\*

Liu Gengnian<sup>1</sup>, Xiong Heigang<sup>2</sup> and Cui Zhijiu<sup>1</sup>

<sup>1</sup>Department of Geography, Beijing University, Beijing, China

<sup>2</sup>Department of Geography, Xinjiang University, Xinjiang, China

According to the 1980 data measured in three points at Tianshan Mountains, it can be reflected that the denudation rates by gelifraction at the high altitude of Tianshan Mountains (3200-4000 m) are 0.0014 m<sup>3</sup>/m<sup>2</sup>·yr, 0.015 m<sup>3</sup>/m<sup>2</sup>·yr and 0.00018 m<sup>3</sup>/m<sup>2</sup>·yr, respectively. The rate goes higher with high altitude, but the petrology, structure and humidity may make this tendency complicated. The rates on southern slopes are higher than those on northern slopes. Higher precipitation and air humidity may make the rate higher. It shows by comparison that the alpine periglacial environments in middle latitude are the favorable for denudation by gelifraction.

## INTRODUCTION

The Bing Pass (also known as Shengli Pass), 4010 m a.s.l., is situated on the Urumqi-Kuerle highway, 135 km south of Urumqi. This highway was put into use in the late fifties and was abandoned in 1959 because a section of the highway near the Bing Pass was built on the lateral moraine of No.4 Glacier that, when melted, made the road sink and collapse. The abandoned road received the gelifractioned debris, providing an ideal place for measuring the denudation rate of gelifraction.

The Haxilegen Pass, 3580 m a.s.l., is situated on the Dushanzi-Kuche Highway, 110 km south of Dushanzi. Yuximolegai Pass, 3428 m a.s.l., is situated on the Dashanzi-Kuche Highway, 175 km south of Dushanzi City. The Dushanzi-Kuche Highway began construction in 1974 and the section going through the pass was finished in 1981. The gelifractioned debris falls and are amassed on the road from the slope beside the road, also providing a good research location.

## METHOD AND RESULTS OF MEASUREMENT

The measurements include the length and width of the debris spread on the road, the height and slope of the debris hill, the height, slope, slope orientation, petrology and tectonics of the bedrock in the source region. The distance between measured points is 10 m. The cross profile of the gelifractioned debris hill beside the road can be taken as a triangle. The porosity of the gelifractioned debris is averaged at 0.8, so the volume of the debris hill on the road can be calculated as this:

$$1/2 * L(m) * W(m) * H(m) * 0.8$$

\*The research is supported by NSFC and Tianshan Glacial Observation Station.

L: Length of the debris hill (length of the road with debris on it)  
W: Width of the debris hill  
H: Height of the debris hill

and the denudation rate of gelifraction can be calculated as follows:

$$V(m^3)/S(m^2)/T(yr)$$

V: Volume of the debris hill  
S: Area of the source region  
T: Years in succession

1980 data has been measured in those three points. Because this number is too big, only the statistic data of different sections are listed. Table 1. shows the data for the debris in Haxilegen Pass, Table 2 for that in Yuximolegai Pass, Table 3 and Table 4 for that in Bing Pass.

It can be reflected from Table 1, through Table 4 that the denudation rate of gelifraction in Yuximolegai Pass is the fastest. The rate varies among 0.005-0.0392 m<sup>3</sup>/m<sup>2</sup>·yr with the mean value of 0.0115 m<sup>3</sup>/m<sup>2</sup>·yr. The denudation rate of gelifraction in Haxilegen Pass is between those in Yuxilegen Pass and Bing Pass, varying from 0.0045-0.084 m<sup>3</sup>/m<sup>2</sup>·yr, with the mean value of 0.0014 m<sup>3</sup>/m<sup>2</sup>·yr. Bing Pass, the easternmost of the three passes, is lower in the denudation rate of gelifraction. The rate is between 0.000002 m<sup>3</sup>/m<sup>2</sup>·yr and 0.0018 m<sup>3</sup>/m<sup>2</sup>·yr, with the mean value of 0.00018 m<sup>3</sup>/m<sup>2</sup>·yr.

## CHARACTERS AND INFLUENTIAL FACTORS OF DENUDATION

The denudation rate by gelifraction in the cold mountains, plateaus and polar regions is a principal theoretical problem in Geomorphology. And along with the expansion of the human activities, the study of denudation by gelifraction has become a practical problem in the construction field, such as the building of roads,



Table 1. Depositional amount of gelifraction debris and the denudation rate at Haxilegen Pass (average for the year of 1981 to 1990)

Part	Altitude m	Length of Road m	Debris Body			Source Region				Total Amount of Deposition m <sup>3</sup>	Area of Source Region m <sup>2</sup>	Denudation Rate m <sup>3</sup> m <sup>-2</sup> yr <sup>-1</sup>	Rate of Slope Retreat (mean value) mm·yr <sup>-1</sup>
			W (mean value) m	H (mean value) m	S (mean value) °	HS (mean value) m	LS (mean value) m	S (mean value) °	OS (mean value) °				
S UP	3510-3490	58	1.9	0.88	25	4.5	8	34	152	38.79	464	0.0084	8.4
S MP	3490-3421	200	3.0	0.7	14	18.9	30	39	205	168.00	6000	0.0028	2.8
S LP	3421-3400	60	2.6	0.5	11	54.1	86	39	205	31.2	5160	0.0006	0.6
N UP	3510-3480	190	4.1	1.39	20	30.8	50	38	330	433.12	9500	0.0046	4.6
N TP	3480-3430	65	2.3	1.50	41	15.0	25	37	218	89.70	1625	0.0055	5.5
S SP	3430-3400	276	2.7	0.375	8	50.3	90	34	340	109.14	24030	0.00045	0.45
S LP	3400-3385	217	4.3	0.38	5	70.7	110	40	0	141.83	23970	0.00059	0.59

Note: SS: southern slope NS: northern slope UP: upper part MP: middle part SP: second part TP: third part LP: lower part W: width H: height S: slope HS: height of slope LS: length of slope OS: orientation of slope

Table 2. Depositional amount of gelifraction debris and the denudation rate at Yuximolegai Pass (average for the year of 1981 to 1990)

Part	Altitude m	Length of Road m	Debris Body			Source Region				Total Amount of Deposition m <sup>3</sup>	Area of Source Region m <sup>2</sup>	Denudation Rate m <sup>3</sup> m <sup>-2</sup> yr <sup>-1</sup>	Rate of Slope Retreat (mean value) mm·yr <sup>-1</sup>
			W (mean value) m	H (mean value) m	S (mean value) °	HS (mean value) m	LS (mean value) m	S (mean value) °	OS (mean value) °				
UP	3428-3398	368.1	2.55	2.33	41	5.25	6.06	56	158	874.83	2231	0.0392	39.2
S TP	3380-3398	225	2.00	1.40	42	9.50	10.97	54	80	252.00	2468	0.0102	10.2
S SP	3329-3380	623.5	1.23	1.59	37	6.43	7.43	51	145	487.75	4633	0.0105	10.5
S LP	3280-3329	601.8	0.90	1.44	35	9.05	10.45	56	65	311.97	6288.8	0.0050	5.0
N UP	3428-3392	78	2.05	1.725	34	9.0	10.40	67	266	110.33	702	0.0157	15.7
S LP	3392-3280	253.5	0.9	1.715	30	9.5	10.97	74	38	156.51	2781	0.0056	5.6

Note: SS: southern slope NS: northern slope UP: upper part MP: middle part SP: Second part TP: third part LP: lower part W: width H: height S: slope HS: height of slope LS: length of slope OS: orientation of slope

Table 4. Depositional amount of gelifraction debris and the denudation rate at Bing Pass (average for the years of 1981 to 1990)

Part	Altitude m	Length of Road m	Total Amount of Deposition m <sup>3</sup>	Area of Source Region m <sup>2</sup>	Denudation Rate m <sup>3</sup> m <sup>-2</sup> yr <sup>-1</sup>	Rate of Slope Retreat mm·yr <sup>-1</sup>
S AB	3920-4010	1720	2004.7	230030	0.00029	0.29
S CD	3880	536	447.28	26426.8	0.00056	0.56
S DE	3800-3880	713	999.11	42637.4	0.00078	0.78
S EF	3760-3800	1062	981.29	106093.8	0.00031	0.31
S FG	3600-3760	1258	109.19	213952.5	0.00002	0.02
N GH	3960-4010	1270	1104.93	192470	0.00019	0.19
N HI	3900-3960	1110	1186.9	65580	0.0006	0.6
S IJ	3800-3900	280	218.44	7280	0.00052	0.52
S JK	3850-3880	170	135.61	3230	0.00028	0.28
S KL	3589-3850	1670	272.31	486800	0.00002	0.02

Note: SS: southern slope NS: northern slope

Table 3. Depositional amount of gelifraction debris and the denudation rate at Bing Pass (average for the years of 1981 to 1990)

Part	Altitude m	Length of Road m	Debris Body			Source Region		Total Amount of Deposition m <sup>3</sup>	Area of Source Region m <sup>2</sup>	Denudation Rate m <sup>3</sup> /m <sup>2</sup> ·yr <sup>-1</sup>	Rate of Slope Retreat (mean value) mm·yr <sup>-1</sup>	
			W (mean value) m	H (mean value) m	S °	LS (mean value) m	OS (mean value) °					
S	AB	3920-4010	170	1.32	1.00	37	76	219	89.76	12920	0.00023	0.23
			370	2.28	1.78	38	191	172	600.64	70670	0.00028	0.28
			370	1.43	1.12	38	157	170	237.04	58090	0.00014	0.14
			360	2.17	1.90	38	75	171	528.09	27000	0.00065	0.65
			290	2.11	1.59	37	115	176	389.17	33350	0.00039	0.39
			160	2.00	1.25	32	175	200	160.00	28000	0.00019	0.19
			536	1.83	1.14	32	49.3	158	447.28	26424.81	0.00056	0.56
DE	3800-3880	713	2.32	1.51	33	59.8	160	999.11	42637.4	0.00078	0.78	
EF	3760-3800	1062	1.75	1.32	37	99.9	167	981.29	106093.8	0.00031	0.31	
FG	3600-3760	1285	0.70	0.31	24	166.5	182	109.19	213952.5	0.00002	0.02	
GH	3960-4010	320	1.98	1.34	34	81	83	339.61	25920	0.00044	0.44	
		360	1.89	1.23	33	238	92	334.76	85680	0.00013	0.13	
		370	0.84	0.59	35	171	92	73.73	63270	0.00004	0.04	
		220	2.36	1.72	36	80	90	357.21	17600	0.00068	0.68	
N	HI	3900-3960	300	2.67	1.80	34	35	85	576.72	10500	0.0018	1.8
			350	1.56	1.09	35	50	85	238.06	17500	0.00045	0.45
			360	1.58	1.03	33	73	85	234.35	26280	0.0003	0.3
			100	2.18	1.58	36	113	80	137.78	11300	0.00041	0.41
S	IJ	3880-3900	280	1.84	1.06	30	50	150	218.44	14000	0.00052	0.52
	JK	3850-3880	170	1.69	1.18	35	95	95	135.61	16150	0.00028	0.28
KL	3589-3850	240	0.25	0.15	31	275	115	3.6	66000	0.000002	0.002	
		340	1.45	0.94	33	320	90	185.37	108800	0.00006	0.06	
		200	1.24	0.84	34	340	90	83.33	68000	0.00004	0.04	
		410	0	0	25	200	35	0	82000	0	0	
		280	0.01	0.01	25	200	35	0.0112	56000	0	0	
		200	0	0	15	200	30	0	40000	0	0	

railways, oil and gas channels, tourist outfits and scientific stations (Harris, 1986). This problem has been paid much attention in the world and various methods have been engaged to study the denudation rate by gelifraction and the main influential factors (French, 1986; Barsch, 1977; Gray, 1973; Jahn, 1976; Luckman, 1972). Li Shude et al. (1981) noted the denudation rates for the three sections, 300 m long in total, of different altitudes and slope orientations.

#### Altitude

In regards to the influence of altitude on the intensity and speed, the intensity and speed become more and denudation rate becomes higher as the altitude gets higher (see Table 1-4). From 3400 to 3510 m on the southern slope in Haxilegen Pass, the denudation rate changes from 0.0006 m<sup>3</sup>/m<sup>2</sup>·yr and 0.0028 m<sup>3</sup>/m<sup>2</sup>·yr in the lower part, to 0.0084 m<sup>3</sup>/m<sup>2</sup>·yr in the upper part, getting 14 times higher. On the northern slope, the rate changes from 0.00059 m<sup>3</sup>/m<sup>2</sup>·yr to 0.0046 m<sup>3</sup>/m<sup>2</sup>·yr, getting 7.8 times higher. In the lower part (3280-3329 m) on the southern slope in Yuximolegai Pass, the rate is 0.005 m<sup>3</sup>/m<sup>2</sup>·yr, and the rate gets higher with the altitude, 0.0105 m<sup>3</sup>/m<sup>2</sup>·yr, 0.0102 m<sup>3</sup>/m<sup>2</sup>·yr and 0.0392 m<sup>3</sup>/m<sup>2</sup>·yr at the divide (3398-3428 m). The rate of the upper part is 7.8 times of that of the lower part. In the lower part (3280-3392 m) on the northern slope, the mean denudation rate is 0.0056 m<sup>3</sup>/m<sup>2</sup>·yr and the rate becomes 0.0157

m<sup>3</sup>/m<sup>2</sup>·yr for the upper part, getting 2.8 times higher. The denudation rate on the southern slope in Bing Pass changes from 0.0002 m<sup>3</sup>/m<sup>2</sup>·yr at 3600 m to 0.00078 m<sup>3</sup>/m<sup>2</sup>·yr at 3880 m, then getting a little lower from 0.00078 m<sup>3</sup>/m<sup>2</sup>·yr at 3880 m to 0.00029 m<sup>3</sup>/m<sup>2</sup>·yr at 4010 m. The rate on the northern slope changes from 0.00002 m<sup>3</sup>/m<sup>2</sup>·yr at 3589 m to 0.0006 m<sup>3</sup>/m<sup>2</sup>·yr at 3960 m, then getting lower too to 0.00019 m<sup>3</sup>/m<sup>2</sup>·yr for the part between 3960 m and 4010 m. The changing tendency of the denudation rate gets higher with altitude, and after reaching an extreme value, the rate gets lower gradually. This pattern has something to do with the petrology, tectonics and humidity.

#### Slope Orientation and Slope Dip

Table 1 through Table 4 show clearly the influence of slope orientation on the denudation rate by gelifraction that the rate on the southern slope is higher than that on the northern slope. The influence of slope orientation on the denudation rate works by its influence from the temperature and precipitation. On the southern slope, the daily temperature difference is more obvious, especially on the surface of the rocks that are directly exposed to the sun. It is more frequent for the temperature to vary around zero degree centigrade, making the rocks have more opportunity to freeze and melt, thus is favorable for the rocks to collapse. In Haxilegen Pass, the mean rate on the southern slope is 0.002 m<sup>3</sup>/m<sup>2</sup>·yr and that on the northern slope is

0.0013 m<sup>3</sup>/m<sup>2</sup>·yr, the former is 1.6 times of the latter. In the Yuximolegai Pass, the rates on the southern and northern slopes are 0.012 m<sup>3</sup>/m<sup>2</sup>·yr and 0.0077 m<sup>3</sup>/m<sup>2</sup>·yr respectively, the former is 1.54 times that of the latter. In Bing Pass, it is 0.00024 m<sup>3</sup>/m<sup>2</sup>·yr and 0.0123 m<sup>3</sup>/m<sup>2</sup>·yr respectively for the southern and northern slopes, the former is 1.85 m<sup>3</sup>/m<sup>2</sup>·yr. The above data show the obvious influence of slope orientation on the denudation rate.

Tables 1 through 4 don't show a clear tendency of the influence of slope dip on the denudation rate. The denudation rate doesn't get higher with a higher slope dip. In fact, the influence of slope dip on the denudation rate is covered up by the petrology and tectonics.

#### Temperature and Humidity

The climatic data in Tianshan Mountain is rare. Up to now, the data available is from Daxigou Meteorological Station in the source area of Urumqi River, Tianshan glacial observation station of Academia Sinica, Gongnaisi River Snow Avalanche Observation Station of Academia Sinica and Dushanzi Meteorological Station. As well, Liu Chaohai et al. (1988) noted the change of the summer temperature in Tianshan glacial area. Zhang Jinhua et al. have studied the temperature steps in the source area of Urumqi River (see Qiu Guoqing, 1983). Their studies are also helpful to the study of temperature analysis in the above three passes. Daxigou Meteorological Station below Bing Pass is 3540 m a.s.l. The annual mean temperature is -5.34°C and the annual mean precipitation is 430 mm. The average occurrences of air temperature oscillating above and below 0°C is 130. In the source area, the temperature gradient is 0.33-0.37°C/100 m from 1830 to 3000 m, 0.66°C/100 m from 3000 to 4000 m. The Snow Avalanche Observation Station of Academia Sinica (43°21'N, 84°39'E) at the foot of the southern slope of Yuximolegai Pass is 1776 m a.s.l. The annual mean temperature is 1.3°C and the annual mean precipitation is 840 mm (Hu Ruji, 1989). Dushanzi north to Haxilegen Pass is 700 m. The annual temperature is 7.5°C. Table 5 shows the temperature and humidity data in the investigated areas based on the data in the above three places. The temperatures in the three places are similar,

falling in below the snowline and permafrost environments. The precipitation is obviously different, with that in Yuximolegai as the highest and that in Bing Pass as the lowest. Precipitation is directly proportional to the denudation rate by gelifraction, reflecting that humidity is a key factor affecting the gelifraction. Denudation rate on the southern slope is higher than that on the northern slope though the mean temperature on the southern slope is higher than that on the northern slope. This phenomenon shows that the relationship between temperature and denudation rate is not simple. In low temperature conditions, the weathering intensity is controlled by the times of temperature vibration around 0°C and the speed of temperature change. Therefore, a wide scope of temperature difference is favorable for gelifraction.

#### Petrology and Tectonics and Topography

Table 6 gives the statistics of denudation rates for the intensively gelifracted sections in the areas of the three passes. On the southern slope of Haxilegen Pass, the denudation rate is 0.0084 m<sup>3</sup>/m<sup>2</sup>·yr the highest, for the upper part (3490-3510 m), 0.00764 m<sup>3</sup>/m<sup>2</sup>·yr higher than the mean value of 0.0028 m<sup>3</sup>/m<sup>2</sup>·yr for ninety meter long section of the middle part (3421-3490 m) where joints are intensive. On the northern slope of Haxilegen Pass, the denudation rate is the highest in the section where the joints are intensive, the rate is 0.0054 m<sup>3</sup>/m<sup>2</sup>·yr for the lower part (3385-3400 m), 0.0011 m<sup>3</sup>/m<sup>2</sup>·yr and 0.00078 m<sup>3</sup>/m<sup>2</sup>·yr for the second part. They are 9.15, 1.73 and 2.44 times respectively that of the mean value. In Yuximolegai Pass, the part with the fastest denudation rate is the upper part, for both the southern and northern slopes. They are 0.0496 m<sup>3</sup>/m<sup>2</sup>·yr and 0.0346 m<sup>3</sup>/m<sup>2</sup>·yr, 1.27 and 2.2 times that of the mean value respectively. The reason is that the igneous rocks here are subject to collapse. The rate for some sections is much higher than the mean value as shown in Table 6. The intensity of joint development plays an important role in controlling the denudation rate, especially for those areas with a fault belt passing through, such as the denudation rate in Yuximolegai Pass is quite fast. Petrological influences on the denudation are also obvious. In Bing Pass, the

Table 5. Climatic Data of the Investigated Areas

Place	Altitude m	Slope Orientation	Annual Mean Temperature °C	Annual Mean Precipitation mm
Haxilegen Pass	3385-3510	Southern Slope Northern Slope	-5.2 — -6.0 -5.8 — -6.7	500-600
Yuximolegai Pass	3280-3420	Mean	-4.8 — -5.7	600-700
Bing Pass	3589-4010	Northern Slope	-5.6 — -8.4	430

Table 6. Measurement Data of Specially Strong Gelifraction Sites

Location	Slope	Part	Length of Road m	Width of Debris Body m	Height of Debris Body m	Slope of Debris Body °	Slope Length of Resource Region m	Total Amount of Deposition m <sup>3</sup>	Denudation Rate m <sup>3</sup> m <sup>-2</sup> yr <sup>-1</sup>	
HP	SS	UP	58	1.9	0.88	25	8	38.79	0.0084	
		MP	60	3.2	1.79	34	30	137.5	0.00764	
	NS	SP	100	3.8	0.65	34	90	98.8	0.0011	
			87	4.4	0.4	10	90	61.2	0.00078	
		LP	90	4.5	1.5	20	50	243	0.0054	
YP	SS		225	3.3	3.1	37	8.25	920.7	0.0496	
	NS		57	2.7	2.4	36	7.5	147.7	0.0346	
BP		AB	10	3.6	2.22	32	75	32	0.00142	
		CD	30	3.9	2.07	28	12	96.9	0.00897	
	SS	DE	263	2.4	1.2	27	10	303	0.00384	
			90	2.5	1.4	30	45	126	0.0014	
		EF	60	3.9	1.8	25	7	168.5	0.0134	
		FG	50	1.7	0.53	18	85	18	0.00014	
		GH		10	3.1	2.01	33	54	24.9	0.00154
				50	3.3	1.75	28	70	115.5	0.0011
				10	3.9	2.29	30	66	35.7	0.0018
	NS	HI	10	4.7	2.63	29	20	49.4	0.00824	
Ij		3	3.5	1.75	27	17	7.35	0.0048		
JK		5	3.0	1.68	30	8	10.1	0.0084		
	KL		20	1.7	0.9	28	300	12.2	0.00007	
			20	3.8	2.56	34	340	77.8	0.00038	

Note: HP: Haxilegen Pass YP: Yuximolegai Pass BP: Bing Pass SS: southern slope NS: northern slope

augen gneiss is easier to collapse than the schist. Besides, the rate maybe higher in some low places (depressions) perhaps because those places provide more suitable humidity and temperature conditions, such as the EF part on the southern slope and JK part on the northern slope in Bing Pass (ref. Table 6).

The denudation rates in certain places may be quite high due to the influence of tectonics, petrology and topography. In Haxilegen Pass, the highest rate on the southern slope is 0.00764 m<sup>3</sup>/m<sup>2</sup>·yr, 3.8 times that of the mean value, the highest rate on the northern slope is 0.0054 m<sup>3</sup>/m<sup>2</sup>·yr, 4.2 times that of the mean value. In Yuximolegai Pass, the highest rate on the southern slope is 0.0496 m<sup>3</sup>/m<sup>2</sup>·yr, 4 times of the mean value, the highest rate on the northern slope is 0.03455 m<sup>3</sup>/m<sup>2</sup>·yr, 4.5 times of the mean value. In Bing Pass, the highest rate on the southern slope is 37 times the mean value and that on the northern slope is 65 times the mean value.

#### SUMMARY

The following conclusions can be made based on the above analysis:

1. The denudation rates by gelifraction at the high altitude of Tianshan Mountains (3200-4000 m) are 0.0014 m<sup>3</sup>/m<sup>2</sup>·yr in Haxilegen Pass,

0.015 m<sup>3</sup>/m<sup>2</sup>·yr in Yuximolegai Pass, 0.00018 m<sup>3</sup>/m<sup>2</sup>·yr in Bing Pass.

2. The major factors affecting denudation rate are altitude, slope orientation, temperature, precipitation, petrology and topography. The rate is higher with a higher altitude, but the petrology, structure and humidity may make this tendency complicated. The rates on southern slopes are higher than those on northern slopes. The following factors make the rate higher: more intensity and times of temperature change around 0°C, higher precipitation and air humidity, coarser particles, more complicated composition, more tectonic fractured rocks and some lower depression may make the rate higher. It is shown by global comparison that the alpine periglacial environments in middle latitude are favorable for denudation by gelifraction.

#### REFERENCES

- Barsch, D., (1977) Eine Abschätzung Von Schattproduktion und Schuttransport im Bereich aktiver Blockgletscher der Schweizer Alpen, Zeitschrift für Geomorphologie, 21, pp79-86.
- French, H.W., (1976) The Periglacial Environment. ppl48, Table 7.4.
- Gray, J.T., (1973) Geomorphic effects of avalanches and rock-falls on steep mountain slopes in the central Yukon Territory, in

- Fahey, B.D. and Thompson, R.O. (eds), Research in Polar and Alpine Geomorphology, Geo Abstracts, Norwich, pp107-117.
- Harris, S.A., (1986) The Permafrost Environment. Groom Helm, London and Sydney.
- Hu Ruji, (1989) Snow catastrophe protection and management in mountainous areas, Science and Technology Press (in Chinese).
- John, A., (1976) Geomorphological modelling and nature protection in Arctic and sub-Arctic environment Geoforum, 7, pp121-137.
- Li Shude, et al., (1981) Preliminary study on weathering rate of rock in Shengli Daban at the head of Urumqi River, Tianshan, Journal of Glaciology and Cryopedology 3, Special Issue, (in Chinese).
- Liu Chaohai, et al., (1988) A primary calculation of temperature and precipitation in Tianshan Mountains, China, Journal of Glaciology and Cryopedology, 10(2) (in Chinese).
- Luckman, B.H., (1972) Some observations on the erosion of talus slopes by snow avalanches in Slaymaker and McPherson (eds.), Mountain Geomorphology, Tantalus Research, Vancouver, pp85-100.
- Qu Guoqing, et al., (1983) General characteristics of permafrost in Tianshan Mountains, China, Collection of Second National Permafrost Conference of China (in Chinese).

DISCUSSION ON THE DISTRIBUTION OF TANGENTIAL FROST-HEAVING FORCE ALONG THE LATERAL SURFACE OF PILE

Liu Hongxu

Heilongjiang Province Low Temperature Construction Science Research Institute, Harbin, China

By means of experiments the distribution pattern of tangential frost-heaving force along the lateral surface of pile has been found. The results show that its peak value moves gradually downwards to the freezing interface as the freezing depth is developing, and the stress-relaxation feature emerges in the frost-heaving force as the frozen soil displacement is increasing along the trial pile, but the reasons and the conditions for producing the displacement can not be further discovered. A new explanation is put forward as follows to make such problems clearer in this paper: Due to the temperature-dropping shrinkage in foundation soil, the tensile stress and cracks appear later to reduce the freezing strength greatly, and the tangential frost-heaving force is also reduced correspondingly.

INTRODUCTION

It is very important in practical permafrost engineering to study the distribution of tangential frost-heaving force along the lateral surface of pile, and the changing pattern of the distribution with elapsed time in seasonal frozen areas. Scholars from the former Soviet Union have done a lot of research work on this topic. Among them, Darmatov, B.Y. got results in this field for the first time in Yikarkar (Darmatov, 1957). There are also other scholars who had discussed this topic (Orlov, 1962, 1977; Czutovitch, 1972).

Some Chinese scholars have made a series of experiments on the distribution of tangential frost-heaving force along the lateral surface of pile on the Qinghai-Tibetan Plateau.

THE EXPERIMENTAL RESULTS AND ANALYSES

Egalev, K.E., a researcher from the former Soviet Union, got the distribution curves of relative tangential frost-heaving force along the trial pile in the silty sandy clay located in the seasonal active layer in Yikarkar (Fig.1).

After analyzing the distribution curves shown in Fig.1, the following conclusions can be drawn:

(1) The maximum value of relative tangential frost-heaving force initially appears near the ground surface, and then moves downwards to the freezing interface as the freezing depth is increasing, and finally the maximum value emerges at about 2/3 of the whole frost depth.

(2) The average unit tangential frost-heaving force increases gradually with temperatures dropping in the frozen soil layer, and stress relaxation occurs as the frozen soil displacement along the trial pile is increasing (Czutovitch, 1972).

When the shear displacement occurs in the soil of the foundation, the reduction of tangen-

tial frost-heaving force is due to the partial destruction of the ice crystals at the ice-contact points of the foundation, and to the crystal-orientation in the process of recrystallization in the direction of reducing the capability of resistance to the frozen soil displacement of the foundation (Darmatov, 1957; Viylov, 1959; Orlov, 1962, 1977).

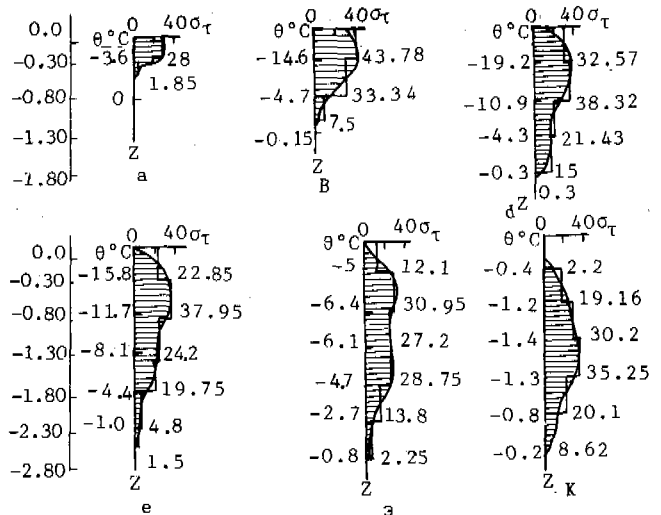


Figure 1. Distribution curves of relative tangential frost-heaving force  $\sigma_T$  (NX10/cm) along the trial pile (taken from K.E.Egalev)

Researchers, from Lanzhou Institute of Glaciology and Geocryology, Chinese Academy of Sciences, also made such experiments at the observation station on Qinghai-Tibetan Plateau in 1975, and obtained similar results on this

topic. They divided the whole freezing process of the soil contacted to the foundation in the same depth into four stages, which are the initial freezing stage, active freezing, cooling, and overcooling. The increasing of tangential frost-heaving force mainly occurred in the stages of initial and active freezing, and in the 3rd stage such increasing became very limited (Tong Changjiang, 1982).

The tangential frost-heaving force increased with the soil temperatures descending from the initial freezing point to  $-5^{\circ}\text{C}$ , the relationship between them could be considered a linear one, and such relationship could still be taken as an increasing one in a direct proportion until the temperature reaches  $-10^{\circ}\text{C}$ . After that, the reduction of tangential frost-heaving force would be dominant in the following process as time progressed (Tong Changjiang, et al, 1985), see Fig.2.

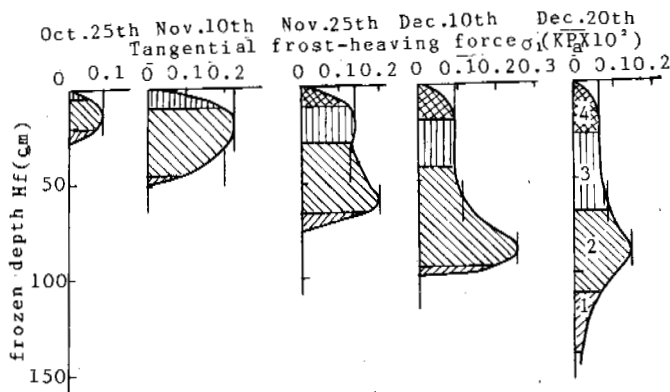


Figure 2. Distribution of tangential frost-heaving force along lateral surface of foundation (from Tong Changjiang, et al, 1985)

1. initial freezing stage;
2. active freezing stage;
3. cooling stage;
4. overcooling stage.

#### THE AUTHOR'S EXPLANATIONS OF THE EXPERIMENTAL RESULTS

The additional freezing strength found by the researchers, from Lanzhou Institute of Glaciology and Geocryology, Chinese Academy of Sciences, by means of indoor experiments is nearly in direct proportion to the negative temperatures at the common changing scope in the foundation. If calculated according to  $-5^{\circ}\text{C}$ , then the long-term additional freezing strength is not lower than 0.4 MPa, and the maximum value of tangential frost-heaving force is not higher than 0.3 MPa. The slump is unlikely to occur under the condition of tangential frost-heaving force not exceeding the long-term additional freezing strength.

The developing process of tangential frost-heaving force should be as follows:

The tangential frost-heaving force produced during soil freezing is located near the freezing interface (in the drastic phase-transformation areas). Because of the volume expansion of soil while freezing, and the foundation remaining stationary even if the freezing makes the soil and the foundation into a whole, the tangential frost-heaving force emerges. The

force is determined by the following three factors: (1) the classification of soil which depends on the soil frost susceptibility, the water content in soil, and the ground-water level. (2) the additional freezing strength along the lateral surface of the foundation while freezing makes the soil and the foundation into a whole, and the strength depends on the negative temperature, the value of the normal compressive stress on the surface, and the surface roughness. (3) the thickness of the frozen layer.

If the soil is of strong frost susceptibility in the foundation, and the additional freezing strength between the soil and the foundation is large enough, then the thicker the frozen soil layer, the greater the stiffness (namely, the bend-resistance capability) of the frozen soil layer, and the larger the distribution area of the effective frost-heaving stress, and finally the larger the tangential frost-heaving force. In fact, this is a loaded system of a two-layer foundation (shown in Fig.3).

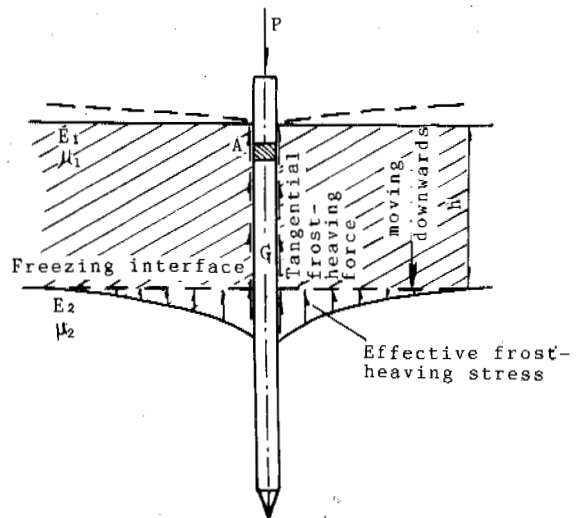


Figure 3. Diagram for the developing process of tangential frost-heaving force

While the air temperature gets lower and lower (except for the rebounding of air temperatures in the following spring), the freezing interface moves downwards, and the ground temperatures continue to drop everywhere along the lateral surface of the foundation (all these places remain firm, e.g. the point "A"). The freezing strength increases in direct proportion to the negative temperatures with the soil temperatures descending, and then the tangential frost-heaving force should become steadily larger and larger, and distribute with the trends and features of being bigger at the upper section and smaller at the lower one as the thickness and the rigidity of the frozen layer increase, but in fact it isn't like that described above.

The main reason for this is that the soil at the upper section is easily and greatly influenced by the air-temperature fluctuations. At the beginning of the freezing period, the

temperature is not very low, and the frost heaving and frost-heaving force of the soil in the drastic phase-transformation areas increases in a linear relation to the negative temperature. The horizontal frost-heaving force in the frozen layer is a compressive stress, so it makes the direct stress on the shear plane between the frozen soil and the lateral surface of the foundation much larger. After the increase of direct stress the shear strength is also enhanced correspondingly, so the capability of transferring tangential force becomes stronger. Because the thickness of the frozen layer increases gradually, the value of tangential frost-heaving force also rises.

The stress-condition changing process in the horizontal direction near to the upper layer is as follows: At the beginning of the freezing period the horizontal frost-heaving compressive stress is very large, and the temperature-drop shrinking stress is relatively small, and the compressive stress becomes larger and larger, furthermore it reaches its maximum value when the horizontal frost-heaving force stops increasing. This compressive stress is balanced by the temperature-drop shrinking stress, so the zero-stress condition emerges. If the temperature-drop shrinkage continues, the large tensile stress will be produced, and also when the horizontal tensile stress is larger than the limited value (exceeds the ultimate tensile strength), the frost cracks will occur because of the fragile failure of the frozen soil load due to the tensile stress (Viyalov, et al, 1981), more over these cracks will continue to develop (most of the cracks are in polygons in the seasonal active layer) (Liu Hongxu, 1990), see Fig.4.

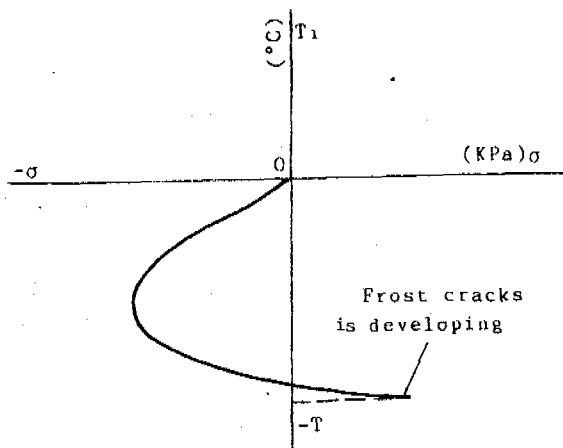


Figure 4. Diagram for changing conditions of horizontal frost-heaving force (from Liu Hongxu, 1990)

In such an obviously changing period from the early winter when the quite large compressive stress emerges to the deep winter when the quite large tensile stress appears in the horizontal direction, the additional freezing strength and the vertical shear strength are also changing, the tangential frost-heaving force will finally vary in correspondence.

After the horizontal tensile stress appears in the frozen layer, the shear-resistance capability between the frozen soil and the lateral surface of pile will reduce greatly, in other

words, the additional freezing strength will lower by a large degree. Although the frost-heaving force, which occurs at the constantly descending freezing interface, is gradually decreasing, the thickness of the frozen layer is continuously enlarging, and the active area of the effective frost-heaving force is rapidly increasing, and the increase of total frost-heaving force is far larger than the decrease of frost-heaving force due to the descending of the freezing interface. So the tangential frost-heaving force becomes larger and larger, and when the force is too great to be endured by the frozen soil, the relative displacement will take place. The displacement will make the additional freezing strength at the interface relax further, this characteristic is exhibited through the decrease of tangential frost-heaving force. The displacement will stop developing when the time of the tangential frost-heaving force is equal to the freezing strength.

On the lateral surface of pile in the foundation at the upper frost-heaving section of the seasonal active layer, the additional freezing strength of the in situ test is identical with that gained by indoor (model) experiments when the soil temperatures are higher than  $-10^{\circ}\text{C}$  (that is the later part of the slow phase-transformation areas), but the additional freezing strength of the sample gained by freezing in the model under the unlimited condition is smaller. The additional freezing strength in situ will be much smaller than that gained by the indoor experiments when the soil temperatures are lower than  $-15^{\circ}\text{C}$  in the direction of a negative temperature.

#### CONCLUSIONS

(1) The peak value of tangential frost-heaving force moves downwards along the lateral surface of pile, and meanwhile this value decreases near to the ground surface. The main reason for that is that the freezing layer expands at first during freezing, and then shrinks with the temperatures decreasing, and the additional freezing strength increases initially and decreases finally.

(2) The additional freezing strength gained by indoor experiments can not be used directly in practical engineering design if the process of the freezing expansion and the temperature-drop shrinkage of the frozen layer in the horizontal direction aren't regarded.

(3) The tangential frost-heaving force obtained by means of indoor experiments cannot be directly put into use in practical engineering design if the changing process of the additional freezing strength between the soil and the lateral surface of foundation is not regarded.

(4) To the shear strength in the frozen layer, which is easily influenced by climate, the frozen layer in the upper part of foundation has a property of anisotropy, and the vertical shear strength is closely related to the horizontal stress in soil, so it must be fully considered in practice.

(5) If an indoor simulation experiment is to be made in an engineering project in seasonal frozen soil, and the changing processes of the expansion and the shrinkage stress in the frozen layer in the horizontal direction aren't considered, the experimental results can be utilized only after analyses has been done about the



influential degree of the processes to the results:

#### REFERENCES

- Czutovitch, N.A. (1972) Frost soil mechanics, Moscow, "Colleges and Universities".
- Darmatov, B. I. (1957) Effecton of soil frost-heaving on building foundation, Leningrad, "National Construction Committee Publishing House".
- Liu Hongxu, (1990) Discussion on some problems of frost-heaving mechanics in freezing process of soil. J. Glaci. & Geocry. No.3.
- Orlov, V.O., (1962) Expansion of fine granular soil at low temperature, "The Russian Academy of Sciences Publishing House".
- Orlov, V.O., (1977) Effecton of soil frost-heaving on building foundation, Lenigrad, "Construction Engineering Publishing House".
- Tong Changjiang, (1982) Frost-heaving force of foundation, Proc. Symp. Glaci. Geocry. Geophys. Soc. China, The Science Press.
- Tong Changjiang, et al, (1985) Frost heave of soil and frost-damage prevention to buildings, The Water Resources & Electric Power Press, China.
- Viyalov, S.S., (1959) Creep fluidity and load capacity of frozen soil, "The Russian Academy of Sciences Publishing House".
- Viyalov, S.S., et al, (1981) Calculation of strength and creep of artificial frozen soil, CCCP.

## STUDY OF THE LAW OF THE DISTRIBUTION OF PERMAFROST AND VEGETATION IN DA HINGGAN LING, NORTHEAST OF CHINA

Liu Qingren<sup>1</sup>, Sun Zhenkun<sup>1</sup>, Cui Yongsheng<sup>1</sup>,  
Liu Jiongde<sup>1</sup> and Chen Dongfang<sup>2</sup>

<sup>1</sup>Heilongjiang Institute of Forestry Design, China

<sup>2</sup>Heilongjiang Institute of City Planning, Prospecting and Design, China

Da Hinggan Ling forest region is located on the southern edge of northeast permafrost belts and is in the most northern permafrost region. From the large amount of information about hydrogeological and engineering geological prospecting and tests, the distribution and the depth of permafrost has a close relation with the vegetation. So, to research the objective conditions of the distribution of permafrost and vegetation succession is important for us be able to protect natural ecological equilibrium and the economic developments in this region.

### INTRODUCTION OF REGIONAL GEOGRAPHY

Da Hinggan Ling forest region borders Heilongjiang River and faces Eluosi in the northern part, borders Eergunan River and Hailaer platform in the western part, Aer mountain in the southern part and western Songlong plateau in the eastern part. The region crosses seven latitudes (46°10' - 53°30'). Alignment of the ridges in the region is in a N.N.E. direction and extends to a S.S.W. direction. The length is about 800 km and the width is 300 km (115°30'N-126°30'E).

#### 1. Meteorology

Da Hinggan Ling forest region is the coldest in northeast China. It experiences a temperate-frigid climate. From Mehe meteorological information and Heilongjiang meteorological atlas, the mean annual air temperature is -5.3 - -1.3°C, mean annual ground temperature is -4.8 - -1.0°C. The extreme low temperature is -52.3°C and the highest temperature is 36.8°C. The yearly precipitation is 350-490 mm. The maximum thickness of snow cover is 30-50 cm. The lasting time of snow is up to seven months. The freezing stage of rivers is six months. The frost-free stage, in whole, is 90 days. Weather in winter is very frigid and there is less precipitation. Influenced by the Mongolia high pressure air mass, snow fall occurs when a very cold air mass comes through the area. Temperature in summer is mild and precipitation is heavy. The humid marine current from southeast meets the cold current in this region and forms rain fall which composes of about 85-90% of whole year's precipitation. The characteristics of a warm and heavy precipitation form a suitable environment for vegetation to grow.

#### 2. Topography, Geomorphology and Soil

The topography in Da Hinggan Ling forest region belongs to denuded and eroded low ridges and tundra phenomenon. The characteristic of it

is flat. From the recorded investigation report in 1954 in Da Hinggan Ling, in the area of the slope the gradient is less than 10° is 69% of the region, 11-15° is 10%, 16-25° is 9% and more than 29° is 2%. The valley is comparatively wide. It can be divided into two types, first is the wide and shallow valleys in which the discharge is less. Most parts of those valleys appear swampy; second is the "V" form valleys, they have a flat bottom and steep cliffs. On the bottom stratum is mainly debris which has a bad sorting index. There are a lot of tussock hummocks on the ground surface. From Yilihuli mountain to Heilongjiang River, there is a large tundra area. It controlled by the rise of Eerguna River and the fault of Heilongjiang River. The strata of Da Hinggan Ling is mainly igneous rock. The direction of main ridges of Da Hinggan Ling is N.N.E. — S.S.W. direction. The eastern side of the ridge is bounded by Songlong plateau, the western side borders the Mongolia plateau and the ratio of slope is more than that on the western side. The strata from old to new appears in this region. There are slate, and metamorphic sand andesite, basalt from Mesozonic erathem sand, tuff, oil shale and coal layer from Jurassic period. Quaternary deposits are eluvium slope wash, alluvium and diluvium. The lithology is humus layer, peat and sandy clay. Surface layer is brownish loam layer. The soil is not fertile. The status degree of soil is from III to IV. It can be divided into four types on the ridges and the northern slope of Da Hinggan Ling, it is brownish and black-brownish aciaelisiluae soil and the status degree of soil is IV. On the western slope, it is brownish aciaelisiluae soil. The status degree of soil is from III to V. On southern slope, it is dark-brownish soil, the status degree of soil is from II to V.

### THE RELATIONSHIP BETWEEN THE DISTRIBUTION OF PERMAFROST AND VEGETATION DIVISION

The permafrost in Da Hinggan has good relation with the cold climate. But the types, depths and distribution of permafrost relates to the factors of geomorphology, topography, lithology, soil, water, etc. At same time, its characteristics is represented by the vegetation, which means that there is a rule between permafrost and vegetation. In large areas, permafrost appears uniform, but in local areas, its presence is different. In order to bring the forest into full play, we ought to take different means to manage the different areas differently. The permafrost types and characteristics of vegetation, and the details are described below (see Fig.1)

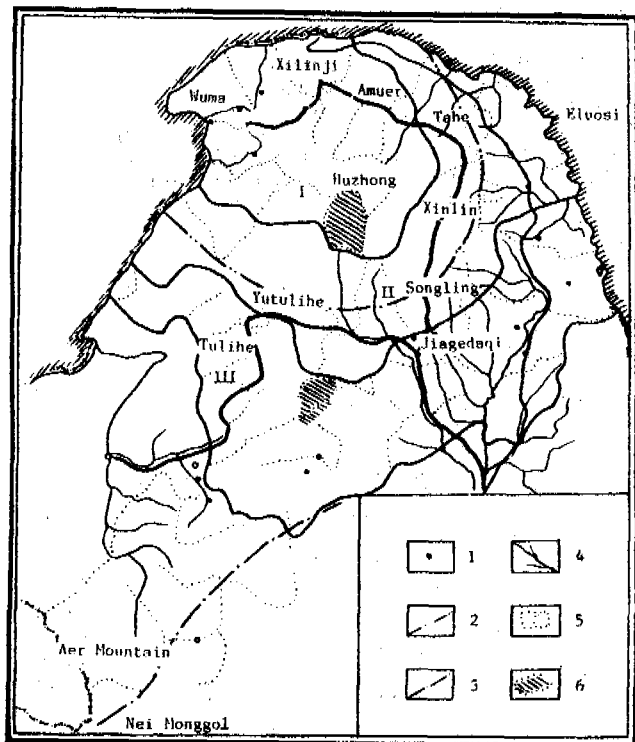


Figure 1. Distribution of permafrost and the management and division of forest

1. County (Banner) government area;
2. Southern limit of continuous permafrost;
3. Sporadic permafrost;
4. River;
5. A foresting Bureau limit;
6. Protected Natural Area.

I. Division A: It lies in the northeast part of this forest region and in a continuous permafrost area. The areas include the bureaus of Fukeshan, Xilinji, Tuqiang, Amuer, Huzhong, Wuma, Qiqian, Jiliu River, along mountain, Magui, etc. The total area is 4293000 hectares. The elevation in this region is the highest in Da Hinggan Ling (i.e. the elevation in Dabai mountain is 1529 m a.s.l.). Topography belongs to ridges and declines to the northeast. The region faces cold currents from Siberia, it experiences a cold climate. The mean annual air temperature is  $-5.3^{\circ}\text{C}$ , mean annual ground temperature is  $-4.8^{\circ}\text{C}$ . The minimum air temperature ever reached was  $-52.3^{\circ}\text{C}$ . The frost-free period is less than three months. The long freezing and short thawing periods make the deterioration of the

permafrost slow and form the widespread permafrost. In valleys and swamps, the depth of permafrost is the thickest. From borehole H<sub>8-24</sub>, the depth is up to 130 m. The depth is 112.6 m from borehole H<sub>8-7</sub>, seasonally thawed depth in general is 0.3-10 m. The depth of permafrost on footslope is 15-30 m and the seasonally thawed depth is 1-3 m. The depth is 15 m on slope and seasonally thawed depth is comparatively deep. The details are listed in Table 1.

In addition, the depth of permafrost relates to geomorphological position and slope exposure. The temperature on northern slope is comparatively higher and the seasonally thawed depth is thick, the permafrost in this area is 0-30 m. The temperature on the southern slope is lower than on the northern slope and the seasonally thawed depth is shallow (see Table 2).

The differences of the topography and air temperatures is listed in Table 2 must be presented for the types of vegetation. The vegetation in Da Hinggan Ling belongs to the southern part of eastern Siberian light aciculiferae, in Chinese. It is called temperate-frigid aciculiferae. In this region, the vegetation is *Pinus pumila-Larixmelini*. There is a little *Rhododendron dauricum-Larixmelini*. In swamps, there are a lot of tussock hummocks. Along river banks, there are *Chosenia macrolepis*, *Populus suaveolens* and *Alnus manshurica*, the species of shrubs are *Juniperus dahurica*; *Rhododendron dahuricum*, *Betula fruticosa* and *Vaccinium Vitis-idea*, in addition to *Empetrum sibiricum*, *Pyrola incarnata*, etc.

*Larixmelini* has a good adaption to the environment and its ability of natural recovery is good. It is distributed from valley, slope to crests. The details of vegetation, soil lithology and topography are presented in Fig.2.

2. Division B: Complex frozen ground area. The types of frozen ground are continuous and sporadic permafrost, in some areas, there are taliks. It lies in the middle of the region which includes the bureaus of Tahe, Shiba Station, Angelin, Genghe, Tulihe, etc. The total forest area is 998000 hectares.

The height of topography in this region is less than in division one. It tends to the northern slope. The degree of cold is less than in division one. The mean annual air temperature is  $-4 - -2^{\circ}\text{C}$  and the mean annual ground temperature is  $-3 - -1.5^{\circ}\text{C}$ . The depth of permafrost in this division is less than in division one. The depth near the border of division one is only 30-70 m. The depth is becoming less and less from the border to the south, at the same time, taliks increase; near the border of division C, it is mostly the sporadic permafrost.

The lesser degree of cold in this area makes the growing period of vegetation longer (90-100 days) and the species of vegetation increase. The representative species on the slope are mainly *Rhododendron dauricum-Larixmelini*. There are *Populus davodiana* and *Betula daurica*, except for the species in division A. The increment percent is increased, too. On eastern part of this division, *Cpicea boraiensis*, *Quercus Mongolica* and a few *Ulmus propingua*, *Phellodendron amurense*, etc. appear. But the growing of few species is not good. Shrubs are exuberant and dense.

The main species is *Rhododendron dauricum*. The number of *Lespedeza bicolor* and *Corylus heterophylla* increases, at same time, there are a few *Alnus manshurica*, *Spiraea sericea*, *Rosa acicularis*, etc. The thin layer is mainly

Table 1. The relationship between the depth of permafrost and topographical position

Position	Valley & swamp			Footslope			Tectonic composition	On slope
	H <sub>S-7</sub>	H <sub>S-13</sub>	H <sub>S-24</sub>	H <sub>Z-1</sub>	H <sub>Z-5</sub>	S-1		
Borehole No.	H <sub>S-7</sub>	H <sub>S-13</sub>	H <sub>S-24</sub>	H <sub>Z-1</sub>	H <sub>Z-5</sub>	S-1	H <sub>Z-6</sub>	H <sub>Z-10</sub>
Depth of permafrost(m)	112.6	122.6	130.0	31.0	14.9	25.0	29.7	16.0
Seasonally thawed depth(m)	3- .8	3- .8	3-1.0	1-2.5	1-3	1-2.5	1-2.5	1-3
Welling water amount (t/d)				1002.15	1.744		1229.82	985.22

Table 2. The characteristics of distribution and the depth of widespread permafrost

Position	East-west river valley			South-north river valley		
	N. slope	Valley	S. slope	W. slope	Valley	E. slope
Mean annual ground temp. (°C)	0 - -1.0	-2 - -4.2	-1 - -2	0 - -1	-2 - -4.2	0 - -0.5
Depth of permafrost (m)	0 - 20	50 - 150	20 - 50	10 - 30	50 - 100	0 - 20
Seasonally thawed depth (m)	2 - 4	0.5 - 1	1 - 1.5	1.0 - 2.0	0.5 - 1	1.0 - 3.0

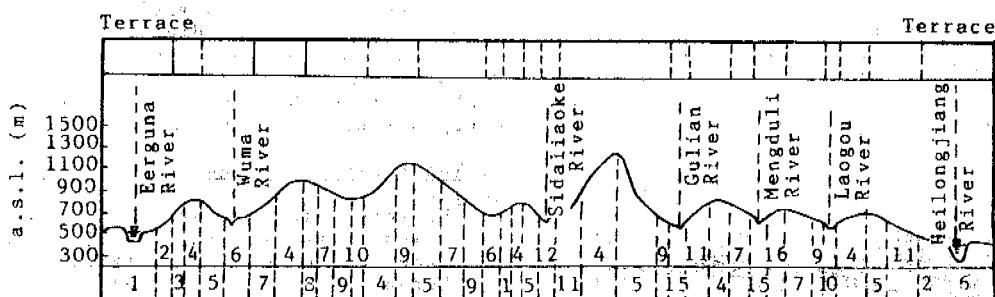


Figure 2. Profile of forest, soil, lithology and topography in Da Hinggan Ling forest region (Zhang, 1986)

1. Swamp with moss; Peat gleysol;
2. Marshland, Black peat;
3. Meadow, Grassland soil;
4. Rhododendron dahuricum and Pinus, Brown coniferous soil;
5. Rhododendron dahuricum and Larixgmelini, Weathered coniferous soil;
6. Swamp with Deyeuxia sorbifolia and Deyeuxia Langsdorffii;
7. Grass and Larixgmelini, brown coniferous soil;
8. Rhododendron dahuricum and Betula plutyphylla;
9. Ledum palustre and Larixgmelini, Shallow layer of brown coniferous soil;
10. Cornus albal. and Larixgmelini, coniferous soil;
11. Grass and Pinus, Brown coniferous soil;
12. Swamp with Betula fruticosa, Peat gleysol;
13. Pinus pumila and Larixgmelini, coniferous soil;
14. Ledum palustre and Betula dahurica, Shallow layer of coniferous soil;
15. Moss and Larixgmelini;
16. Grass and Betula dahurica, Brown coniferous soil;
17. N-Northern slope;
18. S-Southern slope.

Vaccinium uliginosum mixed with mosses, Pyrola in Cornata and Cdeyuxia sp. On the lowland, there are Lespedeza michx and mosses in a dot-distribution. Along river banks, there are swamps in which the water is gradually stored up and not easily drained. In this area, permafrost is developed. On ground surface, there are

a lot of tussock hummocks.

3. Division C: It belongs to sporadic permafrost and lies in the southern part of the region. It includes the bureau's of Kulongsi, Dayangshu, Tulihe, Wuerqian, Bilage, etc. Total area is 5519000 hectares.

This division belongs to low ridges. Tempera-

ture is comparatively higher than in division B. The mean annual air temperature is about  $-1.5 - -1.0^{\circ}\text{C}$ , the freezing period is six months. This area is mostly on the northern slope and belongs to seasonally frozen ground and permafrost-free ground. In swamp or wet land, the drainage condition is not good and the grasses are covered by tussock hummocks; there is sporadic permafrost in this area. We can divide the division C into C1 and C2 sub-divisions, which respectively, have a steep northern slope and a gentle southern slope. The air temperature and humidity in division C1 are higher than in division C2. As a result, the characteristics of permafrost and vegetation are different, too.

4. Division C1: Sporadic permafrost region. The depth of permafrost from northwest to southeast is gradually decreasing, the vegetation is in a transition from *Quercus mongolica*-*Larix gmelini* to *Quercus mongolica* or *Alnus mandshurica* and prairie. The plants in the undisturbed area are exuberant.

5. Division C2: Sporadic permafrost that is deteriorating from northeast to southwest in this region and the vegetation transfers from *Betula platyphylla*-*Larix gmelini* to *Betula platyphylla*, *Betula platyphylla* and grass land. In general, the relation between permafrost and vegetation goes along with the changing of vegetation, the depth of permafrost from northwest to southeast is from the continuous and deep, to the discontinuous and shallow, or disappearing (see Fig.3 of the distributing tendencies of permafrost). Another characteristic is that the depth of permafrost in the same latitude is the same, such as in Huola basin, the depth in the control area is 130 m and on the edge or on the footslope of the basin it is about 30 m. The vegetation also changes too. The vegetation on northwest and west slopes is sparse and on southeast and east slope is dense and exuberant. According to this, when we exploit, manage, utilize and protect forest, we ought to put the forest into full play.

The forest resource in the permafrost forest region of Da Hinggan Ling is rich. It's ecological environment and economic value are significant. From above, we propose some advice:

### 1. Draw up the Laws of Protecting Forest and Ecology in Time

To forest industries, we ought to make some rules for long term destination. For activities of mining, railway, highway and electric power constructions in forest region which relate to the destruction of the forest and disturb permafrost, we should formulate some means to recover the destroyed vegetation before construction. The rules or laws must be put into effect under the local government's provision. To the departments or organizations which don't abide by the rules or laws, we must give them severe punishments in order to protect forest resources and the ecological environment.

### 2. Reasonable Management of Forest Resources from a Long-term Point of View

The departments in this region greatly depend on forests. Forest resource is very important for them. We must do less cutting and increase afforesting in order to create an equilibrium between them. For the cutting area, it is necessary for us to afforest in a given time. To the naked mountains, we should create plans to recover forest on them. We should be monitoring the plant diseases, insect pests and forest fires, seriously. In exploiting the forest, we deal with it according to its ecopheno-type, and same time lay down scientific cutting plans and effectively control the decreasing tendency of wood-reserves. The amount of burned wood caused by the man-made or natural fire is very large. From investigated information in five forest bureaus managed by Da Hinggan Ling forest bureau, the actual burned wood amount, per year, is 90700, more than 3.18 times of the statistics numbers (from Zhou Honglie's information, Da Hinggan Ling Institute of Forestry Planning).

### 3. The Ecological Significance of Protecting the Ecology

The forest in Da Hinggan Ling has the characteristics of storing and adjusting the water resources of Heilongjiang River, Longjiang River and Bergulan River, and hinders and decreases the invasion of Siberian cold current and the wind and sand from the Mongolia Plateau. It nourishes the Longjiang Plateau, the prosperous Hulongbeier League and protects the water and soil losses, and at the same time, provides important wood resource and protects the environment in Da Hinggan Ling.

### REFERENCE

Zhang Wanru, (1986) Chinese Forest and Soil, Published by Chinese Sciences.

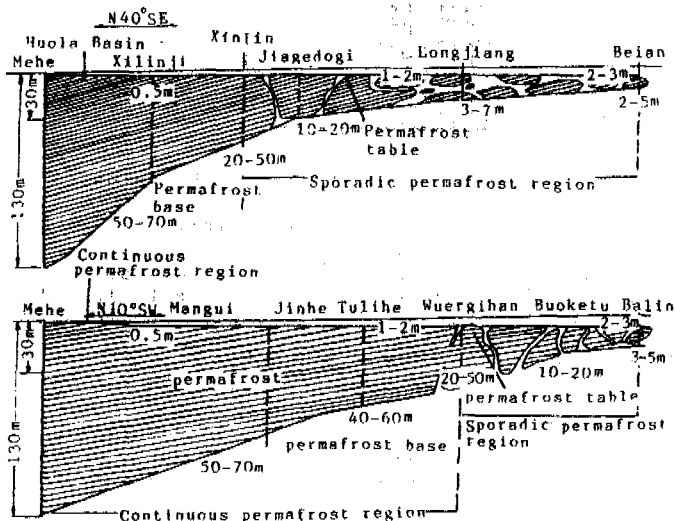


Figure 3. Tendency of vertical distribution of permafrost in Da Hinggan Ling

### SOME IDEAS ABOUT FOREST EXPLOITATION AND PROTECTION IN PERMAFROST REGION

## CRYOGENIC PROCESSES AND PHENOMENA IN MONGOLIA

R. Lomborinchen

Institute of Geography and Geocryology, Academy of Sciences of Mongolia

In the territory of the Republic of Mongolia, 63% of the area is underlain by permafrost. Cryogenic processes and phenomena, including the frost heavings, frost crackings, icings and several kinds of the cryogenic slope processes are widely seen both in the present permafrost regions and the seasonal frost regions. With the degradation of permafrost, the thermokarst processes are activated in the Holocene.

### INTRODUCTION

The southern limit of the Eurasian continental permafrost zone passes through the territory of the Republic of Mongolia, of which 63% is underlain by permafrost. Generally, the middle-high mountains in Mongolia are of an extremely continental cold climate.

There, the mean annual air temperature is usually lower than 0°C. The minimum temperature in permafrost was recorded by the Soviet and Mongolian researchers as low as -4°C to -5°C.

The southern part of Mongolia belongs to the seasonal frost zone.

The average thickness of permafrost varies from 25 to 50 m. In the Mt. Prihubsugul, the permafrost was recorded as thick as 250 m. Permafrost is covered by the seasonally frozen ground with a thickness of 4 m in the north. In Mongolia, the frozen ground is usually characterized by its low ice content, although the segregated and intrusive ground ices are widely distributed. Recently, ice-wedges were found in the Darhat basin.

### FROST HEAVING

In our country, the frost heaving of the dispersal soils, due to the increase in volume of the frozen water and the increase in ice content, can occur locally and regionally. Some results of observations on the northern slope of the Mt. Bogdo-ul are summarized in Table 1, the intensity of frost heaving of sandy clay and silty sand with a low ice content is only tenths of millimeters.

The whole territory of Mongolia is subject to seasonal frost and thus to frost heaving. When refreezing, the active layer is usually in an open system with moisture migration and water flow. Sometimes, the seasonal (one year) migratory frost mound and hydrolaccolith are formed. At the boundary of Hurumtin Somon, Khubsugul Aimak, such one year hydrolaccoliths occurred in groups in the cold season, and disappeared completely in May and June. The native herdsmen call it "Mesen dov" or ice mound. The signs of perennial frost heaving mounds can be seen at the valley bottom of the great rivers and the dep-

Table 1 Intensity of seasonal frost heaving on northern slope of Mt. Bogdo-ul (1600m a.s.l., Steepness 18-20)

No.	Height of control piles(cm)		Up or down (cm)	Mean annual value of heaving (cm)
	Sept, 23, 1981	Sept. 7, 1991		
2	5.0	7.0	2.0	0.2
3	5.0	7.0	2.0	0.2
4	5.0	5.4	0.4	0.04
5	5.0	5.7	0.7	0.07
6	5.0	6.9	1.9	±0.2
7	5.0	5.0	0.0	0.00
8	5.0	5.3	0.3	0.03
9	5.0	4.2	-0.8	±-0.1
10	5.0	5.4	0.4	0.04

ressions in northern Mongolia, for example, the Rivers Chulut, Tes, Sharga, Arsai, Zelter, Shilustei, etc..

They also occur at the bottom of lacustrine depressions: Tonshil-nur, Hutag-nur, Darhat Lake basin, etc.. The frost heaving mounds can be divided into two types: the segregated and intrusive ones. Usually, the perennial heaving mounds are not very big in volume, the biggest one found near the Sangin-dalai nur is 30 to 40 m in height, 150-200 m in diameter at its base (Photo 1). The small mounds, e.g. the turf hummocks, are widely distributed in Mongolia.

#### FROST CRACKINGS AND POLYGONAL FORMS

Under the strong continental climate, one of the widely-distributed processes in Mongolia is the thermal deformation (frost crackings) and thus the polygonal form (from micro to macro polygons). The width of the cracks can be from several millimeters to 10-12 centimeters or more. The penetrating depth of the frost crackings would be limited within the active layer, but in certain conditions, the cracks can penetrate into the permafrost, forming the check-like cryogenic texture.

Macropolygons (maybe with ice wedges) were found by Professor A.P.Gorbunov in Darhat basin of Prihubsugul. These kinds of macropolygons are widely distributed in Darhat basin and the intermontane depressions of Mt. Khangai, Mt. Khentei and other places. The small polygonal forms develop everywhere, i.e. in the flood lands, valleys and terraces, foothills and slopes (Photo 2). The small polygon with a distance of 10-15 cm between the cracks at an elevation of 2500-2600 m on the northern slope of Mt. Altai is the least of all micropolygons observed by the author. Both the nonsorted and sorted polygons were encountered, the nonsorted polygonal forms were widely distributed, the sorted ones--in Mt. Khangai, Prihubsugul and other places (Photo 3).

#### THERMOKARST

The signs of thermokarst, including the round-shaped small lake formed by the melting of ground ice, were often seen at the bottom of lacustrine basins and river valleys. The negative landforms (without water) and the lakes were located at the places with perennial frost heaving mounds.

Because of the climatic optimum in Holocene, the valley-glaciers and the alpine glaciers in Mongolia retreated, the permafrost degenerated and the thermokarst processes began to develop. The signs of such thermokarst processes could be seen not only in the permafrost region, but also in the south, i.e. the seasonal frost zone of the Central Khangai Upland and other places. The development of thermokarst at the climatic optimum period of Holocene accounted for the increase of mean annual air temperature the warming of permafrost, the thickening of the seasonal thaw layer and the increase of the buried depth of ground ice or the ice-rich frozen ground.

Nowadays, thermokarst is still developing and can be seen in the valley of River Changan-turutin-gol of Bajanhongor Aimak (South Khangai), and in the nearby region of Dadal Somon, Khentei Aimak (northeast of Mongolia). In these region, some small drained depressions, 1.5 m in depth and 4-5 m in diameter, were found. This evidently provided for the development of the thermokarst processes. With the entering of water, the

melting of ice would become activated, the settlement of ground would be faster and the small pond would be enlarged.

#### THERMAL EROSION

In Mongolia, thermal erosion usually occurs as a small ditch; when the ice-rich frozen ground or ground ice is subject to erosion, the thermal erosion stream could occur.

In Northern Mongolia, especially in the Darhat basin, because of the intensive snow-melting and the temporary intensive surface flow, the U-shaped ditches develop actively, and thus the seasonal thawing-freezing layer is scoured, the upper part of permafrost is eroded. This causes not only the enlargement of the ditch, but also the intensive settlement of ground. The intensity of the ditch enlargement and the destruction of the river bank composed of ice-rich sandy clay and silty sand can be 1 to 3 m.

Thermal erosions were found in those places, where the ice core (segregated or intrusive) of a frost heaving mound was washed and destroyed by river discharge. This was observed at the valley bottom of River Olgin-gol and River Chargon-Turutin-gol, where a group of perennially frost heaving mounds were encountered. The left bank of River Olgoin-gol was intensively scoured by water, the following profile could be an example:

0-2.2 m Silty sand and sandy clay, dark brown, with plant roots, thawed (seasonal thawing and freezing layer).

2.2-8.0 m Frozen silt, blue, rich in ice, with a bedded and irregular netted cryogenic texture.

At the meander belt of the river, the frozen silt was intensively eroded and thus the river bank was destroyed. In 1988, the author found that it had collapsed into the water, the collapsed section was 3-4 m in width.

#### CRYOGENIC SLOPE PROCESSES AND PHENOMENA

In our country, the most active form to prepare the block materials moving on slopes is Cryogenic Weathering. Sometimes, it is called cryohydration weathering. As a basic result of cryogenic weathering, the large blocks were formed (Photo 4). The cause of cryogenic weathering accounted not only for the fluctuation of ground temperature (in Mongolia it is considerable), but also for the water freezing in the rock joints. A large number of block fields and kurums in mountain regions of our country proved the intensity of cryogenic weathering. In Mt. Khangai, the active cryogenic weathering belt starts from 1500 m a.s.l..

By means of the catcher, the author observed the intensity of cryogenic weathering in the offshoot of Mt. Khangai in the crystalline schist region, River Segnegerin-gol basin, during 1978-1983. In the catcher, 0.5 m in area, two boulders, some gravel and silt were obtained.

As a result of cryogenic weathering, some fine-graded materials occurred. Field observations by means of the catcher were carried out in Mt. Emgant-in-hushu, Hutag Somon, Bulgan Aimak, from 1977-1978. The retreat of the rock-wall caused by weathering, indicated a very low intensity. One example is shown in Table 2.

Kurum is one of the widely distributed forms on slope of the middle-high mountain with continuous, discontinuous, and even sporadic permafrost in our country.

Table 2 Result of observation on the intensity of cryogenic weathering in orthogneiss, Mt. Emgantín-hushu

Duration	Rock	Area of catcher (cm)	Materials into catcher (g)	Working condition of catcher
1977-78	Orthogneiss	400	2.6	shaded

Kurums develop on the slopes with a steepness from 3-5° to 40-45°. For example, in the Mt. Bogdo-gul near the Ulan-Bator City, they generally occur on the north, northeast and northwest slopes. At the upper part of slope, kurums are generally composed of sharp angular blocks and big boulders; at the middle part of slope, they generally consist of angular-rounded big to middle boulders (Photo 5). In the gorge area, the lower part of slope is rather steep (40-45°), the kurums become stone streams, where the velocity of downward movement of the blocks is still considerable (Table 3).

Table 3 Movement of block materials in stone stream at Mt. Bogdo-ul, 1982-1983

Classification of block	Small boulder	Very coarse pebble	Coarse pebble	Middle pebble
Size (cm)	40-20	20-10	10-6	6-4
Moving distance per year (cm)	17.5	21.7	34.1	22.6

As shown in Table 3, the moving speed of the smaller materials is higher than that of the coarser ones. Kurums develop actively in the upper part of the Mongolian high mountains, for example, on the upper part of the planation landform, the ancient planation surface, especially the cryoplanation terraces (with several steps) in the Mt. Bogdo-ul (2100 m) and Buglan-Pusger (2100 m) of the Mt. Khantai and other mountains. Kurums actively develop mainly on stepped cryoplanation terraces, thus the terrace scars would retreat backwards and the lateral cutting would occur.

Cryogenic creeping develops on the slopes and the planed hilltop of the middle and high mountains where the goes ice and snow is melting. The repeated upheaving (caused by the ice formation) and settlement (caused by the ice melting) of a kurum body leads to the block material downslope movement. The moving velocity of cryogenic creeping is very slow and was observed to be several millimeters per year. Usually, cryogenic creeping develops at the upper part of mountains or the planed hilltop and plays an important role in the planation of the summit surface of the middle-high mountains in Mongolia.

Solifluction widely develop in northern Mongolia, mainly on the north-facing slope, on the planed summit and the foothills, in the silty-sandy clay with some coarse-graded debris (Photo 6).

Solifluction can be subdivided into slow and rapid ones. The velocity of the slow plasticoviscous movement of the slope deposits is as low as several centimeters per year. At the upper part of the high mountains without any impeding effects, the solifluctions can occur on all sides of slopes, especially on south-facing slope of Mt. Khentei.

The movement of the silty-sandy clay and silty

sand with some debris on the northeast slope of Mt. Bogdo-ul (with a steepness of 10-29°) is 1.5-2.8 cm per year. The results of observations on the soil-ground movement are listed in Table 4.

Table 4 Observations on the soil-ground movement in the slow solifluctions in Mongolia

Region	Slope steepness	Soil-ground movement	Observer
Mt. Khangai	3-7	25-30	Suhodrvckii, 1974
Mt. Sert-ul	6-7	5	D. Luvsandagva
Mt. Darsin-nuru	12-28	2-7	R. Lomborinchen, 1978
Mt. Bogdo-ul	10-29	24-28	R. Lomborinchen, 1985

The rapid solifluctions were seldom seen, but their signs were observed at Zavkhan, Arkhangai, Bulgan and the Central Aimak. One of the rapid solifluctions took place in the Mt. Turge of Zavkhan Aimak, August 1, 1961. On the northern slope of this mountain, 15-18° in steepness, the root layer was eroded rapidly, becoming a thick slurry moving out on the frozen base on the slope. The solifluctional body was 15-20 m in width and 150 m in length. Being transported downwards along the northern slope the solifluctional deposit formed at the foothills.

In the permafrost region, especially on the northern slope of middle-high mountains, solifluctional landforms, including the tongue, flow, terraces, etc., are widely distributed.

#### ICINGS

icings, small to middle in size, are widely distributed in the middle to middle-high mountain regions of northern Mongolia and can be divided into seasonal (one year) and perennial ones. The seasonal icings are the basic forms, which occur in late Autumn, reach the maximum size in January and February, and disappear in Spring to Summer. The perennial icings are seldom seen. They mainly occur in Khubsugul Aimak and have a local name "Gjalan mes" (brilliant ice). One of the perennial icings was observed by the author in Rinchilhubz Somon, Khucugul Aimak. At maximum, it is 500 m in width, 1.2 km in length and with ice-cracks 2.0-2.5 m in width.

River icings (Photo 7), lake icings and ground water icings are widely distributed, supplied by surface-water, ground water or both.

#### ROCK GLACIER

The mean annual air temperature in Northern Mongolia is as low as -4°C to -6°C. In the alpine region, it is much colder. This is favourable to the development of rock glaciers. Rock glaciers are encountered in Mt. Khangai, Mt. Khentei, of the Pribhugsul, Mt. Altai and the Tavan-Bogdo (4374 m a.s.l.) (Photo 8).

The rock glacier at the valley of southern Tavan-Bogdo is a mature one 200 m in width, 500 m in length, 10-15 m in thickness and with scars about 30° in steepness. It is composed of angular-rounded blocks and boulders. Up to now, there was almost no detailed investigation on rock glaciers in Mongolia.

#### CONCLUSION

In Mongolia, in the semitransitional seasonal



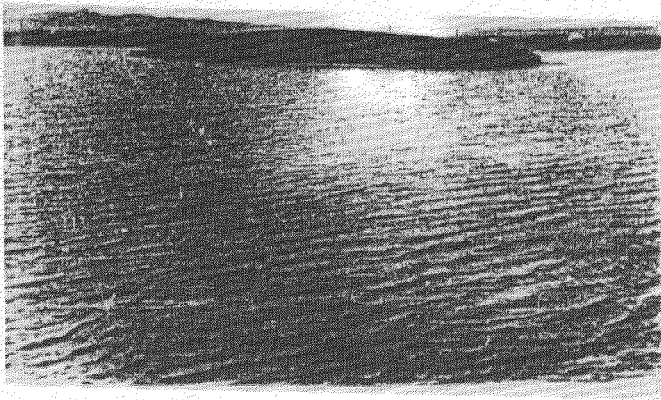


Photo 1 Frost mound in lake Bus-nur, near by Ulan-Bator  
(R.Lomborinchen's photo)

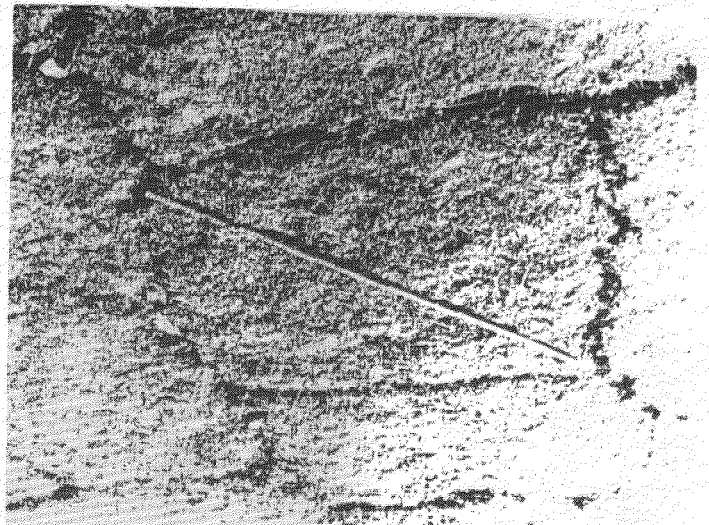


Photo 2 Frost cracks near by Somon Tsagan-ul, Khubsugul district (R.Lomborinchen's photo)

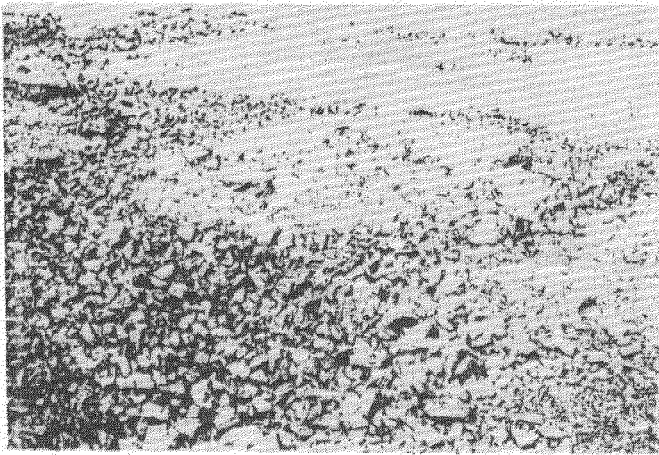


Photo 3 Sorted polygons in river head of Orkhon  
(R.Lomborinchen's photo)

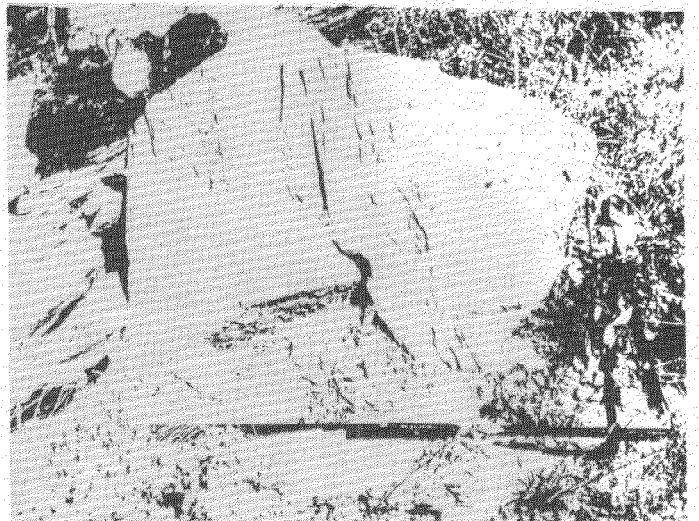


Photo 4 Frost weathering in crystalline slate of Khen-tei's piedmont (R.Lomborinchen's photo)



Photo 5 Block slopes in m. Bogd-ul (Ulan-Bator)  
(S.B.Bazarowa's photo)

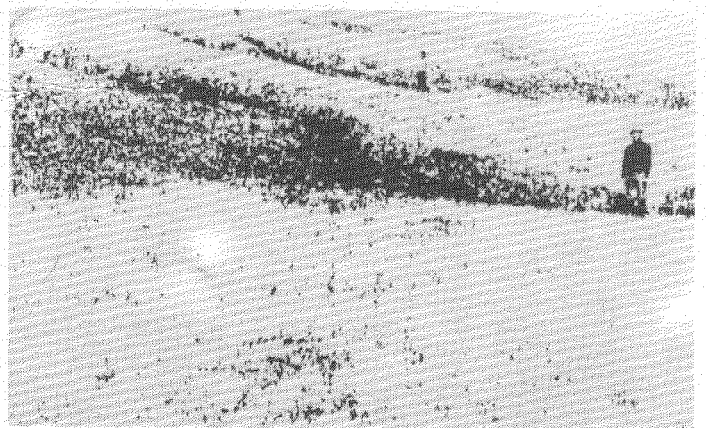


Photo 6 Solifluctions tongue in m. Khangai  
(R.Lomborinchen's photo)

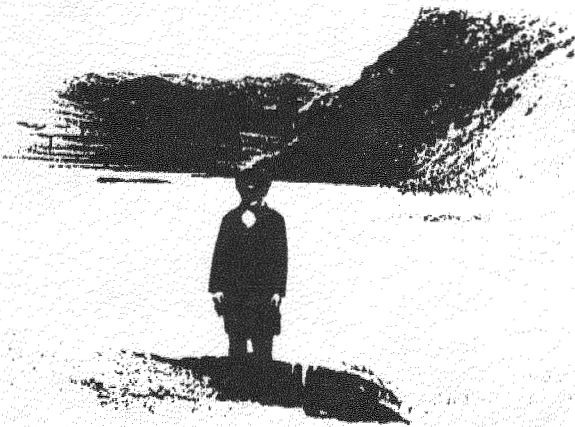


Photo 7 Icing near by Ulan-Bator  
(S.B.Bazarowa's photo)

freezing belt, there occurs almost all kinds of the cryogenic processes and phenomena, the slope processes and phenomem and those related to the activity of water and glaciers. However, the duration of their appearance, their size, intensity and the developing dynamics in Mongolia are different from that in other cryolithologic zones.

The development of periglacial landforms has experienced several stages, the active and degenerated ones. In Hollocene, it is characterized by the tendency of regional degradation of permafrost, so that some kinds of cryogenic processes and phenomena, for example the thermokarst, are activated.

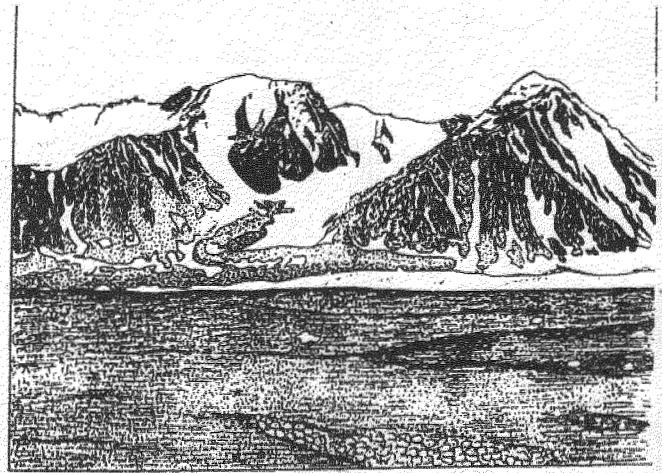


Photo 8 Rock glacier in m. Altai Tavan-Bogd (4374m)

RESEARCH ON TANGENTIAL HEAVING FORCE AND FRICTIONAL RESISTANCE  
AGAINST PULLING UP OF PILE

Lu Xingliang, Yu Shengqing, Xu Bomeng and Hu Shicai

Research Institute of Water Conservancy Committee of Songhua-  
Liaohe Board, 74 Beian Road, Changchun City, China

Based on a great number of the data obtained from many years of in-situ tests of piles with different diameters, structural types and water tables and the practical investigation after overall comprehensive analyzing, the effects of water conditions, soil properties and temperature factors on the frost heaving were discussed; the relationship between frost depth, heaving and water table, the design values of tangential heaving force, and the calculating method are presented in this paper. With the method of using heaving force to pull pile, the long-term frictional resistance of warm soil to the pile was measured, and its design values agreeable to the piles operating conditions in winter were determined.

INTRODUCTION

In seasonally frozen zones, the pile foundation is acted on by the frost heaving of soil. Consequently, the phenomena of its drawing out and breaking away are often brought about. For a long time, in quite a few localities, the measure of increasing the embedded depth of pile was adopted to prevent it from pulling up, which often produced an increase in the cost. Thus, it still remains a problem to be resolved on how to prevent pile foundation from being pulled up by frost heaving of soil and to determine a reasonable embedded depth.

Viewed in this context, we have carried out in-situ test since 1983. The test site is located at a distance of about 60 km from Changchun city, Jiling province. The soil of this site is clayey.

Based on the observation data, the relationship among tangential frost heaving forces and the frost depth, heaving amount and water table was analyzed, the value range of tangential frost heaving force and limited frictional resistance to the pile foundation are presented in this paper.

THE RELATIONSHIP BETWEEN FROST DEPTH, HEAVING AND WATER TABLE

The frost depth is associated with air temperature, soil property, covering condition and water table, etc. For the region without covering and with approximately the same air temperature and soil property, the water table may be taken as the main factor dominating frost depth. According to the results of statistical analysis made by means of observed data years ago, the relation between frozen depth and water table was established (Fig.1).

Recently, in the engineering design, the standard frozen depth was often taken as a design frozen depth. However, there is a certain dif-

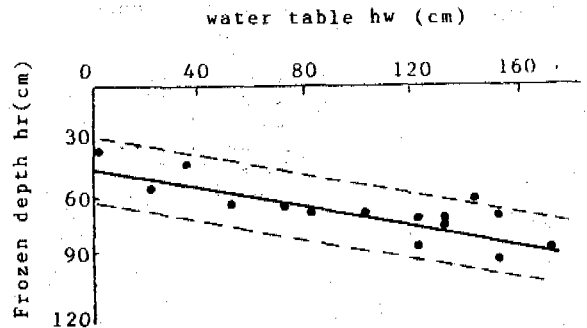


Fig.1 Relation between frozen depth and the water table

Linear equation  $h_f = 104.68 + 0.25h_w$   
Correlation coefficient  $r = 0.84$   
Standard deviation  $S = 8.8$

ference between them. From the linear law in Fig.1 by using the regression analysis and taking influenced distance 180 cm of water table (on the basis of capillary height obtained from laboratory and in-situ tests), the experimental formula for calculating design frozen depth can be derived as follows:

$$h_d = h_s - B(180 - h_w) \quad (1)$$

where  $h_d$  is design frozen depth (cm);  $h_s$  is multiannual maximum frozen depth found out from meteorological data (cm);  $h_w$  is depth of water table from ground surface (cm); B is regression coefficient, taking as 0.25.

The free heaving amount of ground surface depends upon the complicated water migration conditions and processes in the course of soil freezing. But, the key factors governing the degree of water migration and frost heaving is the distance of the ground water level to the freezing front. According to the observation

date with the statistical analysis, the relationship of the heaving ratio to water ground level is obtained in Fig.2 and may be calculated as

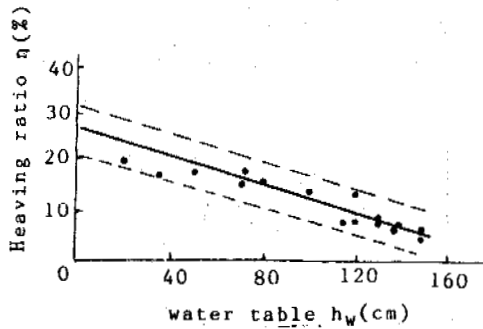


Fig.2 Relationship between the heaving ratio and the water table

Linear equation  $\eta = 26.552 - 0.137h_w$   
 Correlation coefficient  $r = 0.94$   
 Standard deviation  $S = 2.58$

follows:

$$\eta = 26.552 - 0.137 h_w \quad (2)$$

where  $\eta$  is ratio of heave (%); the other symbols are the same as previous.

Both formulas mentioned above can be used to evaluate the frost susceptibility of the construction project site (with clayey soil in an open system, and a ground water level less than 180 cm from the ground surface and drops with the frozen depth development).

**THE FACTORS AFFECTING TANGENTIAL FROST HEAVING FORCE**

**Frost Depth**

From observation data of past years it can be seen that the frost heaving force starts to occur when the frozen depth reaches 20-30 cm, which basically corresponds to the time of frost appearing. Then, as the frozen depth develops, tangential frost heaving forces increase with a quicker rate and in the form of a fluctuation under the action of air temperature variation. Usually, the maximum value occurs in the second week of December to the first week of January next year, but there also exists individual exceptions, earlier or later than that of above. After reaching the maximum value, tangential frost force generally tend to drop, and quickly reduces from the third week of March until it disappears. The date of tangential frost heaving force disappearing comes commonly at the end of March, sometimes delayed to the second week of April. Fig.3 shows the observation results of pile No.7 in the test site during the winter of 1986-1987. From this figure, the process mentioned above can be seen. For years, the other test piles performed similarly to pile No.7. As shown in Fig.3, the frost heaving increases with the frozen depth development and follows the maximum when the frozen depth reaches the maximum, but the maximum value of tangential frost heaving force takes place not at the same time as the maximum frozen depth.

Fig.4 shows the tangential frost heaving force as a function of the ratio of corresponding frost depth. It can be seen from this figure

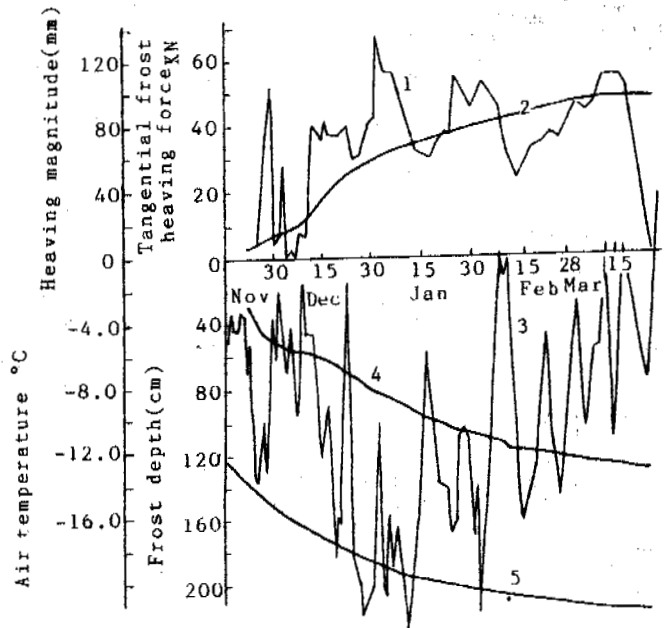


Fig.3 The process of tangential frost heaving force, heaving magnitude, frost depth, water table and air temperature

1 is tangential frost heaving force; 2 is heaving magnitude; 3 is average daily air temperature; 4 is frost depth; 5 is water table (pile No.7, 1986, 1987)

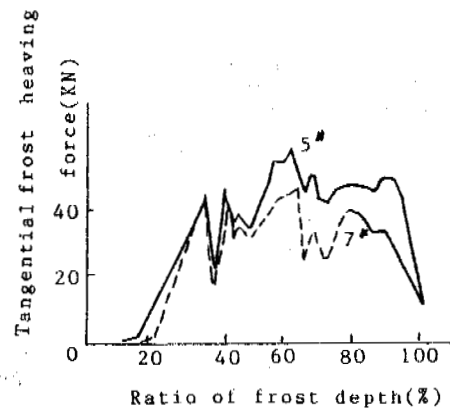


Fig.4 Relationship between tangential frost heaving force and frost depth

that before frost depth reaches 20% of its maximum, the tangential force is very little; when the frost depth is 20-35% of its maximum, it rapidly increases; as the frost depth reaches 60% of its maximum or 80% in individual cases, the tangential frost heaving force reaches the maximum. The cases mentioned above show that the design value of frost depth should be corrected when the unit of tangential frost heaving force is determined and the frost depth is calculated. At this time, the value of 0.6 ( $h_w = 180\text{cm}$ ) to 0.8 ( $h_w = 0$ ) may be taken as the correction coefficient.

### Air Temperature

It can be also seen from Fig.3 that air temperature in winter varied obviously, consequently, tangential frost heaving force appears as a wavelike development with the air temperature changes. According to the meteorological observation data for twenty years in Gongzhuling city and twenty seven years in Shangliao county, the index of negative air temperature accumulation is 1326 and 1336°C.d, respectively. During our observation period, the maximum of this index is 1409.5°C.d (1985-1986), the minimum is 1009.4°C.d (1988-1989). Thus, it may be considered that, so far as the influence of air temperature is concerned, the measurement value of tangential frost heaving force are basically representative.

### Ground Water Level

The heaving of frost soil increases with the ground water level rising (Fig.2). The in-situ observation data indicates that the closer the water table is to the freezing front, the greater the tangential frost heaving force. In the course of approximately a ten year observation, the depth of the water table at the time of frost beginning in each year was from the minimum of zero to the maximum of 150 cm, and the maximum unit tangential frost heaving force was 118 kPa and 40-60 kPa, respectively. In the years with relatively stable ground water, the difference of tangential frost heaving force was not significant. It shows that water table plays an important part in producing tangential frost heaving force.

### DESIGN VALUE OF TANGENTIAL FROST HEAVING FORCE

According to the data obtained from long term in-situ tests and practical investigation, it is demonstrated that the magnitude of tangential frost heaving force is dependent upon a combination of different factors, including ground water level, frost depth, frost heaving ratio, air temperature, roughness of pile, etc..

Based on the continuous observation of the 24 test piles and prototype examination, and taking the water table and frost heaving ratio as the main parameter, the design value of unit tangential frost heaving force is presented in Table 1.

Table 1 Design value of unit tangential frost heaving force

Water table before freezing (m)	Heaving ratio (%)	Unit tangential heaving force (kPa)
>1.5	<6	<60
1.5-0.7	6-18	60-80
0.7-0	>18	80-120

- Notes: 1. The values in this table are applicable to the piles grouted used within the framework otherwise it should be multiplied with a roughness coefficient of 1.2-1.5;  
2. When the total tangential frost heaving force is computed, design frost depth should be calculated with formula (1) and then multiplied by the correction coefficient of 0.6-0.8.

### DESIGN VALUE OF FRICTIONAL RESISTANCE

In order to gain the long-term frictional

resistance between thawing and the foundation, two prototype piles of natural scale are embedded at the Gongzhuling test site, by utilizing frost heaving force as the pulling-up force. After two years of measurement, the limit values of two piles are 213 kN and 240 kN, respectively. The force vs. displacement of piles is shown in Fig. 5. It is illustrated in this figure that before

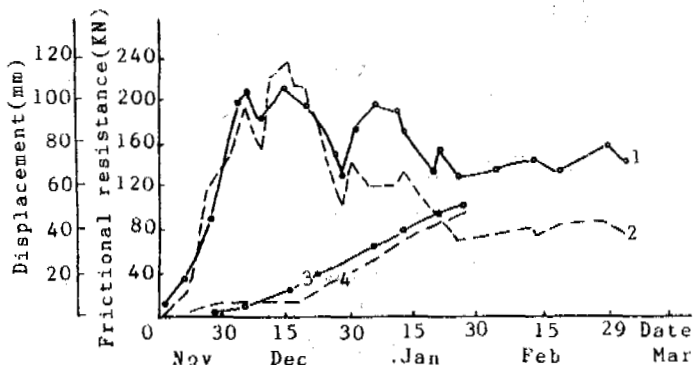


Fig.5 Graph of friction resistance and displacement of piles (1987-1988)

- 1,2--friction resistance of piles No.11 and No.10 respectively;  
3,4--displacement of piles No.11 and No.10 respectively.

reaching the limited value, resistibilities to pulling-up rapidly increase; after reaching the limited value, it falls quickly, at the same time, displacement of piles linearly increases obviously. It indicates that once the pile is pulled to move, resistibility would drop down, very quickly and finally tend to a stable value.

According to the observed values, the average frictional resistance of two piles in thawing soil is 10.7 kPa and 12.6 kPa, respectively. Thus, for the cast-in-place pile foundation embedded in clayey soil, the limited friction resistance against pulling-up may be taken as 11-13 kPa. The ratio of the above value to the unit friction resistance of 30-35 kPa provided for corresponding soils and compression piles in Regulation JGJ 4-80 is 0.4. Therefore, this coefficient may be used to calculate frictional resistance against pulling-up of other soils by using the following formula:

$$F = 0.4S \sum h_i f_i \quad (3)$$

where F is frictional resistance against pulling-up of warm soil layers (kN); S is perimeter of pile (m);  $h_i$  is the thickness of each soil layer (m);  $f_i$  is the unit frictional resistance of compression pile in each soil layer (kPa).

### CONCLUSION

Based on the continuous observation results obtained from the test site for years and the present observation data collected in Jiling province, the relationship between frost depth, frost heaving and ground water level is presented, the design value and computation method of unit tangential frost heaving force and frictional resistance against pulling-up are determined in this paper. These test results have been popularized and applied all over Jiling province, having achieved considerable economic

benefits, at the same time, the reliability of these results have also undergone an examination.

#### REFERENCES

Xu Bomeng and Lu Xingliang (1986) Influence of Moisture Condition on Frost Heave in Clay, Journal of Glaciology and Geocryology, Vol.8, No.3, Sept, pp217-222.

"Design and Construction Regulation of Boring-Cast-in-Place pile in Industry and Civil Constructions" (1980) (JGJ 4-80), Beijing.

Sun Yuliang and Wang Liang (1989) Tangential Frost Heaving Forces and Examination of Anti-Frost Uplift of Reinforced Concrete Piles, Proc. Third Chinese Conference on Permafrost pp150-156.

## Permafrost Formation Time

Virgil J. Lunardini

U.S. Army Cold regions Research and Engineering Laboratory  
Hanover, New Hampshire 03755-1290

The age of permafrost is related to the time required for soil systems to freeze since permafrost is at least as old as its formation time. Freeze/thaw cycles complicate the relation between freeze rate and age. A pure conduction heat transfer with freeze/thaw model is used to predict the time needed to form a given thickness of permafrost. The formation time is a function of the long-term geothermal gradient, the ratios of the frozen- to- thawed thermal properties, and the temperature history of the upper surface of the permafrost. The simple theory leads to universal graphs that predict the formation time. Realistic soil property ratios and paleo- temperature scenarios then lead to estimates of the formation time of permafrost. The model indicates that deep permafrost requires formation times on the order of the complete Quaternary Period.

### INTRODUCTION

Permafrost is a result of the history and the present state of the earth's surface energy balance and the geothermal heat flow. Given the same yearly net gain of energy, however, one region may have permafrost while another will not, due to the sites different thermal histories. Thus, the present energy flows may be such that permafrost cannot exist in one region, whereas it will subsist in another as "relic permafrost." Since the energy balance involves meteorological conditions, surface vegetation, topography, and soil conditions, no simple correlation has been found for the existence of permafrost in the marginal or discontinuous regions.

The thermal history of permafrost depends upon the long-term temperature variations at its upper surface. Mean global temperatures deduced from oxygen isotope data for the past 180 million years suggest that little permafrost existed prior to the late Tertiary Period and none for the 100 million years before the long-term cooling that began 35 million years before the present (MYBP) (Eddy and Bradley, 1991). During the Pliocene (2-5 MYBP), temperatures oscillated up to 4°C above present values (Folland et al., 1990), and permafrost was probably present at locations that now have mean temperatures less than -8°C.

The Quaternary Period has been marked by greatly reduced temperatures, massive glaciations, and ice ages of 100 to 120 thousand years' duration. The Holocene interglacial is somewhat cooler than the previous one and the solar record would seem to indicate the next significant temperature move should be downward with a new ice age evolving (Budyko, 1974; Budd and Smith, 1981). The quantitative temperature record from isotope analysis for the past million years (Folland et al., 1990) indicates at least 4 or 5 glacial periods with the last one (Wisconsin) ending in North America some 12,000 years ago; temperature departures from present values swung from highs of +3°C during interglacials to lows of about -10°C during the

glacial maximums. Analysis of the Vostok (Antarctic) core indicates maximum temperature excess of the past 160,000 years of about 3°C (Jouzel et al., 1987). Temperature variations of 8 to 12°C during the last glaciation have also been reported from Greenland ice cores (Dansgaard and Oeschger, 1989). If the temperature variations deduced from ocean and ice cores were global, then the paleotemperature history at a site could be reconstructed. This has been done for Prudhoe Bay by Osterkamp and Gosink (1991) as shown in Figure 1, based on the work of Brigham and Miller (1983); other scenarios used data from Maximova and Romanovsky (1989), Jouzel et al. (1987), and Sun and Li (1988).

Isotopic data infer that temperatures at a given site could have dropped as much as 12°C below present values; paleotemperature excursions on this order of magnitude should be used with the permafrost formation models. Rapid growth of permafrost should not be explained simply by extraordinarily low paleotemperatures. Figure 2 shows one example of average paleotemperatures

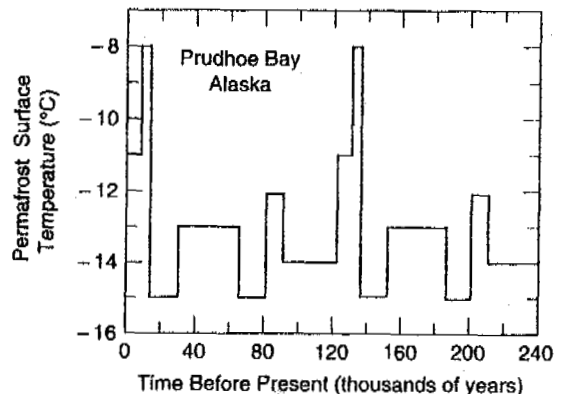


Figure 1. Permafrost Surface Paleotemperature Model for Prudhoe Bay, Alaska, after Osterkamp and Gosink (1991), Brigham and Miller (1983).

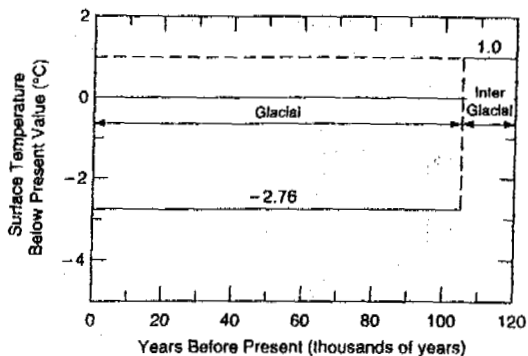


Figure 2. Mean Paleotemperature Departure, Prudhoe Bay, Alaska, One Glacial Cycle, Brigham and Miller (1983) Data,  $\Delta T = -2.54^\circ\text{C}$

for a glacial cycle of 120,000 years for Prudhoe Bay, Alaska, with the temperature variations presented by Osterkamp and Gosink (1991).

The age of a deposit of permafrost is the time that has elapsed during and since the freezing of the soil system. Different cycles of thawing and freezing occur at different places and the age of two "similar" deposits of permafrost may be quite different. It is probable that some permafrost had its origin at the beginning of the Pleistocene era (Brown, 1964), but the intervening thermal conditions were also important.

There have been few systematic thermal studies of the origin of permafrost and its formation time. Osterkamp and Gosink (1991) studied the response of permafrost due to surface temperature variations using quasi-steady, perturbation, and finite element models to predict the position of the permafrost bottom. However, they were mainly interested in deducing paleotemperatures from the present permafrost data at Prudhoe Bay, Alaska. Allen et al. (1988) used a quasi-steady model, based on the work of Lachenbruch et al. (1982) for the same purpose in the Mackenzie Delta region of Canada. Romanovsky et al. (1988) noted qualitative aspects of the origin and disappearance of permafrost in the Transbaikalian area of Russia. Katasonov (1988) used "cryogenic structures" to argue for the origin of permafrost early in the Quaternary.

This paper predicts the rate of permafrost formation, using a simple conduction model and realistic paleo-temperatures.

#### THEORY

Solidification phase change problems are inherently nonlinear with few exact solutions. A solution for a constant initial temperature, semi-infinite medium which undergoes a step change of surface temperature was given by Neumann (1860) and expanded upon by Carslaw and Jaeger (1959). The search for practical solutions has led to approximate solution methods; the heat balance integral technique solves the energy equation on average over a space volume (Goodman, 1958). The method has been applied to constant initial temperature problems of the semi-infinite slab (Lunardini and Varotta, 1981), while a modification of the integral method utilizing a single integration over an entire nonconstant property volume has yielded accurate solutions (Yuen, 1980; Lunardini, 1981a, 1982). The integral method has been used with initial

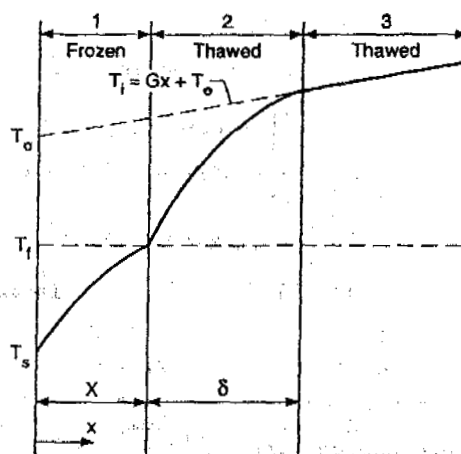


Figure 3. Region With Linear Initial Temperature

temperature distributions but limited to shallow freeze depths (Lunardini, 1984).

Figure 3 shows an infinite layer of soil with a linear initial temperature distribution. The soil is homogeneous and conduction is the only mode of energy transfer. At zero time the surface temperature drops to  $T_s$  and freezing commences. The time it takes for the surface temperature to drop to the freezing point is neglected since this will be small compared to the formation time; thus an acceptable scenario is that for which  $T_0 = T_f$ . The governing equations are

$$\alpha_i \frac{\partial^2 T_i}{\partial x^2} = \frac{\partial T_i}{\partial t} \begin{cases} i = 1 & 0 < x < X \\ i = 2 & X < x < X + \delta \end{cases} \quad (1)$$

$$T_1(0, t) = T_s(t) \quad (1b)$$

$$T_1(X, t) = T_f \quad (2a)$$

$T_s(t)$  is the paleotemperature transient. The heat balance integral method assumes that no thermal changes occur below the thermal disturbance depth  $X + \delta$ , thus,

$$\frac{\partial T_2(X + \delta, t)}{\partial x} = G \quad (2c)$$

$$T_2(X + \delta, t) = (X + \delta)G + T_0 \quad (2d)$$

The temperature at the beginning of freeze is

$$T_2(x, 0) = T_0 + Gx \quad (3)$$

The energy balance at the phase change interface, for the freeze process, is

$$k_1(\partial T_1 / \partial x) - k_2(\partial T_2 / \partial x) = \rho_2 L dx/dt \quad (4)$$

Convection due to density difference is a secondary effect. Because of the initial temperature distribution, during freeze, the heat flow to the freeze interface from the thawed region will exceed the geothermal heat flow until equilibrium is established. Integration of the energy equations over the region where temperature changes are occurring,  $0 < x < X + \delta$ , (Lunardini, 1991), is

$$\frac{d}{dt} \left[ \rho_1 c_1 \int_0^X T_1(x, t) dx + \rho_2 c_2 \int_0^{X+\delta} T_2(x, t) dx - \rho_1 L x \right] + (\rho_2 c_2 - \rho_1 c_1) T_f X - \rho_2 c_2 (X + \delta) \left\{ T_0 + \frac{G}{2} (X + \delta) \right\}$$



$$= -k_1 (\partial T_1 (0, t) / \partial x) + k_2 G. \quad (5)$$

The energy balance at the freezing front is:

$$-k_1 \frac{\partial T_1}{\partial x} \frac{\partial T_2}{\partial x} + k_2 \left[ \frac{\partial T_2}{\partial x} \right]^2 = \rho_2 \lambda \alpha_2 \frac{\partial^2 T_2}{\partial x^2}. \quad (6)$$

Quadratic temperature profiles which satisfy the boundary conditions are

$$T_1 = T_f + a_1 X \left( \frac{X-X_f}{X} \right) + (a_1 X - \Delta T_1) \left( \frac{X-X_f}{X} \right)^2 \quad (7)$$

$$T_2 = T_f + [G(\delta+2X) + 2\Delta T] \frac{X-X_f}{\delta} - (GX + \Delta T) \frac{(X-X_f)^2}{\delta^2} \quad (8)$$

where  $a_1 X = \frac{\Delta T_1}{g}$ ,  $g = \frac{\alpha_{21} (\Delta T + GX) X}{\delta [G(\delta+2X) + 2\Delta T]} + 1$ . The ac-

curacy increases as the polynomial order increases. For the Neumann problem, with quadratic temperature choice, errors in  $X$  of less than 5% occur (Lunardini, 1991). Equation (6) leads to:

$$\beta/g - k_{21} [\sigma(\beta+2) + 2\phi] = 2\rho_{21}\beta(g-1)/S_T. \quad (9)$$

The nondimensional energy equation is:

$$\tau = \int_0^\sigma K d\sigma \quad (10)$$

$$K = \frac{b_1 + b_2 \beta - \frac{1}{6g} \left( 1 - \frac{\sigma g'}{g^2} \right) - C_{21} \sigma \left( \frac{2\beta+1}{3} \right) - \frac{C_{21}}{3} (\sigma + \phi) \sigma \beta'}{\frac{1}{\sigma} \left( \frac{1}{g} - 2 \right) + k_{21}} \quad (11)$$

$$\frac{d\beta}{d\sigma} = \beta' = \frac{a_5 + a_1 a_4}{a_3 + a_2 a_4} \quad (12)$$

$$\frac{dg}{d\sigma} = g' = a_1 - a_2 \beta' \quad (13)$$

$$\text{where } a_1 = \frac{\alpha_{21}}{m} \left[ 1 - \frac{(\sigma + \phi)\beta(\beta+2)}{m} \right], a_4 = \left( \frac{2\rho_{21}}{S_T} + \frac{1}{g^2} \right) \beta$$

$$a_2 = \frac{\alpha_{21}(\sigma + \phi)}{m^2} [2\sigma(\beta+1) + 2\phi], a_3 = \frac{1}{g} - \frac{2\rho_{21}(g-1)}{S_T} - k_{21}\sigma$$

$a_5 = k_{21}(\beta+2)$ ,  $b_1 = -\left[ \frac{1}{3} + \frac{1}{S_T} + C_{21}\phi \right]$ ,  $b_2 = -\frac{1}{3} C_{21}\phi$ ,  $m = \beta[\sigma(\beta+2) + 2\phi]$ . Only the ratios of the thawed-to-frozen values of thermal conductivity, specific heat capacity, and density are needed. These can be estimated with good accuracy for many permafrost soils, see Appendix 1.

Unlike the Neumann solution, the permafrost zone for this case reaches an equilibrium value.

$$X_\infty = \Delta T_1 / (k_{21} G). \quad (14)$$

The ratio of the sensible to the latent heat is quite large and tends to increase as the freeze depth increases. This will cause the permafrost to grow at a far slower rate than for a soil with no geothermal gradient.

#### Effect of Quaternary Freeze/Thaw Cycles

The theory assumes that the soil was initially unfrozen. However, cyclic warming and cooling tend to cool the ground after each thaw event. The time to reach equilibrium will be greatly changed by the initial temperature of the soil but not the final equilibrium thickness. When surface warming occurs, geothermal heat flow melts permafrost and also warms the soil in a growing region near the original freeze/thaw interface. Maximum thaw would occur if all of the geothermal heat flow went into melting, but this is physically impossible. Given sufficient time, the entire permafrost volume would melt and the

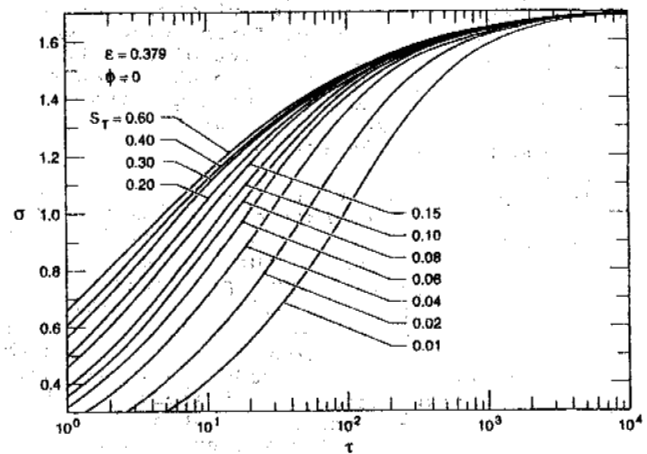
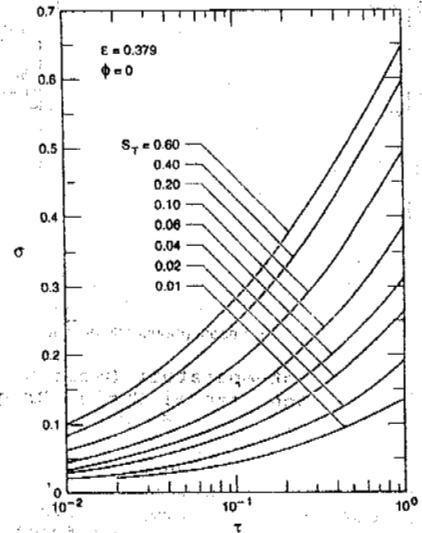


Figure 4. Freeze Time of Saturated Mineral Soils

soil temperature would be less than that of eq.(3). Clearly the sensible heat which must be removed in the modulated case will be less than that for the original freeze, and the cooled soil will freeze much faster with the same mean surface temperature. The concepts and solution are further discussed in Lunardini (1992).

#### DISCUSSION

Equation (10) was solved numerically resulting in values of the permafrost depth versus time as a function of  $S_T$ ,  $\epsilon$ ,  $\phi$ , and the thermal property ratios. Results are graphed in Figure 4 for a soil porosity of 0.379 (Prudhoe Bay, Alaska value); more extensive graphs are given in Lunardini (1992). Figure 4 can be used to estimate permafrost formation times for arbitrary surface temperatures and geothermal gradients. Figure 5 shows the time needed to reach 90% of the equilibrium permafrost thickness. The graphs are only valid for the particular soil ratios given, however, this does not affect the model itself. Any site can be modeled by using site-specific property ratios.

Considerable information is available from exploratory wells at Prudhoe Bay, Alaska; the actual permafrost data show that the property

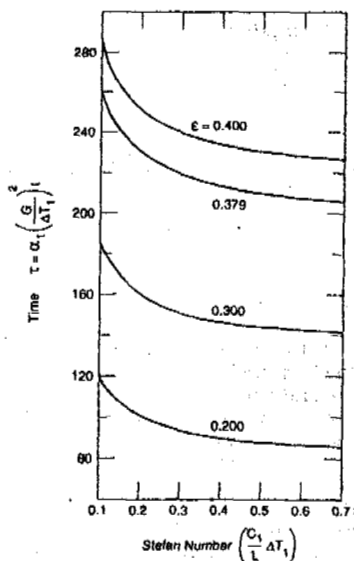


Figure 5. Time to Reach 90% Equilibrium Depth

ratios for  $\epsilon = 0.379$  are close to measured values (Lachenbruch et al., 1982). Some temperature scenarios for Prudhoe are listed in Table 1.

**Example 1.** At Prudhoe Bay, Alaska the permafrost has the conditions:  $T_s = -10.99^\circ\text{C}$ ,  $T_g = -1^\circ\text{C}$ ,  $G = .0286^\circ\text{C}/\text{m}$ ,  $\epsilon = 0.379$ ,  $S_T = 0.1440$ ,  $\alpha_1 = 58.89 \text{ m}^2/\text{yr}$ ,  $k_g = 4.34 \text{ W}/\text{m}\cdot\text{K}$ , measured  $k_{2,1} = 0.5795$ , measured permafrost thickness 599.3m. The equilibrium permafrost thickness is  $X_\infty = 602.8\text{m}$ . From Figure 5 we note that the time to reach 90% of equilibrium (surface temperature held at  $-10.99^\circ\text{C}$ ) is 500,740 yrs. This suggests that the present climate of Prudhoe Bay is considerably warmer today than it has been on average over the past 15,000 years is widely accepted.

**Example 2.** Prudhoe Bay, with the Brigham and Miller (1983) paleotemperature scenario:  $T_s$

Table 1. Paleotemperature scenarios, Prudhoe Bay, Alaska (Osterkamp and Gosink 1991).

Scenario	$T_s$ $^\circ\text{C}$	Time before present (kiloyears)
Present, Lachenbruch(1982)	-10.99	10-150
Brigham and Miller(1983)	-13.69	240
Matteucci(1989)	-11	300
Robin(1983)**	-16	160
Maximova et al.(1988)**	-11.3	170

\* Average value of the surface temperature.  
\*\* Fitted to present Prudhoe Bay temperature.

$= -13.69^\circ\text{C}$  for 225,000 years before warming to  $-11^\circ\text{C}$  in the last 15,000 years;  $X_\infty = 763.5\text{m}$ . For  $t = 225,000$  years ( $r = 67.3$ ), from Figure 5 with  $S_T = 0.1827$ , we read  $\sigma = 1.412$ . Thus the permafrost will grow to 626.5m. This value will then slowly decay to the new equilibrium of 602.8m over 15,000 years. Note that a cooler surface temperature will greatly accelerate growth since a much larger fraction of the growth will be during the early, rapid growth stage.

Figure 6 shows the permafrost thickness at Prudhoe Bay after six glacial cycles. The upper curve predicts rapid initial permafrost growth, reaching a thickness of 570m after 120 kyr, with the paleotemperature model of Fig. 2. The thickness then slowly approaches an equilibrium value

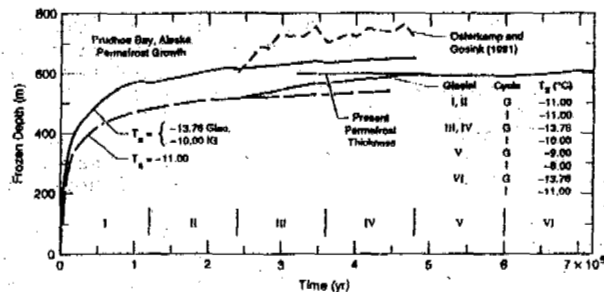


Figure 6. Effect of Paleotemperature on Prudhoe Bay, Alaska, Permafrost Growth

of 739m surpassing the present thickness of 600m after about 185 kyr; this paleotemperature model will yield permafrost that is too thick. Also shown is the prediction of Osterkamp and Gosink (1991) -using Figure 1 and starting with 600m of permafrost- that indicates much faster permafrost growth and thicker permafrost. Their quasi-steady model neglects sensible heat, assumes fixed geothermal heat flow to the freezing interface, and starts with permafrost depth far less than equilibrium; these approximations overestimate the freeze rate. The lower curve of Figure 6 shows the large effect if the paleotemperature model is only slightly modified for different glacial cycles. The predicted permafrost thickness will reach present values after about 645 kyr and will then tend to oscillate about this value.

**Example 3.** Consider the case of very thick permafrost, on the order of 1600m. Let the properties be those of Prudhoe Bay but  $\epsilon = 0.4$ ,  $\Delta T_1 = 29.27^\circ\text{C}$ ,  $G = .0286^\circ\text{C}/\text{m}$ ,  $\alpha_1 = 57.99 \text{ m}^2/\text{y}$ , then  $X_\infty = 1813\text{m}$ . The value of the surface temperature chosen is about  $12^\circ\text{C}$  colder than present winter temperatures in Canada, Russia, and Greenland. To find the time required to form 90% of the permafrost (1632m), the calculations are as before with  $S_T = 0.4$ . The results in Table 2 illustrate the long time needed to form deep permafrost by conduction alone.

Table 2. Formation Time of 1632m Permafrost.

Case	G	Time kyear	Comment
no pre-cool	0.0286	4190.6	Uses eq. (10)
Pre-cool	0.0220	488.9	Uses eq. (10)
Pre-cool	0.0286	358.9	Pre-cool solution
Neumann	0.0286	4250	Equivalent $T$ used
Neumann	0.0	64.8	Minimum time <sup>o</sup>

\*Prudhoe Bay soil,  $\Delta T_1 = 29.3^\circ\text{C}$ ,  $X_\infty = 1813\text{m}$ .

Table 3. Extreme Predicted Permafrost Thickness

Time (years)	r	$\sigma$	Depth (meters)
100,000	2.279	0.769	1488.4
532,257	12.513	1.033	2000.0
1,000,000	22.786	1.1011	2132.0
2,000,000	45.572	1.1643	2254.5
infinity	-	-	2600.2

**Example 4.** Consider the conditions for the maximum probable permafrost thickness; the frozen thermal conductivity is large, the geothermal heat flow and latent heat are low, and the surface temperature is minimal. Let  $\epsilon = 0.2$ ,  $T_s = -23.5^\circ\text{C}$ ,  $q_g = 0.042 \text{ w}/\text{m}^2$ , and soil with  $k_g = 5.86$

W/m-K. The results are shown in Table 3. The permafrost reaches a thickness of 2132m after one million years and a value of 2255m after two million years. Balobaev et al. (1978) note that the greatest permafrost thicknesses recorded are on the East Siberian platform with maximum permafrost thicknesses of 1500m. These thicknesses are on the order of the values predicted here and it is not likely permafrost much thicker than this has ever existed, since the required time exceeds the plausible time available. These extreme thicknesses are not in thermal equilibrium with the present surface temperatures and are slowly thawing.

#### CONCLUSIONS

The calculations and examples indicate that the growth of permafrost, with pure conduction heat transfer, is governed by the transient surface temperature, the geothermal heat flow, and the soil thermal properties. Permafrost grows very rapidly for an initial phase and then asymptotically approaches a steady state value after time spans of immense length. Very thick permafrost may have required the total Quaternary Period to form. It is likely that permafrost is not in equilibrium at most sites. The bottom growth and decay of permafrost are so slow that accurate field methods of detecting which is occurring (or if equilibrium exists) are not available. Permafrost less than 600m can grow within 50,000 years, with surface temperatures only slightly lower than present values, but deeper permafrost depths require time scales of several ice ages and quite low temperatures to form. The oldest permafrost in a given volume will be located at an intermediate depth since thaw occurs first at the upper and lower boundaries.

#### APPENDIX 1. SOIL PROPERTIES AND RATIOS

The thermal conductivity of a mixture can be estimated with the geometric mean (Lachenbruch et al., 1982; Gold and Lachenbruch, 1973; Lunardini, 1981). For a general soil this is

$$k = (k_g)^{x_g} (k_w)^{x_w} (k_a)^{x_a} (k_i)^{x_i} \quad (15)$$

where  $k_a$ ,  $k_g$ ,  $k_i$ ,  $k_w$  are the thermal conductivities of air, soil solids, ice, and water;  $x_j$  is the volumetric fraction of component j.

If the soil is always saturated, has a constant void ratio  $\epsilon$ , and all of the water freezes, then  $x_w = \epsilon$  and the conductivity ratio is

$$k_u/k_f = k_{21} = \gamma (1-\epsilon) (k_w/k_i)^\epsilon \quad (16)$$

where  $\gamma = .9825$  is a temperature correction (Lachenbruch et al., 1982). The presence of unfrozen water and the expansion of water upon freezing lead to second order effects. The volumetric specific and latent heats, density, and thermal diffusivity ratios may be calculated following standard techniques (Lunardini, 1981). For soil systems, the property ratios can be described as functions of the soil void ratio  $\epsilon$  (Lunardini and Varotta, 1981). Using the thermal conductivities of Table 4, the property ratios used in the graphs were calculated for  $\epsilon = 0.379$ . The thermal conductivity ratio will be representative of soil that is not too dry; the ratios should be acceptable if  $\epsilon \geq 0.2$ , Kersten (1949).

Table 4. Thermal conductivity of materials.

Substance	k	W/(m <sup>2</sup> ·C)
Water	0.561	
ice	2.281	
air	0.0237	
siliceous soil solids	4.29-5.87	

#### NOMENCLATURE

c	= specific heat
$c_{1,2}$	= $c_1/c_2$
C	= $\rho c$ , volumetric specific heat
G	= geothermal gradient
k	= thermal conductivity
l	= latent heat of solidification
$q_g$	= geothermal energy flow
$S_T$	= $c_1(T_f - T_s)/l$ , Stefan Number
t	= time
T	= temperature
x	= depth coordinate
X	= permafrost thickness
$\alpha$	= thermal diffusivity
$\beta$	= $\delta/X$
$\delta$	= depth of temperature disturbance
$\epsilon$	= soil porosity
$\Delta T$	= $T - T_f$
$\Delta T_1$	= $T_0 - T_f$
$\rho$	= density
$\sigma$	= $G/\Delta T_1$
$\tau$	= $\alpha_1 (G/\Delta T_1)^2 t$
$\phi$	= $(T_0 - T_f)/(T_f - T_s)$

#### REFERENCES

- Allen, D., F. Michel and A. Judge, (1988) "Paleoclimate and Permafrost in the Mackenzie Delta," Proceedings Fifth International Conference on Permafrost, Vol. I, pp. 33-38.
- Balobaev, V.T., V.N. Devyatkin and I.M. Kutasov, (1978) "Contemporary Geothermal Conditions of the Existence and Development of Permafrost," Proceedings of the Second International Conference on Permafrost, USSR Contribution, pp. 8-12, National Academy of Sciences Press, Washington, D.C.
- Barnosky, C.W., P.M. Anderson and P.J. Bartlein, (1987) "The Northwestern U.S. During deglaciation; Vegetational history and Paleoclimatic implications," in Geology of North America, Vol. K-3, edited by W.F. Ruddiman and H.E. Wright, Jr., pp. 289-321, Geological Society of America, Boulder, CO.
- Brown, R.J.E. (1964) "Permafrost investigations on the Mackenzie Highway in Alberta and Mackenzie District," NRC 7885, Ottawa, Canada.
- Brigham, J.K., and G.H. Miller, (1983) "Paleotemperature Estimates of the Alaskan Arctic Coastal Plain During the Last 125,000 years," Proceedings of the Fourth International Conference on Permafrost, pp. 80-85, National Academy Press, Washington, D.C.
- Budd, W.F., and I.N. Smith, (1981) "The Growth and Retreat of Ice Sheets in Response to Orbital Radiation Changes," Proceedings of Sea Level, Ice, and Climatic Change Symposium, I. Allison, ed., IAHS Publication 131, Wallingford, Oxfordshire.
- Budyko, M.I., (1959) "Climate and Life," Academic Press, New York and London.

- Carslaw, H.S., and Jaeger, C.J., (1959) "Conduction of Heat in Solids," 2nd Edition, Oxford at the Clarendon Press.
- COHMAP Members, (1988) "Climatic Changes of the Last 18,000 Years: Observations and Model Simulations," Science, Vol. 241, 1043-1052.
- Dansgaard, W. and H. Oeschger, (1989) "Past Environmental Long-term Records From the Arctic," pp. 288-317, in The Environmental Record in Glaciers and Ice Sheets, H. Oeschger and C.C. Langway, Eds., John Wiley and Sons.
- Eddy, J.A. and R.S. Bradley, (1991) "Changes in Time of the Temperature of the Earth," EarthQuest, Vol. 5(1).
- Folland, C.K., T.R. Karl, and K.YA. Vinnikov, (1990) "Observed Climate Variations and Change," Ch. 7, Climate Change, The IPCC Scientific Assessment, J.T. Houghton, G.J. Jenkins and J.J. Ephraums, Eds., Cambridge Univ. Press, Cambridge.
- Gold, L.W. and A.H. Lachenbruch, (1973) "Thermal Conditions in Permafrost--A Review of North America Literature," Proceedings of the Second International Conference on Permafrost, Yakutsk, July 1973, North American Contribution, pp. 3-25, National Academy of Sciences, National Research Council, Washington, DC.
- Goodman, T.R., (1958) "The Heat-Balance Integral and Its Application to Problems Involving a Change of Phase," ASME Transactions, 80, pp. 335-342.
- Jouzel, J., C. Lorius, J.R. Petit, C. Genthon, N.I. Barkov, V.M. Kotlyakov, and V.N. Petrov, (1987) "Vostok Ice Core: A Continuous Isotope Temperature Record Over the Last Climatic Cycle (160,000 years)," Nature, 329, 403-408.
- Katasnov, E.M., (1988) "Continuous Persistence of the Permafrost Zone During the Quaternary Period," Proceedings Fifth International Conference Permafrost, Vol. I, pp. 801-804.
- Kersten, M.S., (1949) "Thermal Properties of Soils," Univ of Minnesota Experimental Station, Bulletin no. 28.
- Lachenbruch, A.H., and B.V. Marshall, (1986) "Changing Climate: Geothermal Evidence From Permafrost in the Alaskan Arctic," Science, 234, 689-696.
- Lachenbruch, A.H., J.H. Sass, B.V. Marshall, and T.H. Moses, Jr., (1982) "Permafrost, Heat Flow, and the Geothermal Regime at Prudhoe Bay, Alaska," J. Geophys. Res., Vol. 87(B11), 9301-9316.
- Lachenbruch, A.H., T.T. Cladouhos, and R.W. Saltus, (1988) "Permafrost Temperature and the Changing Climate," Proceedings of the Fifth International Conference on Permafrost, Vol. 3, pp. 9-17, Norwegian Institute of Technology, Trondheim, Norway.
- Lunardini, V.J., (1992) "Formation time permafrost," U.S.A. CRREL Internal Report 1120, Hanover, NH.
- Lunardini, V.J., (1991) "Heat Transfer With Freezing and Thawing," Elsevier Science Publishers, Amsterdam, Holland.
- Lunardini, V.J. (1984) "Freezing of a Semi-infinite Medium With Initial Temperature Gradient," J. Energy Resources Technology, Vol. 106, pp. 103-106.
- Lunardini, V.J., (1981) "Heat Transfer in Cold Climates," Van Nostrand Reinhold, New York.
- Lunardini, V.J., (1981a) "Application of the Heat Balance Integral to Conduction Phase Change Problems," U.S.A. CRREL Report 81-25, Hanover, NH.
- Lunardini, V.J., (1982) "Freezing of Soil with Surface Convection," Proceedings Third International Symposium on Ground Freezing, pp. 205-213.
- Lunardini, V.J., and Varotta, R., (1981) "Approximate Solution to Neumann Problem for Soils Systems," ASME Journal of Energy Resources Technology, Vol. 103, No. 1, p. 76-81.
- Matteucci, G., (1989) "Orbital Forcing in a Stochastic Resonance Model of the Late-Pleistocene Climatic Variations," Clim. Dyn., 3, 179-190.
- Maximova, L.N., and V.Y. Romanovsky, (1988) "A Hypothesis for the Holocene Permafrost Evolution," Proceedings of the Fifth International Conference on Permafrost, Vol. 1, pp. 102-106, Norwegian Institute of Technology, Trondheim, Norway.
- Mercer, J.H. (1984) "Simultaneous Climatic Change in Both Hemispheres and Similar Bipolar Interglacial Warming: Evidence and Implications," Climate Processes and Climate Sensitivity, Geophys. Monogr. Ser., Vol. 29, edited by J.E. Hansen and T. Takahashi, pp. 307-314, AGU, Washington, D.C.
- Neumann, F., (c1860) Lectures given in 1860's, cf. Reimann-Weber, "Die partiellen Differentialgleichungen," Physik, Edition 5, Vol. 2, 1912, p. 121.
- Osterkamp, T.E. and J.P. Gosink (1991) "Variations in Permafrost Thickness in Response to Changes in Paleoclimate," Journal of Geophysical Research, Vol. 96, no. B3, pp. 4423-4434.
- Robin, G. de Q., (1983) "The Climate Record in Polar Ice Sheets," Cambridge University Press, New York.
- Romanovsky, N.N., V.N. Zaitsev, S.Yu. Volchenkoc, V.P. Volkova and O.M. Lisitsina, (1988) "New data on Permafrost of Kodar-Chara-Udokan Region," Proceedings Fifth International Conference on Permafrost, Vol. I, pp. 233-236.
- Sun, Jianzhong and Li, Xinguo, (1988) "Division and Temperature Condition of the Last Glaciation in Northern China," Proceedings Fifth International Conference on Permafrost, Vol. I, pp. 107-112.
- Yuen, W.W., (1980) "Application of the Heat Balance Integral to Melting Problems with Initial Subcooling," International Journal of Heat Mass Transfer, Vol. 23, pp. 1157-1160.

ORIGIN AND TREATMENT OF THE ICINGS IN GULIAN REGION,  
NORTHERN DA HINGGAN LING, NORTHEAST CHINA

Luo Minru, Zhou Xinqing and Na Yunlong

Da Hinggan Ling Institute of Prospecting and Design,  
Ministry of Forestry, China

The residential area of the Gulian Coal Mine is located in a talik in the predominantly continuous permafrost zone of the northern Da Hinggan Ling. The severe cold climate and the plentiful ground water lead to the development of seasonal spring icings. Practice verified the availability of the "frozen ditch" in the treatment of icings.

INTRODUCTION

Buildings would be harmed by icings in the cold regions. In order to find the effective measures for the treatment of icings, an understanding of the origin of icings is necessary. During the construction of the foundation of a residential building, water gushed out and icings were formed in October, 1990. This not only affected the rate of construction but also endangered the foundation. A frozen ditch was dug after a lot of investigation and studies on the genesis of the icings. The water flow was stopped from November, 1991 to May, 1992. So the icing problem has been solved successfully. This indicated that the frozen ditch was effective in controlling the water-gush in the foundation pit and in treating the icings.

A SURVEY OF THE WORKING AREA

Geography and Geology

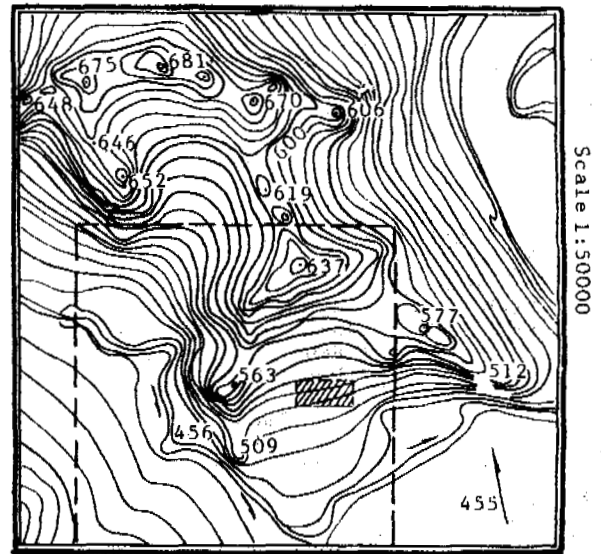
The residential area of Gulian Coal Mine is located in the north part of the Mt. Da Hinggan Ling, at 52°57'-52°59'N, 122°20'-122°23'E and 440-600 m a.s.l., on a denudated-deposited south-facing gentle slope, the Gulian River and Dalin River run through this area and flow into the Amur River — a tributary of the Heilongjiang River (Fig.1).

The working area is in a continental frigid-temperate zone. According to the observations during 1976-1991 in the Mohe Meteorological Station, 10 km from the Gulian Coal Mine, it is known that:

\*the mean annual air temperature is as low as -4.5°C, the minimum -52.3°C, and the maximum -36.8°C;

\*the frost-free period is less than one hundred days, the freezing period lasts about 8 months of the year;

\*the mean annual ground temperature is -4.2°C, the precipitation is concentrated in the period




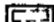
-  1 Residential building area
-  2 Hydrogeological survey area

Figure 1. Topographic map of the investigated area

from July to September and averages 400-500 mm per year.

Such a climate is favourable to the ground freezing and the permafrost development.

The working area is located in the Erguna Fold Belt, a part of the Varisian Fold System. The Late Varisian Granite is widely-distributed in the southern and western parts of this area, forming the base of the Quaternary system and the Cretaceous system. The Lower Cretaceous

tuffaceous breccias and tuffs are in conformity with the granite conglomerate; the Quaternary system, composed of the humus soils, silty clay, sandy soils, pebble and elastics, is widely developed in flood land and gentle slopes.

### Features of Frozen Ground

Generally, this region belongs to the predominantly continuous permafrost zone in the northern Da Hinggan Ling. The development and distribution varies with terrain. The perennially frozen ground as thick as 50-70 m or more and rich in ground ice, is well-developed in the swampy lowland at the bottom of valleys or basins, while the upper-middle part of slopes and the structural denudation ranges are generally occupied by taliks with a few isolated permafrost masses, small and thin (Guo et al, 1989). The residential area of the Gulian Coal Mine is located in a talik on south-facing gentle slope, only a 40 m thick permafrost was observed in the Borehole SZ-4 at its southeast.

The seasonal freezing depth also varies with terrain. For example, it is 2.55 m in Borehole SZ-5 at 497.66 m a.s.l. and 3.20 m in Borehole SZ-6 at 480.54 m a.s.l.

The distribution of frozen ground is shown in Fig.2.

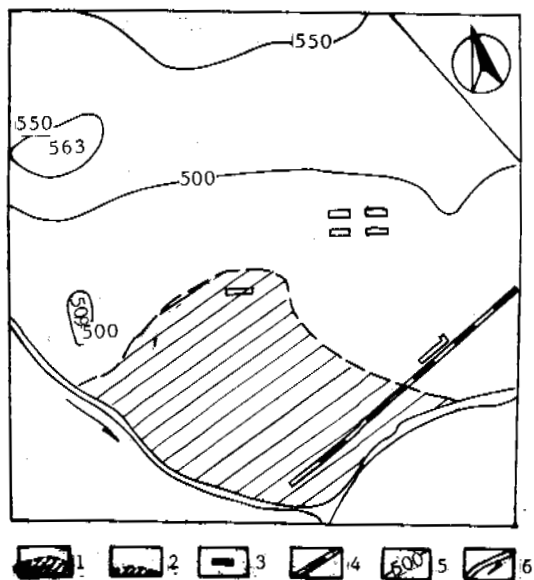


Figure 2. Sketch map showing distribution of permafrost

1. permafrost region
2. permafrost melt region
3. buildings
4. railroad
5. contour
6. river

### Hydrogeological Condition

#### Types and features of ground water

In the permafrost area, the ground water can be divided into the suprapermafrost water and the subpermafrost water; within the talik, there develops the talik water. According to the composition and characteristics of aquifers, the ground water can be divided into the pore-phreatic water in Quaternary sediments in river valley, the pore-crevice phreatic water in the incomplete talik, the structural-crevice water in granite and the pore-crevice water in the tuffaceous breccias.

As the cryogenic impermeable layer, the permafrost can be the obstruction to the water movement leading to concentration of the ground water on the northern part of the working area, seeping out as spring like Springs 1 and 2, forming the spring icings in winter (Fig.3).

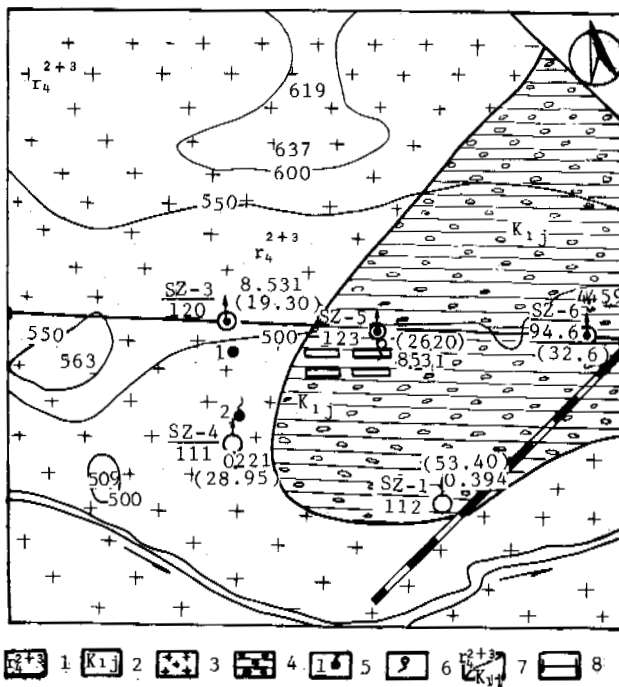


Figure 3. Hydrogeological sketch map

1. granite;
2. Jiu Feng mountain series of cretaceous system;
3. granite;
4. conglomerate;
5. perennial spring;
6. seasonal spring;
7. geological boundary line;
8. profile line.

The aquifer of suprapermafrost water in river valley is generally 1.0-1.5 m in thickness and is frozen partially or completely in winter, showing an obvious seasonal variation, thus, it can only be used as a small scale seasonal water resource.

In the incomplete talik along the railroad, the pore-crevice phreatic water is in a position between the seasonally frozen layer and the perennially frozen ground. It doesn't outcrop on to the ground surface; in winter, it seeps out from the steep side of the subgrade, forming a series of beaded icings. Such kind of ground water, although of little interest in utilization, is an important supply of the deeper aquifer.

Dependent upon the position nature and crevice development of the aquifer and the distribution of permafrost, the water-abundance of the granitic structural crevice artesian aquifer varies considerably. For example, as observed in Borehole SZ-3, 120 m in depth, through the well-creviced granite with a tattered belt 88.5 m in thickness it wells as plentiful as 737.04 m<sup>3</sup>/day when the water table drops for 17.5 m. At the Gulian River, as observed by Borehole SZ-1 down to a depth of 112 m through the granite poor-cracked,

it wells 34.54 m<sup>3</sup>/day when the water table drops for 53.4 m. The abundance of the pore- crevice artesian water in the tuffaceous breccias aquifer is also dependent upon the above factors. For example, it wells in high quantity in Boreholes SZ-5 and SZ-6. Such kind of ground water also distributes in the gentle slope. Based on pumping test unique-borehole in wet season and the pumping test in boreholes in dry season it is known that the amount of the talik artesian water season is 1800-2300 m<sup>3</sup>/day in the wet season.

#### Supply, runoff and drainage of ground water

The precipitation infiltrates into the taliks, forming the pore- crevice phreatic water; then, the phreatic water moves down through the weathering, sedimentary and structural cracks of bedrocks forming the talik artesian water or the subpermafrost artesian water — that is the major way of supply and runoff of the ground water (Yang et al, 1985).

The ground water is drained through two ways: first, drainage through the Dalin River and the Gulian River; second, drainage as springs, forming icings in winter.

In sum, the basic condition for the supply, runoff and drainage is that the pores and cracks are well-developed in the bedrock; and the existence of permafrost as the cryogenic impermeable body is one of the important factors that determine the distribution, supply, runoff and drainage of ground water.

#### ORIGIN OF SPRINGS

The seasonal springs come from the well-permeable aquifer of the weathered granitic conglomerates. Their formation begins in middle November and stops in March next year. During the warm season, the aquifer is very well in containing water while in winter, with the gradually thickening of the seasonal frozen ground, the aquifer reduces in its volume, the ground water is pushed up onto the ground surface under the cryostatic pressure, and frozen under a cold climate forming icings.

The artesian water is usually fed by the pore- crevice phreatic water in taliks, and, under a certain condition the phreatic water can be fed by the artesian water. The Spring 1, 300 m to the west of the building flows 16 m<sup>3</sup>/day all the year round. Such a spring is located in granite area, and can also feed the pore- crevice phreatic water through the fault and the weathered zone of the granite. The amount of the ground water is one of the causes of the seasonal spring-icings.

The occurrence of spring-icings has a close relation to the climate, especially to the precipitation. According to the observation in the Mohe Meteorological Station, the precipitation was 537.9 mm in 1989 and 503.0 mm in 1990, while the mean annual value — only 445.7 mm. During these humid years, for example, since November 1990, all the icings in this area are larger than usual. It follows that the precipitation is the direct supply of the pore- crevice phreatic water in taliks.

#### TREATMENT MEASURES OF ICINGS

Because the spring is fed by the pore- crevice phreatic water in a thin aquifer underlain by impermeable layer, the crosswise slope is gentle, the method of digging a frozen ditch

could be available to prevent the building from the endangering of icings. The frozen ditch was arranged 25 m to the north of the buildings and was 2.0 m in depth, 4.0 m in width, 100 m in length. In this sector, the seasonal frost depth is 2.55 m, so the ditch was cut into the most part of the seasonal frost belt. It was observed that at the depth of 1.5 m there was a well-permeable gravel belt, 0.4 m in width and 0.5 m in height, being a good channel for ground water movement, while beneath a depth of 2-3 m, a poor-permeable granitic conglomerate was found. Thus, the frozen ditch was dug into the aquifer, forming a wall cutting off the ground water.

According to the observation in November and December 1991, some small seasonal spring-icings occurred nearby after the digging of the ditch (Fig.4). This might result from the transfer of the water channel.

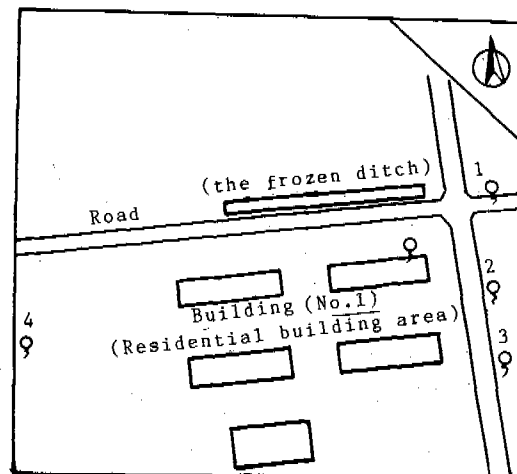


Figure 4. Distribution of the frozen ditch

#### CONCLUSIONS

1. In order to treat the icings, an understanding in hydrogeological condition and in the origin of icings is necessary for the selection of the suitable measures.
2. The frozen ditch method is available to treat the icings fed by the pore- crevice phreatic water coming from the incomplete talik.

#### REFERENCES

- Guo Dongxin, Huang Yizhi, Wang Jiacheng, et al, (1989) Engineering geological conditions of permafrost at the Gulian Coal Mine Area in the Da Hinggan Ling region. Proceedings of the 3rd Chinese National Conference on Permafrost. Science Press. pp.2-15 (in Chinese).
- Yang Rentian and Lin Fengtong, (1986) Hydrogeology and engineering geology of permafrost area. Publishing House of the Dong Bei Forestry University. 398p. (in Chinese).

## EFFECTS OF SNOW COVER ON THERMAL REGIME OF FROZEN SOILS

Ma Hong, Liu Zongchao and Liu Yifeng  
Xinjiang Institute of Geography, Chinese Academy of Sciences, Urumqi 830011, China  
Yang Zhian  
Department of Physics, Xinjiang University, Urumqi 830052, China

This study demonstrates the snow cover has a significant effect on thermal state of underlying frozen soils. The existence of snow will not only insulate the heat loss from ground, thus raising the ground temperature, but also delay the effects of external conditions on thermal state of frozen soil due to its low conductivity and large capacity of heat. The variation of frozen soil depth is closely related to varying air temperature and solar radiation. Therefore, geographical location probably plays a more dominant role in affecting the process of energy exchange between ground and atmosphere, and hence the thermal regime of underlying frozen soil.

### INTRODUCTION

The seasonal frozen soil is widely distributed in the Chinese portion of the Tien Shan mountains, which is almost totally covered by seasonal snow throughout the winters. And snow will alter the boundary conditions and, therefore, change the thermal regime of underlying frozen ground significantly. It is essential to get sufficient data in order to enable an understanding and, further, to permit reliable quantitative analysis of the effects of snow cover on the thermal state of frozen soils. For this purpose, this paper presents some results from field measurements and describes the seasonal variation of frozen soil depth under different external conditions. The results are derived from detail measurements at two experimental sites and from years of field observations. In addition, the effects of air temperature and solar radiation on thermal state of snow and the underlying frozen soil are also discussed, from a theoretical perspective.

### STUDY AREA AND DATA COLLECTION

The study area was located in the mid-mountain zone of the western Tien Shan mountains, near the Tien Shan Snow and Avalanche Research (TSAR) Station (43°16'N, 84°24'E; 1776 m a.s.l.) of the Xinjiang Institute of Geography, Chinese Academy of Sciences. This area, referred to locally as the "wet island in arid lands", has a temperate and humid climate. Mean annual air temperature recorded at the TSAR Station is 1.3 °C (1973-1986), and average annual maximum and minimum temperatures are 12.6 and -14.4 °C in July and January, respectively. Mean annual precipitation is 827.3 mm with a maximum of 1139.7 mm. This area has a mean winter snow depth of 0.86 m with a maximum of 1.52 m. It is estimated that snowfall accounts for about 30% of annual precipitation. Winter lasts for about 4 to 5

months and the snow cover is extremely uneven. The dominant surface materials are drab forest soil and meadow soil covered by dense vegetation. Frost soil occurs at a depth ranging from 0.2 to 1.5 m, depending on slope orientation, slope materials, and surface cover.

Field experiment was carried out in the winter of 1986-87. The measurements of temperature profiles were made using the HP-3497A Digital Data Collection System at two experimental sites. One (site A) was located on a south-facing, gentle slope of about 7°, the other (site B, 50 m apart from site A) was on the flat terrace shaded entirely by mountains. At each site, snow temperatures and temperatures of underlying frozen soil were measured using thermistors at 10 cm intervals. An extra array of thermistors was used near site A to measure only the temperature profiles of frozen ground, with the overlying snow removed soon after each snowfall event. This configuration allows a comparison between thermal regimes of frozen ground under different external conditions.

### RESULTS AND DISCUSSION

The winter of 1986/87 was slightly colder than normal. The lowest air temperature and the maximum snow depth occurred, as usual, in mid-January and early March, respectively. Freezing temperatures began in mid-October and were maintained up to late March. Snowfall began in mid-October and reached its maximum depth of 79 cm in early March, but the frequent melting events delayed the formation of frozen soil for about 20 days. Snowmelt started in late March and was completed in 3 weeks. Surface melting of frozen soils in bare ground advanced by about 15 days than in snow covered site. Forests and shaded slopes retained a snow cover for longer duration. Thus, the surface melting of snow and frozen soil delayed for about a month or even longer, depending on the surface cover and local



topography.

Fig.1 shows the air temperatures, snow depth,

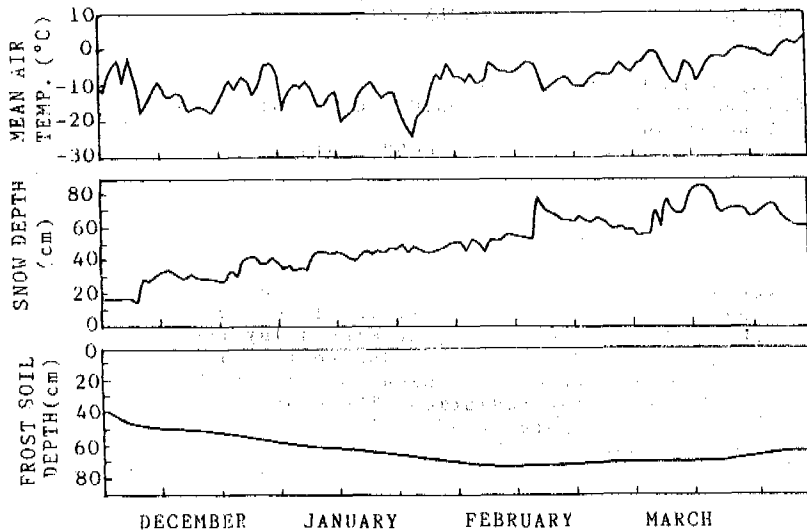


Fig.1 Variation of air temperature, snow depth, and the depth of frozen soil measured at site B during the winter of 1986/87

and the depth of frozen soil from December 1986 to April 1987 measured at site A. From this figure, snow depth increased gradually as the season progressed, and decreased rapidly in late March due to rapid snowmelt. Depth of frozen soil increased as air temperature decreased during the early stage of snow accumulation period, and decreased as increasing air temperature during the late part of winter. The variation of frozen soil depth was closely correlated to that of air temperature if a lag time of about 20 days is taken into consideration. This indicates a close relationship between air temperature and the depth of frozen soils.

Fig.2 shows a comparison between the depths of frozen soil of a snow covered plot (Fig.2a) and a snow-free plot (Fig.2b) measured at site A. These two plots were 5 meters apart and, hence, are considered to be under the same external atmospheric conditions. At snow covered plot, the depth of frozen soil were much thinner than that at snow-free plot, and varied less sensitively than that at snow-free plot in response to varying air temperature. Although snow will reflect a large part of incoming solar radiation and reduce the energy input to snow, the low conductivity and large heat capacity of snow will insulate the energy loss from snow and underlying frozen soil, and, hence, delaying the effects of external atmospheric conditions on thermal state of frozen soil sizeably.

As a poor heat conductor with high albedo for incoming solar radiation, low conductivity, and large heat capacity, the existence of a snow cover will alter the external conditions of frozen soil greatly, thus modifying the energy exchanges at the snow-soil interface. It is therefore important to understanding firstly the

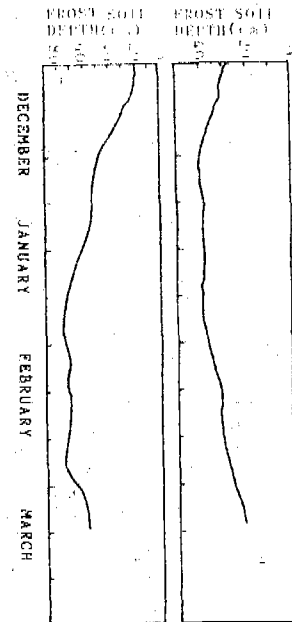


Fig.2 Comparison of frozen soil depths between a snow covered plot (a) and a snow-free plot (b) measured at site A during the winter of 1986/87

thermal regime of snow cover in response to external atmospheric conditions, i.e. to varying surface temperature and periodic solar radiation. Ma Hong and others (1991) developed a model with which the temperature profiles of a snow cover at site A were simulated for 16 February, 1987. Results shown in Fig.3 demonstrate that significant diurnal variation in snow temperature only occur in the top layers of a snow cover, at a depth of about 20 cm below the surface, while temperature in the basal layers is comparatively stable in spite of the large temperature fluctuation and strong solar radiation.

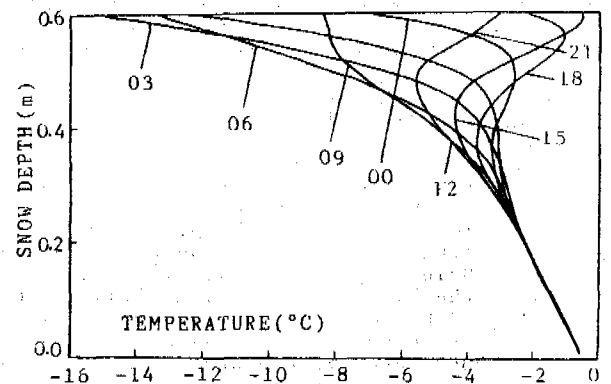


Fig.3 Temperature profiles calculated for site A, 16 February 1987. Time is given in hours of local solar time

indicating the process of energy exchange mainly occur in the top layers of a snow cover, have a minor effect on external factors of thermal regime of deep layers of snow and the underlying frozen soil if the thickness of overlying snow exceeds 30 cm. The energy loss from snow surface at night may be balanced to some extent by rising air temperature and solar input during the day, but the net loss or gain of energy in top layers of a snow cover may affect the thermal regime of deep layers of snow and frozen soil through heat conduction, because this process is rather slow due to low conductivity of snow and frozen soil, and so the existence of snow will delay the effects of external atmospheric conditions and retard the heat loss from basal layers of a snow cover and from the underlying frozen ground.

The effect of solar radiation on thermal regime of snow has been discussed in detail by Colbeck (1989). He reached the conclusion that the amount of solar radiation absorbed beneath the surface of a snow cover can introduce more energy into the snow than can be readily conducted away. Therefore, the sub-surface temperature increases over what it would be in the absence of solar input. To show this experimentally, the snow temperature-profiles (Fig.4) measured at site B for 16 February, 1987 are used here to make a comparison with Fig.3. Despite the results shown in Fig.3 from the

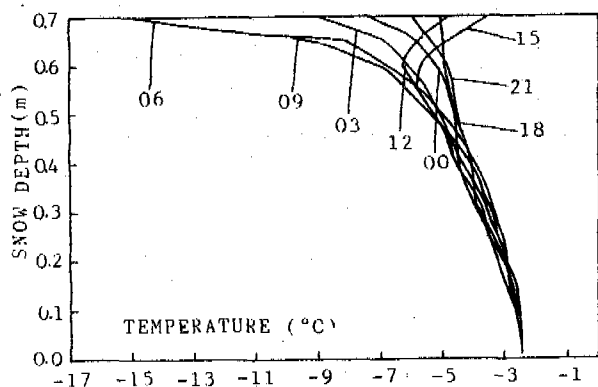


Fig.4 Temperature profiles measured at site B, 16 February 1987. Time is given in hours of local solar time

theoretical calculations, they are still comparable because these results have been tested against the observed data from site A, and showed a good agreement between them. Clearly, the solar radiation shifts the temperature near the surface from lower values shown in Fig.4 to higher values shown in Fig.3 during day time. It seems that there is no effect of solar input on snow temperature in the basal layers because there is no noticeable variation in temperature between the day and night. However, while radiation increases the average temperature and temperature gradient just below the surface in snow, it decreases the average temperature gradient in an intermediate layer below that (Colbeck, 1989). The effect of this is to decrease the heat loss from the basal layers, and hence, to increase the temperature in the basal layers of a snow cover and underlying frozen soil. From Fig.3 and 4, for example, the temperatures at the snow-

soil interface of site A and site B were, respectively,  $-0.5^{\circ}\text{C}$  and  $-2.7^{\circ}\text{C}$ , and the measured depths of frozen soil underlying the two snow covers were, respectively, 25 cm and 75 cm. These differences are considered only due to the effects of solar radiation because the two sites were under the same external conditions except for the solar radiation received. From this it can be seen that the solar radiation affects snow temperature, not only in the upper layers of a snow cover, but also in deeper layers. This is not because the solar radiation penetrates directly to the deeper layers and heats the snow by absorption (because penetrating solar radiation reaches a limited depth of about 30 cm below the snow surface), but because the solar radiation warms the snow temperature near the surface and decreases the average temperature-gradient below that. This decreased temperature-gradient allows more heat energy to be accumulated and less to be lost, and, therefore, increases the temperature in deeper layers of the snow cover, or even in the underlying frozen ground.

#### REFERENCES

- Ma Hong, Liu Zongchao, and Yang Zhian (1991) Temperature regime studies and mathematical calculations for dry snow cover in the western Tien Shan mountains, China. *Annals of Glaciology*, Vol.16.
- Colbeck, S.C. (1989) Snow-crystal growth with varying surface temperature and radiation penetration. *Journal of Glaciology*, 35(119), 23-29.

## STRENGTH AND YIELD CRITERIA OF FROZEN SOIL

Ma Wei, Wu Ziwang and Zhang Changqing

State Key Laboratory of Frozen Soil Engineering, Lanzhou Institute of  
Glaciology and Geocryology, Chinese Academy of Science, China

Limitation has been showed for linear yield criteria of frozen soil which we often continue to use, such as, Mohr-Coulomb, Von Mises-Botkin or Drucker-Prager Criteria. Under combined stress state, as confining pressure is increased the strength increases to maximum value and then decreases with a continued increase in confining pressure. The failure surface in the principal stress space forms a parabolic, the shape of which depends upon the cohesion and the friction angle and their change with temperature. Based on test data, this paper has given a parabolic yield criteria and relevant parameters. At low stress levels, the criteria can transform into linear criteria.

### INTRODUCTION

As a porous materials, frozen soil, which are composed of heterogeneous matters and is highly sensitive to phase change, is very complicated. So far, the more and more scholars have been drawn to work for studying strength problem of frozen soil. It is believed generally that, under the same conditions, the bigger confining pressure applied on frozen soil, the bigger its strength. This conclusion has laid a foundation for many of strength criteria, for instance Mohr-Coulomb Criteria (Terzaghi and peck, 1968), Drucker-Prager (1952) and Von Mises-Botkin Criteria etc. (Vyalov et al., 1962, 1981). Meanwhile some of non-linear criterias also are put forward one after another by Ladanyi (1972), Gorodetskii (1975), Vyalov (1985), Lade et al., (1980), Vyalov and Slepak (1988) et al.

With further thorough studying, a lot of scholars (Chamberlain et al., 1972; Parameswarn and Jones, 1981; Baker et al., 1982; Jones, 1982) found that as confining pressure was increased, the strength increased to maximum value and then decreased with a continued increase in confining pressure. This conclusion also is verified by our tests. It is necessary for us to put forward new strength criteria which is suited to new problem. When Nadai (1950) studied solid material, Reinicke and Reaston (Hausler, 1983) studied sea ice, they found that parabolic functions are applicable as strength criteria of materials. As theory, Fish (1991) has developed such functions into frozen soil. From our experimental results, it is seen that the failure surface of frozen soil forms a paraboloid in the principal stress space (Fig.1, Fig.2 and Fig.3). Based on test data, this paper gives a parabolic yield criteria and relevant parameter.

### RESULTS OF TEST

Keeping loading rate and water contents, we carried out axial compression tests to frozen Lanzhou sandy soil, frozen Huaibei clay soil (in the depth of 177.5 m) and frozen Huaibei sandy soil (in the depth of 143 m). From tests, we found that the shear strength of frozen reaches a maximum value at a certain level of confining pressure, further increase of the pressure leads to a decrease of strength. Its position of maximum value is different with change of temperature and soil property (Fig.1). Fig.2, Fig.3 and Fig.4 show their Mohr's envelopes.

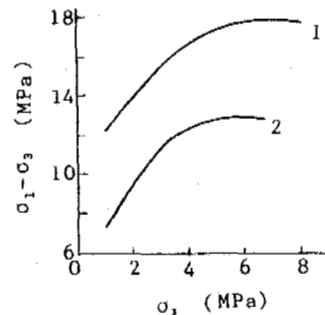


Figure 1. The relation of the shear strength and confining pressure at  $-5^{\circ}\text{C}$  (Loading rate is  $10\text{T}/\text{min}$ )  
1 - Lanzhou sandy soil;  
2 - Huaibei sandy soil.

It is seen that the shear strength  $\tau$  approximately is linear with the mean normal stress  $\sigma$  at low stress level, once confining pressure further increases, this curves show parabolic pattern.

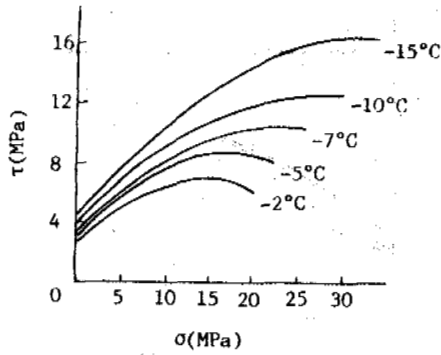


Figure 2. The Mohr's envelopes of Lanzhou sandy soil under different negative temperature

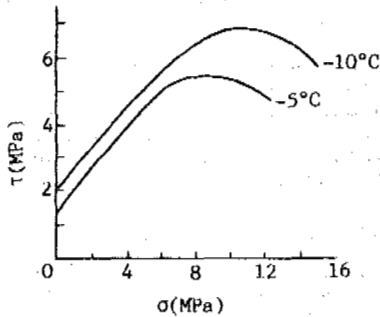


Figure 3. The Mohr's envelopes of Huaibei sandy soil under different negative temperature

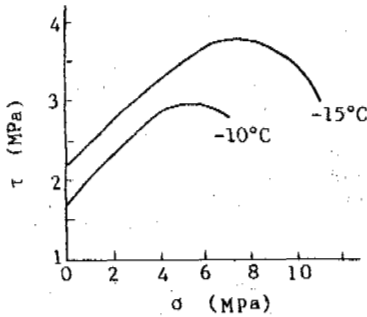


Figure 4. The Mohr's envelopes of Huaibei clay soil under different negative temperature

#### YIELD CRITERIA

For establishing connections between laboratory conditions and multiaxial stress at fields, we should use the invariant function of stress

$$f(I_1, I_2, I_3) = 0 \quad (1)$$

to express yield condition of materials. Where  $I_1$ ,  $I_2$  and  $I_3$  are the first, the second and the third invariant of the stress tensor respectively. When material is considered to be homogeneous and isotropic, we can use eq.(2) to show yield condition of materials:

$$f(J_1, J_2) = 0 \quad (2)$$

Where  $J$  and  $J$  are the first and second invariant of the stress deviator. On octahedral plane, the locus can be expressed in the form

$$f(p, q) = 0 \quad (3)$$

Where

$$p = \frac{1}{3} J_1 = \sigma_1 + \sigma_2 + \sigma_3;$$

$$q = \sqrt{3} J_2 = \frac{1}{\sqrt{2}} [(\sigma_1 - \sigma_2)^2 + (\sigma_1 - \sigma_3)^2 + (\sigma_3 - \sigma_1)^2]^{1/2};$$

Under stress state of axial symmetry,

$$q = \sigma_1 - \sigma_3, \quad p = \frac{1}{3} (\sigma_1 + 2\sigma_3)$$

In the principal stress space, eq.(1) and eq.(3) describe a failure surface, the shape of which is defined by a type of the yield function

$$q = f_1(p) \quad (4)$$

Based on tests, the parabolic function can be selected as a yield criterion for frozen soil (Fish, 1991), (Fig.5)

$$q = c + bp - \frac{b}{2p_m} p^2 \quad (5)$$

Where,  $c$  - resistance associated with soil cohesion on the octahedral plane;

$b = \text{tg}\phi$ ,  $\phi$  is angle of internal friction on the octahedral plane when  $p=0$ ;

$p_m$  - the value of the mean normal stress which the shear strength of frozen soil reaches a maximum value  $q_m$

$$q_m = c + \frac{b}{2} p_m \quad (6)$$

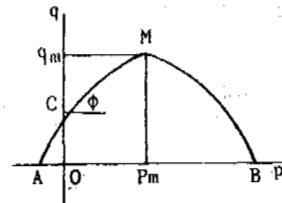


Figure 5. Yield criteria of frozen soil

From eq.(5), it is seen that eq.(5) may transform into the Drucker-Prager yield criterion,  $q=c+bp$ , when  $p_m \rightarrow \infty$ ; For frictionless materials ( $b=0$ ),  $q=c$ , eq.(5) reduces into Von Mises yield criterion.

Thus, the strength of frozen soil under triaxial stress state is described by a yield criterion [eq.(5)], these parameters of which  $c$ ,  $\phi$  and  $p_m$ , can be obtained through test data.

#### DETERMINATION OF PARAMETERS

For frozen Lanzhou sandy soil, the changing relation of  $c$ ,  $\theta$  and  $p_m$  with temperature are as follows (Fig.6, 7 and 8)

$$c = -0.417\theta + 2.255 \quad (7)$$

$$\theta = -0.697\theta + 27.27 \quad (8)$$

$$p_m = (-65.79\theta + 45.61)^{1/2} \quad (9)$$

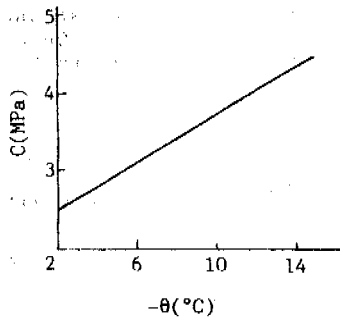


Figure 6. The relation of cohesive resistance and temperature

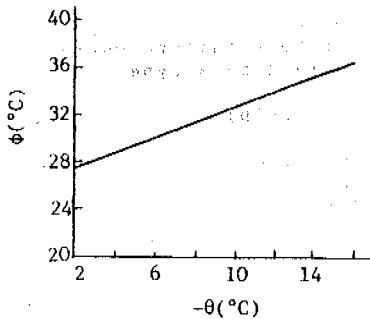


Figure 7. The relation of angle of internal friction and temperature

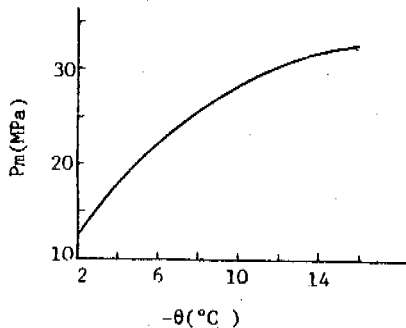


Figure 8. The relation of  $p_m$  and temperature

So eq.(5), (7), (8) and (9) give yield criterion of frozen Lanzhou sandy soil. Through simulated calculation, we found that calculated values are less than test values (shown in dotted line of Fig.9), and the lower temperature, the more calculated values approach test values. This is caused by hypotheses of homogeneity and isotrope. The lower temperature, the more frozen soils approach isotropic materials.

When stress is lower, let  $p_m \rightarrow \infty$  in eq.(5), we can obtain

$$q = c + bp \quad (10)$$

Eq.(10) can be considered as yield criterion of frozen soil under low stress levels. In this moment, the calculated values more approach test values.

#### CONCLUSION

1. Through comparison of calculated values

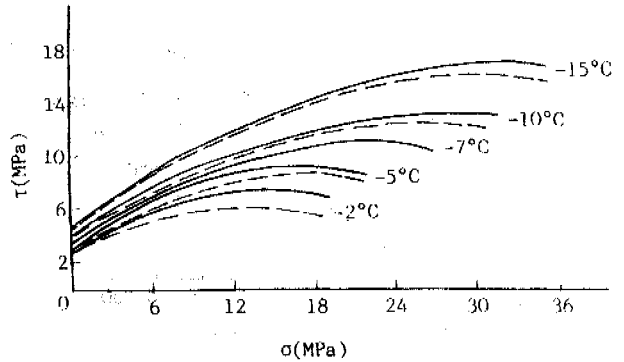


Figure 9. Under different negative temperature, the comparison of calculated values and test values

and test values, this parabolic yield criterion is feasible. When temperature is lower, the criterion more approach practical condition.

2. When stress is lower, we may use Drucker-Prager yield criterion to describe strength change of frozen soil.

#### REFERENCES

- Baker, T.H.W., Jones, S.J. and Parameswaran, V.R. (1982) Confined and unconfined compression tests of frozen sand. Proc. 4th Canada Permafrost Conf., National Research Council of Canada, pp.387-392.
- Chamberlain, E., Groves, C. and Perham, R. (1972) The mechanical behavior of frozen earth materials under high pressure triaxial test conditions. J. of Geotechnique, Vol.22, No.3, pp.469-483.
- Drucker, D.C. and Prager, W. (1952) Soil mechanics and plastic analysis of limit design, Quart. of Appl. Math., Vol.10, pp.157-165.
- Fish, A.M. (1991) Strength of frozen soil under a combined stress state. Proc. 6th Int. Symp. on Ground Freezing, Vol.1, pp.135-145.
- Gorodetskii, S.E. (1975) Creep and strength of frozen soils under combined stress. J. of Soil Mechanics and Foundation Engineering, Vol.12, No.3, pp.205-209.
- Hausner, F.U. (1983) Comparison between different yield function for ice. Int. Glaciological Society, Annals of Glaciology, Vol.4, pp.105-109.
- Jones, S.J. (1982) The confined compressive strength of polycrystalline ice. J. of Glaciology, Vol.28, No.98, pp.171-177.
- Lade, P.V., Jessberger, H.L. and Diekmann, N. (1980) Stress-strain and volumetric behavior of frozen soil. Proc. 2nd Int. Symp. on Ground Freezing, pp.48-64.
- Nadai, A. (1950) The theory of flow and fracture of solids. McGraw-Hill Book Co., New York, Vol.1, pp.572.
- Parameswaran, V.R., and Jones, S.J. (1981) Triaxial testing of frozen sand. J. of Glaciology, Vol.27, No.95, pp.147-155.
- Terzaghi, K. and Peck, R.B. (1968) Soil mechanics in engineering practice. John Wiley and Sons. New York.
- Vyalov, S.S., Zaretskii, Yu. K. and Gorodetskii S.E. (1981) Strength and creep analyses in ground freezing problem. Strogizdat, Leningard, pp.200.

Vyalov, S.S. (1986) Rheological fundamentals of soil mechanics. Elsevier Publ. House Netherlands.

Vyalov, S.S. and Slepak, M.E. (1988) Rheological regularities in frozen soil mechanics and their application in engineering calculations, Int. Conf. on Rheology and Soil Mechanics, Coventry, U.K., Elsevier Applied Science, New York, pp.219-226.

## GEOLOGICAL - ENGINEERING CONDITIONS OF YAMAL PENINSULA ALONG DESIGNING RAILROAD

Anatoly P. Manzelev<sup>1</sup> and Felix E. Are<sup>2</sup>

<sup>1</sup>State Survey and Desing Institute LENGIPROTRANS Moskovsky av.,143, Saint-Petersburg 196105, Russia.

<sup>2</sup>Petersburg Institute of Railway Engineers, Moskovsky av.,9,Saint-Petersburg 190031,Russia.

The geological and engineering conditions of the southern half of the Yamal peninsula were explored for the purpose of road building. The results of this investigation brought to light a number of geological-engineering peculiarities of the region that will hamper the road construction considerably. The report comprises the most important special features of this kind that characterize the composition and the structure of the upper section of the geological column, salinity of the grounds, cryopaigs, the temperature of the grounds, the carrying capabilities of argillaceous grounds, spreading and amounts of the wedge and the sheet ground ice as well as the cryogenic slumping of slopes.

### INTRODUCTION

An extensive volume of geological-engineering survey works for the purpose of building railways in the southern half of the Yamal peninsula up to latitude 70.5° North (Mordyyakha river) was brought about in 1985-1991. In particular, 20 thousand boreholes with the total length of 130 km were bored of which 3000 ones were from 20 m to 40 m deep. Figure 1 shows the layout of location of the routes that were explored.



Figure 1. Layout of railway routes on Yamal Peninsula: 1 - actual railroad; 2 - railroad under construction; 3 - routes versions explored.

The Yamal peninsula is the extreme north-west part of the West Siberian lowland. From the point of view of geomorphology, this is an aggradation plain with a step-like topography which had been formed in the course of the retreat of the sea that was in progressing state since the Middle Pleistocene. The water shed areas of the Yamal peninsula are occupied with the Salekhard Plain with the absolute marks from 65 m to 95 m and with the Kazantsevskaya Plain whose height reaches 45 to 65 m. These plains are fringed with the third marine terrace (22 to 35 m) and with the second (14 to 20 m) and the first (7 to 12 m) terraces preserved partially. Along the whole coast, laida up to 5 m high is spread. As a whole, the peninsula structure consists of a thick layer of the Quaternary sea deposits. The thickness of the permafrost in the middle areas of the peninsula reaches, according to the data of V.V.Baulin, 500 m, and it decreases in the direction of the coast. The thickness of the frozen grounds is limited by their salinization, and due to that it does not exceed 10 m in several areas. The border-line of spread of the frozen grounds coincides, approximately, with the outer border-line of adfreezing of the sea ice and the bottom.

### COMPOSITION OF GROUNDS

The explored top section of the geological column consists of all the geomorphologic levels of dusty sands and of more small-dispersed grounds up to the heavy sandy clays inclusive. Therefore the composition of the grounds is rather monotonous as a whole. But as to the limits mentioned above, the structure of the grounds is characterized by a startling lithologic variety both in the column and along the strike. The upper layers of the grounds are sandy and clay-sandy mainly, while argillaceous grounds begin prevailing as the depth increases. There are more argillaceous grounds on the Salekhard and the Kazantsevskaya Plains, and they are

encountered more frequently close to the surface than on the lower marine terraces. One may see the logic increase of the dispersivity of grounds in the direction from south to north.

Neither ground of the Yamal peninsula may be used for building the earth roadbed without a number of requirements to their humidity and to the technological preparation and erection of the embankment of the railroad-bed are met.

#### SALINITY OF GROUNDS

All the grounds, with the exception of the top layer washed out with surface water and the recent waterborn continental sediments, are characterized with salinity. Salinity of the sands lies within the limits from 0.05 to 0.1 or 0.2% but sometimes it is as high as from 0.3 to 0.6%. Salinity of the sandy clays is from 0.1 to 0.8 or 1.0%, or up to 1.5% in some cases. Salinity of the sands is the same on all the geomorphological levels, with the exception of the laida. The degree of salinity along the strike and to the vertical extent is distributed rather irregularly. Salinity of all the grounds increases as the depth increases. This relationship in the sands can be observed in the form of a feebly seen tendency, and as the dispersivity of the grounds increases this tendency becomes apparent more distinctly while it is visible rather clearly in the heavy sandy clays. The maximum vertical gradients of salinity can be observed in the heavy sandy clays, for example, 0.11% / m. The above difference in the regularity of variation of salinity of sands and sandy clays as the depth increases becomes apparent by the fact that the degree of salinity is less in the sand interbeds in sandy clays considerable as compared to the enclosing grounds. So far as the regions and the territories are concerned, salinity of the grounds increases from south to north and from east to west. In the eastern areas of the peninsula the salinity of all the lithological varieties of grounds is much less as compared to the western territories.

Due to the salinity, almost all the frozen grounds occurring below the layer with annual variation of temperature are in the plastic frozen state even at the lowest temperatures, which reduces their carrying capability sharply. So salinity increase with the depth leads to the decrease of the carrying capability of the grounds with the depth.

The grounds that from the flood-plains of the rivers flowing into the Kara Sea on the western coast of the Yamal are also salinized. For example, in the valley of the biggest river of the Yamal peninsula, the Yuribay, all the grounds making up the flood-plain are salinized at the distance up to 65 km from the mouth in a straightline, with the exception of the upper section of the sand layer in the river bed and the taliks under the large lakes that do not freeze through down to the bottom. Some geomorphological, geological and hydrological signs confirm the fact that the salinization of the grounds in the flood-plain of the Yuribay river occurred during the Holocene marine transgression which converted the valley of this river into a gulf. Judging by the marks of the flood-plain at the distance of 65 km from the sea, the sea level relative to the land in the course of the peak of that transgression was located approximately 8 m

higher as compared to the present one. Decoding of the pictures made from the space shows that the transgression penetrated into the valleys of all the rivers of the Yamal peninsula that flew into the Kara Sea at the western and the northern coasts but the most extensive flooding took place on the valleys in the southern part of the Baidaratskaya Bay.

#### CRYOPAIGS

On the flood-plains and the marine terraces in the salinized sands on the marks below the sea-level there are encountered pressure cryopaigs of marine origin. Best of all they have been explored in the valley of the Yuribay river and its vicinities. The thickness of the layers filled with cryopaigs does not exceed 20 to 30 cm. In the valley of the river they can be seen, as a rule, 10 cm and more below the sea-level. As to the marine terraces, those layers are located 20 m below the sea-level. The cryopaigs are confined to sands only, and for the time being no one has managed to find out any connection of their spread with other geological, geomorphological, hydrological or geobotanical conditions. They have no continuous areal extent. Their area and depth distribution is of incidental nature. As a rule, the cryopaigs have got heads but the heads are different from layer to layer, and from the point of view of regularity, they have nothing to do with the depth of occurrence. All that confirms the fact that the sands saturated with cryopaigs are scattered closed lenses which dimensions are relatively small.

Figure 2 illustrates the graph of mineralization of cryopaigs versus the latter's temperature plotted on the basis of studying the specimens of cryopaigs sampled from 18 boreholes and the basis of measuring the temperatures in the same boreholes. The graph is approximated by the equation given hereafter:

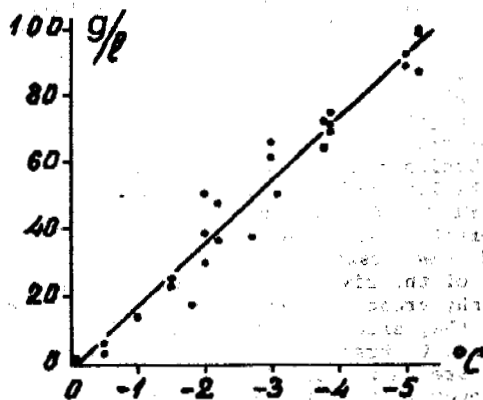


Figure 2. Graph of mineralization of cryopaigs versus their temperature.

$$M = 18.77t - 1.21$$

with the correlation coefficient equal to 0.98.

The data show in Figure 2 indicate that the availability or the unavailability of cryopaigs in grounds does not depend upon their temperature. Cryopaigs were discovered practically within the whole range of temperatures observed



in the area being investigated, that is, from 0°C to -5.2°C. Evidently, there exists a thermochemical equilibrium between the cryopaigs and the permafrost grounds which is regulated by the temperature while the cryopaigs are saturated solutions which concentration correspond to their chemical composition and temperature.

The cryopaigs were formed in the process of epigenetic freezing of the sandy rocks that left the areas from under the sea-level at the regression. It is well known that at freezing from above not all the salts dissolved in the subterranean water become included into the ice. Some parts of them get squeezed out from the freezing area downwards, to the thaw zone. The negative isothermal lines move downwards through the zone of elevated mineralization of the pore solution and enter, again, the initial mineralization area, where the second zone of ice formation comes into existence. Thus the first (the upper) zone of elevated mineralization remains behind of the freezing front. A layer of cryopaigs gets formed which is limited by frozen grounds from above and from below. Because of the non-uniformity of the stratification of grounds, the layers of cryopaigs become limited along the strike, which results in formation of closed layers or lenses. The temperature of the cryopaigs decreases in the process of further freezing of the water-saturated layers. In this case the water contained in the closed layer of sand with cryopaigs increases their head.

#### TEMPERATURE OF GROUNDS

The temperature of grounds on the explored territory was measured at the depth of the zero annual amplitudes lies within the range from 0 to -6°C. Its distribution in plan is characterized by considerable non-uniformity, and anomalies are often encountered so far as the depth is concerned. Visual inspection of the surface conditions near 43 geothermal bore-holes showed that the temperature value depends, mainly, upon the three interrelated factors listed hereafter: microrelief, vegetation and the depth of the snow cover. Under the normal tundra conditions, that is, on the vast flat surfaces without bushes, or with scattered bushes of birch trees and willows which height does not exceed 30 cm, the temperature of grounds, at a considerable distance from water basins and stream flows, is in compliance with the latitudinal zonation law, and it varies from -4°C to -6°C in the meridional direction on the territory explored.

On the watershed plains and on the floodplains of the rivers there can be seen vast willow bushy areas. In some places on the floodplains they exceed the man's height, and they are difficult to traverse. In winter time all the bushes are snow-bound to their whole height. The snow cover in the shrubs is very loose (man falls through it) and is a very reliable thermo-insulating layer preventing the grounds from being frozen in winter. Therefore in the shrubs one can see an elevated temperature of grounds which is close to 0°C sometimes. Snow accumulation is also formed in the negative depressions of the terrain. The gullies and the narrow deep valleys of small rivers are snow-bound completely. Along the steep precipices eroded by the rivers and the lakes, along the steep slopes of the terraces and the thermokarst lacustrine depressions extensive

snow drifts get formed. Those accumulations of snow also call forth the increase of temperature of the grounds. The temperatures of grounds on various geomorphological levels under the similar surface conditions do not differ very much from one another.

There may be defined three types of temperature distribution in depth that are characterized not only by rather a definite pattern of the distribution curves but also by the temperature ranges at the depth of zero annual amplitudes (Figure 3). The first type (normal) corresponds to the theoretical conception of the one-dimensional temperature pattern under the steady state conditions. The temperature increases as the depth also increases, that is, the direction of the heat flow is upward. The vertical gradient of the temperature is close to 0.01°C/m. The temperature depth distribution is linear. On the single distribution curves the waves of winter cooling and those of summer heating are similarly distinct. The temperature at the depth of 18 m lies within the limits from -2.3°C to -5.4°C (in the basin of the Yuribay river).

The second type is characterized by the fact that the temperature of the ground becomes lower

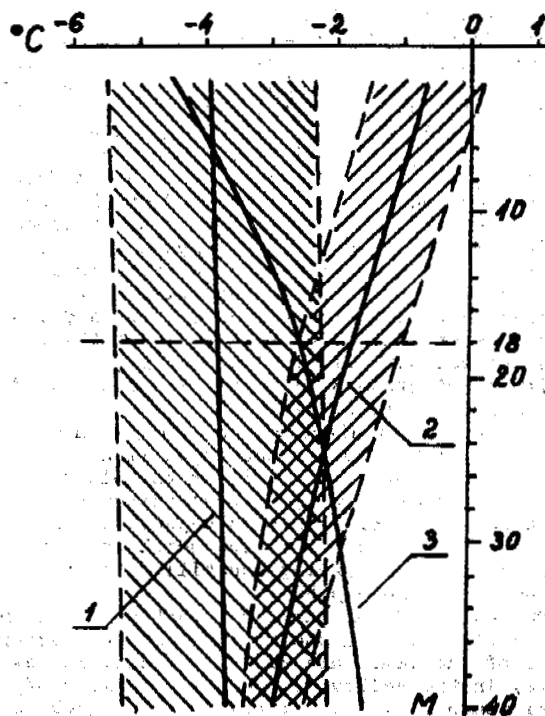


Figure 3. Diagram showing types of distribution of average annual temperature of grounds depending on depth in the Yuribay river basin: 1 - 1st type; 2 - 2nd type; 3 - 3rd type.

as depth increases. Direction of the heat flow is downward. The vertical gradient of the temperature ranges at the depth of the zero annual amplitudes from 0.06 to 0.08°C/m.

The distribution of the temperatures is curvilinear. The distribution single graphs show that the wave of winter cooling is either not quite distinct or it is unavailable at all. The

temperature at the depth of 18 m lies within the range from  $-1^{\circ}$  to  $-2.6^{\circ}\text{C}$ . The pattern of curves 1 and 2 illustrated in Figure 3 shows that the curves approach each other with the depth and that, evidently, they meet at a certain depth.

The third type of distribution, like the first one, is characterized by the temperature decrease with the depth, but the vertical temperature gradient is several times, sometimes ten times as much as compared to the first type. Direction of the heat flow is upward, and its extent is abnormally high. The temperature distribution in respect of the depth is curvilinear. The waves of the winter cooling and the summer warming-up of the grounds are seen very distinctly in the single temperature distribution graphs. The temperature measured at the depth of 18 m lies in a very broad range from  $-0.7^{\circ}\text{C}$  to  $-4.5^{\circ}\text{C}$  and may be even positive. It is no use to illustrate such a range in a graph.

The first type of temperature distribution can be seen at the vast open and even areas that are rather far from water basins and stream flows and that are situated beyond the borders of continuous brushwood of bushes over 30 cm high. The second type is encountered in the thick bushes over 30 cm high in the negative topographic forms, in the vicinity of steep and high benches, terraces, coasts etc. The third type was found in the areas of recently frozen taliks below river beds and below lakes.

In accordance with the data obtained after surveying the surface conditions around the geothermal bore-holes, a graph of ground temperature at the depth of 18 m in the basin of the Yuribay river versus the height of continuous bushes (Figure 4) has been plotted.

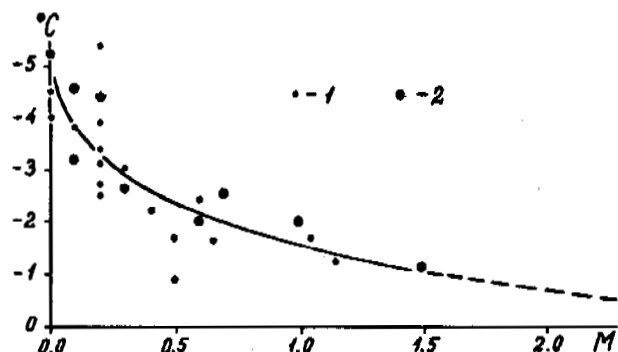


Figure 4. Temperature of grounds versus height of bushes in the Yuribay river basin: 1 - on the flood-plains; 2 - on the marine terraces and on the Kazantsevskaya plain.

This relationship is approximated by the parabola of

$$t = 7.4(h+0.03)^{0.18} - 9 \quad (2)$$

where  $h$  - shrub height in meters. According to Figure 4, the extrapolation of the parabola up to the highest possible height of the shrub equal to 2.5 m shows that the bushes in the areas of the Yamal peninsula being analyzed cannot be the

cause of degradation of the permafrost or that of formation of local taliks in the unsalinized grounds.

The materials set forth above testify to the availability of the climatic reserve of the negative temperature of grounds for many territories of the Yamal peninsula that are characterized by an elevated temperature. Removal of shrubs, draining of the terrain and measures to be taken to avert snow-drifts will make it possible to reduce considerably the temperature of the grounds for engineering purposes.

#### GASES IN GROUNDS

In many geological-engineering bore-holes drilled along the draft line of the railway being planned, emission of combustible gas could be observed, sometimes for rather a long time. In one of the wells in the valley of the Yuribay river the gas flame was burning one month and a half. Weak emission of gas was observed in many bore-holes even a year later after the drilling was over. In the course of field explorations of the grounds one could see that some samples of the sandy clays have the density which is somewhat lower as compared to the conventional values at the same humidity. At the field description of sandy clays cores and at their laboratory analyses, cavities of various shapes with the vertical dimensions up to 12 mm were found many times (Figure 5).



Figure 5. Dusty clay extracted from the depth of 15 m on the Kazantsevskaya plain.

Calculations of gas content (air porosity) in some individual samples of sandy clays out of the cores of bore-holes with taking into consideration their salinity and the content of unfrozen water allowed to find out at various sections of the route separate layers of sandyclays with an elevated air porosity of some 5 to 7% as an average value in the column and up to 10% in individual samples. Calculation of the air porosity of the sandy clays nondestructed structure with approximate taking into account the content of unfrozen water made on the basis of the initial data obtained by the radio-isotope logging method also made it possible to detect individual layers of sandy clays with an elevated air porosity. In this case the highest air porosity equal to 50%

approximately was detected on the 579 kilometer of the route (Figure 6).

The actual materials that are available are insufficient for profound generalizations though they are of principal significance since they testify to the fact that on the territories that were explored sandy clays with an elevated air porosity are encountered. In such grounds the pores are sometimes combined in large hydraulically single systems. The order of the values of air porosity is high enough to affect considerably on the settlement of sandy clays under structures both at thaw and in the plastic frozen state.

#### SUBSURFACE ICE

The distribution and the volumetric content of all the kinds of subsurface ice on the Yamal peninsula, both in top view and in cross-section, are extremely irregular (Figure 6). In general, ice micro-content and the content of wedge ice increase regularly in the direction from south to north and with the height of geomorphological level.

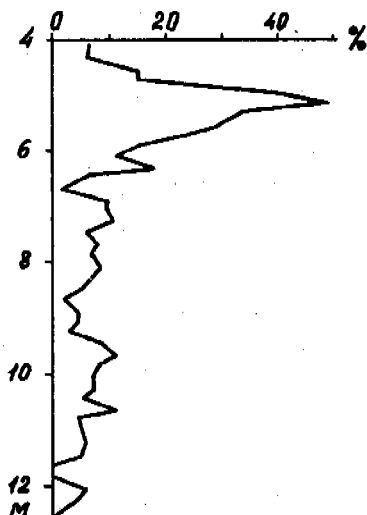


Figure 6. Distribution of air porosity depending on depth in borehole No. 6 on the 579th km of the route.

For example, the ice content of the sands on the marine terraces within the area of the Yuribay river does not exceed too much their full moisture capacity in the thawed state as a rule. Dusty sands with the gravimetric humidity up to 65% can be encountered on the Kazantsevskaya plain. They acquire fluent state at thawing. Their settlement at thawing lies within the range from 0.2 to 0.4.

To the south away from latitude 68° North (the Yuribay river mouth), the volumetric content of wedge ice in the grounds is not very high as a rule. For example, on the marine terraces in the lower reaches of the Yuribay river the size of polygons ranges from 15 to 20 m, the thickness of the ice veins on the top is up to 0.5 m, the vertical size accounts for 5 or 6 m. On the Kazantsevskaya plain, to the north from the Yuribay river, there could be observed ice veins up to 3 m wide and up to 10 m high while the

dimensions of the polygons measured 15 x 15 m. Here the volumetric content of the wedge ice sometimes exceeds 25%.

The amazing peculiarity of the Yamal peninsula consists in the local thick polygonal wedge ice texture spread on some areas whose size does not exceed only several dozens of meters. They can be observed from time to time on the vast territories composed of grounds with low ice content without wedge ice or with its low content. On the edges of river valleys and on the erodible banks of the rivers they are characterized by two or three huge cemetery mounds up to 20 m high (Figure 7).

Sometimes local (patch) peat-beds 2 or 3 m thick are confined to them.

The greatest danger to the building is in the sheet ground ice (injected ice, segregated ice, glacier ice, the ice sheet of water basins and stream-flows) which is not marked as a rule in the topography on the plain surfaces of the terrain.

Up to nowadays the scientists cannot understand the appropriateness of the spreading of the ice of that kind. The ice can be encountered at a depth of 2, 3 or several dozens of meters from the surface (Figure 8).

The thickness of the ice body may reach 20 to 30 m, the horizontal dimensions may be equal to several hundreds of meters or even exceed a kilometer.

In the course of surveying the railroads, there were found two areas of mass contamination of the territory with sheet ice on the third marine terrace: in the basin of the mouth reaches of the Erkatayakha river (latitude 68° North) and to the extreme North of the explored territory, in the region of future railway station Bovanenkovo. The availability of sheet ice may be detected by the geomorphological signs seen on the slopes of the river valleys and the lake depressions, which is favoured due to the erosive ruggedness of relief. The reliable indicators of the availability of sheet ice are the thermocirques and the termoterraces on the slopes and the small thermokarst depressions both on the slopes and on the watershed surfaces.

#### CRYOGENIC SLUMPING OF SLOPES

In August 1989 near the Bovanenkovo station there occurred mass slumping of the grounds of the seasonally thawed layer on these slopes which steepness does not exceed 15° which aroused the engineers anxiety. The slumping can be externally exposed in different ways, from small territorial exposures of frozen grounds in the upper parts of the slopes (Figure 9.) and up to mud-torrents 1000 m long.

The main reason causing the slumping is the moistening of the grounds of the seasonally thawed layer in the bottom parts of the slopes due to the summer atmospheric precipitation and the thawing of the ice-rich grounds near the base of the seasonally thawed layer. Slumping is favoured by the double layer structure of the seasonally thawed layer: a sand layer lying on sandy clay.

Thus, the optimum conditions for mass development of cryogenic slumping appear during the years with the unusually warm summer and with an abnormally great amount of summer atmospheric precipitation. Such conditions were observed in

1989. The summer of 1990 was warmer than the summer of 1989 but the amount of atmospheric precipitation decreased sharply, and the slumping of the grounds ceased.

The top part of the seasonally thawed layer in the vicinity of Bovanenkovo consists, as a rule, of thixotropic sands that, since they are unfrozen and water-saturated, are easily converted into the quicksand state due to the effect of dynamic loads. Hence, the movement of trains and other dynamic loads being applied to the grounds can cause their cryogenic slumping in the summer time. The mass slumping of the slopes in the area of the Bovanenkovo in 1989 happened everywhere on the same days.

Taking into account the above physical mechanism of cryogenic slumping, one may offer two principal methods of engineering protection of the structures against the phenomenon described above: 1) deriving of the surface water and draining of the grounds of the seasonally thawed layer on the slopes for the purpose of dewatering them, and 2) erection of special constructions on the slopes that could hinder the slumping. For example, the stability of the grounds may be improved by erecting vertical piles in staggered rows on the slopes with their penetration into the permafrost grounds for preventing them from frost heave.

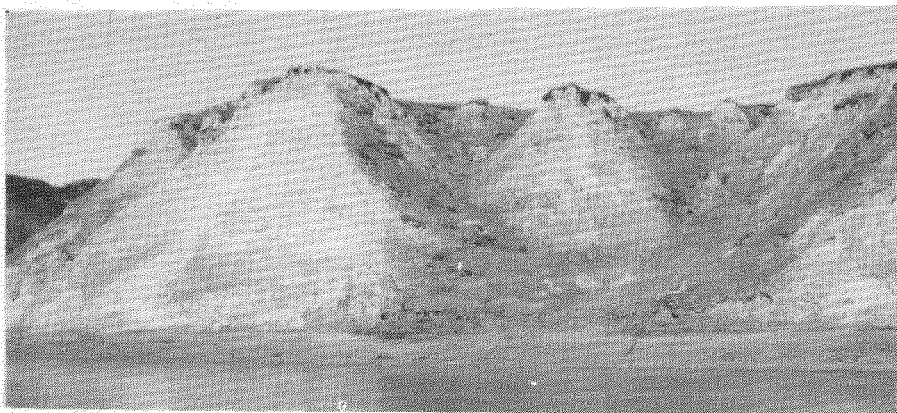


Figure 7. Cemetery mounds on the bank of Erkatayakha river, the 3th marine terrace.

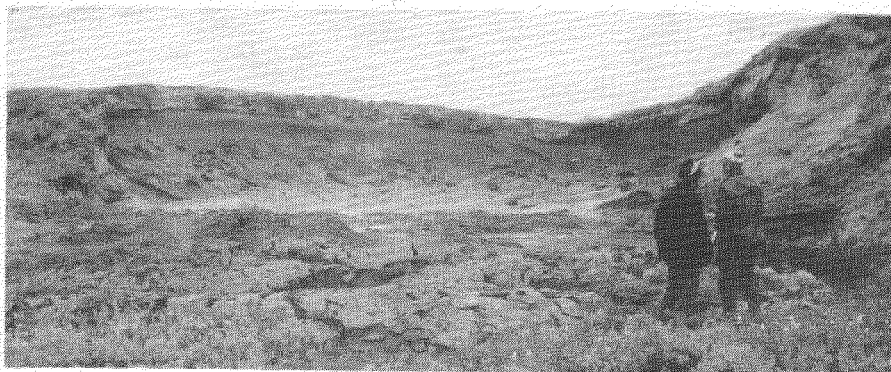


Figure 8. Sheet ice exposure near Bovanenkovo.



Figure 9. Cryogenic Landslip near Bovanenkovo

# INFILTRATION OF MELT WATER INTO FROZEN SOILS IN A CONTINUOUS PERMAFROST ENVIRONMENT

Philip Marsh<sup>1</sup> and Ming-ko Woo<sup>2</sup>

<sup>1</sup>National Hydrology Research Institute, Saskatoon, Sask., Canada S7N 3H5

<sup>2</sup>Department of Geography, McMaster University, Hamilton, Ontario, Canada L8S 4K1

Observations using a gamma density meter showed that total infiltration during snowmelt at two sites near Resolute, N.W.T. varied from 9 to 12 mm of water, or 6% of the initial snowpack water equivalent. At a site with a deeper snow cover, infiltration was 38 mm in 1988 and 34 mm in 1989, representing 13 and 6% of the snowpack water equivalent. Asynchronous timing of infiltration at gamma, TDR, and thermistor sites suggests significant spatial variability in infiltration. The empirical frozen-soil infiltration model of Gray et al. (1985), applicable for sites with limited infiltration, over-predicted total infiltration at sites near Resolute. It is believed that this occurred because the soil temperature was colder and the snow water equivalent was larger, at the Resolute sites than in the Prairies where the equation was developed. As a result, the model requires further calibration before it can be used in runoff models for permafrost areas.

## INTRODUCTION

During snowmelt runoff, meltwater may either infiltrate into the soil directly beneath the snowpack, or runoff laterally as overland flow in a saturated layer at the snow/soil interface. The relative importance of these two flow paths greatly influences the timing and magnitude of snowmelt runoff, and also affects soil temperature through the transfer of sensible and latent heat. In extreme conditions, either the soil is impermeable and all meltwater leaves the snowpack as saturated overland flow, or the soil is sufficiently permeable that all meltwater enters the soil. It is more likely however, that conditions are between these two extremes, with the relative importance of infiltration vs. overland flow varying within a basin, and from year to year. In this situation, it is very difficult to accurately predict the timing and magnitude of snowmelt runoff.

Since infiltration into frozen soils plays an important role in controlling snowmelt runoff, considerable work has been carried out in regions where soils are seasonally frozen. This includes field measurements (Kane, 1980; Kane and Stein, 1983; Granger et al., 1984) and model development/testing (Harlan, 1972; Alexeev et al., 1972; Gray et al., 1985). However, only a few studies have considered the unique aspects of meltwater infiltration in permafrost environments (Marsh, 1988; Woo and Marsh, 1990). Some of the important differences include, colder ground temperatures and the existence of a frozen substrate of extremely low permeability at a shallow depth.

It is the purpose of this paper to determine variations in frozen soil infiltration for three typical soil types at a site in the zone of continuous permafrost. Specifically, this paper will:

- (1) describe variations in both total and unfrozen soil moisture during the melt period,
- (2) determine total soil infiltration, and
- (3) test a simple soil infiltration model developed for seasonally frozen soils.

## STUDY AREAS AND FIELD TECHNIQUES

Field work was carried out near Resolute, Northwest Territories (74° 55'N, 94° 51'W), where the annual mean daily temperature is -16.6°C. Resolute is in the zone of continuous permafrost, with typical active layer thicknesses between 0.2

and 0.7 m. Mean total precipitation reported by the weather station is 131 mm/yr, of which 79 mm falls as snow, and the ground is snow covered for about 9 months each year. However, Woo et al. (1983a) showed that snow storage in the study area is 1.3 to 3.0 times greater than the snowfall reported at the weather station. Woo et al. (1983b) found that snowmelt runoff dominates the annual hydrograph in the Resolute area.

During the spring of 1988 and 1989 field work was carried out at three sites within 1 km of each other (see Woo and Marsh, 1990 for site map), and approximately 5 km from the Resolute airport. These sites include three typical surficial materials found in the area (Cruickshank, 1971), including polar desert soil which is a mixture of pebbles and loam (site A), bog or wetland soil (site B), and lithosol or gravelly materials (site C). The properties of the soils at each site are given in Table 1. Since the wetland site is fed by snowmelt throughout the summer, it is referred to as the fen site. A more complete description of these sites is provided by Woo and Marsh (1990).

At each study site, gamma access tubes, TDR probes and thermistors were installed down to the permafrost table at a depth of approximately 35 cm (fen) and 50 cm (polar desert and gravel) in late August 1987. Unfortunately these instruments could not be placed at exactly the same sites, but instead were installed within 2 to 3 metres of each other. A twin-probe gamma density meter was used to measure soil density, with measurements obtained at 5 cm increments. These values were then used to determine relative changes in soil moisture (assuming that changes in density were due solely to changes in liquid content). Since bulk density was measured at each site, gamma densities were also converted to volumetric soil moisture. The relative and absolute measurements include both frozen and unfrozen water. The changes in relative soil moisture are accurate to  $\pm 2$  mm of water, but there is considerable uncertainty in the absolute soil moisture due to vertical variations in bulk density. However, for infiltration, it is the relative changes which are most important. TDR probes were installed horizontally at depths of 10, 25, and 45 cm. Calculations of unfrozen soil moisture followed the procedure described by Topp et al. (1980). However, for the polar desert and gravel sites, a relationship developed by Smith (personal communication) for gravel soils was used. At all three study sites, ground

Table 1 - Soil properties for the three soil types typical of the study sites near Resolute.  $\phi$  is the soil porosity. (Woo and Marsh, 1990)

Site	Clastic Portion				Bulk Density (kg m <sup>-3</sup> )	$\phi$	Organic Content (%)	Hydraulic Conductivity (m s <sup>-1</sup> )
	Clay %	Silt %	Sand %	Gravel %				
Polar desert	9	19	42	30	1709	.37	2	2.4*10 <sup>-4</sup>
Fen	21	53	23	3	1683	.38	15	--
Gravel	3	9	18	70	1709	.37	.0	1.9*10 <sup>-1</sup>

temperatures were measured at depths of 2, 5, 10, 25, and 50 cm. At a nearby site, snow depth and properties were measured in snow pits following the procedure described by Marsh and Woo (1984). These data were used to determine when meltwater first reached the snowpack base and was therefore available for infiltration.

Measurement problems which limited the data analysis for the fen site in 1988 and 1989, and the polar desert site in 1989 include: (1) at the fen site in 1988 and the polar desert site in 1989, the wet soil density as measured by the twin tube gamma probe, were often less than the measured soil bulk density. This likely occurred because of the development of ice lenses within the soil, which would have resulted in a reduction in soil density. As a result, the gamma measurements could only be used for relative changes in soil water storage. They could not be converted into volumetric soil moisture, and (2) the gamma tubes at the fen site ruptured during the winter of 1988/89, and as a result the tubes were flooded in the spring of 1989 and could not be used.

A meteorological station was located at a site midway between the polar desert and the gravel sites to measure air temperature, relative humidity, wind speed, solar radiation, and rainfall. These data, recorded at hourly intervals by a Campbell CR21 data logger, are considered to be representative of the three study sites. The meteorological data were used to compute snowmelt using the technique described by Heron and Woo (1978). These data were used to determine the beginning of the melt period.

## RESULTS

### Soil moisture and temperature during snow melt

During 1988, snowmelt began on June 25 (day 175), but due to significant refreezing within the cold snowcover (Marsh and Woo, 1984) it took approximately 3 to 4 days for melt water to percolate through the snowpack and to reach the snowpack base. During this period the total soil moisture, as measured by the twin probe gamma density meter, remained constant at all three sites (see Figures 1 and 2 for data from the polar desert and gravel sites). At both the polar desert and gravel sites, the soil moisture was between 20 and 30% by volume at a depth of 10 cm, and about 5 to 10% by volume at a depth of 25 cm. The drier soils at depth may have resulted from moisture migration during the winter, although it may also be due to the uncertainty in the absolute moisture when the gamma densities are converted to moisture by volume.

At all sites, and all depths, the unfrozen water component, as measured by TDR, was between 2 and 5% (see Figure 1 and 2 for gravel and polar desert sites). Given that soil temperatures were between -8 and -12°C, these values seem slightly high, but are possible considering the potential freezing point depression (Tice et al., 1978). In addition, since typical errors for TDR are approximately 2%, these values are certainly within the error bounds of the measurement technique.

During the period before liquid water reached the snowpack base, soil temperatures increased slowly (Figures 1 and 2). However, as liquid water reached the base of the snowpack, soil temperatures increased more rapidly at most depths, with the effect decreasing slightly with increasing depth (Figures 1 and 2). A similar, rapid increase also occurred at the fen site (Woo and Marsh, 1990). It would be expected that this rapid increase in soil temperature is related to the release of latent heat during refreezing of infiltrated melt water. However, as Figures 1 and 2 show, neither the gamma or TDR showed any increase in soil moisture at this time. Since this rapid increase in soil temperature could not be due to heat conduction alone, other possibilities are likely. For example, meltwater may have infiltrated preferentially down the ground thermistor rod, or infiltration may be spatially variable. This will be addressed more fully in the discussion section.

At both the polar desert and gravel sites, it was not until near the end of the melt period that soil moisture increased significantly (Figures 1 and 2). At the polar desert site, for example, soil moisture, both frozen and unfrozen as indicated by the gamma meter, increased 5 to 10% by volume at both the 10 and 25 cm depths, while unfrozen content as indicated by TDR, showed an anomalously large increase at the 10 cm level. Again, this may be due to spatial variations in soil infiltration, or since the measured soil moisture is larger than the porosity, it may indicate the occurrence of large pores surrounding the TDR probe. One possibility for the occurrence of such pores, is the potential for thawed ice lenses remaining as water-filled macropores as hypothesized by Dyke and Egginton (1990). At the gravel site, similar increases in total moisture occurred. However, the increase in liquid water showed a more reasonable increase (Figure 2).

### Cumulative Infiltration during snow melt

The maximum increase in soil moisture during the 1988 melt period varied from 38 mm at the gravel site, to 12 mm at the fen site, to only 9

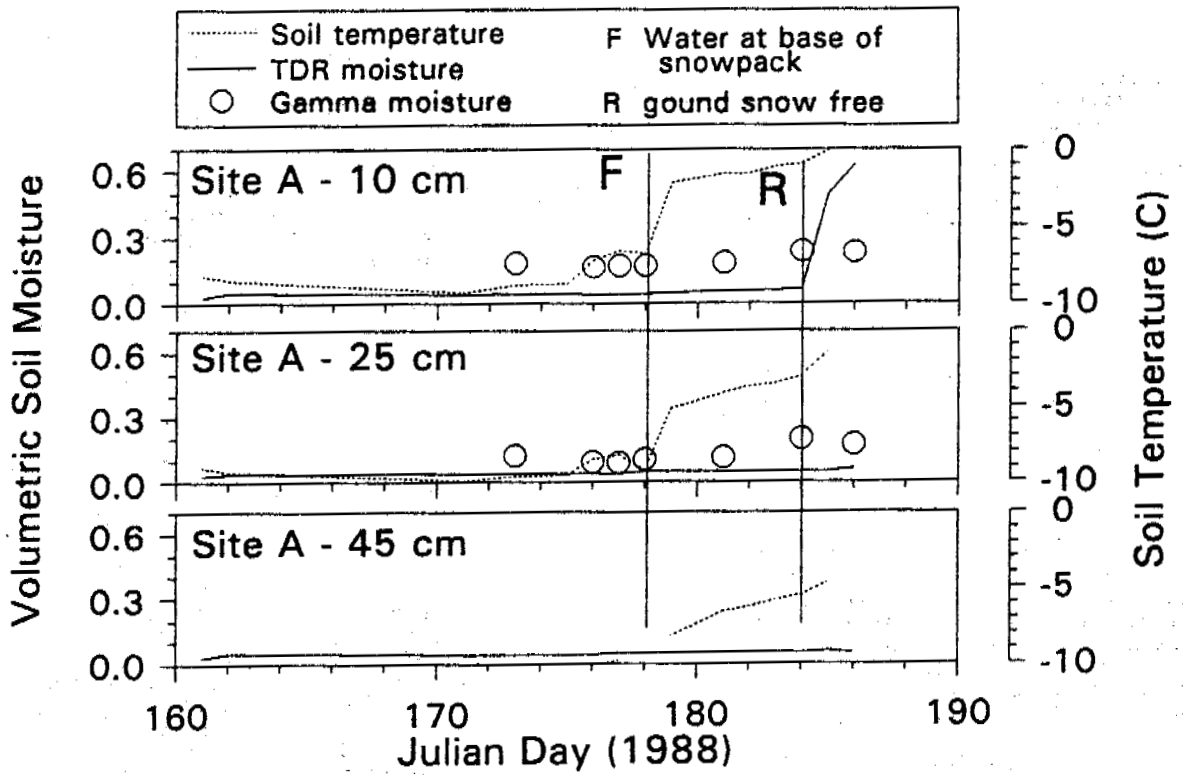


Figure 1. Change in total soil moisture, unfrozen soil moisture, and temperature at depths of 10, 25, and 45 cm at the polar desert site in 1988.

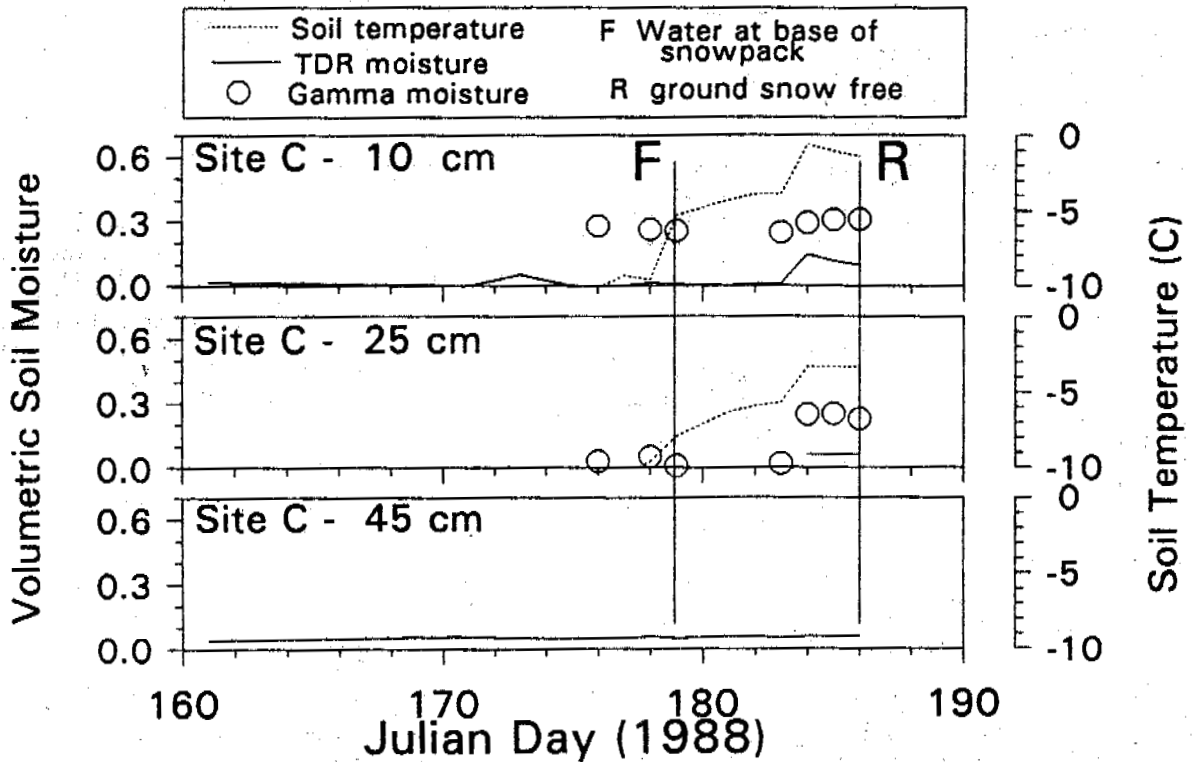


Figure 2. Change in total soil moisture, unfrozen soil moisture, and temperature at depths of 10, 25, and 45 cm at the gravel site in 1988.



mm at the polar desert site (Table 2). As expected, the cumulative infiltration curve for the fen site (Figure 3) shows that the majority of infiltration occurred at approximately the same time that melt water first reached the snowpack base. However, at both the gravel and polar desert sites, the majority of infiltration occurred near the end of the melt period. Normally, infiltration would occur when water first reached the snow/soil interface. However, this may have been affected by the existence of basal ice at the beginning of the 1988 melt period. This basal ice resulted from an unusually early snowmelt during May, followed by heavy snowfall and low temperatures which refroze the meltwater as ice layers and basal ice. At the fen and polar desert sites, the basal ice layer was nearly continuous, while at the gravel site it was sporadic. It is quite likely, therefore, that basal ice played a role in blocking the entrance of June meltwater into the soil. Only later in the melt period, when the basal ice layer reached an isothermal condition, did it become sufficiently permeable to allow meltwater to penetrate the ice. Since we have no measurements of change in soil moisture during the May melt event, it is unknown if soil infiltration occurred at that time. It is possible, though, that the soil was sufficiently cold to freeze all meltwater as soon as it came in contact with the soil. As a result, the infiltration capacity of the soil would not have been filled during the May melt.

In 1989, total soil infiltration at the polar desert and gravel sites, was similar to that in 1988 with 10 mm and 34 mm respectively. However, the spring melt sequence in 1989 was more typical of long term conditions at Resolute, with an abrupt start to the melt during June. In this case there was no basal ice when meltwater reached the soil surface in June. The timing of infiltration at the polar desert site relative to snowmelt was similar to what occurred in 1988. However, the gravel site was considerably different, with infiltration beginning as soon as meltwater reached the snowpack base (Figure 3). In addition to this first peak, it appears that there was another peak in infiltration during the latter parts of the melt period, similar to 1988.

#### MODELLING

Gray et al. (1985) describe three basic soil infiltration classes in the Canadian Prairies: restricted, limited and unlimited infiltration. In the restricted case, virtually no infiltration occurs due to a blocking layer near the soil surface. In the unlimited case, all of the snowpack may infiltrate the frozen soils due to the existence of large, air filled pores, or macropores. Marsh (1988) described soils which fall into the unlimited class in the Mackenzie Delta region, while Marsh and Woo (1984) reported soils which fall into the limited classes for the Resolute area. Both of these sites are in the zone of continuous permafrost.

For soils with limited infiltration, Gray et al. (1985) noted that there is an inverse relationship between infiltration and the frozen soil moisture content for medium to fine-textured, frozen prairie soils, and Gray et al. (1989) showed that the soil is usually

not saturated at the end of the melt period, but instead the "degree of saturation" is typically  $\theta_s = 0.60 + 0.40 \theta_p$ , where  $\theta_s$  and  $\theta_p$  are the saturation limit and premelt moisture content, with both expressed as the degree of pore saturation. In addition, they noted that meltwater typically penetrated the frozen soil to a depth of only 30 cm. When taken together, these two conditions imply that the infiltration capacity of these soils is small. For limited soils, Gray et al. (1985) suggest that infiltration is primarily determined by the snowpack water equivalent and the frozen water content of the upper 30 cm of the soil as:

$$(1) \quad INF = 5(1 - \theta_p) SWE^{0.564}$$

where INF is the total soil infiltration (mm) and SWE is the premelt snowpack water equivalent (mm).

#### Application to Resolute Study Sites

In order to apply equation 1, soil infiltration must only occur into the upper 30 cm of the soil. Woo and Marsh (1990) present data which illustrates that at the polar desert and gravel sites, the largest increases in water storage occurs at a depth of between 25 and 35 cm, with little or no apparent changes below that depth. At the fen site, moisture increase, although small, occurred at all depths down to 35 cm at the base of the active layer. At all three sites, therefore, the depth to which significant infiltration occurred is very similar to that found in the studies of Gray et al. (1985), suggesting that their equation may be applicable.

Equation 1 was applied to the polar desert and gravel sites to predict infiltration in 1988 and for the gravel site in 1989 (Table 2). The predicted value for these sites were 54, 80, and 69 mm respectively, compared to measured values of 9, 38, and 34 mm (Table 2). This apparent over prediction may be due to either differences in the soil type, soil temperature, or snow water equivalent between the Resolute sites and the study area of Gray et al. (1985). It would be expected that soil temperature plays an important role in limiting meltwater infiltration. Since soils in the zone of continuous permafrost are considerably colder at all depths than in the Canadian Prairies, it would be expected that  $\theta_s$  would be considerably lower, thereby affecting the relationship between  $\theta_p$ , SWE and INF. Further work is required.

#### DISCUSSION

Comparison of the timing of changes in soil temperature, frozen and unfrozen soil moisture (gamma), and unfrozen soil moisture (TDR) show that they are non-synchronous by as much as several days in many cases. As suggested earlier, one possible reason for this is differential infiltration at the three instrument sites, even though they were separated by only a few metres. Such variation in the timing of infiltration may be related to small scale variations in the availability of water at the snow/soil interface due to the occurrence of flow fingers in the snowpack (Marsh and Woo, 1984). If infiltration is

Table 2 - Snow water equivalent (SWE), soil moisture, and infiltration at the three study sites in 1988 and 1989. The predicted soil infiltration is from equation 1. Julian days are in brackets.

Year	Site	Snow Water Equivalent		Vol. Soil Moisture			Infiltration		
		Date	mm	Date	%	$\theta_p$	Obs. (mm)	% of SWE	Pred. (mm)
1988	Polar desert	June 24 (175)	150	June 25 (176)	16	.42	9	6	79
	Fen	June 24 (175)	217	June 25 (176)	----	----	12	6	----
	Gravel	June 24 (175)	289	June 25 (176)	16	.42	38	13	116
1989	Polar desert	June 15 (166)	174	June 15 (166)	----	----	10	6	----
	Fen	June 15 (166)	189	-----	----	----	-----	----	----
	Gravel	June 16 (167)	612	June 16 (167)	25	.68	34	6	159

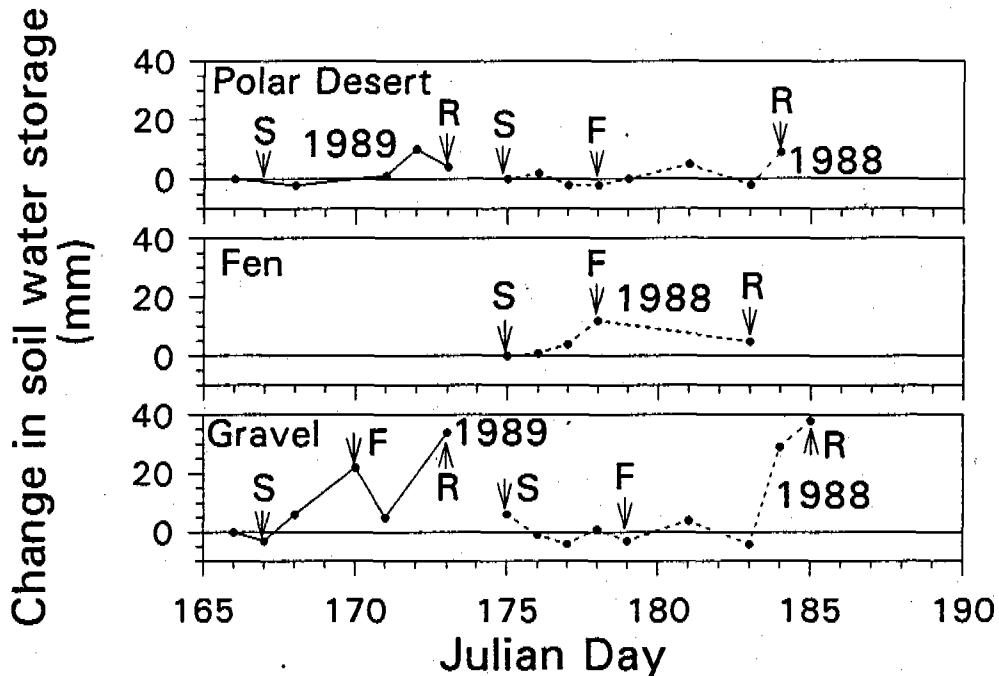


Figure 3. Cumulative change in frozen and unfrozen soil water storage at the polar desert, fen, and gravel sites in 1988 and 1989. Also shown are the start of snowmelt (S), the first day melt water reached the snowpack base (F), and the date on which the snow cover was removed (R).

spatially variable, with large differences over very short distances, this has implications to the representativeness of existing measurement techniques, which generally average over distances of only tens of cm.

Since total infiltration may represent a considerable proportion of the total snowpack, frozen soil infiltration has a significant impact on both the timing and volume of snowmelt runoff. As a result, there is a need for simple models to predict infiltration, both for basin scale hydrologic models and for larger scale hydrologic models which are required to interact with Global Circulation Models for predicting climate change. One of the few models of frozen soil infiltration which is sufficiently simple in terms of data requirements, is that developed by Gray et al. (1985) for the Canadian Prairies. Although this type of model may apply to permafrost areas, comparison with field data from Resolute shows that more information is required in order to apply it to permafrost soils. An additional limitation of the Gray et al. (1985) model is that it is only applicable to the class of soils they call "limited infiltration" soils. There is a need for simple techniques to differentiate between the unlimited, limited and restricted infiltration soils, all of which may occur in permafrost areas.

#### ACKNOWLEDGEMENTS

This research was supported by the National Hydrology Research Institute and by a grant from the Natural Sciences and Engineering Research Council. We acknowledge the generous logistical support of the Polar Continental Shelf Project of the Department of Energy, Mine, and Resources. The indispensable assistance of Mary Ferguson, Philip Giles, Kathy Young and Kelly Thompson are gratefully acknowledged.

#### REFERENCES

- Alexeev, G.A., Kalyuzhnyy, I.L., Kulik, V. Ya., Pavlova, K.K., and Romanov, V.V. 1972. Infiltration of snowmelt water into frozen soil. In *The role of snow and ice in hydrology*. Proceedings, Banff Symposium, UNESCO-WMO-IAHS, Vol. 1, 313-325.
- Cruickshank, J. 1971. Soil and terrain units around Resolute, Cornwallis Island. *Arctic*, 24, 195-209.
- Dyke, L. and Egginton, P. 1990. Influence of ice lens fabric on the hydraulic conductivity of thawing soil. in: *Permafrost - Canada*, Proceedings of the Fifth Canadian Permafrost Conference, Collection Nordicana, No. 54, Universite Laval, Quebec, 137-141.
- Granger, R.J., Gray, D.M., and Dyck, G.E. 1984. Snowmelt infiltration to frozen Prairie soils. *Canadian Journal of Earth Science*, 21, 669-677.
- Gray, D.M., Landine, P.G., and Granger, R.J. 1985. Simulating infiltration into frozen Prairie soils in streamflow models. *Canadian Journal of Earth Science*, 22, 464-472.
- Gray, D.M., Pomeroy, J.W., and Granger, R.J. 1989. Modelling snow transport, snowmelt, and meltwater infiltration in open, northern regions. In: *Northern Lakes and Rivers*, W.C. Mackay (editor), Boreal Institute for Northern Studies, University of Alberta, Occasional Publication Number 22, 8-22.
- Harlan, R.L. 1972. Ground conditioning and groundwater response to surface freezing. In: *The role of snow and ice in hydrology*. Proceedings, Banff Symposium, UNESCO-WMO-IAHS, Vol. 1, 326-341.
- Heron, R. and Woo, M.K. 1978. Snowmelt computation for a High Arctic site. Proceedings 35th Eastern Snow Conference, Hanover, 162-172.
- Kane, D.L. 1980. Snowmelt infiltration into seasonally frozen soils. *Cold Regions Science and Technology*, 3, 153-161.
- Kane, D.L. and Stein, J., 1983. Water movement into seasonally frozen soils. *Water Resources Research*, 19, 1547-1557.
- Marsh, P. 1988. Soil infiltration and snow-melt run-off in the Mackenzie Delta, N.W.T. Proceedings 5th International Conference on Permafrost, Trondheim, Norway, 618-621.
- Marsh, P. and Woo, M.K. 1984. Wetting front advance and freezing of meltwater within a snow cover, 1. Observations in the Canadian Arctic. *Water Resources Research*, 16, 1853-1864.
- Smith, M. personal communication. Dept. of Geography, Carleton University, Ottawa, Ontario.
- Tice, A.R., Burrows, C.M., and Anderson, D.M. 1978. Determination of unfrozen water in frozen soil by pulsed nuclear magnetic resonance. In: *Third International Conference on Permafrost*, Edmonton, Canada, 150-155.
- Topp, G.C., Davis, J.L., and Annan, A.P. 1980. Electromagnetic determination of soil water content: Measurements in coaxial transmission lines. *Water Resources Research*, 16, 574-582.
- Woo, M.K., Heron, R., Marsh, P., and Steer, P. 1983a. Comparison of weather station snowfall with winter snow accumulation in High Arctic basins. *Atmosphere-Ocean*, 21, 312-325.
- Woo, M.K., Marsh, P., and Steer, P. 1983b. Basin water balance in a continuous permafrost environment. In: *Permafrost: Fourth International Conference*, Proceedings, Fairbanks, U.S.A., 1407-1411.
- Woo, M.K. and Marsh, P. 1990. Response of soil moisture change to hydrological processes in a continuous permafrost environment. *Nordic Hydrology*, 21, 235-252.

## CRITICAL POLYGON SIZE FOR ICE-WEDGE FORMATION IN SVALBARD AND ANTARCTICA

Norikazu Matsuoka<sup>1</sup> and Kazuomi Hirakawa<sup>2</sup>

<sup>1</sup>Institute of Geoscience, University of Tsukuba  
Tsukuba, Ibaraki 305, Japan

<sup>2</sup>Department of Geography, Tokyo Metropolitan University  
Hachioji, Tokyo 192-03, Japan

Dimensions and character of polygons and the underlying wedge structures were investigated in three permafrost regions. Polygons in the Sør Rondane Mountains, Antarctica, are 3-15 m in diameter and mainly underlain by ice wedges. In Adventdalen, Svalbard, large polygons (7-30 m in diameter) accompany ice wedges, whereas smaller ones have only active-layer soil wedges. Despite large diameters (5-30 m), polygons in Linnédalen, Svalbard, are only underlain by active layer soil wedges. The depth of wedge is, on the whole, proportional to the spacing, but the relationship between the two dimensions is expressed by distinct regression lines for continuous and discontinuous permafrost regions. These results show that the polygon size can be indicative of the existence of an ice wedge, if the depth to the permafrost table and the temperature of permafrost are known.

### INTRODUCTION

Thermal contraction cracking in frozen soils produces polygonal patterns on the ground surface underlain by subsurface wedges. The wedges growing in contemporary periglacial regions are classified into several types (e.g. French, 1976; Washburn, 1979; Permafrost Subcommittee, 1988). Cracks extending downward into permafrost yield permafrost wedges, which are subdivided into ice, composite and permafrost soil wedges with respect to composition (Washburn, 1979, 114, Table 4.4): the type of the fillings depends mainly on soil humidity. Cracks confined to seasonal freeze-thaw layers result in active-layer soil wedges in permafrost regions or seasonally frozen-ground soil wedges in non-permafrost regions: in the following, these wedges are collectively referred to as seasonal frost wedges. Romanovskij (1985) displayed zonation of permafrost and seasonal frost wedges. Ice wedges concentrate in cold permafrost regions, while active-layer soil wedges occur mainly in warm permafrost regions. This is because, with falling ground temperature, the depth of thermal contraction cracks tends to deepen while that of the active layer thins.

Permafrost and seasonal frost wedges also occur simultaneously within a small area. For instance, Romanovskij (1973) indicated that an ice-wedge polygon often includes several smaller polygons underlain by active-layer soil wedges. In such a case, permafrost wedges tend to develop beneath larger polygons than do seasonal frost wedges (Fig. 1). The question then arises as to whether permafrost and seasonal frost wedges can be identified by means of the polygon size. The visco-elastic theory of thermal contraction cracks led Lachenbruch (1962) to state that deeper cracks relieve thermal stress over wider areas, resulting in larger polygons. His theory suggests that there is a certain relation between depth and spacing of thermal contraction cracks. Consequently, the polygon size may be indicative of the wedge type.

From this viewpoint, we investigated the rela-

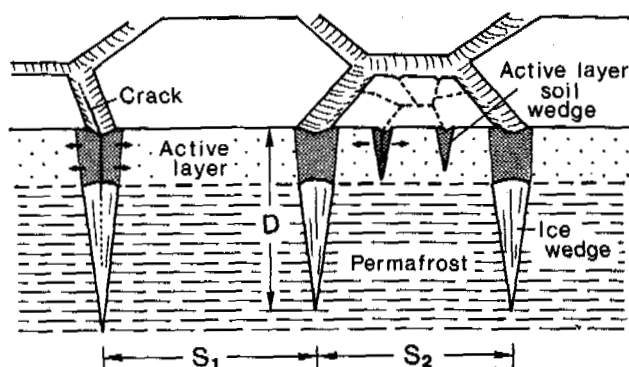


Figure 1. Schematic diagram indicating the relationship between the polygon size and the type of wedge.

tionship between depth and spacing of wedges originating from thermal contraction cracks, the type of wedge and the depth of the active layer in three permafrost regions: Linnédalen and Adventdalen in Svalbard and the Sør Rondane Mountains in Antarctica. These regions are different in permafrost temperatures and depth of the active layer.

### STUDY AREAS

Antarctic study sites lie in ice-free areas of the Sør Rondane Mountains, East Queen Maud Land, which stand above the Antarctic Ice Sheet. The mountains are located ca. 200 km south of the nearest coastline and dominated by continental climates. Air temperature never rises above 0°C throughout the year and mean annual air temperature (MAAT) is -19°C at Asuka Camp, 40 km north of the mountain front. However, strong insolation in summer sometimes thaws the ground surface, yielding an active layer no deeper than 40 cm, which is

underlain by thick permafrost (Matsuoka et al., 1990; Matsuoka and Moriwaki, 1992). The depth to the permafrost table is commonly 30 cm in dry, sandy till. The amount of snowfall is quite small, and much of the snow sublimates, which keeps the ground surface dry. Whereas permafrost wedges have been intensively studied in Victoria Land (e.g. Berg and Black, 1986), only a brief description of polygons has been made in the Sør Rondane Mountains (Van Autenboer, 1984). Polygons occur on till consisting mainly of gravelly sand. In particular, typical forms develop on moraines older than 1 million years (Moriwaki et al., 1991). Younger moraines, most of which are considered to be ice-cored, exhibit only irregular polygonal forms which may be deformed by decaying ice-cores.

Polygons are extensively developed in Svalbard. Some of them are described as ice- or soil-wedge polygons (Jahn, 1983; Akerman, 1987), but detailed studies on wedge structures are very few. The two study areas lie along Isfjorden, central Spitsbergen. Adventdalen is a wide U-shaped valley extending to the fjord. Polygons of a variety of sizes are developed on river terraces along the Adventelba River and on gentle valley slopes. Ice wedges were found beneath some of the polygons (Svensson, 1988). The river terraces are rock terraces with a thin cover of loamy till and outwash deposits (Ono et al., 1991). In some swampy areas, peat covers the terraces. Thermal contraction cracks are formed in the till, outwash and peat deposits. Meteorological data at Longyearbyen, located on the coast 25 km west of this area, indicate that MAAT is  $-5.8^{\circ}\text{C}$  (Akerman, 1987). MAAT at the study area is probably slightly lower than  $-6^{\circ}\text{C}$ , because most polygons occur 100 to 300 m higher than the Longyearbyen station. Thus, permafrost here is thought to be continuous, but not very thick in places as suggested by open-system pingos on river beds. The depth to the permafrost table averages 100 cm and varies from 80 to 120 cm, depending on soils and local climate.

Linnédalen is located at the southwest entrance to Isfjorden. A number of polygons are developed on a series of Holocene coastal terraces (7 to 35 m a.s.l.), which lie between the present coast and the Lake Linnévatnet. The whole area was covered with a glacier during Last Glacial Maximum, submerged in the sea following deglaciation and transgression, and then exposed by isostatic uplift between 9600 and 8000 yr B.P. (Svendsen et al., 1989). The uppermost layer of the terraces consists of marine sand and gravel, which partly incorporate a lodgement till up to 3 m thick (Lønne and Mangerud, 1991). Meteorological data at Isfjorden Radio Station, located at the northern end of Linnédalen, show that MAAT is  $-4.7^{\circ}\text{C}$  (Akerman, 1987). Polygons occur primarily where the ground is underlain by permafrost. However, there are a number of thermokarst lakes lacking permafrost (Salvigsen and Elgersma, 1985), which suggests that the permafrost is discontinuous. The frost table in marine deposits lies commonly at a depth of 100 to 110 cm in July, and probably deepen to 130±20 cm by the end of summer.

#### DIMENSIONS AND CHARACTER OF POLYGONS AND WEDGES

##### Definition of Dimensions

Dimensions of a polygon and the underlying wedge are expressed by the spacing,  $S$ , and the depth,  $D$ , of the wedge (Fig. 1). The  $S$  value is defined by the mean diameter of two adjacent polygons bordered by the wedge, i.e.,  $S = (S_1 + S_2) / 2$ . The  $D$  value is represented by the wedge depth measured from the rim of the furrow. These measurements were adopted

for polygons with a diameter greater than 1 m. For smaller polygons mostly lacking wedge structures, the  $D$  value is expressed by the depth of open cracks.

##### Sør Rondane Mountains, Antarctica

Polygons in the Sør Rondane Mountains are small, commonly 3-15 m in diameter. Furrows dividing polygons are obvious, averaging 50 cm wide and 10 cm deep. Six furrows were excavated, and ice wedges were found in five of them. Open cracks, which are the direct evidence for active cracking, are rare in the furrows. However, ice-wedge tops at 30-40 cm depth approximate the present permafrost table, indicating that the ice wedges are active, or that they have rarely experienced climate warmer than the present since they became inactive. These ice wedges are at most 90 cm wide and 80 cm in the vertical dimension. The maximum crack depth (i.e., the maximum thaw depth plus vertical extent of the ice wedge) was 110 cm (Fig. 2a: SR4). The crack depth tends to be proportional to the crack spacing (Table 1). The smallest polygon ( $S = 3.7$  m) accompanies a crack 56 cm deep, the lowest portion of which is occupied by a miniature ice wedge 6 cm wide and 20 cm in the vertical dimension (Fig. 2a: SR5). These ice wedges underlie dry active layers. Measurements of soil moisture at the center of an ice-wedge polygon (SR1) showed that the active layer was very dry (1-3 % water/wt dry soil) in summer months when diurnal thawing often took place. In contrast, the top of permafrost showed comparatively large ice content (15-30 % water/wt dry soil).

The excavated furrow without an ice wedge was underlain by a wedge of poorly sorted gravelly sand (Fig. 2a: SR8). Traced downward to a depth of 124 cm from the surface, the wedge penetrated well below the present permafrost table. Thus, this wedge may be a permafrost soil wedge with primary filling, i.e., a sand wedge described by Péwé (1959). However, the wedge contained a number of pebbles and cobbles, which seemed to be too large to fall into a narrow thermal crack. The polygon had a wider (220 cm) and deeper (24 cm) furrow in comparison with the ice-wedge polygons, and the edges of the furrow were rounded. As a result, this polygon exhibited a domelike shape. Most polygons around this furrow showed similar shapes. Both the wedge and its host permafrost showed very low ice content, which may indicate that ice content was reduced by sublimation. Thus, an alternative hypothesis is that the wedge was initiated as an ice wedge or a composite wedge (Berg and Black, 1986), and a subsequent arid climate caused sublimation of ice from both the wedge and host permafrost, resulting in a special kind of ice-wedge cast.

##### Adventdalen in Svalbard

Polygons in this area are grouped into large, medium and small sizes. Large-size polygons ( $S = 7-30$  m) are bordered by wide (1-5 m), vegetated furrows. New, open cracks (mostly <1 cm wide) were found in a quarter of the furrows. Digging to the frost table in early summer exposed ice veinlets (commonly 2-3 mm wide) below the open cracks, and further digging showed the ice veinlets extending into permafrost. Although the frequency of cracking has yet to be checked by long-term observations (e.g. Mackay, 1992), these features seem to indicate active thermal cracking under the present climate. Large polygons are often subdivided into several medium-size polygons ( $S = 1-5$  m), which also occur independently of the large polygons. These medium-size polygons show similar open

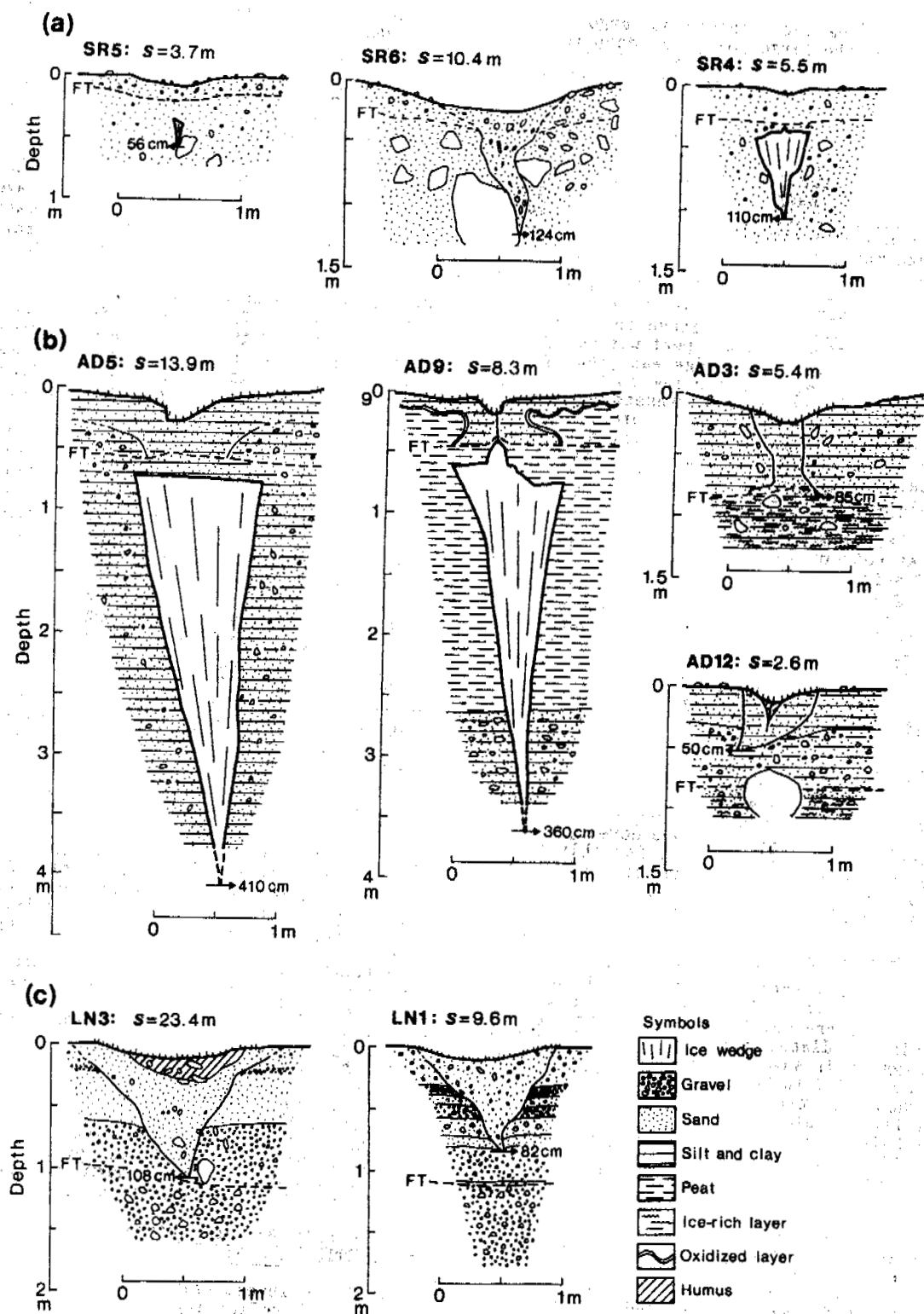


Figure 2. Sketches of wedges in (a) the Sør Rondane Mountains, Antarctica, (b) Adventdalen and (c) Linnédalen, Svalbard. FT indicates the frost table on the excavated day in mid-summer.

cracks with underlying ice veinlets as large as those accompanying the large polygons, despite having narrower furrows (0.6–2 m wide). Small-size polygons ( $S = 0.1\text{--}1\text{ m}$ ) are also formed within larger ones or independently of them.

Four sections of large polygons were observed. Two of them were exposed along a river bank and the others were artificially excavated to the bottom of wedge structures. All the polygons accompanied large ice wedges 85–220 cm wide with vertical dimensions of 225–490 cm (Fig. 2b, Table 1). The  $S$ - $D$  ratios of ice wedges occurring in fine soils (loam and peat) are similar to those in coarse materials (sand and gravel), although data are extremely limited (Table 1). One ice wedge displayed a syngenetic structure in which a small wedge 15 cm wide protruded 20 cm above the main wedge (AD9), suggesting that the peat was being deposited while the small ice wedge was growing. The other three ice wedges, occurring in till or outwash deposits, showed neither syngenetic nor anti-syngenetic (Mackay, 1990) structures.

Five medium-size polygons were excavated well into permafrost, but none accompanied an ice wedge. Instead, the furrows between the polygons were underlain by a soil wedge confined to the active layer (Fig. 2b: AD3, AD12). Some soil wedges had a broad flat bottom (AD3) rather than a pointed end. Such flat bottoms may reflect lateral displacement of soils by cryoturbation in the active layer abutting the permafrost table (Jetchick and Allard, 1990; Van Vliet-Lanoë, 1991). Indeed, since both the soil wedges and host soils were abundant in silts and clays, they were frost susceptible. With regard to surface morphology, these medium-size polygons are hardly distinguishable from the smallest ice-wedge polygons ( $S = 3\text{--}4\text{ m}$ ) in the very different soils of Sør Rondane Mountains. In addition, both polygons have similar  $S$ - $D$  ratios ( $S/D = 5$ ; Table 1).

Distinct furrows and wedge structures were rarely found in the small-size polygons. These polygons were bordered by open cracks in the active layer only, no deeper than 40 cm and developed on both the bare and vegetated ground. Possibly those on the bare ground were desiccation cracks. However, the regularity of the surface forms is quite similar to those of larger polygons.

#### Linnédalen in Svalbard

Polygons (mostly  $S = 5\text{--}30\text{ m}$ ) are extensively developed on coastal terraces. No significant difference in the size and form of polygons was found among the terraces. Most of the polygons exhibited similar diameter and geometrical pattern to large polygons in Adventdalen, although furrows of the former tended to be narrower and shallower.

Wedge structures were observed in five polygons. None of the five displayed an ice wedge, despite all of them being accompanied by an active-layer soil wedge (Fig. 2c). For example, the largest excavated polygon (LN3;  $S = 23.4\text{ m}$ ), described as an ice-wedge polygon by Akerman (1987), was excavated to a depth of 160 cm. Nevertheless, the furrow was underlain by a soil wedge ( $D = 108\text{ cm}$ ) only, which was confined to the active layer. The depth of these soil wedges ranges from 51 to 108 cm, roughly proportional to the polygon sizes, and the  $S$ - $D$  ratios here ( $S/D > 10$ ) are much greater than the other two areas (Table 1).

The wedges, consisting mainly of sand and silt with a few pebbles, displayed a vertical orientation, which was quite different from the host materials composed of horizontal layers of marine sand and gravel. The fillings were probably derived from both the host and wind-brown fine mate-

Table 1. Dimensions and characteristics of excavated wedges.

Wedge ID	S (m)	D (m)	S/D	Wedge <sup>a</sup> type	Host materials
Sør Rondane Mountains, Antarctica					
SR1	7.1	>0.65	—	IW	Gravelly sand
SR2	5.2	1.20	4.3	IW	Gravelly sand
SR3	5.3	1.05	5.0	IW	Gravelly sand
SR4	5.5	1.10	5.0	IW	Gravelly sand
SR5	3.7	0.56	6.6	IW	Gravelly sand
SR6	10.4	1.24	8.4	PSW	Gravelly sand
Adventdalen, Svalbard					
AD1	2.2	0.71	3.1	ASW	Loam
AD2	0.30	0.18	1.7	AOC	Loam
AD3	5.4	0.85	6.4	ASW	Loam
AD4	0.93	0.29	3.2	AOC	Loam
AD5	13.9	4.10	3.4	IW	Loam
AD6	0.14	0.05	2.8	AOC	Loam
AD7	3.8	0.72	5.1	ASW	Loam
AD8	22.5	3.45	6.5	IW	Sand/gravel <sup>b</sup>
AD9	8.3	3.60	2.3	IW	Peat and loam
AD10	3.8	0.72	5.3	ASW	Loam
AD11	19.0	5.80	3.3	IW	Sand/gravel
AD12	2.55	0.50	5.1	ASW	Loam
Linnédalen, Svalbard					
LN1	9.6	0.82	12	ASW	Sand/gravel
LN2	19.3	0.90	21	ASW	Sand/gravel
LN3	23.4	1.08	22	ASW	Sand/gravel
LN4	7.0	0.58	12	ASW	Sand/gravel
LN5	9.0	0.51	18	ASW	Sand/gravel

<sup>a</sup> IW= ice wedge, PSW= permafrost soil wedge, ASW= active layer soil wedge, AOC= open crack in the active layer.

<sup>b</sup> Alternation of sand and gravel

rials. Unlike the flat-bottomed soil wedges in Adventdalen, these wedges had a pointed bottom (Fig. 2c). Such a typical wedge shape suggests that the non-frost susceptible host materials rarely allowed deformation of the wedges by cryoturbation.

Although the excavations to date are limited to five sites, the lack of wedge penetration into permafrost suggests that these polygons mainly accompany active-layer soil wedges regardless of the polygon size. After the ground was uplifted above the sea level (9600–8000 B.P.), ice wedges may have occurred when the active layer was considerably shallower than the present and then melted by warming. Shallow furrows between most of the polygons, however, hardly indicate subsidence due to the ice-wedge melting. New, open cracks found in some furrows suggest that thermal cracking which initiated the soil wedges is still active.

#### RELATIONSHIP BETWEEN SPACING AND DEPTH OF THERMAL CONTRACTION CRACKS

The field investigation suggests that wedges have a depth reflecting their spacing for each study area or for similar thermal environments. The data on the relation between depth and spacing are compiled to evaluate the influence of thermal condition (Fig. 3). Data points for small polygons ( $S < 1\text{ m}$ ) represent the mean values for more than ten adjacent cracks. Regardless of soil types, a

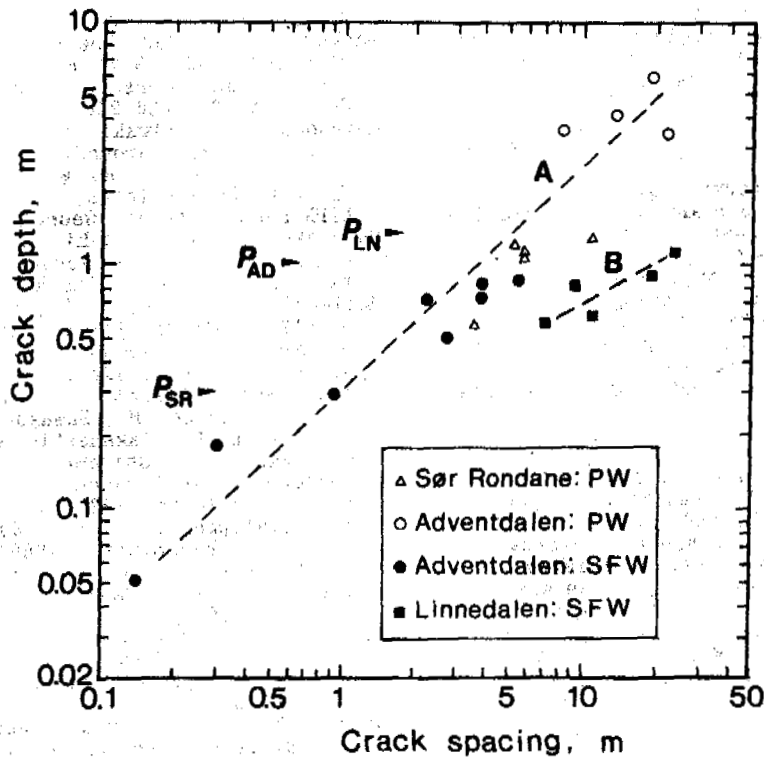


Figure 3. Relationship between the depth and spacing of thermal contraction cracks.  $P_{SR}$ ,  $P_{AD}$  and  $P_{LN}$  indicate the average depths to the permafrost table for the Sør Rondane Mountains, Adventdalen and Linnédalen, respectively. PW= permafrost wedge (ice or permafrost soil wedge). SFW= seasonal frost wedge (active-layer soil wedge or open crack in the active layer). Lines A and B are explained in the text.

good relation can be seen for data from the two regions of continuous permafrost, as indicated by Line A. Data from the discontinuous permafrost region (Linnédalen) are plotted as Line B, indicating that for the same  $S$  value the  $D$  value here is smaller than in the continuous permafrost regions.

The two lines in Fig. 3 are believed to reflect chiefly the difference in permafrost temperatures, because soil types here as at Adventdalen do not seem to affect the  $S$ - $D$  ratios very much. There are two possible effects of permafrost temperatures on the ratios. One is that warmer permafrost is relatively plastic which would tend to arrest the crack extension and result in shallower cracks (Lachenbruch, 1962, 37). The other effect is that cooling leads to contraction of frozen ground when freezing of most of the water and the resultant expansion is complete (Romanovskij, 1973). The temperature at which the soil contracts rather than expands may lie between  $-0.5$  and  $-8^{\circ}\text{C}$ , depending on grain sizes and water content of the soil (Williams and Smith, 1989, 169). Unless the frozen ground is cooled below this critical temperature, thermal contraction cracks never appear. Both effects suggest that cracks do not penetrate into warm permafrost, winter temperature of which falls no lower than several degrees below  $0^{\circ}\text{C}$ .

Lower MAAT and continentality in Adventdalen suggest that winter permafrost temperature is considerably lower than that in Linnédalen. The lower temperature in the former may allow deeper penetration of the thermal contraction cracks into the ground. By contrast, only shallow cracks can be

formed in Linnédalen. This is one possible explanation for the scarcity of active ice wedges in regions of discontinuous permafrost. Indeed, only active-layer soil wedges extending no deeper than 1.5 m have been found beneath large polygons ( $S = 10$ -50 m) in a variety of discontinuous permafrost regions, regardless of soil types: tephra and sandy silty soils in Iceland (Friedman, et al., 1971), volcanic sand and gravel in northern Japan (Sone et al., 1988), and sandy till in Québec (Jetchick and Allard, 1990). The  $S$ - $D$  ratios for these regions seem to exceed ten and lie around Line B in Fig. 3.

By contrast, Line A indicates that permafrost temperatures in winter are low enough to produce deep contraction cracks in both of the continuous permafrost regions. The results agree well with the previous studies from other continuous permafrost regions, which state that ice wedges are usually found beneath polygons larger than 10 m in diameter (e.g. Berg and Black, 1988; Black, 1974; Mackay, 1974), whereas active-layer soil wedges are often found beneath smaller polygons, for example, those smaller than 6 m in Svalbard (Jahn, 1983).

The average depth to the permafrost table,  $P$ , for each area is also indicated on Fig. 3. The intersection between the  $S$ - $D$  line and  $P$  value gives approximately the critical spacing for permafrost-wedge formation. The effect of the  $P$  values on the critical spacing is seen, for example, in the medium-size polygons ( $S = 3$ -4 m), which accompanies permafrost wedges in the Sør Rondane Mountains where  $P = 0.3$  m, but not at Adventdalen



where  $P = 1.0$  m. Because the  $P$  values rarely exceed 2 m in continuous permafrost regions, Fig. 3 demonstrates that active-layer soil wedges mainly occur where  $S < 10$  m in continuous permafrost regions, while they can develop where  $S > 10$  m in discontinuous permafrost regions.

Figure 3 enables us to predict the existence of ice (or permafrost) wedges in terms of polygon size, if the depth to the permafrost table and the temperature of permafrost are known. This relation is also applicable to the identification of the type of fossil wedges, where  $S$ ,  $D$  and  $P$  values at the time of wedge formation can be evaluated. Also soil type cannot be ruled out as being responsible for some of the scatter in Fig. 3, even though it may not be a major factor. Improving the accuracy of the  $S$ - $D$  ratios will require more data on  $S$  and  $D$  values from a variety of soil and climatic regimes.

#### ACKNOWLEDGEMENTS

The field work in Antarctica was supported by Japanese Antarctic Research Expedition, National Institute of Polar Research, and that in Svalbard was funded by Kyoikusha Co., Tokyo and International Scientific Research Program, Ministry of Education, Science and Culture, Japan. We acknowledge the field assistance and helpful comments of T. Koaze, Y. Ono, K. Moriwaki, S. Iwata, T. Watanabe, S. Sawaguchi, H. Hasegawa, K. Shiraiwa, T. Sawagaki, A. Harada and Y. Ebina.

#### REFERENCES

- Akerman, J. (1987) Periglacial forms of Svalbard: a review. In: J. Boardman, ed. *Periglacial Processes and Landforms in Britain and Ireland*. Cambridge University Press, Cambridge, pp. 9-25.
- Berg, T. E. and Black, R. F. (1986) Preliminary measurements of growth of nonsorted polygons, Victoria Land, Antarctica. In: J. C. F. Tedrow, ed. *Antarctic Soils and Soil Forming Processes*. American Geophysical Union, Antarctic Research Series, No. 8, pp. 61-108.
- Black, R. F. (1974) Periglacial features indicative of permafrost: ice and soil wedges. *Quaternary Research*, 6, 3-28.
- French, H. M. (1976) *The Periglacial Environment*. 309 pp. Longman, London.
- Friedman, J. D., Johansson, C. E., Oskarsson, N., Svengsson, H., Thorarinsson, S. and Williams, R. S. Jr. (1971) Observation on Icelandic polygon surfaces and palsa areas: photo interpretation and field studies. *Geografiska Annaler*, 53A, 115-145.
- Jahn, A. (1983) Soil wedges on Spitsbergen. *Proc. 4th Intl. Conf. Permafrost*. National Academy Press, Washington, D. C., pp. 525-530.
- Jetchick, E. and Allard, M. (1990) Soil wedge polygons in Northern Québec: description and paleoclimatic significance. *Boreas*, 19, 353-367.
- Lachenbruch, A. H. (1962) Mechanics of thermal contraction cracks and ice-wedge polygons in permafrost. *Geological Society of America Special Paper*, No. 70, 69 pp.
- Lønne, I. and Mangerud, J. (1991) An Early or Middle Weichselian sequence of proglacial, shallow marine sediments on western Svalbard. *Boreas*, 20, 85-104.
- Mackay, J. R. (1974) Ice-wedge cracks, Garry Island, Northwest Territories. *Canadian Journal of Earth Sciences*, 11, 1366-1383.
- Mackay, J. R. (1990) Some observations on the growth and deformation of epigenetic, syngenetic and anti-syngenetic ice wedges. *Permafrost and Periglacial Processes*, 1, 15-29.
- Mackay, J. R. (1992) The frequency of ice-wedge cracking (1987-1987) at Garry Island, western Arctic coast, Canada. *Canadian Journal of Earth Sciences*, 29, 236-248.
- Matsuoka, N., Moriwaki, K., Iwata, S. and Hirakawa, K. (1990) Ground temperature regimes and their relation to periglacial processes in the Sør Rondane Mountains, East Antarctica. *Proc. NIPR Symp. Antarct. Geosci.*, 4, 55-66.
- Matsuoka, N. and Moriwaki, K. (1992) Frost heave and creep in the Sør Rondane Mountains, Antarctica. *Arctic and Alpine Research*, 24, 271-280.
- Moriwaki, K., Hirakawa, K., Iwata, S. and Hayashi, M. (1991) Glacial history in the Sør-Rondane Mountains, East Antarctica: thick tills and evidence of warmer climate in the past. *Abstr. 6th Intl. Symp. Antarct. Earth Sci.*, pp. 418-422.
- Ono, Y., Matsuoka, N., Sawaguchi, S., Shimokawa, K., Fukuda, M., Takahashi, N., Shiraiwa, T., Hasegawa, Y., Yoshikawa, K. and Muto, H. (1991) Geomorphological results of the Japanese Expedition to Svalbard, 1988-1989. *Mountain Research and Development*, 11, 259-269.
- Permafrost Subcommittee (1988) *Glossary of Permafrost and Related Ground-Ice Terms*. National Research Council Canada, Technical Memorandum, No. 142, 158 pp.
- Péwé, T. L. (1959) Sand-wedge polygons (tessellations) in the McMurdo Sound Region, Antarctica: a progress report. *American Journal of Science*, 257, 545-552.
- Romanovskij, N. N. (1973) Regularities in formation of frost-fissures and development of frost-fissure polygons. *Biuletyn Peryglacjalny*, 23, 237-277.
- Romanovskij, N. N. (1985) Distribution of recently active ice and soil wedges in the USSR. In: M. Church and S. Slaymaker, eds. *Field and Theory: Lectures in Geocryology*. University of British Columbia Press, Vancouver, pp. 154-165.
- Salvigsen, O. and Elgersma, A. (1985) Large-scale karst features and open taliks at Vardeborgsletta, outer Isfjorden, Svalbard. *Polar Research*, 3, 145-153.
- Sone, T., Takahashi, N. and Fukuda, M. (1988) Alpine permafrost occurrence at Mt. Taisetsu, central Hokkaido, in northern Japan. In: K. Senneset, ed. *Proc. 5th Intl. Conf. Permafrost*, Vol. 1. Tapir Publishers, Trondheim, pp. 253-258.
- Svendsen, J. I., Mangerud, J. and Miller, G. H. (1989) Denudation rates in the Arctic estimated from lake sediments on Spitsbergen, Svalbard. *Palaeogeography, Palaeoclimatology, Palaeoecology*, 76, 153-168.
- Svensson, H. (1988) Ice-wedge casts and relict polygonal patterns in Scandinavia. *Journal of Quaternary Science*, 3, 67-87.
- Van Autenboer, T. (1984) The geomorphology and glacial geology of the Sør Rondane, Dronning Maud Land, Antarctica. *Mededelingen van de Koninklijke Vlaamse Academie voor Wetenschappen, Letteren en Schone Kunsten van België*, No. 8, 91pp.
- Van Vliet-Lanoë, B. (1991) Chronostratigraphy and paleoclimatic meaning of cryogenic deformations in the central European Loess. *GeoJournal*, 24, 157-163.
- Washburn, A. L. (1979) *Geocryology: A Survey of Periglacial Processes and Environments*. 408pp. Edward Arnold, London.
- Williams, P. J. and Smith, M. W. (1989) *The Frozen Earth: Fundamentals of Geocryology*. 306 pp. Cambridge University Press, Cambridge.

PECULIARITIES OF FORMATION AND THAWING OF ICE ORIGINATED FROM COLLOID SOLUTIONS  
AND REGULATING OF THE PHASE CONDITIONS OF WATER IN THE CRYOSPHERE

Vladimir Melnikov and Gennadi Smorygin

Institute of the Earth's Cryosphere, Tyumen, Russia

Experiments show that freezing of colloid solutions results in a notable, if not irreversible, re-distribution in their structure and changes in their behavior. When the distance between gel and ice reaches  $10^{-4}$ - $10^{-5}$  cm, the disjoining pressure is induced in a water film that hinders future movement of the gel closer to the ice. The gel inclusion into the ice depends upon the two parameters: the specific hydroconductivity of growing gel films and their thickness. There exists a certain dependence of crystallization rate upon the temperature of the cooled ice surface. If the solution contains highly grained mineral particles freezing will be accompanied by their re-distribution. An ice embryo is necessary for the crystallization to begin, otherwise the solution gets overcooled due to the heat emission. The destruction of frozen colloid systems with the layered structure during thawing occurs in the following way. A temperature increase causes thawing of cells containing substantial quantities of admixtures.

Colloid systems are rather wide-spread in nature. The best known examples are dispersions of clay and other mineral particles, surfactant solutions of high molecular compounds as a part of sewage, soil and other natural formations.

Experiments show that freezing of colloid solutions results in a notable, if not irreversible, re-distribution in their structure and changes in their behavior.

Let us consider freezing of colloid solutions containing gel forming high molecular compounds (Fig.1). During crystallization polymer molecules will accumulate at a non-stationary boundary, since polymer solubility in ice is much lower than in water. At the same time polymer diffusion into non-crystallized water will occur. Their stationary distribution is possible with time ahead of an advancing front. But a stationary concentration of admixture near the front of crystallization can be associated with non-interacting molecules. Beyond some critical concentrations polymer molecules tend to be bound with each other and form gels. Water transport to the front is possible through forming gel (filtration). During filtration a hydrodynamic force is induced that presses a gel layer to the phase boundary.

When the distance between gel and ice reaches  $10^{-4}$ - $10^{-5}$  cm forces of the disjoining pressure are induced in a water film that hinders further moving of gel closer to ice. Depending upon these forces a gel layer can be incorporated into the ice or expelled into the solution.

Processes associated with gel formation near the surface of a growing crystal seem to be analogous to dynamic membrane formation. The latter are formed by coming through a porous layer within solutions containing membrane-forming substrates, the pores' size being of  $3 \times 10^{-7}$ - $5 \times 10^{-4}$  cm (Bryk and Tsapjuk, 1989). The following compounds can serve as membrane-generating substances: neutral organic polymers

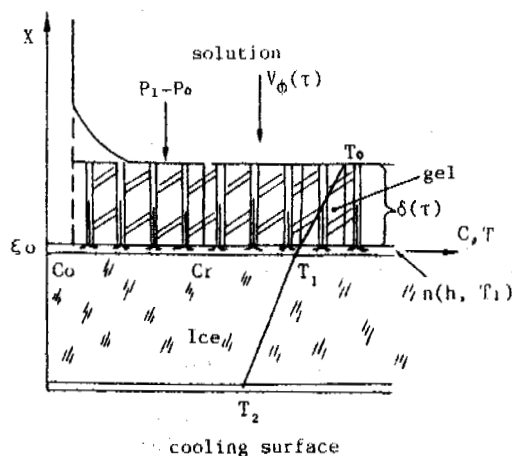


Figure 1. The scheme of a gel layer  $\delta(\tau)$  formation on the surface of growing ice.  $P_1$  is the external pressure;  $P_0$  is the atmospheric pressure,  $V_f$  is the filtration rate,  $\delta$  is the thickness of a gel layer,  $C_0$  and  $C_r$  are polymer concentrations in the initial solution and the critical of gel formation,  $\Pi(h)$  is the disjoining pressure,  $T_2$  is the temperature of the refrigerator,  $\xi$  is the thickness of an ice layer

(polyvinyl alcohol, starch, dextrans), organic and non-organic ion-exchangers (bentonite, highly dispersed ionites), polyelectrolytes (huminoacids, polyacrilic acid, gelatine and the like), hydroxides of multicharged metals.

Dynamic membranes are capable of incorporating low-molecular substances present in the solution (secondary detaining).

One of the most important characteristics of the dynamic membranes, including those originated

from gelatine, is their high compressibility. At pressures exceeding 4 MPa the filtration slightly increases, and at pressures more than 6 MPa it remains practically constant. So, the detaining of magnesium chloride by a starch dynamic membrane makes up 10% at the pressure 1 MPa and 60% at P=6 MPa. The reason of the pressure dependent increase in secondary detaining can be attributed to compressibility of a membrane layer that increases the contribution of the interface forces to the distribution.

The above mentioned reasons can have a significant influence upon freezing of closed cells of colloid solutions at the nucleus pressure up to dozens of atmospheres.

The formation of dynamic membranes during crystallization of surfactants requires special conditions. Molecules of surfactants form true solutions at concentrations lower than the critical concentration of micelle formation. On reaching a critical concentration aggregate-micelles are generated from single molecules present as micro-compounds of different shapes. A colloid micelle is a semi-penetrable system, since some substances, being introduced into the solution and according to their chemical nature, can spontaneously diffuse through a monolayer and accumulate in the nucleus up to high concentrations. The mechanism of their transfer inside the micelle is analogous to that in biologic membranes.

Let us consider the formation of a concentrated polymer layer at the initial stage, i.e. the concentration near the phase boundary is lower than Cr (a critical concentration of gel formation). A non-stationary transfer is described by the equation of the convective diffusion in the coordinate system connected with the boundary of ice growth:

$$\frac{\partial C}{\partial \tau} - V_0 \frac{\partial C}{\partial x} = D \frac{\partial^2 C}{\partial x^2} \quad (1)$$

with the following initial and boundary conditions:

$$\begin{aligned} C(\tau, \infty) &= C_0, & C(0, x) &= C_0, \\ D \frac{\partial C}{\partial x} + V_0 C &= 0, & x=0, \end{aligned} \quad (2)$$

where  $C_0$  is the polymer concentration in the initial solution (or on the infinity);  $D$  is the diffusion coefficient of the polymer in water;  $V_0$  is the rate of ice growth;  $x$  is a coordinate;  $\tau$  is time.

The solution for a set of equations (1) and (2) is of the form (Amelkin, Smorygin; 1989):

$$\begin{aligned} C(x, \tau) = C_0 \left( 1 + \frac{V_0}{D^{0.5}} \exp\left(-\frac{V_0 x}{2D}\right) \int_0^\tau [(\pi t)^{-0.5} \exp\left(-\frac{x^2}{4Dt}\right) \exp\left(-\frac{V_0^2 t}{4D}\right) + \frac{V_0}{2D^{0.5}} \exp\left(-\frac{V_0 x}{2D}\right) \operatorname{erfc}\left(\frac{x}{2(Dt)^{0.5}} - \frac{V_0 t^{0.5}}{2D^{0.5}}\right)] dt \right) \end{aligned} \quad (3)$$

and at the ice surface ( $x=0$ ):

$$\begin{aligned} C(0, \tau) = C_0 \left[ 1 + \operatorname{erf}(0.5 V_0 (\tau/D)^{0.5}) \right] \left( 1 + \frac{V_0 \tau}{2D} \right) + V_0 \left( \frac{\tau}{\pi D} \right)^{0.5} \exp\left(-\frac{V_0^2 \tau}{4D}\right) \end{aligned} \quad (4)$$

It can be seen from expression (4) that an unlimited increase in concentration near the ice-solution interface can be observed at  $\tau \rightarrow \infty$  and at the ultimate rate of ice growth.

Let us find an equation to describe the changes in the level of a determined concentration  $Cr(x(\tau), \tau)$  in order to define the distance from the ice surface at which the concentration is enough for gel formation ( $Cr$ ). Setting the full time derivative of  $Cr$  to null and using equation (1) we derive:

$$\frac{dx}{d\tau} = \frac{V_0}{\Delta} \exp\left[-\left(V_0 + \frac{dx}{d\tau}\right) \frac{x}{D}\right],$$

$$\Delta = Cr/Co - 1; \quad C(0, \tau_0) = Cr; \quad x(\tau_0) = 0,$$

where  $\tau_0$  is the moment of detachment of the concentration level  $Cr$  from the crystallization front. For the concentration  $Cr \gg Co$  we have:

$$x = \frac{D}{V_0} \ln\left[\frac{V_0^2}{D\Delta} (\tau - \tau_0) + 1\right] \quad (5)$$

At  $\tau_0 = \frac{D\Delta}{V_0^2}$  we derive:

$$x = \frac{D}{V_0} \ln\left[\frac{V_0^2 \tau}{D\Delta}\right] \quad (5')$$

Calculations show that the thickness of a gel layer makes up  $71 \times 10^{-6}$  m at crystallization rates near  $10^{-4}$  m/s; the minimum time of formation is 17 min. The time of  $10^7$  sec is necessary for the formation of more thick gel layers (up to 1 mm) at the above mentioned rate. At high rates of ice growth ( $10^{-4}$  m/s) during the interval of  $10 \times 10^{-6}$  m is formed. According to (3) the polymer concentration in gel alters. So, after the interval of 3.16 sec the value of  $C(0, \tau)$  exceeds the initial concentration 300 times at the interphase boundary, and at a distance of  $5 \times 10^{-6}$  m from the boundary the concentration of dissolved molecules does not differ from the initial concentration (Fig.2). Such a sharp decrease in concentration near the phase surface is not characteristic of gel-forming substances. Hence, the system (1)-(2) can serve exclusively for estimation. The initial layer formed from connected molecules presents an obstacle for other polymer molecules. This specific filter lets through water molecules and dissolved low-molecular compounds, and detains large polymer molecules. Meanwhile a gel membrane increasing in time is formed with the thickness of  $\delta(\tau)$ . The hydroporemeability  $K$  is a decreasing time function. In this case, taking into consideration non-stationary growth of a gel layer, the problem will be written in the following way:

$$\frac{\partial C}{\partial \tau} = D \frac{\partial^2 C}{\partial x^2} + V(\tau) \frac{\partial C}{\partial x} \quad (6)$$

$$C_m \frac{\partial \delta(\tau)}{\partial \tau} = D \frac{\partial C}{\partial x} + V(\tau) C; \quad x = \delta(\tau) \quad (7)$$

$$C(\tau, \infty) = C_0; \quad C(\tau, \delta(\tau)) = Cr; \quad (8)$$

$$\delta(\tau_k) = 0;$$

where  $C_m$  is the polymer concentration in a gel layer;  $V(\tau)$  is the filtration rate of water;  $\tau_k$  is the time necessary for the initial gel layer formation (the first approximation for  $\tau_k$  can be derived from (5')).

The polymer concentration  $C_m$  in a gel layer depends upon a lot of factors, i.e. upon the

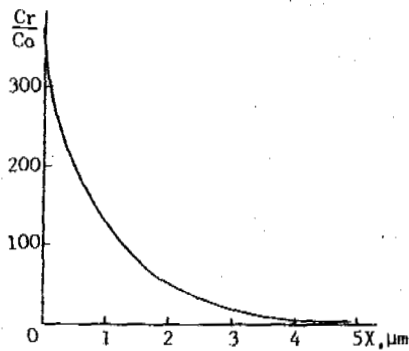


Figure 2. The distribution of a relative polymer concentration  $C_r/C_0$  from the surface to the depth of the solution

critical concentration  $C_r$  of gel formation which, in its turn, is governed by gel-forming properties of the polymer; upon temperature; upon the filtration rate and pressure etc.

The solution of the system (6)-(8) is of the form:

$$\delta(\tau) = z D^{1/2} (\tau - \tau_K)^{-1/2} \quad (9)$$

$$\frac{C_m}{2(C_r - C_0)} z \approx \frac{K_0}{Dz} \Delta P \left( \frac{C_r}{C_r - C_0} \right) - \frac{\exp[-(z/2 + K_0 \Delta P / 2Dz)^2]}{\pi^{1/2} \operatorname{erfc}(z/2 + K_0 \Delta P / 2Dz)} \quad (10)$$

In expression (10) it is assumed that

$$\Delta P = \frac{V_f(\tau) \delta(\tau)}{K_0}$$

where  $K_0$  is the permeability of a thickness unit in a gel layer [ $m^4 N^{-1} sec^{-1}$ ];  $P$  is the difference of pressures in the solution and in an unfrozen water film between gel and ice.

The analysis of expression (10) shows that there exists a critical value of the specific hydroconductivity  $K_0 \leq 1.2 \cdot 10^{-16} m^4 N^{-1} sec^{-1}$ , under which a gel layer cannot appear ( $\delta=0$ ).  $\Delta P = 10^5 Pa$ ,  $C_0 = 0.1\%$ ,  $C_m = 0.5\%$  gel layer with the  $\delta = 13 \cdot 10^{-6} m$  ( $K_0 = 2 \cdot 10^{-16} m^4 N^{-1} sec^{-1}$ );  $\delta = 40 \cdot 10^{-6} m$  ( $K_0 = 10^{-15}$ ); and  $\delta = 150 \cdot 10^{-6} m$  ( $K_0 = 10^{-14}$ ) is formed during 100 sec (Fig.3) at  $\Delta P = 10^5 Pa$ ;  $C_0 = 0.1\%$ ;  $C_m = 0.5\%$ , and under complete detachment of polymer molecules from ice. At the initial polymer concentration  $C_0 = 0.01\%$  and at  $K_0 = 10^{-15} m^4 N^{-1} sec^{-1}$  the thickness of a gel layer amounts to  $4 \cdot 10^{-6} m$  for 100 sec, which approximately 3 times lower than at  $C_0 = 0.1\%$ . Thus, a gel layer, capable of influencing further mass exchange, is formed near the ice surface in some tenths of seconds.

The hydroconductivity of a layer  $\delta(\tau)$  (a concentrated polymer solution) decreases with further gel formation, and water inflow to growing ice diminishes. This results in disbalance of the thermodynamic equilibrium, and the temperature  $T_i$  of the phase transfer (the temperature of an unfrozen layer) decreases and goes lower than 273 K.

Let us derive the equation of the thermodyna-

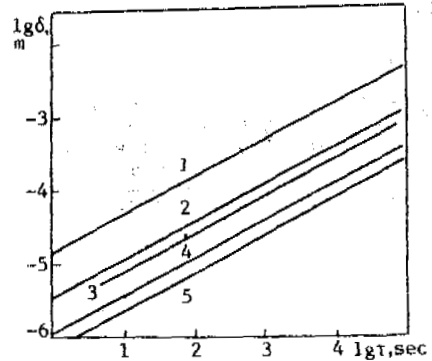


Figure 3. Time dependence of a gel layer thickness ( $\delta$ ) ( $\delta$ -m,  $\tau$ -sec,  $V_0$ -m/sec,  $K_0$ - $m^4 N^{-1} sec^{-1}$ ,  $C$ -%,  $P=10^5 Pa$ ):

1 - is the initial filtration rate  $V_0 = 6.6 \cdot 10^{-5}$ ,  $K_0 = 10^{-14}$ ,  $C_m = 0.5$ ,  $C_0 = 0.1$ ; 2 -  $V_0 = 2.8 \cdot 10^{-5}$ ,  $K_0 = 10^{-15}$ ,  $C_m = 0.5$ ,  $C_0 = 0.1$ ; 3 -  $V_0 = 2.8 \cdot 10^{-5}$ ,  $K_0 = 10^{-15}$ ,  $C_m = 1.0$ ,  $C_0 = 0.1$ ; 4 -  $V_0 = 1.7 \cdot 10^{-5}$ ,  $K_0 = 2 \cdot 10^{-16}$ ,  $C_m = 0.5$ ,  $C_0 = 0.1$ ; 5 -  $V_0 = 1.4 \cdot 10^{-4}$ ,  $K_0 = 10^{-15}$ ,  $C_m = 1.0$ ,  $C_0 = 0.01$ .

mic equilibrium at the interphase boundaries gel - unfrozen water film - ice (Fig.1). The expression for the free energy ( $G_B$ ) of water near the gel surface is:

$$G_w = G_{w0} + V_w P_w - S_w T_w - g(x) + P_{10} V_w \quad (11)$$

where  $G_{w0}$  is the free energy of water;  $V_w$ ,  $S_w$  are the specific volume and water entropy;  $g(x)$  is a characteristic of the gel surface impact;  $P_w = P_{wg} - P_0$  is the pressure within a water layer;  $P_{wg}$  is the pressure near the gel surface;  $T_w = T_{wg} - T_0$  is temperature;  $T_{wg}$  is the water temperature in a layer near the gel surface;  $P_0$ ,  $T_0$  are the pressure and the temperature under normal conditions;  $P_{10}$  is the hydrostatic pressure of the solution ( $P_{10} = P_{10} - P_0$ ).

The free energy of ice at the boundary with the unfrozen water can be written:

$$G_i = G_{i0} + V_i P_i - S_i T_i \quad (12)$$

where  $G_{i0}$  is the free energy of ice;  $P_i$  and  $T_i$  are the pressure and the temperature of ice near the phase boundary.

By making equal the free energies near the phase surface, and assuming that  $h$  (a distance between phase surfaces gel-ice (unfrozen water)) is small, and by introducing  $T_w = T_i = T_1$ ;  $P_w = P_i = P_c$ , we obtain:

$$\Delta V P_c - (S_w - S_i) T_1 + P_{10} V_w = g(h) \quad (13)$$

$$\Delta V = V_w - V_i$$

Taking into consideration that  $(S_w - S_i) T_0 = L$ , where  $L$  is the latent heat of the phase transfer ice-water, and considering the correlation (Gilpin, 1980)

$$P_c = V_w^{-1} g(h)$$

we obtain from (13):

$$V_w P_{10} = V_i P_c + \frac{L T_1}{T_0} \quad (14)$$

The condition for the mechanic equilibrium of the system under consideration (Fig.1) can be obviously written:

$$P_{10} = P_c + \Pi(h) \quad (15)$$

where  $\Pi(h) = B/h^2$  is the disjoining pressure; B is the constant (Derjagin and Churajev, 1980).

Using (14) and (15) we can write:

$$\Pi(h) = (1 - \frac{v_w}{v_i}) P_{10} + \frac{L T_1}{v_i T_0} \quad (16)$$

The rate of filtration through gel is determined by the expression:

$$V_f(\tau) = K \Delta P \quad (17)$$

where K is the hydroconductivity coefficient of gel channels and of an unfrozen layer (Fig.1);  $\Delta P = P_{10} - P_c$ . The hydroconductivity coefficient is usually determined by the formula:

$$K^{-1} = (K^*)^{-1} + \delta/K_0 \quad (18)$$

where  $K^*$  is the hydroconductivity of an unfrozen layer. The following dependence was suggested by R. Gilpin (1980) for water transport between the discs with the radius R and growing ice:

$$\frac{1}{K^*} = \frac{1}{Ah^2} = \frac{3}{2} \frac{v_w \eta R^2}{gh^3} (1 - 3 \frac{1}{2} \pi r^2/R^2) \quad (18')$$

where A is a constant; r is the effective radius of the pores;  $\eta$  is viscosity; g is the acceleration of gravity. The value h is defined from the expression:

$$h = \left[ \frac{v_i K_0 B}{v_w \delta v_i} \right]^{\frac{1}{2}} \quad (19)$$

The pressure upon the layer from the side of a moving solution is balanced by the disjoining pressure  $\Pi(h)$ . Thus,

$$\frac{v_f}{K} = \Pi(h) \quad (20)$$

By substituting the expression for  $\Pi(h)$  we derive from (16):

$$\frac{v_f}{K} = (1 - \frac{\rho_i}{\rho_w}) P_{10} + \frac{\rho_i L T}{T_0} \quad (21)$$

Let us connect the filtration rate with the rate of a moving phase boundary ice-solution. The heat transfer (ice formation) being rather slow, we shall make use of the quasistationary field condition for the temperatures in ice and in a gel layer. If, for the sake of simplicity, the temperature of the solution  $T_0$  is assumed to be equal to the temperature of the equilibrium phase transfer, we obtain (Fig.1):

$$\left[ \frac{\lambda_w}{\delta(\tau)} + \frac{\lambda_i}{\xi(\tau)} \right] T_1 - \left[ \frac{\lambda_w T_0}{\delta(\tau)} + \frac{\lambda_i T_2}{\xi(\tau)} \right] = L \rho_w v_i(\tau) \quad (22)$$

where  $\lambda_w$  and  $\lambda_i$  are heat conductivity coefficients of water and ice;  $T_1$  is the temperature of water in an unfrozen layer;  $T_2$  is the temperature of the cooled ice surface;  $\xi$  is the ice thickness.

We define the temperature in an unfrozen layer from correlation (22):

$$T_1 = \frac{L \rho_w v_i + \lambda_w T_0 / \delta + \lambda_i T_2 / \xi}{\lambda_w / \delta + \lambda_i / \xi} \quad (23)$$

Substituting the expression for temperature (23) into (21), and taking into consideration the connection  $v_i = v_f w / i$ , we define the crystallization rate  $v_i^*$  beyond which gel will be incorporated into the ice:

$$\frac{\rho_i v_i^*}{wK} = (1 - \rho_i / \rho_w) P_{10} + \rho_i L - \frac{\rho_i L}{T_0} \left( \frac{L \rho_w v_i^* + \lambda_w T_0 / \delta + \lambda_i T_2 / \xi}{\lambda_w / \delta + \lambda_i / \xi} \right) \quad (24)$$

Let us use the dependence in (18), (18') and in (19) to define K:

$$\frac{1}{K} = \frac{1}{A \left[ \frac{\rho_w K_0 B}{\rho_i \delta v_i} \right]^{3/2}} + \frac{\delta}{K_0} \quad (25)$$

By transformation of (24) with respect to (25) we obtain the ultimate expression for the definition of  $v_i^*$ :

$$\left[ \frac{\rho_w}{\rho_i} \right]^{\frac{1}{2}} \frac{v_i^{*5/2}}{A \left[ \frac{K_0 B}{\rho_i \delta v_i} \right]^{3/2}} + v_i^* \left\{ \frac{\delta}{K_0} + \frac{\rho_w \rho_i L^2}{T_0 (\lambda_w / \delta + \lambda_i / \xi)} \right\} = \left[ 1 - \frac{\rho_i}{\rho_w} \right] P_{10} + \rho_i L \left[ 1 - \frac{\lambda_w T_0 / \delta + \lambda_i T_2 / \xi}{T_0 (\lambda_w / \delta + \lambda_i / \xi)} \right] \quad (26)$$

The analysis of equation (26) shows that the gel inclusion into the ice depends, mostly, upon the two parameters: the specific hydroconductivity of growing gel films ( $K_0$ ) and their thickness ( $\delta$ ) (Fig.4). There exists a certain dependence of  $v_i^*$  upon the basis temperature  $T_2$ . Up to  $-2.5^\circ\text{C}$  ice formation is governed by the water inflow through a gel layer (the first left member prevails). Above this temperature the rate of ice growth is limited by the heat exchange (the second left member). If the external pressure slightly deviates from the atmospheric pressure ( $P_{10} = 0$ ), and  $T_2$  tends to  $T_1$ , the process is determined by the second right member and the rate of ice growth tends to 0. In fact, equation (26) can be re-written in the form:

$$a v_i^{*5/2} + b v_i^* = 0 \quad (27)$$

Removing  $v_i$  out of the brackets we derive two equations:

$$v_i^* = 0; \quad v_i^{*3/2} = -\frac{b}{a}$$

Since the coefficients a and b are positive in the last equation, the rate appears to be negative, which is obviously a sharp contradiction in terms. Thus, at  $T_2 = T_0$   $v_i^* = 0$ .

In this connection, in order to define the critical rate of the gel inclusion into the ice it is necessary to use the range of temperatures from  $-10^\circ\text{C}$  to  $-2.5^\circ\text{C}$  (Fig.4), within which the process is governed by both the mass- and heat exchange. This temperature range can extend to higher temperatures at other values of  $\delta$ ,  $K_0$  and  $\xi$ .

An impact of the external pressure upon the increasing critical rate appears to become notable beginning with  $P_{10} = 5$  MPa and at  $T_2$  being above  $-3^\circ\text{C}$ .

Thus, critical rates are rather low and make

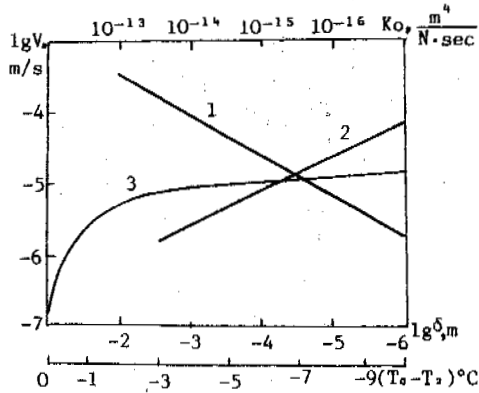


Figure 4. The dependence of a critical rate of ice growing ( $V_i^*$ ) upon temperature ( $T_0 - T_2$ ), specific hydroconductivity ( $K_0$ ) and a gel layer thickness ( $\delta$ ).  
 1- $V_i^* = V_i^*(K_0)$  at  $T = -1^\circ\text{C}$ ,  $\delta = 10^{-5}\text{ m}$ ,  $\xi = 10^{-3}\text{ m}$ ;  
 2- $V_i^* = V_i^*(\delta)$  at  $T = -1^\circ\text{C}$ ,  $\xi = 10^{-3}\text{ m}$ ,  $K_0 = 10^{-15}\text{ m}^4\text{ N}^{-1}\text{ sec}^{-1}$ ;  
 3- $V_i^* = V_i^*(\Delta T)$  at  $\xi = 10^{-2}$ ,  $\delta = 10^{-5}$ ,  $K_0 = 10^{-15}\text{ m}^4\text{ N}^{-1}\text{ sec}^{-1}$ .

up to  $10^{-6}\text{ m/s}$  under the most common conditions ( $K_0 = 10^{-15}$ ,  $\delta = 10^{-4}$ ,  $\Delta T = -1^\circ\text{C}$ ). Detachment of gel and concentration of ice layers are possible at lower rates.

If the solution contains highly grained mineral particles, i.e. a colloid fraction of soils (with the particle size less than  $0.25 \times 10^{-6}\text{ m}$ ), silt ( $0.25 - 1\ \mu\text{m}$ ), clay ( $1 - 10\ \mu\text{m}$ ), freezing will be accompanied by their re-distribution. A correlation has been found between the critical rate of the particles inclusion and their radii  $R$  (Cisse, Bolling; 1971).

$$V_i^* R^3 = \frac{4\phi K T \sigma a_0}{9\pi\eta^2} \quad (28)$$

where  $\eta$  is the viscosity of water;  $\sigma = 1.6 \times 10^{-2}\text{ J sm}^{-2}$  is the free surface energy at the phase boundary;  $a_0 = 3.8 \text{ \AA}$  is the molecular distance in water;  $\phi = 0.34$  is a dimensionless constant;  $K$  is the Boltzmann constant;  $T$  is temperature. There is a linear dependence of  $V_i^*$  upon  $R$  in the logarithmic coordinates (Fig. 5). Calculations show that colloid fractions of soil and silt particles will be incorporated into the ice at crystallization rates of  $10^{-5} - 10^{-4}\text{ m/s}$ . Since, at rates of  $10^{-6} - 10^{-7}\text{ m/s}$ , when a gel layer detachment is observed, these particles will be expelled by growing ice and will concentrate near the phase boundary together with the polymer. On reaching a critical concentration individual properties of mineral particles become lost (they are connected with the polymer), and the behavior of the gel - particles system will be controlled by hydroconductivity and the size of a gel layer.

Let us pay attention to the following important factor. An ice embryo is necessary for the crystallization to begin, otherwise the solution gets overcooled due to the heat emission. The solution can remain interminably in a supercooled state, until an embryo spontaneously

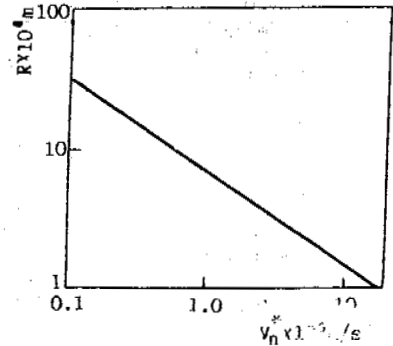


Figure 5. The dependence of a critical rate upon the particles' radii.

nucleates. It is very soon followed by a net of ice dendrites, which accumulate ice originated from water advancing through gel membranes. In this case ice layers (without gel) are located in what seems to be a chaotic order in respect to the surface of cooling.

If a cooled surface is covered with solid ice, pure ice crystals will grow in a sheet-like form perpendicular to the surface of the heat emission. This may be a result of the phase boundary instability, which manifests itself in the appearance of spontaneous protuberances and their penetration into a better nutrition media. The higher the rate of the heat emission, the more probable the process is.

Layered structures described above cause the aggregation and distabilization of stable colloid systems. A concentration of dispersed particles takes place with their further aggregation in between pure ice layers.

The destruction of frozen colloid systems with the layered structure during thawing occurs in the following way. A temperature increase causes thawing of cells containing substantial quantities of admixtures. But a melted gel layer with small solid particles is not subjected to destruction and tends to remain bounded. After thawing of pure ice layers gel cells, being more heavy, precipitate in the capacity, i.e. the distribution of the colloid solution takes place.

The process of ice growth (freezing) in soils and rocks containing highly molecular compounds, though in tiniest quantities, favours their concentration and accumulation near the daily surface. This as well can be referred to the freezing of water reservoirs. Here two cases are possible. Aggregates of polymer molecules are heavier than water, so they precipitate. But the tiniest mineral particles, non-soluble organic substances (oil emulsions) and gas bubbles can be found in dirty water alongside with soluble polymers. Concentrated mineral particles connected with the polymer are heavier than water and will precipitate during thawing. Oil emulsions and gas bubbles incorporated into the polymer can come to the surface and remain there or precipitate. This is conditioned by a quantitative correlation between compounds in aggregates.

Polymer molecules are incorporated into the ice practically without their re-distribution in the solution at rates  $V_i^* > 5 \times 10^{-5}\text{ m/s}$  (Fig. 3). In this case a polymer is proportionally distributed in ice, which results in formation of a specific ice-composed material. During thawing, of this material incorporated molecular chains

become exposed and remain connected from the side of ice, and form gel or a highly viscous layer from the side of a thawing phase. This layer hinders or limits the water flow near the ice surface.

It is known that a turbulent flow consists of a viscous layer, a transitional zone and a turbulent nucleus. Melting polymer molecules form a zone that causes a significant shift in the profile of the turbulent flow at the boundary ice-water. This causes an increase in the thickness of a layer immediately adjacent to the walls that connects a viscous layer and a transitional zone (Fig.6). An increased thickness of an adjacent layer should result in a decrease in the heat emission coefficient and, hence, in a decrease of ice thawing intensity. The other reason for a decrease in ice thawing intensity is a turbulence extinction caused by polymer molecules penetrating into the flow during thawing.

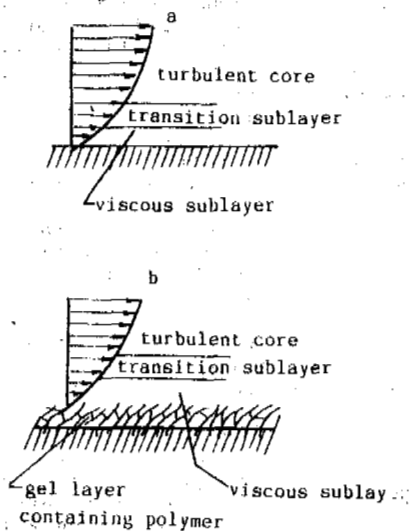


Figure 6. The turbulent flow structure near the wall during ice thawing  
a- near the pure ice surface;  
b- ice containing polymer.

Experiments on a transitional layer, on ice thawing and heat exchange were carried out on a closed hydrodynamic contour, the operating channels being made of transparent organic glass. The flow rate was changed from 0.1 to 4 m/s. The analysis of the pictures shows that the thickness of a transitional layer varies from 1.5 to 7 mm for different polymers. Coefficients of heat emission depend upon the flow velocity and differ in three times or more for pure ice as compared to ice with polymer (Fig.7).

Criterion analysis of experimental data for pure ice gives a correlation:

$$Nu = 0.0138 Pe^{0.8}$$

for ice containing 0.5% of gelatine:

$$Nu = 0.005 Pe^{0.8}$$

and for ice with 0.5% of polyoxyethylen:

$$Nu = 0.006 Pe^{0.8}$$

where Nu, Pe are the Nusselt and Peckle numbers.

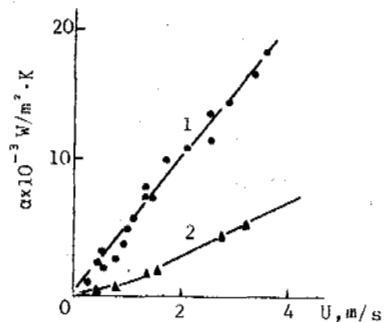


Figure 7. The dependence of the heat emission coefficient upon the flow rate  
1 is pure ice;  
2 is ice containing 0.5% of gelatine.

As the intensity of ice thawing is directly proportional to Nu, the introduction of 0.5% of gelatine decreases ice thawing in 3.3 times, the introduction of 0.5% of polyoxide-in 2.7 times as compared with pure ice.

#### REFERENCES

- Bryk M.T., Tsapjuk E.A., (1989) Ultrafiltratsija. - Kijev, Naukova Dumka. 288p.  
Amelkin S.V., Smorygin G.I., (1989) Gazokineticheskiye prozessy pri l'dobrazovanii. - V kn.: Inzhenerno-geokriologicheskoye obespechenije stroitel'stva sooruzhenii.-Novosibirsk, Nauka. p.63-71.  
Gilpin R.R., (1980) A Model for the Prediction of Ice Lensing and Frost Heave in Soils.- Water resources research. Vol.16, No.5, p.918-930.  
Derjagin B.V., Churajev N.V., (1980) Techenije nezamerzajuschikh proslojek vody i moroznoje razrushenije poristykh tel. - Kolloidnyi zhurnal. t17, n 5, p.842-852.  
Tolling J.F., Cisse J. (1971) A Theory for the Interaction of Particles with a solidifying front. - J. of Crystal growth. Vol.10, p.56-66.

## THE CHANGE OF THE ARTIFICIAL PERMAFROST TABLE UNDER THE ROADBED AND EFFECT ON THE ROADBED

Mi Haizheng and Wang Shaoling

Lanzhou Institute of Glaciology and Geocryology,  
Chinese Academy of Sciences, China

The paper analyzes the change of the artificial permafrost table and the roadbed stability after asphalt pavement was laid in the Qinghai-Xizang Plateau permafrost region. The main effect factors of the artificial table are as follows: roadbed height, water on the highway sides, ice content of the permafrost, air temperature and dynamic load etc. The changes of the artificial permafrost table affects directly the roadbed stability. On the basis of investigation data the paper summarizes the change law, in addition, the authors put forward some suggestions on protecting the permafrost with an aim of keeping the roadbed stabilized.

### INTRODUCTION

At present there are no reliable and cost saving techniques for building asphalt pavement in permafrost areas. The Qinghai-Xizang Highway passes through a continuous permafrost region. From 1979 to 1984 the asphalt pavement was laid and the highway has been running for eleven years. Now about 300 km (section) of the highway is damaged in varying degrees, compromising 55% of the total length. For this reason in 1991 engineering renovations were prepared for the damaged section, and therefore drilling investigations were conducted for permafrost. For engineering the most important thing is to find the influencing factors and change law of the artificial table and the influence of the artificial table on roadbed stability. In the paper the authors discuss the problems from investigation data and experience, and propose some suggestions on protecting the permafrost in engineering.

### INFLUENCING FACTORS OF THE ARTIFICIAL TABLE

After the asphalt pavement was laid, the permafrost table under the roadbed started to descend. The thaw settlement causes deformation to appear in the roadbed, this is a basic reason for highway failure. There are many influencing factors of the permafrost table change. The main factors are as follows:

#### Roadbed Height

As the highway is built in a permafrost area, increasing the roadbed height has the action of protecting permafrost. The artificial table changes with the roadbed height, and the change of the artificial table with roadbed height can be described as follows (Fig.1)

$$\Delta h_1 = k_1 H + b \quad (1)$$

where,  $\Delta h_1$  — permafrost table change (m), positive is descendant, negative is ascendant;

H — roadbed height (m);

$k_1, b$  — statistical constants.

From various highway sections the values of  $k_1$  and  $b$  are given in Table 1.

It should be pointed out, the roadbed height influences the heat conducted into the permafrost under the roadbed. This is a leading factor. In addition, the change of the artificial table with the roadbed height is affected by water on the highway sides and roadbed soil characteristics. Therefore, the statistics are slightly rough, but the law is right.

#### Water on the Highway Sides

In the building process the original ground surface at the roadbed slope foot was damaged in some sections. Due to precipitation water pits were formed, causing the permafrost table to descend. For example, at Erdaogou, in same the landforms and same soil group there are two drill holes at a distance of 750 meters, one drill hole is located at the section where there is no water at the highway sides, another drill hole is located at the section where there is water at the highway sides. The artificial table of the former is 4.10 m, that of the latter is 5.60 m where the natural permafrost table is 2.30 m. This shows that the influence of water is very serious. It is very difficult to calculate the heat magnitude caused by water, but the heat amount is very great, lake taliks are an extreme example of this condition.

#### Ice Content of Permafrost

This is the ice content near the permafrost table. Usually the permafrost table descends less at high ice content sections (Wu Ziwan, 1982), because changing ice into water requires



Table 1. The values of  $k_1$  and  $b$

Place	Kunlun N-slope	Kunlun Basin	Chumaer River	Kekexili	Fenhuo Mount.	Kaixinlin South	Tuotuo River
$k_1$	-1.40	-1.11	-1.61	-1.09	-1.20	-2.01	-1.39
$b$	2.35	2.19	3.64	2.21	2.39	3.87	3.24

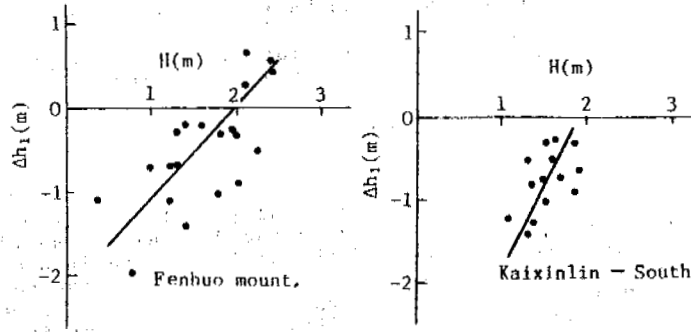


Figure 1. The relationship of  $\Delta h_1$  and  $H$

a great amount of latent heat; on the contrary, the permafrost table descends more at low ice content sections. For example, at somewhere there are two drill holes, the distance is 800 m, where the roadbed is the same i.e. 1.35 m, soil classification is the same i.e. clayey soil, and where the natural permafrost table is 1.70 m. The artificial table is 5.00 m and 3.60 m, respectively, correspondingly the water content is 33.9% and 72.1%. The difference of the two artificial tables is 1.40 m.

Air Temperature

Mean annual air temperature is a controlling factor, it controls permafrost formation and development. Along the highway the air temperature depends on elevation height. Through exploration it is indicated that the permafrost under the roadbed appears in a similar state in some mountain ridges, and in a unstimular state in basin and plain sections, where the thaw layer has developed. This shows that the seasonal thaw depth is more than the seasonal freezing depth. Based on this fact it is deduced reasonably when the mean annual air temperature reaches a certain value the permafrost under asphalt pavement will descend. Because of absorption heat in asphalt pavement the thaw date of the seasonal frozen ground under roadbed is earlier. Comparing the temperature data of observation drill hole (Fig.2) it is seen that the thaw date is earlier than in the past, and the corresponding thaw depth increased, this causes the permafrost table to increase gradually year by year, this indicates the change of ground temperature in the roadbed which does not appear in a cyclical change year by year, so a thaw layer was formed. The result is a accumulative effect of ground temperature increase.

Dynamic Load

Taking a k3051+220 original sand-gravel highway as an example we analyze the influence of dynamic load, where the original artificial

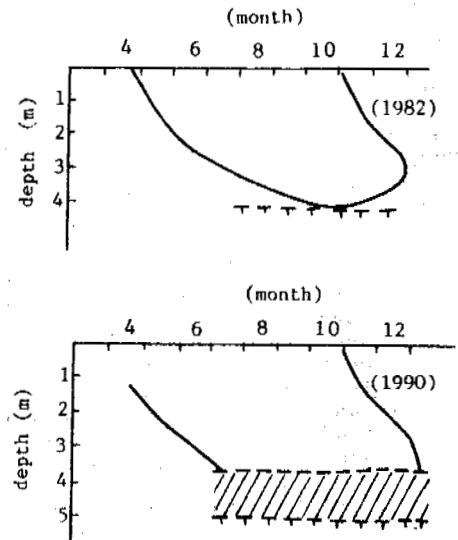


Figure 2. Thaw-freeze process of the highway center drill hole permafrost table  
 ---- 0°C ground temp.  
 //// thaw layer

table was 2.70 m during highway use, now the section of highway has been abandoned for 8 years, the permafrost table has become 2.20 m, and the natural permafrost table is 2.00 m. From this it is seen that the influence of dynamic load is 22.7% of the original permafrost table. This factor should be payed attention to.

LAW OF ARTIFICIAL PERMAFROST TABLE DESCENT AND EFFECT ON THE ROADBED

The descence of the artificial permafrost

table is usually uniform, and depends on the soil classification, ice content, time and roadbed highness, etc. The depth of the artificial table with time appears as follows:

$$h = k_2 N^\alpha \quad (N \geq 1) \quad (2)$$

where,  $h$  — artificial permafrost table depth(m)  
 $N$  — time after asphalt pavement was laid (y)

$k_2, \alpha$  — statistical constants

So, the change of artificial table with time is

$$\Delta h_2 = k_2(N^\alpha - (N-1)^\alpha) \quad (3)$$

The values of statistic content  $k_2, \alpha$  are given in Table 2.

Table 2: The values of  $k_2$  and  $\alpha$

Place	Roadbed height (m)	Time (y)	$k_2$	$\alpha$
Kunlun Basin	1.60	6	3.38	0.104
GG station	1.80	6	3.71	0.109
Wudaoliang	1.60	12	3.76	0.110
Kekexili South	1.95	10	3.33	0.117
Fenghou Mount.	2.40	6	2.85	0.064

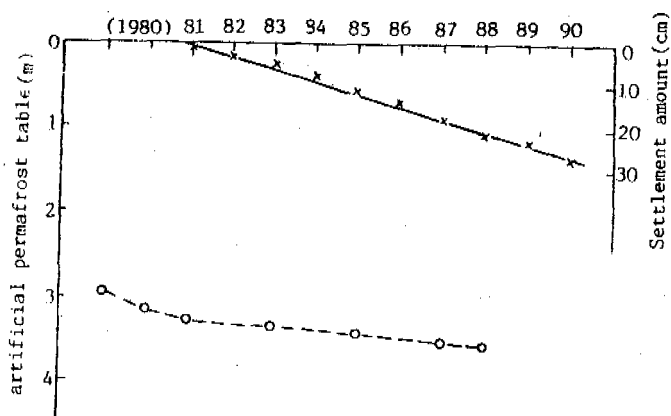


Figure 3. The relationship of the artificial table and time (from Xian First Highway Exploration Design Academy)

x — roadbed descence  
o — change of artificial table

The change in the permafrost table causes inevitably roadbed deformation. From Fig.3 it is seen that the pavement deformation appear approximately in a linear law:

$$\Delta H = k_3 N \quad (4)$$

where,  $\Delta H$  — pavement settlement value (m)  
 $N$  — time after asphalt pavement was laid (y)  
 $k_3$  — statistic constant

Comparing  $k_2$  with  $k_3$  it is known that if the descence of the permafrost table is great, the roadbed settlement is great also. This shows the descence of the permafrost table affects directly the roadbed deformation and stability.

## PRELIMINARY CONCLUSIONS AND QUESTIONS

### Preliminary Conclusions

(1) After asphalt pavement was laid in the permafrost region a great change occurred, the permafrost table descends and the thaw layer deepens. These changes cause roadbed non-stability.

(2) Thaw time under asphalt pavement is earlier than before, thaw date increases, therefore the change of the soil temperature under the roadbed does not appear in cyclical changes year by year, the soil temperature has an accumulative effect.

There are many effect factors of the artificial permafrost table change, the leading factor is heat thaw, secondly, the water on the highway sides is very significant.

The change of the artificial permafrost table with time is

$$\Delta h_2 = k_2(N^\alpha - (N-1)^\alpha)$$

The change of artificial permafrost table with the roadbed height is:

$$\Delta h_1 = k_1 H + b$$

### Questions and Suggestions

One of key problems in road engineering is roadbed stability. So, it is necessary to further study the following problems: the maximum thaw depth under the roadbed, the steady time and conditions of the artificial permafrost table, and the changes of permafrost under the combined actions of heat and load, so that permafrost problems in road engineering can be solved thoroughly.

The authors who took part in this exploration investigation of permafrost damage, propose the following suggestions: (1) Elimination of water on the highway sides, facts prove that, the pavement appeared settled or damaged in the sections where the highway sides of the original ground surface were destroyed and water pits were formed. Therefore, it is very important to install culverts and drainage ditches. (2) The berm and slope should be paved, the optimum material is sod. This not only decreases heat but also prevents rainwater from entering the roadbed from two sides. These actions help protect the permafrost. (3) Choosing suitable roadbed materials. The roadbed must meet the needs of load and frost heave during winter. Usually, the coarse grained soils are suitable materials. Silty and cohesive soils should be avoided. (4) Treating the non filled and excavation sections. It has been proved all these sections were damaged. So these sections have to be treated specially. From the present situation there are several methods: laying a partition heat layer under the roadbed, laying aeration pipes, or replacing fine grained soils with coarse grained soils. From many facts it has been shown that the permafrost with a culvert on two sides is maintained in its original state. Through practical investigation these ways have been shown to be successful.

### ACKNOWLEDGMENT

The authors greatly appreciate Xian First Highway exploration design Academy for providing a convenient site for field work and part data.

## REFERENCES

- Wu Ziwang, (1982) Engineering classification on permafrost. Journal of Glaciology and Geocryology, Vol.4, No.4.
- Yu Wenxue and Wu Jingmin, (1986) The roadbed highness problem of asphalt pavement in permafrost area of Qinghai-Xizang Highway. Journal of Xian Highway College, 86-1.
- Research Group of Permafrost Roadbed for Qinghai-Xizang Highway, (1988) Roadbed Engineering in Permafrost Region. Lanzhou University Publishing House, p61-85.
- G.H. Johnston, (1981) Permafrost Engineering Design and Construction, Hunter Rose Company Ltd, Canada, p345-378.

## PHENOMENOLOGICAL MODELLING OF FROST-SUSCEPTIBLE SOILS

Radoslaw L. Michalowski

Department of Civil Engineering, The Johns Hopkins University  
Baltimore, MD 21218, U.S.A.

A constitutive model for saturated frost-susceptible soils is presented. The growth of ice during freezing is simulated through introducing a function representing the rate of porosity growth, rather than simulating formation of single ice lenses. A hypothetical form for the porosity rate function is proposed. Distinct features associated with soil freezing are captured: dependence of heave on the temperature, temperature gradient, magnitude of porosity, and stress state. The model is targeted at qualitative and quantitative predictions of frost heave, not at explaining the physics of the phenomenon itself.

### INTRODUCTION

Two frost-heave models which have been advocated the most in the past decade or so are the *rigid ice model* (Miller, 1978) and the *segregation potential model* (Konrad and Morgenstern, 1980). A reliable quantitative description of the effects of freezing in frost-susceptible soils is still to be achieved. While the rigid ice model is the one most widely accepted in the scientific community, the model based on introduction of the segregation potential has proved to be a more useful engineering tool. Both models are based on micromechanics considerations. The formation of a single ice lens is modelled, and the Clausius-Clapeyron equation is used to relate the pressure in ice and water. Neither model is capable of predicting the macroscopic stress state in the soil skeleton and ice. They include the influence of the stress only in terms of "overburden pressure", which is meaningful only in one-dimensional freezing processes. Besides the two mentioned above, other useful models can be found in the literature (e.g., Shen and Ladanyi, 1987, Guymon et al., 1984).

The model which is presented in this paper is closely related to that proposed by Blanchard and Frémond (1985), and is very different from the other models in its approach. Instead of concentrating on the mechanism of a single ice lens growth, the concept of a *porosity rate function* is adopted. The influence of temperature, temperature gradient, current value of porosity, and the stress state on the porosity increase is taken into account.

The model is not targeted at explaining the frost heave phenomenon, but is aimed at qualitative and quantitative predictions of the frost heave itself. While considerations

of the microscopic mechanisms (interactions between ice, water, and soil skeleton) are useful for indicating the qualitative tendencies the model should predict, the model itself does not need to be derived directly from analysis of the micromechanical processes. This statement is certainly true in the mechanics of solids, where constitutive relations have been formulated on the basis of macroscopic effects observed on the samples, rather than on the basis of microscopic processes. Such models are not expected to explain the nature of the phenomenon, but to predict the magnitude of the macroscopic effect. For instance, the classical model of elasticity does not explain why some materials (in a certain stress range) behave elastically, but, if they do, this model predicts deformation of these materials quite accurately. There is no reason why such approach to modeling frost heave in soils should be dismissed.

### POROSITY INCREASE IN FREEZING FROST-SUSCEPTIBLE SOIL

It is assumed that the soil is fully saturated. Water coming from the unfrozen side of the freezing zone feeds the growing ice lenses. Individual ice lenses are not modelled here; instead, the increase in volume of a frost susceptible soil during freezing is described by a rate of porosity change, here called a *porosity rate function*. The ice fraction in a representative volume of the skeleton-water-ice mixture will be increasing due to influx of water and freezing. The porosity rate function describing this increase is postulated in the following form, where  $\dot{n}$  is the rate of porosity change ( $\partial n / \partial t$ ),  $T$  is the temperature (in °C), and  $\Phi(\sigma_{xx}^{(i)})$  is a function dependent on the first

invariant of the stress tensor in ice

$$\dot{n} = \dot{n}_m \frac{T - T_0}{T_m} e^{-\frac{T - T_0}{T_m}} (1 - e^{\alpha \frac{\partial T}{\partial l}}) (1 - n)^\beta \Phi(\sigma_{kk}^{(i)});$$

$$T < T_0, \quad \frac{\partial T}{\partial l} < 0 \quad (1)$$

Function  $\dot{n}$  (eq. (1)) is a proposed hypothetical function which accounts for the distinct features associated with soil freezing known from laboratory experiments. Parameters  $\dot{n}_m$  and  $T_m$  are the maximum porosity rate and the temperature at which that maximum occurs, respectively, and  $\alpha$  and  $\beta$  are also material parameters. Figure 1 shows the porosity rate (based on eq. (1)) as a function of temperature, all other parameters held constant. By selecting a proper combination of parameters  $\dot{n}_m$  and  $T_m$ , the characteristic features of different soils can be modelled. For instance, selecting a large value of  $\dot{n}_m$ , and  $T_m$  only slightly below freezing temperature  $T_0$ , is typical of silts where the frost heave is very intensive but tapers down very quickly with a decrease in temperature. Clay, on the other hand, would be better modelled with a lesser value of  $\dot{n}_m$  and lower  $T_m$ .

Phenomenological description of the porosity increase dependent on only two parameters ( $\dot{n}_m$  and  $T_m$ ) was suggested earlier by Frémond (1987), and a simulation of a boundary value problem was shown by Li et al. (1989).

Note that the rapid growth of porosity at temperatures slightly below the freezing temperature is characteristic of the growth of ice lenses at the freezing front, while the lower rate of ice growth at temperatures well below freezing can be interpreted as secondary frost heave.

Porosity increase as a function of temperature alone cannot accurately predict the volume expansion due to ice growth in frost susceptible soils. This porosity increase must also be a function of the temperature gradient, porosity itself, and the stress state in ice. The expression in the first pair of parentheses (eq. (1)) accounts for the influence of the temperature gradient. At the temperature gradient equal to zero ( $\partial T / \partial l = 0$ ,  $l$  coincides with the heat flow line at the point where  $\dot{n}$  is calculated), the ice (or porosity) growth ceases as this expression becomes zero. At temperature gradients significantly lower than zero, this expression approaches unity. The expression in the second set of parentheses in eq. (1) takes the current porosity into account: the larger the porosity, the lower the rate of porosity increase. When porosity reaches

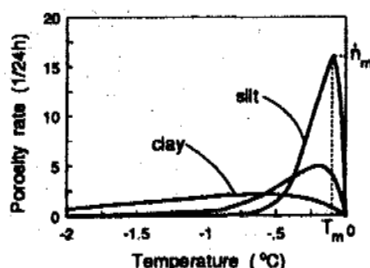


Fig. 1. Illustration of porosity rate function.

unity, the entire volume is filled with ice and the porosity rate drops to zero.

As the porosity increases due to growth of ice in the soil, the increasing stress state in the ice will inhibit the ice growth. It is postulated that the deviatoric part of the stress tensor in ice has no influence on  $\dot{n}$ , and function  $\Phi$  in eq. (1) is made dependent only on the first invariant of the microscopic stress in ice ( $\sigma_{kk}^{(i)}$ ). Function  $\Phi(\sigma_{kk}^{(i)})$  is not specified here in detail. At this stage of model development it is doubtful whether function  $\Phi(\sigma_{kk}^{(i)})$  can be estimated with a precision good enough to be of any practical value. This is because the calculations of the stress state in ice involve equilibrium of all three phases (water, ice, and soil skeleton), and the calculations of water suction are inherently imprecise due to inaccuracies in estimates of hydraulic conductivity as a function of temperature. Therefore, for simulation purposes, function  $\Phi(\sigma_{kk}^{(i)})$  in eq. (1) was replaced with a function dependent on the total stress in soil,  $\bar{\sigma}_{kk}$  (eq. 17).

Growth of ice in freezing soils has an anisotropic character, i.e., the increase of the volume cannot be represented by a scalar quantity. The volumetric strain of the soil due to ice lens growth is relatively large in the direction of the heat flow lines, and it is likely to be small in the direction of the isothermal lines. To capture the anisotropic character of void growth, the porosity growth tensor is introduced as

$$\dot{n}_{k2} = \dot{n} \begin{vmatrix} \xi & 0 & 0 \\ 0 & \frac{1}{2}(1-\xi) & 0 \\ 0 & 0 & \frac{1}{2}(1-\xi) \end{vmatrix} \quad (2)$$

where  $0.33 \leq \xi \leq 1.0$ . The two limit values of  $\xi$  (0.33 and 1.0) describe the isotropic growth and unidirectional growth of ice lenses (in the direction of heat flow lines), respectively. Tensor  $\dot{n}_{k2}$  is identical to the strain rate tensor for the entire frozen composite due to ice growth.

#### UNFROZEN WATER CONTENT

The second material function which is very important to the model presented is the unfrozen water content in frozen soil. A three-parameter function is postulated here in the form

$$w = w^* + (\bar{w} - w^*) e^{a(T - T_0)}; \quad T < T_0 \quad (3)$$

where  $w$  is the unfrozen water content as a fraction of the dry weight,  $w^*$  is the residual unfrozen water content at some very low reference temperature,  $\bar{w}$  is the minimum unfrozen water content at freezing temperature  $T_0$ , and  $a$  is the third material parameter. Experimental data confirming this type of relation can be found in the literature (e.g., Anderson and Tice, 1973). This paper considers only the freezing process; during a thawing process the unfrozen water content can

also be expressed by eq. (3), but parameters  $\bar{w}$  and  $a$  are likely to be different.

#### A MODEL FOR FROST HEAVE SIMULATIONS

To present the principles of conservation for the freezing skeleton-water-ice mixture, quantities  $\theta^{(s)}$ ,  $\theta^{(w)}$ , and  $\theta^{(i)}$  describing the volume fractions of skeleton, water, and ice, are introduced

$$\begin{aligned} \theta^{(s)} &= \frac{V^{(s)}}{V} = 1 - n, & \theta^{(w)} &= \frac{V^{(w)}}{V} = v n, \\ \theta^{(i)} &= \frac{V^{(i)}}{V} = n(1 - v) \end{aligned} \quad (4)$$

where  $V^{(s)}$ ,  $V^{(w)}$ , and  $V^{(i)}$  are the volumes of the soil skeleton, unfrozen water, and ice, respectively, and  $V = V^{(s)} + V^{(w)} + V^{(i)}$ .  $v$  is the unfrozen water concentration in frozen soil

$$v = \frac{V^{(w)}}{V^{(s)} + V^{(w)}} \quad (5)$$

The soil is assumed to be saturated, and the density of the mixture,  $\bar{\rho}$ , can be represented as

$$\begin{aligned} \bar{\rho} &= \theta^{(s)} \rho^{(s)} + \theta^{(w)} \rho^{(w)} + \theta^{(i)} \rho^{(i)} = \\ &= (1 - n) \rho^{(s)} + v n \rho^{(w)} + n(1 - v) \rho^{(i)} \end{aligned} \quad (6)$$

where  $\rho^{(s)}$ ,  $\rho^{(w)}$ , and  $\rho^{(i)}$  are the densities of the three components of the mixture, respectively. The heat capacity of the mixture per unit volume is

$$C = (1 - n) \rho^{(s)} C^{(s)} + v n \rho^{(w)} C^{(w)} + n(1 - v) \rho^{(i)} C^{(i)} \quad (7)$$

where  $C^{(s)}$ ,  $C^{(w)}$ , and  $C^{(i)}$  are the mass heat capacities of the soil skeleton, water, and ice, respectively. Due to changing proportions of the components in the freezing soil, the heat capacity will vary.

The heat flow is assumed to be governed by the Fourier law of heat conduction with thermal conductivity  $\lambda$  being a function of temperature ( $\lambda(T)$ )

$$Q_i = -\lambda(T) \frac{\partial T}{\partial x_i} \quad (8)$$

$Q_i$  is the heat flux vector,  $T$  is the temperature, and  $x_i$  is the space co-ordinate. Heat conductivity  $\lambda(T)$  is a property of the soil-water-ice mixture. Temperature  $T$  is the temperature of the frozen composite, and no differentiation is made among the temperatures of all three phases. Water transport is described by Darcy's law

$$q_i = -k(T) \frac{\partial h}{\partial x_i} \quad (9)$$

where  $q_i$  is the flow rate vector,  $h$  is the hydraulic head, and  $k(T)$  is the hydraulic conductivity (a function of temperature). The

total stress in composite  $\bar{\sigma}_{ij}$  is

$$\begin{aligned} \bar{\sigma}_{ij} &= \bar{\sigma}_{ij}^{(s)} + \bar{\sigma}_{ij}^{(i)} + \bar{p} \delta_{ij} = \\ &= \theta^{(s)} \sigma_{ij}^{(s)} + \theta^{(i)} \bar{\sigma}_{ij}^{(s)} + \theta^{(w)} u \delta_{ij} \end{aligned} \quad (10)$$

where  $u$  is the pressure in water,  $\delta_{ij}$  is Kronecker's symbol, and stresses with bars are related to the cross-section of the entire composite (macrostresses), while the symbols without bars represent the microstresses. Deformability of the frozen composite is described by a hypoelastic-type constitutive law

$$\bar{\sigma}_{ij} = B(T)_{ijkl} \bar{\epsilon}_{kl} \quad (11)$$

where  $\bar{\epsilon}_{kl}$  is the strain tensor and  $B(T)_{ijkl}$  is the constitutive tensor for the composite. A similar relation describes the deformability of the skeleton itself

$$\bar{\sigma}_{ij}^{(s)} = B(T)_{ijkl}^{(s)} \bar{\epsilon}_{kl}^{(s)} \quad (12)$$

where  $\bar{\epsilon}_{kl}^{(s)}$  is the strain tensor and  $B(T)_{ijkl}^{(s)}$  is the constitutive tensor of the skeleton. Note that the strain tensor of the composite is equal to the macrostrain tensor in the skeleton.

The principle of energy conservation takes the form

$$C \frac{\partial T}{\partial t} - l \frac{\partial \theta^{(i)}}{\partial t} \rho^{(i)} - \nabla \cdot (\lambda \nabla T) = 0 \quad (13)$$

where  $l$  is the latent heat of fusion of water per unit mass and  $\theta^{(i)}$  is the fraction of ice (eq. (4)). It needs to be mentioned that eq. (13) contains no term due to heat transport by water flow. It also neglects the terms due to mechanical work. These terms are considered small compared to the latent heat released during freezing. The mass conservation principle can be expressed as

$$\begin{aligned} (\rho^{(i)} - \rho^{(s)}) \frac{\partial n}{\partial t} + (\rho^{(w)} - \rho^{(i)}) \frac{\partial (nv)}{\partial t} - \\ - \rho^{(w)} \nabla \cdot (k \nabla h) = 0 \end{aligned} \quad (14)$$

The momentum conservation principle for the entire mixture (in terms of the total composite stress  $\bar{\sigma}_{ij}$ ) is

$$\frac{\partial \bar{\sigma}_{ij}}{\partial x_j} + \bar{p} g_i = 0 \quad (15)$$

where  $g_i$  is the gravity acceleration vector; and for the skeleton

$$\frac{\partial \bar{\sigma}_{ij}^{(s)}}{\partial x_j} - \rho^{(w)} g_i \nabla h + (\bar{p} - \rho^{(w)}) g_i = 0 \quad (16)$$

Equation (10) allows one to find the stress in ice after the total stress and the macrostress in the skeleton are calculated from eqs. (11), (12), (15), and (16), and pressure  $u$  (suction) is calculated after the hydraulic head is obtained. Such estimate of the stress

in ice, though theoretically consistent, may be inaccurate, since  $u$  is very sensitive to hydraulic conductivity, which changes with temperature. For this reason, function  $\Phi(\bar{\sigma}_{ij})$  in eq. (1) is replaced here by a function of the total composite stress, and it is postulated in the following form

$$\Phi(\bar{\sigma}_{ij}) = e^{-\frac{\bar{\sigma}_{kk}}{\tau_0}} \quad (17)$$

where  $\bar{\sigma}_{kk}$  is the first invariant of the total stress tensor (compression taken as positive),  $\zeta$  is a material parameter, and  $n$  is the porosity. The function in eq. (17) is a hypothetical function which accounts for the descending tendency of the porosity growth with an increase in the stress state. Thus, the rate of frost heave decreases with the increase in stress  $\bar{\sigma}_{kk}$ .

#### MATERIAL PARAMETERS

An application of the proposed model in the simulation of a one-dimensional freezing process is shown in the next section. Model parameters are assumed to be known. The more standard parameters, such as the unfrozen water content (a function of temperature), hydraulic and thermal conductivity, initial porosity, and densities of the components of the mixture, are assumed to be known from independent tests. It is the parameters of the porosity rate function that require some explanation as to their possible methods of estimation. It is suggested that these parameters be derived from tests with "ramping temperatures". When the rate of boundary temperature change is sufficiently slow, such tests allow a nearly constant temperature gradient to be maintained in the freezing sample, and, thus, the process in the freezing zone can be considered as approximately stationary with respect to the co-ordinate system attached to the moving freezing front (due to geometrical changes the process is not strictly stationary). The heave rate is then expected to be nearly constant. The heave rate obtained from experiments can be described as

$$\frac{dH}{dt} = \int_0^h n_{zz} dz = \text{const} \quad (18)$$

where  $H$  is the height of the sample, and  $n_{zz}$  is expressed by eqs. (1) and (2). Porosity rate  $n$  for material under a negligible stress state is a function of parameters  $n_m$ ,  $T_m$ ,  $\alpha$ , and  $\beta$ ; thus, a minimum of four tests are needed, each with a different temperature gradient. Four separate experiments are suggested rather than one with a varying temperature gradient to avoid difficulties in interpretation of the non-stationary porosity growth. Parameter  $\zeta$  needs to be evaluated from additional tests where the sample is loaded with an external load. While, theoretically, five separate tests are needed to evaluate the five parameters, more tests are desirable to obtain a reliable set of parameters. Determining the model parameters then reduces to a "curve

fitting" process with five free parameters. The tests used to determine the parameters must not be used to verify the adequacy of the model.

In the simulation shown below the porosity growth will be assumed to be anisotropic with  $\xi = 1$  (no lateral growth of ice lenses, eq. (2)). Neglecting the weight of the sample, the first invariant of the total stress tensor is calculated as

$$\bar{\sigma}_{kk} = p \frac{1+\mu}{1-\mu} \quad (19)$$

where  $p$  is the load per unit area applied to the sample, and  $\mu$  is Poisson's ratio of the frozen mixture.  $\bar{\sigma}_{kk}$  from eq. (19) will be used to calculate function  $\Phi$  (eq. (17)), which has an inhibiting effect on porosity growth in the freezing soil.

Hydraulic conductivity undergoes large changes in quantity during freezing. These changes can be incorporated into the calculations easily, however, only two values of hydraulic conductivity  $k$  will be used here: one for unfrozen soil, and one for frozen soil. Also, two values of thermal conductivity will be used rather than a smooth function of temperature.

No exact model parameters were available for simulation, therefore, reasonable values of parameters such as thermal conductivity were assumed, and the characteristic parameters in eqs. (1) and (2) were selected in such a way so that the result of the numerical simulation would match the experimental result reported by Konrad and Morgenstern (1980). This, of course, cannot be regarded as verification of the model.

Heat conductivity of the mixture was estimated as  $\lambda = 145 \text{ kJ/24h}\cdot\text{m}\cdot^\circ\text{C}$  for the unfrozen mixture and  $\lambda = 175 \text{ kJ/24h}\cdot\text{m}\cdot^\circ\text{C}$  for the frozen composite. Heat capacity per unit mass of the skeleton was assumed to be  $900 \text{ J/kg}\cdot^\circ\text{C}$ . Hydraulic conductivity was estimated as  $k = 10^{-6} \text{ m/24h}$  for the frozen material, and  $k = 10^{-2} \text{ m/24h}$  for the unfrozen mixture. Note that the value for the frozen soil is two orders of magnitude lower than that reported by Konrad and Morgenstern (1980); this is because the value they reported was for the frozen fringe, while here it is an estimate of the value for the frozen soil. The maximum of the porosity rate was assumed as  $n_m = 15 / 24h$ , and the related temperature as  $T_m = -0.15^\circ$ , and  $\alpha = 0.2$  and  $\beta = 5.0$ . The parameters in the function representing the unfrozen water content in frozen soil (eq. (2)) were assumed as:  $\bar{w} = 0.15$ ,  $w^* = 0.02$ ,  $a = 0.9 / ^\circ\text{C}$ , and  $T_0 = 0^\circ\text{C}$ . The density of the skeleton in the calculations was  $\rho^{(s)} = 2.7 \text{ Mg/m}^3$ .

#### SIMULATION OF A 1-D SINGLE-STEP FREEZING PROCESS

A freezing process of a soil sample was simulated using the model described in this paper. The initial height of the sample was 18 cm. This freezing process is similar to that described by Konrad and Morgenstern in their 1980 paper (test NS-10). A one-step freezing process was simulated where the initial temperature of the entire sample was

1°C, and at time  $t = t_0$ , the temperature of the top boundary was dropped to -6°C. The freezing process was then allowed to continue for 10 days.

Calculations were performed replacing the freezing soil sample with an assembly of control volumes, with the heat and mass flow occurring between these volumes. The temperatures of the boundary volumes were adjusted to be equal to the prescribed boundary temperatures. The diffusion process was numerically generated through an explicit scheme (independently calculated fluxes between the control volumes). The number of elements (control volumes) was 20.

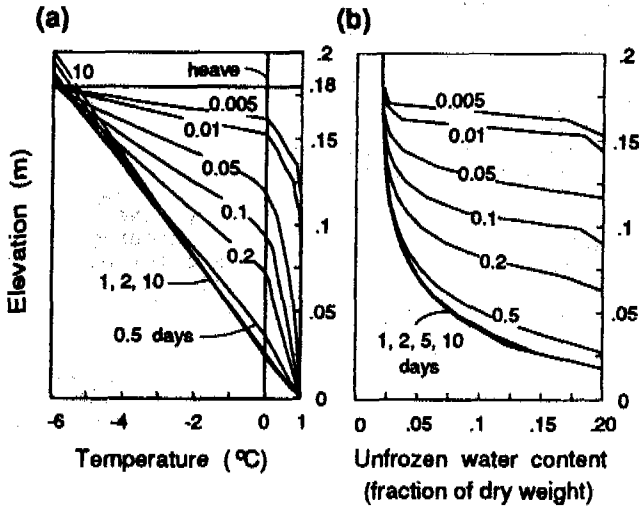


Fig. 2. (a) Temperature variation during freezing; (b) unfrozen water content.

Fig. 2 presents the variation of the temperature throughout the sample at different times of the process, and the unfrozen water distribution (a fraction of the dry weight). The initial porosity of the material was assumed to be homogeneous, and equal to 0.35, which, assuming full saturation of the sample before freezing, led to an initial moisture content of 0.199. Under given boundary conditions, the heat flow process becomes almost steady after one day (Fig. 2(a)). The variation in the unfrozen water content is related to the temperature changes. The drop in unfrozen water content with decreasing temperature affects the heat diffusion process through the release of latent heat (this coupling leads to iterative numerical procedures for solving the freezing process).

Fig. 3(a) shows the porosity increase throughout the sample due to freezing, and Fig. 3(b) shows the increase of the ice content. Appearance of ice lenses is modelled here as regions of increased porosity. The quick advancement of the freezing zone in the first four hours of the process results in freezing *in situ* where no significant increase in void volume is observed. Once the speed of the 0°C isotherm becomes relatively small, the process of porosity growth becomes very pronounced. The ice content increases significantly in the neighborhood of the nearly-stationary freezing zone, which is indicated by the increasing "bulb" in ice

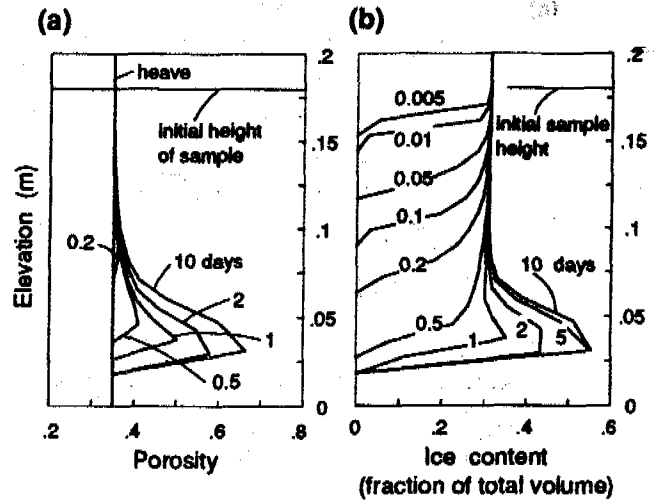


Fig. 3. (a) Variation of porosity during freezing process; (b) ice content.

content distribution curves in Fig. 3(b). The peak in the ice content distribution can be interpreted as the "final" ice lens formed during step freezing, while the increased ice content above that indicates a lower average ice concentration, e.g., thinner and widely spaced lenses. The constant ice content distribution in the upper part of the sample indicates freezing *in situ* of that part.

The model presented does not require calculations of hydraulic head (suction) to simulate heave. This is because the porosity rate function becomes independent of the suction if the influence of the stress state in ice is neglected. It is possible, however, to back-calculate suction assuming that the water transfer is governed by Darcy's law. Hydraulic conductivity in frozen soil is very much dependent on temperature (especially in the region of intensive porosity increase), and its exact variation is seldom tested for practical purposes. Back calculations of suction based on approximately estimated hydraulic conductivity are not very accurate, but they are presented here so some qualitative conclusions can be drawn. The level of the hydraulic head at the bottom of the sample was assumed to be zero. The hydraulic head and its gradient for the simulated step freezing process are presented in Fig. 4. The distribution of the cryogenic suction changes during the process, and it reaches its maximum before a big concentration of increased porosity is formed. As expected, the maximum of the suction gradient is related to the maximum heave rate, and the suction gradient decrease coincides with a decrease in the heave rate. Some oscillations in the magnitude of the cryogenic suction and suction gradient were observed during the process (see, for example, the sequence of results for 2, 5, and 10 days). These oscillations seem to be of a numeric nature and become smaller with a decrease in time step.

The heave of the sample as a function of time is shown in Fig. 5. During the step freezing process the heave rate (derivative of



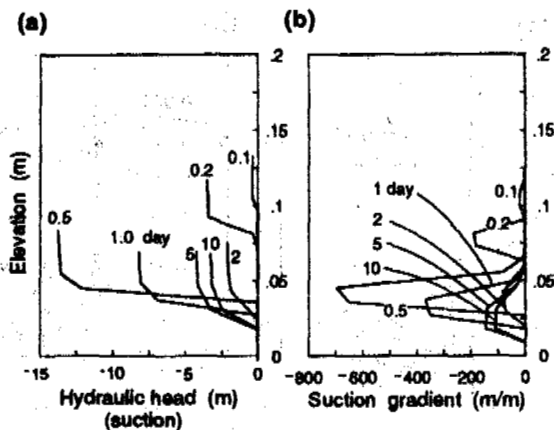


Fig. 4. (a) Hydraulic head during freezing; (b) hydraulic gradient.

30, 100, 200, and 300 kPa, respectively. As mentioned earlier, the stress state in ice, which is likely to be a governing factor in decreasing the heave rate, cannot be calculated accurately. Therefore, the decrease in the porosity rate due to an elevated stress level was expressed as a function of the first invariant of the total stress state  $\bar{\sigma}_{kk}$  (the following parameters were used in eq. (18) and (19):  $\mu = 0.3$ ,  $\zeta = 0.333$ ). This hypothesis requires more study, though the reduction in frost heave shown in Fig. 5(a) due to overburden seems to be reasonable.

#### FINAL REMARKS

The model presented in this paper has a phenomenological character and it is not derived from micromechanical processes. The primary reason for formulation of this model is to create a predictive tool for qualitative and quantitative estimates of frost heave, not to explain the phenomenon itself.

While no experimental data is available to verify the model quantitatively, the qualitative results are quite encouraging. Simulations were also performed for processes with multi-step boundary conditions (Michalowski, 1992), and with ramped temperatures. The qualitative results are equally promising.

Further development of the model needs to concentrate on experimental verification of the porosity rate function, and on a more precise capturing of the influence of the stress state in frozen soils.

#### REFERENCES

- Anderson, D.M. and Tice, A.R. (1973). The unfrozen interfacial phase in frozen water systems. In: Ecological Studies: Analysis and Synthesis. ed. A. Hadar, vol.4, 107-124.
- Blanchard, D. and Frémond, M. (1985). Soil frost heaving and thaw settlement, 4th Int. Symp. Ground Freezing, Sapporo, 209-216.
- Frémond, M. (1987). Personal communication.
- Guymon, G.L., Hromadka, T.V. and Berg, R.L. (1984). Two dimensional model of coupled heat and moisture transport in frost-heaving soils, *J. Energy Res. Technol.*, 106, 336-343.
- Li, Y., Michalowski, R.L., Dasgupta, B. and Sterling, R.L. (1989). Preliminary results of simulation of retaining wall displacement by frost action. 5th Int. Conf. Cold Reg. Eng., ed. R.L. Michalowski, Minneapolis.
- Konrad, J.M. and Morgenstern, N.R. (1980). A mechanistic theory of ice lens formation in fine-grained soils, *Can. Geot. J.*, 17, 473-486.
- Michalowski, R.L. (1992). A constitutive model for frost susceptible soils. 4th Int. Symp. Num. Meth. in Geomech., eds. G.N. Pande & S. Pietruszczak, Swansea, 159-167.
- Miller, R.D. (1978). Frost heaving in non-colloidal soils, 3rd Int. Conf. Permafrost, 707-713.
- Shen, M. and Ladanyi, B. (1987). Modelling of coupled heat, moisture and stress field in freezing soil, *Cold. Reg. Sci. Technol.*, 14, 237-246.

the heave curve) tapers down once the freezing zone becomes almost stationary. Such behavior of the simulated sample is to be expected, since it is postulated in eq. (2) that the porosity rate decreases with an increase in porosity itself. The heave rate reaches its maximum somewhere at the beginning of the process, but not at the very start of freezing. The temperature gradient is highest in the frozen part of the sample at the beginning of step freezing. The porosity rate increases with an increase in  $|\partial T/\partial z|$ . Heave of the sample, however, is the integral of the volume increase over the frozen part of the sample, and this frozen part is small at first, when the magnitude of the temperature gradient is high. Consequently, the sample (during step freezing) reaches the maximum heave rate not at the very start of the process, but shortly after, see Fig. 5(b) (some fluctuations in the simulated heave rate were also observed, due to discretization of the sample for numerical calculations).

Discrete points in Fig. 5(a) represent the heave measured by Konrad and Morgenstern (1980). While such simulation cannot be considered a verification of the model, the numerical results indicate that the model produces very reasonable qualitative results. The four curves for  $p > 0$  in Fig. 5(a) represent heaving for overburden pressures of

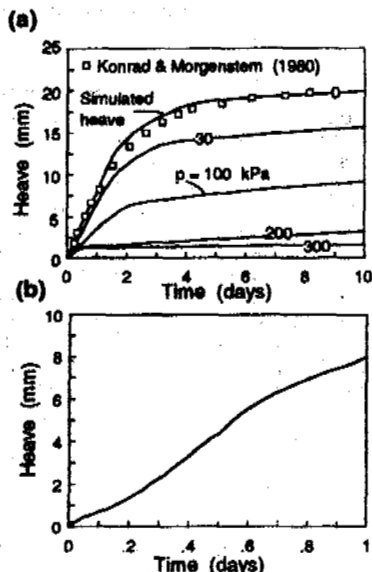


Fig. 5. Simulated heave.

## TRANS ALASKA PIPELINE REINSULATION IN ATIGUN PASS

Keith F. Mobley, P.E.<sup>1</sup> and John E. Ferrell<sup>2</sup>

- (1) Engineering Project Leader on contract to Alyeska Pipeline Service Co., Anchorage, Alaska.
- (2) Civil Engineering Coordinator, Alyeska Pipeline Service Co., Anchorage, Alaska.

Approximately 520 meters of the Trans Alaska Pipeline in the Brooks Range of Alaska were reinsulated in 1990. The remote mountainous site and the harsh arctic climate made the project difficult to construct. This paper discusses how the insulation design and materials selection were driven by the environmental constraints. Several insulation systems were evaluated as a part of the design process of the second phase of construction. Water and water vapor absorption, durability and construction factors were considered. It was found that plastic waterproof insulations will absorb significant quantities of water vapor under conditions similar to those expected at the project site. A simple laboratory test was developed to compare vapor absorption capabilities of the different insulations. The tests did not provide enough information to predict how the insulation would actually perform in the field. A test section of the three leading insulations systems was constructed and instrumented to provide long-term performance evaluation.

### INTRODUCTION

Approximately 520 m (1700 feet) of the Trans Alaska Pipeline in the Brooks Range of Alaska was reinsulated in 1990 because of deterioration of the original insulation system. The decision to replace the original insulation was based on monitoring data and visual observations during maintenance projects. Beyond the physical constraints imposed by the pipe itself, the remote mountainous site and harsh arctic climate influenced how the construction was to be completed.

As a part of the design, five proposed insulation types were evaluated for their suitability. Water and water vapor absorption, durability, and construction factors were used to determine the final insulation selection. A simple laboratory test was developed to compare vapor absorption potential of the different insulation systems. Based on the results of this testing, an insulation system was designed and constructed which included the above mentioned factors.

The laboratory testing did not provide enough information to predict the long-term performance of the insulation in the field. To provide additional field information, a test section of the three best insulations systems was constructed and instrumented. Periodic readings of the monitoring instruments continue to be made.

### HISTORICAL BACKGROUND

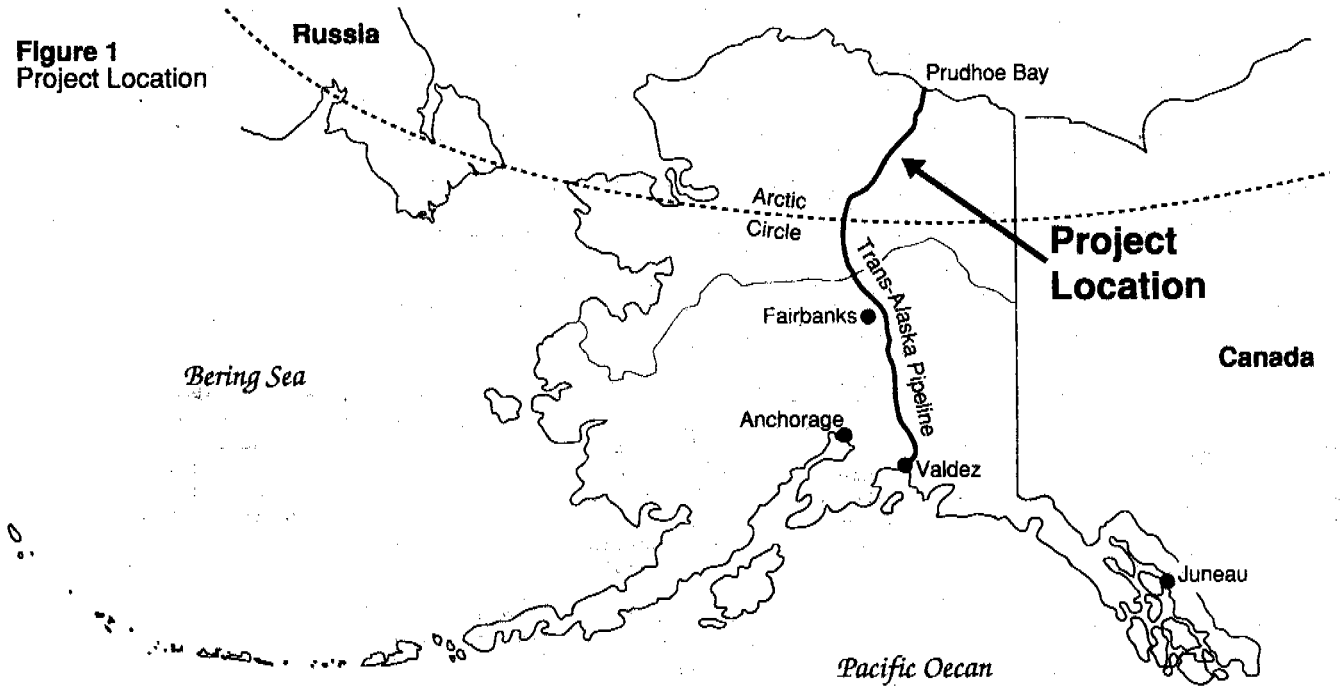
Atigun Pass is located on the continental divide in the Brooks Range in northern Alaska (Figure 1). This pass provided the best overall route for the Trans Alaska Pipeline to bring warm (50° - 60° C) crude oil from Prudhoe Bay to Valdez. The arctic/continental climate in the region consists of brief, cool summers from June through August and winter dominating the remainder of the year.

The work site is located on the south side of the pass about 2.5 km from the top. The drainageway through which the pipeline is located is steep and narrow with about a 200 m drop in 1.5 km. Sideslopes range from 30 to 80%. Soils consist of avalanche and rockfall deposits from 3 to 50 m thick. Clear ice lenses up to 2 m thick have been encountered in boreholes drilled at the site.

Prior to pipeline construction, geotechnical exploration revealed several areas of ice-rich, thaw-unstable permafrost along the proposed pipeline route. Under normal construction conditions, the pipeline would have been built in an above-ground mode. Due to snow avalanche and rockfall hazards, however, two insulated boxes, one each for the north and south side of the pass, were designed to allow below-ground construction in the zones where thaw-unstable soils were found (Ref 5). Each insulated box consisted of 53 cm (21 inches) of rigid board insulation surrounding the pipe, supported by a concrete pad. The space between the box walls and the pipe was filled with a cement grout (See Fig. 2A). Embedded within the box were sacrificial magnesium anodes for cathodic protection.

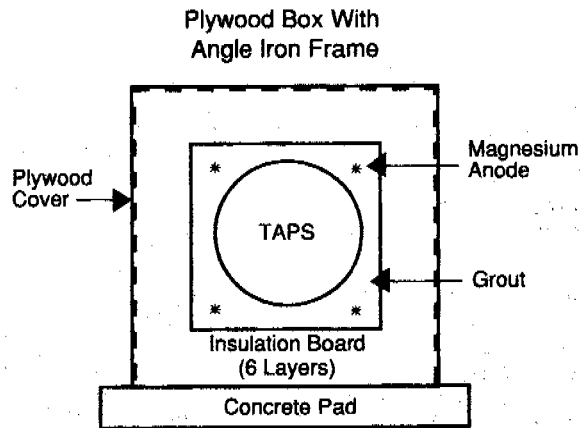
In 1979, about 2 years after completion of pipeline construction, a pipe leak resulting from thaw-settlement was discovered in Atigun Pass (Ref 2). A major repair effort, coupled with extensive exploration and monitoring program enhancements, was conducted from 1979 through 1981. Several sections of the insulated box were found to have experienced significant settlement caused by degradation of the underlying permafrost. Repair work included lifting the pipeline to reduce stresses, construction of below-ground supports, soil grouting, dewatering wells and drainage ditches to control water, and mechanical refreezing to restore the permafrost. Thermosyphons were also installed to maintain the frozen soil in critical

**Figure 1**  
Project Location

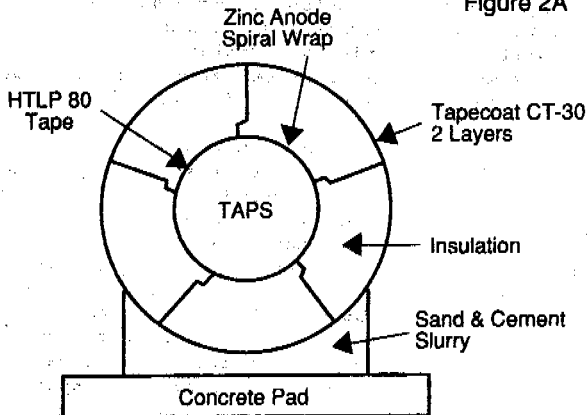


**Figure 2**  
Cross-Section Schematics  
of Insulation Systems

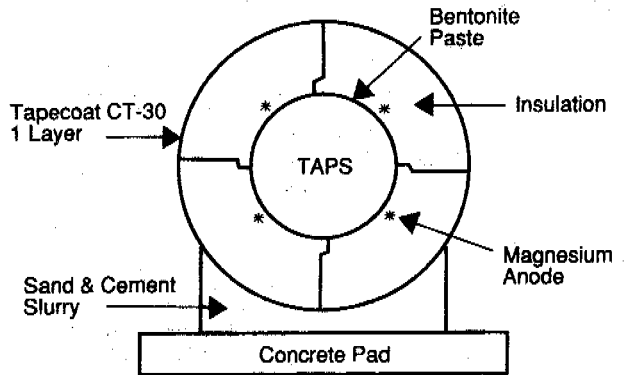
Scale In Meters



Original Insulated Box AS-31  
Figure 2A



Polystyrene Annular Insulation  
Figure 2B



PVC Foam Annular Insulation  
Figure 2C

areas (Ref 6). An extensive monitoring system consisting of thermistor strings and survey rods attached to the pipe was established during this time.

Subsequent monitoring indicated that three areas in the south side insulated box, encompassing about 275 m (900 feet), were continuing to settle and that stresses in the pipe were approaching maximum allowable values (Ref 4). In 1988 these three areas were excavated and relevelled. Because the insulated box in these areas was damaged, the insulation was replaced with 41 cm (16 in.) of annular extruded polystyrene insulation (See Fig 2B).

During earlier repair work, it was concluded that one of the major causes of the permafrost degradation was groundwater flowing along the uninsulated portion of the pipeline trench above the insulated boxes, transporting heat through the trench outside the insulation. As the permafrost thawed, the pipeline and insulated box settled. The settlement tended to crack the concrete and grout and to spread the joints in the insulation. This movement in turn allowed more water to come in contact with the warm pipe, exacerbating the thawing.

During the 1988 reinsulation and releveling work, water was found trapped against the pipe, in the insulation joints and in the insulation pore spaces. The protective tape coating was deteriorated and exterior corrosion was noted. Also the sacrificial magnesium anodes had severed due to the settlement. Based on these observations, it was recommended that all of the remaining portion of the south insulated box be replaced. To reduce further corrosion potential, the pipe will be recoated and the cathodic protection system repaired. The last portion of the project to replace this insulated box is tentatively scheduled for 1994.

#### INSULATION EVALUATION

The insulation used to replace the insulated box needs to be able to tolerate a wet environment and pipe movements associated with settlement, pipe pulses and thermal expansions and contractions. The annular insulation system is more forgiving for minor movements than the rigid, brittle insulated box. Board stock insulations maintain their thermal properties by resisting moisture infiltration, while other insulations rely upon a waterproof jacket to protect the underlying insulation.

Plastic board stock insulations are known to uptake moisture in the pores despite their allegedly being waterproof (Ref 3). Laboratory testing subjects the insulation samples to immersion in water for

varying lengths of time. This test shows whether the insulation is essentially waterproof. Field conditions, however, subject the insulation to a different environment than submersion. In the field, water infiltrates cracks and joints and gets heated in proximity to the pipe. Some of the water changes to the vapor phase and is driven by the temperature differential into the pore spaces of the insulation. Because the inside and outside temperatures are inherently different and not constant, the vapor partial pressure differential is not constant. When the partial pressure in a given pore decreases to the dew point, the excess vapor is changed back to the liquid phase. This change alters the thermal conductivity of the insulation which further alters the vapor pressure differential. By continuous recycling of this complex mechanism, water vapor is forced farther and farther into the insulation cross section. Over time, the effectiveness of the insulation deteriorates.

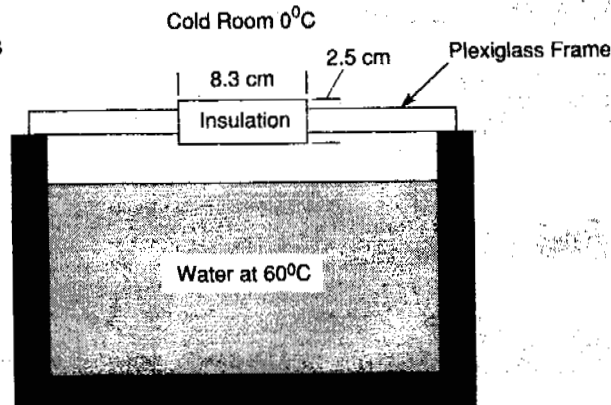
To evaluate different insulations for their resistance to vapor absorption, a simple laboratory test program was developed. Due to time constraints, only a single set of tests was performed. The simple tests provided only comparative test results of the insulation samples.

The five different insulation samples were first oven-dried, and their dry conductivity was tested using a constant energy thermal probe inserted into the sample. Power was applied for ten minutes, and the temperature changes were recorded and thermal conductivity calculated. The results matched the manufacturers' published conductivity values. The insulation samples were cut into 8.3 cm diameter by 2.5 cm thick disks and were mounted in a plexiglass support frame with both flat faces of the insulation exposed. The support frame was placed over a sealed water bath and the entire apparatus placed in a cold room. The water bath was maintained at 60° C, and the cold room was maintained at 0° C. This test thermal range approximated actual field temperatures previously measured. Figure 3 shows a schematic of the test apparatus.

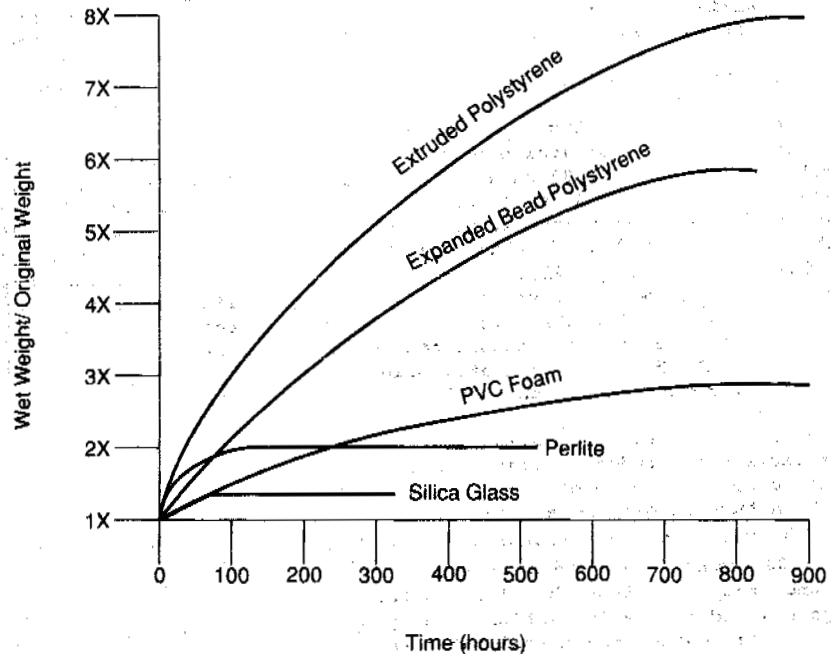
The insulation was kept in the test apparatus for 4 weeks. Periodically during the testing the samples were removed, the surface blotted dry, and the sample weighed. The increase in weight was plotted as water uptake. See Figure 4. At the end of the test period, all of the samples were tested for a moist thermal conductivity using the same procedure as the oven-dry samples. The results of this testing are presented in Figure 5.

To determine the thickness of insulation required to keep the foundation soils in thermal equilibrium,

Figure 3  
Schematic of Insulation Test Apparatus



**Figure 4**  
Water Vapor Absorption

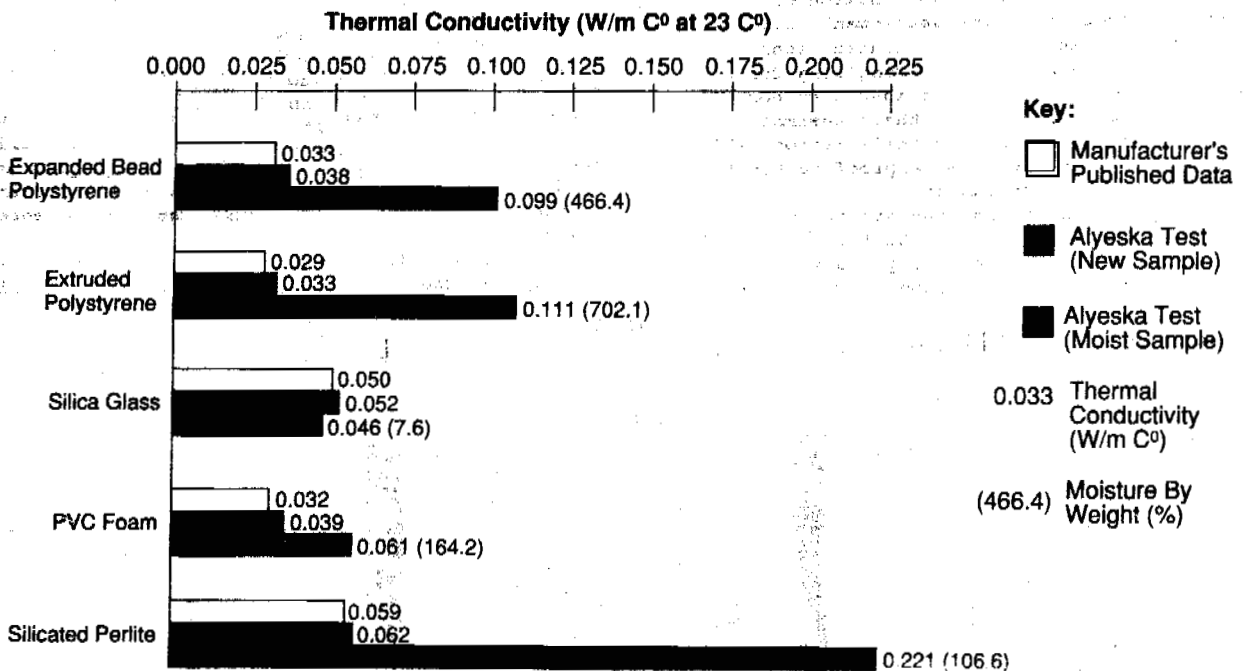


a two dimensional finite element analysis was performed (Ref 1). Several different models were computed providing the range of thaw and refreezing that might be expected in the field. Because actual soil and air temperatures and the effect of moving water were not known, the soil thermal parameters were estimated and the results of the modelling were considered approximate.

**DESIGN AND CONSTRUCTION**

The results of the laboratory testing indicated the sodium silica glass insulation maintained its thermal conductivity the best, followed by PVC foam. In evaluating the construction techniques, the design life of the project and the shipping requirements, the PVC foam was chosen for the project. The PVC

**Figure 5**  
Wet & Dry Thermal Conductivity



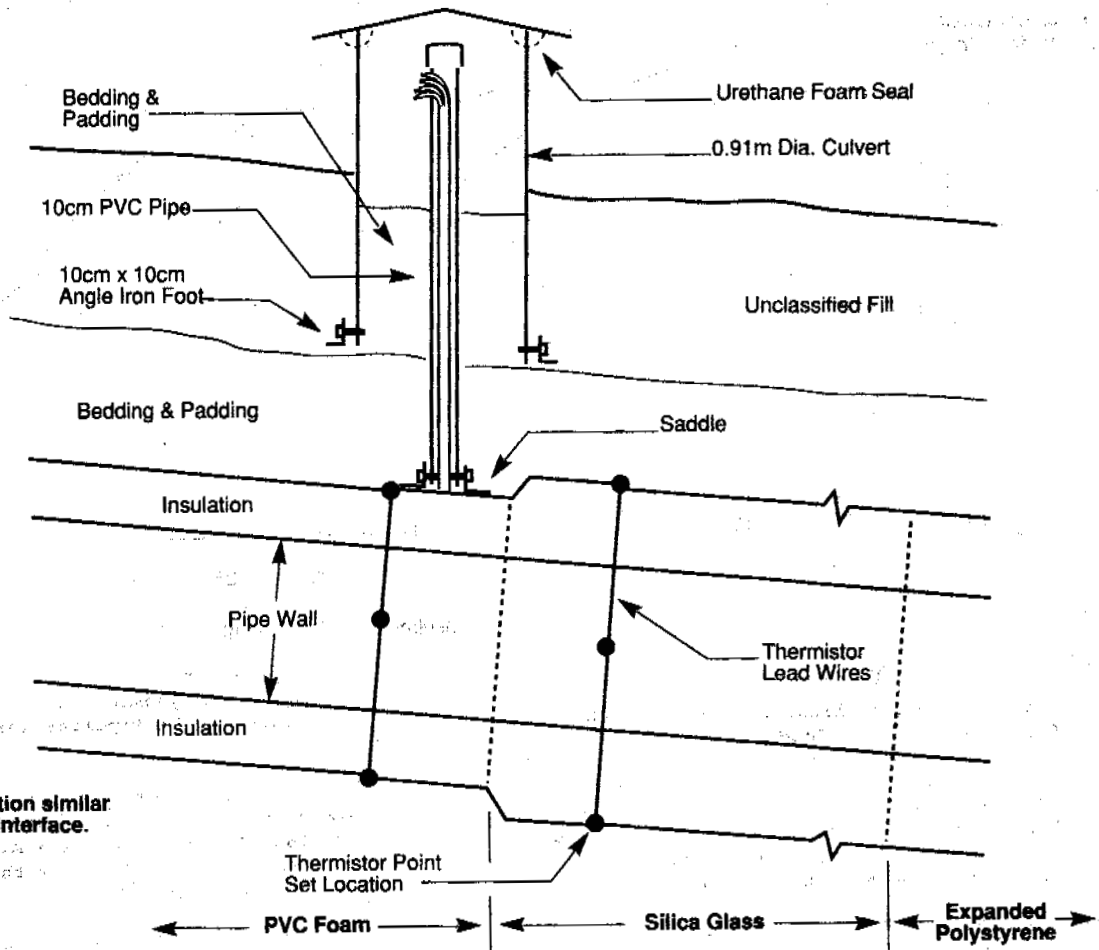
insulation cross section was built of three laminated layers. Thin and denser inside and outside layers sandwiched a thicker, more fragile and less conductive center. The dense inside layer was designed to reduce vapor transport. The dense exterior shell was designed to protect the insulation from construction damage during burial. The insulation design is shown in Figure 2C. The thickness of the insulation system was based primarily on the wet conductivity values obtained in the laboratory testing.

**FIELD TEST SECTION**

As part of the construction project to install the PVC foam insulation, a field test section was constructed to further evaluate the PVC foam and silica glass insulation. The expanded polystyrene annular insulation placed on the pipe in 1988 was also included in the test. The test section was chosen based on location of the existing polystyrene insulation, groundwater conditions, and absence of known avalanche run-out zones. The absence of potential avalanches was to protect above-ground monitoring instrumentation.

Approximately 3 meters of cellular silica glass insulation was installed between the PVC foam and the existing polystyrene foam. Figure 6 presents a

**Figure 6**  
Schematic of Thermistor Installation



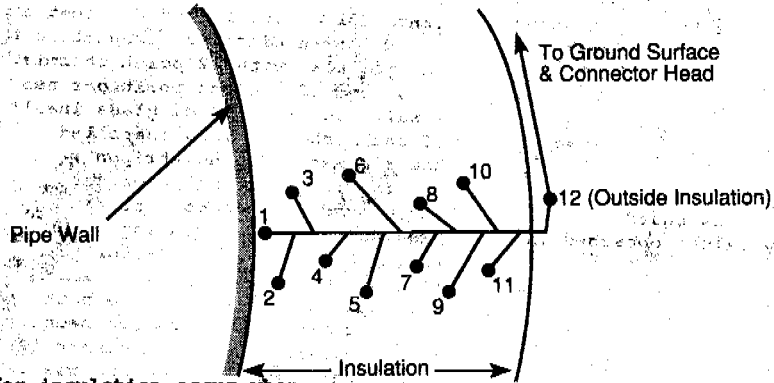
longitudinal section of the test area.

The three different insulation types were instrumented with 12 point thermistor strings at the 3, 6, and 12 o'clock positions near each face of the insulation. The silica glass insulation had two sets of thermistor strings installed, one at each end of the 3 m section. The strings were installed about 0.6 meters from the insulation change joint to ensure that boundary effects were minimized. Figure 7 presents the configuration of the thermistor installation. The thermistor points collectively are accurate to 0.1° C per the manufacturers data sheet. This was confirmed with ice bath tests. The thermistor strings have been read periodically since installation in September 1990. To date, little change has been detected, as was expected from the design. In the future, as the insulation becomes wetter, the thermal conductivity is expected to increase, thereby increasing the temperature in the insulation profile and the adjacent soil. Figure 8 presents a predicted graphic illustration of the insulation performance over time.

**CONCLUSIONS**

Evaluating insulation in an environment where vapor absorption can occur is not currently possible using data derived from existing test methods. The

**Figure 7**  
Thermistor Point Layout  
(3 o'clock position x-section)



most detrimental conditions for insulation occur when a warm, moist enclosed space is to be insulated from a cold, freely circulating environment. The buried Trans Alaska Pipeline, in areas where ground water is in contact with the pipe, is such an environment. Similar conditions exist in humidified living spaces in cold regions. To date, vapor barriers have been used to protect the insulation, sometimes with less than optimum results. No vapor barrier is 100% effective, and moisture will permeate into the surrounding insulation. In critical applications, insulation should be evaluated on a

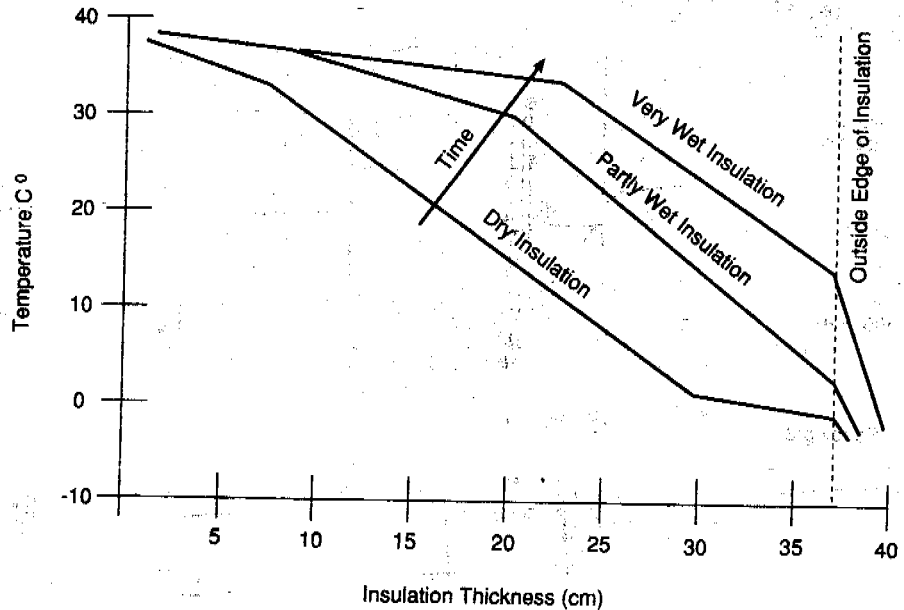
wetted condition to ensure its thermal performance.

We recommend that a standardized test for vapor absorption into insulation be developed. Engineers will then have a tool by which insulation systems can be evaluated for expected useful life and economic considerations.

**ACKNOWLEDGEMENTS**

The authors wish to express their appreciation to Alyeska Pipeline Service Company for permission to publish this paper.

**Figure 8**  
Insulation Effectiveness  
v.s. Water Content



**REFERENCES**

1. Goering, D.J. and Zarling, J.P., 1985, "TDEC, Two Dimensional Heat Conduction," Computer Model, University of Alaska, Fairbanks
2. Johnson, E.R., 1981, "Buried Oil Pipeline Design and Operation in the Arctic - Lessons Learned on the Alyeska Pipeline," Proceedings of the 37th Petroleum and Mechanical Conference
3. McFadden, T., 1986, "Moisture Effects on Extruded Polystyrene Insulation," Proceedings of the 4th International Conference on Cold Regions Engineering
4. Simmons, G.G. and Alto, J.V., 1988, "Pipeline Curvature by Polynomial Approximation," Proceedings of the Pipeline Infrastructure Conference
5. Stanley, J.M. and Cronin, J.E., 1983, "Investigations and Implications of Subsurface Conditions Beneath the Trans Alaska Pipeline in Atigun Pass," Proceedings of the 4th International Ground-Freezing Symposium
6. Thomas, H.P., et al, 1982, "Pipeline Stabilization Project at Atigun Pass," Proceeding of the 3rd International Ground Freezing Symposium

## CAST IN PLACE CONCRETE PILES IN PERMAFROST

Truls Mølmann<sup>1</sup> and Kaare Senneset<sup>2</sup>

<sup>1</sup>Barlindhaug AS, Tromsø, Norway

<sup>2</sup>Geotechnical Division, The Norwegian Institute of Technology, Trondheim, Norway

### SYNOPSIS

In Norway, Svalbard is the only stable permafrost region. During the past decades different foundation principles have been tested. Among these, wooden and to some extent prefabricated concrete piles in drilled holes (with slurry) have proved to be favourable both geotechnically as well as economically. Long transport and thus high material costs on piles, initiated the studies at The Norwegian Institute of Technology of alternative construction methods of foundations in frozen ground. This report deals with the first step of a study aimed at a relatively easy and low cost method of concrete foundations in permafrost regions.

### INTRODUCTION

Due to recent Norwegian progress in the field of concrete technology and the fact that Longyearbyen has a concrete plant, the development of bored cast in situ concrete piles is of great interest.

For decades dwelling houses in Spitzbergen have been built on wooden pile foundations, but the development towards heavier and more complex constructions in permafrost has necessitated heavier foundations. Prefabricated concrete piles have mainly been used, but distance of transport has resulted in relatively high installation costs. This research program was therefore initiated to develop a more economic and flexible method of pile foundation.

The principle is to drill a hole with diameter 200 mm and depth from 5 m - 10 m, install reinforcement and fill up with fresh concrete. During the hardening and curing period, the frozen adjacent ground will act as a formwork. Our studies have dealt with below 0 °C concrete technology as well as geotechnical frozen ground problems.

This study also continues the research work done by Bredeesen, Pushmann and Gregersen, published in the Permafrost Proceedings, Vol. 2, from the V. International Conference on Permafrost in Trondheim, Norway, August 1988. This was a "Long term settlement test for concrete piles in permafrost", and one of the three test piles was in fact a cast in situ reinforced concrete pile.

World wide research studies on this subject have contributed very little to our knowledge of the bearing capacity of piles installed by this method. It has been suggested that cast in situ piles produce an excessive thermal disturbance of frozen ground during concrete curing, and in this way cause effects at the pile/natural permafrost interface which will reduce the bearing capacity.

Our laboratory research work has therefore been concentrated on the extent to which the thermal conditions in the frozen ground will be influenced by the relatively warm (fresh and hardening) concrete.

Fig. 1 is an illustration of the expected influenced zone adjacent to the pile surface.

Of the ground parameters determining the bearing capacity, our main interest was the possible change of ice content and salinity of the frozen ground surrounding the piles owing to the thawing and freezing process. Our main concern was the eventuality of migration of moisture towards the pile, and forming a thin layer of ice coating at the pile surface. The bearing capacity design might then be that of a pile in pure ice.

Likewise we wanted to investigate whether there was a detectable migration of salt towards the pile surface. Salt is known to depress the freezing point of pure water thus accelerating the creep rate and reducing the shear strength of frozen soil at the pile interface.

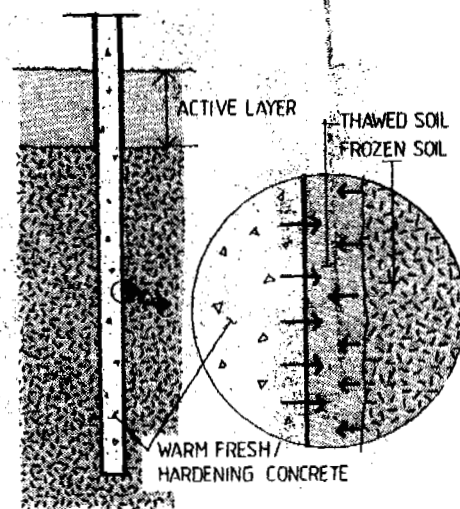


Fig. 1. Expected migration of moisture and salt.



## TEST PROCEDURE

Initially we had to develop a test procedure which simulated the natural conditions of a cast in situ concrete construction in frozen soil material. The idea of a circular steel tank came from BIGGAR and SEGO's "Ciment Fondu based grout test" published in the Proceedings of the Fifth Canadian Permafrost Conference.

Fig. 2 illustrates the investigated section of a pile cast in frozen ground.

The tests were carried out in a steel tank containing approximately 0.5 m<sup>3</sup> of soil material, and during freezing of the soil material a hole (Ø 215 mm, h = 300 mm) in the centre was made by using a formwork of cardboard material. The size of our test tank was determined from practical handling and storing considerations as well as preliminary calculations of thermal conditions in curing concrete.

After having established stable thermal conditions in the frozen soil sample, the formwork was removed, and the remaining hole was filled with concrete.

The diameter of the concrete pile section was taken as an average of those installed to date in permafrost areas.

The 50 mm glycol - filled refrigerant chamber surrounding the test soil was to secure a controlled temperature at the outer edge of the soil material. At the bottom and on top of the soil a PVC-membrane and 100 mm polystyren insulation were precautions made to simulate field temperature and moist conditions.

In the laboratory at the Norwegian Institute of Technology we have simulated the concrete casting and hardening process in ice-poor frozen ground at temperatures -1 °C, -5 °C and -10 °C. These temperatures were characteristic temperatures from the seasonal ground temperature profiles in Longyearbyen. The temperature span from -1 °C to -10 °C covers both summer and winter permafrost conditions. Our aim was to test a pile foundation method which could be carried out at any time of the year.

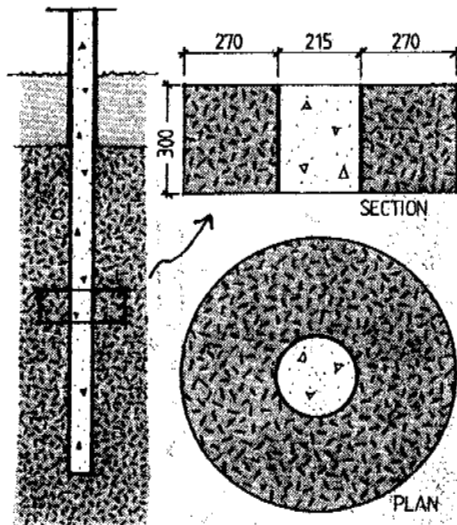


Fig. 2 Illustration of pile section.

Fig. 3 is an illustration of test temperatures of this program related to a schematic graph of the ground temperature profile in Longyearbyen.

Initially after casting, temperature surveillance and registration started both in the concrete pile section as well as in the surrounding frozen soil.

Our research work was carried out in two parallel series. One with concrete mixed with an anti-freeze additive, and the other with concrete having a heating cable placed vertically in the centre of the pile model.

This was to ensure the thermal hardening conditions of concrete cast in frozen soil material.

Tests were also made on two different soil materials. One coarse sand/gravel material with approximately 12% water content. The other was a silt/clay material from Longyearbyen with a 25% - 30% water content. Both were ice-poor soils with frozen bulk density more than 1,7 g/cm<sup>3</sup>.

All tests were made using the same concrete recipe, w/c ratio 0,45 (C35).

Temperature variations during a 120 hour period after casting were recorded in the concrete test pile model as well as in the surrounding frozen soil. Tests were also made on concrete strength and migration of water and salt towards the pile/soil interface.

Fig.4 shows the plan and section of test tank with the location of temperature sensors.

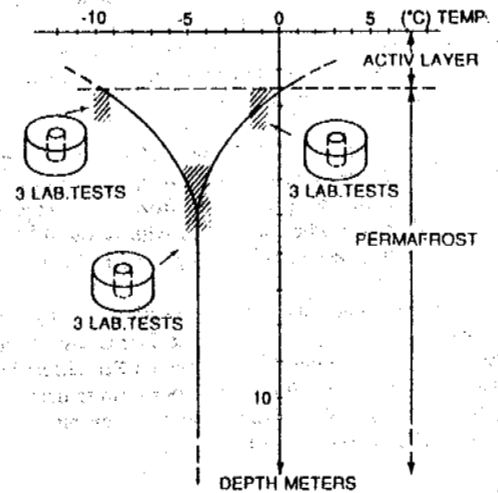


Fig. 3 Test temperatures related to seasonal ground temperature profile in Longyearbyen.

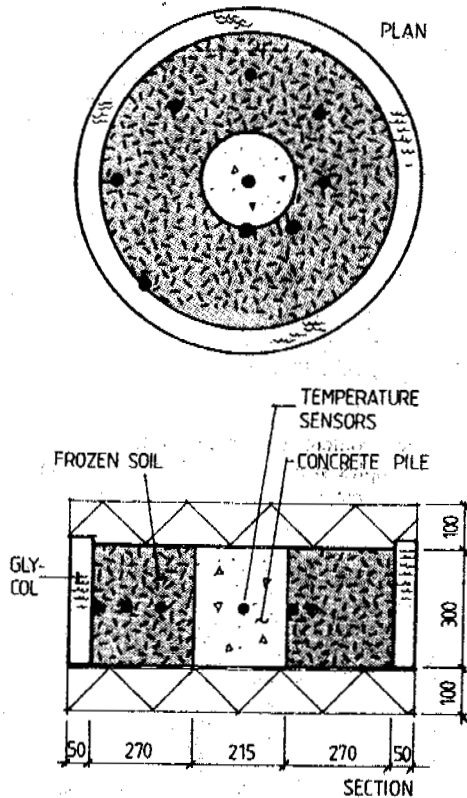


Fig. 4 Plan and section of test tank with the location of temperature sensors (pile centre, pile/frozen soil interface, 25 mm, 50 mm, 100 mm, 150 mm, 220 mm and 270 mm from pile surface).

## TEST RESULTS

We will here give a brief summary of test results of two representative tests with soil temperature  $-5^{\circ}\text{C}$ .

### Concrete mix with 5% anti-frost additive

Before casting, the temperature in the homogenous frozen soil sample was constant at  $-4,7^{\circ}\text{C}$ .

The temperature in the fresh concrete at the moment of casting was  $+20^{\circ}\text{C}$ . After  $4\frac{1}{2}$  hours the temperature was below  $0^{\circ}\text{C}$ , and the concrete pile section started freezing.

Fig. 5 shows the concrete temperature variation in cubes stored in water at  $+20^{\circ}\text{C}$ , and in the concrete pile section cast in frozen soil. Additionally we have indicated the development of cube compressive strength in cubes stored in water at  $+20^{\circ}\text{C}$ , as well as in cubes cut from the concrete pile.

In spite of the rapid temperature fall, concrete curing and hardening continued, with a relative rapid increase in compressive strength from day 2. After 7 days the strength of concrete cast in frozen soil was close to that of concrete cubes stored at normal standard conditions, in water with constant temperature  $+20^{\circ}\text{C}$ .

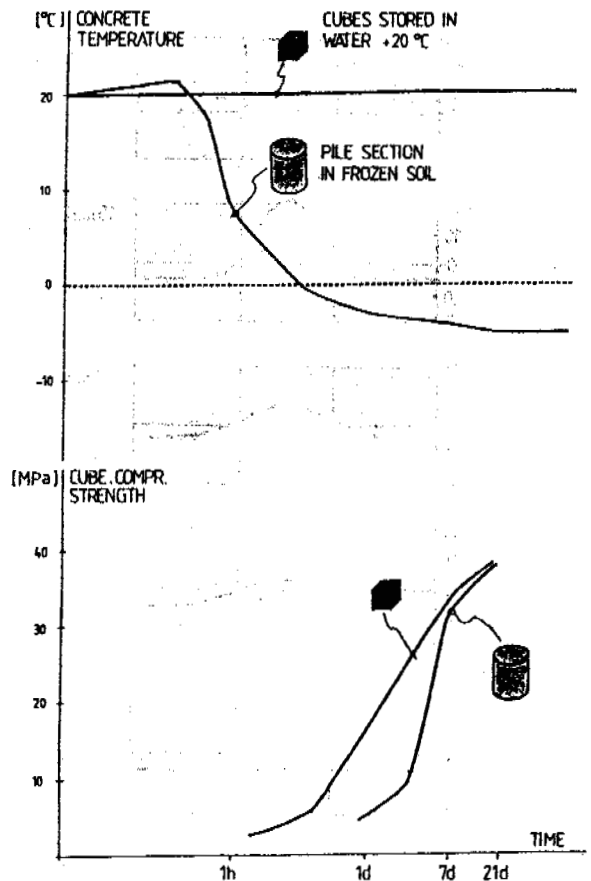


Fig. 5 Temperature variation and cube compressive concrete strength versus time. (Concrete mix with 5% antifrost additive).

The above is of great interest for Svalbard conditions since permafrost temperature below 4-5 m under terrain surface is constant approximately  $-5^{\circ}\text{C}$ . The lab-test indicates that by this method it is possible to establish a cast in place concrete pile with acceptable strength by using a standard concrete mix with 5% anti-frost additive.

Fig. 6 shows temperature in the concrete pile during hardening and curing as well as in the surrounding soil. At the pile-soil interface a 10 mm - 20 mm zone, measured radially from the pile surface, thawed due to the warm concrete.

The period, in which the soil around the pile surface was thawed was less than 5 hours and this indicated that both the amount of free water (and salt) and the time period of possible migration towards the pile surface are limited.

Fig. 7 (and Fig. 10) show ice content and salinity of drilled core samples of the frozen soil 5 days after concrete casting. None of our tests indicated any detectable migration of either water or salt towards the pile surface due to the concrete casting and curing process.

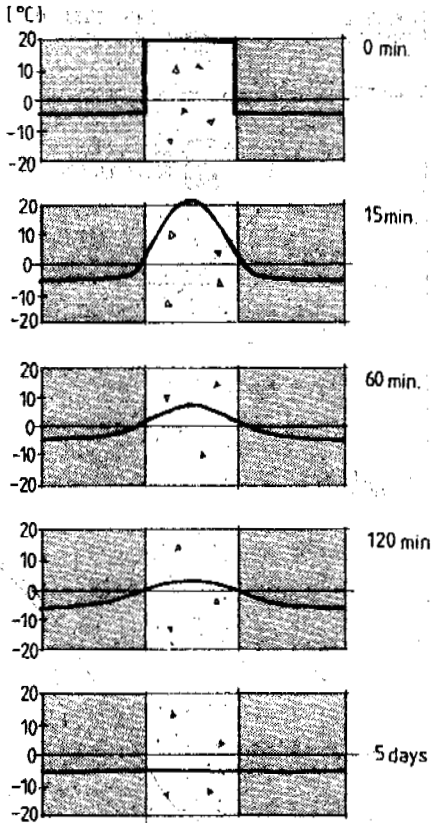


Fig. 6 Temperature profiles in concrete and soil at given time intervals. (Concrete mix with 5% antifrost additive).

#### Concrete pile section with a cast in heating cable

This was a standard concrete mix without any anti-frost additives, but with a heating cable to support the curing process.

Initially the fresh concrete had a temperature of 23.4 °C, but after 5½ hours the temperature in the centre of the pile fell to just below 6 °C. At the pile/soil interface the temperature at this time was -1 °C, and these temperature conditions both in the concrete pile section and in the surrounding frozen soil remained steady throughout the whole test period (5 days).

These are optimal thermal conditions since in this temperature range concrete is curing rapidly and at the same time the soil at the pile surface remains frozen.

Fig. 8 shows the development of temperature and concrete hardening. The concrete compressive strength of the test pile section develop close to parallel to the strength of cubes stored in water at +20 °C.

The thermal disturbance of the surrounding soil is also negligible since the temperature at the pile surface at no time in the test period exceeded -1 °C. This is shown in Fig. 9.

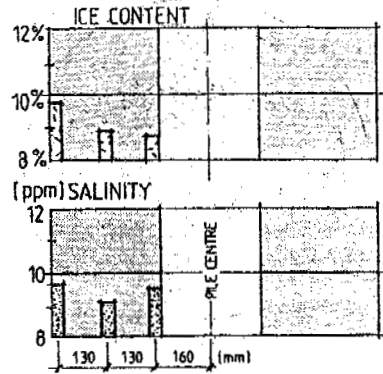


Fig. 7 Ice content and salinity after 5 days in frozen soil samples at locations indicated. (Concrete mix with 5% antifrost additive).

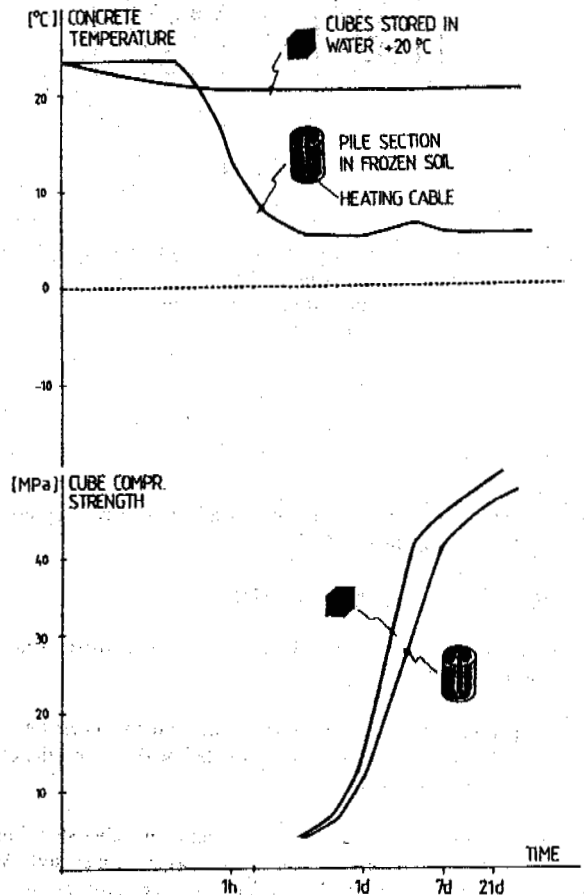


Fig. 8 Temperature variation and cube compressive concrete strength. (Concrete with heating cable).

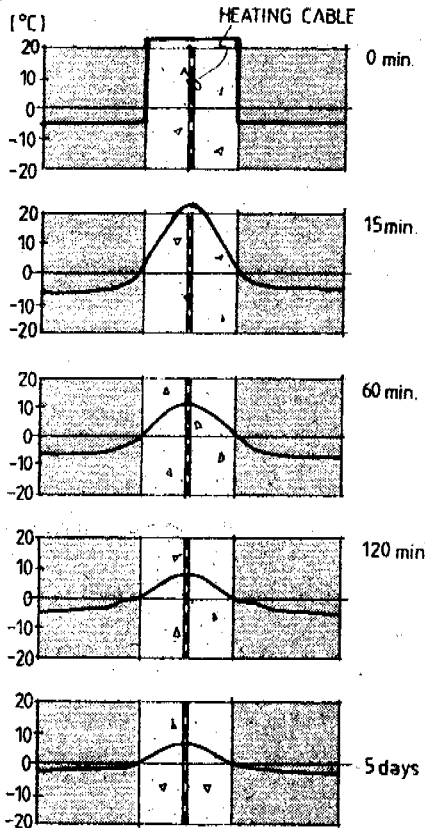


Fig. 9 Temperature profiles in concrete and soil at given time intervals. (Concrete with heating cable).

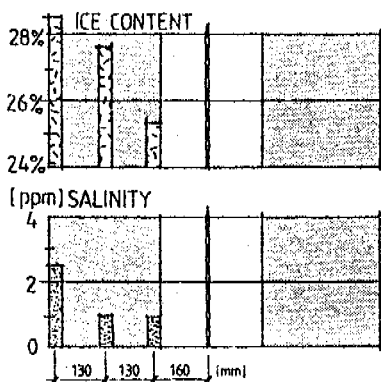


Fig. 10 Ice content and salinity after 5 days in frozen soil samples at locations indicated. (Concrete with heating cable).

## COMMENTS

So far our studies have shown that for ice-poor frozen soils at temperatures between  $-1^{\circ}\text{C}$  and  $-10^{\circ}\text{C}$  there are no significant changes of the frozen soil due to the cast in situ installation method.

Fig. 7 and 10 indicate higher ice contents at the outer radius of the frozen soil, but we are at this stage unable to conclude other than that this variation occurs due to inaccuracy of measurements or the initial soil freezing process.

We made however two important observations:

- (i) The zone around the pile which thawed due to the "warm" concrete was very small (less than 60 mm measured radially from the pile surface). This means that the amount of free water and salt to migrate is limited.
- (ii) The period during which the soil surrounding the pile had a temperature above  $0^{\circ}\text{C}$  was relatively short (less than 6.5 hours).

The conclusion is, therefore, that there is just a limited range of thermal disturbance on the surrounding ground due to the cast in situ process. At this stage of our studies we are of the opinion that the load-bearing capacity of concrete piles in permafrost within the thermal, water and salinity regimes tested here, is relatively indifferent to the installation method (cast in situ or installation of ready made concrete piles in drilled holes with slurry). This also means that the known models for theoretical calculations of concrete piles in permafrost may be applied with no corrections for the cast in situ piles of these tests.

## REFERENCES

- Bredesen, Puschmann and Gregersen (1988)  
 Long Term Settlement Test (3 years).  
 For Concrete Piles In Permafrost.  
 Proceedings Vol. 1; 5th. International Conference on Permafrost in Trondheim, Norway.
- Biggar and Sego (1990)  
 The curing and strength characteristics of cold setting cement foru gront.  
 PERMAFROST-CANADA, Proceedings of the Fifth Canadian Permafrost Conference.
- B. Ladanyi (1988)  
 Short- and long-term behaviour of axially loaded bored piles in permafrost.  
 Deep Foundations on Bored and Anger Piles, 1988, Rotterdam, ISBN 9061918146.
- T. Mølmann (1991)  
 Cast-in-situ piles in frozen soil.  
 Master thesis, Geotechnical Division, Norwegian Institute for Technology, University of Trondheim

SAND WEDGES AND PERMAFROST HISTORY, CRUMBLING POINT,  
PLEISTOCENE MACKENZIE DELTA, CANADA

Julian B. Murton and Hugh M. French

Department of Geology, University of Ottawa and  
Ottawa-Carleton Geoscience Centre, Ottawa, Ontario K1N 6N5, Canada

Large sand wedges (≤10m deep and ≤4m wide) at Crumbling Point, Summer Island, penetrate deformed icy sediments and massive ice and underlie a discontinuous veneer of aeolian sand. The wedges probably formed under cold, dry conditions in the Middle to Late Wisconsinan. During the late Wisconsinan-early Holocene warm interval, regional thermokarst formed a secondary thaw contact beneath melt-out diamiction. Since the warm interval, ice veins and wedges have formed, many superimposed within sand wedges.

### INTRODUCTION

Along the coastline of the Pleistocene Mackenzie Delta, retrogressive thaw slumping locally exposes sand wedges. At Crumbling Point, on northern Summer Island (Figure 1), we have examined more than 50 sand wedges and their adjacent cryostratigraphy. By placing them in their cryostratigraphic and regional contexts, we reconstruct the late Quaternary permafrost history of Crumbling Point and discuss the regional significance of the sand wedges.

In several ways, the sand wedges at Crumbling Point are unusual. First, sand wedges are rarely described from the western North American Arctic (see e.g. Mackay, 1974; Hodgson, 1982, p.27; Carter, 1983). Instead, they are usually described from permafrost environments that are very cold and arid (e.g. Berg and Black, 1966; Bennike, 1987) or from areas where permafrost no longer exists (e.g. Gozdzik, 1973; Mears, 1987). Second, the sand wedges at Crumbling Point are singularly large (≤10m deep and ≤4m wide). Third, many host ice veins and wedges. However, unlike other descriptions of composite ice-sand wedges of primary infilling (e.g. Berg and Black, 1966), where the ice and sand are essentially coeval, the sand wedges and ice wedges at Crumbling Point formed at different times and under different climates. Fourth, the sand wedges penetrate a thick body of icy sediments and massive ice. Similar icy bodies, common in western arctic Canada, are generally interpreted either as intrasedimental ice, formed during permafrost aggradation (e.g. Mackay, 1971; Mackay and Dallimore, 1992), or glacier ice buried during either ice stagnation or glacier retreat (e.g. French and Harry, 1988, 1990). To our knowledge, sand wedges in icy sediments or massive ice have been described solely from Antarctica, where they penetrate stagnant glacier ice (Péwé, 1959).

### LOCATION

Crumbling Point (69°36'N;133°54'W) is in the zone of continuous permafrost. The permafrost thickness is 600-700m and the mean annual ground temperature is c.-8°C to -9°C. The site lies just within the Early Wisconsinan (Toker Point Stade) glacial limit but beyond that of the Late Wisconsinan (Sitidgi Stade; Figure 1; Rampton, 1988, map 1647A; Vincent, 1989, Figure 2.7).

The Point itself is the rapidly retreating headland of an ice-rich plateau (c.20m asl). Along c.1km, the plateau is truncated by large thaw slumps that expose numerous sand wedges.

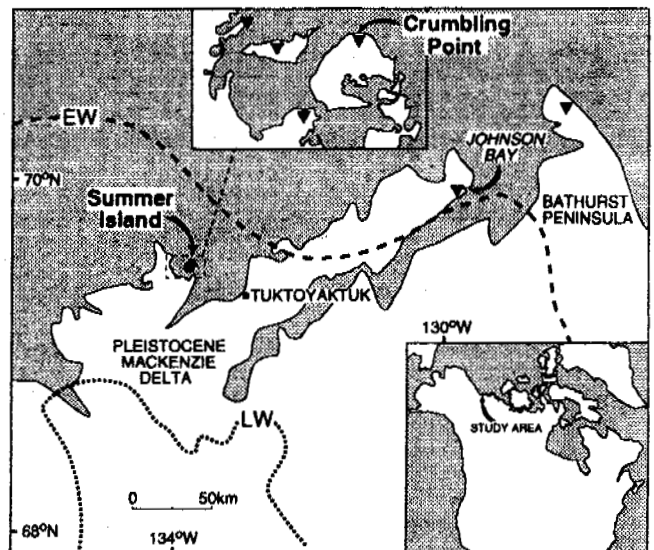


Figure 1. Location map of the Tuktoyaktuk Coastlands. Triangles mark the locations of sand wedges. 'EW' and 'LW' denote the probable Early and Late Wisconsinan glacial limits.

### SAND WEDGES

The sand wedges penetrate a thick (15+m) unit of layered and deformed icy sediments and massive ice (Figure 2). The icy layers (c.0.01-0.40m thick and c.2-60+m long) have volumetric ice contents locally exceeding 95%; their sediments comprise sand and muddy diamiction.

The sand wedges form a polygonal network of downward-tapering bodies whose average spacing is c.10m (Figure 2). Most are steeply to vertically laminated (Figure 3A). The laminae (1-7mm thick and 0.05-3+m long) parallel or subparallel the wedge sides, and many display low-angle cross-cutting relationships. Some wedges contain distinct bundles of sand laminae, the bundles forming wedge-in-wedge structures (Figure 3A; cf. Williams and Tonkin, 1985; Nissen and Mears, 1990). The bundles (0.05-0.5m thick, 0.3-3.5m long

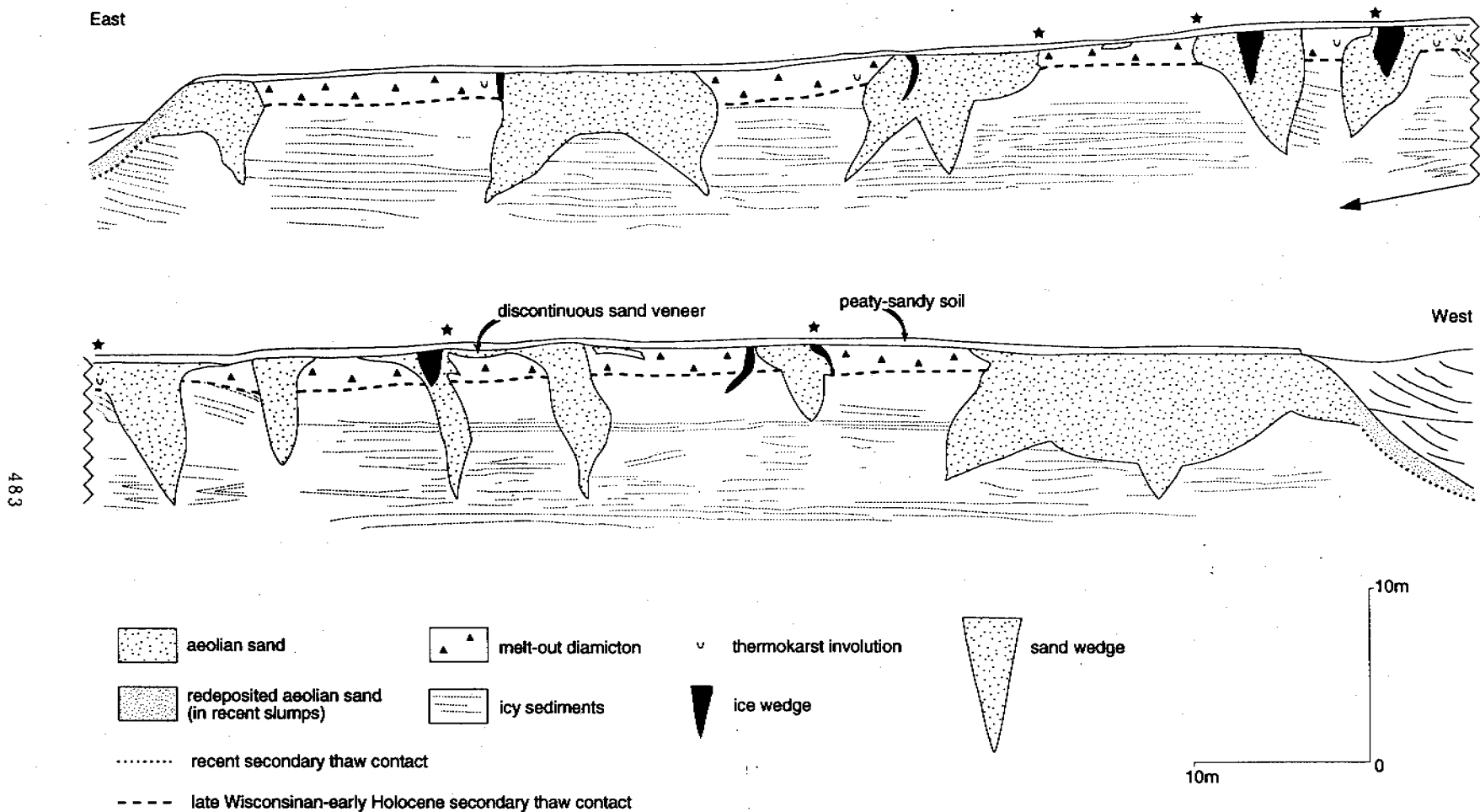


Figure 2. Cryostratigraphic sketch of sand wedges penetrating deformed icy sediments at Crumbling Point (July 7 1990). Ice wedges occur both within and between the sand wedges. The geometry of the latter is due to the variable angles at which their axial planes intersect the curved headwall; there are three examples of convergent wedges. The sites at which  $^{14}\text{C}$  dates were obtained are a few hundred metres east of this section. At both ends of the headwall occur recent stabilised slumps. '\*' denotes sand wedges with deformed tops.

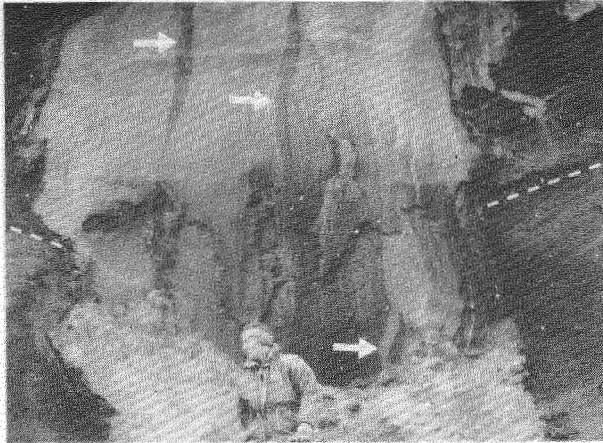


Figure 3A. Sand wedge (c.3m in true width) with well-developed vertical sand laminae and wedge-in-wedge structures (arrows). Above the secondary thaw contact (dashed line), the top of the wedge is deformed (June 7 1991).



Figure 3B. Sand wedge containing two ice wedges. Above the secondary thaw contact (dashed line), sand ball-and-pillow structures (arrows) are suspended in melt-out diamicton (June 7 1991).

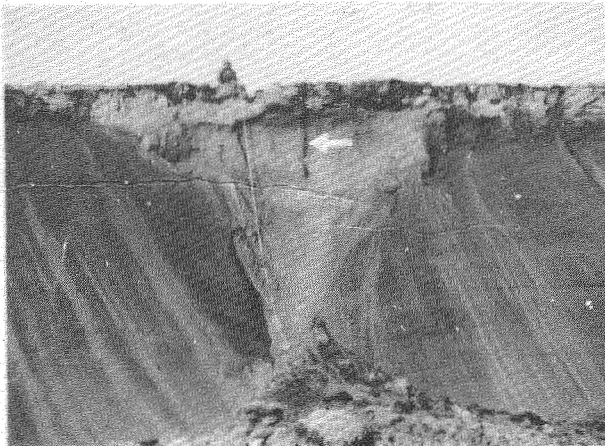


Figure 3C. Sand wedge (c.7.5m deep) whose top merges into a veneer of aeolian sand. In the upper centre of the sand wedge is a thin ice wedge (arrow; July 4 1990).

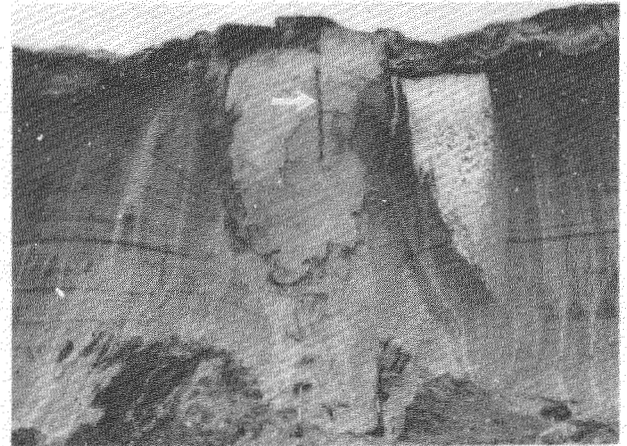


Figure 3D. Adjacent sand wedge (c.7m deep) and ice wedge. A second ice wedge (arrow) occurs within the sand wedge (June 3 1991).

and generally containing a few to several tens of laminae) reflect grain-size variations.

The sand infill is fine grained and well sorted, similar to local Pleistocene and aeolian dune sand (Figure 4). SEM analysis of grains from the infill reveals numerous equant depressions, rounded edges and upturned plates (Figure 5A), all signs of aeolian abrasion (e.g. Krinsley and Doornkamp, 1973). But many grains also display V-shaped patterns and bulbous edges (Figure 5B), signs of subaqueous abrasion (Krinsley and Marshall, 1987). Wherever aeolian and subaqueous textures coexist, the former are superimposed on the latter (Figure 5; cf. Krinsley and Cavallero, 1970), suggesting that subaqueously abraded sand was later abraded in an aeolian environment.

The sand wedges are thought to have formed by the infilling of thermal contraction cracks with aeolian sand. This is indicated by the large-scale polygonal pattern of the wedges, by the sand laminae within the infill, by grain-surface textures characteristic of aeolian abrasion and by a textural similarity between the sand infill and local aeolian dune sand. Individual laminae show that the wedges grew incrementally; bundles of sand laminae suggest that sand supply and/or wind velocity/direction changed episodically. The unusually large size of the wedges is problematic, but it may reflect high thermal coefficients of linear expansion and contraction of the ice-rich host materials.

## CRYOSTRATIGRAPHY

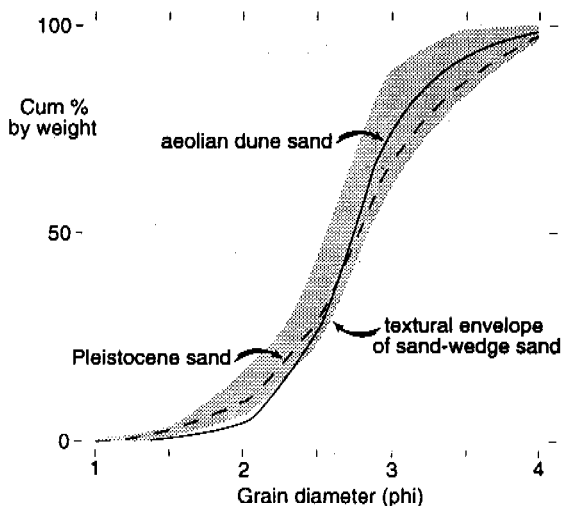


Figure 4. Textural envelope of sand-wedge sand (based on 10 samples) in the Summer Island area. Individual grain-size curves show local Pleistocene and aeolian dune sand.

The cryostratigraphic horizon beside the tops of the wedges comprises sand and diamicton (Figure 2). In texture and grain-surface features, the sand resembles that within the wedges, suggesting that it too is aeolian. The diamicton (c.0.2-2.5m thick) is mud-rich, texturally identical to that within the underlying icy sediments; but its volumetric ice content is lower ( $<c.50\%$ ) and its clast density higher. The sand and diamicton horizon has several distinctive features. First, it contains many soft-sediment deformation structures (diapirs, load casts, pseudo-nodules and ball-and-pillow structures; Figure 3B). Second, within this horizon the tops of some sand wedges are deformed (Figures 2 and 3A). Third, the diamicton locally underlies a veneer ( $\leq 1.5$ m thick) of sand that is contiguous with the sand wedges (Figures 2 and 3C). Fourth, there are abrupt lateral facies changes: diamicton is absent where sand wedges occur, and sand is locally absent between them (Figure 2).

The lower contact of the diamicton (average depth=2.3m;  $n=37$ ) is sharp and planar to gently curved (Figure 2). While much of the contact is conformable with bands in the underlying icy materials, it locally forms an angular unconformity. Across the contact is an isotopic discontinuity: the average  $\delta^{18}O$  value of ground ice above it is  $-24.73\text{‰}$  ( $n=4$ ;  $\sigma=1.55\text{‰}$ ), that below it  $-29.95\text{‰}$  ( $n=7$ ;  $\sigma=0.58\text{‰}$ ).

Because of the angular unconformity and the isotopic discontinuity, the contact must be a thaw (or erosional) contact; and because it is younger and lower than the tops of the sand wedges, the thaw contact must be secondary. This would explain (1) the abundance of soft-sediment deformation structures (i.e. thermokarst involutions; Murton, 1993), (2) the deformed tops of some sand wedges and (3) the relatively low ice-content of the diamicton. The contact represents the base of an ancient thaw layer in which diamicton melted out from the underlying icy sediments and massive ice.

Ice veins and wedges ( $\leq 1.5$ m wide and  $\leq 4$ m deep) penetrate each cryostratigraphic unit (Figure 2). They appear to be epigenetic and related to the present ground surface. Many are superimposed within the sand wedges (Figures 3B-3D).

## DISCUSSION

### Age Control

Assuming that the deformed host icy materials were deformed glaciectonically (cf. Mackay et al., 1972) during the Early Wisconsinan (Rampton, 1988, p.66; Vincent, 1989, Figure 2.7), then the undeformed sand wedges postdate this time.

The thaw layer, melt-out diamicton and underlying secondary thaw contact likely formed during the late Wisconsinan-early Holocene warm interval. This is suggested by two  $^{14}C$  dates of 9,480  $\pm$  100 years B.P. (Beta-46224) and 8,860  $\pm$  180 years B.P. (Beta-46223) from wood fragments above the contact. The first was from the bottom of a 40cm thick layer of fibric peat overlying a 1.0-1.5m thick sand lens separated from the underlying secondary thaw contact by 2-3cm of melt-out diamicton. The second was from a root suspended in slump-floor deposits above a slump-

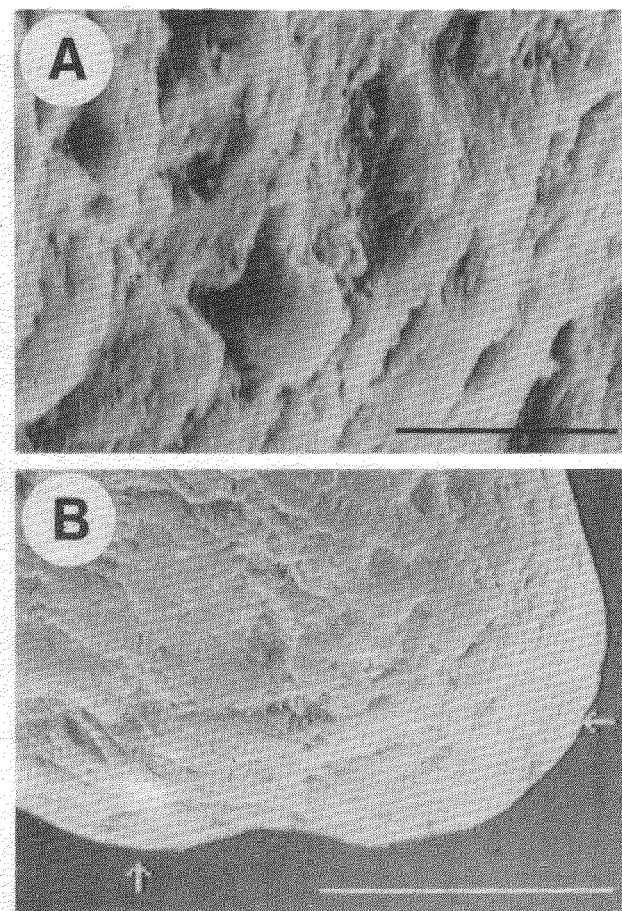


Figure 5. Scanning electron micrographs of a sand grain from a sand wedge. Upturned plates (A) are superimposed on bulbous edges (B; arrows). Scale bars are respectively 5µm and 100µm.



floor secondary thaw contact. The simplest interpretation of these dates is that the wood grew during the warm interval which triggered the thaw slumping and which formed both the melt-out diamicton and the underlying thaw contact. This interval was probably the late Wisconsinan-early Holocene, a time when western arctic Canada experienced regional thermokarst (e.g. Mackay, 1978; French et al., 1982; Rampton, 1982, p.33; 1988, pp.74-76, Figure 66; Burn et al., 1986; Harry et al., 1988).

Two lines of evidence indicate that the sand wedges predate the episode of thawing. First, since one of the <sup>14</sup>C-dated wood fragments overlies the sand, and the other occurs in slump-floor sediments that include redeposited sand, both dates provide minimum ages for the cessation of aeolian sand deposition. Second, sand wedges whose tops are deformed in the thaw layer (Figure 3A) must predate it.

In short, the age of the wedges is likely Middle to Late Wisconsinan.

#### Late Quaternary History of Crumbling Point

The deformed icy sediments and massive ice are probably Early Wisconsinan in age or older. However, whether these materials are buried glacier ice (e.g. see French and Harry, 1988; 1990) or intrasedimental ice that was glacially deformed (cf. Mackay et al., 1972) is beyond the scope of this paper.

By the Middle Wisconsinan, the northwest margin of the Laurentide Ice sheet had probably retreated southeast of the Tuktoyaktuk Coastlands (J-S Vincent, personal communication, November 1992), exposing the ground surface to thermal contraction cracking and aeolian activity. During the Middle to Late Wisconsinan, aeolian sand derived locally from Pleistocene deposits (Figure 4; see Rampton, 1988, map 1647A) accumulated both in thermal contraction cracks, forming sand wedges, and on the ground surface, a veneer. Because the late Wisconsinan-early Holocene thaw layer had not yet formed, the veneer likely accumulated directly on the icy sediments and massive ice.

During the late Wisconsinan-early Holocene warm interval, Crumbling Point experienced regional thermokarst. The plateau was isolated on at least three sides by thermokarst basins and thaw slumps, and the uppermost icy sediments and massive ice melted within a thick thaw layer. Thawing was accompanied by (1) the formation of the melt-out diamicton above a secondary thaw contact and (2) the deformation of the sand veneer and the tops of some sand wedges. As no ice wedges extend down from the thaw contact, thermal contraction cracking had likely ceased.

Since the warm interval, permafrost has aggraded into the base of the thaw layer, and thermal contraction cracking has recommenced. But instead of infilling with sand, the cracks have infilled mainly with water (ice), because the modern climate is wetter and warmer than that of the Middle to Late Wisconsinan (e.g. Ritchie, 1984, p.155). Equally important, however, is that during the Holocene, the sand supply has likely decreased, reflecting plant colonisation of, and pedogenesis within, the top of the sand veneer.

#### Regional Significance

This paper is the first to describe Wisconsinan-age sand wedges of primary infilling from the Tuktoyaktuk Coastlands. The wedges must be distinguished from (A) the small Early Wisconsinan or older sand wedges of secondary infilling (see Mackay and Matthews, 1983) and (B) modern sand wedges of primary infilling forming in the sandy floors of drained lakes (see Mackay, 1974; personal communication, August 1991). Besides the wedges at Crumbling Point, we have observed large sand wedges at three other sites near Summer Island, and single wedges elsewhere (near Johnson Bay and on Bathurst Peninsula; Figure 1). Why these features have not been described before is probably due to poor exposures, many wedges being obscured by slumped sand.

Our study implies that sand wedges are likely to be common in those sandy areas of the Tuktoyaktuk Coastlands which were unglaciated during the Late (and ?Middle) Wisconsinan. In many parts of the Coastlands, sand of pre-Middle Wisconsinan age is abundant (see Rampton, 1988, map 1647A). Furthermore, by analogy with modern ice-free areas bordering large ice-caps (e.g. Berg and Black, 1966; Bennike, 1987), the Late Wisconsinan climate here was probably very windy, with cold katabatic winds sweeping across the ice-free areas northwest of the Laurentide ice margin. The Late Wisconsinan environment probably resembled that of adjacent Beringia (see Hopkins, 1982). However, the Coastlands lay relatively close to the margin of the Laurentide Ice sheet - a setting likely analogous to present, sandy ice-marginal areas of Antarctica and northern Greenland, where sand wedges form today (e.g. Berg and Black, 1966; Bennike, 1987). In these sandy environments, and probably in those of Late Wisconsinan Beringia and the Tuktoyaktuk Coastlands, thermal contraction cracking would have coincided with aeolian activity.

#### CONCLUSIONS

Large sand wedges at Crumbling Point penetrate icy sediments and massive ice. The wedges are interpreted as thermal contraction cracks infilled with locally derived aeolian sand. They likely formed during the Middle to Late Wisconsinan. Sand wedges of this age are probably widespread in those areas of the Tuktoyaktuk Coastlands which were unglaciated during the Middle to Late Wisconsinan and which possessed abundant Pleistocene sand. The closest modern environmental analogues to that of Late (and ?Middle) Wisconsinan Crumbling Point are probably the sandy ice-marginal areas of Antarctica and northern Greenland.

#### ACKNOWLEDGEMENTS

Fieldwork during the summers of 1989 to 1991 was supported by NSERC grant A-8367 (H.M. French); The Geological Survey of Canada; The Inuvik Research Centre, Science Institute of the Northwest Territories; and The Polar Continental Shelf Project, Energy, Mines and Resources Canada. The authors are grateful to S.R. Dallimore, D.G. Harry, W.H. Johnson, J.R. Mackay, J.V. Matthews Jr., J. Shaw, A. Sher, W.W. Shilts, A.A. Velitchko and J-S Vincent for their comments about the sand wedges at Crumbling Point, and to L.D. Carter and

E.A. Koster for reviewing this manuscript. Andy Green and Bruce Lowe assisted with the fieldwork, and Edward Hearn the cartography.

#### REFERENCES

- Bennike, O. (1987) Quaternary geology and biology of the Jorgen Bronlund Fjord area, North Greenland. *Meddelelser om Gronland, Geoscience*, 18, 23pp.
- Berg, T.E. and R.F. Black (1966) Preliminary measurements of growth of non-sorted polygons, Victoria Land, Antarctica. In: (ed. J.C.F. Tedrow) *Antarctic Soils and Soil-Forming Processes, American Geophysical Union Antarctic Research Series*, 8, pp.61-108.
- Burn, C.R., F.A. Michel, and M.W. Smith (1986) Stratigraphic, isotopic and mineralogical evidence for an early Holocene thaw unconformity at Mayo, Yukon Territory. *Canadian Journal of Earth Sciences*, 23, 794-803.
- Carter, L.D. (1983) Fossil sand wedges on the Alaskan Arctic Coastal Plain and their paleoenvironmental significance. In: *Permafrost, Proc. 4<sup>th</sup> Int. Conf., National Academy Press, Washington, D.C.*, pp.109-114.
- French, H.M. and D.G. Harry (1988) Nature and origin of ground ice, Sandhills Moraine, southwest Banks Island, Western Canadian Arctic. *Journal of Quaternary Science*, 3, 19-30.
- French, H.M. and D.G. Harry (1990) Observations on buried glacier ice and massive segregated ice, western Arctic coast, Canada. *Permafrost and Periglacial Processes*, 1, 31-43.
- French, H.M., D.G. Harry, and M.J. Clark (1982) Ground-ice stratigraphy and late-Quaternary events, southwest Banks Island, Canadian Arctic. In: (ed. H.M. French) *The R.J.E. Brown Memorial Volume, Proc. 4<sup>th</sup> Can. Perm. Conf., National Research Council of Canada, Ottawa*, pp.81-90.
- Gozdzik, J. (1973) Geneza i pozycja stratygraficzna struktur peryglacjalnych w srodkowej Polsce (Origin and stratigraphical position of periglacial structures in middle Poland, Polish with English summary), *Acta Geographica Lodziensia*, 31, 119pp.
- Harry, D.G., H.M. French, and W.H. Pollard (1988) Massive ground ice and ice-cored terrain near Sabine Point, Yukon Coastal Plain. *Canadian Journal of Earth Sciences*, 25, 1846-1856.
- Hodgson, D.A. (1982) Surficial materials and geomorphological processes, western Sverdrup and adjacent islands, District of Franklin. *Geological Survey of Canada Paper 81-9*, 44pp.
- Hopkins, D.M. (1982) Aspects of the paleogeography of Beringia during the late Pleistocene. In: (eds D.M. Hopkins, J.V. Matthews Jr., C.E. Schweger, and S.B. Young) *Paleoecology of Beringia*. Academic Press, New York, pp.3-28.
- Krinsley, D.H. and J.R. Marshall (1987) Sand grain textural analysis: an assessment. In: (ed. J.R. Marshall) *Clastic Particles: Scanning Electron Microscopy and Shape Analysis of Sedimentary and Volcanic Clasts*. Van Nostrand Reinhold, New York, pp.2-15.
- Krinsley, D.H. and L. Cavallero (1970) Scanning electron microscopic examination of periglacial eolian sands from Long Island, New York. *Journal of Sedimentary Petrology*, 40, 1345-1350.
- Krinsley, D.H. and J. C. Doornkamp (1973) *Atlas of Quartz Sand Surface Textures*. 91pp. Cambridge University Press, Cambridge.
- Mackay, J.R. (1971) The origin of massive icy beds in permafrost, western Arctic coast, Canada. *Canadian Journal of Earth Sciences*, 8, 397-422.
- Mackay, J.R. (1974) The rapidity of tundra-polygon growth and destruction, Tuktoyaktuk Peninsula-Richards Island area, N.W.T. In: *Current Research, Part A, Geological Survey of Canada Paper 74-1*, pp.391-392.
- Mackay, J.R. (1978) Freshwater shelled invertebrate indicators of paleoclimate in northwestern Canada during late glacial times: Discussion. *Canadian Journal of Earth Sciences*, 15, 461-462.
- Mackay, J.R. and S.R. Dallimore (1992) Massive ice of the Tuktoyaktuk area, western Arctic coast, Canada. *Canadian Journal of Earth Sciences*, 29, 1235-1249.
- Mackay, J.R. and J.V. Matthews Jr. (1983) Pleistocene ice and sand wedges, Hooper Island, Northwest Territories. *Canadian Journal of Earth Sciences*, 20, 1087-1097.
- Mackay, J.R., V.N. Rampton, and J.G. Fyles (1972) Relic Pleistocene permafrost, western Arctic, Canada. *Science*, 176, 1321-1323.
- Mears, B.Jr. (1987) Late Pleistocene periglacial wedge sites in Wyoming: an illustrated compendium. 77pp. *The Geological Survey of Wyoming, Memoir 3*.
- Murton, J.B. (1993) *Thermokarst Sedimentology of the Tuktoyaktuk Coastlands, NWT*. 187pp. Unpublished PhD thesis, University of Ottawa.
- Nissen, T.C. and B. Mears Jr. (1990) Late Pleistocene ice-wedge casts and sand-wedge relics in the Wyoming Basins, USA. *Permafrost and Periglacial Processes*, 1, 201-219.
- Péwé, T.L. (1959) Sand-wedge polygons (tessellations) in the McMurdo Sound Region, Antarctica - a progress report. *American Journal of Science*, 257, 545-552.
- Rampton, V.N. (1982) *Quaternary Geology of the Yukon Coastal Plain*. 49pp. *Geological Survey of Canada Bulletin*, 317.
- Rampton, V.N. (1988) *Quaternary Geology of the Tuktoyaktuk Coastlands, Northwest Territories*. 98pp. *Geological Survey of Canada, Memoir 423*.
- Ritchie, J.C. (1984) *Past and Present Vegetation of the Far Northwest of Canada*. 251pp. University of Toronto Press, Toronto.
- Vincent, J-S. (1989) Quaternary geology of the northern Canadian Interior Plains. In: (ed. R.J. Fulton) *Quaternary Geology of Canada and Greenland*. *Geological Survey of Canada, Geology of Canada*, no. 1, pp.100-137.
- Williams, G.E. and D.G. Tonkin (1985) Periglacial structures and palaeoclimatic significance of a late Precambrian block field in the Cattle Grid copper mine, Mount Gunson, South Australia. *Australian Journal of Earth Sciences*, 32, 287-300.

## Effects of Climatic Warming on the Active Layer

T. Nakayama, T. Sone and M. Fukuda

Institute of Low Temperature Science, Hokkaido University,  
Sapporo, 060, Japan

**SYNOPSIS** Under a climatic warming trend, the thickness of the active layer over permafrost will increase. Changes in the thickness and thawing period of the active layer are important, because a thickened active layer may produce positive feedback effects with respect to future climate. In this paper, we compute ground temperature profiles using a one-dimensional heat conduction solution and estimate active layer thickness under appropriate conditions with respect to alpine permafrost in Hokkaido, northern Japan. Applying results obtained by this model to global permafrost regions, the following consideration is obtained. If warming of climate occurs in all permafrost regions, the increase of active layer thickness near the southern limit is larger than in arctic regions. If the ground surface temperature increases linearly, active layer thickness will also increase proportionally. However, active layer index which is derived from accumulating value of each day thawing depth (cm·days) will increase exponentially. As this index is an appropriate indicator of positive feedback to warming of climate, the result of this estimation suggests that the feedback effect will increase rapidly year by year.

## INTRODUCTION

Recently it has been reported based on meteorological observation that global climatic warming is occurring. (Jones and Wigley, 1990) and that warming will be greatest in polar regions of the northern hemisphere (Yamamoto and Hoshiai, 1980; Hansen and Lebedeff, 1987). Most climatic models also have predicted that air temperature increases mainly in high latitude of northern hemisphere, especially in winter (Manabe and Stouffer, 1980; Washington and Meehl, 1984; Hansen et al., 1988; Schlesinger and Mitchell, 1955). An increase of air temperature probably results in increases of ground surface temperature and ground thermal regime, disregarding changes of snow, humidity, vegetation, and so on. In permafrost areas, higher ground temperature may cause a decrease of permafrost thickness, an increase of active layer thickness, and a resultant poleward retreat of permafrost boundaries. Climatic change causes significant effects on permafrost environments.

Changes of active layer thickness, especially in alpine and polar regions, are the focus of our study. Both thickening of the active layer and increases in the thawing period cause changes near the permafrost table and these changes in turn produce some effects on climate. In high latitude regions, when the temperature above the upper permafrost is above zero during summer, the seasonal wetlands are formed on permafrost. The

peat in the active layer begins to decay under anaerobic conditions and methane gas is produced there and released to the atmosphere. The production of methane gas probably increases due to both an increase of active layer thickness and longer thawing period. Because methane is a prominent greenhouse gas, an increase of its emission from active layer may cause further global warming. The thickening of the active layer also causes melting of excess ground ice, and discharged water will affect surrounding hydrological environments. Increased water volume leads to changes in vegetation and, additionally, changes of albedo and evapotranspiration from plants in that area. It is therefore important to evaluate the magnitude of thickening and the prolonged period of thawing of active layer under recent trends of climatic warming.

One of the objectives of this study is to ascertain how future warming will affect the active layer, especially related to the changes of thickness and thawing period in the active layer. To estimate those changes, a method using numerical analysis was adopted. The simulation was performed in regard to alpine permafrost in Hokkaido, northern Japan, where fluctuations of ground temperature have been monitored. Additionally, we applied results derived from this model to global permafrost and considered positive climatic feedback effects due to changes in active layer.

## STUDY SITE

In mid-latitude regions like Japan, alpine permafrost exists on high mountains. The Daisetsu mountains are located in central Hokkaido, northern Japan. These mountains are composite volcanoes and their highest peak is Mt. Asahidake, which is 2,290 m above sea level. On the Hokkai-daira plateau, which is 2,070 m a.s.l. (Fig.1), the existence of some alpine permafrost and periglacial features such as frost-fissure polygons were previously reported (Fukuda and Kinoshita, 1974). The material of surface sediment is mostly of volcanic origin and with some organic materials. The basal rock is some kind of volcanic rocks.

Fluctuations of air and ground temperatures have been monitored since 1985 in this site (Sone et al., 1988). The mean annual air temperature is  $-3.7^{\circ}\text{C}$  (the average of 1951-1990) and the temperatures were monitored at the ground surface and at depths of 40cm, 90cm, 140cm, 220cm and 300cm. Owing to the flatness of the plateau and severe prevailing westerly winds in winter, there is little snow cover accumulation on the ground surface. The ground surface temperature regime is therefore similar to air temperature (Fig.2).

The depth of the bottom of permafrost at the site has not been measured directly as yet. However it was estimated as somewhere between 5 and 10 m deep based on an analysis of ground temperature gradient and geo-electrical resistivity survey (Sone et al., 1988; Fukuda and Sone, 1992). The depth of thaw in soil is inferred from ground temperature profiles mentioned above. Thawing of frozen

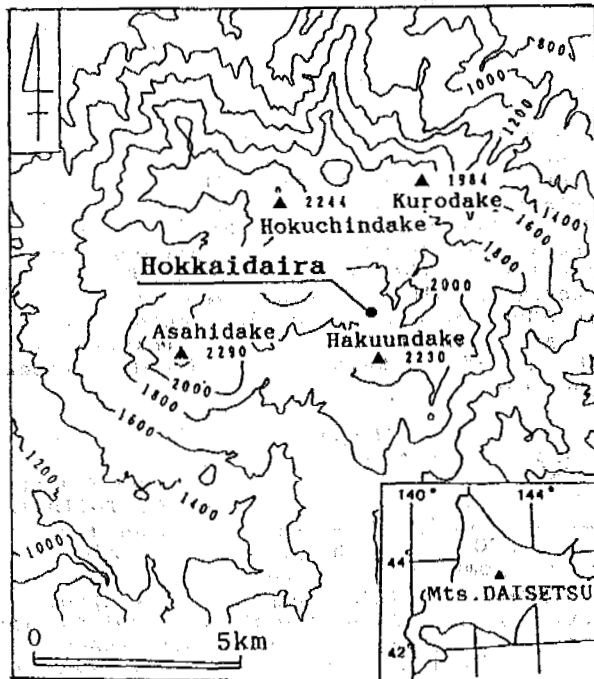


Fig.1 Location map of Hokkai-daira plateau, Mts.Daisetsu, Hokkaido.

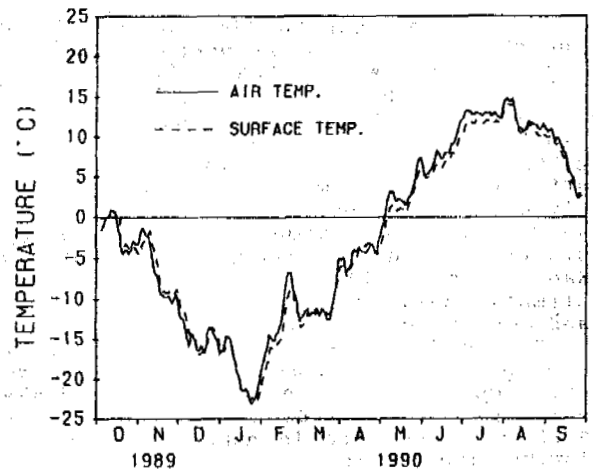


Fig.2 Air temperature and ground surface temperature on Hokkai-daira plateau in 1989-1990.

ground begins in early May and the maximum thaw depth occurs at 1 - 1.5 m deep in between late September and early October.

## NUMERICAL MODEL

To predict the response of the active layer to climatic warming, it is necessary to estimate ground temperature profiles under given boundary conditions. Ground temperature as a function of time was obtained based on the heat conduction equation with phase changes terms as a non-linear heat transport equation. In this study, the heat transport by moving ground water is neglected. The basic equation is a one dimensional, differential equation of heat conduction :

$$\frac{\partial T}{\partial t} = a_u \frac{\partial^2 T}{\partial x^2} \quad (t > 0^{\circ}\text{C}) \quad (1)$$

$$\frac{\partial T}{\partial t} = a_f \frac{\partial^2 T}{\partial x^2} \quad (t < 0^{\circ}\text{C}) \quad (2)$$

where  $x$  is the coordinate in the vertical direction,  $T$  is ground temperature,  $t$  is time and  $a$  is thermal diffusivity. The subscripts,  $u$  and  $f$  denote as unfrozen and frozen states, respectively. These equations were solved numerically using an implicit finite difference method. The grid spacing is 10 cm and numerical solution is made with one day time step.

The amount of latent heat at phase change is treated as an apparent heat capacity. Latent heat is substituted for heat capacity with equivalent amounts, when freezing temperature stands within given temperature range. The following parameters is used for numerical simulation. The first is some properties of the sediment, such as thermal conductivity, volumetric heat capacity and volumetric water content. Sediments near the surface and at 1 m depth were sampled and their volumetric water content and thermal conductivity were measured in the laboratory.

But we sampled only one time and didn't treat the changes of these properties with time. Heat capacity was estimated based on water content and specific heat of the dry soil. Secondary, as the upper boundary condition, fluctuation of ground surface temperature is given in sinusoidal form. As the lower boundary condition, temperature at 10 m deep is given as a constant value, which is equal to annual mean air temperature. Based upon similar procedures, Goodwin et al. (1984) and Kane et al. (1991) examined the effect of climatic warming on permafrost temperature and active layer thickness in Alaska.

To verify the accuracy of the solution, simulated active layer thicknesses were compared with that measured on the Hokkai-daira plateau in 1986 and 1990. The ground surface temperature is approximated by following sine curve:

$$T(n) = AMP \cdot \sin ( 2n / 365 + PH ) + AT \quad (3)$$

where  $n$  is elapsed day, AMP and AT are amplitude of annual variation and annual mean value in ground surface temperature and PH is phase difference. On Hokkai-daira plateau, AMP is  $14.5^{\circ}\text{C}$  and AT changes year by year, for example  $-4.5^{\circ}\text{C}$  in 1986 and  $-2.3^{\circ}\text{C}$  in 1990. Ground temperature profiles under these assumptions were obtained computationally and the active layers are calculated for two years. Comparisons of active layer thicknesses between simulated and measured ones are shown in Fig.3. The simulated values of active layer thickness coincide with measured ones.

Particularly first day of thawing and rate of thaw penetration in frozen layer are well-simulated. As a consequence, this model is applicable to predict changes of thickness and thawing period of active layer under specific, relatively simple condition (e.g. homogeneous soils, snow-free surface).

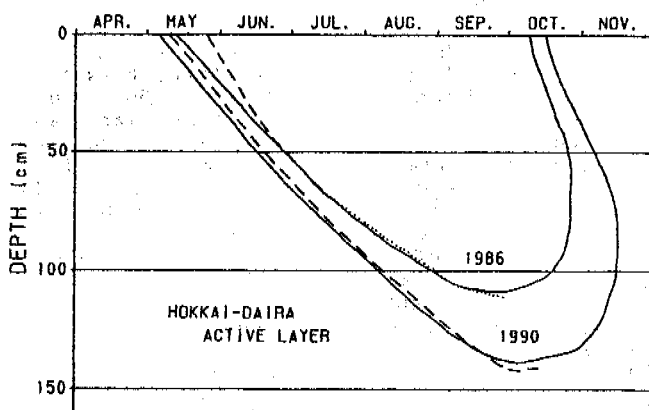


Fig.3 Comparison between measured and simulated active layer thicknesses on Hokkai-daira plateau in 1986 and 1990.

## CLIMATIC WARMING AND ACTIVE LAYER CHANGE

### The case of the Daisetsu Mountains

In general, it is reported that global warming of  $0.3^{\circ}\text{C} - 0.7^{\circ}\text{C}/100$  years has occurred during the past century (WMO, 1986). Over the last few decades, some climatic models have been developed and future warming has been predicted. No definite predictions have been made due to difficulties and uncertainty in the numerical analysis. However according to recent atmospheric general circulation models which are coupled to a mixed-layer ocean, if the concentrations of greenhouse gases continue to increase at the present rate, the increment of the global mean air temperature will reach  $1.5^{\circ}\text{C}$  and  $3.5^{\circ}\text{C}$  in the 2030s (Meteorological Agency, 1989).

The regional warming in Hokkaido has not been studied. Thus the minimum value of global average ( $1.5^{\circ}\text{C} / 50\text{yr}$ ) was adopted as the rate of warming for this study. At the same time, the warming trend was assumed to be a linear increase, with a constant annual variation. In general, the ground surface temperature is different from air temperature. However, we assumed that the ground surface temperature was equal to air temperature. This assumption is appropriate on Hokkai-daira plateau, because of the lack of accumulation of snow and vegetation on the ground surface. We computed the change of ground temperature profile and estimated the increase of thickness and thawing period in the active layer with the ground surface temperature warming over the next 100 years. The ground surface temperature, which is given as the upper boundary condition, is obtained from the approximated sine curve of eq.3. AMP is steady at  $14.5^{\circ}\text{C}$ , but AT is temporal function as follows:

$$AT = 3.0 / 100 \cdot Y - 3.7 \quad (4)$$

where  $Y$  is the elapsed year. As the lower boundary condition, the temperature at a depth of 10 m is given as the same value as obtained by eq.4. The result is shown in Fig.4. The active layer thickness increases gradually in response to ground surface warming at the rate of  $3^{\circ}\text{C} / 100$  yr. The increased value of thickening of active layer is 53cm and thawing period becomes 37days longer than present. It is noteworthy that the trend of this line indicates linear increase.

### Sensitivity of the active layer to climatic change

We assume that the ground surface temperature rises by one degree in two following manners. In the first case, it rises from  $-10^{\circ}\text{C}$  to  $-9^{\circ}\text{C}$  and in the second from  $-3^{\circ}\text{C}$  to  $-2^{\circ}\text{C}$ . By comparison of these two cases, the influence of initial temperature to change of active layer thickness might be obtained. The term "sensitivity of active layer change" is defined by the authors as the increase of active layer thickness caused by one degree temperature rise.

With respect to Hokkai-daira plateau, ten thawing curves (in fig.5) were drawn by

computations using mean annual ground surface temperatures, which vary from  $-10^{\circ}\text{C}$  to  $-1^{\circ}\text{C}$ , with the same value of AMP as  $14.5^{\circ}\text{C}$ . In fig.6, the relations between initial ground surface temperature and increase of active layer thickness with  $1^{\circ}\text{C}$  increments of temperature are plotted. In proportion to the increase of initial ground surface temperature, the thickness of the active layer increases exponentially. The higher initial ground surface temperature corresponds to the southern margins of the permafrost regions in the northern hemisphere. Thus an uniform increase of temperature causes greater thickening of active layer in southern regions than in Arctic regions.

#### Active layer index

Under a climatic warming trend, the thickness and the thawing period of the active layer in permafrost area will increase. It is convenient to introduce the term "active layer index" to evaluate the effects of the degrees of active layer change under a warming trend. This index is defined as the integrated value of the daily thawing depth from beginning to end during thaw period (cm-days). The value is equivalent to the area of thawing curves, for example, which is shaded in Fig.5. Because the active layer index represents both the values of thickness and thawing period in the active layer, it is a very appropriate indicator in considering the interaction between changes of active layer and climate. We consider that this index with relation to permafrost in high latitude areas, may represent the positive feedback effect on climate in the following path.

The active layer in high latitude areas, which exhibits seasonal wetland characteristics during summer, plays an important role as the major source of methane gas. The methane gas is produced by decay of organic materials under anaerobic condition. High amounts of organic material are commonly

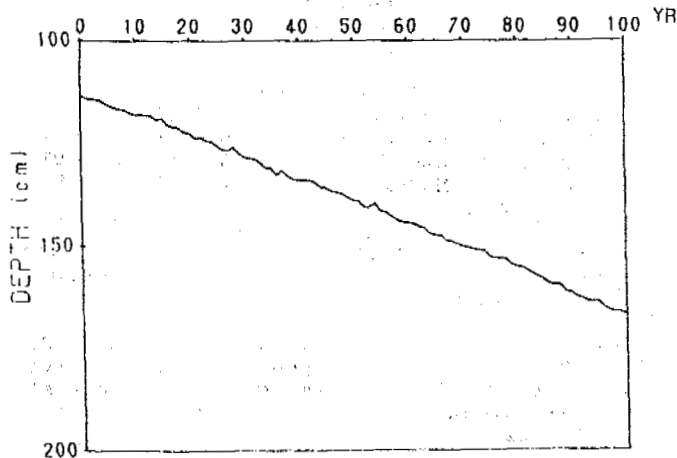


Fig.4 Change of active layer thickness under a climatic warming with the rate of  $3^{\circ}\text{C} / 100 \text{ yr}$  on Hokkai-daira plateau.

stored in the active layer, and this is the primary source of methane. Permafrost beneath active layer may contain "locked" organic materials. If the depth of the active layer exceeds the previous maximum depth and no change of the hydrological condition such as ground water level occurs during climatic warming period, rapid decay of organic materials from "locked" layer might occur. A large amount of methane gas may then be released from that layer. It is predicted

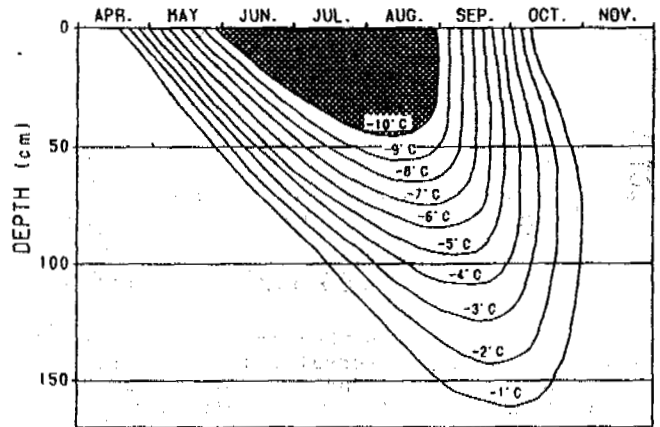


Fig.5 Seasonal changes of thawing depth for different annual mean ground surface temperatures. An area of shaded portion is equivalent to active layer index value when ground surface temperature is  $-10^{\circ}\text{C}$ .

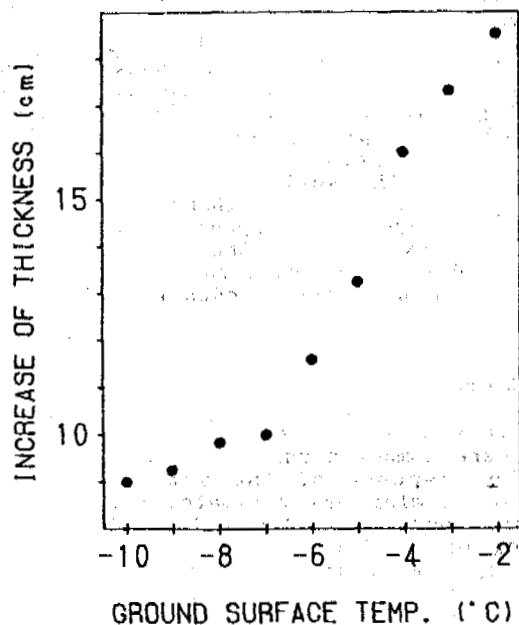


Fig.6 Relations between initial ground surface temperature and increase of active layer thickness with temperature rise by  $1^{\circ}\text{C}$ .

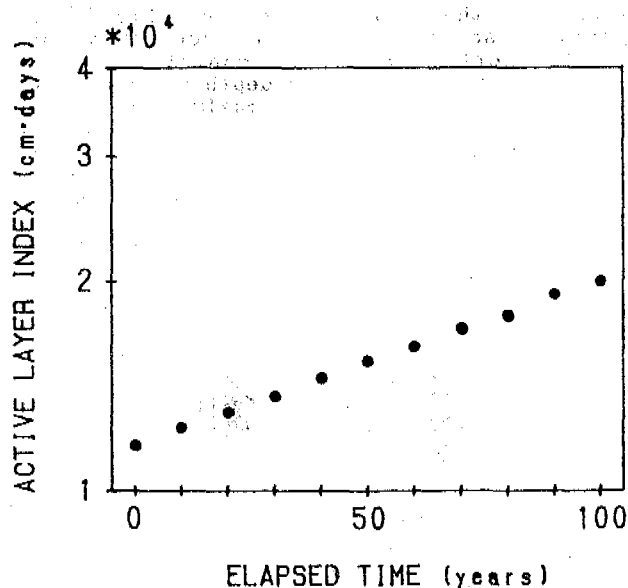


Fig.7 Change of active layer index under warming trend at intervals of ten years for one hundred years. The rate of warming is constant as  $3^{\circ}\text{C} / 100 \text{ yr}$  and initial temperature is  $-3.7^{\circ}\text{C}$ .

that the thickening of the active layer and prolonging of the seasonal thaw cause additional production of methane gas.

With respect to Hokkai-daira plateau, using the value of the initial ground surface temperature as  $-3.7^{\circ}\text{C}$ , the calculations of active layer index were made at ten year interval for 100 years with an increase rate of  $3^{\circ}\text{C} / 100 \text{ yr}$  (Fig.7). This figure indicates that the active layer index increases exponentially with a linear temperature rise. Assuming that this result is applicable to not only the alpine permafrost in mid-latitude but the permafrost regions in high latitude and the active layer index represents the indicator of methane emission from the active layer, the exponentially increase of this index suggests that the warming of the ground at a constant rate may result in accelerated positive feedback effects to climate.

## CONCLUSION

In this study, ground temperature profiles were computed using numerical analysis and the response of the active layer to climatic warming was estimated under simple boundary conditions. The effect of climatic warming on active layer is concluded in following summarizing sentences:

1. If the mean annual ground surface temperature in the Daisetsu Mountains, Hokkaido, increases linearly by  $3^{\circ}\text{C}$  over the coming 100 years, the thickness and the thawing period of the active layer will increase by 53 cm and 37 days respectively.

2. The thickening of the active layer in a warming trend depends on initial tempera-

ture conditions. An increase in active layer thickness with a temperature rise of  $1^{\circ}\text{C}$  becomes larger in response to an increase of initial temperature. It implies that in southern regions of permafrost, the thickening of active layer will occur more dramatically than in Arctic regions under uniform warming occurs in both regions.

3. The active layer index is newly proposed by the authors as an indicator of the degree of change in the active layer under warming trend. This index is derived from an integration of thaw depth values at each day (cm-days). The results of calculations with respect to the Daisetsu Mountains suggest that this index value exponentially increases in accordance with a linear increase of mean annual ground surface temperature. From this fact, it may be suggested that some positive feedback effects will accelerate year by year. To clarify the interaction between the permafrost and climatic change in future, it is necessary to ascertain the changes of the methane emission, the hydrological condition and other factors with the change of active layer thickness.

## REFERENCES

- Fukuda, M., and Kinoshita, S. (1974) Permafrost at Mt. Daisetsu, Hokkaido and its climatic environment. *The Quat. Res.*, 12, 192-202.
- Fukuda, M., and Sone, T. (1992) Some characteristics of alpine permafrost at Mt. Daisetsu, central Hokkaido, Northern Japan. *Geografiska Annaler*, 74A, 159-167.
- Goodwin, C.W., Brown, J., and Outcalt, S.I. (1984) Potential response of permafrost to climatic warming. In: J.H. McBeach (Editor), *Proc. The potential effect of carbon dioxide-induced, climatic change in Alaska*. Misc. Publ., 83-1, 93-105.
- Hansen, J., and Lebedeff, S. (1987) Global trends of measured surface air temperature. *J. Geophys. Res.*, 92, 13345-13372.
- Hansen, J., Fung, I., Lacis, A., Rind, D., Lebedeff, R., Ruedy, R., and Russell, G. (1988) Global Climate Changes as Forecast by Goddard Institute for Space Studies Three Dimensional Model. *J. Geophys. Res.*, 93, 9341-9364.
- Jones, P.D., and Wigley, M.L. (1990) Global warming trends. *Scientific American*, August 1990, 66-73.
- Kane, D.L., Hinzman, L.D., and Zarling, J.P. (1991) Thermal response of the active layer to climatic warming in a permafrost environment. *Cold Reg. Sci. Technol.*, 19, 111-122.
- Manabe, S., and Stouffer, R.J. (1980) Sensitivity of a global climate model to an increase of  $\text{CO}_2$  concentration in the atmosphere. *J. Geophys. Res.*, 85, 5529-5554.

Meteorological Agency of Japan (1989) Abnormal weather report. 433pp.

Schlesinger, M.E., and Mitchell, J.F.B. (1987) Climate model simulations of the equilibrium climate response to increased carbon dioxide. Rev. Geophys., 25, 760-798.

Sone, T., Takahashi, N., and Fukuda, M. (1988) Alpine permafrost occurrence at Mt. Daisetsu, Central Hokkaido, in Northern Japan. in Proceedings, Fifth International Conference on Permafrost, 253-258.

WMO (1986) Report of international conference on the assessment of the role of the carbon dioxide and of other greenhouse gases in climatic variations and associated impacts. WMO-No.661, 78pp.

Washington, W.D., and Meehl, G.A. (1984) Seasonal cycle experiment on the climate sensitivity due to a doubling of CO<sub>2</sub> with an atmospheric general circulation model coupled to a simple mixed-layer ocean model. J. Geophys. Res., 89, 9457-9503.

Yamamoto, R., and Hoshiai, M. (1980) Fluctuations of northern hemisphere mean surface air temperature during recent 100 years, estimated by optimum interpolation. J. Meteor. Soc. Japan, 58, 3, 187-193.



## UPLIFT RESISTANCE OF PIPELINES BURIED IN FROZEN GROUND

J.F. (Derick) Nixon<sup>1</sup> and Beez Hazen<sup>2</sup>

<sup>1</sup>Nixon Geotech Limited  
Calgary, Alberta, Canada  
<sup>2</sup>Yukon Pacific Corporation  
Anchorage, Alaska, USA

Design of buried chilled pipelines in frost heaving terrain requires a knowledge of the uplift resistance of pipes buried in frozen ground. As the chilled pipe crosses from unfrozen (heaving) terrain to frozen (non-heaving) ground in discontinuous permafrost areas, the frozen soil generates considerable resistance to upward pipe movement. If these uplift resistance forces are very high, then the resulting curvatures and strains induced in the pipe near the interface between frozen and unfrozen ground will tend to be higher. This paper describes the load-resistance response as a pipe is displaced upwards through frozen ground. A series of six tests have been carried out, providing the general shape of the load-displacement curve, and the effects of backfill type, displacement rate and temperature. Interesting crack patterns in the frozen soil around the pipe have been observed, and their role in limiting or controlling peak and residual uplift resistance is discussed.

### INTRODUCTION

#### Background

A large diameter pipeline may be subject to frost heave displacements of a meter or more, if the pipe is buried in initially unfrozen soil, and is operated continuously at temperatures significantly below 0°C (Nixon et al, 1990). Considerable study has been carried out into predicting frost heave itself, and future laboratory and field studies will further refine predictions.

frozen soil in the frost bulb around the pipe is capable of providing very large resistances to pipe movement near the interface, and therefore strains and curvatures in the pipe may develop more rapidly across such a transition.

To date, the uplift resistance side of the transition has received considerably less attention than the frost heave side. In short, there are no available data in the public domain for this important parameter.

The uplift resistance is most simply introduced into a PIPELIN or equivalent structural pipeline analysis as an elastic-plastic load-displacement relationship, which may also have a post-peak reduction, or residual level at larger displacements. The peak uplift resistance is very important in determining the allowable frost heave for design purposes. For example, if the peak uplift resistance for a large diameter pipe were increased from 300 to 600 kN/m length of pipe, the allowable frost heave before a design strain limit were achieved might be reduced from 1 m to 0.6 m.

Also of considerable importance is the summer versus winter values of uplift resistance. If the soil over the pipe is allowed to thaw to some depth close to the pipe each summer, a large reduction in uplift resistance, and consequent relaxation in pipe strains could be expected.

A full scale test on a section of large diameter pipe, tested at very low vertical displacement rates over both summer and winter seasons would be costly, and the alternative of carrying out mid-scale laboratory model pipe tests was selected. The one-sixth or so scale test considered here would require only a small fraction of the cost and elapsed time that would be associated with a full scale field test.

The test program was designed to increase the level of confidence in the value of the peak uplift resistance and nature of the load-displacement function to be used in pipeline structural analysis for frost heave design. In addition, visual observations were made to determine the mode of failure of the soil around the pipe during the test. It has been suggested that cracks may form around the pipe that would tend to reduce the uplift resistance (See Nixon et al, 1984). However, this may be appropriate for more rapid rates of upward displacement, and a brittle mode of soil failure. It may transpire that slower and more realistic vertical displacements result in a more ductile, creep mode

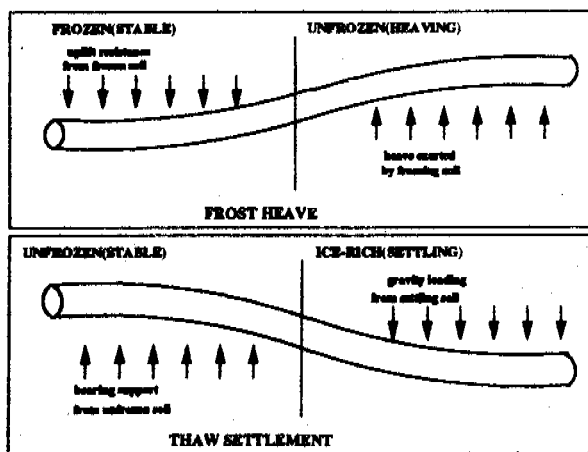


Figure 1. Freezing and thawing effects on pipeline in discontinuous permafrost

As shown on Figure 1, another major input required for frost heave-pipeline interaction analysis is the uplift resistance offered to upward motion of the pipe by the frozen soil. If the uplift resistance were low (as in the case of unfrozen soil), the pipe heave near an interface between two soils of different heave potential would occur gradually across a transition, and strains and curvatures induced in the pipe would be of less concern. However, where the transition occurs between frozen and unfrozen soil, the unfrozen zone may be capable of large frost heave. The adjacent frozen zone will be stable, and does not normally heave to any significant extent. The

of failure. If the peak uplift resistance is strongly a function of displacement rate, then it would be more appropriate to use a viscous creep function to model uplift resistance within the pipeline structural analysis. This could have major ramifications (hopefully beneficial) for the allowable frost heave determined for a pipeline project.

**TEST EQUIPMENT**

The pipe was 140 mm in diameter, fabricated from a heavy walled steel pipe having a wall thickness of 19 mm. The pipe protruded a short distance from both ends of the soil container, and was loaded on the underside of each protruding end. Initial testing did not apply a different temperature in the pipe, other than that maintained in the surrounding soil.

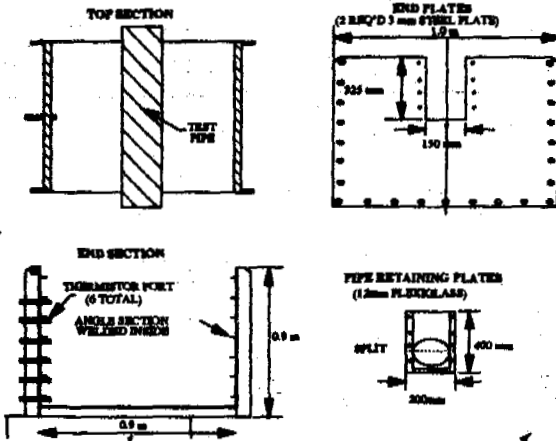


Figure 2. Soil container for pipe stress experiments

The soil container was approximately a cube, 0.9m on a side. It was made from welded steel plate 3 mm thick on two sides and the base, with two end plates bolted on to allow for removal following sample freezing (See Figure 2). Steel ribs were welded to the inner sides of the box to prevent vertical slipping of the soil mass during loading. During freezing, the two end plates were bolted in place. Part of each end plate was designed to be removed during loading from time to time for observation and photography.

The soil container was assembled and operated in a small walk-in cold room. No temperature control was applied to the soil container itself, other than the cold room environment, which controls ambient temperatures to about +/- 1°C. The effective temperature control within the soil mass was much better than this, i.e. to a tenth of a degree or so, because of the thermal damping effects of the soil mass.

**Soil Sample and test set-up**

A large volume of a local clayey silt was available at the nearby University of Calgary, and approximately one cubic meter of this material was air-dried for the testing. This is the same material that was present at the Calgary frost heave test site.

The bulk soil sample was homogenized in a concrete mixer, and blended with about 22% water by dry weight. The cold room was set initially at around -10°C, and lifts about 0.15 m thick were placed in the soil container and allowed to freeze over a 24 hour period. The wet soil was lightly compacted using a hand compaction device to remove most of the air voids. No effort was made to allow the soil to consolidate prior to freezing. Random horizontal ice lenses similar to those found under field conditions formed in the soil during

freezing. However, the overall moisture content of the soil remained much the same, due to the essentially closed system nature of the freezing.

Approximately 4 lifts were placed and allowed to freeze. The pipe section was then placed and the next lift of soil placed around the pipe. Finally, a 0.15 m lift of soil was placed over the pipe to final elevation, to simulate a scaled thickness of overburden over the pipe. The second and subsequent tests investigated the effects of using the same soil from Test 1, ditching a scaled trench in the frozen soil, placing the pipe in the trench, backfilling to final elevation with frozen soil chips, and then saturating the backfill with water prior to final freezing.

The protruding ends of the pipe were connected to the reaction frame and loading assembly, and the cold room reset to -5°C to equilibrate at the desired test temperature. Samples of the frozen soil were taken at the beginning and end of the test to determine moisture content and dry density.

**Loading System**

A reaction frame was constructed from steel sections, and employed two mechanical actuators (screw jacks) rated for a total load of 20 tonnes each. These were turned by a 1/4 HP DC motor with variable power supply, and a gear reduction system. The gear reduction system was designed to achieve a near constant displacement rate of around 1 mm/day or less, which is similar to the maximum rate of displacement experienced by a pipe under field conditions. The motor turned the gear reduction system, which was equipped with a double output shaft. Each shaft turned an actuator at each end of the pipe section at a rate of around one revolution per day, corresponding to the target displacement rate of 1 mm/day or less. The actuators were Duff-Norton Model 9820, and the gear reducer system was a 120,000:1 triple reduction worm gear unit. Original designs for the loading system had considered a hydraulic loading system, but this was discarded in favour of the mechanical system, due to potential problems with unequal loading and tilting of the pipe.

**Instrumentation and data acquisition**

Two load cells on the protruding pipe ends monitored the loads actually being applied to the test pipe. Two LVDTs (linear voltage displacement transducers) monitored the displacements being experienced by the pipe. A third LVDT measured the vertical displacement of the soil surface. This third LVDT was changed to measure the central deflection of the pipe in the second and subsequent tests, as a concern for bending of the pipe existed. These sensors had a total travel of 50 mm, with an accuracy of about 0.025 mm. The location of these sensors is given on Figure 3.

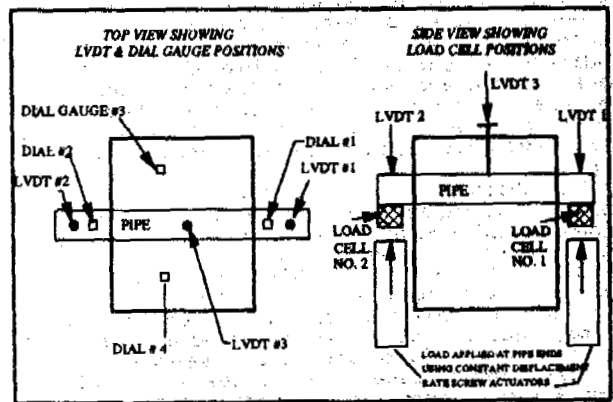


Figure 3. Sensor locations

A total of 9 thermistors in the soil and pipe, and another thermistor in the room were used to monitor temperatures throughout the test. They were located in the soil around, over and beneath the pipe to observe any temperature variations throughout the soil mass.

The thermistors, together with 2 LVDTs and 2 load cells were monitored every hour using a data acquisition system and PC computer. The data acquisition system used was an interactive program for the PC that allows regular sampling of various sensors, storage to hard disk, and formatting for later processing using a spreadsheet program. A real time display on the PC screen was obtained during testing. The data were stored on floppy disks, and post-processed using a simple FORTRAN program written for the PC.

### TEST PROCEDURES AND SCHEDULE

After freezing, the ends of the container were removed. Insulation was placed around the container. A plastic sheet was placed on the soil surface to prevent sublimation of ice from the soil. The top anchor beams as shown on Figure 3 were placed across the top of the container. The actuators and LVDTs were positioned, and the data acquisition started. The motor was activated, and controlled to obtain approximately the target displacement rate.

During the test, the end sheets of insulation were occasionally removed, to observe and photograph the pipe, soil and deformation patterns. The tests was terminated when total displacements exceeded around 50 mm, and when a significant reduction in total load had been observed.

Following the test, observations of the soil and ice conditions around the pipe were made. It was possible to re-use the majority of the soil in the test container for all of the 6 tests. It was necessary to remove the soil around the pipe and reconstruct a 'trench' in the soil, so that the pipe could be replaced and backfilled at the start of each new test.

The first test involved a uniform soil and constant displacement rate for the duration of the test. The soil and pipe temperature were controlled at  $-5.5^{\circ}\text{C}$ . This test was designed to observe peak and residual loads at large displacement, and to observe the general characteristics of load versus time for a slow displacement rate.

The second test involved removing the highly disturbed frozen soil around and over the pipe to a width of about one diameter on either side of the pipe, and processing the frozen material by breaking it down and sieving in the frozen condition to obtain a uniform size. The pipe was then replaced in the trench, and the frozen backfill placed around and over the pipe. The backfill was saturated with water, and allowed to freeze in the cold room. The second test then proceeded as before. Fortunately, this test indicated almost no discernible effects of backfill replacement of the load-displacement response of the pipe, and this permitted future tests to re-use the majority of the frozen soil mass, and only replace the soil zone around the pipe.

The third test used the same configuration as Test 2, and explored the effects of different slower displacement rates during the same test. The test was started at a displacement rate of 1 mm/day, until about one-third of the anticipated peak load was observed on the pipe. The displacement rate was then decreased to around 0.2 mm/day, and run past the peak load at this rate. In this way, information on the dependence of load on displacement rate (i.e. creep) was obtained.

Test 3 experienced some temperature fluctuations, and was repeated in Test 5. Consequently, only the results of Test 5 at the slow displacement rate

are reported here.

The fourth test investigated the effects of increased soil temperature of  $-2^{\circ}\text{C}$  around the pipe. This could be caused by increased ground and/or pipe operating temperature, for example.

Test 6 applied a warming cycle to the soil surface, while maintaining a controlled pipe temperature of around  $-5^{\circ}\text{C}$  as before. This was to simulate the effects of summer warming on the pipe uplift resistance.

### RESULTS

A summary of the key results and background data for each of the 5 tests is given on Table 1.

Table 1. Summary of test conditions

TEST #	COND'N	TEMP. (C)	TIME (hr)	DISPL. RATE (mm/hr)	PEAK LOAD (kN)	DISPL AT PEAK (mm)	RESIDUAL LOAD (kN)
1	U	-5.5	29	0.6-1.0	187.3	7.0	44.0(-)
2	R	-5.5	36	0.6-1.0	178.4	6.5	36.0(-)
4	R	-2.1	23	0.6-1.0	76.0	2.4	40.0(-)
5	R	-5.5	75	0.15-0.2	147.0	4.0	76.0(-)
6	R	-5.5*	27	0.6-1.0	140.0	3.2	20.0(-)

- Note that the peak and residual loads reported on this table refer to the total load on both ends of the 0.9 m length of pipe.
  - \* Surface warming cycle imposed during test.
- U-uniform backfill condition; R-reworked backfill

The moisture content of the lightly compacted soil used below the pipe for all experiments was in the range of 18.5-20 % by dry weight. The water content of the replaced and reworked soil in the backfill trench in the last 4 experiments was 22-25% by dry weight.

#### Test # 1 - Control test on uniform silt

The load peaked about  $2 \times 93.6$  kN at a time of 10 days, with a displacement of about 7 mm, as shown on Figure 4. The unit load corresponds to about 208 kN/m at this displacement rate. The test exhibited a relatively brittle post-peak phase, after which the load tended to stabilize at some residual level after a few days.

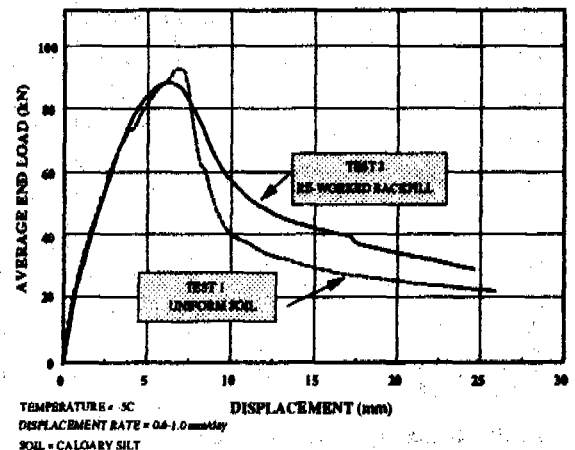


Figure 4. Pipe load-displacement for tests 1 and 2 - effect of backfill type

The soil surface displacement rate increased dramatically after peak load, and this is likely due to cracking along the soil surface over the pipe. Finally, soil temperatures remained quite stable throughout the test, varying by about  $0.1^{\circ}\text{C}$ . At the end of the loading phase, the loading apparatus was switched off, and the relaxation of load was monitored for 2 days. After completion, the soil around and over the pipe was removed and broken down in the frozen state, backfilled, flooded with warm water, and re-

frozen. The second uplift resistance test was then carried out under the same conditions as the first, to see the effects of the replaced, partially thawed and re-frozen backfill around the pipe.

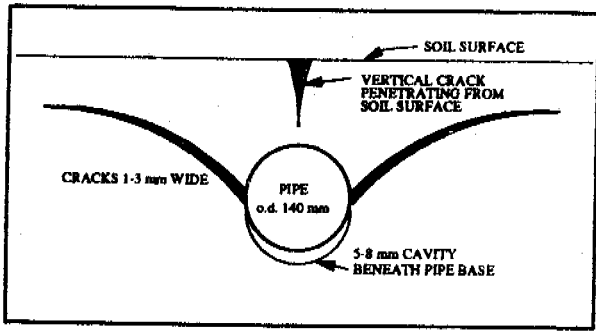


Figure 5. Pattern of cracking in soil around pipe for Test # 1

The pattern of cracks was mapped twice, (at 11 days and at the end of the test), and then photographed. The patterns did not change since the first mapping at 11 days (See Figure 5), with the exception that the crack over the center of the pipe penetrated from the soil surface almost to the pipe.

**Test # 2 - Re-worked backfill**

Results for Test # 2, which is a typical or control test, are given in Figures 6-10. The backfill around the pipe was reworked as described earlier. The purpose of the test was to examine the effects of backfill method on the frozen uplift resistance.

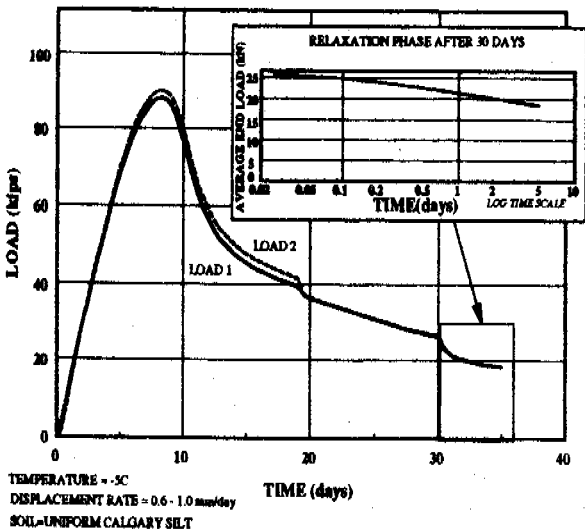


Figure 6. Pipe end load with time for test # 2

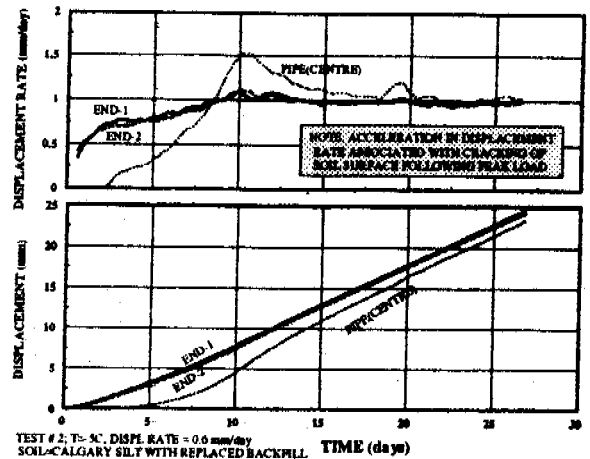


Figure 7. Pipe displacement with time for test # 2

The load versus time plot as given on Figure 6 is very similar to the first test with the homogeneous backfill. The peak load is almost the same at 90 kN for each end of the pipe, although it occurred at a slightly smaller displacement of 8.5 mm, as shown on Figure 4. The residual load remained somewhat higher than test # 1. The displacement at the center of the pipe was measured directly from a small rod welded to the pipe using an LVDT. This displacement clearly lagged behind the applied end displacements by up to 3 mm, as shown on Figure 7. Except for a period of rapid load build-up at the beginning of the test, the displacement plot with time is quite linear, indicating the success of the mechanical screw actuator system in maintaining near constant displacement rates. The displacement rates obtained at the center and ends of the pipe vary from about 0.6 mm/day while the load was increasing on the system to around 1.0 mm/day as load on the system was reducing. Finally, the difference in end minus center displacements was plotted on Figure 8 with the average end load on the system. The plot indicates that the displacement lag appears to be linearly elastic and recoverable.

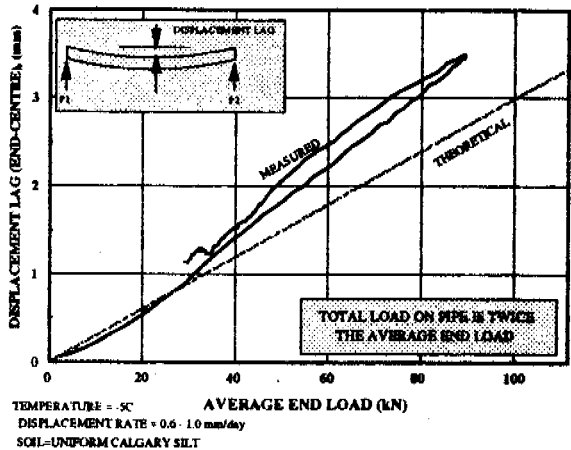


Figure 8. Displacement lag vs end load, test # 2

The loading apparatus was then switched off, and the relaxation of load was monitored for a 5-day period. This final segment of the load time curve as indicated on Figure 6 has been replotted as a straight line on a semi-log plot, and indicates the lengthy time period that would be required for the load to stabilize. This behavior certainly indicates a time-dependent or creep response in the pipe-soil system. The crack over

the center of the pipe penetrated from the soil surface almost to the pipe. The cracks on either side of the pipe developed almost horizontally from the spring line of the pipe, with the crack on one side not so well developed as the one on the other side.

**Test # 4 - Effects of warmer soil temperature**

Test # 4 had a nominal soil temperature of -2°C, which was significantly warmer than the previous tests. A nominal displacement rate of 0.6-1.0 mm/day was selected for similarity with Tests 1 and 2 at -5.5°C.

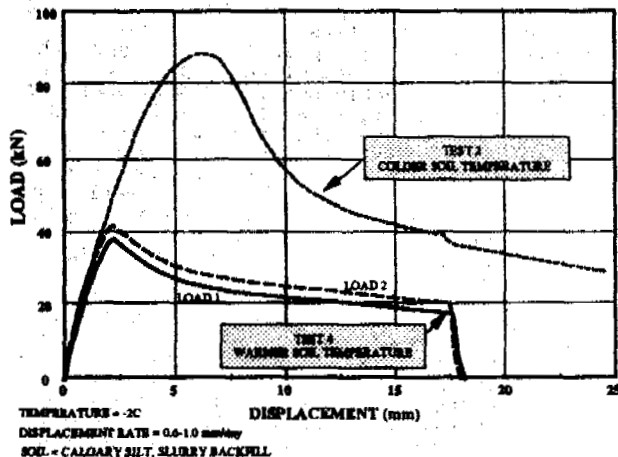


Figure 9. Load-displacement for test 4 - effects of warmer soil temperature

Figure 9 shows the load-displacement plot. Comparison with results for Test # 2 indicate that the same shape of curve was obtained, although the peak load was about one-half of the value obtained from the tests at -5.5°C. The displacement with time shows that the ends were displaced at a relatively uniform rate, with the center of the pipe lagging 1-2 mm behind the ends, as observed previously. Aside from a temperature fluctuation of about 1.0°C in the early stages of the test, the temperature remained relatively constant at around -2.1 to -2.2°C. The peak displacement was realized at a displacement of around 2 mm, as compared with 7mm for the tests at -5.5°C. Also, the peak-to-residual reduction in load does not seem as pronounced in this test, indicating a less brittle response. At about 5 days, some small cracks in the soil were first noted close to the pipe springline, but these did not seem to penetrate very far into the soil. Around day 18 at the conclusion of the test, the end was removed from the soil box, and only two relatively minor cracks were observed in the soil starting at the pipe springline, and rising at about 60° to the horizontal part way to the soil surface. These cracks did not penetrate all the way to the surface. The usual large gap between pipe and soil was present at the base of pipe, roughly equal in size to the applied displacement of 18 mm. The crack noted over the pipe was up to a few mm wide, and did not penetrate all the way to the pipe.

From day 18 to day 20, the displacement rate was stopped to observe relaxation, and the load decayed from about 18.7 kN to about 14.3 kN at each end of the pipe. At day 20, the cold room was switched off, and the soil allowed to warm up and thaw. Within about 1 day, the soil over the pipe thawed, and the load fell essentially to zero, as would be expected. This phase of the test simply demonstrates that if thawing of the soil around and over the pipe can be induced (however temporary), then the uplift resistance will drop to practically zero. This may be very beneficial when considering practical measures to reduce uplift resistance, and thereby increase the

allowable frost heave of a buried pipeline.

**Test 5 - Slower displacement rate.**

This test was a repeat of Test 3, which experienced some temperature control problems. Test 5, however ran successfully for a duration of 75 days, with an applied displacement rate of 0.15-0.2 mm/day, and excellent temperature control. The load-displacement curve for this test is given on Figure 10. Also shown is the equivalent curve for the control Test 2 for comparative purposes. It is seen that Test 2 at the higher displacement rate exhibited a higher peak and residual load, and also peaked at a somewhat higher pipe displacement. These observations are consistent with the idea that at least some of the uplift resistance depends on the creep properties of the frozen soil, and that lower displacement rates will result in lower uplift resistance values.

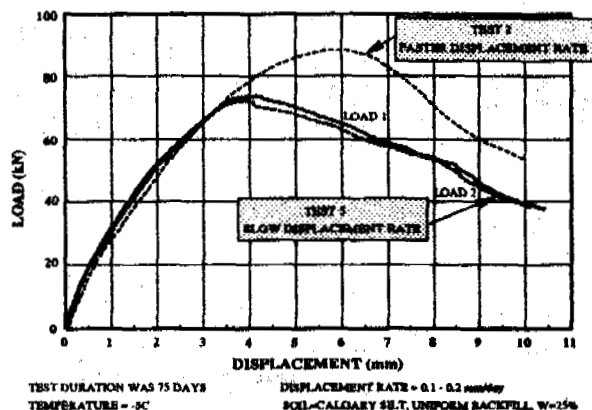


Figure 10. Test 5 - slow displacement rate

It is important to note that the amount of soil cracking observed around the pipe was greatly reduced at the end of this test. Even though the peak pipe load had been achieved some considerable time previously, the magnitude and extent of soil cracking adjacent to the soil springline was minimal. A few minor cracks extending 30-60 mm away from the pipe were noted. A significant crack was present at the soil surface directly over the pipe, however, in all tests. This crack was the first to develop, and extended about half way from the soil surface to the pipe.

**Test 6 - Surface warming cycle**

Figure 11 shows the load-displacement curve for Test 6, where the usual displacement rate of around 1 mm/day was imposed on the pipe ends until about 2/3 of the peak load was attained. At this time, when a load of about 70 kN on each end of the pipe was reached, a surface warming cycle was imposed on the soil surface, to simulate the effects of surface seasonal warming in the field. This was done by placing a grid of closely spaced plastic pipes on the soil surface, and covering them with a 25 mm thick layer of dry, fine silt. This provided a thermal contact between the surface heating grid and the soil surface. The grid of heating pipes was connected to a constant temperature circulating bath controlled at +5°C. The pipe was controlled at a constant temperature of -5°C during the same time period when the surface temperature warming cycle was imposed. The surface warming was applied for a 12-day period in the middle of the test. Almost immediately after application of the surface temperature increase, the pipe load on each end fell rapidly from about 70 kN to 12 kN. After this, the temperatures were allowed to return to their original value of -5°C. A slight recovery of the pipe end load was observed, followed by a continuing decay in the pipe loads. The effects of surface warming were

dramatic and immediate, which will be of interest to pipeline designers concerned with mitigating the effects of curvatures induced by frost heave on a buried pipeline.

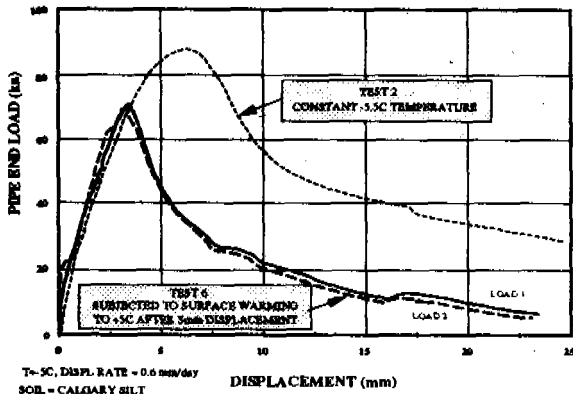


Figure 11. Load-displacement for test 6 - effects of surface warming cycle

Tensile testing of frozen soil.

Clearly, the peak load and initiation of soil cracking are limited to a large extent by the tensile strength of the frozen soil adjacent to and over the pipe. Tensile cracks seem to open at a time corresponding to the peak load experienced by the pipe. In order to interpret the peak pipe loads using some basic soil property such as tensile strength, a series of uniaxial tensile strength tests were carried out. As noted by many investigators in the past, the strength of frozen soils (in tension or compression) is time dependent, and decreases significantly with increasing time to failure or loading rate. A series of 7 uniaxial tests were carried out in a specially designed tension apparatus, that applied a constant dead load to a dumbbell shaped specimen, similar to Zhu and Carbee (1987). The tests were all carried out in a cold room at -5°C, at varying stress levels. The reciprocal of stress was plotted against the logarithm of the time to failure as shown on Figure 12, according to the Vialov plotting procedure. A well defined straight line was obtained, allowing the uniaxial tensile strength to be obtained as a function of the time to failure. The strain at failure for all tests was in the range of 1%, indicating a rather brittle response to tensile stresses. For example, for times to failure of 8 and 32 days, the tensile strength is estimated to be 350 and 311 kPa respectively. Future analysis will employ these values in correlating the observed pipe load in the uplift resistance tests with the uniaxial test results.

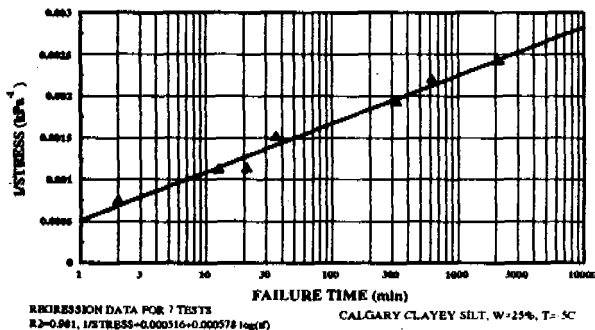


Figure 12. Uniaxial tensile testing of frozen soil

SUMMARY AND CONCLUSIONS

A new loading device and soil container to measure pipe uplift resistance in frozen soil has been successfully designed, fabricated and instrumented. A series of 6 tests have been completed, and have investigated the effects of different backfill types, displacement rates and soil temperatures.

A pronounced peak load and post-peak reduction in load was noted in all tests, although warmer temperatures and slower displacement rates seem to result in less pronounced post-peak reductions in load. Cracking in the soil followed two general trends. Initial cracking commenced from the soil surface over the pipe, propagating downwards towards the pipe as the test progressed. Meanwhile, at some displacement at or just after peak load, cracks propagated outwards and sometimes upwards from the pipe springline. Only minor cracking in the soil adjacent to the pipe was observed in the slowest test at a displacement rate of 0.2 mm/day, suggesting that cracks may not occur at very slow rates of displacement where the soil behavior is more ductile, rather than brittle.

Relaxation of load occurs when the applied displacement rate is set equal to zero. This implies that a significant component of the load is creep-related, or dependent on the rate of displacement. Surface warming is extremely effective in reducing the uplift resistance experienced by the buried pipe.

A series of tensile tests have been completed on the frozen soil in order to provide basic data on the tensile properties of the frozen soil. This will allow correlation of the observed uplift resistance tests with the tensile strength of the material surrounding the pipe.

Future tests will investigate the effects of shallower pipe burial, larger pipe diameters, and the effects of surface thawing and re-freezing. Finite element analyses will be undertaken to understand the mode of failure in the soil around the pipe, and reconcile the uplift resistance values with more basic properties such as the tensile strength and creep properties of the frozen soil.

ACKNOWLEDGEMENTS

The authors are grateful to their colleagues at Imperial Oil Limited in Calgary and Yukon Pacific Corporation in Anchorage for support and permission to publish the results of this investigation. Mr Geoff Spedding ran many of the tests, and Mr. Ken Croasdale provided extensive advice and support. Mr. Chris Heuer, Mr. Jim Caldwell and Mr. Todd Dunnivant of Exxon Production Research in Houston provided review comments. Mr. Stephen Lord of the National Energy Board has provided financial support for later testing in the series.

REFERENCES

Nixon, J., Stuchly, J., and Pick, A. 1984. Design of Norman Wells pipeline for frost heave and thaw settlement. Proc 3rd Intl. OMAE Symposium, New Orleans, La, Feb 12-16.  
 Nixon, J., Sortland, K. and James, D. 1990. Geotechnical aspects of northern gas pipeline design. Proc 5th Canadian Permafrost conference, pp. 209-307. Laval University, Quebec, June.  
 Zhu, and Carbee, 1987. Tensile strength of frozen silt. U.S. Army CRREL Report, 87-15, Hanover, N.H.

POTENTIAL OCCURRENCE OF PERMAFROST AND GAS HYDRATES  
IN THE CONTINENTAL SHELF NEAR LONELY, ALASKA

T.E. Osterkamp and T. Fei

Geophysical Institute  
University of Alaska Fairbanks  
Fairbanks, Alaska 99775-0800

A two-dimensional finite element model was used to investigate the thermal response of subsea permafrost and gas hydrates to changes in sea level and climate over a 121 Kyr time period along a line offshore from Lonely, Alaska. For subsea permafrost containing brines, the spatial distribution of the ice-bearing permafrost (IBP) is predicted to be wedge shaped and to extend only 19 km offshore. There is significant lateral heat flow throughout the IBP section offshore and the depth to the IBP table increases almost linearly with distance offshore. For subsea permafrost with constant thermal parameters, IBP is predicted to extend 52 km offshore (water depth ~ 50 m) and is nearly isothermal beyond 4 km offshore. Depth to the IBP table increases almost linearly with distance offshore and then becomes relatively shallow and nearly constant in depth. Seabed temperatures and the assumed sea level history curve are especially important in determining the current distribution of subsea permafrost. The full thickness of IBP onshore can be modeled better using constant thermal parameters. Depth to the IBP table offshore may be modeled better when it is assumed that the permafrost contains brines. The predicted depth zone for stability of methane gas hydrates is between 220 m and 650 m near shore. For subsea permafrost containing brines, this zone extends 32 km offshore compared to 54 km (to the 55 m water depth) for constant thermal parameters. The time scale for producing methane gas from destabilized gas hydrates in the continental shelf near Lonely is on the order of  $10^4$  years, much longer than previously predicted.

INTRODUCTION

During the past million years, there is evidence for repeated glaciations about every  $10^5$  years (Shackleton and Opdyke, 1977). The continental shelves of the Arctic Ocean were emergent during these glaciations, up to current water depths of 120 m (Bard et al., 1990). Cold climates during periods of emergence favored the formation of permafrost and the stabilization of gas hydrates in the shelves. Rising sea levels during interglacial periods replaced the cold air temperatures on the shelves by much warmer sea water temperatures. As a result, the permafrost and thawed sediments would have warmed at all depths, and permafrost would have started to thaw from both the top and the bottom. Eventually, gas hydrates would have been destabilized, providing a potential source of methane gas to the atmosphere.

Since permafrost thaws very slowly in response to the new surface boundary conditions after submergence, considerable time (on the order of tens of millennia) may be required to completely thaw the permafrost. Consequently, ice-bearing permafrost (IBP) and gas hydrates may still exist in parts of the continental shelves of the Arctic Ocean. The existence of subsea permafrost and the presence of ice in these continental shelves has been confirmed by drilling in shallow water (usually a few tens of meters or less in depth) off the coasts of the USSR (Molochushkin, 1978), Alaska (Lewellen, 1973), and Canada (Mackay, 1972). Subsea permafrost is also indicated in the interpretations of offshore seismic data (Hunter et al., 1976) and of geophysical logs in offshore petroleum exploration wells (Osterkamp et al., 1985). Destabilization of gas hydrates (by warming the sediments in the continental shelves) during periods of high sea level may be a periodic source of atmospheric methane over geological time (Clarke et al., 1986; MacDonald, 1990). Warming of the permafrost and sediments and permafrost

thawing eventually causes gas hydrates to become unstable resulting in the liberation of large volumes of gas. However, the permafrost may act as a seal (because of ice in the pores) preventing the gases from escaping until sufficient ice has been thawed to generate escape routes for the gas. MacDonald (1990) has investigated the time scales for the response of the permafrost to submergence using a one-dimensional analytical model. Since the model did not include latent heat effects, the predicted time scales are expected to be much too short. This means that his predictions regarding the time scales for production of atmospheric methane gas by destabilization of gas hydrates in continental shelves affected by permafrost are not correct.

Calculations using one-dimensional analytical models (e.g. Mackay, 1972; Lachenbruch et al., 1982) and numerical models (Outcalt, 1985; Nixon, 1986) for the transient response of permafrost to submergence generally suggest the presence of relatively thick subsea permafrost even in areas of deeper water. The occurrence of subsea permafrost implies the potential presence of stability zones for gas hydrates. However, one-dimensional models are not completely satisfactory because of possible lateral heat flow in the subsea permafrost particularly near shore. In some cases, it may also be necessary to include distributed latent heat effects and variable thermal parameters associated with the potential presence of saline pore fluids in the permafrost, which do not appear to have been done.

This paper presents the results of two-dimensional numerical modeling of the thermal response of permafrost to changes in sea level and climate, which includes the effects of saline pore fluids on latent heat and thermal parameters. The region considered was the continental shelf of Alaska near Lonely. Results of these simulations are used to evaluate, at the present time, the spatial distribution of IBP in the continental shelf near Lonely and the stability zones of gas

hydrates that may exist within or under the permafrost.

Additional information on the numerical simulations, study site, choice of parameters, initial conditions, boundary conditions, and other simulations may be found in Fei (1992).

#### STUDY SITE

The study site, offshore from Lonely which is about 135 km southeast of Barrow, Alaska, was chosen because of the availability of data from other research and from onshore and offshore petroleum exploration wells. Available data consist of geophysical logs and samples from the J.W. Dalton-1 (JWD) well onshore and the Antares well offshore (Collett et al., 1989; Deming et al., 1992), results of thermal studies in five shallow drill holes along an offshore line to the northwest from Lonely (Harrison and Osterkamp, 1981), and results of bottom sampling and shoreline erosion studies (Hopkins and Hartz, 1978).

The onshore surficial deposits were mapped as interglacial nearshore and lagoon sand, silty fine sand, and pebbly sand (Hopkins and Hartz, 1978). Shallow offshore drilling data (Harrison and Osterkamp, 1981) indicate that the seabed sediments are fine-grained to about the 30 m depth. At the JWD well, the deeper well logs indicate relatively coarse material (conglomerate and sandstone) down to the 270 m to 300 m depth or so overlying finer material (siltstone) (Collett et al., 1989). There is a change in the temperature gradient in this depth interval (Lachenbruch and Marshall, 1986). We interpret the base of the IBP to be at 360 m to 366 m (about  $-2.2^{\circ}\text{C}$ ) where slight changes in the resistivity log and the temperature gradient occur. Other onshore wells in this region indicate a similar lithology but generally with somewhat finer material.

The nearest offshore well (Antares, EXXON) is about 24 km distant on a line bearing  $\text{N}55^{\circ}\text{E}$  from Lonely in about 15 m of water. Well logs indicate that relatively fine-grained material exists in the upper section (above 190 m) where permafrost might be expected with some coarser material from 190 m to 312 m. The use of geophysical logs to determine the presence or absence of IBP is very difficult because of the lack of contrast in physical properties between the thawed material and any warm and marginally ice-bearing permafrost which would be thawing from both the top and bottom. According to the gamma ray log, there are two similar sections just above 272 m and 305 m. Increases in the resistivity log (DIL) above 272 m but not above 305 m suggest that IBP may exist above 272 m which is our interpretation of the log. However, other factors (e.g., changes in pore fluid salinity) besides permafrost could produce these increases.

The harmonic mean thermal conductivity determined from drill cuttings from the JWD well in the frozen interval from 113 m to 269 m is  $2.57 \text{ W(mK)}^{-1}$  (Deming et al., 1992). Values of  $2.5 \text{ W(mK)}^{-1}$  and  $1.7 \text{ W(mK)}^{-1}$  were used for the frozen and unfrozen material respectively. The porosity was assumed to be 0.2. For fine-grained sediments containing brines, the temperature-dependent thermal parameters were calculated using an unfrozen water content,  $\theta_u = AT^B$ , where  $T$  is the magnitude of the temperature ( $^{\circ}\text{C}$ ) and  $A$  and  $B$  are empirical constants ( $A = 0.1435$ ,  $B = -0.902$ ) (Fei, 1992). Freezing point depression was assumed to be  $-1.63^{\circ}\text{C}$ . The volumetric heat capacity and the thermal diffusivity were calculated according to the methods used by Osterkamp (1987).

Deming et al. (1992) suggest a large heat flow of  $\approx 80 \text{ mW-m}^{-2}$  for the JWD well. However, the average measured temperature gradient and the above frozen conductivity yield a more normal value of  $\approx 54 \text{ mW-m}^{-2}$  in the upper interval. For the simulations, a compromise value of  $65 \text{ mW-m}^{-2}$  was used.

Information on the near surface seabed sediments, temperatures, and depth to IBP was obtained in five shallow drill holes which were rotary jet drilled along a line bearing  $\text{N}32^{\circ}\text{W}$  near the DEW site at Lonely (Harrison and Osterkamp, 1981). Distances from shore were paced and may contain significant errors.

Figure 1 shows temperature profiles measured in these holes, two to three weeks after drilling, which are thought to be within a few hundredths degree of equilibrium values. The profiles show a decreasing thermal gradient with distance (time) offshore. Assuming the current average shoreline erosion rate ( $4.7 \text{ m-yr}^{-1}$ ), the hole at 7770 m offshore has been submerged for about seventeen centuries. Approximate mean seabed temperatures can be obtained by projecting the thermal gradients in the deeper part of the holes up to the seabed. However, the presence of a phase boundary often makes it difficult to do this reliably.

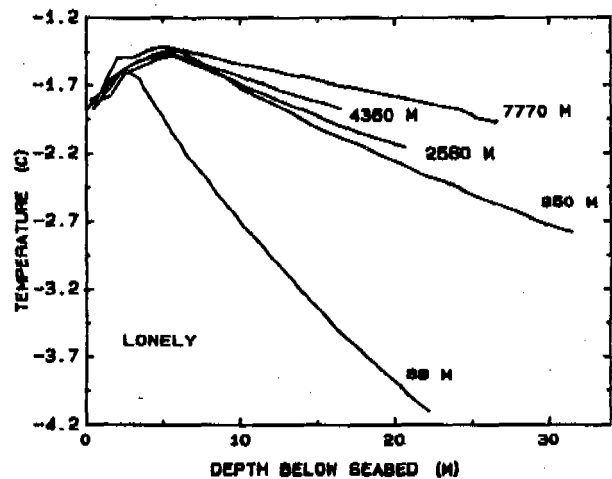


Figure 1. Subsea permafrost temperatures measured in five, shallow, offshore holes along a line bearing  $\text{N}32^{\circ}\text{W}$  at Lonely, Alaska. The numbers next to the profiles are the estimated distances offshore which were paced and may contain significant errors.

In warm subsea permafrost which contains brines, the amount of ice appears to increase gradually with depth (Osterkamp and Harrison, 1982; Osterkamp et al., 1989). Consequently, there is no distinct change in temperature gradient nor properties at the IBP table but only a gradual curvature of the temperature profile which makes it difficult to detect the presence of ice from the drilling data or the temperature data (Fig. 1). Therefore, the holes were heated to determine the presence of ice using the method described by Osterkamp and Harrison (1980). Our interpretation of the results of drilling and heating the holes indicate that the IBP table occurs between 6 m and 15 m below the seabed along this line (Table 1).



Table 1. Data for holes drilled at Lonely along a line N32°W starting at a point on the shoreline which was N66°W from the DEW site radar dome. The hole number is the distance from shore in meters determined by pacing.

Hole Number	Drilling Date	Water Depth	Sea Ice Thickness	Ice-Bearing Permafrost Table	
				Depth	Temperature
88	5/8/80	1.98 m	1.45 m	6-7 m	-2.2°C
950	5/9/80	3.12 m	1.58 m	7-14 m	-1.6 to -1.9°C
2560	5/10/80	4.80 m	1.47 m	8-13 m	-1.6 to -1.9°C
4360	5/11/80	6.50 m	2.1 m (rafted?)	7-12 m	-1.5 to -1.7°C
7770	5/13/80	7.70 m	1.39 m	7-15 m	-1.5 to -1.7°C

Simulations were done for two lines, one bearing N32°W (Table 1) which crosses the shelf at an angle and one bearing N20°E which is perpendicular to the depth contours and passes about 15 km to the west of the Antares well. Seabed profiles for these lines were constructed using results from the above studies and bathymetric maps. Two simulations for the latter line are reported herein, one for sediments with fresh-water pore fluids and one for sediments containing sea water brines. Our strategy was to perform two simulations for two near-extreme cases with regard to their effects on the thermal state of the permafrost. Additional details and simulations are discussed in Fei (1992).

#### INITIAL AND BOUNDARY CONDITIONS

The initial thermal conditions are unknown. However, the simulations were started using steady state conditions (Lachenbruch, 1957) far enough into the past (121 Kyr BP) to allow any transients (Osterkamp and Gosink, 1991) associated with the initial conditions to disappear. The surface boundary condition depends on whether the surface is emergent or submergent. For the emergent surface temperature, the paleoclimatic temperature history of Maximova and Romanovsky (1988), modified for the Lonely region (Osterkamp and Gosink 1991), was used. Their history gives good agreement with the current permafrost thickness at Prudhoe Bay (Osterkamp and Gosink, 1991). Since there does not appear to be a sea level history curve for this portion of the Beaufort Sea shelf, the timing for emergence and submergence was obtained from the sea level history curve of Bard et al. (1990) modified to take shoreline erosion into account (Fei, 1992). This procedure produces depths to the seabed that are somewhat shallower than observed up to 20 km offshore. For the submerged surface, current seabed temperatures determined from measurements in shallow drill holes at Prudhoe Bay, Barrow, and Lonely, adjusted for water depth, were used (Fig. 1 and Osterkamp and Harrison, 1982, 1985). Additional information is provided by Fei (1992).

#### RESULTS AND DISCUSSION

##### Fine-Grained Material Containing Brines

Figure 2 shows the predicted current temperature distribution in the continental shelf along the line bearing N20°E from Lonely. The uneven character of the isotherms in Figure 2 is caused by the plotting algorithm. IBP (-1.6°C isotherm) is predicted to extend only about 19 km offshore. This surprising prediction is a result of the relatively large heat flow and low ice content assumed for the IBP.

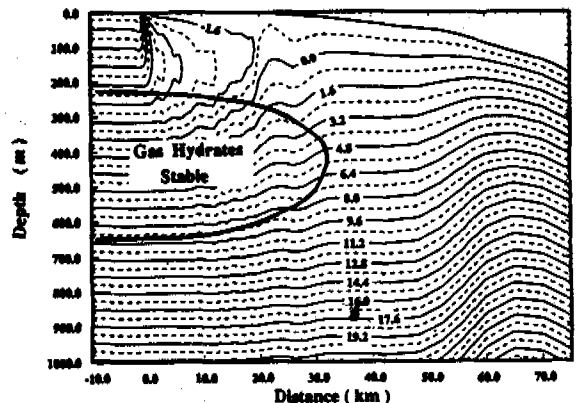


Figure 2. Predicted offshore temperature distribution and stability zone for gas hydrates at the present time near Lonely for fine-grained sediments containing brines. The ice-bearing permafrost is defined by the -1.6°C isotherm.

Lateral heat flow is large in the IBP near the coast, but it is also significant in the rest of the IBP and in the thawed material under it and seaward of it. Beyond 50 km offshore, at deeper depths the curved isotherms and associated lateral heat flow appear to be the result of recently thawed IBP near the seabed. These results suggest that one-dimensional thermal models that assume there is no lateral heat flow may not correctly predict the thermal regime of subsea permafrost containing brines.

The predicted depth to the base of IBP onshore is 318 m compared to the observed depth of 366 m, a difference of 13%. In the offshore region, the base of the IBP rises rapidly with distance offshore. A comparison with the Antares well is difficult since it is about 15 km east of this profile in a water depth of 15 m. If water depth is used as a criterion, this calculated profile predicts an absence of IBP at the Antares well. However, if distance offshore is used, IBP at the Antares well would be predicted to a depth of about 200 m compared to the 272 m observed.

Depth to the IBP table increases almost linearly with distance offshore to about 66 m below the seabed at 19 km offshore. At 7.8 km offshore, the predicted thickness of the thawed layer at the seabed is 21 m. At the same distance offshore, along the line bearing N32°W, the observed thickness is 7 m to 15 m (Table 1). If water depth were used as a criterion, the difference between observed and calculated values would be greater.

### Fine-grained Material with Constant Thermal Properties

Figure 3 shows the predicted current temperature distribution along the line bearing N20°E from Lonely. A nearly isothermal IBP section extends from 4 km to 52 km offshore where the water depth is about 50 m. Up to about 24 km offshore, the IBP section is wedge-shaped and beyond 24 km it is nearly tabular with a relatively flat vertical tip. The relatively thick tabular section appears to be a result of the assumed sea level curve. This curve indicates that depths of less than 50 m were continuously exposed to cold air temperatures for more than 70 kyr and only submerged during the last 11 kyr. This would produce a thick section of IBP out to the current 50 m isobath.

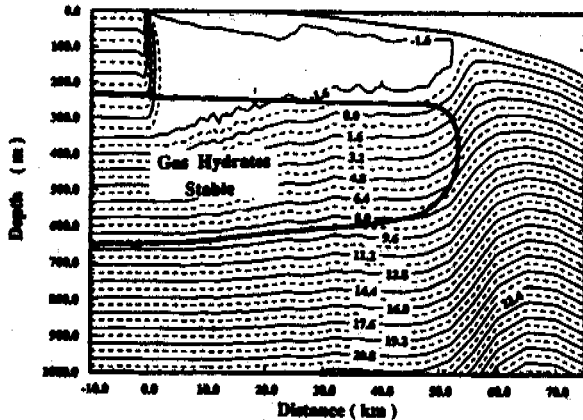


Figure 3. Predicted offshore temperature distribution and stability zone for gas hydrates at the present time near Lonely for fine-grained sediments with constant thermal parameters. The ice-bearing permafrost is defined by the  $-1.6^{\circ}\text{C}$  isotherm.

Lateral heat flow is large within 4 km of shore and in the thawed material beyond and under the tip of the IBP. Predicted depth to the base of the IBP onshore (355 m) is close to the observed value (366 m). This suggests that the full thickness of the IBP may be modeled better with constant thermal properties than with temperature-dependent properties and distributed latent heat effects associated with the presence of brines in the permafrost. A similar result was found by Osterkamp and Gosink (1991) when modeling changes in permafrost thickness at Prudhoe Bay in response to changes in paleoclimate. In the offshore region, the predicted base of the IBP rises rapidly to 24 km offshore and then more slowly farther offshore. Comparison with the Antares well is again difficult. At the equivalent water depth (15 m), the predicted base of the IBP would be at about 210 m below sea level, and at the equivalent distance offshore, about 270 m compared to the observed depth of 272 m.

Depth to the IBP table increases almost linearly with distance offshore and reaches a maximum value of 66 m below the seabed at 22 km offshore. It then rises to within 30 m of the seabed and remains at nearly a constant depth to the tip of the IBP. This behavior is the combined result of the sea level history curve and seabed temperatures. Sea levels rose rapidly from the glacial minimum less than 20 kyr BP to about 4 kyr

BP. As a result, the shelf was rapidly covered with deep cold water (about  $-1.5^{\circ}\text{C}$ ). In the last 4 kyr, submergence (due to sea level rise and shoreline erosion) occurred in shallow warm water (about  $-1^{\circ}\text{C}$ ). In the shallow water, the larger temperature gradient in the thawed material between the seabed and the IBP table ( $-1.63^{\circ}\text{C}$ ) allows for greater heat flow and therefore a faster thawing rate. The predicted thickness of the thawed layer below the seabed is 38m at 7.8 km offshore, much greater than observed along our line of shallow holes (Table 1.). While thawing near the seabed for this case is initially greater than when brines are present, by 19 km offshore the thicknesses of the thawed layers are about equal.

Simulations for both materials were carried out along our line of shallow holes (N32°W) using the above parameters and conditions except for a larger geothermal heat flow of  $80 \text{ mW}\cdot\text{m}^{-2}$  as suggested by Deming et al. (1992). In these cases, predictions for the depth to the base of IBP onshore were much too shallow suggesting that this choice of heat flow may be too large for Lonely.

### Stability Zone for Gas Hydrates

Gas hydrates are stable over a limited range of pressures and temperatures that can be found in association with permafrost, including subsea permafrost (e.g. Kvenvolden and McMenamin, 1980; Collett et al., 1988). The stable region can be determined from the phase equilibrium diagram (Sloan, 1990). It was assumed that the only gas in the hydrate was methane and that pressures could be converted to depth using hydrostatic conditions in the sediments. Latent heat effects due to formation or decay of the gas hydrates were neglected. With these assumptions, the current approximate stability regions for methane gas hydrates in the continental shelf near Lonely were mapped on the two-dimensional depth-temperature diagrams in Fig. 2 and 3.

In fine-grained sediments containing brines, gas hydrates can potentially exist up to 32 km offshore. The stability zone is below 220 m and above 650 m near shore, about the same as that shown in Lachenbruch et al. (1988) for the JWD well. For constant thermal parameters, the depth range of the stability zone near shore is similar; however, the stability zone extends up to about 54 km offshore where the water depth is about 55 m. Using the sea level history curve of Bard et al. (1990), depths of 50 m to 55 m were submerged about  $10^4$  years ago. Thus, the time scale for producing methane gas from destabilized gas hydrates in the continental shelf near Lonely (for constant thermal parameters) is about four times greater than predicted by MacDonald (1990).

### SUMMARY

A two-dimensional finite element model was used to evaluate the thermal response and current thermal regime of permafrost to changes in sea level and climate. This information was used to calculate the current stability zone for gas hydrates in the continental shelf. The study site, offshore from Lonely, was chosen because of the availability of data from other research and from two oil exploration wells, one onshore and one offshore. These data were used to provide information on sediment types, depths to the permafrost table and base, thermal properties of the sediments, heat flow, shoreline erosion rate, and boundary conditions for modeling. Simulations were carried out for two extreme cases, permafrost with constant thermal parameters and permafrost containing sea water brines which introduce distributed latent heat effects and cause the

thermal parameters to have a strong dependence on temperature. These two cases span a wide range of thermal parameters and produce results for the thermal states of the permafrost which are quite different.

For the case when the permafrost contains brines, ice-bearing permafrost (IBP) is predicted to extend only 19 km offshore. This is a result of the relatively large heat flow ( $65 \text{ mW}\cdot\text{m}^{-2}$ ) and low ice content (porosity) assumed for the IBP. Lateral heat flow is significant throughout the IBP and in the thawed material under it and seaward of it. This suggests that one-dimensional thermal models may not correctly predict the thermal regime of subsea permafrost containing brine. Depth to the IBP table increases almost linearly with distance offshore and, at 7.8 km, is 28 m compared to the 7 m to 15 m observed along another line at the same distance offshore.

For the case when thermal properties are constant, IBP is predicted to extend 52 km offshore where the water depth is 50 m. The IBP is primarily isothermal, wedge shaped to 24 km offshore, nearly tabular beyond 24 km offshore, and has a relatively flat vertical tip. Depth to the IBP table increases almost linearly with distance offshore over the wedge shaped section and is relatively shallow and nearly constant over the tabular section. This behavior is the combined result of the assumed sea level history curve and seabed temperatures. At 7.8 km offshore, the predicted thickness of the thawed layer at the seabed is 38 m compared to 7 m to 15 m observed along another line at the same distance offshore.

Predicted depth to the base of IBP onshore obtained by applying the model with constant thermal properties (355 m) is in better agreement with the observed value (366 m) compared to the prediction using temperature-dependent thermal properties (318 m). This suggests that the full thickness of the IBP can be modeled better with constant thermal properties. However, the depth to the IBP table appears to be predicted better using the model where the permafrost contains brines. While thawing of subsea permafrost is a complex process possibly involving convective heat flow by movement of the brines, this suggests that most of the deeper permafrost may be relatively free of brines but that the near-surface permafrost contains brines, although other factors may play a role.

Simulations using the large heat flow ( $80 \text{ mW}\cdot\text{m}^{-2}$ ) suggested by Deming et al. (1992) resulted in predictions for the base of the IBP which were much too shallow.

The predicted zone for stability of methane gas hydrates is below about 220 m and above about 650 m near shore. When the permafrost contains brines, this stability zone extends 32 km offshore. For permafrost with constant thermal properties, the stability zone extends 54 km offshore to the 55 m water depth. Submergence occurred at this water depth about  $10^4$  years ago. This indicates that the time scale for producing methane gas from destabilized gas hydrates in the continental shelf near Lonely is about four times greater than predicted by MacDonald (1990).

#### ACKNOWLEDGMENTS

We wish to thank T.S. Collett and Dr. J.P. Gosink for their comments on this research. The finite element model used for these simulations was developed by Dr. J.P. Gosink. This research was funded by the Army Research Office, National Science Foundation, U.S. Geological Survey and by the State of Alaska.

#### REFERENCES

- Bard, E., B. Hamelin, and R.G. Fairbanks (1990) U-Th ages obtained by mass spectrometry in corals from Barbados: sea level during the past 130,000 years, *Nature*, 346, 456-458.
- Clarke, J.W., P.S. Amand, and M. Matson (1986) Possible cause of plumes from Bennett Island, Soviet Far Arctic, *Bull. Am. Assoc. Pet. Geol.*, 70(5), 574.
- Collett, T.S., K.J. Bird, K.A. Kvenvolden, and L.B. Magoon (1988) Geologic interrelations relative to gas hydrates within the North Slope of Alaska, Open-File Rept. 88-389, USGS, Menlo Park, CA.
- Collett, T.S., K.J. Bird, K.J. Kvenvolden, and L.B. Magoon (1989) Map showing the depth to base of the deepest ice-bearing permafrost as determined from well logs, North Slope, Alaska, U.S.G.S., Oil and Gas Investigations, Map OM-222.
- Deming, D., J.H. Sass, A.H. Lachenbruch, and R.F. DeRito (1992) Heat flow and subsurface temperature as evidence for basin scale groundwater flow, North Slope of Alaska, *GSA Bull.*, 104, 528-542.
- Fei, T. (1992) A theoretical study of the effects of sea level and climatic change on permafrost temperatures and gas hydrates, unpublished M.S. Thesis, 102 pp., Univ. of Alaska, Fairbanks, AK.
- Harrison, W.D., and T.E. Osterkamp (1981) Subsea permafrost: probing, thermal regime, and data analyses, Annual Rept. to NOAA, ERL, Boulder, CO.
- Hopkins, D.M., and R.W. Hartz (1978) Shoreline history of Chukchi and Beaufort Seas as an aid to predicting offshore permafrost conditions, Environmental Assessment of the Alaskan Continental Shelf, Annual Rept., 12, 503-575.
- Hunter, J.A.M., A.S. Judge, H.A. MacAulay, R.L. Good, R. M. Gagne, and R.A. Burns (1976) Permafrost and frozen sub-seabottom materials in the Southern Beaufort Sea, Tech. Rept. 22, Beaufort Sea Project, Dept. of the Environment, Victoria, B.C.
- Kvenvolden, K.A., and M.A. McMenamin (1980) Hydrates of natural gas: A review of their geological occurrence, USGS Circular 825, Arlington, VA.
- Lachenbruch, A.H. (1957) Thermal effects of the ocean on permafrost, *GSA Bull.*, 68, 1515-1530.
- Lachenbruch, A.H., J. H. Sass, B.V. Marshall, and T. H. Moses Jr. (1982) Permafrost, heat flow, and the geothermal regime at Prudhoe Bay, Alaska, *J. Geophys. Res.*, 87 (B11), 9301-9316.
- Lachenbruch, A.H., and B.V. Marshall (1986) Changing climate; geothermal evidence from permafrost in the Alaskan Arctic, *Science*, 234, 689-696.
- Lachenbruch, A.H. and others (1988) Temperature and depth of permafrost on the Arctic Slope of Alaska, in U.S.G.S. Prof. Paper 1399, p. 645-656.
- Lewellen, R.I. (1973) The occurrence and characteristics of nearshore permafrost, Northern Alaska, Proc. Second Int. Conf. on Permafrost, 131-135, NAS, Washington, D.C.
- MacDonald, G.J. (1990) Role of methane clathrates in past and future climates, *Climatic Change*, 16, 247-281.
- Mackay, J.R. (1972) Offshore permafrost and ground ice, Southern Beaufort Sea, Canada, *Can. J. Earth Sci.*, 9(11), 1550-1561.
- Maximova, L.N., and V.E. Romanovsky (1988) A hypothesis for the Holocene permafrost evolution, Proc. of the Fifth Int. Conf. on Permafrost, 1, 102-106, Norwegian Inst. of Tech., Trondheim, Norway.

- Molochushkin, E.N. (1978) The effect of thermal abrasion on the temperature of the permafrost in the coastal zone of the Laptev Sea, p. 90-93, *USSR Contribution, Permafrost, Second Int. Conf.*, July 13-28, 1973, NAS, Washington, D.C.
- Nixon, J.F. (1986) Thermal simulation of subsea permafrost, *Can. J. Earth Sci.*, 23, 2039-2046.
- Osterkamp, T.E. (1987) Freezing and thawing of soils and permafrost containing unfrozen water or brine, *Water Resources Res.*, 23(12), 2279-2285.
- Osterkamp, T.E., and W.D. Harrison (1980) Subsea permafrost: probing, thermal regime, and data analyses, Annual Rept. to NOAA, ERL, Boulder, CO.
- Osterkamp, T.E., and W.D. Harrison (1982) Temperature measurements in subsea permafrost off the coast of Alaska, Proc. Fourth Canadian Permafrost Conf., pp. 238-248, National Research Council of Canada, Ottawa, Canada.
- Osterkamp, T.E., and W.D. Harrison (1985) Subsea permafrost: probing, thermal regime, and data analyses, 1975-1981, Rept. UAGR301, 108 pp., Geophys. Inst., Univ. of Alaska, Fairbanks, AK.
- Osterkamp, T.E., J.K. Petersen, and T.S. Collett (1985) Permafrost thicknesses in the Oligotok Point, Prudhoe Bay, and Mikkelson bay areas of Alaska, *Cold Reg. Sci. and Eng.*, 11, 99-105.
- Osterkamp, T.E., G.C. Baker, W.D. Harrison, and T. Matava (1989) Characteristics of the active layer and subsea permafrost, *J. Geophys. Res.*, 94(C11), 16,227-16,236.
- Osterkamp, T.E., and J.P. Gosink (1991) Variations in permafrost thickness in response to changes in paleoclimate, *J. Geophys. Res.*, 96(B3), 4423-4434.
- Outcalt, S. (1985) A numerical model of subsea permafrost in freezing and thawing of soil-water systems, TCCRE Monograph, D.M. Anderson and P.J. Williams, eds., ASCE, New York, NY.
- Shackleton, N.J., and N.D. Opdyke (1977) Oxygen isotope and paleomagnetic evidence for early northern hemisphere glaciation, *Nature*, 270, 216-219.
- Sloan, E.D., Jr. (1990) Clathrate hydrates of natural gases, 641 pp., Marcel Dekker, Inc., New York, NY.

## THE ION EXCHANGE INTENSITY BETWEEN SOIL AND SNOW

Ostroumov V.E., Demidov V.V., Butsenko A.N., Makeev O.V. and Gershevich V.D.

Institute of Soil Science and Photosynthesis,  
Russian Academy of Sciences, Pushchino, Russia

The present paper deals with the intensity of ion transfer in the frozen soil - snow boundary. The contribution of ice crystal surface to the ion transfer in frozen soils is considered by example of snow. The comparison is made of the intensity of fluxes of chemical elements in to snow from different sources: underlying soil, precipitation, local fluxes of soil particles due to the weathering. The role of mass transfer on the boundary soil - snow in the balance of chemical elements of soil is evaluated. The quantitative contribution of this process to the run-off elements from soils with thawing fluxes is estimated.

### INTRODUCTION

The intensity of chemical elements transfer between snow and frozen soils is determined by their permeability (transfer coefficients) as well as concentration and temperature gradients. Frozen soils and, to a greater extent, snow are permeable for mobile components. The diffusion coefficients of water vapour in frozen soils vary within the range from  $10^{-7}$  to  $10^{-3}$   $m^2/s$  depending on their composition and structure (Ostroumov, 1989). Snow is characterized by high gas permeability which, according to Kolyakov (from Saveliev, 1991) makes up 1-2 m/s. In fresh snow the water vapour diffusion coefficient is as high as  $5.6 \cdot 10^{-5}$   $m^2/s$  (Fedoseeva et al., 1986). In many cases a liquid component of the permeability of frozen soils and snow is also significant. In frozen ice saturated soils, where the unfrozen liquid is present as thin films on the surface of silicates and organic matter, the liquid water diffusion coefficients are  $10^{-6}$  to  $10^{-10}$   $m^2/s$  (Ostroumov, 1988). In snow the intensity of liquid transfer makes up a hundredth part of the gas flux.

The concentrations of porous solutions in soils are usually higher than in snow. For example, in sandy podzolic soils, potassium concentration in the porous solution varies from 7.0 to 112.0 mg/l (Kanunnikova et al., 1981), and is ten times lower in snow (Fedoseeva et al., 1986). There is a concentration gradient between soil and snow. The diffusion flux of dissolved substances caused by this gradient is directed from soil into snow. The existence of such a flux is confirmed by Jonasson and Allan (1972), Makarov et al., (1990) and others. Alongside with transfer from soil into snow, there is a reverse process associated with temperature gradient (Makarov, Fedoseeva and Fedoseev, 1990). The transfer of mobile components and exchange of chemical elements are continuously going in frozen soils and snow due to the permeability and gradients of concentration and temperature. The intensity of fluxes and the factors determining it still remain obscure.

The transfer of elements in frozen soils occurs mainly in the unfrozen water films (Cary and Mayland, 1970). The ions are the most active participants in liquid transfer. This is confirmed by a high electric conductivity of frozen soils, which is of an ionic type (Maeno, 1988; Frolov, 1976). Under the influence of temperature gradient, the transfer of ions and water in frozen soils occurs in the direction of the thermal flux. The experimental evidences show that the intensities of ions transfer in frozen, not icy clays and sands, are approximately equal. The contents of unfrozen liquid on silicate surface are different in these case. In addition, in the frozen samples, at moisture content approximating the maximal molecular capacity, the transfer coefficients are only slightly lower than in similar but thawed samples (Ostroumov, 1988). This is probably due to the fact that ion transfer happens mostly not in the unfrozen moisture films on the silicate surface, but in those on the ice surface. To verify this supposition, one should define the trend and quantity of the intensity of ion transfer in snow, which in such case can be considered as a model of porous ice in frozen soils. The element transfer within the system soil-snow is employed in geochemical investigations. For instance, the quantity of mobile components in snow is used as the method in mineral resources prospecting. Their anomalies point out, and with high probability, to the localisation of deposits of mineral resources in zones of hypergenesis. The records of the content of gas and volatile components of oil in snow are used in the oil and gas prospecting. The analysis of the distribution of rare and scattered element is used in prospecting of metals, specifically tungsten, platinum, gold (Makarov et al., 1990).

The results of the observations of contaminants in the snow cover are widely used to study their fluxes from the atmosphere to soil. It is the most important method in ecology which yields data on the accumulation of heavy metals, organic and inorganic acids, and other technogenic substances on the soil surface (Vasilenko, Nazarov and Friedman, 1988). However,

it disregards the flux of elements from soil into snow, which contributes to the total flux of contaminants on the surface. To avoid the errors, e.g. Viersma (1982) examined the uppermost 5 cm layer of snow on the glacial surface. The works of Vasilenko et al. (1988) and Viersma (1982) are examples of different attitude to the problem of the flux of elements from soil into snow and shows that it remains unsolved. A credit part of the balance of water soluble components includes fluxes to the underlying layers of rocks with infiltration, lateral run-off, run-off of elements due to erosion, fluxes to plants and soil covers. The field observations confirm that in spring the loss of chemical elements with melting water flows and run-offs from the surface of cultivated lands may be very high (Bulatkin, 1986; Eryomina and Ershova, 1978). The contribution of these processes to the elemental balance of soils may be estimated by the comparison of fluxes participating in mass transfer.

#### OBJECTS AND METHODS

To evaluate the intensity of elemental fluxes from soil to snow one could use the data obtained from their examination in field experiments. They are known however for their special heterogeneity. Without taking into consideration this fact it is impossible to obtain the reliable data on changes of the distribution of elements with time. The latter requires a labour consuming analytical work since more observation sites are needed. To decrease the amount of work, observations were carried out on specially prepared homogenous objects.

Experiment. A 2 cm layer of the paste made of preliminary grinded and sieved material sampled from the ploughed horizon of sandy-loam grey forest soil was placed in rectangular polyvinylchloride vessels. The paste was preliminarily brought to the state approximating the capillar moisture capacity using the lithium chloride solution at a concentration of about 50 g/l. The chloride of a lithium salt as a label is explained by the two reasons: firstly, its transfer coefficients in soils are similar to such widely spread elements as potassium as an indicator of the ion transfer; secondly, unlike the other elements, lithium does not practically fall on the soil surface together with precipitation (Voitkevich et al., 1990) and is not found in fresh snow, except for the regions of local technogenic discharges. In our experiment it may only arrive into snow from the underlying soil paste.

In the above mentioned vessels, the homogenous soil paste was frozen during 4 hrs at cryogenic texture which pointed out to the homogenous distribution of moisture and others mobile components. The soil paste was then covered with snow. In the control vessels without the paste, the snow was placed directly on the bottom. During the observations, the temperature at the bottom of the vessels was adjusted to about -3° C. The walls were heaped with snow for thermoinsulation. One of the vessels had 4 inertion thermometers installed (time constant 20 min) to follow the temperature throughout the snow thickness. The snow layer both in the control and experimental vassels was 15 cm.

The snow was sampled 0, 67, 95, 100 and 167 hrs after the beginning of the experiment. Short

periods allowed us to follow the fluxes from soil to snow at the beginning of the possible saturation of the latter due to the action of the diffusion mechanism. In the course of time, the concentrations of elements in soil and snow may become equal causing the abatement of diffusion. Therefore our data on the intensity of the flux from soil into snow are overestimations, compared to the values obtained for longer periods. The transfer of elements may change its direction and intensity under the action of the temperature gradient. In our experiments the change of the temperature gradient sign from negative to positive (snow heating from above) decreased rapidly the concentration of ions in the snow layer on the border with the soil paste. It is probably associated with the ion migration from snow into soil and points out to the fact that the processes of the transfer within the system soil-snow are rather dynamic.

The snow samples were taken layer by layer (at a depth of 0-7, 7-11, 11-13, 13-14, 14-15 cm). Snow was melted in polyethylene packets at room temperature. The resulting water was filtrated (red line) to separate large particles. In the filtrate, we determined the quantity of lithium and others elements. For the analytical determinations, the elements were chosen to enable the characterization of migrating agents having the most diverse mobility. For instance, lithium was chosen as the mobile cation of a small radius ( $0.6 \cdot 10^{-10}$  m, according to Poling, see (Voitkevich et al., 1990)), and potassium having a larger radius ( $1.33 \cdot 10^{-10}$  m). Calcium ion occupies an intermediate position ( $r=0.99 \cdot 10^{-10}$  m). Bivalent copper was chosen as an example of inactive cation having a small ion radius ( $0.70 \cdot 10^{-10}$  m), cadmium ( $2+$ ,  $r=0.97 \cdot 10^{-10}$  m) and lead ( $2+$ ,  $r=1.21 \cdot 10^{-10}$  m) as larger slow cations. Lead, cadmium and others heavy metals only migrate in solid disperse phase soils, not in the form of ions. However the mobility of these elements correlates with the parameters of corresponding ions. Of all the anions, chlorine was taken for determinations.

The quantity of lithium and potassium in the filtrate was determined by the emission technique in the flame of an acetylene burner. Calcium concentration was determined by the atom absorption method with flame atomization of samples. Copper, lead, and cadmium concentrations were also determined by the atom absorption technique, using however an electrothermal method to atomize the samples. All determinations of the cation quantity were made with an atom absorption spectrophotometer AAS -3. The quantity of chlorine atoms was -12°C. This resulted in the formation of the determined by the standard technique of argentometric titration. The diversity of the results obtained for each sample was no higher than 2% for cations, and 8% for chlorine, compared to the total quantity.

The same determinations were made on the water extract of the soil paste underlying snow in the experimental vessels.

From the data on the distribution of elements in the snow layers in the control and experimental vessels, we calculated the intensities of their fluxes from soil into snow ( $I$ ,  $g/m^2 \cdot hr$ ) according to the formula:

$$I = (C_1 \cdot l_1 + C_2 \cdot l_2 + \dots + C_n \cdot l_n) \cdot b - (C_1 \cdot l_1 + C_2 \cdot l_2 + \dots + C_n \cdot l_n) \cdot k_j \cdot p_s / T \cdot p_w,$$

where  $C_1, C_2, \dots, C_n$  ( $g/m^2$ ) - are the concentra-

tion of element in the filtrate of the snow from layers 1, 2, ..., n from the experimental (b) and control (k) vessels; T (hr) is the time period from the arrangement of the vessels to the snow sampling;  $\rho_s$ ,  $\rho_w$  ( $\text{kg/m}^3$ ) - is snow and water density;  $l_1, l_2, \dots, l_n$  (m) - is the depth of the snow layers 1, 2, ..., n.

The experimental and control vessels were under equal condition of the flux of elements from atmosphere. The comparison of the content of elements in both ones, makes it possible to obtain the data on the fluxes from the soil paste to snow disregarding the effect of their fluxes from the atmosphere.

The intensity of the above fluxes was determined from the same formula. The comparison was made of snow samples taken from the control vessels at different time intervals. The resulting intensity of e.g. potassium flux makes up  $1.4 \cdot 10^{-5} \text{ g/m}^2 \cdot \text{hr}$ .

We made also an attempt to evaluate the share of the element run-off, including some byophils, from soil with melting snow. The field experiments were carried out on the slope of grey forest soil with 1.8-2.3% humus content. The total amount of consumed bases changes from 12.5 to 18.9 mg-eq/100 g. This soil is characterized by the medium quantity of mobile forms of nitrogen, phosphorus, and potassium,  $\text{pH}=6.5-6.8$ . The soil of this region was subjected to crop rotation during 8 years without application of fertilizers. The estimation of the quantity of chemical elements in snow and thaw were made by the water-balance method using run-off grounds within the framework of the complex programme of soil erosion investigations.

The determination of run-off flux of elements was made by calculation. To calculate the run-off flux we used a data of measurements of element concentration in the snow cover. The nitrogen concentration in filtrate was determined by potentiometric techniques. To measure all others element concentrations was used method described, above.

## RESULTS AND DISCUSSION

The figure 1 shows a typical distribution of elements in the control (dotted line) and experimental (solid line) snow samples. The curves showing the distribution of all the elements under the study take the alike form. Therefore, for the illustration we took lithium and potassium for the time period 67 hrs beginning from the vessel arrangement. The highest amounts of all the elements were observed in the lower snow level in control vessels at the contact with the underlying frozen soil paste. Such a distribution character points out that the flux of elements is directed from soil into snow.

The curve of potassium distribution (Figure 1) and of other elements except for lithium demonstrates a slight increase of their concentration in the uppermost layer. It is associated with the element transfer from fresh snow. This is confirmed by the absence of such an increase in case of lithium.

Table 1 contains the data on the intensity of lithium flux from soil to snow at different average temperatures of snow, and temperature gradient. The negative values of the gradient mean that the temperature in the upper layer is

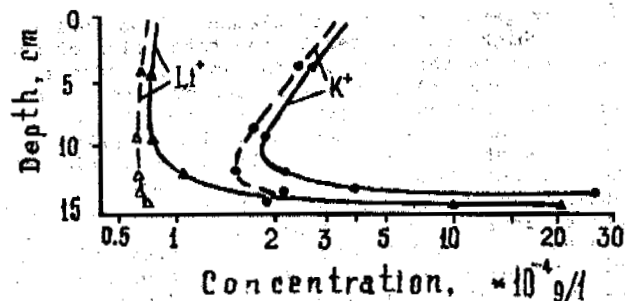


Figure 1. The distribution of lithium and potassium ions in the snow

lower than in the lower one, due to its cooling by the ambient air.

The temperature elevation from  $-8.2$  to  $-1.8^\circ\text{C}$  makes increase the flux intensity from  $0.155 \cdot 10^{-5}$  to  $3.42 \cdot 10^{-5} \text{ g/m}^2 \cdot \text{hr}$ . This is connected with the increase of the coefficients of liquid transfer as far as the snow temperature increases, and happens due to the enlargement of the film on the ice crystals and probably due to its mobility (Kvlividze et al., 1970).

The increase of the absolute value of temperature gradient (from  $-0.6$  to  $-1.1 \text{ grad/cm}$ ) also makes increase the flux intensity (from  $0.155 \cdot 10^{-5}$  to  $0.762 \cdot 10^{-5} \text{ g/m}^2 \cdot \text{hr}$ ) in spite of the drop of temperature. Evidently with the temperature range lower than  $-8.2^\circ\text{C}$  the role of the gradient as a transfer factor becomes more important compared to the temperature. This is confirmed by the exponential form of the curve denoting the dependence of the liquid film width on temperature (Ershov, Akimov et al., 1979). The increasing flux intensity as far as the absolute value of the temperature gradient increases points out to the fact that the ions are transferred in the same direction as the heat flux. The same occurs with the ion flux, in frozen non-saline soils (Ostroumov, 1988) within the limits of the inner liquid layer adjacent to the solid phase surface. The coincidence of the direction of non-isothermal ion transfer in cryosoil and snow samples points out to an important role of the common for these objects mechanism of the migration, i.e. the ion transport within the layer of liquid on the crystal surface. The participation of this mechanism in mass transfer explains a comparatively high permeability of frozen unsaturated with ice sand samples having a very small quantity of unfrozen water on the surface of a solid silicate component.

The results presented in table 2 make it possible to compare the intensities of fluxes of different ions. The elements are arranged in the decreasing order of their fluxes in the snow, which reflects the decrease of their transfer ability in the snow. These data are given for average snow temperatures  $-12.1^\circ\text{C}$  and gradient  $1.1 \text{ grad/cm}$ .

The transfer intensity of ions depends on radius (r), atomic weight (M) and electric charge (Q) of ions. The flux of ions decreases with growth of these parameters product (Figure 2).

The experimental evidences show that soils have a higher mobility of ions compared to cations (Ostroumov, 1988). This is explained by the fact that cations are more rigidly sorbed on the negatively charged silicate surface. Probably a comparatively low mobility of a chlorine ion

Table 1. Dependence of the intensity of lithium flux from soil to snow on snow temperature and its gradient. Notes: a - date of vessels arrangement; b - date of snow sampling; T - duration of the snow contact with the frozen soil paste in experimental and control vessels; t - snow temperature averaged by time and depth; q - snow temperature gradient averaged by time; i - intensity of lithium flux to snow averaged by time.

a	b	T, hr	t, °C	q, grad/cm	I, *10 <sup>-5</sup> g/m <sup>2</sup> *hr
13.01.92	16.01.92	67	-12.1	-1.1	0.762
13.01.92	17.01.92	95	-8.2	-0.6	0.155
13.01.92	20.01.92	167	-4.0	-0.2	2.13
16.01.92	20.01.92	100	-1.8	-0.2	3.42

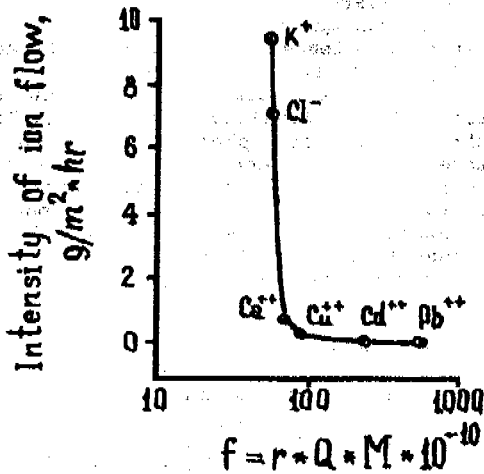


Figure 2. Impact of ion radius, charge, and atomic weight on the intensity of elements flux in snow

within the system soil-snow as compared to a potassium ion is due to the analogous effect. A charge of the ice crystal surface is usually positive which is connected with the excess of positively charged lattice defects in its structure. Due to this fact, the anions in snow are sorbed on the surface of ice particles more tightly than cations and their mobility relatively drops.

To determine the flux of elements with thaw which brings them from the slope to the accumulating components of the landscape, we analysed the snow cover before thawing. The snow contained the following concentrations of elements (mg/l): nitrogen - 1.5, chlorine - 1.24, calcium - 1.00, sodium - 0.60, potassium, magnesium, phosphorus - 0.20, 0.15 and 0.10, respectively; or calculated per 1 hectare they were (kg/ha 1.77, 0.80, 0.65, 0.39, 0.13, 0.10, 0.06 respectively).

During snow melting, ammonium concentration varies from 1.1 to 0.2 mg/l, being maximal in the beginning. The same holds true to potassium (1.7 - 0.7 mg/l). The concentration of nitrates changes from 2.0 to 3.4 mg/l, of calcium from 8.2 to 14.7 mg/l. Their concentration increases at the end of the thaw. Phosphorus is almost absent (0.16 mg/l and less), chlorine (2.8 - 5.3 mg/l) and mad-

Table 2. A succession of ions in the order of the intensities of their flux from soil to snow

Ions	K	Cl	Li	Ca
I, g/m <sup>2</sup> *hr	9.83	6.89	0.762	0.54
Ions	Cu	Cd	Pb	
I, g/m <sup>2</sup> *hr	0.288	0.0007	<0.0007	

nesium (less than 1.95 mg/l) concentrations show slight changes. The same was observed with sodium concentration which varied within the range from 1.0 to 1.4 mg/l. The ionometric determinations of the reaction of the medium showed its proximity to the neutral one (pH=6.45-6.78).

The calculation of the element run-off with thaw allowed us to arrange elements in the decreasing order (kg/hr per a thaw period, (Table 3).

Table 3. The loss of elements (m) by grey forest soil during snow melting (by data on run-off grounds)

Elements	Ca	N	Cl	Mg
M, kg/ha	1.83	0.72	0.37	0.35
Elements	Na	K	P	
M, kg/ha	0.25	0.23	0.04	

The run-off of elements from the surface with thaw fluxes is equivalent to the annual average of fluxes given in Table 4. It contains some data which allows the comparison of the intensity of elements flux from soil into snow and other their influences and effluxes.

Table 4. The intensity of element fluxes (I\*10<sup>-5</sup> g/m<sup>2</sup>\*hr) connected with the snow cover ("-" no data)

Flux	K	Na	Ca	Mg
Soil-snow	9.83	-	0.53	-
Atmosphere-snow	1.42	-	0.02	-
With thawing water	0.26	-	2.08	0.40
Flux	Cd	N	Cl	
Soil-snow	0.0007	-	6.89	
Atmosphere-snow	0.004	-	-	
With thawing water	-	0.82	0.42	

The fluxes within the system soil-snow and atmosphere-snow were determined according to the above described method.

These data show that the intensity of the element transfer at the soil-snow boundary is not less than the other sources of their efflux and influx to soil.

#### CONCLUSION

The described experiments showed the distribution of chemical elements in the homogenous snow layer contacting the frozen soil. Their maximal concentration in snow is found in the place of their contact with soil. The calculations of the intensity of element fluxes from soil to snow showed that they depend on temperature, as well



as temperature gradients and element concentration. The ions are transferred to snow in the same direction as the heat flux. The coincidence of the direction of ion fluxes in snow and frozen soil is connected with their transport within the liquid layer on the ice crystal surface. The composition of the element flux at the boundary soil-snow and their run-off with thaw showed that the former is not a determining factor in the landscape cycle of matter.

#### REFERENCES

- Bulatkin G.A. (1986). Ecological and energy aspects of agrocenoses productivity, Pushchino, 209 p.
- Cary I.W., and Mayland H.S. (1972). Salt and Water Movement in Unsaturated Frozen Soil. - Soil Science Society of America Proc., N 36, 549 - 555.
- Eremina R.F., and Ershova V.G. (1978). Effect of terraces on nutrient concentration and their efflux with surface thaw. Soil Protection Against Erosion, 4 (19), Kursk, 49 - 54.
- Ershov E.D., Akimov Yu.P., Cheverev V.G., Kouchoukov E.S. (1979). The phase composition of moisture in cryorocks. Moscow State University, 190 p.
- Fedoseeva V.I., Fedoseev N.F. (1988). Estimation of vapour diffusion coefficient in the snow cover (by example of Central Yakutia). Meteorologia i Gidrologia, 2, 132 - 135.
- Fedoseeva V.I., Makarov V.N., Fedoseev N.F. (1984). Mineralisation of the snow cover. Meteorologia i Gidrologia, 4, 75 - 79.
- Frolov A.D. (1976). Electric and elastic properties of cryorocks. Moscow, 254 p.
- Jonasson J.R., and Allan R.J. (1972). Snow: a sampling medium in hidrogeochemical prospecting in temperature and medium regions. - Geochemical Exploration, 161 - 176.
- Kanunnikova N.A., Kovrigo V.P., and Dzyuin G.P. (1981). Dynamics of potassium potentials of soil solution. Pochvovedenie, 11, 61 - 70.
- Kvividse V.I., Kiselyov V.F., and Ushakova L.A. (1970). Quasiliquid film on the ice surface. Doklady Acad. Nauk, v. 191, 5, 1088 - 1090.
- Maeno M. (1988). Ice science. Moscow, Mir publishers, 230 p.
- Makarov V.N., Fedoseev N.F., and Fedoseeva W.I. (1990). Geochemistry of Yakutia snow cover. Yakutsk, 148 p.
- Ostroumov V.E. (1988). Thermodiffuse ion transfer in grounds. Permafrost Proc., v.1. Trondheim, 425 - 430.
- Ostroumov V.E. (1989). The transfer of dissociated salts in frozen grounds under the influence of temperature gradients. Geocryological Research, Moscow State University, 63 - 74.
- Saveliev B.A. (1991). Glaciology. Moscow State University, 288 p. Savelieva E.M. (1986). Effect of the water-ice phase transition on hydrometeorological processes within the system atmosphere - soil. Ph.D.thesis, Leningrad, 17 p.
- Vasilenko V.N., Nazarov I.M., and Freedman M.D. (1988). Monitoring of snow cover contamination. Environmental analysis. Proceeding of V Soviet - American symposium. Leningrad, Gydrometeoizdat, 61 - 71.
- Viersma D.B. (1982). Complex monitoring of contaminants in National Park Olympic. The USA Biosphere Reserve. Complex global monitoring of environmental contamination. Leningrad, Gidrometeoizdat, 94 - 105.
- Voitkevich G.V., Kokin A.B., Miroshnikov A.E., and Prokhorov V.G. (1990). Reference book on geochemistry. Moscow, Nedra, 480 p.

QUANTITATIVE ESTIMATION OF MASS-TRANSFER  
IN LANDSCAPE COMPLEXES OF NORTHERN RUSSIA

A.V.Pavlov

All-Russian Research Institute of Hydrogeology and Engineering Geology,  
Zeleny Village, Noginsk district, Moscow region 142452 Russia

The paper presents a quantitative estimation of mass-transfer for wide variety of landscape complexes and their most important component. A simplified method is suggested to calculate the coefficient of thermal conductivity of snow as function of its density and temperature. Thermal protection ability of surface covers (moss, lichen) is discussed. Heat-exchange of water basins with atmosphere is analyzed for an annual cycle. It is shown that temperature at the bottom of arctic lakes is lower than the temperature corresponding to the highest density of water (+4°C). It is established, how forests effect heat balance of the earth's surface and thermal regime of soil. Examples are shown for changes in heat-transfer of landscape complexes under typical anthropogenic impacts.

INTRODUCTION

Thermal factor is decisive in preservation of natural situation in the North under anthropogenic development. Temperature of soil and freezing and thawing of this soil are controlled by it interaction with atmosphere and surface covers. Quantitative study of heat-transfer in landscape complexes is an important task of geocryological prediction and monitoring. Under supervision of the author, a detailed study of thermal regime of landscape complexes was carried out in permafrost covering 70% of Russian territory. The experiment embraced chiefly the regions of continuous permafrost (Central Yakutia, north of West Siberia) and discontinuous permafrost (Yenisey River North, Bolshezemel skaya tundra).

Snow as a Function of Temperature

Specific features of snow cover include a continuous evolution of the texture due to metamorphism and good thermal protection properties. Conductive exchange in snow cover is always supplemented by heat-exchange induced by thermal diffusion.

Thus, intensity of heat-transfer depends on effective coefficient of thermal conductivity. Thermal conductivity and thermal protection properties of snow to a great extent depend on temperature. For a long time the researchers did not take this fact into consideration. Since the time when the publication of G.F.Abel's (1883) appeared a number of formulae were obtained (Iansson 1904; Iosida, 1955; Proskuryakov, 1956, et al) in which coefficient of snow, thermal conductivity ( $\lambda$ ) was related to density ( $\rho$ ). The comparison of these formulae shows a high scattering in the  $\lambda$ -values at the same discrete values of  $\rho$  (Pavlov, 1979). So, the use of only one  $\lambda$ -

factor is not enough to calculate  $\lambda$ -value. The same is shown by the analysis of the results obtained at the geocryological monitoring stations in Russia (Figure 1). For example, in Solyony settlement (northern West Siberia) and especially in Yakutsk where the temperature of air and snow cover is in general lower than in Igarka, the  $\lambda$ -values are on the average lower (see Figure 1). The author (Pavlov, 1975, 1984) has shown the dependence of  $\lambda$  value on both density  $\rho_{sn}$  and snow temperature  $T_{sn}$ . Generally, this dependence on the both factors is linear. For relatively narrow range of densities (0.12 g/cm<sup>3</sup> - 0.35 g/cm<sup>3</sup>) one can obtain the following simplified calculating formula:

$$\lambda_{sn} = \begin{cases} 0.04 + \chi \rho_{sn}, & T_{sn} < -10^{\circ}\text{C} \\ \chi \rho_{sn}, & -10^{\circ}\text{C} > T_{sn} > -20^{\circ}\text{C} \\ -0.04 + \chi \rho_{sn}, & T_{sn} < -20^{\circ}\text{C} \end{cases} \quad (1)$$

where  $\lambda_{sn}$  - in W/(m°C),  $\chi$  - dimensional coefficient (in the accepted system of dimensions  $\chi = 1^{\circ} [W / (m.K)] / (g/cm^3)$ ). The lower is density of snow and the higher is temperature, the more is its influence upon the coefficient of thermal conductivity and total heat-transfer. A  $\lambda_{sn}$ -change due to temperature is one of mechanisms of selfregulation in thermal regime of landscape complexes in winter.

At temperature of -25°C and lower the  $\lambda_{sn}$ -values are actually not dependent on snow temperature and correspond to conductive heat transfer. According to the experimental results obtained in Yakutsk, the coefficient of purely conductive heat transfer is considerably lower than that calculated by formula (1) and is equal to 0.05; 0.12 and 0.19 W<sub>t</sub>/(m°C) at  $\rho_{sn} = 0.1; 0.2$  and  $0.3 \text{ g/cm}^3$  respectively.

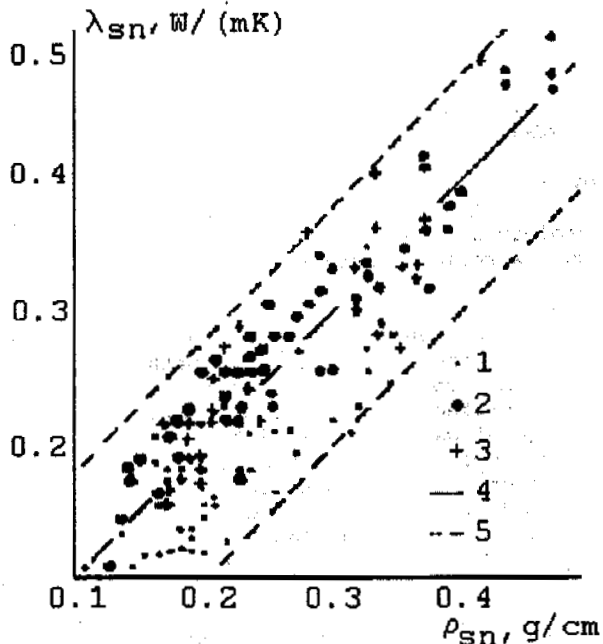


Figure 1. Thermal conductivity coefficient of snow cover  $\lambda_{sn}$  as function of density  $\rho_{sn}$  according to the experimental data for Yakutsk (1), Igarka (2), Solyony (3); 4 - line  $\lambda_{sn} = \rho_{sn}$ ; 5 - lines of confining range

Temperature of snow cover at meteorological stations and geocryological-monitoring points is not measured as a rule. Therefore, the relationships obtained are similar to (1), where instead of  $v_{sn}$  value, the air temperature  $v_a$  is used (Pavlov, 1981). As the Yakutian experiments have shown, the  $\lambda_{sn}$  value increases with a rise in snow crystal sizes. So, the metamorphosed snow is characterized by a slightly higher  $\lambda_{sn}$  -value than a fresh snow. However, this difference is not large.

Thus, heat transfer in a snow cover, as well as the rate of recrystallization depends both on vertical gradient of temperature and on temperature itself. An optimal growth of snow crystals is observed at negative temperatures (5 to 15°C), and the most intensive diffusion and heat transfer are observed within 0 to -2°C.

#### Thermal Conductivity and Cooling Effect of Surface Soils

Organic covers (i.e. moss, moss-lichen, moss-peat) overlying the mineral soils are usually called by Russian geocryologists as on-topsoil covers. While being in a thawed state they serve as a natural thermal insulator because their thermal conductivity is 10-20 times lower than the soil.

Thermal conductivity and heat-proof ability of the surface soil cover and peat was studied by R.I.Gavriliev and S.V.Eliseev (1970),

A.A.Konovalev and L.T.Roman (1973), A.A.Mandarov and P.N.Skryabin (1978), A.V.Pavlov (1979), V.P.Chernyadiev, et al (1984). Lichen and forest layers in a thawed state are less heat conductive than other surface covers (thermal conductivity) coefficient is not more than 0,25 W/(m.K). Thermal conductivity coefficient of sphagnum and peat in a saturated state may reach 0,6 to 0,75 W/(m.K).

A cooling effect of surface covers is manifested itself most of all during the first half of warm season (5 to 8°C at a cover thickness of 4 to 6 cm). In winter this effect is less than in summer, as the thermal conductivity of surface soil covers increases with freezing by a factor of 2 to 4. On the average, the covers cool the soil by 0,5 to 1,5°C per year and per summer season.

#### Specificity of Heat Exchange between Soil and Atmosphere

Annual contribution of solar radiation to the territory of Russia is 25\$10 to 50\$10 MJ/m². The western regions of this country obtain at the same latitudes, due to a greater cloudiness caused by air masses coming from the Atlantic Ocean, a slightly lesser solar radiation totally for a year than in the east.

Radiation balance R of the natural earth's surface varies within the permafrost zone from 600 to 800 MJ/(year.sq.m) at high latitudes (the coast of the Arctic Ocean) to 1600 MJ/(year.sq.m) in the south of Siberia. The annual radiation balance R does not exceed 40% from the total radiation. Negative R-values are observed during 5-6 months (since October to March or April).

Annual change of Q, R, turbulent heat-exchange P, heat losses for evaporation  $\omega E$  (where  $\omega$  - heat, E - intensity of evaporation) for different landscape complexes in the North (e.g. variegated-grass meadows) moss-lichen tundra, forests, water basin) is well known. Maximum values of these components fall on June-July. In winter, the R, P,  $\omega E$ -values are from 5 to 15 times lower than in summer.

Most studied are the components of the external heat transfer for an open area. Heat losses for evaporation are equal to 15-40% (from the total radiation) during the warm months and 11-33% during the cold months. The P/R ratio in the tundra during the warm season is in general the same as in the steppe. A decrease in R-value with a rise in latitudes determines a general tendency of reducing evaporation E from the soil surface. Not only the E-value decreases here, but E/R ratio as well, in spite of that the soil is over moisture.

Heat flux B into a soil essentially increases in the northern regions as compared with the moderate latitudes. The B-values during the entire warm season may reach 5-6% relative to Q and 10-14% relative to R. The peak of B-values falls on the beginning of soil thawing. Heat yield is the highest in the

beginning of winter.

Temperature of soil surface  $v_s$  is a resultant of the heat interaction between external components of heat balance and internal component B. Average monthly difference between the  $v_s$  values (for an open flat area with a natural surface) and the  $v_a$  values do not exceed  $5^\circ\text{C}$ . The  $\delta = v_s/v_a$  ratio to a considerable extent depends on the continentality of the climate. So, for the vicinity of Yakutsk a value of  $\delta \sim 0.95-1.2$ . For the Arctic coastal areas the  $\delta$  value increases to 1.5-2. Besides, one observes here considerable interyear  $\delta$  variations. During relatively cold summer time,  $\delta$  values increase and in warm time decrease. Temperature of snow cover surface is usually lower than the temperature of air. On the average during winter season this decrease amounts typically to not more than  $1-1.8^\circ\text{C}$ .

The formation of average annual temperature of soils at the top and base of a layer of annual heat-circulation  $v_0$  over local areas is controlled to a great degree by geomorphological conditions, lithology, vegetation. The same concerns the depth of seasonal thawing  $\xi_{th}$ . The importance of the first two factors is most clearly seen in the Arctic. In particular, in the West Yamal the  $\xi_{th}$  value varies from 0.45 to 0.75 on polygonal peatbogs to 1.5 to 1.7 m on sand-blowing areas. The highest temperatures  $v_0$  (from  $-2^\circ\text{C}$  to  $-4^\circ\text{C}$ ) are typical of bogged lowlands, leeward slopes and ravine bottoms, where the thickness of snow deposits reaches 1.5 to 2 m (up to 4 m). The lowest temperatures of soils ( $-5^\circ\text{C}$  to  $-7.5^\circ\text{C}$ ) are observed on sand-blowing areas and bare windward slopes.

Of the highest multi-year variability among thermal parameters of the lithogenic basis of a landscape complex is usually the temperature of a soil surface  $v_s$ , of the lowest one is the  $\xi_{th}$  value. According to the computer-modelled results, the limits of changes in average annual temperature for the past 30-40 years are as follows in Central Yakutia - from  $+0.5^\circ\text{C}$  to  $-8.9^\circ\text{C}$ ; in the Yenisey River North - from  $+2^\circ\text{C}$  to  $-4.8^\circ\text{C}$ ; in the north-east of West Siberia - from  $-4^\circ\text{C}$  to  $-12^\circ\text{C}$ . Multi-years variations in the  $\xi_{th}$  value are higher for organic soils than for mineral ones. The  $\Delta\xi_T/\xi_T$  values are equal, according to the results of multi-year observations conducted in West Yamal, to from 32 to 73% for peat, 15-16% for sands and from 18 to 24% for sands loam.

#### Forest Effect on Thermal Regime of Soil

Among all the landscape complexes of the North coniferous forests and water basins have

the lowest values of albedo during a warm season ranging from 10 to 14% and 6 to 12%, respectively. Albedo of closed forests in permafrost (e.g. larch, fir-tree, pine, birch) is 6 to 11% for summer season and 18 to 20% for winter season lower as compared with an open area (Pavlov, 1979). An annually summed effective radiation of forest-covered and forest-free areas is approximately the same and is equal to 31-33% from Q value. In winter, the effective radiation of forests prevails and in summer that of meadows. An annual sum of radiation balance of forest R<sub>S</sub> increases by a factor of 1.4 to 1.6 as compared with the radiation balance of forest-free (bare) territory R<sub>p</sub>. Forest-covered areas usually show an increase in moisture circulation.

Forest influence on thermal regime of a soil is due mainly to the shading effect, a change in snow deposition, existence of a heat-proof forest layer. In forests there is a smaller depth of seasonal thawing and lower annual heat transfer in soil. According to the experimental data obtained for Central Yakutia, the heat transfer in a deciduous forest amounted to only 70 to 76% as compared to the heat transfer in an open area. In the taiga zone where the wood vegetation has a well-developed top crown, during a warm season and annually the effect of forest on a soil is as a whole a cooling one. That is why in the areas near the southern boundary of the permafrost zone no taliks exist in the forests. Sparsely growing forests and shrubs have, as a rule, a warming effect on a soil. This is typical of forest-tundra zone due to snow blowing away at the open areas of its retention by wood vegetation. In the forest-tundra zone of West Siberia, continuous frozen soils are often absent.

#### Heat Balance and Thermal Regime of Lakes

The detailed year-round study of watersurface heat balance was carried out for the first time at Syrdakh Lake in Central Yakutia (Pavlov, Are, 1984). One of the basic features in the formation of lake heat-balance is a considerable growth in radiation balance, evaporation, seasonal accumulation of heat by a water mass as compared with adjacent shoreline. Radiation balance of lakes during an open-water period rises by a factor of 1.1-1.3 and by 20 to 25% during a year. Heat accumulation becomes 7-8 times higher at a depth of water of 5 to 6 m.

In Central Yakutia during a spring season a considerable radiation warming occurs of water beneath the ice up to  $10^\circ\text{C}$  (Are, 1974). Due to the intensive water warming in spring the melting of ice cover from below is comparable with melting from above. During the ice-melting period the heat accumulation by a lake reaches almost the radiation balance. In summer period, shallow lakes (up to 1.52 m deep) have typically approximately the same temperature ( $15$  to  $20^\circ\text{C}$  and higher) throughout their

thickness. Water temperature in the lakes that are less than 3-4 m deep decreases with depth due to lack of wind mixing. Thus, a stable dense stratification is formed. An annual average temperature at a lake bottom  $v_{bt}$  is equal to 6 to 8°C within a rather wide depth interval (1.5 to 3.5 m). At a water depth of 50 to 80 m, it approaches to +4°C.

During several recent years the thermal year-round observations have been conducted at the lakes of Gydan and Yamal peninsulas (i.e. Krugloye, Parisento, Zagadochnoye, Syurtyav-Malto). These lakes are characterized by a deep mixing of open water masses (to 10-12m and more) and a lower temperature of the bottom sediments (by 3 to 4°C) as compared with the lakes of the Yakutian taiga zone. The lakes of the tundra zone show in winter a general increase in water temperature with depth. A stable dense stratification of water masses is formed. In the deep lakes during a period, prior to ice melting, the temperature distribution in the central part of a water mass becomes close to isothermal. At the same time, the water masses under the ice and in the near-bottom layer are characterized by a notable vertical-directed heterogeneity in temperature. Such temperature distribution indicates the existence of free convection in this central part of water mass. This interesting fact of convective mixing of water masses under the ice at the isothermal state was reported earlier for the Vanda Lake in Antarctica (Hoare, 1969). The temperature does not reach the level which would correspond to the maximum density.

Radiation warming of water below the ice in the lakes of Gydan and Yamal is expressed poorly. Therefore, the ice melts away chiefly from above. After the ice cover is melted completely, a rapid heating of water begins. Isotherm is formed throughout the entire water mass. Maximum heating of water reaches 14 to 18°C (July, August). Temperature at a bottom surface within the freezing-free period, in general, actually does not depend on the depth both in shallow and relatively deep lakes (Figure 2). An annual average increase in temperature of the bottom is 2.8 to 3.8°C within a depth interval of 1.8 to 2 m. At a water depth of more than 2 m an  $v_{bt}$  increase with depth is not large (see Figure 2).

**Anthropogenic Impact on Heat Transfer in Landscape Complexes.** The areas in the Russian North that are under intensive development suffer from the following widely spread anthropogenic actions on the surface of landscape complexes: disturbance (or removal) of turf and vegetation layers; compaction (clearance) of snow; use of admixtures (fillings) and artificial coverings. Changes in a natural complex are most active during the first several years after the development. According to the observations conducted in the north of West Siberia (Pavlov, Sergeev, Skryabin, 1979; "Impact of Territory

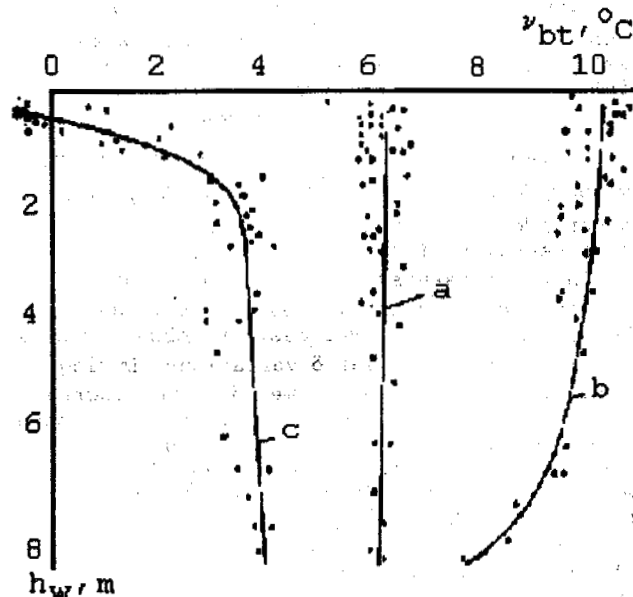


Figure 2. Temperature change in bottom surface  $v_{bt}$  with depth of water  $h_w$  in the lakes of West Yamal, averaged for a freeze-free period: (a), July (b) and annual (c)

Development..." in Proc. of Third Inter.Conf. on Permafrost, 1978), a disturbance or removal of tundra covers leads during a warm period to a decrease in earth's surface albedo by a factor of 1.5 to 2 and more (from 0.2-0.35 to 0.08-0.1) and in turbulent heat-exchange by a factor of 1.4 to 6.3. An increase is observed in evaporation (by 1.3 to 2 times), radiation balance (by 5 to 15%), heat accumulation by a soil (to 60%). This kind of anthropogenic impact in the areas with high-ice soils results in thawing of ice rich soil, accumulation of water and subsidence of the earth's surface. In a few years after a disturbance, a depth of seasonal thawing may become 2 to 4 times greater as compared to the initial value.

Cardinal changes in heat transfer begin when forest vegetation is removed. This is well studied for a taiga zone (Pavlov, 1979). As a rule, in this case a growth is observed in reflecting ability and a drop in radiation balance of the territory. Due to an increase in evaporation, there is a general moisture-circulation decline. On the contrary, heat accumulation by the soil and thawing depth increase.

A great heating effect is observed when a snow cover is affected. In particular, in the Arctic each artificial 10 cm decrease in a height of snow cover (with natural density preserved) causes a reduction of an annual average temperature of soils  $v_0$  by 0.5 to 1.5°C. At a complete removal of snow the heat-circulations increased by a factor of 1.5 to 2 and more.

Table 1. Temperature of air and surface of sandy loam under natural and disturbed conditions according to long-term data from the Yakutian Geocryological Observation Station, °C

Experimental site	January	July	Annual
<u>Air temperature</u>			
In all sites	-42.5	20.2	-10.5
<u>Temperature of soil surface</u>			
In a bare site with natural snow cover	-20.8	23.2	-2.2
In pine forest	-24.3	18.1	-5.1
Soil with turf-vegetation and snow covers removed	-32.9	23.6	-6.0
Ventilated cellar (without heating sources)	-32.4	17.0	-8.4
Ventilated cellar plus a 0.1 m thick foam plastic cover on a soil	-12.4	2.8	-4.3
Snow cover plus a foam plastic cover over soil, of a thickness: 0.07 m	-10.5	8.3	-2.9
0.2 m	-2.8	0.6	-1.8
0.3 m	-2.7	0.6	-1.9
With a polyethylene cover	-12.7	26.7	1.7

The use of artificial covers (e.g. heatisolation and transparent materials), fillings and ventilated cellars may greatly affect the temperature and thawing/freezing of soils. The most complete quantitative estimation of efficiency of surface influence on the thermal regime of the permafrost zone is obtained for Yakutsk. Thus, the temperature of soil surface in a ventilated cellar was estimated for July and annually on the average by 6.6°C and 2.4°C lower as compared to the  $v_s$  values in the bare site (see Table 1). The depth of seasonal thawing  $\xi_{th}$  in the ventilated cellar dropped by 10 to 12% against the natural conditions. When a soil was overlain by an additional foam-plastic layer 0.1 m thick, the  $\xi$  value in the same cellar decreased by a factor of 2.6 to 2.9. On the whole (see Table 2), foam plastic covers have the most considerable effect on soil temperature both in summer and winter, and on the depth of seasonal thawing as compared with other kinds of surface effects. In Yakutsk, the soil covered by a 0.25-0.3m foam-plastic layer thaws during the whole summer not more than to 0.1-0.25 m. A transparent polyethylene cover spread over the soil surface raises the summer temperature of a soil in June-July by 3 to 6°C and may lead to a disconnection of a seasonally frozen layer and permafrost strata. Intensive development of the territory can result in the formation of natural and technical complexes (systems) unstable in thermal term. Their stabilization sometimes takes dozens of years.

Table 2. Dynamics of seasonal thawing of sandy loam under natural and disturbed conditions according to long-term data from the Yakutian Geocryological Observation Station, m

Experimental site	Date	1.06	1.07	1.08	15.09
In an open site with grass cover		0.89	1.40	1.76	1.84
In pine forest		0.57	1.06	1.40	1.53
Soil with turf-vegetation cover removed		0.96	1.38	1.72	1.85
Ventilated cellar (without heating source)		0.42	0.91	1.39	1.76
Ventilated cellar plus a 0.1 m thick foam plastic cover on a soil		0.04	0.12	0.46	0.65
A foam plastic cover over soil, of a thickness: 0.07 m	0.09	0.24	0.75	1.02	
0.2 m	0.03	0.06	0.32	0.51	
0.3 m	0	0.01	0.11	0.16	
With a polyethylene cover		1.02	1.76	2.25	2.24

\*)End of thawing season

#### REFERENCES

- Abel's, G.F. A daily trend of snow temperature and relationship between heat conductivity of snow and its density. Proc., 65p. (Meteorol. Proc., v.IV, Annex to V.72, West Russ. Academy of Sciences).
- Are, F.E. (1974) Heat regime of shallow lakes in the taiga zone of East Siberia (on the example of Central Yakutia). In: Lakes in the Cryolitozone of Siberia. Novosibirsk, Nauka, 98-116.
- Chernyadiev, V.P., A.L. Chekhovskiy A.Y. Stremyakov, V.A. Pakulin. (1984) Prediction of thermal state of soils under development in the northern regions. Moscow, Nauka, 137 pp.
- Gavriliev, R.I., S.V. Eliseev (1970) Thermal properties of peat. In: Methods for Determination of Thermal Properties of Rocks. Moscow, Nauka, 145-153.
- Hoare, R.A. (1968) Thermoline convection in Lake Vanda: Antarctica. J.Geophys.Res., Vol.73, No.2, 607-612.
- Iansson, M. (1904) Om varmeledningsformogangen hos snö. Uppsala. Impact of territory development on heat balance and thermo-moisture regime of soils in the north of West Siberia. (1978) /Moskalenko, N.G., V.B. Slavin-Borovsky, Y.L. Snur, et al./ In: Third Inter. Conf. on Permafrost. Edmonton, Alberta, Canada. Proc., Vol.1, 55-60.
- Iosida, Z. (1955) Physical studies on

deposited snow. Thermal Properties  
Contrib. Inst. Snow. Temperat. Sci.,  
No.7, 19-74.

Kononov, A.A., L.T. Roman (1973) On thermo-  
physical properties of peats. Base  
ments, Foundations and Rock Mechanics.  
No.3, 21-22.

Mandarov, A.A., P.N. Skryabin (1978) Heat  
conductivity of soils in the North  
Yenisey River area and its seasonal dy-  
namics. In: Geothermophysical Studies  
in Siberia. Novosibirsk, Nayka, 74-82.

Pavlov, A.V. (1975) Heat exchange between a  
soil and atmosphere in the northern  
and moderate latitudes of the USSR  
territory. Yakutsk, Book Publ.House,  
302 pp.

Pavlov, A.V. (1979) Thermophysics of Lands  
capes. Novosibirsk, Nauka, 285 pp.

Pavlov, A.V. (1984) Energy-exchange in the  
landscape sphere of the Earth.  
Novosibirsk, Nauka, 256 pp.

Pavlov, A.V. (1981) Thermophysical studies  
of naturel and disturbed landscape  
complexes in the North of the USSR.  
Cold Regions and Technology, 4, 129-  
135.

Pavlov, A.V. Are F.E. (1984) The thermal re-  
gime of thermokarst lakes in Central  
Yakutia. In: Permafrost, Fourth  
International Conference. Final  
Proceedings. National Academy Press  
Washington, D.C.,

Proskuryakov, B.V. (1956) Instructions on  
preparation of a soil for development  
in the winter conditions. Publ.  
Technical Assistance Bureau of  
Gorselstroy Research Institute.

## SOIL CLASSIFICATION AND CLIMATIC ZONES OF ALASKA

C.L. Ping<sup>1</sup> and J.P. Moore<sup>2</sup>

<sup>1</sup>Agricultural and Forestry Experiment Station, University of Alaska Fairbanks  
Palmer Research Center, 533 E. Fireweed, Palmer, Alaska 99645 USA

<sup>2</sup>U.S. Department of Agriculture, Soil Conservation Service  
949 E. 36th Ave. Suite 400, Anchorage, Alaska 99508 USA

Approximately 80 percent of Alaska is underlain by permafrost which controls the soil temperature regime and often the soil moisture regime. Three soil climatic zones in Alaska roughly correspond to the three established permafrost zones. The cryic climatic zone corresponds to the zone free of permafrost, with a maritime climate. Soils in this zone have mean annual soil temperature (MAST) measured at 50 cm depth of  $>0^{\circ}$  to  $8^{\circ}\text{C}$ , and mean annual precipitation (MAP) of 40 to 500 cm. The cryic-pergelic climatic zone corresponds to the zone of discontinuous permafrost, with a strong continental climate. This zone is composed of a complex mosaic of permafrost soils and permafrost-free soils with MAST of  $>-4^{\circ}$  to  $2^{\circ}\text{C}$ , and MAP of 30 to 45 cm. The pergelic climatic zone corresponds to the zone of continuous permafrost, and has MAST from  $-4^{\circ}$  to  $-10^{\circ}\text{C}$ , with MAP of 12 to 50 cm.

### INTRODUCTION

Soil temperature and precipitation and their distribution are important factors in controlling the biological and chemical activities, as well as physical processes such as permafrost formation, in soils. In the U.S., agricultural practices are closely related to soil climate, and thus, soil temperature and soil moisture were recognized as differentiae in *Soil Taxonomy* and used at various categoric levels (Smith, 1986). Mean annual soil temperature measured at 50 cm was introduced as a diagnostic soil property at the suborder, great group, subgroup, and family categoric levels in *Soil Taxonomy* (Soil Survey Staff, 1992). The frigid and cryic temperature regimes share the same range of MAST of  $> 0^{\circ}\text{C}$  to  $8^{\circ}\text{C}$ ; the former have a mean summer soil temperature (MSST) at least  $5^{\circ}$  warmer than the mean winter soil temperature (MWST). The pergelic soil temperature regime is defined as MAST of  $0^{\circ}$  or less regardless of the presence of permafrost. As defined in *Soil Taxonomy*, permafrost is a substance in which the temperature is perennially at or below  $0^{\circ}\text{C}$ , whether the consistency is very hard or loose. Soils with permafrost have pergelic temperature regimes [mean annual soil temperature (MAST)  $<0^{\circ}\text{C}$ ] and are placed in pergelic subgroups. It is important to note that pergelic and permafrost are not synonymous. A soil with MAST  $<0^{\circ}\text{C}$  at the 50 cm depth may not have a thermal condition perennially equal to or below  $0^{\circ}\text{C}$ . Permafrost soils are encountered consistently in the zone of continuous permafrost of northern arctic Alaska and inconsistently in the zone of discontinuous permafrost of interior subarctic Alaska, but not in the coastal zone of southern Alaska (Péwé, 1975).

In a general overview, soils from the northern arctic region that currently classify

in pergelic subgroups have permafrost within 1 m. This is true regardless of the thickness of the surface organic mat. Soil temperature and permafrost are the dominant soil properties affecting land use and management practice. Management is usually directed at preserving the current status of permafrost.

In the interior subarctic region, a dynamic relationship exists between the surface organic mat thickness, soil temperature, and depth to permafrost (Viereck, 1973). Many soils, under climax native vegetation, have a thick layer of mosses and organic matter on the surface. This organic mat acts as an effective insulator against changes in soil temperature. The MAST is perennially  $<0^{\circ}\text{C}$  in these soils. If the surface organic mat is disturbed, either by technogenic activities, or more commonly by wildfire, the soil temperature will begin to rise and the permafrost table will lower (Viereck, 1973; Foote, 1976). If the disturbance is significant, MAST may, within a few years, rise above  $0^{\circ}\text{C}$  and the permafrost table recede to well below 1 m (Moore and Ping, 1989). With natural succession of the vegetation toward climax, the surface organic mat may reestablish and thicken, and the MAST may decrease below  $0^{\circ}\text{C}$  again.

The current definitions and taxonomic keys in *Soil Taxonomy* (Soil Survey Staff, 1992) do not adequately address many of the cryic and pergelic soils of high latitudes. As stated throughout *Soil Taxonomy and Conversations in Soil Taxonomy* (Smith, 1986), the existing concepts of soils of high latitudes are tentative and need to be revised as research continues. On-going research and progressive soil surveys are bearing out these statements. The use of current *Soil Taxonomy* concepts on many high-latitude soils and even high-altitude soils (Bockheim and Burns, 1991) with perma-



frost does not adequately aid the transfer of soil knowledge. As pointed out by Moore et al. (1992), nearly 65 percent of the soils in northern Alaska can be covered by only two subgroups, either Periglacial Cryaquepts or Ruptic-Histic Periglacial Cryaquepts. The purpose of this paper is to review and summarize current data on soil climate in Alaska and to formulate soil climatic zones. These climatic zones would aid the improvement of soil classification in high latitudes.

#### METHOD

The soil climate data are reviewed from published journal articles, professional papers, government documents, and unpublished data of on-going research projects. The climatological data (air temperature, precipitation, and growing season) are primarily from *Climatological Data-Annual Summary* (NOAA, 1990). The primary sources for thickness and temperature of permafrost are from that of Péwé (1975) and Lachenbruch et al. (1989). The primary sources of soil temperature are from that of published data of Ping (1987) and unpublished data from on-going soil temperature and wet soils monitoring projects of Ping. The boundaries of soil climate zones are approximated with reference to Lachenbruch et al. (1989), Washburn (1973), Péwé (1975), and NOAA (1990).

#### RESULTS AND DISCUSSION

##### Periglacial Soil Climatic Zone

This zone generally corresponds to the zone of continuous permafrost which includes the Arctic Coastal Plain, the Arctic Foothills, and the Brooks Range (Péwé, 1975). The area has strong arctic influence. The MAAT is generally less than  $-8^{\circ}\text{C}$ , and as low as  $-12^{\circ}\text{C}$  in Barrow (Owenby and Ezell, 1992). The MAP ranges from 12 to 20 cm along the Arctic Coast to 50 cm in the Brooks Range. Permafrost thickness ranges from 200 to 650 m on the coastal plain, but decreases to 280 to 310 m in the foothills of the Brooks Range (Brown et al., 1980; Lachenbruch et al., 1989; Péwé, 1975; and Williams, 1970). Lachenbruch et al. (1989) estimated the long-term mean surface temperature ( $0^{\circ}$ ) of this zone based on 21 exploratory drilling wells. The MAST of permafrost soils are thus estimated to be  $-7^{\circ}$  to  $-9^{\circ}\text{C}$  on the Arctic Coastal Plain, and  $-4^{\circ}$  to  $-7^{\circ}\text{C}$  in the Foothills and  $-4^{\circ}$  to  $-5^{\circ}\text{C}$  along the northern slopes of the Brooks Range (Lachenbruch et al., 1989; Osterkamp, 1988; Péwé, 1975; and Williams, 1970). Therefore, the MAST in this periglacial zone ranges from  $-4^{\circ}$  to  $-10^{\circ}\text{C}$ .

In this zone, the thermal balance of the soil is maintained, to a major degree, by the insulating properties of the surface organic mat. Disturbance of the organic mat will result in an increase in soil temperature. As a result, the active layer will thicken and the permafrost table will lower. Rarely, however, will the permafrost table lower completely below the soil profile. The permafrost table will remain as an impermeable layer usually within 1 m. Water released by the thickened active layer during thaw will perch on the permafrost table. Barrow is located at the northern tip of this zone, with

the lowest MAP of 12 cm, and water budget is less than 0.1 cm (Bovis and Barry, 1974). Yet soils in the Barrow area have an aquatic moisture regime because the soils are saturated much of the growing season (Soil Survey Staff, 1992) due to the presence of the permafrost table impeding internal drainage. Therefore, many shallow lakes dominate the coastal landscape. Any lowering of the stable permafrost tables is a major concern in engineering interpretation. The primary land management goal is to insulate the permafrost against any change in heat and thus to maintain a stable thermal regime (Linell and Tedrow, 1981; Johanson, 1990).

##### Cryic-Periglacial Soil Climatic Zone

This zone corresponds to the zone of discontinuous permafrost according to Péwé (1975), and it lies mainly in interior Alaska, bounded by the Brooks Range on the north and the Alaska Range on the south. In this climate zone, permafrost soils are interspersed with permafrost-free soils. The relative proportion of permafrost soils decreases from north to south throughout the zone. The southern boundary of the Zone of Discontinuous Permafrost is approximated by the  $0^{\circ}\text{C}$  mean annual air isotherm (Péwé, 1975). This zone has a strong continental influence, and the soil climate is transitional between cryic and periglacial. The MAAT ranges from  $0^{\circ}\text{C}$  to  $-7^{\circ}\text{C}$ , and the MAP ranges from 17 to 45 cm along a south to north gradient (NOAA, 1990). The recorded permafrost temperatures at 15 to 25 m at Fairbanks, Glennallen, Kuskokwim Delta, and near Nenana are, respectively,  $-0.9^{\circ}\text{C}$ ,  $-1.5^{\circ}\text{C}$ ,  $-0.1^{\circ}\text{C}$ , and  $-0.3^{\circ}\text{C}$ , and the thickness of permafrost in this zone ranges from 3 m to 40 m (Péwé, 1975). Williams (1970) compiled data from well-drilling logs and found the permafrost temperature ranges from  $-0.3$  to  $-1.2^{\circ}\text{C}$  in the Interior. In similar latitudes to interior Alaska, Burns and Smith (1988) measured the MAST of six sites near Mayo, Yukon Territory ranging from  $-0.5^{\circ}$  to  $-1.5^{\circ}\text{C}$  with permafrost thickness of 74 to 110 m. In general, the temperature of permafrost at 15 to 25 m ranges from  $0^{\circ}\text{C}$  along the southern boundary to less than  $-5^{\circ}\text{C}$  along the northern boundary of this zone (Péwé, 1975).

The MAST of an undisturbed permafrost soil at Fairbanks is  $-1.3^{\circ}\text{C}$  (Ping, 1987), which is  $0.4^{\circ}\text{C}$  lower than that of the receding permafrost. The MAST of another permafrost soil on the Copper River Plateau is  $-1.0^{\circ}\text{C}$ , but a few years after land clearing, the MAST rose to  $2^{\circ}\text{C}$  and the soil became well drained. (Clark and Kautz, in press). In areas like interior Alaska, slope aspect plays an important role in the occurrence of permafrost (Péwé, 1954; Rieger et al., 1963). The south facing slopes are generally well drained and free of permafrost, and the north facing slopes are usually underlain by permafrost with thickness ranging from as little as a few centimeters near the ridge tops to more than 80 m in the valley bottom (Osterkamp, personal communication). Kawosaki and Osterkamp (1988) measured MAST of  $1^{\circ}\text{C}$  on south facing hillsides and  $-3^{\circ}\text{C}$  in bottomland areas. The MAST on some sites north of Fort Yukon are less than  $-1^{\circ}\text{C}$  with MAST of  $14^{\circ}\text{C}$  or more indicating active layer deeper than 50 cm (Ping, unpublished data). The permafrost-free soils in this zone have MAST

above 0°C. Thus, the MAST of this zone is estimated to range from >-4 to 2°C.

The thermal balance of the soils is maintained primarily by the insulating properties of the surface organic mat. However a dynamic relationship exists between the surface organic mat thickness, soil temperature, and depth to permafrost as described by Moore and Ping (1989). Any disturbance of the organic mat, naturally occurring such as wildfire, or man-induced such as cultivation, can result in sufficient soil temperature increase (Ping, 1987; Kallio and Rieger, 1969) to lower the permafrost table 2 m or more below the soil surface. Water released from the active layer during thaw often will drain freely, and the MAST will rise above 0°C. In areas with permafrost, the active layer is often saturated during the growing season, and has an aquic soil moisture regime. Areas free of permafrost usually have well-drained soils, and a udic soil moisture regime (Soil Survey Staff, 1992). Interior Alaska has summer storms which prevent the soils from drying out during the growing season.

#### Cryic Soil Climatic Zone

This climatic zone corresponds to the sporadic permafrost and permafrost-free zones as defined by Pévé (1975). This is the southern coastal zone having strong marine influence, including southeastern Alaska, lowlands of the southcentral Alaska mountains, the Cook Inlet-Susitna Lowland, the Alaska Peninsula, and southwestern islands. These areas are generally free of permafrost except at high altitudes and on ice fields. The northern boundary of this zone corresponds to the MAAT of the -2°C isotherm based on data from Pévé (1975) and from climatological data (NOAA, 1990). Soils in this zone have a cryic soil temperature regime (Ping, 1987; Rieger, 1983; Smith et al., 1964). Soils with forest cover generally have low summer soil temperatures, but seasonal frost penetration is as little as a few centimeters due to the insulating effect of snow cover (Rieger, 1973). Some soils in this zone, due to localized strong winds which remove the snow cover, have deeper frost penetration. The recorded MAST ranges from 0° to 6°C (Ping, 1987; Smith et al., 1964; Alexander, 1991). The MAAT in this zone ranges from -2° to 8°C. Most of this zone has a udic soil moisture regime with MAP ranging from 40 to 150 cm. In southeast Alaska and along the Gulf of Alaska where the MAP ranges from 150 to 450 cm, the soils have a perudic moisture regime due to precipitation exceeding evapotranspiration in all months of most years (Soil Survey Staff, 1992).

#### CONCLUSION

Based on extent of permafrost, soil temperature and soil moisture regimes and other climatic data, Alaska can be provisionally divided into three soil climatic zones (Fig. 1), and the soil climate of selected areas and sites are summarized in Table 1.

(1) Pergelic zone. This zone includes the Arctic Coastal Plain, the Arctic Foothills, and the northern slopes of the Brooks Range. The MAAT ranges from -8°C to <-12°C, and MAP ranges from 12 to 50 cm. The esti-

mated MAST ranges from -4° to -10°C. It has a pergelic soil temperature regime and a predominantly aquic soil moisture regime.

(2) Cryic-pergelic zone. This climatic zone is transitional between cryic and pergelic. The MAP ranges from 17 to 45 cm and the MAAT ranges from -7° to -2°C. The MAST ranges from >-4° to 2°C. It is dominated by aquic and udic moisture regimes.

(3) Cryic zone. This zone is free of permafrost with MAP ranging from 45 to 450 cm and MAAT ranging from -2° to 8°C. The MAST ranges from >0° to 8°C. The dominant moisture regime is udic where the MAP is less than 150 cm, and perudic where the MAP is more than 150 cm.

Soil climatic zones of areas with permafrost such as Alaska are not adequately addressed in *Soil Taxonomy*. The recent focus on the effects of global change on biogeochemical soil processes in relation to environmental quality and long-term ecological implications certainly has created more demand for the inventory and research of permafrost soils. A well-defined soil climatic zone would improve the soil classification system, which would in turn facilitate soil-based technology transfer.

Table 1. Soil climate of selected areas and sites in Alaska.

Area/Site	Lat. °N	Elev. m	MAP cm	MAAT °C	MAST+ °C	MSST °C	Source of MAST
<u>Pergelic zone</u>							
Arctic coastal plain	69°30'	—	18-22	-12.8 to -10.6	-5.5 to -9.8	—	(1)
Barrow	71°16'	9	12	-11.5	-7.7 to -7.3	—	(1), (10)
Arctic Foothills	68°-69°	—	14-27	-11.1 to -9.0	-7.3	—	(1), (6)
Anaktuvuk Pass	68°9'	1800	30	-10.3	—	—	(2)
Brooks Range	67°-69°	—	30-50	-6.9 to -5.9	-4.3 to -5.1	—	(9)
Umiat	69°22'	81	15	-12.0	-6.5	—	(2)
<u>Cryic-Pergelic zone</u>							
Interior	62°-67°	—	17-45	-6.9 to -3.7	—	—	
Fairbanks	64°51'	135	29	-2.6	-1.3 (V) 2.1 (D)	9.5	(3)
Copper River	61°48'	400	37	-3.1	-1.5 (V) 2.4 (D)	8.6	(5)
Fort Yukon	66°35'	127	17	-6.3	-1.3	—	(8)
<u>Cryic zone</u>							
Cook Inlet							
Palmer	61°36'	68	38	1.3	1.4 (V) 3.0 (D)	13.1	(3)
Juneau	58°22'	4	135	4.4	6.0	—	(4)
Sitka	57°03'	20	250	5.8	—	—	(7)

(1) Lachenbruch et al., 1989; (2) Rieger et al., 1979; (3) Ping, 1987; (4) Alexander, 1991; (5) Clark and Kautz, in press; (6) Osterkamp, 1988; (7) NOAA, 1990; (8) Ping, unpublished; (9) Péwé, 1975; (10) Brown et al., 1980.

+ (V) Forested; (D) Cleared ground

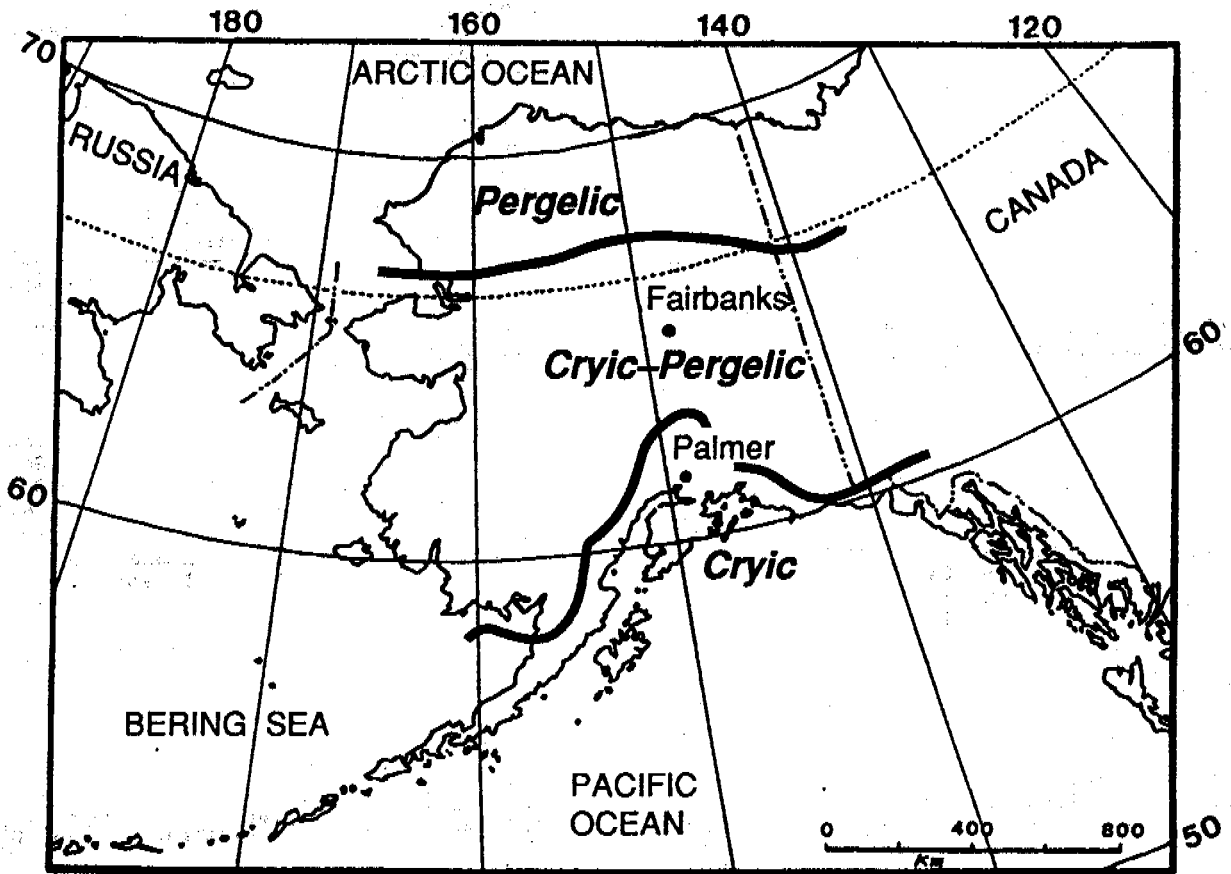


Figure 1. Soil climatic zones of Alaska.

## REFERENCES

- Alexander, E.B. 1991. Soil temperatures in forest and muskeg on Douglas Island; south-east Alaska. *Soil Survey Horizon* 32:108-116.
- Bockheim, J.G., and S.F. Burns. 1991. Pergelic soils of the western contiguous United States: distribution and taxonomy. *Arctic and Alpine Res.* 23:206-212.
- Bovis, M.J., and R.G. Bary. 1974. A climatological analysis of north polar desert areas, p. 23-32. In T.L. Smiley and J.H. Zuberger (eds.) *Polar Deserts and Modern Man*. The University of Arizona Press. Tucson, AZ, p. 178.
- Brown, J., K.R. Everett, P.J. Webber, S.F. MacLean Jr., and D.F. Murray. 1980. The coastal tundra at Barrow, Alaska. p. 1-29. In J. Brown, P.C. Miller, L.L. Tieszen, and F.L. Bunnell (eds.) *An arctic ecosystem: the coastal tundra at Barrow, Alaska*. The Institute of Ecology. Dowden, Hutchinson & Ross, Stroudsburg, Pennsylvania.
- Burns, C.R., and C.A.S. Smith. 1988. Observations of the "thermal off-set" in near-surface mean annual ground temperatures at several sites near Mayo, Yukon Territory, Canada. *Arctic* 41:99-104.
- Clark, M.H., and D. Kautz. (In press.) Soil survey of the Copper River Area, Alaska. USDA-SCS. U.S. Government Printing Office, Washington, D.C.
- Foot, M.J. 1976. Classification, description, and dynamics of plant communities following fire in the taiga of Interior Alaska. Fire effects study. USDA Forest Serv., Inst. Northern Forestry, Fairbanks, AK.
- Johansen, N.J. 1990. Engineering problems associated with permafrost. In *Proceedings of Western Regional Cooperative Soil Survey Conference*, 511 N.W. Broadway, Portland, OR.
- Kallio, A., and S. Rieger. 1969. Recession of permafrost in a cultivated soil of Interior Alaska. *Soil Sci. Soc. Am. Proc.* 33:430-432.
- Kawasaki, K., and T.E. Osterkamp. 1988. Mapping shallow permafrost by electromagnetic induction-practical considerations. *Cold Region Science and Technology* 15:279-288.
- Lachenbruch, A.H., Sass, J.H., Lawyer, L.A., Brewer, M.C., Marshall, B.V., Munroe, R.J., Kennelly, J.P., Jr., Galanis S.P., Jr., and Moses, T.H., Jr. 1989. Temperature and depth of permafrost on the Arctic Slope of Alaska, in Gryc, G., ed., *Geology and exploration of the National Petroleum Reserve in Alaska, 1974 to 1982*: U.S. Geological Survey Professional Paper 1399, p. 645-656.
- Linell, K.A., and J.C.F. Tedrow. 1981. *Soil and permafrost surveys in the Arctic*. Clarendon Press, Oxford. 263 pp.
- Moore, J.P., D.K. Swanson, and C.L. Ping. 1992. Warm permafrost soils in interior Alaska. In *Proceedings, First International Conference on Cryopedology*, Pushchino, Moscow Region, Nov. 10-14, 1992. Russian Academy of Science. Moscow, Russia. (in press).
- Moore, J.P., and C.L. Ping. 1989. Classification of permafrost soils. *Soil Survey Horizons* 30:98-104.
- NOAA. 1990. *Climatological Data - Annual Summary, Alaska, Vol. 76, No. 13*. U.S. Department of Commerce, National Climatic Data Center. Asheville, NC.
- Osterkamp, T.E. 1988. Permafrost temperatures in the Arctic National Wildlife Refuge. *Cold regions Sci. and Technol.* 15:191-193.
- Owenby, J.R., and D.S. Ezell. 1992. Monthly station normals of temperature, precipitation, and heating and cooling degree days, 1961-90. *Climatography of the U.S. No. 81*. U.S. Dept. of Commerce. NOAA - National Climatic Data Center. Asheville, North Carolina.
- Péwé, T.L. 1954. Effect of permafrost on cultivated field, Fairbanks, Area, Alaska. U.S. Geol. Survey Bull. 989-F. U.S. Government Printing Office, Washington, D.C.
- Péwé, T.L. 1975. Quaternary geology of Alaska. U.S. Geol. Survey Prof. paper 835. U.S. Government Printing Office, Washington, D.C.
- Ping, C.L. 1987. Soil temperature profiles of two Alaskan soils. *Soil Sci. Soc. Am. J.* 51:1010-1018.
- Rieger, S. 1973. Temperature regimes and classification of some well-drained alpine soils in Alaska. *Soil Sci. Soc. Am. Proc.* 37:806-807.
- Rieger, S. 1983. *The genesis and classification of cold soils*. Academic Press, New York.
- Rieger, S., J.A. DeMent, and D. Sanders. 1963. Soil survey of Fairbanks Area, Alaska. USDA-SCS, U.S. Government Printing Office, Washington, D.C.
- Smith, G.D., F. Newhall, L.H. Robinson, and D. Swanson. 1964. Soil-temperature regimes-Their characteristics and predictability. USDA-SCS-TP-144. U.S. Government Printing Office, Washington, D.C.
- Smith, G.D. 1986. *Conversations in soil taxonomy - Original transcriptions of taped conversations by Guy D. Smith*. In T.R. Forbes (ed.) *The Guy Smith interviews: Rationale for concepts in Soil Taxonomy*, Cornell Univ., Ithaca, NY.
- Soil Survey Staff. 1992. *Keys to Soil Taxonomy*. SMSS Technical Monograph No. 19, 5th ed. Pocahontas Press, Inc., Blacksburg, VA.
- Viereck, L.A. 1973. Wildfire in the taiga of Alaska. *Quat. Res.* 3:465-495.
- Washburn, A.L. 1973. *Periglacial processes and environments*. St. Martin's Press, New York. (320 pp.).
- Williams, J.R. 1970. Ground water in the permafrost regions of Alaska. Geological survey professional paper 696. U.S. Government Printing Office, Washington, D.C.

## DILATOMETRY OF POROUS LIMESTONES UNDERGOING FREEZING AND THAWING.

A. PISSART<sup>1</sup>, A. PRICK<sup>1-2</sup>, J. Cl. OZOUF<sup>3</sup>

<sup>1</sup>Laboratoire de Géomorphologie et de Géologie du Quaternaire,  
Université de Liège, Belgium

<sup>2</sup>Aspirante du Fonds National Belge de la Recherche Scientifique

<sup>3</sup>Centre de Géomorphologie du CNRS, Caen, France.

The dilatometrical behaviour of calcareous rocks cylinders was measured in diameter and in length during freeze-thaw cycles. These measurements have shown intricate and non-isotropic variations in the dimensions of the rocks which are in connection with migrations of unfrozen water within the samples at negative temperatures. These migrations can be regarded as responsible for contractions instead of the global expansion which was previously expected. These experiments stress the importance of factors which have been acknowledged by many authors, ie the water content in the sample, its lithology, the rate of cooling and the slight alterations of the experimental device.

### INTRODUCTION

A very important dilatometric research on materials undergoing freezing and thawing was published by Thomas (1938). He has observed complicated curves of variations in length of some rocks, bricks and tiles samples when they are freezing. He tried to explain these variations but had some difficulties to understand why some wet materials undergo contraction under freezing. He explained that inside these samples, the pressure given by the newly-formed ice induces liquefaction for the ice in favourable position, and that this process promotes intrusion of water into unfilled pores.

Lehmann (1955) has described a similar contraction of wet bricks under freezing. His observations became explicable in the papers of Powers and Helmuth (1953) and Powers (1958) on the dilatometric variations of cement pastes (figure 1). They have shown that, if microscopic bubbles are inside the cement pastes (the bubbles must be so numerous that they are separated by layers of paste of only a few thousandths of an inch thick), the freezing produces shrinkage rather than dilatation. And they proposed to explain this shrinkage by transfer of water from the paste to the air bubbles.

This migration of water by cryosuction gives an explanation for some part of the dilatometric curves recorded in experiments carried out with porous limestone. With these explanations, the dilatometric curves enable one to see what happens during the freezing of wet material and the process of gelifraction.

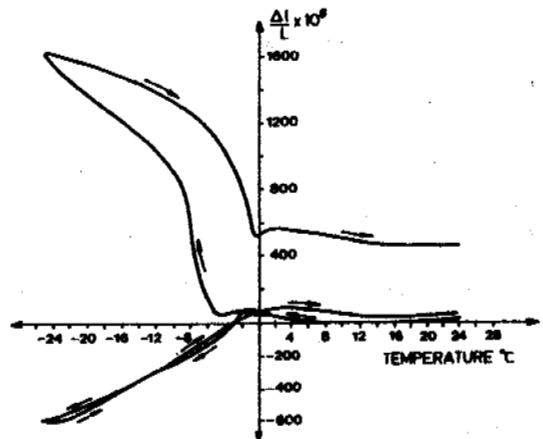


Figure 1 : Dilatometric curves of cement pastes - Upper curve shows dilatation produced in paste containing no air bubbles. Lower curve shows same paste with entrained air.  $DL/L$  = length change in millionths (Powers, 1958).

### OUR MEASUREMENTS

Figure 2 shows the experimental device with which we have made dilatometric measurements. The experiment samples are cylinders of limestone  $\pm 10$  cm in length and 4 cm in diameter. The main peculiarity of our system is that we not only measure the variations in length of cylindrical sample in one place but in several locations : in the central point of the circular base, near the border of the same base, and also on two points which are facing each other on the sides of the cylinder. With all these measurements, we register not only

the variations in length of the cylinder but also its variations in diameter.

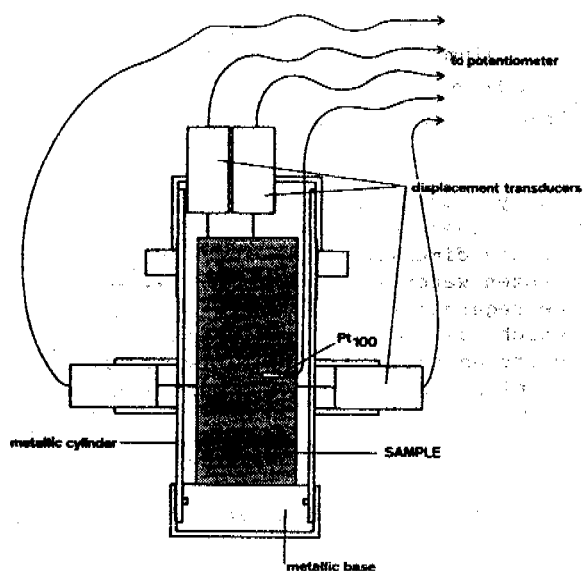


Figure 2 : Experimental device used in our experiments.

The experiments that we present below were made with two kinds of rock : the stone of Caen which is a bathonian bioclastic limestone and a turonian "Tuffeau" called Brézé. The porosity of the stone of Caen is between 32 and 33,2 %; for the Brézé, the value is between 46,6 and 48 %.

The measurements were made with linear electronic displacement transducers made by Schlumberger (Sangamo) which give variations in length with an accuracy of 1 mm or less. The bases of the studied samples were stuck inside a steel cylinder on which the displacement transducers were set. The dilatation curves that we present below were corrected for the coefficient of expansion of the steel cylinder.

#### Results of our Measurements

The interpretations of dilatometric curves obtained during freezing and thawing were illuminated by the results of dilatometric measurements made on the same calcareous rocks during dessiccation experiments (Pissart and Lautridou, 1984; Hamès et al., 1987). In these papers we have shown that important changes in the length of cylinders of the same rocks occur when the water content fluctuates. Variations in length are at the highest when the water moves in or out of the thinner fissures of the rocks. This result was demonstrated when we observed that the loss of

a very small amount of water gives in samples with very little water an important dilatometric shrinkage. This contraction in length was by far less important when the sample held more water and lost the same weight by dessiccation.

The presentation of dilatometric curves that we give below will demonstrate the influence of the water content, of the porosity of the rock, of the slight alterations of the experimental device and the rate of cooling, all factors which are well known as controlling gelifraction processes.

#### Influence of the Water Content inside the Sample

We shall see the effect of variations in the water content of Brézé samples through the comparison of dilatometric curves recorded for a cylinder which contains 56,8 g of water (which represents 98 % of the full saturation) with a cylinder which held 42,1 g of water that is to say 72 % of its full saturation. The rate of change in temperature during both experiments was 2 °C/h.

Figure 3 gives a view of the variation in length and in diameter observed for the sample with 98 % of his full saturation. On this graph, we recognize the successive phases :

1. Contraction of 20 mm in length and dilatation of 10 mm in diameter when the sample goes from 20 °C to 0 °C.
2. Great increase in length and in diameter when the sample remains at 0 °C (zero curtain).
3. Small increase in length when the temperature of the sample goes down until -10,7 °C; the diameter increases during a longer time.
4. Low shrinkage in length and in diameter during the 16 hours when the sample remains at a temperature of -12,5 °C.
5. Important contraction during the warming until 0 °C and the zero curtain.
6. Increase in length and in diameter when the warming occurs above 0 °C.

These different parts of the curve may probably be explained by the processes described now, taking into account the numbers given above :

1. Thermic contraction and migration of water inside the sample by the formation of a gradient of temperature inside the cylinder.
2. Freezing of the free water in the rock almost at the full saturation.
3. The adsorbed water freezes at temperatures below 0 °C.
4. Unfrozen water remains at -12,5 °C. Some of this water is moving inside of the sample to pores which are void.

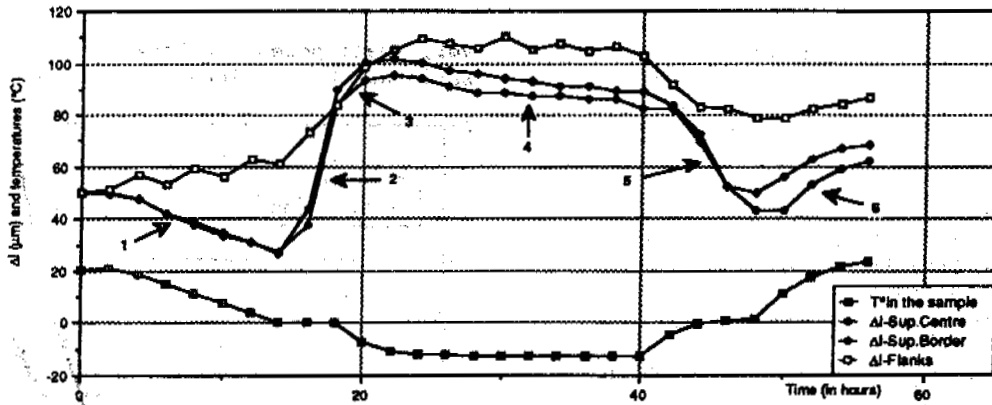


Figure 3 : Dilatometric curves recorded for a cylinder of "tuffeau de Brézé" with 98 % of the full saturation. Rate of cooling 2 °C/h. The numbers indicate the different phases described in the text.

Legend :  $T^\circ$  in the sample = temperature measured with Pt100 inside the sample;  $\Delta l$  = dilatometric variations in  $\mu\text{m}$ ; Sup.Centre = measure on the central point of the superior face of the cylinder; Sup.Border = measure on the border of the superior face of the cylinder; Flanks = sum of the measures made on the sides of the cylinder.

All our dilatometrical measurements are put to the initial value of 50 in order to facilitate the comparison between curves.

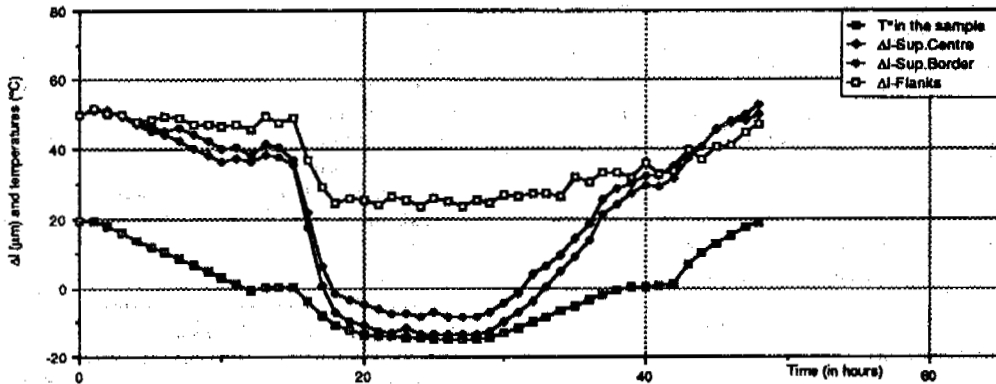


Figure 4 : Dilatometric curves recorded for a cylinder of "tuffeau de Brézé" with 72 % of the full saturation. Rate of cooling -2 °C/h. See legend below figure 3.

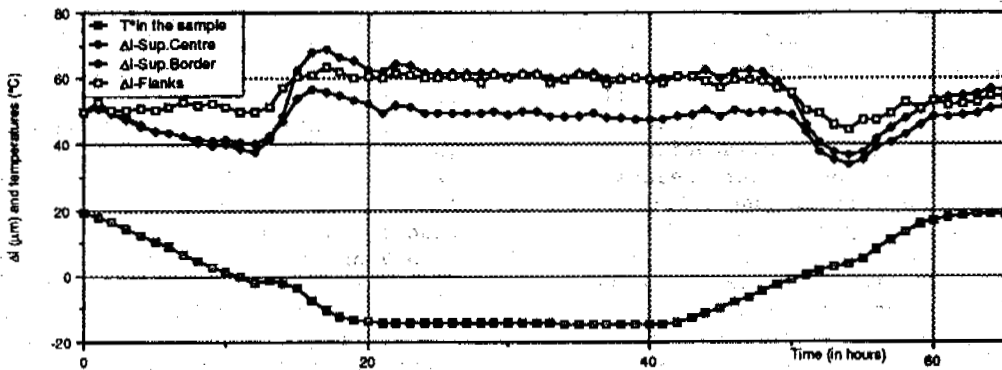


Figure 5 : Dilatometric curves recorded for a cylinder of stone of Caen with 77 % of the full saturation. Rate of cooling -2 °C/h. See legend below figure 3.



5. During the warming when the temperature remains below 0 °C, the ice which is under pressure and which is in contact with some salts begins to melt or allows a shrinkage of the rock.

6. The water which comes from the melting of the ice goes back into the thinner pores of the rock and gives a dilatation. At the same time a thermal dilatation occurs.

With 72 % of the full saturation, below 0 °C, the dilatometric curve becomes completely different (figure 4) :

The retraction of the sample above 0 °C is related mainly to the thermal coefficient of dilatation. The freezing of the free water which occurs at 0 °C (zero curtain) did not give any dilatation because there were enough voids without water inside the sample to accept the change in volume of the freezing water without a significant increase in pressure. After the zero curtain, the sample undergoes a very important retraction which is the same phenomenon as the one described by Thomas (1938) that we have mentioned in the introduction of this paper. The variation in diameter is similar to the variation in length if it is remembered that the length of the studied cylinder is 10 cm and its diameter 4 cm. By comparison with the interpretation of Powers (1958) we believe that this retraction results from the migration of water from the very thin fissures present in the rock to the nearest empty larger pores where ice crystals are growing.

A slow migration of water goes on when the temperature oscillates around -15 °C.

During the warming, the movement of the water going back into the thin fissures is the main reason why dilatation occurs.

#### Influence of the Porosity of the Rock

With a similar amount of water (77 % of the full saturation), the curves recorded with a cylinder of stone de Caen (figure 5) do not show the shrinkage we have seen under the same conditions in the sample of Brézé (figure 4). As soon as the freezing begins (moment clearly visible on the temperature curve by the small increase in temperature which occurs inside the sample), we observe a small dilatation which continues until the temperature reaches -1 °C. Below this temperature a contraction occurs and this probably appears when the migration of water from the smaller pores and fissures exceeds the dilatation related to the increase in volume by water freezing.

The different responses of the Caen and Brézé stones must be seen in connection with the characteristics of porosity of the two rocks (figure 6). The Brézé stone has a great number of pores smaller than 0,05 mm. These

very small pores are known to induce important shrinkage by dessiccation.

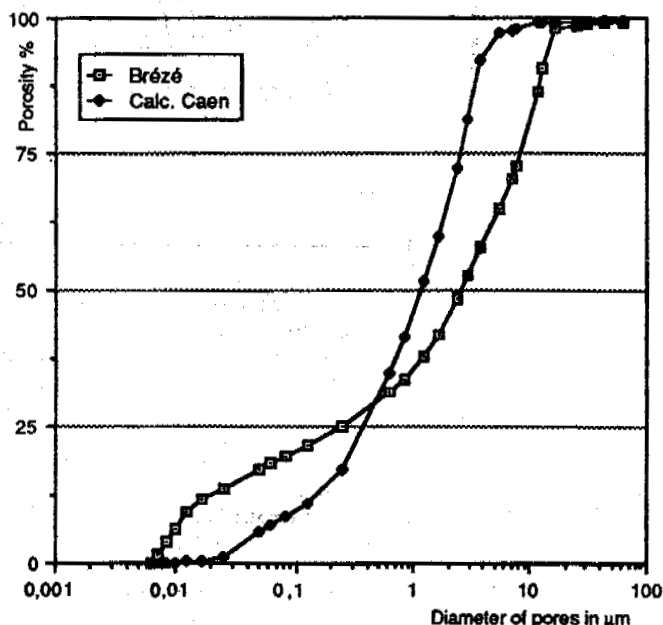


Figure 6 : Distribution of the pore size in stones of Caen and in "tuffeaux de Brézé" as they are measured with a mercury porosimeter. The percentage of the pores under 0,15 mm is higher in the "Brézé" than in the stone of Caen. The difference between these two limestones is greater for the pores below 0,025 mm.

#### Significant Influence of Slight Alterations of the Experimental Device

The experiment presented in figure 5 like the other ones we have presented till now had occurred in our refrigerator in which there is no ventilation system. For the experiment shown in figure 7, an electric fan was set inside the cold room to mix the air during the entire experiment. These cooling conditions, with a cold air current which blows horizontally, are different from the conditions used for the previous experiments, and consequently we notice differences in the dilatometrical behaviour.

We had seen on figure 5 a pronounced dilatation in length and in diameter in connection with the freezing of free water. Figure 7 shows a dilatometrical response in length which is different from that in diameter, if we remember that the length of the cylinder is 10 cm, and its diameter, 4 cm. The behaviour shown on this figure is very different from the one observed on figure 5. This seems normal since it is known that these behaviours are related to different water

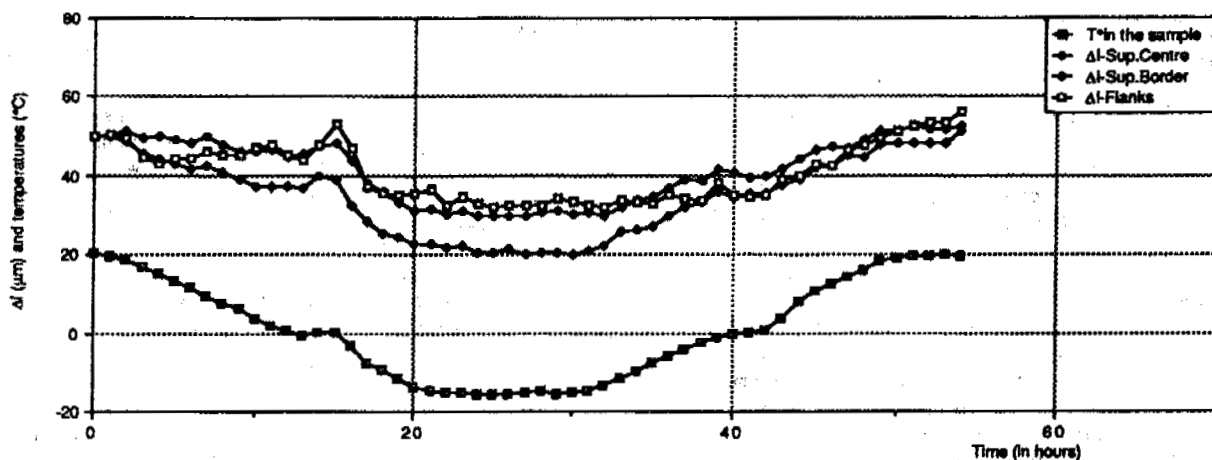


Figure 7 : Dilatometric curves for a stone of Caen with 77 % of the full saturation. Rate of cooling  $-2\text{ }^{\circ}\text{C/h}$ . An electric fan has mixed the air in the refrigerator during the entire experiment. See legend below figure 3.

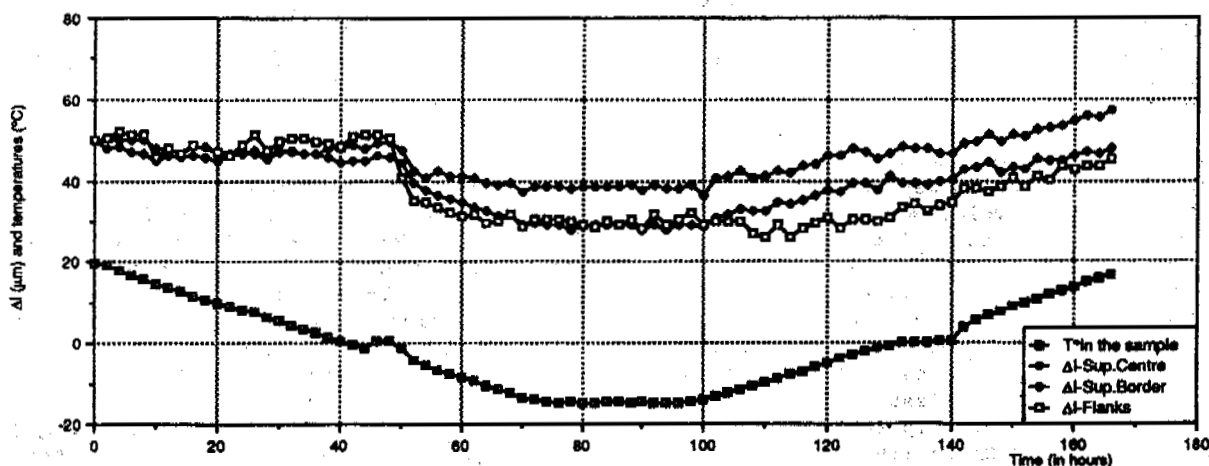


Figure 8 : Dilatometric curves for a stone of Caen with 72 % of the full saturation. Rate of cooling  $-0,5\text{ }^{\circ}\text{C/h}$ . See legend below figure 3.

migrations induced by different directions of the freezing front propagation.

Measurements of the distribution of  $\text{H}_2\text{O}$  inside a cylinder of Brézé frozen under the same conditions have shown that some water was moving from the center of the cylinder to the sides. This migration of water, induced by the location of a lateral gradient of temperature during the freezing explains the anisotropic character of the dilatation of the sample. These observations show clearly that it is impossible to understand the dilatometric response of a rock if measurements are not made in different directions.

#### Influence of the Rate of Cooling

The comparison of the dilatometric curves given on the figures 5 and 8 illustrates the influences of the rate of cooling of the samples. With a rate of  $2\text{ }^{\circ}\text{C/h}$  a dilatation was observed during the freezing. With an amount of water that is not very different (72 % against 77 %), the experiment shown on figure 8 with a rate of cooling of  $0,5\text{ }^{\circ}\text{C/h}$  provokes only a contraction of the sample. It seems that with a very slow freezing, the gradient of temperature was not important enough to give migrations of water and a dilatation. However, a slow freezing allows

the migration of water from the narrow fissures to the large pores where it freezes.

#### CONCLUSIONS

These experiments show the complexity of the dilatometric variations of wet samples of rocks undergoing freezing and thawing. The increase in volume related to the transformation of water in ice is the main mechanism when the sample is close to saturation; it becomes less important when the voids in the rocks are not filled with water. In this case, the migration of water becomes the main process. Transformation of water in ice gives a dilatation of the rock; migration of water from the small pores and fissures to larger empty pores gives a contraction of the rock.

It has been known for many years that the factors we have discussed here, i.e. the content of water in the sample, the distribution of the porosity in the rock, the influence of slight alterations of the experimental device and the rate of freezing are important parameters in the gelification of the rocks.

Here, we have shown that these influences may be seen on dilatometric curves and that their role in gelification may be approached in a single freezing cycle. We believe that the dilatometric research will become an important method to analyze the gelification process in different materials. Because it clearly shows the influence of the displacement of water inside the rocks which correspond to a process of desiccation and hydration in the smallest fissures, the dilatometric research may help answer the aggressive question of White (1976): "Is frost action really only hydration shattering?".

#### REFERENCES

- Hames, V., Lautridou, J.-P., Ozer, A. & Pissart, A. (1987) Variations dilatométriques de roches soumises à des cycles "humidification - séchage". *Géographie Physique et Quaternaire*, 41 (3), 345 - 354.
- Lehmann, H. (1955) Die Beurteilung der Frost Beständigkeit grobkeramischer Erzeugnisse mit Hilfe dilatometrischer Messungen. *Ziegelindustrie*, 8 (15), 569-574.
- Pissart, A. & Lautridou, J.-P. (1984) Variations de longueur de cylindres de pierre de Caen (calcaire bathonien) sous l'effet de séchage et d'humidification. *Zeitschrift für Geomorphologie N. F.*, suppl. Bd. 49, Berlin - Stuttgart, 111 - 116.
- Powers, T.C. & Helmuth, R.A. (1953) Theory of volume changes in hardened Portland Cement Paste during freezing. *Materials and Construction*, 285-297.
- Powers, T.C. (1958) Structure and physical properties of hardened Portland Cement Paste. *Journal of the American Ceramic Society*, 41 (1), 1-6.
- Prick A., Pissart A. & Ozouf J.-C. (1992) Variations dilatométriques de cylindres de roches calcaires subissant des cycles de gel/dégel. *Permafrost and Periglacial Processes*, 3, 15 p. (sous presse).
- Thomas, W.N. (1938) Experiments on the freezing of certain building materials. Department of Scientific and Industrial Research, Building Research Station, Technical Paper, 17, 146 p.
- White, S.E. (1976) Is frost action really only hydration shattering? A review, *Arctic and Alpine Research*, 8 (1), 1 - 6.

## DISCUSSION OF DESTRUCTIVE CAUSE ON THE SOIL DAM BANK OF RESERVIORS AND ITS PREVENTATIVE STEPS

Qiao Dianshi<sup>1</sup>, Xu Jingguang<sup>2</sup> and Zhang Xikun<sup>3</sup>

<sup>1</sup>Suihua Area Hydraulic Bureau, Heilongjiang, China

<sup>2</sup>Lanxi Country Hydraulic Bureau, Heilongjiang, China

<sup>3</sup>Qinggang Country Hydraulic Bureau, Heilongjiang, China

According to observation data of ice pressure and dam frost heave of large-middle type reserviors for many years in the region, the ice condition law of reserviors is analyzed. The destructive causes of reservior soil dams were primary studied, its preventative steps are presented below.

### INSTRUCTION

Heilongjiang Province is located in a high frigid region, the winter is long, and the changing amplitudes of air temperature are large. Yearly average temperature is below 0°C and the lowest temperature is -50°C. Soil freezing lasts as long as 7-9 months. The period of reservior freezing is as long as six months. The average maximum depth of frozen soil is 1.5-2.5 m, maximum ice thickness is 0.9-1.5 m (Qiao Dianshi, 1986). The damage to the reservior soil dam bank that is produced by frost damage is very serious. Nowadays, many scholars believe that the main cause of the damage of the reservior soil dam bank is produced by static ice pressure, so steps of preventing ice pressure are presented.

According to observation data on ice pressure and dam frost heave of reserviors over many years, the main cause of the destruction of reservior banks is produced by frost heave and ice pull force. If there is enough thickness for the bank and the construction quality can be determined, damage can be prevented.

### ANALYZED OBSERVATION DATA ON ICE PRESSURE OF RESERVIORS AND FROST HEAVE OF DAMS

#### Analyzed Observation Data of Ice Pressure on the Reservior

Ice pressure on the reservior is produced by heat expansion of the reservior ice layer when constrained, ice pressure is relative not only to the limited conditions of the ice layer (banks and forms of reservior surface), but to temperature, ice temperature and ice thickness, as well (Xu Bemeng, 1983). Ten years of observation data on ice pressure of the Shenli reservior in Qinggang of Heilongjiang from 1980-1990, shows the following law:

#### Ice pressure under different temperatures and

#### maximum ice pressure

With different temperature changes, the ice pressure is different. According to many years of observation data on ice pressure of the Shenli reservior, temperature change is divided into three types:

(1) The general weather at daily variations, the ice temperature starts to increase at 8:00 and arrives at the maximum value at 14:00, then decreases and arrives at the minimum at night. The second day is similar to the first day. Expansion pressure between ice layers is not synchronized, they constrain each other, so the ice pressure is not large. The result of practical observation shows that ice pressure is at a maximum at 14:00 every day, at about 100 KPa.

(2) The temperature in a successive decrease. Ice pressure is smaller in this condition. This is because non-uniform contractions of the ice layers are produced by a temperature decrease and there are many irregular fissures. In fact, the ice field has not been an integral mass in the condition of the cross fissures. When the new ice mass is formed by water in those fissures or the temperature increases the definite value, free expansion is limited by the ice layers and the ice layers expand again, and ice pressure is formed. So ice pressure in a successive decrease of temperature is smaller.

(3) The weather of a successive rising in temperature: Ice pressure is at its yearly maximum value. Before creep didn't take place in the ice layers, ice temperature increased with the temperature rising, and the ice mass and pressure expands. According to the observation results of several years, the weather of a successive rise in temperature is often shown twice, once in the last ten days of the 11th month, the thickness of the layer is about 20-30 cm. The other is at the end of the second month and early days of the third month, temperature largely increases, ice pressure is at its maximum value of the year. Maximum observation

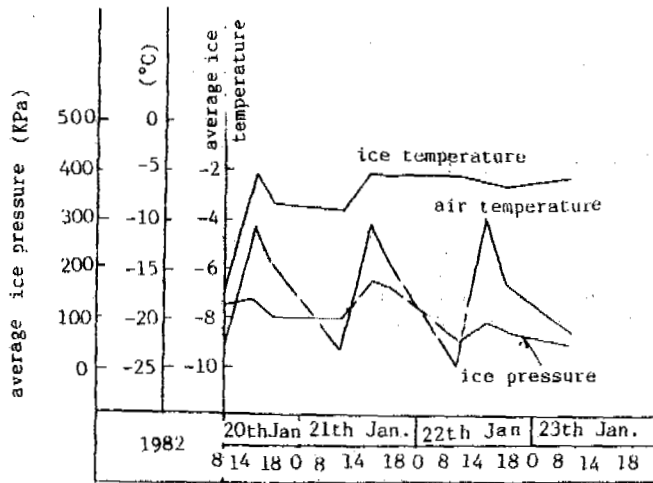


Figure 1. The process line of general temperature, ice temperature and ice pressure in the daily changes at Shenli reservoir

lating ice pressure on the section is an average value of kind points. The average calculation of ice pressure on the section is about 150-200 KPa, when the maximum ice pressure appears.

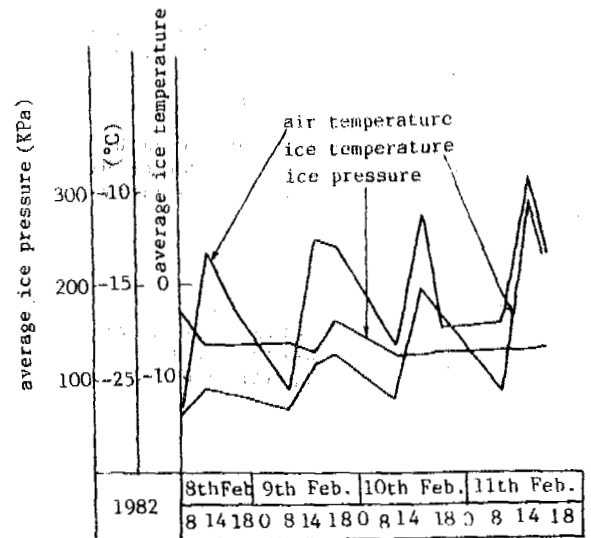


Figure 3. Process line of temperature, ice temperature and ice pressure of the weather in a successive rise in temperature at Shenli reservoir

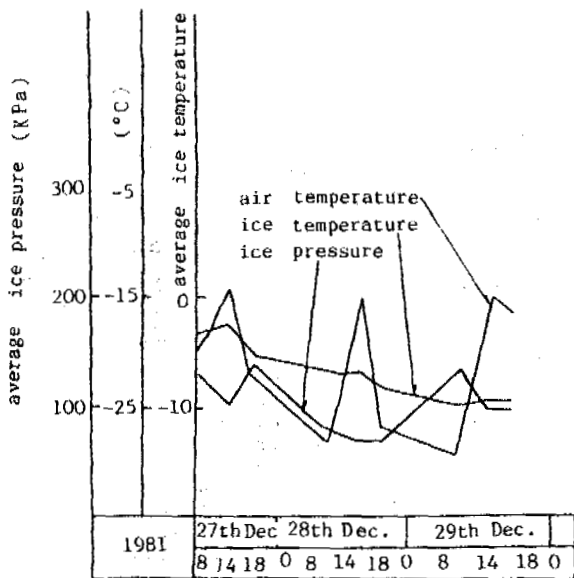


Figure 2. The process line of temperature, ice temperature and ice pressure in a successive decrease of temperature weather at Shenli reservoir

values of a section are generally 300-400 KPa.

The distribution law of ice pressure is found with the thickness of the ice layer and by calculating the value of ice pressure

According to the observation data of several years, ice pressure of different depths of the ice layer is not identical (Fig.4). Maximum ice pressure appears at 20-30 cm in places. Because of the free linking surface of the ice body, the expansion of the ice layer at the depth of 20-30 cm endures smaller constraints, thus ice pressure is smaller than that of the lower layer. The triangle distribution is equal to zero at the maximum ice thickness. Because of different ice pressures on the section, calcu-

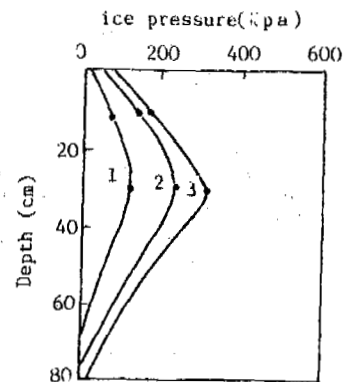


Figure 4. Changing of ice pressure with depth

Observation Analyses of Dam Frost Heave

The soil dam of Shenli reservoir in Qinggang country and the Nihe reservoir in Lanxi country are isotropic soil dams. The banks are constructed with dregs-soil concrete of 7 cm thickness above the water table of Xingli in the last ten days of the month. The banks use concrete placements of 100 cm\*50 cm in area and 10 cm thickness below the water table of Xingli, asphalt liquid of 2 cm thickness is paved under the concrete plate, dregs soil concrete of 7 cm thickness is paved under the asphalt liquid, total thickness is 19 cm. There are dam fills of clayey soil (plastic index is 14-17) under the dregs-soil concrete. The soil dam of Luhe reservoir in Qinggan country is an isotropic soil dam of clayey soil, this dam uses a bank of dry building stones, its thickness is 30 cm, under it there is 20 cm of gravel and 15 cm of coarse

sand.

According to the dam observation of several years for the mentioned three reservoirs, after freezing, the three dams produce frost heave to a different extent, the dams surface rises, banks slip and fissures increase. The maximum frost heave amount of the dams appears in the surface at 1.5-2.0 m above the water table, the frost heave amount is 20-30 cm. This is because the capillary water still successively migrates forward to the freezing front and forms ice crystals in the dam after the dam freezes and the soil water forms ice crystals. From the view of the frost heave process, frost heave in the first stage develops quickly, that of later period becomes slow (Fig.5, Fig.6).

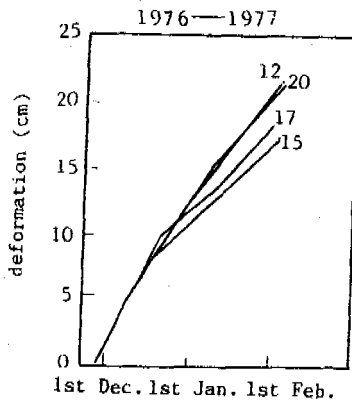


Figure 5. The process line of frost heave deformation of Shenli reservoir dam

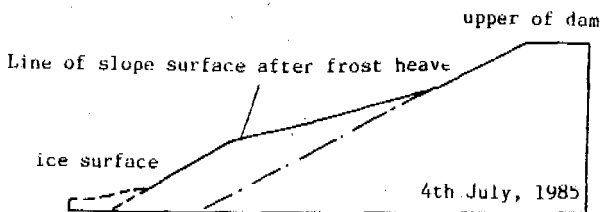


Figure 6. The example of frost heave of the dams slope at Luhe reservoir

#### PRIMARY ANALYSES OF THE CAUSES OF SOIL DAM DAMAGE

Frost damage of the dam bank is produced by several acting factors. By analyzing all of the factors of bank damage, such as ice push force, dam frost heave and bank quality, the main destructive causes can be found.

#### Analysing the Ice Push Force Acting on the Dam Slope — (An Example of a Dry Building Stones Bank)

$t$  is the thickness of the dry stones bank.  $T$  is ice pressure, its condition of bearing force is as follows.

According to the force balance, the bank safety coefficient of the resisting slide is:

$$K = \frac{W' \cdot \sin\alpha + (T \cdot \sin\alpha + W' \cdot \cos\alpha) \cdot f}{T \cdot \cos\alpha} \quad (1)$$

where  $W'$ —the weight of bed ice layer and deducted buoyancy.

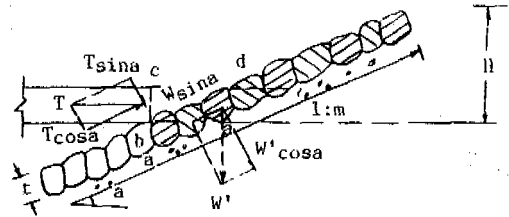


Figure 7. Calculation figure of dry building stones bearing the ice push force

$$W' = r_k \cdot \sqrt{1+m^2} H t - \frac{m}{2} t^2 - \sqrt{1+m^2} t \cdot \alpha \quad (2)$$

$f$ —friction coefficient between the dry building stones bank and the pad layer;  
 $\alpha$ —the cross angle between the slope surface and horizontal line

$$\alpha = \text{tg}^{-1} \frac{1}{m}$$

$r_k$ —stones capacity.  
 Reducing equation (1)

$$K = \frac{r_k \sqrt{1+m^2} H t - \frac{m}{2} t^2 - \sqrt{1+m^2} t \delta + \frac{f}{m}}{T} \left( \frac{1}{m} + f \right) + \frac{f}{m} \quad (3)$$

If  $K=1$ , the thickness of ice layer  $\delta=1$  m,  $T=200$  KPa,  $t=0.4$  m  $r_k=26$  KN/m<sup>3</sup>,  $m=3$ ,  $f=0.8$ . Ice push force can be resisted by a bank of 3.9 m height above the ice surface.

$$H = 4.39 \text{ m} = \frac{1}{r_k \sqrt{1+m^2}} \left\{ \frac{K m - f}{1 + m f} T + \sqrt{1+m^2} t \delta + \frac{m}{2} t^2 \right\} \quad (4)$$

The dam of general middle-heights have the bank height conditions. If bank thickness is large enough and the building stones of the bank are compacted, ice push force can be resisted. The reservoir using dry building stones banks and with a high quality of building stones has been constructed for 10-20 years in our region and banks have no inflicted damage.

#### The Effect of Dam Frost Heave on Bank Damage

For the soil dams of frigid regions, the dam pad under the bank is of silty clay and loam with strong frost heave properties, if the dam surface does not have a thick enough protection layer of sand shale, non uniform frost heave is easily produced in surface soil of soil dams during freezing and causes the building mass of the bank due to the rising and fissuring cannot exactly reset before the ice thaw in spring and the frozen soil doesn't reset during the thaw. It's easily eroded to the filter pad under the building stones, finally causing the bank to slump. The dregs-soil concrete bank of the soil dam in Shenli reservoir (Qinggang country) was built in 1975. Tensile strength of the dregs-soil concrete is 100 KN/cm at the temperature of -20°C and compression strength is 1000 N/cm. When tensile stress produced by the frost heaving force of the dam is more than 100 KN/cm, fissures of frost heave are immediately produced in the bank surface of dregs-soil concrete. On April 29, 1983, the reservoir suffered due to seven large storms, frost heave fissures of the dregs-soil in the concrete bank didn't reset and close, soil grains of the dam were eroded by waves, maximum erosion depth was 2.1 m, this caused the banks of dregs-soil concrete to sink

and break. 18 banks of the dams were damaged and the damage area was 2000 square meters. Nihe reservoir in Lanxi county was built in 1976. Because of frost heave of the dam in 1984, banks of dregs-soil concrete were damaged and lost their effectiveness.

Recently, the soil dam of the Dongfanghong reservoir used stone pads of 1.5 m thickness under the bank, weathering granite with 5 m thickness is the replacement material under the pad. A large volume core-wall dam is used in Xiangyang reservoir, sand shell is used below the pad. Three layer pads of stones, gravel and sand (thickness is 1.15 m) are used below the bank at Dongfanghong reservoir. These reservoirs have been running for many years. The frost heave amount of the dams is very small, though preventative steps are not taken the banks are still in good condition.

#### Effects of the Engineering Quality on the Destruction of Banks

From observation, bank damage of many soil dams is relative with the engineering quality. It is irrational to the design, if the building quality, proper running, etc., is not ensured.

1. The demand of preventative frost heave in the design is not considered. If the pad thickness is not enough, the soil dam banks of reservoirs in seasonally frozen soil regions must consider the thickness of the bank and pad from the view of preventing frost heave. But many designs of soil dam banks don't consider this point. In 1965 the bank design of the Lianlai reservoir in Hailun city used concrete prefabricated slabs of 50\*50\*18 cubic centimeters and gravel and fine sand of 10 cm in thickness were paved under it, it was destroyed in less than three years. The 500 m long bank of Weixin reservoir in Wangan county used concrete prefabricated slabs of 100\*100\*20 cubic centimeters and a two layers filler ditch 30 cm in thickness, which were set up in the joint in 1966. It was damaged in less than two years after being built and in 1967 concrete prefabricated slabs of 100\*50\*20 cubic centimeters were used, gravel and fine sand 10 cm in thickness were set up under the slab, most of the bank was damaged in two years after being built.

2. Building quality cannot be ensured. The stone size of dry the building stones bank is on the small side, and a "close, tight and smooth" stones building isn't accomplished. It is common to have a loose joint between every stone, causing the building to rise and be uneven.

Natural filter material is used in the pad, the grain-size analysis is not finished, the gradation and the coefficient among layers cannot meet the demand of the design. It is more serious to the phenomenon if the thickness and mingling levels are not uniform.

Poor running and maintenance levels. Some parts and small areas of damage in the bank were found later and were not repaired and reinforced in time. Due to large waves, the bank is destroyed and there is a large scale collapse.

In summary, the main destructive causes of the soil dam bank in the reservoirs in seasonally frozen soil regions is because effective steps to prevent frost heave of the soil dam are not taken. The external factors of bank destruction are due to the inferior quality of bank engineering. If the mentioned two conditions are met, damage caused by ice push force can be prevented.

#### DISCUSSION OF PREVENTATIVE STEPS OF FROST DAMAGE IN THE RESERVIOR BANK

From the view of preventing ice push force, preventative steps in frost damage of reservoir banks have many methods at home and abroad. There are ice breaking methods (mechanical and artificial methods), slide methods using a plastic film, the method of regulating the water table etc. Static ice pressure is the main cause of the bank destruction. So the direct action of separating the ice and the bank cause the ice mass to have a free surface or friction between the ice and bank are decreased to make ice freely expand to achieve the goal of decreasing ice pressure. In order to prevent bank destruction by ice push force, the bank must have a definite thickness and be closely constructed to prevent ice push force in the engineering structure. From the observation data of many years at Shenli reservoir in Heilongjiang it is shown that maximum ice pressure of the section is less than 200 KPa and the friction coefficient between the pad and building stones is equal to 0.8, bank thickness is designed according to equation (3).

The frost damage of the soil dam bank of reservoirs in seasonally frozen soil regions should take the measures to prevent frost heave of the soil dam surface with the engineering design. It is suggested that the structure of the soil dam be improved and the sand shell or pad thickness be increased except for in loam fill materials to prevent frost heave. It is an essential step to prevent the soil dam bank destruction. The thickness of the protecting layer is determined according to the depth of frozen ground and the capacity height in the location.

In addition, the engineering quality must be ensured in the design and construction of bank engineering. The thickness of the pad and building mass and composition of the layers must meet the relevant standards.

#### CONCLUSIONS

1. Discussion of the destructive causes of the soil dam bank is the premise by which the measures to prevent frost damage are taken.
2. The main destructive cause of the soil dam bank is frost heave of the soil dam in the thesis. External destructive factors of the soil dam bank is the inferior quality of bank and pad construction.
3. The steps of preventing ice at present, for example, mechanical and artificial ice breaking or the plastic film producing slide, prove that the main destructive causes of the soil dam bank is the static ice pressure, and much money is spent every year. These steps of prevent ice are feasible for some low soil dams.

#### REFERENCES

- Xu Bemeng, (1983) Expand pressure of ice layer of reservoir. Proceedings of the sixth international symposium on Ice Situation.
- Qiao Dianshi, Any Yongchang and Zhang Xikun, (1984) Ice Situation, Ice pressure and preventing steps of ice damage in Shenli reservoir. J. of Engineering and Frozen soil. 1986, 2.

DEVELOPMENT CONDITION OF ALPINE PERMAFROST  
IN THE MT. TIANSHAN, CHINA\*

Qiu Guoqing

Lanzhou Institute of Glaciology and Geocryology,  
Chinese Academy of Sciences, China

The three-dimensional variation of mean annual air temperature in the Mt. Tianshan, China leads to a descent of the lower limit of alpine permafrost northwards and eastwards and the thickening and colding of perennially frozen ground upwards. The mean annual air temperature  $T_a$  at the lower limit of alpine permafrost should be  $-1.83^\circ\text{C}$  according to statistics. Since the Gorczynski's continentality is generally lower than 50, the permafrost in Chinese Tianshan should not be considered as the "continental" one. Because the lower limit of permafrost can be located at the positions with different values of continentality, it seems that the continentality is not the only factor that determines the distribution of permafrost. The variation in the amount, distribution and form of precipitation might be an important reason resulting in the difference of permafrost distribution in West and East Tianshan.

INTRODUCTION

The Tianshan is a grand mountain system in the Central Asia, of which 1700 km stretches in the Chiense territory, acrossing  $21^\circ$  in longitude. There are many ridges and fault basins controlled by the WNW and ENE tectonic lines and other factors. Most of the ridges are higher than 4000 m a.s.l.

Alpine permafrost and glaciers are widely distributed in this mountain system, the former occuples a total area of  $63000 \text{ km}^2$  (Qiu et al, 1983), and the latter —  $9548.45 \text{ km}^2$  (Shi et al, 1988).

It is recognized that the altitudinal zonation of air temperature is the major factor for the development of permafrost in alpine region. Gorbunov (1978) and Harris (1989) emphasized the importance of the continentality or the annual range of air temperature in the development of permafrost. Xu and Fu (1983) suggested a regression equation, on the basis of data from 29 meteorological stations spread from 34.5 to 2136.9 m a.s.l. in the whole territory of Xinjiang, to show the dependence of air temperature on latitude and altitude and to decide the permafrost distribution in the high mountain above 2800 m a.s.l.

In this paper, the author would like to discuss the influence of climatic factor on the development of alpine permafrost. For this purpose some equations are suggested to express the variation of precipitation and the mean annual value and annual range of air temperature in three-dimensions.

MEAN ANNUAL AIR TEMPERATURE AND GROUND SURFACE TEMPERATURE

\*This project is supported by the National Natural Science Foundation of China and by the Tianshan Glaciological Station of Academia Sinica.

Generally, the mean annual air temperature will decrease with the rising of altitude. Because of the temperature inversion in winter in the lower part of Tianshan, the gradient of mean annual air temperature varies in different altitudinal zones. For example, along the Urumqi River, the mean annual air temperature will decrease  $0.3^\circ\text{C}$  to  $0.4^\circ\text{C}$  as the elevation arising 100 m at the area from 900 to 3000 m a.s.l., where the temperature inversion is obvious in winter; from 3000 to 4000 m a.s.l., the gradient is  $0.6^\circ$  to  $0.7^\circ\text{C}/100 \text{ m}$ .

For a general understanding of the variation of mean annual air temperature in three-dimensions, statistics was made by using data observed in 17 meteorological stations in/around Tianshan ( $41^\circ10'$  to  $44^\circ54' \text{N}$ ,  $80^\circ14'$  to  $94^\circ42' \text{E}$ , 468.2 to 3539 m a.s.l.). The result is as follows:

$$T_a = 109.3 - 2.19X_1 - 0.024X_2 - 0.0051X_3 \quad (1)$$

where,  $T_a$  — mean annual air temperature ( $^\circ\text{C}$ );  
 $X_1$  — latitude ( $^\circ\text{N}$ );  
 $X_2$  — longitude ( $^\circ\text{E}$ );  
 $X_3$  — altitude (m a.s.l.).

The correlation coefficient of Equation (1) is 0.9596.

As shown in Equation (1), the mean annual air temperature will decrease  $2.2^\circ\text{C}$  with each  $1^\circ$  increase in latitude,  $0.02^\circ\text{C}$  with each  $1^\circ$  increase in longitude and  $0.51^\circ\text{C}$  with each 100 m increase in altitude. This result can roughly tell why the lower limit of alpine permafrost descends from south to north and from west to east (Qiu et al, 1983).

In order to compare the significance of the factors, the standard regression coefficient were calculated:

$$B_i = b_i \sqrt{(\sum X_i^2 - (\sum X_i)^2/n) / (\sum T_a^2 - (\sum T_a)^2/n)}$$

where,  $n$  — number of stations.



Correspondingly, for latitude  $X_1, B_1 = -0.47$ ; for longitude  $X_2, B_2 = -0.025$ ; for altitude  $X_3, B_3 = -0.93$ .

Since  $|B_3| > |B_1| > |B_2|$ , it can be believed that the altitude is the most significant factor that affects the mean annual air temperature, then the latitude, and then the longitude.

The development and distribution of permafrost, however, is not directly dependent upon the air- but the ground-surface-temperature. The necessary condition for the development of permafrost is that the mean annual temperature on ground surface is equal to or lower than  $0^\circ\text{C}$ .

Based on the statistics by using the data from 15 meteorological stations in/around the Tianshan, it is known that the relationship between the mean annual ground surface temperature  $T_s$  and the mean annual air temperature  $T_a$  is as follows:

$$T_s = 1.86 + 1.02 T_a \quad (2)$$

The correlation coefficient of Equation (2) is 0.9673.

If  $T_s = 0$ , then the mean annual air temperature should be:

$$T_{ac} = -1.86/1.02 = -1.83^\circ \approx -2^\circ\text{C}$$

In other words, the mean annual air temperature at the lower limit of permafrost should be around  $-2^\circ\text{C}$ , statistically.

At the Summer Camp of the Tianshan Glaciological Station or the Daxigou Meteorological Station (3539 m a.s.l.), the mean annual air temperature is  $-5.4^\circ\text{C}$ , the gradient is  $0.63^\circ\text{C}/100\text{ m}$ , thus, at an elevation of 2972 m the mean annual air temperature would be  $-1.83^\circ\text{C}$ , and at 3000 m a.s.l., it would be  $-2^\circ\text{C}$ . Therefore, it is easy to understand why the lower limit of alpine permafrost in the upper reach of the Urumqi River is at about 3000 m a.s.l. (3250 m on the south-facing slope and about 2900 m on the north-facing slope).

In the Kuixian Daban region, the mean annual air temperature was observed to be  $-1.1^\circ\text{C}$  at the Dongdesala Meteorological Station (2921.3 m a.s.l.,  $42^\circ 51'$  in latitude and  $86^\circ 54'$  in longitude). If the gradient is  $0.6^\circ\text{C}/100\text{ m}$ , then the mean annual air temperature at an elevation of 3050 m (south-facing slope) should be  $-2^\circ\text{C}$ . This can tell why the permafrost lower limit at south-facing slope was observed to lie on 3100 m a.s.l.

The variation of air temperature in three-dimensions leads to the northward and eastward descent of the lower limit of permafrost, and especially, to the thickening and colding of the perennially frozen ground upwards. For example, along the Urumqi River, the ground temperature at the level of zero annual amplitude is  $-0.7^\circ\text{C}$  at 3348 m a.s.l.,  $-1.6^\circ\text{C}$  at 3497 m a.s.l. and  $-4.9^\circ\text{C}$  at 3900 m a.s.l.

Thermal regime of ground also depends on the local conditions, such as the slope orientation and surface cover especially the snow cover (Table 1).

As shown in Table 1, at a same elevation the maximum ground surface temperature on south-facing slope was much higher than that on the north-facing slope, while the minimum — close to each other. This indicates a much higher heat-input on the south-facing slope. The difference of heat-balance on slopes also leads to a differentiation of permafrost lower limit. For example, in the Kuixian Daban region, the lowest

position for permafrost occurrence on north-facing slope was observed to be at an elevation of 2700 m a.s.l. and 400 m lower than that on the south-facing slope (Qiu and Zhang, 1981).

## CONTINENTALITY

Recently, the importance of continentality was emphasized in some literatures. Gorbunov (1978) suggested that the alpine permafrost be divided into the maritime and continental types, according to the continentality. The former developing under a maritime climate might be characterized by that its lower limit is close to the snowline, while the latter developing under continental climate — the snowline is much higher than the permafrost lower limit. The distance between the snowline and the lower limit will enlarge with the increase of continentality and the Mt. Tianshan, according to Gorbunov, is the typical continental permafrost region. Harris (1989) agreed to Gorbunov's idea and considered a quantitative relationship between continentality and the altitude of permafrost lower limit.

Of course, Tianshan is far from ocean and the places at the hillfoot of Tianshan are in an environment of continental climate. The index commonly used for evaluating the continental extent of climate in a certain region is the CONTINENTALITY  $K$  suggested by Gorczyński (Zhang and Lin, 1985):

$$K = 1.7 A/\sin X_1 - 20.4$$

where,  $A$  — annual range of air temperature  $^\circ\text{C}$ ;  
 $X_1$  — latitude.

At the foot of Tianshan, in the Urumqi City (918 m a.s.l.),  $A$  is  $40.9^\circ\text{C}$ , the continentality  $K$  is 79.9. As the altitude rising,  $A$  and  $K$  become lower and lower. Along the Urumqi River, for example, at the Base of the Tianshan Glaciological Station (2130 m a.s.l.),  $A$  is  $26^\circ\text{C}$  and  $K$  is 44.1; at the Summer Camp of the Tianshan Glaciological Station or the Daxigou Meteorological Station (3539 m a.s.l.),  $A$  is  $20.6^\circ\text{C}$ ,  $K$  is 30.8; and at the Dry Cirque (3820 m a.s.l.), it is  $20.3^\circ\text{C}$  in  $A$  and 30.1 in  $K$ . Usually, in a region with a typical continental climate, the  $K$  value should be greater than 50. Thus, the permafrost region along the Urumqi River is not continental climatically.

For an approximate understanding of the dependence of annual range of air temperature  $A$  on the latitude  $X_1$ , longitude  $X_2$  and altitude  $X_3$ , statistics based on the data from 19 stations in/around Tianshan has the following result:

$$A = -27.62 + 0.74X_1 + 0.41X_2 - 0.0059X_3 \quad (3)$$

The correlation coefficient of Equation (3) is 0.8899. The corresponding standard regression coefficients are: for factor latitude  $X_1, B_1 = 0.098$ ; for factor longitude  $X_2, B_2 = 0.269$ ; and for the factor altitude  $X_3, B_3 = -0.847$ . Since  $|B_3| > |B_2| > |B_1|$ , it can be recognized that the factor altitude  $X_3$  is the most significant one, the longitude  $X_2$  is the second, and the latitude  $X_1$  — the third. That is to say, the annual range of air temperature will decrease for  $0.59^\circ\text{C}$  with each 100 m increase of altitude, ascend  $0.74^\circ\text{C}$  or  $0.41^\circ\text{C}$  with each  $1^\circ$  increase in latitude or  $1^\circ$  increase in longitude respectively.

Based on Equation (3) and the Gorczyński's

Table 1. Ground surface temperature at 2960 m a.s.l. in Kuixian Daban region (after Qiu and Zhang, 1981)

Date	Slope orientation	Ground surface temperature °C		
		Max.	Min.	Daily amplitude
Aug. 4, 1972	North-facing	31.6	4.6	27.0
	South-facing	51.7	4.0	47.7
Oct. 21, 1972	North-facing Exposed	21.5	-12.0	33.5
	Beneath 10 cm snow	0.3	-5.8	6.1
	South-facing	31.0	-12.3	43.3

definition, a nomograph showing the variation of continentality in three-dimensions can be made; also, based on the Equation (1) and (2), the statistical lower limit of alpine permafrost or the position possibly with a mean annual air temperature of  $-1.83^{\circ}\text{C}$  can be determined (Fig.1).

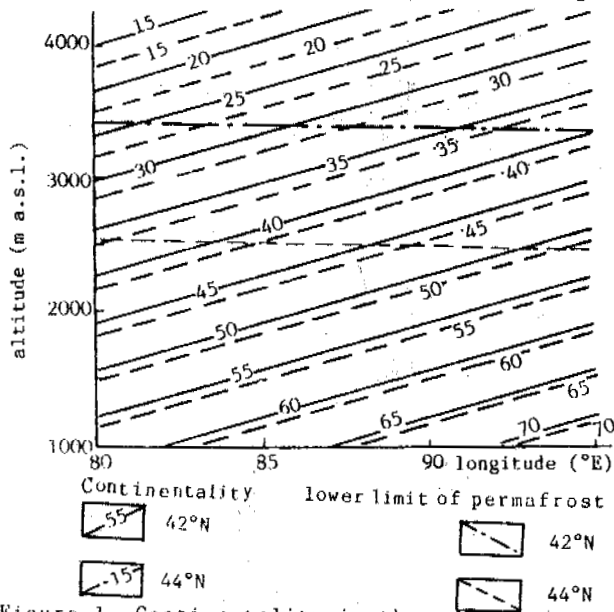


Figure 1. Continentality in three-dimensions in/around the Mt. Tianshan

From the Fig.1, one can see that in most of the alpine permafrost area the continentality is less than 50, therefore it should not be considered that the alpine permafrost in Tianshan belongs to the continental type developing under a continental climate. Also, since the continentality in regions higher than the glacier terminus (above 3600 m) is much lower than 50, the glaciers in Tianshan should not be considered as the continental type either. Because the line of the statistical lower limit of alpine permafrost can run through the positions with different continentality, for example at  $44^{\circ}\text{N}$  the K-value at the lower limit varies from 35 to 50, it seems that the continentality is not the only factor that determines the distribution of alpine permafrost.

#### PRECIPITATION

There is no denying the importance of temper-

ature amplitude on the development of frozen ground. With a same value of mean annual air temperature, a higher range of air temperature indicates a colder winter favourable to ground freezing and a warmer summer favourable to ground thawing. The penetrating depth and process of freezing-thawing, however, depends not only on air temperature but also on the surface cover especially the snow cover, the lithological characteristics of ground and other factors. Here, the amount, distribution of precipitation might have an important effect on the development of frozen ground.

If the precipitation is concentrated on cold season, then under a thick and stable snow cover the ground and the ground-surface must be much warmer than the atmosphere because of the insulation effect of the snow, even though in a considerable cold winter, the freezing process of ground would be limited, not able to penetrate to a considerable depth. In an arid and warm summer, on the other hand, there would not be a hamper to the thawing process of ground. Thus, the higher the annual range of air temperature, the deeper the depth of ground thawing in summer. Therefore, the perennially frozen ground must be developed under a mean annual air temperature cold enough.

If precipitation is concentrated on a warm summer in liquid state, there is not a thick and stable snow cover in winter, with a higher annual range of air temperature, it is possible to form a thick frozen ground in the cold and dry winter, but in the rainy warmer summer, under the thermal effect of the higher temperature and the rainfall, there must be a considerable thawing depth of ground. This is also unfavourable to the development of permafrost.

If the precipitation is concentrated on warm season mainly in solid state, then in the winter time with a few snowfall there would not be a stable and thick snow cover. The major effect of the thin and unstable snow cover in winter is to reflect the solar radiation. Thus, under a low temperature the freezing process is allowed to penetrate down to a considerable depth. In the relatively warm summer, it is impossible to form a thick and stable snow cover either. The solar radiation would be reflected by the temporary snow surface and consumed with the snow melting. This would be unfavourable to the thawing of ground but favourable to the development and preservation of permafrost.

Thus, it is necessary to discuss the spatial and seasonal distribution of precipitation. Based on the statistics by using data from

18 stations in/around the Mt. Tianshan, the dependence of precipitation P on latitude X1, longitude X2 and altitude X3 is known as follows.

$$P = -2669.12 + 99.81X_1 - 18.70X_2 + 0.1383X_3 \quad (4)$$

The correlation coefficient of Equation (4) is 0.8077. The corresponding standard regression coefficient B1 for factor X1 is 0.51, B2 for X2 is -0.48, and B3 for X3 is 0.63. So, the order of significance of factors can be listed as X3 → X1 → X2. The Equation (4) shows a general tendency that the precipitation decrease eastwards and increases northwards and upwards. However, the spatial distribution of precipitation is not completely coincided with the linear regulation. There are high-precipitation belts at the middle-altitude and at the modern snow-line. Although the precipitation decreases eastwards in general, it would be changed by the local terrain, e.g. it is 326 mm in Yining (770 m a.s.l.), then increases to 460 mm in Xinyuan (928.2 m a.s.l.), reaches up to a value as high as 827.3 mm at the Tianshan Snow Station (1776 m a.s.l.), then drops again eastwards to 285 mm in Bayanbluk (2458 m a.s.l.) and down to 86.7 mm in Yiwu (1728.6 m a.s.l.) at the eastern end of Tianshan. So, the Equation (4) can only express a general tendency of precipitation distribution.

A comparison between the East and West Tianshan (Fig.2) showed that either the annual value or the precipitation in the season with a mean monthly air temperature <0°C in the west are generally much higher than that in the east. The snow cover in winter could restrict the freezing of ground. For example, according to the observation at 2700 m a.s.l. in the Balshaya Almatinka Permafrost Station, Zayiliskii Alatau, Kazakhstan during 1975-1976, in the center of a wind-drifted snow bank (120 to 160 cm in thickness), the freezing depth of ground was only 45 cm; at the edge of the snow bank with a thickness of 80 cm at the most and 30 to 40 cm from November to February, the freezing depth of ground penetrated down to 1.4 m; at the position 20 m from the snow bank, where the snow cover was 0 to 30 cm and occasionally 40 cm at late spring, the freezing depth of ground penetrated down to 2.4 m (Fig.3) (Severskiy and Severskiy, 1990). In the East Tianshan, the observation in the Tianshan Snow Station showed that under a 50 cm snow cover, the ground only froze down to a depth of 60 cm (Hu and Jiang, 1989). Thus, in the snow-rich West Tianshan and the Yili valley of the East Tianshan, it is necessary to have a colder temperature for the development of permafrost. For example, at an elevation of 3300 m in the Balshaya Almatinka River basin, the permafrost with a thickness of 20-40 m or so is discontinuously confined in the north-facing valley filled with till, although the mean annual air temperature is as low as -3.4°C (Severskiy, 1978). In the most parts of the East Tianshan, it is more favourable to the development of permafrost. For instance, in the upper reach of the Urumqi River, 76.5% of the annual precipitation is concentrated in the relatively warmer season from June to September in solid state, the snow cover usually exists no more than two days; as mentioned above, this is favourable to the preservation of the frozen ground. In the coldest season from November to February, the monthly precipitation is usually

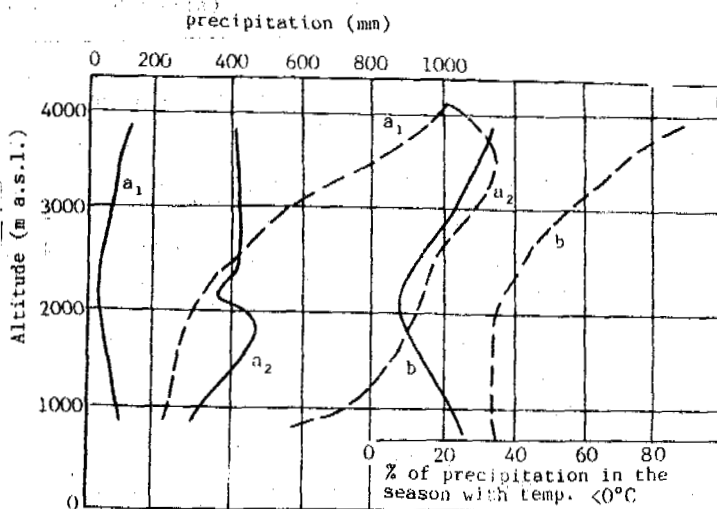


Figure 2. Dependence of precipitation on altitude along the Balshaya Almatinka River and the Urumqi River

- a<sub>1</sub> - precipitation (mm) in the season <0°C;
- a<sub>2</sub> - annual precipitation (mm);
- b - percentage of precipitation in the season <0°C;

dotted line - Balshaya Almatinka River (after Severskiy, 1978; with modification);  
thick line - Urumqi River.

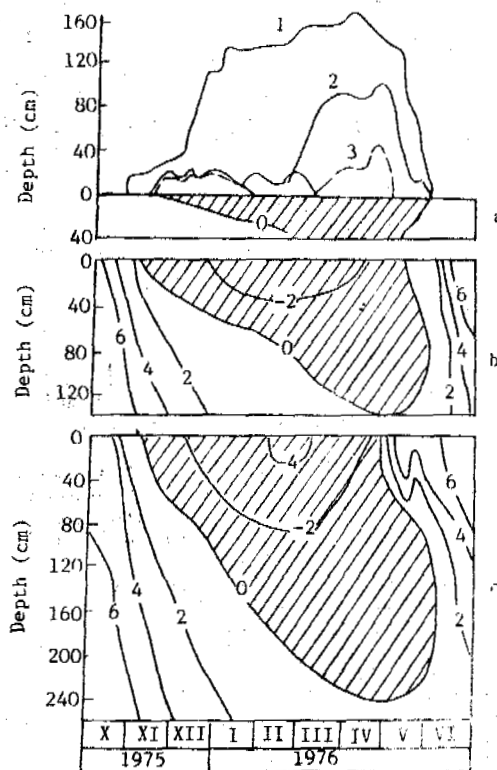


Figure 3. Isotherms in ground under or surrounding the snow bank (after Severskiy et al, 1990)  
a. under the center of snow bank; b. at the edge of snow bank; c. 20 m from the snow bank. Height of snow bank: 1. center of the snow bank; 2. at the edge of the snow bank; 3. 20 m from the snow bank.

less than 5 mm (Table 2). Without a thick and stable snow cover in winter, the freezing process is allowed to penetrate to a considerable depth. Under such a favourable condition, at an elevation of 3348 m at the upper reach of Urumqi River, the permafrost can be as thick as 50 m with a ground temperature of  $-0.7^{\circ}\text{C}$  at the level of zero annual amplitude.

In the much drier Kuixian Daban region to the south of the Urumqi River basin, according to the observation at the Dongdesala Meteorological Station (2912.3 m a.s.l.), the total value of precipitation in the coldest season is only 5 mm or the 2.2% of the annual precipitation (Table 2). The lower limit of permafrost there lies at 2700 m a.s.l. on north-facing slope and at 3100 m a.s.l. on south-facing slope (Qiu and Zhang, 1981) and is about 200 m lower than that in the Urumqi River basin. At the elevation of 3300 m, the ground temperature at the level of zero annual amplitude was observed to be  $-2.0^{\circ}\text{C}$  and is  $1.3^{\circ}\text{C}$  lower than that at the same elevation at the Urumqi River basin.

It should be considered that the precipitation in winter would increase with the increase of annual amount northwards and westwards in the East Tianshan, although the precipitation there is generally relatively concentrated on the warmer season. This would reduce the northward descent of permafrost lower limit and enhance its eastward descent. In some places, the condition for permafrost development would be more favourable than in the area bordered on its north because of the difference in precipitation. The story in the Kuixian Daban and the Urumqi River basin might be one of the examples.

Thus, the amount, distribution and form of precipitation might have an important effect on the development of the frozen ground and might be an important reason resulting in the difference of permafrost distribution in the west and East Tianshan and within the East Tianshan itself.

## CONCLUSION

### 1. The development and distribution of alpine

permafrost are influenced by the combined effect of the natural factors. The altitudinal variation of the air temperature is the most important factor that leads to the altitudinal zonation of frozen ground. The decrease of the mean annual air temperature from south to north and from west to east would lead to a descent of permafrost lower limit at the same direction; the increase of precipitation northwards and westwards would lead to an ascent of permafrost lower limit from south to north and from east to west. Thus, the northward descent of permafrost lower limit caused by the decrease of mean annual air temperature would be reduced by the increase of precipitation at a same direction, while the descent of the lower limit eastwards caused by the decrease of the mean annual air temperature would be enhanced by the decrease of precipitation west to east. As a result, the actual northward descent of permafrost lower limit would be less than that calculated by the Equation (1) and (2); the actual variation of the lower limit from west to east would be greater than the calculated one.

2. The seasonal distribution of precipitation has an important effect on the development of frozen ground. The snowfall in winter would restrict the ground freezing, while the snowfall in summer would be favourable to the preservation of frozen ground. The spatial and seasonal difference in precipitation distribution might be an important reason that causes the difference in permafrost distribution between the East and the West Tianshan and within the East Tianshan itself.

3. Since the continentality is usually less than 50, it would be inappropriate to consider the permafrost there as the "continental type". Because the lower limit of alpine permafrost runs through the places different in continentality, it seems that the continentality is not the only factor that determines the distribution of permafrost.

Table 2. Precipitation (mm) in selected stations

Station (m a.s.l.)	Month	Jan.	Feb.	March	Apr.	May	June	July	Aug.	Sept.	Oct.	Nov.	Dec.	Year
Urumqi (918)		7.7	10.1	20.0	34.1	34.7	41.4	21.7	19.6	26.8	28.6	19.2	14.0	277.7
Heroic Bridge (1650)		5.5	6.4	10.5	40.7	64.7	110.3	92.0	53.6	44.1	22.4	12.2	6.4	468.8
Bas of TGS (2130)		0.7	3.4	5.6	21.7	52.6	82.3	87.9	44.3	25.9	15.4	9.6	3.9	353.2
Yaojin Bridge (2400)		1.2	2.5	8.6	17.9	59.1	106.2	97.8	40.2	54.7	16.7	7.6	3.9	416.6
Summer Camp of TGS (3539)		2.7	3.6	7.3	22.6	47.7	90.6	106.0	81.2	45.1	11.0	2.5	1.7	421.9
Dry Cirque (3820)		1.8	4.5	7.1	13.6	54.9	80.2	116.2	73.5	24.1	25.3	0.6	1.7	403.5
Dongdesala (2921.3)		0.4	0.3	1.1	1.3	6.4	34.0	37.5	118.8	16.9	2.6	0.0	0.7	220.0

## REFERENCES

- Gorbuinov, A.P., (1978) Permafrost investigations in high mountain regions. *Journal of Arctic and Alpine Research*, Vol.10, No.2, pp.238-294.
- Harris, S.A., (1989) Continentality index: its uses and limitations in the Canada Cordillera. *Physical Geography*, Vol.10, No.3, pp.270-284.
- Hu Ruji and Jiang Fengqing, (1989) Snow avalanche and its control in Tianshan, China. People's Transportation Publishing House, Beijing, 167p. (in Chinese).
- Qiu Guoqing and Zhang Changqing, (1981) Distributive features of permafrost near the Kuyxian Daban in the Tianshan Mountains. in: *Memoirs of Lanzhou Institute of Glaciology and Cryopedology*, Academia Sinica, No.2, Science Press, Beijing, pp.1-14 (in Chinese).
- Qiu Guoqing, Huang Yizhi and Li Zuofu, (1983) Alpine permafrost in Tianshan, China. in: *Proceedings of the 4th International Conference on Permafrost*. National Academy Press, Washington D.C., U.S.A. pp.1021-1023.
- Shi Yafeng, Huang Maohuan, Ren Binghui, et al, (1988) An introduction to the glaciers in China. Science Press, Beijing, 243p. (in Chinese).
- Xu Xiaozhu and Fu Liandi, (1983) Conversion of parameters in air-ground system and determination of maximum of both seasonal frost and thaw depth. in: *Proceedings of the Second Chinese National Conference on Permafrost*. Gansu People's Publishing House, Lanzhou, pp.108-120 (in Chinese).
- Zhang Jiacheng and Lin Ziguang, (1985) Climate in China. Shanghai Science and Technology Publishing House, 603p (in Chinese).
- Severskiy, I.V., (1978) Snow avalanche in the Zailiyskii Alatau. *Hauka*, Alma-Ata, 255p. (in Russian).
- Severskiy, I.V. and Severskiy, E.V., (1990) Snow cover and seasonal frost of soils in northern Tianshan. Permafrost Institute, Siberian Branch, Academy of Sciences, USSR, Iakutsk, 182p. (in Russian).

## REPAIR OF A ROAD BUILT ON PERMAFROST AT KILPISJÄRVI, NORTHERN FINLAND

Seppo Saarelainen Dr.Tech. (Civ.Eng.),  
Senior Research Scientist

Technical Research Centre of Finland,  
Road, Traffic and Geotechnical Laboratory  
P.O. BOX 108, SF-02151 Espoo  
FINLAND

This paper deals with a repaired, insulated road structure on permafrost in Peera, Northern Finland. The road section was built in 1987. It was monitored since then in years 1988 - 1991. The depth of frost and thaw penetration and thawing in and below the insulated road, frost heave and thaw settlement, as well as changes in the moisture content of the subgrade were monitored by field measurements. The freeze and thaw behaviour of the road was compared to that of old road before repair. Thaw settlements have occurred even after the repair, but at a lower rate.

### INTRODUCTION

The specific problems in cold climate are connected to frost heaving and thaw compression in freezing and thawing soils, and accumulation of snow and ice to communications, roads and other structures.

The stable state of the ground in seasonal frost areas is an unfrozen one, while in permafrost areas the ground is frozen. Freezing of unfrozen, frost-susceptible ground, as well as thawing of frozen, ice-rich ground may cause volume changes in the ground, and displacements at the ground surface and the structures upon it.

The stability of structures in permafrost is normally maintained by limited freezing and thawing of the frost-susceptible ground in the active zone. An engineering structure, i.e. a road, causes changes to thermal conditions at the ground surface zone. The main effects are due to the raised pavement temperatures in warm seasons and lowering of temperatures in winter by exposure of snowless pavement. The snow accumulation on the road and side slopes can cause instability of embankment shoulders. In summer, the ponding of runoff as well as the all embankment surfaces may cause local heating effects to the underlying permafrost.

In the late 80'ies, a research project dealing with cold climate problems in Northern Finland, was carried out (Fig. 1). It included experiments and design solutions for the control of frost heave, prevention of snow accumulation on road, mitigating icing on road, and limiting the excess thaw settlements of the road underlain by permafrost (Lehtonen & Saarelainen 1989, Saarelainen 1990a, 1990b, Saarelainen & Kivikoski 1990, Lehtonen 1991, Kivikoski 1990).

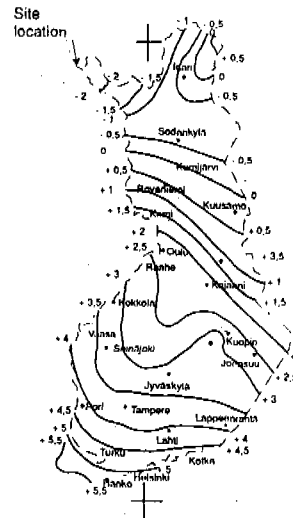


Fig. 1. Site location. Mean annual air temperatures in Finland (Talonrakennuksen routasuojausohjeet 1987).

### LOCAL CONDITIONS

The mean annual air temperature at the site is about  $-2.5^{\circ}\text{C}$ . The mean freezing index is 42 000  $\text{h}^{\circ}\text{C}$ , maximum once in 10 years about 50 000  $\text{h}^{\circ}\text{C}$ , and the estimated maximum once in 50 years about 60 000  $\text{h}^{\circ}\text{C}$ . The thawing index according to air temperatures is about 25 000  $\text{h}^{\circ}\text{C}$ .

The site, an old road embankment on palsa, was located close to the edge of peatland. The depth to the base of permafrost beneath the palsa was according to site investigations

about 7-8 metres. The generalized longitudinal profile is illustrated in Fig. 2. The the old road embankment was underlain by thawed peat to the depth of 2 metres. The permanently frozen horizon consisted of a top layer of frozen peat, about 1 - 2 metres thick, underlain by frozen silt, changing at a greater depth to till. According to geophysical soundings, the base rock was at the depth of about 10 metres.

The road is an old transportation route, that was constructed for car traffic during World War II. The road had been paved with oil-gravel layer in 1962. The maximum thaw settlement for the period of 1962 - 1987 was about 1,8 metres. This could be detected

during test construction, as the maximum thickness of the pavement layer was exposed (Fig. 3). The oil-gravel thickness resulted from the continuous maintenance and raising of the surface with pavement material.

The thaw compression of frozen peat in laboratory thaw-compression tests was about 70 %. If a thaw settlement was 1,8 metres, the corresponding, cumulative thaw penetration in the peat subgrade had been about 2,5 metres. This means that an average rate of excess thaw penetration in frozen peat was about 100 mm/year, and the annual rate of thaw settlement about 70 mm/year. The thaw damage was concentrated at the edge of palsa.

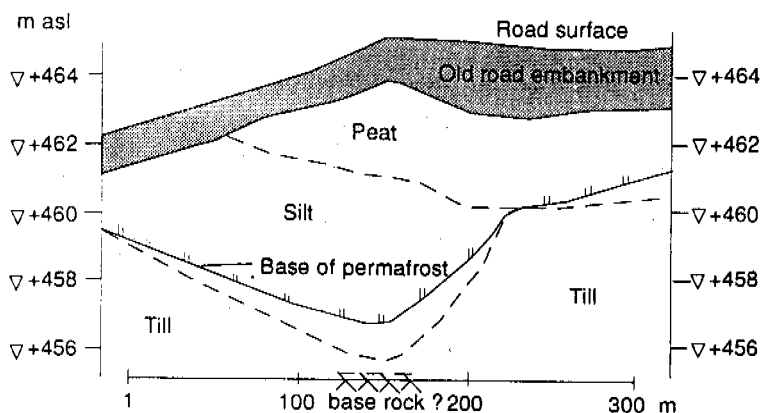


Fig. 2. Longitudinal profile of palsa ground at Peera test section.



Fig. 3. Old, exposed oil-gravel layers with thickness of 1.8 metres on Peera palsa.

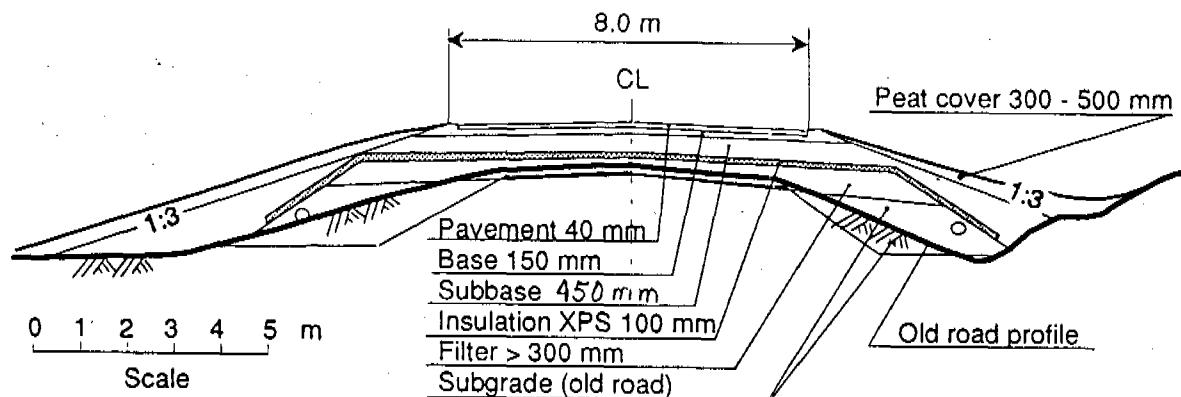


Fig. 4. Structural section of the planned test road at Peera, palsa.

#### THE TEST STRUCTURE

The goal of test construction at the site was to find and test an approach, in which the thaw settlements could be limited, and the rate of settlement could be reduced to a tolerable level.

At the site conditions, this means, in principle, either replacement of the frozen peat at the top of the palsa with stable fill or limiting the thaw penetration using thermally insulated structure. The heating effect was to be reduced using a light-coloured pavement aggregate.

The excavation of frozen or pre-thawed peat, and replacement with a stable gravel fill was seen too laborious and expensive. Thus, the experimentation was concentrated into the design and testing of a thermally insulated road embankment.

In order to ensure the proper freeze-thaw behaviour, the embankment was planned with thermal insulation. The insulated structure was designed by thermal analysis, in which, starting from the initial temperature conditions and thaw depth, the seasonal thaw and frost penetrations were calculated applying on the pavement assumed surface temperatures. In winter, the temperatures were assumed to follow air temperatures, as to thawing and warm season, the air temperatures were multiplied by 1.5. The analysis was run over three freeze-thaw cycles. The insulation was selected so that the freeze-thaw depth was limited to coarse-grained, stable embankment. An illustration of the road section is illustrated in Fig. 4 and the freeze-thaw prediction in Fig. 5.

The thermal insulation, 100mm thick extruded polystyrene foam board, was covered with upper subbase and base layers overlain with oil-gravel pavement, and underlain with levelling layer of gravel. The original road embankment was spread to the subgrade in order to form a stable layer for the delayed thaw under the insulation. The slopes were covered with a 0.3 - 0.5 metres thick layer of peat for the vegeta-

tion and for the reduction of thaw penetration during warm season. The pavement was mixed using light-coloured quartzite aggregate.

#### CONSTRUCTION

The old pavement was removed and the old embankment spread on the subgrade in autumn 1986. The subgrade was exposed for freezing in winter 1986 - 1987. The new embankment with thermal insulation was constructed in May 1987, and the pavement was laid in August 1987. The schedule was determined in order to create freeze-thaw conditions, in which the thermal behaviour of the insulated embankment is approaching the balance from the cold side.

#### MONITORED BEHAVIOUR

The temperature profiles as well as freeze and thaw depths were monitored at two points of the section, at locations of 30 280 m and 30 320 m from the border to Norway, 1.5 metres aside from the centre line, in years 1987-1989. Temperatures were measured using copper-constantan thermocouples, and freeze-thaw depths using frost tubes filled with 1:2000 methylene blue solution. The vertical displacement of the pavement was measured by monthly levelling of the pavement at two locations.

An example of the monthly variation of temperatures in the freeze-thaw season 1987 - 1988 is illustrated in Figs. 6, and the observed freeze-thaw development in the same season at the two observation points in Fig. 7. According to measurements, the thawed horizon was frozen to the permafrost table, as to the following thaw penetration was about 2 - 2.4 metres, while the actual thickness of the embankment was 2-2.2 metres.



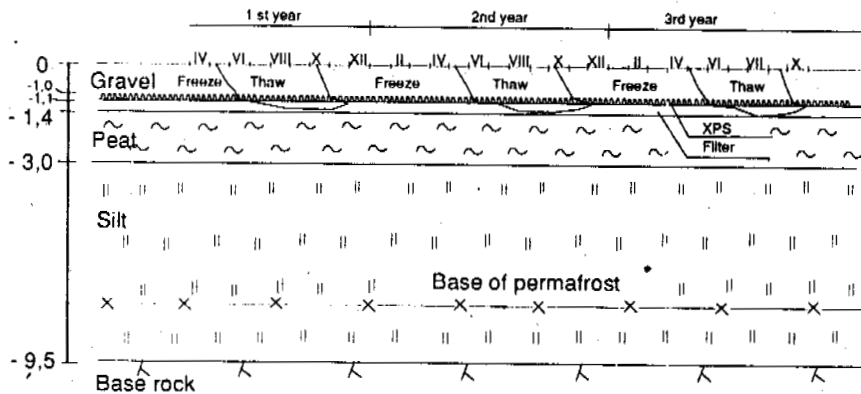
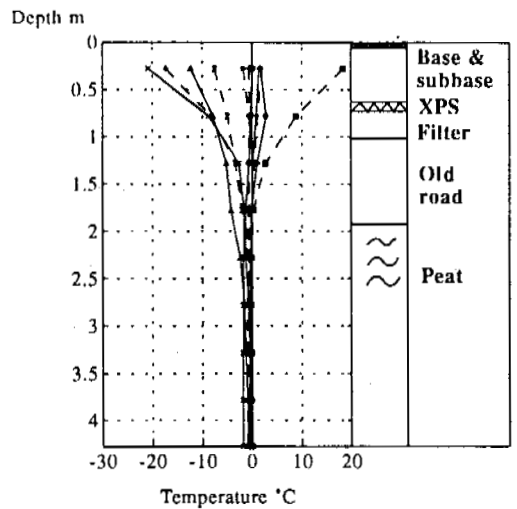


Fig. 5. Calculated frost and thaw penetration in the designed road section over three freeze-thaw cycles at Peera, palsa.

a)

p. 30280



b)

p. 30320

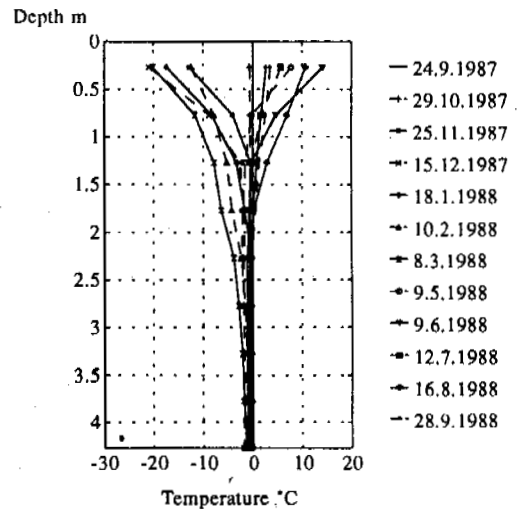


Fig. 6. Measured ground temperatures in the test section at Peera, palsa, during freeze - thaw season in winter 1987 - 1988 at points 30280 (a) and 30320 (b)

DISCUSSION AND CONCLUSIONS

Frost penetrated at the observation points down to the permafrost table during the freezing period of the winter 1987 - 1988. The thaw penetration at the monitoring points of the test section in the late summer of 1988 was roughly the same (about 2 metres) than for the original embankment. In the old embankment with the thickness of 1 - 1.8 metres, the late thaw penetrated into the ice-saturated peat. In the test structure, thaw penetration was limited almost totally within the thermally insulated embankment. Moreover, the thawing index in summer 1988 was high (28 900 h°C) compared to the long-term average (about 25 000 h°C). In the back-analysis of thaw penetration, a n-coefficient value about 1.25 was estimated.

This means a distinct effect of pavement colour on the thawing index, as values cited in literature are normally higher than 1.4 (Lunardini 1978). The corresponding n-coefficients varied on other, normally paved test sections in the close vicinity, at a distance of 100 - 300 metres in the same area, in the range of 1.33 - 2.0.

As a conclusion, it could be stated that the harmful thaw settlement can be limited using a proper, insulated embankment. The insulation thickness 100 mm extruded polystyrene was satisfactory in the conditions of the site. The use of light-coloured pavement aggregate decreases pavement temperatures during thawing season.

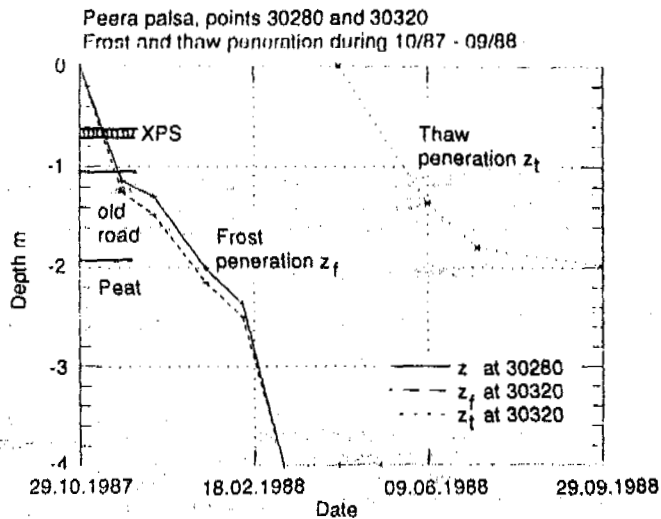


Fig. 7. Measured frost and thaw penetration in the period of autumn 1987 - autumn 1988 at the observation points.

The structure has to be designed using the data about local ground conditions and local climate. The design should cover a reasonable amount of freeze-thaw seasons to provide the description of long-term behaviour.

The insulation material should be of low-permeable type like the extruded poly-styrene, and the subdrainage should be provided in order to maintain the long-term functioning of the insulation.

#### REFERENCES

Kivikoski H., Repair of a road built on permafrost on main road 21 in Peera. Dimensioning, building and monitoring during 1987 - 1988. Espoo, Technical Research Centre of Finland, Research Notes 1030. 46.p. + app. 23 p. (In Finnish with English summary).

Lehtonen J., Improvement of icing on main road 21 at Haukijoki, Muotkataikka, Saarikoski and Pitkäranta. Construction and monitoring in 1986 - 1988. Espoo, Technical Research Centre of Finland, Research Notes 1218. 60 p. (In Finnish with English summary).

Saarelainen S., Repair structures of frost damage on main road 21 at Peera, Northern Finland. Design, construction and monitoring during 1986 - 1988. Espoo, Technical Research Centre of Finland, Research Notes 1102. 62 p. + app. 15 p. (In Finnish with English summary).

Saarelainen S., Repair of frost damage on main road 21 at Tulli, Kilpisjärvi. Design, construction and monitoring in 1987 - 1988. Espoo, Technical Research Centre of Finland, Research Notes 1107. 54 p. + app. 52 p. (In Finnish with English summary).

Saarelainen S. & Kivikoski H., Prevention of snow drifting with the help of road levelling and design. Experimental structure on main road 21 at Jeänkkash. Espoo, Technical Research

Centre of Finland, Research Notes 1096. 36 p. (In Finnish with English summary).

Talonrakennuksen routasuojausohjeet. (Instructions for frost protection in building construction). Helsinki, VTT, Geotechnical Laboratory & Rakentajain Kustannus Oy. 95 p. (In Finnish).

Lunardini V.J., Theory of n-factors and correlation of data. Proc. III Int. Conf. on Permafrost, Edmonton, Alberta, July 1978, Vol. 1, pp. 40 - 46.

**GLOBAL CLIMATIC CHANGE AND SOME POSSIBLE GEOMORPHOLOGICAL AND ECOLOGICAL EFFECTS  
IN ARCTIC PERMAFROST ENVIRONMENTS,  
ISFJORDEN AND LIEFEDEFJORDEN, NORTHERN SPITSBERGEN.**

Elisabeth Schmitt

Geographisches Institut, Justus-Liebig-Universität, D-6300 Giessen, Germany

Radiation, through its effect on temperature is the most important and differentiating ecological factor controlling the development of (and interactions between) vegetation, permafrost and geomorphology in the Arctic. To get some information on what may happen to the arctic permafrost environment in case of a global warming, two areas with different geocological conditions have been investigated: Liefdefjorden (80°N) and Isfjorden (78°N). Climatological, ecological and vegetation gradients from inner to outer fiord areas are presented. The role of solifluction and permafrost deserves special interest in this context. A comparative analysis includes the vegetational and ecological patterns, the macro- and local climate, and the microclimatic, geomorphological and pedological site conditions. It allows an interpretation of imaginable environmental aspects of a possible climatic change in these permafrost areas.

**INTRODUCTION AND AIM OF THE STUDY**

In the arctic, radiation through its effect on temperature is the most important factor controlling the development of permafrost, geomorphic features, vegetation and their interactions. To get some information regarding what may happen to the arctic permafrost environment in case of a global atmospheric warming, which is expected to be most pronounced at arctic latitudes (MAXWELL, 1991) two areas on Spitsbergen with different macroclimatic and geocological conditions have been investigated (Figure 1): Isfjord (78°N) and Liefdefjord (80°N).

The comparative investigation of these two areas with the vegetational and ecological distribution patterns and their regional variations as a function of meso- and microclimatic as well as geomorphological and pedological site conditions should allow an interpretation of some environmental aspects of a possible climatic change in these arctic permafrost areas.

**METHODS**

The ecological data on which the paper is based have been recorded during three field seasons on Spitsbergen (August 1989 - northwest coast of Spitsbergen, summer 1990 - Liefdefjord, summer 1991 - Isfjord). All locations and areas mentioned here have been visited. The vegetation has been recorded and mapped with the method of BRAUN-BLANQUET (1964,). Altogether more than 150 vegetation records have been done in the Isfjord area and about 100 records at the coasts of the Liefdefjord. The size of the homogeneous test areas was about 25m<sup>2</sup> per record. The cover was estimated for each vascular plant species and for the group of mosses and lichens. To get an explanation for the evident differences in the vegetation within each of both fiord areas and

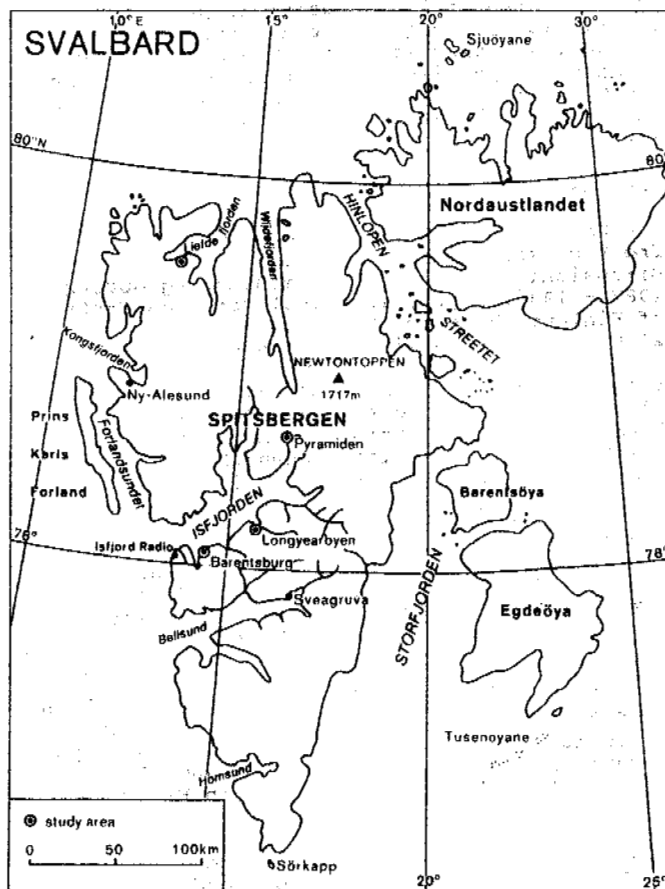


Figure 1. Location of the study areas in Isfjord and Liefdefjord

Table 1. Climatic gradient in the Isfjord attributed to the gradient in continentality

location	27.7.91	28.7.91	R	MJ	MS
Radio Isfjord	7.3°C weakly foggy, diffuse sunshine	7.2°C weakly foggy, diffuse sunshine	5986 cal/cm <sup>2</sup>	4.6/4.7°C	2.6/2.8°C
Barentsburg	9.1°C sky slightly overcasted to cloudy	11.2°C slightly cloudy with some clearings	7423 cal/cm <sup>2</sup>	5.1/5.1°C	3.1/3.3°C
Longyear	10.0°C sky slightly overcasted to cloudy	15.0°C sunny with single clouds	10785 cal/cm <sup>2</sup>	6.1/6.3°C	4.2/4.1°C
Pyramiden	15.2°C sunny	17.1°C sunny	14271 cal/cm <sup>2</sup>	7.6/7.8°C*	6.8/6.6°C*

R = mean global radiation July 1991

MJ = mean temperature July 1991/mean temperature July 1956-1976

MS = mean temperature summer season 1991/mean temperature summer season 1956-1976

\* = mean temperature summer season 1986-1990

increasing temperature  
 decreasing degree in cloudiness  
 increasing degree in continentality

between them, relevant ecological site conditions such as substrate, soil, geomorphology, permafrost, hydrology and climatic factors have also been recorded with special reference to the meso- and microclimate. The meso- and microclimatic situation of the investigated areas has been registered with several weather stations. In the Liefdefjord six electronic data logger recorded global radiation, air temperature, soil temperature in different depth, wind velocity, wind direction and relative humidity in different ecological sites. In the Isfjord one automatic weather station was set up in the vicinity of Longyearbyen. The climatic data of Barentsburg and Pyramiden have been recorded and provided to me by the Russian Arktikugol coal mining company. The data of Isfjord Radio were given by the local weather station and the long-term mean values of Longyearbyen and Isfjord Radio refer to AUNE (1982).

#### PRESENT ECOLOGICAL SITUATION

##### Ecological gradients in the research areas

As one passes up the Isfjord which deeply intersect the interior of Spitsbergen a gradual change in climate takes place. Sea fogs do not penetrate far into the fiord and low-lying clouds are often dispersed by the heat from the land near the entrance. As a result, clear weather is more frequent and insolation and temperature are higher than in the outer part.

This phenomenon is also true for the Liefdefjord, where cases of non-penetration of fog and clouds from the sea were observed at 80% of the days in July and August 1990. An additional factor, which probably exerts an important effect in producing these climatic gradients (particularly in Liefdefjord) is the prevalence of föhn winds blowing down the Monacobreen, a mighty glacier calving at the head of the fiord. On the whole, the climatic gradient is more pronounced in the very long Isfjord than in the much shorter Liefdefjord.

Table 1 shows the enormous differences in global radiation, temperature and wind velocity owing to the pronounced gradient in continentality from the mouth to the head of the Isfjord.

Corresponding to this climatic gradient in both investigation areas are gradients in vegetation which are also much more impressive in the Isfjord than in the Liefdefjord. It is a gradient in both, number of species and plant communities which is shown for the Isfjord in Table 2. According to the climate four climatic and vegetation zones on flat areas can be distinguished:

1. moss and lichen dominated zone: In the exterior coastal regions of Spitsbergen influenced by the Gulf stream, the fog abundance and the number of overcast days is very high (20 to 25 days in July). These less favourable climatic conditions during the summer allow only a few flowering plants to exist. Here more or less closed communities dominated by mosses, lichens and grass species seem to form the climax (moss and lichen heaths, cp. EUROLA, 1968).

2. Grass and herb mat zone: Further up the fiord and less exposed to the sea fog, climatic conditions become more favourable and allow the occurrence of a relatively closed vegetation cover richer in flowering plants.

3. Dryas zone: The Dryas zone is situated in the parts of the fiords protected from fog to a certain extent. The most highly developed vegetation form in this area is a dwarf-shrub heath of *Dryas octopetala*.

4. Cassiope zone: The inner fiord areas where coastal fog occurs rarely, heaths of *Cassiope tetragona* occur, provided that edaphic and topographical conditions are favorable.

Table 2. Vegetation gradient in the Isfjord due to the climatic gradient with special reference to the characteristic floristic structures

	Isfjord Radio	Barentsburg	Longyearbyen	Pyramiden
Typical Dryadion communities	fragmentary occurrence	Polari-Dryadetum	Tetragonae-Dryadetum	Tetragonae-Dryadetum
Degree in vegetation cover (vascular plants)	ca. 20%	40-50%	60-70%	above 70%
Occurrence of <i>Dryas oct.</i>	missing	rare	frequent	very frequent
Occurrence of <i>Cassiope tetragona</i>	missing	missing	frequent	very frequent
Vitality of dwarf shrubs	weak	moderate to weak	good to very good	very good
Proportion of grass species to dwarf shrubs	4:1	2:1	1:2	1:3
Diversity in vascular plant species	low	middle	high to very high	very high

In the Isfjord it is possible to trace the gradual appearance of *Cassiope* (Table 2) due to the existing gradient in temperature (Table 1). The plant is missing in areas near the fiord mouth. Further to the interior it forms extensive and luxuriant heaths and is accompanied by a flora of increasing diversity. Some of the attendant species occur exclusively in these inner fiord areas, e.g. *Empetrum hermaphroditum*, *Rubus chamaemorus* (dwarf shrub and fresh-moss heaths). Others, such as *Dryas octopetala*, *Alopecurus alpinus*, *Papaver dahlianum* and *Pedicularis hirsuta* (dry moss heath) are concentrated mainly in this part. In comparison, species which are more concentrated in the outer parts of the fiord are rather rare, e.g. *Poa alpina*, *Saxifraga cernua* (dry moss heath) and *Saxifraga oppositifolia* which is much more frequent and reaches a higher cover here than in the interior parts of the fiord. The communities of *Dryas octopetala* (*Nardino-Dryadetum*, *Rupestri-Dryadetum*, *Polari-Dryadetum* and *Tetragonae-Dryadetum* - RÖNNING, 1965) are concentrated in the "inland" areas (cp. EUROLA, 1968).

At present *Cassiope tetragona* forms communities of limited extent but SUMMERHAYES and ELTON (1928) assumed it would form heaths if the climate was slightly warmer. This richest type of vegetation, also characterized by species such as *Rubus chamaemorus*, *Vaccinium uliginosum* and *Betula nana*, seems to be most developed in the surroundings of Pyramiden (cp. Figure 1). Large areas of the Isfjord are part of the *Cassiope* zone, a smaller part belongs to the very well developed *Dryas* zone and only the outer fiord belongs to a moss and lichen dominated tundra. The border between the inner fiord area and less favorable areas may be located in Colesbukta.

Table 3. Alteration of significant ecological factors due to an increasing latitude and the effects on vegetation

	Isfjord		Licdefjord
Latitude	78°	←	79,9°
sun angle (21.6.)	35,5°	→	33,5°
radiation (cal/cm <sup>2</sup> /min) on a plane surface (21.6.)	1,16	→	1,1
mean July air temp.	6,3°	→	4,6°
snow-free areas mid-June (17.6.91)	100%	→	20-30%
period of ground thawing	begin of June - end of August	→	mid-June - mid-August
thawing depth	2,5 m	→	1,8 m
vegetation season	84 days	→	62 days
diversity in vascular plants	132 species	→	102 species
height of vegetation	20-30 cm	→	10-15 (20) cm
mean vegetation cover	75%	→	40-45%
vegetation pattern	continuous	→	patchy
structural vegetation diversity	high	→	medium
plant productivity	3-4 salix leaves per year	→	1-2 salix leaves per year
regeneration potential	higher	→	lower

→ arrow shows direction of decrease

The climatic conditions and thus the ecological situation in the Liefdefjord is comparably less favourable than in the Isfjord because of its position about 200 km further north (Table 3). The vegetation cover here is less dense and communities dominated by *Dryas octopetala* (not as well developed as in the Isfjord) are the climax. *Cassiope tetragona* is confined entirely to the interior of the fiord and even here it is not abundant and the individuals are not particularly luxuriant. The occurrence of *Cassiope*, even of *Empetrum hermaphroditum* at one place, and of additional 102 plant species, however, indicate advantageous meso- and microclimatic conditions in spite of the high latitude.

There are not only ecological gradients within the fiords due to the degree of continentality but also north-south gradients in important ecological factors. Table 3 shows the alteration of significant ecological factors due to an increasing latitude and their effects on vegetation.

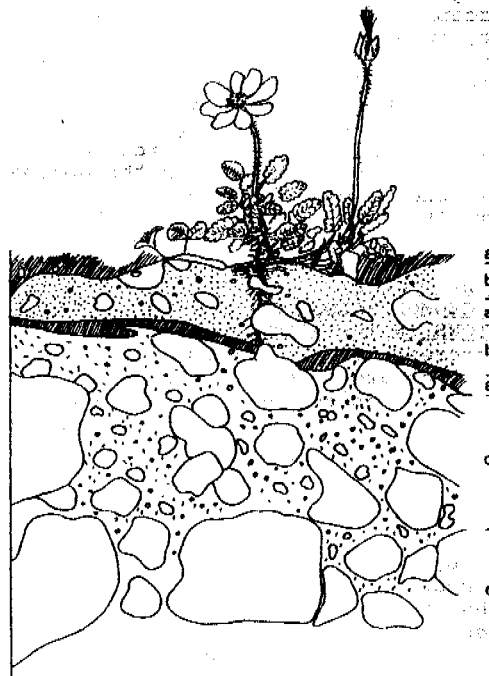
#### VEGETATION PATTERNS, SOLIFLUCTION AND PERMAFROST

At first sight the extramontane areas of the Liefdefjord seem to be very homogeneous with regard to vegetation and geomorphology. These patterns are primarily the result of the relations between water budget, microclimatic conditions, geomorphic processes and their influence on site stability over permafrost. The predominantly intact vegetation cover seems to indicate this area is geomorphologically inactive. However, detailed analysis of soil profiles, rhizospheres and plant societies indicate widespread occurrence of solifluction under vegetation cover.

The distribution of particular plants, especially *Dryas octopetala* and *Silene acaulis* seems to be a reliable indicator of the presence (*Silene acaulis*) or predominant absence (*Dryas octopetala*) of surficial solifluction processes (especially frost creep). Investigation of vegetation and soils in the Liefdefjord and the adjacent Bockfjord showed that *Dryas* is not competitive on poorly drained soils with pronounced surficial solifluction. The plant possesses a strong main root up to 0.3 m long which can be separated by the shear stress between upper and lower horizons during solifluction or by shearing over stones and stone flakes (cp. Figure 2). This phenomenon was evident in more than 70 pits exposing the root system of *Dryas*, which seemingly died out without cause.

In contrast, sites of active solifluction in the research area can be recognized at high numbers and intensive regrowth of *Silene acaulis*. The ability of this arctic-alpine radial cushion plant to discard the main root every two years (HEGI, 1979) makes it very competitive on unstable ground. In addition the studies in Liefdefjord showed that *Silene acaulis* does not even form a true main root but only a fine but dense and shallow root net. So the cushion can move with the upper few centimeters of the soil without suffering damage. With sufficient water saturation solifluction starts on gradients of 1° as

microsolifluction (TROLL, 1944) Clearly visible miniature solifluction lobes with a diameter of a few centimeters or tens of centimeters appeared on slopes greater than 5°. Characteristic of the visibly active zone is an increasing dominance of grassy species (*Poa alpina*, *Poa arctica*, *Alopecurus alpinus*), of *Oxyria digyna* and *Polygonum viviparum* (besides *Silene acaulis*). *Cassiope tetragona* shrubs also seem to be able to survive soil sliding or flow without suffering serious damage.



- a 1 to 8 cm thick layer of blackish-brown organic material with dark brown fine grained, slightly loamy substrate
- a<sub>1</sub> buried organic material
- b brown, slightly loamy substrate with a percentage of gravels and stones of about 15 Vol%
- c greyish-brown, slightly loamy substrate; soil pores filled with water; more than 80 Vol% gravels and stones
- d boulders of a diameter of about 50 cm rather no fine grained substrate

Figure 2. Separation of the strong main root of *Dryas octopetala* at sites with solifluction under vegetation (Liefdefjord). The main root of the plant has been cut at a depth of 3 to 4 cm. Only the unfrozen horizons a and b are moving. The drawing is made after a photograph taken in summer 1990 and displays a very typical situation.

Microclimate and soil type are essential factors controlling solifluction. The influence of both factors is particularly evident on a SSW-facing 10° slope in Liefdefjord with substrates consisting of silty sand to sandy loam. The relatively high summer temperatures (soil temperatures of 23° were frequent during summer 1990) and the good drainage resulted in deep desiccation of the substrate during the summer. As a result ground ice formation and frost action are reduced during the winter. Even at a depth of 40 - 45 cm the substrate was moderately dry. Due to the lack of water, solifluidal processes are reduced even at high slope angles. Among comparable soil conditions, there seems to be a gradient in solifluction activity in extramoral areas from the outer parts of the fiords to the inner parts. This phenomenon could be traced particularly well in the Isfjord. However, this gradient has no validity for intramoral areas where intensive thermal erosion (increased by high radiation and temperatures) is the dominant ecologic and geomorphic process (KING & SCHMITT, 1993).

#### GLOBAL WARMING AND SOME POSSIBLE ALTERATIONS IN RECENT GEOMORPHOLOGICAL AND ECOLOGICAL CONDITIONS IN THE ARCTIC

At present it is not possible to accurately predict what arctic climate changes will result from global changes (BLISS & MATVEYEVA, 1991). Global models predict that winter temperatures will rise more than summer temperatures (GAMMON et al., 1985). This assumption has already been true for the past secular temperature changes which have been more pronounced in Spitsbergen than in north-west Europe (HESSELBERG & BIRKELAND, 1940). In Spitsbergen, the increase in the mean annual temperature in about 50 years has been calculated to be 2 - 3° C. This has been mainly due to an increase in the winter temperature which has risen up by about 5° C. The temperature increase in July as the warmest month has been insignificant. Because the summer temperature is by far the most important climatic factor for the plant growth in Spitsbergen the change that has taken place has scarcely had such a great effect on the vegetation as one might expect judging from the rise of the mean annual temperature (HÖEG, 1956).

If the prediction of MAXWELL (1991) comes true and the mean annual temperature increase in the Arctic is about 3° or 4° C and winter temperatures rise about 7° to 9° C, the summer warming will be significant and will have important effects on the arctic ecology. Then, the following alterations in the arctic environment of Spitsbergen are imaginable:

1. In the near future the greatest changes probably will occur in processes related to permafrost (MAXWELL, 1991). These will be indirect changes resulting from an increase in the active layer thickness. It is expected that these short-term effects of a climatic warming differ widely from intramoral to extramoral sites:

Geomorphologically intramoral areas are characterized by a widespread thermal erosion today (KING, 1993) which may certainly be enhanced by a future warming. Consequently

substrate instability will be intensified so that no ecological development can take place - in contrast a degeneration of the present, weakly developed ecosystems will be promoted by an increase in radiation and temperature. In extramoral areas increasing temperatures will immediately favour plant growth, plant survival, the development of a more dense and continuous vegetation cover (as the ecological gradients of today show us). As a result of improved conditions for plant growth, vegetation will be enabled to retard and minimize erosion associated with the melting of ground ice. At the same time higher temperatures will also increase the maturity degree and the differentiation of the scarcely developed soil profiles.

2. As a longterm effect, a partial displacement of the inner arctic zonation (Low, Middle and High Arctic) with their structural characteristics towards north is to be expected because "floristic zones are correlated with the amount of summer warmth to the point that other ecological factors are insignificant in comparison" (YOUNG, 1971 in BILLINGS, 1991). In the case of Spitsbergen as a high arctic area there will be a displacement of vegetation zones along the described gradients with an extension of warm-loving Cassiope tetragona and Dryas octopetala communities.

3. In the most favourable areas of Spitsbergen (inner fiord areas) the vegetation cover will experience incisive structural and floristic changes. Empetrum hermaphroditum which presently occurs to a limited extent will form true heaths if the climatic conditions improve. The occurrence of plants such as Betula nana, Rubus chamaemorus and Vaccinium uliginosum together with Sphagnum species (SUMMERHAYES & ELTON, 1928) indicates that a relatively slight amelioration of the present climate would produce tundra vegetation of the typical subarctic type, here.

The final extent to which climatic changes will affect these permafrost environments depends on the physiological reactions of arctic wildlife to a changing climate and even more than this on the nature of feedbacks coupling vegetation, substrate stability and geomorphological processes (see CHAPIN, 1991).

#### ACKNOWLEDGEMENTS:

Sincere thanks are due to the German Research Foundation (DFG) for financial support of my research work. Many thanks are also given to the people of Barentsburg for their friendly welcome and readily given valuable informations and to Prof. Dr. L. King for introducing me to the Arctic, geomorphological advice and supplying the necessary climatological instruments.

## References:

- AUNE, B. (1982): The climate at Norwegian Arctic Stations. - Klima, 5, Norsk Meteorologiske Institutt.
- BILLINGS, W. D. (1991): Phytogeographic and evolutionary potential of the arctic flora. - In: F. S. Chapin et al. (eds.): Arctic ecosystems in a changing climate: 91-106 London.
- BLISS, L. C. & K. M. PETERSON (1991): Plant succession, competition and the physiological constraints of species in the Arctic. - In: F. S. Chapin et al. (eds.): Arctic ecosystems in a changing climate: 111-133. London
- BLISS, L. C. & N. V. MATVEYEVA (1991): Circumpolar vegetation. - In: F. S. Chapin et al. (eds.): Arctic ecosystems in a changing climate: 59-86. London.
- BRAUN-BLANQUET, J. (1964): Pflanzensoziologie. Grundzüge der Vegetationskunde. Wien
- CHAPIN, F. S. et al. (1991): Arctic plant physiological ecology: a challenge for the future. - In: F. S. Chapin et al (eds.): Arctic ecosystems in a changing climate: 3-7. London.
- EUROLA, S. (1968): Über die Fjeldheide-vegetation in den Gebieten von Isfjorden und Hornsund in Westspitzbergen. Bot.Inst. Universität Oulu, Finnland.
- GAMMON, R. H. et al (1985): History of Carbon dioxide in the atmosphere. - In: J.R. Trabalka (ed.): Carbon dioxide and the global carbon cycle: 25-62. Math. Tech. Info. Serv. Springfield, Virginia.
- HEGI, G. (1979): Illustrierte Flora von Mitteleuropa III, 2, 812 pp, Berlin
- HESELBERG, Th. & B. J. BIRKELAND (1940): Säkulare Schwankungen des Klimas von Norwegen. Die Lufttemperatur. - Geophysikalische Publikationen 14,4.
- HÖEG, O.A. (1956): The present and past vegetation of Spitsbergen. - Proceedings of the Linnean Society of London 166 (1-2): 144-149. London.
- KING, L. (1993): Examples of geomorphological changes in glacially sculptured high arctic permafrost areas from Svalbard and the Queen Elizabeth Islands, Canada. (this volume)
- KING, L. & E. SCHMITT (1993): Solifluction and thermal erosion in high arctic ecosystems, Northern Spitsbergen: Processes and effects. - In: B. Frenzel (ed.): Palaeoclimate Research, in print.
- MAXWELL, B. (1991): Arctic climate: potential for change under global warming. - In: F. S. Chapin et al (eds.): Arctic ecosystems in a changing climate: 11-31. London.
- RÖNNING, O. (1965): Studies in Dryadion of Svalbard. - Norsk Polarinstittutt Skrifter 134: 1-52.
- SCHMITT, E. (1992): Ökologische Untersuchungen zur Vegetationsdifferenzierung und -dynamik im Liefdefjord. - Stuttgarter Geographische Studien 117: 133-140.
- SUMMERHAYES, V. S. and C. S. ELTON (1928): Further contribution of the ecology of Spitsbergen. - Journal of ecology 16 (2): 193-268. Cambridge.
- TROLL, C. (1944): Strukturböden, Solifluktion und Frostklimate der Erde. - Geologische Rundschau XXXIV: 546-694. Berlin.
- WÜTHRICH, C. (1991): Landschaftsökologische Umweltforschung: Beiträge zu den Wechselwirkungen zwischen biotischen und abiotischen Faktoren im hocharktischen Ökosystem (Spitzbergen). - Die Erde 122 (4): 335-352. Berlin.



# Correct Use of the Segregation Potential Concept for Two-Dimensional Frost Heave Simulation

Mu Shen and J.-M. Konrad

Dept. of Civil Engineering, Laval University, Quebec, PQ, G1K 7P4, Canada

The segregation potential of a soil can be used as an input to predict the moisture content increase due to ice lens growth during freezing. It is an efficient phenomenological parameter that can readily be used in a two-dimensional numerical simulating heat and mass transfer model.

This paper discusses modifications to conventional heat flow models in order to determine the temperature gradient in the frozen fringe with sufficient accuracy and without oscillations despite spatial discretization. A new technique for calculating the temperature gradient in the frozen fringe has proven to be a satisfactory approach for applying correctly the SP functions to soil freezing. This technique is especially applicable for soils characterized by sharp transitions between the unfrozen and frozen state.

## INTRODUCTION

Konrad and Morgenstern (1980, 1981, 1982) introduced the segregation potential,  $SP$ , to characterize freezing in fine-grained soils, and showed that this concept is very useful for engineering predictions. According to the Konrad-Morgenstern  $SP$  theory, frost heave results from two components: the water transported to the frost front to form ice lenses, and the in situ freezing of the pore water. The water intake flux to the active ice lens is proportional to the temperature gradient in the frozen fringe

$$v = SP \cdot gradT \quad (1)$$

where  $v$  is the velocity of water intake ( $m/s$ ),  $gradT$  is the temperature gradient in the frozen fringe ( $^{\circ}C/m$ ), and  $SP$  is the segregation potential ( $m^2/^{\circ}C \cdot s$ ), which can be determined from laboratory freezing tests. A detailed procedure for experimental determination of the segregation potential has been described by Konrad (1987). Konrad and Morgenstern (1982) established that the segregation potential of a given freezing soil decreases with increasing applied pressure as follows

$$SP = SP_0 \cdot e^{-a\sigma_n} \quad (2)$$

where  $SP_0$  is the value of  $SP$  obtained for zero applied pressure,  $\sigma_n$  is the stress normal to frost front, and  $a$  is a soil's constant. The  $SP$  frost heave model in its simplest form only requires a precise knowledge of the temperature gradient in the frozen fringe. In recent years, the

segregation potential concept has been successfully applied for predicting frost heaving from chilled pipelines and artificial ground freezing in one-dimensional cases (Nixon, 1982; Konrad and Morgenstern, 1984). However, calculations of the adequate temperature gradient and the stress-heave interaction in two-dimensional cases are much more complex than in one-dimensional cases. The thermal analysis by Konrad and Morgenstern (1984) for predicting frost heave around chilled buried pipelines was based on a one-dimensional, axially symmetrical finite difference method. This implied that the thermal effects from the ground surface were not taken into account with this approach. Nixon (1986) developed a two-dimensional thermal simulator incorporated with the  $SP$  concept. In this simulator, the temperature gradient and position of active lensing were obtained by using a quadratic fit to the temperatures in the elements adjacent to the frost front. However, this method is limited to the case where the frost front is approximately orthogonal to the grid lines of the rectangular mesh. Coutts (1991) used the control volume finite element method (CVFEM) incorporated with the  $SP$  concept to simulate the temperature and stress fields in freezing soil around a chilled pipeline. Because of the spatial discretization, the calculated temperature gradient in this numerical model oscillates with time. To reduce the amplitude of oscillations, Coutts (1991) proposed that the temperature gradients used to calculate the water intake should be determined at the isotherm of the coldest temperature in the phase change range. Obviously, this approach may not eliminate completely the oscillations, but

reduce their amplitudes.

This paper describes a numerical technique for determining the temperature gradient in the frozen fringe with sufficient accuracy and without oscillation.

### OUTLINE OF THE THERMAL MODEL

The basic heat transfer equation in a freezing soil is governed by the following partial differential equation

$$\frac{\partial H}{\partial t} - \nabla \cdot (\lambda \nabla T) - Q = 0 \quad (3)$$

where  $H$  denotes the enthalpy per unit volume ( $J/m^3$ ),  $\lambda$  is the thermal conductivity ( $W/m^\circ C$ ),  $T$  is the soil temperature ( $^\circ C$ ),  $t$  is time ( $s$ ), and  $Q$  is the internal heat source ( $W/m^3$ ). Convection within the soil is neglected, since the conductive components are often 2 or 3 orders of magnitude greater than the convective components (Nixon, 1975).

Alternatively, eqn.(3) can be expressed as

$$\bar{C} \frac{\partial T}{\partial t} - \nabla \cdot (\lambda \nabla T) - Q = 0 \quad (4)$$

where is  $\bar{C}$  an apparent heat capacity, defined as

$$\bar{C} \equiv \frac{dH}{dt} \quad (5)$$

Bonacina et al. (1973) assumed that latent heat during phase change is released over a very narrow temperature range,  $T_2 - T_1$  ( $T_1 < T_f < T_2$ ). It has been found that numerical results are sensitive to the selection and implementation of the  $T_2 - T_1$  interval. Instead, O'Neill (1983) suggested that the phase change occurs at a discrete temperature,  $T_f$ , without any artificial spreading of the phase front, i.e.

$$\bar{C} = C + L\delta(T - T_f) \quad (6)$$

where  $L$  denotes the latent heat of fusion per unit volume of the soil ( $J/m^3$ ), and  $\delta$  is the Dirac delta function.

### FINITE ELEMENT PROCEDURE

Using the Galerkin finite element method, one multiplies the governing equation (4) by a weighting function  $N_i$  and integrates over the whole domain

$$\begin{aligned} \int_A N_i \left[ \bar{C} \frac{\partial T}{\partial t} - \nabla \cdot (\lambda \nabla T) - Q \right] dA = \\ \int_A [N_i \bar{C} \frac{\partial T}{\partial t} + \nabla N_i \cdot \lambda \nabla T] dA - \int_S N_i \lambda \frac{\partial T}{\partial n} dS \\ - \int_A N_i Q dA = 0 \end{aligned} \quad (7)$$

where  $A$  designates the spatial domain, and  $S$  is its boundary with normal direction  $n$ . The finite element discretization is accomplished using triangular elements. The unknown function  $T$  can be approximated throughout the solution domain at any time  $t$  by the relationship

$$T \approx \sum_{j=1}^N T_j(t) N_j(x, y) \quad (8)$$

where  $T_j(t)$  are nodal temperatures to be determined, and  $N_j$  are interpolation functions, which are chosen to be identical to the weighting functions. Substituting the approximation (8) in (7) provides  $N$  equations for solving  $N$  unknown nodal temperatures  $T_j$ , once the boundary conditions have been applied

$$[N]\{T\} + [K]\{T\} = \{F\} \quad (9)$$

where

$$\begin{aligned} [N] &= \int_A \bar{C} N_i N_j dA \\ [K] &= \int_A \nabla N_i \cdot \lambda \nabla N_j dA \\ \{F\} &= \int_A N_i Q dA \end{aligned}$$

The greatest difficulty in solving latent heat effects is the evaluation of matrix  $[N]$ , which contains the integral of the apparent heat capacity. O'Neill (1983) proposed an approach for obtaining the matrix  $[N]$  associated with the  $\delta$  function in the heat capacity

$$[N] = \int_A C N_i N_j dx dy + L \int_A N_i N_j \delta(T - T_f) dx dy \quad (10)$$

The second term of the right hand side in eqn.(10) is nonzero only when an element contains the  $T_f$  isotherm. Using two-dimensional linear triangular finite elements, the temperature gradient in each element is constant, and all isotherms in the element are parallel. However, considering a new coordinate system ( $x', y'$ ) for each element, in which  $x'$  is perpendicular to the  $T_f$  isotherm and  $y'$  extends along this isotherm, the temperature distribution function,  $T$ , can then be expressed to be only a function of  $x'$

$$\frac{dT}{dx'} = gradT = \sqrt{\left(\frac{\partial T}{\partial x}\right)^2 + \left(\frac{\partial T}{\partial y}\right)^2} \quad (11)$$

$$\frac{dT}{dy'} = 0$$

Applying the characteristics of  $\delta$  function, the integral including latent heat may be transformed as

$$\begin{aligned} L \int_{\Delta} N_i N_j \delta(T - T_f) dx dy &= L \int_{\Delta} N_i N_j \delta(T - T_f) dx' dy' \\ &= L \int_{y'} \int_{x'} N_i N_j \delta(T - T_f) \frac{dx'}{dT} dT dy' \\ &= \frac{L}{gradT} \int_{x'_1}^{x'_2} N_i N_j |_{T=T_f} dy' \end{aligned} \quad (12)$$

where the subscripts 1 and 2 are two intersection points of the  $T_f$  isotherm with two of the three element sides. The above integral is then evaluated approximately by using Simpson's rule. In phase change elements, thermophysical properties  $\lambda$  and  $C$  are evaluated from the weighted area method. This procedure provides a latent heat contribution to the matrix  $[N]$ , after which one may proceed as usual.

Because the thermophysical properties are related to temperature, the system of differential equations (9) is nonlinear and an iterative procedure is normally required to upgrade the estimate of  $[N]$  and  $[K]$  at each time step. However, these coefficients may also be evaluated using the temperature distribution of the previous time step without iteration. Evidently, some errors are introduced as compared with a solution obtained by a fully iterative procedure, but these errors are of the same nature as the truncation errors in any finite difference procedure and hence can be reduced to an acceptable level by using relatively small time steps during the period of rapidly-changing temperature.

### SINGULARITY IN THE TEMPERATURE GRADIENT

The gradient used in the *SP* concept (eqn.(1)) for water intake velocity to the frost front is the temperature gradient in the frozen soil nearest to the  $T_f$  isotherm. Because of the discontinuity in temperature gradients at the frozen-unfrozen interface, the temperature gradient within an individual heating element, as determined from eqn.(11), does not vary monotonically with time, as it would in a real system, but instead oscillates. This phenomenon occurs in

all fixed-mesh finite element models. To illustrate this phenomenon, a one-dimensional thermal simulation with phase change was performed on a soil column discretized using two-dimensional triangular elements. The soil column was 2m high, and the top boundary temperature was held at  $-1^\circ\text{C}$ . The bottom and sides of the column were specified as zero-flux boundaries. The temperature gradient of the element containing the  $T_f = 0^\circ\text{C}$  isotherm varying with time was presented by the dotted line 2 in Figure (1).

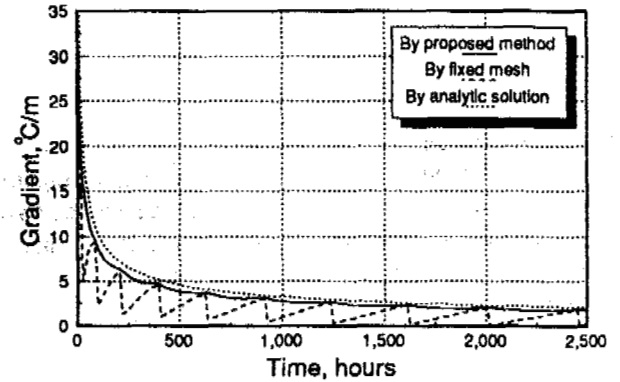


Figure 1: Comparison of temperature gradients calculated by using different methods.

As seen in this figure, the temperature gradient at phase change elements fluctuates significantly. This arises from the fact that when the frost front crosses an element boundary, the resulting temperature gradient is an average of the temperature gradients in the frozen and unfrozen portions of the element. As the frost front progresses through the element, the temperature gradient increases since the area of the frozen portion increases. This continues until the  $T_f$  isotherm crosses the next element boundary. Then, the temperature gradient suddenly drops, because the frozen area in the "new" element becomes much less than in the "old" element.

To avoid oscillations of the temperature gradient used in the *SP* concept during computations, the temperature gradient should be determined from a completely frozen element adjacent the frost front. This can be done by using a locally moving mesh technique as illustrated in Figure (2). Consider that the frost front intersects the shaded triangular element *JE* at points 1 and 2 as shown. From the mid point of segment 1-2, an orthogonal line, *A-B*, is drawn. All the triangular elements having a common node with the shaded element *JE* are searched (elements *E1* to *E12* as shown). From these elements, the nodes which are in the frozen zones (nodes *k1* to *k4*) are searched and

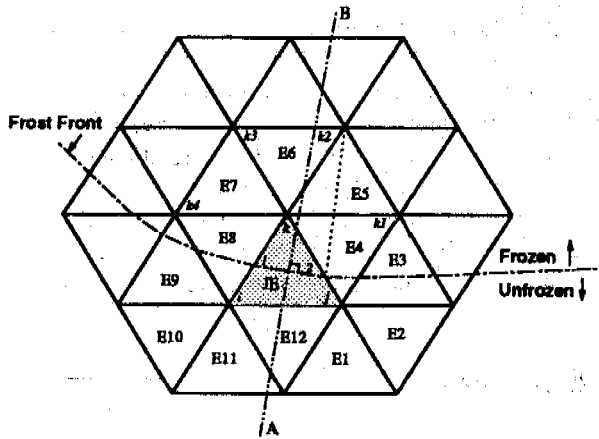


Figure 2: Illustration of the proposed method.

stored. The node with the shortest distance normal to the line A-B (node  $k_2$ ) is selected. A temporary triangular element joined by points 1, 2 and  $k_2$  is now created, from which the temperature gradient in the frozen side of the frost front segment 1-2 can be determined by using eqn.(11). This gradient is then used to calculate water intake flux  $v$  to the heaving element  $JE$  (shaded) from the SP function.

### CALCULATION OF THE FROST HEAVE

Frost heave in a freezing soil usually has two components, in-situ heave and segregational heave. For heaving element,  $JE$  (shaded element as shown in Figure (2)), the total volumetric strain increment,  $d\epsilon^v$ , in a particular time step is

$$d\epsilon^v = d\epsilon_{in}^v + d\epsilon_s^v \quad (13)$$

where  $d\epsilon_{in}^v$  and  $d\epsilon_s^v$  are the element volumetric strain increments due to in-situ heave and segregational heave, respectively. The in-situ expansion in the element is caused by freezing and expansion of the pore water in the soil, given by

$$d\epsilon_{in}^v = \frac{\Delta V_{in}}{V} = \left(\frac{\rho_w}{\rho_i} - 1\right)(W_0 - W_u) \frac{\rho_d}{\rho_w} \Delta\chi \quad (14)$$

where  $\Delta V_{in}$  is the element volumetric expansion increment due to the in-situ heave,  $V$  is the total volume of the element,  $\rho_i$ ,  $\rho_w$  are densities of the ice and water, respectively,  $W_0$ ,  $W_u$  are initial water content and unfrozen water content, respectively,  $\rho_d$  is the dry density of the soil,

and  $\Delta\chi$  is the change in the proportional of the fractional area frozen in the element over the time step.

With the frost front position given by the temperature solution for the time step, the temperature gradient determined by using the proposed technique, and the length of the segregational freezing front isotherm  $l$ , in the element (length of the segment 1-2 as shown in Figure (2)), may be used to calculate the volumetric strain increment due to the segregational heave using the SP function

$$d\epsilon_s^v = \frac{\Delta V_s}{V} = \frac{\rho_w}{\rho_i} l v \frac{\Delta t}{A} \quad (15)$$

where  $\Delta V_s$  is the element volumetric expansion increment due to the segregational heave,  $A$  is the element area,  $\Delta t$  is the time step, and  $v$  is the water intake flux to the heaving element obtained by using the eqn.(2).

For the case of plane strain, the initial strain is affected by the elastic constants. The element isotropic volumetric heave strain increment may be written as

$$d\{\epsilon^v\} = \begin{Bmatrix} d\epsilon_x^v \\ d\epsilon_y^v \\ d\epsilon_{xy}^v \end{Bmatrix} = \frac{(1+\mu)d\epsilon^v}{3} \begin{Bmatrix} 1 \\ 1 \\ 0 \end{Bmatrix} \quad (16)$$

where  $\mu$  is the Poisson's ratio. More detail on the mechanical finite element procedure will appear in an upcoming paper, where anisotropic heave is also discussed.

### NUMERICAL EXAMPLES

The accuracy of the numerical thermal model has been verified against the results of Neumann solution for a one-dimensional freezing problem using the two-dimensional triangular finite elements. The region considered is initially unfrozen at a  $1^\circ\text{C}$  and the freezing temperature is taken as

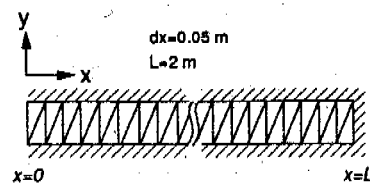


Figure 3: Finite element mesh 1-D freezing problem.

0°C. The finite element mesh used is shown in Figure (3). The following parameter values are used in this numerical test

$$T|_{x=0, t>0} = -1^{\circ}\text{C}$$

$$\lambda_f = 1.22 \qquad \lambda_u = 1.09 \text{ W/m}^{\circ}\text{C}$$

$$C_f = 2.07 \qquad C_u = 2.5 \text{ MJ/m}^3$$

$$L = 75.42 \text{ MJ/m}^3$$

The progress of the frost penetration is compared with the Neumann solution in Figure (4). As shown in this figure,

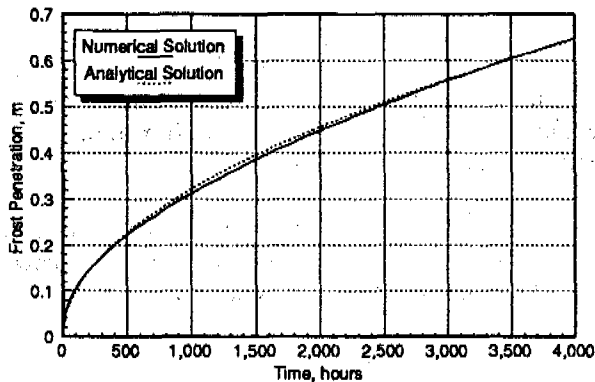


Figure 4: Comparison between calculated and analytical (Neumann) frost penetration.

the numerical result agrees well with the analytic solution. Figure (1) shows the temperature gradients for calculating water intake flux to the heaving element varying with time, using three different methods. The dotted line 3 in this figure presents the analytic solution of the temperature gradient in frozen zone, which is obtained by using the exact location of the frost front incorporated with the linear temperature profile in frozen zone. The solid line 1 shows the temperature gradient in the frozen soil close to the frost front calculated using the proposed technique. The precision of the numerical results based on the proposed method is shown to be quite satisfactory when compared with the analytical solution.

The model has been used to simulate the first phase of the Canada-France pipeline ground freezing experiment described by Williams (1983). In this experiment, the temperature of the pipe was held constant at  $-2^{\circ}\text{C}$ , and the temperature of the ground surface was at  $-0.75^{\circ}\text{C}$ . The initial temperature was  $4^{\circ}\text{C}$  and the moisture content was 40% ( $\text{m}^3/\text{m}^3$ ). A  $SP_0$  value of  $145 \times 10^{-5} \text{ (mm}^2/\text{C}\cdot\text{s)}$  was selected, and the parameter  $a$  in the eqn.(2) was given as  $2.0 \text{ (MPa}^{-1}\text{)}$  (Coutts, 1991). In this numerical test, we have only considered an extreme pipe-confinement case in which

the pipe is assumed to be free floating.

Figure (5) and (6) show the simulated isotherms and the moisture content after 6000 hours, respectively. From these two figures, it is found that a significant moisture accumulation occurs below the pipe and behind the advancing freezing front. More detail on the mechanical model and simulation results will be presented in a subsequent paper, because of the limitation of space.

## CONCLUSION

Most of the two-dimensional thermal models use a fixed finite element mesh and simulate fairly well the location of the frost front. However, the fixed finite element mesh leads to oscillations in temperature gradient in the phase change element, which in turn may lead to oscillations in frost heave computations if SP concept is used. A new approach for determining the temperature gradient in the frozen fringe without oscillations due to spatial discretization has been described. This technique was used to calculate the temperature gradient in the frozen soil near the frost front for a one-dimensional freezing problem using a two-dimensional mesh. It was established that the numerical results agree well with the analytic solution.

## REFERENCE

- Bonacina, C., Comini, G., Fasano, A. and Primicerio, M., 1973, Numerical solution of phase-change problems, *Int. J. Heat Mass Transfer*, 16, pp.1825-1832.
- Coutts, R.J., 1991, Development of a Two-dimensional Finite Element Model to Calculate Temperatures and Stresses in Frost Susceptible Soil around a Chilled Pipeline, M.Sc. Thesis, Univ. of Waterloo.
- Konrad, J.-M. and Morgenstern, N.R., 1980, A Mechanistic Theory of Ice Lens Formation in Fine-grained Soils, *Can. Geotech. J.*, 17, pp.473-486.
- Konrad, J.-M. and Morgenstern, N.R., 1981, The Segregation Potential of a Freezing Soil, *Can. Geotech. J.*, 18, pp.482-491.
- Konrad, J.-M. and Morgenstern, N.R., 1982, Effects of Applied Pressure on Freezing Soils, *Can. Geotech. J.*, 19, pp.494-505.
- Konrad, J.-M. and Morgenstern, N.R., 1984, Frost Heave Prediction of Chilled Pipelines Buried in Unfrozen Soils, *Can. Geotech. J.*, 21, pp.100-115.
- Konrad, J.-M., 1987, Procedure for Determining the Segregation Potential of Freezing Soils, *ASTM Geotechnical Testing Journal*, pp.51-58.
- Nixon, J.F., 1975, The Role of Convective Heat Transport

in the Thawing Soils, *Can. Geotech. J.*, 12, pp.425-429.  
 Nixon, J.F., 1982, Field Frost Heave Prediction Using the Segregation Potential Concept, *Can. Geotech. J.*, 19, pp.526-529.  
 Nixon, J.F., 1986, Pipeline Frost Heave Predictions Using a 2-D Thermal Models, *ASCE Res. on Transportation Facilities in Cold Regions*, pp. 67-82.  
 O'Neill, K., 1983, Fixed Mesh Finite Element Solution for Cartesian Two-dimensional Phase Change, *J. of Energy Resources Techno.*, ASME, 105, pp.436-441.

Shen Mu, 1988, Numerical Analysis of Temperature Field in a Thawing Embankment in Permafrost, *Can. Geotech. J.*, 25, pp.163-166.  
 Shen Mu and Ladanyi, B., 1991, Soil-pipe Interaction During Frost Heaving around a Buried Chilled Pipeline, *Proc. of 6th ASCE Cold Regions Eng. Conf.*, West Lebanon, NH, pp.11-21.  
 Williams, P.J., 1983, Investigation of Soil Freezing in Association with a Buried Chilled pipeline in a Large-scale Test Facility - Phase 2 (Final Report) for Earth Physics Branch, EMRC.

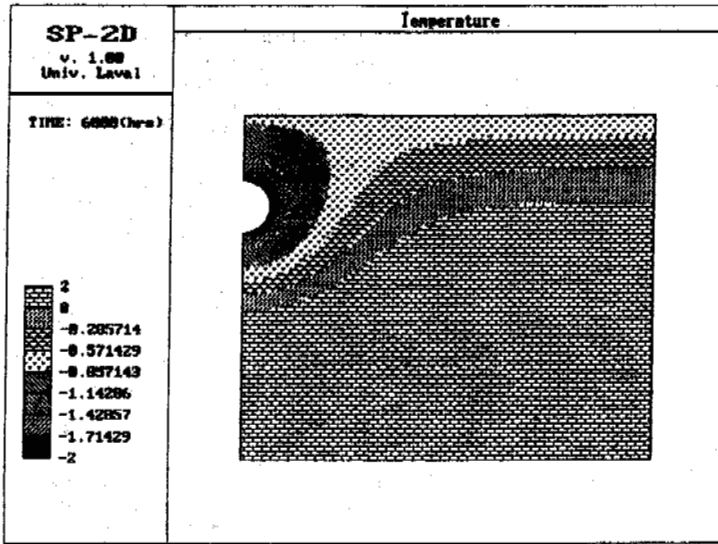


Figure 5: Simulated isotherms after 6000 hours.

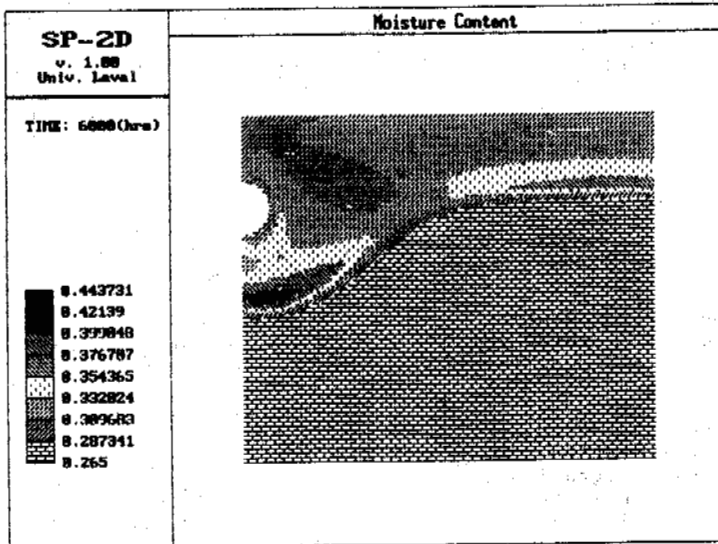


Figure 6: Simulated moisture distribution after 6000 hours

## A MODEL OF MIGRATION POTENTIAL FOR MOISTURE MIGRATION DURING SOIL FREEZING

Sheng Yu, Ma Wei and Hou Zhongjie

State Key Laboratory of Frozen Soil Engineering, Lanzhou Institute of  
Glaciology and Geocryology, Chinese Academy of Sciences, China

A model for moisture migration during soil freezing is proposed. According to the model, the moisture migration in freezing fringe can be determined through introducing the concept of migration potential  $M_p$  (extended segregation potential) which can be given by tests. The uncertainty can be avoided for estimating the hydraulic conductivity within freezing fringe in general models. Experimental method of migration potential is given.

### INTRODUCTION

When a column of soil freezes from cold side to warm side, the moisture migration occurs, and the moisture field redistributes. Both theory and practice prove that moisture migration occurs mainly in freezing fringe, and the amount of the migration depends on temperature gradient, moisture content and soil properties. Many mathematical models have been proposed. The model for coupled heat and moisture is presented by Harlan (1973) in which moisture migration is calculated, through introducing Darcy's law into frozen soil. The theory of segregation potential ( $S_p$ ) (Konard and Morgenstern, 1981) simply determines the moisture migration during the formation of the final ice lens. In this paper, the concept of  $S_p$  is extended to freezing soil and renamed as migration potential ( $M_p$ ). Combining  $M_p$  and Harlan's model, a new mathematical model for determining the moisture field is proposed during soil freezing. The relation between  $M_p$  and the penetration rate is obtained in open system.

### GENERAL MATHEMATICAL MODELS

According to the law of moisture migration, a column of soil can be divided into three zones (shown in Figure 1): unfrozen zone, freezing fringe and frozen zone. In unfrozen zone, there does not exist ice, the moisture distribution is defined by the soil water potential. Freezing fringe is a important zone for migration, although it is thin. The moisture migration is mainly controlled by the zone. That is the most intense zone among the three zone during freezing. In frozen zone, soil have been completely frozen, the structure of the soil is comparatively steady. The amount of the moisture migration is very less.

Many mathematical models have been proposed to calculate the moisture migration in freezing

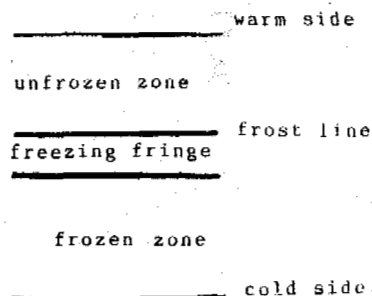


Figure 1. Schematic diagram of freezing soil

soil. The moisture equation combining Darcy's law with Clapeyron equation is the most common. Darcy's law is as follow:

$$V = K \frac{\partial \psi}{\partial x} \quad (1)$$

Where:  $V$  - the rate of migration (cm/s)  
 $K$  - moisture conductivity (cm/m)  
 $\psi$  - soil water potential (cm)  
 $x$  - coordinate (cm)

Based on the calculation of soil water potential, we get:

$$\psi = P_w + \chi \quad (2)$$

here,  $P_w$  is the water pressure. So that:

$$\frac{\partial \psi}{\partial x} = \frac{\partial P}{\partial \theta} \frac{\partial \theta}{\partial x} \quad (3)$$

$$K \frac{\partial P}{\partial \theta} = D \quad (4)$$

where,  $D$  is diffusivity, (cm<sup>2</sup>/s),  $\theta$  is moisture content

In frozen zone and freezing fringe, the Clapeyron equation is expressed as:

$$\frac{dP_w}{\rho_w} - \frac{dP_i}{\rho_i} = L \frac{dT}{T_k} \quad (5)$$

Where:  $P_i$  - ice pressure  
 $L$  - latent heat  
 $T_k$  - absolute temperature  
 $T$  - temperature  
 $\rho_w, \rho_i$  - density of water and ice, respectively.  
 If  $P_i=0$ , and the darcy's law is still correct, substituting equation (2) and (5) into equation (1) yields:

$$V = \frac{\rho_w K L}{T_k} \frac{dT}{dx} \quad (6)$$

It is difficult to determine the moisture conductivity in the frozen and freezing soil by experiment. In order to carry out numerical simulation, it is often assumed that the moisture conductivity is a function of moisture content or temperature in some models. The effect of the moisture conductivity on the calculation is small for the frozen zone because of its steady structure. However, the assumption has a great influence on the calculation for freezing fringe, because the unfrozen moisture content has a rapid decreases and the decreasing process can't be determined by experiment. Therefore, if the assumption  $K=f(\theta)$  or  $K=f(T)$  is used to calculate moisture field, there would be a less reliability, and the accuracy of the model is doubtful.

#### MIGRATION POTENTIAL MODEL

##### Segregation Potential

In order to avoid the uncertainty and sensitivity of the moisture conductivity, a simple method is proposed to predict the frost heave by Konard and Morgenstern (1981). It is pointed out that moisture migration rate ( $V$ ) is in inverse proportion to the temperature gradient ( $Gr$ ) in freezing fringe during the formation of final ice lens, and the proportional coefficient is defined as segregation potential ( $Sp$ ), that is:

$$V = Sp \cdot Gr \quad (7)$$

The process of the formation of ice lens can be considered as a steady process. When the boundary condition is constant, the segregation potential is proximately constant. Using equation (7), moisture migration can be obtained after  $Sp$  is determined.

##### Migration Potential Model

Segregation potential is constant only in steady process. When soil freezes continuously,  $Sp$  is obviously changeable. The changes of penetration rate, moisture distribution of unfrozen zone and overburden certainly effected the change of  $Sp$ , and the concept of segregation is not suitable at this moment. In order to predict the moisture migration under nonsteady condition, the concept of migration potential is proposed in the paper. Assuming that equation (8) is still correct, the proportional coefficient is not a constant, but a function of penetration rate, moisture content and overburden. The function is expressed as follow:

$$V = M_p(V_f, \theta, P_{ov}) \times Gr \quad (8)$$

where:  $V_f$  - penetration rate, (cm/hr.)  
 $P_{ov}$  - overburden (Kpa)

The function is defined as migration potential -  $M_p$ . Using equation (8), the moisture migration in freezing fringe can be expressed during dynamic freezing. Combining equation (3), (6) and (8), the moisture field of the three zone of freezing soil is determined.

##### Preliminary Experimental Research

When a one-way freezing experiment in which the temperatures of both sides of the sample are controlled is conducted, the temperature field  $T(x,t)$  is taken. If the relation between the freezing point and unfrozen moisture content is known, the frost line can be determined. The temperature gradient ( $Gf$ ) in freezing fringe is replaced with the gradient at frost line, that is  $Gf=(dT/dx)|_{T=T_f}$ . After the test is completed, the change of the moisture content is measured, the moisture migration rate is gotten by:

$$V = \gamma_d \Delta \theta V_f \quad (9)$$

here,  $\gamma_d$  is the dry density of the soil. Using equation (8),  $M_p$  is calculated. Discussing data from many groups of experiments, the function  $M_p(V_f, \theta, P_{ov})$  can be found.

This paper gives a preliminary result for Lanzhou loess. The test is conducted in open system under constant overburden. The sample is saturated during soil freezing, thus the moisture content at the top of freezing fringe is constant. Therefore,  $M_p$  is only the function of penetration rate  $V_f$ . It becomes feasible to find the relation between  $M_p$  and  $V_f$  with experimental data from the same test. Some initial conditions in the test are listed in Table 1.

Table 1. Initial conditions

Initial moisture content(%)	Overburden (Kpa)	Dry density (g/cm <sup>3</sup> )	Freezing point (°C)
27.7	28.57	1.53	-0.15

The process of the penetration is shown in Figure 2. Using a regression analysis, the process is repressed as equation (10).

$$H_f = \frac{t}{At+B} \quad (10)$$

Where,  $t$  is time, hour;  $A$  and  $B$  are empirical constants, and  $A=0.11983$ ,  $B=0.8688$ . The penetration rate is calculated from equation (11).

$$V_f = \frac{dH_f}{dt} \quad (11)$$

The temperature gradient at frost line is obtained from temperature distribution during soil freezing. If the moisture migration is ignored in frozen zone, the change of the moisture content can be determined from the moisture distribution that is shown in Figure 3 after test.  $\Delta \theta = \theta|_{x=H_f} - \theta_0$ .  $\theta_0$  is the initial moisture content.

Thus, the migration rate is calculated with equation (9), and the migration potential is determined with equation (8). After analyzing, the relation between migration potential ( $M_p$ ) and penetration rate ( $V_f$ ) is as follow: (Fig.4)



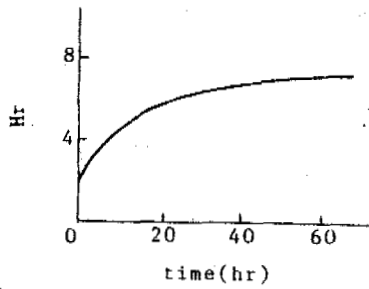


Figure 2. The process of penetration

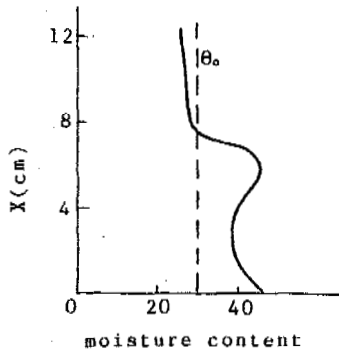


Figure 3. Moisture distribution after testing

$$\begin{aligned}
 M_p &= 128.07 \times V_f - 0.261 & \text{for } V_f < 0.1 \text{ (cm/hr)} \\
 M_p &= 94.77 \sqrt[3]{V_f} - 31.26 & \text{for } V_f > 0.1 \text{ (cm/hr)}
 \end{aligned}
 \quad (12)$$

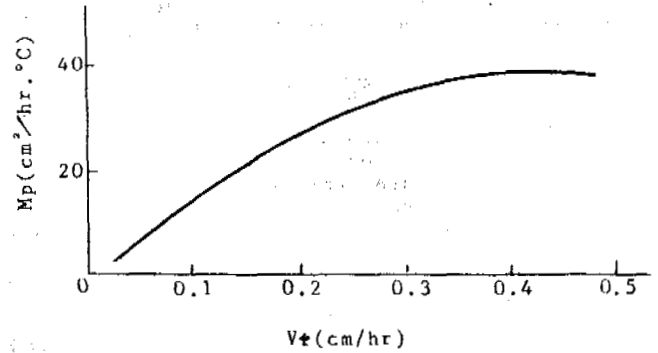


Figure 4. Relation between  $M_p$  and  $V_f$  in open system

### CONCLUSION

The model simplifies the calculation of moisture migration, and has the advantage that it is independent upon the moisture conductivity. Further research later, the model can be hoped to predict moisture migration in accordance with the condition of frozen soil in field, and furthermore it will provide the theoretical basis for the frost heave.

### REFERENCES

- Harlan, R. (1973) Analysis of coupled heat-fluid transport in partially frozen soil. *Water Resources Research*, No.9, pp.1314-1322.
- Konard, J. and Morgenstern, N. (1981) The segregation potential of freezing soil. *Can. Geotech. J.*, No.18, pp.482-491.
- Xu Xiaozu and Deng Yousheng (1991) Experimental research on moisture migration in frozen soil. Published by Sciences.

## EFFECT OF SOIL THAW ON OFF-ROAD VEHICLE TRACTION

Sally A. Shoop

Cold Regions Research and Engineering Laboratory  
Hanover, New Hampshire, USA 03755-1290

To determine the effects of thawing on vehicle mobility, an instrumented vehicle was used to measure traction on a variety of thawing conditions of a frost-susceptible, silty sand. The tests were performed in a large soil test basin where temperature and moisture conditions were controlled.

Thawing causes a layering of the soil that is most pronounced when the soil is very wet and, therefore, the thawed layer is extremely weak. Traction decreases substantially when the water content of the thawed layer is above the liquid limit of the soil. Traction also decreases as the thaw depth increases until a critical depth is attained, beyond which no further traction is lost. For dry and intermediate water contents, trafficking the soil increases the obtainable traction, but for wet soils, trafficking increases traction only if it creates a favorable rut geometry.

### INTRODUCTION

Driving a vehicle on thawing ground is difficult because of the low strength of thawing soil. Weak soil conditions are primarily caused by water drawn into the soil during freezing, or added to the surface while drainage is restricted by the underlying impermeable frozen soil. The result is a weak, thawed layer over a strong, frozen base. During thaw, road traffic is often restricted and off-road travel is virtually impossible. Also, vehicle traffic on thawing ground can result in extensive rutting and environmental damage.

Thawing soils experience an extreme change in strength during thawing and, with both frozen and thawed soil present, must be studied as layered media. The objective of this study was to determine how soil conditions influence vehicle mobility on thawing ground. An experimental approach was taken using an instrumented vehicle to measure vehicle traction for a variety of thawing conditions of a frost-susceptible silty sand. The tests were run in a large soil test basin where temperature and moisture conditions could be varied and controlled.

### EXPERIMENTAL METHOD

The experimental design focused on the factors controlling soil strength, because strength is the single most important soil property controlling off-road vehicle mobility. The same test technique and vehicle were used for all mobility tests so that applied strain rate and loading were constant. Because a single test soil was used, the strength of the thawing soil could be varied by controlling the water content, density, and thaw depth. Many other parameters (such as freeze rate, freeze depth, thaw rate, depth to water table, ice segregation, frost heaving, and initial soil conditions) were also simultaneously controlled or monitored, as discussed in Shoop and Henry, 1991.

#### Thawing Soils Test Basin

The mobility test basin is 36 by 13 meters by 3.5 meters deep. Its bottom is filled with 2.4 meters of gravelly sand, which can be used to control the water table. The sand is covered by a geotextile to separate the base fill and the overlying one meter of test soil. The basin is instrumented with tensiometers and thermistors to monitor soil moisture and temperatures throughout the basin.

The test soil used in these experiments is a fine-grained, silty sand typical of river bed sands in the northeastern United States. Because of the fine-grained fraction and the high permeability, this soil is highly susceptible to frost heaving and subsequent thaw weakening. In the test basin, it simulates off-road or trail conditions.

Before freezing, the test soil is tilled and compacted to a specified density. The surface of the soil is then covered with refrigeration panels to freeze the soil from the surface downward. Panel temperatures are adjusted to control freeze rate, frost heave, moisture migration, and frost depth. To thaw the soil, the panels are removed and the thaw rate is controlled by the air temperature in the building. The conditions of the thaw depend on the soil's water content and density before freezing, the amount of moisture migration and frost heave during freezing, and thaw reconsolidation.

The water content is controlled by initially drying or wetting the soil prior to freezing, by adjusting freeze rate, by adding a water table, and by sprinkling water on the thawing soil surface to simulate snow melt and spring rains. The test basin and experimental method is more fully described in Shoop et al., 1991.

Each time traction tests are performed, soil properties such as moisture, density, thaw depth, resistance to cone penetration, and shear strength are measured. Density and moisture measurements are taken throughout the test basin and averaged to represent the overall soil condition. For deep thaws, samples are taken at the surface and at various depths to define the moisture and density profile. Moisture conditions deeper than 0.3 meters are calculated from the tensiometer readings using a soil moisture characteristic curve. Thaw depth is obtained from the soil temperature profile and cone penetration measurements or test pits. Generally, at least 15 penetration measurements are made throughout the test basin to determine the homogeneity of the soil strength and thaw. Soil shear strength is measured with an in-situ shear annulus device, or by direct shear and triaxial testing in the laboratory.

To simulate a site that has been trafficked by many vehicles (such as a company of the Army), additional traction tests were performed after the soil was trafficked 50 passes with a five-ton truck. Experience has shown that after 50 passes, additional traffic does not affect soil strength.

### Vehicle Traction Testing

Vehicle tests were performed using a vehicle instrumented to measure the forces generated at the tire-soil interface, as well as the speed of each wheel and the true vehicle speed. The test vehicle equipment and its use are fully described in Berliner and Shoop, 1991; Shoop, 1992; and Blaisdell, 1983. For this test series, a mud and snow radial tire was used (Table 1).

**Table 1. Tire Characteristics**

Diameter .....	73.7 cm
Inflation Pressure.....	103 kPa
Contact Area .....	509.7 cm <sup>2</sup>
Tread Width .....	15.7 cm
Deflection .....	6.2 cm (38 percent)

Driving traction is the force generated at the tire-soil interface as a result of increasing the torque applied to the wheel. The tractive force varies with the slip of the wheel, but for comparison among soil conditions, the data is reduced to an average peak traction value and converted into a tractive coefficient by dividing by the vertical force on the wheel. At least three traction tests are performed at each soil condition; because two of the wheels are instrumented, a minimum of six independent measurements are obtained.

### SOIL CONDITIONS TESTED

Table 2 summarizes the soil conditions tested (expressed as thaw depth, water content, dry density, cone penetration index, and cone gradient), along with the corresponding traction obtained on

each surface. Data are grouped according to test conditions. Aside from the thirteen undisturbed thawing conditions, traction also was measured when the soil was totally frozen, and again with no frost layer present. To clarify the effects of density, the soil was also tested after tilling (similar to a farm field). The final grouping consists of the six thawing conditions tested after the soil was trafficked. The data in the table, as well as in all subsequent graphs, are averages of all traction and soil measurements for that test condition.

The range of the thawing soil conditions tested are displayed in Figure 1, which also illustrates the range of combinations of each of the variables, which forms the basis of the experimental design concept. The shaded area represents the conditions tested (with the exception of the tilled soil). The blank area is in the region representing a deep thaw in wet soil, which was difficult to obtain because the sandy soil (which has a relatively high permeability) begins to drain laterally as the thaw depth increases, as also happens in nature. A deep, wet thaw occurs naturally in less permeable soils.

### PARAMETRIC ANALYSIS

With the soil type held constant, the soil parameters that significantly affect vehicle mobility (and soil strength) are moisture, depth of thaw, and density. The only vehicle parameter varied was repetitive loading (trafficking). The effects of each of these parameters are discussed below.

### Soil Moisture

The fact that soil moisture affects soil strength and, therefore, vehicle mobility, has been known for quite some time (Casagrande, 1932; Ayers,

**Table 2. Soil parameters and vehicle traction for each test condition.**

	Gross Traction Coefficient	Thaw Depth (cm)	Water Content (%)	Dry Density (g/cm <sup>3</sup> )	Cone Index	Cone Gradient
<b>Undisturbed Thawing Soil</b>						
4 May 88	0.651	5.7	9.7	1.48	270	158
5 May 88	0.582	11.4	6.8	1.50	206	82
18 May 88	0.610	8.9	11.8	1.51	206	102
9 Jun 88	0.667	10.2	21.0	1.58	235	102
10 Jun 88	0.657	14.0	17.5	1.65	182	60
19 Jul 88	0.665	2.5	24.8	1.48	291	163
20 Jul 88	0.636	5.6	17.7	1.63	181	78
9 Nov 88	0.633	3.8	19.9	1.51	155	105
10 Nov 88	0.460	12.7	23.4	1.55	113	65
28 Dec 88	0.484	4.4	24.2	1.52	145	93
20 Jul 89	0.665	16.9	18.1	1.71	222	72
7 Nov 89	0.671	17.8	17.6	1.62	111	38
15 Nov 89	0.585	1.3	20.8		300	
<b>No frost present</b>						
20 Dec 88	0.662	0.0	13.0	1.70	203	53
27 Dec 88	0.649	0.0	9.0	1.61	210	53
<b>Totally frozen</b>						
3 Nov 89	0.689	0.0	10.5	1.62	300	
<b>Tilled for low density</b>						
20 Nov 89	0.546	0.0	9.2	1.08	9	2
<b>Trafficked thawing soil</b>						
10 Nov 88	0.518	12.7	28.6	1.52	218	105
30 Dec 88	0.486	5.1	27.1	1.55	117	59
7 Nov 89	0.740	17.8	17.4	1.75	174	49
16 Nov 89	0.666	8.9	13.7	1.77	214	67
17 Nov 89	0.712	16.5	13.0	1.79	210	59
20 Nov 89	0.744	35.1	12.7	1.83	275	57

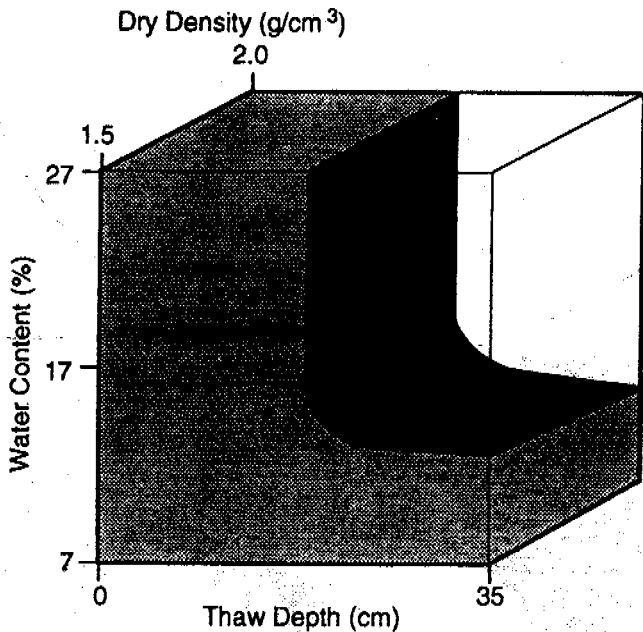


Figure 1. Test design concept showing range of soil parameters tested.

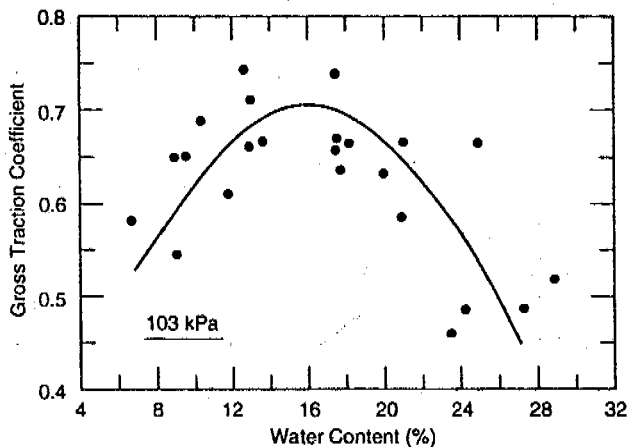


Figure 2. Traction versus water content.

1987; Ageikin, 1987; Shoop, 1989b). In fact, the mobility models used by the U.S. Army use soil moisture to predict soil strength and consequently vehicle mobility (Kennedy et al., 1988). It is not surprising then to see also a strong relationship between soil moisture and vehicle performance (traction) for thawing soils. The major difference in thawing ground is that the moisture content can reach levels much higher than those normally seen in unfrozen soil. For instance, a normally free-draining, high-permeability sand can become super-saturated during thaws because of drainage restriction caused by the underlying frozen soil.

The effect of water content on vehicle performance can be seen by plotting the peak tractive coefficient with water content as shown in Figure 2 for all 23 soil conditions tested. The graph clearly indicates an increase in traction with increasing soil moisture until the water content reaches approximately 18 percent; traction then drops

rapidly as the water content increases beyond the liquid limit of the soil (20 percent). An exception occurs when the soil is wet (above the liquid limit), but the thaw is very shallow (less than three cm), such as the conditions tested on 19 July 1988. In this case, high traction was obtained, despite a high water content, because of the strength provided by the close proximity of the underlying frozen soil and the ability of the spinning tire to dig through the weak, thawed layer to the strong, frozen soil below.

#### Thaw Depth

Traction and soil strength are strongly influenced by layering. This is particularly true of thawing soils because the strength of the frozen soil is significantly greater than the thawed soil. To observe the effect of the thaw depth (depth to the top of the competent frozen soil) directly, without confounding the other soil parameters, the data collected on undisturbed thawing soil were grouped by similar water content (low water content ranging from 6 to 13 percent; intermediate water content, 17 to 21 percent; and high water content, more than 23 percent) and are plotted in Figure 3. The most significant effects are for very wet soils where the traction decreases rapidly (by one third) as the thaw increases, and then levels off to a nearly constant value at a thaw depth of ten cm. At this depth, the strong frozen layer is too deep to provide additional traction for the tire, and the thawed layer is too thick to be scraped away by the spinning wheel. When the moisture content is low (less than 13 percent), there is a similar but lesser effect on traction, but at intermediate water content there is no loss of traction with thaw. The effects of layering at the dry and intermediate water contents are less pronounced because the strength of the thawed soil is greater (at the lower moistures); thus, the strength difference between the thawed and frozen layers is less, particularly at the intermediate soil moisture levels.

The effects of the freeze/thaw layering on gross traction are more clearly understood by considering the nature of the soil failure beneath a spinning tire. A typical failure zone for the tire and soil conditions tested was calculated using the finite difference plasticity analysis described in Karafath and Nowatzki, 1978. For a tire slip of five

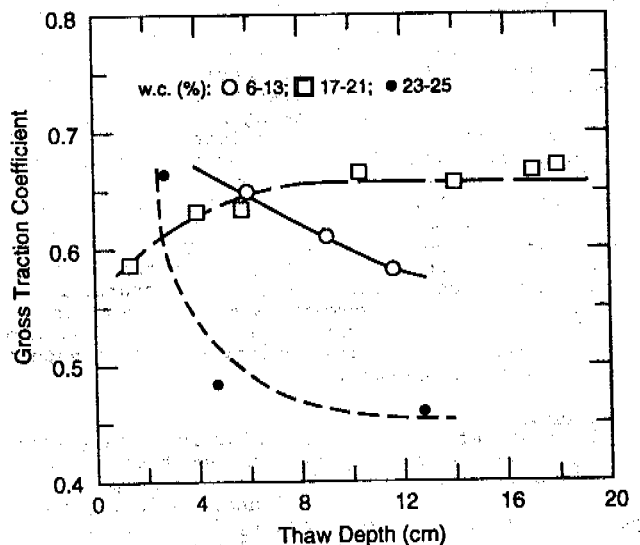


Figure 3. Traction versus thaw depth

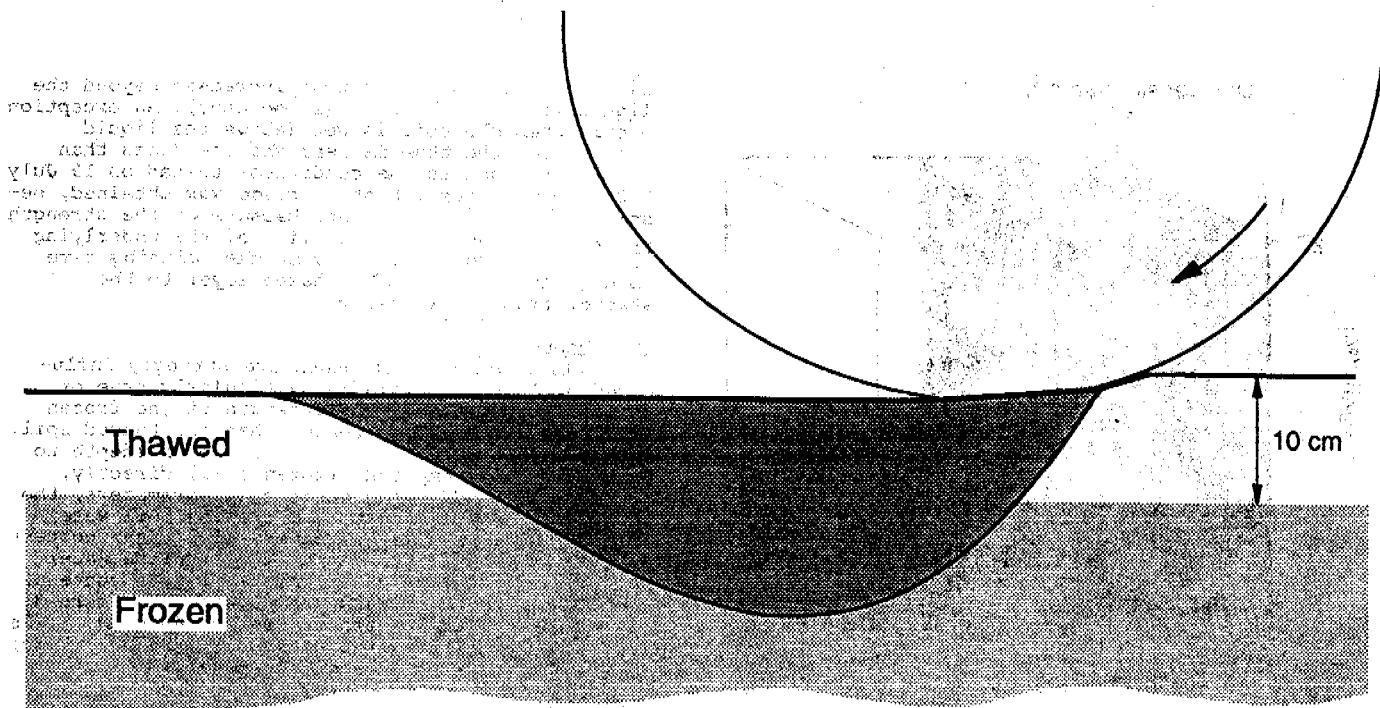


Figure 4. Geometry of the soil failure zone generated by a spinning tire. The presence of a strong frozen soil within this zone will affect the vehicle traction.

percent, the plastic failure in a homogeneous soil, with properties of the thawed sand, extends to a depth of approximately 17 cm (shown in Figure 4). For thawing conditions, a frozen layer would be added; because of the strength of the frozen soil, the failure is confined to the thawed layer. Potentially, therefore, any frozen layer within 17 cm of the surface would add to the traction available to the tire. In reality, the frozen soil has little influence until it is well within the theoretical failure zone (within ten cm of the surface, as indicated by the flattening of the curve in Figure 3).

#### Soil Density

Density also affects vehicle performance, but its contributions are strongly overshadowed by the influence of moisture and thaw depth for the range of densities tested. The dry density ( $\gamma_d$ ) of the thawing soils ranged from 1.48 to 1.83 g/cm<sup>3</sup>. Although the freezing and thawing process changes the density slightly, the range of initial soil density (prior to freezing) is limited by the flat response of the soil to various water contents and compactive efforts. Therefore, to evaluate density affects, a traction test was performed on tilled soil. The low density tilled soil ( $\gamma_d = 1.08$  g/cm<sup>3</sup>) yielded 16 percent less traction than the corresponding compacted soil (same soil moisture, but  $\gamma_d = 1.61$  g/cm<sup>3</sup>, 27 December 1988). However, these are dry soils (water content of nine percent), and the traction loss for low-density wet soils should be considerably greater.

#### Trafficking

The major effect of trafficking is rutting generated by compaction and mass movement of the soil. The repeated load of the five-ton truck applies a compactive effort to the soil and, as in any compactive effort, the soil density increases as a function of the water content. The water contents and densities obtained after trafficking are shown

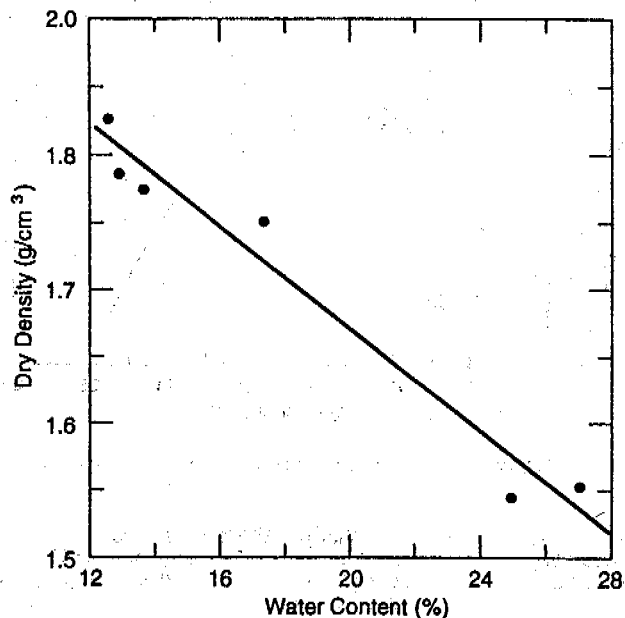


Figure 5. Density of trafficked soil is a function of water content.

in Figure 5. The optimum water content for compacting this soil, as determined by ASTM standard compaction testing, is approximately 13 percent, and this is where the high densities occur. At the other end of the graph, the very wet thawing soil behaves as an incompressible fluid, and although rutting is extensive due to soil flow around the wheels, density remains on the low side.

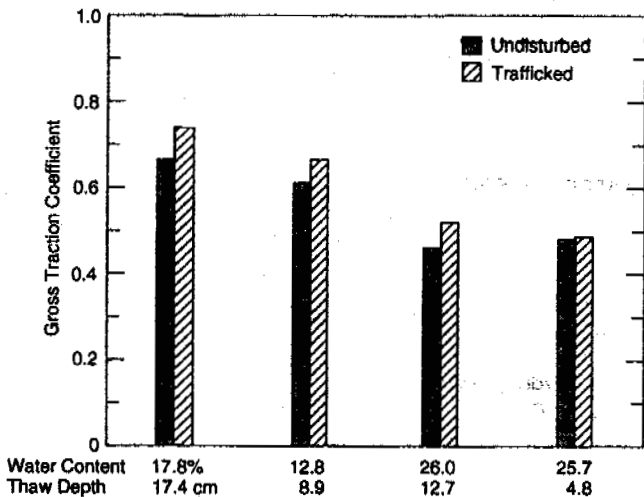


Figure 6. Effect of traffic on vehicle traction for comparable thawing soil conditions.

The effect of trafficking on traction can be seen by comparing tests on trafficked and untrafficked soil for similar thaw conditions (same thaw depth and water content). This was possible for four of the trafficked soil tests; the other two tests had no similar untrafficked conditions. The traction values for the four comparable data sets are shown in Figure 6, along with average soil conditions. In general, trafficking increases the traction by approximately ten percent. On wet soils, however, as trafficking does not increase soil density, an increase in traction depends on whether the trafficking leaves ruts that are cleared of wet soil (as happened in the third comparison in the figure), or the wet soil covers the ruts of the previous pass, yielding uniformly slippery soil (and no traction increase as shown in the last comparison in Figure 6).

#### SUMMARY AND CONCLUSIONS

Vehicle traction was tested on several different conditions of frozen/thawing sand using an instrumented vehicle in a moisture- and temperature-controlled test basin. The purpose of the study was to determine how soil parameters influence vehicle mobility in thawing ground. The results of the experiments can be summarized as follows:

1. Water content has a strong influence on traction because of its effect on the strength of the soil. Traction (and shear resistance of the soil) increases with soil moisture to a maximum value at intermediate water contents and then decreases rapidly at moisture levels beyond the liquid limit.
2. Soil thawing causes layering of the soil profile (weak, thawing soil over a strong, frozen base) and therefore, thaw depth also has a major influence on vehicle performance. The effects are most pronounced when the thawing soil is very wet and weak. Traction decreases with increasing thaw depth as the strength provided by the frozen layer becomes less influential and the thawed layer becomes too thick for the tire to scrape away. Once a critical thaw depth is reached (ten cm), no further reduction in traction is observed.
3. Traction increases with soil density; however, the effect of density is small compared to the influence of moisture and thaw depth over the relatively narrow range of densities obtainable on sandy soil.

4. At low and intermediate moisture levels, trafficking increases soil density and therefore increases traction. For incompressible, wet soils, however, trafficking results in mass movement of the soil without compaction, and vehicle performance depends on whether resulting ruts are cleared of the slippery, wet soil.

#### REFERENCES

Ageikin, I.S. (1987) Off-the-road wheeled and combined traction devices: Theory and calculation, Amerind Publishing Co. Pvt. Ltd., New Delhi.

Ayers, P.D. (1987) Moisture and density effects on soil shear strength parameters for coarse grained soils, Trans. ASAE, 30(5), 1282-1287.

Berliner, E. and S. Shoop, 1991, Instrumentation for vehicle mobility testing in the Frost Effects Research Facility, Proceedings of the 2nd International Symposium on the State of the Art of Pavement Response Monitoring Systems for Roads and Airfields, ASCE, September 1991.

Blaisdell, G.L. (1983) The CRREL instrumented vehicle, CRREL Special Report No. 83-3.

Casagrande, A. (1932) Research on the Atterberg limits of soils. Public Roads, vol. 13, p. 121-136.

Karafiath, L.L., and E.A. Nowatzki (1978) Soil mechanics for off-road vehicle engineering. Claus-thal, Germany: Trans Tech Publications.

Kennedy, J.G., et al. (1988) Updated soil moisture-strength prediction (SMSP) Methodology, WES Technical Report, GL-88-13.

Shoop, S.A., E. Berliner, and S. Decato (1991) An experimental method for vehicle mobility testing on freezing/thawing soil, Proceedings of the Engineering Foundation Winter Mobility Conference, Santa Barbara, CA, June 1991.

Shoop, S.A. (1989a) Vehicle mobility on thawing soils, Interim Report on CRREL's Test Program, CRREL Special Report No. 89-31.

Shoop, S.A. (1989b) Thawing soil strength measurements for predicting vehicle performance, Proceedings of the North American Conference of the International Society for Terrain Vehicle Systems, Victoria, BC, Canada, April 1989. Also CRREL Report 92-17.

Shoop, S.A., and K.S. Henry (1991) Effect of a geotextile on water migration and frost heave in a large-scale test basin, Transportation Research Record 1307, 309-318.

Shoop, S.A. (1992) Precision analysis and recommended test procedures for mobility measurements made with an instrumented vehicle, CRREL Special Report No. 92-7.

#### ACKNOWLEDGEMENTS

The author thanks Steve Decato and Rosanne Stoops, who contributed extensively to the experimental program in the mobility test basin; George Blaisdell and Dr. Bernard Alkire for their helpful comments on the text; Matt Pacillo for drafting the figures; and Gioia Cattabriga for editing and layout.

## N-FACTOR MAPS OF RUSSIAN PERMAFROST REGION

Y.L. Shur<sup>1</sup>, V.B. Slavin-Borovskiy<sup>2</sup>

<sup>1</sup>Palmer Research Center, University of Alaska Fairbanks  
Palmer, Alaska USA 99845

<sup>2</sup>All-Russian Scientific-Research Institute of Hydrogeology  
and Engineering Geology (VSEGINGEO)  
Zeleny vil., Noginsk dist., Moscow reg., 142452, Russia

The n-factor is the ratio of surface temperature to air temperature (both integrated over time) for any period - usually for summer and winter. The summer n-factor is of special interest to engineers. The authors have conducted long-term experimental studies of n-factor in West Siberia. In addition, they have determined n-factors (summer) for the Russian permafrost region on the basis of data from more than 800 meteorological stations. These results are determined from sandy and fine-grained surfaces without plant cover. Generally, the n-factor increases from south to north. Time variation of the n-factor integrated for short periods is considerable during the summer. The total summer n-factor variation among different years is slight. The summer n-factor maps for the Russian permafrost region are presented in this report.

### INTRODUCTION

In the summertime the temperatures of most of the natural surfaces and disturbed surfaces are higher than the air temperature. In the wintertime the snow cover's temperature is slightly less than the air temperature. The latter usually is not very important in the prediction of permafrost prediction temperature.

The difference between the temperature of the soil surface and the air is found as a rule from an energy balance at the earth's surface. For this purpose the following equation is used:

$$t_s - t_a = \frac{R - LE}{\alpha} ;$$

where:

- $t_s$  - temperature of the surface;
- $t_a$  - air temperature;
- R - net radiation balance at the surface;
- LE - heat spent in evaporation;
- $\alpha$  - convective heat exchange coefficient.

This method is effective enough for theoretical analysis. Its practical use meets many difficulties. Firstly, the net radiation balance at the ground surface can differ in the same area from spot to spot by 20-30 % and more. Secondly, the quantity of the heat consumed in evaporation

changes by several times depending on the moisture conditions of the subsurface's layer. The calculation of LE as the component of the heat balance equation usually doesn't give the correct results (Lazareva, 1978). Thirdly, the largest errors (1.5-2 times) are related to the determination of the convective exchange coefficient.

### FIELD STUDY

The difficulties mentioned above forced us to study the temperature regime of various soil surfaces by the experimental method. Measurements of temperatures of hundreds of undisturbed and disturbed surfaces were obtained during eight summer seasons in different areas of West Siberia by the authors of this report and N. Moskalenko (Moskalenko, 1983). It was found that a fairly constant relationship was obtained between the sums of the summer air temperatures and the sums of the soil surface temperatures. The ratio of the sum of the soil surface temperature to the sum of the air temperature is known in permafrost literature as the n-factor.

### DATA ANALYSIS

The n-factor was used for the calculation of the depth of the active layer by H. Carlson (1952). This approach has been used many times in different countries. American data were generalized by Lunardini (1978). He also developed the n-factor theory. Special investigation of the

n-factor was made by the authors of this report (Slavin-Borovskiy, Shur, 1977).

After the comparison of our data and data of other researchers we came to the conclusion that the n-factor for the whole summer is stable from year to year and there is definite regularity in its geographical variation. Based on this hypothesis we calculated the summer n-factor for the Russian permafrost region. For this purpose we used data from more than 800 meteorological stations which are located throughout the entire permafrost region or close to its southern border. Meteorological record books from which we took the information contained monthly data about the soil surface and air temperature averaged for a long period. We also found detailed information from 10 stations and studied the n-factor change during the summer seasons 1961 - 1974 (Figure 1). According to Figure 1, where the n-factor is rounded to 0.1, the n-factor is very stable. The limit of divergence from the n-factor value averaged for a long period is not more than 10 %.

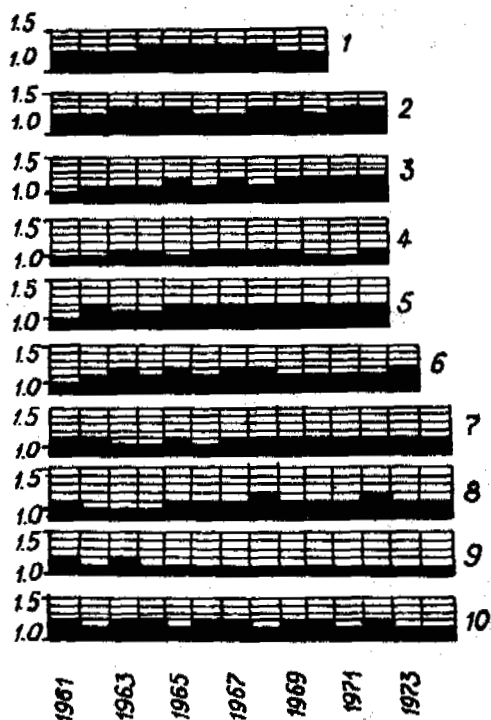


Figure 1. The n-factor (summer) change during 1961 - 1974 for 10 meteorological stations of the Russia permafrost region.

From place to place the n-factor changes noticeably under the influence of several factors: subsurface material, the position of the site in relief, its distance from the sea or large lake and other local factors.

The n-factor distribution for plains can be estimated easily and can be expressed on maps by isolines. The n-factors of bald mountains everywhere are equivalent to 1.0-1.1. In

valleys, n-factors depend on the location of the site within the valley. Slope exposure, depth of the valley and of the site to a river are also important. For example, the n-factor increases on the south facing slopes, and inside deep (300-500 m) hollows and valleys, if the site is open enough to the horizon.

The influence of the seas is seen well on those plains which are open to seas. The greatest n-factor in all land situations is found on the seacoast. On arctic islands according to the data of Meteorological record books the n-factor can be incredibly high compared with continental locations. As one moves into the continent he can see that the n-factors decrease regularly. The influence of the northern seas determines the decrease of the n-factor from north to south. In the summer basic air masses are forming above the northern seas and moving into the continent. The soil surface which absorbs solar radiation is considerably warmer than the air. This difference between these temperatures is relatively reduced into the continent.

Local factors such as the location of the site in microrelief, the moisture condition of the soil surface, artificial covering of the soil surface, and building development around the site can be very important. The n-factor depends on the granulometric composition of the soil. It increases in the following order of soil types: peat, clay, silt, sand, gravel. But moisture conditions of the soil's surface and subsurface layer are very important and often change this regularity, because the n-factor of the wet surface is considerably less than that of the dry one.

The impact of a microrelief on the n-factor was studied on a sand embankment with a height of about 1.5 m. On the north facing slope of the embankment  $n = 1.05$ ; on its horizontal part  $n = 1.2$ ; on its south facing slope  $n = 1.3$ . Artificial coverings, such as concrete or asphalt completely change the heat balance in any area, and n-factors for this kind of surface are the greatest of any studied. In an area surrounded by buildings the turbulent heat exchange is decreased and the n-factor is therefore greater than that of open space.

#### N-FACTOR MAPPING

The schematic maps, Figure 2, represent the n-factor isolines of the Russian permafrost region. The maps were derived from data obtained from bare surfaces which had coarse (Figure 2-a) and fine (Figure 2-b) subsurface materials, according to record books of Russian meteorological data. For the plains, the n-factor distribution is shown by isolines  $n = 1.1$ ; 1.2; 1.3; 1.4; 2.0. For the mountain areas, only the most reliable regularities are given. They relate to large valleys, hollows and gentle slopes. The n-factors of the upper parts of slopes, bald mountains, passes and tops are usually more than 1 and less than 1.1.

According to data from the meteorological record books and the maps in Fig. 2 the n-factor everywhere is more than 1.0, because meteorological stations are usually



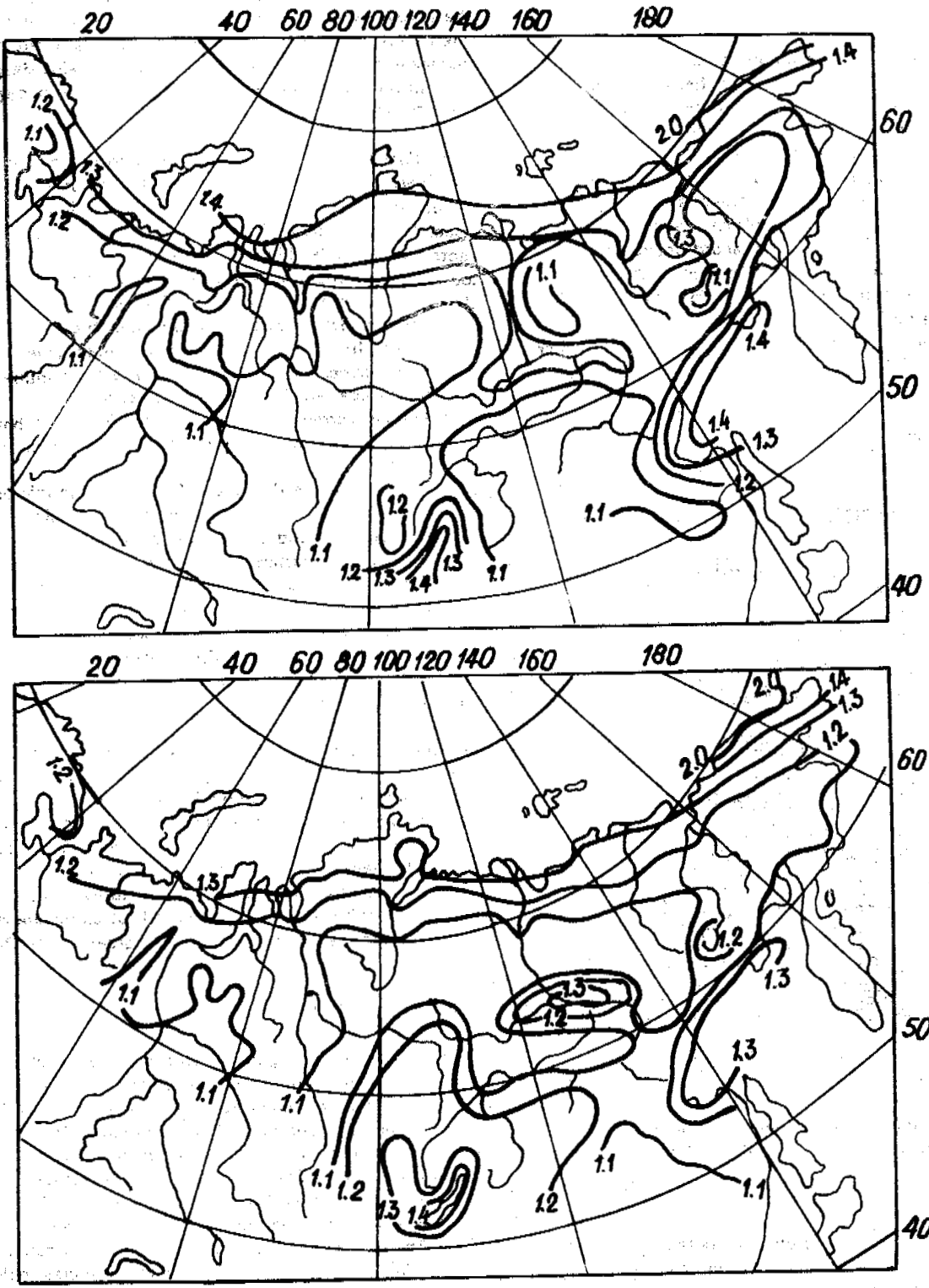


Figure 2. Schematic n-factor maps of the Russia permafrost region. The soil surface without plant cover.  
 a - clay soil; b - sandy soil.

located on dry and sunlit places. However, the n-factor of swampy spots or shady slopes can be equal to or less than one.

The regularities which are shown on the maps are true only for the whole summer period; they are not true for shorter periods of time, such as 1 month, 10 days, and especially, 24 hours.

We studied especially the n-factor's change during the summer season. Both the instantaneous value and the value which was averaged for a short period (24 hours, 1 week) were changing considerably in an irregular manner. The changes depended on the moisture of the soil surface, the meteorological conditions, and some other factors. The accumulated value, however, was changing quite regularly. For dry surfaces it was at its maximum in the first summer month and it decreased to its limit (the n-factor for the whole summer) by the end of the summer. For the constantly wet surfaces, and especially the surface of water, the regularity of the n-factor's change was the exact opposite, and the accumulated value of the n-factor increased to its limit during the summer season.

**ADDITIONAL APPLICATIONS**

Based on the climate data n-factor values were calculated as functions of the latitude of the site and the calendar time. The result of this calculation for sand surfaces in West Siberia is shown in the nomogram (Figure 3).

The nomogram was used for the determination of the temperature of the soil surface for any summer month and calculation of the active layer's change during the summer. For this purpose the following formula can be used:

$$t_{s,i} = \sum_{j=1}^i t_{a,j} (n_i - n_{i-1}) + n_{i-1} t_{a,i} \quad ;$$

where:

$\sum t_{a,j}$  - the sum of the air temperatures from the beginning of the period with the air temperature above 0° C including the month for which the soil surface temperature must be predicted;

$n_i, n_{i-1}$  - the n-factor value for the present and previous months.

The prediction of the n-factor value for artificial covering is one of the very serious questions in the engineering permafrost prediction. In a few areas (Fairbanks, Alaska - USA for example), n-factors have been studied extensively, but for many areas we still don't have any information at all. Using the maps and the graphs in Figure 3 we can extrapolate the information from the areas where the n-factor values are known into the area where the n-factor value is unknown. As a first approximation the following

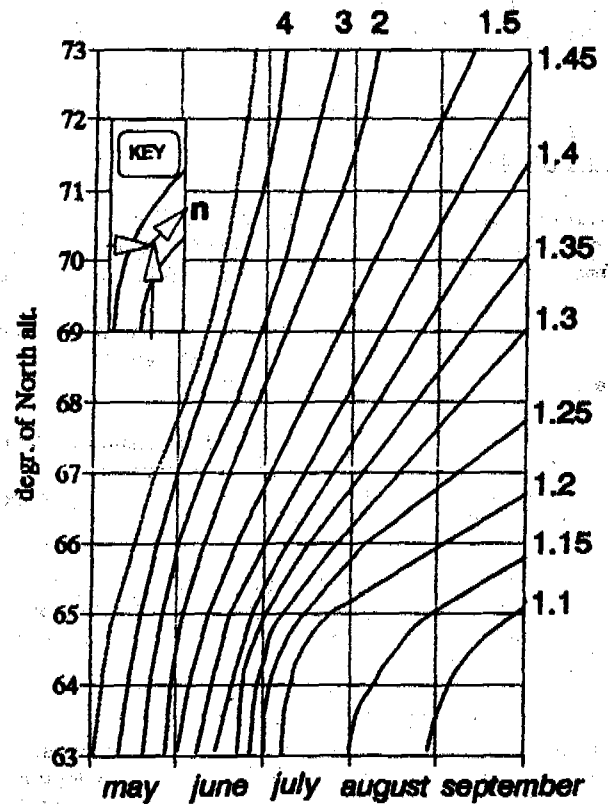


Figure 3. The n-factor nomogram for any period of time.

formula can be helpful:

$$n_s = \frac{n'_s}{n'_m} \cdot n_m \quad ;$$

where:

- $n_s$  - n-factor value for a predicted situation;
- $n'_s$  - n-factor value of the same kind of surface in any area where n-factor value is known;
- $n'_m$  - n-factor map value (Fig. 2) at the same area as  $n'_s$ ;
- $n_m$  - n-factor map value (Fig. 2) at the same area as  $n_s$ .

For example, it is necessary to know the n-factor of a concrete surface in North Chukotka and there is this kind of information for Yakutsk. If  $n'_s = 1.6$ ;  $n'_m = 1.2$  and  $n_m = 2$  then  $n_s = 2.7$ .

The n-factor maps can be used in many ways, in particular for the prediction of the impact of global climate change on permafrost.

## ACKNOWLEDGMENTS

The authors are grateful to Ray Kreig of R.A. Kreig & Associates for advice and support.

## REFERENCES

Carlson H. and Kersten M. Calculation of depth of thaw in frozen ground. Highway Research Board, Special report 2, Frost action in soils. Washington, D.C., 1952, pp. 192-223

Lazareva N.A. Results of calculations of the turbulent heat and moisture flows. Main Geophysical Observatory, Leningrad, 1978, Vol. 402, pp.49-86

Lunardini V.J. Theory of n-factors and correlation of data. Proc. 3rd International Conference on Permafrost, Edmonton, Alta., Canada, 1978, National Research Council, Vol. 1, pp. 41-46

Moskalenko N.G., Slavin-Borovskiy V.B. and Shur Y.L. Temperature regime and active layer. Permafrost Prediction for West Siberia Oil and Gas Regions. Novosibirsk. Nauka, 1983, pp. 58-68

Slavin-Borovskiy V.B. and Shur Y.L. The temperature of the soil surface without a plant cover in the summer time. All-Russian Scientific-Research Institute of Hydrogeology and Engineering Geology, Moscow, 1977, Vol.113, pp. 11-20.

ALUMINAS IN QUATERNARY SEDIMENTARY ROCKS OF YAKUTIA:  
NEW FINDINGS CONCERNING MINERAL FORMATION IN PERMAFROST REGIONS

Christine Siegert

Alfred-Wegener-Institut für Polar- und Meeresforschung  
Forschungsstelle Potsdam  
Telegrafenberg A43, D-0-1561 Potsdam, Gemany

Newly-formed aluminas were found by cryolithological investigations in ice-rich Quaternary deposits in Yakutia. The results of detailed mineralogical examinations have shown that these aluminas can be assigned to the modifications  $\alpha$ -Al<sub>2</sub>O<sub>3</sub> (corundum),  $\delta$ -Al<sub>2</sub>O<sub>3</sub> and  $\theta$ -Al<sub>2</sub>O<sub>3</sub>. The crystallization of these phases in syngenetic frozen sediments takes place under quite unusual thermodynamic conditions. It points to the fact that cryogenous dehydration processes are of great influence on the diagenetic transformation of sediments within the permafrost zone.

#### INTRODUCTION

In the frame work of long-term cryolithologic research activities in various regions of Yakutia special investigations have been carried out concerning the formation of minerals under permafrost conditions. Besides regional factors which are controlled by the geological setting of a region and the special landscape attached thereto these results reflect that cryogenic processes have a decisive impact on mineral formation.

Cryolithogenic deposits which have been developed under various conditions are characterized not only by distinguished characteristic facies-caused frost effects as cryogenic structures, ice wedges and various other frost-action phenomena, but also by certain parageneses of authigenic minerals (Siegert, 1981, 1987).

Geochemical processes, which lead to new formation of minerals reach their highest intensity in sediments of active layers and in small taliks, where seasonal and long-periodical variations of climatic factors are most effective. The manifold repeating phase transitions of water, and the various cryogenic processes connected therewith, as well as significant seasonal changes in the biological activity, lead to a profound chemical nonequilibrium within the sediment milieu and stimulate precipitation and crystallization of mineral substances. Within the upper permafrost layer, that is subjected to seasonal and longterm temperature variations, cryogenic mineral forming processes continue. Along with it authigenic phases may be formed reflecting specific cryogenic processes. The

metastable newly formed aluminas, which we proved in quaternary frozen rocks of Yakutia, belong to them and are going to be presented here.

#### FINDING CONDITIONS OF ALUMINAS

Authigenic aluminas were found in the area of the Lena delta as well as in several regions of the Central Yakutian lowland in loess-like deposits of Late Pleistocene and Holocene ice complexes. All horizons with aluminas show distinct characteristics for cryogenic hydromorphic soil formation. Besides aluminas, Fe and Mn hydroxides, sulfides (greigite, mackinavite) and also manganese calcites occur as new formations. The observed mineral parageneses and the total content of authigenic components characterize a high hydrogen accumulation rate within active layers prior to their permafrost transition.

Within the Central Yakutian lowland, the sediments which carry newly formed aluminas have developed in valleys of small rivers. The composition of the allochthonous components indicates that slope processes play an important role in their accumulation. The erosional areas are composed of Mesozoic, pyrite containing argillites and subarkoses. Therefore, suprapermafrost waters enriched in sulphate and fulvo acids can be formed (Katasonova and Siegert, 1982). They cause mobilisation and transport of aluminium and enable its enrichment in certain geochemical barriers within those areas in this environment which are characterized by accumulation.

In the eastern part of the Lena delta newly formed aluminas were found in Late

Pleistocene sediments which were strongly overthrust by cryogenic soil formation. In this case the erosional products of argillites as supplier of matter again played an important role (Slagoda, 1989).

#### MINERALOGICAL CHARACTERIZATION OF NEWLY FORMED ALUMINAS

Aluminas occur as white and yellow dums, which exhibit a glass or pearl lustre. Their mean diameter is 0.1-0.2 mm. In the investigated samples the total content of the dums does not exceed 0.0n%, however, in the heavy mineral fraction it rises in average up to 1-3% and reaches maximum values of 10-30% (sample series taken from the eastern Lena delta). Detailed microscopical investigations have shown that the dum-shaped grains were formed by adhesion of fine crystals (Fig. 1). Sometimes, aluminas have grown on plant detritus which is a definite proof for their authigenic character. The great grain brittleness is an additional argument against their redeposition. When exerting slight pressure they crumble to a great number of crystallites.

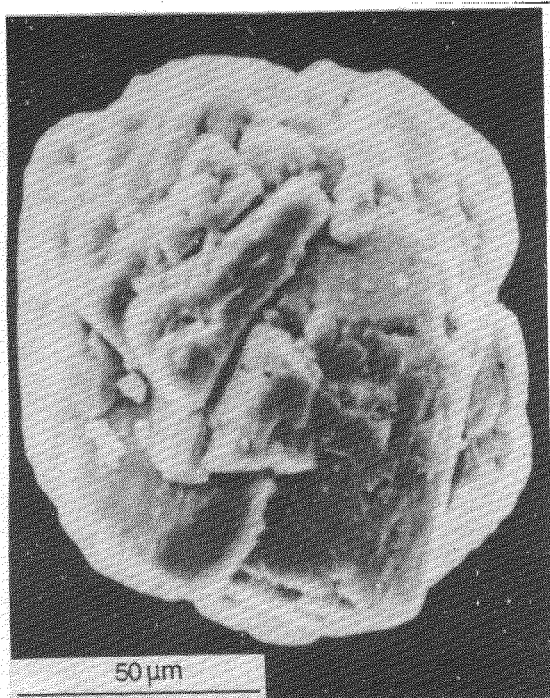


Figure 1. Scanning electron micrograph of alumina grain (transition phase)

According to their light refraction the newly formed aggregates are inhomogeneous. In mono-chromatic light ( $\lambda = 589\text{nm}$ ) values of 1.698 to 1.754 have been measured for  $n$ . The double refraction reached

a maximum of 0.005-0.006. Since the microprobe was only able to prove aluminium one might assume that the aluminum hydroxides diaspore was newly formed. X-ray diffraction analysis, however, showed that these newly formed phases in fact are three different alumina modifications  $\alpha$ - $\text{Al}_2\text{O}_3$  (corundum),  $\delta$ - $\text{Al}_2\text{O}_3$  and  $\theta$ - $\text{Al}_2\text{O}_3$ . This result deserves special attention as the last two phases were only known so far as artificial metastable products which develop by dehydration of aluminum hydroxides under the influence of high temperatures (Lippens, 1961). Corundum will be formed as the stable end product.

In order to trace possible crystallographic differences between each alumina modifications within the deposits investigated by us a great number of individual grains of different origin were analyzed by X-ray diffraction (Debye camera) and Camebax microprobe. The result was that according to their crystal structure all purely white grains were in fact corundum ( $\alpha$ - $\text{Al}_2\text{O}_3$ ). Two types of Debye-grammes were obtained from the yellowish grains (Table 1).

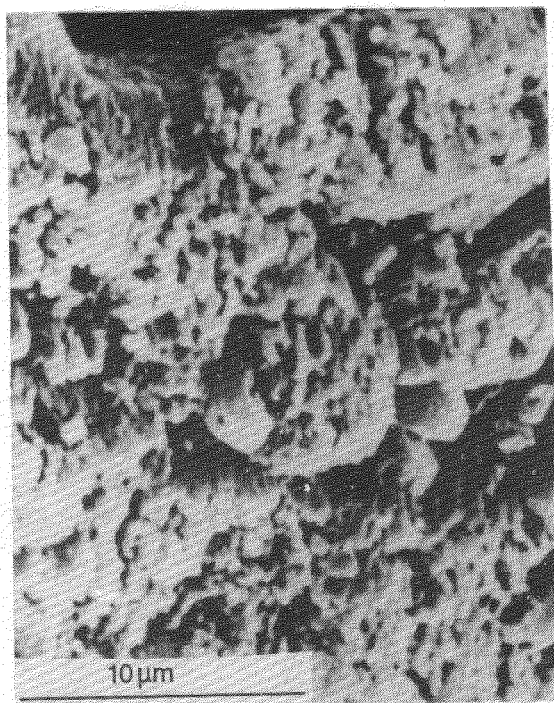


Figure 2. Scanning electron micrograph showing the porosity of the inner zone of a corundum grain

The first ( $\delta$ - $\text{Al}_2\text{O}_3$ ) differ by weak faded lines, whereas sharp intensive reflexes are characteristic for  $\theta$ - $\text{Al}_2\text{O}_3$ . These crystallographic peculiarities also apply to artificial test pills (Powder

Tabelle 1. X-ray diffraction data of aluminas

$\delta$ -Al <sub>2</sub> O <sub>3</sub>				$\theta$ -Al <sub>2</sub> O <sub>3</sub>				$\alpha$ -Al <sub>2</sub> O <sub>3</sub> *)		
G-5-5		Etalon No 16-384		G-5-25		Etalon No 4-875		U-19-1		
I	d	I	d	I	d	I	d	I	d	
		4	7,6							
		4	6,4							
		4	5,53							
		8	5,10	1	5,47	20	5,25			
		12	4,57	1	4,58	60	4,55			
		12	4,07							
		4	3,61			10	3,56	8	3,53	
		4	3,23							
		4	3,05							
		8	2,881	4	2,88	80	2,87			
2	2,76	30	2,728	6	2,71	80	2,74			
1	2,59	25	2,601	1	2,56	20	2,58	10	2,56	
3	2,43	60	2,460	4	2,42	80	2,45			
		16	2,402					4	2,40	
		8	2,315			60	2,33			
2	2,30	40	2,279	3	2,28	60	2,26			
1	2,11	4	2,16			?	2,17			
						5	2,13			
3	2,01	75	1,986	4	2,01	80	2,03	10	2,09	
2	1,96	40	1,953							
		12	1,914	2	1,895	40	1,92			
		4	1,827							
		8	1,810	1	1,791	20	1,81			
				1	1,728	5	1,75	5	1,734	
		8	1,628	1	1,610	10	1,63			
		4	1,604					10	1,605	
		8	1,538	3	1,537	60	1,55			
1	1,52	16	1,517	1	1,480	40	1,50	1	1,514	
		8	1,456	1	1,447	40	1,46			
						5	1,44			
		50	1,407	1	1,419	60	1,41			
10	1,39	100	1,396	10	1,386	100	1,40	5	1,400	
						5	1,35	6	1,375	
					1	1,290	20	1,29		
						10	1,27			
					1	1,246	10	1,24	4	1,236
							?	1,19	1	1,187
					1	1,141	5	1,16	1	1,141
					1	1,102	10	1,11	1	1,20
								1	1,096	
							5	1,07	1	1,077
							10	1,04	3	1,041
					1	1,029	20	1,02	1	1,014
					2	0,995	20	1,00	3	0,996
					1	0,969	10	0,977		
					1	0,948	10	0,957		
					1	0,927	10	0,938	1	0,933
							5	0,919		
							5	0,910	3	0,905
							10	0,893	1	0,898
							5	0,857	3	0,857
								1	0,850	
								1	0,845	
					1	0,825		4	0,829	
					1	0,806		2	0,807	
								2	0,805	
								3	0,797	
								1	0,795	

\*)X-ray diffraction data of sample U-19-1 totally equal etalon of corundum No.19-173. Etalon according to Powder Diffraction File, 1977, JCPDS, USA

Diffraction File, 1977). The Al<sub>2</sub>O<sub>3</sub> content for all modifications amounts to 83-87 mass%, whereas the content of traces is always less than 1% (Table 2).

Considering the fact that the examinations were carried out with great care, the low oxide sums and Al<sub>2</sub>O<sub>3</sub> contents only can be explained by very high micro-porosities of the new phases which is typical especially for the inner regions of the micro-aggregates. The rather high micro-porosity of the corundum grains (Fig. 2) is an obstacle when preparing the samples for the microanalyses. We believe that the Cr<sub>2</sub>O<sub>3</sub> contents in the α-Al<sub>2</sub>O<sub>3</sub> modification are a result of remaining polishing paste. The investigation conditions are described in our paper (Siebert et al., 1990).

examined by us are similar to the corundum described from the bauxites.

2. In the recent subpolar environment aluminum is released by weathering of soils. Evidence is given for this fact by the relatively high content of water- and oxalate-soluble aluminum within certain horizons of gley tundra soils (Zvereva and Ignatenko, 1983) and alas soils (Desyatkin, 1984). The fulvo acids, which commonly prevail within the cryogenic soils, favour the formation of soluble Al-organometallic compounds and enable mobility and transport of aluminum. In case the permafrost is close to the surface, the transport of dissolved components from the active layer is limited. As a result of cryogenic changes in the composition of the pore solution

Tabelle 2. Chemical composition of the authigenic aluminas, mass %

Colour	yellow						white		
	δ-Al <sub>2</sub> O <sub>3</sub>			θ-Al <sub>2</sub> O <sub>3</sub>			α-Al <sub>2</sub> O <sub>3</sub>		
Modifi- cation, Sample	δ-19-21			U-19-24			G-5-1		
Al <sub>2</sub> O <sub>3</sub>	85,04	82,92	87,09	84,81	82,77	86,41	86,35	83,78	82,86
FeO	-	0,09	-	-	-	-	-	-	-
MnO	-	0,13	-	-	-	-	-	-	-
MgO	-	0,09	-	-	-	0,11	-	-	-
CaO	-	0,36	0,29	0,28	0,28	0,31	-	-	-
Na <sub>2</sub> O	-	0,08	-	-	0,09	0,11	-	-	-
Cr <sub>2</sub> O <sub>3</sub>	-	-	-	-	-	-	0,21	0,97	0,64
total	85,04	83,67	87,38	85,09	83,14	86,94	86,56	84,75	83,50

#### DISCUSSION OF THE FORMATION CONDITIONS

The presence of authigenic corundum and the natural equivalents of the modifications δ-Al<sub>2</sub>O<sub>3</sub> and θ-Al<sub>2</sub>O<sub>3</sub> in syngenetic frozen sedimentary deposits shows that undoubtedly these phases must have been formed outside their stability fields at negative or low positive temperatures. The following facts may be discussed for the explanation of the genesis under such thermodynamic conditions which are unusual for them:

1. "Low-temperature corundum" is already known as a rare weathering product. Terent'eva et al. (1961) have described a hypergene fine-crystalline corundum from Russian bauxite deposits which had not been influenced metamorphically. Low-temperature corundum from such bauxites is characterized as a metastable product that was formed in the course of natural ageing of klichites and which easily hydrates into gibbsite under surface conditions. With respect to their optical and micromorphological properties the authigenic aluminas

even an initially low content of dissolved substances may lead to a slow enrichment and precipitation within the soils. For this reason, the formation of klichite as well as various crystalline aluminium hydroxides (gibbsite, boehmite) was observed (Zvereva and Ignatenko, 1983; Gradusov and Urusevskaya, 1987).

3. Since aluminas have been found in frozen rocks which are rich in ice it can be assumed that cryogenic processes must have played an important role in their crystallization. The effects of freezing processes on structural changes of hydrogels are known in colloid chemistry for a long time. Coagulates of metal hydroxides adopt granular character after freezing. The porosity, filtration and sorption ability of the precipitates increase considerably. Later activities investigated the effect of individual factors (freezing temperature, freezing velocity, foreign ion content, pH) on structural changes of the coagulates (Komarov et al., 1982 a,b). Comparing investigations have shown that adsorbents grown out of klichites reach their optimum properties

at a freezing temperature of  $-4^{\circ}\text{C}$ . Lower negative temperatures, which accelerate ice crystallization, reduce the structure formation of hydrogels

#### CONCLUSION

Only cryogenic processes enable the formation of the alumina modifications under such unusual thermodynamic conditions. A longterm influence of negative temperatures might intensify dehydration of coagulates. It may be assumed that the slow reaction velocity in frozen systems is responsible for obtaining the metastable transition phases  $\delta$ - and  $\theta$ - $\text{Al}_2\text{O}_3$  besides corundum.

Hence, the presented investigations improve our knowledge of new mineral formation in sediments within the permafrost zone and reflect the special role of cryogenic processes on phase balances. They underline that cryogenic dehydration processes have great influence on the diagenesis of cryolithogenic sediments.

#### ACKNOWLEDGEMENT

The investigations presented were conducted during my stay at the Laboratory for Cryolithology of the Institute for Permafrost in Yakutsk. During my field work and sample preparation I was assisted by members of the Laboratory for Cryolithology. The crystalstructural and microprobe analyses were carried out by A.L. Shirokov, L.V. Nikishova and L.A. Pavlova at the Institute for Geosciences in Yakutsk. I wish to express my sincere thanks to all of them.

#### REFERENCES

- Desyatkin, R.V. (1984). Alas soils of the Lena- Amga-watershed. Yakutsk, ed. Yakutian Department of the Siberian Branch USSR Acad. Sci., 168 pp. (in Russian)
- Gradusov, B.P. and I.S. Urusevskaya (1987). Mineralogy of fine substances in soils of forest tundra and of the northern Taiga of the Cola Peninsula. Vestnik MGU, ser. Soil Sci., No 2, 9-7 (in Russian)
- Katasonova, E.G. and H.G. Zigert (Ch. Siegert) (1982). Slope deposits in river valleys of Central Yakutia. In "Geology of the Cenozoic of Yakutia". Yakutsk, ed. Yakutian Department of the Siberian branch USSR Acad. Sci., 122-132 (in Russian)
- Komarov, V.S. and O.F. Skurko (1982). Structure formation in frozen hydrogels in presence of cations with a 2 to 3 valency. Izvestiya Akad. Sciences BSSR, ser. Chemical Sci., No 2, 31-33 (in Russian)
- Komarov, V.S., O.F. Skurko and N.S. Repina (1982). The influence of the pH-value on the pore structure of frozen hydrogels. Izvestiya Akad. Sciences BSSR, ser. Chemical Sci., No. 3, 24-27 (in Russian)
- Lippens, B.C. (1961). Structure and texture of Aluminas. Delft, 179 pp. Powder Diffraction File (1977), USA, JCPDS.
- Siegert, Ch. (1981). Mineral formation under permafrost conditions. In: "Structure and heat regime of frozen rocks". Nauka Publ., Novosibirsk, 14-21 (in Russian)
- Siegert, Ch. (1987). Greigite and mackinavite in quaternary perennally frozen rocks of Central Yakutia. Mineral. zhurn., 9, No.5, 75-81 (in Russian)
- Siegert, Ch., A.L. Shirokov, L.V. Nikishova, L.A. Pavlova and O.A. Babiy (1990). Natural equivalents of alumina modifications  $\delta$ - $\text{Al}_2\text{O}_3$  and  $\theta$ - $\text{Al}_2\text{O}_3$  in sediments of permafrost regions. Doklady Acad. Sci. USSR, 313, No.3, 689-692 (in Russian)
- Slagoda, E.A. (1989). Structure and texture peculiarities of the ice-complex deposits in North Yakutia. In: "Theory of soil cryogenesis". Abstracts, 5. Conference USSR, Pushchino, 48-49 (in Russian).
- Terent'eva, K.F., F.G. Pasova and G.A. Sidorenko (1961). On fine-dispersed corundum in bauxites. Mineral'noe syr'e, vyp.2, 108-116 (in Russian).
- Zvereva, T.S. and I.V. Ignatenko (1983). Soil weathering of the minerals in tundra and forest-tundra regions. Nauka Publ., Moscow, 232 pp., (in Russian)

This is contribution No. 607 of the Alfred-Wegener-Institute.



## HYDROLOGIC AND WATER QUALITY CHARACTERISTICS OF A DEGRADING OPEN-SYSTEM PINGO

Charles W. Slaughter and Ronald J. Hartzmann

Land/Water Interactions Research Program  
Pacific Northwest Research Station  
USDA Forest Service, Fairbanks, Alaska 99775 USA

Flow regime and selected water quality attributes of water flowing from a thermally and geomorphically degrading open-system pingo in central Alaska (zone of discontinuous permafrost) have been monitored over four summer runoff seasons. Water discharge was not responsive to summer precipitation, and did not appear directly related to ambient air temperature. Chemistry of pingo outflow was consistently different from and apparently unrelated to chemistry of streamflow in a closely adjacent first-order stream. We suggest that water yielded from this thermally degrading pingo is derived from subpermafrost groundwater, initially infiltrated at higher elevations in the landscape. Such thermally sensitive pingos offer an opportunity for monitoring the consequences of possible global warming on permafrost-underlain landscapes.

### INTRODUCTION

"Pingo" is an Eskimo name for large mounds or small hills which are ice-cored (Holmes et al. 1968), and which can be conspicuous in the low-relief terrain of North America's Arctic Coastal Plain and Mackenzie Delta (Mackay 1981). Muller (1959) proposed the currently accepted classification of pingos according to mode of formation. Closed-system pingos, those typical of the Arctic and most widely studied (e.g., Mackay 1973, 1981; Rykborst 1975; Walker et al. 1985), commonly form in drained lakebeds in the continuous permafrost zone. As heat is lost from the ground beneath a former shallow arctic lake, permafrost encroaches on the unfrozen groundwater beneath the lake bed. The water in this increasingly confined unfrozen zone (termed a talik) moves upward vertically in the soil toward the now-cold (subsequent to lake drainage) surface and freezes. Expansion of water on freezing forces the overburden upward to form a surface mound. This process may continue until the finite subsurface water supply is exhausted. Such closed-system pingos may become as much as 40 m high with basal diameters up to 700 m (Holmes et al. 1968).

Open-system pingos form when unfrozen subpermafrost groundwater (or perhaps occasionally intrapermafrost water (Holmes et al. 1968)) under

confined piezometric head penetrates upward to permafrost, thereupon freezing, expanding, and with continuing water supply eventually heaving up the overlying surface to form a mound or small hill. Open-system pingos have received less attention than closed-system pingos; Holmes et al. (1968) suggest that this is because (1) open-system pingos occur primarily in the discontinuous-permafrost zone (i.e. central Alaska) which has more heterogeneous relief than the Arctic coastal plain and is largely vegetated by forest or tall shrubs, making these land forms less conspicuous, (2) pingos may be mistaken for other land forms such as landslide debris or erosional remnants, and (3) the general region of their occurrence may have received less attention by surficial geologists than has the Arctic.

This paper reports observations of hydrologic and water quality attributes of a thawing open-system pingo in the discontinuous-permafrost Yukon-Tanana Uplands of central Alaska.

### SETTING AND DESCRIPTION

The Caribou-Poker Creeks Research Watershed (CPCRW) lies in the Yukon-Tanana Uplands of central Alaska at 65°10'N, 147°30'W. The dendritic drainage pattern of the 104-km<sup>2</sup> CPCRW is

developed in unglaciated Birch Creek schist. Elevations range from 226 to 826 m. Slopes are mantled with a relatively thin veneer of loess, deeper on south-facing than on north-facing slopes, derived from river floodplains to the south. Toeslopes and valleys have accumulations of ice-rich fine-grained retransported colluvium intermixed with organics. Ridges, north slopes, and valleys are underlain by permafrost at shallow depth; south-facing slopes are generally free of permafrost.

Vegetation is typical of the northern boreal forest (Van Cleve et al. 1986). Productive stands of white spruce (*Picea glauca*), birch (*Betula papyrifera*) and aspen (*Populus tremuloides*) grow on south-facing, well-drained slopes; permafrost-underlain north-facing slopes and valleys support low-productivity open black spruce (*P. mariana*) woodland with minor components of larch (*Larix laricina*) and occasional balsam poplar (*Populus balsamifera*). Riparian zones are occupied by mixed open woodland and tall shrub communities, with willow (*Salix* spp.), dwarf birch (*B. glandulosa*) and alder (*Alnus crispa*) major components.

Two pingos occur on the immediate south side of Caribou Creek in southeast CPRW, situated about 1200 m apart at the base of a steep north-facing hillslope at 240 m elevation. One pingo is completely vegetated and lacks a thaw pond or surface drainage. The second pingo is "mature" in the sense of Holmes et al. (1968); this pingo is vegetated by white and black spruce, birch and balsam poplar trees with an understory of shrubs, forbs, and a deep organic forest floor. This pingo has a small pond in a central crater, and evidently is thermally and geomorphically degrading. It appears similar to the "Discovery Pingo" described by Holmes et al. (1968, p. H27-H29).

When first observed in the early 1970's the thawing pingo had a small central crater and pond and was assumed to be degrading thermally (A. Helmers and F. Lotspeich, pers. comm.). This pingo was subsequently studied during the period 1987-1990. Surface topography was surveyed; vegetation development was monitored at fixed points; pond stage, channeled surface runoff, and water quality were monitored during the summer (open water) season.

## METHODS

The pingo pond drains to the northwest through a natural surface outlet; runoff water was channeled through a 5.1-cm (throat width) prefabricated fiberglass Parshall flume installed in the outlet stream. The

Parshall flume was chosen for this installation because its hydraulic design and structural stability are appropriate for installation in thermally sensitive stream sections, it is fairly insensitive to approach velocity, and does not require a pool at the inlet (Slaughter 1981). Water stage was recorded utilizing an electronic data logger coupled by a potentiometer to a float in the stilling well of the flume, and was also periodically recorded manually by field technicians. We did not attempt to measure subsurface water which may have left the pond by infiltration through the soil mantle.

Water quality attributes were determined for grab samples collected in the thaw pond, normally within one meter of the bank. Samples were collected in 500-ml pre-washed Nalgene bottles which were capped under water and kept cool and dark during transport to Fairbanks for analysis. Specific conductance was measured with a Beckman Solubridge meter; total alkalinity was determined by titration to pH 5.1 using a Hach digital titrator; pH was determined with a DigiSense LED pH meter; turbidity was determined utilizing a Hach analytical nephelometer.

Air and water temperature were measured with a pre-calibrated glass thermometer at the pingo at time of site visits. Precipitation was recorded by a tipping-bucket precipitation gage permanently located in the Caribou Creek valley 1000 m east of the pingo. Concurrent streamflow measurements were available from a north-aspect 5.7-km<sup>2</sup> catchment (C-3) located 2400 m west of the pingo.

During occasional winter visits to the site extensive ice accumulation in the lower reaches of the runoff channel, similar to aufeis deposits commonly found in other sectors of the research watershed (Kane and Slaughter 1973a; Slaughter 1990), provided evidence of water outflow during winter months.

## RESULTS AND DISCUSSION

Data for 1989 are presented, as representative of the four years of study.

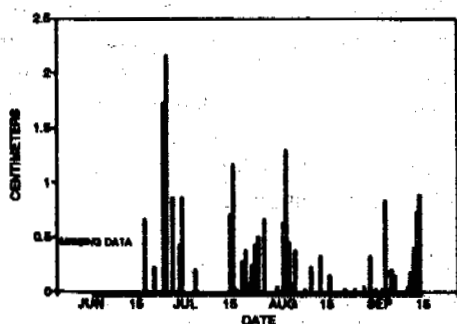
### Water yield:

The summer flow of water from the pingo thaw

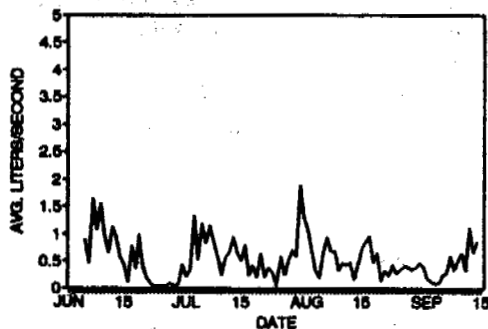
pond through the runoff channel varied from 0.3 to 2.5 l/s in 1987, zero to 4.1 l/s in 1988, zero to 1.8 l/s in

precipitation (Haugen et al. 1982). The lack of pingo flow response to precipitation suggests that the water source is subpermafrost groundwater.

### 1989 PRECIPITATION



### 1989 PINGO DAILY DISCHARGE



### 1989 C-3 DAILY DISCHARGE

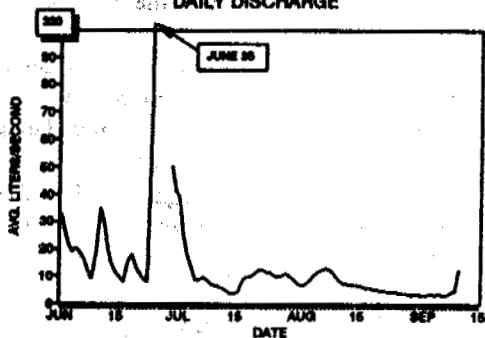


Figure 1. Precipitation, pingo discharge, and C-3 stream discharge, 1989.

1989, and zero to 0.9 l/s in 1990. Discharge from the pingo was not responsive to precipitation (Figure 1) and shows no correlation with streamflow of a nearby first-order stream in catchment C-3 (Figure 2). Streamflow in C-3 is highly responsive to summer

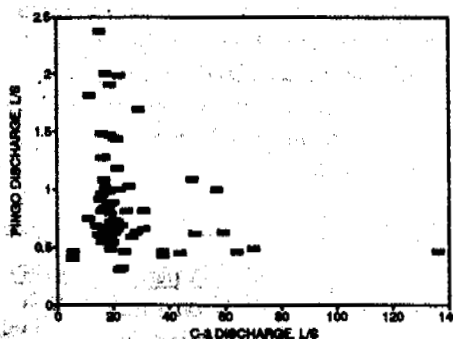


Figure 2. Pingo discharge vs C-3 discharge for concurrent dates, 1987.

Since this water is presumably derived from subpermafrost groundwater, it is not appropriate to infer a "catchment area" for the water source. Groundwater in the uplands near Fairbanks (including the region of this study) is recharged primarily by snowmelt on high-elevation ridges where soils are thin and the bedrock is fractured and permeable (Cederstrom 1963). Lawson et al. (1991) utilized ground-penetrating radar to investigate suspected bedrock fractures and jointing on Caribou Peak, in the center of the research watershed; they concluded that an extensive fracture zone allowed groundwater recharge to a sub-permafrost aquifer. Recharge from either snowmelt or summer precipitation is presumed to be minor to non-existent on permafrost-underlain slopes such as the hillslope immediately south of this pingo; the active layer (zone of seasonal thaw at the surface) in such settings is only 50-80 cm, and the permafrost probably extends to at least 75+ m depth (site-specific permafrost depth data are not available). Ice-rich frozen ground is effectively impermeable to movement of water (although frozen ground may in some cases have "low but finite permeability" (Williams and van Everdingen 1973). Therefore the permafrost which occupies the hillslope above the pingo acts as a confining layer. It would consequently be expected that water escaping to the surface at the slope base, as in the pingo pond, might be under considerable artesian pressure (Williams and van Everdingen 1973). The pingo pond surface is ca. 5 m above the surrounding terrain, and potentially subject to as much as 250 m hydraulic head (the elevation difference between pond surface and the ridgeline where recharge is

presumed to occur). While the topographic situation is dissimilar, it is relevant to note that Kane and Slaughter (1973b) documented recharge of a thaw lake (for which there is no visible evidence of having been a pingo) by groundwater flow upwards through a thawed zone penetrating at least 40 m of permafrost.

Williams and van Everdingen (1973) cite Holmes et al. (1968) in suggesting that conditions required for formation of open-system pingos include (1) a continuous, confining impermeable layer which might well be permafrost, (2) restricted, but continuing, groundwater flow ("...too large a flow rate would prevent freezing of the pingo"); (3) ground temperature close to 0°C to produce minimal tensile strength of frozen ground and to reduce opportunity for groundwater freezing at great depth. They suggest that the combined forces of artesian pressure and freezing pressures of groundwater would be required to provide the uplifting force required to raise the mounds which become pingos. These conditions appear to be met in the case of the CPCRW pingos: the contributing slope (south of the pingo) is underlain by permafrost at shallow depth; the recharge zone, while undetermined, is most likely confined to the narrow (<250 m) ridgeline, so groundwater recharge is presumably slow and of relatively low volume; permafrost temperature measured elsewhere in the research watershed varied from -2 to -3°C at 12 m depth in a valley location ca. 1200 m east of the pingo, and was -1°C at 5 m depth at an alpine site in the center of the research basin (Collins et al. 1988).

Water quality:

During the four summers of study, the range in pH was 6.4 to 8.2. Measured pH was below 7.0 only during summer 1988. Alkalinity ranged from 75 to 159 mg/l. Specific conductance reached a maximum value of 661 micromhos/cm in 1987, and in 1988-1990 was in the range 283-482 micromhos/cm. Turbidity was generally in the range of 5-100 NTUs, but was as low as <1 NTU and as high as 200 NTUs (1988). The seasonal course of these attributes for 1989 is depicted in Figure 3.

These characteristics of water quality differ notably from the water in the nearby C-3 stream (Hilgert and Slaughter 1983, 1987). During summer 1989 values for pH, alkalinity, turbidity and specific conductance of pingo waters consistently exceeded those for C-3 streamflow on concurrent sampling dates (Figure 3).

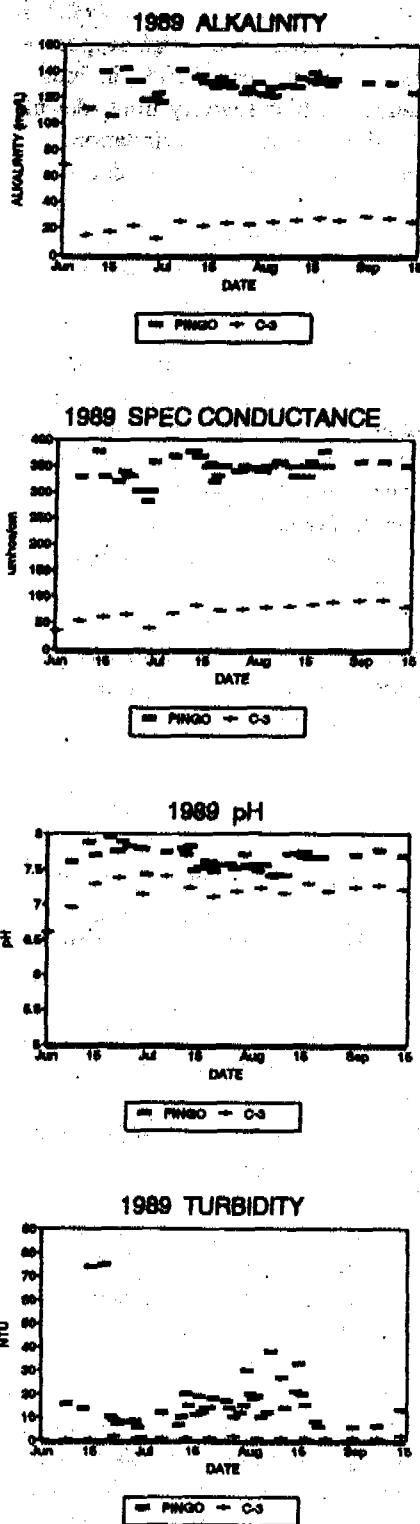


Figure 3. Seasonal course of pingo water quality attributes, 1989.

This first order catchment (C-3) is very responsive to snowmelt and to summer precipitation, and is considered a "flashy" stream (Haugen et al 1982); its rapid response is conditioned by the high proportion of permafrost in the catchment area (>50%, including the entire stream channel), which severely limits detention storage and infiltration of summer precipitation. Summer low flows in this small basin are dominated by groundwater (base flow); yet even at base flow the water does not appear to reflect the same subsurface processing as has been exerted on water issuing from the pingo (see Figure 3). This difference may be partially attributed to the mingling of C-3 baseflow with interflow and surface runoff during transit in the open channel downstream to the point of sampling -- the stream length above the C-3 gaging station is ca. 1500 m. Water yielded through the pingo pond has been in contact with subsurface geologic formations from time of initial infiltration to reaching the pond surface. We have no estimate of transit time for this water.

Pingo water quality attributes appear insensitive to summer precipitation. This is hardly surprising, given the small surface area of the pond (about 50 m<sup>2</sup>).

## CONCLUSIONS

Holmes et al. (1968) reported observations on about 270 pingos in central Alaska, in varying stages of growth or decay. The thawing and geomorphically degrading pingo described in this paper is probably not atypical of many in the subarctic, discontinuous zone of central Alaska and northwest Canada. However, in contrast to Holmes' et al. (1968) observation that pingos predominantly occur at the base of gentle south-facing slopes, the two pingos in CPRW are at the base of steep north-facing, permafrost-underlain slopes.

The volumetric flow contribution of this thawing pingo to the larger Caribou Creek is negligible in terms of affecting total water yield of the catchment. This pingo and similar features are probably important hydrologically only in a very localized sense. Similarly, the dissolved inorganic loading contributed to the larger stream system is not significant in relation to total stream loading. However, analysis of this pingo outflow is useful in providing some insight into the groundwater relationships in a locale which has received virtually no study of groundwater recharge or yield.

This thawing pingo, along with the companion pingo

which is not (yet?) thawing and degrading, provides an opportunity to monitor ice-cored, thermally sensitive geomorphic landforms in a controlled setting. Permafrost terrain, particularly in the zone of discontinuous permafrost in central Alaska, is extremely sensitive to possible global warming (Lachenbruch and Marshall 1986; Post 1989). Monitoring the hydrologic and geomorphic status of these pingos over the coming decade may allow early clarification of whether such warming is indeed occurring, at least in this specific environmental setting. In this context, the pingos and the landscape-scale catchment/stream system of Caribou-Poker Creeks Research Watershed are incorporated into the Pacific Global Change Research Plan of the USDA Forest Service Global Change Research Program (Science Policy Associates 1990).

## ACKNOWLEDGEMENTS

This research was supported by the Pacific Northwest Research Station, USDA Forest Service. Field sampling was largely accomplished with support of volunteers from EARTHWATCH, The Center for Field Research, Watertown, Mass. Brigitte Jaeger, Lisa Reeber, Laura Larsen and William Wood were instrumental in guiding the efforts of volunteers, and in acquisition and analysis of data. Scott Ray and Michelle Smith provided invaluable field and laboratory assistance with this research.

## REFERENCES

- Cederstrom, D.J. (1963) Ground water resources of the Fairbanks area, Alaska. U.S. Department of the Interior, Geological Survey. Water Supply Paper 1590, 84 p.
- Collins, C.M., R.K. Haugen, and R.A. Kreig (1988) Natural ground temperatures in upland bedrock terrain, interior Alaska. Proceedings 5th International Conference on Permafrost. Trondheim, Norway. National Academy of Sciences, 56-60.
- Haugen, R.K., C.W. Slaughter, K.E. Howe, and S.L. Dingman (1982) Hydrology and climatology of the Caribou-Poker Creeks Research Watershed, Alaska. CRREL Report 82-26. Hanover, NH: U.S. Army Cold Regions Research and Engineering

- Laboratory, 42 p.
- Hilgert, J.W. and C.W. Slaughter (1987) Water quality and streamflow in the Caribou-Poker Creeks Research Watershed, Central Alaska, 1979. Research Note PNW-RN-463. Portland, OR: U.S. Department of Agriculture, Forest Service, Pacific Northwest Research Station, 34 p.
- Holmes, W.G., D.M. Hopkins, and H.L. Foster (1968) Pingos in central Alaska. Bulletin 1241-H. U.S. Department of Interior, Geological Survey. 34 p.
- Kane, D.L. and C.W. Slaughter (1973a) Seasonal regime and hydrological significance of stream icings in central Alaska. pp. 528-540 IN Proceedings, The role of snow and ice in hydrology. Banff, Alberta. UNESCO/WMO/IASH.
- Kane, D.L. and C.W. Slaughter (1973b) Recharge of a central Alaska lake by subpermafrost groundwater. North America contribution -- Permafrost Second International Conference. National Academy of Sciences, 458-462.
- Lachenbruch, A.H. and B.V. Marshall (1986) Changing climate: geothermal evidence from permafrost in the Alaskan Arctic. *Science* 234, 689-696.
- Lawson, D.E., S.A. Arcone, and C.M. Collins (1991) Geophysical investigations of an anomalous unfrozen zone, Caribou Peak, Alaska. CRREL Report 91-17. Hanover, NH: U.S. Army Cold Regions Research and Engineering Laboratory, 23 p.
- Mackay, J.R. (1973) The growth of pingos, western arctic coast, Canada. *Canadian Journal of Earth Sciences* 10, 979-1004.
- Mackay, J.R. (1981) Aklisuktuk (Growing Fast) Pingo, Tuktoyaktuk Peninsula, Northwest Territories, Canada. *Arctic* 34, 270-273.
- Muller, F. (1959) Beobachtungen uber Pingos. *Meddeleser om Gronland* 153(3):1-127. Translated by D.A. Sinclair: 1963. Observations on pingos. National Research Council of Canada Technical Translation 1073, 117 p.
- Post, W.M. (ed.) (1989) Report of a workshop on climate feedbacks and the role of peatlands, tundra, and boreal ecosystems in the global carbon cycle. Office of Health and Environmental Research, Assistant Secretary for Environment, U.S. Department of Energy, 28 p.
- Ryckborst, H. (1975) On the origin of pingos. *Journal of Hydrology* 26, 303-314.
- Science Policy Associates (1990) Global change research program plan. U.S. Department of Agriculture, Forest Service, 76 p.
- Slaughter, C.W. (1981) Streamflow measurement with pre-fabricated Parshall flumes in a permafrost-dominated watershed. Research Note 382. Portland, OR: U.S. Department of Agriculture, Forest Service, Pacific Northwest Forest and Range Experiment Station, 8 p.
- Slaughter, C.W. (1990) Aufeis formation and prevention. p. 433-458 IN Ryan, W.L., and Crissman, R.D. (eds.) *Cold Regions Hydrology and Hydraulics*. Technical Council on Cold Regions Engineering Monograph, American Society of Civil Engineers, New York, NY.
- Van Cleve, K., F.S. Chapin, P.W. Flanagan, L.A. Viereck, and C.T. Dyrness (eds) (1986) *Forest ecosystems in the Alaskan taiga*. Ecological Studies 57. Springer-Verlag, New York, 230 p.
- Walker, D.A., M.D. Walker, K.R. Everett, and P.J. Webber (1985) Pingos of the Prudhoe Bay region, Alaska. *Arctic and Alpine Research* 17, 321-336.
- Williams, J.R., and R.O. van Everdingen (1973) Groundwater investigations in permafrost regions of North America: a review. North American Contribution -- Permafrost Second International Conference. National Academy of Sciences, pp. 435-446.

LABORATORY SIMULATION OF DOLOMITE AND LIMESTONE DISSOLUTION:  
RATES, YIELD, AND MINERALOGY OF FINE-GRAINED RESIDUE

Ronald S. Sletten

University of Washington  
Civil Engineering, Mail Stop FX-10  
Seattle, WA 98105 USA

Dissolution of carbonate rocks is a primary mechanism underlying the production of fine-grained material that is important for development of soil profiles and for driving diverse geomorphic phenomena. Experiments were designed to simulate limestone and dolomite dissolution at the acidity of precipitation and snowmelt (pH 5-5.5). Dolomite dissolved to produce fine-textured residues (<0.05 mm diameter particles), primarily of dolomite mineralogy, amounting to 8-14% by weight of the sample dissolved. In contrast, dissolution of limestone yielded <1-3% fines, primarily of silicates. Dolomite dissolved approximately 2 times slower than limestone, however, chemical weathering of carbonate rocks in soils is limited by water availability rather than dissolution kinetics. The effect of rock type and chemical weathering on frost shattering is discussed.

#### INTRODUCTION

Soils in the High Arctic developed on dolomite<sup>1</sup> parent material are often quite striking due their tendency to form sorted features. These soils generally have abundant silt-size fines<sup>2</sup> primarily of dolomite mineralogy (Tedrow and Krug 1979; Foreman and Miller 1984; Mann et al. 1986; Etzelmüller and Sollid 1991; Dredge 1992). They have been observed to be very actively undergoing cryoturbation and develop into some of the most picturesque sorted features (Washburn 1980; Hallet and Prestrud 1986; van Vliet-Lancée 1988). In contrast, High Arctic soils on limestone are not generally noted to contain significant quantities of fines, and the fines that are present tend to be silicates. In order to gain insight into the soil processes that lead to the development of these soils, several questions were posed. What is the primary mechanism for producing the silt-size dolomite particles in soils developed on dolomite? Can the fines be accounted for by chemical dissolution, or are physical weathering or transport processes necessary to account for the fines present? This study presents results from laboratory experiments designed to simulate chemical weathering, and discusses alternative sources of

fines in soils developed on carbonate rock parent material.

Soil forming processes in the High Arctic and Antarctic are limited by the cold conditions and low precipitation. Weathering of silicate rocks to form clay minerals and metal oxides occurs very slowly, whereas dissolution of carbonate rocks occurs relatively rapidly (Ugolini 1986; Bockheim and Ugolini 1990; Doner and Lynn 1989). Dissolution of carbonate rocks to produce a fine-textured residue has been proposed as a major mechanism for formation of fines in the Arctic where carbonate rocks are widespread (Ugolini and Tedrow 1963; Tedrow 1977; Forman and Miller 1984). Although accumulation of fines in soils developed on carbonate rocks have been observed, little work has focused on determining rates, yield, and mineralogy of fines produced under weakly acidic conditions. The focus of this paper is to establish yields and mineralogy of the residue remaining after dissolution of carbonate rock under mildly acidic conditions expected in High Arctic soils. This study provides a quantitative estimate of the production of fine-textured residue produced from dolomite dissolution and contrasts this with the residue produced by limestone dissolution, in order to better understand processes of soil genesis.

In addition to the laboratory study, a case study of silt accumulation in a soil developed on dolomite parent material is presented. Since chemical weathering may be insufficient to produce the silt accumulation found in this soil, other potential sources of fines are discussed.

<sup>1</sup> Dolomite may refer to either the mineral dolomite or sedimentary rock containing predominantly dolomite; herein dolomite refers to the rock unless stated otherwise. Limestone is a sedimentary rock whose primary carbonate mineral is calcite. (Bates and Jackson 1984)

<sup>2</sup> For the examples and experiments described here, the fines have been determined to contain >80% silt-size particles (2-50  $\mu\text{m}$ ), therefore the terms fines and silt are used interchangeably.

## METHODS

### Chemical Dissolution

Five samples of dolomite and limestone were selected from Brøggerhalvøya, Spitsbergen (78°55'N, 11°25'E) and Svartknausflya, Nordaustlandet (79°25'N, 22°20'E), both in the Svalbard archipelago. X-ray diffraction patterns of random powder mounts indicate that the dolomite contains about 5-10% quartz and <5% plagioclase, while the limestone was composed primarily of calcite with variable amounts of quartz and minor amounts of plagioclase (Table 2). To compare only fresh unweathered surfaces, rock samples were broken to remove weathering rinds, if present, and crushed. The unweathered surfaces might be expected to weather more rapidly than when a rind is present, but using freshly exposed surfaces allows a more consistent comparison to be made between different samples. In addition, weathering of fresh surface may better represent conditions present early in soil development. The crushed rock was sieved to keep only the 0.5 to 0.25 mm size fraction and rinsed with distilled water to remove any adhering finer size fragments.

One gram samples were placed in 100 ml beakers and 60 ml of distilled water was added. The beakers were sealed to minimize evaporation except for a pH probe and burette tip to add acid. A Teflon coated magnet was suspended from the beaker stopper by latex tubing and the beaker was placed on a magnetic stirrer, allowing the solution to be stirred without the sample being abraded. The pH was maintained at either 5.0 or 5.5 utilizing a pH-stat setup (Radiometer Model PHM 62 pH meter fitted with Radiometer Model ABU11 autoburette, TTA60 titration assembly (Radiometer America, Inc., Westlake, OH)). The pH was maintained at the set value by the addition of 0.25 N HCl; during the course of the experiments the amount of acid added to maintain the pH was recorded as a function of time. A pH value of 5.5 was used for the majority of the experiments since pH values of precipitation and snowmelt are typically between 5 and 6 (Mann et al. 1986; Sletten 1988, unpublished data). A pH value of 5.0 was chosen for one experiment to explore the effects of slightly more acidic conditions. The experiments were conducted for periods up to 509 hours, generally until approximately 20% of the original sample had dissolved.

### Collection and Analysis of Residue

At the completion of the experiment the solution was passed through a 0.1  $\mu$ m polycarbonate filter membrane to collect the residue. The residue was sieved at 0.05 mm. The <0.05 mm fraction indicates the proportion that is silt-sized or smaller. Previous results (Mann et al. 1986; Sletten, unpublished data) indicate that clay size particles (<0.002 mm) typically comprise less than 20% of the <0.05 mm fraction in soils developed on the rock types investigated here. Therefore, the <0.05 mm fraction in these experiments is assumed to consist primarily of fragments greater than clay size. The weights of sample dissolved and fine-textured residue produced were determined.

## RESULTS

### Residue Yields and Mineralogy

The yields of the residues are shown in Table 1. The dolomite samples dissolved at pH 5.5 produced an average 10.6 $\pm$ 3.0% fines (<0.05 mm), while the limestone samples yielded an average of 1.8% for the two samples tested. Dolomite sample 1 dissolved at pH 5.0 produced only 3.1% fines, compared to 14% fines at pH 5.5. Dolomite sample 2 was dissolved for two time periods resulting in the dissolution of 15 and of 20% of the original sample, and producing 9.9 and 8.1% fines residue.

Table 1. Amount of fine-textured residue (<0.05 mm in diameter) produced based on the amount of sample dissolved. The original sample consisted of 1.0 g of 0.5-0.25 mm rock fragments (chips).

Sample	pH	sample dissolved (mg)	silt-size residue (%)
dolomite 1a	5.0	210	3.1
dolomite 1a	5.5	156	14.0
dolomite 2a	5.5	145	9.9
dolomite 2b	5.5	190	8.1
limestone 3a	5.5	210	0.5
limestone 4a	5.5	254	3.0

In addition to normalizing the amount of fine-textured residue produced to the amount of sample dissolved as shown in Table 1, the residue produced can be normalized to the amount of calcium solubilized by rock dissolution; these values are given in Table 2.

Table 2. Average yields in mg silt (<0.05 mm diameter) per meq Ca dissolved into solution.

Sample	pH	silt yield
dolomite 1a	5.0	2.4 mg silt/meq Ca <sup>2+</sup>
dolomite 1a	5.5	10.0 "
dolomite 2a	5.5	8.5 "
dolomite 2b	5.5	7.7 "
limestone 3a	5.5	0.25 "
limestone 4a	5.5	1.6 "

Results of x-ray diffraction analysis are shown in Table 3. The dolomite and limestone both contained silicate minerals. The mineralogy of the dolomite residue was very similar to the original rock, reflecting a silt-size fraction primarily composed of dolomite. In contrast, the dissolution of limestone preferentially removed calcite and produced a residue primarily composed of silicate minerals. Both residues contained traces of feldspar that were not noted in the x-ray diffraction patterns of the original samples. Most likely this is due to the fact that the silicates are present in greater relative abundance in the residue, and hence are detectable in the residue, but not in the whole rock sample.



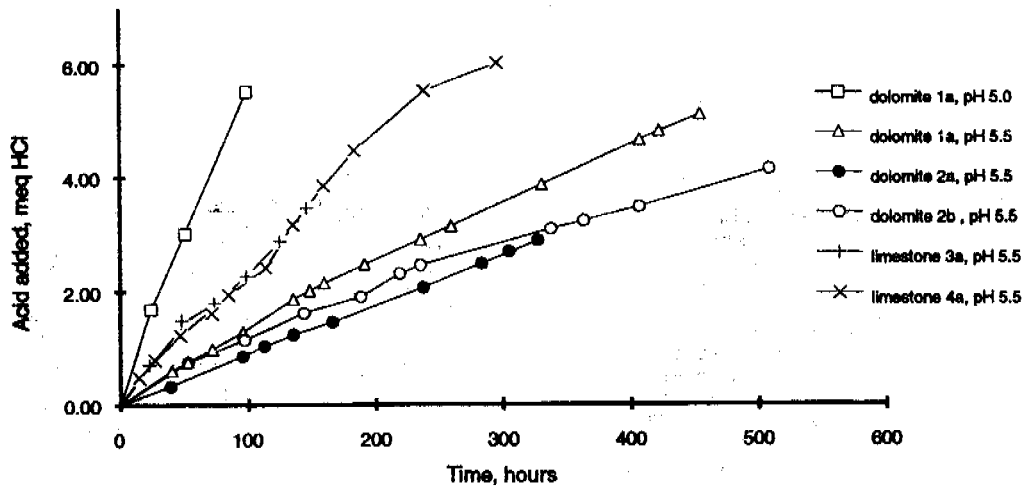


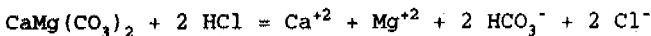
Figure 1. Acid added versus time of dissolution for dolomite and limestone samples.

Table 3. X-ray diffraction analysis of original rock samples and of the <0.05 mm size residue produced after dissolution. Relative abundance based on the 100 peak height: - = no peak, + = trace, ++ = moderate, +++ = major. Note: minerals present at less than about 5% abundance may not be detected. (qz = quartz, dolo = dolomite, cal = calcite, feld = feldspar, plag = plagioclase, res = residue after dissolution.

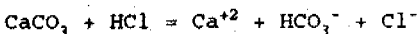
Sample	qz	dolo	cal	feld	plag
dolo rock	++	+++	-	-	+
dolo res	++	+++	-	+	+
lime rock	++	-	+++	-	-
lime res	+++	-	+ / ++	+	-

#### Rate of Dissolution and Acid Consumed

The rate of acid addition is proportional to the carbonate dissolution rate (Figure 1). The amount of acid added can be utilized to estimate the amount of rock dissolved depending on the rock type. The amount of pure dolomite dissolved is 0.46 mg per meq acid added according to the equation:



While the amount of calcite dissolved is 0.5 mg per meq acid added according to the equation:



The slopes of the lines allow estimates of the dissolution rates to be calculated. The rates are 25 µg/hr for dolomite at pH 5.0; 4.5 ± 1.7 µg/hr for dolomite at pH 5.5; and 12 ± 1.2 µg/hr for limestone at pH 5.5. The limestone dissolves approximately twice as fast as the dolomite sample at pH 5.5. The single dolomite sample tested at pH 5.0 dissolved approximately 6 times more rapidly than at pH 5.5.

#### DISCUSSION

##### Dissolution Rate and Silt Yield

Dissolution rates determined here were compared with rates determined using pure minerals of dolomite and calcite (Table 4), given in a review by Wollast (1990). The dissolution rate for the dolomite sample tested in this study was greater and the rate was more sensitivity to hydrogen ion activity. This may be due to the samples analyzed being less crystalline or incompletely dolomitized. Analysis of dissolution products support this contention since greater amounts of  $\text{Ca}^{2+}$  on a molar basis were produced than were  $\text{Mg}^{2+}$  for some of the samples tested. Dissolution of limestone compared to pure calcite at pH 5.5 was approximately 4 times less. The calcite in the limestone was pure according to x-ray diffraction analyses and the dissolution products contained only traces of magnesium, therefore the difference do not appear to be attributable to differences in mineral purity. There may be differences in surface characteristics and estimates of surface area.

The pH conditions used for most of the dissolution experiments were selected to approximate the hydrogen activity of precipitation and snowmelt, as discussed above. When meteoric water contacts carbonate rocks in

Table 4. Average dissolution rates ( $\text{mol} \cdot \text{cm}^{-2} \cdot \text{s}^{-1}$ ) determined in this study compared to those presented by Wollast (1990). ND = not determined.

Rock type	pH	Dissolution rate	
		This study	Wollast
dolomite	5.0	$10^{-10.0}$	$10^{-10.2}$
dolomite	5.5	$10^{-10.8}$	$10^{-10.5}$
limestone	5.5	$10^{-10.4}$	ND
calcite	5.5	ND	$10^{-9.8}$

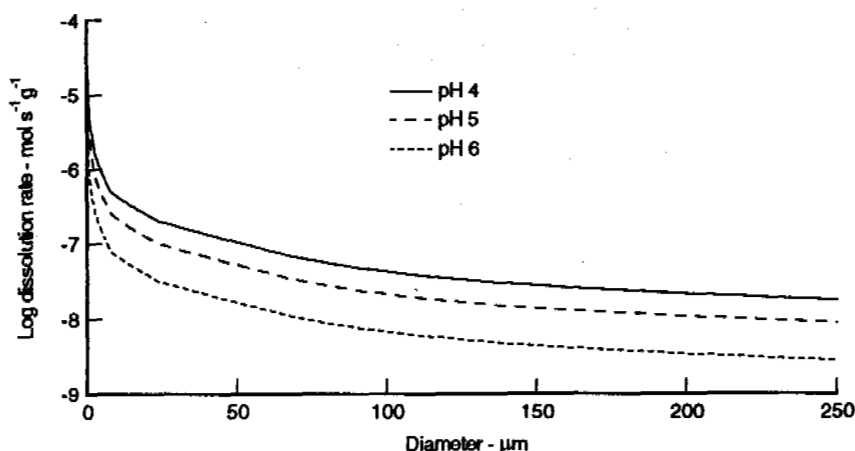


Figure 3. Dolomite dissolution rate as a function of particle size at various pH values. Rate constants used to generate these graphs are from review by Wollast (1990).

the soil the pH increases, along with  $\text{Ca}^{2+}$  and  $\text{HCO}_3^-$ . Soil solutions, collected by tension lysimeters, were found to approach saturation with respect to carbonate minerals near the surface (Mann et al. 1986; Sletten 1988).

The tendency of dolomite to form fine-grained material is related to its fine-grained matrix, revealed clearly in a thin section (Figure 2). For a given composition, larger grains are relatively stable and smaller crystals will dissolve more quickly since dissolution rates increase sharply with decreasing particle size as shown in Figure 3. Particles less than a few  $\mu\text{m}$  in diameter dissolve particularly quickly; perhaps accounting for the paucity of clay size particles of carbonate minerals in these soils.

#### Soils on Limestone and Dolomite

According to the experiments performed here, accumulation dolomitic fines are sensitive to slight changes in pH since dissolution at pH 5.0 produced less residue than at pH 5.5. This helps explain why dolomitic fines accumulate and

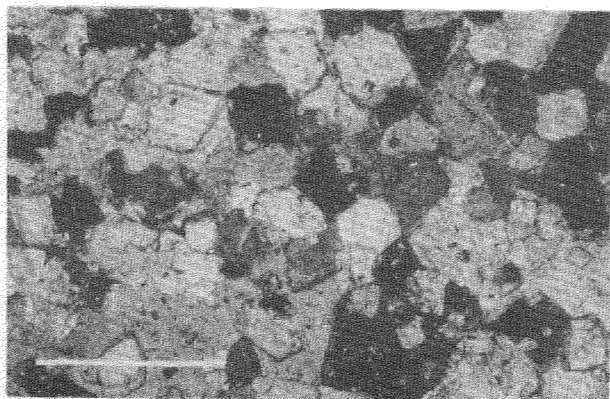


Figure 2. Thin section of dolomite sample 1a viewed under plane polarized light. Grain sizes range from  $<50$  to  $>200$   $\mu\text{m}$ . White bar is 390  $\mu\text{m}$  in length.

are abundant in Arctic regions where chemical weathering is weak. Under more intense weathering conditions, such as occurring in temperate climates, dolomite dissolves more completely, including its dolomitic fines, and less residue is expected, but the residue that is produced will have a relatively greater proportion of silicate minerals.

Soils developed on carbonate parent material in the High Arctic often are barren of vegetation and are classified as Polar Desert soils (Tedrow 1977; Bliss and Matveyeva 1992). Soils on silicate parent rocks under the same climatic conditions generally have richer vegetation. The barren conditions may be related to soil instability due to cryoturbation, rock instability by dissolution, and the alkaline conditions and limited availability of nutrients. In limestone terrain only small quantities of fines are produced and the soils are often very gravelly and not very conducive to plant colonization. On the other hand, soils on dolomite parent material contain an abundance of silts that allow rapid "wicking" of water, as is evident during collection of soil solutions using tension lysimeters and from extensive frost-heave of the surface which may disrupt vegetation.

#### Case Study - Soil Developed on Dolomite

The amount of silt produced per equivalent of  $\text{Ca}^{2+}$  solubilized, along with values of  $\text{Ca}^{2+}$  in soil solutions, can be used to estimate rates of silt formation in soils. For example, consider soils developed on reworked beach deposits primarily of dolomite at Brøggerhalvøya, Spitsbergen (Forman and Miller 1984; Mann et al. 1986). For this example, assume that climatic conditions have been similar to present, all water from precipitation has percolated through the soil, and the weathering intensity has been constant.

The soil considered in this example developed on the crest of a raised beach ridge that dates to 11 kBP and, based on analogy to modern-day beach deposits, did not inherit silt. In contrast, swales between the beach ridges have abundant silt; presumably due to accumulation after deposition and original back shore deposits. These soils have developed a

horizon enriched in silt-size particles (Mann et al. 1986). Micromorphology of this horizon were interpreted by van Vliet-Lanoë (personal communication, 1992) to be pedogenic in origin and not due to sedimentation in a marine environment.

An estimate of the maximum production of fines due to chemical weathering can be made from climatic and soil solution data. The current mean annual precipitation is 385 mm, estimated from the weather station at NyÅlesund. Assume all water from precipitation percolates through the soil and dissolves 25 mg  $\text{Ca}^{2+}$ /l, the concentration of  $\text{Ca}^{2+}$  measured in soil solutions collected by tension lysimeters exiting the silt horizon (Mann et al. 1986; Sletten 1988). This amounts to 5.3 keq  $\text{Ca}^{2+}$  per square meter over 11,000 years. Using the average of the values for dolomite dissolution at pH 5.5 (Table 2), 8.7 mg of silt produced per meq  $\text{Ca}^{2+}$  dissolved, leads to an estimate of 46 kg of silt per  $\text{m}^2$  over the time period specified. In actuality, soil profiles from Brøggerhalvøya contain approximately 64 kg silt/ $\text{m}^2$  (15 cm thick horizon with silt accumulation containing 25% silt with a bulk density of 1.7  $\text{g}/\text{cm}^3$ ).

These calculations suggest that dolomite dissolution can account for a major amount of the fines present. It is important to consider the validity of the assumptions. Since most of the precipitation occurs as snow and much of the water from snowmelt flows overland, the assumption that all the water from precipitation percolates through the soil may be an overestimate. On the other hand, the amount of silt produced in the soil may be greater than that produced in the experiments at pH 5.5, since the stability of the silt-size dolomite is quite sensitive to pH conditions and the soil pH is typically higher than 5.5. The silt accumulated in the silt horizon can also be subject to dissolution, although the dissolution here is expected to be minimal since the soil solutions approach saturation with respect to dolomite near the soil surface (Sletten 1988). Other potential sources of fines are discussed below.

Additional sources leading to the observed silt accumulation in the soils presented in the case study include: (1) fine-grained material inherited with the parent material; (2) eolian input of silt; or (3) physical weathering processes, in addition to chemical dissolution, to produce silt. As discussed above, it does appear that, since these soils occur on beach ridges, they did not inherit much fines, so the first possibility is excluded. With respect to eolian input, soils in other locations on Svalbard have been noted to have a significant input of loess (Sletten 1990). There are no local loess sources for the soil presented here and nearby soils developed on non-carbonate parent material do not contain dolomitic silt, therefore it appears unlikely that eolian input could account for much of the silt accumulation.

#### Physical Weathering

An alternative mechanism for producing fines from dolomite in periglacial environments is physical weathering. Considerable experimental work suggests that the production of fines by freezing depends on the total porosity, pore size distribution, saturation coefficient, permeability, and strength of the material (Lautridou and Ozouf 1982; Whalley and

McGreevy 1983; Latridou 1988; Hall and Latridou 1991). Frost weathering is often believed to be due to volumetric expansion of water during freeze-thaw cycles, but such cycles may not be necessary since growth of ice at sustained freezing temperatures are sufficient to produce pressures adequate to comminute rocks (Hallet et al. 1991). The effect of water is also important in non-freezing environments since clay minerals in dolomite rocks tend to concentrate at grain boundaries and thereby, due to expansion by water adsorption as rocks are wetted, are susceptible to breakdown. Clays in non-dolomitic limestone tend to be disseminated and do not display the same tendency (Dunn and Hudec 1966; Fahey and Dagrèsse 1984).

Dolomite may gain porosity during recrystallization from limestone due to a 13% contraction when  $\text{Mg}^{2+}$  stoichiometrically substitutes for  $\text{Ca}^{2+}$ ; typical porosities of dolomite are even greater than this (Murray 1960; Moore 1989). Murray (1960) showed that rocks with increasing dolomite mineral content (from 50 to 90%) had increasing porosity (from 10 to 30%), and that dolomite in general had significantly greater porosity than limestone (5 to 15%). The greater porosity of dolomite versus limestone suggests that it may be more likely to frost-shatter.

Although it appears reasonable that dolomite is susceptible to breakdown by water due to frost shattering and water adsorption, in experiments it is not noted to be particularly prone to frost shattering. The combined effects of chemical and physical weathering may be important in producing silt from dolomite. Dissolution of smaller grains between larger grains in dolomite could increase the porosity in the small pore size range leading to enhanced susceptibility to physical weathering by freezing. This process would be expected to be more important near the surface, where water is least saturated with respect to carbonates and dissolution will occur more rapidly. This is consistent with field observations that rocks near the surface display considerable pitting and fracturing, while rocks within the soil profile show few signs of weathering.

#### CONCLUSIONS

Dissolution of dolomite by dilute acid produced a fines residue up to 14% by weight of the amount of rock dissolved, primarily of dolomite mineralogy. Limestone produced much less fine-textured material and the fines were composed primarily of silicates. The accumulation and persistence of dolomitic silt-size particles in High Arctic soils is explained by the weakly acidic conditions; particles less than silt-size are especially unstable toward dissolution and even under these conditions do not persist.

Despite the high yield of dolomitic fines produced by chemical weathering, this may be insufficient to explain the amount of fines accumulated for the "case study" soil developed on dolomite. It is suggested that the porosity of dolomite relative to limestone, particularly for small size pores, is enhanced by chemical weathering and that this may render dolomite more susceptible to frost weathering. Additional studies are in order to consider the

interactions of chemical and physical weathering in producing fines from carbonate rocks.

#### ACKNOWLEDGMENTS

I appreciate the numerous stimulating discussions I have had with B. Hallet, D. Mann, F.C. Ugolini, and A.L. Washburn regarding the formation of fines in Arctic soils. I thank B. van Vliet-Lanoe for performing and interpreting the micromorphology of silt-rich horizons. I am grateful to F.C. Ugolini, B. Hallet, R. Reanier and the anonymous reviewers for their comments on the manuscript, and to C. Pitz for preparing and interpreting dolomite thin sections. I appreciate the cooperation of the Norwegian Polar Institute in field logistics. Funding for this work was provided by National Science Foundation Grant DPP 8303624 and DPP 9100080.

#### REFERENCES

- Bates, R.L. and J.A. Jackson, ed., 1984, *Dictionary of Geological Terms 3rd Ed*, American Geological Institute, NY.
- Bliss, L.C. and N.V. Matveyeva (1992) Circumpolar Arctic Vegetation. In F.S. Chapin, R.L. Jefferies, J.F. Reynolds, G.R. Shaver, and J. Svoboda, ed., *Arctic Ecosystems in a Changing Climate*, Academic Press, San Diego, California, pp. 59-90.
- Bockheim, J.G. and F.C. Ugolini (1990) A review of pedogenic zonation in well-drained soils of the southern circumpolar region. *Quaternary Research* 34:47-66.
- Doner, H.E. and W.C. Lynn (1989) Carbonate minerals. In J. Dixon and S. Weed, ed., *Minerals in the Soil Environment*, Soil Science Society of America, Madison, Wisconsin, pp. 279-330.
- Dredge, L.A. (1992) Breakup of limestone bedrock by frost shattering and chemical weathering, Eastern Canadian Arctic. *Arctic and Alpine Research* 24:314-323.
- Dunn, J.R. and P.P. Hudec (1966) Water, clay, and rock soundness. *The Ohio Journal of Science* 66:153-168.
- Etzelmüller, B. and J.L. Sollid (1991) The role of weathering and pedological processes for the development of sorted circles on Kvadehuksleta, Svalbard—a short report. *Polar Research* 9:181-191.
- Fahey, B.D. and D.F. Dagesse (1984) An experimental study of the effect of humidity and temperature variations on the granular disintegration of argillaceous carbonate rocks in cold climates. *Arctic and Alpine Research* 16:291-298.
- Forman, S.L. and G.H. Miller (1984) Time-dependent soil morphologies and pedogenic processes on raised beaches, Brøggerhalvøya, Spitsbergen, Svalbard archipelago. *Arctic and Alpine Research* 16:381-394.
- Hall, K. and J.P. Latridou (1991) Introduction-cryogenic weathering. *Permafrost and Periglacial Processes* 2:269-270.
- Hallet, B. and S. Prestrud (1986) Dynamics of periglacial sorted circles in western Spitsbergen. *Quaternary Research* 26:81-99.
- Hallet, B., J.S. Walder, and C.W. Stubbs (1991) Weathering by segregation ice growth in microcracks at sustained subzero temperatures: verification from an experimental study using acoustic emissions. *Permafrost and Periglacial Processes* 2:283-300.
- Latridou, J.P. and J.C. Ozouf (1982) Experimental frost shattering: 15 years of research at the Centre de Géomorphologie du CNRS. *Progress in Physical Geography* 6: 215-232.
- Latridou, J.P. (1988) Recent advances in cryogenic weathering. In: M.J. Clark, ed., *Advances in Periglacial Geomorphology*, John Wiley, New York, pp. 33-47.
- Mann, D.H., R.S. Sletten, and F.C. Ugolini (1986) Soil development at Kongsfjorden, Spitsbergen. *Polar Research* 4:1-16.
- Moore, C.H. (1989) Carbonate diagenesis and porosity. *Developments in Sedimentology* 46. Elsevier, Amsterdam. 338 pp.
- Murray, R.C. (1960) Origin of porosity in carbonate rocks. *Journal of Sedimentary Petrology* 30:59-84.
- Sletten, R.S. (1988) The formation of pedogenic carbonates on Svalbard: the influence of cold temperatures and freezing. In K. Senneset, ed. *Proceedings, Fifth International Conference on Permafrost. The Norwegian Committee on Permafrost, Norwegian Institute of Technology, Trondheim*, pp. 467-472.
- Sletten, R.S. (1990) Pedogenic processes in well-drained soils of Spitsbergen and Nordaustlandet. *Inter-nord* 19:465-470.
- Tedrow, J.C.F. (1977) *Soils of the Polar Landscape*. Rutgers University Press, New Brunswick, New Jersey. 638 pp.
- Tedrow, J.C.F. and E.C. Krug (1979) Weathered limestone accumulations in the high Arctic. *Biuletyn Peryglacjalny* 29-10: 143-146.
- Ugolini, F.C. (1986) Pedogenic zonation in the well-drained soils of the Arctic regions. *Quaternary Research* 26:100-120.
- Ugolini, F.C. and J.C.F. Tedrow (1963) Soils of the Brooks Range, Alaska: 3 Rendzina of the Arctic. *Soil Science* 96:121-127.
- van Vliet-Lanoe, B. (1988) The origin of patterned ground in N.W. Svalbard. In K. Senneset, ed. *Proceedings, Fifth International Conference on Permafrost. The Norwegian Committee on Permafrost, Norwegian Institute of Technology, Trondheim*, pp. 1008-1013.
- Washburn, A.L. (1980) *Geocryology: A survey of Periglacial Processes and Environment*. Arnold, Washington, 406 pp.
- Whalley, W.B. and J.P. McGreevy, J.P. (1983) Weathering. *Progress in Physical Geography*, 7:559-586.
- Wollast, R. (1990) Rate and mechanism of dissolution of carbonates in the system  $\text{CaCO}_3\text{-MgCO}_3$ . In W. Stumm, ed., *Aquatic Chemical Kinetics*, John Wiley, New York, pp. 431-445.

ANALYSIS OF TEMPERATURE EFFECTS ON THE FLEXURAL BEHAVIOR OF FROZEN SOIL

Sweanum Soo<sup>1</sup> and Tsung-Ping Fang<sup>2</sup>

<sup>1</sup>Associate Professor, <sup>2</sup>Graduate Assistant  
Department of Civil Engineering and Construction  
Bradley University  
Peoria, Illinois, U.S.A.

The mechanical properties of a frozen soil depend heavily on its temperature distribution in situ. At different temperatures, frozen soil exhibits different creep rates under the same load. In addition, the creep rates under tension are different from those under compression even if the magnitudes of stresses are the same. The creep strain rates of frozen soil are usually calculated by a power law but with different parameters for tension and compression. This paper evaluates the temperature effects on the flexural behavior of frozen soil using analytical equations and finite element analysis. Vyalov's equation is used to account for the temperature effect on creep strain rates of frozen soil. Analytical equations were derived to analyze frozen soil beams with linear temperature distributions. A finite element method was used to analyze an artificially frozen retaining wall to study the temperature effect on the design of frozen soil retaining walls.

**INTRODUCTION**

The mechanical properties of a frozen soil depend heavily on its temperature distribution in situ. At different temperatures, frozen soil exhibits different creep rates under the same load. In addition, the creep rate under tension is different from that under compression even when the magnitudes of stresses are the same.

The flexural behavior of frozen soil under constant and uniform temperature distributions was analyzed by Soo et. al. (1986). Since the temperature distribution of frozen soil in situ is seldom uniform, a study of the temperature effects on the flexural behavior is important.

This paper evaluates the temperature effects on the flexural behavior of frozen soil using two methods. First, analytical equations were derived to analyze frozen soil beams with linear temperature variations. The temperature is assumed at its lowest at the top of the beam and varies linearly to the bottom or vice versa. An example solution is presented. This situation is similar to frozen ground under seasonal temperature changes.

Second, an artificially frozen soil retaining wall was analyzed utilizing a finite element method. As shown in Fig. 1 the temperature is at its lowest at the location of freezing pipes and gradually warms up with increasing distance from the pipes. Artificially frozen soil retaining walls have been used for large excavation for more than a hundred years. This technique has been proven to be cost effective for soft ground and high water table conditions. A design method assuming a uniform temperature distribution was presented by Soo and Muvdi (1992) but the temperature effects were not well understood. This paper evaluates the temperature effects on the wall design with a computer analysis.

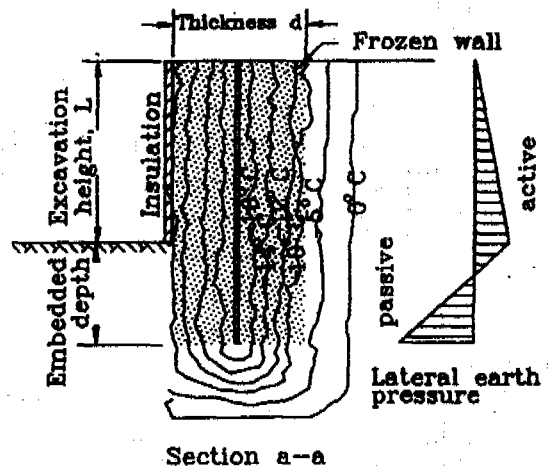
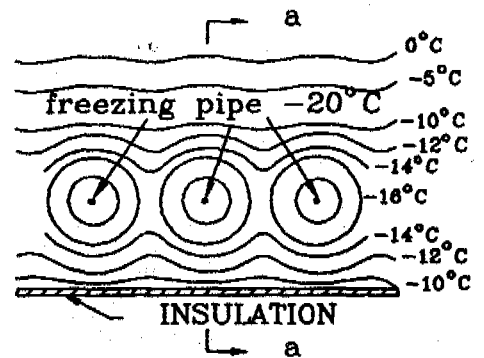


FIG 1. A FROZEN SOIL RETAINING WALL

A commercial computer program ANSYS was used to analyze the temperature distributions. According to the different temperature distributions, three cross-sections with different wall depths were chosen for the stress-strain analysis. A two dimensional finite element program specially designed for frozen soil was used for stress-strain analysis. Material properties were included according to the temperature distribution. Results for all three sections are presented and compared.

### MATERIAL PROPERTIES OF FROZEN SOIL

The mechanical properties of frozen soil is dominated by creep behavior and is sensitive to temperature change. Unlike most materials that exhibit creep (eg. metal), frozen soil exhibits different creep behavior in tension than in compression. Creep of frozen soil is usually divided into three stages: primary creep, secondary creep, and tertiary creep. Under a constant temperature, the creep strain can be calculated by a creep equation as (Andersland, et al 1978, Ladanyi, 1972)

$$\epsilon = \epsilon_0 (\sigma / \sigma_0)^n t^b \quad [1]$$

where  $\epsilon$  is the creep strain,  $\sigma$  is the stress,  $\epsilon_0$  is an arbitrary strain rate selected for convenience in computation (proof strain rate),  $\sigma_0$  is a temperature-dependent proof stress for normalization of dimensions,  $n$  is the exponential parameter for stress,  $t$  is time, and  $b$  is the exponential parameter for time  $t$ .

When  $b < 1$ , Eq. 1 represents primary creep and when  $b = 1$ , equation Eq. 1 represents secondary creep. Frozen soil is considered failed when the tertiary creep stage is reached. The primary creep stage is usually of short duration for high stress levels and the creep behavior is dominated by the apparent secondary creep stage. Therefore, creep strain can be approximated by secondary creep alone. Under the secondary creep stage, Eq. 1 becomes

$$\epsilon = \epsilon_0 (\sigma / \sigma_0)^n t \quad [2]$$

Since frozen soil has a different creep behavior under tension from that under compression, Eq 1 (and so also Eq. 2) will need two sets of parameters to describe the creep behavior of frozen soil, one for tension and the other for compression. These parameters may be obtained by conducting separate tensile and compressive creep tests in the laboratory (Eckardt, 1981).

Temperature has a large influence on the creep behavior of frozen soil. A decrease in temperature will generally increase the strength of frozen soil and will also increase its brittleness. To model the effect of temperature on the mechanical properties of frozen soil, an empirical power law has been commonly used (Vyalov, et al. 1962). The equation is as follows

$$\sigma_0 = \sigma_n (T / T_n)^k \quad [3]$$

where  $T$  and  $\sigma_0$  are the desired temperature and the corresponding stress,  $T_n$  and  $\sigma_n$  are the reference temperature and the corresponding proof stress,  $k$  is a parameter for the temperature effect. For most frozen soil  $k$

varies from 0.9 to 1. For frozen soil with a small temperature variation,  $k$  can be assumed as 1 (Andersland et al, 1978).

### ANALYSIS OF FROZEN SOIL BEAM WITH LINEAR TEMPERATURE DISTRIBUTION

Since frozen soil has different material properties in tension than in compression, the neutral axis of a frozen soil beam is not necessarily located along the center of the beam as in the case for creep of metal beams. An important objective for the analysis of frozen soil beam is to determine the location of the neutral axis. Once, the location of the neutral axis is determined, the stresses, strains and deflections can be calculated.

### Derivation of Analytical Equation

Consider a frozen soil beam subjected to pure bending as shown in Fig. 2(a). Temperature is assumed to vary linearly across the section as shown in Fig 2(b). Assume the neutral axis is located at a distance  $h_c$  from the top surface of the beam. Assuming that plane sections remain plane after deformation, the strain will vary linearly across the section as shown in Fig. 2(c).

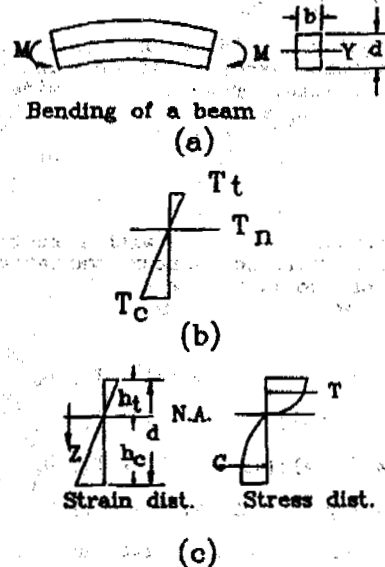


FIG 2. A FROZEN SOIL BEAM

To simplify the analysis, only the secondary creep stage is considered and the stress-strain rate relationship is used in stead of stress-strain relationship. Because of the different creep properties in tension and compression, Eq. 2 is expanded to two power law equations and the taken derivatives with respect to time are then taken. The equations become

$$\epsilon_c = \epsilon_{oc} (\sigma_c / \sigma_{oc})^{n_c} \quad \text{for compression} \quad [4a]$$

$$\epsilon_t = \epsilon_{ot} (\sigma_t / \sigma_{ot})^{n_t} \quad \text{for tension} \quad [4b]$$

$$h_c = h_t (\epsilon_{oc}/\epsilon_{ot}) (\sigma_c/\sigma_t) \left[ \frac{k_t}{k_c} \right]^{n_c} \left[ \frac{\sigma_{nt}}{\sigma_{nc}} \right]^{n_c} \left[ \frac{I_c}{I_t} \right]^{k_c} \quad [19]$$

Substituting Eq. 19 into Eq. 17, yields

$$h_t = \frac{1/m_t}{\sigma_t} \left[ \frac{k_t}{k_c} \right]^{n_c} \left[ \frac{\sigma_{nt}}{\sigma_{nc}} \right]^{n_c} \left[ \frac{I_c}{I_t} \right]^{k_c} A \quad [20]$$

where

$$A = \frac{p}{(\epsilon_{oc}/\epsilon_{ot}) \sigma_{nt}} \frac{1/(m_c - m_t)}{\sigma_{nc}} \quad [20]$$

and

$$p = m_c / (m_c - m_t)$$

Substituting Eq. 16b into Eq. 20, and rearranging terms, we obtain

$$J_c (I_t/I_c)^p + J_t (I_t/I_c)^q = D M \quad [21]$$

where

$$q = m_c / (m_c - m_t)$$

$$D = \frac{A}{(\epsilon_{oc}/\epsilon_{ot})} \frac{p/m_t - p}{\sigma_{nt}} \frac{q}{\sigma_{nc}} \quad [22]$$

The right hand side of Eq. 21 contains the creep parameters, external moment, and known temperature values. The left hand side contains  $I_c$ ,  $I_t$ ,  $J_c$  and  $J_t$  which are defined integrals of  $z$ , and hence functions of  $h_c$  and  $h_t$ . If  $I_c$ ,  $I_t$ ,  $J_c$  and  $J_t$  are integrable, then, the location of the neutral axis can be calculated.

For a frozen soil beam with a rectangular section, with small temperature variations and  $k_c$  and  $k_t$  close to 1, the terms,  $I_c$ ,  $I_t$ ,  $J_c$  and  $J_t$  can be integrated as follows:

$$I_c = [b/(m_c+1)(m_c+2)] [ |T_c| (m_c+2) - K h_c ] h_c^{m_c+1} \quad [23a]$$

$$I_t = [b/(m_t+1)(m_t+2)] [ |T_t| (m_t+2) + K h_t ] h_t^{m_t+1} \quad [23b]$$

$$J_c = [b/(m_c+2)(m_c+3)] [ |T_c| (m_c+3) - K h_c ] h_c^{m_c+2} \quad [24a]$$

$$J_t = [b/(m_t+2)(m_t+3)] [ |T_t| (m_t+3) + K h_t ] h_t^{m_t+2} \quad [24b]$$

Substituting Eqs. 23a, 23b, 24a, and 24b into Eq. 22, we obtain

$$A_1 \{ (a_1 - K h_c) [(a_1 + K h_c)/(a_3 - K h_c)]^p \} h_t^i h_c^{i-1} + A_2 \{ (a_2 + K h_t) [(a_2 + K h_t)/(a_3 - K h_c)]^q \} h_t^{i+1} h_c^{-1} = D M / b \quad [25]$$

where

$$A_1 = \frac{[(m_c+1)(m_c+2)/(m_c+1)(m_c+2)]^p}{[(m_c+2)(m_c+3)]}$$

$$A_2 = \frac{[(m_t+1)(m_t+2)/(m_t+1)(m_t+2)]^q}{[(m_t+2)(m_t+3)]}$$

$$a_1 = \frac{|T_c| (m_c+3)}{|T_c| (m_c+2)}$$

$$a_2 = \frac{|T_t| (m_t+3)}{|T_t| (m_t+2)}$$

$$a_3 = \frac{|T_c| (m_c+2)}{|T_t| (m_t+2)}$$

$$i = \frac{[m_c(m_c+1)]}{(m_c - m_t)}$$

$$j = \frac{[m_t(m_t+1)]}{(m_c - m_t)}$$

### Example

A frozen soil beam 12 inch (30.48 cm) wide and 40 inch (101.6 cm) deep is subjected to a moment  $M = 77.64$  kip-ft (105.26 kN-m). The temperatures at the top and the bottom of the beam are  $-8^\circ\text{C}$ . and  $-12^\circ\text{C}$  respectively. The material parameters are as follows:

$$\begin{aligned} \sigma_{nt} &= 140 \text{ psi (965.16 kN/m}^2\text{) at } T_n = 1^\circ\text{C} \\ \sigma_{nc} &= 1400 \text{ psi (9651.6 kN/m}^2\text{) at } T_n = 1^\circ\text{C} \\ \epsilon_{oc} &= \epsilon_{ot} = 1 \text{ hr}^{-1} \\ m_c &= 0.2, \quad m_t = 0.6 \end{aligned}$$

Eq. 25 becomes

$$0.2113 (43.2 - 0.1 h_c) [(17.6 + 0.1 h_t)/(31.2 - 0.1 h_c)]^{1.5} h_t^{1.5} h_c^{0.2} + 0.1783 (25.6 + 0.1 h_t) [(17.6 + 0.1 h_t)/(31.2 - 0.1 h_c)]^{0.5} h_t^{2.6} h_c^{-0.8} = 1753 \text{ in}^2 \quad (11309.65 \text{ cm}^2) \quad [26]$$

Solving Eq. 26 by trial-and-error gives  $h_c = 25$  in. (63.5 cm),  $h_t = 15$  in. (38.1 cm). From Eqs. 16a and 16b;  $\sigma_c = 227.5$  psi (1568.4 kN/m<sup>2</sup>),  $\sigma_t = 241$  psi (1661.5 kN/m<sup>2</sup>).

### FINITE ELEMENT ANALYSIS OF A FROZEN SOIL RETAINING WALL

In an artificially frozen soil retaining wall, temperature is at its lowest at the freezing pipes and increases with distance from the pipes as shown in Fig. 1. The first step in designing a frozen soil retaining wall is to determine the wall thickness based on the applied load, the temperature below freezing and soil condition. A designer will need to determine wall thickness for his analysis. A thicker wall will result a smaller temperature gradient while a thinner wall results a larger temperature gradient if the freezing pipe temperature are the same for both. If a thicker wall is assumed, the temperature at the outer reaches of the wall will be warmer and frozen soil will creep at a faster rate. On the other hand, the applied stress will be smaller when a thick wall is assumed. The result is reversed when a thinner wall is used. To study the temperature effect on the design of a frozen soil retaining wall, temperature variations were first determined. Then, three different wall thicknesses at three different temperature ranges were analyzed and compared.

#### Analysis of temperature distribution

A commercially available computer program, ANSYS, was used to analyze the temperature variation around freezing pipes. Temperatures along the length of the pipes were assumed uniform, as were temperatures along the height of the retaining wall. Therefore, only two dimensional analysis is needed. Fig. 3 shows a top view of a frozen soil retaining wall with five freezing pipes and temperature contours around the pipes. The temperature at the freezing pipes is  $-30$  degree C. The spacing of the freezing pipes is 3 feet (0.91 m). The heat conductivity coefficient is 1.25 watt/ft<sup>2</sup>C (4.1 watt/m<sup>2</sup>C). The boundary at the excavation side of the retaining wall is insulated. The other three sides are assumed unfrozen.

where  $\epsilon_c$  and  $\epsilon_t$  are creep strain rates,  $\sigma_c$  and  $\sigma_t$  are applied stresses,  $\epsilon_{oc}$  and  $\epsilon_{ot}$  are arbitrarily chosen proof strain rates,  $\sigma_{oc}$  and  $\sigma_{ot}$  are proof stresses, and  $n_c$  and  $n_t$  are constants that depend on material properties. The subscript c and t denote the compression zone and the tension zone, respectively.

The effect of temperature distribution on creep strain rate at any fiber of a beam is accounted for by varying the proof stress in the power law as shown in Eq. 3. To consider the difference in compression and in tension, Eq. 3 is expanded to two new equations as follows:

$$\sigma_{oc} = \sigma_{nc} (T_c/T_n)^{k_c} \quad \text{for compression} \quad [5a]$$

$$\sigma_{ot} = \sigma_{nt} (T_t/T_n)^{k_t} \quad \text{for tension} \quad [5b]$$

where  $T_c$  and  $T_t$  are the temperatures in degree C below the freezing point of water at any fiber in the compression zone and in the tension zone, respectively,  $T_n$  is a chosen reference temperature at -1 degree C, and  $k_c$  and  $k_t$  are constants that depend on material properties,  $\sigma_{nc}$  and  $\sigma_{nt}$  are the proof stresses in compression and in tension at reference temperature,  $T_n$ .

At an extreme fiber Eqs. 4a, 4b, 5a, and 5b become

$$\underline{\epsilon}_c = \epsilon_{oc} (\underline{\sigma}_c / \sigma_{oc})^{n_c} \quad [6a]$$

$$\underline{\epsilon}_t = \epsilon_{ot} (\underline{\sigma}_t / \sigma_{ot})^{n_t} \quad [6b]$$

$$\underline{\sigma}_c = \sigma_{nc} (T_c/T_n)^{k_c} = \sigma_{nc} |\underline{T}_c|^{k_c} \quad [7a]$$

$$\underline{\sigma}_t = \sigma_{nt} (T_t/T_n)^{k_t} = \sigma_{nt} |\underline{T}_t|^{k_t} \quad [7b]$$

where the underline symbol " " denotes the stresses, strains, and temperatures at the extreme fibers.

From Fig. 2(c) the strain rates are

$$\epsilon_c = \underline{\epsilon}_c (|z|/h_c) \quad [8a]$$

$$\epsilon_t = \underline{\epsilon}_t (|z|/h_t) \quad [8b]$$

where  $\underline{\epsilon}_c$  and  $\underline{\epsilon}_t$  are the strain rates at the extreme fibers, and  $z$ ,  $h_c$  and  $h_t$  are as defined in Fig. 2(c).

Writing the stresses in terms of strain rates in Eqs. 4a and 4b, and substituting Eqs. 5a, 5b, 8a and 8b into these equations, one obtains:

$$\sigma_c = \underline{\sigma}_c (|\underline{T}_c|/|\underline{T}_c|)^{k_c} (|z|/h_c)^{m_c} \quad [9a]$$

$$\sigma_t = \underline{\sigma}_t (|\underline{T}_t|/|\underline{T}_t|)^{k_t} (|z|/h_t)^{m_t} \quad [9b]$$

where  $m_c = 1/n_c$ , and  $m_t = 1/n_t$ .

Since temperature varies linearly with  $z$ ,  $|\underline{T}_c| = |\underline{T}_x| + K|z|$  and  $|\underline{T}_t| = |\underline{T}_x| - K|z|$  where  $\underline{T}_x$  is the temperature at the neutral axis,  $K = (|\underline{T}_c| - |\underline{T}_t|)/d$  is the temperature gradient,  $d = h_c + h_t$  is the total depth of the beam. Therefore,

Eqs. 9a and 9b become

$$\sigma_c = [\underline{\sigma}_c / (|\underline{T}_c|^{k_c} h_c^{m_c})] (|\underline{T}_x| + K|z|)^{k_c} |z|^{m_c} \quad [10a]$$

$$\sigma_t = [\underline{\sigma}_t / (|\underline{T}_t|^{k_t} h_t^{m_t})] (|\underline{T}_x| - K|z|)^{k_t} |z|^{m_t} \quad [10b]$$

The total resultant forces C and T in the compression and tension zones can be obtained by integration. Thus,

$$C = [\underline{\sigma}_c / (|\underline{T}_c|^{k_c} h_c^{m_c})] I_c \quad [11a]$$

$$T = [\underline{\sigma}_t / (|\underline{T}_t|^{k_t} h_t^{m_t})] I_t \quad [11b]$$

where

$$I_c = \int_0^{h_c} (|\underline{T}_x| + K|z|)^{k_c} |z|^{m_c} b \, dz \quad [12a]$$

$$I_t = \int_0^{h_t} (|\underline{T}_x| - K|z|)^{k_t} |z|^{m_t} b \, dz \quad [12b]$$

and  $b$  is the width of the section as shown in Fig 2(a).

The location of the resultant forces in the compression and tension zones can be determined by

$$Z_c = J_c / I_c \quad [13a]$$

$$Z_t = J_t / I_t \quad [13b]$$

where

$$J_c = \int_0^{h_c} (|\underline{T}_x| + K|z|)^{k_c} |z|^{m_c+1} b \, dz \quad [14a]$$

$$J_t = \int_0^{h_t} (|\underline{T}_x| - K|z|)^{k_t} |z|^{m_t+1} b \, dz \quad [14b]$$

The external moment is equal to the resultant forces, C, multiplying by the moment arm,  $Z_c + Z_t$ . Thus,

$$M = [\underline{\sigma}_c / (|\underline{T}_c|^{k_c} h_c^{m_c})] I_c (J_c/I_c + J_t/I_t) \quad [15]$$

From Eq. 15, we can write the stress in the extreme fibers, leading to

$$\underline{\sigma}_c = [M |\underline{T}_c|^{k_c} h_c^{m_c}] / [I_c (J_c/I_c + J_t/I_t)] \quad [16a]$$

Similarly,

$$\underline{\sigma}_t = [M |\underline{T}_t|^{k_t} h_t^{m_t}] / [I_t (J_c/I_c + J_t/I_t)] \quad [16b]$$

From Eqs. 11a and 11b, we let  $C = T$ , and obtain

$$h_t / h_c = (\underline{\sigma}_t / \underline{\sigma}_c) (I_c / I_t) (|\underline{T}_c|^{k_c} / |\underline{T}_t|^{k_t}) \quad [17]$$

From Fig. 2(c), we have

$$h_t / h_c = \underline{\epsilon}_t / \underline{\epsilon}_c \quad [18]$$

Substituting Eqs. 6a, 6b, 7a, and 7b into Eq. 18, we obtain



From Fig. 3, three sections along the center pipe were chosen for stress-strain analysis. Case I covers the temperature range from -30 degree C to -20 degree C. The thickness of the wall considered is from point A to the left edge of the wall as shown in Fig. 4. Case II covers the temperature range from -30 degree C to -10 degree C. The thickness considered is from point B to the left edge of the wall. Case III covers the temperature range from -30 degree C to -5 degree C. The thickness considered is from point C to the left edge of the wall:

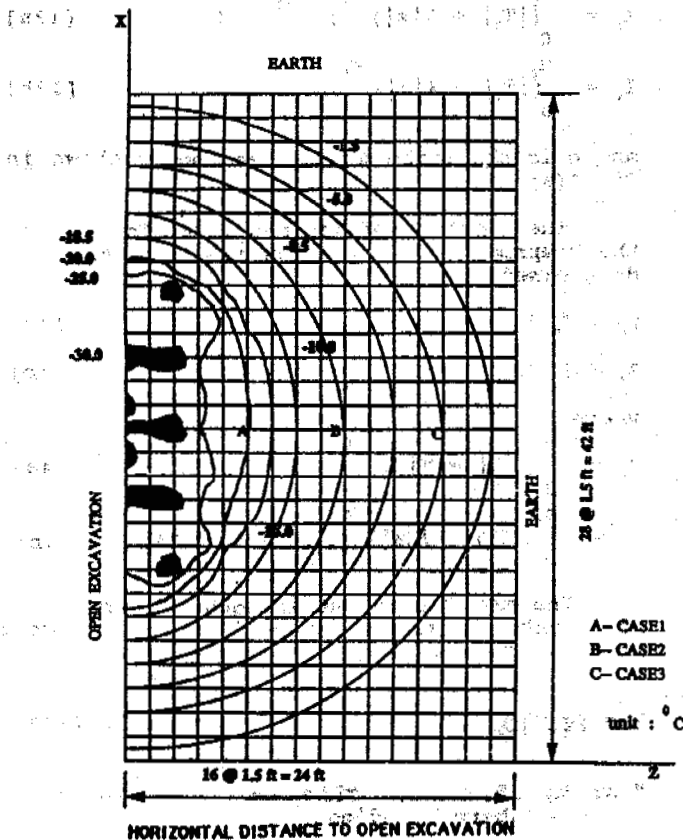


FIG. 3 TEMPERATURE DISTRIBUTION IN RETAINING WALL (TOP VIEW)

### Stress-strain analysis

The stress, strain and displacements in the three sections selected in Fig. 3 are analyzed utilizing a finite element program, FEMFSL, which was developed specially for frozen soil. The program uses a common finite element procedure for creep analysis, which can be found in many texts such as Zienkiewicz (1977) for example. The difference between FEMFSL and common FEM creep analysis programs is that FEMFSL considers the difference in material properties in tension and in compression. When the element is in tension, tensile properties are used and vice versa.

A finite element grid used for case III is shown in Fig. 4. The FEM grids for cases I and II are similar but with fewer elements along the z direction. Element properties are calculated by Eq. 3 based on element temperatures. The creep properties used for the calculations were obtained from experimental results published by Eckardt (1981) for frozen sand and are listed below.

$$\begin{aligned} \sigma_{nt} &= 136 \text{ psi } (949.82 \text{ kN/m}^2) \text{ at } T_n = 1^\circ\text{C} \\ \sigma_{nc} &= 1360 \text{ psi } (9498.2 \text{ kN/m}^2) \text{ at } T_n = 1^\circ\text{C} \\ \epsilon_{oc} &= \epsilon_{ot} = 1 \text{ hr}^{-1} \\ n_t &= 5, n_c = 1.61 \\ k_c &= k_t = 1 \\ b_c &= 0.26, b_t = 0.55 \end{aligned}$$

where  $b_c$  and  $b_t$  are exponential parameters for time  $t$  in compression and in tension as shown in Eq. 1. The elastic moduli for both compressive and tension are  $3.8 \times 10^6$  psi ( $2.62 \times 10^6$  kN/m<sup>2</sup>) and  $3.8 \times 10^6$  psi ( $2.62 \times 10^6$  kN/m<sup>2</sup>) respectively as determined by Soo (1984).

### Results

Creep displacements at the top left corner of the retaining wall are listed in Table 1 and shown in Fig. 5. The creep displacement from 0 to 160 hours for cases I, II and III are  $0.41 \times 10^{-5}$  m,  $0.294 \times 10^{-5}$  m, and  $0.9543 \times 10^{-5}$  m. The creep deformation is larger for case III than those of cases I and II. For the type of frozen soil where its displacement is dominated by creep displacement, a thicker retaining wall would yield a more conservative analysis.

The stress contour for stresses in y directions at 160 hour are shown in Fig. 6. Note that the maximum compressive stresses are located near the warmest temperatures. This explains why case III has larger creep deformations.

Table 1 Horizontal creep displacement at top of the retaining wall (x10<sup>-5</sup> m)

Time(hr)	Case I	Case II	Case III
0	0	0	0
20	0.1725	0.1253	0.7549
40	0.2538	0.1932	0.9387
60	0.3051	0.2154	0.9436
80	0.3428	0.2331	0.9480
100	0.3701	0.2500	0.9501
120	0.3889	0.2658	0.9516
140	0.4016	0.2805	0.9530
160	0.4100	0.2940	0.9543

### CONCLUSION

1. An analytical equation for a frozen soil beam with a linear temperature variation was derived.
2. The temperature effect on a frozen soil retaining wall for a type of frozen soil was studied. According to the results, if the displacements of the frozen soil retaining wall were dominated by creep displacement, then, a thicker wall may be used for analysis so that the analysis result can be conservative.

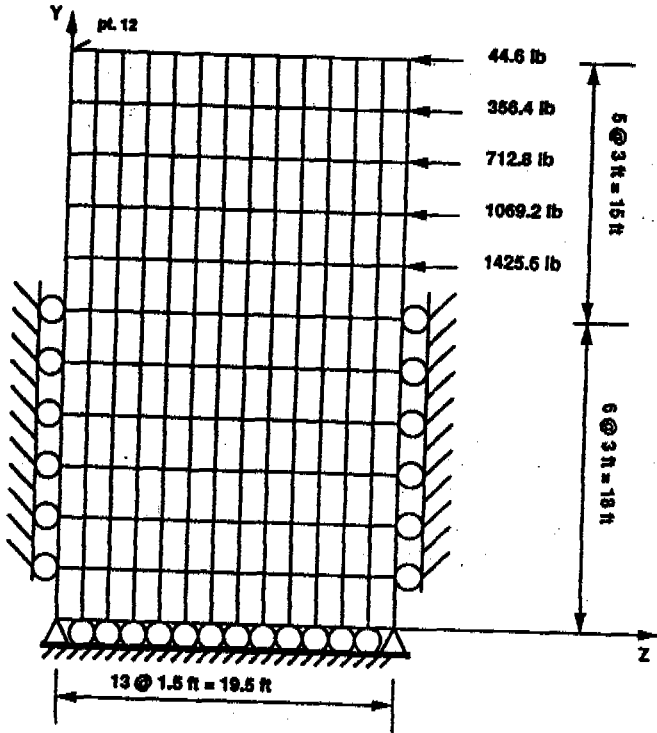


FIG. 4. FINITE ELEMENT GRID

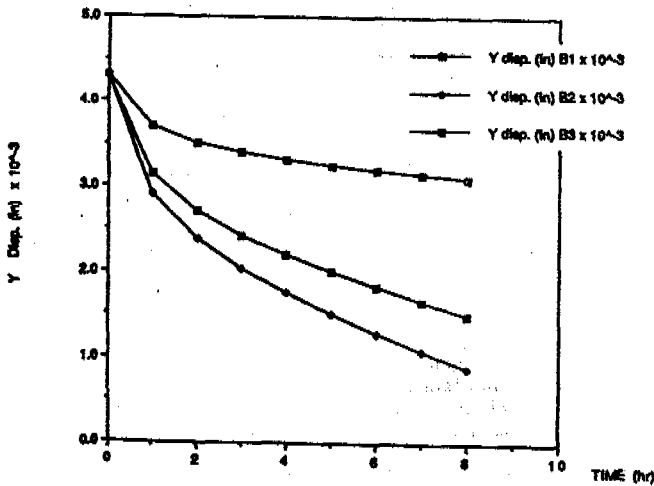


FIG. 5. DISPLACEMENT AT FROZEN SOIL RETAINING WALL

**ACKNOWLEDGMENT**

This material is based upon work supported by the National Science Foundation under Grant number MSS-9111021. The authors wish to express their appreciation to the National Science Foundation and Bradley University for supporting this project and to Dr. B. B. Muvdi for reviewing this text.

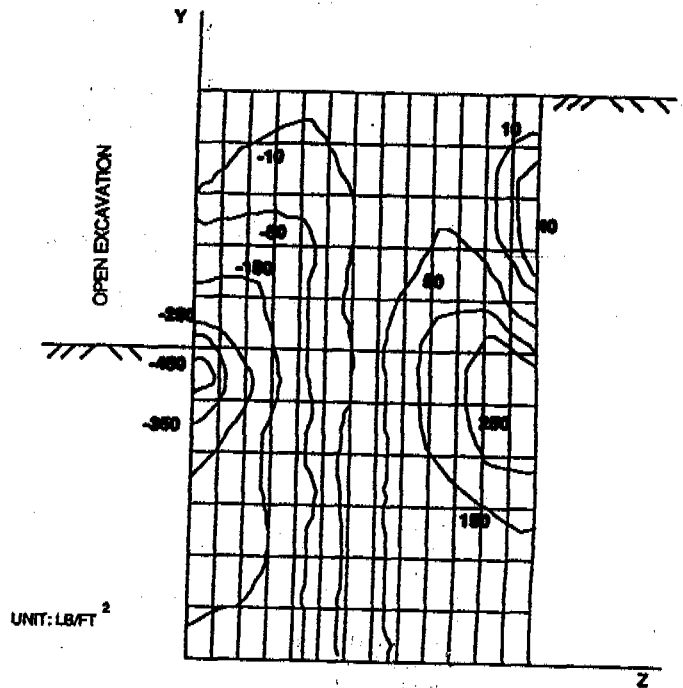


FIG. 6. STRESS CONTOURS

**REFERENCE**

Andersland, O. B., Sayles, F. H., JR., and Ladanyi, B. 1978. Mechanical properties of frozen ground. In Geotechnical engineering for cold regions. Edited by Andersland, O. B. and Anderson, D. M. McGraw-Hill Book Co., New York, N.Y., Chapter 5.

EcKardt, H. 1981. Creep tests with frozen soils under uniaxial tension and uniaxial compression. Proceedings of the 4th Canadian Permafrost Conference, Calgary, Alberta, March 2-6. Edited by H. M. French. National Research Council of Canada, Ottawa, PP 365-373.

Ladanyi, B. 1972. An Engineering theory of creep of frozen soils. Canadian Geotechnical Journal, V 9 pp63-80.

Soo, S. 1984. Studies of Plain and Reinforced Frozen Soil Structures. Ph.D. thesis, Michigan State University, East Lansing, Michigan, U.S.A.

Soo, S., Wan, R. K., and Andersland, O. B. 1986. Flexural behavior of frozen soil. Canadian Geotechnical Journal, v. 23, p 355-361.

Soo, S. and Muvdi, B. B. 1992. Design method for frozen soil retaining walls. ASCE Cold Regions Engineering Journal, Vol. 6 No. 2, pp73-89.

Vyalov, S. S. 1962. The strength and creep of frozen soil and calculations for ice-soil retaining structures. U.S. Army Cold Regions Engineering Laboratory, Trans. 76, Hanover, N.H.

Zienkiewicz, O. C. 1977. The Finite Element Method. McGraw-Hill Book Co., London, England.

THE METHOD OF DETERMINED DESIGN VALUES OF HORIZONTAL HEAVE FORCE ON  
RETAINING WALLS IN SEASONALLY FROZEN GROUND AREA

Sui Tieling, Na Wenjie, Li Dazhou and Jiang Weiqiang

Heilongjiang Hydraulic Research Institute, Harbin, China

After 5 years of field tests the values of horizontal heave force of retaining walls and its distribution pattern along the walls was obtained. Using the statistical analysis method of an external enveloping graph the authors changed the pressure graph of horizontal heave force of the retaining wall with a non-steady state into that of a steady state. After correcting the pressure, deformation, slope, etc., the method of determining design values and calculating the formula of horizontal heave force of the retaining wall were obtained. A new method of determining the dominant design load is provided for preventing frost heave in the seasonally frozen ground areas.

INTRODUCTION

The seasonally frozen ground with a freezing depth above 0.5 m and permafrost occupy about 68.6% of Chinese territory (Tong Changjiang et al., 1985). The retaining soil structures and buildings are mainly distributed in the Northeast, Northwest, and North of China. Traditionally these structures and buildings were designed as the main load with soil pressure. In cold regions the frost heave of the earth behind the retaining walls was not taken into account, according to investigation data frost damage of the retaining walls is about 40%. Therefore, in the cold regions the retaining walls were designed not only with common soil pressure, but also with the horizontal heave force as the main load for preventing frost damage.

At the frozen ground test site in Harbin the horizontal heave force value and distribution pattern of the fully constrained retaining wall was measured (Sui Tieling et al., 1987; Sui Tieling et al., 1989), through statistical analysis of the space-time distribution law of the horizontal heave force. After correcting pressure, deformation, and slope, this paper gives the method of taking the design values and calculating the formula of the horizontal heave force of retaining walls.

BASIC EFFECT FACTORS

Effect of the Bidirectional Freezing State

The earth behind the retaining wall was affected by negative air temperature from the earth surface, the wall surface and wall foot, and was gradually frozen. The freezing outline changes from one-directional freezing to bidirectional freezing parallel to the wall top. The outline of the freezing process (0°C isothermal curve) is plotted in Fig.1.

Because the heave force is an internal stress

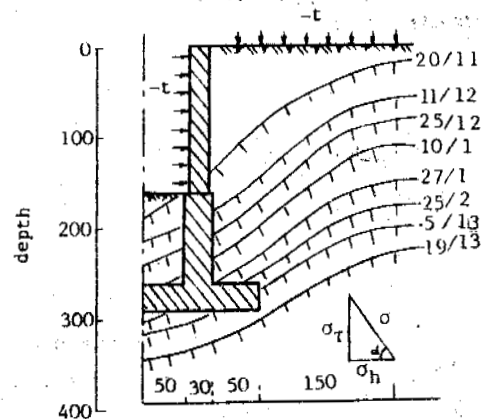


Fig.1 The signal figure of 0°C isothermal curves and heave force of the tested restraining wall during 1986-1987

- σ -heave force
- t-negative temp.
- σ<sub>τ</sub>-tangential heave force
- σ<sub>h</sub>-horizontal heave force
- 27/1-day/month
- size unit:cm

from the earth frost, its action is vertical to the isothermal line, the horizontal heave force acting on the retaining wall is a horizontal component of the frost force, i.e.,  $\sigma_h = \sigma \cdot \cos \alpha$ . Therefore, the magnitude of the horizontal heave force changes with the movement of the isothermal curve.

Effects of the wall height on the heave of force have been confirmed by the practical measurement of the distribution law of the horizontal heave force and by an electric resistance network analog test. The development of the frozen front can be simulated numerically. Its numerical solution is shown on the computer. After verification with the practical measured data the method of determining the design value

and horizontal heave force values given by this paper are only suitable in the range of wall heights less than 5 m and three times that of the designed frozen depth.

Effects of the Wall Constraint Degree (deformation)

As the frost heave is not constrained by structures the frost heave amount appears in macroscopic observation, but there is no frost force. The structures containing the earth bears the heave force, and the heave force changes with the constraint degree. On the basis of heave force and the deformation relationship, through testing and results from home and abroad, 7 groups of heave force and deformation data were analyzed, the results are shown in Fig.2. For

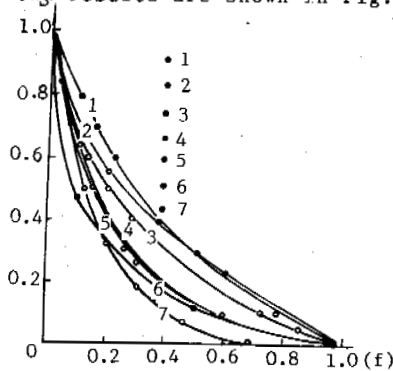


Fig.2 The relationship of deformation and heave force

1. Low Temperature Research Institute of Heilongjiang
2. Heilongjiang Hydraulic Research Institute
3. Heilongjiang Hydraulic Research Institute
4. Heilongjiang Hydraulic Research Institute
5. Lanzhou Institute of Glaciology and Geocryology
6. Japan
7. Jilin Hydraulic Research Institute

engineering safety the disadvantages are taken into account. The empirical formula is given as follows:

$$f = 1 - S^{0.5} \quad (1)$$

where f--heave force coefficient, equal to the proportion value of the semi-constrained state (there is deformation) with the complete constraint state (there is not deformation); S--deformation coefficient, equal to the proportional value of deformation of the constrained structure with the frost amount of natural earth.

Effect of the Soil Frost Characteristics

The horizontal heave force is a action force caused by the soil frost, so, the strength of

the soil frost effects directly the value of horizontal heave force on the retaining wall. In engineering practice, it is a very complex problem to evaluate the soil frost strength because there are many effect factors. As a result of "engineering classification of foundation soil frost for hydraulic structures in seasonally frozen ground", our institute gathered several hundred measured samples of soil frost which were affected by many factors. The statistical method of the semi-empirical formula was proposed. In the formula, latitude, load, water content, and soil characteristic factors were considered, and according to the frost amount, the frost engineering classification of hydraulic foundation soil is given. According to site test data for 5 years in complete constraint, Table 1 gives the maximum horizontal heave force values of the retaining wall in complete constraint by synthetic analysis on the frost classification of foundation soils.

From the calculations or the measured frost values of natural conditions at the engineering areas, the maximum horizontal heave forces of the nondeformation retaining wall can be determined from Table 1.

THE EMPIRICAL PRESSURE FIGURE OF THE MAXIMUM HORIZONTAL HEAVE FORCE OF RETAINING WALLS

The pressure figure of the horizontal heave force of the retaining wall is a non-steady pressure figure which changes with time and space. To obtain steady pressure figures that can be used in practical engineering design, it is necessary to find the distribution law of the non-steady horizontal heave force. The distribution law can be obtained by analyzing the measured data. A coordinate system is chosen with the horizontal heave force and the wall height above the ground, and the maximum heave force of every month each year is plotted in the coordinates, the maximum external envelope line of the pressure distribution was plotted in Fig.3. For the purpose of practical engineering design, the maximum values of horizontal heave force of each year were enveloped on a broken line for fine soil, the distribution law of horizontal heave force along the wall height was obtained (Fig.3).

Fig.4 is the empirical pressure figure which is obtained from the distribution law of the horizontal heave force, the figure is plotted by the following steps: 1) Finding the maximum value of horizontal heave force of the complete constraint retaining wall on the soil classification; 2) Calculating respectively the relative wall height of these feature points, i.e. 0.375 h, 0.75 h, ...h; 3) After the horizontal heave force corresponding to the feature points is determined in coordinates, these points are connected with the line, and the figure is ob-

Table 1 The maximum horizontal heave force values of retaining walls in complete constraint

Frost type	I	II	III	IV	V
Frost amount (cm)	$\Delta h < 2$	$2 < \Delta h \leq 5$	$5 < \Delta h \leq 12$	$12 < \Delta h \leq 22$	$\Delta h > 22$
Horizontal heave force (kPa)	<50	50-100	100-150	150-200	200-250

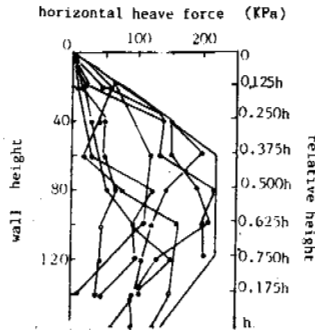


Fig. 3 External envelope of horizontal heave force of retaining wall

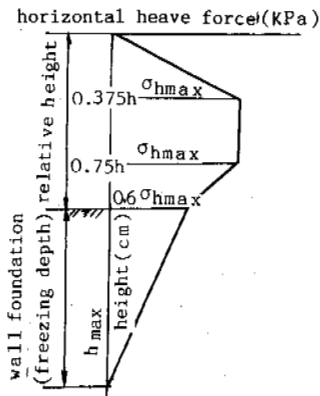


Fig. 4 The maximum empirical pressure figure of horizontal heave force of complete constraint retaining wall

tained.

#### CALCULATING DESIGN VALUES OF HORIZONTAL HEAVE FORCE

The figure 4 can not be applied directly to the structure design with deformation. So, it is necessary to correct the pressure, deformation, and slope for the horizontal heave force, and then the design value can be calculated.

#### Correction of the Maximum Horizontal Heave Force With Pressure

Comparing the maximum measured value during 1982-1987 with the maximum empirical static value given on the distribution law of horizontal heave force monthly, first, the correction coefficients of every month are calculated, then, the mean value of the months each year is taken, these are the correction coefficients of the maximum horizontal heave pressure (Table 2).

For improving the calculation precision of the correction coefficient C, the correction

Table 2 Correction coefficients of horizontal heave force of each year

Year	1982-1983	1983-1984	1984-1985	1985-1986	1986-1987
Maximum pressure(kPa) (measured value)	100	66	220	192	200
Mean pressure(kPa) (measured values)	53	34	128	92	102
Mean pressure(kPa) (correction values)	76.2	50.3	168	146	153
Correction coefficients	0.7	0.68	0.76	0.63	0.67

coefficient is calculated in practical measured values every 20 months, and the coefficient is 0.7.

#### Correction of the Horizontal Heave Force With Different Deformation

The horizontal heave force is an external stress on frozen ground in the horizontal heave force there appears a decreasing tendency with the deformation increasing. For the retaining wall with deformation the maximum horizontal heave force in complete constraint is corrected on the allowable deformation degree of the wall. Its value is calculated in formula (1).

#### Correction of Horizontal Heave Force With the Slope

Because the horizontal heave force acts perpendicularly on the wall, when the wall displacement appears, the force will decrease. The slope coefficient may be found in Table 3.

#### Step of Taking Design Value of Horizontal Heave Force

1. The frost amount is calculated or measured at 1/2 of the wall height from the ground, then the maximum horizontal heave force in a complete constraint state is found from Table 1.

2. According to the wall design height, structural form, structural material, etc.. The allowable deformation of the respective wall height is determined by the present standard, the heave force coefficient is calculated by using formula (1).

3. On the slope rate the slope correction coefficient is found in Table 3.

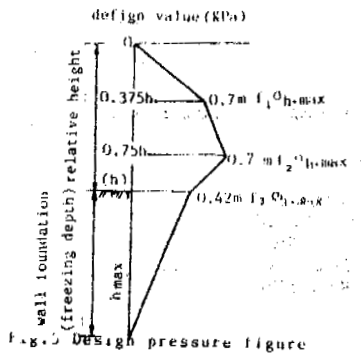
4. In the complete constraint state the pressure, deformation, and slope are corrected by the horizontal heave force. The design value of the horizontal heave force of the retaining wall is calculated with formula (2):

$$\sigma_h = C M F \sigma_{h \max} \quad (2)$$

5. Respective wall height and the design value of horizontal heave force are plotted in Fig.5. From Fig.5 the design pressure figure is obtained.

Table 3 Slope correction coefficients

Slope rate	0	0.1	0.2	0.3	0.4	0.5	0.6	0.7	0.8	0.9	1.0
Correction coefficients	1.0	0.9	0.85	0.81	0.79	0.785	0.78	0.775	0.77	0.765	0.76



**REFERENCES**

Tong Changjiang, Guan Fengnian (1985) Frost Heave of Soils and Prevention of Constructures Frost Damage, Hydraulic Power Publishing House.

Sui Tieling, Na Wenjie (1987) Test Method of Horizontal Heave Force of Retaining Wall in Field, Journal of Glaciology and Cryopedology, Vol.9, No.2.

Sui Tieling, Na Wenjie (1989) Study of Horizontal Heave Force of Retaining Wall in Seasonally Frozen Ground, Proceedings of the Third China Symposium on Permafrost, Science Publishing House.

## CRITICAL SEGREGATION POTENTIAL - FROST HEAVE UPPER LIMIT

Otto J. Svec<sup>1</sup>, Yen Chang<sup>2</sup>

<sup>1</sup>Institute for Research in Construction  
National Research Council of Canada  
Ottawa, Ontario, Canada, K1A 0R6

<sup>2</sup>Civil Engineering Department, Carleton University  
Ottawa, Ontario, Canada, K1S 5B6

The experimental laboratory technique described in this paper is based on a concept that cooling of the soil sample can be described by a temperature gradient and a frost penetration rate. Experimental results from a series of frost heave tests using a ramping technique were integrated in a data base. The data base includes the cooling rate, temperature gradient and water intake for a particular soil. A new approach is presented in this paper combining this data base (interpolated by a cubical spline technique) and numerical modelling, to predict frost heave in the field. The resulting finite element computer program was validated against examples of laboratory experiments and data from the field. This novel approach is shown to have potential for use in engineering practice.

### INTRODUCTION

Structural and geotechnical designs of civil engineering structures, such as roads, airfields, and buried pipelines in cold climates require a knowledge of the classification of frost susceptibility of soils. Unfortunately, it is very difficult to determine the frost susceptibility of soils to a satisfactory level of confidence. The complexity of frost heave prediction is a consequence of the many factors that influence soil behaviour. One group of factors is related to soil characteristics; for example type of soil (size and shapes of mineral particles), density, moisture content and permeability. Another group of factors is related to external conditions, such as mechanical loads, thermal gradients and cooling rates (both based on thermal and climatic boundary conditions), and availability of soil water. The frost susceptibility of soils should include all these factors and, therefore, a selected susceptibility index can vary considerably. As a result, the prediction of frost heave (based on this index) could lead to misleading design parameters, so that additional freezing tests for a particular soil and project are often required.

Practical commercial tests must be simple, of short duration and inexpensive. To satisfy these conditions commercial frost heave tests have been based on testing conditions and processes which, in some cases, are unrealistic. For example, the thermal conditions for the cold and warm boundaries of the soil sample are constant and the values are completely out of the range of real engineering and practical conditions. The thermal gradients used during tests are normally several times higher than those developed in the field. The resulting frost heave or susceptibility index, determined in such a commercial test, could be far from reality. What is really needed is to be able to determine frost heave upper and lower bounds (or only the upper bound). Even better, the key need is to predict or realistically estimate an expected real heave. This is the main objective of the authors' approach.

### FROST-SUSCEPTIBILITY INDEX TESTS

Chamberlain (1981) performed a comprehensive survey of frost-susceptibility index tests used by transportation departments throughout the world. He concluded that most of these agencies have used their own criteria. Freezing tests employed for this purpose are normally poorly designed and executed. In addition, only frost heave or thaw weakening, rather than both, are used. As a result, the frost-susceptibility index does not represent the actual heaving or thawing or thaw-weakening potential, particularly for marginally frost-susceptible soils. Recognizing this problem, Chamberlain (1987) developed and proposed a new five-day freezing test based on two freeze-thaw cycles and the California Bearing Ratio (CBR) test. The frost susceptibility index is then defined as the heave rate at the end of the first eight hours of each two-day freeze-thaw cycle. The repetition of the freeze-thaw cycle accounts for the changes in susceptibility to frost heave in frost virgin material. The CBR test, which is performed after the second thaw, yields the thaw-weakening index. Both of these tests are then used to determine the frost-heave potential.

The main drawback of these tests is the fact demonstrated below, that the frost heave rate is heavily dependent on the test specifications and its performance. For example, the heave rate of a soil during a classical one-step change test, depends on thermal gradient, i.e., on cold and warm boundary conditions. If these conditions are constant, not only the thermal gradient will change rapidly as the test progresses, but also the specimen cooling and frost penetration will be continuously changing. In addition, the temperature gradients used in frost susceptibility index tests are so high, that they do not reflect conditions frequently occurring in nature.

### EXPERIMENTAL PROGRAM

Before the testing program carried out in this paper is described, several aspects of frost action will be discussed in detail. The elements of frost action are important, because the new

computer model has been designed to closely simulate actual frost penetration.

#### Ice Segregation

Frost heave in soils is caused not only by freezing of in-situ pore water but also by freezing of migratory water. This water transfer, which is in addition to natural water movement caused by gravity and elevation heads, is due to suction developed in the "freezing fringe". This is a partly frozen zone between the zero-degree isotherm and the growing ice lens. Water migration depends on the capillary characteristics of soil, chemical potential, osmotic forces, pneumatic and elevation heads, and overburden pressure, but the main agent generating suction potential is the change in the adsorbed water layer surrounding the soil particles. As this water freezes and becomes thinner, a negative pressure within the layer is generated. The resulting suction causes water to flow through the freezing fringe and to accumulate in form of an ice lens. This process is known as ice segregation and occurs at the location where an optimum thermodynamic condition develops for ice lens growth. This condition combines suction, hydraulic conductivity and temperature (including latent heat). It is also influenced by the fact that within the freezing fringe the suction pressure and soil hydraulic conductivity vary exponentially with temperature but in opposite direction.

The processes of ice segregation in soils are now reasonably understood, but their quantitative determination and engineering prediction are not yet at hand. The segregation process leading to multiple, or rhythmic ice-lenses can be described as follows.

During the growth of an ice lens the segregation temperature as well as the ice-lens location remain constant due to a balance between the release of latent heat from the freezing of the inflowing water and the heat flux. The zero-degree isotherm, however, moves as cooling continues. Consequently, the width of the freezing fringe increases and the overall "effective" hydraulic conductivity decreases. The water flow towards the ice lens can be calculated as a product of the hydraulic conductivity and the suction potential. Since the suction gradient remains more or less constant, it is the low hydraulic conductivity and the "long" path through the freezing fringe that eventually retard the water movement. At such a time, the thermal and hydraulic balance is disturbed and fast freezing results. The entire fringe then moves further, with continuing cooling until a new segregation location, with suitable thermal and hydraulic conditions develops.

#### Importance of Temperature Gradient

The above description of the segregation process can also explain the important influence of temperature gradient on the rate of heave. The segregation temperature, i.e., the temperature of the growing ice lens on its active boundary, can be considered constant with respect to changes in the temperature gradient. This temperature is unique for a given soil, i.e., it depends on soil type, percentage of fines, and porosity, and certainly on the overburden pressure. Therefore, the segregation temperature is dependent on suction pressures in the adsorbed water layers or, in other words, on the water/ice pressure differential. The segregation temperature is more or less independent of the temperature gradient. However, since the depth of freezing fringe is a strong function of temperature gradient, the water migration and resulting frost heave also heavily depend on the temperature gradient. In addition, the resulting frost heave is a function of the hydraulic conductivity, the suction potential and,

in general, the path the water has to migrate through to reach the freezing fringe.

#### Segregation Potential

Instead of using the complex factors presented above and because there are serious difficulties associated with their determination, Konrad and Morgenstern (1981) proposed an engineering parameter called "Segregation Potential", SP. The definition of SP is based on their experimental observation: at the time of formation of the final ice lens, the flow of water,  $v$ , is proportional to the thermal gradient,  $dT/dz$ , in the frozen soil, so:

$$v = SP \cdot dT/dz$$

Another very important parameter strongly influencing the water migration is the cooling rate (Svec, 1989) and is utilized as follows. If the soil cooling is expressed in terms of temperature gradient and frost penetration as two independent variables, (forced to be independent, as for example, in ramping freezing laboratory tests), i.e.:

$$\frac{\partial T}{\partial t} = \frac{\partial T}{\partial x} \cdot \frac{\partial x}{\partial t}$$

where  $X$  represents the frost penetration,  $t$  is time; then the importance of the rate of cooling can be observed.

#### Rate of Cooling

The importance of the rate of cooling can be explained as follows. At a constant temperature gradient,  $\partial T/\partial x$ , the rate of frost penetration is directly proportional to the rate of cooling. At low cooling (i.e., frost-penetration) rates, once the ice-segregation site is established, the rate of heave is also low because the freezing fringe is very thick. The low frost-penetration rates do not act to force the segregation site to relocate. As well, the release of latent heat from the freezing of inflowing water keeps the thermodynamic processes relatively steady. The amount of time required to relocate the ice-segregation site (i.e., start of a new ice lens) is relatively very long. In the middle range of frost-penetration rates, the above process is faster which, in a dynamic sense, allows a thinner freezing fringe to form. Moreover, the segregation temperature decreases with the increase in penetration rate. A thinner freezing fringe accompanied by a lower segregation temperature will result in a higher rate of heave. In the high range of frost-penetration rates, the freezing process becomes so fast that there is not enough time to establish significant water flow between successive locations of ice segregation sites. As a result, the heave rate must decrease.

#### FREEZING TESTS

In the vast majority of experimental one-step freezing tests, constant boundary conditions are used. In contrast, the testing procedure described in this paper is based on the so-called "ramping" technique. In this method the temperatures at the cold and warm ends of the sample are simultaneously decreased according to a pre-programmed function. Authors have strong experimental evidence shown below that if the temperatures of both ends follow the same linear function of time, a "ramp", then the frost heave vs. time will also be a straight line. This relationship persists as long as the temperature gradient is constant (dependent on rate of cooling). The rate of heave then clearly becomes a



constant. In other words, a constant cooling rate results in a constant heave rate. It is shown below that the rate of heave, however, is highly dependent on cooling rate.

The frost heave cell used in this study was described by Penner (1986), Figure 1. All the tests were carried out using the same soil, classified as clayey silt. Soil samples were prepared from a slurry (moisture content about 2% above the liquid limit) by consolidating the sample under 400 kPa vertical stress and allowing it to rebound under 20 kPa.

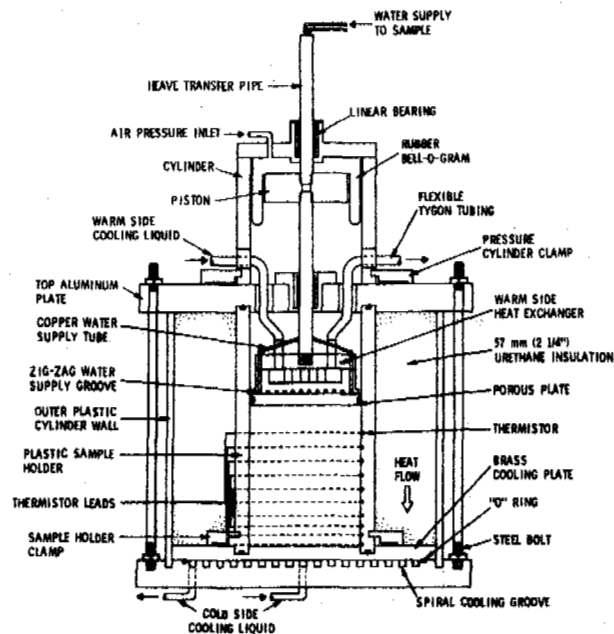


Figure 1. NRC Freezing Cell

Prior to frost heave testing, a prescribed thermal gradient was established. The soil sample was then supercooled in order to initiate ice crystallization. Upon initialization of ice crystallization, the temperature rapidly increased due to the release of the latent heat of fusion. The soil sample was then thermally stabilized and the temperature gradient was forced to return to the initial condition.

Fresh samples were prepared for each individual test. Two freeze/thaw cycles were performed for each test to account for the changes in susceptibility to frost heave in freezing virgin material. During each test the temperature gradient and the cooling rate were both kept constant. This was achieved by controlling the boundary conditions in ramping fashion using 0.05°C temperature increments, (Figure 2). Figures 3a and 3b show the results of the position of the zero degree isotherm, and the development of frost heave and water intake, respectively, during a typical test.

Four sets of tests based on three constant temperature gradients (0.035, 0.05, 0.075 and 0.1°C/cm) have been performed. Most of the results from the first two sets of experiments using two constant temperature gradients 0.035 and 0.05°C/cm were described by Svec (1989). Results from a third set of tests based on a 0.075°C/cm temperature gradient are shown in Figure 4. The fourth set using 0.1°C/cm has not been completed at the writing of this paper. The purpose of these tests has been to provide an experimental data base as an input for a computer prediction model.

Test Series III, No.2 Boundary Condition  
Temperature gradient 0.075°C/cm, Ramping rate 0.2°C/day

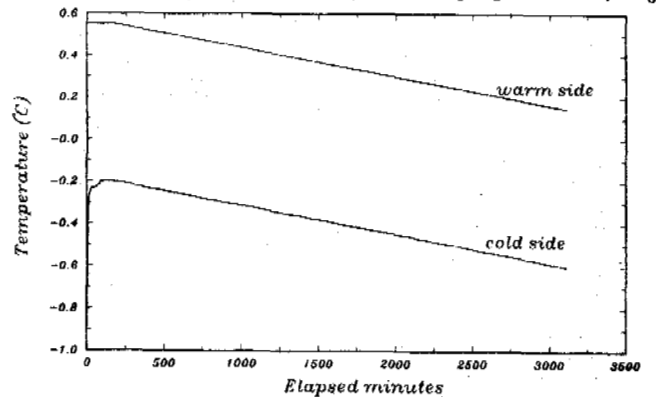
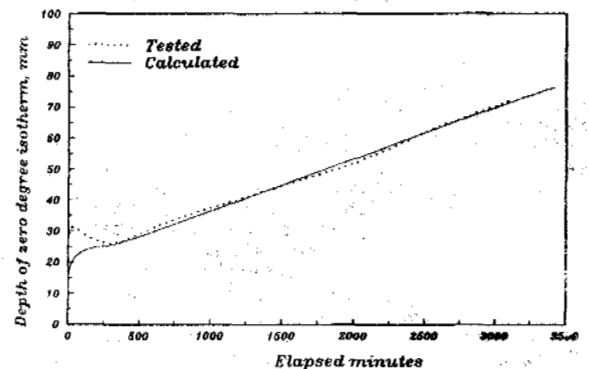


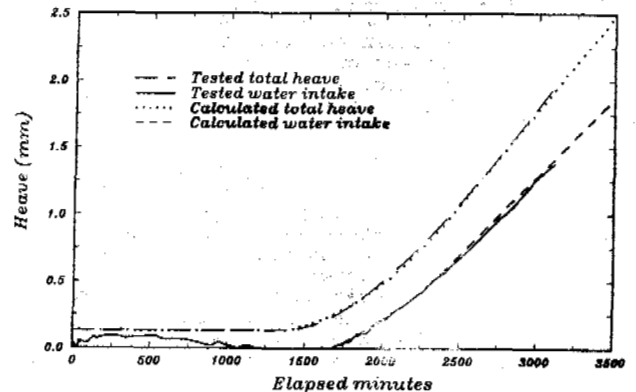
Figure 2. Boundary Conditions in a Ramping Test

Test Series III, No.2 Depth of Zero Degree Isotherm vs. time  
Temperature gradient 0.075°C/cm, Ramping rate of 0.2°C/day



(a)

Test Series III, No.2, Heave vs. time  
Temperature gradient 0.075°C/cm, Ramping rate 0.2°C/day



(b)

Figures 3a & b. Results of a Typical Ramping Test and Compared to Computer Model

### Heave Rate vs. Cooling Rate

Test series III with temperature gradient of 0.075°C/cm

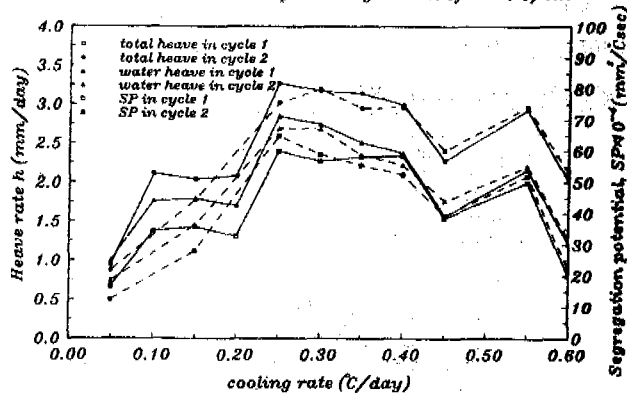


Figure 4. The Third Set of Tests Based on Temperature Gradient of 0.075°C/cm

### PROPOSED APPROACH

The proposed experimental-computer integrated frost heave prediction model is based on testing as described above. Sets of tests using constant temperature gradients, and increasing cooling (frost-penetration) rates will be performed for major soil types, (e.g., clay, silt, silty clay), resulting in a set of functions (one function for each temperature gradient). These functions, whose form will be similar to those in Svec (1989) and in Figure 5, will then be assembled into a data base and by using splines (or some other extrapolation technique), a 3-D surface envelope will then be constructed. If necessary, however, for specific site, project and climatic conditions, additional tests could be performed as follows: by observation, a thermal gradient and cooling rate will be selected that would lead to the worst frost-heaving conditions. The results of a freezing test using these parameters will give the highest possible potential to heave, called the "Critical Segregation Potential", CSP, of the soil representing the selected major soil type. Similarly, as suggested by Chamberlain (1987), these additional freezing tests should consist of two freeze/thaw cycles, followed by a CBR test.

The results of future experimental programs assembled in data bases, which is graphically shown in Figure 5, will be used in combination with our new computer model described below.

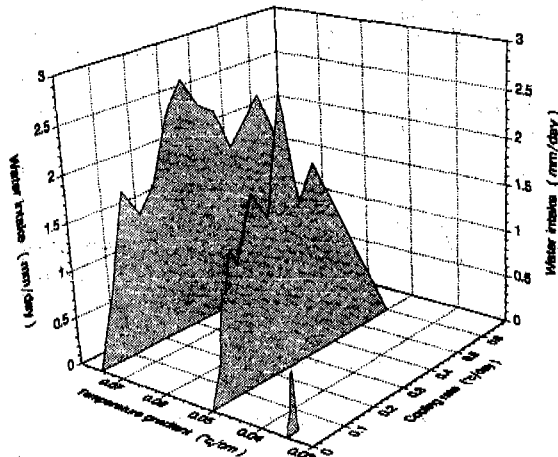
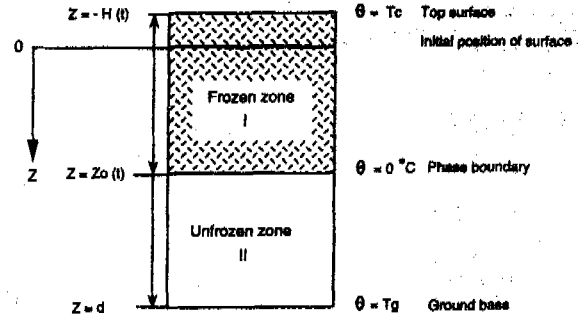


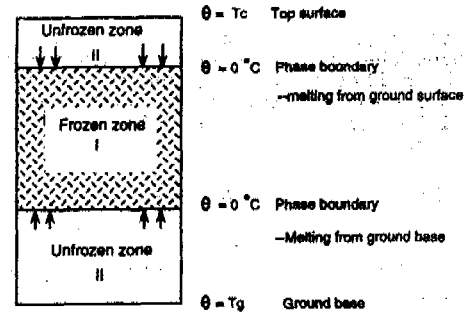
Figure 5. 3-D Data Base as a Result of Experimental Program, Fig. 4, Svec. 1989

### INTEGRATED EXPERIMENTAL-MATHEMATICAL MODEL

A one-dimensional finite element model proposed in this study is shown in Figure 6. The solution is sought in two, finite saturated soil regions: the frozen zone (I) and the unfrozen zone (II) (before freezing and after thawing).



6(a) -- freezing action; Conduction only using experimental data base



6(b) -- Melting process; Zone I - Conduction, Zone II - Conduction and convection

Figure 6. One-dimensional model for seasonal ground freezing and thawing

#### Zone (I) - Frozen Zone

In this zone the soil/ice mixture is assumed to be rigid (e.g., without any water migration) and the heat transfer is by conduction alone.

#### Zone (II.a) - Freezing Zone - Frost Action

During freezing action in this zone heat transfer is by conduction alone, but water migration is determined from experimental data base as described above. The concept of this model for this zone is based on utilizing the water intake, as an experimental determined 3-D function, Figure 5, which depends on cooling rates and temperature gradients. Both these variables are determined in each time step and in each element. The cooling rate is calculated based on results of the last two time steps, while the temperature gradient is calculated on the result of the last step only. These two variables are then used to determine the water flow, entering into appropriate elements from the data base shown in Figure 5. In a point form this process is as follows:

- (1) Calculate temperature gradient and cooling rate at each time step in each finite element;
- (2) Use these two values to determine the water intake from the experimental data base;

- (3) Use the water intake for the next time step in all elements as new water level and latent heat load;
- (4) Use an iterative process in the next time step and calculate temperature distribution, frost penetration and resulting heave.

**Zone (II.b) - Thawing Zone**

During thawing, full conduction and convection heat transfer calculations are performed as described by field equations below:

**Field Equations:**

The fixed vertical coordinate system is denoted by Z. The coordinate of the soil surface at time t, on which temperature  $\theta_s$  is applied, is  $Z = -H(t)$ . H represents the amount of heave. The coordinate of the phase change boundary is  $Z = Z_0(t)$  where the temperature is  $\theta_0$ . Since the influence of live loads on frost heave in a road application can be considered negligible, the overburden pressure is assumed constant (20 kPa). Boundary conditions representing a prescribed temperature at the surface and phase change at the interface have been included.

Field equation in the frozen **Zone I**:

$$\text{Energy balance: } \rho_{oi} \frac{\partial \theta}{\partial t} = k_{oi} \frac{\partial^2 \theta}{\partial z^2}$$

where  $\theta$  represents temperature, z is depth,  $\rho_{oi}$  denotes the average heat capacity per unit volume of the soil/ice mixture, and  $k_{oi}$  is the average thermal conductivity of the soil/ice mixture.

Field equation in the unfrozen **Zone II**, during freezing:

$$(\rho_1 c_1 + \rho_2 c_2) \frac{\partial \theta}{\partial t} + (\rho_1 c_1 \frac{\partial w}{\partial t} + \rho_2 c_2 \frac{\partial w}{\partial t}) \frac{\partial \theta}{\partial z} = k_o \frac{\partial^2 \theta}{\partial z^2}$$

Field equation in the unfrozen **Zone II**, during melting:

Equilibrium  $\frac{\partial \sigma'}{\partial z} + \frac{\partial p}{\partial z} - \gamma_s = 0$

Stress-strain  $\sigma' = -\frac{1}{m_v} \frac{\partial w}{\partial z}$

Continuity:  $\frac{\partial^2 W}{\partial z \partial t} + \frac{\partial^2 w}{\partial z \partial t} = 0$

Darcy's law:  $\frac{\partial W}{\partial t} - \frac{\partial w}{\partial t} = -k_p \left[ \frac{\partial p}{\partial z} + \gamma_w \alpha (\theta - \theta_0) \right]$

Energy balance:  $(\rho_1 c_1 + \rho_2 c_2) \frac{\partial \theta}{\partial t} + (\rho_1 c_1 \frac{\partial w}{\partial t} + \rho_2 c_2 \frac{\partial w}{\partial t}) \frac{\partial \theta}{\partial z} = k_o \frac{\partial^2 \theta}{\partial z^2}$

where  $\sigma'(z,t)$  = effective stress;  $\gamma_s, \gamma_w$  = submerged soil unit weight, water density;  $p(z,t)$  = pore pressure (or excess);  $m_v$  = coefficient of volume compressibility;  $w$  = soil displacement;  $W$  = water displacement;  $k_p$  = coefficient of permeability;  $\theta(z,t)$  = temperature of the mixture;  $\rho_1 c_1$  = heat capacity of soil;  $\rho_2 c_2$  = heat capacity of water in soil;  $k_o$  = average thermal conductivity of the soil/water mixture;  $\alpha$  = coefficient of volumetric expansion of water;  $\theta_0$  = reference temperature;

Galerkin's weighted residual method was applied using third order polynomial functions in Z and linear finite - difference step in time. Substituting these functions into a linearized version of the above equations and using the Galerkin approach yields a set of 16 algebraic equations.

This model was compared to the results of an independent (e.g., variable boundary conditions)

laboratory freezing test, and as well to the frost heave data from the field-experimental road soils. These validations are described in the next section.

**RESULTS OF MODEL TESTING**

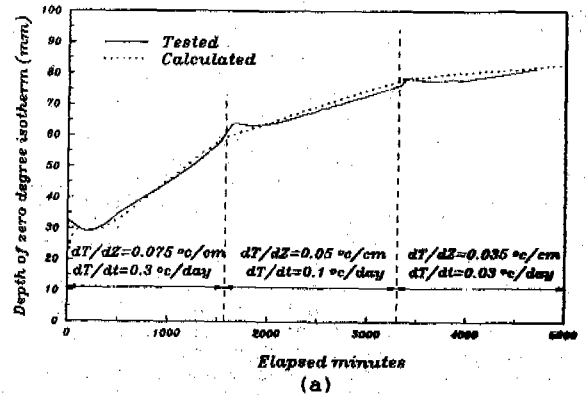
**Laboratory Freezing Tests**

The first step in the evaluation of the finite element model was to carry out individual laboratory freezing tests. The water intake was calculated from the data base described above for each time step, and then used as a load in the model subjected to freezing. The earlier Figure 3a shows a comparison between experimental and calculated results for the depth of the zero degree isotherm, while Figure 3b shows the results for the heave. These two figures represent typical results in this approach. As can be seen, the model coincides remarkably closely with the experiments. The evaluations of all of the results from all test series were similar, indicating that the computer model performed rather well.

**Independent Laboratory Test**

In the second step the proposed approach was further extended to evaluate an "independent" test (Test Series IV), where temperature gradients and cooling rates were changed in time. For the fourth set of experiments, the variable temperature gradients and cooling rates during each individual test were chosen. (Fig. 7)

Test Series IV, No.2, Depth of Zero Degree Isotherm vs. Time



Test Series IV, No.2, Total Heave vs. Time

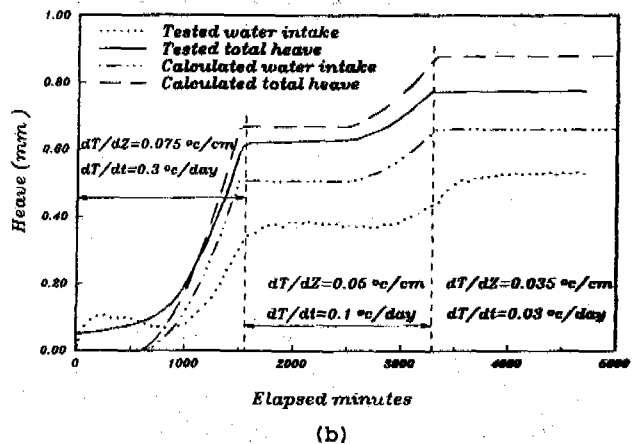


Figure 7. Independent test

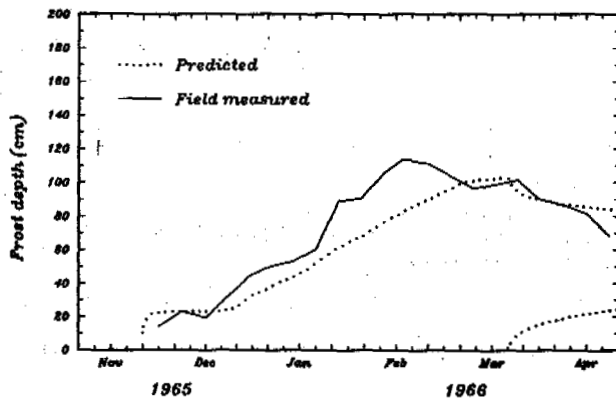
The test described in this paper was based on co-activation of three different consecutive

temperature gradients 0.075, 0.05 and 0.035°C/cm and three different consecutive cooling rates 0.3, 0.1 and 0.03°C/day. Figure 7a shows experimental and calculated results for the depth of the zero degree isotherm, while Figure 7b shows the calculated and experimental water intake and total heave. A good agreement between the model and the experimental results was achieved. This evaluation is still in process. A large number of evaluation tests are planned.

#### Road Field Data Predictions

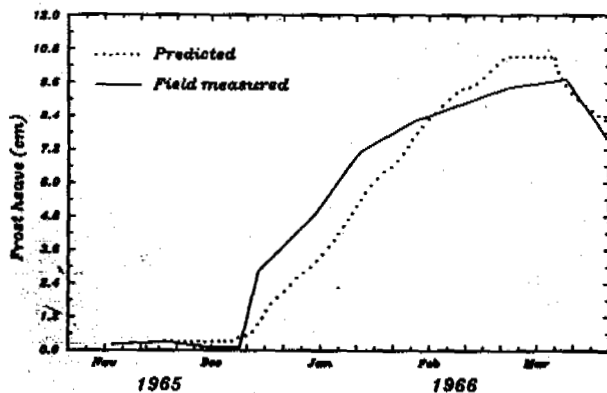
Data from a road test section built on the NRC campus in 1965, Penner (1967) were used in another evaluation of proposed model. As can be seen in Figure 8, both the frost penetration and total heave coincide well with field data. It can be concluded, even based on these rather limited and only preliminary results, that using proposed approach accurate frost heave prediction for engineering projects will be possible.

Zero Degree Isotherm vs. Time



(a)

Frost Heave vs. Time



(b)

Figure 8. Comparison Between Proposed Model and Field Road Data by Penner, 1965

#### CONCLUSIONS

This paper is based on the Critical Segregation Potential concept. The experimental program, using laboratory freezing tests of clayey silt with controlled temperature gradients and cooling rates, resulted in a data base for water intake. The combination of this data base and a finite element computer model was used to develop a novel approach to predict frost heave. The preliminary laboratory results indicate that this new model could lead to prediction of frost heave in freezing soil in the field.

It must be stressed, however, that a large (but not impractical) number of tests must be performed to complete the data base for clayey silt. In order to make this method generally acceptable in engineering practice, similar data bases must be developed for other soil types.

#### ACKNOWLEDGMENT

The authors express their deep appreciation to Mr. David Eldred of IRC/NRC, for his technical help in this project. Acknowledgement and gratitude are also due to NSERC and IRC/NRC for their financial support.

#### REFERENCES

- Chamberlain, E.J., 1981. Frost susceptibility of soil, review of index tests, CRREL Monogr., 81-2.
- Chamberlain, E.J., 1987. A freeze-thaw test to determine the frost susceptibility of soils. CRREL, Spec. Rep. 87-1.
- Konrad, J.-M and Morgenstern, N.R., 1981. The segregation potential of freezing soil. Can. Geotech. J., 18 (4): 482-491.
- Penner, E.P., 1986. Aspects of ice lens growth in soils. Cold Reg. Sci. Technol., 13(1): 91-100.
- Penner, E.P., 1967. Experimental pavement structure insulated with a polyurethane and extruded polystyrene foam. Proc. of the Int. Conf. on Low Temperature Science, 1966, Sapporo, Japan, Vol. 1, Part 2, pp. 1311-1322.
- Svec, O.J., 1989. A new concept of frost-heave characteristics of soils. Cold Regions Science and Technology, Vol. 16, No. 3, 1989, pp. 271-279.

CALCULATION OF FROST HEAVE STRESS ACTING  
ON THE FOUNDATION BOTTOM

Tang Shuchun

Da Qing Oil Field Constuction Design  
Research Institute, China

The frost heave stress acting on the foundation bottom is one of the important parameters of the depth of structural foundations. On the basis of the energy balance principle the paper deduces the method of determining the frost heave stress on various foundation forms. The problem is of great significance for shallow foundations.

INTRODUCTION

In seasonally frozen ground regions, because of the effect of frost heave on structural foundations the depth of the foundation has to be buried below the frost depth, due to horizontal frost heave non-frost soils are filled into the foundation sides, this method is not only an economical waste but is also complex in construction. Therefore it is a significant problem to determine a reasonable depth of foundation above the seasonally frozen ground. The key to this problem is predicting the frost heave stress acting on the foundation bottom. The energy balance principle balances the effects caused by foundation frost heave against the potential energy caused by the structural deformation, with a mathematical method the paper obtains the analytical solution for this problem.

For solving the problem the following assumptions were made:

(1) The freezing process of the seasonally frozen foundation is one-direction plane freezing, i.e. the freezing depth develops gradually from the surface downward, after the structures are built, the heat transmission process of the frozen foundation is changed, it decreases the freezing depth of the foundation but the plane freezing state is not changed.

(2) It is assumed that the frozen soil under the foundation is uniform the ground temperature gradient is constant during the freezing process. So, the frost energy caused by the unit frozen soil layer at any depth is the same, that is, under the foundation the frost energy from the first unit soil layer is equal to that of unit soil layers at other depths, it can be described as the following (Tang Shuchun, 1990):

$$\Delta h_1 \delta_1 = \Delta h_2 \delta_2 = \dots = \Delta h_n \delta_n \quad (1)$$

where:  $\Delta h_1 \delta_1, \Delta h_2 \delta_2, \dots, \Delta h_n \delta_n$  indicates the frost energy from first, second, third, ...nth

unit soil layer, respectively.

Under natural conditions formula (1) can be written as follows:

$$\Delta h_1 \gamma_1 \Delta H = \Delta h_2 \gamma_2 \Delta H = \dots = \Delta h_n \gamma_n \Delta H \quad (2)$$

where:  $\Delta h_1, \dots, \Delta h_n$  -- frost amount from 1-n unit soil layer (m)  
 $\gamma_1, \dots, \gamma_n$  -- unit weight of 1-n unit soil layer (KN/m)  
 $\delta_1, \dots, \delta_n$  -- soil weight raised by 1-n unit soil layer frost (KN/m<sup>3</sup>)  
 $\Delta H_1, \dots, \Delta H_n$  -- the thickness of unit soil layer (m)

The following equations are obtained from formula (2)

$$\Delta h_2 = \frac{\Delta h_1 \gamma_1}{2 \gamma_2} \quad (3)$$

$$\Delta h_3 = \frac{\Delta h_1 \gamma_1}{3 \gamma_3} \quad (4)$$

$$\Delta h_n = \frac{\Delta h_1 \gamma_1}{n \gamma_n} \quad (5)$$

Equations (3), (4), (5) indicate that  $\Delta h_1, \Delta h_2, \dots, \Delta h_n$  has a linear relationship for uniform soil, the frost amount at negative temperature decreases linearly along the foundation depth.

(3) Interface stress at the frost front is equal to or less than the bearing capacity of the foundation, and the frost stress acting on the foundation bottom by the frozen soil layer is determined by the stress spread principal.

From above these basic assumptions on energy balance principles on the effects of soil frost heave on structures shall balance with the potential energy caused by structural deformation. This can be written as the following formula:

$$[W1] = [W2] \quad (6)$$

where [W1] -- Effect of soil frost on structure, KJ.

[W2] -- Potential energy caused by the structural deformation, KJ.

**FORMULA DEDUCTION**

When the structure and the frozen soil foundation are working at the same time, the frost deformation caused by the frozen soil effects the structure. The structure affected by the frost action has deformation potential energy. This energy balances with the frost energy. Within the two energies the soil frost energy plays a dominant role. It is of important significance for the design of the structures on frozen foundations to determine the energy magnitude.

The sum of frost energy ( $W_i$ ) caused by unit soil frost under the foundation is the frost energy acting on the foundation bottom (Fig.1). It can be described as follows:

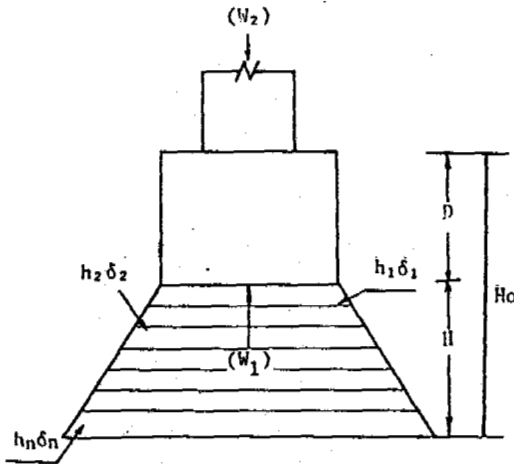


Figure 1.  $[W1] = \sum_{i=1}^n W_i = W1 + W2 + \dots + Wn$

this equation can be replaced with the following equations:

$$\begin{aligned} W1 &= (V_0 Y_0 + V_1 Y_1) h_1 \\ W2 &= (V_0 Y_0 + V_1 Y_1 + V_2 Y_2) h_2 \\ W3 &= (V_0 Y_0 + V_1 Y_1 + V_2 Y_2 + V_3 Y_3) h_3 \\ &\dots\dots \\ Wn &= (V_0 Y_0 + V_1 Y_1 + \dots + Vn Yn) hn \end{aligned}$$

where,  $V_0, Y_0$  -- frozen soil weight above the foundation bottom, KN

$V_1, Y_1 - Vn Yn$  -- 1 - n soil layers weight under the foundation bottom, KN

The above equations may be varied to the following form:

$$\begin{aligned} W_0' &= V_0 Y_0 (h_1 + h_2 + h_3 + \dots + h_n) \\ W_1' &= V_1 Y_1 (h_1 + h_2 + h_3 + \dots + h_n) \\ W_2' &= V_2 Y_2 (h_2 + h_3 + \dots + h_n) \\ &\dots\dots \\ W_n' &= V_n Y_n (h_n) \end{aligned}$$

Due to the stress spread action the value of  $W_i$  relates to the shape of the structural foundation. Here taking a strip foundation as an

example we state simply the reduction method of frost energy under the foundation.

For the strip foundation:

$$\begin{aligned} V_0 &= B D b \\ V_1 &= \Delta H (B + \frac{\Delta H}{tg \alpha}) b \\ V_2 &= \Delta H [(B + \frac{2 \cdot 1 \Delta H}{tg \alpha}) + \frac{\Delta H}{tg \alpha}] b \\ V_3 &= \Delta H [(B + \frac{2 \cdot 2 \Delta H}{tg \alpha}) + \frac{\Delta H}{tg \alpha}] b \\ &\dots\dots \\ V_n &= \Delta H [(B + \frac{2 \cdot (n-1) \Delta H}{tg \alpha}) + \frac{\Delta H}{tg \alpha}] b \end{aligned}$$

Replace  $V_0, V_1 \dots Vn$  into equations of  $W_0', W_1', \dots, Wn'$ , we obtain:

$$\begin{aligned} W_0' &= B D b Y_0 (h_1 + h_2 + h_3 + \dots + h_n) \\ W_1' &= \Delta H (B + \frac{\Delta H}{tg \alpha}) b Y_1 (h_1 + h_2 + \dots + h_n) \\ W_2' &= \Delta H [(B + \frac{2 \cdot 1 \Delta H}{tg \alpha}) + \frac{\Delta H}{tg \alpha}] b Y_2 (h_2 + h_3 + \dots + h_n) \\ W_3' &= \Delta H [(B + \frac{2 \cdot 2 \Delta H}{tg \alpha}) + \frac{\Delta H}{tg \alpha}] b Y_3 (h_3 + h_4 + \dots + h_n) \\ &\dots\dots \\ W_n' &= \Delta H [(B + \frac{2 \cdot (n-1) \Delta H}{tg \alpha}) + \frac{\Delta H}{tg \alpha}] b Y_n h_n \end{aligned}$$

Above equations can be written as the following form

$$\begin{aligned} W_1'' &= B D b Y_0 h \\ W_2'' &= \Delta H B b (h_1 Y_1 + 2 h_2 Y_2 + 3 h_3 Y_3 + \dots + n h_n Y_n) \\ W_3'' &= \frac{\Delta H^2}{tg \alpha} b (h_1 Y_1 + 2 h_2 Y_2 + 3 h_3 Y_3 + \dots + n h_n Y_n) \\ W_4'' &= \frac{\Delta H^2}{tg \alpha} b \cdot 2 [(h_2 Y_2 + h_3 Y_3 + h_4 Y_4 + \dots + h_n Y_n) \\ &\quad + 2 (h_3 Y_3 + h_4 Y_4 + \dots + h_n Y_n) \\ &\quad + 3 (h_4 Y_4 + \dots + h_n Y_n) \\ &\quad + \dots\dots \\ &\quad + (n-1) h_n Y_n] \end{aligned}$$

Because  $h, h \dots h_n$  tend gradually to zero with the development of frozen depth, and there appears a distribution of upside-down trigonometry, therefore:

$$h_1 Y_1 + h_2 Y_2 + h_3 Y_3 + \dots + h_n Y_n = h \bar{Y} \tag{7}$$

where,  $h$  -- total frost deformation amount of frozen soil layer under strip foundation, m;  
 $\bar{Y}$  -- mean unit weight of the frozen soil layer under strip foundation, KN/m<sup>2</sup>;  
 $B$  -- width of strip foundation, m;  
 $D$  -- depth of strip foundation, m;  
 $b$  -- calculation length of strip foundation, is 1 m.

From equation (7) and through mathematical treatment, we get:

$$\begin{aligned} W_1'' &= B D b Y_0 h \\ W_2'' &= H B b \bar{Y} \frac{h}{2} \\ W_3'' &= 0 \\ W_4'' &= \frac{H^2 h \bar{Y} h}{2 tg \alpha} \end{aligned}$$

where H -- frozen soil layer thickness under strip foundation, m.  
 since,  $[W_1] = W_1^1 + W_2^1 + W_3^1 + W_4^1$   
 thus,

$$[W_1] = \frac{(2BDtg\alpha \cdot Y_0 + BHtg\alpha \cdot \bar{Y} + H^2 \bar{Y})bh}{2tg\alpha} \quad (8)$$

replacing  $Y_0$  with  $Y_1$ ,  $b=1$ , Eqs.(8) becomes

$$[W_1] = \frac{(2BDtg\alpha + BHtg\alpha + H^2)h\bar{Y}}{2tg\alpha} = \eta h\bar{Y} \quad (9)$$

where

$$\eta = \frac{2BDtg\alpha + BHtg\alpha + H^2}{2tg\alpha}$$

$\eta$  is the comprehensive effect coefficient, it is related to the foundation bottom shape, size, and thickness of the frozen soil layer under the foundation and angle of stress spread, its dimension is in  $m^3$ .

With the same method it can be obtained the frost energy expression under circular and rectangular foundation bottoms the expression pattern is the same as in formula (9), but the value of  $\eta$  is different.

For rectangular foundations:

$$\eta = \frac{ABHtg^3\alpha + AH^3tg^3\alpha + BH^3tg^3\alpha + H^3 + 2ABDtg^2\alpha}{2tg^3\alpha}$$

For circular foundations:

$$\eta = \frac{\pi(4R^3Htg^3\alpha + 4RH^3tg^3\alpha + H^3 + 8R^3Dtg^2\alpha)}{8tg^3\alpha}$$

where, A, B -- rectangular foundation side length, m;

R -- radius of circular foundation, m;

H -- frozen soil layer thickness under foundation, m;

D -- foundation depth, m.

After structures are built, soil frost heave under the foundation is restrained by the load of the structure. The effects of soil frost heave causes the potential energy of the structural deformation, the two energies are in a balanced state during the soil frost heave process. When the effects of soil frost heave causes structural deformation, as long as the deformation is not greater than structural allowance or the demanded deformation amount, the structure will be in a safe state. Therefore, the allowable deformation potential energy caused by soil frost heave under the foundation can be indicated as follows:

$$[W_2] = F\delta f \quad (10)$$

where, F -- foundation bottom area,  $m^2$ ;

$\delta$  -- frost stress acting on foundation bottom,  $KN/m^2$ ;

f -- allowable deformation of structure by the action of frost heave stress, usually taken as 0.01 m.

From formula (6), we obtain:

$$\eta h\bar{Y} = F\delta f$$

From this we obtain the calculation formula for frost heave stress:

$$\delta = \frac{\eta h\bar{Y}}{Ff} \quad (11)$$

## CONCLUSION

The frost heave stress acting on the foundation bottom is obtained with the energy balance principle, this is a new attempt. The theoretical calculation result compares favourably with practical engineering. The calculation method given by the paper may be used for the calculation of dam foundation stability and other structural foundations.

## REFERENCES

- Tang Shuchun, (1990) Application of expansion mechanics in oil field engineering, oil field ground engineering. Vol.9, No.2,  
 Tang Shuchun, (1990) Determining the depth of constructure foundation in cold region with energy method. Harbin Industrial University Journal.

## EXPERIMENT AND APPLICATION OF HEAVY TAMPING METHOD TO PREVENT A HIGHWAY FROM FROST HEAVING AND BOILING

Tang Xiaobo

Heilongjiang Province Low Temperature Construction  
Science Research Institute, Harbin, China

It is low-costed, effective and easy to manipulate in practice to consolidate a roadbed by using heavy tamping method in prevention of frost heaving and boiling of highway in cold regions.

### INTRODUCTION

In the cold regions of northern China, the frost disasters of highways are very serious. The frost heaving and thawing settlement of the seasonal active layers cause the road boiling to influence the normal traffic, and sometimes make the traffic interrupted, so the expenditures on road maintenances and repairs are very large. In order to search for an effective, simple, and low-costed approach to prevent highways from frost heaving and boiling, one trial section was taken from a highway, in which the frost heaving and boiling developed, to use the heavy tamping method to treat the roadbed. The experimental process was carried out at the same time as the road section was rebuilt. The experimental results showed that the heavy tamping method had a good effect in prevention of frost heaving and boiling of a highway.

### SURVEY OF THE ENGINEERING CONDITION AT THE TRIAL SECTION

This engineering project was located in the central part of Longfeng district of Daqing city in Heilongjiang Province. The experimental section was selected at the main line of Tuanjie road, in which the frost heaving and boiling were most serious. The section was 275 m long, 12 m wide, and 3300 m<sup>2</sup> in area. The Tuanjie road is topographically low, the groundwater level is -0.5 m, the drainage condition was not very smooth. The soils in the roadbed were clay and lam with a high frost-heaving property. The pavement was made of sand and stones. Since the road was built in 1961, the frost heaving and boiling had occurred every year. Although a large amount of rubbles, crushed stones, limestone powder, and lay cinder was used to pave the road in the one year, the boiling still emerged in the next year. The road was rebuilt by applying the heavy tamping method to treat

the roadbed in 1984, and the pavement was concrete instead of sand and stones.

### THE HEAVY TAMPING CONSTRUCTION, TEST AND OBSERVATION

In the construction of this engineering project by using the heavy tamping method, a 15T crawler crane was used, as well as a hammer and an auto-unhooked equipment designed and made by ourselves. In order to avoid the occurrence of crane's backward declination with tamping while the crane arm being in a large tilt angle, a Dongfanghong 100-type bulldozer was used to pull the crane forwards, meanwhile the bulldozer was also used to smoothen the roadbed. All the heavy tamping parameters are shown in Table 1.

During the tamping construction all the tamping-pit bottoms must be controlled to be higher than the bottom of the road trough, and also the tamping settlements must be limited within 0.94 m by adding some soil constantly into the tamping pits. Meanwhile, the heavy tamping numbers were counted by calculating the last two times' average settlement to be no more than 0.03 m. The method of pump drainage and artificial drainage were adopted because the drainage ditches along two sides of the road were not completed at that time. After the tamping construction, the bending settlement test was made according to the highway construction standards. The results listed in Table 2 met the design requirements.

In 1985 and 1986, the observation on freezing and thawing deformation was done during the winters and springs after the heavy tamping construction. The largest frost heaving value was 0.188 m in the untamped beds of Tuanjie road, and the value, by contrast, was 0.054 m in the tamped beds of the same road. Compared with that at the untamped section the largest frost-heaving deformation reduced about 70% at the heavy tamped section (Table 3). Fig.1 has



Table 1. The heavy tamping parameters at the trial section of Tuanjie road

Hammer weight	Hammer's dropping distance	Center-line distance between every two tamping pits	Average tamping settlement at every pits	Average impact energy per unit area	Average ground settlement in all the tamping areas
115 (KN)	9-10 (m)	3.25 (m)	0.945 (m)	600 (KNm/m <sup>2</sup> )	0.3 (m)

Table 2. The results of bending settlement test in the bed of Tuanjie road after the tamping construction.

Test site No.	1	2	3	4	5	6	7
Coordinate	0+610	0+570	0+530	0+490	0+450	0+410	0+370
Bending settlement (mm)	1.40	1.60	1.24	1.30	1.24	1.42	1.22

Table 3.

Observation sites	The untamped section							The heavy tamped section								
	1	2	3	4	5	6	7	1	2	3	4	5	6	7	8	9
Frost-heaving value (mm)	78.8	65.7	71.4	71.3	67.2	70.1	61.0	8.8	17.1	35.0	46.3	35.4	29.3	25.0	35.6	12.4

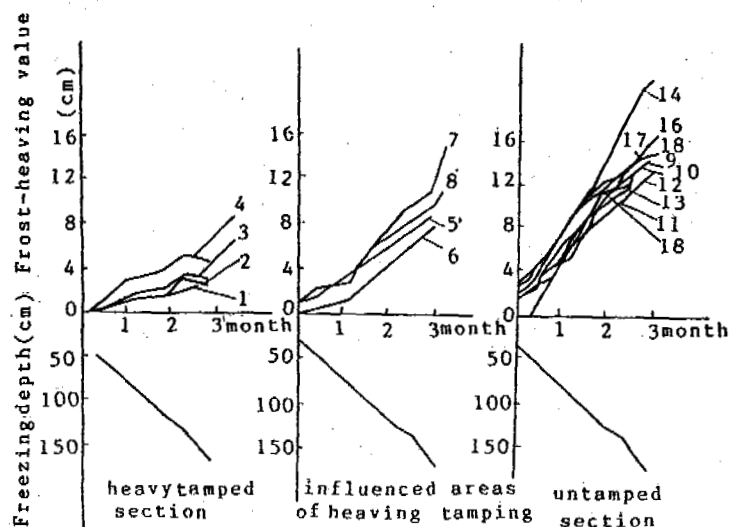


Figure 1. The frost-heaving deformation curves at the observation sites of the heavy tamped and the untamped road sections

shown how the frost-heaving deformation changed with time and freezing depth.

#### ANALYSIS AND RESEARCH OF THE TEST RESULTS

The test results showed that the heavy tamping method was very effective in the prevention of frost heaving, it could greatly diminish the possibility of the road damage caused by frost heaving and boiling in the roadbed.

The frost-heaving swell is the expansion action in volume during the freezing of the soil. Except for the expansion in volume while the origin water in soil is freezing into ice, the swell is mainly caused by the relative displacement which happens due to the volume expansion of ice as water constantly migrates and accumulates from the unfrozen areas to the frontal areas of freezing. It is also defined as the so-called frost heaving. The road boiling is the frost-caused phenomenon that the water content in soil will increase a lot when the separated ice is thawed, and the soil in the roadbed will be in saturation because so much thawed water is unlikely to slake out in a short period, but meanwhile the deeper part of the roadbed is still in freezing, so the soil gets softer and softer, its strength becomes lower and lower. As a result, the spring-like deformation emerges in the pavement under the repeated loads produced by running vehicles, finally cracks, and drumlins will appear and mud will flow out. Both the frost heaving and the ice separating only can occur under the three conditions as followed: the first is that the soil must be sensitive to freezing, the second is that the frozen depth must reach to the easily frozen soil, and the third is enough water supply. Among these three conditions the water supply is the foremost. All the enough water can come from the ground water, and the partial rainfall which penetrates into the roadbed through the pavement or the road shoulders, so if the water supply can be stopped, the frost heaving of the roadbed soil will be surely reduced, and the occurrence of frost heaving and boiling will be effectively prevented. The heavy tamping method can meet this requirement. Under the strong impact force of heavy tamping, the soil will be consolidated quickly, and the soil porosity will be lessened. A large amount of experiments and engineering practices demonstrated that the inner stress field will be changed when the impact energy of heavy tamping is spreading into the roadbed soil as various waves, and the pore water pressure will be increased. After such an energy reaches to some value, many cracks will appear in the soil. The free water, the capillary water, and the partial loosely bound water will permeate towards low-pressured places through the cracks under the action of the pressure differences, the water content of the soil will decrease consequently, as well as the soil permeability being low down. The coefficient of permeability of the soil (clay or lam) as commonly in  $1 \times 10^{-5}$  before the soil being tamped, and was smaller than  $1 \times 10^{-8}$  after tamped. Besides this, the heavy tamping could also lower the ground-water level down, the level was -0.5 m before tamped by contrast to the -3 m after tamped. Meanwhile, large amounts of backfill soil, crushed stones was tamped into the roadbed, this led to the reducing of the frost heaving property of the soil. From Fig.1, the following

fact can be figured out, which was that the frost-heaving deformation of the tamped roadbed was very little, and the frost-heaving deformation of the untamped roadbed developed continuously when the frozen depth exceeded the structural layer of the roadbed, this illustrates that the frost-heaving degree of the tamped soil has changed. The density-increased soil formed a water-resisting layer in a certain range and depth and this layer cut the passages of the water supply to the roadbed completely or partially, and made the ice separation impossible, so the road boiling in spring time could be prevented. After the practical examinations on Tuanjie road through total three cycles of freezing and thawing, it was testified that the features such as fissure of displacement, swell, and surface cracks were very common at the untamped road section, by contrast, any such similar features happened at the tamped section.

#### CONCLUSION

The heavy tamping is a simple, low-costed, easily manipulated method with splendid prespectives of further development for the prevention of the frost heaving and boiling of a highway in the cold regions, although it was the first time for the method to be applied in this field. It can be carried out by using a lot of local materials such as sand, stones, constructional refuse, and industrial wastes, etc. So it can transfer the harms into the benefits.

The mechanism and the long-term effectiveness of the heavy tamping method in prevention of the frost heaving and boiling of highways need to be further tested.

#### ACKNOWLEDGEMENT

The author would like to thank Guo Mingzhu and Han Huaguang who participated in the experimental work.

#### REFERENCES

- Han Huaguang, et al. (1989) Research and application of heavy tamping method in prevention of frost heaving. Proceedings of the Third National Symposium on Permafrost of China, Science Press.

## A METHOD TO MEASURE HEAT CONDUCTIVITY WITH A HEAT FLOW METER

Tao Zhaoxiang, Zhang Lixin and Hou Zhongjie

State Key Laboratory of Frozen Soil Engineering, Lanzhou Institute of  
Glaciology and Geocryology, Chinese Academy of Sciences, China

The method determining the thermal conductivity of frozen soil with the heat flow meter is based on the principle of steady heat conduction. The temperature of one side of the sample is kept higher and the other lower by cooling baths. After the steady heat situation is set up, the difference of the temperature of the two sample sides and the heat flow transferring through the sample can be determined. Then the thermal conductivity can be calculated with a datataker.

### INTRODUCTION

With the development of construction, new types of building materials and insulators are continuously invented. One of the main indexes that reflect the properties of the insulator is heat conductivity. In order to accurately measure the heat conductivity, the heat flow meter method is proposed for the local requirements and experiences. It makes up for the lack of present devices.

### EXPERIMENTAL PRINCIPLE

The method of the heat flow meter belongs to one of the measuring methods of the principle of steady heat conducting that is commensurate with the case of steady heat conduction across double decked plate. Keeping constant the difference of temperature between the two sides of the sample, when the heat flow is in the steady state, the heat conductivity can be calculated by measuring the difference of temperature and heat flux across the sample:

$$\lambda = \frac{E}{C} \cdot \frac{\Delta h}{t_1 - t_2}$$

where:  $\lambda$  — heat conductivity, W/m·°C;  
 $C$  — coefficient of heat flow meter, mv m<sup>2</sup>/W;  
 $E$  — heat flow meter reading, mv;  
 $\Delta h$  — interval between thermocouples, m;  
 $t_1, t_2$  — thermocouples indications, °C.

### EXPERIMENTAL DEVICES AND OPERATING PROCESSES

There are two systems of experimental devices.

#### Constant Temperature System

The system consists of a thermostatic box and two low temperature calculators (the ranges of

temperature: -50 - 40°C and -20 - 10°C; controlling accuracy: ±0.05°C).

The change of the temperature on the surface of the thermostatic box can't surpass: ±0.11°C. Details are shown in Fig.1 (Tao Zhaoxiang, 1983)

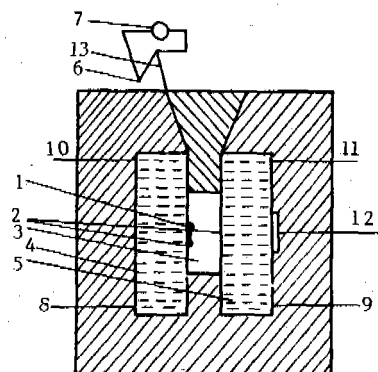


Figure 1.

1-heat flow meter; 2-thermalcouple;  
 3-sample; 4-thermostat A;  
 5-thermostat B; 6-zero point of  
 7-datataker; thermalcouple;  
 8,9-inlets of circulated alcohol;  
 10,11-outlets of circulated alcohol;  
 12-screw for tightening;  
 13-leading lines of the thermalcouple and heat  
 flow meter.

#### Systems of Measuring Heat and Temperature

The sensors of heat and temperature form of a heat flow meter and two thermalcouples. The secondary instrument is used as datataker.

The operating processes are as follows:

1). Preparing sample: The size of the sample is 25X25X25 cm<sup>3</sup>. It is demanded that there not be granulars of bumps and holes on the two larger

surfaces of the sample. The sample is put into the test box in which the sides and bottom are made of copper with a size of 25X25X5 cm<sup>3</sup>.

2). Positioning of the heat flow meter and the sensor of the thermocouples: The sensors of thermocouple are positioned respectively on the two bigger surfaces of the sample where a small trough is carved in advance. And a small trough that has the shape of the heat flow meter is carved on one of the bigger surfaces to attach the heat flow meter, and the sensor and heat flow meter are placed in the centre of the surface. When the sample is granular or powdery, the sensors and the heat flow meter are directly placed in the internal surfaces of the copper.

3). After the sample is put into the thermostatic box, it is clipped as tightly as possible, so that it is very close to the walls.

4). Turn on the thermocouple, heat flow meter and circulators, and set the temperature of the circulators; 20°C in A, 3°C in B for positive temperature; -20°C in A, -3°C in B for negative temperature. Then the experiment begins.

5). After the data of temperature and heat flux are displayed on the screen and reach a steady state, data is retrieved and the heat conductivity is calculated.

6). It is feasible to put two samples together into thermostatic box, so that two results can be measured at the same time.

## RESULTS AND DISCUSSION

### Experimental Results

Through multiple experiments of seven kinds of materials, the method is proved to be feasible. Table 1 and Table 2 list the results that are approached with the data measured with TC-22 type digital heat conductivity meter made in Japan.

Table 1. Comparison of the results of two test methods

The units of heat conductivity: W/m °C

Sample name	Density dry (kg/m)	Meter heat flow		TC-22		Absolute error	
		$\lambda$	$\lambda$	$\lambda$	$\lambda$	$\lambda$	$\lambda$
Foamed polystyrene	34	0.034	0.034	0.02	0.02	-0.005	-0.005
Foamed polystyrene	35	0.035	0.03	0.03	0.03	-0.004	-0.004
Foamed polystyrene	32	0.036	0.03	0.03	0.03	-0.005	-0.004
Polyurethane	36	0.019	0.02	0.01	0.01	-0.004	-0.006
Polyurethane	47	0.015	0.01	0.01	0.01	-0.001	-0.003
Glass wool	32	0.036	0.03	0.03	0.03	-0.001	-0.003
Glass wool	32	0.034	0.03	0.03	0.03	0.001	0.000
Perlite concrete	930	0.231	0.23	0.23	0.23	0.008	-0.004
Perlite concrete	940	0.228	0.22	0.22	0.22	-0.003	-0.005
Pearlite concrete	1220	0.331	0.34	0.32	0.32	-0.008	-0.021
Pearlite concrete	1460	0.345	0.35	0.32	0.33	-0.018	-0.025
Quartz sand	1680	0.302	0.25	0.30	0.28	0.001	0.030

\*--water content is zero.

### Discussions

The measured materials include several types of plastics, granular and powder, concrete and metal. All the materials didn't contain moisture. The absolute errors of both the methods are within the range of 30%.

Following conclusions may be obtained:

(1). What are measured are dry samples of granular and powder, massive materials such as insulator and plastic, anisotropic material of granular, etc.

(2). The measuring range: 0.010-0.600 W/m, °C.

(3). Two samples can be measured at the same time.

(4) Accuracy: 3%.

### CONCLUSIONS

Most of the present methods to measure heat conductivity, no matter if the basis is steady or not, are used through stabilizing the boundary temperature or heating sample. These methods can not measure samples with some water and anisotropic materials. Compared with other methods, the heat flow meter has following advantages:

1. It can measure the heat conductivities in both positive and negative temperatures.

2. It overcomes the problem of the water content being redistributed and results in the distortion of data by heating in other methods.

3. Anisotropic materials of granular and massive samples can be measured.

4. Both dry and humid samples can be measured.

Table 2. Test results of complex samples

The units of heat conductivity: W/m °C

Sample name	Dry density (kg/m)	Sample 1		Sample 2	
		$\lambda$	$\lambda$	$\lambda$	$\lambda$
Foamed polystyrene	35	0.033	0.038		
Foamed polystyrene	34			0.035	0.035
Polyurethane	36	0.017	0.017		
Polyurethane	47			0.020	0.021
Perlite concrete	940	0.231	0.226		
Perlite concrete	930			0.230	0.222
Foamed polystyrene	35	0.030	0.033		
Perlite concrete	930			0.204	0.219

\*--water content is zero.

REFERENCE

Tao Zhaoxiang and Wang Maohai, (1983) The Comparative Method used for Determining Thermal Conductivity of Soil. Professional Papers on Permafrost Studies of Qinghai-Xizang Plateau, Publishing by Science Press House, pp.149-151.

ULTRASONIC MEASUREMENTS IN FROZEN SOILS TO  $-120^{\circ}\text{C}$  :  
RESULTS AND INTERPRETATION USING DIFFERENT THEORETICAL MODELS

THIMUS, J.F.<sup>1</sup>, AGUIRRE-PUENTE, J.<sup>2</sup>, COHEN-TENOUDJI, F.<sup>3</sup> and  
LECLAIRE, Ph.<sup>3</sup>

<sup>1</sup>Département de Génie Civil, Université Catholique de Louvain,  
Louvain-la-Neuve, Belgium

<sup>2</sup>Laboratoire d'Aérothermique du C.N.R.S., Meudon, France

<sup>3</sup>Laboratoire Universitaire d'Applications de la Physique,  
Université de Paris 7, Paris, France

Transmission experiments of ultrasonic longitudinal impulses have been carried out in three geological samples of different nature, from ambient temperature down to  $-120^{\circ}\text{C}$ . In this range of temperatures the whole domain of phase transition is included. Values of measured velocities for completely frozen and unfrozen states allow testing of the different ultrasonic wave propagation models in the two limits of application. Evidence is shown that the solid matrix undergoes consolidation process due to the ice formation. Assuming a matrix consolidation percolation process, wave velocity is predicted in function of the unfrozen water content. With this value on one hand, and the experimental velocity vs temperature curve on the other hand, a relationship between the water content and the temperature is then obtained. For one of the studied samples, a comparison of results and a detailed discussion are made in relation to other existing predictions.

## INTRODUCTION

The important reservoirs of hydrocarbon resources in arctic regions and the research which must be made in the Antarctic require the construction of big structures on the land (roads, pipelines, buildings) as well as upon the sea floor (artificial islands, off-shore structures, gas or oil exploration and production wells). The technologies present important challenges due to difficulties caused by the extreme climate conditions and the freezing susceptibility of soils (water suction, frost heave).

Indeed, the grounds of these permafrost regions are frequently composed of very fine-grained soils with high water content. The annual variations of the climate act upon the ground, and the soil undergoes thawing and freezing cycles which continuously modify the porous medium and its mechanical properties.

Engineers are required to provide important data for the design of structures and the prediction of the ground-structure system behaviour. The proposed structures and building procedures must respect the natural permafrost characteristics and the environment.

Proper design will require a good knowledge of the complex phenomena which determine the behaviour of soils during freezing and thawing processes and their different thermo-physical properties. One of the most important properties is the unfrozen water content which affects the local thermal response to low temperatures and consequently the global thermal behaviour of the system as frost heave, mechanical resistance, ground-structure interactions, a.s.o. Determination of the unfrozen water content will affect the prediction of the in situ behaviour of materials, the scope of laboratory experiments and the interpretation of tests conducted in the field or in the laboratory. Non-destructive tests are often required and acoustic techniques appear to provide very good information allowing the

determination of the thermo-physical characteristics and a best knowledge of the freezing or thawing phenomena.

Laboratory investigations in this field have recently been done and semi-empirical models were widely tested. In certain cases, satisfying practical results were obtained, but only with the help of laboratory experiments conducted over a large range of temperature in order to adjust the models using the totally frozen and unfrozen conditions of the soils. Leclaire (1991, 1993) have proposed a rigorous theory, presented in a companion paper at this conference, in order to get a generalized solution of the freezing soil acoustic problem.

The aim of the present paper is to submit results of the most recent experimental research, to describe and interpret measurements using the practical semi-empirical methods and to discuss results in view of this new theoretical research.

## SEMI-EMPIRICAL APPROACH

Deschâtres (1989) and Thimus (1991) have proposed several semi-empirical approaches to determine the relationship between unfrozen water content and temperature. The authors have observed that the Timur's model (in  $1/v$ ) (1968) and the Wyllie et al second model (in  $1/\rho v^2$ ) (1956) give erroneous values of ultrasonic velocities for fine-grained soils in respectively totally unfrozen or totally frozen states. These discrepancies could be explained by physico-chemical changes at the boundaries of the clay flakes which occur during the cooling of the sample at temperatures below  $0^{\circ}\text{C}$  and lead to changes of the mechanical characteristics of the grains forming the solid matrix. Consequently, the authors have proposed a new approach which considers a continuous linear variation of the unfrozen water content with the  $1/v$  or the  $1/v^2$  parameters between the two extreme situations. The authors have measured the ultrasonic velocity during the thermal process, determined the

unfrozen water content and observed a good agreement with values given by other approaches such as calorimetric and NMR methods. The description of performed tests, the characteristics of studied soil (Boom clay) and the results are described below. These two practical methods give results which do not differ greatly for the Boom clay. Nevertheless, the authors felt the necessity to confirm the validity of this approach studying other types of soils. This paper describes new measurements conducted on silt and another clay samples and compares them with those carried out on the Boom clay samples.

### THEORETICAL APPROACH

As shown in previous papers by Deschâtres (1989) and Thimus (1991), semi-empirical approaches allow to obtain interesting results for specific types of soils. However, a given available model was unable to explain the entire suite of measurements. In particular, these models could not give a good estimate of the ultrasonic velocity for both consolidated and unconsolidated media, and were unable to calculate the acoustic waves attenuation coefficient. An acoustical theoretical model has been developed in collaboration between Paris 7 University LUAP and CNRS Aerothermic Laboratory by Leclaire et al. This theoretical model is discussed in another paper presented at this Conference (Leclaire, 1993). Biot's theory of sound propagation in porous media without phase change has been developed for a complex medium where a variable proportion of two phases, ice and water, fills the pores of the solid porous matrix. With the help of this theoretical model, one is able to predict for any porous medium, the velocities and attenuations of the different waves (3 longitudinal and 2 transverse) which can propagate through the porous medium. These waves properties depend directly on proportions of the water and ice as a function of temperature. Consequently, the theoretical prediction of velocities can be used to interpret experimental results as discussed by Leclaire (1993).

### SOILS PROPERTIES

The paper presents results obtained for three different types of soils, two clays and one silt :

- a tertiary overconsolidated clay of Rupelian age (Boom clay)
- a tertiary clay of Ypresian age (ypresian clay)
- a quaternary eolian loess (weichselian silt).

The main physical characteristics of these soils have been determined and are given in Table 1.

### PERFORMED TESTS

Test procedure and results obtained for Boom clay specimen have been already presented (Leclaire, 1991). The procedure used to study other soils is more sophisticated. Two soil specimens are placed in a box in the cold room of Civil Engineering Laboratory (LGC - UCL). This box is cooled by dispersion of liquefied nitrogen. During the cooling, the temperature decreased at a 3 K/hour rate between 20 and -20 °C and a 12 K/hour rate below -20°C. The thawing of the specimens is obtained naturally. The temperature is measured inside and outside of the

Table 1 : Physical characteristics of soils

	Boom clay	Ypresian clay	Silt
Mineralogical content	Kaolinite 40% Illite 25% Montmorill. 20% Montmor-Ill 15%	Smectite 50% Illite 25% Kaolinite 25%	Quartz Smectite Illite Kaolinite
Clay content (%)	45	23	25
Specific Area (m <sup>2</sup> /gr)	39.1	~ 39	~ 1.5
W <sub>L</sub> (%)	67.50	77.50	31.20
W <sub>p</sub> (%)	26.20	25.80	20.70
I <sub>p</sub> (%)	41.30	51.70	10.40
γ <sub>s</sub> (kN/m <sup>3</sup> )	20.14	20.49	20.47
γ <sub>w</sub> (kN/m <sup>3</sup> )	16.32	16.11	16.93
γ <sub>d</sub> (kN/m <sup>3</sup> )	26.40	26.96	26.38
W <sub>w</sub> <sup>mc</sup> (%)	22.20	21.39	17.28
W <sub>w</sub> <sup>mc</sup> (%)	26.78	24.22	19.74
S <sub>r</sub> (%)	100.00	85.63	81.70
n (%)	39.00	40.30	35.20
W <sub>L</sub> : liquid limit W <sub>p</sub> : plastic limit I <sub>p</sub> : plasticity index γ <sub>s</sub> : unit weight of soil γ <sub>d</sub> : unit weight of dry soil			γ <sub>s</sub> : unit weight of solid particles w : water content S <sub>r</sub> : degree of saturation n : porosity

first specimen by thermistors and/or thermocouples. The ultrasonic velocity is measured by two sensors placed on the ends of the other specimen. Contact between the sensors (54 kHz frequency) and the sample is provided by spring. The testing equipment is shown on Figure 1. A personal computer allows a continuous acquisition of data : temperature within the box, temperature of sample, travel time and acoustic signal. This acquisition allows not only the study of travel time but also detailed interpretations of the acoustic signal using Fourier analysis, amplitude and attenuation. Two different tests were carried out on ypresian clay and silt specimens with same results. Figure 2 shows the change of ultrasonic velocity for the three soils. It is observed that the two clay specimens reach the totally frozen state at only -100°C. The silt specimen is not totally frozen at -85°C. An hysteresis phenomenon appears also clearly for the three soils between the freezing and thawing processes. The delay observed for beginning of freezing could be explained by the undercooling phenomenon.

### INTERPRETATION OF RESULTS

Several comments can be made based on comparative analysis of the velocity curves for the silt and the clays.

As shown by Johnson and Plona (1992) for a two phase medium (solid-liquid), the sound velocity increases with the consolidation of the medium. Its minimum value, when the solid is unconsolidated, is given by the Wood-Wyllie formula (1956) using the averaged bulk moduli.

The three samples are slightly consolidated at room temperature as shown by the low values of observed Young modulus, 30, 90 and 150 MPa. These low values are not sufficient to significantly increase velocities from the values given by the Wood-Wyllie formula.

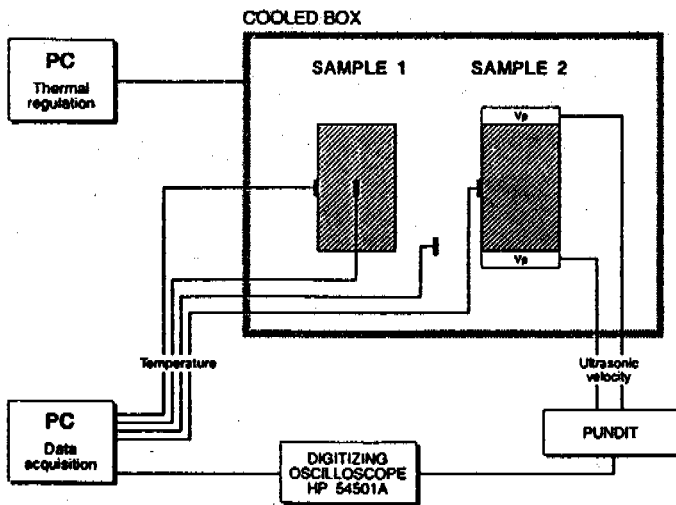


Figure 1 : Testing apparatus at LGC-UCL

**Silt sample :**

Using the Leclaire model (1993), the predicted velocity, for silt where the solid is slightly consolidated and when the water is totally frozen, should be 3495 m/s, while the measured experimental values were higher than 4500 m/s. The consolidation of the solid matrix is then a required condition to explain the discrepancy between the experimental and theoretical results. This fact has already been described, as occurring in Boom clay, by Thimus (1991).

Starting with the experimental velocity at low temperature, numerical simulations done with the Leclaire et al theoretical model (1993) predict that the elastic coefficients of the solid matrix should be  $K_{sm} = 2 \cdot 10^{10}$  Pa and  $G_{sm} = 1.2 \cdot 10^{10}$  Pa. These high values are inconsistent with the low velocity values found in the unfrozen sample. Our interpretation is that the elastic coefficients must change during the freezing process due to the fact that the forming ice tends to occupy a greater volume than water and then exerts a compactness force on the surrounding solid particles. If we use the Kuster and Toksöz model (1974) to evaluate the elastic coefficients of a connected solid matrix with the same porosity of the silt sample, we find that, when using bulk coefficients of fused silica, the elastic coefficients are  $K_{sm} = 2.208 \cdot 10^{10}$  Pa and  $G_{sm} = 1.421 \cdot 10^{10}$  Pa. These values are noticeably near the values expected by Leclaire et al model (1993) using the experimental value as in input. This result strengthens the idea of consolidation, caused by the ice formation, of the solid matrix and then of the medium as a whole.

The knowledge of the degree of consolidation induced by ice for a given temperature is necessary to evaluate the unfrozen water content at a given temperature. In absence of this knowledge provided by a more general model, one may only try to estimate the variation of the solid matrix coefficient with temperature (or in absence of a thermodynamical state equation, with the unfrozen water content).

Using a power variation law for the description of dependence of the elastic constants of solid matrix with the unfrozen water content, expression  $K_{sm}$  is determined as :

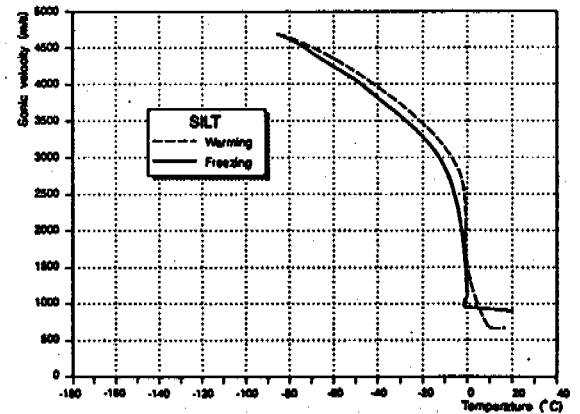
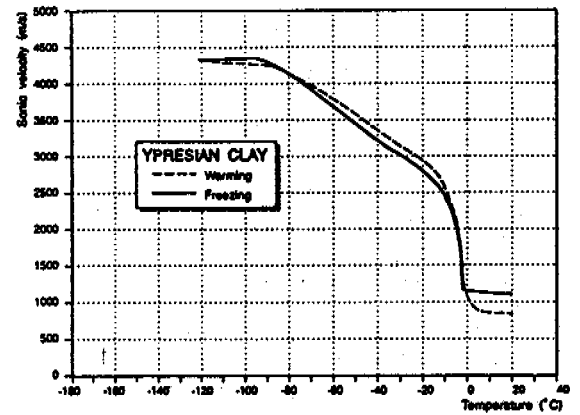
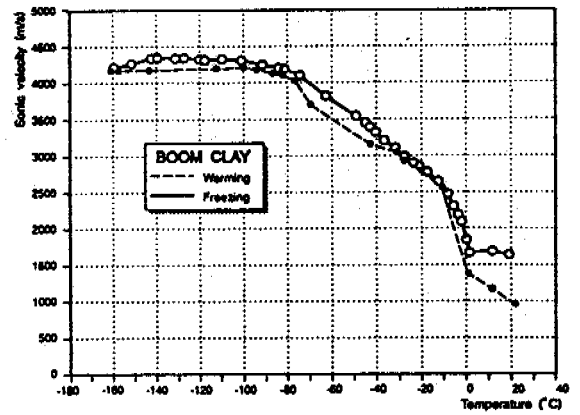


Figure 2 : Ultrasonic velocity versus temperature

$$K_{sm} = K_{smT} (1 - x)^r \text{, using } x = \phi_w/n$$

where

$K_{smT}$  is the bulk modulus of the solid matrix induced by ice for the totally frozen case,  
 $\phi_w$  is the unfrozen water volume proportion,  
 $r$  is a constant, and  
 $n$  is the porosity.

The simplest possible value for  $r$  is 1 for a linear dependency but no strong physical argument favours it. It is interesting to describe the



consolidation of the solid matrix, as a percolation effect : the formation of ice induces expansion forces which establish contacts between solid particles which strengthen the matrix. The critical exponent  $r = 3.8$  has been proposed (De Gennes, 1976) to describe the variation of the coefficients of elasticity in a power law of the number of contact points above a certain number threshold  $p_0$ . This law takes the form  $\Delta K_{em} \approx (p - p_0)^r$ . We arbitrary assume here that the number of contact points above threshold is proportional to the ice volume fraction which leads to the law  $K_{em} = K_{emT} (1-x)^r$  with  $r = 3.8$ . Using this law, the longitudinal wave velocity calculated with the model of Leclaire (1993) is plotted in figure 3.

**Clay samples :**

As with the silt sample, the measured velocities are higher than the predicted velocities when all water is frozen and the matrix is slightly consolidated. The Kuster and Toksöz model allows the evaluation of the elastic constants of a porous connected matrix using porosity  $n$  given in Table 1. Assuming coefficient  $r = 3.8$ , the numerical simulation, made with the model of Leclaire (1993), of the longitudinal wave velocity can be determined as a function of the unfrozen volume ratio (Figure 3).

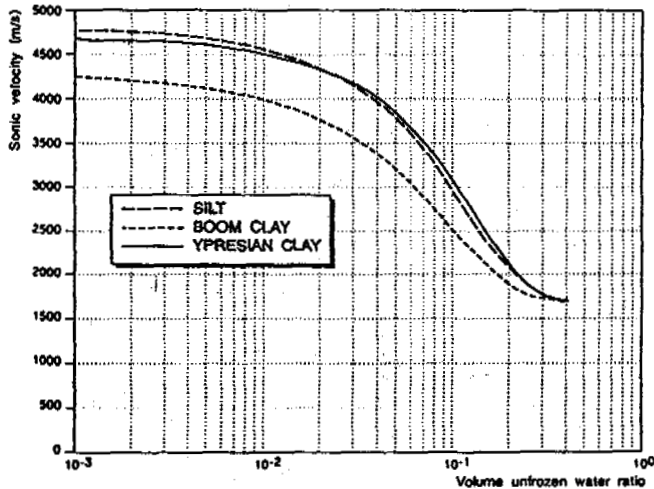


Figure 3 : Numerical simulation of sonic velocity

**COMPARISON OF PREDICTED AND EXPERIMENTAL VELOCITIES**

The predicted velocity for temperatures above 0°C (totally unfrozen water) (figure 3) is greater than the experimental value for the samples of silt and ypresian clay (figure 2). This difference can be explained by the presence of air which has the effect of drastically reducing the velocity in the sample. On the other hand, a good correlation was observed for the Boom clay specimen which was completely saturated.

For temperatures below 0°C (totally frozen water), the predicted values are in relative agreement with the experimental values.

**COMPARISON OF PREDICTED UNFROZEN WATER CONTENTS**

An exploitation of the figures 1 and 2 conducts to the relationship between the volume unfrozen

water ratio and the temperature, and using the relation between the water content  $w$ , the porosity  $n$  and the degree of saturation  $S_r$ , figure 4 represents the unfrozen water content (instead of volume unfrozen water ratio) vs temperature. This figure shows that the water content behaviour of Boom clay and ypresian clay is very similar : the two clay samples are totally frozen only at -100 °C and Boom clay seems to freeze more slowly than ypresian clay; silt sample freezes more quickly than the two clays but, at -80 °C, the sample is not yet totally frozen; these observations appear consistent with the fine-grained characteristics of two clays and silt samples.

It seems very important to compare the predicted values with those obtained by thermodynamical Gilpin's law (Gilpin, 1980), by law based on liquid limit determination (Tice, 1976) or by semi-empirical approach based on velocity values for totally frozen and unfrozen water states (Thimus, 1991).

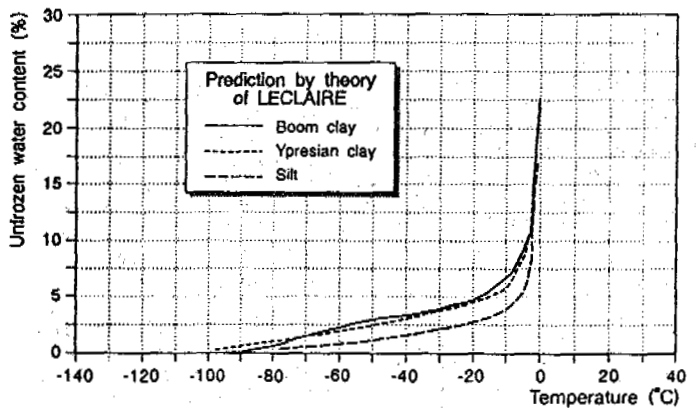


Figure 4 : Predicted unfrozen water content

Figure 5 shows the comparison of results. The following observations have been made :

**Boom clay :**

- the predicted values by Tice, Anderson, and Banin, and by Gilpin do not allow for a totally frozen state of soil;
- the probable reason is the nature of the laws (power law) and the high value of liquid limit;
- the predicted values based on velocity measures are in better agreement except for temperatures between -5 and -50 °C.

**Ypresian clay :**

- the same comments as for Boom clay can be made regarding the laws by Tice, Anderson, and Banin and by Gilpin;
- the predicted values based on velocity measures are very similar.

**Silt :**

- because of the very low value of specific surface area, the law proposed by Gilpin does not give reliable values of unfrozen water content;
- the predicted values by Tice, Anderson and Banin seem reasonable, probably because of low values of liquid limit;
- the predicted values based on velocity measurements are very similar and very close to prediction of Tice, Anderson and Banin.

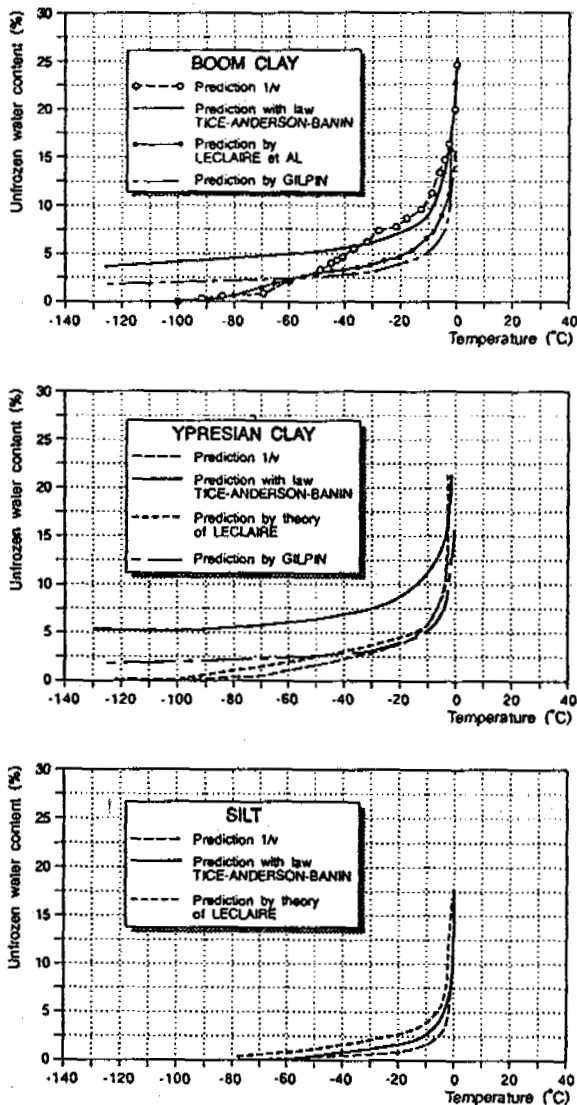


Figure 5 : Comparison of predicted unfrozen water content

#### COMPARISON OF PREDICTED AND EXPERIMENTAL UNFROZEN WATER CONTENTS

The comparison of predicted and experimental unfrozen water contents can be made only for Boom clay. Ouvry (1986) has determined for this clay the relationship between the unfrozen water content and temperature using the calorimetry method (DSC) and nuclear magnetic resonance method (NMR), although only to  $-45^{\circ}\text{C}$ . Quinn (1991) have determined this relationship for the Boom clay using NMR method to  $-100^{\circ}\text{C}$ . Figure 6 shows the experimental unfrozen water content versus temperature given by these authors. The predicted values using semi-empirical approach Thimus (1991) and theoretical law by Leclaire (1991) are also indicated.

One can observe the great differences between the results of experimental measurements :  
 -the results of Ouvry (1986) confirm the prediction by semi-empirical approach but are limited to the temperature range between  $-20$  and  $-45^{\circ}\text{C}$ , depending on the technique used;

-the results of Quinn (1991) show a slower freezing of clay. The only agreement with the predicted unfrozen water content is observed for the temperature of totally frozen state at  $-100^{\circ}\text{C}$ . Nevertheless due to the difference with all other results, these results must be taken with qualification.

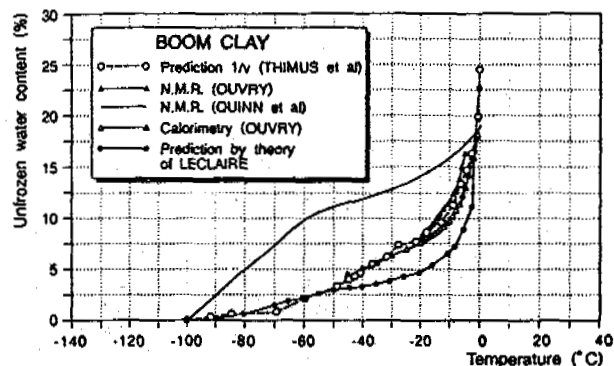


Figure 6 : Comparison of predicted and experimental unfrozen water content

#### CONCLUSIONS

The theoretical approach proposed by Leclaire (1991, 1993) confirms the prediction in  $1/v$  given by semi-empirical approach proposed by Thimus (1991). The results appear in relative agreement for the three studied soils.

The prediction based on thermodynamical Gilpin's law or on the liquid limit determination seems in agreement only for particular conditions concerning the specific surface area, the granulometry, and the liquid limit. These limitations restrict the use of these techniques for particular types of soils.

The performed tests indicate the importance of ultrasonic velocity measurements survey to determine the changes of unfrozen water content of a soil during the freezing process.

In the future, the authors will continue to study and to develop the theoretical law presented by Leclaire et al and will test to explain and to solve the discrepancy observed between the theoretical results and measurements (NMR) for fine grained soils.

#### REFERENCES

- De Gennes P.G., (1976), On a relation between percolation theory and the elasticity of gels, *J. Physique Lett.*, pp. L1-L2.
- Deschâtres M.H., Cohen-Ténoudji F., Aguirre-Puente J. and Thimus J.F., (1989), Ultrasonic propagation through frozen porous media. Liquid phase content determination, *Ultrasonic Int. Conf. Proc.*, Madrid, pp. 158-163.
- Gilpin R.R., (1980), Wire regulation at low temperatures, *Journal of Colloid and Interface Science*, Vol 77, n° 2, pp 435-448.
- Johnson D.L. and Plona T.J., (1982), Acoustic slow waves and the consolidation transition, *J. Acoust. Soc. Am.*, 72 (2), pp. 556-565.
- Kuster G.T. and Toksöz M.N., (1974), Velocity and attenuation of seismic waves in two phase media, Part I and II, *Geophysics*, Vol 39, pp 587-618.

- Leclaire Ph., Cohen-Tenoudji Fr., Aguirre-Puente J., (1991), Etude de la propagation acoustique dans les milieux poreux soumis au gel. Modélisation et expérience, XVIIIth International Congress of Refrigeration, Montreal, Canada, Vol II, pp 814-819.
- Leclaire Ph., Cohen-Ténoudji F., Aguirre-Puente J., (1993), Model of elastic wave propagation in frozen media. Comparison with experiment, Vith International Conference on Permafrost, Beijing, China.
- Ouvry J.Fr., (1986), Etude physique et rhéologique des argiles congelées - Application à l'argile de Boom, Document BRGM, Vol 103, pp 1-207.
- Quinn F.X., Weldon V.L., McBrierty V.J., Kruijssen A.A., and Unsworth J.F., (1991), Cryogenic properties of soils and rocks - 1. Anomalous behaviour of water, Géotechnique 41, N° 2, pp 195-209.
- Thimus J.F., Aguirre-Puente J. and Cohen-Ténoudji F., (1991), Determination of unfrozen water content of an overconsolidated clay down to -160°C by sonic approaches. Comparison with classical methods, Proc. Vith Int. Symp. on Ground Freezing, Beijing, China, pp. 83-88.
- Tice A.R., Anderson D.M., Banin A., (1976), The prediction of water contents in frozen soils from liquid limit determinations, CRREL Report 82-15, pp 1-9.
- Timur A., (1968), Velocity of compressional waves in porous media at permafrost temperatures, Geophysics, Vol. 33, n° 4, pp. 584-595.
- Wyllie M.R., Gregory A.E., Gardner L.W., (1956), Elastic wave velocity in heterogeneous and porous media, Geophysics, Vol. 21, n° 1, pp. 41-70.

## ICE WEDGES IN NORTHEASTERN CHINA

Tong Boliang

Lanzhou Institute of Glaciology and Geocryology,  
Chinese Academy of Sciences, China

A group of well-preserved inactive ice wedges were first discovered in the I-level terrace of the Yilijiqi River in Wuma area (52°45'N, 120°45'E), in the northwestern part of Mt. Daxinganling of China. The ice wedges were being formed during the late glacial period of the late Pleistocene, and stopped developing in the end of late Pleistocene epoch. From the ice wedges, we can derive that the mean annual air temperature in this area at that time was at least 4.6-7.6°C lower than today; and it was no more than 0.6-1.4°C during the hypsithermal interval of the Holocene, while the mean annual ground temperature was approximately 0-1.9°C, indicating a periglacial environment within the period.

### INTRODUCTION

The Chinese scholars of the Quaternary Earth Sciences had only found sand wedges and soil wedges in the territory of China before the mid-1980s, and reported them as a sign of ice wedges. However actual ice wedges were not found until 1987, when they were discovered by Jia Minchao and Cheng Guodong in the I-level terrace on the right bank of Yitulihe River in Daxinganling prefecture of China. They were 1-1.32 m wide at the top and 0.9-1.5 m deep, and distributed in wetlands with a humus silt mud covering. The <sup>14</sup>C datings yielded that they were products of the Neoglaciation following the hypsithermal interval of the Holocene (Peng Haiyun and Cheng Guodong, 1990). This strongly demonstrates that the permafrost in Daxinganling prefecture experienced a developed stage during the Neoglaciation.

It is generally assumed that permafrost with a thickness of 60-100 m is not only formed within the approximate 3000 years of the Holocene. Unfortunately, we couldn't directly prove the presence of permafrost in the Pleistocene because of the dearth of evidence. Whether the permafrost existed in the late Pleistocene or melted away entirely, or has not survived has been an unsettled problem for a long time.

### CHARACTERISTICS OF THE ICE WEDGE

In the summer of 1990, we discovered seven ice wedges in the I-level terrace of the right bank of Yilijiqi River, a tributary of Wuma River, in Qiqian town, northwestern part of Daxinganling prefecture. The ice wedges vary in width, of which five are from 1 m to 3.3 m, and the maximum could reach 5 m. The visible height of the ice wedges is 2 m and they are 1.6-2 meters beneath the ground surface. The wedge ice is characterized by vertical foliation and is fairly pure, transparent, with rich oval gas

bubbles of 1-2 mm in diameter. Hence it appears to be opalescent on the surface. The adjacent sediments of the ice wedges are ice-rich gravel sand and ice-rich gravel silt soil, and they exhibit an upward bending resulting from lateral squeezing forces (photograph). The ice and silt, ordered in alternate layers, are 3-15 cm and 2-6 cm in thickness respectively, and usually the thickness of ice layer is 4-5 cm, while the silt layer is 2-3 cm. The adjacent sediment between two ice wedges is in a horizontal form. At the top 70 cm of the ice wedges, there are traces of patch melting and refreezing, and 2 or 3 semicircle melting troughs which are usually 15-55 cm deep and 30-57 cm wide at the trough mouth. There is sandy gravel of poor roundness deposited in the troughs. Fig.1 shows the section of sediments at the spot where the ice wedges are covered.

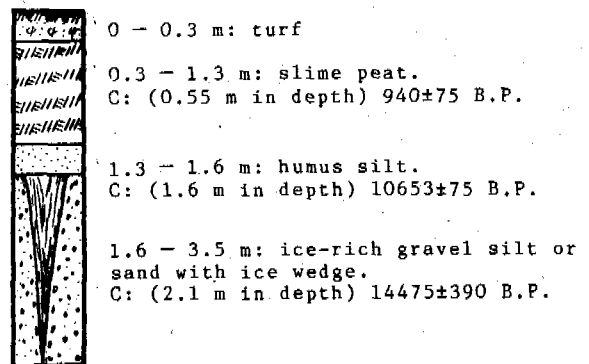
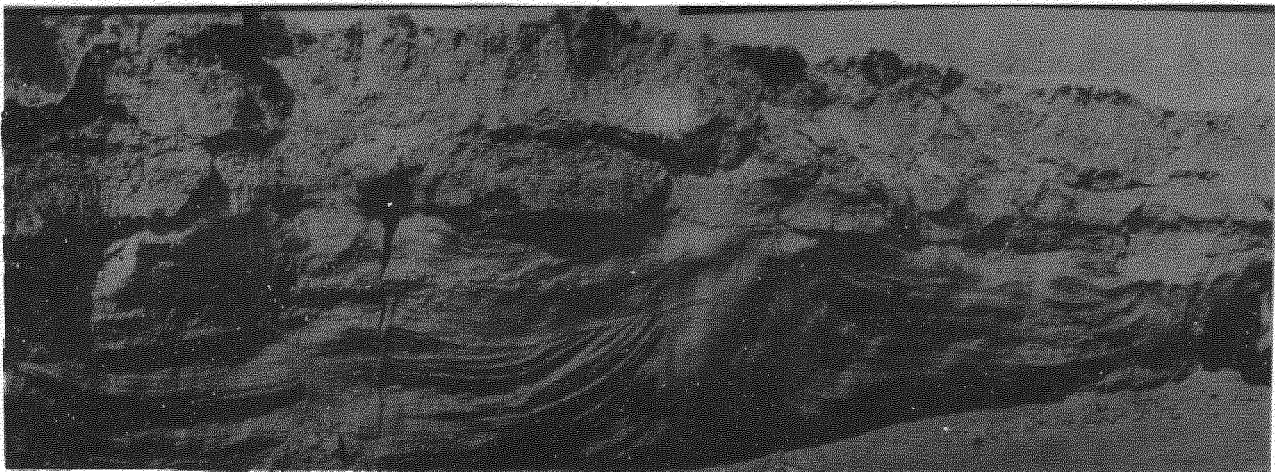


Figure 1. Profile of sediments at the spot of ice wedge covering



Photograph. Ice wedge in Wuma

The sediments are characterized by material of fluvial flat facies. They become coarse-grained at the lower reaches of the river, while rapidly disappear towards the upper reaches due to the rising of the bedrock surface. From the horizontal form of the overburden above the ice wedges, we can see that there were neither grid frost cracks nor a fissure trench on the ground surface, and the wedges were inactive.

#### NATURAL CONDITION AT THE SITE OF THE ICE WEDGES

In the Yilijiqi River basin of Wuma area, the mountain ridge runs from north to east. Its altitude is generally 600-700 m a.s.l. and the minimum is 423 m; the relative height amplitude is 200-300 m. The mountain slope is asymmetrical with a southeast and southwest-facing slope which is steep whereas the northeast and northwest-facing slope is gentle. The Yilijiqi River, 28 km long, flows sinuously from north to south and joins the Wuma River first and then empties into the Erguna River. The river valley is 1500-3000 m wide while the river bed is only 3-8 m wide. The river depth is less than 1 m. The ground surface of the floodplain is flat. There is a widely developed wetland which has shrub vegetation and secondary birch woods.

Controlled under the high air pressure of Siberia and Mongolia in the winter, the area is bitterly cold with a mean monthly air temperature of  $-28.3^{\circ}\text{C}$  in January and is usually clear with little moisture and cold northeast winds. In contrast, it is affected by the monsoon from the Pacific Ocean in summer, it is hot with monthly air temperature of  $16.5^{\circ}\text{C}$  in July. It is an extreme continental climate. The mean annual air temperature is  $-4.4^{\circ}\text{C}$  (1966-1988) and the yearly amplitude of air temperature is  $44.8^{\circ}\text{C}$ . The air temperature is below  $0^{\circ}\text{C}$  from October to April, gaining 3394-centigrade  $\cdot$  day in frozen index, whereas the 170 days of warm season contributes only 1829.3-centigrade  $\cdot$  day in melting index. The annual precipitation is 300-400 mm among which the precipitation in the warm season (May-Sept.) accounts for 86.55%, and that of July and Aug. is 197.22 mm, 55.45% of the whole year. The thickness of snow deposit in winter (Dec.-Feb.) is usually 10-20 cm, equal to 10.78 mm of precipitation and only making up 3.03% of

the yearly total. The snow cover period lasts from the last ten days of October to April or the beginning of May, which is 195 days in average. The bitterly cold winter and short hot summer is favourable for the preservation of ice wedges in this area. In addition, the thin snow cover and the April snowfall which can delay the rising of ground surface temperature also contribute to the preservation of ice wedges.

Wuma area is situated in the lower reaches of the Erguna River. It belongs to a discontinuous permafrost zone. In general, there is no permafrost on the sunward slope. Permafrost is widely distributed on the shady slope only with exception of river talik and tectonic talik. The permafrost is usually 50-80 m in thickness and occasionally up to 100 m. The mean annual ground temperature is  $-1$  to  $-1.5^{\circ}\text{C}$  and the minimum can reach  $-2^{\circ}\text{C}$ . The seasonal thaw depth varies from 0.5-3.7 m in different geomorphologic positions. It is 0.5-0.9 m, the least, in the marshlands at the valley bottom, 0.7-1.2 m on the shady slope; and 1.2-1.7 m in swampy floodplains.

#### TYPES OF ICE WEDGES

There are three types of ice wedges in accordance with the formation: syngenetic, epigenetic and complex. The classification is mainly based on the principle of growth relationship between the ice wedge and its adjacent sediments. The principle is of great significance in age-dating the wedges. Of the seven ice wedges discovered in Wuma, five are more than 1 m in width, and they are 1 m, 1.8 m, 3.3 m, 3.5 m and 5 m, respectively. The height of all ice wedges is over 2 m. The adjacent sediment is gravel silt soil, and it alternates with the segregated ice layers. The silt soil layer is 2-3 cm in thickness, while the ice layer is 4-5 cm. The volume ice content is rather large. This suggests that the sedimental environment at that time was cold and fairly stable. The silt soil deposits frozen from bottom to top. The frozen ground is syngenetic. The ice wedges, considered from their size, have a different order of genesis, i.e. the one with wide top formed earlier than those with a narrow top. This corresponds to the formation law of frost cracks.

From the relationship between the ice wedges

and their adjacent sediments, we can see that all the ice-rich silt soil that touches the side of wedge of over 1 m wide exhibits an upward bending, and only that in the middle position appears to be a horizontal form (photograph). N.N. Romanovskij regards it as one of the marks of a syngenetic ice wedge (1977, p.106). On the top 70 cm of an ice wedge with 1 m width, there are several layers of segregated ice, 4-5 cm thick, connecting the wedge and its adjacent sediment. This indicates that the ice wedge experienced partial thaw truncation at its top during the warm season in the course of formation, and was simultaneous with the formation of the seasonal thaw layer of the adjoining soil. When the seasonal thaw layer freezes from the bottom to the top, the top of ice wedge also freezes simultaneously, producing the same layer of segregated ice. Then due to the climate cooling and aggradation action, the seasonal thaw depth becomes shallow so that the above segregated ice layer could be preserved. This is another mark of a syngenetic ice wedge.

Only one epigenetic ice wedge was discovered in Wuma area. It is located between the two syngenetic wedges and is only 8 cm in width. The adjacent sediment is in a horizontal form. On the top of the wedge, there is a vertical crack filled with 30 cm depth of overburden soil, i.e. humus silt. This shows that it was formed after the formation of syngenetic wedges and at the time of an air temperature drop which was the frigid period of the beginning of the Holocene epoch, 10,000 years ago.

#### PALEOENVIRONMENT INDICATED BY ICE WEDGE

It is worth noting that the syngenetic ice wedges with different width and a different order of formation are products of the same sedimental age.  $^{14}\text{C}$  datings for the adjacent sediment and the top overburden soil have proven that the ice wedges were formed between 14475±340 to 10668±257 years ago, which was the end of late Pleistocene. And they are products of the early period of the Late Glaciation in the upper Pleistocene.

It is a prerequisite for the formation of ice wedge in sandy soil that the mean annual ground temperature should be no higher than  $-5 - -7^{\circ}\text{C}$  (Romanovskij N.N., 1977). This can allow the bottom of the active layer to freeze from bottom to top in the process of sediment accumulation. The mean annual ground temperature in Wuma area at present is  $-1 - -1.5^{\circ}\text{C}$  and the minimum does not go below  $-2^{\circ}\text{C}$ . Obviously, it does not fit the condition of ice wedge formation, but it could reflect that the mean annual ground temperature at the time of ice wedge-forming was 4-5.5 $^{\circ}\text{C}$  lower than today. To consider the difference between ground temperature and air temperature at the same geomorphologic unit in Daxinganling prefecture (Table 1), we know that the air temperature then could not be higher than  $-9 - -12^{\circ}\text{C}$  and was at least 4.6-7.6 $^{\circ}\text{C}$  lower than that at present. This is equivalent to the present physical condition of the areas of Northern Yakuchika city ( $-10^{\circ}\text{C}$  in the mean annual air temperature) in Russia.

The ground surface soil layer must have a gradient of 100 $^{\circ}\text{C}/\text{m}$  in the course of frost cracking (Romanovskij N.N., 1977). We can thus estimate that the climate then was dry with little precipitation, and particularly the snow deposits in winter were less and the vegetation

Table 1. Difference between the mean annual ground temperature and the air temperature in Daxinganling prefecture

Site	North latitude	Ground temp. ( $^{\circ}\text{C}$ )	Air temp. ( $^{\circ}\text{C}$ )	Difference ( $^{\circ}\text{C}$ )
Gulian	53 $^{\circ}$ 03'	-0.5 - -1	-4.8	3.8-4.3
Mangui	51 $^{\circ}$ 59'	-1.1 - -1.6	-5.4	3.8-4.3
Yitulihe	50 $^{\circ}$ 32'	-1.2	-5	3.8

on ground surface was sparse. This was caused by the high air pressure of Siberia and Mongolia at that time, of which the controlling time was longer, and the effect larger, and the continental climate was more extreme. The data from Wang Manhua (1990) also indicates that the amplitude of the mean annual air temperature drop from present to the pleniglacial period (20000-11000 years B.P.) increases in the North-east Plain from south to north. It is 5.4 $^{\circ}\text{C}$  in Liaohe Plain, 6.9 $^{\circ}\text{C}$  in Shunnan Plain and up to 7.6 $^{\circ}\text{C}$  in Shanjiang Plain. Generally, the amplitude of the air temperature drop increases 0.7 $^{\circ}\text{C}$  per latitude toward north. Computed by this, it will reach 11.7 $^{\circ}\text{C}$  to Wuma area, and it approximates to our previous inference.

Based on the pollen analysis data at Huanggangliang in the southern part of Daxinganling prefecture (Xie Youwu, 1984), we can obtain that the herb pollen content was as high as 90% among which the content of Artemisia and Chenopodium genera increased to 50-70%, while woody plants were less than before, among which the pollen of conifer amounted to 2-3%. The content of calcium sulphate was as high as 3.15%, indicating a fairly weak Lixiviation at that time. The content of soluble salt in soil accounted for 0.04-0.38% and the pocked quartz made up 10-40%. This indicates that the whole Daxinganling prefecture at that time was in a dry and cold climatic condition. The wind power was strong and thus favourable for the ground surface to crack and the temperature to drop quickly, and subsequently also favourable for the growth of ice wedges. It was the dry and cold climate condition that made the southern boundary of the permafrost move south to 38-42 $^{\circ}\text{N}$  (Xu Shuying et al., 1989). This was more southerly than that of Europe (43-44 $^{\circ}\text{N}$ ) and Siberia (47-50 $^{\circ}\text{N}$ ).

In the end of late Pleistocene, the climate in East China became warm, hot and humid, or warm and arid after entering into the Holocene epoch. However, there occurred an obvious low temperature period 9,000 years ago (Yang Huaijen and Xie Zhiren, 1985). The epigenetic ice wedge found in Wuma might not be formed later than this period. After then along with the gentle rising of the whole area and the undercutting action of the Yilijiqi River, the terrace surface emerged up to 5-6 m above the water level, which halted the development of the wedges in a relatively high ground temperature condition. In the Hypsithermal interval, there developed widespread peat from south to north in northeastern China (Li Handing and Gao Fengqi, 1991). In Wuma area, peat, one metre in depth, was deposited at the valley bottom. Under such a background of high air temperature, the seasonal thaw depth in Wuma area increased, and resulted in patches of deformation on the top of

ice wedges. Consequently some varying degrees of semicircle thermal melting troughs of 15-55 cm deep were formed and served as the seasonal drainage channel on the ground surface during the warm season at that time. There accumulated sandy gravel of poor roundness in these troughs. From these thermal melting troughs and accumulated gravels, we can see that at that time the thaw depth was not deep, ground temperature not high, water amount limited, flowing speed quick but passing time short. Therefore, it had not much effect on the melting of the ice wedges. All of this reveals that the weather in Wuma area was relatively warm but with limited rise in temperature during the Hypsithermal. Wang Manhua proposed that the air temperature in Shanjiang plain of Northeastern China during the Hypsithermal was 3-5°C higher than today. Hence the air temperature in Wuma area at that time couldn't be higher than 0.6-1.4°C. The whole area was still under the periglacial environment. The swampy ground surface, developed peat and thicket mosses halted greatly the rise of ground temperature caused by climate warming. Based on the data of the adjacent outer Bakar (Geocryology USSR, 1989), mosses could make the mean annual ground temperature decrease more than 2-3°C. In addition, peat could contribute 2.5-4°C drop of ground temperature. As a result, a decrease of 4.5-7°C in ground temperature was caused by both of the above factors. Therefore the mean annual ground temperature in Wuma area at that time couldn't be higher than 0-1.9°C. This provided a perfect natural condition for ice wedge to pass through the Hypsithermal interval of the Holocene. Further more, the latent heat fusion of ice in ice-rich silt soil and ice wedge itself was also a favourable factor for wedge preservation.

In another case, there were a large amount of debris in the deposits of the Hypsithermal in Amur region on the eastern slope of Mt. Daxinganling. It reflects that although the air temperature rose to some degree at that time, it was still under a periglacial environment. The permafrost zone retreated northwards to Mangui-Amur line (Guo Dongxin et al., 1981). Wuma was still within the permafrost region.

The air temperature in 68° of northern latitude, west Siberia, north of Wuma, was 2.8-4°C higher than today. The southern limit of permafrost retreated northwards by 16-19° lat. to the vicinity of 66°N. In the area of 62-64°N, the upper table of permafrost descended to 100-150 m below the ground surface (Baulin V.V. et al., 1981). There was widely developed subcommittee ice wedges, lowlying land and plate-shape low-lying land. The southern limit of permafrost in China only retreated northwards by 10-12° lat. It seems that the permafrost in China has a relatively stronger stability.

Cold periods occurred in 8200-7000, 5800-4800 and about 4000 years ago in the Holocene (Yang Huaijen et al., 1985). Ice wedges of 1.5 m and 0.9 m deep (4518±90 B.P. — 3644±90 B.P.) were formed in the bottom of Yiliji River Valley of Daxinganling prefecture (Peng Haiyun and Cheng Guodong, 1990). Periglacial phenomena formed during these periods have been found in regions of both the south and north bank of the Heilongjiang River Basin. It was severely dry about 3000 years ago and Zhu Kezhen called it the coldest period in the 10th century B.C. In 960-1276 and 1650-1700 A.D. the climate tended to be colder. Consequently the permafrost in China gained another period of development and

moved southwards by 5-6° latitudes, establishing the present pattern of permafrost distribution in northeastern China. In places with suitable conditions, e.g. the bottom of Yitulihe River valley, there grew ice wedges of 40 cm in width, whereas there was no such occurrence in Wuma area because of the ascending bedrock surface and the Quaternary overburden layer being thin (5-8 m). Nevertheless, both the permafrost and the ice wedges formed in the late Pleistocene have been preserved to the present due to such favourable factors as the periglacial environment, ground surface swamp, vegetation of mosses as well as little snow in winters, etc.

## CONCLUSION

1. The permafrost and ice wedge in Wuma area, northern part of Mt. Daxinganling, northeastern China was formed at least 14,000-10,000 years ago, i.e. the late glacial period of the end of upper pleistocene, and are inactive at present. They experienced patches of thaw truncation during the Hypsithermal of the Holocene but favored by the periglacial environment, they were able to be preserved to the present time.

2. The syngenetic ice wedge is the major type in Wuma area, while the epigenetic one is rather rare and its size is smaller than the former one. They are distributed commonly in the I-level terrace at valley bottom which is characterized by wetlands with thicket mosses. The lithological property in ice-rich frozen ground is mainly characterized by silt and clay soil.

3. The mean annual air temperature in the northern part of Daxinganling prefecture in the end of late Pleistocene was 4.6-7.6°C lower than today and the climate was dry and cold. This can be illustrated by the presence of ice wedge and permafrost at that time, and by the dynamic shifting of the southern boundary of permafrost during the late Pleistocene to the Holocene. Compared with the North Europe and Siberia, the permafrost in northeastern China has relatively stronger stability since the Hypsithermal interval of the Holocene.

## ACKNOWLEDGEMENTS

I would like to thank Mr. Wang Yinxue, Ding Linlong and Ms. Liu Jinren for their assistance in the field work.

## REFERENCES

- Baulin, V.V., Chekhovskiy, A.L., Sukhodolskiy, S.E., (1981) Main stage of permafrost development in the European North-East and Western Siberia. History of Development of Permafrost of the Eurasia on the Example of Separate Regions, "Nauka" Moscow, 41-59.
- Geocryology USSR. Eastern Siberia and Far East, 398-411.
- Guo Dongxin and Li Zuofu, (1981) Preliminary approach to the history and age of permafrost in northeast China. Journal of Glaciology and Geocryology, Vol.3, No.4, 1-16.
- Jia Mingchao, Yuan Fu and Cheng Guodong, (1987) First discovery of ice wedges in northeast China. Journal of Glaciology and Geocryology, Vol.9, No.3, 257-260.
- Li Handing and Gao Fengqi, (1991) Peat development and peatification periods since the late stage of late Pleistocene in east China. Correction of Onshore and Offshore Quaternary in China, 217-221.

- Peng Haiyun and Cheng Guodong, (1990) The ice wedge in daxinganling prefecture, Northeast China and their paleoclimatic significance. Proceedings of Fourth National Conference on Glaciology and Geocryology (Selection, Geocryology) 9-16.
- Romanovskij, N.N. (1977) Formation of polygon-wedge structures. Novosibirsk, Nauka 215pp.
- Wang Manhua, (1990) Preliminary study on paleovegetation and paleoclimatic index in the period of the late Pleistocene in the Northeast Plain of China. Formation and Evolution of Natural Environment of Quaternary in Northeast Plain of China, Harbin Map, Publishing House, 51-59.
- Xie Youyu, (1984) Periglacial sedimentary environment of Huanggangliang region, the Main peak of Daxinganling in the late Pleistocene. Journal of Glaciology and Geocryology, Vol.6, No.4, 69-74.
- Xu Shuying and Xu Defu et al., (1989) The boundary of permafrost region in east China during last Glacial Epoch. Proceedings of the Third Chinese Conference on Permafrost (selection), 105-113.
- Yang Huai-jen and Xie Zhiren, (1985) Sea-level changes and climatic fluctuations over the last 20000 years in China. Proceedings of Quaternary Glaciation and Geology, Vol.2, 1-18.



## SHALLOW FOUNDATION IN THE REGION OF FROZEN GROUND

Tong Changjiang<sup>1</sup> and Luo Mingru<sup>2</sup>

<sup>1</sup>Lanzhou Institute of Glaciology and Geocryology,  
Chinese Academy of Science, China

<sup>2</sup>Prospecting Academia of Management Bureau of  
Da Hinggan Ling, Forestry Ministry, China

Shallow foundation, which its bottom is buried within maximum depth of seasonally freezing, was successfully used in deep seasonally frozen ground region in 1982. By being improved in 1989, the experiments were taken in permafrost region and talik of Da Hinggan Ling, its results showed that foundation embedded depth of building could be reasonably determined according to property of frost heave and thaw settlement, state of ground water, tangential and normal frost heaving force, building load and restraining action of load on frost heave of subsoil. Moving condition of building in permafrost and deep seasonally frozen ground region show that foundation of building can be shallowly buried and meet and demand of building stability.

### INTRODUCTION

Foundation type of building and its embedded depth are continuously taken attention to engineering circle in permafrost and sporadic permafrost region of Da Hinggan Ling and deep seasonally frozen ground of Hei Long Jiang and Nei Meng Gu. The experiments which foundation of buildings shallowly buried have even been taken since fifty years. But for knowledge on theory of frost heave being not enough, some buildings are successful, some produce destroy of different extent for freezing and thaw action. So some rules provide that foundation bottom must be put in 10-20 cm place under maximum depth of freezing. Deep pile foundation is used in permafrost zone. In early stage of 70 ages, advancing embedded depth of foundation can be within seasonally freezing depth after constructed, but residual frozen ground layer under foundation is not permitted to be preserved during constructing. From later stage of 70 ages to early stage of 80 ages, many institutes early or later continued to develop experimental research in this aspect. <<Design standard of subgrade foundation of building in frozen ground region>> is written by seven units, GBJT-89 standards further perfected. Experimental research of shallow foundation show, although engineering geological condition of frozen soil in the location and theory of frost heave are fully mastered, shallow foundation can be locally used in not only deep seasonally frozen ground region but talik of Da Hinggan Ling.

### DESIGN FACTORS OF SHALLOW FOUNDATION

It is extensively distributed to open and close talik of permafrost and talik of sporadic permafrost in Da Hinggan Ling. Maximum depth of seasonally freezing is 2.0-2.5 m. Trivial buildings of many years in these regions testify that foundation can be shallowly buried in freezing

stratum within depth of seasonally freezing, residual freezing stratum is permitted to preserve in bottom of foundation.

Foundation reasonably shallowly buried is determined by following factors:

#### 1. Frost Heave Property of Subsoil

A large number of field data show that the frost heave amount of subsoil increase with freezing depth increasing in freezing process and its increment is not constant value, it change with soil, moisture and freezing condition. Most distributed law of frost heave amount of subsoil alone freezing depth appear larger in upper and small in lower (Tong Changjiang and Guan Fengnian, 1985). See Fig.1. Fig.1 shows that coefficient of frost heave ( $\eta$ ) of lower soil in freezing depth is all smaller. If calculation by  $\eta=2\%$ , its distributed depth make up nearly 20-30 per cent of total freezing depth. Frost heave property of this subsoil cannot obviously affect enough stability of building.

#### 2. Restrained Action of Building Load on Frost Heave of Subsoil

Experimental results show that upper loads have obviously restrained action on frost heave of subsoil (Fig.2). Frost heave of subsoil decrease with surcharge load increasing, ( $M_p$ ) is used to indicate their relation.

$$M_p = 1 - \frac{(\Delta h_0 - \Delta h_p)}{\Delta h_0} \quad (1)$$

Where  $\Delta h_0$  - frost heave amount of the same layer nature subsoil under the action of dead weight.

$\Delta h_p$  - frost heave amount of the same subsoil under the action of surcharge load.

According to the relationship between restraining coefficient ( $M_p$ ) under action of different load and the thickness of freezing ground under

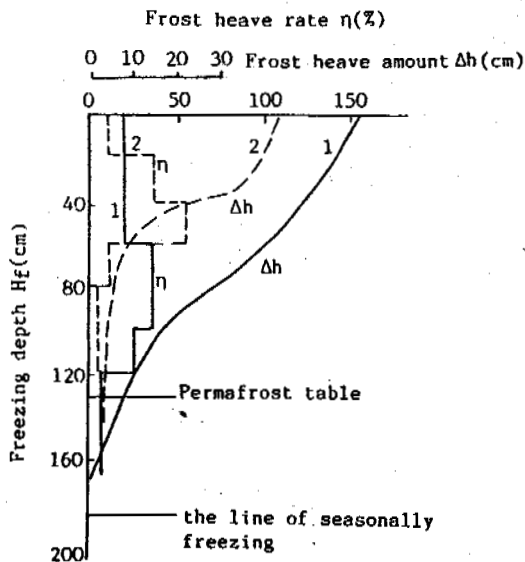


Figure 1. Distribution of frost heave rate and frost heave amount vs freezing depth

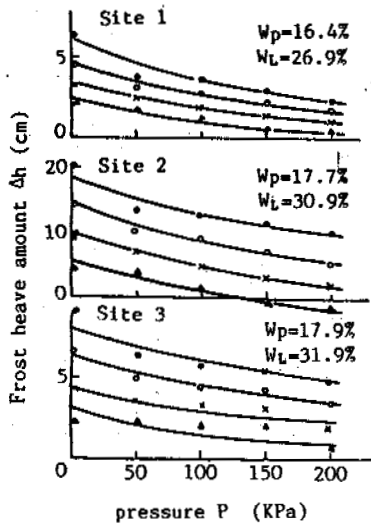


Figure 2. Frost heave amount vs applied load for various buried depths  
 o — 40 cm; o — 70 cm;  
 x — 100 cm; Δ — 130 cm.

foundation ( $\delta f$ ), design value\* of restraining coefficient different subsoil of frost heave can be given to provide design and using of shallow foundation. Restraining action of surcharge load can obviously decrease destructive action of frost heave of subsoil on building.

### 3. Effect of Heating System on Freezing Depth

Reasonably installing heating system can decrease refreezing depth of subsoil and destroy action of frost heave in heating building. Effect coefficient of heating is relative with refilling height of indoor, its value can refer

\*Lanzhou Institute of Glaciology and Geocryology, Academia Sinica and Daqing Institute of design and Construction of Oil Field, 1985, <<Information manual of frozen soil subgrade of industrial and civil building design in Daqing region.>>.

to standard GBJT-89. In general, indoor surface is 75 cm high than outdoor surface, the influence action of heating system cannot be considered. Thus, standard maximum depth of freezing given according to rule\*\* should multiply affect coefficient of heating ( $\phi_{zh}$ ), soil ( $\phi_{zs}$ ), frost heave of subsoil ( $\phi_{zw}$ ) and environment ( $\phi_{zc}$ ) which the rule give to gain design depth of freezing ( $H_f$ ).

According to the statistics of building structure and using condition, permitting deformation value of brick-wood building or brick-concrete building can be controlled at 10 mm (Jiang Hongju & Cheng Enyuan, 1989). So, frost heave deformation produce for refreezing of residual frozen soil in second years must meet the demand of following equation:

$$d \cdot \eta \cdot M_p \leq [\Delta h] \quad (2)$$

Where,  $d$  — thickness of residual frozen ground.  
 $\eta$  — average heave coefficient of upper subsoil within maximum freezing depth (decimal calculating).

$M_p$  — restraining coefficient of surcharge load on frost heave of subsoil (decimal calculation).

$[\Delta h]$  — permitting non-uniform deformation value of building (cm or mm).

So permitting thickness of residual frozen ground under foundation is:

$$d \leq \frac{[\Delta h]}{\eta \cdot M_p} \quad (3)$$

Embedded depth of foundation is:

$$[H] = H_f - d \quad (4)$$

In order to preventing refreezing of residual frozen ground and frost heaving force produced by subsoil freezing beside foundation from affecting stability of building, checking computation of resisting frost heaving force must be taken. In other words, foundation of building must meet the demand of stability under the action of tangential and normal frost heaving force. Design value of tangential frost heaving force can refer to reference of Dai Huiming and Tie deting (1989), standard value of normal frost heaving force can refer to reference of Tong Changjiang and Cheng Enyuan (1989). These values are taken successive revision of foundation bottom area, permitting deformation and freezing depth by their demand to be designed value.

If it cannot meet the demand. First, 20 centimeters thick gravel soil are filled in foundation side to weaken action of tangential frost heaving force; second, residual thickness of frozen soil can be reasonably decreased.

Because the present constructed stage is all advanced to spring, residual frozen ground gradually thaw in constructed stage, thawing coefficient is determined by soil, dry unit weight and water content of residual frozen ground to calculate its subsidence amount (Tong Changjiang and et al, 1987; Zhu Yuanlin, 1983).

### CONCLUSION

In talik of permafrost and deep seasonally frozen ground region, according to water content,

\*\*Heilongjiang Institute of Construction of Low Temperature, 1991. Design rule of construction of subgrade and foundation.

dry unit weight, frost heave property of subsoil, thaw settlement property of frozen ground, local freezing depth and etc., embedded depth of foundation is locally calculated for all kinds of more uniform subgrad. So that foundation is reasonably shallowly buried and hold stability of building. The rule which foundation bottom must be put under freezing depth is broken through.

According to the mentioned method, practice of experiment in Daqing and Jiagedaqi region and constructing houses are testified, design of shallowly buried foundation is reasonable, reliable and can be used in design before and after construction. Its engineering cost can be nearly decreased 10 per cent.

#### REFERENCES

- Tong Changjiang & Guan Fennian, (1985) Frost heave of soil and prevention of building. Publishing House of Hydroelectricity.
- Tong Changjiang & Yu Chongyun, (1990) Effect of Overcharge Pressure on Frost Heave of Shallow Foundation. J. of Glaciology and Geocryology, Vol.12, No.13, 193-199.
- Jiang Hongju & Cheng Enyuan, (1989) Calculation of the Minimum Buried Depth of Building Foundations in Consideration of the Frost Susceptibility of Subsoil. Proceeding of the Third Chinese Conference on Permafrost, Publishing House of Science, pp.266-271.
- Dai Huiming & Tie Deting et al., (1989) Study on tangential frost heave force on the reinforced concrete bridge pile foundation, Proceeding of the Third Chinese Conference on Permafrost, Publishing House of Science, pp.141-149.
- Tong Changjiang and Yu Chongyun, (1989) Test standard and design value of normal frost heaving force. Proceeding of the Third Chinese Conference on Permafrost, Publishing House of Science, pp.157-160.
- Tong Changjiang and Cheng Enyuan, (1987) Property of thaw compress of seasonally frozen ground. J. of Glaciology and Geocryology, Vol.9(3): 221-228.
- Zhu Yanlin and Zhang Jiayi, et al., (1983) Calculation of thaw compress of frozen ground subgrade. Proceedings of Permafrost Research in Qinghai-Tibet, Publishing House of Science, 134-138.

**INFLUENCE OF MOUNTAIN PERMAFROST ON CONSTRUCTION  
IN THE ZUGSPITZE MOUNTAINS, BAVARIAN ALPS, GERMANY**

Roland Ulrich<sup>1</sup> and Lorenz King<sup>2</sup>

<sup>1</sup> Bauingenieur- und Vermessungswesen, Universität der Bundeswehr D-8000  
MÜNCHEN, Germany

<sup>2</sup> Geographisches Institut, Justus Liebig-Universität,  
D-6300 GIESSEN, Germany

During construction of a cable car station, two entranceways with 8 m penetrations were blasted at 2449 m a.s.l. Approximately 10 cm wide open joints filled with frozen weathered loam and ice were discovered in the limestone. According to the high degree of cleavage and the rooflike structure of the rock profile of the Zugspitze crest, the chosen construction directed the force vector (resulting from the weight of the structure and the force of the tow-line) into the core of the mountain. The stabilizing effect of permafrost was maintained by restricting the temperature influence of the building and the direct solar impact. During construction of a railway tunnel in 1985, an ice-filled sink hole with a diameter of 15 m was penetrated at an altitude of 2560 m. The ice-body was insulated. Effects of atmospheric warming on the permafrost temperature and thickness could also be observed during construction of a new cable-way to the top of the Zugspitze.

**INTRODUCTION**

The widespread occurrence of permafrost in the Alps is well known for countries as Switzerland (BARSCH 1977, HAEBERLI 1985), France (EVIN in KING et al. 1992), Italy (CARTON et al. 1988, BELLONI et al. 1993) and Austria (HAEBERLI & PATZELT 1982), where mountains often reach altitudes of more than 3500 m or even 4500 m a.s.l. In contrast to the mentioned regions (HAEBERLI 1992), the highest mountain in the German Alps, the Zugspitze, reaches less than 3000 m (Figure 1) and studies of active permafrost were little known until recently. This paper describes three construction sites in the Bavarian Alps and shows how the occurrence of permafrost in morphologically exposed high mountain bedrock has to be accommodated with special construction techniques. The discovery of this permafrost occurrence was unexpected for the leading engineers and geologists. Today the existence of permafrost is known for the area and the planning of constructions can be done accordingly thus limiting construction risks as well as financial risks.

**THE CABLE CAR EIBSEE - ZUGSPITZE**

The cable car system has a length of 3353 m, was constructed in 1961 and shows an altitudinal difference of 1949 m between the valley and the mountain station at 2943 m a.s.l. (Figure 2). The foundation of the mountain station is located in a narrow crest formed by two differently inclined rock surfaces consisting of thickly banked and massive Wetterstein limestones (Middle Alpine Trias). This bedrock forms the northern edge of a basin structure dipping in ENE direction (strike of bedding planes: N 60 -70° E, dip: 25 to 35° towards S).

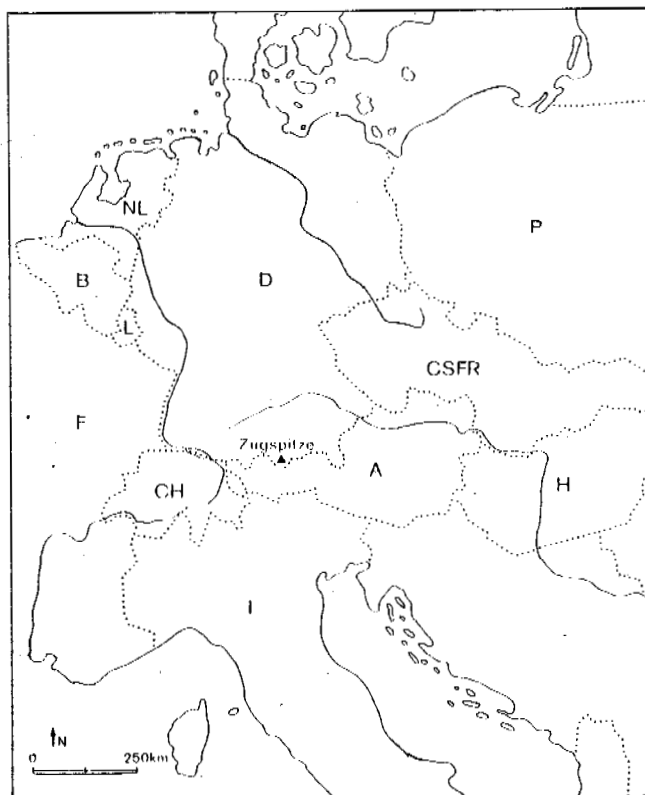


Figure 1. Location of the Zugspitze mountains.

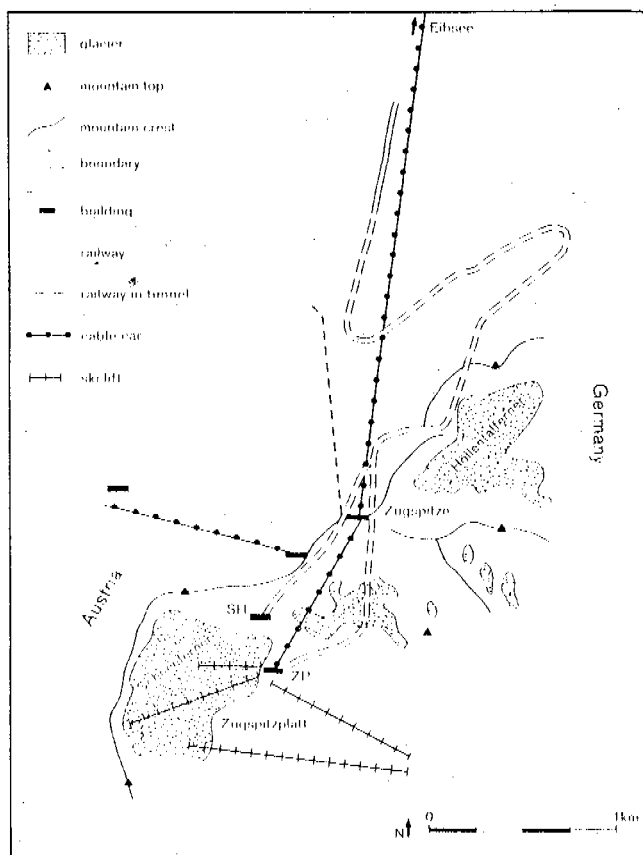


Figure 2. Location of the construction area at the mountain crest forming the border between Austria in the western half and Germany in the eastern half of the figure. Zugspitze, the highest mountain in Germany (2963 m a.s.l.) can be reached with the Eibsee cable car constructed in 1961 or via the new railway tunnel constructed in 1985 and leading to the new ski center Zugspitzplatt (ZP, 2585 m a.s.l.) and the new cable car constructed in 1991-93. The old railway tunnel leads to the Hotel Schneefernerhaus (SH, 2.665 m a.s.l.). The outlines of the glaciers (Schneeferner, Höllentalferner) display the situation in 1961; they are much smaller today.

Strong mechanical stress during orogenic processes produced a broken rock formation, whereby strong disturbances running NNE and crosswise to the crest intensely crushed the bedrock up to the order of decimeters. Knowing well these fundamental characteristics already during the planning stage, the construction design was drawn up according to these unfavourable fractured rock conditions. The loads of a steel-portal frame construction that had to be directed into the bedrock should correspond to the weight of the bedrock broken for the entranceways, so that no additional loads had to be directed into the subsurface.

During the excavation of the 8 m deep and 7 m broad openings for the entranceways a fact was discovered that caused additional problems for the long term static safety of the

construction: Perennially frozen weathered loam and up to 10 cm thick ice lenses filled the NNE-running cleavages at the foundation level: Thus the Zugspitze mountain top had to be regarded as a permafrost area and conventional rock construction techniques couldn't be used, e.g. injections of concrete for consolidation, or the application of prestressed rock anchors (cf. MÜLLER 1963, KEUSEN & HAEBERLI 1983). The functioning of these two methods was unreliable or impossible due to permafrost and ice-filled bedrock joints. The design of the foundation construction was developed in a way that avoids forces directed outwards for all possible cases of loads and all load points. The required load direction at the northerly foundations is enforced by a special support construction with a roller bearing principle similar to that used in bridge constructions. A joint bearing at the southerly foundations thus creates forces at both sides of the roof-like mountain crest that are directed towards the mountain core. These forces press together the mountain crest without e.g. prestressed rock anchors and approximately restore the original load conditions of the mountain crest prior to the construction (cf. Fig. 3). In addition, it was decided that the foundations should furthermore be exposed to the natural atmospheric conditions in order to preserve the stabilizing effect of the permafrost. This could be realized for the northern foundation without further preventive measures, but at the southern foundation exposed to the direct solar radiation it was decided to construct in addition a sun terrace that shaded the critical area thus evading problems by hydrology and thermal erosion (cp. KÖRNER & ULRICH 1965).

#### THE CABLE CAR ZUGSPITZPLATT - ZUGSPITZE MOUNTAIN TOP

With the construction of this new cable car (1991-93) from the Zugspitze mountain top towards south the availability of the ski area at the Zugspitzplatt will be facilitated. An altitudinal difference of 360 m will be surmounted with an oblique length of 1.000 meters. The top station of this new cable car is located beside the Eibsee cable car station to the west in order to allow its level connection. However, the foundation of the building was constructed in the less steeply inclined (35°) southerly slope of the Zugspitze crest in bedrock relatively little dissected by joints.

Already in an early stage, the construction of the new building could be planned according to the now known rock properties and permafrost conditions. A similar design was originally planned at the neighbouring Eibsee top station, placing the rope bollard into the northern slope. However, limited space and architectural circumstances required that the foundation of the building had to be placed entirely on the southern slope of the mountain crest (cf. Figure 4).

During July/August 1991 the excavations for the stressing pit - through which the main load of the building would be directed into the rock subsurface - were done. The exposed layer joints below the rock surface were filled with ice down to a depth of 3 meters. On the other

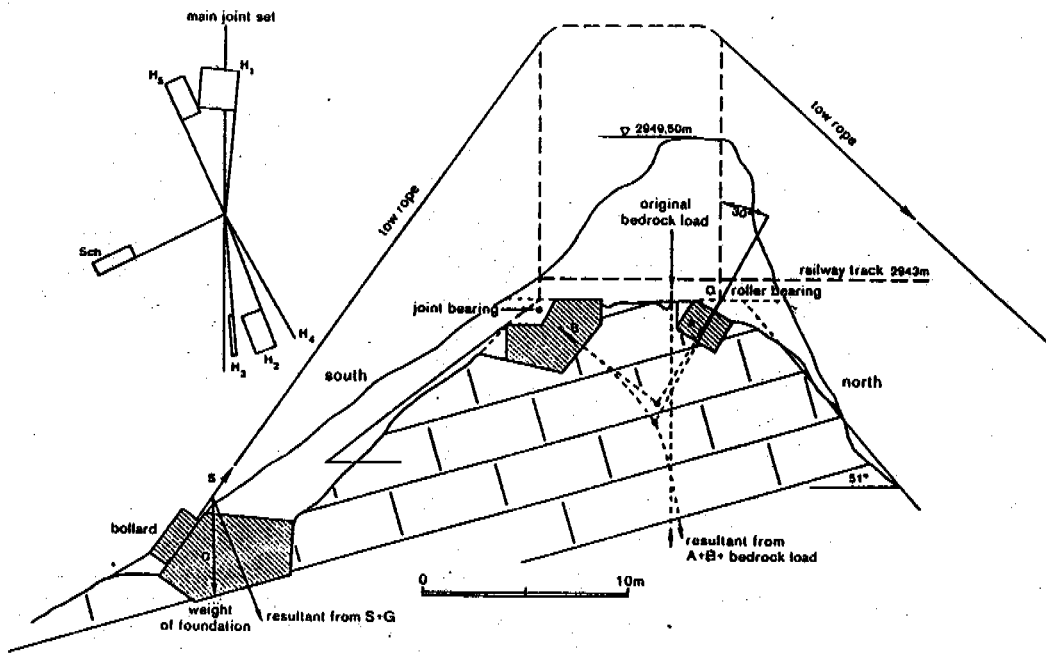


Figure 3. Section across the mountain crest with foundations of the cable car Eibsee - Zugspitze at the mountain top station.

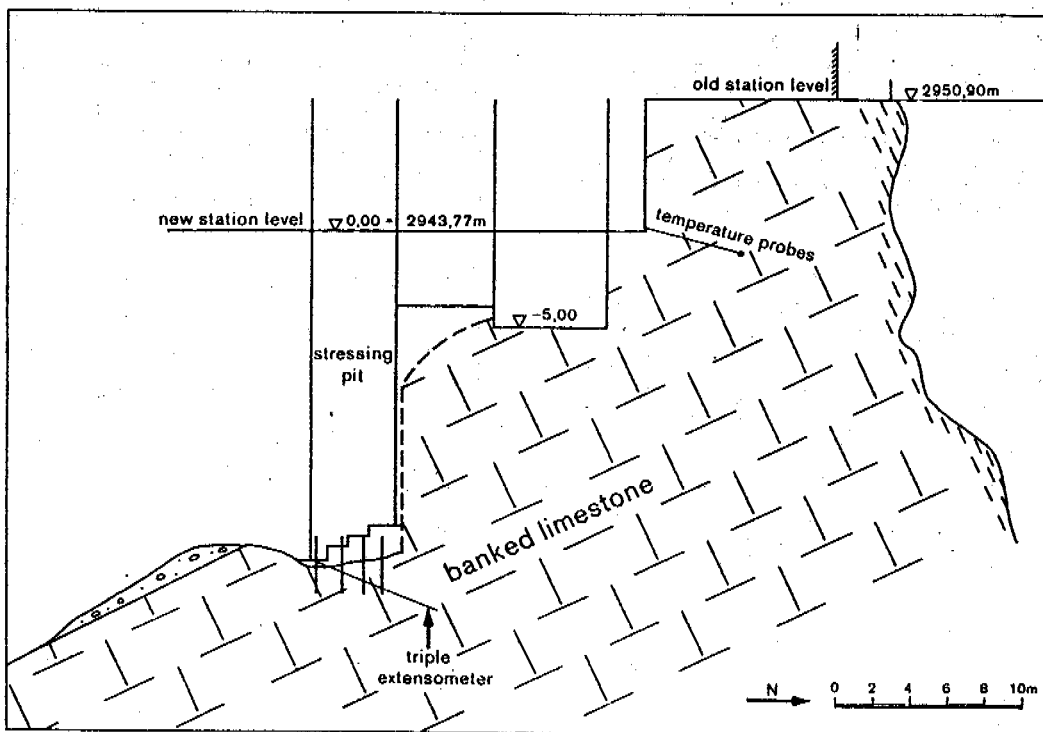


Figure 4. Foundation of the cable car Zugspitzplatt - Zugspitze at the mountain top station with locations of the triple extensometer and the probes for temperature measurements in bedrock.

hand the weathered loam in the little pronounced and NNE-running transverse disturbances was unfrozen. The layer joints had to be regarded as potential sliding planes and the excavations for the stressing pit were therefore deepened down to depths where the occurrence of open, ice-filled joints was highly improbable. In addition an extensive plugging (one three-meter rock bolt per m<sup>2</sup>) between the foundation concrete and the bedrock was applied in order to increase the shear stability. A "triple extensometer" with lengths of 5, 10 and 15 meters for the observation of the bedrock below the stressing pit was also installed, because the stability could not be evaluated clearly and because the construction site was extremely exposed. The installation allows to judge during the construction the increasing influence of the load to the subsurface. According to the new data obtained at the southern slope of the Zugspitze mountain top, the use of rock anchors in the bottom zone of the stressing pit would be possible, because the extensometer drilling didn't hint to the occurrence of deep reaching permafrost. At the end of the year 1992, a drilling directed towards the north wall will be done in order to install thermistors to monitor rock temperatures.

The construction of the new cable car required the demolition of the sun terrace at the mountain top station of the Eibsee funicular. There, it could be observed, that extensive ground ice had formed in the excavation material since its deposition about 30 years ago. The ice formation continued into the open joints of the bedrock. As expected, the (tritium) dating of the ice gave a very young age (after 1965).

Actual formation of permafrost and ground ice at this site is well understandable at this shaded site with little ventilation and evaporation, and may also be expected when considering the air temperatures (Figure 5) measured at the nearby official weather station of the German Weather Service (DWD). The ten

year mean temperatures show a slight increase from -5.25° in the first decade of this century to -4.9° C in the sixties and seventies and to -4.6° C during the last ten years. According to KING (1983, 1986, 1990) and others, this means that permafrost occurrences are probably quite widespread here, and that a considerable permafrost thickness may be expected at least in slopes exposed towards north.

A comparison of the precipitation values between the first 30 years of this century and the period 1961 to 1989 reveals also remarkable results: The precipitation total has significantly increased from 1332 mm per year to 2009 mm per year (Figure 6). During these 90 years the glacier tongue at the Zugspitzplatt has receded continuously and is located today at 2.570 m a.s.l. A detailed climatological analysis shows, that especially winter temperatures have increased in the fifties and seventies, and that quite a considerable amount of precipitation has probably fallen as rain instead of snow, providing an explanation for the continuous negative mass balance and glacier retreat.

THE CONSTRUCTION OF A NEW RAILWAY TUNNEL TO THE ZUGSPITZPLATT

This rack-railway, originally constructed in the year 1930, leads from Garmisch-Patenkirchen (994 m a.s.l.) to the Zugspitze Hotel Schneefernerhaus at 2665 m a.s.l.. An additional railway branch leading to the ski center at the Zugspitzplatt and with a length of 800 m was added in the year 1985. The new tunnel was explored in an area with little roof cover by 5 boreholes. It was discovered then, that below up to 15 m morainic material there is primarily solid limestone bedrock. On the other hand it was known that karst features occur in the basin-like "Zugspitzplatt" (e.g. sink holes and ponors), which were sometimes filled with ice. It was however by pure hazard that the tunneling after only about 100 meters entered an area with massive ice over its whole

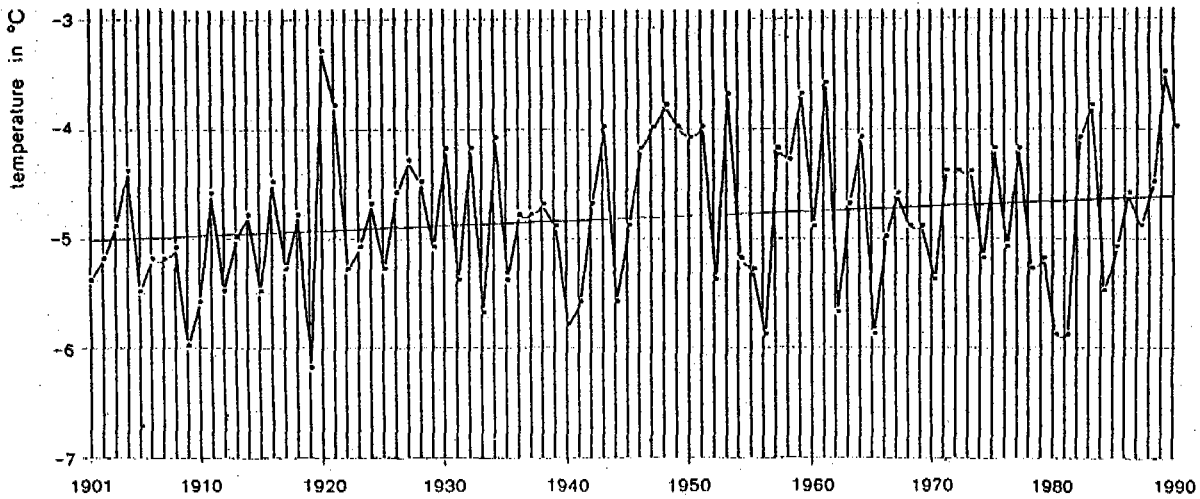


Figure 5. Mean annual air temperatures 1901 to 1990 and linear regression at Zugspitze, 2960 m a.s.l.

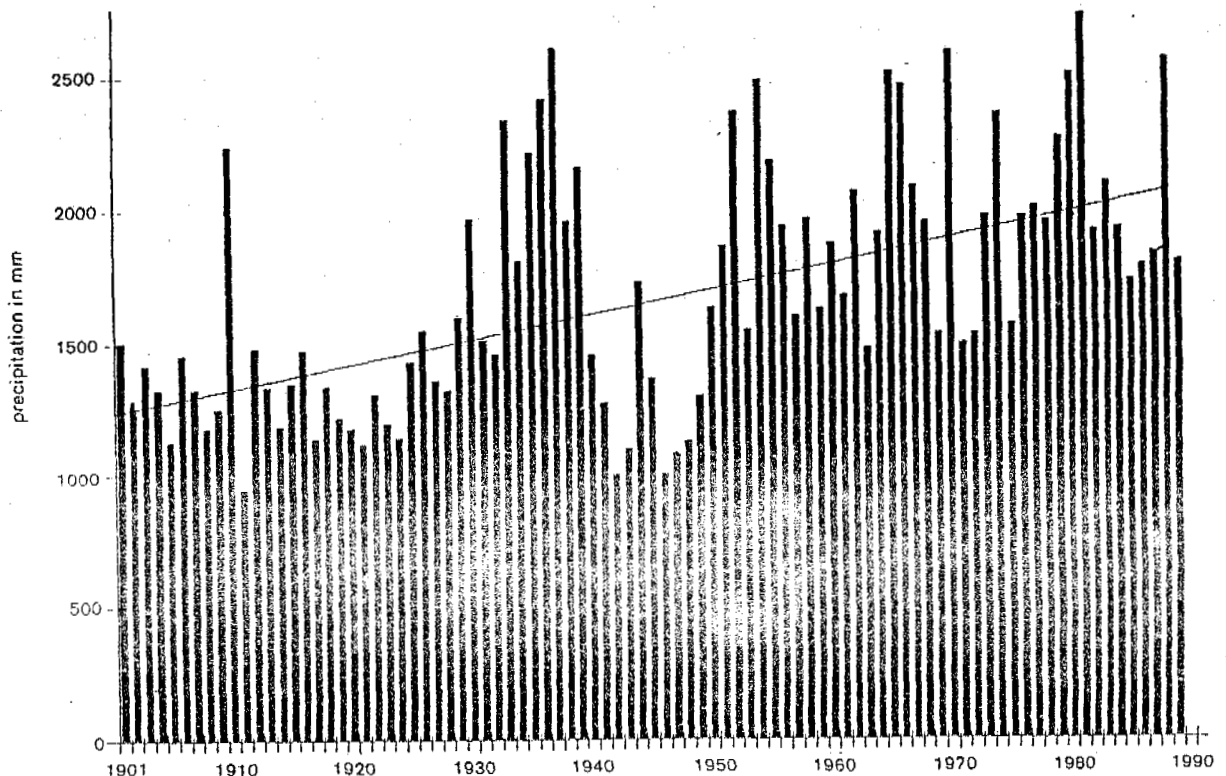


Figure 6. Annual precipitation 1901 to 1990 at Zugspitze, 2960 m a.s.l., and linear regression line.

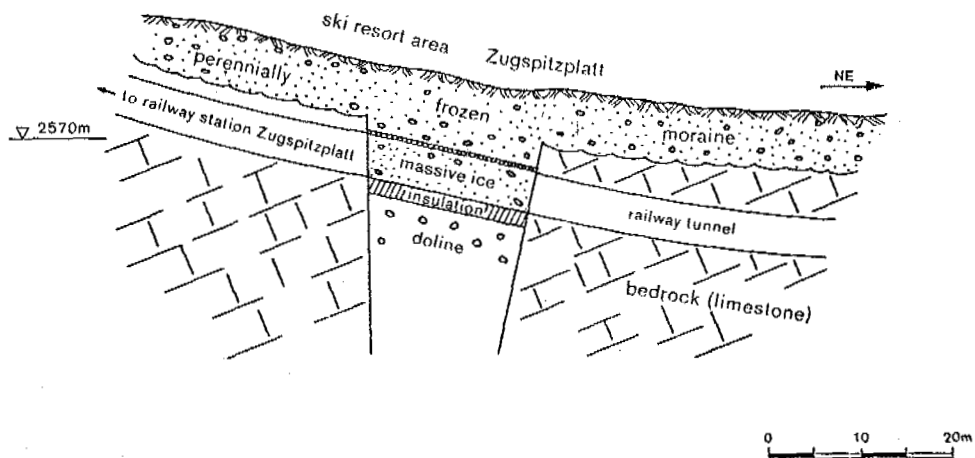


Figure 7. Tunnel track in the area with the ice-filled doline. The moraine cover is perennally frozen and the frozen debris shows thick ice lenses and massive ice. The tunnel track entered an area mainly with massive ice. The railway track was well insulated (cf. text).

diameter. Rock particles marked a 45° stratification at its left hand side, flattening towards the right hand side. The tunneling undoubtedly established the fact that an ice-filled sink hole was hit, a massive ice body of unknown size. Test borings then revealed ice for a distance of 19 meters (cf. Figure 7).

The foundation for the rack-railway track, extremely sensitive to settlement, required intensive investigations into the problem of

heat exchange between the heated tunnel air and the ice. It had to be reliably determined that melting of the ice and future thaw settlement of the railway track could be excluded. Assuming an air temperature of +6° C and an ice temperature of -1.5° C, heat flow calculations revealed a progressive melting of the ice along the whole tunnel soffit. In order to avoid this, the use of insulation material below the heavily loaded railway track was required as follows:



- 1 m thick gravel bearing layer on
- 0.1 m damming layer of foam glass (i.e. pure glass based on aluminum and silicon, acid resistant, compressive strength 0.5 N/mm<sup>2</sup>),
- 0.3 m gravel bed with sleepers.

The tunnel wall was insulated with a 0.3 m thick layer of shotcrete on the ice and 0.1 m thick slabs of rockwool at the inner surface of the tunnel. The temperature in the massive ice body is continuously recorded at 6 sites. The ice temperatures just behind the tunnel cover show mean annual values of -0.5° C (measured over a period of 6 years). Until now, there was no detrimental influence of the tunnel statics and the railway track due to melting processes.

A final remark concerns the origin and age of the ice: The tunnel area investigated was still ice covered in 1856 and became ice-free after about 1892 (FINSTERWALDER 1950). The karst morphology of the Zugspitze area have been formed between the Pliocene and the Lower Pleistocene. The weathering loams at the Zugspitze mountain top originate from an older cover above the actual mountain crest and are not a weathering product of the limestone ("Wettersteinkalk").

#### CONCLUSIONS

Construction experience shows that permafrost in bedrock plays only a minor role concerning the stability, because the cleavage volume filled with ice is limited. The described construction measures have shown, that a critical examination of the structure stability in areas of mountain permafrost has to consider primarily the joint set of the rock (set-up and degree of separation) and the morphological circumstances of the construction site. However, permafrost may have a long lasting stabilizing effect, if at least partly cohesive joint fillings occur, that would have negative effects for the shearing strength of unfrozen rock.

According to the actual climatic trend, a reduction of the permafrost extent may be expected, and instruments recording the temperature development and the rock compression have been installed therefore at the foundation level. If the observations point out, that the conserving effect of the permafrost diminishes in course of time, a stepwise replacement by grout injections and tie-rods is intended.

In contrast to bedrock, ice in frozen debris (moraines, slope material) often forms the effective matrix and therefore strongly influences the load capacity and shear strength with ice temperatures of about -3° C. In bedrock and frozen debris, some difficulties may be encountered with the corresponding techniques described in this paper.

#### ACKNOWLEDGEMENTS

The authors acknowledge the continuous support for this study from the Zugspitzbahn AG and the permission to publish the obtained results. Special thanks to Dipl.-Ing. P. Huber for his cooperation and his numerous technical advice.

#### REFERENCES

- BARSCH, D. (1977): *Alpiner Permafrost - ein Beitrag zur Verbreitung, zum Charakter und zur Ökologie am Beispiel der Schweizer Alpen*. - *Abhandlungen der Akademie der Wissenschaften, Göttingen, Math.-phys. Kl. 3*: 118-141.
- BELLONI, S. et al. (1993): *Distribution of rock glaciers as discontinuous permafrost indicators in the alpine belt, Italy*. - *Proceedings of the Sixth International Permafrost Conference, Peking (this volume)*.
- CARTON, A., F. DRAMIS & C. SMIRAGLIA (1988): *A first approach to the systematic study of the rock glaciers in the Italian Alps*. - *Proceedings of the Fifth International Permafrost Conference, August 1988*: 712-717.
- FINSTERWALDER, R. (1950): *Die Gletscher der Bayerischen Alpen*. - *Jahrbuch des DVGAV 76, Innsbruck*: 60-66.
- HAEBERLI, W. (1985): *Creep of Mountain Permafrost: Internal Structure and Flow of Alpine Rock Glaciers*. - *Mitteilungen der Versuchsanstalt für Wasserbau, Hydrologie und Glaziologie, ETH Zürich 77*: 142 pp.
- HAEBERLI, W. (1992). *Permafrost research sites in the Alps. Field guide for the excursions of the International Workshop on permafrost and periglacial environments in mountain areas*. - *IPA workshop, Interlaken, October 1991*.
- HAEBERLI, W. & G. PATZELT (1982): *Permafrost-Kartierung im Gebiet der Hochebenkar-Blockgletscher, Obergurgl, Ötztaler Alpen*. - *Zeitschrift für Gletscherkunde und Glazialgeologie 18, 2*: 127-150.
- KEUSEN, H.R. & W. HAEBERLI (1983): *Site investigations and foundation design aspects of cable car construction in Alpine Permafrost at the "Chli Matterhorn", Wallis, Swiss Alps*. - *In: Permafrost, Proceedings Fourth International Conference. National Academy Press, Washington, D.C.*: 601-605.
- KING, L. (1983): *High mountain permafrost in Scandinavia*. - *In: Permafrost, Proceedings Fourth International Conference. National Academy Press, Washington, D.C.*: 612-617.
- KING, L. (1986): *Zonation and ecology of high mountain permafrost in Scandinavia*. - *Geografiska Annaler 68 A*: 131-139.
- KING, L. (1990): *Soil and Rock Temperatures in Discontinuous Permafrost: Gornergrat and Unterrothorn, Wallis, Swiss Alps*. - *Permafrost and Periglacial Processes 1*: 177-188.
- KING, L., A.P. GORBUNOV & M. EVIN (1992): *Prospecting and Mapping of Mountain Permafrost and Associated Phenomena*. - *Permafrost and Periglacial Processes 3*: 73-81.
- KÖRNER, H. & R. ULRICH (1965): *Geologische und felsmechanische Untersuchungen für die Gipfelstation der Seilbahn Eibsee-Zugspitze*. - *Geologica Bavarica 55*: 404-421.
- MÜLLER, L. (1963): *Der Felsbau, Band 1*. - *Stuttgart, Enke-Verlag*.

## PERMAFROST AND PERIGLACIAL FORMS IN THE ROMANIAN CARPATHIANS

Petru Urdea

Department of Geography, University of Timisoara  
1900 Timisoara, Romania

This paper outlines recent advances in our understanding of some periglacial processes and forms in the Romanian Carpathians, as well as the existence of permafrost. Landform investigated include: rock glaciers, cryoplanation terraces, stone rivers, thermal contraction cracks in peat, ice caves, thufurs, ploughing blocks and other solifluxional forms. The spread of these forms is closely correlated to the ecological and microclimatic conditions particularly. Taking into account the climatic conditions, the presence of segregated ice, the spreading and evolution of the mentioned periglacial forms, the results of the application of the BTS method and having in view the summer temperatures of the springs situated at the fronts of rock glaciers, indicate the existence of permafrost-patchy and sporadic in the research areas. The ice caves, characteristic of the extrazonal permafrost, are a real presence in all the major subdivisions of Romanian Carpathians.

### INTRODUCTION

Romanian geomorphologists have not paid sufficient attention to the existence of permafrost in the Romanian Carpathians. Aside from its inclusion as part of the presentation of Romanian glacial epoch's conditions (e.g. Ichim, 1980, 1983) which included the analysis and presentation of rock glacier in the Southern Carpathians, the current existence of the permafrost in the Romanian Carpathians has not been discussed (Urdea, 1985, 1988, 1992).

Alpine or mountain permafrost refers to areas of ground that are predominantly underlain by permafrost in mountain regions, in areas where permafrost is absent in the adjacent lowlands (cf. Harris and Corte, 1992). Mountain permafrost exists in a close and complex interaction with a large number of geocological factors (altitude, slope, exposure, climatic conditions, vegetations, etc.).

### SITE CONDITIONS

The Romanian Carpathians (spread over 66.303 km<sup>2</sup> area, i.e. 27,8% of Romanian's surface) are situated between 44°30' and 48° N and 21°22' and 26°41' E, the maximum altitude being 2544 m in Moldoveanu Peak in Fagaras Mountains (Southern Carpathians) (Fig. 1). If on the whole, the 2000 m altitude relief represents 3% of the surface, in the Southern Carpathians higher than 2000 m relief represents more than 10%.

In many parts of the Romanian Carpathians, high mountain areas exhibit glacial sculpture, with cirques, steep slopes and U-shaped valleys, or/and rounded mountain tops and interfluves.

The climatic conditions specific for the high zone of the Romanian Carpathians are cold; median temperatures under 0°C at more than 2000 m altitude, and the absolute minimum is -38°C. The box-

plot of monthly temperatures at selected meteorological stations from the Romanian Carpathians

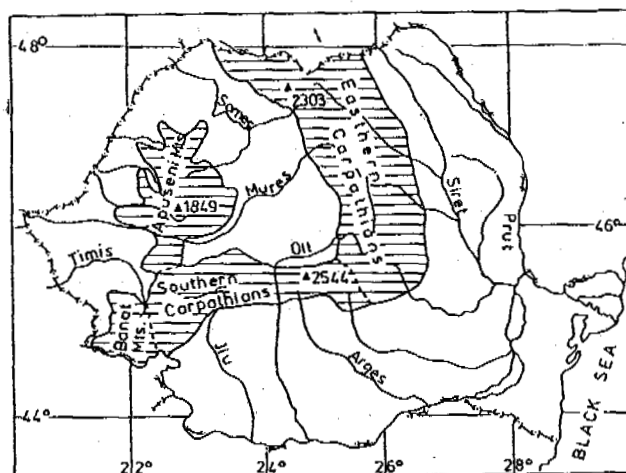


Figure 1. Location map of study area.

gives the range in monthly air temperatures during the year, conditions characteristic for most stations in Romanian Carpathians (Fig. 2). The number of days with frost ( $T_{min} \leq 0^\circ C$ ) is 200-254 (Table 1) and the number of frost-thawing cycles is more than 125, frost being possible during the whole year. The mean monthly wind speed is more than 10 m/s on the high summits (Omu and Tarcu -10,6 m/s, Ceahlau -10,4 m/s), with maximum speeds exceeding 40 m/s. Winds of more than 6 m/s (i.e., capable of redistributing snow) have a 60% frequency, but during the winter months this frequency reaches 80%. The

prevalent winds are those from the west and north-west.

Table 1. Mean winter (1), summer (2), annual (3) and absolute minimum air temperature (4), (°C), days with frost (5) and annual precipitations (mm)(6) of selected Romanian Carpathians stations.

Station and period	Location	m.a.s.l.	1	2	3	4	5	6
Baisoara 1931-1970	Apuseni Mts.	1385	-4,3	+12,7	+4,4	-25,3	157	842
Vladeasa 1896-1975	Apuseni Mts.	1836	-7,5	+9,1	+1,1	-30,0	191	1058
Tarcu 1931-1970	Southern Carp.	2180	-7,8	+7,7	-0,5	-28,2	179	1178
Omu 1896-1975	Southern Carp.	2505	-10,0	+4,8	-2,5	-38,0	255	1278
Ceahlau 1931-1970	Eastern Carp.	1897	-8,1	+8,3	+0,6	-28,2	193	738
Iezer 1931-1970	Eastern Carp.	1785	-6,2	+9,1	+1,6	-29,0	193	1330

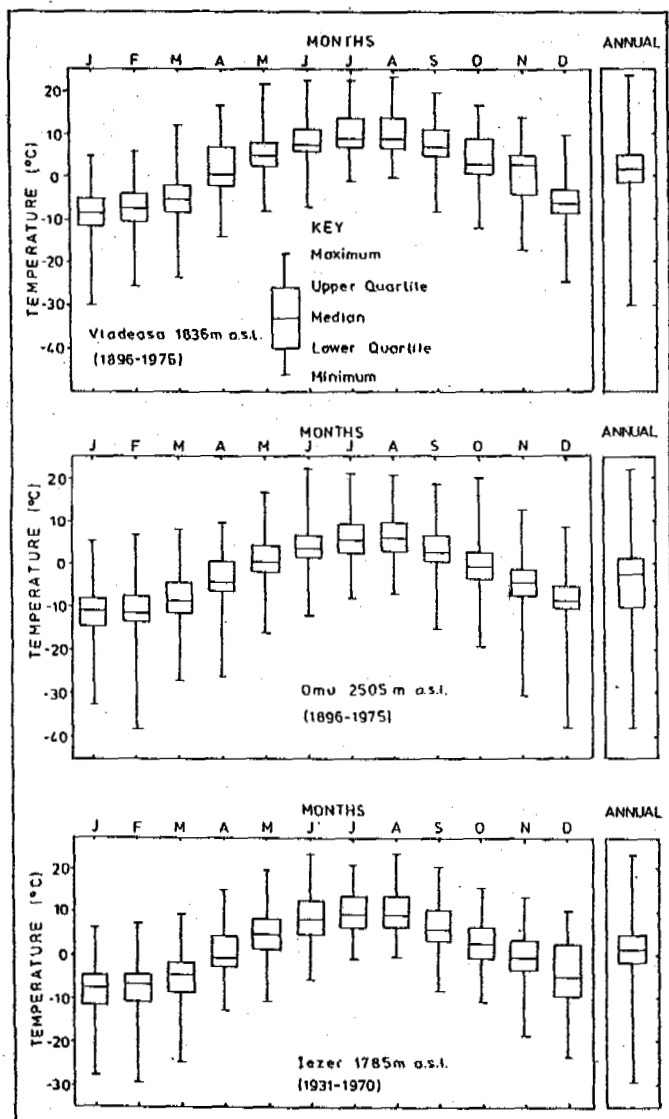


Figure 2. Box-plots of the distribution in monthly temperatures, at some selected meteorological stations from the Romanian Carpathians: Vladeasa, (Apuseni Mts.), Omu (Southern Carpathians) and Iezer (Eastern Carpathians).

Snow accumulation (snow thickness, duration of snow cover) on the ground surface is another important factor for the occurrence of permafrost. Due to the high frequency and speed of the winds, on the displayed surfaces the snow may not exist or it has reduced thickness, up to 50 cm, while in other places the thickness of the layer can be more than 370 cm. The maximum thickness are achieved in March, after the period of the lowest temperatures, and as a consequence of frost penetration into the ground, this favors conservations of permafrost.

The high limit of the forest is situated between 1750-1850 m in the south of the mountain area and between 1600-1750 in the north, climbing mainly on the South displayed versants and descending on the North displayed ones.

#### FIELD OBSERVATIONS AND DISCUSSION

Mountain permafrost occurs as a regular phenomenon in the periglacial belt of all high mountain systems.

Although many periglacial features have been identified in the Romanian Carpathians (Morariu, 1959, Iancu, 1961, Niculescu and Nedelcu, 1961, Cotet, 1964, Morariu et al., 1964, Ichim, 1973, 1983 Urdea, 1985, 1992), not all are currently active: rock glaciers, cryoplanation terraces, rock streams, thermal contraction cracks in peat, thufurs, ploughing blocks and other solifluxional forms.

Because permafrost can develop where the seasonal depth of freezing is larger than that of thawing (Sone, 1990), we have calculated freezing index (FI) and thawing index (TI) (cf. Harris, 1982) and using the Stefan equations:

$$Df = a \sqrt{FI} \quad (1)$$

$$Dt = a \sqrt{TI} \quad (2)$$

we calculated the depth of the winter freezing (Df) and that of the summer thawing (Dt) (Table 2). The altitude where the depth of winter freezing is larger than that of summer thawing is estimated as around 1800 m.a.s.l. (Fig. 3), an altitude that generally corresponds to the high limit of the forests. This altitude is considered as the lower limit of permafrost in the ideal conditions, because in reality the local conditions have a major influence over the formation of permafrost (cf. King, 1986, Haerberli et al., 1991).

Rock glaciers represent very favorable sites for maintenance of permafrost. The large extent of the glacial relief on the north versant of the Southern Carpathians and Rodnei Mountains favors the formation of rock glaciers in glacial cirques

and valleys (Urdea,1992).

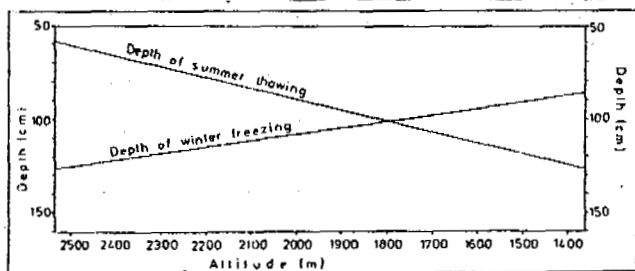


Figure 3. Potential depth of seasonal freezing and thawing versus altitude in the Romanian Carpathians.

Table 2. Freezing (FI) and thawing indexes (TI), depth of seasonal freezing (Df) and thawing (Dt) in the Romanian Carpathians.

Stations	m.a.s.l.	FI	TI	Df	Dt
Omu	2505	1768,9	404,9	126,2	60,4
Tarcu	2180	1297,8	874,3	108,1	88,7
Ceahlau	1897	1364,0	1067,9	110,8	98,0
Vladeasa	1837	1282,5	1113,5	107,4	100,1
Iezer	1785	1390,7	1128,1	111,9	100,7
Baisoara	1385	826,8	1815,4	86,3	127,8

Situated at the foot steep, shaded slopes, the steep walls protect the rock glaciers from direct solar radiation and also offer a large quantity of frost shattered blocks. The microclimatic conditions favorable for the spreading of rock glaciers were also generated by the intense cooling of air masses that rise on the north and north-west versant of these mountains, the dominant circulation of air being in this direction, up to the level of condensation after the dry adiabatic gradient ( $-1^{\circ}\text{C}/100\text{ m}$ ), and higher after the wet adiabatic gradient ( $-0,65^{\circ}\text{C}/100\text{ m}$ ). The high degree of higrical continentality (60-64) favors the spreading of rock glaciers (cf. Höllermann, 1983). Glacial cirques also experience frequent thermal inversions during both winter and summer, which favors the maintainance of permafrost in these places.

Taking into consideration that rock glaciers indicate permafrost, in the absence of using geophysical methods (seismic, geoelectrical, radio-eco sounding, etc.) the application of the BTS (bottom temperature of winter snow cover) method and having in view the summer temperatures of the springs situated at the fronts of rock glaciers, the resulting values indicate the existence of permafrost in the research areas. Thus, except for the frontal and marginal zones of rock glaciers (points 1,2,3,17 and 18) the BTS values are between  $-5,6$  and  $-8,5^{\circ}\text{C}$ , which indicates the presence of underground ice (cf. Haerberli, 1978, Haerberli and Epifani, 1986) and presumably permafrost (Table 3).

The temperatures measured in July and August 1986 and 1987 in the springs situated at the fronts of rock glaciers Pietrele, Valea Rea and Galeasu (Retezat Mountains) were under  $2^{\circ}\text{C}$ , values that are independent of air temperature. The low values of the spring temperatures, which are close

to the ice point suggest that these waters come from the melting of ice within rock glaciers (Table 4), (cf. Haerberli, 1983).

Table 3. Results of BTS measurements in the Retezat Mountains (10-13.II.1992)

Point	Snow thickness (cm)	BTS ( $^{\circ}\text{C}$ )	Point	Snow thickness (cm)	BTS ( $^{\circ}\text{C}$ )
1	84	-0,7	10	119	-8,4
2	90	-1,3	11	53	-8,0
3	155	-0,8	12	120	-7,7
4	140	-5,6	13	100	-6,2
5	120	-8,5	14	98	-6,8
6	130	-8,1	15	110	-6,2
7	72	-6,0	16	150	-5,8
8	100	-5,8	17	147	-0,9
9	70	-8,0	18	120	-1,4

Table 4. Temperatures of the springs situated at the base of some rock glaciers front from Retezat Mountains.

Date	Temperatures of the springs ( $^{\circ}\text{C}$ )					Air temperature ( $^{\circ}\text{C}$ )
	1	2	3	4	5	
21.08.'86	1,2	1,8	1,5	-	-	14,2
22.08.'86	-	1,7	1,4	1,7	1,3	12,1
23.08.'86	1,7	-	-	1,6	1,4	16,0
24.08.'86	1,5	1,7	1,2	-	-	12,9
19.07.'87	1,1	1,5	1,3	-	-	13,7
20.07.'87	-	1,3	1,2	1,4	1,2	18,2
21.07.'87	1,3	-	-	1,4	0,9	14,9

Using data obtained by the two methods presented above, we attempted to predict the occurrence of permafrost in Pietrele-Galesu zone from Retezat Mountains, (Fig.4.). The existence in the Paring, Tarcu, Fagaras and Rodna Mountains of some rock glaciers, which are situated in the same conditions that have been mentioned in the Retezat Mountains, with a topography that is characteristic for these forms, we believe that permafrost also exists in these mountains. In fact, ice has been discovered during July, August and September in a cave from the rock glacier Doamnele at 2050 and 2124 m (Giurgiu, 1990), with measured temperatures in the caves from Fagaras and Bucegi Mountains during July and August being  $0-2,5^{\circ}\text{C}$  (Giurgiu, 1990).

Freezing and thawing indexes (Harris,1982) calculated at each meteorological station between 1385 m a.s.l. (Baisoara) and 2505 m a.s.l.(Omu) with the range of  $\pm 1^{\circ}\text{C}$  in mean annual air temperature in the Romanian Carpathians are plotted on the diagram of Harris (1982). Use of these diagrams offers the opportunity of studying the possibilities of some periglacial forms existence in the Romanian Carpathians, (Fig. 5).

Thus, thermal contraction cracks in peat, existing at more than 1900 m a.s.l. are also specific to sporadic and patchy permafrost, thufurs occur at more than 1700 m, and the rock glaciers are developing up to the low limit of patchy permafrost (Fig. 5 b and c). Cryoplanation terraces, which are present in Retezat, Tarcu, Paring, Fagaras, Calimani and Rodna Mountains, are represented

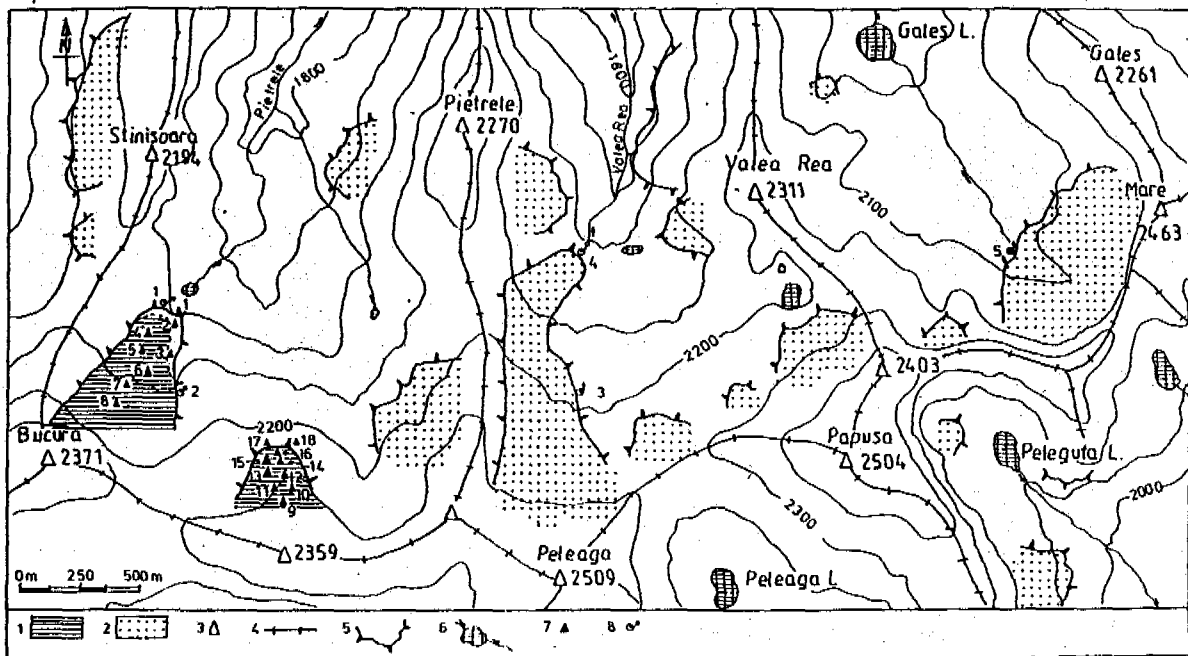


Figure 4. Permafrost occurrence in the area Pietrele-Galesu (Retezat Mountains) on the basis of BTS measurements and estival temperature of the springs situated at the base of rock glaciers front: 1-permafrost present, 2-permafrost possible, 3- peak, 4-ridge, 5-rock glaciers, 6-rivers and lakes, 7-BTS mesurement, 8-spring measurement.

by shapes situated at over 2000 m in full evolution proved by the freshness of cliffs and the presence of solifluxional processes on the surface of these terraces. These terraces are situated inside the areal delimited by the  $-1^{\circ}\text{C}$  isotherm, which corresponds to the lower limit of these forms developing (Karte, 1982).

Rock streams or stone rivers, elements especially characteristic of geomorphological landscapes of the zone situated above the forest limit in the Romanian Carpathians, are periglacial phenomena of the permafrost zones (cf. Romanovski and Turin, 1986). Some of the constituent blocks of the stone rivers situated at more than 2100 m have a yearly maximum motion of up to 8-12 cm (Urdea, 1989).

In order to make a correct estimation of the presence and spreading of permafrost in Romanian Carpathians, we believe that special attention should be given to the ice and perennial snow caves, known by the local population but also by tourists and eloquently called "glacier" or "ice cave" or "snow cave".

From over 11000 caves existing in Romania, 40 contain ice and perennial snow, being situated in all three divisions of the Romanian Carpathians, at altitudes between 900 and 2506 m a.s.l. (Table 5). It is important to mention that some of these store the huge quantities of ice, Focul Viu Glacier - 25000  $\text{m}^3$ , Bortigu Glacier - 30000  $\text{m}^3$ , The Aven with ice in Albele - 30000  $\text{m}^3$  and 60 m thickness, and Scarisoara Glacier - 75000  $\text{m}^3$ , with a 18 m ice thickness (Fig. 6). The ice formations, stalagmites, stalactites and columns, change from season to season, with a thaw during summer when the temperature rises up to  $+1^{\circ}\text{C}$ , and with a reconstruction during winter, the mean temperature being  $-7^{\circ}\text{C}$ , (Viehmann et al. 1968).

Pollen analysis of the ice at Scarisoara and Focul Viu suggests that the accumulation of ice masses began in the first part of Subatlantic, 3000 years ago (Pop and Ciobanu, 1950) and is not relict ice from the glacial period.

The presence of ice and perennial snow in many caves, the great quantity in some caves, as well as the permanent refreshment of these ice and snow masses even in those zones where the climatic conditions involve longterm mean annual temperatures of  $6-7^{\circ}\text{C}$ , suggest that the topographic and microclimatic local conditions are decisive for the appearance of this type of frost. The absence of air current allows the preservation of cold air in these cavities, the snow mass gathered during winter as well as ice and snow that existed previously maintaining a low temperature the whole year.

#### CONCLUSIONS

Taking into account the zone of mountain permafrost in the Romanian Carpathians, considering the presentation of the above realities we consider that up to 2100-2200 m a.s.l. there is patchy permafrost. In the lower area we can also find extremely sporadic permafrost, either in talus cones in shady places, some of them covered with snow patches that are preserved a long time, sometimes even from one winter to another, or in peat deposits.

Considering that ice and perennial snows from the caves are a special form of the permafrost's existence, conditioned by strict local factors that don't obey to the laws of the zonality (in this case vertical zonality), i.e. with widespread vertical distribution, we propose the name of extrazonal permafrost. This extrazonal

Table 5. Caves with ice and/or perennial snow at the Romanian Carpathians

Cave	Location	Altitude m.a.s.l.
1. Glacier Scarisoara	Bihar Mts.	1165
2. Glacier Bortigu		1200
3. Glacier Focul Viu		1165
4. Glacier from Virtop		1200
5. Cave with ice		1090
6. Glacier Zgurasti		900
7. Pit with snow from Virtop		1254
8. Aven with snow from Virtop		1240
9. Cave with ice of Valea Seaca		1300
10. Glacier Virtop		1310
11. Glacier from Zapodie		1100
12. Glacier Barsa		1136
13. Glacier Aven		1210
14. Virtop with ice		1200
15. Glacier Cave	Vladeasa Mts.	1330
16. Aven with ice of Rol	Aninei Mts.	950
17. Aven with snow of Stanuleti-Piule Mts.		1900
18. Aven with ice of Albele		1925
19. Aven with ice of Piule		2000
20. Aven with snow of Scorota Seaca		1960
21. Cave with ice of Dilma cu Brazii		1390
22. Cave nr.1 with ice of Cheile Jiului		1110
23. Cave nr.2 with ice of Cheile Jiului		1125
24. Cave nr.3 with ice of Cheile Jiului		1150
25. Aven with ice of Dilma cu Brazii		1750
26. Aven of Scocu Stanuleti		900
27. Aven of Bradul Strimb		1200
28. Cave L6 of Tirnovu	Capatinii Mts.	1625
29. Cave below Negoiu	Fagaras Mts.	2240
30. Cave nr.4 of Lespezi		2506
31. Cave nr.6 of Lespezi		2498
32. Cave nr.7 of Lespezi		2490
33. Cave of Doamnele Cirque		2124
34. Aven of Doamnele		2050
35. Cave with ice of Piatra Mare	Birsei Mts.	1400
36. Cave with ice of Piatra Singuratica	Hasmas Mts.	1585
37. Aven nr.2 of Piatra Alba		1540
38. Cave with snow of Hasmasu Negru		1500
39. Cave with ice of Ocolas Ceahlau Mts.		1620
40. Cave with ice of Borsec	Giurgeu Mts.	990

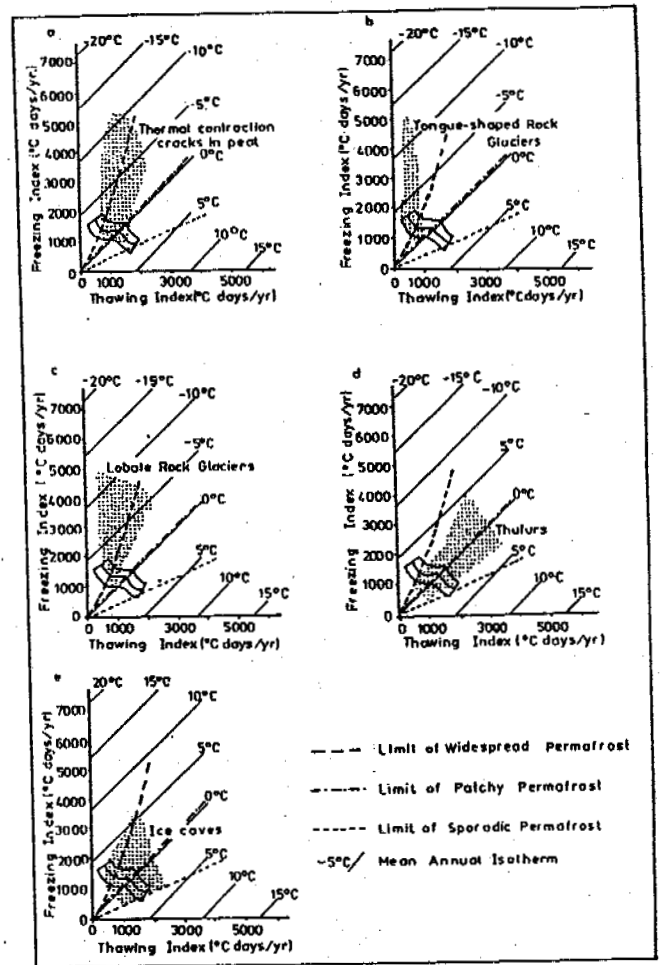


Figure 5. Possibility of the occurrence for frost cracks in peat (a), tongue-shaped rock glaciers (b), lobate rock glaciers (c), thufurs (d) and ice caves (e) in the Romanian Carpathians in relation to freezing and thawing indexes.

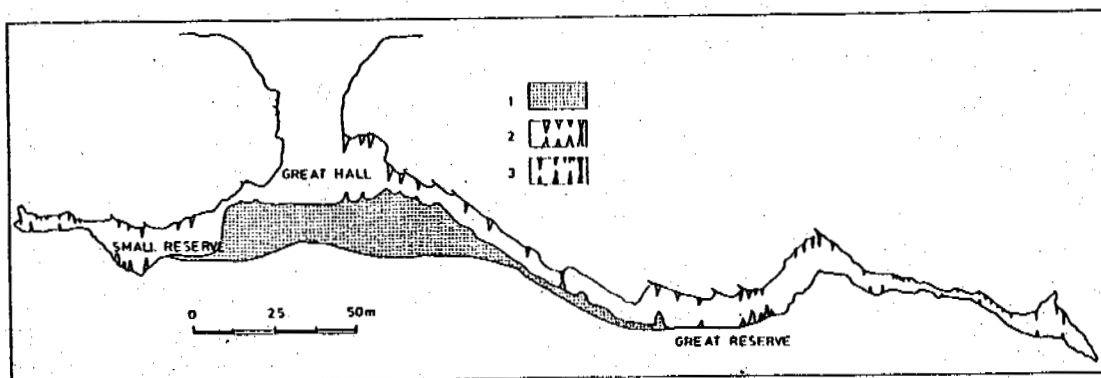


Figure 6. Glacier Scarisoara Cave-cross section: 1-ice, 2-ice formation(stalagmites, stalactites, columns), 3-limestone formations.

permafrost is as we have already noticed, well represented in all the major subdivisions of Romanian Carpathians, but especially in Apuseni Mountains and in Southern Carpathians (Fig.7).

#### REFERENCES

Barsch, D.(1978) Active rock glaciers as indicator for discontinuous permafrost. An example

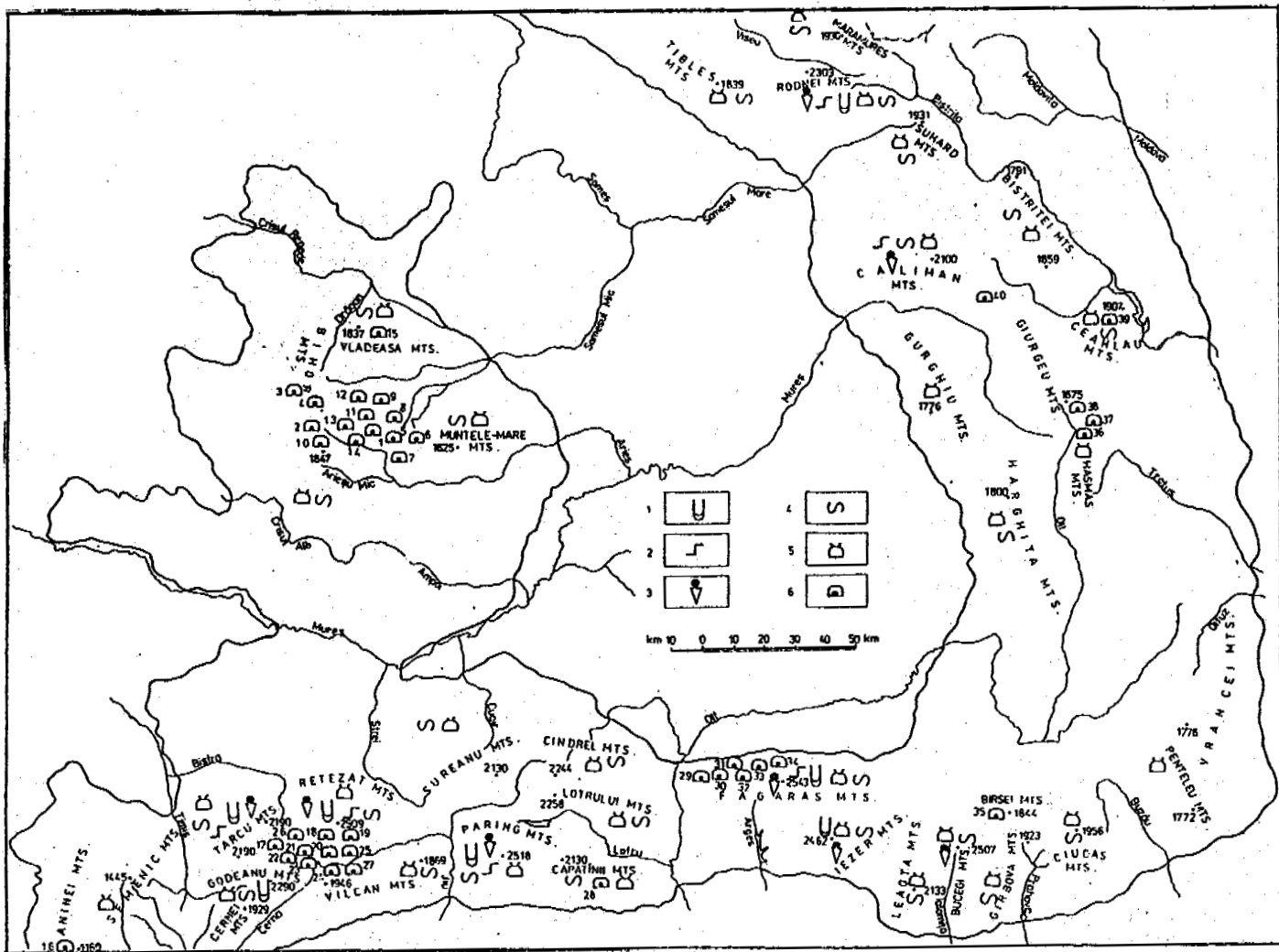


Figure 7. Spreading of some periglacial forms and ice caves in the Romanian Carpathians: 1-rock glaciers, 2-cryoplanation terraces, 3-stone rivers, 4-solifluxional forms, 5-thufurs, 6-ice caves.

from the Swiss Alps. In Proceedings Third International Conference on Permafrost, Vol. 1. National Research Council of Canada, Ottawa, pp.349-352.

Corte, A.(1976) Rock glaciers, *Biuletyn Peryglacjalny*, 26, pp.175-205.

Cotet, P.(1964) Formes de relief périglaciaire en Roumanie, *Revue Roumaine de Géologie-Géophysique-Géographie, Géographie*, 8, pp.111-119.

Evin, M., Fabre, D.(1990) The Distribution of permafrost in rock glaciers of the southern Alps, *France, Geomorphology*, 3, pp.57-71.

Giurgiu, I.(1990) Pesterile din Romania descoperite la peste 2000 m altitudine-completare esentiala a imaginii carstului din tara noastra, *Buletinul Clubului de Speologie „Emil Racovita Bucuresti*, 13, pp.62-75.

Haerberli, W.(1978) Special aspects of high mountain permafrost methodology and zonation in the Alps. In Proceedings Third International Conference on Permafrost, Vol.1. National Research

Council of Canada, Ottawa, pp.379-384.

Haerberli, W.(1983) Blockgletscher and Permafrost, *Schweiz Grün, Das Gelbe Heft*, Zürich, pp.19-20.

Haerberli, W.(1985) Creep of mountain permafrost: internal structure and flow of alpine rock glaciers, *Mitteilungen der Versuchsanstalt für Wasserbau, Hydrologie und Glaziologie, ETH Zürich*, No. 77, 142pp.

Haerberli, W., Epifani, F.(1986) Mapping the distribution of buried glacier ice - an example from Lago delle Locce, Monte Rosa, Italian Alps, *Annals of Glaciology*, 8, pp.78-81.

Haerberli, W., Harris, S. A., Guodong, C., Gorbunov, A. P.(1991) Mountain permafrost and climatic change, Report of IPA Workshop 1991, „Permafrost and periglacial environment in mountain areas”, 21pp.

Harris, S.A.(1982) Distribution of zonal permafrost landforms with freezing and thawing indices, *Biuletyn Peryglacjalny*, 29, pp.163-182.

Harris, S.A., Corte, A.(1992) Interaction and

- relations between mountain permafrost, glaciers snow and water, *Permafrost and Periglacial Processes*, Vol. 3, pp.103-110.
- Iancu, S.(1961) Elemente periglaciare in Masivul Paringului, *Probleme de geografie*, 3, pp.191-203.
- Ichim, I.(1973) Problema teraselor de crioplanatie din Masivul Calimani; *Lucrarile Statiiunii „Stejarul” Geologie-Geografie*, pp.83-92.
- Ichim, I.(1973) Cu privire la unele fenomene periglaciare din Carpatii Orientali, *Realizari in Geografia României*, Editura Stiintifica, Bucuresti, pp.65-75.
- Ichim, I.(1978) Preliminary observations on the rock glaciers phenomenon in the Romanian Carpathians, *Révue Roumaine Géologie-Géophysique-Géographie*, 23(2), pp.295-299.
- Ichim, I.(1980) Probleme ale cercetarii periglaciariului din România, *Studii si cercetari de geologie, geozica, geografie, Geografie*, 7(1) pp.18-23.
- Ichim, I.(1983) Relieful periglaciari, In *Geografia României-I Geografia fizica*, Editura Academiei, Bucuresti, pp.141-144.
- Karte, J.(1982) Development and present state of german periglacial research in arctic and alpine environments, *Biuletyn Peryglacjalny*, 29, pp.203-206.
- King, L.(1986) Zonation and ecology of high mountain permafrost in Scandinavia, *Geografiska Annaler*, 68A (3), pp.131-139.
- Morariu, T.(1959) Fenomene periglaciare din R.P. R., in stadiul actual de cercetare, *Studia Universitatis Babeş-Bolyai, Seria II, Fasciculus I Geologia-Geographia*, pp.139-152.
- Morariu, T., Savu, A.(1964) Nouvelle contribution à l'étude du périglaciaire en Roumanie, *Révue Roumaine Géologie-Géophysique-Géographie, Géographie*, 8, pp.103-110.
- Niculescu, G., Nedelcu, E.(1961) Contributii la studiul microreliefului crio-nival din zona inalta a Muntilor Retezat-Godeanu-Tarcu si Fagaras-Iezer, *Probleme de geografie*, 8, pp.87-121.
- Orghidan, T., Negrea, S., Racovita, G., Lascu, C. (1984) *Pesteri din Romania*, Editura Sport-Turism Bucuresti, 454 pp.
- Pancza, A.(1989) Un pergélisol actuel dans le Jura Neuchâtelois, *Bulletin de la Société neuchâteloise de géographie*, No. 32-33, 129-140.
- Pissart, A.(1987) *Geomorphologie Periglaciaire*, Rijkuniversiteit Gent, Belgische FRANQUI Leerstoel 1987, 135 pp.
- Pop, E., Ciobanu, I.(1950) Analize de polen in gheata de la Scarisoara, *Analele Academiei Române, Sectiunea geologie-geografie, stiinte tehnice si agricole*; an 3, nr.2, 30 pp.
- Romanovski, N.N., Turin, A.I.(1986) Kurums, *Biuletyn Peryglacjalny*, 31, pp.122-127.
- Sone, T.(1990) The permafrost environment of the Daisetsu Mountains, Central Hokkaido, Northern Japan, *Environmental Science, Hokkaido University*, 13(2), pp.1-28.
- Urdea, P.(1985) Citeva aspecte ale reliefului periglaciari din Muntii Retezat, *Analele Stiintifice Universitatea „Al. I. Cuza” Iasi, Sectiunea II, T.2, 2*, pp.73-76.
- Urdea, P.(1988) Considération sur les glaciers des pierres des Montagnes du Retezat, *Analele Stiintifice Universitatea „Al. I. Cuza” Iasi, Sectiunea II, b, 34*, pp.65-69.
- Urdea, P.(1989) Muntii Retezat. *Studiu geomorfologic*, Teza de doctorat, Universitatea „Al. I. Cuza” Iasi, 186pp.
- Urdea, P.(1992) Rock glaciers and periglacial phenomena in the Southern Carpathians, *Permafrost and Periglacial Processes*, in press.
- Viehmann, I., Racovita, G., Serban, M.(1968) *Ghetarul de la Scarisoara*, Editura Meridiane, Bucuresti, 78pp.



## A MULTI-LINGUAL INDEX OF PERMAFROST TERMS

Robert O. van Everdingen

The Arctic Institute of North America, The University of Calgary  
Calgary, Alberta, Canada T2N 1N4

The Terminology Working Group of the International Permafrost Association is preparing a multi-lingual index of the main and secondary terms contained in the "Glossary of Permafrost and Related Ground-Ice Terms" (Permafrost Subcommittee, 1988). The index covers terms in English, French, German, Italian, Spanish, and Russian; Scandinavian terms still have to be added. For each language, a separate section of the index will have the terms arranged alphabetically in that language, with each term followed by its equivalents in the other languages. Transliterated Russian is included for added convenience. To simplify editing and updating, the index is being prepared as a database, using WordPerfect version 5.1 for IBM-compatible computers. Printouts of the current draft version of the index are available for distribution in hard-copy format.

### INTRODUCTION

During the 5th International Permafrost Conference, held in Trondheim (Norway) in August 1988, the Council of the International Permafrost Association (IPA) authorized the establishment of a Terminology Working Group with the mandate "to develop a set of internationally accepted permafrost terms for use in engineering and science, with equivalents in various languages, and to disseminate and encourage the use of such terminology". The Terminology Working Group was established in the fall of 1988, with members from Argentina, Canada, China, Finland, France, Germany, the USA, and the (former) USSR.

The Working Group agreed to use as the basis for its work the "Glossary of Permafrost and Related Ground-Ice Terms", which had just been published (Permafrost Subcommittee, 1988). The initial effort was directed towards the preparation of a multi-lingual index incorporating the primary and secondary terms in the Glossary, and a number of synonyms. The languages to be covered by the index were to be English, French, German, Spanish, and Russian. Other languages were to be added if desirable. This effort was coordinated by the author.

At about the same time, work started in Lanzhou (China) on a Chinese-English-Russian list of permafrost and frozen-ground terms.

### RESULTS / TRANSLATIONS

#### French

At the time of publication of the Glossary (Permafrost Subcommittee, 1988), a French translation was also published (Sous-comité de Pergélisol, 1988). From this, most of the French equivalents of the primary and secondary terms were incorporated in the glossary index without change. Changes were made for 46 of the terms, following suggestions from the French Commission for the Study of Periglacial Phenomena

(Commission Française pour l'Etude des Phénomènes Périglaciaires), which were received from J.-P. Lautridou (Caen, France) in January 1991. Examples of the changes include: "couche active" instead of "mollisol"; "géli-adhérence" instead of "congélation adhérente"; and "frange gelante" instead of "frange gelée".

#### German

A German translation of "Permafrost Terminology" (Brown and Kupsch, 1974) had been prepared in 1982 by J. Karte (Bonn, Germany). The German equivalent terms from that translation were incorporated in the glossary index, with a number of corrections and additions provided by J. Karte in September 1991.

#### Spanish

The Spanish translation of the glossary terms was prepared by A. E. Corte and E. Buk (Mendoza, Argentina). Their listing of the Spanish equivalents of the primary terms was received in February 1990; secondary terms were added in May 1990.

#### Russian

A copy of the Russian translation of the whole Glossary, prepared by N. N. Romanovskiy, G. Rozenbaum, and V. N. Konishchev (Moscow, Russia), was received in February 1991. The Russian equivalents of the primary and secondary terms have been incorporated in the multi-lingual index. Since that time, a much expanded glossary of Russian terms, with English equivalents (if available) has been compiled by Romanovskiy and his co-workers. Currently, the definitions and comments in that expanded Russian glossary are being translated into English, with support from the IPA.

#### Transliteration

Transliterations of Russian equivalent terms, from the Cyrillic alphabet to the Latin

alphabet, using the Library of Congress system, have been added to the terminology index for the convenience of non-Russian users.

#### Italian

Italian translations of the Glossary terms were prepared by C. Ottone (Pavia, Italy) and F. Dramis (Camerino, Italy) in 1992, and incorporated in the index after they were formally accepted in November 1992 by the Italian adhering body for IPA.

#### Scandinavian

Preparation of a listing of Scandinavian terms for the index did not get underway until the fall of 1992. Only five terms had been included in the index at the time this paper was prepared. It is anticipated that a more complete set of Scandinavian terms will be incorporated in samples of the index to be exhibited during the Conference.

#### Synonyms

A number of synonyms (including terms designated as "not recommended" in the Glossary) have been included in the current terminology index, because many of these terms are found in the early permafrost literature.

#### WORD PROCESSING / PRINTING

To simplify editing and updating, the index was prepared as a database, using WordPerfect version 5.1 (for IBM and compatible computers). The index is maintained as a master list of records, in which each record comprises the following fields:

(1) a number, corresponding to the sequential location of the English term in the Glossary (Permafrost Subcommittee, 1988); (2) the English term; (3) the French equivalent; (4) the German equivalent; (5) the Italian equivalent; (6) the Scandinavian equivalent(s); (7) the Spanish equivalent; (8) the Russian equivalent; and (9) the transliterated Russian equivalent.

In order to avoid possible confusion of entries such as "ice, wedge" and "ice wedge", all multi-word terms have been entered in the index using the natural word sequence (i.e. "wedge ice" and "ice wedge" for the above example). The elimination of commas also improves the quality of machine sorting.

The database can be sorted alphabetically for any of the seven languages. Small files of layout specifications can then be used to print separate versions of the index for each of the seven languages, with the terms in the selected language as the prime entries (see Figures 1 to 7). In individual printouts, the sequence of the secondary entries can be varied as desired, but the Russian terms and their transliterations have here been listed after the other languages, to minimize printer commands in the layout specifications. A utility program (Lines, Boxes Etc., from MAP Systems, Houston) is used by the author to display the Cyrillic characters on the screen, and to enhance print quality and printing speed on dot-matrix printers.

Currently, the database occupies about 147,000 bytes on diskette; individual language sections with layout specifications each occupy between 136,000 and 161,000 bytes on diskette, and 17 to 22 single-spaced pages in print-out.

#### DISTRIBUTION / PUBLICATION

Photocopies of printouts of the current draft of the multi-lingual terminology index can be obtained from the author, at a nominal cost of US\$6.00 per language section. At the time of writing of this paper, no decision had been made regarding the eventual publication of the index.

acoustically-defined permafrost (- ice-bonded permafrost)  
active air-cooled thermal pile

F..pieu thermique à circulation d'air froid.

G..Kühlpfahl mit Luftzirkulation. I..pilone attivo con refrigerante ad aria fredda. S..pila térmica activa a circulación de aire frío. R..активная термосвая система с холодным воздухом [aktivnaia termosvaia sistema s kholodnym vozdukhom].

active construction methods in permafrost

F..méthodes actives de construction dans le pergélisol.

G..active Bauverfahren für Permafrost. I..metodi attivi di costruzione nel permafrost. S..métodos activos de construcción en permafrost. R..активные методы строительства на вечной мерзлоте [aktivnye metody stroitel'stva na vechnoi merzlotte].

active frost (- seasonal frost)

active layer

F..couche active. G..Auftauboden. I..strato attivo.

S..capa activa. R..деятельный слой [deiatel'nyi sloi].

active-layer failure

F..décollement dans la couche active.

G..Auftauboden-Rutschung. I..collasso dello strato attivo. S..ruptura o deslizamiento de la capa activa. R..смещение деятельного слоя [smeshchenie deiatel'nogo sloia].

active-layer glide (- active-layer failure)

active liquid-refrigerant thermal pile

F..pieu thermique à réfrigérant liquide. G..Kühlpfahl mit flüssigem Kühlmittel. I..pilone attivo con refrigerante a liquido freddo. S..pila térmica activa a refrigerante líquido. R..активная термосвая система с жидким охлаждением [aktivnaia termosvaia sistema s zhidkim okhlazhdeniem].

active zone (- active layer)

adfreeze / adfreezing

F..géli-adhérence. G..Anfrieren. I..congelamento aderente.

S..congelamento aderente. R..смерзаться / смерзание [smerzats'ia / smerzanie].

adfreeze strength

F..résistance de la géli-adhérence.

G..Anfrierungsfestigkeit. I..resistenza per congelamento aderente. S..fuerza de la congelación adherente. R..сила смерзания [sila smerzaniia].

adfreezing force (- adfreeze strength)

aggradational ice

F..glace d'aggradation (d'accroissement).

G..Aggradationseis. I..ghiaccio di aggradazione. S..hielo aggradacional. R..аградационный лед [agradatsionnyi led].

air freezing index (- freezing index)

air thawing index (- thawing index)

alás / alass

F..alass. G..Alas / Alass. I..alás. S..alass. R..алас [alás].

alpine permafrost (- mountain permafrost)

altiplanation terrace (- cryoplanation terrace)

annual frost zone (- active layer)

annually frozen/thawed layer (- active layer)

apparent heat capacity

F..capacité calorifique apparente. G..scheinbare

Wärmekapazität. I..capacità termica apparente.

S..capacidad de calor aparente. R..эффeктивная теплоемкость [effektivnaia teploemkost'].

Figure 1. Sample of the English version.

**abaissement du point de congélation**  
 E..freezing-point depression.  
 G..Gefrierpunktserniedrigung. I..abbassamento del punto di congelamento. S..depresión del punto de congelamiento. R..понижение точки заморзания [ponizhenie točki zamerzaniia].

**action du gel (- gélivation)**

**affaiblissement dû au dégel**  
 E..thaw weakening. G..auftau bedingte Abschwächung. I..indebolimento da disgelo. S..debilitación por descongelamiento. R..ослабление прочности грунта при протаивании [oslablenie prochnosti grunta pri protaivanii].

**affaissement de dégel**  
 E..thaw sink. G..Tausenke. I..cavità di disgelo. S..dolina de descongelamiento. R..понижение обусловленное протаиванием [ponizhenie obuslovennoe protaivaniem].

**agradation du pergélisol**  
 E..permafrost aggradation. G..Permafrost-Aggradation. I..aggradazione del permafrost. S..agradación del permafrost. R..аградация вечной мерзлоты [agradatsiia vechnoi merzloty].

**aiguille de glace (- pipkrake)**

**alass**  
 E..alas / alass. G..Alas / Alass. I..alas. S..alass. R..алас [alas].

**aquiclude cryogénique (- piégeage aqueux cryogénique)**

**aufeis (- glaçage)**

**baidjarakh (- butte de thermokarst)**

**base du pergélisol (- plancher du pergélisol)**

**béton de glace / géliment**  
 E..permacrete. G..Frostbeton. I..permacrete. S..gelicemento. R..искусственно приготовленные блоки (кирпичи) из мерзлого грунта [iskusstvenno prigotovlennye bloki (kirpichi) iz merzlogo grunta].

**bulbe de dégel**  
 E..thaw bulb. G..Tau-Aureole. I..bulbo di disgelo. S..bulbo de descongelamiento. R..орол протаивания [oreol protaivaniia].

**butte cryogénique**  
 E..frost mound. G..Frost-Hügel. I..monticello criogenico. S..domo de congelamiento. R..бугор пучения [bugor puchenii].

**butte de glaçage**  
 E..icing mound. G..Aufeis-Hügel. I..monticello da ghiacciamento superficiale. S..montículo de englamiento. R..наледный бугор [nalednyi bugor].

**butte de terre**  
 E..earth hummock. G..Erdbülte. I..cuscinetto di terra. S..domo de tierra. R..земляная кочка (бугорок) [zemlianaia kochka (bugorok)].

**butte de thermokarst**  
 E..thermokarst mound. G..Thermokarst-Hügel. I..monticello termocarsico. S..monticulo de termocarst. R..байджерах [baidzherakh].

**butte gazonnée**  
 E..turf hummock. G..Torfbülte. I..cuscinetto erboso. S..domo de turba. R..дёрновая кочка [dernovaia kochka].

**capacité calorifique apparente**  
 E..apparent heat capacity. G..scheinbare Wärmekapazität. I..capacità termica apparente. S..capacidad de calor aparente. R..эффективная теплоемкость [effektivnaia teploemkost'].

Figure 2. Sample of the French version.

**Abscherung**  
 E..detachment failure. F..rupture par décollement. I..frana di distacco. S..ruptura por despegamiento. R..смещение с отрывом [smeshchenie s otrivom].

**active Bauverfahren für Permafrost**  
 E..active construction methods in permafrost. F..méthodes actives de construction dans le pergélisol. I..metodi attivi di costruzione nel permafrost. S..métodos activos de construcción en permafrost. R..активные методы строительства на вечной мерзлоте [aktivnye metody stroitel'stva na vechnoi merzlote].

**Adereis (- Veneneis)**

**Aggradationseis**  
 E..aggradational ice. F..glace d'aggradation (d'accroissement). I..ghiaccio di aggradazione. S..hielo agradacional. R..аградационный лед [agradatsionnyi led].

**Alas / Alass**  
 E..alas / alass. F..alass. I..alas. S..alass. R..алас [alas].

**alpiner Permafrost (- Hochgebirgspermafrost)**

**Anfrieren**  
 E..adfreeze / adfreezing. F..géli-adhérence. I..congelamento aderente. S..congelamiento adherente. R..смерзаться / смерзание [smerzats'ia / smerzanie].

**Anfrierngsfestigkeit**  
 E..adfreeze strength. F..résistance de la géli-adhérence. I..resistenza per congelamento aderente. S..fuerza de la congelación adherente. R..сила смерзания [sila smerzaniia].

**approximativer Auftauindex**  
 E..approximate thawing index. F..indice de dégel approximatif. I..indice di disgelo approssimato. S..indice de descongelamiento aproximado. R..приближенный индекс протаивания [priblizhennyi indeks protaivaniia].

**approximativer Gefrierindex**  
 E..approximate freezing index. F..indice de gel approximatif. I..indice approssimato di congelamento. S..indice de congelamiento aproximado. R..приближенный индекс промерзания [priblizhennyi indeks promerzaniia].

**Aufeis**  
 E..icing. F..glaçage. I..ghiacciamento superficiale. S..englamiento. R..наледь [naled'].

**Aufeis-Hügel**  
 E..icing mound. F..butte de glaçage. I..monticello da ghiacciamento superficiale. S..montículo de englamiento. R..наледный бугор [nalednyi bugor].

**Aufeisblase**  
 E..icing blister. F..dôme de glaçage. I..blister da ghiacciamento superficiale. S..domo de englamiento. R..наледный бугор [nalednyi bugor].

**Auffrieren**  
 E..frost jacking. F..éjection gélivale. I..eiezione criogenica. S..eyección por congelamiento. R..криогенное (морозное) выпучивание (вымораживание) [kriogennoe (moroznoe) vypuchivanie (vymorazhivanie)].

**aufgetauter Boden**  
 E..thawed ground. F..sol dégelé. I..suolo disgelato. S..suelo descongelado. R..талый грунт (отложение, порода) [talyi grunt (otlozhenie, poroda)].

Figure 3. Sample of the German version.

**abbassamento del punto di congelamento**  
 E..freezing-point depression. F..abaissement du point de congélation. G..Gefrierpunktserniedrigung. S..depresión del punto de congelamiento. R..понижение точки заморзания [ponizhenie točki zamerzaniia].

**acqua di interfaccia (~ acqua interstiziale)**

**acqua di intrapermafrost**  
 E..intrapermafrost water. F..eau intrapergélisol. G..Intrapermafrostwasser. S..agua de intrapermafrost. R..межмерзлотные воды [meshmerzlotnye vody].

**acqua di soprapermafrost**  
 E..suprapermafrost water. F..eau suprapergélisol. G..Suprapermafrostwasser. S..agua de suprapermafrost. R..надмерзлотные воды [nadmerzlotnye vody].

**acqua di sottopermafrost**  
 E..subpermafrost water. F..eau infrapergélisol. G..Subpermafrostwasser. S..agua de subpermafrost. R..подмерзлотные воды [podmerzlotnye vody].

**acqua interstiziale**  
 E..pore water. F..eau interstitielle. G..Porenwasser. S..agua intersticial. R..вода поровая [voda porovaia].

**acqua libera (~ acqua interstiziale)**

**acquicluda criogenico**  
 E..cryogenic aquicluda. F..piégeage aqueux cryogénique. G..kryogener Grundwasserstauer. S..acuicluda criogenica. R..криогенный водоупор [kriogennyi vodoupur].

**aggradazione del permafrost**  
 E..permafrost aggradation. F..agradation du pergélisol. G..Permafrost-Aggradation. S..agradación del permafrost. R..аградация вечной мерзлоты [agradatsiia vechnoi merzloty].

**alás**  
 E..alás / alass. F..alass. G..Alas / Alass. S..alass. R..алас [alás].

**assestamente del suolo per fusione (~ compressione da disgelo)**

**assestamento da disgelo**  
 E..thaw settlement. F..tassement dû au dégel. G..auftau bedingte Setzung. S..asentamiento por descongelamiento. R..осадка при оттаивании [osadka pri ottaivani].

**azione del gelo**  
 E..frost action. F..gélivation. G..Frostwirkung. S..acción de congelamiento. R..криогенные процессы [kriogennye protsessy].

**azione del gelo/disgelo (~ azione del gelo)**

**barrens**  
 E..barrens. F..désert de gélivation. G... S... R... .

**base del permafrost**  
 E..permafrost base. F..plancher du pergélisol. G..Permafrostuntergrenze. S..base del permafrost. R..подошва вечной мерзлоты [podoshva vechnoi merzloty].

**blister criogenico**  
 E..frost blister. F..hydrolaccolite saisonnier. G..Frostblase. S..domo de congelamiento estacional con nucleo de hielo. R..гидролакколит [gidrolakkolit].

**blister da ghiacciamento superficiale**  
 E..icing blister. F..dôme de glaçage. G..Aufeisblase. S..domo de engelamiento. R..наледный бугор [nalednyi bugor].

Figure 4. Sample of the Italian version.

**аградационный лёд [agradatsionnyi led]**  
 E..aggradational ice. F..glace d'agradation (d'accroissement). G..Aggradationseis. I..ghiaccio di aggradazione. S..hielo aggradacional.

**аградация вечной мерзлоты [agradatsiia vechnoi merzloty]**  
 E..permafrost aggradation. F..agradation du pergélisol. G..Permafrost-Aggradation. I..aggradazione del permafrost. S..agradación del permafrost.

**агрегатная криогенная микроструктура [agregatnaia kriogennaia mikrostruktura]**  
 E..fragmic cryogenic fabric. F..microstructure cryogénique angulaire. G..fragmische kryogenes Gefüge. I..struttura criogenica a frammenti. S..fábrica criogénica frágmica.

**агрегатоподобная криогенная микроструктура [agregatopodobnaia kriogennaia mikrostruktura]**  
 E..fragmoidal cryogenic fabric. F..microstructure cryogénique subangulaire. G..fragmoidales kryogenes Gefüge. I..struttura criogenica fragmoidale. S..fábrica criogénica fragmoidal.

**активная термосвая система с жидким охлаждением [aktivnaia termosvaia sistema s zhidkim okhlazhdeniem]**  
 E..active liquid-refrigerant thermal pile. F..pieu thermique à réfrigérant liquide. G..Kühlpfahl mit flüssigem Kühlmittel. I..pilone attivo con refrigerante a liquido freddo. S..pila térmica activa a refrigerante líquido.

**активная термосвая система с холодным воздухом [aktivnaia termosvaia sistema s kholodnym vozdukhom]**  
 E..active air-cooled thermal pile. F..pieu thermique à circulation d'air froid. G..Kühlpfahl mit Luftzirkulation. I..pilone attivo con refrigerante ad aria fredda. S..pila térmica activa a circulación de aire frío.

**активные методы строительства на вечной мерзлоте [aktivnye metody stroitel'stva na vechnoi merzlote]**  
 E..active construction methods in permafrost. F..méthodes actives de construction dans le pergélisol. G..active Bauverfahren für Permafrost. I..metodi attivi di costruzione nel permafrost. S..métodos activos de construcción en permafrost.

**алас [alás]**  
 E..alás / alass. F..alass. G..Alas / Alass. I..alás. S..alass.

**байджерах [baidzherakh]**  
 E..thermokarst mound. F..butte de thermokarst. G..Thermokarst-Hügel. I..monticello termocarsico. S..montículo de termocarst.

**бугор пучения [bugor puchenii]**  
 E..frost mound. F..butte cryogénique. G..Frost-Hügel. I..monticello criogenico. S..domo de congelamiento.

**булгуннях [bulgunniakh]**  
 E..closed-system pingo. F..pingo en système fermé. G..Pingo vom geschlossenen System. I..pingo a sistema chiuso. S..pingo de sistema cerrado.

**булгуннях [bulgunniakh]**  
 E..pingo. F..pingo. G..Pingo. I..pingo. S..pingo.

**вечная (постоянная, многолетняя) мерзлота [vechnaia (postoiannaia, mnogoletnaia) merzlot]**  
 E..permafrost. F..pergélisol. G..Permafrost. I..permafrost. S..permafrost.

**вечная мерзлота альпийская (~ высокогорная мерзлота) [vechnaia merzlot]**  
 E..permafrost. F..pergélisol. G..Permafrost. I..permafrost. S..permafrost.

**вечная мерзлота альпийская (~ высокогорная мерзлота) [vechnaia merzlot]**  
 E..permafrost. F..pergélisol. G..Permafrost. I..permafrost. S..permafrost.

Figure 5. Sample of the Russian version.

**acción de congelamiento**  
 E..frost action. F..gélivation. G..Frostwirkung.  
 I..azione del gelo. R..криогенные процессы  
 [kriogennye protsessy].

**acuiclusa criogénica**  
 E..cryogenic aquiclude. F..piégeage aqueux  
 cryogénique. G..kryogener Grundwasserstauer.  
 I..acquicluda criogénico. R..криогенный водоупор  
 [kriogennyi vodoupor].

**agradación del permafrost**  
 E..permafrost aggradation. F..agradation du  
 pergélisol. G..Permafrost-Aggradation.  
 I..aggradazione del permafrost. R..аградация  
 вечной мерзлоты [agradatsiia vechnoi merzloty].

**agua de intrapermafrost**  
 E..intrapermafrost water. F..eau intrapergélisol.  
 G..Intrapermafrostwasser. I..acqua di intrapermafrost.  
 R..межмерзлотной воды [mezmerzlotnye vody].

**agua de subpermafrost**  
 E..subpermafrost water. F..eau infrapergélisol.  
 G..Subpermafrostwasser. I..acqua di sottopermafrost.  
 R..подмерзлотные воды [podmerzlotnye vody].

**agua de suprapermafrost**  
 E..suprapermafrost water. F..eau suprapergélisol.  
 G..Suprapermafrostwasser. I..acqua di  
 soprapermafrost. R..надмерзлотной воды  
 [nadmerzlotnye vody].

**agua intersticial**  
 E..pore water. F..eau interstitielle. G..Porenwasser.  
 I..acqua interstiziale. R..вода поровая [voda porovaiia].

**alass**  
 E..alas / alass. F..alass. G..Alas / Alass. I..alas.  
 R..алас [alas].

**asentamiento por descongelamiento**  
 E..thaw settlement. F..tassement dû au dégel.  
 G..aufaubedingte Setzung. I..assestamento da disgelo.  
 R..осадка при оттаивании [osadka pri ottaivanii].

**barrera cero**  
 E..zero curtain. F..période zéro. G..Nullschleier.  
 I..periodo zero. R..нулевая завеса [nulevaia zavesa].

**base del permafrost**  
 E..permafrost base. F..plancher du pergélisol.  
 G..Permafrostuntergrenze. I..base del permafrost.  
 R..подшва вечной мерзлоты [podoshva vechnoi  
 merzloty].

**bulbo de descongelamiento**  
 E..thaw bulb. F..bulbe de dégel. G..Tau-Aureole.  
 I..bulbo di disgelo. R..ореол протаивания [oreol  
 protaivaniia].

**bulbo de hielo**  
 E..frost bulb. F..manchon de gel. G..Frost-Aureole.  
 I..nucleo di gelo. R..ореол промерзания [oreol  
 promerzaniia].

**calor latente de fusión volumétrico**  
 E..volumetric latent heat of fusion. F..chaleur latente  
 volumique de fusion. G..Schmelzwärme. I..calore  
 latente volumetrico di fusione. R..объемная скрытая  
 теплота плавления [obъемnaya skrytaia teplota  
 plavleniia].

**campo de bloques**  
 E..block field. F..champ de blocs. G..Blockfeld.  
 I..campo di pietre. R..каменное (глибовое) поле  
 [kamennoe (glybovoe) pole].

Figure 6. Sample of the Spanish version.

**is**  
 E..ice. F..glace. G..Eis. I..ghiaccio. S..hielo. R..лед  
 [led].

**palsa**  
 E..palsa. F..palse. G..Palsa. I..palsa. S..palsa.  
 R..палса (пальса, пальза) [palsa (pal'sa, pal'za)].

**perenne tjäle**  
 E..permafrost. F..pergélisol. G..Permafrost.  
 I..permafrost. S..permafrost. R..вечная  
 (постоянная, многолетняя) мерзлота [vechnaia  
 (postoiannaia, mnogoletniia) merzlota].

**sträng myr**  
 E..string fen. F..tourbière réticulée. G..Strangmoor.  
 I..torbiera a cordoni. S..turbera reticulada.  
 R..грядово-мочажинное болото [griadovo-mochazhinnoe  
 boloto].

**tjäle**  
 E..frozen ground. F..gélisol. G..gefrorener Boden.  
 I..suolo gelato. S..suelo congelado. R..мерзлый грунт  
 (порода, отложение) [merzlyi grunt (poroda,  
 otlozhenie)].

Figure 7. Sample of the Scandinavian Version

#### REFERENCES

- Brown, R.J.E., and Kupsch, W. 1974. Permafrost Terminology. Associate Committee on Geotechnical Research, National Research Council of Canada, Ottawa, Technical Memorandum No. 111, 70p.
- Permafrost Subcommittee. 1988. Glossary of Permafrost and Related Ground-Ice Terms. Associate Committee on Geotechnical Research, National Research Council of Canada, Ottawa, Technical Memorandum No. 142, 156p.
- Sous-comité de pergélisol. 1988. La terminologie du pergélisol et notions connexes. Comité associé de recherches géotechniques, Conseil national de recherches du Canada, Ottawa, Note de service technique No. 142, 154p.

PERIODIC ICE-WEDGE FORMATION AND WEICHSELIAN COLD-CLIMATE  
FLOODPLAIN SEDIMENTATION IN THE NETHERLANDS

J. Vandenberghe & C. Kasse

Institute of Earth Sciences, Vrije Universiteit,  
De Boelelaan 1085, 1081 HV Amsterdam, The Netherlands.

A radiocarbon-dated, seven metres thick, Weichselian Pleniglacial fluvial sediment sequence indicates seven periods when permafrost aggraded and degraded. The previous existence of permafrost is testified by the presence of ice-wedge casts, while the corresponding permafrost degradation is manifested by cryoturbations. The sedimentary sequence is characterized by cycles of overbank deposition (sand and silt) followed by periods of land surface stability (organic sediment). During the latter phases permafrost aggraded on the floodplain. Floodplain submersion, however, resulted in degradation of the (top of the) permafrost and subsequent formation of cryoturbations. The periods of inundation lasted several hundreds to thousands of years. After withdrawal of water from the floodplain, permafrost re-established and new ice wedge polygons developed, often above the old wedges and penetrating the previously cryoturbated zone. The latter are a special kind of syngenetic ice wedges because their upward growth was interrupted by cyclic fluvial flooding, resulting in the downward thawing of the ice wedges and cryoturbation.

INTRODUCTION

Ice wedges have been subdivided classically into two main categories: epigenetic and syngenetic ice wedges (e.g. French 1976; Harry 1988; French & Gozdzik 1988; Mackay 1990). For the epigenetic type the surface level is supposed to remain constant during the complete development of the wedge. Epigenetic ice-wedge casts have been recorded by far as the most numerous ice-wedge casts (Harry & Gozdzik 1988).

The development of syngenetic wedges, conversely, takes place during slow but generally continuous deposition at the surface. In the case of slow sedimentation rates the growth of the ice veins keep pace with the sediment aggradation and the wedges grow progressively in vertical direction. In some cases, the rate of deposition on top of the wedges is discontinuous resulting in thickness variations of the ice wedge and a more or less developed wedge-in-wedge structure originates (Dostovalov & Popov 1963; French & Gozdzik 1988; Vandenberghe & Van Huissteden 1988). Generally, the syngenetic ice wedges are not disturbed by the sedimentation process. In this paper, another type of syngenetic ice wedge formation is described which is characterized not only by the temporary interruption of wedge growth but also by partial melting which is caused by flooding.

The ice-wedge casts which were studied were formed in fine-grained, fluvial and aeolian sediments dating from the last glacial. The deposits were exposed in two tunnel construction pits besides the Prinses Margriet Canal near Grouw in the northern Netherlands (53°04'45''N, 5°49'54''E; Figure 1).

Geological setting

A condensed geological section is presented in fig. 2. The basal part is formed by a gree



Figure 1 Location map of study area.

nish till consisting of sandy clay with dispersed pebbles and cobbles and dating from the end of the penultimate glacial (Saalian). Its top is weathered by soil formation and covered by peat and sandy or clayey peat from the Eemian and Early Weichselian. During the subsequent Weichselian Pleniglacial fluvial deposition occurred in the headwater of a local small river catchment. This catchment drains the

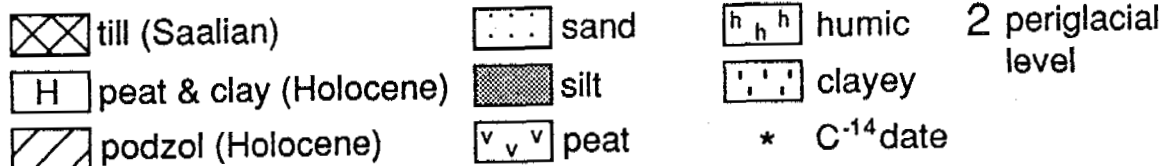
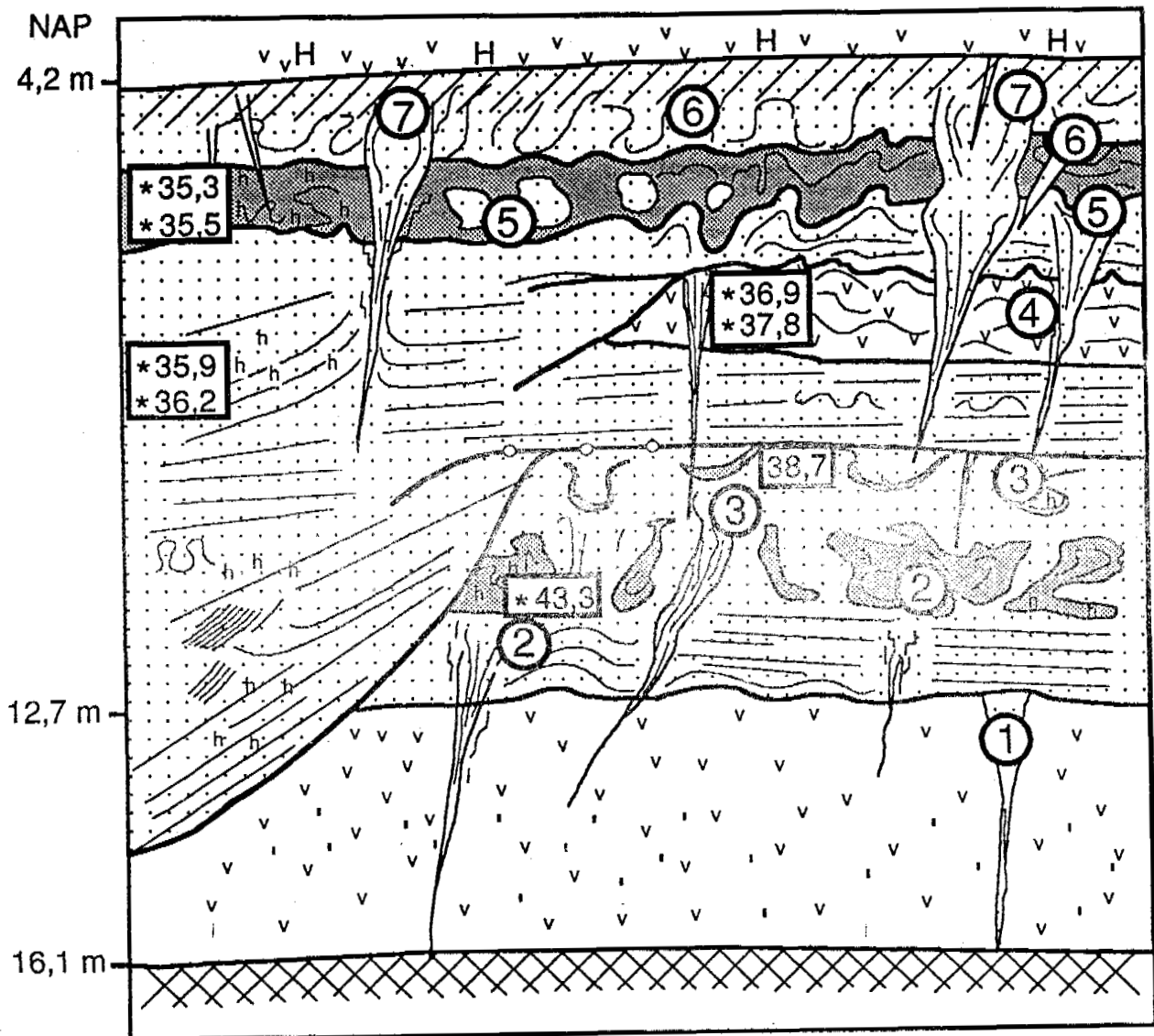


Figure 2 Simplified section of the Late Pleistocene sequence at Grouw.

higher Saalian till regions, approximately 20 to 40km south and east of the exposure. The sediments consist predominantly of fine sands alternating with (humic) silts and peat. They contain numerous levels of ice-wedge casts, each associated with cryoturbations. The presence of peaty layers enables accurate datation. The residue components and the humic extract of each organic sample have been dated in order to determine the effect of eventual humus infiltration. Only the residue dates are presented in Figure 2. The Pleistocene sediments

and their morphology are covered by about 3.5 m of clay and peat which formed in the Holocene coastal plain.

Cyclic periglacial river activity during the Weichselian Pleniglacial

Two main sedimentary facies are distinguished. The first occurs in channels which incised the older Pleniglacial fluvial deposits, Eemian peat and locally the Saalian till (Figure 2, left part). This facies is characterized by a stacked sequence of channel sediments which reveal a general fining-upward of about 7 m. Fine to medium sand with large-scale cross-

bedded sets are common at the base. Higher in the sequence, the sands are fine-grained and intercalated with many humic silt beds. Horizontal and low-angle channel fill cross-bedding are dominant. Individual sand and silt beds reveal small-scale current ripple cross-lamination and climbing ripple lamination. A rhythmic alternation of fine sand grading into sandy silt with reworked organic material is regularly found. Locally the sands show a patchy outlook and are apparently homogenized by fluidization. Isolated small-amplitude (dm-scale) cryoturbations and frost cracks are found occasionally in the channel facies. All these characteristics point to channel deposition with large and repetitive (seasonal?) discharge fluctuations in a periglacial environment.

The second facies occurs outside the channels as a complex of extended sheets, each having a thickness of a few dm to 1.5 m. Five superposed sheets are recognized in the Grouw exposures. The topmost two units also extend over the channel facies. The individual sheets consist of a fining-upward sequence of fine sands grading into sandy silts, humic silts and sometimes (clayey) peat (Figure 2, right part). These sheets are interpreted as overbank deposits. Generally, they are not erosive, in contrast to the channel deposits. Lateral transitions from channel to overbank facies are preserved occasionally, but often they are eroded. It follows that it is not always possible to connect individual overbank units to the corresponding channel unit. The overbank deposits are characterized by cryoturbations and ice-wedge casts.

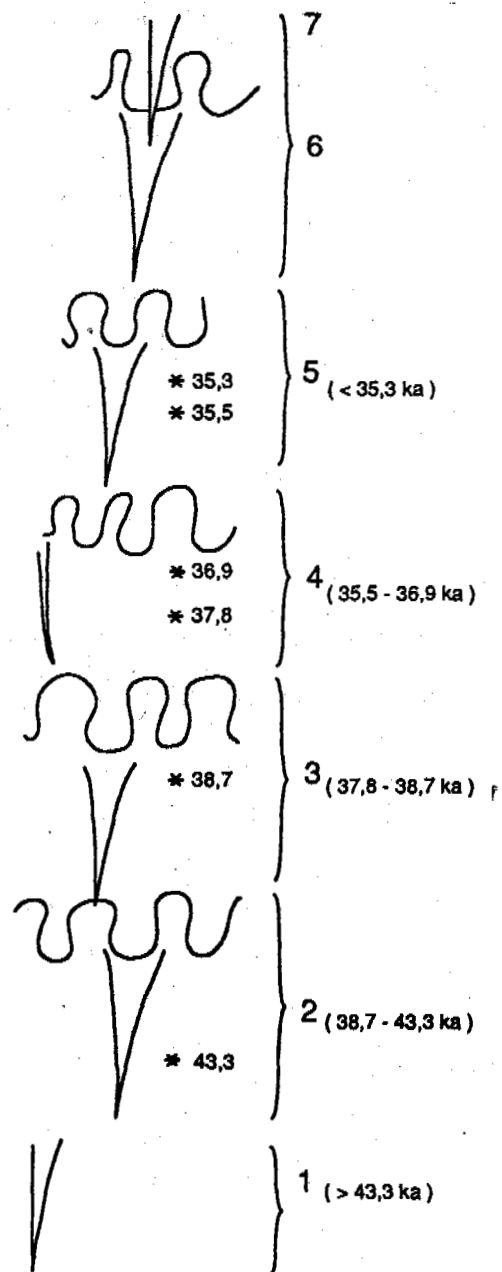
The fluvial dynamics can be conceived as a repetitive system of channel flow accompanied by flooding. The exposures did not permit identification of pointbar deposits and it was impossible to find out if the river was one- or multi-channelled. However, as channel infilling was rather fast, as indicated by the sedimentary structures, and because erosion was lateral only, the river was probably a quick lateral migrating type.

According to the general lithostratigraphy of the region (Vandenberghe 1985; Vandenberghe & Van Huissteden 1988) and radiocarbon analyses, the fluvial sediments date from the Weichselian Pleniglacial.

Cyclic development of periglacial structures during the Weichselian Pleniglacial

As shown above, a number of fluvial cycles is distinguished in the overbank series. Each of them is associated with a level of periglacial deformations, i.e. ice-wedge casts and cryoturbations. The latter levels are successively described below (see Figures 2 and 3).

The lowest level of periglacial activity (1) consists only of ice-wedge casts; they have developed on top of fine fluvial sands. As the wedges were filled by this sand, the ice wedges postdated the fluvial deposition. These sands and the ice-wedge casts are both younger than Eemian (the age of the underlying peat), On the other hand, they are overlain by a widespread erosional pebble horizon, which dates from the end of the Early Pleniglacial (Vandenberghe 1985) and by a humic layer radiocarbon dated at 43.3 ka. Thus, it is concluded that the ice wedges as well as the fluvial sands which form



\* C<sup>14</sup> - date      w w cryoturbation      Y ice - wedge cast

Figure 3 Schematic representation of the Weichselian periglacial cycles at Grouw.

the fill of these wedges date from the Early Pleniglacial (72-61 ka). This period represents the first cold phase of the last glacial in Europe with continuous permafrost.

The second level consists of numerous casts of different size overlain by a zone of cryoturbation, 80 to 110cm in amplitude. Some of the casts are fully developed while others seem to have been interrupted in a young stage. As demonstrated earlier (Vandenberghe 1983), the



ice-wedge casts and cryoturbations formed in a single time span during permafrost degradation; remnants of the ice wedges continued to exist below the permafrost table while the involutions formed in the deepening active layer. This means that the involuted organic silt, although it overlies the ice-wedge casts, is at least as old as, or older, than the ice- The organic layer is dated at c. 43.3 ka while another overlying organic silt, which is not affected by the cryoturbation, is dated at c. 38.7 ka. It follows that permafrost established and (partially) disappeared between these two dates.

The third level shows many similarities with the second. It consists of ice-wedge casts with overlying cryoturbations (amplitude 50 - 100 cm). Dating of this phase of permafrost aggradation is possible by considering the age of the organic layer deformed by the cryoturbations of this phase (38.7 ka) and the age of the base of an overlying peat layer which is not deformed (37.8 ka). Permafrost re-established and degraded at this site during this 900 years period.

The fourth level is characterized by involutions, about 70 cm in vertical extent, on top of a peat layer. Only a few ice-wedge casts have been found.

Although somewhat less expressed, these periglacial features point again to the development of permafrost and its subsequent degradation. The top of the peat, which formed before the ice-wedge growth, is dated at c. 36.9 ka while the next youngest organic layer, formed with certainty after the degradation of that permafrost, is 35.5 ka old.

Fully developed ice-wedge casts and associated well-expressed cryoturbations (amplitude 100 cm) characterize the fifth level. This level postdates a deformed organic layer the top of which is dated at c. 35.3 ka. Thus, the development and degradation of permafrost is slightly younger than this date.

The sixth phase mainly consists of extensive cryoturbations (c. 70 cm amplitude) which are developed in the uppermost fluvial sands. Only a few ice-wedge casts have been observed. Unfortunately, levels 6 and 7 cannot be dated absolutely, because of the absence of organic matter.

The uppermost level (7) is composed only of large ice-wedge casts. The overlying (cryoturbated) sediments have been removed by erosion (possibly deflation) during the Weichselian Late Pleniglacial or Late Glacial. The Holocene podzol was formed in this eroded Weichselian surface (see fig. 2). The wedge casts of level 7 form together with the casts from the underlying levels classical examples of syngenetic ice-wedge casts: they form a wedge-in-wedge structure (Vandenberghe & Van Huissteden 1988; Mackay 1990). The wedges of level 7 may have been formed shortly after the older levels, this means shortly after 35 ka. Otherwise, it is also possible that the last two periglacial levels developed during the last glacial maximum around 23-17 ka.

#### Relation between sedimentary environment and permafrost development/degradation

The overbank facies reveals a sedimentary and a periglacial cyclicity. The sedimentary cycles consist of fining-upward sequences from

fine or medium sands into (humic) silts or (clayey) peat. These sedimentary cycles are stacked upon each other without interruption or they are separated by concordant erosion levels. According to the regular sedimentation sequence it seems that the eroded volumes were very small (except for the lower- and uppermost levels).

The periglacial levels normally consist of ice-wedge casts associated with overlying cryoturbations. It is striking that the periglacial levels correspond with the sedimentary cycles and both systems run perfectly parallel. The topographic surface at the time of permafrost development probably coincides with the top of the fining-upward sequence. However, the upper surfaces of the cryoturbated zones do not necessarily correlate with the top of the fining-upward series. Instead, they generally occur in the lower sandy part of the overlying sediment cycle. The cryoturbated zones mostly consist of an intermingling of silt/peat (top of the lower fining-upward sequence) and sand (base of the overlying fining-upward sequence). This indicates that permafrost degradation occurred during flooding at the beginning of a new overbank sedimentation cycle. The bottom of the cryoturbations marks the minimum depth of permafrost degradation.

#### Model of permafrost development on a periglacial floodplain

A model of periglacial river activity and permafrost development is proposed.

The fluvial system is subdivided into channel and adjacent overbank environments. The overbank environment is characterized by cyclic deposition. Flooding of the river plain (deposition of sand by running water) is followed by a period of decreasing flow and standing water conditions (deposition of sandy to clayey silts) and finally transformation of the ponds into marshes (organic silts, peat).

During the latter phase of stable conditions permafrost becomes established and ice wedges form. This development continues until the next invasion of the floodplain. At that point sands are deposited while permafrost thaws as a consequence of the water on the floodplain. Then wedge ice melts, as well as the top of the ice-rich permafrost, resulting in the transformation of ice-wedges to ice-wedge casts and the formation of cryoturbations in the top sediments. The sedimentation cycle continues by deposition of fines in the backswamps while permafrost (at least) partially disappears depending on its thickness and the duration of flooding.

This twofold cycle has been recognized at least seven times. The frequent presence of organic backswamp deposits allows detailed dating of the events. This holds especially for the cycles 2, 3 and 4 which are bracketed accurately between radiocarbon dates. It is striking that the periglacial cycles 3 and 4 and their parallel sedimentary cycles were established in a short time: in less than about 0.9 ka and 1.4 ka respectively.

#### Synthesis

Ice-wedge growth in the Weichselian periglacial floodplain was interrupted by flooding phases with partial melting of the permafrost.



Figure 4 Ice-wedge cast and associated cryoturbation from level 3 overlain by ice-wedge cast from level 4. The cryoturbated zone at the base of the photo belongs to periglacial level 2.

After an inundation event, when the floodplain fell dry, the buried remnants of the ice wedges were reactivated. Ice-wedge casts from one level are found on top of wedge casts from an older level and partially penetrating into them (Figure 4). This mechanism of cyclic syngenetic ice-wedge growth differs from classical syngenetic ice-wedge formation, described by French & Gozdzik 1988, which is characterized by more continuous deposition and simultaneous upward growth of the ice wedge (Figure 5). Cyclic syngenetic ice-wedge formation, as described here, is characterized by a more steplike development. This is caused by substantial sedimentation in between the different phases of ice-wedge development and by the partial melting of the wedge ice from a previous growth phase. In this way, cyclic syngenetic ice-wedge casts can be distinguished in the field.

#### References

Dostovalov, B.N. and A.L. Popov (1963) Polygonal systems of ice wedges and conditions of their development. In 'Proceedings International Conference on Permafrost', Lafayette, Indiana. Nat. Res. Council, Washington D.C., 102-105.

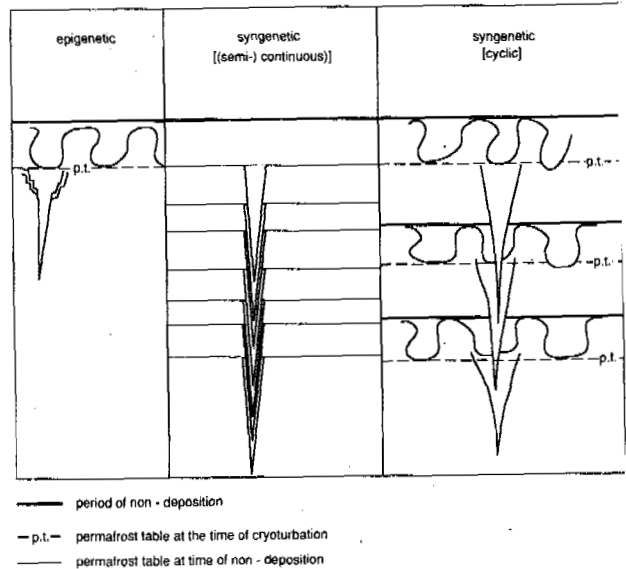


Figure 5 The main characteristics of cyclic syngenetic ice-wedge casts and cryoturbations compared with syngenetic and epigenetic forms.

- French, H.M. (1976) The periglacial environment. Longman, London.
- French, H.M. and J.S. Gozdzik (1988) Pleistocene epigenetic and syngenetic frost fissures, Belchatów, Poland. *Can. J. Earth Sci.* 25, 2017-2027.
- Harry, D.G. (1988) Ground ice and permafrost. In Clark, M.J. (ed.) 'Advances in Periglacial Geomorphology', Wiley, Chichester, 113-149.
- Harry, D.G. and J. Gozdzik (1988) Ice wedges: growth, thaw transformation, and paleoenvironmental significance. *Journ. of Quatern. Science* 3, 39-55.
- Mackay, J.R. (1990) Some observations on the growth and deformation of epigenetic, syngenetic and anti-syngenetic ice wedges. *Permafrost and Periglacial Processes* 1, 15-29.
- Vandenberghe, J. (1983) Ice-wedge casts and involutions as permafrost indicators and their stratigraphic position in the Weichselian. *Proc. 4th Int. Conf. Permafrost I*, Fairbanks, 1298-1302.
- Vandenberghe, J. (1985) Paleoenvironment and stratigraphy during the Last Glacial in the Belgian-Dutch border region. *Quaternary Research* 24, 23-38.
- Vandenberghe, J. and J. Van Huissteden (1988) Fluvio-aeolian interaction in a region of continuous permafrost. *Proc. 5th Int. Conf. Permafrost, Trondheim*, 876-881.

PAVEMENT PERFORMANCE AND LOW TEMPERATURE  
CRACKING OF SUBARCTIC AND ARCTIC AIRFIELDS

Ted S. Vinson<sup>1</sup>, DuHwoe Jung<sup>2</sup>, and James W. Rooney<sup>3</sup>

<sup>1,2</sup>Professor and Graduate Research Assistant, respectively,  
Department of Civil Engineering, Oregon State University, Corvallis, OR 97331  
<sup>3</sup>President, R and M Consultants, Inc., Anchorage, Alaska

Airfields are the primary element supporting the transportation network in the subarctic and arctic. Since the number of paved airfields in the subarctic and arctic is not great, their performance and factors which cause distress to asphalt concrete may not be fully appreciated by professionals involved in airfield design and construction.

Airfield pavement performance in cold regions may be categorized with respect to four modes of distress: (1) distortion and pavement faulting, (2) disintegration, (3) inadequate skid resistance, and (4) cracking. Cracking may be traffic/load associated or non-traffic/load associated. With respect to asphalt concrete airfield pavements, non-traffic/load cracking, specifically low temperature cracking, is predominant.

## INTRODUCTION

Airfields are the primary element of the transportation network in the subarctic and arctic. A recent example is the network of 12 airports to serve the Inuit villages in Quebec north of 55° north latitude (Tremblay 1989). The network was part of the James Bay and Northern Quebec Agreement signed in 1983. It is scheduled for completion in 1992.

Virtually all permanent airfields were initially constructed of a gravel fill placed directly on the existing vegetation to take advantage of the insulation and latent heat capacity of the surface organic layer (Crory 1988). It has generally been the case that the airfield was unpaved in its early history and a bearing surface was created by adding fines to "bind" the gravel, which was then compacted and graded. The binder material was necessary because the aggregates which were used were not crushed. Difficulties arose, however, due to ingestion of surface particles into aircraft engines, and severe rutting of the surface as the ground thaws and softens when attempts are made to extend operations into the summer season (Linell and Johnston 1973). Consequently, when equipment can be barged or airlifted to the site, and as commercial air service increases, consideration is given to paving the airfield, which in North America is almost exclusively associated with the use of asphalt concrete.

Since the number of paved airfields in the subarctic and arctic is not great, their performance and factors which cause distress to asphalt concrete may not be fully appreciated by professionals involved in their design and construction. The purpose of this paper is to provide a review of the performance of paved airfields in the subarctic and arctic and to identify a design methodology to relate to one major distress mode, namely, low temperature cracking.

## PERFORMANCE OF PAVED AIRFIELDS IN THE SUBARCTIC AND ARCTIC

Airfield pavement performance in cold regions may be categorized with respect to four modes of distress (Vinson, et al. 1986): (1) distortion and pavement faulting, (2) disintegration, (3) inadequate skid resistance, and (4) cracking. A brief background of these distress modes together with a limited review of the current state-of-the-art of research and/or practice is presented in the discussion that follows.

### Distortion and Pavement Faulting

Frost heave and thaw degradation of permanent frost are primary causes of distortion and faulting of airfield pavements in the arctic and subarctic. Distortion distress is also associated with buried structures "jacking out" of the ground under successive freeze-thaw cycles or remaining fixed while the surrounding soil heaves. Berg and Johnson (1983) noted that drains, culverts, or utility ducts placed under pavements on frost susceptible subgrades often experience differential heave and should be avoided.

Rice (1975) succinctly identified the causes of frost heave as the three W's: winter, water, wick (i.e., cold temperatures, access to water, a frost susceptible soil). It is universally recognized that mitigation of distress related to frost heave involves the elimination of one or more of these factors. Considering the evolutionary history of most airfields it may not be practical to remove frost susceptible soils since they often comprise most of the embankment. Consequently, insulation is experiencing increased use to prevent the advance of the freezing front into the embankment (Kestler and Berg 1989). However, the use of insulation on runways is not a common practice since it can produce surface icing and, therefore, result in concerns for aircraft safety on landings.

In general, a consideration of frost heave suggests the related problem of thaw weakening in the pavement structure (i.e., base and subgrade). Pavement deterioration under repeated loads is a process of cumulative damage. During spring thaw, the supporting capacity of a pavement surface layer provided by the base, sub-base, and/or subgrade, can be reduced owing to excess porewater in the supporting layers. Under these conditions damage accumulation for a given traffic volume and load is greatest and can lead to a substantial reduction in overall pavement life (Rutherford and Mahoney 1986). An example calculation which follows the mechanistic approach to pavement design (Mahoney and Vinson 1983) suggests the magnitude of the problem at the Nome Airfield (Vinson and Rooney 1991). Considering the potential for a fatigue failure in the asphalt concrete under three design aircraft loadings at the Nome Airfield, it was demonstrated that 85% of the annual damage occurs in a one-month "typical" spring thaw condition. Berg and Johnson (1983) recommend a minimum 10 cm drainage layer be placed between the asphalt concrete pavement and the base course. The drainage layer should not have more than 2% passing the number 200 sieve. Impedance of subsurface drainage elements caused by frozen soils must be considered in the design process.

Distortion distress of airfields in the sub-arctic and arctic caused by thaw-consolidation of underlying ice-rich permafrost is related to conductive and/or convective heat transport processes. Representative case histories which document this problem have been presented for the Nome (Rooney et al. 1988), Kotzebue (Esch and Rhode 1976), and Bethel (McFadden and Seibe 1986) airfields.

It is extremely important when seeking a solution to a permafrost degradation problem to identify the contribution related to conductive versus convective heat transport processes. Permafrost degradation related to conduction may be associated with an inadequate thickness of gravel fill and/or the change in albedo of the surface when the airfield is paved. Traditional solutions for a conduction problem are to increase the thickness of the fill (Hennion and Lobacz 1973) or insulate the problem area (Esch 1973, 1986; Esch and Rhode 1976; Rooney et al. 1988). Non-traditional solutions include changing the surface albedo using paint (Fulweider and Aitken 1963; Berg and Aitken 1973; Berg and Esch 1983), the use of thermoprobes (or thermosyphons) (McFadden and Siebe 1986), prevention of snow acting as an insulation blanket during the winter (Zarling et al. 1988), use of air-duct systems (Zarling et al. 1983), and pre-thawing followed by dynamic consolidation (Rooney et al. 1988).

Permafrost degradation related to convective heat transport is associated with ground water flow beneath the airfield or through the embankment. The influence of convection is to cause a positive inflow of heat into the system, thereby slowing down or preventing long-term freeze back; or alternatively, accelerating the depth of thaw. The solution to a convective heat transport problem generally involves the modification of an existing subdrain system, and/or the enhancement of subsurface drainage away from the runway.

Rutting distortion can occur in the asphalt concrete surface layer under aircraft tire loading. If rutting is likely to occur, it is gener-

ally associated with taxiways and parking aprons. Janco (1989) discusses rutting related to the use of low viscosity asphalt cements in cold regions. He notes that rutting is related primarily to the aggregate in the mix and to a much lesser degree the grade of the asphalt cement. To minimize the potential for rutting, a well-graded angular aggregate (with two or more fracture faces) is recommended. The practice of adding one-half percent to the design asphalt cement content should be avoided as it may contribute substantially to rutting.

#### Disintegration

Disintegration is the breakup of a pavement into small, loose particles. Disintegration may be accelerated by freeze-thaw cycles, or traffic loading, especially adjacent to cracks. In an asphalt concrete pavement, disintegration is generally related to insufficient asphalt cement content in the mix, poor compaction of the mix (which may be related to cold weather construction (Eaton and Berg 1978)), overheating of the mix, or stripping in the asphalt mixture. The first three problems can be avoided by carefully following conventional mix design practice and conscientiously supervising the construction of the pavement. The potential for stripping may be overlooked.

Stripping of an asphalt concrete pavement is the loss of adhesion between the asphalt cement and the aggregate. Stripping is due to the action of water or water vapor in the asphalt concrete pavement. Specifically, water gets between the asphalt cement film and the aggregate surface. Since the aggregate surface often has a greater attraction for water than asphalt, the water is drawn between the asphalt cement and aggregate surface and strips the asphalt away from the aggregate. The rate at which stripping takes place depends on the temperature, type of aggregate, and viscosity and composition of the asphalt (Tyler 1938). A summary and evaluation of laboratory test procedures used to identify the potential for stripping has been prepared by Terrel and Shute (1989).

#### Skid Resistance

Good surface friction or skid resistance of airfield pavements under all weather conditions is necessary to insure safe operations. Loss of skid resistance can be related to aggregates which polish under traffic and the buildup of rubber deposits over a period of time. Loss of skid resistance in asphalt concrete pavements may also be associated with "bleeding" typically caused by too much asphalt in the mix. Hydroplaning (i.e., the buildup of a thin layer of water between the pavement and tire) is often associated with loss of skid resistance.

Lack of skid resistance related to skidding on an icy surface is usually the greatest concern. Very little information is found in the literature on means for improving skid resistance on icy runway pavement surfaces. Reckard (1986) used hot sand to improve the traction on icy roads. ADOT/PF has recently used rubber aggregate asphalt at some selected highway locations to assess the influence of the rubber particle flexing on breaking ice bonding under repeated traffic loadings (Takallou et al. 1989).

## Cracking

By far the most prevalent airfield pavement performance problem is cracking. Cracking may be traffic/load associated or non-traffic/load associated. With respect to airfield pavements, non-traffic/load associated problems related to changes in temperature in the pavement structure and underlying ground are predominant.

Traffic/load associated cracking in airfield pavements is not common. In the subarctic and arctic, traffic/load associated cracking is often associated with snow plow wheel loading early or late in the snowfall season, before the subgrade is frozen or after it has thawed. Fatigue cracking also may occur under aircraft loading in the wheel path of a taxiway.

Reflection cracks are an expression of the crack pattern in an underlying pavement. They are caused by horizontal and/or vertical movements in the pavement beneath an overlay. Reflection cracks may be observed in both asphalt concrete overlays on old PCC and asphalt concrete pavements. Despite extensive work using techniques such as stress and strain relief interlayers, geotextiles, or reinforcing in the overlay, an economic solution to prevent reflection cracks does not exist. Reflection cracks have been observed within 6 to 12 months after construction of an overlay on a 50 mm asphalt concrete surface that was cold milled to an initial thickness of 12 mm (Vinson et al. 1986). The only way to completely eliminate reflection cracking is to remove the old pavement.

Reflection cracks have been associated with the use of a cement treated base (CTB). However, Vita et al. (1988) did not find this to be the case at the Bethel, Alaska, airfield which consists of a CTB underlying an asphalt concrete pavement. CTB reflection cracks did not appear to be a serious problem at Bethel. In fact, the construction and performance of CTB in cold regions has been very successful and it should be considered for more routine use in the future (Vinson et al. 1984).

Two distress mechanisms are believed to cause thermal cracking in the subarctic and arctic (Fromm and Phang 1972; Esch and Franklin 1989; Tian and Dai 1988). First, transverse cracks may be caused by the overall contraction of the entire pavement structure and/or underlying subgrade. This mechanism may cause the crack to extend through the entire pavement structure and into the subgrade. The crack can be several centimeters wide and extend across the pavement surface into the shoulder. This type of transverse crack is associated with the thermal contraction of soil (in the base, subbase, and/or subgrade) rather than the asphalt concrete surface layer. In fact, they can occur in both paved and unpaved roads and airfields at intervals of 12 to 90 m and depths extending to 2 m (Esch and Franklin 1989).

Second, low temperature cracking is attributed to tensile stresses induced in the asphalt concrete pavement as the temperature drops to an extremely low temperature. If the pavement is cooled to a low temperature, tensile stresses develop as a result of the pavement's tendency to contract. Friction between the pavement and the base layer resists the contraction. When the tensile stress induced in the pavement equals the tensile strength of the asphalt concrete mixture at that temperature, a microcrack develops at the edge and surface of the pavement. Under repeated temperature cycles or the occur-

rence of colder temperatures, the crack penetrates the full depth and across the asphalt concrete layer. Tian and Dai (1988) note that it may be possible for a thermal crack to reflect up through the asphalt concrete layer from an underlying stabilized layer if the coefficient of contraction of the stabilized layer is greater than that of the asphalt concrete layer.

The primary pattern of low temperature cracking is transverse to the longitudinal axis of the paving lane and is fairly regularly spaced at intervals of 30 to 60 m for new pavements to less than 5 m for older pavements. If the transverse crack spacing is less than the width of the pavement, longitudinal cracking may occur, and a block pattern can develop. The complex pattern of cracking that may be observed in many older airfield pavements is a result of (1) the increase in stiffness (i.e., hardening) of the asphalt cement with age, and (2) the change in the geometry of the pavement slab. On the taxiway at Fairbanks Airfield a 3 m "block pattern" developed on the taxiway associated with longitudinal and transverse thermal cracks (Esch and Franklin 1989).

Fromm and Phang (1972) noted that the transverse cracks caused by the overall contraction of the pavement structure and subgrade are not as serious as cracks occurring wholly in the asphalt concrete surface layer. Cracks restricted to the asphalt concrete surface layer allow ingress of water which in turn increases the rate of stripping, and allows pumping of a fine granular base course and load associated cracking. Water entering the crack during the winter may result in the formation of an ice lens below the crack which produces upward lipping at the crack edge. Also, de-icing salts may enter the crack and cause localized thawing of the base which, in turn, may result in a depression around the crack. Cedergren and Godfrey (1974) noted that 70% of surface runoff can enter a crack one mm wide.

## LOW TEMPERATURE CRACKING OF AIRFIELDS

### Identification of Low Temperature Cracking

It is inevitable that low temperature cracking will occur in airfield pavements constructed in the subarctic or arctic. Esch and Franklin (1989) state that all pavements in Alaska, with the possible exception of those in the south-coastal areas, can be expected to suffer from thermal contraction cracking. Therefore, design engineers involved in establishing the requirements for airfield pavements must identify an asphalt concrete mixture that will minimize low temperature cracking without compromising other performance characteristics, for example, resistance to rutting. Three approaches may be employed to identify the low temperature cracking resistance of an asphalt concrete mixture: (1) regression equations, (2) mechanistic predictions, and (3) simulation measurements.

Based on an analysis of data from 26 airfields in Canada, Haas, et al., (1987) established regression equations to predict the average transverse crack spacing based, in part, on P<sub>VN</sub> (McLeod 1972, 1987) and the minimum temperature at a site. The 26 airfields considered were south of the 50° north latitude. Fifteen were "coastal associated" airports. Approximately half of the observations were made for pavement overlays. Finally, extracted (not "origi-

nal") asphalt cement properties were used to develop the regression equation(s).

In the mechanistic prediction it is hypothesized that low temperature cracking occurs in the surface layer when the thermally induced tensile stress (owing to the pavement's tendency to contract with decreasing temperature which is resisted by friction at the pavement/base course interface) equals the tensile strength of the asphalt concrete mixture. The thermally induced tensile stress is generally calculated from a pseudo-elastic beam analysis equation (Hills and Brien 1966) which employs two input parameters: (1) the coefficient of thermal concentration, and (2) the asphalt concrete mix stiffness. The tensile strength of the asphalt concrete mix may be estimated or measured in the laboratory in either direct or indirect tension.

The determination of both the asphalt concrete mix stiffness and the tensile strength requires that the rate of cooling in the field (and the associated development of tensile stresses and strength) must be related to a rate of loading or deformation in the laboratory (or in the case of a creep test, a time after initial loading). To date, a procedure to accomplish this task has not been convincingly demonstrated to the pavement engineering community.

#### Simulation Measurement

Monismith et al. (1965) were the first to suggest that the thermally induced stress, strength, and temperature at failure could be measured in a laboratory test which simulated the conditions to which a pavement slab was subjected in the field. The basic requirement for the test system is that it maintains the test specimen at constant length during cooling. Initial efforts to accomplish this involved the use of "fixed frames" constructed from invar steel (Monismith et al. 1965; Fabb 1974; Janoo 1989; and Kanerva and Nurmi 1991). In general, these devices were not satisfactory for larger specimens owing to the fact that as the temperature decreased the load in the specimen caused the frame to deflect to a degree that the stresses relaxed and the specimen didn't fail! Arand (1987) made a substantial improvement to the test system by inserting a displacement "feedback" loop which insured that the stresses in the specimen would not relax because the specimen length was continuously corrected during the test. A modified version of Arand's system, fabricated at Oregon State University under Contract A-003A of the Strategic Highway Research Program (SHRP), is shown in Figure 1 (Jung and Vinson 1991).

A typical result from a thermal stress restrained specimen test (TSRST) is shown in Figure 2. The thermally induced stress gradually increases as temperature decreases until the specimen fractures. At the break point, the stress reaches its maximum value, which is referred to as the fracture strength, with a corresponding fracture temperature. The slope of the stress-temperature curve,  $dS/dT$ , increases until it reaches a maximum value. At colder temperatures,  $dS/dT$  becomes constant and the stress-temperature curve is linear. The transition temperature divides the curve into two parts, relaxation and nonrelaxation. As the temperature approaches the fracture temperature, the asphalt cement becomes stiffer and the thermally induced stresses are not relaxed beyond this temperature. The slope tends to

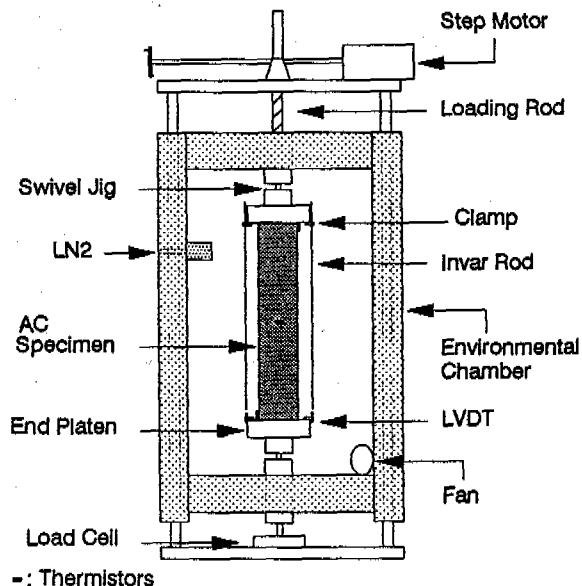


Figure 1. Schematic of thermal stress restrained specimen test (TSRST) apparatus.

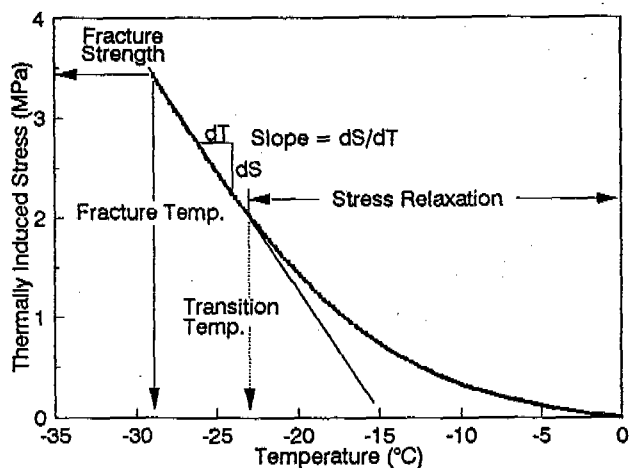


Figure 2. Typical TSRST results for monotonic cooling.

decrease again when the specimen is close to fracture due to the stiffness of the asphalt cement or the development of microcracks.

Representative TSRST results for mixtures with two asphalt cements and two aggregates are shown in Figure 3. Fracture temperatures for the 5 x 5 x 25 cm beam specimens subjected to a 10°C/hr rate of cooling are plotted against the air voids content. The ranking for the mixture response is in agreement with the ranking based on the physical properties of the asphalt cements. Specifically, AAK2 (AC-10) exhibits the coldest fracture temperature and AAG1 (AR4000) exhibits the warmest fracture temperature.

TSRSTs are generally conducted at a rate of cooling of 10°C/hr. The slower the rate of cooling the colder the fracture temperature. The difference may be as great as 5°C for a rate of cooling of 1°C/hr compared to 10°C/hr. The rate of cooling apparently does not have a signifi-

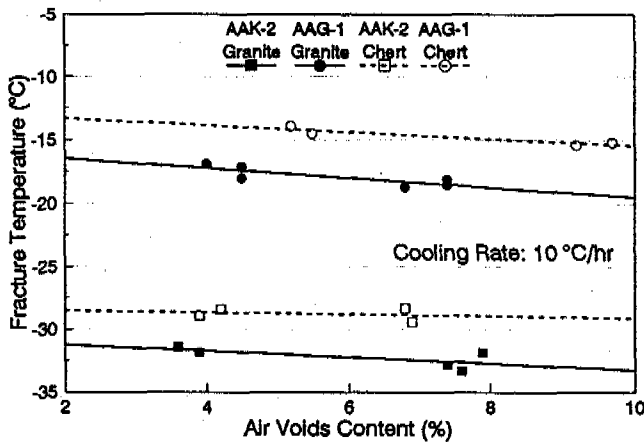


Figure 3. Fracture temperature versus air voids content.

cant influence on the TSRST results for rates of cooling faster than 5°C/hr (Sugawara and Moriyoshi 1984). Field rates of cooling are less than 1°C/hr (Janoo et al. 1990).

TSRSTs are conducted under long- and short-term age conditioning. The greater the degree of age conditioning the warmer the fracture temperature. The long term oven age (LTOA) conditioning is believed to represent aging which occurs during the construction of the pavement through a 5 to 10 yr time period thereafter. The fracture temperature of a short-term specimen is of the order of 5°C colder than a long-term specimen, which is very significant.

#### EVALUATION OF LOW TEMPERATURE CRACKING OF AIRFIELD PAVEMENTS IN THE SUBARCTIC AND ARCTIC

Considering the limitations of existing regression equations and mechanistic predictions, it appears the potential occurrence of low temperature cracking is best evaluated with a simulation measurement. Figure 4 presents a framework to evaluate low temperature cracking based on TSRST results. Implicit in the framework is the assumption that the TSRST fracture temperature is equivalent to the field fracture temperature of an airfield pavement. The design air temperature should be based on the probability of occurrence of a given low temperature at the airfield location. For example, the design temperature might be the coldest expected temperature with an annual probability less than or equal to 2%. This means that the temperature will only drop this low once every 50 years.

The pavement surface temperature may be calculated from the air temperature (Goering and Zarling 1985) or established from empirical correlations. In general, the pavement temperature will be several degrees warmer than the air temperature. At the St. Anne test road the pavement temperature was approximately 5°C warmer than the air temperature (Deme et al. 1975).

The other elements of the framework have been discussed above. The acceptable mix design determined is most likely conservative since it is based on a fully aged mix, whereas field aging will occur gradually over the life of the pavement.

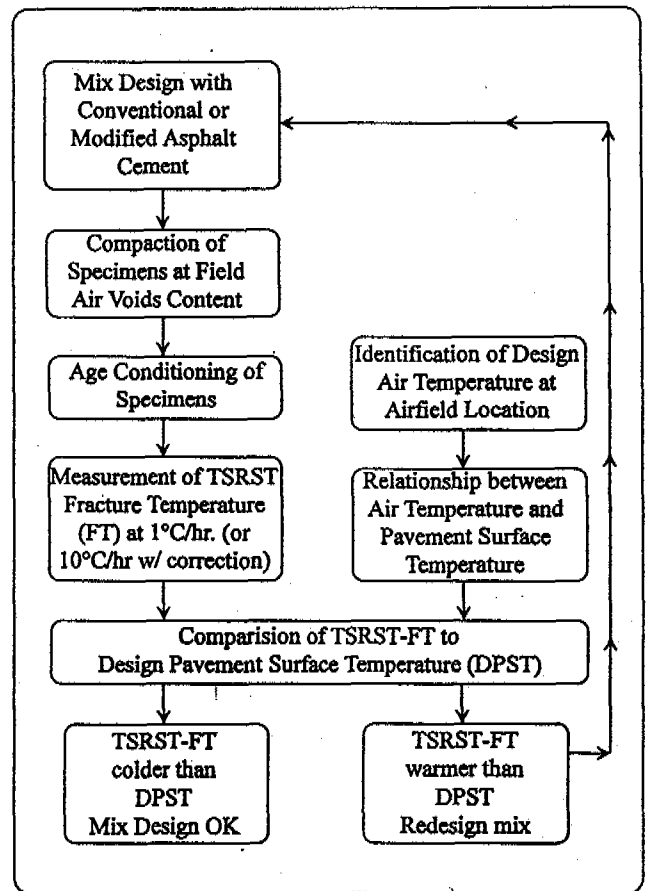


Figure 4. Framework to evaluate low temperature cracking of airfield pavements.

#### SUMMARY AND CONCLUSIONS

Professionals involved with the design of airfield pavements in the subarctic and arctic must be concerned with four modes of distress: (1) distortion and pavement faulting, (2) disintegration, (3) inadequate skid resistance, and (4) cracking.

A framework to evaluate the potential for low temperature cracking at subarctic and arctic airfields is presented. The framework employs the results from the thermal stress restrained specimen test, the aging characteristics of the asphalt concrete mix, the field cooling rate, and the probability of occurrence of an extreme low temperature at a given location. The mix design which is determined to be acceptable is most likely conservative since the design is based on a fully-aged mix, whereas aging in the field will occur gradually over the life of the pavement.

#### REFERENCES

- Arand, W. (1987) Influence of bitumen hardness on the fatigue behavior of asphalt pavements of different thickness due to bearing capacity of subbase, traffic loading, and temperature. Proc. 6th Intl. Conf. on Structural Design of Asphalt Pavements, Univ. of MI.

- Berg, R. and T. Johnson (1983) Revised procedure for pavement design under seasonal frost conditions. Special Report 83-27, USACRREL.
- Berg, R.L. and G.W. Aitken (1973) Some passive methods of controlling geocryological conditions in roadway construction. Proc. North American Contribution, 2nd Intl. Conf. on Permafrost (ICPF).
- Berg, R.L. and D.C. Esch (1983) Effect of color and texture on the surface temperature of asphalt concrete pavements. Proc. 4th ICPF.
- Cedergren, H.R. and K.A. Godfrey (1974) Water: Key Cause of Pavement Failure. Civil Engrg. Magazine, ASCE.
- Crory, F.E. (1988) Airfields in arctic Alaska. Proc. 5th ICPF.
- Deme, I., F.D. Young, and R.W. Culley (1975) Low temperature performance of composite asphalt concrete pavements. Proc. CTAA.
- Eaton, Robert A. and Richard L. Berg (1978) Temperature effects in compacting an asphalt concrete overlay. Proc. Cold Regions Specialty Conf., Anchorage, AK, ASCE.
- Esch, D.C. (1973) Control of permafrost degradation beneath a roadway by subgrade insulation. Proc. North American Cont., 2nd ICPF.
- Esch, D.C. (1986) Insulation performance beneath roads and airfields in Alaska. Proc. 4th Intl. Conf. on Cold Regions. Engrg. (ICCRE), ASCE.
- Esch, D.C. and D. Franklin (1989) Asphalt pavement crack control at Fairbanks Intl. Airfield. Proc. 5th ICCRE, ASCE.
- Esch, D.C. and J.J. Rhode (1976) Kotzebue Airfield, runway insulation over permafrost. Proc. 2nd Intl. Symp. on Cold Regions Engrg.
- Fabb, T.R.J. (1974) The influence of mix composition, binder properties and cooling rate on asphalt cracking at low-temperature. Proc. AAPT, Vol. 43.
- Fromm, H.J. and W.A. Phang (1972) A study of transverse cracking of bituminous pavements. Proc. AAPT, Vol. 41.
- Fulwider, C.W. G.W. Aitken (1963) Effect of surface color on thaw penetration beneath a pavement in the arctic. Proc. 1st Intl. Conf. on the Structural Design of Asphalt Pvmts.
- Goering, D.J. and J.P. Zarling (1985) Geotechnical thermal analysis with a microcomputer. Proc. Arctic '85, ASCE.
- Haas, R., F. Meyer, G. Assaf, and H. Lee (1987) A comprehensive study of cold climate airfield pavement cracking. Proc. AAPT, Vol. 56.
- Hennion, F.B. and E.F. Lobacz (1973) Corps of Engineers technology related to design of pavements in areas of permafrost. Proc. North American Cont. 2nd ICPF.
- Hills, J.F. and D. Brien (1966) The fracture of bitumens and asphalt mixes by temperature induced stresses. Proc. AAPT, Vol. 35.
- Janoo, V.C. (1989) Use of low viscosity asphalts in cold regions. Proc. 5th ICCRE, ASCE.
- Janoo, V., T.S. Vinson, R. Haas, and J. Boyen (1990) Test methods to characterize low temperature cracking. Proc. 4th Paving in Cold Areas Mini-Workshop (PCAMW).
- Jung, D.-H. and T.S. Vinson (1991) Low temperature cracking -- test selection. Final report, Strategic Highway Research Program (SHRP), TM-OSU-A-003A-92-20.
- Kanerva, H. and T. Nurmi (1991) Effects of asphalt properties on low temperatures cracking of asphalt pavements. Proc. ASTO Conf., Espoo, Finland.
- Kestler, M. and R. Berg (1989) Comparison of insulated and noninsulated pavements. Proc. 5th ICCRE, ASCE.
- Linell, K.A. and G.H. Johnston (1973) Engineering design and construction in permafrost regions: a review. Proc. North American Cont. 2nd ICPF.
- Mahoney, J.P. and T.S. Vinson (1983) A mechanistic approach to pavement design in cold regions. Proc. 4th ICPF.
- McFadden, T. and C. Siebe (1986) Stabilization of permafrost subsidence in the airfield runway at Bethel, Alaska. Proc. 4th ICCRE, ASCE.
- McLeod, N.W. (1972) A four year survey of low temperature transverse pavement cracking on three Ontario test roads. Proc. AAPT, Vol. 41.
- McLeod, N.W. (1987) Pen-vis number (PVN) as a measure of paving asphalt temperature susceptibility and its application to pavement design. Proc. PCAMW, Vol. 1.
- Monismith, C.L., G.A. Secor, and K.E. Secor (1965) Temperature induced stresses and deformations in asphalt concrete. Proc. AAPT, Vol. 34.
- Reckard, M. (1986) Hot sand for improved traction on icy Roads. Proc. 4th ICCRE, ASCE.
- Rice, E. (1975) Building in the North. Monograph, The Geophysical Institute, Univ. of Alaska, Fairbanks, AK.
- Rooney, J.W., J.F. Nixon, C.H. Riddle, and E.G. Johnson (1988) Airfield runway deformation at Nome, Alaska. Proc. 5th ICPF.
- Rutherford, M. and J.P. Mahoney (1986) A thermal analysis of pavement thawing. Proc. 4th ICCRE, ASCE.
- Sugawara, T. and A. Moriyoshi (1984) Thermal fracture of bituminous mixtures. Proc. PCAMW.
- Takallou, H., R.G. Hicks, D. Esch, and T. Vinson (1989) Performance of rubber-modified asphalt pavements in cold climates. Proc. 5th ICCRE, ASCE.
- Terrel, R.L. and J.W. Shute (1989) Summary report on water sensitivity. SHRP, National Research Council, SHRP - A/IR-89-1003, Washington, DC.
- Tian, D. and H. Dai (1988) Cold cracking of asphalt pavement on highway. Proc. 5th ICPF.
- Tremblay, C. (1989) Airfield construction in northern Quebec, and permafrost research. Proc. 5th Canadian Permafrost Conf.
- Tyler, O.R. (1938) Adhesion of bituminous films to aggregates. Purdue Univ. Research Bulletin, No. 62, Vol. 22.
- Vinson, T.S., J.P. Mahoney, and M. Kaminski. (1984) Cement stabilization for road construction in cold regions. Proc. 3rd ICCRE, ASCE.
- Vinson, Ted S., R. Berg Zomerman, and H. Tomita (1986) Survey of airfield pavement distress in cold regions. Proc. 4th ICCRE.
- Vinson, T.S. and J.R. Rooney (1991) A mechanistic approach to pavement design for Nome Airfield. Proc. 6th ICCRE, ASCE.
- Vita, C.L., J.W. Rooney, and T.S. Vinson (1988) Bethel Airfield, CTB pavement performance analysis. Proc. 5th ICPF.
- Zarling, J.P., W.A. Braley, and D. Esch, (1988) Thaw stabilization of roadway embankments. Proc. Permafrost: 5th ICPF.
- Zarling, J.P., B. Connor, and D.J. Goering (1983) Air duct systems for roadway stabilization over permafrost areas. Proc. 4th ICPF.



GEOPHYSICAL AND PHOTOGRAMMETRICAL INVESTIGATION OF  
ROCK GLACIER MURAGL I, UPPER ENGADIN, SWISS ALPS.

Daniel S. Vonder Mühll and Willy Schmid

Laboratory of Hydraulics, Hydrology and Glaciology,  
VAW -ETH Zentrum  
CH - 8092 Zürich, Switzerland

Muragl I is one of five rock glaciers investigated within a recently established permafrost monitoring program. The physical parameters of Muragl I were determined by two geophysical methods. Seismic refraction surveys revealed a typical three-layer case: active layer (2 m to 7 m thick) with a velocity of about 1000 m/s or less and a near-surface refractor with 3200 m/s to 3700 m/s representing the permafrost. With long profiles, bedrock (~5000 m/s) was reached at depths of about 50 m. DC resistivity soundings showed the presence of a layer with several hundreds of k $\Omega$ m, indicating the rock glaciers permafrost consisting of congelation ice. First results of the aerophotogrammetrical studies in the time period 1981/1985/1990 are also presented. Evaluation was performed with an analytical plotter by simultaneously comparing two pictures of the same area, but at different dates. Surface movements were consistently in the range of 1 - 2 decimeters per year. Acceleration and thickness change of the creeping permafrost body were calculated.

#### INTRODUCTION

Located in the eastern Swiss Alps, Muragl I is one of the five rock glaciers that are studied within the scope of the permafrost monitoring program initiated recently (Haeberli et al. 1993). The investigated rock glacier is approximately 750 m long and 150 m wide, and has pronounced lobes, furrows, and ridges caused by compression flow. The lobes show several societies of vegetation and lichen, and hence have developed most likely over several generations. The rock glacier flows from a small cirque into the main valley of Muragl. The flow direction turns sharply from NNE to NW (see Figures 1 and 5).

The two rock glaciers in the Val Muragl are already described by Salomon (1929) and Domaradzki (1951). Barsch (1973) investigated the frontal part of rock glacier Muragl I by the refraction seismic method with a sledgehammer. At the front, the active layer thickness of up to 20 m indicated that the permafrost in the rock glacier is inactive. However, Barsch supposed that 80 m behind the front, the active layer thickness is about four meters. Barsch and Hell (1975) measured in the frontal part a horizontal velocity of 21 cm/a and a vertical displacement of 10 cm/a. BTS-measurements (Haeberli 1992) showed that the entire rock glacier area is under permafrost conditions, and calculations with the digital permafrost distribution program PERMAKART (Keller 1992) indicated that rock glacier Muragl I lies at the margin of the discontinuous permafrost area.

It is the aim of the monitoring network to survey the rock glaciers by means of aerial photos and to use the corresponding data processing possibilities of the analytical plotter. Aerial photos from this region are available for the years 1981, 1985 and 1990. A direct comparison of the same area for two dif-

ferent years enables to determine changes in altitude and displacements.

In order to obtain additional information about the physical parameters of the permafrost body of rock glacier Muragl I, seismic refraction and DC resistivity soundings were carried out in the summer of 1991. The knowledge of seismic wave velocities, thickness of the active layer, depth to the bedrock and resistivity of the rock glacier permafrost increases the understanding of the processes in this periglacial area. Very low frequency resistivity (VLF-R) measurements were performed to test capability of this method in permafrost areas. Results remain ambiguous but with further measurements it is hoped that results will provide valuable information.

#### GEOPHYSICAL MEASUREMENTS

In summer 1991, seismic refraction measurements and DC resistivity soundings were carried out on rock glacier Muragl I. Figure 1 gives an overview of the investigations performed. A significant difficulty of geophysical measurements on blocky permafrost surfaces arises from the difficult contact between the sources, the sensors and the ground.

For seismic purposes, explosives are usually detonated in boreholes in order to introduce an optimum amount of energy into the ground. Since the surface of rock glaciers is covered with big boulders, explosives could only be placed underneath them. Geophones were pressed into fissures or between the boulders.

DC resistivity soundings are usually done by putting steel sticks into the ground to generate an electrical potential field which is surveyed by the potential electrodes made of clay pots. On rock glaciers the contact resistivity between the steel sticks and the underground is generally too high. To create the electrical field in the subsurface, saltwater

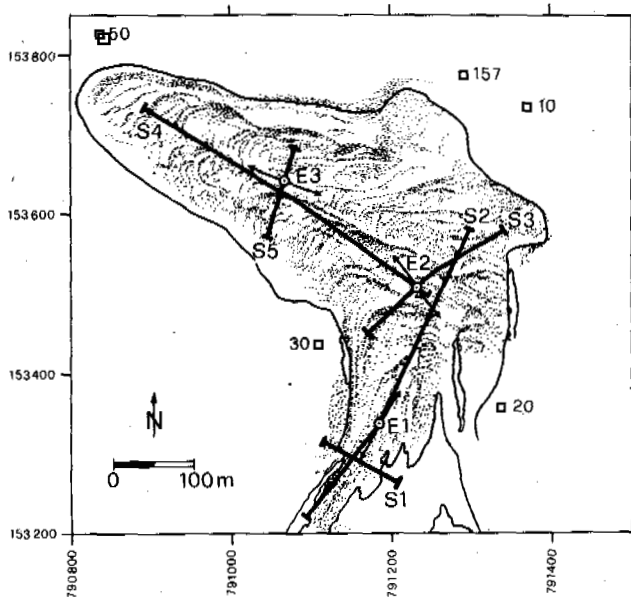


FIGURE 1. Geophysical measurements on rock glacier Muragl I in the summer of 1991. The grid corresponds to the orthogonal Swiss Coordinate System (unit in meters).

saturated sponges were used as current electrodes. The clay pots have to be placed very carefully with the help of mud and water.

Rock glaciers are three-dimensional bodies which change their physical properties over short distances, so it is difficult to calculate a detailed stratigraphy.

Nevertheless, a rough structure can be derived (cf. Fisch et al. 1977; King et al. 1987; Evin et al. 1990).

#### Seismic Refraction

Five seismic refraction profiles were carried out. In order to calculate the thickness of the active layer, geophones were placed at 5 m intervals on the crossing profiles and 10 m on the profiles which are parallel to the flow line direction. The location of each geophone and shot point was determined by geodetic survey. The acoustic waves were generated by explosives (Telsit A, up to 1 kg per shot). The registration was made with a 24 channel ABEM TERRALOC Mk II. For the investigations of the permafrost refractor, the Generalized Reciprocal Method (Palmer 1980, Palmer 1986) was used. The method, based on Hagedoorns Plus-Minus method (Hagedoorn 1959), takes migration into account. The two profiles along the main flow-line direction should enable the determination of the bedrock depth.

Since especially the profiles in flow line direction had a strong average inclination, a coordinate transformation was performed first. The new distance axis is the linear regression line calculated for the distance along the profile and the altitude of the geophones in order to obtain minimal topographic effects. The number of layers and their structures is determined from the time-distance curve defined by the new coordinate system.

Velocity of the active layer is calculated by dividing the direct distance between the shot points and the nearest geophones by the

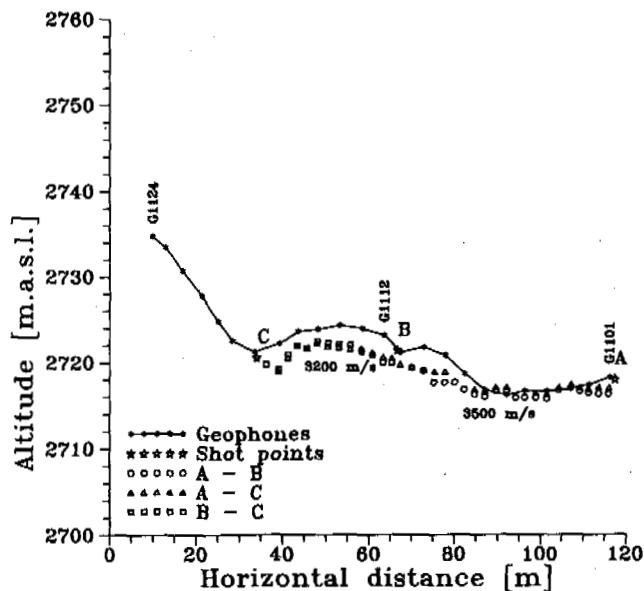


FIGURE 2. Depth of the permafrost table on profile MGL S1 (difference of elevation between geophones and refracting elements of different shots). On the right side, a perennial snow patch exists and hence thickness of the active layer is very slight. Note that at the furrows, thickness of the active layer is decreased.

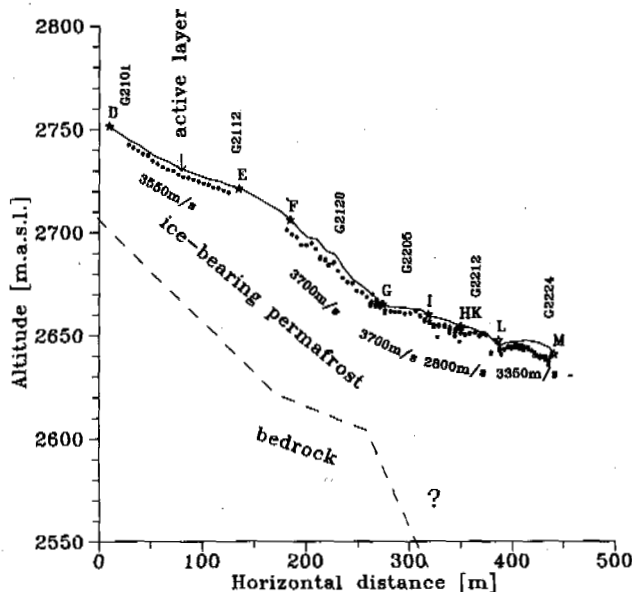


FIGURE 3. Structure under the seismic refraction profile MGL S2. The long distance between the shot points provided signals from the bedrock, which lies at a depth of about 40 to 60 m.

travel times. Values vary between 400 and 1300 m/s. In the upper part of the rock glacier with predominantly boulders and perennially snow patches, velocities of the active layer

are higher than in the middle and lower part where there is more fine-grained material and even some vegetation. Haerberli and Patzelt (1982) observed a similar relation at the rock glacier Hochebenkar (Austria). Since rock glaciers are moving downslope, altitude corresponds roughly to the age of rock glacier material. The boulders falling onto the uppermost part of the creeping permafrost surface, weather during the transport downvalley and the near surface structure allows even vegetation to grow.

Figure 2 shows results of seismic profile S1. The profile strikes approximately East-West and crosses the rock glacier in the cirque. A perennial snow patch occurs at the eastern part of the rock glacier (on the right of Figure 2). Velocities are 1200 m/s to 1300 m/s and 3200 to 3500 m/s for the active layer and the permafrost body, respectively. At the perennially frozen snow patch, the calculated depth of the refractor (permafrost table) roughly coincides with the surface. The thickness of the active layer decreases also at the furrow near shot point B. The same effect is encountered by seismic refraction measurements on rock glacier Murtel I (Vonder Mühl in prep.): Generally the active layer thickness increases at convex topographic forms and decreases at concave forms.

On rock glacier Muragl I it varies between 0 m (profile S1, Figure 2) and about 7 m in the marginal parts of the rock glacier (profiles S2, S3 and S5). The velocity of the permafrost refractor varies between 2600 m/s (in the lower part of the rock glacier) and 4050 m/s in the middle and upper part. High values are observed on the long distances between the two shot points and vice versa. This is a consequence of the increasing velocity with depth: the greater the distance between the shot points, the greater the penetration depth of the seismic waves.

Shots over long distances of up to 500 m were recorded on the two profiles along the flow line. Refracted signals from bedrock are observed on profile 2. Bedrock velocity lies between 4300 m/s and 5700 m/s. In profile S4, a faster refractor is indicated but bedrock depth could not be calculated. Figure 3 shows the results for profile S2. The thickness of the active layer increases with decreasing altitude, and is relatively thin near the furrows. Bedrock lies 40 to 60 m below the surface. Where the rock glacier turns its flow direction, bedrock depth seems to increase dramatically. It can be inferred that there is probably a low velocity layer between the frozen material and the bedrock.

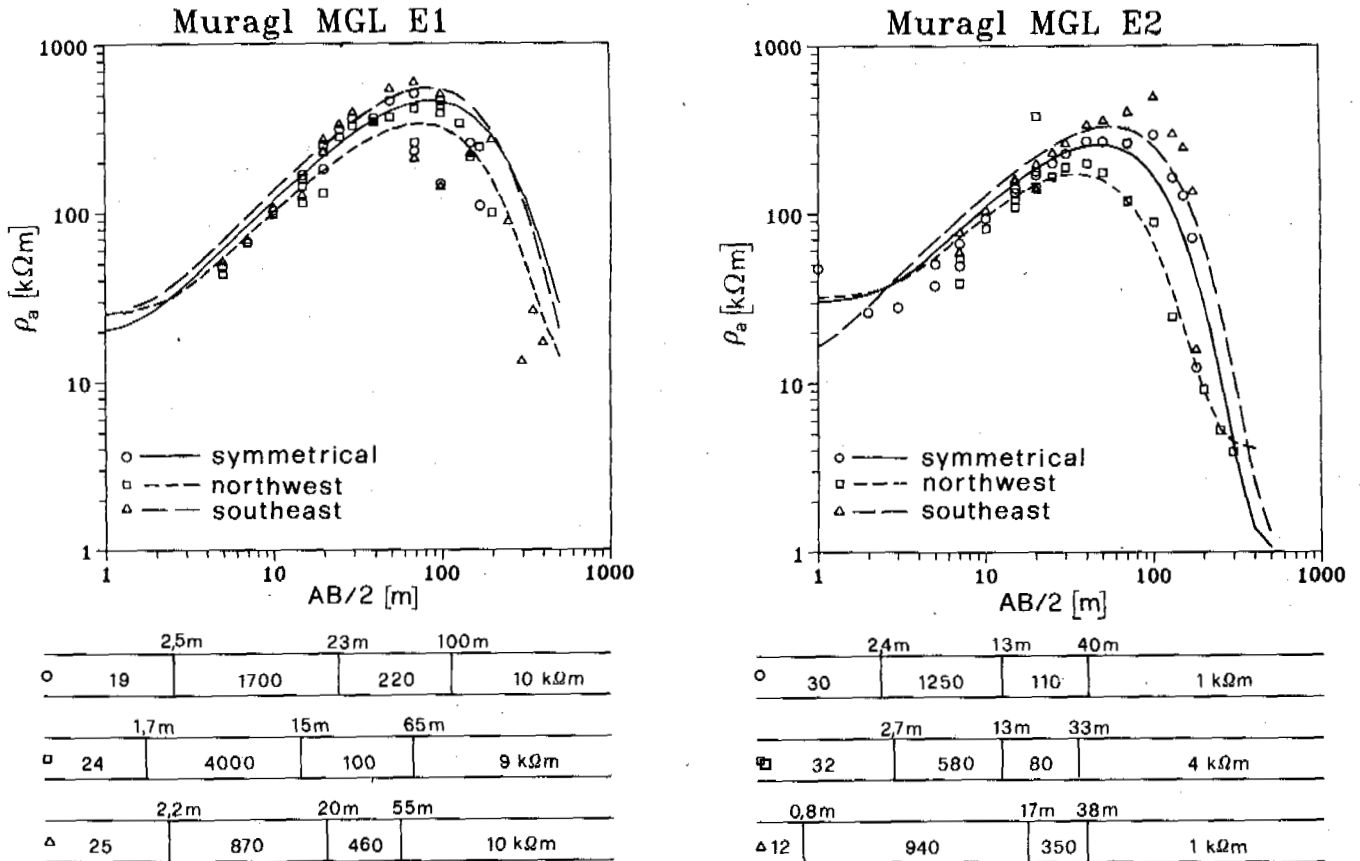


FIGURE 4. DC resistivity soundings on rock glacier Muragl I.

### DC Resistivity Sounding

DC resistivity of congelation ice in permafrost (cf. Shumskii 1964) ranges from  $k\Omega m$  to a few  $M\Omega m$  (Fisch et al. 1977). In contrast, temperate glacier ice (sedimentary ice) shows typical values of more than  $10 M\Omega m$  (Röthlisberger and Vöggtli 1967). Therefore, DC resistivity sounding is an appropriate method to classify the frozen material.

King et al. (1987) mention with regard to the special problems of resistivity measurements in permafrost: (i) Lateral effects can cause an oversteepened sounding graph (in particular in its decreasing part). (ii) Layers have to have a minimum thickness to be detectable. (iii) Formation resistivity depends on temperature (Hoekstra and McNeill 1973). The resistivity rises with decreasing temperature, particularly around  $0^{\circ}C$  and the real permafrost thickness may, therefore, be underestimated and only a minimum depth of the frozen body is derived. (iv) Since different multi-layer structures generate similar sounding graphs, interpretation of DC resistivity measurements reveals a range of resistivity and thickness models. In addition, the high resistivity (around  $M\Omega m$ ) of ice rich permafrost is mainly a consequence of frozen water in the pores and fractures. Bedrock with negative temperatures near the freezing point of water and a low ice content may show values far below  $100 k\Omega m$ .

Measurements were carried out with the Hummel-Schlumberger array. This method provides three values for each AB/2 - position (one for the symmetrical, one for the left side and one for the right side). The asymmetrical array (Hummel array) allows measurements up to great distances (AB/2) despite unfavorable topography (steep walls, etc). Moreover, differences between the left and the right side indicate the lateral variation of the underground (see sounding MGL E2, Figure 4). It is important to measure the oversteepened decreasing part of the curve so that the thickness of the high resistivity layer can be modelled. Interpretations are made on a personal computer using algorithms based on Koefoed (1979).

On rock glacier Muragl I three DC, resistivity soundings were carried out (see Figure 1). The lowermost one (MGL E3) is situated at the transition between the active and inactive part (vegetation appears downhill). Observed values of apparent resistivity were contradictory. The two other resistivity soundings furnished the typical form of electrical measurements in permafrost. After a smooth increase of the apparent resistivity with electrode spacing AB/2, a sudden decrease of one to two orders of magnitude occurs. Initial interpretations provide a three-layer case where the active layer has several  $k\Omega m$ , the highly resistive frozen ground several  $100 k\Omega m$ , and the unfrozen bedrock several  $100 \Omega m$ . Referring to permafrost boreholes in the Alps (Vonder Mühl and Holub 1992), ice content in the permafrost tends to decrease with depth. Therefore, the second layer of the three-layer model is separated into two: one with a higher resistivity (corresponding to the ice rich, cold part), and one with a moderate permafrost resistivity.

Figure 4 shows measured values and interpreted curves. In order to determine maximum and minimum values for resistivity and thickness, several extreme models were calculated.

Sounding MGL E1 is located at the end of the cirque in the uppermost and often shaded part of the rock glacier. It revealed underneath a 2 m thick active layer with a resistivity of  $25 k\Omega m$ , a high resistivity layer. The resistivity of the second layer lies between  $200 k\Omega m$  and  $4 M\Omega m$ , and the layer is between 50 and 70 m thick. The two asymmetrical curves (north and south) are similar. For a three layer case, the thickness of the high resistivity layer (ice-bearing permafrost) is not more than 50 m. If this layer is separated into two layers, one with a  $M\Omega m$ - and the other with a  $100 k\Omega m$ -resistivity, thickness of these two layers together may be up to 100 m. Inserting a third layer of  $20 k\Omega m$  the total thickness of these three layers could be more than 100 m without contradiction to the measured data. On the other hand, a high-resistivity layer with  $4 M\Omega m$  could not be thicker than 5 m. Within these extreme values there are hundreds of possibilities for models. Reasonable values for the permafrost body may be around 60 m thickness and about  $1 M\Omega m$  at this site.

Sounding MGL E2 is located at the point where the rock glacier turns to the Northwest. It shows two asymmetrical curves which are quite different. The thickness of the high resistivity layer in the northwestern part (downvalley) appears to be thinner than in the southeastern part, which ends at the steep rock wall. Resistivity values vary between  $100 k\Omega m$  and  $3 M\Omega m$ . Thicknesses depend on the insertion of a second permafrost layer with a  $100 k\Omega m$  resistivity. However, layer thickness may be up to 40 m but not more. The layer below has a much lower resistivity (several  $100 \Omega m$ ) than the one in sounding MGL E1 because the curve is strongly oversteepened.

### PHOTOGRAMMETRICAL INVESTIGATIONS

#### Methods

In 1900 Buchholz recognized that displacement can be determined by comparing two pictures for which the orientation is known. Finsterwalder (1931), Hofmann (1958) and Kick (1966) developed methods for the calculations. Flotron (1979) refined the concept and adapted it to digital interpretation devices with which the displacement can be measured directly. Photogrammetrical investigations of Muragl rock glacier were performed on the KERN DSR 15-18 analytical plotter, which is a digitally controlled stereo restitution instrument.

Creep velocity of rock glacier permafrost is generally in the order of decimeter per year. The vertical accuracy of the interpretation of an aerial photo taken from approximately 900 m (corresponding to a scale of 1:6,000) is less than 0.01% of the altitude above ground. The horizontal accuracy is about 5 cm, which means that total displacement accuracy is about 10 cm/a. Thus, in order to measure significant displacements the necessary time interval is 4 to 5 years. Moreover, the surface of a rock glacier is undulating and extremely irregular and hence is not clearly defined.

First, each stereo terrain model of the years 1981, 1985 and 1990 was processed digitally with a grid distance of 20 m. Then, two pictures of a different date were put together to

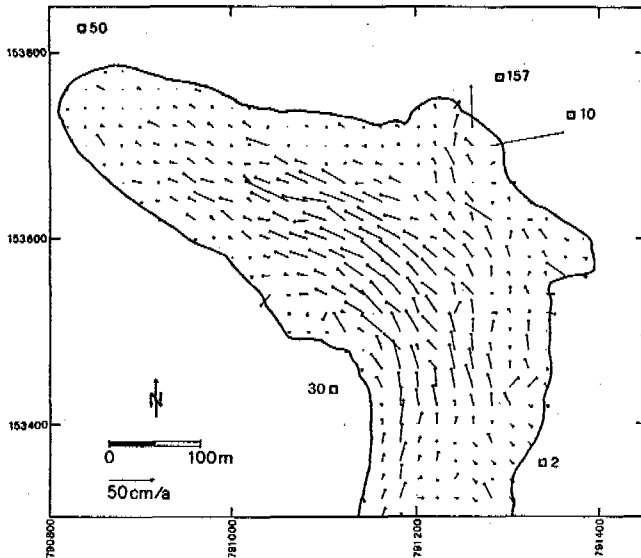


FIGURE 5. Displacement vectors on rock glacier Muragl I between the years 1985 and 1990.

form a stereo model. At the grid points, which are localized automatically by the analytical plotter, the parallaxes which are caused by the movement of the rock glacier are measured and the corresponding displacements calculated. These basic data enable the subsequent calculations of velocity, changes in surface altitude ( $\Delta h$ ), and strain rates to be made.

### Results

The vectors of displacement between 1985 and 1990 are presented in Figure 5. The velocities decrease towards the margins. The sharp turn of the feature is also visible in the direction of the vectors. Maximum values of 30 cm/a occur in the center of the rock glacier. The lowermost part, where Barsch (1973) performed seismic refraction measurements, shows very small movements. There, a higher rate of displacement is observed in the period 1981/1985 than in 1985/1990. The same tendency is observed in the marginal parts. This indicates an ongoing slowdown of the rock glacier movement in its frontal part as well as at the margins.

Several exceptional points are measured, especially in the marginal and frontal parts. These points are caused by blocks falling down a break line.

The calculation of the vertical variations of the altitude per year between 1981 and 1990 revealed that areas which rise or subside occur randomly over the rock glacier. Vertical movement of the surface is less than 20 cm/a. The only exception is the slow moving area in the transition zone between the cirque and the valley on the eastern part with subsidence rates of up to 40 cm/a.

Since the vector plots of the two periods 1981/85 and 1985/90 are quite different, especially in the frontal and marginal parts, acceleration of the rock glacier can be calculated, i.e. the velocity changes between the two time intervals. The observed trend of a stopping of the rock glaciers movement in the lowermost part is not confirmed, most likely due to the exceptional points. Values vary

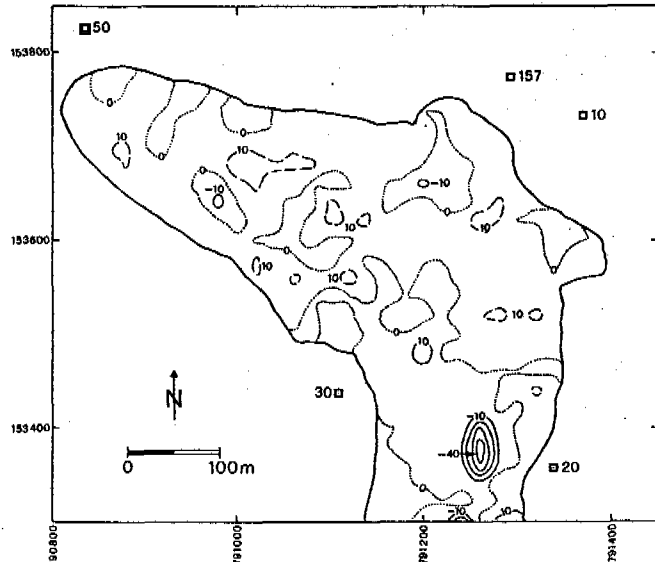


FIGURE 6. Rates of changing surface altitude ( $\Delta h/\Delta t$ ) between the years 1981 and 1990 in centimeters.

within 20 cm/a<sup>2</sup>, i.e. within the uncertainty interval. The results imply unwieldiness of the permafrost body.

In order to obtain better results from the photogrammetrical study, measurements with increased intervals are recommended. The movement of rock glacier Muragl I is about 3 to 4 times slower than that of the Gruben rock glacier (Haeberli and Schmid 1988), so the survey periods should be approximately twice to three times longer.

### CONCLUSIONS

The combined geophysical and photogrammetrical study of rock glacier Muragl I revealed that typical seismic velocities in the permafrost are approximately 1000 m/s for the active layer, 2800 - 3900 m/s for the ice-bearing permafrost, and 5000 m/s for bedrock. Thicknesses of the active layer vary between 1 and 7 m with higher values near the rock glacier front. DC resistivity values for the active layer are about 20 k $\Omega$ m and 100 - 2000 k $\Omega$ m for the ice-bearing, highly resistive permafrost. The thickness of this high-resistivity layer may be up to 100 m and decreases from the upper part of the rock glacier to its lower part, which is of the same order as the values derived from the seismic survey. The permafrost body creeps with a velocity of 10-30 cm/a in a predominantly compressing mode. The overall flow direction changes drastically (about 90°). Variations in altitude and velocity between the two periods remain within measuring accuracy. Subsiding and rising areas are randomly distributed. The marginal and frontal parts of the rock glacier appear to slow down.

### ACKNOWLEDGEMENTS

Thanks are due to all colleagues who helped during the field work in the Val Muragl; to Wilfried Haeberli for many productive discussions; to Hermann Bösch for supporting the

calculations on the analytical plotter; to Bruno Nedela for preparing the Figures; to Jörg Ansonge for critically reading the manuscript and to Susan Braun-Clarke for editing the English. The Institute of Geophysics (ETH Zurich) provided the instruments for the geophysical surveys.

#### REFERENCES

- Barsch, D. (1973) Refraktionsseismische Bestimmungen der Obergrenze des gefrorenen Schuttkörpers in verschiedenen Blockgletschern Graubündens. *Z'schrift für Gletscherkunde und Glazialgeologie IX* (1-2), 143-167.
- Barsch, D. und G. Hell (1975) Photogrammetrische Bewegungsmessungen am Blockgletscher Murtél I, Oberengadin, Schweizer Alpen. *Z'schrift für Gletscherkunde und Glazialgeologie XI* (2), 111-142.
- Domaradzki, J. (1951) Blockströme im Kanton Graubünden. Ergebnisse der wissenschaftlichen Untersuchungen des Schweizerischen Nationalparks. Komm. der Schweiz. Naturforschenden Gesellschaft III (24), 177-235.
- Evin, M., A. Assier et D. Fabre (1990) Les glaciers rocheux du Marinét (Haute-Ubaye, F). *Revue de géomorphologie dynamique XXXIX* (4), 139-155.
- Finstervalder, R. (1931) Geschwindigkeitsmessungen an Gletschern mittels Photogrammetrie. *Z'schrift für Gletscherkunde IX*, 251-262.
- Fisch, W. Sen., W. Fisch Jun. and W. Haeberli (1977) Electrical D.C. resistivity soundings with long profiles on rock glaciers and moraines in the Alps of Switzerland. *Z'schrift für Gletscherkunde und Glazialgeologie XIII* (1/2), 239-260.
- Flotron, A. (1979) Verschiebungsmessungen aus Luftbildern. Mitteilung VAW-ETH Zürich 41, 39-44.
- Haeberli, W. (1992) Possible effects of climatic change on the evolution of Alpine permafrost. Ed. M. Boer and E. Koster. *Catena Supplement 22*, 23-35.
- Haeberli, W., M. Hoelzle, F. Keller, W. Schmid, D. Vonder Mühll and S. Wagner (1993) Monitoring the long-term evolution of mountain permafrost in the Swiss Alps. Proc. 6th International Conference on Permafrost.
- Haeberli, W. und G. Patzelt (1982) Permafrostkartierung im Gebiet der Hochebenkar-Blockgletscher, Obergurgel, Ötztaler Alpen. *Z'schrift für Gletscherkunde und Glazialgeologie XVIII* (2), 127-150.
- Haeberli, W. and W. Schmid (1988) Aerophotogrammetrical monitoring of rock glaciers. Proc. (1) 5th International Conference on Permafrost, 764-769.
- Hagedoorn, J.G. (1959) The plus-minus method of interpreting seismic refraction sections. *Geophysical Prospecting VII*, 158-182.
- Hoekstra, P. and D. McNeill (1973) Electromagnetic probing of permafrost. Proc. 2nd International Conference on Permafrost. 517-526.
- Hofmann, W. (1958) Bestimmung von Gletschergeschwindigkeiten aus Luftbildern. *Bildmessung und Luftbildwesen*, 71-88.
- Keller, F. (1992) Automated mapping of mountain permafrost using the program PERMAKART within the geographical information system ARC/INFO. *Permafrost and Periglacial Processes 3* (2), 133-138.
- Kick, W. (1966) Measuring and mapping of glacier variations. *Canadian Journal of Earth Sciences 3* (6), 775-781.
- King, L., W. Fisch, W. Haeberli and H.P. Wächter (1987) Comparison of resistivity and radio-echo soundings on rock glacier permafrost. *Z'schrift für Gletscherkunde und Glazialgeologie XXIII* (2), 77-97.
- Koefoed, O. (1979) Geosounding principles, 1. Resistivity sounding measurements. 276 pp. Elsevier Scientific
- Palmer, D. (1980) The generalized reciprocal method of seismic refraction interpretation. 104 pp. Society of Exploration Geophysicists, Tulsa.
- Palmer, D. (1986) Refraction Seismics. Handbook of Geophysical Exploration, Section I Seismic Expl. By Klaus Helblig and Sven Treitel 13, 269 pp.
- Röthlisberger, H. and K. Vögtli (1967) Recent DC resistivity soundings on Swiss glaciers. *Journal of Glaciology 6* (47), 607-621.
- Salomon, W. (1929) Arktische Bodenformen in den Alpen. *Sitzungsberichte der Heidelberger Akademie der Wissenschaften. Math.-naturwiss. Klasse 5*. 34 pp.
- Shukmskii, P.A. (1964) Principles of structural glaciology. 497 pp. Dover Publications, Inc., New York.
- Vonder Mühll, D. (in prep.) Geophysikalische Untersuchungen im Permafrost des Oberengadins, Graubünden. Ph D thesis ETH Zurich.
- Vonder Mühll, D. and P. Holub (1992) Borehole logging in Alpine permafrost, Upper Engadin, Swiss Alps. *Permafrost and Periglacial Processes 3* (2), 125-132.

## RAPID SOLIFLUCTION AS A STAGE OF THE TRANSITION FROM COVERED SOLIFLUCTION TO THE FREE SOLIFLUCTION

E. A. Vtyurina, S. G. Guevorkian, V. L. Poznanin

Industrial and Research Institute for Engineering Investigations of Construction,  
18, Okruzhnoy, Moscow, Russia

In this paper the rapid solifluction is shown as a process of the transition from covered solifluction to the open one. Two kinds of the rapid solifluction are distinguished according to the mechanism of the thawed soil's movement down the slope. The first kind corresponds to the case of the movement like the flow of viscous Newtonian media, and the second kind corresponds to the movement of visco-plastic Binghamian media. The causes of thawed soil's local instability on the slope are revealed, and critical conditions, necessary for the rupture of the turf layer and its swift descent down the slope are analysed.

The problem of rapid solifluction on slope in the zone of permafrost has been insufficiently developed as yet, despite its negative impact on the development of the territory. Saying about the rapid solifluction (or spliv in Russian terminology; that signifies the rapidly floating turf on the slope) we imply the phenomenon of the rupture of the turf layer and its swift descent downwards the slope. Because the term spliv better corresponds to the essence of this phenomenon, below we use this term instead of the term rapid solifluction. Most researchers consider the splivs as one of the types of solifluction (Kaplina, 1965; Popov, 1967; Zhigarev, 1975, 1978; Geocryology of the USSR, 1989), but, however, the main distinguishing feature which would enable us to rank the spliv with other types of solifluction (closed or covered, open or free) has not been shown yet. The difference between the covered and free solifluction is in the conditions of soil flow. Covered solifluction concerns the soil flow under the turf. In the case of free solifluction the soil flows over the turf or the turf is lacking (Fig. 1).

In a contrast with the view by (Kaplina, 1965; Zhigarev, 1978), the specific character of the splivs, its difference from closed and free solifluction may be shown only if we take into consideration the presence and behaviour of the turf layer (turf-peat horizon) during the process of the spliv. The velocity of soil's flow and the time of soil's movement appearance don't give the possibility to reveal the peculiarities of the spliv, because the velocity of the spliv is comparable with the velocity of the free solifluction, and besides that the splivs may appear at any season. In nature, when the slopes are largely covered with turf, the immediate transition from closed solifluction to the open one is impossible. First, some process should cause the turf removal on a site of the slope. The spliv is such a process. Hence, the closed solifluction is the flow of soil under the turf; the spliv is the flow of soil together with the turf, floated on the soil downward the slope; and the free solifluction is the flow of soil having

no turf or a little bit of it over. The above-mentioned three types of solifluction form the common range of its developmental stages in which they replace closed solifluction, then the spliv, and, lastly, the open solifluction. It is the closed solifluction that can arise independently and separately from the other two types. The spliv is impossible without preceding development of the closed solifluction. The free solifluction is also impossible without preceding developments of closed solifluction and of the spliv (with its fullest display, when the ruptured turf is swept down the slope with the flowing soil). In case of reduced spliv the effusion of water-saturated soil occurs through the gap in the slightly displaced turf.

Hence, the flow of soil under the turf on the slopes is the necessary condition for the spliv emergence. But this condition is sufficient only for the development of closed solifluction, but not for the spliv. The second necessary condition of spliv emergence is the breaking of turf under the influence of flowing soil and the passive flowing of turf with flowing soil down the slope. It is this condition that accounts for the spliv emergence. Therefore, the solution of spliv problem requires the consideration of two important questions: a) the conditions and mechanism of solifluction soil flowing on the slopes under the turf and b) the conditions necessary for breaking the turf along the inclination of the slope and across it and the flowing down of turf together with the flowing soil.

Of these two questions a special attention is paid in connection with rapid progress of closed solifluction in the field of permafrost and its negative influence on the development of slopes. In 1938, Lukashov pointed out the conditions necessary for solifluction soil flowing. Later those conditions were confirmed and supplemented: the slope of the surface, sand composition of thawed soil, its extension beyond soil liquid limit at some moment, and the definite ice content of thawed soil. The splivs as well as other types of solifluction progress in seasonally cryogenic soils (SCS). It should be noted that

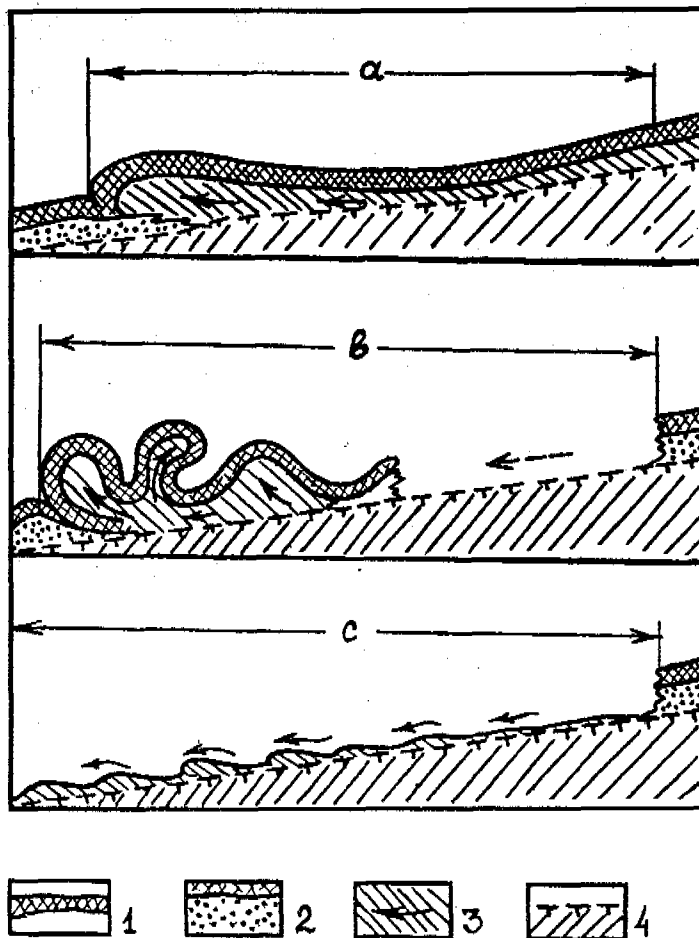


Figure 1. Forms of the solifluction:  
 a) Free solifluction;  
 b) Rapid solifluction (criogenic splay);  
 c) Closed solifluction.  
 1 - turf; 2 - plastic soil; 3 - fluid soil;  
 4 - thawing boundary of the frozen ground.

the dominating composition of seasonally cryogenic soils (SCS) thawed in the course of summer, their moisture and thickness meet the requirements necessary for the development of viscous-plastic soil on the slopes of different steepness. They mostly consist of sand in the whole section or in the separate horizons. The moisture of seasonally cryogenic soils or their different horizons may exceed the soil liquid limit during summer period (Vtyurina, 1984). Therefore, the thawed soils on the slopes in the zone of permafrost may flow. The role of soil thickness in the development of solifluction flowing is estimated according to the flowing mechanism. Nowadays it is considered that the viscous-plastic flowing is similar to the flowing of Bingham media (Kaplina, 1965; Zhigarev, 1967, 1975, 1978). Hence, the necessary thickness of thawed soils is one of the obligatory conditions of viscous-plastic flowing on the slopes.

When solving the splay problem one might just use this idea if nature of thawed soils flow on

the slopes. This idea has not been objected to and one could not touch the wider problem of soil flowing on the slopes at all. It was established long ago that the splays emerge not only in autumn (Zhigarev, 1978) but in spring-summer period (Kaplina, 1965; Scrilnic, 1975) when the thickness of thawed soils is less than necessary for the Bingham media and the Newtonian liquid. This is also proved by the regularities of the cryogenic structure of SCS (Vtyurina, 1984, 1985), by the ice content in them, and the thawing of which ensures the definite moisture of thawed soils. As it was shown in the analysis and summary of actual data, the upper horizon of the sand-suglinok of SCS in the whole zone of permafrost and also all SCS may be beyond the moisture limit of yield only because of ice thawing in these soils. The composition and moisture do not limit their flowing down the slopes in the course of thawing as in the case of the Newtonian liquid. The splay development similar to the Bingham media is typical of the autumn splays when



the lower icy horizon of SCS is in the larger zone of permafrost and the middle horizon has a low ice content.

Therefore, one can distinguish two types of soil flowing; the first one - splivs developing similar to the flowing of the Newtonian liquid and the second one - splivs developing similar to the flowing of the Bingham media. This enables us to reconsider the role of permafrost in the splivs development. Its role does not prove the fact that the splivs are allegedly possible only in autumn with the beginning of permafrost thawing (Shigarev, 1978) and that permafrost is a water confining stratum.

The main thing is that the presence of permafrost and its temperature differences determine the regularities of cryogenic composition of sand SCS, the amount and distribution of ice in SCS being the reason for primary moistening the soils with thawing (Vtyurina, 1984, 1985).

The differences in the character of soil flowing under the turf determine the different conditions for breaking the turf across the slope and its shearing along the inclination of the slope. When the soil is flowing as the Newtonian liquid, turf breaking and shearing depend on the thickness of turf (H), its resistance limit to breaking ( $\delta_b$ ) and lateral shear ( $\delta_s$ ), its density ( $\rho_t$ ), thickness (h) and density ( $\rho_s$ ) of thawed soils under it. When the soil is flowing as the Bingham media, the turf breaking and shear and the development of splivs of the second type also depend upon the shear resistance limit of thawed soils ( $\tau$ ). Finally, taking into account these indices makes it possible to determine the critical length (L) along the inclination and the width (B) across the slope with turf. Those indices are necessary for turf breaking and shear, and therefore, for its downward flow on condition that the soil is flowing under the whole area of that site at given moment of thawing.

During the seasonal thawing of mineral soils in spring when ( $h=0, \delta_b > \delta_s$ ), it is possible to determine the critical length of the slope for the first type splivs by the formula:

$$L = \frac{\delta_b}{g \cdot \rho_t \cdot \sin \alpha} \quad (1)$$

where  $\alpha$ -steepness of the slope, g-free fall acceleration (the rest of the symbols are in the text).

Accepting ( $\delta_b > \delta_s$ ) is possible in case of turf disturbance, but in nature the turf is usually undisturbed. On condition that ( $\delta_b = \delta_s$ ) and ( $h=0$ ), the possibility of spliv is determined not only by (L) but also by (B), i.e. by the length of the turf breaking and the slope width. In this case (L) is calculated by the formula:

$$L = \frac{2 \cdot \delta_b}{(\rho_t + 0,25\rho_s \cdot h/H)g \cdot \sin \alpha} \quad (2)$$

and B by formula:

$$B = \frac{4 \cdot \delta_b}{(\rho_t + 0,25\rho_s \cdot h/H)g \cdot \sin \alpha} \quad (3)$$

The analysis showed that depending on the thickness of turf and flowing thawed soil under it, their physico-mechanical indices and the slope steepness, the values L and B change from some meters to hundreds and even thousands, increasing, other things being equal, with decreasing of slope steepness.

The flowing of thawed soils as the Bingham media under the turf on condition that ( $\delta_b > \delta_s$ ), the critical length of the slope for the spliv of the second type is determined by formula:

$$L = \frac{\delta_b}{(1,25\rho_t + 0,25\rho_s \cdot h/H)g \cdot \sin \alpha - 0,25 \cdot \tau/H} \quad (4)$$

If having the undisturbed turf, then  $\delta_b = \delta_s$ , L and B are determined by the formula:

$$L = \frac{2 \cdot \delta_b}{(1,25\rho_t + 0,25\rho_s \cdot h/H)g \cdot \sin \alpha - 0,25 \cdot \tau/H} \quad (5)$$

$$B = \frac{4 \cdot \delta_b}{(1,25\rho_t + 0,25\rho_s \cdot h/H)g \cdot \sin \alpha - 0,25 \cdot \tau/H} \quad (6)$$

The time registration and the spliv mechanism enable us to suggest a new classification: a) the spring splivs are only of the first type; b) the summer splivs are mainly of the first type, rarely, of the second type; c) the autumn splivs on the most part of permafrost zone are largely of the second type, rarely, of the first type, except the extreme Northern regions.

Depending on the spliv type the analysis of L and B may be done by the equalities (1), (2) and (3); the state of turf being taken into account and h (splivs of the first type) or by the equalities (4), 5 and (6) (splivs of the second type).

It should be noted that the timely assessment of the spliv hazard of slopes is extremely important. The sites where the splivs have occurred may be considered to be nonhazardous in the course of 20-30 years. The other cryogenic processes are likely to develop on the above-mentioned sites but the splivs may again occur only after the turf renewal.

On detail investigation of the thickness and turf properties and the thawed soil under the turf on the slope investigated, the obtained data on L and B make it possible to estimate the actual spliv hazard of the slopes. In 1992 the author first suggested the criteria, assessment methods and principles of cartographic representation of potential spliv hazard of slope. Due to the spatial heterogeneity of thickness and turf properties and thawed soil on the slopes, the actual spliv hazard, as a rule is less than the potential one. Especially if it refers to the spring splivs. Potentially, they occur rarely as their development depends on the turf thickness and its relationship with thaw depth in spring. The sites of the slopes on which the turf thickness is equal or more than the thaw depth in spring are nonhazardous at that season of the year.

The summer splivs of the first type on the part of permafrost zone mainly depend on summer rains. Therefore, the most considerable differences between potential and actual summer spliv hazard of slopes are likely to be in dry summer.

The least difference between the potential and actual spliv hazard of slopes should be in autumn. Being determined largely by ice content and, consequently, by the moisture of the lower horizon of SCS thawing in autumn, the autumn spliv hazard is not practically influenced by the heterogeneity of turf thickness and the rainy autumn season. The temporary changes of cryogenic structure of sand SCS is the main reason for the differences between potential and actual autumn spliv hazard of slopes on the most part of permafrost zone. Perennial changes of thaw depth in

different years in autumn cause thawing the horizons of various content of ice and, in addition, the SCS ice-content horizons of various thickness in the same site of the slope.

The actual spliv hazard of slopes is likely to be less than the potential one in cold summer-autumn period and higher in the following warm ice content horizon of SCS which exceeds the average potential spliv hazard for a period of many years.

Mapping the potential spliv hazard of slopes i. e. the possibility of spliv emergence under given conditions makes it possible to develop the rational method of natural investigation necessary for actual spliv hazard assessment.

#### REFERENCES

Geocryology of the USSR. Western Siberia, 1989, Moscow, Nedra, 232 pp.

Kaplina T. N. 1965. Cryogenic slope processes. Moscow, Nauka, 296 pp.

Popov A. I. 1967. Cryolitology, Moscow, Moscow University Press, 304 pp.

Skrilnik G. P. 1975. Peculiarities of the forming processes of some slopes on the South of the Middle and Eastern Siberia, In: Investigations of the interactions in the systems. Vladivostok, 106-113 pp.

Vtyurina E. A. 1984. The seasonal cryogenic rocks, Moscow, Nauka, 120 pp.

Vtyurina E. A. 1985. The underground ice of the seasonal cryogenic rocks. Essay of the dissertation. Moscow, 44 pp.

Zhigarev L. A. 1967. The mechanism and causes of the solifluction's development. Moscow, Nauka, 140 pp.

Zhigarev L. A. 1975. Processes of the thermodenudation and thawing soils behavior during the deformation. Moscow, Nauka, 110 pp.

Zhigarev L. A. 1978. Postcryogenic splives of the soils on the slopes and shores. In: The General Geocryology. The Materials for the III International Conference on Permafrost. Novosibirsk, Nauka, 141-151 pp.

# A NUMERICAL SIMULATION OF COASTAL RETREAT AND PERMAFROST CONDITIONS, MACKENZIE DELTA REGION, CANADA

Baolai Wang

Department of Geology, University of Ottawa, and Ottawa-Carleton  
Geoscience Centre, Ottawa, Ontario, Canada K1N 6N5

The proximity of the Beaufort Sea influences permafrost in the Mackenzie Delta region in at least two ways: 1) thermal erosion and rapid coastal retreat of unconsolidated ice-rich sediments leaves an offshore zone of relict permafrost beneath shallow water, and 2) the thermal regime in such areas progressively adjusts to the new upper boundary zone created by the coastal retreat. To understand these implications more fully, a numerical model is applied to simulate the thermal conditions of the Mackenzie Delta littoral environment. The model predicts permafrost preservation in the nearshore following coastal retreat. This layer of relict permafrost will vary in thickness, depending upon distance offshore, but its temperature will be 3 to 5°C warmer than adjacent terrestrial permafrost.

## INTRODUCTION

Subsea permafrost in the nearshore areas of the Arctic Ocean has been documented by Russian (e.g. Are 1983; Molochushkin 1978), Canadian (e.g. Hunter 1988; Mackay 1972), and American scientists (e.g. Lachenbruch and Marshall 1977; Osterkamp and Harrison 1982). Its origin is closely related to an emergence-submergence mechanism which states that permafrost formed on exposed shelf areas during the Pleistocene when sea level was lower (Mackay 1972; Vigdorichik 1980). The ground thermal regime of subsea permafrost depends largely upon the stability of the shorelines. In areas where the shoreline has been relatively stable for long periods of time, the thickness and temperature of subsea permafrost approach an equilibrium state. However, the time required for subsea permafrost to reach this equilibrium state after a rapid sea-level transgression and/or coastal retreat is probably more than 10,000 years (Lachenbruch 1957). Shorelines developed in unconsolidated and ice-rich permafrost sediments will unlikely remain stationary during such a long time period. Therefore, the study of littoral nearshore permafrost is most realistic if a retreating shoreline is assumed. This can be justified in the Mackenzie Delta region where extensive areas are underlain by unconsolidated ice-rich sediments and massive ground ice. In this paper a numerical model, applicable to the littoral zone of the Mackenzie Delta region, is used to simulate the ground thermal regime of nearshore permafrost under the influence of continuous coastal retreat.

## EVIDENCE FOR COASTAL RETREAT

Coastal recession, caused by thermal

erosion of ice-rich and unconsolidated sediments has been reported from many areas of northern Alaska (e.g. Vigdorichik 1980; Walker 1988), northern Siberia (e.g. Are 1983), and the Western Canadian Arctic (e.g. Dyke 1991; Harry, French and Clark 1983; Mackay 1963, 1986). In the Laptev Sea, certain islands have disappeared in historic times, on account of extremely rapid coastal recession (Barr 1976). On the Yukon Coastal Plain, the grave of a member of Amundsen's expedition had to be moved landward several times due to coastal retreat (Mackay, 1963). Recent field observations along the Beaufort Sea coast in the Mackenzie Delta region indicate that the retreat rate varies between less than one metre to more than 8 m per year (Figs. 1 and 2) (Dallimore et al. 1988; Mackay 1986), depending mainly on ice content, degree of lithification of the sediments and the activity of storm surges and longshore currents. Elsewhere, maximum retreat rates of 15 to 20 m/year have been documented for parts of the Laptev Sea coast, Siberia (Molochushkin 1978).

## NUMERICAL MODELLING

### Seafloor Temperature

Mean annual seafloor temperature (MAST) is taken as a boundary condition in this model. For the Mackenzie Delta region, a mean annual ground surface temperature of -8.0 °C is typical (Allen et al. 1988; Judge 1973). Recent studies indicate that seafloor temperature decreases with increasing water depth and remains below 0°C for much of the year (Dyke 1991; Hunter 1988; Sellmann et al. 1992). In the Mackenzie Delta region of the Beaufort Sea the MAST ranges mostly between 0 and -2°C. In this study values of MAST of between -1 and -2°C are assumed for all areas between Herschel Island and King Point, plus the

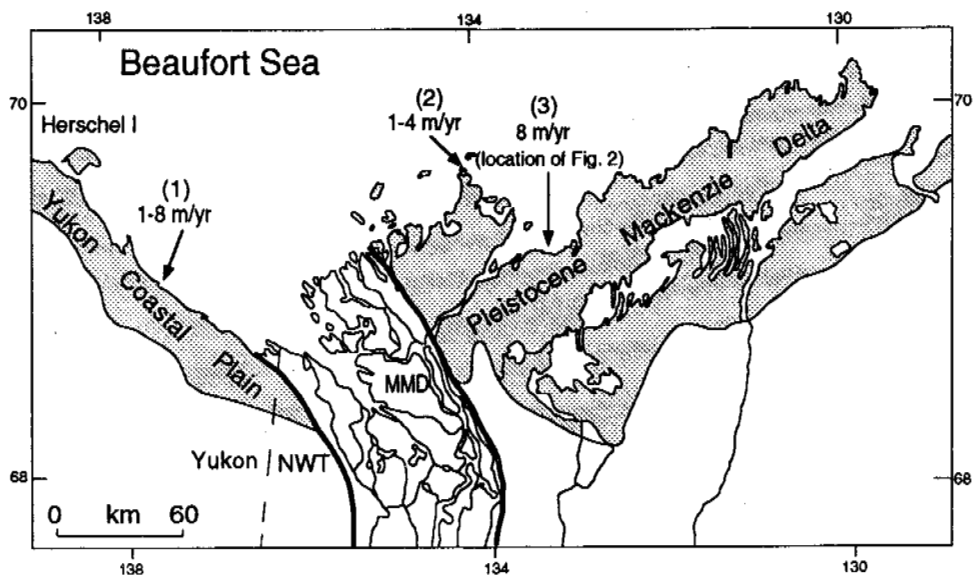


Figure 1. Location map of the Mackenzie Delta region, showing typical rates of coastal retreat: (1) King Point, (2) North Head, and (3) Peninsula Point and Tuk 3 site. Coastal retreat data according to Mackay (1963, 1986) and Dallimore et al. (1988); MMD - Modern Mackenzie Delta.

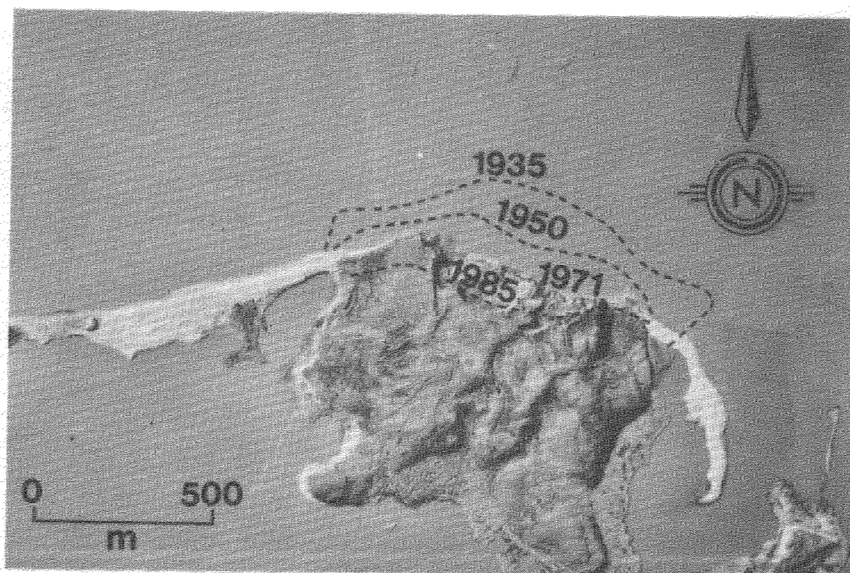


Figure 2. A 1971 air photo (A22535) of Peninsula Point, showing the shoreline positions at different times (1935, 1950, and 1985) (Source: Mackay 1986).

offshore areas of the Pleistocene Mackenzie Delta (Fig. 1). The discharge of the Mackenzie River mixes with sea water to give above  $0^{\circ}\text{C}$  temperatures, but this effect is restricted to shallow depths only (Dyke 1991; Hunter 1988). The MAST in this area is assumed to be  $0$  to  $-1^{\circ}\text{C}$ . Following shoreline retreat the submerged permafrost is subject to degradation although MAST can be below  $0^{\circ}\text{C}$  (Nixon 1986). The depth of thaw has been

discussed by Dyke (1991), Hunter (1988) and Nixon (1986). This paper, however, focuses mainly on the temperature variations of nearshore permafrost after rapid coastal retreat, regardless of the phase change.

#### The Model

The first problem to consider is the ground-temperature disturbance due to the ocean, where the shoreline is supposed to

have shifted during some brief interval of time in the past, and to have since remained stable. The earth's surface can be considered as a plane ( $Z = 0$ ), composed of the land surface and the ocean bottom. Neglecting relief in this way can be justified along the Western Arctic Coast of Canada because of the gently sloping continental shelf and low relative relief. In a two-dimensional model, the shoreline is represented by a vertical line ( $Z = 0, X = 0$ ), the land surface by  $Z = 0, X < 0$ , and the ocean bottom by  $Z = 0, X > 0$  (Fig. 3).

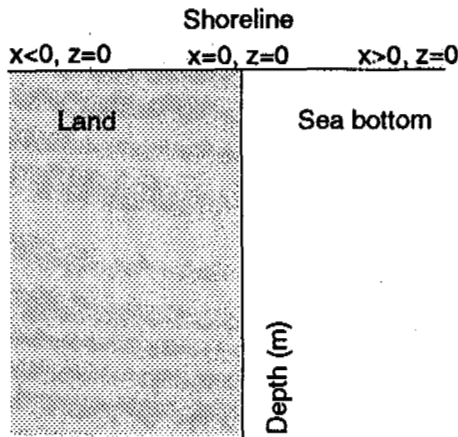


Figure 3. Coordinates of the model (see text).

The basic equation describing the heat distribution is the two dimensional Fourier equation (Lachenbruch 1957):

$$\frac{\partial^2 \theta}{\partial x^2} + \frac{\partial^2 \theta}{\partial z^2} = \frac{1}{\alpha} \frac{\partial \theta}{\partial t} \quad (z > 0) \quad (1)$$

The problem is to find the increase in temperature ( $\theta$ ) caused by coastal retreat, at any subsurface point ( $x, z$ ) that satisfies equation (1). At the same time, the model needs to satisfy several conditions. First, it is assumed that prior to initiation of coastal retreat, there was no thermal disturbance, i.e.:

$$\theta(x, z, 0) = 0 \quad (z > 0, t = 0) \quad (2)$$

Second, after the beginning of retreat, although thermal disturbance at the sea bottom occurs, it is assumed that there is no change in ground surface temperature (i.e.  $T_s$  remains constant). The sea bottom disturbance is the difference between the mean annual temperatures of the land surface and ocean bottom, represented by  $A$ . Furthermore, at an infinite depth beneath land ( $z = \infty$ ), it is assumed that

the thermal disturbance caused by coastal retreat is zero. These assumptions are expressed as follows:

$$\theta(x, 0, t) = 0 \quad (t > 0, x < 0, z = 0) \quad (3)$$

$$\theta(x, 0, t) = A \quad (t > 0, x > 0, z = 0) \quad (4)$$

$$\theta(x, \infty, t) = 0 \quad (t > 0, x < 0) \quad (5)$$

Equation (2) is an initial condition; while (3) to (5) are boundary conditions. The solution to the problem can be written in the form (Lachenbruch 1957):

$$\theta(x, z, t) = A \Psi\left(\frac{x}{z}, m\right) \quad (6)$$

where

$$\Psi = \frac{1}{2} \operatorname{erfc} \sqrt{m} +$$

$$\frac{1}{\pi} \int_0^{\frac{x}{z}} \exp[-m(1+v^2)] \frac{dv}{1+v^2} \quad (7)$$

where  $m = z^2/4\alpha t$ ;  $\alpha$  = thermal diffusivity,  $\text{cm}^2/\text{sec}$ ,  $t$  = time since coastal retreat, yr,  $v$  = integration variable.

The restriction that a shoreline moves suddenly, at  $t = 0$ , to a new position,  $x = 0$ , can be removed by superposition of solutions of the form of (6). In the general case when  $n$  stages of shoreline retreat are considered, solution (6) becomes (Lachenbruch 1957):

$$\theta = A \left[ \sum_{i=1}^{n-1} \left[ \Psi\left(\frac{x-x_{i+1}}{z}, m_i\right) - \right. \right.$$

$$\left. \Psi\left(\frac{x-x_i}{z}, m_i\right) \right] + \Psi\left(\frac{x-x_1}{z}, m\right) \quad (8)$$

Therefore, the ground temperature at any point ( $x, z$ ) is the temperature before disturbance ( $T_u$ ) plus the temperature increase caused by shoreline retreat:

$$T(x, z, t) = T_u + \theta = T_s + T_g * Z + \theta \quad (9)$$

where  $T_g$  is the ground thermal gradient ( $^{\circ}\text{C}/\text{m}$ ).

The model simulates the thermal regime of permafrost by tracing shoreline retreat over the last 300 years. Assuming a maximum rate of 8 m/yr as typical of exceptionally rapid retreat, the coastline of certain part of the Mackenzie Delta region would have been 2400 m seaward of its present position.

This retreat of the coastline during the last 300 years can be divided into several stages: when the coastline moves from (1)  $x = \infty$  to  $x_1 = 2,400$  m at  $t = 0$ ; (2)  $x_1 = 2,400$  m to  $x_2 = 1,600$  m at  $t_1 = 100$  years; (3)  $x_2 = 1,600$  m to  $x_3 = 800$  m at  $t_2 = 200$  years; and (4)  $x_3 = 800$  m to  $x_4 = 0$  at  $t_3 = 300$  years. For such a four-stage retreat model from  $t = 0$  (i.e. 300 years ago) to  $t = 300$  yr (i.e. present), the general form (8) becomes:

$$\theta = A\left[\Psi\left(\frac{x-x_2}{z}, m_1\right) - \Psi\left(\frac{x-x_1}{z}, m_1\right) + \Psi\left(\frac{x-x_3}{z}, m_2\right) - \Psi\left(\frac{x-x_2}{z}, m_2\right) + \Psi\left(\frac{x-x_4}{z}, m_3\right) + \Psi\left(\frac{x-x_3}{z}, m_3\right) + \Psi\left(\frac{x-x_1}{z}, m\right)\right] \quad (10)$$

where  $m_i = z^2/4\alpha(t-t_i)$ .

Solution to the equations is made by routine calculations following the methods of Smith (1953) and Lachenbruch (1957). A major problem in the model is the calculation of the disturbance function  $\Psi$  from equation (7). This involves the complementary function  $\text{erfc}(x)$  which itself relates to an error function  $\text{erf}(x)$ . Solution of these functions can be found in engineering mathematics textbooks (e.g. Kreyszig 1966). A second problem relates to the second term of equation (7) which is an integral. Smith (1953) has made a solution in the form of a series expansion.

### Results

The thermal regime of nearshore permafrost in the coastal retreating zone is finally predicted by equation (9) under three different seafloor temperatures (Tsf). The results are shown in Figs. 4 and 5. These diagrams indicate that, although there is a minor difference in permafrost thickness between land and sea, the temperature beneath the sea is warmer than beneath land. For example, the offshore ground temperature predicted under the condition of Tsf=0°C is mostly above -4°C. By contrast, the temperature beneath land 500 m away from the shoreline may be as low as -7°C.

Fig. 4 shows that permafrost can be expected to persist at a significant distances offshore following rapid coastal

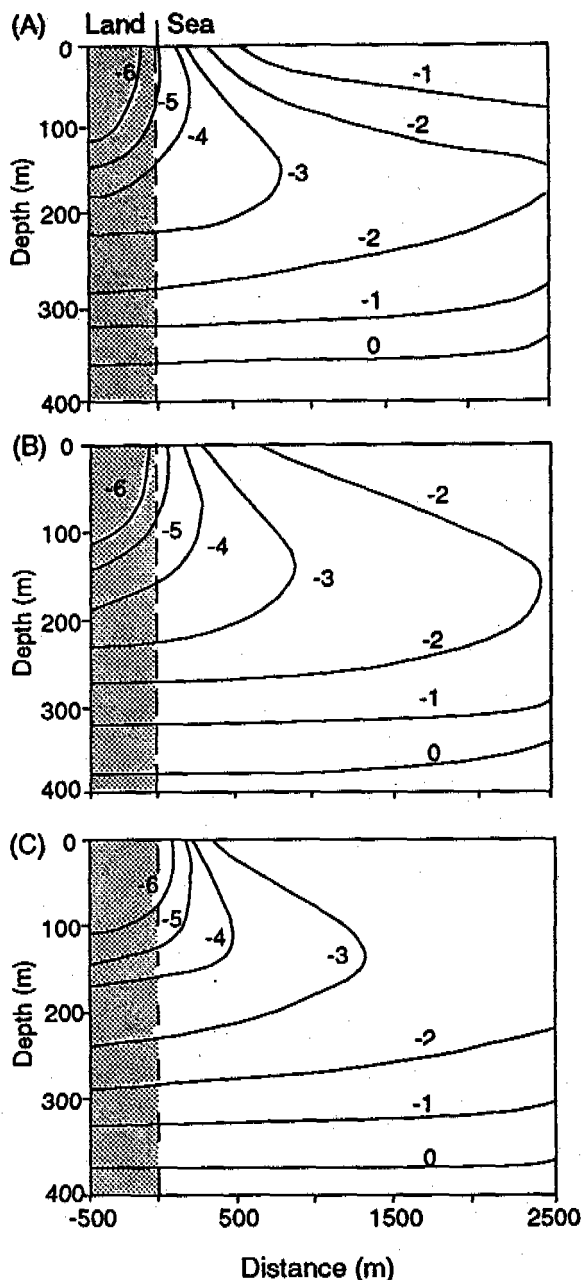


Figure 4. Predicted ground temperature for rapid retreating shorelines: A-seafloor temperature (Tsf) = 0°C, B-Tsf = -1°C, and C-Tsf = -2°C.

retreat. This has been proven offshore of Tuktoyaktuk Peninsula where drilling has indicated subsea permafrost several tens of km offshore (Hunter et al. 1976; Mackay 1972). Such extensive subsea permafrost may be due partly to rapid coastal retreat. This inference is supported by the temperature data from Norton Sound area of the Bering Sea, where nearshore subsea permafrost is present only in areas of rapid coastal retreat (Osterkamp and Harrison 1982).

Fig. 5 indicates, not surprisingly,

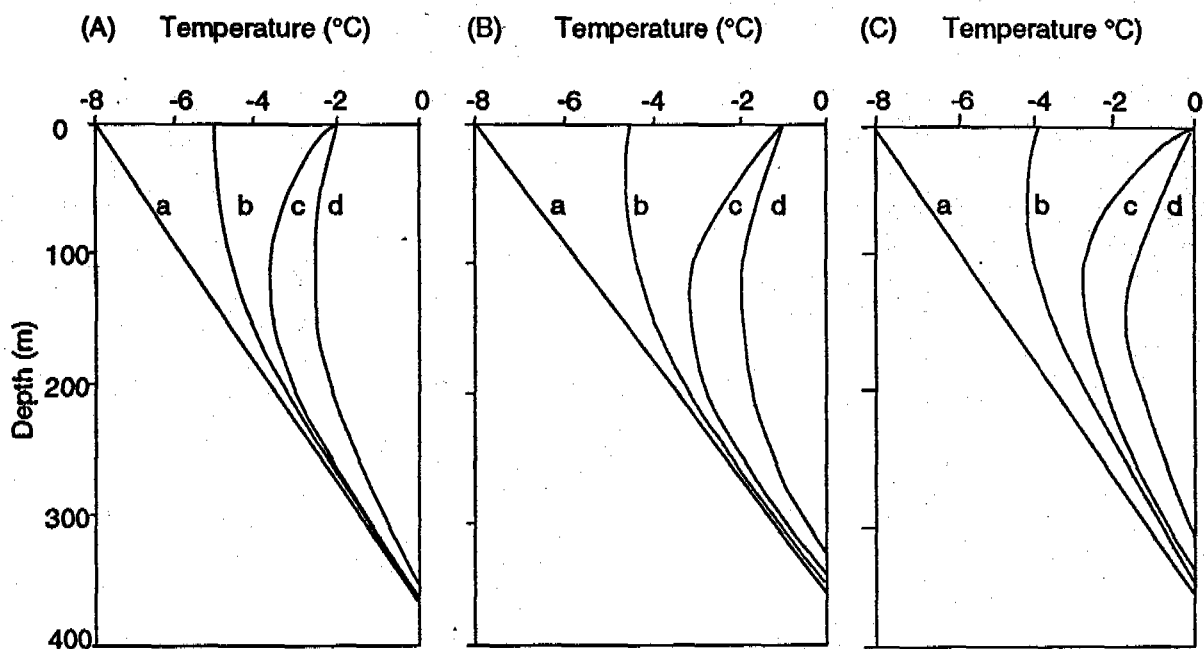


Figure 5. Ground temperature profiles predicted for different locations: A-Tsf = 0°C, B-Tsf = -1°C, and C-Tsf = -2°C; curve a-500 m landward of shoreline, curve b-at shoreline, c-500 offshore, and d-2500 m offshore.

that the most significant increase in temperature occurs near the surface (i.e., seafloor). The temperature increase within 100 m of the sea bottom may be as much as 4-6°C during the first several hundred years of submergence caused by coastal retreat. Data which support the model have been reported from the Laptev Sea, USSR (Molochushkin 1978), and from Prudhoe Bay, Alaska (Lachenbruch and Marshall 1977).

The model also indicates that the geothermal gradient of subsea permafrost becomes smaller subsequent to submergence, and that it decreases gradually from the land to the offshore. Another phenomenon associated with coastal retreat (or submergence) is the presence of a negative geothermal gradient in the upper 100 m of subsea permafrost.

#### DISCUSSION

By definition, permafrost, or perennially cryotic ground, need not contain ice even though its temperature remains below 0°C. Therefore, the permafrost base does not always coincide with the lower limit of ice-bonded permafrost. This model delineates the boundary between cryotic and noncryotic ground in the sea bed using the 0°C isotherm (Permafrost Subcommittee 1988). However, the lower limit of ice-bonded permafrost cannot be directly predicted by the model because the freezing point of the sea bed changes considerably with soil type, salinity, pressure, etc.. Investigations carried out by Lachenbruch et al. (1982) indicate that the distance between the base of ice-bonded permafrost

and 0°C isotherm ranges from 20 to 45 m at Prudhoe Bay, Alaska.

Because seafloor temperatures are mostly between -1 and -2°C (i.e. about 6 to 7 °C higher than Ts), much subsea permafrost must be relict and is degrading. If a geothermal gradient of 0.01 °C/m is assumed for the sea bottom, the equilibrium thickness of permafrost would be 200 m. Thus, one can infer that the thickness of relict degrading offshore permafrost may be as much as 150 m. As a regional maximum rate of shoreline retreat has been assumed in this simulation, areas with slower retreat rates will have thinner relict permafrost, and the thermal cross-section will be also different.

#### CONCLUSIONS

Areas of littoral and offshore permafrost exist in the Mackenzie Delta region due to rapid coastal retreat. Consequent upon retreat, submerged permafrost adjusts to higher seafloor temperatures. However, it never reaches its equilibrium thermal condition since the moving shoreline always creates a new upper boundary. The most significant increase of temperature takes place near the seafloor rather than at the base of permafrost. The numerical model discussed in this paper illustrates that the temperature of subsea permafrost, under rapid coastal retreat conditions, is at least 3°C higher than in adjacent land permafrost. This can have significant implications for all geotechnical activities in the littoral zone nearshore.

## ACKNOWLEDGEMENTS

Logistical support was provided by the Polar Continental Shelf Project, Energy, Mines and Resources Canada, the Inuvik Research Centre, Science Institute of the Northwest Territories, and the University of Ottawa Northern Research Group. This study, in part funded by the Natural Sciences and Engineering Research Council of Canada (grant A-8367 to H.M. French) is part of a Ph.D. thesis which is being undertaken at the University of Ottawa. The author wishes to thank an anonymous reviewer for his helpful comments on the manuscript.

## REFERENCES

- Allen, D.M., Michel, F.A., and Judge, A.S. (1988) The permafrost regime in the Mackenzie Delta, Beaufort Sea region, N.W.T. and its significance to the reconstruction of the paleoclimatic history. *Journal of Quaternary Science*, 3: 3-13.
- Are, F.E. (1983) Thermal abrasion of coasts. *Proceedings of the Fourth International Conference on Permafrost*, National Academy Press, Washington, D.C., 24-28.
- Barr, W. (1976) Retreating coasts and disappearing islands in the Arctic. *Musk-Ox*, 18, 103-111.
- Dallimore, S.R., Kurfurst, P.J., and Hunter, J.A.M. (1988) Geotechnical and geothermal conditions of near-shore sediments, southern Beaufort Sea, Northwest Territories, Canada. *Permafrost: Proceedings of the Fifth International Conference on Permafrost*, Trondheim, Norway. Tapir publishers, vol.1, 127-131.
- Dyke, L.D. (1991) Temperature changes and thaw of permafrost adjacent to Richards Island, Mackenzie Delta, N.W.T.. *Canadian Journal of Earth Sciences*, 28, 1834-1842.
- Harry, D.G., French, H.M., and Clark, M.J. (1983) Coastal conditions and processes, Sachs Harbour, Banks Island, Western Canadian Arctic. *Zeitschrift fur Geomorphologie*, Supplementband 47, 1-26.
- Hunter, J.A. (1988) Permafrost aggradation and degradation on arctic coasts of North America. *Permafrost: Proceedings of the Fifth International Conference on Permafrost*, Trondheim, Norway. Tapir Publishers, Vol.3, 27-33.
- Hunter, J.A., Judge, A.S., MacAulay, H.A., Good, R.L., Gagne, R.M., and Burns, R. A. (1976) The occurrence of permafrost and frozen subsea bottom materials in the southern Beaufort Sea. Canada Department of Environment, Beaufort Sea Project. Technical Report no.22, 174pp.
- Judge, A.S. (1973) The thermal regime of the Mackenzie Valley: Observations of the natural state. Environmental-social program, Northern pipelines, Information Canada, Cat. No. R72-11973.
- Kreyszig, E. (1966) *Advanced engineering mathematics*. John Wiley and Sons, 777pp.
- Lachenbruch, A.H. (1957) Thermal effect of the ocean on permafrost. *Bulletin of the Geological Society of America*, 68, 1515-1530.
- Lachenbruch, A.H. and Marshall, B.V., (1977) Sub-sea temperature and a tentative model for offshore permafrost at Prudhoe Bay, Alaska. United States Department of the Interior Geological Survey, Open-file report 77-395, 54pp.
- Lachenbruch, A.H., Sass, J.H., Marshall, B.V. and Moses, T.H. Jr. (1982) Permafrost, heat flow, and the geothermal regime at Prudhoe Bay, Alaska. *Journal of Geophysical Research*, 87, B11, 9301-9316.
- Mackay, J.R. (1963) Notes on the shoreline recession along the coast of Yukon Territory. *Arctic*, 16, 195-197.
- Mackay, J.R. (1972) Offshore permafrost and ground ice, southern Beaufort Sea, Canada. *Canadian Journal of Earth Sciences*, 9, 1550-1561.
- Mackay, J.R. (1986) Fifty years (1935 to 1985) of coastal retreat west of Tuktoyaktuk, District of Mackenzie. In: *Current Research, Part A*, Geological Survey of Canada, Paper 86-1A, 727-735.
- Molochushkin, E.N. (1978) The effect of thermal abrasion on the temperature of the permafrost in the coastal zone of the Laptev Sea. *Permafrost*, Second International Conference, Yakutsk, USSR, 1973. USSR Contribution, National Academy Press, Washington, D.C., 90-93.
- Nixon, J.F. (1986) Thermal simulation of subsea permafrost. *Canadian Journal of Earth Sciences*, 23, 2039-2046.
- Osterkamp, T.E. and Harrison, W.D. (1982) Temperature measurements in subsea permafrost off the coast of Alaska. The Roger J.E. Brown Memorial Volume - *Proceedings of the Fourth Canadian Permafrost Conference* (edited by H.M. French). National Research Council of Canada, Ottawa, 238-248.
- Permafrost Subcommittee, Associate Committee on Geotechnical Research (1988) Glossary of permafrost and related ground-ice terms. National Research Council of Canada, Technical Memorandum 142.
- Sellmann, P.V., Delaney, A.J. Chamberlain, E.J. and Dunton, K.H. (1992) Seafloor temperature and conductivity data from Stefansson Sound, Alaska. *Cold Regions Science and Technology*, 20, 271-288.
- Smith, R.C.T. (1953) Conduction of heat in the semi-infinite solid, with a short table of an important integral. *Australian Journal of Physics*, 6, Melbourne, 127-129.
- Vigdorichik, M.E. (1980) *Submarine permafrost on the Alaskan continental shelf*. Boulder, Colorado, Westview Press, 118pp.
- Walker, H.J. (1988) Permafrost and coastal processes. *Permafrost: Proceedings of the Fifth International Conference on Permafrost*, Trondheim, Norway. Tapir Publishers, vol.3, 35-42.



## CORRELATION OF FREEZE-THAW ACTION TO THE FORMATION AND EXPLORATION OF QUATERNARY GOLD PLACERS

Wang Chunhe

Natural Resources Section of Changchun Institute of Geography,  
Chinese Academy of Sciences, Changchun 130021

It is generally accepted that gold placers are the comprehensive products of manifold natural agents in geologic history. When scientists discuss the concrete agents, however, they often neglect the effect of temperature factors. We have been studying the Quaternary gold placers in the northern part of the Greater and Lesser Hinggan mountain region where there develops freezing, denudation, frost weathering, nivation, freeze-thaw sorting, freeze-thaw action and thaw action, etc. These actions played very important and unneglectable roles in the formation, preservation and exploration of gold placers. Based on the exploration experiences of gold placers in this periglacial frost region, we will give our views on the correlation of freeze-thaw action to the formation and exploration of Quaternary gold placers in the northern part of the Greater and Lesser Hinggan mountain region.

### INTRODUCTION

The Greater and Lesser Hinggan mountain region is located in Northeast China. Geotectonically, it lies in the northeast end of East-Asia-Hinggan-Mongolia Fold region. The stratigraphy of the studied region are mainly the metamorphic rocks of Proterozoic and Paleozoic Erathem, medium-acidic volcanic assemblage and coal-bearing sedimentary rocks among inland basins of Mesozoic Erathem, and elastic sediment of Cenozoic Erathem. The regional tectogenesis of post-Mesozoic Erathem was chiefly in a perpendicular up and down movement. The neotectonic movement has been active there.

The region of interest develops almost all kinds of geomorphological units, but low mountain and hill dominate. Because of the Tertiary peneplanation process, the mountains have been denudated and shaped round and smooth. This region widely developed a very thick weathering crust of the Hinggan penplain (Late Tertiary Period) and Buxi penplain (early pleistocene Epoch). They are eroded by the tributaries of the Heilongjiang (Amur) river basin. The main branches are: Nengan, Humar, Ermur, etc..

On the surface the main growth is Hinggan larch, Camphor pine, Asian white birch, etc.. As well, there are swamp plants and miscellaneous herbs. The soils are brown conifer forest soil, dark brown soil, tundra soil, etc..

The studied region is characteristic of the continental monsoon climate of the frigid-temperate zone. In winter, it is very cold, dry and long. The extreme lowest temperature is  $-52.3^{\circ}\text{C}$ . The frozen period lasts 7 to 8 months. It's yearly average temperature is  $-1$  to  $-5^{\circ}\text{C}$ . The temperature difference of a whole year is  $41.8$  to  $53.5^{\circ}\text{C}$ , which is the most extreme in the country. It snows heavily, with an average depth of  $0.3$  to  $0.4$  m. The blowing snow piles can reach a thickness of  $0.8$  to  $1.5$  m. In this region, the snow-retaining time can last 6 to 7 months. The studied region develops continuous

permafrost in the north and gradually becomes discontinuous island-like permafrost and thaw areas in the south. Its annual precipitation is  $400$  to  $500$  mm.

Since the periglacial environment dominates many kinds of modern periglacial landscapes and ancient periglacial occurrences develop widely

1. Freezing, nivation and frost weathering promoted the fragmentation of gold-bearing geologic bodies, which supplied large amounts of fragmental materials for the formation of gold placers.

Different minerals and rocks have quite different thermal stress indices, such as thermal conductivity, thermal capacity, coefficient of thermal expansion, etc.. During the long-term temperature variations and frequent freezing actions, when the thermal stress of rocks and soils is larger than the tensile stress of the selves, the frost weathering fissures are formed, which splits the hard rocks. Especially, when the leakage water freezes along the joint beddings or cracks, the volume of ice is 9% larger than that of water with the same weight which can produce a great swelling pressure. During the congelation, if all the restricted ice crystals are not allowed to expand, their bulk expansion pressure (at  $-22^{\circ}\text{C}$ ) can reach  $2115$   $\text{kg}/\text{cm}^2$  (Tstovich, N.A., 1973). In temperate zones, the pressure exerted on the pore wall of rocks by frozen water or ice can reach  $960$   $\text{kg}/\text{cm}^2$ . It is measured that the normal swelling force of frozen soil attains  $50$ - $60$   $\text{kg}/\text{cm}^2$  (Tong Changjian, 1983). Such gigantic frost pressures and heavy forces may destroy any hard rocks. In particular, during the seasons of day-thaw and night-freeze, at day time, the precipitation and meltwater of ice and snow filters into all kinds of minor fissures; at night, they swell and produce gigantic ice-splitting forces which chop gold-bearing geologic bodies. After the physical and chemical weathering of repeated freeze-thaw actions in

geologic history, a large amount of gold-bearing fragmental materials were formed. In the region of interest, the periglacial geologic products of such a process are: frost altiplanation terraces, periglacial talus, block fields, stone strips, stone streams, etc.. They greatly promoted the formation of gold placers.

In the studied region, the accretion time of snow lasts 5 to 6 months. The thickness of the snow mantle varies in different places. The thickest places are specific accumulating depressions, lee shelters, blowing snow piles and snow ridges, with a depth of 0.8-1.5 m. From precipitation to accumulation, with the prolonging of overstocking, snow gradually becomes more concentrated and its density increases, with the measurement of on-the-spot, from 0.2g/cm<sup>3</sup> of primary snow to 0.3g/cm<sup>3</sup>, 0.5g/cm<sup>3</sup>, and 0.6g/cm<sup>3</sup>. During the spring-thaw, snow gradually melts and recrystallizes. At the same time, snow meltwater permeates into snow. All the processes increase the snow density up to 0.7-0.8g/cm<sup>3</sup>, which becomes firm ice (see table 2). Like glacier ice (average density is 0.83g/cm<sup>3</sup>), while melting, the hard firm ice slides along the slope and ploughs and excavates the underlying rocks. Together with the sheetwash denudation and corrosion of ice-snow meltwater, they formed many nivation trough valleys and depressions, with the shapes of hemicycle, chair, or dustpan, etc.. These geomorphological units inlay between crests or hang on mountain sides, below which is often accompanied by ice-snow drift fans, with the shapes of fan or dish, which became the convenient passways for the transportation of placer gold and supplied large amounts of gold-bearing fragmental materials. These typical periglacial geomorphological landscapes are widely seen in this region. For example, there is a groove with running water a length of less than 3 km in warm seasons, where develops a branch valley gold placer. The enrichment of placer gold has a close relationship with 5 large nivation trough valleys, depressions and their corresponding snow drift fans developed on the northwestern upper slopes, which supplied large amounts of fragmental materials for the formation of the gold placer.

2. Freeze-thaw action and the torrent of ice-snow meltwater promoted the migration and enrichment of placer gold-bearing fragments.

Due to the diversity of material components, grade, and water-bearing nature, the surface rocks and soils have distinctively different thermal characters. During the process of repeated freeze-thaw actions, they produced quite different capacities of frost-expansion and thaw-sink which caused uneven displacements, rearrangements and combinations. As a result, on the surface there appears the microgeomorphological landscapes of stone stream, stone strips, polygon spotten tjaele, and stone rings, etc.. In particular, under the effect of slope torrents caused by ice-snow meltwater, the stone streams can move faster. There was a catastrophic fire in the forests of the studied region in 1987. Only 4 years later, we observed that, with the combined effect of the torrent of ice-snow meltwater and freeze-thaw uplift, many blocks of the stone stream climbed onto the burned stumps. The uneven freeze-uplift action made blocks emerge out of the soils and push the dead trunks down.

These freeze-thaw sorting and uneven freeze-uplift actions played very important roles in

the sorting and transporting of placer gold-bearing fragments on slopes. For instance, in a mesotype gold placer of the studied region, there are many stone streams with the width of 0.3-0.4 m on the base of valley slopes. These stone streams directly transported a lot of placer gold-bearing fragments into the riverbeds and promoted the formation of gold placers.

Accompanying the surface freeze-expansion, a frozen soil or rock grain on slopes can rise with a little height perpendicular to the slope face. When thawing, this grain will fall vertically due to its gravitation. In this process of the freeze-thaw action, the grain creeps a minor distance down on the slope. Because of the repeated freeze-thaw action in geologic history, the texture of soil bodies became loose. The soil bodies on slopes would wriggle and crumple along the humid thawing surface or upper limit of permafrost (Wang Chunhe, 1982), which formed congeliturbation flows or congeliturbation terraces. In the studied region, congeliturbation flows frequently appear on the low-angle slopes of 2°-10°, in particular, on the rectilinear slopes of the dark side. Some developed into congeliturbation terraces with a grade of 3 or 4, which are distributed in a scaly form on the low-angle slopes.

In profile, the congeliturbation flow is a mixture consisting of gravels, broken rocks, sands, soils, sticky muds, mucky paleo soils, etc.. Under the effect of paleoperiglacial environments, sands, rocks, muds and gravels in congeliturbation flows inlay and alternate on another, like kneading doughs, forming variegated soils with miscellaneous colours of black, yellow, brown, etc.. We once dated the congeliturbation flow, with an age between 15830±243 a B.P. and 36400±490 a B.P. which corresponds to the forming time of gold placers in this region. This indicates that under the effect of paleoperiglacial environments, congeliturbation flows supplied a lot of materials to gold placers. For example, the congeliturbation flow in a gold placer of the studied region has moved over the valley terrace of grade 1 and stretched to the high flood plain. In particular, some parts of it has crept up on the river bank and like a conveying belt, it directly supplied large amounts of fragmental materials for the washing, transporting and sorting by river water. This process has more rapid movement than that of slope wash only on slopes (Table 2).

The stability of vegetation, soils and rocks on the base of hillslope is destroyed by fetching soils for constructing roads, river erosion on the bank and forest fire, etc., the primary natural thermal equilibrium of permafrost will be broken, which causes huge-ice tjaele to lose equilibrium, esp. the base of slope where there develops underground ice. Therefore, on the edges of slopes, the thawing tjaele collapse or slide suddenly in masses. This kind of thermo-thaw slumping develops more rapidly than the congeliturbation flow does, which directly supplied fragmental materials for the formation of gold placers. For instance, in a gold placer of the region, because workers fetched soils for constructing roads, the stability of slope base and thermal equilibrium were broken. In only 3 years, the thermo-thaw olistostrome was formed with a width of 4 to 5 meters and an intermittent elongation of several hundred meters.

The snowfall which accumulates during the whole winter may reach a thickness of 0.3-0.4m,

Table 1 Roles of freeze-thaw actions in the formation of gold placers

stages of the formation of gold placers	ordinary view	roles of freeze-thaw actions(as additions)
1.preparation of materials	main external agents: running water, wind, living things, sea breakers, glaciers	1.freezing, nivations and freeze-thaw actions cause mighty freeze pressure, heaving forces ice-snow excavating,which produce the relevant fragments.
2.migration of gold-bearing fragments slopes	main transferring agents and media: gravitation,running water, gravitation, running water, glaciers, meltwater, wind	2.freeze-thaw sorting stone stream as carrier 3.freeze-thaw action: congeliturbation flow and congelifraction slump as carrier 4.torrent of meltwater and snowdrift fan as carrier
3.transportation, sorting washing up and concentrating of placer gold	main agents:running water in river	5.torrent of ice-snow melt-water caused spring flood
4.burying and preservation of gold placers	sediments accumulated and buried gold placers	6.frozen for many years protect ore bodies from destruction

some blowing snow piles and snow ridges can reach a thickness of over 0.8-1.5 m. In the first several days of sudden warmth in the spring, snow melts completely. At that time, the vegetation under the trees has not germinated and the surface is exposed without resistance. Therefore, the mighty spring slope torrents caused by the ice-snow meltwater, especially in the afternoon, scour the slopes more violently than summer storms do.

During a site observation, after a torrent of spring meltwater, on the exposed slope of a relative catchment, the scour channel was 0.2-0.3 m deep. On the valley below the base of the slope formed a minor proluvial fan with a length of over ten meters. Along the slope, the torrent of ice-snow meltwater scoured and pushed the gold-bearing fragments down straight to the riverbed and supplied it with large amounts of materials. The mighty spring flood can scour and transport many more materials than summer precipitation with dense vegetation can do.

Above all, the repeated actions and corresponding periglacial products of gelivation, swelling, ice-splitting, nivation, ice-snow excavation and denudation, freeze-thaw sorting, freeze-thaw action and the subsurface erosion by the torrent of ice-snow meltwater, play very important roles in every stage of forming placer gold, either in the pulverization of gold-bearing rocks, or in the disassociation of gold from rocks, or in the migration of gold-bearing fragmental materials on slopes, or in the transportation and enrichment of placer gold, or in the preservation of frozen gold placers from destruction, etc.(Table 1).

3. In the formation of gold placers, the agents of nivation, freeze-thaw action, gravitation and running water, etc. superimposed one another and alternated in geologic history.

(1) The cold-warm fluctuation in geologic history

In the Quaternary Period, periglacial climates

and interperiglacial climates alternated many times in the studied region.

During the relatively cold stages, gelivation, ice-splitting, nivation, etc. dominated, which is favourable to pulverize gold-bearing geologic bodies and dissociate gold from them. The formed block field, talus, snowdrift fans, etc. stored sufficient fragmental materials for the formation of gold placers. The stone streams, congeliturbation flows, stone rings, congelifraction slumps, etc. became very important media for the migration of gold-bearing fragments on slopes.

During relatively warm stages, the temperature rises, and ice and snow thaw. The mighty torrent of meltwater caused the dominant transportation of slope sheetwash and denudation, etc. which transferred the stored gold-bearing fragments of relatively cold states to the riverbed. Such a cold-warm alternation in geologic history helped the formation of gold placers.

(2) Seasonal cold-warm alternation in a year

There is a distinctive seasonal change in this region. In frigid winter, the lowest temperature is -40 to -50°C. There are very strong gelivation, ice-splitting, nivation, bearing, etc.. After the winter, ice and snowthaw, the congeliturbation and subsurface erosion of lamellar flow and the torrent of meltwater strengthen. Hereafter, in summer, rain takes the place of snow, the running water dominates (see Table 2). Year in, year out. Such a cold-warm alternation helped the formation of gold placers.

(3) Differences of daily temperature cause the alternation day-thaw and night-freeze actions.

There is an annual average daily temperature difference of 48.4°C in the studied region. There are nearly three months of the year in which the temperature fluctuates around 0°C. The large daily temperature difference caused the positive and negative temperatures of day and night to vary violently. The alternation of day-

Table 2 Time alternative relationship of external agents, such as nivation, freeze-thaw, gravitation, running water, etc. in modern periglacial environments

seasons content months of items	late autumn	early winter	frigid winter	early spring	spring	early summer	summer & autumn
	late Sept. to early Oct.	middle Oct. to Nov.	Dec. to next early Feb.	middle Feb. to middle Mar.	middle Mar. to early Apr.	middle Apr. to late Apr.	May to Sept.
behaviour of snow mantle	unstable	thin layer of snow mantle	snow mantle becomes thicker blowing snow piles appear	snow mantle begins to thaw	snow mantle thaw	meltwater permeate	precipitation(rain)
state of snow mantle		cottony	granular	firm	firm ice	snow-ice	running water
bulk density of snow mantle(g/cm)		cottony 0.18-0.22	granular 0.2-0.33	firm 0.3-0.4	firm ice 0.4-0.53	snow-ice 0.5-0.81	running water 1.0
surface freeze-thaw	occasional-ly freeze	night-freeze day-thaw	stable freeze	occasional-ly thaw	day-thaw night-freeze	stably thaw	thaw depth becomes bigger
transporting way of water	surficial evaporation and permeation	slight evaporation, migrate to the frozen	migrate to the frozen face, accumulating ice	first melt-water seep	meltwater seeps and evaporates	permeate, evaporate, sheetwash	sheetwash, permeate, evaporate
result of actions	evaporate to dry	heaving, fracture	ice-splitting, nivation, heaving	slight erosion of melt-water	erosion of meltwater	lamellar flow of ice-snow meltwater, undercutting	washing out of running water

thaw and night-freeze made surface soils and rocks freeze and thaw repeatedly. In particular, at day time, free water in soils and rocks thaw and permeate into minor joints and fractures. At night, they freeze to form ice bodies, which produces gigantic ice-splitting forces and gravitation pressure. These freeze-thaw actions smash rocks or gold-bearing geologic bodies, which promotes the formation of gold placers.

"The present is the key to the past". Either cold-warm alternations in geologic history, or seasonal alternations in a year, or frequent alternations of day-thaw and night-freeze in a day, all could make freeze-thaw actions alternate in time. They are favourable for the pulverization of gold-bearing fragments on slopes, which promoted the enrichment of placer gold.

4. In the formation of free gold, the external agents of nivation, freeze-thaw action, gravitation and running water are relayed in space.

Based on our experiences of research and prospecting of gold placers, we conclude that the forming process of gold placers can be described in this way: from ridges to slopes to valleys, successively appear the supply zone of pulverization and disassociation of gold-bearing materials, the migration zone of gold-bearing fragments on slopes, the transporting, washing, sorting and sedimentation zone of free gold. The alternation of gold placers mutually deliver and relay from up to down (see Fig.1).

In the supply zone of gold-bearing materials, the actions of freezing, nivations, and gravitation caused heaving, frost work, ice-splitting and denudation, which smashed gold-bearing geologic bodies and promoted gold dissociation. As a result, the relevant products of talus, block field and snowdrift fan, etc. appeared. They were

moved further down to the migration zone.

In the migration zone of fragments, due to the actions of freeze-thaw sorting, the torrent of meltwater and freeze-thaw action, the products of congeliturbation flow, snowdrift fan, congelifraction olistostrome, etc. became the carriers of gold-bearing fragments. Like conveyor belts, they delivered the fragments from hill tops and slopes into river valleys.

In river valleys, by means of running water, the fragments were transported, washed up and sorted. Therefore, free gold was enriched in convenient places.

In brief, the above agents were mutually relayed and delivered, which took place in the whole forming process of valley gold placers in frigid areas.

5. Evaluation on the positive and negative aspects of freeze-thaw action in the exploring and mining of gold placers.

(1) Permafrost is as hard as rock and always forbids exploration work. Prospecting gold placers in this region, either by drilling, or excavating, or digging shallow wells, is very difficult. When prospecting gold placers, we usually utilize the chopper of a shocking bore, which pounds the tjaele to pieces. We also pour hot water and vapour into the drilling hole, which becomes effective to the work. In this way, if the underground ice is met, the footage of drilling may increase greatly, but the sampling rate reduces greatly, too. It even affects the reserves of gold placers.

(2) In early spring, land and rivers are still frozen in this region. So the exploring and mining people use meltwater from accumulating snow, ice pinnacle, river ice, small lake ice, to wash up heavy placer minerals or for drinking. In remote mountain areas, ice cone or seasonal thaw spring is better for drinking. Only

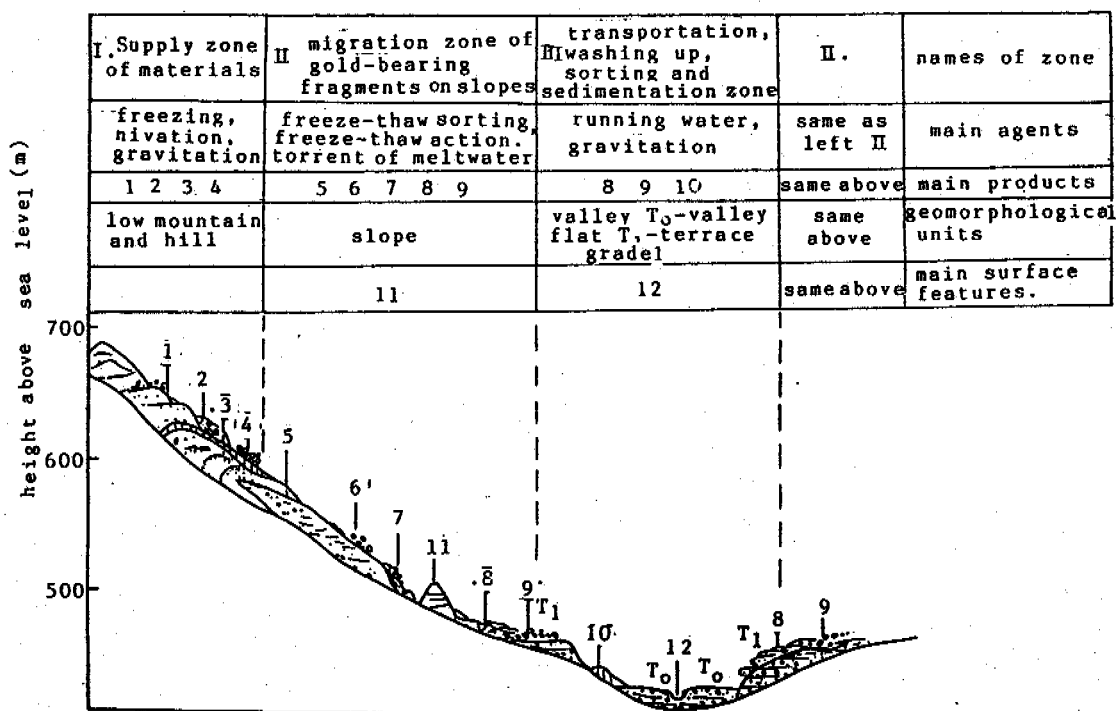


Fig.1 Diagram of spatial relay and deliver of external agents, such as freezing nivitation, thaw, gravitation, running water in the formation of gold placers

1 altiplanation; 2 block field; 3 nivitation depression; 4 talus; 5 snowdrift fan; 6 stone strip; 7 congelifraction slump; 8 congeliturbation flow; 9 stone stream; 10 swelling hillock; 11 road; 12 river

in those large mining regions can the deep underground water under the permafrost layer be used for drinking.

(3) In this region, from late spring to early summer, as the weather becomes warmer, the active layer becomes thinner. We use blasting to excavate test pits, ditches or shallow wells. Because the walls of pits or ditches are frozen solidly, the border slopes are stable and can prevent water from seeping. During this time, it is neither necessary to use supports to prevent the walls from collapsing, nor to build cofferes to avoid soaking. So it is faster to drill and convenient to sample or take measurements. If we miss such a good time, the test pits, ditches and shallow wells become soaked. As the frozen layers of walls thaw, they collapse. So it is very difficult to construct, collect samples or take measurements.

(4) Since it is very difficult to dig in permafrost areas, the local manual workers throw baked stones or burning charcoal into mining galleries to melt the tjaele, which is called "scalding method of baked stone" and is very effective. In many mining districts, it is generally done to root up grass and peat layer by bulldozers in spring. With the help of summer sunlight, the frozen nongold-bearing swamp layer thaws naturally. When it thaws, the bulldozers strip the soils. The upper frozen layer becomes soft and is favourable to excavate, the lower layer is still frozen and has a high intensity, on which the bulldozers do not get bogged down. This way of prethawing and stripping is very effective. After many experiments, we found that the everyday thawing thickness can reach 1.8-2.5 cm, which increases one fold more than natural

thawing.

(5) In ordinary valleys of the studied region, swamp and permafrost exist together and depend on each other. In summer and autumn, the active layer becomes thicker. It is difficult to travel on. Therefore, the gold miners have to send their drilling tools, outfits, provisions and staff by tractors which drag sledges in late winter or early spring. They work there for more than half a year. When land is frozen in winter, workers and machines can withdraw. We did so when we made explorations of several gold placers in this region.

(6) In the studied region, there are still miscellaneous negative effects of exploring and mining of gold placers, such as frost heave, freeze injury, snow hindrance, ice pasts, freeze destruction of bridges and house buildings in mining field, et..

#### REFERENCES

- Tstovich, N.A. (1973) The mechanics of Frozen Ground, Higher Education Publisher.  
 Tong Changjiang (1983) The normal heaving force when the seasonally active layer freezes in the Fenghuoshan permafrost region, "Collected works on Qinghai-Tibet tjaele", Science Press.  
 Wang Chunhe (1982) The upper limit of permafrost and underground ice in northern part of the Greater Hinggan mountains, "Collected works of symposium on Ice and Tjaele, China's Geographic Association", Science Press.

# INFLUENCE OF POROUS CHARACTERISTIC OF MATERIAL ON DISPLACEMENT DURING FREEZING

Wang Jiacheng and Cheng Guodong

State Key Laboratory of Frozen Soil Engineering, IGCAS, PRC

The displacement of various materials was determined under different temperature gradients by the controlled freezing tests, and the porous characteristic of them was also determined by Porosizer. It was found that the porous diameter ranging from 0.1 to 10 microns is available for material moving during freezing, those greater than 10 microns or less than 0.1 microns difficult for moving and those ranging from 1 to 5 microns optimal for moving. There exists optimal initial temperature for a certain kind of materials to move.

## INTRODUCTION

Frost action induces water migration and ice segregation of wet soils so as to displacement of soil particles and other materials in soils. Research on frost heaving mechanism has been lasted for several decades and large amount of scientific articles have been published (Corte, A.E., 1963; Penner E., 1966; Miller E.D., 1980). Previous results verify that silt is the serious one for water migration and frost heaving among various types of soils. More attention was put on the influence of grained size of soils and temperature conditions.

In our opinion, the displacement of materials during freezing mainly depends on the degree of water migration and ice segregation, which related to porous characteristic. Therefore, the displacement of materials was observed by the controlled freezing test and the porous characteristic determined. The purpose of this paper is to describe the relationship between the displacement and porous characteristic.

## EXPERIMENTATION

Before testing, the materials used in the test, including brick, ceramic, zeolite, gneiss, tuff, slate, sandstone and glass balls, are soaked into distilled water for one night to let them be saturated.

The distilled water is poured into the sample box to the height of 3 cm and quickly frozen under the temperature of  $-20^{\circ}\text{C}$ . Then, the tested samples are put on the surface of ice body and the distilled water with temperature of  $0^{\circ}\text{C}$  is poured again into the sample box to the height of 10 cm. The thermocouples are inserted into the sample box with the interval of every centimeter. Afterwards, the side of the sample box is surrounded with insulation materials with the thickness of 10 cm and the box is put into the chamber with constant temperature. Finally, the

circulating tubes at the bottom end of the box are connected with the refrigerated circulating bath and the plastic film covered on the top of the box.

The temperature at the bottom of sample is set and adjusted according to the requirement of test and freezing will be from the bottom upwards.

The freezing front and sample displacement are determined during testing and the porous characteristic of materials determined after testing.

## RESULT AND ANALYSIS

Table 1 shows the amount of displacement of

Table 1 Displacement value of materials for one day under different temperatures, cm

name of material	Bottom temperature, $^{\circ}\text{C}$				
	-2.2	-1.7	-1.2	-0.7	-0.2
brick	0.6	2.5	1.7	1.5	0.2
ceramic	0.3	0.9	1.4	1.0	0.0
zeolite	0.2	1.0	0.8	0.5	0.0
gneiss	0.0	0.2	0.2	0.1	0.0
slate	0.0	0.0	0.1-0.2	0.1-0.2	0.0
tuff	0.0	0.0	0.0	0.0	0.0
sandstone	0.0	0.0	0.0	0.0	0.0
glass ball	0.0	0.0	0.0	0.0	0.0

materials during one day when the chamber temperature keeps at  $3.2^{\circ}\text{C}$  and the bottom temperature of sample is different. From table 1 it can be seen that the frost displacement occurs for some materials such as brick, ceramic, zeolite, gneiss and slate with moving of freezing front of water under different bottom temperature, but for other materials such as tuff, sandstone and glass balls do not occur.

When the end temperature conditions are the

Table 2 Porous characteristic of materials

name of material	total porous volume, ml/g	porosity ratio, %	average dia. $\mu\text{m}$	porous diameter distribution, %					
				>100	100-10	10-5	5-1	1-0.1	<0.1
brick	0.2810	41.08	1.3422	0	7	0	80	13	0
ceramic	0.2061	33.34	0.2399	0	2	0	0	95	3
zeolite	0.1185	20.70	1.0746	0	0	20	50	12	8
gneiss	0.0374	10.36	0.0585	0	0	2	17	44	37
slate	0.0250	6.36		0	12	52	7	0	29
tuff	0.1291	23.90	1.9751	90	3	1	2	4	0
sandstone	0.0019	1.00		9	38	0	2	3	48
glass ball	0.0100	2.52		23	64	0	0	0	13

same, the amount of displacement changes with materials and follows the order from high to low as: brick > ceramic > zeolite > gneiss > slate. If the material is the same, the amount of displacement changes with end temperature and has its maximum.

Basically, there two conditions for saturated materials moving up with freezing front of water: the material must be permeable and the hydraulic conductivity greater than the freezing rate. When these two conditions are satisfied, water can go through the pores and reach to the interface between material and ice and freeze there. Then material can move up from time to time. Otherwise, the material will be engulfed by the advancing freezing front and stop moving.

According to Darcy's law, the flux of water migration through porous materials is proportional to the hydraulic conductivity and hydraulic pressure gradient. These two parameters depend on the size, shape, quantity and continuity of material. The freezing rate depends on the temperature gradient between both ends of the sample. When the temperature at the upper end of the sample keeps constant, the freezing rate depends on the temperature at the bottom end of the sample.

Table 2 shows the porous characteristic of various materials. It can be seen that among the five movable materials mentioned above, the content of porous diameter ranging from 0.1 to 10 microns is greater than 59% and the total porous volume is greater than 0.02 ml/g, respectively. For the three unmoved materials, the content of porous diameter greater than 10 microns and less than 0.1 microns is greater than 93% and the total porous volume is less than 0.01 ml/g, except for the tuff. Therefore, from engineering application point of view, the porous diameter ranging from 0.1 to 10 microns can be considered to be the extent for materials moving during freezing and both the diameters greater than 10 microns and less than 0.1 microns are the extent for materials unable to move. The comparison of two kinds of materials, brick and ceramic, further indicates that even the total porous volume and the content of porous diameter ranging from 0.1 to 5 microns are very close to each other, the amount of displacement is quite different under the same temperature conditions. So the extent of porous diameter ranging from 1 to 5 microns can be considered to be the optimal extent for frost displacement of materials. In contrast of Table 1 to Table 2 it is found that the amount of displacement during freezing is related to the total porous volume. Brick has both the maximum of displacement and total porous volume, ceramic and zeolite in the middle,

and gneiss and slate in the minimum except for the tuff. Although tuff has greater total porous volume, about 90% of porous diameter are greater than 100 microns and its capillary potential is very low.

Table 3 shows the result of frost displacement of brick in relation to the bottom temperature. From the third column of Table 3 it can be

Table 3 Displacement of brick in relation to end temperature

test No.	Chamber Temp, °C	bottom temperature(°C)/displacement(cm)				
		1st day	2nd day	3rd day	4th day	5th day
W1		-0.7/1.5	-0.7/1.0	-0.7/0.4	-0.7/0.4	-0.7/0.3
W2		-1.7/2.5	-2.0/2.0	-2.4/2.0	-2.2/1.1	
W5	3.2	-0.7/1.5	-1.0/1.2	-1.4/1.5	-1.8/1.5	-2.4/1.5
W6		-2.2/0.6				
W7		-0.2/0.2				

seen that there exists an optimal bottom temperature, at which the frost displacement has its maximum. When the temperature is greater or less than the optimal value, the displacement becomes less (Fig.1). If temperature at both ends of the sample keeps constant, the displacement decreases with decreasing of temperature gradient in ice (Fig.2). If the bottom temperature is decreased during testing, it is possible to keep the displacement constant (Fig.3).

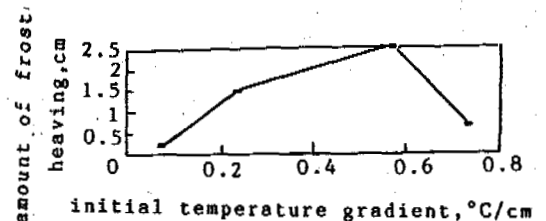


Fig.1 Curve of heave amount of brick vs. initial temperature gradient

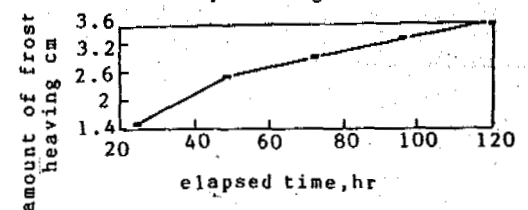


Fig.2 Curve of heave amount vs. elapsed time under condition of end temperature constant (W1)

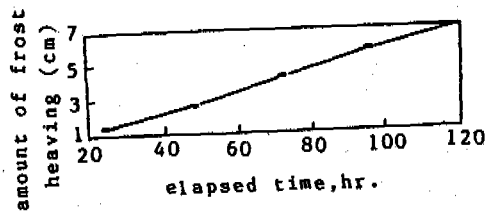


Fig.3 Curve of heave amount vs. elapsed time under condition of end temperature decreasing (W5)

### CONCLUSIONS

1. Two parameters of porous diameter and its content are the main factors as the porous characteristic of materials influencing the displacement during freezing, the porous diameter ranging from 0.1 to 10 microns can be considered to be the extent for porous material moving during freezing; those greater than 10 microns or less than 0.1 microns to be the extent for porous material unable to move and those ranging from 1 to 5 microns to be the optimal extent for porous materials to move. The total porous volume must be greater than 0.025 ml/g for porous materials to move.

2. There exists an optimal initial end temperature (or temperature gradient) for materials to move during freezing. The displacement will be reduced when the end temperature is greater or less than the optimal value.

### REFERENCES

- Corte A.E.(1963) Vertical migration of particles in front of a moving freezing plane, CRREL Research Report 105.
- Penner E.(1966) Pressure developed during the unidirectional freezing of water-saturated porous materials, Physics of Snow and Ice, Sapporo Conference. part 2,1401-1412.
- Uhlmann D.R.and Jackson K.(1966) Frost heave in soils: the influence of particles on soil dification, Physics of Snow and Ice, Sapporo Conference, part 2,1361-1373.
- Miller R.D.(1980) Freezing phenomena in soils (in application of Soil Physics, ed. by Hillel, D., Academic Press, 254-299.
- Kinosita S.(1985) Physics of frozen soils, Translated by Wang Yi and Zhang Ziquang, Jiling Scientific and Technical Press.



## THREE-DIMENSIONAL FINITE ELEMENT ANALYSIS OF STRESS AND DEFORMATION OF FROZEN WALLS IN DEEP THICK CLAY LAYERS

Wang Jianping, Wang Zengting and Wu Qijian

Central Coal Mining Research Institute, Beijing People's Republic of China

The deformation of frozen walls, stress, and bottom heave are calculated by using the ADINA program. The influence of the height of the section, of exposing time and temperature are analyzed. And the results are compared with measurements in frozen shaft construction. That indicated that calculating results of three dimensional models are similar with reality. So the results of the paper can be used as a reference of the mechanical state of frozen walls under similar conditions.

### INTRODUCTION

Stress and deformation of frozen walls is one of the main reasons affecting the quality of sinkings and build shaft linings in frozen shaft construction. Proved by practice, if this problem is tackled badly, it would impair the quality of the project, hold up the project and increase the cost of the project, even probably endanger the construction (Cheng Wenbao et al., 1988).

In the construction of frozen shafts, especially when the shaft is sunk through a clay layer, accidents occasionally take place such as the extra deformation of the frozen wall. In recent years, some shafts in constructing coal fields would sink through 200 - 400 m of unsteady alluvium in our country. In the stratum, generally there are deep and thick clay layers. The thickness of the largest single layer is over 100 m, successive thickness is over 200 m. The clay layer has poor thermal conduction, and low frozen strength. When the shaft sinks through the stratum, under the crustal stress, generally there are freeze pipes broken, caused by extra deformation of the frozen wall. This makes normal construction of sinking shafts confusing impairing the quality of construction, holding up the construction and increasing the price of construction. So, research of strength and deformation of frozen shafts in deep and thick clay layers is very necessary.

Sinking and building the shaft lining of the frozen shaft is a complicated physical mechanics process. Stress and deformation of the frozen wall are both verified with time and space, especially affected by sinking. Sinking the shaft breaks the balance of the initial crustal stress field. As the crustal stress always exists, the deformation of the frozen wall exists as well. Only when the inner lining has been built, does the deformation of the frozen wall basically stop.

### MATHEMATICAL-MECHANICAL MODEL OF THE FROZEN WALL

The frozen wall is an irregular cylinder frozen soil wall and a form which is a temporary support for sinking. Therefore, the character of mechanics and shape of the frozen wall are not regular vertically and radially as the slope of borehole and the varied characteristics of soil layers are.

The irregularity of the frozen wall shape and varied characteristics of soil make research of the frozen shaft very difficult. By analyzing the frozen wall of the main shaft in Xieqiao mine Huainan, complicated stress and deformation of the frozen wall are researched by using ADINA program. Some assumptions in the research are made as follows:

(1) The paper take the placement of the frozen wall by finite length cylinder and clay is the only material for the frozen wall. The distance between freeze pipes in the frozen wall and the radius at which the freeze pipes are arranged is the same. The inner boundary of the frozen wall is determined by the maximum radius of sinking. The outer boundary is determined by  $-2^{\circ}\text{C}$  (Yu Chuhou etc., 1989). There is no slope of freeze pipes. This shown in Fig.1.

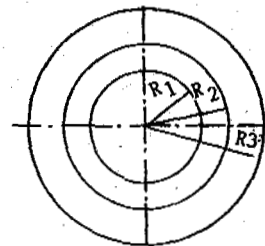


Fig.1 Section of frozen wall

$R_1$ --radius of sinking  
 $R_2$ --radius at which freeze pipe arranged  
 $R_3$ --radius of out boundary of frozen wall

(2) The distribution of temperature changes very little with time, so the changes can be neglected. The temperature does not change in a vertical direction, shown in Fig.2.

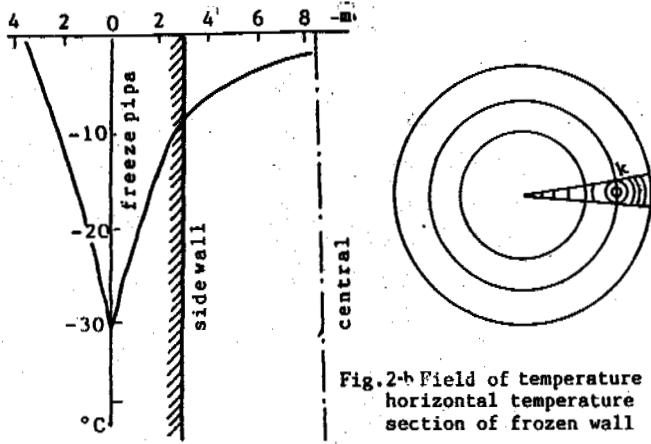


Fig.2-a Field of temperature in vertical section temperature of frozen wall

Isotherms in the frozen wall present concentric circles which use the frozen pipe as the center of the circle, but the temperature in the influenced region of varied freeze pipes mixes together. The temperature in the model is obtained by considering the real situation and calculating the value.

For testing the accuracy of temperature in the model, use formula:

$$t_k = t_p (0.73 + d/S - 0.55 S/E) \quad (1)$$

$t_k$ --temperature of point K (shown in Fig.2b);  
 $t_p$ --temperature of salt water in freeze pipe;  
 $d$ --diameter of freeze pipe;  $S$ --distance between freeze pipes;  $E$ --the thickness of frozen wall.

The temperature of point K is calculated, the result indicates that calculation and determination are the same, proving that temperature determined by measurement and regulation of distribution of temperature is a reality.

(3) The vertical length of the model is 12.4 m, the thickness of the frozen wall is 6.3 m. Shown in Fig.3. The distance between pipes is 2.08 m, from the temperature distribution of the shaft cross section in Fig.2, although the distribution of temperature of the shaft is not on axial symmetry, the freeze hole layout is at the same distance, therefore the temperature distribution in the frozen wall consists of many similar sectors. One of them is chosen for calculation. A mesh of finite elements in calculations is three dimensional and has eight nodes, the total number of mesh are 192. The period of calculating lasted 144h.

(4) The average unit weight of overburden in the Huainan mine region which is below the surface about 200 m is 1.8 g/cm<sup>3</sup> (Lanzhou Institute of Glaciology and Geocryology, Sinking Company of Coal Ministry, 1988), the vertical pressure on the frozen wall is 4.580 MPa. The pressure on the side face is expressed by the empirical formula:

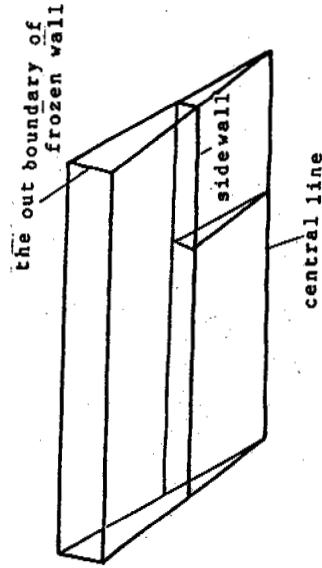


Fig.3 Three dimensional model of frozen wall

$$P = 0.0127 H \quad (\text{MPa})$$

Where 0.0127 is an empirical coefficient, and H denotes the depth of the calculation level.

(5) The material is creep and elastic-plastic solid. The parameter is as follows:

The site parameter:

$$\mu = 0.4 - 0.008 |T| \quad (2)$$

Elastic modulus from experiment as in Table 1, the curve of it is shown in Fig.4.

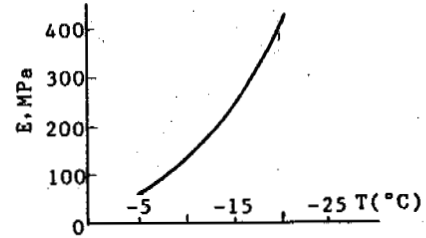


Fig.4 Elastic modulus of frozen clay vs the temperature

Table 1 Temperature vs elastic modulus

Temperature (°C)	Elastic modulus
-5	57.59
-10	138.40
-15	243.24
-20	437.84

The creep function:

$$\psi(\epsilon) = \sigma(t)/E + \int_0^t K(t-t_0)\sigma(t_0)dt_0 \quad (3)$$

$\sigma(t)/E$ : elastica strain

$\int_0^t K(t-t_0)\sigma(t_0)dt_0$ : creep strain

The material function which fits the paper:

$$k(t) = \alpha \delta t^{\alpha-1} \quad \psi(t) = H \delta t^{\alpha}$$

$\alpha < 1$ ,  $\delta$  the parameter,  $t$ : time.

Under the condition of constant pressure, the following formula is derived from the above formula:

$$\epsilon = \sigma(t) / E + A(T) \sigma B t^C \quad (4)$$

$A(T)$ : the experimental parameters which depend on temperature,  $B, C$ : experimental parameter.

The parameters in the formula come from reference (Lanzhou Institute of Glaciology and Geocryology, Sinking Company of Coal Ministry, 1988):

$$B=1.47 \quad C=0.217 \quad A(T)=0.7255|T|^2$$

Under the constant pressure, the strength of frozen soil decreases with the increase of time, shown in Fig.5. Therefore the strength of frozen soil can be classified into instantaneous

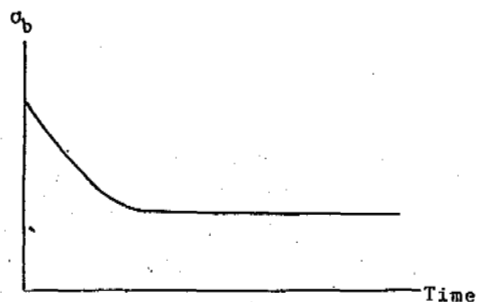


Fig.5 Strength of frozen clay vs the time

strength and long-term strength. Long-term strength applied in engineering is not the only concept. When the long-term strength of frozen soil is determined for structures on permafrost, the criterion of time to failure has to be taken for very long, while for the construction on the temporary frozen soil such as the frozen shaft, the time is relatively short. Considering the time at which the frozen wall is working the long-term strength is usually determined as follows (Beijing Research Institute of Mine Construction, Central Coal Mining Research Institute, 1989; China University of Mining and Technology, Shaft Sinking of Special Techniques, Coal Industry Publishing House):

$$\sigma_B = 1.73 + 0.392 |T| \quad (5)$$

#### THE CALCULATION RESULTS OF DEFORMATION AND ANALYSIS

(1) Influence of the height of sinking sector on deformation of the freeze wall:

Influence on deformation of the frozen wall at three heights of the section (4.4, 3.3 and 2.2 m) are compared. The calculated results are shown in Fig.6. The results indicated the height of the section has an obvious influence on deformation of the frozen wall, and the influence increased as time increased, but the relative difference was not changed. The maximum value of deformation of the frozen wall generally appears near the working face. The largest deformation of the different heights of the section and time are shown in Table 2.

From that, deformation of the frozen wall is

Table 2 The maximum value of displacement vs height of section

Time	Height of section		
	2.2m	3.3m	4.4m
12h	10.3mm	19.3mm	18.4mm
24h	17.4mm	20.9mm	26.0mm
36h	22.3mm		33.8mm

increased one time as the height of the section is doubled. Therefore, it is obvious that the height of the section has an influence on deformation. From the Fig.6 lead deformation is influenced by the height of section, the deformation of 2.2 m height of section reached about 2 m below the working face, but at the height of 4.4 m and 3.3 m it will reach about 5 m. So the section height has an obvious influence on lead deformation, as shown in Fig.6.

(2) The influence of time on deformation of the frozen wall and bottom heave:

The more time the frozen wall is exposed, the larger the deformation is, but the speed of increase is decreased. It indicated the deformation is attenuation deformation, so the frozen wall is steady if the amount of deformation is not larger than the permitted value, and it will meet the needs of construction. If a decrease of the deformation of the frozen wall is expected, it is necessary to speed up the construction, and decrease the exposure time of the frozen wall. At the beginning, the displacement of 3.3 m and 4.4 m height of section accomplished in the same time are similar, but larger than the 2.2 m section. Accomplish time, and influences of the height of the section are larger and larger, shown in Fig.7.

When the lining of the shaft has been built and the sinking, has stopped the longer the time is, the larger the deformation is, shown in Fig.8. But in the condition of strengthening freezing, the speed of bottom heave is decreased, similar to deformation of the frozen wall, so long as the amount of bottom heave is smaller than the permitted value, the shaft is secure. It indicated the strengthening freezing has restrained the non-attenuation deformation, the largest speed of bottom heave is 47.4 mm/h, it appeared at the beginning of the stop in sinking. The radius is larger, and the bottom heave is larger. The deeper, the smaller bottom heave is. And the scope of influence is restricted by time as well, as shown in Fig.9, therefore, there are many factors influencing lead deformation.

(3) The deformation in frozen walls:

The deformation in frozen walls is smaller than deformation of side walls, and its curves are comparatively smooth and have no inflective points. This proves the process of shaft sinking has more influence on the sidewall than the inner frozen wall. Although the inner lining has basically no displacement, the frozen wall near the freeze pipes have little displacement, it indicated the frozen wall would have little displacement after the inner lining has been built, shown in Fig.10.

The distribution of displacement in the frozen wall shown in Fig.11, from that, the influence of time on displacement of the side wall is larger than that of the inner frozen wall.

(4) Comparison of calculating results and measurement:

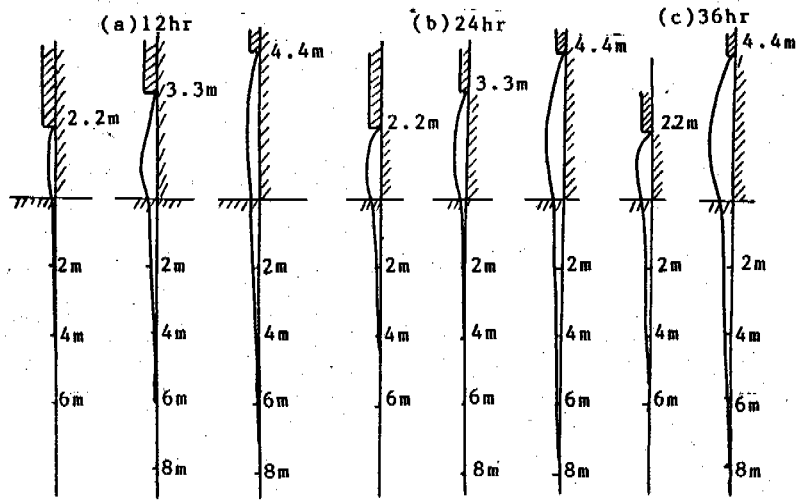


Fig.6 The deformation of frozen wall along depth for different height sections at exposure time equal to:

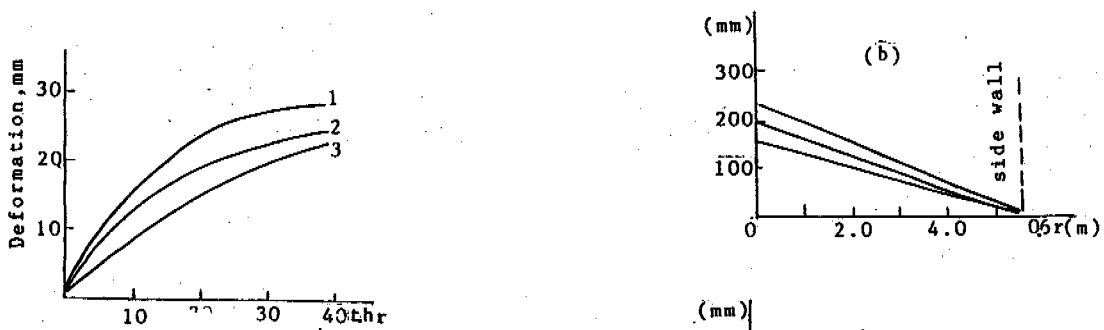


Fig.7 The maximum value of deformation vs time

- 1--height of section =4.4 m
- 2--height of section =3.3 m
- 3--height of section =2.2 m

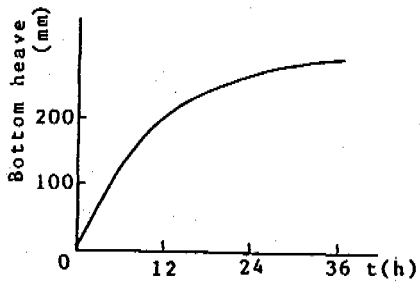


Fig.8 bottom heave vs time

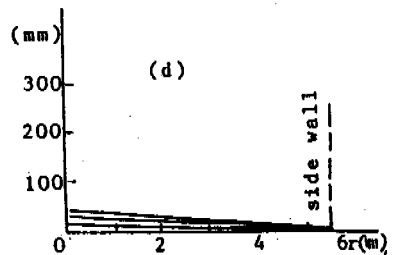
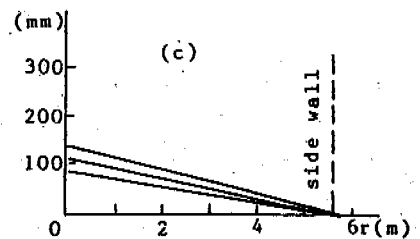
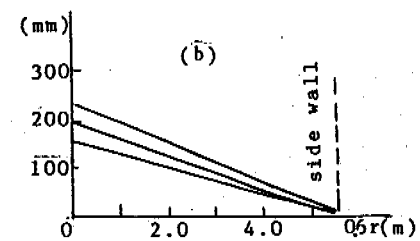
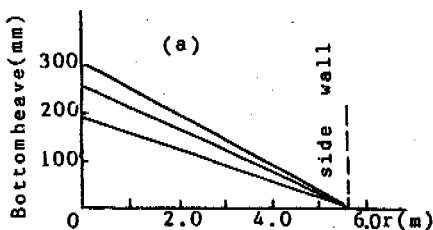


Fig.9 Bottom heave vs radius of shaft at different distances under working face: (a) 0; (b) 2.2 m; (c) 4.2 m; (d) 6.2 m

The Xieqiao main shaft is Xieqiao's hoisting shaft, it's finished radius is 7.6 m, total depth is 732.2 m. Shaft sinking through Quaternary overburden has a thickness of 291.3 m. Sand strata is 54.47%, clay strata is 45.53%. The characteristics of the clay strata is that it is buried deep, it has larger thickness of a single layer and more content of film water, it

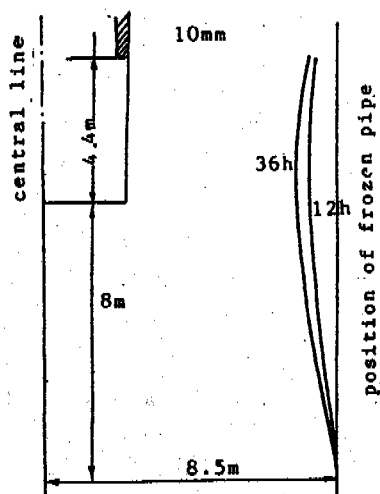


Fig. 10 Displacement of frozen wall at freezing pipe

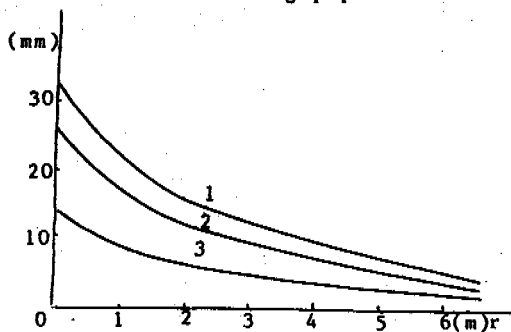


Fig. 11 Deformation of frozen wall vs thickness of frozen wall for 1--36 hour ; 2--24 hour ; 3--12 hour

is difficult to freeze and has a low strength after freezing. It obviously has the characteristics of creep. The largest thickness of the lining in the frozen section is 1.8 m. The largest radius of sinking is 5.4 m. After strength freezing, the distribution of temperature between two freezing pipes is shown in Fig. 2. The model is similar to construction. The depth of the model was from 260 m to 272.4 m. The temperature of the outer boundary was  $-2^{\circ}\text{C}$ . Thickness of the frozen wall was 6.3 m. The speed of sinking was 1.1 m/d.

From Table 3, the measurement in construction: bottom heave is 200 mm, the deformation of the frozen wall is 30 mm during 36 hour, and the

Table 3 Measurement in construction and calculation results

Item	measurement	calculation
Bottom heave	200mm	275mm
Displacement	30mm	32mm

calculating result is that deformation of the frozen wall is 30 mm and bottom heave is 275 mm. Therefore the calculation and measurement of displacement of the frozen wall are basically the same. That proves the model can be used to

simulate the shaft in a deep and thick clay layer. Certainly, the calculation and measurement of bottom heave have a great difference. This is because the measurement of bottom heave is not precise, some assumptions are different from the real conditions, and the error in calculating, etc. For detail, see reference (China University of Mining and Technology etc.). In addition, the model size, especially the size under the working face has an influence on bottom heave, it is an important factor.

### STRESS

The stress of every node is an average value of nearby gauss nodes. The distribution of strength and elastic modulus in the frozen wall are shown in Fig. 12 and Fig. 13.

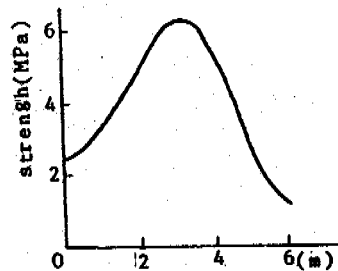


Fig. 12 Strength vs thickness of frozen wall

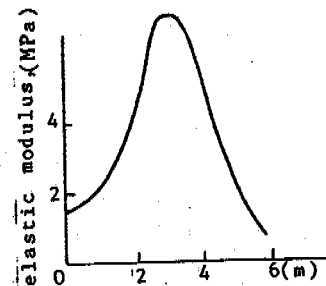


Fig. 13 Elastic modulus vs thickness of frozen wall

(1) Distribution of stress in frozen wall:

The distribution of  $\sigma_z$  (the vertical stress of shaft) and the radius direction,  $\sigma_{\theta}$  (tangential stress) are basically the same, they both reach the largest value at the place where freeze pipes are and their amounts are the same too. Only  $\sigma_r$  (radial stress) increases according to the radius increase. But it is much smaller than  $\sigma_z$  plus  $\sigma_{\theta}$ . The distribution of stress is the same with the distribution of strength in the frozen wall. This explains the cause of no plastic region appearing in the frozen wall. At same time, it proves that calculations, according to assumption of well-distribution of the frozen wall, have a great difference with the real situation that makes real capacity of load-bearing larger than that of the calculation.

From that, the distribution of mechanical characteristics have an influence on the stress field in the frozen wall, but the distribution of temperature has an influence on distribution of mechanical characteristics. Therefore, a reasonable temperature field can be designed for raising the capacity of load bearing. That must be noted for the same temperature field, the

mechanical characteristics would be different if the nature of soil is different. So the nature of the soil is an important factor.

From the results, the shear stress is smaller than stress, its absolute value is smaller than 0.15 MPa, so it can be neglected. The distribution of stress in a vertical direction is well-distributed. In changes near the working face and near the bottom of the inner lining, this indicated that the change of restraint conditions of the frozen wall affected the stress in the frozen wall a little, but not obviously.

Distribution of elastic modulus, yield stress and creep parameters have an influence on the stress field in the frozen wall directly, and the stress field would be determined whether the plastic region appeared, its size and where it appeared. Especially, the plastic region does not always appear in the inner circle and extend to the outer circle. It appeared in regions near the freeze pipes sometimes. This is mainly because the distribution of mechanical characteristics are not well-distributed.

(2) Influence of time and height of section on stress:

As influence by the characteristics of creep material and the sinking of the shaft, the stress in the frozen wall is always changed. From Fig.14, no matter what the height of the section, the time of frozen wall exposure has little influence on the stress in the frozen wall. But sinking of the shaft is a process which changes the restraint conditions of the frozen wall, so the stress changed a lot in the process of sinking, see Table 4.

Table 4 Time & height of section vs stress

Height of section	Stress $\sigma_z$ (MPa)		Stress $\sigma_\theta$ (MPa)	
	12h	24h	12h	24h
2.2m	5.442	5.428	5.294	5.288
3.3m	6.071	6.0919	5.920	5.945
4.4m	6.230	6.2425	6.225	6.172

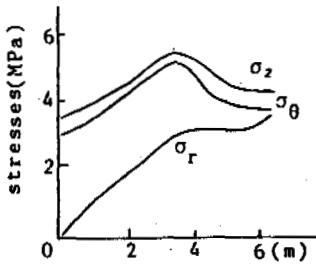


Fig.14a Height of section =2.2m exposing time t=0

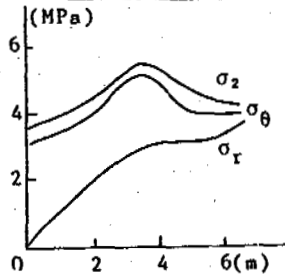


Fig.14b Height of section =2.2m exposing time t=24

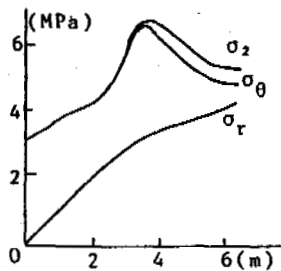


Fig.14c Height of section =3.3m exposing time t=0

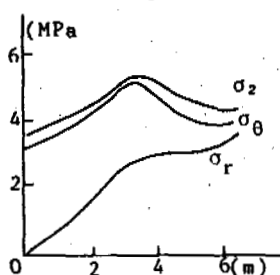


Fig.14d Height of section =3.3m exposing time t=14.4

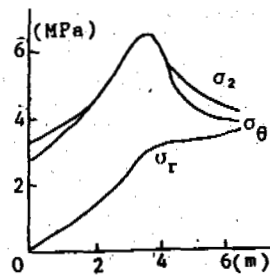


Fig.14f Height of section =4.4m exposing time t=9.6

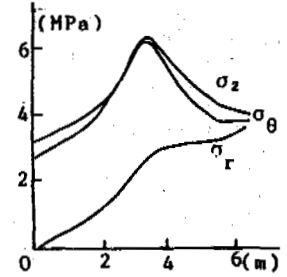


Fig.14e Height of section =4.4m exposing time t=0

### CONCLUSION

The article made use of finite element method to calculate and some helpful conclusion were obtained:

(1) Three-dimensional model of frozen shaft was proved practically and was able to solve the problems of strength and deformation in the frozen shaft.

(2) The lead deformation of the frozen shaft was affected by many factors, for example: the process of sinking, the height of section, and the time for building the lining. The range of the lead deformation is about two times the radius under the conditions of the paper.

(3) The deformation of the frozen shaft is greatly affected by the height of the section. When the height of the section decreases by half, the deformation of the frozen wall reduced by the same amount. The nearer to the side wall, the bigger the deformation is. And the deformation is influenced by time greatly, the farther from the side wall, the smaller the influence is.

(4) According to calculations, there are very few number nodes in the plastic state. This explains why plastic deformation ceases at the same time the frozen wall is basically in an elastic state. But the plastic region in the frozen wall does not always appear in the inner circle of the frozen wall, its determined by the distribution of mechanical characteristics. This results in great differences with ordinary mechanical calculating. The maximum stress in the frozen wall exposed section) increases as the height of the sinking section increases. The value of stress increases 15% as the height of section doubled.

(5) The process of sinking has a great influence on the changes of stress, but the time of exposure of the frozen wall has little influence on the stress. Shear stress could be neglected compared to stress.

### ACKNOWLEDGMENTS

The authors wish to express their appreciation to senior engineer Chai Zhongxiong (The Center of Calculating, Chinese Academy of Sciences) and Su Lifan (Central Coal Mining Research Institute, Beijing) for their helpful advice on the calculating and writing of the paper. Thanks are also given to the authors whose paper are quoted.

### REFERENCES

Cheng Wenbao, Xu Guangji and Tang Zhibin (1988) Reason and counter-measures of broken freezing pipe in deep shaft.

Yu Chuhou etc. (1989) The Research strength of frozen wall and its parameter.  
Lanzhou Institute of Glaciology and Geocryology  
Sinking Company of Coal Ministry (1988)  
Engineering Behavior of Frozen Wall, Frozen Shaft Sinking, Lanzhou University Press.  
Beijing Research Institute of Mine Construction, Central Coal Mining Research Institute (1989)  
Researching of character of Frozen Clay.  
China University of Mining and Technology, Shaft Sinking of Special Techniques, Coal Industry Publishing House.  
Lou Genda (1985) Data Simulating of Process of Frozen Wall Creep-Analysis of Finite element.  
China University of Mining and Technology etc.  
Researching of Parament of Measurement of Deformation of Frozen Wall.

# THE PREVENTION, CONTROL, AND EVALUATION OF FROST DAMAGE ON THE BUILDINGS OF CANAL SYSTEMS IN SEASONAL FROZEN GROUND AREAS

Wang Wenkai and Lin Chuanwei

Sui Hua Water Conservancy Bureau of Hei Longjiang Province

This paper analyzes the reasons and measures of prevention and control of frost damage of canal systems in seasonal frozen ground areas, and makes a suggestions for problems awaiting research.

## INTRODUCTION

At Hei Longjiang Province, most of the area is seasonal frozen ground. The degree of frost damage on the buildings of canal systems is 53% at Mei Ling County and 83% at Northern Cha Ha Yang Guan area. The retaining wall is one of the structures in which damage is most serious, then the bottom plate of Drops, Floodgates and Pump Stations, etc.

For engineering purposes, if we pay attention to the overall arrangements of structure and the reasonable measures of local prevention and control of frost heave, frost damage of the buildings of canal systems can be avoided. The reasons for frost damage, although there are a lot of different views, most scholars think that the main factors causing frost damage in canal systems are soil, water, temperature and stress. So engineering circles adopt the following methods to prevent and control frost damage.

## METHOD OF WHOLE STRUCTURE

Frost damage is most serious in the middle and small buildings of canal systems. In the overall arrangement of building canal systems, first we should reduce the contact area with the structural foundation in order to decrease the probability of frost heave, this is called the "avoiding" method of frost heave.

1. In order to reduce plane size of the building structure, we should shorten, as far as possible, the retaining wall or adopt a wall structure of "-" type (Fig.1), which is buried under the frozen layer, so that vertical anti-permeating is combined with the horizontal anti-permeating and the effect of normal frost heave can be avoided. If reducing the energy with sieves is used, frost damage in the structures can be solved, because its reduced energy is sufficient and the protecting bottom of the reducing energy pool is built with separated concrete, which has

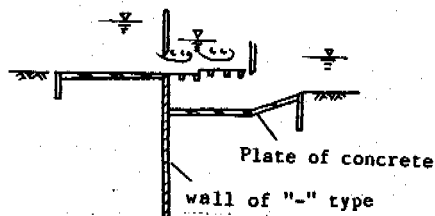


Fig.1 Floodgate of "-" type

a strong adaption to the deformation of frost heave. At Sui Hua and Wu Chang, etc. area, structure of "-" type was used many times at the drops and floodgate, in which the longest using time is 20 years and the effect of reducing energy and preventing and controlling frost damage, etc., was very good, and more than 50% of the structural amount can be decreased. For the middle to small structures used in water conservancy, this measure is not only applicable, but also is accepted easily and is feasible for theory.

2. Adopting a structure built on stilts. At Sui Hua, etc. area, the aqueduct drops and aqueduct pump stations are adopted (Fig.2), this arrangement changed the plane type into the cubic type and may cancel or shorten a lot of the retaining wall and make the contacted area between the building and frozen ground concentration on several props of the aqueduct so as to avoid frost heave. For example, at Sui Hua area, when the area has normal and shear force of frost heave it decreased respectively by 3% and 18% in former area, frost damage of drops reduced considerably. Meanwhile 60% of the structural amount was decreased.

3. At Sui Hua and Mu Lan etc. area, reducing energy with a deeply buried shaft was adopted, it can also obtain results of reducing the struc-



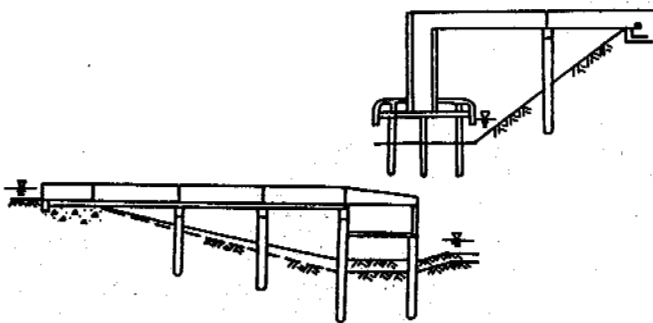


Fig. 2 Aqueeduct drops and aqueeduct pump station

tural area and frost damage.

So it is seen that frost damage can be avoided or reduced if we adopt new technology, according to the different characteristics of buildings and local conditions, and as far as possible reduce plane sizes of structures, for example, adopting the reducing energy of shaft or wall of "-" type or a structure built on stilts, etc.,

4. For some of the buildings where the water head is not high, if we do not want to adopt the "avoiding method", we may change the retaining wall to a structure of a vacant box built by concrete (Fig. 3). Engineering practices at



Fig. 3 Retaining wall built by concrete

Sui Hua and Xing Jiang, etc., area has verified that the built structure will allow for certain deformations in order to make the force of frost heave reduce greatly; After the forces of frost heave vanish, its deformation can be recovered. Since the function of drainage in the cracks of equipment is good, frost heave is very small, so we may neglect additional forces of frost heave on the structural design. In some areas where hoisting occurs, it is feasible to use the built structure to avoid frost damage of some small structures.

The above measures may be separated into allowable and unallowable deformations. The proceeding three kinds of methods produce no deformations or very small deformations, the fourth allows the production of certain deformations. The two kinds of functions for preventing and controlling frost damage are good.

#### LOCAL MEASURES OF PREVENTING AND CONTROLLING FROST HEAVE

In the overall arrangement of the structures, although the above methods may avoid frost heave, there is still some areas of the foundation contacting the frozen ground. We must treat seriously this position. The concrete methods are as follows:

##### Exchanging Soil, Damming Water and Drainage

One of the measures to prevent and control frost damage is through an exchange of foundation soil in a frost heave zone. This is economical and practical in a seasonal frozen ground

area. We must take into consideration the structural hydrology and practical conditions so we can obtain satisfactory effects.

During the freezing process, with a change of boundary conditions, the route of water migration from a normal source causes an increase of frost heave, or drainage produced by the frost heave.

1. When there is a gravel layer which doesn't have pressure water under the foundation, the foundation pit should be dug to the gravel layer, then change the fine soil to pure gravel (size of foundation pit must be larger than size of foundation), or we may use a blind shaft which is filled with gravel in order to connect the foundation pit with the gravel layer under the foundation as a passageway for drainage (Fig. 4).

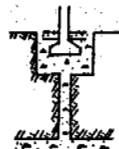


Fig. 4 Blind shaft drainage

Only when the distance between the groundwater level and the frost front is larger than 0.5 m under the frost front, is this method suitable. Only when the range of penetration is 0.6 times at the sides of the structure, must we change the foundation soil to gravel soil of frost non-susceptibility in order to eliminate the effects of the shear force of frost heave which act on the foundation sides.

2. When the foundation soil is frost heave soil, according to the conditions of the groundwater level, we should adopt different measures:

(1) When distance between the groundwater level and frost front is larger than the withdrawn height of foundation soil to the groundwater, the above method is good.

(2) When groundwater level is higher, we should adopt the layer-fill method to change soil, in which the soil is dug out from the foundation pit and dried slightly by airing, and a plastic membrane is used for layer-fill damming water so as to form "layer-fill closed foundation". We know that during the frost heave process, formation of an ice layer is a result of the continuous migration of water. Within the range of the frost heave zone, we must use a plastic membrane to dam water, meanwhile we still must make the plastic membrane extend outside the foundation side so as to eliminate shear frost heave. According to observations of many years on the use of plastic membrane for anti-permeating at home and abroad, we think that it is very good material. But we notice its fault in not allowing the inner water to drain out.

It is seen that the key to exchanging soil is "water". So long as we watch closely the water and the area's conditions and adopt different methods of exchanging soil, a good effect of preventing and controlling frost heave can be obtained.

For exchanging soil behind a retaining wall, we also may adopt a similar method.

At Sui Hua area, in the canal and the embankment of the canal there are pillow beams 50 cm in height and under the beams is a gravel layer

70 cm in thickness (Fig.5), the bridge plank is

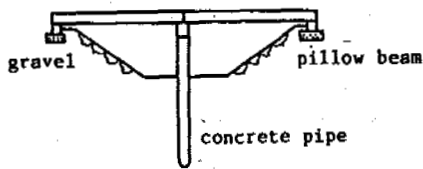


Fig.5 Pillow beam bridge of shallow foundation

laid upon the pillow beams. When canal water recedes, the water in the gravel layer under the beams is drained quickly, so the frost heave of beams is small, this is caused by good drainage.

Strictly speaking, during the process of exchanging soil, we must consider simultaneously the drainage and damming of water, otherwise frost damage can not be prevented or controlled.

#### Temperature-retaining Measure

The temperature-retaining measure is a recently perfected method of preventing and controlling frost heave (Fig.6). It is based on changing the temperature field of the base and using

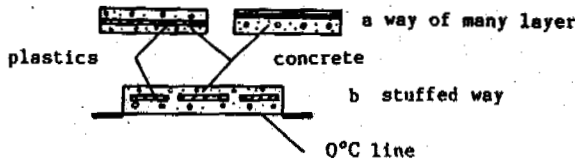


Fig.6 Temperature-retaining foundation

some materials as a temperature-retaining foundation, for example, a rigid foamed plastic plate of polystyrene, perlite and water, etc.. In conditions of thick sandy clay and groundwater of unconfined water, the freezing time of soil is postponed because of temperature-retaining measures of the foundation, and there will be a lot of time for a drop in the groundwater level, so the amount of water migration is reduced. But the velocity of the frost front beyond the temperature-retaining base is still quicker. A crosswise negative temperature gradient is formed between warm and frozen soil, meanwhile, the direction of water migration is changed. So it is necessary to reduce the effect of frost heave of soil around the foundation.

1. Using rigid foamed plastics of polystyrene. At Harbin, etc., area, through using this material of 10 cm thickness for horizontal temperature-retaining of many layers, soil under the foundation can't freeze. For eliminating the effects of frost heave of soil around the foundation, the horizontal temperature-retaining layer should be extended beyond the foundation at about a penetration of 0.6-0.8 times. When base pressure is 294 KPa, deformation of this material may be controlled at less than 10% (its density is larger than 0.03 g/cm<sup>3</sup>). The amount of deformation may satisfy the requirements of middle and small structures.

2. Using ceramsite perlite. Without water, conductivity of this material is less than 0.23 W/m·°C. At water conservancy structures, water-proofing is difficult. When this material is soaked, its temperature-retaining properties decrease obviously.

3. Using water. When the structures foundation is lower and the canal at winter still has water, we may adopt a temperature-retaining

water layer. Data of Hei Longjiang Institute of Water Conservancy Science showed that a water layer 1 unit in thickness may eliminate a frozen soil layer of 1.5 units in thickness. But this method is only suitable for canals in which the water depth can be assured in winter.

4. Using the method of an air fill-layer. This method can retain temperature, but it is not an ideal method because of the strong convection of air and the difficulty of construction.

Based on above-mentioned analyses, we think that it is better to use a rigid foamed plastic plate. In small structures, we should go as far as possible to use this method.

#### Measure of Mechanical Balance

Under conditions of not allowing the deformation of structures, a larger force of frost heave will be produced. It is not a good method of self-resistance, because this method can not prevent and control frost heave. When contact between the structural foundation and frozen ground is concentrative comparatively, we may adopt the following method to prevent and control frost heave through using the principle of mechanical balance.

1. Measure of self-anchor. Forces and counter forces of frost heave are a couple of forces in which the size is the same and direction is opposite. So we may lay up a plate or wood pile to offset the counter force of frost heave under the frozen layer (Fig.7). Based on the same

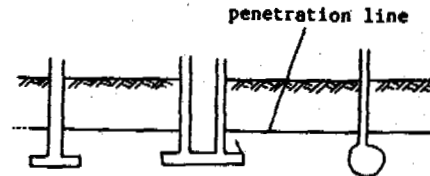


Fig.7 Pile fixed by anchor

reasons, the bottom plate of the retaining wall that is cantilever also may offset counter forces of frost heave and strengthen the stability of the retaining wall.

2. Increasing the buried depth of frictional pile. When the groundwater level of the foundation pit is higher it is difficult to dig a big foundation pit with a plate fixed by an anchor, we may adopt the use of piles in drilled holes. This measure also may reach the goal of offsetting counter forces of frost heave. Compared with the measure of a self-anchor, the structural amount is larger, but it is an acceptable method because this method has the characteristics of quick mechanical hole drilling and uses simple technology. The above-mentioned measures of "overall arrangement" and "local prevention and control" are divided, artificially by us, according to engineering design and construction practice. If we notice their characteristics and suitable conditions and adopt a suitable arrangement of structures, we may prevent and control frost damage and obtain a good economical effect.

#### FUTURE RESEARCH DIRECTION

For resolving effectively the problem of frost damage, we should pay attention to the following problems.

1. Relation between air temperature and penetration. Based on the former results of research which have given the standard methods, for exam-

ple, relation between negative temperature index and penetration, etc., we can obtain quickly the standard penetration and the penetration of structural design. If we can draw an isogram of the average frost index of many years, according to local data of air temperature, we can obtain the exact standard penetration of the engineering site. If we know the property of foundation soil, groundwater level and load, etc., we can obtain the amount of frost heave and relevant forces of frost heave. So it is important to obtain an isogram of the average frost index of many years.

2. Relation between the force of frost heave and allowable deformation of different buildings. We know that the force of frost heave changes with the change of allowable deformation values. Although there is some relation between the force of frost heave and allowable deformation, we have not determined how much allowable deformation should be chosen and how much the degree of attenuation of force of frost heave is. So we think that it is worth researching the problem to find the relationship between the amount of frost heave, allowable deformation and attenuation of force of frost heave.

3. Freezing-thawing damage of slope protection at the exit of the hydroelectric station. Since hydroelectric station needs many years to generate electricity and the current velocity of the exit is fast, it causes serious freezing-thawing damage of the slope protection. So this also is worth further research.

#### REFERENCE

- Wang Wenkai & Lin Chuanwei (1982) Method of prevention and control of frost damage on buildings of canal system at seasonal frozen ground area.
- Lin Chuanwei et al. (1984) Design of floodgate of "-" type, Irrigation and Water Conservancy and Small Hydroelectricity.
- Cheng Xiaobai et al. (1980) Pore water pressure of saturated gravel during freezing. Journal of Glaciology and Geocryology, Vol.2, No.4.
- Hei Longjiang Institute of Water Conservancy Science (1985) Research and engineering practice of closed foundation of floodgate built-layer.
- Lin Chuanwei (1989) Evaluation on prevention and control of frost damage of building of canal system, Irrigation and Water Conservancy and Small Hydroelectricity.
- Water Conservancy Board of China (1991) Standard method of design on preventing frost heave of canal system engineering, Publishing House of Water Conservancy and Electric Power.

## PROFILES OF FREEZING POINT AND UNFROZEN WATER CONTENT AROUND CGWS, ANTARCTICA

Wang Ya-qing and Chen Xiao-bai

Lanzhou Institute of Glaciology and Geocryology,  
Chinese Academy of Sciences, China

The variation of freezing point, unfrozen water content of soils along depth could usually indicate indirectly the change of grading size, mineral and chemical compositions, consequently, the sedimental and environment condition as well. Experimental results show that the extreme value of freezing point and unfrozen water content occurs at different depth of sedimental cores which might reflect some events at the China Great Wall Station, Antarctica for reconstructing the climate change and environmental development in Late Pleistocene.

### INTRODUCTION

One of the authors, Chen, has gotten rather complete sedimental cores and measured the ground temperature with the depth of 0 to 3 m to 6 m in the end of February or the early of March in the China Great Wall Station, Antarctica (CGWS) while he was a member of the 5th China Antarctic Expedition in 1988 to 1989 which provides a possibility to study the environmental change and climate development for Late Pleistocene (Chen). Determining the profiles of freezing point,  $T_f$ , and unfrozen water content,  $W_{unf}$ , of the sedimental cores is one of the task which was discussed in this paper.

The profiles of  $T_f$  and  $W_{unf}$  depend on not only the moisture and ground temperature, but also the grading size, ion content and type as well. Therefore, any sudden variation of  $T_f$  and  $W_{unf}$  of soil core along depth might reflect the different sedimental condition, and consequently, might provide more evidence for the reconstruction of climate and environmental condition.

### MEASUREMENT AND APPARATUS

#### Measurement

Freezing point  $T_f$  of samples was conducted by the well known supercooling method. And unfrozen water content  $W_{unf}$  was determined as the moisture beginning freezing at given temperature.

#### Apparatus

The temperature controlled by the cycle refrigerator bath with a sensitivity of  $\pm 0.02^\circ\text{C}$  and an accuracy of  $\pm 0.1^\circ\text{C}$ , made in NESLAB Co. USA, and determined by thermocouples collected by HP 3054-S Automatic Data Acquisition System with a speed of 100 per second and a sensitivity of  $\pm 1\mu\text{V}$  which is correspondent to  $\pm 0.025^\circ\text{C}$ .

### EXPERIMENTAL RESULTS

The tests of  $T_f$  and  $W_{unf}$  were conducted with 76 samples collected from Yenwu Lake, West Hill, East side of West Lake and a sorted circle nearby the scientific building of the CGWS.

As well known,  $T_f$  or  $W_{unf}$  mainly depends on water content  $W$ , temperature  $T$  respectively (Qiu and Wang). After determining and analyzing 5 to 9 correspondent value of  $T_f$  and  $W$  or  $W_{unf}$  and  $T$  for each sample, a regression function could be expressed by:

$$T_f = -A_1 W^{A_2} \quad (1)$$

$$W_{unf} = B_1 |T|^{B_2} \quad (2)$$

The constants  $A_1$ ,  $A_2$ ,  $B_1$  and  $B_2$  in fitting Eq. (1) and (2) and their correlation coefficient  $r$  for each sample are listed in Table 1 to 4. Most of correlation coefficient is available with the value of more than 0.9.

### ANALYSE AND DISCUSSION

The distribution of  $T_f$  and  $W_{unf}$  along the depth for the sedimental cores were calculated by means of Eq.(1) and (2) with the constants listed in Table 1 to 4. And the moisture and ground temperature profiles measures in situ as well.

The profiles of geological column,  $T_f$  and  $W_{unf}$  for the cores collected from Yenwu Lake, West Hill, East side of west Lake and a sorted circle were shown in Fig.1 to 3 and Table 5 respectively. From Fig.1 to 3, we know that the peak value of freezing point is correspondent to the peak one of unfrozen water content at given depth.

For the profile of  $T_f$  and  $W_{unf}$  in Yenwu Lake (Fig.1) with elevation of 14.5 m a.s.l., the  $W_{unf}$  of sandy gravel layer at the depth of 1.15 m to 1.24 m, 2.00 m to 2.10 m, 2.10 m to 2.30 m and 3.47 m to 3.55 m is 28.53%, 13.71%, 13.24%

Table 1. Constants in Eq.(1) & (2) for core profile collected from Yenu Lake, CGSW

Depth (cm)	Test Number	$T_f = -A_1 W^{A_2}$		$W_{unf} = B_1  T ^{B_2}$		r
		A <sub>1</sub>	A <sub>2</sub>	B <sub>1</sub>	B <sub>2</sub>	
20-40	6	763272	5.607	11.408	.170	.976
105-115	6	431175	5.196	12.644	.170	.939
115-124	6	821.63	2.669	12.485	.365	.987
187-193	9	2295	4.463	5.804	.216	.963
200-210	9	266.78	2.493	10.520	.332	.909
235-250	6	15.77	2.066	3.997	.467	.982
264-270	7	387.02	3.392	6.013	.278	.971
285-292	5	816.08	3.857	6.814	.219	.919
313-325	6	170.57	1.824	17.089	.475	.931
329-335	5	1926046	5.627	13.667	.164	.960
335-340	6	236.34	2.079	14.323	.433	.949
347-355	8	694.39	2.582	13.087	.358	.961
398-405	8	143630	4.875	11.575	.200	.988
415-423	7	516.70	2.541	12.041	.370	.969
450-455	7	1951	3.008	13.069	.289	.929
460-463	6	494.93	2.678	11.180	.298	.894
463-470	7	178922	5.059	11.091	.191	.983
493-499	6	295328	5.295	11.397	.168	.943
536-540	5	156.66	2.998	5.407	.321	.981
566-571	6	213.51	2.396	9.416	.401	.980
580-585	6	25677	3.983	13.544	.225	.947
626-632	8	3347	2.701	22.338	.303	.905
675-687	8	580.11	3.267	7.382	.288	.971
702-707	9	931.09	2.324	19.427	.407	.973
708-715	7	22938	4.254	11.991	.191	.902
722-729	9	368.05	1.864	24.466	.465	.931
736-744	7	84874	4.093	16.462	.227	.963

Table 2. Constants in Eq.(1) & (2) for core profile collected from West Hill, CGSW

Depth (cm)	Test Number	$T_f = -A W^A$		$W_{unf} = B  T ^B$		r
		A	A	B	B	
0-10	6	330.05	2.273	13.896	.371	.919
20-30	6	71964	4.353	13.329	.215	.968
40-50	6	26182	4.182	11.740	.224	.937
55-60	6	8537	4.075	9.463	.233	.976
75-85	7	2527	3.548	11.151	.190	.822
95-100	6	101655	4.697	12.190	.185	.932
110-120	8	113129	4.446	13.903	.213	.972
140-145	8	20861	3.890	13.259	.239	.963
150-160	7	2317	3.233	12.542	.223	.849
228-234	5	38.73	1.747	8.251	.556	.986
237-241	5	981.77	2.563	15.946	.296	.871
273-275	6	106.00	2.177	9.076	.376	.905
275-278	5	2656	3.291	11.303	.266	.935
310-318	5	59.21	1.464	16.427	.619	.952
318-325	6	781.45	2.659	13.400	.292	.880
335-345	5	9625	3.927	12.067	.162	.798

and 16.77% which is much more than its preservation capacity of soil moisture ( $W_{pc}=10\%$ ) where  $T_f$  is nearby  $-1.0^\circ\text{C}$ . The  $T_f$  of former three is close to  $0^\circ\text{C}$  because its water content reaches 40% by weight. The preservation capacity of soil moisture, 3.47 m to 3.55 m in depth, is less than that of former three, its  $T_f$  is  $-0.15^\circ\text{C}$  while its water content is more than 25%. Consequently, there is much more content of soluble ion contained in above sandy gravel layers.

The unfrozen water content of sandy gravel or fine sand layers at the depth of 4.70 m to 4.75 m, 5.66 m to 5.71 m, 5.80 m to 5.85 m and 6.75 m

to 6.87 m is 12.76%, 12.86%, 16.17% and 9.41% respectively which is more than that of its moisture preservation capacity. The fact shows that the soluble ion content contained in above layers is rather more.

For clayey soil layer, the freezing point  $T_f$  at the depth of 3.19 m to 3.25 m, 3.35 m to 3.40 m, 3.47 m to 3.70 m and 4.05 m to 4.63 m is  $-0.61^\circ\text{C}$ ,  $-0.35^\circ\text{C}$ ,  $-0.1^\circ\text{C}$  and  $-0.1^\circ\text{C}$  respectively which indicates there might be much more ion content contained in above layers. The sedimental cores collected from above layers were usually in thawing state containing few

Table 3. Constants in Eq.(1) & (2) for core profile collected from the East side of West Lake, CGWS

Depth (cm)	Test Number	$T_f = -A_1 W^{B_2}$		$W_{unf} = B_1  T ^{B_2}$		r
		A <sub>1</sub>	A <sub>2</sub>	B <sub>1</sub>	B <sub>2</sub>	
0-15	7	201.40	2.492	9.764	.315	.887
15-30	8	8780	3.739	12.344	.226	.919
35-45	5	63808	4.630	11.523	.196	.953
45-55	6	161.37	2.099	12.931	.385	.899
60-70	6	395.70	2.521	11.196	.362	.921
70-80	6	2049	3.328	11.011	.238	.889
80-90	8	40.50	2.010	8.002	.391	.886
95-105	7	325.50	2.770	9.231	.293	.901
105-120	6	27.44	1.834	7.529	.437	.895
130-140	5	14047530	6.349	13.503	.148	.969
140-155	6	161878	4.611	13.810	.176	.902
160-170	5	234716	4.917	12.440	.189	.964
170-185	5	43788	4.207	12.730	.227	.977
185-200	6	16544342	6.662	12.380	.129	.924
210-220	5	974847	5.527	12.340	.166	.957
220-240	5	165481	4.785	12.390	.194	.964
240-255	5	1087444	5.242	14.240	.185	.986
255-275	5	52483	3.899	16.320	.233	.953
275-285	5	82447	4.325	13.703	.230	.998
285-295	5	937677	5.152	14.440	.191	.992
295-302	5	824242	5.076	14.650	.193	.990

Table 4. Constants in Eq.(1) & (2) for core profile collected a sorted circle, CGWS

Depth (cm)	Test Number	$T_f = -A_1 W^{B_2}$		$W_{unf} = B_1  T ^{B_2}$		r
		A <sub>1</sub>	A <sub>2</sub>	B <sub>1</sub>	B <sub>2</sub>	
1-5	5	16495	4.304	9.639	.224	.983
11-14	5	8841	3.750	11.350	.249	.966
34-36	5	1970	3.016	12.570	.316	.976
45-47	5	4193	3.526	10.790	.274	.982
54-56	5	654345	5.567	11.210	.170	.973
64-66	5	234719	5.143	11.340	.173	.944
74-76	5	170.43	2.021	12.704	.489	.995
81-82	7	777.40	2.729	11.565	.348	.974
91-93	5	10035.92	3.445	14.484	.282	.985
98-100	5	1079.86	2.645	14.013	.376	.998
107-110	5	1347.96	2.824	12.832	.351	.996

Table 5. Freezing point and unfrozen water content profile of depth of a sorted circle, CGWS

Depth (cm)	Water content (%)	Freezing point (°C)	Depth (cm)	Water content (%)	Freezing point (°C)
0-3	172	0	64-67	68	0
3-5	57	0	74.5-76	66	-0.036
9-13.5	65	-0.001	81-82.5	58	-0.012
34-36	50	-0.015	91-94	30	-0.082
45-47	58	-0.003	98-100	30	-0.134
54-56	61	0	107-110	31.5	-0.079

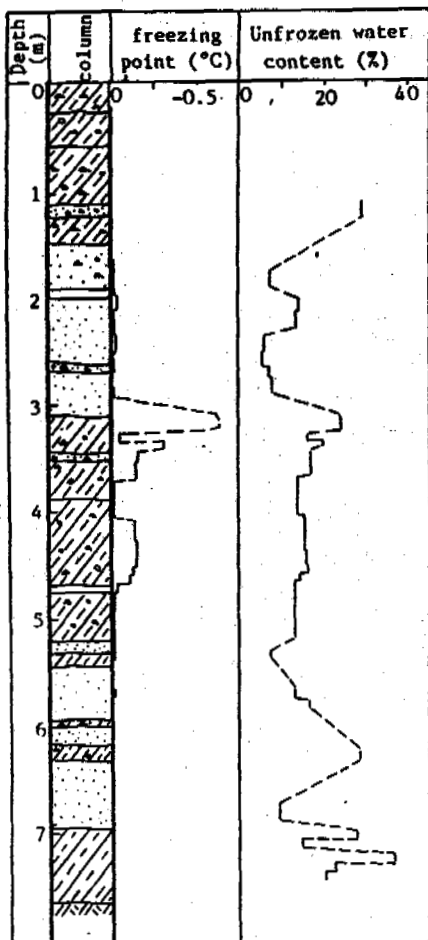


Figure 1. Freezing point and unfrozen water content profile of sedimental core collected from Yenu Lake, CGWS

ice crystals. Besides above, the unfrozen water content  $W_{unf}$  at the depth of 6.26 m to 6.32 m, 7.02 m to 7.07 m, 7.22 m to 7.29 m and 7.29 m to 7.44 m is 27.65%, 36.70%, 22.41% and more than 20% respectively. The fact of an alternating variation of  $W_{unf}$  might reflect the event on the sudden change of the sedimental environment and climate.

After analyzing the profile of  $T_f$  and  $W_{unf}$  of sedimental core collected at the West Hill with an elevation of 24 m a.s.l. at the surface (Fig.2), it is shown that the  $T_f$  at the depth of 0 to 0.5 m is less than  $-0.3^\circ\text{C}$ , the  $T_f$  of medium sand layer at the depth of 0.55 m to 0.60 m is  $-0.11^\circ\text{C}$ . As well known,  $T_f$  for sand without any ion content is close to  $0^\circ\text{C}$ . Looking forwards to the deeper part,  $T_f$  at the depth of 0.95 m to 1.0 m and 1.10 m to 1.20 m is also less than  $-0.30^\circ\text{C}$ . This is because of the similar condition between the upper and lower parts.

The  $T_f$  at the depth of 1.20 m to 1.30 m is extreme lower of  $-19.78^\circ\text{C}$ . The reason might be much more ion content on one hand, and on the other hand, its water migrated to the upper part and lower part (permafrost table at the depth of 1.5 m to 1.6 m) both for a long time which made it dehydrated ( $W=7\%$ ). Beneath the thick mass ice (from 1.90 m to 2.22 m), the soil moisture at the depth of 2.37 m to 2.41 m is the similar to that at 1.20 m to 1.31 m

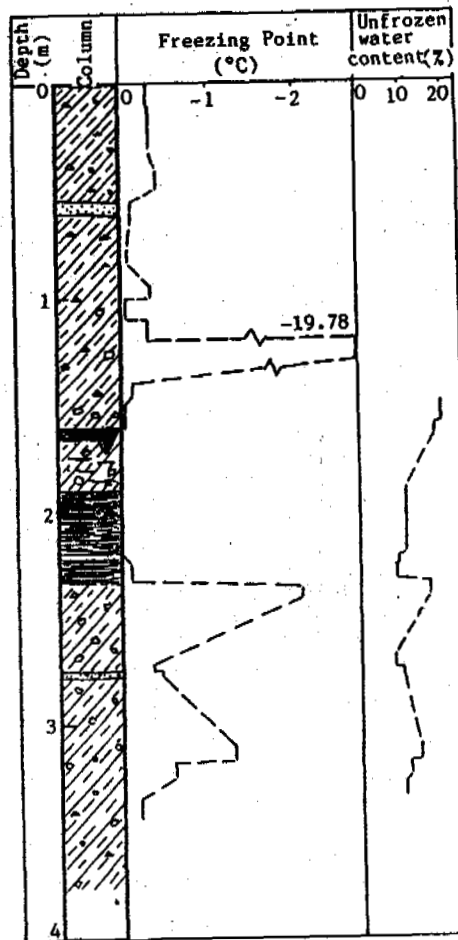


Figure 2. Freezing point and unfrozen water content profile of sedimental core collected from West Hill, CGWS

except its ion content is rather more.  $W_{unf}$  and  $T_f$  of sandy gravel layer at the depth of 2.75 m to 2.78 m is 11.1% and  $-0.45^\circ\text{C}$  which could be only existed while its ion content is rather more also. The peak value of  $T_f$  at the depth of 3.10 m to 3.18 m and 3.18 m to 3.25 m occurs  $-1.31^\circ\text{C}$  and  $-0.58^\circ\text{C}$  respectively which indicate the event of ancient environmental and climate variation also.

The profile of  $T_f$  and  $W_{unf}$  of the east side of West Lake with an elevation of 16.90 m a.s.l. is shown in Fig.3. In the seasonally thawing layer, 0 to 1.20 m in depth, the variation of  $T_f$  is rather small because it is affected by the Lake water nowadays which is not useful for indicating ancient environmental change. The water content of sandy clay with gravel developed at the depth 1.30 m to 3.00 m is not big which indicates the freezing speed might be very fast without water supply during freezing. The  $W_{unf}$  at the depth of 1.30 m to 1.40 m (very close to permafrost table) is 18.98% because of rather higher ground temperature. The  $W_{unf}$  at the depth of 1.40 m to 1.55 m and 2.40 m to 3.02 m is 18.68% and 17.98% while ground temperature is  $-0.3^\circ\text{C}$  and  $-0.7^\circ\text{C}$  to  $-0.8^\circ\text{C}$  respectively which might be able to indicate the sedimental conditions.

The sorted circle mentioned above is located at the inside of the second marine terrace with

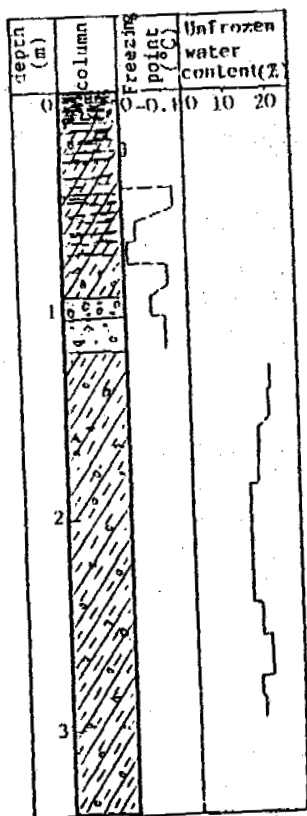


Figure 3. Freezing point and unfrozen water content profile of sedimental core collected from the East side of West Lake, CGWS

a snow cover of 1.5 m to 2.0 m in winter season and 30 cm on January 11, 1989. Its distribution of water content and  $T_f$  along depth is listed in Table 4 to 5. The  $T_f = -0.04^\circ\text{C}$  at the depth of 0.74 m to 0.76 m while  $W=66\%$  is rather lower than that of others, 0 m to 0.82 m in depth. Besides,  $T_f$  becomes  $-0.08^\circ\text{C}$  to  $-0.13^\circ\text{C}$  at the depth of 0.91 m to 1.10 m. During collecting, the thawing layer was found below the depth of 0.87 m with much lower water content. Compared with the ground temperature profiles, the thickness of permafrost here might be more than 20 m. Thus, existence of thawing layer shows that there is much more ion content in the layer on one hand, and on other hand, the thawing intercalation occurs in permafrost because of thick snow cover which makes ground temperature raised.

#### CONCLUSIONS

The systematic experimental study on the profiles of freezing point and unfrozen water content for sedimental cores with different landforms in the China Great Wall Station is the important part of the physico-mechanical properties of frozen ground, Antarctica. The results show that the extreme value of the freezing point  $T_f$  of soil is correspondent to the peak value of unfrozen water content at the given depth, and the sudden variation of  $T_f$  and  $W_{unf}$  along depth is the important index for indicating the change of the ancient climate and environment at Fildes Peninsula, the south of King George Island, Antarctica, which will be helpful for their reconstruction by using

radioisotope and geochemical analyses.

#### ACKNOWLEDGMENT

This project was supported by The China Antarctic Expedition Committee.

#### REFERENCES

- Chen, X.B., (1993) Permafrost around CGWS, Antarctica, Proc. of VI ICOP, 84-88.  
 Qiu, G.Q., Wang, Y.Q. et al, (1990) Freezing point of loess in Lanzhou, China. J. of Glaciology & Geocryology, Vol.12, No.2, 115-122.



PERMAFROST AND PERIGLACIAL WINDS AROUND THE WISCONSINAN  
ICE MARGIN IN THE NORTHERN PLAINS OF THE USA

William J. Wayne<sup>1</sup>, and Robert S. Guthrie<sup>2</sup>

<sup>1</sup>University of Nebraska, Lincoln, NE 68588-0340, U.S.A.  
<sup>2</sup>Bay West Inc., 5 Empire Dr., St. Paul, MN 55103, U.S.A.

Ice-wedge casts, relict sand wedges, ventifacts, deflation surfaces, and aligned landforms record permafrost around the Wisconsinan ice sheet margin in the United States from Montana to Indiana. From Montana to northeastern Nebraska, northwesterly winds were compressed into a narrowing zone with increasing velocity, keeping upland surfaces free of snow so that permafrost could develop, and forming yardangs. Sand deflated from desiccated snow-free ridges dropped into open thermal contraction cracks, producing sand wedges. Eastward the strong winds deflated soils to produce the Iowan Erosion Surface, leaving the paha as ridges. Permafrost may have been continuous in Wisconsin and Minnesota 23 to 18 ka, but was discontinuous or sporadic to the southeast in Illinois and Indiana.

## INTRODUCTION

During the Wisconsinan glaciation, and perhaps during earlier glaciations, a periglacial zone in the northern Great Plains and Central Lowland is evident from ice-wedge casts, relict sand wedges, involutions, and patterned ground. Other indicators of periglacial conditions, although not necessarily of permafrost, include extensive solifluction and other forms of mass wasting phenomena and wind-oriented fluted landforms and deflation basins. Fossil evidence in sediments includes assemblages of boreal and tundra mammals, snails, beetles, diatoms, and pollen typical of modern arctic and subarctic environments.

For many years, few features had been documented that suggested a severe frost climate around the Laurentide ice margin. During the 1950's and earlier, some workers, particularly palynologists, argued that they found no evidence of such conditions. In contrast, some physical geographers had proposed a wide band of tundra, with permafrost, along the glacial margin during the Wisconsinan maximum (Dillon, 1956; Manley, 1955).

In Wisconsin, Black (1965) reported ice wedge casts in the re-entrant between the lobes that approached the "Driftless Area" from both east and west. Scattered observations in Illinois (Sharp, 1942; Frye and Willman, 1958) were compiled by Wayne (1967) along with his records of patterned ground, relict solifluction features, and tundra mollusks in Indiana to interpret presence of sporadic permafrost around the Wisconsinan ice margin about 20,000 years ago in the Central Lowland. Farther west, Sharp (1949) reported abundant ventifacts in eastern Wyoming; Shafer (1949) recorded ice wedge casts and involutions in eastern Montana in the plains between the mountain front and the edge of the continental glacier; and Tipton and Steece (1965) pointed out probable ice wedge casts in southeastern South Dakota. Péwé (1983) summarized the reported wedge sites across the United States, and proposed that a relatively wide band of continuous and discontinuous permafrost extended across the plains from Ohio to the Rocky Mountain front during the Wisconsinan glaciation. Our report incorporates more recent information and refines

the interpretation of the periglacial environment across the northern Great Plains and the Central Lowlands. New records of biota help confirm interpretations based on geomorphic features.

## NORTHERN GREAT PLAINS

### Montana and Wyoming

Eastern Montana also was within a periglacial region, and permafrost should have been extensive. The only area where geomorphic features resulting from a severe frost environment have been reported, though, is in the trough between the edge of the Laurentide ice sheet and the front of the Rocky Mountains. Shafer (1949) described ice-wedge casts near Choteau and involutions in the same region. Farther north, Karlstrom (1990) described ice-wedge casts along the margin of the ice sheet east of Glacier National Park (Figure 1). Wind-carved yardangs have been reported in southeastern Montana (Colton, 1980).

Ice-wedge casts have been documented in the intermontane basins of Wyoming, (Mears, 1981, 1987), in the southern part of the High Plains of that state near Cheyenne (Figure 1), and in the Powder River Basin (Nissen and Mears, 1990). The strong winds that are characteristic of the modern Wyoming Plains were even more intense during Pleistocene glaciations, when abundant ventifacts were formed near Buffalo (Sharp, 1949). The wind would have swept many areas free of an insulating snow cover so that permafrost could develop on the exposed ground.

The Black Hills lie between the eastern and western parts of the northern Great Plains. Even though the altitude of the Black Hills is greater than that of the surrounding plains, it did not support any glaciers during the Pleistocene. Both its location and altitude should have produced periglacial conditions during the glaciations, but few observations of such features have been reported.

Many of the valley slopes in the Black Hills are smooth and surely were affected by greater rates of solifluction, and permafrost may have existed at least locally. A road cut at Custer, South Dakota exposes micaceous

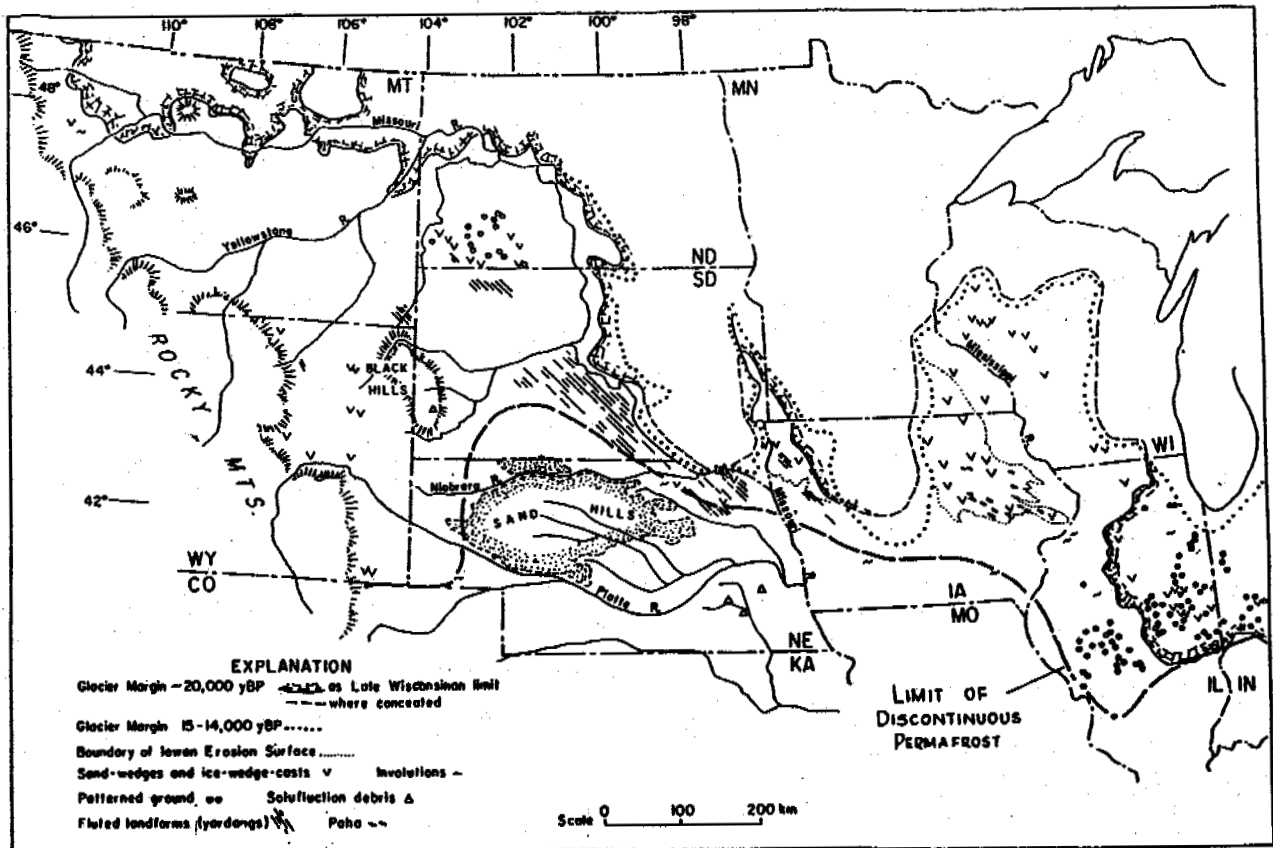


Figure 1. Map of permafrost-related periglacial features between central Indiana and the Rocky Mountain front and probable position of the southern limit of discontinuous/sporadic permafrost. Principal data sources are: Indiana (Wayne, 1967), Illinois (Johnson, 1990), Wisconsin (Black, 1965), Iowa (Guthrie, 1990), Nebraska (Wayne, 1991), South Dakota (Tipton and Speece, 1965), North Dakota (Clayton, 1980), Montana (Shafer, 1949), Wyoming (Mears, 1987).

schist, the steeply dipping foliation of which bends abruptly down slope along a line about 2 m beneath the land surface. Norton and Redden (1960) reported that they had observed "about 15 to 20 exposures" of mica schist in the Custer-Keystone area where a "slip zone" parallel to the surface slope had formed 1 to 3 m below the surface. This abrupt bend and the "slip zones" may mark the base of the active layer at a time when the rock below it was frozen. Increased intensity of frost action may also have contributed to the granular disintegration of the Harney Peak Granite in places like "The Needles."

#### Nebraska, South Dakota, North Dakota

Although a few observations of presumed ice-wedge casts had been published, recent discovery of sand wedges and ice-wedge casts in northeastern Nebraska (Wayne, 1991a,b) adds considerable understanding of the conditions that existed there and in the adjacent parts of South Dakota and northwestern Iowa during the last glacial maximum (Figure 1). These discoveries also give credence to the interpretation that wedge-shaped features near Osmond, Nebraska noted by Todd (1899), those reported by Tipton and Steece (1965) in southeastern South Dakota, and some wedge-shaped structures that penetrate black shale, observed in 1971 in road cuts near Santee, Nebraska, formed in thermal contraction cracks in permafrost at the time of the maximum advance of the last ice sheet.

This late Wisconsinan loess covers older sediments that lack a soil profile on ridge tops in northeastern Nebraska, although in the same area a Sangamon paleosol is buried beneath thicker loess on some former toe slopes. Sublimation of ice in the exposed frozen soil on the ridgetops loosened the surface material (McKenna-Neuman, 1990), making it available for deflation by the strong unidirectional winds (Wayne, 1991a,b). The wind kept the upland surfaces blown free of snow, but drifted it into lower areas, where it protected soils from deflation. A lag of ventifacts on the deflated hilltop surfaces is further evidence of the effectiveness of the ice-marginal winds. Comparison of till features with those where a pre-Wisconsinan soil profile is preserved indicates that as much as 1.5 m of soil and till may have been deflated.

For many years, molluscan and vertebrate fossil material recovered from the Peoria Loess and fluvial sediments provided evidence that colder conditions existed in the plains south of the Wisconsinan ice margin. Most interpretations, however (Leonard, 1952), were that although the environment of loess deposition was cooler than at present, it was not cold. Recent collections from loess that may have been nearly contemporaneous with the formation of sand wedges and wedge casts in northeastern Nebraska contain an assemblage that includes several cold-climate species (Wayne, 1991a). Similar assemblages have been reported from Iowa (Frest and Rhodes, 1981; Baker and others,

1986). Collections of vertebrate remains from fluviatile sediments along the Niobrara River, west of the sites where relict wedges are recorded, are dominated by boreal small mammals (Voorhees and Corner, 1985).

Southwestern North Dakota endured both strong winds and permafrost when it lay within the periglacial zone during the Wisconsin glacialiation. In several papers, Bluemle and Clayton (1986); Clayton (1980); and Clayton, Moran, and Bluemle (1980) have described patterned ground and ice-wedge polygons southwest of the outermost Wisconsin till. Ventifacts are fairly common on the siliceous caps of buttes in the unglaciated part of North Dakota. Aligned trough and ridge topography (yardangs) developed in a belt across central and southern South Dakota (Tipton and Steece, 1965), northeastern Nebraska (Wayne, 1991a), and northwestern Iowa (Hallberg, 1979) from the erosive action of strong wind NW to SE along the glacier margin.

A similar linear pattern can be detected in southeastern Montana (Colton, 1980) and in northwestern South Dakota, but it becomes more evident in the central part of that state, particularly near the Missouri River, where some of the shallow wind-cut troughs have been accentuated by stream erosion. To what extent bedrock structure has affected this pattern is difficult to determine; Rahn and Frazee (1974) pointed out that a major joint pattern in the Pierre Shale has the same orientation, and a recently published map (Thelin and Pike, 1991) shows a NW-SE linear pattern throughout the western part of the Dakotas and in eastern Montana that may be related to rock structure. The pattern is distinctive on thick Quaternary deposits in northeastern Nebraska and western Iowa (Figure 1), however, where bedrock structure is not likely to have influenced it. It disappears at the edge of the younger till of the Des Moines Lobe in central Iowa.

The extensive area of wind-cut ridges and troughs, the many ventifacts, some that lie on deflated surfaces, and the distribution of loess provide geomorphic evidence of strong unidirectional wind along the ice margin during the Wisconsin glacialiation. Wells (1983) identified a similar Wisconsin wind regime from study of dune orientation on the Great Plains. Katabatic winds draining off the glacier undoubtedly contributed to drying the land surface and subliming ice in it. They probably also stressed any exposed vegetation greatly and contributed to reduction of the plant cover. Velocities of katabatic winds may have been great enough at times to deflate the surface close to the ice margin, but it is unlikely that they continued far across the ice-free surface. They certainly could not have produced the yardang-like linear features because they did not flow in the direction necessary to do so (Figure 2).

To produce winds capable of such erosive power, northwesterlies, draining from the trough between the Rocky Mountain Front and the Laurentide glacier rising to the east, could have become a thermally confined current between the rising topography of the glacier and the southern split of the polar jet stream (Kutzbach and Wright, 1985). Northwestern wind constricted between these two limits (Figure 2) would have increased in velocity as it flowed through the narrowing boundaries. It produced ventifacts but only minor deflation and little linear scouring in Montana and North Dakota, but deflation and yardang development increased toward the southeast. Topographic deflection of the NW-SE wind around the west side of the Black Hills (Figure 1, 2) accounts for more northerly wind directions recorded by the ventifact orientations near Buffalo, Wyoming (Sharp, 1949). Similarly the positions of the ice margin and the polar jet stream would have funneled the wind more directly toward the east across Iowa and northwestern Illinois.

This interpretation is not in agreement with the concept that cyclonic disturbances should have formed in the ice-free zone along the edge of the glacier

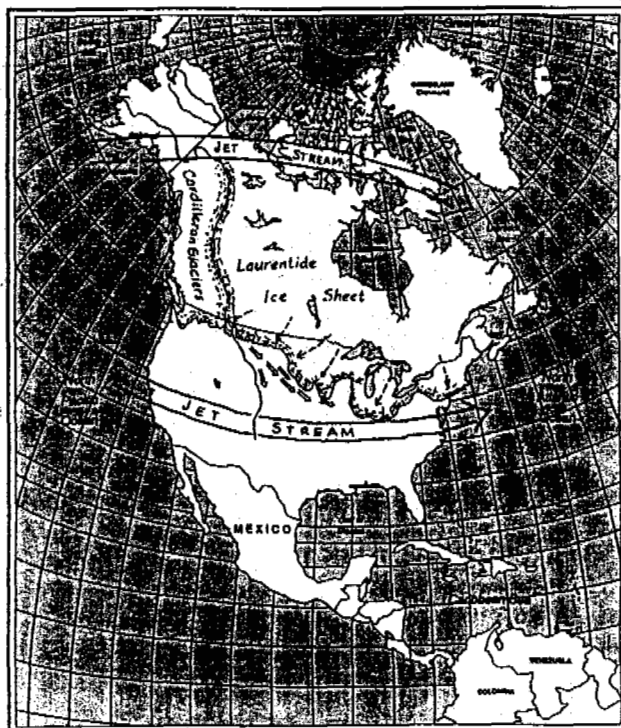


Figure 2. Position of jet stream across North America (after Kutzbach and Wright, 1985) at 20,000 years B.P. Open arrows represent strong ice-marginal wind pattern; dashed arrows show katabatic drainage.

(Liljequist, 1974). Such a condition would create strong wind flow toward the west, rather than toward the southeast; the orientation of the observed wind-cut linear patterns.

Loess is thin on many of the upland surfaces in northeastern Nebraska but thickens noticeably in the transverse valleys between the ridges as well as farther south, where it completely covers the till. Land snails characterize the Peoria Loess, but in many areas, particularly in north-central Nebraska, they are far from abundant. Loess that accumulated on or near streams is more likely to contain shells of fossil land snails than is loess that was deposited on interfluvial areas, which suggests that conditions were too dry for survival of snails except low on the slopes. Farther south, along the Platte River, for example, the Peoria loess is more richly fossiliferous, with snail taxa that are characteristic of cool, not cold, conditions.

#### CENTRAL LOWLAND BETWEEN THE MISSISSIPPI AND MISSOURI RIVERS

Northwestern Iowa, west of the Des Moines Lobe till, displays periglacial features similar to those in northeastern Nebraska. Hallberg (1979) called attention to the NW-SE linear pattern that is evident on aerial photographs, and sand wedges/sand-filled ice-wedge casts have been observed in several places in Iowa and southeastern Minnesota (Ruhe, 1969; Walters, 1992). The Iowan Erosion Surface (IES) is a region both east and west of the Des Moines Lobe till in Iowa where the till is old but lacks a pre-Wisconsin soil profile (Ruhe, 1969; Prior, 1991). Ventifacts have been reported in several places along the till-loess contact (Wilson, 1945).

Knowledge of the vegetation that existed about 20 ka is far better in Iowa than in Nebraska and farther west in the plains. Virtually total absence of pollen records

in the Great Plains during the Wisconsin maximum, 22 - 18 ka, has made it necessary to use proxy data of extensive wind erosion and the habitat requirements of land snails to guess that the ice-marginal zone was largely either barren or partly covered with tundra plants. Records in Iowa, however (Baker and Waln, 1985; Baker and others, 1986), indicate that a boreal forest gave way to tundra-like conditions with scattered conifers, much like that described for ice-marginal conditions in Indiana at the same time (Wayne, 1967). Mollusks and vertebrates collected from full glacial sediments include a significant number of cold-climate taxa, although they also include some that do not require tundra-like conditions. Insect assemblages in an east-central Iowa site have analogues today along the tree-line in northern Canada (Baker and others, 1986).

Through central Iowa, much of the IES is obscured by the younger till of the Des Moines Lobe, but to the east it continues (Figure 1). Remnants of the pre-Wisconsinan surface, with a well developed paleosol beneath a loess cover, exist in the southern part of the IES as isolated elongate ridges or paha. The paha, oriented about N60°W - S60°E, are a further record of the effectiveness of wind erosion/deflation across this part of the state.

Paha are both till-cored and loess-cored. The till-cored paha are deflationary remnants; loess-cored paha are longitudinal loess dunes. Most of these ridges are in the eastern part of the IES (Figure 1) and represent a surface of accretion that was stabilized by vegetation. The IES includes one area covered with thick loess and another, nearer the Wisconsin glacial margin, without a loess cover. The thick loess border extends northward into southern Minnesota, roughly parallel to the Mississippi River. In southeastern Minnesota the thick-loess border is abrupt and, as in Iowa, separates the IES into two parts. The loess-cored paha of southeastern Minnesota have a more northwesterly orientation than those in Iowa, are located on broad uplands near the thick loess border, and are characterized by coarse silt and fine sand.

#### CENTRAL LOWLAND EAST OF THE MISSISSIPPI RIVER

Loess-cored paha, oriented about N60°W, continue eastward across the Mississippi River into northwestern Illinois (Flemel et al, 1972). Johnson (1990) demonstrated that relict nonsorted polygons and ice-wedge casts can be recognized outside the Wisconsin ice limit as well as on the outer parts of the Wisconsin till plain (Figure 1). Across Illinois then, the zone occupied by perennially frozen ground must have been somewhat more extensive than it was in Indiana.

Where the Wisconsin glacier reached its most southerly extent in central Indiana (Figure 1), ice-wedge polygons have not been recognized beyond the glacier boundary, although asymmetrical valleys, which indicate more intensive mass wasting but do not require permafrost, are fairly common along east-west trending valleys. Ice-wedge polygons are noticeable features of the landscape on the till plain between the first (~21,000 B.P.) and a subsequent (~20,000 B.P.) readvance of the glacier (Wayne, 1967). Land snail assemblages recovered from a silt bed that lies between the tills of these two ice advances and dated at 20,000 B.P. are similar to those now living near Churchill, Manitoba, in a region of spruce parkland and discontinuous permafrost (Wayne, 1959, 1967). Some non-sorted polygons are present on the surface of the till plain left by this ice advance, although none are on surfaces near the ice advances that took place about 15,000 B.P. Mass wasting on the still unvegetated central Indiana till plain filled in depressions on the hummocky surface and reduced the relief to less than 1 or 2 m over most of the surface (Wayne, 1968). In this region permafrost was discontinuous or sporadic, existing only where local

conditions permitted development and maintenance of perennial ground ice.

Some of the locations where abundant ice wedge casts have been observed are in Wisconsin, where they are present in pre-Wisconsinan materials (Black, 1965). Although Black considered them to be related to the Wisconsin ice advance that reached the Johnstown Moraine about 15,000 B.P., and Attig and Clayton (1992) pointed out that some patterned ground in the state is even younger, it is likely that permafrost began to form earlier than that. Clayton and Moran (1982) suggested an ice-marginal position across Wisconsin 20,000 years ago that is only slightly less extensive than that of the ice that reached its maximum position at the Johnstown Moraine. The kettle lakes at Madison, Lakes Mendota and Monona, are evidence that large masses of stagnant ice from an earlier glacier advance were buried by the one that built the Johnstown Moraine west of Madison. The re-entrant between the western side of the Lake Michigan-Green Bay Lobe and the east edge of the Des Moines Lobe was undoubtedly a region of intense cold. Permafrost probably was continuous or nearly so throughout this re-entrant.

#### DISCUSSION

Although patterned ground and slope debris of various kinds are well known in the Appalachian Plateau in western New York and in Pennsylvania, no evidence for permafrost has been reported from the Central Lowland in western Ohio. In Indiana, non-sorted patterned ground and thermal contraction wedge casts are restricted to sites near the ice margin and within embayments along its lobate front. This distribution suggests that only sporadic permafrost existed there during the Wisconsin glacial maximum, about 20,000 years ago (Figure 1). Westward, around the glacier margin in Illinois, the zone in which patterned ground is present widens, and in Wisconsin, in the unglaciated region between the Lake Michigan Lobe and the Des Moines Lobe, permafrost probably was continuous.

Ice-wedge casts and deflation landscapes in eastern Iowa and in southeastern Minnesota provide evidence that permafrost was extensive, although whether or not it was continuous can not be determined from data available at this time. Frequent strong winds across the region, though, not only deflated the surface material, producing the Iowan Erosional Surface, but also would have kept it free of an insulating blanket of snow, thus permitting greater frost penetration. Faunal and floral remains corroborate the tundra-like landscape indicated by the geomorphic data.

West of the Des Moines Lobe, yardang-like fluting indicates that strong NW-SE winds were frequent and that extensive deflation took place. Sand wedges and sand-filled ice-wedge casts in northwestern Iowa and northeastern Nebraska were filled with sediment from the nearby deflated till surface. Snow blown from the ridges accumulated in more protected sites in valleys, insulating the surface there and protecting it from deflation. Permafrost probably was discontinuous in this region, although the band of discontinuous and sporadic permafrost widened to at least 100 km in Nebraska (Figure 1).

Extensive records of patterned ground in southwestern North Dakota makes it likely that much of South Dakota was within the zone of at least discontinuous permafrost, in spite of the absence of observations that would confirm its presence. Both the geographic position and altitude surely provided the conditions for permafrost to exist in the Black Hills. In the plains between the Black Hills and the Rocky Mountain front, ice-wedge casts, ventifacts, and deflation hollows provide ample evidence of the greater intensity of the frost environment during the last glaciation. The presence of ice-wedge casts in

the Great Plains in Wyoming makes it probable that eastern Montana was in a region of perennially frozen ground.

The boundaries we are suggesting for the distribution of permafrost during the period when the Wisconsin ice sheet had its greatest influence on the climate of the surrounding region, between about 22,000 and 16,500 years ago, show it to have been somewhat more limited than those suggested by earlier authors. Permafrost probably was sporadic near the ice margin in Indiana and may not have existed in Ohio except in the Appalachian Plateaus. The zone widened across Illinois, and continuous permafrost must have been present in the re-entrant not covered by glacier ice between the Lake Michigan Lobe and the Des Moines Lobe.

#### REFERENCES

- Attig, J. W., and Lee Clayton (1992) Conditions beyond the ice margin in Wisconsin during the last glacial maximum. Geological Society of America, Abstracts with Programs, 24: (4) 3.
- Baker, R.G., and K.A. Waln (1985) Quaternary pollen records from the Great Plains and central United States, in Bryant, V. and Holloway, R., ed., Pollen Records of Late-Quaternary North American Sediments. American Association of Stratigraphic Palynologists Foundation, Dallas, 191-203.
- Baker, R.G., R.S. Rhodes II, D.P. Schwert, A.C. Ashworth, T.J. Frest, G.R. Hallberg, and J.A. Janssens, 1986. A full-glacial biota from southeastern Iowa, U.S.A. Journal of Quaternary Science, 1: (2) 91-107
- Bettis, E.A., III, and T.J. Kemmis (1992) Effects of the last glacial maximum (21,000-16,500 B.P.) on Iowa's landscapes. Geological Society of America, Abstracts with Programs, 24: (4) 5.
- Black, R.F. (1965) Ice-wedge casts of Wisconsin. Wisconsin Academy of Science, Arts and Letters, 54: 187-222.
- Bluemle, J.P., and Lee Clayton (1986) Permafrost features in southwestern North Dakota. North Dakota Academy of Science, Proceedings, 40: 15.
- Clayton, Lee (1980) Geologic map of North Dakota, 1:500,000. U.S. Geological Survey and N.D. Geological Survey.
- Clayton, Lee, and S.R. Moran (1982) Chronology of Late Wisconsinan glaciation in middle North America. Quaternary Science Reviews, 1: 55-82.
- Clayton, Lee, S.R. Moran, and J.P. Bluemle (1980) Explanatory text to accompany the geologic map of North Dakota. North Dakota Geological Survey, Rept. of Investigation No. 68, 93 p.
- Colton, R.B. (1980) Yardangs in southeastern Montana. Geological Society of America, Abstracts with Programs, 12: (6) 270.
- Dillon, L.S. (1956) Wisconsin climate and life zones in North America. Science, 123:167-176.
- Flemal, R.C., S.E. Odom, and R.G. Vail (1972) Stratigraphy and origin of the paha topography of northwestern Illinois. Quaternary Research, 2: 232-243.
- Frest, T.J., and R.S. Rhodes II (1981) *Oreochelix strigosa cooperi* (Binney) in the midwest Pleistocene. The Nautilus, 95: 47-55.
- Frye, J.C., and H.B. Willman (1958) Permafrost features near the Wisconsin glacial margin in Illinois. American Journal of Science, 256 (7) 518-524.
- Guthrie, R.S. (1990) Geology and distribution of oriented landforms and associated features in northeastern Nebraska. University of Nebraska, Department of Geology, Ph.D. dissertation, 125 p.
- Hallberg, G.R. (1979) Wind-aligned drainage in loess in Iowa. Iowa Academy of Science Proceedings, 86: 4-9.
- Johnson, W.H. (1990) Ice-wedge casts and relict patterned ground in central Illinois and their environmental significance. Quaternary Research, 33:(1) 51-72.
- Johnson, W.H. (1992) Periglacial landforms and landscape modification during the last glacial maximum in east-central Illinois. Geological Society of America, Abstracts with Programs, 24:(4) 24.
- Karlstrom, E.C. (1990) Relict periglacial features east of Waterton-Glacier Parks, Alberta and Montana, and their paleoclimatic significance. Permafrost and Periglacial Processes, 1: 221-234.
- Kutzbach, J.E., and H.E. Wright, Jr. (1985) Simulation of the climate of 18,000 years BP: results for the North American/North Atlantic/European sector and comparison with the geologic record of North America. Quaternary Science Reviews, 4: 147-187.
- Leonard, A.B. (1952) Illinoisian and Wisconsinan Molluscan Faunas in Kansas. University of Kansas Paleontological Contributions, Mollusca, Article 4, 38 pp.
- Liljequist, G.H. (1974) Notes on meteorological conditions in connection with continental land-ices in the Pleistocene. Geologiska Foreningens i Stockholm Forhandlingar, Stockholm, 96: 293-298.
- Manley, Gordon (1955) A climatological survey of the retreat of the Laurentide ice sheet. American Journal of Science, 253: 256-273.
- McKenna Neuman, C. (1990) Role of sublimation in particle supply for aeolian transport in cold environments. Geografiska Annaler, 72A: 329-335.
- Mears, Brainerd, Jr. (1981) Periglacial wedges and the late Pleistocene environment of Wyoming's intermontane basins. Quaternary Research, 15: 171-198.
- Mears, Brainerd, Jr. (1987) Late Pleistocene Periglacial wedge sites in Wyoming: An illustrated compendium. Wyoming Geological Survey Memoir No 3, 77 pp.
- Nissen, T.C., and Brainerd Mears, Jr. (1990) Late Pleistocene ice-wedge casts and sand-wedge relics in the Wyoming basins, USA. Permafrost and Periglacial Processes, 1: 201-219.
- Norton, J.J., and J.A. Redden (1960) Structure associated with rock creep in the Black Hills, South Dakota. Geological Society of America, Bulletin 71: 1109-1112
- Pewe, T.L. (1983) The periglacial environment in North America during Wisconsin time, Chapter 9, p. 157-189, in Porter, S.C., ed., The Late Pleistocene, v. 1 of Wright, H.E., Jr. ed., Late-Quaternary Environments of the United States. University of Minnesota Press, Minneapolis, 407 pp.
- Prior, J.C. (1974) Drainage alignment in eastern Pennington County, South Dakota, South Dakota Academy of Science, Proceedings, 53: 61-68.
- Ruhe, R.V. (1969) Quaternary landscapes in Iowa. Ames, Iowa State University Press, 255 p.
- Schafer, J.P. (1949) Some periglacial features in central Montana. Journal of Geology, 57: 154-174.
- Sharp, R.P. (1942) Periglacial involutions in northeastern Illinois. Journal of Geology, 50: 113-133.
- Sharp, R.P. (1949) Pleistocene ventifacts east of the Big Horn Mountains, Wyoming. Journal of Geology, 57: 175-195.
- Thelin, G.P., and R.J. Pike (1991) Landforms of the conterminous United States--a digital shaded-relief portrayal. U.S. Geological Survey, Miscellaneous Investigation Series, Map I-2206.
- Tipton, M.J., and F.V. Steece (1965) Introduction to Pleistocene of Big Sioux River basin in South Dakota, in Schultz, C.B. and Smith, H.T.U. eds., Guidebook for Field Conference C, Upper Mississippi Valley. INQUA Congress VIII, 11-29.
- Todd, J.E. (1899) The moraines of southeastern South Dakota and their attendant deposits. U.S. Geological Survey, Bulletin 158, 171 pp.

- Voorhees, M.R., and R.G. Corner (1985) Small mollusks with boreal affinities in Late Pleistocene (Rancholabrean) deposits of eastern and central Nebraska. *Institute for Tertiary-Quaternary Studies, TER-QUA Symposium Series, 1: 125-142.*
- Walters, J.C. (1992) Ice-wedge casts on the Iowan erosion surface of northeast Iowa. *Geological Society of America, Abstracts with Programs, 24:(4) 70.*
- Wayne, W.J. (1969) Inland mollusks from Hudson Bay, Manitoba. *Nautilus, 72: 90-95.*
- Wayne, W.J. (1967) Periglacial features and climatic gradient in Illinois, Indiana, and western Ohio, east-central United States, in Cushing E.J. and Wright, H.E. Jr., eds, *Quaternary Paleocology, Yale University Press, New Haven, 393-414.*
- Wayne, W.J. (1968) The Erie lobe margin in east-central Indiana during the Wisconsin Glaciation. *Proceedings of the Indiana Academy of Science, 77: 279-291.*
- Wayne, W.J. (1991a) Ice-wedge casts of Wisconsinan age in eastern Nebraska., *Permafrost and Periglacial Processes 2: 211-223.*
- Wayne, W. J. (1991b) Provenience of sand in periglacial sand wedges and sheet sand, northeastern Nebraska, USA. *Symposium Periglacial Environments, IPA Working Group, Amsterdam May 1991, Abstracts, p.18*
- Wells, G.L. (1983) Late-glacial circulation over central North America revealed by aeolian features, in A. Street-Perrott et al (eds.), *Variations in the Global Water Budget, D. Reidel Publishing Company, p. 317-330.*
- Wilson, L.R. (1945) Pebble band ventifacts on Iowa till in Linn County, Iowa, *Iowa Academy of Science, 52: 235-241.*

## MICROSTRUCTURAL ALTERATION OF A FROST HEAVE SUSCEPTIBLE SOIL ADJACENT TO A BURIED CHILLED PIPELINE

T.L. White<sup>1</sup>, P.J. Williams<sup>2</sup>

<sup>1</sup>Institute for Research in Construction  
National Research Council of Canada  
Ottawa, Ontario, Canada, K1A 0R6

<sup>2</sup>Geotechnical Science Laboratories  
Carleton University  
Ottawa, Ontario, K1S 5B6

The thermodynamic conditions within frozen ground at temperatures just below 0°C are such that there is continuing translocation of water and ice, and the displacement of skeleton components. The dynamic nature of frozen ground expresses itself in microstructural changes which take place as a function of freeze-thaw cycling. Micromorphological observations performed after completion of the fourth freeze-thaw cycle of the Canada-France ground freezing experiment reveal evidence of internal movement and reorganization of soil fabric components and pore space distribution. The resultant fabric types are believed to be responsible for changes in hydraulic conductivity, water retention characteristic and for increasing the frost heave susceptibility of the soil.

### BACKGROUND

#### Test Facility/Experimental Conditions

The Canada-France Pipeline Ground Freezing study is carried out in the controlled environment facility of the Centre de Géomorphologie, Caen, France, under the auspices of Centre National de la Recherche Scientifique, Laboratoire Central des Ponts et Chaussées, and Energy, Mines and Resources Canada. The totally enclosed temperature controlled test facility was described in detail by Burgess et al (1982) when the experiment was initially set up, and after additional instrumentation was added by Carleton University (1988).

The facility consists of a refrigerated hall 18 m long by 8 m wide and 5 m high. The base of the trough of the facility is 1.75 m deep and was specially prepared to isolate the thermal and hydraulic regimes and to carefully control experimental conditions.

The experiment is heavily instrumented to monitor both the thermal and hydrological regimes. A network of sensors consisting of thermistors and thermocouples are used to monitor thermal regime, and tensiometers and piezometers are used to monitor the hydrological regime. Additional instrumentation consisting of gloetzl and petur cells are used to monitor total soil pressure. Periodic level surveys are carried out in conjunction with measurements of soil heave using telescoping heave tubes. An 18 m long by 27 cm diameter uninsulated steel pipe was buried in initially unfrozen soil to a depth of 60 cm below surface, so that it transects a frost susceptible silt and non-frost susceptible sand (Figure 1). During freezing periods air temperature was maintained at -0.75°C and pipe temperature at -2°C (first cycle) and -5°C (subsequent cycles).

#### Soil Characteristics/Grain Size Analysis

The frost susceptible silt (Caen silt) had not been frozen prior to the installation of the pipe. The silt is eolian in origin and composed of about 3 to 10 percent sand (2.0 to 0.076 mm), 75 to 85 percent silt (0.076 to 0.002 mm) and 10 to 20

percent clay (<0.002 mm). Atterberg limit determinations of Caen silt placed its liquid limit at 32%, and plastic limit at 21%. It can be designated as ML (silt with low plasticity) by the Unified Soil Classification System.

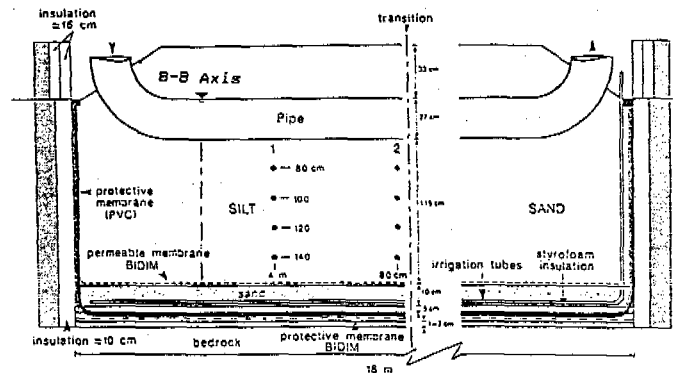


Figure 1. Longitudinal Cross Section of the Caen Experiment

#### Soil Sampling

After four cycles of freezing and thawing (during which part of the silt was frozen), 29 undisturbed Kubiena Box samples were taken for micromorphological analysis, in 1990 twenty-nine hydraulic conductivity core samples were also obtained. The samples were taken from five soil profiles along the B-B axis (in the centre of the silt section of the experiment) located at: centre of pipe, adjacent to side of pipe, 0.5 m from side of pipe, 1.0 m from side of pipe and 3.0 m from the side of the pipe (Figure 2). The samples were taken according to procedures outlined in Sheldrick (1984) and Murphy (1986), and every effort was taken to obtain all samples in an undisturbed condition (that is, to minimize damage to the samples such as stress cracks).

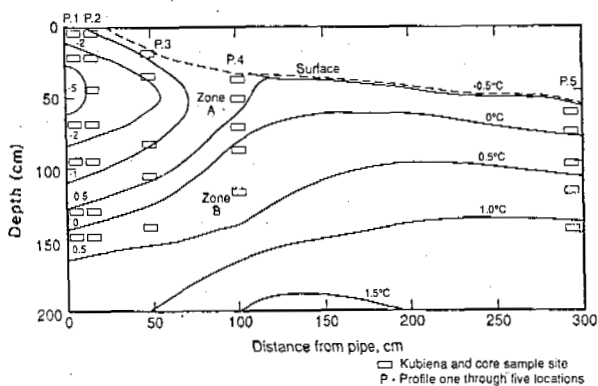


Figure 2. Sample Location in Profiles Along the B-B Axis.  
Position of Isotherms Day 482,  
Fourth Freeze Cycle

All Kubiena box samples and core samples were returned to Canada and placed in storage in a temperature controlled (10°C) and humidity controlled (100%) room at Agriculture Canada.

#### LABORATORY RESEARCH PROGRAM

A test program consisting of the study of the Caen silt's micromorphology (i.e., the arrangement of soil particles and pore space distribution) was then undertaken at Agriculture Canada's Land Resource Research Institute, Ottawa. Physical property tests consisting of saturated hydraulic conductivity determinations and soil-water desorption determinations were undertaken in an attempt to relate the micromorphological features observed in thin sections and block specimens to the physical properties exhibited by the Caen silt.

#### Sample Preparation for Micromorphological Study

Soil water was removed from the soil samples prior to impregnation. Two methods are generally used: first, air drying; second, replacement of soil water with acetone. Air drying may result in substantial shrinkage of the sample. Given the presence of an identified swelling clay mineral (smectite), air drying was deemed unsuitable for the purpose of this study. Exchange with acetone maintains the sample morphology close to sampling conditions, and thus provides greater confidence for characterization of the observed features. Murphy (1982) discusses the advantages of acetone replacement of soil water for pore analysis studies in mineral soils.

Soil thin sections and block specimens were prepared from the undisturbed Kubiena box samples after they had undergone soil water replacement with acetone and then, subsequently, impregnated with a polyester resin containing a fluorescent dye (Uvitex OB, Ciba-Geigy). The methodology for sample impregnation and block sample preparation is widely documented, having been described in detail by Osterkamp (1977), Fitzpatrick (1984), Sheldrick (1984) and White (1991a).

The use of thin sections and block specimens facilitates the description of the arrangement of soil particles and voids as well as provides information on particular features and how these features are interrelated. Characterization of the voids, their shape, size and arrangement may be undertaken and quantitative information obtained by using computerized image analysis instrumentation (Bullock and Thomasson, 1979).

#### Cryogenic and Fabric Observations

Soil micromorphology is the systematic study of the arrangement of the soil constituents and associated pores in an undisturbed state of the soil at a particular time. Micromorphology of the thin sections was described according to Brewer (1964) and a glossary of micromorphological terminology by Howes and White (1991). Soil fabric descriptions were made from vertically oriented thin sections at 6X magnification. This magnification provides an indication of the gross morphology that characterizes the structure of the soil fabric (Fox 1979).

Distinct gross morphologies were observed to have developed in the samples taken from the zone within the soil profile exposed to the four freeze-thaw cycles. Van Vliet-Lanoe (1985) and White (1991b), noted that soil structure developed directly in response to freezing and thawing processes, and that the structures were stable and maintained their distinctive morphology through subsequent disruption.

The dominant morphology which has developed in the zone exposed to repeated freeze-thaw cycles is a fragmoidic fabric, Plate 1 (40 cm below the bottom of pipe). The fragmoidic fabric designates morphology having planar pores and coalesced, often elongated, soil units. Such fabric was interpreted by Van Vliet-Lanoe (1985) to result from ice lens formation, and shown by Pawluk (1988) to form from repeated freeze/thaw cycles. The fragmoidic fabric was observed to change to a fragmic fabric as a function of decreases in the thermal gradient and with increasing depth below and distance away from the buried chilled pipeline, Plate 2 (1.0 m from pipe, 20 cm below surface). The fragmic fabric designates morphology having compact aggregates separated by planar pores. Maximum planar pore widths (up to 0.2 mm) were observed in the fragmoidic fabric in the frost bulb below and immediately adjacent to the buried chilled pipeline and were observed to decrease in width as the fabric changed to a fragmic fabric where maximum pore width (up to 0.07 mm) were observed.

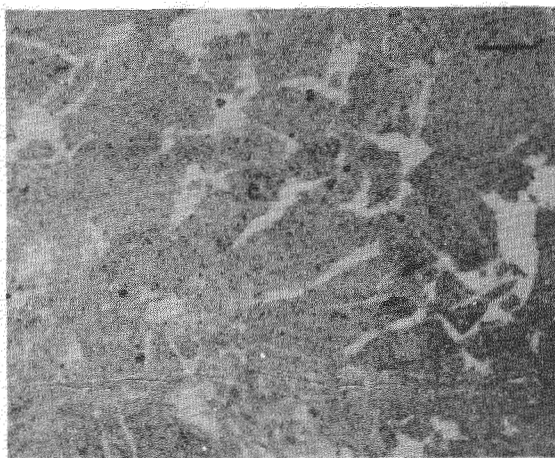


Plate 1: Fragmoidic Morphology  
(40 cm below the below the bottom of pipe)  
Scale length is 1.0 mm

In strong contrast, Plate 3 (80 cm below surface, 0.5 m from the pipe) shows a much denser granular structure which characterizes the soil taken from zones in the profile not exposed to freezing. The dominant morphology in this zone is granoditic fabric with random zones of porphyroskelic fabric. The granoditic fabric



distribution designates morphology having irregular weakly interconnected vughs separating coalesced aggregates.

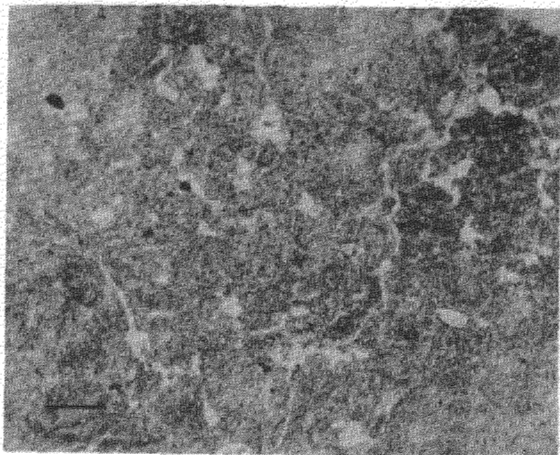


Plate 2 Fragmic Morphology  
(1.0 m from side of pipe  
- 20 cm below surface)  
Scale length is 1.0 mm

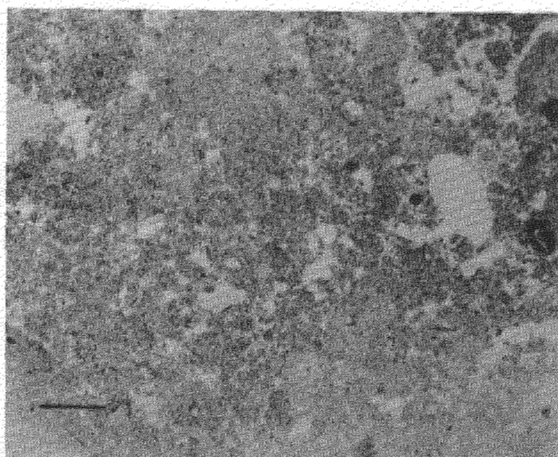


Plate 3 Granodic Morphology  
(80 cm below surface, 0.5 m from pipe)  
Scale length is 1.0 mm

Lithic discontinuities and stratification of sediment first observed by Dumoulin et al (1987) and later confirmed by White (1992) were also evident in the thin sections made from samples taken from the surface above the pipe and at a depth of 60 cm below surface, (the depth at which the pipe was installed) 0.5 m from the pipe. The activity of equipment and people on the ground surface along the pipe caused some additional compaction of the soil. The dominant morphology in the zones, exposed to additional compaction, is porphyroskelic fabric, Plate 4, whose morphology is characterized by a dense ground mass with few to no distinct voids.

#### TESTS OF PHYSICAL PROPERTIES

##### Saturated Hydraulic Conductivity Determinations

Dallimore (1984) reported changes in hydraulic

conductivity of Caen silt after performing detailed analysis of sections of samples exposed to several freeze-thaw cycles. After the first freeze-thaw cycle, it was observed that the

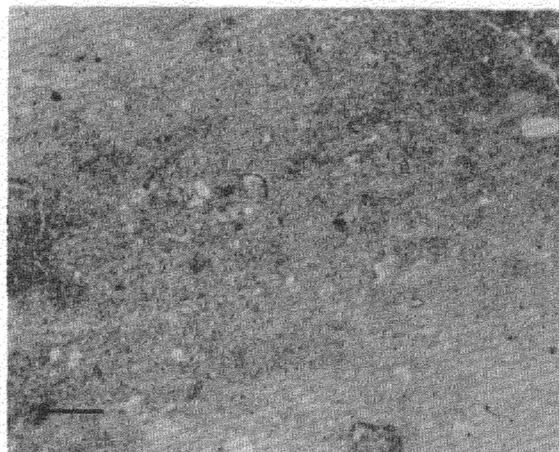


Plate 4 Porphyroskelic Morphology  
(60 cm below surface, side of pipe)  
Scale length is 1.0 mm

vertical permeability of the reconsolidated thawed sample increased from  $8 \times 10^{-8} \text{ cm s}^{-1}$  to  $3 \times 10^{-7} \text{ cm s}^{-1}$ . Detailed examination of sections of the test specimens suggests that the increase in the vertical permeability was due largely to an increase in the hydraulic conductivity in the portion of the sample frozen during the test. Intense ice-lensing, it is believed, is responsible for structural changes which have resulted in paths for increased water flow.

The undisturbed core samples taken from zones of the five profiles which had been exposed to freezing and zones which had not been exposed to freezing were prepared and instrumented with a constant head apparatus developed by Klute (1965) to measure the hydraulic conductivity.

Hydraulic conductivity (K) can be determined from the following equation:

$$K = \frac{QL}{ATH}$$

where K is saturated hydraulic conductivity ( $\text{cm s}^{-1}$ ), Q is the volumetric flow over a period of time T, L is the length of the core specimen (cm), T is time in seconds, A is the cross sectional area of the core ( $\text{cm}^2$ ) and H is the hydraulic head difference in cm.

All test results are plotted on a cross section of the sample site locations along the B-B axis (Figure 3). Overall, the test results indicate a pattern of hydraulic conductivity similar to the changes reported by Dallimore. Hydraulic conductivity values at 3.0 m from the test pipe were  $10^{-4} \text{ cm s}^{-1}$  compared to higher values (one order of magnitude)  $10^{-3} \text{ cm s}^{-1}$  in zones below (in the frost bulb) and immediately adjacent to the pipe where the most intense segregated ice-lensing had been observed by Smith and Williams (1990).

In contrast, much lower hydraulic conductivity values  $10^{-5} \text{ cm s}^{-1}$  were observed immediately above the pipe and in the zone of the soil profile along the B-B axis near the pipe but not subjected to freeze-thaw cycles. These observations were an order of magnitude lower than the base values recorded at 3.0 m from the pipe.

Some variations in hydraulic conductivity from the reported general pattern were also observed. This suggests that, in spite of the elaborate pretreatment of the silt used in the Caen experiment, differences in packing are present in the soil profile. Hydraulic conductivity values in the zones at 60 and 80 cm below surface, 0.5 m from the side of the pipe were one order of magnitude lower. Micromorphological observations indicate that porphyroskelic fabric had developed in this zone where compaction associated with installation of the buried pipe took place.

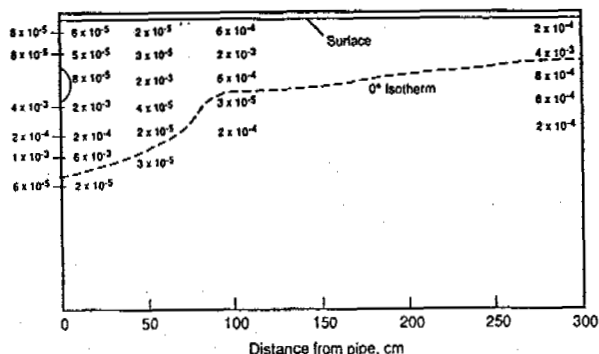


Figure 3. Saturated Hydraulic Conductivities for Sample Profiles along B-B Axis

#### Soil-Water Desorption Determinations

The relationship between the soil water content and the soil water suction is a fundamental part of the characterization of the hydraulic properties of a soil.

Soil-water desorption data provides information on pore size distribution which is valuable for characterizing soils for various applications relating to drainage, liquid waste disposal and frost heave potential.

Soil-water desorption tests are carried out by applying a suction to a specific volume of soil for sufficient time to allow the pores which will drain at the applied suction, to do so. The equilibrated sample is weighed and this value is used to calculate the water content for the applied suction.

Following the completion of hydraulic conductivity determinations, the 29 core samples were prepared for soil-water desorption measurement according to methodology described in detail by Sheldrick (1984).

The suction tank provided a suction medium with both high saturated hydraulic conductivity and a high air-entry value. Glass beads with a medium diameter of 30  $\mu\text{m}$  were used as the suction medium for suction pressure heads from 0 to 100 cm of water, and aluminum oxide powder of 9.5  $\mu\text{m}$  medium diameter was used for suctions from 100 to 350 cm of water.

To achieve desorption of the soil cores, a negative pressure head was applied to the glass bead tank by lowering the constant head burette to give the desired head. When the cores had equilibrated for the appropriate amount of time (Sheldrick, 1984) at the desired pressure head, the samples were removed from the tank's suction plate and weighed.

Desorption curves (Figure 4, above and below the pipe) and Figure 5 (0.5 m from side of pipe), when compared to Figure 6 (1.0 m from side of pipe), show that variations in water retention exist between zones of the profiles which have been exposed to freezing when compared to zones of the profiles not exposed to freezing.

The most significant variation in water

retention at different suctions was observed between the core samples taken from above and below the pipe. Water retention ranged from 20%

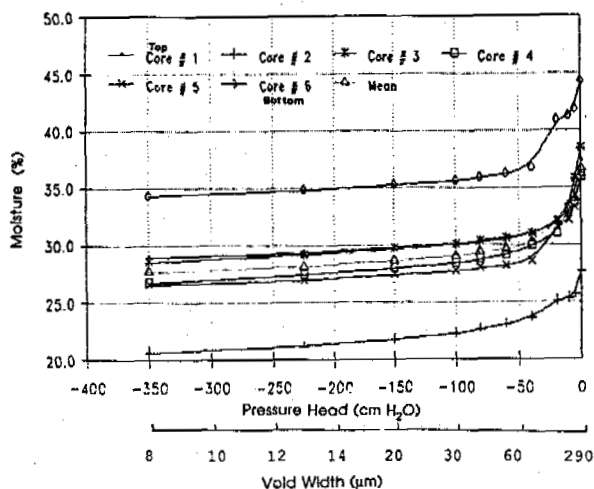


Figure 4. Profile One Desorption Curves for Sample Cores Located (above and below the pipe)

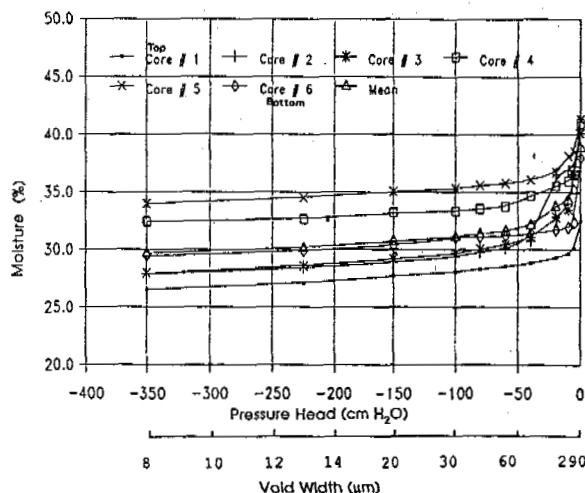


Figure 5. Profile Three Desorption Curves (0.5 m from side of pipe)

for samples located above the pipe to 34% for a sample located below the pipe at a tension of -350 cm of water. A much narrower range of water retentions was exhibited by core samples located 1.0 m from side of pipe (Figure 6) where water retention varied by as little as 2%.

Low porosity values (38%) were observed throughout the surface layer of the sample area and are attributed to the compaction of this zone by equipment and foot traffic over the operating life of the experiment.

Water holding capacity and higher porosity values (46%) within the zones of the soil where intense segregated ice-lensing was observed would create more macro sized pore space (> 60  $\mu\text{m}$ ) which is responsible for this zone's higher water holding capacity. In contrast, water retention and calculated porosity for the profiles located 1.0 m and 3.0 m from the side of the buried chilled

pipe, where little freezing took place, were observed to be more uniform.

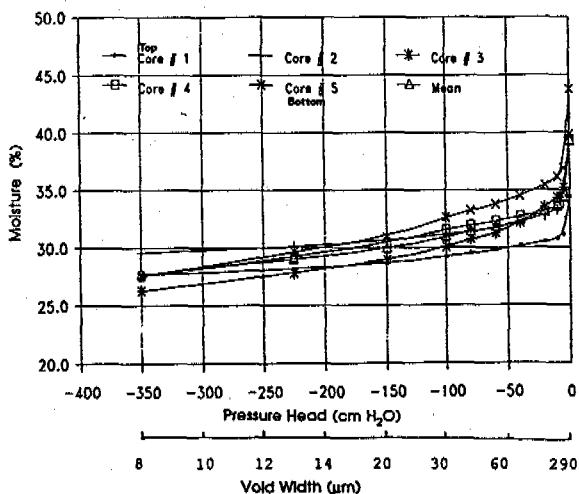


Figure 6. Profile Four Desorption Curves (1.0 m from side of pipe)

#### Implications for Frost Susceptibility

Given that both the carefully controlled thermal and hydraulic regimes for freeze-thaw cycles have remained similar in the Caen experiment, it can be inferred that the reported changes in the soil's fabric and physical properties, (specifically, saturated hydraulic conductivity and water retention characteristics) have altered its heave susceptibility. Chamberlain and Gow (1979) showed that the freezing and thawing of silt and clay slurries caused an increase in the vertical permeability in their test specimens. Chamberlain (1988) observed that changes also occurred in the frost heave potential of compacted soils from the first freeze-thaw cycle to the second and third cycles. Subsequent freeze-thaw permeability test results performed by Chamberlain et al (1990) on four compacted frost susceptible soils also illustrated the extent to which vertical permeability was increased as a function of freeze-thaw cycling.

TABLE 1. Heave of Pipe in Caen Silt (Day 100)

<u>Freeze Cycle</u>	<u>Heave (cm)</u>	<u>% Increase</u>
Second	9.88	-
Third	10.77	9
Four	11.40	5.8

Table 1 indicates how, in successive freeze-thaw cycles of the Caen experiment, the heave susceptibility of the silt continued to increase.

The increasing frost susceptibility of Caen silt may have been brought about by intense segregated ice-lensing which has created the fragmoidic fabric adjacent to and beneath the buried pipe. The observed changes in hydraulic conductivity and water retention attributed to intense ice-lensing (Dyke, L. and P. Egginton 1990) have developed as a result of high soil moisture suctions in the freezing zones. These cause an increase in the effective stress in the region below the freezing front during the formation of segregated ice-lensing.

The ice-lensing has been responsible for increasing the soil's vertical permeability in the near surface layer, permeability which has remained unaltered or possibly been enhanced by each subsequent cycle. Increased porosity is associated with macro pore spaces left behind by

intense ice-lensing.

While the permeability of the zones of Caen silt exposed to freezing have been observed to increase and thus permit increasing amounts of water to migrate to the freezing front where ice accumulation was observed to be greatest, the situation at depth has been observed to be quite different. Consolidation which may be due to frost induced suction has resulted in a full order of magnitude decrease in the silt's hydraulic conductivity, and a reduction in its water retention.

The reported findings for changes in hydraulic conductivity of Caen silt core specimens indicate that zones of the sample profile not exposed to freezing have become less permeable and more dense after several consolidation phases, while conversely, zones of the sample profiles exposed to freezing have experienced an increase in vertical permeability.

#### CONCLUSIONS

Micromorphology observations and physical properties tests performed after the completion of the fourth freeze-thaw cycle of the Canada-France ground freezing experiment have revealed that the dynamic nature of frozen ground is expressed by morphological changes in soil structure and pore size distribution. The cumulative effects of the continuous translocation of water, ice and small displacements of material due to frost creep associated with alternating freeze-thaw cycles has resulted in alteration of this frost susceptible soil's fabric. The reported changes in fabric have resulted in the alteration of both the saturated hydraulic conductivity and the water holding capacity of the soil.

It is clear that the effects of micro structural changes in soil fabric can alter the frost-heave susceptibility of soil and should be taken into consideration in order to better evaluate soil-pipe interactions which will occur in situ in the field.

Finally, more micromorphological research should now be undertaken on various frost susceptible soils. This research would help clarify what cryogenic processes are responsible for alterations of frost susceptible soils' fabric, and would enable a better understanding of the mechanisms responsible for some micromorphological assemblages reported in this paper.

#### ACKNOWLEDGEMENTS

The success of the research presented in this paper is due in part to the willingness of colleagues, especially Dr. K. Torrance to assist through lengthy informative discussions, to Dr. Cathy Fox and Mr. Raymond Guertin, Agriculture Canada's Land Resource Research Institute, and to B. Van Vliet-Lanoe, who were generous with their time and helped tremendously in sorting out many of the technical aspects of micromorphological research.

#### REFERENCES

- Bullock P. and A.J. Thomassen, 1979. Measurement and characterization of macroporosity by image analysis. *Journal of Soil Science*, Vol. 30, pp. 391-413.
- Burgess, M., G. Lemaire, M.W. Smith and P.J. Williams, 1982. Etude du gel sols autour d'une conduite refroidie enterrée dans une station expérimentale-Phase I. Pour Le Ministère d'Énergie, Mines et Ressources, Direction de la Physique du Globe, 62 pp, also as: IR 29, Geotechnical Science Laboratories, Carleton Univ.

- Burgess, Margo. 1985. Permafrost, Large scale research at Calgary and Caen, Geos, 1985/2, 19-22.
- Brewer, R. 1964. Fabric and Mineral Analysis of Soils, Wiley, New York.
- Carleton University, Geotechnical Sciences Laboratories, 1988. The third freeze cycle of the Canada-France ground freezing experiment. Final report to the Permafrost Research Section, Terrain Sciences Division, Geological Survey of Canada (Department of Energy, Mines and Resources), January 1988, 78 pp. also as: IR 54, Geotechnical Science Laboratories, Carleton Univ.
- Chamberlain, E.J. and A.J. Gow, 1979. Effect of freezing and thawing on the permeability and structure of soils. Engineering Geology (Amsterdam, 13: 73-92)
- Chamberlain, E.J., 1988. Effects of freezing and thawing on the permeability of compacted clay. U.S. Army Cold Region Res. and Engineering Lab., Hanover, NH., Draft Rept. prepared for U.S. Dept. of Energy.
- Chamberlain, E.J. 1990. Effect of freeze-thaw cycles on the permeability and macrostructure of soils. Proceedings, International Symposium Frozen Soil Impacts on Agricultural, Range and Forest Lands, Spokane, Washington, pp. 145-155.
- Dallimore, S.R. 1984. Laboratory characterization of frost heaving of Caen silt, Pipelines and Frost Heave. Proceedings of a Seminar at Caen, France, April 25-27, pp. 23-27.
- Dumoulin, R., A. Cupas and J.C. Valeux, 1987. Mesures et interpretation des gonflements internes et des variations de densite des sols par double sonde gamma. 2eme Coloque. Franco-Polonaises, Gel et Genie Civil. Laboratoire Central des Ponts et Chaussees.
- Dyke, L. and P. Egginton, 1990. Influence of ice lens fabric on hydraulic conductivity of thawing soil. Fifth Canadian Permafrost Conference, pp. 137-141. NRC - Centre d'etudes Nordiques, Laval University.
- Fitzpatrick, E.A. 1984. The micromorphology of soils. Chapman and Hall Ltd., New York.
- Fox, C.A. 1979. The soil micromorphology and genesis of the Turbic Cryosols from the MacKenzie River Valley and Yukon Coastal Plane. Ph.D. Thesis (unpubl.), Department Land Resource Science, University of Guelph, Guelph, Ont. 196 pp.
- Howes, J. and T.L. White. 1991. A glossary of micromorphology terminology. IR 61, Carleton University, Geotechnical Science Laboratories, 38 p.
- Klute, A. 1965. Laboratory measurement of hydraulic conductivity of saturated soil. In Methods of Soil Analysis. C.A. Black, ed., Agronomy No. 9, Part 1, American Society of Agronomy, Madison, WI.
- Murphy, C.P. 1982. A comparative study of three methods of water removal prior to resin impregnation of two soils. J. Soil Sc. 33, 719-735.
- Murphy, C.P. 1986. Thin section preparation of soils and sediments. AB Academic Publishers, Berkhamsted, Herts, England, 149 pp.
- Osterkamp, T.E., 1977. A method of cutting and preparing thin sections of frozen soil. Journal of Glaciology, Vol. 18, No. 78.
- Pawluk, S., 1988. Freeze-thaw effects on granular structure reorganization for soil materials of varying texture and moisture contents. Can. J. Soil Sci. 68: 485-494.
- Sheldrick, B.H. (editor), 1984. Analytical methods manual, thin sections. Land Resources Inst., No. 84-30.
- Smith, S.L. and P.J. Williams, 1990. Ice lens orientation around a chilled buried pipe. Proceedings, Fifth Canadian Permafrost Conference, pp. 83-87. NRC - Centre d'etudes Nordiques, Laval University.
- Van Vliet-Lancee, B., 1985. Soils and quaternary landscape evolution: Frost effects in soils. John Wiley and Sons Ltd.
- White, T.L., 1991a. Preservation of frozen soil samples. Procedure Manual, Carleton University, Geotechnical Science Laboratories, Revised LTR 12.
- White, T.L., 1991b. Microstructural genesis of a frost susceptible soil adjacent to a buried chilled pipeline. Proceedings, Canada-France Seminar, Gas and Oil Pipelines and Civil Engineering in Arctic Climates, Caen and Paris, France.
- White, T.L., 1992. Cryogenic alteration of a frost susceptible soil. Geotechnical Science Laboratories, Carleton University, 189 pp.

## INFLUENCE OF SALINITY ON THE COMPRESSIVE STRENGTH BEHAVIOR OF FROZEN SOILS

Harsha Wijeweera<sup>1</sup> and Ramesh C. Joshi<sup>2</sup>

<sup>1</sup>Department of Civil Engineering, The University of Calgary  
Calgary, Alberta, Canada T2N 1N4

<sup>2</sup>Department of Civil Engineering, The University of Calgary  
Calgary, Alberta, Canada T2N 1N4

The primary objective of this study was to evaluate the effects of salinity, temperature and the total water content on the compressive strength of fine-grained frozen soils. Three strength parameters, namely, peak, yield and residual strength, were considered in evaluating the strength characteristics of such soils. The secondary objective was to examine the type of failure frozen saline soils undergo.

### INTRODUCTION

During the past few decades, increasing development has been taking place both in the coastal and off shore regions in the Arctic. The permafrost in these areas contain various levels of salinity. The presence of solutes in the pore fluid considerably affect the strength and deformation behaviour of frozen soils. The geotechnical engineer who has to design and construct structures in saline permafrost should possess a clear understanding of the short-term and long-term strength and deformation behavior of such soils. However, in the literature relatively little data on strength and deformation behavior are available, particularly for frozen fine-grained saline soils.

The short-term strength behavior of frozen saline sand has been investigated by Sego et al. (1982) and Jessberger et al. (1985). Sego et al. (1982) conducted unconfined compression tests at  $-7^{\circ}\text{C}$  with the pore water salinity of the sand varying between 0 and 100 parts per thousand (ppt) while Jessberger et al. (1985) performed triaxial compression tests on fine frozen sand with salinity varying between 0 and 200 ppt and at temperatures ranging from  $-10^{\circ}\text{C}$  and  $-40^{\circ}\text{C}$ . The results from both these studies indicated a marked reduction in the uniaxial compressive strength of frozen sand with increasing salinity. Ogata et al. (1983) also observed similar strength behavior in frozen saline sand at temperatures warmer than  $-20^{\circ}\text{C}$ , based on tests conducted on four sands and three cohesive soils with different salinities, (0 to 30 ppt) and at temperatures between  $-2^{\circ}\text{C}$  and  $-70^{\circ}\text{C}$ . At temperatures below  $-20^{\circ}\text{C}$  Ogata et al. (1983) noticed that the strength of sand with salinity of 30 ppt to be greater than that of the strength of sand with lower salinities. However, the test results from Jessberger et al. (1985) did not indicate such strength increase with increasing salinity below  $-20^{\circ}\text{C}$ .

This paper presents the results of uniaxial compression test on a fine-grained soil, with levels of salinity varying between 0 and 20 ppt. The tests were conducted at temperatures between  $-5^{\circ}\text{C}$  and  $-17^{\circ}\text{C}$  on specimens with different total water contents (i.e. both unfrozen and frozen water content) of between 30% and 56%. Important strength parameters such as peak, yield and residual strength, derived from the stress-strain curves of the specimens under the various testing conditions are considered in this study.

### MATERIALS AND SAMPLE PREPARATION

The fine-grained soil used in this study was Ball clay, a high plastic clay, with a liquid limit of 56.9 and a plastic limit of 24.7. The saturated soil was initially prepared using slurry consolidation technique in a specially fabricated 200 mm internal diameter cell. The steel cell body was coated with a teflon lining to prevent corrosion of the cell due to the presence of salts. The lining also helped in reducing the friction effects on the soil during consolidation. Saturated samples of the soil with water contents of around 52 and 34% were prepared by consolidating the initially de-aired slurry under pressures of 100 and 1200 kPa, respectively. The pore water salinity of the soil slurry was varied by adding sodium chloride at concentration levels of 0, 10 and 20 g/L (or parts per thousand) to distilled water.

From the 200 mm diameter consolidated sample test specimens, 38 mm in diameter and 80 mm in length, were extracted using a core cutting tube. The sample disturbance was minimal. The specimens were then frozen unidirectionally from top to bottom, without access to water at the bottom, in a freezing cabinet with the temperature maintained at  $-73^{\circ}\text{C}$ . Visual examination of sections through the frozen

specimens revealed no ice lenses and no disturbance to the initial unfrozen soil structure. The degree of saturation of the test specimens prepared in this way was greater than 95%. The details of the equipment and the specimen preparation and freezing procedures are contained in Wijeweera (1990).

### UNIAXIAL COMPRESSIVE STRENGTH TESTS

Constant strain-rate uniaxial compression tests were performed on the frozen soil test specimens using a closed-loop control, Material Test System (MTS) machine. A constant strain rate of  $10^{-2} \text{ s}^{-1}$  was used for all tests and the specimens were strained to 20%. A temperature controlled cabinet mounted on to the MTS machine allowed the test temperature to be maintained constant for each test but varied between  $-5^{\circ}\text{C}$  and  $-17^{\circ}\text{C}$  for the test program. During the tests axial load-deformation curves for each specimen were recorded using a x-y plotter. Three tests using separate specimens were conducted for each test condition.

### TEST RESULTS AND DISCUSSION

#### Failure Modes of the Specimens

The frozen soil specimens with total water contents of around 52% and salinity 10 ppt or less tested at temperatures  $-10^{\circ}\text{C}$  and below failed in a brittle manner, exhibiting distinct shear failure planes. However, at a salinity level of 20 ppt, with the other testing conditions remaining the same, the frozen specimens failed in a more ductile manner with only barely visible cracks forming even at strains close to 20%. The frozen saline soil specimens with total water contents of around 32% generally failed in a ductile way with no indication of visible cracks. A ductile type of failure was also observed in all the saline soil specimens tested at  $-5^{\circ}\text{C}$ . Therefore, test results generally indicate that high temperatures (around  $-5^{\circ}\text{C}$ ), high salinity levels (around 20 ppt) and low total water contents (around 34%) in Ball clay will contribute to a ductile type of failure deformation when subjected to rapid compression tests. A more brittle type of failure can be expected in the frozen soil at high total water contents, with low salinities and low temperatures. This type of brittle behavior at low temperatures and high total water contents has also been reported in six non-saline fine-grained frozen soils by Joshi and Wijeweera (1990).

#### Stress-Strain Behavior

Typical stress-strain curves for the specimens tested under various conditions are given in Figures 1 to 4. Figure 1 shows that the strength of the soil increases considerably with decreasing salinity. The stress-strain curves of the non-saline soil specimens exhibits a prominent peak and as the salinity increases the stress-strain curve flattens out with no significant peak visible. A similar behavior was observed at  $-10^{\circ}\text{C}$  as well. The specimens tested at  $-5^{\circ}\text{C}$  did not exhibit prominent peak in their stress-strain curves, particularly for the saline samples (see Figure 2). It was noted that specimens which exhibited a prominent peak in their stress-strain curves failed in a brittle manner while the specimens that failed in a ductile manner generally had

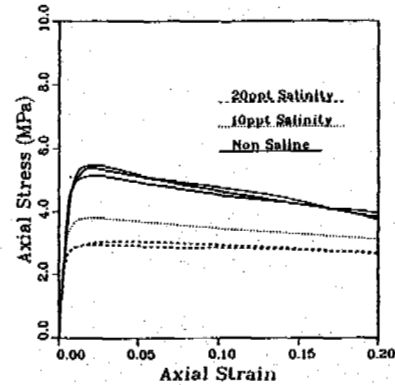


Fig. 1 Effect of salinity on the axial stress-strain deformation behavior of Ball clay specimens with total water content of around 52% and at a temperature of  $-17^{\circ}\text{C}$ .

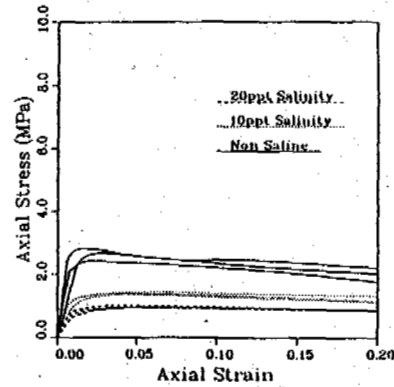


Fig. 2 Effect of salinity on the axial stress-strain behavior of Ball clay specimens with total water content of around 52% and at a temperature of  $-5^{\circ}\text{C}$ .

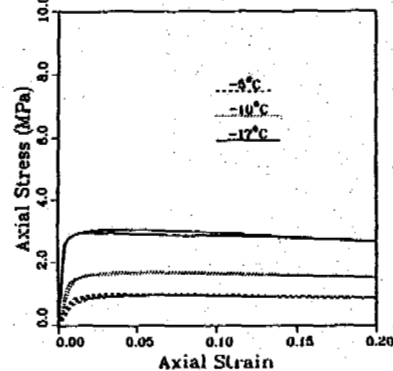


Fig. 3 Effect of temperature on the axial stress-strain behavior of Ball clay specimens with 20 ppt salinity and total water content of around 52%.

stress-strain curves with no prominent peak. The effect of temperature on the stress-strain behavior of frozen soil saline Ball clay is shown in Figure 3. The strength of the soil decreases considerably with increasing temperature. Figure 4 shows typically the effect of total water content on the stress-strain behavior of frozen Ball clay. It can be observed (Figure 4) that at high salinity levels (around 20 ppt) the change in the total

Table 1. Peak Compressive Strength of Ball Clay at Various Temperatures and Salinities

Salinity (ppt)	Total w.s. (%)	$\gamma_d^1$ (kN/m <sup>3</sup> )	Average Strain at Peak Strength			Average Peak Strength (MPa)		
			-5°C	-10°C	-17°C	-5°C	-10°C	-17°C
0	51.81	10.39	0.03	0.03	0.03	2.63	3.63	5.34
0	33.31	13.14	0.07	0.04	0.04	1.84	3.10	4.81
10	55.58	10.07	0.05	0.04	0.02	1.39	2.13	3.82
10	35.23	13.09	0.07	0.08	0.03	1.33	1.99	3.39
20	50.76	10.66	0.07	0.06	0.03	0.97	1.69	3.00
20	34.16	13.19	0.13	0.12	0.09	1.00	1.51	2.71

dry unit weight

water content of the soil has hardly any effect on the strength and stress-strain behavior of the soil. However, for non-saline soil specimens higher strength is exhibited at higher total water contents, Wijeweera and Joshi (1990).

Peak Strength Behavior

The average peak strength and corresponding strain to peak values, for frozen Ball clay under different salinity, temperature and total water content conditions are presented in Table 1. It can be seen that the axial strain at peak strength increases with increasing temperature, particularly in the saline soil specimens. Furthermore, this type of behavior is exhibited more prominently in specimens with low total water content. High values of strain (e.g. 0.09 or more) at peak strength indicate a ductile deformation as evident from the failure modes.

The peak strength data in Table 1 clearly indicate that the strength decreases sharply with both increasing salinity and temperature. The total water content does not effect the peak strength of saline soil specimens

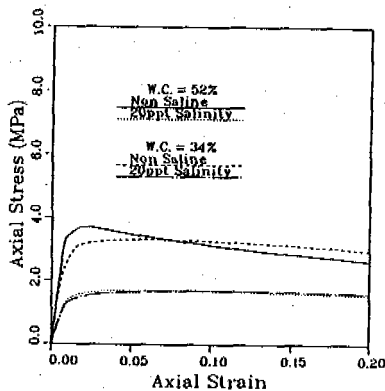


Fig. 4 Effect of total water content on the axial stress-strain behavior of Ball clay specimens at -10°C.

significantly. However, a reduction in peak strength is noticeable in non-saline specimens at low total water contents (see Table 1 and Figure 4).

Figure 5 shows the variation in peak strength with change in temperature for different salinities of the soil. The relationship between peak strength,  $\sigma_m$ , and temperature,  $\theta$ , can be best represented by

$$\sigma_m = A_m (\theta/\theta_0)^{m_m} \tag{1}$$

Table 2. Value of Parameters in the Different Strength-Temperature Relationships

Salinity (ppt)	$\gamma_d$ (kN/m <sup>3</sup> )	Parameters in Eq. (1)		Parameters in Eq. (2)		Parameters in Eq. (3)	
		$A_m$ (MPa)	$m_m$	$A_y$ (MPa)	$m_y$	$A_y$ (MPa)	$m_y$
0	10.39	1.02	0.57	0.80	0.58	0.83	0.54
0	13.14	0.52	0.78	0.22	0.90	0.46	0.79
10	10.07	0.40	0.75	0.20	0.89	0.37	0.69
10	13.09	0.37	0.77	0.17	0.88	0.33	0.76
20	10.66	0.22	0.90	0.07	1.22	0.19	0.91
20	13.19	0.25	0.81	0.11	0.93	0.25	0.80

where  $A_m$  and  $m_m$  are parameters relating the peak strength to the temperature ratio. These are dependent on the properties of the soil and are determined experimentally.  $\theta$  is in degrees Celsius and  $\theta_0$  is a reference temperature, usually -1°C. A similar form of temperature dependence on peak compressive strength of non-saline frozen soils has been reported by Sayles and Haines (1974), Tsytovich (1975), Zhu and Carbee (1987) and Wijeweera and Joshi (1990).

The values of parameters  $A_m$  and  $m_m$  for different dry unit weights and salinities of the soil were derived by regression analysis and are given in Table 2. The correlation coefficient of these two parameters, derived from the analysis, was found to be around 0.98, indicating Eq. (1) to be a reasonable prediction of peak strength at various temperatures.

Yield Strength Behavior

The stress-strain curves of the frozen Ball clay specimens showed yield to occur at axial strains between 0.5 and 0.8%. The yield strain values observed in this study are near the value of 1% reported for polycrystalline ice (Hawkes and Mellor, 1972) and non-saline fine-grained frozen soils (Sayles and Carbee, 1981; and Wijeweera, 1990). The average yield strength values for the frozen Ball clay specimens at various levels of salinity, dry unit weight and temperature are given in Table 3. Figure 6 plots the yield strength data with changing temperature. The data in Table 3 and Figure 6 indicate that the yield strength increases with decreasing temperature and salinity and also with increasing total water content. Furthermore, Figure 6 suggest that the relationship between yield strength and freezing temperature can be expressed as a simple power law:

$$\sigma_y = A_y (\theta/\theta_0)^{m_y} \tag{2}$$

The parameters  $A_y$  and  $m_y$  for various dry unit weights and salinities of the frozen soil were derived by regression analysis, with a correlation coefficient of 0.98, and the values are given in Table 2. The parameters  $A_y$  and  $m_y$  vary in a similar manner with  $A_m$  and  $m_m$  respectively i.e.  $A_y$  decreases and  $m_y$  increases with increasing salinity.

Figure 7 plots the peak strength data versus the yield strength. The data points corresponding to a particular salinity and dry unit weight represent strength values at different temperatures ranging between -5°C and -17°C. The figure clearly indicates that peak strength increases with increasing yield strength and this behavior can be expressed in a linear form:

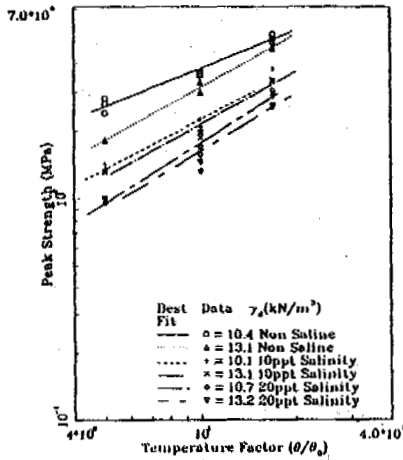


Fig. 5 Temperature dependence of peak strength.

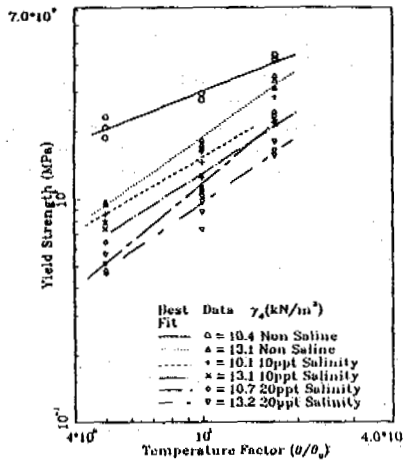


Fig. 6 Temperature dependence of yield strength.

$$\sigma_m = k \sigma_y \quad (3)$$

where  $k$  is a parameter independent of the test temperature. Peak and yield strength data for seven non-saline fine-grained frozen soils followed a relationship of the form given in Eq. (3) (Wijeweera and Joshi, 1990, and Zhu and Carbee, 1987). Wijeweera and Joshi (1990) also reported that Eq. (3) holds true for fine-grained frozen soils with dry unit weights less than  $17 \text{ kN/m}^3$ .

In Figure 8 the peak to yield strength ratio is plotted against the dry unit weight for a number of non-saline and saline fine-grained frozen soils. The strength ratio for non-saline frozen soils have been extracted from Wijeweera (1990). Figure 8 shows that the strength ratio data derived from this study follow the distribution corresponding to non-saline frozen soils. It is also observed that the strength ratio increases with increasing dry unit weight. The strength ratio increases very rapidly beyond a dry unit weight of  $17 \text{ kN/m}^3$ .

The peak to yield strength ratio can also be approximated by the parameter  $k$  in Eq. (3) for soils with a dry unit weight of less than  $17 \text{ kN/m}^3$  (Wijeweera and Joshi, 1990). Wijeweera

Table 3. Yield and Residual Strength of Ball Clay at Various Temperatures and Salinities

Salinity (ppt)	$\gamma_d$ ( $\text{kN/m}^3$ )	Average Yield Strength (MPa)			Average Residual Strength (MPa)			Peak/Residual Strength Ratio		
		-5°C	-10°C	-17°C	-5°C	-10°C	-17°C	-5°C	-10°C	-17°C
0	10.39	2.10	2.83	4.27	2.00	2.79	3.85	1.32	1.30	1.39
0	13.14	0.97	1.75	3.36	1.65	2.74	4.37	1.12	1.13	1.10
10	10.07	0.87	1.45	2.85	1.18	1.65	3.12	1.18	1.29	1.22
10	13.09	0.76	1.17	2.22	1.16	1.86	2.94	1.15	1.07	1.15
20	10.66	0.53	1.09	2.40	0.86	1.54	2.67	1.13	1.10	1.12
20	13.19	0.54	0.90	1.67	0.97	1.44	2.54	1.03	1.05	1.07

and Joshi (1990) also reported that for non-saline fine-grained frozen soils  $k$  can be expressed as

$$k = (1 + \epsilon_m) [0.015 (\gamma_d w_L)^{\frac{1}{3}} + 0.684] \quad (4)$$

where  $\gamma_d$  = dry unit weight in  $\text{kN/m}^3$ ,  
 $w_L$  = liquid limit as a percentage,  
 and  $\epsilon_m$  = average strain at peak strength at temperatures between  $-5^\circ\text{C}$  and  $-17^\circ\text{C}$

Figure 9 compares the predictions made by Eq. (4) with actual  $k$  values. In this figure data for a number of frozen non-saline soils reported by Wijeweera and Joshi (1990) and Zhu and Carbee (1987) along with the  $k$  values obtained from this study are presented. It is evident from Figure 9 that predictions made using the parameter  $k$  agree well with actual data for both the saline and the non-saline frozen fine-grained soils considered. Furthermore, as seen from Figure 7 the peak strength versus yield strength relationship given by Eq. (3) using the predicted  $k$  values, given by Eq. (4), agrees with the data.

#### Residual Strength

In this report, the residual strength is considered as the axial stress at 20% axial strain. The average residual strength data for frozen Ball clay at various salinities, temperatures and dry unit weights are listed in Table 3. The data indicate that the residual strength increases with decreasing salinity and temperature. The effect of total water content on residual strength is found to be not very

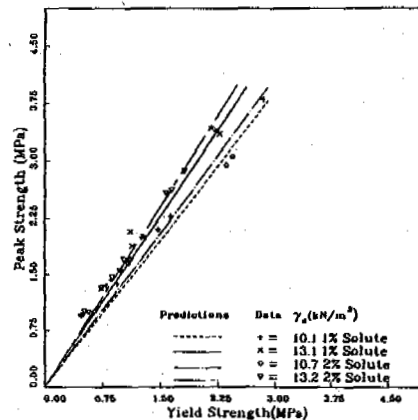


Fig. 7 Peak strength vs. yield strength behavior



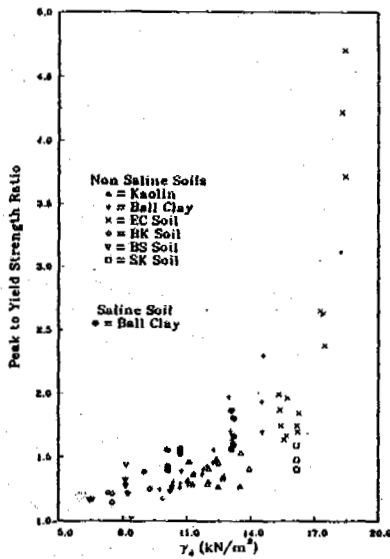


Fig. 8 Effect of dry unit weight on the peak to yield strength ratio.

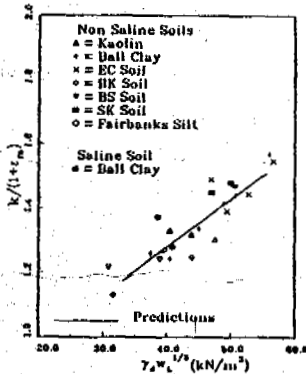


Fig. 9  $k/(1 + \epsilon_m)$  vs.  $\gamma_d w_L^3$

significant, particularly in the case of frozen saline soil.

The residual strength variation with temperature is shown in Figure 10. The relationship between the two can be approximated by a power law, similar to peak or yield strength versus temperature behavior, given by:

$$\sigma_r = A_r (\theta/\theta_0)^{m_r} \quad (5)$$

The values of the parameters  $A_r$  and  $m_r$  derived by regression analysis, with a coefficient of correlation around 0.98, corresponding to different salinities and dry unit weights of the soil are given in Table 2.

The results from this study show that peak, yield and residual strength of the saline frozen soil increases with decreasing temperature in a similar manner and this behavior can be expressed by a simple power law. It is found that the two parameters  $A$  ( $A_m$ ,  $A_y$  and  $A_r$ ) and  $m$  ( $m_m$ ,  $m_y$  and  $m_r$ ) describing the dependence of each strength on temperature are strongly influenced by the salinity but are not

significantly affected by the dry unit weight, particularly in the saline soil specimens. The  $A$  values decrease and the  $m$  values increase sharply with increasing salinity. This behavior suggests that, at temperatures close to freezing, the change in strength (peak, yield or residual) due to change in salinity is much greater than at lower temperatures.

Joshi and Wijeweera (1990) have reported a relationship between peak and residual strength in the form given by Eq. (6) for non-saline frozen fine-grained soils.

$$\frac{\sigma_m}{\sigma_r} = 65.4 (\gamma_d w_L^3)^{-1.052} \quad (6)$$

where  $\sigma_m$  = peak axial compressive strength in MPa,  
 $\sigma_r$  = axial residual strength in MPa,  
 $\gamma_d$  = dry unit weight of the soil in  $\text{kN/m}^3$ ,  
and  $w_L$  = liquid limit of the soil as a percentage.

Figure 11 plots the data corresponding to peak to residual strength ratio at  $-10^\circ\text{C}$  for saline Ball clay derived from this study as well as the data reported by Joshi and Wijeweera (1990) for non-saline frozen soils. The peak to residual strength ratio of all the frozen soils considered, both saline and non-saline, appears to decrease with increasing dry unit weight and this behavior may be approximated by Eq. (6). The best fit curve for all the data points closely follows the predicted values. Similar observations were also made for data corresponding to temperatures  $-5^\circ\text{C}$  and  $-17^\circ\text{C}$ . Joshi and Wijeweera (1990) also reported that the peak to residual strength ratio for non-saline frozen soils is not affected by the temperature. The same appears to hold true for the frozen saline soil used in this study (see Table 3). As seen from Table 3 the peak to residual strength

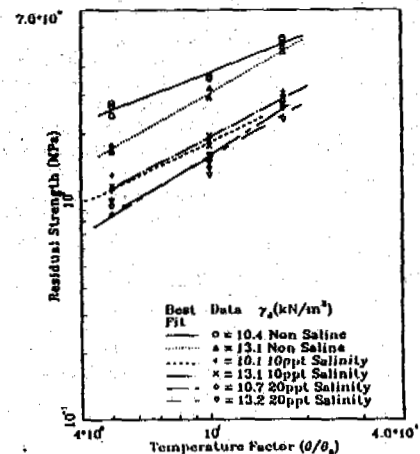


Fig. 10 Temperature dependence of residual strength.

ratio decreases slightly with increasing salinity, particularly in soil specimens with low dry unit weight.

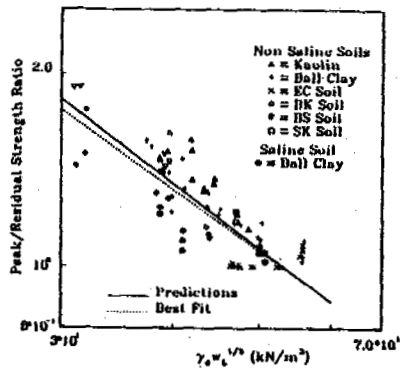


Fig. 11 Behavior of peak to residual strength ratio.

Joshi, R.C. and H. Wijeweera (1990) Post peak axial compressive strength and deformation behavior of fine-grained frozen soils. Collection Nordicana No. 54 (Proceedings, 5th Canadian Permafrost Conference), National Research Council of Canada, 317-325.

Ogata, N., M. Yasuda, and T. Kataoka (1983) Effects of salt concentration on strength and creep behavior of artificially frozen soils, Cold Regions Science and Technology Vol. 8 (2) 139-153.

Sayles, F.H. and D.L. Carbee (1981) Strength of frozen silt as a function of ice content and dry unit weight. Engineering Geology, Vol. 18, 55-66.

Sayles, F.H. and D. Haines (1974) Creep of frozen silt and clay, U.S. Army Cold Regions

## CONCLUSIONS

An increase in the salinity of a frozen fine-grained soil increases its ductility. A ductile type of deformation can be expected in frozen soils with high salinities (20 ppt), low total water contents (34%) and at high temperatures (-5°C).

The peak, yield and residual strength of frozen soils decreases with increasing temperature and this behavior can be represented by a simple power law of the form given by Eq. (1). The temperature dependence of these three types of strength is considerably affected by the change in salinity of the soil, the strengths decreasing sharply with increasing salinity. The effect of salinity on strength is more pronounced at temperatures close to freezing than at lower temperatures.

The peak to residual strength ratio of the saline frozen soil decreases with increasing dry unit weight and this behavior is very similar to that of non-saline frozen soils.

The peak strength increases linearly with increasing yield strength and the relationship between the two takes the form given by Eq. (3). The coefficient  $k$  in this relationship increases with increasing dry unit weight and the expression for  $k$  developed is common to both non-saline and saline fine-grained frozen soils.

The conclusions drawn above are true only for the soil considered in this study. More soils with wide range of properties should be tested to verify the applicability of these conclusions in general to other types of fine-grained frozen saline soils.

## REFERENCES

Hawkes, I. and M. Mellor (1972) Deformation and fracture of ice under uniaxial stress. Journal of Glaciology, Vol. II (61), 103-131.

Jessberger, J.L., W. Ebel, and P. Jordan (1985) Temperature dependent strength and creep behaviour of frozen saline sand. Fourth International Symposium on Ground Freezing, Sapporo, Japan.

## EFFECTS OF TERRAIN DISTURBANCE ON ARCTIC SLOPE HYDROLOGY

Ming-ko Woo<sup>1</sup> and Kathy L. Young<sup>1</sup>

<sup>1</sup>Department of Geography, McMaster University  
Hamilton, Ont. CANADA L8S 4K1

An experiment was conducted in a continuous permafrost area (Resolute, Canada) by placing a berm, a trench and a subsurface flow barrier perpendicular to a slope, and comparing their hydrologic and thermal conditions with two control plots. Differential thawing altered the frost table configurations. The trench created a pond while the water table was often close to the ground surface behind the barrier, but deep beneath the berm. The timing and magnitude of overland flow was modified, with no flow downslope of the berm and reduced flow below the trench. Suprapermafrost groundwater flow was modified by the frozen core of the berm. The trench regulated the outflow to the lower slope, but the subsurface barrier completely interrupted the subsurface flow.

### INTRODUCTION

Development and human settlements in the Arctic cause terrain disturbances and some of the impacts on permafrost have been well documented (e.g. French 1987, Lawson 1986, van Everdingen 1974). Other than a few papers (e.g. Soulis and Reid 1978), the short-term effects of terrain disturbance on permafrost hydrology have received limited attention. There is a need to understand how the thermal and hydrological processes are affected by various slope disturbances and the present paper attempts to address this.

Simple linear structures were set across a slope to observe the 'treatment' effects of arctic terrain disturbance during the course of one summer season. The purpose is to determine how the hydrologic activities, including the water table fluctuations, groundwater and overland flows, are modified when such man-made structures are emplaced across slopes underlain by continuous permafrost. Results of this experimental study can be applied to the planning of roads, ditches and buried linear structures in the continuous permafrost region.

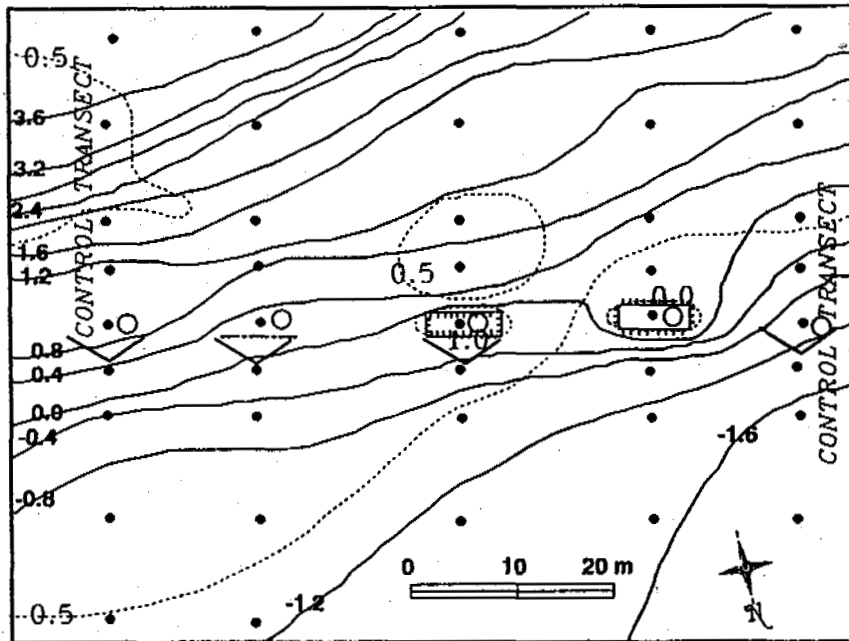
### STUDY AREA AND FIELD METHODS

A field experiment was conducted between June and August 1988, at a site 3 km northeast of Resolute, N.W.T. (74°45'N, 94°50'W) on a north-facing slope of relatively uniform gradient of 0.06. The slope materials can be described as polar desert soil (Cruickshank 1971) which is a mixture of pebbles (33 to 52 percent), sand (41 to 52 percent) and finer materials (these percentages were based on five grab samples from the experimental slope). Hydraulic conductivities, determined using the single auger hole method (Luthin 1966), is  $10^2 \pm 30$  mm/d or

$1.2 \pm 0.3 \times 10^{-3}$  mm/s (based on nine measurements). The active layer on the slope usually reaches 0.6 m, and the vegetation is sparse. These conditions are typical of many areas in the High Arctic.

Three types of slope disturbances were introduced at the end of August 1987, and included a gravel berm 0.75 m high and 1.5 m wide, a trench 0.6 m wide and about 0.3 m deep (uneven floor due to slumping of materials into the trench), and a subsurface barrier consisting of a plastic sheet backed by plywood buried to a depth of 1 m (Fig. 1). These treatments represent features such as roadbeds, ditches and buried impermeable structures. Two undisturbed plots were set up on either side of the experimental slope to serve as controls. All plots were approximately 6 m wide and oriented across the slope, with their centre lines separated from each other by 20 m. Each plot included a series of perforated pipes placed in the active layer to permit groundwater level measurements (at daily intervals). The arrangement of these pipes are shown in Figure 1. Next to each pipe, measurements of frost table were taken by driving a steel rod into the ground until the frozen zone is encountered. In addition, one thermistor string was embedded at each plot to measure ground temperatures daily at five depths (eight for the berm site). Immediately downslope of each disturbance location and also at the lower slopes of the control plots, surface flow was collected by diverting (using corrugated 4 inch wide garden trim) runoff into containers (Lewkowitz and French 1982). The water levels in the containers were recorded by Leupold-Stevens Type F recorders and the rates of rise were converted into flow rates.

The advantage of such experimental design is that all plots have the same topographic setting,



- |           |   |   |                      |
|-----------|---|---|----------------------|
| -----     | SUBSURFACE BARRIER                      |   | TRENCH               |
| - - - - - | 0.5 SNOW DEPTH (m)                      |   | BERM                 |
| 3.6       | CONTOURS<br>(m above arbitrary datum)   |   | OVERLAND FLOW TROUGH |
| •         | FROST AND WATER TABLE OBSERVATION POINT | ○ | THERMISTOR STRING    |

Fig. 1: Experimental slope and treatment plots, deployment of groundwater observation pipes and overland flow gauges, and snow depth (in m) in late June 1988.

uniform surface cover, and similar microclimatic conditions. The disadvantage is their limited horizontal extent so that some edge effects are unavoidable. Since the goal is to examine how these types of disturbances will alter the spatial patterns of slope hydrology, our emphasis is on the relative rates rather than the absolute magnitudes of changes caused by these impacts.

The summer of 1988 was warmer than the 30 year average (Fig. 2), and an early melt event in May ripened most of the winter snow cover, only to be followed by heavy snowfall and low temperatures which refroze the meltwater produced by the early melt. By the time the main melt season arrived (late June), the slope around the experimental plots had an average snow depth of 0.5 m, though the trench site trapped over 1 m of snow and the crest of the berm was bare. All the disturbance plots became snow-free in early July, but a residual snowbank upslope of the plots continued to provide meltwater input throughout July. Summer rainfall, measured by a tipping-bucket rain-gauge, totalled only 26 mm, most of which fell after mid-August. Parts of the field data have been reported in another paper (Woo and

Young 1990). The present paper will compare the overall thermal and hydrologic impacts between the control plots and the plots subject to the three types of disturbances.

#### THERMAL EFFECTS

Figure 2 shows the ground temperatures at the disturbed plots, compared with their adjacent control plots. Of particular hydrologic significance is the position of the frost table below which lies the frozen materials that generally have very low hydraulic conductivity and negligible water storage capacity (Kane and Stein 1983). Changes in the frost table configuration will affect the storage and movement of suprapermafrost groundwater (Woo and Steer 1983).

The maximum active layer depths at the two control plots were comparable, averaging 0.6 m, though the initiation of thaw was delayed by several days on the western flank of the slope due to a deeper snowbank. The gravel berm had no snow on its crest and thawing began earlier than at the other plots. Once started, thawing

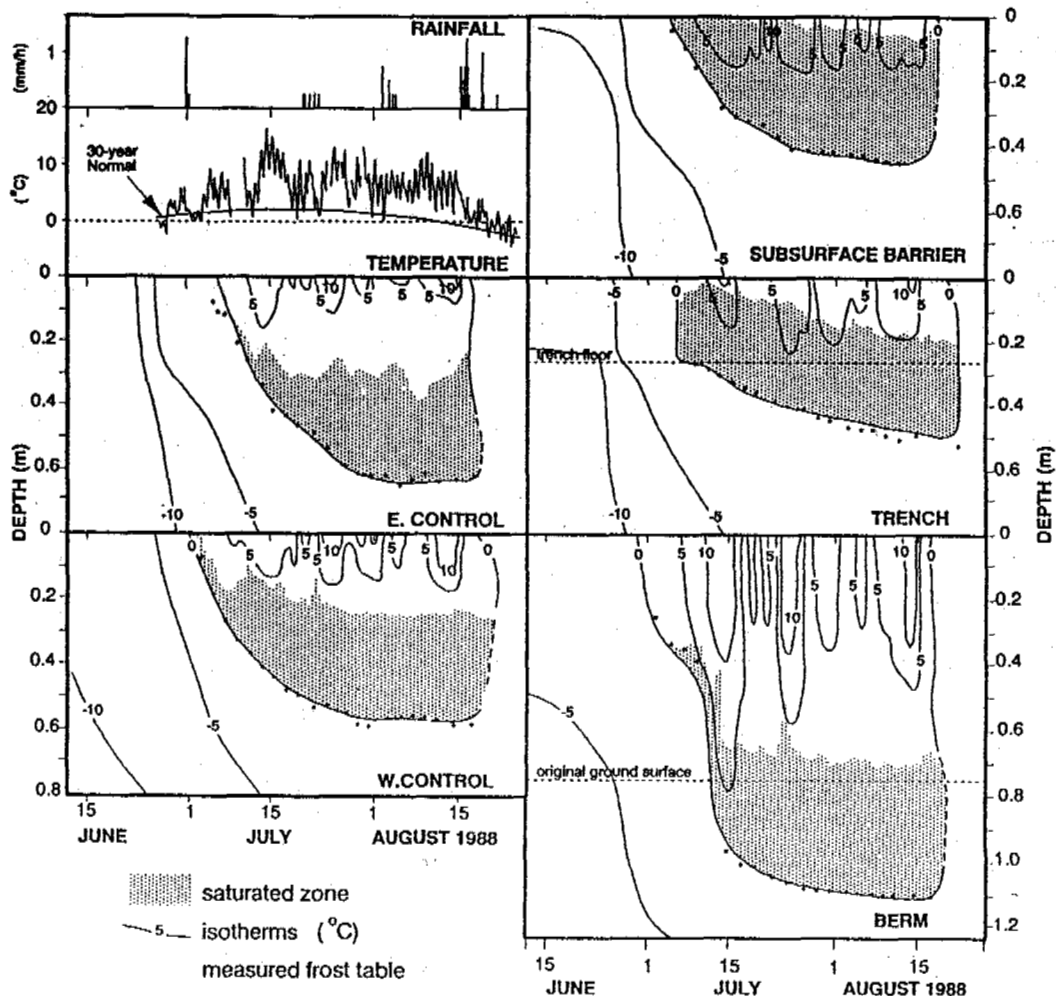


Fig. 2: Air temperature, rainfall, ground temperatures (in °C), frost tables and water tables at five sites.

proceeded rapidly because of the high thermal conductivity of gravels, but when the thawing front reached the original ground materials, thawing was retarded. The maximum thaw depth below the berm surface reached 1.05 m. The subsurface barrier produced a saturated zone upslope, with the water table being close to the ground surface. Thawing front descent was retarded because more heat was used both to warm the groundwater and to thaw the ground ice. The maximum thaw depth reached only 0.42 m. The trench was filled with snow and ice in early July and ground thaw was delayed until the ice melted. It remained flooded throughout the summer and with heat loss to warm the water and possibly to sustain higher evaporation from the open water surfaces, less heat was conducted to the trench floor. This resulted in a shallow active layer below the trench (maximum thaw depth was 0.28 m), but freeze-back of the ground was delayed until the water in the trench froze.

#### HYDROLOGIC EFFECTS

##### Water Table

Figure 3 shows the probabilities (estimated

by relative frequencies using daily observations) of water table positions after the snowmelt period for points located at the disturbance, at +5 m (upslope) and -5 m (downslope) of the disturbed position. The two control sites showed that the water table was often at 0.1 to 0.2 m below the surface, and there were notable variations in the water table positions from site to site.

Water level rose above ground more frequently at the subsurface barrier site, but downslope of it, the water table was more often deeper below the surface, indicating that the barrier usually withheld some of the lateral runoff and denying it to its downslope locations. The trench intercepted the upslope runoff, either storing it in the depression or losing it to evaporation, but was able to alter the flow downslope so that water table positions were less variable than at the upslope positions. During early summer, the berm had a frozen core with an elevation higher than the frost tables beneath its adjacent zones (Woo and Young 1990). This core effectively acted as a subsurface flow barrier but its water table was always below ground because of the elevated berm topography.

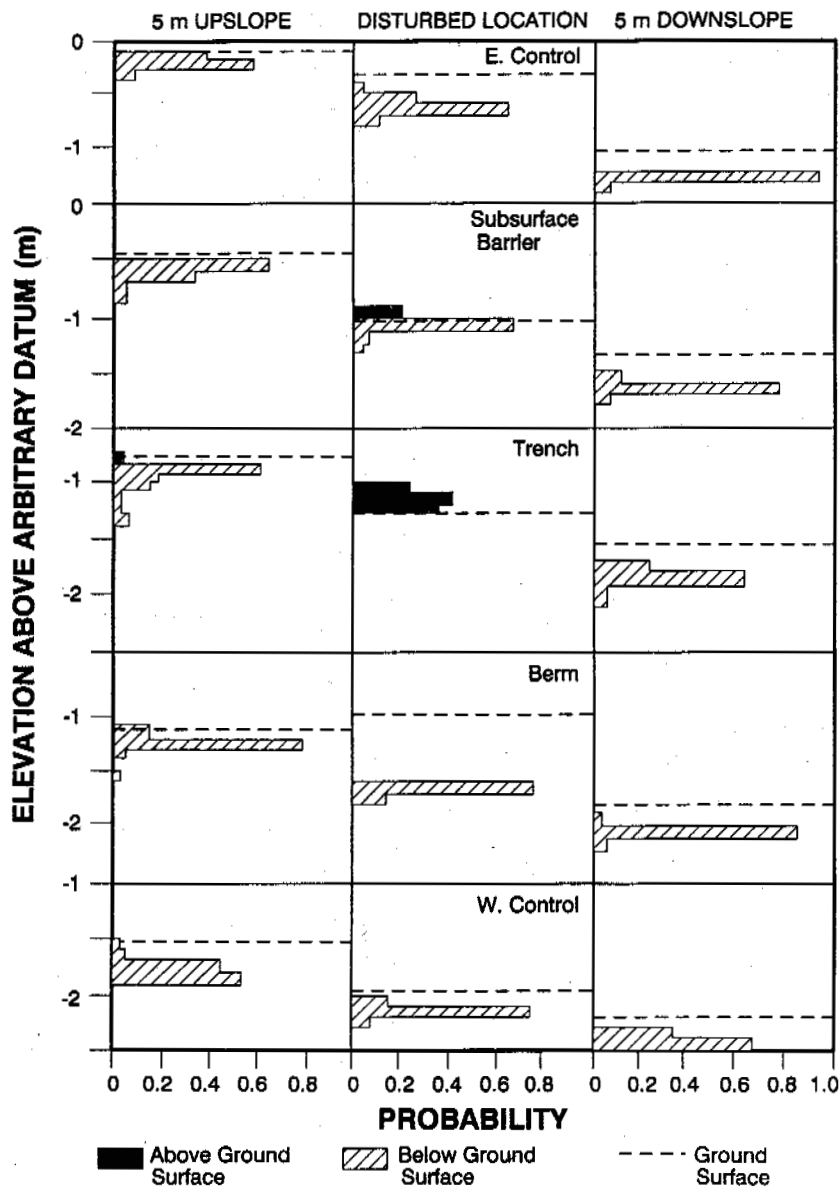


Fig. 3: Probabilities of water table positions relative to the ground surface, at the disturbed and control locations and at 5 m upslope and downslope of these locations.

#### Overland Flow

Overland flow was observed during the snowmelt period downslope of all plots except the berm. The berm, with a frozen core and topographically higher position, intercepted all the flow and impounded it upslope. Surface runoff at the other plots began on 27 June, but the magnitude of flow was less than 0.1 l/m/h (Fig. 4). The snow-filled trench was the first to generate notable amounts of flow (over 5 l/m/h) as water overflowed its brim on 29 June. Continuous melting dropped the water level in the trench (meltwater has much less volume than snow)

and outflow was reduced, ceasing completely by 2 July. The control plots produced large overland flows between 1-3 July during days of intense melt. The subsurface barrier created a high water table upslope, but the downslope zone was relatively unsaturated. Overland flow was able to infiltrate the newly thawed zone until it, too, was saturated. Then, on 3 July, significant overland flow occurred below the barrier site. The constantly saturated zone upslope of the barrier sustained high overland flow on 4 July even when the adjacent control plot yielded no flow. Thus, the barrier modified the timing of flow events.

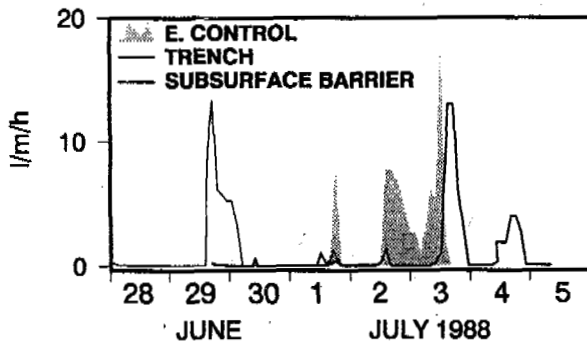


Fig. 4: Hourly overland flow downslope from the western control plot, the trench and the subsurface barrier site.

#### Groundwater Flow

During the summer period, groundwater flow ( $Q$ , as discharge per unit slope width) into and out of the disturbed reaches was calculated by

$$Q = -k (D_d + D_u) / 2 \cdot (h_d - h_u) / dl \quad (1)$$

where  $k$  is measured hydraulic conductivity,  $D$  is thickness of the saturated zone at an observation well, with  $D = (h - f)$ , for  $h$  being the water table and  $f$  being the frost table elevations. The subscripts  $d$  and  $u$  denote an upslope and a downslope observation well and  $dl$  is their distance apart. For each disturbance plot, water table and frost table data from wells at  $-10$  and  $-5$  m, and from wells at  $+10$  and  $+5$  m were taken in pairs to compute inflow and outflow (for the control plots, the wells at  $-10$ ,  $0$  and  $+10$  m were used). Differences in flows entering and leaving the disturbed segments were also calculated for the period 10 July to 14 August (Fig. 5).

At the western control transect, inflow and outflow were similar throughout the summer. The eastern control transect received more inflow than outflow and this was due to the higher water table at the upper slope fed by a late-lying snowbank. The trench received similar amounts of inflow as the eastern control plot but the pool in the trench regulated the outflow such that the net change in flow through this disturbed section was small. The subsurface barrier completely blocked groundwater flow, reducing the outflow to very low values. The net result of excessive inflow was to create a high water table which sometimes rose above the ground surface at this disturbed site (Fig. 2).

Until July 10, the berm had a frozen core with a frost table higher than the water table upslope. This obstructed groundwater movement and built up a thick saturated zone upslope. At this time, groundwater flow downslope of the berm was maintained by meltwater from the snow on the downslope flank. With more rapid thawing of the berm material, the frozen core disappeared in mid-July and groundwater flows along the slope were connected. Inflow benefited from a thick saturated zone while the hydraulic gradient was reduced by the berm; but outflow was compensated by a steepened gradient and the net effect was an

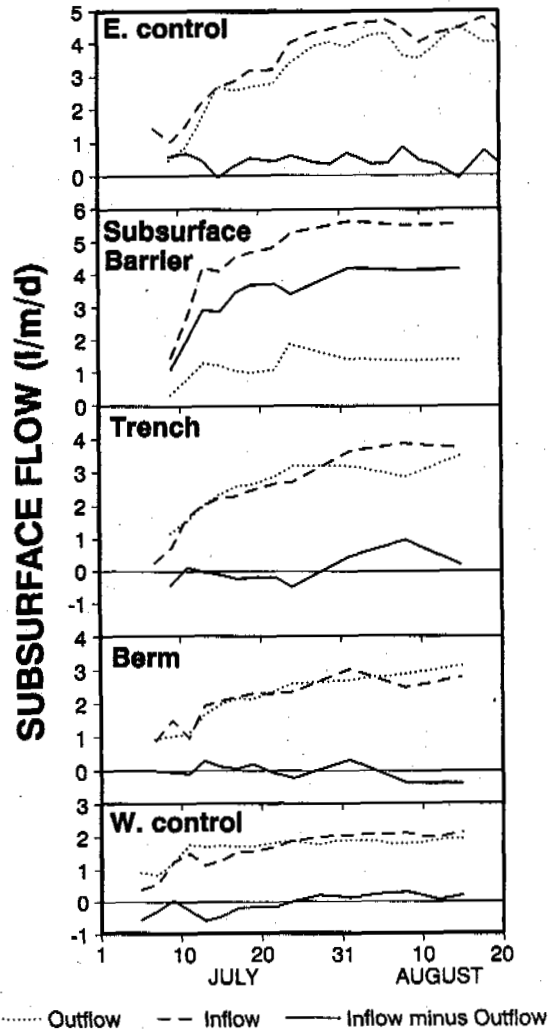


Fig. 5: Calculated groundwater inflow and outflow and difference of flow entering and leaving the disturbed or control segments.

equalization of inflow and outflow. The processes revealed by this experiment suggest that if the berm is higher or if it is made of materials of lower thermal conductivity, an impervious frozen core may persist longer to interrupt groundwater movement. In that case, its effect will be similar to that of the subsurface barrier noted above.

#### CONCLUSIONS

Field experiments demonstrated the effects of slope disturbance on the thermal and hydrological processes in continuous permafrost terrain.

(1) A trench traps more snow which delays ground thaw, while the water in the trench retards thawing front descent in summer. The pond created by the trench regulates downslope groundwater flow.

(2) A subsurface barrier intercepts groundwater flow from upslope and deprives the downslope side of groundwater supply. The timing of overland flow is different from undisturbed terrain, and the saturated zone behind the barrier facilitates saturation overland flow conditions during snowmelt and heavy rain.

(3) Gravels which constitute the berm have a low porosity (Morris and Johnson 1967) and therefore a higher thermal conductivity than materials with greater air or moisture contents (Farouki 1981). This, together with an early disappearance of snow on the berm, results in a deeper active layer. The presence of a frozen core in spring interrupts groundwater flow and impounds water behind the berm. Overland flow is limited to the upslope side of the berm, but groundwater flow along the slope will resume when the frozen core is lower than the upslope water table.

#### ACKNOWLEDGEMENTS

We wish to thank Peter Graham, Philip Giles, Philip Marsh and Zhaojun Xia for field assistance, and we acknowledge the financial support of the Natural Sciences and Engineering Research Council of Canada, and the Department of Indian and Northern Affairs through its Northern Training Grant. We are grateful to the Polar Continental Shelf Project for logistical support.

#### REFERENCES

Cruickshank, J. 1971. Soil and Terrain units around Resolute, Cornwallis Island. *Arctic* 24, 195-209.

Farouki, O.T. 1981. Thermal properties of soils. *U.S. Army CRREL Monograph* 81-1, 136 p.

French, H.M. 1975. Man-induced thermokarst, Sachs Harbour airstrip, Banks Island, N.W.T. *Canadian Journal of Earth Sciences* 12, 132-144.

Kane, D.L. and Stein, J. 1983. Water movement

into seasonally frozen soils. *Water Resources Research* 19, 1547-1557.

Lawson, D.E. 1986. Response of permafrost terrain to disturbance: a synthesis of observations from Northern Alaska. *Arctic and Alpine Research* 7, 420-432.

Lewkowicz, A.G. and French, H.M. 1982. The hydrology of small runoff plots in an area of continuous permafrost, Banks Island, N.W.T. *Proceedings 4th Canadian Permafrost Conference*, Calgary, National Research Council of Canada, 151-162.

Luthin, J.N. 1966. *Drainage Engineering*. Wiley, N.Y. 243 p.

Morris, D.A. and Johnson, A.I. 1967. Summary of hydrologic and physical properties of rock and soil materials, as analyzed by the Hydrologic Laboratory of the U.S. Geological Survey, 1948-60. *U.S. Geological Survey Water Supply Paper* 1839-D, 42 p.

Soulis, E.D. and Reid, D.E. 1978. Impact of interrupting subsurface flow in the northern boreal forest. *Proceedings 3rd International Conference on Permafrost*, Edmonton, Alberta, 225-231.

van Everdingen, R.O. 1979. Potential interaction between pipelines and terrain in a northern environment. *Inland Waters Directorate Technical Bulletin* No. 114, Environment Canada, Ottawa, 7 p.

Woo, M.K. and Steer, P. 1983. Slope hydrology as influenced by thawing of the active layer. *Canadian Journal of Earth Sciences* 20, 978-986.

Woo, M.K. and Young, K.L. 1990. Thermal and hydrological effects of slope disturbances in a continuous permafrost environment. *Proceedings 5th Canadian Permafrost Conference*, Quebec, National Research Council of Canada, 175-180.



**THE RELATIONSHIPS BETWEEN THE LAKE AND FORMING ENVIRONMENT OF PERMAFROST, NORTH REGION, KEKEXILI, QINGHAI**

Wu Qinghai and He Yixiang,  
Lanzhou Institute of Glaciology and Geocryology, Academia Sinica

Kekexili northern region in Qinghai is situated in the hinter of Qinghai-Tibet plateau, it is an empty region of worse nature environment. Lake, glacier and permafrost are extensive distributed and form a intricate system. By a lot of field information of drilling, pit and geophysical prospecting, the relationships between lake and forming environment of permafrost are comprehensive analysed. Effects of lake on permafrost, ground ice forming, cryogenic texture and so on are primarily discussed in the thesis.

**GEOLOGICAL AND GEOGRAPHIC ENVIRONMENT**

Kekexili region in Qinghai is situated in the middle zone between kekexili and kuenlun mountain, it is the subsidence zone of Mesozoic era and about 90°20'-93°25'N, 35°-36°E (Fig.1). It is extensive distributed to the stratum with auriferous quartz vein of Mesozoic era and the red stratum of Tertiary system. There are diluvion, diluvion-alluviation and glacial sediment of Quaternary system that its thickness are generally thinner. Lake and alluvation primarily distribute in morden lake region, wide valley and basin and form the platform of gentle fluctuation. Eroded action of river are caused by Qinghai-Tibet plateau strongly rising in the region and cutting action of flowing water is more weakness. Surface of plateau is completely kept and extreme high mountain as high as 6000 meters is formed for textural difference of the part in the region.

There are no existed complete meteorological information, temperature, precipitation, and relative humidity in August are only observed during expedition. Month average temperature is

4.0°C, month precipitation is more than 70 mm in August. Comparing to the meteorological data of wudaoliang in August (Fig.2). Month average

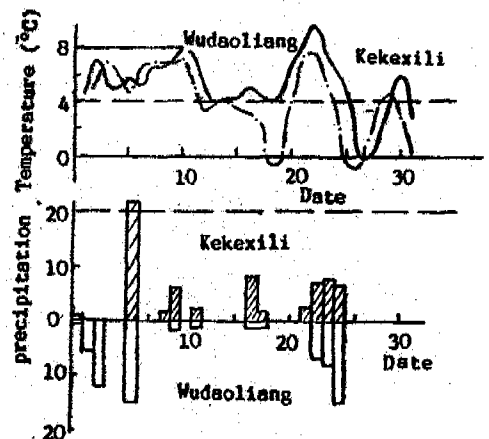


Fig.2 Temperature and precipitation in August, 1990

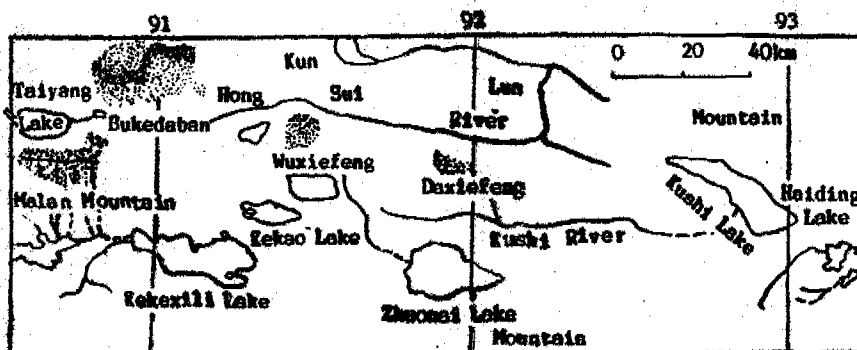


Fig.1 Northern area of Kekexili in Qinghai

Table 1 Analysing result of water chemistry

Sampling site	Water type	ion content (g/l)							Mineralized degree(g/l)
		Cl <sup>-</sup>	SO <sub>4</sub> <sup>2-</sup>	HCO <sub>3</sub> <sup>-</sup>	Na <sup>+</sup>	Ka <sup>+</sup>	Ca <sup>+</sup>	Mg <sup>+</sup>	
Haiding Lake	Lake Water	8.73	0.83	4.12	6.05	0.14	0.16	0.60	20.63
Kushi Lake	Lake Water	7.73	1.28	4.0	6.63	0.18	0.05	0.32	19.89
Kushi River	River Water	0.75	0.19	0.43	0.44	-	0.14	0.07	2.01
Zhounai Lake	Lake Water	4.09	0.24	0.95	2.73	0.00	0.01	0.19	8.22
Zhounai Lake	Lake Water	2.41	0.11	0.18	1.38	-	0.05	0.12	4.25
Kekexili Lake	Lake Water	4.16	0.57	0.15	2.61	0.14	0.03	0.15	7.81
Taiyang Lake	Lake Water	0.11	0.07	0.10	0.12	-	-	-	0.42

temperature is smaller than that of wudaoliang, precipitation is approach and relative humidity is high than that of wudaoliang by 13.3%.

THE CHARACTERISTICS OF LAKE AND WATER CHEMISTRY

It is extensive distributed to lake in the region, such as Haiding lake, kushi lake, Zhounai lake and so on, they are all half-closing lake. Most lake have supple river by ice-snow water forming. The major axis direction of lake is east-west direction and correspond with regional tectonic line. This shows that forming of lake basin are controlled by regional tectonic line, the lakes of northern region at Kekexili are tectonic lake (Shi Chengxi, 1989).

Such as table 1, mineralized degree of lake water gradually decreases from east to west at Kekexili northern in Qinghai, the lake show changing suite from salt lake to saline, saltish water and frash water lake.

Wangping (1986) consider that the bigger air humidity is in glacier area, the smaller mineralized degree is. If it is a desert scene, it is advantage to in-crease mineralized degree of water. The change of mineralized degree in research area mainly related with air humidity, precipitation and supply distances and supply amount of river and are successive decreased with altitude increasing. In order to analysing and discussing succession history of lake, a drilling is made in south bank of Zhounai lake, drilling depth is 30.08 m. The sediment of lake farice is gravel soil from zero to 3.8 m, interbedding of gray clay and gravel soil from 3.8 m to 11 m and gray-black clay with a little gravel soil from 11 m to 30.08 m. According to geophysical profile in Zhounai lake, the sedimental thickness of lake farice is more than 48.7 m and the sediment of lake extend forward to 2 km. This shows the lake was ever in the stage of expanding, then in the stage of retreating. Many paleobank lines are left in the lake bank and their height are primarily approach. This shows that lake has not affected by new tectogenesis since Qinghai-Tibet plateau rising. The major cause of lake retreating is caused by climate gradually becoming drought, lake being gradually precipited.

PERMAFROST CHARACTERISTICS

It is extensive existed to continuous permafrost at northern region of Kekexili in Qinghai.

Distributed pattern of continuous permafrost, open talik of lake bed and close talik of lake bank are formed for the effect on water body of many lakes and river. According to the pit of Taiyang lake and zhuonai lake and drilling of Zhounai lake, the effect range of talik of lake bank is generally 20-40 m, this shows that permafrost of lake bank are directly affected by the heatamount of lake. The lake areas are larger in the region, depth of Taiyang lake is 41 m, that of zhuonai lake more than 50 m and they are textonic lake. So the lake bed of Taiyang lake and Zhounai lake must be open talik. According to water area and textogenesis, open talik of lake bed is easily formed for Kekexili lake, Kushi lake and Haidingnuoer lake. Meanwhile close talik exist in ceitain depth under bottom of supple river of lake in the region. Drilling volumn promulates in Bingguo of Kushi river branch that permafrost are not found in 5 m depth under river bed and all river bed may be close talik (Fig.3). This is because Bingguo is

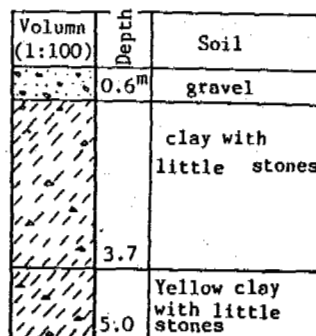


Fig.3 Volumn of 4# drilling in Bingguo

a textonic zone and is affected by surface water. Hongsui river locates in big textonic zone of southslope of Kunlun mountain and heat spings that temperature arrive to 92°C are situated in the frontier of Bukedaban glacier, plused to influence of river, deducing the open talik of Hongsui is formed.

Permafrost table is generally 1.55-2.0 m in the region and ice layer with soils of 5-10 cm thickness is often found around table (Fig.4), permafrost table of the part arrive to 2.5-3.0 m. Such as Kushi lake, permafrost table beside lake affected by high salt amount make permafrost table of bank migrate down. For example Lian

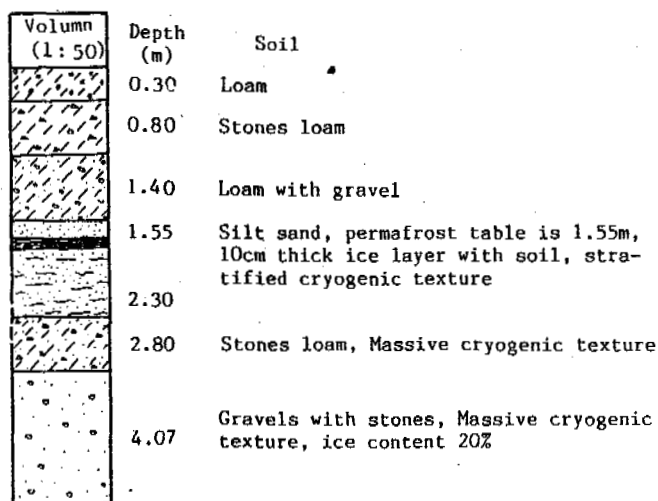


Fig.4 Volumn of 1# drilling in Zhuonai lake

lake, pit prospecting shows that soil under 4 m are frigid soil that soil temperature is  $-4.0^{\circ}\text{C}$  (according to data of Mr. Li Shude). This shows that permafrost table in the effect range of lake bank are obviously affected by high salt amount of lake, but the influence of lake heatamount seem more weaken.

Because of time limiting, thermosensitive resistor is set in 2# drilling of Zhuonai lake and steady geothermal curve is not observed. So the thickness of permafrost cannot be deduced by geothermal gradient. But two geophysical profile are installed in Zhuonai lake and Binggou of branch of Kushi river, according to calculation of electric measuring thickness, the thickness of permafrost is 74.8 m in Zhuonai lake, the thickness of permafrost in Binggou is more than 40 m in upstream and 28 m in downstream. The thickness of permafrost change smaller in wide valley and basin of gentle fluction. The thickness of permafrost is more than the value in the rock area of high mountain. Why do the thickness of permafrost of two mentioned area produce so large difference? The main cause is that permafrost in Binggou may be affected by new tectogenesis in Binggou. For the view of Tong Belling and Li Shude (1983), permafrost in Qinghai-Tibet pleteau show stronger law of vertical zonating of elevation, elevation height increase 100 m, ground temperature decrease  $0.8-0.9^{\circ}\text{C}$ . Comparing with Wudaoliang, elevation of basin in the region is high 120 m than that of Wudaoliang and latitude of two areas are the same, according to the law of vertical zonating of elevation, the thickness of permafrost deduced in wide valley and basin is 65 m, primarily approaching to geophysical projecting data. This shows that permafrost at Kekexili northern region in Qinghai abide the law of vertial zonating of elevation, but the thickness of permafrost in the part are affected by other factors.

#### GROUND ICE AND CRYOGENIC TEXTURE

Ground ice is only formed in lake sediment around lake basin and glacial hill in the region. Ground ice formed in lake sediment is relative with sedimentary environment of lake. Generally, grain of sediment is coarser, thickness of ground ice is thinner; grain of sediment is finer, thick-

ness of ground ice is thicker. For example, ground ice layer of different thickness are existed in the bank of Zhuonai lake, its thickness is generally 5-10 cm, the deepest one arrive to 30 cm and it is pure ice layer which is formed in upper of gray clay. Ice layer with soil is formed in gravel stratum and its thickness is thinner (Fig.5). Thickness of ground ice layer being formed in glacial hill is thicker. For example, Ground ice formed by repeatedly segregating is found in the front of glacial water fan, its thickness is 150 cm (according to Mr. Li Shude). Inductive inference, there are two deformation for ground ice, one is intraneous ice segerated by surface water in process of freezing; other is endagenetic ice for glacial ice, lake ice and river ice buried.

Drilling of Zhuonai lake promulate that cryogenic texture is basically regared as being integral, stratified and basic massive cryogenic terxture, and change with advance and retreat of lake and sedimentary rhythm. In general, lake retreat, integal cryogenic texture is formed for corase soil accumulated and ice content is smaller; Lake advance, basic massive cryogenic texture is formed for fine soil accumulated and ice content is larger. Meanwhile lake repeatly advance and retreat make water succssive migerate to freezing front and thicker ice layer is formed. Sedimentary stratum of lake ferice alternatally change from corase to fine, cryogenic texture gradually change from integal, stratified to basic massive cryogenic texture and there is stratum characteristics of intrusive cryogenic texture (Translated by Guo Dongxing et al, 1988). See Fig.5. Thus, forming of cryogenic texture have inherit relation to sedimentary environment and sucession history of lake.

#### CONCLUSIONS

1. Distributed pattern of continue permafrost, open talik of lake bed and circle-typed close talik of lake bank are formed at northern region of Kekexili in Qinghai.
2. Lake has ceitain influence on permafrost in lake bank, its range of effect is generally in 20-40 m. Salt content of lake have larger effect on permafrost table of lake bank.
3. Cryogenic texture is mainly integal, stratified and basic massive texture in lake bank of the region and there is stratum characteristics of intrusive-cryogenic texture, identital characteristics cannot appear far away from lake basin. Meanwhile cryogenic texture have inherit relation to sedimentary environment sucession history of lake.
4. Ground ice only exited in sedimentary stratum of lake ferice and glacialtill in the region. In general, ground ice is thinner in sedimentary stratum of lake ferice and deeper in glacial till.

#### ACKNOWLEDGEMENT

The author wish to thank associate professor Li Shude for help and guide and very grateful all researcher of the exploring team of sandy gold for accommodation in Kekexili region.

#### REFERENCES

Shi Chengxi et al (1989) An instruction of lake in China, Publishing House of science.

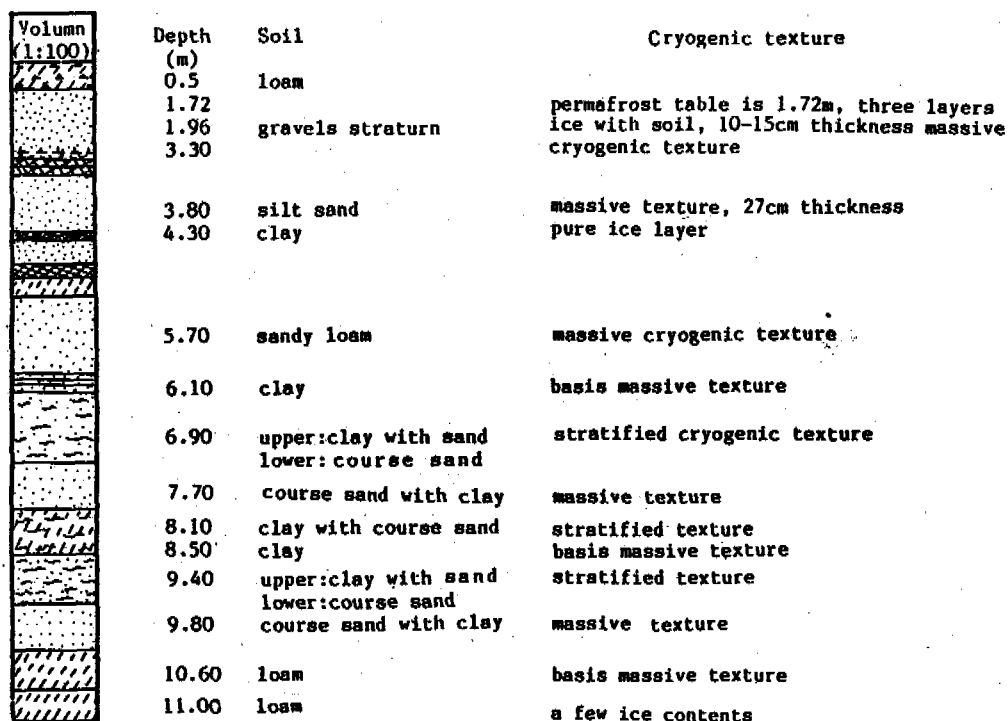


Fig.5 Volumn of 2# drilling in Zhuonai lake

Wang Ping (1986) Research of ice-snow chemistry of glacier in China. Journal of Glaciology and Geocryology, 8(1):40-50.

Tong Beliang and Li Shude (1981) Some characteristics of permafrost and effect factors in Qinghai-Tibet pleteau, Proceedings of permafrost research in Qinghai-Tibet pleteau. Publishing House of science, 1-12.

Li Shude (1991) Record of actual events of permafrost explored in Kekexili region, Acknowledgement of hundreds sciences, 91,5.

Guo Dongxing et al translating (1988) General geocryology (in Russian), Publishing house of science.

EXPERIMENTAL RESEARCH ON DEFORMATION IN MODEL  
OF AN ARTIFICIALLY FROZEN WALL

Wu Ziwang, Ma Wei, Zhang Changqing, Chang Xiaoxiao and Liu Yongzhi

State Key Laboratory of Frozen Soil Engineering, Lanzhou Institute of  
Glaciology and Geocryology, Chinese Academy of Science, China

Based on experimental results of a model of an artificially frozen wall, it was shown that deformation of a frozen wall are related closely with an unsupported height, deviatoric stress and average temperature. It is found that the position of maximum deformation is not fixed, and moves down gradually with increase of deviatoric stress. The change law is:

$$h_0 = B (\sigma_1 - \sigma_3)^A (\sigma_1 + \sigma_3)$$

INTRODUCTION

In freezing sinking of deep shafts, the key technical problem lies with deformation of the frozen wall and the related factors. Since the non-homogeneity of temperature and strength of the frozen wall and the creep deformation affected by conditions of the freezing stratum and parameters of construction, it is difficult to solve this technical problem through a perfect analytic approach. As a result, a modelling approach is proposed to study the whole deformation process of the frozen wall and the related factors. This paper will introduce and discuss mainly study results of this problem.

EXPERIMENTAL SET-UP AND SAMPLE PREPARATIONS

All of the tests are done on low-temperature tri-axial experimental machines, and the data are taken in time and processed by a computer. Both ends of the sample are fixed by a loading plate, which can be allowed to produce a proper deformation. Deformeters are installed according to pattern of Figure 1.

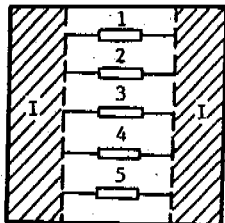


Figure 1. Schematic drawing of deformation installation

Lanzhou loess sample was used in this study. The main physical parameters are as follows:

water contents: 14-15%;  
dry unit weight: 1.77-1.78 g/cm<sup>3</sup>;  
confined pressure: 5.5 MPa;  
temperature: -5, -10, -15°C;  
height of frozen wall: 30-50 cm;  
sizes of sample:  
outer diameter D=40 cm;  
inner diameter d=20 cm;  
thickness of frozen wall e=10 cm.

Table 1. Physical parameter of sample

Soil name	Composition of grain(%)				Grav-ity	Liquid limit (%)	Plastic limit (%)
	>0.1	0.1-0.05	0.05-0.005	<0.005			
Lanzhou loess	1.7	5.4	58.6	34.3	2.7	24.6	17.7

EXPERIMENTAL RESULTS AND ANALYSIS

1. Displacement Law of Frozen Wall

Under a hydrostatic pressure state, distribution law of deformation along the height of the frozen wall are shown in Figure 2. The maximum deformation emerges at upper part of the frozen wall. From upwards to downwards, the amount of deformation reduces gradually.

Figure 3 is deformation curves of the frozen wall vs. time. It is seen that deformation curves are like typical creeping curves. During first creeping stage, the amount of deformation is about 20-35% of total deformation, this deformation is difficult to measure at field construction. Under the same pressure, there are the same type of creeping curves and their deformation is not alike at different positions of the frozen wall (Figure 3); Under a different height and the same pressure, there may be different types of creeping curves, the higher height of

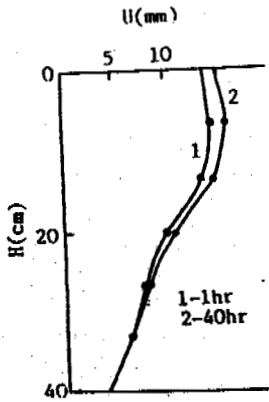


Figure 2. Distribution law of deformation along height of the frozen wall (-10°C)

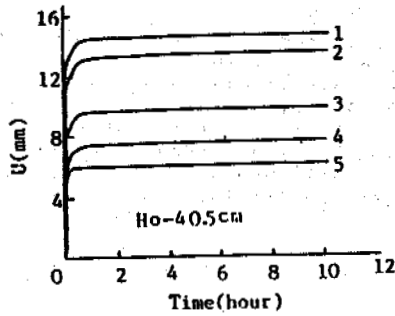


Figure 3. Deformation curves of frozen wall vs. time (-10°C)

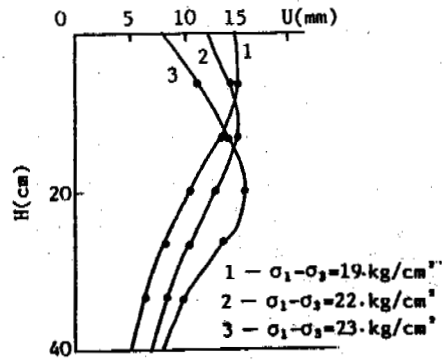


Figure 4. Under different deviator stress, the distribution law of deformation along height of the frozen wall (-10°C)

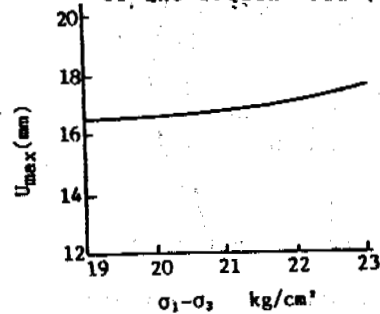


Figure 5. The relation of maximum deformation value and deviator stress (-10°C, 10hr)

the frozen wall, the easier non-attenuated creep emerges (Figure ).

## 2. The Relation of Deviator Stress and Deformation Law to the Frozen Wall

When deviator stress increases, the position of maximum deformation of the frozen wall will gradually move down (Figure 4). From Figure 5, it is found that the amount of deformation increases with increase of deviator stress under confined pressure. The relation of the position of maximum deformation value and deviator stress can be described by following formula:

$$h_0 = B (\sigma_1 - \sigma_3)^A (\sigma_1 - \sigma_3) \quad (1)$$

Where  $h_0$  is distance from upper end of the frozen wall (cm);  $A$  and  $B$ , are test parameters respectively,  $A=8.59 \times 10^{-5}$ ,  $B=3.84 \times 10^{-5}$ .

According to above-mentioned law, we may obtain that the position of maximum deformation is not fixed during practicable construction of the frozen wall, and it moves down with increase of sinking depth. The result is verified by data of No.3 Dong Feng shaft, Panji at Huainan.

## 3. The Relation of Height and Deformation of the Frozen Wall

Under the same pressure and temperature, the height of the frozen wall affects greatly its deformation (Figure 6). When height  $h > 45$  cm, non-attenuated deformation will take place; When  $h < 45$  cm, it will produce attenuated deformation. The bigger height of the frozen wall, the bigger deformation. From Figure 6, it is seen when  $h < 45$  cm, the second creeping stage

occupies an important place. So, we can calculate deformation through the engineering creep theory of frozen soil:

$$U_{max} = U_k \left( \frac{H}{H_k} \right)^k + \dot{U}_e \left( \frac{H}{H_e} \right)^n t \quad (2)$$

Where  $U_{max}$  is maximum deformation value of the frozen wall;  $H$  is height;  $t$  is time;  $H_k$  and  $\dot{U}_e$  are standard reference values;  $U_k$ ,  $H_e$ ,  $k$  and  $n$  are parameters, which they are dependent upon temperature, at  $-10^\circ\text{C}$ ,  $U_k=2.453$ ,  $H_k=10$ ,  $\dot{U}_e=10^{-8}$ ,  $H_e=0.0046$ ,  $k=1.253$ ,  $n=1.81$ .

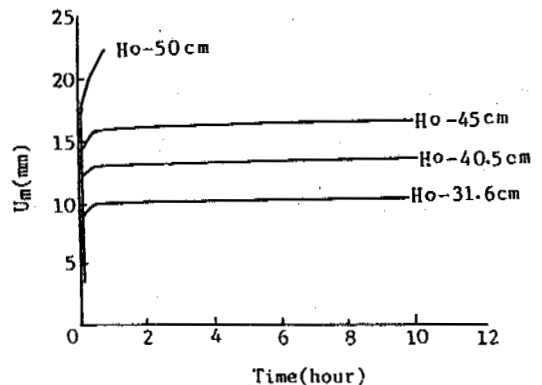


Figure 6. Under different heights of the frozen wall, the curves of maximum deformation vs. time (-10°C)

When creeping time is very long, the first in eq.(2) may be neglected. So eq.(2) becomes:

$$U_{\max} = \dot{U}_e \left( \frac{H}{H_e} \right)^n t \quad (3)$$

#### 4. Effect of Temperature to Deformation of the Frozen Wall

We know that the lower the temperature, the greater strength of frozen soil and smaller its deformation. This law is verified also by our tests. Fig.7 is the curves of deformation of the frozen wall under the same height and pressure.

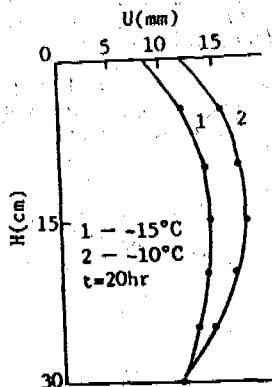


Figure 7. Under different temperature, change of deformation along height of frozen wall

#### CONCLUSION

1. As can be obtained from analyzing the experimental results, the temperature and height affect greatly the deformation of the frozen wall. The lower the temperature, the smaller the deformation, and the smaller the height, the smaller the deformation as well. So special attention should be paid to the selection of these factors in the designing and freezing-sinking of a deep shaft.

2. It is found that the position of maximum deformation is not fixed, and it moves down gradually with increase of deviatoric stress. Its position can be determined by eq.(1), once its position is determined, the maximum deformation value can be calculated by either eq.(2) or (3).

#### REFERENCES

- Ladanyi, B. (1982) A engineering theory of frozen soil creep. J. of Glaciology and Geocryology of the World, No.1, pp.55-77.
- Lanzhou Institute of Glaciology and Geocryology etc. (1988) Engineering behaviour of frozen wall in artificially freezing sinking. Publishing House of Lanzhou University.
- Xu Bingyie, (1981) Mechanics of Elasticity and Plasticity. Publishing House of Engineering Industry.

ACTIVE LAYER THAW CALCULATIONS USING  
SIMPLIFIED THERMAL AND HYDROLOGICAL PARAMETERS

Zhao-jun Xia<sup>1</sup> and Ming-ko Woo<sup>1</sup>

<sup>1</sup>Department of Geography, McMaster University  
Hamilton, Ontario, Canada L8S 4K1

The Green theorem was used to solve the heat flow equation for an active layer zone with the frost table as its lower boundary. The model incorporates the effect of ground ice content in the retardation of thawing front descent, and the moisture status in the calculation of thermal conductivity. The frost table computed for a transect comprising two distinct soil segments compared favourably with measured values. The model was used to assess frost table responses to varying degrees of soil saturation, ice content and air temperatures, and the result demonstrates the need to consider the hydrological variables in thaw calculations.

INTRODUCTION

Ground conditions in continuous permafrost areas may be considered to comprise a number of segments, each underlain by different materials experiencing non-uniform hydrological conditions, and subject to differential surface heating. Year to year fluctuations in the climate and long term climatic change will vary the surface temperature and the hydrology, thus affecting the thawing of the active layer (Smith and Riseborough 1983). In addition, alterations of thermal properties in any portion of the land will affect the frost table depths at its adjacent zones. These changes in thaw depths may have implications on landform development, vegetation growth and the stability of man-made structures.

Given adequate data on the soil properties, the hydrological behaviour and the surface temperature regime, various numerical methods (e.g. Kane et al. 1991) can determine the thaw depth along a stretch of the ground. However, detailed climatic and hydrological data are often not available to run such models. If only mean surface temperature and average hydrological information are available, an alternative method is needed to predict frost table positions under the influence of climatic variability and change. This paper presents an application of the Green theorem to solve the heat flow equation for an active layer zone with the frost table as its lower boundary.

THEORY

The two-dimensional, heat transfer partial-difference equation involving phase change of ground ice is

$$k_x \frac{\partial^2 T}{\partial x^2} + k_z \frac{\partial^2 T}{\partial z^2} - C \frac{\partial T}{\partial t} + \lambda \frac{\partial \theta}{\partial t} \quad (1)$$

where  $k$  is thermal conductivity,  $C$  is heat capacity,  $\lambda$  is volumetric latent heat of fusion,  $\theta$  is ice content,  $T$  is temperature,  $t$  is time, and  $x$  and  $z$  are horizontal and vertical directions. At the thawing front,  $\frac{\partial T}{\partial t} = 0$ .

Let us first suppose that  $k_x = k_z = k$  and neglect  $\frac{\partial \theta}{\partial t}$  for the time being. At the thawing front, equation (1) is reduced to the Laplace equation:

$$\frac{\partial^2 T}{\partial x^2} + \frac{\partial^2 T}{\partial z^2} = 0 \quad (2)$$

The Green function can be applied to solve equation (2) (Fritz 1982). The solution is

$$T(x, z) = \int_{\partial \Omega} \left[ T \cdot \frac{\partial \Gamma}{\partial n} - \Gamma \cdot \frac{\partial T}{\partial n} \right] ds + \int_{\Omega} \Gamma \cdot \Delta T dx dz \quad (3)$$

with  $n$  being the direction normal to the boundary, and

$$\Gamma = \frac{1}{2\pi} \ln \left[ \frac{\sqrt{(x-\xi_1)^2 + (z-\xi_2)^2}}{\sqrt{(x-\xi_1)^2 + (z+\xi_2)^2}} \right] \\ \Omega = \{(x, z) = -\infty < x < \infty, z > 0\} \quad (4)$$



$f$  is the radius from  $(x, z)$  to the boundary, for all  $f \neq x$  and  $f \neq z$ .

Heat flux across the boundary ( $\partial n$ ) is  $k \frac{\partial T}{\partial n}$ , and

$$\nabla^2 = \frac{\partial^2}{\partial x^2} + \frac{\partial^2}{\partial z^2}$$

At the boundary,  $z = 0$  and because of equation (4),  $\Gamma = 0$ . Furthermore,  $\nabla^2 T = 0$  at the thawing front, so that equation (3) is now reduced to

$$T(x, z) = \int_{\partial n} T \frac{\partial \Gamma}{\partial n} ds \quad (5)$$

with

$$\frac{\partial \Gamma}{\partial n} \Big|_{x=0} = \frac{\partial \Gamma}{\partial n} \Big|_{x=\infty} = \frac{\partial \Gamma}{\partial n} \Big|_{z=0} = 0$$

Along the boundary,  $\partial \Gamma / \partial n = 0$  except for the ground surface segment. In other words,  $\partial \Gamma / \partial n \neq 0$  only when  $z = 0$  and  $-\infty < x < \infty$ .  $ds$  can now be replaced by  $df_1$ , and  $\partial \Gamma / \partial n = \partial \Gamma / \partial f_1$ .

$$\frac{\partial \Gamma}{\partial n} \Big|_{z=0} = - \frac{\partial \Gamma}{\partial f_1} \Big|_{z=0} = \frac{1}{\pi} \frac{z}{(x - \xi_1)^2 + z^2}$$

Substituting into (5), we have

$$T(x, z) = \frac{1}{\pi} \int_{-\infty}^{\infty} \frac{T(\xi_1, 0) z}{(x - \xi_1)^2 + z^2} d\xi_1 \quad (6)$$

Introducing heterogeneous materials and non-steady state situation, the condition the thawing front,  $z = h(x, \tau)$ , is

$$T_{(x, h(x, \tau))} = \frac{1}{\pi k_{(x, h(x, \tau))}} \int_{-\infty}^{\infty} \frac{k(\xi, h_{(x, \tau)}) T_0(\xi, \tau) h_{(x, \tau)}}{(x - \xi)^2 + h_{(x, \tau)}^2} d\xi \quad (7)$$

Here,  $f_1$  is replaced by  $f$  for simplicity of presentation; and  $T = T_0$  at  $f_2 = 0$ . It is also assumed that a weighted average  $k$  is applicable to the thawed zone such that  $k(x, z, \tau) = k(x, \tau)$ .

Consider two adjacent segments, labelled A and B, consisting of different soil materials and surface temperature conditions. At the thawing front, we have

$$T_{(x, h)} = \frac{1}{\pi k(x, \tau)} \left[ \int_{-\infty}^0 \frac{k(A, \tau) T_A h}{(x - \xi)^2 + h^2} d\xi + \int_0^{\infty} \frac{k(B, \tau) T_B h}{(x + \xi)^2 + h^2} d\xi \right] \quad (8)$$

with  $h = h(x, \tau)$ .

Next, we examine the situation where the terms on the right hand side of equation (1) is non-zero. Instead of solving the equation directly, we partition the surface ground temperature into two components: one to raise the ground temperature  $T^*$ , and the other ( $T'$ ) to cause

phase change at the thawing front. Then

$$T(x, \tau) = T^*(x, \tau) + T'(x, \tau), \text{ with}$$

$$kT'/z = \lambda dz/d\tau$$

At the thawing front

$$T' = \lambda h^2 / 2k\tau \quad (9)$$

Equation 9 is substituted into equation 8 and integrated to yield an approximate solution to equation 1:

$$\begin{aligned} T(x, h) = & \frac{k(A, \tau) T^*(A, \tau)}{\pi k(x, \tau)} \tan^{-1}[(\xi - x)/h] \Big|_{-\infty}^0 \\ & + \frac{k(B, \tau) T^*(B, \tau)}{\pi k(x, \tau)} \tan^{-1}[(\xi - x)/h] \Big|_0^{\infty} \\ & - \frac{k(A, \tau) T^*(A, \tau)}{\pi k(x, \tau)} [(\pi/2) - \tan^{-1}(x/h)] \\ & + \frac{k(B, \tau) T^*(B, \tau)}{\pi k(x, \tau)} [(\pi/2) + \tan^{-1}(x/h)] \end{aligned} \quad (10)$$

At the thawing front,  $T(x, h) = 0$ . This condition is satisfied when the proper value of  $h$  is obtained for the right-hand-side of equation 10.

#### PARAMETER ESTIMATION

Hydrological status of the soil affects frost table development through the thermal conductivity and the amount of ground ice. Thermal conductivity of earth materials can be estimated by (Farouki 1981):

$$k = \sum_j f_j k_j \quad (11)$$

where  $f$  is the volumetric fractional content of soil component  $j$  which includes elastic materials (m), organic matter (o), water (w), ice (i) and air (a). Their respective thermal conductivities (in W/m°C) are:  $k(m) = 2.93$ ,  $k(o) = 0.25$ ,  $k(w) = 0.57$ ,  $k(i) = 2.20$  and  $k(a) = 0.025$ . For a soil column, the relative contents of  $w, i$  and  $a$  vary with time and depth, depending on the hydrological and thermal conditions.

In the thawed zone, the general moisture profile is considered to be composed of three sections (Fig. 1). At the base is the saturated zone with mean thickness during the period  $(0, T)$  determined by averaging the daily differences between the frost table and water table positions. In the non-saturated zone, moisture content at depth, or  $f_z(w)$ , is assumed to decrease linearly upward to reach the specific retention value,  $f_0(w)$ :

$$f_z(w) = \max[f_0(w), f_s(w) - g(z_s - z)] \quad (12)$$

where  $z$  is the depth at the top of the saturated zone and  $g$  is the gradient of moisture decrease, being 2/m for gravel, 1.5/m for fine sand and clay and 1/m for peaty soils. The estimated

values for saturated moisture content,  $f_s(w)$ , for specific retention,  $f_o(w)$ , are listed in Table 1.

Table 1 Input parameters

	Gravelly Soil	Peaty Soil
$f_s(w)$	0.3	0.4
$f_o(w)$	0.2	0.3
a	1.15	0.87
b	1.23	0.90

\* see text for explanation of symbols

The ice content in a profile is taken as the moisture content frozen at the beginning of the past winter. The zone saturated with ice is obtained by the difference between the water table and frost table at the end of the previous summer season.

Ground surface temperatures ( $T^*$ ) are estimated empirically from air temperatures ( $T_a$ ):

$$T^* = a + b T_a \quad (13)$$

The coefficients were determined from field measurements (Table 1) and the correlation

coefficients were 0.99 for gravels and 0.98 for peaty soils obtained from summer seasons of 1988 and 1989.

#### MODEL TESTING

The model was applied to a transect in the continuous permafrost area near Resolute, N.W.T. (74°43'N, 94°59'W). The 34 m transect consisted of a gravel segment and a segment with peaty soil cover, and their stratigraphy is given in Figure 1. The site was chosen because of the availability of frost and water table measurements for seven summers (Woo and Steer 1983). Two water table wells, one in the gravel and the other in peaty materials, provided inputs for moisture profile estimation. Air temperatures from the nearby Resolute weather station allowed estimations of  $T^*$  using equation 13. In addition, frost tables were monitored at five points along the transect to allow verification of model results.

Mean ground surface temperature and mean thickness of the saturated zone for both soil types were calculated over periods of 15, 35 and 55 days since the beginning of thaw in 1988 and 1989. The initial ice contents were estimated from the water table positions for the end of the previous summers. The thawing depths (h) along the transect (x) for the test periods of various durations were obtained by optimization such that the right-hand-side of equation 10 satisfies the condition  $T(x,h)=0$ .

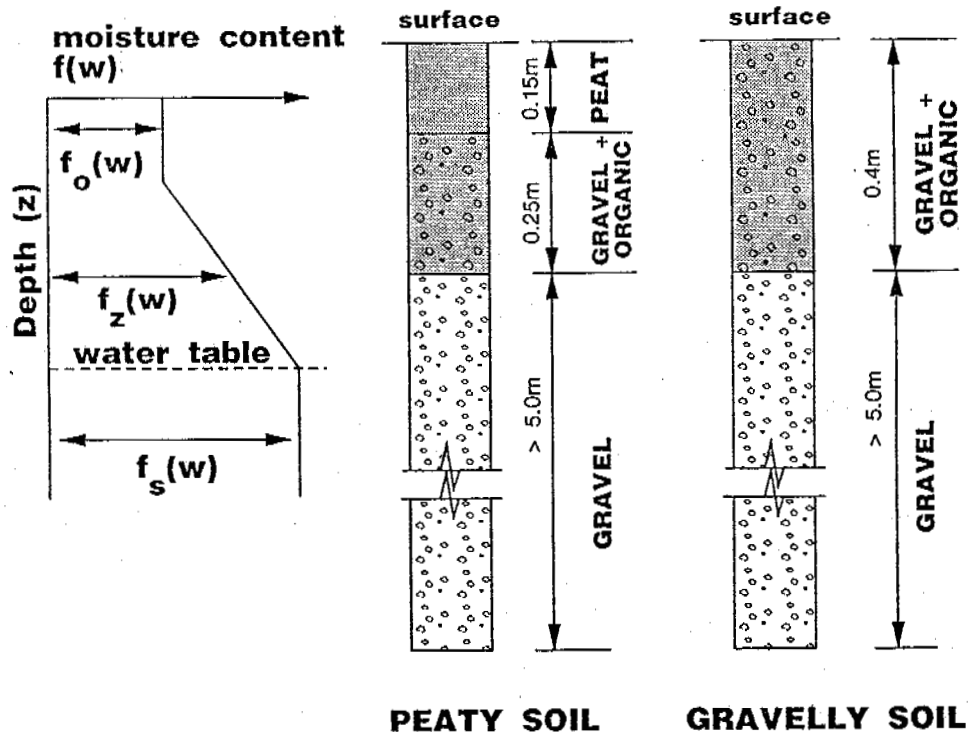


Fig.1

Assumed moisture content profile above and below the suprapermafrost water table and stratigraphic profiles of two soil types used in model testing.

Table 2. Sensitivity of ground thaw to temperature, moisture and ice contents

INPUT VARIABLES			
	Summer Temperature (°C)	Saturated Zone Thickness (m)	Ice-rich zone Thickness (m)
Gravelly soil:			
Maximum	6.62	0.40	0.39
Average	4.35	0.22	0.23
Minimum	2.24	0.04	0.04
Peaty soil:			
Maximum	6.88	0.43	0.42
Average	4.53	0.26	0.29
Minimum	2.35	0.10	0.09

OUTPUT VARIABLES (thawed depth in m)						
	Saturated Zone			Ice-rich Zone		
	Max.	Avg.	Min.	Max.	Avg.	Min.
Gravelly Soil:						
Max. temp.	0.81	0.76	0.71	0.72	0.76	0.81
Avg. temp.	0.67	0.62	0.57	0.58	0.62	0.67
Min. temp.	0.49	0.45	0.40	0.42	0.45	0.49
Peaty Soil:						
Max. temp.	0.59	0.55	0.48	0.50	0.55	0.62
Avg. temp.	0.46	0.42	0.39	0.39	0.42	0.51
Min. temp.	0.35	0.32	0.27	0.26	0.32	0.37

Figure 2 shows part of the transect adjacent to the border between the gravel and the peaty soils. Comparison of the calculated frost table positions (appear as lines in Fig. 2) with the observed values (symbols in Fig. 2) suggests that the model results were very close to the field data for the three time periods during the two years of model testing. The root-mean-square error from all the points was 0.014 m in 1988 and 0.017 m in 1989.

#### SENSITIVITY

Experiments were performed to determine the sensitivity of active layer thaw to varying degrees of soil saturation, ice content and air temperature conditions. Maximum, mean and minimum values were extracted from water level records obtained over seven years at the Resolute experimental site to estimate the saturated moisture content and the ice content for the wettest, average and driest summers. These variables were combined with the warmest, the average and the coolest summers (55 days of the thawed season) reported by the Resolute weather stations to estimate the thawing responses.

Table 2 shows that while thaw depth is controlled by temperatures, it is also significantly affected by the thickness of the saturated zone and by the thickness of the zone

saturated with ice. Given similar summer temperatures, a thick saturated zone will enhance thawing due to higher k value relative to the dry soil; but a large ice content in the soil will retard frost table descent as more heat is needed in ice melt. These experiments demonstrate the hydrological influence on ground thaw.

#### CONCLUSIONS

- (1) As the frost table represents a boundary where the ground temperature is 0, it is feasible to apply the Green theorem to solve the heat flow equation to yield a simple equation. Equation 10 is easily applicable to calculate ground thaw along a transect comprising two distinct segments each with its soil thermal and hydrological characteristics.
- (2) The model result compares well with observed frost table data collected in the continuous permafrost area, along a line that traversed a peaty and a gravelly soil segment.
- (3) Sensitivity experiments using different moisture and ice contents and subjected to various temperature conditions demonstrated that the hydrological status of the soils is

important in modifying the rate of summer thaw. Thus, in terms of permafrost responses to climate warming, it is necessary to consider the wetting or drying scenarios that accompany temperature changes.

**ACKNOWLEDGEMENTS**

This work was supported by the Natural Sciences and Engineering Research Council of Canada. The generous logistical support of the Polar continental Shelf Project is gratefully acknowledged.

**REFERENCES**

Farouki, O.T. 1981. Thermal properties of soils. U.S. Army EQUATION Monograph 81-1, 136p.

Fritz, J. 1982. *Partial Differential Equations*. Springer-Verlag, N.Y., 249p.

Kane, D.L., Hinzman, L.D. and Zarling, J.P. 1991. Thermal response of the active layer to climatic warming in a permafrost environment. *Cold Regions Science and Technology* 19, 111-122.

Smith, M.W. and Riseborough, D.W. 1983. Permafrost sensitivity to climatic change. *Proceedings, Fourth International Conference on Permafrost*, Fairbanks, Alaska, 1178-1183.

Woo, M.K. and Steer, P. 1983. Slope hydrology as influenced by thawing of the active layer, Resolute, N.W.T. *Canadian Journal of Earth Sciences* 20, 978-986.

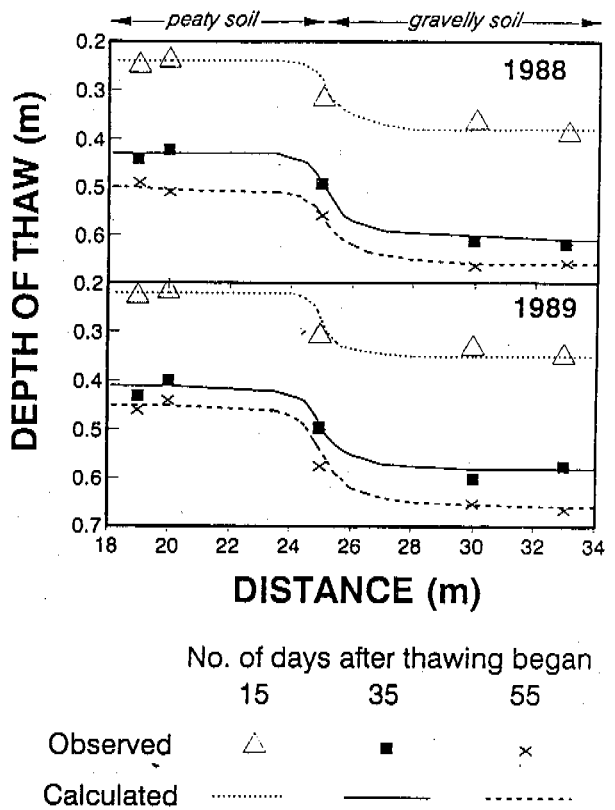


Fig.2 Calculated and measured frost table positions along the test transect near Resolute, 1988 and 1989.

## PROBLEMS OF PERMAFROST IN DEVELOPMENT OF WATER RESOURCES OF THE HENERGUNA AND HEILONGJIANG RIVER

Xu Bomeng<sup>1</sup>, Wang Zeren<sup>1</sup>, A.A. Kagan<sup>2</sup> and N.P. Krivonogova<sup>3</sup>

<sup>1</sup>Northeast Prospect-Design Institute of Ministries of Water Resources, Energy Resources, Changchun, China

<sup>2</sup>Hydro Electric Design Institute, Leningrad Branch, Russia

<sup>3</sup>All-Union Research Institute of Hydraulic Engineering (VNIIG) Leningrad, Russia

In recent years, the Soviet Union and Chinese specialists have conducted an engineering geologic investigation and study of the Henerguna River and boundary reaches of Heilongjiang (Amur) River. In this paper, the permafrost distribution and thickness in those areas are introduced, five permafrost zones were divided, the possible changes of permafrost conditions after hydraulic projects constructed and the effect on the hydraulic projects were evaluated. Analysis indicated that the permafrost is good for developing conditions at the Mohe dam site and permafrost does not exist in the Huma dam site down stream. Construction and operation of hydraulic projects would induce the degeneration of permafrost, but it would not cause various changes of geological conditions at the dam sites.

### INTRODUCTION

During 1987-1991 Soviet Union and Chinese specialists have conducted engineering geological studies for the comprehensive use of water resources of the Henerguna River and the boundary reaches of Heilongjiang (Amur) River. Investigated territory involves a zone with a 250 km width, extending above the rivers from the mountains of East Zabaykal'ye in the west to the low plains of middle Priamur. The development scheme involves Mohe (Amazal), Liangin (Galingga), Shuanghezhan (Tolbuzin), Opu (Kuzniezove), Huma (Nowesklecinove), Hehe (Blakowesinsk) and Taipingou (Shinan) hydroelectric stations.

For composing the planning scheme, one of the most important problems is, based on the permafrost zonation, to predict permafrost conditions, their changes during the operation of each structure and effects on the engineering geological situation and structures.

### DISTRIBUTION AND THICKNESS OF PERMAFROST

Researched territory is located in the south zone of high latitude permafrost within the Europe-Asia continent. Consequently, the distribution of permafrost has complicated and ununiform characteristics. The fundamental factor governing permafrost distribution and thickness is climate. The general tendency for zonation of permafrost distribution, therefore, is to submit to the latitudes, namely air temperature decreases from south to north, from southeast to northwest and the area and thickness of permafrost increases with latitudinal rising. But, affected by human activity and natural factors, such as altitude, microclimate, composition of rocks, vegetation of forest, surface and underground water, exposure, etc. the distribution of permafrost in this territory has obvious regional features, such as: continuous, discontinuous, island, scattered island permafrost and seasonal frozen soil with different thicknesses.

The results of investigation and exploration conducted in recent years indicate that in the last ten years with air temperature rising, human activity increasing and effect of other natural factors as well, degeneration of permafrost has occurred in this territory, expressed by the annual mean ground temperature rising, area of permafrost reducing and thickness thinning. Such phenomenon is not only shown by the changes of permafrost conditions in overall and local ranges of this territory, but also can be visibly found from the results of geological exploration and temperature observations at each dam site.

By referring to the existing data, in combination with engineering geological exploration and permafrost on-the-spot survey and investigation to analyze the general action of air temperature and all natural and artificial factors mentioned, above the principle law of space distribution of permafrost in this territory can be derived as follows:

The continuous permafrost mainly exists in local ranges of the northwestern slopes of the Da Hinggan Ling mountains on the right bank of the Heilongjiang River, in the north-western slopes in the region with medium mountain terrain (absolute elevation of more than 1000 m a.s.l.) of the upland on the left bank, and in the highest peaks of Da Hinggan Ling mountains. It is because in these regions there exists low air temperature, dense vegetation, virgin forest, steep slopes without stable snow cover, deeply dissected intermontane basins, and shady slope surfaces of river and creek valleys. Permafrost thickness varies from 50 to 150 m, sometimes to 200 m. The taliks are mainly developed beneath the river bed and have generally penetrated through the permafrost. On individual gentle slopes with southern exposure the infiltrated taliks of the radiating-thermodynamic type are also found.

Discontinuous permafrost is distributed in large parts of the northwestern slope of Da

Hinggan Ling mountains on the right bank of the Heilongjiang River, in the north and west regions with medium and low mountains with a small area on the left bank, and in the large parts the elevation is less than 100 m a.s.l. Thickness of permafrost is 50 m or so, in the majority and increases to 100 m or so in some sectors. In these regions, taliks distributed on the gentle slopes and flat watershed where the snow cover is thicker and has a thermodynamic effect and can accumulated there, beneath the beds of large rivers, and in the river terraces the deposits are composed of sands and gravels.

Island and scattered island permafrost are widely distributed with a thickness of 10-50 m in general, at the slope with northern and northeastern exposure, especially, at their lower parts, in the valleys and lower terraces with dense vegetation and marshes. This situation depends on the slopes having different exposures the ground surface to large extent is shaded and the top layer is generally composed of loam sediments and peat with lower permeability and greater moisture. In these regions, taliks widely develop. They exist beneath the beds, not only of the large rivers, but also in the tributaries, and widen to larger areas on both banks.

In the southeastern part of the studied territory from the Huma dam site down stream, there is virtually no permafrost because air temperature is higher and rainfall is more abundant in summer. Only in some sections of the lower part of slopes on the right bank and upstream flood land of rivers are there pereletoks to be found. Their thickness may reach 8 m. At the same time, some relicts may be found on the right bank, but the thickness does not generally exceed 3-5 m.

#### ZONATION OF ENGINEERING PERMAFROST

In order to research permafrost conditions affecting the engineering geological situation, a zonation of permafrost in this territory has been made.

The principle of zonation is that the permafrost conditions of the divided zones are extremely different from each other.

The basis of zonation is, the characteristics of permafrost distribution and thickness, annual mean temperature of frozen and thawed ground, seasonal freezing and thawing depth, and cryogenic phenomena, as mentioned above.

According to the principle and basis mentioned above, five permafrost zones were divided, a zoned map with scale of 1:2500000 was plotted (see attached map).

Zone I — zone has virtually no permafrost. Only in the lower boggy terraces, lower parts of northern exposure slopes composed of loam does pereletok or relict permafrost exist.

This zone involves the southern part of the Amul-Zeia plain and all of the Zeia-Bleia plain on the left bank of the Heilongjiang River, the area south of Xinjeiji village, from the eastern slope of the Yilehuli mountains, northeastern slopes of Xiao Hinggan Ling mountains and the massif of their southeast end to the side on the right bank.

Ground temperature in this zone on the erosion slopes with a southern exposure is +1 — +3°C, on the high terraces composed of permeable rocks from the ground surface is +5°C or higher. The seasonal freezing depth depends on the composition and moisture of sediment, and varies between 3-6 m. Cryogenic phenomena are few, only

some remain in the thermal karst basins, terraces of mud flow and little frost mounds that are locally found.

Zone II — zone of scattered island permafrost. This zone encompasses the southwestern and middle mountain sides and part of lower mountains, northwest and southeast on both banks along the Heilongjiang River, and the regions with lower mountains and hills of the Xiao Hinggan Ling mountains.

The thickness of the permafrost is 5-15 m, and sometimes reaches 25 m. Permafrost is mainly distributed in the valley bottom, boggy sections of lower terraces, and lower parts of the northern slopes. It occupies an area of 10-20%. Temperature of permafrost is -0.2 — -0.5°C generally. This zone has characteristics of deep seasonal thaw with depths of 3-5.5 m. In some sections, composed of permeable alluvial rocks, the seasonal thawing depth may reach 8 m, forming frozen layers of the unjoined type.

In this zone, all kinds of cryogenic phenomena widely develop. At the valley bottom there develops frost mounds, pingos and thermal karst, on the slopes there develops mud flows and stony conglomerates.

Zone III — zone of island permafrost. This zone occupies quite a large amount of the middle part of the studied territory. Temperature of the permafrost varies between 0-1.0°C minimum is -2.0°C. Permafrost widely develops at the bottom part of the river valley, intermontane basin and on the slopes with a northern aspect. Its thickness may reach 20-30 m, distribution area is 30-50%. Seasonal freezing-thawing depths are 2.5-3.5 m in the sections composed of loam and clay, and 1.5-2.0 m in the boggy sections. In the sand-gravel sediments of high terraces, the seasonal thawing depth exceeds 3.5 m.

In this zone, cryogenic phenomena widely develops. Icing occurs in all of the rivers and creeks, frost mounds occur at the bottom of valleys and gullies, the lower parts of river valley slopes and on the smooth watershed with marshes; active mud flow is often accompanied with a stony conglomerate on the slopes; polygon vein ice and soil veins are found at the back crack of terraces on the smooth slopes. As well, thermal karst widely develops on the smooth sections of the valley bottom, intermontane basins, and in the river valleys.

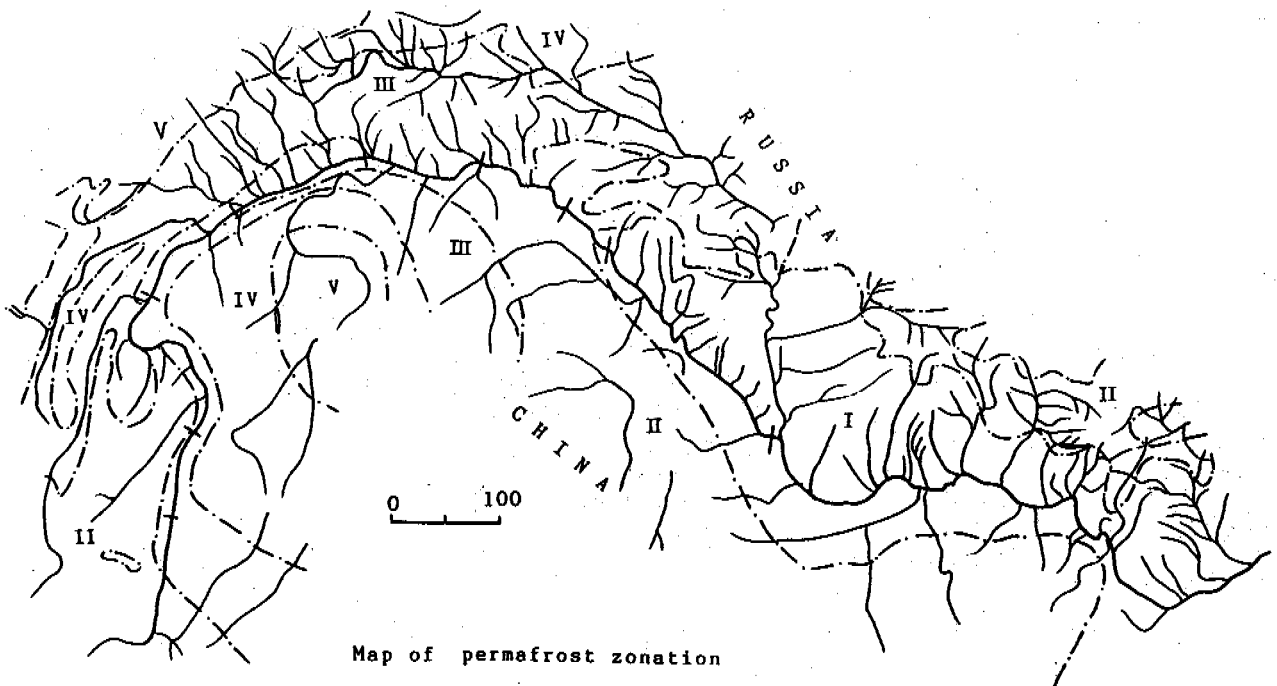
Zone IV — zone of discontinuous permafrost. This zone is comprised of part of the east and north massif on the left bank of the Heilongjiang River, and the wide area of northwestern slopes of Da Hinggan Ling mountains on the right bank. It occupies an area of 70-80%. Temperature of the permafrost is between 0-2°C. Its thickness is generally 60-80 m, at some sites it may reach 100 m. The taliks are present on the sunny slopes with less vegetation cover, smooth lower watersheds composed of permeable rocks (with an elevation of less 1000 m a.s.l.), and in the structural break zones of the river valley. Seasonal freezing and thawing depths vary from 2.0 to 5.0 m, and are approximately 1.0 m in the marshland at the valley bottom.

Cryogenic phenomena is widely developed. On the slopes, stony conglomerate, stone-ring-polygon and mud flow develops; at the lower part there are polygon vein ice, and frost mounds; at the bend of the slope there are pingos; pingos can be seen anywhere in the rivers and creeks; at the intermontane basin and bottom of the river valley, thermal karst and frost mounds, polygon vein ice and soil vein are widely

Legend

Zones	Characteristics	Mean temp. of rock, °C	Thickness of permafrost m	Seasonal frost thaw depth m	Crygenic phenomenon
I	Permafrost actually not, possibly relict or perelotok at lower location of valley bottom.	0 - +5 mainly +1 - +3	Relict or perelotok 3 - 7 sometimes 10	3.0 - 6.0	
II	Scattered island permafrost, area 10-20%	-0.5 - +2.0	0-25	$\frac{3.0-4.5^*}{>5.0}$	Thermal carst, mud flow, stony, pingo frost mound.
III	Island permafrost area 50-60%	-2 - +1 mainly -1 - 0	0-50	$\frac{2.5-3.5}{>3.5}$	Mud flow, stony, thermal carst, pingo, frost mound polygon vein ice.
IV	Discontinuous permafrost, area 70-80%	-3 - 0 mainly -2 - -1	0-100	$\frac{2.0-3.5}{3.5-5.0}$	Mud flow, stony, thermal carst, pingo, frost mound, polyon vein ice, soil vein.
V	Continuous permafrost, area >70-80%	-5 - 0 mainly -3 - -1	0-200 mainly 50-100	$\frac{1.0-2.5}{2.5-3.5}$	Mud flow, stony, frost mound, pingo, polygon vein ice and layered ice

\* Numerator-clayey soil, denominator-rock with good permeability.



developed.

Zone V — zone of continuous permafrost. This zone lies in the local massif of the northwestern slope of Da Hinggan Ling mountains on the right bank of the Heilongjiang River and in the highest part of northwestern mountains on the left bank. Its area exceeds 80%. Temperature of the permafrost is generally  $-1.0 - -3.0^{\circ}\text{C}$ , in an individual location it may reach  $-5.0^{\circ}\text{C}$ . The permafrost thickness is 50-100 m. Seasonal thawing depth in the sector is composed of loam and clay and is 1.0-2.5 m with a minimum of about 0.5 m, in the location composed of sand and gravel it may reach 3.0-3.5 m.

In this zone, cryogenic phenomena widely develops. In the river valleys and intermontane basins, pingos, frost mounds, polygon vein ice, and locally layered ice develop. On the slopes, there are mud flows and stony conglomerates.

#### EVALUATION OF THE EFFECTS OF PERMAFROST CHANGE ON ENGINEERING GEOLOGIC CONDITIONS

In the last thirty years, the permafrost in the territory of Hengerguna River and the upper reaches of Heilongjiang River has been degenerating[6]. During construction and operation of each hydraulic project designed in the development scheme of Heilongjiang River, the permafrost located in the corresponding site would degenerate. But, degeneration of the permafrost would not make the engineering geological condition severely deteriorate because of the cracking degree of rocks at the main projects was comparatively low and its permeability was lower. In the period of construction however some problems associated with the changes in permafrost may occur. Besides, owing to the zonal and local difference, when other construction beyond the main project are made, such problems would also be met. These problem should be studied in the future.

#### CONCLUSTON

The territory of Hengerguna River and the boundary reaches of the Heilongjiang River can be divided into five zones of frozen soil. Upwards from Huma, all dams sites are located in permafrost zones. Among them, the Mohe dam site has the coldest frost conditions. Owing to the fairly low cracking degree of rock at the main project and the lower permeability, the degeneration of permafrost may not cause the engineering geological condition to severely deteriorate. However, during construction of the dams and the other related projects, the problems associated with permafrost will still be met, and should be further studied in the future.

#### REFERENCES

1. Geocryology USSR, (1989) East Siberia and Far East. Ed, A.D. Ealsov. M.
2. Geocryology USSR, (1989) Southern mountain area USSR. Ed. A.D. Ealsov, M.
3. Apstein G.M., (1961) Problem of temperature reverse increase near ground and permafrost distribution of river valley in Zabaykal'ye and PriAmul regions, Prof. Papers (Frost Study", Pub, MSU, pp.71-81.
4. Apstein G.M., (1961) Some laws of seasonal freezing and thawing of ground in the island distribution zone of permafrost (taking upstream valley of Amul River as sample). Prof. Papers "Frost Study", Pub, MSU, pp.45-58.
5. Guo Dongxin at al., Zanation of Permafrost in Big and Xiao Hinggan Ling Mountains, "J. of Glaciology and Cryology", Vol.13, No.3.
6. Shengqing Yu, Shenzhen Wang, (1992) On the degeneration of permafrost in upstream valley region of Heilongjiang River. The paper presented to this Conference.



## A PRIMARY STUDY ON INTERFACE CONDITIONS OF ICE SATURATED CLAY

Xu Xiaozu and Wang Jiacheng  
State Key Laboratory of Frozen Soil Engineering, LIGGAS, PRC  
E.M.Chuvilin and I.U.P.Lebedenko  
Moscow State University, Russia

By using an electronic scanning microscope the interface conditions surrounding ice saturated soil particles, including montmorillonite, kaolinite and multi-mineral Neimong clay, are observed under different temperatures and solution concentrations. Results show that under certain temperatures below zero the shape and the thickness of unfrozen water film surrounding the soil particles changes with soil type, temperature and concentration. The shape of the unfrozen water film surrounding the ice saturated clay particles can be divided into three types: smooth, winding and overflow.

### INTRODUCTION

The interface conditions among soil particles, unfrozen water film, ice and vapor are important contents of the physics of frozen soils. The interface conditions formed under certain conditions result from comprehensive actions of various forces. The study in this area is of great significance for understanding water phase changing, cryogenic structure forming and water migrating in frozen soils, and also for physico-mechanics of frozen soils. For many years, few international studies have been done in this area. For instance, Anenian (1970) pointed out that the bond energy of water surrounding frozen soil particles decreases with an increase in the distance between water molecules and soil particles in the power form. Doctoalov (1973) showed that the structure of water layers changes with the distance to the soil particles and can be divided into three types: an active energy zone of bounded water, a non active energy zone of bounded water and an active energy zone of frozen water. Anderson and Morgenstern (1973) described the existant multi-layers of water surrounding mineral particles, i.e., the disordered zone located both at surfaces of silicate substract and ice, respectively, and the zone of enhanced order

located between two disordered zones. But further research is difficult due to the limitation of study measures.

Recently, Chinese and Russian scientists made a joint effort to research the interface conditions of water surrounding ice saturated soil particles with different temperatures and concentration by using an electronic scanning microscope. The purpose of this paper is to present some observed results.

### SAMPLE PREPARATION

There are three kinds of soils used in the test, i.e., kaolin and montmorillonite (taken from Russia) and multi-mineral Neimong clay (taken from China). The physical properties are shown in Table 1.

The kaolin, montmorillonite and Neimong clay are mixed with distilled water and a solution of natrium chlorite, respectively. The samples are quickly frozen under temperatures of 10 to 15 degree centigrade below zero. Afterwards, the samples are put into a chamber with a constant temperature for 48 hours. Then each sample is split into two pieces by a knife and spreaded on a fresh surface with the plexiglass solution with the same temperature as the sample, and then put away in a chamber with a constant tem-

Table 1 Physical properties of the clay

Soil type	Particle composition %			Liquid limit %	Plastic limit %	Gravity g/cm <sup>3</sup>	Surf. area
	>0.05mm	0.05-0.002	<0.002				
Kaolin	0.5	44.7	54.8	51.0	31.0	2.64	30
Montmori.	0.2	46.7	53.5	114.0	44.0	2.45	560
Neimonclay	0.2	50.8	47.1	32.8	20.4	2.73	28

Table 2 Shape of unfrozen water film under different temperatures and concentration conditions

Soil type	Sample No.	Temperature, °C	Concentration, Mole	Film shape
Kaolin	G-01	-1.5	0	NOT SEEN
	G-02	-1.5	0.1	SMOOTH
Montmori- llonite	M-01	-1.5	0	SMOOTH
	M-02	-1.5	0.1	WINDING
		-1.5	0.1	OVERFLOWING
Neimong clay	N-01	-11	0	NOT SEEN
	N-02	-11	0.1	NOT SEEN
	N-03	-11	0.5	NOT SEEN
	N-04	-11	1.0	SMOOTH
	N-05	-5	0	NOT SEEN
	N-06	-5	0.1	SMOOTH
	N-07	-5	0.5	SMOOTH
	N-08	-3	0	NOT SEEN
	N-09	0.1	0.1	SMOOTH

perature for one or two days to allow the plexiglass solution to dry. Finally, the dried film is taken off the sample and the sample is used for observation on the electric scanning microscope.

#### RESULTS AND ANALYSIS

Table 2 shows the observation results. It can be seen that the unfrozen water film of ice saturated clay is not always observed under various conditions by electronic scanning microscope. For example, the unfrozen water film can not be seen in kaolin without solutes, and with a temperature of  $-1.5^{\circ}\text{C}$ ; for Neimong Clay without solutes and with a temperature of  $-3^{\circ}\text{C}$ . And the thickness of unfrozen water film observed has reached the order of  $\mu\text{m}$ . The fact mentioned above indicates that the use of the electronic scanning microscope to investigate the interface conditions on ice saturated clay has its limitations, the thickness of unfrozen water film must reach the order of  $\mu\text{m}$ . But it also implies that the thickness of unfrozen water film of ice saturated clay is not uniform.

According to the calculation for the ice saturated Neimong clay under the conditions mentioned above, the average thickness of the unfrozen water film is less than 100 angstrom, but the unfrozen water film with the thickness of several microns is observed under the electronic microscope. The existence of unfrozen water film with such a large thickness can not be explained by the double layer theory. Olphen, H.V. (1977) pointed out that the thickness of the electric double layer decreases with an increase in the concentration (see Table 3). One of the possible

Table 3 Approximate value of double layer thickness in relation to concentration under constant surface potential

counter ion concentration mole/dm <sup>3</sup>	thickness of double layer, angstrom	
	one-valence ion	two-valence ion
0.001	1000	500
1.0	100	50
100	10	5

explanations is the freezing point decreases with an increase in concentration.

According to the observations, the interface conditions of ice saturated clay can be divided into three types: smooth, winding and overflowing (see Photos). From the photos it is shown



Photo 1 G-01

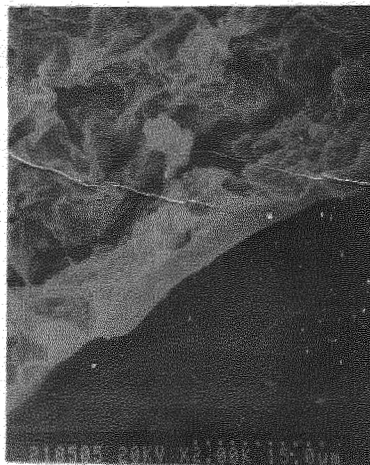


Photo 2 M-01

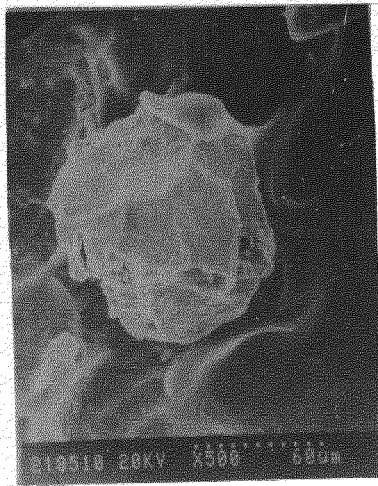


Photo 3 M-02

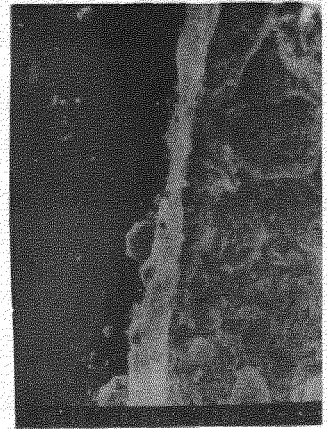


Photo 6 N-07

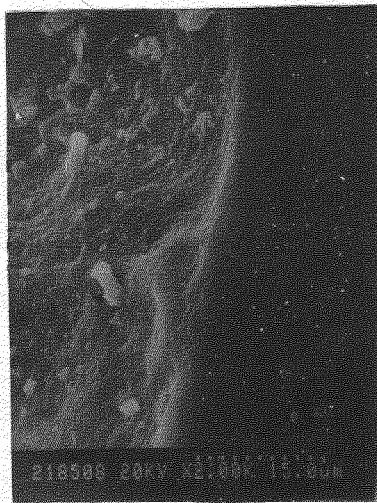


Photo 4 M-02

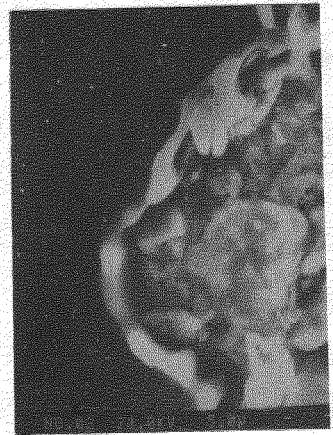


Photo 7 N-06

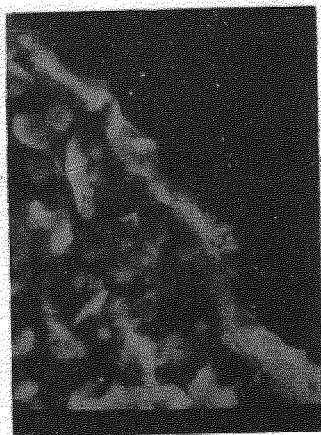


Photo 5 N-04



Photo 8 N-09

hat for the smooth unfrozen water film, there is a white stripe band with uniform thickness surrounding the soil particle. For the winding unfrozen water film, its thickness changes from place to place and may be related to the distribution of charges on the surface of soil particles. For the overflowing unfrozen water film, the stripes of unfrozen water (white) and ice (black) are inlaid.

For montmorillonite all three types of interface conditions can be observed, but for kaolin and multi-mineral Neimong clay, only one type—the smooth one was observed, especially for Neimong clay, it only appears under higher concentration conditions. The fact mentioned above indicates that the interface conditions are related to the surface energy of soil particles. If the specific surface area is great, the complicated interface conditions may occur.

#### SUMMARY

The interface conditions of unfrozen water film is studied by using an electric scanning microscope. Observation shows that three types of interface conditions may occur in montmorillonite: smooth, winding and overflowing. For kaolin and multi-mineral clay with a lower surface energy, only the smooth one can be observed.

By using an electric scanning microscope, the shape of unfrozen water film can be observed only for those with a thickness greater than microns, which may be in the pores. Different methods of studying the interface conditions between particles have to be found.

#### REFERENCES

- Anderson, D.M. & Morgenstern, N.R. (1973) Physics, chemistry and mechanics of frozen ground: a review, Proceedings of 2nd International Conference on Permafrost, p257-288.
- Arshov, A.D. et al. (1979) Water phase composition of frozen soils, Moscow University Press, pp 189.
- Alphen, H.V. (1977) An introduction to clay colloid chemistry, A Wiley-interscience publication, pp281.

THE ROLE OF SNOW IN STREAMFLOW GENERATION  
FROM AN ALPINE PERMAFROST BASIN IN TIANSHAN, NORTHWESTERN CHINA

Daqing Yang<sup>1</sup>, Ming-Ko Woo<sup>2</sup>, Fengjing Liu<sup>1</sup> and Zhenjiang Yang<sup>1</sup>

<sup>1</sup> Lanzhou Institute of Glaciology & Geocryology, Chinese Academy of Sciences, Lanzhou 730000, P.R.China

<sup>2</sup> Department of Geography, McMaster University, Hamilton, Ontario, L8S 4K1, Canada

The winter snow cover in the alpine area of Tianshan, China, is often shallow and unevenly distributed. After correcting for systematic errors in gage measurements, total winter snowfall far exceeds the snow accumulation on the ground because the latter experiences sublimation losses and winter melt on sunny slopes. Melting of the snow cover in May is the main source of spring runoff. After the winter snow is depleted, the active layer thaws rapidly, providing ample storage capacity for suprapermafrost groundwater. From June to August, stream flow is maintained by summer precipitation, producing many high flows which respond readily to rainfall, but lag behind snowfall by 1 to 3 days. For alpine permafrost catchments, it is useful to distinguish between snowmelt runoff (from the winter snow cover) and snowfall runoff (from summer snowfall events) and rainfall runoff (from summer rain events).

**INTRODUCTION**

The snow cover in mountainous areas is characterized by its high albedo, large temporal changes and significant spatial variability. These features have a strong influence on the ground surface energy and water budgets which in turn are closely related to the climate, permafrost characteristics and hydrology of mountain basins. In mid-latitude alpine areas, snowfall can occur during any time of the year, though summer precipitation also occurs as rain or hail. As the bulk of winter snowfall does not melt until spring, the magnitude and timing of snowmelt runoff is controlled by winter snow storage and by weather conditions during melt. In summer, runoff may be sustained by rainfall or by rapid melting of newly fallen snow. Thus, the basin snow cover is expected to have significant influence on mountain hydrology. This paper presents the preliminary results of snow cover observation, surface runoff, active layer thaw and water table variations in an alpine permafrost watershed in Tianshan, northwestern China, and demonstrates the role of snow in runoff generation.

**RESEARCH AREA AND METHODS**

The Urumqi River originates on the north slope of Chinese Tianshan and flows northward to the city of Urumqi, the capital of Xinjiang Autonomous Region. The headwaters of this river lies within the zone of alpine permafrost where the surface cover is dominated by tundra vegetation, rock outcrops, felsenmeer and glaciers. The climate of this area is typically continental, with a mean annual air temperature of -5.4°C and mean annual precipitation of 420 mm at the Daxigou meteorological station (43.06°N, 86.50°E; 3539 m a.s.l.). When corrected for the systematic error caused by wind and wetting loss of the Chinese standard gage, the actual mean annual precipitation should be about 560 mm (Yang et al. 1989). A study basin was selected in the Dry Cirque, a south-facing non-glacierized watershed, 1.5 km long and 1 km wide, surrounded by peaks of about 4300 m elevation on its western, northern and eastern flanks. Most slopes are steep and many parts of the basin are covered by coarse gravels. A hydrometric station was set up at the basin outlet (3804 m a.s.l.) and controls a drainage area of 1.68 km<sup>2</sup>. In addition, air temperature, precipitation and relative humidity have been measured routinely at this station since May 1982 (Fig. 1).

Braun (1991), Cooley (1988), Elder and Dozier (1989, 1990) and Goodison (1981) have discussed methods of snow survey and water equivalent computations. At the Dry Cirque, snow depths were measured once every 7 to 10 days during the snow seasons of 1989-90 and 1990-91, using 42 stakes deployed in the elevation range between 3800 and 3940 m. Snow pits were dug between stakes along rows C and D for density measurements. At several depths in each pit, three to five snow samples were taken using a 100 cm<sup>3</sup> snow sampler, and the samples were weighed by a spring balance accurate to 5 g. A second weather station was set up near the centre of the basin where air temperature and precipitation were observed at 8:00 a.m. everyday during summer. Three frost tubes, each 2 m long, and seven groundwater wells, provided frost table and water table measurements taken at a weekly interval in winter and a daily interval during May to August. Snow and ground temperature data were collected near stake C, and frost tube 2, using two thermistor strings (Fig. 1).

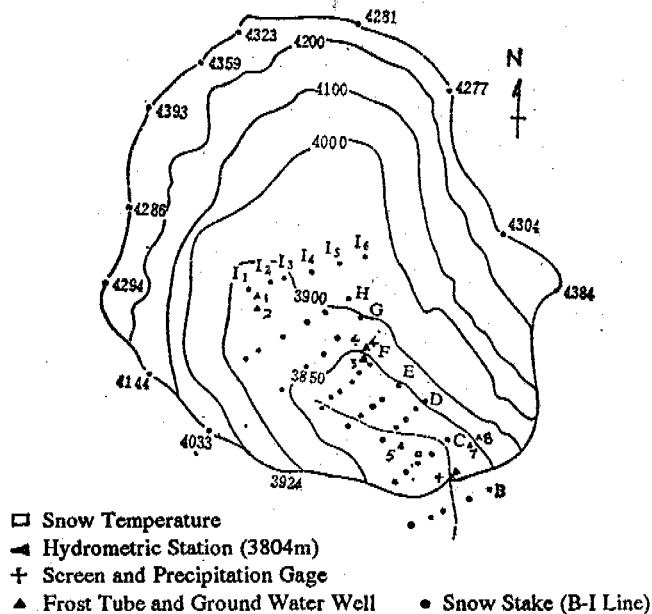


Figure 1. Topography of the Dry Cirque watershed showing the instrumentation and snow stakes

## COMPARISON OF SNOW COVER AND SNOWFALL MEASUREMENTS

Several studies (Goodison 1978, 1989, Sevruk 1985, Woo et al. 1983) have shown that snowfall measurement by all types of ordinary snow gages could produce systematic error as large as 50-100% at windy and exposed sites, but the "ground truth snow" cannot be measured accurately even with shielded gages such as the double fence intercomparison reference gage (DFIR) which was designed as the reference for WMO Solid Precipitation Measurement Intercomparison (WMO 1985). Fortunately, in the study area, wind speed during precipitation is generally low, with 80% of the annual precipitation occurring when daily wind speed is below  $3 \text{ m.s}^{-1}$ . Thus, the spatial distribution of the freshly fallen snow is relatively even, allowing the calculation of new snowfall at the basin stake network during the 1989-90 season. Table 1 shows that the SWE of the new snow, measured soon after snowfall in order to eliminate snow sublimation of 0.1-0.3mm per day (Yang and Zhang, 1992), was always higher than the gage measurement despite winter sublimation from the snow surface. Generally, the ratio of water equivalent of newly fallen snow to gage measurement is less variable for the heavy snow events. For these events, the gage catches 62-88% of the SWE of new snow, and on average, the catch ratio of the Chinese standard gage for dry snow is 73.2% (Tab.1). The 5-year intercomparison measurement of snowfall at the adjacent Glacier No.1 hydrological station indicated that the average catch ratio was around 79% when compared with DFIR (Yang et al. 1989). However, because of the small undercatch of the DFIR at high wind speed during storms (Golubev 1985a, 1985b), we prefer the basin-wide snow survey of both depth and density for winter accumulation estimation.

Table 1 Comparison of SWE measured at stake network and snowfall measurement by Chinese standard gauge, Dry Cirque, 1989/90 winter

Period	New Snow		SWE (mm)	Snowfall (mm)	
	Depth(cm)	Density		Dry Cirque	Daxigou
Oct.06/Oct.16	9.0	0.125	11.3	10.0	10.9
Dec.23/Jan.01	2.2	0.120	2.6	1.0	1.2
Jan.12/Jan.20	1.5	0.100	1.5	0.5	0.7
Feb.14/Feb.20	1.1	0.100	1.1	1.6	2.8
Feb.26/Mar.05	2.1	0.100	2.1	2.1	2.7
Mar.19/Mar.26	6.4	0.135	8.6	6.0	6.3
Apr.16/Apr.22	13.8	0.137	18.9	16.1	17.8
Apr.23/May.04	28.4	0.118	33.5	21.0	21.1
Total	64.5	-	79.6	58.3	63.5
Mean	-	0.117	-	-	-

## TEMPORAL AND SPATIAL VARIATION OF WINTER SNOW COVER

A seasonal snow cover usually develops in early October. Snow accumulates slowly during the dry period of November through March, with mean snow depth ranging from 5 to 10 cm. Precipitation increases significantly in late April and early May and maximum snow depth reaches 50-80 cm. The major snowmelt period begins in early May and the snow cover often disappears completely by late May or early June. The rate of densification of the shallow

snowpack is low: the mean snow density ranges from 150 to 270  $\text{kg.m}^{-3}$  from October to February and increases to 310  $\text{kg.m}^{-3}$  by mid-March, while in late April, it decreases rapidly to 200-215  $\text{kg.m}^{-3}$  because of the addition of large quantities of new snow of low density. When the snow ripens in early May, its density reaches 300-350  $\text{kg.m}^{-3}$ . Snow water equivalent generally increases from October to May and the maximum of 190-200 mm appears at the valley bottom near stake  $C_5$  in early May (Fig. 2).

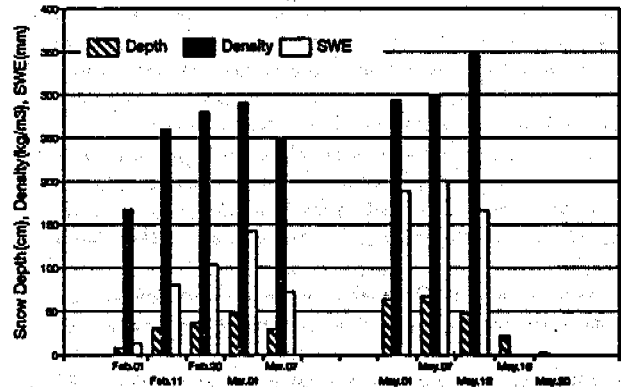


Figure 2. Snow depth, density and SWE at  $C_5$  stake, Dry Cirque, 1991

Snow distribution depends primarily on local wind pattern, vegetation and topography. In order to detect the spatial distribution of snow depth and density and to compute the basin SWE for subsequent runoff analysis, an intensive snow survey was carried out on 1-2 May 1991 along all the stake rows and additional lines, at intervals of 10 m for snow depth and 20 m for snow density. In the Dry Cirque, the deepest snow of 1.0-1.5 m was found at the valley bottom and on the base of the steep slopes. The upper slopes (above 4000 m a.s.l.) were covered by shallower snow of 10-20 cm depth because of losses to avalanches and to wind scour. Snow on south-facing slopes tended to be shallower than those with a northern exposure. Occasionally, the south-facing slopes were bare because of greater sublimation and melt than the other slopes (Fig. 3a).

Snow density at peak accumulation varied considerably in the basin (Yang et al. 1991; Fig. 3b). Density on slopes ranged from 120 to 200  $\text{kg.m}^{-3}$  but on the valley bottom, it reached 400-500  $\text{kg.m}^{-3}$ , because of the ice layers formed by refreezing of meltwater released by mid-winter melt events. Deep snowpacks also have high densities because of snow compaction (Dozier et al. 1989, Hall 1985). On the average, the density of the deepest snowpack varied from 100 to 300  $\text{kg.m}^{-3}$  while the shallower snow had a larger density variation. There is no significant correlation between snow depth and snow density for shallow snow cover (Yang et al. 1991), as was also noted by Goodison (1981).

At Daxigou meteorological station, 1.5 km from the Dry Cirque outlet, the coefficient of variation of snow depth is 3.5 to 4 times that of snow density (Yang et al. 1991). In the Dry Cirque, the coefficients of variation for snow depth and density were 0.59 and 0.30, respectively, suggesting that snow depth is more variable than snow density in the shallow mountain snowpack in Tianshan.

The distribution pattern of SWE was similar to that of snow depth. On south-facing slopes, SWE ranged from 10 to 20 mm and increased to 40-80 mm on the valley bottom, while the maximum of 100-150 mm appeared at the foot of the west slopes (Fig. 3c). On 1 May 1991, the mean SWE for the basin was 28.1 mm.

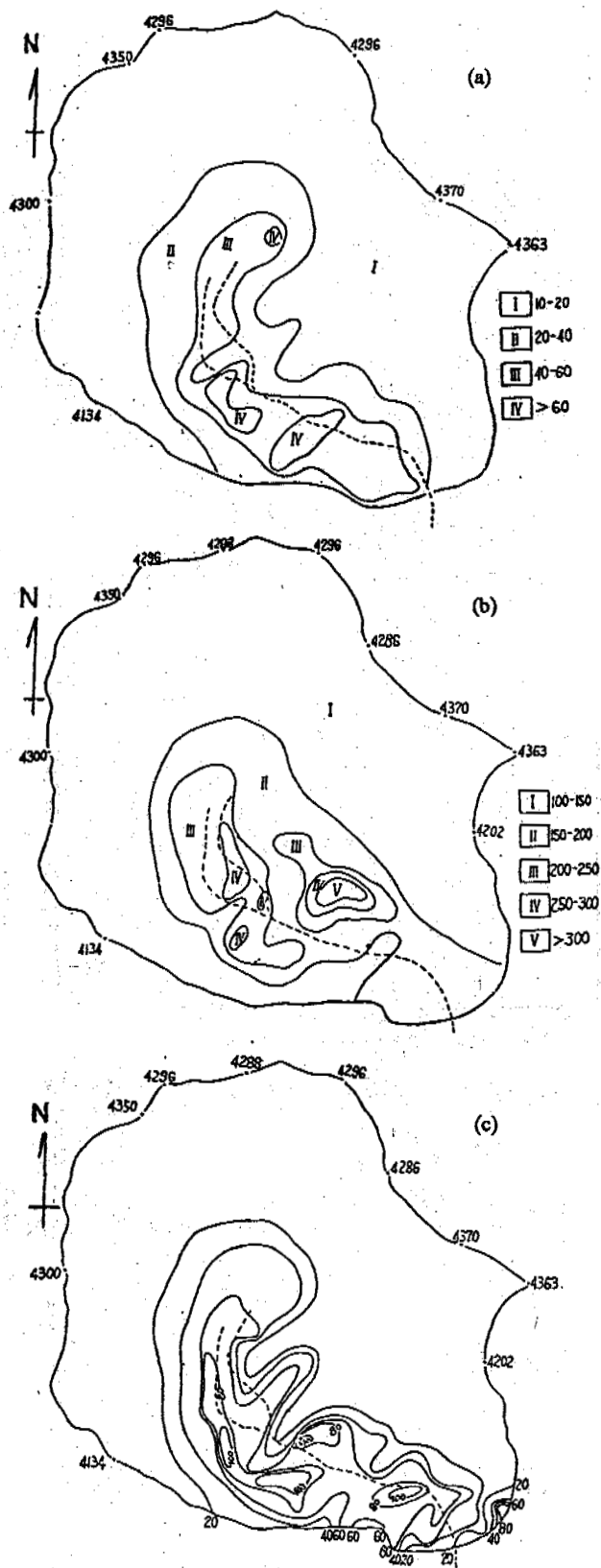


Figure 3. Snow distribution in the Dry Cirque on 1 May 1991: (a) snow depth in cm, (b) snow density in kg/m<sup>3</sup> and (c) snow water equivalent in mm

Snow cover mass balance can be expressed (all terms in mm.) as

$$SWE = P_s + M_s + D - E - Y \quad (1)$$

where  $P_s$  is snowfall,  $M_s$  is mass transfer from the ground to the snowpack,  $D$  is snow redistributed by wind,  $E$  is snow surface sublimation and  $Y$  is drainage of meltwater to the ground in winter. As first approximation,  $M_s$ ,  $D$  and  $Y$  are negligible for the dry, cold snowpack overlying frozen ground of the Dry Cirque where drifting seldom occurs because of low wind speed. Snowfall and sublimation therefore dominate the snow water equivalent on the ground. Winter precipitation at Daxigou meteorological station is a good indicator of the nearby research area since winter is generally dry and precipitation does not change much with elevation. Comparison of the snowpack SWE with precipitation at Daxigou station indicates (Fig. 4): (i) at the stage of snow cover formation in October, SWE was close to cumulative snowfall, (ii) for the relatively dry period of December to February, SWE was less than cumulative precipitation due to sublimation and weak melt during the brief, warm spells, (iii) from mid-February to late March, SWE was close to cumulative precipitation, (iv) by April, significant melt and sublimation decreases the snowpack sharply, the SWE accounts for 10-20% of the total winter precipitation, on the other hand heavy snow storms in May increases the snow cover. Similar conclusions can be applied to the Dry Cirque basin except the delay of snow melt to early May.

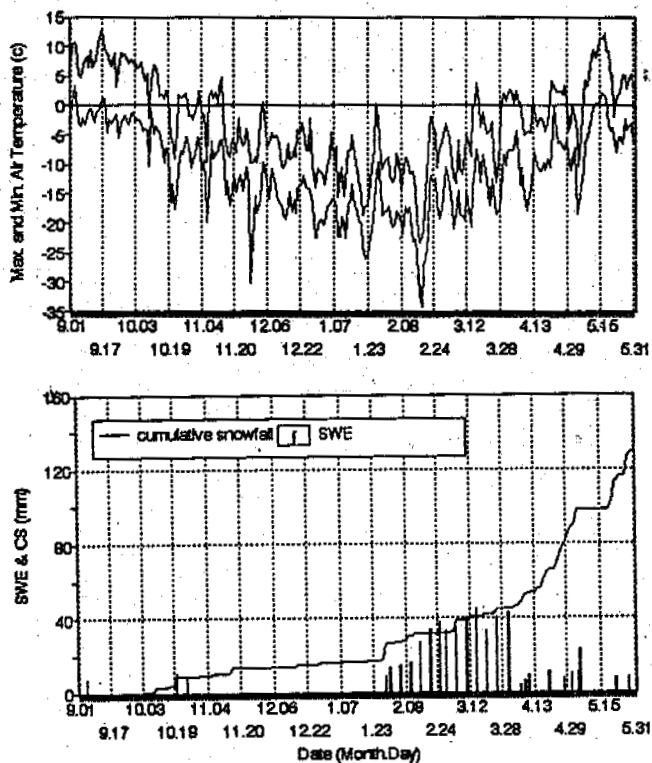


Figure 4. Maximum and minimum air temperature, cumulative snowfall (CS) and water equivalent of snow cover (SWE) at Daxigou station in 1990/91 snow season

#### SNOWMELT RUNOFF IN SPRING

Streamflow records for 1982-91 showed that flow usually began in May and ended in September, with an annual average runoff of 370

mm. The range of runoff was 122-510 mm per year and the coefficient of variation was 0.27. Runoff contribution from May averaged 37 mm, or 10% of the annual total. The May average temperature and precipitation are -7°C and 60 mm, but annual variability of runoff for this month depends on the winter snow accumulation and the weather during melt. A 40-80% variability of precipitation in the winter months suggests that the snow cover is highly variable from year to year. Although the May precipitation is relatively stable, the May air temperature varies greatly, causing a high runoff variation of 0.60.

The shallow snow cover in the Dry Cirque has low temperatures but a large temperature gradient. In the winter of 1989-90, for instance, the minimum recorded snow temperature was -23.4°C and the maximum gradient was -0.58°C.cm<sup>-1</sup> (Yang et al. 1991). Snowmelt begins in early May as the upper layer of the pack reaches 0°C. When the percolating meltwater reaches the cold ground, some refreezing produces basal ice above the ground (Marsh and Woo 1985, Woo et al. 1982), attaining a thickness of 3-15 cm. Despite the low ground temperatures, the coarse gravels that underlie most parts of basin permits infiltration, as in Arctic Canada (Woo and Marsh 1990). Some meltwater is ponded as surface storage while the deep snowpack along the channel retains much meltwater. All these processes and the other factors such as ice formation in stream channel and restoration of high albedo by snowstorms (Kattelmann and Yang, 1992) delay surface runoff and in 1991, streamflow did not begin until 10 May (Fig. 5).

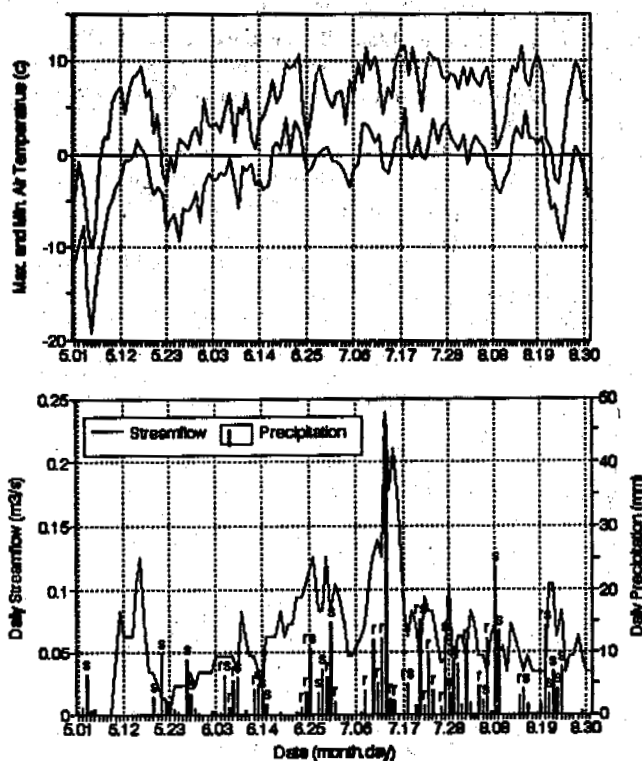


Figure 5. Air temperature, precipitation and streamflow in the Dry Cirque watershed, May - August 1991 (s = snowfall, r = rainfall, rs = rain mixed with snow)

In 1991, thawing of the active layer started as soon as snow disappeared. Thawing began first on south-facing slopes and in areas where the snow was thin. At this stage, the thinly thawed layer was

mostly saturated and supraperafrost groundwater flow occurred, sometimes even underneath a melting snow cover. The completely ripened residual snowpack in the valley bottom melted rapidly, yielding the first peak runoff for several days. From middle May onward, streamflow declined as the melt process ceased. Statistical analysis of two years of daily discharge data for the month of May showed that streamflow (Q) did not change with daily precipitation, but was closely related to daily maximum air temperature (T<sub>max</sub>):

$$Q = 0.044 + 0.048 * T_{max} \quad (n=62, r^2=0.52, \text{confidence level}=0.01, -10.2 < T_{max} < 12.2)$$

This relationship confirms that snowmelt was the main contributor to streamflow during the spring period.

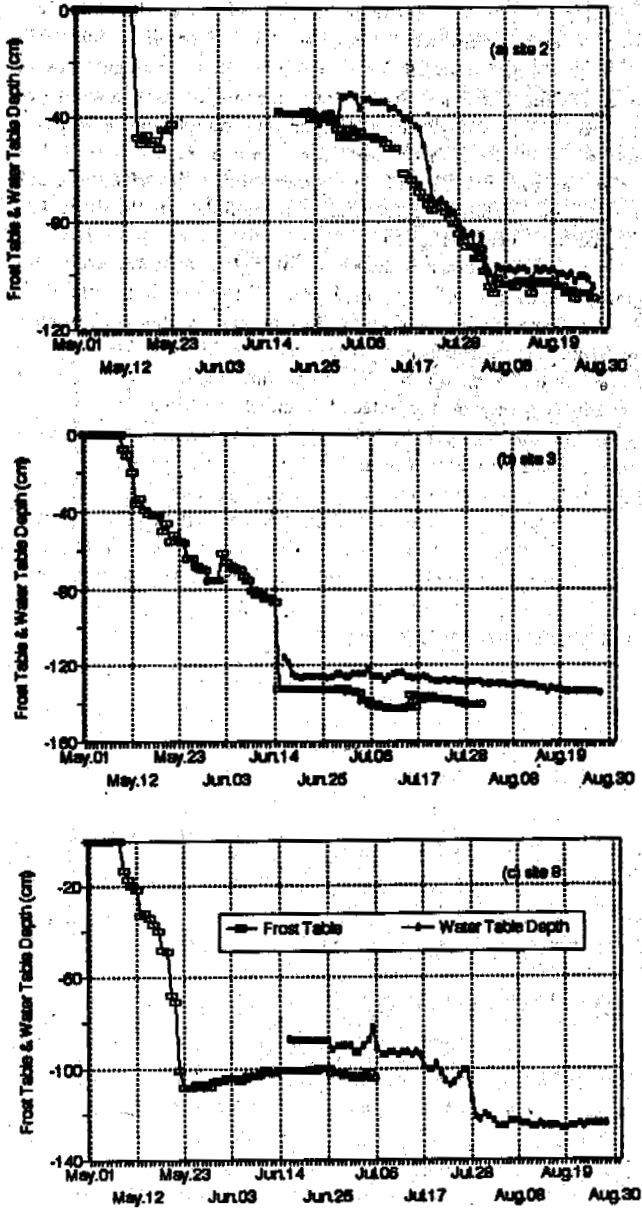


Figure 6. Frost table and water table depth in the Dry Cirque, 1991



## SUMMER RUNOFF

During and immediately after spring melt, the active layer thawed rapidly in the gravelly soils, providing much thawed pore space for infiltration and for suprapermafrost groundwater storage. By late May, the frost table receded to 1.1 m on the sunny slopes (site 3 in Fig. 6), and on slopes where the winter snow cover was shallow but where the soil materials were gravelly (site 8 in Fig. 6). At the lower basin, the thawing front only reached 0.5-0.7 m because of the low thermal conductivity of the fine materials and the high ice content (Xia and Woo 1993). In the valley bottom where the winter snow cover remained long, ground thaw was more gradual and did not reach 1 m until late July (site 2 in Fig. 6).

The steep topography of the alpine catchment and the coarse materials that constitute the active layer permit rapid subsurface delivery of rainwater and summer snowmelt which percolate the thawed zone. Streamflow response to rainfall was therefore very rapid, as was exemplified by the peak runoff event of 13 July 1991 (Fig. 5). Summer snowfall events are also common, though the snow cover seldom persists. Streamflow response to snowfall is often delayed by 1 to 3 days, depending on how rapidly the snow cover melted. Such 'snowfall runoff' events are more common in late spring and towards the end of summer. Examples of hydrograph rises lagging behind the snowfall can be found in the 1991 late summer streamflow (Fig. 5).

From June to August is the period of high runoff, accounting for approximately 85% of the annual total. On the average, runoff is about 130 mm in July and about 90 mm each in June and August. By September, the freezing front descends the active layer as air temperature drops, and streamflow declines also. The hydrograph recession depends on the antecedent moisture storage in the active layer and the weather in September. In general, a long slow recession occurs with warm and wet weather, otherwise the stream stops flowing shortly after the onset of dry, cold days. Monthly runoff for September averages about 20 mm, but the coefficient of variation is 70%. Melt rate of the freshly-fallen snow is low during late September, though some meltwater does infiltrate the coarse materials to raise the soil moisture, and therefore increase the winter ground ice content of the active layer.

## DISCUSSION

The winter snow cover of an alpine basin differs from its summer snow cover in two major respects. There is more time to accumulate the winter cover to greater thickness and for the snow to be redistributed more unevenly over the basin; but the summer snow cover usually is wetter (sometimes the wet snow is mixed with rain) and melts more quickly. The water equivalent of the winter snow cover influences the magnitude of the melt-freshet of the mountain streams while the snow distribution pattern affects the rate of active layer thaw which in turn determines the capacity of suprapermafrost groundwater storage in spring. The summer snow cover delays water delivery to the stream and therefore modifies the rainfall-runoff relationship expected of the summer flow.

In view of the above considerations, one may distinguish between snowmelt runoff generated by melting of the winter snow cover, and snowfall runoff produced by the melt following individual storm events. Much attention has been paid to snowmelt runoff in permafrost regions (e.g. the nival runoff regime first described by Church, 1974). In alpine permafrost areas with high summer

precipitation, runoff may be generated by rainfall, snowfall and a mixture of solid and liquid precipitation. The runoff pattern produced by rainfall will be different from the snowfall-generated discharge which is also distinct from the spring-time snowmelt runoff. To understand better the hydrology of high mountains, the streamflow-generating processes merit further attention.

## ACKNOWLEDGEMENT

Funding for this study was provided by a grant from the National Natural Sciences Foundation of China. The logistic support from the Tianshan Glaciological Station of Lanzhou Institute of Glaciology and Geocryology, Chinese Academy of Sciences, during the field work is gratefully appreciated by the authors.

## REFERENCES

- Church, M. (1974) Hydrology and permafrost with reference to northern North America. Proc. Workshop Seminar on Permafrost Hydrology. Canadian National Committee for IHD, Ottawa, 7-20.
- Cooley, K.R. (1988) Snowpack variability on western rangelands. Proc. of the Western Snow Conference, 56, 1-22.
- Braun, L.N. (1991) Modelling of the snow-water equivalent in the mountain environment. Snow, Hydrology and Forest in High Alpine Areas. IAHS Publ.no.205, 3-18.
- Dozier, J., J. Melack, K. Elder, R. Kattelmann, and M. Williams (1989) Snow, Snowmelt, Rain, Runoff and Chemistry in a Sierra Nevada Watershed. Final Report to California Air Resources Board, 16-26.
- Elder, K. and J. Dozier (1989) Spatial and temporal variation of net snow accumulation in a small watershed, Emerald Lake basin, Sierra Nevada, California, U.S.A.. Annals of Glaciology, 13, 56-63.
- Elder, K. and J. Dozier (1990) Improved methods for measurement and estimation of net snow storage in a small watershed. Hydrology in Mountain Regions I- Hydrological Measurements, The Water Cycle, IAHS Publ.no.193,147-156.
- Golubev, V.S. (1985a) On the problem of standard condition for precipitation gauge installation. Proc. International Workshop on the Correction of Precipitation Measurements, Zurich, Switzerland, 57-59.
- Golubev, V.S. (1985b) On the problem of actual precipitation measurement at the observation site. Proc. International Workshop on the Correction of Precipitation Measurements, Zurich, Switzerland, 61-64.
- Goodison, B.E. (1978) Accuracy of Canadian snow gauge measurements. Journal of Applied Meteorology, 17(10), 1542-1548.
- Goodison, B.E. (1981a) Compatibility of Canadian snowfall and snowcover data. Water Resources Research, 17(4), 893-900.
- Goodison, B.E. (1981b) Measurement and data analysis. Handbook of Snow, Pergamon Press, Toronto, 200-210.
- Goodison, B.E. and J.R. Metcalfe (1989) Canadian participation in the WMO Solid Precipitation Measurement Intercomparison: preliminary results. Proc. International Workshop on Precipitation Measurement, St.Moritz, Switzerland, 121-126.
- Hall, D.K. (1985) Remote Sensing of Ice and Snow. New York, Chapman and Hall Ltd., 26-32.
- Kattelmann, R and D. Yang (1992) Factors delaying spring runoff in

- the upper Urumqi River basin, China. *Annals of Glaciology*, 16, 225-230.
- Marsh, P. and M.K. Woo (1985) Meltwater movement in natural heterogeneous snow cover. *Water Resources Research*, 21(11), 1710-1716.
- Sevruk, B. (1985) Correction of precipitation measurements: summary report. Proc. International Workshop on the Correction of Precipitation Measurements, Zurich, Switzerland, 13-26.
- Yang, D., Y. Shi, E. Kang, and Y. Zhang (1989) Research on analysis and correction of systematic errors in precipitation measurement in Urumqi river basin, Tianshan. Proc. International Workshop on Precipitation Measurement, St. Moritz, Switzerland, 173-179.
- Yang, D., Y. Zhang, Z. Zhang, K. Elder, and R. Kattelmann (1991) Physical properties of snowcover and estimation of snowmelt runoff in a small watershed in high alpine Tianshan. *Snow, Hydrology and forest in High Alpine Areas*. IAHS Publ.no.205, 169-180.
- Yang, D and Y. Zhang (1992) Results of snow surface sublimation measurements in the mountain area of Urumqi river basin. *Journal of Glaciology and Geocryology*, Vol.14, No.2, 122-128.
- WMO, (1985) International Organizing Committee for WMO Solid Precipitation Measurement Intercomparison, Final Report of First Session, Geneva, 31pp.
- Woo, M.K., R. Heron, and P. Marsh (1982) Basal ice in high arctic snowpacks. *Arctic and Alpine Research*, 14, 251-260.
- Woo, M.K., R. Heron, P. Marsh and P. Steer (1983) Comparison of weather station snowfall with winter snow accumulation in high arctic basins. *Atmosphere-Ocean*, 21(3), 312-325.
- Woo, M.K., and P. Marsh (1990) Response of soil moisture change to hydrological processes in a continuous permafrost environment. *Nordic Hydrology*, 21, 235-255.
- Xia, Z.J. and M.K. Woo (1993) Active layer thaw calculation using simplified thermal and hydrological parameters. Proc. Sixth International Conference on Permafrost (this issue).

PERMAFROST HYDROLOGICAL PROCESSES IN BINGGOU  
BASIN OF QILIAN MOUNTAINS\*

Yang Zhenniang, Yang Zhihui, Liang Fangxian and Wang Qiang

Lanzhou Institute of Glaciology and Geocryology, Chinese Academy of Sciences,  
Lanzhou 730000, China

Binggou experimental basin is located on a north slope in the middle section of Qilian Mountains. Its altitude ranges from 3431 to 4401 m a.s.l. and basin area is 30.48 km<sup>2</sup>. Mean annual air temperature is -2.5°C, which corresponds with the area at the limit of permafrost in Qilian Mountains. Meteorological and hydrological research began since 1984, and in recent years, there was further research on ground temperature, ground water and thawing and freezing of the active layer. Analysis shows that hydrologic processes are restricted by the fluxes of heat and water between the ground and the atmosphere. Changes of air temperature, and the freeze-thaw activities vary with the season and the altitude. These processes directly affect the generation and concentration of runoff, the occurrence of hydrologic activities and the characteristics of runoff.

**INTRODUCTION**

Hydrological processes in high cold region of western China are significantly affected by the presence of perennially frozen ground, and its water and heat conditions. Over 50% of the catchment area of alpine rivers in Qilian Mountains are higher than 3500 m a.s.l., where there is abundant permafrost, seasonally frozen ground, perennial firn and glacier. The northern fringe of Qinghai-Xizang plateau has an annual mean air temperature of -2.0 to -3.0°C (Cheng, 1979). Although one quarter of the entire area of China is underlain by permafrost, systematic research on permafrost hydrology in China is a late development. The runoff experimental field site in Binggou basin of the upstream Heihe River at the mid-section of Qilian mountains was established in the 1984 to study "the changes of glacier, climate and runoff in Qilian Mountains". In 1989 to 1991, the Commission of National Natural Sciences Foundation of China provided support to study the physical processes of permafrost hydrology. This paper describes (a) the effect of water and heat on runoff generating processes, (b) the basic hydrologic characteristic of permafrost area, and (c) the result of water balance based on measurements in the Binggou study area.

**STUDY AREA**

Binggou experimental basin is located on the upstream area of Heihe River which lies on a north slope in the middle section of Qilian Mountains, between longitudes 100°12' E to 100°18' E and latitudes 38°01' N to 38°04' N. The elevation ranges from 3431 to 4401 m a.s.l., and the study area has an area of 30.48 km<sup>2</sup> (Fig.1). About half of study area lies between the elevation 3431 to 3900 m a.s.l.. Below the study area lies the forest belt, while at 3500-4000 m a.s.l.

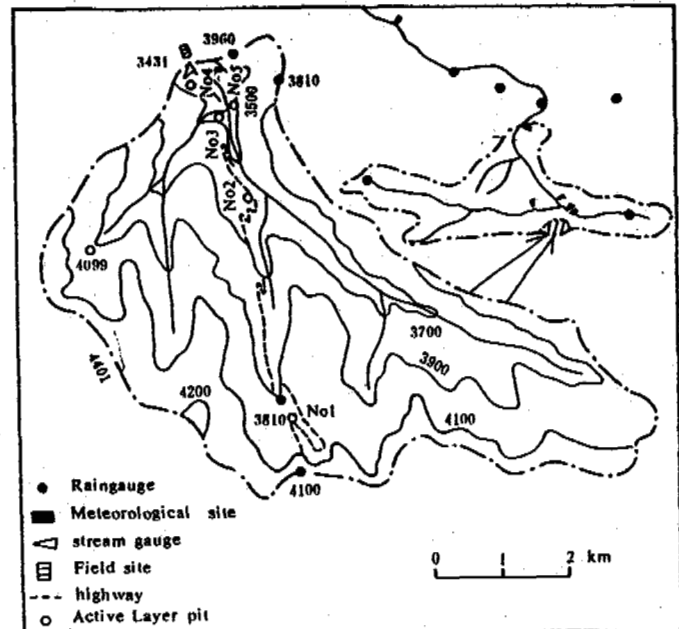


Fig.1 The study area of Binggou basin

there is mountain pasture, vegetation becomes sparse above 4000 m in the alpine desert zone, with burst growing along the streams. The permafrost active layer at the both sides of river bank is about 1.0-1.5 m in depth, and increases toward the hill slope. Mean annual air temperature at the Binggou meteorological site is -2.5°C, the minimum and maximum air temperatures are

\* This project is supported by the Commission of National Natural Sciences Foundation of China.

30.8°C and 24.8°C, respectively. Mean annual air temperature at the upper basin, it is approximately -7.0°C. Mean annual precipitation at the meteorological site of Binggou basin is 686 mm. Solid precipitation occurs in October to April. Snow cover at the upper basin generally is about 0.5 m in depth, and the maximum snow thickness is about 0.8 m. A discharge gauge was set up at 431 m a.s.l.. In addition, there was a hill slope runoff experimental site and a meteorological site (3452 m a.s.l.) that measured air temperature, ground temperature, precipitation, evaporation, humidity, sunshine, wind speed and wind direction. Another meteorological site was set up at 4100 m to measure air temperature and humidity, and five precipitation gauges were erected at different elevation, slope direction. Five points were selected for observation of ground temperature, water table, freezing and thawing of the active layer (Fig.1).

#### THE INFLUENCE OF HEAT AND WATER CONDITION TO RUNOFF GENERATING

##### Air Temperature

Air temperature was used as the main index of heat condition, because it is one of the main considerations for permafrost development and the freeze-thaw processes of the active layer. The distribution of air temperature hence the occurrence of permafrost in western China is governed by latitude and elevation, and various local factors. Data from the meteorological site (1984-1991) from the Binggou experimental basin yielded a mean annual air temperature of -2.5°C. The mean annual air temperature gradient is 0.52°C/100m. Continuous permafrost area lies above 4000 m a.s.l., where the mean annual air temperature is below -5.0°C, the period of below freezing temperature lasts 9 months (Sept. to May). Discontinuous permafrost occurs below this elevation, where below freezing temperature lasts for between October and April. From the course of air temperature shows, air temperature rises stable over 0°C, which begins in late April at the lower part of Binggou basin and is delayed in June at the upper basin (Fig.2), and the

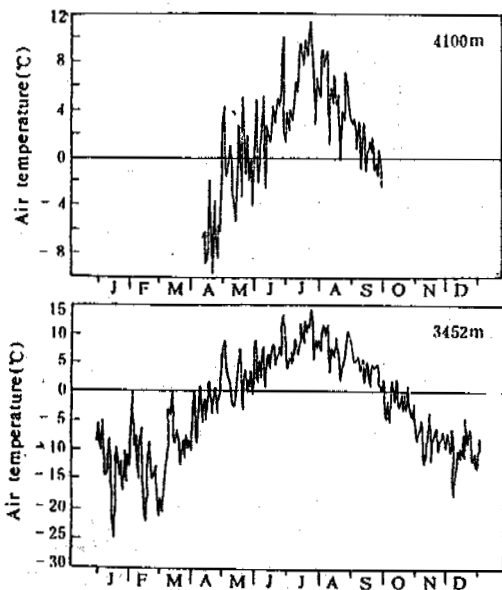


Fig.2 The course of air temperature in Binggou basin (1988)

relationship between air temperature at  $T > 0^{\circ}\text{C}$  and  $T < 0^{\circ}\text{C}$  and different altitudes has been obtained (Fig.3). It shows that the duration of

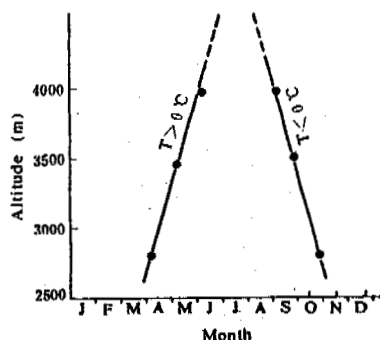


Fig.3 The relationship between air temperature at  $T > 0^{\circ}\text{C}$  and  $T < 0^{\circ}\text{C}$  and different altitudes

thaw decreases with increasing altitude. Runoff terminates at the lower basin in October, and for the upper basin, runoff ceases in September (Yang Z.N., 1991b).

##### Ground Temperature

##### The variation of ground temperature in different seasons

Measurements show that the depth of the active layer is 1.0-1.5 m beneath the north-facing slopes, and wetlands (No1, No3, No5 pit), and is 3.0 m in depth at the first terrace (No4 pit). No permafrost was found on the south-facing slope after digging down to 3.2 m (No2, and meteorological site pit). Ground temperature profile from the meteorological site located on a south-facing slope at 3452 m a.s.l., from January to April, ground temperature is below 0°C from the ground surface down to 3.2 m in depth. The head-surface (0-1.5 m) temperature rises above 0°C in May, but the lower layer (1.5-3.2 m) remains at approximate 0°C in May to June (Fig.4). It shows that ground temperature in deeper layer lags behind air temperature rises for about two months. The ground temperature profile at the first terrace of north-facing, 3440 m a.s.l. (No4 pit), as shown in Fig.5, is similar to Fig.4, but from 0.5 m downward, frozen condition continued in May to June.

##### The variation of thawing and freezing layer in space and time

The depth of active layer is affected by topography, slope direction, elevation, rock properties, soil moisture and surface condition. From Fig.6 shows (1) the date of thawing in the same layer lags with the increasing altitude, (2) the thawing depth in dry ground is much deeper than wetland at the same altitude, (3) the date of thawing on the south-slope is earlier than on the north slope; while for freezing layer is opposite. It is very important for the analysis the generation and concentration of runoff at different altitude area.

In relation to permafrost hydrology, the ground temperature regime has the following implications: (1) there is no runoff generation in early spring when the active layer is freezing. Melting may occur on the snow surface, but

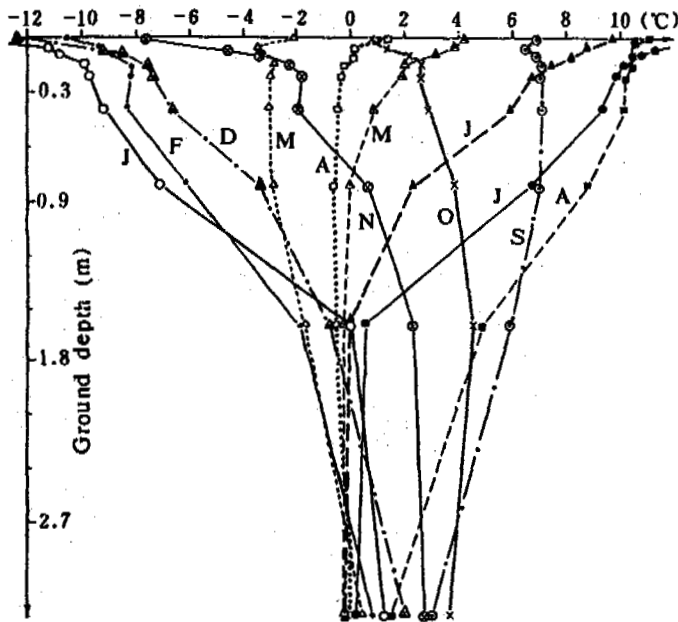


Fig.4 The profile of ground temperature at meteorological site (1991)

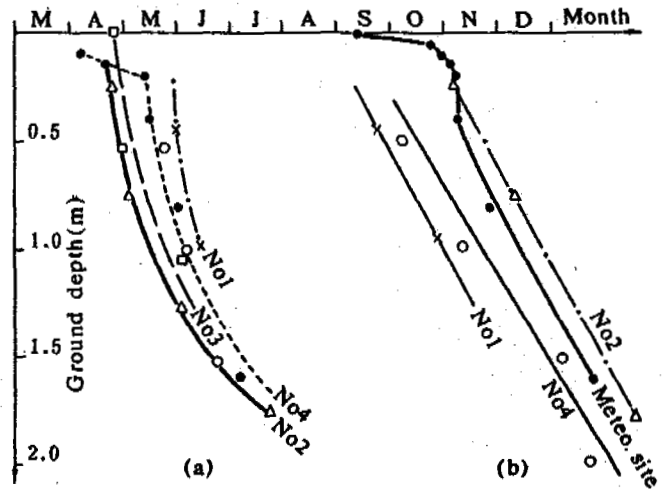


Fig.6 The variation of thawing and freezing layer with season

pit	elevation(m)	
Meteorological site	3452	(a)thawing
No1	3956	
No2	3510	(b)freezing
No3	3473	
No4	3440	

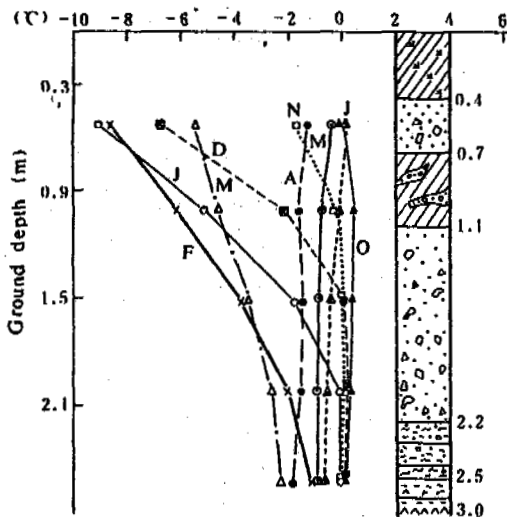


Fig.5 The profile of ground temperature in pit No4 (1991)

- 0.0-0.4 m Brown grass charcoal subclay, wet.
- 0.4-0.7 m Grey green thick sand, crushed stone 50%.
- 0.7-1.1 m Grass charcoal, subclay and crushed gravel.
- 1.1-2.2 m Yellow green, thick sand crushed stone, and its content increases with depth to 70%
- 2.2-3.0 m Grey black, peat layer, 2.2 freezing.

the percolating meltwater is often absorbed by snowcover or depression storage and there is little runoff generated, (2) in late spring the depth of thaw is very shallow. The frozen ground it acts as an aquiclude (Dingman, 1975), therefore after the initial moisture deficit is satisfied, surface runoff occurs. This yields more runoff in spring (Yang Z.N., 1981), (3) in late summer, the seasonal frost disappears, so that the ability of water storage and evaporation in the basin increases. Thus the peak discharge in summer is lower than in spring generally, but except the occurring of heavy rain, and the base flow is extended, (4) in the winter, the spring and ground water supply to valley, icing and river ice are formed as the air temperature is extremely low, and there is no hydrology activity about half of a year.

#### Water Table in the Active Layer

The active layer is very shallow (1.0-1.5 m) along the stream bank and has large water storage which decreases from the two sides of stream bank toward the hill slope. Seasonal variation of ground water in storage in the active layer is particularly noticeable on the upper reach of valley. For example, in pit No1, at elevation 3956 m a.s.l., the depth of active layer is 1.1 m, but the frost table is about 0.5 m in June. Afterward, frost disappeared in July to August, and the water table rises to approximate 1.0 m. As the air temperature falls rapidly in September to October, no meltwater and rainfall on surface, but there is meltwater supply to the ground and as lateral drainage continues, the basin water storage declines and the water table drops and frost table rises (Fig.7a). At the pit on the mountain slope (pit

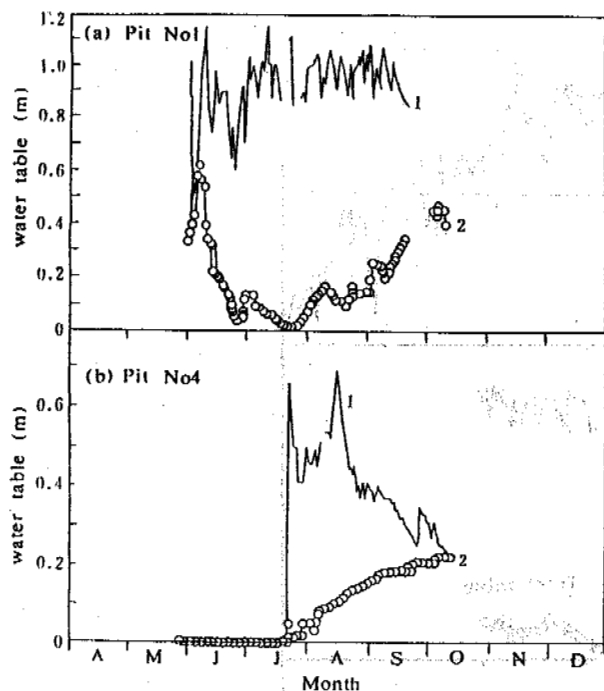


Fig.7 The course of water table in the pit No1 and No4 (1991)

- 1 water table  
2 frost table

No4), the ground water content in the active layer is affected by rainfall. When there is no rainfall, the saturated zone disappears. When the rainfall season comes, the water content of the soil increases, and the corresponding water table rises. In Autumn, air temperature drops below 0°C and the solid precipitation occurs. The amount of water percolation is reduced, and the water table drops accordingly, frost table raise from August to October. These observations indicate that the changes of water table in the active layer is directly affect by frozen soil (Fig.7b).

#### CHARACTERISTIC OF HYDROLOGY PROCESSES IN PERMAFROST AREA

##### Streamflow Regime

Binggou study area lies in the cold region of high mountains. Besides the influence of water and heat regime of the atmosphere, permafrost is also a main factor affecting the hydrologic processes. The melt runoff from snow cover begins from low land and extends to higher elevations; and the thawing of river ice also occurs from downstream to upstream when the air temperature rises in spring (April to May). Air temperature is rather low in early spring. So that the thawing of frozen soil is shallow in spring, the infiltration of meltwater is very weak (Kane and Stein, 1983; Yang Z.N., 1988), meltwaters are absorbed in the snow cover (Woo et al., 1983), then, when the meltwater has satisfied the depression storage, surface runoff will begin (Woo, 1986). Meltwater release follows a strong daily cycle, and as heat supply increases stably in the late spring, so does streamflow discharge. When air temperature is remains higher than 0°C,

a large amount of snowmelt water is produced and spring flood is generated in May to June. The hydrograph of peak discharge during snow melt coincided closely with air temperature. In summer, there is no snow in the study area and rainfall is the main water sources. The thawing depth extends gradually to the entire active layer, allowing rainwater infiltration to raise the water table. Lateral flow concentrates the water into the valley to sustain streamflow, water storage in the basin increases in summer, so the peak discharge is relatively lower than in spring, and the base flow gradually rises. However, catastrophic floods can be generated by heavy rains in summer. For example, a rain event of 50 year return period occurred in July 1989 in Binggou basin, causing landslide, debrisflow and floods that destroyed highways, bridges, and disturbed traffic for more than one month. Air temperature drops rapidly below 0°C in Autumn, ground freezing occurred in both upward and downward direction. Water storage is reduced as less water was added to the basin. Discharge continues to decline upto October which river ice grows. Runoff terminates in late November as river ice and icing block the channels and the outlets of small valley. Winter flow is absent for about half of a year. This streamflow regime (Fig.8) is analogous to the Subarctic nival regime in North America (Church, 1974).

##### Water Balance

The water balance equation of a basin is:

$$P = R + E + \Delta S$$

where: P is mean annual precipitation, R is runoff, E is evaporation and  $\Delta S$  is the changes of water storage, including the changes of ground water in the active layer, ground ice, river ice and snow cover. In general, mean annual precipitation increases with elevation (Fig.9), but during some storms, the center of rainfall may be over the lower basin. For example, the storm of 1-2, July, 1986, deposited 38.7 mm on the low basin, and only 11.8 mm at the upper basin. Fig.9 shows the general trend of elevational increases in precipitation based on mean annual values from 1984-1991. Using this relationship, the precipitation at different elevation is estimated. The area of various elevation bands are also determined to enable the calculation of areally weighted mean precipitation for the basin. Since the measured precipitation underestimated (Yang D.Q., 1988), 20% corrections were made to the measured data of Binggou basin (Yang Z.N., 1991c). For the study period of 1984-1991, mean annual precipitation in the basin was 806 mm, runoff was 568 mm. Assuming that the mean storage change is zero ( $\Delta S=0$ ), evaporation is calculated to be 238 mm.

Table 1 The result of water balance in Binggou

Years	Precipitation*(mm)	Runoff (mm)	Evaporation(mm)	Runoff ratio	Air temperature (°C)
1984	713	529	184	0.74	-2.9
1985	804	548	256	0.68	-2.5
1986	804	682	122	0.85	-2.8
1987	811	595	216	0.73	-1.9
1988	812	704	108	0.87	-2.4
1990	935	568	367	0.60	-2.2
1991	761	348	413	0.46	-2.2
Average	808	568	238	0.70	-2.4

\* added the correction precipitation (20%).

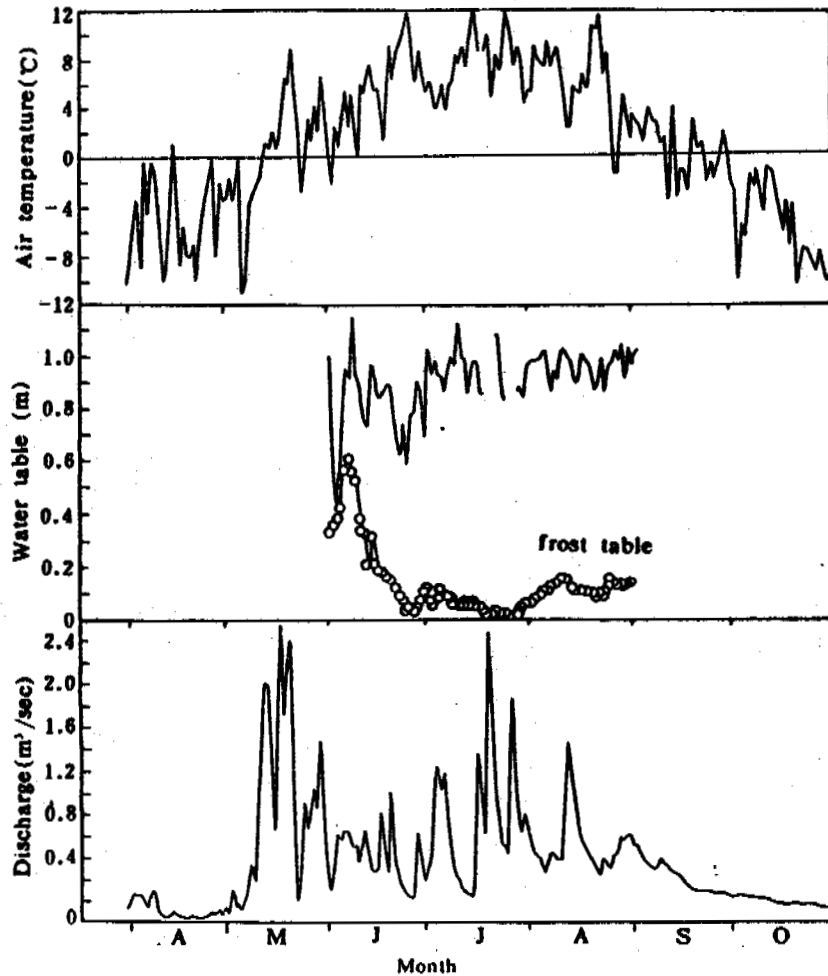


Fig.8 The course of air temperature, water table, frost table and discharge (1991)

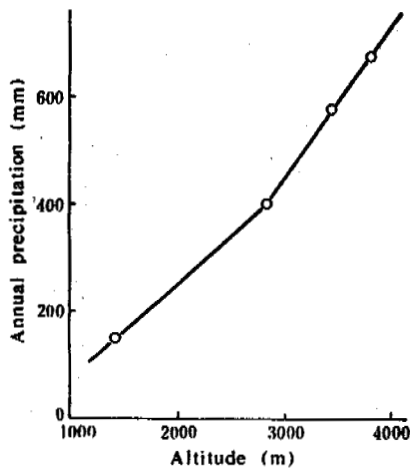


Fig.9 The relationship between mean annual precipitation and altitude

Mean runoff ratio was 0.70, a value that is compatible with the value of in Tianshan Urumqi river (Yang Z.N., 1991a) and the research result in Arctic region (0.7-0.8) (Anderson, 1974, Findlay, 1969, Kane et al., 1973, Woo, 1983). The runoff ratio changes with climate variation. During 1991 when the summer air temperature was above 1.0-1.5 normal and precipitation was below normal, the runoff ratio was reduced to 0.46 (Table 1). This runoff ratio is higher (in permafrost area) than in unpermafrost area.

#### CONCLUSIONS

- (1) The presence of perennially and seasonally frozen soil is a main factor affecting the hydrologic processes in alpine permafrost area. Permafrost behaves as an impermeable medium, and the catchment runoff response to snowmelt and rainfall is strongly modified. This is similar to the finding of (Slaughter et al., 1983).
- (2) The thickness of the active layer is controlled by topography, slope direction, elevation, soil moisture content and surface condition, such as snow cover and vegetation and rock properties. The rate of thaw, the variation of

water table in the active layer influence other hydrological processes in the permafrost zone. The runoff regime is analogous to the subarctic nival regime reported in North America.  
(3) In terms of water balance, over 70% of annual precipitation is lost to runoff and rest to evaporation, but the runoff ratio for individual years can depart significantly from the mean value, as the change of climate.

#### ACKNOWLEDGEMENTS

We are gratefully acknowledged to professor M.K.Woo of McMaster University Canada for his extremely helpful comments and reviews on this manuscript.

#### REFERENCES

- Anderson, J.C.(1974) Permafrost hydrology studies at Boot Creek and Peter Lake watersheds. N.W.T.PROC.workshop seminar on permafrost hydrology, Can.Nat.Comm.IHD., Ottawa, 39-44.
- Cheng Guodong (1979) Some differences between permafrost in Qinghai Xizhang plateau and in the Northern Canada. Journal of Glaciology and Geocryology, Vol.2, 39-42 (in Chinese).
- Church, M.(1974) Hydrology and permafrost with reference to North America. Proc. Workshop Seminar on Permafrost Hydrology, Can. Nat. Comm., IHD, Ottawa, 7-20.
- Dingman (1975) Hydrologic effects of frozen ground. U.S.Amy CRREL Sepc.Rep.128,55.
- Findlay, R.F.(1969) Precipitation in northern Quebec and Labrador: An evaluation of measurement technique, Arctic, 22,140-150.
- Kane, D.L.,R.F.Carlson (1973) Hydrology of the central Arctic River basin of Alaska. Inst. of Water Resources Rep.No.IWR-41, University of Alaska, 55.
- Kane, D.L.and J.Stein (1983) Water movement into Seasonally frozen soils. Water Resour.Res 19: 1547-1557.
- M.K.Woo (1983) Hydrology of frainge basin in the Canadian High Arctic. Am.ASSOS.Am.Geogr.73: 577-596.
- M.K.Woo, Philip Marsh, and Peter Steer (1983) Basin water balance in a continuous permafrost environment. Permafrost Fourth International Conference, Proceedings, 1407-1411, National Academy Press Washington,D.C.
- M.K.Woo (1986) Permafrost hydrology in North America ATMOSPHERE-OCEAN 24 (3), 202.
- Slaughter, C.W., Hilgert and E.H.Culp (1983) Summer streamflow and sediment yield from discontinuous-permafrost headwaters catchments. Proc. Fourth International Conference on Permafrost, Fairbanks, Alaska, pp.1172-1177.
- Yang Daqing, Jiang Tong, Zang Yinsheng and Kang Ersi (1988) Analysis and correction errors in precipitation measurement at head of Urumqi River, Tianshan. Journal of Glaciology and Geocryology, Vol.10, No.4, 384-399 (in Chinese).
- Yang Zhenniag (1981) The types of river in western mountains of China, Journal of Glaciology and Geocryology Vol.3, No.2, 24-31 (in Chinese).
- Yang Zhenniag (1988) Chapter XI Runoff from glacier melting water in China and its nourishment to rivers. AN INTRODUCTION TO THE GLACIERS IN CHINA, 187-204 (in Chinese).
- Yang Zhenniag (1991a) Glacier water resources

in China (monograph). Scientific Techic Publishing House of Gansu, China (in Chinese) 108-110.

- Yang Zhenniag, Yang Zhihui, Wang Qiang (1991b) Characteristic of hydrological processes in a small high mountain. Snow Hydrology and Forests in High Alpine Area, Proceedings of the Vienna Symposium, August, 1991, IAHS publ. No.205, 232-233.
- Yang Zhenniag (1991c) Estimation of Mass-balance and runoff component of Urumqi Glacier No.1 from water-balance analysis. NORTHERN HYDROLOGY, Selected Perspectives, NHRI Symposium No.6, 353-362.



# ESTIMATION AND MEASUREMENTS OF TRANSPORT PROPERTIES OF FROZEN SOILS

Yin-Chao Yen and Yoshisuke Nakano

U.S. Army Cold Regions Research and Engineering Laboratory  
Hanover, New Hampshire 03755, USA

This paper describes the thermal properties, unfrozen water content and hydraulic conductivities of soils in a brief manner. The factors that influence these properties, such as soil composition, structure, water content, temperature level and soil dry density are discussed. A very important and complex constituent of soil is water, which can coexist in several phases, and its effect on these properties is evaluated under a variety of experimental conditions. Methods of evaluating these property functions, which are vital to the understanding of the simultaneous heat and mass transport mechanism in soils, are reviewed and compared with experimentally determined data. In this review, frozen and unfrozen soils, both saturated and unsaturated, are covered and the results are presented either in theoretical or empirical expressions and in graphical form.

## INTRODUCTION

For the advancement of cold regions technology, a comprehensive knowledge of the mechanisms of heat conduction and water migration under isothermal conditions or a temperature gradient, and the effects of soil type, the water content, the temperature on the water migration and heat conduction in saturated and unsaturated frozen soils are needed. This review was undertaken to summarize and analyze briefly the methods of soil thermal conductivity measurement and its prediction equations, the unfrozen water content functions and the development of models to formulate the hydraulic property functions of frozen soils.

## METHODS OF THERMAL CONDUCTIVITY MEASUREMENT

Thermal conductivity measurements can largely be divided into two broad categories, steady and transient methods. In both methods, the soil is assumed to be isotropic.

### Steady State Method

In this method, the measurement will be made until the whole system has reached a pseudo steady state (theoretically it will never reach a steady state in a real sense if the soil is not 100% dry). In the case of moist soil, there is always moisture transfer due to the vapor pressure gradient caused by the imposed temperature gradient. Therefore, in practical sense, we only can consider that a pseudo steady state has been reached. The most commonly used test is the guarded hot plate test (GHPT) in which the thermal conductivity  $k$  can be computed from

$$k = \frac{Q}{A} \frac{\Delta x}{\Delta T} \quad (1)$$

where  $Q$  is the rate of heat flow,  $A$  is the cross-sectional area of the specimen,  $\Delta x$  is the sample length and  $\Delta T$  is temperature drop across the sample. The drawback of this method is not only that it takes a long time to reach a steady state, but that it also needs a rather large temperature differential, which may cause an appreciable moisture migration. Gravitational effects also show up, as in the experimental results on moist Ottawa sand by Woodside and Cliffe (1959).

Thermal conductivity can be measured in cylindrical and spherical configurations. In the cylindrical arrangement, the main heater is in the center and is guarded by upper and lower heaters to reduce heat loss along the longitudinal axis. In the spherical method, the sphere may be hollow or solid and it may be copper or aluminum. If we assume that the depth at which the measurement is made is large compared with the sphere radius, the thermal conductivity of the surrounding soil after a steady state has been attained, is given by

$$k = \frac{Q}{4\pi r(T_1 - T_2)} \quad (2)$$

where  $r$  is the radius, and  $T_1$  and  $T_2$  are temperatures of external surface and the heat sink. In addition, thermal conductivity can also be obtained by measuring the temperature at two points in the soil and the heat flow between the two points with the use of a heat meter.

### Transient Methods

In transient methods, the soil temperature varies with time. Such methods are more versatile and less time consuming than the steady-state methods.

The probe method is widely used in determining thermal conductivity of soils both in laboratory or in situ. Hooper and Lepper (1950), DeVries (1952), Mason and Kurtz (1952), Lachenbruch (1957), Van Rooyen and Winterkorn (1959), Woodside and Messmer (1961), Penner (1970), and McGaw (1974) all have used the probe to determine the thermal conductivity value of soil. They reported some alteration in moisture redistribution due to the short time period of testing and the small rise of the probe temperature.

The probe method is based on the assumption of a line heat source placed in a semi-infinite homogeneous and isotropic medium. If at time  $t = 0$ , a constant rate of  $q$  per unit length of probe is applied to the probe, the temperature rise  $\Delta T$  of the medium (Carslaw and Jaeger, 1959) can be given as

$$\Delta T = \frac{q}{4\pi k} \left[ -Ei \left( -\frac{r^2}{4\alpha t} \right) \right] \quad (3)$$

where  $r$  is the radial distance from the line

source,  $\alpha$  is the thermal diffusivity, and  $Ei(-x)$  is an exponential integral. For large values of time, the temperature rise can be approximated by replacing the  $Ei(-x)$  with the logarithm of time with the assumption of invariant  $k$ , which can be computed from

$$k = \frac{q}{4\pi(T_2 - T_1)} \ln\left(\frac{t_2}{t_1}\right) \quad (4)$$

where  $T_1$  and  $T_2$  are probe temperatures at times  $t_1$  and  $t_2$ , respectively. To conduct laboratory testing properly, Wechsler (1966) provides the following criterion related to the sample radius  $R$  by

$$\exp\left(-\frac{R^2}{4\alpha t}\right) \leq 0.02 \quad (5)$$

An important factor needed to be considered is the temperature gradient setup by the probe heater. If it is too large, it may cause excessive moisture migration in unsaturated soils, and it may cause melting in the case of frozen soils.

The periodic transient method is based on the assumption that the annual variation in temperature at the ground surface can be represented by a sine wave. Analyzing the attenuation and lag of the annual temperature wave in the soil, one can estimate the value of  $\alpha$  (Forbes (1948). Hoekstra et al. (1973) reported values of  $\alpha$  of a cylindrical soil sample by applying a sinusoidal temperature wave to its periphery. This method is especially advantageous for samples where there may be a moisture migration problem or changes in the thermal properties.

Another transient technique is the so-called thermal shock method. Here a sudden change in temperature is imposed on the boundaries of a cylindrical sample and the temperature change is recorded at its center. To compute the thermal conductivity, the value of specific heat must be known beforehand.

In general, the probe method gives somewhat higher thermal conductivity values than the guarded heat plate method.

#### THEORETICAL AND EMPIRICAL EQUATIONS FOR PREDICTING EFFECTIVE THERMAL CONDUCTIVITY

Various models have been developed for predicting effective thermal conductivities,  $k_a$ . The soils are assumed to have isotropic properties; i.e., the value of thermal conductivity does not depend on the direction of heat flow. Most of the prediction equations are purely empirical with some theoretical basis. Farouki (1981) has reviewed exclusively the models developed prior to 1979. These include the simplest theoretical expressions for predicting thermal conductivity, i.e., the series, parallel and geometrical mean models; the Smith (1942) methods for dry soils that assume two heat flow paths to be parallel, with one path consisting entirely of an air column and the other of some series of air and soil grain; the Kersten (1949) equations for unfrozen and frozen silt-day soils; and other models developed by Mickley (1951), Gemant (1952), DeVries (1963), Woodside and Messmer (1961) and McGraw (1969). The most recent prediction models are by Johansen and Frivik (1980), Muzzio and Solaini (1982) and Gori (1983)

#### Comparison of Some Predicted Results

Gori (1983) has computed some results and compared those derived by DeVries (1963) and Johansen and Frivik (1980) with his equations (9, 10 and 11). Figure 1a shows the variation of  $k_{eustf}$  with  $s_r$ . The data points are those of Kersten (1949) on Ramsey sandy loam as reported by Farouki (1982).

As evidenced from the Figure, DeVries' equation gives the highest prediction, while those of Johansen and Frivik fall into the middle. Gori's prediction gives much better agreement with the experimental data up to  $s_r$  around 0.75. Figure 1b provides the variation of  $k_{eustf}$  with  $s_r$  for the case  $V_w/V_v < V_{wa}/V_v$ . As shown in previous figure, the effect of  $u_w$  on  $k_{eustf}$  is much more pronounced than in the equation by DeVries. Johansen and Frivik give much closer results between  $u_w = 0$  and  $u_w \neq 0$ . However, both equations predict much higher  $k_{eustf}$  values than Kersten's results on Fairbanks silty clay loam, as reputed by Farouki (1982). Both predictions give higher  $k_{eustf}$  values, when  $u_w = 0$  for the entire range of  $s_r$ . However, Gori's equation gives a slighter lower value of  $k_{eustf}$  for  $u_w = 0$  and for  $s_r \leq 0.5$ . Not until  $s_r > 0.65$ , does  $k_{eustf}$  for  $u_w = 0$  deviate from  $u_w \neq 0$  and rise steeply. Figure 1c shows the comparison of experimental data of Penner et al. (1975) for three soils classified as 8, 9 and 10. The same conclusions can be drawn from Figure 1c as from Figure 1b, but in general, there is a better agreement between the theoretical prediction and the experimental data.

#### UNFROZEN WATER CONTENT AND APPARENT SPECIFIC HEAT CAPACITY OF FROZEN SOIL

Anderson et al. (1973) reported and summarized the work of Anderson and Tice (1972) on the phase composition curves of 11 representative soils by a simple power equation, i.e.,

$$w_u = \alpha\theta^\beta \quad (6)$$

where  $w_u$  is in g H<sub>2</sub>O/100 g soil,  $\theta$  is the temperature in degrees Celsius below zero, and  $\alpha$  and  $\beta$  are parameter characteristics of each soil for clay-water systems. The least squares expressions for  $\alpha$  and  $\beta$  are respectively given by

$$\ln \alpha = 0.5519 \ln s + 0.2618 \quad (7)$$

and

$$\ln(-\beta) = 0.2640 \ln s + 0.3711$$

Therefore,  $w_u$  can be written in terms of  $s$  (specific surface per unit mass of soil) as

$$\ln w_u = 0.2618 + 0.5519 \ln s - 1.449 s^{-0.264} \ln \theta \quad (8)$$

If we consider that the frozen ground is composed of two components (soil and water) and three phases, i.e., soil particle matrix, ice and unfrozen water, the heat capacity of the system can be expressed (Anderson (1967) as the sum of

$$c_a = c_s + c_1 (w_w - w_u) + c_u w_u + \frac{1}{\Delta\theta} \int_{\theta_1}^{\theta_2} L \left(\frac{\partial w_u}{\partial \theta}\right) d\theta \quad (9)$$

where  $c_a$  is apparent specific heat capacity (cal/°C unit weight of soil),  $c_s$ ,  $c_1$ , and  $c_u$  are the specific heat capacity of soil matrix, ice and unfrozen water, respectively, and  $w_w$  = the total water content.  $\theta_1$  is defined as  $\theta - \Delta\theta/2$ ,  $\theta_2 = \theta + \Delta\theta/2$ ,  $\Delta\theta = \theta_2 - \theta_1$ , and  $L$  is the latent heat of fusion. The final expression of  $c_a$  is

$$c_a = c_s + c_1 w_w + (c_u - c_1) \alpha\theta^\beta + \frac{\alpha L}{\Delta\theta} (\theta_2^\beta - \theta_1^\beta) \quad (10)$$

The calculated results indicate that soils of high specific surface area have much lower  $c_a$  values at low water contents than the coarser soils with lower values of  $s$ .

## HYDRAULIC PROPERTIES OF FROZEN SOILS

Scientific investigations of soil freezing began in the early 1900's. Taber (1929, 1930) empirically showed that when a frost-susceptible soil froze, water was driven toward the freezing front and frost heave occurred primarily because of freezing of incoming water and not simply because of the freezing of in-situ water.

Several mathematical models have been proposed for describing the mechanisms of water transport through frozen soils (Nakano, 1991). Some models were built by simply extending the known percolation laws of unfrozen porous media while others were based on nonequilibrium thermodynamics (Perfect et al., 1991). However, there is no consensus among researchers on the subject because none of these models has been completely validated by experiments. In view of these circumstances, we will focus our discussions on the mechanism of water transport because the quantitative presentation of the hydraulic properties of frozen soils depends on a given model.

### Unsaturated Frozen Soils

In the past, most researchers assumed that the main driving force of water in unsaturated frozen

soils under both isothermal and nonisothermal conditions is the gradient of unfrozen water pressure,  $P$ , if gravitational effects are neglected, and that the mass flux of water,  $J$ , in one direction is given as:

$$J = - K_1 \frac{\partial P}{\partial x} \quad (11)$$

where  $x$  is the space coordinate and  $K_1$  is the conductivity function that generally depends on the composition of a given soil.

Assuming a one-to-one correspondence between  $P$  and the content of unfrozen water (weight based)  $w_u$ , some researchers (Taylor and Luthin, 1978; Jame and Norum, 1980) used an alternative form of Eq. 17 given as:

$$J = - \rho_d D_1 \frac{\partial w_u}{\partial x} \quad (12)$$

where  $\rho_d$  is the dry density of a given soil and  $D_1$  is the diffusivity function defined as:

$$\rho_d D_1 = K_1 \frac{dP}{dw_u} \quad (13)$$

It is clear that Eq. 11 is the same as the well-known Richards equation (Richards, 1931) for water flow through unsaturated and unfrozen soils and that Eqs. 11 and 12 are simple extensions of the flow law through unfrozen soils to frozen soils. The mass flux of water in freezing soils was calculated from measured profiles of water content (Hoekstra, 1966; Dirksen and Miller, 1966). However, the pressure of unfrozen water,  $P$ , was not measured in these experiments, and no quantitative evaluation was made on the mechanism of water transport.

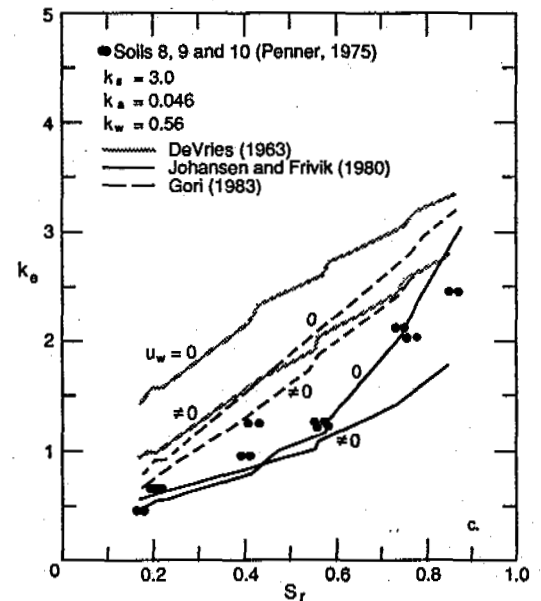
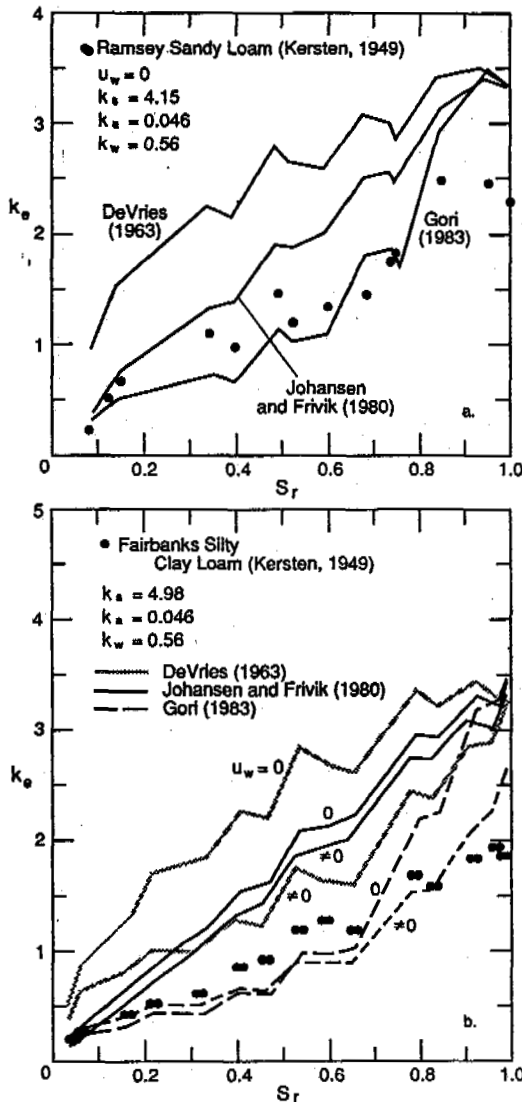


Figure 1. Comparison of experimental data and theoretical predictions vs degree of saturation where  $u_w$  is the ratio of the volume of unfrozen water to the total volume of the cell;  $k_s$ ,  $k_a$  and  $k_w$  are thermal conductivity of solid, air and water, respectively; and  $k_e$  is effective thermal conductivity.

Harlan (1973) introduced a hypothesis that the hydraulic conductivity of a given soil depends on the liquid water content regardless of frozen or unfrozen conditions. This hypothesis was tested by Jame and Norum (1980), Pikul et al. (1989) and Lundin (1990). These results indicate that Harlan's hypothesis grossly overestimates the flux of water and that an empirically determined impedance parameter (or function) is needed to fit experimental data. It appears that no convincing empirical verification of either Eq. 11 or 12 has been provided.

In the early 1980s a series of investigations on the mechanism of water transport through unsaturated frozen soils were initiated at CRREL. Nakano et al. (1982, 1983a, 1983b, 1984a, 1984b, 1984c) and Nakano and Tice (1987) studied the transport of water in frozen clay under isothermal conditions and found that the mass flux of water,  $J$ , can be expressed by:

$$J = -\rho_d D_1 (w, T) \frac{\partial w}{\partial x} \quad (14)$$

where  $w$  is the content of water in all phases. They validated Eq. 14 with a series of experiments in which two long soil columns with two different but uniform initial values of  $w$ ,  $w_1^0$  and  $w_2^0$ , were connected and exposed to a given constant negative temperature  $T$ .

Unfrozen water does not simply flow through a matrix made of soil and ice because ice is not a permanent constituent but it may grow or melt depending on a given conditions. Growing (or melting) ice decreases (or increases) the local flux of unfrozen water, which disrupts ordinary mechanisms of flow through porous media. For instance, when  $w_1^0$  was greater than the equilibrium unfrozen water content  $w^*$  at  $T$  and  $w_2^0$  was negligibly small, Nakano et al. found that water was transported from the wet part to the dry part according to Eq. 14 and that, in the wet part, the unfrozen water content remained constant at  $w^*$  while melting of ice occurred. It is important to mention that the transport of water in the wet part, where  $w > w^*$  under such a condition, usually is accompanied by melting of ice and that the concept of an analogy between mechanisms of water transport in unsaturated soil and those in frozen soil clearly breaks down here.

The data of Hadley and Eisenstadt (1955), Hutcheon (1958) and Oliphant et al. (1983) clearly show that a temperature gradient is an important driving force of water in unsaturated frozen soils. Therefore, the gradient of water content under isothermal conditions and the gradient of temperature are clearly two major driving forces for the transport of water in unsaturated frozen soils. There still remains an important question on whether these two driving forces act independently when the transport of water takes place under nonisothermal conditions.

If  $T$  and  $w$  are independent, the mass flux of water,  $J$ , may be written in the general form given as:

$$J = -\rho_d D_1 \frac{\partial w}{\partial x} - \rho_d D_2 \frac{\partial T}{\partial x} \quad (15)$$

where  $D_1$  and  $D_2$  are empirically determined transport functions that generally depend on  $T$  and  $w$ . If  $T$  and  $w$  are dependent,  $J$  is given as:

$$J = -\rho_d \hat{D}_1 \frac{\partial w}{\partial x} = -\rho_d \hat{D}_2 \frac{\partial T}{\partial x} \quad (16)$$

where  $\hat{D}_1$  and  $\hat{D}_2$  are empirically determined transport functions.

In experimental work of Nakano and Tice (1988, 1990), a column of soil with initially uniform dry density and water content was placed in a linear temperature field. If Eq. 16 holds true, then water must keep moving in the direction of lower temperature. However, according to their experiments, as water moves toward the cold end, the initial uniformity of  $w$  breaks down and a gradient of water content buildup in the column acts against the driving force of water due to a temperature gradient. Sooner or later two driving forces of water tend to balance each other, while the profile of water content in the column asymptotically approaches the stationary profile as time increases. These experimental data confirm the validity of Eq. 15.

Xu et al. (1985) reported experimental results on water migration in unsaturated frozen Morin clay subjected to temperature gradients. The effects of experimental duration,  $t$ , temperature,  $T$ , dry soil density,  $\rho_d$ , and temperature gradient, Grad  $T$ , on water migration flux,  $J$ , can generally be expressed as

$$J = f(t, T, \rho_d, \text{Grad } T) \quad (17)$$

For varying experimental duration,  $t$ , and by maintaining the other variables at specific values under the fixed values of  $T$ ,  $\rho_d$  and Grad  $T$ , the flux  $J$  can be written as

$$J = f(A t^{-1/2} + B) T, \rho_d, \text{Grad } T \quad (18)$$

The value of  $A$  was found to be dependent on the value of  $T$  and increases as  $T$  increases. Contrary to common belief, the value of  $B$  is not zero when  $t$  is zero. For the effect of temperature,  $T$ , the  $J$  value can be expressed by

$$J = (C T^{-D})_{\text{Grad } T, \rho_d, t} \quad (19)$$

The values of  $C$  and  $D$  are found to be complex functions of Grad  $T$ ,  $\rho_d$ ,  $t$  as well as  $w$ . For the effect of Grad  $T$  on  $J$ , a linear relation can be used, i.e.

$$J = (E + F \text{ Grad } T) T, \rho_d, t \quad (20)$$

The effect of  $\rho_d$  on flux  $J$  was unique. For same Grad  $T$  and  $t$ ,  $J$  increases with  $\rho_d$  up to a critical  $\rho_{dc}$  after which  $J$  decreases as  $\rho_d$  increases. For temperature ranged from  $-4^\circ$  to  $1^\circ\text{C}$ . Xu et al. (1985) concluded that the mechanism of water migration in unsaturated frozen soils is similar to the process in unsaturated unfrozen soils.

Recently Deng and Xu (1991) determined hydraulic conductivities,  $K$ , of both saturated and unsaturated soils subjected to freezing and thawing. The hydraulic conductivity of unsaturated soil is found to be related to the soil-water potential and water content and usually can be expressed in terms of an exponential function. For a given water content,  $K$  decreases with an increasing content of fines and dry density. Within a certain region of soil-water potential, the value of  $K$  increases with increasing amount of fines and  $\rho_d$ . For any kinds of saturated soils, the value of  $K$  is larger after going through one cycle of freezing and thawing than prior to freezing. The increase in  $K$  value is more distinctive for fine-grained soils than coarse-grained soils and is larger for greater dry density. The value of  $K$  increases only slightly after repeated cycles of freezing and thawing, and in general, it reaches a limiting value.

### Saturated Frozen Soils

Water in saturated frozen soils generally exists in two phases: unfrozen liquid water and ice. It has been shown empirically that the gradient of temperature  $T$  under uniform pressure fields (Mageau and Morgenstern, 1980; Perfect and Williams, 1980) and the gradient of unfrozen water pressure  $P$  under isothermal conditions (Burt and Williams, 1976; Horiguchi and Miller, 1983) are two major driving forces for the transport of water in saturated frozen soils. An important but unresolved question is whether  $T$  and  $P$  are independent when the transport of heat and water takes place simultaneously.

If  $T$  and  $P$  are independent, the mass flux of water,  $J$ , in one direction may be written as:

$$J = -K_1 \frac{\partial P}{\partial x} - K_2 \frac{\partial T}{\partial x} \quad (21)$$

where  $x$  is the space coordinate, and  $K_1$  and  $K_2$  are empirical functions describing the transport properties of a given soil that generally depend on  $T$  and the composition of the soil. If  $T$  and  $P$  are dependent,  $J$  is given as:

$$J = -\hat{K}_1 \frac{\partial P}{\partial x} = -\hat{K}_2 \frac{\partial T}{\partial x} \quad (22)$$

where  $\hat{K}_1$  and  $\hat{K}_2$  are empirical functions that generally depend on  $T$  and the composition of the soil.

Equation 21 is a generalization of somewhat simpler equations proposed by Ratkje et al. (1982), Derjaguin and Churaev (1986), Horiguchi (1987) and others. Equation 21 implies that the chemical potential of unfrozen water depends on  $T$  and  $P$  independently and that the effect of  $T$  becomes significant at subzero temperatures. Such an effect of  $T$  was explained by either the interaction between unfrozen water and soil surfaces (Horiguchi, 1987) or that between unfrozen water and ice surfaces (Derjaguin and Churaev, 1986; Kuroda, 1987). However, hardly any experimental data exist to support such explanations.

Equation 22 has been popular among researchers. The first equality of Eq. 22 is reduced to Darcy's law provided that the dependence of  $K_1$  on  $T$  becomes negligible for  $T > 0^\circ\text{C}$ . However, the second equality does not hold true for unfrozen porous media. Hence, Eq. 22 is clearly not a simple extension of Darcy's law to frozen saturated soils and Eq. 22 needs empirical verification. The direct empirical verification of either Eq. 21 or 22 requires the accurate measurement of  $P$  under transient conditions. Unfortunately, neither Eq. 21 nor 22 has been directly verified due to the lack of suitable instrumentation for pressure measurements. However, this situation does not necessarily preclude indirect methods of evaluating these flow equations.

Based on recent mathematical and experimental studies of a steady growth layer (Nakano, 1990; Takeda and Nakano, 1990; Nakano and Takeda, 1991), Nakano found that the choice of transport law (Eq. 21 or 22) is the major factor affecting the behavior of the solutions. Comparing the properties of the solutions with reported empirical findings and newly obtained data, it was found that the model based on Eq. 21 is consistent with data while the models based on Eq. 22 contradicts the empirical findings.

### REFERENCES

Anderson, D.M. (1967) The interface between ice and silicate surfaces, *J. Colloid Interface Sci.*, 25:174-191.

- Anderson, D.M. and A.R. Tice (1972) Predicting unfrozen water contents in frozen soils from surface area measurements. Highway Research Board Record no. 393, p. 12-18.
- Anderson, D.M., A.R. Tice and H.L. McKim (1973) The unfrozen water and the specific heat capacity of frozen soils. *Permafrost: Second International Conference, North American Contribution*. National Academy of Sciences, Washington, D.C., p. 289-295.
- Burt, T.P. and P.J. Williams (1976) Hydraulic conductivity in frozen soils. *Earth Surface Processes*, 1(4):349-360.
- Carlsaw, H.S. and J.C. Jaeger (1959) *Conduction of Heat in Solids*, Oxford: Clarendon Press.
- Deng, Yousheng and Xiaozu, Xu (1991) Hydraulic conductivity of unsaturated soil and its changing regularity in saturated soil after freezing-thawing cycles. *Journal of Glaciology and Geocryology*, 13(1):51-59.
- Derjaguin, B.V. and N.V. Churaev (1986) Flow of nonfreezing water interlayers and frost heaving. *Cold Reg. Sci. Tech.*, 12:57-66.
- DeVries, D.A. (1952) A nonstationary method for determining thermal conductivity of soil in situ. *Soil Science*, 73(2):83-89.
- DeVries, D.A. (1963) Thermal properties of soils. In *Physics of Plant Environment* (W.R. VanWijk, ed.) Amsterdam, North Holland Publishing Co.
- Dirksen, C. and R.D. Miller (1966) Closes-system freezing of unsaturated soil. *Proc. Soil Sci. Soc. Amer.*, 30:168-173.
- Farouki, O.T. (1981) Thermal properties of soils. U.S. Army Cold Regions Research and Engineering Laboratory, Monograph 81-1.
- Farouki, O.T. (1982) Evaluation of methods for calculating thermal conductivity, U.S. Army Cold Regions Research and Engineering Laboratory, Report 82-8.
- Forbes, J.D. (1948) Account of some experiments on the temperature of the earth at different depths and in different soils, near Edinburgh. *Transactions of the Royal Society of Edinburgh*, 16:189-236.
- Germant, A. (1952) How to compute thermal soil conductivities. *Heating, Piping and Air Conditioning*, 24(1):122-123.
- Gori, F. (1983) A theoretical model for predicting the effective thermal conductivity of unsaturated frozen soils. *Permafrost: Fourth International Conference, Proceedings*, National Academy Press, Washington, D.C., p. 363-368.
- Hadley, W.A. and R. Eisenstadt (1955) Thermally actuated moisture migration in granular media. *Trans. Amer. Geophysical Union*, 35:615-623.
- Harlan, R.L. (1973) Analysis of coupled heat-fluid transport in partially frozen soil. *Water Resources Res.*, 9:1314-1322.
- Hoekstra, P. (1966) Moisture movement in soils under temperature gradients with the cold side below freezing. *Water Resources Res.*, 2:241-250.
- Hoekstra, P., A. Delaney and R. Atkins (1973) Measuring the thermal properties of cylindrical specimens by the use of sinusoidal temperature waves. USA Cold Regions Research and Engineering Laboratory, Technical Report 244.
- Hooper, F.C. and F.R. Lepper (1950) Transient heat flow apparatus for the determination of thermal conductivities. *Heating, Piping and Air Conditioning*, 22(8):129-134.
- Horiguchi, K. (1987) An osmotic model for soil freezing. *Cold Reg. Sci. Tech.*, 14:13-32.
- Horiguchi, K. and R.D. Miller (1983) Hydraulic conductivity functions of frozen materials. *Proc. 4th Int. Conf. on Permafrost*, Nat. Acad. Sci., Washington, D.C., 504-508.
- Hutcheon, W.L. (1958) Moisture flow induced by thermal gradients within unsaturated soils. *Highway Res. Board Special Rep.*, 40:113-133.

## THE DEGENERATION OF PERMAFROST IN UPSTREAM VALLEY REGION OF HEILONG RIVER

Yu Shengqing and Wang Zhanchen

Research Institute of Song-Liao Water Conservancy Commission,  
74 Beian Road Changchun City, China

The upper reach of the Heilong River is located in a cold region with developed permafrost. Since the 1950's, the state of the permafrost in the valley has to a certain extent changed as human activity has increased and the natural environment has been altered. In this paper, the data observed for more than 30 years and the change of topographical features in this area are analyzed. It indicates that the permafrost is degenerating which is expressed in the average annual ground temperature gradually rising, and the area and thickness of the permafrost reducing. The reasons for permafrost degeneration is revealed. It provides useful information for the further study of the permafrost in this region.

### DISTRIBUTION AND CHARACTERISTICS OF PERMAFROST ALONG THE UPSTREAM VALLEY OF HEILONG RIVER

The upper reach of the Heilong River is 897 km long in total from the confluences of the Shilek and Eerguna rivers to Heihe city. In this region the climate is cold, and permafrost has developed to a large extent. As permafrost is the product of heat exchange between the atmosphere and lithosphere and the general level of heat exchange increases from northwest to southeast along the Heilong river, the area of permafrost distribution and its thickness decrease in this direction, which reflects the zonation of permafrost distribution with latitude. As a result of different topography, and the different conditions of heat exchange, the frozen conditions have different characteristics in the same region.

From the confluence to Xingan village is the coldest in the region, with an ultimate minimum air temperature of  $-52.3^{\circ}\text{C}$ . In the zone beneath the Heilong River bed, penetrating talik develops, in certain ranges of both river banks there exist island and scattered island permafrost. Permafrost layers are distributed mainly at the bottoms of the valley and gullies, in lower boggy depression sections and sheltered slopes and at their bases. Generally, permafrost thickness is 5-15 m, the maximum may reach 25 m. Spreading in the direction of both banks, permafrost changes from scattered island to island and island talik, up to a continuous distribution zone, and its area and thickness gradually increase.

In the range from Xingan village to Xinjieji village, the frost condition is weaker, scattered island permafrost occupies most of the area of both banks. On the right bank, permafrost exists mainly in lower boggy depression sectors composed of clayey soils, bottoms of creek valleys, and in partial sections of the lower part of the northern slopes. Whereas, in the sectors with ground vegetation being severely destroyed,

taliks only exist. On the left bank in partial lower boggy and depression sections, and bottoms of creek valleys, permafrost can also be met. Usually, the thickness of permafrost is 3-15 m, in individual locations slightly more. With spreading in the direction of both banks, the permafrost increases in area and thickness and develops into an island distribution zone.

Starting from Xinjieji village, the upstream valley of the Heilong River enters into a seasonally frozen zone. Within this zone, there is principally no permafrost. Only on the right bank in marshland and locations with thick vegetation and bryophyte are there a very few undegenerated relict frozen layers. The thickness generally is 3-5 m, the maximum may reach 8 m. On the left bank, in lower boggy river terraces and lower parts of northerly slopes composed of loam, there is frost pereletok to be met.

### DEGENERATION OF PERMAFROST ALONG RIVER VALLEY

In the 1950's, a great quantity of permafrost investigation and exploration along the upstream valley of the Heilong River was carried out and much practical data was obtained (G.M. Aposckin, 1962). During 1987-1991, we have again conducted investigation, exploration and observation on permafrost in this region. The results indicate that in the last thirty years, considerable degeneration of permafrost in this region has occurred.

### Moving Upward of Southern Limit of Permafrost in River Valley

What is called the southern limit of permafrost is termed as a zone, in which the permafrost and nonpermafrost may replace each other, only several island thin frost relict layers or pereletoks exist. At the same time, as a result of the short periodic fluctuation of the heat exchange level, in this zone the transitional pattern from permafrost to seasonal frost, or

the reverse, may take place.

The exploration results of the 1950's indicated that the southern limit was located between Huma and Sikejiu dam sites. At that time, in the stratum of loam and clay, the location with thick bryophyte growing and weak bogginess of the upper reach of the creek valley, the sectors covered by many clusters of small grass on lower depression of flood land, there was permafrost or pereletoks with a thickness of generally 3-5 m. Whereas, after thirty years, in this range frost conditions have greatly changed, only few or no ungenerated relict frozen layers are present. Thus, it can be inferred that in the last thirty years, the southern limit of permafrost along the valley of Heilong River has moved upwards approximately 50-100 km.

#### Ground Temperature Rising

Knowing the vertical distribution of the ground temperature makes it possible to not only determine the important factors such as mean annual ground temperature, depth of annual temperature variation layer, thickness of frozen layer etc., but also to define the developing and changing extent of permafrost according to the variation tendency of the ground temperature.

In the course of surveying in the 1950's, on both river banks in the studied region many temperature bore holes were set up. Based on the observation data, the temperature and thickness of frozen soil at that time were obtained. In recent years, using the original holes on the right bank, we have repeated temperature measurement. It was found that ground temperature has changed in a different extent. The main expression is that ground temperature is rising.

The Fig.1 shows the vertical distribution curves of ground temperature measured at one hole on right bank in the upper reach of the Heilong River in 1958 and 1990, respectively. From the curves in this figure it can be seen that in a certain range below a depth of 6 m from the land surface the temperature is or is near 0°C, indicating that at

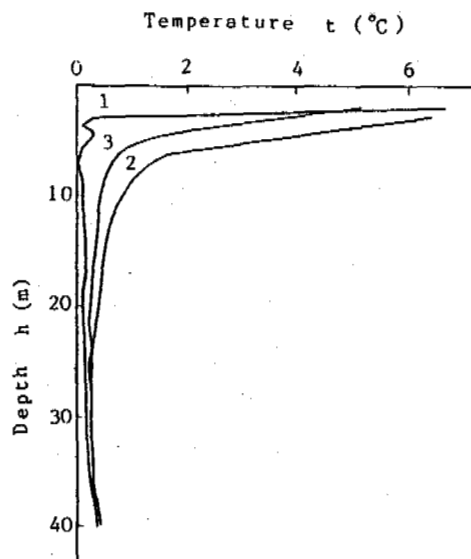


Fig.1 Curve of ground temperature-vs-depth  
1--1959.8.11; 2--1990.7.17; 3--1990.10.2

a given depth at that time there was frozen layer with a high temperature. The curves 2 and 3 show that ground temperature near the earth surface has the greatest variation, with the depth increasing the range of variation gradually reduces. Downwards from a depth of 25 m, these curves coincide in the main, showing the ground temperature below 25 m being stable. Whereas upwards from this depth it obviously rises with an increase of more than 0.2°C. For example, at depth of 10 m, the measured value in 1958 is 0.1°C, but in 1990 reaches 0.4-0.7°C. At present, in that hole there is not permafrost any more.

#### Permafrost Reducing in Area and Thickness

At the same time that the southern limit of permafrost moved upwards along the Heilong River, corresponding changes also took place in island and scattered island permafrost zones. According to the exploration results in the 1950's, in the upstream valley of the studied region at the wide 1st flood plain terrace, the thickness of permafrost was 20-40 m, at the 3rd and 4th terraces the permafrost was of a continuous distribution with a thickness of 30-50 m. Whereas, the exploration results conducted in recent years indicated that the permafrost area currently remains only approximately 10-20%, generally, the thickness is 10-15 m, and the maximum may reach 25 m.

For example, at a 1st terrace in the village near the riverside and adjacent localities on the right bank, in the 1950's there was island distribution of permafrost. However, to date the permafrost has reduced or exists no longer, only in locations with bogginess and dense vegetation does there exist relict permafrost. In the other wide 1st terrace with complicated topography, in the large boggy sectors, in the 1950's surface water remained there year in and year out, thus, human access was difficult. But, in recent years, surface water has considerably decreased, in the third week of September the ground surface is principally without water. Therefore, except the season of successive rainfall, people may pass through there. Degeneration of the bog induces permafrost to degenerate visibly, finding expression in the upper limit of permafrost obviously lowering. In the sectors with vegetation in good condition, the upper limit generally lies at 2 m deep; in the sectors with vegetation in a slightly bad condition, it has dropped down to below 5 m. Based on the above, it can be concluded that the area of permafrost distribution in the upstream valley of the Heilong River is gradually decreasing and the thickness is thinning, which results in the island permafrost zone changing to a scattered island permafrost zone and, subsequently, the latter changing into a seasonally frozen zone.

#### THE CAUSES OF PERMAFROST DEGENERATION

The permafrost exists in a certain environment, thus, the change of natural factors such as climate, topography, terrain features, etc. has a great effect on the permafrost distribution and development. The changes of external factors certainly causes the changes of the permafrost.

#### Rising Air Temperature in Studied Region

Available data indicates that the warming of

the climate over one hundred years is one of the basic causes inducing the permafrost to degenerate. According to the related information over thirty years in the studied region, the air temperature generally tends to increase in the form of a wave. The increase range is more than 1.0°C, being particularly obvious during the twenty years from the early 1970's to the early 1990's. The distinguishing feature of climate warming in the north of our country is the increase of air temperature in the winter season being greater than that in summer. According to the related data, in the most of northeast China and the other regions of northern China, winter average air temperature of the winters in the 1980's was 1.0-1.5°C higher than that in the thirty years before 1980 (Reference Room of NMB, 1991). The increase of the average air temperature of winter in the upper reaches of the Heilong River is much higher.

The large increase of the air temperature in the studied region speeds up the heat exchange between the earths stratum and the atmosphere, induced ground temperature to rise, changed the conditions on which the permafrost relies for existence, and consequently, resulted in permafrost degeneration.

#### Human Activity

Since the 1960's, with the development of the Big Xingan mountains, many tree farms, (mine-fields and residential areas have been set up, and the production scale has continuously expanded, and human activity has continuously increased.

The primeval forest in the river valley has been in a large scale felled and replaced by a new tree generation. To meet the needs of logging and other production activities, highway systems and drainages have been constructed in the region. This situation not only destroyed protophyte conditions, but also enhanced the drainability of ground surface, inducing the surface water to discharge rapidly, moisture content in soil layers to decrease, seasonal thawing depth to increase, and the area of talik to develop continuously.

The many sectors of the terraces with initial vegetation in good conditions were continuously cultivated into farmland. The thick and dense vegetation has deteriorated year after year. For example, in one 1st terrace with a wide topography and residential area, the farmland area is approximately 20-30%; in this terrace, 80-90% of the vegetation has been severely destroyed. This condition remains to be worse off.

Different human activities would cause the ecological balance to be continuously destroyed, resulting in the intensification of heat exchange between the atmosphere and lithosphere, quickening the degeneration of the permafrost.

#### Flood Water

The fluctuation of water level in the tributaries on both banks of the Heilong River certainly causes the change of the ground water level in the 1st and 2nd terraces of the river valley. Particularly, in the high permeable earth stratum, the rising and dropping of the ground water level is basically simultaneous with that of the river level, namely, when the river level rises, the ground water level also rises, and the flowing velocity increases correspondingly. In the sectors with lower land surface and a deeper permafrost limit, when the

ground water level rises over the bottom limit of the permafrost, it causes dissolution of the permafrost. For example, in the wells and vegetable cellars of residential areas, during the low-flow period, the ground water is separated from the permafrost layer; but, during the flood period the ground water level is higher than the bottom limit of the permafrost. By the dissolution action of the ground water, the permafrost thickness gradually decreases.

The other effect of flooding to the permafrost is erosion of the floodplain terrace. There are two flood periods every year in Heilong River. One of them is the spring flood with ice running. During the river thaw with ice running, a large number of ice cakes often pile up in the river channel, forming an ice dam. Consequently, the river level rises up, and the terrace lands are inundated with flood water. The other is the summer flood. At this time, the river overflows, which results in a vast sheet of water on the lower terrace.

As a result of frequent and great floods, not only the permafrost in the terraces was eroded, the vegetation on the inundated sectors was also largely destroyed, which would change the developing conditions of the permafrost.

#### CONCLUSION

The permafrost in the upstream valley of the Heilong River is subject to latitude zonation. At the same time, due to different topography, terrain features and heat exchange levels, etc., there are different frost conditions in different river reaches. In most of the upstream river reaches on both banks there exists scattered island permafrost. Stretching in each directions of both banks along the transverse section, the area and thickness of the permafrost gradually increases, the scattered island distribution of the permafrost changes to island, or island talik types.

The results of exploration and investigation conducted in recent years indicates that obvious degeneration of the permafrost in the studied region has taken place, found the expression in ground temperature rising, area and thickness decreasing, talik expanding, and the southern limit has moved towards the up stream by approximately 50-100 km.

The main cause resulting in permafrost degeneration is the change in the permafrost environment. Increase of human activities and flood inundation have severely destroyed the vegetation, and enhanced the heat exchange process between the atmosphere and lithosphere. With the changing of the permafrost environment, permafrost degeneration in this region will be further sped up.

#### REFERENCES

- G.M.Aposchein (1962) Zonation and Southern Limit of Permafrost in Upstream Valley of Amul river, "Problems of Geologic Structure and Engineering-Geologic Characteristics in Upstream Valley of Amul River", Press of Moscow University.  
Reference Room of NMB (1991) Bulletin of Meteorologic Monitor, No.2.



# USE OF GROUND PENETRATING RADAR FOR THE DETECTION OF PERMAFROST AND DELINEATION OF ITS DISTRIBUTION UNDER THE ASPHALTED ROAD OF QINGHAI-XIZANG HIGHWAY

Zeng Zhonggong, Huang Yizhi and Xia Zhiying  
Lanzhou Institute of Glaciology and Geocryology, Chinese Academy of Sciences  
Maurice-K. Seguin  
Department of Geology, Laval University, Quebec, Canada

The application of ground penetrating radar to plateau permafrost regions along the Qinghai-Xizang highway has proven useful. The methodology is described and typical examples are presented. The area distributions of seasonally frozen ground and permafrost are well discriminated and clearly identified with the help of the ground probing radar method. The radar information gathered is complemented by and correlated with control geological logs from numerous drill holes, as well as results from detailed electrical resistivity soundings. The depths to the permafrost upper table calculated from the GPR data depict a relative error which does not exceed 5%. Numerous problems related to the methodology, field procedure and application of ground penetrating radar for the delineation of plateau permafrost are discussed in this paper.

## INTRODUCTION

The Qinghai-Xizang highway is an important traffic artery which runs from Xining at its northern end, to Lhasa at its southern extremity. According to recent statistics, most of the passengers and goods transported in and out of the Xizang Autonomous Region are carried on this road which is called the "golden bridge"; it is the main connection between Xizang and China's inland provinces.

The construction of the Qinghai-Xizang highway began in 1953. Due to increasing transportation demands, the highway underwent reconstruction in the 1970's and later in the 1980's. The dirt (sand and gravel) road was then replaced by an asphalted highway. The section of the highway which extends from Golmud to Lhasa cuts through Kunlun, Tanggula and Nyanqentanglha mountain ranges and it runs across the Yangtze river head plateau; its total length amounts to 1155 km. The mean height of this section is located over 4100 m a.s.l.; 600 km of the roadbed is situated in permafrost zones. Road damages resulting from permafrost action occurred continuously since the start of its construction in spite of the protection measures taken to halt its degradation. Such measures included increase of roadbed height, improved selection of roadbed materials, etc.. After the highway reconstruction, road stability problems have never been solved satisfactorily. The investigations and statistics put forward by the highway department in 1990 have shown that 343 km of the road surface or roadbed between Golmud and Lhasa exhibit damages at different degrees and that it is difficult to keep the transportation going smoothly in such circumstances.

To satisfy the requirements for repairs and new designs of the roadbed, a knowledge of the distribution of permafrost and the seasonally frozen ground, of the depth of the man-induced

upper frozen table, of the frozen soil texture and especially of the spatial extent of permafrost with a high ice content are required. With these objectives in mind, an integrated geophysical investigation was undertaken between Xidatan and the northern slope of Tanggula Mountains. The geophysical surveys were complemented by temperature measurements in drillholes and geological logs issued as a control. In this paper, we will restrict ourselves to the discussion of the results obtained with the ground probing radar (GPR) survey. This survey was conducted in the period: August to November 1991. A total length of 220 km was surveyed along the highway using a Canadian digital recording Pulse EKKO IV GPR unit with an emission frequency of 50 MHz. For measurements along the longitudinal section to the highway, the antennas separated by a spacing of 1 m were fixed on a wooden sleigh which was towed with a jeep. The speed of the vehicle varied between 7 and 8 km hr<sup>-1</sup>; the distance between two sampled (digitized) points is about 10 m and the measurements were automatically recorded on a continuous basis. Control points were taken every 500 m to insure accurate location of the survey stations. Detailed GPR surveys were done near the site of the drill holes on the side and along the transect direction of the highway in order to correlate the results with the actual position of the man-made upper frozen table. This survey was conducted using the manual mode with measurement steps of 0.5 m. To calculate the velocities of the radar wave in the various soil layers, the common depth point (CDP or WARR) technique was used. In the expanding spread configuration used, the minimum distance between the antennas is 1 m, the maximum 20 m and the distance between the measured points 1 m. For the purpose of comparison and supplement of geoscientific results, over 200 D.C. electrical soundings with small electrode spacings (the maximum half-distance (AB/2) of the current electrodes is equal to 12 m) were

also undertaken to investigate the distribution of permafrost and seasonally frozen ground as well as the depth of the natural upper table of permafrost.

## RESULTS

According to the experience on GPR probings in past years (P.Hoekstra et al.,1975; S.A.Arcone et al.,1984; J.A.Pilon et al.,1985; A.P. Annan et al.,1977; J.A.Pilon et al.,1980; P.V. Sellman et al.,1983; S.A.Arcone et al.,1982), and in order to obtain geological information which is as reliable and objective as possible, a functional methodology is required for tracing the reflectors and correlating with geological objects at the interpretation stage of GPR data (P.Hoekstra et al.,1975; S.A.Arcone et al.,1984; J.A.Pilon et al.,1985; A.P. Annan et al.,1977; J.A.Pilon et al., 1980; P.V.Sellman et al.,1983; S.A.Arcone et al.,1982). The GPR records were analysed throughout the 220 km long section, then compared and correlated with the geological information from about 300 drill holes and over 200 electrical resistivity soundings uniformly distributed along this section and used as control points. The comparison of GPR profiles and CDP sections with drill hole records is most informative. The reflected wave train corresponding to the upper table of permafrost can be established and the taliks outlined thanks to the disappearance of the wave trains on the GPR records. Taliks identified in this manner coincide definitely with the geological logs in the drill holes and the interpreted results of the electrical soundings. In actual fact, this methodological approach was occasionally used to correct some errors encountered in the geological logs. To determine the depth to the upper table of permafrost, the radar wave velocity is calculated making use of the true depth of the upper table revealed by geological and thermal logs on the one hand, and the corresponding wave arrival time on the other hand. In sectors where the geology and geomorphology are uniform, a mean wave velocity value is adopted and the

depth to the upper table of permafrost is calculated at every point in these sectors of the section. The relative error of the calculated depths is less than 5%, only a few points have an absolute error exceeding 0.3-0.4 m. This point will be demonstrated by comparing 5 out 38 sections on which drill hole information is available.

### Example 1:GPR Recordings to the South of Wuli Pass

Radar data were collected to the south of Wuli Mountains where permafrost and isolated taliks alternate. No permafrost was detected on the geological logs of drill holes located at kilometrage:3134 (distance (km) from Beijing)+400 m and 3135-30 m but the geological logs indicated permafrost in drill holes situated at 3135+100 m and 3135+620 m where the depth of the permafrost upper table is 6.0 and 5.6 m respectively (Fig.1). An electrical resistivity sounding (ERS) was conducted beside the drill hole at 3135-30 m. The ERS curves are of the D type (Fig. 2). In the first part of the curve, the resistivity  $\rho_s = 100-120 \Omega\text{-m}$  while at larger electrode separation,  $\rho_s = 100 \Omega\text{-m}$ ; permafrost is thus absent since  $\rho_s$  does not increase at depth. The ERS curve at 3135+70 m located 20 m away and on the right side of the highway is of the A type with  $\rho_s = 40 \Omega\text{-m}$  in the first section of the curve,  $\rho_s = 90 \Omega\text{-m}$  mid-way and  $\rho_s > 130 \Omega\text{-m}$  at larger separation. Another ERS located 3 m away from the right side of the highway at 3135+700m is characterised by a H type curve with  $\rho_s > 200 \Omega\text{-m}$  at the beginning of the curve,  $\rho_s = 100 \Omega\text{-m}$  midway and  $\rho > 170 \Omega\text{-m}$  at larger separation. These two last ERS curves indicate the occurrence of permafrost at the south of Wuli Mountains and depth to the upper table approximately equal to 3.5 m. Similarly, the GPR record shows a significantly different signature between the two segments of this section and a sharp boundary at 3135+50 m. No reflectors are recorded after 100 ns in the northern sector while in the southern sector, six reflectors can be identified before or after 110 ns and the ill-defined six

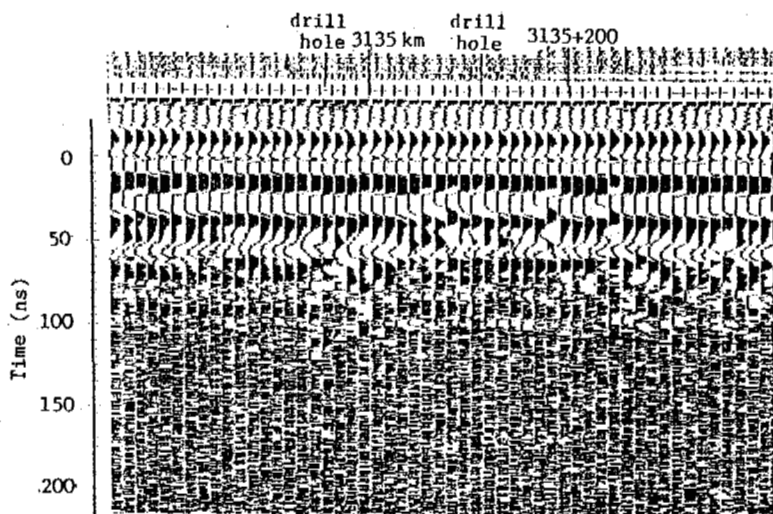


Fig.1 Ground probing radar recordings of a section to the south of Wuli Pass (~3135 km from Beijing)

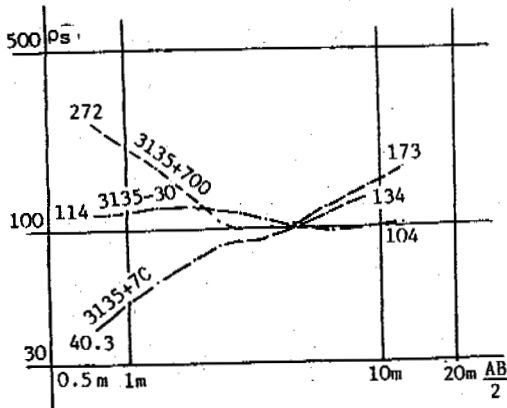


Fig.2 Three electrical resistivity sounding curves in the area south of Wuli Mountains

reflectors become clearer towards the south. This is apparently caused by multilayered ice accumulation near and below the permafrost upper table. Thus, the train of radar waves received is the result of reflections from the permafrost upper table. Between stations 3135+50 m and 3138 km, a radar velocity value ( $V=0.10 \text{ m ns}^{-1}$ ) is adopted for calculating the depth of the upper table and the mean relative error is estimated at 2.2% when compared with the geological logs of the drill holes.

Example 2: GPR Section at Budongquan Army Service Station

Budongquan means unfrozen spring in Chinese. This section is situated in a tectonic belt and as its name implies many hot springs are present there. In 1991, 5 boreholes were drilled between 3115 and 2920 km but no permafrost was detected. This region was thus considered as a large tectonic unfrozen zone (tectonic supertalik in geological terms). Radar recordings from 2917 to

2921 km show contrasted differences in segments bounded by 2917 km+500 m and 2918+800 m, 2919-300 m and 2920 km (Fig.3). These two segments do not depict any observable reflected event after 100 ns. However, a clearly identifiable and continuous fifth reflector is observed in the 3 other segments of this section after 100 ns. The geomorphology of the gentle slope to the south of 2920 km suggests the presence of permafrost. In addition, the highway is damaged at this emplacement. Finally permafrost is found in the flood plain to the north of 2915 km. The radar recordings showing a fifth reflector at 100 ns in these three segments of the section are indicative of the upper table of permafrost. A test borehole was drilled at 2917 km but its depth (4.1 m) was insufficient to reach permafrost. It was then found that on an old army service station located at 2919 km on the right side of the highway, 100 m away from the highway, permafrost had been encountered when digging a well (Wang Shooling personal communication). These observations corroborate the occurrence of permafrost interpreted from the GPR data. A combination of 1) relatively large distance from the hot springs, 2) low topography and 3) fine-grained texture of the deposits explains the preservation of permafrost at 2917 and 2919 km.

Example 3: Radar Section on the Southern Slope of Kaixingling

Predominantly continuous permafrost occupies the area extending from the southern slope of Kaixingling to the northern edge of Tongtian River basin. Clayey sediments and ground ice are widespread in this region. These adverse geological conditions are responsible for thermokarst depressions and large damages to the highway. The roadbed becomes largely unstable during the thawing season.

Fig.4 shows the GPR recordings on the southern slope of Kaixingling. The deep reflectors are unclear as the GPR signal is strongly attenuated due to fine-grained soils and a high moisture content (the space is occupied by swamps).

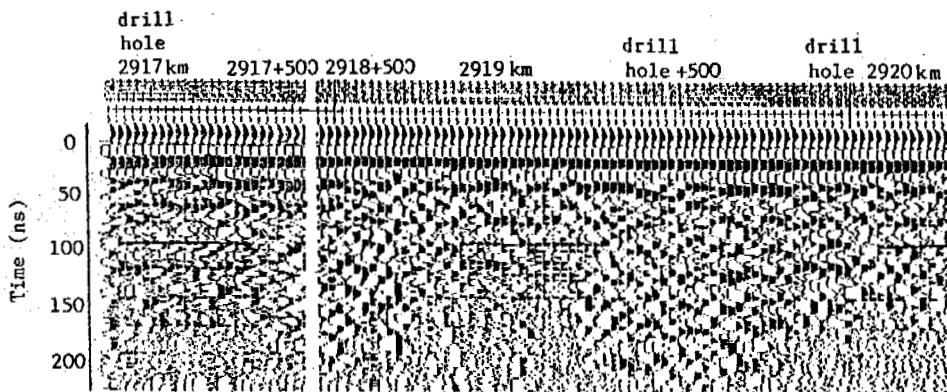


Fig.3 Ground penetrating radar section at Budonquan army service station in a tectonic belt characterised by hot springs

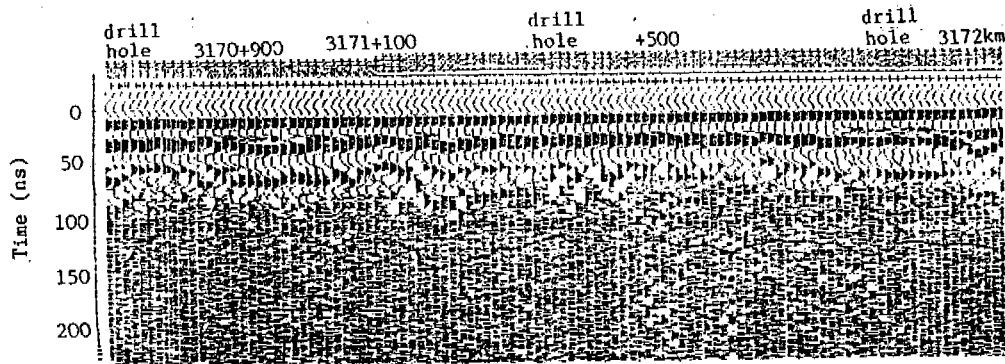


Fig.4 Radar recordings on the southern slope of Kaixingling

Still, the sixth reflector in the 110-150 ns time window is continuous. The depths to the permafrost upper table as determined from borehole geological logs are 5.1, 4.2 and 4.2 m on three points: the corresponding arrival times of the sixth reflector are 134, 115 and 118 ns. Making use of the GPR velocity ( $V=0.075 \text{ m ns}^{-1}$ ), the depth of the permafrost upper table are calculated as 5.04, 4.32 and 4.44 m respectively. The relative error on depth estimations between the GPR results and those obtained from the geological logs at 12 boreholes drilled between 3170 and 3179 km varies between 1.2 and 5.7% (mean: 2.8%).

#### Example 4: GPR Section on the Northern Slope of Tanggula Mountains

This section is characterised by a zone of continuous permafrost in a thick layer of fine-grained sediments containing well developed lenses of ground ice. The GPR method outlines nicely the permafrost distribution and the depth variations of its upper table under the road surface (Fig.5). The northern end of this section is located in Muqu River. The sixth reflector is not present to the north of 3310+400 m indicating the talik caused by the river bed where unfrozen gravel was observed in a drill hole at 3310+150 m down to a depth of 7.1 m. On the other hand, a clearly identified sixth reflector occurs to the south of 3310+400 m. The fifth and sixth reflectors merged in the southern segment of the section as a result of a shallow upper table depth. Radar velocities ( $V=0.078$  and  $0.068 \text{ m ns}^{-1}$ ) were calculated for the segments: 3310-3320 and 3320+50m-3233km respectively. The mean relative error of the calculated results is 3.8% by comparison with those of the geological logs from 11 drill holes available on this section.

In addition to the detection of permafrost distribution and the depth to its upper table, the GPR information can also be used to distinguish sedimentary rocks and/or soil types. For instance, the deposits on the northern section from 3310 to 3313 km and which are located at the foothills of the mountain range are of alluvial-diluvial-glaciofluvial nature, they are mainly composed of gravel with pebbles and cobbles. In the middle segment of the section (from 3313 to 3320 km), i.e. on the lower portion of the slope, clayey silt sediments with a minor fraction of gravel were deposited by diluvial agents. The gravel content increases towards the southern segment of this section near the upper position of the mountain range slope.

On the GPR recordings these changes in sedimentary facies are readily observed. In the northern segment of the section, the GPR recording pattern is relatively disordered (diffuse or disrupted reflectors) due to predominant scattering of the radar wave caused by the occurrence of gravel. The GPR recordings from the middle segment of this section are relatively uniform and the intensity of the sixth reflector indicating the depth to the permafrost upper table is severely attenuated due to strong absorption of the fine-grained and wet soils. Finally, in the southern segment of the section, the GPR pattern is again relatively disordered in view of the increasing content in coarse-grained material.

#### DISCUSSIONS AND CONCLUSION

When integrated with information obtained from D.C.E.R soundings and geological logs in drill holes, the GPR method yielded very useful information along the 220 km-long section of the Qinghai-Xizang highway north of Tanggula Mountains, in particular concerning the permafrost under the roadbed and the ice content in permafrost. The results of this investigation do have a practical significance in the road construction and repair. The depth of the artificial permafrost upper table under the roadbed varies from 3 to 7.5 m along this highway as a result of differences in roadbed heights and soil types and the GPR recordings reflect faithfully the variations in depth of the upper table. A certain number of control drill holes is required since the upper table may correspond to the fourth, fifth or sixth reflector given the differences in soil texture and composition as well as nature of upper table depth. Data on seasonally frozen and thawing depths are essential for construction purposes in cold regions. As these depths are generally smaller than 5 m, they fall in the detection range of the GPR method. Ground penetrating radar is more accurate and faster than the traditional geophysical methods of permafrost investigation such as E.R. soundings or seismics and its application in this field should be more widespread. This GPR survey was undertaken in September and October because the depth of seasonal melting is then near its maximum. Even though radar wave absorption in the soil (wet) is large, the contrast in dielectric constant between the moist zone and permafrost upper table (thawed-frozen interface) is clearly predominant. In North America, GPR investiga-

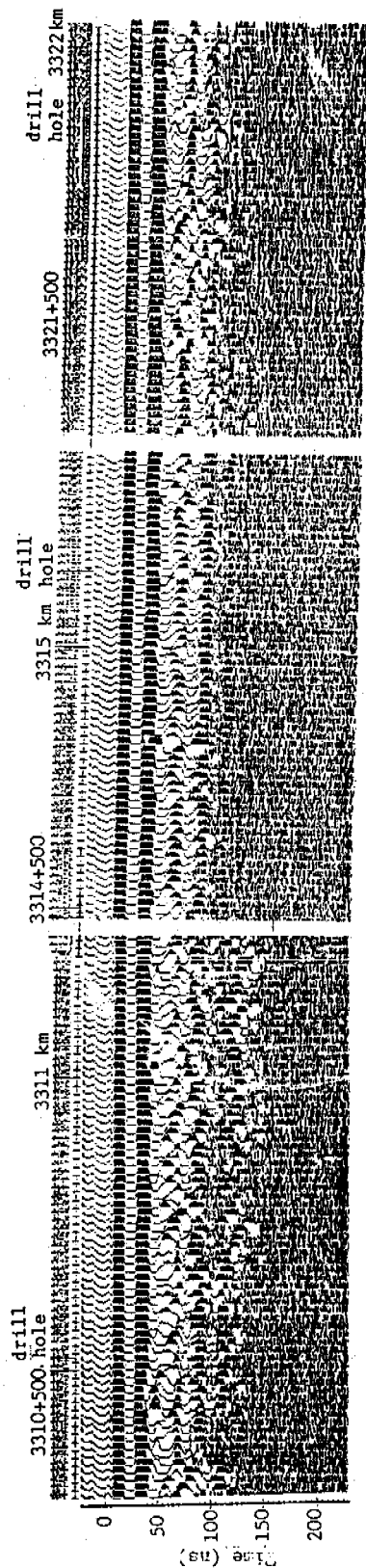


Fig.5 Delineation of the depth to permafrost upper table with the help of a GPR survey carried out on the northern slopes of Tanggula Mountains

tions for permafrost are often carried out in April-May. Even though the soil absorption of radar waves is small since the near-surface sections of soil is in the frozen state, the contrast of electrical properties at the upper table of permafrost is weak and diffuse during this period of the year. So, the selection of an optimum timespan in the year to undertake GPR surveys for permafrost investigation needs additional experimentation, comparison and further discussion.

The travel speed of GPR wave in soil layers is essential to the quantitative interpretation of radar recordings. In the present study, time domain reflectometry was not used in view of the non-availability of the equipment. As mentioned in reference (R.M.Morrey et al.,1985), radar wave velocities obtained through the analysis of CDP records are sometimes higher than the actual ones. A comparison of the velocities inferred from CDP recordings and those obtained from reflectors on radar properties correlated with geological logs from drill holes indicate that they are nearly the same. Sometimes, the former is larger than the latter and sometimes the reverse is true. The explanation of this phenomenon is that in a multilayered medium, radar wave trains cause interferences for large separation ( $> 1$  m) of antennas. It is thus difficult to pinpoint accurately the arrival time and a relatively large error is associated to the calculation of ground radar velocity using the CDP technique.

A glance at Fig.5 shows the differences in radar recording pattern resulting from different lithologies. It is generally found that the radar wave pattern is more irregular at stations nearby rivers and streams. This example and many similar ones demonstrate the possibility of distinguishing types of deposits and sedimentary facies changes. This difference is especially obvious in natural (undisturbed) ground sections. On the highway, this distinction is more difficult as 2-3 m of gravel make up the roadbed.

The history of application of the GPR method goes back to 20 years only. In China, this is the first ground penetrating radar investigation for permafrost, so obviously many problems of theoretical, methodological and practical nature still remain and require further discussion. For instance, an analysis of the radar wave train shows that the fourth, fifth or sixth reflector can delimit the permafrost upper table depending on many factors such as soil type, water content, thickness of roadbed, nature and thickness of seasonally thawed layer. In summary, the first correlated radar signal is undoubtedly the direct air wave travelling from the transmitter to the receiver. The second correlated radar signal (reflector) is due to a reflection from the highway. However its time delay is 25-30 ns which means that the radar wave velocity in the asphalt layer is only  $0.035-0.04 \text{ m ns}^{-1}$  which is clearly too low even though the asphalt is highly porous. The third reflector is commonly unrelated to a change in particle size within the roadbed materials or to the depth corresponding to the interface: bottom of roadbed-underlying soil layer.

#### ACKNOWLEDGEMENTS

The authors would like to thank Ma Zhixue, Guo Xingming, Wang Yujie and Wang Haomo for

their contribution to this study. This investigation was financially supported by the First Highway Designing Institut., Ministry of Communication.

#### REFERENCES

- P.Hoekstra et al.(1975) Dielectric properties of soil at UHF and microwave frequencies. Journal of Geophysical Research. (11): 1699-1708.
- S.A.Arcone et al.(1984) Radar investigations above the trans-Alaskan pipeline near Fairbanks. CRREL Report 84-2.
- J.A.Pilon et al.(1985) Monitoring permafrost ground conditions with ground probing radar (G.P.R.). CRREL Special Report 85-5.
- A.P.Annan et al.(1977) Use of radar and time domain reflectometry in permafrost studies. Proceedings of a symposium on permafrost geophysics 12 October 1976. OTTAWA.
- J.A.Pilon et al.(1980) Comparison of thermal and radar measurements of the active layer thickness in the Leaf Bay area, New Quebec. Proceedings of a Symposium on permafrost geophysics (No.5) 13 and 14 November 1978. OTTAWA.
- P.V.Sellman et al.(1983) Radar profiling of buried reflectors and the groundwater table. CRREL Report 83-11.
- S.A.Arcone et al.(1982) Radar detection of ice wedges in Alaska. CRREL Report 82-43.
- R.M.Morrey et al.(1985) Analysis of wide-angle reflection and reflection measurement. CRREL Report 85-5.

## THE PROBLEMS OF WATER TRANSFER FROM SOUTH TO NORTH CHINA OVER WESTERN PERMAFROST AREAS\*

Zhang Changqing, Zhu Linnan, Zhang Jianming and Liu Yongzhi

State Key Laboratory of Frozen Soil Engineering, Lanzhou Institute of  
Glaciology and Geocryology, Chinese Academy of Sciences, China

The proposal is for a western construction line for water transfer from south to north across continuous permafrost and seasonally frozen ground regions whose geographical condition is complex and ecological environment is weak. From field investigation in the water transfer region, we present a general image about the study of resources and environmental evaluations, specific research contents and technical routes.

### INTRODUCTION

The distribution of water and soil resources are considerably uneven in China. The drainage area of the Yellow River ( $75.2 \times 10^4 \text{ km}^2$ ) in northern China is 42.1% more than that of the Yangzi River ( $178.2 \times 10^4 \text{ km}^2$ ) in southern China.

The mean annual run-off of the former ( $584 \times 10^8 \text{ m}^3$ ) is only about 61.4% of the later ( $9513 \times 10^8 \text{ m}^3$ ). The mean water amount for one person and one hectare, in the former is about 26.4% and 11.5% of the latter respectively (Wang, 1991). The data listed above presents a characteristic of the severe shortage of water resources in the northern part and a comparative surplus of water resources in the southern part. From this, a reasonable balance of water resources is one significant measure in the water-transfer from south to north across drainage areas. As of now, we have worked out programs of water transfer from south to north across drainage areas and some parts of the programs have been put into effect. The western line of construction for the water transfer from the Yangzi River to the Yellow River has great importance in changing the water shortage situation, improving the environment and developing local economies in the northwest area. Some research work is currently under way.

The regions that the proposed western line of construction of water transfer from south to north needs to pass are the Tongtian River and the Dadu River which are located in the headwaters of the Yangzi River (Fig.1). The general water amount transferred is up to  $200\text{--}300 \times 10^8 \text{ m}^3$ . The construction is composed of several water transfer lines which are either in an artesian

mode or a raised mode. A series of diversion junctions that can contain  $100 \times 10^8 \text{ m}^3$  of water and have a height between 200-400 m, water transfer pump stations and diversion culverts of more than 50-100 km, diversion channels and other hydraulic structures are needed. The scale of the construction is very large. Since the construction is located in high altitudes which have an adverse natural circumstances and made communication difficult, there is a little scientific information on this region. Therefore, we must conduct a series of studies about the environmental evaluation of natural resources in water transfer areas and their interaction with the construction, in addition to solving a lot of cold region problems of engineering technology. These studies have a great importance in improving the progress of engineering construction and in rising the scientific level in cold regions.

### PHYSIOGRAPHICAL CONDITIONS AND THE CHARACTERISTICS OF PERMAFROST

The region (32-35N, 95-103E) of the western line of water transfer lies in southeast part of Qinghai-Tibet. The altitude of the region is 2900-5500 m and the physical features lower from west to east. The strike of the ridges in this region appears in N.W.-S.E. direction. Ba Yakala Mountain crosses the hull region. It is also a dividing range of the Yangzi River and Yellow River. In the southern region (the drainage area of Yangzi River), the topography is a considerably eroded area and the difference of elevation is up to 500-1000 m. The area experiences a subfrigid or frigid climate. There are *acculisilvae* and crops distributed in the area. In the northern region (Yellow River drainage area) the topography is gentle.

In the western line of Tequantu-Sangrima in this region, topography is mainly high mountains, shallow and wide valleys and a lot of lakes and swamps. In the east of the line is a high moun-

\*Other research staff are Li Zuofu, Zen Zhong-gong, Guo Xingming, Mi Haizheng, Chang Xiaoxiao, Wang Guirong, An Weidong, Xian Congde and Liu Xingmao.

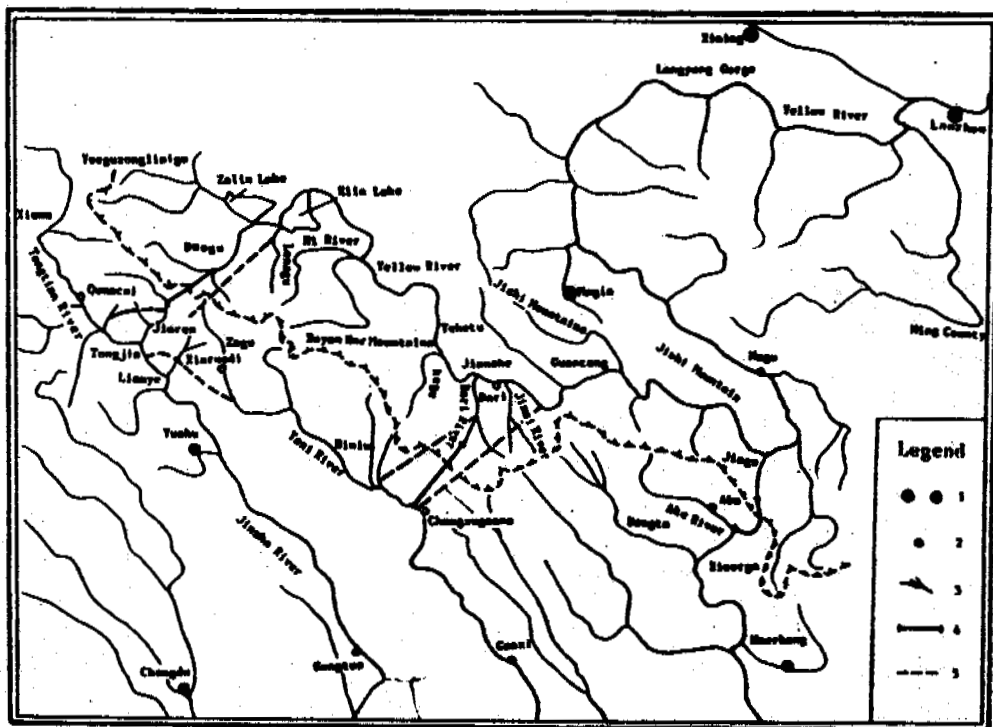


Figure 1. Western line of water transfer from south to north

1. Government areas of prefecture and province;
2. County area;
3. Hydrological station at Dam site;
4. Water transfer line;
5. Artesian water transfer line.

tain area, the difference of altitude is 100-1000 m. In the eastern line of Maqu-Jiaqu, topography is diluvial plateaus and ridges. It experiences a subfrigid and draughty climate and appears a tundra phenomenon (see picture). The geologic structure is complex. New structure movement is very strong, earthquakes are frequent and the Ms is more than 6.0.

The type of permafrost in western line of the water transfer construction belongs to upland permafrost that lies in a transitional belt of continuous permafrost in Qinghai-Tibet Plateau and discontinuous permafrost or seasonal frozen ground. The area of permafrost is about  $14.4 \times 10^4$  km<sup>2</sup> (Wang, 1991), in which the permafrost from Tongqian River to Lianghu water transfer regions contains 70-80% of all the permafrost. Only in river valleys and areas around lakes are there taliks. There is mainly sporadic permafrost from Yalong River to Dari River in water transfer areas. The area is about 40-50% of all the region. There is fragmentary permafrost between the altitude of 4300 and 4400 m from the Dadu River to the Yellow River, its area is less than 20% and it basically belongs to deep seasonal frozen ground. The distribution of permafrost is controlled by altitude. The limit of permafrost in Tongqian River water transfer area is about 4200-4300 m a.s.l. In the Yalong River in the water transfer area, the limit is 4150-4250 m a.s.l. and 4300-4400 m a.s.l. It submits to the law of the change of latitude. The latitude decreases one degree, the sub-limit of perma-

frost rises 130 m. In addition, the difference of geomorphology and vegetation has the same effect on the limit. Owing to the complexity of the natural condition in water transfer areas, the localization of the distribution and the instability of fresh water is obvious.

Up to now, the measured depth of permafrost in the region was little. The maximum depth measured is less than 50 m, the inferred increasing rate of the depth of permafrost is 13-17%. From this, the depth of permafrost at the altitude above 5000 m maybe surpass 100-120 m. But the water transfer construction related to the permafrost in the Tongqian River area is probably within 40-60 m, in the Yalong River area it is probably within 10-20 m. The Dadu River water transfer area only relates to seasonal frozen ground. Cryoturbation, thawed landslide, ground water, frost heaves and pingoes are distributed in water transfer areas, especially in the valley area of Bayakala mountain near the water transfer areas of Tongqian River and Yalong River (see picture), in which the ground water and cryoturbation will jeopardize the hydraulic structures. Pingoes and etc. may damage roads and the running of water transfer lines. In addition, large lakes and swamps may have deep ground water (i.e. there is a thick layered ground water of about 4.45 m at the depth of 20 m) which always threatens the stability and normal running of hydraulic structures. In concluding the characteristic of permafrost, the following statements have a practical significance and must be given



attention.

1. The permafrost in the western line of the water transfer area belongs to high temperature permafrost and has an unstable characteristic except for the western water transfer area of Tongqian River, especially when the foundation is in a rich ground water area in the region, there will be no ending creep and the bearing capacity of foundations is approximately zero (Tstovich, 1973). This type of permafrost is unsuitable for dam foundations and culverts. When the construction doesn't avoid the region, it will need complex techniques and higher expenses to devise the construction so that it will protect the permafrost from thawing or allow the permafrost to thaw.

2. The distribution of permafrost on the flat is very complex at the same construction site, there may be permafrost and seasonal frozen ground, and the frozen and thawed ground crisscrosses because the depth of permafrost in this region is less and lies in the warming condition of modern climate, human impact may induce the deterioration or disappearance of permafrost. In choosing the schemes of water transfer lines and key water control projects, we must pay great attention to this and give it further investigation.

3. Natural conditions in the region have considerable differences and the ecological environment is complex and weak. When its disturbed, it is difficult to recover. For example, the low land in Lianghu area, the area of swamp may spread or disappear, and the degree of salinization of soil may be intensified. The evaluation of the species of plants and animals and epidemics caused by water transfer has complex negative and positive social effects. Owing to this, we ought to give systematic plans in exploiting the water transfer resources.

#### ENVIRONMENTAL AND CONSTRUCTION PROBLEMS IN WATER TRANSFER AREAS

As described above, the scientific information such as permafrost, environment, ecology, and water resources and etc. in the western line of construction of the water transfer area is a little or none. Be confronted with such a significant large great systematic engineering of water and soil amelioration of the scales may be as large as Sanxia engineering of Yangzi River in the processes of planning design and construction. We face many problems to be solved. The main task for us is to predict and evaluate the environmental and water resource conditions before the construction begins, in addition to solving the cold region construction and technology problems. This research can not avoid the delays caused by incorrect evaluations and improve the progress of the construction in water transfer regions, but also enrich the scientific information of Qinghai-Tibet and enhance the research level of Chinese cold region environmental studies.

From the practical information, we divide the problems of water resource, environment and construction of the water transfer areas from south to north into six aspects:

##### 1. Evaluation of Cold Region Engineering Geology in Permafrost Areas

On the basis of permafrost surveys in large areas, the characteristics of the distribution of permafrost and its physiographical model,

monitoring the regimes of water and heat and their dynamic equilibrium in permafrost foundations, defining the local laws of transition belts of frozen ground from permafrost, sporadic permafrost in the active layer, and then predicting the deterioration tendency of permafrost caused by human activities should be determined. Research on the interaction and the relation of water transfer construction including canals, culverts, pump stations and etc. to various harmful geological phenomena. The evaluation criterion of thermal stability methods, constructing principles, and their reasonable uses in key control constructions (dams, weirs and brakes) in permafrost region should be studied. As well as to find and prevent negative effects of water and heat regimes of permafrost in transection belts on construction and ecology. The results of the above problems provide a qualitative basis for choosing and optimizing the scheme of water transfer lines and verifying the possibility of construction.

##### 2. Technological Construction Problems of Rock in Cold Region

This subject can be merged with engineering geocryology in cold region hydraulic structures. The main study is about the form and the condition of thermal transfer in the action of water and heat in the foundations and base of hydraulic structures and their interactive effects, with the structure. Those studies include mechanics, heat, physiochemistry of soil freeze thawing and their processes which can provide data for construction devices. In addition, we must give special and detailed study about some problems in permafrost foundations, such as the law of the distribution of stress field, stress and the criterion of deformation stability of permafrost foundations in different constructed forms and thermal processes, the effect of flowing deformation and the permitted bearing capacity in the long term stress bearing on reservoir banks, weir bases and deep channels; dynamic response and the long term stability of bearing various changing stresses (vibration, impulsive force explosions and etc.) of the permafrost foundation. The pressure density of high temperature permafrost foundations, thermal creeping law and the regime of thermal mechanics (thermal active effect) (Vialov, 1978), in addition to the experiments, analysis, simulation and prediction of stress fields in high stress foundations (high weir base or high stress centre area). The rules and the principles of freezing thaw of the foundation of various hydraulic structures, the thermal prediction of simulation for the reconstruction of reservoir banks in permafrost regions, as well as the frozen damage such as man-made thermal thawing, frost heave, surface depression, and the protecting measures and principles to the water from reservoir banks and water transfer constructions. To resolve and research the above problems effectively will have an advantage to improve the reasonability of the design and construction and will obtain social benefits.

##### 3. Synthetic Use and Soil Research

This subject presents the basic contents of exploiting resources in the water transfer area. It includes water resources (the thawed water of ice, snow, and run-off of rivers), the effects of building hydraulic structures on surface ground water run-off and their inter-

compensation and prediction of their changing tendency; the methods of reasonably exploiting land resources and their optimum in water transfer areas; the temporal and spacial changes of water and soil caused by water transfer across different drainage areas between water resources and water receiving places and the probable redistribution phenomenon of land resources such as the tendency of desertification in water transfer areas, especially in Yangzi River drainage area which is caused by the decrease of water in local areas. The water accepting area (Yellow River drainage area) may increase the intensity of salinized soil which is caused by the rise in ground water level. In some area, new swamps may appear. To study the above problems about the redistribution of water and land resources and the process of their dynamic balance and discuss the means to prevent the negative effects caused by water transfer as a basis of land realignment and schemes in water transfer areas. According to this, we must design and research water transfer construction simultaneously.

#### 4. Evaluation of the Cold Region Environment and Environmental Protection

One direct result of water transfer across different drainage areas is changes in the balance of the ecological environment in the hull of the water transfer areas, even around the boundary areas. To predict the changing effects, we ought to establish a new balance model. This is the main link to protecting the environment and to allow the construction to be put into effect. The three items listed above all can be merged into an environmental construction problem in a broad sense. Only in the narrow sense of the ecological environment, is it the successional rules, the distribution and the consistency of various biological resources, the prediction of the changes of ecological environment after the building of large reservoirs, such as the migration of biological species and the changes of growing rules of vegetation. The effects of water transfer on environmental engineering geology such as the changes of geochemistry, hydrochemistry, the means of construction and biology for environmental protection. On the whole, environmental ecology is a systematic construction, we need to give synthetic adjustment to each link and this may obtain the optimum results. This is a problem of human concern in world, and we must pay attention to it.

#### 5. Prediction of the Changes of Climate in Water Transfer Areas

To master the rules of changing climate and to predict its dynamic state is an important basis for us to reasonably exploit and utilize the water resources. It includes the rule of atmospheric circulation, the prediction of the changes of climate caused by water transfer and its effect on the ecological environment in water transfer areas, in addition to predicting the effects of the change of airflow in low pressure areas, of Songpan and on weather features in Qinghai and Gansu. In western Sichuan (water resource area), drought may intensify the climatic change. The results discussed above can directly be used in the construction scheme in the water transfer areas.

#### 6. The Regime of Geological Environment

Following the construction of a series of large central hydraulic hubs, the geological environment must be changed, and at the same time, the stress field of regional tectonics may also be changed too. The effect of many reservoirs and human activities may induce geological disasters and earthquakes. To research the regimes of the environment and the effects and to give long term monitoring are of great importance for the safety of future construction.

The contents described above are the basic features of the resources environments and construction. Following the engineering practices, will gradually form a research network about central studies of engineering environmental monitoring, and human studies of cold region engineering and water and soil resources. The hull systems will coordinate to the construction of the structure in its different periods. In the period of structural planning, the main tests will find out the physiogeographical models and their changing tendency and their relation to the permafrost environment in permafrost regions and to make test research about the characteristics of heat and mass transfer and the process of the physical and mechanical qualities of the foundation of hydraulic structures. This can be the basis of optimally choosing water transfer lines and evaluating local environments and the benefits of the schemes of water transfer, and finally improve the strategic decisions of water transfer from south to north. We hope the construction will be put into effect earlier.

#### REFERENCES

- Tstovich, N.A., (1973) The Mechanics of Frozen Ground. Higher Education Publisher.  
Vialov, S.S., (1978) Rheological Principles of Soil Mechanics. Higher Education Publisher.  
Wang Shaoling and Luo Xiangrui, (1991) The Distributive Characteristics of Ground in the east Qinghai-Xizang Plateau. Journal of Glaciology and Geocryology, Vol.13, No.2, p.131-140

MECHANISM OF THE ATTENUATION OF STRENGTH FOR LOESS-CEMENT  
UNDER CYCLICAL FREEZING AND THAWING\*

Zhang Huyuan<sup>1,2</sup>, Feng Ke<sup>2</sup>, Zhang Lixin<sup>1</sup>, Wang Yinmei<sup>3</sup> and Zhang Xiangong<sup>4</sup>

<sup>1</sup>State Key Laboratory of Frozen Soil Engineering, LIGG, Academia Sinica

<sup>2</sup>Department of Geology, Lanzhou University, China

<sup>3</sup>Department of Hydrogeology and Engineering Geology, Taiyuan University of Technology, China

<sup>4</sup>Department of Hydrogeology and Engineering Geology, China University of Geosciences, Beijing, China

The durability of loess-cement is assessed with cyclical freezing and thawing tests. After the cyclical test, specimens are cut into layers from which water content is measured and micrographs of SEM are taken. Micrographs show that the cement added to loess is hydrated to produce a lot of pin- or fabric-like crystals between soil particles. This three dimensional crystal framework gives loess-cement an improved strength. During the freezing period, water within the specimen or supported from outside circumstance is found to transport successively to the frozen front and be crystallized out forming some continuous layers of ice in the specimen. In this process, the crystal framework of hydrated cement around ice layers is broken down by tension. As a result, some weak planes appear in the specimen when it is melted.

INTRODUCTION

Loess has a wide distribution with a large thickness in China. The best known examples of collapsing soils, epistocene and holocene loesses have some poor engineering properties including dispersibility, high compressibility and low strength. From the engineering geological point of view, loess may be reinforced by various means so that its engineering performance can be improved. In general, they fall into two categories: mechanical and chemical reinforcement. But loess-cement may be referred to as loess consolidated both mechanically and chemically. When soil is mixed with Portland cement and compacted at an appropriate water content, the mixture forms a hard, durable material known as soil-cement, which has been used in China in the construction of roads, airports, earth dam pavements and foundations of buildings since 1970's (Xiao Lin et al., 1987). Systematic research about loess-cement began in 1987, when Prof. Zhang Xiangong was sponsored by the National Funds for Natural Sciences. It has been found that loess consolidated by cement has improved engineering properties (Wang Yinmei and Zhang Xiangong, 1991). As further research, here is discussed the strength attenuation of loess-cement when it is exposed to cyclical freezing and thawing weather conditions, great attention has been paid to the micro-mechanism of the attenuation so that the results may be used for other kinds of soil-cement.

MATERIALS AND MOULDING OF LOESS-CEMENT

Loess-cement is a mixture of loess, cement and water. The loess used in our experiment is the natural loess soil sampled at five locations

within Lanzhou District, Gansu Province, China, numbered respectively I to V as shown in Table 1. The physical parameters of these loess samples are listed in Table 1. Table 2 shows the chemical composition of loess numbered V. The cement added to loess is a normal silicate cement with grade 425. Tap water is used as pore liquid to hydrate the powder mixture of loess and cement. In case of discussing the effect of additives upon the strength of loess-cement, one of the different additives is dissolved in or mixed with the tap water.

Table 1. Physical Parameters of Loess Samples

Sample	Specific gravity	LL (%)	PL (%)	Granulometric composition(%)		
				>0.05 mm	0.05-0.005 mm	<0.005 mm
I	2.75	26.1	16.0			
II	2.71	23.3	15.4			
III	2.73	25.0	17.6	10	72.6	17.4
IV	2.73	27.1	18.3	22	61	17
V	2.725			21	72.6	6.4

Air-dried loess, passed through 0.5 mm sieve, is mixed with certain percent of cement, by weight of loess, to form a powder mixture, to which a certain percent of tap water, by weight of loess and cement, is then added and mixed together as homogeneously as possible. The selected additive is originally dissolved in the tap water if necessary. Begin the moulding procedure as the whole mixture is completed.

According to the water content of the mixture when all materials are mixed together, there are two ways to mould the mixture to form a loess-cement specimen. If the mixture has a water content near its plastic limit, it is compacted in a mold on a material-testing machine to take a cubic shape, in the case of the compacted loess-

\* This study was supported by the State Key Lab of Frozen Soil Engineering, LIGG, Chinese Academy of Sciences.

Table 2. Chemical Composition of Loess Sample No.V

Constituent	Content(%)	Constituent	Content(%)
SiO <sub>2</sub>	57.74	H <sub>2</sub> O <sup>+</sup>	2.90
Al <sub>2</sub> O <sub>3</sub>	12.00	H <sub>2</sub> O <sup>-</sup>	1.08
Fe <sub>2</sub> O <sub>3</sub>	2.83	CO <sub>2</sub>	6.17
FeO	1.44	TiO <sub>2</sub>	0.62
MgO	3.28	P <sub>2</sub> O <sub>5</sub>	0.15
CaO	8.18	MnO	0.09
K <sub>2</sub> O	2.29	S	0.06
Na <sub>2</sub> O	2.30		

(data from Wang Yongyan et al., 1982)

cement (C). If the mixture has a water content up to or more than its liquid limit, it is thrown into a mold piece by piece and then pushed out three days later, in the case of self-hardening loess-cement. It is found that between compacted and self-hardening loess-cement (SH), except the difference in initial water content and in moulding procedures, there is a similar mechanism of hydration of cement added to loess. All the specimens out of the mold are cured in certain circumstances and for different times as required.

**ENGINEERING PROPERTIES OF LOESS-CEMENT**

When the materials of loess-cement are just mixed together, the loose mixture has no strength. The self-hardening loess-cement, having its strength from the chemical reactions within the loess-cement-water system, can be referred to as chemically consolidated loess. The compacted loess-cement has an initial strength coming from the mechanical compaction effort and an increased strength with time coming from chemical reactions shown in Fig.1. That is, compacted loess-cement is a loess consolidated by both a mechanical and chemical processes.

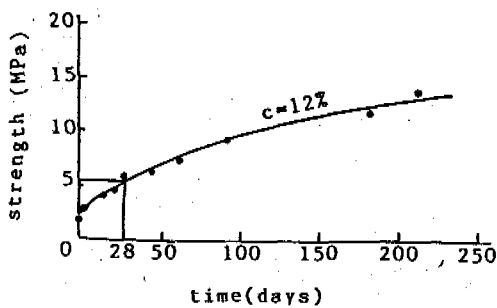


Figure 1. Increase in strength of compacted loess-cement

Unconfined compressive strength, one of the most important parameters for a material, is also used for loess-cement reflecting its quality. Obviously, there are many factors effecting the strength of loess-cement, primarily the

density, percentage of cement added, curing time and the type and the addition of additives used. Similar to that for concrete, a curing period of 28 days is defined for loess-cement when its strength is referred to as the normal strength used for the purpose of engineering design. This does not mean that the increase in strength has ceased at the time, in fact, above that time loess-cement increases its strength considerably shown in Fig.1. Fig.2 shows the effect of increased cement content and dry density on the strength of compacted loess-cement. Fig.3 shows the effect of increased cement content and curing time on the strength of self-hardening loess-cement. From Figs.2 and 3, it can be found that the more the cement content and density and curing time, the higher the strength of loess-cement. It is impractical to increase the strength of loess in construction by infinitely increasing the density or the cement addition due to technical or economical reasons. A reasonable method may be, finding an economically acceptable percentage of added cement, the mixture is compacted to a maximum density as the capacity of a compacting machine could do.

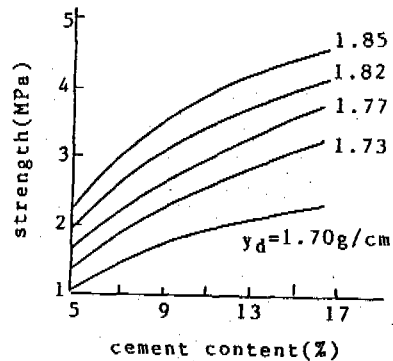


Figure 2. Effect of cement content and dry density (d) on the strength of compacted loess-cement

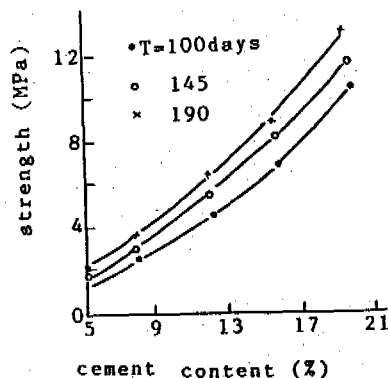


Figure 3. Effect of cement content and curing time (T) on the strength of self-hardening loess-cement

Typical relationships between stress and strain for loess-cement are shown in Fig.4. It can be seen from Fig.4 that loess-cement at first deforms elastically under load and then, after a shorter strain-hardening stage, ceases to resist further deformation and will rupture at the peak

point when it is tested with a machine or rather the stiff machine that was used here. Compared with loess, loess-cement is a higher elastic but lower ductile material.

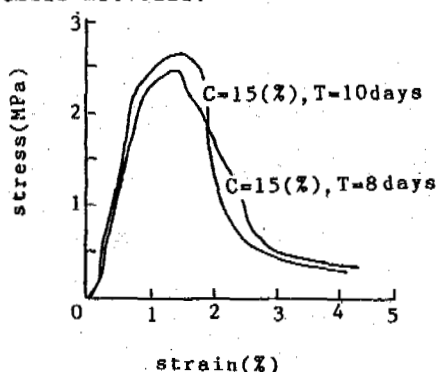


Figure 4. Stress-strain relationship of self-hardening loess-cement

#### DURABILITY OF LOESS-CEMENT

The durability of loess-cement is traditionally assessed with the attenuation of strength after it has been frozen and then thawed 25 times. Table 3 shows the effect of some additives on the durability of loess-cement. From Table 3 it can be found that, without any additives, loess-cement loses more than 30 per cent of its initial strength after 25 circles of freezing and thawing, and that the addition of washing powder makes the loess-cement mostly resist the attenuation more than the others do. Because the loess-cement-additive-water system is very complicated, there is a further need to research the effect of additives on the durability of loess-cement.

Due to its comparatively poor durability, loess-cement is thought to be troublesome in that it, if used under cold weather conditions, it can lose part of its strength and lead to instability of the structures. In order to understand the strength attenuation mechanism, four specimens of two kinds of loess-cement were tested under different conditions as shown in Table 4. A cylindrical specimen,  $\phi 15$  cm x 15 cm, fixed in the testing cell and side-wrapped with foam rubber, is exposed to an accurately controlled gradient of temperature in an axial direction, and then is frozen or cyclically frozen and thawed when the temperature gradient exposed to is adjusted as required. Three of the four specimens, were supplied with outside water through a pipeline in the bottom of the cylinder. After the test above, specimens are removed from the cell and are cut into layers about 1 cm in thickness each, of them half is used to measure their water content and the other half is used to take micrographs with a Scanning Electron Microscope (SEM).

Figs. 5, 6, 7, and 8 show the water distribution profiles for specimen S1, S2, S3 and S4, respectively, after they are tested under the conditions shown in Table 4. The frozen front is in the specimen whether fixed or unfixed as shown in Table 4, and means that part of the specimen tested will be frozen or cyclically frozen and thawed, and another part will not be frozen during the whole testing period. It is easily found that water is transported partly to the frozen end from the unfrozen end (as in S3), or from both the unfrozen end and the outside (as in S1, S2 and S4). It is interesting to note that there are three layers of ice available in specimen S1 after it had been tested, leading to a sharp increase in water content (see Fig.5). Two of the self-hardening loess-cement specimens

Table 3. Effect of Additives on the Durability of Loess-Cement

Sample	Additive		Strength of loess-cement		
	Name	Addition (g)	A(MPa)*	B(MPa)*	C(%)*
III <sub>0</sub>	None	None	7.90	5.31	32.78
III <sub>1</sub>	0.5% washing powder diesel oil	3.16	7.33	6.53	10.91
III <sub>2</sub>	0.5% sodium phosphite	3.16	6.55	5.60	14.50
III <sub>3</sub>	0.6% calcium chloride	3.79	5.96	4.90	17.79
III <sub>4</sub>	0.5% sodium sulfate 0.5% sodium nitrite 1% sodium phosphite	12.64	6.13	5.20	15.17
III <sub>5</sub>	0.5% washing powder	3.16	7.18	6.83	4.87

\* A=initial compressive strength  
B=attenuated compressive strength after 25 circles of freezing and thawing  
C=(A-B)/A, ratio of initial strength loss

Table 4. Characteristics of Loess-Cement and Test Conditions

Characteristics and conditions	Specimen of loess-cement			
	S1	S2	S3	S4
Type of the specimen	SH	C	SH	C
Cement content (%)	15	15	15	15
Initial dry density (g/cm <sup>3</sup> )	1.56	1.91	1.59	1.78
Initial water content (%)	26.0	9.05	26.78	9.38
Curing time (days)	9	9	20	21
Supporting water from outside	yes	yes	no	yes
Freezing only	✓	✓		
25 cycles freezing and thawing			✓	✓
Frozen front in specimen	fixed	fixed	unfixed	unfixed
Total time for testing (hrs)	240	240	370	370

(S1 and S3), having lower initial densities but higher initial water contents, are found to be more easily cut after having been tested than two of the compacted specimens (S2 and S4). From that viewpoint of durability, compacted loess-cement shows a higher freezing-resistance than the of the self-hardening specimens. This is because compacted loess-cement gains its strength from both the compaction effort and the cementing action of cement added, but the self-hardening loess-cement gains its strength from the later only.

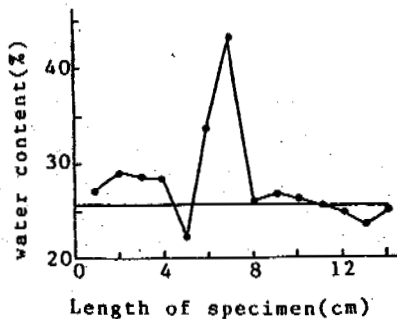


Figure 5. Water distribution profile for S1

The fact of whether or not the self-hardening specimen is complemented with water from the outside environment has an important effect on the durability of the specimen. Due to its lower density, self-hardening loess-cement is more permeable than the compacted specimen, so it can get more water from outside to be frozen and

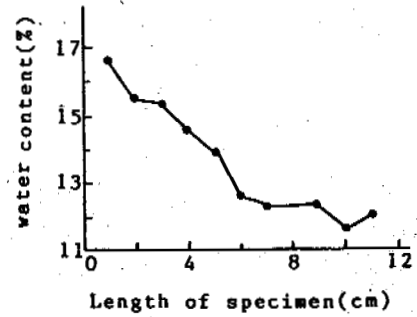


Figure 6. Water distribution profile for S2

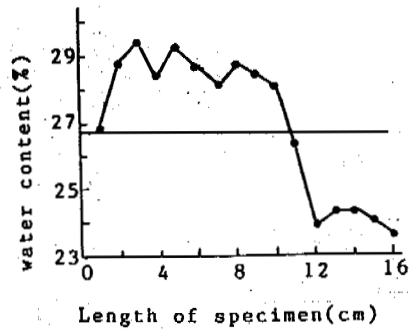


Figure 7. Water distribution profile for S3

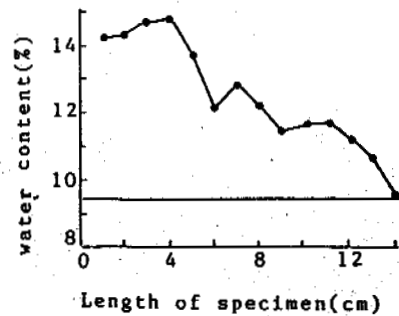


Figure 8. Water distribution profile for S4

has a higher potential to attenuate its strength.

Based on the analysis above, it can be preliminarily concluded that the durability of loess-cement may be improved by the ways as follows:

\* For a given cement addition, the mixture of all component materials of loess-cement should be compacted as hard as possible;

\* High water content of loess-cement should be avoided, whether the water is held in it originally or comes from outside environment secondarily. In other words, dry conditions are suitable to loess-cement;

\* Some additives should be added to loess-cement, such as daily used washing powder.

#### MICROTEXTURE AND ITS CHANGE IN LOESS-CEMENT

Three categories of micrographs were taken by the SEM from loess and loess-cement before and after the freezing-thawing tests to understand: (1) how loess-cement improves its strength from

the cement added, and (2) how loess-cement attenuates its strength when it is frozen or cyclically frozen and thawed.

Micrographs show that silt grains in loess have their "clean" surfaces and distinct outlines, but all of the soil particles in loess-cement have vague surfaces and outlines that can hardly be distinguished from one another. Another obvious phenomenon observed is that there are a lot of pin- or fabric-like crystals between soil particles of loess-cement. These crystals, having their growing points on the surfaces of soil particles, interweave with one another and form a framework in three dimensions. These new grown crystals in loess-cement must be the products of hydrated cement, although their mineral composition is unknown. It is believed that the new-grown three-dimensional crystal framework in loess-cement gives it an improved strength.

After the freezing or cyclical freezing-thawing test, specimens of loess-cement were cut into layers, which then were melted and air-dried in an indoor condition. Typical layers are used to take micrographs comparing with that taken from a similar untested specimens. It is found that the crystals where the frozen front stood have been broken down, this is caused by the tension effect while freezing. It is also found that the higher the increase of water content, the more the degree in which the crystals have been broken down. After the loess-cement is melted, there will be some weak planes where the crystals of hydrated cement have been broken down. It is the failure of the crystals that decreases the durability of loess-cement. If a cement content is given, it is impossible to increase the strength of the crystals of hydrated cement to improve the durability of loess-cement, except by using the alternatives selected: more powerful compaction, or water-proof treatment of loess-cement, or addition of additives, or a combination of them.

#### ACKNOWLEDGMENTS

This study was sponsored by the State Key Laboratory of Frozen Soil Engineering, Lanzhou Institute of Glaciology and Geocryology, Chinese Academy of Sciences. The authors would like to thank the Institute for financial support and the cooperation of the staff in this laboratory. The permission of preparing specimens of loess-cement in the Geotechnical Laboratory, Department of Geology, Lanzhou University, is sincerely appreciated.

#### REFERENCES

- Wang Yinmei and Zhang Xiangong, (1991) The Strength of Loess-Cement and its Effect on Controlling Loess Collapse Hazard. *J. of Geological Hazard and Control*, 2(1), pp.51-63.
- Wang Yongyan et al., (1982) *Loess and Quaternary Geology*. People's Publication House of Shaanxi Province.
- Xiao Lin, Wang Chunyi and Guo Hansheng, (1987) *Soil-Cement as Building Materials*. Hydraulic and Electric Power Publication House.

## ANALYSIS OF THE SECOND PHASE TRANSITION OF SODIUM CHLORIDE SOLUTION IN FREEZING SOIL

Zhang Lixin, Xu Xiaozu, Tao Zhaoxiang and Deng Yousheng  
The State Key Laboratory of Frozen Soil Engineering, Academia Sinica

By determining the unfrozen water content of saline freezing soils, including Lanzhou sand, Lanzhou loess and Inner Mongolia clay, with a different alignment of initial concentration of sodium chloride solution and total water content in a wide range of minus temperature. It is found that when the total water content and initial concentration of the solution in soil reaches an appropriate alignment, there occurs a clear second phase transition with the temperature going down. The beginning temperature in the second phase transition decreases with the particles becoming finer, and increases with the total water content and the initial concentration of the solution in soil rises. On the basis of a great deal of testing, this article has established the quantitative relationship between the beginning temperature of the second phase transition and total water content, as well as the initial concentration of solution in the soil.

### INTRODUCTION

The frozen soil is different from unfrozen soil in some properties, just because there is ice and unfrozen water coexisting in frozen soil at the same time. The ice and unfrozen water content existing in different proportions in frozen soil causes many complex changes of the soil properties, such as the appearance of heaving, creeping, and soliflucting, the changing of strength and thermal properties, and the forming of special cryogenic textures, etc. The existence of electrolytes in the solution of soil will significantly affect the freezing temperature. The proportion of ice and unfrozen water content in frozen soil will also be limited to a large extent at the same temperature.

Up to now, the content and type of the electrolyte as a notable factor influencing the properties of frozen soil, has caused researchers more and more interest. With the opening of the seashore and seabed frozen soil, the problems of the redistribution, the other behaviors and properties of frozen soil becomes vaster. Among them, the effect of the electrolyte on the unfrozen water content is a key one. The study on the problem is not very thorough (A. Bain and D. M. Anderson, 1974; A. R. Tice and Zhu Yuanlin et al, 1984, etc). More detailed work has been done in theory to deduce the relationship between the depression of freezing point to the solution in soil and the type and concentration of the ions in the solution has been deduced theoretically (A. Bain and D. Anderson, 1974). Experimental data shows that the unfrozen water content increases quickly with an increasing molaring of soil solution at the given temperature ( $>-20^{\circ}\text{C}$ ). The mutual relationship between two quantities is well represented by a linear function (Xu Xiaozu et al, 1988). The further experimental work also proves this point and shows that the relationship between the unfrozen water content in soil and total water content in the saline ( $\text{NaCl}$ )

soil, is a linear function at the same temperature ( $>-20^{\circ}\text{C}$ ). When the initial concentration and total water content in soil reach a certain alignment, the unfrozen water content changes sharply with the temperature decreasing further (Zhang Lixin, 1991). This phenomenon of unfrozen water content changing sharply corresponds to the second phase transition in  $\text{NaCl-H}_2\text{O}$  system. This paper will discuss the characteristics and law of the second phase transition in frozen saline ( $\text{NaCl}$ ) soil. There is certain significance to guide us in opening and using frozen soil, in particular, the artificial saline frozen soil. We can determine the temperature at which the second phase transition occurs so as to avoid a sharp change of the frozen soil properties.

### EXPERIMENTAL METHOD AND SAMPLE

In this test, we use Praxis PR-103 Nuclear Magnetic Resonance analyzer to detect unfrozen water content in soil within temperatures of 0 to  $-35^{\circ}\text{C}$ . What related to the operative method of using the analyzer to detect the unfrozen water content has been introduced in detail in some compositions (A. R. Tice et al, 1978, Xu Xiaozu and Deng Yousheng, 1984).

The samples used in the test are Lanzhou sand, Lanzhou loess and clay, which in size composition have some typicality. The size composition, index of plasticity and initial content of salt can be seen in Table 1.

Before compounding the sample, distilled water was used to wash out the salt in Lanzhou sand and Inner Mongolia clay. By detecting the conductivity of the washed liquid and comparing it with the conductivity of distilled water, we find both are almost identical, and use this as standard to determine the content of easily soluble salt near to zero. Since the content of easily soluble salt in Lanzhou loess is very little, it was not washed.

Heating the three soils, respectively, we com-



Table 1 Size composition, plastic index and initial content in samples

Soil Name	Size Analysis				Liquid Limit (%)	Plastic Limit (%)	Initial Content of Salt (%)	The Place Taking Sample
	>0.1 (mm)	0.1-0.05	0.05-0.005	0.005				
Lanzhou Sand	94.78%	3.93	0.37	0.04	-	-	0.146	Lanzhou
Lanzhou Silt	0.48	7.13	75.69	16.70	26.7	17.6	0.08	Lanzhou
Inner Mongolia Clay	0.48	1.64	20.56	77.22	32.8	20.4	0.705	Inner Mongolia

Table 2 The composition of samples

Soil Name	Salt Content	Concentration	Total Water Content				
			0	5	10	15	20
Lanzhou Sand	5	0	0.25	0.5	0.75	1.0	1.25
	7.5	0	0.375	0.75	1.125	1.5	1.875
	10	0	0.5	1.0	1.5	2.0	2.5
	12.5	0	0.625	1.2	1.875	2.5	3.125
	15	0	0.75	1.5	2.25	3.0	3.75
Lanzhou Silt	17.5	0	0.875	1.75	2.625	3.5	4.375
	5	0	0.25	0.5	0.75	1.0	1.25
	10	0	0.50	1.0	1.5	2.0	2.5
	15	0	0.75	1.5	2.25	3.0	3.75
	20	0	1.0	2.0	3.0	4.0	5.0
Inner Mongolia Clay	25	0	1.25	2.5	3.75	5.0	6.25
	30	0	1.30	3.0	4.5	6.0	7.5
	10	0	0.5	1.0	1.5	2.0	2.5
	15	0	1.75	2.25	3.0	3.75	30
	20	0	1.0	2.0	3.0	4.0	5.0

Unit in the table: Salt content, g salt/100g soil;  
Concentration, g salt/100g water;  
Water content, g water/100g soil.

found them into the samples containing Sodium chloride salt which have a different total water content and concentration of liquid percentages. The composition of samples are shown in Table 2.

ANALYSIS OF THE THEORY OF THE SECOND PHASE TRANSITION

The Theory of the Phase Figure to the System of NaCl-H<sub>2</sub>O

Fig.1 is the phase figure of the NaCl-H<sub>2</sub>O, in the figure the CD curve is the solubility of ice, the line of DJ is the solubility of NaCl·2H<sub>2</sub>O. Since there is no maximum point in the medium, the water-compound is unstable, the line of DJ is the solubility of NaCl.

GDE shows the line of common existence of ice, NaCl·2H<sub>2</sub>O and liquid phase. To take advantage of the above curves, the phase figure can be divide into the following areas. I is the area of unsaturated liquid (fully liquid area). The area indicates that unsaturated NaCl liquid does not have a solid phase.

II, IV, V are the areas of the solid-liquid-balance double phase. These areas indicate that some solid phase and unsaturated liquid commonly exist. Among them, II is the ice crystalline

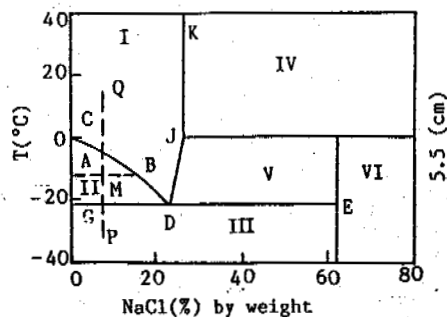


Fig.1 is the phase figure of the NaCl-H<sub>2</sub>O, in Fig.1 NaCl-H<sub>2</sub>O system phase figure(Liang Biaoming, 1986)

area, IV is NaCl crystalline area, V is NaCl·2H<sub>2</sub>O crystalline area.

III, VI are the areas of the fully solid phase. The system in the areas is situated in a double solid phase common existence and no liquid phase. III is Ice+NaCl·2H<sub>2</sub>O area, VI is NaCl2H<sub>2</sub>O+NaCl area.

The Second Phase Transition of the System of

## NaCl-H<sub>2</sub>O

According to the understanding of NaCl-H<sub>2</sub>O systematic phase figure, it is concluded that the sodium chloride solution of certain concentrations under a general temperature will occur in a phase double change with a decrease of temperature. Assuming that the initial location of the systemic point at Q in I area, with the temperature decreasing and going below zero, the systemic point will go along the QP curve into II area, in which there is pure solid phase of ice crystallizing. This is the systemic first phase transition. While the temperature continues to reduce to -21.2°C, the systemic point will go from II area into III area, at this time, since in II area ice is continuously crystallizing the densified NaCl liquid quickly will turn into second phase transition.

### The Discussion of the Text Conclusion about the Second Phase Transition of Solution in Soil

1. The basis of existence of the second phase transition of the solution in soil

In light of the above analysis, we can deduce that the sodium chloride solution in soil following a temperature reduction also should have the phenomenon of a second phase transition. The investigation of unfrozen water content in the frozen soil containing sodium chloride verifies the above deduction.

According to the investigation of unfrozen water content of the three kinds of soil containing sodium chloride, Lanzhou sand, Lanzhou loess and Inner Mongolia clay, we find that the curve of dependence on unfrozen water content and temperatures below zero have two evident changing processes. When temperature reduces to the beginning freezing temperature and overcomes the supercooling phenomenon, the unfrozen water content gradually decreases with the temperature decrement, which has the form  $W_u = A \cdot T^B$ , A, B are parameters related to soil, T is the absolute value of temperatures below zero, °C,  $W_u$  is unfrozen water content, %. When temperature reduces to a value which is inferior to -21.2°C, in unfrozen water content there abruptly occurs a quickly reducing phenomenon, as shown in Fig. 2, 3, 4.

Since unfrozen water content reflects that the solid-liquid ratio of the solution in soil after freezing, we can determine the occurrence of the second phase transition according to the change of unfrozen water content. In Fig. 2, 3, 4 the first section of curve indicates the process which solid ice phase crystal out, corresponding to the first phase transition in the phase figure. The second curve represents the process of NaCl·2H<sub>2</sub>O forming, which should belong to the second

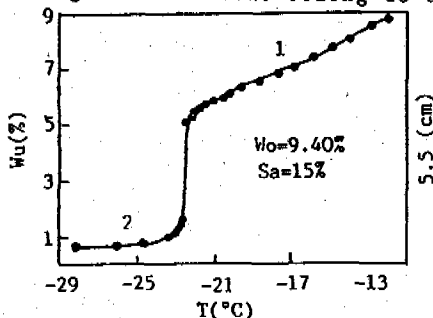


Fig. 2 The character of unfrozen water content with negative temperature changing to Lanzhou Sand

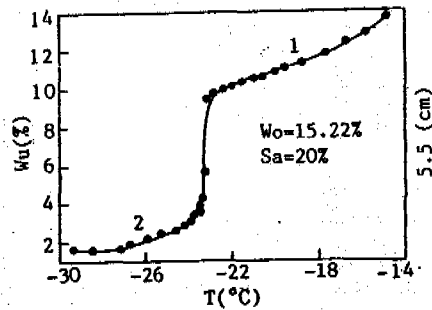


Fig. 3 The character of unfrozen water content with negative temperature changing to Lanzhou loess

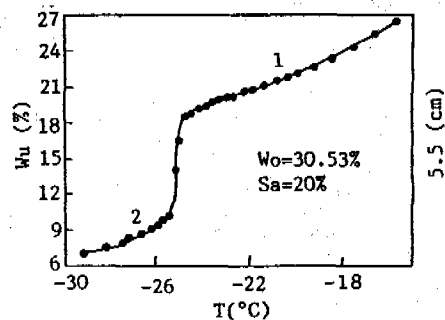


Fig. 4 The character of unfrozen water content with negative temperature changing to Inner Mongolia clay

phase transition.

2. Affecting elements and characters of the second phase transition of the solution in soil

a) The affect of the soil type

The general appearance of the second phase transition of the solution in soil is that the unfrozen water content can abruptly change with the change of unfrozen water content. The actual investigating conclusion shows that with different size composition the abruptly changing phenomenon will have different characters.

In the case of the Lanzhou sand, while the second phase transition is going, the unfrozen water content suddenly falls vertically and quickly reduces to below 2%. To finish this process of abrupt changing it will need a temperature, which is generally high and its range is very narrow, as Fig. 2 show. This indicates that in Lanzhou sand, the process of second phase transition of solution finishes quickly and fully.

Inner Mongolia clay is different from Lanzhou sand. Although the process of the second phase transition of the solution in soil is obvious on the curve dependent on unfrozen water content and temperature, there is a certain successive gradually changing process. The temperature of the second phase transition in the beginning is lower and the range is wider. Phase transition does not finish completely and the unfrozen water content at the bottom is over 8%, as shown in Fig. 4.

The character of the second phase transition of solution of Lanzhou loess is between that of Lanzhou sand and Inner Mongolia clay. After abruptly changing, the unfrozen water content is over 2% as shown in Fig. 3.

The second phase transition of the solution to the above three types of soils has different characters, the main reason is that the size of Lanzhou sand is larger, mainly in quartz, feldspar, mica, their reaction with water is not obvious, adding to the sand specific area very little, so the limiting force of the solution in soil is very little, the characters are particley the same as compared with the standard solution. Inner Mongolia clay particles are very little and fine, mainly are composed of unsolvent second-produced minerals such as kaolinite, montomotillonite, due to the illite in them, since montomotillonite has a special electrovalent bond and electric charge dispersion, the particle action with water is quite obvious. Since its specific area is very large and structure is very complex, so the solution in soil is limited strongly. In quite an extent it is different from the characters of the standard solution.

Lanzhou loess in size composition is in the medium of them, mineral compositions mainly are quartz, feldspar, mica, their content is over 60%. It also contains a few clay mineral, mainly montomorillonite and illite. The loess samples in the experiment according to the plastic index sorting should belong to loess sand clay. The property of solution in loess is in the middle of that of above solution in soils.

(b) The affect of initial concentration of solutions in soils

On the basis of analysis to test data about the abruptly changing phenomenon of unfrozen water content, it is found that in the frozen soil containing sodium chloride the relationship between initial temperature of the second phase transition of the solution in soil and initial percent density of solution in soil have the following form:

$$T = \frac{A}{S_a + B} \quad (1)$$

where  $S_a$  is the initial percent density of solution in soil,  $T$  is initial temperature of the second phase transition, °C,  $A, B$  are parameters related to soil. The Fig.5 reflects the

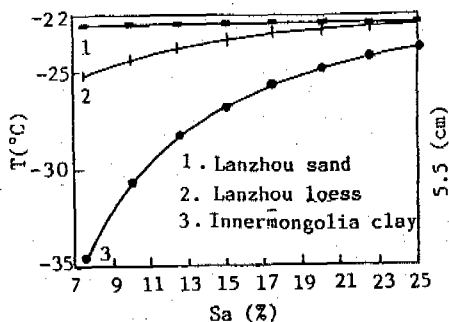


Fig.5 The relationship between the temperature of the second phase transition point and initial concentration of solution in soil

relationship between the point of the second phase transition and concentration of the three types of soil.

(c) The affect of total water content

Similar to the initial concentration of solution in soil, the relationship between total water content and the temperature of the second phase transition beginning also can be approxima-

tely expressed as:

$$T = \frac{C}{W_0 + D} \quad (2)$$

where  $W_0$  is total water content, %,  $C, D$  are parameters related to soil. As Fig.6 showing,

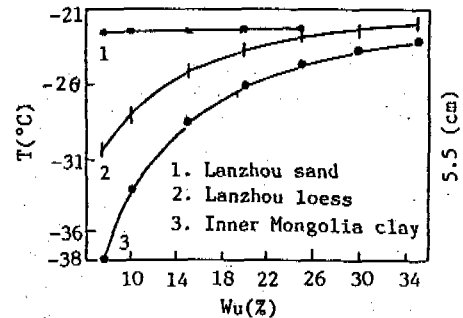


Fig.6 The relationship between the temperature of the second phase transition point and total water content to solution in soil

the figure reflects the relationship between the temperature of the second phase transition point and total water content.

Combining fomula (1) and (2), we can establish the following formula:

$$T = \frac{C \cdot S_a + A \cdot W_0}{2S_a \cdot W_0} \quad (3)$$

In the light of formula (3), it can be seen that the temperature of the second phase transition beginning is strongly limited by total water content and initial concentration of the solution in soil. As one of them approaches zero, it will let the beginning temperature of the second phase transition reduce particley.

## CONCLUSIONS

(1) When the temperature of the solution in frozen soil containing sodium chloride reduces to a certain value, the second phase transition will occur. The general displaying of this phenomenon is that unfrozen water content will reduce quickly.

(2) The size composition of soil has a certain affect. The finer the soil particle is, with the same initial concentration of solution in soil and total water content, the lower the second phase transition temperature is, and the more uncompletely the phase transition is, which is obvious in the process of gradual change.

(3) It is obvious that the affect of total water content and initial concentration of the solution in soil to the second phase transition. The less both are, the lower the point of the second phase transition is. Both of them have a reciprocal relationship.

## REFERENCES

- A.Banin and D.M.Anderson (1974) Effects of Salt Concentration Changes During Freezing on the unfrozen water content of Porous Materials. WATER RESOURCES RESEARCH, 10:124-128.
- A.R.Tice, Zhu Yuanlin and J.L.Oliphant (1984) The Effects of Soluble Salts of the Unfrozen water content of the Lanzhou, P.R.C., Silt. USA CRREL Report 84-16.

Xu Xiaozu, J.L.Oliphant and A.R.Tice (1985)  
Soil Water Potential, Unfrozen water content  
and temperature. *Glaciology and Geocryology*,  
7(1),14.

A.R.Tice, C.M.Burrous and D.M.Anderson (1978)  
Determination of Unfrozen Water in Frozen  
Soil by Proceedings, Third International  
Conference on Permafrost.

Liang Biaomin (1986) Water-salt-system phase  
figure and its appliance. Light Industry  
Publish House Beijing.1-85.

PLANT COMMUNITY ORDINATION AND ITS ENVIRONMENTAL INTERPRETATION FOLLOWING THE  
DISASTROUS FIRE IN AMUR AREA, DAXINGANLING PREFECTURE, NORTHEASTERN CHINA\*

Zhang Qibin, Zhou Youwu, Wang Jiachen, Liang Linben and Gu Zhongwei

Lanzhou Institute of Glaciology and Geocryology, Academia Sinica

In this paper, the plant communities following 1987's turbulent forest fire in Amur Area, northern part of Daxinganling were studied using the methods of TWINS-SPAN polythetic hierarchical divisive classification (TWINS-SPAN program) & DCA ordination (DECORANA program). The results show that DCA axis 1 reflects the gradient of soil characteristics and topography; DCA axis 2 is interpreted as the gradient of forest fire burning degree which can cause changes in both the thaw depth to frozen ground and the soil temperature at shallow layer that are the significant factors for the distribution of plant communities, and a regression equation is produced. In addition, we discussed the direction and stages of plant secondary succession under the influence of permafrost environment development.

## INTRODUCTION

The turbulent forest fire burned in Mt. Daxinganling in the northeast of China during May 6-June 2, 1987 made a great loss of forest resources in this region and it also caused prominent effect on the permafrost environment. In this case, understanding and mastering the relationship between the plant communities and permafrost environment and their developing laws following the fire would have great significance for the renewal of forest resources and promotion of the plant secondary succession. The methods of TWINS-SPAN polythetic hierarchical division classification and DCA ordination are currently one of the advanced methods for multivariate analysis of plant communities. It is the least studied for using this method to analyze the relationship between the plant communities and their permafrost environment following the disastrous forest fire in Mt. Daxinganling. In this paper, we made careful analysis of the data obtained in the field work during May-Aug. 1990 by means of the above method and drew a satisfactory result.

## STUDY AREA

Amur lies in the northern part of Daxinganling prefecture, and belongs to Mohe county. Its geographical position is 52°50'N and 123°11'E.

Amur is characterized by an extremely frigid-temperate zonal continental climate with short summer, long winter, cold and long period of snowing. By the data from the Amur Meteorological Observatory, the mean annual air temperature is -4.9°C, the mean annual maximum air temperature is -31.4°C and the minimum -47.2°C. The annual precipitation is 443.9mm. The frozen period

lasts for 8 months.

The geomorphologic feature of the area is low mountain and wide valley. The valley is widely underlain by unconsolidated sediments deposited during the Quaternary. The main rock is granite and there are also tuff breccia etc.. The main soil is brown conifer soil, and the soil layer is very shallow. There is bog soil in the bottom of valley. The area is permafrost discontinuous distribution region. There can be seen frost heaving, stone stream, drunken forest and other permafrost phenomena.

The area is part of the frigid-temperate zonal conifer forest region in accordance with division of vegetation. There are relatively few vegetation types and poor composition of plant species. The turbulent forest fire burned away a large area of the larch (*Larix gmelinii*) forest in the region and only left a few area of unburned forest. After three years, the plant secondary succession sequences on the burned areas are different with the situation of burning degrees, permafrost conditions and the keeping and invading circumstances of seeds.

## BRIEF INTRODUCTION TO THE RESEARCH METHOD

### Sampling

During May-August, 1990, the authors made a survey of the vegetation and permafrost conditions following the fire in Tahe, Amur, Tuqiang and Xilingji forest bureaus. After then we chose Amur as our field observation site and arranged four transect-observing lines according to the variation of burning degree, topography and the appearance of vegetation. We used typical sampling method to make the sample surveys of each different types of plant communities. Quadrant size of the samples was 10mX10m in wood vegetation, 4mX4m in tall shrub vegetation (h>0.5m),

\* This research project was supported by the National Natural Science Foundation.

2mX2m in short shrub vegetation ( $h < 0.5m$ ) and 1mX1m in meadow vegetation. Certain environmental conditions, species coverage percentage and abundance, community structure and height of layers were recorded for each sample. The plant community type was primarily determined in the field by dominant plants. Environmental factors measured or noted included the thaw depth to frozen ground, water content in soil, ground temperature at shallow layers and soil texture etc.. There were 38 formal plant samples and some supplemental samples, and they embraced the main types of plant communities in the area.

#### Quantitative Classification and Ordination of Plant Communities

Based on the data of field samples, we made the community classification by means of the TWINSpan program according to the percentage coverage of "sample---species data matrix"; and made principle correspondence analysis (PCA) ordination by ORDINA program, reciprocal averaging (RA) and detrended correspondence analysis (DCA) ordination by DECORANA program. In comparison, DCA ordination appeared better than the RA and PCA ordination because it can reveal the relationship between the plant communities and the environmental factors objectively and effectively, and avoid the arch distortion in the RA ordination. Thus DCA ordination was used in this paper to make further environmental interpretation. All of the calculation is accomplished on the VAG11/780 computer at the Lanzhou Institute of plateau atmosphere of the Chinese Academy of Sciences.

#### Correlation and Regression Analysis of Community Ordination Axis on Dominant Environmental Factors

First of all, according to the habitat data of each sampling points and their positions on the ordination figure, we analyzed the ecological meanings shown on the ordination axis. Then we made correlation and regression analysis of the environmental indexes with the DCA sample ordination scores, consequently we worked out the multivariate regression equation and made significance test. As a result, we got the

quantitative relationship between the plant communities and their permafrost environmental factors.

#### WORKING RESULTS

##### TWINSpan Classification

Table 1 is the classification result of the 38 samples and 32 plant species in the survey area by means of TWINSpan polythetic hierarchical division classification.

The selected maximum division level is four and the maximum number of indicating species in each division is four. The lower part shows the division levels and types of samples while the right part shows that of plant species. Twelve types of plant communities were classified in Amur following the fire (Table 2) and the result was basically consistent with that identified by the community structure and appearance feature.

##### DCA Ordination

Fig.1 is the two-dimensional plant community DCA ordination, which indicates perfectly the relationship between plant communities and their environmental factors.

The DCA ordination axis 1 reflects a gradient of soil characteristics and topography. Its character value is 0.733. The plant communities with AX1 scores <180 units are "Pinus sylvestris + Larix gmelinii" and "Rhododendron dauricum + Betula platyphylla + Alnus mandshurica" communities and generally they are situated at the ridge, middle-upper part of mountain or steep slope where it is characterized by thin layer of big-grained dry coarse sandy soil with crushed gravel layer underlain. The porosity is big and the drainage and aeration are well. AX1 scores between 180 and 340 are "Vaccinium vitis-idaea + V. uliginosum + Ledum palustre" and "Artemisia laciniata + Vaccinium vitis-idaea + Sanguisorba officinalis" communities. They are situated at the middle-lower section of the mountain with gentle slope. The soil is eluvial and slope wash crushed gravel subsandy soil and subclay soil. The soil porosity, drainage and aeration are poorer than the former one. The AX1 scores between 340 and 520 are "Larix gmelinii-Rhododend-

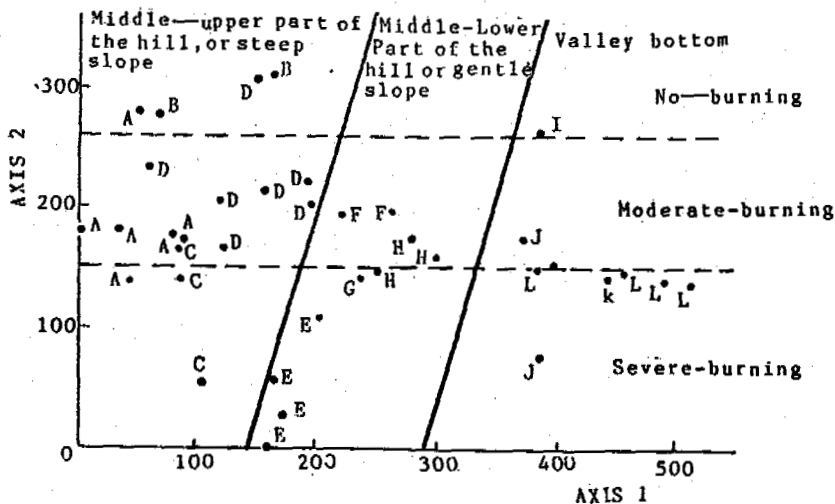


Fig.1 The DCA ordination of plant communities following fire in Amur area, Daxinganling prefecture. The community symbols are defined in Table 2

Table 1 The result of TWINSpan polythetic division and classification for plant communities and species after the disastrous fire in Amur area, Daxinganling prefecture

Plot number	1 1 1 2									1 1 1 3 3			1 2 3		2 4	3 1 2 2 2			1 2 2 2			3 3 3			1 2 2 3			3 3	Division level of species					
	3	5	7	4	8	9	0	1	1	3	3	1	2	3		8	3	1	2	2	6	6	7	8	6	4	5			6	9	0	3	4
Species																												1 2 3 4						
2 Larix gmelinii	7	-	-	-	-	-	-	-	-	-	-	-	-	-	3	7	-	-	-	-	-	-	-	-	-	-	-	-	-	-	6	0 0 0 0		
1 Pinus sylvestris	3	-	-	-	-	-	-	-	-	-	-	-	-	-	-	7	3	-	-	-	-	-	-	-	-	-	-	-	-	-	-	0 0 0 1		
3 Betula platyphylla	3	-	-	-	-	-	-	-	-	-	-	-	-	-	-	3	-	-	-	-	-	-	-	-	-	-	-	-	-	-	-	0 0 0 1		
4 B. platyphylla (clustered)	-	-	3	-	5	-	3	6	5	-	6	-	2	2	1	-	-	-	-	-	-	-	-	-	-	-	-	-	-	-	-	0 0 0 1		
5 Alnus mandshurica	5	-	4	-	-	2	6	4	3	5	-	-	-	-	-	-	2	-	-	-	-	-	-	2	-	-	-	-	-	-	-	0 0 0 1		
6 Populus davidiana	-	-	-	-	-	-	-	-	-	-	-	-	-	-	4	2	-	-	-	-	-	-	-	-	-	-	-	-	-	-	-	0 0 0 1		
8 Rhododendron dauricum	5	5	5	5	4	3	4	6	5	5	6	5	3	4	6	4	4	5	-	3	-	-	-	-	2	-	-	-	-	-	-	0 0 0 1		
15 Rosa davurica	4	-	-	3	-	-	-	3	-	1	3	3	-	-	2	-	-	2	-	-	-	-	-	2	2	-	-	-	-	-	-	0 0 0 1		
17 Sorbaria sorbifolia	2	-	-	-	-	-	-	-	-	-	4	2	-	-	-	-	-	-	-	-	-	-	-	-	-	-	-	-	-	-	-	0 0 0 1		
30 Deyeuxia angustifolia	2	3	2	4	2	-	1	3	7	6	-	2	6	2	1	3	3	1	-	3	1	2	-	1	-	3	2	1	-	-	1	0 0 0 1		
19 Sanguisorba officinalis	-	-	-	1	-	-	1	2	3	2	1	2	1	-	2	2	3	2	-	-	1	3	1	4	2	3	5	4	5	-	-	-	0 0 1 0	
20 Chamaenerion angustifolium	-	-	-	-	1	1	-	-	1	1	-	-	-	-	1	-	-	-	-	-	1	-	1	-	1	2	-	-	-	-	-	-	0 0 1 0	
21 Artemisia laciniata	-	-	1	-	-	-	-	-	7	4	-	-	-	-	7	6	3	3	1	-	-	4	-	3	4	2	5	6	1	-	-	-	0 0 1 0	
23 Pyrola incarnata	1	1	1	1	-	2	1	-	1	-	1	-	1	-	1	-	1	-	-	1	1	-	1	-	3	1	1	-	-	-	-	-	0 0 1 0	
24 Adenophora sp.	-	-	-	-	-	-	-	-	-	-	-	-	-	-	1	1	1	1	-	-	-	1	-	-	1	1	-	-	-	-	-	-	0 0 1 0	
25 Geranium maximowiczii	-	-	1	-	-	-	-	-	1	-	1	-	1	-	3	1	1	1	-	-	1	-	1	1	1	-	-	-	-	-	-	-	0 0 1 0	
26 Aquilegia viridiflora	-	-	-	1	-	-	-	-	1	-	-	-	-	-	1	-	1	1	-	-	-	-	-	1	-	1	-	-	-	-	-	-	0 0 1 0	
27 Vicia baicalensis	-	-	-	-	-	-	-	2	-	-	-	-	-	-	4	-	-	-	-	-	-	3	1	-	1	1	-	-	-	-	-	-	0 0 1 0	
28 Maianthemum bifolium	-	-	1	1	5	-	-	-	2	-	1	-	3	-	-	-	-	-	-	-	-	-	-	2	2	2	-	1	-	-	-	-	0 0 1 0	
14 Vaccinium vitis-idaea	5	6	6	7	7	7	5	5	5	4	5	5	5	5	5	5	8	3	4	5	5	5	4	4	6	2	6	2	2	-	3	-	0 0 1 1	
18 Spiraea salicifolia	-	3	-	-	-	-	-	1	4	-	-	3	3	2	-	1	-	1	-	-	-	-	3	1	2	-	-	-	-	3	-	-	0 0 1 1	
22 Saussurea amurensis	-	-	-	-	-	-	-	-	1	-	-	1	-	-	1	-	1	-	1	2	-	3	3	4	2	1	1	-	2	-	-	-	0 0 1 1	
12 Ledum palustre var. angustum	5	5	6	-	5	5	-	1	-	-	-	-	-	-	-	5	5	3	3	3	2	-	-	6	2	7	5	2	2	2	3	3	0 1	
13 Vaccinium uliginosum	-	-	5	-	-	-	-	-	-	-	-	-	-	-	-	2	5	6	7	8	8	7	-	4	-	3	-	5	4	5	5	2	5 3 0 1	
29 Carex sp.	-	-	-	-	-	-	-	4	-	-	-	4	-	2	1	-	-	3	4	3	-	4	-	5	6	5	7	-	-	-	-	-	0 1	
7 Betula fruticosa	-	-	-	-	-	-	-	-	-	-	-	-	-	-	-	-	-	-	-	-	-	-	-	-	-	5	4	5	5	5	5	6	4 1 0 0	
32 Sphagnum sp.	-	-	-	-	-	-	-	-	-	-	-	-	-	-	-	-	-	-	-	-	-	-	-	-	-	-	7	8	6	4	5	5	6	5 6 1 0 0
10 Salix myrtilloides	-	-	-	-	-	-	-	-	-	-	-	-	-	-	-	-	-	-	-	-	-	-	-	-	-	1	-	-	-	-	-	-	4 1 0 1	
11 S. brachypoda	-	-	-	-	-	-	-	-	-	-	-	-	-	-	-	-	-	-	-	-	-	-	-	-	-	2	-	-	-	2	2	-	3 1 0 1	
16 Dasiphora fruticosa	-	-	-	-	-	-	-	-	-	-	-	-	-	-	-	-	-	-	-	-	-	-	-	-	-	-	-	-	-	1	-	2	2 1 0 1	
31 Eriophorum vaginatum	-	-	-	-	-	-	-	-	-	-	-	-	-	-	-	-	-	-	-	-	-	-	-	-	-	-	-	-	1	-	6	4	7	6 4 1 0 1
9 Rhododendron parvifolium	-	-	-	-	-	-	-	-	-	-	-	-	-	-	-	-	-	-	-	-	-	-	-	-	-	-	1	-	2	2	-	1	5	1 1
Division level of plots	1	0	0	0	0	0	0	0	0	0	0	0	0	0	0	0	0	0	0	0	0	0	0	0	0	1	1	1	1	1	1	1		
	2	0	0	0	0	0	0	0	0	0	0	0	0	0	0	0	0	1	1	1	1	1	1	1	1	0	0	0	0	0	0	0	1	
	3	0	0	0	0	0	0	0	0	0	0	0	1	1	1	1	0	0	0	0	0	0	0	1	1	1	1	0	0	0	0	1		
	4	0	0	0	0	0	0	0	1	1	1	1	1	0	0	0	1	1	0	0	1	1	1	1	0	0	0	0	1					

Table 2 The plant community types after the disastrous fire in Amur area, Daxinganling prefecture

- A: Rhododendron dauricum + Betula platyphylla + Alnus mandshurica
- B: Pinus sylvestris + Larix gmelinii
- C: Rhododendron dauricum-Vaccinium vitis-idaea + Artemisia laciniata
- D: Rhododendron dauricum - Ledum palustre - Vaccinium vitis - idaea
- E: Artemisia laciniata + Vaccinium vitis - idaea - Sanguisorba officinalis
- F: Vaccinium vitis - idaea - V. uliginosum + ledum palustre
- G: Ledum palustre + Carex sp. - Vaccinium vitis - idaea
- H: Vaccinium uliginosum - V. vitis - idaea
- I: Larix gmelinii - Rhododendron parvifolium - Sphagnum
- J: Betula fruticosa - Ledum palustre - Sphagnum
- K: Betula fruticosa - Vaccinium uliginosum - Sphagnum
- L: Betula fruticosa - Eriophorum vaginatum - Sphagnum

ron parvifolium" and "Betula fruticosa-Eriophorum vaginatum-Sphagnum" swamp communities. They are located at the valley bottom. The soil is swamp soil with fine grained, well-developed peat and there is logging water on ground surface.

The above analysis shows that the edaphic or soil characteristics and topography are the most significant factors for the structure and distribution of plant communities along the DCA AX1. The soil characteristic and topography

interrelated with each other by the aluvial, eluvial and slope wash actions.

The character value of DCA Axis 2 is 0.424. The Axis 2 shows a gradient of the forest fire burning degree and can be reflected out by thawing depth to frozen ground and soil temperature at shallow layers in the middle ten-day period of June. In summer the vegetation on permafrost can reduce the direct light shining to the ground surface and decrease the evaporation and the ground temperature (Qin, Z.Y. and Xie, W.Z.,

1987) so as to protect the existence and development of permafrost and slow down the thawing speed of the active layer. Due to the varying degrees of damage of vegetation by fire, the thawing depth to frozen ground and the shallow layer soil temperature changed consequently at different site in different period. The plant communities have a relatively close relationship with their permafrost environment in the middle ten-day period of June because it is the beginning of middle-growth period of plant.

The bottom swamp and the mountain slope have a great difference in ecological conditions. We select the plant communities in the slopes to make multiple analysis. Their characteristics along the DCA ordination AXIS 2 are shown as follows:

The section with AX2 scores <150 units is heavy-burning area where the thawing depth to frozen ground reaches 60-70 cm and the shallow layer soil temperature is 11-14°C (The value is the average of soil temperature at 10 and 20 cm deep. It is the same in the following). The forest here suffered a severe damage. In the composition of plant species of communities, the dry-tolerant and sun plants such as *Artemisia laciniata*, *Chamaenerion angustifolium* etc. grow exuberantly. Besides, some shrub such as seedling of *Betula*, *Alnus* and *Rhododendron* grow vigorously too. AX2 scores between 150-260 is middle-burning area where the thawing depth to frozen ground is 50-60 cm and the shallow layer soil temperature is 9-11°C. The forest is sparse, and some ever-burning trees have resuscitated. The dominant plant species are *Ledum palustre*, *Vaccinium uliginosum*, *V. vitis-idaea*, *Betula platyphylla* and *Alnus mandshurica* etc.. There are also *Artemisia laciniata*, *Chamaenerion angustifolium* and *sanguisorba officinalis* etc. but their abundance is less than that of the heavy burning area. The AX2 scores between 260-320 is no-burning area where the thawing depth to frozen ground is only 40-50 cm and the soil temperature at shallow layer is 8-9°C. The coverage of *Pinus* and *Larix* forest can reach 70 percent or so. The composition of plant species below the forest is poor. There are *Pyrola incarnata*, *Vaccinium vitis-idaea*, *Rosa davurica* and *Vicia* spp. etc..

It is clear that the permafrost environmental changes following the fire have a close relationship with the distribution of plant communities and their species composition. And it can be reflected on the DCA ordination AXIS 2.

The correlation coefficients of DCA AX2 with the thawing depth of frozen ground and the shallow layer soil temperature are as follows:

$$r_1 = -0.72^{**} \quad (p < 0.01)$$
$$r_2 = -0.54^* \quad (p < 0.05)$$

Using the ordination scores of plant communities on DCA AX2 and above two parameters of environment to make regression analysis, we obtained the following two-variable linear regression equation.

$$AX2 = 588.16 - 5.6X_1 - 11.44X_2$$

In which AX2 is the ordination scores of plant communities on DCA AXIS 2.

$X_1$  is the thawing depth to frozen ground  
 $X_2$  is the soil temperature at shallow layer by significance test,  $F = 9.71^{**}$  ( $p < 0.01$ )  
Therefore, the above regression equation

reflects perfectly the relationship between the plant communities on DCA axis 2 and the thawing depth to frozen ground and the shallow layer soil temperature in the middle ten days of June.

## DISCUSSION

### Plant Succession and Permafrost Development

The broad natural forest in the north of Mt. Daxinganling is determined by the climatic conditions in this area, while the permafrost is the product of such special climatic conditions and it has a close relationship with plant growth and root system development. The permafrost environment created special ecological conditions for the natural forest growth, and the forest vegetation, acting as an insulating layer, protects the permafrost existence. They coexist and develop coordinately. The turbulent fire caused changes in both the vegetation type and the permafrost environment. If there will not be any further great and repeated disturbances in the future, the thawing depth to frozen ground and the shallow layer soil temperature will decrease at the same time with the vegetation renewal. From the regression equation we can see that the ordination scores for vegetation type will increase on the DCA AX2. That is, the plant community types will change from the communities dominant by species of *Artemisia laciniata*, *Sanguisorba officinalis*, *Chamaenerion angustifolium*, and *Deyeuxia angustifolia* etc. to that of *Ledum palustre*, *Betula platyphylla* and *Alnus mandshurica* etc.. After the plant self-spreading action and invading growth of conifer trees, it will develop into conifer and broad-leaf mixed forest, and will go on to reach the climax type-- *Larix gmelinii* forest. The permafrost environment will also recover to the pre-fire situation.

After three years of the turbulent fire, the plant succession developed well. It has passed through the herb stage and are developing or has developed into the short shrub or shrub stages and will keep on the succession to the *Betula* or *Betula-Alnus* community types (Sun, H. L. and Feng, Z. W., 1988). In the slight burning areas, many trees have resuscitated and grown well. By avoiding great and repeated disturbances and strengthening the environment conservation and artificial tending, the forest resources and permafrost environment will recover successfully.

### Method Discussion

It is a practicable method to combine the quantitative classification ordination with conventional classification in the research of plant ecology. Some Chinese scholars have used the method in the research of vegetation on Qinghai-Xizang plateau, and alpine tundra types, and have made remarkable results (Zhang, D. H. S. and Gauch, H. G., 1986; Qian, H., 1990). From our research work in Mt. Daxinganling we can see that this method successfully handled the diversity of plant communities, and also provided objective and quantitative relationship between the permafrost environmental factors and the vegetation types following the fire in permafrost area.

There are many environmental factors to affect the plant growth and they are usually interrelated. In this paper we mainly discussed the relationship between the plant communities and their permafrost environment. From the cor-



relation coefficients and the significance test, we can see that the result is perfect. We hope in the future to collect more vegetation and environmental data so as to derive a more precise understanding of vegetation and permafrost environment in Mt. Daxinganling.

#### REFERENCE

- Gauch, H.G. (1982) Multivariate analysis in communities ecology. Cambridge University Press, Cambridge, England.
- Guo Dongxin, Wang Shaolin (1981) Division of Permafrost region in Daoxiao Hingganling Northeast China (In Chinese). Journal of Glaciology and Geocryology. 3(3):1-9.
- Keith van Clear and Leslie A. Viereck (1984) A comparison of successional sequence following fire on permafrost-free site in Interior Alaska. The Fourth International Conference on Permafrost.
- Liou Shener (chief editor) (1959) Checking Table of Plants in Northeast of China (In Chinese). Science Press, Beijing, China.
- Qian Hong (1990) Numerical classification and ordination of plant communities in the alpine tundra of Mt. Changbai (In Chinese). J. Appl. ecol. 1(3):254-263.
- Qin Zhiye, Xie Wenzhong (1987) The relationship between plateau plants and melting soil-layer in the Frozen Season in Tumen prefecture, Xizang (In Chinese). Journal of Glaciology & Geocryology. Lanzhou China. 9(2): 149-156.
- Sun Hongliang, Feng Zhongwei (1988) The characteristics of ecosystem of north Daxinganling Mountains Forest and the ecological principle of its remedy after an extraordinary serious fire-disaster (In Chinese). China Environment Science. Beijing, China. 8(2): 85-61.
- Zhang D.H.S. and Gauch, H.G. (1986) Multivariate analysis of plant communities and its environmental factors in Ngari, Tibet. Ecology. 67 (6): 1568-1575.

## CHANGING CLIMATE AND PERMAFROST TEMPERATURES IN THE ALASKAN ARCTIC

T. Zhang and T. E. Osterkamp

Geophysical Institute  
University of Alaska Fairbanks  
Fairbanks, AK, 99775-0800

Climatological data and modeling are being used to investigate the response of permafrost in the Alaskan Arctic north of the Brooks Range to changes in climate over the last century or so. Air temperatures in this region are strongly correlated, vary with periods of 10 years and 47 years, and follow the same general trends as the North American Arctic. There is no evidence in the Barrow record (1921-1991) for a warming of air temperatures consistent with the 2 to 4°C warming observed at the permafrost surface. Precipitation was primarily snowfall which was greater during cold periods and smaller during warm periods, was poorly correlated between stations, and showed a periodicity of 37 years at Barrow and 34 years at Barter Island. These results suggest that the effects of changes in air temperatures on permafrost temperatures may have been modified by changes in snow cover. A numerical model using North American Arctic air temperatures to represent the permafrost surface temperatures and using Prudhoe Bay conditions showed that the permafrost temperature variations depended strongly on the choice of initial conditions, that air temperature changes were sufficiently large to account for the magnitude of the observed changes, and that air temperature changes predated permafrost temperature changes. An alternative explanation of the last result is that the shallow permafrost temperatures were colder than the assumed initial conditions. For a site near Barrow, the model with Barrow air temperatures applied at the ground surface with no snow cover predicted little change in permafrost temperatures. This result disagrees with observations made in 1949 and confirms that air temperature variations alone (since 1923) cannot account for the observed warming of the permafrost. For the observations and predictions to be compatible when the snow cover was added, the initial ground surface temperature must have been about the same as the mean annual air temperature. This implies a very thin snow cover prior to 1923. Variability in timing, rate of thickening, duration, thickness of the snow cover, and the poor correlations between stations, may explain why different sites show a warming, little or no change, or a cooling of permafrost temperatures. However, there is insufficient data to directly test this hypothesis. Consequently, variations in the magnitude and penetration depth of the permafrost warming signal in Northern Alaska remain to be satisfactorily explained.

### INTRODUCTION

It has been established that the long-term mean surface temperature (MST) of the permafrost, obtained by extrapolating the deep linear portions of temperature profiles to the surface, in Alaska's Arctic Region north of the Brooks Range has recently warmed about 2 to 4°C (Lachenbruch and Marshall, 1986; Lachenbruch et al., 1988; Osterkamp, 1988). Estimates for the start of this warming are generally about 40 to 80 years ago. Weather records for the North American Arctic and Alaska show that there was a cooling trend from about 1940 until the mid-1970s (e.g. Hansen and Lebedeff, 1987). However, there is no evidence for this colder period, which lasted three and one-half decades, in the permafrost temperature profiles. This apparent anomaly suggests that the relationships between air and permafrost temperatures require further investigation.

This paper is a progress report on an investigation into the effects of air temperatures, snow cover, and the active layer on permafrost temperatures. We will review some of the available information on permafrost temperatures and climate in the Alaskan Arctic north of the Brooks Range. Some preliminary modeling results will be presented showing the

effects of using past air temperatures as the boundary condition at the permafrost surface, ground surface, and surface of the snow cover (winter) and ground surface (summer). The effects of initial conditions, the use of linear approximations for the permafrost surface temperature history, and the presence or absence of a snow cover on permafrost temperatures will be discussed.

### PERMAFROST TEMPERATURES

Temperature measurements through permafrost have been made in more than 40 holes on the Arctic Coastal Plain and in the foothills of the Brooks Range generally between Prudhoe Bay and Cape Thompson (Lachenbruch et al., 1962; Lachenbruch et al., 1982; Lachenbruch and Marshall, 1986). Lachenbruch and Marshall (1986) and Lachenbruch et al. (1988) used an analytical model to reconstruct the history of temperature changes at the permafrost surface from these permafrost temperature profiles. Their results show that a variable but widespread warming (typically 2 to 4°C) occurred at the permafrost surface during the 20th century. Specifically, data from their main group of holes show that, for a surface temperature history consisting of a step function, the warming started about 1946 ±13

years with the permafrost surface temperature increasing by  $2.7^\circ \pm 1.0^\circ\text{C}$ . For the linear case, the warming would have started about  $1925 \pm 20$  years with the permafrost surface temperature increasing by  $4.0^\circ \pm 1.6^\circ\text{C}$ . The maximum depth of the climatic disturbance is generally about 100 m. Data from the Prudhoe Bay group show that the warming there started somewhat earlier (step function  $\approx 1924 \pm 13$  years; linear function  $\approx 1912 \pm 9$  years) with the permafrost surface temperature increasing by  $1.9^\circ \pm 0.5^\circ\text{C}$  for a step-function and by  $3.1^\circ \pm 1.1^\circ\text{C}$  for a linear function. The average penetration depth of the climatic disturbance for the Prudhoe Bay group is about  $163 \pm 16$  m. There does not appear to be any evidence for a three and one-half decade long (1940-1976) cooling event in these temperature profiles. Most of these holes show a cooling within the last decade that may be associated with the drilling pad, geomorphic processes, or short-term climatic fluctuations (Lachenbruch and Marshall, 1986; Lachenbruch et al., 1988; Osterkamp and Lachenbruch, 1990).

A few shallow holes ( $\approx 60$  m) have been drilled along the trans-Alaska pipeline and in the Arctic National Wildlife Refuge (ANWR) and temperature measurements made for the purpose of investigating the response of the permafrost to climatic changes (Osterkamp et al., 1987; Osterkamp, 1988). Data from these holes are consistent with the deep holes and show that there has been a long-term warming of permafrost temperatures followed by a cooling of about  $1^\circ\text{C}$  from the time these holes were drilled (1983). This cooling is tentatively attributed to a climatic cooling (Osterkamp and Lachenbruch, 1990). Temperature measurements in ANWR show results that are qualitatively consistent with data at Prudhoe Bay and to the west (Osterkamp, 1988).

In brief, permafrost temperatures in the Alaskan Arctic north of the Brooks Range show that some areas have warmed over the last century but with different magnitudes of warming and with different timing, a few show little or no change, and some areas show a very recent cooling.

#### CLIMATIC HISTORY

Global mean air temperatures over both the land and the oceans of both hemispheres (Jones, et al., 1986) show a marked warming to 1940, relatively steady conditions to the mid-1970s and a subsequent rapid warming. The mean annual air temperature (MAAT) measured at meteorological stations in the northern hemisphere has been increasing since the beginning of recorded data with most of the warming occurring in the period before 1940 (Ellsaesser, et al., 1986). Hansen and Lebedeff (1987) have shown that, in the northern hemisphere, there was a warming about  $0.6^\circ\text{C}$  from 1880 to 1940, a cooling of about  $0.3^\circ\text{C}$  from 1940 to 1970, and a warming of about  $0.3^\circ\text{C}$  from 1970 to 1980. This three decade long cooling period is coincident with the time when the permafrost temperatures indicate a warming. Warming of the air temperatures in the higher latitudes was significantly greater than at low latitudes and the warming was greater in the North American quadrant of the Arctic (Fig. 1C, Hansen and Lebedeff, 1987). The MAAT increased more than  $3^\circ\text{C}$  from the mid-1880s to 1940 in this region. However, fragmentary early data suggest significant cooling prior to the mid-1880s such that 25% to about 50% of the subsequent warming may represent a return to earlier levels (Ellsaesser, et al., 1986).

In Alaska, MAAT have warmed significantly during the twentieth century in a pattern similar to that of the North American Arctic (Hamilton,

1965). Most Alaskan stations warmed suddenly beginning in 1976 and warm winters have been common for most Alaskan stations since then (Hoffman and Osterkamp, 1986). Air temperatures at Barrow, the station with the longest weather record on Alaska's North Slope, shown in Fig. 1A and Barter Island (Fig. 1B) have a similar pattern. For the periods of record, the MAAT at Barrow was  $-12.5 \pm 1.1^\circ\text{C}$  and at Barter Island  $-12.4 \pm 1.2^\circ\text{C}$ . The MAAT at these two stations were closely correlated with each other (correlation coefficient of 0.90) over the period between 1949 and 1988. The MAAT for Barrow show a warming trend to about 1940, a three and one-half decade long cooling trend to about 1976, followed by a warmer period since then. There is no evidence in the Barrow record (1921 to present) for a warming of air temperatures consistent with the 2 to  $4^\circ\text{C}$  warming observed at the permafrost surface.

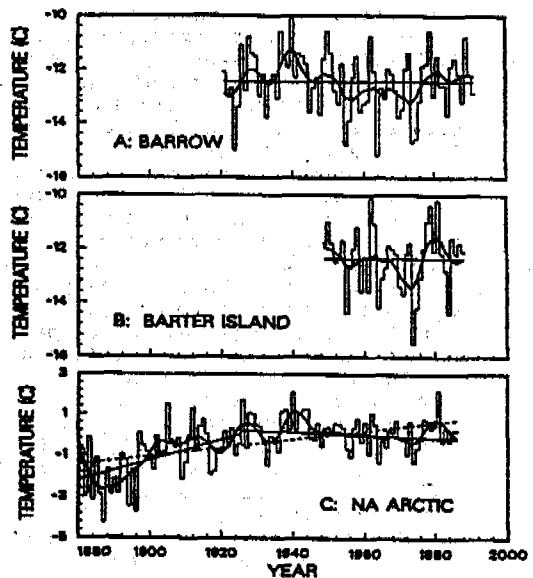


Figure 1. Mean annual air temperatures from the U. S. Weather Bureau at Barrow (A) and at Barter Island (B). The data in (C) represent the temperature variations obtained by Hansen and Lebedeff (1987) for the North American quadrant of the Arctic. These data were smoothed by a low-pass filter with a cut-off frequency of  $0.091 \text{ year}^{-1}$  (dark solid line). The record averages (thin solid lines in A and B) and selected regression lines (thin solid and dashed lines in C) as used by Lachenbruch et al. (1988) are also shown.

The power spectra for the time series of MAAT and snowfall at Barrow and Barter Island are shown in Figure 2. These spectra were calculated using the maximum entropy method (Jenkins and Watts, 1968) with a cut off frequency of  $0.15 \text{ year}^{-1}$ . MAAT varies with periods of 47.3 years and 10.1 years at Barrow and with period of 9.7 years at Barter Island. Lack of a 47 year period at Barter Island may be due to the shortness of the temperature-time series. The 10 year period at both stations confirms the correlation of air temperature variations. Snowfall varies with periods of 37.3 years at Barrow and 33.8 years at Barter Island.

In the Alaskan Arctic north of the Brooks Range, 65% to 80% of the precipitation is snowfall which lasts for nine months (Benson, 1982). Annual average precipitation and snowfall

for the period of record at Barrow were about  $11.0 \pm 4.5$  cm and  $71 \pm 30$  cm, respectively, and about  $15.5 \pm 6.0$  cm and  $107 \pm 47$  cm at Barter Island.

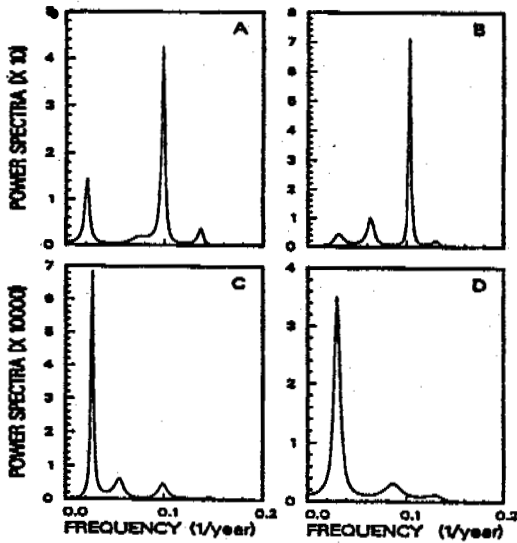


Figure 2. Power spectra for air temperature-time series at Barrow (A) and Barter Island (B) and for snowfall-time series at Barrow (C) and Barter Island (D), using a cut-off frequency of  $0.15 \text{ year}^{-1}$ .

Figure 3 shows deviations of MAAT and snowfall from their long-term means at Barrow and Barter Island, smoothed by a low-pass filter with a cut-off frequency of  $0.091 \text{ year}^{-1}$ . In general, there was a trend with greater snowfall during colder years and smaller snowfall during warmer years except for a period between the mid-1960's and mid-1970's at Barter Island. This reciprocal relationship between air temperature and snowfall also exists in other places in Interior Alaska (Bowling, 1977) and is probably associated with synoptic-scale circulation (Bowling, personal communication). These results and the large annual variations in snowfall suggest, because of the insulating properties of the snow, that the effects of changes in air temperatures on permafrost surface temperatures may have been modified substantially by changes in snow cover.

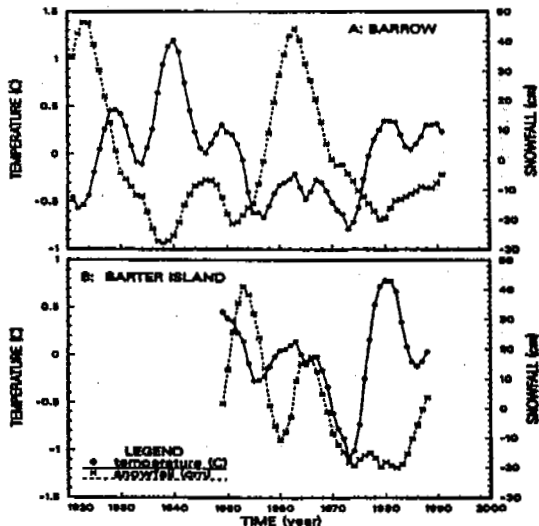


Figure 3. Deviations of the mean annual air temperature and snowfall from their means at Barrow and Barter Island, smoothed by a low-pass filter with a cut-off frequency of  $0.091 \text{ year}^{-1}$ .

#### RELATION OF PERMAFROST TEMPERATURES TO CLIMATIC DATA

A finite difference model for one-dimensional heat flow problems with phase change (Goodrich, 1977, 1982) is being used to investigate the effects of air temperature, snow cover, and active layer on permafrost temperatures. This numerical model has a detailed routine for including the effect of snow cover on soil (active layer and permafrost) temperatures. The model has been modified to use weather data input files and for the long-term calculations needed in this research. Comparisons of model predictions with analytical solutions have been excellent. This numerical model has been calibrated using our unpublished data for conditions near the West Dock at Prudhoe Bay, Alaska which is close to site E of Lachenbruch et al. (1982).

The choice of initial conditions for modeling the response of permafrost to surface temperature changes is often difficult. A constraint is imposed by the long-term MST (obtained by extrapolating deeper temperatures to the surface). The possibility remains that surface temperatures may have been significantly colder or warmer than the long-term mean for periods of several decades. Perturbations in the temperature profiles supporting this idea have not been reported. This problem is inherent in forward modeling of long-term permafrost temperatures.

For the results shown in Figure 4, the air temperature changes for the North American Arctic (Fig. 1C) were used for the surface temperature changes of the permafrost at Prudhoe Bay ( $0^\circ\text{C}$  corresponding to a MST =  $-12.0^\circ\text{C}$ ). Seasonal temperature variations were not included. Lachenbruch et al. (1988) have made similar calculations for their AWUNA site, about 375 km southwest of Prudhoe Bay. Physical and thermal parameters for the active layer and permafrost were based upon data for Prudhoe Bay conditions (Lachenbruch, et al., 1982; Zhang, 1989). Figure 4 shows the calculated permafrost temperature changes for different initial conditions. The initial condition in 1880 was assumed to be an equilibrium temperature profile with different long-term MST. In effect, air temperatures were assumed to be constant with the value of the long-term mean until 1880 and then to vary as shown in Fig. 1C. For case I, the MST =  $-12^\circ\text{C}$  which was changed in increments of  $-1^\circ\text{C}$  for cases II, III and IV. This procedure introduces a step change in 1880 ranging between  $-1^\circ\text{C}$  and  $+2^\circ\text{C}$ . These curves illustrate the effects of air temperature changes and of different choices of the initial condition on changes in the permafrost temperatures. The results show that air temperature variations since 1880 are sufficiently large to account for the geothermal observations provided that a sufficiently cold MST is assumed. Cases III and IV are better matches to the data of Lachenbruch et al. (1982) for the Prudhoe Bay area. Depth of penetration of the curves compared to the data shows that the warming penetrates deeper than observed. Lachenbruch et al. (1988) have suggested that the atmospheric warming started earlier than the permafrost warming. Another possibility is that the shallow permafrost temperatures were colder than the assumed initial conditions. Except for the last possibility, the conclusions for Prudhoe Bay are the same as those reached by Lachenbruch et al. (1988).

These forward modeling results and those of Lachenbruch et al (1988), based on inverse modeling of the temperature data, suggest that the permafrost warming probably began much later than 1880, for Prudhoe Bay about 1920. However,

Fig. 3 suggests that the air temperature trends since 1920 have generally varied by less than 1°C about the mean and the variations were both positive and negative. Therefore, air temperature changes alone (since 1920) do not appear to have been sufficient to account for the observed 2 to 4°C warming of the permafrost.

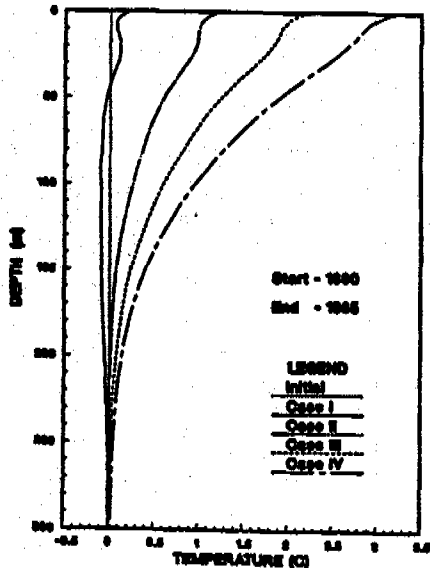


Figure 4. Predicted permafrost temperature changes in 1985, for Prudhoe Bay conditions starting in 1880, using air temperature variations from the North American quadrant of the Arctic for the upper boundary condition at the permafrost surface. For case I, the initial equilibrium surface temperature was set at -12°C which was changed in increments of -1°C for cases II, III and IV.

A comparison was also made between cases where the air temperature data were used for the permafrost surface boundary condition and where these data were approximated by straight lines as in Lachenbruch et al. (1988). The initial conditions were taken to be the starting points of regression lines fitted to the data (Lachenbruch et al., 1988). Case I in Figure 5 used the air temperature data and case II used the single regression line from 1880 to 1985 (Fig. 1C) with the initial MST offset by -1.46°C for both cases. Case III used the air temperature data and case IV used the two regression lines (Fig. 1C) with an initial offset of -2.21°C for both cases. The results in Figure 5 show that the differences between using straight lines to approximate the data and using the actual data are relatively small but generally measurable below about 50 m and may be more significant above this depth.

The use of air temperature variations to represent permafrost surface temperature variations is obviously not realistic given the presence of a seasonal snow cover, the active layer and other effects. A lack of knowledge of the initial snow cover conditions also hinders attempts at forward modeling of this problem. Goodrich (1982) has shown that the equilibrium response of the annual mean temperature at the ground surface is extremely sensitive to the assumptions made in treating the snow cover. For example, for a fine-grained soil with a snow cover reaching a maximum thickness of 0.25 m, the mean annual temperatures at the ground surface

can be increased 3 to 7°C over that of a bare ground surface depending on the rate at which the snow cover reaches its maximum thickness.

Figure 6 shows measurements of the MAAT and the mean annual temperature at the permafrost surface at three sites near Prudhoe Bay from 1986 to 1990. These means were calculated from measurements made at four hour intervals at eleven levels. One measurement was made at 1.5 m above the ground in a radiation shield, one at the ground surface, and nine in the active layer and top 0.4 m of the permafrost (see Zhang, 1989). Generally, these mean annual permafrost surface temperatures were higher than MAAT by about 3 to 6°C. The snow conditions for this period (average maximum thickness of about 17 cm) appear to be less than the average since 1977 based upon measurements of the water equivalent of the snow (Alaska Soil Conservation Service). There is not a well-defined relationship between these temperatures.

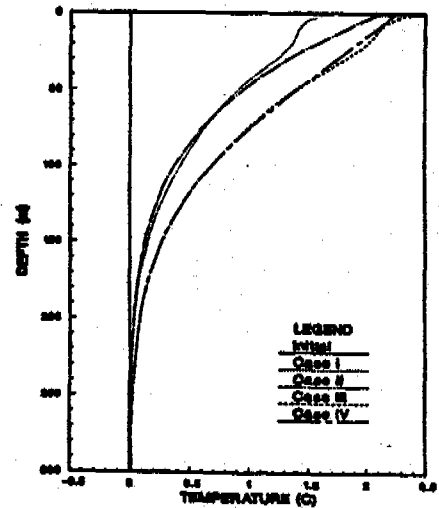


Figure 5. Predicted permafrost temperature changes in 1985 using air temperature data for the North American quadrant of the Arctic (case I, III), the single regression line in Fig. 1C from 1880 to 1985 (case II), and the two regression lines in Fig. 1C (case IV), for the upper boundary condition at the permafrost surface.

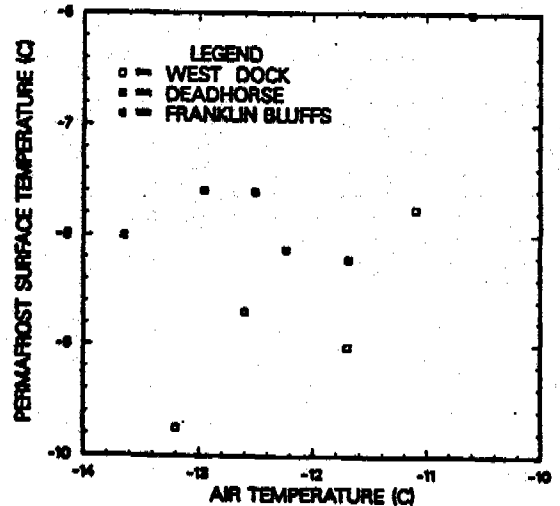


Figure 6. Mean annual air temperature and the permafrost surface temperature from 1986 to 1990 near Prudhoe Bay, Alaska.

The numerical model was also used to evaluate the effects of a snow cover on permafrost temperatures. The calculations (Fig. 7) were made using the air temperatures to drive the ground surface temperatures for cases without and with a snow cover. Barrow weather data (mean daily air temperatures, snowfall and snow cover) for the period from 1923 through 1991 were used in the calculations. Thermal properties of the snow were estimated from the results of Benson (1982) and Sturm (1992). The initial (1923) MST was assumed to be  $-12.2^{\circ}\text{C}$  with a thermal gradient of  $0.03^{\circ}\text{C m}^{-1}$ . The snow surface or ground surface, as appropriate, was taken as the upper boundary. Physical and thermal parameters for the active layer and permafrost were based upon data for Barrow conditions (Brown, 1969; McGaw et al., 1978; Lachenbruch et al., 1988). The dots represent data which were obtained in 1949 (at SB3, Lachenbruch et al., 1962).

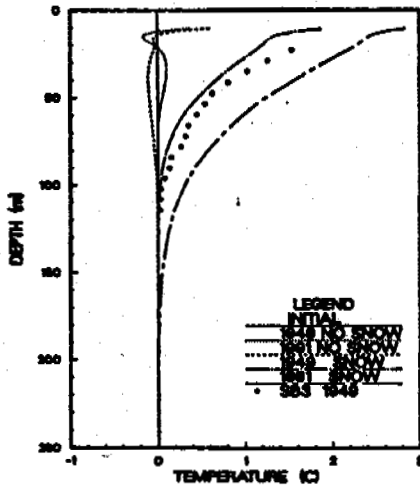


Figure 7. Predicted permafrost temperature changes at site SB3 near Barrow using daily air temperatures from Barrow (starting in 1923) as the upper boundary condition at the ground or snow surface as appropriate. The dots are the approximate permafrost temperature changes at site SB3 in 1949 (Lachenbruch et al., 1962).

With no snow cover, the model predicts a slight warming of permafrost temperatures for 1949 and a slight cooling for 1991. These results do not agree with the observations at SB3 nor at other sites where warming has occurred. Given the assumptions, these calculations show that air temperature variations alone could not have produced the observed permafrost warming.

With the snow cover, the model predicts permafrost temperature changes and a depth of penetration which compare favorably with the measurements at SB3. There is no clear evidence for a cooling of permafrost temperatures from 1940 to the mid-1970's. These results, approximately correct predictions for both the magnitude and penetration depth of permafrost temperature changes, are fortuitous and may be misleading. One of the assumptions of the model was that the initial ground surface temperature ( $-12.2^{\circ}\text{C}$ ) was about the same as the MAAT which is equivalent to assuming a very thin snow cover initially. Thus, the model predictions (and the experimental data of Fig. 6), show that placing a snow cover on bare ground is equivalent to warming the ground surface by several degrees. Therefore, this favorable result is caused by the choice made for the initial ground surface

temperature.

The choice of the MST of the permafrost ( $-12.2^{\circ}\text{C}$ ) for the initial ground surface temperature was indicated by the data of Lachenbruch et al. (1988). A significantly different choice of MST leads to incorrect predictions. MST colder than MAAT are not permissible. If the snow conditions prior to 1923 were similar to those after 1923, then a ground surface temperature several degrees warmer would be appropriate. However, such a warm initial temperature would produce permafrost temperatures that are too warm compared with the data at SB3. For the results and data to be compatible, the initial ground surface temperature must be similar to the MAAT. This implies a very thin snow cover prior to 1923. A similar hypothesis was proposed by Taylor (1991) for the interpretation of permafrost temperatures in the Canadian Arctic Archipelago. However, there does not appear to be other supporting evidence for it.

The results of these simulations and those of Goodrich (1982) indicate that snow cover can play a major role in determining changes in permafrost temperatures. For the same air temperature history, the presence, absence, or changes in thickness and duration of snow cover can result in either a warming or a cooling of permafrost temperatures. These results and the fact that snow cover is not correlated between stations may explain why different permafrost sites in the Alaskan Arctic show a warming, little or no change, or a cooling of permafrost temperatures.

#### SUMMARY

Air temperatures at Barrow and Barter Island generally follow those for Alaska and the North American Arctic showing an increasing trend until 1940, a decreasing trend to the mid-1970's and then an increase to warmer temperatures during the late 1970's and 1980's. The MAAT at Barrow was  $-12.5 \pm 1.1^{\circ}\text{C}$  and at Barter Island about  $-12.4 \pm 1.2^{\circ}\text{C}$ . Power spectra for the temperature-time series show that periods of 47.3 years and 10.1 years exist at Barrow and 9.7 years at Barter Island. There is a strong correlation of air temperatures at both stations. Precipitation is primarily snowfall in the Alaskan Arctic north of the Brooks Range. Power spectra for the snowfall-time series show a period of 37.3 years at Barrow and 33.8 years at Barter Island. During cold periods, snowfall was greater, while during warmer periods, snowfall was smaller. This suggests that the effects of changes in air temperatures may have been modified by changes in snow cover. Correlation of snowfall between stations was poor.

A finite difference model for one-dimensional heat flow problems with phase change (Goodrich, 1977) was used to investigate the effects of air temperature, snowfall, and the active layer on permafrost temperatures. Simulations were carried out using past air temperatures for the boundary conditions at the permafrost surface, ground surface, or surface of the snow cover. The effects of initial conditions, use of approximations for the surface temperature history, and of the active layer and snow cover on permafrost temperatures were examined in this continuing investigation.

When air temperature variations in the North American Arctic were applied to the permafrost surface at Prudhoe Bay, it was found that the permafrost temperature variations depended strongly on the choice of initial conditions (long-term MST). The air temperature variations (since 1880) were sufficiently large to account for the permafrost temperature variations and the

air temperature changes occurred earlier than the permafrost temperature changes. These results were the same as those found by Lachenbruch et al. (1988). An alternative explanation of the last result is that the shallow permafrost temperatures were colder than the assumed initial conditions. The differences between using air temperature data at the permafrost surface compared to using straight line approximations to the data were small but measurable below about 50 m and may be more significant above this depth.

Barrow air temperatures (1923-1991) used for the ground surface boundary condition (active layer but no snow cover) at a site (SB3) near Barrow produced little change in permafrost temperatures from the initial condition. This result disagrees with permafrost temperature observations at SB3 and confirms that air temperature variations alone (since 1923) cannot account for warming of the permafrost. For the observations and predictions to be compatible when the snow cover was added, the initial ground surface temperature must have been about the same as the MAAT. This implies a very thin snow cover prior to 1923. For the same air temperature history, changes in snow cover can result in either a cooling or a warming of the permafrost. The above results and the fact that snow cover is not correlated between stations may explain why different sites in the Alaskan Arctic show a warming, little or no change, or a cooling of permafrost temperatures. However, lack of information on the timing, rate of thickening, maximum thickness, and duration of the snow cover prior to 1923 at Barrow and at other sites does not allow detailed analyses of these effects and hampers forward modeling efforts. Consequently, variations in the magnitude and penetration depth of the permafrost warming signal in Northern Alaska remain to be satisfactorily explained.

#### ACKNOWLEDGMENTS

We wish to thank Dr. L. Goodrich for discussions on the use of his numerical model and Dr. A. H. Lachenbruch and Dr. R. W. Saltus for their discussions and for providing a computer tape with the climatic data of Hansen and Lebedeff (1987). This research was funded by the Division of Polar Programs of the National Science Foundation and by the State of Alaska.

#### REFERENCES

- Alaska Soil Conservation Service, Snow survey: Basin outlook reports. Soil Conservation Service, Anchorage, Alaska.
- Benson, C. S., 1982. Reassessment of winter precipitation on Alaska's Arctic Slope and measurements on the flux of wind blown snow, *Geophysical Institute Report, UAG-R 228*, University of Alaska Fairbanks.
- Bowling, S. A., 1977. Relationships between temperature and snowfall in Interior Alaska, *Arctic*, 30(1), 62-64.
- Brown, J., 1969. Soil properties developed in the complex tundra relief of northern Alaska, *Biuletyn Peryglacjalny*, vol. 18, p. 163-167.
- Ellsaesser, H. W., M. C. MacCracken, J. J. Walton and S. L. Grotch, 1986. Global climatic trends as revealed by the recorded data, *Reviews of Geophysics*, 24, 745-792.
- Goodrich, L. E., 1977. Efficient numerical technique for one-dimensional thermal problems with phase change. *Int. J. of Heat and Mass Transfer*, 21, 615-621.
- Goodrich, L. E., 1982. The influence of snow cover on the ground thermal regime, *Can. Geotech. J.*, 24, 160-163.
- Hamilton, T. D., 1965. Alaskan temperature fluctuations and trends: an analysis of recorded data, *Arctic*, 18(2), 105-117.
- Hansen, J. and S. Lebedeff, 1987. Global trends of measured surface air temperature. *J. Geophys. Res.*, 92, 13,345-13,372.
- Hoffman and Osterkamp, 1986. Bar graphs of climatological data for Alaskan stations: temperature, snowfall, and thawing and freezing degree days for 1949-1982, Interim report to Alaska Department of Transportation and Public Facilities.
- Jenkins, G. M. and D. G. Watts, 1968. *Spectral analysis and its applications*, Holden-Day Inc., London.
- Jones, P. D., T. M. L. Wigley and P. B. Wright, Global temperature variations between 1861 and 1984, *Nature*, 322, 430-434.
- Lachenbruch, A. H., M. C. Brewer, G. W. Greene and B. V. Marshall, 1962. Temperature measurements in permafrost. in *Temperature, Its Measurement and Control in Science and Industry*. New York: Reinhold, vol. 3, pt. 1, p. 791-803.
- Lachenbruch, A. H. and B. V. Marshall, 1986. Changing climate: Geothermal evidence from permafrost in the Alaskan Arctic, *Science*, 234, 689-696.
- Lachenbruch, A. H., J. H. Sass, B. V. Marshall and T. H. Moses Jr., 1982. Permafrost, heat flow, and the geothermal regime at Prudhoe Bay, Alaska, *J. Geophys. Res.*, 87(B11), 9301-9316.
- Lachenbruch, A. H., T. T. Cladouhos and R. W. Saltus, 1988. Permafrost temperature and the changing climate, *Proc. Fifth Int. Conf. Permafrost*, Trondheim, Norway.
- McGaw, R. W., S. I. Outcalt and E. Ng, 1978. Thermal properties of wet tundra soils at Barrow, Alaska. In *Proceeding Third International Conference on Permafrost*, Edmonton, Alberta. National Research Council of Canada, Ottawa, vol. 1, pp. 47-53.
- Osterkamp, T. E., 1988. Permafrost temperatures in the Arctic National Wildlife Range, *Cold Regions Science and Technology*, 15(2), 191-193.
- Osterkamp, T. E., J. P. Gosink and K. Kawasaki, 1987. Measurements of permafrost temperatures to evaluate the consequences of recent climate warming, Report No. 84 NX 203 F 233181, Alaska Dept. of Transp. and Public Facilities, Fairbanks, Alaska.
- Osterkamp, T. E. and A. H. Lachenbruch, 1990. Thermal regime of permafrost in Alaska and predicted global warming, *J. Cold Regions Engineering*, Vol. 4, No. 1, 38-42.
- Sturm, M. and J. B. Johnson, 1992. Thermal conductivity measurements of depth hoar, *J. Geophys. Res.*, 97(B2), 2129-2139.
- Taylor, A. E., 1991. Holocene paleoenvironmental reconstruction from deep ground temperatures: a comparison with paleoclimate derived from the -5180 record in an ice core from the Agassiz Ice Cap, Canadian Arctic Archipelago, *J. of Glaciology*, Vol. 37, No. 126.
- Zhang, T. 1989. Thermal Regime of Permafrost Within the Depth of Annual Temperature Variation at Prudhoe Bay, Alaska, MS thesis,

# RANDOM CHARACTERISTICS OF FROST HEAVE AND APPLICATION TO THE DESIGN OF ANTI-FROST LIFT RELIABILITY OF GROUTING PILE AT BUILDING SITE

Zhang Xin, Zheng Duo and Feng Yanhui

Jinlin Provincial Institute of Water Conservancy Science, Changchun, China

By way of analyzing a series of frost heave data in the same terms at a special site, the random distributed characteristics of frost heave is determined at a uniform building site. The index  $\beta$  of structural reliability of the anti-frost lift stability of grouting pile is calculated by means of the normalization method. The sensitivity of the influence of frost depth  $H$  and frost heave  $h$  on  $\beta$  is analyzed. The results state that the random characteristics of both factors are of the same importance to the failure probability  $P_f$  of the structure. The relation between  $P_f$  and the variation coefficients of the two factors rises monotonously.

## INTRODUCTION

Frost depth and frost heave are the basic factors in anti-frost design. The random characteristic of frost depth was first considered in "Design Specifications of Anti-frost Heave in Canal System Engineering SL 23-91" on May, 1991. The design frost depth was adopted according to its arising frequency and the frost heave was determined as a constant and the design method of a single safety factor was still adopted.

The paper will discuss the random characteristics of frost heave based on the special observed data. Considering the case of design and operation of the bridge around the observation site, the stability of anti-frost lift of the grouting pile is estimated according to the reliability theory. Lastly, the sensitivity of the variation coefficient to the failure probability of the structure is discussed.

## SUMMARY OF THE OBSERVATION OF FROST HEAVE

The observation site is placed on the alluvial plain on the left bank of Dongliao River and located 43°30' north latitude and 124°12' east longitude. The altitude is 138.17 meters on the level of Dalian base. The site is a typical seasonally frost soil region in China and is of broad and smooth terrain. Paddy fields are all over the site. Based on the exploitation of engineering geology, the finite site is considered as a well-distributed site.

The area of the site is 24x24 square metres one hundred and forty four surface frost heave finders are set up at the interval of 2 m. All the finders are made of hard plastics in equal size, and the same methods of setting up and observation are used.

The site maintains a natural snow cover, and the height of grass is limited to 25 cm.

Observations were carried out 53 times in the interval of 10 days in the three cold

seasons from Dec. 1980 to May 1983. More than 7600 data were measured.

## STATISTICAL ANALYSIS AND FITTING INSPECTION OF THE OBSERVED DATA OF FROST HEAVE

All the data for each observation are regarded as a sampling. The maximum value, which is of the most interest for us, of each measuring point is different and does not appear in the same observation. All the maximum values within the same cold season are also regarded as a sampling, we get a total of thirty-nine samplings.

For each sampling, the variations of frost heave are 37.0-170.0 mm, the variations of the variation coefficient are 0.091-0.27 (its mean value is 0.133). The sample capacities are 133-144. When the capacities are less than 144 it is due to the damage of findings. In order to determine the type of random distribution of frost heave  $X$ , the K-S inspection method is adopted. We assume that the distribution are the types of normal, lognormal and extreme I. Let the degree of confidence  $\alpha$  be equal to 0.05, the statistic  $D_n$  and the critical values  $D_{n,0.05}$  are calculated by:

$$D_{n,0.05} = 0.886/\sqrt{n} \quad \text{for normal and lognormal}$$

$$D_{n,0.05} = 0.888/\sqrt{n} \quad \text{for extreme I}$$

The percentages which are not rejected to accept the above three types of distributions ( $D_n < D_{n,0.05}$ ) are 58.97, 48.72 and 10.26, respectively. Obviously, the distribution of observed data is most close to a normal distribution.

In general engineering, it is rare that the sampling capacities are 133-144. In order to estimate the significance of the above conclusions, subsampling in which about 27-29 observed data are taken from each observation are inspected. Let  $\alpha=0.05$ , the percentage of  $D_n < D_{n,0.05}$  are 100, 92.31 and 89.74 for the above



three types of distributions, respectively. The assumption of normal distribution is the best again. Smaller subsampling inspections (n=8-16) are carried out. Finally, we find that the frost heave  $X$  at a well-distributed site submit to a normal distribution. The inspecting results with  $\bar{x}$  method and A-D method also support the above conclusion well.

Except for the three samplings of maximum value and the three samplings of general observation, the correlation coefficient  $r$  between frost heave  $X$  and variation coefficient  $C_v$  of the thirty-three of the thirty nine samplings is  $-0.767$ , and  $C_v$  decreases with the increasing of  $X$ .

Setting up so many measuring point is rare in engineering and that many sets of measuring points are selected to observe is possible. Taking the maximum values of frost heave of each cold season as the totality, 399 samplings are taken with the pseudo-random process, and all the capacities of the samplings is 5. The analysis is below.

The mean of the totality of frost heave in every cold season is expressed as  $\bar{X}$ , variation coefficient as  $C_v$ , the mean of subsampling (n=5) as  $\bar{X}_s$ , the mean of  $C_v$ s is  $\bar{C}_v$  the results are shown in Table 1.

Table 1. The statistical results of maximum value for n=5

Cold season	$\bar{X}_{mm}$	$\bar{X}_s$	$C_v$	$\bar{C}_v$	$C_{v0}$
1980-1981	117.50	116.92	0.1130	0.1037	0.1671
1981-1982	169.97	169.61	0.1073	0.0889	0.1913
1982-1983	167.40	167.82	0.1010	0.0872	0.1514

The results in Table 1 indicate that  $\bar{X}_s \approx \bar{X}$ ,  $\bar{C}_v$ s is close to  $C_v$  and the totality is identical with the totality of observations on the whole. The  $C_{v0}$  in Table 1 represents:  $P(C_v < C_{v0}) = 95\%$ .

#### INFLUENCE OF RANDOM CHARACTERISTIC OF FROST HEAVE ON ANTI FROST LIFT RELIABILITY OF GROUTING PILE

The frost heave of the foundation is the outcome of the combined action of both natural factors and engineering conditions. So the value of the frost heave reflects the frost strength acting on the structure. The frost heave is the only index to estimate the frost susceptibility of foundation in Criterion SL23-91, and it is also the only basis to estimate the standard value of the various units of frost heaving force. For example, the standard value of the unit frost shear stress can be express as:

$$\tau = 308 h^{0.46} \text{ (KPa)} \quad (1)$$

here,  $h$  is the index of frost heave classifying the foundation soil in engineering; its unit is meter. The criterion indicates that  $h$  is determined according to the possible frost heave of the foundation in specific engineering conditions. If there is observation, the value  $h$  is determined with the observed data.

The total frost heaving force applied on the structure is determined by acting strength and frost depth  $H$ .  $H$  and  $h$  are two simultaneous factors. A great deal of previous works (Zhang,

1987; 1983; Ministry of Water Conservancy, 1991) have found out the random characteristics of frost depth is independent upon frost heave. The random characteristics of both  $H$  and  $h$  decided that of the frost heaving force, and they are basic values influencing the structural reliability of building under frost heaving force.

According to the theory of structural reliability, both the resistance of structure and the random characteristics of frost heaving force determine that there must exist a corresponding failure probability  $P_f$ :

$$P_f = 1 - \Phi(\beta) \quad (2)$$

where,  $\beta$  is the index of reliability,  $\Phi(\beta)$  is the value of normal function of the  $\beta$  that is determined by the random combination between structural resistance and frost heaving force. The more the  $\beta$ , the less the  $P_f$ , and the more reliable the structure.

There are many canals constructed around the site. Since the later period of the 70's, the anti-frost reliability has been considered in engineering design, particularly in plinch design in which the frost shear stress is considered as a normal designing load, and the frost damages have decreased obviously. But there still exists a few phenomena of frost lift (Li, 1990). Fig.1 show the typical scheme

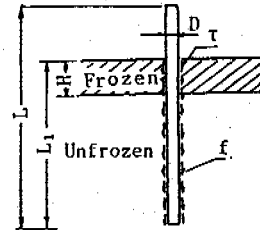


Figure 1. Typical scheme of the verification of anti-frost lift stability of grouting pile

for the verification of anti-frost lift stability of the grouting pile of the bridge at the site. The safety factor  $K$  is calculated as follows:

$$K = \frac{\pi D(L-H)f}{\pi D H \tau - P - G} \quad (3)$$

here,  $D=0.6$  m, design diameter;  
 $H=1.6$  m, design frost depth;  
 $L=8.1$  m, depth of pile below ground surface;  
 $\tau=122.5$  KPa, unit frost shear stress;  
 $f=18.8$  KPa, unit anti-frost lift stress of unfrozen soil;  
 $P=124.5$  KN, overburden on the top of the pile;  
 $G=67.8$  KN, the weight of pile.

From the above values,  $K$  is calculated and equal to 1.3, and it meets the requirement of the design.

According to the criterion SL23-91, the verified value of the safety factor  $K$  is 1.03. The character of the two verifying methods is the same except for the difference in the value of design variation.

Although there is an obvious difference in the safety factors of the two methods, the two results are all considered safe.

According to the statistical data at the site, below will estimate the anti-frost lift stability of the grouting piles, in the view of the structural reliability.

Owing to the criterion SL23-91 that has been issued and put into effect, the unit frost shear stress is calculated from equation (1) in accordance with the observed frost heave. The structural function Z is expressed as follows:

$$Z = \pi D1[(L1-H)f + D1 L1\gamma/4 + \pi \cdot D^2(L-L1)\gamma/4 - 308H h^{0.06}] \quad (4)$$

where, D1 is the diameter of the forming hole of the grouting pile, f is constant and equal to 0.8x18.8 KPa.

The characteristic values of the seven random variations in equation (4) are listed in Table 2. Table 2 is the characteristic values of design variations.

Table 2. Characteristic value of design variations

Variation	H	h	P	$\gamma$	l	l	D
Mean value	1.30	0.17	124.50	24.00	10.000	8.100	0.650
Variation coefficient	0.13	0.19	0.06	0.025	0.033	0.037	0.024

here, H is taken from the standard atlas of frost depth in Jilin Province (Zhang, 1987) and is submitted to normal distribution; h is the maximum value in the Table 1, and it is a normal distribution, too. The other variations are selected from field investigation and data by our institute. D1 is assumed as lognormal distribution, the others are regarded as normal distribution. The limit state equation is:

$$Z = 0 \quad (5)$$

The formula (5) is a non-linear equation with multi-variation, and must be solved with the iterative method.

According to the principle drawn up by The International Committee of Structural Safety (Zheng, 1992), the minimum reliability  $\beta$  is calculated with the normalization method.

Below is what was discussed:

1. It is calculated from seven random variations in Table 2 that  $\beta$  is 0.7725 and  $P_f$  is 0.2199. This indicates that the primary design is of a greater failure probability, which has a relation to the less selected value of anti-frost life stress f, and it also exists in verification according to criterion.

2. It is selected that H and h are random variations, and the others are constant and equal to their mean values, we obtained that  $\beta$  is 0.7874 and  $P_f$  is 0.2155. Compared with the above results,  $P_{r12}/P_f$  equals to 0.98. It is illustrated that the failure probability of grouting pile depends greatly upon the frost depth (H) and frost heave (h).

3. H is selected as the only random variation, the results are  $\beta$  is 0.9367,  $P_{r2}$  is 0.1745 and  $P_{r2}/P_f$  equal to 0.7. We find out that the random characteristic of frost depth (H) is more direct than that of frost heave (h) in calculation.

4. If h is the only random variation, we can obtain that  $\beta$  is 1.0707,  $P_{f2}$  is 0.0474 and  $P_{f2}/P_f$

is equal to 0.21.

Comparing the result 3 with 4, we consider that the effect of random characteristic of frost heave on the reliability is less than that of frost depth according to the data listed in Table 2, but it is not negligible.

In general, it is discussed that the relation between the failure probability ( $P_f$ ) and the variation coefficients ( $C_{vH}$  &  $C_{vh}$ ) of frost depth (H) and frost heave (h). The results are shown in Fig.2 (at this moment, each variation in equation (4) is random), and  $P_f$  rises monotonously with the two variation coefficients.

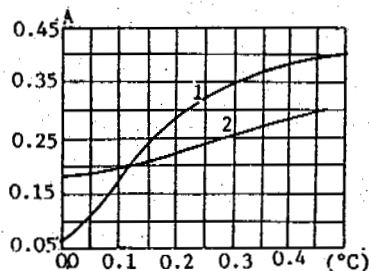


Figure 2. The relation between  $P_f$  and  $C_v$   
1,  $P_f - C_{vH}$   
2,  $P_f - C_{vh}$

When  $C_{vH} > 0.2$ , the slopes of the curves in Fig.2 are very close.

We should give attention to the fact that the lesser the mean of frost depth and frost heave, the greater the variation coefficient (Zhang, 1983; Ministry of Water Conservancy, 1991) (see Table 1). As a result, we can explain why the frost heaving damage of the liner of the canals in the region where the frost depth is shallow, is more serious and occurs mostly in the primary period. In the region where the frost depth is shallow (including northeastern forest area, a low altitude seasonally frozen soil area and a coastal area), the variation coefficient of frost depth will increase, and is often of  $C_{vH} > 0.2$ . In our observation, the variation coefficient of frost heave at the beginning of a cold season is much greater than that at the period when the maximum value appears. However, H and h are all constant in the design of the erected buildings.

It is interesting that when the frost depth (H) is the only random variation,  $P_f$  equals 0.1745 which corresponding to that, the safety factor is 1.03 from Criterion. This means that when K is greater than 1, there still exists a greater failure probability.

## CONCLUSIONS

The observed data cited in the paper indicate that the frost heave is random and submits to normal distribution in the view of geology exploitation in engineering practice.

The random characteristics of both frost depth and frost heave are of the same importance to anti-frost heave stability of the structure.  $P_f$  rises monotonously with the variation coefficients of H and h.

In order to determine exactly the failure probability under the frost heaving force, it is necessary to realize the random variations.

In engineering practice, owing to the fact

that a site is often regarded as well-distributed and a local zone which is represented with a observing site, the above conclusions are significant for actual engineering.

#### REFERENCES

- Li Lianju and Zheng Yongkun, (1990) Damage of Pile-Bridge and Methods of Preventing and Curing. Northeast Hydroelectric.
- Ministry of Water Conservancy, In China, (1991) Criterion of Anti-Frost Heave Design in Canal System Engineering. SL23-91. Published by Hydroelectric Press, Beijing.
- Zhang Xin and Li Yinrong, (1987) 1:2000000 Atlas of Seasonal Frost Depth in Jilin Province. J. of Glaciology and Geocryology.
- Zhang Xie, et al., (1983) Study on the Years-running Dynamic State of Seasonal Frost Depth in Jilin Province. Jilin Provincial Research Institute of Water Conservancy, Changchun.
- Zheng Duo and Wu Shiwei, (1992) Linear Extreme State Equation and Normalization Method. Proceedings of 3rd Conference on Reliability. Nanjin.

## THE FORMATION CHARACTERISTICS OF FROZEN-AREA BOGS IN CHINA

Zhang Zeyou

Peat Society of Jilin Province, P.R. China

In our country, most of the formation environments of bogs belong to the cool-damp type, which is mainly involved in the frozen areas of the Greater and Lesser Xing'an Mountains in the northeast, high mountains in the west and the Qinghai-Xizang Plateau or in the neighboring areas where island-like frozen soils transit to seasonal ones. Among these bogs, the cover-degree and the accumulation intensity are 0.35% and 511.89T/km<sup>2</sup> respectively for the Greater Xing'an Mountains, while for high mountains and plateaus in the west, 0.004-1.57% and 1.14-97.20 T/km<sup>2</sup>, respectively. The values of other areas are very low. Such a distribution pattern has a direct relationship with the surface melting in the frozen areas (Zhou Youwu et al., 1982).

### INTRODUCTION

The formation and development of peat marsh results from the comprehensive actions of various natural factors. Most of the peat marsh in the earth is distributed over the frigid zones and temperate zones of Europe, Asia and North America. It is closely connected with environmental conditions of frozen earth. Its distribution has clear features of latitudinal zonality. Peat marsh on the land surface on the earth shows a north-south symmetry. In the cold moist or cool moist climate, regional rainfall is higher than the regional evaporation capacity, and frozen earth develops. It is the most powerful belt where peat marsh forms and develops. To the north or south of the belt, the forming action of peat marsh weakens. The peatland in the northeast of China is part of the belt. In the Greater and Lesser Xing'an Mountains, the cover-degree of peat marsh is 0.35%, and the accumulation intensity of peat reaches 511.89 T/km<sup>2</sup>. The Qinghai-Xizang plateau is the area where peat marsh develops in vertical regions, and peat in this area is distributed over mountain plains and basins of 3200-4500 miles above sea level.

### THE ENVIRONMENTAL FEATURES THAT FORMS PEAT MARSH

Environmental conditions of water and heat are the basis of peat marsh formation, because water and heat decide the categories and increase amount of plants. Meanwhile, they also restrict decomposition intensity of plant residue. Change of soil temperature and soil moisture restricts the actions of plants and microorganisms directly. Generally, under the condition when the soil temperature is 30°C, the rate of moisture content (the weight of water in soil times 100%) is 30% and the maximum content of soil moisture is 60-80%, the decomposition action of microorganisms is most active (Translated by Shi Hua, 1973). When soil temperature is

below 30°C and the productivity of peat plants is more than the decomposition capacity, it is helpful for the development of peat marsh.

The moist part of northeast China in the frigid-temperate zone and the medi-temperate zone is the region where the distribution and reserves of peat marsh are the largest in the country. The regions are roughly situated between 42°N and 53°N, and includes the Greater and Lesser Xing'an Mountains, the San Jiang Plain, the Chang Bai Mountains and the eastern edge of the NeiMeng Plateau. When peat marsh forms, the most advantageous environmental condition is the climate condition. Except for the north of the Greater and Lesser Xing'an Mountains, which are located in the moist climate region in the frigid temperate zone and have widely continuous perennial frozen earth and island like perennial frozen earth, the others are located in the meditemperate-moist climate region, which is a seasonal frozen soil area. Their main climatic features are shown in Table 1.

We can see from Table 1, in the Greater and Lesser Xing'an Mountains and the eastern edge of the NeiMeng Plateau, the temperature is low, the frozen season of earth surface is long, and there is perennial frozen earth, yielding capacity of vegetation is low, but the decomposition capacity is weak, and forest marsh develops. All these make for a strong accumulations of peat. In the Chang Bai Mountains and the San Jiang Plain, plant grow luxuriantly, there is developed seasonal frozen earth layers that prevent surface water from draining and promote peat marsh formations. In the eastern edge of the NeiMeng Plateau, the surface of earth is wavy, most of the sand dunes are fixed, the river valley and low-lying land among the sand hills are wide and low, spring water accumulates in these low lands, temperature is low, and there is perennial frozen earth. All these work together to make peat marsh develop widely in the area although the area is relatively dry.

The peat marsh in the northeast of China are

Table 1 The environmental features of peat marsh formed in China

grade one area	item grade two area	average temperature(°C)			accumulated temperature Σ°C	annual average rainfall (mm)	dry degree (%)	frozen season (days)	layer of frozen soil
		January	July	annual					
The peat marsh area in the Qinghai-Xizang Plateau	the Greater and Lesser Xing'an Mountains	-30--20	18-22	-4-0	1500-2500	350-500	1.00	250-325	Layers of perennially frozen soil and island-like frozen soil
	the San Jiang Plain	-20--18	22-23	0-2	2500-2800	500-600	1.00	200-250	Layers of seasonally frozen soil
	the Chang Bai Mountains	-18--16	22-24	2-4	2000-3000	600-900	1.0-0.75	180-250	Layers of seasonally frozen soil
	the eastern part of Nei Meng	-16--14	18-22	0-2	2000-3000	400-500	1.5-2.0	250-290	Layers of partially perennial frozen soil
The peat marsh area in the Qinghai-Xizang Plateau	La Sa			7.5	2000-2500	443.6	1.6	200-250	Layers of island-like frozen soil and seasonally frozen soil
	Dang Xiong			1.3	2000-2400	483.1	1.7	210-260	Layers of island-like frozen soil and seasonally frozen soil
	Ruorgai	-10	10-12	0.8-3.3	1000-1200	565-752	1.5-2.0	190-240	Layers of island-like frozen soil and seasonally frozen soil

formed by the climatic, geologic and geomorphologic actions, and it has some features of zonality. For example, high position and middle position peat marsh are mainly distributed in the north and are scarcely distributed in the south. In short, peat marsh is more widely distributed in the Greater and Lesser Xing'an Mountains and has more types. The Chang Bai Mountains is the second. Marsh is also widely distributed in the San Jiang Plain, but the accumulation capacity of peat is low. It is much less in the east of NeiMeng.

The peat marsh in the Qinghai-Xizang Plateau is distributed in the semimoist temperate zone. Especially, the conditions of peat marsh forming are more suitable in the east of the plateau. Peat marsh develops strongly in mountain plains and wide valleys of 3000-5000 m above sea level. For example, the Ruorgai Plateau is the largest highland peat marsh area. At the height that is higher or lower than that of the area peat vegetations are rare or with perennial ice and snow over 5000 miles above sea level. There is a large change in water and heat conditions in a vertical direction because of many differences of cutting degrees caused by the rise of the earth's surface. Generally under favorable geomorphologic and climatic conditions water insulation action from the layers of frozen earth and low temperature provide some good environmental conditions for peat marsh to form. There is 30-60 cm frozen earth layer in 60-100 cm soil layer under ground that is located near 30°N and 4000-4600 m above sea level in the Xizang Plateau. According to the investigation in Zhong Ba county and Dong Xiong from June to July, 1979, these frozen earth layers of the peat marsh are difficult to melt in summer (Song Haiyuan et al., 1985). The accumulative area of peat marsh in the Rurgai Plateau (3400-3600 m above sea level) lies in the northeast of the Qinghai-Xizang

Plateau. It belongs to two branches of the Yellow River, the Black River and the White River. In hilly plains the hills are low and gentle and valleys are wide. So peat marsh is formed at the bottom of valleys, terraces and low-lying land along the shore. The depth of the peat layer is 2-3 m and the maximum reaches over 10 m. The surface area is nearly 3000000ha. The type of peat marsh is singular, which has a relation to high altitude and cold and moist climate in the area. Although temperature is low here, the radiant amount is great (solar radiant amount in a year is 120-150 large calories per square centimeter). So various herb still grow luxuriantly. Seasonally frozen earth is distributed widely. The temperature of the surface soil is low, microorganism's action is weak. All these make it difficult to dissolve dead marshy plants. So peat marsh in large areas is formed.

Peat marsh is distributed widely in the source of the Chang Jiang River and Yellow River where perennial frozen earth develops under the earth surface. Peat marsh in KaMaLong valley in the south of Qinghai province is located at 4000-4300 miles above sea level. Here the climate is cold, and the annual average temperature is 0°C. The growing period of plants is 120 days. Peat marsh is distributed in a plain and straight valley, and its length is 2 km and its width is 0.4 km and its area is about 0.64 km<sup>2</sup>. The thickness in a single layer is 0.85 m, the maximum is 2.2 m. At the bottom is a mud layer, and a frozen earth layer is also seen.

Based on research and environmental analyses made by geologic and mineral departments, the peat marsh was formed from the late pleistocene Epoch to the beginning of the Preboreal Epoch. During the period, glaciers developed and dug the valleys firstly, and then, the climate got warmer, and the glaciers melted, the snowline

rose, a terminal ridge of laid drifts were kept in the end of valley and became th natural dike for accumulating water and marsh. Peat marsh developed and stretched up along the mountain slope under the condition of a relatively cold climate and an existence of frozen earth layers. During the later period the terminal ridge of laid drifts were gradually burst by water flow, peat marsh retreated to the bottom of the valley from the wide and gentle slope and developed into a herbaceous peat marsh landscape.

#### THE TYPE FEATURES OF PEAT MARSH

The northeast of China and the Qinghai-Xizang plateau are the two large distribution areas of peat marsh in our country (Fig.1). Peat marsh from low positions to high positions is formed in the latitudal zone area of frozen earth in the North. Only low position peat marsh is formed in the frozen earth area in the Qinghai-Xizang Plateau.

According to the principles of origination theories, namely, according to the nutritious condition of the process of peat marsh forming and developing and types of marsh vegetations, peat marsh in China is classified into 3 patterns and 14 types (Table 2).

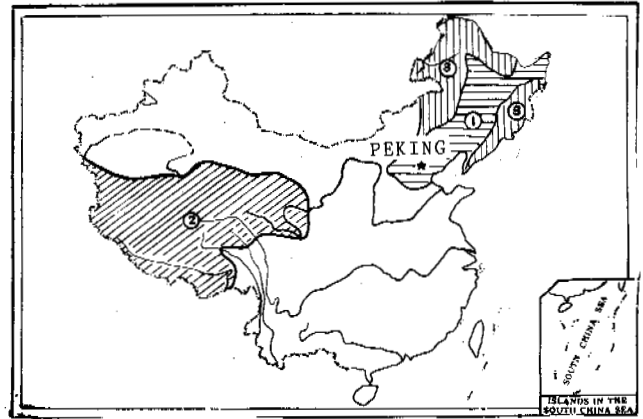


Fig.1 Accumulation area and types of peat in China  
 1. Plainsland  
 2. Plateau land  
 3. Mountainous area

Table 2 Patterns and categories of peat marsh in China

Patterns	Categories
Low position peat marsh patterns	Carex peat marsh category Phragmites peat marsh category carex--Phragmites peat marsh category Kobresia--Carex peat marsh category Carex--Glyceria peat marsh category Aluns--Carex peat marsh category Salix--Carex peat marsh category Larix--Carex peat marsh category
middle position peat marsh patterns	Carex--Sphagnum peat marsh category Larix--Carex--Sphagnum peat marsh category Vaccinium--Eriophorum--Sphagnum peat marsh category Larix--Ledum--Sphagnum peat marsh category
high position peat marsh patterns	Ledum--Sphagnum peat marsh category Sphagnum peat marsh category

Low position peat marsh is widely distributed in our country. Its area is large and reserves are abundant. There is a complete variety of category of peat marsh in the northeast of China. Except for the Carex--Kobresia peat marsh category and Carex--Glyceria peat marsh category that are mainly distributed in the Qinghai-Xizang Plateau, the other twelve categories can all be found in the northeast. Of these categories, Carex peat marsh category covers the maximum surface area of which the major plant species are Carex meyerans, Carex lasiocarpa, Carex schmidtii, Carex pseudocuraica, etc.. The peat marsh is located in flood--plains, terrace, valleys and low-lying land and is usually marsh of seasonal or perennial water keeping, Water--chemical pattern is HCO<sub>3</sub>--Ca--Mg and mineralization degree varies from 50 to 500 mg/l. Most are of a flat and grasshilly microgeomorphology peat marsh landscape (Chai Xiu, 1986). Low position peat marsh can develop to become middle position peat marsh in the course of environmental evolution

and development of the peat marsh itself. The categories that are usually seen in the Greater and Lesser Xing' an Mountains and the Chang Bai mountains area of cold and moist climate are Larix--Carex--Sphagnum peat marsh category. Ledum--Eriophorum--Sphagnum peat marsh category and Carex--Sphagnum peat marsh category. Middle position peat marsh can develop continuously to become high position peat marsh. The categories of high position peat marsh that have been found are Sphagnum peat marsh category and Ledum--Sphagnum peat marsh category. They are only distributed in hilly areas with a cold--moist climate in the northeast of China. Generally the peat marsh protrudes into the central surface. It is higher than its edge by about 1-1.5 m. The central depth of the peat is bigger, and has a variation from position peat marsh to middle position peat marsh to high position peat marsh. Little peat marsh can also be seen in the forest belts of the high--altitude and cold--moist climate. And they are high position peat marsh that is directly formed on perennial frozen earth and has not experienced the stage of low position peat marsh. For example, in the area of Ar Mount and YiErSi in the Greater Xing' an Mountains, the plants on the earth ground are, mainly, Sphagnum, secondly, Paytrchum and hypum, etc., occasionally, Ledum and Vaccinium are associated with them.

Type of peat marsh is singular in the Qinghai-Xizang Plateau. Categories of low position peat marsh in the area are mainly Kobresia--Carex peat marsh category and Carex--Glyceria peat marsh category (You Nusi et al., 1991). Of marsh vegetations, Kobresia tibetica is a special species in the area. The main component of the Carex plant community are Carex muliensis and a few Carex trichocarpa and Blysmus sinocompressus. Usually grasshill microgeomorphy develops. They are the kinds of grass hills that are consisted in Kobresia. Of them, large and small ridgy grass hills are distributed widely. The formation of these ridge grass hills is closely related to the distribution of frozen earth. Just as E.Toler said, the ridgy and moist low-lying land peat marsh is concentrated in the south of today's perennial frozen earth belts

(about 50°-55°N). It is a result of the alternatively freezing and melting action in the frozen earth area. In addition, some peat embankments and peat hills are also formed under the environmental conditions of frozen earth.

#### PEAT MARSH IN THE FROZEN EARTH AREA AND ITS DEVELOPING TENDENCY

Although there are different ideas on which the most developed belt of peat marsh is, either close to the discontinuous belt of perennially frozen earth in the south of perennially frozen earth area or to the south of perennially frozen earth, the opinions that peat marsh benefits by conserving frozen earth are consistent. The forest region of the Greater Xing'an Mountains in the northeast of China is a perennially frozen area, an example is the Gulian valley basin. The depth of perennially frozen earth varies from high to low from the bottom to the edge of the basin. The depth exposed at hydrology No.1 drill hole located at the bottom of the basin is 75 m, but the depth exposed at hydrology No.2 drill hole located on the edge of the basin is only 28 m. There are bushes, low position Carex peat marsh, a thin buried peat layer, and grass-mound microgeomorphology, developed in the low-lying land in the basin. *Betula Platyphylla* and *Larix alternata* on the edge of the basin. *Pinus camphora* is distributed on the top of the mountain. The depth of the loose deposit is the largest at the bottom of the basin and is 7-8 meters, and gets thinner upward gradually. The depth of perennially frozen earth varies from 75 m to 100 m at the bottom of the basin, from 30 m to 40 m at the sloping abdomen, and to 10-20 m on the edge of the basin. Based on the data of the Huola River basin the maximum seasonally melted depth varies from low to high from the bottom to the edge of the basin, it is 0.6-0.8 m at the bottom of the basin and 0.8-1.4 m at the sloping abdomen and 2.2-2.3 m on the top of mountain (Liang Linheng et al., 1991). At the end of August the maximum melted depth of the peat marsh in Mo He forest area is only 0.5 m or so. Especially the melted depth in the high Sphagnum peat marsh area is smaller. The phenomenon is a result of weak heat conductivity of peat. Usually the rate of heat conductivity of peat is very small and is about 0.0015 cal/cm.s.°C, and that of peat with full water is 0.0011 cal/cm.s.°C, and is far lower than that of mineral soil (0.003-0.004 cal/cm.s.°C). Under this condition, peat layers protect the frozen earth layer on one hand, and low temperature and water insulation action of frozen earth layers improve the development of peat marsh on the other hand. So middle position peat marsh and high position peat marsh that formed on the frozen earth layer directly can be seen in the Greater Xing'an Mountains. High position Sphagnum peat marsh is not found in the Qinghai-Xizang Plateau. It is probably a result of strong solar radiation, which is disadvantageous to growth of malnutrient plants such as Sphagnum, etc.. From this we can consider that frozen earth has a close relationship with the formation and development of peat marsh. Just as the scholars on frozen earth study have put forward, that marsh forming and development of peat and layer of Sphagnum can promote the formation of a frozen earth layer, and it is very obvious for the layer of soil in which the temperature is near 0°C. In the Greater Xing'an Mountains, the earth temperature in the peat marsh land is

lower than that in mineral land by about 1-2°C. So a frozen earth island can be almost circled out in the south bounds and lower bounds of the frozen earth area based on the surface outline of peat marsh. On the contrary, in the area where the annual average earth temperature is near 0°C, even the distribution of zero gradient temperature can be seen, and the bottom of the frozen earth is not stable, quarrying peat marsh land must result in an increase in temperature for the frozen earth layer and fall in upper bounds of frozen earth and even degeneration of frozen earth. The period of degeneration of frozen earth is usually the stage of development of peat marsh with rich water resources. At present the total developing tendency of peat marsh in our country, whether in the northeast or in the Qinghai-Xizang plateau, peat marsh on the edge of the Ruorgai Plateau appears to become sand and to dry. Grassy marsh-land plants gradually replace the marshy plants. Little stream and little river are found in the peat marsh land in the Ching Bai Mountains in the northeast of China. Due to water erosion, peat is exposed to the ground. All these have some relation to the arid climate and human activity.

#### REFERENCES

- Zhou Youwu, Guo Dongxin (1982) The main features of frozen earth in our country, "Glaciology and Geocryology", 1.  
Translated by Shi Hua (1973) Types and distribution of peat marsh in the frigid zone and temperate zone in the Northern Hemisphere, "Chinese Translation Bulletin of Geography", 2.  
Song Haiyuan, Wang Debin, etc. (1985) Formation and evolution of peatland in the Xizang Plateau, "Scientia geographica sinica", 2.  
Chai Xiu (1986) Preliminary research on law of formation and distribution of peat in China, "Journal of Geography", 3.  
You Nusi, Yang Fuming, Zhong Fangying (1991) Exploitation and Utilization of peat marsh in the Heng Duan Mountains in the west of Si Chuan province, "Prairie in Si Chuan Province", 2.  
Liang Linheng, Zhou Youwe (1991) Variety of environment of frozen earth after conflagration in the forest area in the Greater Xing'an Mountains, "Glaciology and Geocryology", 3.

# INSTANTANEOUS-STATE DEFORMATION AND STRENGTH BEHAVIOUR OF FROZEN SOIL

Zhang Zhaoxiang<sup>1</sup>, Yu Qun<sup>1</sup>, Xen Zhenya<sup>2</sup> and Lu Heiyen<sup>2</sup>

<sup>1</sup>Beijing Agricultural Engineering University

<sup>2</sup>The First Institute of Engineer Troops

Triaxial compressive tests were conducted on the loam and the sand taken from Jilin and Beijing in a high-speed triaxial test machine. The test results showed, the plastic property of deformation is exhibited in the frozen loam under high strain rate and high confining pressure. But the strength does not depend on strain rate and confining pressure. The failure of brittle shear and axial crack occur in frozen sand. The strength of high density and saturated sample increase linearly with increasing confining pressure. The strength of low density and unsaturated samples presents three stages due to the pressure-injuring of ice. The conception of particle porosity  $\xi$  and particle bond ratio  $(1-\xi)$  were introduced to describe the effect of the degree of ice-particle friction on the frozen soil strength. A strength model of frozen soil was set up. Finally, the reasonableness of the model was verified by means of a series of tests.

## INTRODUCTION

Many test data showed that the strength of frozen soil depends on the strength of ice, the friction between particles and their interaction (Gaughnour, 1986, Chamberlain, 1972, Alkire, 1973, Paramaswaran, 1981, Sayles, 1973). Ting (1983) analyzed qualitatively the mechanism of the interaction of ice and soil particles and the constitution mechanism of the strength of frozen soil. Ladanyi also analyzed the transmissive form of the stress between the frame of soil and pore ice, and by means of the method set by Seed (1967) to analyze the triaxial shear undrained test of unfrozen soil [4], put forward the method to predict the strength of frozen sand (Ladanyi, 1981, 1985, 1990). But the quantitative analysis about the mechanisms is not well resolved. For this reasons, the high-speed triaxial compressive tests were conducted on frozen loam and sand to analyse the properties of deformation, and the strength. This paper discusses the relationship between the strength and some basic physical parameters, such as, the particles friction coefficient, water content and saturated degree.

## SOME BEHAVIOURS OF TRIAXIAL DEFORMATION AND STRENGTH OF FROZEN SOIL

The high-speed triaxial tests in the laboratory were conducted on frozen loam and sand at various constant strain rates ranging from 0.022 S to 0.813 S and under various confining pressures ranging from zero to 8-MPa. The test apparatus, a high-speed triaxial testing machine, was developed by the authors.

Figure 1 shows the particle size distribution curves of the samples tested. The average dry density, plastic limit and liquid limit of samples are 2.72 g/cm<sup>3</sup>, 20% and 39.8% for loam and 2.65 g/cm<sup>3</sup> for sand, respectively. The samples were 39 mm in diameter and 10 cm in length.

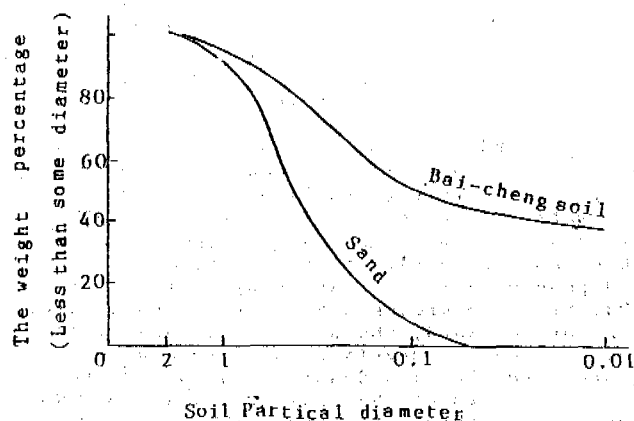


Figure 1. Particle size distribution curve

The typical stress-strain curves of frozen loam and sand under various strain rates and confining pressures is shown in Figure 2. The water content, temperature and density of loam samples are 25.1%, -33.5°C and 1.5 g/cm<sup>3</sup>, respectively. The water content, temperature, strain rates, low-density and high-density of sand samples are 14%, -35.1°C, 1.0 S<sup>-1</sup>, 1.6 g/cm<sup>3</sup> and 1.91 g/cm<sup>3</sup>. The plastic property of frozen loam is displayed under high strain rates ranging from 0.022 S<sup>-1</sup> to 0.813 S<sup>-1</sup> and with a high confining pressure of more than 1.0 MPa. The result is similar to the deformation behaviour of loam at low strain rates (Zhu Yuanlin, 1988). But the deformation behaviour of frozen sand displays brittle failure under various confining pressures, especially, the elastic-brittle failure that occurs to sand under uniaxial compressive conditions. There are obvious remnant strengths for low-density and saturated sand.

The relationships between peak stress,



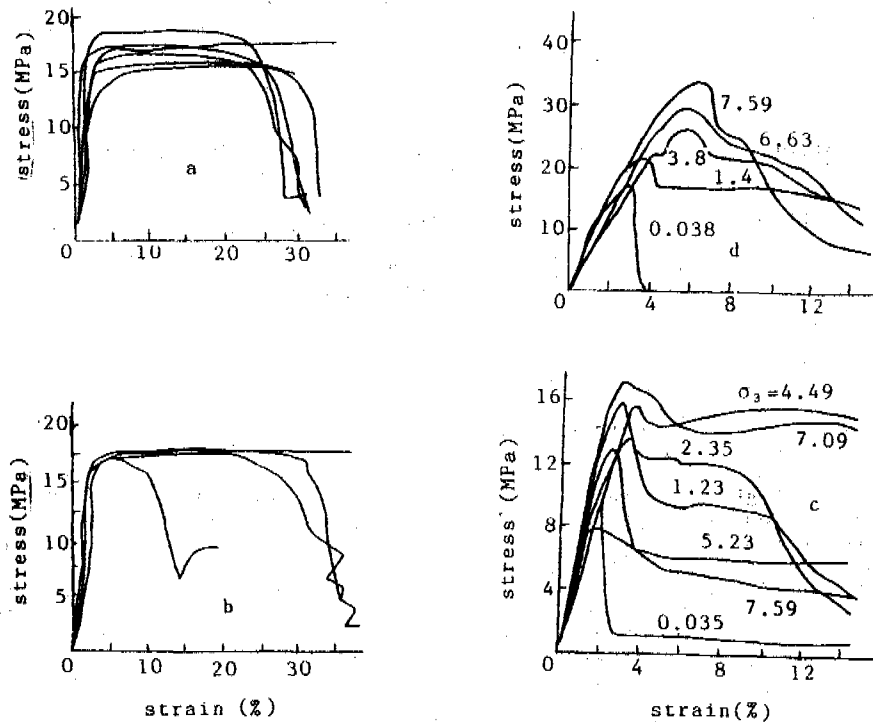


Figure 2. The stress vs. strain (a: loam soil at different strain rates, b: loam soil under different confining pressures, c: low-density sand under different confining pressures, d: high-density sand under different confining pressures)

$(\sigma_1 - \sigma_3)_{max}$  and yield stress, strain rate, and confining pressure, for loam and sand, are given in Figure 3, Figure 4 and Figure 5. Figure 6 shows Mohr's envelope curves of the strength of sand. Figure 3 and Figure 4 indicate that the peak stress and yield stress of frozen loam do not depend on a strain rate ranging from zero to 5 MPa. Figure 5 presents that, for high density and saturated sand, the peak stress and yield stress increase linearly with increasing confining pressure. For low density and unsaturated sand, the curves of the peak, yield and remnant stresses have three processes. The confining pressures that correspond with the maximum and minimum peak stresses are 3.58 MPa and 5.73 MPa, respectively. The maximum value of remnant stress is approximately equal to the maximum value of peak stress, the correspondent confining pressures are 4.49 and 3.58 MPa, respectively, it is indicated that the deformation behaviour of frozen sand is similar to the deformation behaviour of frozen loam when the confining pressure changes from 3.58 MPa to 4.5 MPa. That is, the strength decreases slightly with increasing of deformation.

The angle of internal friction, for high density sand samples, is approximately equal to the value given by Alkire (1973) and Sayles (1973). These are respectively  $31.5^\circ$ ,  $31.4^\circ$  and  $31^\circ$ . Because of different failure types on various confining pressure conditions, the angles are more than the values ( $19.3^\circ$ ,  $12.4^\circ$ ) given by Chamberlain (1972), and V.R. Parameswaran (1973) on high pressure testing conditions.

#### DISCUSSION

E. Chamberlain, (1972), studied the effects

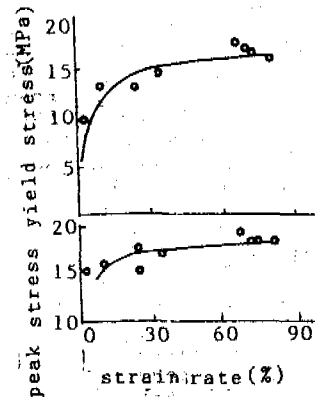


Figure 3. Strength of frozen soil from Bai-Cheng vs. strain rate,  $T = -33^\circ\text{C}$ ,  $W_c = 25.1\%$ ,  $R_d = 1.58 \text{ g/cm}^3$ ,  $P = 4.57 \text{ MPa}$

of confining pressure on the strength of frozen soil. The study showed the strength curve changing with confining pressure has three stages. The confining pressure corresponds with the maximum and minimum peak stresses which are respectively 52.5 MPa and 105 MPa. The result of the strength decreasing with increase of confining pressure is owing to the pressure-melting of ice in frozen soil. But the pressure-melting of ice seems to be impossible in our testing conditions. For low-density and unsaturated frozen sand, because of the pressure-injuring of ice, the strength decreases with increasing of confining pressure.

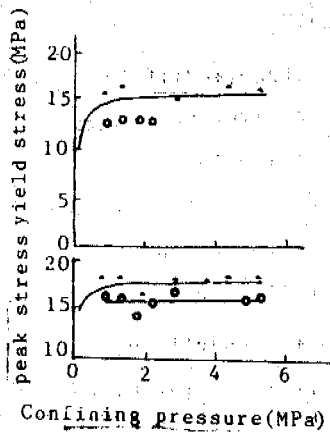


Figure 4. Strength of frozen soil from Bai-Cheng vs. confining pressure.  
 $T = -33^{\circ}\text{C}$   $R_d = 1.4 \text{ g/cm}^3$   $W_c = -27\%$   
 Strain rate/s

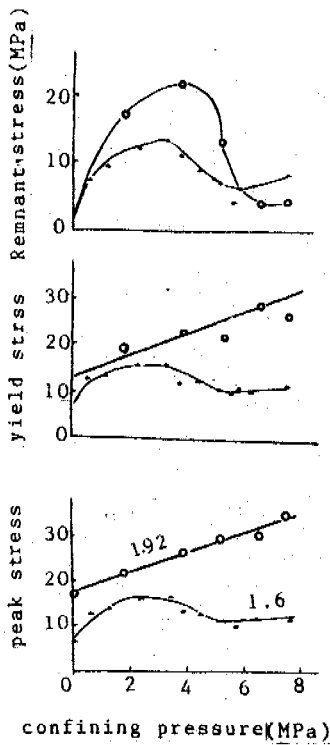


Figure 5. Strength of frozen sand vs. confining pressure  
 $v = 0.896/s$   $T = -36.3^{\circ}\text{C}$   $W_c = 14\%$   
 Dry density  $\text{g/cm}^3$

The frozen soil is of a cementary texture material consisting of ice and particles. The cementary ways and its strength on a micro-cosmic level are different. Stress concentration produced by the different particle friction under hydrostatic pressure causes the injury and failure of the ice-particle cementary force. After a part of cementation is failed, the stress will be redistributed in frozen soil in order to balance the existing stress field. This process occurred by means of the particles

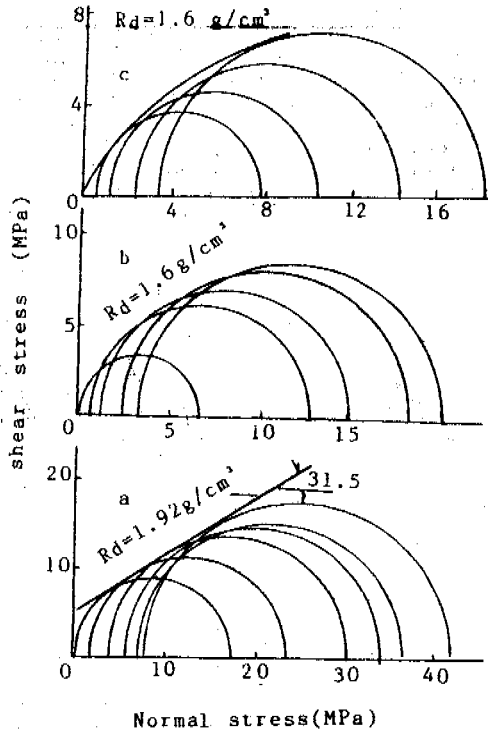


Figure 6. Mohr's envelope curve of the strength of sand

displacement. The end of the process is that ice is broken and strength is lost.

The behaviour of pressure-melting of ice was realized by many researchers. On the basis of the discussions in reports (Ladanyi, 1981, 1985, 1990), it is known there are ice weakening effects under high pressure. If it is said that the soil particles have failed under high pressure, the pressure-injuring of ice will certainly occur under high pressure.

The discussion given above indicates the frozen soil strength behaviours of the three stages in the strength of frozen soil will simultaneously depend on the pressure-injuring and the pressure-melting of ice. For low density and unsaturated frozen soil, the pressure-injuring of ice is the main reason.

#### THEORETICAL ANALYSIS ON THE STRENGTH OF FROZEN SOIL

The frozen soil strength depending on ice is taken into account through ice strength and ice content; furthermore, the frozen soil strength depending on particles is taken into account through particles friction and porosity. For above, the frozen soil strength depending on ice and particle is simultaneously related to porosity. The particles porosity, is defined as:

$$\xi = \frac{V - V_{\min}}{V} = 1 - \frac{V_{\min}}{V} \quad (1)$$

Where,  $V$ ,  $V_{\min}$  — soil volume and minimum soil volume, respectively;

$v$ ,  $v_{\min}$  — soil specific volume and minimum soil specific volume;  
 $1 - \xi$ , is defined as particles contact rates.

From formula (1), if  $v=v_{min}$ , then  $\xi=0$ ; and if  $v \gg v_{min}$ , then  $\xi=1$ . It is said the over-saturated frozen soil will convert into ice samples.

For theoretical analysis, a simplified model of soil texture is shown in Figure 7. Ice in frozen soil can be classified as pore ice and cementing ice. The steady aggregate of soil composed of particles and cementing ice is named as the frozen particles frame work. The unfrozen water content is neglected.

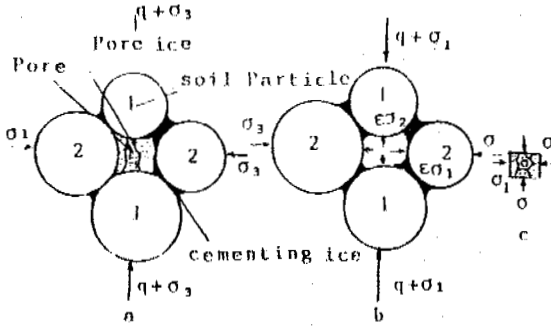


Figure 7. The model of construction of frozen soil

The following conditions are assumed in the analysis:

1) The strength of the frozen particles framework consists of an ice cementation bond and the particles friction. The functions,  $f(\xi)$  and  $g(\xi)$  present the effective degree of the ice cementation bond and the particles friction on the strength of the frozen particles framework.

2) Pore ice is injured under hydrostatic pressure. The injury variable is described with the effective area coefficient of pore ice.

3) When the frozen soil has failed the deformation is small.

4) During the deformation processes of frozen soil, first, the failure of cementing ice occurs. When frozen soil has failed, the pore ice failure types includes tensile, shear and compression. Various conditions are satisfied as follows:

$$\begin{aligned} \text{for tensile failure:} & \quad \sigma_1 = -T_i \\ \text{for shear failure:} & \quad \sigma_2 - \sigma_1 = T_i \\ \text{for compressive failure:} & \quad \sigma_2 = \sigma_i \end{aligned}$$

Where,  $\sigma_1, \sigma_2$  — the maximum and minimum principle stress of pore ice.

$T_i, t_i$  and  $\sigma_i$  — tensile, shear and compressive strength of ice, corresponding deviator stress,  $q_1, q_2$  and  $q_3$  are written:

$$\text{where, } q_i = a_i \sigma_3 + b_i \quad i=1,2,3 \quad (2)$$

$$\begin{aligned} \text{where, } a_1 &= \frac{2(B+\sqrt{2}\xi C)}{A-B} \\ b_1 &= \frac{(A+\sqrt{2}\xi C)[2\xi T_i + \sqrt{2}t_i f(\xi)]}{A-B} \\ a_2 &= \frac{2B}{A-B+\sqrt{2}\xi C} \\ b_2 &= \frac{(A+\sqrt{2}\xi C)[\xi + \sqrt{2}f(\xi)]T_i}{A-B+\sqrt{2}\xi C} \end{aligned} \quad (3)$$

$$a_3 = \frac{2(B-\sqrt{2}\xi C)}{A-B+2\sqrt{2}\xi C}$$

$$b_3 = \frac{(A+\sqrt{2}\xi C)[2\xi T_i + \sqrt{2}t_i f(\xi)]}{A-B+2\sqrt{2}\xi C}$$

Where,  $A = f(\xi) + g(\xi)$

$$B = g(\xi) \cdot f, \quad C = f(\xi) + K g(\xi)$$

$f$  — particles friction coefficient.

$$K = E_1 / E_2$$

$E_1, E_2$  — elastic moduli of ice and particles.

From equation (3), if  $f=0$ , then  $a=0$ . It is shown frozen soil strength does not depend on the confining pressure. In addition, if  $a_1 \geq a_2 \geq a_3$ , i.e. the internal friction angle of frozen soil when tensile failure of pore ice occurs is more than the angle when shear and compressive failure occur.

Especially, if  $\xi=0$ , the equation may be written:

$$q_0 = a_0 \sigma_3 + b_0 \quad (5)$$

where,  $a_0 \equiv a_1 = a_2 = a_3 = \frac{2B}{A-B}$

$$b_0 \equiv b_1 = b_2 = b_3 = \frac{\sqrt{2}\Lambda f(\xi) T_i}{\Lambda - B}$$

Furthermore, if  $\xi=0$ ,  $f(\xi)=0$  and  $g(\xi)=1$ , the equation (5) may be changed into:

$$q_0 = \frac{2f}{1-f} \sigma_3 = (K_p - 1) \sigma_3$$

It is obtained:

$$f = \frac{K_p - 1}{K_p + 1}, \quad K_p = \tan^2\left(\frac{\pi}{4} + \frac{\phi_u}{2}\right) \quad (6)$$

Where,  $\phi_u$  — internal friction angle of unfrozen soil.

It is easy to calculate the  $f$  by using equation (6). e.g. if  $\phi_u=18^\circ$ ,  $f \approx 0.3$ ,  $\phi_u=24^\circ$ ,  $f \approx 0.4$ .

1) The failure condition of pore ice: There are two critical values ( $\sigma_{C1}, \sigma_{C2}$ ) when confining pressure increases. These can be expressed as:

$$\sigma_{C1} = \frac{\sqrt{2}}{4} T_i \left\{ \frac{A-B}{C} (\gamma_2 - 2) - 2[\sqrt{2}\xi + \gamma_2 f(\xi)] \right\} \quad (7)$$

$$\sigma_{C2} = \frac{\sqrt{2}}{4} T_i \left\{ \left( \frac{A-B}{C} + \sqrt{2}\xi \right) (2\gamma_1 - \gamma_2) - \sqrt{2}[\xi + \sqrt{2}f(\xi)] \gamma_2 \right\}$$

That is:

If  $\sigma_3 \leq \sigma_{C1}$ , the tensile failure will occur.

$\sigma_{C1} \leq \sigma_3 \leq \sigma_{C2}$ , the shear failure will occur.

$\sigma_3 > \sigma_{C2}$ , the compressive failure will occur.

2) The frozen soil strength composition:  $\sigma_e$  is denoted as the particles friction effective stress. The frozen soil strength can be written:

$$q_1 = \sqrt{2} f B \sigma_e + t_i f(\xi) + 2\xi T_i + 2\xi C \sigma_e$$

$$q_2 = \sqrt{2} f B \sigma_e + t_i f(\xi) + 2\xi T_i + 0 \quad (8)$$

$$q_3 = \sqrt{2} f B \sigma_e + t_i f(\xi) + 2\xi T_i - 2\xi C \sigma_e$$

From the equation, it is clear that the first term expresses the particles framework strength, the second term expresses the pore ice strength and the third term expresses the strength of interaction on particles and pore ice. Furthermore, the third term is a plus value for tensile failure, a minus value for compression and zero for shear failure.

3) The determination of functions,  $f(\xi)$  and  $g(\xi)$ :

It is obtained by the analysis:

$$f(\xi) = 1 - \text{Exp} \left( \frac{-k_1 \xi (1-\xi)}{(\xi_c - \xi)^2} \right) \quad (9)$$

$$g(\xi) = 1 - \text{Exp} \left( \frac{-k_2 (1-\xi)}{\xi^2} \right)$$

Where,  $k_1, k_2$ , — test parameters.  
 $\xi_c$  — critical porosity depending on soil type.

4) The relationship between  $\xi$  and  $\sigma_3$ :  
 The relationship between  $\xi$  and  $\sigma_3$  is simulated by Figure 8. It is written:

$$\eta \sigma_3 = \frac{4}{3} G \frac{\xi(\xi - S_r)}{S_r(1-\xi)} \quad , \quad (0 \leq \sigma_3 < \sigma_1)$$

$$\eta \sigma_3 = \frac{2}{3} \tau_i \left( \ln \frac{1 - \lambda \beta}{1 + (1-\lambda)\beta - S_2/S_1} + \frac{S_1(\xi - \lambda S_2)}{S_1 - \lambda S_2} \right) \quad , \quad (\sigma_1 \leq \sigma_3 \leq \sigma_2)$$

$$\xi = \lambda \left[ 1 - \text{Exp} \left( 1 - \frac{3\eta \sigma_3}{2\tau_i} \right) \right] \quad (\sigma_3 > \sigma_2)$$

and

$$\beta = \frac{1 - S_r}{1 - \xi}$$

$$S_1 = \frac{S_r(\tau_i + 2G)}{S_r\tau_i + 2G} \quad , \quad S_2 = \frac{S_r(\tau_i + 2G)}{2G}$$

$$\sigma_1 = \frac{2}{3} \frac{\tau_i S_1}{\eta} \quad , \quad \sigma_2 = - \frac{2}{3\eta} \tau_i \ln(1 - S_2)$$

Where,  $G$  — elastic shear modulus of ice.  
 $\tau_i$  — shear strength of ice.  
 $S_r$  — initial ice saturated degree.  
 $\lambda$  — remnant effective area coefficient of ice.

$\eta$  — stress transmit coefficient between pore ice and particle framework.

Figure 9 shows the  $\sigma_3$ - $\xi$  relation curve at various values of  $S_r$  and  $\lambda$ , and  $G=60$  MPa,  $\tau_i=6$  MPa,  $\eta=1$ . From the figures, it is noted that, for  $\lambda < 1$ , the mechanical injuring of ice is a main factor, especially for unsaturated frozen soil. For  $\lambda=1$ , that is, the pressure-injuring of ice does not exist. The ice strength increases with increasing  $\sigma_3$ .

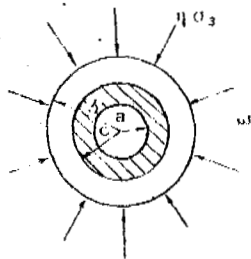


Figure 8. The stress of ice in sphere cavity

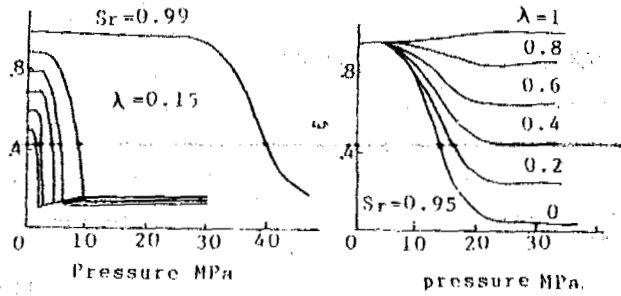


Figure 9.  $\sigma_3$  vs.  $\xi$

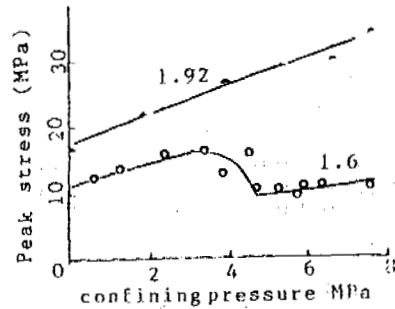


Figure 10. Strength of frozen sand (From Beijing) vs. confining pressure  
 $i=1.03/s$ ,  $T=-35.1^\circ\text{C}$ ,  $W_c=14\%$   
 Dry density

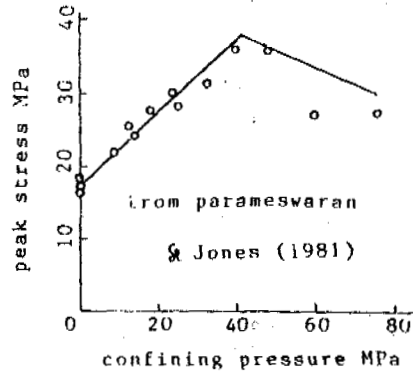


Figure 11. Strength of frozen sand (from Ottawa) vs. confining pressure  
 $i=7.7 \times 10^{-5}$ ,  $T=-10.1^\circ\text{C}$   
 $R_d=1.7 \text{ g/cm}^3$ ,  $W_c=14\%$

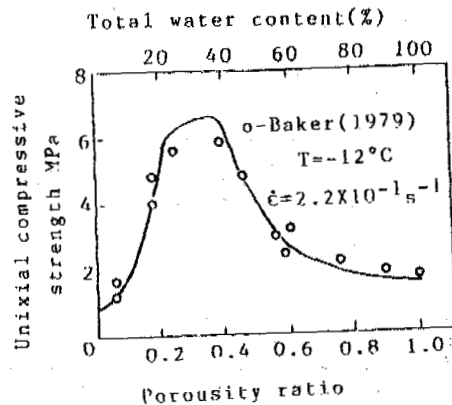


Figure 12. Strength of frozen sand vs. water content

### COMPARISON CALCULATED VALUE WITH TEST VALUE

Figure 10, 11 and 12 show the relationships between frozen soil strength and  $\sigma_3$  as well as water content. The calculation values in Fig. 10, 11 are obtained by  $q_1$ , and  $q_2$  from equation (2), and the value in Figure 12 is from  $q_1 = b_1$ . Simultaneously,  $\xi$  was found by the following formula:

$$\xi = 1 - v_{\min} \left( 1 - \frac{v_w}{v} \right) \quad (11)$$

Where,  $v_w$  — water volume in soil.  
 $v$  — soil volume.

The parameters in Fig. 10, 11, 12 are as follows:

	$\lambda$	$f$	$K$	$K_1$	$K_2$	$T_1$	$T_2$	$G$	$\xi_c$	$v_{\min}$
Fig. 10	0.2	0.30	0.3	0.02	0.04	4.0	7.5	1800	0.25	1.39
Fig. 11	0.2	0.32	0.3	0.02	0.04	3.5	7.5	1800	0.25	1.39
Fig. 12	1	0.32	0.3	0.05	0.15	0.5	1.8		0.30	1.05

Fig. 10, 11, 12 show the calculation values coincide with test values. These also show the reason that the friction angle under high confining pressure is more than the angle under low confining pressure, that is, the reason is from different failures types of pore ice under various confining pressures. In addition, the relationship between dry density ( $R_d$ ) and  $\xi$  is as follows:

$$R_d = (1 - \xi) R_{d\max}$$

Where  $R_{d\max}$  — maximum dry density of soil given.

Figure 12 shows frozen soil strength decreases with increasing  $R_d$ . The results were testified to by many researchers (Zhu Yuanlin, 1987, Sayles, 1981, Wijeweera, 1990).

### CONCLUSION

Under high-speed loading the plastic failure type occurs in frozen loam. The strength does not depend on strain rate ( $\dot{\epsilon} = 0.022s^{-1} \sim 0.813s^{-1}$ ) and confining pressure. The brittle failure occurs in frozen sand and the type of brittle failure is elastic under the uniaxial compressive test. Because of the pressure-injuring of ice, there are three processes in the relationship curve between the strength and confining pressure for low-density unsaturated sand. Owing to different failure types of pore ice under different confining pressure, the friction angle of frozen sand is different.

Equation (2) and (3) can reflect the law of strength of frozen soil. The function  $f(\xi)$  and  $g(\xi)$  can express the effect degree of the friction between ice and particles on the strength of frozen soil.

### REFERENCES

Goughnour, R.R. and Andersland, O.B., (1986) Found Div., 94(4), pp923-950.  
 Chamberlain, E., Groves, C. and Perham, R., (1972) Geotechnique, 22(3), pp469-483.  
 Alkire, B. and Andersland, O.B., (1973) J. of Glaciology, 12, pp469-481.

Parameswaran, V.R. and Jones, S.J., (1981) J. of Glaciology, 27(95), pp147-155.  
 Sayles, F., (1973) 2nd Int. Conf. on Permafrost, pp384-391.  
 Ting, J.M., Martin, R.T. and Ladd, C.C., (1983) J. Geotech. Engr. 109, pp1286-1302.  
 Ladanyi, B., (1981) Proc. Symp. on Free Boundary Problem.  
 Ladanyi, B., (1985) 10th Cancam.  
 Ladanyi, B., (1990) Can. Geotech. J. 27, pp8-18.  
 Zhu Yuanlin and Carbee, D.L., (1988) 5th Int. Symp. on Ground Freezing.  
 Zhu Yuanlin and Carbee, D.L., (1987) CRREL Report pp87-100.  
 Sayles, F.H. and Carbee, D.L., (1981) Engr. Geology, 18, pp55-66.  
 Wijeweera, H. and Joshi, R.C., (1990) Can. Geotech. J., 27, pp472-483.  
 Seed, H.B. and Lee, R.L., (1967) Soil Mech. and Found. Div., 93(SM6), pp333-360.

# CLIMATE FLUCTUATION AND THE PROCESS OF PERMAFROST FORMATION SINCE LAST GLACIATION IN THE SOURCE AREA OF URUMQI RIVER, TIANSHAN, CHINA\*

Zhao Lin, Qiu Guoqing and Jin Huijun

Lanzhou Institute of Glaciology and Geocryology,  
Chinese Academy of Sciences, China

The Source Area of Urumqi River experienced the warm-cold and arid-humid fluctuations after Last Glaciation, with an amplitude smaller than that in Europe and East China. The buried humus soils widely found on the lower part of slope and swampy valley bottom indicated the aggradation of sediments since Last Glaciation with a various aggradating rate from place to place. The aggradating sediments in cold climate were possible to form the syngenetic permafrost. This was confirmed by the data from boreholes and pits, where several ice-rich horizons were found. Based on the mineralogical evidence and comparison with previous work, it is estimated that the lower limit of alpine permafrost along Urumqi River during Last Glaciation be at about 2100 m a.s.l. and 900 m lower than its present position.

## INTRODUCTION

Climate is an important factor in permafrost development. The formation or degeneration, colding or warming, thickening or thinning of permafrost are resultant from climate change. On the other hand, the information of permafrost development or degeneration could be the indicator of climate change, used for the reconstruction of environment. Since few paleo-periglacial features were found out of the present permafrost area, the authors would like to discuss the permafrost change mainly by using the stratigraphical data.

## THE STUDY REGION

The Source Area of Urumqi River is located on the northern side of Mt. Kalawucheng, the middle part of Tianshan (43°07'N, 83°49'E). The ridges are at an elevation of 4000 m or so. The modern snowline is at 3900 to 4100 m a.s.l. The terminus of modern glaciers runs down to 3600 m a.s.l. The lower limit of permafrost is at 2900 m (north-facing slope) to 3250 m a.s.l. (south-facing slope).

Belonging to Tianshan Geosynclinal Folding System, it is composed of Paleozoic igneous rock and metamorphic rocks, including augen, gneiss, diabase, granite and chlorite schist. The glaciated area in late Pleistocene was known to be down to 3000 m a.s.l.

Xinjiang is far from ocean and is generally recognized as an area with typical continental climate. Tianshan, however, lying across the middle of Xinjiang, is relatively humid and with a continentality lower than 50, and thus could not be considered as a region of continental climate. The mean annual air temperature decreases upwards, down to -2°C at 3000 m a.s.l.,

and -5.4°C at 3539 m a.s.l., about -8°C at the ridges of 4000 m a.s.l.

The vegetation zones occur altitudinally: the Picea forest at 1800 to 2700 m a.s.l., the sub-alpine and alpine pelouse mainly composed of *Cobresia filifolia* group at 2700 to 3600 m a.s.l. and steppe belt from 1000 to 1800 m a.s.l. According to the plant sampling and analysis (sampled by Jin Huijun and analyzed by Zhang Guoliang and Zhang Qibin), the vegetation in the modern permafrost area is composed of *Potentilla*, *Leontopodium*, *Helictotrichon*, *Caryophyllaceae*, *Ranunculaceae*, *Carex* etc. In palynological composition of ground surface, the content of *Potentilla* is 75.42%, *Chenopodiaceae* and *Artemisia* — 11.5%, *Ephedra* — 5.4%, *Picea* — 7.1 to 32.8% as well as few *Caryophyllaceae*, *Polygonaceae*, *Chrysanthemum*, *Arster*, *Cruciferae* etc. (Li and Yan, 1990).

## THE AGGRADATION OF QUATERNARY SEDIMENTS

### Distribution of Aggradating Sediments

The buried humus soils were widely found in excavations or Pits of 81-1, 81-3, 89-1, 90-1, 90-2, 90-3, 90-4, 90-5, 90-6 and the Boreholes T-2, 91-1 and 91-3 (Fig.1). Five layers of humus soils were found in Pit 90-4 (Fig.2), and four humus layers in Borehole 91-2.

It is commonly known that the humus soil should be formed at ground surface. The presence of buried humus soils indicates an aggradation of sediments.

According to the characters of sediments, the aggradating sediments can be divided into two types: a. those mainly in talus in the lower part of relatively steep slope; b. those on the relatively gentle slope and swampy lowland composed of slope wash, gelifluctational and glaciofluvial deposits.

### Aggradating Rate of the Sediments

In Pit 89-1, the mean aggradating rate was

\*This project is supported by the National Science Foundation of China and the Tianshan Glaciological Station, Academia Sinica.

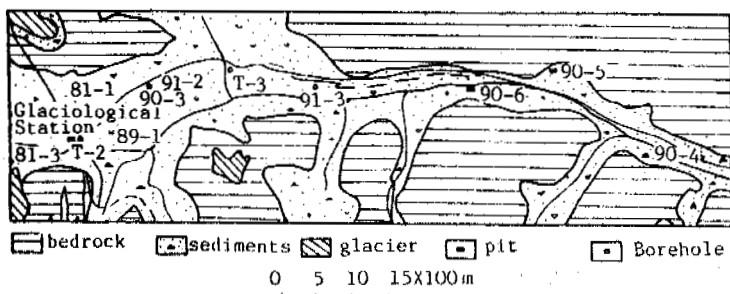


Figure 1. The distributional map of pits and boreholes in the Source Area of Urumqi River

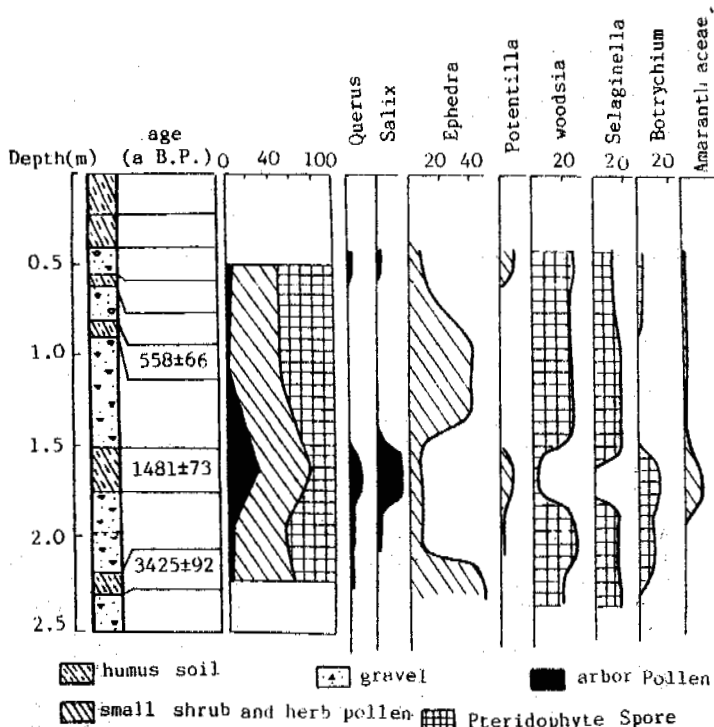


Figure 2. Palynological figure in the section of Pit 90-4

0.24 mm/a at 4300 a B.P. From 4301 to 3211 a B.P., it was 0.16 mm/a; from 3211 to 201 a B.P., it was 0.27 mm/a (Zhao and Qiu, 1991). The aggradating sediments are composed of gravel and sandy clay. It can be considered as the representative aggradating rate in swampy ground in the middle of swampy lowlands.

In Pit 90-4 on the south bank of Urumqi River near the Wangfeng Highway Maintenance Squad, 5 layers of humus soils were found. The lower three layers were formed in 3425±92, 1481±73 and 558±66 a B.P. respectively. Thus the mean aggradating rate was 0.66 mm/a around 3425 a B.P., 0.365 mm/a from 3425 to 1481 a B.P., 0.758 mm/a from 1481 to 558 a B.P. and covered by the aggradating gravelly soils, 1.44 mm/a from 558 a B.P. on. It can be considered as the representative aggradating rate at the lower part of slope.

THE CLIMATE FLUCTUATION AFTER THE LAST GLACIATION  
The Palynological Data and Paleoclimate Informa-

tion from the Section of Pit 90-4

As shown in Table 1 and Fig.2, the total number of pollen and spore grains is 1033, in which 99 grains are of the tree pollens, 478 grains are of the small shrub and herb pollens, and 456 — pteridophyte spores.

The section can be divided into 4 belts, palynologically and stratigraphically.

(1) In the humus soil at the depth from 2.3 to 2.2 m and 3425 a B.P. in age, the pollens and spores are mainly of small shrub, herb and pteridophyte. The content of small shrub and herb pollens is 58.2%, pteridophyte spores — 39.3%. The Ephedra content is as high as 88.7% in the small shrub and herb pollens. Woodsia and Selaginella spores is 50% and 42.6% respectively in pteridophyte spores, the content of tree pollens — only 2.5%.

It is known that the Ephedra, Woodsia and Selaginella are growing in the arid and cold environment. This palynological indicates a climate cold and dry around 3425 a B.P.

(2) In the gravelly sediment 2.2 to 1.62 m in depth and 3425 to 1481 a B.P. in age, the content of tree pollens increases to 6.2%, the Ephedra content abruptly decreases to 28% in total grains of small shrub and herb pollens. The content of Chenopodiaceae, Artemisia and Gramineae pollens increases to 12%, 6% and 8% respectively of the small shrub and herb pollens. Some new pollens, such as Compositae and Potentilla are found. The content of pteridophyte spores, mainly the Woodsia, is 40.2%. The Selaginella content is 21.2%. Botrychium spores occurs in this belt.

Comparing with the first belt, it could be known that there was a slight warming and wetting climatically. Comparing with the modern vegetation (Li and Yan, 1990), the climate condition was still drier and colder than that at present.

(3) In humus soil, 1.62 to 1.40 m in depth and 1481 a B.P. in age, the content of tree pollens increases greatly to 28.6%, mainly including Salix (53.6% of the total tree pollens) and Quercus (30.4%). Within the small shrub and herb pollens (49.8% in total), there are Amarantaceae (23.3%), Potentilla (15.0%), Ephedra (13.3%), Caragana (13.3%), Chenopodiaceae (8.3%), Artemisia (5%). The content of pteridophyte spores decreases to 21.6%. There are Botrychium (55.8%), Woodsia (19.2%), Lycopodium (11.5%).

The great increase in tree pollen, especially the Quercus pollens, and the decrease in Ephedra, the increase in Botrychium spores indicate the warming and wetting around 1481 a B.P.

(4) The upper part of the section (0 to 1.4 m in depth) was formed after 1481 a B.P. Two palynological samples were taken. The tree pollens decrease greatly down to 1.6-7.3%. The pteridophyte spores increase to half of the total pollen content and the spore content — 49.2 to 50.9%, the small shrub and herb pollens — from 41.8 to 49.2%, in which the Ephedra pollens are the most (23.9 to 84.2%), the Potentilla — 0 to 17.6%, Amarantaceae — 2.5 to 4.3%. In the pteridophyte spores, there are mainly Woodsia and Selaginella.

This belt can be divided into two stages: the first, 1.4 to 0.85 m in depth and 1481 to 558 a B.P. in age, the sediments are composed of gravels; in which the palynological composition and climate is similar to Belt 1; the

Table 1. Palynological result of Pit 90-4 in the Source Area of Urumqi River

Sample number	90-4-1		90-4-4		90-4-5		90-4-6		90-4-7	
	Number	Percent	Number	Percent	Number	Percent	Number	Percent	Number	Percent
Name of pollens or spores										
Total number of pollens and spores	110		244		241		194		244	
Tree pollens	8	7.3	4	1.6	69	28.6	12	6.2	6	2.5
Small shrub and herb	46	41.8	120	49.2	120	49.8	50	25.8	142	58.2
Pteridophyte	56	50.9	120	49.2	52	21.6	132	68.0	96	39.3
Picea	1	1			1	0.4	1	0.5		
Taxodiaceae									1	0.4
Quercus	4	3.6	4	1.6	21	8.7	9	4.6	5	2
Betula					3	1.2				
Alnus					5	2.1				
Salix	3	2.7			37	15.4	2	1.0		
Juglans					2	0.8				
Ephedra	11	10	101	41.4	16	6.6	14	7.2	126	51.6
Rhododendron					5	2.1				
Compositae	3	2.7			2	0.8	4	2.1		
Artemisia			2	0.8	6	2.5	3	1.5	2	0.8
Chenopodiaceae	1	1	4	1.6	10	4.1	6	3.1	4	1.6
Caryophyllaceae			2	0.8	1	0.4			1	0.4
Rosaceae	4	3.6	3	1.2					1	0.4
Potentilla	9	8.2			18	7.5	3	1.5		
Lilium	4	3.6	2	0.8	2	0.8	3	1.5	3	1.2
Mimosoideae	5	4.5			2	0.8	3	1.5		
Caragana	4	3.6			16	6.6	6	3.1		
Gramineae	3	2.7	2	0.8	8	3.3	4	2.1	1	0.4
Amaranthaceae	2	1.8	3	1.2	28	11.6				
Ranunculus			1	0.4	1	0.4				
Polygonaceae							3	1.5		
Convolvulus					1	0.4				
Labiatae					3	1.2				
Malva					1	0.4				
Cornu							1	0.5	4	1.6
Woodsia	29	26.4	62	25.4	10	4.1	53	27.3	48	19.7
Drynaria baronii	5	4.5	10	4.1	2	0.8	15	7.7	7	2.9
Botrychium	4	3.6			29	12	19	9.8		
Selaginella	15	13.6	44	18.0			28	14.4	41	16.8
Lycopodium	3	2.7	4	1.6	6	2.5	7	3.6		
Adiantum					5	2.1	9	4.6		
Plagiogyria							1	0.5		

(analyzed by Ma Yuzheng, the Department of Geography, Lanzhou College)

second stage, 0 to 0.85 m in depth and the age — from 558 a B.P. to present, indicates a climate slight warmer in comparison with the Belt 1.

So, the climate fluctuated from cold-dry to a slightly cold-wet, relatively warm-wet, cold-dry since 3425 a B.P. according to Zhou Kunshu (1981), at the Hongwuyue Bridge Section (2520 m a.s.l.) around 4000 a B.P., the vegetations of Ephedra and other herbs being able to grow in cold-dry environment were dominant; after 4000 a B.P., the Picea pollens increased slightly and the Ephedra pollens were still in the most. This indicated a slightly warmer.

#### The Climate Changes Since Last Glaciation

Similar to other places in the world, the Source Area of Urumqi River has experienced the

cold-warm and arid-himid fluctuations since Last Glaciation.

According to Qin Dahe et al (1984), it was cold in 15000 a B.P., the snowline was about 550 m lower than at present, and the glaciers advanced down to about 3000 m a.s.l. and the mean annual air temperature was about 4°C lower than at present. This cold period could be confirmed by mineralogical evidence too. In the mineralogic composition of the Upper Wangfeng moraine, the unstable mineral content was 32.75 to 65.75% in the heavy minerals, of which the hornblende and augite contents were 28.15% and 17.15% respectively. The mean content of stable heavy minerals was 19.6%; the superstable minerals — only 1.1%. In the light mineral composition, the plagioclase content was 51.23% quartz — 32.8%. All of these indicate that the



moraine experienced a cold climate since the Last Glaciation.

After 15000 a B.P., the climate gradually slightly became warmer and drier. In the Early Holocene, it was still cool and dry, and tended to warmer continually (Han, 1985). About 7000 a B.P., it was relatively warm and wet, the area of the Hongwuyue Bridge was covered by Picea forest, the air temperature was about 1°C higher than that at present (Zhou et al, 1981). In Middle Holocene or the Neoglaciation, the first glacier advance was developed between 5700 and 5000 a B.P. The snowline was 240 m lower than that at present (Zhang, 1981). It was estimated that the air temperature was about 1.5°C lower than that at present. Afterwards, the air temperature rose again.

By 3425 a B.P., corresponding to the Zhou-Qin Dynasty Cold Period (Zhu, 1979), the climate in this region became cold and dry. The second glacier advance of the Neoglaciation was performed and the Shanbei Moraine was formed (Chen, 1987). The mineralogical results also indicated a cold climate (Table 2). Then, the climate became slightly warmer. After 1481 a B.P., i.e. 469 D.C., it became relatively warm and wet. The air temperature was estimated to be about 1°C higher than that at present.

Between 469 and 1392 D.C., it became cold and dry. The vegetation was just like that between 3500 and 2900 a B.P., and the air temperature was about 1.5°C lower than that at present. After 1392 D.C., it became slightly warmer. During 16 to 19 centuries or the Little Ice Age, the temperature amplitude was no more than 1°C (Qin et al, 1984).

Comparing with the previous work, it is known that the amplitude of temperature fluctuation in this region was some lower than at the other places in the world. For example, the temperature depression in this region was 4°C at the second stage of the Last Glaciation or 15000 a B.P., and was 6 to 8°C in East China (Yang and Xie, 1985), 10 to 15°C in Central Europe and North America (Frakes, 1979). Around 7000 a B.P., the mean annual air temperature in this region was 1°C higher than that of present (Zhou et al, 1981), while in East China — 2 to 5°C (An et al, 1991). From 5700 to 5000 a B.P., the temperature in this region was 1.5°C lower than that at present, while in East China and North America — 5 to 6°C (Yang and Xie, 1985). In

Sum, the climate in this region is more stable than others (Fig.3).

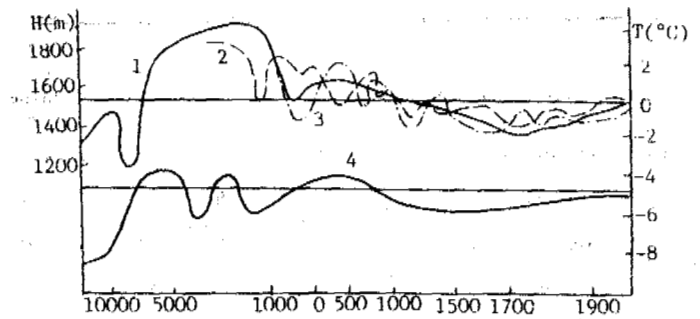


Figure 3. Air temperature curve in the Source Area of Urumqi River in the past of 15000 years  
 1. altitude of snowline in Norway;  
 2. air temperature curve in China;  
 3. air temperature curve in Xinjiang;  
 4. air temperature in the Source of Urumqi River in the past of 15000 years (Zhu, 1979; Li, 1985)

#### THE FORMATION PROCESS OF SYNGENETIC PERMAFROST SINCE LAST GLACIATION

Syngenetic permafrost was defined as the permafrost that formed more or less simultaneously with the deposition of ground in which it occurred (Brown and Kupsch, 1974). Accompanying to the aggradation of sediments, the permafrost table rose, and the sediments that was buried in the seasonally thawing layer was becoming permafrost. The syngenetic permafrost have been formed (Popov et al., 1974).

There are some points should be discussed in detail:

#### The Significance of the Buried Humus Soils

As mentioned above, humus were found in the slope wash at the lower part of slope and in the sediments in swampy lowland. Sometimes it was buried under the permafrost table, for example, in the Pit 81-3, the humus soil with an ice content of 94% was found at the depth of 1.5 to 1.68 m, while the permafrost table — at 1.5 m. In Pit 90-6, humus soil was found at 1.65 m, while the permafrost table — 1.4 m. Sometimes, the humus soils were found above the

Table 2. The mineralogic compositions of the till in the Source Area of Urumqi River

Types Stability Content(%)	Heavy mineral							Light mineral		"B" value of clay
	Unstable				Relatively stable	Stable	Super-stable	Quartz	Plagioclase	
	Mean	Hornblende	Augite	Biotite	Mean	Mean	Mean			
Ice Age										
Little Ice Age	41.71	17.44	9.52	13.09	25.45	27.7	5.14	23.4	52.86	2.25
Neoglaciation	48	39.5	0.25	5.75	28.5	20.5	3.0	27.5	52	0.98
Wangreng Glaciation	54.92	28.15	17.15	4.3	24.38	19.6	1.1	51.33	22.81	1.05-1.07

(Wang Jintai et al, 1981, unpublished)

permafrost table, e.g. Pit 89-1, the humus soil was found at a depth of 0.95 m, the permafrost table — 1.42 m. Usually the humus soil could only be formed by organism at the surface horizon of ground, the occurrence of buried humus soil indicates the aggradation of sediment. Also, the thickness of active layer is usually greater than 1 m in this region, if the permafrost table is higher than or just slightly lower than the humus soil, which could be the indicator of the previous ground surface, then it is possible to consider that the permafrost table has been rising. In other words, the syngenetic process of permafrost has occurred.

#### The Periglacial Environment in this Region Favourable to the Development of Syngenetic Perennially Frozen Ground

The most part of the working area has been in a periglacial environment with some fluctuations since Last Glaciation even though in the hypithermal interval of the Early Holocene, the mean annual air temperature was only 1°C higher than at present. The aggradation of sediments in a periglacial environment could result in the formation of syngenetic perennially frozen ground.

#### Glaciation and Permafrost Development

Nowadays, the glaciers are surrounded by the periglacial alpine permafrost area. The ended and lateral moraines are perennially frozen with buried glacial ice occasionally. The fact that the temperature under ice bed near the equilibrium line of Glacier No.1 was observed to be -1.8°C (Huang et al, 1990) indicated the existence of permafrost in subglacial moraine. Thus, it might be believable that in the ice ages, for example in the Last Glaciation, at the ice advance stages the ended and lateral and subglacial moraines would be syngenetically and perennially frozen, beyond that there would be the periglacial region much larger in area. At the interglacial stage or intervals, the glaciers would retreat, the snowline and permafrost lower limit would rise. In the area above permafrost lower limit, after the melting of the subaerial glacial ice, it was cold enough to develop and preserve the frozen ground, for example, in the Dry Cirque glaciated in Little Ice Age near the Glacier No.1, the mean annual air temperature is -7.2°C nowadays; in the observation site of the Daxigou Meteorological Station, glaciated in Last Glaciation and Neoglaciation, it is now -5.4°C. Under such a cold climate, the aggradation of sediments would result in the formation of syngenetic perennially frozen ground.

#### DISCUSSION: THE POSSIBILITY OF APPLYING THE RATIO OF QUARTZ/FELDSPAR TO RECONSTRUCT THE ALPINE PERMAFROST LOWER LIMIT

According to Konischev (Konischev et al, 1988; Konischev, 1985), the stability of minerals in cold environment is just contrary to that in warm-humid environment. Quartz is less stable in cold environment with a cryogenic cracking size limit of 0.05 to 0.01 mm, while the feldspar — 0.1 to 0.05 mm, biotite — 0.25 to 0.1 mm and muscovite — 0.5 to 0.25 mm. As a result of the longterm intensive procession of freeze-thaw weathering in cold environment, the quartz grains would concentrate on the size of 0.05-0.01 mm, and feldspar grains — 0.05 to 0.1

mm. Konischev suggested a coefficient K to be an environmental index:

$$K = \frac{\text{quartz content (0.05 to 0.01 mm)}}{\text{feldspar content}}$$

$$K = \frac{\text{quartz content (0.1 to 0.05 mm)}}{\text{feldspar content}}$$

Experientially, if  $K > 1$ , the sediments should be formed in a permafrost environment or have ever experienced a permafrost environment after its formation; if  $K < 1$ , the sediments should have never experienced a permafrost environment. Some results of mineral analysis (analyzed by Ma Zhenhai) are shown in Table 3.

Sample 1 with a K-value of 1.134 was obtained in the modern permafrost area. Sample 2 to 5 was formed during Late Pleistocene (Gao and Wang, 1989). According to the above statement, Sample 2 and 3 with a K-value greater than 1 might have experienced a permafrost environment, and the Sample 4 and 5 with a K-value  $< 1$  might be not. Therefore, the permafrost lower limit along Urumqi River during Last Glaciation should be between 2020 and 2200 m a.s.l.

As mentioned above, the mean annual air temperature during Last Glaciation was 4°C lower than that at present. If the temperature gradient was about 0.41°C/100 m, the permafrost lower limit during Last Glaciation should be 900 to 1000 m lower than its present position, and should be between 1900 and 2300 m a.s.l., this is similar to the result by using the K-value. Thus there reveals a possibility of applying the mineralogical technique to reconstruct the permafrost lower limit in a certain period. However, there are still some problems in such a method. First, the criterion of K is only an empirical parameter, and more perfect theoretical basis is necessary. Second, the K-value would be changed with the environment, for example, if the deposit was formed in a very cold environment and most of the quartz grains has reached their size limit, then as the climate warming, more feldspar grains would become smaller, as a result, the K-value would tend to decrease, vice versa. Thus, more evidence is needed for the verifying of the results by this method. Since the working area has never experienced a very warm climate after the Last Glaciation, maybe, this method could be available to search the permafrost lower limit in the past cold period.

#### CONCLUSION

In conclusion, the following points could be made:

1. Buried humus soils in the profiles indicated the aggradation of sediments on slope and the swampy lowland since Last Glaciation.
2. Since Last Glaciation, the amplitude of cold-warm fluctuations in the Source Area of Urumqi River was less than that in East China. The working area has been in a relatively stable cold periglacial environment.
3. The aggradation of sediments in periglacial environment led to the formation of syngenetic permafrost.
4. By the mineralogical method, it is estimated that the permafrost lower limit during Last Glaciation was 900-1000 m lower than that at present. More evidence is needed for verifying such a result.

Table 3. K-value, quartz- and feldspar-content in Selected Sites

Number	1		2		3		4		5	
Sampling site	Near Daxigou Meteorological Station		Hong Wuyue Bridge		Houxia		Houxia		The fourth Team	
Altitude (m)	3530		2520		2200		2020		1600	
Name	Gravel subclay		Sand		Loess		Loess		Loess	
Grain size grade (mm)	0.1-0.05	0.05-0.01	0.1-0.05	0.05-0.01	0.1-0.05	0.05-0.01	0.1-0.05	0.05-0.01	0.1-0.05	0.05-0.01
Quartz content (%)	59.5	62.5	41.5	47.5	41.0	42.5	56.5	55.0	59.5	55.0
Feldspar content (%)	40.5	37.5	58.5	52.5	59.0	57.5	43.5	45.0	40.5	45.0
K	1.134		1.293		1.064		0.941		0.832	

## REFERENCES

- An Zhisheng, Wu Xihao, Lu Yanchou, Zhang De'er, Sun Xiangjun, Dong Guangrong and Wang Sumin, (1991) Paleoenvironmental changes of China during the last 18000 years. *Quaternary Geology and Environment in China*. Science Press, Beijing, China, pp.228-236.
- Brown, R.J.E. and Kupsch, W.O., (1974) Permafrost terminology. National Research Council of Canada, Ottawa, pp.27-29.
- Chen Jiyang, (1987) Preliminary research on Mid- and Late-Holocene glacial fluctuations in Tianger Peak II regions, Tianshan Mountains. *J. of Gla. and Cryo.*, 9(4): pp.347-354 (in Chinese).
- Frakes, L.A., (1979) Chapter B: The Neogene — wide swings and cyclicity. *Climates-throughout Geologic Time*. Elsevier Scientific Publishing Company, New York, pp.217-258.
- Gao Chunhai and Wang Shuji, (1989) Environmental evolution of Late Cenozoic in Urumqi Region. *Geographical Symposium of Arid Zone*, Vol.1, Science Press, Beijing, China, pp.86-93 (in Chinese).
- Han Shuti, (1985) On the sedimentary environment in the northern piedmont of Tianshan Mountains. *Symposium of Quaternary Research in Arid Zone of Xinjiang*. Xinjiang People's Publishing House, pp.32-41 (in Chinese).
- Huang Maohuan, Cai Baolin and Wang Zhongxiang, (1990) The basal conditions of the Glacier No.1 of Urumqi River headwaters. *Proceedings of the 4th Chinese National Conference on Gla. & Geocryology (selection) (Glaciology)*. Science Press, Beijing, pp.59-64 (in Chinese).
- Konischev, V.N., Gogov, V.V. and Poklonny, S.A., (1988) Physical-chemical types of cryogenesis. *Proceedings of 5th Conference on Permafrost*, Trondheim, Norway, Vol.1, Tapir Publishers: pp.381-383.
- Li Wenye and Yan Shun, (1990) Chapter 5: Quaternary spore-pollen study of the Chaiwopu Basin. in: *The Quaternary Climate-environment Changes and Hydrogeological Condition of Chaiwopu in Xinjiang Region*. China Ocean Press, Beijing, pp.46-74 (in Chinese).
- Qin Dahe, Feng Zhaodong and Li Jijun, (1984) Discussion of the fluctuation and the environment since Main Wurm Glaciation in Headwater of Urumqi River, Tianshan. *Journal of Gla. and Cryo.* 6(3), pp.51-62 (in Chinese).
- Yang Huai ren and Xie Zhiren, (1985) The climate fluctuation and sea-level up-down movement during the last 20000 years in China. *Proceedings of the Symposium of Quaternary Glacier and Geology*. Science Press, Vol.2, Beijing, pp.1-18 (in Chinese).
- Zhang Zhenshan, (1981) Changes of snowline at the Head of Urumqi River, Tianshan. *J. of Gla. & Cryo.* 3 (Special Issue), pp.106-113 (in Chinese).
- Zhao Lin and Qiu Guoqing, (1991) Buried humus soil and syngenetic permafrost around the Daxigou Meteorological Station at the Source of Urumqi River, Tianshan. *J. of Gla. & Geocryology*. 13(2), pp.177-180 (in Chinese).
- Zhou Kunshu, Liang Xiulong and Lin Ruiling, (1981) Preliminary study on palynology of glacier ice and Quaternary deposit at the Upper Researches of the Urumqi River, Tianshan. *J. of Gla. & Cryo.* 3 (Special Issue), pp.97-105 (in Chinese).
- Zhu Kezheng, (1979) Preliminary study on climate fluctuation in China during the last 5000 years. in: *The Collection of Zhu Kezheng's Papers*. Science Press, Beijing, pp.475-498 (in Chinese).
- Konischev, V.N., Pogov, V.V., (1985) *Methods for cryolithological studies*. Publishing House of Moscow State University, 150p (in Russian).
- Popov, A.I., Tolstikhin, N.I. and Gravis, G.C., (1974) Ground ice, cryogenic structure and freezing-facies analysis of frozen-ground. in: *General Geocryology*, "Nauka" Press, Novosibirsk, pp.135-160 (in Russian).

THE LOESS AND ITS CLIMATE RECORDS IN KUNLUN SHAN REGION  
SINCE THE LATE PLEISTOCENE

Zhao Xiufeng, Guo Dongxing and Huang Yizhi

Lanzhou Institute of Glaciology and Geocryology, Chinese Academy of Sciences

In this paper, the properties, origin and especially the loess climatic record of the studied loess section has been thoroughly discussed. Based on evidence of climatic changes provided by loess and other periglacial phenomena, the climatic fluctuation in the region from about 24 ka B.P. can be divided into following periods: the cold period in late Pleistocene (24-10.7 ka B.P.), the transitional period in early Holocene (10.7-8.8 ka B.P.), the moist-warm period in middle Holocene (8.8-6.0 ka B.P.), the warm period in middle Holocene (6.0-4.5 ka B.P.) the late Holocene period (since 4.5 ka B.P.) and etc..

INTRODUCTION

Kunlunshan region is located between the southern continuous permafrost region on Qinghai-Xizang Plateau and the northern arid desert regions such as Tarim basin, Qaidam basin and etc.. Its high altitude terrain is accompanied by a predominantly cold and arid climate. The high altitude loess deposit developed in periglacial environment not only occurs on the northern slope of Kunlun Mts, but on the slope valley and river terraces in the interior of Kunlunshan region where the height is above 4000 m a.s.l.. A series of research work on the loess profile in eastern Xidatan have been carried out from 1990 and the research results revealed that the Kunlunshan region have undergone climate fluctuation periods since 24 ka B.P. as following: The cold period in late Pleistocene (24-10.7 ka B.P.); The transitional period in the early Holocene (10.7-8.8 ka B.P.); The relative warm and wet period in the middle Holocene (8.8-6.0 ka B.P.); The warm and arid period in middle Holocene (6.0-4.5 ka B.P.); Climate fluctuation period in late Holocene (since 4.5 ka B.P.).

GENERAL DISCUSSIONS ON THE LOESS PROPERTIES IN KUNLUNSHAN REGION

The loess deposit can be seen from Golmud to Xidatan along the Qinghai-Xizang Highway. Its thickness is generally between 1-2 m and the maximum is about 10 m. The loess is relatively coarse and composed by more silt or fine sand. Gravel layer often appears in the loess profiles. Thick and typical loess deposit developed only in some areas.

The Xidatan fault valley which stretches from east to west situated between 35°40'N to 36°N. According to Xidatan Meteorological Station (4101 m a.s.l.), the mean annual precipitation is 287 mm. The mean annual air temperature is 2.9°C, the mean monthly air temperature in July is 5.9

°C. The primary form of Xidatan was formed in the tectonic movements at the beginning and the middle of middle Pleistocene. During late Pleistocene, it accepted 310 m loose sediments by strong sinking. The loess profile discussed in this paper, which covers on bedrock or late Pleistocene slope sediments and attributed to eolian-slope origin, is located at the foot of southern slope in the joint part of Xidatan and Xiaonanchuan (Fig.1). The absolute altitude at the bottom of the loess profile is 4040 m a.s.l.

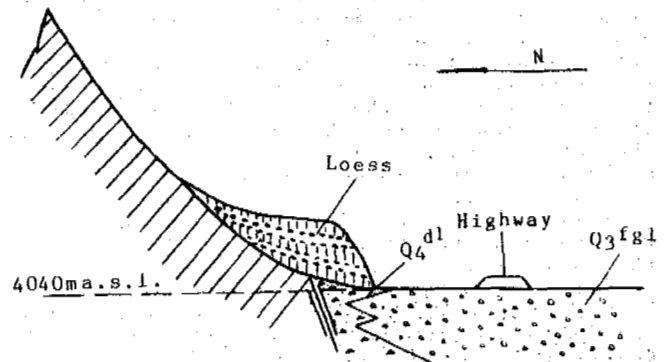


Fig.1 Loess profile in the East of Xidatan

Two gravel belts composed by interlaced loess and gravel bed appears at the depth from 1.5-3.1 m and from 5.9-6.3 m. the gravel which has the same lithologic properties as the slope bedrock differs in size with general diameter about 1-2 cm and the maximum diameter can be 5 cm. The upper, middle and lower part of the loess naturally divided by the two gravel belts are homogeneously, largely unstratified silt with no obvious calcic accumulation occurrence. Compared with the loess deposits in other regions in China, the coarse silt content in Xidatan Profile and

Table 1 Granularity characteristics of the loess in Xidatan

Depth (m)	Percentage (%)					M	$\sigma_1$	SK <sub>1</sub>	Kg	Kd	<sup>14</sup> C or calculated date (y)
	<2	2-4	4-6	6-8	>8						
1.5	1.76	17.43	61.00	11.09	8.72	4.5	1.78	0.39	2.49	7	6343
3.1	1.12	13.96	62.33	12.41	10.18	4.73	1.70	0.41	1.96	6.12	12125+90
4.4	0.12	5.34	68.70	15.91	9.93	4.89	1.60	0.62	1.68	6.92	13658
5.8	0.59	13.38	57.54	16.30	12.19	4.85	1.83	0.45	1.56	4.72	15310+110
6.3	0.22	11.72	62.64	15.14	10.28	4.81	1.67	0.50	1.48	6.10	18210+135
7.4	7.88	36.09	40.49	8.01	6.93	5.73	2.00	0.07	1.90	5.84	24480+765

Table 2 The average content of some heavy minerals of the loess in Xidatan (%)

Depth (m)	Amph.	Pyro.	Epid	Garn	Mica	Meta	Unst.	M.st	stab.	V.st
0.4	37.61	0.86	22.17	3.26	8.26	23.48	35.43	33.69	27.39	3.47
1.5	43.56	1.28	21.03	3.86	5.58	18.45	44.41	30.46	22.73	3.35
3.1	40.69	0.20	20.05	4.29	9.41	20.65	37.62	33.14	25.55	3.68
4.4	38.51	1.03	20.91	3.73	9.52	23.19	35.19	34.99	27.13	2.69
5.8	38.30	0.20	20.08	4.76	15.94	17.81	36.86	38.29	22.99	1.87
6.3	42.13	0.23	19.67	4.63	12.03	18.98	39.35	34.94	24.30	1.38
7.4	30.90	0.85	19.10	3.86	18.24	24.03	33.90	35.83	28.31	1.92

the mean grain size are larger but the clay content is obvious low (Table 1). The skewness (SK<sub>1</sub>), kurtosis (Kg) and the standard deviation ( $\sigma_1$ ) are from 0.3 to 0.7, from 1.5 to 3 and from 1.6 to 2.0 respectively. All of them coincide with eolian transformation and a concentrated granulith on coarse silt.

The heavy minerals in loess deposit in Xidatan are predominantly amphibololite, epidote, mica and metal mineral. The content of unstable minerals and relative stable minerals is higher than that of the loess in eastern China but is similar to that of the loess in the northern slope of Kunlun Mts in Xingjiang Province. This indicates the similarity of the loess properties in periglacial environment. Based on heavy mineral analysis, though the loess material may be partly from the northern Qaidum basin, most of them come from the cryogenic weathering mountainous areas and the loose Quaternary sediment in the region because the west wind is prevalent. The active dune not far from this profile may be an evidence for this conclusion.

From stratigraphic analysis, the occurrence of loess deposit should begin in the latest Pleistocene. The <sup>14</sup>C dating at the bottom of this profile is 24470+765 a B.P., which is coincided with the age of loess on the third terrace of Golmud River (18931±400 a B.P., Wang Shaoling, 1989), the loess on northern slope of Kunlun Mts in Xingjiang Province (about 20 ka B.P., Gao Conghai etc., 1991), the new loess in Gonghe Basin (27600 ± 750 a B.P., Xu Shuying, 1986), and the synchronus sand deposit on Qinghai-Xizang Plateau. Their occurrences are all relevant to the arid trend of climate in plateau and adjacent regions at about 23 ka B.P.. A lot of research works have identified that the Qinghai-Xizang Plateau upheaved to 2000-3000 m a.s.l. from the early to middle Pleistocene and the southwest Monsoon could climb over the not very high Himalaya Mts. then and brought abundant rainfall to the Plateau and even the regions in the north of Kunlun Mts. The Plateau was uplifted

to above 4000 m a.s.l. and the height of Himalaya surpassed 6000 m a.s.l. after Middle Pleistocene. The northern trip of southeast monsoon was so resisted and the Qinghai-Xizang Plateau began its climate evolution in the trend of arid and cold. But before 23 ka B.P., the climate on plateau or in nearby regions was relatively wet which can be verified by the fresh water lacustrine deposit and the developing of large-scale ice-wedges on plateau (Generally, the developing of large-scale ice-wedge requires a relative wet climate condition). After 24 ka B.P., the climate became arid and the Qaidum basin began its second salt depositing period. The desert in Northwestern China expanded and the eolian deposit appeared on plateau. The loess deposit began to appear then in the region and adjacent regions which indicates the cold-arid environmental characteristics began to be gradually formed.

#### THE CLIMATE RECORDS IN LOESS DEPOSIT

##### Lithological Record

The lower gravel belt in the loess profile in Xidatan is located at the depth from 5.9-6.3 m and its age is between 18210±135 to 15310±110 a B.P.. The upper gravel belt is located at the depth from 1.5-3.1 m and its age is between 12125±90 to 6000 a B.P. (Fig.2). This two periods still have arid-moisture fluctuation as showed by the interlaced loess and gravel layer, but they are definitely the most moist periods since 24 ka B.P.. The individual gravel layer appears at 1.8 to 1.9 m, 2.1 to 2.3 m, 2.9, 5.9 m and 6.3 m respectively and they are all corresponded with the susceptibility peaks which shows a synchronous wet-warm feature.

As to the grain-size analysis result, a popular view held by specialists suggests that the 0.05-0.01 mm particle group is the main group of eolian sediment and the particle group <0.005 mm is the additional group of eolian sediment. Arid and cold climate condition is favourable for

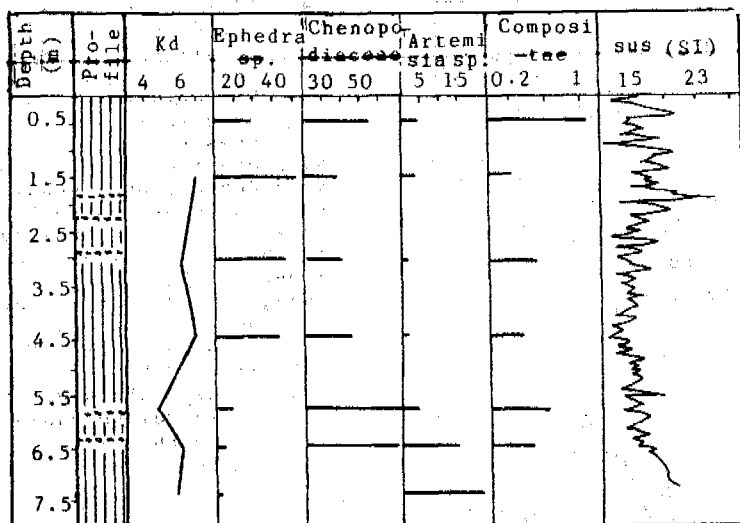


Fig.2 Climate records in the loess profile in Xidatan

coarse silt accumulation but unfavourable for clay accumulation. When loess had deposited, increasing weathering and soil-forming action result in increasing clay content and decreasing coarse silt content. The ratio of them (Kd) can be used for indicating the cold-arid or warm-wet climate condition. Considering the special hypergenesis in cold region, the Kd may have another meaning: In warm-wet climate condition the clay is formed, but in cold-arid climate condition the clay content drops greatly due to irreversible coarsening and coarse silt content increases due to frost cracking of the particle larger than 0.05 mm. The low clay content revealed in the profile just shows a cold climate characteristic. Thus high Kd value indicates arid-cold climate and low Kd value shows warm and wet climate. We can conclude from Fig.2 that the climate gradually became arid-cool from warm-wet between 24-18 ka B.P.. The period from 15 to 12 ka B.P. was extremely arid and cold and the coldest period was at about 13.7 ka B.P.. The climate following this became favourable at 12 ka B.P., and at 7 ka B.P. there was a low temperature event.

#### Pollen and Spore Analysis

In the whole loess profile excluding gravel belts, the pollen content of desert vegetation such as Ephedra sp., Chenopodiaceae and Artemisia sp. can surpass 90% which indicates the loess depositing environment was similar to the modern environment—the desert or desert pasture environment. The pollen content of drought-enduring plant such as Ephedra sp., Chenopodiaceae and Artemisia sp. gradually increase from the bottom to the depth of 6.4 m showing that the climate became arid and cold from 24 to 18 ka B.P.. Though the pollen content from 5.8 m to 3.1 m deep is also mainly composed by the above types, but the pollen types and other pollen content decrease apparently in the middle part which shows the same climate change trend of the grain-size analysis. That is, from arid-cool to arid-cold and then warm-moist during the period from 15-12 ka B.P.. From the depth of 1.5 m to 0.4 m, the pollen content of Ephedra sp. drops and pollen types and other plant pollen content increase gradually and Polypodium appears at 0.4 m depth indicates that the climate condition then

(2 ka B.P.) was greatly improved.

The other analysis results such as weathering coefficient of heavy minerals,  $SiO_2/Al_2O_3$  ratio and etc. have similar reflection for climate fluctuation as the pollen and grain-size analysis.

#### The Susceptibility Record

Though the physical meaning of the susceptibility of loess has not been perfectly solved, its well-correspondence to the  $\delta^{18}O$  record of the deep-sea sediment provides us a useful method to analyse the climate change. Generally, high susceptibility shows warm-moist climate and low susceptibility indicates arid-cold climate condition. By measuring the susceptibility of loess deposit, a continuous climate change curve was made and the ages of arbitrary point at the profile were calculated based on susceptibility.

From the susceptibility curve, we can conclude that the air temperature in Kunlun Mts. region gradually decreased from 24 ka to 15 ka B.P. (Fig.3). But at about 15 ka B.P. there was a temperature increasing event. Then the temperature again dropped and reached the lowest point at about 13.7 ka B.P.. After that the temperature fluctuated frequently and an extreme-cold event occurred at about 10666 a B.P.. Following this event the climate entered its Holocene period. The temperature in Early Holocene increased fastly in fluctuation form and the susceptibility value immediately surpassed its mean value in Holocene (15.6). At about 9 ka B.P. the susceptibility dropped steeply and then increased greatly at about 8.8 ka B.P. to the highest value in Holocene. They indicated one extreme-cold and one strong temperature increasing event respectively. During the period of 8.8-4.5 ka B.P., the susceptibility was over the mean value in Holocene except at about 7 ka and 6.2 ka B.P.. This period should be a warm period and the period from 6.0 to 4.5 ka B.P. should be the optimum climate period for the susceptibility was all above the mean value in Holocene. In the period from 4.5-2.0 ka B.P., the temperature fell frequently and the lowest susceptibility appeared at 3.9 ka B.P.. This period was the Neoglaciation period. The susceptibility

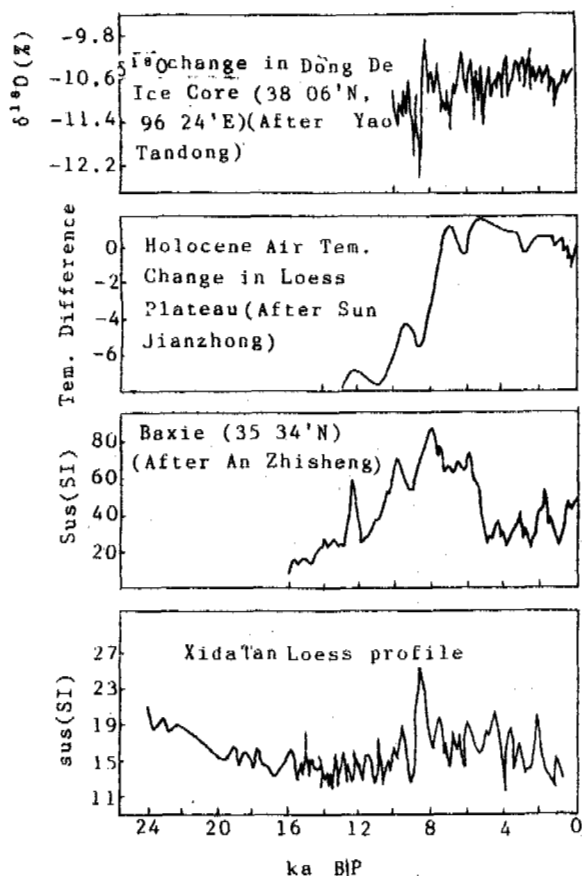


Fig.3 Climate change comparing in different region since 24 ka B.P.

rose at 2 ka B.P. and then fell greatly and entered the modern little glaciation period.

According to preceding analysis, the climate change in Kunlun Mts. region can be divided as following periods: 1) The cold period in Late Pleistocene among which the period from 24-18 ka B.P. was warm-arid, the period from 18-15 ka B.P. was cool-moist, the period from 15-12.5 ka B.P. was cold-arid and period from 12.5-10.5 ka B.P. was wet-cold. 2) The temperature rising period in Early Holocene (10.5-8.8 ka B.P.) characterized by wet-warm climate and violent temperature increasing and decreasing. 3) The wet-warm period in Middle Holocene (8.8-6.0 ka B.P.). 4) The warm-arid period in Middle Holocene (6.0-4.5 ka B.P.) which is the optimum climate period. 5) The period of Late Holocene Since 4.5 ka B.P. and etc..

#### THE COMPARING OF CLIMATE CHANGE SERIES

The climate change sequence showed by the loess deposit in Xidatan is synchronous as a whole to those of other region. But the violent and frequent temperature fluctuation, the cold event reflected by the susceptibility is especially obvious. This may be due to the plateau upheaving effects added on pure climate changes.

The permafrost research showed that the permafrost northern limit had expanded to the region near Nachitai (3550 m a.s.l. at present) in Late Pleistocene. In early Holocene the climate

changed in warm and wet climate, permafrost retreated and humus layer or peat were developed in the valley and basin on Plateau with the age between 10-8 ka B.P.. In the Neoglaciation period the permafrost again expanded its distribution area indicated by involutions and other evidences to the north of modern permafrost northern limit. And through our researches on sand deposit on Qinghai-Xizang Plateau, the warm periods occurred at 9 ka, 5-4 ka, 1 ka B.P.. The above facts are coincided with our conclusions in this paper. The researches on salt lake sediment in Changan Lake revealed that the climate change trend in this region since 24 ka B.P. was wet (before 24 ka B.P.)--> arid (after 24 ka B.P.)--> most arid (16-9 ka B.P.)--> relatively wet (since 9 ka B.P.) (Cheng Kezao, 1986). And Zhang Penxi subdivided the arid period since 5 ka B.P. in Qaidum basin (Zhang Pensi, 1986). According to the high altitude loess study results in Xingjiang, the climate in this region from 1.2-7 ka B.P. was cold-arid or cool-arid while the early period of Early Holocene may be wet-cool, obvious wet climate appeared from 7-5 ka B.P.. The climate condition in Late Holocene was degraded and two cold period occurred in 4.0-2.7 ka B.P. and 19th-17th century (Gao Conghai, 1991). All of the above environmental change series are correspondent with our conclusion apart from some details.

The record of Dongde ice core shows that the climates in Kunlun Mts. and Qilian Mts. which situated in southern and northern side of Qaidum Basin respectively have the most similarity. Especially the coincided extreme-cold event at 8.9-8.7 ka B.P. and so on and the high-temperature event at 2.9 ka B.P. and etc. (Yao Tandong, 1991). The climate change records of the loess deposit in Xidatan is also confirmed by that of the loess in Loess Plateau, especially the cold period occurrences in 8.7-8.9 ka B.P., 7.5 ka B.P., 3 ka B.P. and etc. which are well-correspondent with our research results. It is obvious that the climate record of the loess in the region is of wide-spread meanings and provides a good reference sequence for climate studies in nearby regions and in permafrost regions on Qinghai-Xizang Plateau. Lastly, we give out the comparing of climate change series in different region and end our discussions.

#### REFERENCES

- Liu Dongsheng (1985) Loess and environment. pp. 191-218, 78-81. Science Press. Beijing (in Chinese).
- Gao Conghai (1991) An approach to sedimentary environment of Loess at northern slope of Kunlun Mts. Arid Land Geography. Vol. 14, No. 3, pp. 9-17 (in Chinese).
- Sun Jianzhong (1991) Quaternary of Loess Plateau in China. pp. 113-143, 186-205. Science Press, Beijing, China (in Chinese).
- Zhao Xiufeng (1991) The origin and Environmental Meanings of the sand deposit Along Qinghai-Xizang Plateau. Arid Land Resources and Environment. pp. 61-69. The Inner-Mongolia Printing House of Science and Technology, Hohhot. P.R. China (in Chinese).

## PROTEIN CHANGES AND FUNCTIONS DURING COLD ACCLIMATION OF WINTER WHEAT

Zhao Yutain and Zhao Jun

Institute of Crop Germplasm Resources, Chinese Academy of  
Agricultural Sciences, Beijing 100081, China

The paper presents that there were nine soluble proteins in the cultivar of Jingdong-1 and 13 in Xiaolong-12 that increased markedly in amount during cold acclimation, of which the amount of five proteins with molecular weights of 1000 D, 7000 D (high PI), 18000 D (two kind), and 21000 D in both of the two cultivars presented to be positively correlated with the development of cold hardiness. During the period of cold acclimation, two kind of specific membrane polypeptides of 34500 D and 24000 D were newly synthesized in cultivars of Jingdong-1 and Longda-139; one specific membrane polypeptide of 24000 D was newly synthesized on the cultivar of Xiaolong-12. And the amount of these polypeptides in leaf tissues appeared a positive correlation with the development of cold hardiness. There were six membrane polypeptides in Jingdong-1 and seven in Xiaolong-12 accumulated and the amount in leaf tissues increased proportionally to the increase in cold hardiness.

### INTRODUCTION

In recent years, studies on protein synthesis and changes of winter wheat upon cold conditioning have served as a profile of gene expression alteration to deduce the effect of certain increasingly or newly synthesized specific proteins on the improving of cold hardiness of plants. Cloutier discovered in 1983 that the amount of some soluble proteins of Winter Wheat and Rye increased twice following cold acclimation. In 1987, Guy found that three membrane proteins with molecular weights of 160, 117 and 85 KD were synthesized in spinach during cold acclimation. Mohapatra reported in 1988 that cold treatment to Alfalfa induced the synthesis of ten new membrane proteins. This research demonstrates that the cold-conditioned proteins are positively correlated with the improving of freezing tolerance of plants, and also related to the alteration in gene expression.

Detailed studies on cold-hardened membrane proteins are now in progress on the physiological functions and specific properties of tissues. We attempt here to approach the changing regularity of soluble protein and membrane protein of winter wheat during cold acclimation. Our research objectives also include establishing the relationship between protein changes and the regulation of freezing-resistant gene expression, and furthermore deriving their relationship with the development of freezing tolerance.

### MATERIALS AND METHODS

#### 1. Plant Materials

Sixteen cultivars of wheat with varying degree of cold hardiness were selected for all experiments. They are as follows: Jingdong-1 (JD-1), Jinglong-160 (JL-160), Longda-139 (LD-139), Xiaolong-12 (XL-12), 9-Shi-2/AH1599, Yuandong-8165 (YD-8165), Yuandong-834 (YD-834), Baofeng-

7227 (BF-7227), Xuzhou-21 (XZ-21), 86-005, Ping-007, 9-Shi-5/WH59, 9-Ping-1/AH1059, 9-Ping-9/WH45, 9-Shi-9/H1890, and Yuandong-8756 (YD-8756).

#### 2. Cold Acclimation and Deacclimation

Seedlings grown at 20°C were divided into two groups. one group was maintained at 5-15°C as a contrast, the other group was placed into a controlled environment chamber for cold acclimation for 42 days (day: 2-4°C 12h/night: 0-2°C, 12h). Thereafter, the cold acclimated seedlings were transferred to 5-20°C conditions for deacclimation. All of the experimental seedlings were basically uniform in size.

#### 3. Administration of Freezing Processing

The experimental CH\*, NH, and DH (10 days) seedlings were processed in a freezing environment by the method we described in a previous paper (Zhao and Liang, 1987).

#### 4. Extraction of Soluble Protein and Membrane

The soluble proteins and membrane proteins of winter wheat leaf tissues in CH, NH, and DH seedlings were extracted according to the procedures described by Guy and Cloutier.

#### 5. Gel Electrophoresis

Two-dimensional slab isoelectric focusing/SDS — index pore gradient PAGE technique was used in separating proteins according to the references from Guy (1987) and Zhao (1990).

### RESULTS AND ANALYSES

#### 1. Results of the Freezing Tolerance Evaluation

The survival rates of CH, NH, and DH wheat seedlings following freezing process in a controlled environment chamber at -7°C and -8°C

\*Abbreviations: CH, cold hardened; NH, nonhardened; DH, dehardened.



Table 1. Survival rate of wheats grown in different conditions and processed in -7°C and -8°C conditioning

Cultivar Names	Survival Rate					
	-7°C			-8°C		
	NH	CH	DH	NH	CH	DH
Jingdong-1	15.7	90.2	19.8	0	88.5	23.3
Xiaolong-12	0	76	16.1	0	74	5.2
Jinglong-160	43.5	88.5	51.3	0	89.7	7
Longda-139	42.3	86				
86-005	53.3	85.4		0	80	
Yuandong-8615	57.1	93.3		47	82.4	
Yuandong-834	42.9	95.7				
9-Ping-1/AH1095	68.4	93.7		0	90.9	
9-Shi-5/WCH59	0	85.7		0	80.4	
9-Shi-2/AH1599	22	77.7		19.4	72.7	
9-Shi-9/H1890				23.9	67.8	
9-Ping-9/WH45				7.7	87.5	
Ping-007				0	78	

are listed in Table and Photos 1 and 2. From these results it is clear that compared with the contrast ones, the survival rate of winter wheat following 42 days of cold hardening increased markedly. This indicates that cold hardening can indeed improve the ability of freezing tolerance of winter wheat. If the CH seedlings of JD-1, XL-12 and JL-160 were returned to 5-20°C condition for deacclimation and then placed at -7°C and -8°C for freezing processing, the survival rate would decline significantly, indicating an apparent decrease in the ability of freezing tolerance of these cultivars.

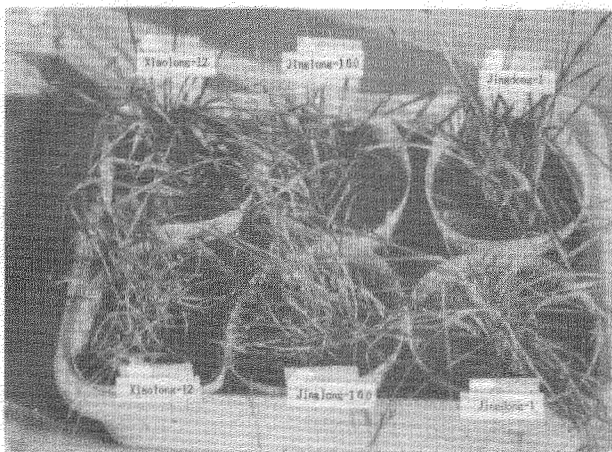


Photo 1. Growing state of 42-day cold hardened and the contrast wheat seedlings at 20°C for 1 week following processing at -8°C.

## 2. Changes and Functions of Soluble Proteins during Cold Acclimation and Deacclimation

### 2.1 Changes and functions of soluble proteins during cold acclimation

The alterations in soluble protein content of leaf tissues in cultivars of JD-1 and XL-12 are presented in Table 2. It can be observed



Photo 2. Growing state of 42-day cold hardened and the contrast wheat seedlings at 20°C for 30 days following processing at -8°C

from Table 2 that there were at least nine soluble proteins of leaf tissues increased in amount in CH seedlings of JD-1, compared with that of NH<sub>1</sub> seedlings. The mol wt of increased proteins included 43, 41, 18 (two kinds), 24, 21, 7 (two kinds with higher PI and lower PI respectively), and 1KD. There were at least thirteen soluble proteins increased in amount in XL-12, among which nine were the same as that of JD-1 and the other four were different kinds with mol wt of 42KD.

It is, therefore, concluded that with the increase in freezing tolerance of CH seedlings, there is a progressive increase in the ability to synthesize soluble proteins. This suggests that the gene that regulates the protein synthesis has altered in the expression mechanism during the cold acclimation.

### 2.2 Changes and functions of soluble proteins during deacclimation

Analysis of the Table 2 reveals that the nine proteins that increased apparently in amount during cold acclimation of JD-1 (thirteen proteins in XL-12) occurred the following changes during deacclimation.

a. Three proteins of 43, 41, and 24 KD in JD-1 increased in amount further, while in the protein of 7KD (high PI) there remained no change. As for the cultivar of XL-12, eight proteins of 42 (four kinds), 41, 43, 24, and 7KD (high PI) accumulated further. By comparison of the soluble protein contents of NH<sub>1</sub> and NH<sub>2</sub> leaf tissues, we found that except the disappearance of 7KD protein, the other three proteins increased in amount in NH<sub>2</sub> leaf tissues of JD-1. All of the eight proteins in leaf tissues of XL-12 presented a marked increase in amount. The results suggest that the amounts of these proteins in leaf tissues are mainly subject to the individual growth development, although they also appear to be affected by temperature and the development of freezing tolerance, which are not closely related.

b. The 7KD (lower PI) protein of JD-1 tended to disappear, while the 18 KD (two kinds) decreased in amount, and the 1 KD protein disappeared completely. In cultivar of XL-12, the 1 KD protein vanished while the protein content of 21 KD and 18 KD (two kinds) declined. By observing

Table 2. Alterations in soluble proteins (increase in amount during cold acclimation) of NH<sub>1</sub>, CH, DH, and NH<sub>2</sub> leaf tissues

Protein Number	Mol wt (Dalton)	A l t e r a t i o n s									
		Jingdong-1					Xiaolong-12				
		NH <sub>1</sub>	CH	DH	NH <sub>2</sub>	RS	NH <sub>1</sub>	CH	DH	NH <sub>2</sub>	RS
1	43000	+	↑	↑	↑	o	+	↑	↑	↑	o
2	42000 (four kinds)	-	-	+	+	o	+	↑	↑	↑	o
3	41000	+	↑	↑	↑	o	+	↑	↑	↑	o
4	24000	+	↑	↑	↑	o	+	↑	↑	↑	o
5	18000 (two kinds)	+	↑	↓	=	Δ	+	↑	↓	=	Δ
6	7000 (higher PI)	+	↑	=	-	o	+	↑	↓	↑	o
7	7000 (lower PI)	+	↑	↓*	=	Δ	+	↑	↓*	↑	▲
8	1000	+	↑	-	=	Δ	+	↑	-	=	Δ
9	21000	+	↑	↓*	-	▲	+	↑	↓	=	Δ

"+" , presence of protein; "-" , absence of protein; "=" , no change; "↑" , increase in amount of protein; "↓" , decrease in amount of protein; "↓\*" , tending to disappear in protein content; "RS" , relationship between protein and freezing tolerance; "o" , the amount of protein is dominantly controlled by the growth development despite its certain less closing relationship with the development of freezing tolerance; "Δ" , the amount of protein is positively related to the development of freezing tolerance, and it is not affected by the individual growth development; "▲" , the amount of protein is positively related to the development of freezing tolerance, and it is also influenced by the individual growth development.

the variation of soluble protein of leaf tissues in NH<sub>1</sub> and NH<sub>2</sub> seedlings, we discovered that the four kinds of proteins in either JD-1 or XL-12 didn't change in amount in NH<sub>2</sub> leaf tissues. This suggested that the amount of these proteins in leaf tissues was positively correlated with the development of freezing tolerance, and was influenced only by temperature, not by individual growth development. Consequently it indicates that these proteins are expressed by specific freezing-resistant gene regulation and is responsible directly for the improving of freezing tolerance.

c. The 21 KD protein in JD-1 and the 7 KD (lower PI) in XL-12 tended to disappear during deacclimation. By observing the variation of soluble protein of leaf tissues in NH<sub>1</sub> and NH<sub>2</sub> seedlings, we discovered that the 21 KD protein of leaf tissues in NH<sub>2</sub> JD-1 disappeared whereas the 7 KD (lower PI) protein in NH<sub>2</sub> XL-12 increased in amount. This suggested that they had double functions, i.e. increasing proportionally to the increase in freezing tolerance and also playing a certain role in the individual growth development. These experimental results show that the gene expression in CH leaf tissues during deacclimation has adjusted remarkably so as to meet the requirements of development at a normal temperature, hence in the mechanism of gene expression there has occurred a crucial alteration during cold hardening.

### 3. Changes and Functions of Membrane Proteins during Cold Acclimation and Deacclimation

#### 3.1 Changes and functions of membrane proteins during cold acclimation

Electrophoretic pattern of membrane proteins from cultivars of JD-1, LD-139 and XL-12 NH and CH leaf tissues is shown in Photo 3 (A,B,C). Alterations in membrane proteins of leaf tissues in JD-1 and XL-12 under different conditions are

listed in Table 3. From Photo 3 and Table 3, we can see that after 42 days of cold acclimation of JD-1, there synthesized two kinds of specific membrane proteins of 34500 D and 24000 D which were absent in the NH<sub>1</sub> leaf tissues. By comparison of the membrane protein changes in CH and NH leaf tissues, we discovered a marked increase in the levels of six membrane polypeptides of 34000 (three kinds), 15000, 7500, and 26000 D. And we also observed a marked decrease in the levels of at least thirteen membrane polypeptides having mol wt of 305000, 10000 (two kinds), 9000 (four kinds), 10500 (two kinds), 42000, 37000, 28000, and 22500 D among which the polypeptides of 10000 (one kind), 9000 (two kinds), 105000 (one kind), 30500, 42000, 37000, and 28000 D tended to disappear. Photo 3(B) illustrated that the membrane polypeptide changes in LD-139 leaf tissues during cold acclimation resembled that of JD-1. From Photo 3(C) and Table 3, we can see that a specific membrane polypeptide of 24000 D was also synthesized in XL-12 leaf tissues during cold acclimation. There were seven membrane polypeptides that increased in amount, compared with that of NH<sub>1</sub> tissues. Their mol wt were 75000 (two kinds), 8000 (two kinds), 34000 (two kinds), and 15000 D. There were at least seven membrane polypeptides that declined in amount markedly. Their mol wt were 10000 (two kinds), 9000 (four kinds) and 10500 D.

From these results it was evident that there occurred dynamic alterations in the composition of membrane protein in winter wheat leaf tissues during cold acclimation. Some normal genes closed whereas some other adaptive genes opened, presenting the inhibition of normal protein synthesis and the induction of stressed protein synthesis. This demonstrated that the gene that controlled the synthesis of these membrane proteins had shown fundamental alterations.

Table 3. Alterations in membrane proteins (changed in amount during cold acclimation of NH<sub>1</sub>, CH, DH, and NH<sub>2</sub> leaf tissues)

Classification of membrane proteins	Protein number	Mol wt (Dalton)	Alterations									
			Jingdong-1				Xiaolong-12					
			NH <sub>1</sub>	CH	DH	NH <sub>2</sub>	NH <sub>1</sub>	CH	DH	NH <sub>2</sub>		
Newly synthesized during cold acclimation	1	34500	-	⊕	-	-	-	-	-	-	-	-
	2	24000	-	⊕⊕	-	-	-	⊕	-	-	-	-
Increased in amount during cold acclimation	3	34000 (3 kinds in JD-1, 2 kinds of higher PI in XL-12)	+	↑	-	-	+	↑	-	-	-	-
	4	15000	+	↑	-	-	+	↑	-	-	-	-
	5	7500 (lower PI)	+	↑	-	-	+	↑	↑*	↓*	↓*	↓*
	6	7500 (higher PI)	+	↑	↓*	-	+	↑	-	-	↓*	↓*
	7	26000	+	↑	-	-	+	↑	↑*	↓*	↓*	↓*
	8	8000 (2 kinds)	+	↑	-	-	+	↑	↑*	↓*	↓*	↓*
Decreased in amount during cold acclimation	9	35000	+	↓*	↑	↓*						
	10	10000 (2 kinds)	+	↓*	↑	↓*	+	↓*	↑		↓	↓
	11	9000 (4 kinds)	+	↓*	↑	↓*	+	↓*	↑		↓	↓
	12	10500 (higher PI)	+	↓*	↑	↓*	+	↓*	↑			=
	13	10500 (lower PI)	+	↓*	↑	=						
	14	42000	+	↓*	↑	↓						
	15	37000	+	↓*	↑	↓						
	16	28000	+	↓*	↑	↓						
	17	22500	+	↓*	↑	↓						

"⊕", newly synthesized; "⊕⊕", newly synthesized in great amount

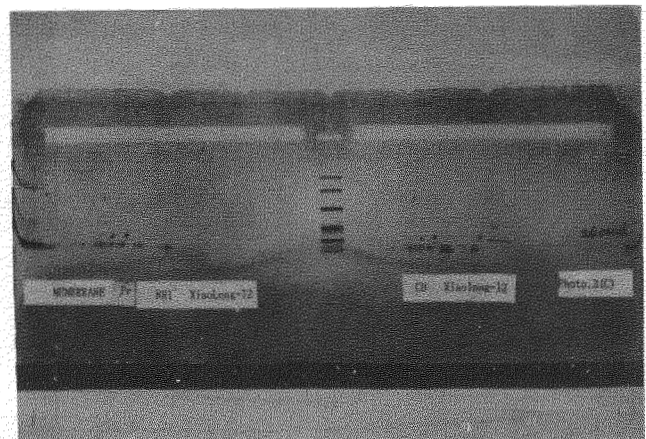
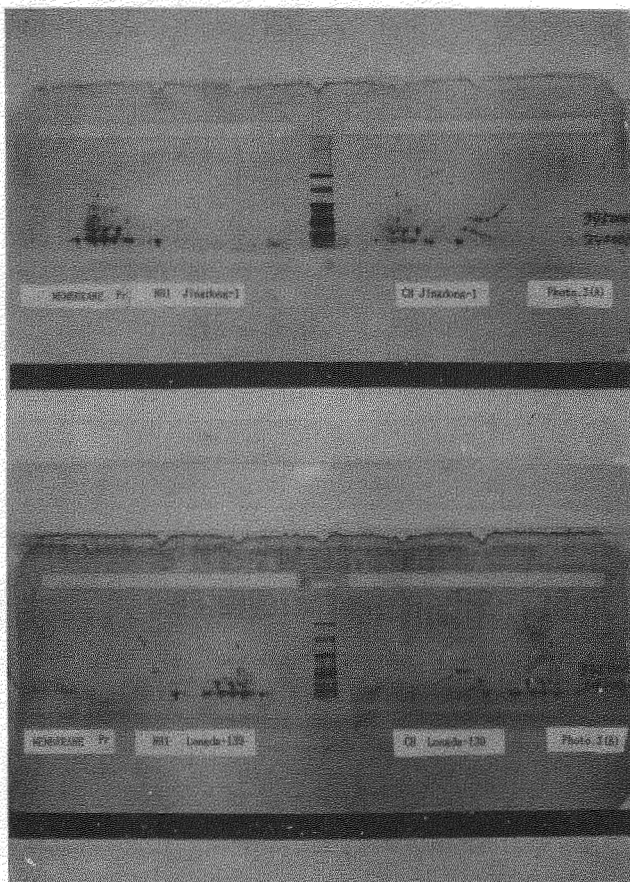


Photo 3 (A, B, and C). Two-dimensional silver-stained gel electrophoretograms of membrane polypeptides. Arrows point out the specific membrane polypeptides.

### 3.2 Changes and functions of membrane proteins during deacclimation

Changes in membrane proteins of leaf tissues during deacclimation of JD-1 and XL-12 are shown in Table 3. It was seen that the two specific membrane proteins of 24000 D and 34500 D which were newly synthesized in leaf tissues of JD-1 during cold acclimation, and that of 24000 D in XL-12, disappeared completely during deacclimation. This suggested that the synthesis and inhibition of the three specific membrane proteins had a close relationship with the increase or decrease of the ability of freezing tolerance. They were essential for the development of freezing resistance. The thirteen membrane

proteins of leaf tissues in JD-1 and seven in XL-12 that declined in amount during cold acclimation showed an increase in amount during deacclimation, indicating a negative relationship between the amount of these proteins in leaf tissues and the development of freezing tolerance.

Of the six membrane proteins of JD-1 that increased in amount during cold acclimation, one protein of 7500 D declined in amount during deacclimation and the other five disappeared. And of the seven increased membrane proteins of XL-12, three proteins of 8000 (two kinds) and 7500 D (lower PI) declined in amount and the other four disappeared completely. By comparison of the variation in membrane proteins of NH<sub>1</sub> and NH<sub>2</sub> leaf tissues from Table 3, we can see that the six membrane proteins of JD-1 disappeared in NH<sub>2</sub> leaves. The proteins of 8000 (two kinds) and 7500 D (two kinds) in XL-12 declined in amount obviously, while the other three vanished. This indicates that the amounts of the six membrane proteins in JD-1, and the seven in XL-12, are affected not only by the temperature but also by the individual growth development, and are present to be a positive correlation with the development of freezing tolerance.

#### DISCUSSIONS AND CONCLUSIONS

Our study of the cold acclimation of winter wheat indicates that the improving of freezing tolerance is accompanied by the alteration in gene expression. The results are similar with those relevant abroad (Gilmour, 1988; Guy, 1987; Mohapatra, 1988). In recent years, it was found that some soluble proteins and membrane proteins were newly synthesized in plant bodies during cold acclimation, hence demonstrated on the levels of protein that the gene expression mechanism altered under freezing stress along with the improving of freezing tolerance. Our experiments showed that the amount of nine soluble proteins in JD-1 and thirteen in XL-12 increased under the low temperature conditioning. This empirical result was first reported in our country and is similar with that obtained from Cloutier's experiments (Cloutier, 1983). Analyses of membrane proteins indicated that during the cold acclimation not only two new membrane proteins of JD-1 were synthesized, but six membrane proteins (seven in XL-12) increased in amount, thirteen membrane proteins (seven in XL-12) declined in amount of which some vanished. This resembles that of Yoshida's study (1984).

We discovered in our experiments that the amount of proteins of 41, 43, 24, 7 (one kind), and 42 KD (four kinds) in leaf tissues were mainly subject to the individual growth development, hence there might be some enzymes responsible for regulation in some metabolic processes. On the other hand, since their content in tissues increased merely with the increase of freezing tolerance but did not decrease with the decrease of freezing tolerance, they could be regarded as having functions in leaf tissue cells at low temperature but not directly participating the metabolic process of freezing-resistant development. As for the 21 KD protein of JD-1 and one kind of 7 KD in XL-12, they were also considered as enzymes responsible for regulation in some metabolic processes because their contents in leaf tissues were affected by the individual growth development. Nevertheless, since the alterations in the protein content paralleled the increase or decrease of freezing tolerance, they were deduced to regulate certain

metabolic process that are directly associated with the development of freezing resistance.

The proteins of 1000, 18000 (two kinds), 7000 (one kind), 21000 D (7000 D in JD-1 and 21000 D in XL-12) were probably some soluble proteins except enzymes, for their contents were not subject to the individual growth development. The amount of these proteins in leaf tissues presented a positive correlation with the development of freezing resistance. Their function was to consolidate the cell capacity of holding water so as to resist the impact of density that resulted from freezing dehydration.

For the two newly synthesized specific membrane proteins in JD-1 (only one protein of 24 KD in XL-12) during cold acclimation, their synthesis and inhibition during the period of acclimation and deacclimation appeared to be positively related to the improving or weakening of the ability of freezing tolerance. The amount of membrane protein of 24000 D in JD-1 leaf was more than that in XL-12, and the membrane protein of 34500 D was not synthesized in XL-12 at all. On this basis, it seemed more reasonable that these specific membrane proteins were freezing-resistant gene proteins produced under the low temperature stress. The functions of these specific membrane proteins are to maintaining the mobility of membrane at low temperature conditioning, preventing protein from conformational changes due to freezing dehydration, and resisting the mechanical impact caused by freezing injury. They are essential and directly responsible for the improving of freezing tolerance, and may provide key information for gene engineering.

We can draw the following conclusions from the above analyses.

(1). The ability of freezing tolerance acquired during cold acclimation of winter wheat is improved obviously compared with that of contrast.

(2). Cold hardening of winter wheat can induce marked increase in the levels of 9 soluble proteins in JD-1 leaf tissues (thirteen in XL-12). Among them, the amount of five proteins with mol wt of 1000 D, 7000 D (one kind), 21000 D, and 18000 D (two kinds) in both two cultivars presents a positive correlation with the development of freezing tolerance.

(3). During cold acclimation, two specific membrane proteins of about 34500 and 24000 D in leaf tissues of both cultivars of JD-1 and LD-139, one specific membrane protein of about 24000 D in XL-12, present a positive relation to the development of freezing tolerance. There are six membrane proteins in JD-1 and seven in XL-12 increased in amount and they are present to be positively correlated with the development of freezing tolerance. There are at least twelve membrane proteins in JD-1 and seven in XL-12 decreased in amount markedly. They are inversely related to the development of freezing tolerance.

(4). The ability of freezing tolerance of plants is subject to the gene expression. Protein is the final product of gene translation and interpretation. The studies of stressed membrane proteins and their relationship with the development of freezing tolerance are of great significance in elucidating the regulating mechanism of gene expression during the process of plant individual growth, in revealing the essence of freezing tolerance, and in sifting the stress-resistant source. Finally it will also be helpful for breeding new cultivars with stress-resistance by means of a combination of

gene engineering with conventional methods of breeding.

#### REFERENCES

- Cloutier, Y. (1983) Changes in the electrophoretic patterns of the soluble proteins of Winter Wheat and Rye following cold acclimation and desiccation stress. *Plant physiol.* 71(2):400-403.
- Gilmour, S.J., Hajela, R.K. and Thomashov, M.F. (1988) Cold acclimation in *Arabidopsis thaliana*. *Plant physiol.* 87(3):745-750.
- Guy, C.L. and Haskell, D. (1987) Induction of freezing tolerance in Spinach is associated with the synthesis of cold acclimation induced proteins. *Plant physiol.* 84(3):872-878.
- Mohapatra, S.S., Polle, R.J. and Dhindsa, R.S. (1987) Changes in protein patterns and translatable messenger RNA population during cold acclimation of Alfalfa. *Plant physiol.* 84(4):1172-1176.
- Uemura, M. and Yoshida, S. (1984) Involvement of Plasma membrane alterations in cold acclimation of Winter Rye seedlings (*Secale cereale* L. cv Puma). *Plant physiol.* 75(3):818-826.
- Zhao, J. (1990) Thesis of M.S. (In Chinese).
- Zhao, Y.T. and Liang, B.W. (1987) Identification of the cold Hardiness of winter wheat (In Chinese). *Scientia Agricultural Sinica*, 20(6):74-80.

## EFFECTS OF FOREST FIRE ON THE HYDRO-THERMAL REGIME OF FROZEN GROUND, THE NORTHERN PART OF DA HINGGAN LING, CHINA\*

Zhou Youwu, Liang Linheng, Gu Zhongwei, Liang Fengxian and Zhang Qibin

Lanzhou Institute of Glaciology and Geocryology,  
Chinese Academy of Sciences, China

The contrast of observations at burned and unburned sites in Amuer region of Da Hinggan Ling indicate that forest fire has obvious effects on permafrost. The local air temperature, ground surface and shallow ground temperatures and mean annual ground temperature increased at burned sites. The increases at burned sites in swamps are more obvious than on slopes. This paper also evaluates the effects of snow cover on the mean annual ground surface temperature and temperature range. Water content at burned sites in earlier stage of thawing is less than at unburned sites and reverses in later stages. The average water content in seasonally thawed layers at burned sites is 20% more than unburned sites in the swamp. The maximum seasonally thawed depths at burned sites is double that of unburned sites in the swamp.

### INTRODUCTION

The effects of forest fire on permafrost has been studied since the 1930s in foreign countries, and there have been some reports about the study recently and in the past. The author of this paper has had a synthetic introduction to this problem (Zhou Youwu et al., 1991)

In order to examine the effects of the disastrous forest fire in 1987 on the permafrost in the northern part of Da Hinggan Ling, China, following the investigation in Gu Lian mining area in 1988 (Liang Linheng, Zhou Youwu, 1991), we gave further investigation to the Amuer region (52°50'N, 123°11'E) in 1990/1992.

The region is characterized by low rolling ridges, ranging in altitude from 500 to 700 m. It is located in a frigid-temperate (boreal) zone. The mean annual air temperature is -4.7°C. The mean monthly air temperature in January and July is -30.0°C and 17.5°C, respectively, and the mean annual temperature range is 47.5°C (Amuer meteorological station in 1975/1990). The yearly precipitation, 83% of it in the summer, is 416 mm. The period of minus air temperature is 211.3 days. Snow can be maintained for about 187 days. There is a temperature inversion in winter. The vegetation in this region is dominated by *Pinus pumila*. The steep southern slope is covered by *Pinus sylvestris*. A big forest fire destroyed a vast area of vegetation in this region in 1987.

The bedrock in this region is composed of volcanic breccia and basalt-andesite of the Mesozonic era. Quaternary unconsolidated deposits are diluvium, alluvium, slope wash alluvium and eluvium. Their depth is from several meters to 20 meters. Permafrost is developed in the swamp and on the gentle slopes of the mountain footslopes in this region. The annual ground

temperature in the swamp is -1.0 — -4.2°C and on the slope is 0.0 — -0.2°C (Dai Jinbo, 1982). The maximum seasonally thawed depth is less than one meter in the swamp and 1.5-4.5 m on slopes and river terraces. The characteristics of permafrost in this region are described in another paper (Gu Zhongwei et al., 1992).

### EFFECTS OF FOREST FIRE ON PERMAFROST

We set up 40 periodic observation sites which contain ground temperature. Water content and thaw depth in the northern valley, in the swamp and on the slope of Amuer forest management bureau in burned and unburned stands. Especially observing 5 sites each with boreholes. We give the micro-meteorological observations on sites 3 (unburned) and 4 (burned) about the air temperature, humidity, ground and ground surface temperatures for each, once every five days, and measured snow cover in March 1991 and in the winter of 1991/1992. In Table 1 are the site conditions.

### Change to the Microclimate

The burned forest has a black underlying surface which decreases its reflectance. According to field investigation at severely burned and unburned sites in the swamp study area on Sept. 13, 1990, the mean daily reflectance at burned and unburned sites is 0.15 and 0.18, respectively, and in the day the radiation balance at burned sites is more than at unburned sites (Zhao Kuiyi, 1991). The changes of reflectance and radiation balance caused by forest fire lead to the changes in the surrounding ground surface air temperature, ground temperature and water regime, and finally result in the changes of frozen ground.

The observed meteorological data (Fig.1) at burned and unburned sites indicate that annual air temperature at burned sites (site 4) is higher than at unburned sites (site 3), on the whole. The difference of air temperature is 0.2-

\*The project was funded by the Chinese Committee of National Sciences

Table 1. Site conditions

No.1	Geom. Position	Vegetation	Lithology
1	Swamp in intermountain	Natural young <i>Pinus pumila</i> with height of 3-5 m and canopy density of 0.4, sparse tussock hummock, litter-layer with depth of 5 cm, <i>Rhododendron parvifolium</i> and moss with a coverage degree of 0.5.	From borehole Z1: 0-1.2 m: Peat layer. 1.2-3.0 m: Icebeds with soil. Sandy clay and ice layers alternated. 3.0-14.1 m: Gravel layer. Contained sand-gravel and sand clay. 14.0-19.6 m: Breccia contained in ice-coating body.
2	Swamp about 50 m apart from No.1.	Burned <i>Pinus pumila</i> . Dead trees have been removed. Now are <i>Betula dehuricaea</i> , <i>Vaccinium</i> , <i>Carex</i> sp. whose coverage degree is 0.2 and a lot of tussock hummocks.	From borehole Z2: Almost as same as above. At depth of 18.0 m is weathering layer.
3	Gentle slope with N.W. exposure and with 6 gradient	Natural young <i>Pinus pumila</i> with height about 10 m and canopy density is 0.7, <i>Rhododendron drucicum</i> , <i>Ledum palustris</i> var. <i>angustum</i> and <i>Vaccinium vitis-idaea</i> communities in addition to sparse <i>Betula d.</i> and <i>Pinus s.</i>	From borehole Z3: 0-0.2 m: Humus soil. 0.2-6.1 m: breccia in which there is aquifer between 1.9 & 2.4m. 6.1-7.0 m: Clay layer contained little gravel. 7.0-13.5 m: Crushed gravel. It is volcanic breccia. 13.5-21.0 m: Weathering volcanic breccia and turf in which crevasse has developed.
4	Gentle slope with N.W. exposure 500 m apart from No.3. The gradient is 4.	Almost all <i>Pinus pumilla</i> was burned and removed except for several ones still alive. There is black ash layer about 1 cm on ground. Now shrubs are prosperous which are mainly <i>Vaccinium uliginosum</i> and <i>Vaccinium vitis-idaea</i> com.	From borehole Z4: 0-0.1 m: Humus soil. 0.1-4.8 m: Breccia with sandy clay. 4.8-6.5 m: Crushed gravel. It is volcanic 6.5-21.0 m: Weathering volcanic breccia with developed crevasse.
5	Gentle slope with S.E. exposure. The gradient is 10.	All burned <i>Pinus pumila</i> have been removed.	From borehole Z5: The lithology is the same as borehole Z4.

0.4°C in summer and 0.6-1.5°C in winter. It also presents, that the gradient of air temperature (0.5-2.0 m) observed at burned sites is higher than at unburned sites. Only in the beginning of spring and the end of autumn, i.e. the beginning and the end of vegetation growing period, the air temperature at burned sites is lower than at unburned sites. From this, we can see that the canopy has a strong effect on air temperature in the forest. And the approximate observation data shows that the mean annual air temperature range at unburned sites in the pine forest is 0.6°C higher than at burned sites.

#### Changes to the Ground Surface and Shallow Ground Temperature

Ground surface temperature is not correspondent with air temperature on the slope from the observations. In the warm season (from mid-June to the mid-September), the ground surface temperature at burned sites is higher than at unburned sites, but in the cold season (after mid-October), the temperature is reversed (Fig.1) at the two sites. Finally, the annual ground surface temperature at burned sites is approximately the same or probably lower than at un-

burned sites and the annual ground surface temperature range at burned sites is 2.4°C higher than at unburned sites.

The changes of shallow ground temperature on the slope is similar to the ground surface temperature. Namely it is higher in the warm season at burned sites than at unburned sites, and is reversed in the cold season at the two sites. Figure 2 indicates that the ground temperature within 20 cm at burned sites is 1.0-2.5°C higher than at unburned sites from May to October, but the temperature is reversed in May-June and Oct. at the two sites. Making a comparison about the accumulated ground temperature and average air temperature in the cold season (Table 2) between burned and unburned sites, we find that minus accumulated ground temperature within the depth of 1.5 m at burned sites is more than in unburned sites and the average air temperature is 0.1-0.5°C lower than in unburned sites. But the ground temperature at burned sites in the swamp is higher than at unburned sites during the whole year. According to field measurements from May to Aug. in 1990, the ground temperature at burned sites is 3.6°C higher than at unburned sites within the depths of 10-40 cm; at a depth

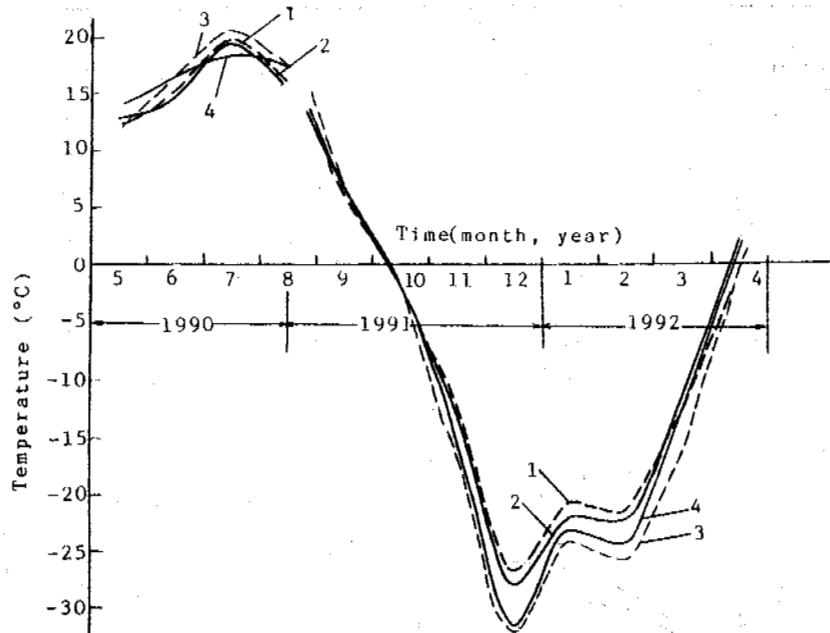


Figure 1. The comparison of air temperature and ground surface temperature between burned and unburned sites on slope  
 1,2 — Air temperature at burned and unburned sites  
 3,4 — Ground surface temperature at burned and unburned sites

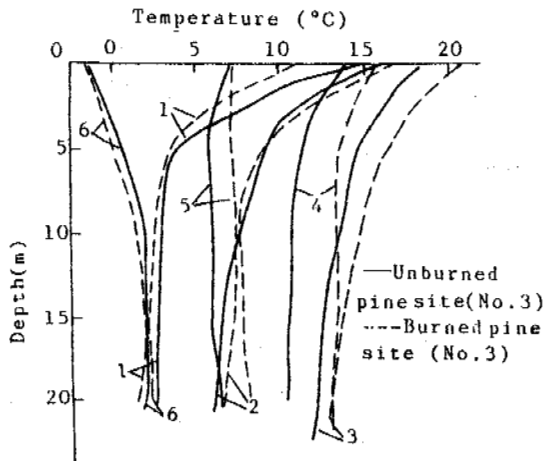


Figure 2. The comparison of shallow ground temperature between burned and unburned sites on slope  
 1-3 The average of the temperature from May to July, 1990.  
 4-6 The average of the temperature from Aug. to Oct., 1991.

of 10 cm, the difference is up to 4-7°C from June to July. In the cold season, the minus accumulated ground temperature at burned sites is less than at unburned sites, but the average temperature is higher than at the unburned site (Table 2).

We can see, from the above, that the vegetation (young *pinus pumila*) in the swamp has an obvious cold effect, but on the slope, it has a cold effect in the warm season and has a warm effect within the depth of 1.5 m in the cold season. The whole year's effect on the slope needs further observation.

#### Changes to the Snow Cover and Its Warm Effect

Through investigation the maximum thickness of snow deposited, in mid-March or late March, is up to 31-33 cm. It was up to 36-40 cm in 1990. Later, following the increasing air temperature, snow cover becomes thinner, and up to mid-April, it has almost thawed completely (Fig.3). In the coldest month (January), the thickness of snow cover is 25-25 cm; the difference of the thickness between burned and unburned sites is that, in the swamp, the thickness at burned sites is 1 cm more than at unburned sites, and on the northern slope the thickness at burned sites is 1 cm less than at unburned sites. The density of snow cover is increasing as the thickness is increasing before mid-March. The changing range of the density is between 127-191 kg/m<sup>3</sup>. The density at burned sites is more than at unburned sites not only in the swamp but also on the slope.

We used V.A. Kudryavtsev's para-empirical formula (E.D. Ershov, et al., 1986)

$$\Delta T_s = \Delta A_s = A / 2(1-1/f)$$

to calculate the value of warm effect ( $\Delta T_s$ ) and the decrease value of ground surface temperature range ( $\Delta A_s$ ). Where A is mean annual range of air temperature, and (1-1/f) is found in the given table by V.A. Kudryavtsev according to the density and thickness of snow cover. The calculated results illustrate that, under the condition that the mean annual air temperature range is 47.5°C, 25-26 cm thickness of snow cover with its density between 155.4-163.0 kg/m<sup>3</sup> can increase mean annual ground surface temperature and decrease the range of mean annual ground surface temperature 3.8-4.0°C. Thus, the mean annual ground surface temperature under snow cover is only -0.7 - -0.9°C, and the temperature range of it is 39.6-40.0°C. When the thickness of snow cover increased 1 cm, it can increase



Table 2. The comparison of ground temperature (°C) at burned and unburned sites in winter (05,11,1991-25,04,1991)

Depth (m)	On slope				In swamp			
	Unburned site		Burned site		Unburned site		Burned site	
	Accu. Temp.	Avg. Temp.	Accu. Temp.	Avg. Temp.	Accu. Temp.	Avg. Temp.	Accu. Temp.	Avg. Temp.
0.5	-79.1	-4.4	-87.5	-4.9	-119.2	-6.6	-118.3	-6.6
1.0	-36.2	-2.0	-38.3	-2.1	-74.8	-4.2	-68.4	-3.8
1.5	-25.7	-1.4	-31.6	-1.8	-77.7	-4.6	-61.7	-3.4
2.0	5.7	0.3	7.0	0.4	-48.0	-2.7	-21.7	-1.2
2.5	7.4	0.4	15.4	0.9	-44.6	-2.5	-14.0	-0.8
3.0	7.7	0.4	24.1	1.3	-37.6	-2.1	-12.3	-0.7
3.5	2.7	0.2	19.9	1.1	-42.5	-2.4	-18.3	-1.0
4.0	6.7	0.4	29.5	1.6	-36.7	-2.0	-16.3	-0.9

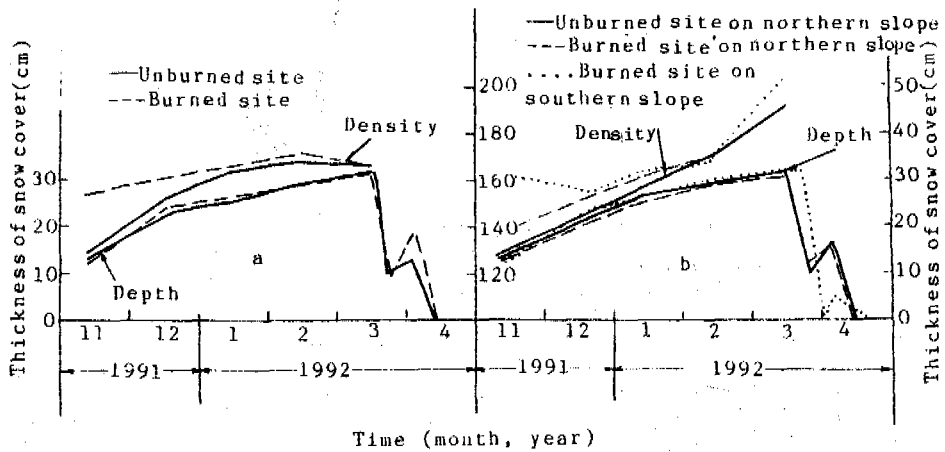


Figure 3. Changes of the density and the thickness of snow cover at burned and unburned sites a-in swamp b-on slope

mean annual ground surface temperature and decrease the range of it by 0.2°C.

**Changes to the Water Content in Ground**

According to numerous measurements about water content, it presents that the water content at burned sites in the swamp is more than unburned sites within the depth of 20 cm before the beginning of July; after this time, the water content is reversed at the two sites. On the slope, the water content at burned and unburned sites changes alternatively before mid-June, after this time, the water content at unburned sites is steadily less than at burned sites (Table 3). Within the depth of 0.9 m on the southern slope and 1.5 m in the swamp, the water content at burned sites is more than at unburned sites, even in mid-October (Fig.4).

For this reason, we divide the changes of water content with time into two periods at burned and unburned sites. In the first period, before the duration from mid-June to mid-July, the transpiration of trees is not comparatively intense, and this makes the water content in the soil layer at unburned sites more than that of burned sites; in the second period, from mid-July to October, i.e. the vegetation growing period, trees have a strong transpiration, and this makes the water content in soil layers at unburned sites less than at burned sites. For example, in the swamp, the value of evaporation (from latent heat flux) at unburned sites is up

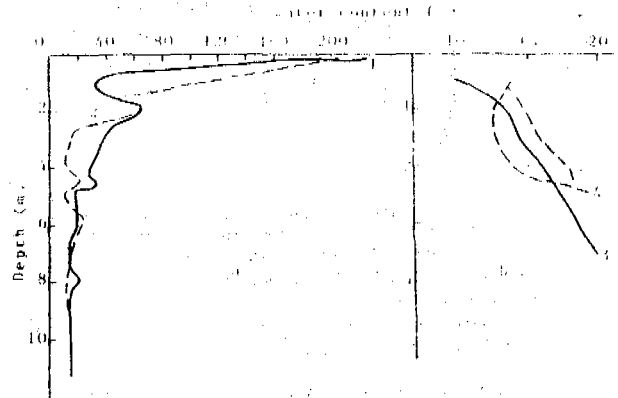


Figure 4. Changes of water content in ground with depth (a-Swamp, b-Slope) 1-5 Boreholes from Z1 to Z5. The solid line is the unburned site. The dashed line is the unburned site.

to 10.92 mm/d, and at burned sites it is only 5.99 mm/d (Zhao Kuiyi, 1991).

Table 3. Changes to the water content in ground at burned and unburned sites

Date (mm-dd-yy)	Depth (m)	Water cont. in swamp (%)		Date (mm-dd-yy)	Depth (m)	Water cont. on southern slope (%)	
		Unburned site (No.1)	Burned site (No.2)			Unburned site (No.3)	Burned site (No.4)
05,17,1990	0.05	436.7	89.1	05,18,1990	0.10	23.9	27.6
06,22	0.20	414.7	177.2	-05,19	0.10	33.1	22.3
07,08	0.10	1770.0	656.2	06,10	0.20	15.5	22.4
07,20	0.10	104.2	441.4	06,19-06,22	0.20	14.4	24.0
	0.20	---	241.5	07,05-07,07	0.20	13.2	21.9
08,03-	0.10	362.0	489.6	08,03	0.20	18.8	30.9
08,05	0.20	185.0	---	08,10	0.10	35.7	59.9
10,10,1991	1.2-1.3	36.7	82.0		0.40	10.4	13.2
-10,18	1.6-1.8	64.5	66.5		0.80	13.5	26.2
	2.0-2.2	61.1	54.9		1.50	12.8	14.2
				10,10,1991	0.50	10.0	14.0
				-10,16	1.00	13.4	12.6
					1.50	14.2	12.6
					2.00	16.1	13.8

The effect of the changes of water content, mentioned above, on the whole seasonally thawed layer can be indicated by the weighted average water content of the seasonally thawed layer. At the five observation sites, the values are 71.5%, 91.6%, 16.0%, 15.7% and 16.3% respectively. It is obvious that the weighted average water content at burned sites is 20% more than at unburned sites in the swamp, and there is relatively little difference on the slope.

Changes to the Mean Annual Ground Temperature

From the curves of borehole temperature (Fig. 5, 6), the mean annual ground temperature at the depth of zero annual amplitude (about 15 m) is -2.1°C at unburned sites and -1.8°C at burned sites in the swamp, 0.1°C at unburned sites and 0.8°C at burned sites on the northern slope, and 1.8°C at burned sites on the southern slope. It is clear that the mean annual ground temperature at burned sites is really higher than at unburned sites, and its difference on the slope is much more distinct. As there are a lot of factors which affect the mean ground temperature, we can conclude that the differences are not only caused by forest fire, but at least, it is one of the main factors.

Changes to the Seasonally Thawed (Frozen) Depth

Through field investigation from May to July 1990, we found that the seasonally thawed depth at burned sites is 7-40 cm deeper than at unburned sites in the swamp, but on the slope, the seasonally thawed depth at burned sites is less than at unburned sites before the end of May, after this time it is reversed. We estimate from Fig.5 that the maximum seasonally thawed depth at unburned and burned sites are 1.3 m and 2.5 m, respectively, in the swamp. The latter is almost twice the former.

On the slope at unburned sites, there is a layer of permafrost at a depth of 5 to 10 cm in which the ground temperature is approximately equal to 0°C. The layer is thin and is unconnected with the seasonally frozen layer (Fig.6). Therefore, on the slope the sites generally belong to a seasonally frozen zone, not seasonally thawed zone. The seasonally frozen process lines illustrate (Fig.7) that the maximum frozen depth at burned and unburned sites are 2.85 m and 3.0 m, respectively, on the slope. It appears

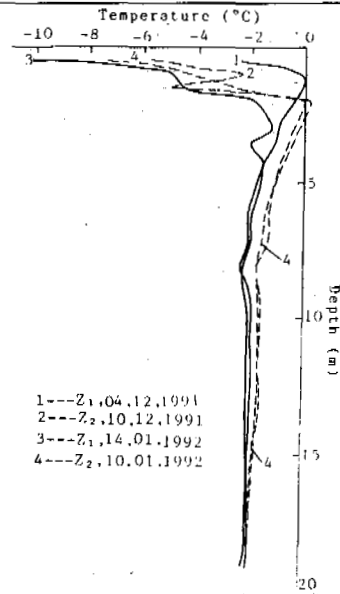


Figure 5. Changes of ground temperature with depth in swamp

The solid line is unburned site (borehole Z1).  
The dashed line is burned site (borehole Z2).

that the depth at burned sites is less than at unburned sites.

It is evident that forest fires have a strong effect on seasonally thawed depths in permafrost-dominated regions and have little effect on seasonally frozen depths in permafrost-free region. After a forest fire, the water content in soil has increased in the swamp. From this, the maximum seasonally thawed depth ought to decrease, but the common effects of increasing ground temperature and the ground surface temperature range play the leading roles in the increase of seasonally thawed depths. The water content is of little difference at burned and unburned sites on the slope. The counteraction of the increasing mean annual ground temperature and the ground surface temperature range made the seasonally

frozen depths change little.

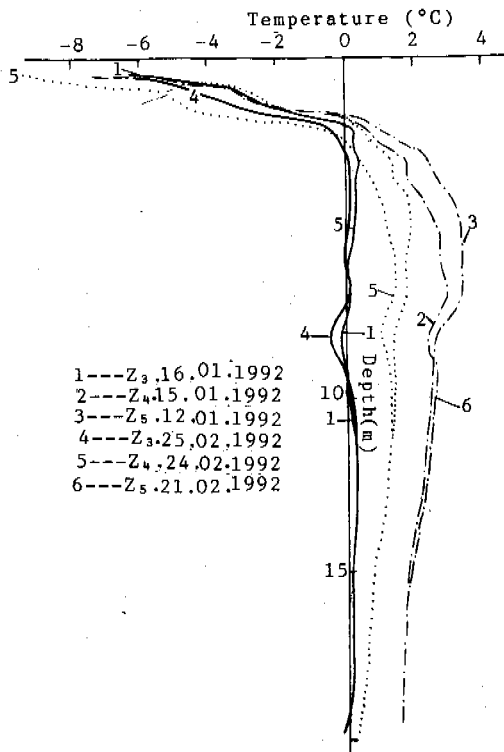


Figure 6. Changes of ground temperature with depth on slope  
 1,4-Borehole Z3 at unburned site on northern slope;  
 2,5-Borehole Z4 at burned site on northern slope;  
 3,6-Borehole Z5 at burned site on southern slope.

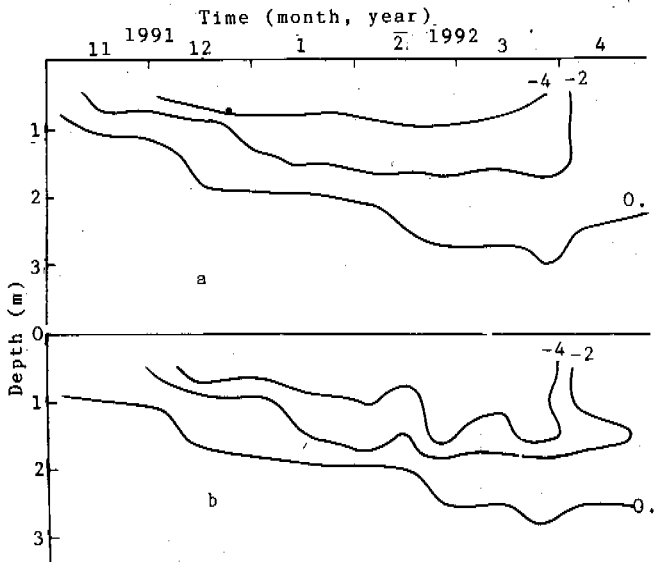


Figure 7. The seasonally freezing process line at unburned(a) and burned(b) sites on northern slope.

### CONCLUSIONS

Forest fire has distinct effect on the hydro-thermal regime of permafrost in Da Hinggan Ling, China. The effect is displayed, as follows, after the fire: Local air temperature has risen, the temperature from ground surface to the depth of zero annual amplitude is increased in the swamp, the temperatures of shallow ground and ground surface at burned and unburned sites have little difference on slopes, but the ground temperature at burned sites is higher than at unburned sites. Snow cover increases the mean annual ground surface temperature and decreases the range of it to 3.8-4.0°C. The difference of the depth of snow cover at burned and unburned sites is 1-2 cm, and can make the mean annual ground surface temperature differ by 0.2°C. Litter layer decreases the mean annual ground surface temperature by 0.1-0.2°C and the range of it is 2.4-5.2°C. The layer of black ash (burned litter layer) can increase ground temperature slightly. The changes of water content during the preceding period of seasonally thawing at burned sites is less than at unburned sites. Later, the average water content in the seasonally thawed layer at burned sites is 20% more than at unburned sites in the swamp. It is of little difference at the two sites on the slope. The maximum seasonally thawed depth at burned sites is twice that of the unburned sites in the swamp. The seasonally frozen depth changed little on the slope. Seasonal thaw types are towards an unstable developing direction.

The increase of thaw depth and water content at burned sites in the swamp are probably to make the swamp-land further the swamping. Owing to the fact that the deteriorated permafrost, coarse soil grains and almost no forest litter on ground surface makes it difficult for water to accumulate, in addition to the low temperature in the afforesting seasons of spring and autumn, which are unfavorable for sapling growth. We can use the regularity of the changes of ground temperature and water content with time on the slope to choose the optimum time to afforest.

The effect of forest fire on permafrost is a complex problem, it is concerned with the hydro-thermal exchanges among the atmosphere, vegetation and the layer of permafrost. It needs further research.

### ACKNOWLEDGEMENTS

The assistance of colleagues is gratefully acknowledged, especially to Associate Profs. Wang Jiacheng and Song Xinbo for site setting and field observations, and Din Dewing and Lou Guo-wei for other help.

### REFERENCES

- Dai Jinpo, (1982) Characteristics of Ground Temperature on Permafrost Areas in the Northern Part of great Xinan Mountain. Journal of Glaciology and Cryopedology, Vol.4, No.3, pp.53-63.
- E.D. Ershov and et al., (1986) Field methods of Geocryological Researches (in Russian). Press of Moscow University, pp.111-119.
- Gu Zhongwei and et al., (1992) The Characteristics and the Changes of Permafrost, Amuer Region, Da Hinggan Ling, China. The Sixth International Conference on Permafrost (to be published).

- Liang Linheng and Zhou Youwu, et al., (1991a) Changes to the Permafrost Environment after Forest Fire in Northeast Region of Chinese Da Hinggan Ling. Making an Example of Gulian Mining Area (in Chinese). Journal of Glaciology and Geocryology, 13(1).
- Liang Linheng and et al., (1991b) Changes to the Permafrost Environment after Forest Fire. Da Hinggan Ling, Gulian Mining Area, China. Permafrost and Periglacial Processes, Vol.2, pp.253-257.
- Zhao Kuiyi, (1991) The Disturbances of Fire of the Da Hinggan Ling on the Swamp Vegetation. Journal of Nanjing University (Natural Sciences Edition), Nov. pp.417-424.
- Zhou Youwu and Liang Linheng, (1991) The Effects of Forest Fire on Permafrost Environment (A Summary of the Study of Foreign Developments) Journal of Developments of Earth Sciences. (1).

A DEVELOPMENT MODEL OF THE PERIGLACIAL LANDFORMS ON SLOPE LAND —  
TAKING THE PHENOMENA OF PERIGLACIAL LANDFORMS IN THE TIANSHAN  
MOUNTAINS, WEST ANTARCTICA AND THE ANDES AS EXAMPLES

Zhu Cheng  
Department of Geo. & Ocean Sciences, Nanjing University

A development model of periglacial landforms on slope land is summarized based on the distribution characteristics of periglacial landforms in the central Tianshan Mountains, Fides Peninsula, King George Island, West Antarctica, and the central Andes. There is an inherent connection among various periglacial types on slope land in view of occurrence. A type at high elevation is a base for types at low elevation in constitution, while a type at low elevation is a succession and development of its neighbouring type at higher elevation; From the development spectrum of the periglacial type along the top — slope — bottom, a progression is characterized of periglaciation and the periglacial processes from simplicity to variety and complexion, and the periglacial types also progresses from common to superior; There is an influence of climate, shape and facing of slope on the development of periglacial landforms.

OUTLINE OF THE DISTRIBUTION OF PERIGLACIAL  
LANDFORMS ON SLOPE LAND IN THE CENTRAL TIANSHAN  
TIANSHAN MOUNTAINS, KING GEORGE ISLAND, WEST  
ANTARCTICA, AND THE CENTRAL ANDES

The Central Tianshan Mountains (Zhu, 1992a)  
(Taking Daxigou Area as an Example, as in Fig.1,  
Showing the Distribution of Periglacial Landforms)

1. On the north slope which is relatively steep and with bare rock, there exists: periglacial tor — rock sea — rock debris (or debris cone) — rock glacier; 2. On the south slope which is relatively gentle and with bare rock, there exists: periglacial tor — rock sea — block slope — sorting terrace — sorting stria net — sorted circle — block stream (or stone-stripes) — upheaving stone (or seasonal pingo)

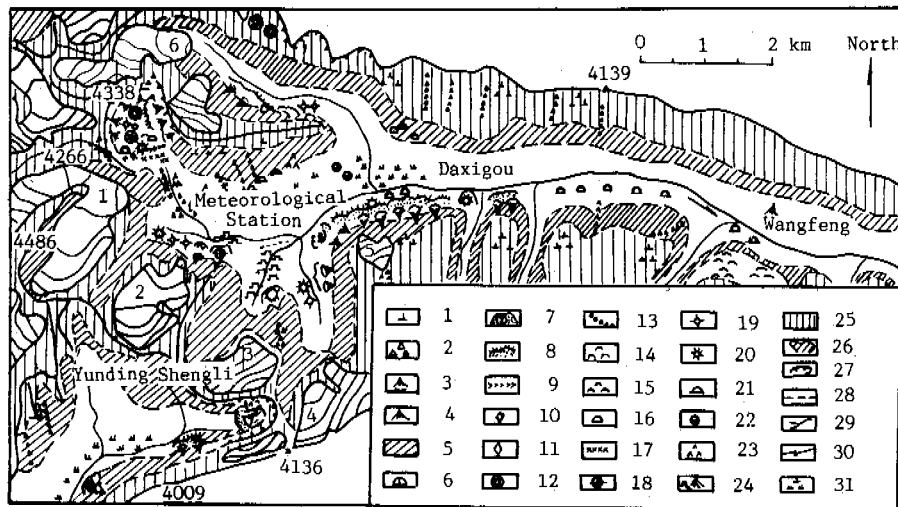


Figure 1. Sketch map showing the distribution of periglacial landforms in Daxigou area, the central Tianshan Mountains  
1 periglaciator; 2 rock sea; 3 rock debris; 4 debris cone; 5 block slope; 6 sorting terrace; 7 a single rock glacier and its number; 8 cluster of rock glaciers; 9 sorted stria; 10 sorting stria net; 11 sorted polygon; 12 sorted circle; 13 block stream; 14 stone spread; 15 gelifluction tongue; 16 gelifluction bench; 17 unsorted stria; 18 unsorted stria net; 19 unsorted polygon; 20 unsorted circle; 21 seasonal pingo; 22 thawing depression; 23 up-heaving stone with its base rock from weathering; 24 denudation of base rock from weathering; 25 base rock slope; 26 a modern glacier and its number; 27 cirque and invation depression; 28 boundary line; 29 river; 30 mountain peak and ridge line; 31 swamp.

— stone spread; 3. On the slope where the soil forming process of slope wash is evident (such as Wang Peak), there exists: periglacial tor — rock sea — gelifluction tongue — gelifluction terrace — sorted stria — unsorted circle (or stria net); 4. Along the valley bottom, there exists: stone spread (the slope of the sediment plane is 3-5°) — thawing depression.

Fides Pininsula, King George Island, West Antarctica (Zhu, 1991a) (Fig.2)

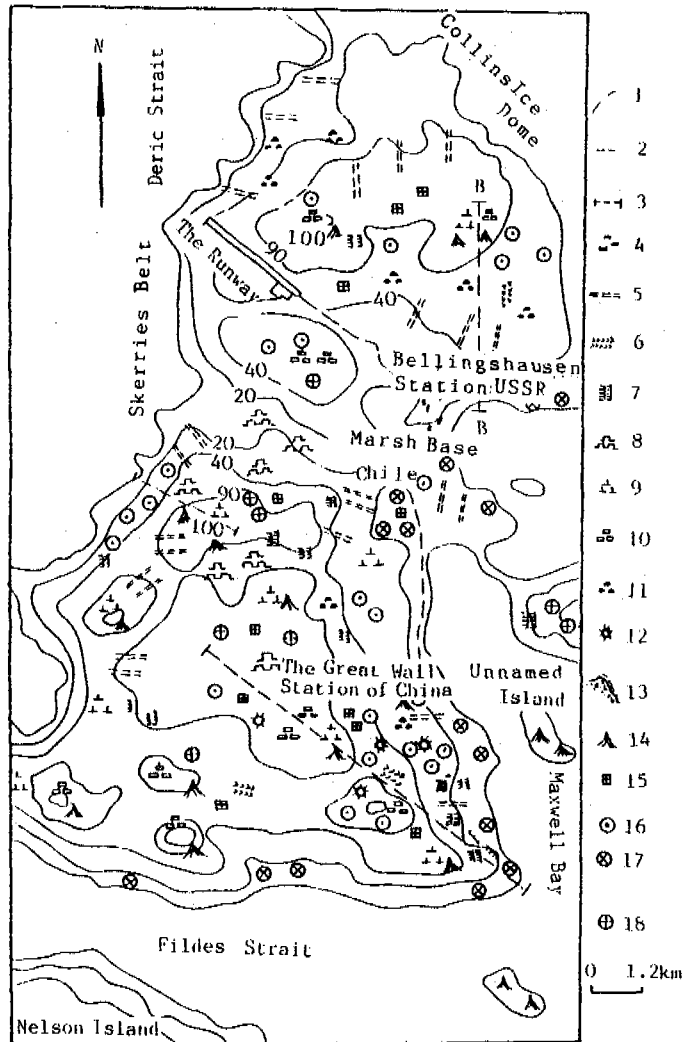


Figure 2. Sketch map showing the distribution of periglacial landforms in Fides Peninsula 1 contour line; 2 seaside road; 3 landform thalweg; 4 station construction; 5 striated soil slope; 6 stone stripe; 7 stone bench; 8 stone spread; 9 periglacial tor; 10 rock sea; 11 gelifluction terrace; 12 stone flower; 13 rock glacier; 14 rock debris and block slope; 15 sorting stria net; 16 sorted circle; 17 sorted circle consisted of beach pebble; 18 debris island.

1. From Shanhaiguan Peak (154.68 m), the top of the south platform where periglacial landform has a relatively dense distribution, to Half Triangle (thalweg A in Fig.2), developments from the top to bottom are: periglacial tor and rock

sea — rock debris and block slope — sorted circle, stone flower and sorting stria net — sorted circle, stone bench and rock glacier — sorted circle consisting of beach pebble;

2. From the highest peak (156 m) of the north platform with a relatively rich and thick plasma sediment, to the seashore near Belinsigaojin Station, USSR (thalweg B in Fig.2), developments from the top to bottom are: periglacial tor and rock sea — rock debris and block slope — rock circle, stone stripe and gelifluction terrace — striated soil slope — sorted circle consisting of beach pebble;

3. From Mingyue Mountain (132.8 m) in the central platform, where there is relatively fine sediment in the middle section, and there exists a relatively large difference of relative heights of the first order bench, to Haibao Beach next to Shongwu Bay on the west coast (thalweg C in Fig.2), a greater difference exists in profile characteristics in comparison with the first two cases, developments from top to bottom are: periglacial tor and rock sea — block slope — stone spread and striated soil slope — rich muddy sorted circle — small snow patch erosion — beach.

The Central Andes (Zhu, 1992b) (Fig.3)

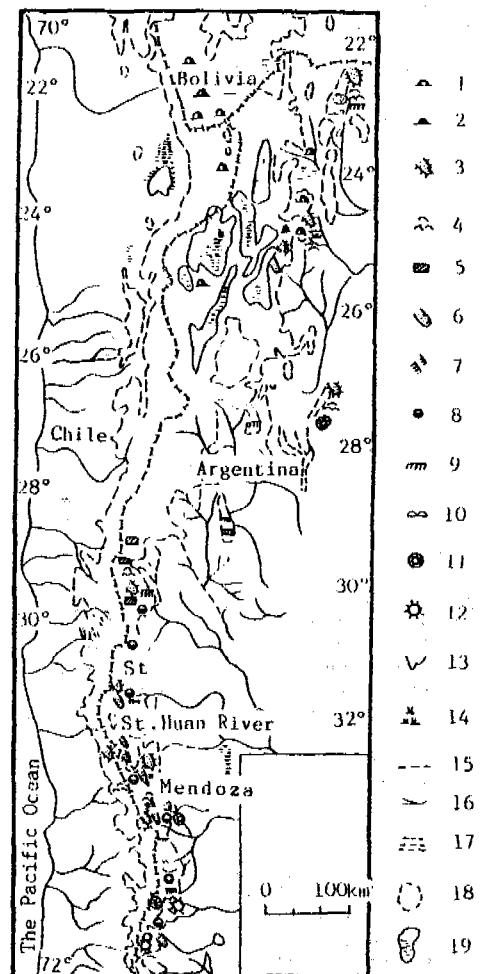


Figure 3. Sketch map showing the distribution of periglacial landforms in the central Andes 1 pingo of reglation type; 2 pingo of peat and swamp type; 3 rock glacier; 4 gelifluction tongue;

5 block slope; 6 rock glacier from glacier retreat; 7 base rock of frost-crack type; 8 thermokarst subsidence; 9 cryoplanation surface; 10 involution; 11 sorted circle and sorting stria net with diameter  $>1$  m; 12 same as above  $<1$  m; 13 asymmetric periglacial valley; 14 peat and swamp of periglacial type; 15 national boundaries; 16 river; 17 swamp; 18 modern periglacial area; 19 lake.

1. The relatively moist periglacial zone on the west side of the central Andes is narrow and with fewer types of periglacial landforms. In the north of the zone, there are only a few pingoes of regulation type, on the south, there are only a small amount of rock glaciers and gelifluction tongues developed; while on the relatively dry east side of the central Andes, the periglacial zone is relatively wide, and with relatively more types of periglacial landforms distributed.

2. Above 3670 m a.s.l., there are pingoes of the large type developed in the dry Puna Plateau ( $22^{\circ}$ - $25^{\circ}$ S). Glaciated rock glaciers and pingoes of peat and swamp types are distributed above 4500 m a.s.l. (Corte, 1988).

3. The area from  $33^{\circ}$ - $35^{\circ}$ S in the central Andes can be divided into two subareas based on the environmental background:

1) The permafrost area: its lower limit is indicated by the end of rock glaciers at 3200 m a.s.l. The types of periglacial landforms distributed from 3200-4700 m a.s.l. are: active rock glacier, large type of solifluction tongue, gelifluction bench, foliated periglacial rock debris, large sorted circles with diameters of 1-4 m, cryoplanation surface, non-symmetric periglacial valley, block slope, thermokarst subsidence.

2) The seasonal frozen ground area: the mean annual air temperature is above  $0^{\circ}$ C, the main types of periglacial landforms are: gelifluction and solifluction, wedge ice immediately under the surface, shifted rock engendering pits and holes left due to vertical sorting and frost weathering, block slope, small sorted circle net with a diameter of 10-20 cm.

#### A PROBE INTO THE DEVELOPMENT MODEL OF THE PERIGLACIAL LANDFORMS ON SLOPE LAND

From the distribution of periglacial landforms in the above mentioned three regions, some characteristics of development of the periglacial landforms on slope land can be drawn:

(a) There is an inherent connection among various types. Such connection displays that: all the main types occur above the lower limit of frozen soil, the material consisting of each type is initially produced from weathering rock, material consisting of a type at high elevation is a material base for types at low elevation is a succession and development of its neighbouring type at a higher elevation.

(b) From the development spectrum of the periglacial types along the top — slope — bottom, a progression is characterized of periglacialization from simplicity to variety and complexness, and periglacial types also progresses from common to superior. Besides cold weathering, block slope and rock debris on rock slope experience gravitation, washing of plasma from snow meltwater and rain, and freeze thaw action from freezing and melting of such-percolated water. On rich muddy slopes, if the slope is relatively large, gelifluction tongue, gelifluction terrace

and gelifluction bench develop with evident gravitation and gelifluction; if the slope is relatively small, streamed striated soil slope develops with evident gelifluction and freeze-thaw sorting and less evident gravitation. At a slope bottom, a variety of periglacialization is more evident, rock glacier develops, mainly under gelifluction accompanied with gravitation, freeze expansion pressing, and freeze-thaw sorting, largely on shaded and half shaded slopes. And pingo develops mainly under frost heaving largely on the sunny slope, or sorted circle, sorting stria net and so on develop mainly under freeze-thaw sorting. Near the bottom of relatively gentle slopes, stone spread develops, mainly under the washing of meltwater and frost heaving, from periglacialization. Besides sorted circles and sorting stria nets developed under freeze-thaw sorting in rich muddy valleys, when the ground ice is exposed due to human activity, thermokarst subsidence easily develops in a headward progression.

(c) There is the influence of climate, shape and facing of slope on the development of periglacial landforms. Usually, in cold and dry climate regions, where the slope is moderate, the longer a distance is from the lower limit of the frozen soil to the snow line, the more types and the more complete the periglacial landforms are on slope land, and, the longer and the more perfect the development spectrum is on slope land. In cold and dry climate regions, where the slope is very steep, periglacial landforms of mass movement types mainly due to gravitation develops predominantly, such as rock debris, debris cone and block slope, while types of gelifluction and freeze-thaw sorting are less developed. The less the distance is from the lower limit of the frozen soil to the snow line, the fewer the types of periglacial landforms on slope land, and the shorter the development spectrum is. In cold and wet climate regions glacier development is predominantly in favor, a main type of the periglacial landforms are of gelifluction, e.g. gelifluction tongue, gelifluction terrace, and rock glacier with tongue shape due to glacier retreat on a relatively large scale.

Based on the above mentioned development characteristics, the author thinks that a development model of periglacial landforms on slope land may be summarized, as shown in Fig.4.

#### DETAILED PRESENTATION OF THE DEVELOPMENT MODEL OF PERIGLACIAL LANDFORMS ON SLOPE LAND IN THE THREE REGIONS

A detailed presentation of the development model of periglacial landforms on slope land differs from one to another due to different conditions of climate, landform, facing, and so on, in the above mentioned three regions.

#### The Periglacial Region in the Central Tianshan Mountains

With a boundary line of  $86^{\circ}$ E, the conditions of landforms and climate in the east area is different from the west area of  $41^{\circ}31'$ - $44^{\circ}20'$ N,  $82^{\circ}10'$ - $88^{\circ}40'$ E in the central Tianshan Mountains, discussed in this paper. In comparison of landforms, the mountain area above 4000 m in the west region is larger than that in the east region (Yilianhabierduo Mountain with 5500 m a.s.l. in the west area has the highest peak within this investigated region). There is a relatively large span from the lower limit of

Periglacial tor (mainly under relatively simple frost weathering)

Mountain top with slope steep mountain slope >38

Relatively gentle mountain slope

Mountain top with gentle slope

Mountain top

Weathering debris gradually becomes fine-grained and mud increases gradually

Periglacial process becomes complicated

Mountain foot

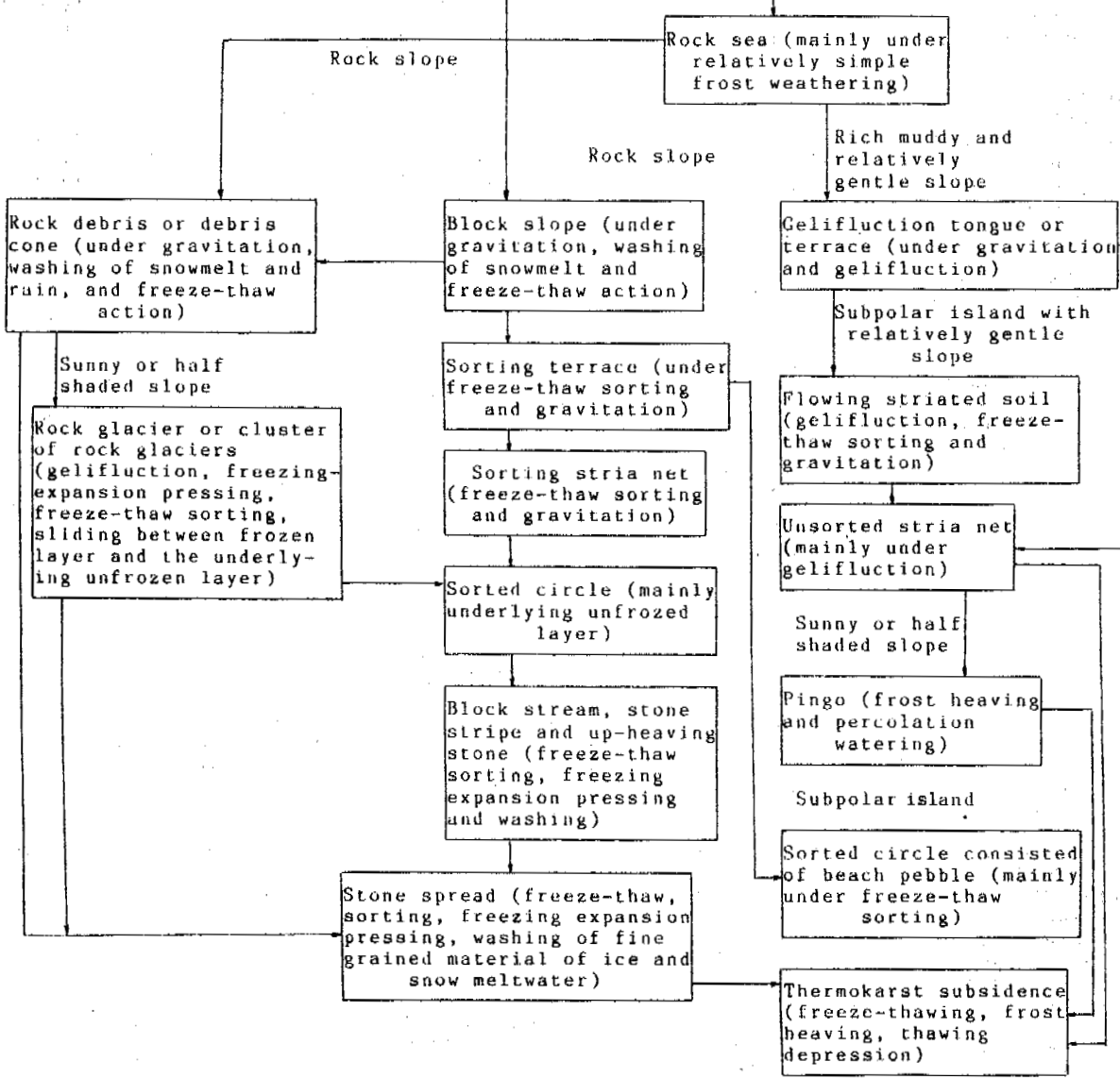


Figure 4. Demonstration of the development model of periglacial model of periglacial landforms on slope land

frozen soil to the snow line in the west region, which seems to imply that there is well developed periglacial landforms on slope land and a long development spectrum, however, there are a relatively large amount of deep canyons. So that the land slope is large, except for the mass movement types of periglacial landforms it is relatively well developed, all the other types on slope land are restrained. Although the span of the periglacial zone in the east region is not as large as that in the west region, there are a relatively small amount of deep canyons (e.g. canyons in Daxigou area are mainly distributed in the zone of 1700-3300 m, slopes on mountain valley land above 3300 m are obviously small), the land slope is relatively

gentle, the development of periglacial landforms on slope land is complete, and the development spectrum on slope land is relatively perfect (Zhu, 1992a). As well, in view of the climate, the precipitation is great in the west region in the central Tianshan Mountains, it decreases gradually towards the east. This indicates that the west part of the central Tianshan Mountains is relatively cold and wet, while the east part is relatively cold and dry. Since a cold and wet climate is favorable to the development of glaciers, a cold and dry climate is favorable to the development of periglacial landforms, therefore, it has resulted in that, in the west part of the region there is a relatively large amount of glaciers and rock glaciers with tongue shapes



in the valley due to glacier retreat, there are relatively few other types of periglacial landforms, common ones are only periglacial tor, rock debris, block slope, gelifluction tongue, block stream and so on. In the east part, modern glaciers are not as well developed as that in the west part, and there are a few rock glaciers with tongue shapes in the valley, however, there is a variety of other types of periglacial landforms, and the development spectrum on slope land is relatively perfect, such as that in the Daxigou area, nearly 20 types of periglacial landforms exist from periglacial tor — rock sea — rock debris — block slope — rock glacier — gelifluction tongue — sorting stria net — stone spread — thermokarst subsidence and so on (see Fig.1).

#### The Periglacial Region in Fides Peninsula

According to 3 year measurements from 1986-1989 at the meteorological station in the Great Wall Station of China built in 1985, the mean annual air temperature is about  $-3.3^{\circ}\text{C}$ , and the mean annual precipitation is 605 mm approximately (Zhu, 1991b). From the above data, such air temperature and precipitation are favorable to the development of periglacial landforms. However, the land of the peninsula is less undulated, which causes the development of periglacial landforms on slope land to be restricted within a relatively low height zone, thus the development spectrum of the periglacial landforms is also compacted in a relatively short distance. Furthermore, the peninsula was influenced by the sea side historically, and the deposits of salt ions arose from the evaporation of modern sea water, there is a high salt concentration within the active layer, which causes the layer to have a far smaller frozen strength and frozen depth compared with those in the central Tianshan Mountains and the central Andes. Therefore, flowing striated soil mainly under gelifluction is the most widely developed type of periglacial landform on slope land, the development of rock debris and rock glaciers of mass movement type, and of pingo and so on mainly under frost heaving, is less widespread. It is worthwhile to note that, during Pleistocene when Antarctic Ice Sheet was advancing, the northwest side of the peninsula was facing the ice advance, the southeast side was facing the ice retreat. The base rock on the southeast side experienced intense drag erosion from regelation, so it was fully broken, and was denuded easily under weathering after the glacial epoch; the side facing the ice advance mainly experienced compressive stress, after the glacial epoch, the base rock mainly experienced stress release which caused the rock surface to be eroded but the extent of the breaking as a whole is far less than that on the side facing the ice retreat. This is the basic reason that, there is a rich source of debris on the southeast side, and there is a relatively large amount of rock debris and periglacial types sorted from coarse grained debris, while on the northwest side there is a poor source of debris, rock debris is not developed, and there are many types sorted from fine grained mud flow (Zhu, 1991b). That is, there is a historically deep reaching band from glacier erosion in the development model of periglacial landform on slope land in this region.

#### The Periglacial Region in the Central Andes

The author thinks that, the most distinguished feature of the development of periglacial land

forms on slope land in the central Andes ( $22^{\circ}$ - $35^{\circ}\text{S}$ ) is the difference of slope facing, that is, on the west side of the mountains, the periglacial zone is narrow, the development spectrum on slope land is short, there is a relatively small amount of periglacial types, and the lower limit of the periglacial zone is in a relatively high elevation, while the situation in the east side is of the contrary. From analysis, this difference is mainly due to climatic reasons.

As mentioned previously, for comparison of the development of periglacial landforms with that of glaciers, the requirements for glaciers is cold and wet, while for periglacial landforms, it is cold and dry. In more detail, a maritime climate region is favorable to the development of glaciers, and not favorable to development of periglacial landforms (Cui, 1980). A continental climate region is not favorable to the development of glaciers, but favorable to development of frozen soil and periglacial landforms. Because the freeze thaw frequency and amplitude in dry regions are larger than those in wet regions in view of space, a periglacial zone in a dry region under a dry climate period is wider than that in a wet region under a wet climate period.

The difference in distribution of periglacial landforms on both the east and west sides in the central Andes is a representation of the inherent regular pattern of the development model of periglacial landforms on the above mentioned slope land. The Andes is not only the longest and most principal mountain range in the southern hemisphere, but also it is an important dividing line for the climate. Although the mean monthly air temperature of the coldest month (July or August) over the mountain region above 3000 m is below  $0^{\circ}\text{C}$ , and that of the warmest month (January or February), is  $0^{\circ}$ - $8^{\circ}\text{C}$ , the east side of the mountain range is mainly influenced under the trade winds from the north-east and southeast, the west side is mainly influenced under the trade winds from the west. Because the east side is relatively far from the sea, it has resulted in that there is more precipitation on the slope facing the wind on the west side than that on the east side. Speaking of the main periglacial areas in the central Andes, its mountain foot on the west side in Chile is under a subtropical Mediterranean climate, with a mean annual precipitation of about 500-1000 mm, while its mountain foot, on the east side in Argentina, is under a dry and half dry subtropical climate, with a mean annual precipitation of only 200-600 mm. Therefore, the east side appears cold and dry, and the west side appears warm and wet.

In the development of permafrost and periglacial landforms, winter is an important accumulation period for two way propagation of a negative cold wave (that is towards the direction of the upper and lower limit of frozen soil) (Cuituowèiqi, 1985). Thickness of frozen soil and uplift amplitude of pingo and so on come to the maximum usually at end of winter or beginning of spring (Zhu, 1990). The west side of the central Andes is situated in a Mediterranean climate region, warm winter with rich rain easily causes the surface to be in a thawing condition, which is not favorable to the full development of frozen soil and periglacial landforms. Year by year, positive accumulated temperature increases the elevation above sea level, of the lower limit of permafrost and terminal of rock glacier increases accordingly,

the amount of periglacial types decreases, and the periglacial zones become narrow. Although the east side of the mountain range is influenced under the Föhn effect to some degree during summer, as the climate is dry, with small amount of cloud, small temperature inversion, large temperature difference between day and night, and large amplitude of air temperature drop during night, and during winter the climate is cold and dry, the cold wave propagates deeply, which are favorable to the development of frozen soil and periglacial landforms, therefore, the lower limit of frozen soil and terminal height of rock glaciers is relatively low, the amount of periglacial types is large and the periglacial zones are wide, so that the development spectrum of the periglacial landforms on slope land is relatively long.

It should be pointed out that, the development model of the periglacial landforms on slope land proposed in this paper is mainly based on the author's field investigation in the above mentioned three regions, together with references of previous related research on periglacial landforms on slope land in the Qinghai-Tibet Plateau (Cui, 1981), Colorado Mountains in North America (White, 1981) and the Andes in South America (Corte, 1988). Further research and discussion are required from colleague scientists to testify whether or not the development model is suitable for the development of periglacial landforms on slope land in other regions in the world.

#### REFERENCES

- Corte, A.E., (1988) Geocryology of the central Andes and rock glaciers, Fifth International Conference on Permafrost, Proceedings Vol.1, Trondheim, Norway, 718-721.
- Cui, Z., (1980) On the periglacial mark in permafrost area and the relation between glaciation and periglaciation, *Glaciology and Cryopedology*, Vol.2, No.2, 1-8.
- Cui, Z., (1981) The basic characteristics of periglacial landform in Qinghai-Tibet Plateau, *China Science*, No.6, 724-733.
- Zhu, C., (1992a) Some problems on periglacial landform in the central Tianshan Mountains, *Mountain Research*, 10(2).
- Zhu, C., Cui, Z. and Xiong, H., (1991a) Analysis of processes of periglacial landform in Fides Peninsula, King George Island, Antarctica, *Antarctic Research*, 3(3), 25-38.
- Zhu, C., (1992b) Characteristics of periglacial landform on slope land in the central Andes, *Geography Science*, (in press).
- Zhu, C., Cui, Z. and Yao, Z., (1992c) On features of rock glacier in the central Tianshan Mountains, *Journal of Geography*, Vol.47, No.3, 233-241.
- Zhu, C. and Cui, Z., (1991b) Characteristics of distribution of periglacial landform in Fides Peninsula and its mutual relations with history of glacier erosion, *Geography Science*, Vol.11, No.4, 336-342.
- Zhu, C., Song, C. and Liu, Y., (1990) Characteristics of seasonal frost heaving mounds at the head of Urumqi River Tianshan, *Journal of Glaciology and Geocryology*, Vol.12, No.1, 55-62.

Cuituoweiqi, H.A., (1985) *Mechanics of frozen soil*, Science Press.

White, S.E., (1981) Alpine mass movement forms, classification, description, and significance, *Arctic and Alpine Research*, 13(2), 127-137.

THE RESEARCH OF THE FOSSIL ICE-WEDGES AND PERIGLACIAL INVOLUTIONS IN THE  
EASTERN PIEDMONT OF THE GREAT XINGAN RANGES, CHINA

Zhu Jinghu, Song Changqing, Tang Zhonghai and Wang Guangzhou

Department of Geography, Harbin Normal University Harbin, P.R.China

The Baitushan platform was developed in the foothill belt on the eastern slopes of the Greater Xingan Ranges. Many fossil ice-wedges and periglacial involutions were extensively developed in the platform. The Baitushan formation stands for the deposition character of an alluvial fan formed by the river in front of the foothill. The Pingtai formation covered the Baitushan formation. The lower part of the strata reflects the character of slope wash deposition, however, the upper part is a weathering crust. A lot of periglacial involutions formed by frost-heaving action are in the lower part of Pingtai formation, and some periglacial involutions are in the top of upper part of the strata covered by the periglacial loess. Periglacial phases occurred in the Mid and Late Pleistocene.

#### INTRODUCTION

Baitushan formations were developed in the foothill belt of the eastern slope of the Greater Xingan Ranges, at the mouth of the Taoer river, Zhouer river, Yalu river, Alen river and Noumin river. They were cut by these rivers to form the platform (Photo 1), the isolated hillock, the landform of ridge about 20-25 m high,



Photo 1 Foothill platform at the mouth of the Taoer river

200-230 m above sea level, however, in the south of the foothill belt of the Taoer river, there is widely developed loess of early, middle, and late Pleistocene. The date of Baitushan formation was determined to be the early Pleistocene by the early regional strata table (The group writing the stratigraphical time table on Heilongjiang province, 1979). Recently, the department of hydrogeology is definite it is the early period of middle Pleistocene. The cause of the formation, is still thought to be glacial, glaciofluvial deposition (Yu Jianzhang, 1964) and was established in the Baitushan period (Sun Diangqing, 1977). Through research in recent years, some people think it belongs to the alluvial deposition, or pluvial deposition (Qu Shanwen, 1983), and some people believe it to be the

deposition of lake facies (Zhang Qingwen, 1981). Baitushan formation is covered by Pingtai formation in the area of Pingan town, Pingtai and the eastern Baitushan. This formation was considered to be the accumulation of an interglacial period. The date was determined to be the middle period of middle Pleistocene. Many fossil ice-wedges and periglacial involutions were extensively developed in the platform and Pingtai formation (Fig.1).

#### THE CHARACTER OF DEPOSITION GROUPS

The strata of the Baitushan formation are grayish white, and grayish yellow gravel, which is accompanied with sand and lens of grayish white clay. The length of the sandy lens is about 20-30 m, the thickness is about 0.5-1.5 m. The length of the grayish white clay lens is about 3-5 m, the thickness is several ten cm. An extensive layer of ferrousdyed phenomenon exists in the connected surface between the gravel and clay layer. There is a grayish green clay stratum or lens under the layer. It has an obvious slanting stratification in the sandy gravel layer. The group of Baitushan strata in the top of the platform changes gradually with the bedrock. In the top of neutral-acid volcanic rock, the grayish white, brownish red and brownish yellow weathering clay has formed, the thickness is 2-3 m.

The composition of the gravel is mainly neutral-acid volcanic rock, for example, rhyolite, dacite and tuff, with some andesite, syenite porphyry, trachyte, granite, vein quartz and opal. The diameter of most gravel is 4-7 cm, the longest is 17 cm, the sphericity of gravel is very sharp, and most of them are round, or sub-round. Few gravels have a polished surface but have no striae. The a-axis of gravels predominantly declines to SSW in Pingan town. Some of them decline to SE, which is vertical to the water flow direction or slant, the oblique angle is 15-24°.

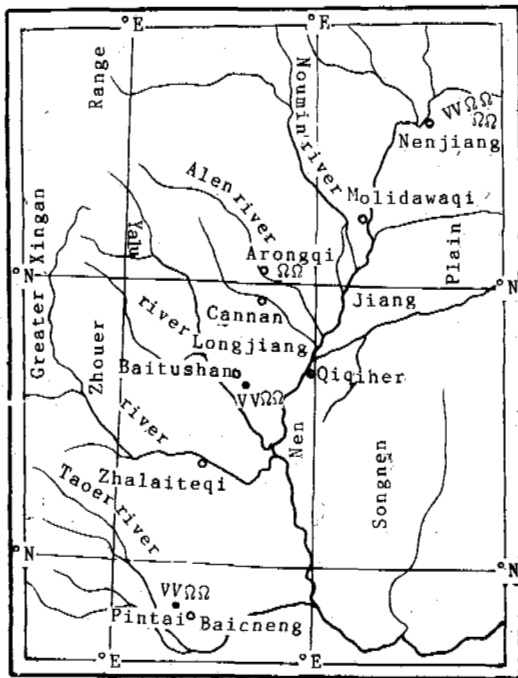


Fig. 1 The distributional map of the fossil ice-wedges and Periglacial involutions in the eastern Piedmont of the Greater Xingan Ranges

VV--fossil ice-wedges

ΩΩ--Periglacial involutions

wedge-shape intrudes into the Baitushan formation, some parts have evident marks of extruding in the both walls of the split, except for the nearly vertical shape, some of the tops are at a regular projection to the north or south. The two walls are symmetrical or not symmetrical. The upper mouth width of the wedge is 40-50cm, the bottom's is 15cm. The average depth is 1.0-2.0m, the deepest is 3.5m. In some place, the distance between two wedges is 0.5-1.3m. The fill of the wedges is the clay of lower part of Pingtai formation containing brownish red gravel. Most of the gravel is arranged erectly. The brownish yellow clay of the upper part of Pingtai formation developed in a level position (Photo 2). The wedge is the



Photo 2 Fossil ice-wedges on the east profile of road side in Pingtai

ab-surface of gravel mainly declines to SW, secondly to SE, normally to the foothill, and the main slanting-angle is 20-50°. The direction of the gravel arranging stands for the deposition characters of alluvial fan formed by river in front of the foothill. The clay of the Baitushan formation is lacustrine in the reduction condition and weathering in the warm-arid climatological condition besides alluvium-diluvium.

The Pingtai formation can be divided into upper and lower parts that cover the Baitushan formation. The lower part is reddish brown clay containing gravel and there is relatively more gravel nearing the bottom. The stratification is not clear. The composition and diameter of gravel are similar to that of the Baitushan formation, the thickness is about 1.0-1.5 m. The upper part is reddish brown clay containing small gravel and the colour turns to brownish yellow gradually from bottom to top, with a thickness of 0.5-1.0 m. The boundary between upper and lower is not clear in the Pingtai formation, Pingtai formation has a discordant contact that is wedge-shaped, bundle-shaped and pot-shaped with Baitushan formation, some parts were covered by brownish yellow loess, the vertical joint is widely developed, 1.8 m thick. The lower part of Pingtai formation reflects the character of slope wash deposition, however, the upper part is weathering crust.

#### CHARACTER OF FOSSIL ICE-WEDGES AND PERIGLACIAL INVOLUTIONS

Fossil ice-wedges are mainly distributed in Pingtai and eastern Baitushan. The split of the

existing mark of paleo-permafrost. It shows the annual mean temperature is -5°C in the eastern slope of the Greater Xingan Ranges in middle Pleistocene of Quaternary. It is normally equal to the present annual mean temperature in Mohe.

Periglacial involutions widely developed in the Baitushan platform of the eastern slope of Greater Xingan ranges. A lot of involutions formed by frost-heaving action are in the lower part of the Pingtai formation. They are pot-shaped, cylinder-shaped, bag-shaped and a string of bead-shaped. The upper opening width of the pot-shape reaches to 1.5-4.0 m. The involution is slightly symmetrical, the burying depth is from about 20-30 cm to 1.7-2.7 m and it shows the thickness of the action layer is from tens of centimeters to 2-3 m. It can be observed that the grayish white gravels of Baitushan formation were enclosed by brownish red clay containing gravels in the pot-shaped periglacial involutions disturbed by frost-thawing in the section of the walls of the Pingtai camp road or the section of the north-west part of the brick factory in Pingan town. Some of the round, circular cone brownish red clay cubes containing gravels were pressed into the white gravel layer (Photo 3). The diameter of the bundle is 20-40 cm, the striking marks of pressing are obvious around its. The pot-shaped periglacial involutions are 70 cm, wide and long, in the top of the upper part of Pingtai formation is covered by the loess in the section of the Longjiang brick factory.

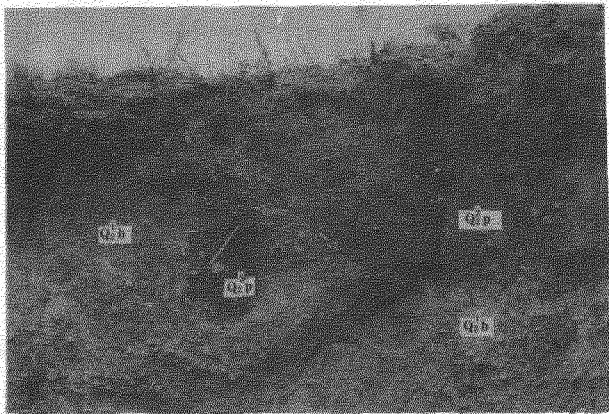


Photo 3 Periglacial involutions on the Pingtai



Photo 4 Dividing of the periglacial ages of Pingtai  
 (1) Periglacial age of Pingtai  
 (2) Periglacial age of the late period of late Pleistocene

#### THE DATE OF THE WEDGES AND PERIGLACIAL INVOLUTIONS

According to the method of geomorphology, stratigraphy, thermoluminescence, paleomagnetic dating, clay mineralogy and spore-pollen analysis, the age of the paleo-ice wedge was determined and also divided into the relevant periglacial age.

The wedges and periglacial involutions developed in the platform of the Baitushan formation of the Greater Xingan Ranges, which formed later than the Baitushan formation. Through thermoluminescence and paleomagnetic dating to date the Longjiang Baitushan strata in recent years, the date of the formation was determined to be 800000-1000000 B.P. (Miao Zhendi, 1982), the middle Pleistocene deposition  $Q_{12b}$ . The main white clay mineral in Baitushan and Pingtai is kaolin and contains a few montmorillonite (Qu Shanwen, 1983; Zhang Qingwen, 1981). The main spore-pollen composition is herbs in this formation, for example, artemisia, lamb's quarters, and urtica. The xylophyta's are few, only several pollens of birch and oak (Qu Shanwen, 1983; Zhang Qingwen, 1981). Vegetation type is grasslands or birch, or oak veld. Both the clay mineral and spore-pollen composition reflects the mild, warm, and slightly dry paleoclimate environment, to show that there does not exist a "Baitushan glacial epoch" in the eastern piedmont of the Greater Xingan Ranges.

The age of the gravel filling in wedges, the disturbed layers of Pingtai formation ( $Q_{2P}$ ) and the same period layers of 61.70 m deep in the east part of Shongnen plain was determined to be  $538000 \pm 8100$  B.P. by thermoluminescence. The lower Harbin Huangshan formation developed periglacial involutions were dated 400000-600000 B.P. by paleomagnetism. The spore-pollen are very abundant in the brownish red clay containing gravel of the Pingtai formation. The spore-pollen of trees are 2.22-6.85%, the main arborees are pine, larch, birch and oak. The grass pollen are artemisia, lamb's quarters, and of the grass family (Zhang Qingwen, 1981). The plant type is larch and birch to reflect the paleoclimate environment of cold and damp. So the Pingtai formation is not the interglacial epoch after "the Baitushan glacial epoch", it is periglacial age equal to Mindel glacial epoch, called Pingtai periglacial age (Photo 4)--the periglacial age trace of middle Pleistocene was

found and determined prior to late Pleistocene in the north-east and north of China.

The periglacial loess covering the Pingtai formation in Longjiang brick factory produced fossil groups of fauna, for example, *Equus przewalskyi*, *Coelodonta* and *Bos primigenius*. *Bos primigenius* was dated  $9520 \pm 130$  B.P. (Miao Zhendi, 1982) by  $C^{14}$ . The periglacial loess with the micro layer structure is 10 m thick and produces fossils of mammoth and North-China *Myospalax* in the upper land near the reservoir of the right front Qi of KerrQin. The periglacial loess and the fossils group of mammoth-coelodonta belong to late periglacial age of late Pleistocene, and could last to the early Holocene in this area.

#### REFERENCES

- The group writing the stratigraphical time table on Heilongjiang province (1979) The stratigraphical time table on North-eastern China, The part of Heilongjiang province, Geological press.
- Yu Jianzhang (1964) Quaternary glacier in the Greater Xingan Ranges, The collection of Quaternary glacier in China, Science press.
- Sun Diangqing (1977) The Quaternary glacier in China, Geological Acta, No.2.
- Qu Shanwen (1983) The discussion on Baitushan glacial period in North-eastern China, Journal of glaciology and geocryology, Vol.5, No.2.
- Zhang Qingwen (1981) The discussion on the reason of Baitushan formation material, Journal of Changchun geological institution.
- Miao Zhendi (1982) Quaternary dating in Heilongjiang province.

SIMULATED ANALYSIS ON A MODELING TEST FOR SOIL FREEZING-  
THAWING PROCESS WITHOUT PRESSURE

Zhu Linna<sup>n</sup>, Li Dongqing and Guo Xingming

State Key Laboratory of Frozen Soil Engineering, LIGG, AS, China

There are the coupled heat-moisture transfer and deformation from thaw-consolidation or frost-heaving in the freezing-thawing process of soil without pressure. We used the theory of simulation for the modeling test to mark system analysis and to suggest the simulated conditions satisfied with modeling.

INTRODUCTION

There are the coupled heat-moisture transfer and deformation from thaw-consolidation or frost-heaving in the periodic freezing-thawing process of soil layers beneath the natural ground surface in permafrost or deep-seasonal frost regions. In order to study the relationship between an engineering construction and its foundation soil in the periodic freezing-thawing process and the stability of construction used in the modeling test method, we first proceed with the simulated analysis without pressure in the freezing-thawing process of natural ground.

In this paper, we have discussed the criteria of the simulated modeling for two cases, that is, unsaturated soil and saturated soil, and suggest the simulation conditions, also is determined by present simulation conditions.

MATHEMATICAL MODEL

Let us consider the problem of the heat-moisture transfer occurring in phase-change and deformation from thaw-consolidation or frost-heaving in porous material, the group of basic differential equations and single conditions can be written as the following:

1. Heat-moisture transfer equations:  
thawed region:

$$C_u \frac{\alpha T_u}{\alpha t} = \frac{\alpha}{\alpha X} (\lambda_u \frac{\alpha T_u}{\alpha X}) \quad (1)$$

$$\frac{\alpha \theta}{\alpha t} = \frac{\alpha}{\alpha X} (D_u \frac{\alpha \theta}{\alpha X}) \quad (2)$$

frost region:

$$C_f \frac{\alpha T_f}{\alpha t} = \frac{\alpha}{\alpha X} (\lambda_f \frac{\alpha T_f}{\alpha X}) \quad (3)$$

$$\frac{\alpha \theta_u}{\alpha t} = \frac{\alpha}{\alpha X} (D_f \frac{\alpha \theta_u}{\alpha X}) \quad (4)$$

2. Coupled conditions on the surface of thawing-freezing (Ding Dewen, 1983):

$$\lambda_f \frac{\alpha T_f}{\alpha x} - \lambda_u \frac{\alpha T_u}{\alpha x} = L \rho_w [\theta_0 - \theta_u + \Delta \theta] \frac{dh}{dt} \quad (5)$$

$$D_u \frac{\alpha \theta}{\alpha x} - D_f \frac{\alpha \theta_u}{\alpha x} = \Delta \theta \frac{dh}{dt} \quad (6)$$

$$\left. \begin{aligned} T_f &= T_u = T_0 \\ \theta &= \theta_u \\ x &= h \end{aligned} \right\} \quad (7)$$

for thawing in form (5)  $\Delta \theta = 0$ .

3. Equation frost-heaving (An Weidong et al., 1990):

$$\epsilon = 0.09(\theta_0 + \Delta \theta - \theta_u) + (\theta_u - n) \quad (8)$$

$$\Delta h = \epsilon \bar{H} \quad (9)$$

4. Equation of thaw-consolidation (chargeless pressure):

$$S = \Lambda_0 \bar{H} \quad (10)$$

5. Boundary conditions and initial conditions:

$$\left. \begin{aligned} X=0, T=T_1(t), \theta &= \theta_1(t) \\ X=H, T=T_{cp}, \theta &= \theta_2(t) \\ t=0, T=T(X), \theta &= \theta(X) \end{aligned} \right\} \quad (11)$$

where  $C_u(C_f)$  is heat capacity of soil, (sign  $u$  means thawed,  $f$  frost),  $\lambda_u(\lambda_f)$  is thermal conductivity,  $T_u, T_f, T_0$  are frozen soil, thawed soil, and phase change temperature,  $D_u(D_f)$  hydraulic diffusivity,  $\theta, \theta_u, \Delta \theta, \theta_0$  are the total

water content, unfrozen water content, transfer water content, initial water content in unit volume,  $t$  time,  $h$  is location of phase surface in depth,  $L$  is potential heat of phase change,  $\rho_w$  is density of water,  $\epsilon$  is ratio of frost heaving,  $\Delta h$  is number of frost heaving,  $A_0$  is coefficient of thaw-consolidation,  $\bar{H}$  is thickness,  $n$  is porosity,  $S_r$  is saturated degree.

#### DERIVATION OF SIMULATED CRITERIA

According to the theory of simulation, the criteria formulations can be obtained from equations (1), (2), (3), (4), used in integral comparison, as in the following:

$$\frac{a_u t}{l^2}, \frac{a_f t}{l^2}, \frac{D_u t}{l^2}, \frac{D_f t}{l^2} \quad (a = \frac{\lambda}{c})$$

from equation (5) (6), obtained:

$$\frac{\lambda T t}{q l^2}, \frac{D \theta t}{\Delta \theta l^2}, \quad (q = L \rho_w (\theta_0 - \theta_u + \Delta \theta))$$

$$\text{and } \frac{\lambda_u}{\lambda_f}, \frac{D_u}{D_f}, \frac{\theta_u}{\Delta \theta}, \frac{T_u}{T_f}, \frac{\theta}{\theta_u}$$

from equation (8) (9), obtained:

$$\frac{\Delta h}{\epsilon \bar{H}}, \frac{\epsilon}{\Delta \theta}, \frac{\theta_u}{n} = S_r$$

from equation (10), obtained:  $\frac{S}{A_0 \bar{H}}$

The aforesaid basic simulated criteria formulations all must be abided by in the modeling test, and would be rewritten by the simplified criteria forms consisting of four forms according to the self modeling property of soil, that is, the parameters of heat and moisture of soil change with temperature and water content and can be satisfied in the freezing or thawing process, then, through substitution among the criteria, the result is as follows:

$$\frac{\Delta h}{\epsilon \bar{H}} \left( \frac{S}{A_0 \bar{H}} \right) = f \left( \frac{\lambda T t}{q l^2}, \frac{D \theta t}{\Delta \theta l^2} \right), \quad (12)$$

This result is true and consummate, and determined by "π dimensional theorem" (Li Zhiguang, 1973), which holds that, the phenomenon described by physical variables 1, which have number of 8 including  $\lambda$ ,  $T$ ,  $t$ ,  $Q$  (quantity of heat),  $\theta$ ,  $D$ , and  $\epsilon$  ( $A_0$ ), while, the basic physical units 2, which have number of 5, including  $T$ ,  $t$ ,  $l$ ,  $Q$ , and  $M$  (quality), so that, the number of undimensional

invariants (that is, simulated criteria)  $m = i - z = 3$ , it tallied with (12) in other words, from (12) instead of the group from (8), (9), (10), (11).

#### ANALYSIS OF SIMULATION CONDITIONS

The indicative forms of simulated ratio can be written from (12), as the following:

$$\frac{c \Delta h}{c \epsilon c \bar{H}} \left( \frac{c_s}{c A_0 c \bar{H}} \right) = 1, \frac{c \lambda c_T c_t}{c_q (c_1)^2} = 1, \frac{c_D c \theta c_t}{c_{\Delta \theta} (c_1)^2} = 1.$$

let us discuss this problem in order of closed conditions and opened conditions, respectively, for moisture transfer replenishment.

#### Moisture Transfer Replenished With Closed Conditions

In this case, the soil layer occurs in an unsaturated state because the ground water level is staccato when the modeling test was used in original soil, the ratio of simulation:

$$c \lambda = c_q = c_D = c \epsilon = c A_0 = 1$$

$$c \Delta h = c \bar{H} = c_1$$

letting  $c_T = c \theta = 1$  (that is, temperature and moisture are the same between natural and model soil), above three criteria can be simplified as the following form (13):

$$\left. \begin{aligned} \frac{c \Delta h}{c \bar{H}} \left( \frac{c_s}{c \bar{H}} \right) &= 1 \\ \frac{c_t}{(c_1)^2} &= 1 \end{aligned} \right\} \quad (13)$$

This result indicates that, the ratio of time equals to the quadratic ratio of geometry in the model when the ratios of temperature and moisture are equal to one. Fig.1 shows the comparison results between the modeling test and field observation; the Lanzhou loess in the model simulates the silty clays in field of the Qinghai-Xizang Plateau. The ratio of time  $c_t = 365$  (that is, one day of model time simulates one year of natural process), the ratio of geometry  $c_1 = \sqrt{c_t} = 19.1$ , (length of model reduces 19.1 time) the upper boundary temperature used in the atmosphere temperature adds the increment of temperature in the adherent surface layer (Wu Ziwan et al., 1988), the lower boundary temperature used in the year average ground temperature, which equals to  $-2.5^\circ\text{C}$ , is located at the depth of 15 meters, where Fig.1a, the seasonal thawing process shows a good coincidence in both the

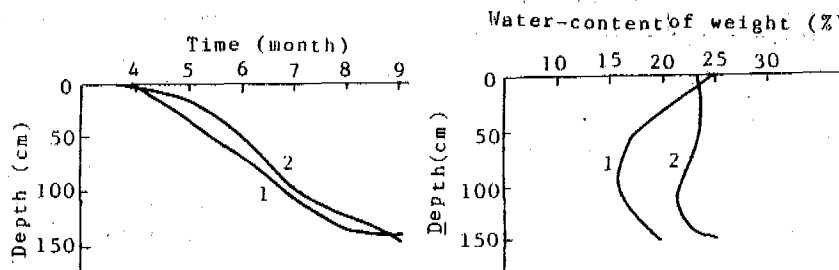


Fig.1 Compared results between modeling test and field observation (Ke Ke Xi Li in Qinhai)  
a. seasonal thawing process, b. curve of water content in end of thawing period  
1. curve of modeling test, 2. curve of field observation

model and natural field, Fig. 1b, the curve of water content in the end of the thawing period shows the same change tendency (that is, the middle of the curve presents a dried situation but there occurs some of deviation), otherwise, the number of thaw-consolidation are not computed because there are no field dates.

#### Moisture Transfer Replenish With Open Conditions

In this case, there is a ground water level used for the source to replenish the soil layer continuously. Comparing the depth  $h'$  of ground water level with the highness  $h_0$  of upper capillary of soil, when  $h' < h_0$  the seasonal thawing-freezing soil layer occurs in a saturated state and is the same in model and in field, then, above simulated conditions, from (13), also can be satisfied and popularized, if  $h' > h_0$ , the section of  $(h' - h_0)$  of seasonal thawing-freezing soil layer occurs in unsaturated state in field, but it is saturated in model because  $(h'/l \ll h_0)$ , where  $h_0$  is a constant of soil and  $h'$  would be reduced by the geometric simulated ratio  $C_1$ , thereby the simulation criteria can not be satisfied and needs to be revised as used in the coefficient  $\alpha = h_0/h'$ , where  $\alpha$  means the ratio compared the saturated layer with total seasonal thawing-freezing layer, in other words, only the layer of  $h_0 = \alpha h'$  in the field is saturation, but total layer  $h'$  in the model has been oversaturated for complete saturate, therefore, the results of test including  $\Delta h_0$  and  $S_0$  need revising and multiply the ratio  $\alpha$ , that is,  $\Delta h = \alpha \Delta h_0$ ,  $S = \alpha S_0$ , which are close to the real deformation of natural soil layer.

#### REFERENCES

- Ding Dewen (1983) Calculation of frost depth and moisture condition in open system, Proceedings of Second National Conference on Permafrost of China.
- An Weidong et al. (1990) Interaction Among Temperature, Moisture and Stress fields in Frozen Soil, the Lanzhou University Press, China.
- Li Zhiguang (1973) Institute Base of Modeling Test for Thermodynamic Equipment, the National Defence Industry Press, China.
- We Ziwang, Cheng Guodong, Zhu Linnan et al. (1988) Roadbed Engineering in Permafrost Region, the Lanzhou University Press, China.



# FROST HEAVE PREVENTION DESIGN FOR THE RIGID CANAL LININGS

Zhu Qiang

Gansu Provincial Research Institute of Water Conservancy

This paper presents a practical way to select the frost heave mitigation measures for the canal linings according to the engineering classification of the frost heave. The frost heave predictions, for the groundwater table when it was shallow or deep seated, are given. Based on the frost heave value predicted, an engineering classification of frost heave as well as the scientific selection of the frost heave prevention measures are made.

## INTRODUCTION

In Gansu Province, China, frost heave is one of the main factors causing damage to the hydraulic structures in the winter time. Especially the rigid canal linings which suffer the most from frost heave owing to the frequent contact with the water as well as the small weight of the linings. The frost damage causes great economic losses. Firstly, the effectiveness of seepage prevention is reduced. Prototype tests show that the seepage lost in the lined canals subjected to a medium frost damage increased by 30% as compared with the undamaged canals. It is estimated that the total amount of the water loss due to this is about  $10^8 \text{m}^3$  in the province. Secondly, the rehabilitation cost for the frost damaged canals is significant. For a medium size irrigated area (5000-10000 hec.) in a frost heave area, the rehabilitation cost may reach 100000-150000 Rmb yuans per year if proper mitigation measures have not been taken. The total cost for the whole province is about 3-4 millions Rmb yuans each year. Finally, the service life of the canal is greatly shortened. Many canals in Gansu have to be rebuilt only after ten year service. So, the economic effect of the investment of the canal construction is greatly reduced owing to the frost action.

Many engineers and researchers have paid great attention to the engineering practices and research works on the mitigation measures for the frost heave of the canals. C.W.Jones et al. of the U.S. Bureau of Reclamation (1982) made a wide investigation on the frost heaving cases in the USBR projects and suggested some corrective measures for the hydraulic structures including the canal linings. Q.Kong (1983) discussed the frost heaving features of the concrete canal linings and put forward a frost heave classification of the soil, as well as damage control measures for the concrete linings. Q.Zhu et al. (1983, 1986, 1988) studied the frost heave characteristics of

the concrete canals and presented many research findings on the gravel-sand replacement and other mitigation measures. A.Li (1988) conducted an experiment on a large U-shaped canal. B.Zhao (1986) presented some results from the field tests on the subsoil replacement using very fine sand collected from the dunes. B.Song (1988) studied the anti-frost-heave behaviors of various types of concrete canal linings. To date, how to scientifically select and design the frost heave mitigation measures for the canal linings is still a problem which the hydraulic engineers have to be faced with. This paper summarizes the engineering experiences and the research findings obtained during the recent years in Gansu and in northern China. After setting up an engineering classification of the frost heaving, a method for the selection and designing of the frost heave control measures for the canal linings is presented.

## PREDICTION OF FROST HEAVE AND ENGINEERING CLASSIFICATION

Since 1980, many field tests have been conducted to determine the frost heave magnitude under various soil and groundwater conditions in the northern provinces of China such as Heilongjiang (Y.Xie et al., 1989), Gansu (Q.Zhu et al., 1988), Xinjiang (D.Zhu et al., 1985), Liaoning (X.Wang, 1985), Shaanxi (A.Li, 1988). These tests showed that the frost heave ratio (ratio between heave value and frost penetration) is mainly related to the soil type, the groundwater table and the soil moisture. The correlation equations to predict the frost heave are divided into two groups, depending on the groundwater condition. When the groundwater table is shallowly seated, the frost heave is related mainly to the groundwater depth in a negative exponential form as follows:

$$f = ae^{-bZ} \quad (1)$$

where  $f$  is the frost heave ratio, in percentage;  $Z$  is the groundwater depth (m);  $a$  and  $b$  are constants, depending on the soil type. According to the above testings,  $a$  and  $b$  can be roughly estimated from Table 1. When the groundwater table is deeply seated, the frost heave is mainly related to the water content in the soil before freezing in a linear form as follow:

$$f = A (w - Bw_p) \quad (2)$$

where  $w$  is the soil moisture before freezing;  $w_p$  is the plastic limit of the soil;  $A$  and  $B$  are constants. From some test results, for loam and sandy loam,  $A$  ranges between 0.37 and 0.5, the more clayey the soil is, the greater value of  $A$  should be adopted.  $B$  ranges between 0.73 and 0.9, the smaller value is suitable for a silt rich soil.

Table 1 Values of  $a$  and  $b$  in equation (1)

Soil type	Groundwater depth $Z$ (m)	$a$	$b$
Clay	$0 < Z <= 1.0$	40-30	1.25
	$1.0 < Z <= 2.5$	27-21	0.85
Heavy and medium loam	$0 < Z <= 2.5$	30-19	1.1
Sandy loam, light loam	$0 < Z <= 1.5$	19-14	1.2

According to Zhu (1990), the critical depth for determining whether the groundwater is deeply or shallowly seated can be found in Table 2.

Table 2 The critical depth for groundwater deeply seated

Soil type	Clay	Heavy and medium loam	Sandy and light loam	Sand
Critical depth(m)	2.5	1.8	0.8	0.5

Then the frost heave can be determined by the following equation:

$$h = fH/100 \quad (3)$$

where  $h$  is the frost heave;  $H$  is the frozen depth.

According to the real situation in Gansu Province, the frost heave of the foundation soil can be divided into four classes by the heave value, as shown in Table 3.

Table 3 The engineering classification of the frost heave

Classification	I	II	III	IV
Frost heave value (cm)	<2	2-6	6-10	>10

In light of the research findings and engineering practices, the frost heave mitigation measures can be classified as structural measure, moisture control measure, subsoil replacement, heat insulation and the adoption of a flexible lining. Table 4 summarizes the applicability of the mitigation measure versus the classification of frost heave.

In Table 4, the mitigation measures suitable for the higher class of frost heave is also effective for the lower class. For instance, the subsoil replacement measure can be adopted in

the class IV as well as the class III but with a smaller replacement depth in the latter case.

### SPECIFIC DESIGN FOR VARIOUS MITIGATION MEASURES

#### The Structural Measures

1. U-shaped canal section: The U-shaped section, being the new favourite for small canals in China in recent years, is usually adopted in a canal with a capacity less than 5 m<sup>3</sup>/s and the curve radius less than 1 m. In most cases, the U-shaped canal lining section is cast with concrete in one piece. For the convenience of construction, prefabricated curved slabs are also used some times but without a joint in the center of the invert. According to field observations, the U-shaped canal is lifted as a whole when subjected to frost heave, so fewer cracks occur. However, when the heaving action is very strong, the heave force on both sides of the U-shaped canal become so large that cracks will occur at the juncture of the circular part and the straight wall. It is concluded that this kind of section can be successfully used in the area with frost heave amounting to 5-6 cm. The U-shaped canal section is shown in Fig.1.

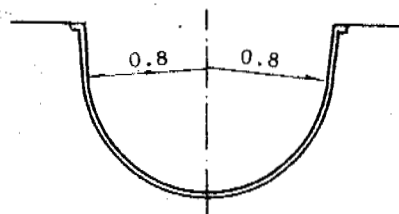


Fig.1 The U-shaped canal section

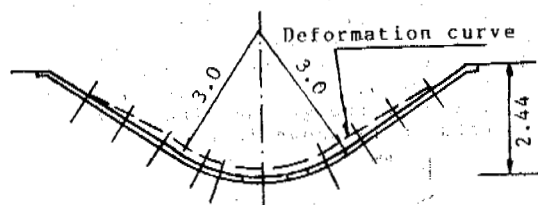


Fig.2 The canal section with an inverted arch bottom

2. Canal with an inverted arch bottom: This kind of canal section shown in Fig.2 has been widely used in Gansu, Xinjiang and other provinces in China. Tests indicated that the deformation in a canal with an inverted arch bottom subjected to the frost heave will be more even than that of a trapezoidal canal with a flat bottom. According to the testing conducted in Gansu, China, the total amount of frost heave for two types of sections is close, but the measured value of angular displacement of the canal lining is only 1/25 of that of the flat bottom. It is concluded that the canal with an inverted arch bottom can safely run in the area with frost heave of up to 5 cm. When the frost heave is very strong, the deformation in the bottom becomes so large that the lining will crack.

3. Beam-slab structure: In recent years, a new type of structure with slabs supported on the beams spaced 0.8 m central to center has been used in Qinghai and Gansu Province. The beams, supporting all the weight of the lining system, has a relatively larger pressure or the

Table 4 The frost heave mitigation measures versus classification of the frost heave

Classification	Frost heave value(cm)	The measures for frost heave mitigation	Applicability
I	<2	No special measure is needed	
II	2-6	Structural measures: 1. U-shaped canal 2. Canal with inverted arch bottom 3. Beam-slab concrete lining 4. Large dimension concrete slab with joints filled with coal-tar polyethylene covered with asphalt	Radius < 1 m and capacity < 5 m <sup>3</sup> /s The bottom chord < 4 m
III	6-10	Moisture control measure 1. Double lining--to put a membrane under concrete slabs 2. Double lining + thin layer of gravel-sand	Groundwater deeply seated, no lateral water source to soil moisture
IV	>10	Subsoil replacement with sand-gravel Heat insulation with polystyrene foam board Flexible lining: geomembrane covered with soil	Flow velocity limited

subsoil than the slabs directly placed on the ground. So the frost heaving is restrained by the pressure from the beams and is decreased. It was observed in the Jintai experiment canal in Gansu, China, that the heave value of the lining is reduced by 1/3 to 1/2 as compared to the heave value of the ground. The beam-slab lining structures is shown in Fig.3.

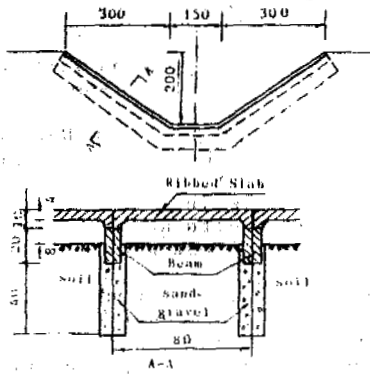


Fig. 3 The beam-slab lining structure

#### The Double Lining

The double lining, is the placement of a membrane under the concrete slab to greatly reduce the seepage through the concrete cracks and joints. This is particularly necessary when the small prefabricated concrete slabs are adopted for canal lining. Then the seepage lost may reach a relatively high amount to replenishing the soil moisture and causing serious damage to the lining in the winter time. Tests showed that

the seepage lost, ranges between 12 to 310 l/m<sup>2</sup> day and is 109 l/m<sup>2</sup>d on average and can be reduced to 7 l/m<sup>2</sup>d on average by placing a membrane under the concrete slabs. Comparative tests showed that the double lining can reduce the frost heave by 35% to 50% as compared with a simple concrete lining. The thickness of the membrane is usually taken as 0.2 mm. To protect the membrane from being punctured by the concrete slab, an interim layer using low grade cement sand with a thickness of 3-5 cm is placed between the slab and the membrane.

The double lining has successfully solved the frost heave problem of many canals originally badly damaged in Gansu and Xinjiang provinces. However, this measure is effective only in the case of the groundwater being deeply seated, no other water supply to the canal bed, neither from the groundwater nor from the irrigated fields or running ditches nearby the canal side.

Although the double lining is very effective in seepage control of the canal, a certain amount of seepage water (average on 7 l/m<sup>2</sup>d) will still occur. If the soil has a very poor drainage performance, after a long period of accumulation in the canal subsoil, the soil moisture can reach a danger value that will cause frost damage in the cold periods. In this case, it is recommended to put a layer of gravel-sand under the membrane. Tests showed that the combination of a double lining and a thin gravel-sand layer can reduce the frost heave by 70% as compared with the simple concrete lining. This measure has been successfully adopted in the Minqin Main Canal, in Gansu, China, with a clayey canal bed, a groundwater table deeper than 3 m and a max frost penetration of 1.4 m in the northern faced slope

Table 5 RR for various soil types and groundwater conditions

Soil type	Depth of water under surface	Upper part of slope	RR(%) Lower part of slope and bottom
Clay	>2.5+H	50-70	70-80
Heavy and medium loam	>1.8+H	50-70	70-80
Light and sandy loam	>1.0+H	40-50	
Clay, heavy and medium loam	Less than above	60-80	80-100
Light and sandy loam	Less than above	50-60	60-80

Note: H is the maximum frozen depth.

(shaded slope) of the canal.

### Subsoil Replacement With Gravel and Sand

This measure is effective in frost heave prevention in various conditions, providing the replacement depth is enough, quality of the material is adequate and proper drainage system is installed, if necessary. According to Q.Zhu et al.(1988), the following 3 criterion should be observed:

1. Depth criterion: According to the in-situ tests conducted on many canals under various soil and groundwater conditions in a 4-6 year period, the more clayey the soil and the shallower the groundwater table is, a greater depth of subsoil replacement is necessary to limit the frost heave value to a safe level. Based on 181 sets of data obtained from the field tests, the replacement ratio (RR), which is the ratio between the replacement depth and the frozen depth, necessary for restricting the heave ratio to less than 2% is shown in Table 5. The replacement depth can be obtained by multiplying RR with the frozen depth. Since the RR and the frost penetration vary with the location of the canal section, the replacement depth designed in this way is nonuniform along the section.

2. Material criterion: According to the research findings and the practical experiences in Gansu, Inner Mongolia and Xinjiang Region, China, it was proved that not only the gravel and gravel-sand but also the sand including very fine sand (average diameter down to 0.13-0.17 mm) can be used as replacement material. But each kind of material should have a limit fine content (diameter < 0.05 mm) to ensure a non-frost-susceptible nature used for replacement. Based on 220 sets of test data from Zhangye Frost Heave Station, Gansu, China, the limit of the fine content is shown in Table 6.

Table 6 Limit of fine content in replacment material

Distance between water table and bottom of frozen soil (m)	>0.5	<0.5
Limit of fine content (weight %)	8	4

3. Drainage criterion: When the replacement material is underlain by an impervious layer, then it will be saturated or partially saturated by the seepage water. The water in the gravel-sand will cause heave action during freezing. In this case, drainage is necessary.

There are two types of drainage systems used in Gansu. One is composed of a longitudinal drainage located at the central line of the replacement bottom and many lateral drainages with a space of 20-30 m to conduct the drainage water

out of the embankment. This design is suitable for a fill section. Otherwise a drainage ditch by the side of the canal is necessary. Another design is suitable when the impervious layer is not thick and a permeable layer lies under it. Then a series of sumps spaced 10-20 m are set at the central line to link the replacement material with the permeable stratum. Fig.4 and Fig.5 illustrates the two types of drainage systems.

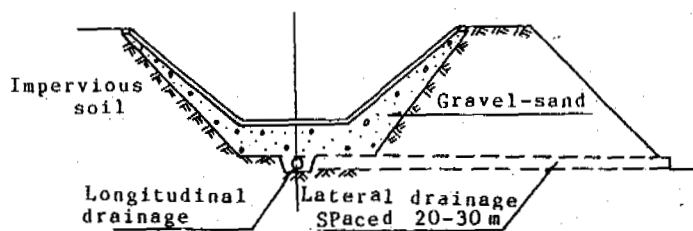


Fig.4 The drainage of subsoil replacement, type 1

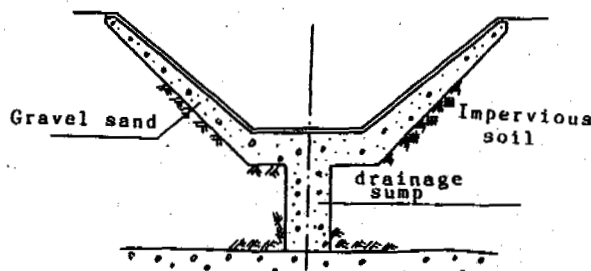


Fig.5 The drainage of subsoil replacement, type 2

### The Heat Insulation

The placement of a polystyrene foam board can obstruct the frost penetration so that frost heave can be reduced to a safe level or thoroughly avoided. The design of the heat insulation can be carried out by the following procedure.

The first step is to determine the frozen depth reduction ratio (FDRR), which can be expressed by the following equation:

$$q = 100 (H - H_1) / H \quad (4)$$

where H is the original frozen depth, H<sub>1</sub> is the frozen depth after the placement of a heat insulation board, q is FDRR. The value of q can be taken as the same with the value of RR in Table 5. Then the reduction of the frozen depth

can be calculated from equation 4. The thickness of the insulation board can be obtained from a heat conduction calculation when the reduced frozen depth  $H_1 = H(1-q/100)$  is given or can be roughly estimated by the following equation:

$$d = (H - H_1)/k \quad (5)$$

where  $d$  is the thickness of the insulation board,  $k$  is a coefficient. According to the field tests,  $k$  ranges between 8 and 12 for the southerly facing slope (sunny slope), 9 and 13 for the canal bottom, 13 and 15 for the northerly facing slope (shaded slope).

Heat insulation is an effective measure for various classes of frost heave but has a limited application for canal linings in China owing to the high cost of the material, except in the large scale water delivery canal in Shandong Province. The insulation board is placed under the concrete slabs at the upper slope while the remaining slope and the bottom under the lowest water level is protected by the water itself which is kept running the whole winter (D.Wang, 1989).

#### The Adoption of a Flexible Linings

In a strong heaving case, it is preferable to use a flexible one instead of a rigid lining. The flexible lining composed of a geomembrane covered with soil or gravel and sand can conform to large deformation caused by frost heaving without any damage. The most commonly used membrane is PE or PVC film of 0.2 mm thick and asphalt grass fabrics which all have relatively lower cost compared with the concrete lining. The disadvantages of flexible lining are the limit allowable flow velocity which is recommended to be less than 0.6 m/s for the soil cover and 0.8-1 m/s for a gravel and sand protection layer. The slope stabilization is also a problem. According to the field tests, to keep the protection layer from sliding, the slope (vertical to horizontal) is recommended to be less than 1: 2-2.5 for a soil cover and 1: 1.75 for gravel sand cover. Because of the flat slope of the flexible lining section, large right-of-way is demanded and increases the construction cost. Recently, the mud-straw cover with thickness of 15-20 cm has been adopted for membrane protection for the small, medium scale and intermittently running canal in Minqin County in Gansu, China. This kind of cover can keep a slope of 1:1.5 for a five year period service with very low cost.

#### CONCLUSIONS

1. The correct determination of the frost heave amount is the base of proper selection of the frost heave mitigation measures. The frost heave prediction can be estimated by some empirical equations obtained from the field tests with enough precision from the engineering viewpoints. These equations can be divided into two groups according to the groundwater condition.
2. The frost heave can be classified into four levels, according to the heave value, which can be related to the proper selection of the frost heave control measures.
3. The frost heave mitigation measures can be divided into structural measure, moisture control measure, subsoil replacement and heat insulation measures. All these measures have their applicability range and should be adopted according to the local conditions.

#### ACKNOWLEDGEMENT

This paper is a summary of a research program supported by the Gansu Science and Technology Committee and the Gansu Provincial Bureau of Water Resources.

#### REFERENCES

- Jones, C.W. et al. (1982) Frost action in soil foundations and control of surface structure heaving, Technical Report No REC-ERC-82-17, U.S. Bureau of Reclamation.
- Kong, Q. (1983) Classification of frost heave soil of concrete channel bed and its anti-heave measure, Proceedings of Second National Conference on Permafrost, pp.462-470.
- Li, A. (1988) A study of frost heave in large U-shaped concrete canals, Proceedings of the 5th International Conference on Permafrost, pp.1110-1115.
- Song, B. et al. (1988) The resistance to frost heave of various concrete lining, Proceedings of the 5th International Conference on Permafrost, pp.1432-1487.
- Xie, Y. et al. (1989) Engineering classification of frost susceptibility of foundation soil of water conservancy structure in seasonal frozen ground region, Proceedings of the Third Chinese Conference on Permafrost (Selection), Academy Press, pp.328-332.
- Wang, D. (1989) An introduction on Huanghe-Qingdao Water Diversion Project. Water Resources and Hydropower Engineering 103:15-18.
- Wang, X. (1985) Design guide of the frost heave damage prevention for the canal linings, Liaoning Provincial Research Institute of Water Resources and Hydropower.
- Zhao, B. et al. (1986) Subsoil replacement using the wind deposited sand for the frost heave prevention of the canal linings, Yellow River, 43:36-37.
- Zhu, D. et al. (1985) Research report of the effect of the soil and moisture conditions on the frost heave of a concrete experiment canal, Water Resources and Hydropower Research Institute of Xinjiang Autonomous Region.
- Zhu, Q. (1983) Frost heave characteristics of the concrete canals in Gansu Province and the measure of subsoil replacement, Proceedings of Second National Conference on Permafrost (Selection), Gansu People's Publishing House, pp.455-461.
- Zhu, Q. (1986) Frost heave control for the canal linings in Gansu Province, Yellow River, 43: 27-30.
- Zhu Q. et al. (1988) Subsoil replacement using sand-gravel for preventing frost heave damage of canal lining, Journal of Glaciology and Geocryology, Vol.10, No.4, pp.400-408.
- Zhu, Q. (1990) Experiments on some basic relationships of the freezing and heaving process of the canal subsoil, Engineering Geocryology 29:10-19.

## PERMAFROST IN THE NORTH OF KOREAN PENINSULA

Viktor An

Institute of Cryosphere of Earth of Russian Academy of Sciences  
f.o.b. 1230, Tyumen, 625000 Russian Federation

The results of the investigation of natural-climatic conditions of the northwestern part of the Korean peninsula are considered based on the possibility of deep freezing. The data testifying to probable presence of the permafrost on the southern and volcanic area.

### INTRODUCTION

The natural-climatic conditions of northwestern part of Korean peninsula on the possibility of the deep ground freezing were studied in 1990. According to the geocryological division of the Euroasian continent into districts this territory is regarded in the zone with the seasonal freezing because of its latitudinal location and the influence of the warm Pacific air mass.

The territory of the volcanic area Pjaktusan presents itself the basaltic plateau on the eastern district of the Kaema tableland with the highest peak of Pjaktusan (2750 m of the altitude). The Chinese name of the area is Chanbai Mountain. It is located on the boundary between China and Korea. A volcano containing a crater, having the same name as Pjaktusan Mountain, is located about 8 km from it and contains the Chendji lake (altitude 2190 m, depth 370 m). The high plateau with the altitude of approximately 2000 m is located to the north and to the east of the volcano. Here stand out the volcanic cones of Sobeksan (2172 m), Kanbeksan (2164 m), Soendzibong (2115 m), Mudubong (1931 m), Djaenzibong (2360 m) and others (Fig. 1).

### THE METEOROLOGICAL DATA

The regular meteorological observations are carried out in this region at a number of the stations, of which the Samchjen has the longest period of measurements (from 1955). The altitude of the station is 1383 m. The average annual air temperature at this station is  $-0.2^{\circ}\text{C}$ . The average monthly temperature in January is  $-17.7^{\circ}\text{C}$ , in July is  $+16.0^{\circ}\text{C}$ . The duration of the warm period is about 193 days, from April to October. The temperature of the soil surface is  $-0.2^{\circ}\text{C}$ . The average sum of the precipitation is 915 mm, and 757 mm of which occurs in the warm period (85% of the annual sum). The greatest monthly sum of the precipitation occurs in July (202 mm) and in August (187 mm). The snow cover begins in the first 10 days of October, when the average temperature is still positive ( $+2.5^{\circ}\text{C}$ ). The depth of the snow cover increases relatively monotonically (Fig. 2), and reaches the maximum (average

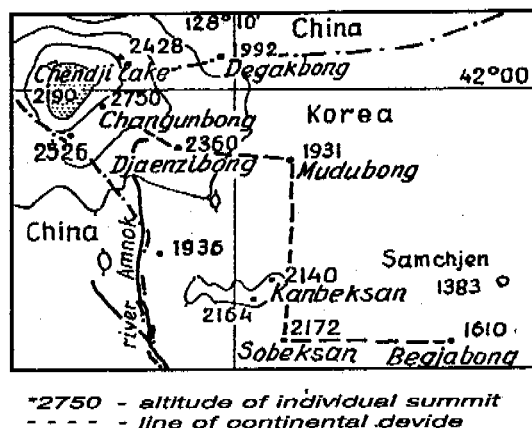


Figure 1. Map of the area of Pjaktusan volcano.

54 cm) by the end of February. The melting of the snow begins at March and melts very rapidly, disappearing entirely by the end of the month.

The freezing of the ground begins in the first days of October, but it stable only after the middle of November. This is because of the insulation by the snow cover of the 10 cm depth. Figure

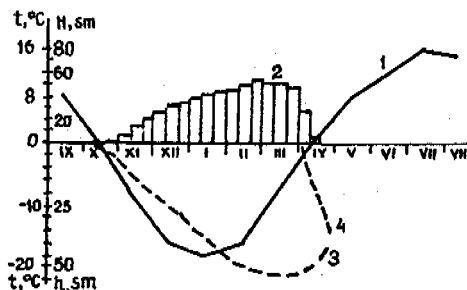


Figure 2. The data of the observations on the Samchjen meteorological station. 1 - average monthly temperature of air; 2 - depth of snow cover in 10 day interval; 3, 4 - curves of freezing and melting of snow.

3 shows the distribution of the average monthly temperature of the soil surface and of the snow based on the data based on many years research at the Samchjen station. Apparently, the mean monthly isotherm of 0°C reaches the maximum depth (of 0.45m) by the end of February. The freezing ends by the middle of March reaching its maximum (0.83 m in 1975 and 0.38 m in 1973). In April, the lower limit of the freezing rises.

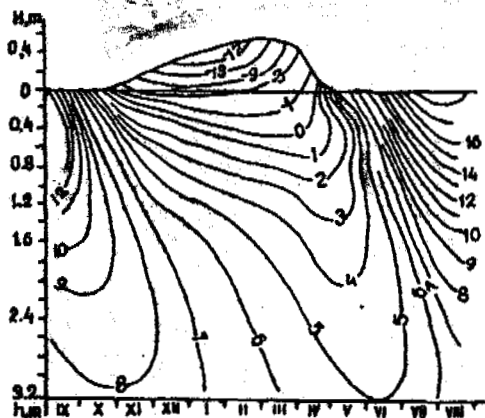


Figure 3. The distribution of average temperature (°C) in the ground and in the snow, Samchjen station.

#### GROUND FREEZING AND PERMAFROST

The curves formed by the data of the temperature's measurement on the grounds of the meteorological station (Fig. 4). Apparently the character of the temperature changes due to the upper horizon's temperature rise in connection with secular changes of the climate and with the air temperature rise as a whole. The character of the average for many years curves in the layer of the zero annual temperature fluctuations (at the depth of 5-7 m) shows that the average temperature is near +5.5°C at the depth of the zero an-

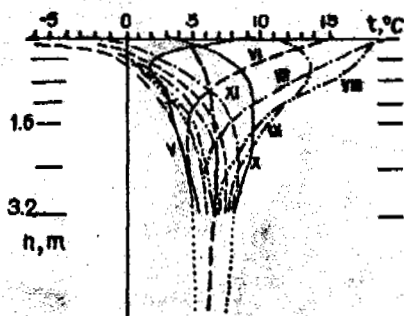


Figure 4. The distribution of the average temperature in the ground, Samchjen station (Roman numerals represent months).

ual amplitude. The seasonal frozen layer of the ground melts intensively in April, 25% of the frozen ground melts from above (Fig. 2). The rest melts from below.

The average annual temperature of the air is observed at the meteorological station in the region of the Pjaktusan volcano also. The tempera-

ture at the altitude 1383 m (Samchjen) is 0.2°C, at the altitude 1500 m -1.5°C and -8.3°C at the altitude 2700 m (Pjaktusan). The hypothermal gradient is 0.006 K/m and corresponds to the gradients of the other areas with the permafrost.

The continental divide passes along the line connecting Begjabong-Sobeksan-Chungangbong-Mudubong-Djaendzibong-Changungbong (Fig. 1). On both sides there were observed the difference of the landscape's conditions. The high plateau with the altitude of nearby 2000 m is located to the north and the northeast of this watershed. This plateau represents the treeless plain, made up of pumicestone of 20 m thickness. Above the altitude of 2000 m the landscape of the plain is alpine tundra. The thickness of the snow here exceeds no more than 0.4-0.5 m, but it is absent here and there in the most northeastern part of the region. Because of the strong and frequent winds the snow blows from the positive and accumulates in the negative elements of the relief. To the southwest of the continental divide the thickness of the pumicestone is no more than 1-2 m and here the dense forests of the larch (*Larix dahurica*) with the admixture of fir and birch are growing on the rocks with a in

weak cover of the red-coloured soils. On the soils, mosses are present at the same time with the bushes (*Rhododendron parvifolium*, *Vaccinium uliginosum* and others). The thickness of the snow cover reaches 1.2 m on an the average.

The permafrost is distributed on an treeless plain on the altitude of more than 2000 m. With regard to the hypsodermical gradient the average annual temperature is -4.5 to -5°C at this altitude. There is the potential for deep freezing of the ground, because the snow cover or its absence. The permafrost's upper limit repeats the relief of the region. On the positive elements of the relief the depth of the permafrost bedding changes from 0.8 to 1.2 m. On the negative elements of the relief the thaw depth can be twice as much because of the concentrated flow of the atmosphere moisture here.

Nearby the Mudubong summit at the altitude of 2000 m has been observed the bearing of the ravine wall. Here the thickness of the detritus of the pumicestone is about 8 m. The soil-vegetation layer lies above the pumicestone and its thickness is less than 0.5 m. The detritus is perennially frozen from the depth of 0.5 m to the bottom and is cemented by the film-crust ice. The visible content of the ice is less than 10%. The bottom of the ravine is filled by perennially snow. The abundance of the water flowing testify that the flow is forming by the melting of ice and the ground water. Below the snow, the bottom is made up of basaltic blocks and boulders. There can be no doubt that the flowing of underground water is concentrated in the hollows. On this country, the thickness of the permafrost is no more than the thickness of the pumicestone material which it is about 10 m.

The permafrost may exist under the banks, from which the snow is blown away and accumulated in the hollows and ravines. It is expected that permafrost has developed under individual summits. The thickness of the permafrost is directly dependent on the altitude. On the Pjaktusan mountains with the individual summits of 2700 m, the average annual temperature of the ground is about -3°C at the depth of 10-15 m based on the hypsodermical gradient. Under normal gradient of

0.015 K/m the thickness of the permafrost can be about 200 m under the Chagunbong summit. The permafrost is absent in the hollow of the Chendji lake because of the insulation of the water and the outflow of the thermal water.

In the altitude range from 1500 to 2000 m, individual islands of the permafrost can be found on areas with the dense forests; predominance of the fir and the moss cover of 0.1 m thick. Although there is insulation of the snow presented in winter, the trees provide shade in the summer. The thick moss cover warms up the soil and accumulates much moisture. The transpiration of the moisture from the soil's cover and the growth of the trees decrease the temperature of the ground surface. Therefore the individual islands of the frozen ground may be developed in those conditions with the thickness of permafrost islands is less than 10 m.

#### THE REASON FOR THE PERMAFROST FORMATION

The primary cause of the permafrost formation is the ecological catastrophe in this region, which occurred in the past. In the present epoch there were 16 cases of the volcanic activity of the Pjaktusan - from 580 to 1898 (Chichagov, Lim, 1990). By far the biggest eruption was in 1703. Following an eruption of the volcano the large pumicestone plain was formed in the limit of the Pjaktusan volcanic plateau. The great primary forests (the needles-broad-leaved forests on the northern slope and mainly the needles on the southern slope) were buried under the thickness of the pumicestone. The trees by the annual rings

are from 320 to 500 years old and more. The buried trees still remained almost undestroyed, thanks to the preserving ability of the grey pumicestone and the frozen ground. By the radiocarbon dating, the age of the buried trees are 650-1000 years old on the south-eastern slope, 1000-1200 years old on the northern, 1400 years old on the eastern (Chichagov, Lim, 1990; Zhao Dachang, 1981). The most powerful phase of the volcanic eruption relates to the end of X - beginning of the XI centuries by the Japanese investigators. The forming of the permafrost began after those eruptions.

#### CONCLUSION

The ecological catastrophe caused the forming of the alpine plain with specific hydroclimatic conditions, this promoted the rise of the high-mountainous tundra. The wind factor caused the deep freezing of the ground and the resulting permafrost.

#### REFERENCES

- Chichagov V.P., Lim Kvon Muk (1990). The volcanic area and Pjaktusan volcano in the PDRK: the modern relief, volcanism and ecological catastrophe. Geography and Natural Resources, No. 2.
- Zhao Dachang (1981). Preliminary investigation on relation between volcano eruption on Chagbai Mountain and the succession of its vegetation. Res. For. Ecosyst., Vol. 2.



## FORECASTING OF RIVER BED DEFORMATIONS IN THE PERMAFROST ZONE

Felix E. Are<sup>1</sup> and Victor A. Savitsky<sup>2</sup>

<sup>1</sup>Petersburg Institute of Railway Engineers, Moskovsky av., 9, St. Petersburg 190031, Russia.

<sup>2</sup>Formerly of the Petersburg Institute of Railway Engineers.

Comparative analysis of the morphometric characteristics of the freely meandering rivers in and outside of permafrost zone showed that the presence of frozen grounds in the river basin does not affect considerably the basic natural laws of river bed deformations in the permafrost zone and the hydromorphological method of forecasting may be applied, in principle, as it has been worked out for the rivers flowing outside of the permafrost zone. Comparison of the rates of natural deformations of the Yamal peninsula rivers and of the rivers located beyond the permafrost zone showed that by the equal width of the river bed the Yamal peninsula rivers differed considerably in lesser rates of deformations.

### INTRODUCTION

Since 1986, the authors have been studying the river bed evolution of the Yamal peninsula rivers with the object of working out the procedure of forecasting the river bed deformations. The grounds of the Yamal peninsula are perennially frozen. The river bed evolution in the permafrost zone has been studied insufficiently, and the methods of forecasting it have not been worked out yet. It is universally recognized that the frozen state of grounds affects the evolution of river bed though there is no single opinion concerning not only the significance of this effect but also about its orientation. Some investigators consider that the frozen state of grounds hinders the river bed deformations while others are of an opposite opinion.

Up to now most of the investigators tried to study the importance of the frozen state of grounds in the evaluation of river bed evolution on the basis of analyzing the erosion of frozen grounds with water streams. Erosion of frozen ground develops due to the combined thermal and mechanical affect onto it by water streams. It is evident that the erosion of frozen grounds is possible only when the stream washes their bare surface. Permanent contact of the stream with the frozen ground in the process of erosion is guaranteed at the water temperature of 0°C. At a positive temperature of the water the ground thaws out, and therefore contact is possible in this case only providing the stream carries away the thawed-out material immediately. The vast observations brought about by the authors on the rivers of the permafrost zone showed that under the natural conditions thawing of grounds outruns the erosion. In this case the surface of the frozen ground is separated from the water stream by the thawed layer, and therefore the frozen state of the grounds does not affect the process of erosion (Are, 1985).

Watching the break-up of rivers in the central part of the Yamal peninsula showed that even in

the very beginning of the break-up the water temperature is above zero. Direct contact of water streams with frozen grounds was observed (1) immediately after the ice cover frozen to the bottom of the river came to the surface, (2) after the snow cover on the banks became eroded, (3) in the course of formation of erosion recesses in the bedding of shore cliffs, (4) at the erosion of collapsed frozen blocks of the shore cliffs. In all the cases listed above, the area of contact of the water stream with the exposed surface of the frozen ground is not large, and it can be seen within a short period of time. Besides, in the first two cases accumulation of thawed sediments can be encountered more frequently as compared to the frozen ground erosion. Therefore there are no grounds for stating that the evolution of the river bed depends to a great extent upon the erosion of the frozen ground. Extensive ice content in the grounds being eroded may appear to be of a greater importance due to the decrease of the volume of the grounds when they thaw out. In some regions of the Yamal peninsula thick sheet ice of vast strike occurs. The river bed evolution may develop in those regions rather peculiarly.

In the course of studying the erosion of frozen grounds, the problem is approached usually from the positions of hydromechanics and thermal physics (Yarshov et al., 1982). The results of those investigations cannot be the basis for working out methods of forecasting the river bed deformations in the permafrost zone not only on the grounds of the above considerations about the importance of frozen state of grounds but also due to the fact that the areas and the duration of direct contact of the bare surface of the frozen ground to the water flow in the river bed of a definite river cannot be defined and used for calculations. Besides, the physical investigations do not take into account the laws of the river development as a phenomenon of nature.

The solution should be searched for from the positions of the hydromorphological theory of the

river bed evolution (Kondratyev et al., 1982) according to which this process is subdivided into 7 types. Each of them is characterized by a number of quantitative morphometrical parameters.

**COMPARISON OF MORPHOMETRICAL PARAMETERS OF FREELY MEANDERING RIVERS IN AND OUTSIDE OF PERMAFROST ZONE.**

All the rivers of the Yamal peninsula develop in conformity with the free meandering type. B.F.Snishtchenko (1979) found out that such rivers beyond the borders of the permafrost zone are characterized by the parameters of river bed evolution type,

$$A = (B_f/B_{ch}) \cdot (I_v/I_r) = 36.6 \pm 11.5 \quad (1)$$

$$A_1 = (B_{mb}/B_{ch}) \cdot (I_v/I_r) = 17.8 \pm 5.5 \quad (2)$$

where:  $B_f$  - width of the flood-plain,  $B_{ch}$  - river bed width,  $B_{mb}$  - meandering belt width (in a general case - width of the river bed formation belt),  $I_v$  - valley bottom gradient,  $I_r$  - gradient of the stream free surface along the thawed line. Figure 1 illustrates the B.F.Snishtchenko's graph showing the morphometrical parameters of rivers with various types of the river bed evolution beyond the borders of the permafrost zone. This graph involves the information about three rivers of the Yamal peninsula (Yuribay, Erkatayakha, Endzoryakha).

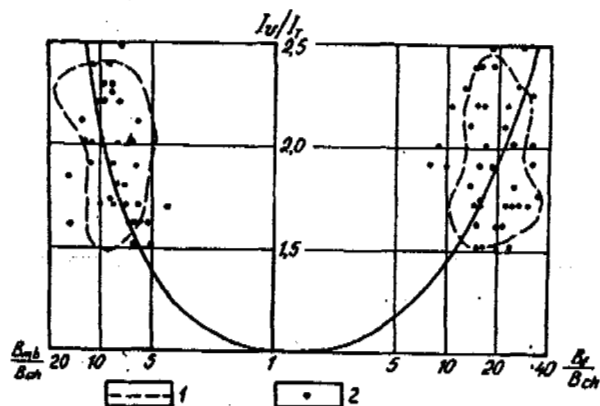


Figure 1. The association of types of river bed evolution with relative gradient  $I_v/I_r$  and relative widths of meandering belt  $B_{mb}/B_{ch}$  and flood-plain  $B_f/B_{ch}$ . 1 - border of the area of existence of free meandering river beds according to B.F.Snishtchenko, 2 - data referring to the freely meandering rivers of the Yamal peninsula.

The overwhelming majority of points appeared to be located within the limits of the region where, in B.F.Snishtchenko's opinion, the free meandering exists.

For the same three rivers of the Yamal peninsula the frequency curves have been plotted that illustrate the relative pitch of meanders,  $\lambda/B_{ch}$ , the angle of turn of the meanders,  $\alpha$ , and the degree of development of the meanders,  $S/\lambda$  ( $\lambda$  - the distance on a straight line between the points of bend of the river bed mean line,  $S$  - length of the meander between the neighbouring points of bending along the middle line of the river bed). The curves are illustrated in Figure 2 together with the similar data of I.V.Popov (1964) for the

Oka, the Irtish and the Ob rivers. The curves of the Yamal peninsula rivers coincide almost completely with the limits of the family of the curves given by I.V.Popov. The same figure illustrates the envelopes of the family of the river bed relative width existence,  $B_{ch}/H$  ( $H$  - depth of the river bed) for the rivers beyond the borders of the permafrost zone according to the I.V.Popov's information (1983) and for six rivers of the Yamal peninsula. The non-coincidence of the lower envelopes can be explained by the fact that the whole river bed width is equal to 4.7 m. The minimum width of the Yamal peninsula rivers shown in the Figure 2 is equal to 100 m. The divergence of the upper envelopes can be explained by the fact that on one of the sections of the Yamal peninsula rivers a very high bank gets eroded. This causes the increase of sediments accumulation, the appearance of islands and the extension of the river bed. As to the other parameters of the data given in Figure 2, they testify to a proper coincidence of the  $B_{ch}/H$  values for the freely meandering rivers beyond the permafrost zone and the rivers of the Yamal peninsula.

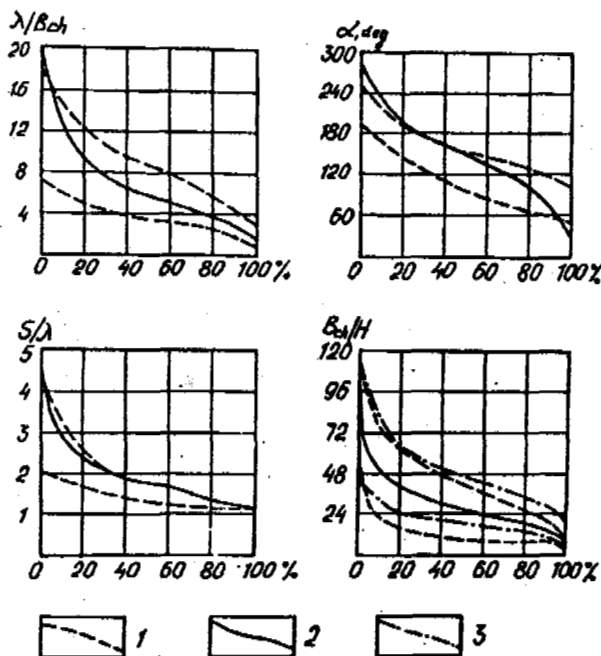


Figure 2. Frequency of the morphometric characteristics of the freely meandering river beds. 1 - envelopes of the family of curves according to the information of I.V.Popov, 2 - averaged curve for the Yamal peninsula rivers, 3 - envelopes of the family of curves for the Yamal peninsula rivers.

No considerable differences were found either in the interrelations of the degree of development of the meanders with the angles of turn and the pitch of meanders with the river bed width (Figure 3). As to the three rivers of the Yamal peninsula that were mentioned above, below given the mathematical expressions of those dependences obtained:

$$S/\lambda = (e^{n\alpha} + e^{-n\alpha})/2 \quad (3)$$

$$\lambda = 18.2 B_{ch}^{0.78} \quad (4)$$

where  $n$  - variable coefficient acquiring the values of 0.007 at  $0 < \alpha < 160^\circ$ , 0.0072 at  $160 < \alpha < 200^\circ$ , and 0.0075 at  $200^\circ < \alpha < 280^\circ$ .

The comparative analysis that was brought about showed that at the macrolevel the development of the freely meandering rivers in the permafrost zone and which beyond the latter's boundaries takes place in compliance with the general conformities to natural laws irrespective of the differences of the climatic and the geocryological conditions within the basins of the rivers.

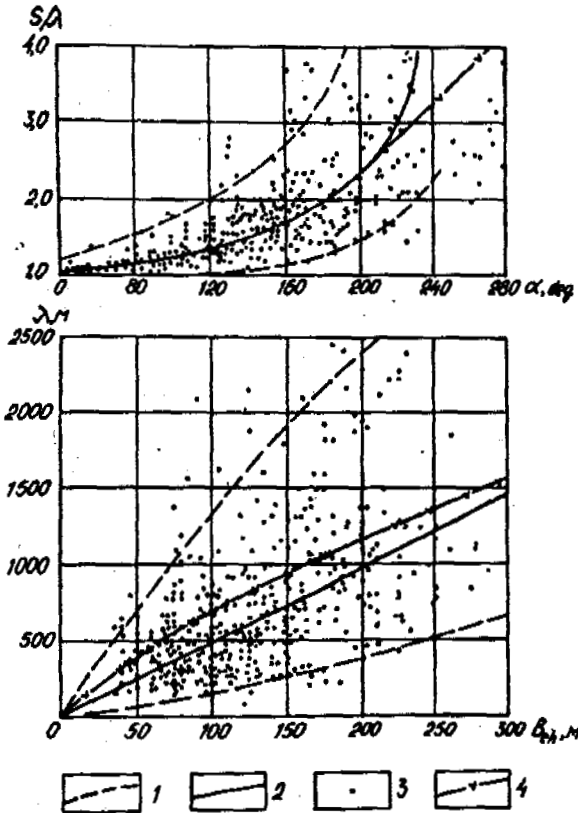


Figure 3. Relations between the parameters, of free meandering. 1 - borders of the range of scattering of the data given by I.V.Popov, 2 - I.V.Popov's generalized dependence, 3 - data referring to the Yamal peninsula rivers, 4 - generalized dependence for the Yamal peninsula rivers.

Hence, the methods of forecasting the horizontal river bed deformations of the freely meandering rivers flowing beyond the permafrost zone borders may be applied, as a matter of principle, also to the similar rivers of the permafrost zone.

#### FORECASTING OF RIVER BED DEFORMATIONS BY THE HYDROMORPHOLOGICAL METHOD

N.E.Kondratyev worked out the hydromorphological method of forecast for the freely meandering rivers and offered the Equation (5):

$$Y = C_{max} \cdot K \cdot T \cdot \frac{h}{h_p} \quad (5)$$

in which  $Y$  - the average long-term horizontal displacement of the concave (being eroded) bank of the meander in the river cross-section being analyzed for the number of years  $T$  in m,  $C_{max}$  - maximum rate of the bank displacement in the meander being analyzed, m/year,  $K$  - empirical coefficient taking into consideration the phase of meander development,  $h$  - maximum depth of the river bed in the cross-section being analyzed,  $h_p$  - maximum depth of the river reach in the meander. The depth values are measured from the average level of the crests of the rifts that limit the meander.

The value of  $C^\circ$  is defined by comparing the aerial photographs or the topographic maps issued in various year of survey, and that is why this value is an integral characteristic which takes into consideration all the hydrological and the other natural factors which the river bed deformations of the river being studied depend upon, including the frozen state of the grounds if the river flows within the permafrost zone.

To use the Equation (5), numerous measurements of the horizontal river bed deformations of 20 rivers of the Yamal peninsula have been taken for the recent 20 years through comparing the aerial photographs (the scales ranged from 1:10000 to 1:45000), the topographic maps at a scale of 1:25000 and the results of the geodetic on-site measurements of the present-day riverbeds location. The geodetic measurements were taken in the course of the route surveying of approximately 300 km of the banks of several rivers.

Processing of the results of those measurements showed that the average long-term rates of the transverse displacements of the flood-plain banks of the greatest river of the Yamal peninsula, the Yuribay (the catchment area is 9100 km<sup>2</sup>, the width of the river bed in the lower reaches ranges from 200 to 250 m, the discharge per year is 4.7 km<sup>3</sup>) account for some 1.7 m/year in the middle sections of the meanders. The absolute maximum average rate for many years of 4.7 m/year was detected at individual short sections of the Yuribay and the Erkayakha rivers.

The results of processing of all the measurements depending upon the average width of the river beds are illustrated in Figure 4. Here the values of the rates for the morphologically homogeneous sections (MHS) of the rivers are shown. Curve 4 illustrates the average rates (the erosion area divided by the total length of the sections being eroded). Curve 3 shows the average maximum rates (the sum of the absolutely maximum rates in each meander divided by the number of meanders in the MHS), while curve 2 shows the absolutely maximum rates of each MHS. The data set forth in Figure 4 testify the fact that the average rates do not exceed, as a rule, 1 m/year, the average maximum rates do not exceed 2 or 3 m/year, and the absolutely maximum rates do not exceed 4 m/year. The dependence of the rates of deformations upon the river bed width is approximated by the regression Equation type

$$C = \sqrt{K \cdot B_{ch}} - m$$

whose parameters are set forth in Table 1.

Figure 4 also illustrates the I.V.Popov's data (Kondratyev et al., 1982) for the rivers flowing beyond the boundaries of the permafrost zone. They testify to the fact that the maximum rates

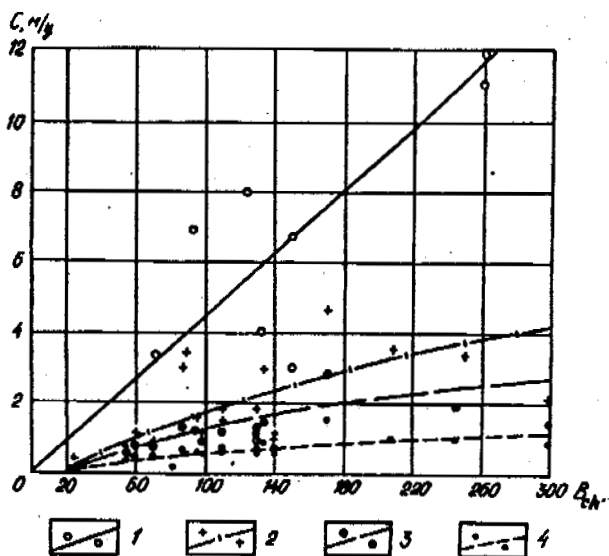


Figure 4. Shore retreat rate versus river bed width. 1 - data and dependence given by I.V. Popov for the rates that are the maximum ones on the section, 2 through 4 - data and dependences for the Yamal peninsula rivers: 2 - maximum rates on the section, 3 - average maximum rates, 4 - mean rates.

of deformations of the Yamal peninsula rivers are two or three times less than those beyond the borders of the permafrost zone. Field observations of the breaking up of the Yuribay river and its tributaries showed that the main cause of that was the affect of the snow cover admitted by all the hidrologists though this feature seems underestimated when applied to the rivers of the tundra zone.

Table 1. Parameters of Equation (6)

C	K	m	Correlation factor
Average	0.01	0.5	0.82
Average maximum	0.05	1.0	0.78
Average maximum	0.11	1.5	0.69

#### THE INFLUENCE OF SNOW COVER ON THE RIVER BED DEFORMATIONS IN TUNDRA

Extensive snow transportation due to wind in the tundra at the poorly expressed prevailing direction of winds results in the fact that along all the bank bluffs of the middle-size rivers (the area of the catchment basin ranges from 2000 to 50000 km<sup>2</sup>) snow drifts appear by the spring, and their maximum thickness is equal to the height of the bluffs. That is, it can reach as much as 20 m. The width of the drifts is three or four times as much as the height of the bluffs. The affect of the snow cover and of the irregularity of its territorial distribution can be seen in several aspects:

1. In the early spring, first of all the open flat areas of the tundra with the least height of snow cover become free from snow. The water from

melted snow flows to the valleys of the channels filled with snow completely or partially, saturates in it and gets filtered in the deflection of the piezometric inclination. It is evident that in this case the water enters the rivers slower and the temperature of the inflowing water is close to the point of freezing. Both these factors decelerate the thermal destruction of the ice cover of the rivers with the water stream and cause a delay of the terms of rivers break-up.

2. Before the beginning of the flood, the ice cover along the shoaly convex banks which was frozen up to the bottom and which has no snow cover becomes thawed due to the effect of the penetrating solar radiation that reaches the drifts lying under the ice and that gets them to thaw too. Therefore, when the water level in the river rises the ice cover on such areas floats to the surface without any obstacle. The snow cover absorbs practically the whole penetrating solar radiation. Therefore, the ice cover which was frozen to the bottom and which was covered with snow does not melt in spite of the availability of penetrating radiation. When the water level in the river rises it does not come to the surface but it sinks and later on is melted due to the effect of the water stream only. In this case the terms of ice melting and floating to the surface are the least on the sections being washed away. As to the accumulation sections, the ice lying on the bottom becomes covered with sediments which slows the thawing, and therefore this ice will come to the surface later. If the layer of sediments is thick enough the ice may not come to the surface at all, and melt in place.

3. Snow drifts along the erosional cliffs lie on the ice cover. They do not let it come to the surface and exclude completely the possibility of washing-out of the banks above the lower mark of the fast ice until this bank protection disappears. So, large snow drifts along the high banks can thus delay the beginning of washing-out terms for a long time. For example, on the Yuribay river, in the Purnado area, in 1987, the high erodible shore became free from the fast ice and the snow drifts on the July 2, 19 days after the beginning of break-up time and in 4 days after its peak phase.

4. After the fast ice and the snow drifts separate from the shore, the water stream enters a direct contact to the frozen grounds and erosion of them takes place. By this time the temperature of water in the river already is 5 - 7°C.

#### CONCLUSIONS

The results of observations set forth above and other results of observations show the different affect of the snow cover on the process of river break-up. Its total effect is reduced to excluding or to decreasing the possibility of direct contact of the water stream to the bare frozen ground both in space and in time. To the greatest extent it applies to the beginning of the spring break-up when the water temperature is the lowest and, hence, when the frozen ground may resist most of all the thermal erosion effect of the water flow. On the whole, the snow cover lessens the part of the frozen state of grounds in the development of the river bed evolution.

The integral affect of the snow cover on the horizontal deformations of the river bed results in their decrease due to:

1) decreasing of high water discharge because of the accumulation of melt water in the snow drifts in the valleys of their small tributaries;

2) decrease of the thermal energy of the river stream because of decreasing temperature of the water coming from the valleys of tributaries filled with snow;

3) decrease of the maximum amount and the period of effect of the river-bed-forming discharges due to retaining the fast ice and the snow drifts on the erosible shores during the peak time of flood.

Retarding of river bed deformations of the Yamal peninsula rivers may be also explained by the short period of high water typical to the permafrost zone rivers caused by the frozen state of grounds in the river basin.

In comparison to the climatic and the hydrological factors mentioned above, the frozen state of grounds does not effect too much the rate of the horizontal river-bed deformations.

#### REFERENCES

- Are F.E. (1985) Forecasting basis of thermoabrasion of banks. Novosibirsk, NAUKA, 173 p.
- Kondratyev N.E., Popov I.V., Shishtchenko B.F. (1982) ) Basis for gydromorphological theory of the river-bed process. Leningrad, Gidrometeoizdat, 272 p.
- Popov I.V. (1964) Quantitative indicex of river-bed process of different kind. Transaction of Gosudarstvennogo gidrolodicheskogo instituta, vypusk 116, p. 32 - 81.
- Popov I.V. (1983) Width and depth correlation of river-bed having differrent types of river-bed process. Transactions of Gosudarstvennogo gidrologicheskogo instituta, vypusk 288, p.3 - 9.
- Snishtchenko B.F. (1979) Relation between river-bed types and shapes of rivers plains. Geomorfologija, No. 1, p. 18 - 25.
- Yershov E.D. et al. (1982) Thermoerosion of dispersed soils. Moskva, Izdatelstvo Moskovskogo universiteta, 192 p.

## PREDICTION OF STABILITY OF SOLUFLUCTION SLOPES AND STRUCTURES ON THEM

G. I. Bondarenko

Research Institute of Bases and Underground Structures  
2-nd Institut'skaya St. 6, 109428 Moscow, Russia

The results of many years of experimental investigations are given in the paper. The calculation methods of stability of the soluflection slopes accounting for the peculiarities of thawing soils deformability on the contact with frozen soil are presented. Dependences of friction and cohesion of thawing soil on water content with shearing at the moment of thawing are given. It has been shown that water content is the main factor governing the stability of the soluflection slopes. The diagrams of the relationships of stable angle of slope, water content and consistency of soil are presented. The steps to improve stability and prediction method of stability of the soluflection slopes and structures on them are recommended.

### RESULTS OF INVESTIGATIONS

Soluflection is wide spread in the regions with cold climate and in the mountainous countries (Chaplain 1965). Industrial and agricultural development not only intensifies soluflection processes, but promotes the appearance and development of these processes on slope where soluflection was not observed earlier.

Study of the conditions of deformations on soluflection slope by (McRoberts 1975, Nixon 1973) and (Zhigarev 1967, Rjabchun 1976) researchers take into consideration that the displacement occurs as sliding of the thawed soil on the underlying frozen soil. Calculations were made accounting that shear-strength is the same for the whole thawed soil and the identical limit-prolonged strength  $\tau_{prol}$  (Zhigarev 1967) or  $\tau=P$  in the stage of viscous flow (Rjabchun 1976). As it was mentioned by the authors, the calculated angles of slopes appeared to be higher than those observed in the natural conditions, even in the cases when the coefficients of filtration and pore pressure were taken into account. The consolidation theory of thawing proposed by the Canadian researchers reflects most completely the peculiarities of deformability of the thawing soil on the slopes when considering filtration of hydrostatic suspension and pore pressure. However, they note the necessity of the detailed study of the geotechnical properties of the soil on the contact with the frozen soil (Nixon 1973).

To develop the calculation methods of stability the authors carried out laboratory and in situ investigations of changing physical and mechanical properties of the soils and the mechanism of the soils deformations while thawing on the slopes. In this case special attention was given to the peculiarities of deformability of the thawing soil on the contact with the frozen soil.

The following main regularities were defined:

- while thawing the upper «overlapping» layer and the lower «near-contact» layer of the soil are created on the boundary with the frozen soil;
- the least strength of shearing is in the (near-contact) layer of the soil, where the maximum loosening, water content and pore pressure were;

strength of shearing of the thawing soil with quick loading action is less than for the long term period;

strength of shearing as well as friction and cohesion are decreased when water content and ice-content are increased; when water content is more than limit of fluidity then strength of shearing is practically absent.

Friction and cohesion of soils were defined in-situ and in laboratory conditions taking the specially developed methods (Bondarenko 1983, 1991) allowed to make the shearing at the moment of thawing. The diagrams of friction and cohesion dependences on water content of soil were made (Figure 1).

One can see from these diagrams clearly that friction and cohesion are decreased when water content is increased. At the same time with equal water content (for example, equalled to 0,36) friction and cohesion for different loams are different and equal correspondingly to:

ferruginous  $-10^\circ$  and 0,08 MPa; dusty  $-5^\circ$  and 0,001 MPa; silty  $-25^\circ$  and 0,04 MPa.

This may be explained that with one value of moisture (0,36) the soils have different consistency: silty loams - hard plasticity one, but dusty loams - fluidity one. 12 types of dispersed soils (loams, sandy loams, dusty sands) from the slopes of the South Yakutiya, Krasnoyarsk region and Yamal were investigated.

It was stated that friction and cohesion of the thawed soils depend not simply on moisture, but on the consistency of soil as well, and they are changed from the maximum values with hard plasticity consistency till the minimum values with fluidity consistency.

The influence of moisture and consistency of soils on the slope stability was investigated. The calculations of stability were made for each type of soil with the given water content.

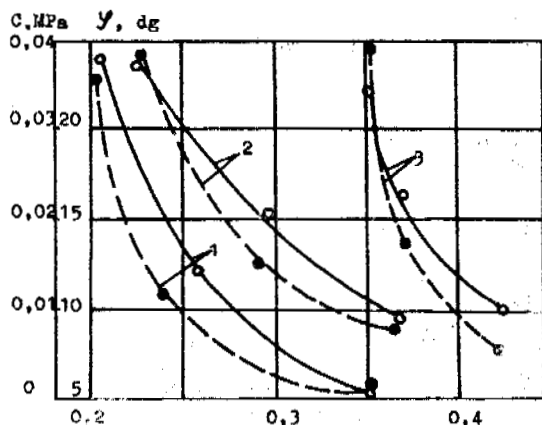


Figure 1. Dependence of friction and cohesion of thawing soil on water content: 1 - dusty ( $W_L=0.31$ ,  $W_p=0.18$ ); 2 - ferruginous ( $W_L=0.38$ ,  $W_p=0.22$ ); 3 - silty ( $W_L=0.43$ ,  $W_p=0.37$ ).

Taking into account the stated regularities the calculations of the stability of slopes, excavations and banks slopes were performed using the scheme of the slope rested against and considering that the line of sliding was given by the depth of thawing. The calculations were performed from the formula:

$$n = \frac{\text{tg}\varphi_{th}}{\text{tg}\alpha} + \frac{C_{th}}{\rho h_{th} \sin\alpha} \geq 1$$

where  $\alpha$  - angle of slope inclination;  $\rho$  - soil density;  $h_{th}$  - depth of soil thawing defined from engineering and geological research or defined from thermotechnical calculations accounting technological action during the period of construction and service operation of structures;  $C_{th}$ ,  $\varphi_{th}$  - cohesion and friction of the thawing soil.

Then basing on these results the diagrams of the dependence of the stable angle of slope on the water content were plotted. It was clear from this diagrams that the stable angle of slope is decreased with the water content increasing. The diagrams in Figure 2 make it possible to define the stable angle of slope for the given type of soil from the data of engineering and geological research with the known values of water content and the depth of thawing. These diagrams make it possible also to predict the value of the angle when the value of water content and the depth of thawing are changed during the period of construction and service operation of structures. The same diagrams of dependence of the stable angle of slope on the different depths of thawing were plotted for the all investigated soils. It was appeared in this case that the values of the stable angle of slope (as well as friction and cohesion) were different for the different soils with the same values of water content. For example, for the investigated loams the values of the stable angle of slope were different with the water content -0.36; for silty loams -12°, for dusty loams

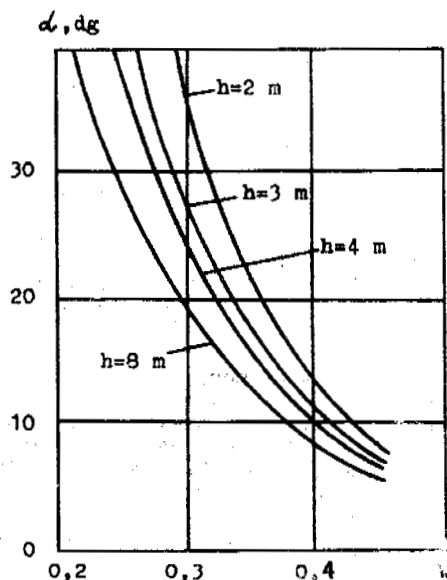


Figure 2. Dependence of stable angle of slope on water content of silty loam with different depth of thawing.

-6°, for ferruginous loams -20°. However, the values of the stable angle of slope are also identical for the same loams with the identical consistency. And hence, the stability of slopes depends not simply on the water content but on the state of soil and primarily on its consistency.

Accounting this the analysis and the determination of the stable slope depending on the consistency (with the change of water content beginning from the limit of rolling out till the limit of fluidity) were performed for 12 types of the investigated soils. It has been appeared that with the identical consistency these soils have practically the same stable angle of slope. The diagrams of dependence of stable angle of slope on consistency of the soil for different depths of thawing were plotted in Figure 3. The values of the stable angle of slope received from the diagrams are well in line with the natural values. The diagrams received permit to define the stable angle of slope from the results of engineering and geological investigations, if the water content at the depth of seasonal thawing is less than the limit of fluidity. If the water content equals or more than the limit of fluidity then the slope is nonstable (Bondarenko 1983).

The depth of thawing may be increased with getting warmer of the climate, leakage of technological waters when vegetable and peat covering is removed. The increase of the depth of thawing leads to the thawing of not deep icy beddings, and this fact initiates the quick solifluction. Moreover the removal of moss and peat covering, trees and bushes, destruction of the upper soil layer during the period of territory development and construction - all this weakens the holding forces of the slope and activates the solifluction processes.

The appearance of solifluction, its action on the surroundings and structures - all this is conditioned by not only the geocryology but the character of the engineering action on the slope as

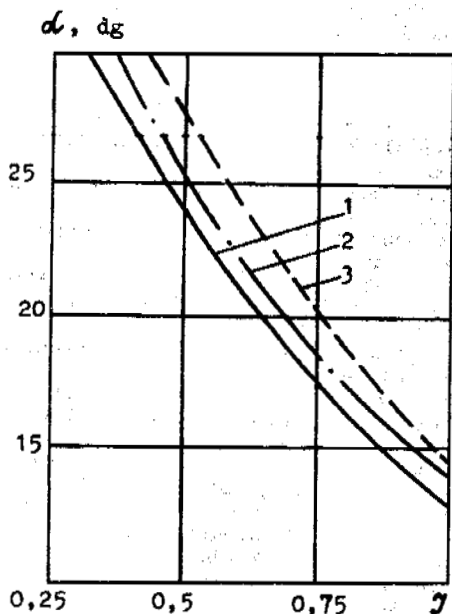


Figure 3. Dependence of stable angle of slope on consistency of loams: 1 - dusty; 2 - ferrous; 3 - silty.

well. Therefore when the stability of the solifluction slopes and the structures on them is defined, then the system «surrounding-structure-slope» should be taken into consideration.

While excavating on the slopes of permafrost dispersed soils the slopes of excavations were swelled up, drainage canals were poured, and this led to the destruction of road-bed and to the interval of transport movement. Landslidings often take place on the slopes of excavations and then heavily iced horizons are exposed during their development. Along with the destruction of local stability of excavation slopes the large-scale landslides take place on the solifluction slopes that lead to the destruction of roads. During the road construction an additional load from the weight of embankments as well as a dynamic load from the rolling stocks act on the slopes. Numerous cases of railways deformation under the action of solifluction are known. Different rates of embankments displacements were observed. Sometimes the road embankment slowly moved together with the seasonally thawed layer during some years. The rates are measured in cm per year. Step-by-step bending of earlier straight sections of road takes place. With strong moistening of soils or with thawing through of heavily ice soils quick landslidings occur as a result of disturbance of turf covering. There are known the cases when the sections of roads with the length of 100 m were displaced along the slope down to 80 m during two days.

The preservation of vegetable covering layer and the use of different types of thermoinsulation decrease the depth of thawing. This not only weakens the displacing forces but keeps the retaining forces at the expense of the vegetable layer and due to prevention of the below located heavily iced horizons from thawing.

The influence of solifluction on the pipelines is explained by the character of the process

(plastic and viscous or viscous flow), by the method of pipeline laying, its thermal regime, by the change of the behaviour of ground waters and the overgraze soil waters. Maximum action on the slope and as the sequence maximum deformations of pipeline take place during underground laying of pipeline. When the route direction and the movement of the flow are coincided then the barring of the pipe may take place. When the pipeline cuts (intersects) the solifluction flow at an angle then the displacement forces of the sliding slope will act upon.

During industrial and residential construction on the solifluction slopes as well as in the immediate vicinity from them trench excavations, cutting of slopes, which take place together with the change of temperature and water content regime in the upper or lower part of them, induce the large landslidings. The most intensive deformations occur at the beginning of construction. The increase of depth of thawing under the structure and the leakage of technogeneous waters may cause not only the disturbance of the local stability but the sliding of the whole slope also.

The moving soil presses considerably on the columns and separate foundations, and pressure can incline them in the direction of slope falling down, if the depth of their embedment in the frozen soil will be nonsufficient or if they have no time to freeze into the soil after their installation.

While construction on the solifluctioned slopes displacements and deformations of small buildings and even small towns on the shallow foundations can be observed.

To prevent the landsliding it is necessary to account the time of construction - the second half of summer and the beginning of autumn, when the maximum thawing takes place. Moreover, it is necessary to choose and design well-grounded the type of foundations, sizes and the depth of embedment. The basic requirement for foundation - not to prevent the natural filtration of water on the slopes in order to exclude the possible formation of icing at the upper part of the slope. Pile foundations, piles-envelopes foundations and columns foundations are the most effective ones for construction on the solifluction slopes.

Two basic types of foundations are recommended for construction on the solifluctioned slopes: 1 - the foundations streamlined by landslide, 2 - the foundations stabilizing landslide. The streamlined foundations are used during the overground communications laying, pipelines, rope roads, electric power lines construction etc., when another methods of road construction round the solifluctioned slope or complete stabilization of the slope are economically nonexpeditious. The design of the foundations streamlined by the thawing soil is carried out on the action of the actual landsliding pressure. The foundation exhibits resistance to plastic deformation.

The construction of stabilizing foundations is one of the radical methods of landslides control. The well-known method of calculation of pore pressure on the stabilizing piles in the nonfrozen soils using the arch effect (Ito 1975) is the cinematically impossible for using at the plastic and viscous pressing through more weak thawing soils. The calculation method by Dr. A.S. Stroganov, developed in Research Institute of Bases and Underground Structures (NIIOSP), is more applicable for the solifluction slopes. This



method is based on the classic theory of plasticity, where the condition of the nonstabilized (nonconsolidated) state of the holding landsliding mass is taken.

#### CONCLUSION

1. While thawing the upper «overlapping» layer and the lower «nearcontacted» layer of soil are created on the boundary with frozen soil. The calculation of the stability of the solifluction soil should be done with account of friction and cohesion with the shearing at the moment of thawing.

2. Water-ice contents on the contact of thawing soil with frozen one is the main factor governing the stability of the solifluction slopes.

3. To predict the slopes stability and structures on them it is recommended to carry out the following:

- to provide engineering surveying for the solifluction investigations;
- to predict stable angle of slope from water content and consistency;
- to calculate slope stability for the system: surroundings-structure slope, taking into account friction and cohesion of thawing soil;
- to develop the complex of antilandsliding measures;

- to select the type of foundation and to calculate the landsliding pressure.

#### REFERENCES

- Bondarenko, G.I. (1983) Prediction of deformations of excavation slopes in permafrost viscous soils. Proc. VNIIOSP, 3-8.
- Bondarenko, G.I. and A.V. Sadovsky (1991) Water content effect of the thawing clay soils on shear strength. Ground Freezing-91, YU 8, Wang(eds), Balkema, Rotterdam, 123-127.
- Ito, T. and T. Matsui (1976) Methods to estimate lateral force acting on stabilizing piles. Soils and Found. 15(4), 43-59.
- Kaplina, T.N. (1965) Cryogeneous slope processes. Publ. House Science, Moscow, p 295.
- McRoberts, E.C. and N.R. Morgenstern (1975) The stability of thawing slopes. Can. Geotech. J., 11(4), 447-469.
- Nixon, J.F. and N.R. Morgenstern (1973) Practical extensions to a theory of consolidation for thawing soil. J. Permafrost. 2-nd Int. Conf. on Permafrost. Yakutsk, Washington, D.C.
- Rjabchun, V.K (1976) Mechanics of viscous solifluction. Proc. of the Institute DVNTS USSR, Issue 74, 81-86.
- Zhigarev, L.A. (1967) Reasons and mechanism of solifluction development. Publ. House Science, Moscow, 117.

## CREATION OF WATER-IMPERVIOUS FROZEN SCREENS IN EARTH DAMS IN CENTRAL YAKUTIA

Rudolf V. Chang and Olga I. Alexeeva

Permafrost Institute, Russia Academy of Sciences Yakutsk 677018, Russia

The results of two field experiments made on the soil dams in Central Yakutia are given in the present paper. The optimum design parameters of fluid-flow thermosiphons have been ascertained for creating reliable antiseepage screens. The efficiency of foam plastic use in combination with thermosiphons is shown.

In the extreme North of Russia small water engineering systems are built with a view to water-supplying the settlements and separate enterprises, to seating reservoir-coolers at the thermal stations and irrigating the land. The low-pressure head dams which are included in the above-said water-engineering systems frequently operate unsatisfactorily and destroy.

The experience has shown that their static and seepage stability should be ensured by means of creating a frozen screen in the body and bed of the dam. The frozen state of the dam might be reached either by natural or artificial freezing of dams stretches for years. One of the most developed and widely used means of the rapid creation of frozen screens is the thermosiphons.

At present the different modifications of thermosiphons are known. They consist of the following parts: the overground part is a heat exchanger dispersing heat into the atmosphere and the soil. As a heatcarrier one can use cold atmospheric air, liquid and steam. As far as the efficiency of soil cooling is concerned they are practically identical. The Yakut builders, for instance, frequently employ kerosene as a heatcarrier. The latter is regarded as the most suitable according to its characteristics such as solubility and corrosin activity with respect to metals. The main feature of fluid-flow thermosiphons compared with other means of soil freezing is the minimum expence on the maintenance and high reliability at long periods of soil freezing.

In Russia there is a great deal of experience of the use of fluid-flow thermosiphons in industrial, civil and hydrotechnical construction. Yakutia is the first region where the above-mentioned installations have undergone industrial testing and been introduced into practice.

Thermosiphons are widely used in the construction of industrial and municipal buildings in the cities of Mirnyi and Yakutsk. An innovative method has been developed: a thermosiphon is placed into a concrete pile (Makarov 1985).

In hydraulic engineering thermosiphons with a liquid coolant were first used in 1973 at the Sitykan water-retaining structure (North-western Yakutia) which was built for water supply in diamond mining operations (Makarov 1985). Later they were used in the water-retaining structure built in the Irelyakh River (Western Yakutia), in

the dams on the Poiiskovy Creek (North-eastern Yakutia) and the Shestakovka River (Central Yakutia).

The Permafrost Institute of Russian Academy of Sciences took immediate part in the development of different structures of thermosiphons and methods of their design, and conducting field tests as well.

Below there are the main results of two tests of such a kind made on the dam of the Maganky River and cut-off dam in the suburbs of the town of Yakutsk. The aim of the investigation was to specify the parameters of the cooling system (arrangement spacing, height of overground exchanger) and the effect assessment of their behaviour in combination with plastic foam heat insulation.

The natural climatic and geocryological conditions of the region in question are characterized by the following data: the average long period air temperature totals 10.3°C below zero; the average monthly temperature of January -45°C below zero, of July +19°C; absolute minimum -64°C, absolute maximum +38°C. The average wind velocity in winter makes 1.8 mps. The amount of precipitation is equal to 247 mm. The long period frozen soils have the thickness to 450 m, temperature ranging from -2.7 to -3°C. There are talics under the lake and river bed.

The dam on the Maganka river was built in 1980 - 82 and it is the reconstruction of the water power station built in 1973 which was twice destroyed (in 1975 and in 1980). It creates the reservoir of long period control with volume of 600 000 cu. m. In summer the water is used for irrigation of 190 ha potatoes and 40 ha of cabbages, in winter-for the watersupply of the airport and the settlement of Magan. The maximum dam height in the bed river section is equal to 11 m, the length along the crest 142 m, the width on the crest 10 m, the base of the upper slope 1:7, the lower base 1:4. The dam body is filled with local dry supes and sandy soils. There is a metal-pipe spillway 1.0 in diameter, 60 m in length with the bucket reinforced concrete stanchion cap.

The soils of the dam bed are characterized by heterogeneous composition. The left side of the valley of the Maganka river is composed of different sands with moisture 0.21 and volume mass 1910 kg/m<sup>3</sup> which thaw to the depth of 5 m. There

are open water-saturated sands in the river bed. The right side of the river valley is composed of suglinoks covered with sands from 1 to 2 m thick. The average moisture is 0.45; the volume mass 1560 kg/m<sup>3</sup>. The seasonally thawed depth varies from 1 to 2 m.

In order to create the frozen antiseepage nucleus in the body and bed of the dam, in December 1982 - January 1983, 30 thermosiphons were set along the upper edge of the dam crest at spacing 2.5 m, from 3.5 to 13 m long. The thermosiphons consist of two pipes coaxially located. The diameter of the exterior pipe of soil heat exchanger is 152 mm, interior 63 mm. The exterior heat exchanger is represented by the ribbed pipe 219 mm in diameter, 2 m in high.

The cut-off dam on the territory of Permafrost Institute was filled in 1965 when making an artificial lake. The lake is an alas depression filled with subpermafrost water. Its capacity is 2500 m<sup>3</sup>, the maximum depth of water is 3.6 m. The original dam dimensions are as follows: the length along the crest 180 m, width 4.5 - 5.0 m, height 3.0 m, the slope base 1:2. The pressure head makes 0.5 m.

The two metre layer of dark grey humus supes with moisture about 0.3. The thickness of grey fine-grain sands with vegetative detritus interlayers with moisture over 0.4. The lateporous sands emerge at the depth of 22 m with moisture 0.2. In order to prevent seepage 37 thermosiphons with spacing 3 m were installed in the body and bed of the dam in September 1982. The external heat exchanger is made of steel pipe 219 in diameter, its height 1.3 m. The soil heat exchanger consisting of two coaxial pipes 159 and 85 mm in diameter are from 7 to 12 m long. In 1984 the plastic foam PCV-1, 6 cm thick was placed on the crest and lower slope of 18 m dam section.

Both hydropower stations were equipped with controlling and measuring devices which enabled one to observe the change of temperature regime. The regular observations on the Magadan dam have been made for 6 years, on the dike for 4 years (1982 - 86).

Figure 1 presents the changes of temperature field of the dam.

The observations showed that the thermosiphons filled with kerosene worked two months in 1983. As a result of it, the soil temperature lowered to 0.2 - 0.4°C at the depth of 7 - 10 m. At the end of January 1984 the reliable close up of the ground ice cylinders along the whole length of the dam was fixed. In the range of the above-said depth in April 1985 - 5 - 6°C. The temperature tend to decrease from year to year. The check boring indicated that the ice ground nucleus to the depth of 11 m is composed of massive texture soils to the depth of 15 m - netted with ice inclusions 1 - 2 mm thick.

The comparative analysis of cryogenic structures points to the conditions of soil freezing: the soils to the depth of 11 m were located in the zone of intensive lateral influence of thermosiphons, below-under the influence of the butts. The dam boring in October 1985 to the depth of 22 m convinced us that the soil ground ice wall formed in the body and bed of the dam.

The observations on the dike of Permafrost Institute showed that the solid frozen screen with the isotherm -1°C was made on the dam bed for two winter seasons; the frozen screen blocked the talic and joined the permafrost soils. The frozen screen thickness in the block sections is 3 - 4 m, the soil temperature in September -1.0 +1.2°C. These parameters of the frozen screen prove its reliability. When using thermosiphons on the dams with low height the problem arises how to preserve the frozen massif in summer. For instance, the depth of seasonal thaw of dam soils makes 2.5 - 3.0 m which is commensurable with its height. It appeared impossible to set up the frozen screen in the dike body only by means of thermosiphons.

Nowadays, highly-efficient heat-insulating materials are being produced-plastic foams on the synthetic resin base. The heat conductivity factor of the above-said materials is 0.02 - 0.04 BTU (m° K). In some countries special types of plastic foams have been developed and widely used for soil thermo-insulation in different climatic zones. In this country the well-known plastic foams of the type PSB and PS, rarely PCV. The ap-

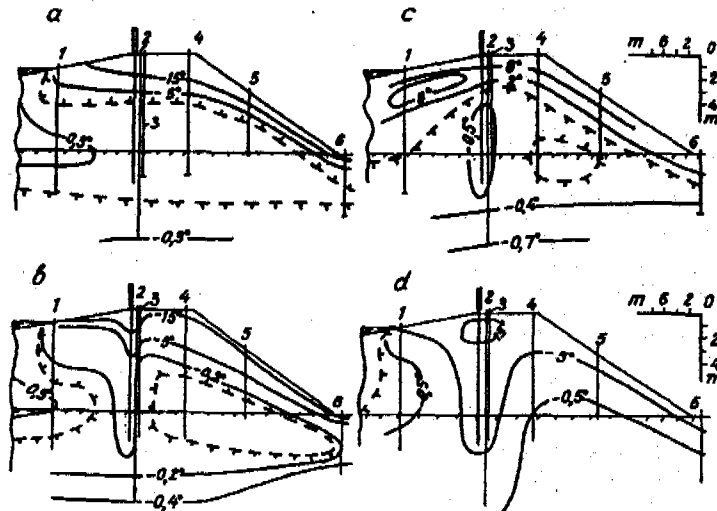


Figure 1. The changes of temperature field in the body and bed of the dam on the Maganka river. a - 02.83; b - 04.83; c - 09.84; d - 03.88 1 - 6 are numbers of thermometric boreholes.

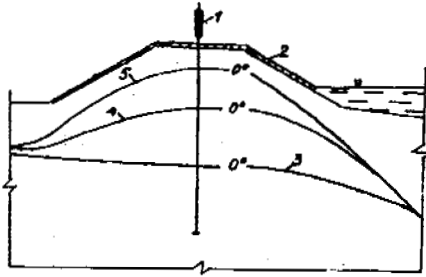


Figure 2. The changes of zero isotherm of the soil dam in the suburbs of Yakutsk. 1 - thermosiphon; 2 - plastic foam cover; 3 - zero isotherm in September 1982 till the installation of the thermosiphons; 4 - zero isotherm in 1984 before placing the plastic foam; 5 - zero isotherm in September 1986.

plication of plastic foams has shown their efficiency in controlling the depth of seasonal thaw of soils.

The observations made on the earth dike dam indicated that after the summer placing of plastic foam on the crest and slopes of the dam the zero isotherms joined approximately a month later than on the sections without plastic foam cover. In

spring one could observe the thaw delay under the plastic foam. The mean annual temperature of the dam surface under the plastic foam have not changed practically and was equal to  $-1.48^{\circ}\text{C}$ . Two years later after placing the plastic foam the average annual temperature lowered to  $-1.1^{\circ}\text{C}$  in the sections without plastic foam cover. The soil temperature has lowered at the depth of 3 m under the plastic foam approximately  $1^{\circ}\text{C}$  (Figure 2) for four years. The changes of soil temperature regime at the depth of 1 m are more evident; the amplitude of annual temperature fluctuations in 1984 - 1985 lowered approximately  $10^{\circ}\text{C}$  compared with 1983 - 84 and in 1986 the temperature curve entirely moved to the range of subzero temperatures. The depth of seasonal thaw of soils under the plastic foam cover decreased three-fold and made 0.5 - 1.0 m. The investigations showed that for the conditions of Central Yakutia the thermosiphons may be set at spacing 2.5 - 3.0 m. The complex application of thermosiphons and efficient heat insulation enables one to make the reliable frozen screen in the body of soil dam and improve its configuration owing to the depth checking of seasonal thaw of soils.

#### REFERENCES

- Makarov, V. (1985) Thermosiphons in construction in the North. 169 p. Nauka, Novosibirsk.

## EVOLUTION OF PERMAFROST ZONE OF NORTH EURASIA IN LATE CENOZOIC AND NEOTECTONIC MOVEMENTS

Igor D. Danilov<sup>1</sup> and Vladislav E. Roujansky<sup>2</sup>

<sup>1</sup>Department of Geocryology, Faculty of Geology, Moscow State University,  
Moscow, 119899 Russia

<sup>2</sup>Ecological Station for Environment Control, World Laboratory Branch 61/1-126 Leninsky Prospect,  
Moscow, 117333 Russia

Role of three types of neotectonic movements in evolution of the permafrost zone in North Eurasia in Late Cenozoic is shown. First, large scale undulatory movements were responsible for the general change of tectonic structure of the Arctic region between Paleogene and Neogene periods and are related to the appearance of the permafrost zone. Second, warping movements resulted in rhythmical structure of sediments and formation of the terrace topography. The transgressions and regressions of the Arctic ocean caused the paleoclimatic changes. Third, small scale local neotectonic movements are landforms patterns.

### INTRODUCTION

One can distinguish three types of tectonic movements which occurred during the new geological stage (Neogene-Pleistocene), namely: large scale undulatory movements, intermediate scale warping movements, and small scale movements related to the formation of local neotectonic structures (Afanasyev et al. 1988). First, undulatory movements create regions of sediment removal and depressions of accumulation. They also determine the thickness of the depositional apron on the platforms and within tectonic basins. Second, warping movements are responsible for the complexity and change of facies, cyclic recurrence, and the stage character of accumulative processes. These movements involve entire continents, or parts of them, which are tectonically uniform. And finally, local tectonic movements, which mainly due to processes of lithogenesis and katagenesis, create local negative and positive structures.

The appearance and development of the present permafrost zone are closely related to the above mentioned neotectonic movements. The general trend of the Earth's climatic cooling in the Late Cenozoic resulted from Alpine orogenic stage and the formation of large mountainous regions of Eurasia and America.

### EVOLUTION OF PERMAFROST ZONE AND WARPING TECTONIC MOVEMENTS

The history of North Eurasia's and the Arctic Ocean's development in the new geologic stage is determined by the warping movements (Afanasyev et al. 1988; Baulin 1985; Danilov 1987). These movements are responsible for changes in the transgressive and regressive development of the Arctic Ocean within the shelf and paleoshelf. They control development of peneplanation surfaces and alluvial and marine terraces.

N.I. Nikolaev (1949) divided the neotectonic

stage into three phases. The first neotectonic (first continental phase) is characterized by the general upward movement. The second phase (marine phase) is characterized by general downward movement. And the third phase (second continental phase) referred to the time of new general upward movement. These three main neotectonic phases occurred in North Eurasia (Figure 1) and caused changes in the paleogeographic environments and the evolution of the permafrost zone in the Late

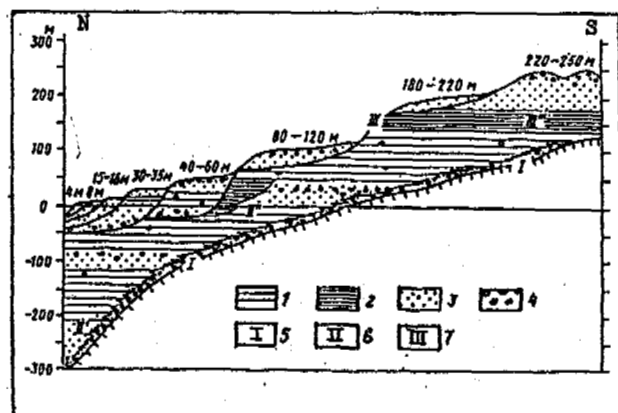


Figure 1. Geologic and geomorphic structure of the northern part of West Siberia with the exposed neotectonic phases: 1-4 - main lithological varieties and facies of basin deposits (1 - relatively deep-water clays and loams; 2 - freshwater and salt-water varved clay and silt; 3 - coastal sands; 4 - littoral gravel sands, shingle beds), I-III - neotectonic phases: I-Miocene - formation of ancient erosional topography, which is buried now; II-Pliocene-Eopleistocene - formation of the main masses of new deposits; III-Quaternary - development of the present topography.

Cenozoic.

The first neotectonic phase, or first continen-

tal phase, which corresponds to the Miocene period, was a time of broad regression of the Polar basin, when almost the entire area of the Arctic shelf had dried. The factors of the over-dependent valleys of the pre-Pliocene and early Pliocene periods are currently buried. They are located at depths from 150 to 250 m in the Pechorskaya lowland, whereas in northern western Siberian lowlands they are located at depths from 300 to 400 m, and within the coastal lowlands of North-East Eurasia they are located at depths from 80 to 100 m below the present sea level. Both seasonal ice on the Arctic Ocean and seasonal ground freezing within the coastal area appeared in the Miocene period (Danilov 1987). Neogenesis of permafrost, i. e. the first formation of the permafrost zone on the dry land, occurred in mountainous regions.

The second neotectonic phase, or marine phase, which corresponds to the Pliocene period, is characterized by sea transgression onto the Arctic shelf and then southward into the adjacent coastal plains of western Eurasia. Thick lagoonal, marine and near shore deposits have accumulated within this region. At the same time, alluvial, deltaic and lagoonal deposits have accumulated within the plains of North Eastern Eurasia. These deposits filled ancient valleys, which now remain buried, and have spatial distribution on watersheds. The stable ice cover on the Arctic Ocean was formed at this time. During the formation of this ice cover, coarse-grained sediments were transported and deposited at the bottom (Clark 1982). Also, permafrost with ground ice appears within lowlands and coastal areas of North Eastern Eurasia (Danilov 1987).

In the third phase, second continental phase, the history of the Arctic and the Subarctic is interpreted in different ways according to the concept of transgressions-glaciations relations. Various geologi-geomorphic data indicate that in the Pleistocene and Holocene periods the leading factors of the Arctic shelf development and that of the adjacent lowlands were the transgressions and regressions of the Arctic Ocean, caused by the warping movements (Danilov 1978; Danilov 1987). In the course of these transgressions, when the amount of warm water flowing into the Arctic Ocean increased, the climate of the surrounding dry land became more humid and moderate. In contrast, during the regressions, when the Arctic Ocean became more isolated, the climate became colder and more continental. These were periods of intensive freezing of solids and the development of extensive permafrost on dried shelf and coastal plains.

Regions of glacier development in the Arctic were limited to mountains. Glaciers extended only to the foothills. At the same time, the cold water sea covered the plains, which have currently an absolute height of up to +250 m, in the maximum stage of the transgression. Vast terrace-like geomorphic levels and terraces were formed in the Late-Pleistocene period.

Thus, permafrost exists within the Arctic and Subarctic plains from the Pliocene period until now. Herewith, periods of predominant continental cryolithomorphogenesis (stages of the regressive development of the Polar basin) and periods of predominant submarine cryolithomorphogenesis (stages of transgressive development of the Polar basin) are distinguished within the plains and shelf of northern Eurasia.

The repeated sequence of transgressive and regressive stages in the Pliocene and Pleistocene periods caused the development of the complex structure of cryogenically transformed sediments. These sediments compose accumulative plains of northern Eurasia. The relationship between the accumulative marine geomorphologic levels of the northern part of the West Siberia and the Pechorskaya lowland and thickness of permafrost, which increases with the age and absolute height of the geomorphologic levels (Trofimov et al. 1980), is due to above mentioned circumstance.

Extremely rigorous climatic conditions in northern Eurasia at the end of the Late-Pleistocene period were related to the stage of the vast pre-Holocene regression. According to the existing estimations (Afanasyev 1988; Danilov 1987) mean annual air temperature, ground temperature and thickness of permafrost have increased about two times. The whole territory of the Former Soviet Union was the part of this ancient permafrost zone. Regions of surficial glaciation in northern Eurasia had comparatively small dimensions and were limited to Fennoscandia, northern and southern parts of the Urals, north-eastern part of the FSU, plateau Putorana and the Arctic islands.

#### PARAGENESIS OF CRYOGENIC GEOMORPHIC PROCESSES WITHIN LOCAL NEOTECTONIC STRUCTURES

There are various types of local neotectonic structures of different sizes within the plains of the permafrost zone, which are composed of thick masses of sediments, e. g. the Pechorskaya lowland, the northern part of West Siberia, the Taymyr lowland etc. Tectonic arches and domes, as well as complex tectonic structures, have been revealed there through the interpretation of remotely sensed data. It was established that the anticlinal domes, which are well-defined in present topography, often inherit ancient positive tectonic structures of the Mesozoic age.

Detailed investigations of the local neotectonic structures in the northern part of the West Siberia have been conducted by many scientists (Sergienko et al. 1983; and others). Our investigations based on interpretation of remotely sensed data allowed to compile the map of neotectonic structures within the Tazovskiy Peninsula, West Siberia (Figure 2). According to the manifestation of neotectonic movements in the present topography, the entire area of the Tazovskiy Peninsula has been subdivided into two main units; areas, which tends to uplift and areas, which tend to subside. In turn, these areas are subdivided into sites with different intensity of neotectonic movements. The main part of the Tazovskiy Peninsula is characterized by a mosaic pattern of sites with different directions and intensity of neotectonic movements.

The comparison of this map with structural and tectonic maps of the region of various formations and levels of platform mantle has shown that in spite of the predominantly inherited character of neotectonic movements in some cases there is the inversion of the trend of the neotectonic movements. Taking into account this circumstance, the map shows local positive and negative inherited neotectonic structures, as well as inversion neotectonic structures of different order.

The local neotectonic structures are responsible for the regional patterns of the per-

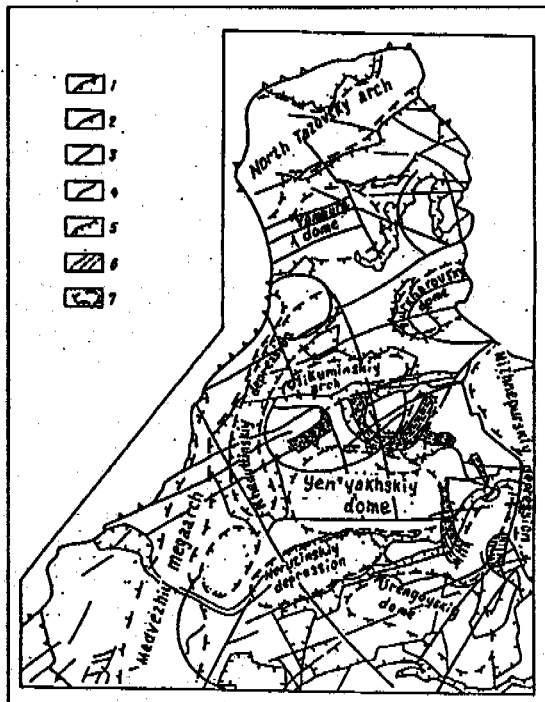


Figure 2. Map of the neotectonic structures within the Tazovskiy Peninsula (northern part of West Siberia): 1 - zones of lineaments, which confine the graben-like river valleys; 2,3 - large lineaments (2-located by the topographic escarpments, 3 - revealed by landscape indicators); 4 - other lineaments; 5 - boundaries of the areas with different trends of neotectonic movements; 6 - sites of the neotectonic structures.

mafrost, thickness of permafrost, as well as spatial distribution and combinations of cryogenic geomorphic processes and landforms. Three types of paragenetic sets of cryogenic geomorphic processes and landforms have been revealed within the Tazovskiy Peninsula depending on inherited character of neotectonic movements in the Pleistocene and Holocene periods.

The first type of the paragenetic sets of cryogenic processes and landforms occurs within the local positive inherited neotectonic structures. It is subdivided into two classes depending on the structure of the lithologic basis of the cryogenic processes and landforms development. First, the accumulative landforms composed of thick masses of the Quaternary sediments. Second, the accumulative-denudational landforms composed of the thin cover of the Quaternary sediments which lied on the consolidated Paleogene clays. First class is characterized by the widespread occurrence of thermoerosional features, solifluction lobes and other slope landforms, epigenetic ice wedges. The areas of positive neotectonic structures in the northern part of the Tazovskiy Peninsula, where permafrost remains unthawed since the Late Pleistocene period, are characterized by the lack of thermokarst lakes and depressions on mineral soils. The positive inherited neotectonic structures within the southern part of the Tazovskiy Peninsula, where permafrost thawed in the Holocene period, are characterized by the occurrence of

thermokarst lakes and other landforms, which are related to thawing of perennially frozen soils. Nevertheless, thermoerosional and slope topography dominates in the northern part of the Tazovskiy Peninsula. Second class occurs within sites, where thin cover of the Quaternary deposits is underlain by Paleogene clays. This class comprises so-called linear ridge topography along with small and deep thermokarst lakes between the ridges, ice wedges, and thermoerosional gullies.

The second type of the paragenetic sets of cryogenic geomorphic processes and landforms occurs within the local negative inherited neotectonic structures, which are characterized by the increased thickness and the high ice content of the Quaternary deposits, predominantly sandy-loamy and loamy. The set includes various thermokarst lakes, pingos, ice wedges, and polygonal peatlands. The high ice content in the deposits and slight dissection of the surface favour wide development of thermokarst lakes and peatlands. As a whole, the inherited negative structures are characterized by highly dynamic contemporary geocryological conditions. Here, the thermokarst process takes place along with the active permafrost neogenesis within the floodplains, thermokarst depressions and swamps.

Finally, the third type of the paragenetic sets of cryogenic processes and landforms occurs within the local neotectonic structures, which changed the direction of their movement in the Late Pleistocene or Holocene periods. The set develops on epigenetic and syngenetic perennially frozen ground, which is characterized by different lithological composition and ice content. The set is intermediate between the two sets described above and includes cryogenic landforms, which are typical for both the positive and negative inherited neotectonic structures. The third type is subdivided into two classes. The first class occurs within the accumulative landforms, which are composed of the Quaternary deposits, and are characterized by the complex combination of the cryogenic processes and landforms. The second class develops within the sites with occurrence of the Paleogene clayey deposits. The second class includes the linear ridge topography, which is well-defined morphologically, various thermokarst lakes, large frost mounds, polygonal peatlands and ice wedges.

#### PROBLEM OF THE ORIGIN OF THE LINEAR RIDGE TOPOGRAPHY

The linear ridge topography widely occurs in the northern part of the West Siberia (Tazovskiy, Gydan and Yamal Peninsulas) within the local sites, where the Paleogene diatomaceous clayey deposits occur near the surface (less than 10 m below the surface) and are overlaid by the Pleistocene sediments. These landforms are the most spectacular in the Tazovskiy Peninsula (Figure 2), where they form curved belts, which represent the system of parallel discontinuous ridges and elongated thermokarst depressions. As to the origin of the linear ridge topography, there is a hypothesis (Arkhipov, Astakhov, Grosvald et al.) according to which the belts of the ridges are considered as the marginal formations, i. e. the frontal moraines of the hypothetical ice sheet of the Late Pleistocene age, which advanced to the dry land from the Kara sea shelf and covered the Tazovskiy Peninsula 16-18 thousand years ago. The

interpretation of various remotely sensed data (satellite and aerial photography), which we carried out, has shown that the distribution and spatial orientation of the belts of the linear ridge topography, are more complex than it was shown by adherents of the glacial hypothesis. The belts are not continuous, and their convex segments do not point out only to south-west, south and south-east direction, i. e. towards the supposed direction of the hypothetical ice sheet movement. The belts of the ridges possess various, predominantly, submeridional orientation. They have a discontinuous pattern and are exclusively located within the limited sites, where the Paleogene clayey deposits occur close (less than 10 m) to the surface and are overlaid by the Pleistocene sediments. This fact is in contradiction with the statement on the continuous character of the linear ridge topography, which indicates the former position of the margin of the ice sheet. Such regularity in the accumulative processes, which were associated with the ice sheet are rather doubtful. Moreover, it was revealed that each particular ridge is a chain of the large frost mounds (Belopukhova et al. 1980). Thus, the linear ridge topography within the Tazovskiy Peninsula is, most probably, of cryogenic and tectonic origin.

**CONCLUSIONS**

Thus, the evolution of the permafrost zone in North Eurasia has been influenced by three types of neotectonic movements: large scale undulatory movements, intermediate scale warping movements and small scale movements related to the formation of local neotectonic structures.

First, undulatory movements are responsible for the general change of the tectonic structure of the Arctic and Subarctic between the Paleogene and Neogene periods. The essential climatic cooling as well as the appearance of the permafrost zone within the dry land in North Eurasia were associated with that change of the entire tectonic structure.

Second, warping movements occurred within the frame of the large scale undulatory movements. The warping movements are responsible for the rhythmical structure of sediments as well as to the formation of the step-like and terrace topography of the coastal plains. The transgressive and regressive stages of the Arctic Ocean were the main cause of the paleoclimatic changes in the region. The climate of North Eurasia became milder and more humid in the course of transgressive

stages, and, on the contrary, it became more rigorous and continental during regressive stages of the Arctic Ocean. The latter were accompanied by broadening of the permafrost zone, decrease in temperature and increase in the thickness of the permafrost.

Third, small scale movements, which are related to the formation of local neotectonic structures, are responsible for the regional specific occurrence of the cryogenic lithomorphogenesis, in particular for spatial differences of the cryogenic geomorphic processes and landforms patterns.

**ACKNOWLEDGMENTS**

The authors express their appreciation and obligedness to Dr. Jerry Brown, Arctic Connections, and Dr. Nikolay Grave, Russian National Permafrost Committee, for their helpful advice, and wish to acknowledge the aid of Kenneth Petersen, Brigham Young University, for his editing of the manuscript.

**REFERENCES**

Afanasyev, B.L., I.D. Danilov and V.A. Dedeev (1982) Methodology of neotectonics. Syktyvkar.  
 Baulin V.V. (1985) Perennially frozen ground within oil and gas fields of the USSR. Moscow.  
 Belopukhova E.B. and A.G. Sukhov (1980) Problem of formation and the history of development of the linear ridge topography within the Tazovskiy Peninsula. Geography and natural resources. 8. 95-101 pp. Novosibirsk.  
 Danilov I.D. (1978) Pleistocene of marine subarctic lowlands. 198 pp., Moscow.  
 Danilov I.D. (1987) The history of development of North Eurasian permafrost zone in the Late Cenozoic. Geocryological Investigations. 45-62 pp. Moscow.  
 Nikolaev N.I. (1949) Neotectonics of the USSR. Moscow/Leningrad.  
 Sergienko V.M. and R.A. Bidgiew (1983) The late Quaternary tectonics of the West Siberian Lowland, northern part. Bulletin MOIP, Section Geology, vol. 58, iss. 6, Moscow.  
 Trofimov V.T., Yu.S. Sadu and G.I. Dubikov (1980) Cryogenic structure and ice content of perennially frozen ground within the West Siberian Plate. Moscow.  
 Clark D.J. (1982) Origin, nature and world climate effect of Arctic Ocean ice cover. Nature, vol. 300, 321-325 pp.



## STRESS-STRAIN STATE OF FROZEN ROCKS AT THEIR THAWING AROUND EXCAVATIONS

Mikhail M. Dubina<sup>1</sup> and Yurii A. Chernyakov<sup>2</sup>

<sup>1</sup>Permafrost Institute, Russian Academy of Sciences Yakutsk, 677018, Russia

<sup>2</sup>Dnepropetrovsk University Dnepropetrovsk, 320036, Ukraine

A stress-strain state dynamics of frozen rocks during their thawing around excavations have been studied. Unlike to the known works, the mechanical behaviour of rocks is described on the basis of plasticity theory methods accounting for microdeformations, microdestruction and dependence of thermomechanical properties of rocks on phase transitions of porous water in the range of its freezing temperature. This approach makes it possible to consider the natural physical peculiarities of rock behaviour and to reveal their effect on service parameters of excavations.

### INTRODUCTION

Among the mostly widespread underground constructions in permafrost are excavations of different applications including mining excavations, cavities, shafts and wellbores. In most cases, the use of such excavations is connected with the fact that the internal temperatures exceed the ice melting point. Under those conditions the frozen rocks surrounding an excavation tend to increase their temperature which leads to formation of a thawed rock zone around the excavation. The values of frozen rock strength properties decrease with temperature and ice content in pores (Dubina and Chernyakov 1990). Thermophysical characteristics show a similar dependence on ice content and temperature. Such a softening of frozen rocks caused by temperature increase results in a higher rock pressure leading to the growth of deformations in unsupported excavations and higher loads to supported ones. Analysis of those deformations and loads is a necessary part of underground construction design. The analysis reliability is determined by a proper choice of physical-mechanical properties in rock behaviour, of their thermomechanical characteristics and by the adequacy of calculation schemes to a real prediction object.

### THERMOMECHANICAL MODELING

In (Dubina and Chernyakov 1990, 1991) we have suggested a model of frozen rock thermomechanical behaviour that was based on the concepts of micromechanics of microinhomogeneous media deformation (Novojilov 1989) which is a characteristic feature of frozen rock according to (Savelyev 1989, Zaretsky 1986). This model equations presented in (Dubina and Chernyakov 1990, 1991) describe the following peculiarities of physical-mechanical structure and behaviour of soils and rocks. First, the properties of plastic deformation under loading associated with a dilatation of shear nature and with an elastic-plastic microcracks opening due to increase of the first invariant of tensor. Second, difference in ten-

sion and compression strengths of rocks, and the Bauschinger effect. Third, macrofracture development based on the macrodeformation theory and, correspondingly, description of rock behaviour at the descending section of loading plot curve. Fourth, damage cumulation and their effect on deformation nature at cyclic loading. Fifth, dependence of thermophysical and mechanical rock properties on the phase composition of porous water in its freezing temperature range as well as a dependence of rock unit volume deformations on temperature and ice content.

The suggested model is based on a concept of a continuous change of soil thermophysical and physical-mechanical properties with its temperature fluctuations from values for a solid frozen state to those for a completely thawed state in conformity with specific ice content. The ice content is described by an ice concentration parameter  $W$  (Tsytoovich 1973) whose temperature dependence can be expressed through the following formula

$$W = \frac{M_i}{M_w + M_i} = \begin{cases} 1 - \frac{1}{1 - A_w T}, & T \leq T_f, \\ 0, & T > T_f \end{cases} \quad (1)$$

where  $M_i$ ,  $M_w$  are mass portions of ice and unfrozen water in a soil element, respectively;  $A_w$  is a parameter characterizing the ice concentration curve pattern and depending on soil type; and  $T_f$  is a temperature at a given soil type starts to freeze up.

The transition of thermomechanical properties values from the solid frozen state to a thawed one can be expressed by any continuous curve depending on soil type. In the general case, this curve can be approximated using a fractional polynomial function. An analysis of empirical data shows an approximation with polynomials up to the third degree to be quite sufficient for obtaining a satisfactory accuracy.

The physical-mechanical parameters of our thermomechanical model were introduced in (Dubina and Chernyakov 1990, 1991) in the form of 6 universal material functions  $B$  describing the diversity of deformation process. Besides, a  $W$  parameter de-

pendence, the universal material functions depend also upon the following two ones:  $\alpha$  - parameter determining the hypercone angle of final loading in the deviator space and characterizing the instantaneous plastic material properties;  $\theta$  - parameter characterizing the material loosening degree as  $\theta = a \cdot \text{tr} \langle \dot{\epsilon}_1 \rangle + b \cdot \text{tr} \langle \dot{\epsilon}_2 \rangle$ , where  $a$  and  $b$  are constants,  $\text{tr}$  is a tensor trace and  $\langle \rangle$  is the averaging sign.

The following form of 6 universal material functions was used in this model

$$\begin{aligned} B_i &= (B_{iT} + (B_{if} - B_{iT})W) \alpha^n; \quad i = 1, 2 \\ B_i &= (1 + B_i\theta)(B_{iT} + (B_{if} - B_{iT})W); \quad i = 3, 4, 5 \\ B_6 &= 1 \end{aligned} \quad (2)$$

where  $B_{iT}$  and  $B_{if}$  - are material constants in thawed and frozen states, respectively; and  $n$  is the approximation constant.

A similar dependence of other mechanical and thermophysical characteristics on ice content was introduced, according to (Dubina et al. 1983, 1990), in the form

$$\begin{aligned} E &= E_T + (E_f - E_T) W, \\ \nu &= \nu_T + (\nu_f - \nu_T) W, \\ \sigma_j^T &= \sigma_{jT}^T + (\sigma_{jf}^T - \sigma_{jT}^T) W, \\ \sigma^B &= \sigma_T^B + (\sigma_f^B - \sigma_T^B) W, \\ C &= C_T + (C_f - C_T) W, \\ \lambda &= \lambda_T + (\lambda_f - \lambda_T) W \end{aligned} \quad (3)$$

where  $E$ ,  $\nu$ ,  $\sigma_j^T$ ,  $\sigma^B$  are elasticity modulus, Poisson's ratio, yield stress and temporary strength, respectively;  $j=1$  and  $j=2$  correspond to microplastic deformation and microdamage cumulation;  $c$ ,  $\lambda$  are specific heat capacity and heat conduction coefficient, respectively; lower indices  $T$  and  $f$  correspond to thawed and solid frozen states of a medium.

The mechanical effect of soil temperature change consists not only in a change of its thermomechanical characteristics as seen from (2), (3), (Dubina and Chernyakov 1991) and (Dubina and Krasovitsky 1983), but also in a change of three-dimensional deformation. In the model considered a relative change of volume  $\epsilon$  represents a sum of three-dimensional deformations resulting from microplastic deformations  $\epsilon_1$ , microdamage cumulation  $\epsilon_2$  temperature deformation  $\epsilon$  and of porous water freezing  $\epsilon_w$  i.e.

$$\begin{aligned} \epsilon &= \epsilon_1 + \epsilon_2 + \epsilon_T + \epsilon_w \cdot \alpha, \\ \epsilon_T &= \alpha_T (T - T_0), \\ \epsilon_w &= \alpha_w \omega W, \end{aligned}$$

where  $\alpha_T$ ,  $\alpha_w$  are coefficients of three-dimensional deformation for the solid mineral skeleton and freezing porous water, respectively;  $\alpha$  is a parameter of porous water solidification taking the value  $\alpha=1$  at freezing and  $\alpha=0$  at soil thawing.

In conclusion for this section describing the model it should be noted the following. First, the theory of microdeformations and microdestruction

considered in this model represents a generalization of existing plasticity theories that can be applied using limiting transitions in the model parameters as shown in (Dubina and Chernyakov 1990). Second, identification of the model parameters for given types of rocks and soils does not require any additional mechanical tests and can be carried out by using ordinary standard tests but under combined loading (Dubina and Chernyakov 1990). Third, a further development of the microdeformation and microdestruction theory will allow not only for describing the rock plastic yielding but also their creeping behaviour which, from the viewpoint of microcracking, is now being considered for frozen soils (Zaretsky 1986).

#### CALCULATIVE PARTICULARITIES

Let us now consider the calculations done according to this model. In order to analyse the dynamics of the stress-strain state (SSS) we have to know the dynamics of media properties change with time which depends on ice content variation  $W(T)$  as a function of temperature. So, SSS is to be calculated at each time step similarly to solving the problem of temperature distribution  $T(t)$ . The temperature field is calculated through a numerical integration of a quasilinear heat conduction equation having a heat capacity value that corresponds to a problem of porous water phase changes in the freezing temperature range (Dubina and Krasovitsky 1983). Since the stresses arising in rocks do not exceed the values at which the SSS effect on temperature field should be considered, the temperature distribution is apart from SSS. Both temperature field and SSS at a general discretization of calculation region on the basis of a basic 8-nodes isoparametric element. The problem of SSS determining is solved in displacement terms by integrating the initial system of equations written in velocity terms with respect to time.

The heat conductivity equation is solved by iteration at each time step. The calculation results obtained using a special computer program are given for nodes of a three-dimensional mesh in the form of isolines of calculated variables at intersections of the calculation region and coordinate surfaces with a given interspacing. In this way it is possible to follow the evolution of  $T(t)$  and SSS for the three-dimensional case of calculation region.

Consider now the applicability of this thermomechanical model to the calculation of SSS in the case of thermal and mechanical interferences of excavations releasing heat into frozen rocks. The commonly used industrial constructions are mostly rather extended along their axis. So, the practical needs would be fairly satisfied through solving two-dimensional thermal plasticity problems for excavations of various cross-sections. The most characteristic features of SSS behaviour are especially markedly seen when calculating the canonic cross-sections such as circle or rectangle. The choice of these cross-sections is due to the availability for them of elastic-plastic problem solutions without formation of a zone of rocks softened by thawing which allows for results comparison. In a series of calculations we have considered singled and coupled closely interspaced circular- and rectangular-shaped excavations. Considered also was the effect of cross-section shape, excavations inter-

spacing, service time, dilatation and loosening on SSS.

#### CALCULATIVE RESULTS

The calculation have given the following results. The SSS development with time was mostly influenced by excavations interspacing and their length. For a muber of excavations there was an interspacing at which their mechanical interaction was ceased (at the excavation depth down to 300 m this interspacing exceeds 5 maximum cross-section sizes for rocks whose specific density is lower than  $2 \text{ t/m}^3$ ). The increase of thawing areas significantly effects the shape of rock plastic deformation region up to areas oversizing the excavation cross-section by an order of magnitude. The prese of a support and the increase of its rigidity decreases the total level of SSS and the sizes of plastic deformation region. The regions of plastic deformations for one excavation row are more developed as compared to the case of two closely interspaced rows. Consideration of rock dilatation gives a considerable decrease in sizes of the plastic deformation region. On the other hand, consideration of microdestruction effects leads to a certain increase of plastic deformation zone. Comparison between the elastic and elastic-plastic models shows that excavation contours can be increased by several orders of magnitude depending on numerical values of calculation parameters. In the case of many years' development of thawing areas the sizes of plastic deformation regions are growing during several first years but then they are diminishing and stabilize in time. Level and sizes of the region of

elevated stress concentration are decreasing with a number of excavations in a certain fixed-sized region up to pillar size of a given minimum value.

Thus, we have developed the model for predicting SSS of frozen rocks around closely interspaced underground excavations and, on this basis, for solving the problems connected with design and service of economically effective and reliable systems of underground constructions.

#### REFERENCES

- Dubina, M. and Y. Chernyakov (1990). Simulation of the thermoplastic deformation of the frozen ground by its thawing around the bore holls. Problems of frozen soil mechanics and permafrost engineering. Strojizdat, Moscow, pp. 76 - 89.
- Dubina, M. and Y. Chernyakov (1991). The simulation and calculation of the thermoplastic state of frozen ground. Novosibirsk, Nauka, 120 p.
- Dubina, M. and B. Krasovitsky (1983). Heat exchange and mechanics of the interaction of the pipelines and bore holls with the ground. Novosibirsk, Nauka, 134 p.
- Grechitchev, S. et al. (1984). The principles of the simulation of the cryogenic physical-geological processes. Moscow, Nauka, 231 p.
- Novojilov, V. (1989). Problems of the mechanics of the solid medium. Leningrad, Sudostroenie, 400 p.
- Savelyev, B. (1989). Physical and chemical mechanics of the frozen ground. Moscow, Nedra, 216 p.
- Tsytoich, N. (1975). Frozen soil mechanics. Moscow, Vyschaya Schola, 448 p.
- Zaretsky, Y. et al. (1986). Viscosity and plasticity of the ice and frozen ground. Novosibirsk, Nauka, 185 p.

## THE TEMPERATURE EFFECT ON THE RE-DISTRIBUTION OF MICROELEMENTS IN THE SOIL MASSIF

Valentina I. Fedoseeva and O. A. Streltsova

Permafrost Institute, Russian Academy of Sciences Yakutsk, 677018, Russia

The tendency of gold redistribution has been estimated having the temperature gradient on the basis of the data obtained investigating the gold absorption on the river sand samples at various temperatures and of the calculation of microelement equilibrium concentrations in frozen and thawed massifs, initial conditions being equal; the solid phase of water is available or lacks.

The considerable part of ore gold deposits in Russia is concentrated in the permafrost zone. At present the geochemical methods of prospecting mineral deposits are being developed in these regions. The methods are based on the soil sampling and soil analysis with a view to revealing dissolved microelements. It is necessary to understand the dissolved elements migration under the conditions of low temperatures and changeable temperature regime as the source of entering microelements is a buried ore body or alluvial deposit.

It is known that the fluid phase in soils exists in some amount at any temperatures under natural conditions. The above-said phase contains microelements forming the diffused haloes in the form of chemical compounds of different composition, the most part of which are able to interact chemically with some active surface centres of dispersive soil components. In our opinion, there is a sense in researching adsorption interactions in heterogeneous soil media and assessing the effect of these phenomena upon the microelement migration. Due to the formation of geochemical fields the particular interest presents the dependence of microelements redistribution between the pore solution and dispersive solid phase of soils upon the ambient temperature. The regularities of the process might be specified when investigating the absorptions of some compounds by the absorption method from the solutions.

The example with alumina (Fedoseeva and Streltsova 1988) has shown that such an important element for prospecting as gold contained in the chloride complex of gold (III) at temperature  $-2^{\circ}\text{C}$  has the adsorption interaction factor with the oxide 3 - 4 times less than at  $+25^{\circ}\text{C}$ . That is to say the absorption affinity of the element to the oxide surface decreases at lower temperatures.

In the present article we have investigated the adsorption interaction of the chloride complex of gold (III) with the natural object river sand at above-zero and below-zero temperatures under conditions approximate to natural ones. For this purpose, the maximum relationship of the solid and fluid phases (20g/20mg) has been chosen which enabled us to sample the sufficient volume of free fluid to analyse it. The gold concentration was determined by spectrophotometrically by

the absorption band of the complex  $\text{AuCl}_4^-$ . In order to prevent the ice formation at  $-2^{\circ}\text{C}$  the initial gold solutions were being prepared in the presence of the background of the electrolyte KCl with concentration 1 mole/l. According to the state diagram of the system  $\text{H}_2\text{O}-\text{KCl}$  the ice starts forming from the solution with such concentration at about  $-3^{\circ}\text{C}$  (Chemist's Reference Book 1965). Taking into account the ability  $\text{HAuCl}_4$  to the hydrolysis (Fedoseeva and Streltsova 1988) the initial solutions after the addition of the required amount of an acid or alkali to get the definite pH (some sand was added) were allowed to stand for 24 hours.

According to the experimental data the curves of gold absorption by the sand surface have been obtained from some initial solutions with different gold concentrations depending on pH and as a result of it the adsorption isotherms at the most common values of pH have been calculated. In order to show the characteristics of the adsorption curves some part of them is given in Figure 1. The adsorption isotherms at pH 6 and 7 given in Figure 2 are the most common adsorption curves characterizing the substance distribution between the solution and solid phase surface subordinate to the adsorption equation by Langmuir (Greg and Sing 1984) (see below) according to which the adsorption constant  $K_L$  can be calculated. It turned out that the gold adsorption constant (III) on the river sand at  $25^{\circ}\text{C}$  exceeds the adsorption constant at  $-2^{\circ}\text{C}$  approximately twofold ( $3.02 \cdot 10^6$  and  $1.6 \cdot 10^6$  l/mole, respectively). That means that at low temperature the ability of the river sand to the gold bond decreases practically twofold.

Taking into consideration these circumstances one can estimate the direction of microelement migration having the constant or changeable temperature gradient in the soil massif and the solid water phase.

Under natural conditions as it was stated above the pore moisture contains the mobile forms of elements. The amount of moisture is easily determined at above-zero temperatures but at below-zero temperatures the value is extremely small that complex determination techniques are required. However, using the published data on the dependence of fluidlike layer thickness on

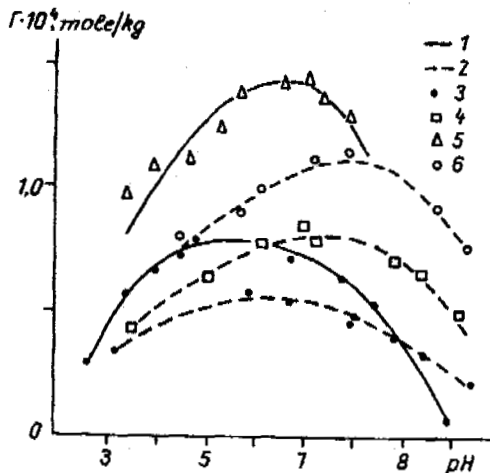


Figure 1. The dependence of gold adsorption on the river sand samples upon pH and temperature for the solutions  $\text{HAuCl}_4$  with initial concentration  $1 \cdot 10^{-4}$  (3),  $1.5 \cdot 10^{-4}$  (4),  $2 \cdot 10^{-4}$  (5),  $3.5 \cdot 10^{-4}$  (6) mole/l. Background - 1 mole/l KCl. 1 -  $25^\circ\text{C}$ , 2 -  $-2^\circ\text{C}$ .

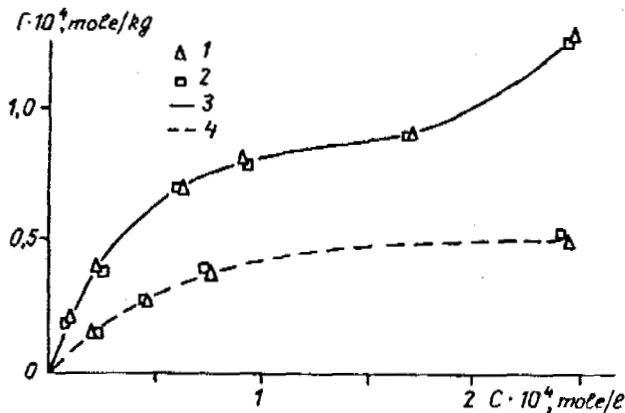


Figure 2. The adsorption gold isotherms from the solutions  $\text{HAuCl}_4$  at pH 6 (1) and 7 (2) at  $25^\circ\text{C}$  (3) and  $-2^\circ\text{C}$  (4).

the interface ice-silicagel (Kvilividze et al. 1974) upon the temperature and on determining experimentally the specific river sand surface by means of the adsorption method from the solutions (Greg and Sing 1984) according to methyl blue, it is quite possible to estimate the amount of fluid-like phase at any below-zero temperature.

To assess the direction of gold migration one should bear in mind that the gold redistribution will occur in the massif with homogeneous initial distribution with the changing temperature in such a way that, firstly, it results in equalizing of the element concentration in the whole fluid phase, secondly, at any soil point the substance amount ratio on the soil particle surface and in the solution corresponds to the temperature.

On the basis of adsorption measurement results we have made calculations of the equilibrium gold concentrations in the river sand massif at different temperatures for the initial gold concentrations  $10^{-4}$  mole/l. The sample moisture is

22%. The concentration of the background electrolyte was taken 1 mole/l both for frozen and thawed soils. The adsorption constants have been calculated on the basis of experimental values  $B$  at  $25$  and  $-2^\circ\text{C}$  and the equation by Arrhenius connecting the constant of any chemical equilibrium with temperature. According to the calculation results shown in Figure 3 (curves 1, 2) it follows that at temperature gradient and considerable microelement adsorption interaction with the surface of dispersive soil components the substance migration in the pore moisture should occur from the cold points system to the warm ones in the thawed and frozen samples. When the temperature of the adjacent blocks is equal (with solid water phase in one of them) the substance movement may occur from the frozen part to the supercool one. Such is the tendency of the microelement migration in the hypothetical pore solution provided the properties and concentration of the background electrolyte do not influence on the adsorption activity of migrating element from.

Actually, the most common concentration of the background electrolyte at above-zero temperatures is  $10^{-2}$  mole/l which increases to several moles per litre. When the systems are freezing leading to reduction of the amount of liquid containing deluted components. Thus, in reality the gold adsorption equilibrium at above-zero temperatures is set in the other media and, therefore, the adsorption constant will be different. Taking into account the fact that the interaction nature of chloride gold complex with the model substance surface is practically similar and the solution composition, the values of pH being equal, is identical one can estimate the adsorption constant correspondence for sand at different background electrolyte concentrations according to the curves of gold adsorption from the solution into the surface of  $\text{Al}_2\text{O}_3$  (Figure 4). It follows from the Figure that at temperature  $25^\circ\text{C}$  the effective adsorption constant at pH 7.0 is over threefold as much for the background media  $10^{-2}$  mole/l KCl compared with onemolar. On calculating the equilibrium concentrations and allowing for the known regularities of adsorption (Greg and Sing 1984) one can determine that the constant increase will be not less than fivefold. Making the corresponding re-calculation of equilibrium concentrations for the thawed samples at different temperatures one can obtain curve 3 in Figure 3. That is to say, the equilibrium concentrations in the thawed part of the massif will appear considerably less than it was supposed.

Thus, on condition of the interaction of the migrating microelement from with the surface of dispersive soil components, as well as the migration form composition, the gold migration ability from the frozen sample part to the adjacent supercool one should increase. In the thawed part of the soil the concentrations are considerably lower than in the frozen one. Consequently, the concentration gradient as the mobile factor of migration will be less, the temperature difference being equal. However, it follows from the assessment of the experimental work results (Mitrofanov et al. 1981) about the gold migration in the mixture of quartz and goethite, the migration degree is twofold at room temperature than at  $-6^\circ\text{C}$ . At the level which is at the distance of 1 cm from the mixture area with gold concentration it was  $9.3 \cdot 10^{-1}\%$  of the total gold content after keeping the samples 6 months at room

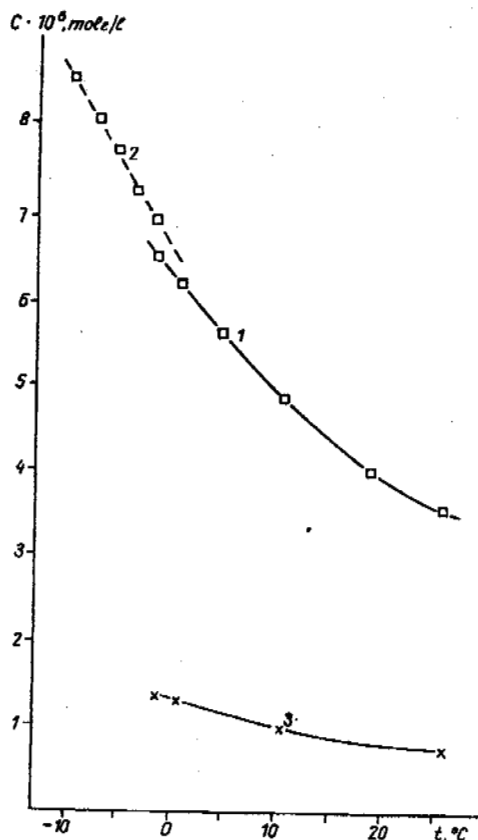


Figure 3. The calculated equilibrium gold concentrations in the pore moisture of thawed (1, 3) and frozen (2) sand samples depending upon the temperature. The background electrolyte concentration taken at calculations, 1 mole/l (1, 2) and  $10^{-2}$  mole/l KCl (3).

temperature and  $4.5 \cdot 10^{-1}\%$  at  $-6^\circ\text{C}$ . It is evident that the result is determined by the qualitative difference of the migration media in the frozen systems. The corresponding contribution is made by the fact that the gold displaces upward on the sample due to the stronger adsorption properties of the solid phase at above-zero temperatures.

The exposure of the quartz sand and goethite mixture at changable temperature regime (from indoor to  $-6^\circ\text{C}$  and inversely) resulted in the gold content of 1.2% of the total gold content at the same level. It is evident that the element migration increases under these conditions. It should be noted that the period are likely to be of great significance when the system passes through  $0^\circ\text{C}$ . The substance migration might mainly occur in the boundary of two adjacent areas with gold concentration, one of which still contains ice and another is thawed.

If we consider adsorption only as a phenomenon governing the element redistribution in the river sand massif with areas with different temperatures ( $-2^\circ\text{C}$  and  $+25^\circ\text{C}$ ), and take into account the regularities mentioned above we can estimate the proportion of gold amount concentrated in these areas in a state of equilibrium.

Let us compare the adsorption equations by Langmuir

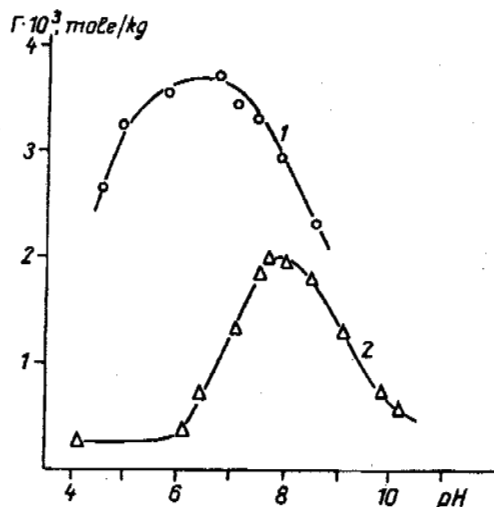


Figure 4. The gold absorption from the solutions  $\text{HAuCl}_4$  by the surface  $\text{Al}_2\text{O}_3$  depending upon pH at different background electrolyte concentrations: 1 -  $10^{-2}$  mole/l KCl, 2 - 1 mole/l KCl. Gold concentration  $2 \cdot 10^{-4}$  mole/l.

$$K_L \cdot C = \Gamma / (\Gamma_M - \Gamma) \quad (1)$$

(Greg and Sing 1984) at two temperatures ( $K_L$  - adsorption constant;  $C$  - equilibrium microelement concentration;  $\Gamma$  - substance quantity adsorbed in equilibrium state;  $\Gamma_M$  - maximum monolayer adsorption capacity). Taking  $C$  from this equation and equalizing the expressions obtained for both temperatures

$$(\Gamma / K_L \cdot (\Gamma_M - \Gamma))_{25^\circ} = (\Gamma / K_L \cdot (\Gamma_M - \Gamma))_{-2^\circ} \quad (2)$$

and taking into account that the value under natural conditions is relatively small, we obtain the relationship

$$\Gamma_{25^\circ} / \Gamma_{-2^\circ} = (K_L \cdot \Gamma_M)_{25^\circ} / (K_L \cdot \Gamma_M)_{-2^\circ} \quad (3)$$

As stated above it is quite evident that the adsorption constant at above-zero temperature exceeds the adsorption constant at  $-2^\circ\text{C}$  not less than tenfold. The maximum monolayer adsorption capacity of the system in question is higher at above-zero temperatures as well. Therefore, it turns out that the gold concentration increases scores of times in the thawed part of sand massif than in the contacting cold part.

The above stated results have been obtained using suppositions favourable for migration; one of them is the similarity of physico-chemical properties of pore moisture of thawed and frozen systems. In reality, a great of many factors arise preventing that. In our opinion, the direction tendency of microelement migration is specified correctly. The migration properties should be taken into account both at even distribution of temperatures (above-zero or below-zero) and at changable temperature regime.

#### REFERENCES

Chemist's Reference Book (1965), v. 3, 1000 pp. Chemistry, Moscow-Leningrad.

Fedoseeva, V. and O. Streltsova (1988), About the temperature effect on the adsorption activity  $AuCl_4^-$  to  $Al_2O_3$ . Geochemistry, no. 3, 449 - 451.

Greg, C. and K. Sing (1984) Adsorption, specific surface, porosity. 310 pp. Mir, Moscow.

Kvilidze, V. et al. (1974) The mobile water phase on ice surface. Surf. Sci., 44, 60 - 68.

Mitrofanov, A. et al. (1981) About possible effect of cryogenic processes on the gold re-distribution in alluvial deposits. Report A. S. USSR, 260 (1), 202 - 205.

## THE MICROBIOLOGICAL AND BIOGEOCHEMICAL RESEARCH IN PERMAFROST: PALEOECOLOGICAL IMPLICATIONS.

David A. Gilichinsky (\*), Elizaveta M. Rivkina, Vladimir A. Samarkin

Laboratory of Soil Cryology (\*), Laboratory of Mass and Energy Transfer, Institute of Soil Science and Photosynthesis, Russian Academy of Sciences, Pushchino, Russia.

Paleoreconstructions of global changes are most apparent in the cryolithosphere, which is a native storehouse of geological, biological and climatic chronicle. But on the some stage of research using traditional methods doesn't give us in the main any new information. It is impossible to obtain the new dates without using the new methods. That is why the scientists now look for new criteria, that can help to solve this problem. The basis of these new methods is the characteristic feature of permafrost - it preserves the material, and the information which it contains. These approaches take into account the cryopreservation of viable microorganisms and some gases in the Late Cenozoic frozen sequences from the moment of sediments freezing.

### INTRODUCTION

The cryolithosphere of the Earth has encoded all the climatic and geological events of the Quaternary period. The permafrost deposits represent the best natural paleobank of geological, biological, ecological, climatic and other data. Their interpretation is not easy because the cryometamorphosed sedimentary cover differs from the original one in both the character of bedding as well as granulometric, mineralogic and geochemical properties. Investigations of their genetic and stratigraphic origin by means of conventional geological methods do not always yield unambiguous results. Moreover, conventional methods are unable to solve the general problem of the historical geocryology, namely they do not determine the age of permafrost and do not describe the paleofrost dynamics in a vertical section, where the ancient levels of melting are found.

The cryolithosphere existence in time and space depends on climatic and geological oscillations. In Pliocene - Pleistocene these oscillations were displayed most clearly as agradation of thick frozen layers during cryochrones and further their degradation during thermochrones. Thermochrones produced stratigraphic levels in the permanently frozen sedimentary cover. The depth of these ancient levels and cups of melting corresponds to the natural situations of that time. After each cooling, the thawed layer refroze and " a young " permafrost was enclosed by " an old " permafrost in one monolith of a frozen section. The border between them, their age and conditions in which they formed can be established from the numerous viable microbial cells and radiative gases in permafrost.

### RESEARCH AREA

Due to its peculiar geocryological and climatic conditions, both ancient and modern ones, the Western part of Beringia (Kolyma - Indigirka lowland) is the most convenient for microbial (Gilichinsky et al, 1992) and gas

investigations (Rivkina et al, 1992). It has six different areas: 1. High Eastern border of lowland on the right bank of the Kolyma in the forest - tundra. This region contains the famous Late Cenozoic exposures. 2. The Late Pleistocene Edoma surface residues on the opposite bank of the river (21600 +/- 200 yr. a, GIN - 4334). 3. The vast sandy plain situated on the left bank of the Kolyma between Kolyma and Konkovaya rivers (Khalarchinskaya tundra). 4. The most abundant uplands constructed by Late Pleistocene deposits of Edoma suite in tundra between the Kolyma and Indigirka rivers. There are a lot of alas levels formed during thawing of Edoma sediments in Holocene. 5. The neotectonic rising with exposures of the most ancient Late Pliocene deposits of Olerion suite. 6. The East Siberian sea coast.

The preliminary results of our geological research, pertaining to the problem discussed, are the following (Gilichinsky, 1992): A/. On the lowland, the glacier cover was absent. Therefore the permafrost thickness thawing was not caused by this factor. B/. The sea sediments are only found in a narrow strip of present - day East Siberian Sea coast. Therefore, the permafrost thawing was not caused by sea transgrations. C/. The climatic conditions of that region also prevented any significant degradation of frozen layers even during optima. Therefore, the permafrost has been preserved in the unchanged form until present time. Kolyma lowland belongs to one of the few regions where the oldest of these thickness were discovered and where sediments frozen in the Late Pliocene did not thaw later, neither as a result of climatic fluctuations no under the influence of geological factors. Its age is more than 3 mln years.

The present-day conditions: influence of external factors and modern processes limited by the depth of the seasonal thaw layer 0.5 - 1.0 m; yearly low temperatures of the sequences (-9 to -13 C°); exceptionally loose sediments cemented with ice (its content is more than 50 % and all pores are closed). In



these closed system, there are no filtration and water horizons; migration of moisture and gases, cells and ions is impossible.

#### METHODS

Samples were taken from the cores of the wells (not from the exposures which are not representative for this kind of research); drilling was performed mechanically without chemicals; the average core temperature was never higher than  $-7\text{ }^{\circ}\text{C}$ . Specimens were placed in sterile aluminum boxes and transported to the laboratory in frozen state. A microbial examination consisted in the study of the qualitative and quantitative diversity of viable cells, their growth at temperatures from  $-10$  to  $+65\text{ }^{\circ}\text{C}$  on dense nutrient media, and response to freezing - thawing stress. The attention was mostly focused on  $\text{CH}_4$ . It was measured in field using a "head-space" technique, on a gas chromatographer XMP-4 supplied with a flameionization detector. The range of  $\text{CH}_4$  values was 5 ppm. Some experiments were done with  $\text{CO}_2$ . Carbon dioxide concentration was measured also under field conditions in the same samples using an infrared analyzer "Infralit"; its range was 5 ppm too. About 2200 samples taken from Late Cenozoic sediments were analyzed for the availability of viable microflora; about 700 samples were tested for the presence of gases. We also studied microbiocenoses and gas phases of modern tundra cryosols as models for paleoreconstructions and interpretation of the data obtained.

#### OBJECTS AND RESULTS

The research was done on layer, particularly the syngenetic frozen one starting from the second half of the Pliocene period until the present time: Wells 2 and 3 (fig.1): The first was drilled to the depth of 20 l, it went throughout the Edoma suite and opened to sands. The average number of viable microorganisms in Edoma sediments was  $1.8 \cdot 10^4$  cells per 1 g; 12% of samples were sterile. The second well is situated in a deep alas depression. Down to 3, 5 l there are alas (6500 +/- 90 yr.a., GIN-4331) and taberal sediments with underlying Edoma suite and then sands. Viable cells were found in all the samples. The number of microorganisms in alas samples is on average higher than in the underlying and surrounding sediments of Edoma suite (up to  $1.6 \cdot 10^6$  cells/g). The transition to Edoma layers is marked by a quantitative peak of viable cell s in the bottom of an alas pack (on the background of the total high quantity) and a drastic drop of the cell number outside the cup of thawing.

Wells 4 and 5 (fig.2): The first was drilled in the alas depression where the main section is represented by alas and taberal sediments with the underlying Edoma suite.

Viable microorganisms were isolated from all the samples of the alas and taberal well 2 (2/84) well 3 (3/84)

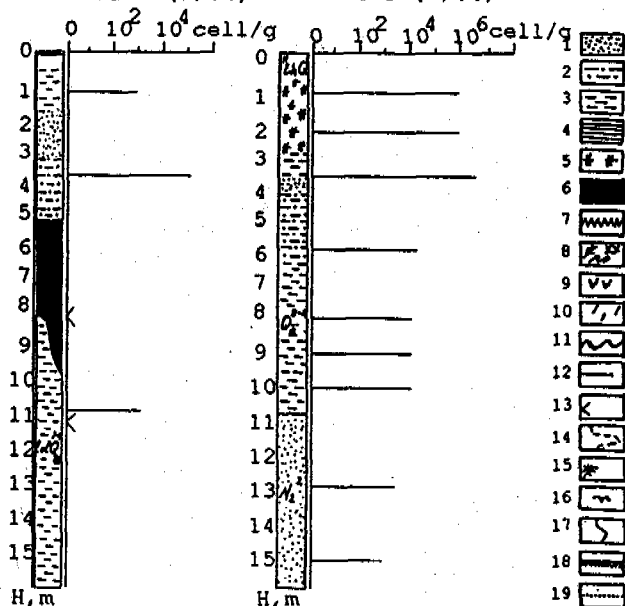


Fig.1. The distribution of viable cells in Edoma and alas sediments of Plakhin Yar. Conditional meanings (fig.1-11: 1 - sands, 2 - loamy sands, 3 - loams, 4 - clays, 5 - peat, 6 - ice, 7 - ice-ground, 8 - organic remains, 9 - sulfide inclusions, 10 - carbonate inclusions, 11 - stratigraphic boundaries, 12 - quantity of viable microorganisms, 13 - sterile samples, 14 -  $\text{CH}_4$ -content, 15 -  $\text{CH}_4 = 0$ ; 16 -  $\text{CH}_4$ - content about 0; 17 -  $\text{CO}_2$ -content, 18 - cover horizon boundary, 19- boundary of the seasonal thawed layer.

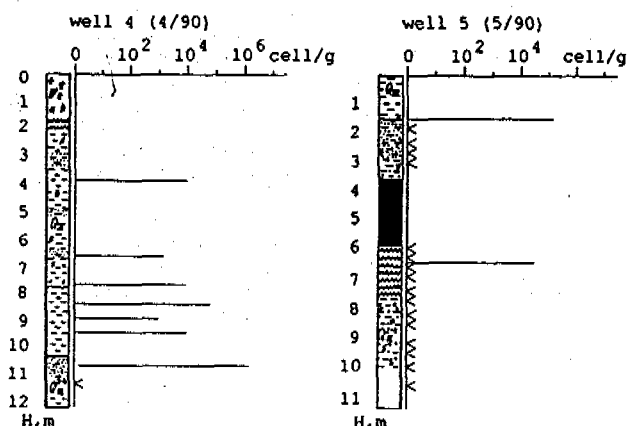


Fig.2. The distribution of viable cells in Edoma and alas sediments of Omolon Yar.

packs, being mostly abundant on the bottom (10.5 m). They grew at all experimental temperatures:  $+65$  to  $+10\text{ }^{\circ}\text{C}$ ; optimum  $+20\text{ }^{\circ}\text{C}$ . A sample from the underlying Edoma suite (11.4 l) was sterile. Well 5 was drilled through icy Edoma sediments. Temperatures of  $+65$ ,  $+45$  and  $+30\text{ }^{\circ}\text{C}$  were unfavorable for the development of

cells from Edoma samples; the cells from the covering 1.5 m horizon were able to grow at +30 C°; the optimum being +10 C°. Well 6 was drilled in the alas depression of one of the north ranges of this Edoma. The alas sediments are underlined by a never thawed Edoma at a depth of 5 m. The average number of viable microorganisms here was  $7 \times 10^5$  cells/g, and  $5 \times 10^3$  in a lower horizon.

Wells 7,10 (fig.3) are a continuation of a well 7 (6/90) well 10 (1/91)

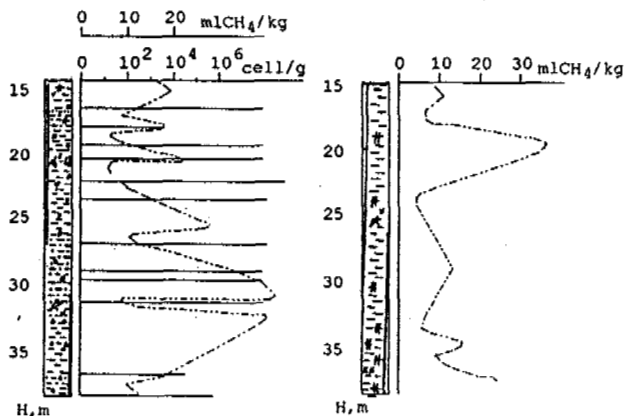


Fig.3. Distribution of viable microorganisms and CH<sub>4</sub>- content in Olerion sediments.

famous stratotype of Olerion suite. Similar results were obtained in both wells. In all the Late Pliocene sediments of Olerion suite there were viable cells ( $10^3 - 10^4$ ;  $9 \times 10^8$  cell/g in mineral and organic layers, respectively) and methane at concentrations from 2.3 to 45.5 ml/kg. The cells did not grow at +65 C°; at 0 C° their number varied from  $3.5 \times 10$  to  $10^5$  cell/g. At this temperature and +10 C°, the cells of 7 out of 19 samples did not grow; at +45 and +30 C°, they were only 4 samples the cells of which were unable to develop, and at +20 C° it was only one such sample. The optimum temperature was between 20 and +30 C°.

Wells 8,9,11 (fig.4) were drilled from the

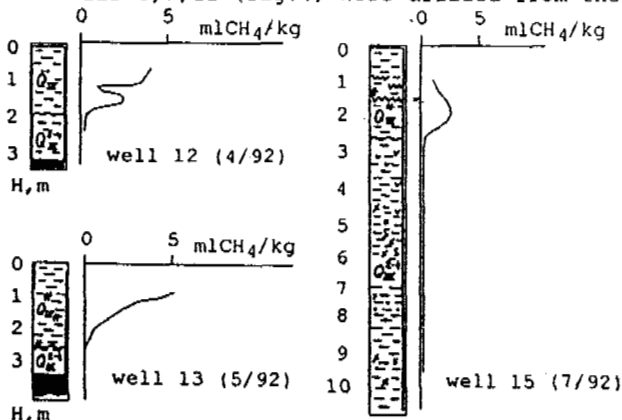


Fig.4. Distribution of viable cells and CH<sub>4</sub>- content in Edoma sediments.

watershed surface: the first opened a 15 m of icy aleurites of Edoma suite; the second, situated in the vicinity, went along the ice vein. In well 8, methane was found only in the covering horizon, its content decreased from 15 ml/kg on the bottom of the seasonally thawing layer to 0.6 ml/kg on the bottom of the Holocene thawing layer. It was absent within the Edoma interval and in samples of the ice-veins taken from well 9. In this well, samely as in the others, the samples of Edoma polyhonal vein ice were completely sterile. At temperatures between +5 and +37 C° in the covering horizon, the number of viable cells varied from  $4$  to  $8 \times 10^5$  cells/g and decreased to  $4 \times 10^3 - 3 \times 10^4$  in the horizon below the border between this layer and underlying nonthawing Edoma suite. Well 11 is situated in the same watershed in a small alas depression. The upper 3.3 m are represented by lake facies with interlayers of turf horizons; the layer from 3.5 m to 4.5 m is represented by taberal sediments; and until the bottom the sediments are represented by aleurites of Edoma suite. CH<sub>4</sub> was present everywhere, at concentrations 1.4 to 9.9 ml/kg in alas sediments. Its quantity dropped to 0.4 - 0.7 ml/kg in taberal deposits at a depth of 3.5 - 4.5 m and to 0 in Edoma suite layers. The average number of viable microorganisms was (optimum being between +10 and +20 C°)  $1 \times 10^4 - 4.5 \times 10^5$  cell/g in alas sediments; the transition to the taberal deposits is marked by a quantitative peak of viable cells ( $7.5 \times 10^5$ ) on the bottom of an alas pack - at the same depth where the CH<sub>4</sub> concentration changes; in lower horizons there were  $8 \times 10^2$  to  $6 \times 10^4$  cells/g.

Wells 12 - 15 (fig.5) were drilled from the watershed surface of Edoma. CH<sub>4</sub> was found in the covering horizon at concentrations 1 to 5 ml/kg and was absent below (in Edoma). Wells 16,17 (fig.6) were drilled in the same place along the exposure wall on the boundary between Olerion and Edoma suits. In the latter, CH<sub>4</sub> was not found; in the contact zone it was found at small concentrations (0.03-0.6 ml/kg); but in Olerion deposits its content changed from 1 to 3.5 ml/kg. CO<sub>2</sub> was present in both suits (1.3-27.3 ml/kg).

Well 18 was drilled in a deep alas depression. The first 4.5 m are represented by alas deposits, then go a thin (1 m) horizon of Edoma suite, and to 44 m deposits of Olerion suite, below (down to 50 m) there are Pliocene sands of TomusYar suite. The CH<sub>4</sub> and CO<sub>2</sub> distribution in the well is following: CO<sub>2</sub> is present in all the samples (1.0 - 23.0 ml/kg); CH<sub>4</sub> is present at a quantity of 1.3-7.7 ml/kg in alas layers, it decreases to 0 in Edoma suite, in Olerion sediments its content varies from 1 to 5 ml/kg and below, in sands, it drops to 1 ml/kg in all the samples.

Wells 19-23 (the bank of the East - Siberian sea).

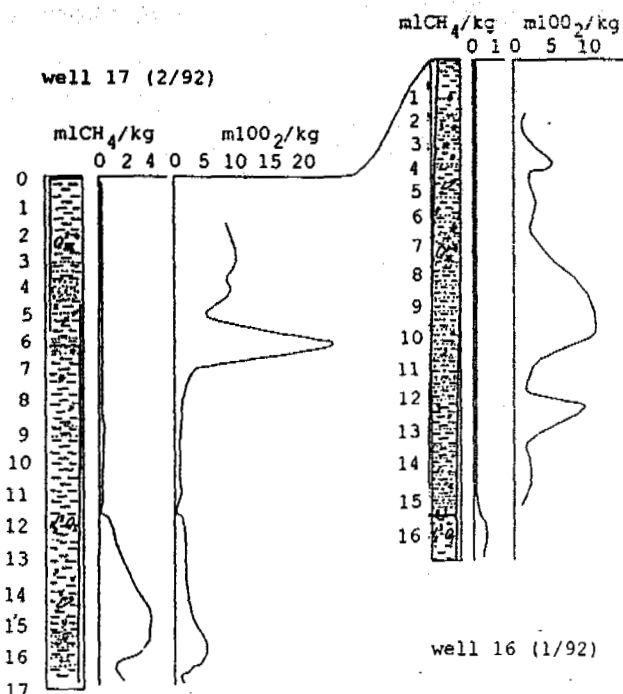


Fig.5. Distribution of viable cells and CH<sub>4</sub>-content in Edoma sediments.

Wells 20,21, 23 are situated on the day surface of the thick Holocene alas. The section of well 19 is represented by taberal sediments with interlayers of peats. The section of well 23 is modern alas deposits within the thickness of Holocene taberal sediments. A 12 m section of well 21 is represented by alas facies; below, to a 20 m depth, they are aleurites of Edoma suite.

In well 20 CH<sub>4</sub> is present throughout the thickness. Down to 7.3 m, the range of concentrations makes up 0.04 - 1.4 ml/kg, below it increases to 2.4 - 10.8 ml/kg. In modern alas sediments, CH<sub>4</sub> is present at a quantity of 0.1 - 1.9 ml/kg. In well 21 on the bottom of the layer of modern seasonal thawing, the methane content is 0.7 ml/kg, and further, within the alas package from 1.3 to 11.4 m it varies from 3.2 to 10.5 ml/kg; in underlying Edoma layers, at a depth 12.5 m, it drops sharply. From 13.5 m and to the well bottom, CH<sub>4</sub> was absent. The cells grow at all temperatures between +10 and +37 °C (10<sup>5</sup> cell/g) in the alas pack and at +20 and +30 °C in underlying Edoma suite (10<sup>3</sup> - 10<sup>4</sup> cells/g). Well 22 was drilled from the watershed surface consisting of icy aleurites of Edoma suite; methane is only found in the upper 2.3 m (a covering layer). Lower it was not found in all the samples. The transition to the Edoma deposits was marked by a quantitative peak of viable cells (3.2 \* 10<sup>5</sup> cell/g) in the bottom of this covering horizon, at the same depth where methane concentration changes. Well 19 to the depth of 4m continues a thick Holocene alas package further under the sea level. It goes through the 20 m thickness of the sea

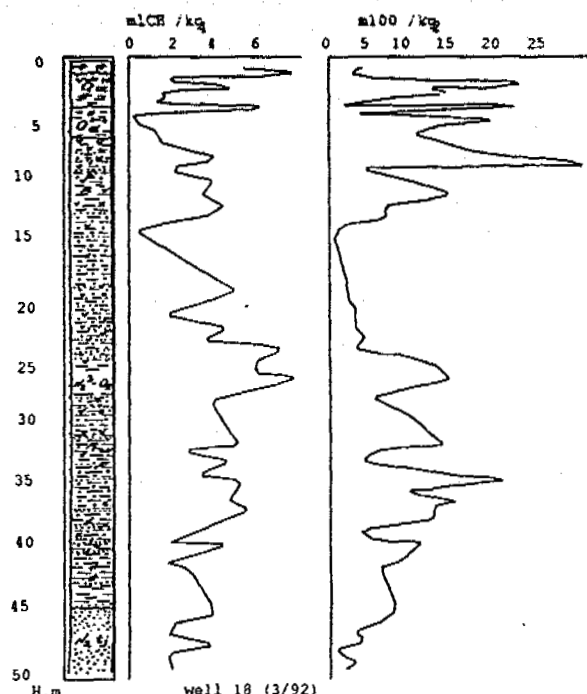


Fig.6. Distribution of CH<sub>4</sub>- & CO<sub>2</sub>- content on the boundary between Edoma and Olerion suits.

sediments and penetrates the continental sands.

More than 60 % of sea samples are sterile; for viable cells from underlying sands the optimum is between +20 and +30 °C (10<sup>4</sup> cell/g). The methane content varies from 1 - 3 to 10 - 13 ml/kg in the sea deposits and decreases to 0 in the sands.

Wells 24 - 27 were drilled in the sands on the south - east of Khalarchinskaya tundra. In well 25, drilled from the surface, methane was absent. The number of viable microorganisms was by 1 - 2 orders lower than in loams. The cells grew within a wide range of temperatures, from 0 to +45 °C, the optimum being +20 to +30 °C in upper horizons and +10 to +20 °C in lower ones. Well 26 was drilled not far from the previous one, in the modern river valley bog situated on the same sands. CH<sub>4</sub> in a small quantity was present throughout the well bog section. Well 24 was drilled from the bottom of the dried lake depression where the uppermost 2 m are represented by the sand lake Holocene facia situated in typical Khalarchin sands. In lake sediments, the bacterial number was 6 \* 10<sup>3</sup> - 2 \* 10<sup>4</sup> cell/g. Below the earlier existed lake talik, the number of viable cells, was similar to that one in Khalarchin sands samples (3 \* 10<sup>3</sup> - 2.4 \* 10<sup>4</sup> cell/g). Well 27. The uppermost 15 m are represented by typical Khalarchin sands, then the well penetrates aleurites of the unknown layer. In the first part of the section, methane was absent; in the second one its content varied 3 to 15 ml/kg.

CH<sub>4</sub> content in the modern tundra cryosols varies from 0 to 5 ml/kg. In the thawed horizons of cryosols, taken from the surface, methane was either absent or present at extremely low concentrations.

An average bacterial number in modern tundra cryosols makes up  $1,5 - 6,0 \cdot 10^6$  cells/g in turf. Down the profile, they become less abundant, their number drops to  $10^4$  and  $10(5)$  in sands and clays, respectively. The bottom of the modern seasonal thawing layer is characterized by the peak of microbial cell number compared with their maximum in surface horizons rich in organic matter.

## DISCUSSION

We managed to reveal the presence of viable cells and radiative gases in permafrost. This fact is important for reconstructions and forecasting of global warming consequences. The most vivid example are thermocarst forms which were widely spread in Holocene. They continue to develop at present and may be taken as a paleoecological model of the results of global warming. The laminarity of CH<sub>4</sub> distribution conditioned by the age and genesis of frozen thickness, eliminates the possibility of its diffusion in them. This methane might be preserved in the thicknesses from the very moment of their transition to the permafrost state and therefore might characterize the biogeochemical situation existed in the sediments by that moment. This is the most important fact for paleoreconstructions (Rivkina et al, 1992).

Methane, alongside with CO<sub>2</sub>, is a powerful absorber of the infrared part of the electromagnetic spectrum. This is its most important role as a "greenhouse" gas. The contribution of methane to the climate warming as a "greenhouse" gas is comfortable with the effect of CO<sub>2</sub>, in spite of its lower concentration. This is explained by the fact that greenhouse effect of CH<sub>4</sub> per a molecule is 25-30 fold higher than of CO<sub>2</sub> (Whalen S.C., and Reeburgh W.S., 1990). The CH<sub>4</sub> formation and emission are affected by the tundra landscapes and make up 7% of the annual total flux of CH<sub>4</sub> to the atmosphere (Cicerone, Oremland, 1988; Fung et al, 1990; Whalen, Reeburgh, 1990). The tundra ecosystems contain about 13% of planetary carbon (Post W.M. et al, 1982), which is mostly found in the seasonally thawing layer and actively participates in the biogeochemical cycles.

A far higher quantity of organic and mineral carbon (in passive form) is present in the permafrost below the thawing layer. CH<sub>4</sub> quantity depends on the genesis of deposits, and type of the cryogenic thickness. It is not found in Edoma suite and Khalarchin sands, however is present in Late Pliocene - Early Pleistocene deposits of Olerion suite sea sediments of the beginning of Late Pleistocene, covering and alas horizons which

thawed during Holocene optimum. CH<sub>4</sub> quantity drastically decreases (almost to zero) on transition from the alas layers to the underlying never thawed deposits of Edoma suite thus marking the border between the frozen sediments of Holocene and Late Pleistocene age. The same border is marked by the peak of the microbial abundance on the top of the permafrost water confining layer which underlies the sediments affected by the thermocarst during Holocene optimum.

The numerous data confirm the idea of a synchronous character of the cycles of thawing and development of thermocarst. According to these evidences, the average July temperatures during Holocene optimum in the North - East Eurasia were by 8 - 9 C° higher than the modern ones. Even at steady winter temperatures, this should sharply increase the depth of seasonal thawing and appearances of thermocarst centers. The further development of the process was flavored by the local factors and primarily by the presence of polygonal ice veins of Edoma suite. It resulted in the increase of the water content in thawed horizons, temperature, and depth of seasonally thawed layer, which promoted the process of methanogenesis. The absence of methane in Edoma deposits is explained by the low water quantity in seasonally thawing layers during their formation, i.e. the prevalence of dry tundra - steppe landscapes. In Holocene, CH<sub>4</sub> generation predominated over CH<sub>4</sub> oxidation which is evidenced by the presence of methane in the above mentioned thawed horizons and its absence in the unthawed Edoma.

The free water appearance and positive temperatures stimulated the revival of cells after cryobiosis, their development and propagation in thawed horizons. The further freezing fixed this outburst of the vital activity and as the result the number of microorganisms in thawed and then frozen deposits is by 2 orders higher than in the underlying syngenetic frozen and not thawed sediments of Edoma suite. This is explained by the fact that during Holocene warming, the depth of seasonally thawing increased. It was accompanied by the transition of viable microorganisms down the section; their number was maximal on top of the underlying never melted frozen Edoma suite. During cool periods, the top of the permafrost went up, and cells accumulated at intermediate depths.

When thermo- and cryochrones occur one after another on the stabilized surface, each new thawing overlaps the previous one. If a new thermochrone causes a deeper thawing, it eliminates the peak of microbial number corresponding to the previous thermochrone and provides the development of a new one at a greater depth. If thawing is less strong, a new peak will develop at a depth lower than the previous one. Therefore, the deeper in the section is the peak of the microbial number, the older is the thermochrone it corresponds to. This was exemplified by the surface

horizon and alas packages thawed during Holocene optimum, i.e. we showed the border between the frozen deposits of Late Holocene age and underlying Late Pleistocene frozen thicknesses. It is interesting that the border is marked not only by the number of viable cells but also by the qualitative variability of microbial spectra and physiological peculiarities.

#### CONCLUSION

Using the microbiological and biogeochemical approaches, as well as traditional and appropriate geological methods, it is possible to distinguish the paleoecological conditions of different geological periods within permafrost areas (Gilichinsky et al, 1988, 1989, Gilichinsky, 1990). In the present work it was shown by example of the boundary between sediments which melted during Holocene optimum and those of Edoma suite. Similarly as the depth of today's summer thawing of tundra cryosols corresponds to the modern climatic conditions, the depth of Holocene thawing also correspond to the climatic regime at that time. The results obtained show that methane is a marker of paleoconditions while, CO<sub>2</sub> distribution in frozen thicknesses cannot serve as that. It is planned to confirm this work to reconstruct the dynamics of frozen soils in the vertical section and to establish the level of thawing of Late Pleistocene and other long-term thermochrones. When determining the depth of thawing it might be unimportant what factor, either climatic or geological, has caused the warm wave. Therefore, the above considered character of the distribution of microorganisms and methane in the subsurface sedimentary thickness conditioned by the climatic optimum, makes it possible to determine the bottom of the earlier existed and then newly frozen lake pseudotalics. The microbiological and biogeochemical data obtained on syngenetic those on epicryogenic thicknesses, make it possible to employ such an approach to establish the paleotalic zones under the prairies and thawing levels of permafrost during sea transgressions.

EXOBIOLICAL SEANCE: Icy caps on Martian poles isolate the underlying rocks from negative temperatures prevailing on the surface (AntArctica or Greenland). The amplitude of their oscillations and the depth of their penetration on equator or middle latitudes reduce sharply because Martian dust (the same way as finely-dispersed soils in Arctic). As a result, in any cases the depth temperatures of Martian permafrost approximate the Earth ones. Therefore Martian cryolithosphere contains the unfrozen water films surrounding the mineral particles and rigidly associated with them. On the Earth, the viable microorganisms are preserved in such an ecological niche "in situ" during the

geological significant period of time up to the first million years. Probably, such a mechanism can work by 2-3 order of time longer: up to billions years. In this case the Earth permafrost - environment inhabited by microbes - can be considered as a model of the Martian one, and the viable cells in permafrost - as the analogues of potential habitants of Martian frozen sequences. The latter protect the cells from the lethal influence of radiation. The CO<sub>2</sub> presence, as well as sharp temperature oscillations across 0 C, is not an unfavorable factor for cells preservation because this gas and these processes are also found in permafrost thickness of the Earth. And if the life existed on Mars during the early stage its development, its traces in the form of microorganisms, might be discovered in the depth of Martian permafrost (Gilichinsky et al, 1992).

#### REFERENCES

- Cicerone R.J., Oremland R.S. Global Biogeochem. Cycles, 1988, vol. 2, N 4, pp. 229-327.
- Gilichinsky D.A., Khlebnikova G.M., Zvyagintsev D.G., Fyodorov-Davydov D.G., and Kudryavtseva N.N. The use of microbiological characteristics of sediments in geocryology. Permafrost Fifth International Conference, Norway, 1988, 1, pp. 749-753.
- Gilichinsky D.A., Khlebnikova G.M., Zvyagintsev D.G., Fyodorov-Davydov D.G., and Kudryavtseva N.N. Microbiological characteristics in studying of sedimentary deposits of cryolithozone. Izv. Akad. Nauk SSSR, Geology Series, 1989, 6, pp. 103-115 (In Russian).
- Gilichinsky D.A. Microbial approach to paleoecological reconstructions in Beringia. Arctic Research. Advances and prospects. Part 2. 1990, Nauka, Moscow, pp. 291-293.
- Gilichinsky D.A., Vorobyova E.A., Erokhina L.G., Fyodorov-Davydov D.G., and Chaikovskaya N.R. Long-term preservation of microbial ecosystems in permafrost. Adv. Space Res., 1992, vol. 12, No. 4, pp. 255-263.
- Gilichinsky D.A. Microbial markers in the cryolithosphere. Geocryology., Nauka-Wiley, 1992, N 1.
- Mathews E., and Fung I. Methane emission from natural wetlands: global distribution area and environmental characteristics of sources. Global Biogeochem. Cycles. N 1, 1987, pp. 61-86.
- Post W.M., Emanuel W.R., Zinke P.J., and Stangerberger A.G. Soil carbon pools and world life zones. Nature, 298, 1982, pp. 156-199.
- Rivkina E.M., Samarkin V.A., and Gilichinsky D.A. Methane in permafrost sediments of Kolyma - Indigirka lowland. Doklady Akad. Nauk, 1992, vol. 323, N 3, pp. 559-562. (In Russian).
- Whalen S.C., and Reeburgh W.S. A methane flux transect along the trans-Alaska pipeline haulroad, Tellus, 42B, 1990, pp. 237-249.

## CONSTRUCTION OF BUILDINGS ERECTED ON SURFACE-TYPE SPACE FOUNDATIONS DESIGNED FOR PERMAFROST

Ju.M.Goncharov

Permafrost Institute of the Siberian Branch  
of the Russian Academy of Sciences Igarskaya Research Permafrost Station

The report covers the problems of construction and use of buildings erected on surface-type space foundations making use of the interlayer, which enables a considerable reduction of cryogenic processes in case of thermal and mechanical interaction of buildings with the frozen base. Observation results related with the use of buildings are presented. The results of providing the thermal conditions for the base soils during construction period are analyzed.

One of the trends in improving foundation engineering on permafrost is the developing and extending the application field of surface type ventilated space foundations making use of the interlayer, which enables a considerable reduction of cryogenic processes in case of thermal and mechanical interaction of buildings with the frozen base.

The interlayer under the space foundation enables:

to confine or eliminate completely the layer of seasonal thawing in the underlying frozen soil of the base in case of the construction according to principle 1;

to reduce considerably the cryogenic processes, which cause soil deformation and heave within the confined depth of seasonal thawing under the footing of the interlayer.

The space structure of the shell-type foundation (A.c. 670683 USSR, MKI D E02 27/02 Foundation (Goncharov Ju.M., Tregubova L.L., Poleshchuk V.L., 1979)) is a folded slab, the folds of which are used for foundation ventilation in order to preserve the frozen state of the base soil. The shell-type foundation is erected of precast members (may be also cast-in-situ) on the interlayer 13 (filled soil), which is arranged between the foundation and the frozen soil of the base formed of non-heaving material.

The shell-type foundation 1 (see Figure 1) is assembled of separate reinforced concrete members with protruding base of working reinforcement around its perimeter. The members consist of the upper thickened horizontal beam for supporting the walls, panels (Figure 1 f) of the building, which turn into two thinner inclined 160 mm slabs, which change into the lower horizontal slabs.

Between the inclined slabs within the internal hollow (cavity) of the member there are strengthening stiffness ribs 2 (Figure 1 c, d, e, f).

The structure of this foundation is rigid enough, therefore the uneven deformations of the base do not practically change the quality of the stress-strain state of foundation members.

The distribution of loads on the foundation in accordance with the deformation properties of inhomogeneous base contributes to the performance of the space structure.

Depending on the structural and technological features of the buildings on intermediate layer there socle part (Figure 1 a, b, g).

For buildings provided with technical floors (for laying engineering pipelines and cables), as well as for connection with engineering pipelines at building floor level, the socle part is designed of the shell-type foundation and the floor slabs (Figure 1, a), which enables to provide cooling of base soils due to the folded shape of the foundation, the upper cavities of which serve for natural cold air ventilation.

For buildings without technical floors and frame-type buildings the folded slab serves as building foundation, and the combination of walls (or safety bracing in frame-type buildings) with floor slabs (Figure 1, b) forms a blown through service space in the socle part of the building used for pipeline laying. This underfloor duct is ventilated through the vents located around the building perimeter. The columns in the frame-type buildings are erected over column footings which are cast-in-situ and installed on a thickened part of the horizontal beams of the shell-type foundation (Figure 1, d). The stiffness of the shell-type foundation in longitudinal direction is provided by the internal and external (Figure 1, b, 7 and 2) stiffness ribs.

In production buildings the socle part of the foundation consists of the ventilated folds in combination with ventilation ducts, which are arranged either on the fill (Figure 1, g) or right inside it (Figure 1 h).

The first buildings on similar foundations have been erected and used in Igarka (in Krasnoyarsk area). This work has been further developed and applied to the industrial region of Norilsk..

Two residential houses on shell-type foundation have been built in Igarka in unfrozen water-saturated clayey silty loams and sandy silty loams with deformation modulus of the base  $E = 3.4$  MPa.

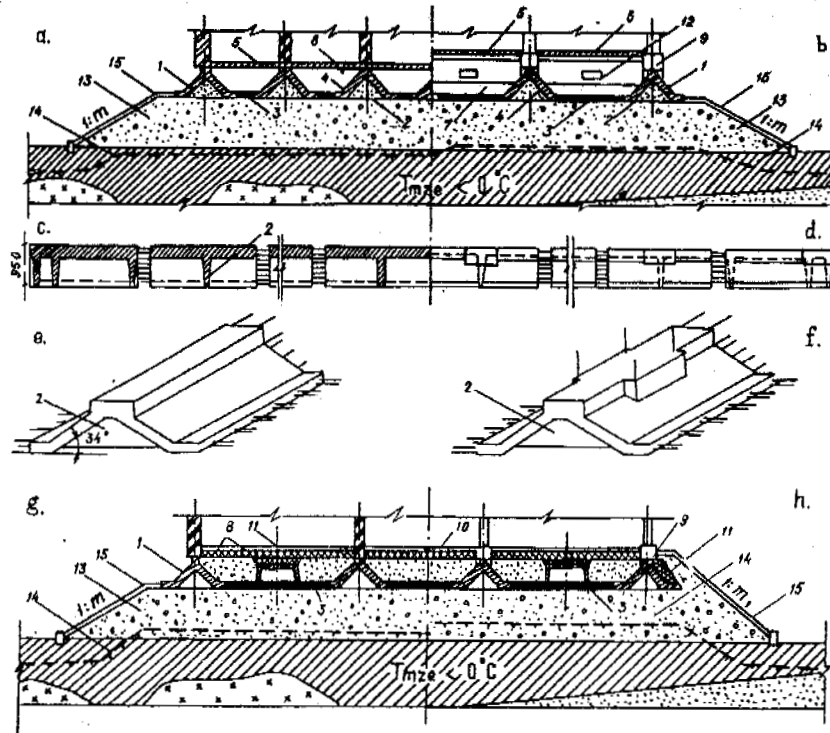


Figure 1. Structural designs of space, ventilated, shell-type foundations  
 a - for bearing walls; b - for columns of framed buildings with an aerated underfloor space; c - longitudinal section of the foundation fold under the bearing walls; d - do, under the columns; e - precast member of the foundation for bearing walls; f - do, under the columns; g - for production buildings with the floors over the soil for the bearing walls; h - do, under the columns.  
 1 - shell-type foundation; 2 - stiffening rib; 3 - cast-in-situ portion; 4 - low-strength filling material; 5 - floor slabs; 6 - wall beam; 7 - stiffening rib; 8 - ventilation duct; 9 - jib cap; 10 - concrete floor; 11 - heat insulation; 12 - vents; 13 - intermediate layer (fill); 14 - top of permafrost; 15 - concrete blind area.

To study the deformation character of the base and the fill and, accordingly, the settlements of the shell-type foundation the residential houses were provided with depth and surface bench marks (Figure 2). Deep marks were located at depths of 1, 2, 3 and 5 m in the middle part of the buildings between the foundation folds, as well as along one of its longitudinal and transverse walls, while the surface marks - in the brickwork of the building socles along the longitudinal and transverse walls at the level of the upper foundation edges.

The maximum non-uniformity (difference) of settlement for house No. 1 (axis B) was 44 mm, and for house No. 2 (axis A) - 33 mm. The non-uniformity of the settlements along the length of the buildings caused the tilt of the foundations which for the two houses was 0.0016 (which is far less than the allowed value of 0.005).

Bend analysis of the shell-type foundation has shown, that there was a slight foundation bend of 0.00043 in house No. 1, and, on the contrary - asymmetrical bend of 0.00072 in house No. 2. The indicated bend values are far less than the ultimate values allowed for brick buildings without the wall reinforcement - 0.001.

From the graphs one can see that the absolute settlement values of house No. 2 foundations ex-

ceed those of house No. 1. The settlements in house No. 1 have almost ceased by the mid of November 1988, whereas in house No. 2 they still occurred.

The average settlements around the building perimeters also vary. In the mid of November 1988 the average settlement in house No. 1 was 8.7 cm and in house No. 2 - 12.7 cm. In house No. 1 the average settlement is less than the ultimate permissible value (10 cm), and in house No. 2 it exceeds this value by 2.7 cm.

The difference between the absolute settlement values and dampening rates is explained by the greater compressibility of the base soil under house No. 2.

Let's examine the base deformations according to the entire depth (Figure 2, e). The measurement has shown that depending on the depth one can observe settlement damping for all the marks.

The deformations of the fill within 1 m and under the foundation footing are as a rule similar. The base under house No. 2 is subjected to greater deformations than that under house No. 1 which resulted in the greater absolute foundation settlements of this house.

The average monthly rate, based on the mean foundation settlement data was 2.8 mm/a month for house No. 1 and 3.8 mm/a month for house No. 2.

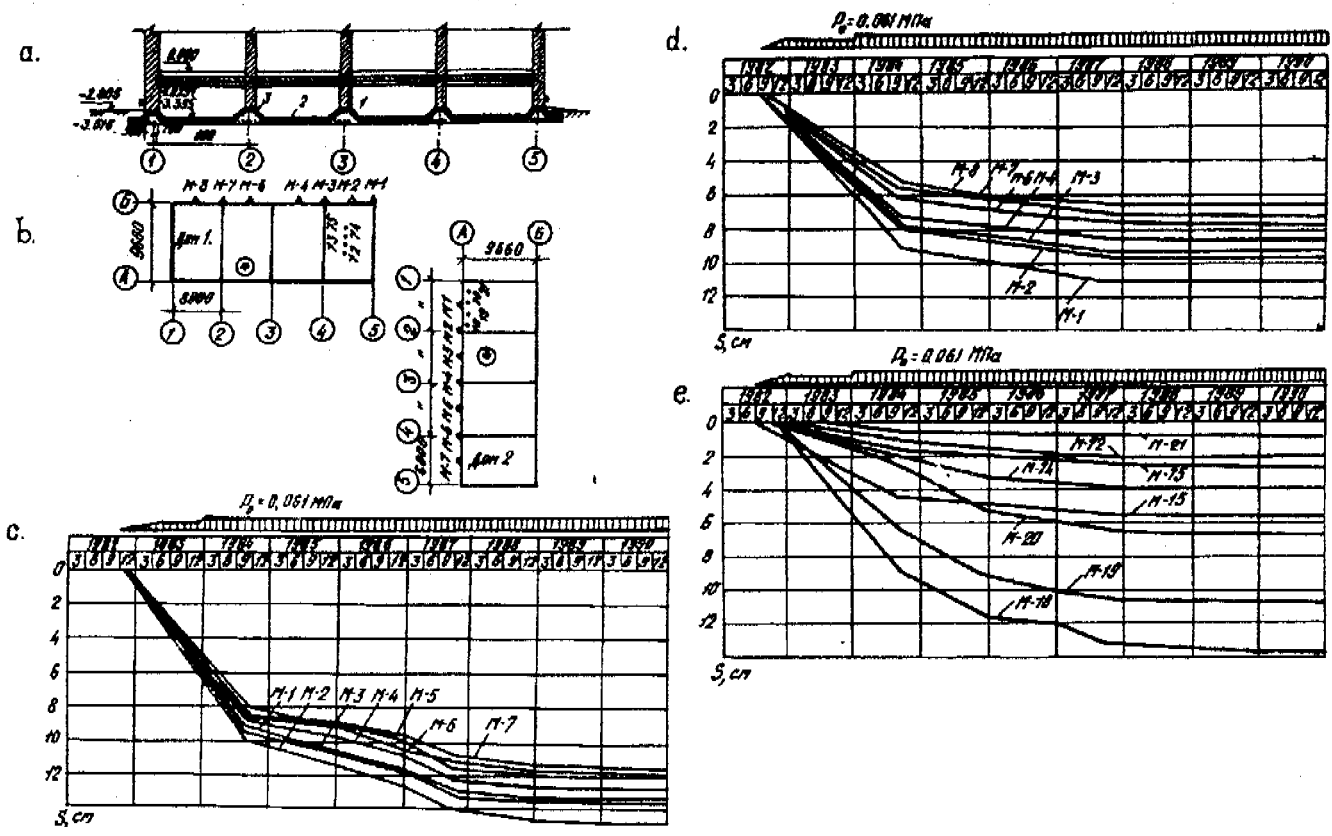


Figure 2. Foundations and soil base settlement curves

a - longitudinal building section; b - layout scheme of experimental houses and deep (a circle), surface (a triangle) marks and a bench mark (a double circle); c - foundation settlement curves for house No. 1; d - do, for house No. 2; e - do, deep marks

1 - foundation fold; 2 - cast-in-situ portion; 3 - insert

During the next years the absolute settlements and their rates have notably reduced. Thus, for instance, the average monthly rates of the settlements for house No. 1 were from 1984 to 1985 - 0.4 since 1985 till 1986 - 0.44, since 1986 till 1987 - 0.26 and since 1987 till 1988 - 0.06 mm/a month, and for house No. 2 accordingly 0.84, 1.1 and 0.14 mm/a month.

A heat-insulated garage building has been erected on ice-rich high-temperature frozen soils. The garage was built on shell-type foundations combined with ventilation ducts in the town of Igarka (according to the structural scheme, shown in Figure 1, g). The three-year use of the building has shown, that during the summer-autumn period no thawing of the frozen base under the intermediate layer (1 m thick) took place. The system of foundation ventilation provides the design temperature conditions of the base and the zero isotherm does not sink below the interlayer footing.

For construction of a building with a non-insulated underfloor space up to 2 m high according to the scheme given in Figure 1, b in the town of Norilsk use has been made of a cast-in-situ shell-type foundation structure.

A frame-type four-storey building with curtain wall panels has 18x54 m plan dimensions.

The shell-type foundation is divided by deformation joints into three blocks. The concentrated loads from building columns are from 10.1 to 21.6 kN.

The intermediate layer was made in two stages. The first stage included soil filling operations to level the site surface; the second stage - making the intermediate layer with an average height of 4 m and ramming in layers.

The first stage operations commenced at negative outside air temperatures and the soil mix temperature (rock fractions from 10 - 15 to 50 - 60 cm with additions of clayey silty loam) averaging to 0.5°C.



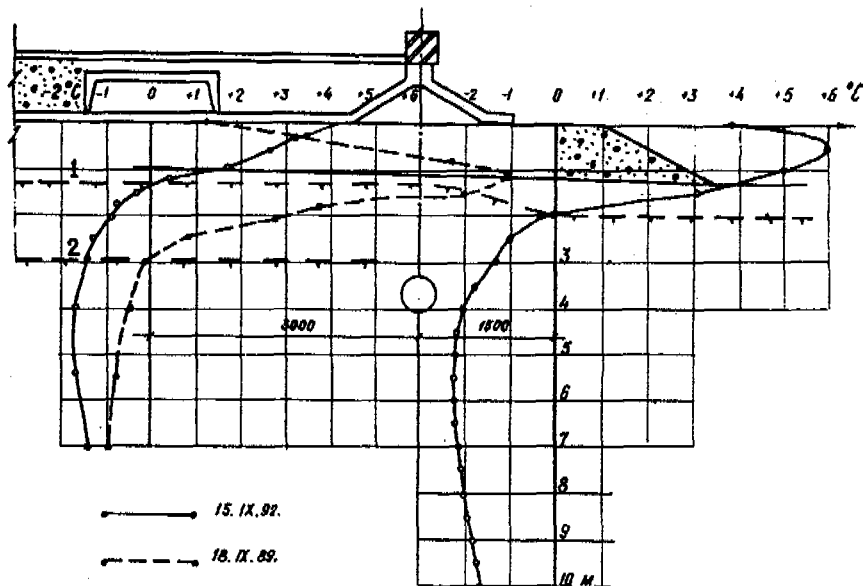


Figure 3. Foundation settlement.  
 1 - top of permafrost - 1992; 2 - top of permafrost - 1989

During the first stage (filling operations) the weather was relatively cold: from  $-8$  to  $-18^{\circ}\text{C}$ .

The fill density was analyzed by determining the soil density in a filled and consolidated state, as well as the granulometric composition, the soil humidity, the content of clayey and silty particles.

The further filling in layers at the second stage was done at a temperature of  $-20^{\circ}\text{C}$ . Use was made of a clean rock with 20 - 30 cm fractions which was consolidated by a vibrating roller to the design elevation.

After the intermediate layer was formed, the operations by making a cast-in-situ shell-type foundation were started.

To provide a continuous concreting of the space foundations the latter was divided into three parts, each of which corresponded to the dimensions of the temperature block. The first technological section on the temperature block of the foundation consisted of horizontal slabs and 1/3 inclined slabs, the second - 2/3 inclined

slabs, horizontal foundation beams and vertical rigidity diaphragms. The concreting of the shell-type foundation was followed by shuttering work, erection of jib cap and wall beam reinforcement with their subsequent concreting.

The observation of the base soil temperatures during the period from 1989 to 1992 inclusively, has shown that: firstly, there occurred a complete soil freezing of the base below the fill footing (before the commencement of work on making the intermediate layer there was a seasonal base thawing) and besides there occurred the lowering of the soil temperature by  $0.2 - 0.5^{\circ}\text{C}$  on the average. The foundation settlements are uniform and do not, as a rule, exceed 2 cm (Figure 3).

#### REFERENCES

- Goncharov Ju.M., Tregubova L.L., Poleshchuk V.L. (1979). Patent 670683 USSR MKI D E02 27/02 Foundations. Discoveries, Inventions N. 24, p. 103.

## MECHANISMS OF LAYER STRUCTURES GROWING DURING GROUND FREEZING

Yakov Gorelik and Vladimir Kolunin

Institute of the Earth's Cryosphere p.b. 1230, Tyumen, 625000, Russia

Experimental data obtained allowed to present characteristic time - dependencies upon the temperature inside a porous filter and the rate of ice growth on the filter's surface. Their correlation was determined during stationary ice growth and during ice penetration onto the filter a pores. The latter is related to a sharp decrease in the rate of ice growth and a sharp increase of the filter's temperature. This obviously proves that the process of a non-streaky zone formation during ground freezing is unstable, whereas ice lensing is a stable process, depending on disturbing factors. On this basis a comprehensive model is suggest for calculation of ice accumulations within freezing ground.

By present two trends for explaining layer grounds proved to be valid both theoretically and experimentally. The first is based on a vacuum filter mechanism of moisture transfer towards a freezing front, and is well illustrated by G.M. Feldman (1988) in his experiments on ground columns freezing. According to this mechanism necessary conditions for ice layer growth in ground are: first, temperature fluctuations on the boundary between thawing and freezing zones within a sample frozen from above, and, second, cohesion of a frozen part of the sample with the walls of a ground containing cassette.

Nevertheless a number of experimental researches demonstrate an alternative mechanism for ice layer growing. Among those researches are experiments on ground columns frozen from beneath (Zhestkova and Schur 1980), on isothermal ice growing above porous filters (Biermans et al. 1978), and the experiments carried out by the authors (Figure 1) in the absence of cohesion. An alternative mechanism is based on power interaction between ice and mineral substances within the ground through the film of unfrozen water. This mechanism presents the second trend accepted by a number of scientists (Gilpin 1980; Gorelik and Kolunin 1989; Grechishcev 1979; Derjaguin and Churaev 1980; O'Neil and Miller 1985). Works Gilpin (1980), O'Neil and Miller (1985) present analytical models for calculating parameters of layer structures formed during ground freezing. Essential in calculations is the presence of frozen fringe beneath a growing ice lens. Re-distribution of tension between solid compounds and unfrozen water results in release of the ground carcass at a certain point within this zone, identifying thus ice lensing. Structures formed according to these models appear to be thin-layered with max. size of ice lenses 1-2 mm. But at a certain depth they are finished up with a thick ice lens corresponding to its stationary growth.

The formation of ice lenses with the ultimate thickness of 1 cm within the framework of these models is hardly ever possible. That is why an



Figure 1. Ice crystal grown on the ceramic filter according to the scheme presented Biermans et al (1978).

analytical description of layer structures within natural ground requires additional studies.

Experiments on ice growth above porous bodies in model systems show that this process is rather stable and can be stopped by destabilizing changes in outside conditions. This determines the most probable mechanism of ice lensing with notable thickness of lenses within frozen ground systems. Experiments by Ozava and Kinoshita (1989) on ice growth on thin porous membranes show that the formation of ice crystals is not followed by their deep penetration into a porous body. This practically means that during stationary ice lensing a freezing zone is absent. This is also proved by the data on thermal regime inside the filter during stationary ice growing and during ice penetration inside the filter unless the process is stable (Figure 2). The general scheme of our experimental layout is analogous to that used Biermans et al. (1978). The operating filter with installed thermocouples was of the diameter 22 mm and of the thickness 5 mm. Besides the device was equipped with automated registration of temperature and moisture levels within the measuring tube bend (Figure 2). During stationary ice growth the temperature at all points inside the filter is lower than the temperature of penetration identified by the fold-point on the curve for level 3 (figure 2). At this point the growth rate of ice decreases to zero, while the temperature at different points within the filter simultaneously goes up to the value corresponding to the freezing temperature of the filter capillaries (curves 1-2). Stationary ice growth can be destabilized by temperature changes or by changes in pressure upon ice. Further increase in liquid level is connected with pressing of water out of capillaries by growing ice crystals. It seems clear that sharp changes in parameters would be impossible if the process were accompanied by ice penetration into the pores with the formation of a frozen zone. The formation of a frozen zone can occur only after stationary ice growth is distorted. At the time  $t_0$  ice crystals penetrated through the filter became visible at the filter's bottom.

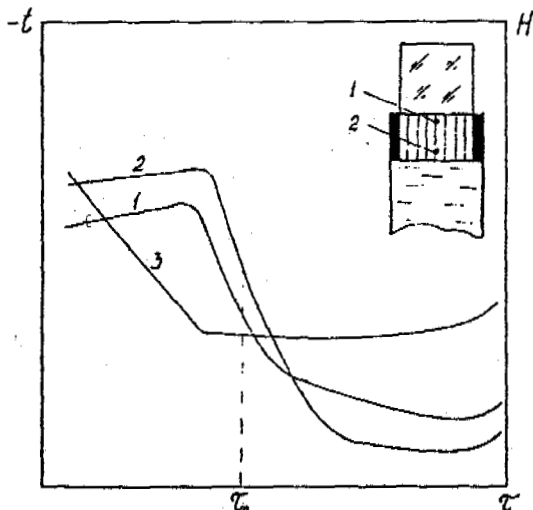


Figure 2. Scheme of installation of thermoregisters inside the filter and changes in temperature (curves 1-2) and in drop of the liquid level in a gauge tube (curve 3).

We suppose that the formation of a layer structure during ground freezing under natural conditions should occur according to the following scheme: growth of an ice lens of a notable thickness proceeds in a stationary regime. The boundary between frozen and thawing ground (freezing front) coincides with the lower boundary of a growing lens, i. e. a frozen zone is absent. During this period the ground temperature monotonously changes with depth from the min value at the front  $t_f < 0^\circ\text{C}$  to the max  $t_g \geq 0^\circ\text{C}$  at a point remote from the ground surface. Water in the ground pores adjacent to a freezing front on the side of thawing ground is super cooled to the temperature lower than the initial freezing temperature of the pores  $t_R < 0^\circ\text{C}$ .

As a result of a cyclic or spontaneous change in outside conditions the stability of ice lens growth is distorted, resulting thus in penetration of ice into the ground pores and partially in the super cooled water zone. Due to instability of this process and in accordance with Fig. 2 the temperature goes up in the initial freezing zone, which contrasts to the data presented Gilpin (1980), O'Neil and Miller (1985), where the calculated temperature monotonously goes down in a frozen zone.

The question of the location of a new lens can be settled on the basis of the criterion for the carcass release ( $\sigma_e = 0$ ,  $\sigma_e$  - tension in the carcass). But the question requires further thorough investigations in compliance with actual.

The present investigation covers only conditions for stationary growth of ice lenses leaving aside aspects related to formation of a new lens.

First, we are interested in a quantitative description of an experiment on ice growth in a pure model situation (Biermans et al. 1978).

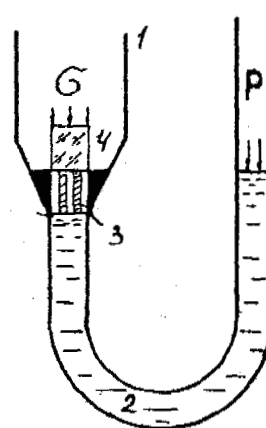


Figure 3. Scheme of experimental layout of Biermans et al. (1978) 1 - a glass tube; 2 - water; 3 - porous filter; 4 - ice column.

The scheme of an experimental device presents a tube of a U-form with a porous filter fixed in its left bend (Figure 3). The initial liquid level allows for a creation of a thin liquid layer above the filter. Independent pressure regulation is designed in the tube channels. The tube was placed in a bath with distilled water used as a thermostat. The temperature in the thermostat was kept constant in the range

-0.01 - -0.06°C. At the initial moment a priming in the form of an ice crystal was put in a liquid layer above the filter. Then the rate of stationary ice growth was measured dependent upon pressure differences in channels at the fixed temperature of surroundings. The authors of the experiment present the necessary parameters and characteristics of the filter used.

Figure 4 shows the diagram for ice-water film equilibrium ( $\Phi_s = 0$ ,  $\sigma = 10^5$  Pa). Figure 5 presents dependence of a summary flow  $\Phi_s$  through the filter upon pressure  $P$  in the right bend of the tube at a constant pressure in the left bend  $\sigma = 10^5$  Pa and at different temperatures of surroundings.

Here are equations for a quantitative analysis of moisture transfer in the discussed experiment. Initial are two correlations for equilibrium at the phase boundary:

$$\sigma = P_f + \Pi(h), \quad (1)$$

$$\frac{\sigma}{\rho_l} - \frac{P_f}{\rho_w} = - \frac{\alpha t_f}{T_0}, \quad (2)$$

which, correspondingly, present the conditions for a mechanic and thermodynamic equilibrium between ice and water film near the solid surface of the filter. Here  $P_f$  is pressure in the film,  $\sigma$  is pressure upon ice,  $\Pi(h)$  is disjoining pressure

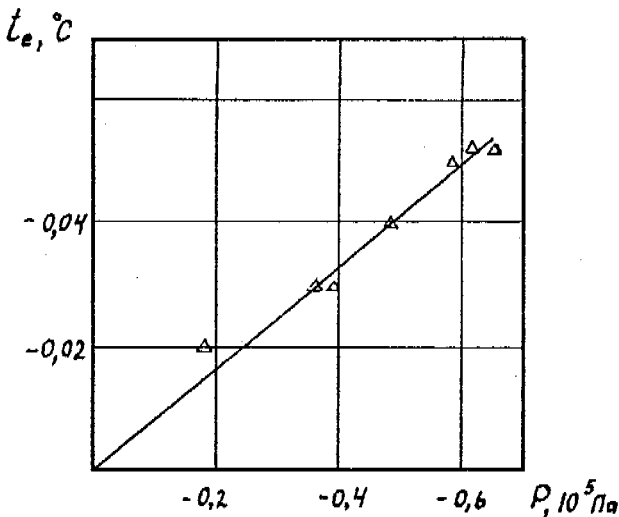


Figure 4. Line of equilibrium between ice and water film.

between solid surfaces dependent upon the film thickness  $h$  (Derjaguin et al. 1985),  $t_f$  is the temperature at the phase boundary,  $T_0$  is the absolute equilibrium temperature of volumetric phases of water and ice at the normal pressure  $P_0 = 10^5$  Pa,  $\rho$  and  $\rho_l$  are ice and water density,  $\alpha$  is specific heat of ice melting. Conditions for a mechanical equilibrium presented in formula (1) indicate the absence of a frozen zone, i. e. the scheme is used without ice penetration into the pores.

For further consideration it is necessary to give a function of the power interaction between solid surface  $\Pi(h)$  (disjoining pressure). It should be noted that at present there are no reli-

able data available for a definite choice of functional dependence  $\Pi(h)$ .

Nevertheless some experimental results, as well as certain approximations of the DLVO theory make it possible to present this dependence in the following generalized way:

$$\Pi(h) = A/h^\alpha, \quad (3)$$

where  $A$  and  $\alpha$  are constants.

Combination of equations (1) and (2) gives the following correlation:

$$\Pi(h) = - \frac{\rho_w \alpha t_f}{T_0} + \left(1 - \frac{\rho_w}{\rho_l}\right) \sigma, \quad (4)$$

which, if (3) is taken into account, determine the dependence of the film thickness upon the outside pressure and the front temperature.

Heat exchange between the phase boundary and surroundings is described by the equation:

$$q = \frac{\lambda}{d}(t_f - t_e), \quad (5)$$

where  $q$  is the heat flow from the phase boundary,  $d$  is the filter thickness,  $t_e$  is the thermostat temperature,  $\lambda$  is the effective coefficient of heat transfer that reflects different conditions of heat exchange between the boundary and surroundings.

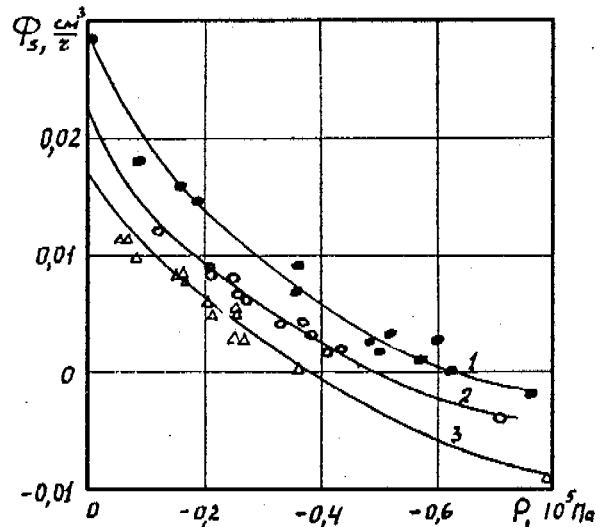


Figure 5. Dependence of the water flow upon pressure at a fixed temperature of the surroundings: O -  $t_e = -0.05^\circ\text{C}$ ;  $\bullet$  -  $t_e = -0.04^\circ\text{C}$ ;  $\Delta$  -  $t_e = -0.03^\circ\text{C}$ . 1, 2, 3 are corresponding calculated curves.

The liquid flow density  $\Phi$  is determined by the equality:

$$\Phi = c(P - P_f), \quad (6)$$

where  $c$  is the coefficient of hydroconductivity of filter - film channels in between ice and the filter surface:

$$c^{-1} = c_g^{-1} + c_f^{-1}, \quad (7)$$

where  $c_g$  is the proper hydroconductivity of a filter section unit,  $c_f$  is the hydroconductivity of

the film that should be calculated by a certain scheme for a liquid flow in the film (Figure 6 a, b).

Liquid coming to the film out of a single capillary spreads over in radial directions from a capillary's mouth and is hampered at the outer contour by counter flows coming out of adjacent capillaries. At the upper film boundary the upstream liquid flow is different from zero. Such a structure of the flow can be described in terms of velocity  $v_r(r, z), v_z(z)$ . The pressure near a single capillary is determined by the function  $P(r, z)$ , where  $r$  and  $z$  are, correspondingly, radial and linear coordinates within an annular zone near the capillary.

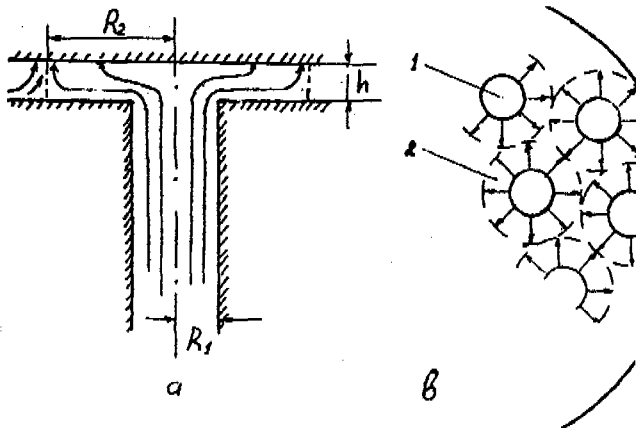


Figure 6. Scheme of the film water flow between ice and water surface; a - separate capillary section; b - plan view; 1 - capillary, 2 - braking zone of flow.

The solution of the task for viscous incompressible liquid flow within the frameworks of the above mentioned scheme allows to express hydroconductivity of the film:

$$c_f = c_f^0 \eta^{-1} n h^3 \equiv c_h H^3, \quad (8)$$

where  $n$  is a number of capillaries per a filter section unit;  $\eta$  is the liquid viscosity;  $c_f^0$  is the numerical multiplier of order 1 dependent only on the correlation of the radii within an annular zone of the liquid flow near a single capillary.

Under the conditions of the stationary flow the values of  $q$  and  $\Phi$  are connected by the correlation:

$$q = \alpha \rho_w \Phi. \quad (9)$$

The set of equations (2), (4), (5), (6) is closed as regards unknown  $\Phi$ ,  $t_f$ ,  $P_f$ ,  $h$  and equalities (3), (7), (8), (9), and makes it possible to investigate the influence of the outside parameters  $\sigma$ ,  $P$ ,  $t_0$  upon the flow  $\Phi$ . The equation for  $t_f$  can be derived from the system:

$$\frac{\lambda}{d}(t_f - t_0) = \alpha \rho_w c \left( P - \frac{\rho_w}{\rho_i} \sigma - \frac{\rho_w \alpha t_f}{T_0} \right), \quad (10)$$

where  $c$  should be expressed through  $t_f$  by correlations (7), (8), (3) and (4).

The analysis of the results should embrace conditions under which the experiment was carried out:  $P < 0$ ,  $\sigma = 0$ . After the solution of equation (1) relatively to  $t_f$ , the flows in the system are described by equations (5) and (6). Let us mark the left side of equation (10) through  $f_h$  (function of the heat flow), and the right side - through  $f_m$  (function of the mass flow). Relative configurations of the functions  $f_h$  and  $f_m$  are shown in Figure 7. The point of intersection of

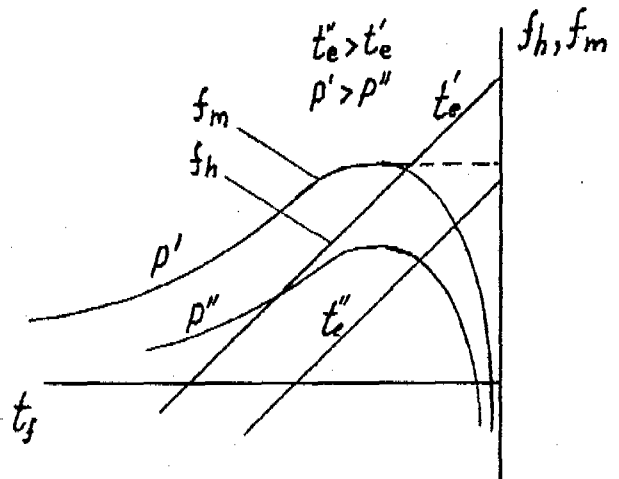


Figure 7. Graphs of the functions of heat and mass flows  $f_h, f_m$ .

the graphs identifies the solution of equation (10). As can be seen from the graphs the flow density  $\Phi$  goes up to the maximum value and then down to zero, provided the temperature of the surroundings  $t_0$  goes down (from  $0^\circ\text{C}$ ) and the pressure  $P$  is constant. Decrease in the pressure  $P$  at a fixed temperature  $t_0$  results in a decrease in the mass flow. For some pressure values the root of equation (10) is  $t_f = t_0$ , while both heat emission and moisture transfer turn to zero ( $q = 0$ ,  $\Phi = 0$ ). The last condition makes it possible to immediately create an experimental graph of equilibrium in the system. With further decrease in pressure the temperature at the front becomes lower than the temperature of the surroundings ( $t_f < t_0$ ) and the flow reverses its sign (ice melting occurs).

These considerations seem to explain a qualitative dependence of the flow  $\Phi$  upon outside factors. Calculations prove that calculated curves can be well applied to experimental coordinates at any value of  $\alpha$  within the range  $1 \leq \alpha \leq 2$ .

Figure 5 demonstrates as an example calculated curves of the flow at  $\alpha = 2$ . The parameter  $A = 4.4 \cdot 10^{-12} \text{N}$  was derived from available experimental data for the thickness of an unfrozen water film at negative temperature. The value of hydroconductivity in (8) was assumed as  $c_h = 7.3 \cdot 10^{12} \text{s}/(\text{kg}\cdot\text{m})$ , and the coefficient of heat conductivity was determined as  $\lambda = 4 \text{ W}/(\text{m}\cdot\text{K})$ .

We should like to mention that the analysis given above proves it valid that hydroconductivity of the film should be chosen in form (8) and disjoining pressure in form (3), which goes

in compliance with the results presented Gilpin (1980). The above mentioned characteristics of the film are further used for the description of ground systems.

It should be noted that at a certain combination of parameters in the system three roots of equation (10) are possible. This situation is conceivable, for example, at small values of the heat emission coefficient or under the conditions  $|t_f| \ll |t_e|$ . In this case two extreme points of intersection in the graph correspond to stable conditions. In fact, time dependence of the film thickness in a non-stationary regime can be represented from some initial value  $h_0$  in the following way:

$$h = h_0 - \int_0^{\tau} \frac{q(\xi)}{\alpha \rho_v} d\xi + \int_0^{\tau} \Phi(\xi) d\xi, \quad (11)$$

where functions  $q(\tau)$  and  $\Phi(\tau)$  are determined by equations (5) and (6) and are time dependent through the temperature  $t_f$ .

After performing differentiation of (11) with respect to time we receive the expression for the rate of changes in the film thickness that can be represented by the functions of  $f_h$  and  $f_m$ .

$$\alpha \cdot \rho_v \frac{dh}{d\tau} = f_m - f_h. \quad (12)$$

Equation (12) readily confirms that small temperature deviations near two extreme roots of equation (10) bring the system back to the initial state. And, vice versa, these deviations near the middle root lead to an increase in deviations.

The question of absolutely stable states associated with the minimum and maximum roots requires special consideration. The experimental evidence however indicates that a decrease in the temperature of the surroundings  $t_e$  leads to an increase of the flow  $\Phi$ , other conditions being equal. This means that in reality this situation corresponds to the maximum root. Besides this, means (and is proved by calculations) that during natural processes the value of  $t_f$  is close to  $0^\circ\text{C}$  (makes up the tiniest parts of a degree). For example during ground freezing the correlation  $|t_f| \ll |t_e|$  is as a rule true, where  $t_e$  should be associated with the temperature at the ground surface. In the latter case the graph of the  $f_h$ -function in Figure 7 presents a straight line parallel to abscissae.

Through monotonous changes in outside parameters (for example a gradual decrease in the temperature  $t_e$ ) it is possible to create such a position that the function of  $f_h$  be a tangent to the function of  $f_m$  at a certain point (a dotted line in Figure 7). The further changes result by a rapid leap in a situation where no stationary solutions are available for equation (10). This can be attributed to the loss of stability and the beginning of ice penetration into ground or filter pores.

In case when the non-equality  $|t_f| \ll |t_e|$  is true and hydroconductivity of the filter can be neglected as compared with that of the film, the stability criterion for the system can be presented obviously:

$$-\lambda t_e / d \leq 2c_h \alpha \rho_v (a/3) 1.5(-P)^{-0.5}. \quad (13)$$

The temperature of penetration at the freezing point is determined by:

$$t_R = 3P \frac{T_0}{\alpha \rho_v}. \quad (14)$$

Condition (13) may as well be a criterion of a stable pushing away of admixture particles from the crystallization front. In this case the violation of condition (13) corresponds to capturing of admixtures. In more complicated cases the determination of stability conditions requires numerical calculations.

In compliance with the above mentioned consideration we shall be able to present the estimation of the size of an ice lens grown at a depth  $z$  during semi-infinitesimal ground freezing with the surface temperature being constantly negative (Figure 8). For the sake of simplicity let us

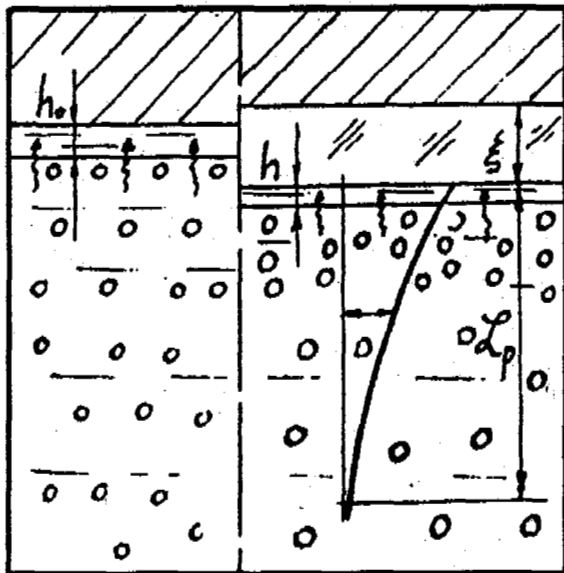


Figure 8. Scheme of ice lensing in the ground system a - at the initial moment; b - during stationary growth.

consider that the thawing part of the ground is homogeneous as regards the moisture content at the initial moment and has the temperature of  $0^\circ\text{C}$ . The process of ice lensing can be divided in two stages. At the first stage the temperature at the bottom of the lens is in the range  $t_R < t_f < 0^\circ\text{C}$  and ice does not penetrate in pores of the thawing ground, i. e. the frozen zone is absent. The second stage begins when the temperature reaches a certain value  $t_R$ , while ice penetration into the thawing ground begins, which causes the formation of the frozen zone of the finite thickness. At this moment the liquid flow on the lens sharply decreases due to an increase in hydroresistance of ground capillaries partially filled in with ice. The further nutrition of the lens proceeds through the frozen zone. The major part of ice within the lens is supposed to accumulate during the first stage.

The pressure distribution in the thawing ground is governed by the equation for the filtration consolidation:

$$\frac{\partial P_w}{\partial t} = c_v \frac{\partial^2 P_w}{\partial z^2}, \quad (15)$$

$$c_v = k_f / (g \rho_w a_0), \quad (16)$$

where  $g$  is the acceleration of gravity;  $k_f$ ,  $a_0$  are correspondingly coefficients of filtration and compressibility of the thawing ground. The pressure in the depth of the thawing zone is  $P_w = 0$ .

Confining to approximate distribution of  $P_w(z, \tau)$  and by introducing the radius of influence  $L_p(\tau)$  (Barenblatt 1954)

$$L_p(\tau) = (c_v \tau)^{1/2}, \quad (17)$$

we can express hydroconductivity of the thawing zone  $c_g$  through its characteristics

$$c_g = B \tau^{-1/2}, \quad (18)$$

where  $B = \{k_f a / (\rho_w g)\}^{1/2}$ .

Thus, a monotonous increase in hydroresistance occurs during lens growth due to involvement of deeper horizons. The maximum of the function of the mass flow  $f_m$  determined by the right side of equation (10) with the coefficient of hydroconductivity  $c$  determined by (7), (8) and (18) monotonously decreases in time due to a decrease in hydroconductivity  $c_g$ . In a certain time interval  $\tau_1$  the stationary lens growth is distorted, and, thus, the determination of the lens size is confined to identification of this time interval.

Dwelling upon consideration for  $\alpha = 1$  we derive for  $\tau_1$ :

$$\tau_1 = (B/\xi')^2 [(2/3)(A^3 c_h)/(3\xi')^{1/2} - \delta]^2, \quad (19)$$

where the rate of freezing  $\xi'$  and pressure upon ice from above the upper ground thickness  $\delta$  is determined:

$$\xi' = -\lambda t_0 / (\alpha \rho_w z); \quad \sigma = \gamma z, \quad (20)$$

where  $\gamma$  is a volumetric ground weight.

The size of an ice lens  $\xi_1$  grown at a depth  $z$  under stationary conditions can be determined through correlation  $\xi_1 = \xi' \tau_1$ . Introducing a clear dependence on  $z$  and taking into consideration (20) we finally derive

$$\xi_1 = [B^2 \gamma z^2 (\phi - z^{1/2})^2] / \beta, \quad (21)$$

where

$$\beta = -\lambda t_0 / (\alpha \rho_w); \quad \phi = 2[A^3 c_h / (27\beta)]^{1/2} \gamma^{-1} \quad (22)$$

The analysis of equation (21) shows that distribution of the sizes of ice lenses according to depth is of non-monotonous character (Figure 9) and at a certain depth turns to zero. Calculations show that this depth determined through parameters of clay formations can make up dozens of meters. The reason for the decrease in the lens size beginning with a certain depth is the prevailing role of pressure from above upper ground horizons that push away the migrating inflow towards the front.

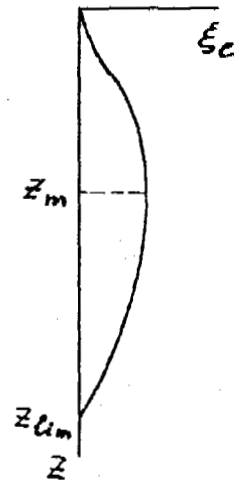


Figure 9. Configuration of the function of the distribution of ice lenses thickness according to the depth of the ground section.

In addition it is necessary to mention that the function of distribution (21) appear to be very sensitive to the configuration of the function of interaction (3). Thus, at  $\alpha = 2$  for small  $z$  there appears a zone free from ice lenses grown in the stationary regime.

#### REFERENCES

- Barenblatt, B.I. (1954) Approximate methods of the theory of one dimension filtration of the fluid by elastic regime. Izv. AN SSSR, OTN, N9, 35-49 (in Russian).
- Biermans, M.B.G.M., K.M. Dijkema, D.A. de Vries (1978) Water movement in porous media towards an ice front. J. Hydrol., v.37, 137-148.
- Derjaguin, V.V., N.V. Churaev (1980) The flow of the unfrozen small water layers and the frost deformations of the porous media. Kolloidnyi zurnal, t. XII, N5, 842-852 (in Russian).
- Derjaguin, B.V., N.V. Churaev, V.M. Muller (1985) The surface forces. M., Nauka, (in Russian).
- Feldman, G.M. (1988) Moisture migration in thaw and freezing soils. Novosibirsk, Nauka, (in Russian).
- Gilpin, R.R. (1980) A model for the prediction of ice lensing and frost heave in soils. Water Resour. Res., v. 16 N 5, 918-930.
- Gorelik, Ya.B., V.S. Kolunin (1980) Moisture migration by freezing of porous media. Geokriologicheskije issledovaniya v arkticheskikh raionakh, vyp. IV, Yamburg, 79-96 (in Russian).
- Grechishcev, S.E. (1979) Interrelation in pore water phase system and a thermodynamic model of frozen ground. Inzhenernaja geologija. N 4, 72-85 (in Russian).
- O'Neill, R., R.D. Miller (1985) Exploration of a rigid ice model of frost heave. Water Resour. Res., v.21, N3, 218-296.
- Ozava, M. S. Kinoshita (1989) Segregated ice growth on a microporous filter. J. Colloid Interface Sci., v.132, N61, 113-124.
- Zhestkova, T.N., Yu.L. Schur (1980) Ground freezing in open system. Merzlotnija issledovaniya. M., MGU, vyp. XIX, 164-177 (in Russian).

OPTIMAL PARAMETERS OF INTERNALLY PRESSURIZED OPENING IN PERMAFROST

Igor E. Guryanov

Permafrost Institute, Russian Academy of Sciences Yakutsk 677018, Russia

The allowable parameter limits for openings pressurized from the inside - depth of openings and minimum pressure - are studied in relation to the value of operating pressure, opening geometry and duration of off-loading. Contours of the limit equilibrium zone of ground, deformation of ground at the opening boundary and in the massif are calculated in the elastic-plastic problems. The equations and plots presented enable one to design openings with optimal parameters under various engineering conditions.

The new methods of low temperature separation of natural gas and condensate generate a need for the construction of underground non-shaft-type storages at a depth of hundreds of meters (Musaev 1983). Thick permafrost ground provides tightness of storages, and the occurrence of sands permits the application of jetting technology for washing out a cavity through a borehole (Gaev et al. 1986).

Our task is to investigate the possibility of constructing underground non-shaft-type storages in the Middle-Viluy gas field area, Yakutia. The generalized geological-lithological profile of this area is composed of the Cretaceous deposits ( $K_2$ ) below the Quaternary cover. Monotypic deposits (sand and unconsolidated sandstone) extent to 850 m depth. Permafrost is 590 m thick; temperature changes with depth can be represented by the form:

$$\Theta = -3.1 + 0.005 \cdot H,$$

where  $\Theta$  - ground temperature, °C; H - depth from the surface, m.

Values of the ultimate long-term strength of frozen ground are normally required to determine the stability of an opening. But we applied the method different from the conventional method which requires much time due to the invariance of rheological curves. Uniaxial compression tests were performed on frozen ground at a continuous loading rate of 5 - 10 kPa/hr; the rate of ultimate deformation was not higher than  $0.001 \text{ hr}^{-1}$ ; and the reaching of ultimate strength was accompanied by a sharp increase in the rate which was greater than that in conventional tests. At  $-5^\circ\text{C}$  the test results are as follows: the mean modulus of sand deformation  $E^* = 60 \text{ MPa}$ , the Poisson's ratio value  $\nu = 0.35$ .

The mean values of the physical characteristics of the frozen sand tested are: porosity coefficient  $e_m = 0.75$ , moisture content  $S_r = 0.96$ , density of pore ice  $\rho_i = 0.86 \text{ g/cm}^3$ . With no air porosity and ice-cement consolidated up to  $\rho_i = 0.92 \text{ g/cm}^3$ , the ultimate volume compressibility of this ground is  $\epsilon_0 = 0.04$ .

The test reveal that the mean stress significantly affects the strength of the sand. So, the results are rationalized according to the

Guber-Mises strength condition relating octahedral tangential stresses  $\tau_0^*$  to normal  $\sigma_0^*$  stresses:

$$\tau_0^* = c^* + \sigma_0^* \text{tg}\varphi = 0.6 + 0.314\sigma_0^*, \text{ MPa.} \quad (2)$$

To extrapolate expression (2) which was solved at  $-5^\circ\text{C}$  to any temperature, taking into account the recommendations given in Manual for Defining Physical, Thermophysical and Mechanical Characteristics of Frozen Ground (Manual 1973) and Structural Design Codes (SNIIP 1990) the angle of internal friction  $\varphi^0$  is assumed to be constant, and cohesion  $c^*$  on account of a narrow temperature range is given by:

$$c^* = 0.2 - 0.08 \Theta, \text{ MPa.} \quad (3)$$

Substituting (1) into (3) we obtain  $c^*$  as a function of depth:

$$c^* = 0.448 - 0.000424 H, \text{ MPa.} \quad (4)$$

From eqn. (4) a change in  $c^*$  is less than 10% for 100 m of depth, which does not exceed the accuracy of strength estimations. Taking into account an increase in density and strength of ground with depth which is reverse to eqn. (4), we think that the strength condition is depth-independent at the mean ground temperature  $\Theta = -2.5^\circ\text{C}$  at the sites of intended openings:

$$\tau_0^* = 0.4 + 0.314\sigma_0^*, \text{ MPa.} \quad (5)$$

Since the considered storages will be the first of this kind, only approximate dimensions of an opening depending on designed capacity are known, while the exact geometry is unknown. So, the stress-strain state of the surrounding ground is calculated for the two extreme geometries of an opening: spherical and cylindrical, and intermediate shapes are estimated according to their similarity to the extreme ones. Since drilling of a borehole amounts to 75% of the total cost of underground storage construction (Musaev 1983), it is necessary to determine the allowable minimum



depth of an opening.

We adopt the depth of an opening and operating pressure in it as operating parameters. As the final task is to find out optimal relationship between these parameters, we must determine the geometry of a plastic zone in the ground massif surrounding an opening, and predict displacement of an opening contour in relation to:

- the depth of an opening at a specified operating pressure in it (higher than natural pressure);
- the operating pressure (lower than natural pressure) at a specified depth of an opening.

Since the effect of the opening depth is controlled by the natural pressure, i.e. ground weight which interacts with the operating pressure in an opening, and this depth is compared with dimensions of an opening, we introduce dimensionless parameters into our analysis.

Linear dimensionless parameters: relative radii and displacements  $\rho = r/r_0$ ;  $k = R/r_0$ ;  $u = U/r_0$ , where  $r_0$  - initial radius of an opening, m;  $r$  - radial coordinate, m;  $R$  - external radius of the calculated zone, m;  $U$  - radial displacement, m; depth of an opening  $h = H/r_0$ , where  $H$  - the distance from the day surface to the center of an opening.

Force dimensionless parameters: natural (ground) pressure  $q_B = p_B/\gamma r_0 = H/r_0 = h$ , where  $\gamma = 0.019 \text{ MN/m}^3$  - volume weight of ground; pressure in an opening  $q = p/\gamma r_0$ ;  $p$  - operating pressure, MPa; modulus of deformation  $E = E^*/\gamma r_0$ ;  $[E^*]$  - MPa; stresses  $\sigma = \sigma^*/\gamma r_0$ ;  $\tau = \tau^*/\gamma r_0$ ;  $[\sigma^*]$ ,  $[\tau^*]$  - MPa; cohesion  $c = c^*/\gamma r_0$ ;  $[c^*]$  - MPa.

In the case of axial (cylindrical) and central (spherical) symmetry of the stress-strain state the Cauchy's formula are:

$$\epsilon_\rho = \frac{\partial u}{\partial \rho}; \quad \epsilon_\alpha = \frac{u}{\rho},$$

where  $\epsilon_\rho$ ,  $\epsilon_\alpha$  - radial deformation and tangential deformation, respectively. In the case of the considered symmetries of the elastic-plastic problem, deformations depend only on the radius. From the Cauchy's formula the deformation continuity equation can be written as:

$$\rho \frac{d\epsilon_\alpha}{d\rho} = \epsilon_\rho - \epsilon_\alpha. \quad (6)$$

We use the Hencky equation:

$$\sigma_i - \sigma_o = \frac{E}{1+\nu} (\epsilon_i - \frac{\epsilon_o}{3}), \quad (7)$$

where  $i = \rho, \alpha$  - radial and tangential indices. We use the difference of main stresses as well, taking into account eqns. (6) and (7):

$$\sigma_i - \sigma_o = \frac{E}{1+\nu} \rho \frac{d\epsilon_\alpha}{d\rho}. \quad (8)$$

For the symmetric problem, the equilibrium equation is:

$$-\rho \frac{d\sigma_\rho}{d\rho} = \sigma_\rho - \sigma_\alpha, \quad (9)$$

where  $i = 1, 2$  correspond to the axial symmetry and central symmetry, respectively. Substituting eqn. (8) into eqn. (9) taking into account eqn.

(7), and calculating eqn. (9) for the case of the central symmetry problem ( $i = 2$ ) gives:

$$3 \frac{1-\nu}{1+\nu} \sigma = C,$$

i.e. the mean stress is radius-independent:  $\sigma_o = \text{const}$ . In the case of the axial symmetry ( $i=1$ ), from eqn. (9) we obtain:

$$\frac{3}{1+\nu} \sigma = C + \sigma_z. \quad (10)$$

Since ground destruction along the contour of an opening is related only to horizontal displacement during vertical deformations

$$\epsilon_z = \frac{h}{E} \left(1 - \frac{2\nu^2}{1+\nu}\right) = \frac{h\beta}{E},$$

and the Hencky equation (7) is complemented by eqn.

$$\sigma_z = \frac{1}{1+\nu} (h\beta + 3\nu\sigma_o),$$

eqn. (10) becomes:

$$3(1-\nu)\sigma_o = C(1+\nu) + h\beta.$$

Again, the mean stress is independent of radius:  $\sigma_o = \text{const}$ .

Thus, the common feature of the stress states in the problems calculated is that the mean stresses are constant. So, the strength conditions (5) can be considered as the plasticity conditions which in the dimensionless form are:

$$\tau_o = c + \sigma_o \text{tg}\varphi = c + 0.314\sigma_o;$$

$$c = 4.21 + 1.75, \quad (11)$$

at the opening radius range  $r_0 = 5 - 12 \text{ m}$ .

Now we consider the stress state of the ground surrounding a spherical or cylindrical opening. The calculated ground massif (a spherical layer or a cylindrical layer) consists of two concentric zones: I - the external elastic zone, and II - the internal plastic zone.

For the case of a spherical layer, from constancy of the mean stress in the elastic zone

$$\sigma_o = \frac{\sigma_\rho + 2\sigma_\alpha}{3} = C_o$$

eqn. (9) becomes:

$$\rho \frac{d\sigma_\rho}{d\rho} + \sigma_\rho = C_o. \quad (12)$$

For the plastic zone, eqn. (9) with eqn. (11) becomes:

$$\rho \frac{d\sigma_\rho}{d\rho} = -3\sqrt{2}(c + \sigma_o \text{tg}\varphi). \quad (13)$$

Calculating eqns. (12) and (13), and equating the stress values at the boundary of the elastic and plastic zones, we obtain the equation for the external radius of the plastic zone (the boundary of zones I and II):

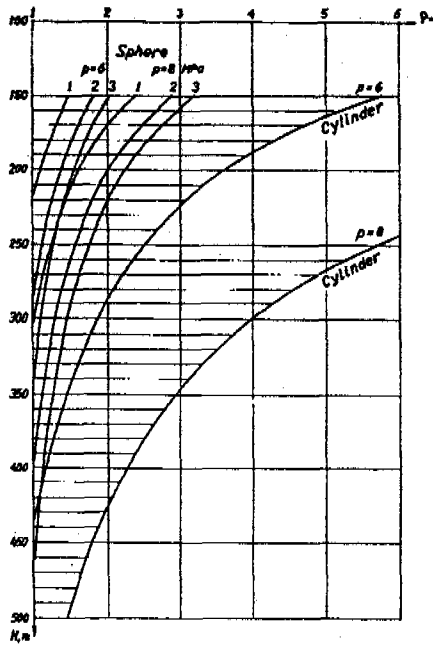


Figure 1. Plastic zone radius  $\rho_{II}$  in the ground mass surrounding spherical and cylindrical openings versus the opening depth  $H$  at different operating pressures  $p$ . Different pressures on the external contour of the spherical calculated area: 1 -  $\sigma_k = h$ ; 2 -  $\sigma_k = 9h/13$ ; 3 -  $\sigma_k = 7h/13$ .

$$\rho_{II} = \exp \left\{ \frac{1}{3} \left[ \frac{0.707(q - \sigma_k \operatorname{sgn}(q - \sigma_k - 1))}{c + \sigma_0 \operatorname{tg} \varphi} \right] \right\}, \quad (14)$$

where  $\operatorname{sgn}$  is a function of the relation between the operating pressure in an opening  $q$  and the natural pressure  $\sigma_k$ .

The mean value of  $\sigma_k$  is

$$\sigma_0 = \frac{1 + \nu}{1 - \nu} \frac{h}{3} = \frac{9}{13} h,$$

and it corresponds to the mean radial depth of zone II around an opening. For the hemisphere which is above or below the equatorial plane, the minimum radial depth (in the key) is determined from eqn. (14) at  $\sigma_k = h$ , and the maximum radial depth (on the horizontal axis) at

$$\sigma_k = \frac{\nu}{1 - \nu} h = \frac{7}{13} h.$$

In the case of a cylindrical layer, from constancy of the mean stress it follows that the sum of radial and tangential stresses is constant:

$$\sigma_r + \sigma_k = 2C_0,$$

i.e. for the elastic zone, eqn. (9) becomes:

$$\frac{\rho}{2} \frac{d\sigma_r}{d\rho} + \sigma_r = C_0. \quad (15)$$

In the plastic zone, eqn. (9) with eqn. (11) gives:

$$\rho \frac{d\sigma_r}{d\rho} = -D, \quad (16)$$

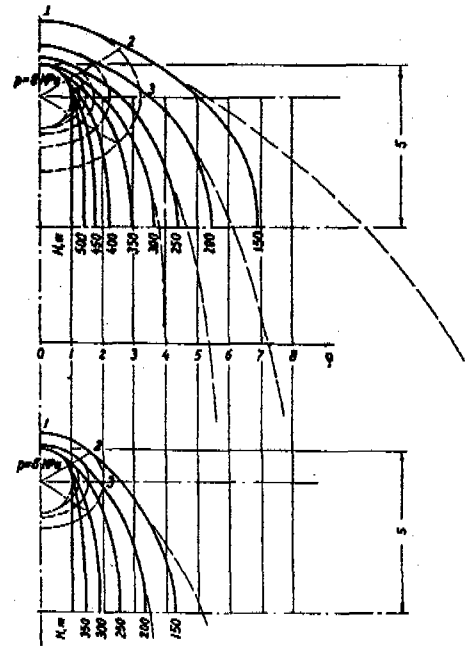


Figure 2. The plastic zone boundaries in the ground mass of a cylindrical opening (height  $L/r_0 = 10$ ) and a spherical opening at different operating pressures  $p$  and depths  $H$ .

where

$$D = \frac{2h}{\sqrt{3(1 - \nu)}} \sqrt{\frac{1}{2} \left[ (1 - \nu) \frac{3c}{h} + (1 + \nu) \operatorname{tg} \varphi \right]^2 - (1 - 2\nu)^2}.$$

Calculating eqns. (15) and (16), and equating stresses at the boundaries of zone I and zone II, we obtain the plastic zone radius expression:

$$\rho_{II} = \left[ \frac{1}{D} \left( q - \frac{\nu h}{1 - \nu} \right) \operatorname{sgn} \left( q - \frac{\nu h}{1 - \nu} \right) - \frac{1}{2} \right]. \quad (17)$$

Figure 1 gives values of the plastic zone radius in the ground mass around a spherical opening versus the opening depth which are calculated by eqn. (14) for different values of  $\sigma_k$  (curves 1, 2, 3), and those around a cylindrical opening which are calculated by eqn. (17). As shown in Figure 1, at a smaller opening depth and greater pressure the plastic zone spreads over a large area of the surrounding ground.

Different variants of loading on the external contour are used in the central symmetry scheme to estimate the effect of ground pressure asymmetry. So, the presented radial depths of the plastic zone must be estimated with consideration for the equivalent angular coordinate of each symmetric calculation (see Figure 2). Since asymmetry of zone II in the transition region between cylindrical and spherical calculations can not exceed curvature of the spherical variant, we introduce increasing heights of a cylindrical opening abutting on a spherical one in Figure 2.

Figures 1 and 2 illustrate behaviour of the ground surrounding a pressurized opening with the operating pressure significantly greater than the

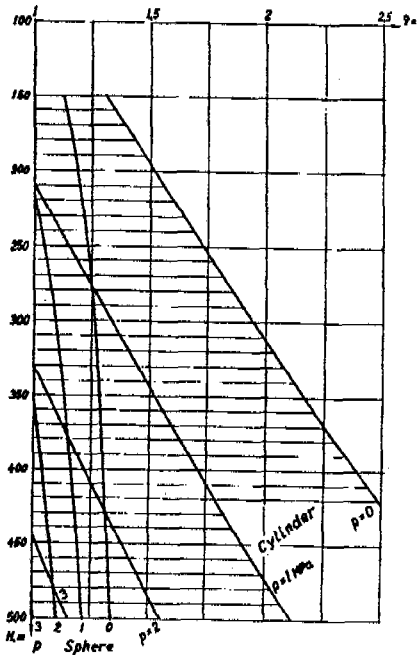


Figure 3. The plastic zone radius  $\rho_{\pi}$  in the ground massif around a spherical opening and a cylindrical opening versus the depth  $H$  at the operating pressure  $p=0, 1, 2, 3$  MPa.

natural (ground) pressure. At a given limited plastic zone radius these relations can be used to determine the minimum depth of an opening.

For the case of an opening with  $q < \sigma_k$ , the natural pressure is a factor controlling ground destruction, and the plastic zone radius increases with increasing depth of an opening (Figure 3). As for the plastic zone geometry, the range of pressure values in an opening which do not impede formation of the plastic zone in the ground, widens with depth. This general regularity is illustrated in Figure 4.

If plastic strain should be avoided, eqns. (14) and (17) enable us to limit the range of safe values of operating pressure in the spherical opening at  $\rho_{\pi} = 1$

$$\sigma_0(1 - \sqrt{2}tg\varphi) - \sqrt{2}c < q < \sigma_0(1 + \sqrt{2}tg\varphi) + \sqrt{2}c, \quad (18)$$

as well as in the cylindrical opening

$$\frac{\nu h}{1 - \nu} - \frac{D}{2} < q < \frac{\nu h}{1 - \nu} + \frac{D}{2}. \quad (19)$$

In expressions (18) and (19), the upper limit is the limit of increasing the allowable pressure in a pressure opening, and the lower limit is allowable off-loading. These expressions enable us to change depths as well. Thus, in a free opening ( $q=0$ ), the maximum depth of a spherical opening  $h = 3.68 c$ , or  $H = 77.4$  m, and that of a cylindrical opening  $h = 3.66 c$ , or  $H = 77$  m. In the case of a pressurized opening with pressure values of 6 - 8 MPa, the minimum depth of a spherical opening is 368 - 504 m, that of a cylindrical opening is 435 - 606 m.

Dimensions of the plastic zone calculated by eqns. (14) and (17) and shown in Figures 2 and 4 are much greater in a cylindrical opening as com-

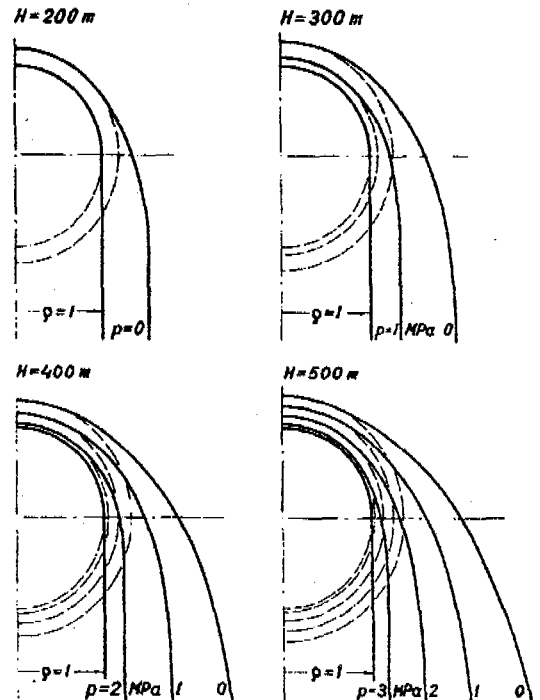


Figure 4. The plastic zone boundaries in the ground massif surrounding a spherical opening and a cylindrical opening at the operating pressures  $p=0, 1, 2, 3$  MPa and depth  $H=200 - 500$  m.

pared to a spherical opening. So,  $1/r_0 = 10$ , the highest value, is taken for the cylindrical opening, and plots of the plastic zone boundary in Figure 1 are limited by curvature of the spherical problem solution.

The first parameter - the depth of an opening - is determined for two values of maximum pressure  $p=6$  MPa and  $p=8$  MPa. The ultimate radial expansion of a cavity equal to 0.5 m is adopted as the requirement for service safety of an opening and an ice wall. Radial displacement of the opening contour is taken as the sum of radial displacement of zones I and II. Assuming the plastic zone to be incompressible (because sand dilatancy is not taken into account), and analyzing the stress-strain state we obtain the expansion for wall displacement of a spherical opening:

$$u = \sqrt[3]{1 + (\rho_{\pi} + u_{\pi})^3 - \rho_0^3} - 1, \quad (20)$$

where  $u_{\pi}$  - radial displacement of the boundary of zone I and zone II which is

$$u_{\pi} = \int_{\rho_{\pi}}^{\infty} \left( \epsilon_{\rho} - \frac{1 - 2\nu}{E} \sigma_0 \right) d\rho = \frac{1 + \nu}{2E} \left[ q - 3\sqrt{2}(c + \sigma_0 tg\varphi) \ln \rho_{\pi} - \sigma_k \right] \rho_{\pi}. \quad (21)$$

Wall displacement of a cylindrical opening is calculated in a similar way:

$$u = \sqrt{1 + u_{\pi}(u_{\pi} + 2\rho_{\pi})} - 1, \quad (22)$$

where

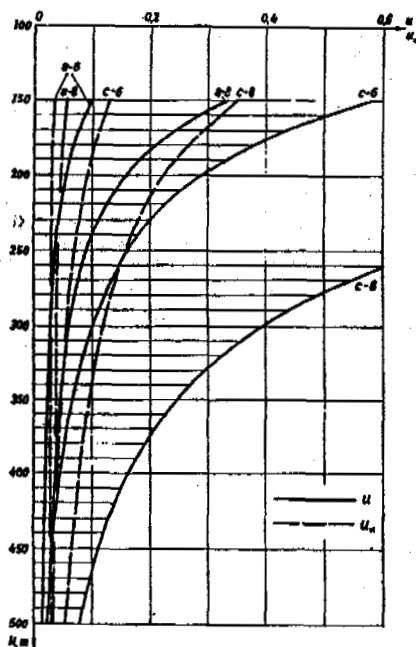


Figure 5. Relative displacement of opening contours  $u$  and the plastic zone  $u_n$  versus depth  $H$ : s-6, s-8 - spherical opening  $p = 6, 8$  MPa; c-6, c-8 - cylindrical opening  $p = 6, 8$  MPa.

$$u_n = \int_{\rho_n}^{\infty} \epsilon \rho d\rho = \frac{1 + \nu}{E} \left( q - D \ln \rho_n - \frac{\nu h}{1 - \nu} \right) \rho_n \quad (23)$$

Table 1. Displacement of the plastic zone contours around an opening

$p, \text{MPa}$	Sphere			Cylinder		
	$r_o = 8 \text{ m}$	$r_o = 8 \text{ m}$	$r_o = 8 \text{ m}$	$r_o = 7.5 \text{ m}$	$r_o = 7.5 \text{ m}$	$r_o = 7.5 \text{ m}$
	$H, \text{m}$	$U, \text{m}$	$U_n, \text{m}$	$H, \text{m}$	$U, \text{m}$	$U_n, \text{m}$
6	190	0.47	0.24	230	0.48	0.34
8	290	0.50	0.30	350	0.51	0.42
	Cylinder $r_o = 5 \text{ m}$			Cylinder $r_o = 7.5 \text{ m}$		
6	300	0.49	0.27	350	0.48	0.34
8	460	0.51	0.31	520	0.51	0.38

Table 2. Minimum allowable pressures in openings, MPa

$r_o, \text{m}$	Sphere				Cylinder			
	8	12	12	350	5	7.5	7.5	520
$h, \text{m}$	190	290	230	350	300	460	350	520
$p_1, \text{MPa}$	0	0.08	0.20	0.74	0.85	2.02	1.46	2.79
$p_2, \text{MPa}$	0.25	1.15	0.88	1.68	1.50	2.82	1.99	3.42

Eqns. (20) - (23) relate ground displacement to the operating pressure and the depth of an opening. Table 1 gives minimum depths of openings calculated using these equations at allowable wall displacement  $u \approx 0.5 \text{ m}$ .

Depths greater than those given in Table 1 are allowable at certain radius and pressure; smaller depth result in wall displacement  $U \approx 0.5 \text{ m}$ . Figure 5 gives the detailed interpretation of these relations. It can be used while choosing depth of an opening from different considerations.

The second parameter - the lower limit of al-

lowable pressure in an opening - can be estimated using plots in Figure 3, or eqns. (14) and (17) on condition that the minimum depth of the plastic zone  $(r_n - 1) r_o \leq 0.5 \text{ m}$  whose ground is held by the lining during displacement toward the cavity.

The limit and duration of short-term off-loading are determined by the rate of contraction of an opening which is assumed to be equal to the rate of volume deformation in the tests:

$$\frac{d\epsilon_o}{dt} = 0.0082t, [t] \sim \text{day}.$$

From it we define the time to reach the ultimate deformation  $\epsilon_o$ .

$$t = \sqrt{244\epsilon_o} = 3.1 \text{ days}.$$

As the tests have shown the time for the entire ground of zone II to reach the ultimate deformation is 1 day (Votyakov 1961), so, the total allowable duration of off-loading is 4 days.

Assuming the linear contraction of an opening allowable in practice to be less than 0.1 m and taking into account the volume deformation of ground, it is easy to determine from eqns. (14) and (17) allowable radial depth of the plastic zone and calculate the minimum pressure during short-term and long-term off-loading of a cavity using the following expressions: for the spherical opening

$$p = 0.01315[H - 1.331(0.333 + \ln \rho_n)(97.1 + H)], \quad (24)$$

for the cylindrical opening

$$p = 0.01023[H - 13.78(0.5 + \ln \rho_n) \sqrt{48.4 + H}], \quad (24)$$

where  $p$  - pressure, MPa;  $H$  - depth, m.

The results of eqns. (24), (25) calculations for the recommended depths of the opening (Table 1) are given in Table 2; the presented values of pressure  $p_1$  are allowable for not longer than 4 days, and the values of  $p_2$  are allowable without time restrictions.

It is evident from Table 2 that spherical openings are preferable not only due to lesser depths but to greater allowable lowering of the operating pressure in an opening as well. Total short-term off-loading is permissible only for the spherical opening constructed at a minimum depth. Moreover, the stress-strain states of the ground in a loaded and off-loaded spherical opening are asymmetric along the perpendicular axes, i.e. the sphere has full stability.

The study of the extreme geometries of an opening - spherical and cylindrical - enables us to estimate the performance of actual oval openings whose shape being an intermediate form between the two extremes is, strictly speaking, unknown and is characterized only by the generalized relationship between diameter and vertical dimensions. The method of an a priori analysis we use which is based on the uncertainty of initial data is called the method of equivalent symmetric solutions. Though the method is approximate, the recommended depths of an opening (Table 1) are twice smaller than those given in a preliminary

design of the gas mining project (Musaev 1983).

It is to be noted that the proposed analysis of continuous variations of the parameters of an internally pressurized opening in relation to depth is valid for the permafrost ground only.

#### REFERENCES

- Gaev, A.Y., V.D.Shugorev and A.P.Butolin (1986). Underground storages: construction, development and performance. 223 pp. Nedra, Leningrad.
- Musaev, R.M. (1983). Gas preparation in underground storages constructed in permafrost. Proc. Conf.

Search, Prospecting and Development of Oil and Gas Fields in Yakutskaya ASSR. Yakutsk, v. 2, 114 - 117.

Manual for defining physical, thermophysical and mechanical characteristics of frozen ground (1973). 191 pp. Stroiizdat, Moscow.

SNiP 2.02.04-88. (1990). Structural design codes 2.02.04-88. Bases and foundations on permafrost. 52 pp. Gosstroi SSSR, Moscow.

Votyakov, I.N. (1961) Physical and mechanical properties of perennially frozen ground in Central Yakutia. 62 pp. Izdatelstvo AN SSSR, Moscow.

## DYNAMICS OF PERMAFROST-HYDROGEOLOGICAL MEDIUM AT PRIMARY (LEDGE) DIAMOND DEPOSIT DEVELOPMENT

Igor V. Klimovsky and Semyon P. Gotovtsev

Permafrost Institute, Russian Academy of Sciences Yakutsk 677018, Russia

The article presents the results of geothermal observations made on technogenic areas (quarries, dumps of enclosing rocks, spoil areas, ground for highly mineralized water storage) of the Udachninsky mining and concentrating plant (the Siberian platform). The possibility of using the geothermal method for singling out water-absorbing collectors in the upper part of the cryogenic layer is justified. The analysis of the dynamics of the temperature field of rocks in the course of area development is given. A dangerous ecological aspect of using the systems of brine burying near watercourse valleys is emphasized.

The primary diamond deposits located in the cryolithozone (permafrost zone) are developed, as a rule, by the open-cut method. As a result, the excavated quarries completely destroy the vegetation and soil surface covers and cause considerable transformation of the day surface. Vast areas are allocated for dumps and tailings. The total area of technogenic surface disturbance is estimated to be dozens of square kilometers. Besides, since the quarries reach the regional level of highly mineralized water - cryopegs (saline water below 0°C) - there is a problem of their drainage and adequate storage of drained brines. Storing of cryopegs in underground collectors is considered to be the most efficient method preventing the contamination of the environment. The following aspects should be considered in this case according to Borisov and Alexeev (198): 1) the well-known property of a brine to remain liquid when subjected to the effect of a wide range of negative temperatures; 2) non-uniformity of the brine on top - ice from bottom system: the brine will inevitably melt the ice if the medium temperature is above its formation point; 3) emptying the collectors space (in case of ice transformation to a liquid and the existence of hollows which are free of ice in permafrost); 4) the effect of a dense convection which consists in fresh brine supply to the point of interaction with ice where its desalinized mixture with dissolved (melted) ice comes to the surface. In this case the process proceeds till complete melting of ice in filtration channels, the concentration gradient in liquid being preserved.

It seems to be useful to examine the raised problems having taken as an example the facilities of the Udachninsky mining and concentrating plant, where primary diamond sources have been being quarried for more than 30 years.

Here is some brief information on the permafrost conditions of the region. The permafrost zone is of a continuous nature: the upper 100-300 m are presented with permafrost containing ice. Below is a layer of frost soil with liquid saline water of negative temperature. The entire thickness of the cryogenic layer ranges from 600 to

1500 m. The cryogenic structure may be largely explained by the lithological and petrographical composition and by the structural and tectonic situation by the time of epigenetic freezing. In crushed areas one may observe fissured, fissure-vein and cryogenic vein structures. The formation of these structures caused the development of a cryogenic disintegration level which spreads deeply to the permafrost bottom. The upper part of the rock layer, i. e. the level of active cryohypergenesis is heavily destroyed. The processes of physical weathering that affected the tectonic jointing have increased clearances in the layer and formed additional hollows for ice formation.

Geothermal features of the cryolithozone have been studied well enough. The first data on the temperature of rocks in an area of the Udachnaya diamond pipe were obtained in the early 1960s. Accordingly to the results of this work there have been made conclusions on the occurrence of a thick permafrost layer and on the complicated character of temperature formation (Klimovsky and Ustinova 1962). It has been discovered that temperature of rocks within the blue ground body varies from -6.0°C to -7.8°C. Relatively lower values in the eastern part of the diamond pipe are explained by the different composition of the blue ground itself and by the location of the diamond pipe in the relief. Later Ustinova stated (1964) that rather low temperatures in the southeastern part of the mine area resulted from brine flow and increased salt concentration, i. e. due to the so-called concentration convection. Numerous factual data were obtained from geothermal observations in 1978-1982 (Devyatkin and Shamshurin 1978). On the basis of the results obtained, morphological parameters of the cryolithozone have been estimated, and, in particular, a sharp bend of isotherms has been discovered which predetermines the position of the zero isotherm, and makes the thickness of the cryogenic layer within a small area vary from 600 m to 1050 m. Of interest is the information on the rock temperature that has been obtained in the course of engineering and survey operations

carried out on the Sytykan River. On the right bank the values at a depth of 15 m within the floodplain area were  $-1.2^{\circ}\text{C}$ , and upwards along the slope of the south-western part they gradually lowered to  $-2.8 - -3.4^{\circ}\text{C}$ . The rock temperature on the slope of the eastern exposure at approximately the same elevations turned out to be anomalously low,  $-8.8^{\circ}\text{C}$ . Such a great temperature drop is probably explained by permafrost conditions: the slopes are covered with deluvial deposits (clayey silt with crushed stone). The thickness of this layer on the left-bank slope is from 2 to 5.8 m, and on the right-bank slope from 1.1 to 2.7 m. Besides, the left-bank clayey silt contains much more ice in the shape of lenses and interlayers.

Geothermal observations of 1986-1991 enable to compare the data which were obtained previously with the newly obtained data (Figure 1 a, b).

Greater changes in the landscape in the process of the deposit development have taken place within the quarry area and in the industrial zone. The area represented formerly a gentle slope covered by trees gradually changing to the valley bed. At present, there are 80 m high dumps around the quarry which occupy large areas; a small valley of the Pirogov Stream, on the slope of which the eastern part of the pipe was exposed, is now covered with dumps, and the vegetational cover has been almost completely destroyed within the range of 2-4 km.

The results of temperature measurements taken in boreholes during 30 years of the deposit development make it possible to get an idea on the trends in the changes of the temperature field in the course of the quarry development. When comparing the results of temperature measurements in borehole 329 (Figure 1 a) we can see that during the five-year period the temperature at a depth of 40 m has lowered from  $-5.1$  to  $6.2^{\circ}\text{C}$  as a result of lateral cooling. The difference in temperatures gradually reduces, and at a depth of 160 m temperatures are almost equal.

The first water-bearing layer of the Upper Cambrian complex was stripped at a depth of 150 m. Temperature measurements taken in boreholes drilled from the depth of 160 m show that there is a temperature rise in the water-bearing rocks during the quarry driving. In the diagram (Figure 1 b) one can see that there is a certain drawing

of the isotherms upwards in the bottom part of the quarry. According to the results of the previous observations the rock temperature on this section steadily decreased from west to east, and the isotherms were directed downwards. Such a marked transformation of temperature in rocks located below the water-bearing layer is, probably, the result of the changed conditions of mining operations. The main reason is probably the increased water content in the lower part of the quarry which results in changes in microclimatic conditions. These conditions change rather rapidly due to various technogenic factors (explosions, transportation operations, etc.). For example, air temperature observations on the edges of technological roads of the quarry show that in winter air temperature in the quarry differs greatly from that in the adjacent area (Potatujeva and Bazavluk 1989). There is a notable winter inversion which results in a decrease in air temperature in the quarry from  $0.2$  to  $5.4^{\circ}\text{C}$  at every 100 m of its depth. The calculations show that in deep quarries the additional cold accumulation in winter makes up to 850 degree-days at every 100 m of depth.

Thus, during the development of the quarries and their deepening to the first water-bearing layer there is lowering of the temperature in the rock mass caused by lateral cooling. After cutting the cryopegs in the lower part of the quarry the rock temperatures increase. This is probably a result of the effect of the heat produced by condensation of water vapours which saturate the air within the quarry. To some extent, it may also be caused by a high technogenic pollution of the atmosphere by gas.

The formation of a temperature regime in dumps and under them is a little bit different. Dumps which occupy large areas may be considered as artificially created mesoforms of the relief. To study dump temperature, boreholes were drilled in two dumps (waste rock) with the height of 80 m and 50 m, respectively, in 1990 (Figure 2). Borehole T-1 is located on the slope of the 80 m high dump, 150-200 m from the edge of its bench. It has been found that the rock is not frozen to the depth of 25 m. The lowest temperatures are observed at the depths of 50 m and 90 m. Seasonal freezing at the end of April reaches 7 m. At this depth the average annual temperature is  $-1.5^{\circ}\text{C}$ .

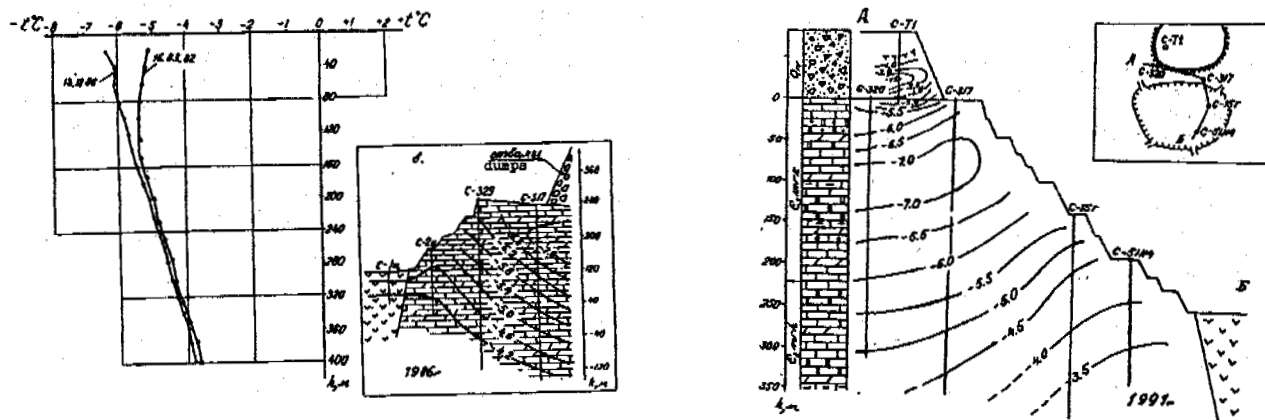


Figure 1. Diagram of temperature change in borehole 329 and the geothermal profiles of the eastern (a) and western (b) sides of the quarry of the Udachnaya pipe.

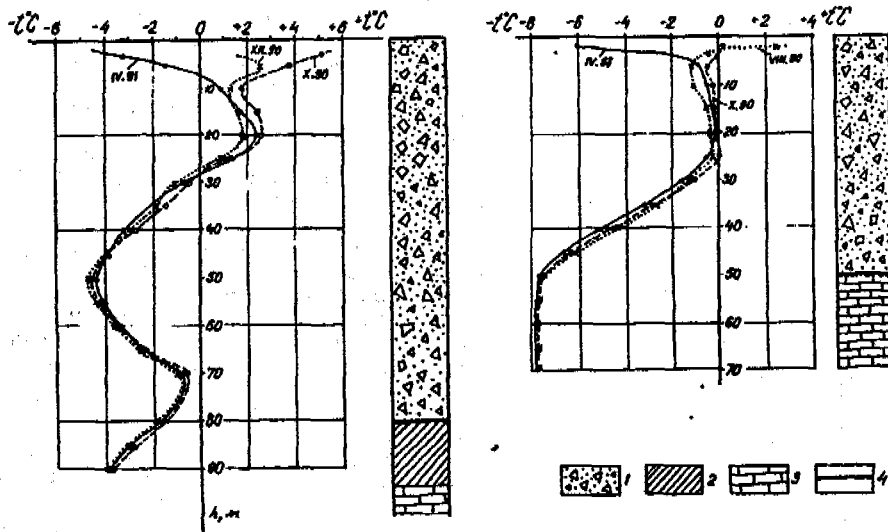


Figure 2. Temperature curves for boreholes T-1 and T-2. 1 - fragmental material of dumps; 2 - alluvial clayey silty loam of the terrace above the Daldyn River flood plain; 3 - bedrock; 4 - ice interlayers.

The permafrost table is on average at the depth of 25 m, and the natural day surface is at the depth of 80 m. At the boundary of large-fragment dump rock and Quaternary clayey silty loam which represents deposits of terrace II above the flood plain of the Daldyn River, the permafrost temperature is rather high ( $-0.5^{\circ}\text{C}$ ); the geothermal curve of the borehole is of a degrading type. This enables us to make a preliminary conclusion that permafrost on the terraces of the Daldyn River which are covered with dumps has not got frozen for the period of 25 years. Therefore, air- and water collecting ducts could exist under them for long time which considerably affect the ecological situation of the landscapes near the river.

Great changes in permafrost and hydrogeological conditions take place during the pumping of the water out of the quarry and its storing. Drainage water of complex hydrochemical composition includes the components which are harmful for the environment and, therefore, is pumped to the brine storages (accumulators), and is discharged through the borehole to the fissured zone of one of the faults. The basic brine absorbing layer is located at a depth of 120-180 m. According to the borehole data the thickness of permafrost cemented by ice is 200-220 m in this area. Thus, ice containing rocks are used as an absorbing system for brine storage.

As an engineering facility, the accumulating structure represents a rather simple system consisting of a small excavation pit of 350x140 sq. m in area and 12 m in depth, and several water intake boreholes located around its parameter. The total area of the ground for burying drainage water is about 6 sq. km.

A preliminary analysis of the geological information show the occurrence of ice-free cavities in the permafrost layer which form drainage water absorption zones connected by fissures-collectors associated, as a rule, with harder rocks (limestone, dolomite). Drainage water is mainly accumulated in clayey varieties of rocks close to their tops. At different portions of the accumulating facility there are 2-3 water-permeable horizons

or active hydrodynamic zones (according to Frolov 1966). The basic form of brine migration is, probably, convection - mechanical transfer caused by the hydraulic gradient; this has been proved by experiments on migration carried out with the use of an indicator (fluorescein). The experiments show that the filtration rate in the horizontal plane of the fissured collector in the upper part of permafrost is up to 0.33 m/min indicating the occurrence of spacious empty cavities.

The results of geothermal observations show that permafrost temperature in the annual cycle is subjected to considerable fluctuations which mainly depend on the temperature of the discharged brines and their amount. These two factors predetermine sharp temperature fluctuations along the depth. Maximum temperature gradients depending on the season have been registered in the brine absorbing intervals. As an illustration one may examine the temperature curves of borehole 41 (Figure 3). The borehole has been drilled in early 1987, and connected with the water discharge system in August 1989. Prior to connection of the borehole to the water conduit rock temperatures at depths of 40, 100, 160 and 200m were  $-3.14$ ,  $-3.06$ ,  $-2.89$  and  $-2.11^{\circ}\text{C}$ , respectively, with an average gradient within the measured interval being  $0.5^{\circ}/100$  m. Some bends of the temperature curves below 140 m indicate the influence of the brines discharged through boreholes 37, 31 and 32 and the direction of their movement. Further observations were made after connecting the borehole to the burying system. The results of geothermal measurements show that rock temperature has slightly lowered (to  $-5.0$ - $-6.5^{\circ}\text{C}$ ), and new temperature anomalies have appeared at the depths of 40-80 m and 160-240 m.

Thus, the absorption intervals in the operating boreholes are notable for temperature values, and form the warm or cold temperature anomalies depending on the season. Similar temperature curves have been registered in other operating boreholes.

As it was expected, the maximum gradients are registered in the operating boreholes (up to



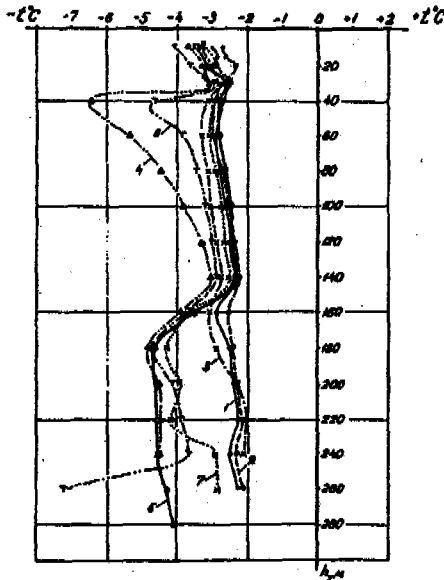


Figure 3. Diagram of temperature changes in operating borehole No. 41. Symbols: measurement dates: 1 - May 13, 1987; 2 - July 21, 1987; 3 - April 7, 1988; 4 - January 16, 1989; 5 - May 8, 1989; 6 - December 15, 1989; 7 - August 21, 1990.

$10^{\circ}/100$  m). In the test boreholes the gradients are 2-3 times lower, and further they are from the operating boreholes, smaller are their values. This fact makes it possible to use the results of geothermal investigations for tracing the location of the brine absorbing collectors. The analysis of temperature gradient changes in borehole 31 reveals that the main brine-absorbing collector is located at the depth of 120-180 m, and, probably, is the only one. In borehole 32 there are two such collectors at the depth of 40-80 m and 100-160 m. In borehole 36 there are three water conducting zones at the depths of 40-60 m, 80-100 m and 120-200 m. One may draw similar conclusions when analyzing the temperature gradients in the test boreholes. This has also been proved by long-term observations of the changes in water level made in hydrogeological boreholes. The water level in borehole 42 have responded rather notably to the water discharge: during the warm period (April) when there is an intensive water discharge, it rises sharply; at the end of May it stabilizes and remains almost unchanged even during the period of intensive water discharge (July-September). From October the water level gradually lowers. In some boreholes (nos. 101 and 55) there is a slight change in the water level; no direct relationship with water discharge intensity is observed.

Thus, the main brine migration within the burying system is non-uniform. Taking into account changes in the water level in the boreholes and the rock temperature, one can single out three horizons or zones of drainage water absorption. The first horizon of ground water (40-80 m) has probably emerged as a result of infiltration of brines discharged right into the accumulating pit, i. e. at the start of the system operation. It caused the concentration of quite large amount of highly mineralized water in the upper part of the rock massif. The formation and persistence of

the water-bearing layer within this system has the most harmful effect on the environment because of its hypsometrical position, since it is located above the local base level of erosion. The second horizon within the range of depths of 120-180 m is the main one. All operating boreholes have been installed in such a way that drainage water is discharged into water intakes and collectors of this horizon. The third horizon has been found at the depth of 220-240 m only in borehole 41; its area is not large.

Additional information on potential occurrence of water-absorbing zones or horizons may be obtained through geothermal observations in so-called blowing boreholes. In this area, vertical air movement was often observed along a borehole shaft. In such cases the results of geothermal observations were affected by air flow. For example, when measurements were made in borehole 41 in January 1989 when it had not been connected to the water discharge system yet, a descending air movement was observed at a rate of 0.4 m/s at its temperature  $-35^{\circ}\text{C}$ . It turned out that in winter the downward movement of air ("suction borehole") causes a decrease in temperature approximately in the same way as in the case of cooled brine discharge (Figure 4, curve 4), i. e. unevenly along the profile. At some depths there are sections and zones with abnormally low temperature values which, as shown by later observations, coincide with the brine absorbing intervals.

During geothermal investigations in the area air convection has been observed in many boreholes located over the entire area. Air flow movement was more frequent and intensive in boreholes 56, 57, 64 drilled in the middle part of the slopes.

Two things should be noted here. First, the boreholes are on average 200-260 m deep, and initially did not reach the natural level of ground water, i. e. they were within the permafrost layer. Therefore, air convection is hardly related to the ground water regime. Second, the observations show that air movement conditions are the same in all boreholes: a descending or ascending air movement is observed at one and the same time which, to our opinion, rules out thermogravitational air convection through the fissured rock and the systems of drilled boreholes. Whereas the ascending air flow normally has the temperature of the horizon which acts as a gas or water collector, the temperature of the descending horizon depends greatly on the season and the time of the day, i. e. depends on the environment temperature. Hence, the effect of the descending air flow is much greater than that of the ascending one, and may act as an additional cooling or heating factor depending on the season.

We have made a series of observations to study the effect of air convection on the results of geothermal investigations and to reveal the fissured zones and air-conducting collectors in rocks. At the very beginning of measurements (8 a.m., 1 May 1990) the borehole sucked the air at a rate of 0.94 m/s. This rate was gradually increasing, and by the end of the experiment lasting 72 hours it reached 13 m/s. During this period the atmospheric pressure steadily lowered from 722 to 699 mm Hg. So, there was an indirect relationship between the changes in the air flow rate in the borehole mouth and the atmospheric pressure. It is in good agreement with earlier investigations (Olovin 1980, 1982). Air temperature

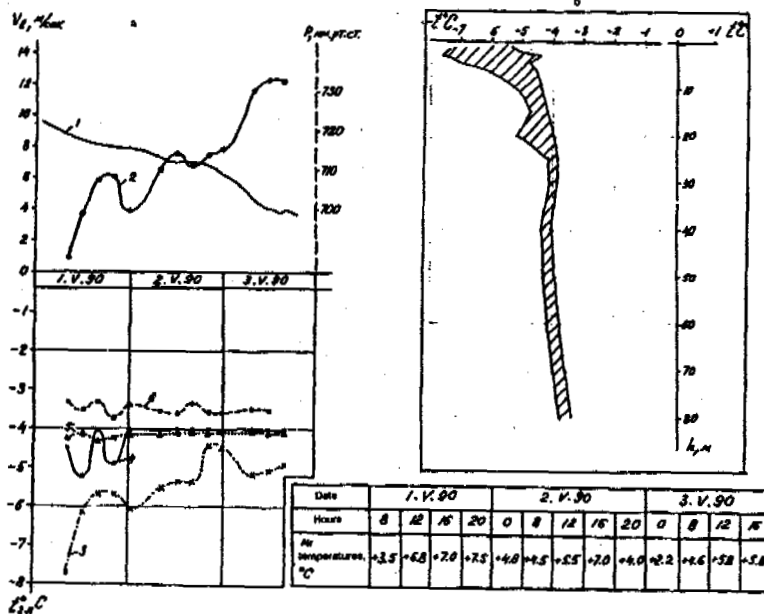


Figure 4. Diagrams (a) of atmospheric pressure change (1), air flow rate (2) and rock temperature change at various depths in borehole 41: (3) - 3 m, (4) - 20 m, (5) - 40 m, (6) - 80 m, and the limits of rock temperature fluctuations in the borehole (b).

at the daytime rose to +7.5°C, and at night lowered to +2.2°C, i. e. warmth was brought to the frozen rocks by air flow. The analysis of the data revealed that rock temperature was in direct relationship with air temperature, this relationship reducing with depth. In the upper part of the quarry it depended on the rate of air flow as well. At the depths of 30 m and 40 m considerable rock temperature fluctuations were registered only during the first hours of the observations, and then the temperature stabilized.

So, detailed geothermal observations find numerous large air- and water conducting collectors in the upper part of a permafrost layer (to a depth of 180 m). These collectors act as drainage brine intakes in permafrost. Being filled with highly mineralized quarry water, they cause melting of ice. The situation is aggravated by the fact that during the period from 1985 till 1991 the quarry water was discharged to the utilization system in growing amount from 200 to 700 thousand cub. m per year. In 1985-1988 it amounted to 1.3 mln. cub. m.

Comparison of temperature measurements of the first two years of investigations (1987-1988) has shown that near some boreholes which are not engaged in brine discharge and are at a small distance away from the quarry, the temperature in the permafrost has undergone notable changes. Rather considerable were seasonal changes in temperature of the brines pumped from the quarry. In summer due to a great water inflow they practically did not stay there; in water they remained there sometimes up to one month. The average temperature values in summer were 5-6°C (the maximum value was 12.5°C in July 1987). During the coldest winter months the brine temperature in the sump lowered to -15 -25°C (at air temperature - 42°C). No notable temperature changes occur during transportation through the pipelines. For

example, in August 1988, when the quarry was drained, the brine temperature in the sump was 5.7°C, and in the top part of the intake boreholes it was 8.1°C. As for the general mineralization, its distribution is different, depending on the season. Whereas in winter time the mineralization of brines is close to the background values, in summer, especially during the period of rains, it decreases to 38-42 g/l. It should be noted that starting from 1985 there have been changes in the background mineralization values of the quarry water as well: in 1985 it was 60-70 g/l, in 1987 - 190-200 g/l, and now it is 230-250 g/l. It might related to the fact that the quarry which is 240 m deep reached the level of highly mineralized water.

Using the information discussed above we can analyze the dynamics of rock temperatures in the upper part of the cryogenic layer in the mining area (Figure 5 a, b, c). At the initial stage of mining, i. e. when the environment had not been disturbed yet, at a depth of 25 m permafrost temperature in divides was -1.7°C, and on north-facing slopes it was -4.0°C. Pumping of highly mineralized water and its infiltration from the quarry has caused total decrease by 1.2°C in rock temperature. At the same time, there is an increase in the concentration of salts and other chemicals in the upper part of the geological medium, i. e. in the layer of frozen ground which might become wet frozen ground, and sharply change its physical properties.

From the ecological point of view, such ground may become traps for suprapermafrost water, and act as water conducting collectors of a pressure-filtration type. It will result in the accumulation of contaminating elements in ground and rocks of the free aeration zone that will undoubtedly affect the permafrost landscape situation. The seasonally thawing layer whose thickness will

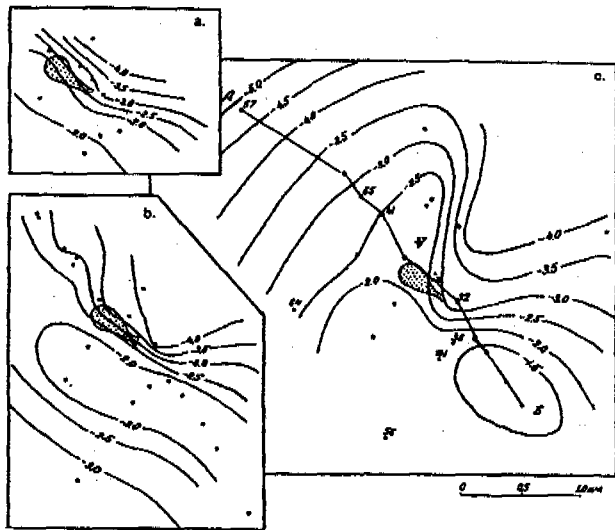


Figure 5. Temperature field of rocks at a depth of 25 m: a) March 1987, b) April 1988, c) May 1989; A-B - location of the geothermal sections.

increase due to salinization, will act in this case as a secondary source of environmental contamination (Goldberg 1985). Moreover, accumulation of brines in the upper part of the geological section, and especially within the layer of annual temperature fluctuations, as well as sharp seasonal fluctuations of rock temperatures will intensify cryogenic disintegration of rocks and, therefore, formation of more fissures and cavities through which pumped brine can drain. Hence, there are real preconditions for the formation of technogenic seasonal icings. Taking into account that in the diamond-bearing area the geological karst phenomenon takes place, as well as seasonal temperature deformations of fissuring in the karst subjected rocks to the quasi-periodical changes in the fissure systems (Timofeev 1985), one may expect a considerable transformation of the hydrogeological conditions of the region and the areas adjacent to the technogenic sections of the Udachnaya diamond pipe.

In the given example, the surface of the ridge where the accumulation pit is located, is 140 m above the water line of the Daldyn River. Assuming the talik under the river bed to be 20 m thick, we can determine the ecologically safe depth for pumping of the quarry water. According to our calculations, it should be about 160 m (285 m a.s.l.). However, according to geothermal and hydrogeological monitoring data, in the

course of the water intake system operation (for a relatively short period of time) a technogenic water-bearing layer has formed at the depth of 40-60 m. Its elevation is higher than the water line of the Sytykan and Daldyn Rivers. Taking into account the north-westerly direction of the Oktyabrsky fault area, we recommend not to discharge drain water to the accumulation facility, since it will cause the explanation of the technogenic water-bearing horizon of aggressive saline water which will inevitably be discharged above the local base level of erosion with subsequent transport to the local river system.

#### REFERENCES

- Borisov, V.N. and S.V. Alexeev (1988) Interaction of brines and permafrost. Abstracts of All-Union Conference on Ground Water of the USSR East. Irkutsk - Juzhno-Sakhalinsk, p. 162.
- Devyatkin, V.N. and V.Y. Shamsurin (1978) Geothermal characteristics of the Sytykan deposit. In: Geothermophysical investigations in Siberia. 142-148 pp. Nauka Publishers, Novosibirsk.
- Prolov, N.M. (1966) Geliothermozone temperature. 160 p. Nedra Publishers, Moscow.
- Goldberg, V.M. (1985) Predicting technogenic changes in hydrochemical conditions of water-bearing systems. In: Comprehensive evaluation and prediction of technogenic changes in the geological medium. 37-42 pp. Nauka Publishers, Moscow.
- Klimovsky, I.V. and Z.G. Ustinova (1962) On peculiarities of permafrost temperature regime in the Udachnaya kimberlite pipe area. In: Permafrost and related phenomena in Yakutia area. 96-106 pp. Nedra Publishers, Moscow.
- Olovin, B.A. (1980) Investigating gas permeability of frozen ground in the massif. In: Permafrost investigations in USSR areas under development. 90-98 pp. Nauka Publishers, Novosibirsk.
- Olovin, B.A. (1982) Permafrost zone dynamics in the Middle Viluy River in relation to hydraulic engineering. Papers of Permafrost Institute, Yakutsk.
- Potatujeva, T.V. and V.A. Bazavluk (1989) Inversion air and rock cooling in deep quarries in Western Yakutia. In: Geocryology of the USSR (Middle Siberia). 375-376 pp. Nedra Publishers, Moscow.
- Timofeev, E.M. (1985) Comprehensive engineering-geological evaluation and stability prediction in karsted areas. In: Comprehensive evaluation and prediction of technogenic changes in the geological medium. 86-89 pp. Nauka Publishers, Moscow.
- Ustinova, Z.G. (1964) Hydrochemistry of kimberlite pipes in Yakutia. In: Problems of ground water geochemistry. 237-252 pp. Nedra Publishers, Moscow.

# ISOTOPIC AND CHEMICAL COMPOSITION OF GROUND ICE IN WEST SIBERIA

L.N.Kritsuk and V.A.Polyakov

All-Russian Research Institute of Hydrogeology and Engineering Geology Zeleny village, Noginsk District, Moscow Region, 142454, Russia.

On the basis of detailed intergrated study of ground ice in West Siberia, widely using hydrochemical and isotope methods, a regional charateristic is obtained for the composition of ground ice and natural water in the study region; regularities in formation, an in ground nature of massive and thick wedge ice. The genetic link with certain types of ground water, frozen under different hydrodynamic and climatic conditions, are established. The mechanism of formation and relative age of different morphological types of ground ice are determined. There is revealed a genetic link between lake water, ground (massive and wedge) ice and cryopegs as different-aged products of cryogenic metamorphization in the course of deep freezing of the lithosphere.

## INTRODUCTION

Isotope investigations in the northern West Siberia have been carried out by VSEGINGEO since 1980 with the aim to determine the genesis of massive ice. As the obtained results show (Anisimova and Kritsuk, 1983; Kritsuk and Polyakov, 1989), more perspective is achieved in the above-mentioned aim by combining hydrochemical and isotope methods. The use of these methods and interpretation of the results obtained were based on the known regular features in the formation of chemical and isotope composition of natural water and ice (Anisimova, 1981; O'Neil, 1968; Souchez and Jouzel, 1984).

As the composition of ground ice is a function of a great number of interconnected natural factors and conditions, to establish the regular features of its formation is possible basing on either large number of analysis of ice-forming phenomena of the same type or detailed testing of a single ice deposit, and employing probabilistic / statistical methods for analytical-data processing.

The work of such kind was performed in the northern West Slieria in the different sites of the Yamal and Gydah peninsulas and Pur-Nadym interfluve (Figure 1). Ground-ice samples were taken from the boreholes 10-15 m deep and natural ground exposures. At the same time, the samples of surface and ground water and precipitation were tested in different sites of the study region. Isotopic and hydrochemical analysis were made in VSEGINGEO. The result obtained are shown in Figures 2-4.

The genetic and paleoclimatic curves were plotted based on the comparison of chemical and isotope composition of ground ice and precipitation. Samples of rain and snow were taken in the coastal area of Marre-Sale, at the shore of Ob Bay (Kamenny Cape and Tadibe-Yakha Peninsula, as well as in the area of Tyurin-to Lake and Nadym City.

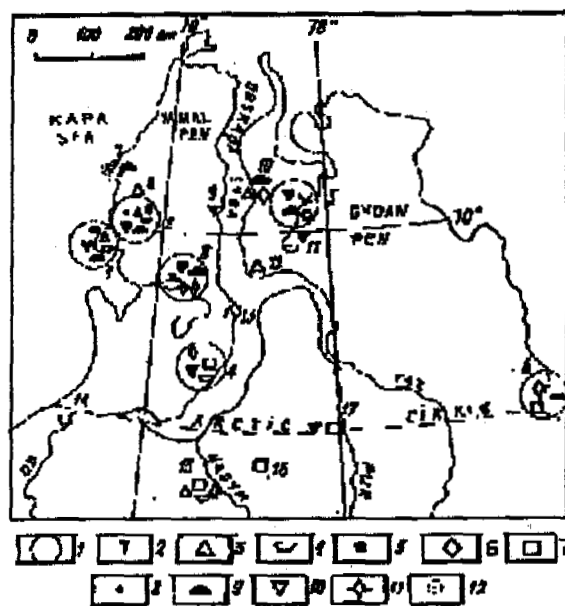


Figure 1. Location of sites for isotope investigation of ground ice in West Siberia. 1- Sites of integrated detailed isotopic and hydrochemical investigation and their number: (1) Marre-Sale Cape; 2) Se-Yakha River Valley (Mutnaya); (3) Nurminskaya structure; (4) Novo-Portovskaya structure; (5) Yuribey River Valley (6) "Ice Mountain" at Yenisey River; 2 - Sites of Individual isotope investigation: (7) Kharasavey Cape; (8) Tyurin-to Lake; (9) Se-Yakha River Mouth (Zelenaya); (10) TidibeYakha River Mouth; (11) Parisento Lake; (12) Antipayuta; (13) Kamenny Cape; (14) Labytnangi; (15) Nadym River; (16) Pangody; (17) Urengoy. Samples of: 3-precipitation; 4-lake water; 5-sea water; 6-river water 7-underground ice; 8-structure-forming ice; 9-massive ice; 10-wedge ice; 11-pingo ice; 12-sea ice.

## RESULTS

Precipitation of West Siberia has an ultrafresh (fresh in coastal area) carbonate sodium-calcium composition with an increased

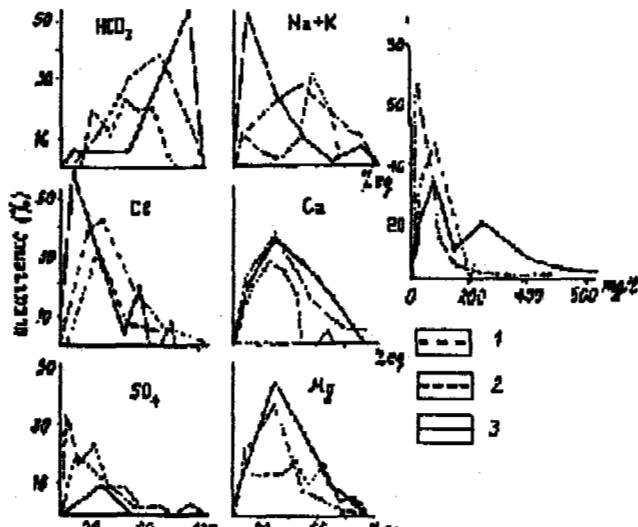


Figure 2. Chemical composition of natural water in West Siberia 1-surface water (n=549) 2-precipitation (n=25); 3-ground water (n>56).

content of Cl and Na in the coastal area and wide variations of Mg and SO due to the latitude of territory, distance from the sea coast and season of the year (Figure 2). Mineralization is usually not more than 60 mg/l and only at the sea coast reaches 200 mg/l.

Isotope composition of precipitation depends on a season and distance from sea coast. The "lightest" precipitation ( $\delta^{18}O$  - 24.1‰;  $\delta D$  - 188‰) was in January in Marre-Sale area, the "heaviest" ( $\delta^{18}O$  - 7.2‰ - in June in Nadym. The variation in  $\delta^{18}O$  and  $\delta D$  content at the coast are in a complete agreement with the trend of average monthly temperature of air (Kritsuk and Polyakov, 1989). Experimental points of isotope composition are located near the calculated line of meteor water (Figure 3).

Surface water isotopic composition was studied in different sites of the regions and in special detail in Yamal. It was established that isotopic composition of surface water contains mainly HCO<sub>3</sub> (excluding the sea coast where there is a high content of Cl, Figure 2) Among the cation at the sea coast, Na prevails, at the Ob Bay shore Mg, and in continental areas - Cl. Mineralization varies from dozens of mg/l (in water of rivers and very large lakes) to several hundreds of mg/l (in lakes of active neotectonic structure). Sulphate are either absent in surface water or have rather low concentrations, associated usually with the lakes, in the shore exposures at which sulphate-containing ice is melting. A sharp increase in sulphate content from 62 to 80% -eq. is observed in the Tadibe-Yakha River Valley and in the lakes of Urengoy structure. Here the ground water is

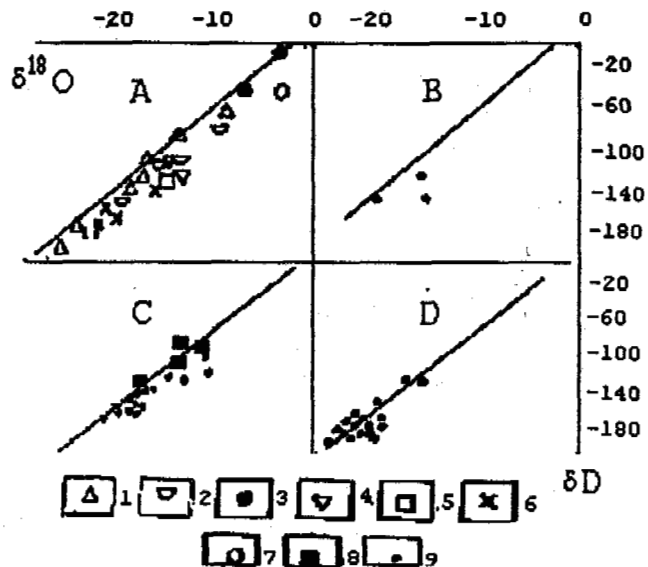


Figure 3. Isotopic composition obtained for: A-natural water; B-ice of pingo; C-massive ice; D-wedge ice. 1-precipitation; 2-lake water; 3-sea water; 4-river water; 5-underground water; 6-icing; 7-sea ice; 8-cryopegs; 9-underground ice.

supposed to be recharged from a zone with a confined water-circulation. Low mineralization indicates prevailing atmospheric recharge.

A specific feature of surface water in West Siberia is its heterogeneous chemical composition, which is confirmed by the elongated shape of distribution curves, low concentrations of different ions, as well as by abnormally high contents of different mineralization components observed in some of the samples (i.e. right-hand side of distribution curves in Figure 2). A reason for the heterogeneity may lie in a different degree of cryogenic metamorphism, connected with seasonal freezing of different amounts of surface water. Special studies, performed within the Nurmisky local tectonic structure, have established a difference in chemical composition of lake water in the dome and wing areas, which was attributed to different depths of the lakes (Kritsuk and Chervova, 1985).

Genetic heterogeneity of surface water in the permafrost of West Siberia is proved by its isotopic composition obtained during the study. Distribution of  $\delta^{18}O$  -values is shown in Figure 5A.

The  $\delta^{18}O$  content in the surface water of West Siberia varies from -6.6 to -18.9‰. Of the heaviest isotopic composition is sea and lake water from the west coast of Yamal. The lightest one is the water of large lakes and rivers in the northern areas of Yamal and Gydan. Considerable variations in  $\delta^{18}O$  values, observed in the lake water of one area having an extremely humid climate, are connected perhaps with a difference in the age of lakes,

the types of lake recharge and with a different cryogenic metamorphization of lake water. Such kind of isotopic composition in lake water was observed in the Bovanenkovo structure ( $\delta^{18}\text{O}$  of -9.7 to -14.7‰), Novo-Portovskaya structure ( $\delta^{18}\text{O}$  of 12.4 to -16.6‰), in the Marre-Sale area ( $\delta^{18}\text{O}$  of -9.0 to -14.3‰).

As a rule,  $\text{HCO}_3$  and Ca prevail in relatively light lake water, but in the heavier lake water a sharp increase of Cl and Na and sometimes of  $\text{NH}_4$  and  $\text{SO}_4$  is observed.

Ground-water composition in the cryolithozone, as a potential source of ice formation, is formed in the paragenetic permafrost-ground water system and reflects a kind of hydraulic connection between ground- and surface water.

Above-permafrost ground water is characterized by ultra-fresh hydrocarbonate calcium composition (chloride-calcium composition at the coast), contains different amounts of silicic acid and is close to the isotopic composition for precipitation of summer and autumn periods ( $\delta^{18}\text{O} = -13.5$  to  $-15.7$ ‰).

Of a notable predominance in the chemical composition of inter-permafrost water are  $\text{HCO}_3$  (to 80 to 90%-eq. and more) and Mg (to 60 to 80%-eq.), which points to a considerable cryogenic metamorphization. A specific feature of this water is a high content of silicic acid (from 20 to 30 to 50 to 60 mg/l) double-valence iron. Mineralization is not high (0.1 to 0.3 g/l), but can, in case of a poor link with surface water, rise to 0.5 g/l (Figure 2). The inter-permafrost water has an atmospheric recharge, which is known by its relatively low mineralization, actual absence of sulphates and isotopic composition of oxygen (Figure 5B).

Freezing-out of inter-permafrost water due to a change in the conditions of heat-exchange of soils with the atmosphere causes a formation of in-permafrost ground water of a chloridesodium or sulphate-magnesium type, differently mineralized (from 3.6 to 6.9 g/l), which has not been once reputed in the central permafrost zone in the north of the Arctic Circle. The analogous lenses of ancient "frozen-out" low-saline (5.4 g/l) chloridesodium ground water which lost its link with surface water (judging by its abnormally light isotopic composition, i.e.  $\delta^{18}\text{O}$  of 21.4 ‰;  $\delta\text{D}$  of 170‰) was found in the south of West Siberia (outside the permafrost zone). According to the radiocarbon analysis, the age of this ground water is more than 10,000 years (Polyakov, 1986).

The in-permafrost mineralized water (i.e., cryopegs) is most widely spread in the northern cryolithozone - Yamal and Gydan Peninsulas, both on the sea coast and in their continental areas, i.e. in the bottoms of drained lakes (hasyreys) and deep narrow bogs. Mineralization range from 1-2 to 80100 g/l. The water is of chloride-sodium type with a high content of

$\text{HCO}_3$  and Mg (20 to 30%-eq., sometimes higher). The  $\delta^{18}\text{O}$  content in the tested cryopegs varies from -5.9 to -18.6‰ (Figure 5B). The experimental point (Figure 3C) of isotopic composition of cryopegs (69-72) are located within the area of cryogenically metamorphized water (above the line of meteor water). This fact, along with its light composition, enabled the authors to conclude that the majority of cryopegs are relicts of the cold climatic epoch when the surface water (and a great part of water in hydrogenic taliks) was found to be frozen. At the same time, the left-hand section of the curve which reflects the composition of deep ground water of oil- and gas fields, surely illustrating a genetic link of the tested samples with sea water.

The ground ice is characterized by fresh (rarely by ultrafresh hydrocarbonate or chloride composition with different content of Ca, Na and Mg (Figure 4). The curves of mineralization components for the ground ice sharply differ from those for natural water in the study regions (see Figure 2) by shape, availability of several peaks in occurrence and rare modal values for the most components of mineralization. Without doubt, these facts point to a heterogeneous composition of frozen water and its different cryogenic metamorphization. A higher (than in surface water and precipitation) mineralization of ground ice gives the basis to suppose an underground source of ice formation.

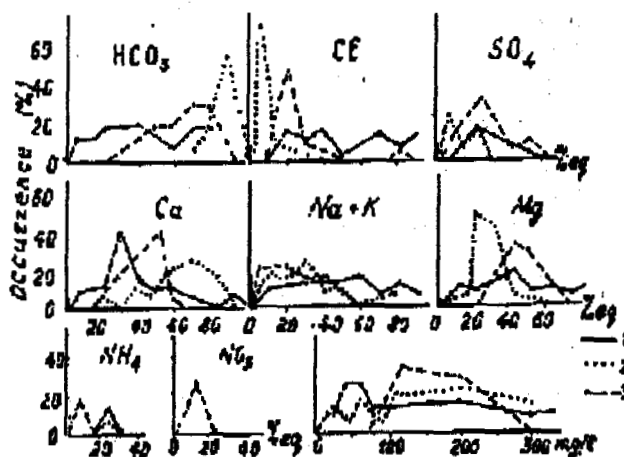


Figure 4. Chemical composition of ground ice. 1 - massive ice in Se-Yakha River Valley (Site 2; n=50); 2 - massive ice of "Ice Mountain" (Site 6; n=32); 3 - wedge ice in Yuribey River Valley (Site 5; n=25).

The content of stable isotopes in ground ice widely varies (Figure 5 C). The location of the experimental points of isotopic composition in Figure 3 provides evidence about the participation of natural water of different genesis in the ice generation, different age of the ice itself, and its formation under a spectrum of air temperature. A combined

analysis of hydrochemical and isotopic results made it possible to establish the genesis, freezing conditions and relative, age of ground ice, as well as to make original paleographic conclusions (Kritsuk, 1990; Kritsuk and Polyakov, 1989).

Ground ice of pingos is of the youngest age. The relief and low hypsometric position (e.g. river valley, bottoms of drained lakes enable the supposition that the formation of pingos is connected with the drop of postoptimal temperatures during Holocene period and freezing of talik ground water. Having a hydrocarbonate sodium ultra-fresh composition, the ice of pingo is characterized by considerable variations in total mineralization along vertical profile, caused by a change in the concentrations of HCO and Na and to a lesser extent of Mg and Ca. As the special detailed hydrochemical investigations of pingo in the south of Gydan showed, the ice of large pingo was

lens-like ice is close to the composition of present-day lake water, and isotopic composition of hydrogen widely varies (Figure 3B). Wedge ice, located usually in the top of pingo, represents the ice of extension figures (Mackey, 1983). Its chemical composition shows an increased Cl and Na content (sometimes of SO<sub>4</sub>), which indicates a high degree of cryogenic metamorphization of frozen water. Isotope composition of wedge ice is much lighter than that of lens-like ice (point 62 in Figure 3 B), which is due to isotope fractioning in freezing water (Souchez and Jouzel, 1984).

Thick massive ice is widely spread in river valleys, on shores of large lakes and sea coast of amal and Gydan, as well as along the eastern periphery of the WestSiberian Plate. It is connected spatially with the zones of abyssal faults, as the analysis of structural-tectonic and aero-space maps shows.

The chemical composition of ice strata is highly heterogeneous both in vertical and horizontal direction (Figure 4). Mineralization ranges from dozens to hundreds mg/l. The analysis revealed a connection between isotopic and chemical compositions of massive ice and between conditions of its occurrence. Of the heaviest composition ( $d^{18}O$  of -9 to -11‰,  $dD$  of -100 to -12‰) is chloridesodium massive ice of the western marginal zone of amal; of a lighter one ( $d^{18}O$  of -13 to -18‰;  $dD$  of -120 to -160‰) hydrocarbonate-calcium (magnesium) ice, developed in the river valleys of Central amal and finally of the lightest composition ( $d^{18}O$  of -20 to 24‰;  $dD$  of 160‰) is thick massive ice of hydrocarbonatemagnesium type, spread on the shores of very large rivers (e.g. Neito, Voivareto Halevto and others). A high content of HCO<sub>3</sub> and Mg, silicic acid (from 2-4 to 10-16 mg/l), and double-valence iron (10 to 15 mg/l), in a number of samples, indicates that the massive ice of amal and Gydan is genetically connected with inter-permafrost water of the southern cryolithozone and availability of SO<sub>4</sub> and NH<sub>4</sub>. This points to a deterioration of water exchange with surface water due to freezing of water in deep hydrogenic talik (Anisimova, 1981). On the contrary, quasi-homogeneous hydrocarbonate-calcium composition of the melting ice of "Ice Mountain" (Site 6 in Figure 1), as well as association of the site with the zone of regional fault, enabled a conclusion to be made about freezing of highly confined fissure water (Kritsuk and Anisimova, 1985).

A genetic link of massive ice with different-type ground water is proved by the isotopic results (Figure 3 C). The experimental point of isotopic composition, grouped around the freezing line (Michel, 1986), were located in several vertical chains, which is an evidence for a genetic relationship between massive ice and ground ice of pingo and for their similarity in the mechanism of formation (Figure 3 B,C). Considerable variations in

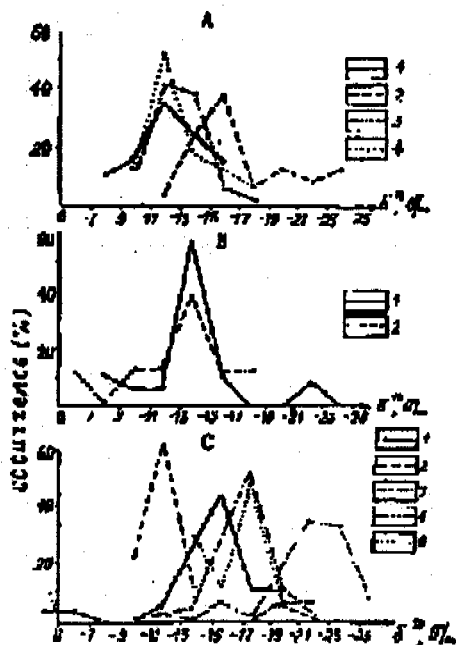


Figure 5. Oxygen isotope composition of natural water and ground ice in West Siberia. A - surface water: 1-rain (n=26) 2 - snow (n=35); 3 - lake water (n=55); 4 - water of rivers and streams (n=17). B - ground water: 1 - ground water of different aquifer (n=17); 2 - cryopegs (n=8). C - ground ice: 1 - structure-forming ice (n=30) pingo (n=13); 3 - massive ice (n=123); wedge ice (n=48); 5 - icings of Putoran and Polar Urals (n=17).

being formed through repeated injections of ground water, frozen in a closed space beneath taliks (Anisimova, 1981).

Among ice types of pingo, there are distinguished massive (lens-like) ice and icewedge bodies. Oxygen-isotope composition of

isotopic composition of massive point to a wide temperature range of ice formation.

A specific feature of thick massive ice is a homogeneity of its isotopic composition in the cross-section (Vaikmyae and Karpov, 1985; Kritsuk and Polyakov, 1989). The ordered location of experimental points in Figure 3 C indicate that large amounts of frozen fresh water, and similarity in the chemical and isotopic compositions of massive ice in different areas of Yamal, about regional distribution of ground water subject to freezing.

The conclusion we have made about in-ground genesis of massive ice of West Siberia and its formation from different-type ground water is confirmed by stable isotopes of carbon

contained in it  $d^{13}C$ : from -17.6 to -10.1‰ (Kritsuk and Polyakov, 1989). The same conclusion was made by the researchers at the "Ice Mountain" (Kuznetsova and Karpov, 1989).

A similarity was established in chemical end isotopic composition of massive ice of Yamal with the composition of water in large lakes inter-permafrost water in the southern cryolitozone and icings along the structural margins of West-Siberian Plate (Figure 5\*). This enables a supposition that this ice is a remainder of a huge underground/on-ground icing, formed during primary freezing of the territory in the areas of discharging ground water with atmospheric recharge. This fact, along with the specific areal distribution of massive ice (i.e. association with the zones of abyssal faults) and the tracers of partial melting of the ice itself, accompanied by formation of secondary contacts of it with the overlying rocks, enable us to consider the massive ice of the northern West Siberia to be the most ancient ice structures (Kritsuk, 1990).

Wedge ice is widely spread in river valleys and lake shores of the peninsulas of Yamal, Gydan and Tazovsky with the thickest occurrence (height > 10 m) associated with the zones of abyssal faults. It is located usually in the well-washed, quartz sands with high inclusion of organics. This kind of ice has a paragenetic link with the underlying massive ice. Ice-bearing sediments for shallow ice veins (< 5 m) are usually lacustrine, marshy highice silty loams overlain by a peat layer and underlain often by lens-like bodies. Actually all the cryological researchers of West Siberia have the same opinion about thick wedge ice as being syngenetic structures, formed due to repeated frost crackings and penetration of surface water into the cracks. However, the isotopic and hydrochemical investigations we have conducted do not confirm this hypothesis. Chemical composition of wedge ice is close to that of massive ice, which indicates a genetic relationship between them (Figure 4). At the same time the thick wedge ice contains an increased content of  $SO_4$  and Mg (to 60%eq.), as well as silicic acid (to 25 mg/l), which is actually absent in surface water and precipitation (Anisimova, 1981),

Along with a relatively high mineralization of wedge ice (to 300 mg/l) and availability of  $NO_3$  end double-valence iron in some samples (unstable in an oxygen medium), the chemical composition of ice veins points to freezing of ground water which has been subjected to a higher cryogenic metamorphization than in massive ice. Thick wedge ice represents the "lightest" ice formations in West Siberia (Figure 3 D).

The samples were taken by the staff from the Polar Ural Expedition and from the Krasnoyarsk Branch of "Priroda" Center, and analyzed in the VSEGINGEO Laboratories. A considerable number of experimental points of wedge ice are located above the line of meteor water. In order to establish the mechanism for formation of ice veins, a detailed hydrochemical testing was performed. Typical vertical distribution of mineral components in a vein is shown in Figure 6 where demonstrates the formation of ground ice due freezing of fresh water in a closed space, accompanied by freezing-out of the salts contained in it (i.e. injection mechanism of ice formation). This conclusion is based on considerable variations in total mineralization of ice in cross-section, connected chiefly with the changes in the concentrations of  $HCO_3$ , Na and at some depths of  $SO_4$  and Mg which are most distinctly expressed in the lower layers of ice. Also, it is confirmed by isotopic studies, i.e. that the lightest composition is the more

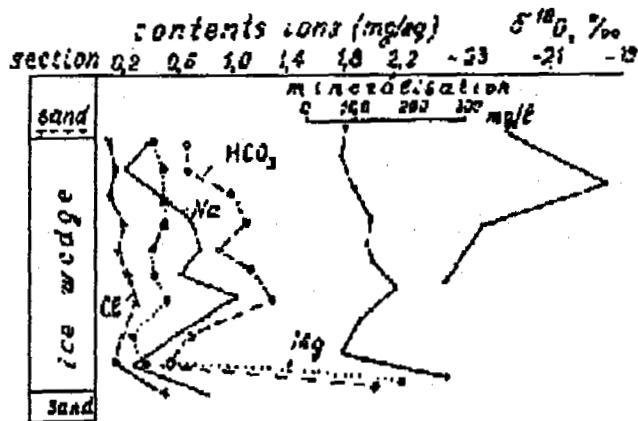


Figure 6. Component changes in mineralization and stable isotopes of ice vein with depth (near-valley area of III terrace of Soty-Yakha River, Site 3) 1 - sand; 2 - ice; 3 - ironing; 4 - perma frost table. mineralized ice (Kritsuk and Polyakov, 1989).

#### SUMMARY

Considering the specific occurrence of the tested ice veins and the established specific features of chemical and isotopic composition of thick wedge ice, a conclusion can be made that it is a secondary in-ground ice, formed under severe climatic conditions from completely frozen cryogenically metamorphized



ground water of deep cryogenic taliks and at penetration of frozen water under high pressure into extension fissures in a frozen mass. The considerable  $\delta^{18}\text{O}$  variations within a narrow  $\delta\text{D}$ -range (Figure 4 D) indicate that the source water in wedge ice is formed under close hydrodynamic conditions and different, climatic conditions with no uniform aquifer available. The  $\delta^{13}\text{C}$  value in the tested vein is equal to  $-14.4\text{‰}$  (Kritsuk and Polyakov, 1989a). The fact that the thick wedge ice is associated with the modern or ancient lakes and river terraces and located above massive ice gives the basis to consider the wedge ice to be younger formations than the latter (Fig.7)

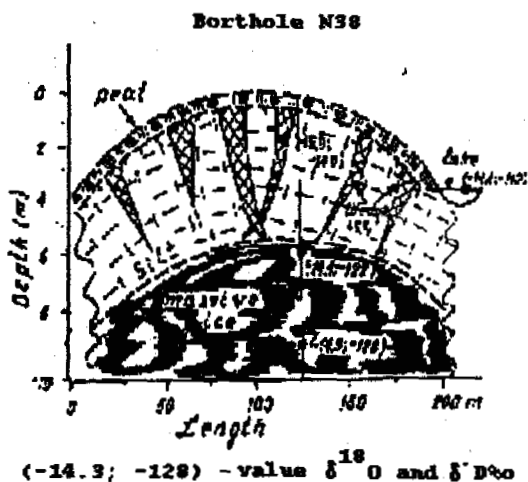


Figure 7. Location of massive ice and ice wedges within the pingo in Soty-Yakha River Valley (site 3) (after V.F. Bolikhovskii)

The isotopic composition of polygonal-wedge ice, widely spread in ancient lake depressions, is close to the composition of ice in pingos and massive ice (left-hand section of the third curve in Figure 5 C). The ice is ultrafresh, HCO and Ca are predominant in its chemical composition, which indicates a genetic link with surface water and precipitation.

Structure-forming ice (ground ice) isotopic composition varies within a wide range (Figure 5 C). Modal  $\delta^{18}\text{O}$  value at the distribution curve ( $-15$  to  $-17\text{‰}$ ) shows that the source water of this ice has been formed at air temperature close to  $0^\circ$  and the ice itself is of a segregated type. At the same time, some samples of structure-forming ice represent probably fissure ice of injection genesis due to the penetration into a frozen ground of the freezing lenses of sea or deep water (lefthand section of the distribution curve) or of the cryogenically metamorphized water from hydrogenic taliks, were freezing during a cold epoch (right-hand section).

#### REFERENCES

Anisimova, N.P. (1981) Cryohydrogeochemi-

cal features of frozen zone. Novosibirsk: Nauka, 153 pp.

Anisimova, N.P. and L.N. Kritsuk (1983) Use of cryochemical data in studying the genesis of ground ice. Problems in Geocryology. Moscow: Nauka, 230-239.

Vaikmyae, R.A. and E.G. Karpov (1985) Study of massive ground ice from the profile of "Ice Mountain" area in the Yenisey River Valley, using oxygen-isotope method. Materials of glaciological investigations. Moscow: No. 52, 135-141.

Kritsuk, L.N. (1990) Ground and surface ice of West Siberia during Pleistocene. Materials of glaciological investigations. Moscow: No. 69, 93-102.

Kritsuk, L.N. and N.P. Anisimova (1985) Chemical composition of massive ice and its connection with ground water. Cryohydrogeological investigations. Yakutsk, 94-108.

Kritsuk, L.N. and V.A. Polyakov (1989) Isotopic investigations of natural water and ice of West Siberia. Engineering Geology, No. 4, 76-94.

Kritsuk, L.N. and V.A. Polyakov (1989) Stable isotopes of carbon in ground ice of West Siberia. Isotopes in Hydrosphere. Abstracts of 3rd All-Union Symposium. Kaunas, 29 May - 1 June, Moscow, 191-192.

Kritsuk, L.N. and E.I. Chervova (1985) Hydrochemical characteristic of surface water and ground ice of the Central Yamal, Cryohydrogeological investigations. Yakutsk, 117-126.

Kuznetsova, T.P. and E.G. Karpov (1989) Conditions for formation of ice and mineral complex "Ice Mountain". Yakutsk, 171 pp.

Polyakov, V.A. (1986) On possible evaluation of a thickness of degraded permafrost strata using isotope and hydrochemical data. IX All-Union Symposium on Isotope Geochemistry. Abstracts. Moscow: GEOCHIM AN SSSR, 277-278.

Mackey, I.R. (1983) Oxygen isotope variations in permafrost, Tuktoyaktuk Peninsula area, Northwest territories: in Current Research Pt B/Geol.Surv.Canad., Paper 83-1B, 67-74.

Michel, F.A. (1986) Isotope geochemistry of frost-blister ice, North Fork Pass, Yukon, Canada, J. Earth Scien. Canad., Vol.23, 543-549.

O'Neil, J.R. (1968) Hydrogen and oxygen isotope fractionation between ice and water. J. Phys. Chem., Vol. 72, 3683-3684.

## ON THE STUDY OF NIVAL DEPOSITS IN YAKUTIA

Viktor V. Kunitsky

Permafrost Institute, Russian Academy of Sciences  
Yakutsk 677018, Russia

From the nival deposits it is suggested to single out the extranivites - peculiar drifts accumulated near a permafrost snow patch as a rule during the surface, flat and small-stream bedless run-off of its melt water under permafrost conditions. There are three main varieties of modern extranivites - deposits near the snow patch bank, deposits near the snow patch cones and deposits near snow patch flood-plain. The article examines some sections of old deposits near snow patches. It has been pointed out that discovery of Pleistocene extranivites and their spread over Yakutia area may witness the development of numerous permanent snow patches on the mountains and plains of this area in the past and prove that accumulation and melting of these snow patches took place under permafrost conditions.

In the regions shown on a schematic map (Figure 1) an attempt was made to find geological features of embrional glaciation, which according to the known hypothesis (Grigorjev 1932) repeatedly covered the area of Yakutia in the Quaternary period and was represented in the mountains and on the plains of this area by vast fields of firn, snow, ice and numerous firn-like snow patches accumulated and melted under permafrost conditions. The author also points out that according to the data available (Shumsky 1947, Solntsev 1961, Osokin 1981) the formation of the firn-like snow patches is taking place up to now in Yakutia and in some of the areas adjacent to it.

The search for the features of embrional glaciation of the Yakutia area was provided in two directions: a) with the use of cryofacial method intended for genetic separation of frozen layers (Katasonov 1954, 1973). Investigated were the sections of the ice complex, i.e. a special horizon with numerous ice veins more or less integral, occupying vast areas but non-uniform in respect to the age, composition, origin and thickness (Solovjov 1959, p.49); b) on the areas adjacent to the permanent snow patches were examined from the cryolithological point of view the original slope drifts similar to those called nival deposits (Ljubimov 1967).

As a result of the investigations the notion of extranivites has been formulated by the author. The data on the composition, cryogenic structure and ice content of the contemporary and old extranivites have been obtained. It was found that extranivites belong to cryolithogenic deposits. The nature of extranivite relationship to other sedimentary rock of the cryolithozone has been specified.

Extranivites (from Latin extra - outside and nivis - snow) are peculiar continental deposits accumulated near a permanent snow patch, as a

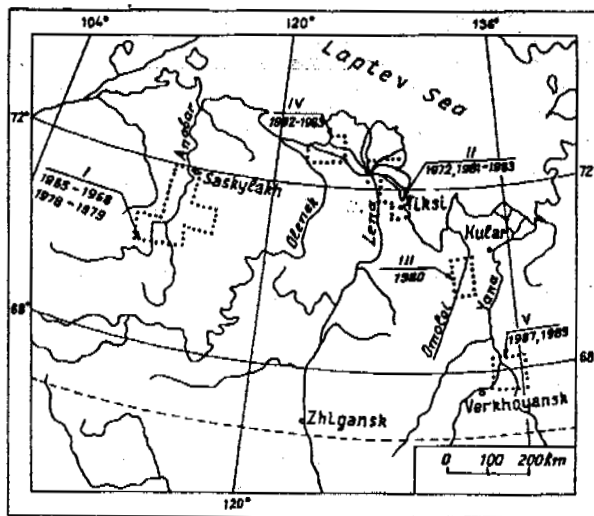


Figure 1. Schematic map of the area under investigation. Extranivite areas are outlined with a dotted line. The fraction of the arrow denotes: numerator - conventional number of the region; I - the region of Prianabarskaya plain; II - the region of Primorskaya bank; III - the region of Omolojskaya Depression; IV - the region of Chekanovsky ridge; V - the region of Kisiljakh ridge; the denominator denotes the year of the author's participation in the field permafrost investigations of the region.

rule, as a result of surface, plain and fine-stream bedless run-off of its melt water under permafrost conditions.

The permanent snow patches include perennial snow patches and drifting snow patches (Shumsky 1976). Both types of snow patches are considered as snow, firn and ice accumulations remaining

throughout the year as compared with seasonal snow patches (spring, early and late summer). The permanent snow patches are peculiar forms of over-ground glaciation. They serve as intermediate link between the seasonal snow cover and glaciers, and differ from them by smaller dimensions, short life, absence of distinct features of movement and division in feed and melt areas.

Snow patches cause nivation (Matthes, 1900) or undersnow erosion (Tolmachjov 1903). It is under stood as a localized rock destruction caused by frost, which includes the processes of its physical and chemical weathering and the processes of ablating the weathering products from snow patches (Chetyrjokhyazychnyj 1980).

In their revision article Embleton and King (1975) point out that nivation efficiency depends on the thickness of the snow patch and on the thermal conditions of the underlying soil. If a snow patch is located on non-frozen soils, the nivation takes place both at its edges and right under it. If the snow patch is underlain by permafrost soils, their nivation is restrained under it and proceeds mainly within a narrow strip along the edges and near the snow patch. With the reduction of its thickness and the occupied area the zone of intensive nivation shifts across the entire surface freed from the snow patch (left by the snow patch).

This dependence helps to understand the mechanism of rock breakage (destruction) caused by snow patches. At the same time it enables classifying the snow patches, singling out at least two main geothermal categories: a) warm snow patches, i.e. located on unfrozen soil; b) cold snow patches - underlain by permafrost. The rock weathering products, which result from nivation, remain on place and subjected to some shifting and sedimentation near the snow patches are called nival deposits (Ljubimov 1967).

According to the data obtained for Bol-shezemelskaya tundra and for mountains of the Caucasus and the Tien Shan (Ljubimov 1967), for the lowlands of Pechjora and West Siberia it is suggested to single out the following types the nival drifts: I - nival-gravitational; II - nival-eolian (epinival); III - nival-eluvial (nival-hypergenic); IV - nival-solifluctional (perinival); V - nival (snow-ice) deposits (Liverovsky and Ljubimov 1972).

This classification covers a wide range of natural phenomena. Among them there are not only the phenomena predetermined by nivation but also those that cause its development - temporary and perennial snow patches which are regarded as nival deposits. Such a proposal is rather disputable, since it contradicts the initial idea of the nival deposits (Ljubimov 1967) and besides, disturbs the casual relationship within the system of notions on snow patches, nivation and nival deposits.

Of special interest within this classification are perinival or nival-solifluctional deposits. They include laminated silt (aleurite) of solifluctional tongues, festoons, pseudo terraces, trails, debris cones below vast snow fields and transverse snow patches on gentle slopes, as well as laminated silt of trails and of debris cones and the material of longitudinal strips with coarse fragments in the trough below the longitudinal snow patches on the slopes of mean steepness and, finally, nonlaminated material of the solifluctional debris cones and

mud-flow coarse fragments and aleurite at cirque-type snow patches on steep slopes (Liverovsky and Ljubimov 1972).

Extranivites might have been referred to perinival deposits. But in this case it should have been noted that genesis of extranivites is associated with the existence of only cold permanent snow patches. Besides, one should mention that the structure and the composition of extranivites is affected not only by nivation and solifluction, but also by other important lithogenetic processes (surface-type, plane-type and fine-stream run-off and alluviation, frost fracturing, frost heave, frost sorting, permafrost), which take place near cold permanent snow patches. Finally, one should mention that accumulation of extranivites is controlled by the seasonally thawing layer processes and not by the nivation and solifluction which according to the available data (Boch 1946, Kaplina 1965, Washburn 1979) take place within the layers of temporary and seasonal freezing of soils and as it is known take part in formation of perinival deposits.

Thus, the idea of perinival deposits is much wider than that of extranivites and differs from it in the contents. This difference is due to the fact that the sense of the notion of perinival deposits is revealed through the determination of the leading factor of rock weathering at places of various snow patch formation, as well as through the judgment on the main process of fragment material shifting from snow patches, irrespective of thermal parameters of the soil under them.

When explaining the sense of the notion on extranivites the priority is given to the idea of a special geocryological situation near the cold permanent snow patches and under them.

According to genetic classification of Quaternary deposits the extranivites represent a peculiar type of continental drifts. They are not so much of a dynamical but rather of a formational category. Therefore, they are also called as snow patch-adjacent deposits.

Now extranivites are found near the cold perennial snow patches on the slopes of mountains and plains. Nival meadows near such snow patches may be regarded as landscape indicators of such deposits.

According to the information related with the investigation of the nival meadows in the tundra area of East Siberia (Tikhomirov 1956) the drifting snow patches on the slopes within Tajmyr Lake resemble small glaciers and provide a peculiar humidification of the adjacent area. In summer the surface of slopes near such snow patches is overwettered. Sometimes it is covered by small mud streams, which sometimes settle here in the form of silt. The grass on these nival meadows is rugged. Since their development is influenced by the streams of meltwater containing suspension matter, the appearance of the nival meadows reminds the surface of the fluvial plains of large rivers and the surfaces of alluvium reworked annually by high water.

This information is similar to the one obtained by the author in Yakutia. It shows that the gently sloping areas adjacent to the cold perennial snow patches in tundra of the Prianabarskaya plain and on the slopes of Primorsky and Chekanovsky mountain range are moistened throughout the warm season by the water of such snow patches.

Melt water in the varying amounts enter the gently sloping surface of altiplanation terraces adjacent to snow patches and flow over it in the form of a continuous film (rather thin) or in the form of stray streams or bedless springs. Such streams do not disturb as a rule the turf (sod) when crossing the terrace. They often split, saturate the seasonally thawed layer, fill cracks in it, stay in microdepressions of the relief and not always reach terrace edge. This water is often turbid. From the lower edge of the perennial cold snow patches they transport nival silt, and sometimes grass, fine crushed stone, gravel grains, fine pebble. Such water more or less evenly irrigates the strip adjacent to the snow patch, the width of which is commensurable with the width of the altiplanation terrace. The snow patch melt water sediment the suspended and fragmental material carried by small streams. As a result of such sedimentation in the nival meadows and adjacent permafrost landscapes near the cold perennial snow patches, peculiar silty deposits are formed on the slopes. These deposits are

patch. Here, the area of snow patch plain deposits is located around the distal periphery of the snow patch debris cones.

Thus, in case of a facial approach one should distinguish three basic varieties of modern extranivites: pseudomoraine or deposits of the snow patch bank; deposits of the snow patch debris cone; deposits of the snow patch plain.

These deposits have an important common feature. The fragmental material of all abovementioned varieties of modern extranivites is deposited without any notable washout on the underlayer surface. No basal horizon is formed on it. At the same time the composition and the structure of each extranivite variety have some peculiar features. Thus, according to the observations made in one of the terraces adjacent to the nival meadow in the tundra of Priyanabarskaya plain, the modern deposits of the snow patch plain had the following peculiar features: a) mainly loessial appearance due to the prevalence of aleurite (silt) particles; b) poorly visible lamination of subhorizontal interlayers containing an abundance of sand particles; c) rare, as a rule, disintegrated grass, gravel, fine crushed stone and small (2-4 cm) pebble rock resistant against weathering; d) numerous threadlike radicles (rootlets), both alive and died off, buried on their place; e) enveloping location on base rock without a basal horizon; f) a small (less than 1 m) depth of seasonal thaw; g) excessive (redundant) humidity in the seasonally thawed layer; h) the traces of intensive processes of shallow and deep frost fracturing. Besides, the same deposits in a frozen state contained cementing, as well as ground ice and wedge ice (Kunitsky 1989). Similar structure is typical of many modern deposits of the snow patch debris cones situated in other areas of the cryolithozone. These analogies are the result of two main reasons. One of the reasons is that all pointed out varieties of modern extranivites belong to cryolithogenic deposits (Katasonov 1972), or to be more exact, to those of them which are accumulated on a seasonally thawing layer. The other reason of these analogies is that one and the same variety of modern extranivites is formed in different regions, in similar though not identical hydrological situation near the thawing cold permanent snow patches on slopes with terraces in these regions (see Figure 1).

According to the opinion of investigators the transportation of fragmental material on the surface of altiplanation terraces in permafrost area is mainly provided by solifluction and by the processes of structural ground formation (Obruchev 1937).

According to the author one should not ignore participation of solifluction in the formation of extranivites. But still in relation to the activity of melt water as a basic agent of transporting the fragmental material of the deposits of snow patch debris cones and snow patch plain, as well as in relation to the mechanism of the primary sedimentation of such material - sedimentation of suspended particles carried by water and their transformation to peculiar drifts deposited on the slopes - the solifluction of such drifts should be considered in most cases as one of the processes within the chain of events that cause accumulation of sediments near snow patches.

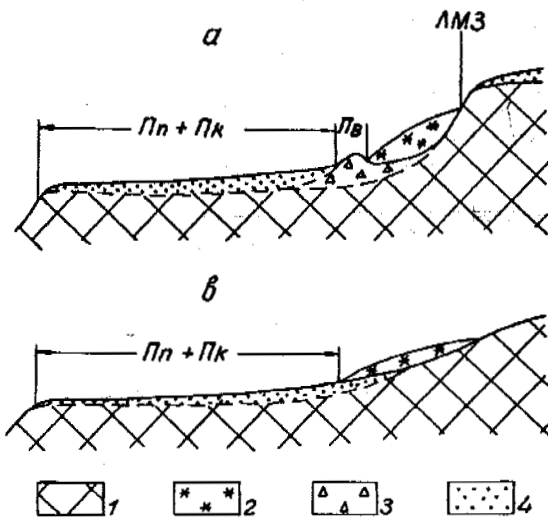


Figure 2. Scheme of extranivite formation: a - in case of snow patch bank; b - in case a snow patch bank is absent.

Symbols: ЛМЗ - the line of intensified frost weathering area (Boch and Krasnov 1943); Πn - protalus rampart (Flint 1963), nival rampart (Ljubimov 1967) or snow patch rampart; Πn + Πk - the area, of the snow patch debris cones and plain; 1 - the soil with underzero mean annual temperature destroyed by nivation; 2 - snow, firn, ice of perennial snow patch; 3 - pseudomoraine (Tolmachev 1903) or snow patch deposits; 4 - the deposits of the snow patch debris cones and the deposits of the snow patch plain (integral deposits).

called modern extranivites, like the material near the snow patch, which substitutes them in accordance with the given scheme (Figure 2).

The area of the existing now deposits near the snow patch plain as well as the area of debris cone deposits near snow patches is located between the bank adjacent to the snow patch and the front edge of the altiplanation terrace (see Figure 2). In the gaps of the nival bank and where it is missing, this area is directly adjacent to the lower edge of the thawing perennial cold snow

A peculiar case of extranivite accumulation is the formation of deposits of a snow patch bank with prevalence of large-fragment material. It is known that such material is accumulated as a result of the slide of rock fragments down the sloped surface of a snow patch from the line of the intensified frost weathering area. Similar slide - solifluction - is observed on the surface of both the warm and the cold snow patches irrespective of their life period.

According to the available data, solifluction, shallow and deep frost fracturing, frost heaving, frost sorting, segregation and wedge ice formation - all these processes take place in modern deposits of snow patch debris cones and snow patch plain. As new layers of such sediments are accumulated, they are subjected to the indicated processes right on the slopes. Strictly speaking, these processes take place at postsedimentation stages of accumulation, when it temporarily stops. The intermittent nature of such sediment accumulation is determined when studying not only modern extranivites but also their ancient analogues observed in the sections of the cryolithozone.

Ancient nival deposits are spread over the area of Yakutia. They are found in the sections of relict altiplanation terraces located, as a rule, below the existing nivation base or below the lower border of its modern development belt (Solntsev 1949). The indicated deposits take part in the structure of cryopediments - gently sloping surface (1-10°) of concaved shape with a 1.5 m thick loose mantle, which differ from altiplanation terraces in the lower part of the water divides of slopes (Czudek and Demek 1973, Czudek 1988). Besides, the ancient nival deposits are found in the sections of almost horizontal areas, which are regarded as permafrost plain pediments (Timofeev 1965) or cryopediments (Timofeev and Vtjurina 1983), and sometimes as terrace ridges (Kartashov 1966) or as syngenetic kind of terrace

ridges (Gravis 1969). Three areas are located, as a rule, near (at) the foot of concaved slopes and differ from cryopediments in greater deposit thickness which is over 1.5 m.

Ancient nival deposit layers were observed in the natural scarps and in the sections of mine openings. Such layers were studied in detail on the slopes of the Frianabarskaya plain and at the foot of the Primorsky bank chain, as well as within the area of the Kisilyakh mountain range (see Figure 1).

Figure 3 shows a cryolithological section of the Prianabarskaya plain area. It enables to make judgements on the structure of one of the altiplanation terraces. The altiplanation terrace investigated by bore pits is probably of a relict character. As shown on the section (see Figure 3), it is rather large. Its rear step is 15 m high, and a gently sloped platform is 1 km wide. This makes an impression of a rather durative nivation on the investigated area provided by probably a big perennial snow patch or by several such patches.

At present, no permanent snow patches are formed on this terrace, though a seasonal snow cover reaches 0.6 m. One may judge about the period of nivation development on this terrace by the comparison of its deposits with the alluvium investigated by boreholes 2266-2268. The formation of this alluvium is said to have taken place at the end of the Sartanskaya epoch or at the beginning of the Holocene. Based on this assumption, the formation of the examined altiplanation terrace should be attributed to the Sartanskaya (Q<sub>3</sub>) or to the earlier epoch. In the rear cusp and on the platform of this altiplanation terrace the boreholes discovered thinly laminated clayey limestone placed almost horizontally. These rocks have a fissured cryostructure formed by a fresh ice with addition of silt, which fills vertical, inclined and horizontal fissures in the limestone. There is a big amount of such ice on the

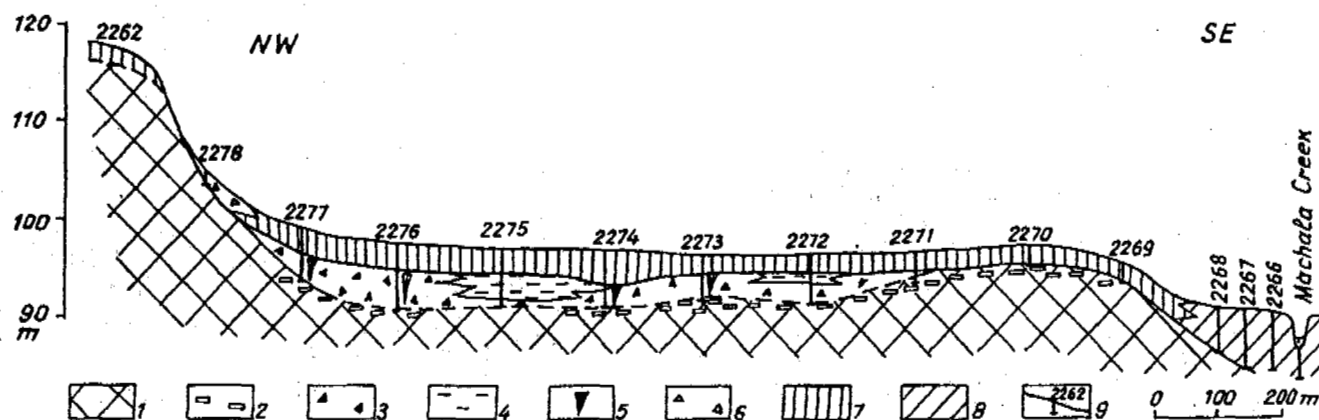


Figure 3. Cryolithological shape of the Prianabarskaya valley area; 1-2 - surface cryogenic eluvium (Katasonov 1965) of limestone: the rock (cliff) with ice-made cracks (1); ice-heaved rock soil (2); 3-5 - Pleistocene (Q<sub>3</sub>) extranivites: deposits of snow patch rampart and snow patch debris cones, integral (3); deposits of snow patch plain (4); deposits of surface and suprapermafrost water from the cold perennial snow patch - ice veins (5); 6 - colluvial-solifluctional crushed rock containing silty loam and clayey loam with a socket-type (socketed) cryostructure; 7 - deluvial-solifluctional sandy silty loam and clayey loam with lens-shaped, latticed cryogenic structure; 8 - alluvium of the modern (Q<sub>4</sub>) horizon: pebble, sand, silty loam, clayey loam, peat, ice veins (wedges); 9 - borehole and its number.

top of the rock mass. In this part of the sections, which resembles a surface-type cryogenic eluvium (Katasonov 1965) the ice-filled cracks (fissures) are up to 2 cm wide and sometimes one may find ice masses with suspended blocks and smaller fragments of limestone located almost horizontally.

The ice complex that covers the eluvium on the platform of the terrace refers to ancient nival deposits. Among them are the deposits of the snow patch plain and integral deposits of the snow patch bank and the snow patch debris cones (see Figure 3).

According to the data provided by boreholes 2271-2277 the integral deposits of the snow patch bank and debris cones contain sandy silty loam and clayey silt. They also contain gross and crushed stone, the amount of which increases with depth. Near the underlying cryogenic eluvium layer one may find limestone blocks. These silty loam and clayey silt include 0.5-2 cm ice sockets and numerous 3 mm thick ice lenses of irregular shape. At greater depth and near ice veins the gaps between limestone fragments are filled with ice with silt inclusions, and a basal cryostructure is observed.

The deposits of the snow patch plain revealed by the boreholes 2272, 2274, 2275 occupy the upper part of the ice complex sections. They are represented by loessial silty loam and clayey silt with numerous thin (1-2 mm) segregated ice lenses. In contrast to the underlying crushed stone silty loam and clayey silt, these deposits contain much less crushed stone and gross, and are characterized by the availability of small black and bluish-black spots, which resemble sulfides that as it is known are typical for silty rock of an ice complex. Horizontal and sometimes concave interlayers of ground ice are attached to the sides of the ice veins of these deposits. The thickness of these interlayers is up to 3 cm.

The ice veins pierced by boreholes 2273-2277 have irregular shape. Their cross-section is similar to large-size boilers made of dirty yellow-brown ice containing subvertical chains of gas bubbles and thin silt layers. In other cases one could observe in similar rocks the asymmetrically split ice veins bent down the slope and ice strips of variable width vertical xenoliths of fine crushed stone and gross.

The upper edges of these ice veins are melted, cut and located below the seasonal thawing layer (Table 1), which makes an impression of antiquity of the wedge ice deposits. Another peculiarity of the examined ice veins is that their side contacts have peculiar steps (projections) - shoulders, which serve as the evidence of geologically simultaneous formation of ice veins and the layers containing these veins. These shoulders also show that accumulation of these underground ice deposits and related extranivites was intermittent by nature.

The sections of the relict terrace end with slope sediments (deposits). They include coluvial-solifluctional rock debris silty loam and clayey loam with cryogenic structure stripped by borehole 2278 and deluvial (talus)-solifluctional silty loam and clayey silt with lens-type, latticed cryogenic structure divided by ice layers and containing numerous remnants of wood (roots, branches, stems) stripped by boreholes 2269-2277 on a gentle slope crossed by dells and occupied by woods.

Table 1. The depth of the maximum seasonal thawing of soils (h) and the depth of ice vein location (H) acc. to borehole data

Borehole No	h, m	H, m
2273	0.40	2.40
2274	0.50	3.65
2275	0.40	2.35
2276	0.50	1.50
2277	0.40	2.40

Note: The depths (h, H) were determined in April 1965. The h-value was determined by means of the cryostructural method.

In the examined section it is suggested to regard the ice complex as the deposits accumulated under the conditions of the Arctic tundra (Gravis 1969). It seems to be correct since no visible vegetation remnants are found in this complex.

It is suggested to regard the ice complex rocks stripped by the borehole 2274 as Quaternary deposits of structural-solifluctional crustoses (Gravis 1969). One may agree with this proposal but it should be reasonable to add that according to the data of borehole 2274 and boreholes 2271-2273 and 2275-2277 the ice complex rock should be regarded as Pleistocenian extranivites.

The ice complex stripped by borehole 2274 is compared with similar deposits investigated previously within the township of Kular (see Figure 1). These deposits fill the small valleys, cover the alluvium of the terraces and form thick layers on the slopes of the mountain ridge Kular up to the outcrop of the bedrock at water divides (Gravis 1969). This comparison and the material presented in this article may prove a wide spread of Pleistocenian extranivites in Yakutia.

According to the available data the ancient extranivites have been preserved not only in the region of the Prianabarskaya plain. The snow patch deposits of the Pleistocene play an important part in the structure of Bykovsky peninsula and Muostakh island in the area of the Primorsky mountain ridge (bank) and occupy some areas within the Chekanovsky ridge. Vast areas are occupied by Pleistocenian extranivites in the Omolojskaya depression and on the slopes of a low mountain range Kisiljakh (see Figure 1).

#### CONCLUSIONS

The hypothesis on the embryonal (East-Siberian) glaciation of Yakutia area in the Quaternary period deserves much attention as paleogeographical and geocryological concept. The judgements on its erroneous nature met in the books on permafrost (Fundamentals of Geocryology 1959) ought to be revised, since the main thesis of this hypothesis on the development in Yakutia (in the past times) of sedentary fields of firn, snow, ice and numerous firnlike snow patches, which existed and melted under permafrost conditions has been proved by the discovered Pleistocenian extranivites and the facts on their wide spread over this area.

#### REFERENCES

- Boch, S.G. and I.I. Krasnov (1943) On Altiplanation terraces, ancient leveling surfaces and related problems. *Izvestia VGO*, V. 75, N 1, 14-25 pp. In Russian

- Boch, S.G. (1946) Snow patches and snow erosion in Northern Urals. *Izvestia VGO*, V. 78, N 2, 207-222. pp. In Russian.
- Encyclopedic four-language glossary of physical geography terms (1980) 704 pp. Sovetskaya Encyclopedia Publishers, Moscow.
- Czudek, T. (1988) Kryopedimente - wichtige Reliefformen der rezenten und pleistozanen Permafrostgebiete. *Petermans Geografische Mitteilungen*, B.132 (3), 161-173.pp.
- Czudek, T. and J. Demek (1973) The valley cryopediments in Eastern Siberia. *Biuletyn Peryglacialny*, 22, 117-130 pp.
- Embleton, C. and C.A.M. King (1975) Periglacial geomorphology. 2nd Edition, V. 2. 203 pp.
- Fundamentals of geocryology (1959) Part I, 460 pp. Izdatelstvo AN SSSR, Moscow. In Russian
- Gravis, G.F. (1969) Slope deposits in Yakutia. 128 pp. Nauka Publishers, Moscow. In Russian
- Kaplina, T.N. (1965) Cryogenic slope processes. 196 pp. Nauka Publishers, Moscow. In Russian
- Kartashov, I.P. (1966) Ridged terraces and the related loose deposits and placers. *DAN SSSR*, V.166, N 2, 424-426 pp. In Russian
- Katasonov, E.M. (1954) Lithology of frozen Quaternary deposits of the Primorskaya Lowland. 25 pp. Avtoreferat dis. kand. geol. miner. nauk, Moscow. In Russian
- Katasonov, E.M. (1965) On the analysis of neotectonic displacements in permafrost area. Abstracts of papers of Workshop on Geomorphology and Neotectonics of Siberia and the Far East. Novosibirsk, 126-128 pp. In Russian
- Katasonov, E.M. (1972) Regularities of cryogenic phenomena development. *Aktualnye voprosy sovremennoi geograficheskoi nauki*. Moscow, 28-35 pp. In Russian
- Katasonov, E.M. (1973) Frost-facies analysis as the main method of cryolithology. *Proc. 2nd Int. Conf. on Permafrost*, V. 3. 29-37 pp. Yakutsk, In Russian
- Kunitsky, V.V. (1989) Cryolithology of the Lower Lena. 162 pp. Yakutsk, In Russian
- Liverovsky, Y.A. and B.P. Ljubimov (1972) Nival lithogenesis in the tundra area exemplified by the northern part of the Pechora River Lowland and Western Siberia. *Problemy kriolitologii*, V. 2. 116-129 pp. Moscow. In Russian
- Ljubimov, B.P. (1967) Mechanisms of nival processes. *Podzemny led*, V. 3. 158-175 pp. Moscow. In Russian
- Matthes, F.E. (1900) Glacial sculpture of the Bighorn Mountains, Wyoming. *US Geol. Survey*, 21st, Ann. Rept., part 2, 173-190 pp.
- Obruchev, S.V. (1937) Solifluctional terraces and their genesis. *Field research in Chukotka krai*. *Problemy Arktiki*, no.3, 27-48, N 4, 57-83 pp. In Russian
- Osokin, N.I. (1981) Snow patches and snow patch systems of low and medium hilled regions of the USSR. 70 pp. Nauka Publishers, Moscow. In Russian
- Shumsky, P.A. (1947) Modern Glaciation of Russian Arctic regions. *Voprosy geografii*, 4. 11-32 pp. Moscow. In Russian
- Shumsky, P.A. (1976) Snow patches. *BSE*. 3d Edition, V. 23. 632-633 pp. Moscow. In Russian
- Solntsev, N.A. (1949) Snow patches as a geomorphological factor. 91 pp. Geografiz Press, Moscow. In Russian
- Solntsev, N.A. (1961) Snow patches and their activity. *Pollee geokriologicheskie (merzlotnye) issledovania. Metodicheskoe rukovodstvo*. 301-308 pp. Izdatelstvo AN SSSR, Moscow, In Russian
- Solovjov, P.A. (1959) Cryolithozone of the northern Lena-Anga interfluve. 142 pp. Izdatelstvo AN SSSR, Moscow. In Russian
- Tikhomirov, B.A. (1956) Some peculiarities of snow cover in the tundra and its effect on vegetation. *Sneg i talye vody*. 206-239 pp. Izdatelstvo AN SSSR, Moscow, In Russian
- Timofeev, D.A. (1965) Middle and low Olekma. 138 pp. Nauka Publishers, Moscow-Leningrad. In Russian
- Timofeev, D.A. and E.A. Vtjurina (1983) Terms on periglacial geomorphology. 233 pp. Nauka Publishers, Moscow. In Russian
- Tolmachjov, I.P. (1903) Geological trip Kuznetsky Alatau in summer 1902. V. 39. 390-436 pp. *Izvestia IRGO*. In Russian
- Washburn, A.L. (1979) *Geocryology. A survey of periglacial processes and environments*. 406 pp. Edward Arnold, London.

## COMPLEX TECHNOLOGY FOR PREPARATION OF PERENNIALY FROZEN PLACERS TO DREDGING

Kurilchik A.F., Samyshin V.K. and Perlshtein G.Z.

All-Russian Science-Research Institute of Gold and Rare Metals, Magadan, 685000, Russia North-Eastern Department of Permafrost Institute, Siberian Branch of Russian Academy of Sciences, Magadan, 685000, Russia

A lot of dredging fields in the North-East of Russia are underlain by inhomogeneous perennially frozen grounds with ice-rich fine-grained deposits substantial thickness at the top of mining massif. A complex technological scheme for preparation of such placers to dredging is worked out. It includes: 1) hydraulic stripping of fine-dispersed seam 2) artificial thawing of alluvial gravel-and-pebble deposits 3) drainage of coarse-grained grounds at depth a bit more greater than seasonal freezing layer thickness. The scheme using will allow to increase the efficiency of dredging in this region.

More than 50 years gold dredging were widely employed in the North-East of Russia. The most part of placers is composed of permafrost deposits that must be thawed to mining. As the main methods of artificial thawing the hydropoint and filtration-drainage ones are generally used. However deposits under mining often include deep lying gold-bearing seam overlapped with inhomogeneous (along vertical section) ground mass. The special complex methods are required for preparation of such deposits to dredging. This paper presents an example of complex technological scheme has been developed specially for some placers in the upper Kolyma river.

The dredge field located in the nameless creek valley is characterized with two-layered section of the deposits to be mined: on the surface there are loams of 2.5-3.0 m thickness underlying with alluvial gravel-and-pebble grounds (6-9 m). Loam ice-content is 600-700 kg/m<sup>3</sup> and that of lower layer is 200-260 kg/m<sup>3</sup>. The region is placed within continues permafrost zone, at an average air temperature -11°C, ground temperature minus 3-5°C and snow thickness 40 cm. The taliks are concentrated only near riverbeds, their seasonal freezing depth achieves 2.5-3.0 m. Hydraulic thawing in this case is quite low-efficient due to the presence of fine-grained deposits of considerable thickness in the upper part of section. These sediments have excess ice-content and negligible permeability in the thawed state. Their removal beyond the contours of the field (using an advance blasting) is too expensive.

Deposits of this type can be effectively mined with help of a complex technological scheme has been worked out in details for similar conditions. All of its elements were thoroughly tested and employed in mining practice. The scheme includes: 1) hydraulic stripping of fine-dispersed seam 2) artificial thawing and subsequent dredging of alluvial coarse grained sediments 3) preparation of so-called "remains" (to be dredged at the beginning of the next summer season).

Performance of the offered technological scheme starts with the removal of a soil and vegetation layer from the field's surface and

simultaneous mounting of water-supply system. The procedures are to be accomplished by the beginning of a summer season, i. e. at time when a hydraulic mining of frozen loamy deposits could be started. Water-pipe system is designed so that it could be used for both hydraulic mining and hydropoint thawing. Hydrojetting of grounds may be performed for instance with the stationary monitors which jets are not more than 50-60 m (Mining World, 1956) Samyshin, 1986). However on the large dredge fields (about 150000 m<sup>2</sup>) it's necessary to have a lot of units acting only 5-9 hours a day that is not efficient enough. Modern technology of frozen deposits hydro-mining calls for using of self-propelled monitor unit joined to a water-main with a flexible rubberized hose of 60-70 m length (Lavrov et al., 1988). That gives it possibility to move over the whole field's area. Self-propelled units have considerable advantages under geocryological conditions of the upper Kolyma.

Hydrojetting is carried out as follows: the field is conventionally divided into several pannels and the unit moving from one pannel to another washes off the thawed layer accumulated on the frozen grounds surface due to action of atmospheric heat. The process allows most rational use of thermal and mechanical energy of water and natural external heat.

The thawed soil is washed off into a specially driven trench and the pulp is transported down to the area of the field worked out before (hydrodump). In case of silting the accumulated layer may be removed by a hydromonitor jet from a close distance. Difficult-to-wash formations can also be washed off by a similar way.

When deposits contain large rock fragments, combined procedures are the most effective and widen considerably the sphere of use for the technology. The main principle of combined operations is separate washing away of fine-grained sediments and transporting of remained large fragments grounds with earth-moving, hauling and other mining equipment (bulldozers, excavators, dredge pump etc.).

The second stage of the complex technology is presented by a hydraulic thawing of gravel-



and pebble deposits. Most versatile method for preparation of frozen grounds to dredging is hydropoint thawing (Miles method). It is used at most dredging sites of the North-East of Russia. Hydropoint thawing is based on the heat exchange between vertical artificial percolation water flows and frozen grounds. The method is performed by drilling holes in frozen massif with subsequent sinking of pipe-points into the holes and water pumping through the points. Drilling marks are arranged in a staggered order at an equal distance from each other. On dredge fields of Kolyma region the ordinary thawing depth is 5-12 m and ice-content is 200-400 kg/m<sup>3</sup>. The distance between hydropoints is commonly set 3.5-4.5 m and water consumption per one point is 1.0-2.5 m<sup>3</sup>/h. At such parameters thaw duration varies in limits 10-50 days.

To prepare a dredge field to mining one may also use filtration-drainage thawing based on heat exchange between seepage flows of mainly horizontal direction and a frozen ground massif. However, the application of this method is limited by the less thawing depth (5-6m) and high standards for hydraulic conductivity (permeability coefficient  $K_p > 2$  m/h).

Nevertheless the method's low cost and availability of fairly large number of placers responding the demands provide it frequent employment. For feeding and draining filtration flows a number of procedures have been developed. Most acceptable are systems with parallel drainage and feeding trenches (of depth 1.5-2.0 and 0.2 m correspondingly) driven at the distance 20-30 m from each other.

Taking into account low rate of filtration-drainage thawing it must be born in mind that the fields prepared in such a way should be mined at the end of a summer season, otherwise the preventing of thawed deposits' freezing is required. At the North-East of Russia thawed ground's protection from freezing is connected with substantial difficulties due to long and very cold winter, comparatively small thickness of snow cover and other natural features. It should be mentioned that the problem of ground stock prepared for dredging in late autumn and especially spring periods remains quite acute for mining enterprises. The availability of such ground stock in spring time provides the possibility of putting up to dredging much more earlier, thus prolonging the dredging season.

This problem can be successfully solved with help of thawed grounds drainage (i.e. producing of so-called "sushentsy" zones) instead of trying to prevent their freezing. Sushentsy are determined as deposits with low moisture content at which they keep loose state even after freezing (Perlshtein, 1979). Technology of artificial sushentsy preparation includes two main elements:

- 1) thawing of frozen grounds by one of the hydraulic methods
- 2) reduction of deposits humidity by

draining to the critical value ( $w_{cr}$ ) that provides loose consistency of grounds in both thawed and frozen state and allows to excavate them all the year round.

Coarse-grained sediments with a sand filler are considered to be proper for preparation of sushentsy zones. In rectangular area of width 200 m and depth 6 m their humidity decreases to  $w_{cr}$  during 10-30 days after draining start. If a filler is presented by light loamy sand, drainage realizes much slower. So, the preliminary calculations are needed to make sure the ground massif with given hydrophysical characteristics can be drained to  $w_{cr}$  before refreezing. For this purpose numerical algorithm and computer program were worked out (Papoport, 1978).

Sushentsy preparation process was successfully employed for placers reclamation to all-the-year-round mining with bulldozers and excavators. The feature of its application for dredging field is an availability of flooded dredge pit. The water level should be lowered and a height of the above-water ground wall must be a bit more than freezing layer thickness. Due to the drainage the upper part of mining massif will be presented by frozen or thawed sushentsy, whereas the lower flooded part (including paygravel layer) will remain in thawed state. Therefore, dredging operations may be started with appearance of first water in the dredge pit by the beginning of spring.

The offered complex technology for preparation of frozen placers to dredging can provide considerable increase in the efficiency of the dredge fleet in the North-East of Russia.

#### REFERENCES

- Lavrov N.P., Perlshtein G.Z., Samyshin V.K. (1988) Results of researches and experience of hydraulic mining of frozen rocks. Proc. 5-th Int. Conf. Permafrost, Trondheim, Norway, p.p.1417-1421
- Mining World (1956), vol.18, N 6, p.p.53-55
- Perlshtein G.Z. (1979) Water-heat reclamation of perennially frozen grounds in the North-East of the USSR.- Novosibirsk, Nauka (Science)
- Samyshin V.K. (1986) Analysis of conditions for application of hydraulic methods of ice-rich deposits mining. Probleme of mining equipment use in the North-East. Proc. VNII-1, Magadan p. p. 14-24

## TECHNOGENIC GEOCHEMICAL FIELDS IN THE PERMAFROST ZONE ON THE EXAMPLE OF YAKUTIA

Vladimir N. Makarov

Permafrost Institute, Russian Academy of Sciences Yakutsk, 677018, Russia

The article examines the peculiarities of technogenic geochemical fields in various natural media of permafrost areas. A weak self-cleaning ability of natural media and high density of technogenic pressure result in a faster formation of contrasting geochemical anomalies in residential and industrial regions. The specific character of technogenic anomalies is dependent on the peculiar migration of chemical elements and compounds. Technogenic anomalies are also registered in the top layer of permafrost.

It is known that the nature of the North is extremely sensitive to human activities. Anthropogenic effect on the permafrost brings about the changes in the Nature's balance, hinders economic activities, causes introduction of large amounts of chemical elements and their compounds to permafrost landscapes. Of particular importance is the study of geochemical processes which determine dispersion and concentration of a substance in the cryolithozone and play an important part in preserving the environment.

### TECHNOGENIC GEOCHEMICAL FIELDS IN THE ATMOSPHERE

Atmospheric pollution is one of notable anthropogenic effects on the natural environment in the permafrost zone. In many regions of the North the climatic peculiarities hinder the spread of pollution agents. They reduce illumination intensity and ultraviolet radiation (by 40-50%) and under northern conditions these factors worsen the living conditions. They reduce the albedo of snow in winter which results in the earlier snow melting on contaminated areas and may result in thermocarst phenomena. It should be noted that the intensity of air pollution is in direct proportion to the number of anticyclonic days and is, therefore, notably expressed in the continental regions of East Siberia. The possibility of self-cleaning of the atmosphere in the northern region is very small; since there is a short growing period, a small biomass and high air humidity. The observations show that the atmosphere of the northern regions is becoming contaminated with various pollutants.

A distinctive feature of the climate in Yakutia is an expressed anticyclonic weather regime in winter and frequent air mass intrusions from the Arctic Ocean. The main feature that determines the character of the climate and salt transfer during the cold period is the spur of the winter Asian anticyclone which almost completely covers the entire territory. The prevailing wind direction during the cold period on the territory of Yakutia are western, northely from Arctic Ocean and relatively local south-western from the Sea of Okhotsk.

The atmospheric transfer of considerable salt masses results in the change of geochemical situation and considerable salination of the permafrost landscapes.

Anthropogenic pollution of the atmosphere in Yakutia reflects the peculiarities of economic development and has a local character, except for the basin of Viljui River, where technogenic pressure is of regional nature because of the atmospheric transfer of sulphur and a number of heavy metals from the territory of Krasnoyarsk area. A short snow-melt period and existence of permafrost rocks causes intensive run-off of meltwater. Therefore, snowmelt play a limited role in feeding underground water on the greatest part of West Yakutia. Intensive accumulation of pollution products in the snow cover has a negative effect on the quality of river water which are mainly fed with melted snow (Viljui and its tributaries Olenek, Anabar). Contamination may also affect the subpermafrost water in areas where geochemical link is provided through talics and underbed, flooded areas with an increased jointing of rocks, which filtrate well the layers of alluvial and fluvioglacial deposits.

The sources of technogenic contamination on the territory of Yakutia determine the local atmospheric pollution. The most typical features of a technogenic pressure (judging by the chemical composition of the snow cover) are the increased content of carbonates sulphur, nitrogen compounds, the transfer of pH values to alkalies, the occurrence of microelements typical of contamination sources. Depending on the intensity of pollution sources the scale of technogenic pressure may be rather considerable. For instance, the technogenic pollution of the atmosphere in Nerjungrinskii-Chjulmanskii industrial district covers an area of about 5000 km<sup>2</sup>, and the total amount of dissolved and solid admixtures that fall on the surface in the region of Nerjungrinskii coal mine reaches 800 t/km<sup>2</sup> a year (Makarov 1990).

Anthropogenic salinization of the permafrost landscapes due the atmospheric transfer of contaminants take place (1) in the regions of high technogenic pressure (2) on the territory of

towns, located in the areas with unfavourable landscape and climate conditions (3) in areas of open-pit mining. The density of technogenic pressure in case of atmospheric pollution may be rather high (Makarov et al. 1990).

Both salts and domestic and processed effluents get into the soil of residential and industrial zones. However, the greater part of them fall on the surface with atmospheric precipitations. For instance, on the territory of Yakutsk, in the area of intensive technogenic effect the amount of the salts that fall out from the atmosphere reaches 44 t/km<sup>2</sup> a year. These are mainly sulphate salts, the concentration of which in the snow-melt water of Yakutsk reaches 1300 mg/l (background content about 0.5 mg/l). Of the total amount of municipal effluents, the atmospheric effluents makes up 19%.

#### TECHNOGENIC GEOCHEMICAL FIELDS IN THE NATURAL WATER

Contamination of the surface water results in the formation of technogenic anomalies, which stretch within the hydraulic system for hundreds and thousands kilometers (the rivers Lena, Viljui, Kolyma). The most extended stream are formed by phenols and oil products. The anomalies of heavy metals in larger rivers are of local nature and result from both the variable economic activities and the high natural concentrations in the rock of the river basins. The mining enterprises have a catastrophic effect on the ecology of the river systems. The greatest negative effects result from the discharge of processed products to the rivers and the rapid increase of the suspended effluent as a result of initiation of thermoerosion processes. The technogenic pollution in this case reach the shelves of northern seas.

Technogenic effect on the environment notably changes hydrogeochemical conditions of water-bearing systems, causes technogenic contamination of natural water, especially fresh suprapermafrost water. The available frozen impermeable layer, located at a small depth from the ground surface as well as low subzero air temperatures make for a peculiar hydrogeochemical situation on the northern territories and wide development of cryogenic metamorphization of ground water in the zone of technogenic pressure consists of the increase in mineralization, chlorides and sulfates in the water and in accumulation of heavy metals. In case of repeated freeze-thawing cycles, the basic amount of soluble products of contamination is concentrated in the gravitational water, thus forming cryopegs. The formation of gryopegs as a result of intensive and durative anthropogenic activity causes their occurrence in the older part of inhabited residential areas (Melnikov, 1963; Anisimova, 1975). A high technogenic load on geosystems during the past years caused the intensified processes of contaminating the soil and suprapermafrost water the formation of cryopegs in the new housing development areas. At the same time the conditions of migration and concentration of chemical elements in the areas of active dynamics of suprapermafrost water was observed. However, slightly contrasting anomalies of contaminating elements were observed in the seasonally thawed layer and in the top permafrost layer.

Observation of the behaviour of soil solutions has enabled to determine the peculiar features of geosystem operation. The most contrasting changes

in the flows of macro- and microelements, the pH value and oxidation-recovery potential, which determine the geochemical migration medium in the upper horizons of the seasonally thawed layer, are observed before and after the cold period, when sharp changes of temperature and staged humidity transfers takes place. Most of the components that form technogenic geochemical fields are accumulated in the upper horizons of the seasonally thawed layer before the cold period. In winter, as a result of cryogenic concentration and migration of soluble contamination products deep into the seasonally thawed layer under the effect of freezing, there occur a depletion of the upper horizons of the seasonally thawed layer; by the beginning of the warm period the concentrations of contaminating components and productivity (component amount in 1 m thick layer) of technogenic anomalies are reduced. The maximum range of seasonal changes in the intensity of geochemical fields is typical of Mo, Cr, Ag, SO<sub>4</sub><sup>-</sup>, Na<sup>+</sup>, Ca<sup>++</sup>, the concentrations of which in soil water change by 5-15 times.

The productivity of technogenic geochemical fields in the upper parts of seasonally thawed layers during the spring and the autumn periods on the territory of Yakutia has been calculated. The difference between the obtained values characterizes the amount of the matter transferred during the winter period to deeper horizons of seasonally thawed layers and to the top of permafrost. One may judge about the scale and the intensity of the processes of cryogenic redistribution of contaminating components by the annual balance of the productivity of technogenic anomalies for the town areas, which makes for SO<sub>4</sub><sup>2-</sup> - 13.8; Cl<sup>-</sup> - 8.8; Na<sup>+</sup> - 7.0; Ca<sup>2+</sup> - 2.4 thou.t. For heavy metals - Cu, Cr, V - these values are 3-4 times lower.

The penetration depth of technogenic anomalies into the top of permafrost depends on the gradient of concentration (component amount in the effluents), geochemical properties of chemical elements, which form the anomaly, and also on geological peculiarities of the section.

The prevalence of intensive anion migration in the left side of the series (SO<sub>4</sub><sup>-</sup>, HCO<sub>3</sub><sup>-</sup>, Cl<sup>-</sup>) proves the experimentally obtained data on a greater mobility of the negative ions in permafrost (Lebedenko 1989).

The distribution of the components in a solid phase is less intensive. Ultimately, the elemental content in the solid and liquid phases of geochemical fields is dependent on a complicated combination of dependent on a complicated combination of simultaneous processes. The most important of them is, probably of the elements by hydrous ferric oxides, hydrous manganese oxides, by organic matter and clay minerals. One may judge about the summary effect of all these processes by the intensity of the aureole zone of chemical elements in solid and liquid phases. For some elements (Zn, Co, Mo, V) there is a prevailing absorption by solid phase, for others (Pb, Mn, Cu) it is in favour of water solution.

Contamination of suprapermafrost water is a considerable danger for the water of the deeper levels, since the geochemical link is realized through taliks. Contamination of the suprapermafrost water is in most cases an irreversible process, resembling a chain reaction and resulting finally in contamination of suprapermafrost water.

## TECHNOGENIC GEOCHEMICAL FIELDS IN SOILS

Beyond the cryolithozone (permafrost) the maximum contamination of soil by the products of the technogenesis is registered on soil surface (Nezhdanova et al. 1984). Soil is regarded as a self-cleaning filter of nature. In the permafrost, however, it practically loses its desinfection properties. The reasons for that are a small thickness of the section, poor drainage, thermohydrogeochemical barrier on the way of contaminant migration, annual freezing that favours the concentration of contaminant in soil water, the prevalence of recovery conditions, weak biochemical and reduced chemical activity of soil (because of low temperatures), a short period of biological life during the year. These conditions effect the acceleration of soil contamination processes in the area of technogenic pressure. The high potential of atmospheric pollution due to climatic peculiarities, limits the scale of contaminant dispersion. As compared with technogenic anomalies in the atmosphere, the lithochemical fields occur on limited areas and have a lesser scale of degradations. In the soil of residential areas there is a high rise of the concentration of Cl<sup>-</sup>, Hg, Pb, P, S, Ag, Sn, Cu, Y, Zn, Cr, the anomalies of which are widely spread, for instance, in Yakutsk and even occur in some regions of such a young and well-developed town as Nerjungri.

The accumulation of the basic mass of solid contaminants take place in the upper part of soils to a depth of 15-20 cm. Depending on the intensity of technogenic pressure source and the intensity of cryogenesis processes the depth of contaminant penetration may reach 2.5-2.7 m, which results from component migration in soil solution and their further settlement (sedimentation) on various adsorbents.

Salt represents the greatest danger for permafrost, as the salinated soils keep the negative temperature, but become thawed, thus reducing the

bearing capacity of building bases and destroying the foundation materials. The anthropogenic salinization of soil may reach the thawing temperature in spite of the fact that annual mean soil temperature remain negative. For instance, if the concentration of pore solution in cleyey silts is 80 g/l, the thawing temperature is equal to -6°C, the soil temperature under natural conditions being about 4-8°C below zero. Therefore a small temperature rise will commence perrenial melting of soil and development of thermokarst. The soil of Yakutsk may serve as an example of high salinization of soil in inhabited areas.

Accumulation of salts in the soils of inhabited points located in more favourable landscapes or with a relatively short period of technogenic pressure proceeds very slowly.

## REFERENCES

- Anisimova, N. (1975) Cryogenic hydrochemical changes in permafrost alluvial deposits discovered during economic development of the Central Yakutia/ Proceedings of the conference on environmental protection held in connection with economic development of the permafrost area, Yakutsk.
- Lebedenko, Yu. (1989) Cryogenic migration of ions and bound water in ice-rich dispersion rocks. Engineering geology, No. 4.
- Makarov, V. (1990) Geochemistry of the snow cover near the mine pit. Geography and natural resources, No. 1.
- Makarov, V. et al. (1990) Geochemistry of the snow cover in Yakutia. Yakutsk.
- Melnikov, P. (1963) The results of geocryological, hydrocryological and engineering-geological survey in Central and Southern Yakutia. M. AS-publishers, p. 84.
- Nezhdanova, I. et al. (1984) Investigating the contamination of urban soil in connection with environmental protection. Bulletin of the Leningrad State University, No. 12.

PHYTO-ECOLOGICAL MAPPING AND BIOGEOCOENOSIS STABILITY OF THE WEST-SIBERIAN PERMAFROST ZONE

Liya I. Meltzer

Institute of Northern Development Russia Academy of Sciences, Siberian Branch  
p.o.b. 2774, Tyumen, 625003, Russia

The paper considers methodological problems of developing phyto-ecological maps on the basis of stability of ecosystems to anthropogenic impacts. The estimation of the stability of biogeocoenosis is based on the study of natural succession and anthropogenic dynamics of vegetation cover.

Ecological problems as well as economic and social problems are among the essential and urgent needs of the Humankind. Solution of ecological problems is impeded by a great number of factors; e.g. in the north of the West Siberia features such as permafrost, short period of vegetation growth, low temperatures, sustained winds, etc; produce highly sensitive ecosystems and low potential for recovery. At the same time a high rate of economic development associated with exploration and exploitation of gas and oil fields results in disturbances of large areas.

Geobotanical investigations of the Western Siberian tundras on the regional level were carried out in 1970 in connection with preparation of the vegetation map of the Western Siberian Plain. The results of investigations were also published in the works describing the plant cover of Yamal-Gydan tundras including the main boundaries of vegetation zones and principles of classification of tundra vegetation (Meltzer, 1977, 1980, 1984, 1985).

Nowadays the necessity for more detailed investigations of environment and large-scale landscape mapping is taking place in connection with economic development of Yamal's North. Methods of ecological mapping rank high among other methods of the environmental research.

We hold with Sochava's term «ecological map» as an approach which describes interaction between biota (vegetation and fauna) and basic environmental conditions (Sochava, 1979).

Field investigations (aerointerpretation and field surveys, together with field ground checks) were planned to cover, to the greatest possible extent the diversity of zonal-provincial features of Yamal's tundras. As a result, a series of large-scale phytoecological maps and maps of biogeocoenosis resistance to mechanical impact were prepared.

The problem of the surface stability arises from the increase in degree of the anthropogenic disturbance. The concept of «stability» is qualitative and at the same time useful approach.

Apparently, this fact has resulted in no well-developed concept of the stability of natural systems (geosystems, ecosystems, landscapes). Insufficient elaboration of theoretical aspects still exist in spite of large number of publications dealing with theoretical and practical questions of the problem (Grave, 1978, 1980; Peres, 1979; Krauklis, 1979; Brown and Grave, 1981; Preobrazhensky, 1983; Kuprijanova, 1983; Glazovskaya, 1988; Isachenko, 1991).

Two aspects are recognized in the problem of surface stability and sensitivity to the anthropogenic impact:

1. Investigations of ground stability and sensitivity to construction (in order to avoid the negative influence of cryogenic processes on engineering constructions).

2. Investigations of the stability of natural systems as a part of the biosphere, i. e. regions of accumulation and transformation of energy and regions of biogeochemical activity of living organisms.

The revealed laws of natural successions and moving forces and trends of anthropogenic vegetation development gives us an opportunity to rank different types of stability of the Yamal biogeocoenosis.

The following criteria were used to distinguish the types of biogeocoenosis stability:

1. The ability of ecosystems (biogeocoenosis) to withstand anthropogenic disturbance and to maintain their initial state (resistance).
2. The ability of biogeocoenosis to recover toward normal (original) regime of functioning after removal of disturbance (resilience).

The final stage of our investigation was the map entitled «Biogeocoenosis resistance to the anthropogenic (mechanical) impact» (Fig. 1). This map was derived from the phyto-ecological map.

The legend of the map is shown on Table 1.

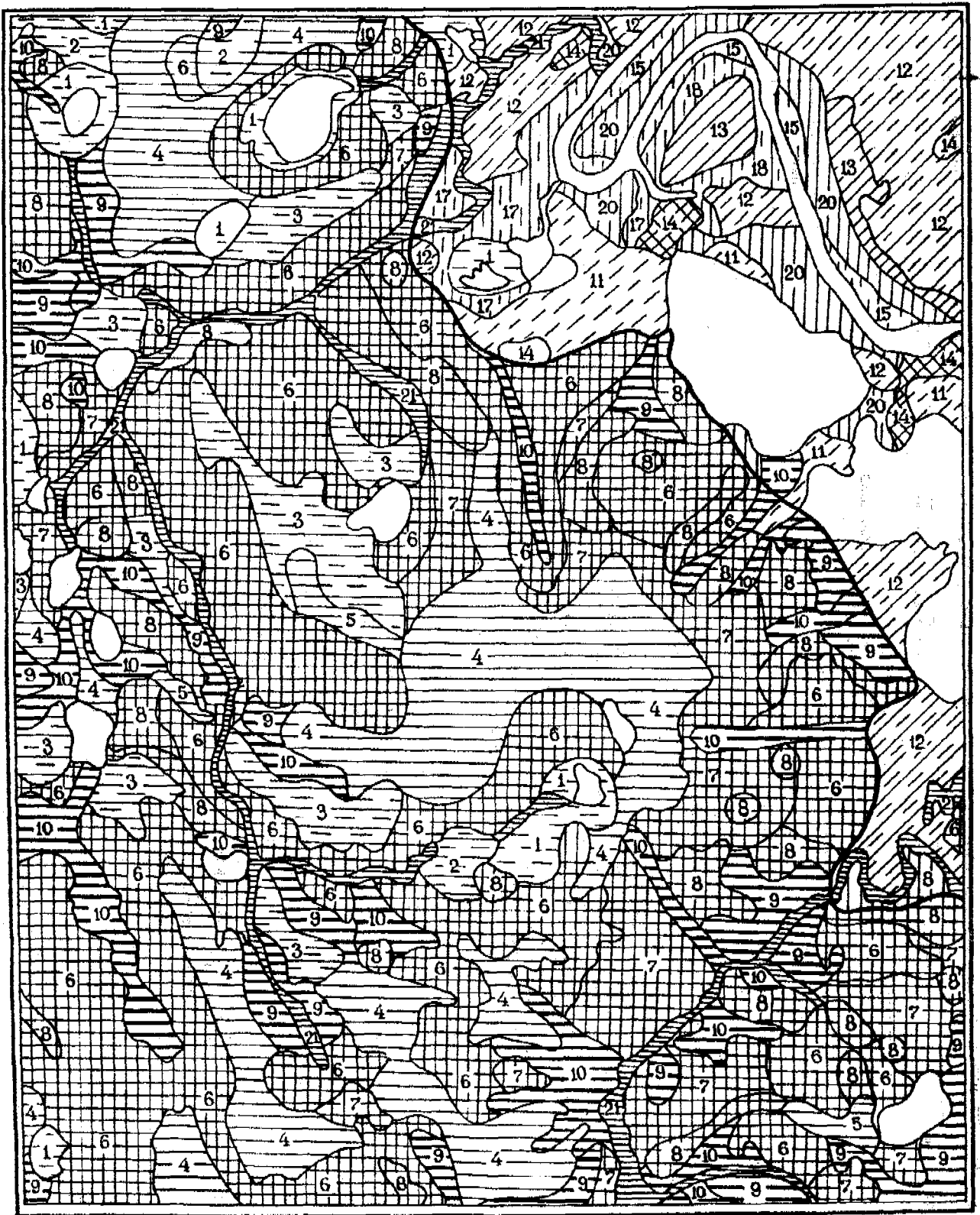


Figure 1. Biogeocoenosis resistance to the antropogenic (mechanical) impact. Fragment of the map (the legend see Table 1.)

Table 1. THE OTHER MAP OF BIOGEOCOENOSIS STABILITY UNDER ANTHROPOGENIC (MECHANICAL) IMPACT (fragment) (continued on next page)

on the map 1	Mapping units 2	Permissible impact 3	Unpermissible impact 4
COMMUNITIES OF EROSIONAL MARINE TERRACES			
I. Relatively stable			
1	Herb, herb-hypnum moss and herb-sphagnum moss communities of lacustrine depressions and drained lake basins	Recovery within 3-7 years in case of slight and insignificant disturbances**	Most severe disturbances cause thermal subsidence, thermokarst
II. Slight stable			
2	Herb-moss with willow paludificated communities of flat-topped uplands	Recovery through plant successions in case of slight and insignificant disturbances	Quite severe disturbances cause increase of swamping, thermal subsidence, partly-thermocarst
3	Dwarf shrub-herb-moss with willow and dwarf birch weakly paludificated tundras of flat-topped, poorly drained uplands	Insignificant disturbances on large territories cause paludification, thermal subsidence	" - "
III. Relatively unstable			
4	Low shrub-herb-moss hillocky polygonal tundras of smoothed poorly-inclined uplands	Slight disturbances on large territories can cause local paludification	Quite severe disturbances on large territories cause activation of CP (thermal subsidence, thermokarst, slumping)
5	Herb-lichen-moss flat palsa mires of flat-topped uplands	Insignificant and quite severe disturbances causes increase of paludification, thermal subsidence. Recovery through plant successions over a long time	" - "
IV. Unstable			
6	Willow and dwarf birch-willow herb-green moss tundras and willow herb-moss communities of slopes	Recovery through plant successions is possible in case of slight disturbances	Activation of CP in case of quite severe disturbances
7	Willow-dwarf birch-dwarf shrub-herb-moss hillocky tundras on upper parts of slopes	" - "	" - "
8	Dwarf shrub-lichen-moss with dwarf willow-dwarf birch hillocky tundras of uplands	" - "	" - "
V. Most unstable			
9	Dwarf shrub-lichen-moss and herb-moss communities of steep side slopes	Slight disturbances on large territories can cause activation of CP	Any anthropogenic impact must be excluded
10	Dwarf shrub-lichen and low shrub-moss communities of gullies	" - "	" - "

on the map 1	Mapping units 2	Permissible impact 3	Unpermissible impact 4
-----------------	--------------------	-------------------------	---------------------------

COMMUNITIES OF FLOODED TERRACES

I. Relatively stable

11	Herb-hypnum moss and sphagnum mores	Insignificant disturbances on large territories cause flooding of localities. Recovery within 3-7 years	Quite severe disturbances cause thermal subsidence, locally-thermokarst
----	-------------------------------------	---	---

II. Slight stable

12	Dwarf shrub-herb-sphagnum moss flat palsa mires and birch polygonal mires	Insignificant disturbance causes development of herb-hypnum moss communities	Palsas and low-centre ice-wedge polygons are destroyed at first in case of severe impact
----	---	--	--

III. Relatively unstable

13	Willow-herb-moss paludificated tundras of flat-topped uplands	Insignificant disturbances cause increase of flooding and development of cotton-grass-hypnum moss communities	Quite severe disturbances cause thermal subsidence on small localities, thermokarst on large territories
----	---	---	--

IV. Unstable

14	Dwarf birch and willow-dwarf shrub-moss and herb-moss communities of flat localities and gentle slopes	Slight and insignificant disturbances cause the replacement of shrubby tundras by herb-moss tundras	Thermoerosional processes (thermokarst, thermoerosion) in case of insignificant and quite severe disturbances
----	--	---	---



## REFERENCES

- Brown J., Grave N.A. (1981) Surface disturbance and protection in northern development. Novosibirsk: Nauka, 88 p. (in Russian)
- Grave N.A. (1978) Sensitivity of surface to the anthropogenic impact in the permafrost zone, ways and methods reflection on the maps. // Metodika ingenerno-geologicheskikh issledovaniy i kartirovaniya oblasti vechnoy merzloty. Yakutsk, pp. 16-33. (in Russian)
- Grave N.A. (1980) Significance and direction of geocryological investigations for the problem of environmental protection and rational use of natural resources in the permafrost region. // Ustoychivost poverhnosti k technogennym vozdeystviyam v oblasti vechnoy merzloty. Yakutsk, pp. 6-12. (in Russian)
- Glazovskaya M.A. (1988) Geochemistry of natural and anthropogenic landscapes of the USSR. M.: Vysshaya shkola, 328 p. (in Russian)
- Isachenko A.G. (1991) Landscapetology and physical-geographical division into districts. M.: Vysshaya shkola, 366 p. (in Russian)
- Krauklis A.A. (1979) Problems of experimental landscapetology. Novosibirsk: Nauka, 232 p. (in Russian)
- Kupriyanova T.P. (1983) The review of ideas about physico-geographical systems stability. // Ustoichivost geosistem. M.: Nauka, pp. 7-13. (in Russian)
- Meltzer L.I. (1977) Mapping of tundra vegetation of the West Siberia. Teoreticheskiye i metodicheskiye voprosy kartografii. Irkutsk, pp. 77-79. (in Russian)
- Meltzer L.I. (1980) The representation of heterogeneous vegetation of West-Siberian tundras on middle-scale maps. Geobotanicheskoye kartografirovaniye, L.: Nauka, pp. 11-24. (in Russian)
- Meltzer L.I. (1984) Zonal division of tundra vegetation of the West-Siberian Plain. Rastitelnost Zapadnoy Sibiri i eyo kartografirovaniye. Novosibirsk, Nauka, pp. 7-19. (in Russian)
- Meltzer L.I. (1985) Tundra vegetation. Arctic tundras. Northern subarctic tundras. Southern subarctic tundras. // Rastitelnyi pokrov Zapadnosibirskoy ravniny. Novosibirsk, pp. 41-54. (in Russian)
- Peres K.T. (1979) Limits of ecosystem resistance. Chelovek i biosfera, vol. 3, Moskovsky Universitet, pp. 90-95. (in Russian)
- Preobrazhensky V.S. (1983) Problems of geosystem stability. // Ustiychivost geosistem. M.: Nauka, pp. 4-7. (in Russian)
- Sochava V.B. (1979) Plant cover on thematic maps. Novosibirsk, Nauka, 189 p. (in Russian) I. (1985) Tundra vegetation. Arctic tundras. Northern subarctic tundras. Southern subarctic tundras. // Rastitelnyi pokrov Zapadnosibirskoy ravniny. Novosibirsk, pp. 41-54. (in Russian)
- Peres K.T. (1979) Limits of ecosystem resistance. Chelovek i biosfera, vol. 3, Moskovsky Universitet, pp. 90-95. (in Russian)
- Preobrazhensky V.S. (1983) Problems of geosystem stability. // Ustiychivost geosistem. M.: Nauka, pp. 4-7. (in Russian)
- Sochava V.B. (1979) Plant cover on thematic maps. Novosibirsk, Nauka, 189 p. (in Russian).

## ROLE OF CLIMATE ON ACTIVE LAYER VARIATIONS, SVALBARD

Krzysztof Migala

Institute of Geography, University of Wrocław  
University Square 1, 50-135 Wrocław, Poland

The main objective of this study is to utilize an empirically-derived equation to estimate the annual depth of the active layer over a 28-year period. The impact of freeze-thaw cycles on bedrock weathering and vertical stratification of the active layer is also addressed. Both the equation and prediction were derived on the basis of mean daily air temperatures and daily liquid precipitation amounts from two western Spitsbergen (Svalbard) stations. Because of strong spatial differentiation of soil features in the unglaciated area, the predictions show only the general trend of the processes and may not be applicable to all types of ground materials.

### INTRODUCTION

Previous investigations of active layer thickness have shown a strong seasonal variability in the operative processes which are often influenced by precipitation (Marciniak and Szczepanik 1983; Olszewski 1986; Migala 1988; 1990; 1990 unpubl.). Migala (1990) has derived a general equation relating annual depth of the active layer to seasonally-fluctuating summer duration and liquid precipitation amounts.

The main objective of this study is to utilize the empirically-derived equation to estimate the annual depth of the active layer over a 29-year period. The impact of freeze-thaw cycles on bedrock weathering and vertical stratification of the active layer will also be addressed.

### METHOD

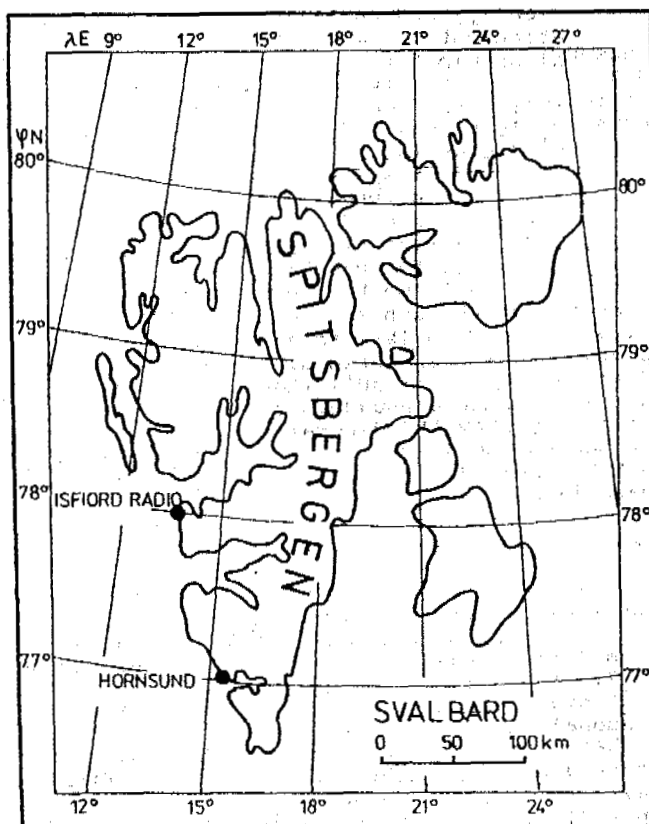
Prediction of annual active layer thickness at the Hornsund Fiord area was empirically derived using meteorological and ground temperature data, and utilized to predict active layer thickness at the Isfiord Radio Station (Map 1). The 29-year record at Isfiord extends from 1947-1975 and is applied to predict active layer development for the years 1948-1975 (Norsk Meteo. Arobk 1947). Both the equation and the prediction utilize mean daily air temperatures and daily precipitation (rain) amounts.

Annual maximum thaw depth ( $h$ ) was calculated using Eq. 1, originally proposed by Migala (1990).

$$h = 0.5 \ln T - (0.364 R_j R_c^{-1} - 0.288) \quad \text{Eq. 1}$$

where:

- $h$  = maximum annual depth of thaw (m)
- $T$  = duration of summer thawing (days)
- $R_j$  = total rain (mm) during previous autumn
- $R_c$  = total rain (mm) during current thaw season



Map 1. Area of investigation, Svalbard (Norway)

It is assumed that the ground thaws when the mean daily air temperature ( $t$ ) rises above  $0^{\circ}\text{C}$ . The duration of seasonal thaw ( $T$ ) commences from this date and continues until  $t$  returns to  $0^{\circ}\text{C}$ . The autumn and summer precipitation periods are determined on the basis of the following criteria (Baranowski 1968):

autumn  $2.5^{\circ}\text{C} > t > -2.5^{\circ}\text{C}$   
 summer  $t \geq 2.5^{\circ}\text{C}$

These periods are defined only to calculate the total sum of liquid precipitation (rain and melted, episodic snowfall). The criterion for the summer defines the period of active rain. The criterion for the autumn period is justified since snowfall does not play a significant role in the Svalbard and the value of  $-2.5^{\circ}\text{C}$  appears to be the limit of ground cooling prior to the final winter freezing of the active layer (Migala 1988; 1990; 1991; Chmal et al. 1988; Migala et al. 1988).

Equation 1 was derived and calibrated using daily ground temperatures and meteorological data for the period 1979-88 at Hornsund Fiord. The seasonal penetration of the  $0^{\circ}\text{C}$  isotherm was analyzed on the basis of ground temperatures at depths of 0.05, 0.1, 0.2, 0.5, 0.8 and 1.0 m.

Next, the impact of meteorological data on the dynamics of  $0^{\circ}\text{C}$  penetration was tested statistically, and indicate a significant correlation between maximum thaw depth and seasonal precipitation amounts at Hornsund;  $r = 0.87$ ,  $F = 17.88$ , with a critical value of 13.75 at ( $p = .01$ ). The standard error of the estimated equation is 0.1023 and the standard error of the regression coefficient is 0.0746.

The ground temperature measurements used in the equation were obtained from a sandy-gravel marine terrace about 20 m asl in the vicinity of the Polish Polar Station in Hornsund Fiord (Szerszen 1965; Baranowski 1968). These terraces occur frequently on the unglaciated coast of western Spitsbergen and, despite the 120 km distance between Isfiord and Hornsund, they probably exist in Isfiord. The strong spatial differentiation of soil features in the unglaciated area suggests that the predictions will only show the general trend of the processes and role of precipitation; they will not be applicable to all types of ground materials.

## RESULTS

The pluviothermal effect on active layer development over the years 1947-75 have been estimated on the basis of meteorological data from Isfiord Radio Station (Norsk Meteo. Arobk 1947...). From Table 1 it is interesting to note that over the period 1947-75, the duration of seasonal thaw ( $T$ , column 1) varied from 86 days (1968) to 151 days (1957). Soil thawing usually started between the end of May and the first ten days of June, and ceased in mid-September or, sporadically, by the beginning of October. The high variability of precipitation should also be noted (columns 4 and 5). The lowest amount of summer precipitation was observed in 1966 (21 mm) and the rainiest period was the thaw season of 1972, with a total of 236 mm. Autumn precipitation fluctuated from 2 mm in 1966 to 138 mm in 1961.

Using the Isfiord meteorological data (Table 1) and Eq. 1, it was estimated that the

Year	T	S	A	Ri	Rj
1947	138	89	26	109	58
1948	124	89	36	92	28
1949	100	66	26	60	47
1950	109	89	32	96	31
1951	94	86	39	93	92
1952	113	90	41	99	55
1953	102	85	67	100	110
1954	92	94	35	86	30
1955	118	110	11	160	10
1956	119	72	56	31	52
1957	151	92	52	97	73
1958	107	85	18	88	59
1959	116	82	38	115	90
1960	121	98	11	145	22
1961	104	79	48	85	138
1962	94	56	56	43	98
1963	113	84	28	134	34
1964			lack of data		
1965	91	77	22	57	2
1966	93	67	29	21	7
1967	105	80	22	172	99
1968	86	64	23	93	58
1969	114	83	26	129	105
1970	94	64	55	135	73
1971	121	88	26	113	33
1972	117	106	22	236	83
1973	103	73	35	148	46
1974	113	73	34	139	41
1975	93	78	30	75	38

Table 1. Pluviothermal conditions for the years 1947-75 at Isfiord Radio Station, Spitsbergen.

ground usually thawed to a depth of 1.5-1.8 m and, sporadically, less than 1.5 m and more than 2.0 m. The only exceptional case was 1962, when the estimated thaw reached a depth of only 0.8 m (Figure 1). The average for the entire population is 1.81 m, with a standard deviation of 0.23 m; if the anomalous case of 1962 is excluded, the average depth is 1.85 m and the standard deviation is 0.12 m.

On the basis of the estimates, the frequency of thaw cycles within the ground was calculated at 0.1 m depth increments (Figure 2). The results suggest that the annual thaw layer extends to a depth of 1.5 m nearly 100% of the time; the only anomalous year was 1962, which had an exceptionally short thaw period. Active layer development to a depth of 1.9 m occurred in 50% of the years. The frequency of thaw therefore diminishes exponentially with depth.

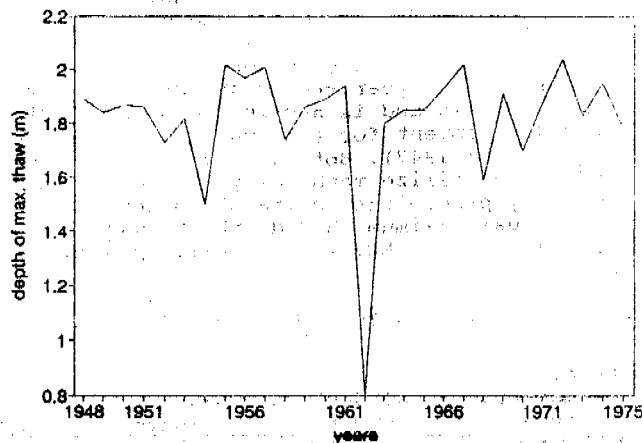


Figure 1. Estimated maximum depth of the active layer, Isfiord Radio.

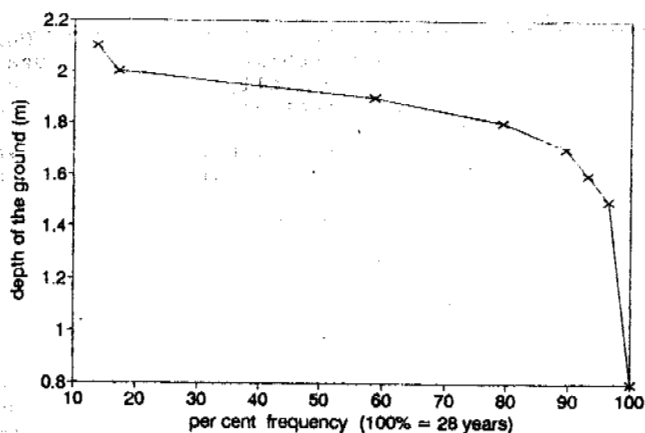


Figure 2. Estimated frequency of freeze-thaw cycles with depth, 1947-75 at Isfiord Radio Station.

The temporal trend of the active layer thickness is shown in Figure 3. The gradual deepening of the active layer above permafrost may reflect the slight global tendency toward warming. The annual variability suggests different intervals of thaw periodicity, but any relationship should be verified by detailed field analysis.

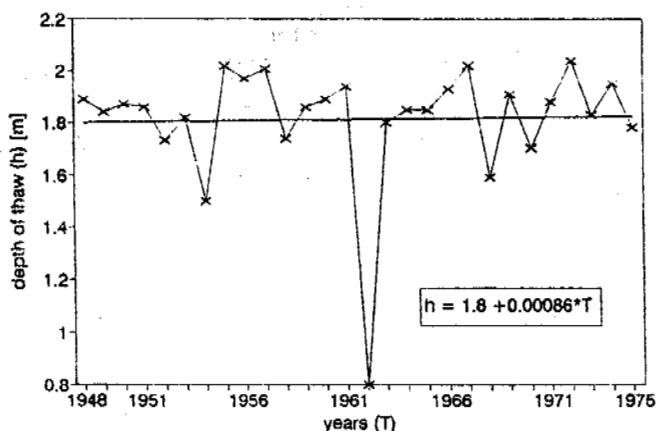


Figure 3. Best-fit trend of seasonal active layer depth, Isfiord Radio Station.

## DISCUSSION

The results show strong variability of annual thaw, which is partially dependent on seasonal liquid precipitation (rain) during the current summer and previous autumn. Preliminary accounts by Chmal et al. (1988) and Migala (1990), and the empirical equation derived at the Hornsund area, indicate favorable correlations and support of these findings. However, these estimates must be verified by extensive field research and spatial analysis.

The problem of precipitation trends and variability in the Svalbard area was analyzed by Baranowski (1975), Houghton (1984) and Brazdil (1988). They concluded that both monthly and annual sums of precipitation fluctuate with periodicities of 3-10 years. Steffensen (1982) and Pereyma (1983) analyzed differences in the spatial distribution of precipitation. Yearly precipitation sums in central Spitsbergen are estimated to be one-half to one-third the amounts received in the western portion of the island. Strong spatial patterns of precipitation are apparent but difficult to correlate empirically owing to local moderation by atmospheric circulation, orographic effects, and the complexity of the varied underlying surfaces including rock, glaciers and snowfields, as well as water and sea ice (Baranowski 1975; Brazdil 1988; Niedzwiedz and Ustrnul 1988; Gluza and Plasecki 1989). In addition, the strong maritime (Gulf Stream) influence on the western side of the island, where this study took place, is noticeably lacking on the eastern (lee) side.

On the basis of the above discussion, the following hypotheses are advanced: (1) the spatial distribution of rainfall plays a major role in the topoclimatic differences of active layer development, and (2) there exists the probability of time sequence correlation between seasonal precipitation magnitudes and the thickness of the active layer. (The role of the "snow-curtain effect" during melting, and the role of snow as an insulator in heat exchange, are well-known and is not discussed in this study).

There are about 80-90 freeze-thaw cycles each year in the near-ground air layer (0.5-1.0 m), and about 50-60 cycles at the ground surface (after Baranowski, 1968). There are usually 10-20 freeze-thaw cycles at a depth of 10 cm, 5 cycles at a depth of 50 cm and 1-2 freeze-thaw cycles each year at greater depths. The freeze-thaw cycles near the surface are not very effective owing to the timing of the maximum frequency (spring and autumn), and because of the very short duration (a few hours) and episodic nature of the events.

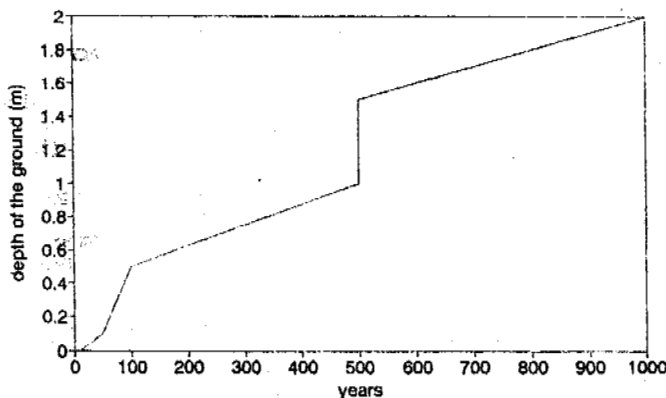


Figure 4. The assumed partial rock disintegration curve for metamorphic schist (after Martini 1986).

Martini (1986) estimated, on the basis of experimental work, that metamorphic schist around the Hornsund Fiord becomes partially disintegrated after about 250-500 freeze-thaw cycles. The time required to partially disintegrate schist by frost weathering within the active layer can be evaluated on the basis of the frequency of thaw with depth, as shown in Figure 2, and the data of Baranowski (1968) and Martini (1986). The estimated curve of frost weathering rates is shown in Figure 4, and seems to reflect a characteristic feature of the active layer: parts of structure in vertical profile, or its "triplicity". The three parts of structure were distinguished by the authors on the basis of the different criteria: distribution of water and ice inclusions (by Zhestkova 1961, after Washburn 1979), thermal conditions, and moisture features (by Czeppe 1966). The precipitation of late summer or autumn period can play an important role in building ice inclusions (lenses, veins, pore ice) in the active layer where, the following season, they will alter the bulk thermal properties and conditions (heat exchange, zero-curtain effect, and latent heat) and moisture distribution in the ground.

In consequence, the vertical structure is affected by the frequency of thaw cycles in each region of the ground. The process is conditioned by thermophysical soil features and distribution of moisture.

#### CONCLUSIONS

Based on the results and discussion presented above, it is concluded that (1) the trend of estimated seasonal active layer thaw depth corresponds to the global warming tendency; (2) the frequency of thaw cycles within the active layer is vertically dependant; and (3) the curve of the frost weathering rate reflects the "triplicity" of the active layer. This fundamental characteristic of the active layer is affected by the frequency of thaw cycles and moisture distribution in the ground.

Two hypotheses can be advanced which will require further research to verify: (1) the spatial distribution of precipitation plays the main role in the topoclimatic differences of active layer development, and (2) there exists the probability of time sequence correlation between liquid precipitation magnitudes and active layer thickness.

#### ACKNOWLEDGEMENTS

The author wishes to thank an anonymous U.S. reviewer for assistance in the preparation of this manuscript.

#### REFERENCES

- Baranowski, S. (1968). Thermic Conditions of Periglacial Tundra, SW Spitsbergen. *Acta Univ. Wratisl.*, 68, 75 pp.
- Brazdil, R. (1988). Variation of air temperature and atmospheric precipitation in the region of Svalbard. In: (Brazdil et al.) *Results of Investigations of the Geographical Research Expedition "Spitsbergen 1985"*, University J. E. Purkyne, Brno, 295-323.
- Czeppe, Z. (1966). The course of the main morphogenetic processes on the SW Spitsbergen. *Prace Instytutu Geograficznego Uniwersytetu Jagiellońskiego*, 35.
- Gluz, A. F., and Piasecki, J. (1989). The role of atmospheric circulation in climate features forming in S Bellsund, Spitsbergen. In: *Wyprawy Geograficzne UMCS na Spitsbergen 1986-1988*, UMCS, Lublin, 9-19.
- Marciniak, K., and Szczepanik, W. (1983). Results of investigations over the summer ground thawing in the Kaffioyra, NW Spitsbergen. *Acta Univ. Nicolai Copernici. Geografia* 18, 69-97.
- Martini, A. (1986). Contemporary periglacial weathering processes of mountain massifs in the vicinity of Hornsund, SW Spitsbergen. *Acta Univ. Wratisl.*, 966, 45-73.
- Migala, K. (1988). The role of snow cover in the active layer development in the Hornsund Area, SW Spitsbergen. In: *XV Sympozjum Polarne*, Wrocław, University of Wrocław, 230-239.
- Migala, K. (1990). Active layer of permafrost in the light of Hornsund climatic conditions, SW Spitsbergen. In: *Spitsbergen Geographical Expeditions of UMCS*, Lublin, 215-226.
- Migala, K. (1990 unpubl). Active layer development in the light of Hornsund climatic conditions, SW Spitsbergen. Ph.D. dissertation, University of Wrocław.
- Niedzwiedz, T., and Ustrnul, Z. (1988). The synoptic situations influence on the pluvial conditions in Hornsund, Spitsbergen. In: *XV Sympozjum Polarne*. Wrocław, University of Wrocław, 196-202.
- Olszewski, A. (1986). The chosen problems of seasonal and roof fluctuations of many years permafrost. *Acta Univ. Nicolai Copernici. Geografia* 19, 47-68.
- Pereyma, J. (1983). Climatological Problems of the Hornsund Area, Spitsbergen. *Acta Univ. Wratisl.*, 714, 134 pp.
- Steffensen, E. L. (1982). The Climate at Norwegian Arctic Stations. *Klima, Det Norske Meteorologiske Institutt*, 5, 44 pp.

## DEGRADATION OF CRYOGENIC STRATA IN LARGE WATER STORAGE AREAS

Boris A. Olovin and Rostislav M. Kamensky

Permafrost Institute, Russian Academy of Sciences Yakutsk 677018, Russia

Results of long-term experimental observation (1969-1992) of thawing dynamics of the frozen ground composing the water reservoir bed of the hydroelectric power plant, constructed on the Viluy River in 1968 are presented. The main components of the thermal balance in the water reservoir, their effect on microclimatic conditions of the near-shore area and water temperature in the lower reach are analyzed. It is found out that the depth of seasonal thaw may increase in the near-shore area resulting in intensive development of thermal erosion of shores.

Main factors causing permafrost degradation are the following: direct thermal effect of the water impounded in a reservoir on the permafrost table, indirect effect manifesting itself in changes in microclimatic conditions of a reservoir and near-shore area, changes in the hydrodynamic regime of ground water and changes in the profile of a shore slope as a result of wave action. These factors affect different sites of a reservoir interruptedly and nonuniformly due to the heterogeneous lithological structure of rocks, the influence of horizontal and vertical inhomogeneity of meteorological characteristics in the near-surface air layer, the variability of water flow into a reservoir due to variability of a precipitation amount in different years, changes in a shore-line position and a shore profile. The study of the thermal regime in the "reservoir-environment" system began 20 years ago for one of the largest water reservoirs constructed on permafrost. Some results have been previously reported (Kamensky and Konstantinov 1972, Melnikov and Olovin 1983).

The water reservoir we investigate (Figure 1) was impounded by the dam erected for the Viluy Hydroelectric Power Plant on the middle reach of the Viluy River. Its total storage is about 36 km<sup>3</sup> and water plane area is 2170 km<sup>2</sup>. The reservoir has (in plan) lake-like widened sections up to 10-18 km in width which are connected by narrower sections 1-2 km in width. The depth of the reservoir ranges from 5-10 m at the backup site to 70 m near the dam, and averages 18 m. Narrower sections of the water body are at sites where trap outcrops occur, wide sections are at the sites composed of thick Mesozoic and Paleozoic deposits.

The total annual inflow into the reservoir is approximately 20 km<sup>3</sup>, half of this value is account for by the Viluy River. The annual runoff of the Chona Creek, largest tributary of the Viluy, constitutes about 1/4 of the Viluy inflow. About half of the annual runoff of the small rivers is in May, that of the Viluy in June. The flowage coefficient of the reservoir is 0.7.

Frozen ground temperature on watersheds with an absolute elevation of 300-400 m is -2...-3°C, the mean annual air temperature,  $t_a$ , is about -

8°C. Site to site variability of  $t_a$  in this area is insignificant; air temperature decreases by 0.71°C northward and by 0.09°C eastward at every 100 km. Air temperature variations with altitude are more significant due to sinking of cold winter air to the low river valley. A considerable difference in the mean annual air temperature between watershed areas and bottoms of river valleys (3°C difference in the investigating area) results from winter inversion in the near-surface air layer and in the free atmosphere. Frozen ground temperatures in the valley range from -1°C to -10°C depending on the altitude, slope angle, exposure and lithology of rocks. Mean annual values of the elasticity of water vapour,  $e_a$ , 2 m above the surface slightly depend

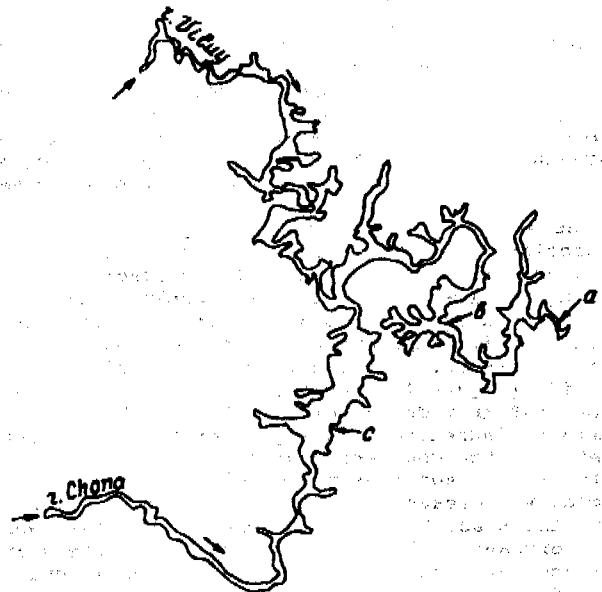


Figure 1. Scheme of water reservoir on the Viluy River: a, b, c - sites of meteorological measurements.

on the altitude: in the elevation range from 160 to 430 m  $e_a$  decreases linearly with altitude at an approximate rate of  $3 \cdot 10^{-4}$  millibar/m. The mean annual wind velocity in river valleys increases linearly from 1 to 3.3 m/sec in the elevation range 160-530 m, while on watershed  $v_a$  is constant 3.3-3.4 m/sec. The main annual precipitation value,  $G_a$ , does not vary in the elevation range 160-350 m. At higher sites with the elevation over 420 m  $G_a$  may considerably increase, as indicated by observation data available from the climate station located at the elevation of 416 m. Prior to the impoundment at the station site  $G_a$  was greater than that in other areas.

The near-shore area. Changes in microclimatic conditions of the near shore area caused by the impoundment are accompanied by changes in the surface thermal balance, an increase in the depth of seasonal thaw, and a rise of frozen ground temperatures. These changes can be estimated using data available from the climatic stations in the near-shore area of the reservoir (Figure 1, sites a, b, c). These stations are located at the elevation of 250 m above sea level, i. e. at the elevation which corresponds to the height of the dam crest of the Viluy Hydroelectric Power Plant.

The most significant changes in the near-shore are changes in air temperature,  $t_a$ , and absolute air humidity,  $e_a$ . During the ice-free period (May-October) the mean air temperature ( $t_a$ ) and air humidity ( $e_a$ ) are greater than those at the sites with the same elevation located far from the water reservoir ( $t_o$ ,  $e_o$ ); these differences depend on the size of a reservoir section: the wider is the reservoir section the greater is the difference. The effect of the reservoir on the microclimatic conditions in the near-shore varies throughout the year (Figure 2); during the freeze-up period the air temperature,  $t_a$ , and air humidity,  $e_a$ , do not differ from those observed at unaffected sites ( $t_o$ ,  $e_o$ ); in May-June the air temperature difference  $t_a - t_o$  in the near-shore zone is lower by 1.5-3°C (Figure 2); in July-August it approaches zero and reaches its maximum ( $t_a - t_o = 1.5-2.5^\circ\text{C}$ ) in October. The air humidity difference  $e_a - e_o$  increases sharply in May-June, reaches its maximum in July ( $e_a - e_o = 2-3 \text{ mb}$ ), then it decreases down to zero by November.

The effect of the reservoir on the microclimatic conditions is determined to a greater extent by the width of the reservoir; during the ice-free period the absolute air humidity increases by 0.3 mb, with the constant value of air temperature or even a slight 0.5°C temperature drop, at the reservoir sections 1-2 km wide (Figure 1, site a); at the reservoir sections 5-6 km wide (Figure 1, site b) the air humidity increases more significantly - by about 1 mb with the constant mean annual air temperature; at the sections up to 10-15 km wide the air humidity increases by 1.5 mb and the air temperature increases by 1.5°C. In winter the heat- and mass exchange between the reservoir and the near-surface air layer is almost the same as in unaffected areas due to the insulating effect of ice and snow covers; and microclimatic conditions above the reservoir are the same as those in unaffected areas at the same elevations.

So, from these facts it follows that a geometrical shape of the near-surface layer in which the significant transformation of

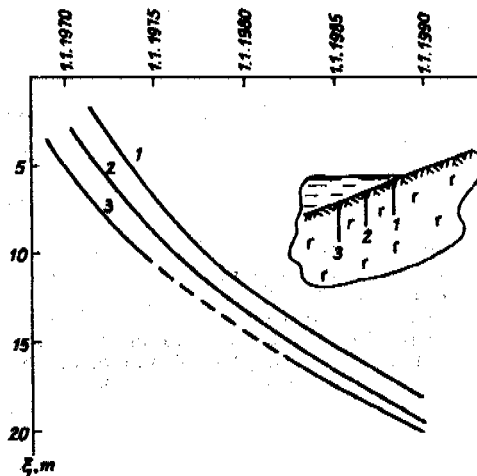


Figure 2. Frozen rock thawing dynamics in the bed of the Viluy water reservoir in the boreholes 1, 2, 3.

meteorological fields related to the impoundment occurs, is system of flattened semi-spheres with a diameter being by 20-30% greater than the width of the reservoir. These semi-spheres are poorly connected with each other at narrower sections of the reservoir; they exist only during the ice-free period; the maximum extent of these zones in terms of the air temperature is in June and October, in terms of the air humidity in July-August. An area affected by the reservoir is estimated to be about 1 km wide, though in some seasons it may be tens of kilometers, particularly during the periods of steady winds with stable direction. The fact that the area affected by the reservoir is rather small can be explained by an increase in the virtual temperature of a near-surface air layer, a shift of the near-water layer stratification toward the super-balanced one and intensified vertical transport.

The impoundment is expected to lead to a slight increase (by 2-4%) in the depth of seasonal thaw in the near-shore of the reservoir (Olovin et al. 1987). Greater changes are expected to occur in the ground temperature regime resulting from the disturbance of natural vegetation due to thermoerosional processes and man's activity in the near-shore zone. Thickness of a layer of seasonal thawing increases 1.5-2 times, frozen ground temperature rises by 3-4°C.

The flooded area. Thawing of frozen rocks composing the bed of the Viluy reservoir has been studied for over 20 years starting from 1968 at a gentle slope site ( $\alpha = 10^\circ$ ) located at a distance of 0.8 km from the plant's dam and water inlet. Three geothermal boreholes were drilled in the flooded area and spaced at 40 m intervals. The borehole were at depths of 6 m (borehole 1), 12 m (borehole 2) and 18 m (borehole 3) from the reservoir surface at a normal water level. Rocks in the reservoir bed are composed of weak-jointed dolerites with the moisture content of about 50 kg/m<sup>3</sup>. Heat and temperature conductivity of dolerites in the massive are  $\alpha = 2.8 \cdot 10^{-4} \text{ m}^2/\text{hr}$ ,  $\lambda = 2.27 \text{ W/m}\cdot\text{K}$ . In the areas we investigated the rate of frozen ground does not depend on the location of a borehole (Figure 3) and changes in

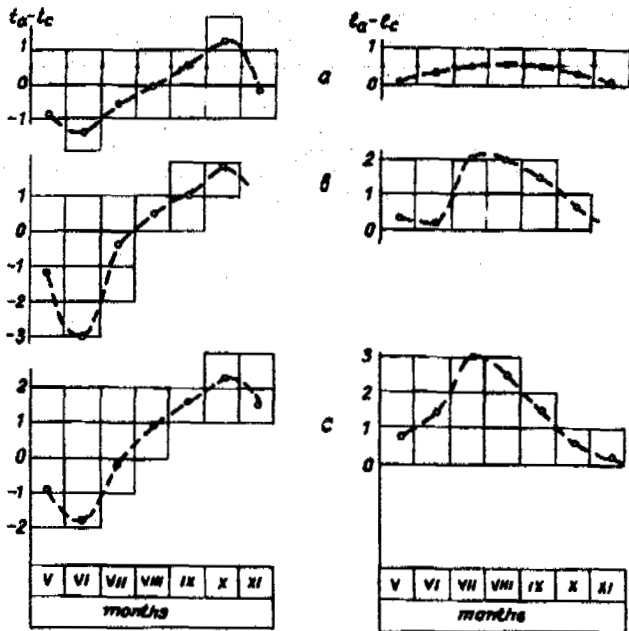


Figure 3. Difference between temperature  $t^{\circ}\text{C}$  and elasticity of water vapour  $e$ , mb, above the water reservoir -  $t_a$ ,  $e_a$ , and those at a considerable distance from it -  $t_c$ ,  $e_c$ ; when the width of the water reservoir is a) 1.5-2 km; b) 5-6 km; c) 10-12 (measurements of meteorological elements were made at the height of 2 m from the ground surface level).

direct proportion to  $r^{0.5}$ . Differences in total thawing depth are resulting mainly from the fact that the borehole sites were flooded at different periods of time: borehole 3 was flooded in May 1969, borehole 2 in May 1970, borehole 1 in June 1974.

Intensity of frozen ground thawing depends on the mean annual temperature of a near-bottom water layer in the reservoir. This temperature is difficult to predict since it depends on many factors determining the water- and heat balance of the reservoir: the hydrological and hydrothermal regimes of the tributaries, intensity of vertical mixing and an average rate of flow, work-load of the plant facilities, operation regime of water outlet structures, etc.

Surface temperature of flooded rocks near the dam is close to the mean annual temperature  $t_w$  of water flowing into the power station units. This mean annual water temperature may be estimated using the equation for the heat balance of the reservoir:

$$Q_w = \frac{V \cdot C_w \cdot K_f}{\Delta T} (T'_w - T_w)$$

where  $V$  is the total storage of the reservoir;  $C_w$  - the heat capacity of water;  $K_f = Q_w/V$  - the flowage coefficient;  $Q_w$  - the annual runoff;  $\Delta T$  - the period of time measured in years;  $T'_w$ ,  $T_w$  - the average temperature of water flowing into the reservoir and flowing out to the downstream;  $S$  - the water surface area in the reservoir.

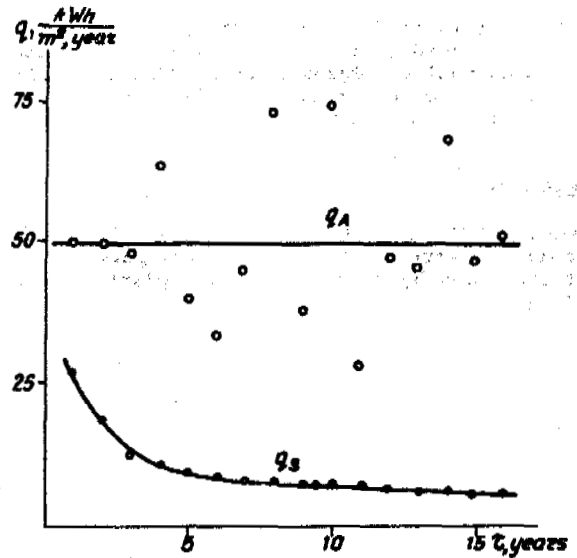


Figure 4. Heat-balance component of the water reservoir: heat exchange with the atmosphere  $q_A$  and heat flow to the underlying rocks  $q_s$ .

Intensity of heat exchange between the reservoir and the atmosphere,  $q_A = Q_A/S$ , (Figure 4) has not been changing for several years and average  $45.8 \pm 13.3 \text{ kWh/m}^2 \cdot \text{yr}$ ; the heat flow in the reservoir bed has been decreasing from  $24.4 \text{ kWh/m}^2 \cdot \text{yr}$  in 1967 to  $5.2 \text{ kWh/m}^2 \cdot \text{yr}$  in 1983-1984. Thus, during the operation of the power plant with an annual power generation output of  $2.6 \cdot 10^9 \text{ kWh}$  the thermal energy of about  $110 \cdot 10^9 \text{ kWh/yr}$  is withdrawn additionally from the Viluy River. A part of this amount of energy ( $11.4 \cdot 10^9 \text{ kWh/yr}$  in the 20th year of the plant operation) is expended for warming and thawing of frozen ground in the reservoir bed; and another part ( $99.4 \cdot 10^9 \text{ kWh/yr}$ , which is the amount of total heat flow into the atmosphere averaged over the past 20 years) is expended for changing the climatic conditions in adjacent areas.

At some sites located near the dam a very high rate of thawing is observed due to water filtration in thawing ground. At these sites the rate of thawing is greater by an order as compared to that observed in the reservoir bed (see Figure 3).

Recently, several regularities governing the talk formation in the water reservoir bed have been revealed depending on inhomogeneity of morphology, composition and structure of frozen ground within separate lithogenic facies and in endomorphic zones. For example, in the areas with the system of cavities and fissures partly filled with ice, irregular or long-period harmonic fluctuations of thawing ground temperatures are observed with an amplitude of up to  $1^{\circ}\text{C}$ . This was being observed during 6 years at borehole no.3 (Figure 2) at the depth of 11 m to 16 m from the surface (the interval of irregular temperature fluctuations is shown by a dotted line). Monotonous long-period fluctuations of thawing ground temperatures (with the period of over 1 year) were found on the right-side bank of the dam base at the Viluy power station. Periodical temperature fluctuations seem to be caused by the transformation of a filtration rate field as the



ice filling large fissures thaw. At present, the study is focused on the quantitative interpretation of thermal and hydrodynamic effects in thawing ground in order to specify the composition and filtration properties of the permafrost massif.

**REFERENCES**

Kamensky, R.M. and I.P. Konstantinov (1972) Thermal regime of water reservoir and its permafrost bed at the Viluy hydroelectric power plant. Kolyma 8, 30-33.

Melnikov, P.I. and B.A. Olovin (1983) Permafrost dynamics in the area of Viluy River Hydroelectric Scheme. Proc. Fourth Int. Conf. on Permafrost, Washington, D.C., Nat. Acad. Press, 838-842.  
Olovin, B.A., B.I. Kolmakov and V.I. Fedoryan (1987) Man induced changes in natural conditions in Far North hydroengineering structure-environment systems. The influence of Hydros on the Environment in the Far North. Yakutsk, 42-57.

# REGULARITIES OF PERENNIALY FROZEN GROUND FORMING IN SOUTHERN ZABAİKALIE

P.I. SALNIKOV

Chita Department of Permafrost Institute  
p. box 539, 672010 Chita, Russia

The report is based on a complex approach and the result of processing and analyzing the data of a 30-year period of observation on meteorological elements affecting the temperature regime of the lower air layer and generalization of new data on frozen grounds. The revealed regularities of permafrost formation in Southern Zabaikalie are considered in relationship with physico-geographical and geologico-geocryological factors.

Southern Zabaikalie is the territory with the state boundary of Russia in the south and east, the Khamar-Daban and Ulan-Burgasy ridges in the west and in the north it is limited by 53° of northern latitude not including the Dauria highland. The main factor determining the peculiarity of the Southern Zabaikalie climate are radiation regime, atmospheric circulation peculiarities, relief with hollows and mountains, remoteness from oceans.

On the territory in question the mean annual air temperature is  $-0.2 \dots -5.7^{\circ}\text{C}$ , the soil surface temperature is  $+1 \dots -5^{\circ}\text{C}$ . Geocryological conditions of the area are complex and diverse, they are due to the interaction of different nature factors: climate, relief, exposure and steepness of slopes, snow cover and vegetation, surface and subterranean waters, lithologic composition and peculiarities of ground structure and texture. All these factors, in the long run, lead to a great variety of temperature regime and thickness of seasonally thawed, seasonally frozen and perennially frozen grounds. Frozen grounds are represented by deep seasonally thawed-frozen grounds, mainly by sporadic high temperature perennially frozen grounds (PFG). The latter are in limit equilibrium to the factors stipulating permafrost existence and are characterized by unstable thermal conditions, availability of continuous, discontinuous and sometimes layered permafrost and taret soil taken in vertical section. Thickness of seasonal thawing and freezing depends upon soil surface temperature, lithologic ground composition, ground humidity on the eve of winter, texture density, regime of ground and temporary waters. Maximum depth of seasonal freezing is registered in large-gritty little-wet grounds and reaches 6 m. In fine grained slightly frost heaving grounds the depth of seasonal freezing reaches 4.5 m, and the depth of seasonal thawing - 4 m. The PFG temperature is  $0 \dots -2^{\circ}\text{C}$ , the thickness is from tens of centimetres to 100 m. The PFG lie in original rocks and Quaternary deposits. Original rocks are represented by bundles of aleurolites, sandstones and argillites, and Quaternary deposits are characterized by alternation of layers with different lithologic composition, represented by argillaceous, sandy and coarse detrital grounds which are quite different in

thickness and strike, often even within one layer.

The factors influencing permafrost formation have been determined on a basis of a approach and discovering system-forming factors. To estimate the regime and common regularities of meteorological elements influencing air and soil surface temperature regime the data of 71 meteorological stations of southern Zabaikalie since 1954 to 1988 have been systematized. This period of observation is representative for the evaluation of meteorological regime due to physical development of processes (Lorents, 1977) and makes it possible to determine basic quantitative and qualitative peculiarities of meteorological processes affecting the formation of temperature regime of lower atmospheric layer, to estimate their time variation and obtain comparable data for revealing regularities of their space changing. The values of meteorological ranges considerably on the territory. Thus, in January the mean monthly values are: atmospheric pressure 1029.8 (the station of Byerka)  $\dots$  1048.1 hPa (the station Udinsk), air temperature  $-19.7^{\circ}\text{C}$  (the station of Sedlovaya)  $\dots$   $-33.2^{\circ}\text{C}$  (the station of Gorbitsa), wind speed 0.2 m/sec (Gorbitsa)  $\dots$  3.7 m/sec (the station of Garskatsan). Systematization and analysis of meteorological data was based on air and soil surface temperature, precipitation, atmospheric pressure, air humidity and wind. Heat transfer into ground and influence of subterranean waters have been established in the result of field investigations, geological prospecting and scientific generalization of literature data. It was established that physico-geographical and geologico-geocryological factors affect PFG forming.

The radiation regime is characterized by a considerable value of total solar radiation and prevalence of direct solar radiation. Equal values of solar radiation are observed in all latitudinal direction. On passing to 1° of northern latitude solar radiation changes by 4%. Total solar radiation in the north of the area equals 4255, and in the south - 4972 MJ/m<sup>2</sup> a year. The direct solar radiation makes up 55% of the total one. The research done by V.A. Lyubchenko and T.I. Palanova (1974) resulted in the finding that scattered radiation reaching the horizontal surface in the shade is

2 times less than in the open.

In addition to solar radiation the energy of atmospheric circulation also affects the heat exchange on the boundary "atmosphere-ground". The total planetary air current system creates total atmospheric circulation due to which the exchange of large air masses is done in horizontal and vertical directions on account of temperature difference between different latitudes, including circulation in the system of anticyclones and cyclones as well. In Zabaikalie there prevail continental arctic air masses, their centres being in the middle and sub-arctic latitudes of both hemispheres. In winter radiation cooling in anticyclone prevails, in summer convection types of weather are predominant. The frequency of the regions of high pressure anticyclones and ridges over Zabaikalie is registered more often than the regions of low pressure cyclones and troughs. The anticyclonic circulation averages 55% of the total number of days, the cyclonic one - 42% (Climate ..., 1982). Due to the atmospheric air mass circulation and the Earth's revolution from the west to the east a settled Siberian anticyclone with the highest winter atmospheric pressure of the Asian continent (the pressure in the centre is up to 1050 hPa) prevailing for almost half a year (Polovinkin, 1946) is formed in a cold period of a year over the territory of Zabaikalie and Northern Mongolia. In this period one can observe small solar heat flow, intensive radiation cooling of lower air layers and their stagnation that provide temperature air inversion reaching 1 ... 2 km in vertical direction. (Pribaikalie ..., 1965). The temperature in this layer can increase with the height to 2° and more per 100 m. In the Siberian anticyclone the formation of continental air takes place, the air in lower layers being even colder than the arctic air, and it provides great temperature inversions. The lowest temperatures on January are registered at a minimum absolute altitude and the temperature increases with an increase of an altitude. It is registered that the temperature of a lower air layer decreases in the regions of high atmospheric pressure. The anticyclone pressure has the maximum value in the centre and decreases to its sides.

In a warm period of the year as compared with the rest of the territory one can observe soil surface temperature increase in the valleys of the Selenga river and its tributaries Khilok and Krasny Chikoi (in the lower course), the Jida and the Uda (in the middle and lower course) as well as the Onon river (in the middle and lower course), the Ingoda and the Shilka (from the station of Karymskaya to the station of Sretensk).

The temperature also increases in the Torey, Klichka and Argun hollows in the south - east and in the Nerchinsk - Olovsk hollow in the north. The mean monthly temperature of the soil surface in these areas in a warm period equals 15°C, both in the south (the stations of Kyakhta, Uruk, Nizny Tsasuchey) and in the

north (the stations of Khorinsk, Shilka, Nerchinsk Sretensk). Here the soil temperature regime is influenced by air flows which are due to an air circulation in the cyclone system. The polar front separating the air of temperate latitudes occupies the northern position; in the front part of cyclones coming from the Middle Asia, Mongolia and China to southern Zabaikalie (Sorochan, 1961) the warm air passes along river valleys and territories with the flatland and mountainous relief. The mountain ranges prevent warm air from penetrating in the areas of middle-mountainous relief, and here the mean monthly temperature of the soil surface in a warm period equals 12 ... 13°C in the south of the territory (the stations of Gheremkhovo, Alexandrovsky zavod) and in the north (the stations of Mogzon, Zilovo).

Under the influence of circulation in the lower air layer and its interaction with the peculiarities of orography and underlying surface there appears local circulation depending upon variety of the relief forms, altitude and proximity to large reservoirs. The temperature change, air humidity and amount of transferred heat depends on the speed of wind. The relief and underlying surface affect the speed of wind. Thus, for instance, an open flat country in the Torey hollow with treeless and steppe vegetation is characterized as the area with the greatest wind activity in Zabaikalie. Here the maximum wind speeds, possible once a 15-year period, reaches 32 ... 42 m/sec.

The speed of wind increases in the places of approaching its current lines and, on the contrary, it decreases in their passing. The increase of the wind speed is registered on the mountain peaks and watersheds, on the slopes exposed to wind or parallel to wind. The character and the degree of influence of the wind regime on the thermal regime of soil surface is determined by the peculiarities of macro- and microforms of the relief, their exposition, absolute and relative heights, length of hollows, depressions and valleys, their width, break, orographic closing (flowing through and vegetation).

The heating influence of large reservoirs on the temperature regime of the adjoining territory was established due to their heat liberation and absorption in the result of phase transition of water into ice and back during the complete freezing and ice break of lakes. It was established that near the stations of Novoselenginsk, Sosnovo-Ozersk, Beklemishevo and Solovyevsk situated on the shore or in the direct proximity from the lakes, the temperature in the period of complete freezing and ice break is correspondingly 1 ... 2°C higher or lower than near the stations outside the zone of their influence. The influence of lake Baikal on the soil surface temperature at the stations in the nearest proximity to it was not established. A number of researchers states that the Baikal influence is spread only on a rather narrow belt due to the proximity of mountain ranges

(Reference book ...,1967). K.A.Losev (1985) also supposes that the lake affects the microclimate of the area which is little larger than the lake itself.

**The atmospheric precipitation distribution** in the area is characterized by considerable unevenness. The mean annual precipitation has the least values (200 ... 350 mm) on the bottoms and lower parts of hollow slopes and river valleys in the middle- and low-mountainous relief, as well as in plains and hills, and the mean ten-day period snow cover depth is 3 ... 12 cm (7 cm on an average), the absolute height of hollow and valley bottoms being of little significance. Precipitation increases with the height on the slopes of mountain ridges in the range of 25 ... 30 mm per 100 m of height a year (Reference book ...,1968). 80 ... 90% of the annual precipitation falls to a warm period of a year. Snow does not affect the ground on low relief elements due to its little thickness, duration of snow covering from 49 to 92% of the cold period and ice crust formation on its surface (from the middle of February) promoting the elimination of snow heating influence in the first 2/3 of winter. Rain precipitation is spread unevenly on relief elements in a mountainous cross-country locality. Precipitation is less on the positive relief forms than on the negative ones because they promote the delay of surface waters streaming down the slopes and contribute to the additional ground damping. The flow of additional moisture from the slopes reaches its maximum values at the foot and in the valleys and the value depends in the duration, slope steepness and its hydraulic characteristics. The ground temperature decrease is greatly influenced by the evaporation from the soil surface which consumes 53 ... 59% of the radiation balance.

Atmospheric total and local air circulation and the relief with mountains and hollows, occupying 2/3 of the area, have a great influence on the heat and moisture distribution and on the regularity breaking of the latitude zonation and the altitude belts.

The PFG formation and development in Southern Zabaikalie took place in the Quaternary period (Geocryology ...,1989). The ground temperature regime on the depth of 40 ... 70 m is known to be formed for the last 30 ... 40 years (Field Geological Research ...,1961). Judging from the fact that an annual heat flow from the Earth interior to its surface averages 1970 kJ/m<sup>2</sup> (Gavrilova, 1978) which is 1.7 thousand times less than a mean annual flow of the solar energy heat at the land surface of Southern Zabaikalie (3277 MJ/m<sup>2</sup>) and taking into account that the PFG maximum thickness here is up to 100 m, we can draw the conclusion that at present the PFG existence is in close interdependence with up-to-date physico-geographical and geologicogeocryological factors. Here PFG is represented by epicryogenic and syncryogenic

grounds, the epicryogenic ones prevailing. In the epicryogenic PFG we can observe the largest ice inclusions in argillaceous grounds in the form of interlayers and lenses up to 30 mm thick. Syncryogenic deposits are to a large extent of an argillaceous sand composition and have the high ice saturation. Maximum inclusions of ice layers or veins are registered in sand loams and sand clays up to 30 ... 40 cm, in slays up to 40 ... 60 cm, and in medium sands up to 100 cm.

The basic geological parameters that stipulate thermophysical properties of grounds are their composition, humidity and density. In some hollows of the Zabaikal type L.M.Demidyuk (1968) discovered a close connection of the character of distributions thickness and temperature regime of PFG with the peculiarities of the tectonic structure of these hollows.

The greatest heat influence of underground waters on PFG is registered in their direct contact. Suprapermafrost waters affect the upper PFG horizon, interpermafrost waters have only a local influence, and subpermafrost waters can substantially change the PFG thickness and temperature.

#### REFERENCES

- Gavrilova M.K. Climate and Perennial Freeze Up of Rocks.- Novosibirsk: Nauka, 1978. 212 pp.
- USSR Geocryology. Mountainous Countries of the USSR South / E.D.Ershov (editor-in-chief). -M.: Nedra, 1989. - 359 pp.
- Demidyuk L.M. Role of Tectonic Structures Heat Regime Formation of Rocks in Intermontane Hollows of the Zabaikal Type / Permafrost Research. -M.: Moscow State University, 1968, N 8. - pp. 215-220
- Chita Climate. - L.: Hydrometeo Publishers, 1982. - 248 pp.
- Lorents E.N. Climate Predictability / Physical Bases of Theory of Climate and its Modelling. Transl. from English. - L.: 1977. - pp. 137-141
- Losev K.S. Climate: Yesterday, Today ... and Tomorrow? - L.: Hydrometeo Publishers, 1986. 17b pp.
- Lyubchenko V.A., Palanova T.M. Some Results of Observing Short - Wave Radiation in the City Construction Zones of Northern Residential Areas. - L.: 1974. - pp. 70-79
- Field Geocryological (Permafrost) Research. - M.: USSR Academy of Sciences, 1961. - 323 p.
- Polovinkin A.A. Climate Peculiarities in Zabaikalie, Priamurie and Primorie / Problems of Geography, 1946, N 1, - pp. 107-120
- Pribaikalie and Zabaikalie. - M.: Nauka, 1965. - 492 pp.
- Sorochan O.G. Some Peculiarities of Monsoon Circulation of Eastern Asia / Works of Chief Geophysical Observatory, 1961, N 192. - pp. 3-11
- USSR Climate Reference Book, N 23, parts II, IV. - L.: Hydrometeo Publishers, 1966, 1968. - 318, 328 pp.

# MASSIVE ICE BEDS OF WESTERN SIBERIA: STRUCTURE AND HISTORY IN PLEISTOCENE

N. A. Shpolyanskaya

Department of Geography, Moscow State University Leninskie Gory, 119899, Moscow, Russia

An analysis is given of the structure and texture of a number of typical underground massive ice bodies in Western Siberia. Four main types of massive ice are revealed: the buried glaciers, the epigenetic injectional the syngenetic near offshore-marine, and the syngenetic submarine ice bodies. For the latter the way of ice formation by freezing of deep-water sediments is proposed.

A certain regularity in the natural occurrence of the above-mentioned types of massive ice is revealed. A reconstruction of the Pleistocene paleogeographical pattern in Western Siberia as well as of the conditions under which the formation of the massive ice take place, is described.

## INTRODUCTION

Massive ice beds are frequently encountered in Western Siberia. These large underground ice bodies are not identical neither by age, nor by genesis. The investigation of the distribution of massive ice shows a certain regularity, which is, in turn, closely connected with the geological history of Western Siberia and with the paleogeographical conditions of past epochs. Both the mechanisms of ice formation and the peculiarities of the respective epochs reflected themselves in the individual features of ice structure. The author is trying to reveal the genesis of several ice bodies of the region, investigated by the author himself and described in the literature. The regularities of massive ice formation in Pleistocene in the north of the Western Siberia are considered here. Since massive ice is wide-spread in many other regions of the Subarctic as well, the applicability of the analysis proposed goes beyond the regional framework.

## THE ANALYSIS OF MASSIVE ICE TEXTURE

The investigation of the texture of several massive ice bodies in various regions of Western Siberia gave the following results.

The Ermacovo's massive ice body, known as the Ice mount, is disposed on the right coast of Yenisei river at the latitude of the Arctic Circle. This is a large ice body, having several hundred meters in diameter and several tens meters thickness. It is disclosed in the section of the 50-m Yenisei's terrace. The ice body is overlaid by the Zyryan till (III<sub>2</sub>) it is 79±20 thousand years old (abs. age - RTL-318 MGU). The ice body itself is represented by the transparent monolithic coarse-crystalline ice, the crystals having size from 10-20 to 50-60 cm of irregular form and their orientation being chaotic. Appreciable inclusions of air and soil inside the ice are absent. There are series of thin parallel fissures in the ice mass, which are filled with the

ice and loamy soil, analogous to the overlying deposits. The width of fissures comes to be a few millimeters. The ice-ground zones are characterized by a comparatively fine crystalline structure (the crystals are 1-4 cm in diameter) filled with air bubbles.

The structure and texture of this ice body can be explained from the position of the glacial hypothesis (Shpolyanskaya et al. 1987). It looks like the dirty ice described by Lavrushin (1976) for many regions. Such an ice texture is formed by dragging rocks of glacier's couch along a flow cleavage with bedding. The latter are formed during the glacier motion.

The new cleavages arise during ice flow. The fissures are filled by soil. In addition, layers of regelational ice are formed there. The transparent ice layers and ice layers with soil lenses and ice schlierens are mutually alternating. Such a structure is typical for the edge parts of glaciers. It has been observed by the author (Shpolyanskaya et al. 1987) for buried glaciers of the mountains Tien-Shan. Thus the Ermacovo's massive ice body is probably a buried remainder of some neighbouring outlet glacier of the Zyryan epoch.

Another massive ice near the village I n n o k e n t y e v s k o y e on the left coast of lower stream of the Yenisei river is disclosed in the section of 50-m Yenisei's terrace. The structure of the ice is similar to the glaciers' (Karpov 1986). The ice body is a large monolithic of 40 m thick. It lies at 0.6-0.8 m depth from the surface. In the ice there are series of thin arclike fissures filled with the loamy soil and the ice body is subvertically stripped. The enclosing sediments are represented by the ice saturated till. Apparently this ice body also has been formed by outlet glaciers from a neighbouring mountain glaciation. It should be noted that the ice of the structure described above, is encountered nowhere in West Siberia except for the regions next to Yenisei river.

Quite a different shape has another ice layer near the village T u b - S a l e. It is disposed

on the left coast of Yenisei in its lower stream. This layer of ice is described by Karpov (1986). The ice body is disclosed in the section of 20-m Kargin (III<sub>3</sub>) terraces. It is overlaid by the varves clay 10 m thick and is underlaid by fine-granular sands. The thickness of the ice body exceeds 15 m, its extent is as much as 1070 m. The ice transparent, contains no air bubbles up to 5 m depth, possesses inclusions of varve bits which amount decreases sharply with the depth. Ground layers, similar to those in the ice bodies described above, are absent here. A hollow of 0.5 m height was uncovered below the ice by the drill hole. The hollow is filled with sublimation ice and is similar to the same hollows of the injected frost mound of Yakutiya (bulgunniakh).

In contrast to another massive ice, the body in exposure Tub-Sale has complicated contacts with overlaying varves. The ice stocks in the form of a mushroom are observed and the clay layers are broken there and shifted with an amplitude up to 1 m on both sides of the ice stock. More or less lengthy layers of ground are absent in the ice. Such a structure of the ice body indicates an interground injection mechanism of its formation by intrusion of the underground water in the upper layers of the freezing groundmass. This leads inevitably to a deformation of soil layers, breaking of them, tearing-off of varve particles, intrusion of diluted soil, etc.

The giant bulgunniakh near the village M e s s o y a k h a (height - 22.5 m and basis - 286x176 m) is described by Karpov (1986). Its core is more than 20 m thick and is represented by a massive glass-like transparent ice without mineral inclusions and with rare air bubbles. The character of ice in the bulgunniakh is similar to the ice body in Tub-Sale.

The geological exposure S e l y k i n o is also in the lower stream of Yenisei river near the village Ust-Port (Tumel, Shpolyanskaya 1983). This massive ice sharply differs from both types described above. The deposits of Middle- and Upper-Pleistocene age form a 40-60 m terrain level. The lower part of the strata is formed by the poor-icy marine aleurites of Middle Pleistocene (II<sub>2</sub>). The boulder loams of regressive stage of the sea (II<sub>4</sub>) are bedding above. The near offshore-marine Kazantsev Upper-Pleistocene sands (III<sub>1</sub>) overlie the latter ones. These deposits include the layers of ice, which are represented by a series of thick ice schliers (15-60 cm), separated by ground layers 15-20 cm thick, seldom up to 30 cm. The ice is transparent, dense, glass-like, sometimes with inclusions of small-particle of soil. The ice texture is coarse-crystalline with crystals, which are 5-6 up to 10-12 cm).

The cryogenic construction of the enclosing sediments as well as the texture of the ice indicate a segregational-cementic mechanism of ice-formation during syngenetic freezing of the near offshore-marine sand deposits. It may be supposed that in the Kazantsev epoch, when the average temperature of the air at that latitude was -9°C (Shpolyanskaya 1981), the near offshore-marine sediments accumulated and froze simultaneously (syngenetic). The ice schliers observed in that part of the exposure have segregational-cementic origin and formed in the basis of the active layer of the permanently accumulated coarse-granular sediment saturated by the suprapar-

mafrost water. This is confirmed also by the fact that the described ice is practically encountered nowhere in the form of single isolated layers, but only in the form of series of conformed layers which evidently have been formed during process of sedimentation.

Similar massive ice beds are described also for the central parts of Yamal (Baulin 1967). Apparently these massive ice also have been formed in a similar way.

The ice layers in the exposure in the valley of river T a d i b e y a k h a at the Western Gydan are disclosed from the depth of 15 m in the section of the Kazantsev (III<sub>1</sub>) strata. Its visible thickness is 5-6 m and its extent is 100-150 m. The ice body is pierced by thin (0.3-1.0 cm) ground layers. In this ice-ground mass we can trace intricately deformed thicker ice layers and thinner ground layers, forming a single conformed pattern. The thickness of the ice layers changes from 2-3 to 10-15, frequently up to 20 cm.

The uniform and thin stratification of the ground and of the ice, and the high conformity of the layers could be formed only in subaquatic conditions at sufficiently large water depth. Taking into account the marine origin of the enclosing deposits one may suggest that such a type of ice has been formed in the Arctic shelf sea as the result of syngenetic freezing of accumulated marine sediments at the comparatively greater depth.

A possibility of such a type of freezing has been considered in details by the author earlier (Shpolyanskaya 1989).

The temperature of the near seabed water in the Arctic seas at the depths from 35-up to 100 m, reaching -1.6° - -1.8°C can provide the freezing of the ground. The salt concentration in pore water of the bottom sediments, preventing their freezing, decreases with depth (a fact well-known in marine hydrochemistry). Thus at a certain depth the freezing of bottom sediments can occur, forming a stratified ice-ground deposits.

These massive ice beds of the Tadibeyakha type have been formed in submarine conditions through simultaneous (syngenetic) accumulation and freezing of sediments. Apparently, similar massive ice which is described for Yamal and Gydan (see e.g. Velikotsky 1987) also has been formed in a similar way.

#### THE REGULARITIES OF MASSIVE ICE DISTRIBUTION

The most ancient and wide-spread ice bodies are evidently included in the Kazantsev sediments. This ice has synergetic submarine and near offshore-marine origin. The ice bodies differently, depending on the specific conditions such as the distance from the shore, depth of the sea, etc. In the outer parts of Yamal and Gydan which were covered by a deep-sea at that epoch, the ice of submarine origin is wide-spread. In the inner parts of Yamal and Gydan which became free from the sea earlier, the ice of near offshore-marine origin is typical.

The buried ice is associated with Zyryan deposits (III<sub>2</sub>) and is encountered near the Yenisei river only.

The injectional ice is apparently the youngest one. It is encountered mainly in the Kargin deposits (III<sub>3</sub>) and has been formed in course of their epigenetic freezing during the subsequent severe Sartan epoch (III<sub>4</sub>). It is encountered

mainly near Yenisei river.

The above-obtained distribution of the different character massive ice is evidently connected with the peculiarities of development of Western Siberia in the Pleistocene.

#### THE HISTORICAL FEATURES OF THE WESTERN SIBERIA IN PLEISTOCENE AND THE UNDERGROUND ICE

Three large cold waves and three large warm waves have been mutually alternating during the Pleistocene and Golocene as it is supposed by the modern paleogeography. The cold epoches are: the epoch of maximum glaciation (II<sub>2-4</sub>), the Zyryan epoch (III<sub>2</sub>) and Sartan epoch (III<sub>4</sub>). The warm epoch are the Kazantsev (III<sub>1</sub>), Kargin (III<sub>3</sub>) one and the Golocene thermal maximum epoch (IV). The development of permafrost and underground ice proceeded under the combined action of the climatic changes and of the subemergence-emergence rhythm of stratification of the Arctic sea.

The most ancient deposits in the region are the marine sediments of Salekhard suite (II<sub>2-4</sub>). They have been formed in the epoch of maximum Yamal transgression, which stretched up to 60-62° N (Danilov 1978; Lazukov 1972; Popov 1959).

The characteristic features of this epoch were the synchronic development of the long transgression and the Middle-Pleistocene glaciation, the accumulation of sediments during tectonic submergence, the formation of sediments at low-temperature conditions. The Salekhard loam-clayish (80-90%) deposits contain little ice, their cryogenic texture is always of epigenetic type.

The Salekhard deposits do not include a layered ice at all. Apparently it is connected with the lithological features of the deposits. A homogeneous thin sediment was accumulated undergoing an active diagenetic process. As a result the sediment was compacted and deprived of water still in subsea conditions. It is possible that the high saltiness of water (which is indicated by some fauna complexes (Lazukov 1972) prevented the freezing of bottom sediments.

The subsequent Kazantsev epoch (III<sub>1</sub>) was characterized by a regressive stage of sea development. The sea level has lowered by 30-50 m although it still remained 60-70 m higher than at present time. The size of the Kazantsev sea has been reduced, it has occupied the territory of modern Yawl, Guyed, Tazovsky Peninsula, and had inoffensively spread into the valleys of the river Ob, Pöle, Poor, Taz. In that sea (depth 50-100 m) with a strongly cut-out coast line and with many islands, an accumulation of clayey and sandy sediments took place. A characteristic feature of deposits of this epoch is a frequent change of the lithologic horizons and a good degree of sorting of sediments.

In the Kazantsev deposits in contrast to the Salekhard ones the syngenetic layered ice is frequently encountered. This can be explained probably by the comparatively coarse-grained composition of the Kazantsev deposits, thanks to which they did not condense rapidly and remained for a long time water supplied. The saltiness of water, noted by the paleogeographers for the Kazantsev sea was also of importance. All this is favorable for the subsea freezing of the accumulating sediments accompanied by formation of large ice bodies.

The larger number of islands in the Kazantsev sea caused a larger diversity of its depths and thus of the conditions for syngenetic freezing of

the accumulating sediments: far from the islands at deeper parts of the sea the sub-marine ice was formed, while at the shallow parts near the islands the near offshore-marine ice was occurred.

The Kazantsev epoch is believed to be a warm one. Its maximum many-year average air temperature exceeded its present value by 3°. For the extreme northern regions of Western Siberia with present air temperature -9° - -11°C this was not of large importance. The temperature remained low enough. For more warm regions, already near Arctic Circle, such a rise of temperature prevented freezing of the bottom ground. Equally, the shallow narrow bays along the modern rivers well-warmed during summer did not contribute to freezing of sediments at that latitudes. Therefore in the Kazantsev deposits massive ice beds are encountered only to

the North of the latitude 68-69° N.

The Zyryan epoch (III<sub>2</sub>) which replaced the Kazantsev one was characterized by a cold climate and a subaerial development of practically all the region. Only the most northern regions of Yamal and Gydan remained under the sea level. Accordingly the Zyryan deposits are represented by non-sorted sand-gravel lake-alluvial and boulder sand-clay glacier and glaci-fluvial material. In the mountains framing Western Siberia a mountain-valley glaciation developed, whose tongues descended the near-Ural and near-Yenisei parts of the region by low-temperature conditions and by deep freezing of the ground, the separate parts of the ice tongues could be easily buried by its own moraine, thus forming underground massive ice beds. The Ermacovo's massive ice described above is probably a buried tongue of the valley glacier from Putoran mounts and the Innokentevskoye massive ice is a tongue from the mountains Byrrang.

In the Zyryan deposits of Yamal and Gydan represented by laid sediments the buried ice is absent. This may indicate the absence of glaciation cover in Western Siberia.

In the Kargin epoch (III<sub>3</sub>) some reverse sea transgression took place which formed an independent terrace level especially extensive along Yenisei river up to the Arctic Circle. This epoch is believed to be relatively warm, remaining the present one. Therefore on Yamal the peaty deposits with thick syngenetic polygonal-wedge ice were formed while in the southern continental regions, e.g. at Yenisei, non-frozen basin sediments were occurred.

Nevertheless the Kargin deposits are frequently accompanied by layered ice of injactional origin. This is especially true for the near-Yenisei part of the Western Siberia. This can be explained only by taking into account that the Kargin deposits began to freeze in the subsequent Sartan epoch (III<sub>4</sub>), marked by a deep regression of the Arctic sea and by an extremely low air temperature. The freezing was accompanied by a non-uniform displacement of appreciable masses of underground water, their freezing and formation of massive ice. The region of Yenisei is most favourable for this. There is a zone which separates two tectonic structures, namely the Western Siberia plain and the Middle Siberia platform. This fractured zone is a discharge area of deep water horizons.

The ancient ice was conserved up to present time, despite the existence in the recent past of the Golocene thermal maximum. A calculation (Shpolyanskaya 1981) has shown that in Western

north of 66°N for its eastern part the frozen ground did not thaw from above neither in Upper Pleistocene nor in Holocene. In Holocene the climate was sharply continental and in the near-Yenisei part the Siberian anticyclone retained its importance, which caused low temperatures and low winter precipitations.

#### REFERENCES

- Baulin, V.V., G.I. Dubikov, E.B. Belopukhova, and L.A. Schmelyov (1967) Geological conditions of Western Siberia. Nauka, Moscow, 212 p.
- Danilov, I.D. (1978) Pleistocene of marine Subarctic plain. Moscow University Press, Moscow, 200 p.
- Karpov, E.G. (1986) Underground ice of the Yenisei North. Nauka, Novosibirsk, 131 p.
- Lavrushin, Yu.A. (1976) The structure and the formation of morainic debris of glacial sheet. Nauka, Moscow, 238 p.
- Lazukov, G.I. (1972) The antropogen of the North of Western Siberia (paleogeography). Moscow University Press, Moscow, 235 p.

Siberia. // Glacier period at the European territory of USSR and Siberia. Moscow University Press, Moscow, pp 360 - 384.

Shpolyanskaya, N.A. (1981) Permafrost of Western Siberia and the trends of its development. Moscow University Press, Moscow, 167 p.

Shpolyanskaya, N.A. (1989) The possibility of freezing of bottom deposits in the Arctic sea. // Vestnik of the Moscow University, Geography, No 5, pp 72 - 78.

Shpolyanskaya, N.A., V.F. Koklin, A.V. Korzun, and V.T. Khlap (1987) Ermacovo's massive ice on the Yenisei. Its structure and possible genesis. // Cryogenic processes. Moscow University Press, Moscow.

Tumel, N.V., N.A. Shpolyanskaya (1983) The cryolithogenesis of Pleistocene deposits in the lower stream of Yenisei (for the example Selyakino). // The problems of cryolithology, vol. 11. Moscow University Press, Moscow, pp 116 - 137.

Velikotsky, M.A. (1987) Dislocation and massive ice in Quaternary deposits of Yamal. // Cryogenic processes. Moscow University, Moscow, pp 48 - 60.



## BOREHOLE ELECTROMETRY OF PERMAFROST ZONE

A. M. Snegirev

Vilyui Permafrost Research Station Permafrost Institute Siberian Branch, Russian Academy of Science.  
VNIMS, Chernyshevsky, 678185, Republic of Sakha (Yakutia), Russia

The borehole electrometry in geocryology is considered as one of the long-term scientific trends, determined by specific aspect of the tasks, the necessary adaptation of technological and informational possibilities of the well-known geophysical methods. Some possibilities of this trend are illustrated with the examples of settled up by the borehole electrometry new peculiarities of electromagnetic field in cryolithozone. Specifically, the existence of the intensive natural electromagnetic field in stationary part of the cryolithozone caused stationary physico-chemical processes is emphasized.

### INTRODUCTION

The modern stage of geocryology aimed at developing the science related to lithosphere cryogenesis includes prediction of undesirable cryogenic process development and elaboration of the methods for controlling these processes. The complicated nature of the stage necessitates the increase of information of geophysical methods by arranging them according to complexes and by increasing sensitivity and accuracy of measurements.

The fact that the borehole electrometry is regarded as a separate section of cryolithozone geophysics can be mainly explained by its peculiar position in respect to the ground and aerospace investigations, as well as by the peculiar aspects of frozen rock survey in boreholes. The complex interpretation of experimental materials makes it possible to determine the internal structure of the cryolithozone, their composition and trends of changing in space and time. Besides, the parameters of electromagnetic fields, measured in boreholes during time periods with an assigned frequency, are very important for predicting possible changes in geocryological sections.

Frozen rock, as object of investigation, is examined in borehole shaft (electrical logging) and within the borehole space, i.e. adjacent space (borehole prospecting). The study of changes in the structure, composition, properties and state are considered to be the main purpose of the investigations.

To achieve this goal one has to solve two sets of problems, which differ greatly and are inter-conditional: the tasks aimed at developing the methods of borehole electrometry and the tasks aimed at extending the use of these methods in geocryology.

The variability (time-space) of a certain geoelectrical section which is the subject of investigation, is determined by external physical, geographical, climatic and antropogenic factors

and identified due to the changes in the parameters of electrophysical processes which occur when artificial electromagnetic field;

- correlative links between the electromagnetic parameters and properties of the medium under consideration;

- and as a final result based on these characteristics:

- structural changes in geocryological section as a result of external effects; and
- structure and lithological composition of geocryological sections.

The methods of borehole electrometry of the frozen lithosphere zone were and are formed taking into account the achievements of prospecting geophysics and the results of experimental investigations in the areas of cryolithozone development. With accumulation of the experience and revealing the conditions for making measurements, the number of methods steadily increased and they were specialized conformably to the new investigation conditions by way of further development of the theory, methods and technological means of measurement, as well as by searching for new methods and physical parameters of a project.

The development of the methods of borehole electrometry is based on the following features:

- the tasks, necessitated by the problem of cryogenesis of lithosphere and the development of the Extreme North regions;

- understanding of differentiation of electrophysical properties of rocks at negative temperatures;

- the peculiarities of physico-chemical processes in frozen rock;

- variability of the state of geoelectrical and geocryological sections under the effect of factors;

- the results of theoretical and experimental of the relations between the electromagnetic field and the investigated object;

- the achievements of electronics, instrument and tool-making industry, drilling technology etc.

The improvement, application and development of borehole electrometry methods was based on the tasks and the peculiarities of investigation object, the presence of ice and unfrozen water in the rock. It is not yet possible to determine strict regularities for this object, which could enable predicting electrophysical properties according to the quantity of certain phases contained in them, their mutual location and taking into account the outside thermodynamic parameters. The existing way of investigations consisted in a direct experimental determination of electrophysical parameters of rock in laboratory and under field conditions. This circumstance, as well as the existing theoretical basis of some methods have contributed to the priority of the experiment at the presents stage.

The borehole electrometry is most efficient for investigation of cryolithozones in hole made with a minimum disturbance of the natural thermodynamic state of rock during drilling operations.

This important feature may be observed as a rule, by using the cooled air as a cleaning agent the process of drilling. On the other hand the investigation of such boreholes limits the possibilities of the known methods of geophysics because of the conditions of the hole wall and the negative temperatures. This problem has been discussed in detail in our papers (Snegirev 1983, 1987). It has contributed to the development of special borehole electrodes, to the methods of preparing borehole wall for observation by conduction methods, complete elimination of conductive and inductive mutual effect of measuring and generating devices, and development of measuring equipment which is capable of working under low temperatures and high electrical resistances.

The experimental materials obtained by means of the investigations provide some new peculiarities of electromagnetic field in the cryolithozone and allow the planning of a more profound study of cryolithozone properties. The illustrations emphasize the above-mentioned peculiarities which are basically as follows:

1. In the stationary part of the cryolithozone there is a natural electrical field which varies in time and space. In general, it is the sum of electrical fields, formed in various sections depending on concrete conditions and reaches the values of 200 mV. Positive, negative and variable-type anomalies are registered with maximum amplitude up to 100 mV (Figure 1).

The existence of variable and stable (time) anomalies of the natural electrical field makes it possible to speak of various sources for their origin. One of the sources of the natural electrical field in the cryolithozone is the phase surface of the line; frozen - thawed rock (Figure 2) which specifies the subject of investigation of cryolithozone by the method.

According to the existing opinions one may suppose that variability of relatively time-stable anomalies of EH-processes is pretermined by permanent physico-chemical processes, which when excited by external factors may serve as peculiar indicators within the cryolithozone monitoring system.

2. The borders between thawed and frozen rocks are not always registered according to electric logging data by changes in electric conductivity, which in the vertical section depends on the temperature, humidity and saline composition in

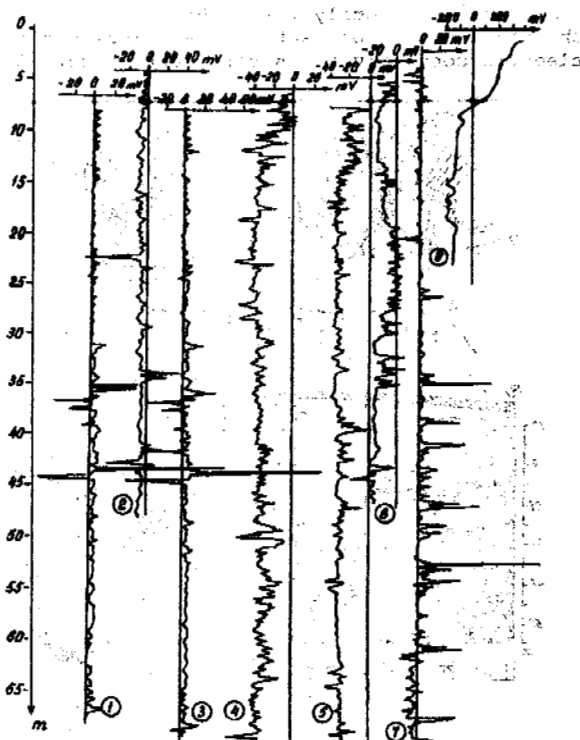


Figure 1. Typical curves EP. 1, 2, 3 - gradient-potential MW=1 m; 4, 5, 6, 7, 8 - potential EP.

the pore solution. Indication of this border according to the data of resistance method may be sometimes possible only in the course of observations, when the anomaly moves after the shifting phase border (Figure 2).

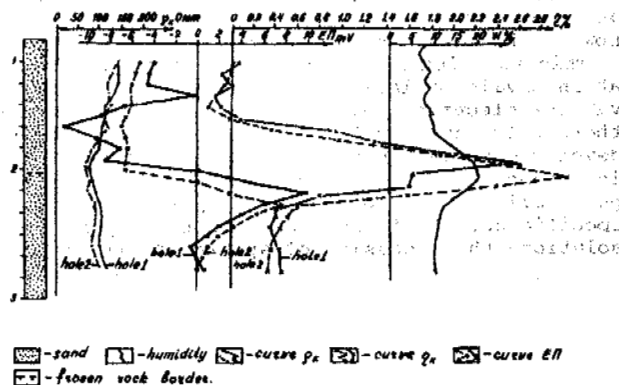


Figure 2. The results of a complex determination of rock properties within the divide surface thaw-frozen rocks in active layer.

3. Geoelectrical and geocryological sections, drawn according to the data of borehole electrometry, mainly reflect the geological and cryolithological permafrost structure. The effect of the spatial distribution of negative temperature in the permanent part of cryolithozone is of a peculiar nature, reflects upon the values of

electric conductivity and does not cause the change of the anomaly form. The correlation in the distribution of isotherms and isolines of electric conductivity is very weak (Figure 3).

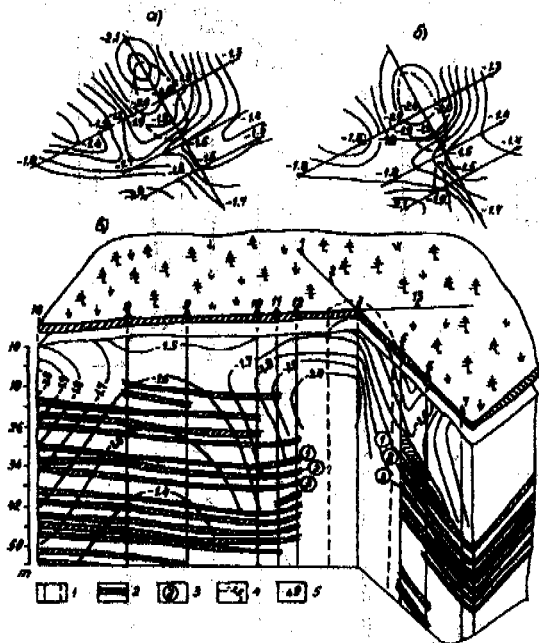


Figure 3. Kimberlite deposit temp. field at various isothermal horizons. a=25m, b=50m, c=interpet. results. 1 - pipe outline (contour), 2 - increased resistance lev., 3 - bearing horizon Nos., 4 - isotherm lines, 5 - hole numbers.

4. In the frozen rock there exist remaining durative potentials of polarization, which occur after the excitation of BH-field by direct current impulse (Figure 4) and which change the sign in case it changes its polarity. This shows the ability of frozen rock to accumulate electric power like electric capacitor.

This revealed peculiarity is found, as a rule at intervals of laminated ice-rich rock of various electric conductivity and should be more thoroughly investigated in the future. Thus, the developed procedure of frozen rock investigation in boreholes by electrometry methods, the peculiarities of frozen rock properties, the specific aspect of the tasks and their peculiar solution (the necessity of special drilling, the

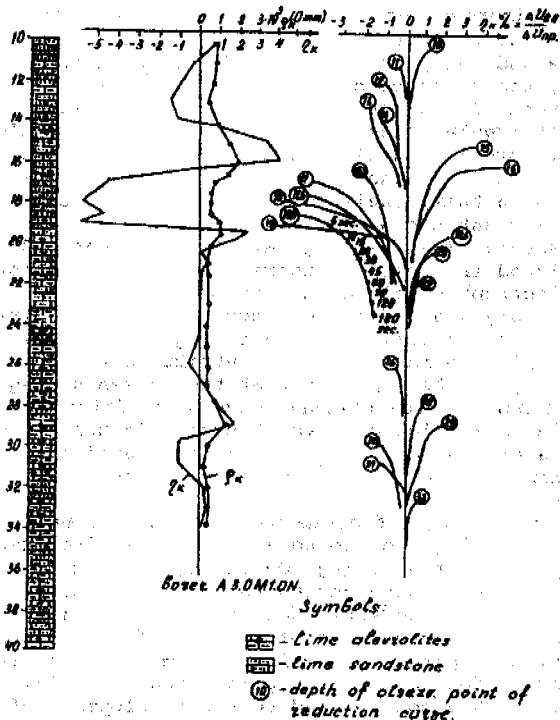


Figure 4. Typical curves of frozen rock polarization reduction in a dry hole and the data of electrical coring (loggings).

development of new structural and functional elements of measuring equipment, etc.) and the results of the experiments enable us to speak about the formation of a new scientific trend in geocryology - the borehole electrometry of the frozen zone of lithosphere.

#### REFERENCES

- Snegirev, A.M. and S.A. Velkin (1987) Elektrokarrotazh, soprotivleniya merzlykh porod v suhikh skvazhinah. Yakutsk. Institute merzlotovedeniya SO RAN, p. 102.  
 Snegirev, A.M. (1983) Electrical coring (logging) of frozen rock. In IV Intern. Conf. on Permafrost. M., pp. 89-93.

## STRATIGRAPHY, AGE AND ORIGIN OF MASSIVE ICE, YAMAL PENINSULA, WEST SIBERIA

V.I. Solomatin, M.A. Koniakhin

Department of Geography, Moscow State University, 119899 Moscow, Russia

New data concerning the age, stratigraphy and origin of massive ice were obtained recently for Yamal Peninsula from an extensive program on geological and engineering boring for gas field development. The complex of analytic results of drill core samples provides the basis for the new conclusions concerning the origin of massive ice.

### INTRODUCTION

This paper is based on geological and analytic materials collected by the authors in the process of personal and joint work with many organizations and colleagues on the problem of massive ice, its origin, age and influence on stability of permafrost as a result of industrial development and human activity on the North. Some aspects of our investigation and valuable materials were produced in collaboration with scientists from Canada - Dr. F. Michel and Dr. W. Macheny, and Estonia - Dr. R. Vajkmae.

Massive ice as an individual morphogenetic type was discovered at the beginning of sixties (Dubicov, Korejsha, 1964; Mackay, 1971). In the middle of the seventies (Solomatin, 1976) it was argued that many features of geomorphological, geological position as well as petrology of massive ice contradicted the injection or segregation idea and may be explained only with the help of buried glacial origin of the ice (Solomatin, 1976). The problem of the massive ice is the key for many problems in Quaternary geology, paleogeographical reconstruction besides its meaning for fundamental permafrost science. There are many of attempts to get any explanation for younger segregated origin of massive ice, but many of them are too speculative and don't correspond with actual data which we possess.

We would like to show evidence which could be further used for discussion of these problems.

The region of our investigation (so called Bovanenkovo gas-field area) is situated in the West of the central part of Yamal Peninsula, near to merging of Mordiyacha and Seyacha rivers. This region is well-known in literature because of wide massive ice distribution. And here was the massive ice body, explored for the first time in Russia.

1. The distribution, dimensions and bedding of massive ice.

Hundreds of drill holes on Bovanenkovo gas field indicate the distribution of actual bodies of massive ice, their upper and bottom surface boundaries and correspondence with geomorphological and geological conditions. The surface of Bovanenkovo districts is formed by remains of a marine terrain eroded by thermokarst and ther-

moerosion, with altitude 20 - 40 m above sea level and the alluvial terrace of 15 - 20 m (above sea level). Those remains are surrounded by lacustrine-alluvial level of 4 - 6 m.

The peculiarities of the terrain consist of many closed lake basins located on different levels and many thermokarst feature on slopes which cut into underground ice.

The drill hole data testify to the wide distribution of massive ice, so that they are found in all sections above levels and what is remarkable - under contemporary river stream and flood plains.

The ice forms a core it hills remains and is partly preserved under frozen deposits of the younger geomorphological levels (Figures 1 and 2). We may say too that modern relief including the river valley, as well, was formed by thermoerosion of the initial surface which was built by icy sediments. A separate part of ice were conserved by new sedimentation.

The area of massive ice bodies reaches more than 100 square kilometers and its diameter - some ten kilometers. The maximum known thickness of ice on Bovanenkovo area is 39.6 m; thickness decreases from high levels to lower ones.

On the basis of data from 76 drill holes we can give the percentage of massive ice thickness: less than 5 m - 47%; 5 - 10 m - 24%; 10 - 15 m - 16%; 15 - 20 m - 9%; more than 20 m - 4%.

The depth to upper boundary of ice bodies from the soil surface varies from 1.5 to 20 m. In most cases it is 2 - 5 m. Evidently this is the reason for thermokarst and thermoerosion forms which are widely distributed on the Bovanenkovo area. An absolute altitude of ice body base varies from +18 to -28.6 m and it changes in correlation with relief of contemporary soil surface: it rises high level surface and is descending under lowered territory (Figures 1 and 3). An altitude of upper ice boundary varies from +30.3 m to +18 m.

There is good correspondence between their boundary and soil surface altitude (Figure 3). From our point of view, it indicates the geological youth of massive ice and of main relief features of Bovanenkovo area. In any other case we couldn't see this evidence because of high rate of ice melting and relief reconstruction.

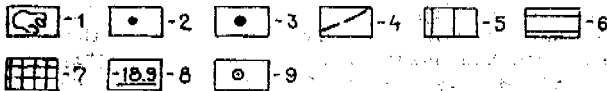
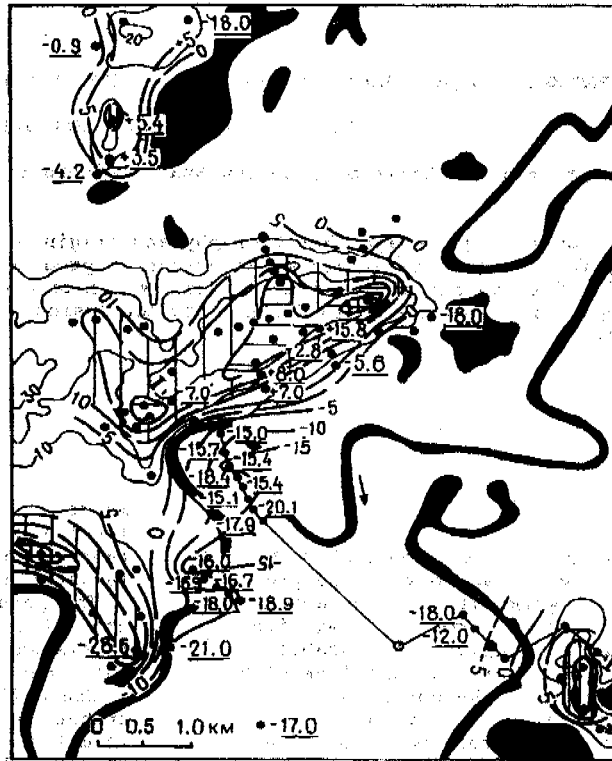


Figure 1. The scheme of soil surface relief and dept of upper and bottom boundaries of massive ice in central part of Bovanenkov area. 1). Relief contour (absolute altitude, meters). 2). Boreholes which have encountered a massive ice. 3). Borehole of 300 m depth. 4). Contours of the upper boundary of massive ice (absolute altitude, meters). (5 - 7). The plots of: 5). massive ice bodies with upper boundary absolute altitude from 10 to 20 m; 6). the same, from 20 to 30 m; 7). the same, more then 30 m. 8). The absolute altitude of massive ice bottom boundary (meters). 9). The boreholes without massive ice. (1 - 1 - geological profile, see Figure 2)

The position of massive ice on a rough surface of underlain by sandy horizon testifies to an identical age of all ice bodies on Bovanenkov territory and possibly a uniform initial strata of ice which was secondary eroded and now is presented by separated remains. Such peculiarities of geological position of massive ice testify to a glacial buried ice origin and don't correspond to an origin by ground water freezing.

2. Stratigraphy and age of massive ice. The detail results of complex analysis of samples from many exposures and boreholes including one with depth 300 m (Figure 4) permits us to give some conclusions concerning the stratigraphic position and age of massive ice.

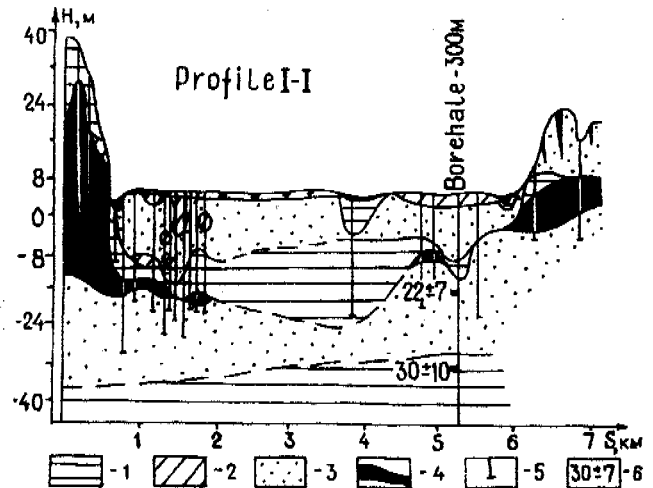


Figure 2. Geological profile across the valley of Sejacha river. (The line 1 - 1 see; Figure 1) 1 - clay; 2 - silt; 3 - sand; 4 - ice; 5 - borehole; 6 - abs. age (TLM)

a) TLM definition shows that the age of sediments underlying the massive ice is 22 ka BP. Based on the depth of 155 m per one thousand year, the sediments on the depth 260 m are aged 115 ka BP.

b) Paleomagnetic analysis of 108 core samples from depth of 50 - 235 m shows that all strata of permafrost have straight magnization, unstable polarity and belong to Brunnes epoch, e. g. to Pleistocene. There is a paleomagnetic episode on the depth near 180 m.

c) Spore-pollen spectrum do not change throughout the main part of the crosssection. The age of sediments is undoubtedly Pleistocene the but mix content of species does not allow more detail stratification. The composition of spectrum is similar to contemporary sediments of Ob River abound of mix species from far regions and availability of Tertiary species permits to suppose a wash away of ancient deposits and poor local sources of spore and pollen.

d) Grain size analysis: massive ice is overlain by silt and clay, probably due to shore lagoonal sedimentation. Under massive ice lies a fine sand, lower-sandy silt, then silty clay with horizons of sand. The grain size analysis testify to a more active sorting material more dynamic conditions of sedimentation in the upper part (to the depth of 250 m) of crosssection than in the lower one. Between them there is the erosional contact - a coarse sand with high level of sorting.

The coefficient of cryogenetic contrast which reflects a relative cryogenetic stability of basic mineral components of ground was calculated by V.Konistchev and V.Rogov: quartz and feldspar in two grain size fraction (0.1 - 0.05 and 0.05 - 0.01 mm); maximal size of cryogenetic subdivision. It was shown that the greater the value of this coefficient the greater stage of cryogenetic transformation in mineralogy of sediments. There are two maximum points of this coef-

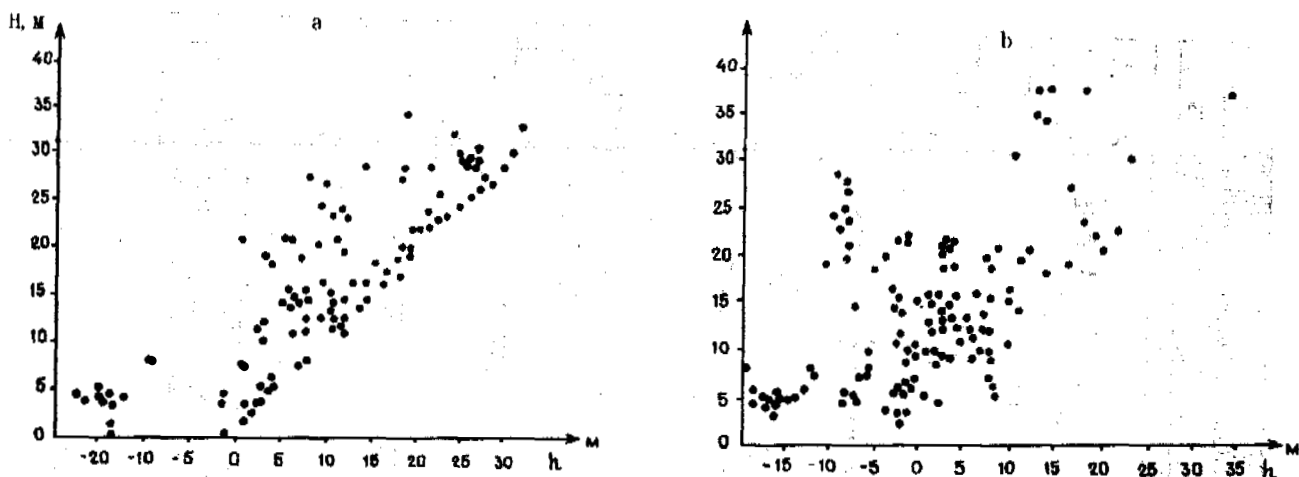


Figure 3. The correlation between massive ice (a) upper and (b) bottom boundary and soil surface, absolute altitude.

ficient at the depth of 80.5 m (5.1 - 5.0) and on the depth of 253 m (2.68). These maximum points correlate with the periods of temperature decrease.

W. Macheny (York University, Canada) carried out the morphostructural analysis of two samples by scanning microscopy for quartz grain surface. He pointed out that the ground was subjected to abrasion by fluvial processes and then passed into a subaerial weathering. V-shaped percussion scars on grain surface show a consequence of water transport and later of weathering. The high number of rounded grains present allow the suggestion that fluvial transport was long and reasonably intense prior to weathering. The impression gained from the range of particles analyzed is that many of them were first transported by ice where they obtained the bulk of fracture features on their surface. Over 80% of the grains with fracture features carry an abundance of adhering particles that may have accumulated from the grinding of rock material at the base of the ice.

e) Chemical content of pore water: the silt and clay above massive ice have a high salinity of pore water. The massive ice is ultrafresh. The salinity of sand under ice consists of 0.06%. With depth a salinity of silt and clay changes rhythmically, maximum reaching to 1.07% and average of 0.5 - 0.6%. The chemical composition here is similar to marine environment.

f) The complex of foraminifer shells includes the genus: *Gyroidinoides globulina pseudoparrella*; *Textularia gavelinopsis*; *Dentalina lenticulina*; *Quinqueloculina*; *Hoeglundina*; *Melonis* - in intervals of section 279 - 255.5 m and 239 - 231.2 m. The absence of Quaternary species in this strata, taking in account TLM data, testifies that it is a replacing complex from out-washed deposits.

In the interval 192 - 157 m occur: *Islandiella norcrossi*; *Islandiella helena*; *Elphidium subclavatum*; *Protelphidium orbiculare*; *Bassidulina reniforme*; *Astrononion gallowayi*; *Quinqueloculina* sp.; *Korrieriella* sp. Probably it is a horizon of marine transgression. In higher horizons a fossil microfauna is absent.

g) Diatom fossils were found in some samples from 62 investigated ones. Mainly the species belong to the thickwall shells which are widely distributed in Tertiary sediments of West Siberia: *Melosira orhata grunow*; *Coscinodiscus moelleri*. On the depth 75 m were found mostly freshwater species: *Melozira* sp.; *Tabellaria fenestrata* (Kutz); brackishwater species - *Stephanodis hautzschii grun*, and a few *Melozira sulcata* ehr (Kutz) - marine diatom. Only freshwater diatom were found in sand underlayered the massive ice: *Eunotia praerupta* var; *Muscicola Boye P.*; *Stauroneis anceps* ehr.; *Caloeis silicula* ehr and others.

h) The existence of beetles in one of samples assumes a closeness of land to an area of sedimentation.

A joint interpretation of all above pointed and other analytical results confirm with a confidence the estuarine conditions of sedimentation of main part of underlain by ice horizons.

Marine conditions in the lower part of thickness changed to delta deposition in more or less brackish water basin. Three horizons may be distinguished in section from a top to the depth under massive ice: first - late Wisconsin (20 - 25 ka BP) sands with the limit on depth 31.7 m; second - interglacial silt (30 - 40 ka BP) to the depth 185 m; third - sandy clay and silt (100 - 120 ka BP).

The isotope oxygen analysis is carried out by F. Michel, N. Kritzuk and by R. Vajkmae (on our sampling) shows that a content of heavy isotope oxygen varies from -12‰ to -23‰ with -18‰ - -21‰. The value of isotope composition has not trend in crosssection but it changes rhythmically. This evidence does not correspond to the volumetric water crystallization.

Conclusions: 1). The massive ice of the district of Yamal peninsula described lies under marine silt and clay and above delta sand. Such type of stratification, silt (clay) - ice - sand is known in most regions of massive ice distribution. This evidence reflects both genetic and stratigraphic behaviour of massive ice. 2). The age of described massive ice is a late Pleistocene. 3). The filling bed of ice in depressions

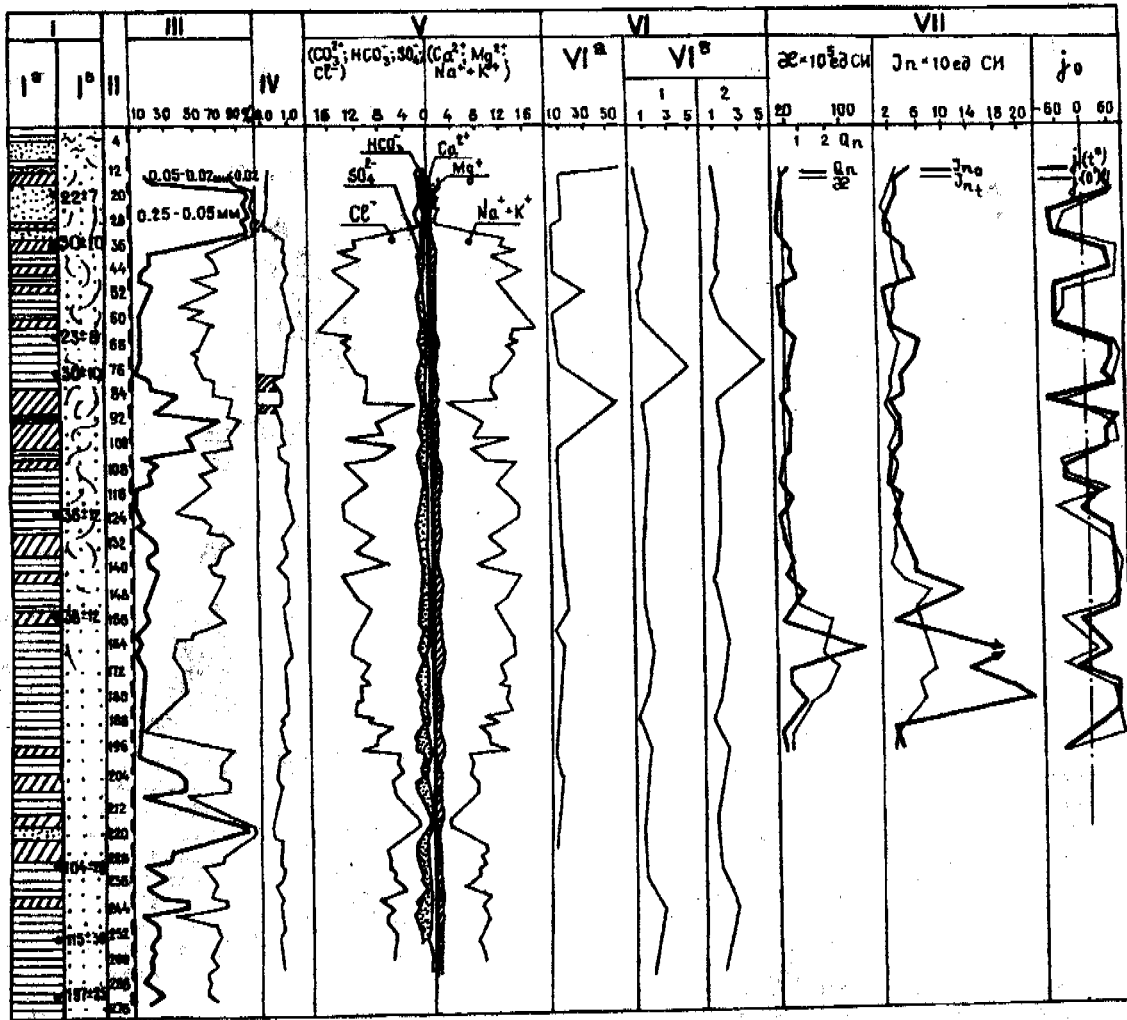


Figure 4. The analytic data of borehole core investigation. I). Geological profile, Ia - lithology and dates of absolute age by thermoluminescence analysis; Ib - cryogenetic structure. II). Depth scale, metr from soil surface (abs. altitude +5 m). III). Grain size content of ground (mm) paterhn. IV). Salinity of ground in percent (signed non-salted layers). V). Ground pore water ionic content, mg/ecv. VI). The coefficients of mineral cryogenetic stability; VIa - in the grain size fraction 0.1 - 0.05 mm; VIb - coefficient of cryogenetic mineralogical contrast, common; VIb\* - the same, individual. VII). Paleomagnetic characteristics; Qn-Kenigsberger factor; magnetic suscseptibility; Jno-magnetic amount before cleaning; Jnt-the same, after cleaning; jo-angle of inclination before cleaning; j(t)- the same, after cleaning.

of beneath deposits indicates a formation of ice on this soil surface. 4). The distribution of massive ice in sections of all geomorphological levels opposes any idea of intraground growth of ice, because the latter process is possible only under geomorphological control. 5). An unconformity of top contact of ice with structure of over laying deposits and with a relief of soil surface as well as a witness of ice roof erosion testifies to a buried ice origin. 6). The large dimension of massive ice body contradicts an intraground origin. 7). The dynamomethamorphic type of ice structure shown in previous works (Solomatin, 1976, 1986) and manifested by macro- and microdeformations which are uncorrelated with structure of contained sediments confirm a glacial nature of the massive ice.

#### REFERENCES

- Dubikov G.I., Korejsha M.M. (1964). The fossil injection ice on Yamal peninsula. Proceeding Acad. of Sci. USSR, Ser. Geograph., N. 5, Moscow, pp. 58 - 65.
- Mackay J.R. (1971). The origin of massive ice beds in permafrost; Western Arctic Coast, Canada. Can. J. of Earth Sci., v. 8, N. 4, pp. 397 - 422.
- Solomatin V.I. (1986). Retrogenesis of underground ice. Novosibirsk. 215 p.
- Solomatin V.I. (1976). Massive ice in down stream of Enisej river. Problems of cryolitology. Moscow, N. 5, pp. 87 - 94.

# PECULIARITIES OF PILE BEHAVIOR IN THAWING SOILS

Y. Y. Torgashov

Chita Department of Permafrost Institute p. Box 539, 672010 Chita, Russia

The results of field investigations of piles in thawing soils are described. Nine stages of interaction of system elements "pile-soil" have been established, every stage being analyzed. The experimental values of negative friction forces influencing on the pile are obtained, their comparison with standard values is made. Some peculiarities of thermo-mechanical interaction of piles with thawing soils are stated.

Pile foundations of buildings and structures constructed on permafrost soils on principle II (assuming the soils thaw in structure service) undergo nine stages of interaction with the base.

In the first stage (Fig. 1. a) the bearing

capacity of pile base is determined by design pressure on frozen ground under the lower end of the pile and design shear strength of soil or soil solution along the lateral surface of pile freezing.

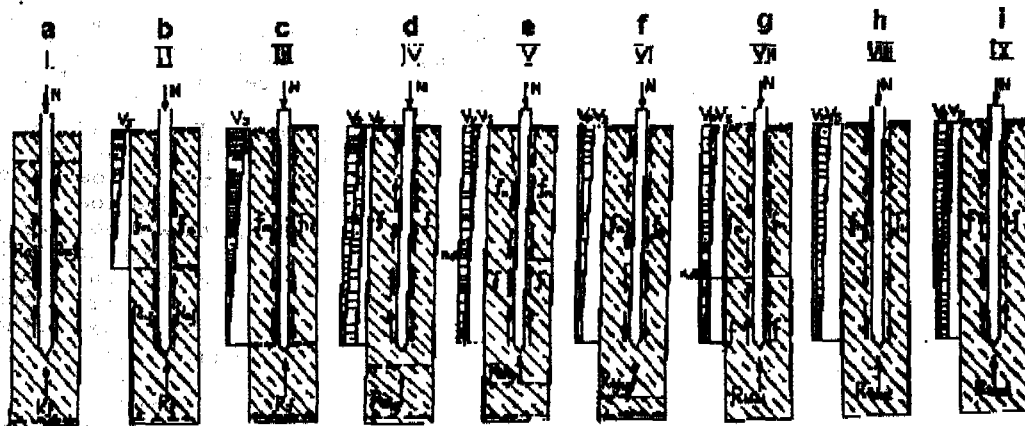


Fig. 1. Stages of pile interaction with permafrost soil of base when used on principle II, assuming the thawing during structure service.

The pile load capacity,  $F_u$ , is determined by the familiar formula (Bases and Foundations.... 1990).

The second stage (Fig. 1. b) is characterized by the beginning of thawing of permafrost soils surrounding the pile.

In the third stage (Fig. 1. c) the halo of thawing has already reached the pile tip.

The fourth stage is characterized by the movement of thawing halo below the pile tip (Fig. 1. d).

Intensive soil compaction and pile settlement occur due to the soil thawing under the pile tip.

In the fifth stage (Fig. 1. e) the thawing halo is lowered to the considerable depth from the pile tip. The rate of soil thawing and compaction under the lower end of the pile is markedly decreased and accordingly the rate of pile settlement being reduced. Within the upper part of the pile body the rate of the thawed soil settlement ( $V_s$ ), surrounding the pile, exceeds the rate of pile settlement ( $V_p$ ), and vice versa, below a certain point we call "zero" (Dalmatov et. al., 1975) the rate of pile settlement exceeds the rate of soil settlement.

With the further advance of thawing halo into the soil below the pile tip (stage VI. Fig. 1. f) the rate of soil thawing and pile settlement becomes minimal. While soil compaction and, accordingly, soil settlement located above the pile tip continues, soil displacement in relation to the pile body occurs, and the development of negative friction results.

Stage VII (Fig. 1. g) is characterized by the complete soil thawing under the pile tip. the development of positive and negative friction forces on the lateral surface of the pile.

In the eighth stage (Fig. 1. h) that thawed soil compaction under the lower end of the pile is coming to an end and soil compaction located above the pile tip is still continuing, that contributes to negative friction development on the lateral surface of the pile.

The ninth stage of interaction of pile with the base soil develops as the soil consolidation at the pile base is completed (both above and below the pile tip (Fig.1.i).

Analyzing the pile load capacity of nine stages of its interaction with the base soil it should be noted that the most unfavorable



conditions for pile behavior are to be found in IV... VIII stages. Let us consider each of the above stages separately.

In the IV stage (Fig. 1. d) the thawing halo having reached the pile tip is moving down. The bearing capacity of the thawed soils under the pile tip is determined by the parameters of ultimate shear strength of the soil condition acquired immediately after thawing (Cthg, Fthg) (Tsitovich, 1973).

Cohesion, in particular, can be determined by the ball method of testing and must correspond to ultimate resistance long Ctho. The angle of internal friction (Ftha) is determined by the quick shear test for undrained and uncompacted soil condition.

The bearing capacity of thawed soils must be estimated in the most dangerous physical state for the pile foundation stability when the soil under the load has not been compacted yet. Considering that at the moment of soil thawing its strength characteristics (Cthg, Fthg) have been considerably reduced at the moment of soil thawing (Mikhailov, Bredjuk, 1966; Shusherina et al. 1983) (depending on the type of soil, its moisture, cryogenic texture, composition, structure, condition), it is evident that the bearing capacity of thawed soil under the pile tip in stage IV is minimal. Therefore, if the load transmitted by the pile tip exceeds some limit value for the given soil, the loss of bearing capacity of soil under the pile tip will occur, and will be accompanied by the pile slide and maximum development of positive friction forces,  $f$ , on its lateral surface.

The fifth stage (Fig. 1. e) is characterized by gradual compaction of the soil under the pile tip, slow pile settlement under the load, development of negative friction forces on the lateral surface of the pile, which in their turn cause additional pile settlement. In case negative friction forces of high value appear, the loss of bearing capacity of thawed soil under the pile tip and pile slide are possible.

In the sixth stage (Fig. 1. f), negative friction forces act within the limits of the entire lateral surface of the pile and reach maximum in their development. The entire load acting on the pile is transmitted to the base soil through the pile tip. This results in high normal and tangential stresses in the soil causing its additional compaction and pile settlement, development of zones of limit equilibrium in the soil and in certain cases, involving either loss of pile load capacity and pile slide or pile fracture. The latter is highly dangerous in case of long built piles (Sobolevsky, 1988).

The results of investigations carried out

by Y. A. and D. Y. Sobolevsky (1988) showed that in analyzing the pile behavior and designing their load capacity it is necessary to consider the influence of dilatancy on the conditions of developing contact filtration and negative friction along the pile body.

By the beginning of the seventh stage (Fig. 1. g) the soil at the pile base has melted entirely. The soil consolidation under the pile tip is gradually being completed. The soil above the pile tip still continues consolidating, especially in upper levels. In these conditions zero point dividing action zones of positive and negative friction is slowly displaced downwards.

The slowing down of soil consolidation located above the pile tip is due to the fact that the soil compaction occurs mostly under the action of its dead load while soil underlying the pile tip is compacted not only under the dead load but also due to the action of the load transmitted by the pile tip. By the end of the stage zero point reaches the level of pile tip.

The eighth stage (Fig. 1. h) is distinguished by the fact that the stresses taken by the pile (external load, negative friction) and also its dead load are transmitted onto the thawed soil by the pile tip. In this case the thickness of the soil located above the pile tip would hand on the pile. This is the case similar to the sixth stage. However, unlike the sixth stage, in the given case the load transmitted by the pile tip acts on the thawed, compacted soil, which consolidation has been practically completed. In this case the probability of large additional settlement is small, however, the probability of fracture of long piles increases repeatedly. Considering all the stages of interaction of system element "pile-soil" it should be noted that the greatest probability of long piles fracture exists in stages III, VI and VIII of interaction of pile with thawing and thawed base soils.

Probability of loss of bearing capacity of thawed soil under the pile tip is especially high in the sixth stage.

Considering that pile behavior in thawing soils is the least studied field in engineering geocology, experimental tests in natural condition of interaction of piles with the thawing soils have been conducted. Thawing argillaceous, sandy and coarse rock soils were subjected to static pressure load tests. The total moisture of the given soils under the pile tip was 0.142... 0.273; 0.089 ...0.240; 0.056 ...0.219, respectively. Cryogenic texture of the soils under investigation was more often massive, seldom layer, net and also crust (sandy and coarse rock soils with sand filler).

Table 1. Comparison of experimental values of unit negative friction forces with the values obtained by design according to the standard formulas.

N test piles	N test	Unit value of negative friction	of negative friction	Excess of negative friction forces obtained by the design versus experimental values, %
		by the result of the experiment	by standard formulas 2.02.03-85	by standard formulas 2.02.04-88
1	1	0.0193	0.0254	31.6 / 86.5
1	2	0.0201	0.0254	26.4 / 79.1
2	11	0.0170	0.0200	17.6 / 111.8

Precast reinforced prismatic piles of square section 0.3\*0.3; 0.35,0.35 m, 6-16 m long, solid and built were used in the tests. The tests were conducted in three stages. In

the first stage the test was conducted in frozen ground, in the second stage - in thawing soil, and in the third stage - in the thawed soil. The pile load

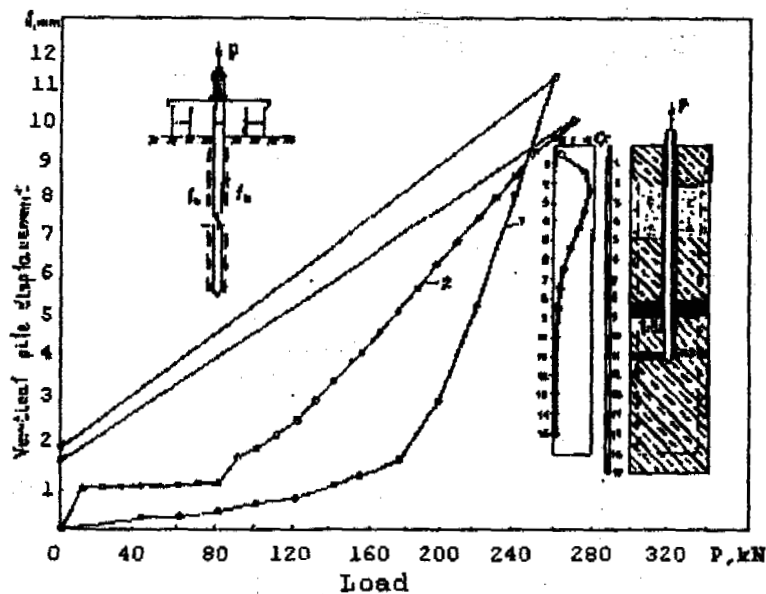


Fig. 2. Dependence of pile N1 displacement on vertically tension pile load.

capacity in different frost-soil conditions the resistance of the thawing soil under the pile tip, the pile and near-the-pile soil settlement were determined. Thawed soils were subjected to tension pile load, the unit values of negative friction forces presented in Table 1 being determined.

The diagrams of dependence of pile N1 displacement on vertical tension pile load made on the results of two tests are presented in Fig. 2. Diagram 1 is characterized by the presence of three zones. In the first zone the dependence of pile displacement upon the load is practically linear. At the point corresponding to the load of 120 kN, there is a change in the diagram and the dependence becomes curvilinear. Under the load of 200 kN the curve becomes straight line steeply going up.

In diagram 2 the curve change corresponds to the load of 80 kN (2.3 times less than in test N1). One of the reasons of early

appearance of the curve change in diagram "load-displacement" in test N2 is incomplete restoration of structural relations between the particles of soil surrounding the pile in 7 days after the Test N1.

A series of tests an estimation of negative friction forces were conducted upon the pile N2 (Fig. 3).

The tests were conducted by the quick test. The diagrams of six tests (from 6th to 11th) are represented in Fig. 3. The intervals between the end of the former and the beginning of the next test lasted for about 25 minutes.

Comparison of unit values of negative friction forces obtained experimentally with the values obtained by the design in accordance with the existing standards shows their considerable difference (on the average 43%).

Taking into consideration a small number of test values of negative friction forces it is necessary to continue field experiments with piles of different length in various

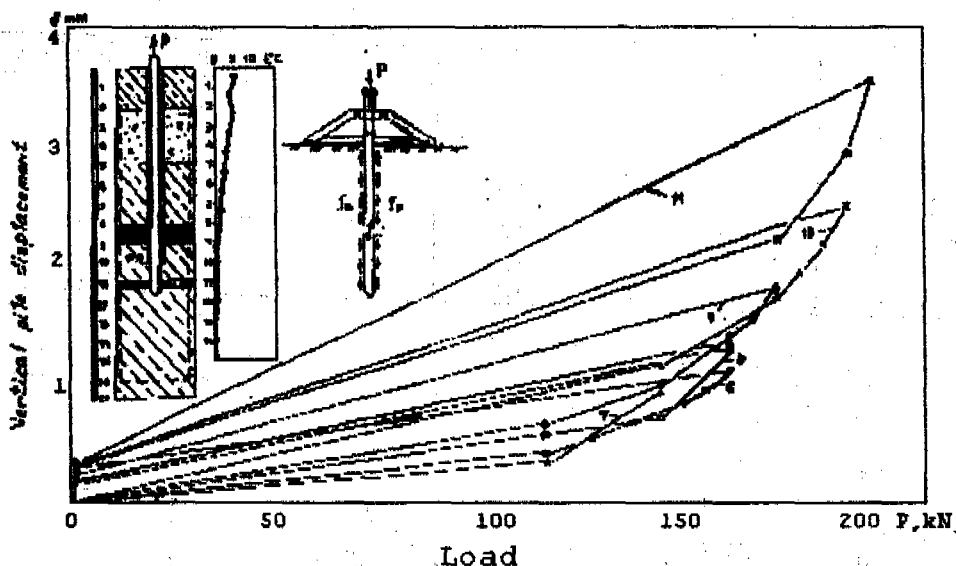


Fig. 3. Dependence of pile N2 displacement on vertically tension pile load

frost soil conditions. Accumulation of experimental data and their processing will allow to compile regional tables of unit values of negative friction forces that will contribute to the reliability of pile foundations in thawing soils.

Analysis of results of pile tests of static push-in loads (with simultaneous thaw of permafrost soils) in situ allow draw next conclusions. Low bearing capacity (50... 300 kN) under pile edge have following types of permafrost soils:

residual clay soils (loam and clay) massive, seldom layer, net cryogenic texture with total moisture more 0. 22, under thaw from tightplastic to currentplastic consistency; fine grained and flour sands massive cryogenic texture with total moisture more 0. 20, under thaw saturated;

frost heaving highicing medium, coarse, gravel sands crust and basal cryogenic texture with total moisture more 0. 15, under that saturated;

highicing gravel and crushed stone with sanding aggregate under thaw saturated, with total moisture 0. 145... 0. 122.

High bearing capacity (700... 1100 kN) under pile edge marked by next types of permafrost soils;

eluvial loams massive cryogenic texture under thaw hard consistency, with total moisture not more 0. 15;

eluvial coarse and gravel sands massive cryogenic texture (tight, seldom medium tight) with total moisture up to 0. 12;

crushed stone soils with loaming aggregate massive cryogenic texture with total moisture 0. 056... 0. 102, under thaw hard consistency.

#### REFERENCES

1. Dalmatov B. I., Lapshin F. K., Rossikbin G. V. Design of pile foundations in soft soils. - L. : Construction Publishing House, 1975. - 240 p.
2. Mikhailov G. D., Bredjuk G. P. Shear Strength of argillaceous soils in thawing. //Paper of the 8th All union inter - department meeting on geocreeology. - Yakutsk: 1966, V. 5. p. 51-60
3. Shusherina E. P., Maksimyak R. V., Martynowa G. P. Shear strength of permafrost soils in thwing. // Problems of geocreeology. M. : Nauka, 1983. p. 100-107.
4. Sobolevsky G. A., Sobolevsky D. G. On dila tant nature of contact filtration and nega tive friction along the pile body. // Papers of the second Baltic Conference on mecha nics of Soils and foundation Constructions. - Tallinn, 1988, V. I, p. 143-149
5. Standards 2. 02. 04 - 88 - Bases and founda tions on permafrost soils. State Construc tion of the USSR. - M. : CNTP of the USSR State Construction, 1990. - 56 p.
6. Tsitovich N. A. Mechanics of frozen ground. : Higher School, 1973. - 448 p.

## NORTHERN ASIA CRYOLITHOZONE EVOLUTION IN LATE QUATERNARY

Yurij K. Vasil'chuk

Theoretical Problems Department,  
The Russian Academy of Sciences, Vesnina 12, 121002, Moscow, RUSSIA

There were studied about 50 base sequences. Oxygen isotope analysis of syngenetic ice wedges allowed to reconstruct winter temperatures which were lower than modern ones about 8-10°C (total winter temperatures) and stayed quite severe and closed to modern ones during Holocene. The correlation analysis of extend massive of palynologic data permitted to evaluate the summer paleotemperatures. They were lower about 1-5°C than modern ones in Late Pleistocene cryochron just during warmest epoch of summer temperatures could be about 1-3°C warmer than modern ones. The summer temperatures were exceeded modern summer temperatures about 4-5°C in Holocene optimum. The total temperatures of naked frozen grounds were lower about 5-9°C during Late Pleistocene cryochron and were close to modern ones in Holocene optimum.

### INTRODUCTION

There are four environmental events attracted the most attention of investigators of the last 40-50 Kyr history. These are Ocean level changes, dynamics of cover glaciations, cryolithozone changes, climatic fluctuations. All of them are interacted more or less. The new information about each other gives knowledge about all the other. So we believed the new data of cryolithozone dynamics which were received last years can be useful for study of adjacent fields.

The main attention we have spared for investigations of basis sequences of syncryogenic thicknesses by complex of conjugated methods named the complex isotope paleogeocryologic analysis. It includes both well-known methods (such as pollen, diatoms, microfauna, paleobotany, hydrochemistry et al.) and the new method i.e. the study of oxygen and hydrogen composition of ground ice. All basis sequences were dated as complete as possible by radiocarbon of any organic matter. It is allowed to make chronologic correlation reliable enough. The deuterium composition data from ground ice had been received more than 40 years ago by R. Teis but regular study of stable isotopes in permafrost began more late. However we must marked that our investigations are differed from other ones by the obligatory procedure i.e. radiocarbon dating of syncryogenic thicknesses containing ice wedges. (Vasil'chuk, 1982; 1988-1992) This is provided the dating both of the frozen thickness and syngenetic ice wedges. The technique of this procedure were described earlier in detail (Vasil'chuk, 1991, 1992).

### STABLE ISOTOPES DISTRIBUTION IN GROUND ICE-WEDGE

The interpolation method was used for dating of single sample or series of samples or part of isotope diagram too. It is provided discount of formation character of concrete ground ice

deposit. One of the most interest paleogeographic and paleoclimatic objects are the Late Pleistocene sequences with thick syngenetic ice wedges which were forming continuously during last 40 Kyr in North of Asia. This fact is allowed to reconsider the accepted paleoclimatic views according to latter the noticeable warming occurred during the Middle of Wurm (Weichelian, Wisconsin, Devensian) and Early and Middle Holocene. As it is found by our study that was not correct for North of Asia. The syncryolithogen processes were took place quite actively during last 40 Kyr including Middle Wurm and Early and Middle Holocene too. The using of complex isotope paleogeocryologic analysis is allowed to receive the quantitative character of syncryolithogenesis geotemperature conditions in North of Asia during last 40 Kyr. Oxygen isotope diagrams received from Late Pleistocene (Figure 1) and Holocene (Figure 2) syngenetic ice wedges of Northern Asia are the base of such paleoreconstructions. The distribution trend has been determined for the Northern Asia ice wedges of different age.

- The  $\delta^{18}O$  trend in Late Pleistocene ice wedges was similar to modern one i.e.  $\delta^{18}O$  became more negative from West toward East by 8-10 ‰, from -19 ‰ -25 ‰ in Western Siberia ice wedges to -30 ‰ -35 ‰ in Northern Yakutia then it is became as high as -28 ‰ -33 ‰ in North of Chuckotka and Central areas of Magadan Region (by 2-3 ‰), and as high as -23 ‰ -29 ‰ in the East of Chuckotka (by 6-8 ‰). These data are evidenced the Air mass Transportation was similar to modern one in the end of Late Pleistocene through Asia Subarctic. West direction of Air mass Transportation was dominated in the considerable part of Eurasia continent. Atlantic influence was essential from Jamal peninsula to North-East Yakutia, but it was possible weaker than modern one due to more frequent cold and dry Arctic air mass advection. The influence of Pacific air masses were probably

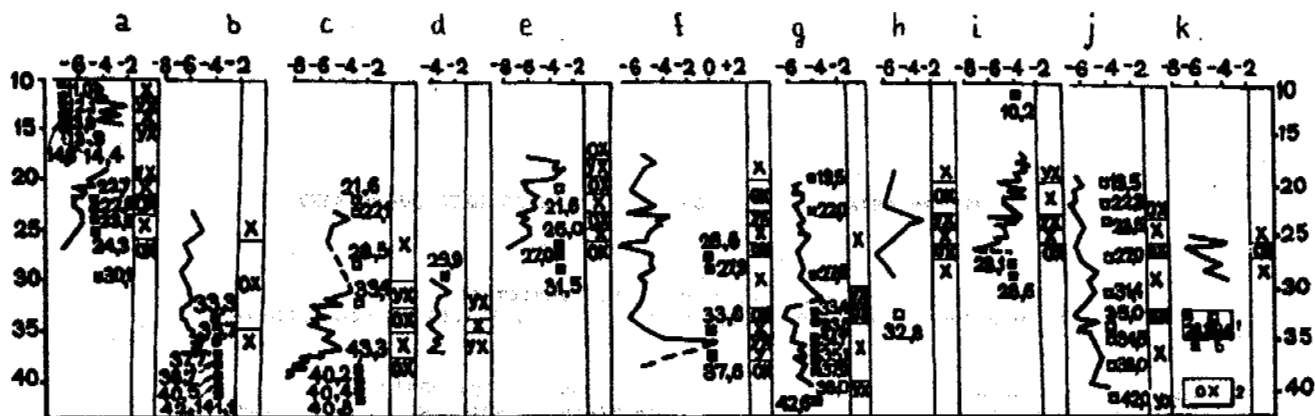


Fig. 1. Interregional oxygen isotope diagram correlation of Late Pleistocene ice wedges of different regions of Eurasia cryolithozone: a-k - ice wedges diagrams: a - near Gyda settlement (up) and near Seyaha settlement (down) in the North of Western Siberia; b - in depression near Kular settlement, c - Bykovsky peninsula in the mouth of Lena river; d-g - in the North of Yakutia: d - Lower Omolon river, e - Plakhinsky Yar natural exposure, f - near Zeleny Mys settlement, g - Duvanny Yar natural exposure; h - Central Yakutia, natural exposure in valley of Viluy river near mouth of Tyalychima river; i-k - Chukotka: i - in the Aion island, j - natural exposure Ledovy Obryv in Main river, k - near Anadyr town; 1 - C-14 date of organic matter from thickness which synchronous to ice wedges; a - author's data, b - literature data; 2 - oxygen isotope zone indexes: Y - temperate (close to present conditions); YX - temperate cold; X - cold; OX - very cold. Ordinate axis is radiocarbon age, received by interpolation of radiocarbon dates, horizontal coordinate is  $\Delta\delta^{18}O - \delta^{18}O$  difference between value  $\delta^{18}O$  from ice wedges and from active ice growth veins from flood plain, laida and peat bogs the same region, where Pleistocene ice wedges were found. Mean value  $\delta^{18}O$  for active ice growth veins is: a: -18%; b-g: -26%; h: -24,5%; i: -26% (the later displacement of isotope provinces has been taken in consideration); j: -22%; k: -16%.

less than present in the east areas of Northern Asia. The continental anticyclonic regime dominated here in winters particularly.

The Holocene ice wedges have preserved the same tendency in  $\delta^{18}O$  distribution i.e. decrease of  $\delta^{18}O$  values was up to 6-8‰ to the East from -14 + -20‰ in Western Siberia ice wedges to -23 + -28‰ in Northern Yakutia ones. However the values of  $\delta^{18}O$  in Chukotka ice wedges increased up to -

15 + -21‰. The modern distribution of oxygen-18 in recent ice vein shoots and in snow cover (average winter values) is closed to Holocene.

Division to oxygen isotope zones which had been offered earlier (Vasil'chuk, 1991) was used for correlation of oxygen isotope diagrams.

#### EQUATIONS OF PALAEOTEMPERATURE CORRELATIONS

The study of dependence of oxygen isotope parameters in recent ice wedges ( $\delta^{18}O$ ) from

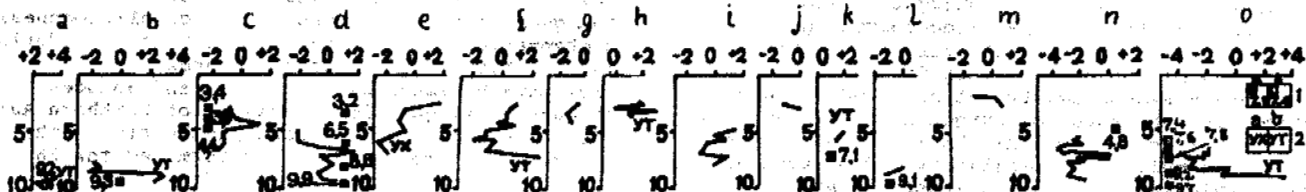


Fig. 2. Interregional oxygen isotope diagram correlation of Holocene ice wedges of different regions of Eurasia cryolitho- zone: a-o - ice wedges diagrams: a-d in the North of Western Siberia: a - near settlement Kharasaway (the first terrace), b - near settlement Seyaha (peat on the third terrace), c - near settlement Gyda (peat on the first terrace), d - near trading station Matjujsale (peat on the second terrace); e - Bykovsky peninsula in the mouth of Lena river (peat on the second terrace); f-i - in North Yakutia: f - mouth of Omolon river (flood plain), g - near exposure Plakhinsky Yar (flood plain), h - near settlement Zeleny Mys (flood plain), i - near exposure Duvanny Yar (alas), j-l - in Chukotka: j - island Aion (peat on the third terrace), k - on the Main river (alas i.e. peat on the ice wedge complex), l - near Anadyr town (peat on the first terrace); m-n - in Central Yakutia: m - flood plain of Viluy river near mouth of Tyalychima river, n - natural exposure Mamontova Gora (lacustrin sediments in upper part 60 - m terrace), o - exposure of the first terrace Chara river, Northern Zabajkalje; 1 - C-14 date of organic matter from thickness which synchronous to ice wedges, a - author's data, b - literature data; 2 - oxygen isotope zone indexes: YX - cold-temperate, YT - warm-temperate, the rest values of  $\delta^{18}O$  belong to zone Y, i.e. temperate, close to modern condition. On the ordinate axis radiocarbon age of the ice wedges, on the horizontal coordinate  $\delta^{18}O$  i.e. difference between value of  $\delta^{18}O$  from ice wedge and from ice growth veins; mean value  $\delta^{18}O$  for ice growth veins are for a-d: -18%, for e-i: -26%, for j: -21%, for k: -22%, for l: -16%, for m: -24,5%, for n: -26%, for o: -21,5%.

## NORTHERN ASIA CRYOLITHOZONE EVOLUTION IN LATE QUATERNARY

Yurij K. Vasil'chuk

Theoretical Problems Department,  
The Russian Academy of Sciences, Vesnina 12, 121002, Moscow, RUSSIA

There were studied about 50 base sequences. Oxygen isotope analysis of syngenetic ice wedges allowed to reconstruct winter temperatures which were lower than modern ones about 8-10°C (total winter temperatures) and stayed quite severe and closed to modern ones during Holocene. The correlation analysis of extend massive of palynologic data permitted to evaluate the summer paleotemperatures. They were lower about 1-5°C than modern ones in Late Pleistocene cryochron just during warmest epoch of summer temperatures could be about 1-3°C warmer than modern ones. The summer temperatures were exceeded modern summer temperatures about 4-5°C in Holocene optimum. The total temperatures of naked frozen grounds were lower about 5-9°C during Late Pleistocene cryochron and were close to modern ones in Holocene optimum.

### INTRODUCTION

There are four environmental events attracted the most attention of investigators of the last 40-50 Kyr history. These are Ocean level changes, dynamics of cover glaciations, cryolithozone changes, climatic fluctuations. All of them are interacted more or less. The new information about each other gives knowledge about all the other. So we believed the new data of cryolithozone dynamics which were received last years can be useful for study of adjacent fields.

The main attention we have spared for investigations of basis sequences of syncryogenic thicknesses by complex of conjugated methods named the complex isotope paleogeocryologic analysis. It includes both well-known methods (such as pollen, diatoms, microfauna, paleobotany, hydrochemistry et al.) and the new method i.e. the study of oxygen and hydrogen composition of ground ice. All basis sequences were dated as complete as possible by radiocarbon of any organic matter. It is allowed to make chronologic correlation reliable enough. The deuterium composition data from ground ice had been received more than 40 years ago by R. Teis but regular study of stable isotopes in permafrost began more late. However we must marked that our investigations are differed from other ones by the obligatory procedure i.e. radiocarbon dating of syncryogenic thicknesses containing ice wedges. (Vasil'chuk, 1982; 1988-1992) This is provided the dating both of the frozen thickness and syngenetic ice wedges. The technique of this procedure were described earlier in detail (Vasil'chuk, 1991, 1992).

### STABLE ISOTOPES DISTRIBUTION IN GROUND ICE-WEDGE

The interpolation method was used for dating of single sample or series of samples or part of isotope diagram too. It is provided discount of formation character of concrete ground ice

deposit. One of the most interest paleogeographic and paleoclimatic objects are the Late Pleistocene sequences with thick syngenetic ice wedges which were forming continuously during last 40 Kyr in North of Asia. This fact is allowed to reconsider the accepted paleoclimatic views according to latter the noticeable warming occurred during the Middle of Wurm (Weichelian, Wisconsin, Devensian) and Early and Middle Holocene. As it is found by our study that was not correct for North of Asia. The syncryolithogen processes were took place quite actively during last 40 Kyr including Middle Wurm and Early and Middle Holocene too. The using of complex isotope paleogeocryologic analysis is allowed to receive the quantitative character of syncryolithogenesis geotemperature conditions in North of Asia during last 40 Kyr. Oxygen isotope diagrams received from Late Pleistocene (Figure 1) and Holocene (Figure 2) syngenetic ice wedges of Northern Asia are the base of such paleoreconstructions. The distribution trend has been determined for the Northern Asia ice wedges of different age.

- The  $\delta^{18}O$  trend in Late Pleistocene ice wedges was similar to modern one i.e.  $\delta^{18}O$  became more negative from West toward East by 8-10 ‰, from -19 ‰ to -25 ‰ in Western Siberia ice wedges to -30 ‰ to -35 ‰ in Northern Yakutia then it is became as high as -28 ‰ to -33 ‰ in North of Chuckotka and Central areas of Magadan Region (by 2-3 ‰), and as high as -23 ‰ to -29 ‰ in the East of Chuckotka (by 6-8 ‰). These data are evidenced the Air mass Transportation was similar to modern one in the end of Late Pleistocene through Asia Subarctic. West direction of Air mass Transportation was dominated in the considerable part of Eurasia continent. Atlantic influence was essential from Jamal peninsula to North-East Yakutia, but it was possible weaker than modern one due to more frequent cold and dry Arctic air mass advection. The influence of Pacific air masses were probably

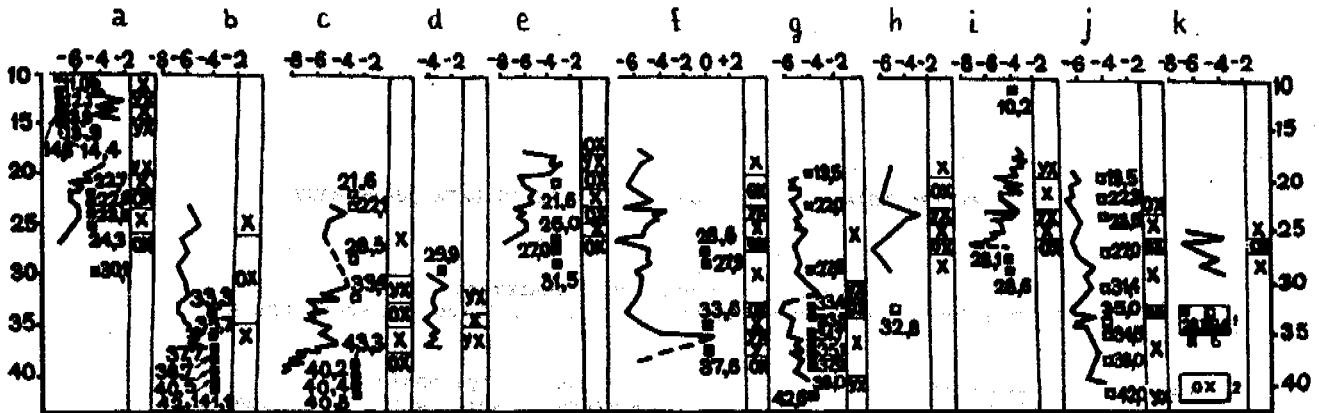


Fig.1. Interregional oxygen isotope diagram correlation of Late Pleistocene ice wedges of different regions of Eurasia cryolithozone: a-k - ice wedges diagrams: a - near Gyda settlement (up) and near Seyaha settlement (down) in the North of Western Siberia; b - in depression near Kular settlement, c - Bykovsky peninsula in the mouth of Lena river; d-g - in the North of Yakutia: d - Lower Omolon river, e - Plakhinsky Yar natural exposure, f - near Zeleny Mys settlement, g - Duvanny Yar natural exposure; h - Central Yacutia, natural exposure in valley of Viluy river near mouth of Tyalychima river; i-k - Chukotka: i - in the Aion island, j - natural exposure Ledovy Obryv in Main river, k - near Anadyr town; 1 - C-14 date of organic matter from thickness which synchronous to ice wedges; a - author's data, b - literature data; 2 - oxygen isotope zone indexes: Y - temperate (close to present conditions); YX - temperate cold; X - cold; OX - very cold. Ordinate axis is radiocarbon age, received by interpolation of radiocarbon dates, horizontal coordinate is  $\Delta\delta^{18}\text{O} - \delta^{18}\text{O}$  difference between value  $\delta^{18}\text{O}$  from ice wedges and from active ice growth veins from flood plain, laida and peat bogs the same region, where Pleistocene ice wedges were found. Mean value  $\delta^{18}\text{O}$  for active ice growth veins is: a : -18% ; b-g : -26% , h : -24,5% , i : -26% (the later displacement of isotope provinces has been taken in consideration); j : -22% ; k : -16% .

less than present in the east areas of Northern Asia. The continental anticyclonic regime dominated here in winters particularly.

The Holocene ice wedges have preserved the same tendency in  $\delta^{18}\text{O}$  distribution i.e. decrease of  $\delta^{18}\text{O}$  values was up to 6-8% to the East from -14 + -20% in Western Siberia ice wedges to -23 + -28% in Northern Yakutia ones. However the values of  $\delta^{18}\text{O}$  in Chukotka ice wedges increased up to

15 + -21% . The modern distribution of oxygen-18 in recent ice vein shoots and in snow cover (average winter values) is closed to Holocene.

Division to oxygen isotope zones which had been offered earlier (Vasil'chuk, 1991) was used for correlation of oxygen isotope diagrams.

#### EQUATIONS OF PALAEOTEMPERATURE CORRELATIONS

The study of dependence of oxygen isotope parameters in recent ice wedges ( $\delta^{18}\text{O}$ ) from

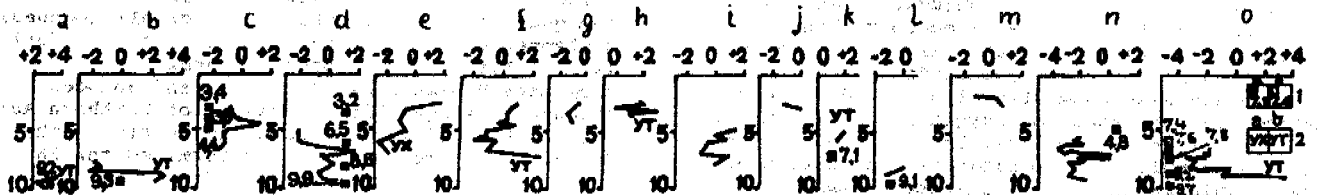


Fig.2. Interregional oxygen isotope diagram correlation of Holocene ice wedges of different regions of Eurasia cryolitho- zone: a-o - ice wedges diagrams: a-d in the North of Western Siberia: a - near settlement Kharasaway (the first terrace), b - near settlement Seyaha (peat on the third terrace), c - near settlement Gyda (peat on the first terrace), d - near trading station Matjujsale (peat on the second terrace); e - Bykovsky peninsula in the mouth of Lena river (peat on the second terrace), f-i - in North Yakutia: f - mouth of Omolon river (flood plain), g - near exposure Plakhinsky Yar (flood plain), h - near settlement Zeleny Mys (flood plain), i - near exposure Duvanny Yar (alas), j-l - in Chukotka: j - island Aion (peat on the third terrace), k - on the Main river ( alas i.e. peat on the ice wedge complex), l - near Anadyr town (peat on the first terrace); m-n - in Central Yakutia: m - flood plain of Viluy river near mouth of Tyalychima river, n - natural exposure Mamontova Gora ( lacustrin sediments in upper part 60 - m terrace ), o - exposure of the first terrace Chara river, Northern Zabajkalje; 1 - C-14 date of organic matter from thickness which synchronous to ice wedges, a - author's data, b - literature data; 2 - oxygen isotope zone indexes: YX - cold-temperate, YT - warm-temperate, the rest values of  $\delta^{18}\text{O}$  belong to zone Y, i.e. temperate, close to modern condition. On the ordinate axis radiocarbon age of the ice wedges, on the horizontal coordinate  $\delta^{18}\text{O}$  i.e. difference between value of  $\delta^{18}\text{O}$  from ice wedge and from ice growth veins; mean value  $\delta^{18}\text{O}$  for ice growth veins are for a-d : -18% , for e-i : -26% , for j : -21% , for k : -22% , for l : -16% , for m : -24,5% , for n : -26% , for o : -21,5%

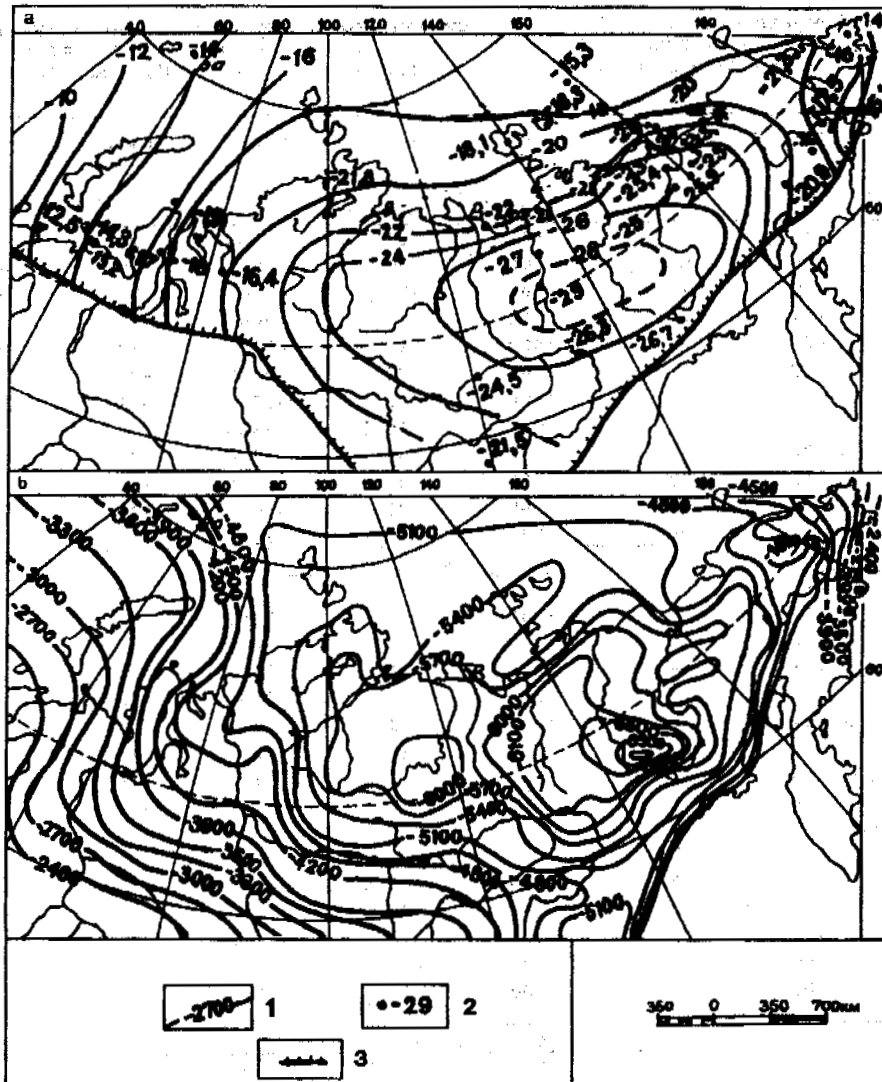


Fig.3. Comparison of character variations oxygen -18 content from recent ice growth veins (which were formed during last 100 years) (a) and total winter temperatures (b) averaging at last 60 - 100 years. Iso-lines : 1 - surely down, 2 - supposed down, 3 - South boundary of present active growth of ice veins.

winter temperatures of the air<sup>n</sup> is demonstrated the close relationship of these characteristics (figure.3). So it is allowed to derive a simple equations of regression.

$$t^{\circ}_{m. winter} = \delta^{18}O_{vein} (\pm 2^{\circ}C) \quad (1)$$

$$t^{\circ}_{m. january} = 1,5 \delta^{18}O_{vein} (\pm 3^{\circ}C) \quad (2)$$

$$S t^{\circ}_{winter} = 250 \delta^{18}O_{vein} (\pm 500^{\circ}C) \quad (3)$$

These equations were used for interpretation of oxygen isotope data to winter paleotemperature values (Table.1). The mean winter temperatures were less by 8-10° C than modern ones during epoch of Late Pleistocene cryochron (40-10 Kyr B.P.), while Holocene winter temperatures were closed to modern ones even during Holocene "optimum". The mean January temperatures were oscillated symbatially too, as they were by 11-16° C

lower than modern ones and the total winter temperatures were less than modern ones by 2000-3000°C in Late Pleistocene cryochron while Holocene temperatures were close to the modern ones.

The numerous palynologic data were provided the reconstruction of summer temperature characteristics. Subfossil pollen spectra were studied and compared with vegetation season temperatures. It is performed the existence of steady relationship for total value (P<sub>t</sub>) of tree pollen (without value of far transported pollen of Pinus sibirica and Pinus silvestris) in flood plain, watte, marsh deposits from total positive temperatures. This dependence may be expressed by follow equation but approximately:

$$S t^{\circ}_{summer} = 40 P_t (\pm 300^{\circ}C) \quad (4)$$



Table 1. The ground temperatures ( $t_{gr}$ , °C - the snow and vegetation cover taken away) in the North Eurasia cryolitotozone in Late Quaternary total summer ( $St_s$ ) and total winter ( $St_w$ ) air temperatures (degree · day) and values  $\delta^{18}O$  in ice wedges (in ‰ to SMOW), mean air winter ( $t_{m.w.}$ , °C) and mean January ( $t_j$ , °C) air temperatures

N on the fig.4A, location of the sequences.	$t_{gr}$	P <sub>tr</sub>	$St_s$	$\delta^{18}O$ , ‰	$St_w$	$t_{m.w.}$	$t_j$	$t_{present}$ grounds
30 - 25 Kyr B.P.								
1. Seyaha river	-15	13	+800	-24	-6000	-24	-36	-10
2. Island Kotel'ny	-19	8	+500	-29	-7250	-29	-43	-14
3. Peninsula Bykovsky	-19	2	+500	-30	-7500	-30	-45	-13
4. Settlm. Kular	-21	2	+500	-32	-8000	-32	-48	-15
5. Vorontsovsky Yar	-21	2	+500	-31,5	-7825	-32	-47	-14
6. Plakhinsky Yar	-22	1	+500	-33	-8250	-33	-49	-13
7. Duvanny Yar	-21	2	+500	-31	-7750	-31	-46	-12
8. Lower Omolon	-20	1	+500	-29,5	-7400	-30	-44	-12
9. Settlm. Zeleny Mys	-20	3	+500	-32	-8000	-32	-48	-12
10. Island Aion	-19	13	+900	-31	-7750	-31	-46	-12
11. Main river	-17	3	+500	-28	-7000	-28	-42	-9
12. Viluj river	-18	30	+1200	-30,5	-7600	-31	-46	-10
22 - 14 Kyr B.P.								
13. Seyaha river	-12	7	+500	-22	-5500	-22	-33	-10
14. Gyda river	-13	7	+500	-21	-5250	-32	-32	-10
15. Island Kotel'ny	-16	6	+500	-25	-6250	-25	-37	-14
16. Settlm. Kular	-21	4	+500	-31	-7750	-31	-46	-14
17. Plakhinsky Yar	-21	1	+500	-32	-8000	-32	-48	-13
18. Settlm. Zeleny Mys	-21	1	+500	-31	-7750	-31	-46	-12
19. Duvanny Yar	-20	2	+500	-31,5	-7900	-32	-47	-12
20. Krasivoe sequence	-19	3	+500	-31	-7750	-31	-46	-12
21. Lower Omolon	-18	2	+500	-29	-7250	-29	-43	-12
22. Aljoshkinskaya ter-ce	-19	3	+500	-31	-7750	-31	-46	-12
23. Island Aion	-18	2	+500	-29,5	-7400	-30	-44	-12
24. Town Anadyr	-12	4	+500	-20,5	-5100	-21	-31	-7
25. Main river	-16	1	+500	-28,5	-7100	-29	-43	-9
26. Viluj river	-18	12	+800	-29,5	-7400	-30	-44	-10
27. Seq. Fenix , Kolyma	Wp0	4	+500	-31,5	-7900	-32	-47	-11
10 - 5 Kyr B.P.								
1. Settlm. Kharasaway	-8	20	+1000	-15,5	-3900	-16	-23	-6
2. Settlm. Seyaha	-10	15	+1000	-19,5	-4900	-20	-29	-10
3. Ngarkatnedayakh R.	-10	9	+900	-17,5	-4400	-18	-27	-10
4. Settlement Gyda	-11	17	+1000	-19	-4750	-19	-28	-10
5. Settlm. Matjujsale	-12	13	+900	-19,5	-4900	-20	-29	-11
6. Island Maly Ljakhovski	-13	6	+600	-21	-5250	-21	-32	-14
7. Bykovsky peninsula	-16	8	+800	-27,5	-9900	-28	-41	-13
8. Zagadochnye lakes	-13	7	+1000	-25	-6250	-25	-37	-12
9. Alas of Plakhinski Yar	-16	13	+900	-27	-6750	-27	-40	-13
10. Alas of Duvanny Yar	-15	12	+900	-26	-6500	-26	-39	-12
11. Alas near s. Kolymskoe	-16	11	+900	-27	-6750	-27	-40	-13
12. Aljoshkinskaya ter-ce	-14	13	+1000	-25,5	-6400	-26	-38	-12
13. Mamontova Gora	-15	70	+1800	-28,5	-7100	-29	-43	-12
14. Chara river	-11	72	+1600	-23	-5750	-23	-34	-8
15. Island Aion	-12	8	+600	-22	-5400	-22	-33	-13
16. Town Anadyr	-7	15	+1200	-17	-4250	-17	-26	-7
17. Main river	-9	25	+1200	-20	-5000	-20	-30	-9

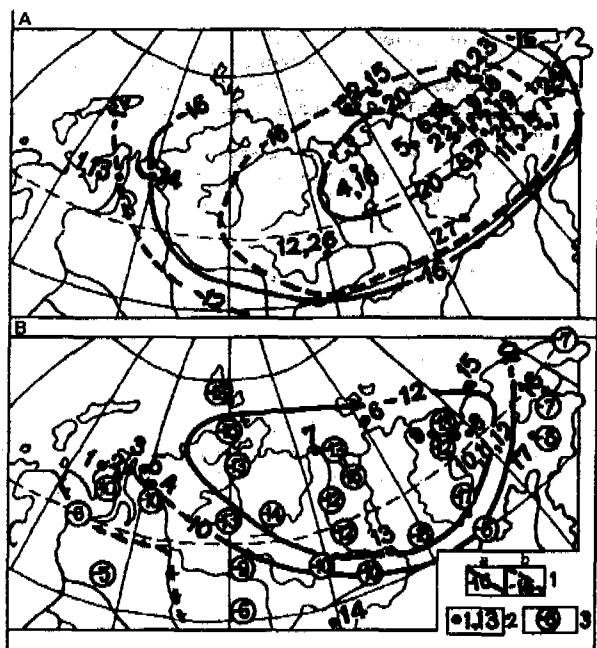


Fig.4. Mean annual temperatures distribution character (the snow and vegetation cover taken away) on permafrost ground surface : A - during Late Pleistocene cryochron: a - 30-25 Kyr (continued lines), b - 22-14 Kyr (dotted lines); B - during Holocene optimum 1 - temperature isolines; 2 - p of evaluated temperatures; for A and B see Table 1; 3 - present temperatures on ground surface

Pollen tree values were determinate from the same sequences as oxygen isotope sampling had carried out in ice wedges. In isolated case the neighboring sequences were used for such examinations. These data having been averaged in the most interest time intervals and processed as values of summer paleotemperatures are presented in Table.1. too. So it is showed summer temperatures were less stable than winter ones. However they were lower than modern temperatures (by 1-5°C for mean summer temperatures and by 200-500°C for total vegetation season temperatures). But there were some short periods of summer warming in Late Pleistocene cryochron 40-10 Kyr B. P., when mean summer temperatures were higher by 1-3°C and total summer temperatures were more by 200-300°C than modern ones.

The calculation of summer temperatures determination is not such accurate as winter, but this fact does not influence on general temperature course due to difference between duration of summer and winter periods. Summer lasts 2-4 months while winter as a rule lasts 8-10 months. So absolute values of total winter temperatures are 6-10 times much than summer ones and even twice or three time increase of total summer temperatures does not influenced on annual temperature course. It is the dynamic of winter temperatures was determined and is determining now changes of temperature field of Northern Asia permafrost.

#### GROUND PALEOTEMPERATURES

We have estimated annual ground temperatures having taken total summer and winter temperatures into consideration. We have abstracted from the winterizing influence of vegetation and snow cover intentionally. These data is showed in Table 1 and Figure 4. The temperatures are showed for conventionally naked ground. One can see the permafrost grounds were colder than modern one by 5-10°C during Late Pleistocene cryochron over all area of Northern Asia cryolithozone. The temperatures of naked permafrost grounds were about -12 ÷ -17°C in the North of Western Siberia (Yamal and Gydan peninsulas); -18 ÷ -22°C in Northern Yakutia; -16 ÷ -20°C in Central Yakutia; -12 ÷ -17°C in Chuckotka.

The temperatures of naked permafrost grounds were close to modern ones in Holocene including optimum. They were about -8 ÷ -12°C in Yamal and Gydan peninsulas; -11 ÷ -16°C in Northern Yakutia; -10 ÷ -15°C in Central Yakutia; -8 ÷ -12°C in Transbaikal region; -6 ÷ -10°C in Chuckotka.

#### CONCLUSIONS

This temperature model is explained the development features of syncryogenic permafrost thickness quite enough. The permafrost thicknesses were forming more southern in Late Pleistocene cryochron than present. Their area has decreased in Holocene. Now they are forming over all Cryolithozone in areas of recent accumulation such as flood-plains, watters, marshes and bogs.

The role of syncryogenic permafrost as paleogeographical indicator is important for the paleoglaciologic reconstructions. This factor is disregarded frequently for paleoglaciologic reconstructions of the end of Late Pleistocene. However the thick non-deformed syngenetic ice wedges are spread over Seaside Subarctic Plains everywhere. They were forming continuously 40-10 Kyr B.P., and could not cover by Ice sheets neither during forming of ice wedges as thick ice cover prevented from the frost cracking the bottom ground, no subsequently as ice sheet pressure should to deform ice wedges. But there is no any deformations even for shallow ice wedges which is lied from depth about 1-2 meters.

So, there is summary of new notion received as a result of study of Late Quaternary syncryogenic permafrost of Northern Asia by the complex oxygen isotope paleogeocryologic analysis. Execution of analogous investigations in Northern areas of Finland, Sweden, Norway (where Holocene permafrost is spread) and Northern Canada and Alaska (where Late Pleistocene syncryogenic thicknesses are spread as much as in Northern Asia) may to complete the notion of paleocryologic evolution of Northern Hemisphere. It have to answer to some difficult questions of Cover Glaciation dynamic, sea level changes and environmental changes as a whole.

#### REFERENCES

- Vasil'chuk Yu. K. (1982) Regularities of development of engineering geology conditions in the north of Western Siberia in the Holocene. Summary of Ph.D. Thesis (in geology and mineralogy) Moscow State University. Moscow. 27 p. Nauka publ. (305 p. is volume of Thesis) (In Russian).

Vasil'chuk Yu. K. (1988) Paleogeocryological interpretation of oxygen isotope composition of Late Pleistocene and Holocene reformed ice-wedges of Yakutia. In Transactions (Doklady) of the USSR Academy of Sciences. Vol. 298. No. 2. p. 425-429. (In Russian).

Vasil'chuk Yu. K. (1989) Formation conditions of the Late Pleistocene and Holocene ice-wedges of Chukotka (isotope-cryolithological and chronological analysis). In Transactions (Doklady) of the USSR Academy of Sciences. Vol. 309 No 4. 920-924. (In Russian).

Vasil'chuk Yu. K. (1990) Isotope geochemical characteristics of the Late Pleistocene ice-wedge complex of Cular depression. In Transactions (Doklady) of the USSR Academy of Sciences. Vol. 310. No. 1. p. 154-157. (In Russian).

Vasil'chuk Yu K. (1991) Late Quaternary syncryogenic permafrost sediments of Northern Eurasia: Structure, oxygen-isotope composition and forming

conditions. Summary of Dr.Sci. Thesis (in geology and mineralogy) Permafrost Institute of Siberian Branch Academy of Science of USSR. Moscow. 48 p. (622 p. is volume I and 244 p.- volume 2 of Thesis (In Russian).

Vasil'chuk Yu.K. (1992) Oxygen isotope composition of ground ice (application to paleogeocryological reconstructions). Moscow. Vol. 1.-421 p. Vol.2.-264 p.(In Russian).

Vasil'chuk Yu.K. (1992) Contradictoriness of modern palaeoclimatic and palaeoglacilogic models of Late Pleistocene in the light of permafrost data. In Buried glacier ice and permafrost in glaciated areas. Termination of Pleistocene in permafrost areas. Abstracts working group meeting IGCP Project 253. Tallinn. June 8-13, 1992. p.15-16.

Vasil'chuk Yu.K. (1992) Correlation of paleoclimate events in Eurasia last 40 Kyr B. P. In 29th International Geological Congress. Kyoto. Japan. 24 Aug.-2 Sep.1992. Vol.2. p.388.

ENGINEERING AND GEOCRYOLOGICAL PECULIARITIES OF USING  
PILE FOUNDATIONS IN MAGADAN AREA

Vladimir P. Vlasov

North-Eastern Department of Permafrost Institute,  
Magadan 685000, Russia

The problem of providing the stability of building and structures erected on frozen ground remains acute. Successful construction under such conditions in Magadan (the North-East of Russia) may be regarded as a positive example. The use of pile foundations here has enabled a safe and efficient construction.

The problem of providing the stability of buildings and structures erected on frozen ground remains acute. It will become still more important in the nearest future because of the global rise in the earth climate temperature. Therefore the search for technical designs, that may increase the safety and durability of bases and foundations is one of the important tasks of engineering geocriology. In this connection the experience of foundation engineering on permanently frozen soil with unsteady temperatures may be of use (Konash 1977, Vlasov 1988).

The town Magadan, founded in 1939, was developing as the administrative, cultural and research centre of the Magadan area the economy of which is based on the mining industry.

The area is characterized by a deep seasonal frost penetration (2.5...3.5 m) and by the presens of discontinuous permafrost, that occurs in the form of lens-shaped portions of 100 to 10000 m and more indiameter between the sites with frozen soil. The thickness of the frozen lenses is, as a rule, 2...10 m and in some cases - up to 30 m. Their temperature ranges from zero to 1°C. The margins of certain islands and lenses of frozen soil are very unsteady since any changes in the heat exchange at the ground surface immediately cause the displacement of the frozen soil margins.

The distribution of ice in the ground is not regular as compared to the areas of continuous permafrost. At the depths of more than 6-8 m, except rare cases, the frozen soils have a relatively small ice content and when thawed give slight settlements. The frozen soil of the upper layers, which have a rather high total humidity, is often susceptible to consolidation by thawing and its subsidence may reach 18 cm/m.

Thus, the relatively small dimensions of the frozen soil lenses, their relatively high tem-

perature and unstable state caused by man's activity as well as the location of stable frozen and unfrozen soil rather close to the surface have created adequate prerequisites for using pile foundations. The many year investigations carried out in Magadan by the author in collaboration with the municipal building organizations has enabled the specification of the problems related with the design and erection of pile foundations in this region. The basic results of these investigations are given below.

At present, depending on the permafrost and hydrogeological conditions of construction sites, here are in use the bored piles with after-driving, as well as of bored sunk constrained and combined piles.

The bored, after-driven piles are such r.c. piles which are sunk into the holes that have been bored up to the design bearing layer of thawed or frozen soils and are after-driven by a diesel-hammer. They are used in any soils which enable driving below the bottom plug of boreholes to a depth of no less than 0.5 m.

The bored sunken constrained r.c. piles are sunk into the boreholes drilled to the design bearing layer of unfrozen or frozen ground and provided with consolidated bottom. The lower ends of the piles are embedded in a concrete casing which should be no less than three borehole diameter high.

The bored sunk combined-type piles are arranged in the boreholes, drilled to the designed bearing layer of unfrozen or frozen ground. Their bottom part consists of the cast-in-situ concrete post, supported by the consolidated borehole bottom, whereas the upper part is designed of a r.c. post embedded in the cast-in-situ concrete to a depth of no less than three borehole diameters.

The characteristic feature of arranging the after-driven piles in unfrozen soil is that one can quick reach the test refusals in case of driving in the soil 0,5 to 4 m below the bore-

hole bottom. Only in some rare cases one can manage to drive piles from the borehole bottoms 6 m deeper on the sites the base of which is composed of dust-like clay or loose sand soil with a small content of coarse grains.

The bored, after-driven piles supported by frozen coarse grain and sandy soil should be handled with special care. In this case there is no need to follow special instructions on the minimum depth of pile drive below the borehole bottom. Rather often it is allowed that the cone of a r.c. pile only penetrates the borehole bottom. Therefore, pile refusal obtained in this case, may not serve as a criterium for evaluation of its bearing capacity and only shows the safety of the lower pile end connection with the frozen soil at the level of the borehole bottom. To prevent piles from breakage during the driving process it is recommended to observe the following rules: in order to make smooth the pile cone penetration - to fill the borehole bottom with unfrozen sand to a height of 0,5 - 1 m or to thaw the soil to the same depth in the borehole base; after the pile reaches the borehole base one should limit the further driving to 30 diesel-hammer strokes. It is recommended to use in this case piles with adequate reinforcement. They should be made of a high-grade concrete and provided with metal caps.

The bored, sunk and combined-type piles are used in case they rest on unfrozen and frozen large-fragment rock, gravel, coarse and medium-grade sands, as well as on dusty clay soil with flow index  $j_i \leq 0.4$ . The use of combined piles is economically reasonable in case of pile depth of no less than 12 m. Consolidation of borehole bases for these piles is provided by ramming their bottom, as a rule, with the use of crushed stone to reinforce the residue of the bore mud.

The length of the sunk r.c. posts of the combined piles is chosen taking into account the fact that they should cut all layers of the frozen soils, that create negative friction forces during thawing and settling. The empty space (hollows) between the walls of the boreholes and the piles are filled with concrete, cement or soil (mud) mortars depending on the horizontal loads and negative friction forces.

The general requirement to all types of piles, used in Magadan, is that in case the construction site is regarded as a seismic zone of 6 points and more, they should be driven to a depth of no less than four meters from the soil surface and in case of water saturated dusty sands in foundation bases - no less than 8 m. The advantage of the above-mentioned pile designs is the suitability of piles to perform under negative friction. Pile arrangement in the boreholes the diameter of which exceeds the largest cross-section of piles by 2 - 15 cm, enables to use any antifrictional filling material that reduces negative friction. In Magadan, for instance, pile hollows are filled, as a rule, with bore mud. This enables saving of concrete and cement as well as to reduce the negative friction forces on the side surface of piles by 40% and thus to increase their bearing capacity.

Depending on engineering and geocryological conditions of construction sites, the examined types of piles may be designed as end-bearing or friction piles. Their design bearing capacity is determined taking into account additional

preload due to the negative friction forces in case of penetration through frozen soil layers which settle during thawing. For calculations of regional values of soil design resistance  $R$  under the lower ends of friction, bored after-driven and bored sunk piles one can use Table I and along the side surface  $f$  of all pile types - Table 2. For piles resting on rock, unweathered and slightly weathered, large-fragment unfrozen and permafrost soil (gravel-shingle, crushed stone and gruss with sand filler)  $R = 20000$  KPa irrespective of their depth. Regional values  $R$  and  $f$  have been obtained on the basis of the results of more than 1000 field tests carried out on various construction and experimental sites of Magadan.

As a design bearing layer one should take the soils which have at thawing under the load the total settlement which does not exceeds the one, allowed for the given type of engineering structures.

Correction factors  $\gamma_{ca}$  and  $\gamma_{cf}$  obtained experimentally, have been introduced in the calculation formula of pile bearing capacity for  $R$  and  $f$ . The factor  $\gamma_{ca}$  considers the way the piles are rested. For bored, after-driven piles it is equal to 1, for bored sunk piles without borehole bottom consolidation - 0.9, and with consolidation I.I. The factor  $\gamma_{cf}$  considers the conditions of pile sinking and the material for filling the hollows. For bored, after-driven piles the side surface of which is below the borehole bottom and is in direct contact with unfrozen soil it is equal to 1, for bored sunk piles the hollows of which are filled with concrete or cement mortar, as well as for combined piles within the limits of the lower part made of cast-in-situ concrete - 0.8. In case of hollow filling with mud mortar for all pile types  $\gamma_{cf} = 0.6$ .

The design value of the total negative friction force  $F_{me}$  (KN), which occurs on the side surface of pile in case of soil thawing around the pile and reduces the design bearing capacity of piles is determined by the data given in Table 3. For calculation of soil base performance one can use factor  $\gamma_b$ , which considers the extent of negative friction reduction depending on the type of material or the type of pile side surface contact with the soil around the pile. For concrete surface of bored after-driven, bored sunk constrained and combined piles with hollows filled with concrete, cement and other similar mortars  $\gamma_b = 1$ , and in case of filling them with mud mortar - 0.6.

The design bearing capacity of piles is checked and specified by means of dynamic (for bored after-driven piles) and static tests according to the standard methods taking into account the following peculiarities.

Bored, after-driven piles are tested by dynamic, pressing and pulling out static loads in unfrozen large-fragment soils and sands 3 days after their driving, in dusty sands and sandy silty loam - 15 days after driving, in clayey loams and clays - 30 days after driving. Bored sunk constrained and combined piles are tested after the cast-in-situ concrete reaches its design strength in 28 days, and in case of using electric heating - after 12 days. The piles with hollows filled with mud mortar are tested for horizontal load not earlier than after 50 days. In this case the soil around the pile should be unfrozen to a depth of no less than five borehole diameters  $d$  and within the radius

Table I

Design resistance R of unfrozen and thawed of medium-density soil under the lower ends of piles, KPa							
Sinking depth of the lower pile end, m	sandy soils						
	semi-gravel	coarse grained	-	medium grained	fine-grained	dust-like	-
	dusty-clay soil with flow index $J_L$ equal to						
	0	0.1	0.2	0.3	0.4	0.5	0.6
Bored after-driven piles							
4	10800	7100	5700	4000	2700	2500	1400
6	12000	9200	6200	5100	3600	2700	1600
8	12900	9800	6800	5400	3900	2850	1700
10	13600	10200	7500	5600	4100	2950	1800
12	14300	10350	7900	5900	4300	3050	1900
14	14900	10450	8200	6200	4600	3150	2000
15	15200	10500	8400	6400	4800	3200	2050
Combined piles							
4	5000*	4100	3400	2700	1900	-	-
	4000	3600	3100	2500	1500	-	-
8	6400	5600	4000	3900	2600	-	-
	4900	4300	3700	3000	2000	-	-
12	7200	6400	5400	4400	3700	-	-
	5400	4800	4200	3600	2800	-	-
14	7600	6600	5800	4900	4000	-	-
	5600	500	4400	3800	3000	-	-
16	7800	6800	6000	5100	4200	-	-
	5800	5200	4600	4000	3100	-	-
18	8000	6900	6100	5200	4300	-	-
	5900	5300	4700	4100	3200	-	-
20	8200	7100	6200	5300	4400	-	-
	6100	5400	4800	4200	3300	-	-

\* For sandy soils the values of R are given in the numerator, and for dusty-clay soils - in denominator.

Table 3

Design negative friction forces $f_n$ of thawing soils, KPa			
Mean depth of soil layer location, m	large-fragment and sandy soils		
	large-fragment, gravel	coarse and medium-grain sands	fine and dusty sand
	dusty-clay soils with flow index J equal to		
	0	0,3	0,5
1	15	10	7
2	20	15	10
3	24	17	12
4	26	19	13
5	28	20	14
6	30	21	15
7	32	22	16
8	34	23	17
9	36	24	18
10	38	25	19

Table 2

Design resistances f of unfrozen and thawed of medium-density soils along the side surfaces of piles, KPa							
Mean depth of soil layer location, m	sandy soils						
	semi-gravel, large and medium grain size	fine	dusty	-	-	-	-
	dusty-clay, with flow index $J_L$ equal to						
	$\geq 0,2$	0,3	0,4	0,5	0,6	0,7	
4	58	42	30	24	18	8	
6	63	45	33	27	20	10	
8	67	48	36	29	22	12	
10	71	51	38	31	24	14	
12	75	53	40	33	26	16	

$$R_0 = 1.5d + 0.5 \text{ m.}$$

To determine the bearing capacity of bored after-driven and bored sunk piles in thawing soils the following method of static tests is recommended. The pile is sunk up to the designed level and the gap between its side surface and the frozen soil, that causes negative friction forces during thawing, and is filled with a casing. The internal diameter of the casing exceeds the maximum size of the pile cross-section. The external surface of the casing is in contact with the frozen soil and takes up negative friction forces  $F_{neg}$ , originated during the soil thawing and settling. The casing sinking depth should correspond to the thickness of the frozen soil layers having the total design settlement of no less than 5 cm during thawing.

A metal pipe thrust into the frozen soil to measure  $F_{neg}$  can be used. In this case for calculation of negative friction forces on piles which will be directly used for foundations the obtained value  $F_{neg}$  is multiplied by the conversion factor of friction  $K_f$ . For piles with hollows filled with concrete or cement mortars  $K_f$  is equal to 1.35, and for those filled with soil mortar - 0.8.

The tests include thawing of the frozen soil around the pile, measurement of the negative friction forces on the casing (metal pipe), thrusting of the pile by static loads and assumption of negative friction forces when calculating the bearing capacity of the pile. The value is determined by hanging the casing on a dynamometer. The soil around the pile should be unfrozen for the entire casing depth within the range  $R_0$ , which will exclude the effect of unfrozen soil interaction at the vertical thawing border with the frozen soil on the development of negative friction forces. The value  $R_0$  is determined by calculation (Instruction, 1988).

The ground below the casing is unfrozen within any radius equal or less than  $R_0$ , as the purpose of the thawing is to eliminate the freezing forces on the side surface of the pile and to prepare the bearing soil layer at pile

base for determining the strength and deformation properties under the action of thrusting static loads.

The indicated method of pile testing for statics in thawing soils does not exclude the use of other methods. For instance, for end-bearing piles the negative friction may be measured according to the test results of the same piles for pulling out from unfrozen soil within the radius  $R_0$ . Instead of measuring the negative friction forces on the casing, one may measure them on an additional piles installed near the basic one.

The above-stated features have formed the basis of the regional building standards and codes (Instruction, 1988). Their efficiency has been proved by almost five-year experience of using them in Magadan. As compared with the previous standards the design bearing capacity of bored after-driven and bored sunk constrained piles has been increased by 30 - 50%, and that of bored sunk combined piles - by 2 - 3 times. This has enabled to determine the optimum quantity and the sinking depth of piles in foundations of various buildings and engineering construction sites. An important reserve for increasing the efficiency of pile foundations in Magadan is the transfer to a more productive drilling of boreholes and mechanized methods of concreting at erection of substructure.

#### REFERENCES

Instructions on design and erection of pile foundations in unfrozen and thawing soils of Magadan area (Building Codes II0-OIO-87. - M.: Minvostokstroy USSR, 1988. - 38 p.

Konash V.E. 1977. Pile foundation on permafrost islands (example of Magadan). - L.: Stroyizdat. - 135 p.

Vlasov V.P. 1988. The experience of pile foundation engineering in Magadan area / Bases, foundations and soil mechanics. - No.4, p.2-4.

ENSURING STRUCTURAL STABILITY AND DURABILITY IN  
PERMAFROST GROUND AREAS AT GLOBAL WARMING OF THE EARTH'S CLIMATE

Vyalov S.S.<sup>1</sup>, Gerasimov A.S.<sup>2</sup>, Zolotar' A.J.<sup>2</sup>, Fotiev S.M.<sup>3</sup>

<sup>1</sup>Kuibyshev Civil Engineering Institute, Moscow, Russia

<sup>2</sup>Research Institute of experimental design of Constraction, St.-Peterburg, Russia

<sup>3</sup>Industrial and Research Institute for Engineering Investigation of Construction, Moscow, Russia

The paper discusses variations in frozen ground temperature conditions and load capacity under a warmer climate, listing techniques to ensure structural safety for buildings. The paper describes analogue simulation for frozen ground temperature and thawing depth changes and consequent durability deterioration under an increase in annual average air temperature of 2 and 4°C. Numerical calculations were performed with respect to four geothermal zones comprising the cryogenic region, in relation to annual average ground temperature. The paper demonstrates warming effects as negligible in northern zones, and fairly pronounce in southern zones, particularly in discontinuous permafrost, including total degradation.

Climatologists have predicted that the coming century will bring global warming of the Earth's climate, caused by a greenhouse effect from increased CO content in the atmosphere, partially resulting from human activities. The warming will undoubtedly affect the temperature and mechanical condition of permafrost masses.

Despite contradictions in the predicted numerical values, the has come engineers to define the directions of change in the mechanical properties of permafrost and to discuss potential approaches for neutralizing the changes, ensure stability of engineering structures in permafrost areas, both operational and newly constructed.

The issues of prospective climate warming have been discussed extensive by in the climatologic literature, reviewed, in particular, in papers (Anthropogenic..., 1987; Borisenkov, Kondrat'ev, 1988). Whereas the rates, values and even character of the warming vary considerably from one model to another, the majority of scientists seem to agree that, with a doubling of CO in the atmosphere, annual average air temperature increment by the middle of the next century will increase from 2 to 4°C. We have chosen these figures as our reference point. Budiko (1980) argues very forcefully, that warming will be strongest in high-latitude regions.

In evaluating the effects of a rise of annual average air temperature on permafrost ground conditions, one should bear in mind that both annual average air temperature and the temperature and thickness of ground ice vary meridionally. Consequently, the response and air-temperature sensitivity of the frozen layer will also vary with latitude. Thus, in northern latitudes, where thick permafrost contains large stores of cold, the warming effect will be negligible, while southern permafrost areas will be affected to the utmost degree. On the strength of the above stated, we have applied a latitude-zone principle

to categorize the whole cryogenic region in four geothermal zones, based upon the degree to which permafrost will resist 1 - 3°C annual average air temperature rise. As a criterion for the categorization, we have selected the permafrost ground annual average temperature  $T_z$ . Zone I - very unstable, comprises permafrost ground areas with temperature  $T_z$  from 0 to -1°C, zone II - mildly unstable, transitional, comprises the area with  $T_z$  from -1 to -3°C, zone III - stable, comprises the area with  $T_z$  from -3 to -7°C, and zone IV - very stable, comprises the area with  $T_z$  below -7°C.

Figure 1 is a map showing isothermic lines for permafrost ground annual average temperatures and geothermal zone boundaries. Figure 2 demonstrates the profiles marked in thick lines in Figure 1, along the 70°E meridian. The profile indicates permafrost ground thickness and annual average air and frozen ground temperatures, as well as geothermal zone boundaries. A characteristic feature of zone I, second in size, is the discontinuous, intermittent, almost insular character of permafrost ground; with permafrost ground there comprising from 5% at the southern to 50% at the northern boundary. Subsequently, frozen ground in the zone is fairly unstable with rises in air temperature. Zone II represents a narrow strip, with frozen ground comprising from 50% at the southern to 90 - 100% at the northern boundary, also unstable, although to a lesser degree. The zone seems to be transitional to stable zone III. The latter is characterized by continuous permafrost, comprising 95 - 100% of the area. Zone IV, the largest and very stable, is characterized by continuous low-temperature permafrost.

Mathematical simulations of warming effects on permafrost ground temperature and mechanical conditions was performed with respect to profile in Figure 2 for six geographical localities bent for the profile.



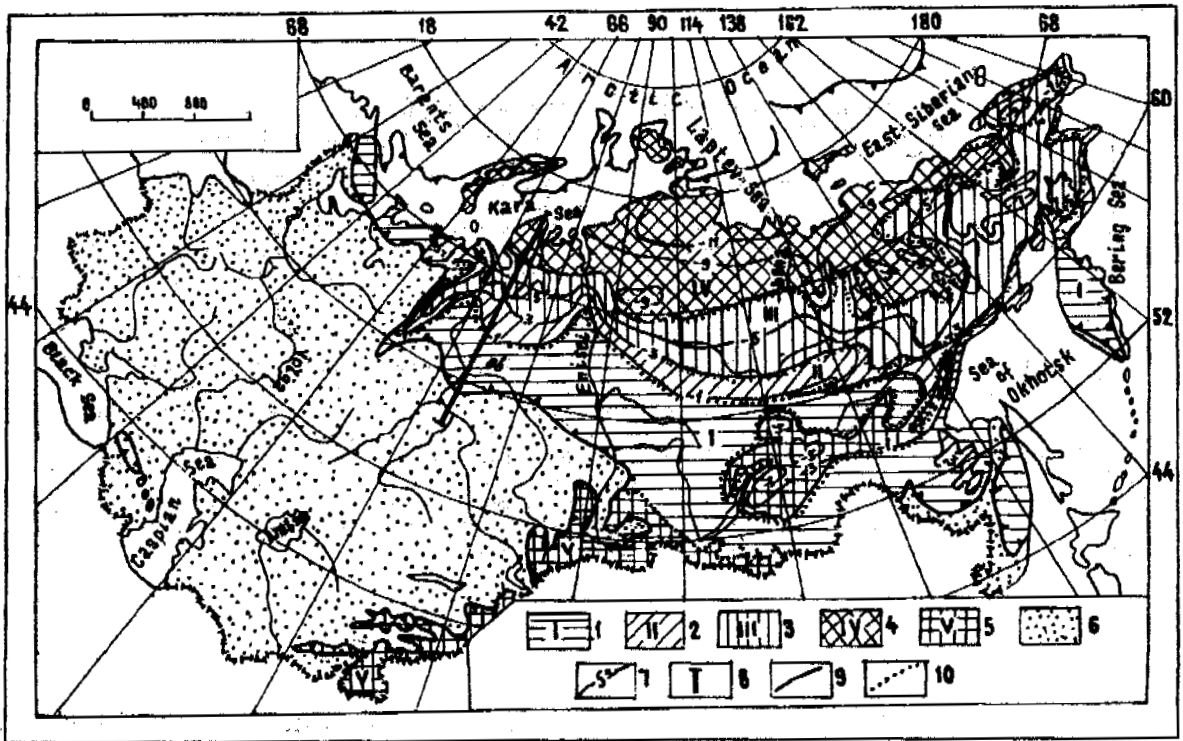


Figure 1. Chart of cryogenic region with defined geothermal zones: 1 - 5 - geothermal zones: 1 - zone I - Tz from 0 to -1°C; 2 - zone II - Tz from -1 to -3°C; 3 - zone III - Tz from -3 to -7°C; 4 - zone IV - Tz below -7°C; 5 - mountain frozen ground; 6 - positive-temperature grounds; 7 - isothermic lines for annual average ground temperature; 8 - profile with number; 9 - cryogeic region boundary; 10 - geothermal zone boundary. (Compiler Fotiev S.M.)

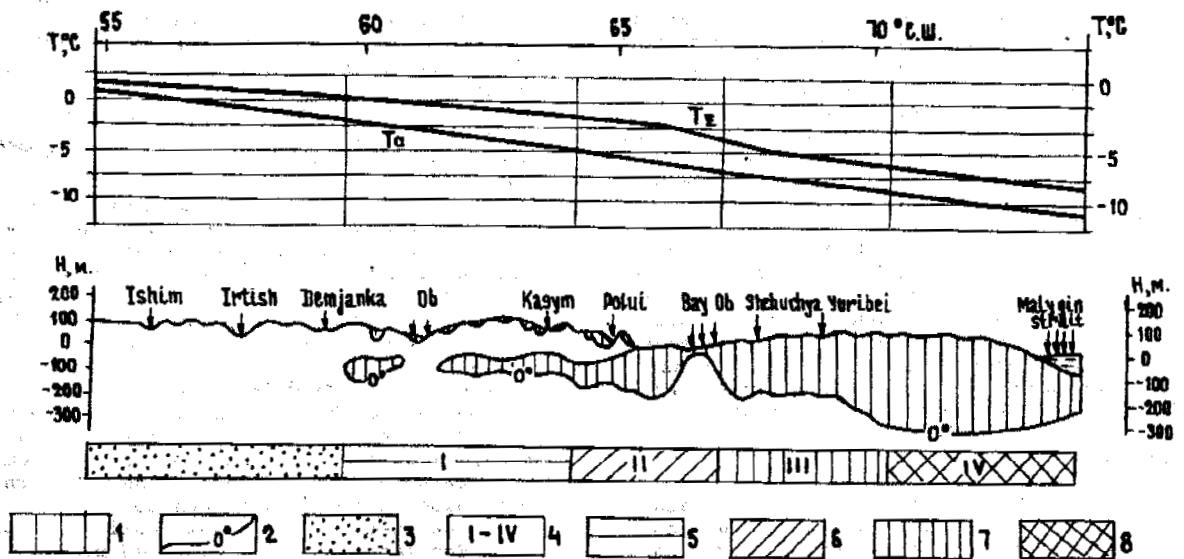


Figure 2. Profile of latitude-zone variations in annual average air temperature ( $T_a$ ) and permafrost ground temperature ( $T_z$ ), thickness and prevalence of permafrost layer along 70 EL (Western Siberia Designations): 1 - permafrost ground; 2 - isothermic line 0°C (Permafrost layer bottom); 3 - geothermal zone with temperature  $T_z$  from 0°C to +2°C and more; 4 - number for geothermal zones cryogenic region; 5 - 8 - geothermal zones with temperatures  $T_z$ , 5 - zone I  $T_z$  from 0 to -1°C; 6 - zone II -  $T_z$  from -1 to -3°C; 7 - zone III -  $T_z$  from -5 to -7°C; 8 - zone IV -  $T_z$  below -7°C. (Compiler Fotiev S.M.)

The annual average air  $T_a$  and ground  $T_z$  temperature (at the depth of 10 m) involved were as follows: for zone IV - Kharasovei,  $T_a = -9.9^\circ\text{C}$  and  $T_z = -7.8^\circ\text{C}$  and Dudinka  $T_a = -10.2^\circ\text{C}$  and  $T_z = -7.5^\circ\text{C}$ ; for zone III - Samur,  $T_a = -8.6^\circ\text{C}$  and  $T_z = -3.5^\circ\text{C}$ ; for zone II - Urangoi  $T_a = -7.5^\circ\text{C}$  and  $T_z = -1.5^\circ\text{C}$ ; for zone I - Numto  $T_a = -5.4^\circ\text{C}$  and  $T_z = -0.8^\circ\text{C}$ .

The simulation was performed by numerical computation in the modified programme developed in Research Institute of experiment design of Construction (St.-Peterburg). The annual average air temperature rise was assumed with the annual trend of 0.033 and 0.066°C, ensuring 60-year increments  $T_a = 2$  and  $4^\circ\text{C}$ , and remaining stable for the 10 years to follow.

Annual average air temperature variations were superimposed by seasonal fluctuations in the form of successive winter and summer sine curves. To provide for the set annual average temperature rise, winter and summer curve amplitudes received appropriate annual increments in the proportion 2:1.

The programme took account for snow (solid in northern and loose in southern zones) and vegetation cover. Soil was assumed to be loam, typical for the upper permafrost layers in Yamal.

Numerical calculations for selected localities defined frozen mass annual average temperatures and their fluctuations in time and depth, accounting for seasonal fluctuations. We also evaluated the role of snow-vegetation cover.

To evaluate changes in frozen ground stability characteristics, we developed a special unit using the obtained temperature variables and corresponding stability characteristics for frozen ground. In doing so, we also accounted for durability variations in time. Thus, in evaluating frozen ground load capacities and their variations with warming, we considered the following processes varying with time  $t$ :

- rock temperature variations in time and frozen layer thickness:

$$T = T(t, z) \quad (1)$$

- frozen ground durability  $R$  variations in time and depth, in accordance with law (Vialov, 1978)

$$R = \frac{\beta(T)}{\ln(t_f/B)} \quad (2)$$

where  $t_f$  - time before destruction,  $\beta$  - parameter dependent on ground temperature;  $B$  - soil constant;  
- durability-temperature relationship, according to the law

$$R = a + b \sqrt{|T(t)|} \quad (3)$$

Paper (Vialov, 1978) describes joint solution for the three equations obtainable from the integral equation

$$I \geq \int_0^{t_u} \frac{dt}{T_f(R, T)} \quad (4)$$

where  $t_u$  - structural service life, and  $t_f$  - time before destruction, correlation to the durability limit by (Borisenzov, Kondrat'ev, 1988).

Numerical evaluation using equation (Vialov, 1978) can define, for each time moment in

the warming process, and for each point in the frozen layer the permafrost ground durability and load capacity.

Simulation findings for changes of ground temperature in cryogenic regions for 50-year annual average air temperature rise are presented in Figure 3. They are:

- frozen ground annual average temperature at the depth of 10 m in localities examined at  $T_a = 2$  and  $4^\circ\text{C}$  will rise from  $-8$  to  $-6.5^\circ\text{C}$  and  $-5^\circ\text{C}$  in the 4th geothermal zone, from  $-1.3$  to  $-1.1$  and  $-1.0^\circ\text{C}$  in the 2th zone, and from  $-0.8$  to  $-0.7$  and  $-0.6^\circ\text{C}$  in the 1th zone (Figure 3a);

- depth of permafrost layers upper line (thawing depth) will increase by 15 - 30 cm in zone IV, by 28 - 85 cm in zone III, by 60 - 345 cm in zone II, and by 450 - 790 cm in zone I (Figure 3b,c). The underlined figures mean that thawing processes is progressive, generating discontinuous frozen ground;

- the thawing rate for frozen ground in the geothermal zones is 2.5 - 5.0 mm per year for zone IV; 3.0 - 14 mm per year for zone III; 10 - 60 mm per year for zone II and 75 - 130 mm per year for zone I.

Thus, for geothermal zones IV and III, the warming will merely result in slightly greater thawing depth, with no radical changes involving permafrost conditions. In zones II and, particularly, I the warming will have more tangible effects, resulting in overall generation of discontinuous frozen ground and taliks, with a tendency for complete degradation of existing ground ice. Eventually, if warming assumes an age-long character, the permafrost line can be drawn further north by 500 km along 70 EL and 1200 and even more km along the 100 EL. But, of course, the thawing can only occur if the climate is getting warmer for a very long (geological) period. Indeed, even at a thawing rate as high as 100 mm per year, thawing of a 10 m frozen layer in zone I will take 100 years. In this case, it will thaw gradually, with the rate lowered from south to north.

Of considerable interest is comparison of the predicted thawing rates with warming effects occurring in the Holocene, beginning 10.5 - 10 thousand years ago and lasting for 4 - 5000 years. In that period, with the air getting 3 - 4°C warmer, permafrost ground 200 m thick in 60 latitude and 50 - 100 m thick in 66 latitude completely, with permafrost line drawn north from 47 to 67 NL. The melting rate, therefore, comprised from 7 to 60 mm per year. Apparently, the previous and predicted thawing rates are of the same order, which - with all the assumptions involved in our forecasts, testify to their plausibility (Geocryology USSR, 1989, Fotiev, 1978).

Let us now discuss predicted changes in frozen ground durability in the course of warming. Numerical evaluations, using equation (Vialov, 1984) indicates, for example, ground-pile freezing durability limit - one of the basic frozen ground strength characteristics, to change in the 60-year design time within the following limits. In zone IV the maximum decrease will be by 3% with a temperature rise of  $2^\circ\text{C}$ , and 3 - 16% with rise of  $4^\circ\text{C}$ ; in zone III the decrease will comprise 8 - 17% at  $\Delta T_a = 2^\circ\text{C}$  and 35 - 50% at  $\Delta T_a = 4^\circ\text{C}$ ; in zone II durability will decrease by 20 - 37% at  $\Delta T_a = 2^\circ\text{C}$  and 46 - 53% at  $\Delta T = 4^\circ\text{C}$ .

As regards zone I, accounting for permafrost degradation, freezing durability decrease will

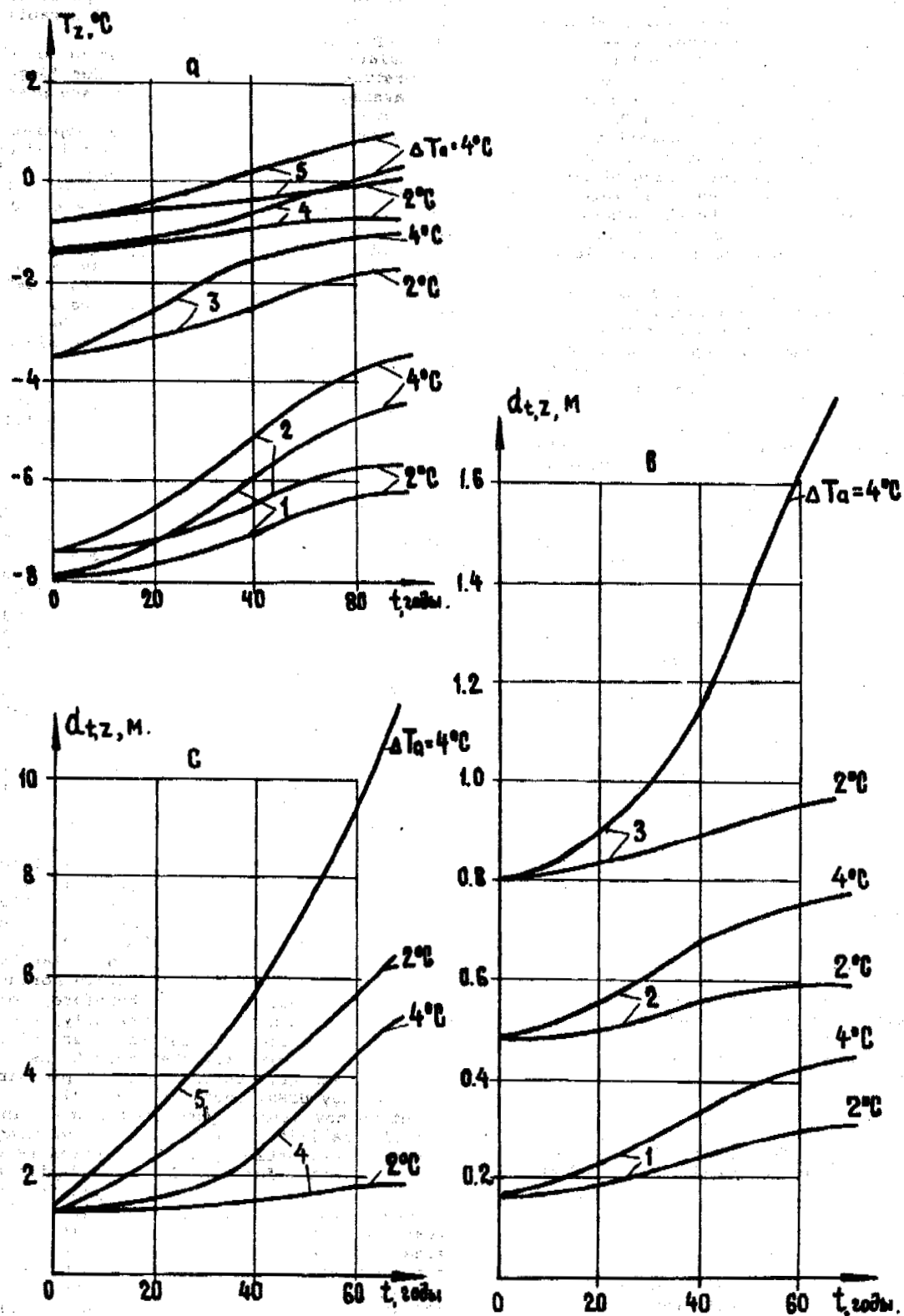


Figure 3. Changes in frozen ground annual average temperature,  $T_z$  (a) and upper line depth  $d_t$  (b,c) at  $T_a = 2^\circ\text{C}$  and  $4^\circ\text{C}$  temperature rise for localities: 1 - Kharasovei, 2 - Dudinka, 3 - Samburg, 4 - Uragoi, 5 - Numto.

comprise from 50% to 100%, so that structural reliability will require either special base cooling procedures, or the use of the second construction principle - allowing thawing.

The effects of potential climate warming in relation to structural stability and durability on permafrost grounds can be summed up as follows:

Within geothermal zone IV there will be a fairly slight deterioration of permafrost ground load capacity, to be easily balanced by some lowering in foundation temperatures to described below.

Within zone III, and particularly zone II, the warming will cause more tangible adverse effects on the stability and durability of structures.

Nevertheless, the warming effects can be neutralized by using the severity - of the northern climate. Indeed, annual average air temperature has always been 2 - 7°C lower than annual average permafrost ground temperature, so that, if the temperature difference can be introduced in the frozen layer, this can, if even partially, balance the air warming effect. Temperature condition control and temperature lowering in permafrost ground by utilizing natural cold can be managed by several techniques.

One is pre-construction ground cooling from the surface, by removing snow. Numerical evaluations indicate that with the surface cleaned of snow-vegetation cover, annual average frozen ground temperatures decrease as follows: in Kharasovei and Dudinka (zone IV) by 2.4 - 3.3°C respectively, in Samburg (zone III, loose snow cover) - by 5.9°C. In zone I (Vialov, 1984 and others) preliminary snow-clearance cooling in the 1st winter ensured an annual average frozen ground temperature decrease from -0.3 to -1.2°C and subsequent cooling in the service period brought the temperature in three years to -2.4°C, increasing overall freezing durability from 0.036 MPa to 0.150 MPa.

In-service base ground cooling is achieved through several strategies. The first is a traditional ventilated basement, with natural and sometimes forced winter air input. Our experience of many years has shown this to achieve a 1 - 3°C decrease in annual average frozen ground temperature. Another technique involves installing ventilation ducts in the ground under the floor of the building, with a natural, or if necessary a forced cold air input. If the structures are not very heavy, then of course we can use ventilated surface foundations set on bedding courses.

The most effective measure, however, is the use of seasonal thermal siphons and thermal piles with steam-fluid coolant. In winter the agent is circulated by density difference in the surface and subsurface sections of the plants. Put another way, the plants require no engines. They can be either fitted in the pile body (thermal piles), or fixed horizontally under the floor. In special cases (spacious structures), foundations can be cooled with the use of engines installed in summer.

The best results in improving frozen ground load capacity can be attained by combining the abovescribed measures for ground cooling using natural cold. Thus, the measures were utilized at the construction of an integrated house-building factory in Yakutsk. The construction site had extremely unfavourable frozen-ground conditions, the ground being high-temperature and highly saline, with extensive thawing zones. The temperature was -1.2 - -1.9°C, which, with the high

salinity, is close to the freezing point, exceeding it in the thawing zone, and in many places subzero grounds were thawing at the same time. Under the conditions, the following measures were taken to lower ground temperatures. First, before the construction works began, the ground was cooled from the surface, both by regular snow clearance and by forcing cold air through previously drilled (for subsequent pile setting) holes. For in-service cooling, a tall basement (from 1.2 to 2.5 m) with a forced ventilation system was installed, with thermal piles about the building perimeter. As a result, for five years oil service life only, base ground temperatures were 4°C lower and the whole base ground layer was completely frozen.

In conclusion, we would like to observe that, accounting for the coming climate warming, construction works in zones II - IV should generally be oriented toward preserving frozen foundations. This is important even if the construction principle permits ground temperature conditions control, using natural cold. This can be performed both for buildings under construction and completed (for example, by fitting thermal siphons).

This will be more complicated in zone I, with discontinuous and insular frozen ground degradation. Apparently, structure built in the zone according to the principle of allowable frozen ground thawing, or to the principle of preserving the frozen condition, will be subjected to greater deformations from climate warming, particularly in the latter case. To prevent deformations in completed structures, thawing process should be slowed down by cooling the grounds with thermal siphons, and even using engine-driven cooling plants. As regards structures in the course of construction, the construction principle should be selected from engineering-economical comparisons. In doing so, the principle of preserving ground frozen will require the most effective, combined base ground cooling procedures. With allowable thawing, on the one hand, one should aim at decreasing the sinking properties of thawing ground, which can usually be attained by preliminary thawing-overal or local (depending on the circumstances). But on the other hand, surface structures should be strengthened and integral functioning of the whole surface structure-foundation-base system ensured.

In conclusion, the prospective climate warming will undoubtedly cause changes in the properties of permafrost negligible in the northern and tangible in the southern section of cryogenic region. Nevertheless, warming effects can be balanced by utilizing the natural cold of northern regions. Meanwhile, appropriate measures should be developed in anticipation of climate warming. In doing so, an absolute requirement is to organize at all large units in permafrost areas regular monitoring of ground temperature conditions and structural deformations. And, of course, climatologists are responsible for specifications of numerical warming effects to be assumed as reference points for engineering design.

#### REFERENCES

- Anthropogenic Climatic Change (ed. by Budyko M.I. and Izrael' Yu.A.), (1987), Leningrad: Gidrometeoizdat, 406pp.

Borisencov E.P., Kondrat'ev K.Ia., (1988), Carbon Turnover and Climate, Leningrad: Gidrometeoizdat, 319 pp.  
Budyko M.I., (1980), Past and future climat, Leningrad: Gidrometeoizdat, 352 pp.  
Fotiev S.M., (1978), Hydrogeothermal peculiarity cryogenic region USSR, Moscow: Nauka, 136 pp.  
Geocryology USSR. Western Siberia, (1989), Moscow: Nedra, 454 pp.

Vialov S.S., (1979), Rheological Principles of Frozen Ground Mechanics, Moscow: Vysshiaia Shkola, 418 pp.  
Vialov S.S., Aleksandrov Iu.A., Gorodetskii S.E., Mirenburg Iu.S., Khrustalev L.N., (1984), Thermal Piles in Construction Engineering., Leningrad: Stroizdat, 148 pp.

## Author Index

- Aguirre Puente J., 611, 368  
 Akseennov V.I., 1  
 Alexeeva Olga I., 855  
 Allard Michel, 5, 182  
 An Viktor, 843  
 An Weidong, 11  
 Are Felix E., 436, 846  
 Ares R., 286  
 Aziz A., 17  
 Barry R.G., 23  
 Barsch Dietrich, 27  
 Bartoszewski Stefan A., 32  
 Belloni S., 36  
 Biggar Kevin W., 42  
 Bird Kenneth J., 94  
 Bondarenko G.I., 851  
 Brennan A.M., 23  
 Brewer M.C., 48  
 Brudie E.L., 244  
 Bruskov A.V., 1  
 Burgess M.M., 54  
 Burn C.R., 60  
 Burns R.A., 66  
 Butsenko A.N., 506  
 Calderoni G., 72  
 Caldwell J.B., 244  
 carter L. David, 48, 78  
 Carton A., 36  
 Cater Timothy C., 316  
 Chang Rudolf V., 855  
 Chang Xiaoxiao, 722  
 Chang Yen, 596  
 Chen Hongzhe, 105  
 Chen Xiaobai, 84, 143, 689  
 Cheng Enyuan, 302  
 Cheng Guodong, 675  
 Cheng Qinghua, 383  
 Chernyakov Yuri A., 862  
 Chuvilin E.M., 89, 160  
 Cohen Tenoudji F., 611  
 Collett Timothy S., 94  
 Corapcioglu M. Yavuz, 100  
 Cui Jianheng, 105  
 Cui Yongsheng, 407  
 Cui Zhijiu, 111, 397  
 Dai Baoguo, 116  
 Dai Chuntian, 116  
 Dai Huimin, 120  
 Dai Pin, 116  
 Dallimore S.R., 125  
 Danilov Igor D., 858  
 Demidov V.V., 506  
 Deng Yousheng, 131, 773  
 Devjatkin, V.N., 134  
 Ding Jingkan, 138  
 Ding Yongqin, 143  
 Domaschuk L., 149  
 Dramis F., 36  
 Du Chengxian, 116  
 Dubina Mikhail M., 862  
 Dubreuil Marie-Andree, 255  
 Duchkov A.D., 134  
 Dydysko P.L., 155  
 Ershov E.D., 89, 160  
 Esch David C., 164  
 Everett Kaye R., 267  
 Fang Tsung Ping, 586  
 Fediukin Igor V., 170  
 Fedoseeva Valentina J., 865  
 Fei T., 500  
 Feng Ke, 768  
 Feng Yanhui, 789  
 Ferrell John E., 471  
 Forbes Bruce C., 176  
 Fortier Richard, 182  
 Fotiev S.M., 955  
 Frech Hugh M., 482  
 Frolov Anatoly D., 170  
 Frydecki Janusz, 5  
 Fukuda M., 488  
 Gao Xingwang, 188  
 Garneau R.R., 286  
 Gerasimov A.S., 955  
 Gershevich V.D., 506  
 Gilichinsky David A., 869  
 Glenn R., 48  
 Goncharov Ju.M., 875  
 Gorelik Yakov, 879  
 Gorainov N.N., 66  
 Gotovtsev Semyon P., 891  
 Gray James T., 192  
 Grechishchev Stanislav E., 54, 198  
 Gu Zhongwei, 204, 388, 778, 819  
 Guevorkian S.G., 660  
 Guglielmin M., 72  
 Guo Dongxing, 210, 282, 809  
 Guo Xingming, 835  
 Guryanov Igor E., 885  
 Guthrie Robert S., 694  
 Haerberli Wilfried, 214, 272  
 Hall Kevin J., 220  
 Hallet B., 226  
 Hansueli Gubler, 332  
 Harris Charles, 232  
 Harris Stuart A., 238  
 Hartzmann Ronald J., 574  
 Hazen Beez, 244, 494  
 He Ping, 250  
 He Yixiang, 718  
 Heginbottom J. Alan, 255  
 Heuer C.F., 244  
 Hinkel Kenneth M., 261  
 Hinzman Larry D., 267, 326  
 Hirzkawa Kazuomi, 449  
 Hivon Elisabeth G., 42  
 Hoelzle Martin, 214, 272  
 Hou Zhongjie, 556, 608  
 Hu Shicai, 416  
 Huang Maohuan, 278  
 Huang Yizhi, 210, 282, 758, 809  
 Huneault P.A., 286  
 Hunter J.A., 66  
 Iordanescu M., 286  
 Jakob Matthias, 27  
 Janoo Vincent, 292  
 Jian Gong, 298  
 Jiang Hongju, 302  
 Jiang Weiqiang, 592  
 Jin Huijun, 307, 803  
 Jin Naichui, 312  
 Jin Zhengmei, 278  
 Jorgenson M. Torre, 316  
 Joshi Ramesh C., 706  
 Joyce Michael R., 316  
 Jr Bayer John, 292  
 Judge A.S., 11, 66  
 Jung Duhwoe, 648  
 Kagan A.A., 730  
 Kamensky Rosteslav M., 322  
 Kane Douglas L., 267, 326  
 Kasse C., 643  
 Keller Felix, 214, 272, 332  
 Kershaw G.Peter, 338  
 King Lorenz, 344, 625  
 Klimovsky Igor V., 891  
 Klimowicz Zbigniew, 350  
 Kolunin Vladimir, 879  
 Kondratyev V.G., 155  
 Koniakhin M.A., 937  
 Konrad J.M., 550  
 Konstantinov Innokentii P., 322  
 Kritsuk L.N., 897  
 Krivonogova N.P., 730  
 Kunitsky Viktor V., 903  
 Kurfurst P.J., 54, 356  
 Kurilchik A.F., 909  
 Kutasov I.M., 362  
 Kwok R., 149  
 Lauriol Bernard, 192  
 Lebedenko Yu.P., 160  
 Leclair P., 368, 611  
 Lehmann Rainer, 374  
 Leibman M.O., 380  
 Lewkowicz Antoni G., 232  
 Li Anguo, 383  
 Li Dazhou, 592  
 Li Dongqing, 835  
 Li Gang, 278  
 Li Hao, 383  
 Liang Fengxian, 204, 388, 744, 819  
 Liang Linheng, 204, 393, 778, 819  
 Lilly E.K., 326  
 Lin Chuanwei, 685  
 Lin Ying, 312  
 Liu Fengjing, 738  
 Liu Gengnian, 397  
 Liu Hongxu, 403  
 Liu Qingren, 116, 407  
 Liu Yifeng, 429  
 Liu Yongzhi, 722, 764  
 Liu Zongchao, 429  
 Lomborinchen R., 411  
 Lou Anjin, 138  
 Lozej A., 72  
 Lu Heiyen, 797  
 Lu Xingliang, 416  
 Lunardini Virgil J., 17, 420  
 Luo Minru, 426, 622  
 Ma Hong, 429  
 Ma Wei, 432, 556, 722  
 Magierski Jan, 32  
 Makarov Vladimir N., 911  
 Makeev O.V., 506  
 Mamzelev Anatoly P., 436  
 Marsh Philip, 443  
 Matsuoka Norikazu, 449  
 Malke Jerzy, 350  
 Melnikov E.S., 54, 356  
 Melnikov Vladimir, 455

Meltzer Liya I., 914  
Mi Haizheng, 461  
Miao Lina, 278  
Michalczyk Zdzislaw, 32  
Michalowski Radoslaw L., 465  
Migala Krzysztof, 919  
Mobley Keith F., 471  
Molmann Truls, 477  
Moore J.P., 517  
Moskalenko N.G., 54  
Murashko A.A., 89  
Murray D.F., 48  
Murton Julian B., 482  
Na Wenjie, 592  
Na Yunlong, 426  
Nakano Yoshisuke, 750  
Nakayama T., 488  
Nelson Frederick E., 261  
Nixon J.F., (Derick), 244, 494  
Olovin Boris A., 923  
Osterkamp T.E., 783, 500  
Ostroumov V.E., 506  
Outcalt Samuel I., 261  
Ozouf J.C.I., 523  
Panday Sorab M., 100  
Pavlov A.V., 511  
Perlshtein G.Z., 909  
Pilon Jean A., 5  
Ping C.L., 517  
Pissart A., 523  
Polyakov V.A., 897  
Popov Kiktor A., 322  
Poznanin V.L., 660  
Prick A., 523  
Prigoda V.Ya., 155  
Qiao Dianshi, 529  
Qiu Guoqing, 307, 533, 803  
Qu Xiangming, 312  
Rasmussen L.A., 226  
Rivkin, F.M., 380  
Rivkina Elizaveta M., 869  
Rooney James W., 648  
Roujansky Vladislav E., 858  
Sadakova M.N., 155  
Salnikov P.I., 927  
Samarkin Vladimir A., 869  
Samyshin V.K., 909  
Sarrelainen Seppo, 539  
Saveliv V.S., 380  
Savitsky Victor A., 846  
Schmid Willy, 214, 654  
Schmitt Elisabeth, 544  
Sego Dave C., 42  
Seguin Maurice-K., 182  
Senneset Kaare, 477  
Shankov Vladimir V., 198  
Shen Mu, 550  
Sheng Yu, 556  
Sheng Zhongyan, 250  
Shields D.H., 149  
Shoop Sally A., 559  
Shpolyanskaya N.A., 930  
Shur Y.L., 564  
Siegert Christine, 569  
Skaret Kevin D., 338  
Skvortsov A.G., 66  
Slaughter Charles W., 574  
Slavin Borovskiy V.B., 564  
Sletten Ronald S., 580  
Smiraglia C., 36  
Smorygin Gennadi, 455  
Snegirev A.M., 934  
Sokolova L.S., 134  
Solomatin V.I., 937  
Sone T., 488  
Song Changqing, 111, 832  
Soo Sweanum, 586  
Streltsova O.A., 865  
Sui Tieling, 592  
Sun Zhenkun, 407  
Svec Otto J., 596  
Tang Shuchun, 602  
Tang Xiaobo, 605  
Tang Zhonghai, 832  
Tao Zhaoxiang, 608, 773  
Tarasov A.M., 356  
Taylor A.E., 125  
Tellini C., 72  
Tenoudji F. Cohen, 368  
Thimus J.F., 611  
Timofeev V.M., 66  
Todd B.J., 66  
Tomita Hsiao, 292  
Tong Boliang, 617  
Tong Changjiang, 622  
Torgashov Y.Y., 941  
Tremblay Clement, 5  
Tschervova E.I., 356  
Ulrich Roland, 625  
Urdea Petru, 631  
Uziak Stanislaw, 350  
Valuyev A.S., 155  
Van Everdingen Robert O., 638  
Vandenbergh J., 643  
Vasil'chuk Yuriy K., 945  
Vasilyev M.L., 155  
Vinson Ted S., 648  
Vlasov Vladimir P., 951  
Vonder Muhll Daniel S., 214, 654  
Vtyurina E.A., 660  
Vyalov S.S., 955  
Wagner S., 214  
Walsh Michael, 292  
Wang Baolai, 664  
Wang Chunhe, 670  
Wang Guangzhou, 832  
Wang Jiacheng, 675, 734, 778  
Wang Jianping, 678  
Wang Qiang, 744  
Wang Shaoling, 461  
Wang Shujuan, 307  
Wang Wenkai, 685  
Wang X.L., 120  
Wang Yaqing, 689  
Wang Yinmei, 768  
Wang Zengting, 678  
Wang Zeren, 730  
Wang Zhanchen, 755  
Wayne William J., 694  
White T.L., 700  
Wijeweera Harsha, 706  
Williams P.J., 700  
Woo Ming-Ko, 443, 712, 725, 738  
Wu Jinming, 138  
Wu Qijian, 678  
Wu Qingbai, 718  
Wu Ziwang, 11, 432, 722  
Xen Zhenyao, 797  
Xia Zhaojun, 725  
Xia Zhiying, 758  
Xiong Heigang, 397  
Xu Bomeng, 416, 730  
Xu Dongzhou, 105  
Xu Jingguang, 529  
Xu Xiaozu, 131, 734, 773  
Yakushev V.S., 160  
Yang Daqing, 738  
Yang Zhenniang, 738, 744  
Yang Zhihuai, 744  
Yen Yinchao, 750  
Yi Qun, 797  
Young Kathy L., 712  
Yu Qihao, 250  
Yu Shengqing, 416, 755  
Zeng Zhonggong, 307, 758  
Zhang Changqing, 432, 722, 764  
Zhang Duo, 789  
Zhang Huyuan, 768  
Zhang Jianming, 764  
Zhang Jiayi, 250  
Zhang Jingzhao, 138  
Zhang Lixin, 131, 608, 773  
Zhang Qibin, 204, 778, 819  
Zhang T., 783  
Zhang Xianggong, 768  
Zhang Xikun, 529  
Zhang Xin, 789  
Zhang Yuanyou, 312  
Zhang Zeyou, 793  
Zhang Zhaoxiang, 797  
Zhao Jun, 813  
Zhao Lin, 307, 803  
Zhao Xiufeng, 210, 282, 809  
Zhao Yutain, 813  
Zhou Xinqing, 426  
Zhou Youwu, 204, 393, 778, 819  
Zhu Cheng, 826  
Zhu Jinghu, 832  
Zhu Linnan, 764, 835  
Zhu Qiang, 838  
Zhu Yuanlin, 11, 250  
Zolotar A.J., 955

## General Subject--Senior Author Index

### CANAL

Chang Rudolf V., 855  
Jian Gong, 298  
Jin Naichui, 312  
Li Anguo, 383  
Qiao Dianshi, 529  
Wang Wenkai, 685  
Xu Bomeng, 730  
Zhang Changqing, 764  
Zhu Qiang, 838

### CHEMISTRY OF FROZEN SOILS

Deng Yousheng, 131  
Ershov E.D., 160  
Melnikov Vladimir, 455  
Osterkamp T.E., 500  
Ostroumov V.E., 506

### CIVIL ENGINEERING

Aksenov V.I., 1  
Goncharov Ju.M., 875  
Huneault P.A., 286  
Kutasov I.M., 362  
Sui Tieling, 592  
Tang Shuchun, 602  
Tong Changjiang, 622  
Torgashov Y.Y., 941  
Ulrich Roland, 625  
Vlasov Vladimir P., 951  
Vyalov S.S., 955

### CLIMATE CHANGE

Carter L. David, 78  
Nakayama T., 488  
Schmitt Elisabeth, 544  
Zhang T., 783  
Zhao Xiufeng, 809

### DISASTER AND ENVIRONMENT PROTECTION

Forbes Bruce C., 176  
Huang Yizhi, 282  
Jorgenson M. Torre, 316  
Kamensky R.M., 322  
Makarov Vladimir N., 911  
Olovin Boris A., 923  
Zhang Qibin, 778  
Zhou Youwu, 819

### ECOLOGY

Dai Chuntian, 116  
Gilichinsky David A., 869  
Liu Qingren, 407  
Meltzer Liya I., 914  
Zhao Yutian, 813

### EQUIPMENT

Fottier Richard, 182  
Tao Zhaoxiang, 608

### FROST HEAVING

Dai Huimin, 120  
Ding Yongqin, 143  
Grechishchev S.E., 198  
Jiang Hongju, 302  
Michalowski R.L., 465  
Pissart A., 523  
Shen Mu, 550  
Svec Otto J., 596

### GENERAL

Barry R.G., 23  
Van Everdingen R.O., 638

### GEOPHYSICAL PROSPECTING

Snegirev A.M., 934  
Zeng Zhonggong, 758

### GEOTECHNICAL PROPERTIES

Lu Xingliang, 416

### HEAT-MASS TRANSFER

Gao Xingwang, 188  
Hallet B., 226  
Hoelzle Martin, 272  
Sheng Yu, 556  
Xia Zhao Jun, 725  
Xu Xiaozu, 734  
Yen Yin-Chao, 750  
Zhang Lixin, 773

### HYDROLOGY AND WATER RESOURCE

Bartoszewski S.A., 32  
Brewer M.C., 48  
Hinzman Larry D., 267  
Kane D.L., 326  
Marsh Philip, 443  
Woo Ming-Ko, 712  
Yang Daqing, 738  
Yang Zhenniangu, 744

### MINING

Dubina Mikhail M., 862  
Wang Jianping, 678

### PERIGLACIAL PHENOMENA

Barsch Dietrich, 27  
Bondarenko G.I., 851  
Burn C.R., 60  
Calderoni G., 72  
Cui Zhijiu, 111  
Guo Dongxin, 210  
Harris Charles, 232  
Harris Stuart A., 238  
Kritsuk L.N., 897  
Kunitsky Viktor V., 903  
Leibman M.O., 380  
Liu Gennian, 397

Luo Minru, 426  
Matsuoka Norikazu, 449  
Murton Julian B., 482  
Shpolyanskaya N.A., 930  
Slaughter Charles W., 574  
Solomatin V.I., 937  
Soo Sweanum, 586  
Tong Boliang, 617  
Vonder Muhll D.S., 654  
Vtyurina E.A., 660  
Wang Baolai, 664  
Wang Chunhe, 670  
Wayne William J., 694  
Zhu Cheng, 826  
Zhu Jinghu, 832

### PHYSICS OF FROZEN SOILS

Chuvilin E.M., 89  
Corapcioglu M.Y., 100  
Fediukin Igor V., 170  
Fedoseeva V.I., 865  
Gorelik Yakov, 879  
Guryanov Igor E., 885  
He Ping, 250  
Huang Maohuan, 278  
Janoo Vincent, 292  
Leclaire P., 368  
Ma Wei, 432  
Sletten Ronald S., 580  
Thimus J.F., 611  
Wang Jiacheng, 675  
White T.L., 700  
Wijeweera Harsha, 706  
Wu Ziwang, 722  
Zhang Huyuan, 768  
Zhang Zhaoxiang, 797  
Zhu Linnan, 835

### PIPELINE

Biggar Kevin W., 42  
Burgess M.M., 54  
Ding Jingkan, 138  
Domaschuk L., 149  
Liu Hongxu, 403  
Mobley Keith F., 471  
Molmann Truls, 477  
Nixon J.F., 494  
Zhang Xin, 789

### REGIONAL GEOCRYOLOGY

Allard Michel, 5  
An Viktor, 843  
Are Felix E., 846  
Aziz A., 17  
Belloni S., 36  
Chen Xiaobai, 84  
Collett Timothy S., 94  
Dallimore S.R., 125  
Danilov Igor D., 858  
Devjatkin V.N., 134  
Gray James T., 192  
Gu Zhongwei, 204  
Haerberli Wilfried, 214



Hall Kevin J., 220  
Hazen Beez, 244  
Heginbottom J. Alan, 255  
Hinkel K.M., 261  
Jin Huijun, 307  
Keller Felix, 332  
Kershaw G. Peter, 338  
King Lorenz, 344  
Klimovsky Igor V., 891  
Klimowicz Zbigniew, 350  
Kurfurst P.J., 356  
Lehmann Rainer, 374  
Liang Linheng, 393  
Lomborinchen R., 411  
Lunardini Virgil J., 420  
Ma Hong, 429  
Manzelev A.P., 436

Migala Krzysztof, 919  
Pavlov A.V., 511  
Ping C.L., 517  
Qiu Guoqing, 533  
Salnikov P.I., 927  
Shur Y.L., 564  
Stegert Christine, 569  
Urdea Petru, 631  
Vandenberghe J., 643  
Vasil'chuk Yuriy K., 945  
Wang Yaqing, 689  
Wu Qingbai, 718  
Yu Shengqing, 755  
Zhang Zeyou, 793  
Zhao Lin, 803

#### REMOTE SENSING AND MAPPING

Burns R.A., 66  
Liang Fengxian, 388

#### ROADS

An Weidong, 11  
Cui Jianheng, 105  
Dydysenko P.I., 155  
Esch David C., 164  
Kurilchik A.F., 909  
Mi Haizhen, 461  
Saarelainen Seppo, 539  
Shoop Sally A., 559  
Tang Xiaobo, 605  
Vinson Ted S., 648